

**EVALUATION OF PRESSURE AND THERMAL DATA  
FROM A WIND TUNNEL TEST OF A  
LARGE-SCALE, POWERED, STOL FIGHTER MODEL**

(NASA-CR-166170) EVALUATION OF PRESSURE AND THERMAL DATA FROM A WIND TUNNEL TEST OF A LARGE-SCALE, POWERED, STOL FIGHTER MODEL Final Report, 4 Jun. 1980 - 4 Jun. 1981 (General Dynamics Corp.) 987 p

N81-33162

HC A99/MF AD1

Unclass

G3/02 38214

By

G. A. Howell  
E. L. Crosthwait  
M. C. Witte

June 1981

Prepared under Contract No. NAS2-10649

By

GENERAL DYNAMICS  
Fort Worth Division

For

AMES RESEARCH CENTER  
NATIONAL AERONAUTICS AND SPACE ADMINISTRATION



57

**EVALUATION OF PRESSURE AND THERMAL DATA  
FROM A WIND TUNNEL TEST OF A  
LARGE-SCALE, POWERED, STOL FIGHTER MODEL**

**By**

**G. A. Howell  
E. L. Crosthwait  
M. C. Witte**

**June 1981**

**Prepared under Contract No. NAS2-10649**

**By**

**GENERAL DYNAMICS  
Fort Worth Division**

**For**

**AMES RESEARCH CENTER  
NATIONAL AERONAUTICS AND SPACE ADMINISTRATION**



1. Report No. NASA CR-166170		2. Government Accession No.		3. Recipient's Catalog No.	
4. Title and Subtitle EVALUATION OF PRESSURE AND THERMAL DATA FROM A WIND TUNNEL TEST OF A LARGE-SCALE, POWERED, STOL FIGHTER MODEL				5. Report Date June, 1981	
				6. Performing Organization Code	
7. Author(s) G. A. Howell E. L. Crosthwait M. C. Witte				8. Performing Organization Report No.	
9. Performing Organization Name and Address  General Dynamics Fort Worth Division P. O. Box 748, Fort Worth, Texas 76101				10. Work Unit No.	
				11. Contract or Grant No. NAS2-10649	
12. Sponsoring Agency Name and Address Ames Research Center Moffett Field, CA 94035				13. Type of Report and Period Covered Contractor Final Report June 4, 1980-June 4, 1981	
				14. Sponsoring Agency Code	
15. Supplementary Notes  Ames Research Center Technical Monitor: Michael D. Falarski (415) 965-5046					
16. Abstract  A STOL fighter model employing the Vectored-Engine-Over Wing concept was tested at low speeds in the NASA/Ames 40x80-Foot Wind Tunnel. The model, approximately 0.75 scale of an operational fighter, was powered by two General Electric J-97 turbojet engines. Limited pressure and thermal instrumentation were provided to measure power effects (chordwise and spanwise blowing) and control-surface-deflection effects.  An indepth study of the pressure and temperature data revealed many flowfield features - the foremost being wing and canard leading-edge vortices. These vortices delineated regions of attached and separated flow, and their movements were often keys to an understanding of flow-field changes caused by power and control-surface variations.  Chordwise blowing increased wing lift and caused a modest aft shift in the center of pressure. The induced effects of chordwise blowing extended forward to the canard and significantly increased the canard lift when the surface was stalled. Spanwise blowing effectively enhanced the wing leading-edge vortex, thereby increasing lift and causing a forward shift in the center of pressure.  The effects of power on the pressures and forces on the model were estimated with two analytical methods; test-to-theory comparisons are presented for each method.					
17. Key Words (Suggested by Author(s)) Powered-lift Prediction Methods Spanwise Blowing STOL Aerodynamics				18. Distribution Statement	
19. Security Classif. (of this report) Unclassified		20. Security Classif. (of this page) Unclassified		21. No. of Pages 956	
				22. Price*	

For sale by the National Technical Information Service, Springfield, Virginia 22161

## TABLE OF CONTENTS

<u>Section</u>	<u>Page</u>
SYMBOLS	iv
LIST OF FIGURES	vi
LIST OF TABLES	xxviii
1. INTRODUCTION	1
2. DESCRIPTION OF MODEL AND TEST PROGRAM	3
2.1 Model Description	3
2.2 Instrumentation	4
2.3 Test Conditions	4
3. FLOW FIELD ANALYSIS	23
3.1 Overview	23
3.2 Wing and Canard Results	
3.2.1 Key Flow Features	39
3.2.2 Wing Without Canard	41
3.2.2.1 Basic Flowfield Characteristics and Flap Effects	41
3.2.2.2 Power Effects Without Spanwise Blowing	43
3.2.2.3 Spanwise Blowing Effects	46
3.2.3 Canard	231
3.2.3.1 Basic Flowfield Characteristics and Flap Effects	231
3.2.3.2 Wing-Induced Effects	233
3.2.4 Wing With Canard	321
3.2.4.1 Basic Flowfield Characteristics and Data Preview	321
3.2.4.2 Canard Effects	322
3.2.4.3 Wing Flap Effects	331
3.2.4.4 Power Effects Without Spanwise Blowing	333
3.2.4.5 Spanwise Blowing Effects	335
3.2.5 Correlation with Small-Scale Model	815

## TABLE OF CONTENTS (Cont'd)

<u>Section</u>	<u>Page</u>
3.3 Strake Results	851
3.4 Beaver Tail Results	873
3.5 Nozzle Flap Results	885
3.6 Thermal Analysis and Correlation with Pressure Data	891
3.6.1 Wing Upper Surface	891
3.6.2 Beaver Tail	893
4. ANALYTICAL EVALUATION	923
4.1 Elementary Vortex Distribution Method	923
4.2 Powered-Lift Prediction Method	939
5. CONCLUSIONS AND RECOMMENDATIONS	949
5.1 Flowfield	949
5.2 Configuration Design	950
5.3 Instrumentation	951
5.4 Test Procedures	952
5.5 Analytical Methods	953
REFERENCES	955

## LIST OF SYMBOLS

$B, b$	Wing span
$Y, y$	Spanwise station
$C_D$	Drag coefficient
$C_L$	Lift coefficient
$C_M$	Pitching moment coefficient
$C_{l'}, C_{l'}$	Section lift coefficient ( $C_N \cos \alpha$ )
$C_{l'_c}$	Canard section lift coefficient
$C_p$	Pressure coefficient
$C_{p_l}$	Pressure coefficient, lower surface
$C_{p_u}$	Pressure coefficient, upper surface
$C_T$	Thrust coefficient
EPR	Engine duct pressure ratio
ITEF, $\delta TE_i$	Inboard trailing-edge flap deflection
OTEF, $\delta TE_o$	Outboard trailing-edge flap deflection
$q$	Dynamic pressure
Re	Reynolds number
$S$	Wing area
SWB	Spanwise blowing
TEDFTP	Total engine duct fore temperature, port engine
$\Delta T$	Incremental temperature above tunnel temperature
$T$	Thrust
$x$	Longitudinal distance from leading edge
$c$	Local chord
$(x/c)_{cp}$	Center of pressure location
$\alpha$	Angle of attack
$\delta_c$	Canard deflection
$\delta_l, \delta_{l'}$	Canard leading-edge deflection

$\delta_t$	Canard trailing-edge deflection
$\alpha_l^* , \alpha_l^*$	Angle of attack when leading-edge stall first occurs
$\alpha_t^*$	Angle of attack when leading-edge vortex first reaches trailing edge
$\eta$	$2y/b$
$\delta_{TE}$	Trailing-edge flap deflection (Inboard/Outboard)
$\Delta C_p$	$C_{p_u} - C_{p_l}$
$\delta \Delta C_p$	Change in $\Delta C_p$

## LIST OF FIGURES

Figure		Page
2-1	STOL Fighter Model in NASA/Ames 40 x 80-Foot Wind Tunnel, Upper View	16
2-2	STOL Fighter Model in NASA/Ames 40 x 80-Foot Wind Tunnel, Lower View	17
2-3	STOL Fighter Model Geometry	18
2-4	Port Nozzle Geometry	19
2-5	Pressure Tap Locations	20
2-6	Rake Installation	21
3.1-1	Common Pressure Distributions, Alpha = 4 deg	25
3.1-2	Common Pressure Distributions, Alpha = 20 deg	26
3.1-3(a)	Reynolds Number Effects, Alpha = 4 deg	27
3.1-3(b)	Reynolds Number Effects, Alpha = 8 deg	28
3.1-4(a)	Canard Effects, Alpha = 4 deg	29
3.1-4(b)	Canard Effects, Alpha = 8 deg	30
3.1-5	Wing Flap Effects	31
3.1-6(a)	Power Effects, Alpha = 4 deg	32
3.1-6(b)	Power Effects, Alpha = 29 deg	33
3.1-7(a)	Spanwise Blowing Effects, Alpha = 0 deg	34
3.1-7(b)	Spanwise Blowing Effects, Alpha = 12 deg	35
3.1-7(c)	Spanwise Blowing Effects, Alpha = 21 deg	36
3.1-8	Beaver Tail Deflection Effects	37

## LIST OF FIGURES

Figure		Page
3.2.2	Angle of Attack Effects, Power Off	49
-1	Flaps Neutral, Inboard	
-2	Flaps Neutral, Outboard	
-3	Flaps Neutral, Spanwise	
-4	Flaps Deflected, Inboard	
-5	Flaps Deflected, Outboard	
-6	Flaps Deflected, Spanwise	
3.2.2-7	Origin of Wing Leading-Edge Vortex, Canard Off	
3.2.2	Wing Trailing-Edge Flap Effects, Power Off	56
-8	Alpha = 0 deg, Inboard	
-9	Alpha = 8 deg, Inboard	
-10	Alpha = 12 deg, Inboard	
-11	Alpha = 16 deg, Inboard	
-12	Alpha = 0 deg, Outboard	
-13	Alpha = 8 deg, Outboard	
-14	Alpha = 12 deg, Outboard	
-15	Alpha = 16 deg, Outboard	
-16	Alpha = 0 deg, Spanwise	
-17	Alpha = 8 deg, Spanwise	
-18	Alpha = 12 deg, Spanwise	
-19	Alpha = 16 deg, Spanwise	
-20	Inboard, Integrated Section Properties	
-21	Outboard, Integrated Section Properties	
3.2.2	Wing Trailing-Edge Flap Effects, Power On,	70
-22	Inboard, Alpha = 0 deg	
-23	Inboard, Alpha = 4 deg	
-24	Inboard, Alpha = 8 deg	
-25	Inboard, Alpha = 12 deg	
-26	Inboard, Alpha = 16 deg	
-27	Outboard, Alpha = 0 deg	
-28	Outboard, Alpha = 4 deg	
-29	Outboard, Alpha = 8 deg	
-30	Outboard, Alpha = 12 deg	
-31	Outboard, Alpha = 16 deg	
-32	Spanwise, Alpha = 0 deg	
-33	Spanwise, Alpha = 4 deg	
-34	Spanwise, Alpha = 8 deg	
-35	Spanwise, Alpha = 12 deg	
-36	Spanwise, Alpha = 16 deg	
-37	Inboard, Integrated Section Properties	
-38	Outboard, Integrated Section Properties	
3.2.2	Power Effects, Flaps Neutral	87
-39	Inboard, Alpha = 0 deg	
-40	Inboard, Alpha = 4 deg	
-41	Inboard, Alpha = 8 deg	

## LIST OF FIGURES

Figure		Page
3.2.2	Power Effects, Flaps Neutral (cont'd)	
-42	Inboard, Alpha = 12 deg	90
-43	Inboard, Alpha = 16 deg	
-44	Inboard, Alpha = 20 deg	
-45	Inboard, Alpha = 24 deg	
-46	Inboard, Alpha = 28 deg	
-47	Inboard, Alpha = 32 deg	
-48	Outboard, Alpha = 0 deg	
-49	Outboard, Alpha = 4 deg	
-50	Outboard, Alpha = 8 deg	
-51	Outboard, Alpha = 12 deg	
-52	Outboard, Alpha = 16 deg	
-53	Outboard, Alpha = 20 deg	
-54	Outboard, Alpha = 24 deg	
-55	Outboard, Alpha = 28 deg	
-56	Outboard, Alpha = 32 deg	
-57	Spanwise, Alpha = 0 deg	
-58	Spanwise, Alpha = 4 deg	
-59	Spanwise, Alpha = 8 deg	
-60	Spanwise, Alpha = 12 deg	
-61	Spanwise, Alpha = 16 deg	
-62	Spanwise, Alpha = 20 deg	
-63	Spanwise, Alpha = 24 deg	
-64	Spanwise, Alpha = 28 deg	
-65	Spanwise, Alpha = 32 deg	
3.2.2	Power-off/Power-on Comparison, Flaps Neutral	114
-66	Inboard, Alpha = 0 deg	
-67	Inboard, Alpha = 8 deg	
-68	Inboard, Alpha = 12 deg	
-69	Inboard, Alpha = 16 deg	
-70	Outboard, Alpha = 0 deg	
-71	Outboard, Alpha = 8 deg	
-72	Outboard, Alpha = 12 deg	
-73	Outboard, Alpha = 16 deg	
-74	Spanwise, Alpha = 0 deg	
-75	Spanwise, Alpha = 8 deg	
-76	Spanwise, Alpha = 12 deg	
-77	Spanwise, Alpha = 16 deg	
-78	Inboard, Integrated Section Properties	
-79	Outboard, Integrated Section Properties	
3.2.2	Power Effects, Flaps Deflected	128
-80	Inboard, Alpha = 0 deg	
-81	Inboard, Alpha = 4 deg	
-82	Inboard, Alpha = 8 deg	
-83	Inboard, Alpha = 12 deg	
-84	Inboard, Alpha = 16 deg	
-85	Inboard, Alpha = 20 deg	



## LIST OF FIGURES

Figure		Page
3.2.2	Power Effects, Flaps Deflected (cont'd)	
-86	Inboard, Alpha = 24 deg	134
-87	Inboard, Alpha = 28 deg	
-88	Inboard, Alpha = 32 deg	
-89	Outboard, Alpha = 0 deg	
-90	Outboard, Alpha = 4 deg	
-91	Outboard, Alpha = 8 deg	
-92	Outboard, Alpha = 12 deg	
-93	Outboard, Alpha = 16 deg	
-94	Outboard, Alpha = 20 deg	
-95	Outboard, Alpha = 24 deg	
-96	Outboard, Alpha = 28 deg	
-97	Outboard, Alpha = 32 deg	
-98	Spanwise, Alpha = 0 deg	
-99	Spanwise, Alpha = 4 deg	
-100	Spanwise, Alpha = 8 deg	
-101	Spanwise, Alpha = 12 deg	
-102	Spanwise, Alpha = 16 deg	
-103	Spanwise, Alpha = 20 deg	
-104	Spanwise, Alpha = 24 deg	
-105	Spanwise, Alpha = 28 deg	
-106	Spanwise, Alpha = 32 deg	
3.2.2	Power-off/Power-on Comparison, Flaps Deflected	155
-107	Inboard, Alpha = 0 deg	
-108	Inboard, Alpha = 4 deg	
-109	Inboard, Alpha = 8 deg	
-110	Inboard, Alpha = 12 deg	
-111	Inboard, Alpha = 16 deg	
-112	Outboard, Alpha = 0 deg	
-113	Outboard, Alpha = 4 deg	
-114	Outboard, Alpha = 8 deg	
-115	Outboard, Alpha = 12 deg	
-116	Outboard, Alpha = 16 deg	
-117	Spanwise, Alpha = 0 deg	
-118	Spanwise, Alpha = 4 deg	
-119	Spanwise, Alpha = 8 deg	
-120	Spanwise, Alpha = 12 deg	
-121	Spanwise, Alpha = 16 deg	
-122	Inboard, Integrated Section Properties	
-123	Outboard, Integrated Section Properties	
3.2.2	Spanwise Blowing Effects, Flaps Deflected, $C_T = 0.9$	172
-124	Inboard, Alpha = 0 deg	
-125	Inboard, Alpha = 4 deg	
-126	Inboard, Alpha = 8 deg	
-127	Inboard, Alpha = 12 deg	
-128	Inboard, Alpha = 16 deg	
-129	Inboard, Alpha = 20 deg	

## LIST OF FIGURES

Figure		Page
3.2.2	Spanwise Blowing Effects, Flaps Deflected, $C_T = 0.9$ (cont'd)	
-130	Inboard, Alpha = 24 deg	178
-131	Inboard, Alpha = 28 deg	
-132	Inboard, Alpha = 32 deg	
-133	Outboard, Alpha = 0 deg	
-134	Outboard, Alpha = 4 deg	
-135	Outboard, Alpha = 8 deg	
-136	Outboard, Alpha = 12 deg	
-137	Outboard, Alpha = 16 deg	
-138	Outboard, Alpha = 20 deg	
-139	Outboard, Alpha = 24 deg	
-140	Outboard, Alpha = 28 deg	
-141	Outboard, Alpha = 32 deg	
-142	Spanwise, Alpha = 0 deg	
-143	Spanwise, Alpha = 4 deg	
-144	Spanwise, Alpha = 8 deg	
-145	Spanwise, Alpha = 12 deg	
-146	Spanwise, Alpha = 16 deg	
-147	Spanwise, Alpha = 20 deg	
-148	Spanwise, Alpha = 24 deg	
-149	Spanwise, Alpha = 28 deg	
-150	Spanwise, Alpha = 32 deg	
-151	Inboard, Integrated Section Properties	
-152	Outboard, Integrated Section Properties	
3.2.2	Spanwise Blowing Effects, Flaps Deflected, $C_T = 1.8$	201
-153	Inboard, Alpha = 0 deg	
-154	Inboard, Alpha = 4 deg	
-155	Inboard, Alpha = 8 deg	
-156	Inboard, Alpha = 12 deg	
-157	Inboard, Alpha = 16 deg	
-158	Inboard, Alpha = 20 deg	
-159	Inboard, Alpha = 24 deg	
-160	Inboard, Alpha = 28 deg	
-161	Inboard, Alpha = 32 deg	
-162	Outboard, Alpha = 0 deg	
-163	Outboard, Alpha = 4 deg	
-164	Outboard, Alpha = 8 deg	
-165	Outboard, Alpha = 12 deg	
-166	Outboard, Alpha = 16 deg	
-167	Outboard, Alpha = 20 deg	
-168	Outboard, Alpha = 24 deg	
-169	Outboard, Alpha = 28 deg	
-170	Outboard, Alpha = 32 deg	
-171	Spanwise, Alpha = 0 deg	
-172	Spanwise, Alpha = 4 deg	
-173	Spanwise, Alpha = 8 deg	
-174	Spanwise, Alpha = 12 deg	
-175	Spanwise, Alpha = 16 deg	
-176	Spanwise, Alpha = 20 deg	
-177	Spanwise, Alpha = 24 deg	

## LIST OF FIGURES

Figure		Page
3.2.2	Spanwise Blowing Effects, Flaps Deflected, $C_T = 1.8$ (cont'd)	
-178	Spanwise, Alpha = 28 deg	226
-179	Spanwise, Alpha = 32 deg	
-180	Inboard, Integrated Section Properties	
-181	Outboard, Integrated Section Properties	
3.2.3	Angle of Attack Effects on Canard	237
-1	Power Off, Flaps Neutral	
-2	Power Off, Flaps Deflected	
-3	$C_T = 0.9$ , Flaps Neutral	
-4	$C_T = 0.9$ , Flaps Deflected	
3.2.3	Wing Trailing-edge Flap Effects on Canard,	241
-5	Power Off, Integrated Section Properties	
-6	$C_T 0.9$ , Integrated Section Properties	
3.2.3-7	Canard Deflection Effects	243
3.2.3-8	Canard Leading-Edge Deflection Effects	244
3.2.3-9	Canard Leading- and Trailing-Edge Deflection Effects	245
3.2.3-10	Canard Leading-Edge Deflection Effects, Canard Deflected	246
3.2.3-11	Canard Leading- and Trailing-Edge Deflection Effects, Integrated Section Properties	247
3.2.3-12	Canard Leading-Edge Deflection Effects, Integrated Section Properties	248
3.2.3-13	Effect of Fuselage/Nacelle Orientation on Canard Pressures	249
3.2.3	Canard Fore/Aft Comparison	250
-14	Power on, Alpha = 0 deg	
-15	Power on, Alpha = 4 deg	
-16	Power on, Alpha = 8 deg	
-17	Power on, Alpha = 12 deg	
-18	Power on, Alpha = 16 deg	
-19	Power on, Alpha = 20 deg	
-20	Integrated Section Properties	
-21	Power off, Alpha = 0 deg	
-22	Power off, Alpha = 4 deg	
-23	Power off, Alpha = 8 deg	
-24	Power off, Alpha = 12 deg	
-25	Power off, Alpha = 16 deg	
-26	Power off, Alpha = 20 deg	
-27	Power off, Integrated Section Properties	

## LIST OF FIGURES

Figure		Page
3.2.3	Wing Trailing-Edge Flap Effects on Canard,	264
-28	Alpha = 4 deg	
-29	Alpha = 8 deg	
-30	Alpha = 12 deg	
-31	Alpha = 16 deg	
-32	Alpha = 20 deg	
-33	Integrated Section Properties	
3.2.3	Dynamic Pressure Effects	270
-34	Alpha = 0 deg	
-35	Alpha = 4 deg	
-36	Alpha = 8 deg	
-37	Alpha = 12 deg	
3.2.3	Power-off/Power-on Comparisons,	274
-38	Wing Flaps Neutral, Alpha = 0 deg	
-39	Wing Flaps Neutral, Alpha = 4 deg	
-40	Wing Flaps Neutral, Alpha = 8 deg	
-41	Wing Flaps Neutral, Alpha = 12 deg	
-42	Wing Flaps Neutral, Alpha = 16 deg	
-43	Wing Flaps Neutral, Alpha = 20 deg	
-44	Wing Flaps Neutral, Alpha = 36 deg	
-45	Wing Flaps Neutral, Integrated Section Properties	
-46	Wing Flaps Deflected, Alpha = 0 deg	
-47	Wing Flaps Deflected, Alpha = 4 deg	
-48	Wing Flaps Deflected, Alpha = 8 deg	
-49	Wing Flaps Deflected, Alpha = 12 deg	
-50	Wing Flaps Deflected, Alpha = 16 deg	
-51	Wing Flaps Deflected, Alpha = 20 deg	
-52	Wing Flaps Deflected, Alpha = 28 deg	
-53	Wing Flaps Deflected Integrated Section Properties	
3.2.3	Power Effects, Wing Flaps Neutral	290
-54	Alpha = 4 deg	
-55	Alpha = 8 deg	
-56	Alpha = 12 deg	
-57	Alpha = 16 deg	
-58	Alpha = 20 deg	
-59	Alpha = 32 deg	
-60	Integrated Section Properties	

## LIST OF FIGURES

Figure		Page
3.2.3	Power Effects, Wing Flaps Deflected	297
-61	Alpha = 4 deg	
-62	Alpha = 8 deg	
-63	Alpha = 12 deg	
-64	Alpha = 16 deg	
-65	Alpha = 20 deg	
-66	Alpha = 28 deg	
-67	Integrated Section Properties	
3.2.3	Spanwise Blowing Effects	304
-68	$C_T = 0.9$ , Alpha = 0 deg	
-69	$C_T = 0.9$ , Alpha = 4 deg	
-70	$C_T = 0.9$ , Alpha = 8 deg	
-71	$C_T = 0.9$ , Alpha = 12 deg	
-72	$C_T = 0.9$ , Alpha = 16 deg	
-73	$C_T = 0.9$ , Alpha = 20 deg	
-74	$C_T = 0.9$ , Alpha = 36 deg	
-75	$C_T = 1.8$ , Alpha = 0 deg	
-76	$C_T = 1.8$ , Alpha = 4 deg	
-77	$C_T = 1.8$ , Alpha = 8 deg	
-78	$C_T = 1.8$ , Alpha = 12 deg	
-79	$C_T = 1.8$ , Alpha = 16 deg	
-80	$C_T = 1.8$ , Alpha = 20 deg	
-81	$C_T = 1.8$ , Alpha = 28 deg	
-82	$C_T = 0.9$ , Integrated Section Properties	
-83	$C_T = 1.8$ , Integrated Section Properties	
3.2.4	Angle of Attack Effects, Power off,	338
-1	Inboard, Flaps Neutral, Low Alpha	
-2	Inboard, Flaps Neutral, High Alpha	
-3	Outboard, Flaps Neutral, Low Alpha	
-4	Outboard, Flaps Neutral, High Alpha	
-5	Spanwise, Flaps Neutral, Low Alpha	
-6	Spanwise, Flaps Neutral, High Alpha	
-7	Inboard, Flaps Deflected, Low Alpha	
-8	Inboard, Flaps Deflected, High Alpha	
-9	Outboard, Flaps Deflected, Low Alpha	
-10	Outboard, Flaps Deflected, High Alpha	
-11	Spanwise, Flaps Deflected, Low Alpha	
-12	Spanwise, Flaps Deflected, High Alpha	
3.2.4-13	Origin Of Leading-Edge Vortex	350
3.2.4	Angle of Attack Effects, $C_T = 0.9$	351
-14	Inboard, Flaps Neutral, Low Alpha	
-15	Inboard, Flaps Neutral, High Alpha	
-16	Outboard, Flaps Neutral, Low Alpha	
-17	Outboard, Flaps Neutral, High Alpha	
-18	Spanwise, Flaps Neutral, Low Alpha	

## LIST OF FIGURES

Figure		Page
3.2.4	Angle of Attack Effects, $C_T = 0.9$ (cont'd)	
-19	Spanwise, Flaps Neutral, High Alpha	356
-20	Inboard, Flaps Deflected, Low Alpha	
-21	Inboard, Flaps Deflected, High Alpha	
-22	Outboard, Flaps Deflected, Low Alpha	
-23	Outboard, Flaps Deflected, High Alpha	
-24	Spanwise, Flaps Deflected, Low Alpha	
-25	Spanwise, Flaps Deflected, High Alpha	
3.2.4	Canard On/Off Effects	363
-26	Inboard, Power Off, Flaps Neutral, Alpha = 0 deg	
-27	Inboard, Power Off, Flaps Neutral, Alpha = 8 deg	
-28	Inboard, Power Off, Flaps Neutral, Alpha = 12 deg	
-29	Inboard, Power Off, Flaps Neutral, Alpha = 16 deg	
-30	Inboard, Power Off, Flaps Neutral, Alpha = 20 deg	
-31	Inboard, Power Off, Flaps Neutral, Alpha = 24 deg	
-32	Inboard, Power Off, Flaps Neutral, Alpha = 28 deg	
-33	Inboard, Power Off, Flaps Neutral, Alpha = 32 deg	
-34	Outboard, Power Off, Flaps Neutral, Alpha = 0 deg	
-35	Outboard, Power Off, Flaps Neutral, Alpha = 8 deg	
-36	Outboard, Power Off, Flaps Neutral, Alpha = 12 deg	
-37	Outboard, Power Off, Flaps Neutral, Alpha = 16 deg	
-38	Outboard, Power Off, Flaps Neutral, Alpha = 20 deg	
-39	Outboard, Power Off, Flaps Neutral, Alpha = 24 deg	
-40	Outboard, Power Off, Flaps Neutral, Alpha = 28 deg	
-41	Outboard, Power Off, Flaps Neutral, Alpha = 32 deg	
-42	Spanwise, Power Off, Flaps Neutral, Alpha = 0 deg	
-43	Spanwise, Power Off, Flaps Neutral, Alpha = 8 deg	
-44	Spanwise, Power Off, Flaps Neutral, Alpha = 12 deg	
-45	Spanwise, Power Off, Flaps Neutral, Alpha = 16 deg	
-46	Spanwise, Power Off, Flaps Neutral, Alpha = 20 deg	
-47	Spanwise, Power Off, Flaps Neutral, Alpha = 24 deg	
-48	Spanwise, Power Off, Flaps Neutral, Alpha = 28 deg	
-49	Spanwise, Power Off, Flaps Neutral, Alpha = 32 deg	
-50	Inboard, Power Off, Flaps Neutral, Integrated	
	Section Properties	
-51	Outboard, Power Off, Flaps Neutral, Integrated	
	Section Properties	
-52	Inboard, Power Off, Flaps Deflected, Alpha = 0 deg	
-53	Inboard, Power Off, Flaps Deflected, Alpha = 4 deg	
-54	Inboard, Power Off, Flaps Deflected, Alpha = 8 deg	
-55	Inboard, Power Off, Flaps Deflected, Alpha = 12 deg	
-56	Inboard, Power Off, Flaps Deflected, Alpha = 16 deg	
-57	Inboard, Power Off, Flaps Deflected, Alpha = 20 deg	
-58	Inboard, Power Off, Flaps Deflected, Alpha = 24 deg	
-59	Inboard, Power Off, Flaps Deflected, Alpha = 28 deg	

## LIST OF FIGURES

Figure		Page
3.2.4	Canard On/Off Effects (cont'd)	
-60	Outboard, Power Off, Flaps Deflected, Alpha = 0 deg	397
-61	Outboard, Power Off, Flaps Deflected, Alpha = 4 deg	
-62	Outboard, Power Off, Flaps Deflected, Alpha = 8 deg	
-63	Outboard, Power Off, Flaps Deflected, Alpha = 12 deg	
-64	Outboard, Power Off, Flaps Deflected, Alpha = 16 deg	
-65	Outboard, Power Off, Flaps Deflected, Alpha = 20 deg	
-66	Outboard, Power Off, Flaps Deflected, Alpha = 24 deg	
-67	Outboard, Power Off, Flaps Deflected, Alpha = 28 deg	
-68	Spanwise, Power Off, Flaps Deflected, Alpha = 0 deg	
-69	Spanwise, Power Off, Flaps Deflected, Alpha = 4 deg	
-70	Spanwise, Power Off, Flaps Deflected, Alpha = 8 deg	
-71	Spanwise, Power Off, Flaps Deflected, Alpha = 12 deg	
-72	Spanwise, Power Off, Flaps Deflected, Alpha = 16 deg	
-73	Spanwise, Power Off, Flaps Deflected, Alpha = 20 deg	
-74	Spanwise, Power Off, Flaps Deflected, Alpha = 24 deg	
-75	Spanwise, Power Off, Flaps Deflected, Alpha = 28 deg	
-76	Inboard, Power Off, Flaps Deflected, Integrated Section Properties	
-77	Outboard, Power Off, Flaps Deflected, Integrated Section Properties	
-78	Inboard, $C_T = 0.9$ , Flaps Neutral, Alpha = 0 deg	
-79	Inboard, $C_T = 0.9$ , Flaps Neutral, Alpha = 4 deg	
-80	Inboard, $C_T = 0.9$ , Flaps Neutral, Alpha = 8 deg	
-81	Inboard, $C_T = 0.9$ , Flaps Neutral, Alpha = 12 deg	
-82	Inboard, $C_T = 0.9$ , Flaps Neutral, Alpha = 16 deg	
-83	Inboard, $C_T = 0.9$ , Flaps Neutral, Alpha = 20 deg	
-84	Inboard, $C_T = 0.9$ , Flaps Neutral, Alpha = 24 deg	
-85	Inboard, $C_T = 0.9$ , Flaps Neutral, Alpha = 28 deg	
-86	Inboard, $C_T = 0.9$ , Flaps Neutral, Alpha = 32 deg	
-87	Inboard, $C_T = 0.9$ , Flaps Neutral, Alpha = 36 deg	
-88	Outboard, $C_T = 0.9$ , Flaps Neutral, Alpha = 0 deg	
-89	Outboard, $C_T = 0.9$ , Flaps Neutral, Alpha = 4 deg	
-90	Outboard, $C_T = 0.9$ , Flaps Neutral, Alpha = 8 deg	
-91	Outboard, $C_T = 0.9$ , Flaps Neutral, Alpha = 12 deg	
-92	Outboard, $C_T = 0.9$ , Flaps Neutral, Alpha = 16 deg	
-93	Outboard, $C_T = 0.9$ , Flaps Neutral, Alpha = 20 deg	
-94	Outboard, $C_T = 0.9$ , Flaps Neutral, Alpha = 24 deg	
-95	Outboard, $C_T = 0.9$ , Flaps Neutral, Alpha = 28 deg	
-96	Outboard, $C_T = 0.9$ , Flaps Neutral, Alpha = 32 deg	
-97	Outboard, $C_T = 0.9$ , Flaps Neutral, Alpha = 36 deg	
-98	Spanwise, $C_T = 0.9$ , Flaps Neutral, Alpha = 0 deg	
-99	Spanwise, $C_T = 0.9$ , Flaps Neutral, Alpha = 4 deg	
-100	Spanwise, $C_T = 0.9$ , Flaps Neutral, Alpha = 8 deg	
-101	Spanwise, $C_T = 0.9$ , Flaps Neutral, Alpha = 12 deg	
-102	Spanwise, $C_T = 0.9$ , Flaps Neutral, Alpha = 16 deg	
-103	Spanwise, $C_T = 0.9$ , Flaps Neutral, Alpha = 20 deg	
-104	Spanwise, $C_T = 0.9$ , Flaps Neutral, Alpha = 24 deg	
-105	Spanwise, $C_T = 0.9$ , Flaps Neutral, Alpha = 28 deg	
-106	Spanwise, $C_T = 0.9$ , Flaps Neutral, Alpha = 32 deg	

## LIST OF FIGURES

Figure		Page
3.2.4	Canard On/Off Effects (cont'd)	
-107	Spanwise, $C_T = 0.9$ , Flaps Neutral, Alpha = 36 deg	444
-108	Inboard, $C_T = 0.9$ , Flaps Neutral, Integrated Section Properties	
-109	Outboard, $C_T = 0.9$ , Flaps Neutral, Integrated Section Properties	
-110	Inboard, $C_T = 0.9$ , Flaps Deflected, Alpha = 0 deg	
-111	Inboard, $C_T = 0.9$ , Flaps Deflected, Alpha = 4 deg	
-112	Inboard, $C_T = 0.9$ , Flaps Deflected, Alpha = 8 deg	
-113	Inboard, $C_T = 0.9$ , Flaps Deflected, Alpha = 12 deg	
-114	Inboard, $C_T = 0.9$ , Flaps Deflected, Alpha = 16 deg	
-115	Inboard, $C_T = 0.9$ , Flaps Deflected, Alpha = 20 deg	
-116	Inboard, $C_T = 0.9$ , Flaps Deflected, Alpha = 24 deg	
-117	Inboard, $C_T = 0.9$ , Flaps Deflected, Alpha = 28 deg	
-118	Inboard, $C_T = 0.9$ , Flaps Deflected, Alpha = 32 deg	
-119	Outboard, $C_T = 0.9$ , Flaps Deflected, Alpha = 0 deg	
-120	Outboard, $C_T = 0.9$ , Flaps Deflected, Alpha = 4 deg	
-121	Outboard, $C_T = 0.9$ , Flaps Deflected, Alpha = 8 deg	
-122	Outboard, $C_T = 0.9$ , Flaps Deflected, Alpha = 12 deg	
-123	Outboard, $C_T = 0.9$ , Flaps Deflected, Alpha = 16 deg	
-124	Outboard, $C_T = 0.9$ , Flaps Deflected, Alpha = 20 deg	
-125	Outboard, $C_T = 0.9$ , Flaps Deflected, Alpha = 24 deg	
-126	Outboard, $C_T = 0.9$ , Flaps Deflected, Alpha = 28 deg	
-127	Outboard, $C_T = 0.9$ , Flaps Deflected, Alpha = 32 deg	
-128	Spanwise, $C_T = 0.9$ , Flaps Deflected, Alpha = 0 deg	
-129	Spanwise, $C_T = 0.9$ , Flaps Deflected, Alpha = 4 deg	
-130	Spanwise, $C_T = 0.9$ , Flaps Deflected, Alpha = 8 deg	
-131	Spanwise, $C_T = 0.9$ , Flaps Deflected, Alpha = 12 deg	
-132	Spanwise, $C_T = 0.9$ , Flaps Deflected, Alpha = 16 deg	
-133	Spanwise, $C_T = 0.9$ , Flaps Deflected, Alpha = 20 deg	
-134	Spanwise, $C_T = 0.9$ , Flaps Deflected, Alpha = 24 deg	
-135	Spanwise, $C_T = 0.9$ , Flaps Deflected, Alpha = 28 deg	
-136	Spanwise, $C_T = 0.9$ , Flaps Deflected, Alpha = 32 deg	
-137	Inboard, $C_T = 0.9$ , Flaps Deflected, Integrated Section Properties	
-138	Outboard, $C_T = 0.9$ , Flaps Deflected, Integrated Section Properties	
3.2.4	Canard On/Off Effects, Forward Position	476
-139	Inboard, Power Off, Alpha = 12 deg	
-140	Inboard, Power Off, Alpha = 16 deg	
-141	Inboard, Power Off, Alpha = 20 deg	
-142	Outboard, Power Off, Alpha = 12 deg	
-143	Outboard, Power Off, Alpha = 16 deg	
-144	Outboard, Power Off, Alpha = 20 deg	
-145	Inboard, $C_T = 0.9$ , Alpha = 12 deg	
-146	Inboard, $C_T = 0.9$ , Alpha = 16 deg	
-147	Inboard, $C_T = 0.9$ , Alpha = 20 deg	
-148	Outboard, $C_T = 0.9$ , Alpha = 12 deg	
-149	Outboard, $C_T = 0.9$ , Alpha = 16 deg	



## LIST OF FIGURES

Figure		Page
3.2.4	Canard On/Off Effects, Forward Position (cont'd)	
-150	Outboard, $C_T = 0.9$ , Alpha = 20 deg	487
-151	Inboard, $C_T = 0.9$ , Integrated Section Properties	
-152	Outboard, $C_T = 0.9$ , Integrated Section Properties	
3.2.4	Canard Deflection Effects	490
-153	Wing Inboard, Alpha = 4 deg	
-154	Wing Inboard, Alpha = 8 deg	
-155	Wing Inboard, Alpha = 12 deg	
-156	Wing Outboard, Alpha = 4 deg	
-157	Wing Outboard, Alpha = 8 deg	
-158	Wing Outboard, Alpha = 12 deg	
-159	Wing Spanwise, Alpha = 4 deg	
-160	Wing Spanwise, Alpha = 8 deg	
-161	Wing Spanwise, Alpha = 12 deg	
-162	Inboard, Flaps Deflected, Integrated Section Properties	
-163	Outboard, Flaps Deflected, Integrated Section Properties	
3.2.4	Canard Leading-Edge Flap Deflection Effects, $C_T = 0.9$	501
-164	Inboard, Canard Neutral, Alpha = 0 deg	
-165	Inboard, Canard Neutral, Alpha = 4 deg	
-166	Inboard, Canard Neutral, Alpha = 8 deg	
-167	Inboard, Canard Neutral, Alpha = 12 deg	
-168	Inboard, Canard Neutral, Alpha = 16 deg	
-169	Outboard, Canard Neutral, Alpha = 0 deg	
-170	Outboard, Canard Neutral, Alpha = 4 deg	
-171	Outboard, Canard Neutral, Alpha = 8 deg	
-172	Outboard, Canard Neutral, Alpha = 12 deg	
-173	Outboard, Canard Neutral, Alpha = 16 deg	
-174	Spanwise, Canard Neutral, Alpha = 0 deg	
-175	Spanwise, Canard Neutral, Alpha = 4 deg	
-176	Spanwise, Canard Neutral, Alpha = 8 deg	
-177	Spanwise, Canard Neutral, Alpha = 12 deg	
-178	Spanwise, Canard Neutral, Alpha = 16 deg	
-179	Inboard, Canard Deflected, Alpha = 4 deg	
-180	Inboard, Canard Deflected, Alpha = 8 deg	
-181	Inboard, Canard Deflected, Alpha = 12 deg	
-182	Inboard, Canard Deflected, Alpha = 16 deg	
-183	Outboard, Canard Deflected, Alpha = 4 deg	
-184	Outboard, Canard Deflected, Alpha = 8 deg	
-185	Outboard, Canard Deflected, Alpha = 12 deg	
-186	Outboard, Canard Deflected, Alpha = 16 deg	
-187	Spanwise, Canard Deflected, Alpha = 4 deg	
-188	Spanwise, Canard Deflected, Alpha = 8 deg	
-189	Spanwise, Canard Deflected, Alpha = 12 deg	
-190	Spanwise, Canard Deflected, Alpha = 16 deg	
3.2.4	Combined Canard Flap Deflection Effects	528
-191	Inboard, Alpha = 0 deg	
-192	Inboard, Alpha = 4 deg	

## LIST OF FIGURES

Figure		Page
3.2.4	Combined Canard Flap Deflection Effects (cont'd)	530
-193	Inboard, Alpha = 8 deg	
-194	Inboard, Alpha = 12 deg	
-195	Inboard, Alpha = 16 deg	
-196	Outboard, Alpha = 0 deg	
-197	Outboard, Alpha = 4 deg	
-198	Outboard, Alpha = 8 deg	
-199	Outboard, Alpha = 12 deg	
-200	Outboard, Alpha = 16 deg	
-201	Spanwise, Alpha = 0 deg	
-202	Spanwise, Alpha = 4 deg	
-203	Spanwise, Alpha = 8 deg	
-204	Spanwise, Alpha = 12 deg	
-205	Spanwise, Alpha = 16 deg	
-206	Inboard, Integrated Section Properties	
-207	Outboard, Integrated Section Properties	
3.2.4	Canard Position Effects	545
-208	Inboard, Power Off, Alpha = 0 deg	
-209	Inboard, Power Off, Alpha = 4 deg	
-210	Inboard, Power Off, Alpha = 8 deg	
-211	Inboard, Power Off, Alpha = 12 deg	
-212	Inboard, Power Off, Alpha = 16 deg	
-213	Inboard, Power Off, Alpha = 20 deg	
-214	Outboard, Power Off, Alpha = 0 deg	
-215	Outboard, Power Off, Alpha = 4 deg	
-216	Outboard, Power Off, Alpha = 8 deg	
-217	Outboard, Power Off, Alpha = 12 deg	
-218	Outboard, Power Off, Alpha = 16 deg	
-219	Outboard, Power Off, Alpha = 20 deg	
-220	Spanwise, Power Off, Alpha = 0 deg	
-221	Spanwise, Power Off, Alpha = 4 deg	
-222	Spanwise, Power Off, Alpha = 8 deg	
-223	Spanwise, Power Off, Alpha = 12 deg	
-224	Spanwise, Power Off, Alpha = 16 deg	
-225	Spanwise, Power Off, Alpha = 20 deg	
-226	Inboard, $C_T = 0.9$ , Alpha = 0 deg	
-227	Inboard, $C_T = 0.9$ , Alpha = 4 deg	
-228	Inboard, $C_T = 0.9$ , Alpha = 8 deg	
-229	Inboard, $C_T = 0.9$ , Alpha = 12 deg	
-230	Inboard, $C_T = 0.9$ , Alpha = 16 deg	
-231	Inboard, $C_T = 0.9$ , Alpha = 20 deg	
-232	Outboard, $C_T = 0.9$ , Alpha = 0 deg	
-233	Outboard, $C_T = 0.9$ , Alpha = 4 deg	
-234	Outboard, $C_T = 0.9$ , Alpha = 8 deg	
-235	Outboard, $C_T = 0.9$ , Alpha = 12 deg	
-236	Outboard, $C_T = 0.9$ , Alpha = 16 deg	
-237	Outboard, $C_T = 0.9$ , Alpha = 20 deg	
-238	Spanwise, $C_T = 0.9$ , Alpha = 0 deg	
-239	Spanwise, $C_T = 0.9$ , Alpha = 4 deg	
-240	Spanwise, $C_T = 0.9$ , Alpha = 8 deg	
-241	Spanwise, $C_T = 0.9$ , Alpha = 12 deg	
-242	Spanwise, $C_T = 0.9$ , Alpha = 16 deg	
-243	Spanwise, $C_T = 0.9$ , Alpha = 20 deg	

## LIST OF FIGURES

Figure		Page
3.2.4	Wing Flap Effects	581
-244	Inboard, Power Off, Alpha = 4 deg	
-245	Inboard, Power Off, Alpha = 8 deg	
-246	Inboard, Power Off, Alpha = 12 deg	
-247	Inboard, Power Off, Alpha = 16 deg	
-248	Inboard, Power Off, Alpha = 20 deg	
-249	Outboard, Power Off, Alpha = 4 deg	
-250	Outboard, Power Off, Alpha = 8 deg	
-251	Outboard, Power Off, Alpha = 12 deg	
-252	Outboard, Power Off, Alpha = 16 deg	
-253	Outboard, Power Off, Alpha = 20 deg	
-254	Spanwise, Power Off, Alpha = 4 deg	
-255	Spanwise, Power Off, Alpha = 8 deg	
-256	Spanwise, Power Off, Alpha = 12 deg	
-257	Spanwise, Power Off, Alpha = 16 deg	
-258	Spanwise, Power Off, Alpha = 20 deg	
-259	Inboard, Power Off, Integrated Section Properties	
-260	Outboard, Power Off, Integrated Section Properties	
-261	Inboard, $C_T = 0.9$ , Alpha = 4 deg	
-262	Inboard, $C_T = 0.9$ , Alpha = 8 deg	
-263	Inboard, $C_T = 0.9$ , Alpha = 12 deg	
-264	Inboard, $C_T = 0.9$ , Alpha = 16 deg	
-265	Inboard, $C_T = 0.9$ , Alpha = 20 deg	
-266	Outboard, $C_T = 0.9$ , Alpha = 4 deg	
-267	Outboard, $C_T = 0.9$ , Alpha = 8 deg	
-268	Outboard, $C_T = 0.9$ , Alpha = 12 deg	
-269	Outboard, $C_T = 0.9$ , Alpha = 16 deg	
-270	Outboard, $C_T = 0.9$ , Alpha = 20 deg	
-271	Spanwise, $C_T = 0.9$ , Alpha = 4 deg	
-272	Spanwise, $C_T = 0.9$ , Alpha = 8 deg	
-273	Spanwise, $C_T = 0.9$ , Alpha = 12 deg	
-274	Spanwise, $C_T = 0.9$ , Alpha = 16 deg	
-275	Spanwise, $C_T = 0.9$ , Alpha = 20 deg	
-276	Inboard, $C_T = 0.9$ , Integrated Section Properties	
-277	Outboard, $C_T = 0.9$ , Integrated Section Properties	
-278	Inboard, $C_T = 1.9$ , Alpha = 4 deg	
-279	Inboard, $C_T = 1.9$ , Alpha = 8 deg	
-280	Inboard, $C_T = 1.9$ , Alpha = 12 deg	
-281	Inboard, $C_T = 1.9$ , Alpha = 16 deg	
-282	Inboard, $C_T = 1.9$ , Alpha = 20 deg	
-283	Outboard, $C_T = 1.9$ , Alpha = 4 deg	
-284	Outboard, $C_T = 1.9$ , Alpha = 8 deg	
-285	Outboard, $C_T = 1.9$ , Alpha = 12 deg	
-286	Outboard, $C_T = 1.9$ , Alpha = 16 deg	
-287	Outboard, $C_T = 1.9$ , Alpha = 20 deg	
-288	Spanwise, $C_T = 1.9$ , Alpha = 4 deg	
-289	Spanwise, $C_T = 1.9$ , Alpha = 8 deg	
-290	Spanwise, $C_T = 1.9$ , Alpha = 12 deg	
-291	Spanwise, $C_T = 1.9$ , Alpha = 16 deg	
-292	Spanwise, $C_T = 1.9$ , Alpha = 20 deg	
-293	Inboard, $C_T = 1.9$ , Integrated Section Properties	
-294	Outboard, $C_T = 1.9$ , Integrated Section Properties	

## LIST OF FIGURES

Figure		Page
3.2.4	Dynamic Pressure Effects, Flaps Deflected, Power Off	632
-295	Inboard, Alpha = 0 deg	
-296	Inboard, Alpha = 4 deg	
-297	Inboard, Alpha = 8 deg	
-298	Inboard, Alpha = 12 deg	
-299	Outboard, Alpha = 0 deg	
-300	Outboard, Alpha = 4 deg	
-301	Outboard, Alpha = 8 deg	
-302	Outboard, Alpha = 12 deg	
-303	Spanwise, Alpha = 0 deg	
-304	Spanwise, Alpha = 4 deg	
-305	Spanwise, Alpha = 8 deg	
-306	Spanwise, Alpha = 12 deg	
3.2.4	Power Effects	644
-307	Flaps Neutral, Inboard, Alpha = 0 deg	
-308	Flaps Neutral, Inboard, Alpha = 4 deg	
-309	Flaps Neutral, Inboard, Alpha = 8 deg	
-310	Flaps Neutral, Inboard, Alpha = 12 deg	
-311	Flaps Neutral, Inboard, Alpha = 16 deg	
-312	Flaps Neutral, Inboard, Alpha = 20 deg	
-313	Flaps Neutral, Inboard, Alpha = 24 deg	
-314	Flaps Neutral, Inboard, Alpha = 28 deg	
-315	Flaps Neutral, Outboard, Alpha = 0 deg	
-316	Flaps Neutral, Outboard, Alpha = 4 deg	
-317	Flaps Neutral, Outboard, Alpha = 8 deg	
-318	Flaps Neutral, Outboard, Alpha = 12 deg	
-319	Flaps Neutral, Outboard, Alpha = 16 deg	
-320	Flaps Neutral, Outboard, Alpha = 20 deg	
-321	Flaps Neutral, Outboard, Alpha = 24 deg	
-322	Flaps Neutral, Outboard, Alpha = 28 deg	
-323	Flaps Neutral, Spanwise, Alpha = 0 deg	
-324	Flaps Neutral, Spanwise, Alpha = 4 deg	
-325	Flaps Neutral, Spanwise, Alpha = 8 deg	
-326	Flaps Neutral, Spanwise, Alpha = 12 deg	
-327	Flaps Neutral, Spanwise, Alpha = 16 deg	
-328	Flaps Neutral, Spanwise, Alpha = 20 deg	
-329	Flaps Neutral, Spanwise, Alpha = 24 deg	
-330	Flaps Neutral, Spanwise, Alpha = 28 deg	
-331	Inboard, Integrated Section Properties	
-332	Outboard, Integrated Section Properties	
-333	Inboard, Alpha = 0 deg	
-334	Inboard, Alpha = 4 deg	
-335	Inboard, Alpha = 8 deg	
-336	Inboard, Alpha = 12 deg	
-337	Inboard, Alpha = 16 deg	
-338	Inboard, Alpha = 20 deg	
-339	Inboard, Alpha = 24 deg	
-340	Inboard, Alpha = 28 deg	

## LIST OF FIGURES

Figure		Page
3.2.4	Power Effects (cont'd)	
-341	Outboard, Alpha = 0 deg	678
-342	Outboard, Alpha = 4 deg	
-343	Outboard, Alpha = 8 deg	
-344	Outboard, Alpha = 12 deg	
-345	Outboard, Alpha = 16 deg	
-346	Outboard, Alpha = 20 deg	
-347	Outboard, Alpha = 24 deg	
-348	Outboard, Alpha = 28 deg	
-349	Spanwise, Alpha = 0 deg	
-350	Spanwise, Alpha = 4 deg	
-351	Spanwise, Alpha = 8 deg	
-352	Spanwise, Alpha = 12 deg	
-353	Spanwise, Alpha = 16 deg	
-354	Spanwise, Alpha = 20 deg	
-355	Spanwise, Alpha = 24 deg	
-356	Spanwise, Alpha = 28 deg	
-357	Inboard, Flaps Deflected, Integrated Section Properties	
-358	Outboard, Flaps Deflected, Integrated Section Properties	
3.2.4	Power Buildup	696
-359	Flaps Neutral, Inboard, Alpha = 4 deg	
-360	Flaps Neutral, Inboard, Alpha = 8 deg	
-361	Flaps Neutral, Inboard, Alpha = 12 deg	
-362	Flaps Neutral, Inboard, Alpha = 16 deg	
-363	Flaps Neutral, Inboard, Alpha = 20 deg	
-364	Flaps Neutral, Inboard, Alpha = 24 deg	
-365	Flaps Neutral, Inboard, Alpha = 28 deg	
-366	Flaps Neutral, Inboard, Alpha = 32 deg	
-367	Flaps Neutral, Outboard, Alpha = 4 deg	
-368	Flaps Neutral, Outboard, Alpha = 8 deg	
-369	Flaps Neutral, Outboard, Alpha = 12 deg	
-370	Flaps Neutral, Outboard, Alpha = 16 deg	
-371	Flaps Neutral, Outboard, Alpha = 20 deg	
-372	Flaps Neutral, Outboard, Alpha = 24 deg	
-373	Flaps Neutral, Outboard, Alpha = 28 deg	
-374	Flaps Neutral, Outboard, Alpha = 32 deg	
-375	Flaps Neutral, Spanwise, Alpha = 4 deg	
-376	Flaps Neutral, Spanwise, Alpha = 8 deg	
-377	Flaps Neutral, Spanwise, Alpha = 12 deg	
-378	Flaps Neutral, Spanwise, Alpha = 16 deg	
-379	Flaps Neutral, Spanwise, Alpha = 20 deg	
-380	Flaps Neutral, Spanwise, Alpha = 24 deg	
-381	Flaps Neutral, Spanwise, Alpha = 28 deg	
-382	Flaps Neutral, Spanwise, Alpha = 32 deg	
-383	Inboard, Flaps Neutral, Integrated Section Properties	
-384	Outboard, Flaps Neutral, Integrated Section Properties	
-385	Flaps Deflected, Inboard, Alpha = 4 deg	
-386	Flaps Deflected, Inboard, Alpha = 8 deg	
-387	Flaps Deflected, Inboard, Alpha = 12 deg	

## LIST OF FIGURES

Figure		Page
3.2.4	Power Buildup (cont'd)	
-388	Flaps Deflected, Inboard, Alpha = 16 deg	725
-389	Flaps Deflected, Inboard, Alpha = 20 deg	
-390	Flaps Deflected, Inboard, Alpha = 24 deg	
-391	Flaps Deflected, Inboard, Alpha = 28 deg	
-392	Flaps Deflected, Outboard, Alpha = 4 deg	
-393	Flaps Deflected, Outboard, Alpha = 8 deg	
-394	Flaps Deflected, Outboard, Alpha = 12 deg	
-395	Flaps Deflected, Outboard, Alpha = 16 deg	
-396	Flaps Deflected, Outboard, Alpha = 20 deg	
-397	Flaps Deflected, Outboard, Alpha = 24 deg	
-398	Flaps Deflected, Outboard, Alpha = 28 deg	
-399	Flaps Deflected, Spanwise, Alpha = 4 deg	
-400	Flaps Deflected, Spanwise, Alpha = 8 deg	
-401	Flaps Deflected, Spanwise, Alpha = 12 deg	
-402	Flaps Deflected, Spanwise, Alpha = 16 deg	
-403	Flaps Deflected, Spanwise, Alpha = 20 deg	
-404	Flaps Deflected, Spanwise, Alpha = 24 deg	
-405	Flaps Deflected, Spanwise, Alpha = 28 deg	
-406	Inboard, Flaps Deflected, Integrated Section Properties	
-407	Outboard, Flaps Deflected, Integrated Section Properties	
3.2.4	Spanwise Blowing Effects	745
-408	Inboard, $C_T = 0.9$ , Alpha = 0 deg	
-409	Inboard, $C_T = 0.9$ , Alpha = 4 deg	
-410	Inboard, $C_T = 0.9$ , Alpha = 8 deg	
-411	Inboard, $C_T = 0.9$ , Alpha = 12 deg	
-412	Inboard, $C_T = 0.9$ , Alpha = 16 deg	
-413	Inboard, $C_T = 0.9$ , Alpha = 20 deg	
-414	Inboard, $C_T = 0.9$ , Alpha = 24 deg	
-415	Inboard, $C_T = 0.9$ , Alpha = 28 deg	
-416	Inboard, $C_T = 0.9$ , Alpha = 32 deg	
-417	Outboard, $C_T = 0.9$ , Alpha = 0 deg	
-418	Outboard, $C_T = 0.9$ , Alpha = 4 deg	
-419	Outboard, $C_T = 0.9$ , Alpha = 8 deg	
-420	Outboard, $C_T = 0.9$ , Alpha = 12 deg	
-421	Outboard, $C_T = 0.9$ , Alpha = 16 deg	
-422	Outboard, $C_T = 0.9$ , Alpha = 20 deg	
-423	Outboard, $C_T = 0.9$ , Alpha = 24 deg	
-424	Outboard, $C_T = 0.9$ , Alpha = 28 deg	
-425	Outboard, $C_T = 0.9$ , Alpha = 32 deg	
-426	Spanwise, $C_T = 0.9$ , Alpha = 0 deg	
-427	Spanwise, $C_T = 0.9$ , Alpha = 4 deg	
-428	Spanwise, $C_T = 0.9$ , Alpha = 8 deg	
-429	Spanwise, $C_T = 0.9$ , Alpha = 12 deg	
-430	Spanwise, $C_T = 0.9$ , Alpha = 16 deg	
-431	Spanwise, $C_T = 0.9$ , Alpha = 20 deg	
-432	Spanwise, $C_T = 0.9$ , Alpha = 24 deg	
-433	Spanwise, $C_T = 0.9$ , Alpha = 28 deg	

## LIST OF FIGURES

Figure		Page
3.2.4	Spanwise Blowing Effects (cont'd)	
-434	Spanwise, $C_T = 0.9$ , Alpha = 32 deg	771
-435	Inboard, $C_T = 0.9$ , Integrated Section Properties	
-436	Outboard, $C_T = 0.9$ , Integrated Section Properties	
-437	Inboard, $C_T = 1.9$ , Alpha = 0 deg	
-438	Inboard, $C_T = 1.9$ , Alpha = 4 deg	
-439	Inboard, $C_T = 1.9$ , Alpha = 8 deg	
-440	Inboard, $C_T = 1.9$ , Alpha = 12 deg	
-441	Inboard, $C_T = 1.9$ , Alpha = 16 deg	
-442	Inboard, $C_T = 1.9$ , Alpha = 20 deg	
-443	Inboard, $C_T = 1.9$ , Alpha = 24 deg	
-444	Inboard, $C_T = 1.9$ , Alpha = 28 deg	
-445	Outboard, $C_T = 1.9$ , Alpha = 0 deg	
-446	Outboard, $C_T = 1.9$ , Alpha = 4 deg	
-447	Outboard, $C_T = 1.9$ , Alpha = 8 deg	
-448	Outboard, $C_T = 1.9$ , Alpha = 12 deg	
-449	Outboard, $C_T = 1.9$ , Alpha = 16 deg	
-450	Outboard, $C_T = 1.9$ , Alpha = 20 deg	
-451	Outboard, $C_T = 1.9$ , Alpha = 24 deg	
-452	Outboard, $C_T = 1.9$ , Alpha = 28 deg	
-453	Spanwise, $C_T = 1.9$ , Alpha = 0 deg	
-454	Spanwise, $C_T = 1.9$ , Alpha = 4 deg	
-455	Spanwise, $C_T = 1.9$ , Alpha = 8 deg	
-456	Spanwise, $C_T = 1.9$ , Alpha = 12 deg	
-457	Spanwise, $C_T = 1.9$ , Alpha = 16 deg	
-458	Spanwise, $C_T = 1.9$ , Alpha = 20 deg	
-459	Spanwise, $C_T = 1.9$ , Alpha = 24 deg	
-460	Spanwise, $C_T = 1.9$ , Alpha = 28 deg	
-461	Inboard, $C_T = 1.9$ , Integrated Section Properties	
-462	Outboard, $C_T = 1.9$ , Integrated Section Properties	
3.2.4	Power Buildup, Spanwise Blowing On	800
-463	Inboard, Alpha = 4 deg	
-464	Inboard, Alpha = 12 deg	
-465	Inboard, Alpha = 20 deg	
-466	Inboard, Alpha = 28 deg	
-467	Outboard, Alpha = 4 deg	
-468	Outboard, Alpha = 12 deg	
-469	Outboard, Alpha = 20 deg	
-470	Outboard, Alpha = 28 deg	
-471	Spanwise, Alpha = 4 deg	
-472	Spanwise, Alpha = 12 deg	
-473	Spanwise, Alpha = 20 deg	
-474	Spanwise, Alpha = 28 deg	
-475	Inboard, Integrated Section Properties	
-476	Outboard, Integrated Section Properties	

## LIST OF FIGURES

Figure		Page
3.2.5-1	General Dynamics Small-Scale VEO-Wing Research Model Installed in the NASA/Langley V/STOL Tunnel	820
3.2.5-2	STOL Fighter Model and VEO-Wing Research Model Planform Comparison	821
3.2.5	Comparison of Alpha Effects	822
-3	Canards off, Flaps Undeflected, Power Off	
-4	Canards off, Flaps Undeflected, Power On	
-5	Canards on, Flaps Undeflected, Power Off	
-6	Canards on, Flaps Undeflected, Power On	
-7	Canards on, Flaps 30 deg, Power Off	
-8	Canards on, Flaps 30 deg, Power On	
3.2.5	Comparison of Canard On/Off Effects,	828
-9	Power Off, Alpha = 4 deg	
-10	Power Off, Alpha = 12 deg	
-11	Power Off, Alpha = 20 deg	
-12	Power On, Alpha = 4 deg	
-13	Power On, Alpha = 12 deg	
-14	Power On, Alpha = 20 deg	
3.2.5	Comparison of Trailing-Edge Flap Effects,	834
-15	Power Off, Alpha = 4 deg	
-16	Power Off, Alpha = 12 deg	
-17	Power On, Alpha = 4 deg	
-18	Power On, Alpha = 12 deg	
3.2.5	Comparison of Power Effects,	838
-19	Flaps Undeflected, Alpha = 4 deg	
-20	Flaps Undeflected, Alpha = 8 deg	
-21	Flaps Undeflected, Alpha = 12 deg	
-22	Flaps Undeflected, Alpha = 24 deg	
-23	Flaps 30 deg, Alpha = 4 deg	
-24	Flaps 30 deg, Alpha = 8 deg	
-25	Flaps 30 deg, Alpha = 12 deg	
-26	Flaps 30 deg, Alpha = 16 deg	
3.2.5	Comparison of Spanwise Blowing Effects,	846
-27	$C_T = 0.9$ , Alpha = 4 deg	
-28	$C_T = 0.9$ , Alpha = 12deg	
-29	$C_T = 1.9$ , Alpha = 4 deg	
-30	$C_T = 1.9$ , Alpha = 12 deg	



## LIST OF FIGURES

Figure		Page
3.3	Power Effects on Strake Pressures, Wing Flaps Neutral	853
-1	Alpha = 4 deg	
-2	Alpha = 8 deg	
-3	Alpha = 12 deg	
-4	Alpha = 21 deg	
-5	Alpha = 29 deg	
3.3	Power Effects on Strake Pressures, Wing Flaps Deflected	858
-6	Alpha = 4 deg	
-7	Alpha = 8 deg	
-8	Alpha = 12 deg	
-9	Alpha = 21 deg	
-10	Alpha = 29 deg	
3.3-11	Strake Vortex Development	863
3.3-12	Wing Flap Effects on Strake Pressures, Power Off	864
3.3-13	Wing Flap Effects on Strake Pressures, Power On	865
3.3	Spanwise Blowing Effect on Strake Pressures	866
-14	Alpha = 0 deg	
-15	Alpha = 4 deg	
-16	Alpha = 8 deg	
-17	Alpha = 12 deg	
-18	Alpha = 21 deg	
-19	Alpha = 29 deg	
3.3-20	Power Effect on Strake Pressures	872
3.4	Angle of Attack Effects, Power Off, Beaver Tail Neutral	875
-1	Wing Flaps Neutral	
-2	Wing Flaps Deflected	
3.4	Wing Flap Deflection Effects,	877
-3	Power Off	
-4	Power On	
3.4-5	Beaver Tail Deflection Effects, Power Off	879
3.4-6	Angle of Attack Effects, Power Off, Beaver Tail Deflected	880
3.4-7	Beaver Tail Deflection Effects, Power On	881
3.4-8	Alpha Effects, Power On, Beaver Tail Deflected	882
3.4	Power Effects,	883
-9	Wing Flaps Neutral	
-10	Wing Flaps Deflected	

## LIST OF FIGURES

Figure		Page
3.5-1	Angle of Attack Effects on Nozzle Flap, Power Off	886
3.5-2	Nozzle Flap Deflection Effects, Power Off	887
3.5-3	Dynamic Pressure Effects on Nozzle Flap, Power On	888
3.5-4	Nozzle Flap Deflection Effects, Power On	889
3.5-5	Angle of Attack Effects on Nozzle Flap, Power On	890
3.6	Wing Temperature Profiles at Static Conditions,	895
-1	EPR = 1.4	
-2	EPR = 1.8	
-3	EPR = 2.0	
-4	EPR = 2.2	
3.6-5	Family of Wing Temperature Profiles at Static Conditions	899
3.6	Isotherms at Static Conditions	900
-6	EPR = 1.4 and 1.8	
-7	EPR = 2.0 and 2.2	
3.6	Wing Temperature Profiles,	902
-8	Alpha = 0 deg	
-9	Alpha = 4 deg	
-10	Alpha = 8 deg	
-11	Alpha = 12 deg	
-12	Alpha = 17 deg	
-13	Alpha = 21 deg	
-14	Alpha = 25 deg	
-15	Alpha = 29 deg	
3.6-16	Family of Wing Temperature Profiles	910
3.6	Comparison of Wing Isotherm and Isobar Patterns,	911
-17	Alpha = 0 deg	
-18	Alpha = 4 deg	
-19	Alpha = 8 deg	
-20	Alpha = 12 deg	
-21	Alpha = 17 deg	
-22	Alpha = 21 deg	
-23	Alpha = 25 deg	
-24	Alpha = 29 deg	
3.6-25	Power Effects on Beaver Tail Pressures and Temperatures	919

## LIST OF FIGURES

Figure		Page
3.6-26	Wing Trailing-Edge Flap Effects on Beaver Tail Pressures and Temperatures	920
3.6-27	Beaver Tail Deflection Effects on Pressures and Temperatures	921
4-1	Illustration of the EVD Jet-Wing Method	928
4-2	Paneling Scheme for STOL Fighter Model	929
4	Comparisons of Data and EVD Method Predictions For	930
-3	Camber and Twist	
-4	8 deg Angle of Attack	
-5	30 deg Trailing-Edge Flap Deflection	
-6	Power Effects, Wing Inboard, Flaps Neutral	
-7	Power Effects, Wing Outboard, Flaps Neutral	
-8	Power Effects, Wing Spanwise, Flaps Neutral	
-9	Power Effects, Wing Inboard, Flaps Deflected	
-10	Power Effects, Wing Outboard, Flaps Deflected	
-11	Power Effects, Wing Spanwise, Flaps Deflected	
4	Comparison of Data and General Dynamics Prediction Method For	941
-12	Lift, Flaps Neutral	
-13	Pitching Moment, Flaps Neutral	
-14	Polar Shape, Flaps Neutral	
-15	Lift, Flaps Deflected	
-16	Pitching Moment, Flaps Deflected	
-17	Polar Shape, Flaps Deflected	
-18	Lift and Moment Increments Due to Power	

## LIST OF TABLES

<u>Table</u>		<u>Page</u>
1	STOL Fighter Model Geometric Parameters	5
2	Pressure Tap Locations	6
3	Thermocouple Locations	8
4	Thrust and Dynamic Pressure Test Values	8
5	Run Schedule For Test 537	9
6	Run Schedule For Test 543	11
7	Run Schedule For Test 546	13
8	Tunnel Conditions With Power Variations	235
9	Pressure Tap Locations on the Small-Scale VEO-Wing Model	815

## 1 INTRODUCTION

Battle scenarios for the 1990's and beyond place stringent requirements upon tactical aircraft if they are to survive and operate effectively against the severe threats that will likely be encountered. In order to meet the demands that will be placed upon them, it is crucial that new and improved technologies be integrated into these new aircraft to improve performance capabilities. For example, high-maneuver load factors will be required to be competitive with other high-performance fighters, and Short Take-off and Landing (STOL) capability will be required to counter runway denial tactics. Technologies that provide both of these capabilities were integrated into a model that was recently tested in the Ames 40 x 80-Foot Wind Tunnel Facility. This model, the STOL Fighter Model, was based on the General Dynamics Vectored-Engine-Over-Wing (VEO-Wing) concept, which for several years has been investigated through analytical studies and small-scale experimental tests. Documentation of several of the VEO-Wing studies and tests is presented in References 1 through 11.

To assure that the analytical studies that defined the capabilities of the VEO-Wing concept were realistic and that the tests were not adversely affected by the small scale of the previously tested model, NASA/Ames undertook the task of constructing and testing a large-scale model of this concept with full-scale, operating engines. The VEO-Wing integrated airframe/propulsion system concept, that employed on the STOL Fighter Model, utilized the full engine momentum from over-wing-mounted engines to augment the external aerodynamic characteristics through a jet-flap effect. In a flight-rate vehicle, the nozzle exhaust vectoring would be scheduled with Mach number and angle of attack to obtain optimum performance. The model also included spanwise blowing, where a portion of the engine flow was exhausted through a nozzle in the side of the nacelle to produce leading-edge vortex augmentation and enhance the overall circulation around the wing/canard lifting system.

Tests of the large-scale STOL Fighter Model were conducted at the Static Test Facility (Reference 12) and in the 40 x 80-Foot Wind Tunnel at the Ames Research Center. Force, pressure, and thermal data were acquired in a series of three wind tunnel test entries, the force data were previously presented in Reference 13 and this report addresses analysis of the pressure and thermal data.

The primary objective in the pressure data analysis was to determine the mechanisms by which chordwise and spanwise blowing affected the external aerodynamic characteristics of the model flowfield. In a cursory analysis of two sets of pressure data on the complete model with power off and power on, there seemed to be many inconsistencies and "unexplainable" phenomena because of what, in retrospect, was only a scant understanding of the flowfield. It was only through a methodical approach that scrutinized first the wing alone, then the canard, and finally the wing plus canard that the finer details of the flow were unraveled.

Many of the flow features that have been investigated in this study (e.g., canard downwash, leading-edge vortices, tip vortices, flap effects, and others) were only stepping stones to a comprehensive understanding of the power effects. However, it is felt that a knowledge of these features could prove helpful to a serious airplane designer. Consequently, the data and findings relating to these features are discussed in detail in Section 3. A considerable amount of pressure data is presented in this section so it will also serve as a limited data documentation for these tests. The reading of some of the details is somewhat laborious, so an overview is provided in Section 3.1 to give a general presentation of the key findings. The remainder of Section 3. may be of keener interest to the "hard-core" aerodynamicists.

The final section in this report presents a discussion of the results obtained from two analytical methods. A finite-element paneling technique was evaluated to determine its applicability as a pre-design tool for the estimation of the induced pressures caused by the exhaust jet of over-wing mounted engines. The predictions matched the data reasonably well at low angles of attack, where the flow was attached. At higher angles of attack, the flow separated and caused pressure patterns that were quite dissimilar to those predicted by the potential-flow method. A semi-empirical method was used to estimate the power-induced lift, drag, and pitching moment. Reasonable correlations with the data were obtained at all conditions.

## 2 DESCRIPTION OF MODEL AND TEST PROGRAM

### 2.1 MODEL DESCRIPTION

The STOL Fighter Model employed in these tests was designed to be representative of a high-performance supersonic fighter aircraft. Off-the-shelf General Electric J-97 turbojet engines were installed in podded nacelles over the wings. Since the engines were existing hardware, and the model was sized to accommodate them, the resulting model scale was approximately 75% of that of an operational fighter aircraft designed to perform an air superiority mission. Photographs of the model installed in the NASA/Ames 40 x 80-Foot Wind Tunnel are shown in Figures 2-1 and 2-2, and a drawing of the model is shown in Figure 2-3.

The model was equipped with a full set of variable control surfaces providing the capability for a thorough evaluation of the aerodynamic characteristics, particularly at STOL conditions. Control surface deflections that could be varied were those of the canard, canard leading-edge flap, canard trailing-edge flap, wing trailing-edge flap (inboard and outboard), beaver tail, and rudder. The canard deflection, which was motor-driven and remotely controlled from the control room, had a deflection range from -20 to +25 deg. The canard leading-edge and trailing-edge devices (simple flaps) were variable from 0 to 30 deg. Wing inboard and outboard trailing-edge devices were also simple flaps that could be varied independently with a deflection range in 10-deg increments from -20 deg (trailing edge up) to 30 deg (trailing edge down). The beaver tail surface, which was designed to provide a nose-up pitching moment, was deflectable with trailing-edge-up angles of 20 and 40 deg. The rudder was deflectable to angles of 20 deg. The fore and aft longitudinal-canard positions provided for on the model are shown in Figure 2-3. The forward position was tested exclusively in Test 537; the aft position was tested exclusively in Tests 543 and 546. A third, intermediate position was not tested. Some of the geometric parameters of the model that may be of interest to the reader are listed in Table 2-1.

The primary nozzles were constructed to simulate the flight configuration during STOL operation. These nozzles, which are illustrated in Figure 2-4, were two-dimensional, convergent-divergent, wedge nozzles with a throat cross-sectional aspect ratio of eight. The internal contour of the nozzle duct had a throat area of  $774 \text{ cm}^2$  ( $120 \text{ in}^2$ ), a fixed diffusion ratio of 1.09, and an exit angle of 25 deg downward. The primary-nozzle exit plane was located directly above the wing inboard-flap hinge-line.

The model was also equipped with provisions for spanwise blowing (SWB). This was accomplished by ducting a portion of the primary nozzle flow through a rectangular, convergent nozzle in the side of the nacelle. The SWB nozzles had an aspect ratio of four and were flush-mounted in the outboard fairings of each nacelle with the nozzle beginning at 23% of the wing root. The nozzle centerline was 9.07 cm (3.57 in) above the wing surface and directed aft at an angle of 40 deg. The throat area of the SWB nozzle was  $129 \text{ cm}^2$  ( $20 \text{ in}^2$ ), which was 17% of the standard primary-nozzle exit area. When the SWB nozzles were installed, alternate primary nozzles with smaller exit areas were also installed so that the combined exit area of the primary and SWB nozzles would be held constant at  $774 \text{ cm}^2$  ( $120 \text{ in}^2$ ) per side. This was accomplished by installing cowl plates along the upper, internal surface of each primary nozzle to reduce the throat area to  $645 \text{ cm}^2$  ( $100 \text{ in}^2$ ).

Each General Electric J-97 turbojet engine was rated at a thrust of 14,011 N (3150 lb) at a nozzle pressure ratio of 2.7 and an exhaust gas temperature of  $650^\circ\text{C}$ . A complete analysis of the operation of the engines and nozzles at static conditions is presented

in the static data report (Reference 12). This reference includes analyses of the normal, side, and axial forces developed during engine operation with the primary and SWB nozzles at various operating settings. The turning angles and efficiencies of each nozzle are also presented in this report.

## 2.2 INSTRUMENTATION

The model was mounted in the Ames 40 x 80-Foot Wind Tunnel (Figures 2-1 and 2-2) on a six-component balance system, from which force and moment data were determined. Instrumentation was also included to obtain a limited amount of pressure and temperature data. All pressure taps were installed on the port side of the model; their locations are pictorially indicated by the dark lines on the model in Figures 2-1 and 2-2. A clearer definition of the pressure tap locations is shown schematically in Figure 2-5, and their precise locations are listed in Table 2-2.

The thermocouples are flush-mounted on the wing and beaver tail upper surfaces. Those on the beaver tail measured the temperature impact of the primary exhaust, and those on the wing measured the effects of the SWB exhaust. The thermocouples were insulated from the model structure so that the temperature of the air (not the temperature of the model) would be measured. They were also installed on the port side of the model and alternated with the pressure taps along the same chordwise and spanwise rows. Table 2-3 lists the coordinates of the thermocouples.

A nozzle pressure rake and a flap pressure rake were installed on the port side to measure the total pressure characteristics of the flow from the primary nozzle. The nozzle rake (shown in Figure 2-6) had a total of 18 total pressure probes. It extended from the ramp to the upper wall of the nozzle and beyond the upper wall an additional 13.3 cm (5.25 in) into the freestream flow. The flap rake (also in Figure 2-6) had a total of 23 total pressure probes and extended to a height of 25.4 cm (10 in) above the flap surface. It measured the total pressure of the flow parallel to the upper surface of the flap. Total pressure at the spanwise nozzle was measured by a 12-probe rake mounted longitudinally along the centerline of the nozzle exit.

## 2.3 TEST CONDITIONS

Low-speed aerodynamic data on the STOL Fighter Model were acquired in the Ames 40 x 80-Foot Wind Tunnel. The angle of attack was varied from -8 deg to 33 deg; the angle of sideslip was varied from -10 deg to 30 deg. Because of difficulties in changing the thrust ( $T$ ) of the engines, the thrust coefficient ( $C_T$ ) was generally varied by the adjustment of the tunnel dynamic pressure ( $q$ ). From the equation  $C_T = T/qS$ , it is seen that decreasing  $q$  increased  $C_T$ . Only two values of thrust were used throughout the tests. Table 2-4 shows the values of  $T$  and  $q$  that were used to simulate a complete power sweep ( $C_T$  variation).

The wind-on tests were conducted in three separate entries in the tunnel. The first test (Test 537) included both SWB-off and SWB-on runs. The second test (Test 543) was conducted entirely with the SWB off, and the third test (Test 546) had the SWB on for most of the test. Run schedules for these three tests are presented in Table 2-5, 2-6, and 2-7.



Table 1 STOL FIGHTER MODEL GEOMETRIC PARAMETERS

Overall Length	10.24 m (33.60 ft)
Overall Width	7.28 m (23.88 ft)
Overall Height	2.27 m (7.45 ft)
Moment Reference	$X_{cg}$ ; FS 609.55 cm (239.98 in)
	$Z_{cg}$ ; 2.08 cm (.82 in) above thrust line

Wing

Reference Area	16.91 m <sup>2</sup> (182 ft <sup>2</sup> )
Aspect Ratio	3.13
Taper Ratio	0.243
Leading Edge Sweep	40 deg
Wing Span	7.28 m (23.88 ft)
Airfoil Section	NACA 64A204
Mean Aerodynamic Chord	2.61 m (8.56 ft)
Leading Edge M.A.C.	FS = 609.55 cm (239.98 in)
	BL = 145.14 cm (57.14 in)
	WL = 71.17 cm (28.02 in)
Root Chord	3.73 m (12.25 ft)
Dihedral	0°
Geometric Twist	4°
Ailerons (outboard flap)	20% chord plain T.E. flap

Canard

Area	3.53 m <sup>2</sup> (37.98 ft <sup>2</sup> )
Aspect Ratio	2.07
Taper Ratio	0.419
Leading-edge Sweep	45 deg
Span	6.04 m (19.82 ft)
Airfoil Section	NACA 64A004
Mean Aerodynamic Chord	1.37 m (4.52 ft)
Leading-edge M.A.C.	FS 396.9 cm (156.26 in)
	BL 228.5 cm (89.97 in)
	WL 106.9 cm (42.10 in)
Root Chord	1.84 m (6.04 ft)
Dihedral	3 deg
Pivot Point Forward	FS 421.64 cm (166.00 in)
Pivot Point Aft	FS 482.60 cm (190.00 in)

Table 2 PRESSURE TAP LOCATIONS

LOCATION	x/c	2y/b	COMMENT	LOCATION	x/c	2y/b	COMMENT	LOCATION	x/c	2y/b	COMMENT
CANARD	0	.75	L. E. UPPER SURF.	CANARD	.060	.75	LOWER SURF.	WING OUTBOARD	0	.84	L. E. UPPER SURF.
	.012				.042				.013		
	.023				.023				.026		
	.042				.012				.039		
	.060			STRAKE	.010		UPPER L. E.		.052		
	.078				.031		UPPER SURF.		.065		
	.097				.072				.117		
	.112				.114				.163		
	.191				.200				.200		
	.251				.280				.349		
	.312				.362				.399		
	.372				.444				.420		
	.523				.527				.462		
	.562				.610				.527		
	.599				.692				.597		
	.635				.734				.653		
	.728				.775				.704		
	.765				.817				.747		
	.802				.858				.840		
	.839				.920				.859		
	.876				.941				.896		UPPER T. E.
	.913				.961				.915		LOWER T. E.
	.951				.982		UPPER T. E.		.915		LOWER T. E.
	.988		L. E.		.982		LOWER T. E.		.896		LOWER SURF.
	.951		LOWER SURF.		.961				.859		
	.913				.941				.840		
	.876				.920				.747		
	.839				.858				.653		
	.802				.817				.527		
	.765				.775				.420		
	.728				.734				.349		
	.635				.692				.200		
	.599				.610				.163		
	.562				.527				.117		
	.523				.444				.039		
	.372				.362				.026		
	.312				.279				.013		LOWER L. E.
	.251				.196			WING INBOARD	0	.64	L. E.
	.191				.114				.013		UPPER SURF.
	.112				.072				.026		
	.097				.031				.039		
	.078				.010		LOWER L. E.		.052		

Table 2 PRESSURE TAP LOCATIONS (Continued)

LOCATION	x/c	2y/b	COMMENT	LOCATION	x/c	2y/b	COMMENT	LOCATION	x/c	2y/b	COMMENT
WING INBOARD	.063	.64	UPPER SURF.	BVR TL SPAN	.588	.523	UPPER SURF.	INBOARD FLAP	.261		UPPER L.E.
	.117					.376		FLAP RAKE	$\alpha$ (Cm)		
	.163					.229			1.27		FLAP SURF.
	.201					.064			2.54		
	.331					.468			3.81		POSITIVE
	.378					.762			5.08		UPWARD
	.520					.908		UPPER LEFT	7.62		
	.462					.908		LOWER LEFT	10.16		
	.527					.762		LOWER SURF	12.70		
	.597					.468			15.24		
	.653					.064		CENTER LINE	17.78		
	.703					.229			20.32		
	.747					.376			22.86		
	.840					.523			25.40		
	.859					.816		CONFL RAKE	0.32		INSIDE
	.896					.890			1.59		NOZZLE
	.915		UPPER T.E.			.963		LOWER LEFT	2.86		UPPER PLATE
	.915		LOWER T.E.	WING SPANWISE	.50	.59	UPPER ROOT		4.13		
	.896		LOWER SURF.			.61		UPPER SURF.	5.40		POS. DOWN
	.840					.64			6.67		
	.747					.66			7.94		PLUG SURF.
	.653					.69		CONFL RAKE	1.90		OUTSIDE
	.527					.71			3.18		NOZZLE
	.420					.74			4.44		UPPER PLATE
	.349					.76			5.72		
	.200					.79			6.98		POS. UP
	.163					.82			8.26		
	.117					.84			9.52		
	.039					.87			10.80		
	.026					.89			12.06		
	.013		LOWER L.E.			.92			13.34		
BVR TL CHORD	.163	.106	UPPER L.E.			.94					
	.349		UPPER SURF.			.97					
	.535					.99		UPPER TIP			
	.721		UPPER T.E.	INBOARD FLAP	.972		UPPER T.E.				
	.721		LOWER T.E.		.883		UPPER SURF.				
	.535		LOWER SURF.		.749						
	.349				.706						
	.163		LOWER L.E.		.617						
BVR TL SPAN	.588	.963	UPPER RIGHT		.528						
		.890	UPPER SURF.		.439						
		.816			.350						

**Table 3 THERMOCOUPLE LOCATIONS**

LOCATION	$x/c$	$2y/b$
WING OUTBOARD	.182	.84
↓	.340	↓
	.443	
	.564	
↓	.662	↓
	.737	
WING INBOARD	.182	.64
↓	.340	↓
	.443	
	.564	
↓	.662	↓
	.737	
WING SPANWISE	.50	.62
↓		.65
		.67
		.70
		.73
		.75
		.78
		.80
		.83
		.85
↓		.87
		.90

**Table 4 THRUST AND DYNAMIC PRESSURE TEST VALUES**

THRUST (lb)	$q$ (psf)	NOMINAL $C_T$
0	15	0
3370	61.8	0.3
3370	37.0	0.5
3860	31.4	0.7
3860	23.0	0.9
3860	15.3	1.4
3860	11.5	1.8

Table 5 RUN SCHEDULE FOR TEST 537 (Continued)

RUN	WING		CANARD			$\delta_r$	$\delta_{bt}$	POWER		$\alpha$	$\beta$	$q$	COMMENTS
	$\delta_{TL1}$	$\delta_{TL0}$	$\delta_c$	$\delta_l$	$\delta_t$			$C_T$	SWB				
46	30	30	0	0	0	0	0	C	ON	0	0	0	RH ENGINE CAL.
47								2.18		A		10.4	
48								1.63				13.9	
49								1.0				22.6	
50								0.5				37.0	
51								0.3				61.8	
52								0.3				61.8	
53								2.0		↓	↓	11.33	
54								0.5		0	B	37	
55								0.5		20		37	
56								2.0		20	↓	11.33	
57			↓	↓	↓			0	↓	A	0	15	INLETS OPEN
59			OFF	OFF	OFF			2.0	OFF			11.5	
60								1.5				15.3	
61								1.0				23.0	
62								0.5				36.8	
63								0.3		↓	↓	61.3	
64								2.0		0	B	11.5	
65								2.0		20		11.5	
66	↓	↓	↓	↓	↓	↓	↓	0	↓	0	↓	15	

RUN	WING		CANARD			$\delta_r$	$\delta_{bt}$	POWER		$\alpha$	$\beta$	$q$	COMMENTS
	$\delta_{TL1}$	$\delta_{TL0}$	$\delta_c$	$\delta_l$	$\delta_t$			$C_T$	SWB				
67	30	30	OFF	OFF	OFF	0	0	0	OFF	10	B	15	
68										20	↓		
69	↓	↓								A	0		
70	0	0						↓				↓	
71								2.0				11.5	
72								1.0				23	
73								0.5				36.8	
74								0				15	
75								1.5				15.3	
76								0.3		↓	↓	61.3	
77								2.0		0	B	11.5	
78								0		20		15	
79								2.0		0		11.5	
80								2.0		20		11.5	
81	↓	↓	↓	↓	↓	↓	↓	0.5	↓	0	↓	36.8	

A = Nominal  $\alpha$  = -8, -4, 0, 4, 8, 12, 16, 20, 24, 28, 32  
 B = Nominal  $\beta$  = -10, -5, 0, 5, 10, 15, 20, 25, 30  
 C = Nominal EPR = 1→2.8

Table 5 RUN SCHEDULE FOR TEST 537

RUN	WING		CANARD			$\delta_r$	$\delta_{de}$	POWER		$\alpha$	$\beta$	$q$	COMMENTS
	$\delta_{TE1}$	$\delta_{TE2}$	$\delta_c$	$\delta_l$	$\delta_t$			$C_T$	SWB				
3	30	30	0	0	0	0	0	C	OFF	0	0	0	LEFT ENGINE ONLY
4													RIGHT ENGINE ONLY
5								↓		↓		↓	LEFT ENGINE ONLY
8								2.0		A		7.3	BOTH ENGINES
9												18.0	
10												11.5	
11			↓					↓				9.5	
12			0					0				15	INLET BLOCKED
13			-10										
14			-20										
15			10										
16			20									↓	
17			0									7	
18										↓	↓	40	
20										0	B	15	
21										10			
22										20			
23										30			
24			-20						↓	0			
25	↓	↓	↓	↓	↓	↓	↓	↓		10	↓	↓	↓

RUN	WING		CANARD			$\delta_r$	$\delta_{de}$	POWER		$\alpha$	$\beta$	$q$	COMMENTS
	$\delta_{TE1}$	$\delta_{TE2}$	$\delta_c$	$\delta_l$	$\delta_t$			$C_T$	SWB				
26	30	30	0	0	0	0	0	C	OFF	0	0	0	RECAL. OF L. ENG. RPM VAR.
27								↓		↓		↓	RECAL. OF R. ENG. RPM VAR.
28								2.0		A		11.5	
29								.46				40	
30								2.5				9.2	
31								1.5				15.3	
32								1.0				23.0	
33								.5				36.8	
34								3		↓	↓	61.3	
35								2.0				11.5	
36								↓		10			
37								↓		20		↓	
38								.5		0		36.8	
39								↓		10			
40								↓		20		↓	
41								2.0		A	0	11.5	
42								1.0				23	
43								0.5		↓	↓	36.8	
44			↓					↓	↓	0	B	↓	
45	↓	↓	0	↓	↓	↓	↓	C	ON	A	0	0	LH ENGINE CAL

Table 6 RUN SCHEDULE FOR TEST 543

RUN	WING		CANARD			$\delta_r$	$\delta_{br}$	POWER		$\alpha$	$\beta$	$q$	COMMENTS
	$\delta_{\pi_1}$	$\delta_{\pi_0}$	$\delta_c$	$\delta_L$	$\delta_t$			$C_T$	SWB				
4	30	30	0	0	0	0	0	2.0	OFF	A	0	11.5	
5								1.5				15.3	
6								1.0				23.0	
7								0.7				31.4	
8								0.5				37	
9								0.3				61.8	
10								0.3				61.8	
11								0		▼	▼	15	
15								2.0		0	B	11.5	
16								1.0				23.0	
17								0.5				37	
18								0		▼		15	
19								2.0		20		11.5	
20			▼					0		▼	▼	15	
21			20					1.0		A	0	23	
22			-10							▼			
23			S							0			
24			S	▼						16			
25			0	10						A			
26	▼	▼	20	▼	▼	▼	▼	▼	▼	▼	▼	▼	

RUN	WING		CANARD			$\delta_r$	$\delta_{br}$	POWER		$\alpha$	$\beta$	$q$	COMMENTS
	$\delta_{\pi_1}$	$\delta_{\pi_0}$	$\delta_c$	$\delta_L$	$\delta_t$			$C_T$	SWB				
27	30	30	S	10	0	0	0	1.0	OFF	0	0	23	
29			0	30						A			
31			20							▼			
32			5					▼		0		▼	
33			0		▼			0		A		15	
34			▼		30			1.0				23	
35			20										
36			0					0		▼		15	
37			S					1.0		0		23	
38		▼	0					2.0				11.5	
39		0						▼				▼	
40								0				15	
41								1.0		▼	▼	23	
44								2.0		0	B	11.5	
45		▼		▼	▼		▼			20	▼		
46		30		0	0		40	▼		A	0	▼	
47								1.0				23	
48								0				15	
49							20	2.0				11.5	
50	▼	▼	▼	▼	▼	▼	▼	1.0	▼	▼	▼	23	

Table 6 RUN SCHEDULE FOR TEST 543 (Continued)

RUN	WING		CANARD			$\delta_r$	$\delta_{bt}$	POWER		$\alpha$	$\beta$	$q$	COMMENTS
	$\delta_{TL_1}$	$\delta_{TL_0}$	$\delta_c$	$\delta_L$	$\delta_t$			$C_T$	SWB				
51	30	30	0	0	0	0	20	0	OFF	A	0	15	
52	0	0						2.0				11.5	
53								1.0				23	
54								0				15	
55							40	2.0				11.5	
56								1.0				23	
57								0				15	
58								2.0				11.5	
59								1.5				15.3	
60								1.0				23	
62								0.5				37	
63								0				15	
64			↓					0.3				61.8	
65			-10					0				15	
66	↓	↓	↓					1.0				23	
67	20	20	0					2.0				11.5	
68								1.0				23	
69								0				15	
70	↓	↓						0.5				37	
72	-10	0	↓	↓	↓	↓	↓	2.0	↓	↓	↓	11.5	

RUN	WING		CANARD			$\delta_r$	$\delta_{bt}$	POWER		$\alpha$	$\beta$	$q$	COMMENTS
	$\delta_{TL_1}$	$\delta_{TL_0}$	$\delta_c$	$\delta_L$	$\delta_t$			$C_T$	SWB				
73	-10	0	0	0	0	0	0	1.5	OFF	A	0	15.3	
74								1.0				23	
75								0.5				37	
76								0				15	
77								0.3		↓	↓	61.8	
79								2.0		0	B	11.5	
80	↓	↓								20	B		
81	10	10						↓		A	0	↓	
82								1.0				23	
83								0				15	
84								0.5				37	
85	-20	-20						2.0				11.5	
86								1.0				23	
87								0.5				37	
88	↓	↓	↓	↓	↓	↓	↓	0	↓	↓	↓	15	

A = Nominal  $\alpha$  = 8, -4, 0.4, 8, 12, 16, 20, 24, 28, 32  
 B = Nominal  $\beta$  = -10, -5, 0, 5, 10, 15, 20, 25, 30  
 S = Nominal  $\delta_c$  = -20, -10, 0, 10, 20



Table 7 RUN SCHEDULE FOR TEST 546

RUN	WING		CANARD			$\delta_r$	$\delta_{\delta r}$	POWER		$\alpha$	$\beta$	$q$	COMMENTS
	$\delta_{TL1}$	$\delta_{TL0}$	$\delta_c$	$\delta_L$	$\delta_t$			$C_T$	SWB				
1	30	30	0	0	0	0	0	C	ON	0	0	$\approx 0$	TRANSDUCER COVERED
2								C		A		$\approx 0$	TRANSDUCER UNCOVERED
3								2.0				11.5	
4								1.5				15.3	
5								1.0				23	
6								0.7				31.4	
7								0.5				37	
8								0.3		↓	↓	61.8	
9								2.0		0	B	11.5	
10								0.5		↓		37	
11								2.0		20		11.5	
12								0.5		↓	↓	37	
13								2.0		A	20	11.5	
14								1.0			0	23	STARBOARD ENGINE OUT
15								0.7				31.4	
16								0.5		↓	↓	37	
17								1.0		0	B	23	
18			↓							20	↓		
19			S							0, 12, 20	0		
20	↓	↓	20	↓	↓	↓	↓	↓	↓	A	↓	↓	↓

RUN	WING		CANARD			$\delta_r$	$\delta_{\delta r}$	POWER		$\alpha$	$\beta$	$q$	COMMENTS
	$\delta_{TL1}$	$\delta_{TL0}$	$\delta_c$	$\delta_L$	$\delta_t$			$C_T$	SWB				
21	30	30	20	0	0	0	0	.3	ON	A	0	61.8	STARBOARD ENGINE OUT
22	↓	↓	↓					1.0				23	PORT ENGINE OUT
24	-10	0	0					2.0				11.5	
25								1.5				15.3	
26								↓				↓	
27								1.0				23	
28								0				15	
29								0.3				61.8	
30								0.5		↓	↓	37	
31								2.0		0	B	11.5	
32								0.5		↓		37	
33								2.0		20		11.5	
34								0.5		↓	↓	37	
35			↓					2.0		A	20	11.5	
36			20					1.0		↓	0	23	
37			S	↓	↓			↓		0, 12, 20	↓	↓	
38			OFF	OFF	OFF			0		A	B	0	WEIGHT STATIC
39								2.0		A	0	11.5	
40								1.5				15.3	
41	↓	↓	↓	↓	↓	↓	↓	1.0	↓	↓	↓	23	

Table 7 RUN SCHEDULE FOR TEST 546 (Continued)

RUN	WING		CANARD			$\delta_r$	$\delta_{bt}$	POWER		$\alpha$	$\beta$	q	COMMENTS
	$\delta_{TE1}$	$\delta_{TE0}$	$\delta_c$	$\delta_l$	$\delta_e$			$C_T$	SWB				
42	-10	0	OFF	OFF	OFF	0	0	0.5	ON	A	0	37	
43								0.3				61.7	
44	↓	↓						0				15	
45	30	30						2.0				11.5	
46								1.5				15.3	
47								1.0				23	
48								0.5				37	
49	↓	↓	↓	↓	↓			0				15	
50	20	20	0	0	0			2.0				11.5	
51								1.5				15.3	
52								0				15	
53								1.0				23	
54	↓	↓						0.5				37	
55	10	10						2.0				11.5	
56								1.5				15.3	
57								1.0				23	
58								0.5				37	
59	↓	↓	↓	↓	↓			0	↓	↓		15	
60	30	30	-5/+5						OFF	0, 12, 20			CANARD ROLL EFFECT
61	↓	↓	-10/+20	↓	↓	↓	↓	↓	↓	A	↓	↓	↓

RUN	WING		CANARD			$\delta_r$	$\delta_{bt}$	POWER		$\alpha$	$\beta$	q	COMMENTS
	$\delta_{TE1}$	$\delta_{TE0}$	$\delta_c$	$\delta_l$	$\delta_e$			$C_T$	SWB				
62	30	30	-10/+20	0	0	0	0	0	OFF	0	B	15	CANARD ROLL EFFECT
63			↓							20	↓		↓
64		-10/+20	0							A	0		AILERON ROLL EFFECT
65										0	B		↓
66		↓						↓		20	↓	↓	↓
67		30						1.0		A	0	23	STARBOARD ENGINE OUT
68								0.7				31.4	
69								0.5				37	
70								0.3		↓	↓	61.8	
71								1.0		0	B	23	
72						↓		↓		20	↓	↓	↓
73						-10		0		A	0	15	RUDDER EFFECT
74										0	B		
75						↓				20			
76						-20				-20			
77											↓		
78										A	0		
79						0		↓		↓	↓	↓	↓
80								0.5		0	B	37	STARBOARD ENGINE OUT
81	↓	↓	↓	↓	↓	↓	↓	↓	↓	20	↓	↓	↓

Table 7 RUN SCHEDULE FOR TEST 546 (Continued)

RUN	WING		CANARD			$\delta_r$	$\delta_{bt}$	POWER		$\alpha$	$\beta$	$q$	COMMENTS
	$\delta_{TE_1}$	$\delta_{TE_2}$	$\delta_c$	$\delta_l$	$\delta_t$			$C_T$	SWB				
82	30	30	0	0	0	0	0	1.0	OFF	A	20	23	STARBOARD ENGINE OUT
86	-10/-20	-30/-20	-20/-20			-20		0		A	0	15	
87								1.0		↓	↓	23	STARBOARD ENGINE OUT
88			↓					↓		0	B	↓	↓
89			0					0		↓		15	
90										20	↓		
91			↓							A	0		
92			-20/-20							↓	20		
93										0	B		
94	↓	↓	↓	↓	↓	↓	↓	↓	↓	20	↓	↓	

A = Nominal  $\alpha$  = -8, 4, 0, 4, 8, 12, 16, 20, 24, 28, 32  
 B = Nominal  $\beta$  = -10, -5, 0, 5, 10, 15, 20, 25, 30  
 C = Nominal EPR = 1→2.8  
 S = Nominal  $\delta_c$  = -20, -10, 0, 10, 20

ORIGINAL PAGE 16  
OF POOR QUALITY



Figure 2-1 STOL Fighter Model in NASA/Ames 40 x 80-Foot Wind Tunnel, Upper View



Figure 2-2 STOL Fighter Model in NASA/Ames 40 x 80-Foot Wind Tunnel, Lower View

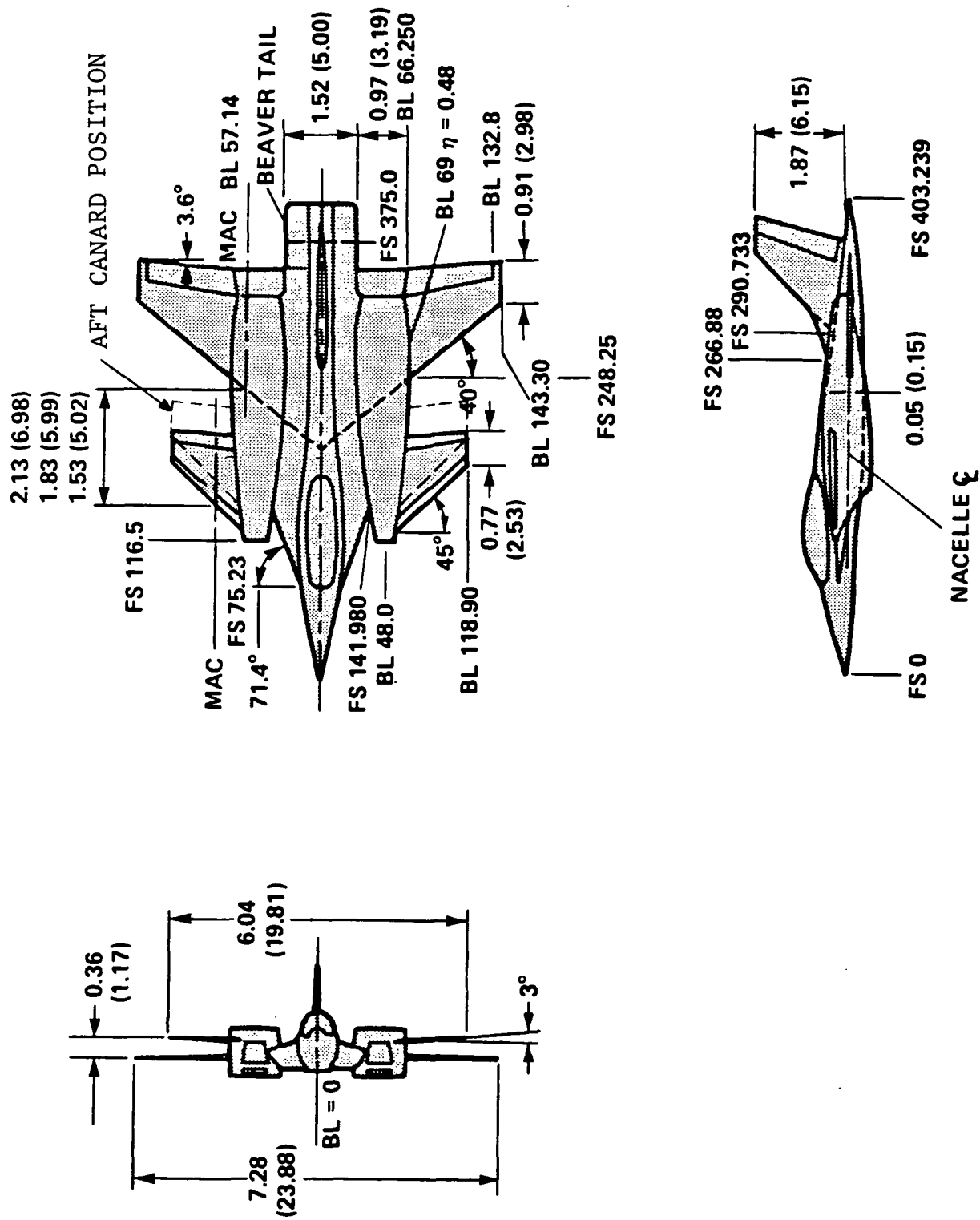


Figure 2-3 STOL Fighter Model Geometry ALL DIMENSIONS IN m (ft)

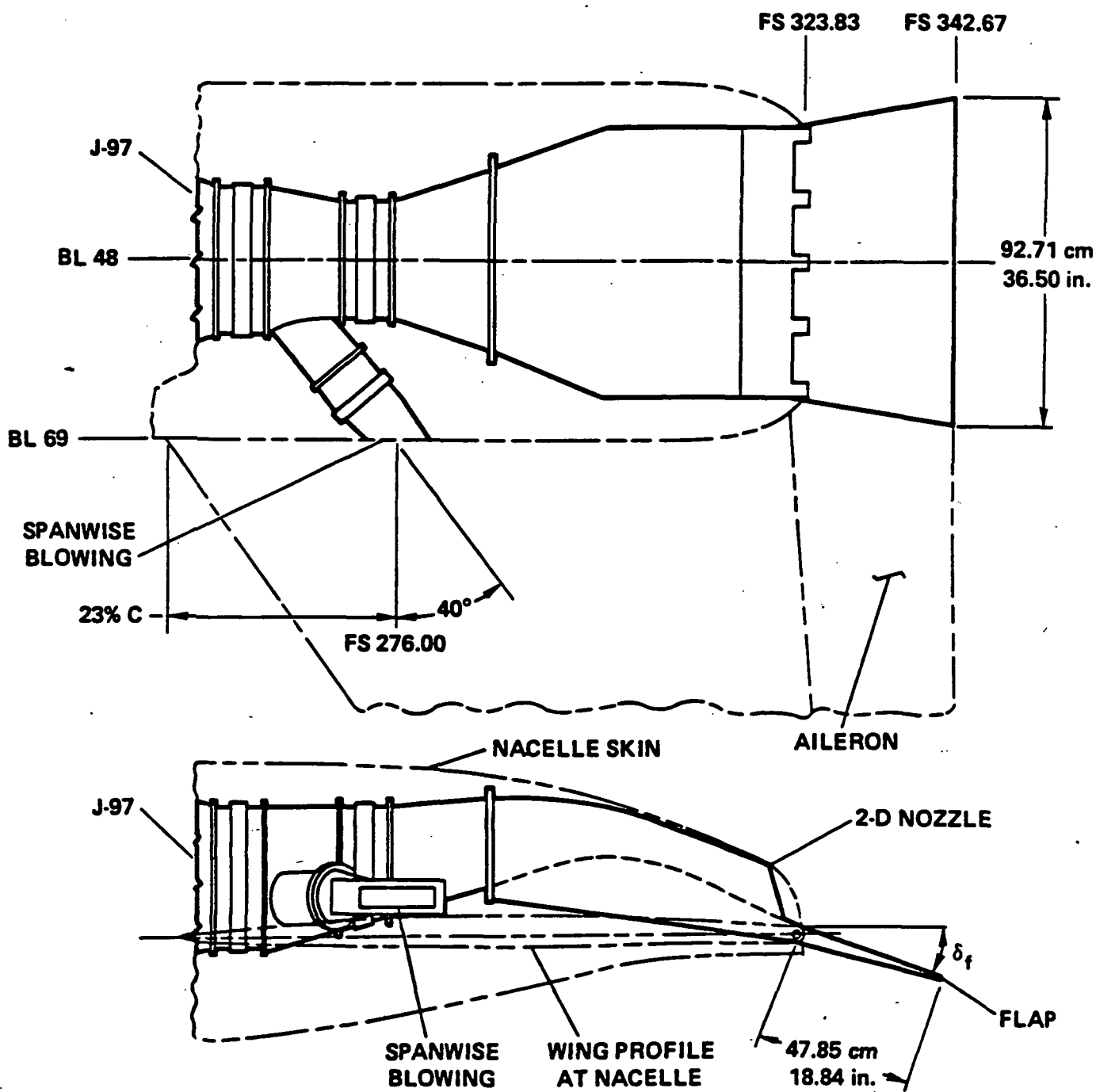


Figure 2-4 Port Nozzle Geometry

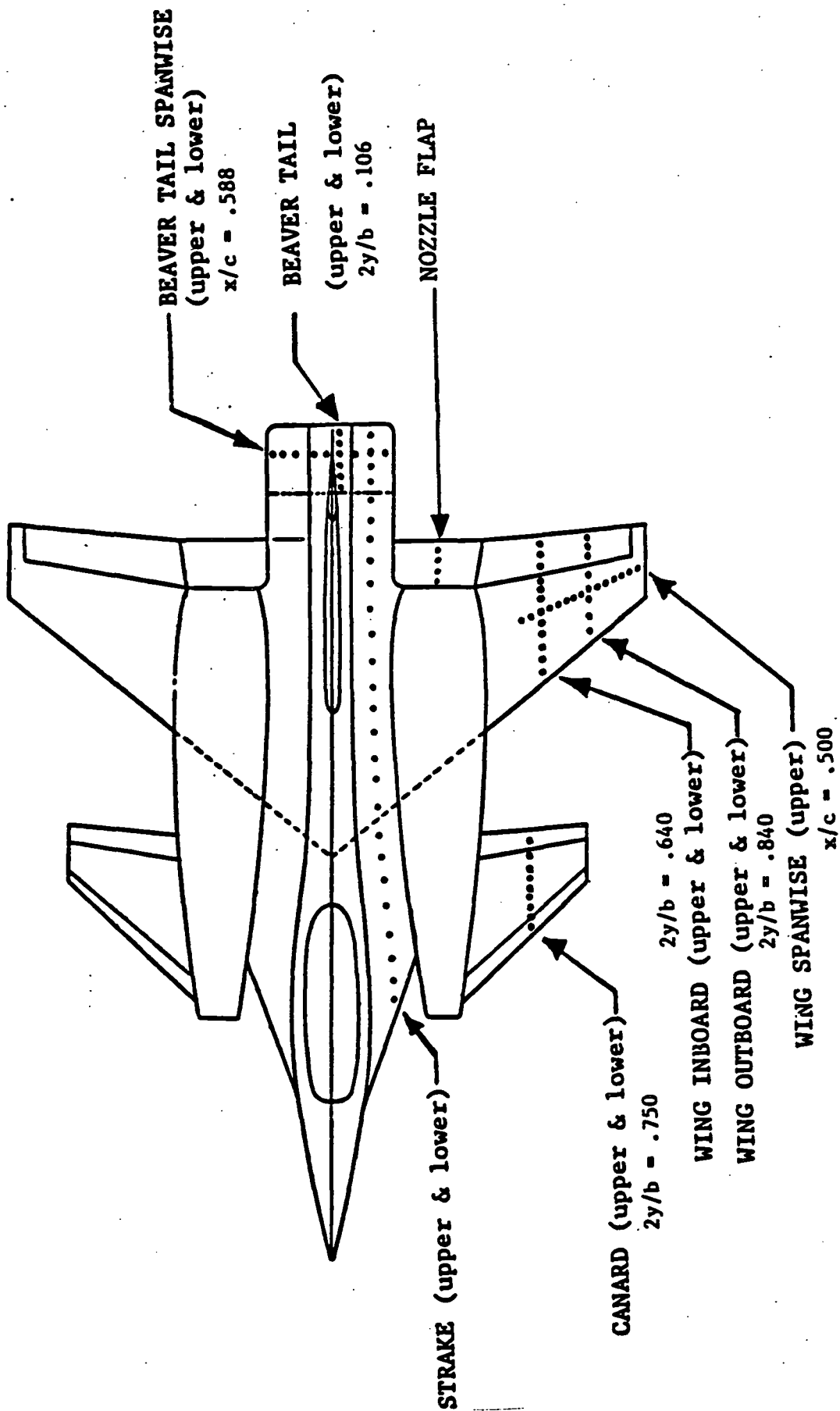


Figure 2-5 Pressure Tap Locations



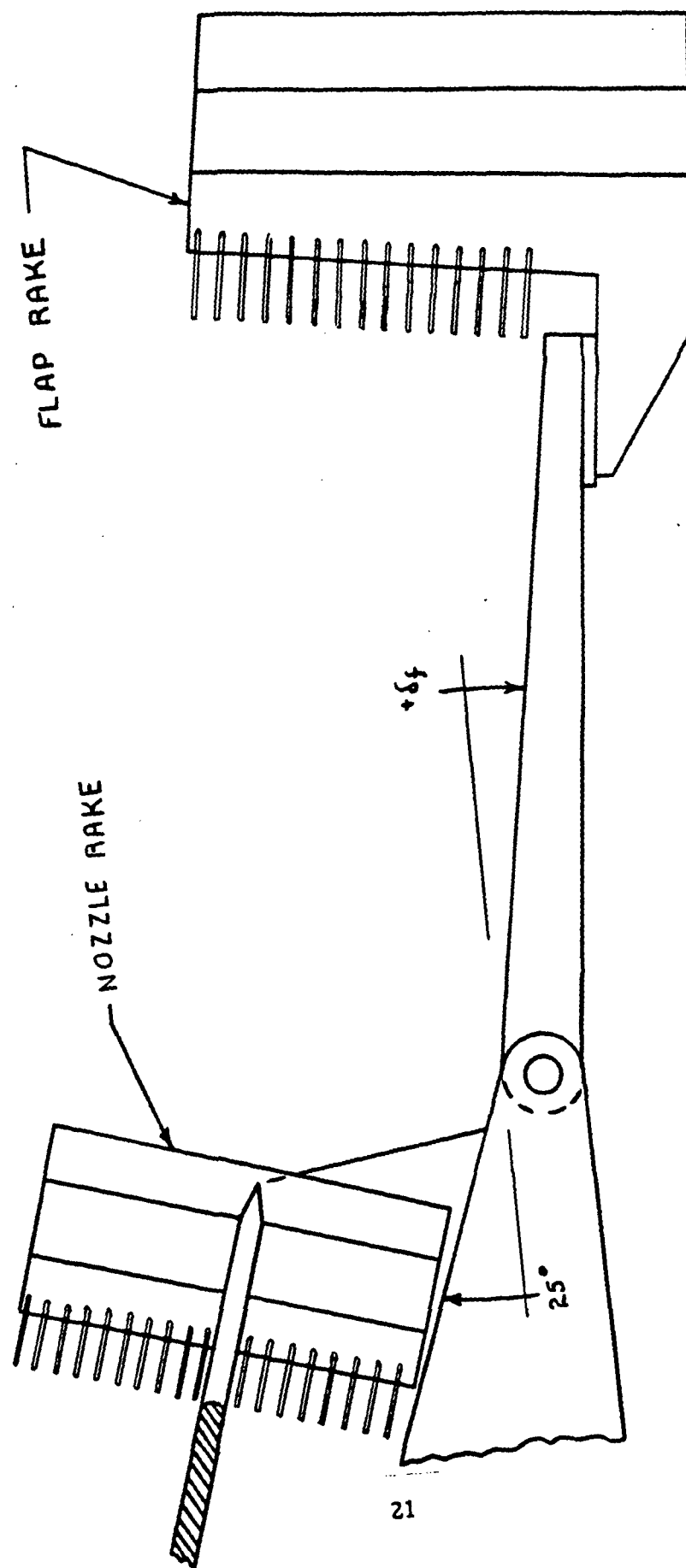


Figure 2-6 Rake Installation

**(This page intentionally left blank.)**

### 3. FLOW FIELD ANALYSIS

#### 3.1 OVERVIEW

The basic lifting-surface elements of the AMES STOL Fighter Model, the wing and canard, are not unusual or unique in their behavior as thin, low-aspect-ratio, mid-sweep panels. The canard full-span leading-edge and trailing-edge flaps and the wing/nacelle two-element trailing-edge flaps bore few surprises. This is not to imply that the flow structure pertaining to the wing and canard was so traditional as to be predictable, or even eminently recognizable, in the very limited diagnostic pressure and temperature measurements available for this purpose. Rather, piecing together a cogent model of the flowfield was compounded by a common nemesis of conventional aerodynamics - uncontrolled separated flow. Once the presence of this phenomenon had been recognized, a means was at hand to tackle the question most pertinent to this vehicle, namely: What effects did power have on the key flowfield features?

Subsections 3.2 through 3.6 present a large portion of the available surface static-pressure and temperature data. Fewer data plots could suffice to highlight the key results, but it is intended that the reader also have an orderly, comprehensive set of test results on hand for his own interpretive analysis. Hence, with clarity foremost in mind, a general description of the wing and canard basic-flow features is presented first (Subsection 3.2.1). This description includes illustrations of the pressure distribution trends that served to identify separation and the presence of a leading-edge vortex. Next (Subsection 3.2.2), results for the wing without a canard are closely examined, particularly where the leading-edge or "free" vortex played a key role. The same is then done with the canard in the presence of the wing (Subsection 3.2.3) and with the wing in the presence of the canard (Subsection 3.2.4). Other component results are treated last. Pressure distribution data for the wing and canard, presented at the beginning of each subsection following Subsection 3.2.1, show typical results with varying angle of attack in order to establish the basic aerodynamic traits of that component. The  $C_p$  changes caused by individual variables, such as flap deflection, canard on/off, and power on/off, are then examined at discrete angles of attack. This treatise is frequently supplemented by computed values of section lift coefficient and center of pressure on the basis of the same chordwise pressure data.

In order to introduce the reader to the  $C_p$  data and their sources, typical results are previewed here in a composite, three-dimensional, 3/4-perspective view (Figures 3.1-1 through 3.1-8). Lower-surface pressures have been omitted since the upper surface was where major effects appeared. Even so, several key features that have a bearing on the flow mechanism cannot be readily identified in these small-scale pressure plots because the clues were often subtle. For example, the onset of leading-edge separation was not a catastrophic condition; generally, the subsequent vortex it formed produced footprints that distorted radically within an  $\alpha$  change of four deg - the interval at which data were acquired. Frequently, the cause of upper-surface pressure changes (i.e., the governing flowfield model) could not be proffered with confidence unless small changes in lower-surface pressure clearly confirmed the diagnosis.

The diligent reader who wades through Sections 3.2 through 3.6 may recognize the following flow features (though not in the same order).

1. The wing and canard at low  $\alpha$ s exhibited chordwise  $C_p$  distributions common to attached flow. Characteristically, they consisted of a low-pressure buildup at the upper-surface leading edge followed by rapid compression towards the trailing edge (Figure 3.1-1).

2. At high alphas, the outboard regions of the wing and canard were largely stalled, but in the inboard regions, there remained a significant, semi-stalled lifting load (Figure 3.1-2).
3. Leading-edge separation first occurred outboard at low alpha and spread inboard with increased alpha. This phenomena generated a weak vortex with a path that was nearly parallel to the leading edge near the innermost stall point, but the path then curved downstream at the more outboard span stations. Where it crossed a chord, static pressures beneath the vortex were reduced in the forward area and increased in the aft area (like a sine wave), and its development was hastened by increased circulation (via increased alpha, flap deflection, etc.) or by reduced  $R_e$  (Figure 3.1-3a shows that a reduction in  $R_e$  brought on stall and a vortex on the wing outboard and on the canard; Figure 3.1-3b shows the same flow pattern on the wing inboard).
4. Pressure distribution and vortex development on the canard were comparable to those on the wing alone, but (a) canard downwash greatly reduced the effective angle of attack of the inboard region of the wing (Figure 3.1-4a), thus (b) postponing local stall onset inboard and outboard to a higher alpha (Figure 3.1-4b). Canard-tip vortex interactions at the wing outboard station were sometimes significant, but more often they were not.
5. When wing trailing-edge flaps were deflected down, the increased circulation sharply reduced leading-edge pressures where stall was not already present. This caused local separation to occur at a lower alpha and the leading-edge vortex to be positioned further inboard at each alpha than it was with flaps undeflected (Figure 3.1-5). Canard loads also were raised.
6. Power applied at the wing-inboard-trailing-edge flap, without spanwise blowing, induced these changes: (a) significant inboard- and outboard-lift benefits that were greatest at high alphas; (b) a modest aft shift in center of pressure; (c) much larger lift gains with flaps deflected than neutral; and (d) substantial canard-lift benefits at highest alphas, even though stalled (Figures 3.1-6a and 3.1-6b).
7. Spanwise blowing over the wing produced: (a) at low alphas, increased circulation plus localized pressure reductions beneath the jet near the midchord and aft areas (Figure 3.1-7a); (b) at mid alphas in addition to (a) leading-edge vortex enhancement (Figure 3.1-7b); (c) at higher alphas, strong jet-vortex interactions (though uncoupled) with an unsweeping of both streams, more lift increase outboard than inboard, a forward shift in center-of-pressure, and an increase in canard loading (Figure 3.1-7c).
8. Beaver-tail deflection created an increase in upper-surface pressures on the beaver tail and somewhat forward on the strake to approximately the wing flap station (Figure 3.1-8). Pressure reductions on the lower surface of the beaver tail (not shown) were even greater in magnitude.
9. Strake pressures, in general, were slightly decreased by any variable that increased circulation, for instance, trailing-edge flap deflection (Figure 3.1-5), power (Figure 3.1-6b), and spanwise blowing (Figure 3.1-7a).

# AMES FIGHTER MODEL

LINE	TEST	RUN	ALPHA	CT	ITEF	OTEF	CAN	SWB
—	543	63	4.2	0.00	0	0	0	OFF

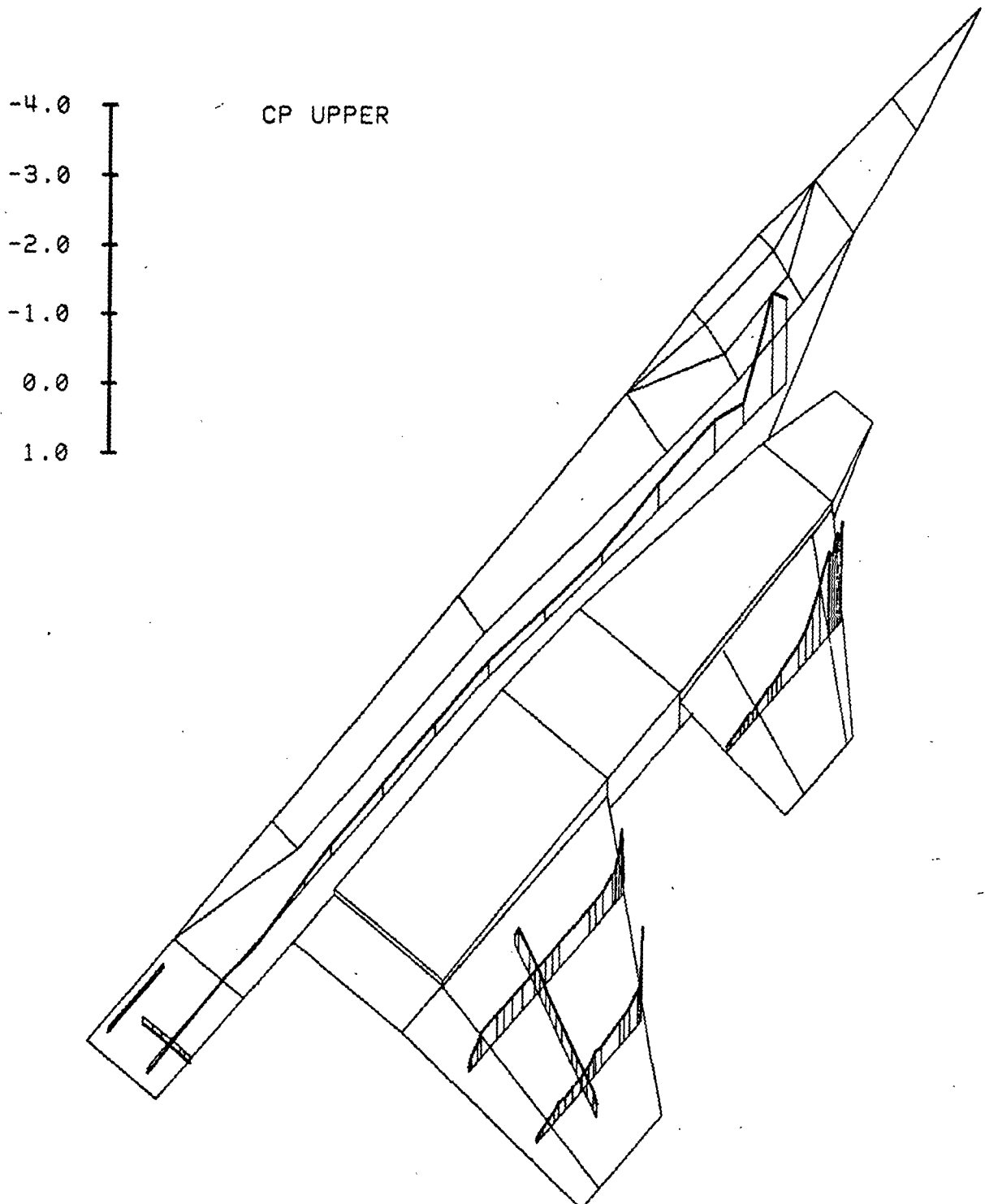


Figure 3.1-1

Common Pressure Distributions, Alpha = 4 deg

## AMES FIGHTER MODEL

LINE	TEST	RUN	ALPHA	CT	ITEF	OTEF	CAN	SWB
—	543	63	20.7	0.00	0	0	0	OFF

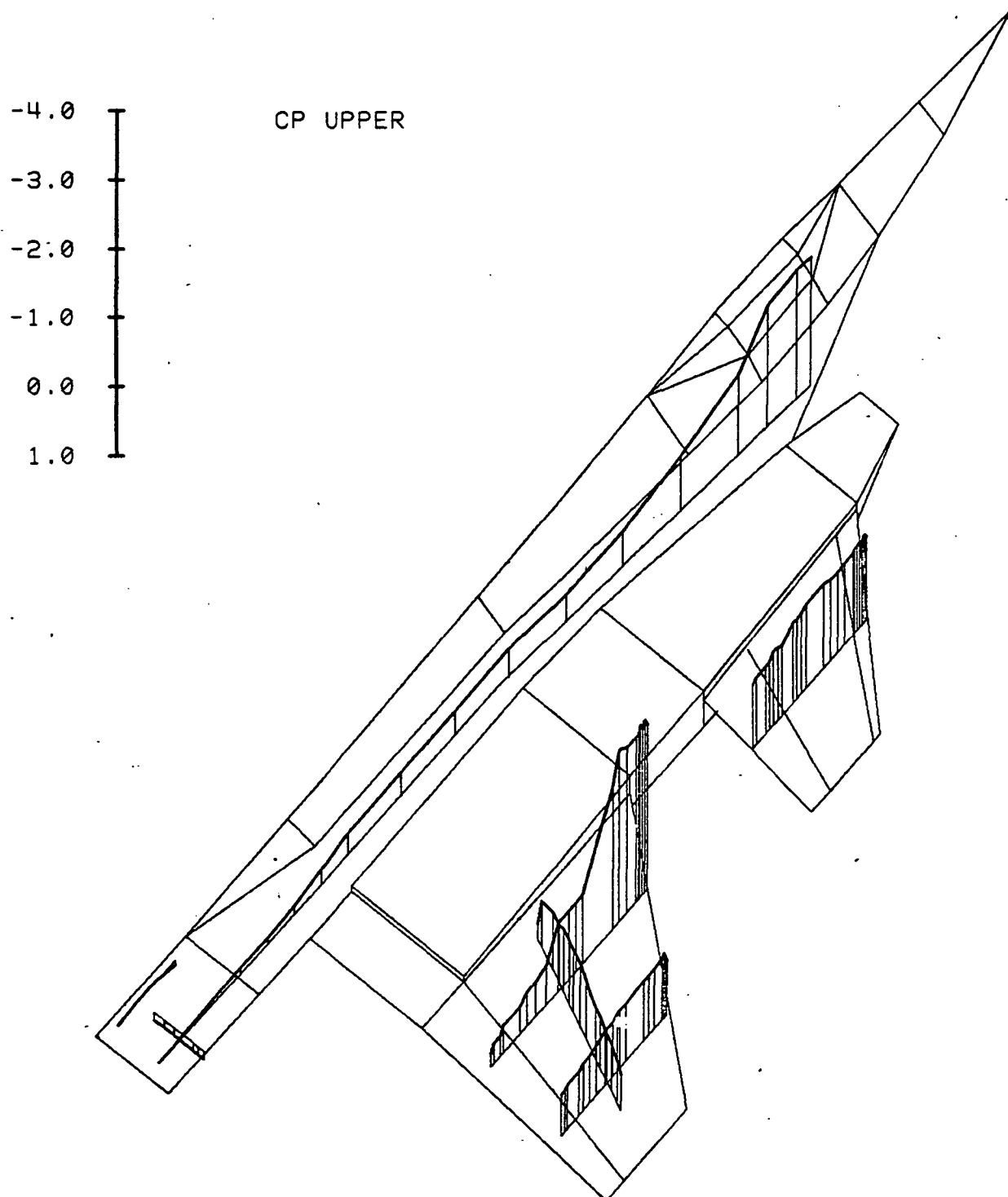


Figure 3.1-2

Common Pressure Distributions, Alpha = 20 deg

## AMES FIGHTER MODEL

LINE	TEST	RUN	ALPHA	CT	ITEF	OTEF	CAN	SWB	q
—	537	18	4.4	0.00	30	30	0	OFF	7
.....	537	17	4.4	0.00	30	30	0	OFF	40

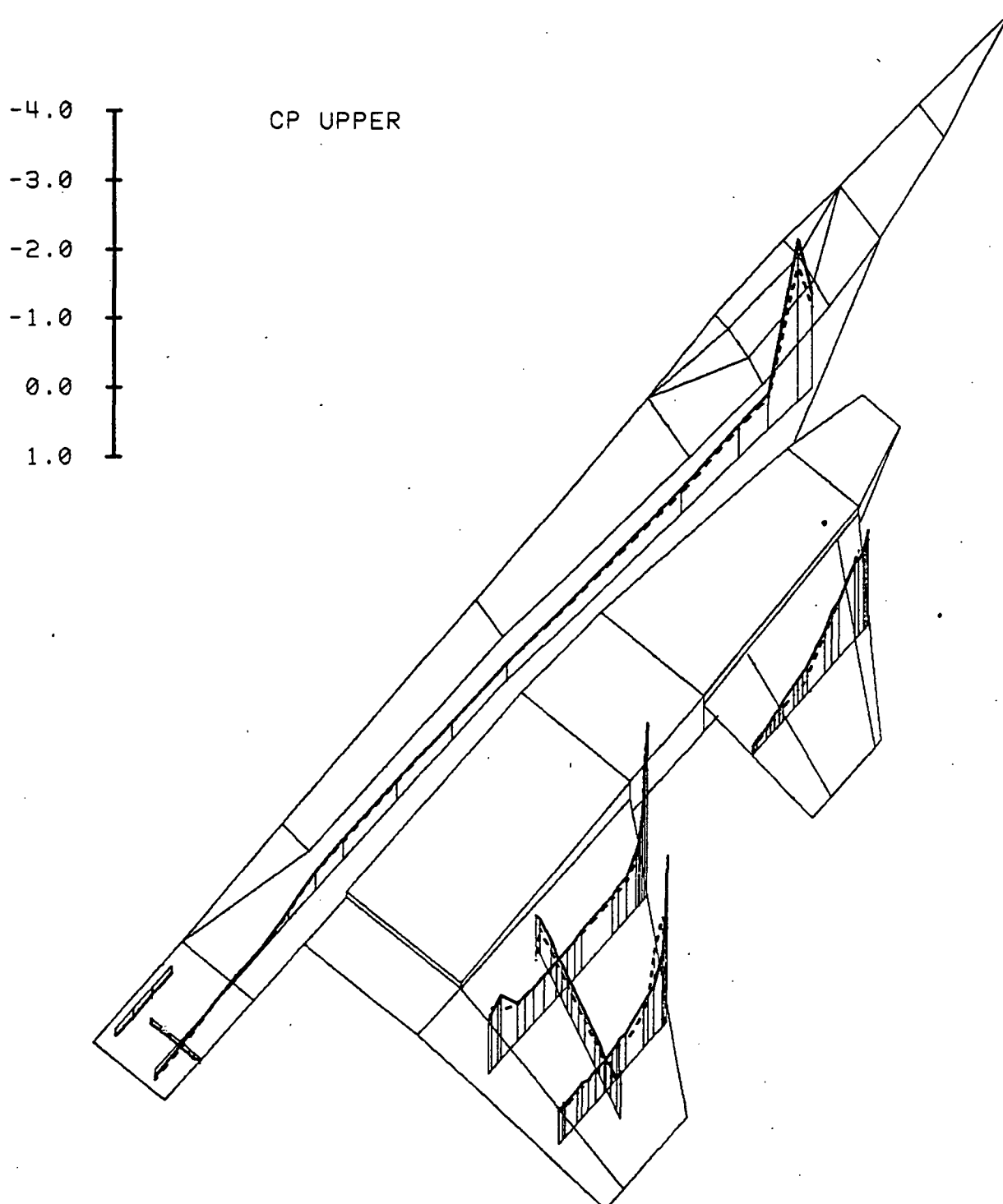


Figure 3.1-3(a) Reynolds Number Effects, Alpha = 4 deg

## AMES FIGHTER MODEL

LINE	TEST	RUN	ALPHA	CT	ITEF	OTEF	CAN	SWB	q
—	537	18	8.5	0.00	30	30	0	OFF	7
.....	537	17	8.5	0.00	30	30	0	OFF	40

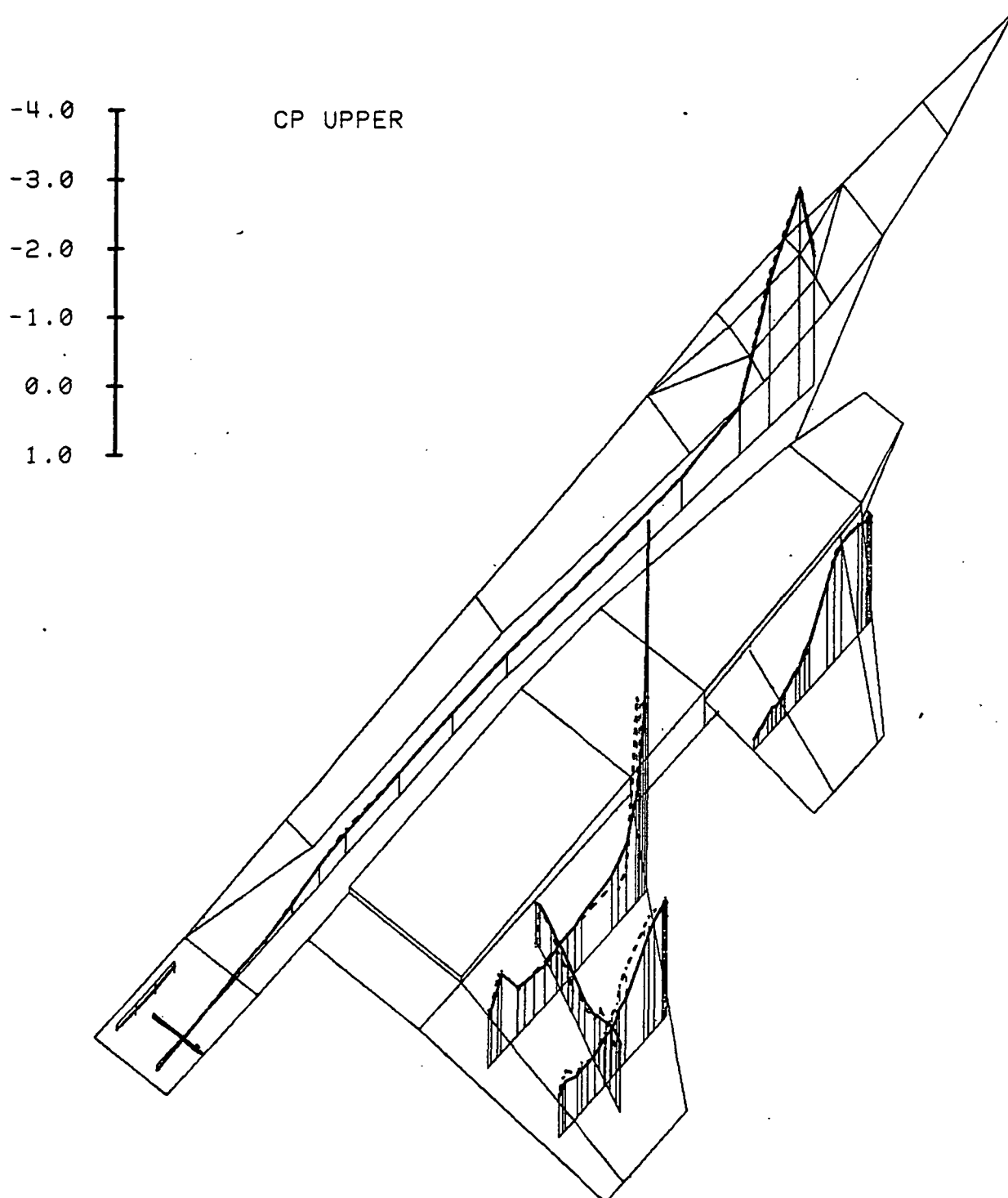


Figure 3.1-3(b) Reynolds Number Effects, Alpha = 8 deg



# AMES FIGHTER MODEL

LINE	TEST	RUN	ALPHA	CT	ITEF	OTEF	CAN	SWB
—	543	11	4.4	0.00	30	30	0	OFF
.....	537	69	4.3	0.00	30	30	OFF	OFF

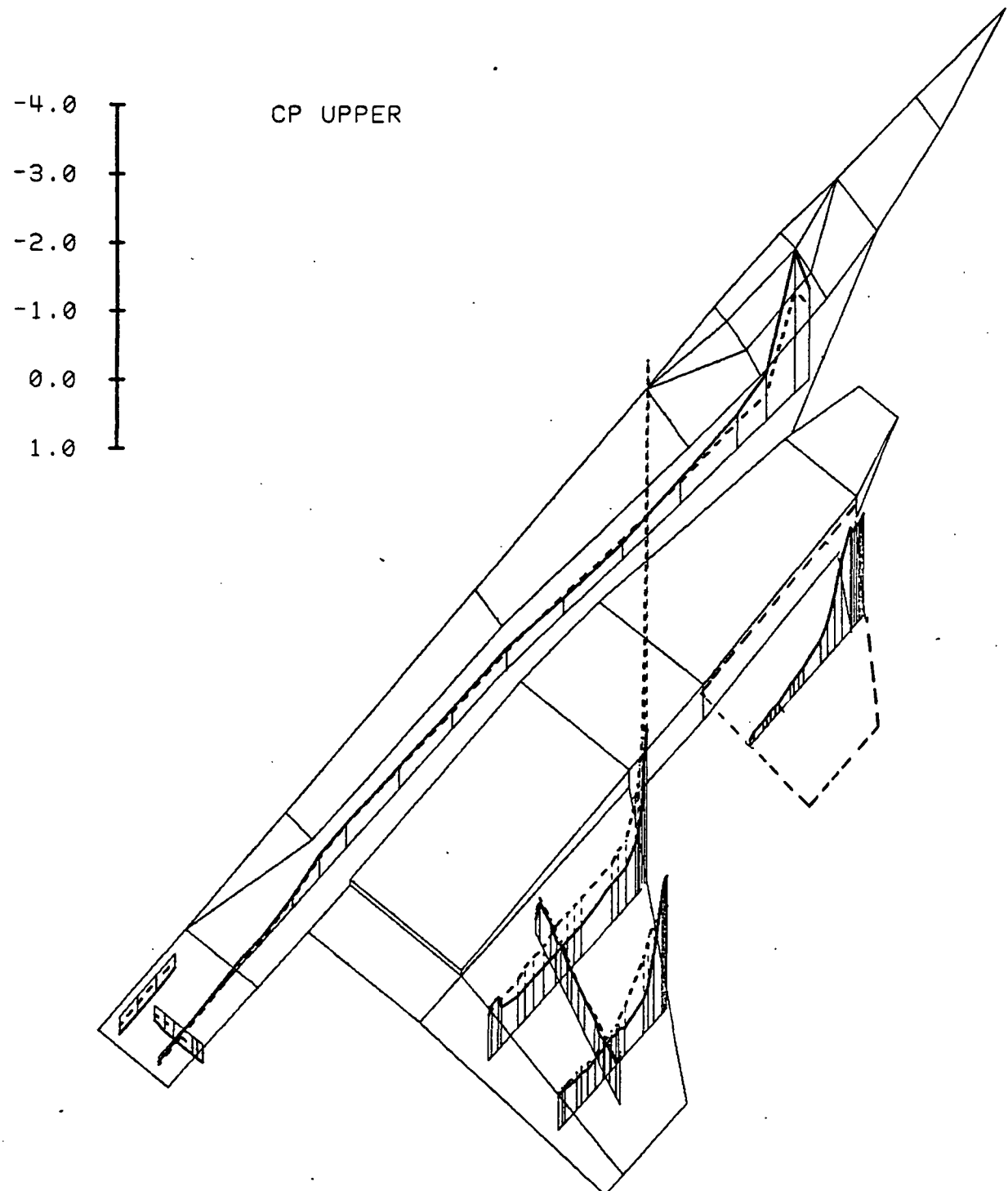


Figure 3.1-4(a) Canard Effects, Alpha = 4 deg

# AMES FIGHTER MODEL

LINE	TEST	RUN	ALPHA	CT	ITEF	OTEF	CAN	SWB
—	543	11	8.5	0.00	30	30	0	OFF
-----	537	69	8.5	0.00	30	30	OFF	OFF

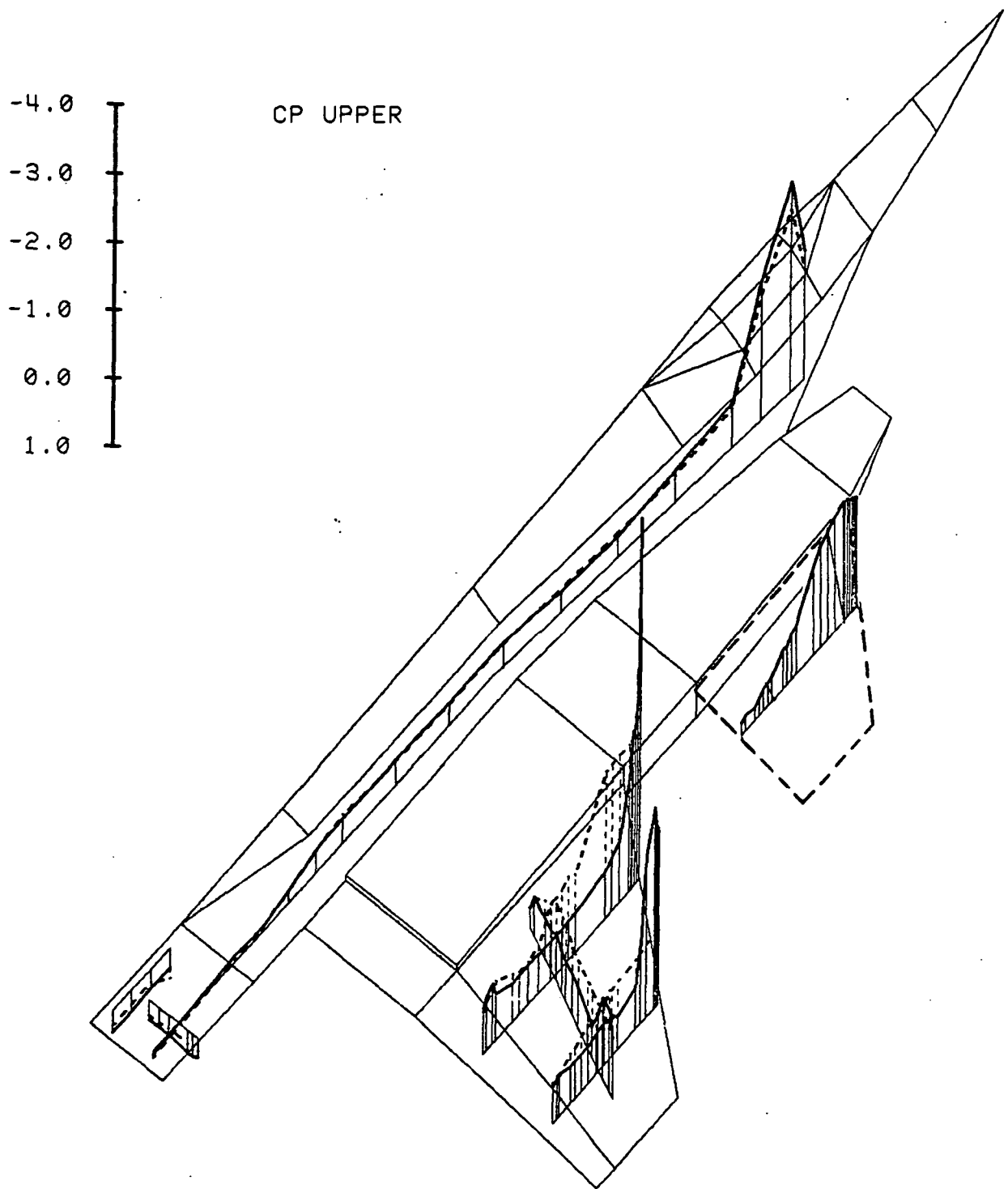


Figure 3.1-4(b) Canard Effects, Alpha = 8 deg

# AMES FIGHTER MODEL

LINE	TEST	RUN	ALPHA	CT	ITEF	OTEF	CAN	SWB
—	543	60	8.4	0.94	0	0	0	OFF
-----	543	6	8.6	0.91	30	30	0	OFF

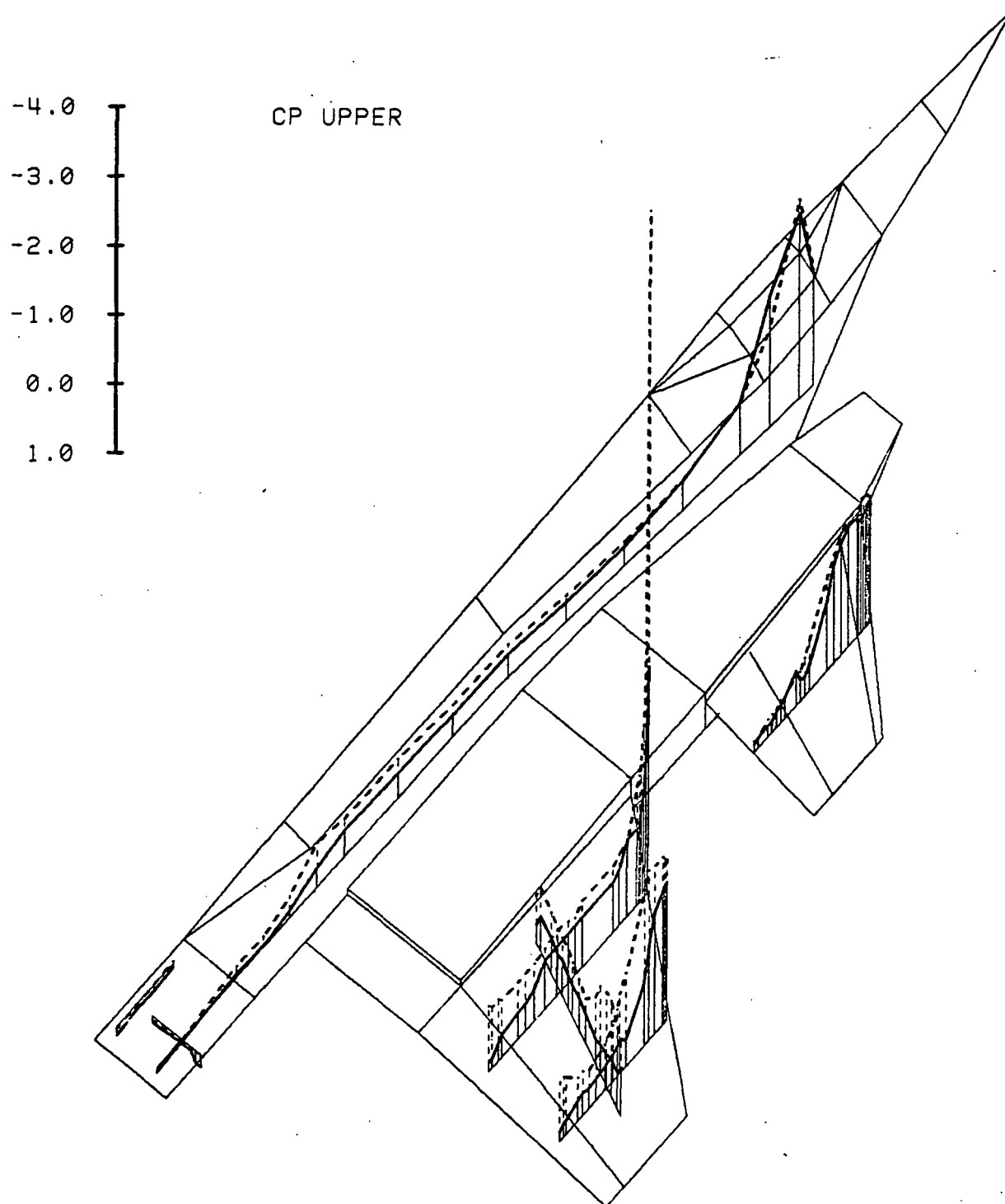


Figure 3.1-5

Wing Flap Effects

## AMES FIGHTER MODEL

LINE	TEST	RUN	ALPHA	CT	ITEF	OTEF	CAN	SWB
—	543	11	4.4	0.00	30	30	0	OFF
-----	543	5	4.5	1.40	30	30	0	OFF

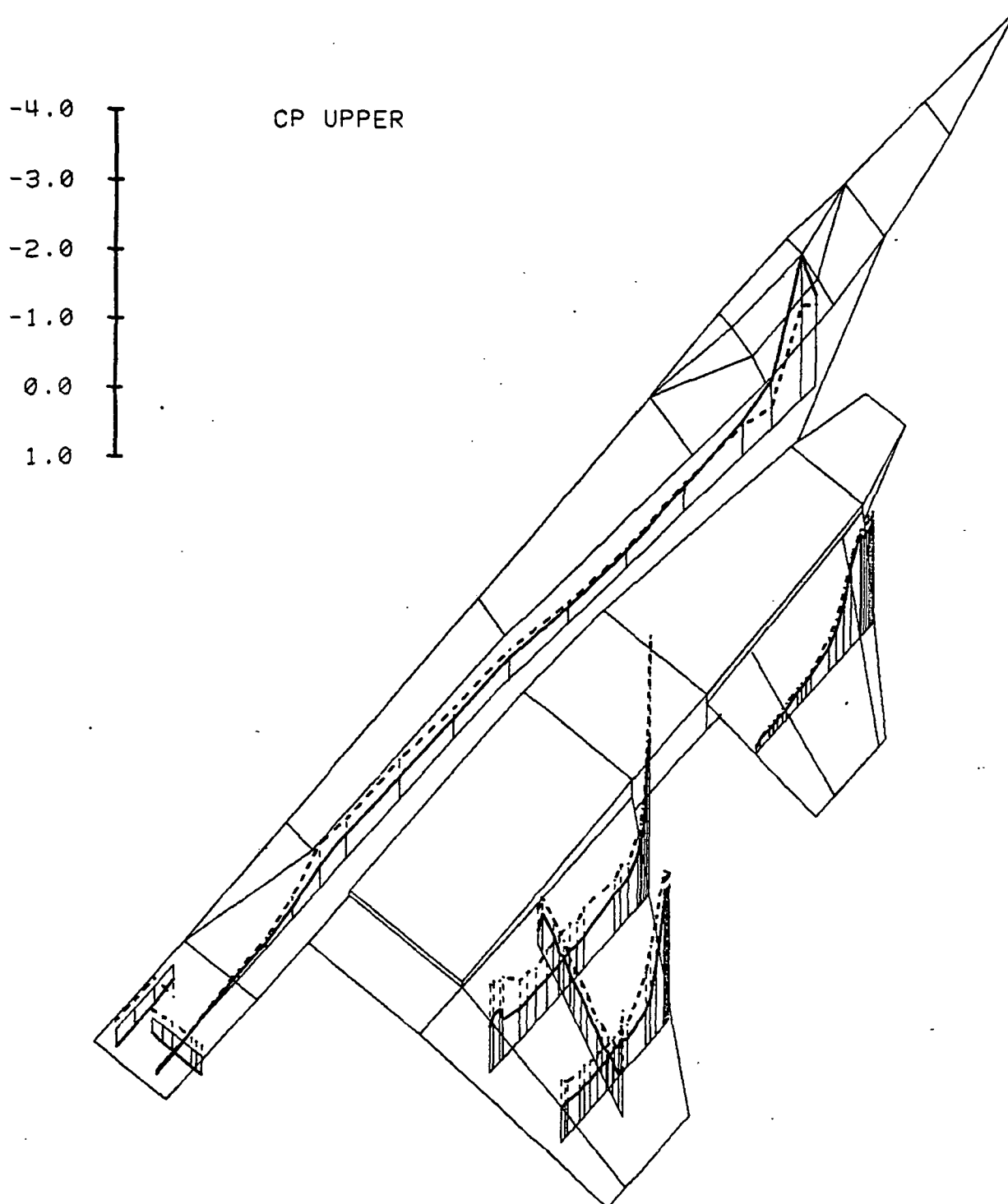


Figure 3.1-6(a) Power Effects, Alpha = 4 deg

## AMES FIGHTER MODEL

LINE	TEST	RUN	ALPHA	CT	ITEF	OTEF	CAN	SWB
—	543	11	28.9	0.00	30	30	0	OFF
-----	543	5	29.2	1.39	30	30	0	OFF

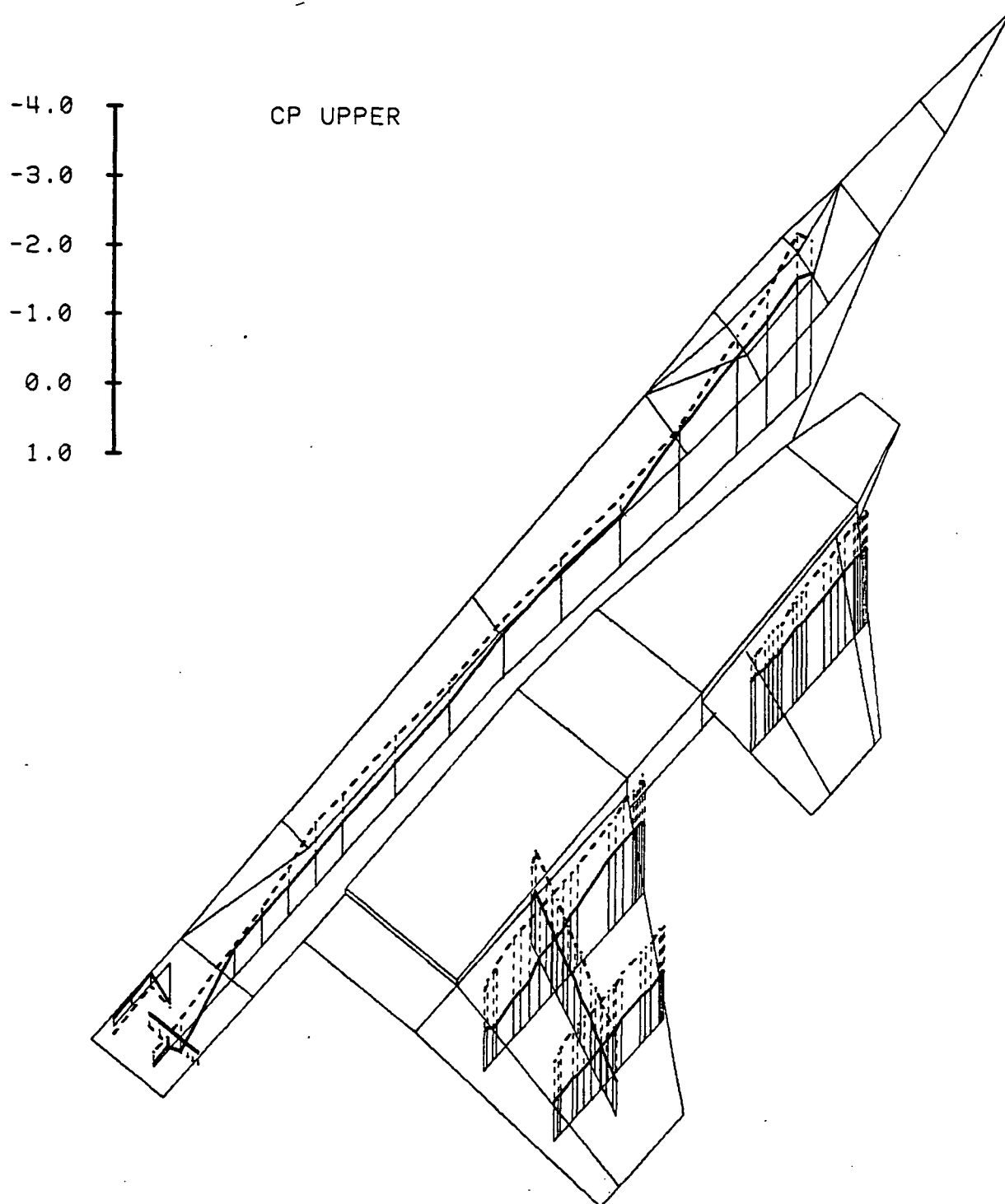


Figure 3.1-6(b) Power Effects, Alpha = 29 deg

# AMES FIGHTER MODEL

LINE	TEST	RUN	ALPHA	CT	ITEF	OTEF	CAN	SWB
—	537	28	0.3	1.89	30	30	0	OFF
-----	537	53	0.4	1.81	30	30	0	ON

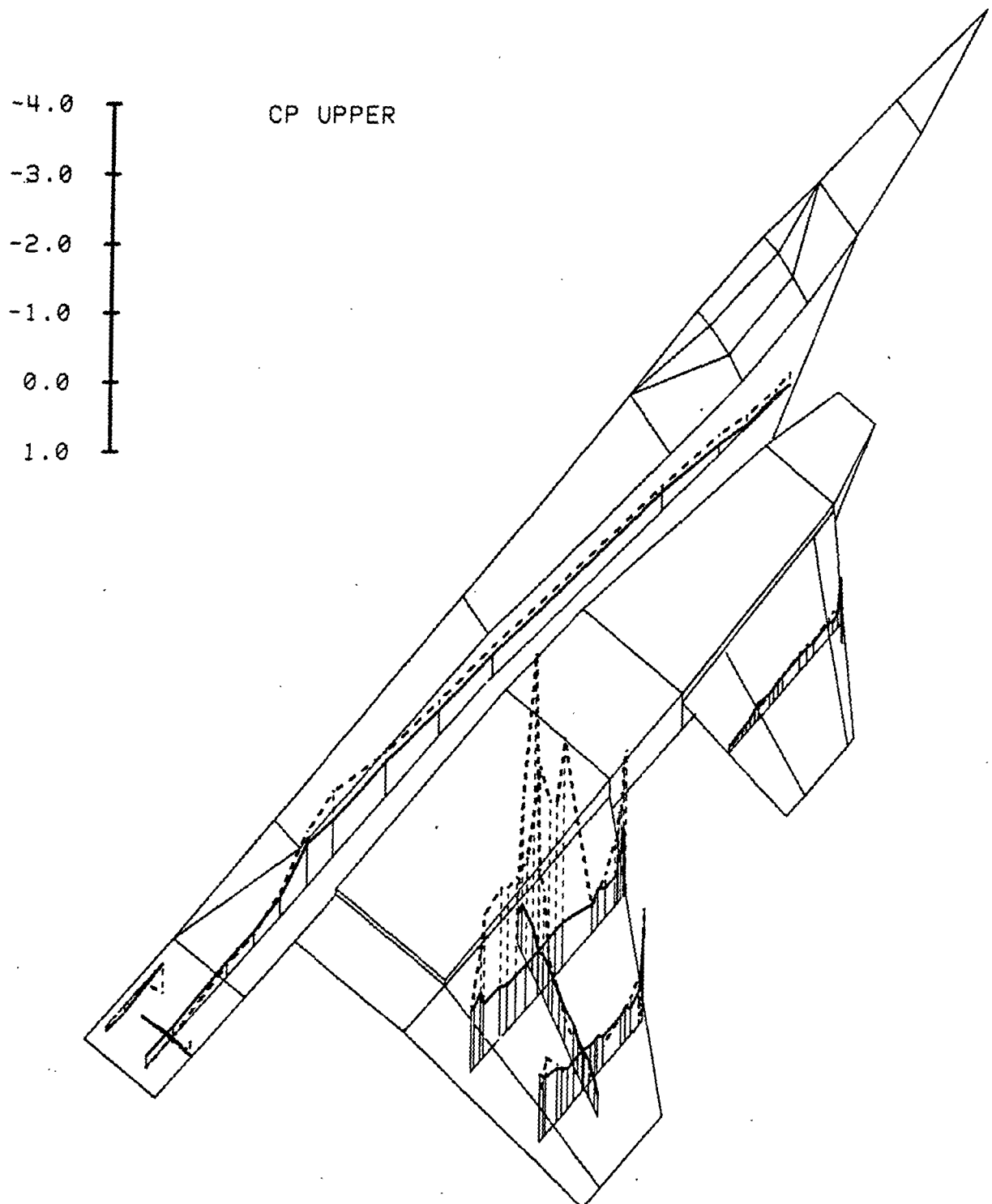


Figure 3.1-7(a) Spanwise Blowing Effects, Alpha = 0 deg

## AMES FIGHTER MODEL

LINE	TEST	RUN	ALPHA	CT	ITEF	OTEF	CAN	SWB
—	537	28	12.8	1.82	30	30	0	OFF
----	537	53	12.9	1.82	30	30	0	ON

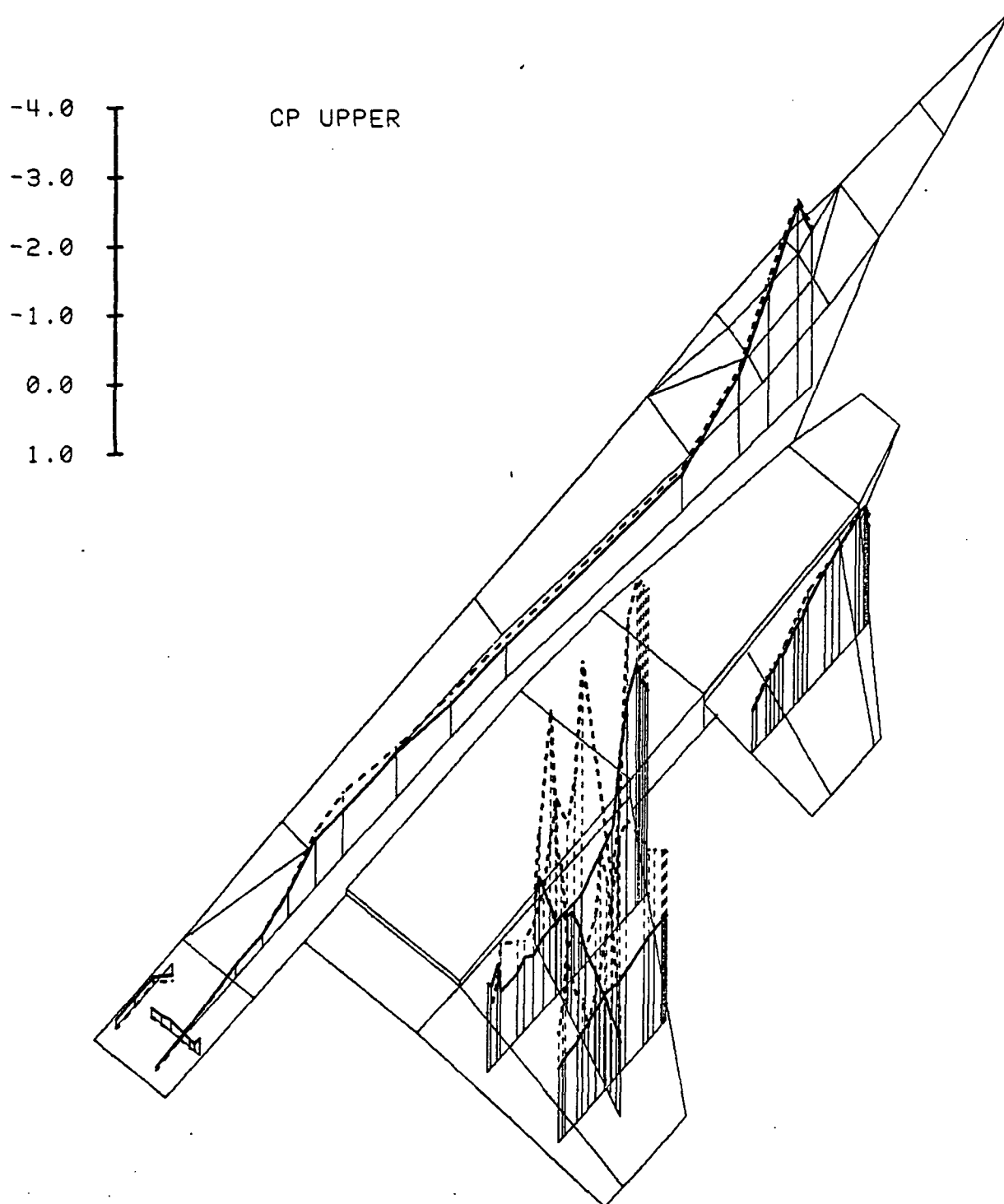


Figure 3.1-7(b) Spanwise Blowing Effects, Alpha = 12 deg

## AMES FIGHTER MODEL

LINE	TEST	RUN	ALPHA	CT	ITEF	OTEF	CAN	SWB
—	537	28	21.0	1.83	30	30	0	OFF
.....	537	53	21.2	1.83	30	30	0	ON

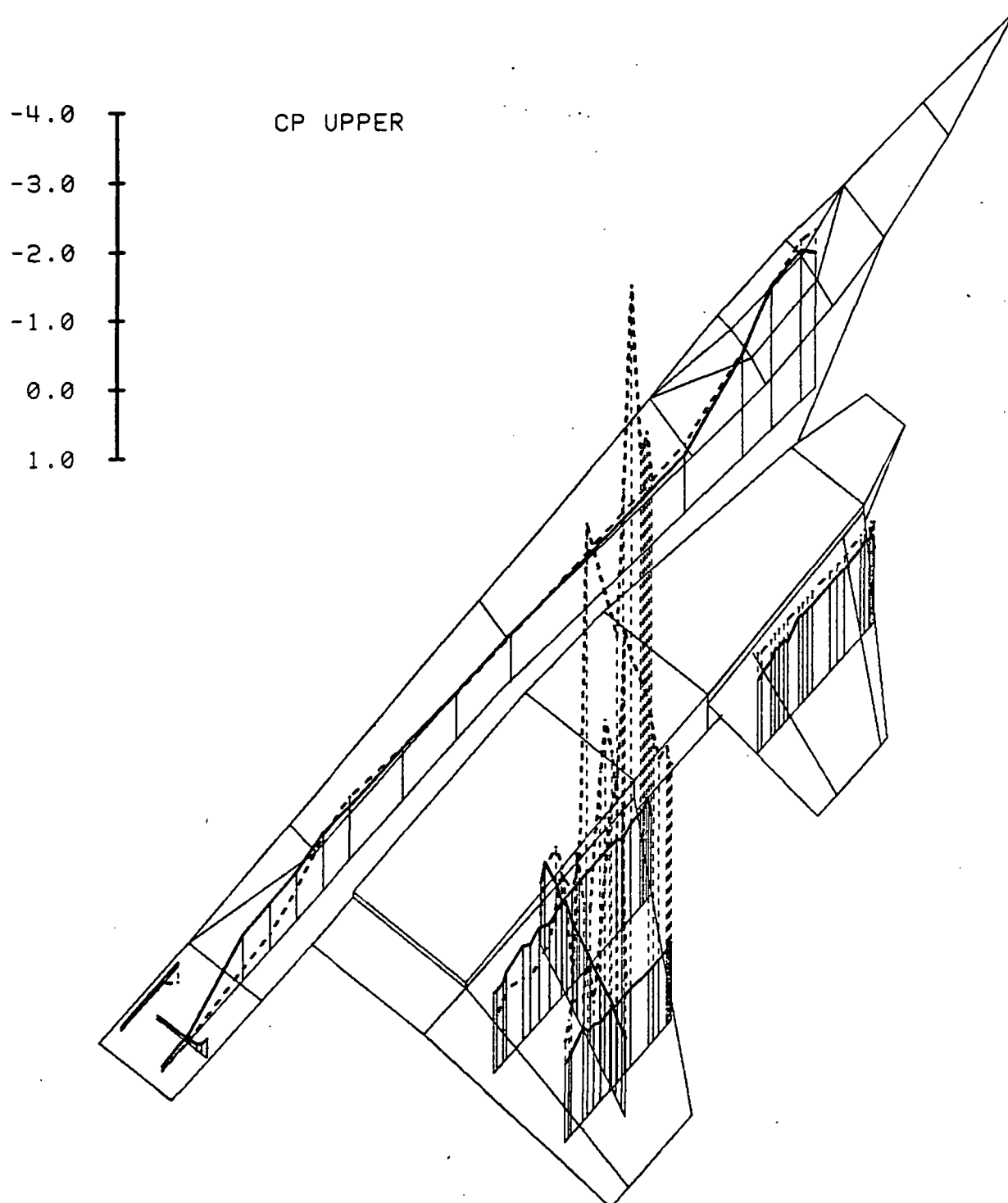


Figure 3.1-7(c) Spanwise Blowing Effects, Alpha = 21 deg



# AMES FIGHTER MODEL

LINE	TEST	RUN	ALPHA	CT	ITEF	OTEF	CAN	SWB	$\delta_{BT}$
—	543	4	4.5	1.90	30	30	0	OFF	0
-----	543	46	4.4	1.90	30	30	0	OFF	40

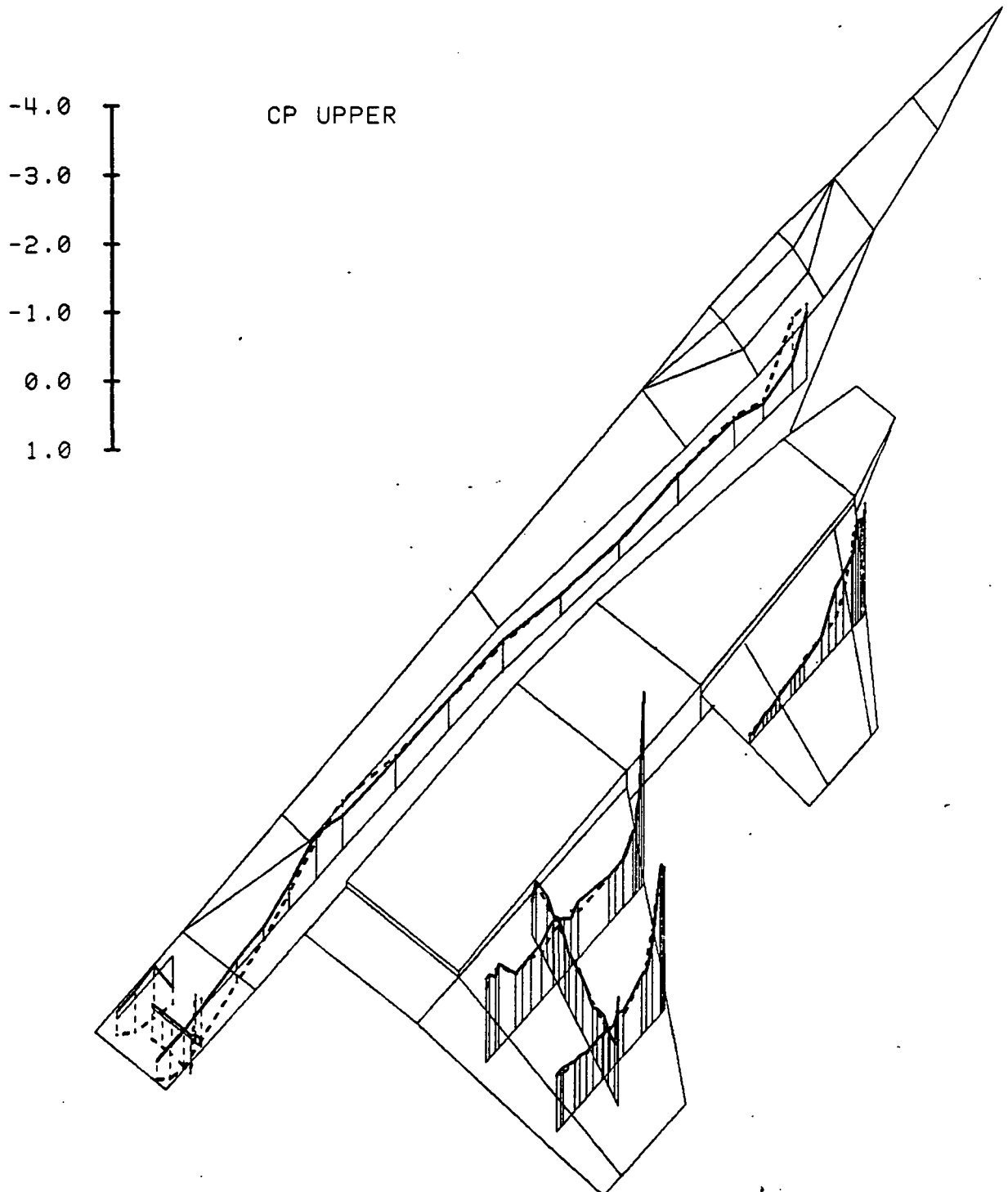


Figure 3.1-8

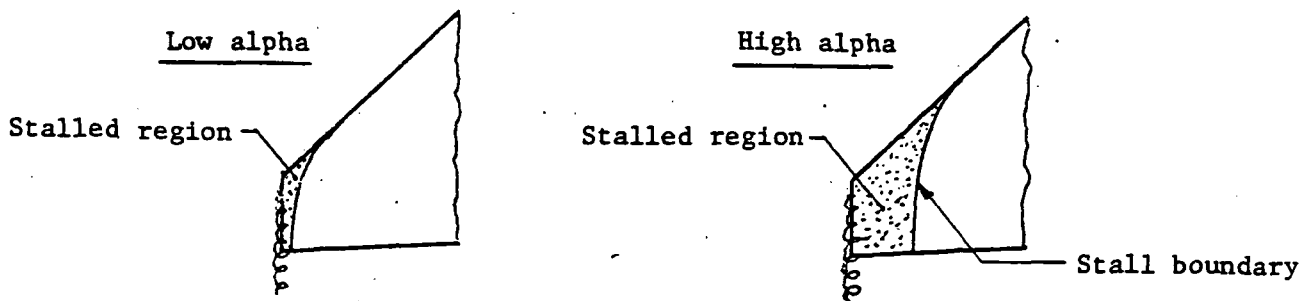
Beaver Tail Deflection Effects

**(This page intentionally left blank.)**

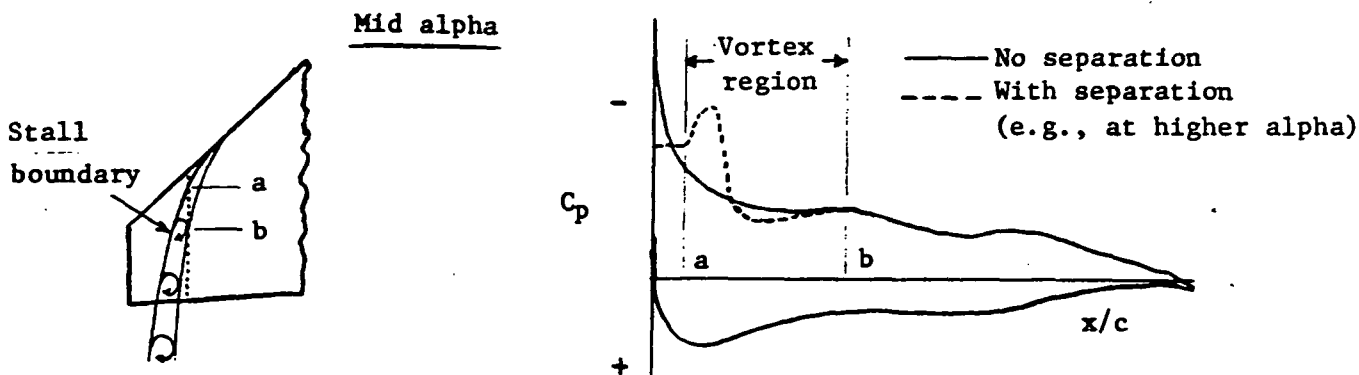
## 3.2 WING AND CANARD RESULTS

### 3.2.1 Key Flow Features

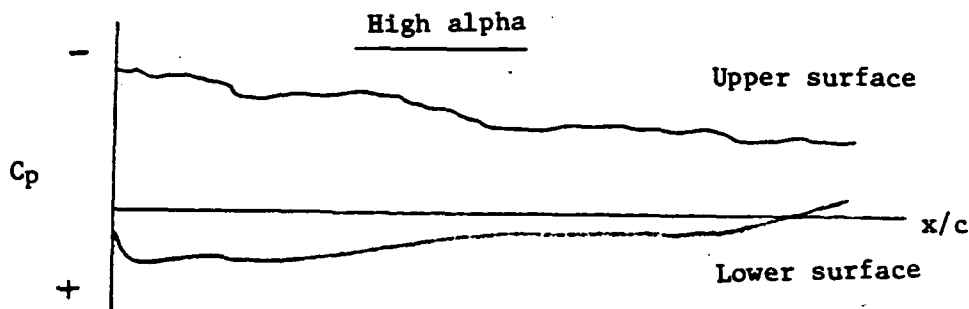
The flowfields generated by the wing and by the canard were similar in several respects since the exposed planforms were similar, differing principally in leading-edge sweep (wing sweep was 40 deg., canard sweep was 45 deg.). From the limited pressure measurements with flaps undeflected and power off, it has been deduced that both the wing alone (canard off) and the canard in the presence of the wing behaved "normally" at one-degree or two-degrees angle of attack. That is, as in potential flow theory, upper-surface pressure was characterized by a suction peak near the leading edge followed by rapid compression downstream, with upper and lower static pressures approaching a common value (nearly ambient) at the trailing edge in accordance with the Kutta condition. A tip vortex was of course present. With increasing  $\alpha$ , however, it was evident that boundary layer separation soon set in at the leading edge somewhere near the tip, grew chordwise, and developed progressively further inboard. When this stall region first reached a chordwise row of taps, its appearance there was revealed by a pronounced reduction in the suction peak at the leading edge. Evidently, separation was the short-bubble type at first, downstream of which the boundary layer reattached. At yet higher  $\alpha$ , the bubble grew chordwise, and static pressure within the bubble remained fairly constant downstream to the end of the bubble. Thus, reattachment formed a boundary, forward and outboard of which the upper surface was stalled. For the overall planform at a fixed  $\alpha$ , this stall boundary appeared to be curved toward the trailing edge, as illustrated below.



The stall boundary also formed the primary separation line of a free vortex situated alongside and inboard of that boundary. The magnitude of the pressure variation beneath this leading-edge vortex suggested it was weak. (In contrast, the leading-edge vortex of high-sweep, sharp-edged wings is strong and produces large pressure changes.) Within its bounds, as it passed over the forward portion of a chordwise row of taps, the vortex produced a reduction in pressure just behind the separation line, and this was followed by a mild compression region that terminated at the vortex reattachment line, as sketched below.



As angle of attack was increased, reattachment at a fixed span station occurred further aft as the vortex grew, moved inboard, and became diffused; soon there was little evidence of reattachment present at that span station. Eventually, the entire chord was within the stalled region as the vortex moved inboard, and the Kutta condition was perhaps no longer satisfied at the trailing edge (upper and lower  $C_p$  values sometimes were evidently unequal). Occasionally a suction peak did not appear, presumably, because the vortex core was well above the surface and/or inboard of this span station, but section lift would still be higher as a result of vortex-induced effects outside the vortex core.



The vortex was sometimes evident at the lower alphas when it passed over the wing mid-chord row of spanwise taps, but by then the vortex had enlarged and weakened to the extent that local static pressures were usually less affected, and the boundaries were less clearly defined.

Vortex flow development over a moderate-sweep wing or canard is not unusual. Similar characteristics are reported in Reference 14, for example, for a model approximating the F-4 Phantom wing planform ( $AR = 2.8$ ,  $\Lambda = 38.5^\circ$ ). But for the NASA AMES Fighter Model, recognition of this phenomenon was an aid in the interpretation of test results of other variables such as flap deflection, power, and spanwise blowing. For example, with leading-edge stall not present, lowering trailing-edge flaps ordinarily would

be expected to reduce upper surface pressure along an entire chord due to induced circulation. When stall was eminent on this model, however, flap deflection caused premature leading-edge separation and an inboard movement of the vortex origin. Or, with a vortex already present at a particular span station and angle of attack, leading-edge stall was exacerbated, and the vortex was made larger there since the vortex origin was then further inboard.

In the discussion to follow, it will be noted that the wing and canard experienced strong flowfield interactions. As one might expect, the canard wake had a direct influence on wing pressure distributions. Surprising, however, may be the degree to which changes on the wing due to flaps, blowing, etc., induced a reaction on the canard. How the induced change in canard flow first affected the wing, and hence in turn again the canard and so forth, cannot even be inferred by the steady-state pressure measurements since they comprised the end result of all interplay. The data were also insufficient to isolate and quantify the effects on wing pressure produced by the canard leading-edge vortex and tip vortex, but significant interactions seemed to influence the behavior of the wing leading-edge vortex itself. Wing variables that increased wing lift, such as power, also tended to increase canard section lift at the single chordwise row of taps, and this influence was strongest at high  $\alpha$ , where both the wing and canard were experiencing widespread stall.

Finally, a few anomalies in the data included occasional chordwise regions of constant pressure along the wing inboard station and, also, some lack of agreement where the inboard row and spanwise row of taps intersect. In spite of these minor problems and some data trends that were at times inconsistent and unexplainable, it is felt that the overall flow model presented herein is a valid representation of the important features.

### **3.2.2 Wing Without Canard**

#### **3.2.2.1. Basic Flowfield Characteristics and Flap Effects**

The limited number of test runs conducted with the canard off provided data that were helpful in understanding wing-canard interactions. In most respects, the wing demonstrated flow features similar to those produced by the canard at low  $\alpha$  where wing-induced effects were smallest. Thus, the development of leading-edge separation and a free, leading-edge vortex were the predominant wing flow features. Induced effects caused by flap deflection were also significant.

**3.2.2.1.1 Flowfield Features.** Wing  $C_p$  data with power off and with the flap and aileron (the outboard flap) neutral were presented in Figures 3.2.2-1, -2, and -3 for the inboard span station ( $2y/b = .64$ ), the outboard span station ( $2y/b = .84$ ) and the spanwise row ( $x/c = 0.5$ ), respectively, at nominal  $\alpha$  settings of 0, 8, 12, and 16 deg (data were unavailable at  $\alpha = 4$  deg). Comparable data with the flap and aileron deflected down 30 deg are shown in Figures 3.2.2-4 thru -6 (including  $\alpha = 4$  deg).

With flaps undeflected, modeling the flowfield was encumbered by the lack of data at  $\alpha = 4$  deg, near which significant changes took place locally, it seems. For example, there is no separation indicated at the inboard or outboard stations (Figures 3.2.2-1 and -2) at  $\alpha = 0$  deg, but stall is evident at  $\alpha = 8$  deg and above. With flaps deflected, the situation is the same at  $\alpha = 0$  and 8 deg. At  $\alpha = 4$  deg, the inboard station (Figure 3.2.2-4) demonstrated a high leading-edge suction, hence no stall, but this was not so for the outboard station (Figure 3.2.2-5). Therefore, with flaps neutral, it can be inferred that inboard stall-onset also occurred at an  $\alpha$  less than 8 deg and that outboard stall-

onset occurred at an even lower alpha, much as it did with flaps deflected. The spanwise data (Figures 3.2.2-3 and -6) provide few clues as to the nature of the flowfield. The general trends suggest that a low-pressure region that formed outboard at low alpha, subsequently, moved inboard with increase alpha. While an increase in inboard lift loading is not uncommon for conventional wings that first stall in the tip region, it has been deduced from the whole body of test data that this trend was also being influenced by a free vortex.

It has been deduced from the data shown in Figures 3.2.2-1 through -6 and from power-on data, to be discussed subsequently, (Subsection 3.2.2.2) that not only did leading-edge separation set in at the outboard station at a lower alpha than at the inboard station but also that inboard and outboard stall-onset occurred at a lower alpha with the trailing edge down than with the trailing edge up. The approximate alpha at which separation first appeared at the leading edge, denoted as  $\alpha_1^*$ , is shown in Figure 3.2.2-7. Since data was obtained at alpha intervals of 4 deg, these values of  $\alpha_1^*$  were deduced from not only the test results shown in Figures 3.2.2-1 through -6 but also from the large body of data with other canard variables as well. Note in Figure 3.2.2-7 that the separation origin moved inboard from span station .84 to .64 in an alpha increase of less than 2 deg. Also, in Figures 3.2.2-3 and 3.2.2-6, note the tip influence indicated at  $\alpha = 12$  deg. The wing-flowfield model, thence, deduced from these data features a leading-edge vortex. As for the canard, the vortex developed as a consequence of leading-edge separation, occurring first near the tip and then progressively further inboard with increased alpha, with the weak vortex tracing a path outboard over the wing and turning downstream with increased curvature. See the illustration in Subsection 3.2.1.

**3.2.2.1.2 Flap Deflection Effects.** When the trailing edge was deflected down, an earlier leading-edge separation was precipitated. That is, at each span station, the onset of stall occurred at a lower alpha. With increasing alpha, therefore, the vortex crossed the outboard station, for example, and eventually was positioned entirely inboard of it at a lower alpha than occurred with the trailing edge neutral. With  $C_T = 0$ , the flap effect on the leading-edge vortex position is more clearly evident when pressure distributions are directly compared at fixed alpha values, as done in Figures 3.2.2-8 thru -19, and when section lift coefficient,  $C_l'$ , and center of pressure,  $(x/c)_{cp}$ , are compared, as done in Figures 3.2.2-20 and -21. Because data were lacking at  $\alpha = 4$  deg, further comparisons with  $C_T = 0.9$  are presented in Figures 3.2.2-22 through -38. The  $C_T$  incremental effects are discussed in Subsection 3.2.2.2.

Evidently, the flap upper surface with 30-deg deflection and  $C_T = 0$  maintained attached flow only at  $\alpha \leq 8$  deg since the only indications of an expansion at the hingeline ( $x/c \approx .80$ ), followed by a recompression, were at the inboard station at  $\alpha = 0$  and 8 deg (Figures 3.2.2-8 and -9). However, by virtue of lower pressures along most of the upper surface and higher pressures along most of the lower surface (principally on the flap), section lift was increased significantly by flap deflection (Figures 3.2.2-20 and -21). With  $C_T = 0.9$ , attached-flow indicators were not noticeably different at  $\alpha \leq 8$  deg (Figures 3.2.2-22 through -24), but section lift (Figures -37 and -38) generally was increased more by flap deflection with power than it was without power. Also, lift at the outboard station was only a little less than at the inboard station, regardless of power.

The above values of section lift coefficient and center of pressure were derived from the measured pressure coefficients by means of numerical chordwise integrations. The corresponding integral equations were the following:

$$C_l' = \cos(\alpha) \int_0^1 (C_{p_l} - C_{p_u}) d(x/c) \quad \text{Equation (1)}$$

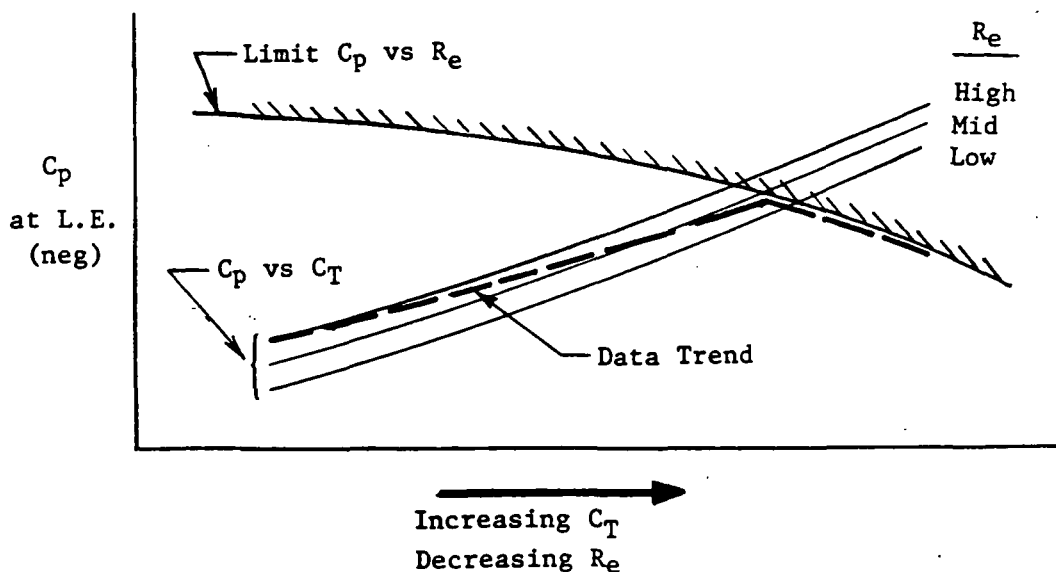
$$(x/c)_{cp} = \frac{\cos(\alpha)}{C_l'} \int_0^1 (C_{p_l} - C_{p_u}) (x/c) d(x/c) \quad \text{Equation (2)}$$

For convenience, a linear distribution between data points was used, and the value at the trailing edge was assumed equal to the average of the rearmost upper- and lower-surface data readings. No attempt was made to determine the axial force contribution to lift since geometric inaccuracies are inherent when integrating  $(C_{p1} - C_{pu})d(x/c)$  for a thin, cambered airfoil. It is for principally this last reason that the notation  $C_l$  has been used instead of simply  $C_l$ .

### 3.2.2.2 Power Effects Without Spanwise Blowing

Power effects on wing  $C_p$  and  $C_l'$  and  $(x/c)cp$  without spanwise blowing or a canard are summarized in Figures 3.2.2-39 through -79 with zero trailing-edge deflection and in Figures 3.2.2-80 through -123 with 30-deg deflection of the flap and aileron. In each case, the results are again discussed in turn for the inboard-station-chordwise-pressure data, outboard-station-chordwise-pressure data, and spanwise row of midchord pressure measurements with results for all  $C_T$  values presented first. Then, because the  $C_T$  changes were accompanied by  $R_e$  variations that obscured the pure power effects (see subsection 3.2.3.2-3 for a related discussion),  $C_p$  comparisons are shown for only  $C_T = 0$  and 1.4 having had the same  $R_e$ .

**3.2.2.2.1 Zero Flap Deflection.** With trailing edge neutral, the inboard station at zero alpha (Figure 3.2.2-39) exhibited little systematic  $C_p$  trend with increased  $C_T$  except at  $x/c = 0$ , where pressure changed inversely with thrust (due to increased circulation). At  $\alpha = 4$  deg (Figure 3.2.2-40), these power-induced flow effects at the leading edge were very strong and increased the negative  $C_p$  levels with increased power up to  $C_T = 1.35$ . At the highest power setting, however, the trend was reversed due to viscous effects, and these set in prematurely because tunnel  $R_e$  was decreasing with increased  $C_T$  (test conditions are discussed in Section 2.3). If  $C_T$  variations had been obtained at the highest  $R_e$  and  $q$ , which corresponded to  $C_T = 0.26$ , it is believed that a higher suction peak would have been realized at all higher  $C_T$  levels, even perhaps at  $C_T = 1.81$ . However, with  $R_e$  having been lowered with each successive  $C_T$  increase, leading-edge separation was caused to occur relatively sooner (at a lower  $C_T$ ), with the consequence that the pressure reduction was curtailed at a  $C_T$  near 1.35, and the trend was reversed with further increases in  $C_T$ . The influence of  $R_e$  on limit  $C_p$  has been recognized before (e.g., References 15 and 16). The following sketch depicts the conflicting factors believed to have been involved in this test program.



Downstream of the leading edge at  $\alpha = 4$  deg, Figure 3.2.2-40 shows that upper-surface lift loading increased progressively further aft as power was increased without much effect on the lower surface. The  $C_p$  trend at  $C_T = 0.26$  (the lowest value tested at  $\alpha = 4$  deg) does not indicate the presence of a weak or separated boundary layer. Therefore, the effect of increased  $C_T$  was not primarily a boundary-layer cleanup phenomenon, otherwise an improved loading would likely have occurred first in closest proximity to the jet (i.e., at the trailing edge). Figure 3.2.2-40 shows no such tendency. In a similar vein, it might be conjectured that the aft boundary layer deteriorated as  $R_e$  decreased with increased  $C_T$ , thereby allowing more corrective benefit of  $C_T$  to be realized (i.e., higher loading). Evidently, this did not exclusively occur either because (1) increased  $C_T$  would at best have then corrected  $C_p$  to the levels of the highest  $R_e$  data ( $C_T = 0.26$ ), and (2) results at  $C_T = 0$  and  $C_T = 1.4$  (same  $R_e$ ) would have shown no benefit of power, which subsequent comparisons clearly contradict (Figures 3.2.2-66 through -77).

The inboard station results at  $\alpha = 8$  deg (Figure 3.2.2-41) appear to be irregular, but on close examination, a degree of order is discernible. Leading-edge stall is evident at  $C_T = 0$ , but it was reduced and the vortex moved outboard at  $C_T = 0.26$  (higher  $R_e$ ). At  $C_T = 0.52$ , the leading-edge loading increased, and stall became slightly more acute. At  $C_T = 0.92$  and  $1.36$ , the vortex, which was clearly evident at  $x/c = 0.09$ , was drawn inboard at the higher of these power settings, thus passing over more of the instrumented chord and lowering  $C_p$  back to the trailing edge. In contrast, the data at  $C_T = 1.84$  resemble more the levels at  $C_T = 0.52$  for reasons unknown. This anomaly disappeared at  $\alpha = 12.4$  deg (Figure 3.2.2-42) and then reemerged intermittently at higher angles (Figures -43 through -46). At  $\alpha = 32$  deg (Figure -47), the effects of  $C_T$  were again rather orderly and, indeed startling, in view of the general stall condition prevailing on the wing. Note in Figures 3.2.2-45 through -47 that lower-surface  $C_p$  at high  $\alpha$  was influenced more by  $C_T$  than it was a low  $\alpha$  and that the trends with  $C_T$  were not consistent.

Data for the outboard wing station with trailing edge neutral (Figures 3.2.2-48 through -56) exhibit much the same tendencies as the inboard station data, but stall and the associated phenomena appeared at a lower  $\alpha$ . At  $\alpha = 8$  deg, for example, (Figure 3.2.2-50), stall was alleviated somewhat at  $C_T = 0.26$  due to higher  $R_e$ , but the overall  $C_p$  distribution shows that most of the section lay within the vortex boundaries (compare Figure 3.2.2-51). Lower surface pressure was less affected by power, but again the influence on upper surface  $C_p$  at higher  $\alpha$  was substantial (Figures 3.2.2-52 through -56).

Spanwise pressure distributions at  $x/c = 0.50$  (Figures 3.2.2-57 through -65) revealed that the leading-edge vortex was drawn inboard slightly by power and by reduced  $R_e$ . Otherwise, they were rather uninformative, with little to confirm the conclusions gleaned from chordwise data. Evidently, the vortex was rather weak this far aft on the wing.

Figures 3.2.2-66 through -77 present  $C_p$  comparisons showing power effects for only a  $C_T$  value of  $1.4$  (nom.) in order to exclude  $R_e$  differences (tunnel  $q$  was  $15$  psf at both  $C_T = 0$  and  $1.4$ ) and to illustrate that the jet efflux alone induced significant flowfield changes on the wing both inboard and outboard from leading edge to trailing edge. Since the flaps were undeflected, there was probably little boundary-layer separation to begin with (power off). It follows that no significant power-induced, viscous-flow interactions in the aft area of the wing were likely, and so the jet benefits are credited, herein, to induced circulation.

Values of the approximate section lift coefficient,  $C_l'$ , and center of pressure,  $(x/c)_{cp}$ , are presented in Figures 3.2.2-78 and -79 for the power-series data discussed above. For clarity, results with  $C_T = 0.26$  have been omitted. Noteworthy in Figures -78 and -79 are



(1) the modest (but significant) increase in lift due to power at low  $\alpha$ , with a little more benefit inboard than outboard up to  $\alpha = 12$  deg; (2) the very significant benefits at  $\alpha > 12$  deg, with increased max  $C_l$  and stall  $\alpha$ ; and (3) a generally moderate aft shift in center of pressure due to power.

**3.2.2.2.2 Flaps Deflected.** Canard-off effects of power with the flap and aileron deflected 30 deg are summarized in Figures 3.2.2-80 through -101 for all  $C_T$  values. At near-zero  $\alpha$  (Figure 3.2.2-80), inboard upper-surface  $C_p$  trends generally were as irregular as they were with flaps neutral (Figure 3.2.2-39). These trends differ at high  $C_T$ , where a substantial increase in aft loading is noted. Aileron effectiveness was evidently enhanced at all power levels. Increased circulation is also more evident in the leading-edge pressure buildup.  $R_e$  effects overcame the power benefits sooner (at lower  $C_T$ ) than when the trailing-edge flap was neutral at  $\alpha = 0$  or 4 deg (Figure 3.2.2-40). At  $\alpha = 4$  deg and  $C_T = 0$  (Figure -81) increased flow around the leading edge caused by flap deflection was evidently as much as the inboard section could subtend without incurring boundary-layer separation, so applying power immediately reduced the suction peak, and this was followed by an attendant vortex encroachment. An inexplicable anomaly occurred at  $C_T = 1.88$  (see Figure 3.2.2-81). Whereas extensive stall was evident at  $C_T = 1.42$ , it disappeared at  $C_T = 1.88$ , and aileron load was also reduced. Stall then returned at  $\alpha = 8$  deg (Figure 3.2.2-82), but aileron load was restored. The reason for this behavior could not be ascertained from these data. Note also the erratic lower-surface pressure trends compared with trailing-edge neutral (Figure 3.2.2-41). However, at high  $\alpha$  (Figure 3.2.2-86 through -88) the power benefits were again as large and consistent as they were with zero trailing-edge deflection.

Outboard chordwise pressures (Figures 3.2.2-89 through -97) with flap/aileron down contrast with those for trailing-edge neutral in a similar manner as do the inboard pressures. It is significant, however, that applying power at near-zero  $\alpha$  reduced upper surface  $C_p$  even more than it did inboard except up forward at the highest  $C_T$  (compare Figures 3.2.2-89 and -80). The load distribution on the aileron (aft of  $x/c \approx .80$ ) is still not indicative of an efficient flow expansion at the hingeline, so the changes in  $C_p$  suggest that the jet imposed an increase in circulation rather than a boundary layer intrainment, which likely would have been manifested nearer the trailing edge. At  $\alpha = 4$  deg (Figure 3.2.2-90), power effects were still greater with flap/aileron down (compare Figure -49) even though the leading edge was stalled. This difference became even larger as  $\alpha$  was increased (Figures 3.2.2-91 thru -97 vs -50 through -66).

Spanwise data with the flap/aileron down and power on (Figures 3.2.2-98 through -106) are of little more diagnostic benefit than with the trailing edge neutral except to suggest there was now (1) a stronger jet influence on  $C_p$ , (2) an earlier leading-edge-vortex interaction near the tip, and (3) perhaps a more pronounced inboard movement of the vortex with increased  $C_T$ . In a comparison of Figures 3.2.2-99 and -58, for example, the  $C_p$  levels across the entire span were elevated more by power, especially near the tip, when the flaps were down. To begin with, the free vortex was already in evidence near the tip with power off and flaps down (Figure -99); therefore, power had a visible, reinforcing influence, but this was clearly not the case with flaps up (Figure 3.2.2-58). At  $\alpha = 8$  deg, Figures 3.2.2-100 and -59, power effects with flaps down were again stronger everywhere even though the free vortex had already been moved inboard somewhat just by flap deflection. The various "humps" do not necessarily pinpoint the location of a free vortex; perhaps they identify areas of influence, which power obviously magnified. The disappearance of a  $C_p$  rise at the tip at higher  $\alpha$ s (Figures 3.2.2-101 through -106) shows that the unavoidable tip vortex was not identifiable by these spanwise, midchord, pressure measurements (and likely not at any  $\alpha$ ). Figures 3.2.2-107 through -121 present power effects at  $C_T$  values of 0 and 1.4 for clarity ( $q$  and  $R_e$  essentially constant).

Section integrated results, Figures 3.2.2-122 and -123, when compared with Figures 3.2.2-78 and -79, show convincingly that power applied with trailing-edge down produced (1) a greater increase in section lift at low  $\alpha$ , (2) less increase in maximum lift, (inboard only), and (3) less aft shift in  $x_{cp}$  at both the inboard and outboard stations.

### 3.2.2.3 Spanwise Blowing Effect

The effects of spanwise blowing (SWB) on wing-alone pressure distributions and section integrated properties with  $C_T = 0.9$  are depicted in Figures 3.2.2-124 through -152 and with  $C_T = 1.8$  in Figures -153 through -181. Inboard, outboard, and spanwise  $C_p$  results are included, each for the complete  $\alpha$  range, with SWB-off and SWB-on distributions compared directly at each  $\alpha$ . At the conclusion of each  $C_T$  condition, the off-on comparison is concluded with summary plots of  $C_l$  and  $(x/c)_{cp}$ .

**3.2.2.3.1  $C_T = 0.9$ .** Pressure distributions at the inboard chordwise row of taps, Figures 3.2.2-124 through -132, show that SWB generated a large, liftwise, load increase in the aft area on the wing and an upwash increase at all angles of attack except zero. An induced upwash was to be expected because SWB increased lift significantly at all  $\alpha$  settings, thus elevating overall circulation. Note the anomaly in Figure 3.2.2-124: the upper-surface pressures forward of  $x/c = 0.38$  were increased by SWB, while lower-surface pressures were decreased. Canard-on results, presented in Subsection 3.2.4.5.1, showed the opposite result near the leading edge and forward of  $x/c = 0.4$  on the lower surface. The wing-alone data presented further anomalies at  $\alpha = 4$  deg (Figure 3.2.2-125) because lower-surface  $C_p$  values were all increased, as expected, and the forward upper-surface levels showed evidence of induced leading-edge stall because of SWB, as expected; the latter result was not accompanied by an attendant leading-edge vortex. Note also that the aft loading increase was less than at  $\alpha = 0$  deg. It is perhaps relevant that it was at  $\alpha = 4$  deg, with SWB off, that other inconsistencies in power trends have been noted (see Subsection 3.2.2.2.2). At  $\alpha = 8$  deg (Figure 3.2.2-126) this annoyance disappeared, as an enhanced leading-edge vortex was clearly evident. The enhancement and aft loading increase were the significant SWB results, anyway. As  $\alpha$  was increased beyond 8 deg, the induced aft loading decreased and became irregular, even negative, but vortex enhancement diminished only when  $\alpha$  exceeded 20 deg and, thus, remained the distinct effect of SWB at the inboard station.

At the outboard station, Figures 3.2.2-133 through -141, a decrease in upwash caused by SWB was again shown at  $\alpha = 0$  deg, followed by an increase at all other angles. The significant result was the change which upper-surface loadings underwent at  $\alpha \geq 12$  deg. At  $\alpha = 4$  and 8 deg it seems the changes reflected the consequences of the increased circulation that SWB induced inboard, with little evidence of a direct SWB interaction. Note at  $\alpha = 8$  deg (Figure 3.2.2-135) that the stalled character of the upper-surface loading was altered only near the trailing edge; indicating that the leading-edge vortex virtually blanketed the chord. At  $\alpha = 12$  deg (Figure -136) it appears that the SWB jet interacted more directly with the leading-edge vortex. This evidently reduced the sweep-back of the vortex and pushed it back across the outboard chord station (the vortex had been positioned inboard of that span station without SWB). It also energized the vortex, just as the inboard data indicated SWB had done (Figure 3.2.2-127). This interaction persisted at  $\alpha = 16$  deg (Figure -137), with the peak  $C_p$  occurring at the same chordwise position,  $x/c = 0.4$ . This is significant because it occurred again at higher  $\alpha$  settings. Pressures further forward were also reduced at higher  $\alpha$ s. The flow model, which is inferred from these trends and from temperature distributions reported in Subsection 3.2.6, positions the SWB jet beneath the vortex. The jet, thus, enhanced the vortex strength and stabilized its spanwise position. The low-pressure spike at  $x/c = 0.4$  probably does not denote the location of either the jet or the vortex as they traversed the chord. A

similar region was identified with the canard on (see Subsection 3.2.6) as the consequence of a complex flow interaction. SWB effects were much reduced at  $\alpha \geq 24$  deg, Figure 3.2.2-111, because the vortex was positioned well above the wing surface and the jet energy at this moderate power setting had perhaps been somewhat dissipated.

Spanwise  $C_p$  distributions along the wing midchord have been an imprecise gauge of vortex position and strength because the vortex was usually weaker and much enlarged when it crossed the row of taps. However, Figures 3.2.2-142 through -150 seem to depict a flowfield development with increased  $\alpha$  that is reasonably supportive of the above SWB interpretations. For example, at  $\alpha \leq 12$  deg the low-pressure regions inboard suggest that the SWB jet was separate from the leading-edge vortex, which was not significantly altered until  $\alpha = 8$  deg (Figure 3.2.2-144). Strong vortex enhancement with an outboard displacement is indicated at  $\alpha = 12$  deg (Figure -145). At increased  $\alpha$ , the SWB jet unswept and crossed the midchord row of taps further out, and the vortex was also centered further outboard, or so it might be inferred at  $\alpha = 12$  and 16 deg (Figures 3.2.2-145 and -146). Thereafter neither the jet nor the vortex could be individually detected from surface instrumentation since the jet was positioned beneath the vortex.

$C_l'$  and  $(x/c)_{cp}$  results, Figures 3.2.2-151 and -152, show that SWB caused a substantial increase in lift at the inboard and outboard stations at angles of attack greater than four degrees and with the centroid of the added lift positioned forward of the basic wing  $(x/c)_{cp}$ . (Note that the  $C_l'$  scale is double that shown in earlier section-lift-coefficient plots.) At  $\alpha \leq 4$  deg, SWB induced little net change at the outboard station, but it caused a large percent increase in lift inboard except at 4 deg, the condition that produced the anomalous pressure distribution trends discussed above. Beyond  $\alpha = 16$  deg, near which the maximum  $C_l'$  was obtained, the gain due to SWB diminished rapidly, which is additional evidence that the leading-edge vortex was displaced upward and became less beneficial. Another trend that bears on the inferred flowfield model was the inboard  $(x/c)_{cp}$  change caused by SWB: a shift aft at low  $\alpha$  because of the direct suction effects of the SWB jet on the aft portion of the wing, and a shift forward at higher  $\alpha$  as the SWB jet unswept and the strength of leading-edge vortex increased.

**3.2.2.3.2  $C_T = 1.8$ .** At the higher power setting, SWB generated such a large influence on the inboard, upper-surface pressures, Figures 3.2.2-153 through -161, that there was no ambiguity in discerning an increase in upwash (large variations in lower-surface pressure notwithstanding), earlier vortex enhancement, and a less-distinct delineation between the vortex and jet regions of influence. Of the last two features, for example, Figure 3.2.2-155 indicates that SWB at  $\alpha = 8$  deg drew the vortex origin inboard and enhanced it with the jet located roughly between  $x/c = .5$  and  $.8$ . By  $\alpha = 20$  deg (Figure -158), the two flows were so proximate that the aft download that SWB produced suggests this was recompression from a vortical-type flow that transcended both regions. Stated another way, flow external to the vortex and jet was pulled down to the surface, after passing over both, due to a peripheral impetus provided by the leading-edge vortex.

Outboard data (Figures 3.2.2-162 through -170) as they had with  $C_T = .9$ , reflected the changes at low  $\alpha$  that SWB had engendered inboard. Again, large interactions between the enhanced vortex and the jet began at  $\alpha = 12$  deg (Figure -165). At this and higher angles of attack the incremental effects were magnified by the higher power setting, but not as much change occurred inboard. The low-pressure spike at  $x/c = 0.4$  persisted. This suggests that the flowfield model was not significantly different than it was at  $C_T = 0.9$ .

The same broad conclusions can be inferred from the spanwise data, Figures 3.2.2-171 through -179, except that with  $C_T = 1.8$  the trends suggest that the vortex was

unswept more and that the jet influence persisted to high alphas. A noteworthy difference was the large increase in pressure induced far inboard at  $\alpha = 20$  and  $24$  deg. This, evidently, was reflecting the recompression phenomenon alluded to in the above discussion of the inboard results.

A comparison of  $C_l'$  and  $(x/c)_{cp}$  results (Figures 3.2.2-180 and -181) and those with  $C_T = 0.9$  (Figures -151 and -152) emphasizes the greater lift benefits at moderate alpha and the further-forward lift centroid produced by the stronger jet at  $C_T = 1.8$ . It also shows that twice the power did not materially postpone max  $C_l$  to a higher alpha or alleviate the sharp lift dropoff at high angles of attack.

SYM	TEST	RUN	ALPHA	CT	ITEF	OTEF	CAN	SWB
⊕	537	74	0.1	0.00	0	0	OFF	OFF
⊞	537	74	8.3	0.00	0	0	OFF	OFF
△	537	74	12.4	0.00	0	0	OFF	OFF
⊕	537	74	16.5	0.00	0	0	OFF	OFF

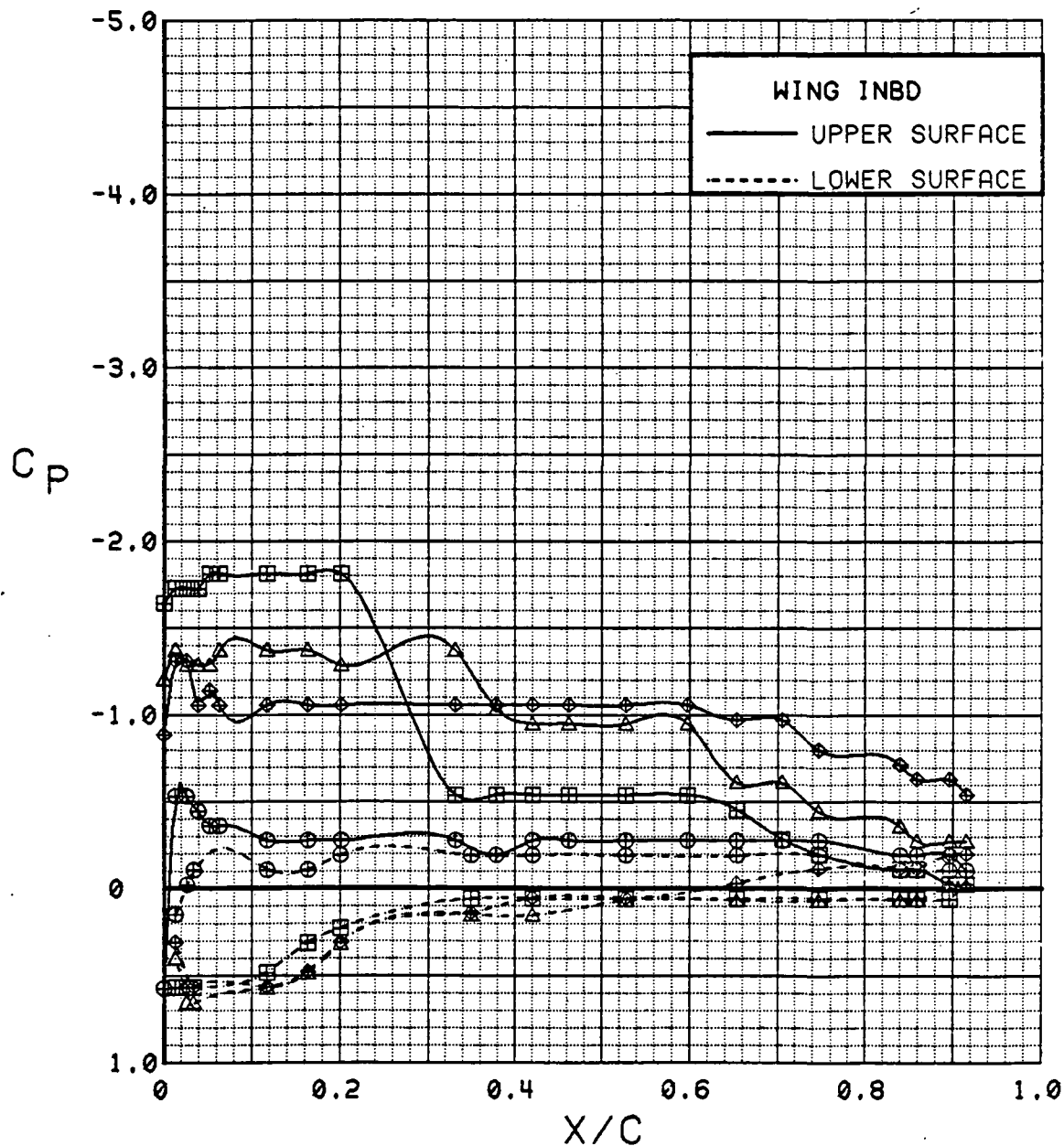


Figure 3.2.2-1 Angle of Attack Effects, Power Off, Flaps Neutral, Inboard

SYM	TEST	RUN	ALPHA	CT	ITEF	OTEF	CAN	SWB
⊕	537	74	0.1	0.00	0	0	OFF	OFF
⊞	537	74	8.3	0.00	0	0	OFF	OFF
△	537	74	12.4	0.00	0	0	OFF	OFF
⬠	537	74	16.5	0.00	0	0	OFF	OFF

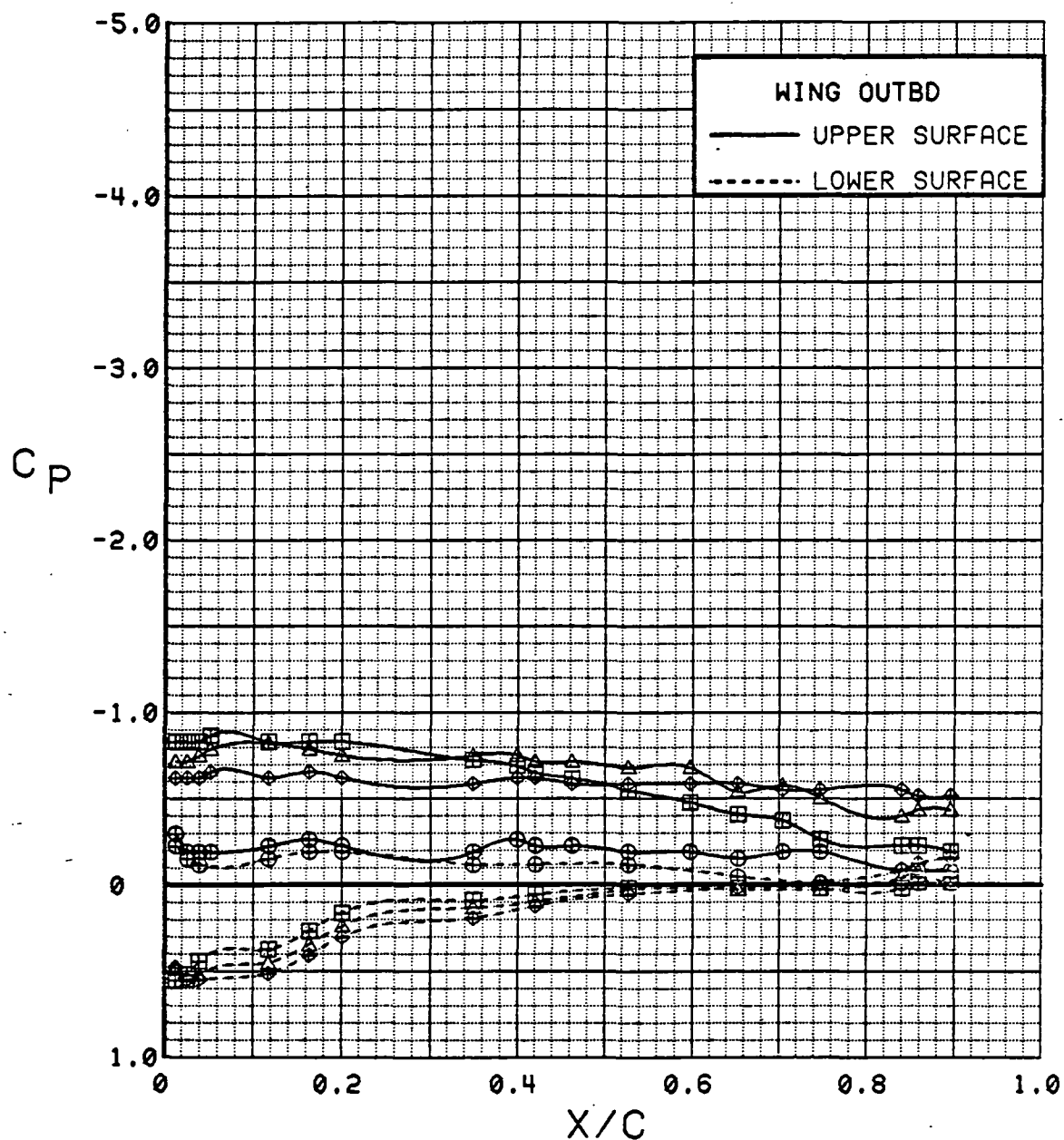


Figure 3.2.2-2 Angle of Attack Effects, Power Off, Flaps Neutral, Outboard

SYM	TEST	RUN	ALPHA	CT	ITEF	OTEF	CAN	SWB
⊕	537	74	0.1	0.00	0	0	OFF	OFF
⊞	537	74	8.3	0.00	0	0	OFF	OFF
△	537	74	12.4	0.00	0	0	OFF	OFF
◆	537	74	16.5	0.00	0	0	OFF	OFF

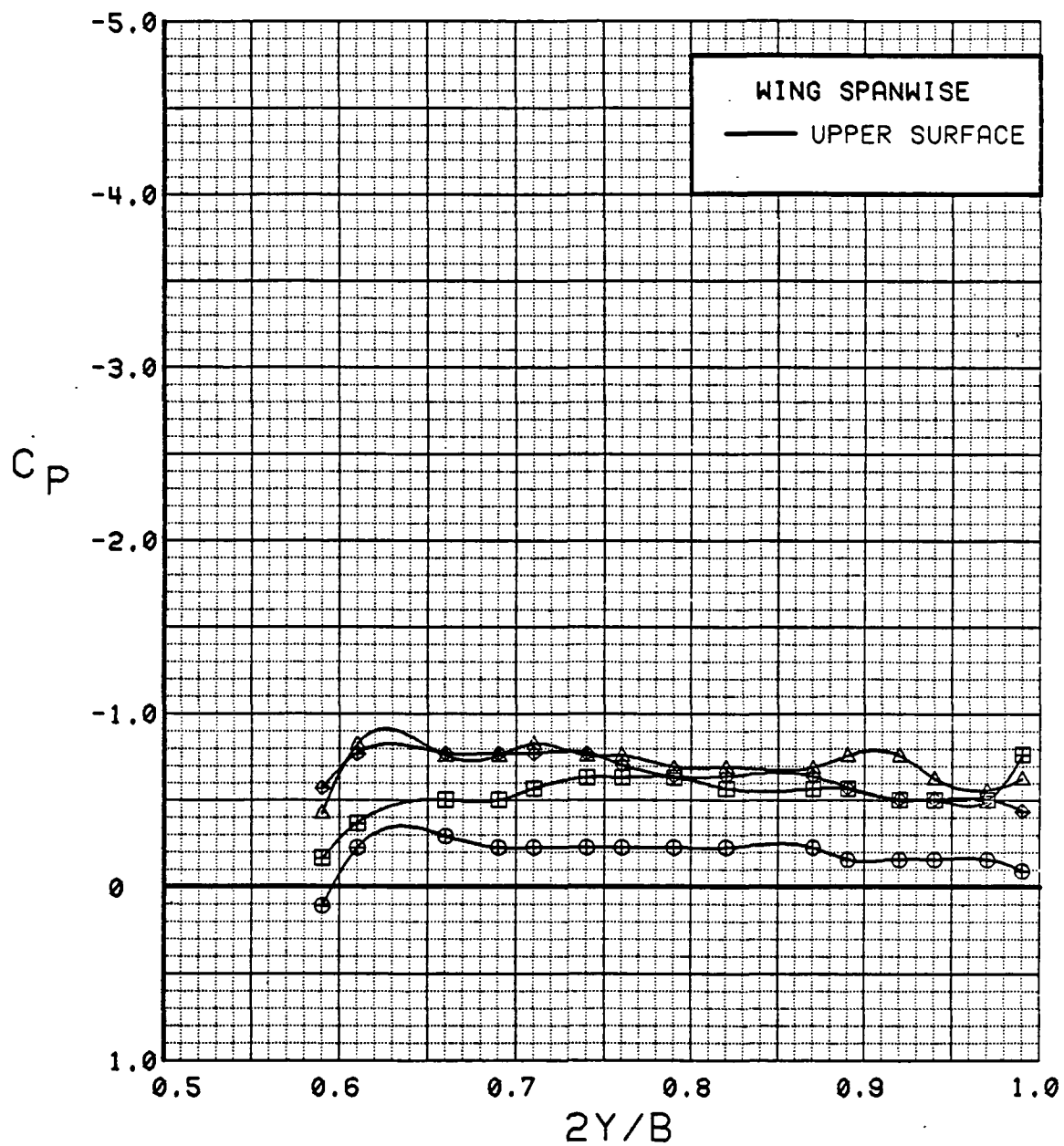


Figure 3.2.2-3 Angle of Attack Effects, Power Off, Flaps Neutral, Spanwise

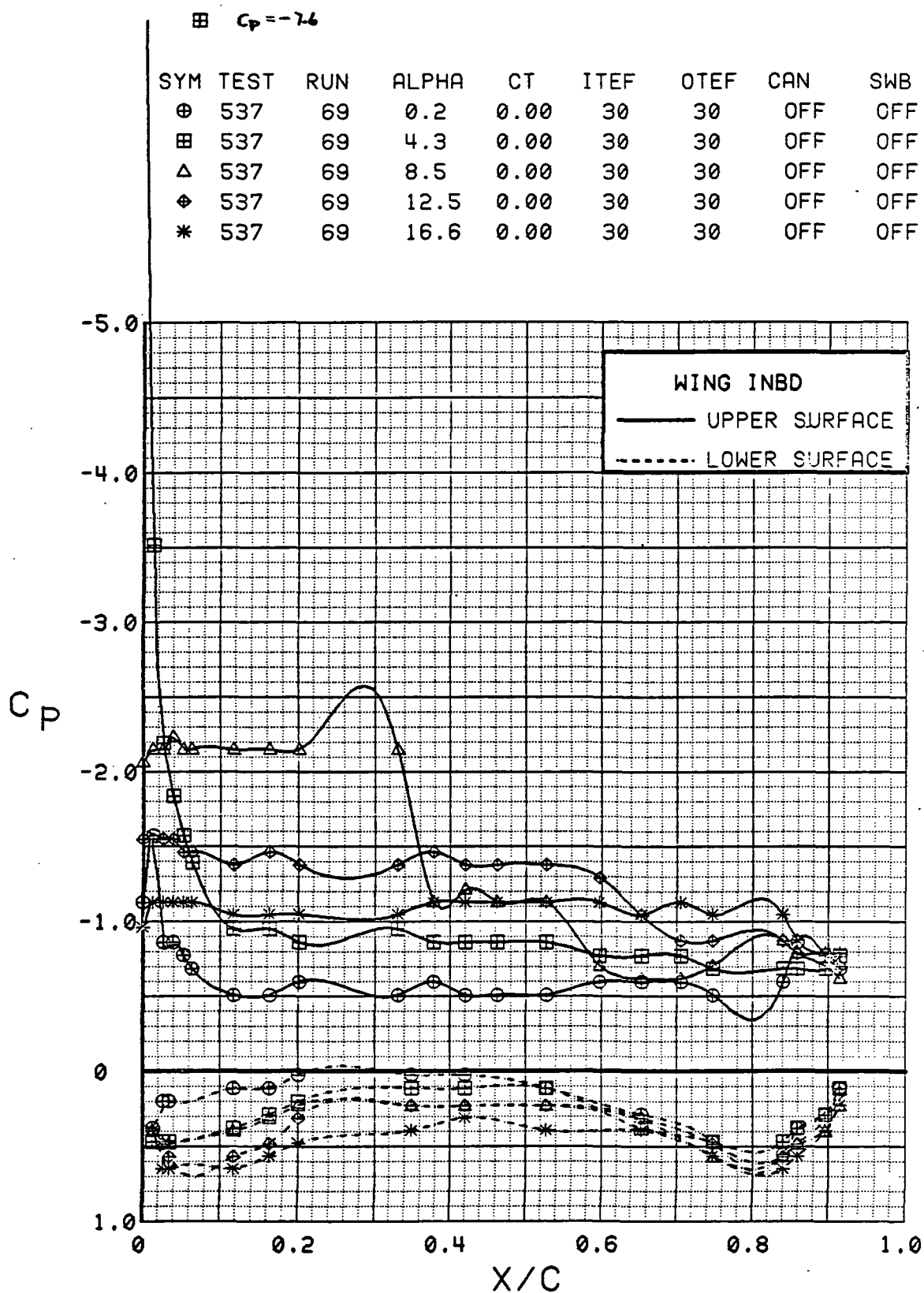


Figure 3.2.2-4 Angle of Attack Effects, Power Off, Flaps Deflected, Inboard



SYM	TEST	RUN	ALPHA	CT	ITEF	OTEF	CAN	SWB
⊕	537	69	0.2	0.00	30	30	OFF	OFF
⊞	537	69	4.3	0.00	30	30	OFF	OFF
△	537	69	8.5	0.00	30	30	OFF	OFF
◆	537	69	12.5	0.00	30	30	OFF	OFF
*	537	69	16.6	0.00	30	30	OFF	OFF

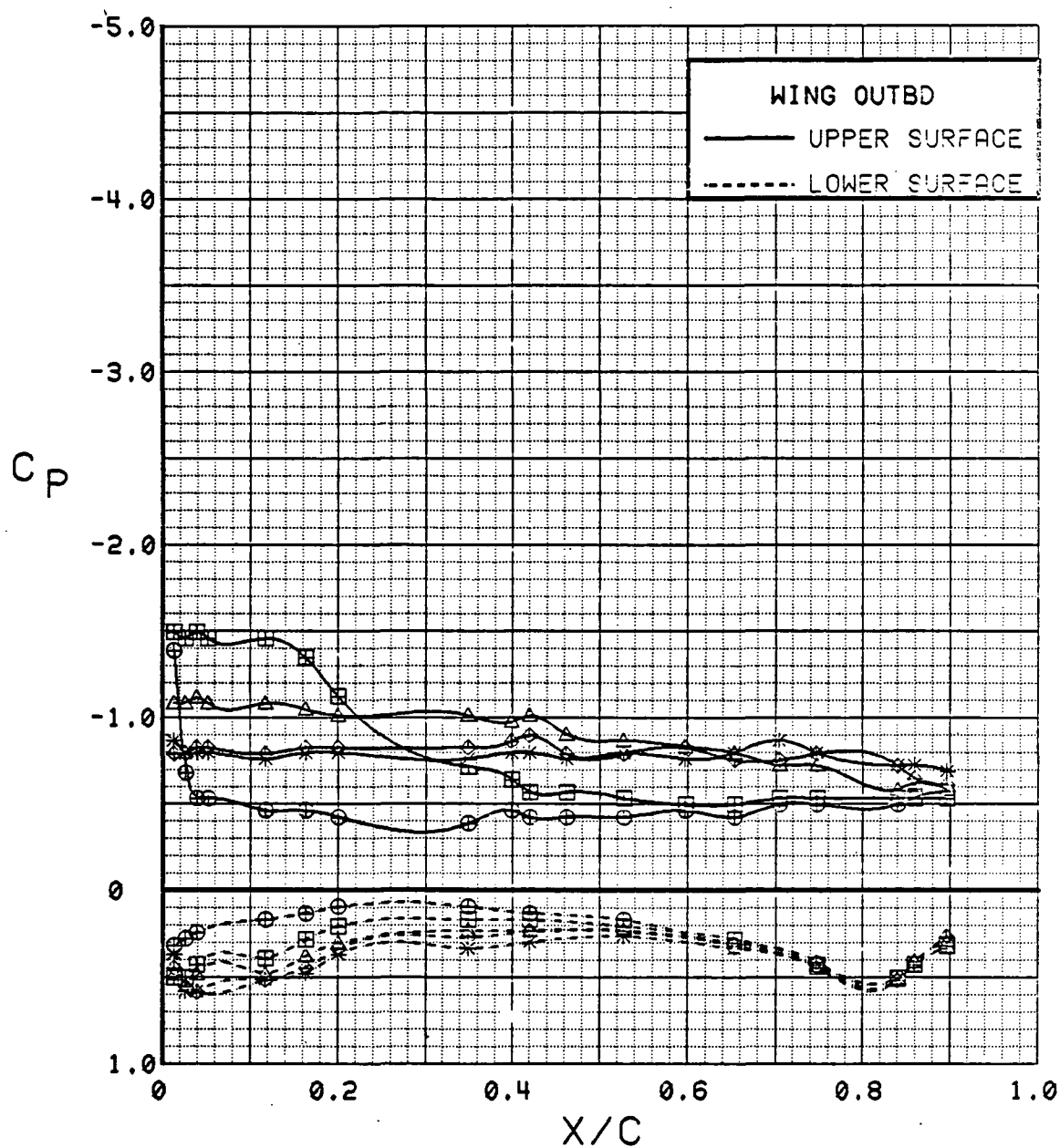


Figure 3.2.2-5 Angle of Attack Effects, Power Off, Flaps Deflected, Outboard

SYM	TEST	RUN	ALPHA	CT	ITEF	OTEF	CAN	SWB
⊕	537	69	0.2	0.00	30	30	OFF	OFF
⊞	537	69	4.3	0.00	30	30	OFF	OFF
△	537	69	8.5	0.00	30	30	OFF	OFF
◆	537	69	12.5	0.00	30	30	OFF	OFF
*	537	69	16.6	0.00	30	30	OFF	OFF

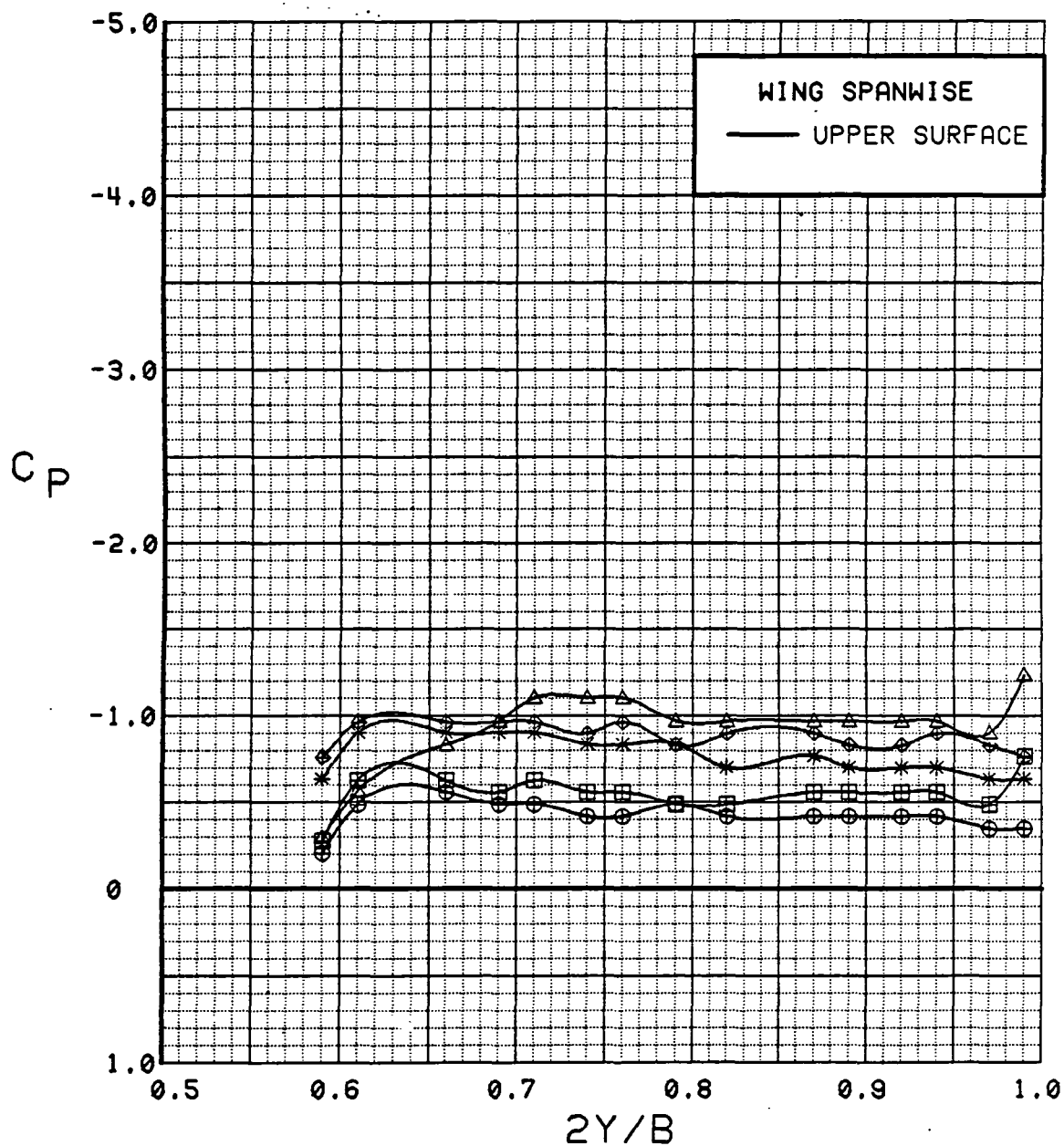
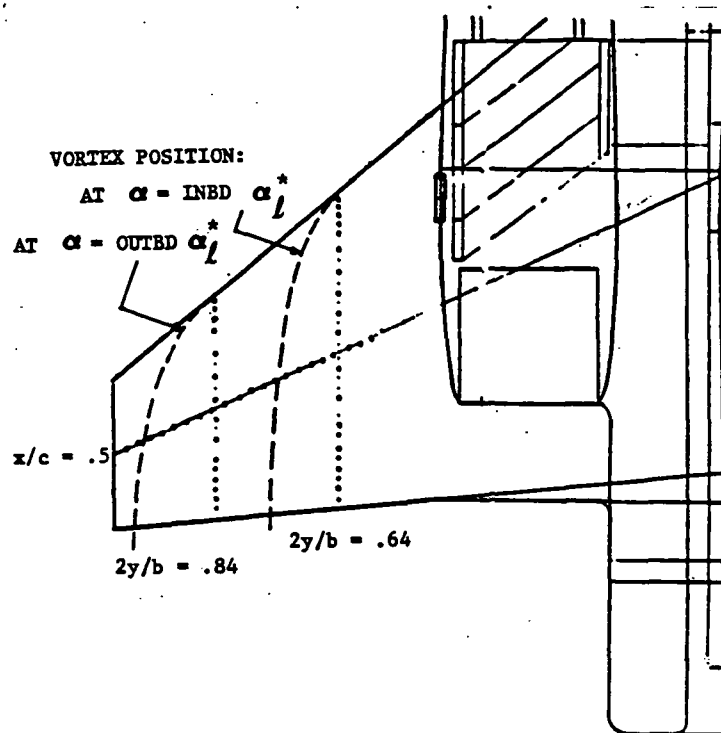


Figure 3.2.2-6 Angle of Attack Effects, Power Off, Flaps Deflected, Spanwise



ORIGINAL PAGE IS  
OF POOR QUALITY

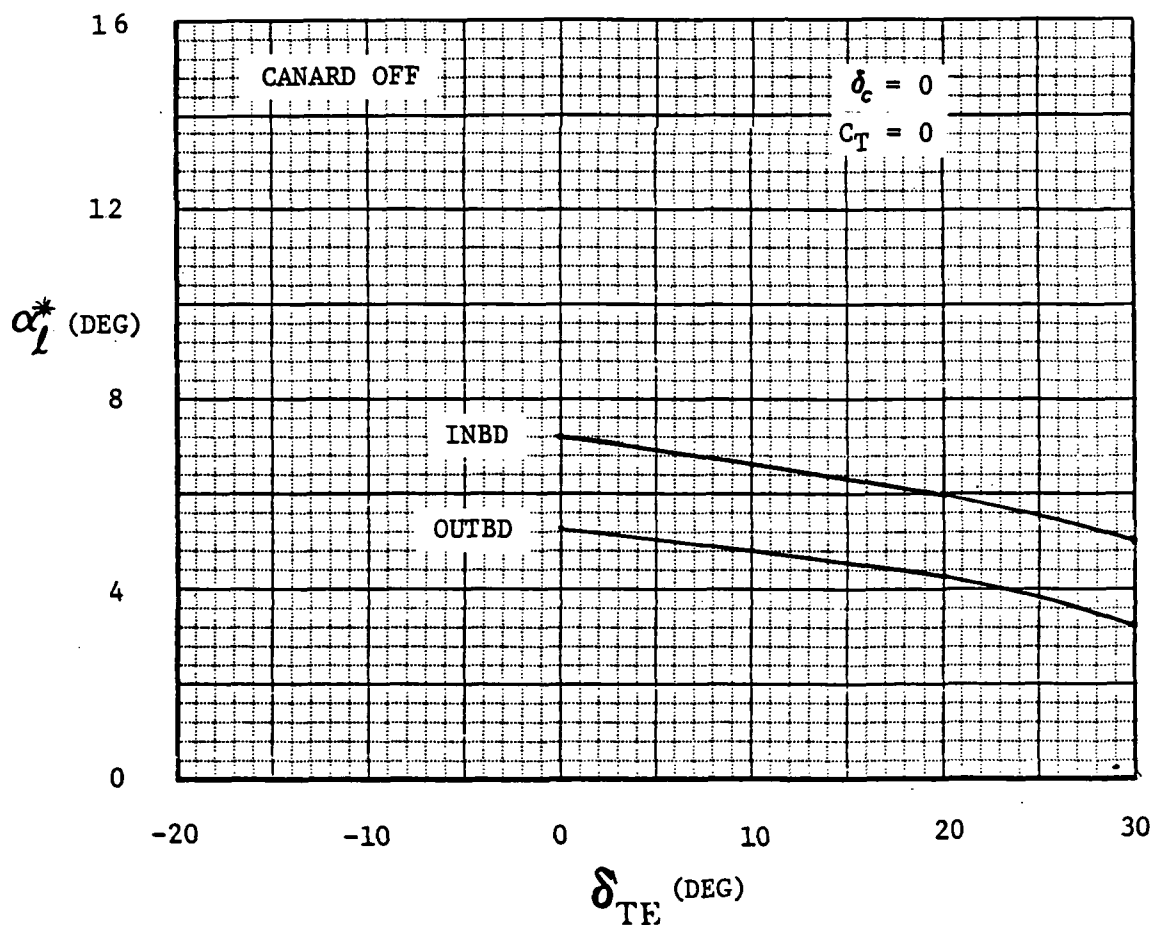


Figure 3.2.2-7 Origin of Wing Leading-Edge Vortex, Canard Off

SYM	TEST	RUN	ALPHA	CT	ITEF	OTEF	CAN	SWB
⊕	537	74	0.1	0.00	0	0	OFF	OFF
⊞	537	69	0.2	0.00	30	30	OFF	OFF

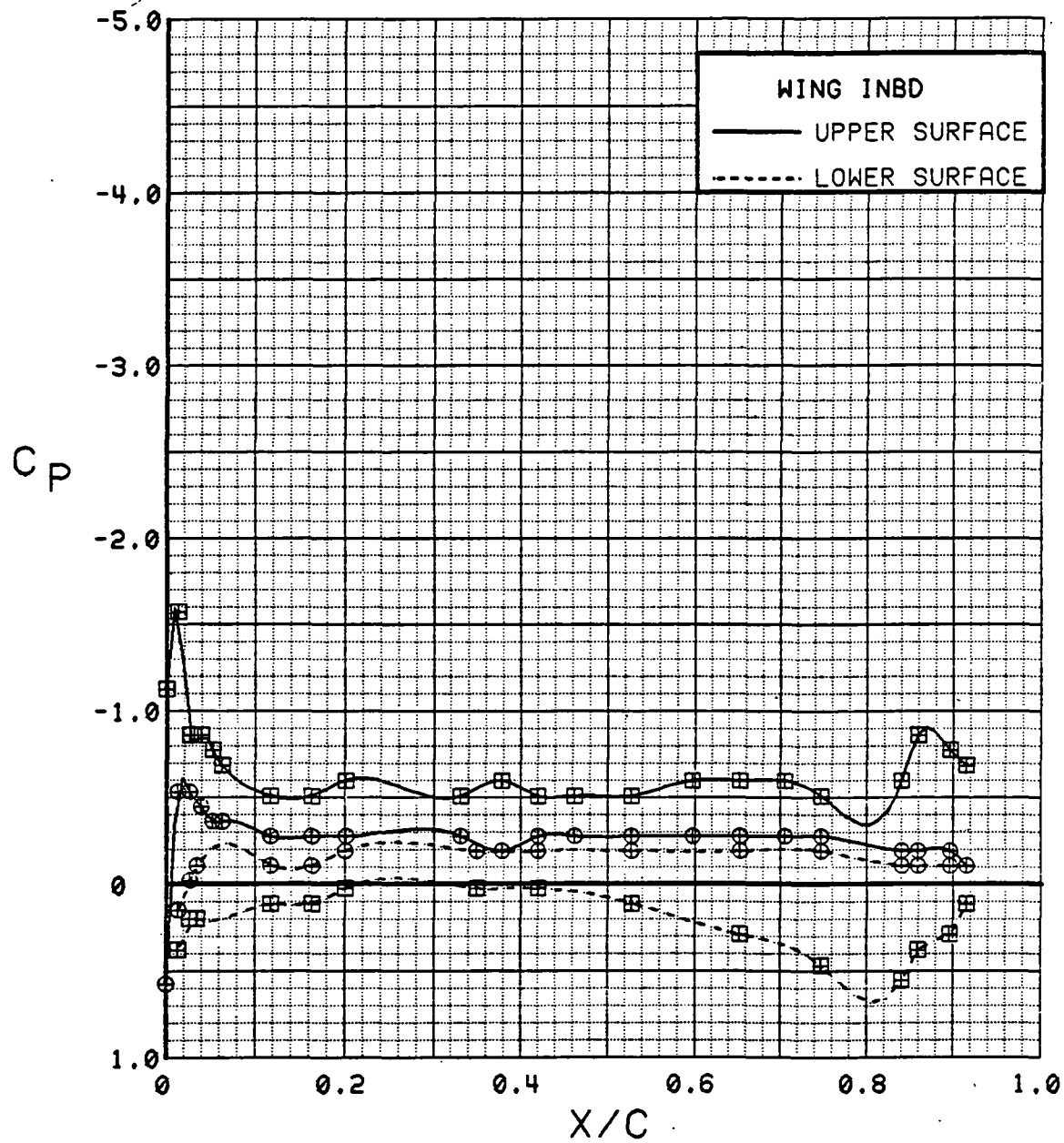


Figure 3.2.2-8 Wing Trailing-Edge Flap Effects, Power Off, Alpha = 0 deg, Inboard

SYM	TEST	RUN	ALPHA	CT	ITEF	OTEF	CAN	SWB
⊕	537	74	8.3	0.00	0	0	OFF	OFF
⊞	537	69	8.5	0.00	30	30	OFF	OFF

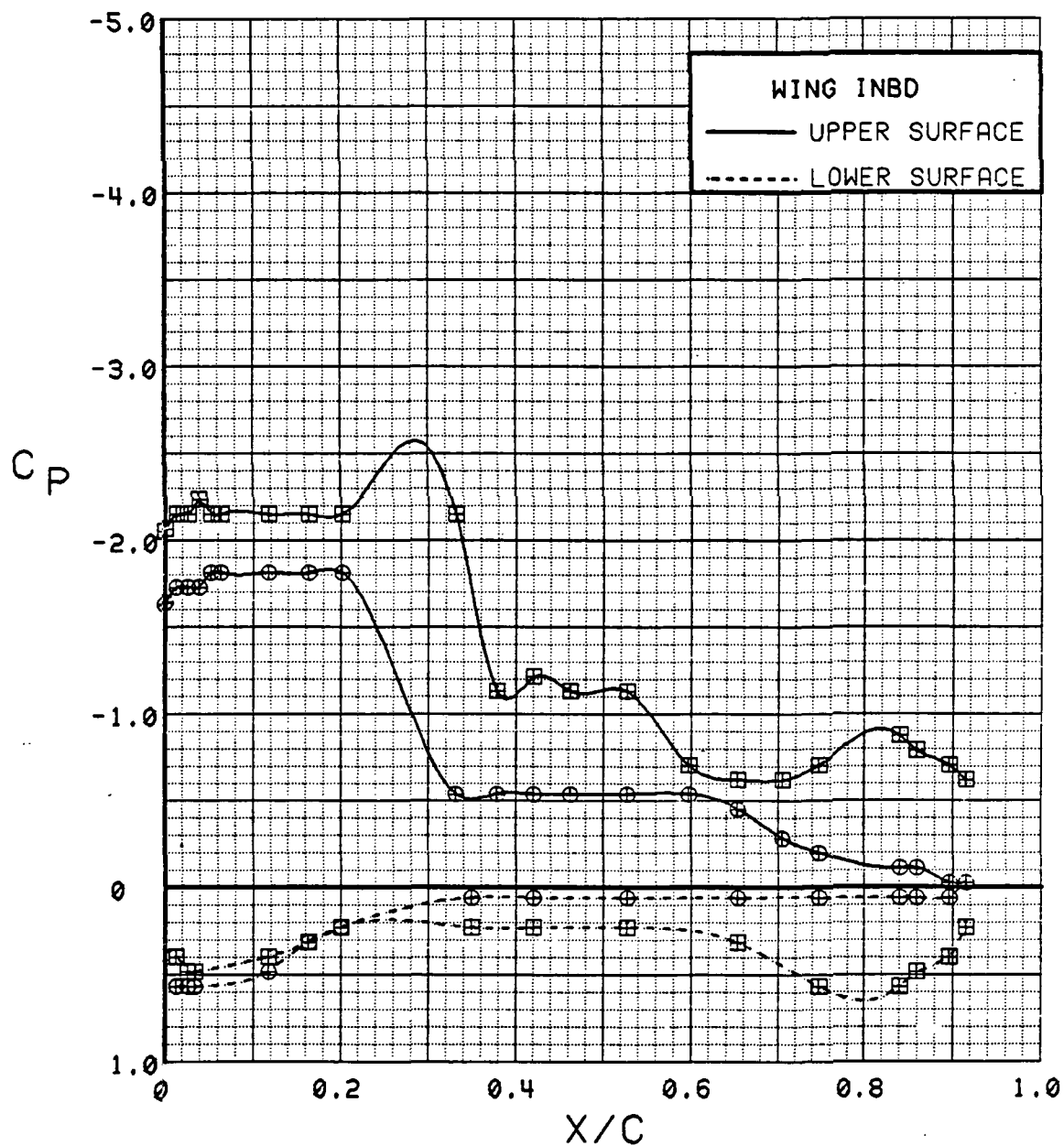


Figure 3.2.2-9

Wing Trailing-Edge Flap Effects, Power Off, Alpha = 8 deg, Inboard

SYM	TEST	RUN	ALPHA	CT	ITEF	OTEF	CAN	SWB
⊕	537	74	12.4	0.00	0	0	OFF	OFF
⊞	537	69	12.5	0.00	30	30	OFF	OFF

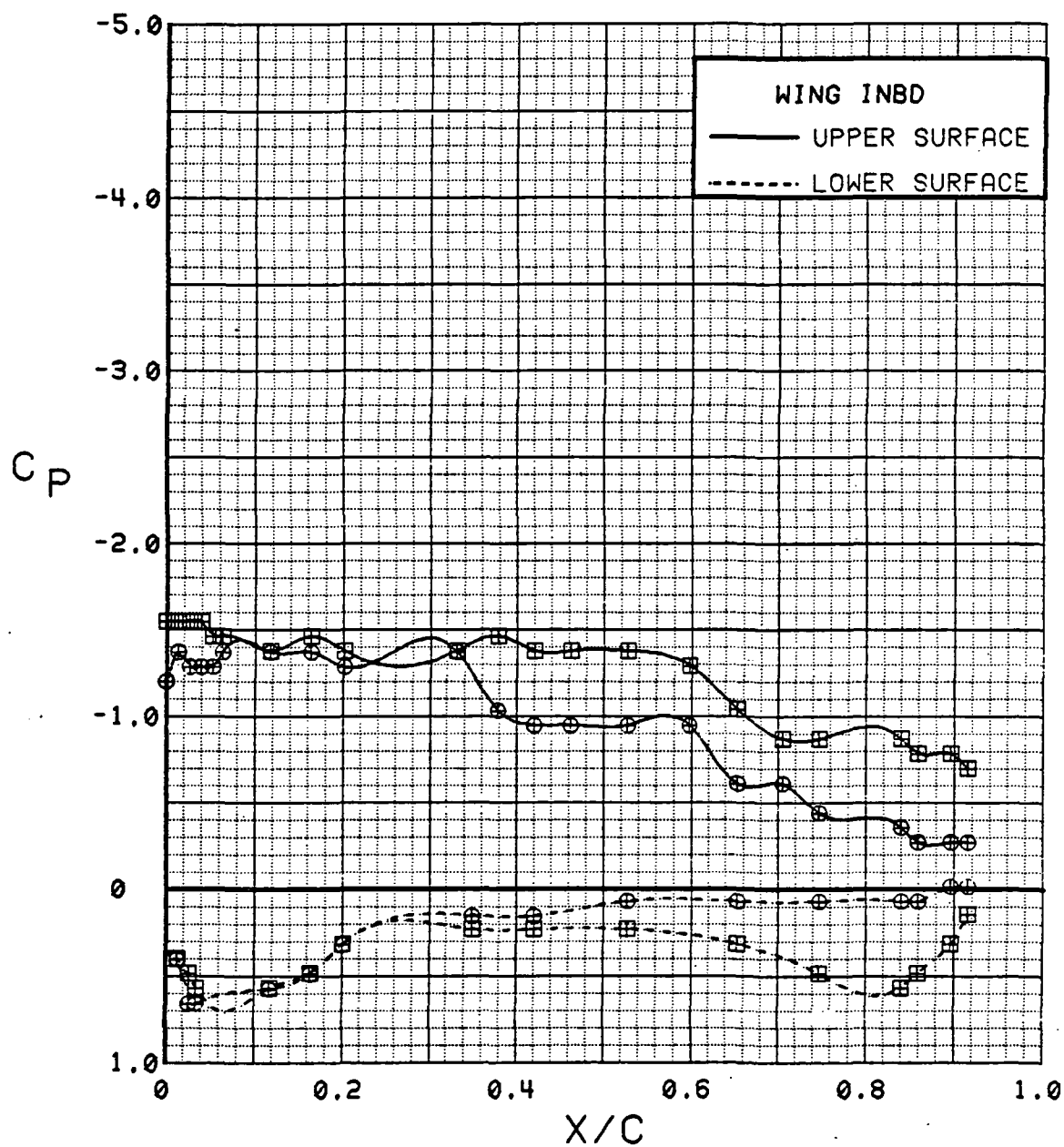


Figure 3.2.2-10 Wing Trailing-Edge Flap Effects, Power Off, Alpha = 12 deg, Inboard

SYM	TEST	RUN	ALPHA	CT	ITEF	OTEF	CAN	SWB
⊕	537	74	16.5	0.00	0	0	OFF	OFF
⊞	537	69	16.6	0.00	30	30	OFF	OFF

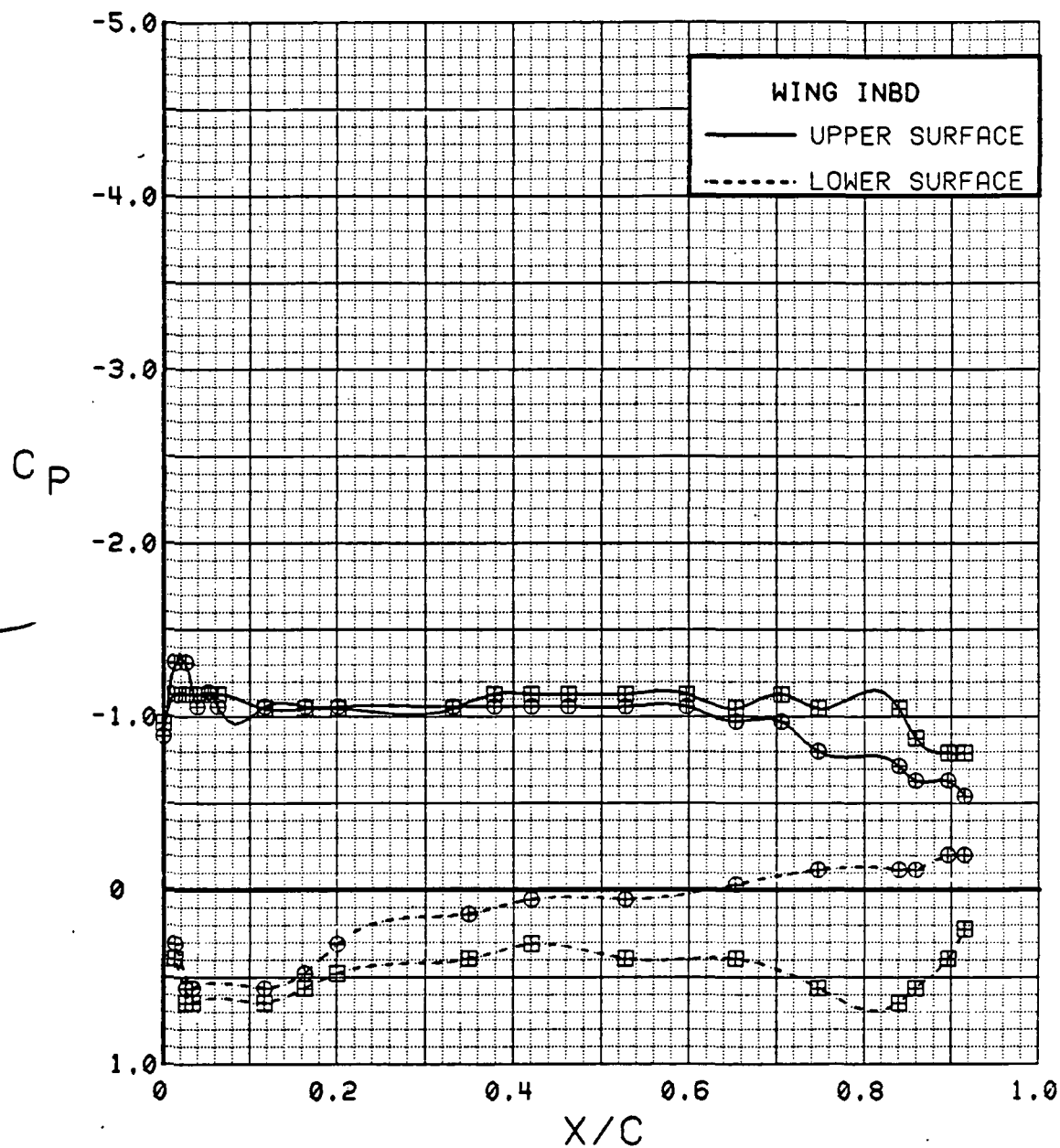


Figure 3.2.2-11 Wing Trailing-Edge Flap Effects, Power Off, Alpha = 16 deg, Inboard

SYM	TEST	RUN	ALPHA	CT	ITEF	OTEF	CAN	SWB
⊕	537	74	0.1	0.00	0	0	OFF	OFF
⊞	537	69	0.2	0.00	30	30	OFF	OFF

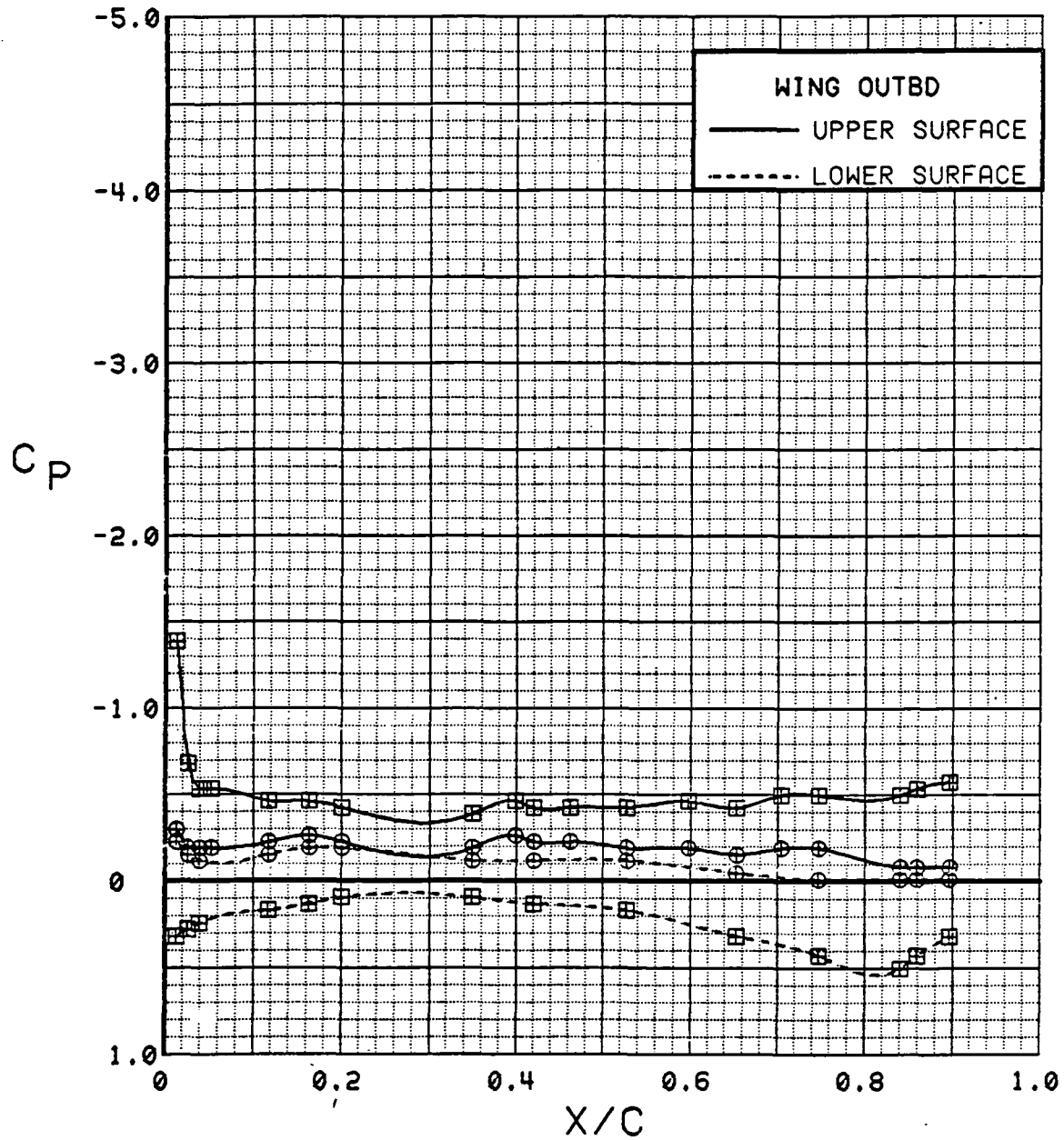


Figure 3.2.2-12 Wing Trailing-Edge Flap Effects, Power Off, Alpha = 0 deg, Outboard



SYM	TEST	RUN	ALPHA	CT	ITEF	OTEF	CAN	SWB
⊕	537	74	8.3	0.00	0	0	OFF	OFF
⊞	537	69	8.5	0.00	30	30	OFF	OFF

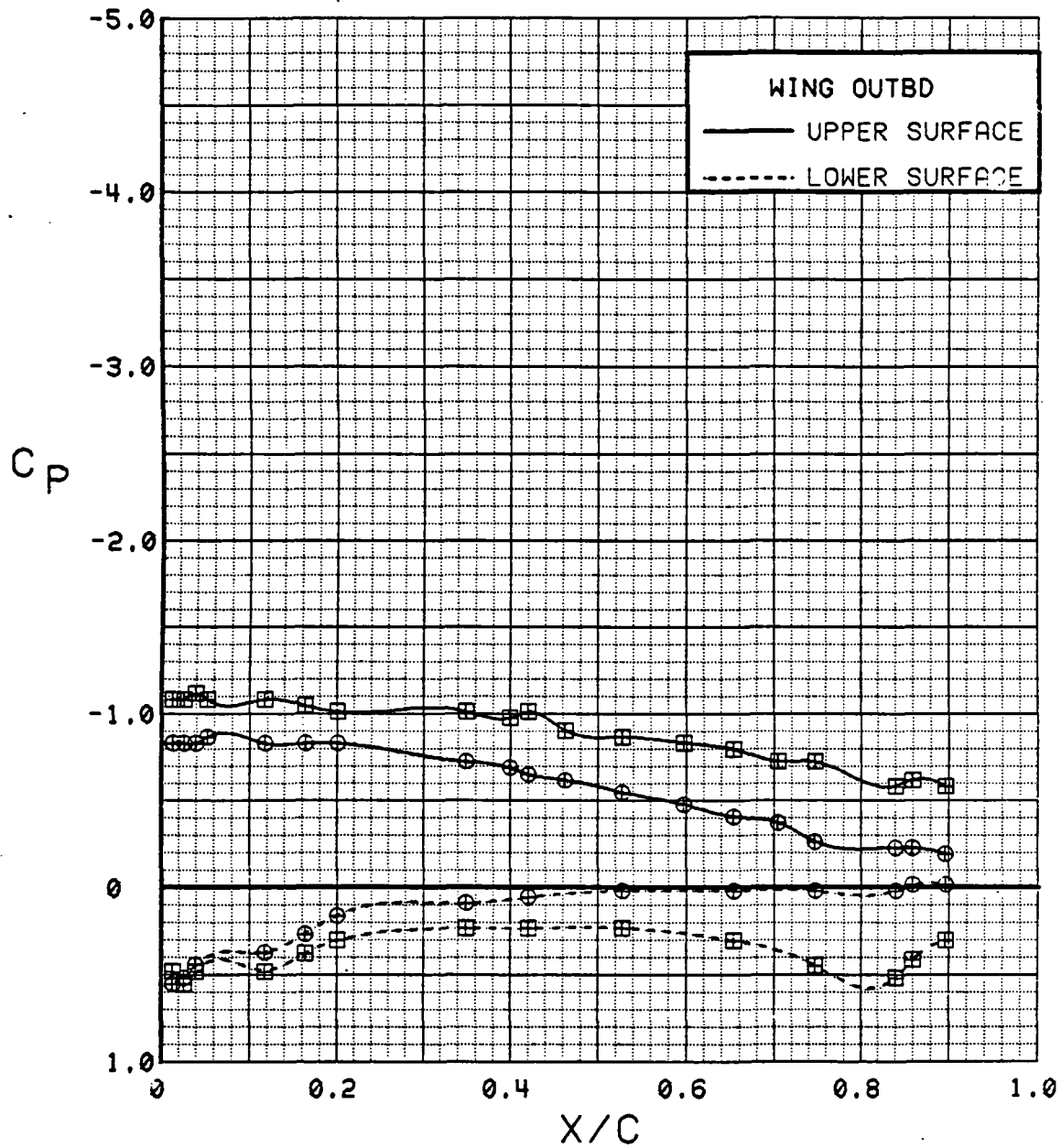


Figure 3.2.2-13 Wing Trailing-Edge Flap Effects, Power Off, Alpha = 8 deg, Outboard

SYM	TEST	RUN	ALPHA	CT	ITEF	OTEF	CAN	SWB
⊕	537	74	12.4	0.00	0	0	OFF	OFF
⊞	537	69	12.5	0.00	30	30	OFF	OFF

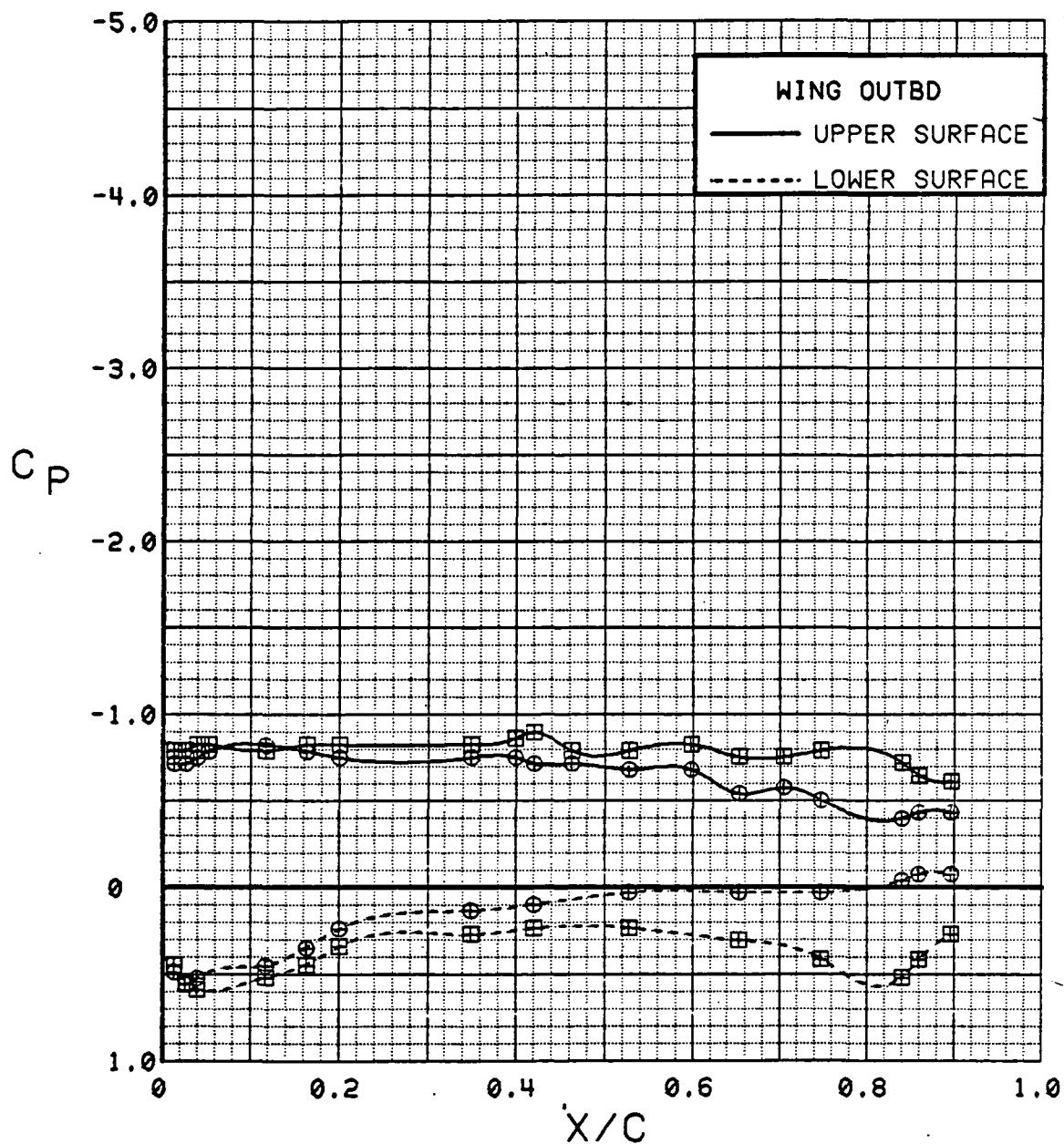


Figure 3.2.2-14 Wing Trailing-Edge Flap Effects, Power Off, Alpha = 12 deg,  
Outboard

SYM	TEST	RUN	ALPHA	CT	ITEF	OTEF	CAN	SWB
⊕	537	74	16.5	0.00	0	0	OFF	OFF
⊞	537	69	16.6	0.00	30	30	OFF	OFF

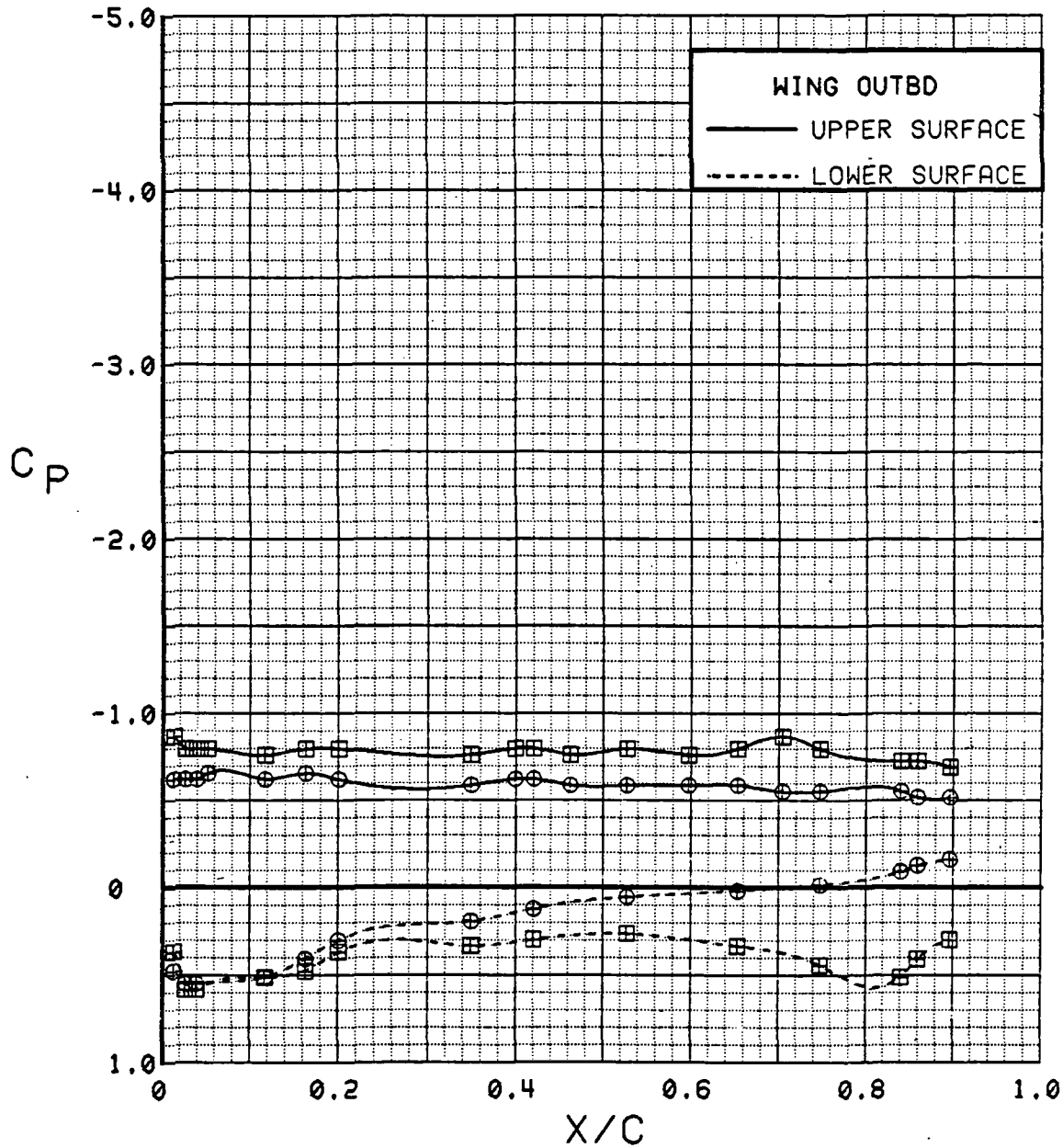


Figure 3.2.2-15 Wing Trailing-Edge Flap Effects, Power Off, Alpha = 16 deg,  
Outboard

SYM	TEST	RUN	ALPHA	CT	ITEF	OTEF	CAN	SWB
⊕	537	74	0.1	0.00	0	0	OFF	OFF
⊞	537	69	0.2	0.00	30	30	OFF	OFF

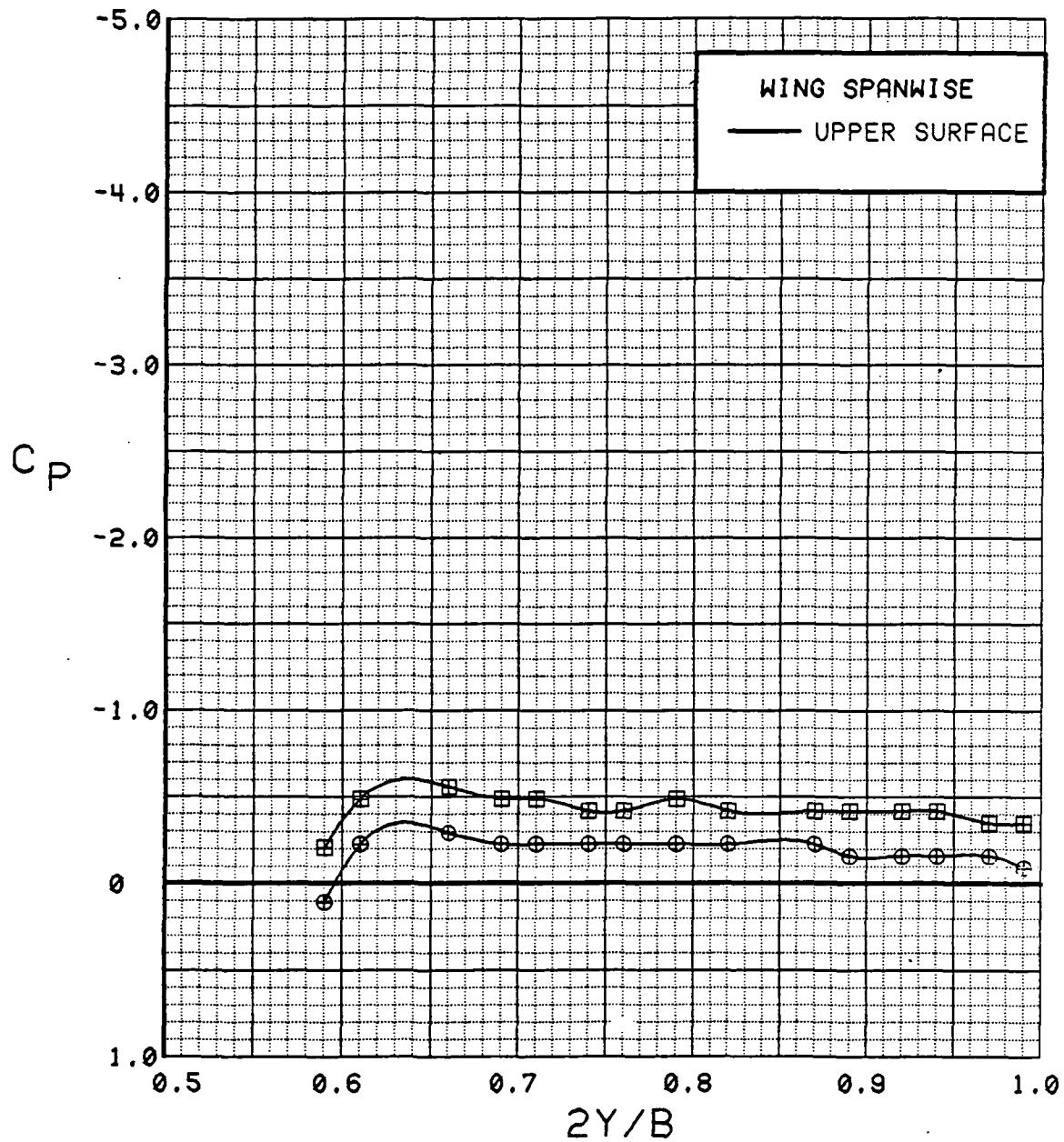


Figure 3.2.2-16 Wing Trailing-Edge Flap Effects, Power Off, Alpha = 0 deg, Spanwise

SYM	TEST	RUN	ALPHA	CT	ITEF	OTEF	CAN	SWB
⊙	537	74	8.3	0.00	0	0	OFF	OFF
⊠	537	69	8.5	0.00	30	30	OFF	OFF

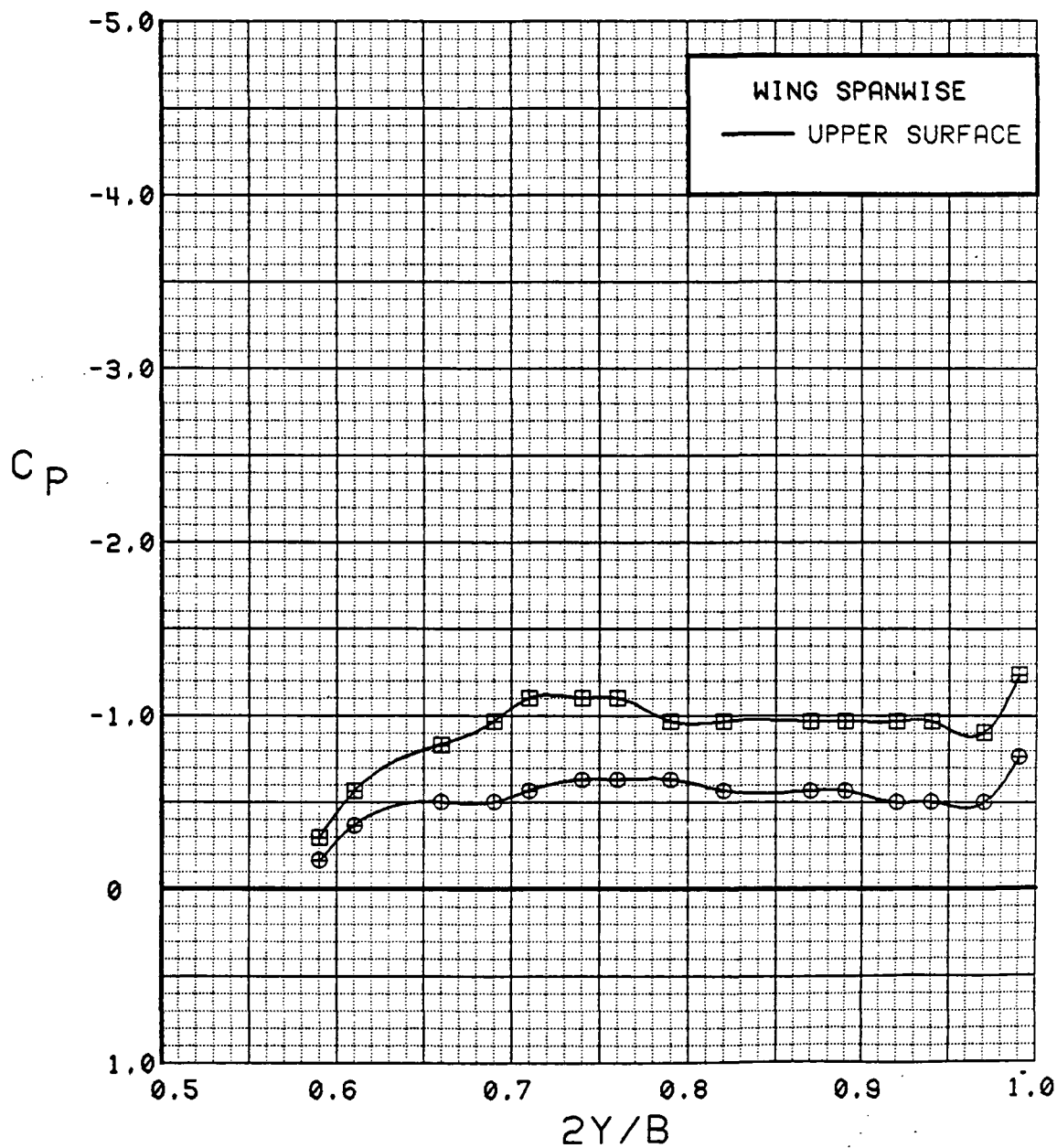


Figure 3.2.2-17 Wing Trailing-Edge Flap Effects, Power Off, Alpha = 8 deg, Spanwise

SYM	TEST	RUN	ALPHA	CT	ITEF	OTEF	CAN	SWB
⊕	537	74	12.4	0.00	0	0	OFF	OFF
⊞	537	69	12.5	0.00	30	30	OFF	OFF

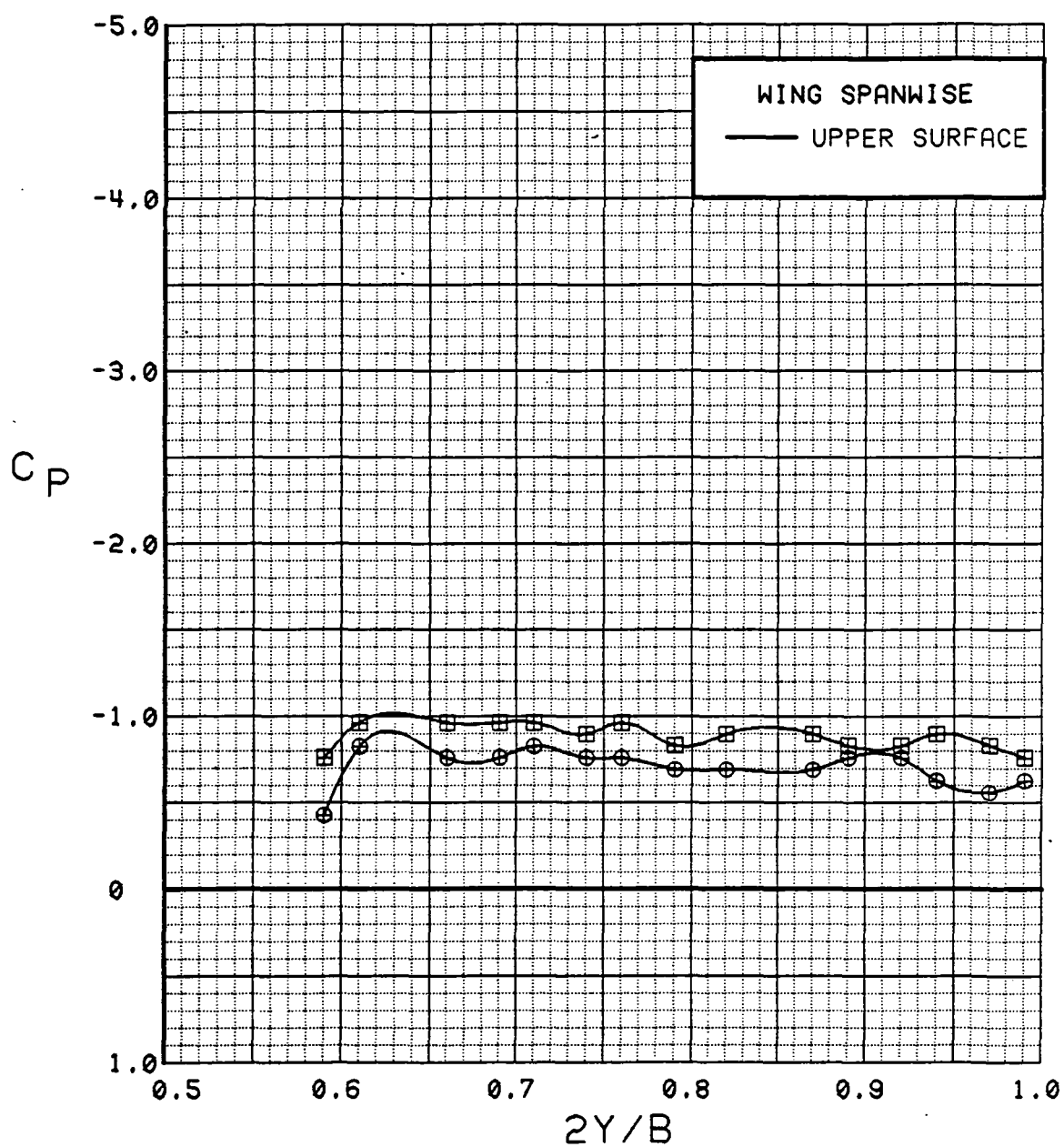


Figure 3.2.2-18 Wing Trailing-Edge Flap Effects, Power Off, Alpha = 12 deg,  
Spanwise

SYM	TEST	RUN	ALPHA	CT	ITEF	OTEF	CAN	SWB
⊕	537	74	16.5	0.00	0	0	OFF	OFF
⊞	537	69	16.6	0.00	30	30	OFF	OFF

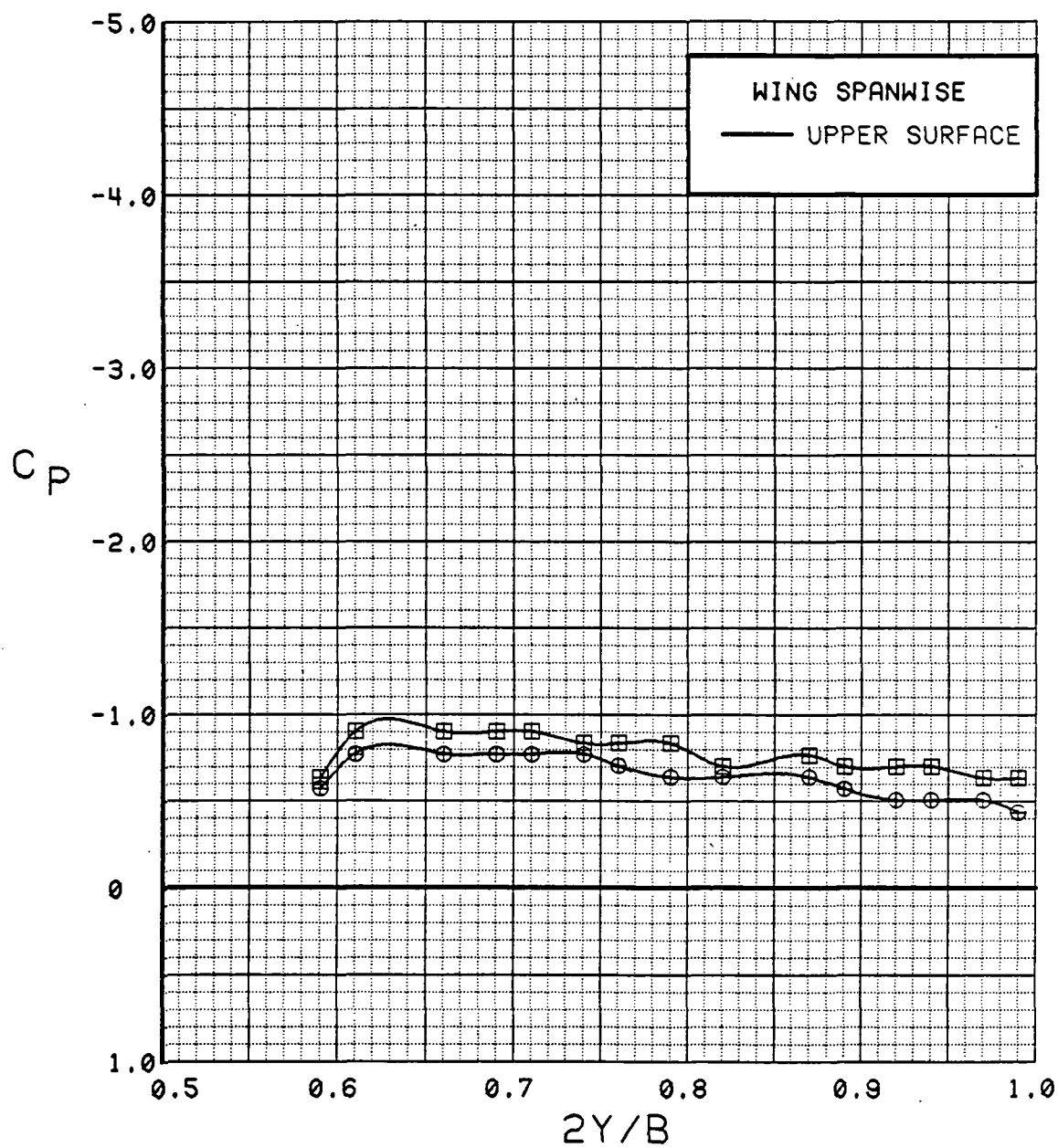


Figure 3.2.2-19 Wing Trailing-Edge Flap Effects, Power Off, Alpha = 16 deg,  
Spanwise

## WING INBOARD

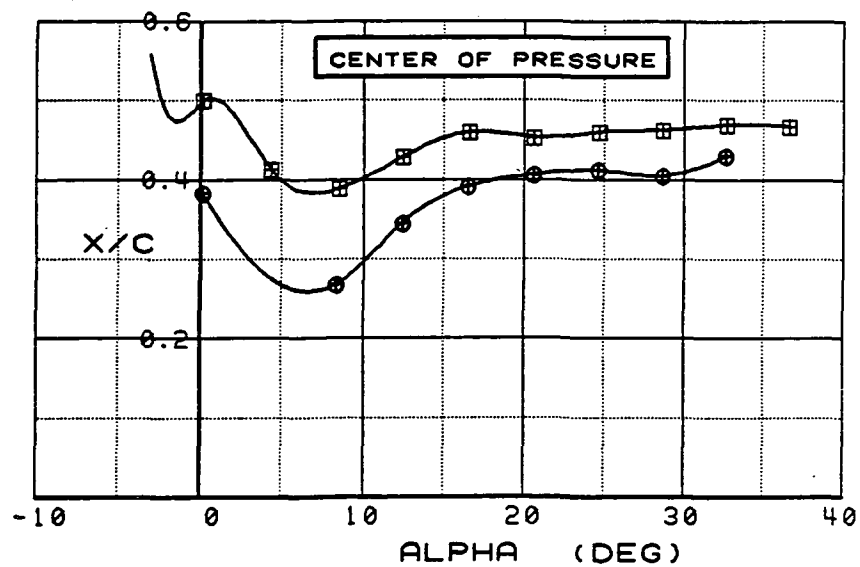
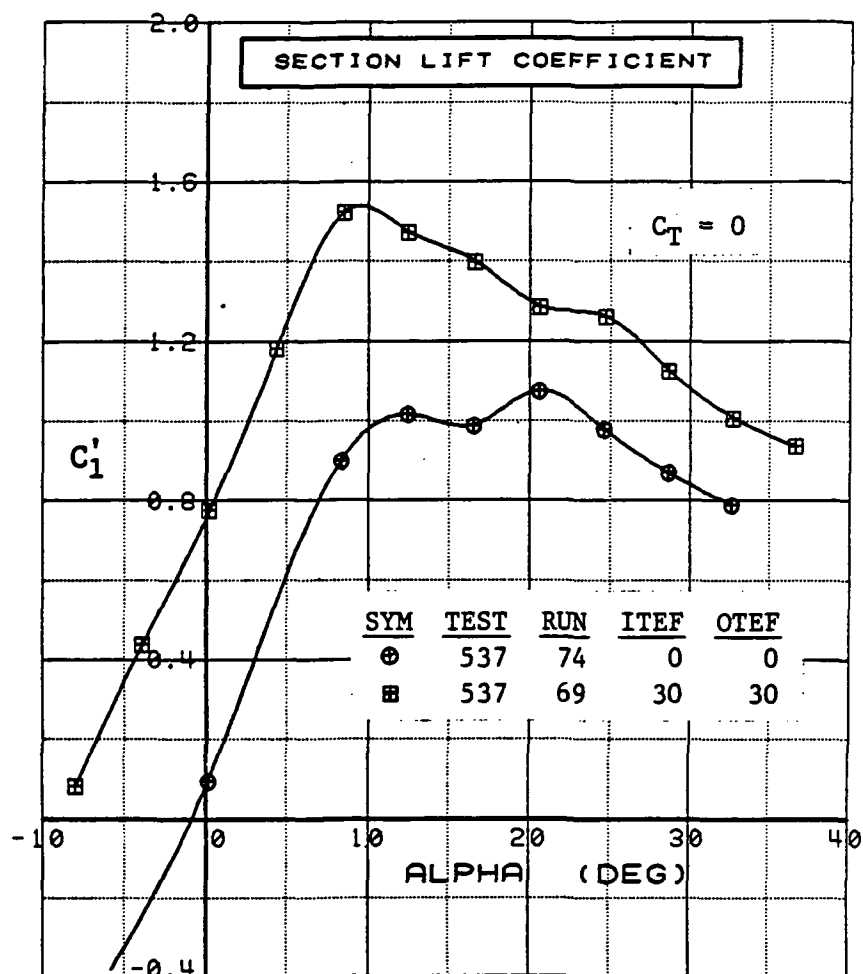


Figure 3.2.2-20 Wing Trailing-Edge Flap Effects, Power Off, Inboard, Integrated Section Properties



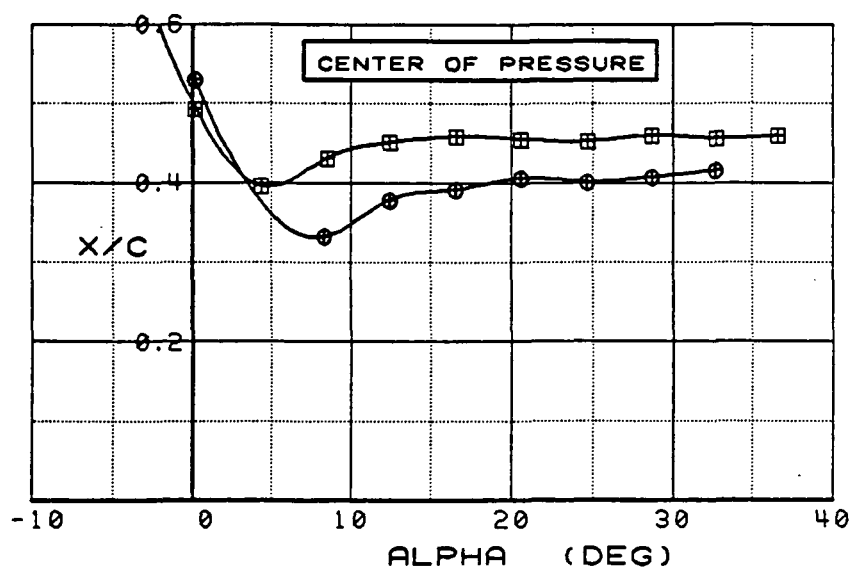
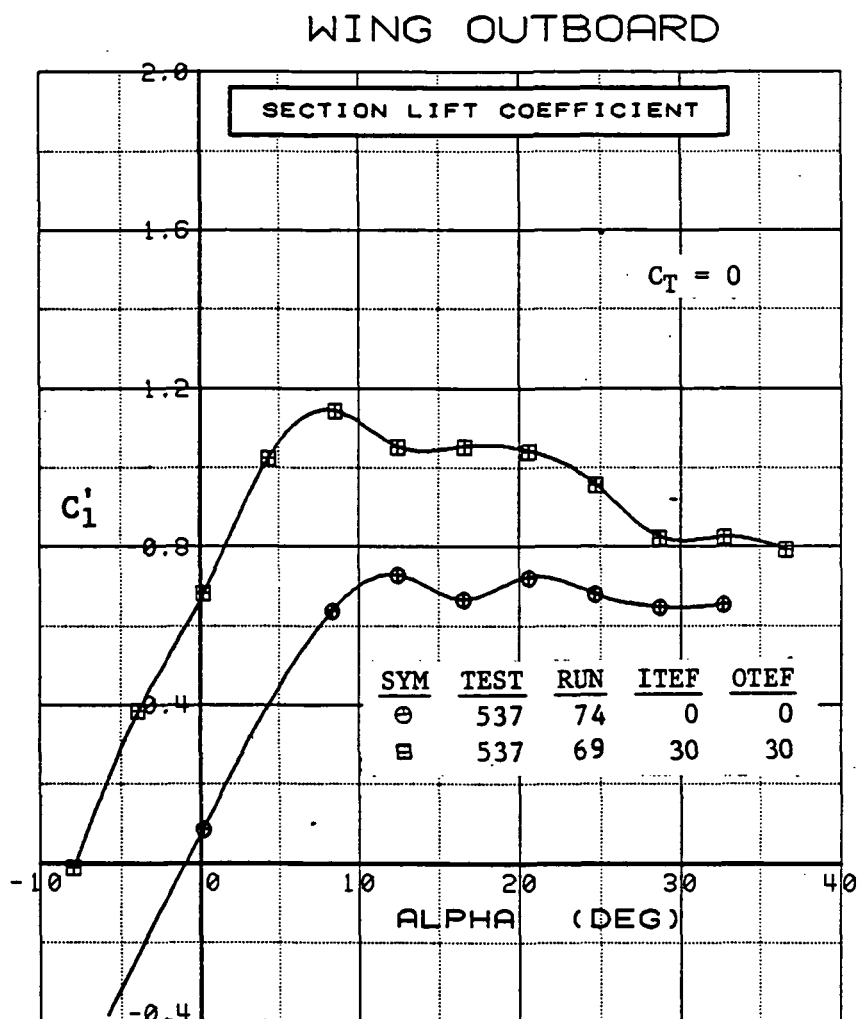


Figure 3.2.2-21 Wing Trailing-Edge Flap Effects, Power Off, Outboard, Integrated Section Properties

SYM	TEST	RUN	ALPHA	CT	ITEF	OTEF	CAN	SWB
⊕	537	72	0.1	0.89	0	0	OFF	OFF
⊞	537	61	0.4	0.94	30	30	OFF	OFF

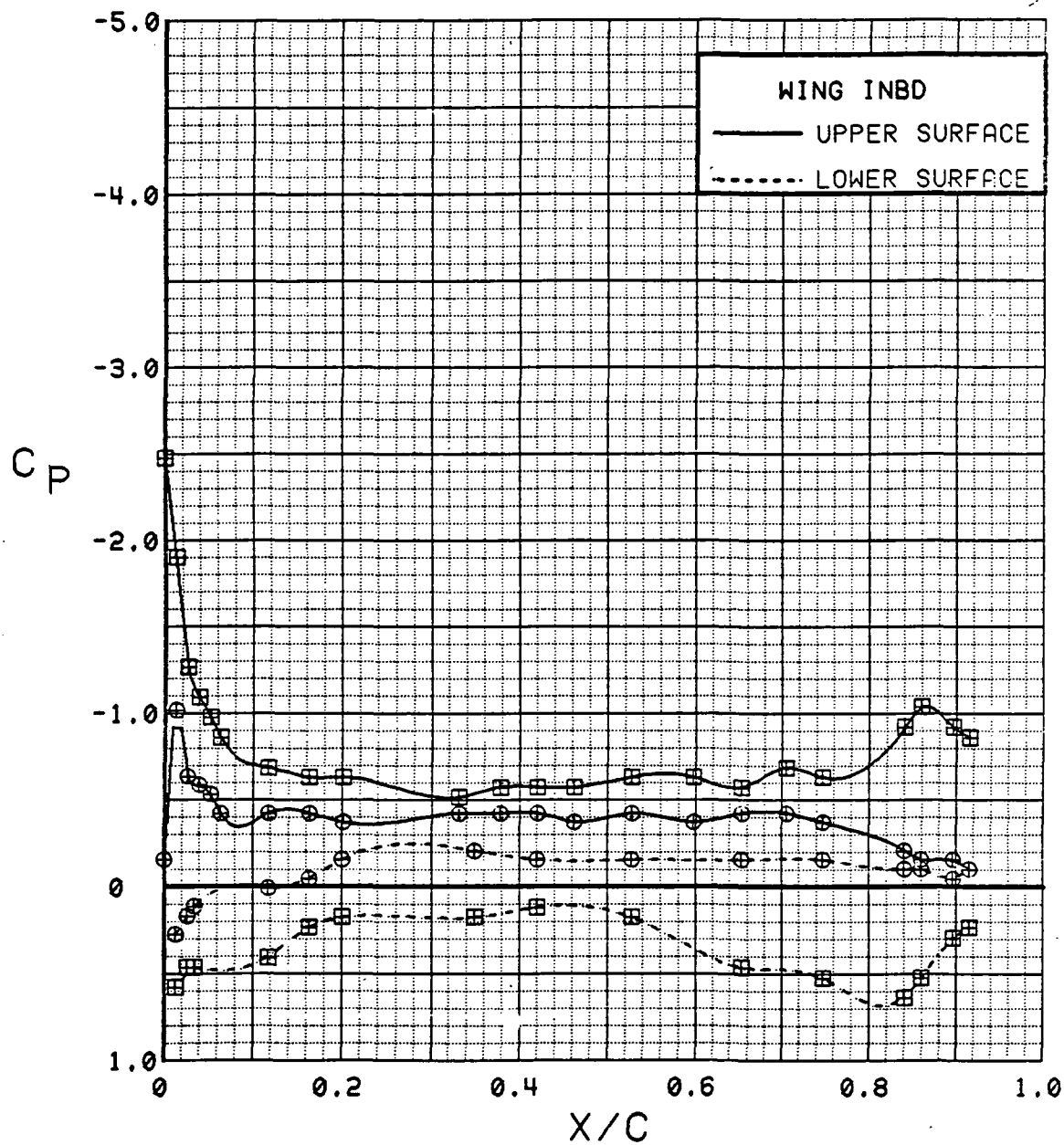


Figure 3.2.2-22 Wing Trailing-Edge Flap Effects, Power On, Inboard, Alpha = 0 deg

C-2

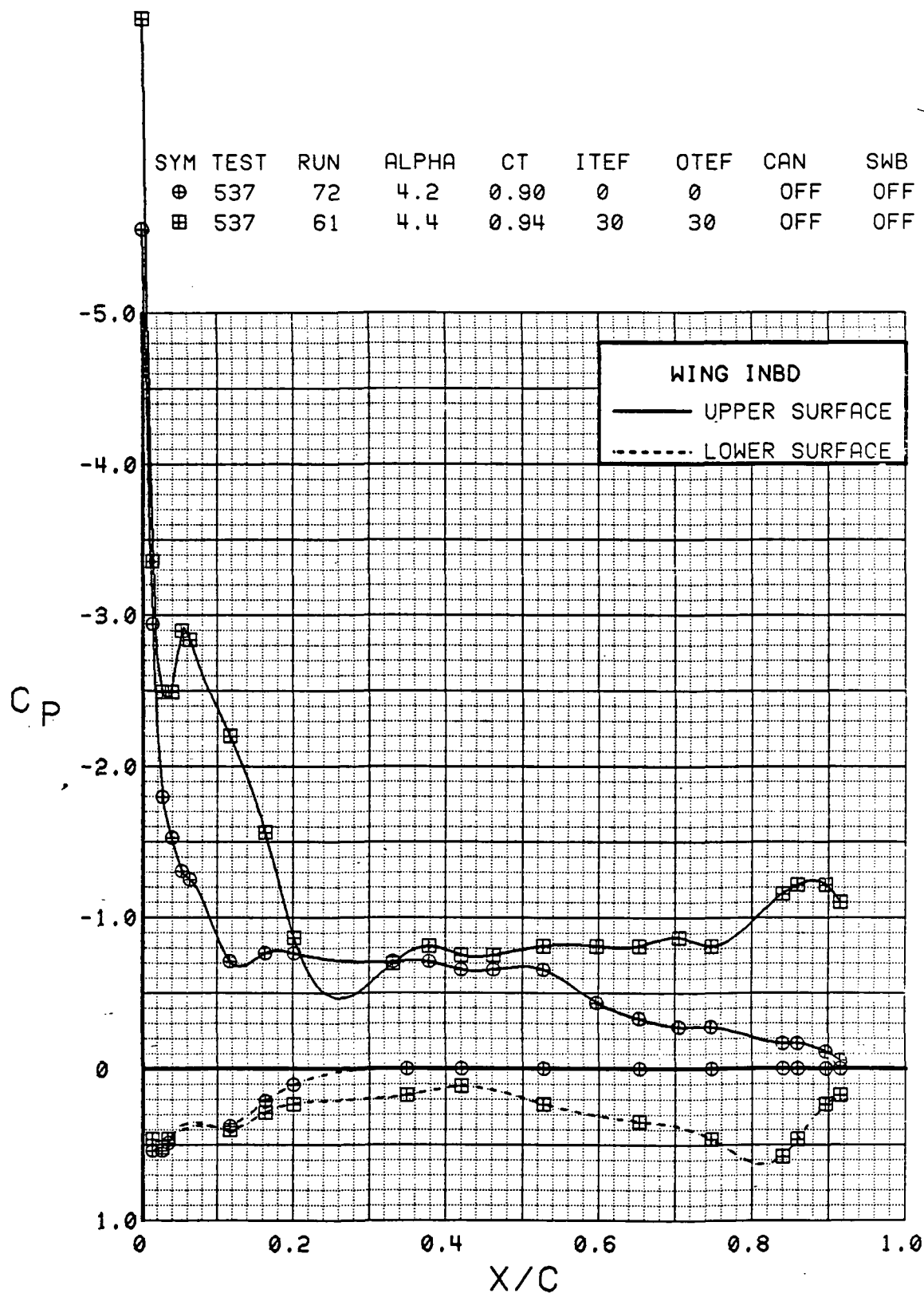


Figure 3.2.2-23 Wing Trailing-Edge Flap Effects, Power On, Inboard, Alpha = 4 deg

SYM	TEST	RUN	ALPHA	CT	ITEF	OTEF	CAN	SWB
⊕	537	72	8.3	0.92	0	0	OFF	OFF
⊞	537	61	8.5	0.94	30	30	OFF	OFF

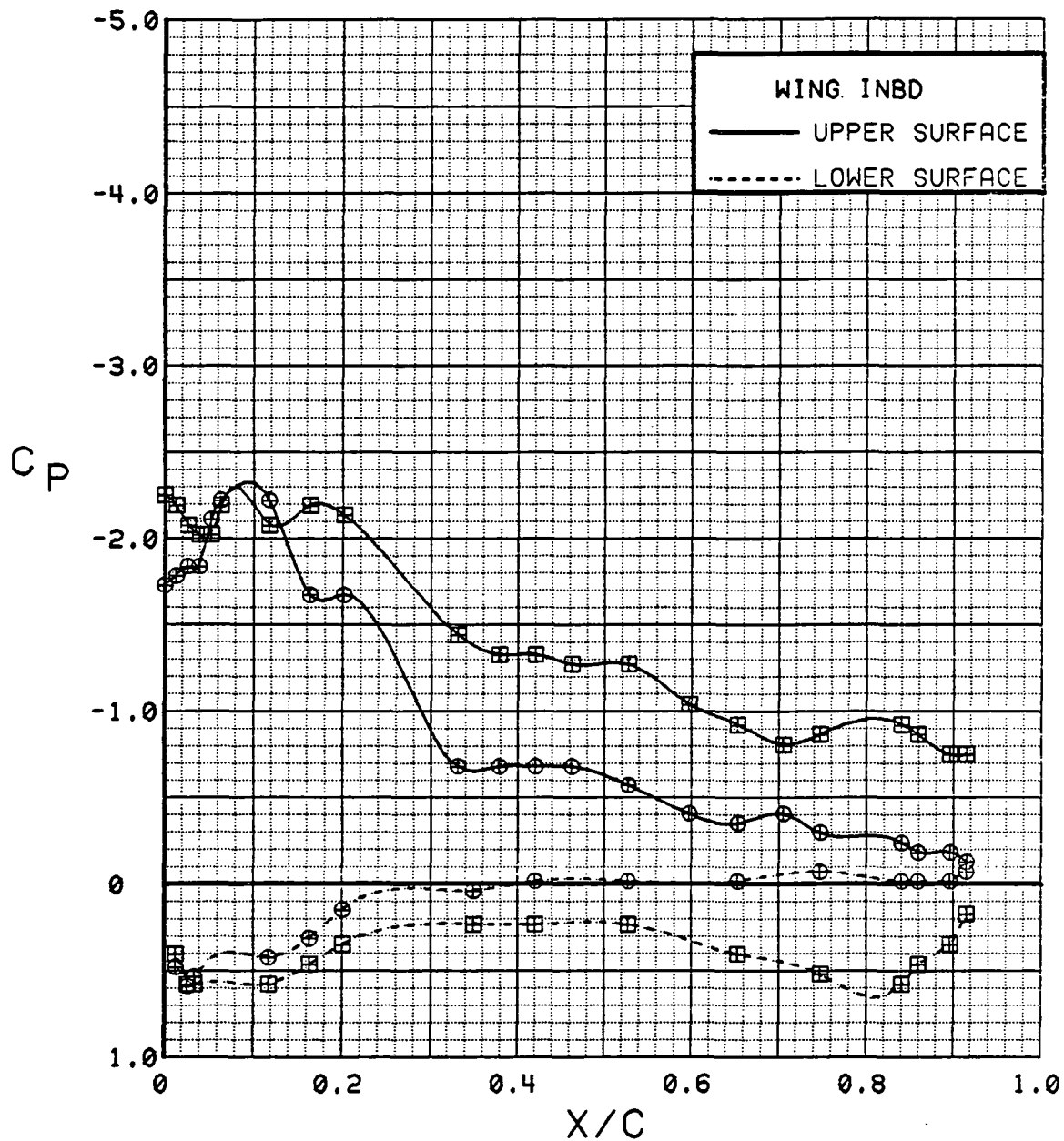


Figure 3.2.2-24 Wing Trailing-Edge Flap Effects, Power On, Inboard, Alpha = 8 deg

SYM	TEST	RUN	ALPHA	CT	ITEF	OTEF	CAN	SWB
⊕	537	72	12.4	0.91	0	0	OFF	OFF
⊞	537	61	12.6	0.92	30	30	OFF	OFF

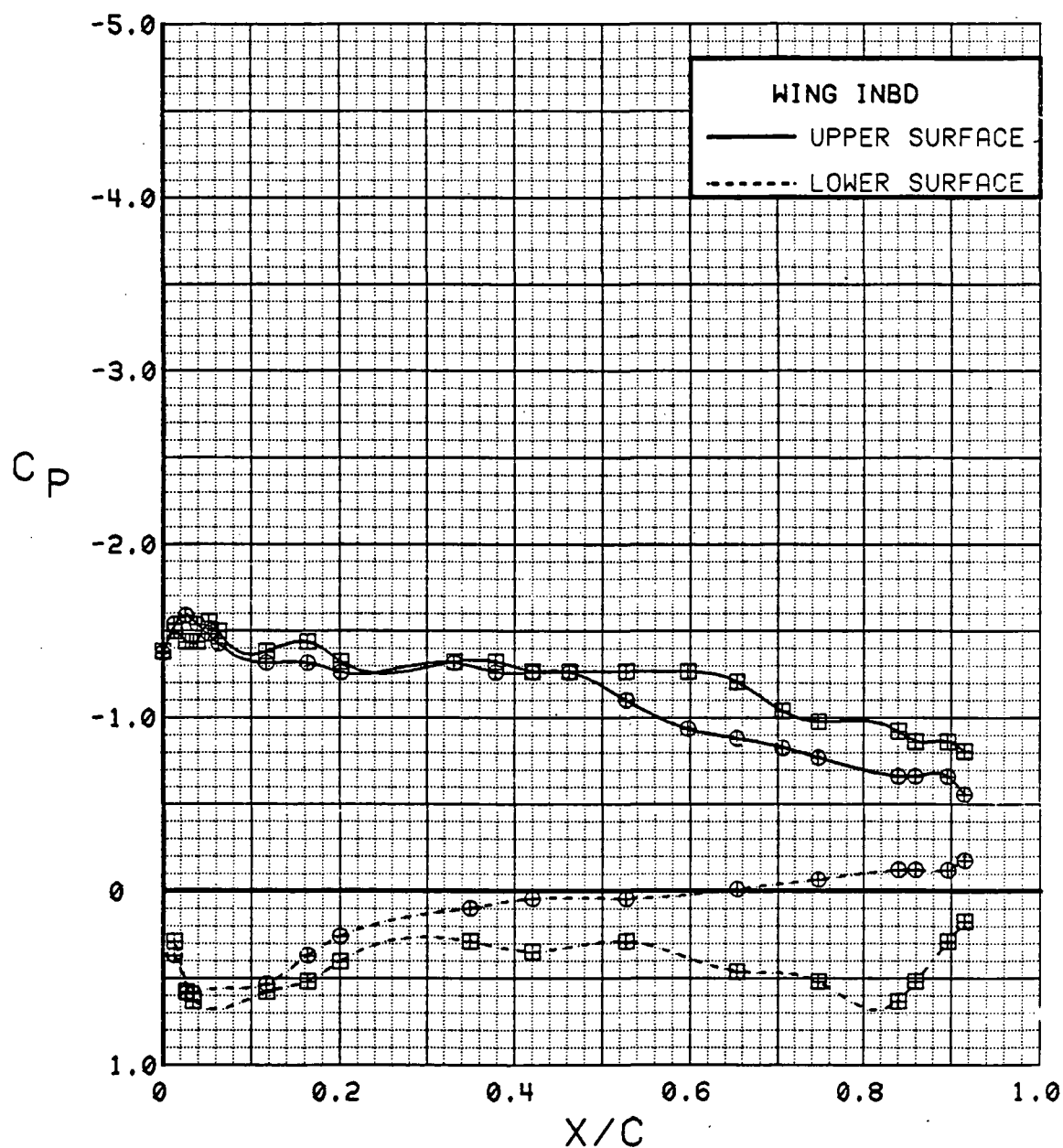


Figure 3.2.2-25 Wing Trailing-Edge Flap Effects, Power On, Inboard, Alpha = 12 deg

SYM	TEST	RUN	ALPHA	CT	ITEF	OTEF	CAN	SWB
⊕	537	72	16.5	0.91	0	0	OFF	OFF
⊞	537	61	16.7	0.94	30	30	OFF	OFF

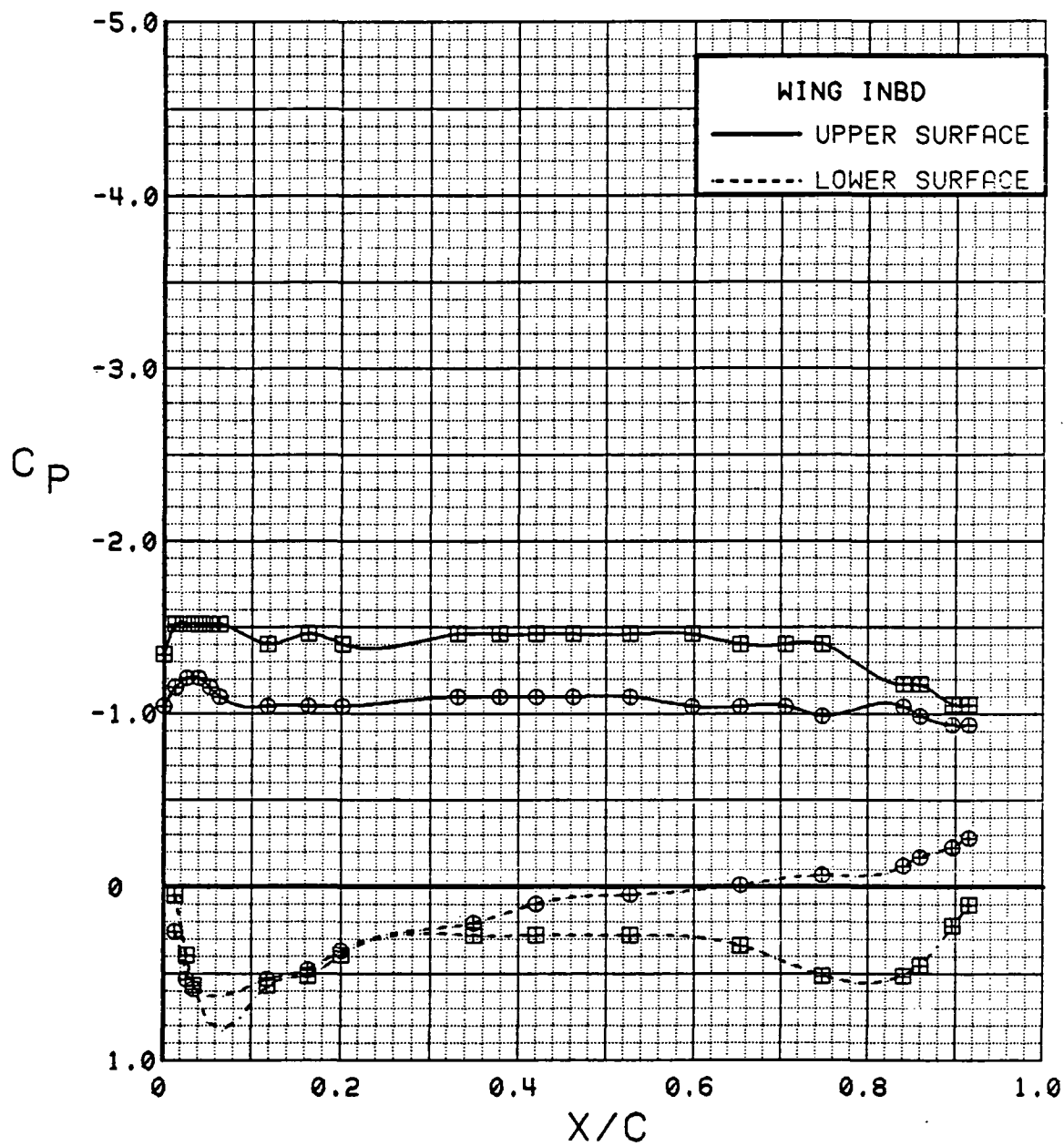


Figure 3.2.2-26 Wing Trailing-Edge Flap Effects, Power On, Inboard, Alpha = 16 deg

SYM	TEST	RUN	ALPHA	CT	ITEF	OTEF	CAN	SWB
⊕	537	72	0.1	0.89	0	0	OFF	OFF
⊞	537	61	0.4	0.94	30	30	OFF	OFF

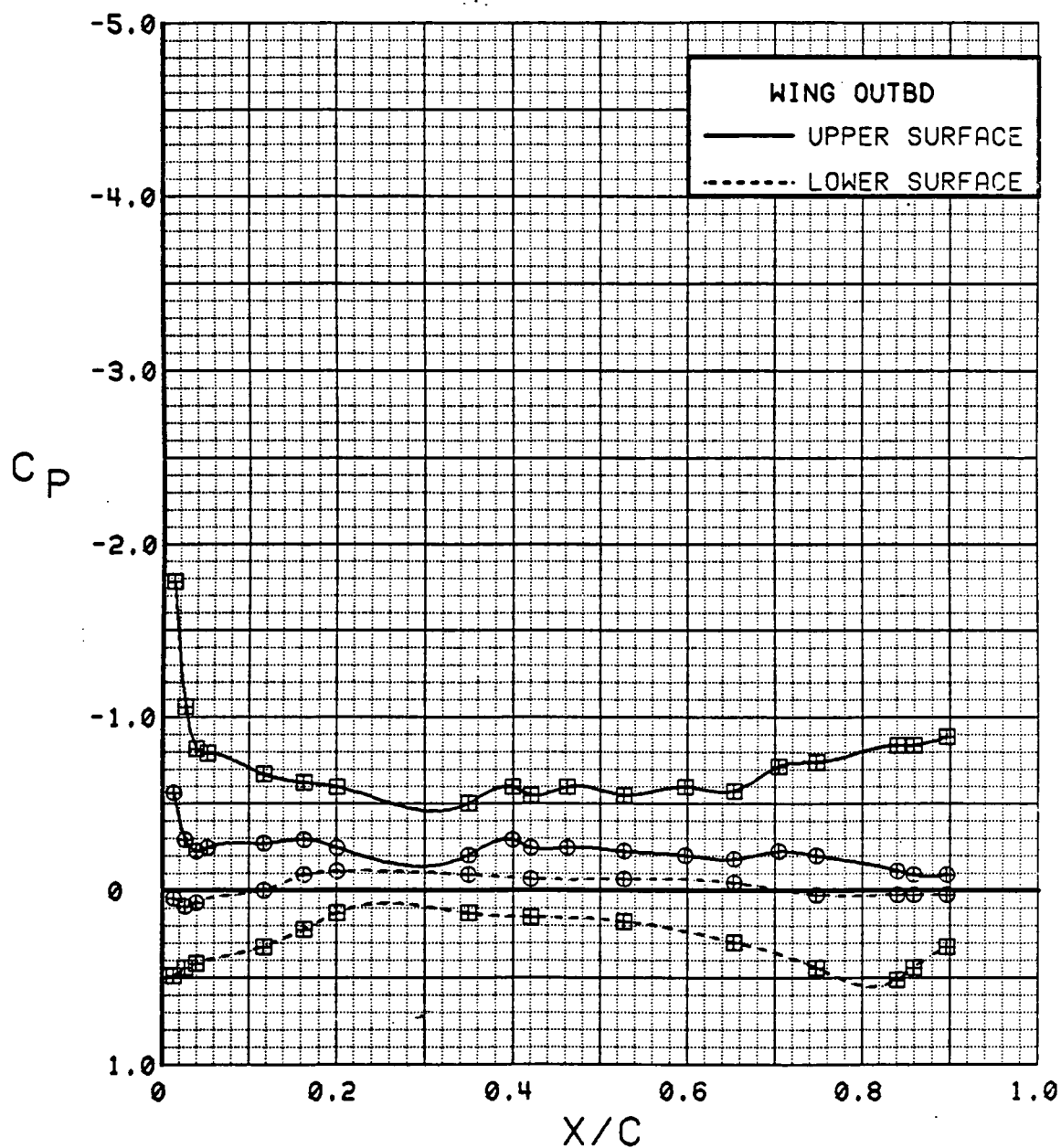


Figure 3.2.2-27 Wing Trailing-Edge Flap Effects, Power On, Outboard, Alpha = 0 deg

SYM	TEST	RUN	ALPHA	CT	ITEF	OTEF	CAN	SWB
⊕	537	72	4.2	0.90	0	0	OFF	OFF
⊞	537	61	4.4	0.94	30	30	OFF	OFF

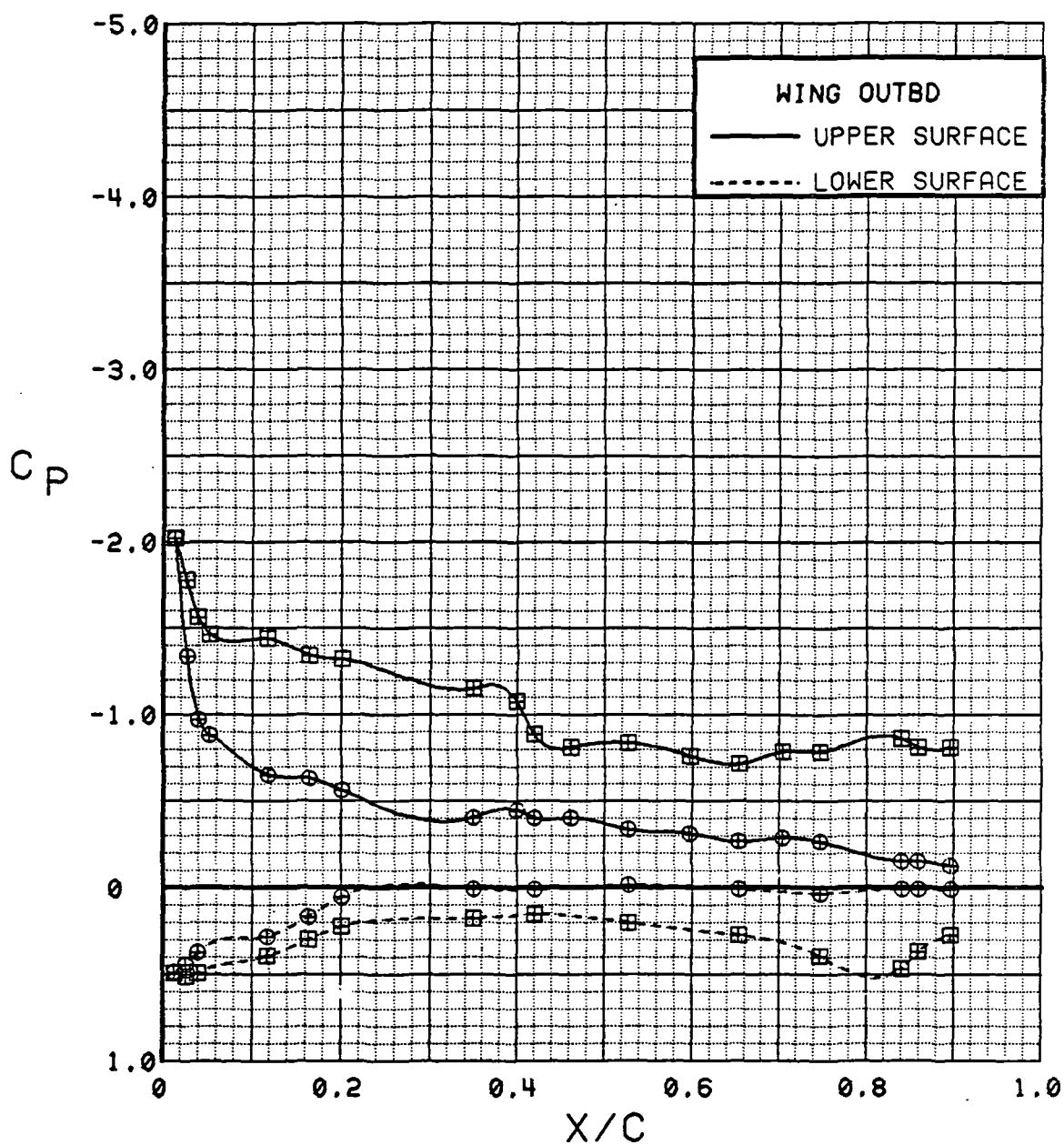


Figure 3.2.2-28 Wing Trailing-Edge Flap Effects, Power On, Outboard, Alpha = 4 deg



SYM	TEST	RUN	ALPHA	CT	ITEF	OTEF	CAN	SWB
⊕	537	72	8.3	0.92	0	0	OFF	OFF
⊞	537	61	8.5	0.94	30	30	OFF	OFF

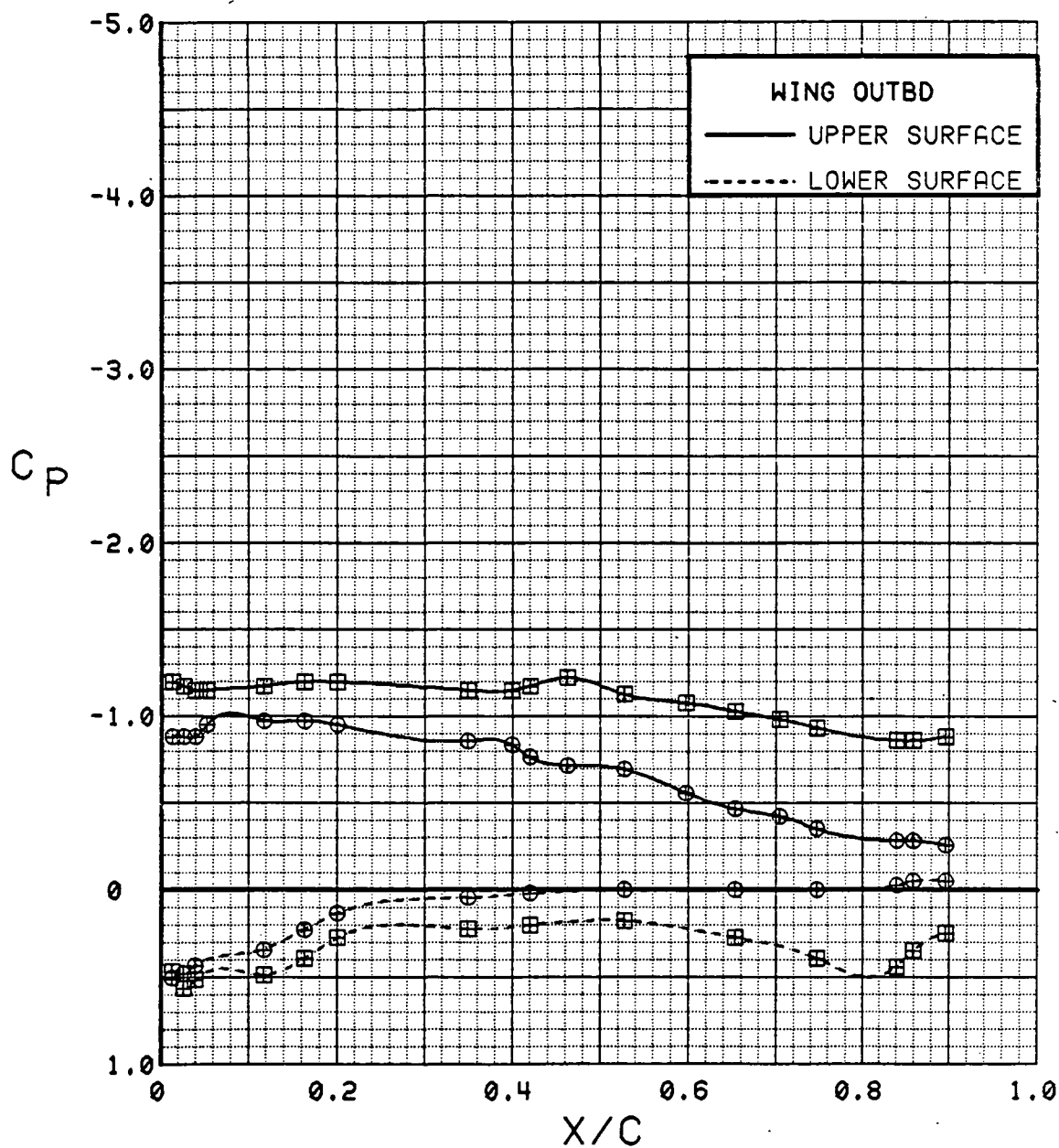


Figure 3.2.2-29 Wing Trailing-Edge Flap Effects, Power On, Outboard, Alpha = 8 deg

SYM	TEST	RUN	ALPHA	CT	ITEF	OTEF	CAN	SWB
⊕	537	72	12.4	0.91	0	0	OFF	OFF
⊞	537	61	12.6	0.92	30	30	OFF	OFF

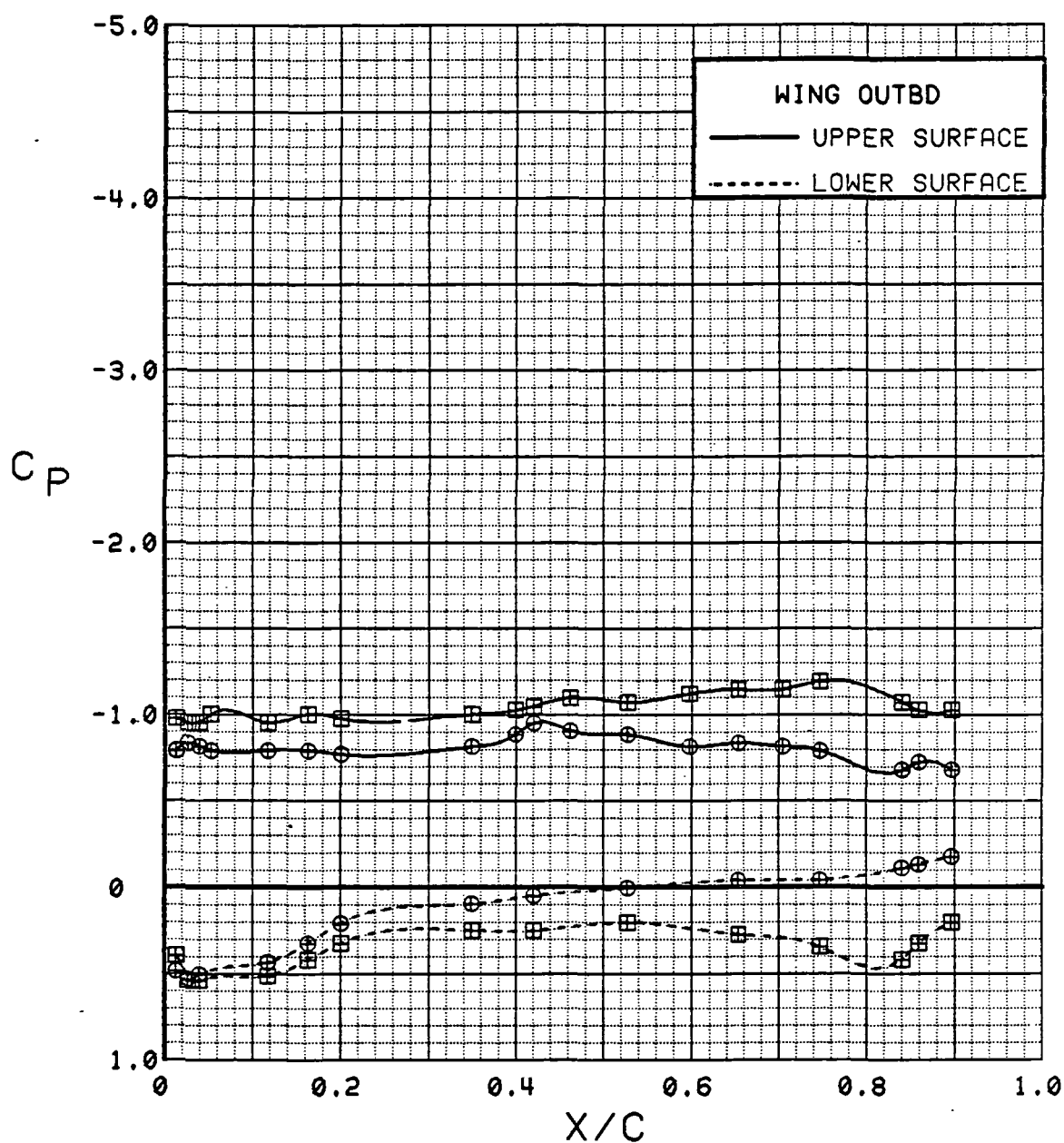


Figure 3.2.2-30 Wing Trailing-Edge Flap Effects, Power On, Outboard, Alpha = 12 deg

SYM	TEST	RUN	ALPHA	CT	ITEF	OTEF	CAN	SWB
⊕	537	72	16.5	0.91	0	0	OFF	OFF
⊞	537	61	16.7	0.94	30	30	OFF	OFF

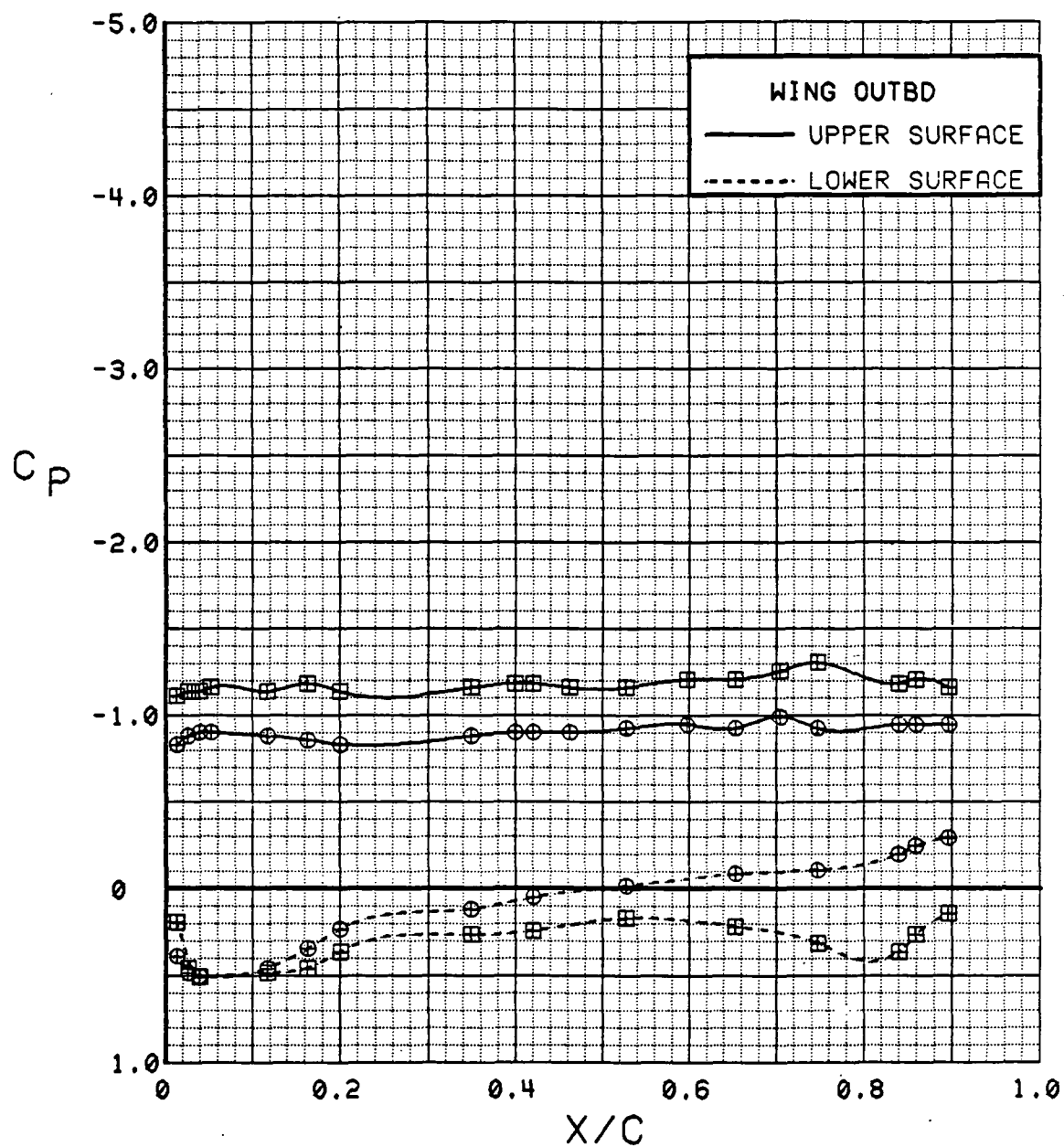


Figure 3.2.2-31 Wing Trailing-Edge Flap Effects, Power On, Outboard, Alpha = 16 deg

SYM	TEST	RUN	ALPHA	CT	ITEF	OTEF	CAN	SWB
⊕	537	72	0.1	0.89	0	0	OFF	OFF
⊞	537	61	0.4	0.94	30	30	OFF	OFF

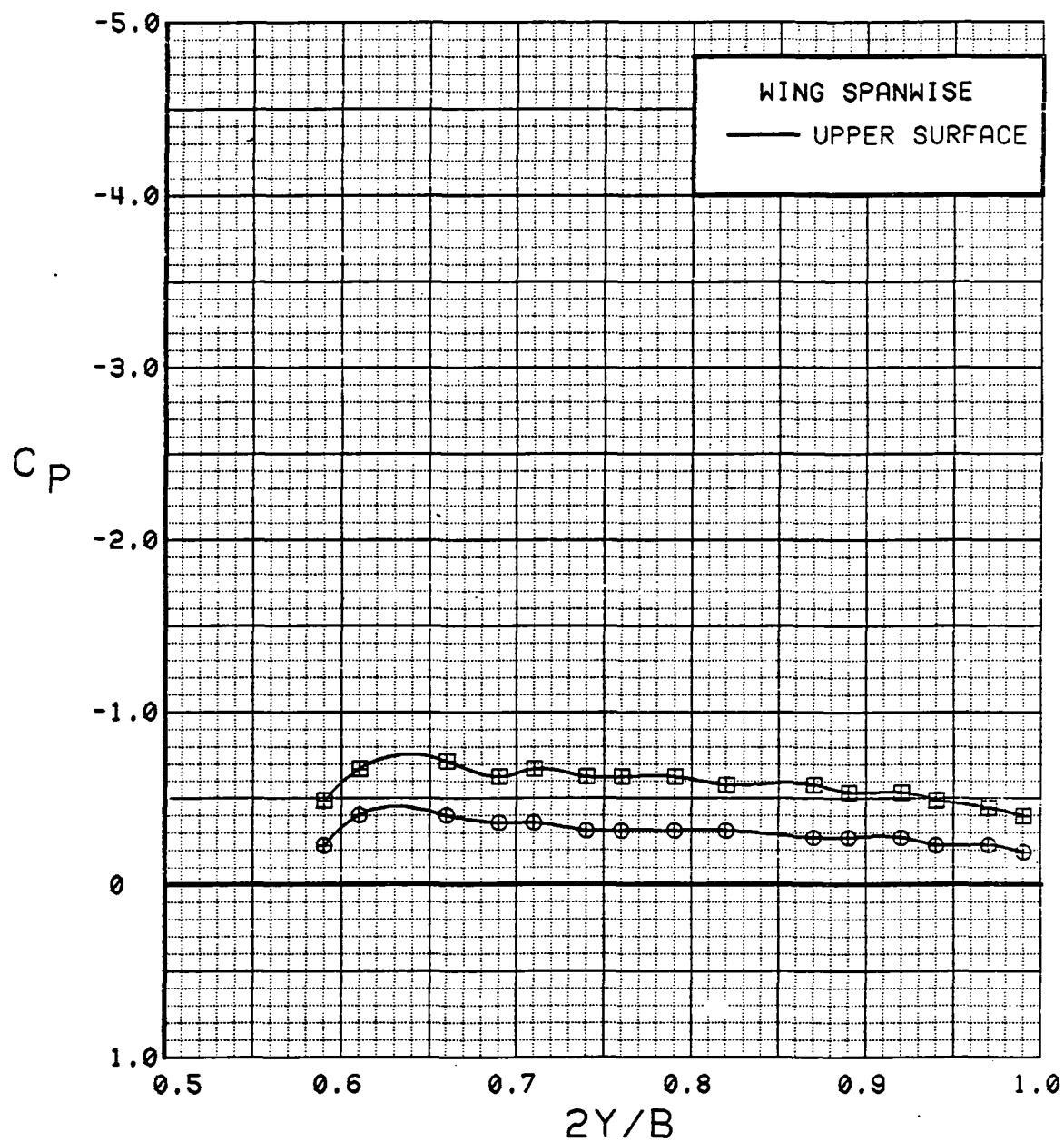


Figure 3.2.2-32 Wing Trailing-Edge Flap Effects, Power On, Spanwise, Alpha = 0 deg

SYM	TEST	RUN	ALPHA	CT	ITEF	OTEF	CAN	SWB
⊕	537	72	4.2	0.90	0	0	OFF	OFF
⊞	537	61	4.4	0.94	30	30	OFF	OFF

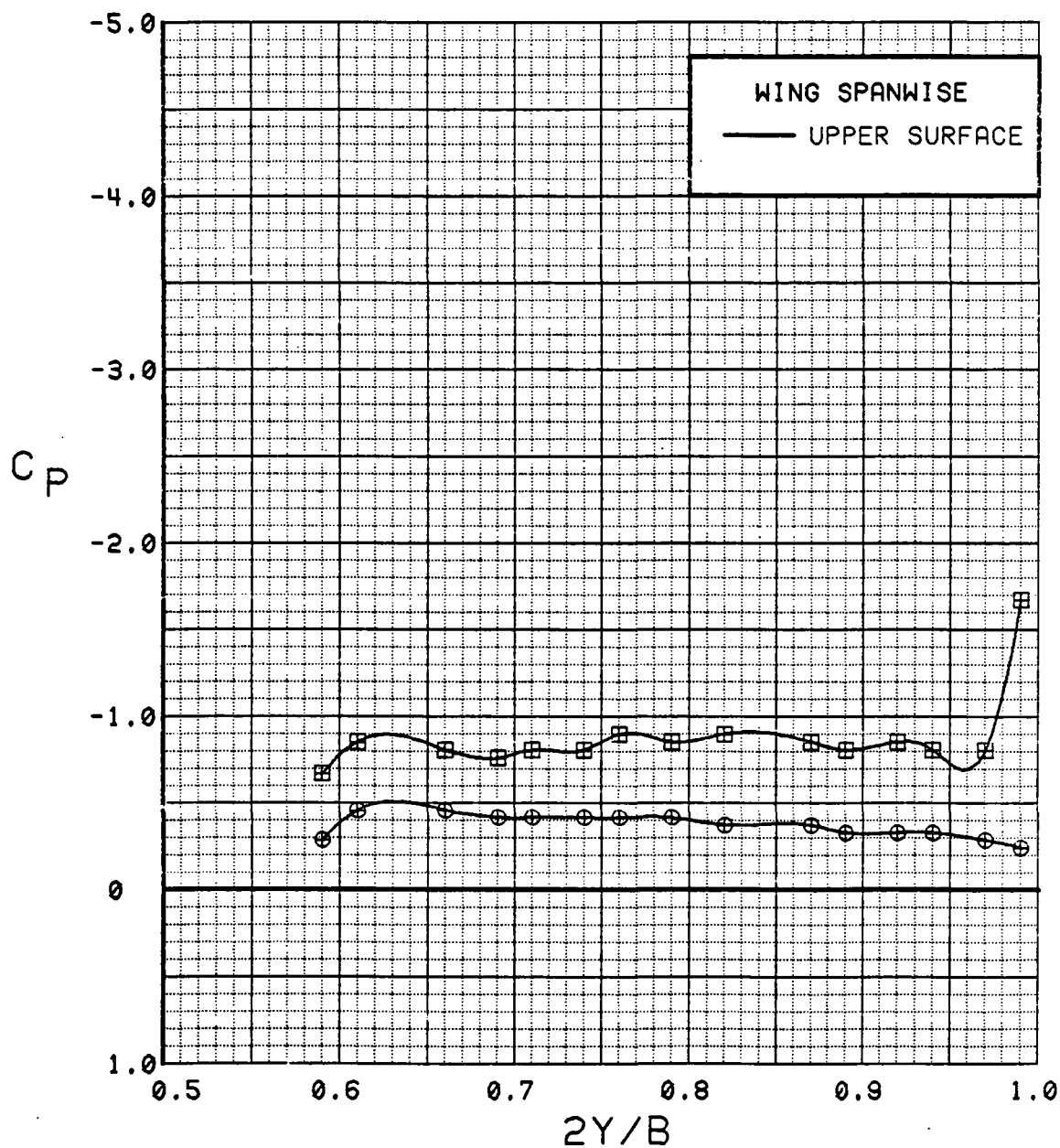


Figure 3.2.2-33 Wing Trailing-Edge Flap Effects, Power On, Spanwise, Alpha = 4 deg

SYM	TEST	RUN	ALPHA	CT	ITEF	OTEF	CAN	SWB
⊕	537	72	8.3	0.92	0	0	OFF	OFF
⊞	537	61	8.5	0.94	30	30	OFF	OFF

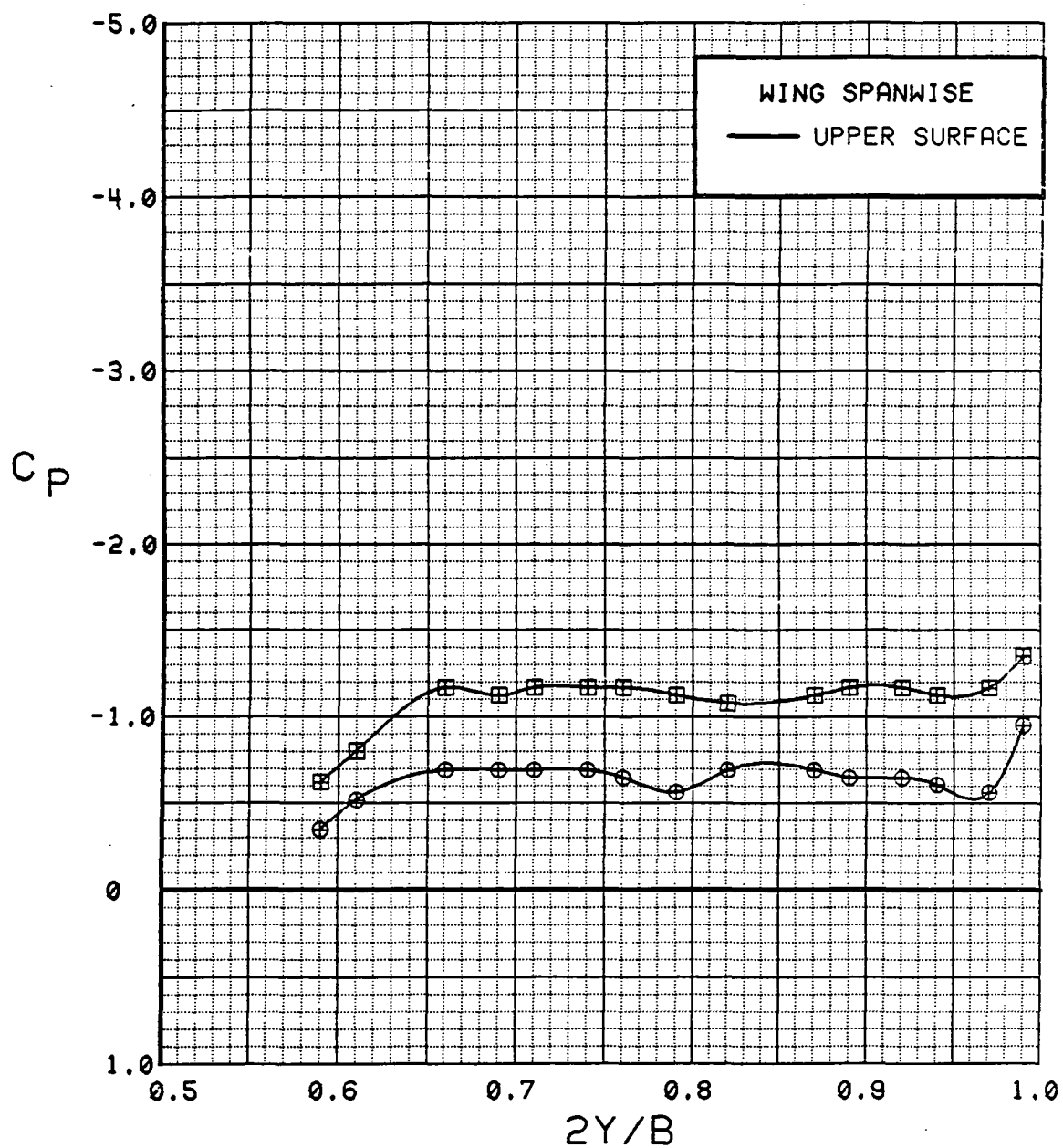


Figure 3.2.2-34 Wing Trailing-Edge Flap Effects, Power On, Spanwise, Alpha = 8 deg

SYM	TEST	RUN	ALPHA	CT	ITEF	OTEF	CAN	SWB
⊗	537	72	12.4	0.91	0	0	OFF	OFF
⊠	537	61	12.6	0.92	30	30	OFF	OFF

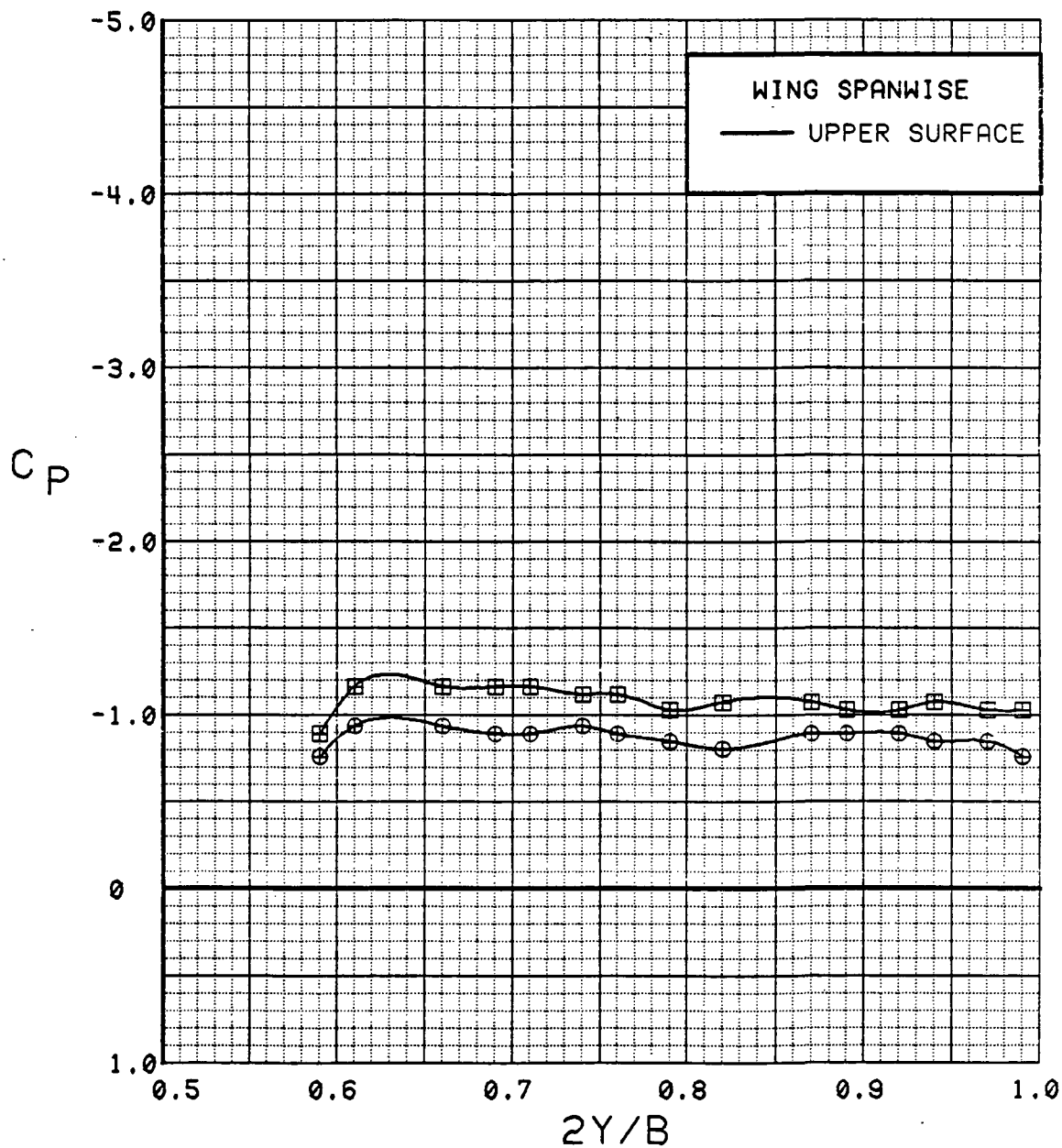


Figure 3.2.2-35 Wing Trailing-Edge Flap Effects, Power On, Spanwise, Alpha = 12 deg

SYM	TEST	RUN	ALPHA	CT	ITEF	OTEF	CAN	SWB
⊕	537	72	16.5	0.91	0	0	OFF	OFF
⊞	537	61	16.7	0.94	30	30	OFF	OFF

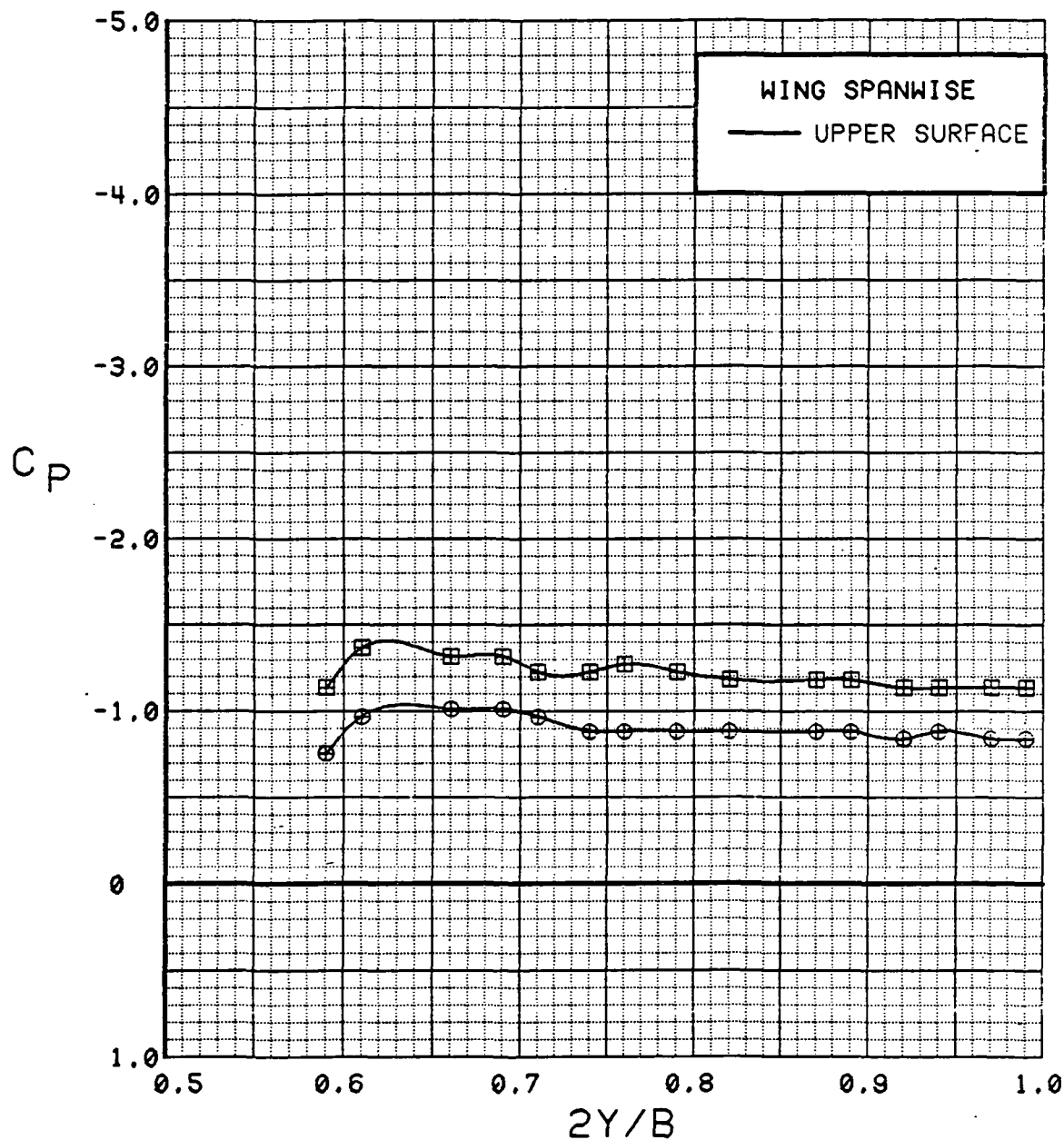


Figure 3.2.2-36 Wing Trailing-Edge Flap Effects, Power On, Spanwise, Alpha = 16 deg



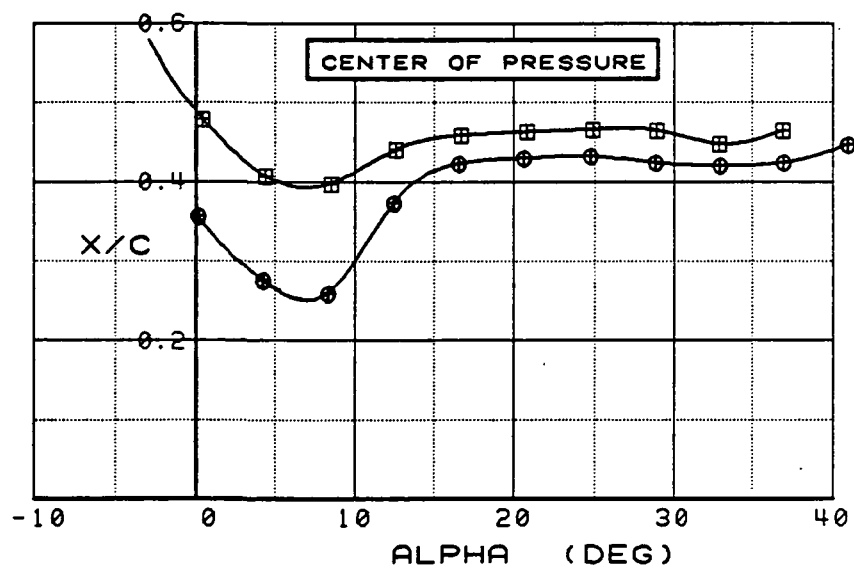
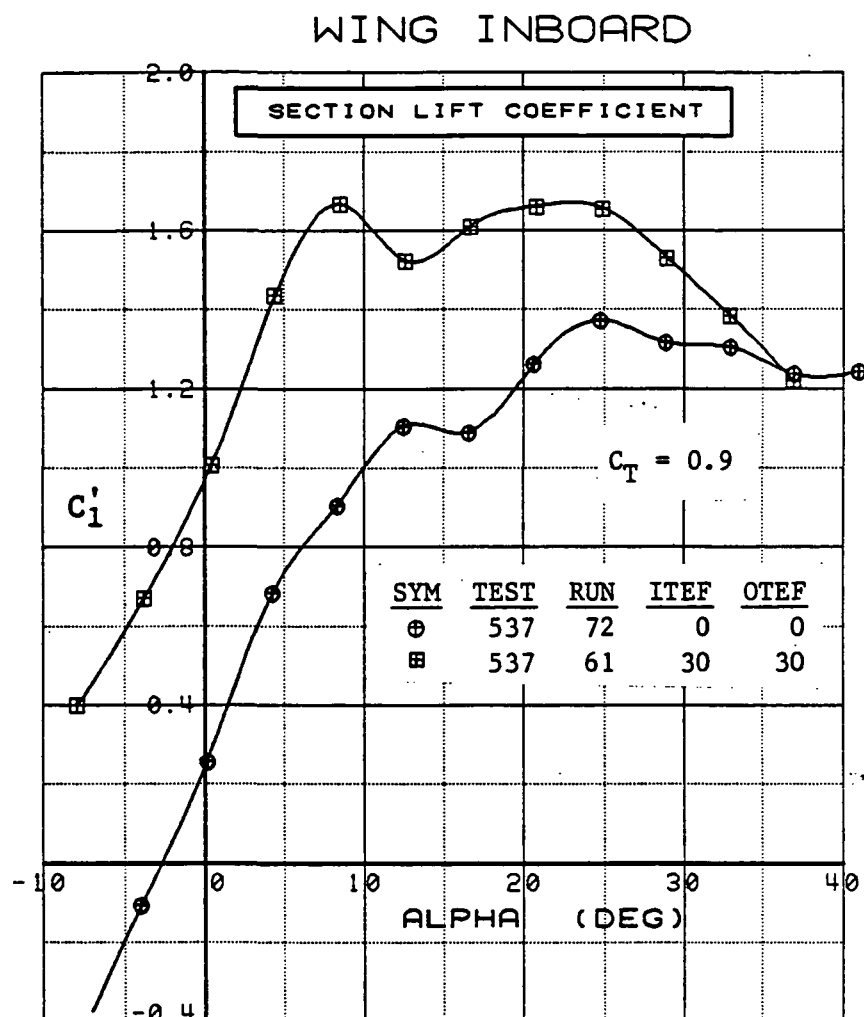


Figure 3.2.2-37 Wing Trailing-Edge Flap Effects, Power On, Inboard, Integrated Section Properties

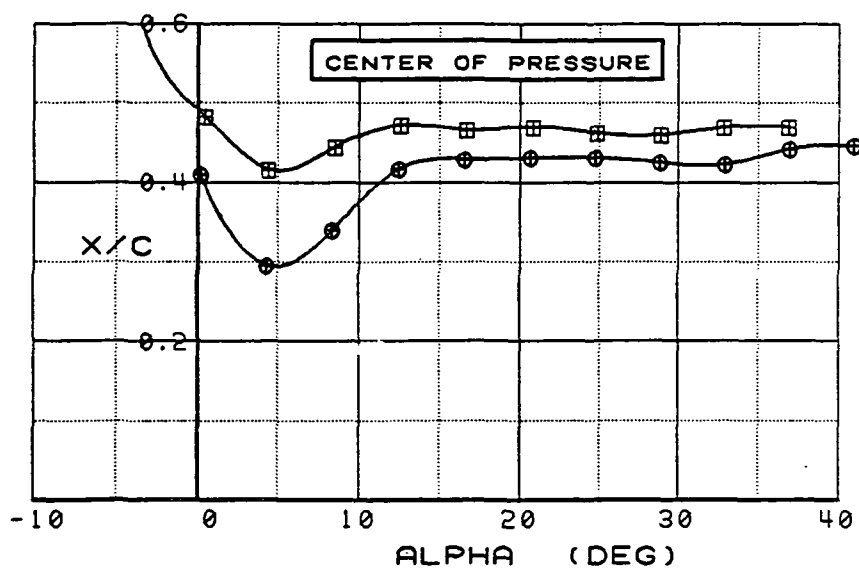
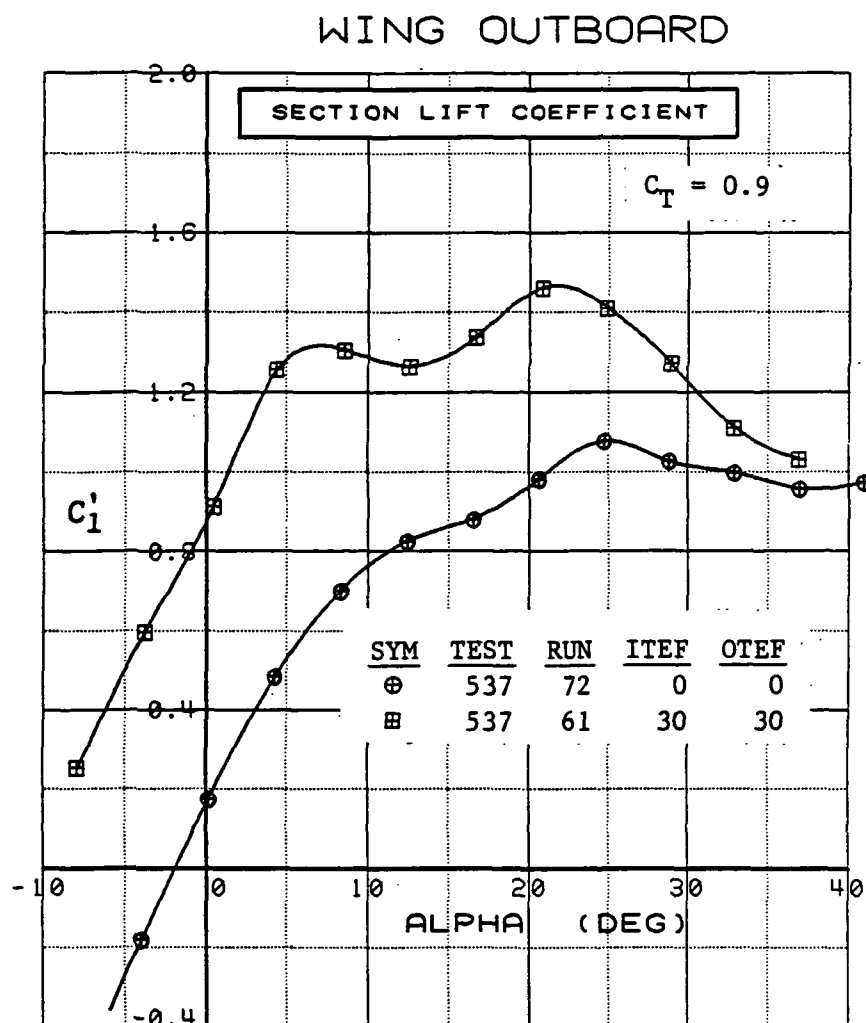


Figure 3.2.2-38 Wing Trailing-Edge Effects, Power On, Outboard, Integrated Section Properties

SYM	TEST	RUN	ALPHA	CT	ITEF	OTEF	CAN	SWB
⊕	537	74	0.1	0.00	0	0	OFF	OFF
⊞	537	76	0.1	0.26	0	0	OFF	OFF
△	537	73	0.1	0.51	0	0	OFF	OFF
◆	537	72	0.1	0.89	0	0	OFF	OFF
*	537	75	0.1	1.31	0	0	OFF	OFF
+	537	71	0.1	1.75	0	0	OFF	OFF

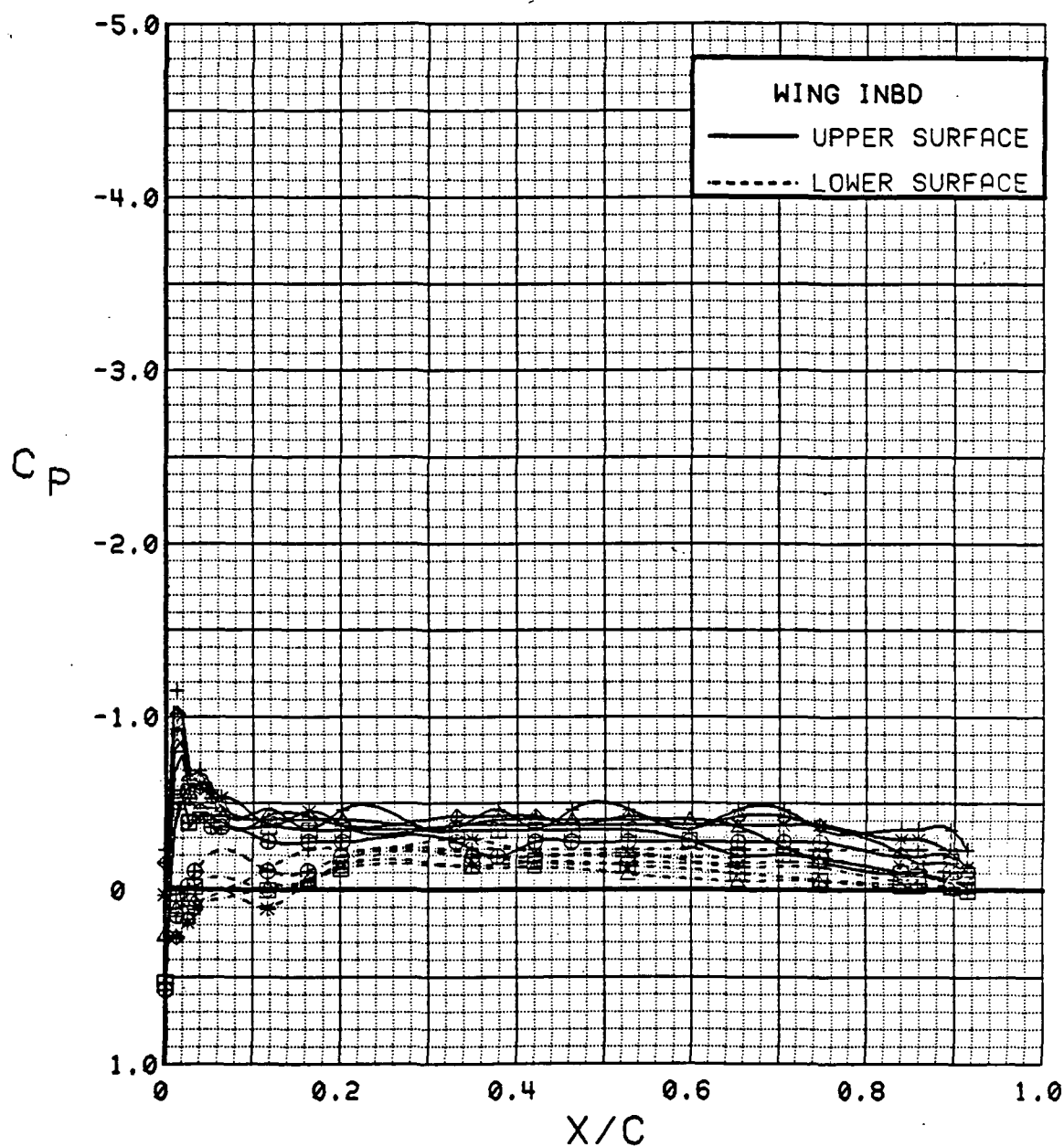


Figure 3.2.2-39 Power Effects, Flaps Neutral, Inboard, Alpha = 0 deg

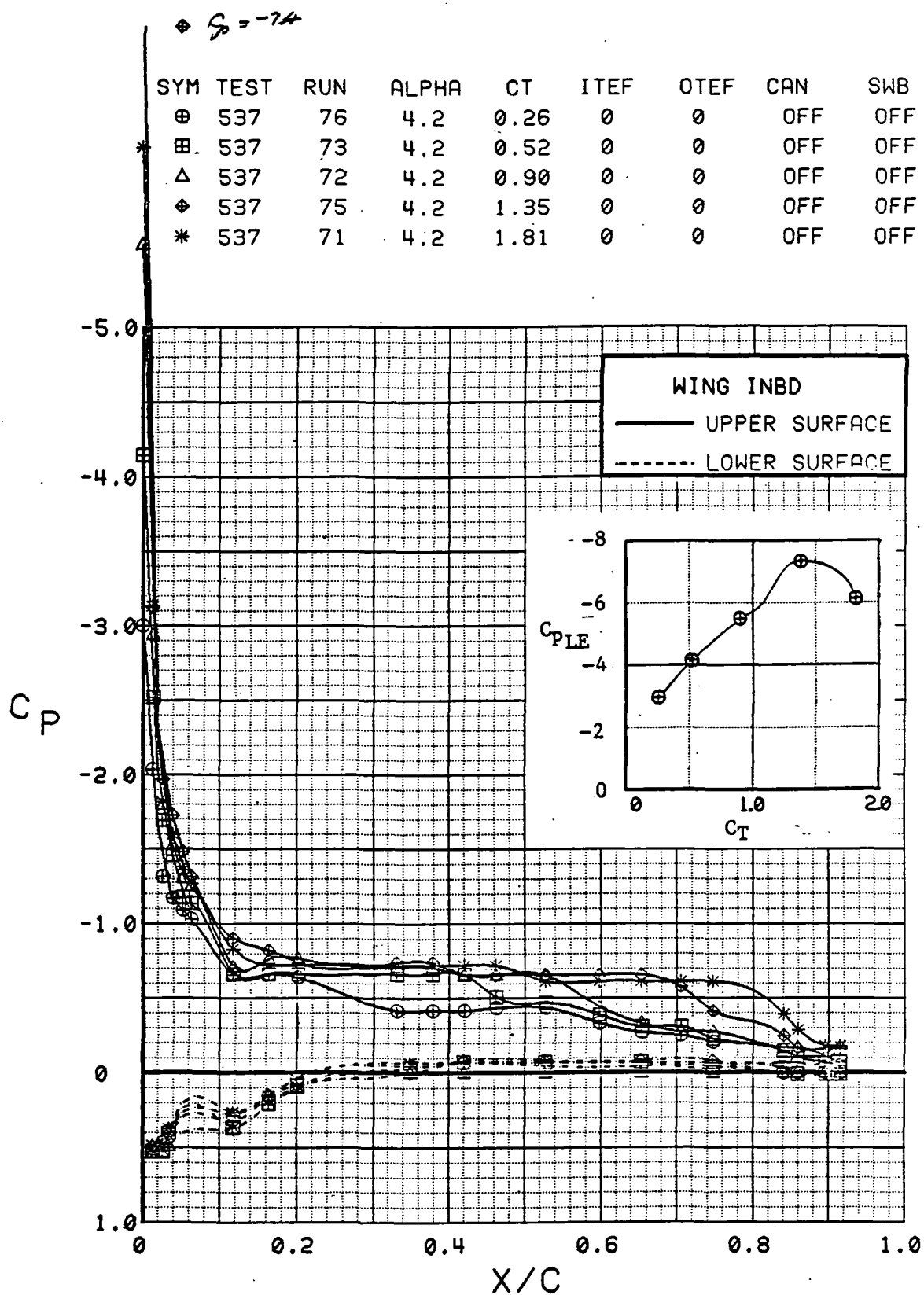


Figure 3.2.2-40 Power Effects, Flaps Neutral, Inboard, Alpha = 4 deg

SYM	TEST	RUN	ALPHA	CT	ITEF	OTEF	CAN	SWB
⊕	537	74	8.3	0.00	0	0	OFF	OFF
⊞	537	76	8.3	0.26	0	0	OFF	OFF
△	537	73	8.3	0.52	0	0	OFF	OFF
⬠	537	72	8.3	0.92	0	0	OFF	OFF
*	537	75	8.3	1.36	0	0	OFF	OFF
+	537	71	8.3	1.84	0	0	OFF	OFF

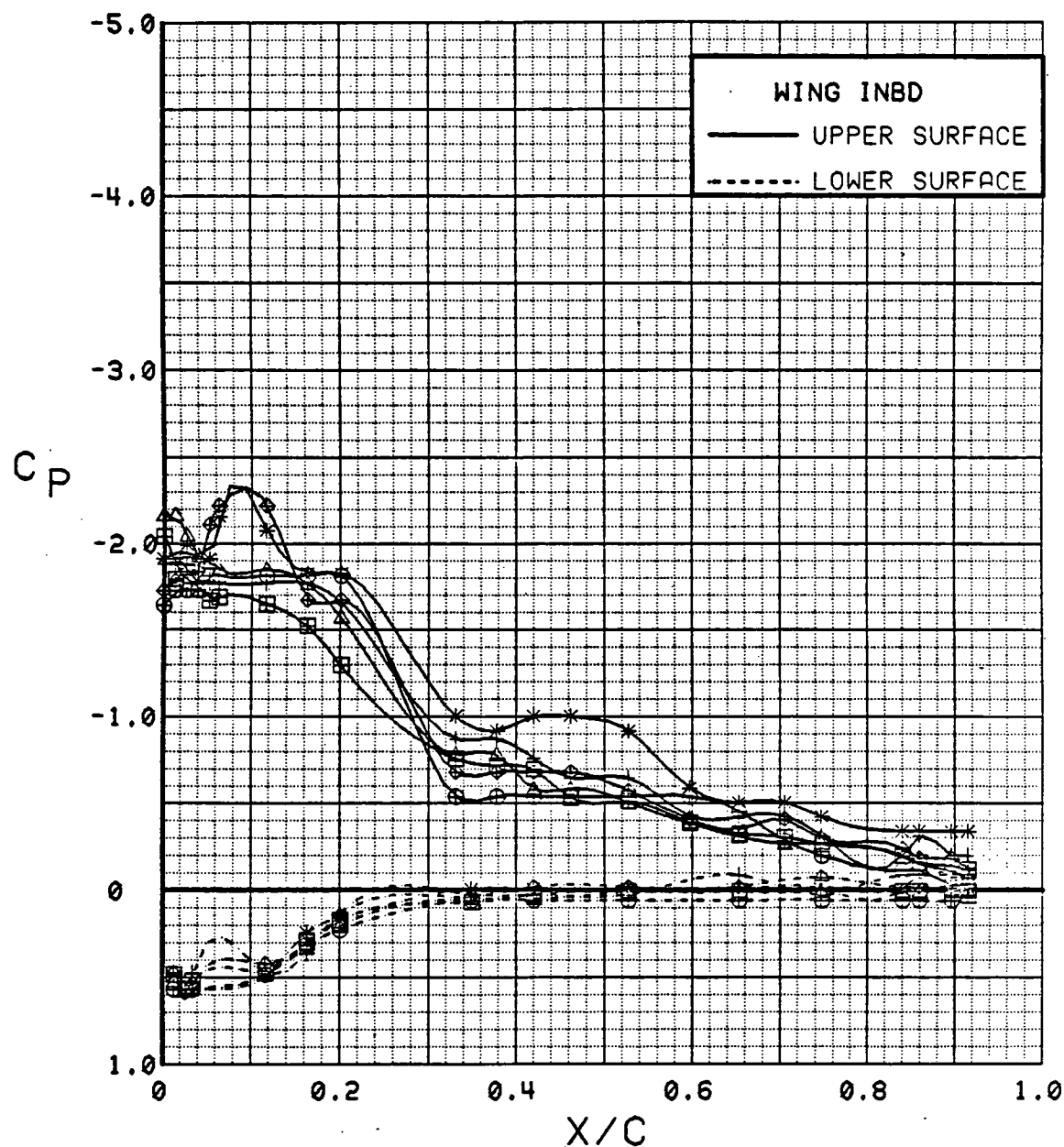


Figure 3.2.2-41 Power Effects, Flaps Neutral, Inboard, Alpha = 8 deg

SYM	TEST	RUN	ALPHA	CT	ITEF	OTEF	CAN	SWB
⊕	537	74	12.4	0.00	0	0	OFF	OFF
⊞	537	76	12.4	0.26	0	0	OFF	OFF
△	537	73	12.4	0.52	0	0	OFF	OFF
⬠	537	72	12.4	0.91	0	0	OFF	OFF
*	537	75	12.5	1.35	0	0	OFF	OFF
+	537	71	12.5	1.85	0	0	OFF	OFF

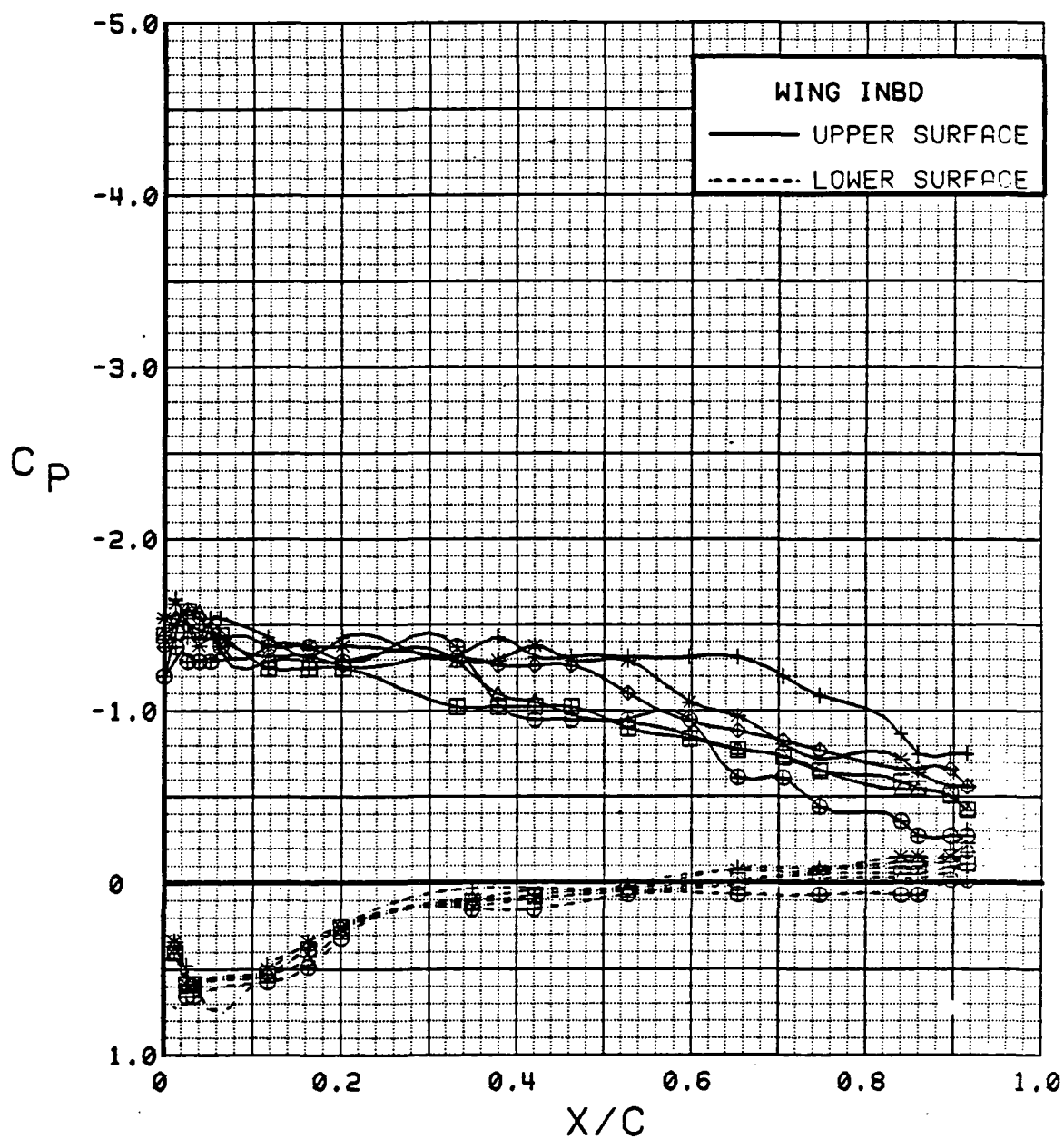


Figure 3.2.2-42 Power Effects, Flaps Neutral, Inboard, Alpha = 12 deg

SYM	TEST	RUN	ALPHA	CT	ITEF	OTEF	CAN	SWB
⊕	537	74	16.5	0.00	0	0	OFF	OFF
⊞	537	76	16.5	0.26	0	0	OFF	OFF
△	537	73	16.5	0.52	0	0	OFF	OFF
⊕	537	72	16.5	0.91	0	0	OFF	OFF
*	537	75	16.6	1.34	0	0	OFF	OFF
+	537	71	16.6	1.82	0	0	OFF	OFF

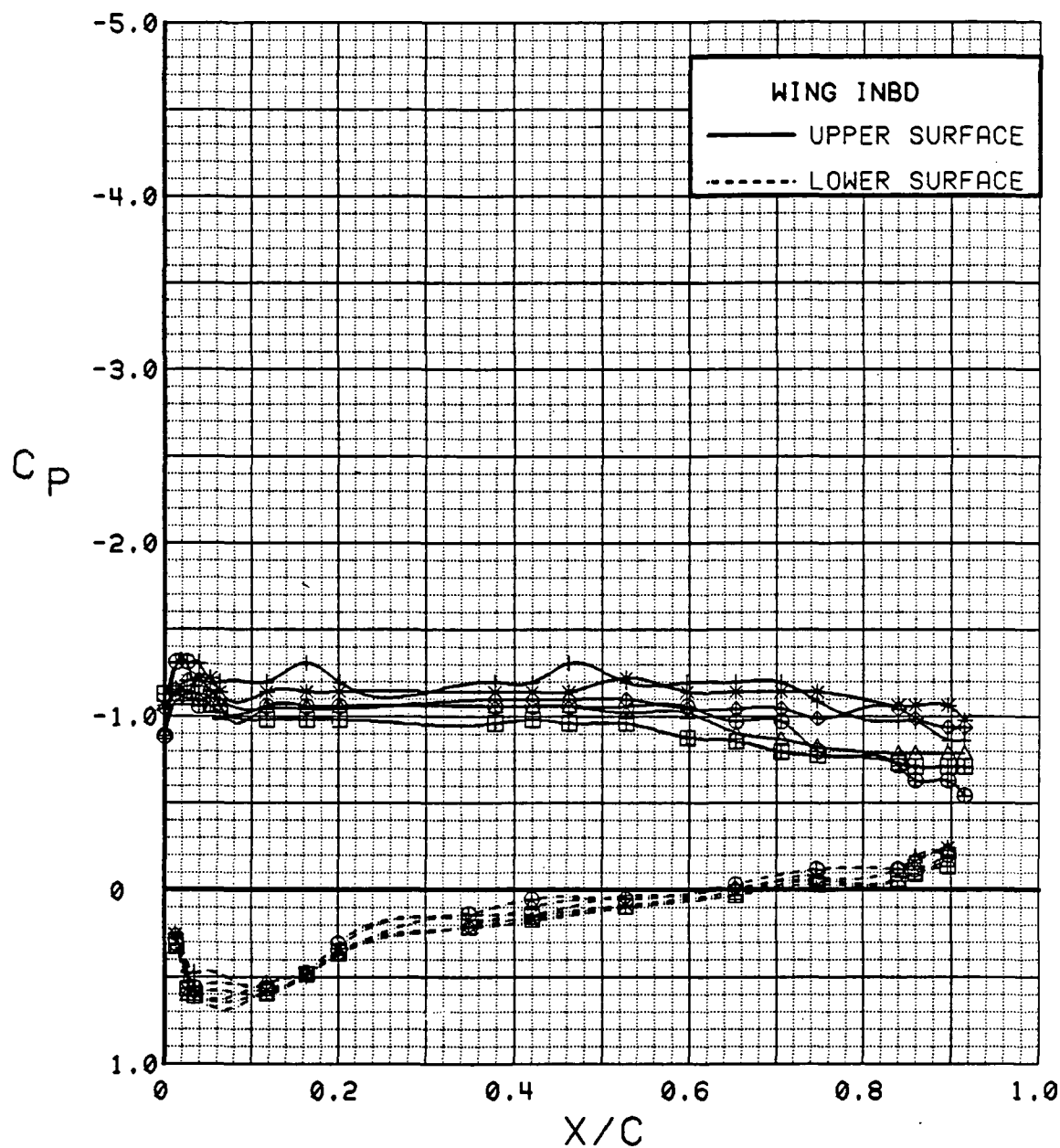


Figure 3.2.2-43 Power Effects, Flaps Neutral, Inboard, Alpha = 16 deg

SYM	TEST	RUN	ALPHA	CT	ITEF	OTEF	CAN	SWB
⊕	537	74	20.5	0.00	0	0	OFF	OFF
⊞	537	76	20.6	0.26	0	0	OFF	OFF
△	537	73	20.6	0.52	0	0	OFF	OFF
⬠	537	72	20.6	0.93	0	0	OFF	OFF
*	537	75	20.7	1.37	0	0	OFF	OFF
+	537	71	20.7	1.93	0	0	OFF	OFF

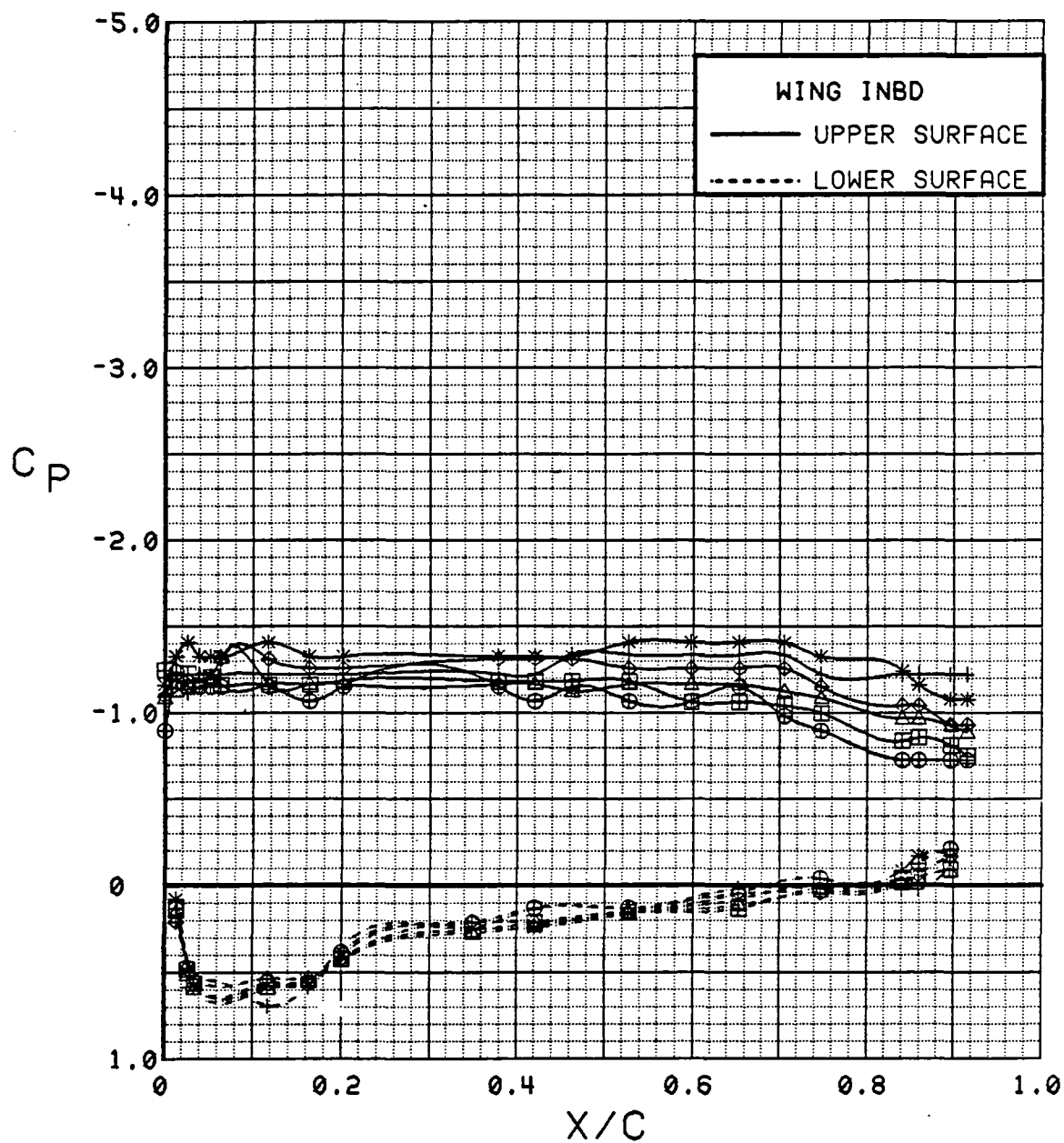


Figure 3.2.2-44 Power Effects, Flaps Neutral, Inboard, Alpha = 20 deg



SYM	TEST	RUN	ALPHA	CT	ITEF	OTEF	CAN	SWB
⊕	537	74	24.6	0.00	0	0	OFF	OFF
⊞	537	76	24.7	0.26	0	0	OFF	OFF
△	537	73	24.7	0.52	0	0	OFF	OFF
⬠	537	72	24.7	0.91	0	0	OFF	OFF
*	537	75	24.8	1.36	0	0	OFF	OFF
+	537	71	24.8	1.79	0	0	OFF	OFF

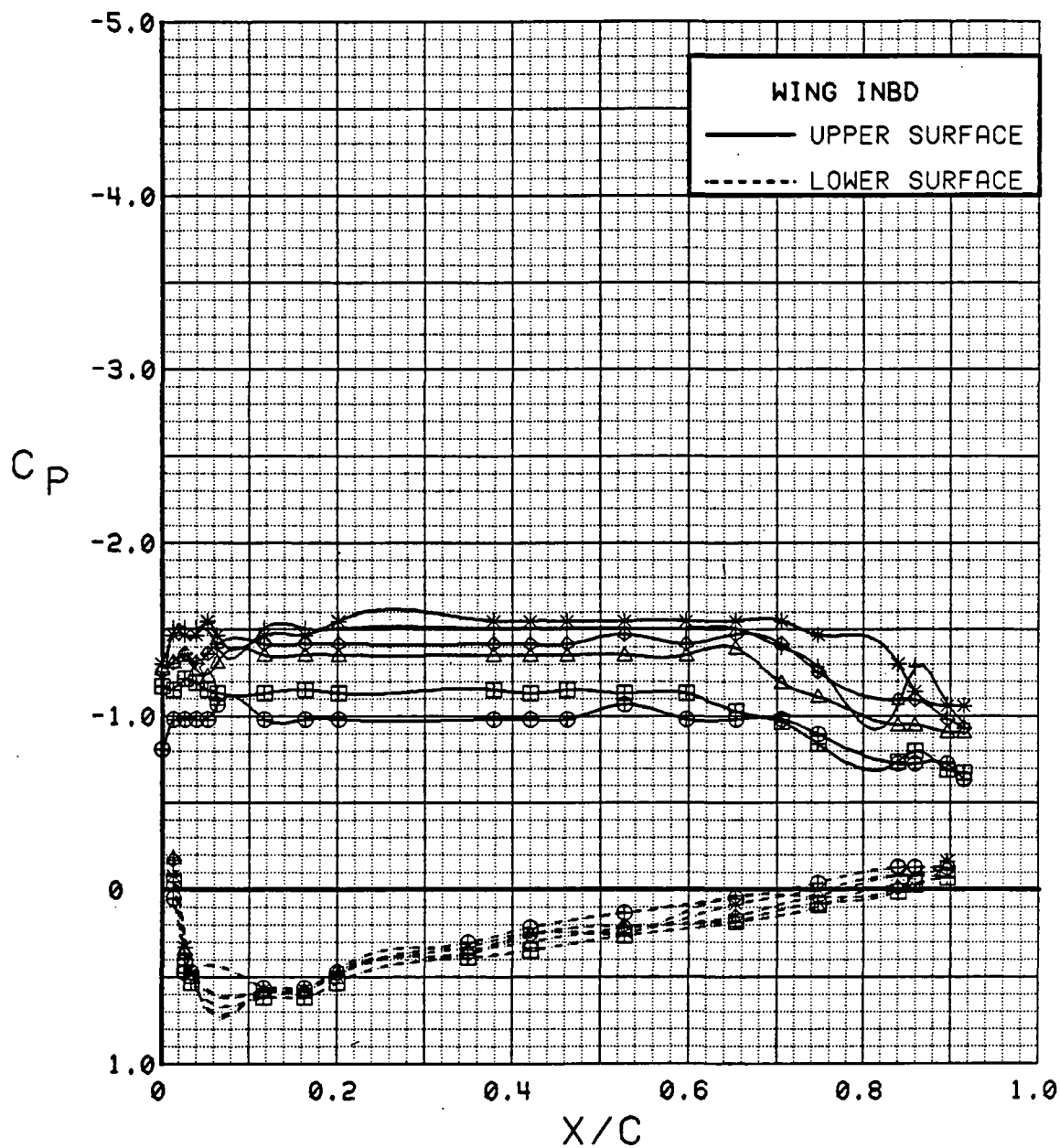


Figure 3.2.2-45 Power Effects, Flaps Neutral, Inboard, Alpha = 24 deg

SYM	TEST	RUN	ALPHA	CT	ITEF	OTEF	CAN	SWB
⊕	537	74	28.6	0.00	0	0	OFF	OFF
⊞	537	76	28.7	0.26	0	0	OFF	OFF
△	537	73	28.8	0.51	0	0	OFF	OFF
⊕	537	72	28.8	0.91	0	0	OFF	OFF
*	537	75	28.9	1.29	0	0	OFF	OFF
+	537	71	28.9	1.81	0	0	OFF	OFF

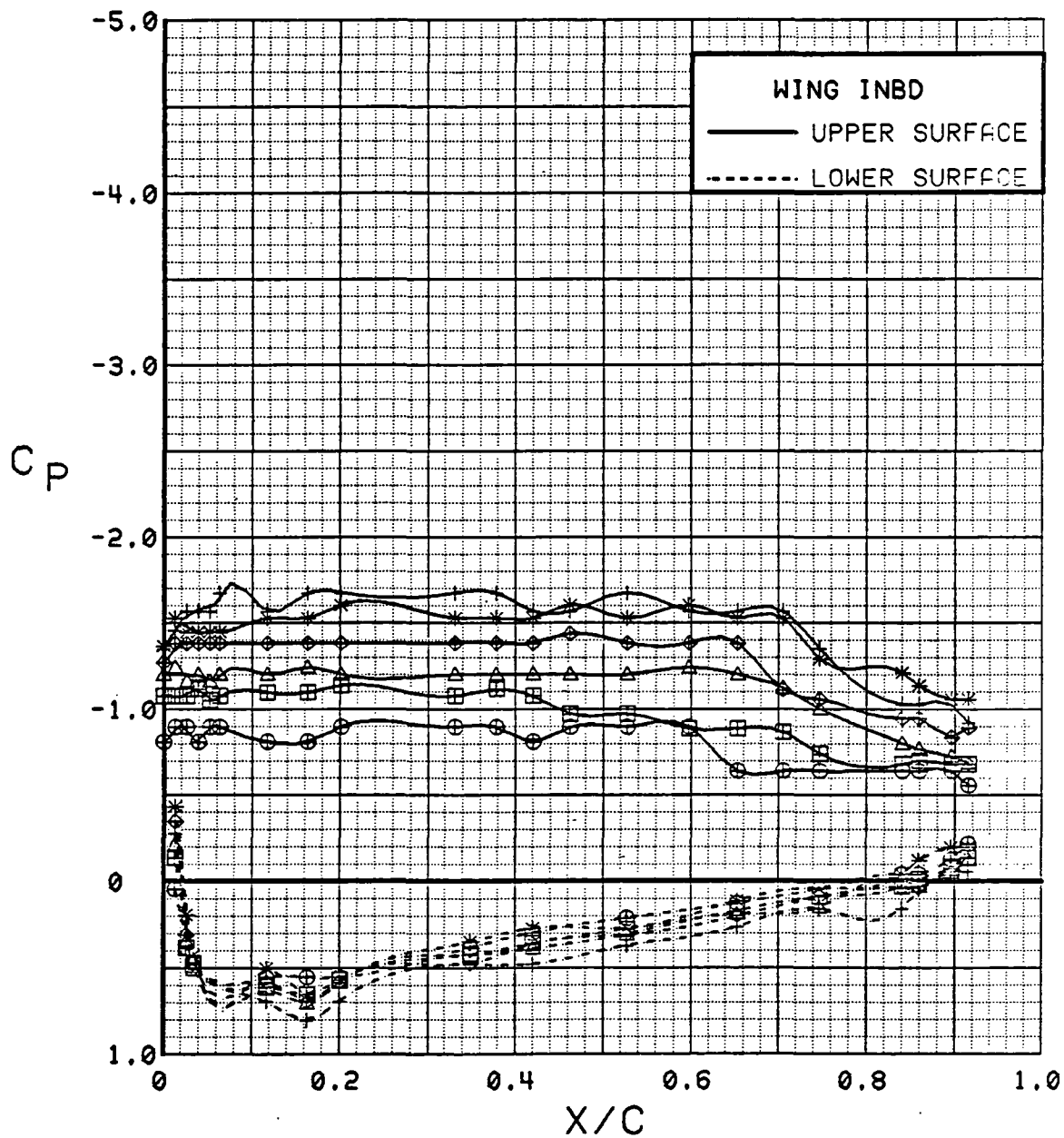


Figure 3.2.2-46 Power Effects, Flaps Neutral, Inboard, Alpha = 28 deg

SYM	TEST	RUN	ALPHA	CT	ITEF	OTEF	CAN	SWB
⊕	537	74	32.6	0.00	0	0	OFF	OFF
⊞	537	76	32.7	0.26	0	0	OFF	OFF
△	537	72	32.9	0.92	0	0	OFF	OFF
◆	537	75	32.9	1.32	0	0	OFF	OFF
*	537	71	33.0	1.82	0	0	OFF	OFF

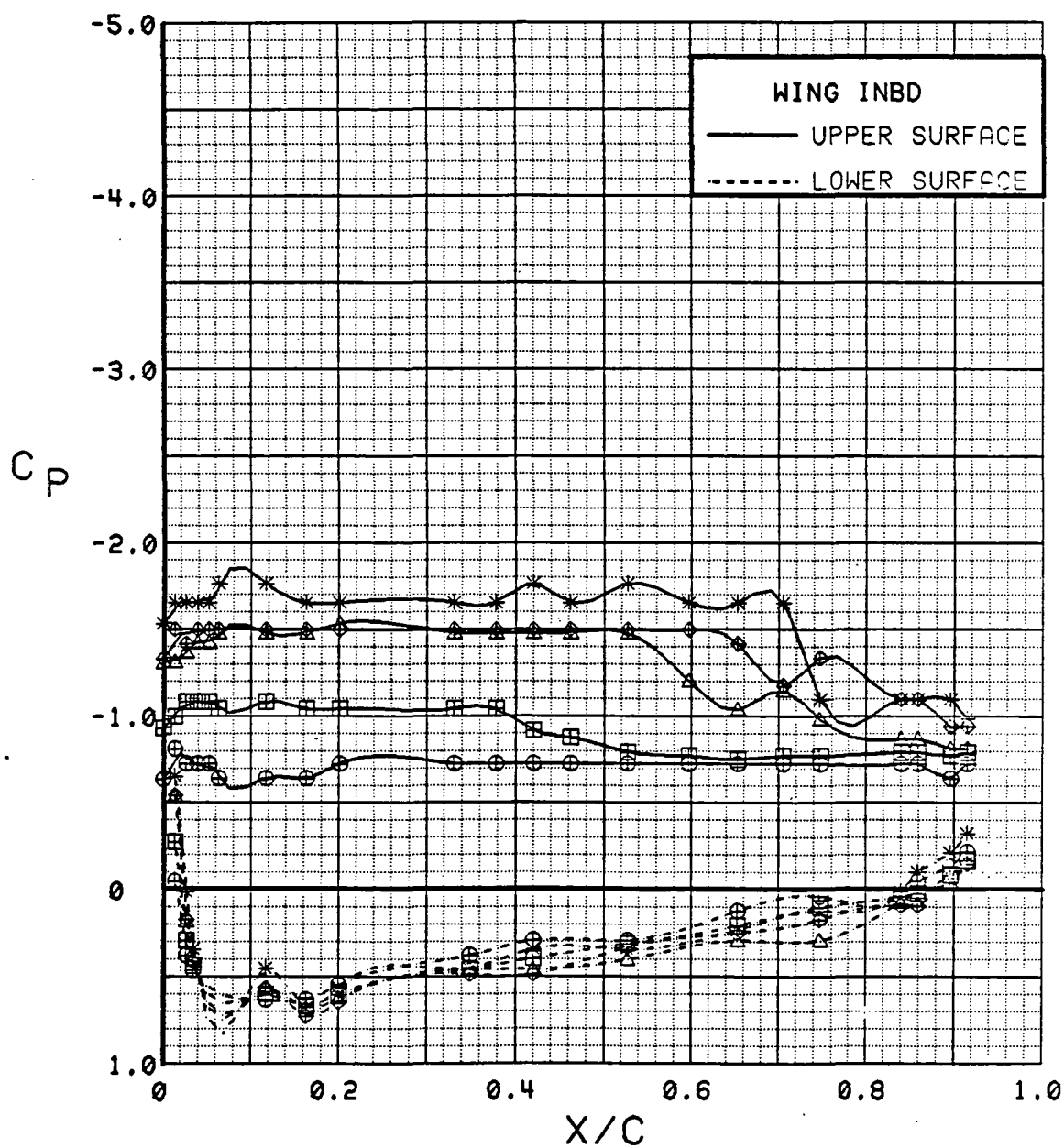


Figure 3.2.2-47 Power Effects, Flaps Neutral, Inboard, Alpha = 32 deg

SYM	TEST	RUN	ALPHA	CT	ITEF	OTEF	CAN	SWB
⊕	537	74	0.1	0.00	0	0	OFF	OFF
⊞	537	76	0.1	0.26	0	0	OFF	OFF
△	537	73	0.1	0.51	0	0	OFF	OFF
◆	537	72	0.1	0.89	0	0	OFF	OFF
*	537	75	0.1	1.31	0	0	OFF	OFF
+	537	71	0.1	1.75	0	0	OFF	OFF

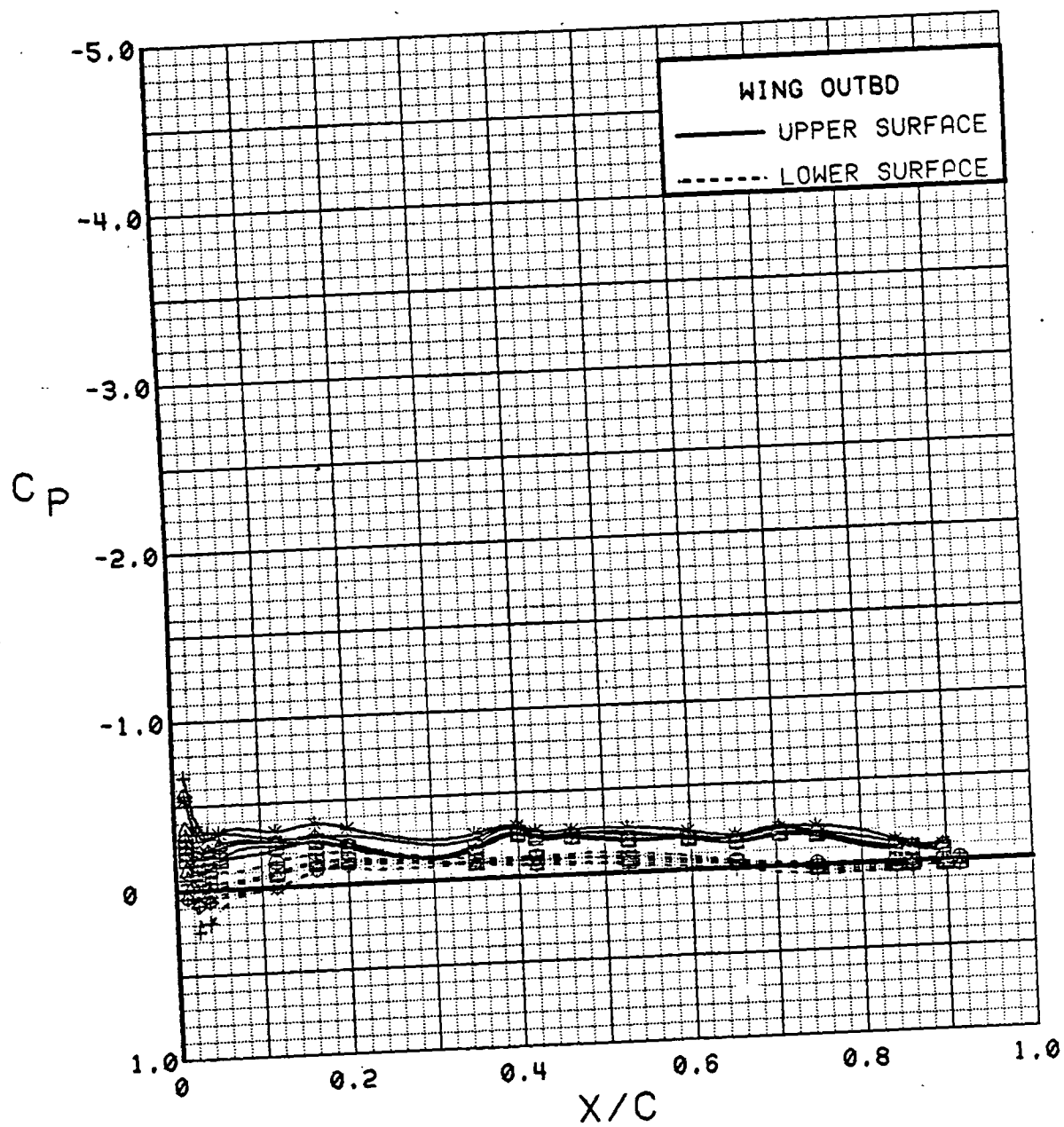


Figure 3.2.2-48 Power Effects, Flaps Neutral, Outboard, Alpha = 0 deg

SYM	TEST	RUN	ALPHA	CT	ITEF	OTEF	CAN	SWB
⊕	537	76	4.2	0.26	0	0	OFF	OFF
⊞	537	73	4.2	0.52	0	0	OFF	OFF
△	537	72	4.2	0.90	0	0	OFF	OFF
◆	537	75	4.2	1.35	0	0	OFF	CFF
*	537	71	4.2	1.81	0	0	OFF	OFF

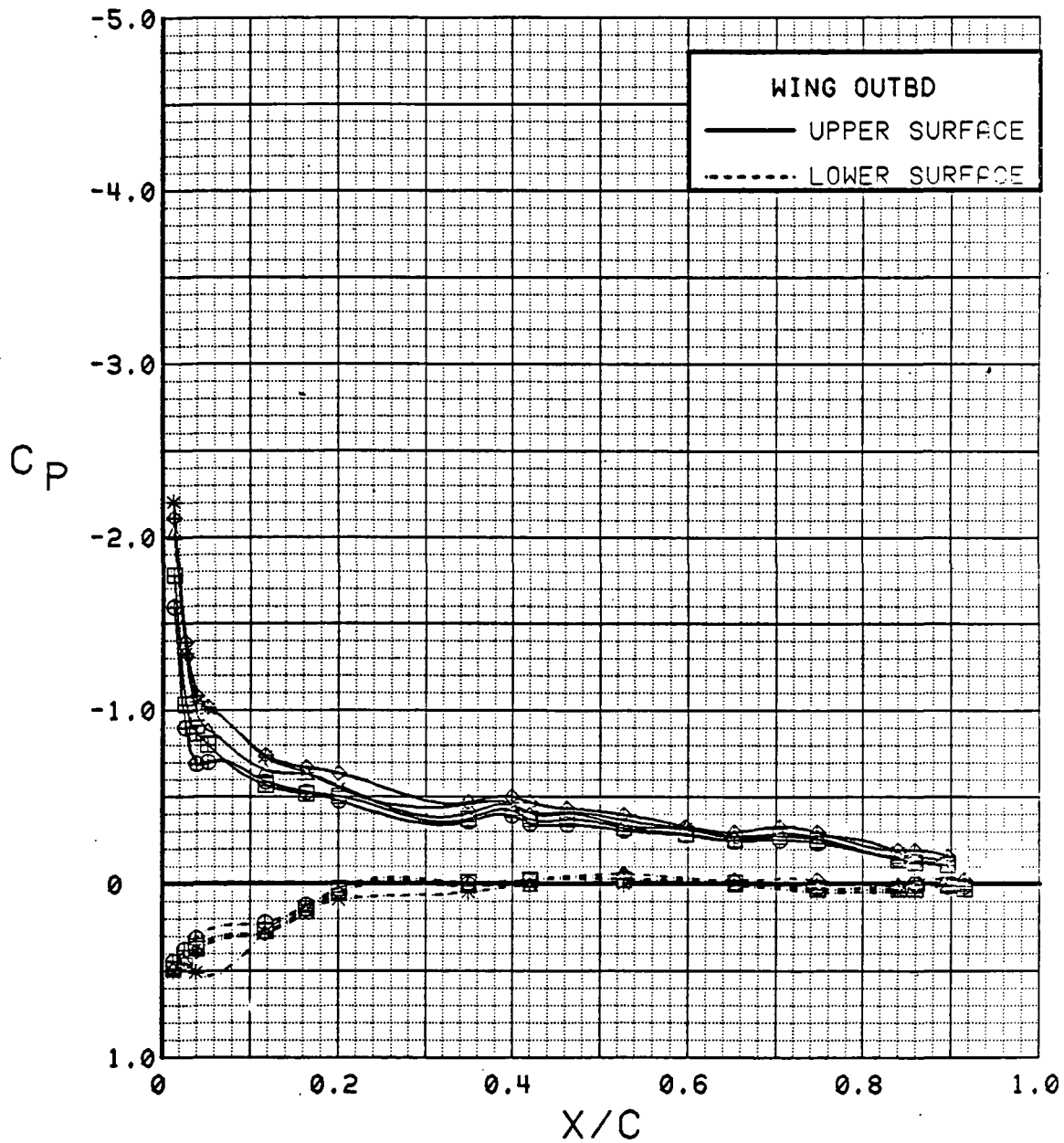


Figure 3.2.2-49 Power Effects, Flaps Neutral, Outboard, Alpha = 4 deg

SYM	TEST	RUN	ALPHA	CT	ITEF	OTEF	CAN	SWB
⊕	537	74	8.3	0.00	0	0	OFF	OFF
⊞	537	76	8.3	0.26	0	0	OFF	OFF
△	537	73	8.3	0.52	0	0	OFF	OFF
⊕	537	72	8.3	0.92	0	0	OFF	OFF
*	537	75	8.3	1.36	0	0	OFF	OFF
+	537	71	8.3	1.84	0	0	OFF	OFF

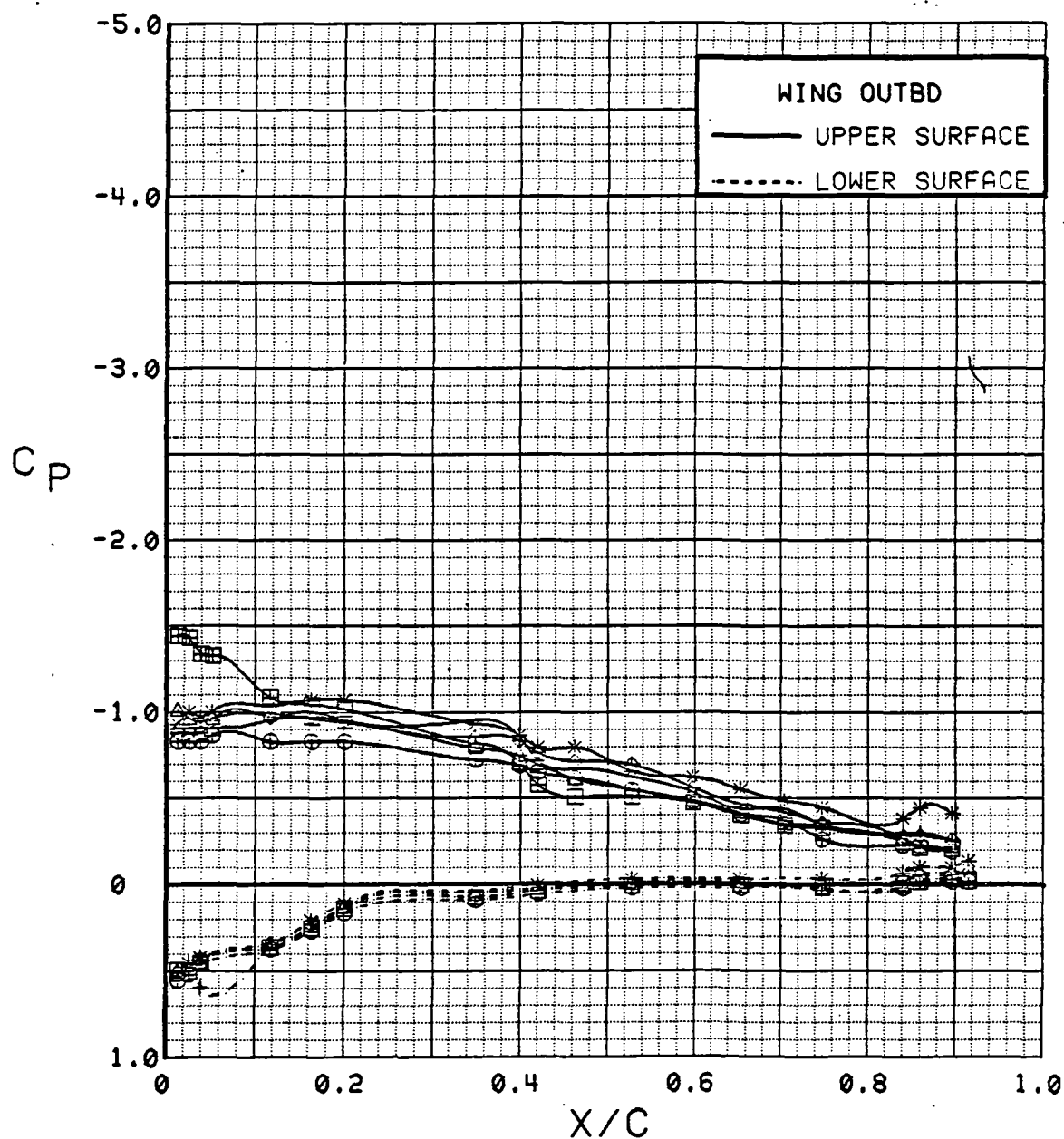


Figure 3.2.2-50 Power Effects, Flaps Neutral, Outboard, Alpha = 8 deg

SYM	TEST	RUN	ALPHA	CT	ITEF	OTEF	CAN	SWB
⊕	537	74	12.4	0.00	0	0	OFF	OFF
⊞	537	76	12.4	0.26	0	0	OFF	OFF
△	537	73	12.4	0.52	0	0	OFF	OFF
⊕	537	72	12.4	0.91	0	0	OFF	OFF
*	537	75	12.5	1.35	0	0	OFF	OFF
+	537	71	12.5	1.85	0	0	OFF	OFF

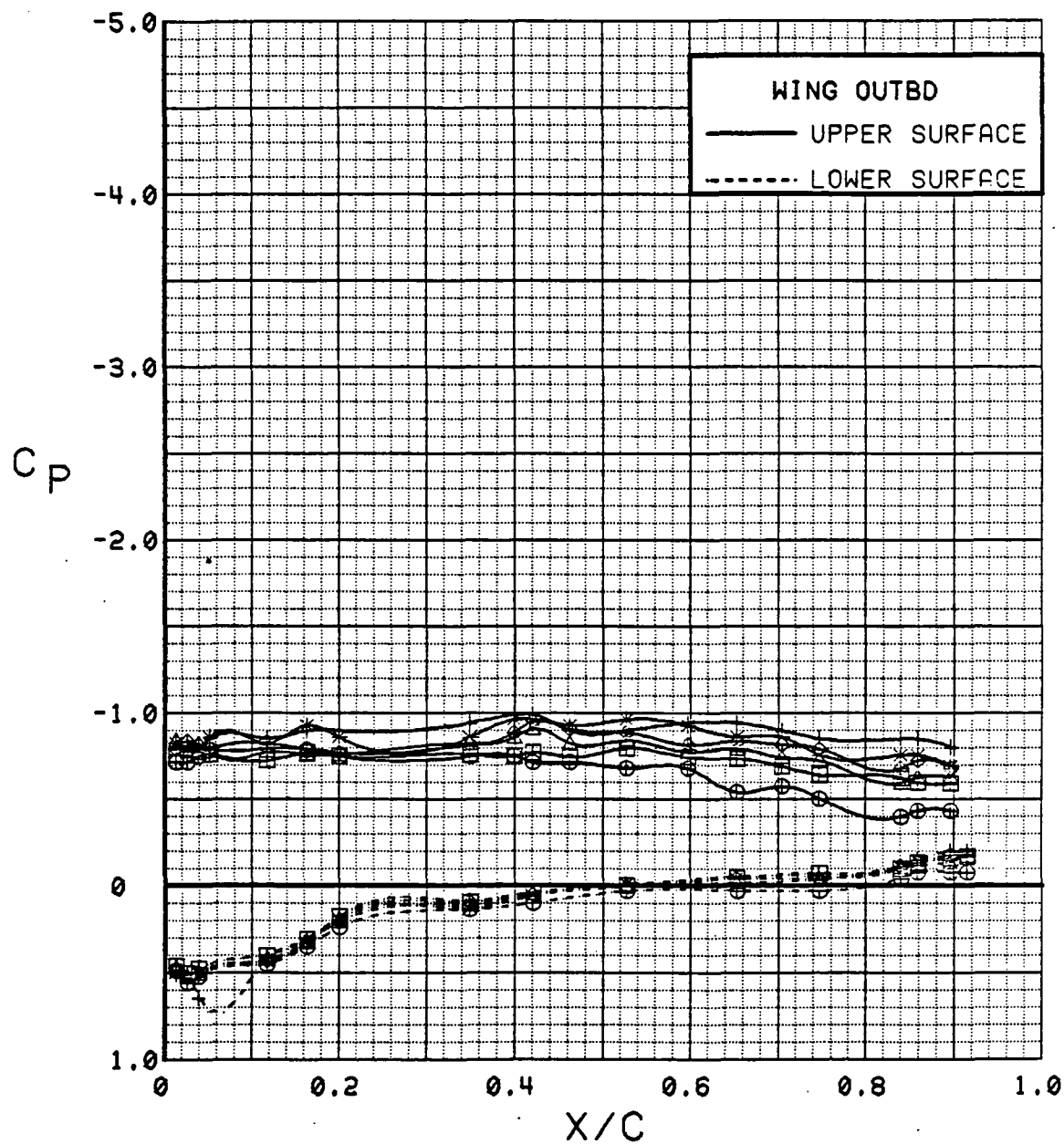


Figure 3.2.2-51 Power Effects, Flaps Neutral, Outboard, Alpha = 12 deg

SYM	TEST	RUN	ALPHA	CT	ITEF	OTEF	CAN	SWB
⊕	537	74	16.5	0.00	0	0	OFF	OFF
⊞	537	76	16.5	0.26	0	0	OFF	OFF
△	537	73	16.5	0.52	0	0	OFF	OFF
⬠	537	72	16.5	0.91	0	0	OFF	OFF
*	537	75	16.6	1.34	0	0	OFF	OFF
+	537	71	16.6	1.82	0	0	OFF	OFF

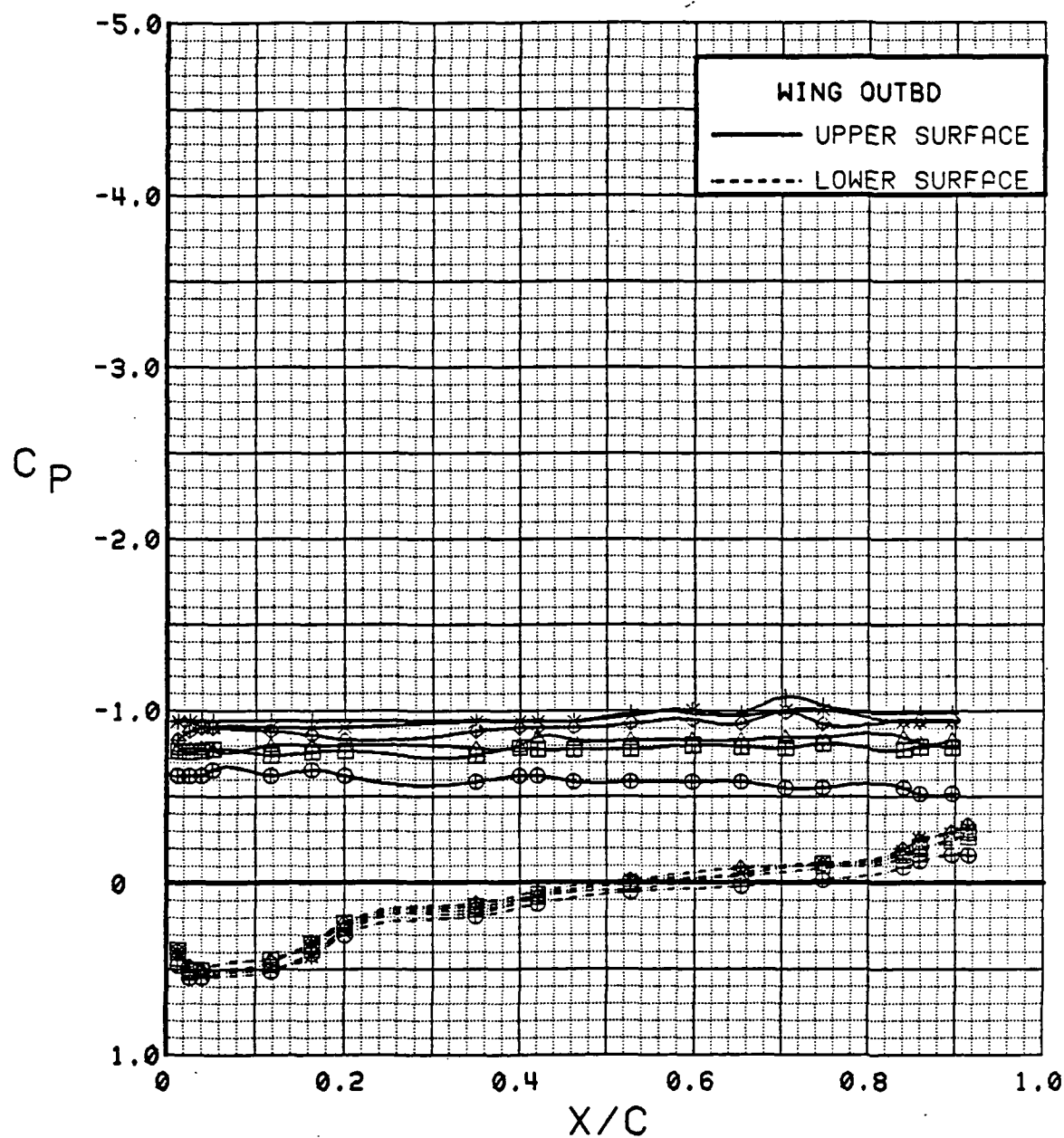


Figure 3.2.2-52 Power Effects, Flaps Neutral, Outboard, Alpha = 16 deg



SYM	TEST	RUN	ALPHA	CT	ITEF	OTEF	CAN	SWB
⊕	537	74	20.5	0.00	0	0	OFF	OFF
⊞	537	76	20.6	0.26	0	0	OFF	OFF
△	537	73	20.6	0.52	0	0	OFF	OFF
⬠	537	72	20.6	0.93	0	0	OFF	OFF
*	537	75	20.7	1.37	0	0	OFF	OFF
+	537	71	20.7	1.93	0	0	OFF	OFF

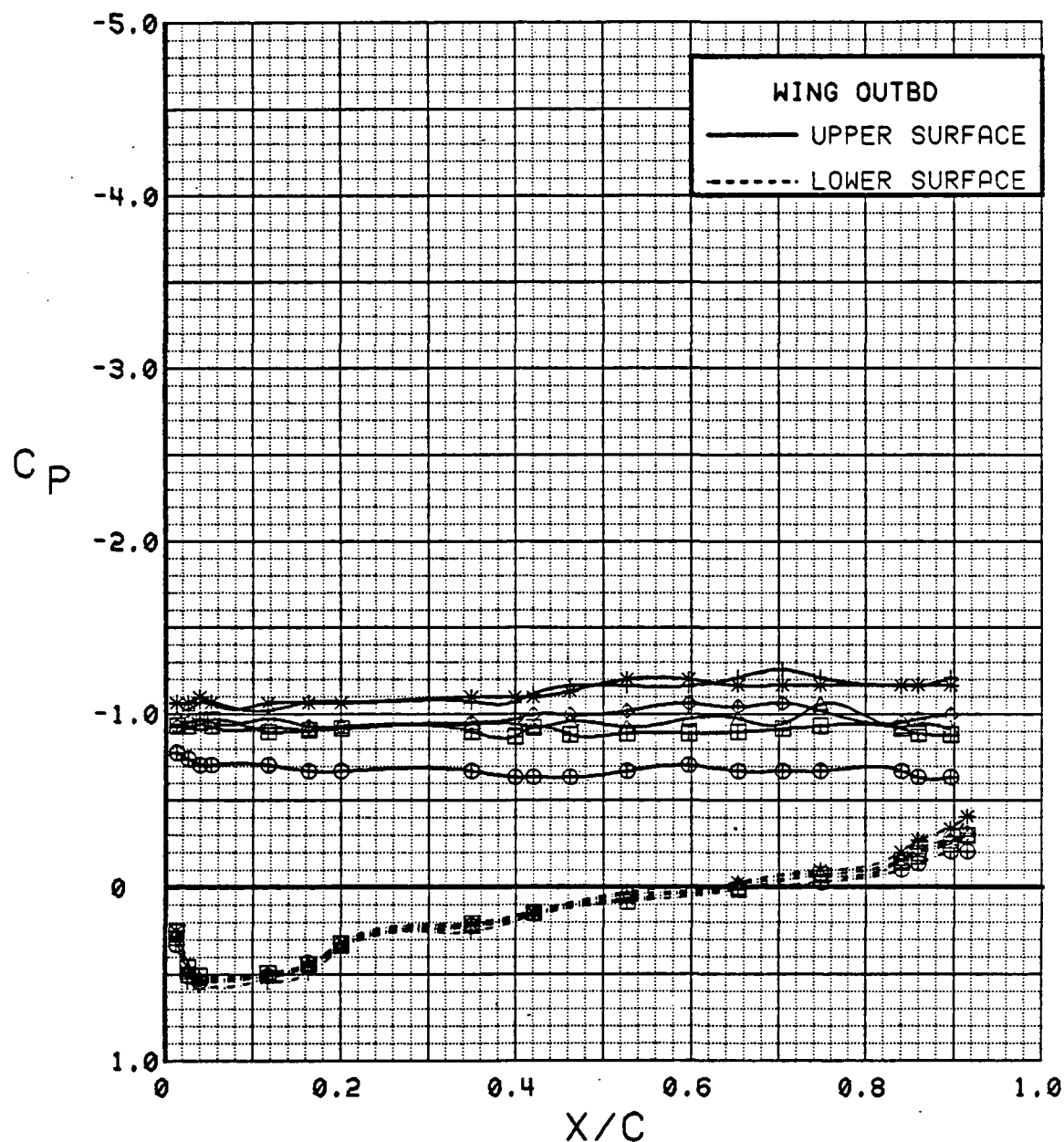


Figure 3.2.2-53 Power Effects, Flaps Neutral, Outboard, Alpha = 20 deg

SYM	TEST	RUN	ALPHA	CT	ITEF	OTEF	CAN	SWB
⊕	537	74	24.6	0.00	0	0	OFF	OFF
⊞	537	76	24.7	0.26	0	0	OFF	OFF
△	537	73	24.7	0.52	0	0	OFF	OFF
⊕	537	72	24.7	0.91	0	0	OFF	OFF
*	537	75	24.8	1.36	0	0	OFF	OFF
+	537	71	24.8	1.79	0	0	OFF	OFF

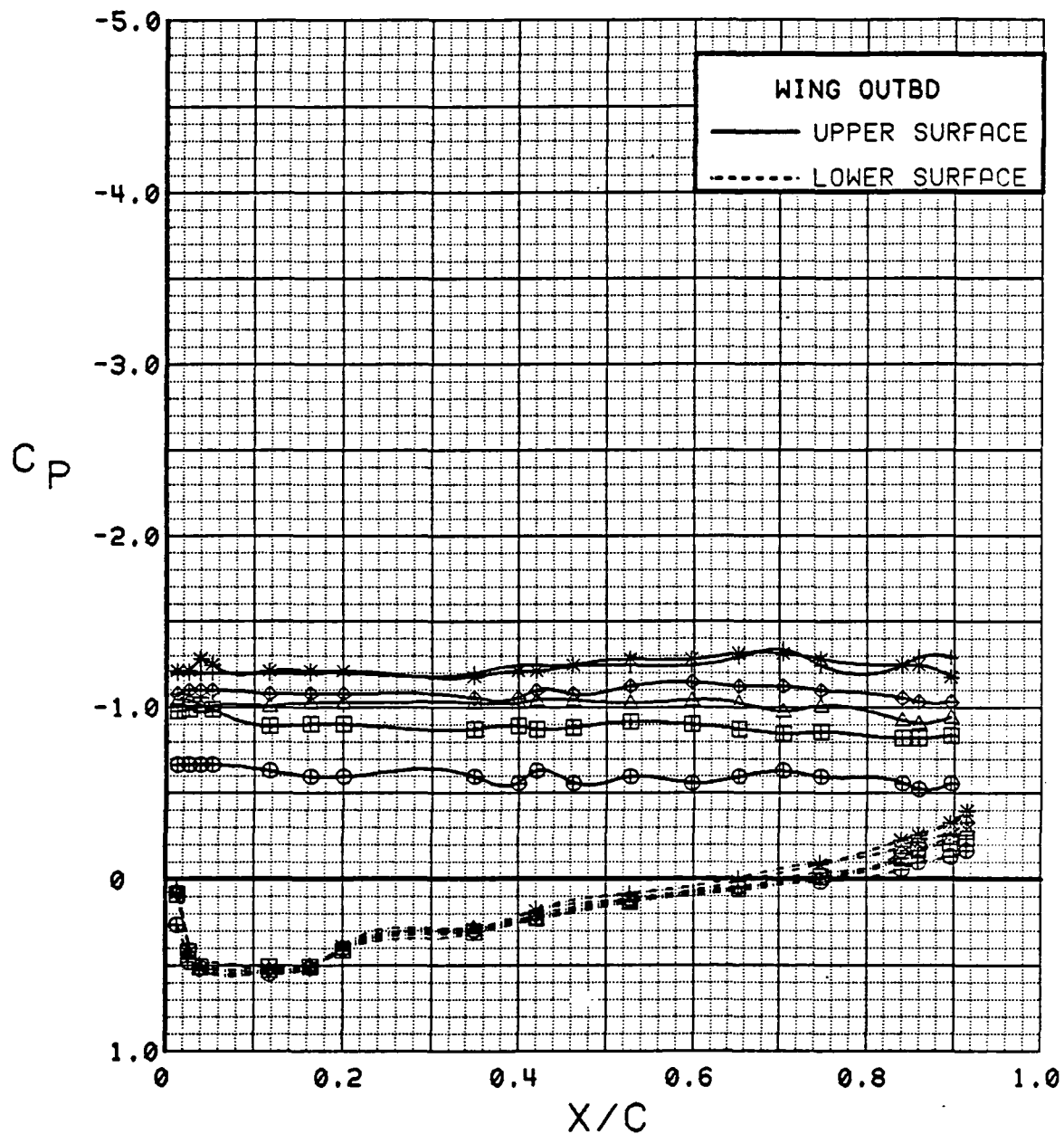


Figure 3.2.2-54 Power Effects, Flaps Neutral, Outboard, Alpha = 24 deg

SYM	TEST	RUN	ALPHA	CT	ITEF	OTEF	CAN	SWB
⊕	537	74	28.6	0.00	0	0	OFF	OFF
⊞	537	76	28.7	0.26	0	0	OFF	OFF
△	537	73	28.8	0.51	0	0	OFF	OFF
◆	537	72	28.8	0.91	0	0	OFF	OFF
*	537	75	28.9	1.29	0	0	OFF	OFF
+	537	71	28.9	1.81	0	0	OFF	OFF

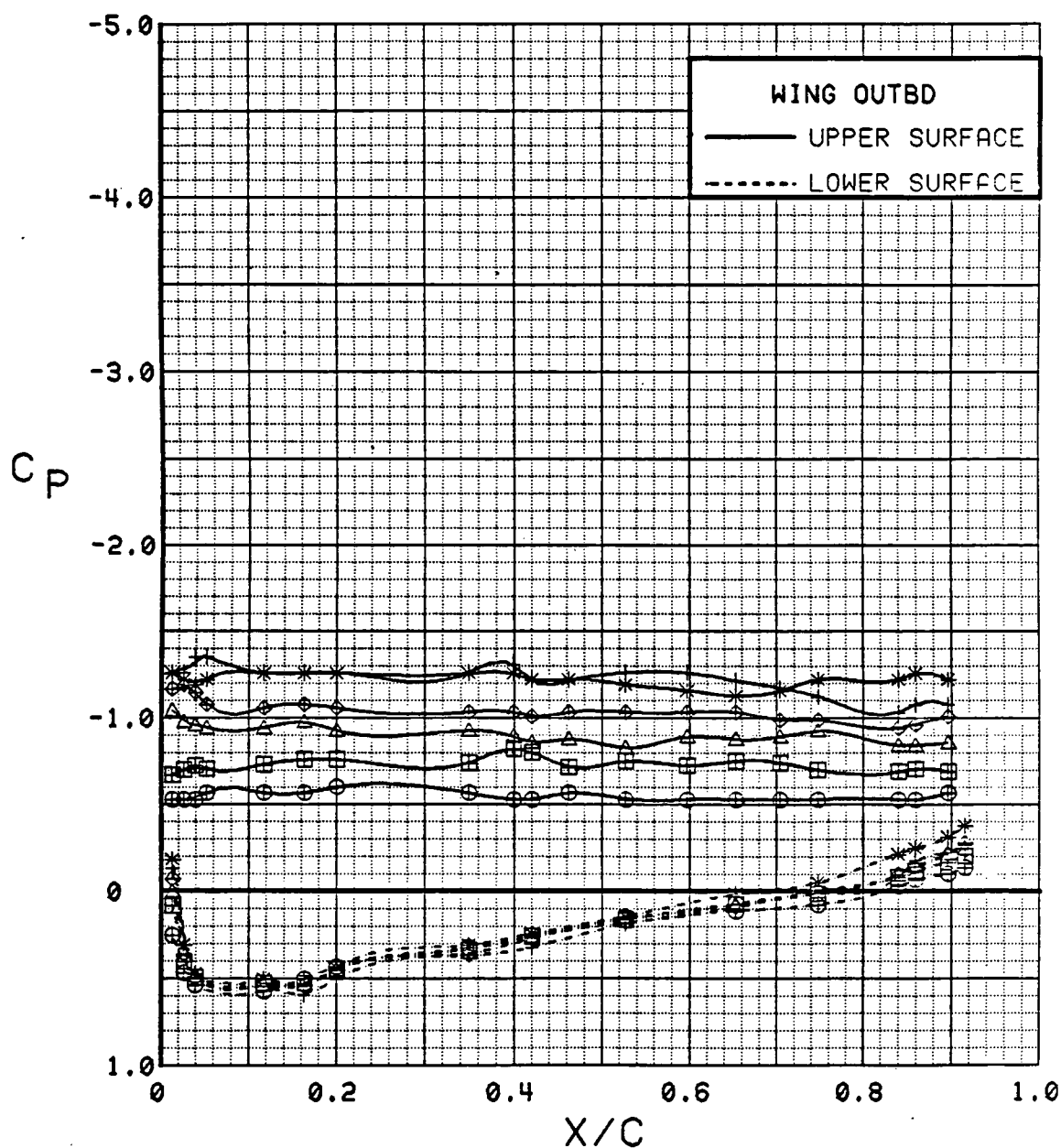


Figure 3.2.2-55 Power Effects, Flaps Neutral, Outboard, Alpha = 28 deg

SYM	TEST	RUN	ALPHA	CT	ITEF	OTEF	CAN	SWB
⊕	537	74	32.6	0.00	0	0	OFF	OFF
⊞	537	76	32.7	0.26	0	0	OFF	OFF
△	537	72	32.9	0.92	0	0	OFF	OFF
⊕	537	75	32.9	1.32	0	0	OFF	OFF
*	537	71	33.0	1.82	0	0	OFF	OFF

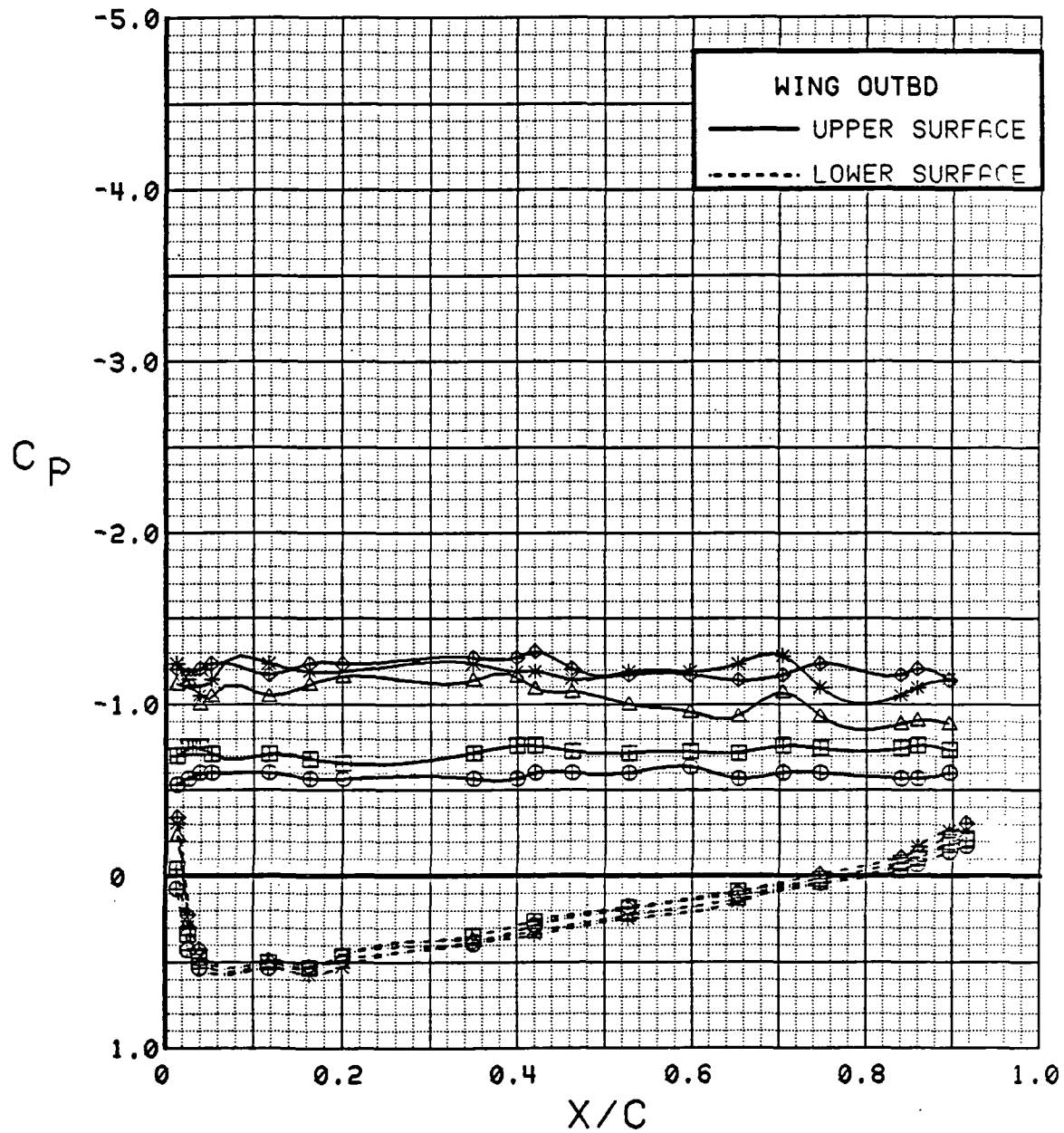


Figure 3.2.2-56

Power Effects, Flaps Neutral, Outboard, Alpha = 32 deg

SYM	TEST	RUN	ALPHA	CT	ITEF	OTEF	CAN	SWB
⊕	537	74	0.1	0.00	0	0	OFF	OFF
⊞	537	76	0.1	0.26	0	0	OFF	OFF
△	537	73	0.1	0.51	0	0	OFF	OFF
◆	537	75	0.1	1.31	0	0	OFF	OFF
*	537	71	0.1	1.75	0	0	OFF	OFF

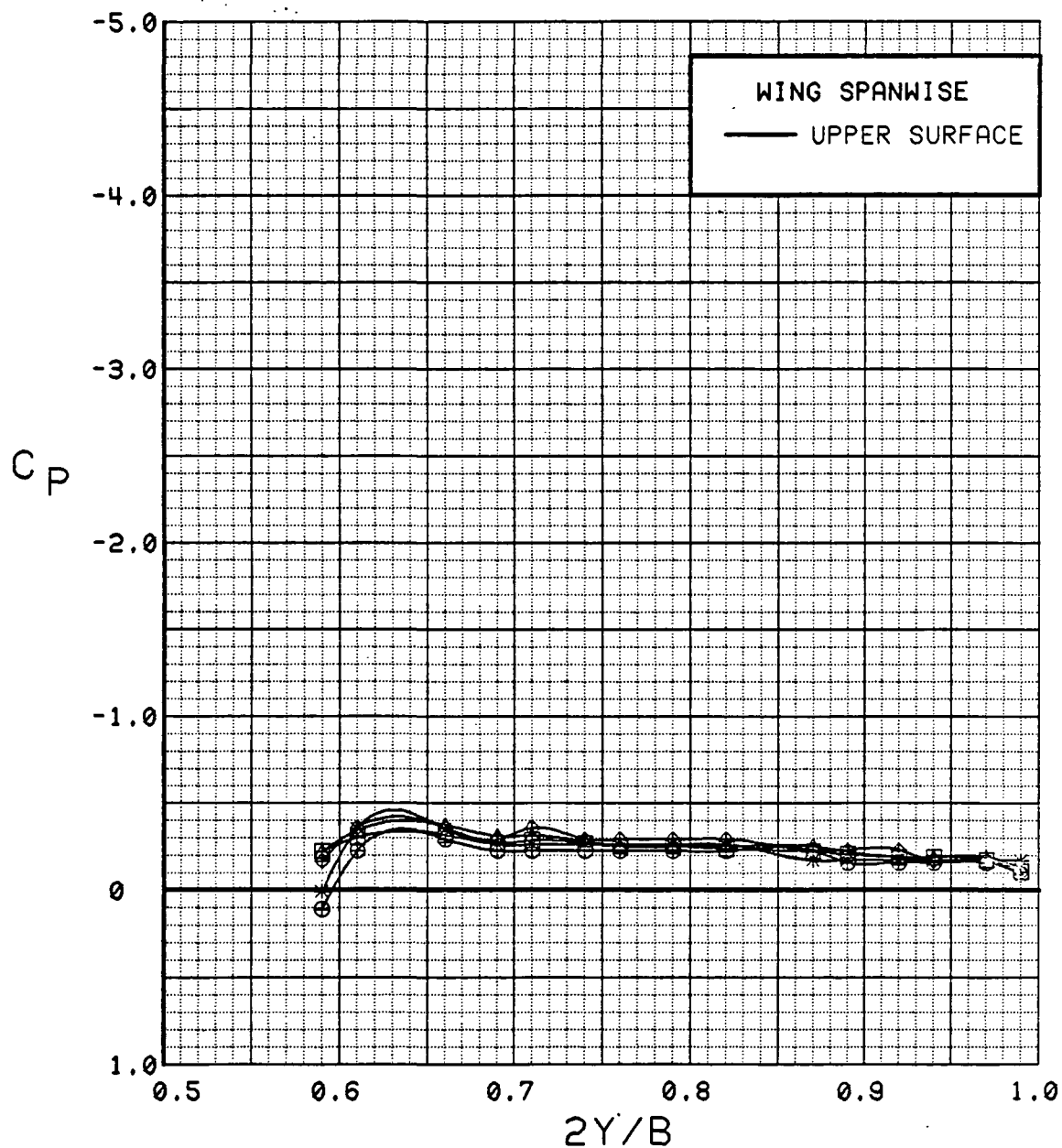


Figure 3.2.2-57 Power Effects, Flaps Neutral, Spanwise, Alpha = 0 deg

SYM	TEST	RUN	ALPHA	CT	ITEF	OTEF	CAN	SWB
⊕	537	76	4.2	0.26	0	0	OFF	OFF
⊞	537	73	4.2	0.52	0	0	OFF	OFF
△	537	72	4.2	0.90	0	0	OFF	OFF
◆	537	75	4.2	1.35	0	0	OFF	OFF
*	537	71	4.2	1.81	0	0	OFF	OFF

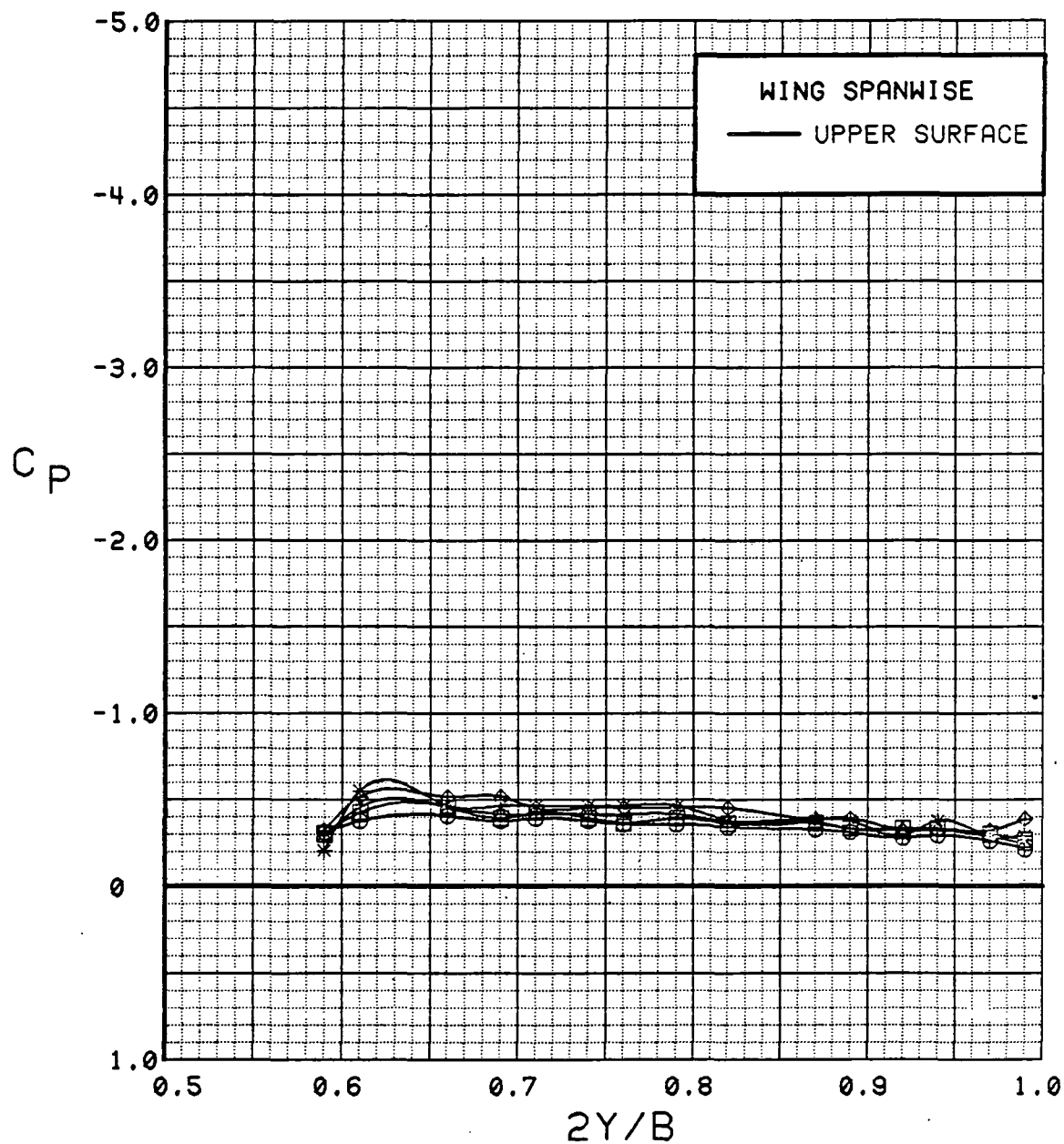


Figure 3.2.2-58 Power Effects, Flaps Neutral, Spanwise, Alpha = 4 deg

SYM	TEST	RUN	ALPHA	CT	ITEF	OTEF	CAN	SWB
⊕	537	74	8.3	0.00	0	0	OFF	OFF
⊞	537	76	8.3	0.26	0	0	OFF	OFF
△	537	73	8.3	0.52	0	0	OFF	OFF
◆	537	72	8.3	0.92	0	0	OFF	OFF
*	537	75	8.3	1.36	0	0	OFF	OFF
+	537	71	8.3	1.84	0	0	OFF	OFF

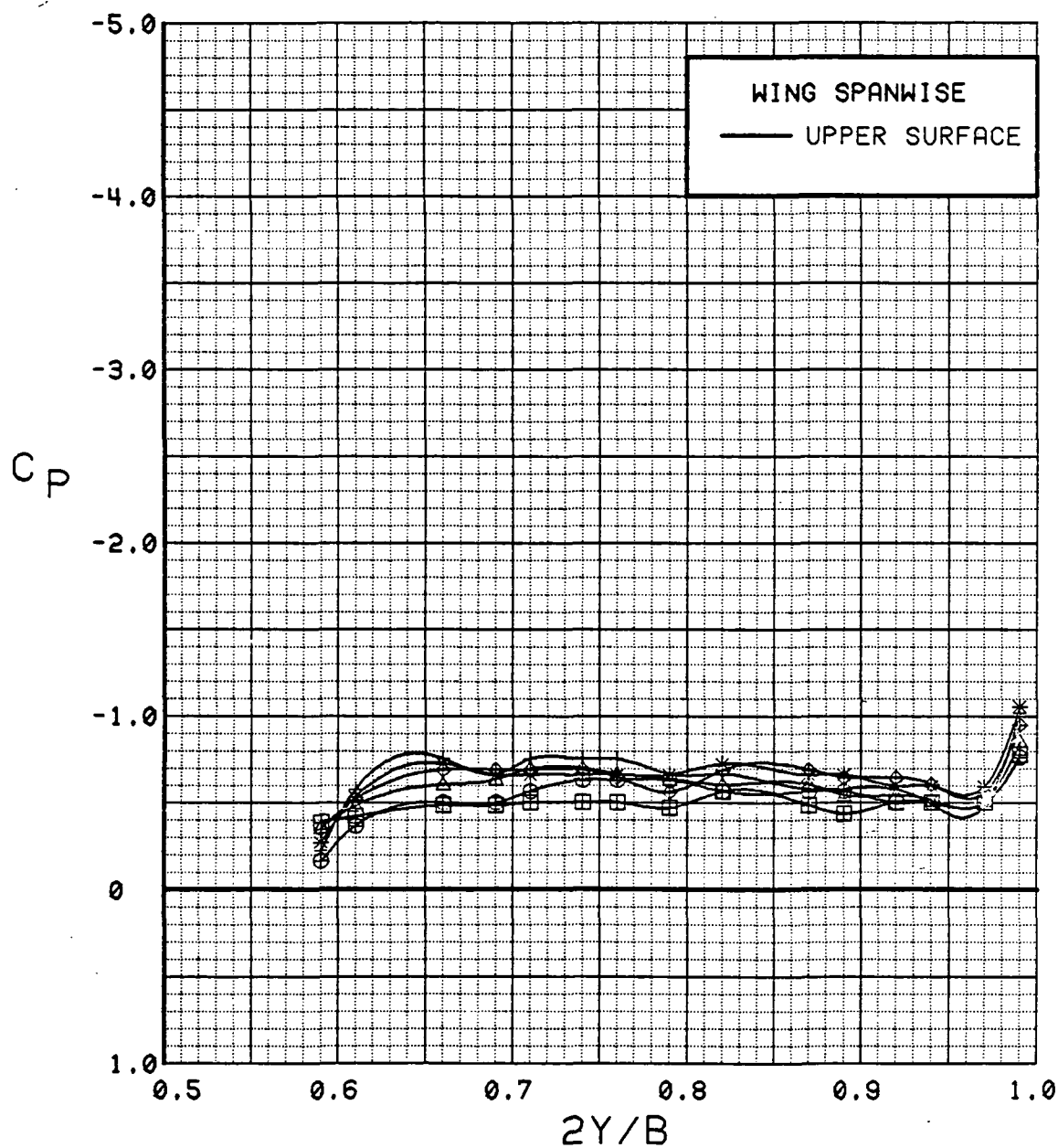


Figure 3.2.2-59 Power Effects, Flaps Neutral, Spanwise, Alpha = 8 deg

SYM	TEST	RUN	ALPHA	CT	ITEF	OTEF	CAN	SWB
⊙	537	74	12.4	0.00	0	0	OFF	OFF
⊠	537	76	12.4	0.26	0	0	OFF	OFF
△	537	73	12.4	0.52	0	0	OFF	OFF
◆	537	72	12.4	0.91	0	0	OFF	OFF
*	537	75	12.5	1.35	0	0	OFF	OFF
+	537	71	12.5	1.85	0	0	OFF	OFF

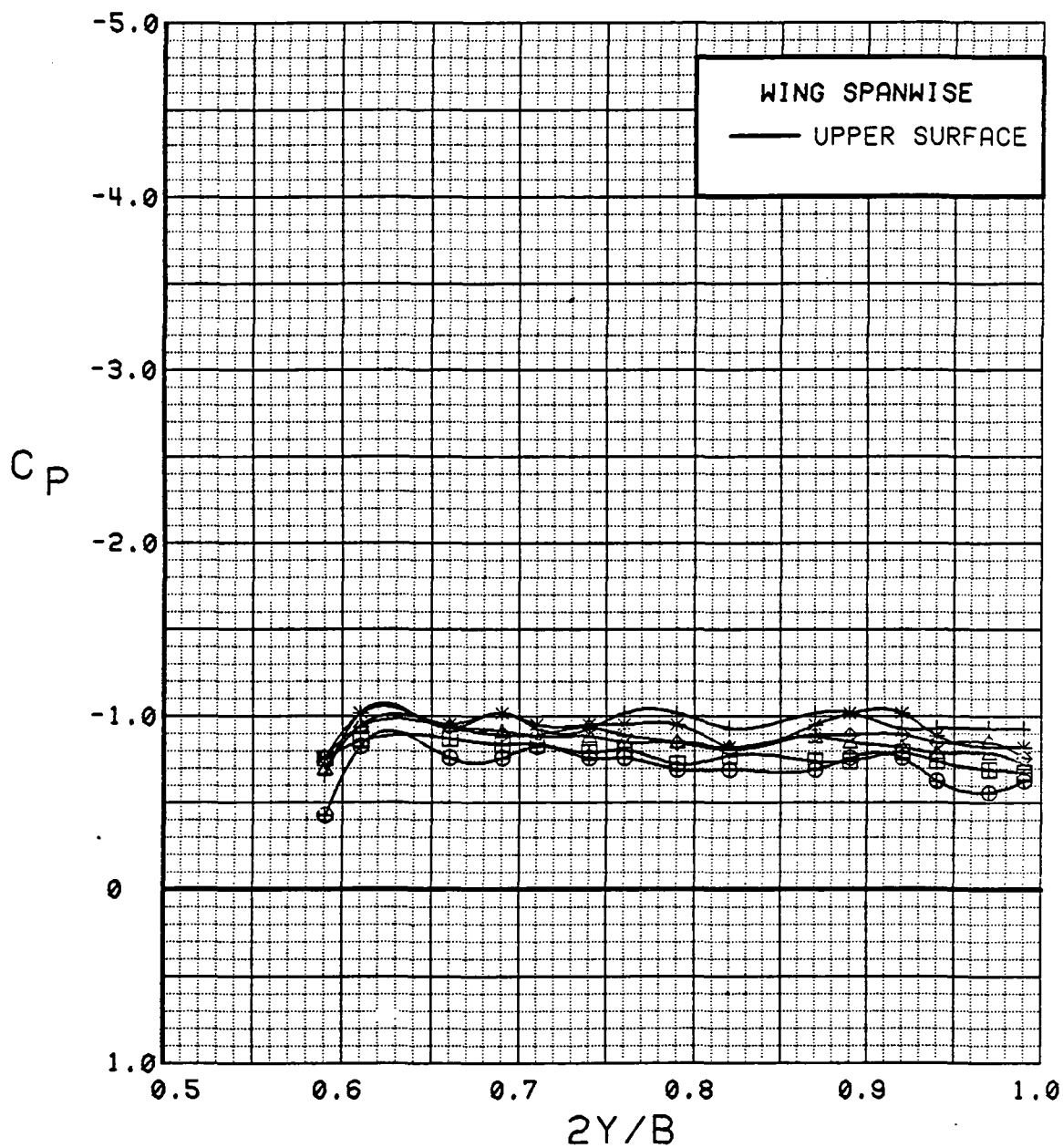


Figure 3.2.2-60 Power Effects, Flaps Neutral, Spanwise, Alpha = 12 deg



SYM	TEST	RUN	ALPHA	CT	ITEF	OTEF	CAN	SWB
⊕	537	74	16.5	0.00	0	0	OFF	OFF
⊞	537	76	16.5	0.26	0	0	OFF	OFF
△	537	73	16.5	0.52	0	0	OFF	OFF
◆	537	72	16.5	0.91	0	0	OFF	OFF
*	537	75	16.6	1.34	0	0	OFF	OFF
+	537	71	16.6	1.82	0	0	OFF	OFF

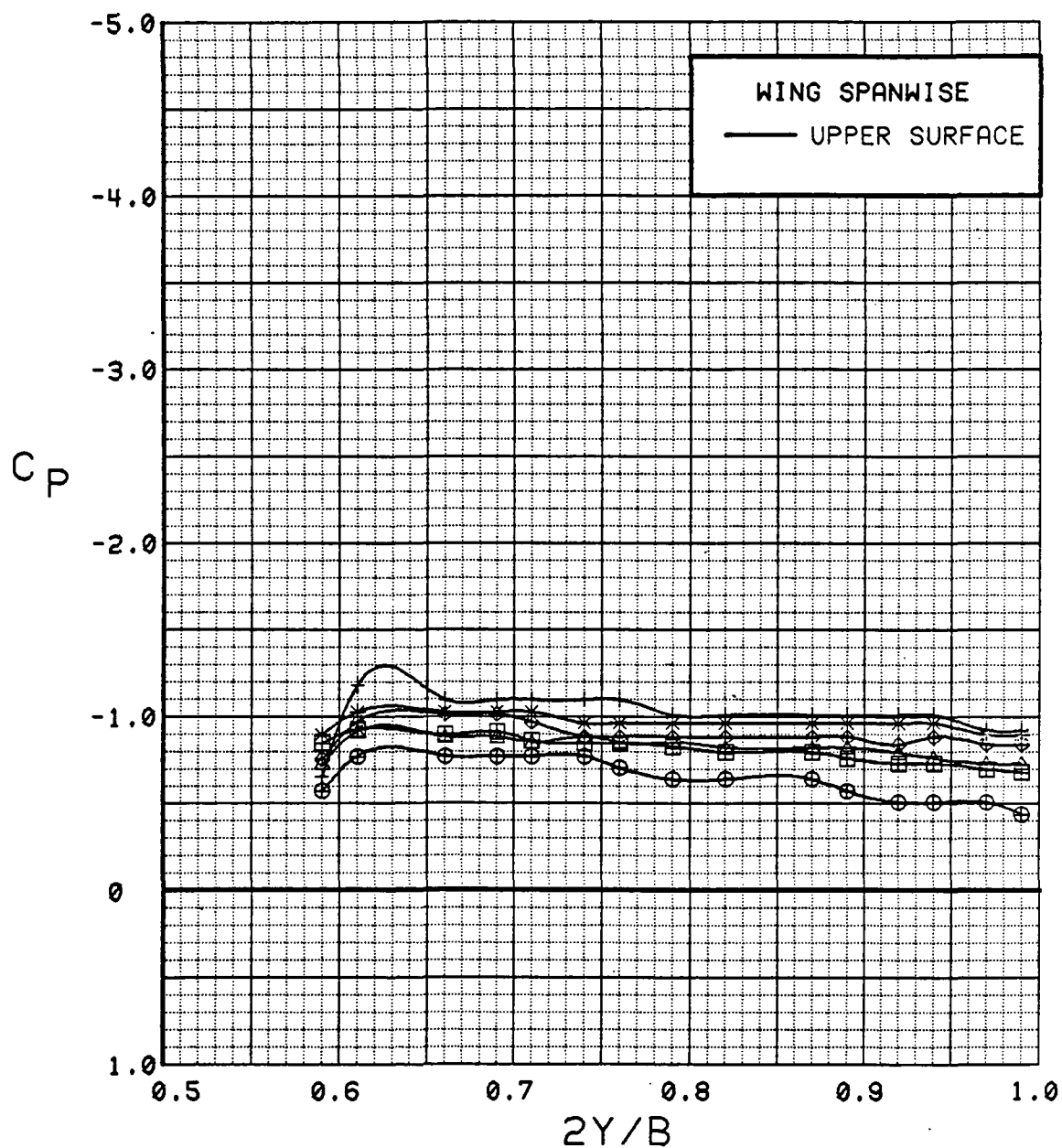


Figure 3.2.2-61 Power Effects, Flaps Neutral, Spanwise, Alpha = 16 deg

SYM	TEST	RUN	ALPHA	CT	ITEF	OTEF	CAN	SWB
⊕	537	74	20.5	0.00	0	0	OFF	OFF
⊞	537	76	20.6	0.26	0	0	OFF	OFF
△	537	73	20.6	0.52	0	0	OFF	OFF
◆	537	72	20.6	0.93	0	0	OFF	OFF
*	537	75	20.7	1.37	0	0	OFF	OFF
+	537	71	20.7	1.93	0	0	OFF	OFF

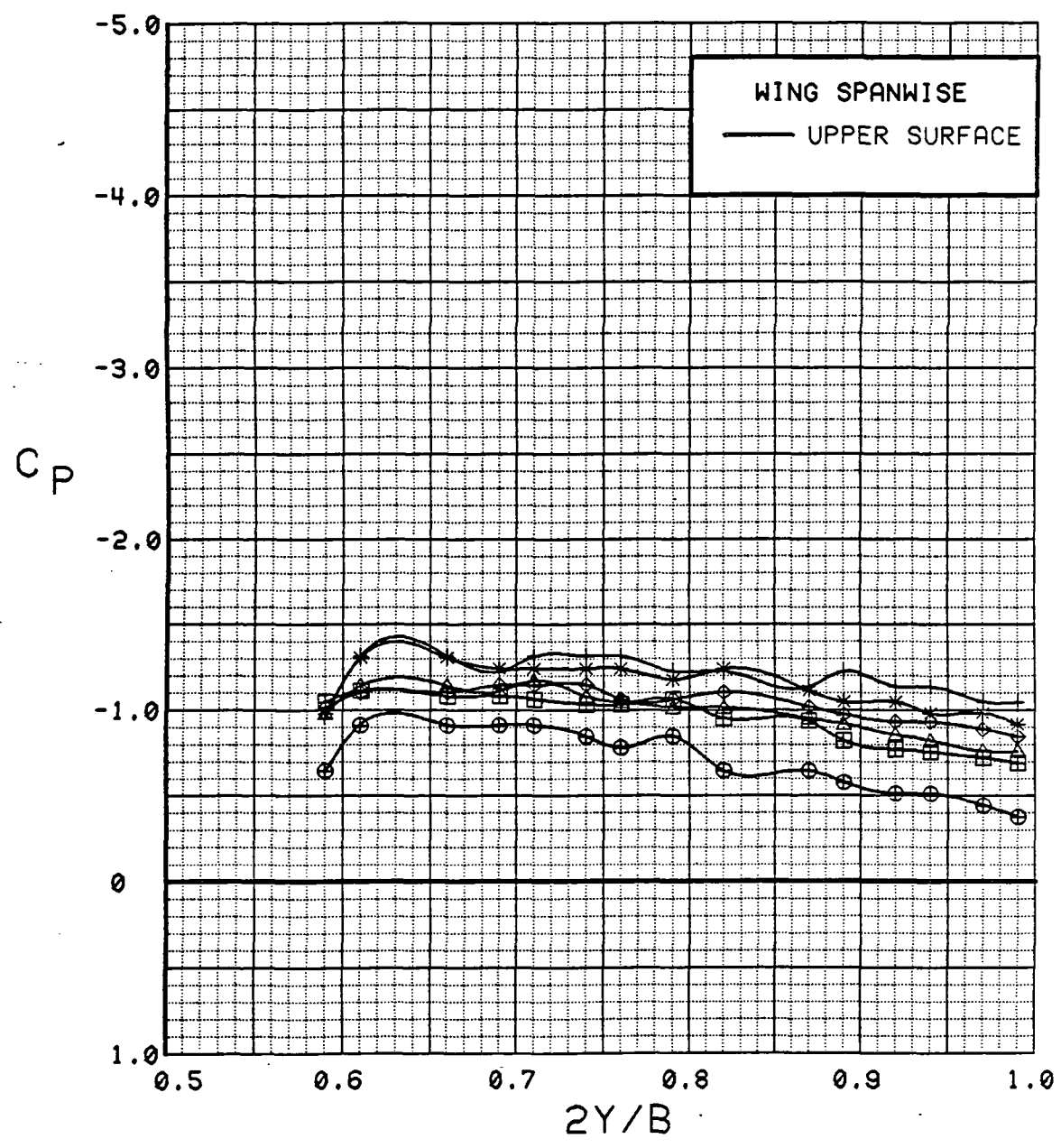


Figure 3.2.2-62 Power Effects, Flaps Neutral, Spanwise, Alpha = 20 deg

SYM	TEST	RUN	ALPHA	CT	ITEF	OTEF	CAN	SWB
⊕	537	74	24.6	0.00	0	0	OFF	OFF
⊞	537	76	24.7	0.26	0	0	OFF	OFF
△	537	73	24.7	0.52	0	0	OFF	OFF
◆	537	72	24.7	0.91	0	0	OFF	OFF
*	537	75	24.8	1.36	0	0	OFF	OFF
+	537	71	24.8	1.79	0	0	OFF	OFF

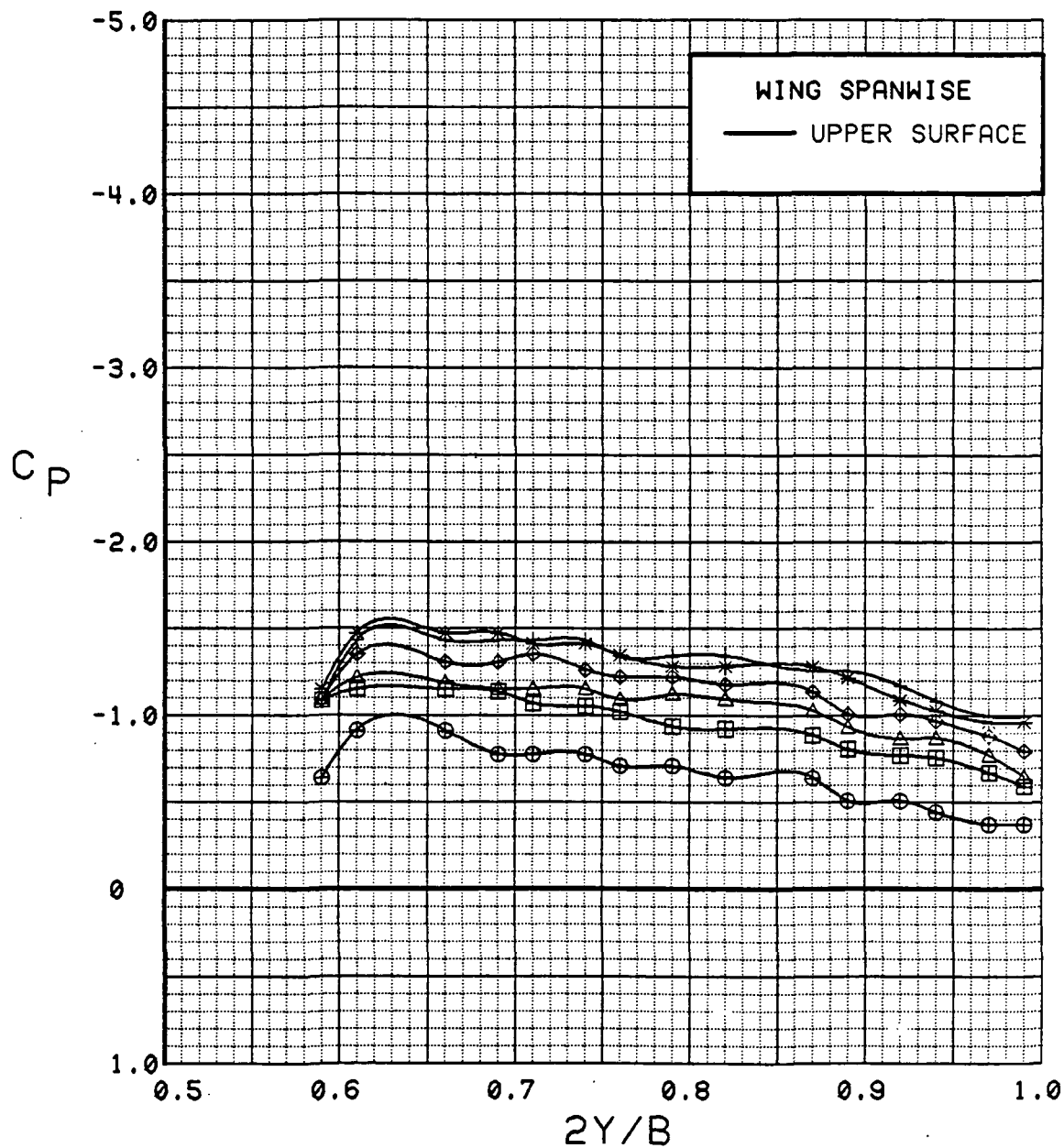


Figure 3.2.2-63 Power Effects, Flaps Neutral, Spanwise, Alpha = 24 deg

SYM	TEST	RUN	ALPHA	CT	ITEF	OTEF	CAN	SWB
⊕	537	74	28.6	0.00	0	0	OFF	OFF
⊞	537	76	28.7	0.26	0	0	OFF	OFF
△	537	73	28.8	0.51	0	0	OFF	OFF
◆	537	72	28.8	0.91	0	0	OFF	OFF
*	537	75	28.9	1.29	0	0	OFF	OFF
+	537	71	28.9	1.81	0	0	OFF	OFF

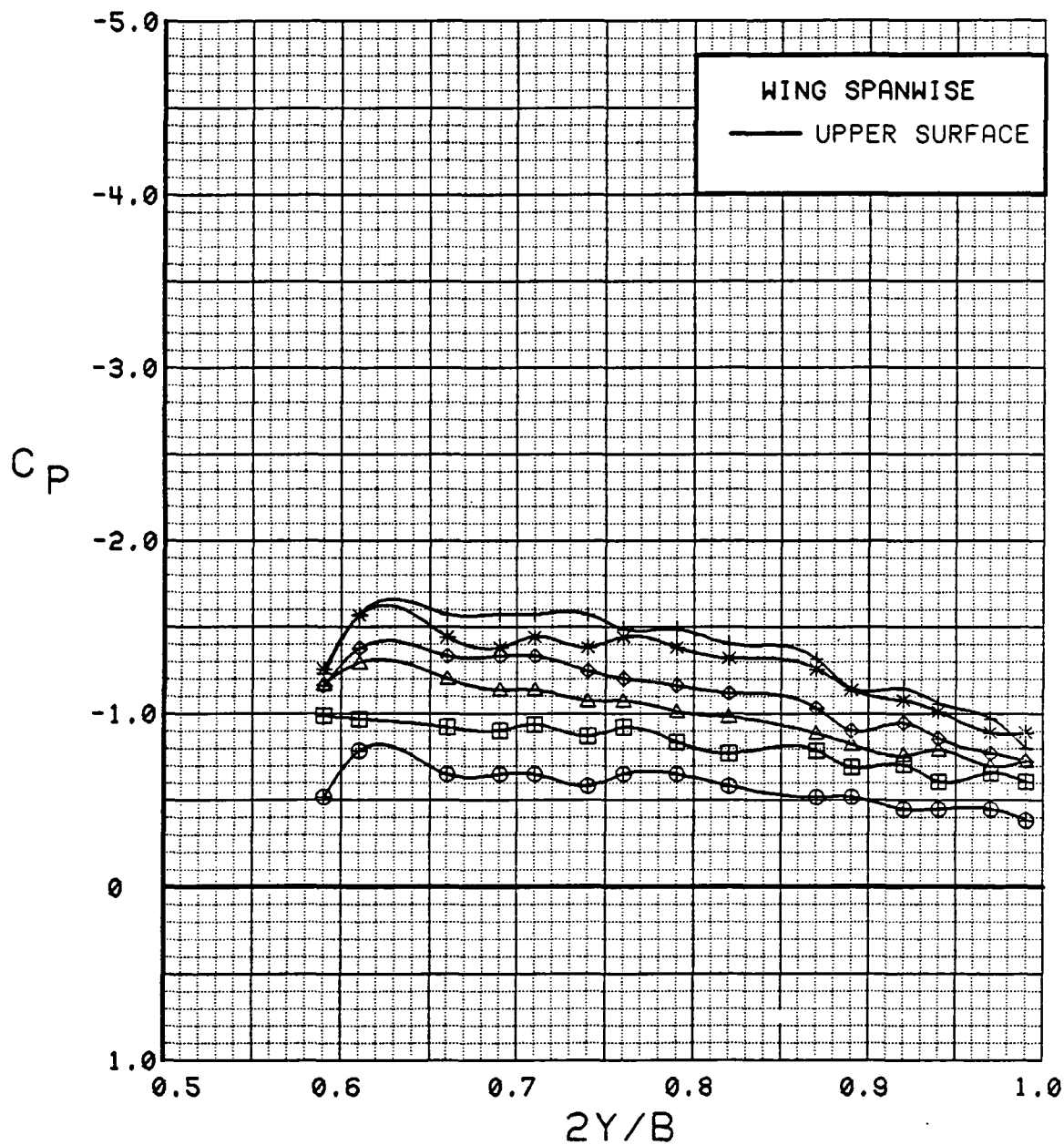


Figure 3.2.2-64 Power Effects, Flaps Neutral, Spanwise, Alpha = 28 deg

SYM	TEST	RUN	ALPHA	CT	ITEF	OTEF	CAN	SWB
⊙	537	74	32.6	0.00	0	0	OFF	OFF
⊠	537	76	32.7	0.26	0	0	OFF	OFF
△	537	72	32.9	0.92	0	0	OFF	OFF
◆	537	75	32.9	1.32	0	0	OFF	OFF
*	537	71	33.0	1.82	0	0	OFF	OFF

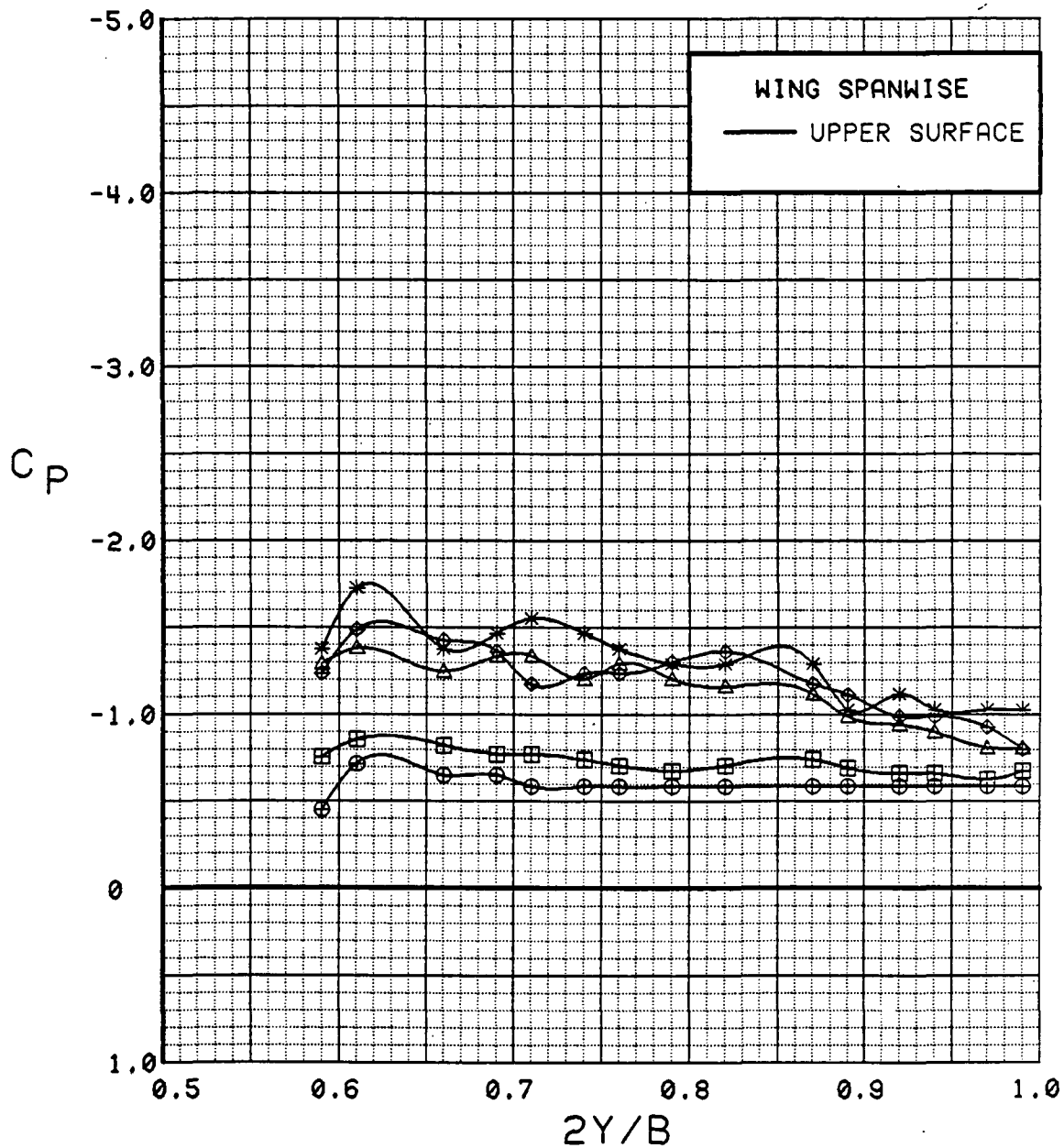


Figure 3.2.2-65 Power Effects, Flaps Neutral, Spanwise, Alpha = 32 deg

SYM	TEST	RUN	ALPHA	CT	ITEF	OTEF	CAN	SWB
⊕	537	74	0.1	0.00	0	0	OFF	OFF
⊞	537	75	0.1	1.31	0	0	OFF	OFF

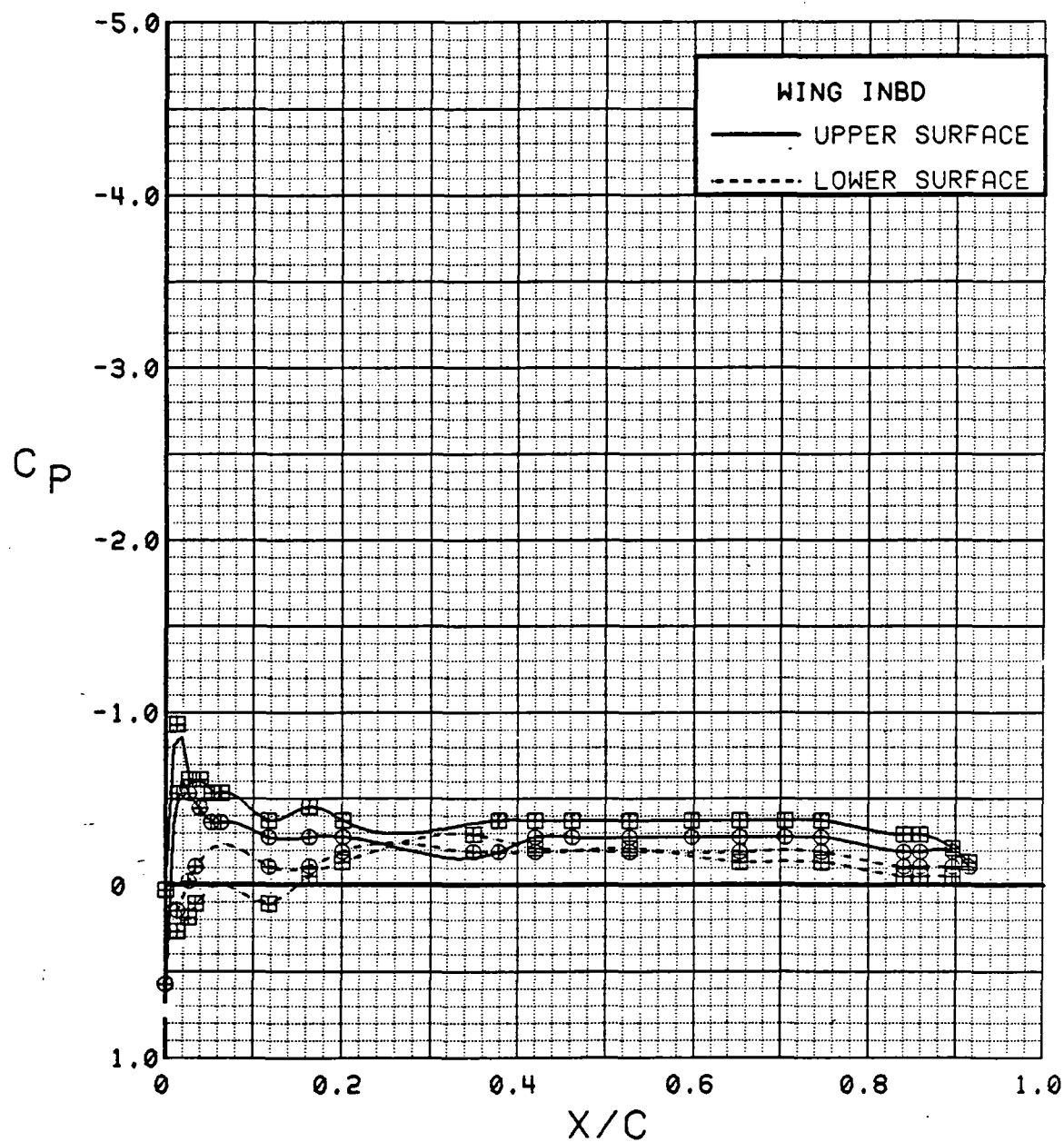


Figure 3.2.2-66 Power-off/Power-on Comparison, Flaps Neutral, Inboard, Alpha = 0 deg

SYM	TEST	RUN	ALPHA	CT	ITEF	OTEF	CAN	SWB
⊕	537	74	8.3	0.00	0	0	OFF	OFF
⊞	537	75	8.3	1.36	0	0	OFF	OFF

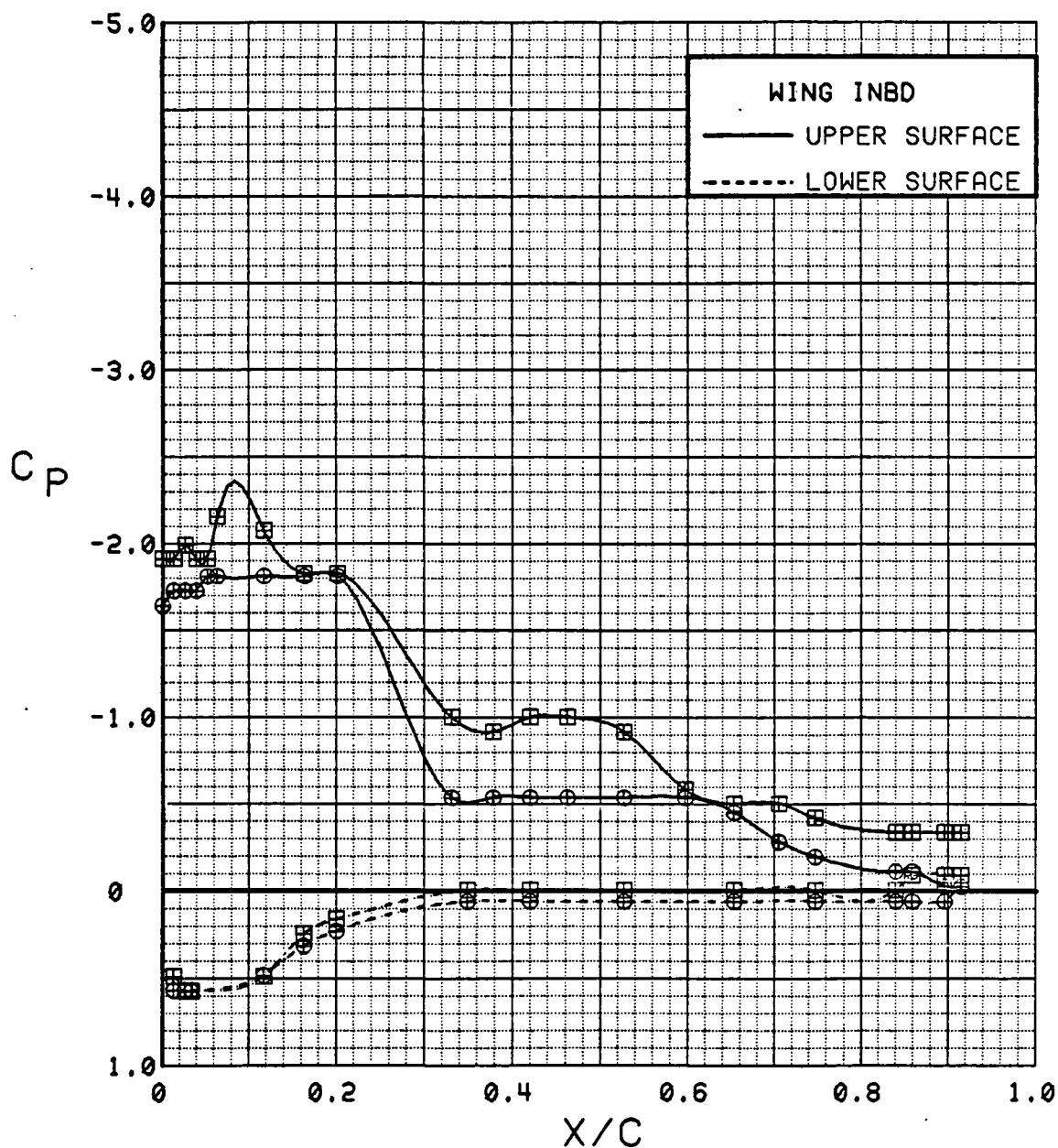


Figure 3.2.2-67 Power-off/Power-on Comparison, Flaps Neutral, Inboard, Alpha = 8 deg

SYM	TEST	RUN	ALPHA	CT	ITEF	OTEF	CAN	SWB
⊕	537	74	12.4	0.00	0	0	OFF	OFF
⊞	537	75	12.5	1.35	0	0	OFF	OFF

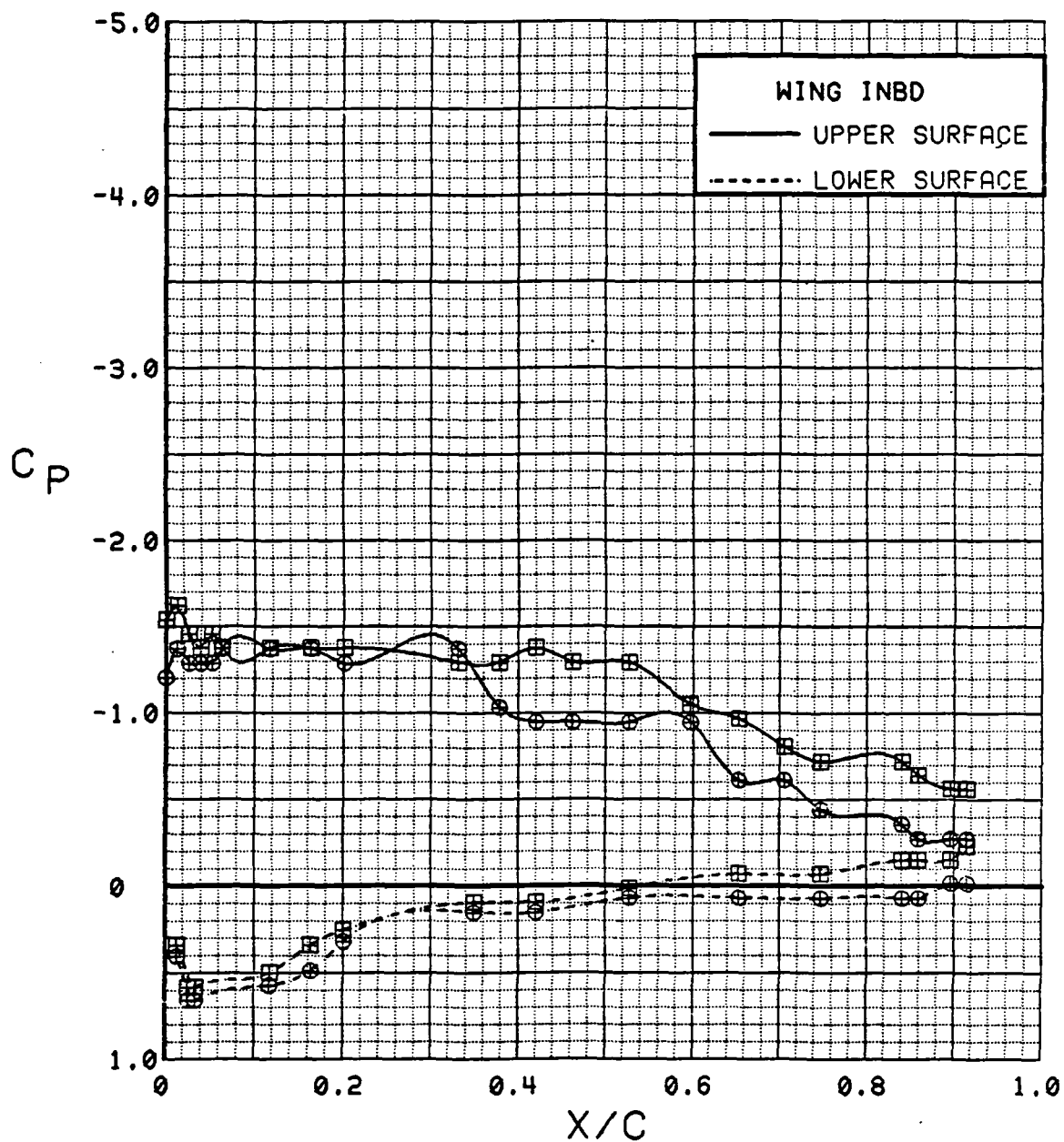


Figure 3.2.2-68 Power-off/Power-on Comparison, Flaps Neutral, Inboard, Alpha = 12 deg



SYM	TEST	RUN	ALPHA	CT	ITEF	OTEF	CAN	SWB
⊕	537	74	16.5	0.00	0	0	OFF	OFF
⊞	537	75	16.6	1.34	0	0	OFF	OFF

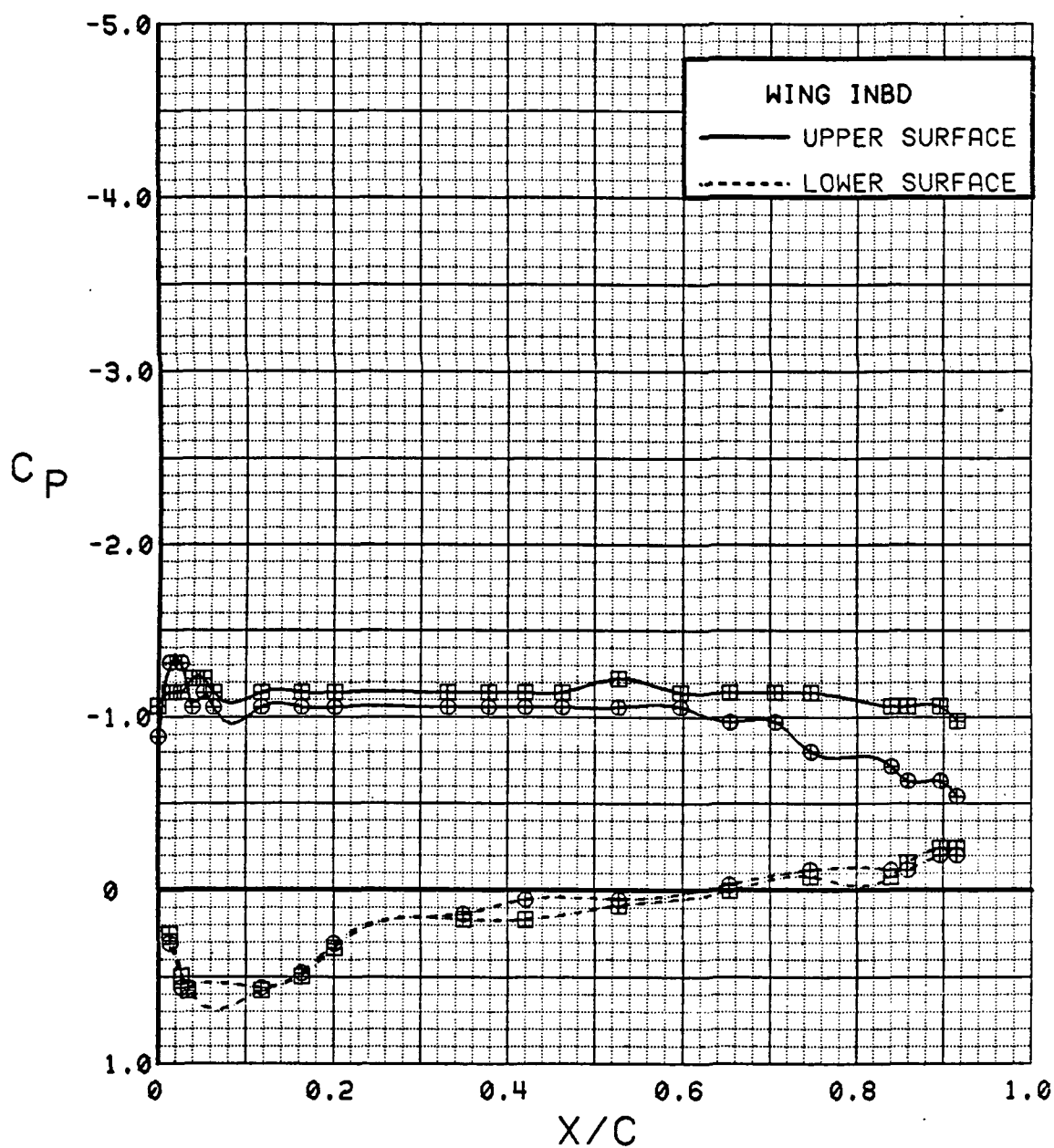


Figure 3.2.2-69 Power-off/Power-on Comparison, Flaps Neutral, Inboard, Alpha = 16 deg

SYM	TEST	RUN	ALPHA	CT	ITEF	OTEF	CAN	SWB
⊕	537	74	0.1	0.00	0	0	OFF	OFF
⊞	537	75	0.1	1.31	0	0	OFF	OFF

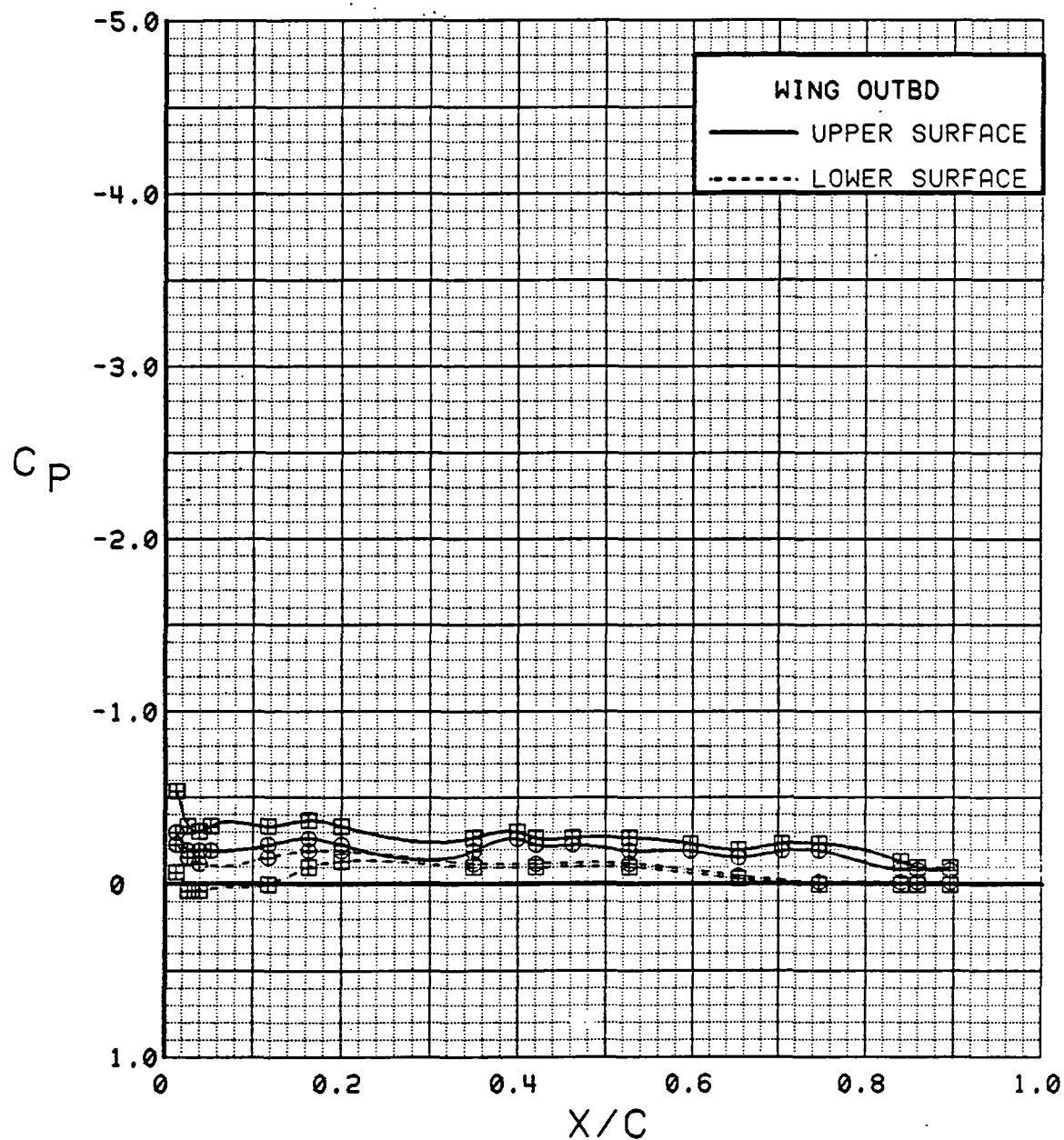


Figure 3.2.2-70 Power-off/Power-on Comparison, Flaps Neutral, Outboard, Alpha = 0 deg

SYM	TEST	RUN	ALPHA	CT	ITEF	OTEF	CAN	SWB
⊕	537	74	8.3	0.00	0	0	OFF	OFF
⊞	537	75	8.3	1.36	0	0	OFF	OFF

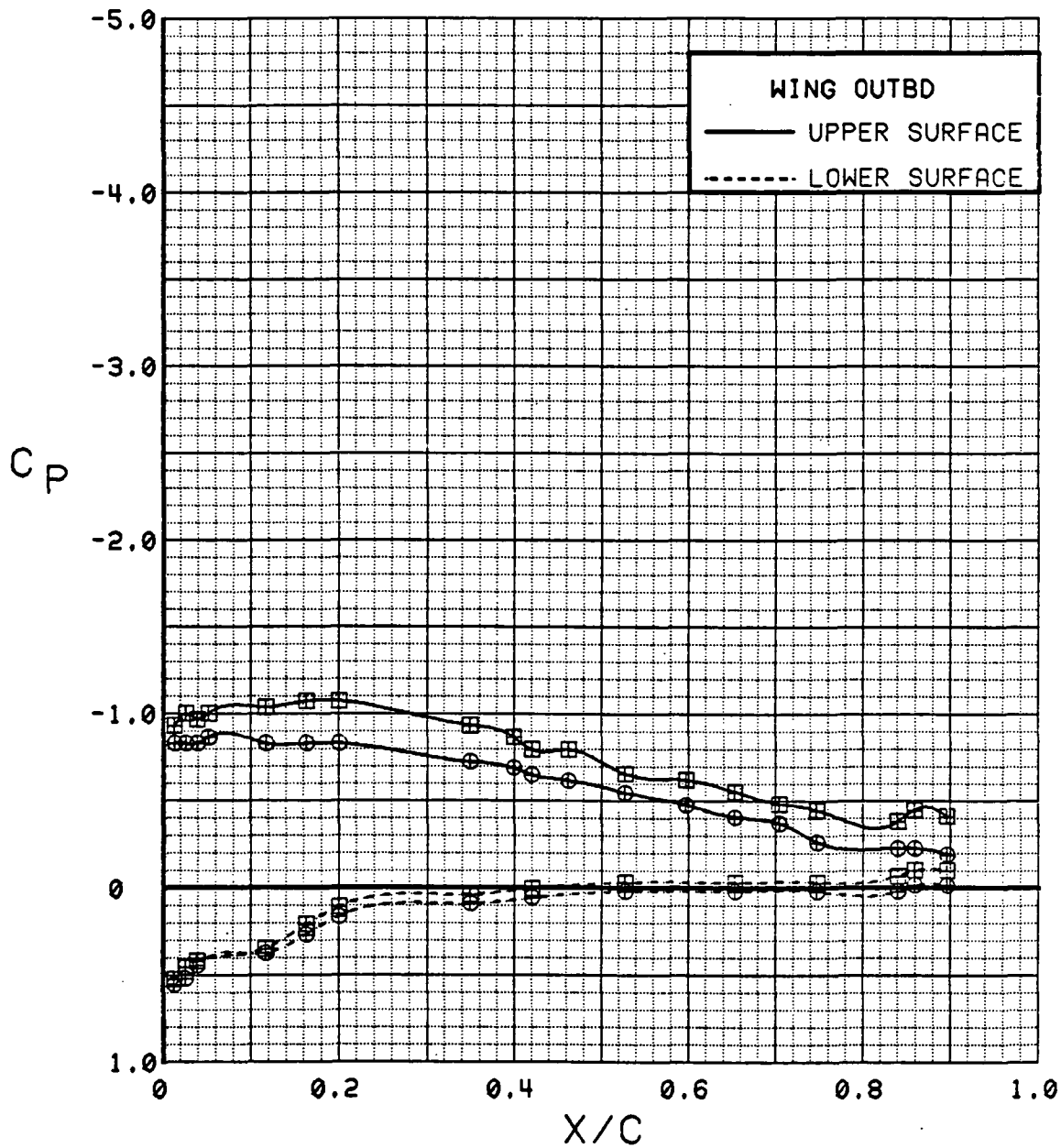


Figure 3.2.2-71 Power-off/Power-on Comparison, Flaps Neutral, Outboard, Alpha = 8 deg

SYM	TEST	RUN	ALPHA	CT	ITEF	OTEF	CAN	SWB
⊕	537	74	12.4	0.00	0	0	OFF	OFF
⊞	537	75	12.5	1.35	0	0	OFF	OFF

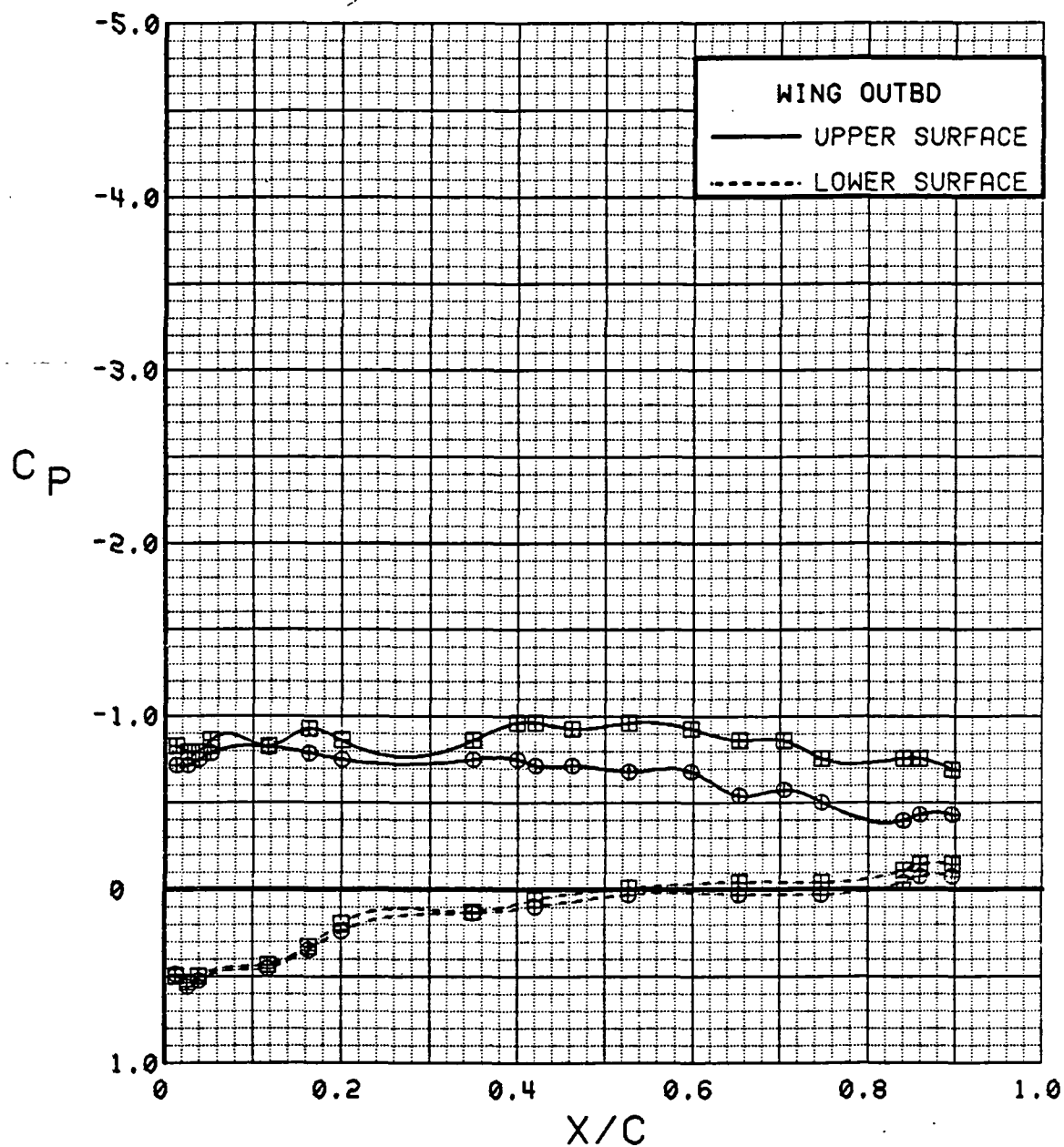


Figure 3.2.2-72 Power-off/Power-on Comparison, Flaps Neutral, Outboard, Alpha = 12 deg

SYM	TEST	RUN	ALPHA	CT	ITEF	OTEF	CAN	SWB
⊕	537	74	16.5	0.00	0	0	OFF	OFF
⊗	537	75	16.6	1.34	0	0	OFF	OFF

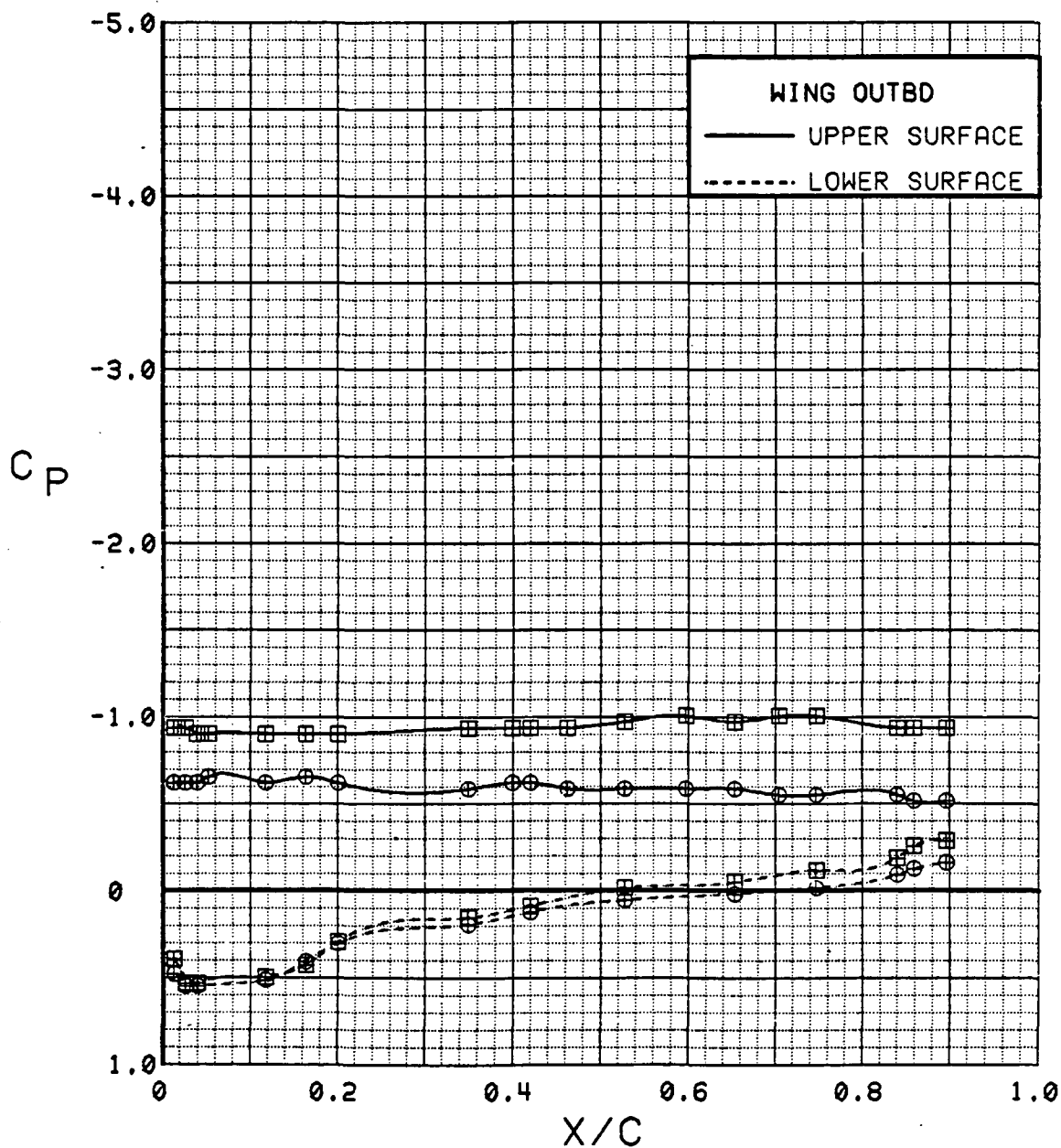


Figure 3.2.2-73 Power-off/Power-on Comparison, Flaps Neutral, Outboard, Alpha = 16 deg

SYM	TEST	RUN	ALPHA	CT	ITEF	OTEF	CAN	SWB
⊕	537	74	0.1	0.00	0	0	OFF	OFF
⊞	537	75	0.1	1.31	0	0	OFF	OFF

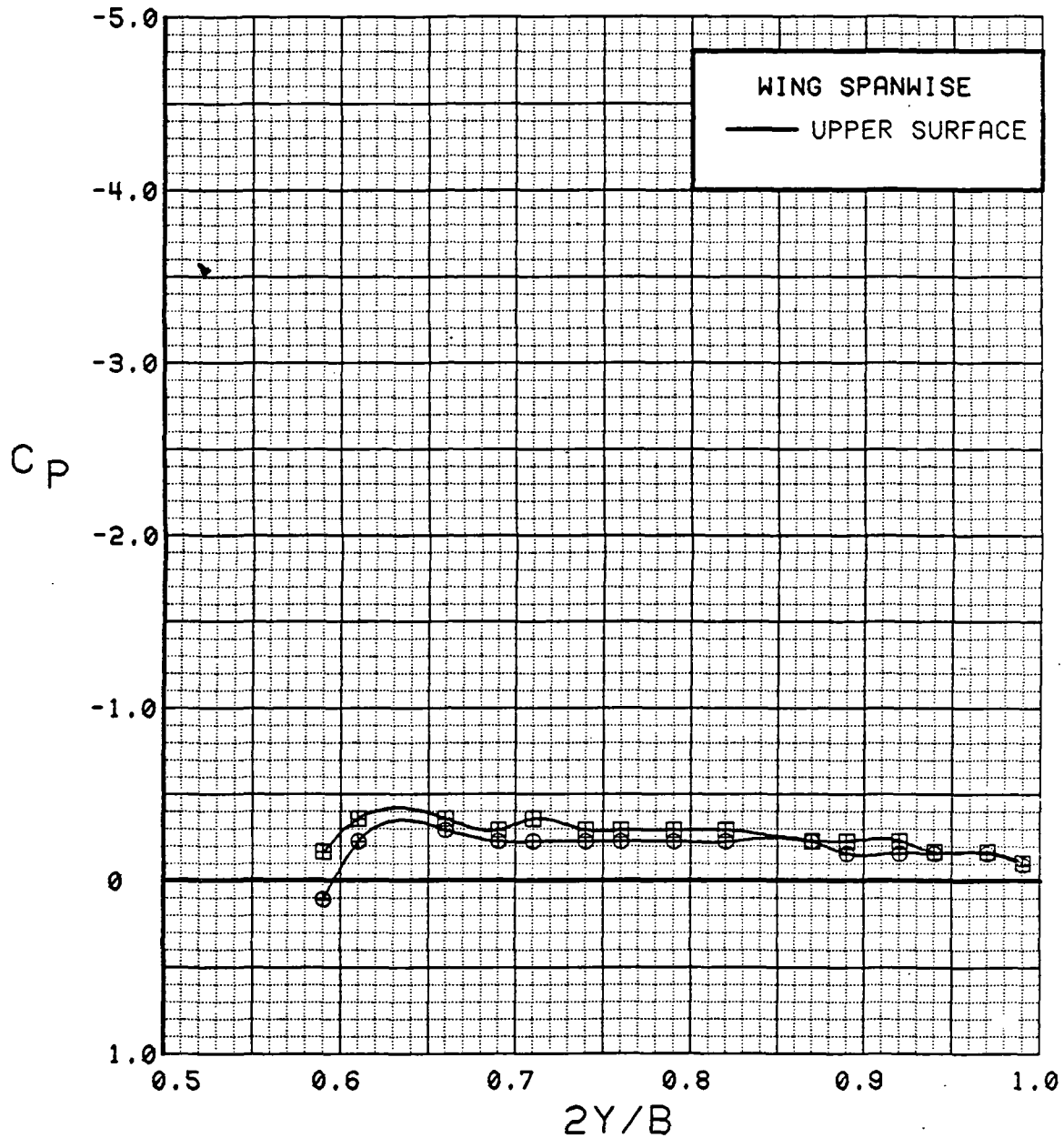


Figure 3.2.2-74

Power-off/Power-on Comparison, Flaps Neutral,  
Spanwise, Alpha = 0 deg

SYM	TEST	RUN	ALPHA	CT	ITEF	OTEF	CAN	SWB
●	537	74	8.3	0.00	0	0	OFF	OFF
■	537	75	8.3	1.36	0	0	OFF	OFF

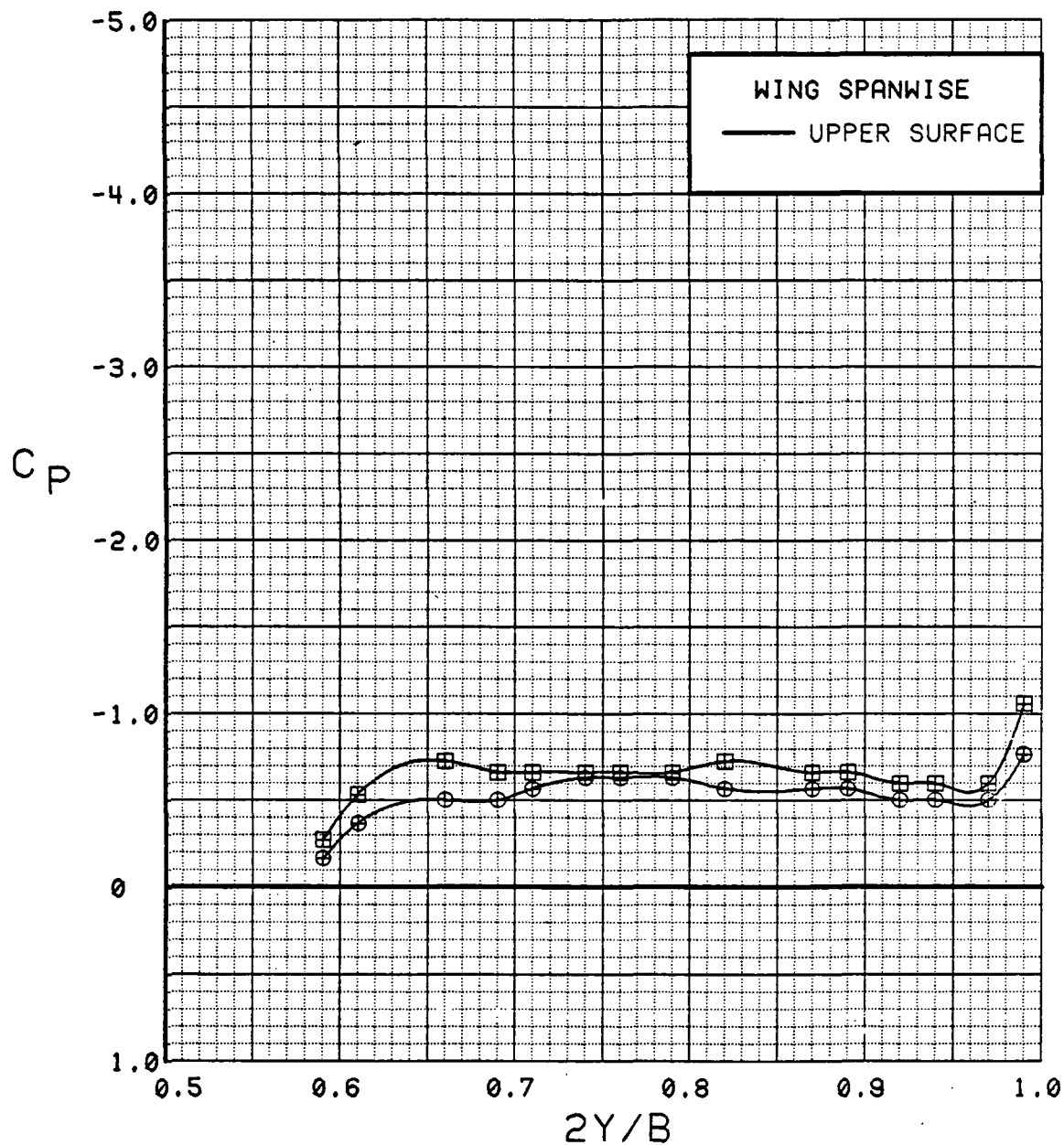


Figure 3.2.2-75 Power-off/Power-on Comparison, Flaps Neutral, Spanwise, Alpha = 8 deg

SYM	TEST	RUN	ALPHA	CT	ITEF	OTEF	CAN	SWB
⊕	537	74	12.4	0.00	0	0	OFF	OFF
⊞	537	75	12.5	1.35	0	0	OFF	OFF

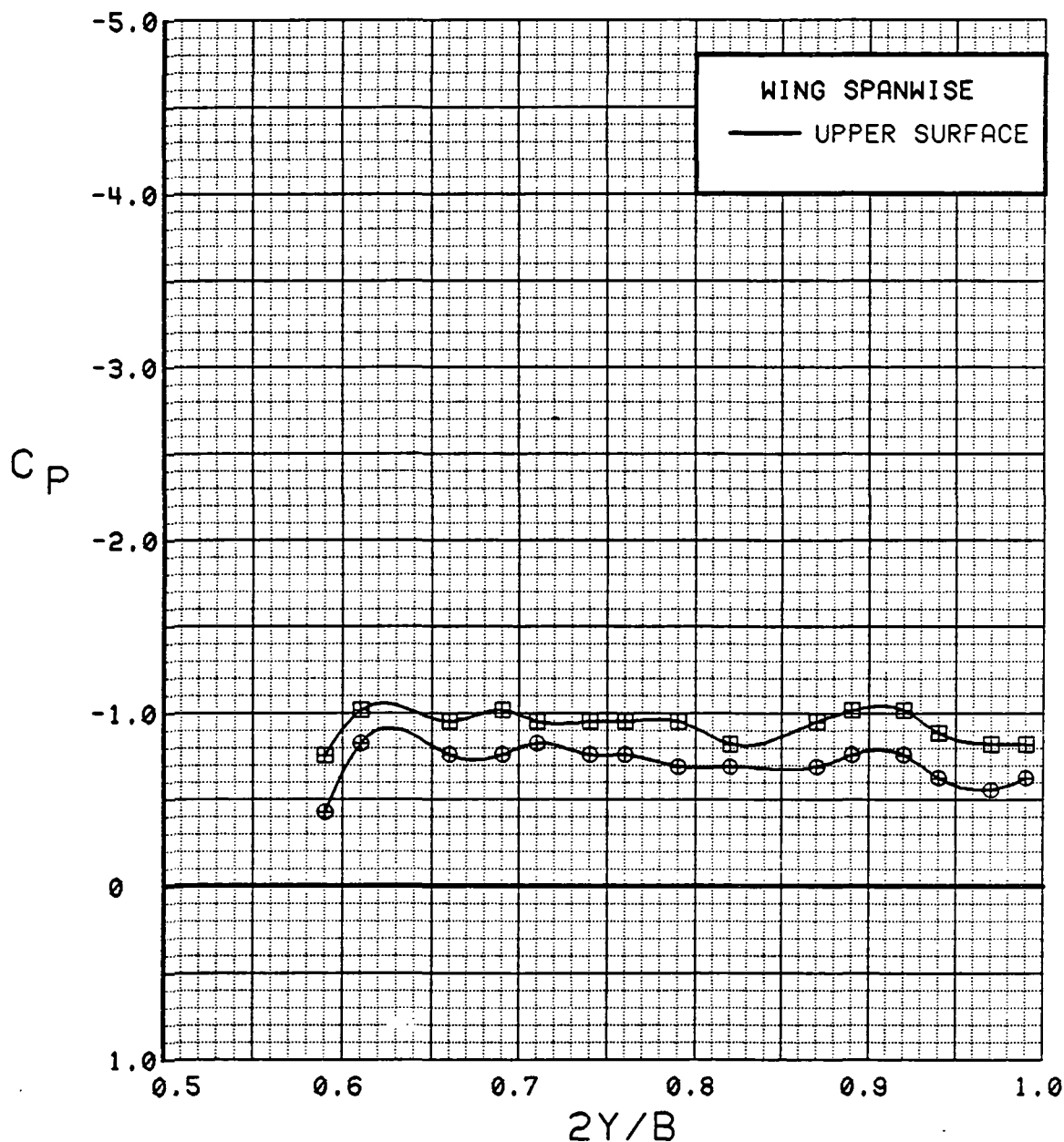


Figure 3.2.2-76

Power-off/Power-on Comparison, Flaps Neutral,  
Spanwise, Alpha = 12 deg



SYM	TEST	RUN	ALPHA	CT	ITEF	OTEF	CAN	.SWB
⊙	537	74	16.5	0.00	0	0	OFF	OFF
⊠	537	75	16.6	1.34	0	0	OFF	OFF

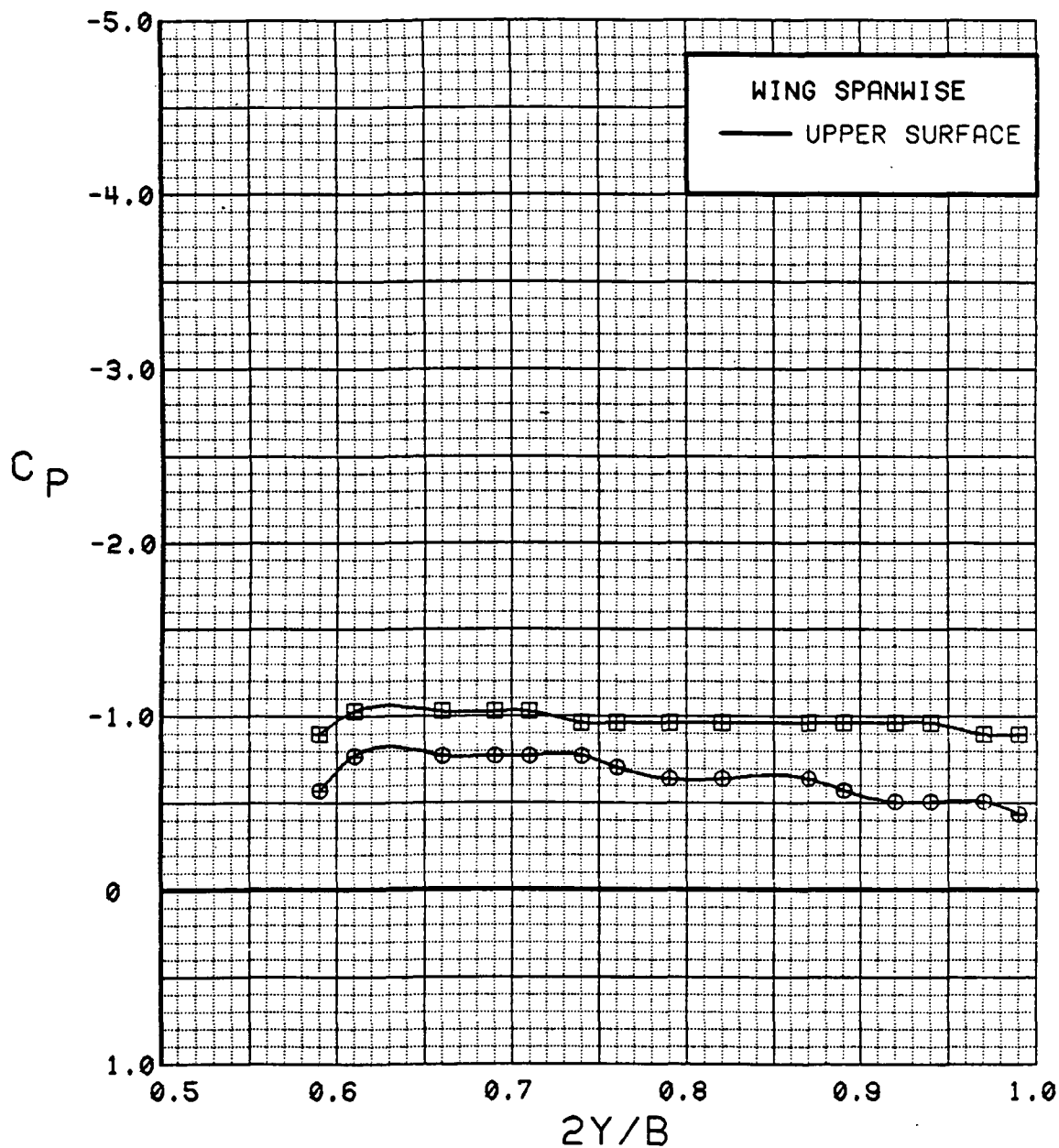


Figure 3.2.2-77 Power-off/Power-on Comparison, Flaps Neutral, Spanwise, Alpha = 16 deg

# WING INBOARD

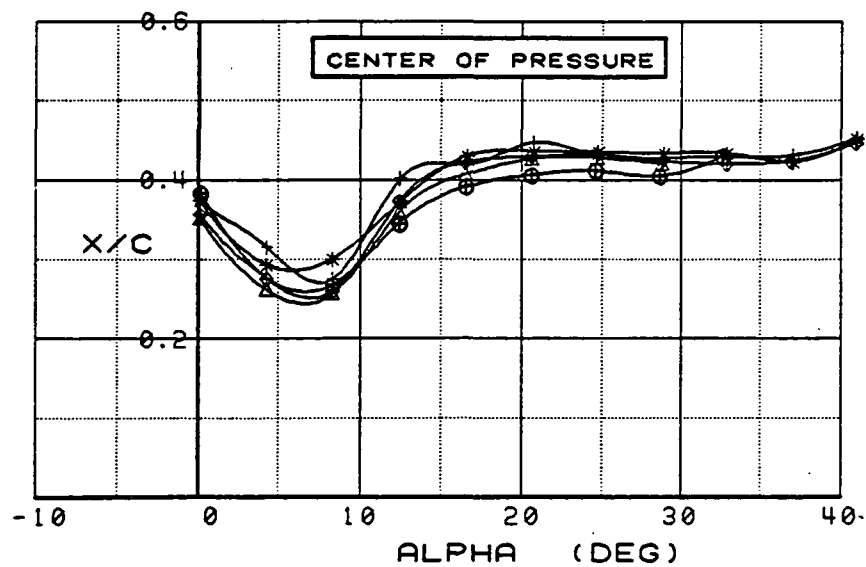
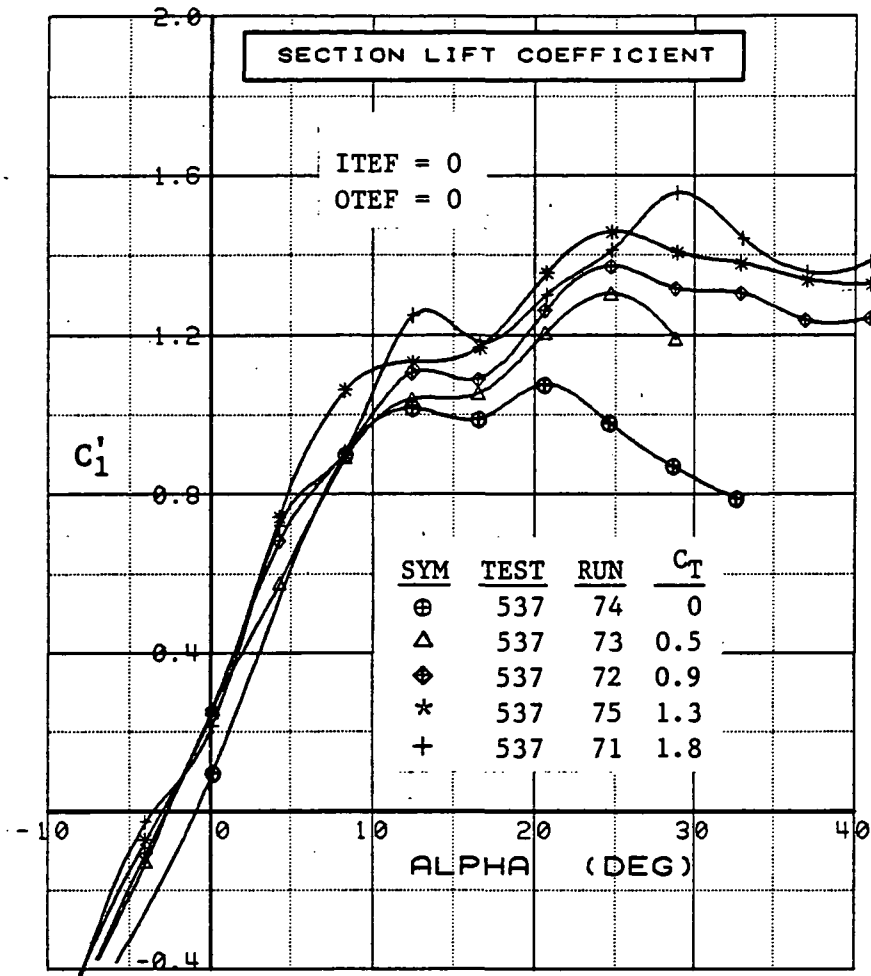


Figure 3.2-2-78 Power-off/Power-on Comparison, Flaps Neutral, Inboard, Integrated Section Properties

# WING OUTBOARD

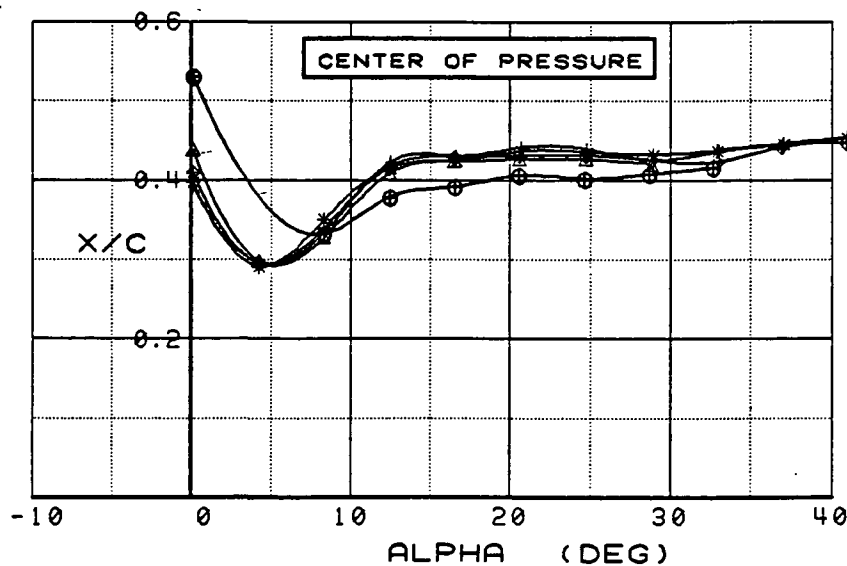
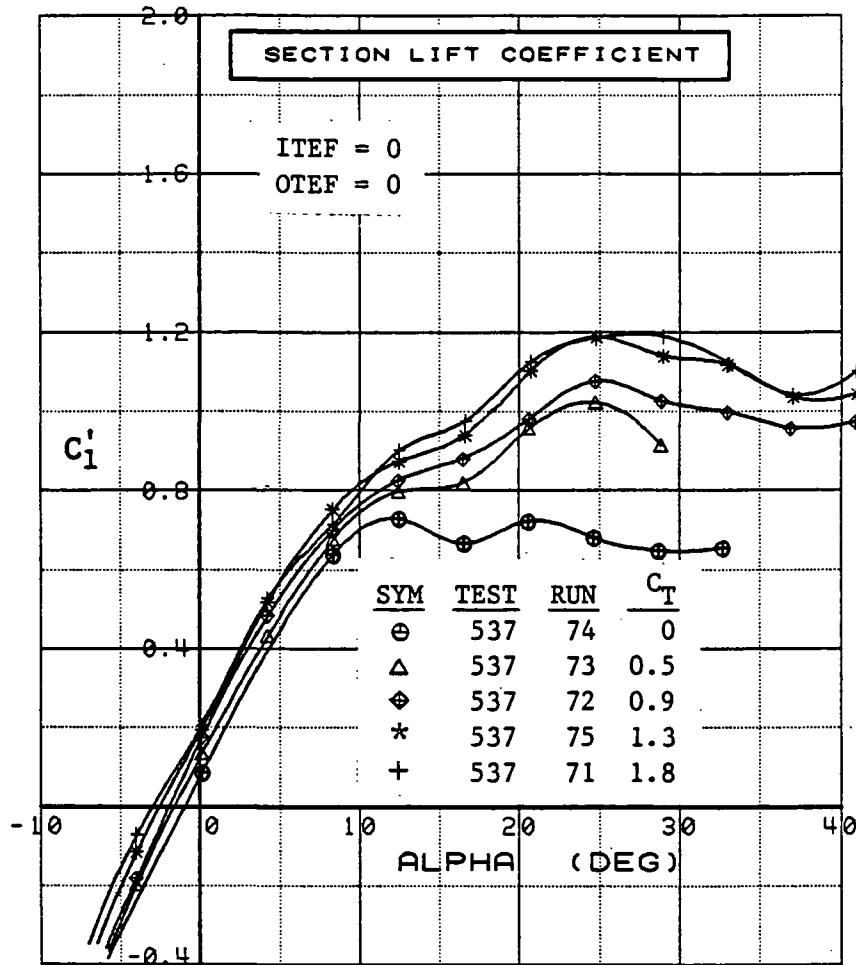


Figure 3.2-2-79 Power-off/Power-on Comparison, Flaps Neutral, Outboard, Integrated Section Properties

SYM	TEST	RUN	ALPHA	CT	ITEF	OTEF	CAN	SWB
⊕	537	69	0.2	0.00	30	30	OFF	OFF
⊞	537	63	0.3	0.28	30	30	OFF	OFF
△	537	62	0.3	0.46	30	30	OFF	OFF
⊕	537	61	0.4	0.94	30	30	OFF	OFF
*	537	60	0.3	1.42	30	30	OFF	OFF
+	537	59	0.3	1.88	30	30	OFF	OFF

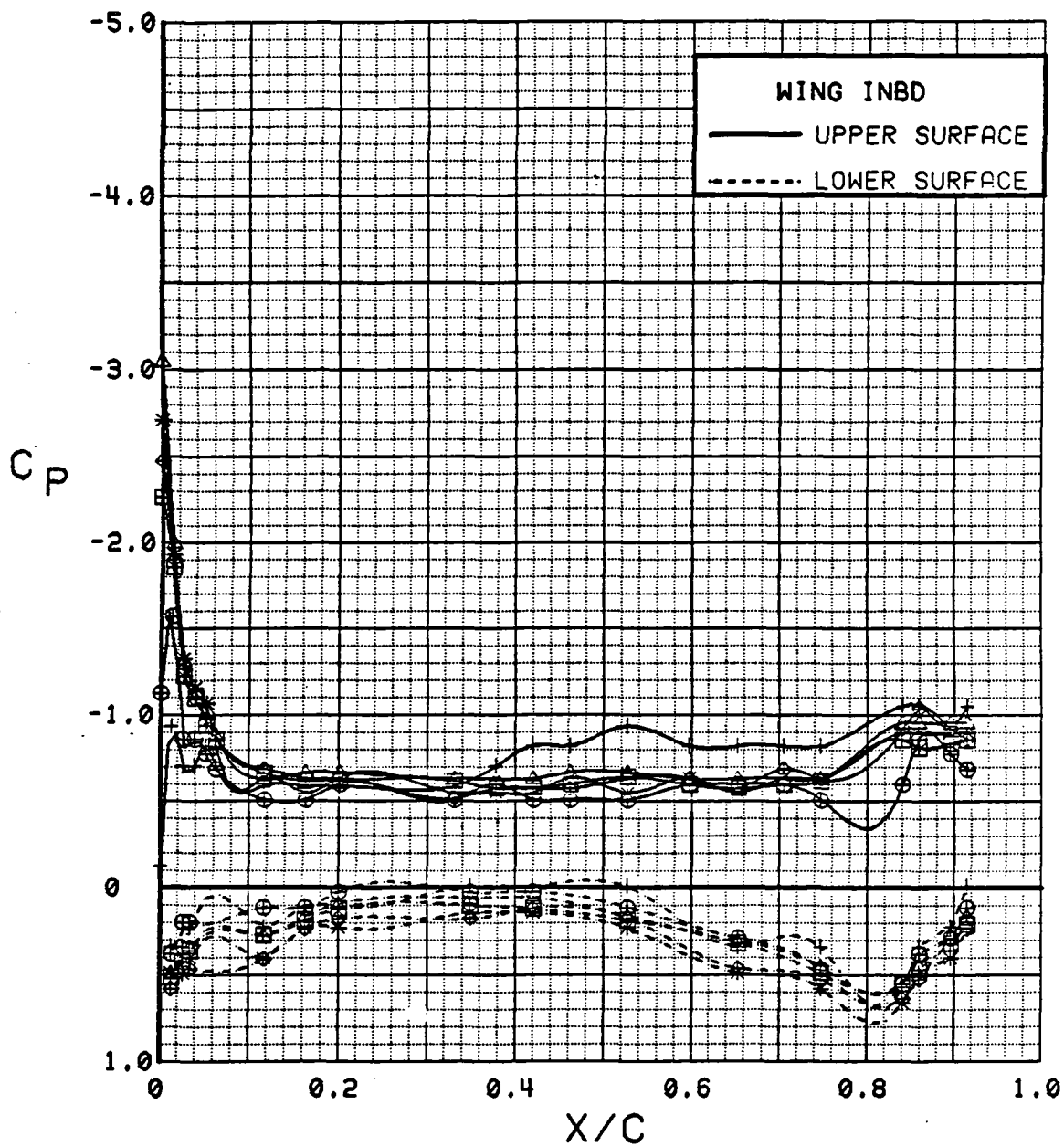


Figure 3.2.2-80 Power Effects, Flaps Deflected, Inboard, Alpha = 0 deg

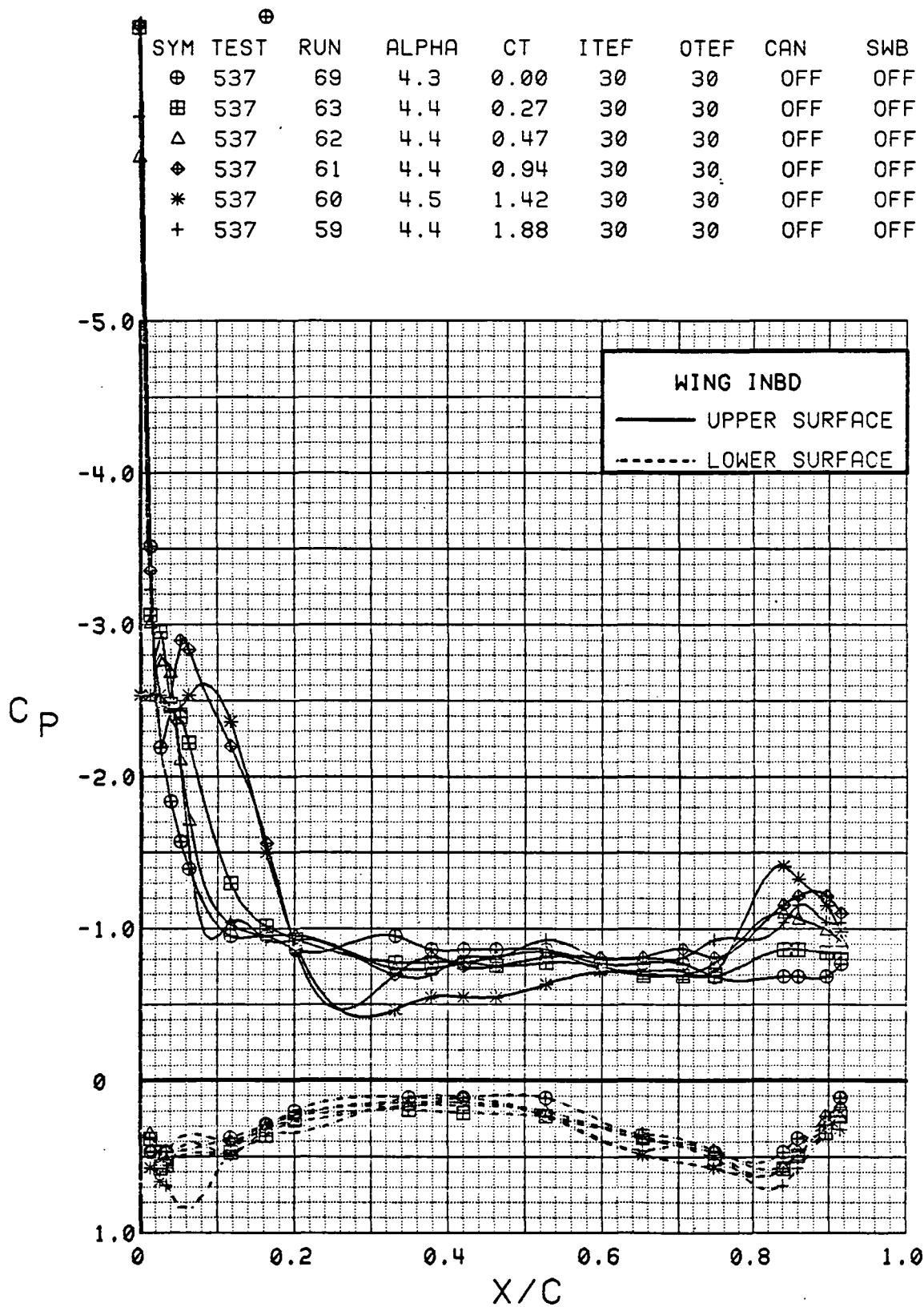


Figure 3.2.2-81 Power Effects, Flaps Deflected, Inboard, Alpha = 4 deg

SYM	TEST	RUN	ALPHA	CT	ITEF	OTEF	CAN	SWB
⊕	537	69	8.5	0.00	30	30	OFF	OFF
⊞	537	63	8.5	0.27	30	30	OFF	OFF
△	537	62	8.5	0.46	30	30	OFF	OFF
⊕	537	61	8.5	0.94	30	30	OFF	OFF
*	537	60	8.6	1.43	30	30	OFF	OFF
+	537	59	8.6	1.88	30	30	OFF	OFF

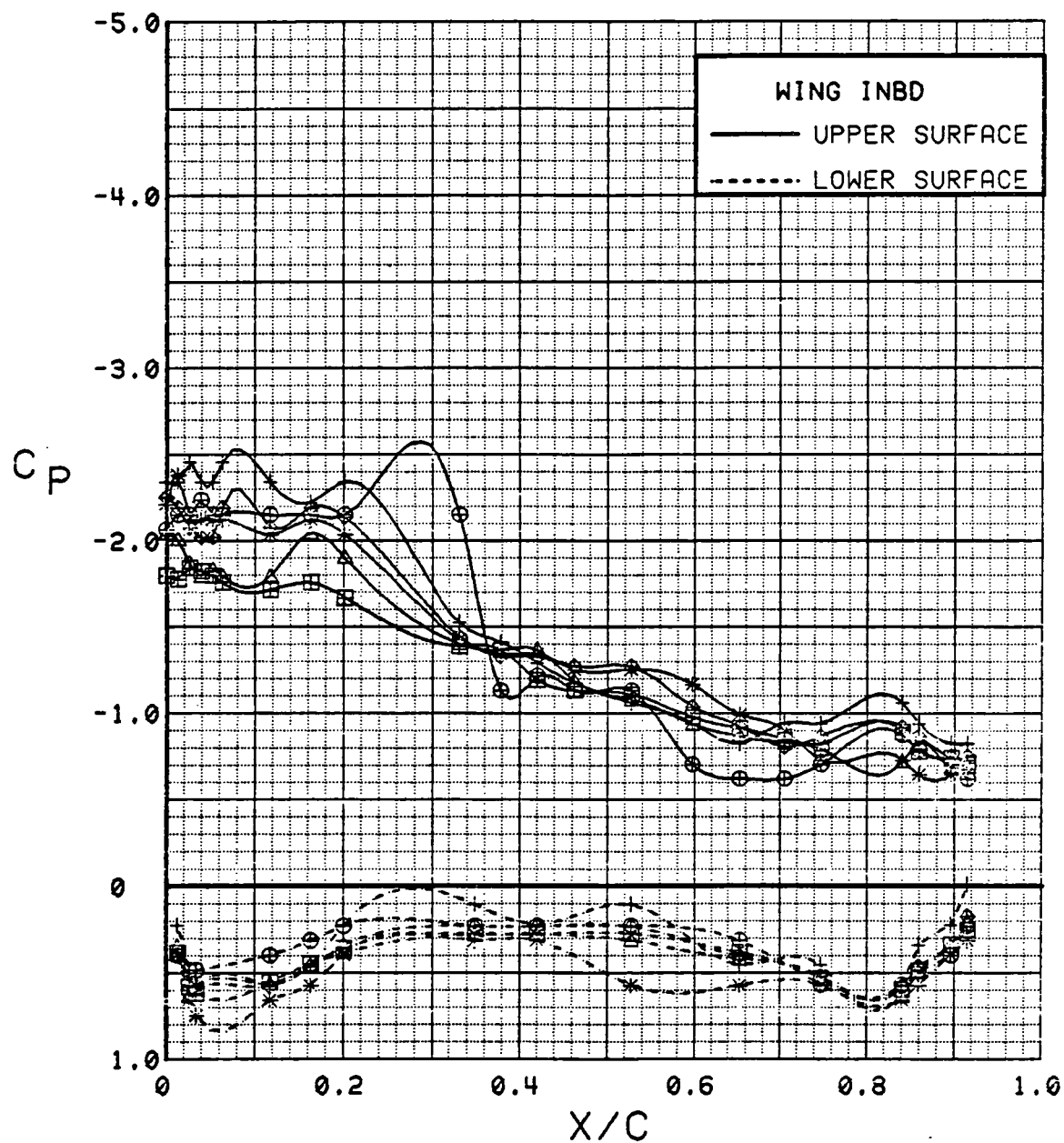


Figure 3.2.2-82 Power Effects, Flaps Deflected, Inboard, Alpha = 8 deg

SYM	TEST	RUN	ALPHA	CT	ITEF	OTEF	CAN	SWB
⊕	537	69	12.5	0.00	30	30	OFF	OFF
⊞	537	63	12.6	0.27	30	30	OFF	OFF
△	537	62	12.6	0.46	30	30	OFF	OFF
⬢	537	61	12.6	0.92	30	30	OFF	OFF
*	537	60	12.6	1.40	30	30	OFF	OFF
+	537	59	12.6	1.88	30	30	OFF	OFF

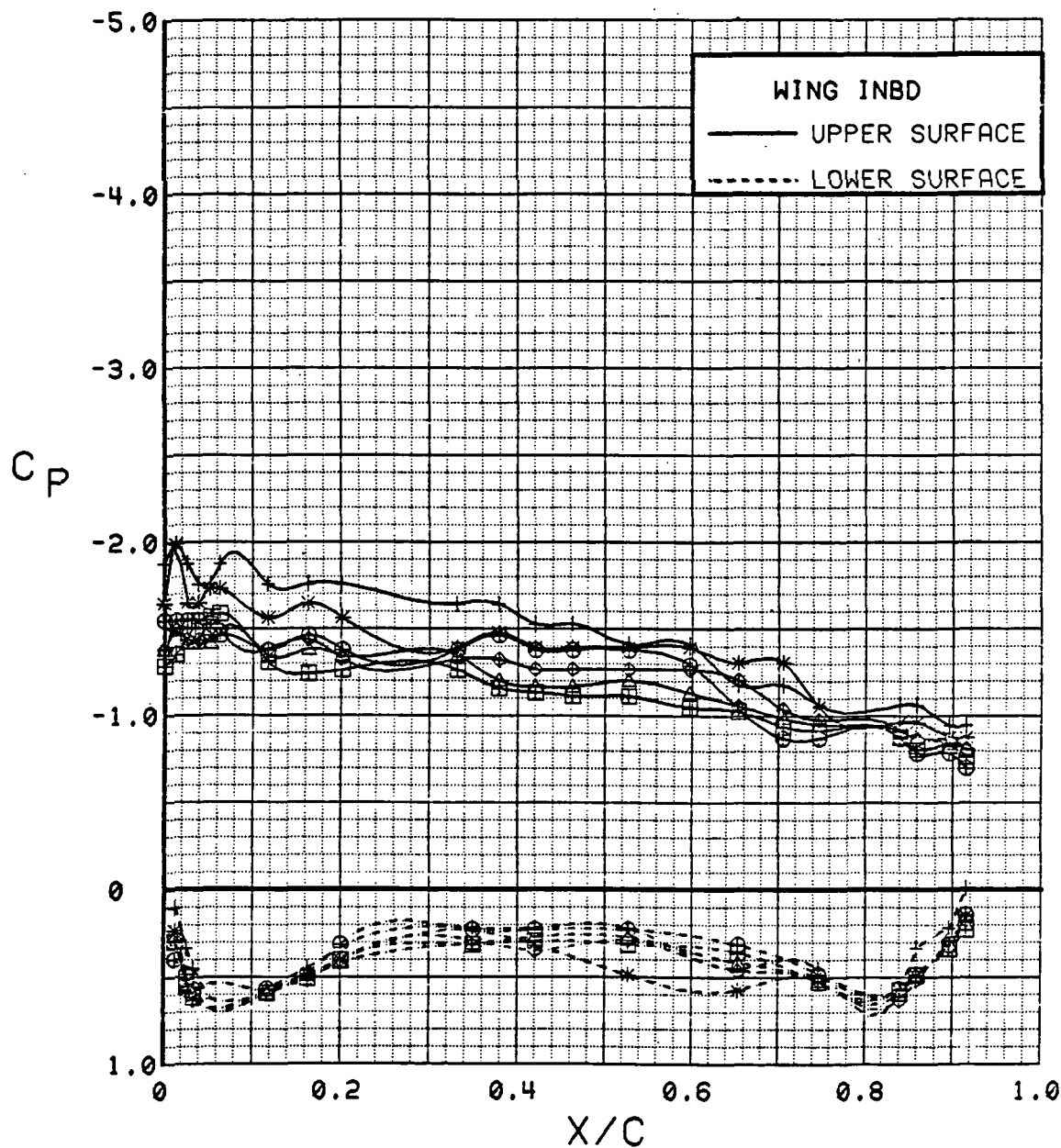


Figure 3.2.2-83

Power Effects, Flaps Deflected, Inboard, Alpha = 12 deg

ORIGINAL PAGE IS  
OF POOR QUALITY

SYM	TEST	RUN	ALPHA	CT	ITEF	OTEF	CAN	SWB
⊕	537	69	16.6	0.00	30	30	OFF	OFF
⊞	537	63	16.7	0.27	30	30	OFF	OFF
△	537	62	16.7	0.46	30	30	OFF	OFF
⊕	537	61	16.7	0.94	30	30	OFF	OFF
*	537	60	16.7	1.40	30	30	OFF	OFF
+	537	59	16.8	1.78	30	30	OFF	OFF

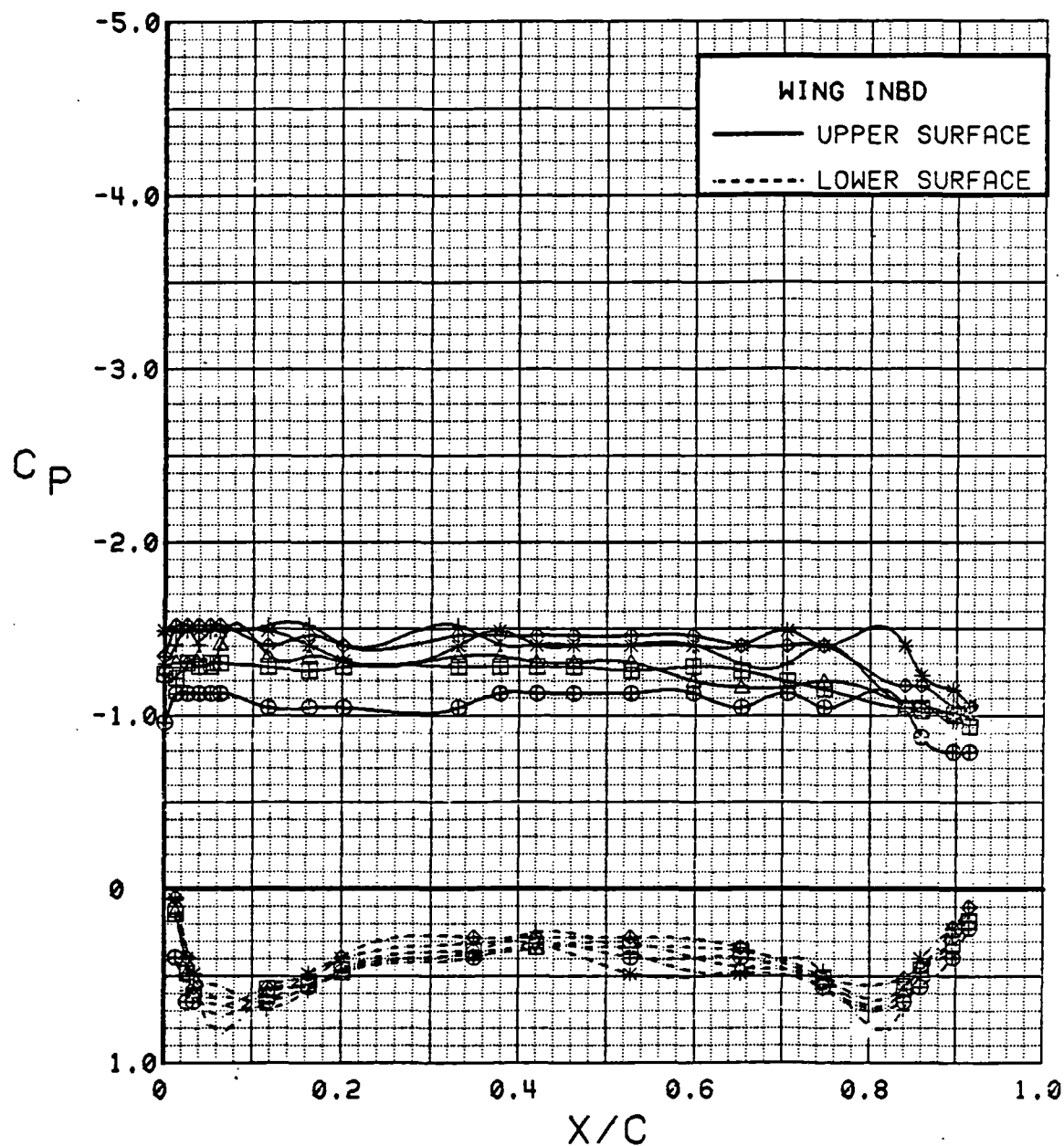


Figure 3.2.2-84 Power Effects, Flaps Deflected, Inboard, Alpha = 16 deg



SYM	TEST	RUN	ALPHA	CT	ITEF	OTEF	CAN	SWB
⊕	537	69	20.6	0.00	30	30	OFF	OFF
⊞	537	63	20.8	0.27	30	30	OFF	OFF
△	537	62	20.8	0.46	30	30	OFF	OFF
⬠	537	61	20.8	0.92	30	30	OFF	OFF
*	537	60	20.8	1.40	30	30	OFF	OFF
+	537	59	20.9	1.84	30	30	OFF	OFF

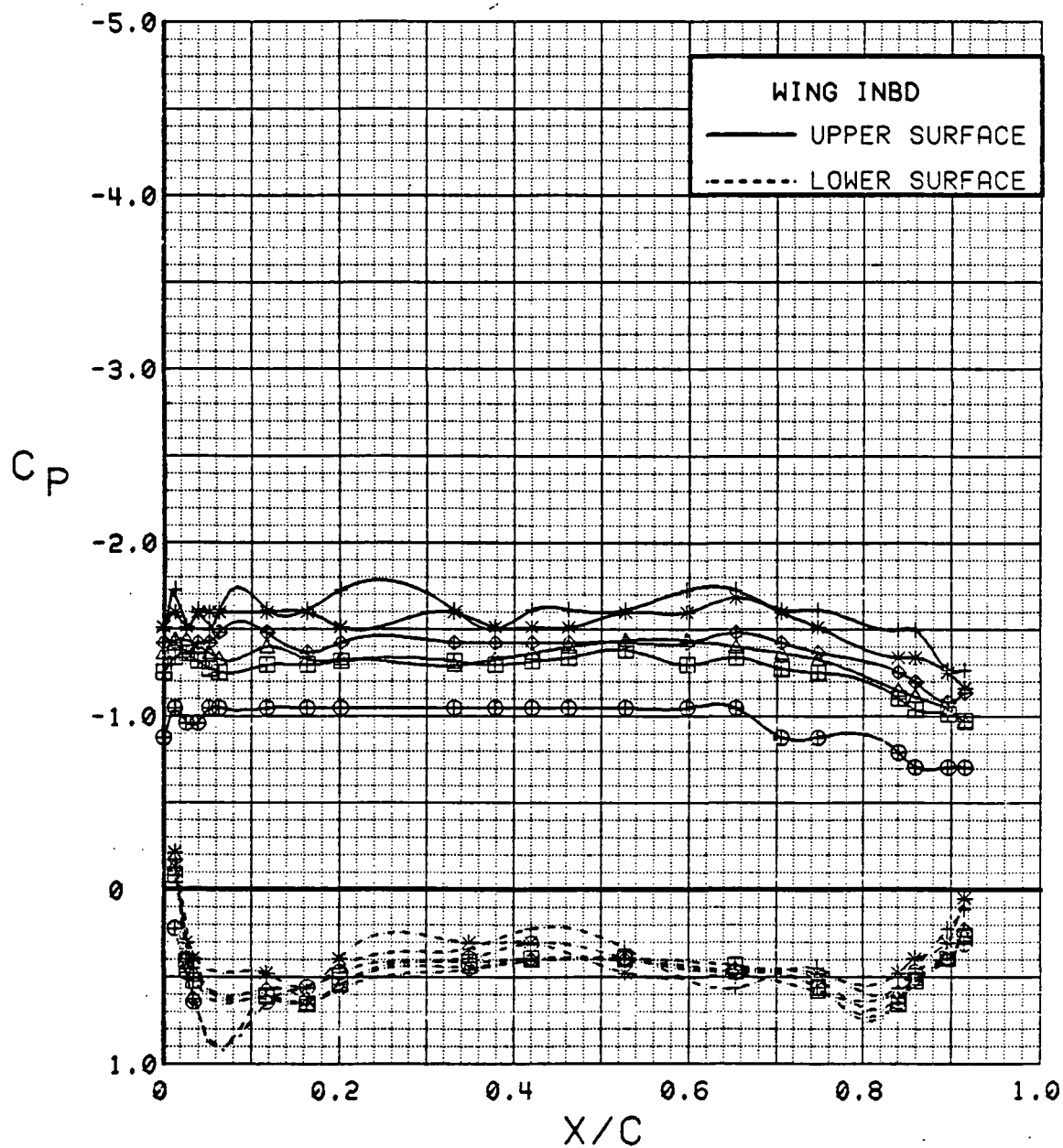


Figure 3.2.2-85 Power Effects, Flaps Deflected, Inboard, Alpha = 20 deg

SYM	TEST	RUN	ALPHA	CT	ITEF	OTEF	CAN	SWB
⊕	537	69	24.7	0.00	30	30	OFF	OFF
⊞	537	63	24.8	0.27	30	30	OFF	OFF
△	537	62	24.8	0.46	30	30	OFF	OFF
⊕	537	61	24.9	0.92	30	30	OFF	OFF
*	537	60	24.9	1.41	30	30	OFF	OFF
+	537	59	24.9	1.89	30	30	OFF	OFF

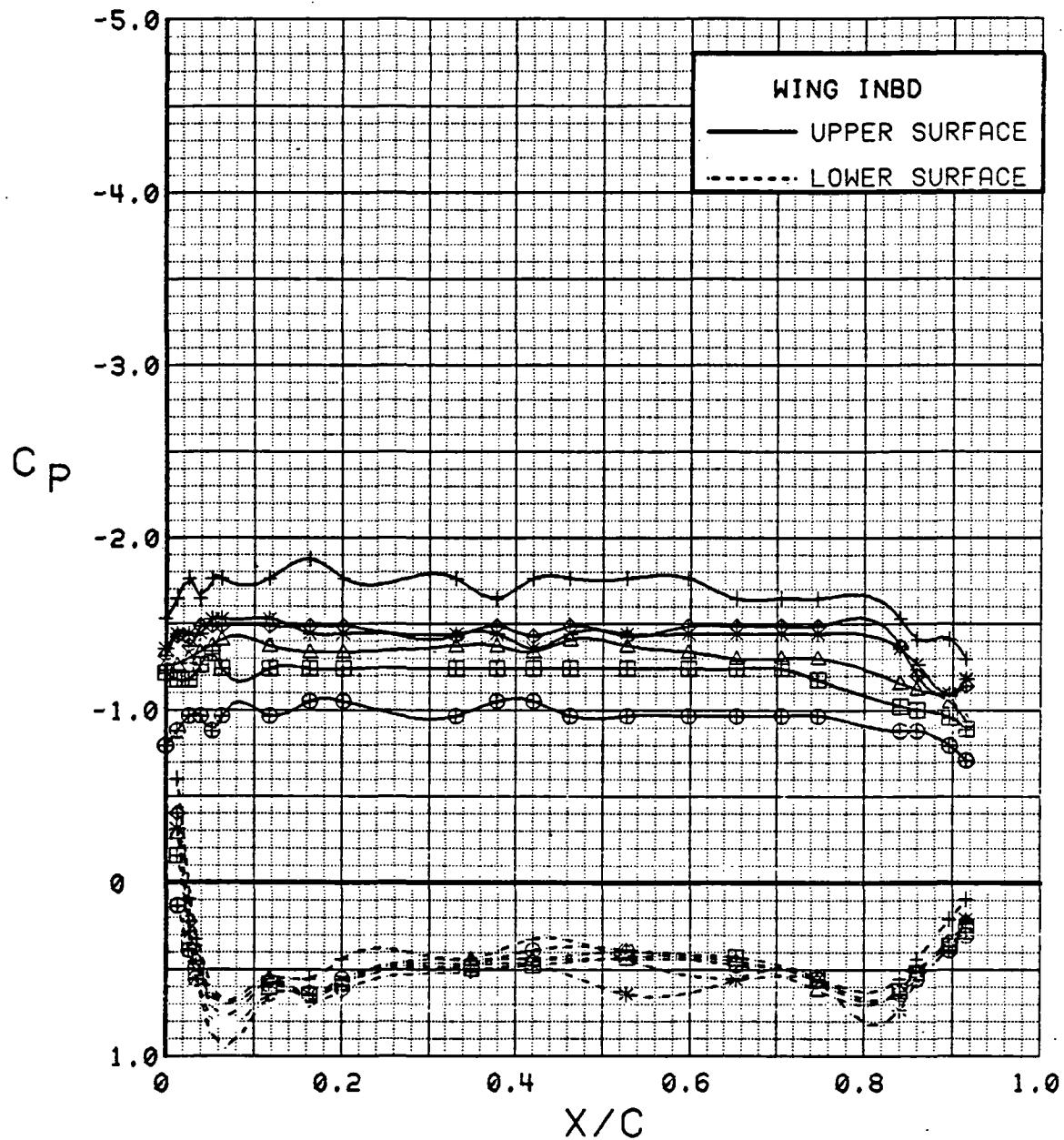


Figure 3.2.2-86 Power Effects, Flaps Deflected, Inboard, Alpha = 24 deg

SYM	TEST	RUN	ALPHA	CT	ITEF	OTEF	CAN	SWB
⊕	537	69	28.7	0.00	30	30	OFF	OFF
⊞	537	63	28.8	0.27	30	30	OFF	OFF
△	537	62	28.9	0.46	30	30	OFF	OFF
⬠	537	61	28.9	0.93	30	30	OFF	OFF
*	537	60	28.9	1.41	30	30	OFF	OFF
+	537	59	29.0	1.84	30	30	OFF	OFF

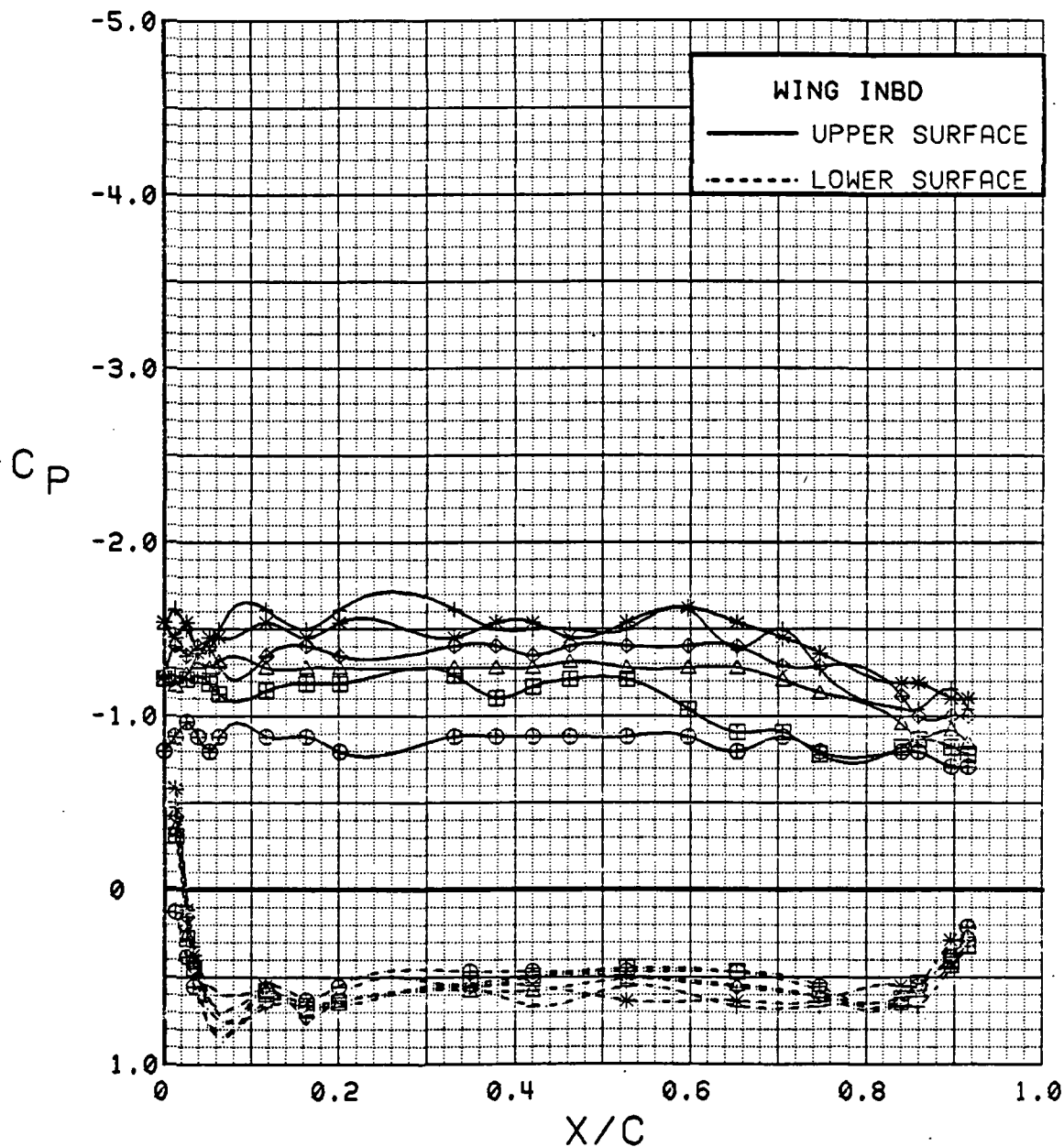


Figure 3.2.2-87 Power Effects, Flaps Deflected, Inboard, Alpha = 28 deg

SYM	TEST	RUN	ALPHA	CT	ITEF	OTEF	CAN	SWB
⊕	537	69	32.7	0.00	30	30	OFF	OFF
⊞	537	62	32.8	0.46	30	30	OFF	OFF
△	537	61	32.9	0.93	30	30	OFF	OFF
⬢	537	60	33.0	1.40	30	30	OFF	OFF
*	537	59	33.0	1.87	30	30	OFF	OFF

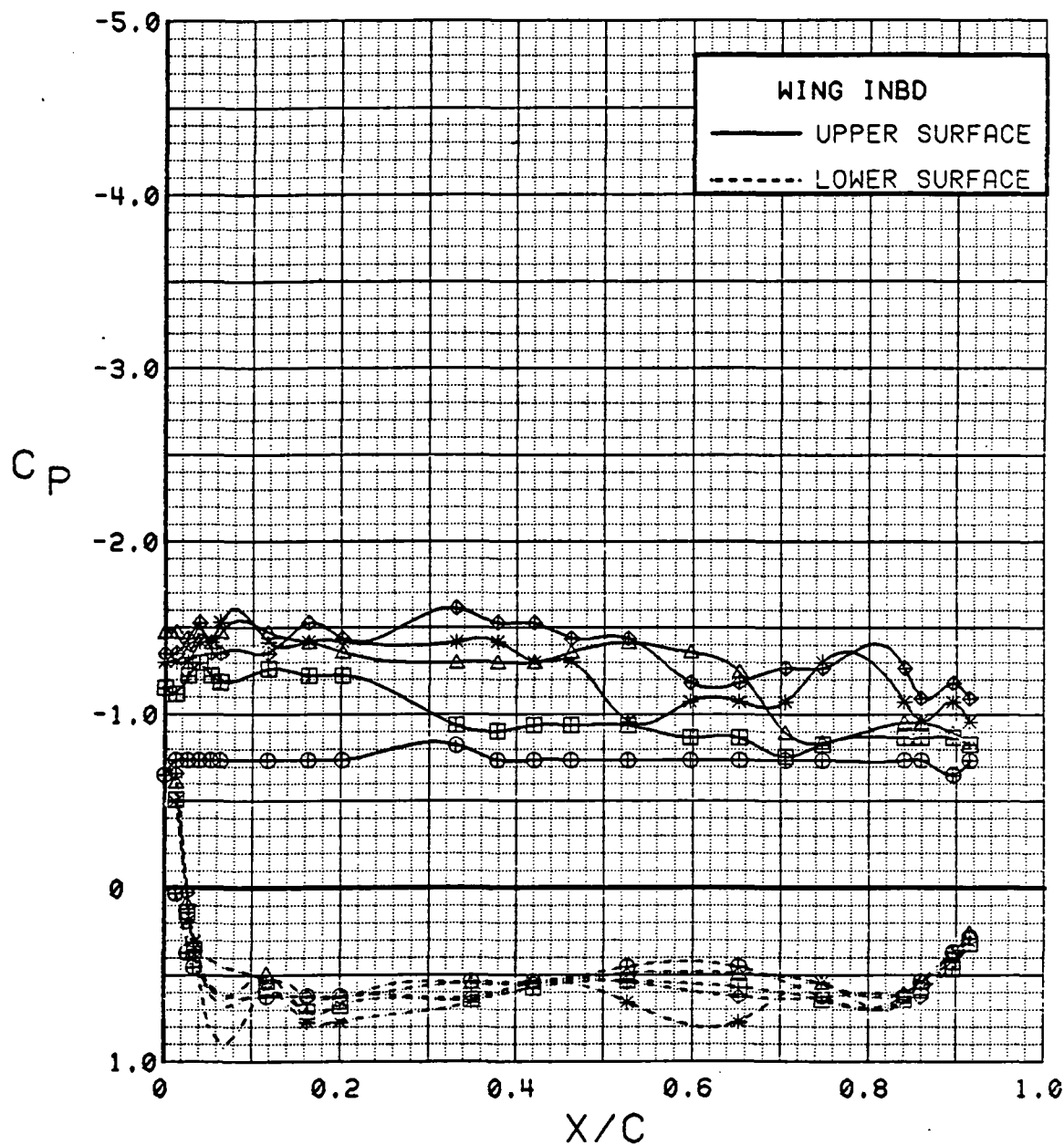


Figure 3.2.2-88 Power Effects, Flaps Deflected, Inboard, Alpha = 32 deg

SYM	TEST	RUN	ALPHA	CT	ITEF	OTEF	CAN	SWB
⊕	537	69	0.2	0.00	30	30	OFF	OFF
⊞	537	63	0.3	0.28	30	30	OFF	OFF
△	537	62	0.3	0.46	30	30	OFF	OFF
⊕	537	61	0.4	0.94	30	30	OFF	OFF
*	537	60	0.3	1.42	30	30	OFF	OFF
+	537	59	0.3	1.88	30	30	OFF	OFF

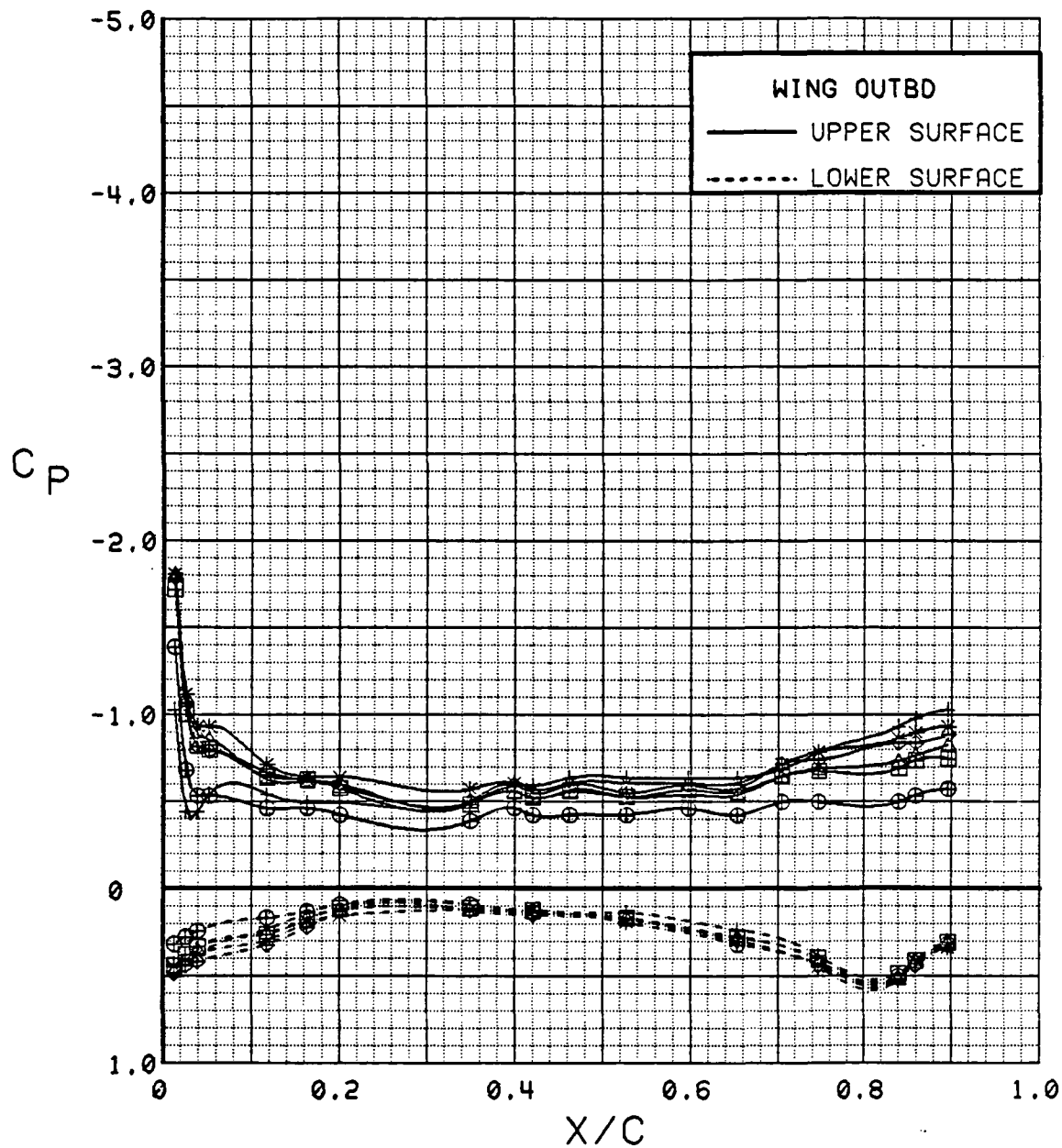


Figure 3.2.2-89 Power Effects, Flaps Deflected, Outboard, Alpha = 0 deg

SYM	TEST	RUN	ALPHA	CT	ITEF	OTEF	CAN	SWB
⊕	537	69	4.3	0.00	30	30	OFF	OFF
⊞	537	63	4.4	0.27	30	30	OFF	OFF
△	537	62	4.4	0.47	30	30	OFF	OFF
⬢	537	61	4.4	0.94	30	30	OFF	OFF
*	537	60	4.5	1.42	30	30	OFF	OFF
+	537	59	4.4	1.88	30	30	OFF	OFF

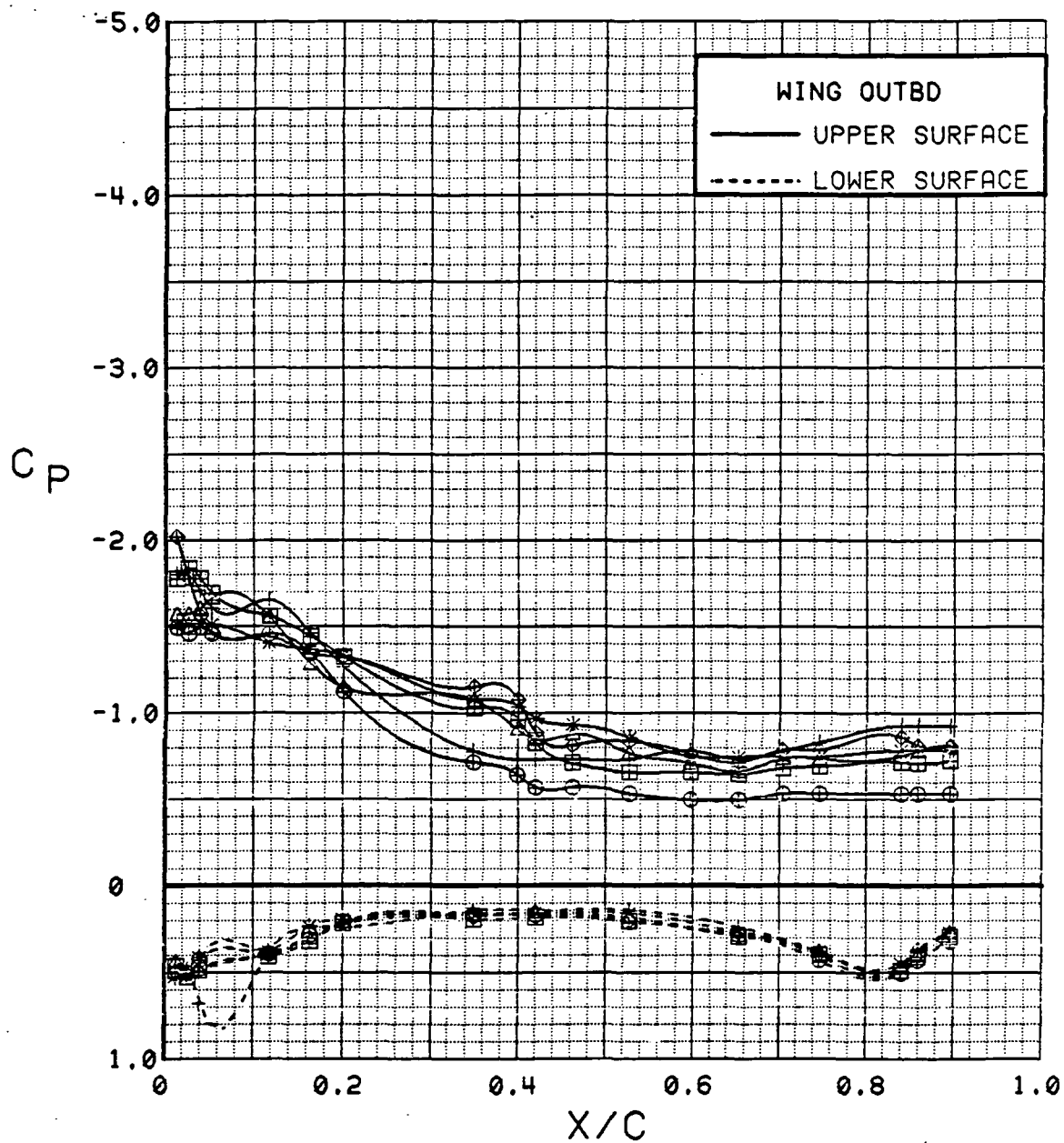


Figure 3.2.2-90 Power Effects, Flaps Deflected, Outboard, Alpha = 4 deg

SYM	TEST	RUN	ALPHA	CT	ITEF	OTEF	CAN	SWB
⊕	537	69	8.5	0.00	30	30	OFF	OFF
⊞	537	63	8.5	0.27	30	30	OFF	OFF
△	537	62	8.5	0.46	30	30	OFF	OFF
⊕	537	61	8.5	0.94	30	30	OFF	OFF
*	537	60	8.6	1.43	30	30	OFF	OFF
+	537	59	8.6	1.88	30	30	OFF	OFF

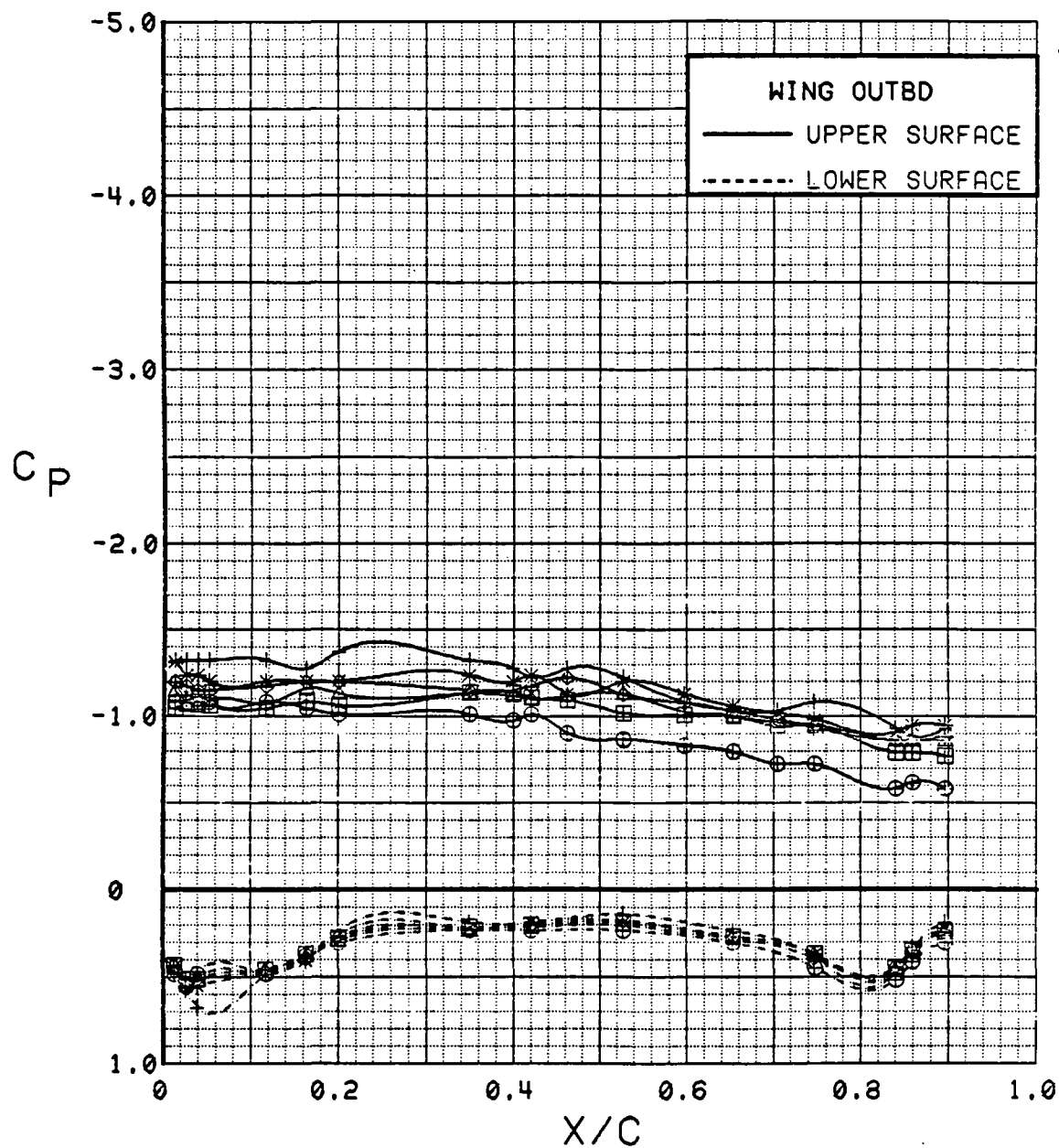


Figure 3.2.2-91 Power Effects, Flaps Deflected, Outboard, Alpha = 8 deg

SYM	TEST	RUN	ALPHA	CT	ITEF	OTEF	CAN	SWB
⊕	537	69	12.5	0.00	30	30	OFF	OFF
⊞	537	63	12.6	0.27	30	30	OFF	OFF
△	537	62	12.6	0.46	30	30	OFF	OFF
⊕	537	61	12.6	0.92	30	30	OFF	OFF
*	537	60	12.6	1.40	30	30	OFF	OFF
+	537	59	12.6	1.88	30	30	OFF	OFF

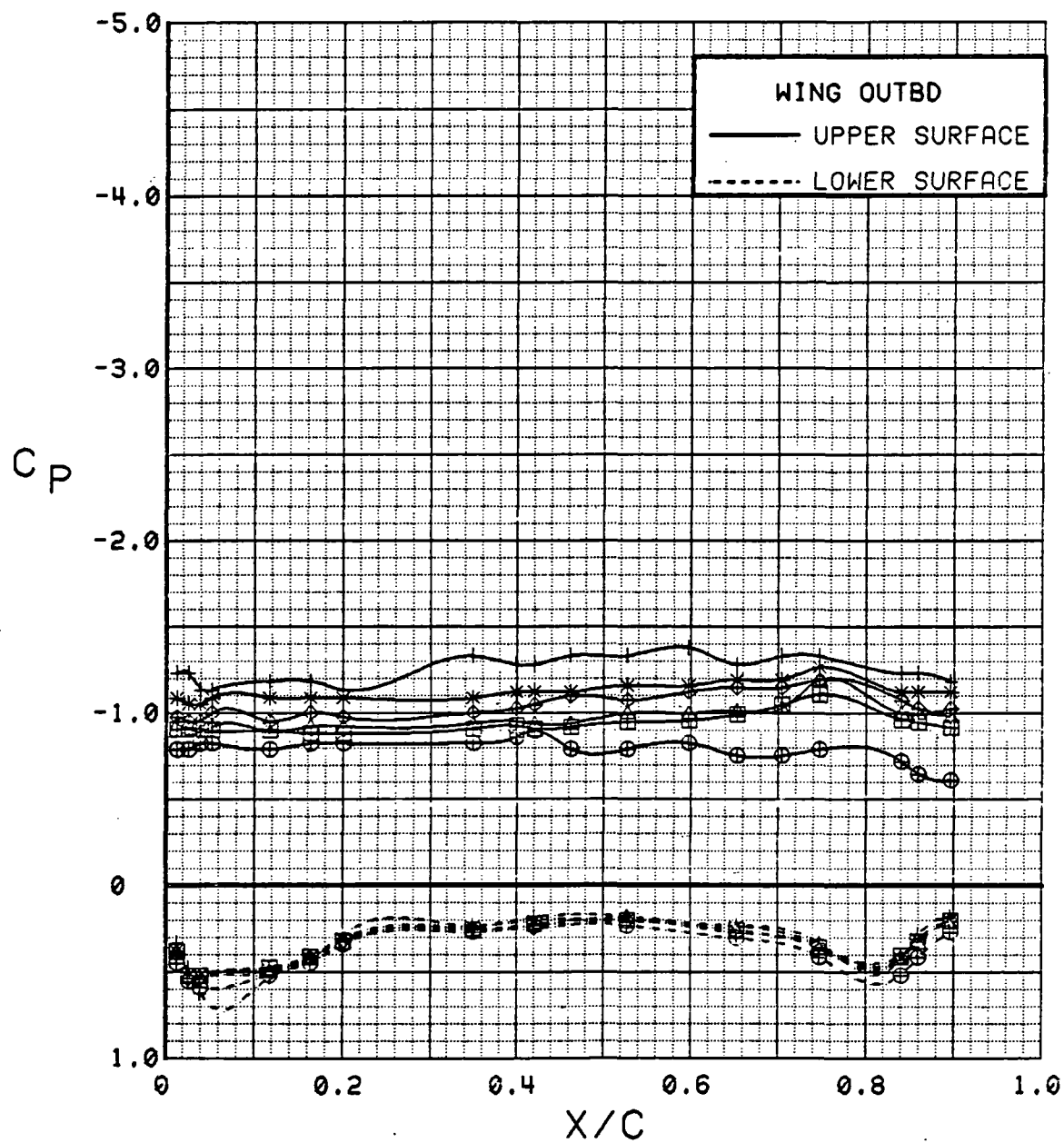


Figure 3.2.2-92 Power Effects, Flaps Deflected, Outboard, Alpha = 12 deg



SYM	TEST	RUN	ALPHA	CT	ITEF	OTEF	CAN	SWB
⊕	537	69	16.6	0.00	30	30	OFF	OFF
⊞	537	63	16.7	0.27	30	30	OFF	OFF
△	537	62	16.7	0.46	30	30	OFF	OFF
⬠	537	61	16.7	0.94	30	30	OFF	OFF
*	537	60	16.7	1.40	30	30	OFF	OFF
+	537	59	16.8	1.78	30	30	OFF	OFF

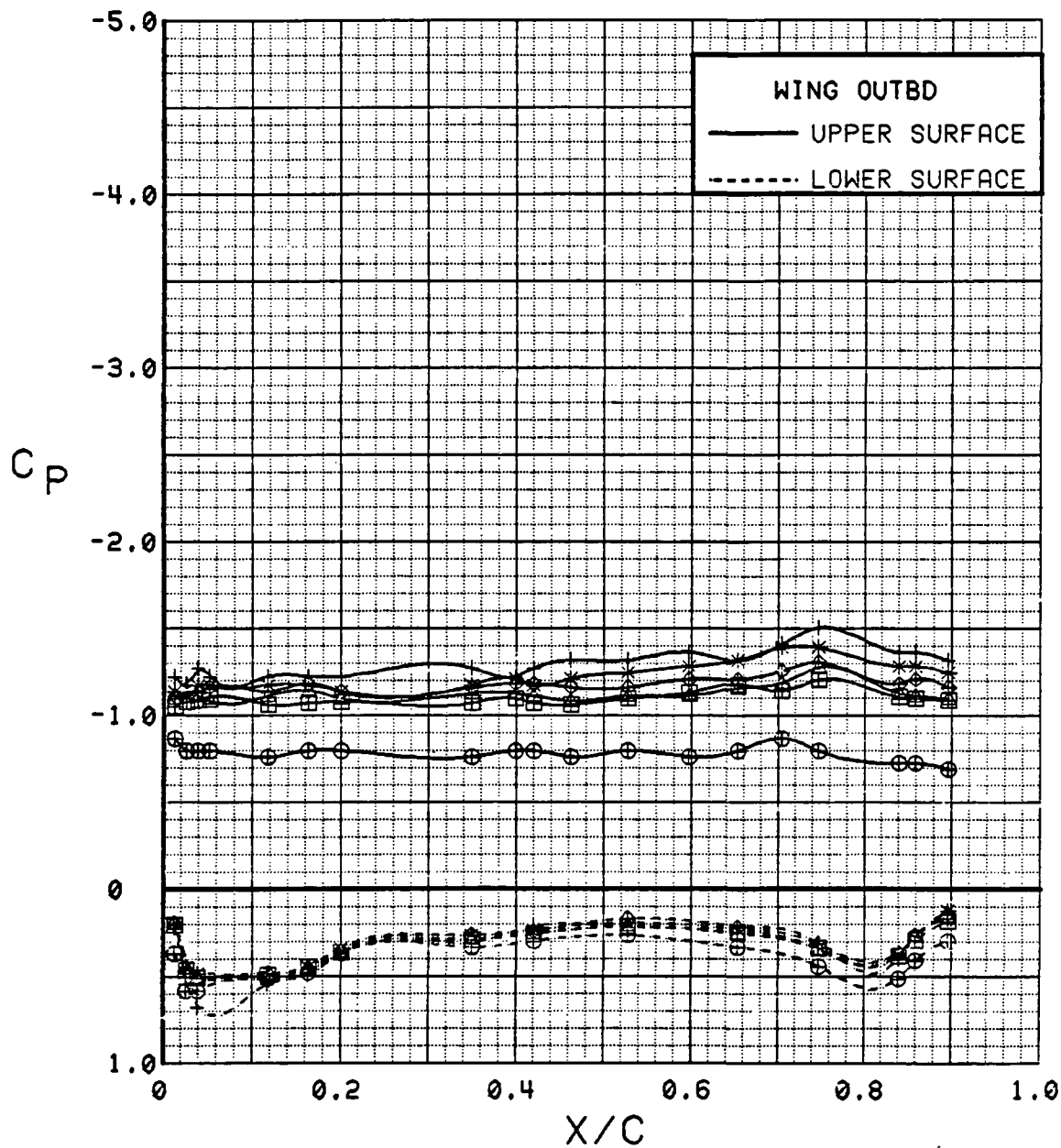


Figure 3.2.2-93 Power Effects, Flaps Deflected, Outboard, Alpha = 16 deg

SYM	TEST	RUN	ALPHA	CT	ITEF	OTEF	CAN	SWB
⊕	537	69	20.6	0.00	30	30	OFF	OFF
⊞	537	63	20.8	0.27	30	30	OFF	OFF
△	537	62	20.8	0.46	30	30	OFF	OFF
◆	537	61	20.8	0.92	30	30	OFF	OFF
*	537	60	20.8	1.40	30	30	OFF	OFF
+	537	59	20.9	1.84	30	30	OFF	OFF

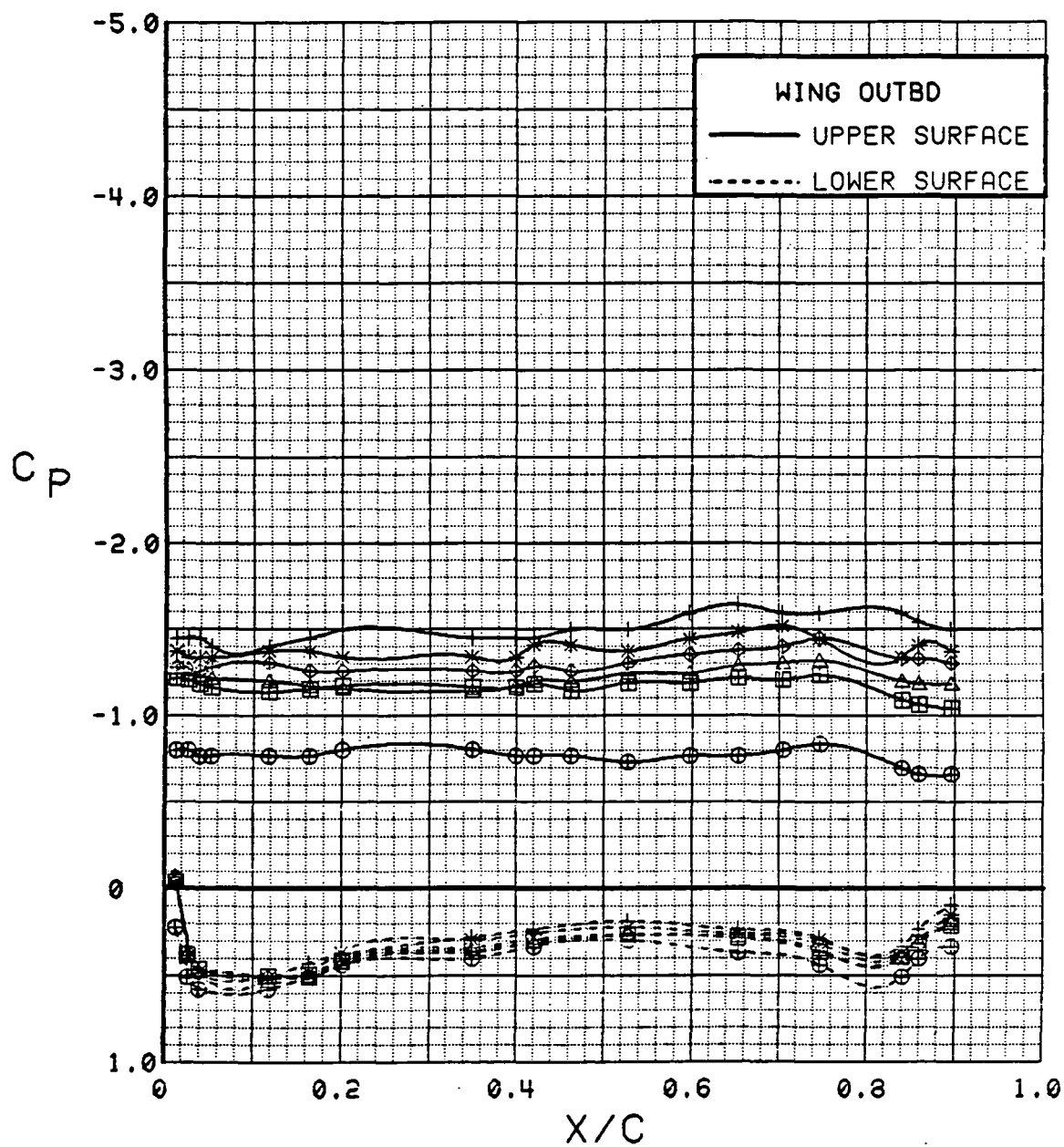


Figure 3.2.2-94 Power Effects, Flaps Deflected, Outboard, Alpha = 20 deg

SYM	TEST	RUN	ALPHA	CT	ITEF	OTEF	CAN	SWB
⊕	537	69	24.7	0.00	30	30	OFF	OFF
⊞	537	63	24.8	0.27	30	30	OFF	OFF
△	537	62	24.8	0.46	30	30	OFF	OFF
⊕	537	61	24.9	0.92	30	30	OFF	OFF
*	537	60	24.9	1.41	30	30	OFF	OFF
+	537	59	24.9	1.89	30	30	OFF	OFF

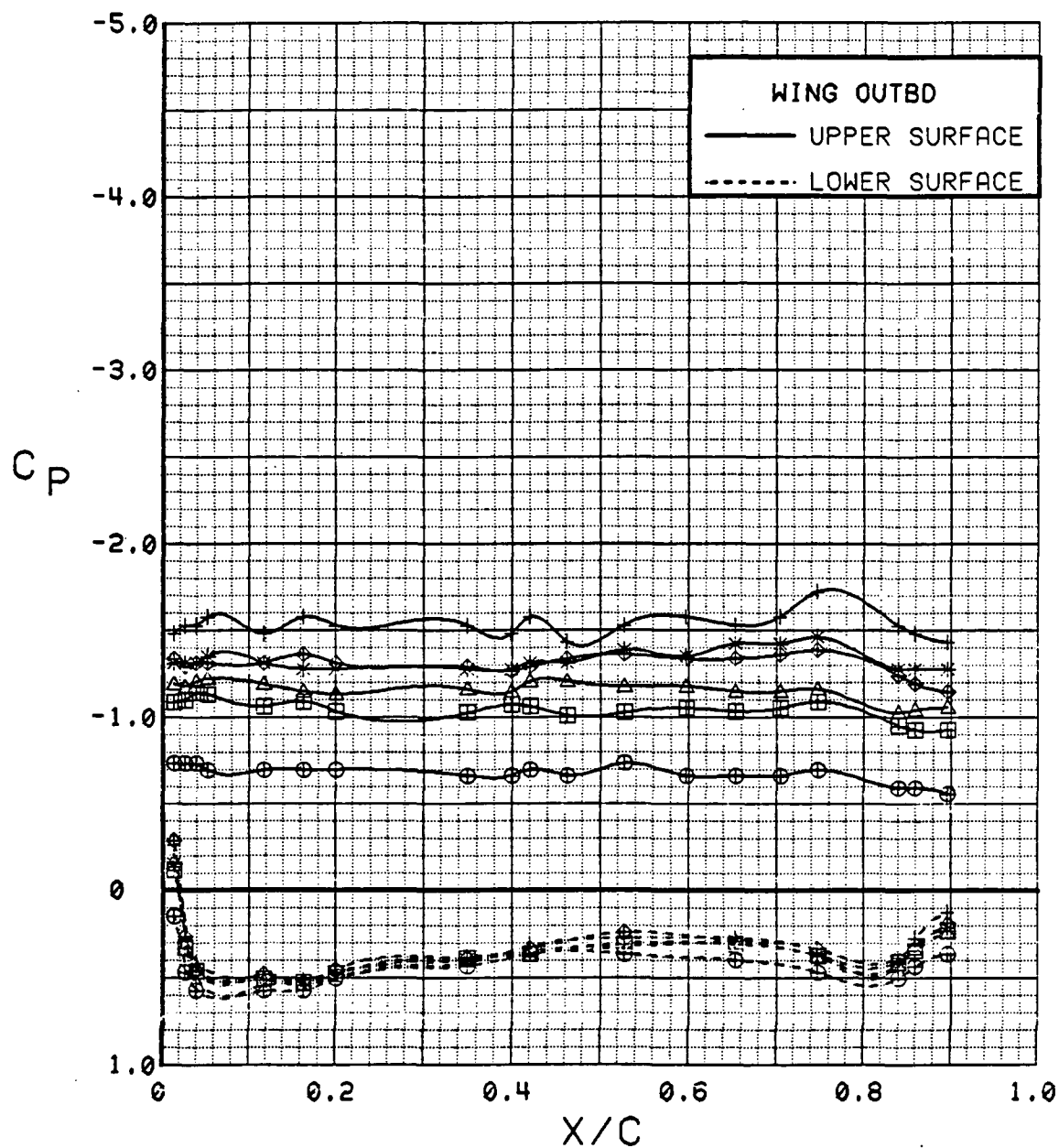


Figure 3.2.2-95 Power Effects, Flaps Deflected, Outboard, Alpha = 24 deg

SYM	TEST	RUN	ALPHA	CT	ITEF	OTEF	CAN	SWB
⊕	537	69	28.7	0.00	30	30	OFF	OFF
⊞	537	63	28.8	0.27	30	30	OFF	OFF
△	537	62	28.9	0.46	30	30	OFF	OFF
⬢	537	61	28.9	0.93	30	30	OFF	OFF
*	537	60	28.9	1.41	30	30	OFF	OFF
+	537	59	29.0	1.84	30	30	OFF	OFF

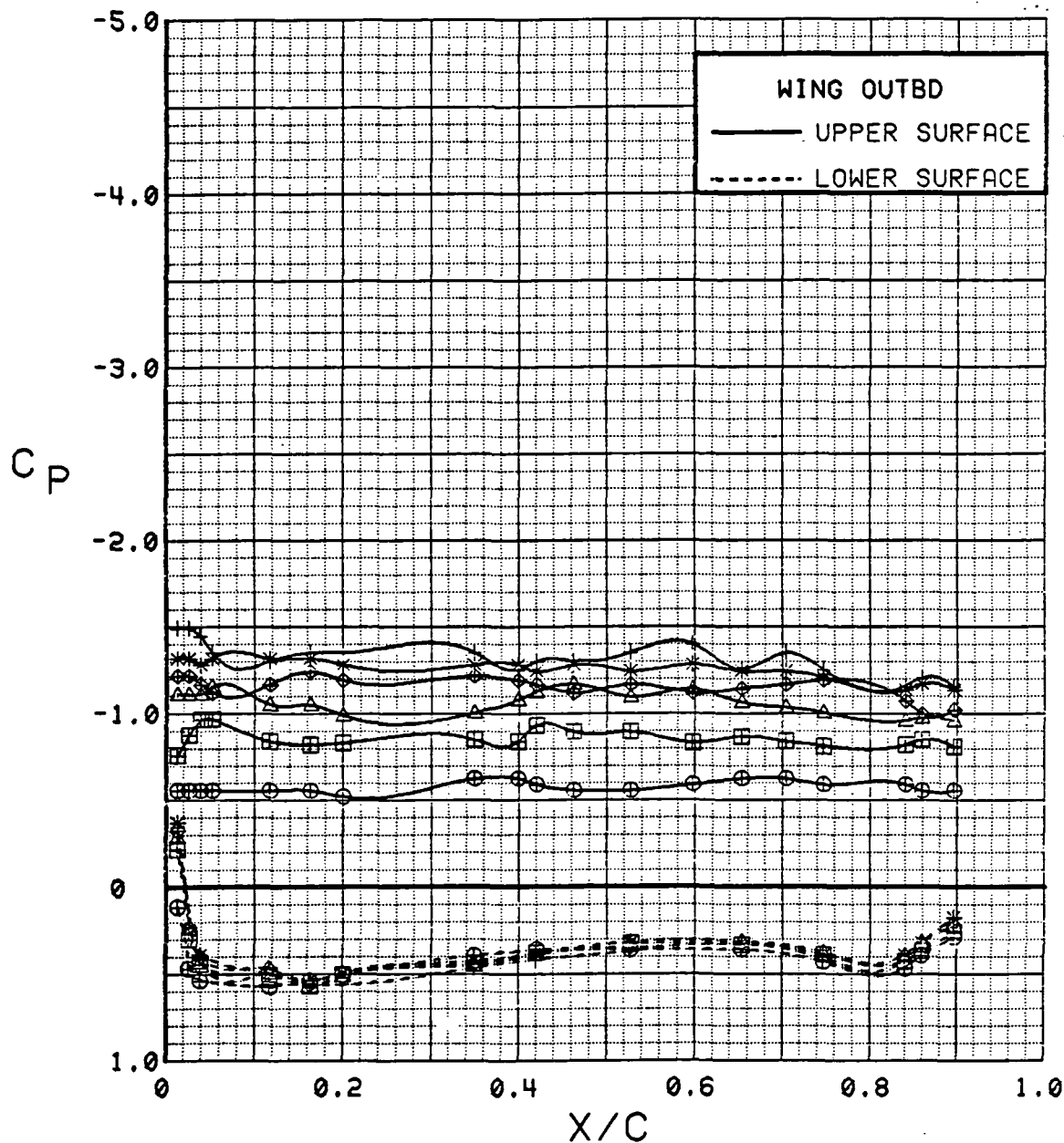


Figure 3.2.2-96 Power Effects, Flaps Deflected, Outboard, Alpha = 28 deg

SYM	TEST	RUN	ALPHA	CT	ITEF	OTEF	CAN	SWB
⊕	537	69	32.7	0.00	30	30	OFF	OFF
⊞	537	62	32.8	0.46	30	30	OFF	OFF
△	537	61	32.9	0.93	30	30	OFF	OFF
⊕	537	60	33.0	1.40	30	30	OFF	OFF
*	537	59	33.0	1.87	30	30	OFF	OFF

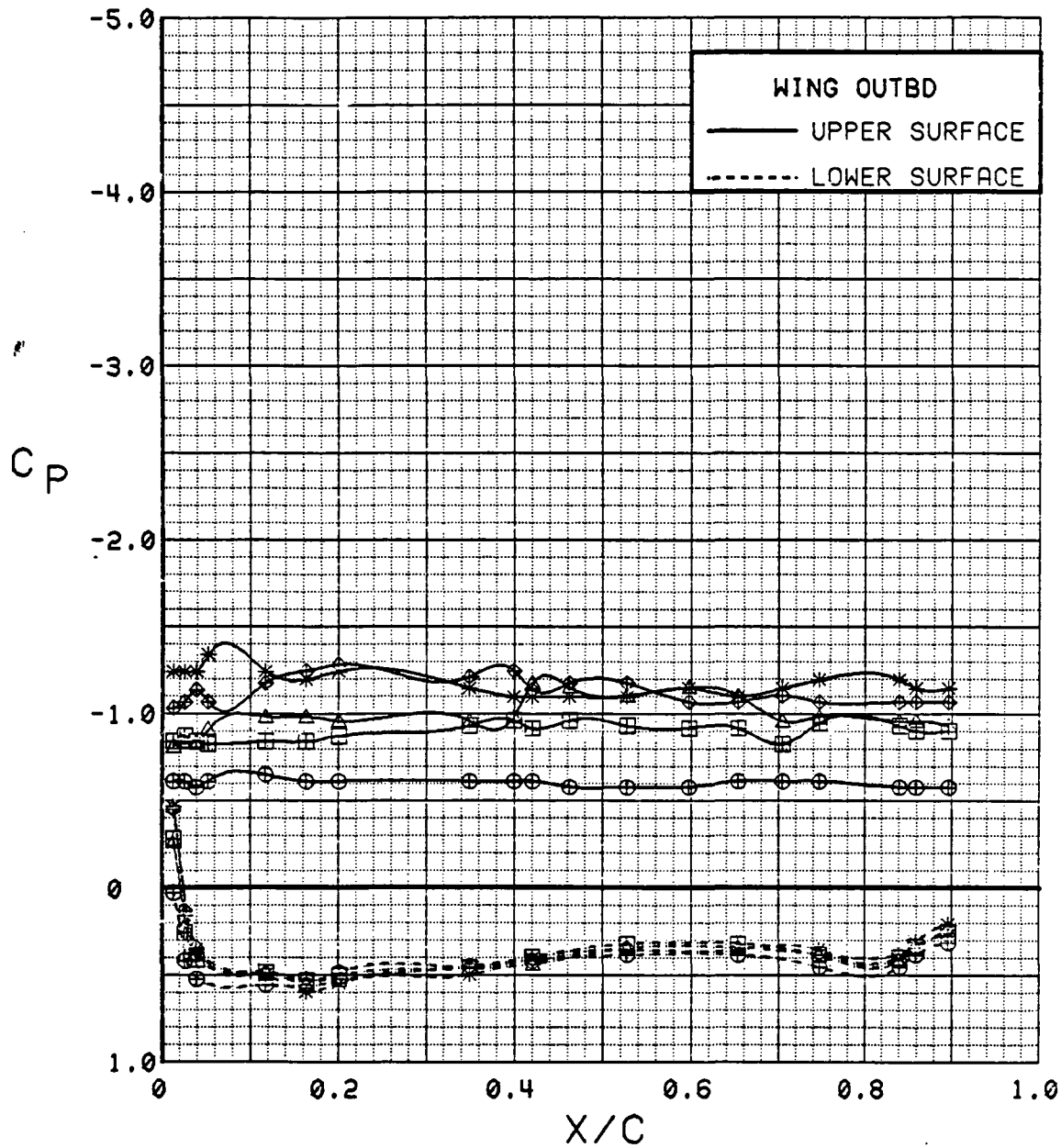


Figure 3.2.2-97 Power Effects, Flaps Deflected, Outboard, Alpha = 32 deg

SYM	TEST	RUN	ALPHA	CT	ITEF	OTEF	CAN	SWB
⊙	537	69	0.2	0.00	30	30	OFF	OFF
⊠	537	63	0.3	0.28	30	30	OFF	OFF
△	537	62	0.3	0.46	30	30	OFF	OFF
◆	537	61	0.4	0.94	30	30	OFF	OFF
*	537	60	0.3	1.42	30	30	OFF	OFF
+	537	59	0.3	1.88	30	30	OFF	OFF

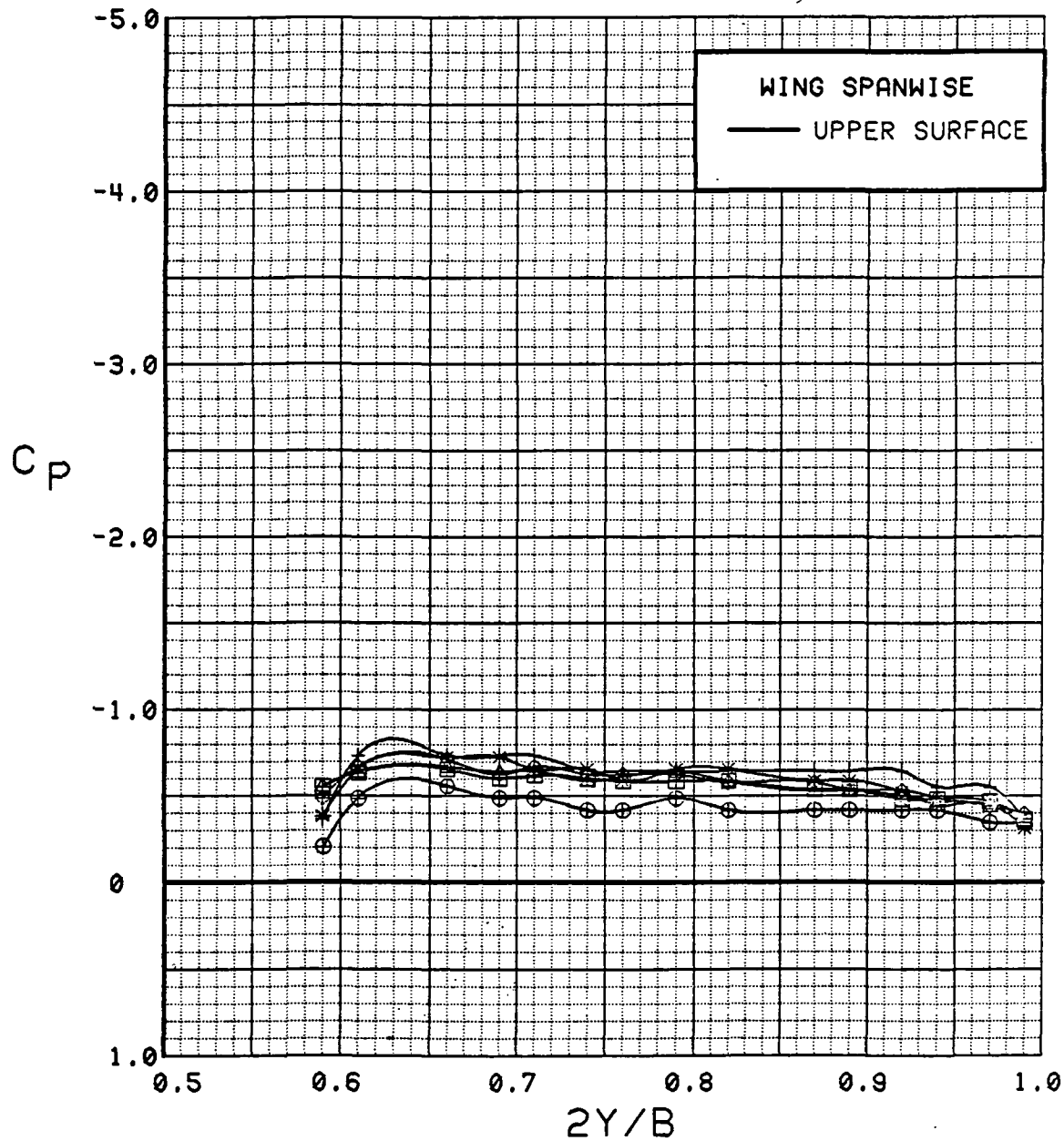


Figure 3.2.2-98 Power Effects, Flaps Deflected, Spanwise, Alpha = 0 deg

SYM	TEST	RUN	ALPHA	CT	ITEF	OTEF	CAN	SWB
⊕	537	69	4.3	0.00	30	30	OFF	OFF
⊞	537	63	4.4	0.27	30	30	OFF	OFF
△	537	62	4.4	0.47	30	30	OFF	OFF
◆	537	61	4.4	0.94	30	30	OFF	OFF
*	537	60	4.5	1.42	30	30	OFF	OFF
+	537	59	4.4	1.88	30	30	OFF	OFF

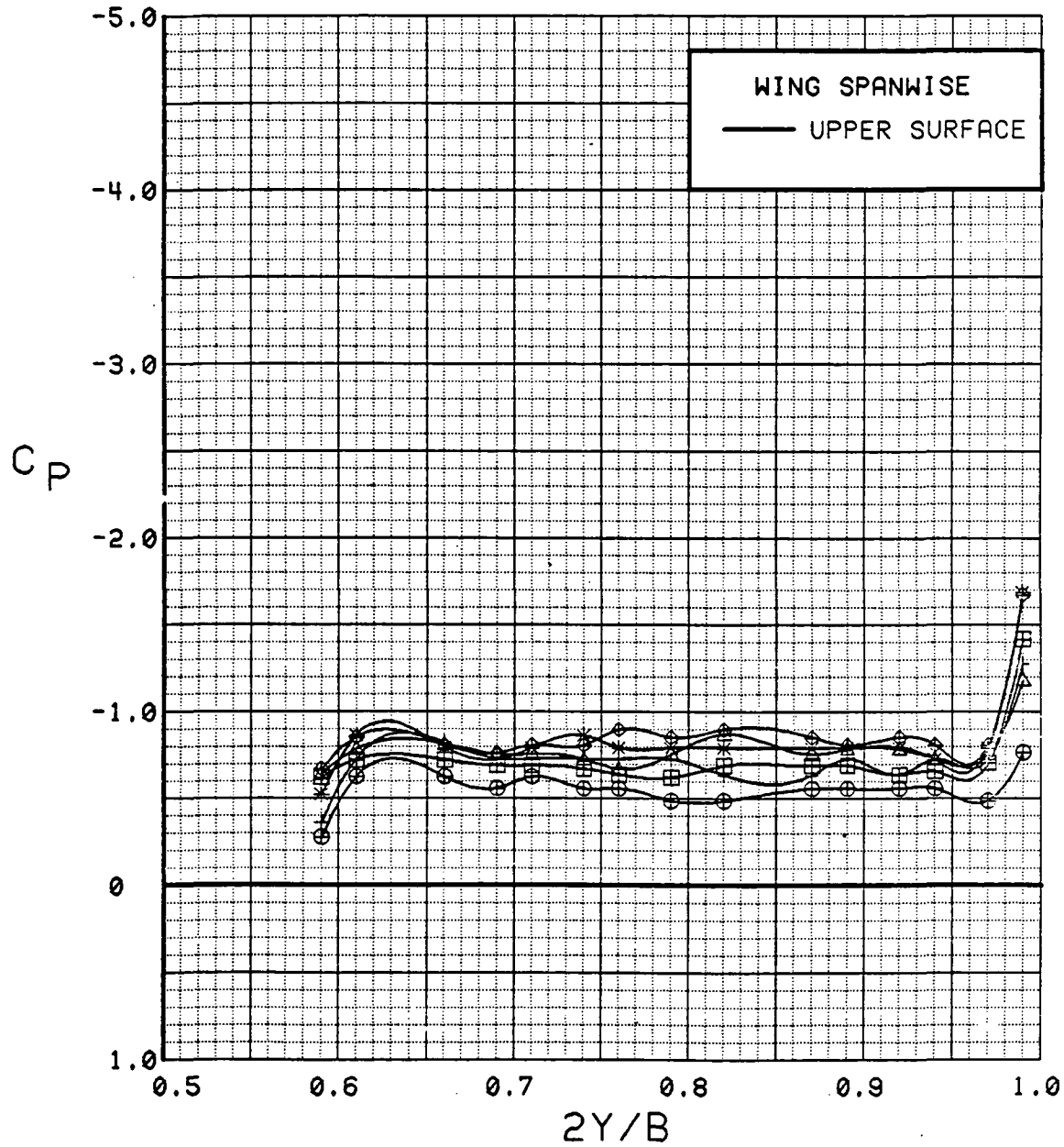


Figure 3.2.2-99 Power Effects, Flaps Deflected, Spanwise, Alpha = 4 deg

SYM	TEST	RUN	ALPHA	CT	ITEF	OTEF	CAN	SWB
⊕	537	69	8.5	0.00	30	30	OFF	OFF
⊞	537	63	8.5	0.27	30	30	OFF	OFF
△	537	62	8.5	0.46	30	30	OFF	OFF
◆	537	61	8.5	0.94	30	30	OFF	OFF
*	537	60	8.6	1.43	30	30	OFF	OFF
+	537	59	8.6	1.88	30	30	OFF	OFF

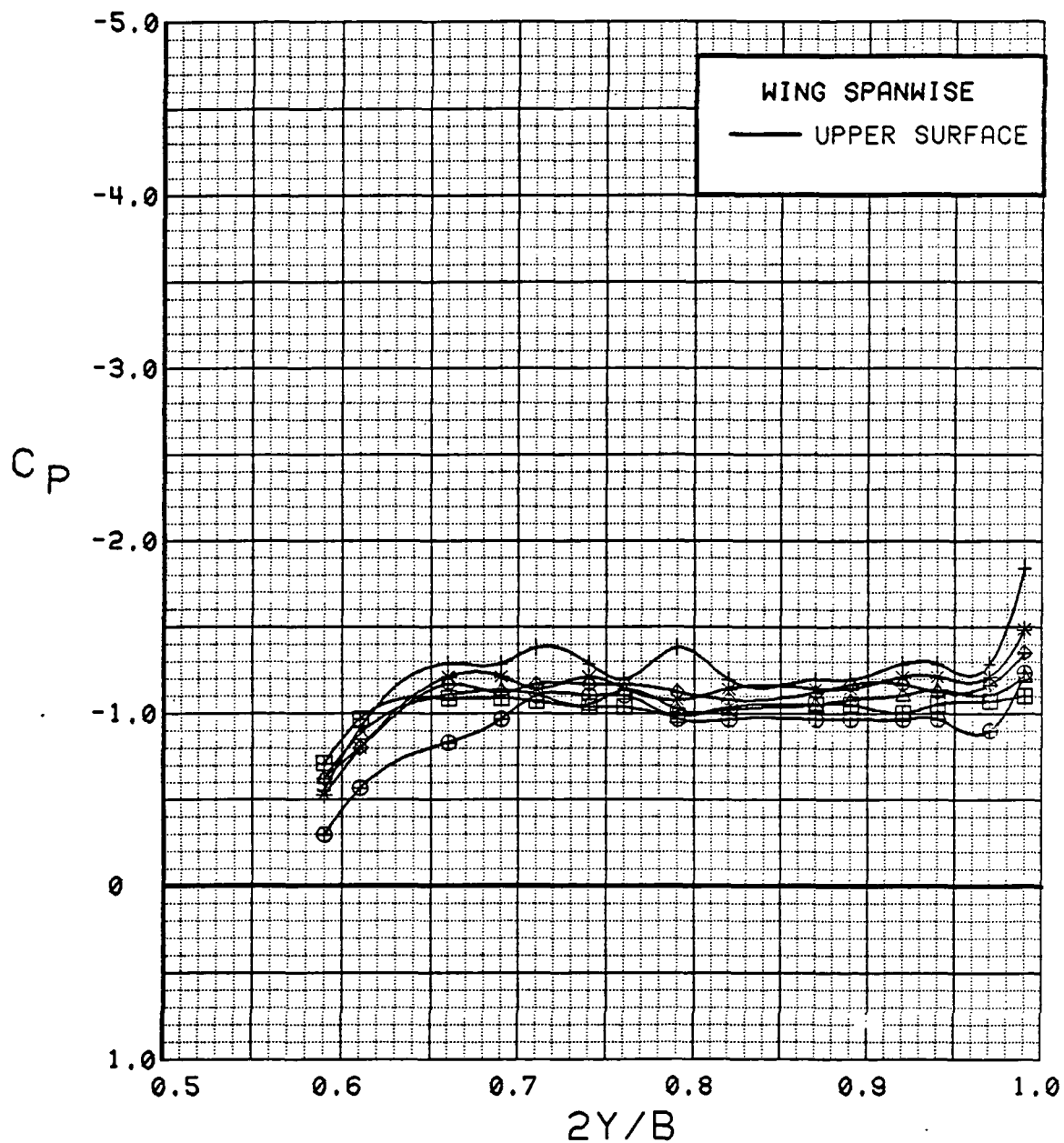


Figure 3.2.2-100 Power Effects, Flaps Deflected, Spanwise, Alpha = 8 deg



SYM	TEST	RUN	ALPHA	CT	ITEF	OTEF	CAN	SWB
⊕	537	69	12.5	0.00	30	30	OFF	OFF
⊞	537	63	12.6	0.27	30	30	OFF	OFF
△	537	62	12.6	0.46	30	30	OFF	OFF
◆	537	61	12.6	0.92	30	30	OFF	OFF
*	537	60	12.6	1.40	30	30	OFF	OFF
+	537	59	12.6	1.88	30	30	OFF	OFF

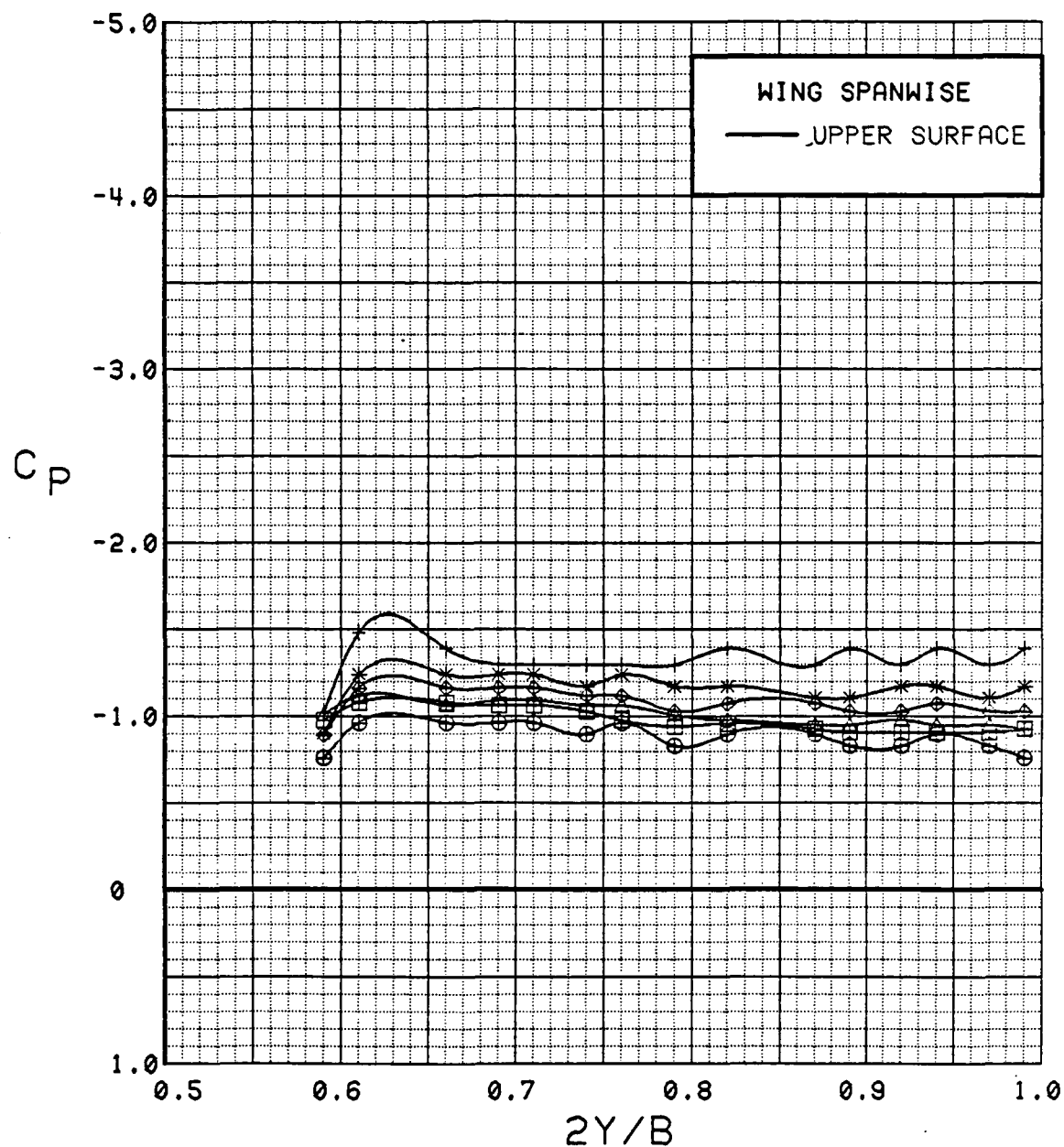


Figure 3.2.2-101 Power Effects, Flaps Deflected, Spanwise, Alpha = 12 deg

SYM	TEST	RUN	ALPHA	CT	ITEF	OTEF	CAN	SWB
⊕	537	69	16.6	0.00	30	30	OFF	OFF
⊞	537	63	16.7	0.27	30	30	OFF	OFF
△	537	62	16.7	0.46	30	30	OFF	OFF
◆	537	61	16.7	0.94	30	30	OFF	OFF
*	537	60	16.7	1.40	30	30	OFF	OFF
+	537	59	16.8	1.78	30	30	OFF	OFF

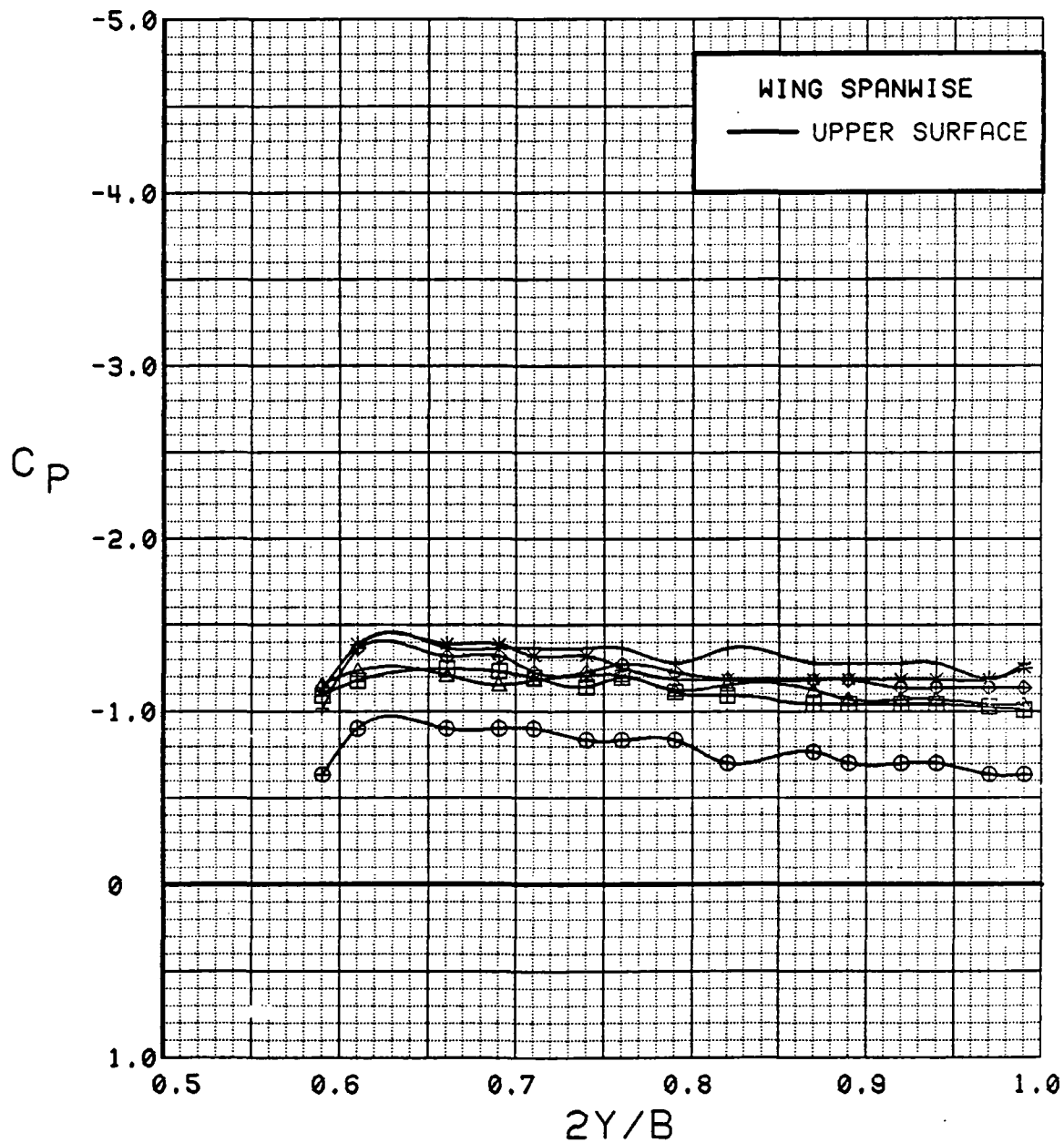


Figure 3.2.2-102 Power Effects, Flaps Deflected, Spanwise, Alpha = 16 deg

SYM	TEST	RUN	ALPHA	CT	ITEF	OTEF	CAN	SWB
⊕	537	69	20.6	0.00	30	30	OFF	OFF
⊞	537	63	20.8	0.27	30	30	OFF	OFF
△	537	62	20.8	0.46	30	30	OFF	OFF
◆	537	61	20.8	0.92	30	30	OFF	OFF
*	537	60	20.8	1.40	30	30	OFF	OFF
+	537	59	20.9	1.84	30	30	OFF	OFF

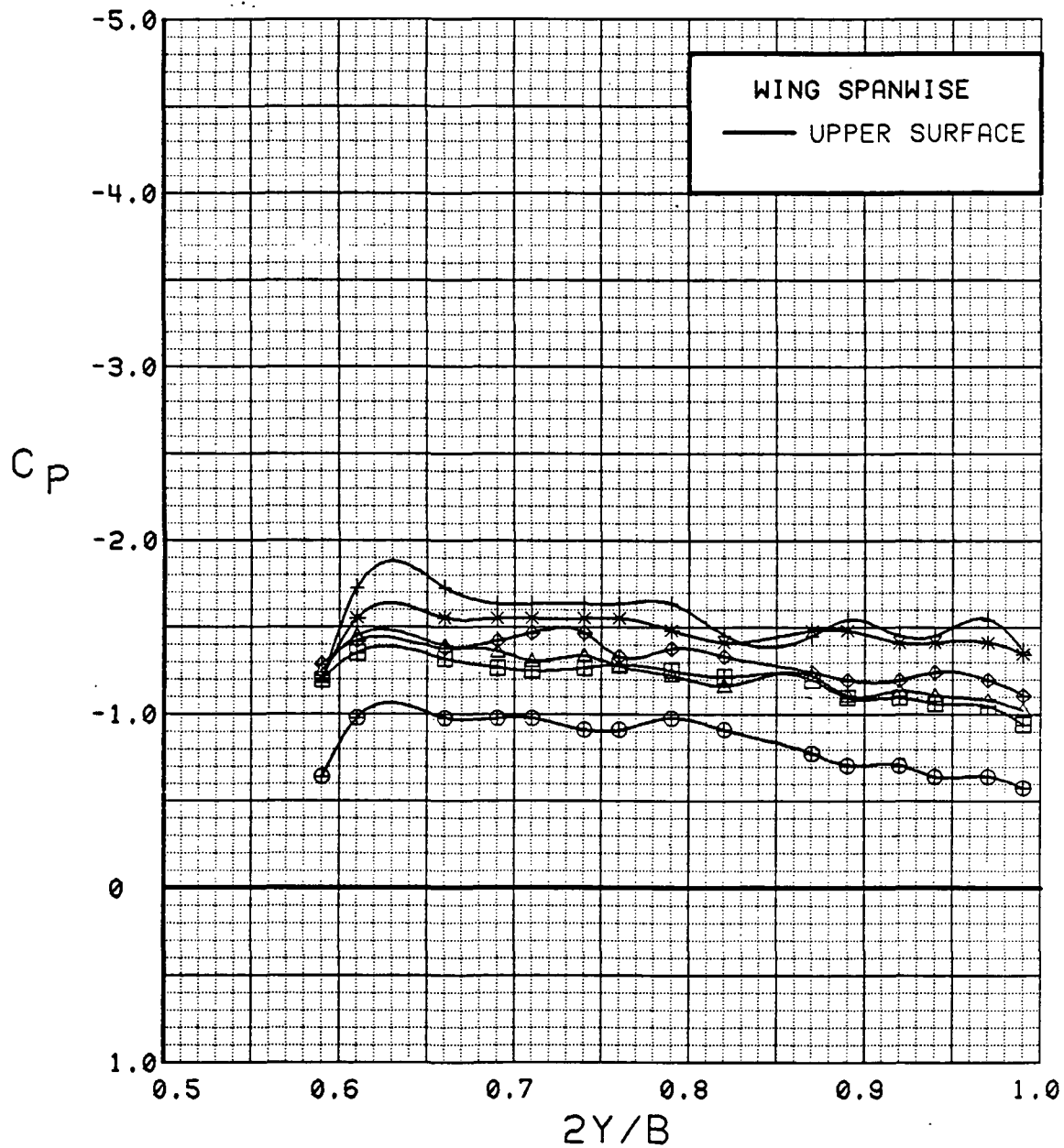


Figure 3.2.2-103 Power Effects, Flaps Deflected, Spanwise, Alpha = 20 deg

SYM	TEST	RUN	ALPHA	CT	ITEF	OTEF	CAN	SWB
⊕	537	69	24.7	0.00	30	30	OFF	OFF
⊞	537	63	24.8	0.27	30	30	OFF	OFF
△	537	62	24.8	0.46	30	30	OFF	OFF
◆	537	61	24.9	0.92	30	30	OFF	OFF
*	537	60	24.9	1.41	30	30	OFF	OFF
+	537	59	24.9	1.89	30	30	OFF	OFF

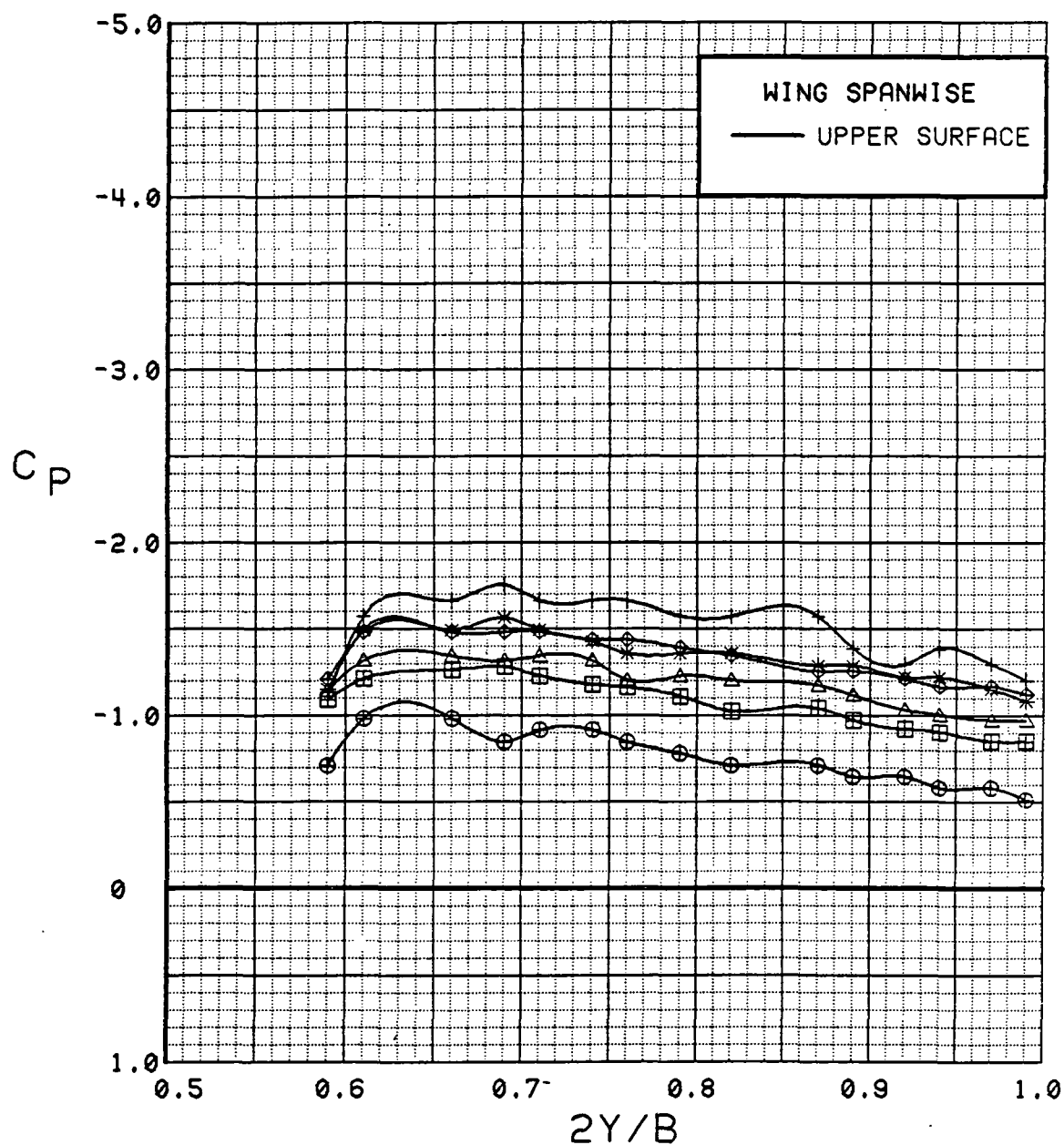


Figure 3.2.2-104 Power Effects, Flaps Deflected, Spanwise, Alpha = 24 deg

SYM	TEST	RUN	ALPHA	CT	ITEF	OTEF	CAN	SWB
⊕	537	69	28.7	0.00	30	30	OFF	OFF
⊞	537	63	28.8	0.27	30	30	OFF	OFF
△	537	62	28.9	0.46	30	30	OFF	OFF
◆	537	61	28.9	0.93	30	30	OFF	OFF
*	537	60	28.9	1.41	30	30	OFF	OFF
+	537	59	29.0	1.84	30	30	OFF	OFF

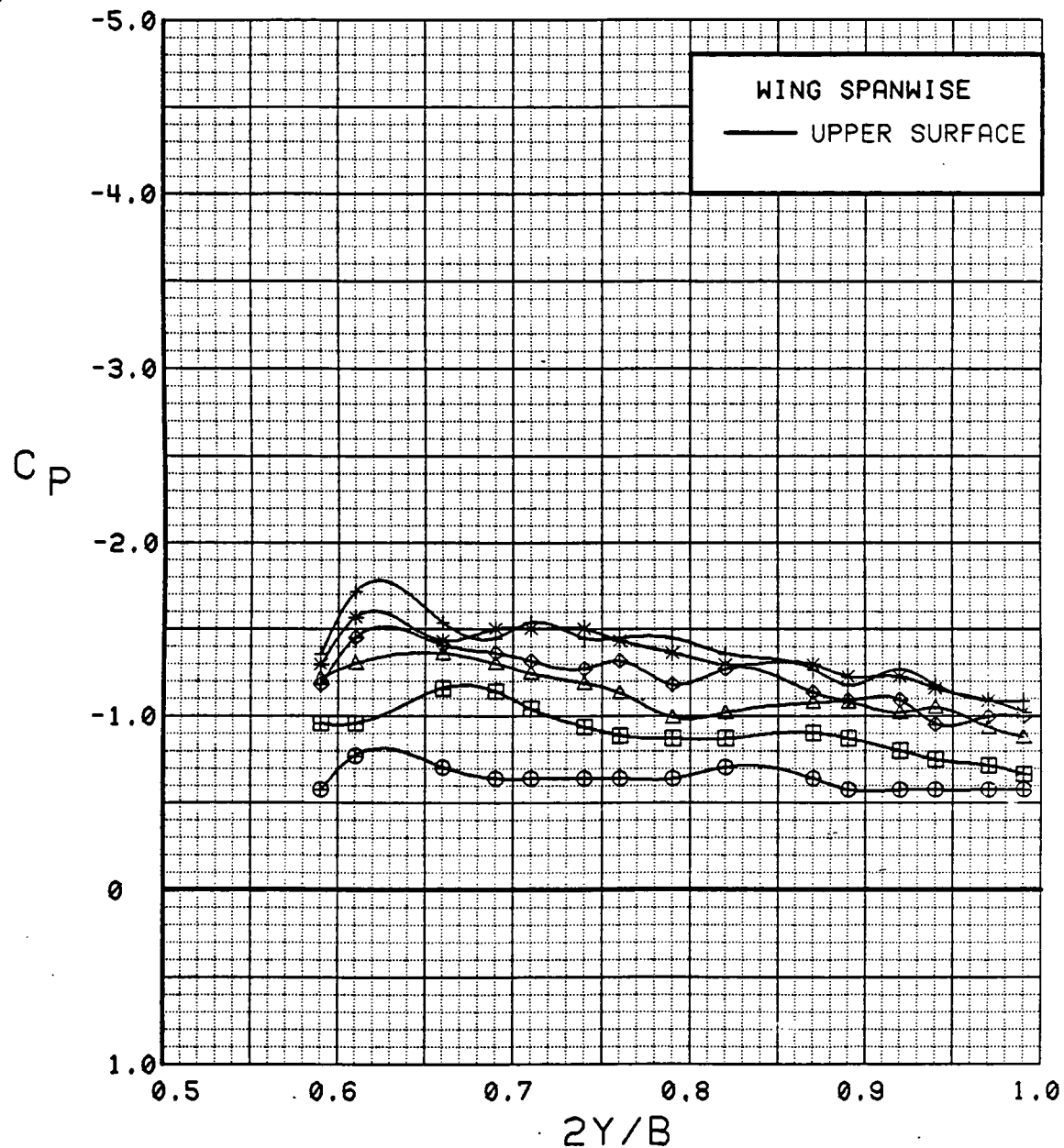


Figure 3.2.2-105 Power Effects, Flaps Deflected, Spanwise, Alpha = 28 deg

SYM	TEST	RUN	ALPHA	CT	ITEF	OTEF	CAN	SWB
⊕	537	69	32.7	0.00	30	30	OFF	OFF
⊞	537	62	32.8	0.46	30	30	OFF	OFF
△	537	61	32.9	0.93	30	30	OFF	OFF
◆	537	60	33.0	1.40	30	30	OFF	OFF
*	537	59	33.0	1.87	30	30	OFF	OFF

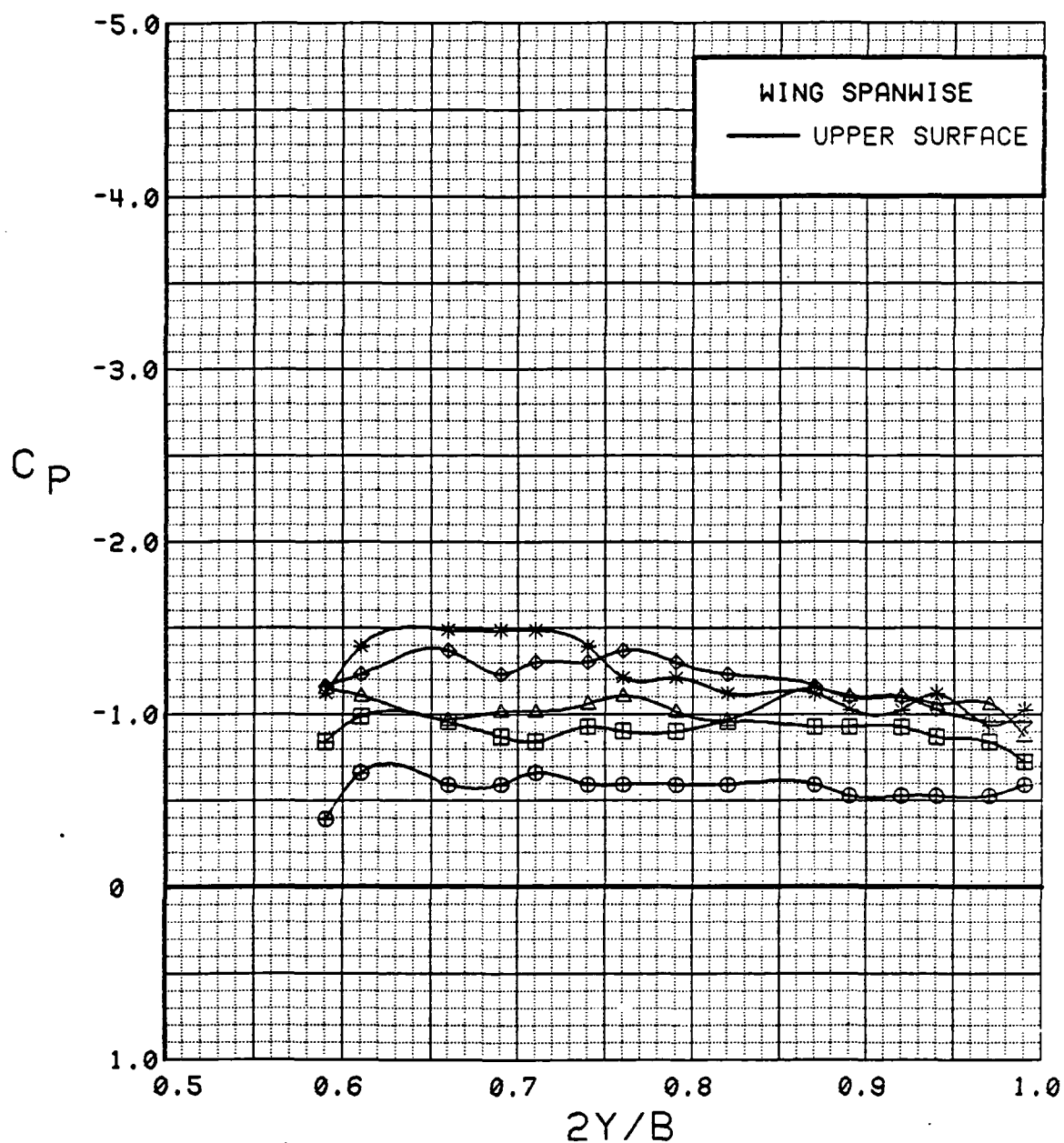


Figure 3.2.2-106 Power Effects, Flaps Deflected, Spanwise, Alpha = 32 deg

SYM	TEST	RUN	ALPHA	CT	ITEF	OTEF	CAN	SWB
⊕	537	69	0.2	0.00	30	30	OFF	OFF
⊞	537	60	0.3	1.42	30	30	OFF	OFF

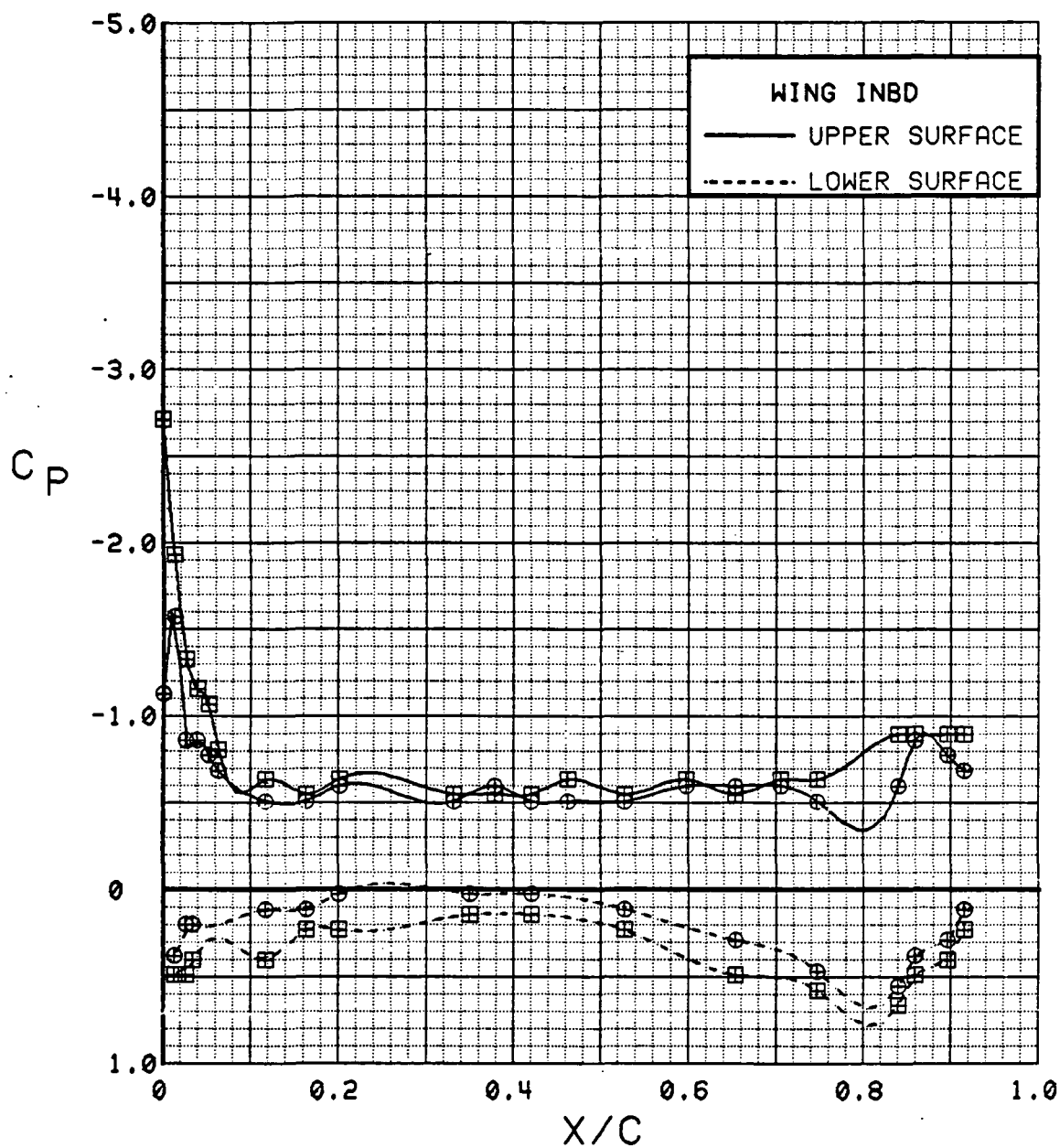


Figure 3.2.2-107 Power-Off/Power-on Comparison, Flaps Deflected, Inboard, Alpha = 0 deg

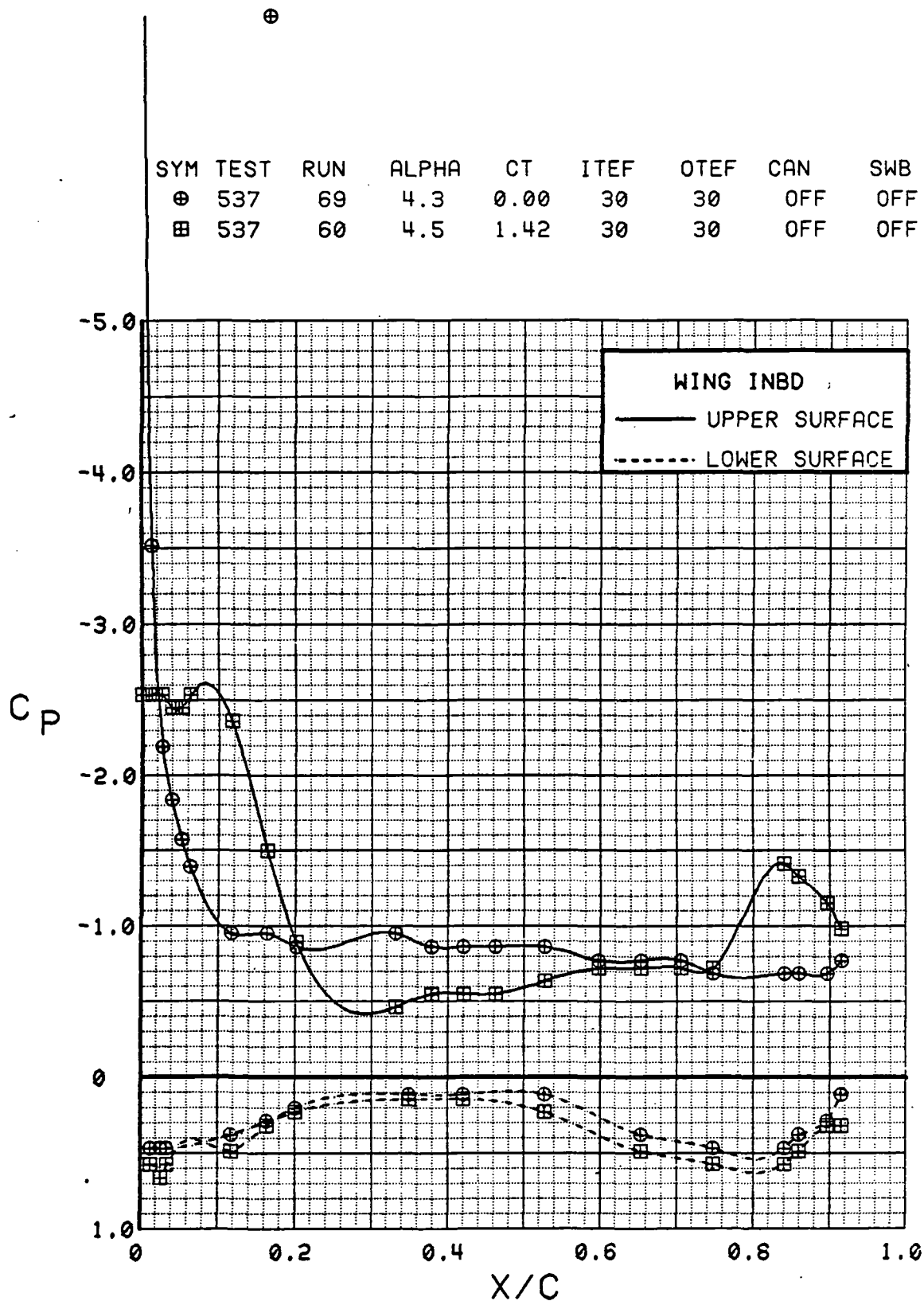


Figure 3.2.2-108 Power-off/Power-on Comparison, Flaps Deflected, Inboard, Alpha = 4 deg



SYM	TEST	RUN	ALPHA	CT	ITEF	OTEF	CAN	SWB
⊕	537	69	8.5	0.00	30	30	OFF	OFF
⊞	537	60	8.6	1.43	30	30	OFF	OFF

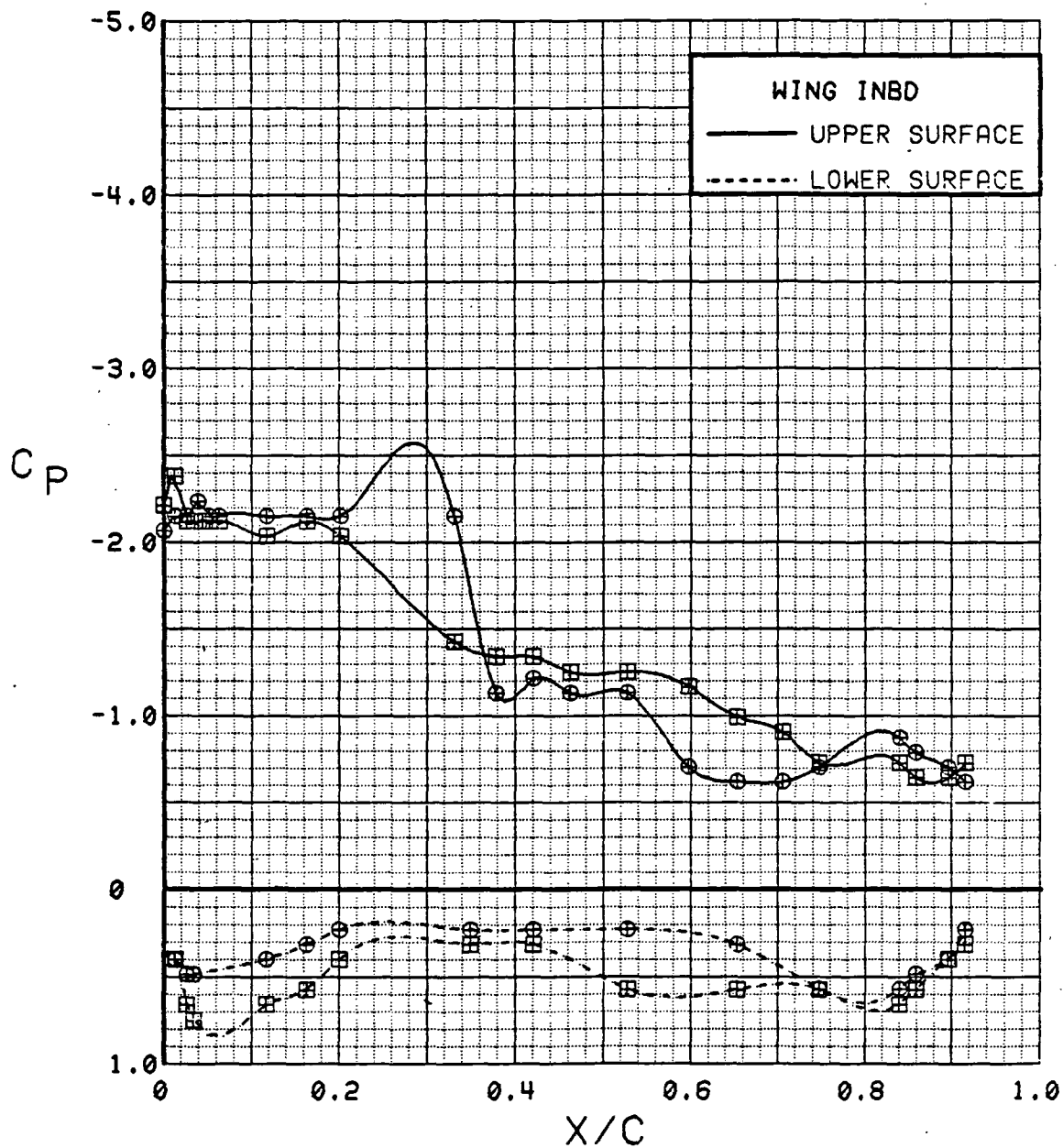


Figure 3.2.2-109 Power-off/Power-on Comparison, Flaps Deflected, Inboard, Alpha = 8 deg

SYM	TEST	RUN	ALPHA	CT	ITEF	OTEF	CAN	SWB
⊕	537	69	12.5	0.00	30	30	OFF	OFF
⊞	537	60	12.6	1.40	30	30	OFF	OFF

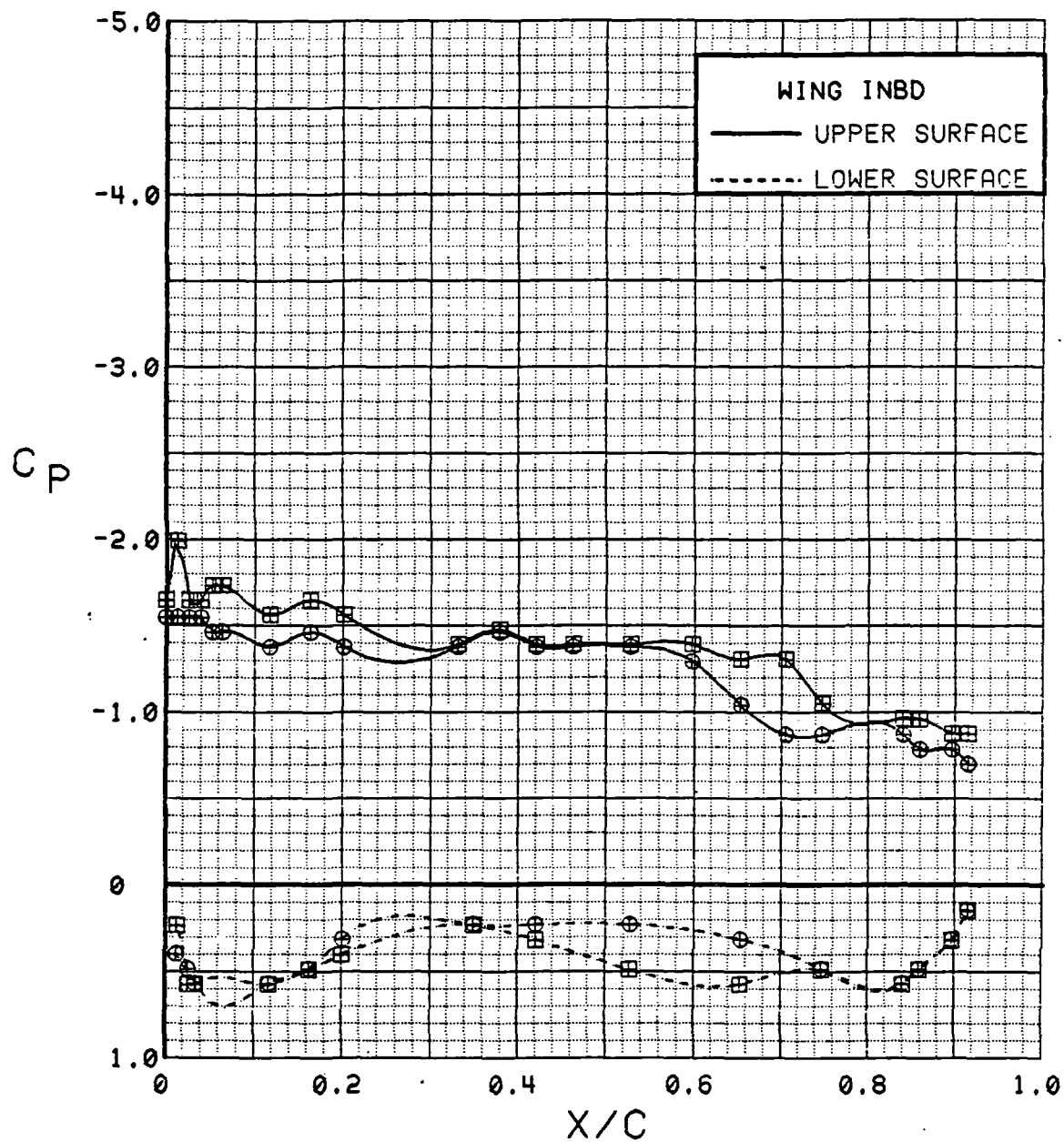


Figure 3.2.2-110 Power-off/Power-on Comparison, Flaps Deflected, Inboard, Alpha = 12 deg

SYM	TEST	RUN	ALPHA	CT	ITEF	OTEF	CAN	SWB
⊕	537	69	16.6	0.00	30	30	OFF	OFF
⊞	537	60	16.7	1.40	30	30	OFF	OFF

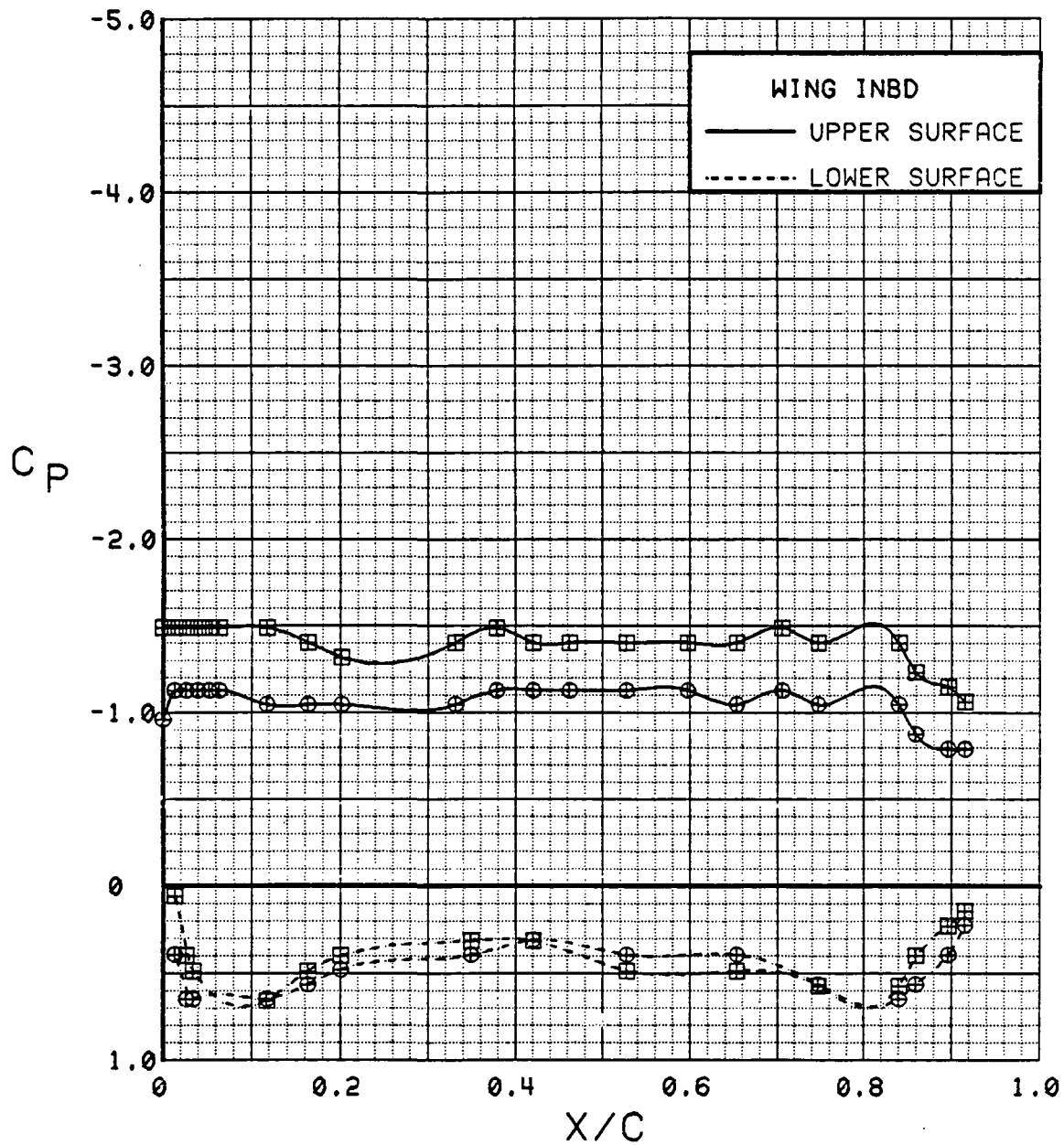


Figure 3.2.2-111 Power-off/Power-on Comparison, Flaps Deflected, Inboard, Alpha = 16 deg

SYM	TEST	RUN	ALPHA	CT	ITEF	OTEF	CAN	SWB
⊕	537	69	0.2	0.00	30	30	OFF	OFF
⊞	537	60	0.3	1.42	30	30	OFF	OFF

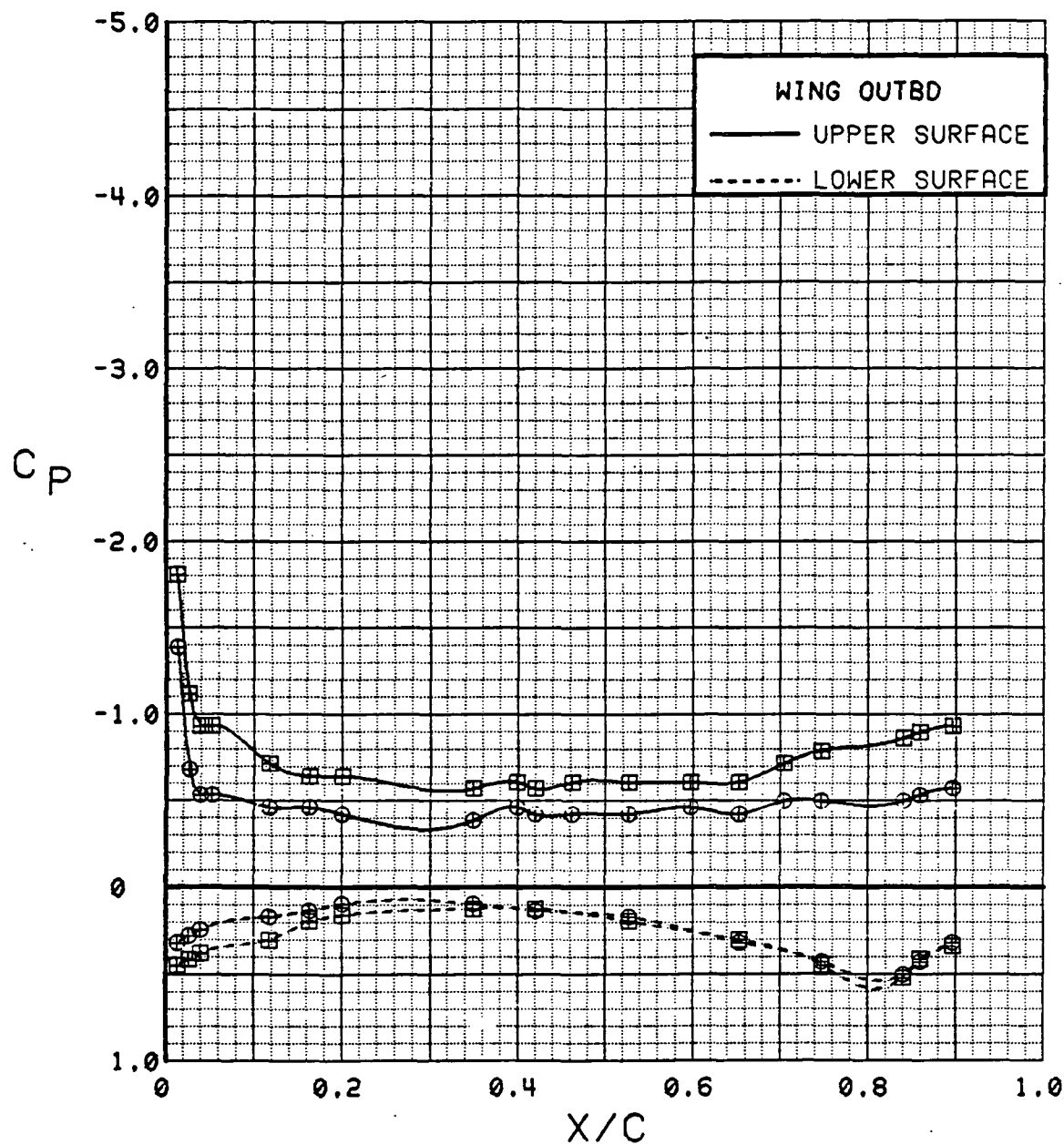


Figure 3.2.2-112 Power-off/Power-on Comparison, Flaps Deflected, Outboard, Alpha = 0 deg

SYM	TEST	RUN	ALPHA	CT	ITEF	OTEF	CAN	SWB
⊕	537	69	4.3	0.00	30	30	OFF	OFF
⊞	537	60	4.5	1.42	30	30	OFF	OFF

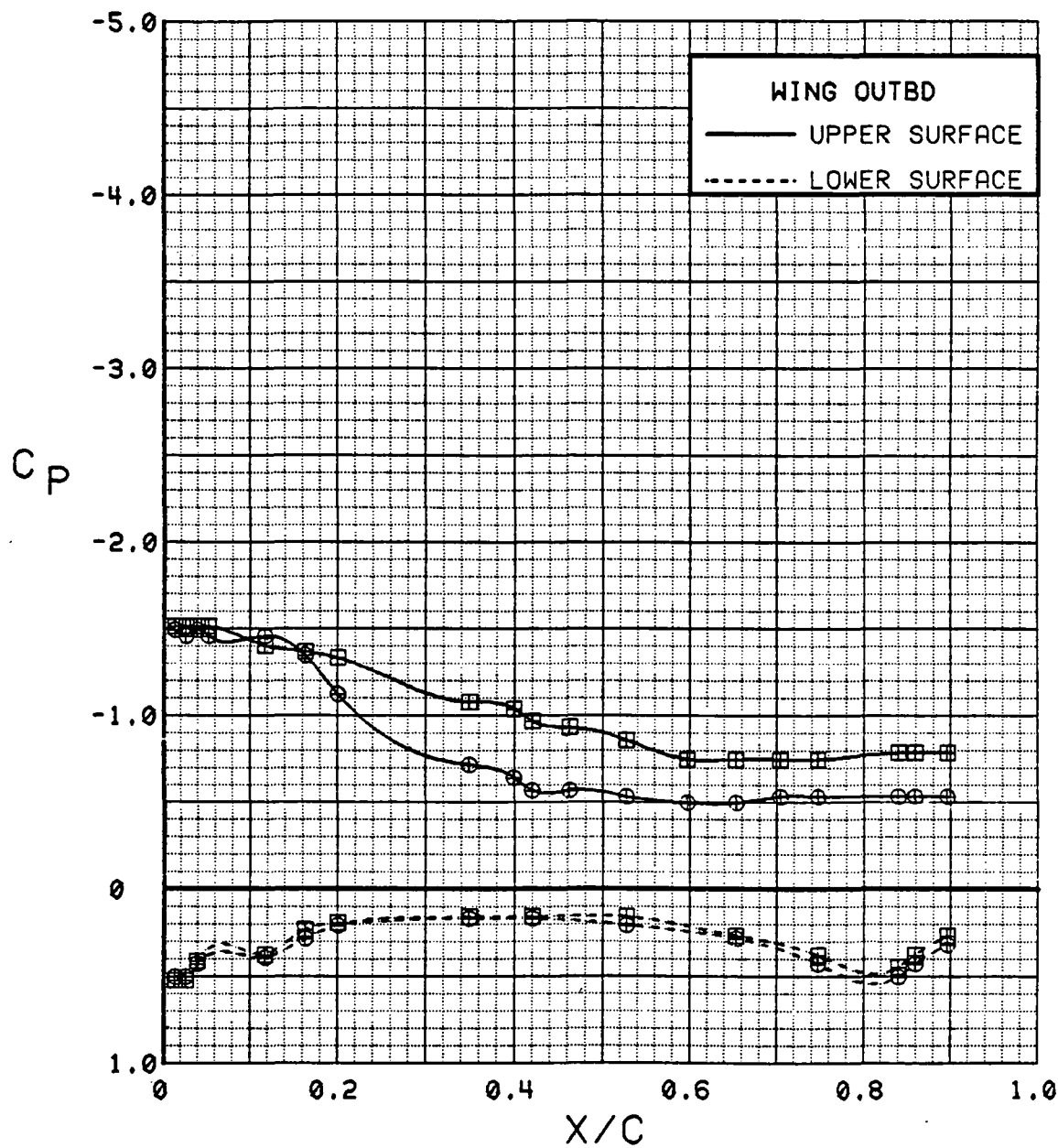


Figure 3.2.2-113 Power-off/Power-on Comparison, Flaps Deflected, Outboard, Alpha = 4 deg

SYM	TEST	RUN	ALPHA	CT	ITEF	OTEF	CAN	SWB
⊕	537	69	8.5	0.00	30	30	OFF	OFF
⊞	537	60	8.6	1.43	30	30	OFF	OFF

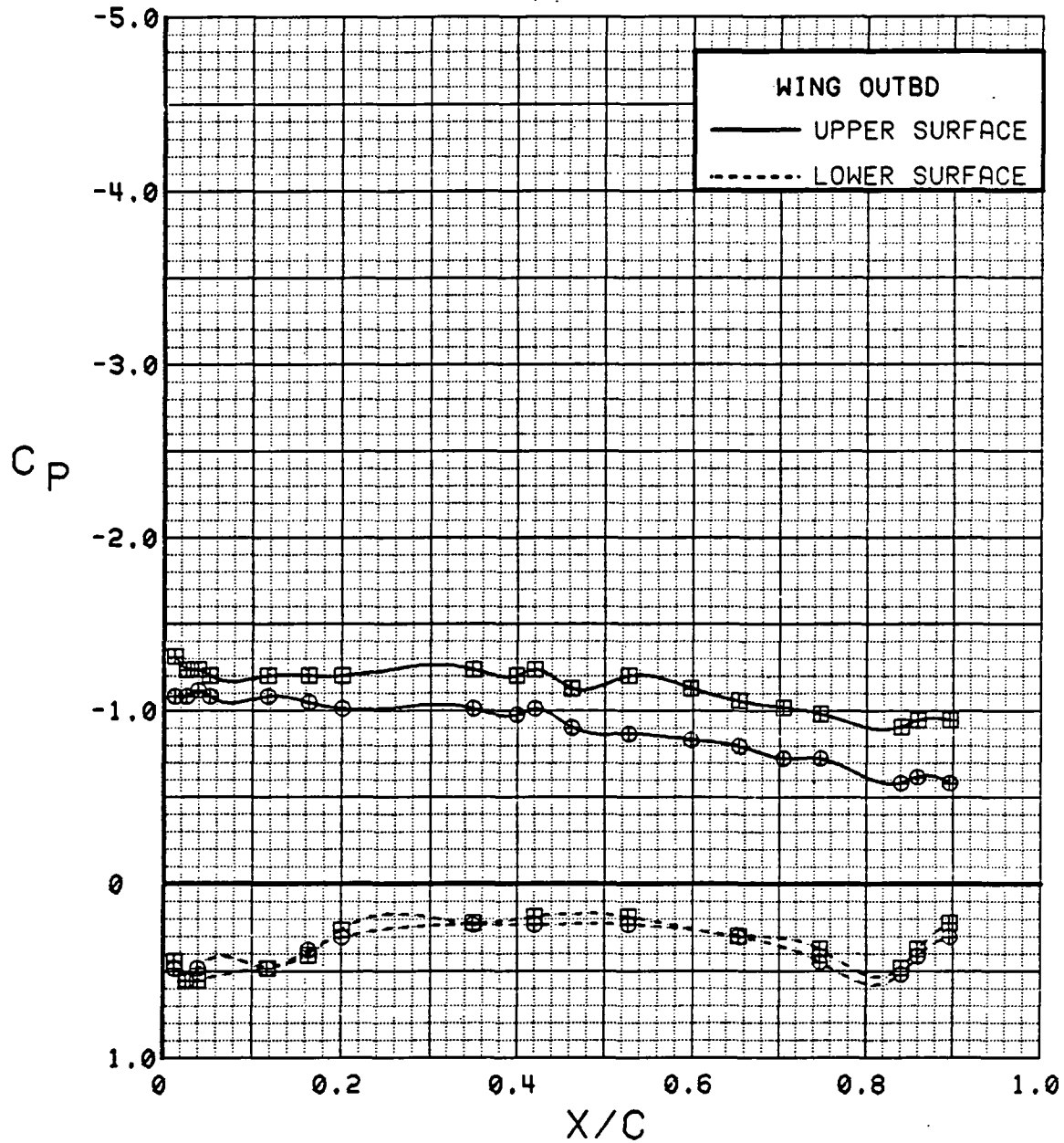


Figure 3.2.2-114 Power-off/Power-on Comparison, Flaps Deflected, Outboard, Alpha = 8 deg

SYM	TEST	RUN	ALPHA	CT	ITEF	OTEF	CAN	SWB
⊕	537	69	12.5	0.00	30	30	OFF	OFF
⊞	537	60	12.6	1.40	30	30	OFF	OFF

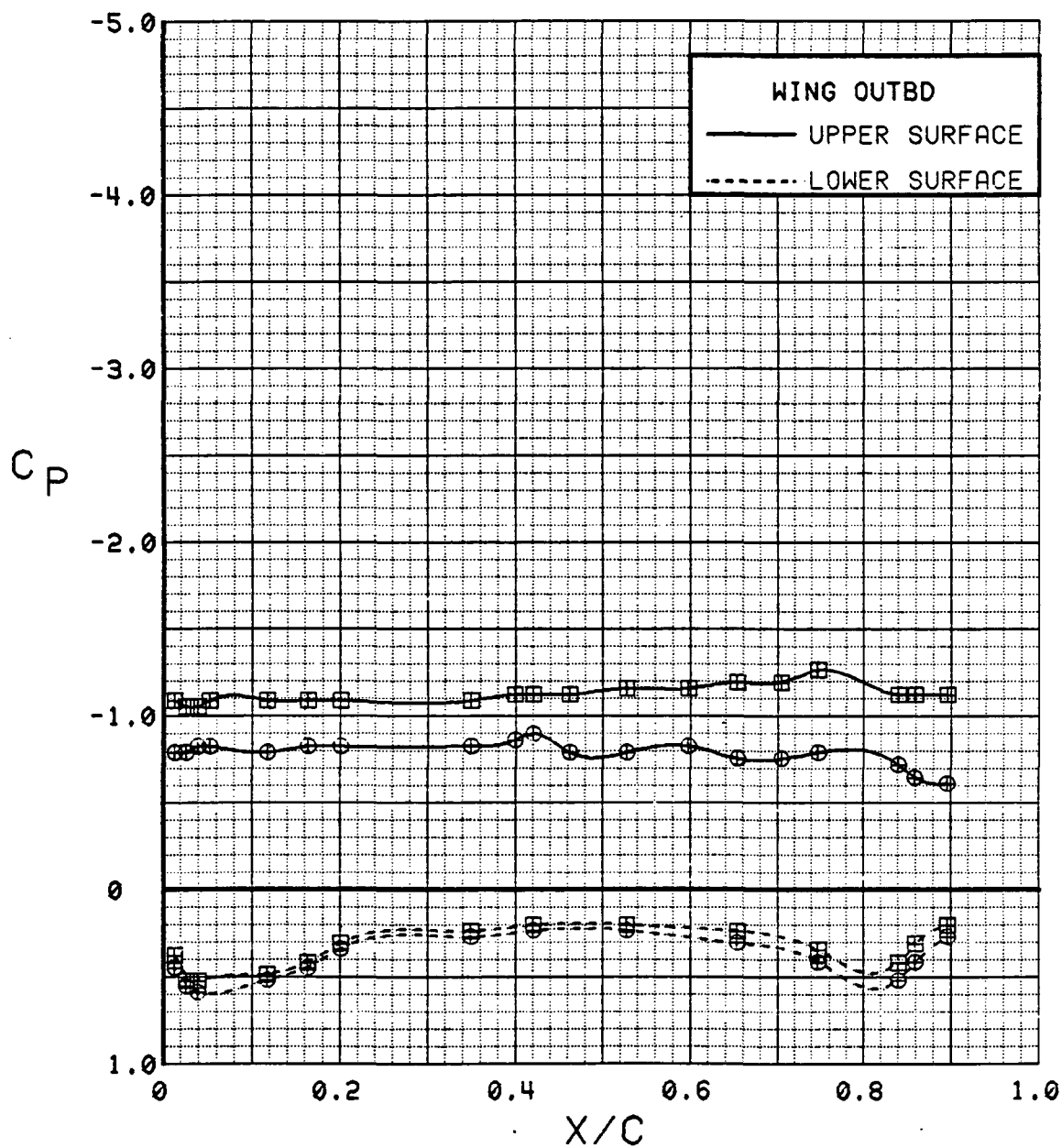


Figure 3.2.2-115 Power-off/Power-on Comparison, Flaps Deflected, Outboard, Alpha = 12 deg

SYM	TEST	RUN	ALPHA	CT	ITEF	OTEF	CAN	SWB
⊕	537	69	16.6	0.00	30	30	OFF	OFF
⊞	537	60	16.7	1.40	30	30	OFF	OFF

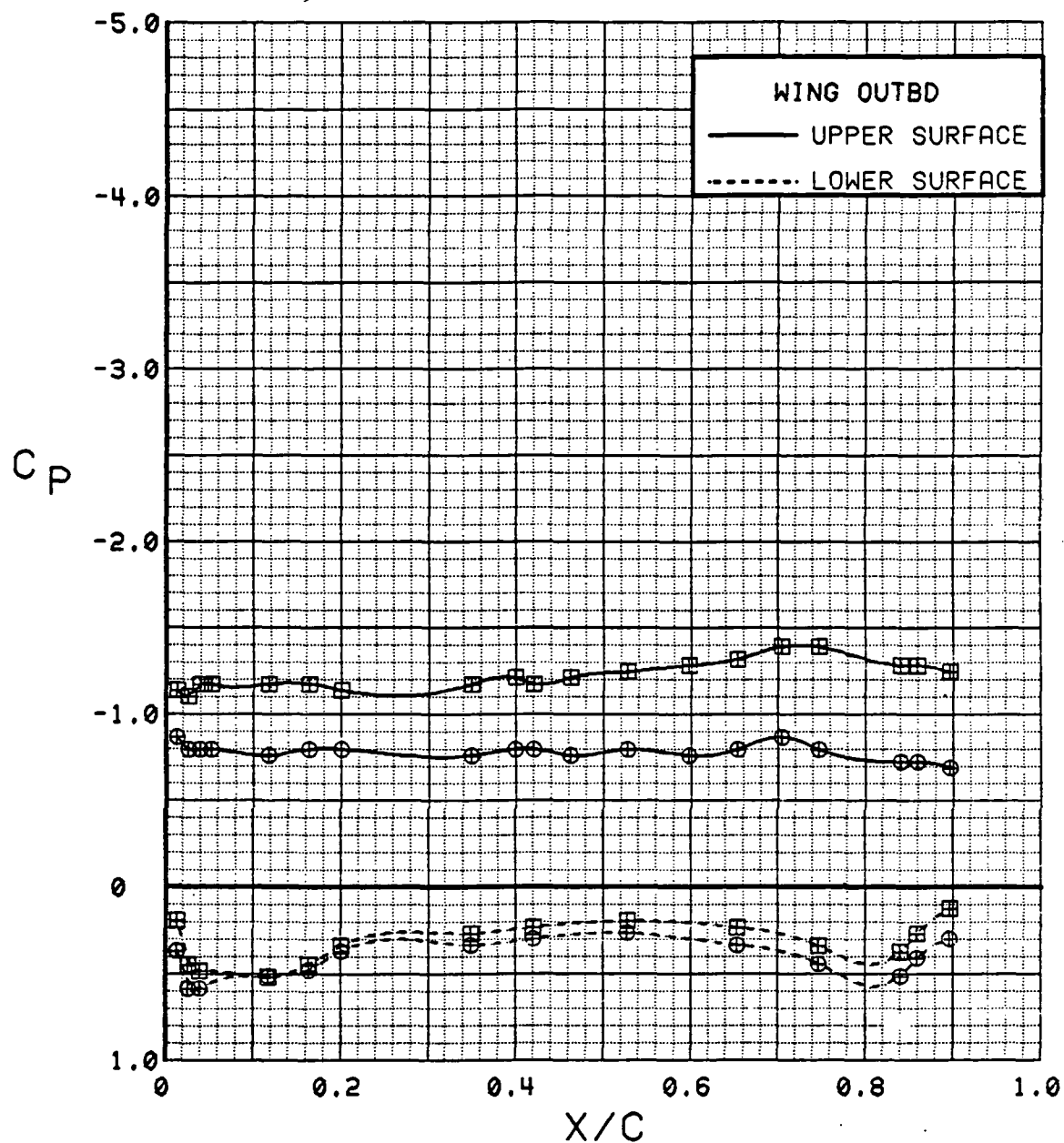


Figure 3.2.2-116 Power-off/Power-on Comparison, Flaps Deflected, Outboard, Alpha = 16 deg



SYM	TEST	RUN	ALPHA	CT	ITEF	OTEF	CAN	SWB
⊕	537	69	0.2	0.00	30	30	OFF	OFF
⊞	537	60	0.3	1.42	30	30	OFF	OFF

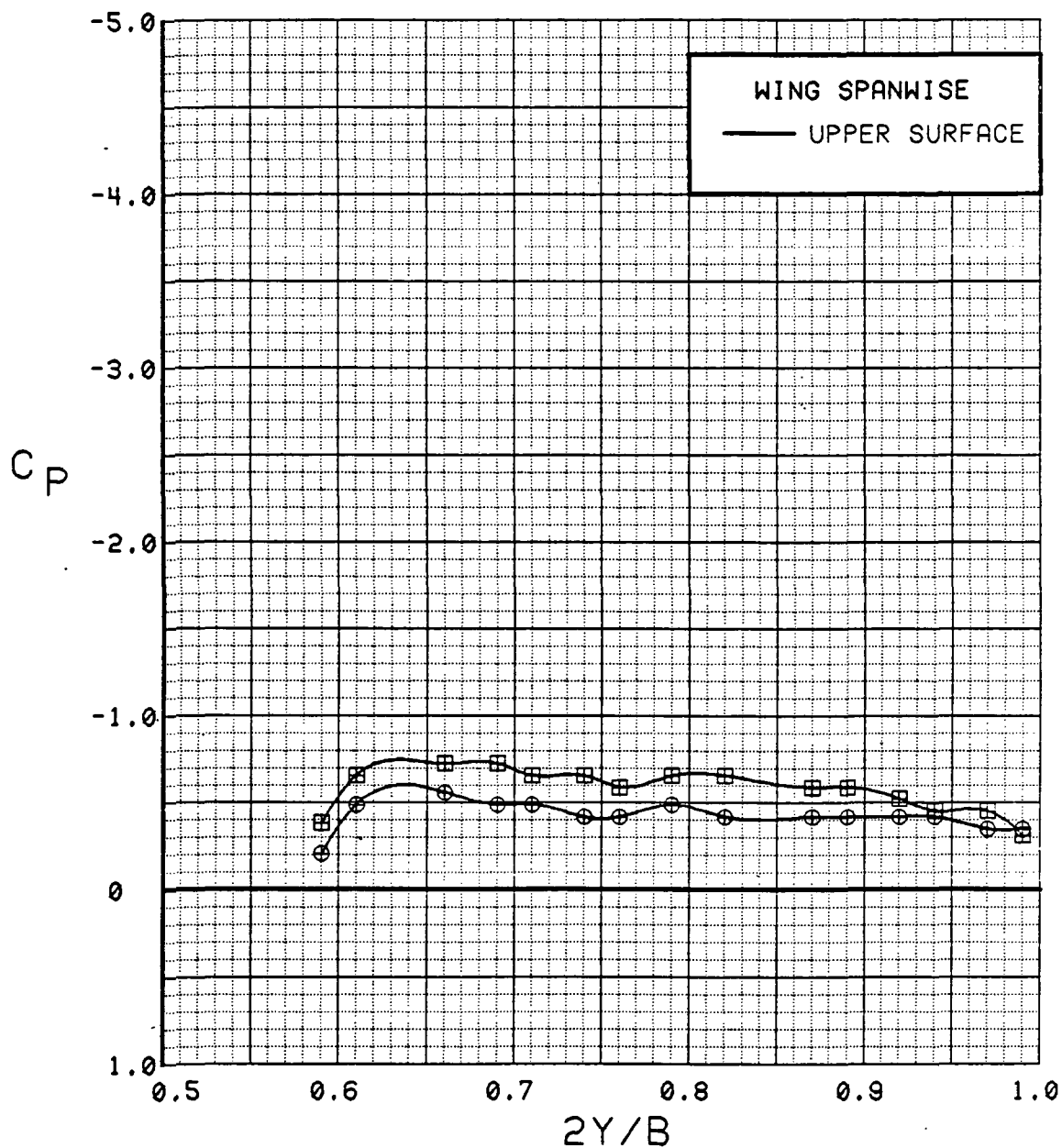


Figure 3.2.2-117 Power-off/Power-on Comparison, Flaps Deflected, Spanwise, Alpha = 0 deg

SYM	TEST	RUN	ALPHA	CT	ITEF	OTEF	CAN	SWB
⊙	537	69	4.3	0.00	30	30	OFF	OFF
⊠	537	60	4.5	1.42	30	30	OFF	OFF

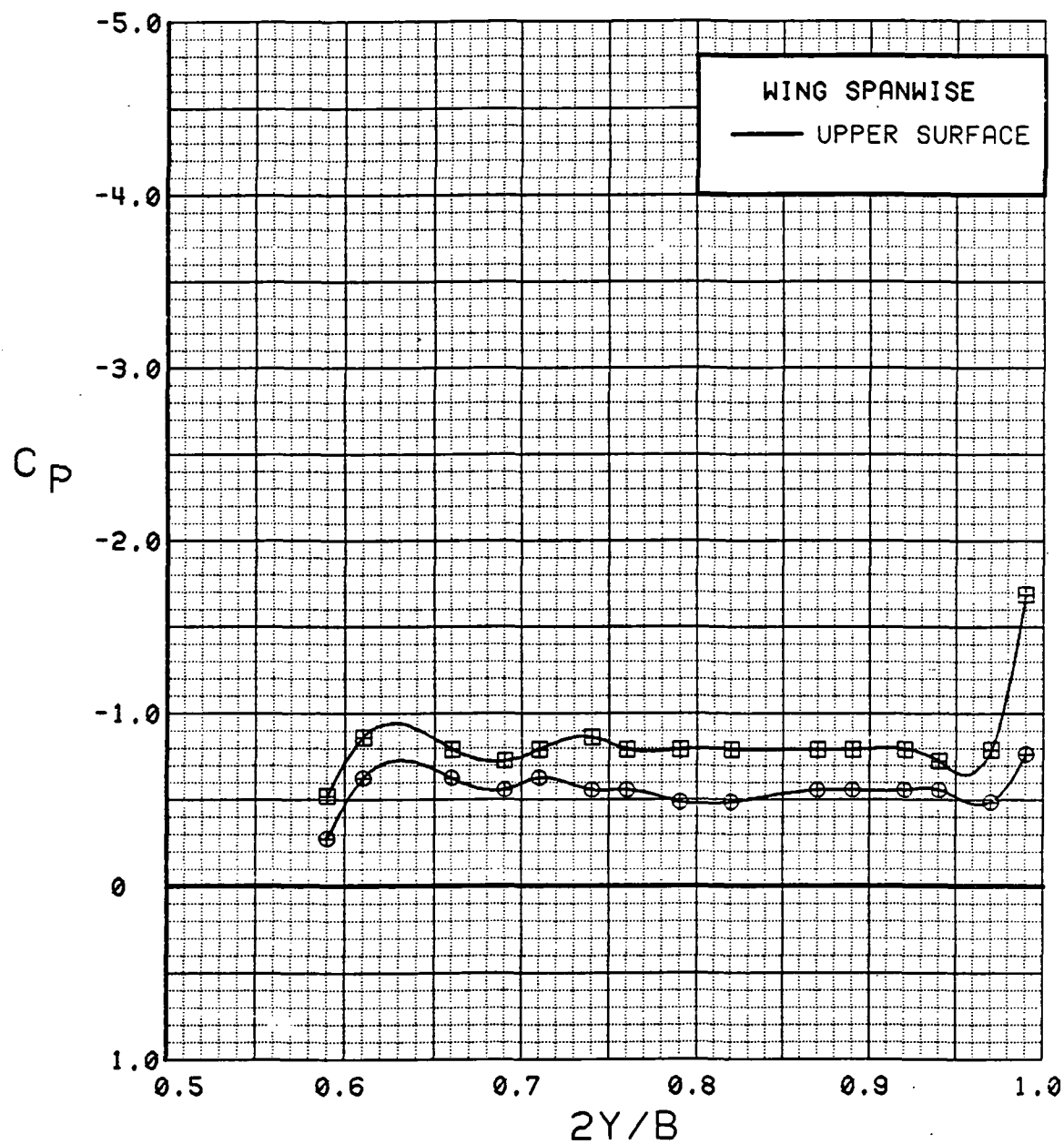


Figure 3.2.2-118 Power-off/Power-on Comparison, Flaps Deflected, Spanwise, Alpha = 4 deg

SYM	TEST	RUN	ALPHA	CT	ITEF	OTEF	CAN	SWB
⊙	537	69	8.5	0.00	30	30	OFF	OFF
⊠	537	60	8.6	1.43	30	30	OFF	OFF

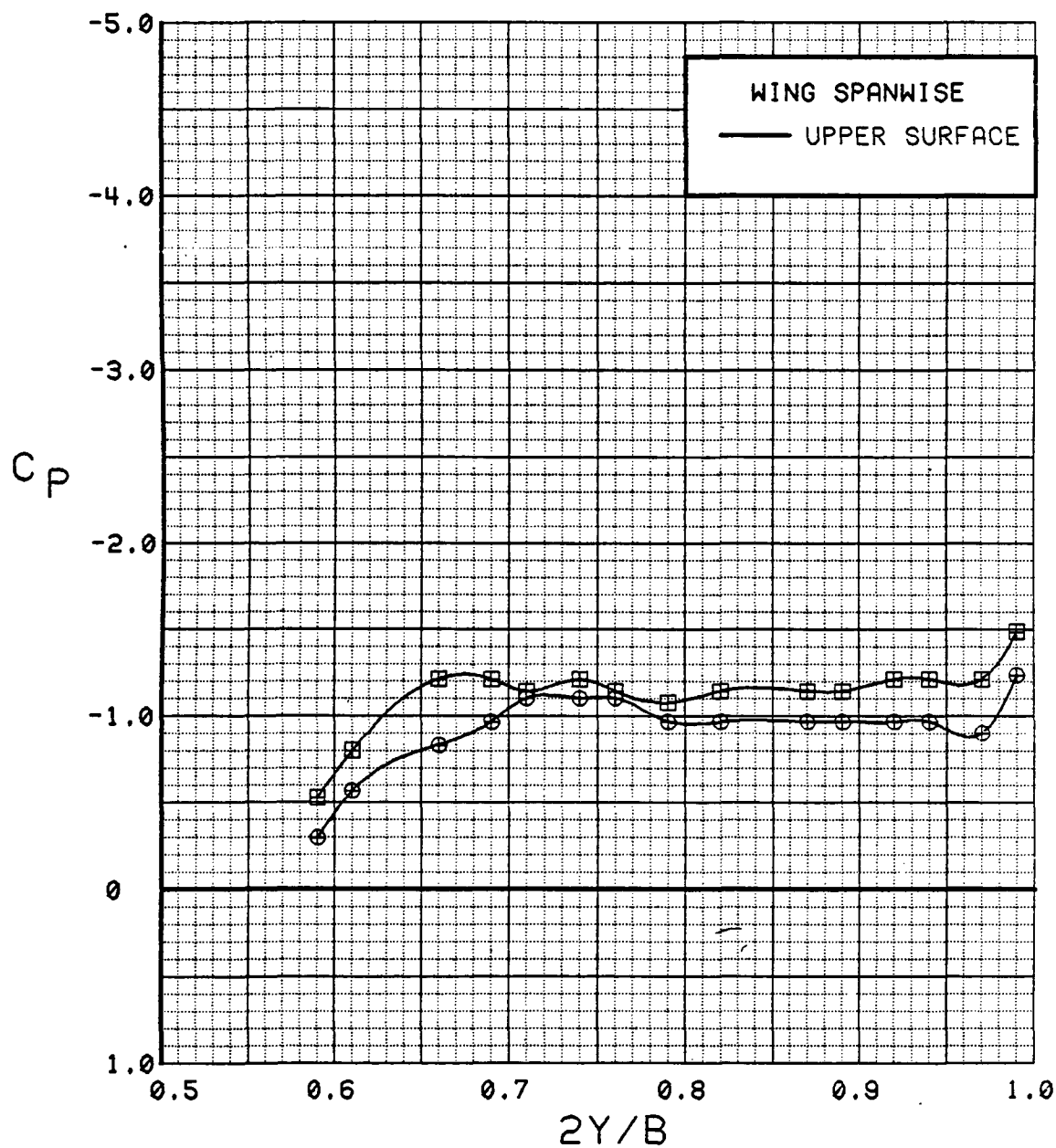


Figure 3.2.2-119 Power-off/Power-on Comparison, Flaps Deflected, Spanwise, Alpha = 8 deg

C - 3

ORIGINAL PAGE  
OF POOR QUALITY

SYM	TEST	RUN	ALPHA	CT	ITEF	OTEF	CAN	SWB
⊕	537	69	12.5	0.00	30	30	OFF	OFF
⊞	537	60	12.6	1.40	30	30	OFF	OFF

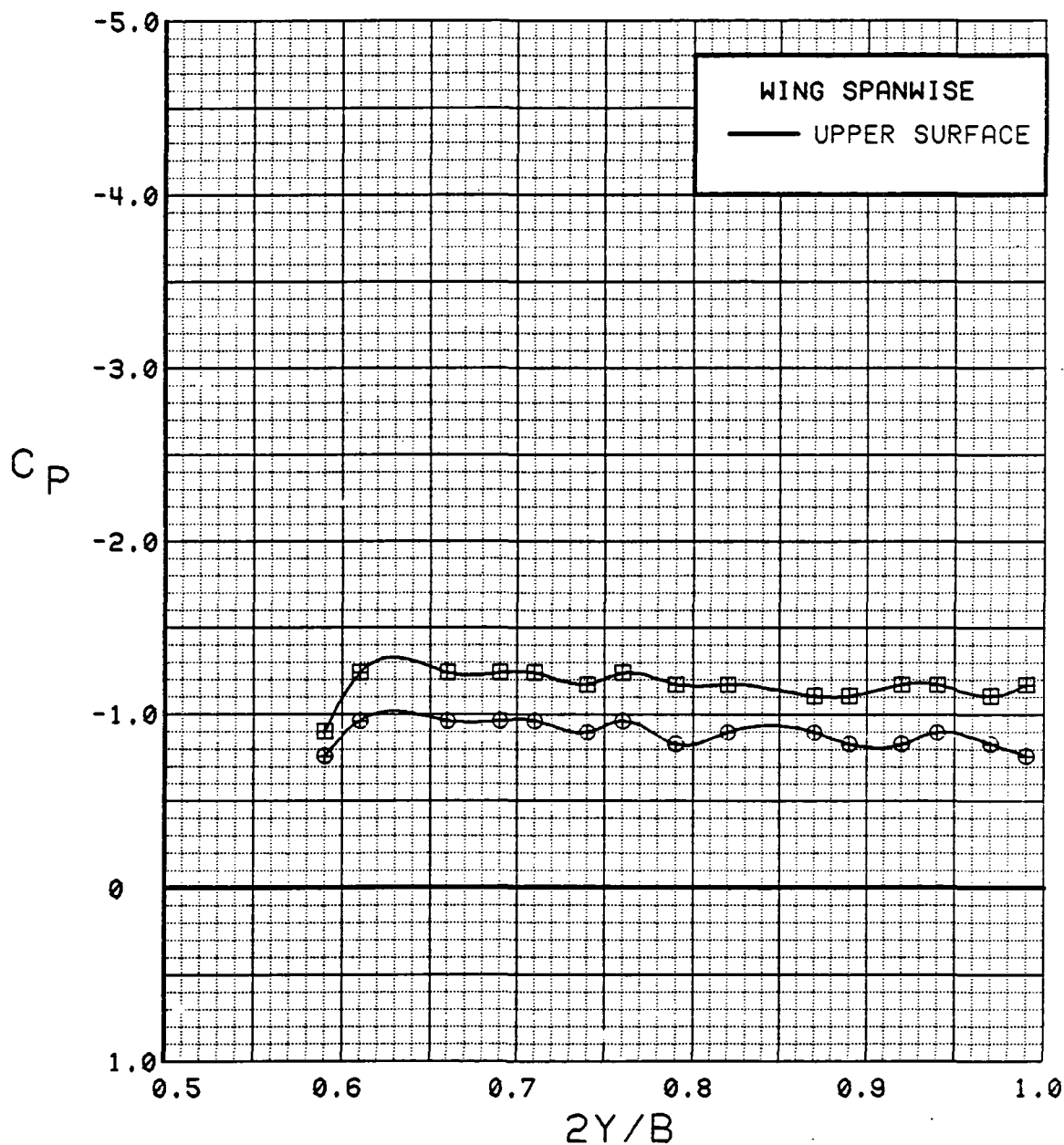


Figure 3.2.2-120 Power-off/Power-on Comparison, Flaps Deflected, Spanwise, Alpha = 12 deg

SYM	TEST	RUN	ALPHA	CT	ITEF	OTEF	CAN	SWB
⊕	537	69	16.6	0.00	30	30	OFF	OFF
⊞	537	60	16.7	1.40	30	30	OFF	OFF

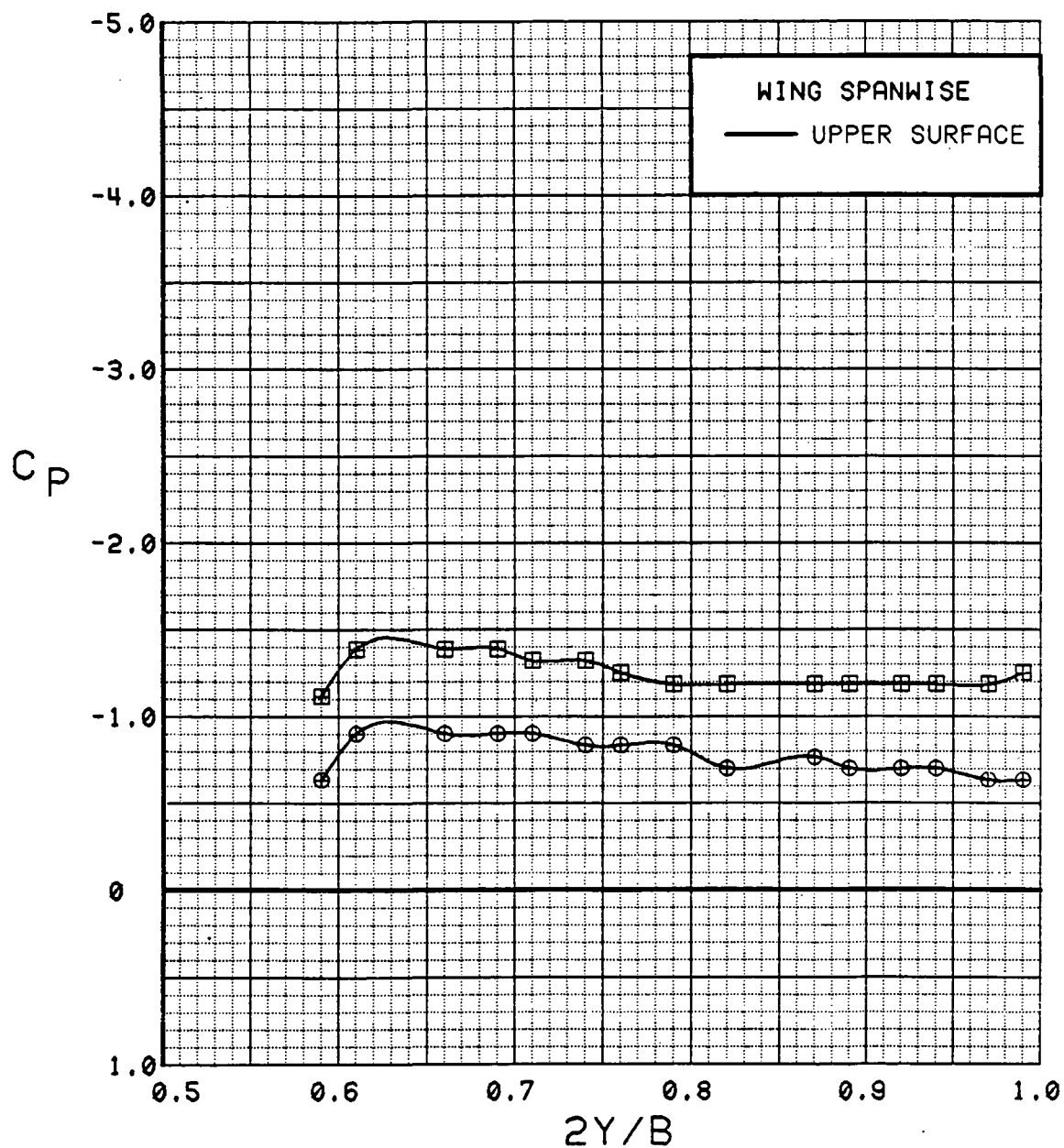


Figure 3.2.2-121 Power-off/Power-on Comparison, Flaps Deflected, Spanwise, Alpha = 16 deg

# WING INBOARD

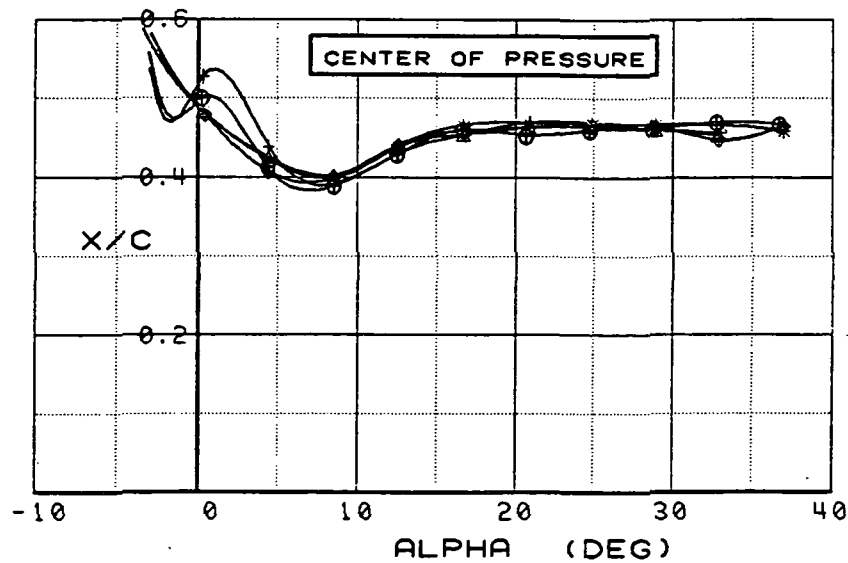
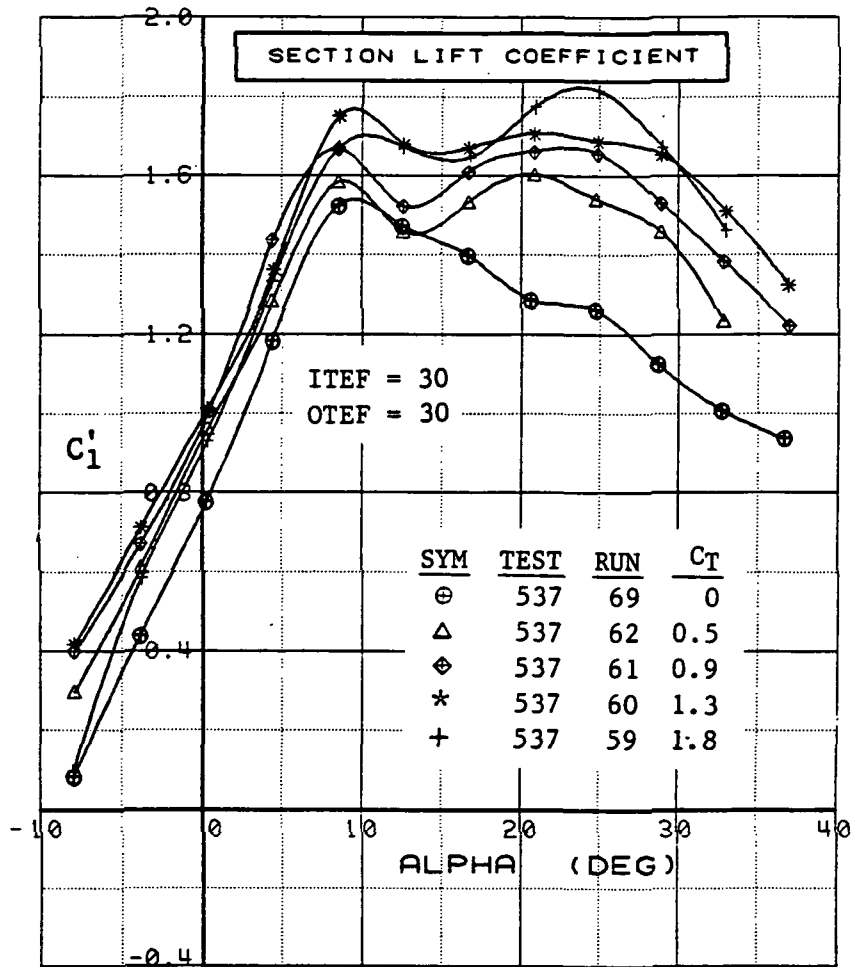


Figure 3.2.2-122 Power-off/Power-on Comparison, Flaps Deflected, Inboard, Integrated Section Properties

# WING OUTBOARD

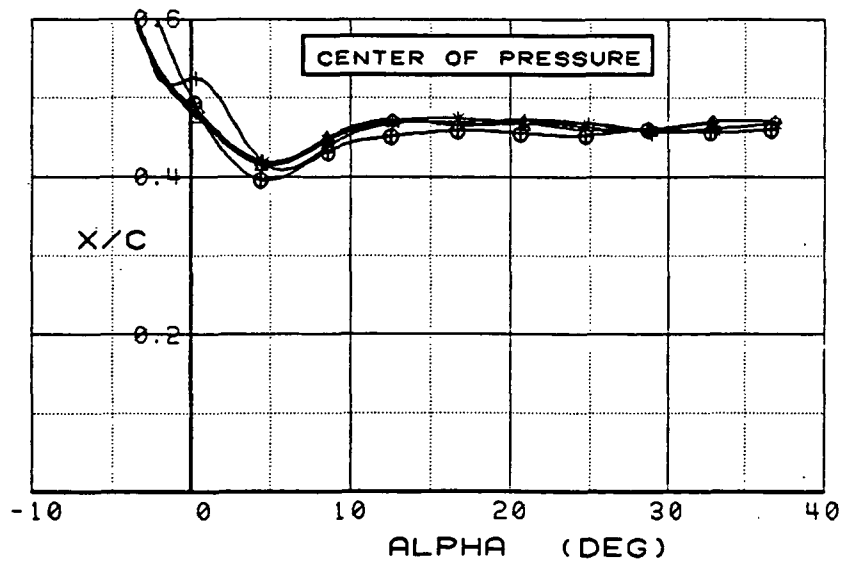
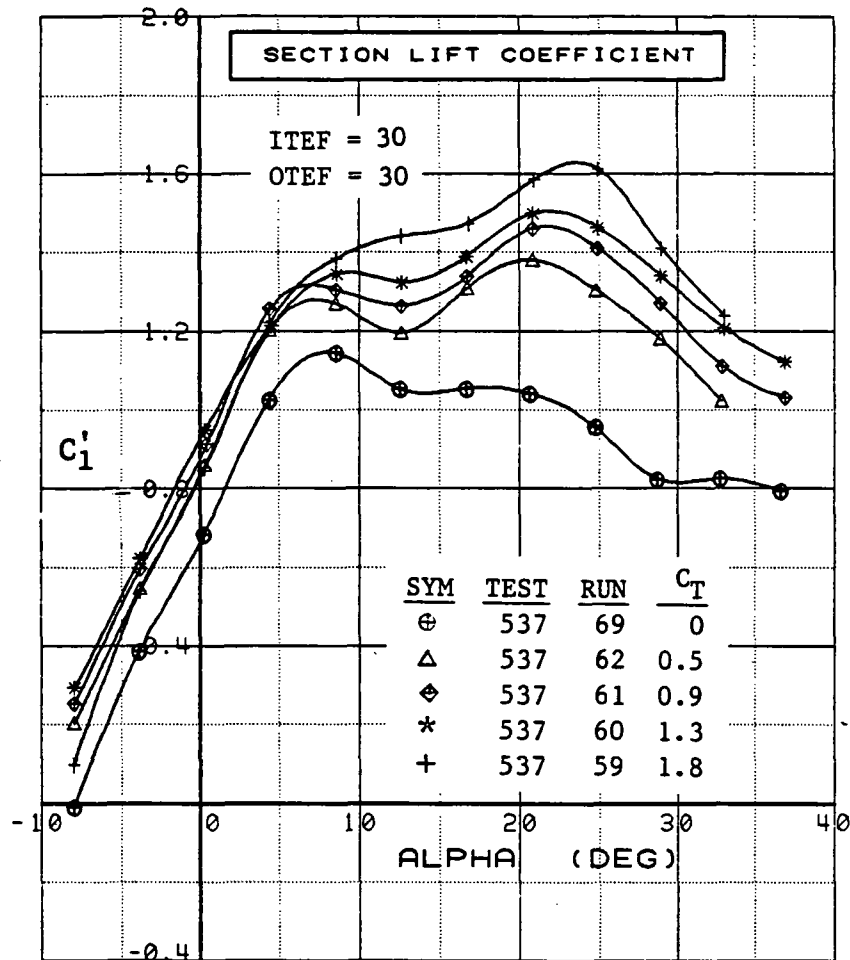


Figure 3.2.2-123 Power-off/Power-on Comparison, Flaps Deflected, Outboard, Integrated Section Properties

SYM	TEST	RUN	ALPHA	CT	ITEF	OTEF	CAN	SWB
⊕	537	61	0.4	0.94	30	30	OFF	OFF
⊞	546	47	0.4	0.96	30	30	OFF	ON

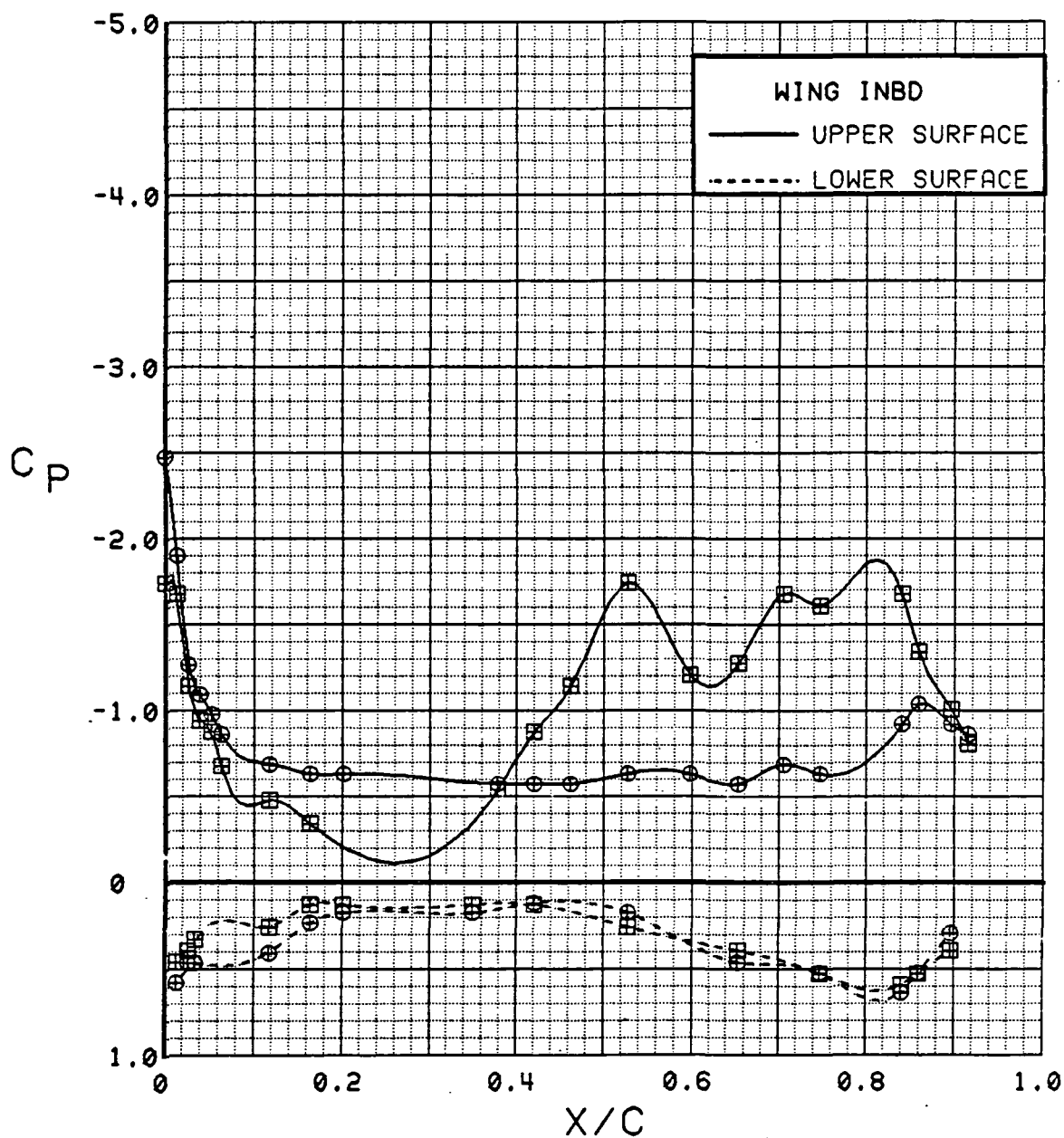


Figure 3.2.2-124 Spanwise Blowing Effects, Flaps Deflected,  $C_T = 0.9$ , Inboard, Alpha = 0 deg



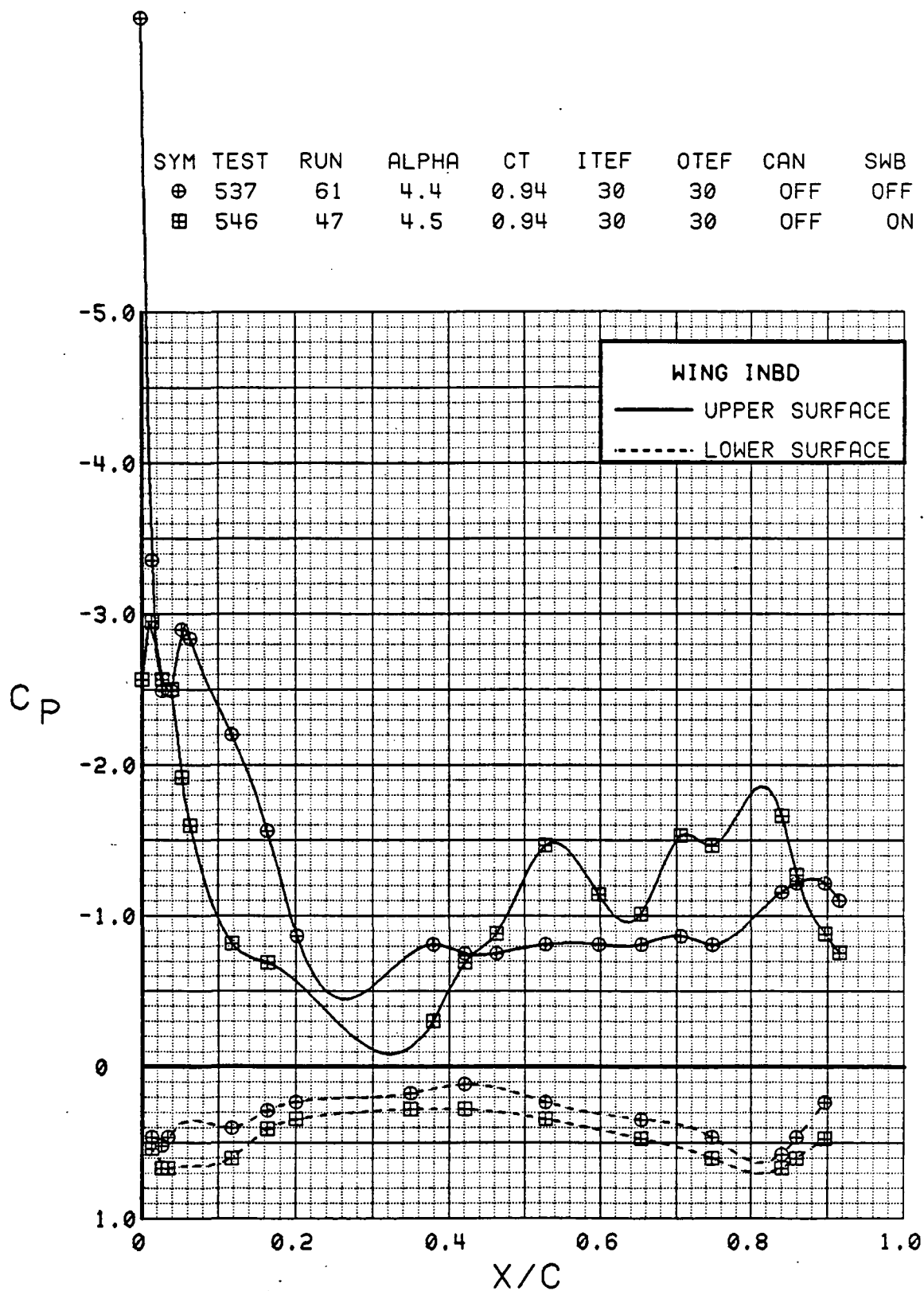


Figure 3.2.2-125 Spanwise Blowing Effects, Flaps Deflected,  
 $C_T = 0.9$ , Inboard, Alpha = 4 deg

SYM	TEST	RUN	ALPHA	CT	ITEF	OTEF	CAN	SWB
⊕	537	61	8.5	0.94	30	30	OFF	OFF
⊞	546	47	8.6	0.94	30	30	OFF	ON

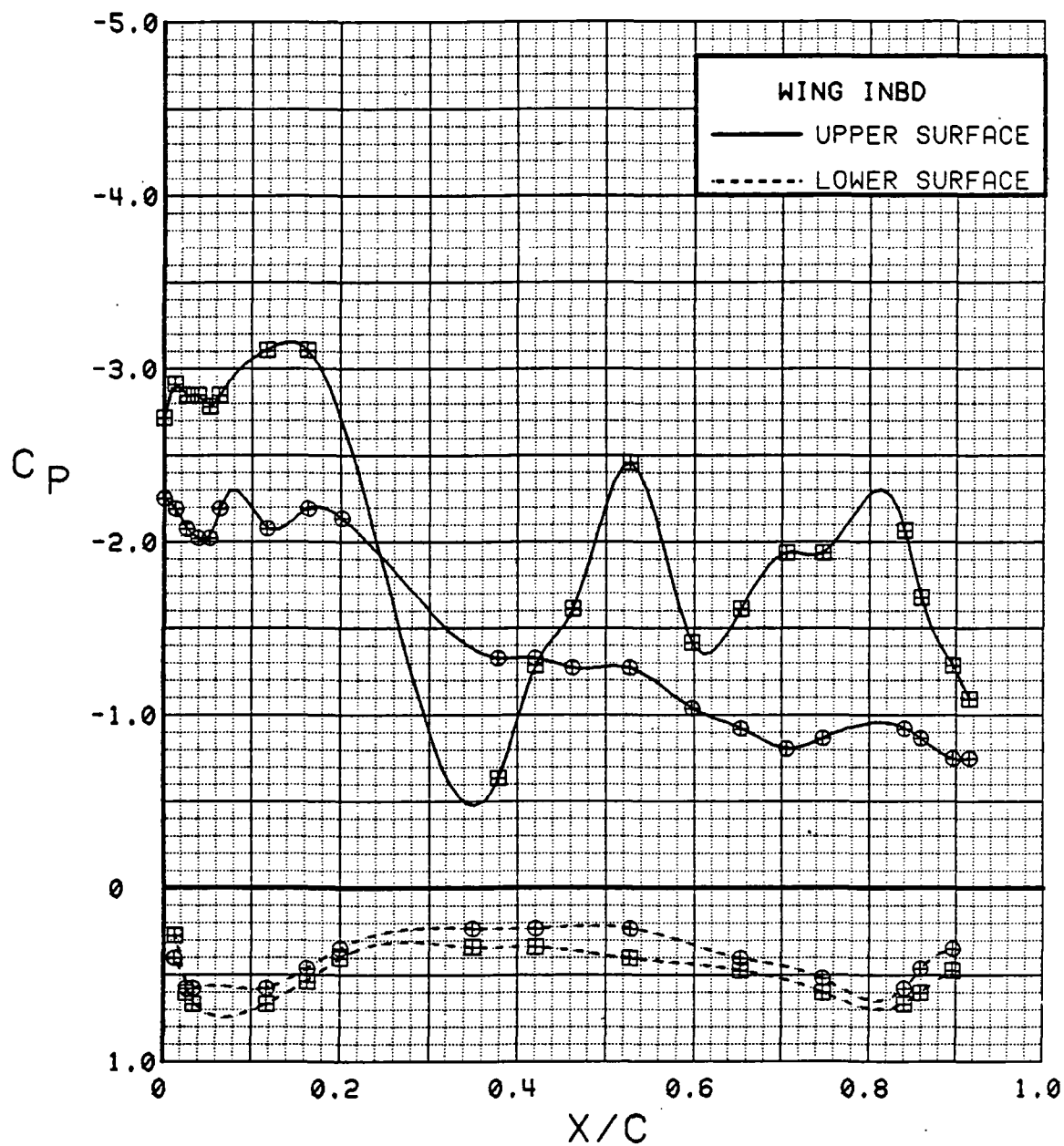


Figure 3.2.2-126 Spanwise Blowing Effects, Flaps Deflected,  $C_T = 0.9$ , Inboard, Alpha = 8 deg

SYM	TEST	RUN	ALPHA	CT	ITEF	OTEF	CAN	SWB
⊕	537	61	12.6	0.92	30	30	OFF	OFF
⊞	546	47	12.8	0.93	30	30	OFF	ON

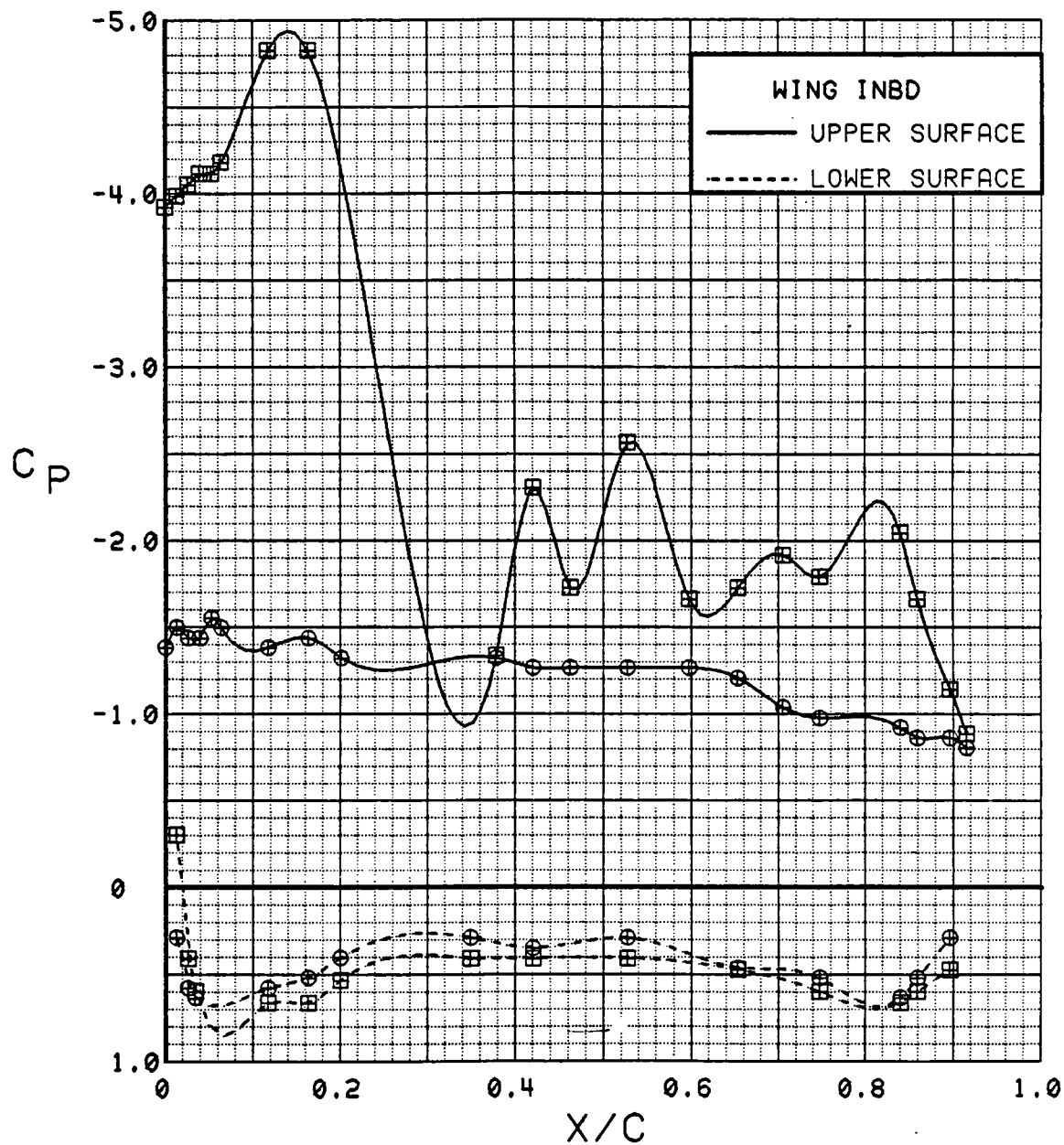


Figure 3.2.2-127 Spanwise Blowing Effects, Flaps Deflected,  $C_T = 0.9$ , Inboard, Alpha = 12 deg

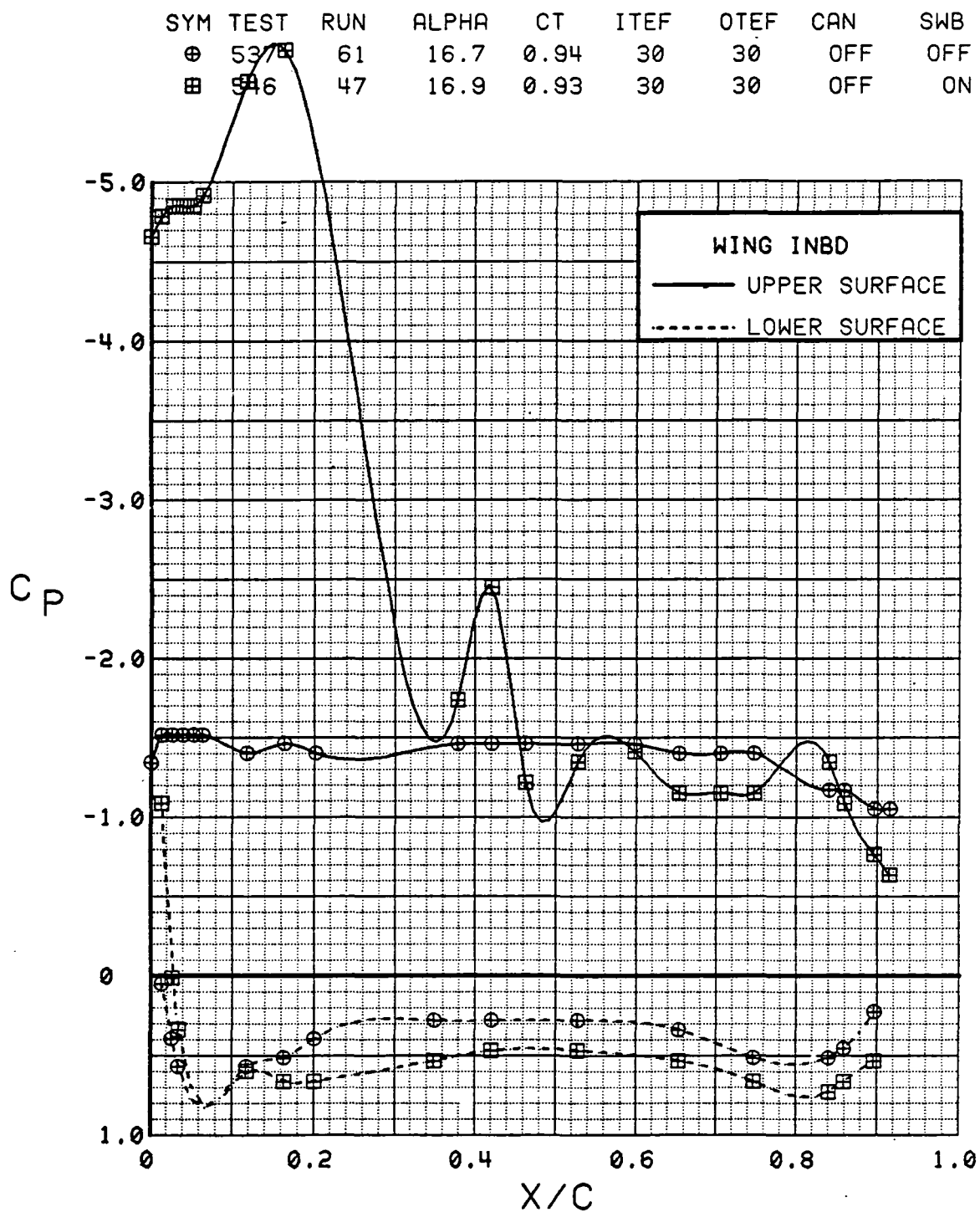


Figure 3.2.2-128 Spanwise Blowing Effects, Flaps Deflected,  
 $C_T = 0.9$ , Inboard, Alpha = 16 deg

SYM	TEST	RUN	ALPHA	CT	ITEF	OTEF	CAN	SWB
⊕	537	61	20.8	0.92	30	30	OFF	OFF
⊞	546	47	20.9	0.94	30	30	OFF	ON

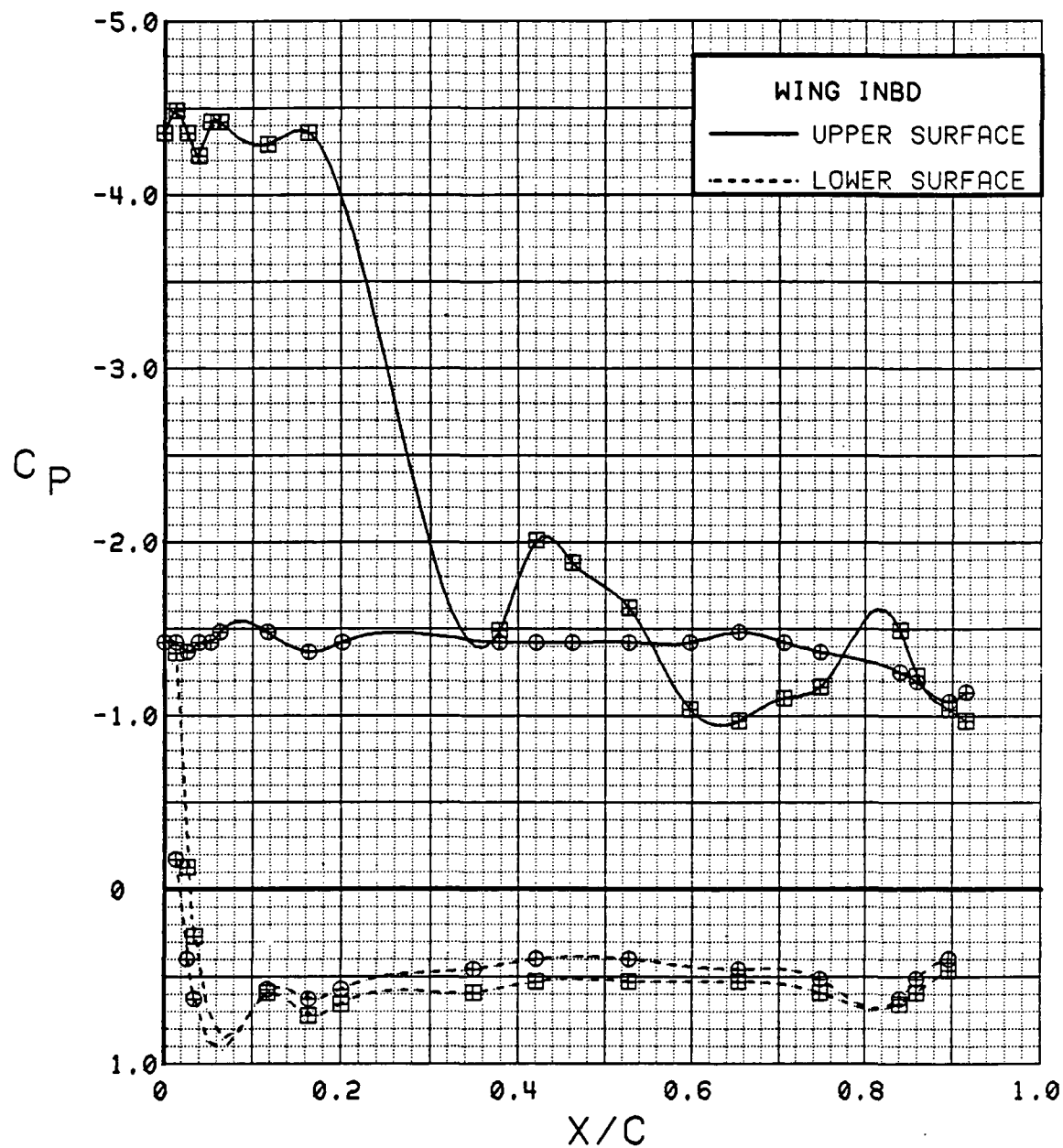


Figure 3.2.2-129 Spanwise Blowing Effects, Flaps Deflected,  $C_T = 0.9$ , Inboard, Alpha = 20 deg

SYM	TEST	RUN	ALPHA	CT	ITEF	OTEF	CAN	SWB
⊕	537	61	24.9	0.92	30	30	OFF	OFF
⊞	546	47	24.9	0.93	30	30	OFF	ON

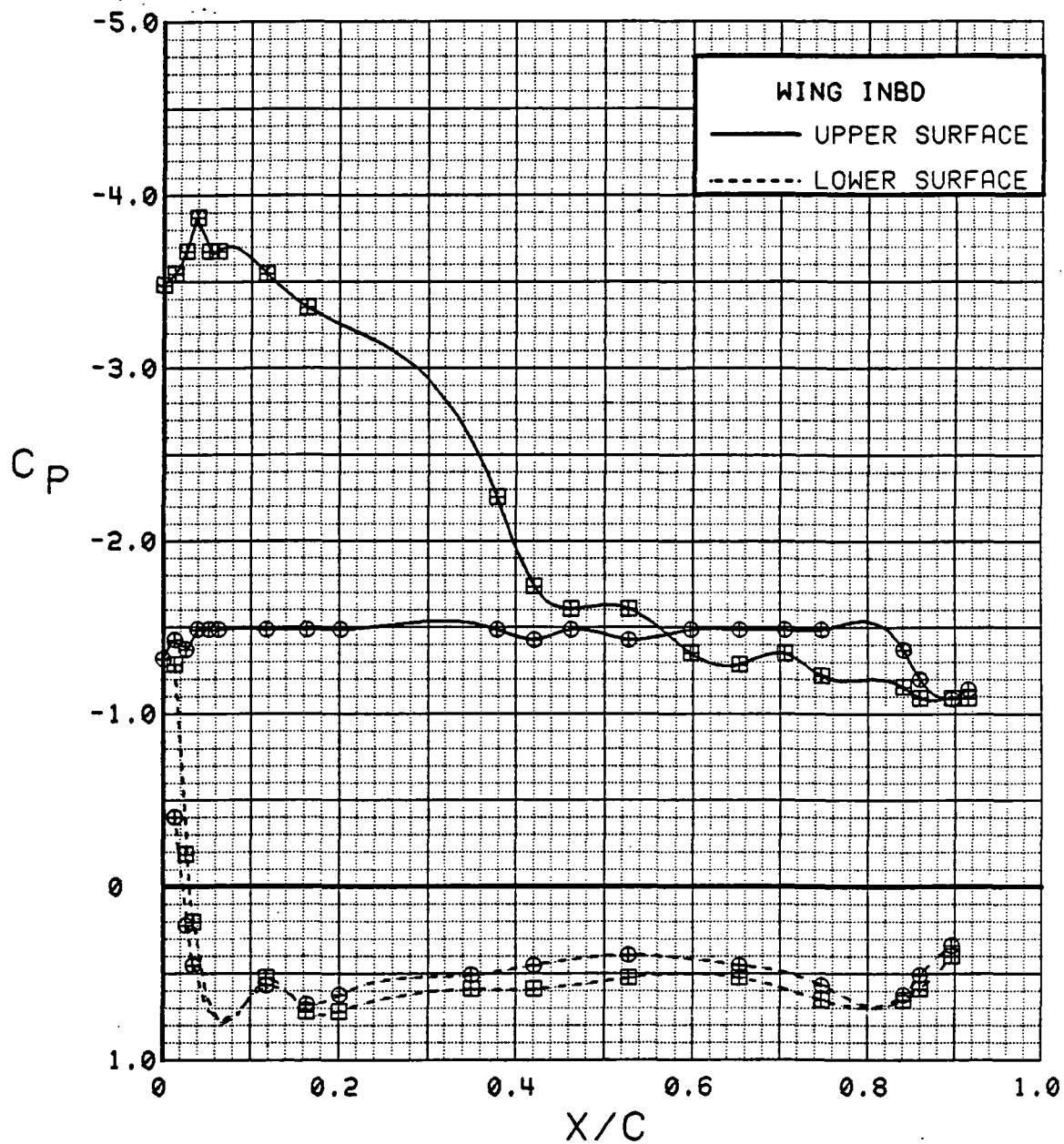


Figure 3.2.2-130 Spanwise Blowing Effects, Flaps Deflected,  $C_T = 0.9$ , Inboard, Alpha = 24 deg

SYM	TEST	RUN	ALPHA	CT	ITEF	OTEF	CAN	SWB
⊕	537	61	28.9	0.93	30	30	OFF	OFF
⊞	546	47	29.0	0.94	30	30	OFF	ON

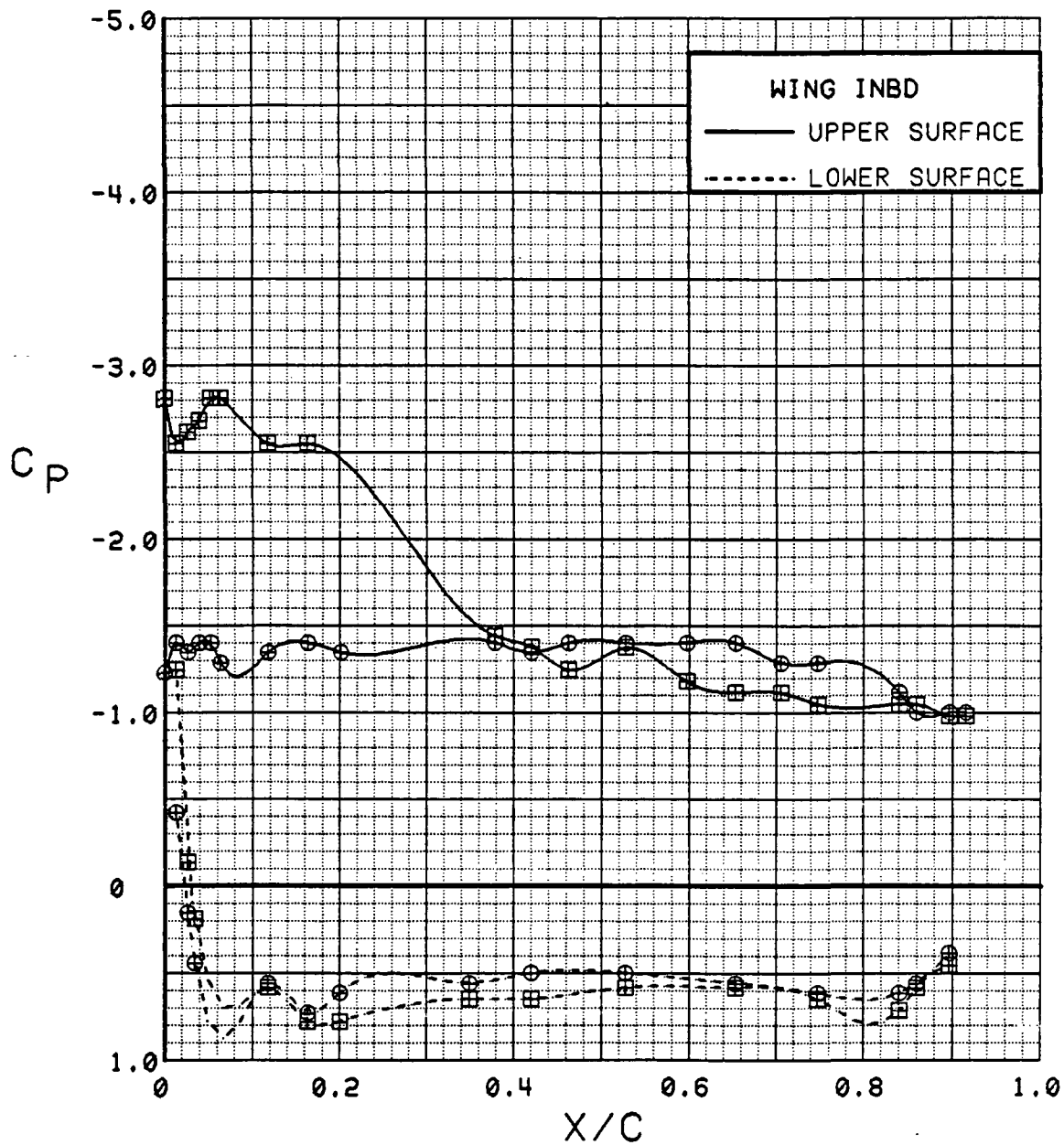


Figure 3.2.2-131 Spanwise Blowing Effects, Flaps Deflected,  
 $C_T = 0.9$ , Inboard, Alpha = 28 deg

SYM	TEST	RUN	ALPHA	CT	ITEF	OTEF	CAN	SWB
⊕	537	61	32.9	0.93	30	30	OFF	OFF
⊞	546	47	32.9	0.94	30	30	OFF	ON

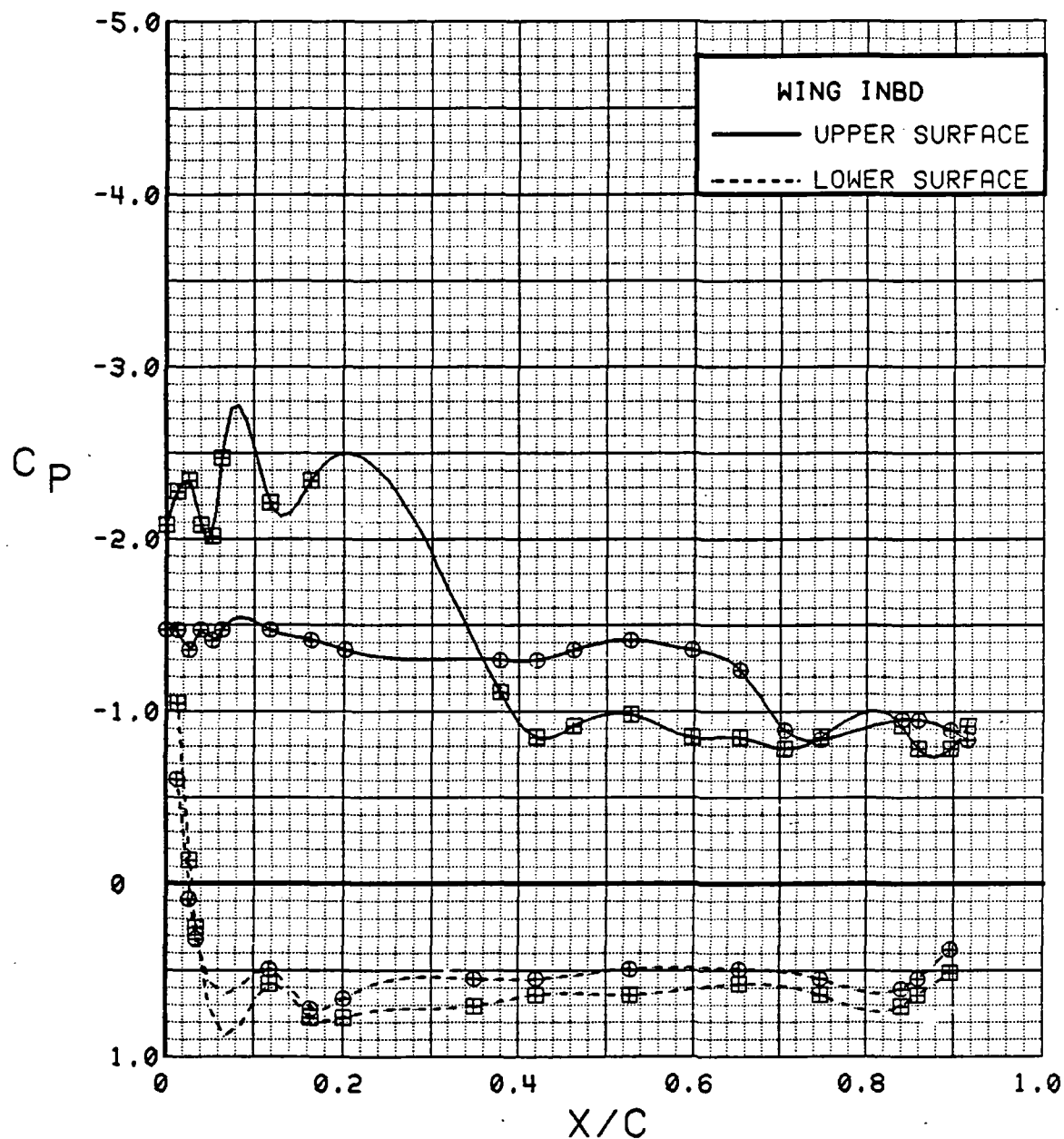


Figure 3.2.2-132 Spanwise Blowing Effects, Flaps Deflected,  
 $C_T = 0.9$ , Inboard, Alpha = 32 deg



SYM	TEST	RUN	ALPHA	CT	ITEF	OTEF	CAN	SWB
⊕	537	61	0.4	0.94	30	30	OFF	OFF
⊞	546	47	0.4	0.96	30	30	OFF	ON

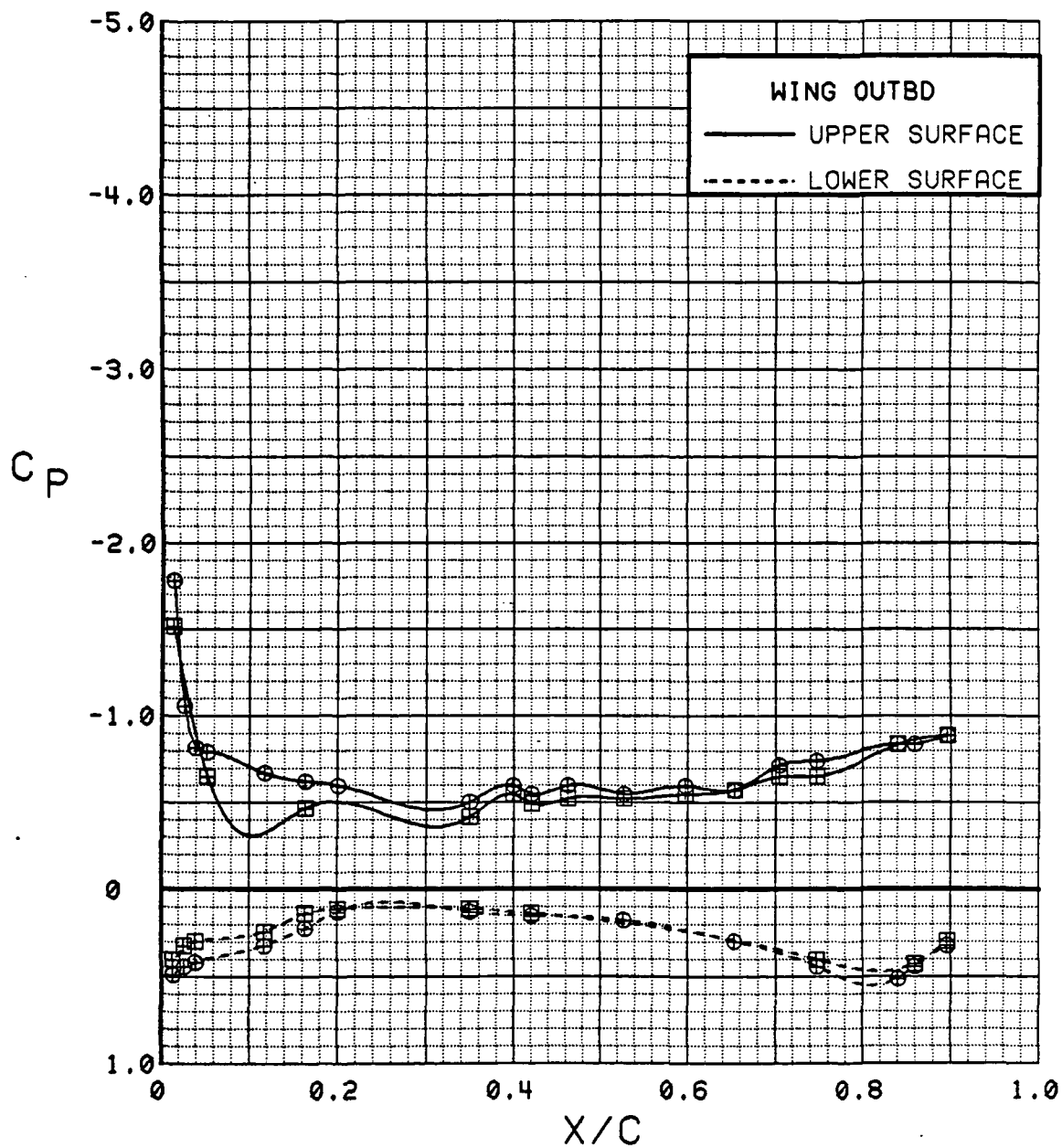


Figure 3.2.2-133 Spanwise Blowing Effects, Flaps Deflected,  
 $C_T = 0.9$ , Outboard, Alpha = 0 deg

SYM	TEST	RUN	ALPHA	CT	ITEF	OTEF	CAN	SWB
⊕	537	61	4.4	0.94	30	30	OFF	OFF
⊞	546	47	4.5	0.94	30	30	OFF	ON

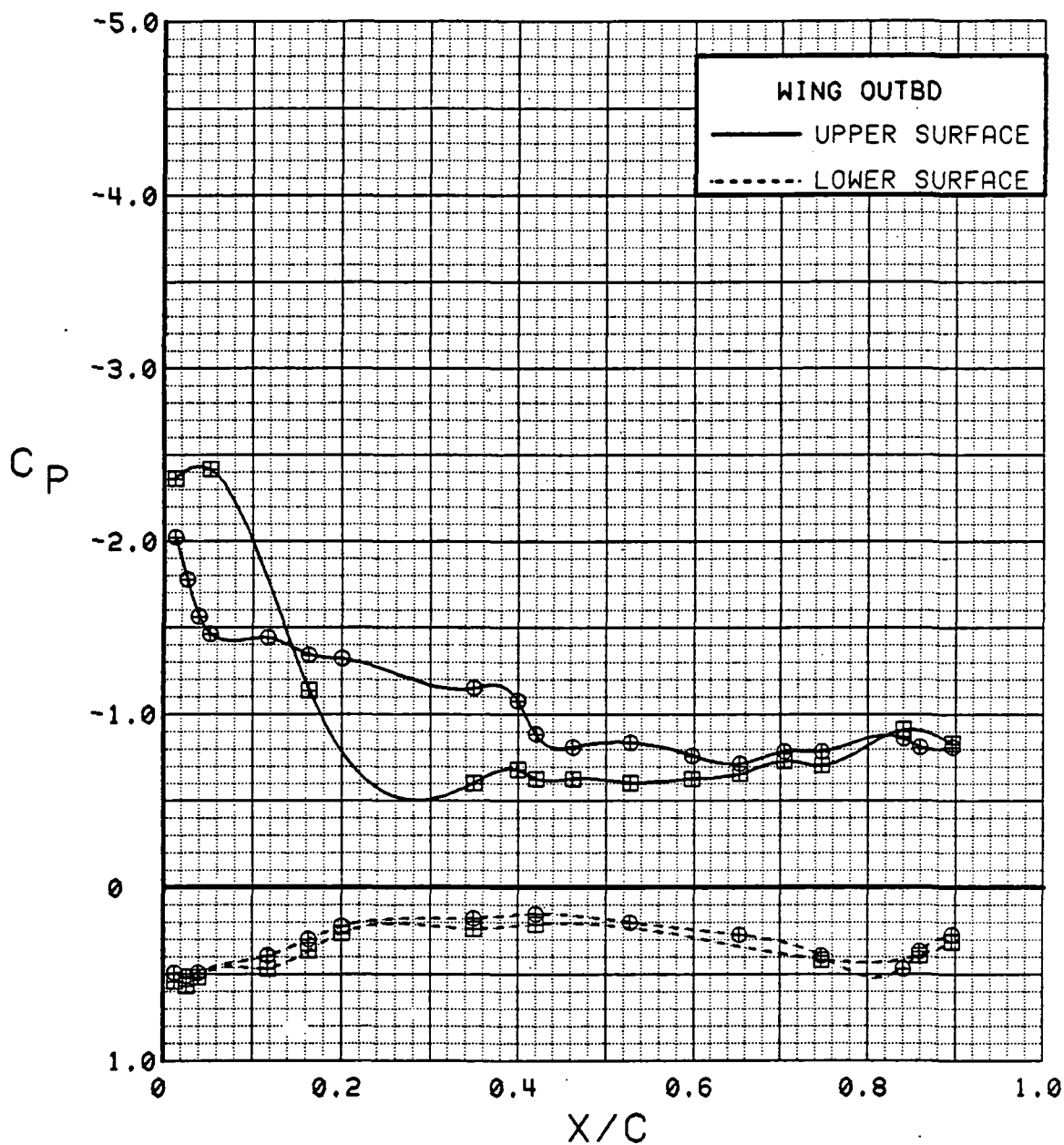


Figure 3.2.2-134 Spanwise Blowing Effects, Flaps Deflected,  
 $C_T = 0.9$ , Outboard, Alpha = 4 deg

SYM	TEST	RUN	ALPHA	CT	ITEF	OTEF	CAN	SWB
⊕	537	61	8.5	0.94	30	30	OFF	OFF
⊞	546	47	8.6	0.94	30	30	OFF	ON

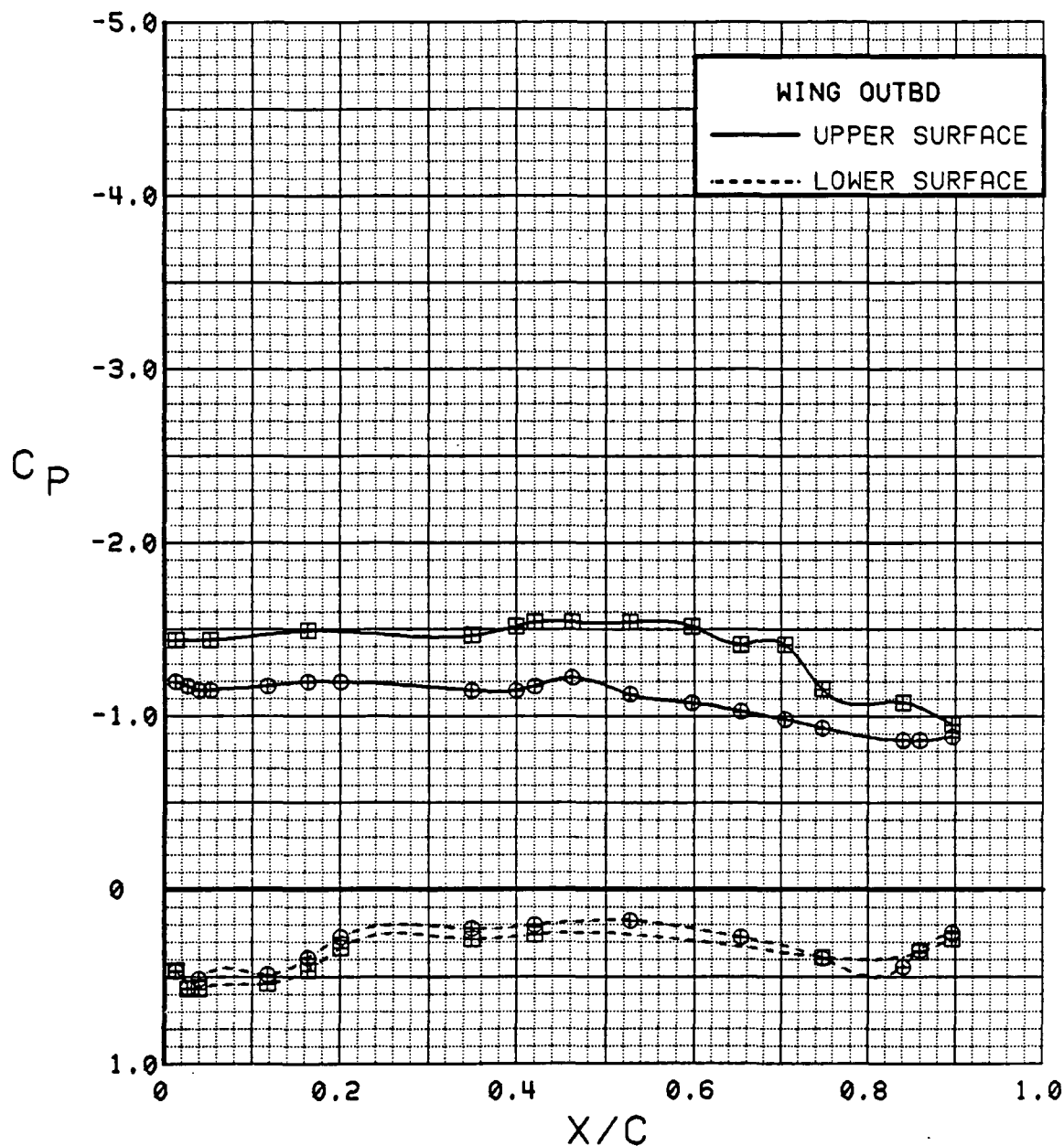


Figure 3.2.2-135 Spanwise Blowing Effects, Flaps Deflected,  
 $C_T = 0.9$ , Outboard, Alpha = 8 deg

SYM	TEST	RUN	ALPHA	CT	ITEF	OTEF	CAN	SWB
⊕	537	61	12.6	0.92	30	30	OFF	OFF
⊞	546	47	12.8	0.93	30	30	OFF	ON

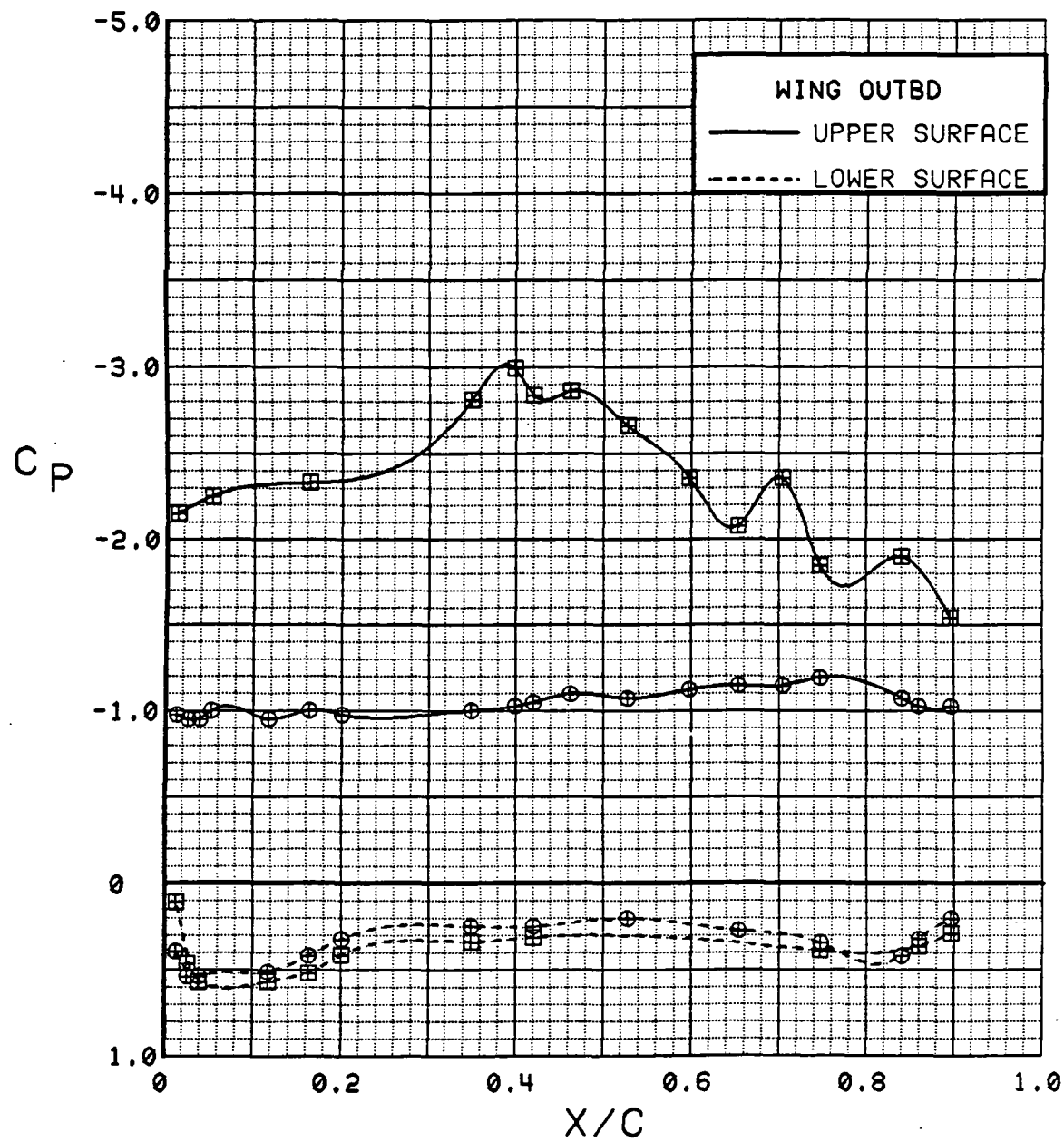


Figure 3.2.2-136 Spanwise Blowing Effects, Flaps Deflected,  $C_T = 0.9$ , Outboard, Alpha = 12 deg

SYM	TEST	RUN	ALPHA	CT.	ITEF	OTEF	CAN	SWB
⊕	537	61	16.7	0.94	30	30	OFF	OFF
⊞	546	47	16.9	0.93	30	30	OFF	ON

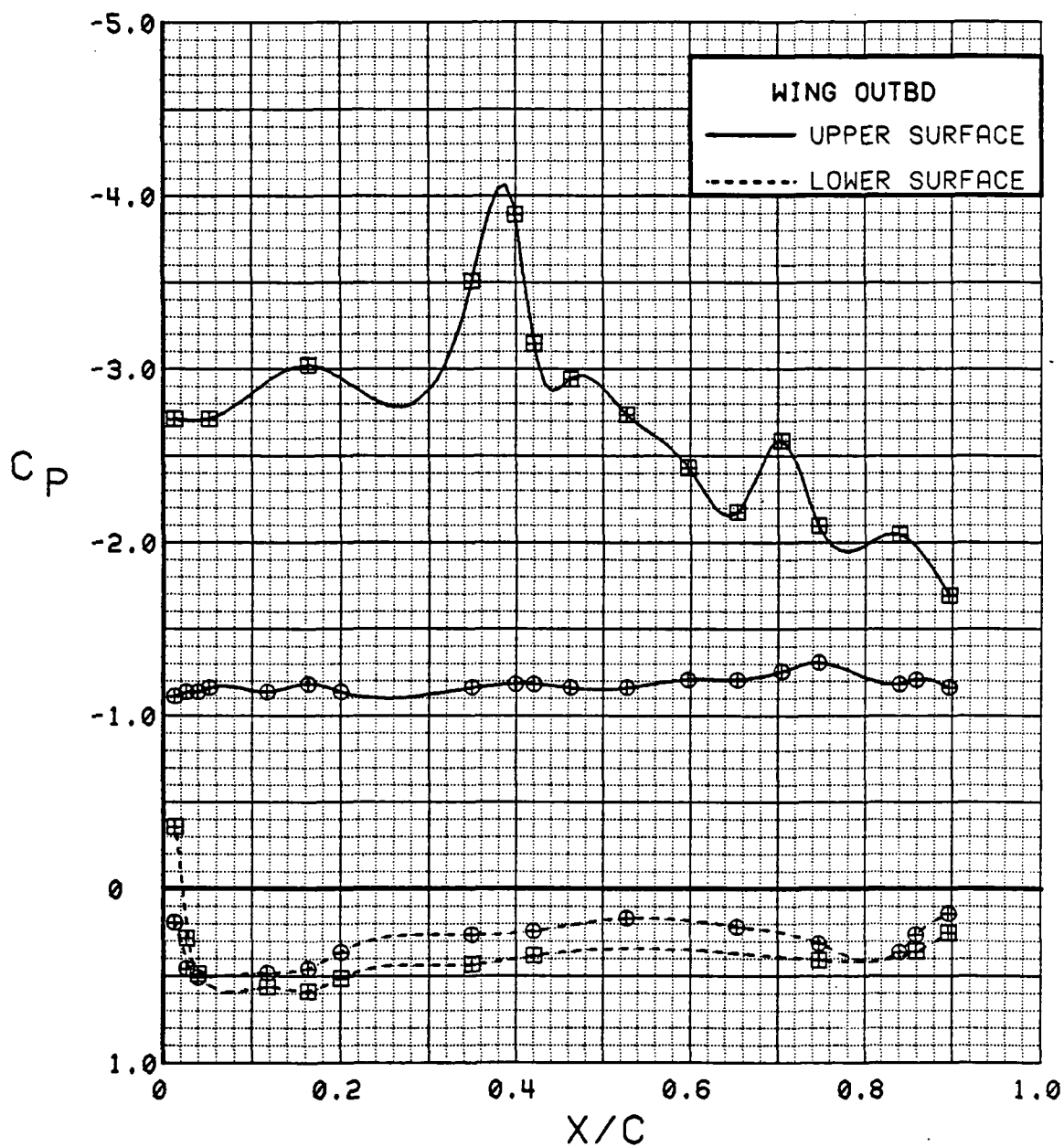


Figure 3.2.2-137 Spanwise Blowing Effects, Flaps Deflected,  
 $C_T = 0.9$ , Outboard, Alpha = 16 deg

SYM	TEST	RUN	ALPHA	CT	ITEF	OTEF	CAN	SWB
⊕	537	61	20.8	0.92	30	30	OFF	OFF
⊞	546	47	20.9	0.94	30	30	OFF	ON

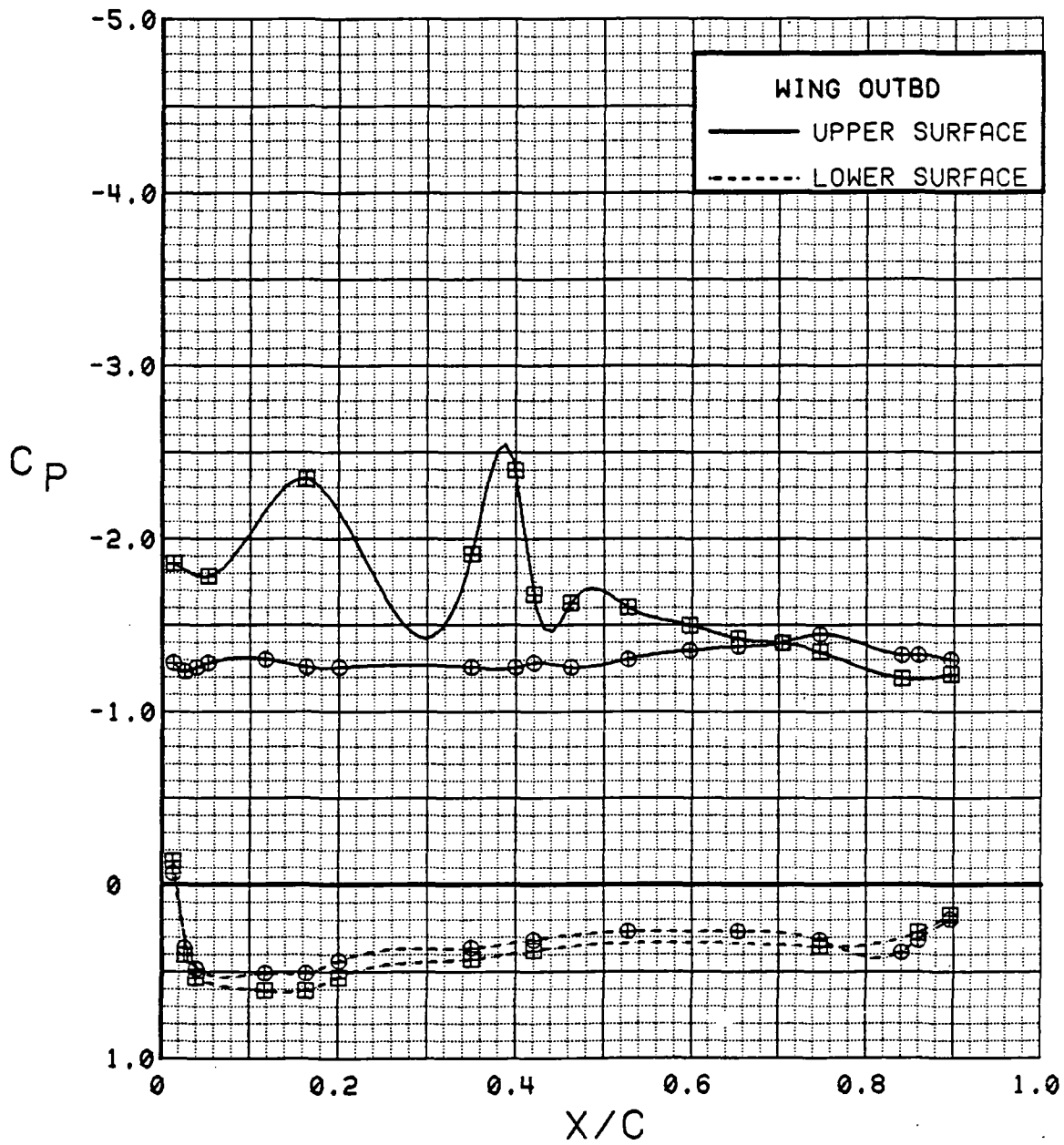


Figure 3.2.2-138 Spanwise Blowing Effects, Flaps Deflected,  $C_T = 0.9$ , Outboard, Alpha = 20 deg

SYM	TEST	RUN	ALPHA	CT	ITEF	OTEF	CAN	SWB
⊕	537	61	24.9	0.92	30	30	OFF	OFF
⊞	546	47	24.9	0.93	30	30	OFF	ON

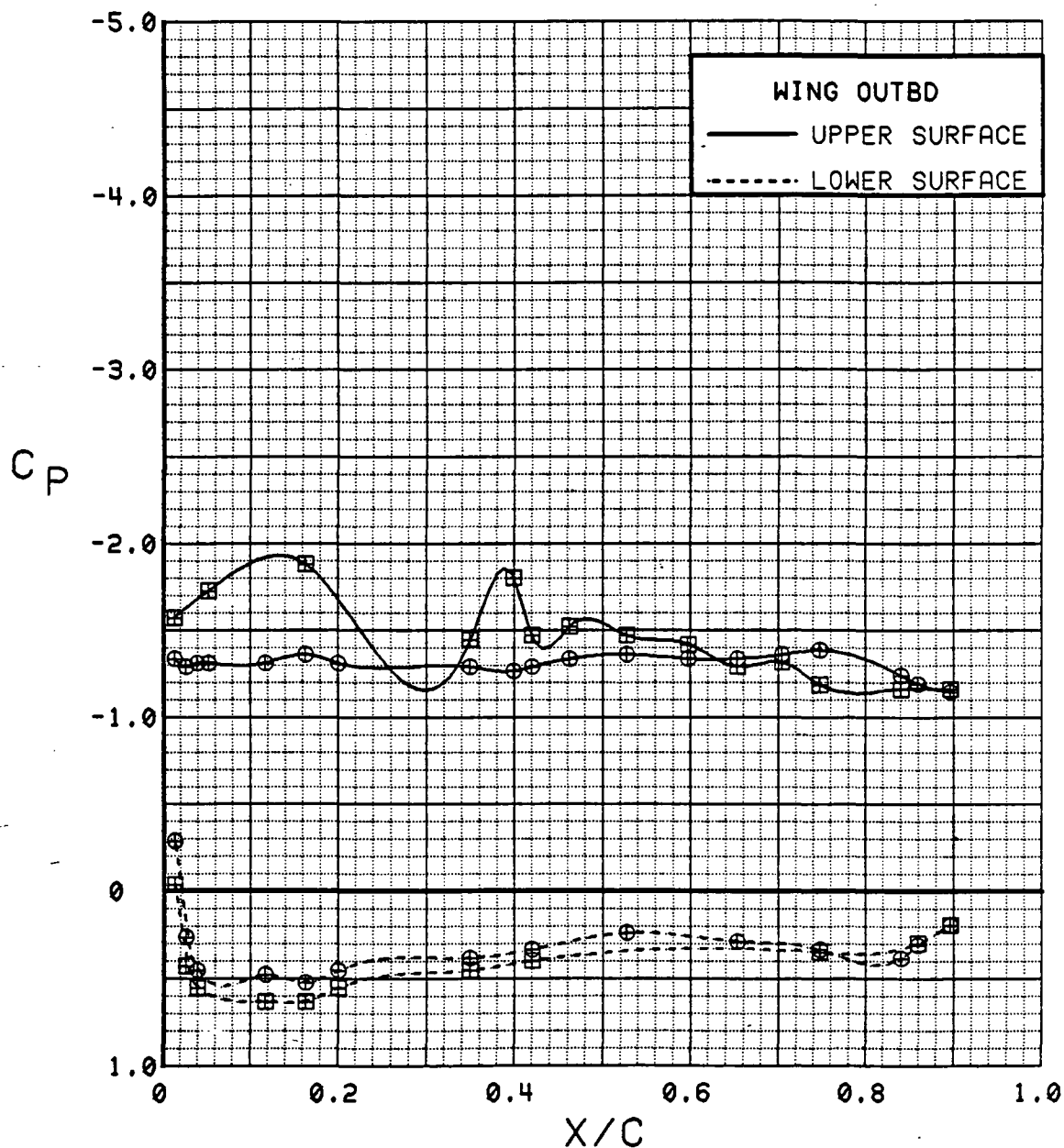


Figure 3.2.2-139 Spanwise Blowing Effects, Flaps Deflected,  $C_T = 0.9$ , Outboard, Alpha = 24 deg

SYM	TEST	RUN	ALPHA	CT	ITEF	OTEF	CAN	SWB
⊕	537	61	28.9	0.93	30	30	OFF	OFF
⊞	546	47	29.0	0.94	30	30	OFF	ON

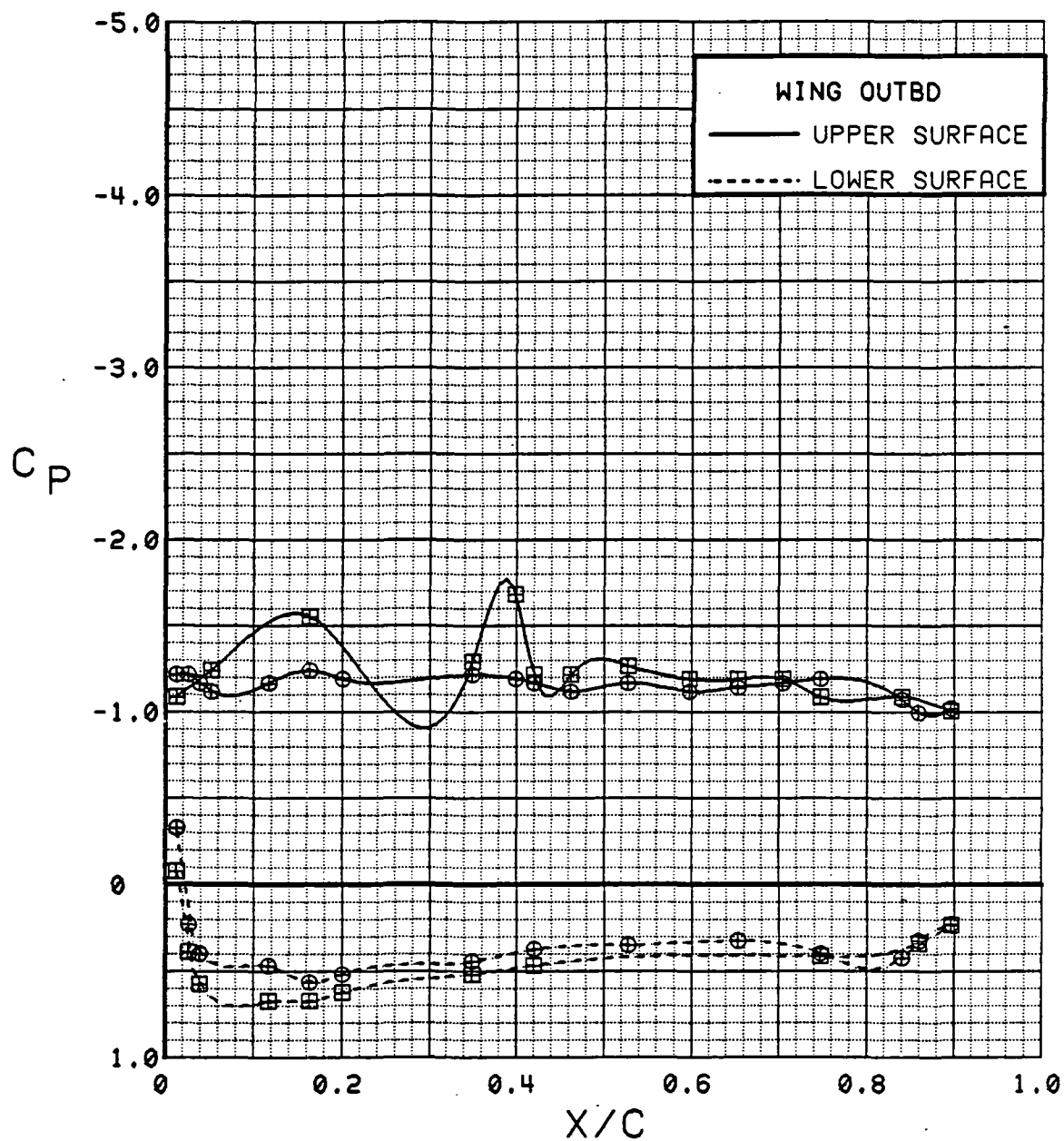


Figure 3.2.2-140 Spanwise Blowing Effects, Flaps Deflected,  $C_T = 0.9$ , Outboard, Alpha = 28 deg



SYM	TEST	RUN	ALPHA	CT	ITEF	OTEF	CAN	SWB
⊕	537	61	32.9	0.93	30	30	OFF	OFF
⊞	546	47	32.9	0.94	30	30	OFF	ON

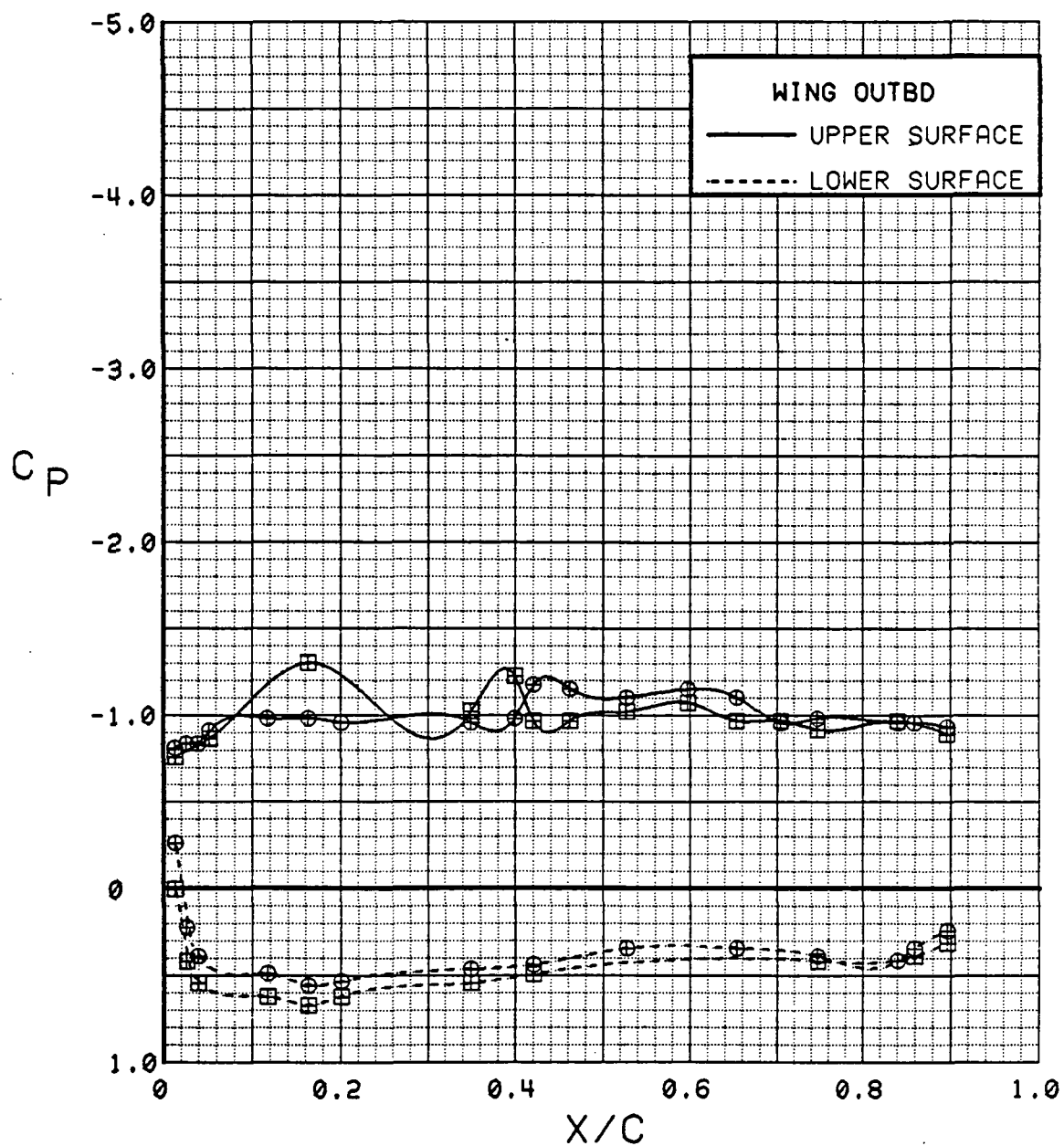


Figure 3.2.2-141 Spanwise Blowing Effects, Flaps Deflected,  $C_T = 0.9$ , Outboard, Alpha = 32 deg

SYM	TEST	RUN	ALPHA	CT	ITEF	OTEF	CAN	SWB
●	537	61	0.4	0.94	30	30	OFF	OFF
■	546	47	0.4	0.96	30	30	OFF	ON

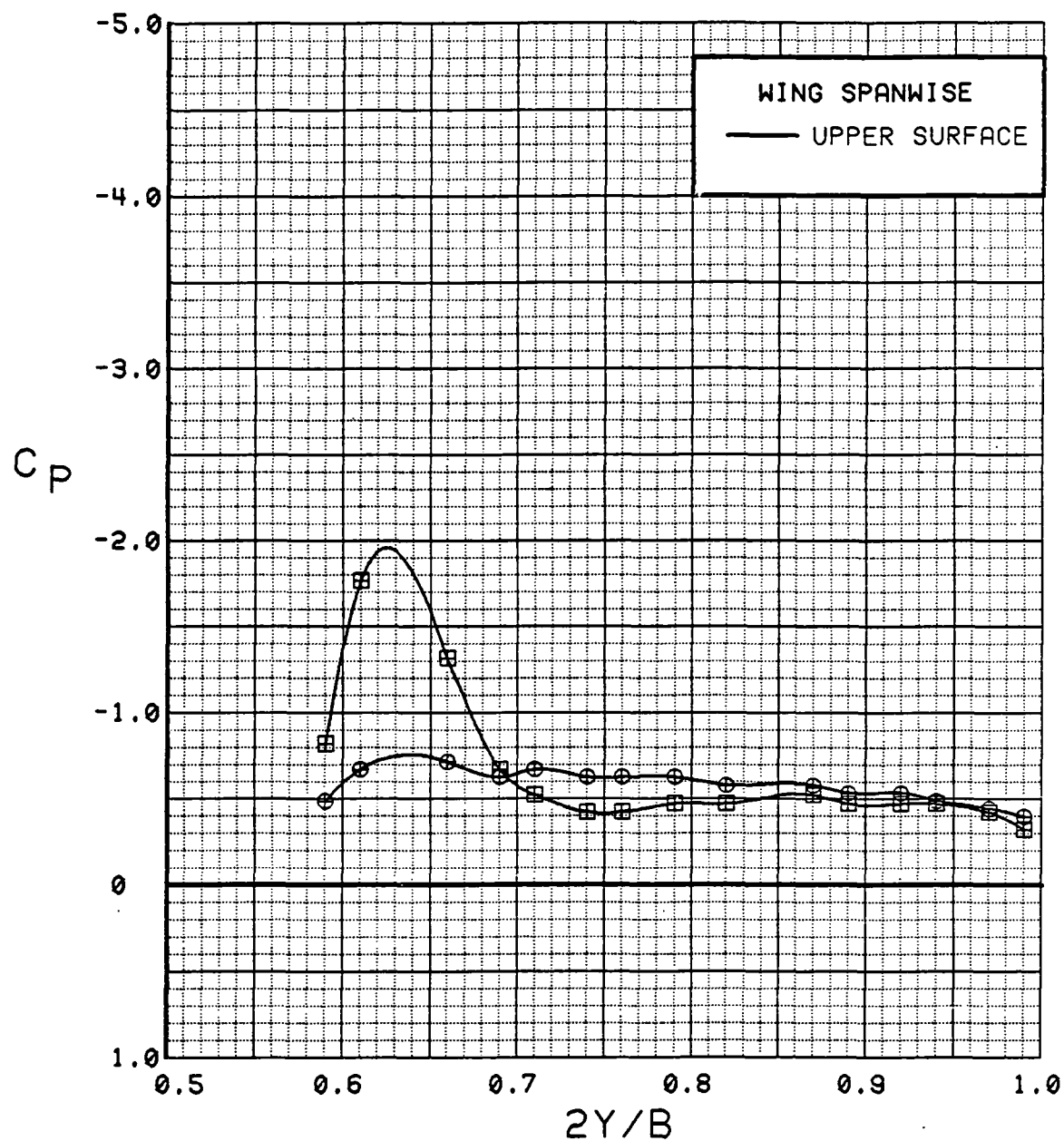


Figure 3.2.2-142 Spanwise Blowing Effects, Flaps Deflected,  
 $C_T = 0.9$ , Spanwise, Alpha = 0 deg

SYM	TEST	RUN	ALPHA	CT	ITEF	OTEF	CAN	SWB
⊙	537	61	4.4	0.94	30	30	OFF	OFF
⊠	546	47	4.5	0.94	30	30	OFF	ON

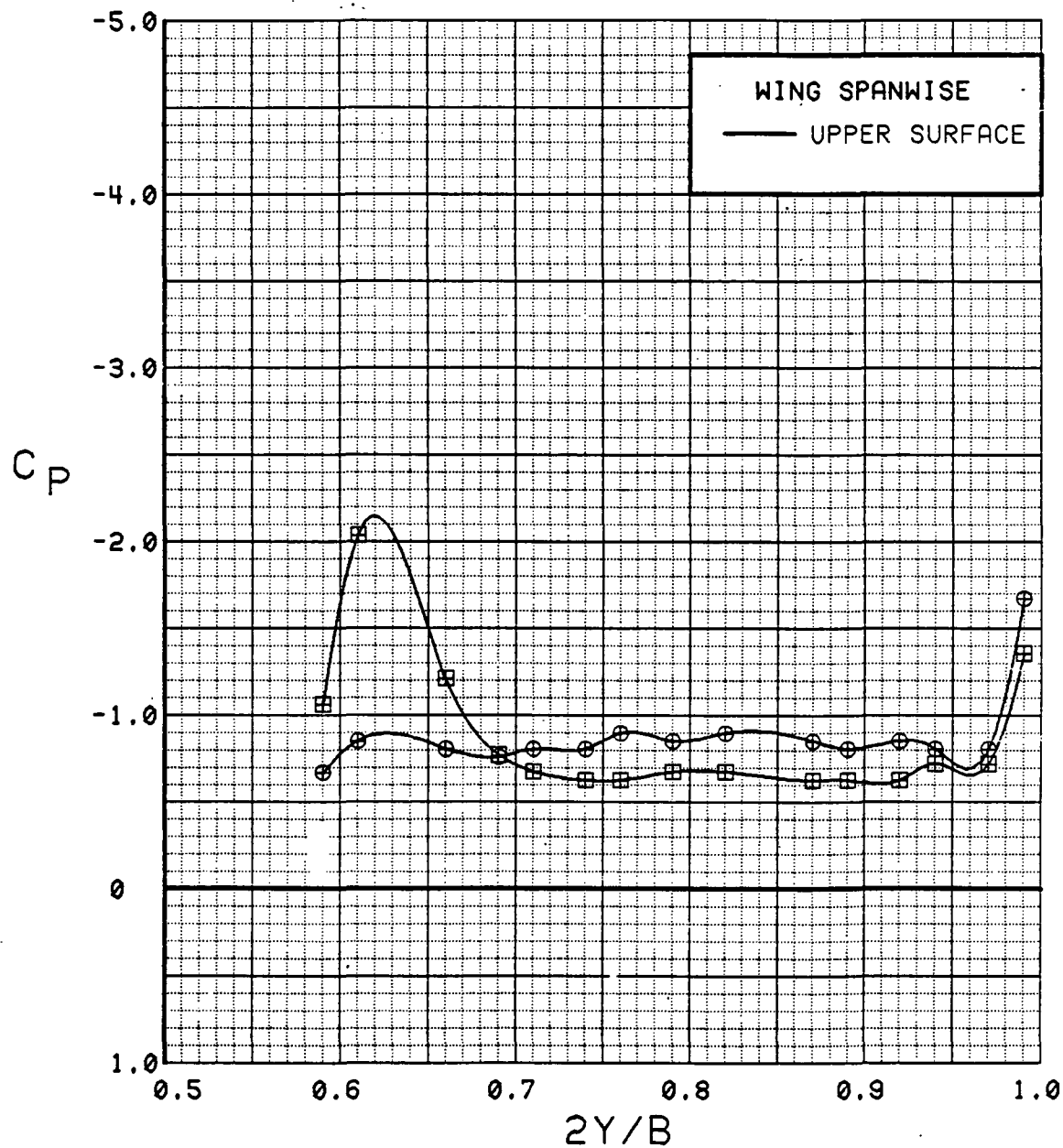


Figure 3.2.2-143 Spanwise Blowing Effects, Flaps Deflected,  
 $C_T = 0.9$ , Spanwise, Alpha = 4 deg

SYM	TEST	RUN	ALPHA	CT	ITEF	OTEF	CAN	SWB
⊙	537	61	8.5	0.94	30	30	OFF	OFF
⊠	546	47	8.6	0.94	30	30	OFF	ON

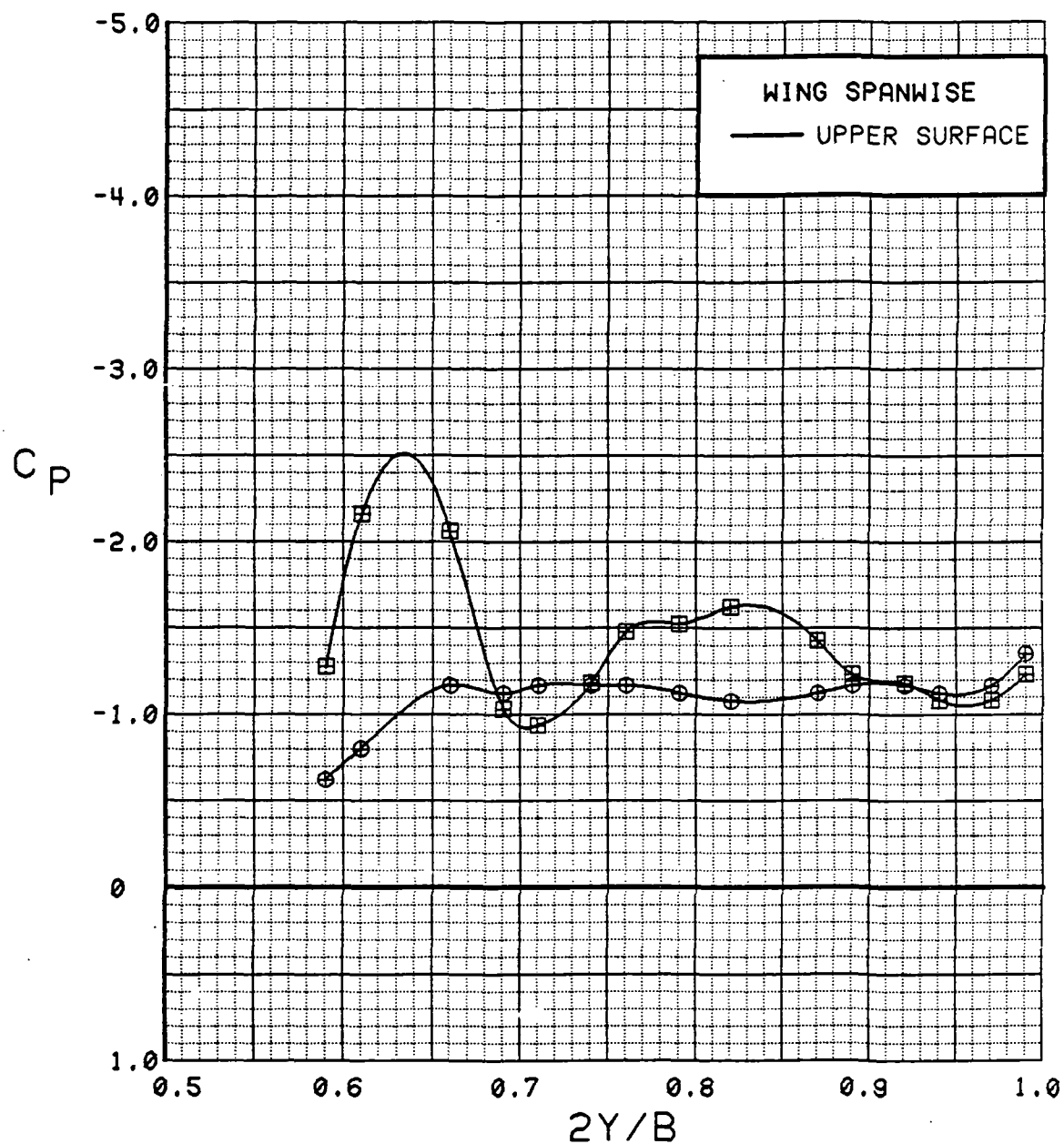


Figure 3.2.2-144 Spanwise Blowing Effects, Flaps Deflected,  
C<sub>T</sub> = 0.9, Spanwise, Alpha = 8 deg

SYM	TEST	RUN	ALPHA	CT	ITEF	OTEF	CAN	SWB
⊕	537	61	12.6	0.92	30	30	OFF	OFF
⊞	546	47	12.8	0.93	30	30	OFF	ON

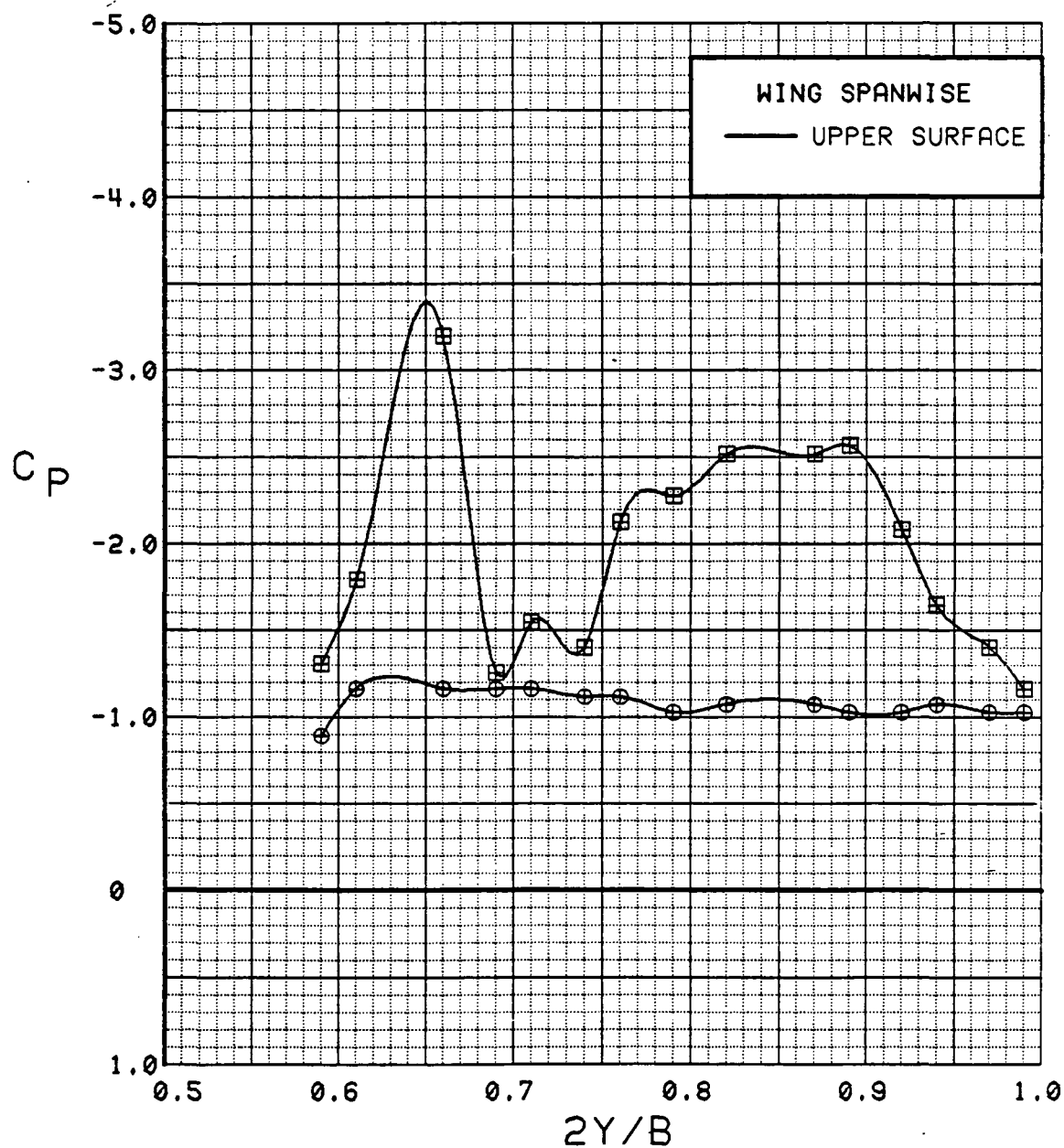


Figure 3.2.2-145 Spanwise Blowing Effects, Flaps Deflected,  
 $C_T = 0.9$ , Spanwise, Alpha = 12 deg

SYM	TEST	RUN	ALPHA	CT	ITEF	OTEF	CAN	SWB
⊕	537	61	16.7	0.94	30	30	OFF	OFF
⊞	546	47	16.9	0.93	30	30	OFF	ON

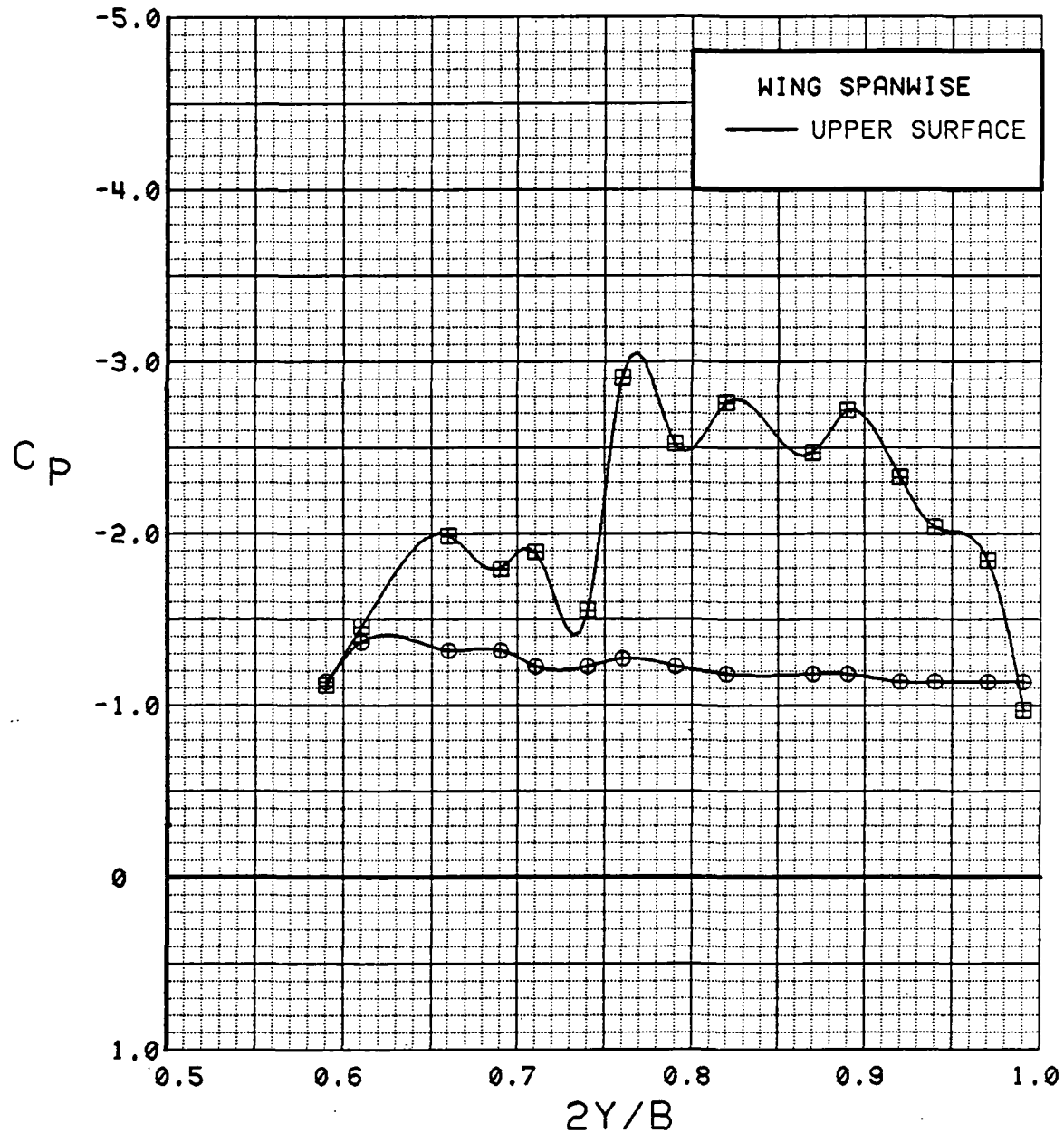


Figure 3.2.2-146 Spanwise Blowing Effects, Flaps Deflected,  
C<sub>T</sub> = 0.9, Spanwise, Alpha = 16 deg

SYM	TEST	RUN	ALPHA	CT	ITEF	OTEF	CAN	SWB
●	537	61	20.8	0.92	30	30	OFF	OFF
■	546	47	20.9	0.94	30	30	OFF	ON

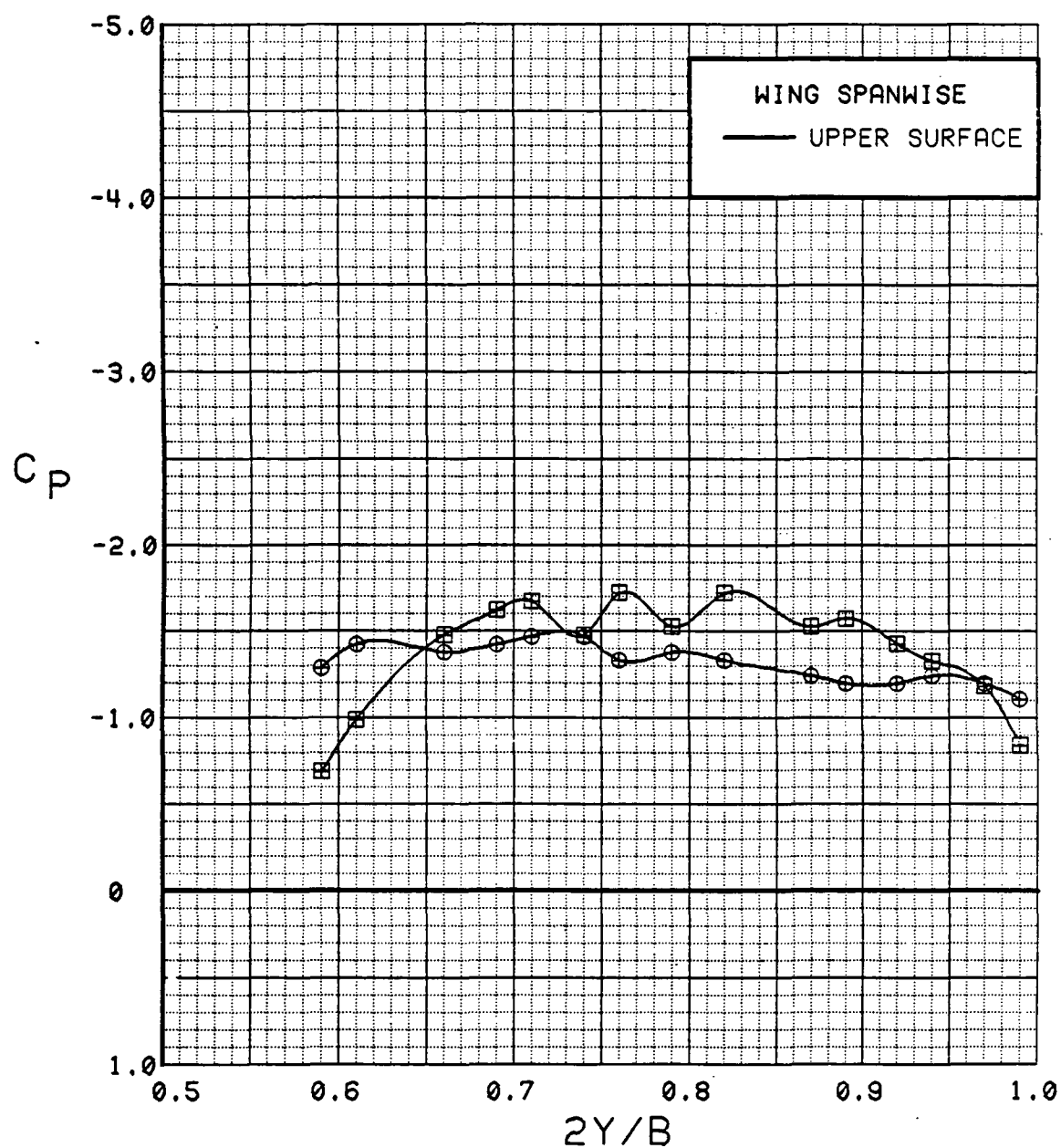


Figure 3.2.2-147 Spanwise Blowing Effects, Flaps Deflected,  
 $C_T = 0.9$ , Spanwise, Alpha = 20 deg

SYM	TEST	RUN	ALPHA	CT	ITEF	OTEF	CAN	SWB
⊙	537	61	24.9	0.92	30	30	OFF	OFF
⊠	546	47	24.9	0.93	30	30	OFF	ON

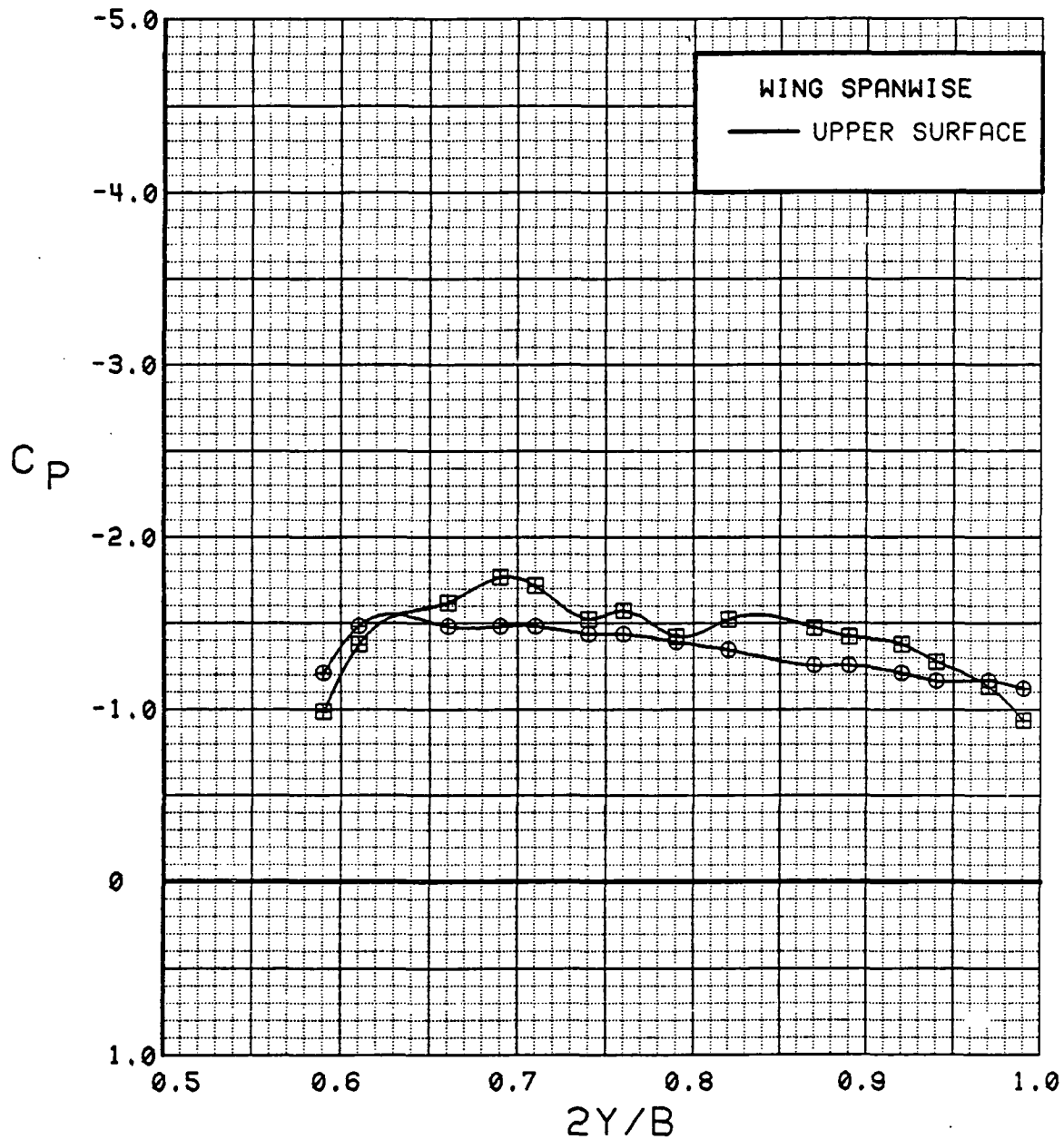


Figure 3.2.2-148 Spanwise Blowing Effects, Flaps Deflected,  
C<sub>T</sub> = 0.9, Spanwise, Alpha = 24 deg



SYM	TEST	RUN	ALPHA	CT	ITEF	OTEF	CAN	SWB
⊕	537	61	28.9	0.93	30	30	OFF	OFF
⊞	546	47	29.0	0.94	30	30	OFF	ON

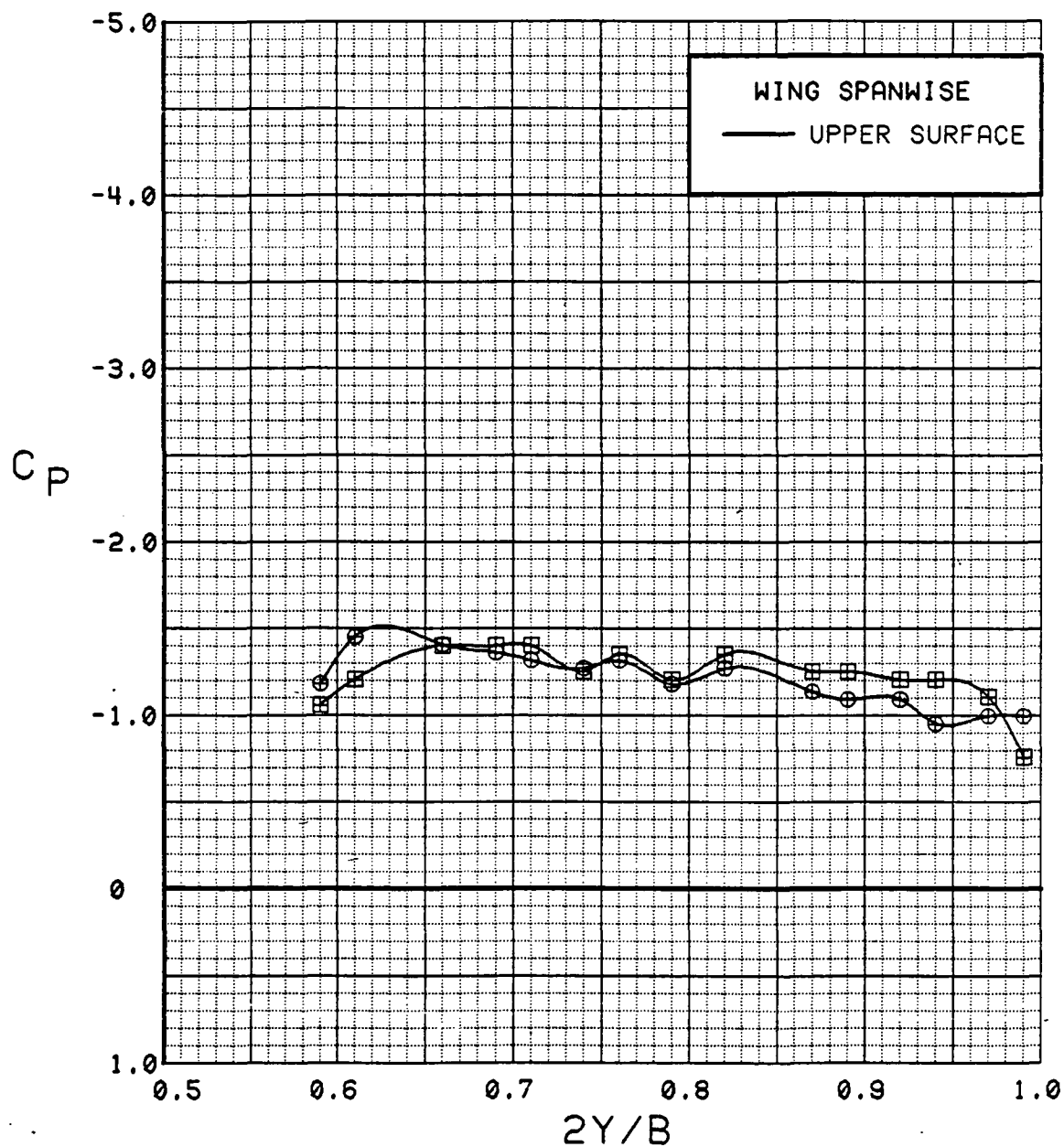


Figure 3.2.2-149 Spanwise Blowing Effects, Flaps Deflected,  
 $C_T = 0.9$ , Spanwise, Alpha = 28 deg

SYM	TEST	RUN	ALPHA	CT	ITEF	OTEF	CAN	SWB
⊕	537	61	32.9	0.93	30	30	OFF	OFF
⊞	546	47	32.9	0.94	30	30	OFF	ON

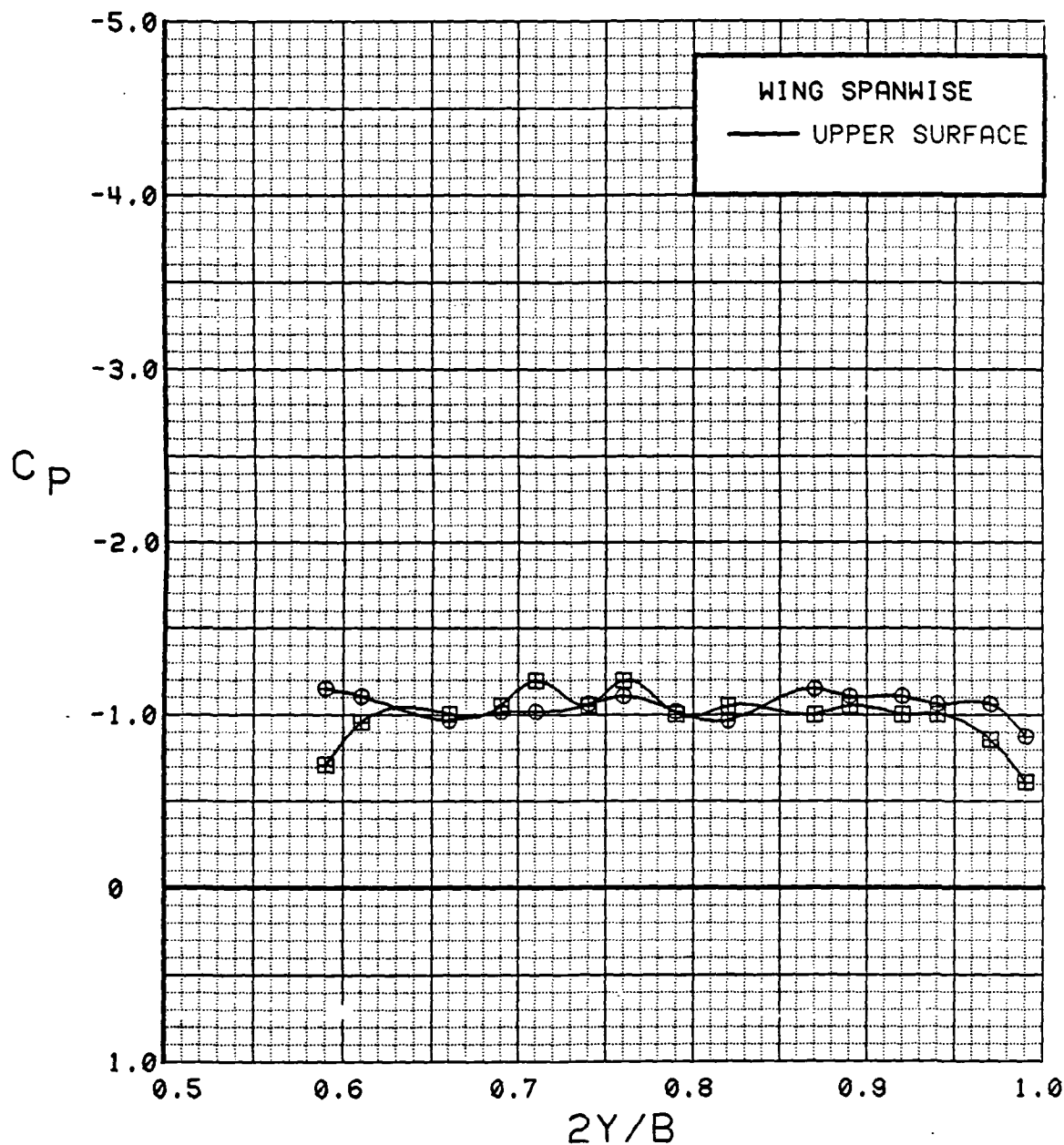


Figure 3.2.2-150 Spanwise Blowing Effects, Flaps Deflected,  $C_T = 0.9$ , Spanwise, Alpha = 32 deg

## WING INBOARD

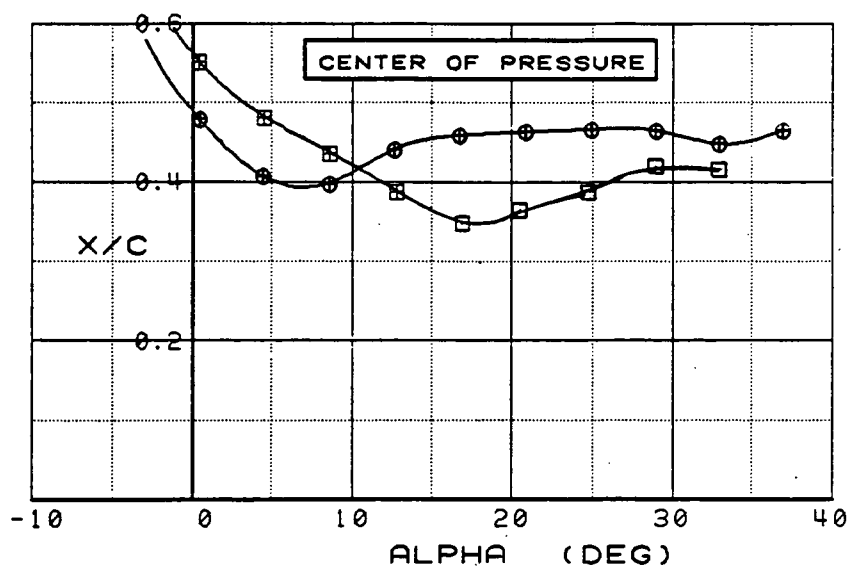
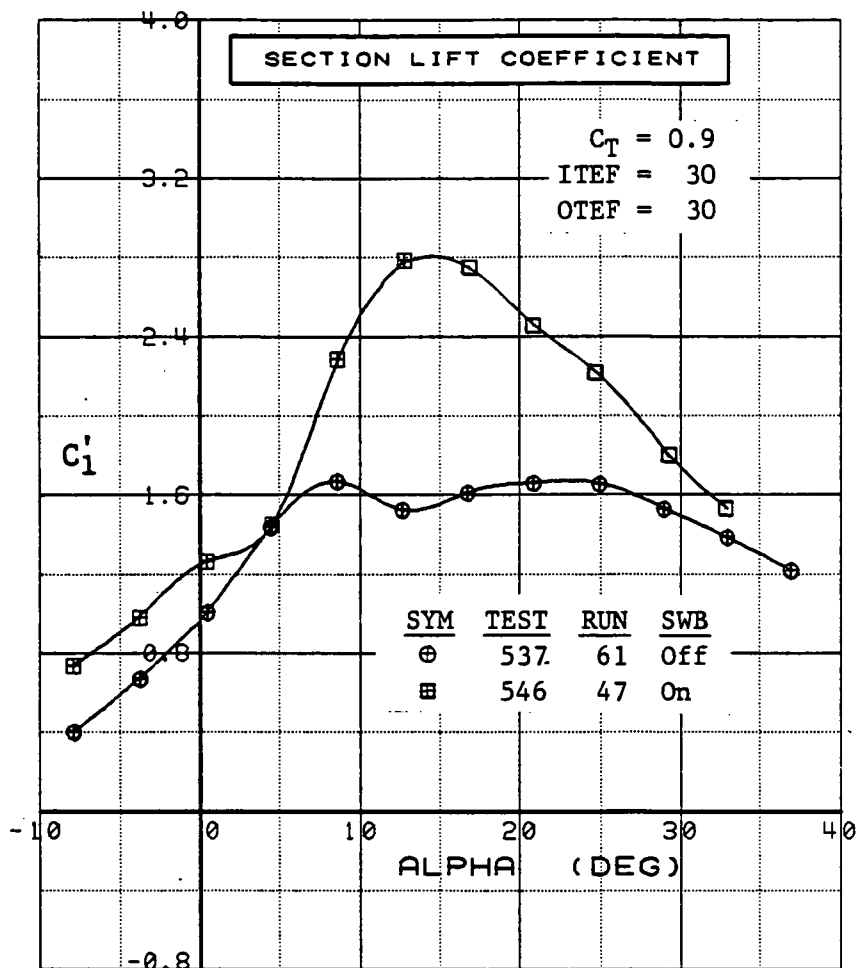


Figure 3.2.2-151 Spanwise Blowing Effects, Flaps Deflected,  
 $C_T = 0.9$ , Inboard, Integrated Section Properties

## WING OUTBOARD

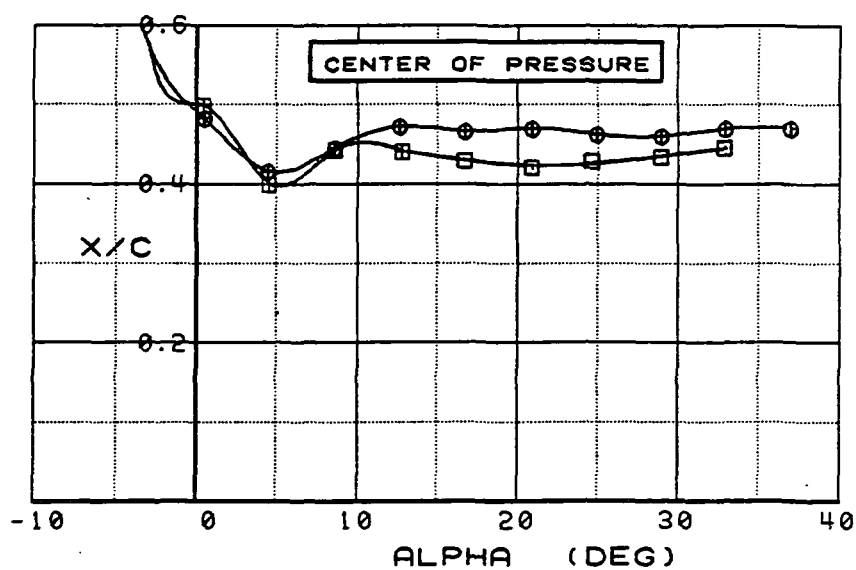
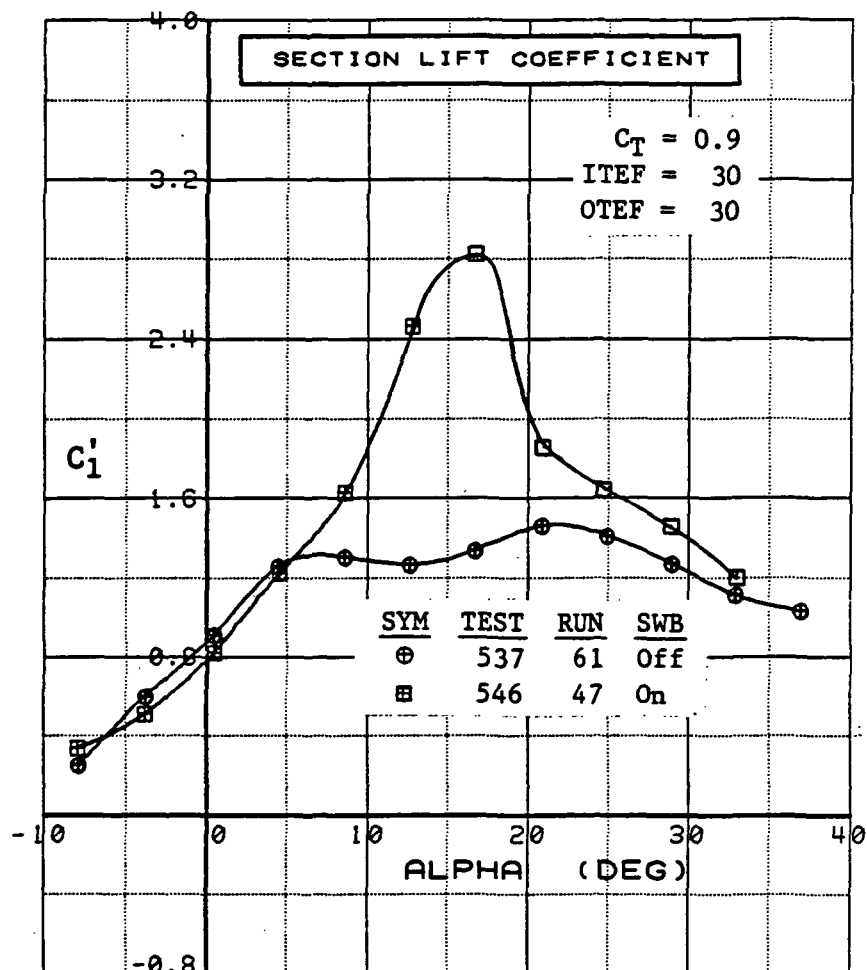


Figure 3.2.2-152 Spanwise Blowing Effects, Flaps Deflected,  
 $C_T = 0.9$ , Outboard, Integrated Section Properties

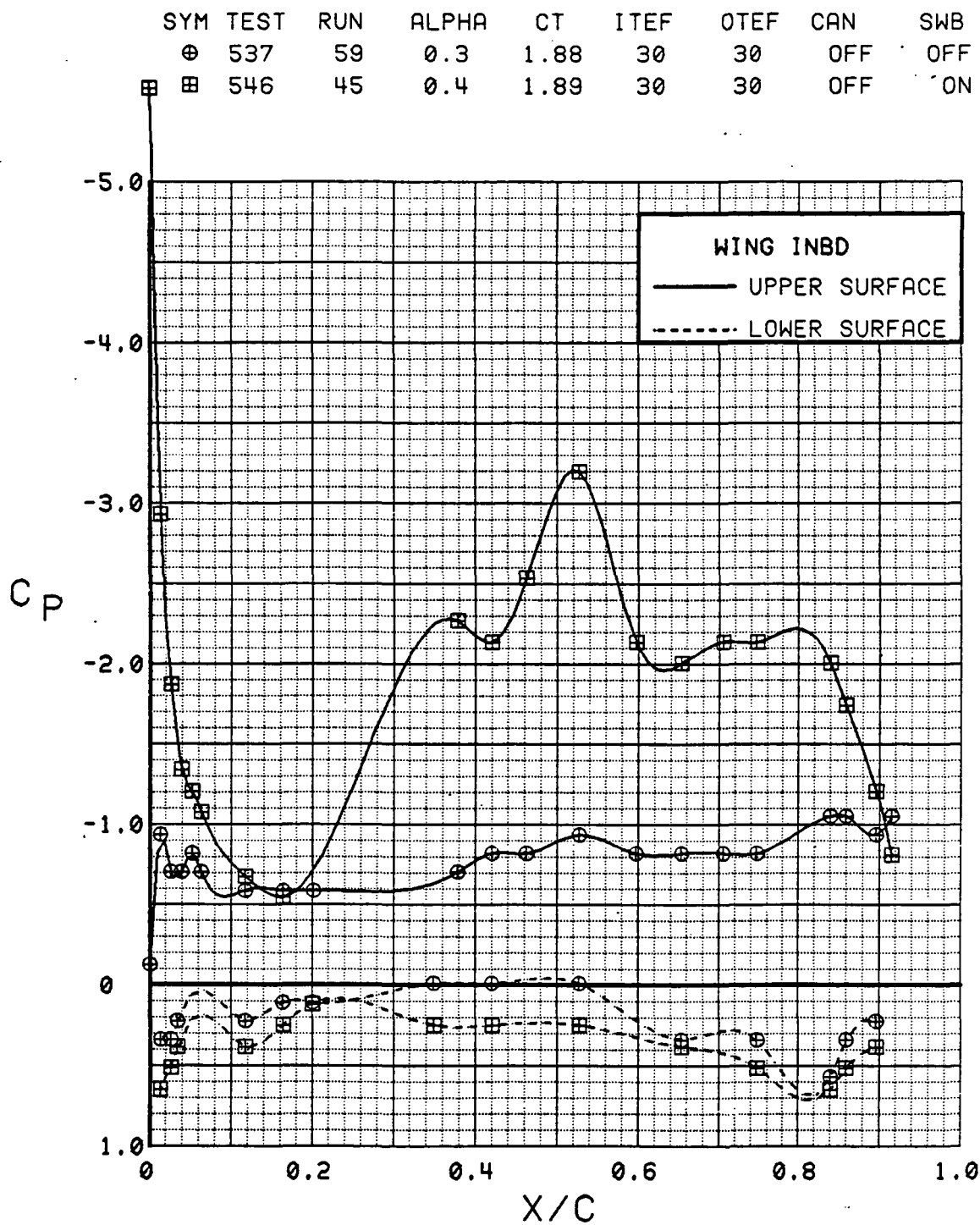


Figure 3.2.2-153 Spanwise Blowing Effects, Flaps Deflected,  
 $C_T = 1.8$ , Inboard, Alpha = 0 deg

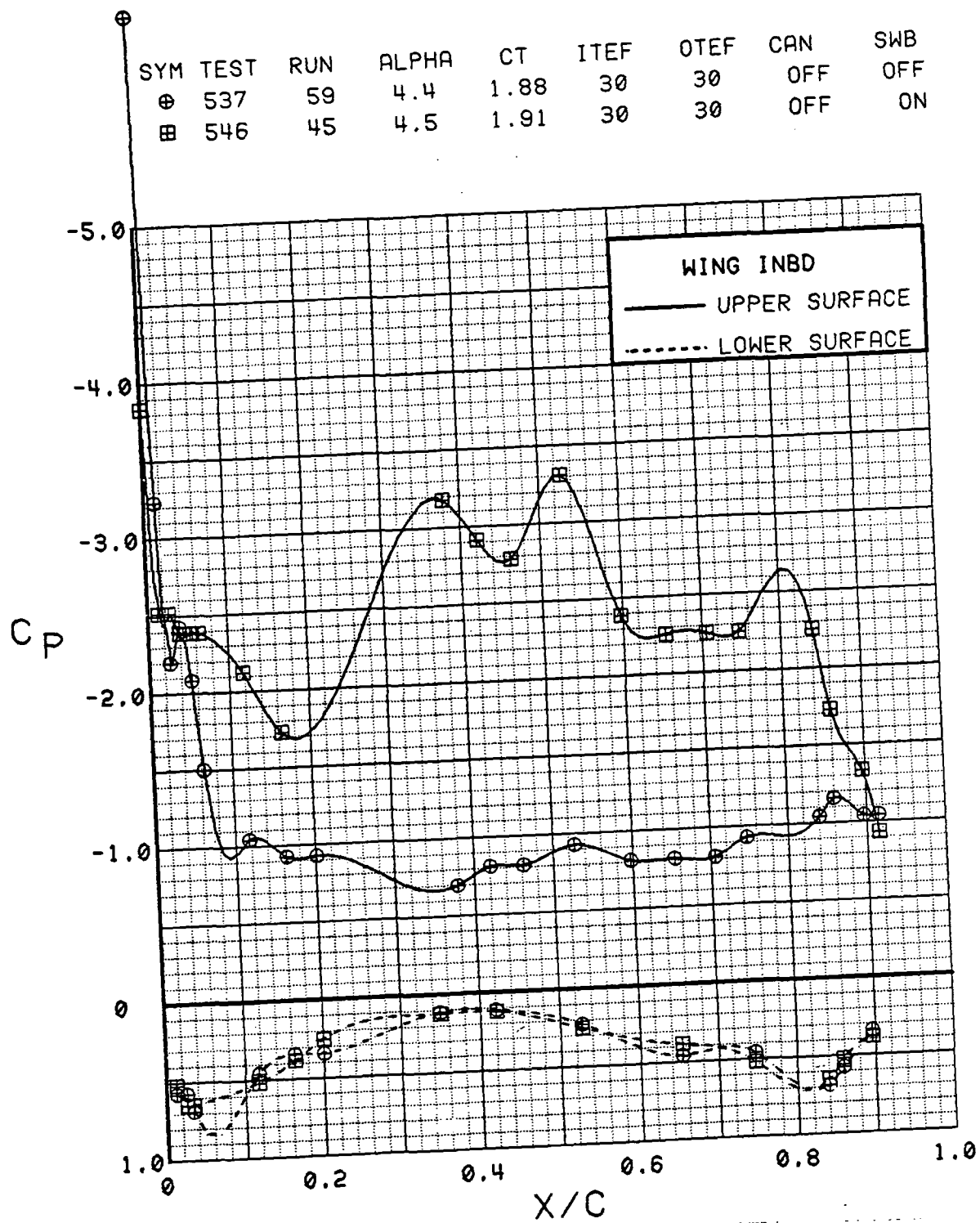


Figure 3.2.2-154 Spanwise Blowing Effects, Flaps Deflected,  
 $C_T = 1.8$ , Inboard, Alpha = 4 deg

SYM	TEST	RUN	ALPHA	CT	ITEF	OTEF	CAN	SWB
⊕	537	59	8.6	1.88	30	30	OFF	OFF
⊞	546	45	8.7	1.90	30	30	OFF	ON

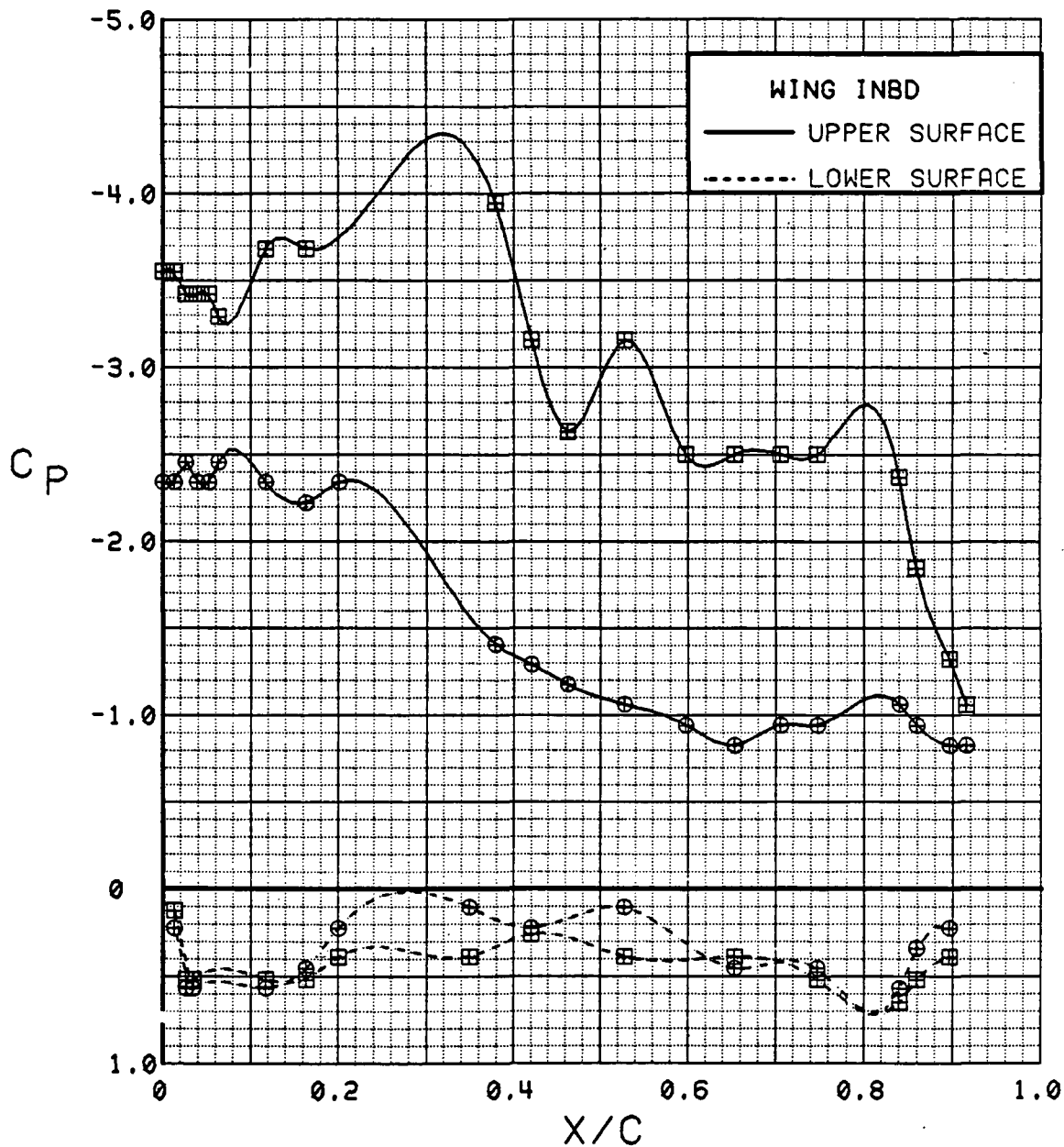


Figure 3.2.2-155 Spanwise Blowing Effects, Flaps Deflected,  
 $C_T = 1.8$ , Inboard,  $\alpha = 8$  deg

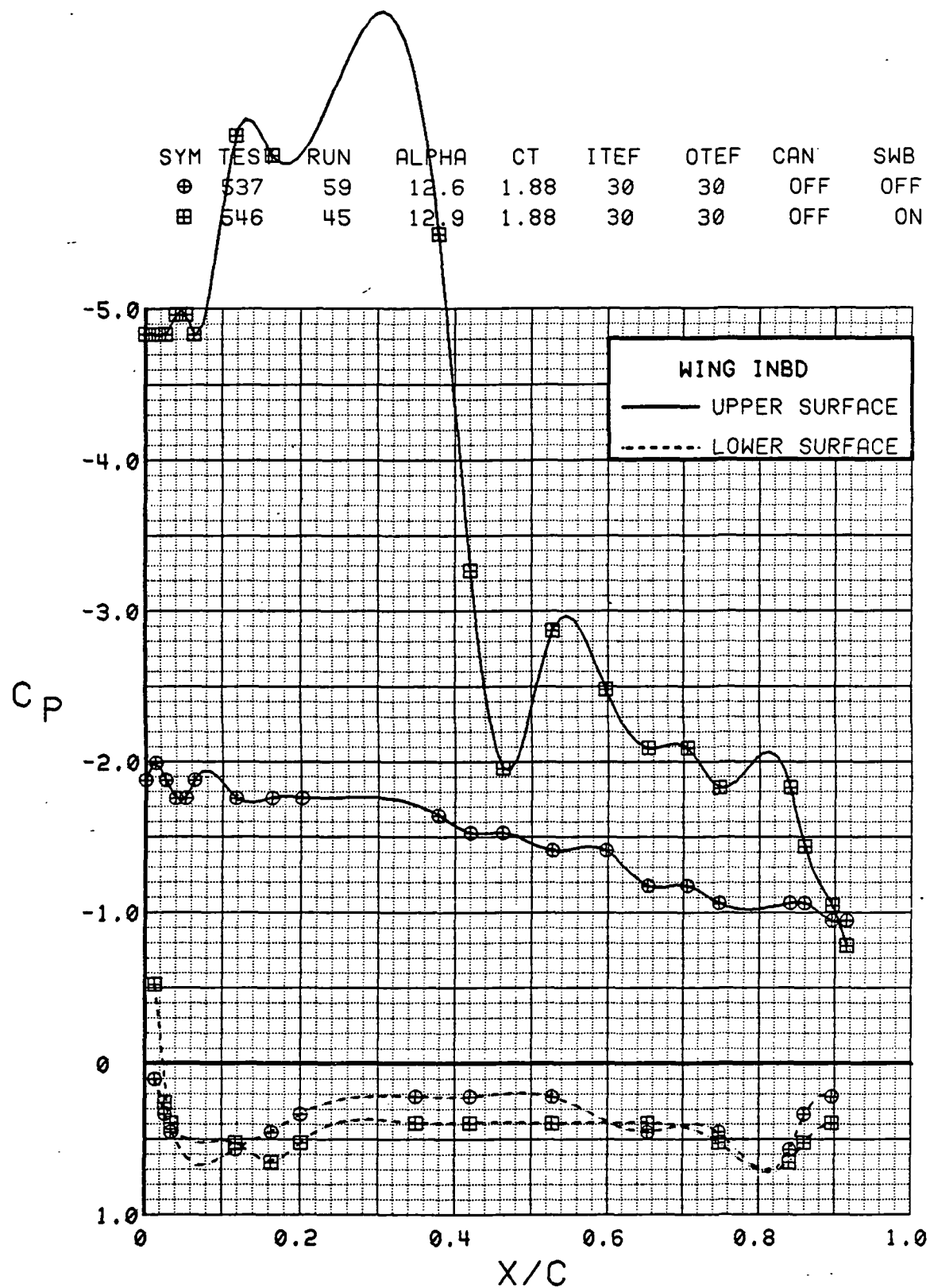


Figure 3.2.2-156 Spanwise Blowing Effects, Flaps Deflected,  
 $C_T = 1.8$ , Inboard, Alpha = 12 deg



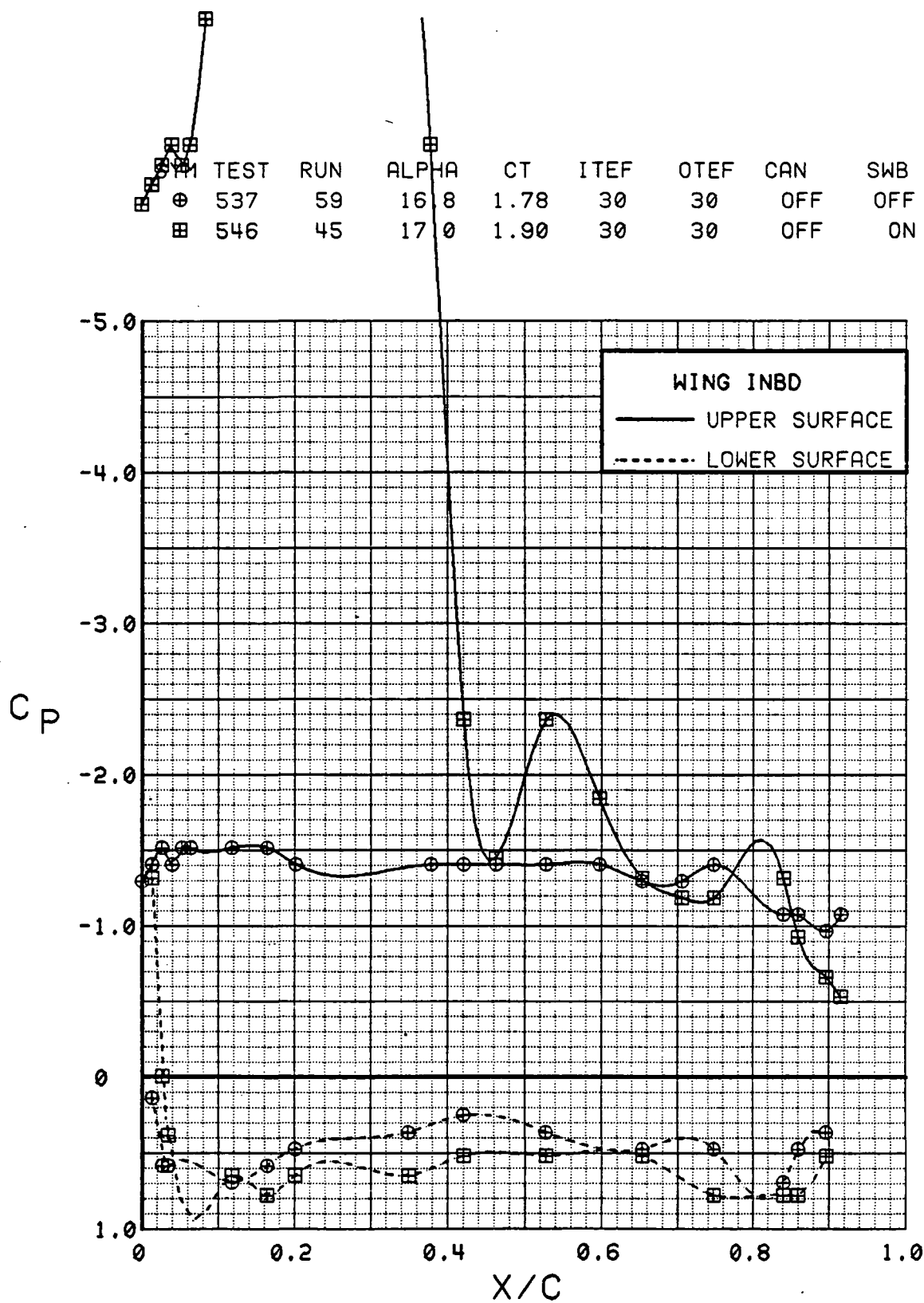


Figure 3.2.2-157 Spanwise Blowing Effects, Flaps Deflected,  
 $C_T = 1.8$ , Inboard, Alpha = 16 deg

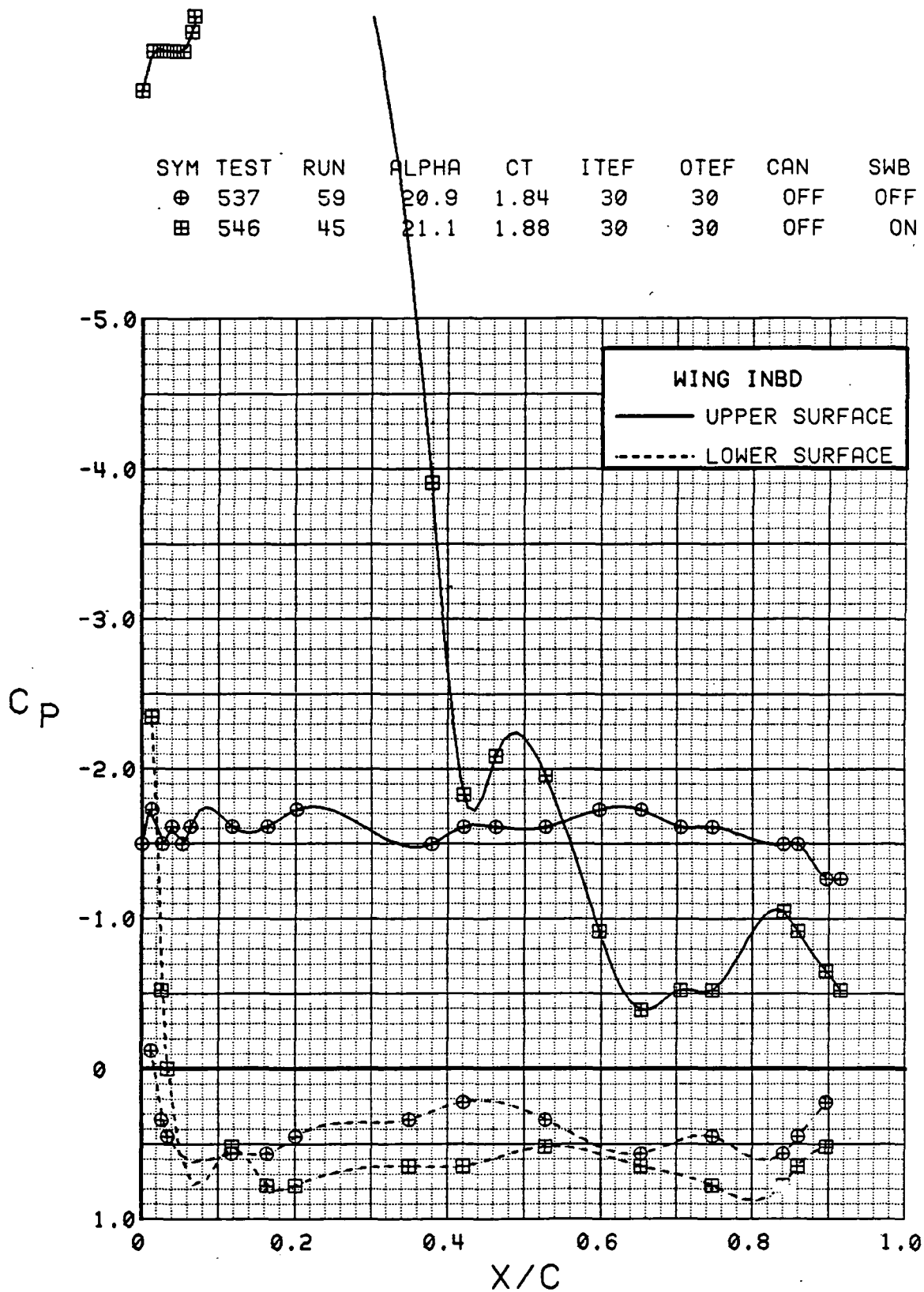


Figure 3.2.2-158 Spanwise Blowing Effects, Flaps Deflected,  
 $C_T = 1.8$ , Inboard, Alpha = 20 deg

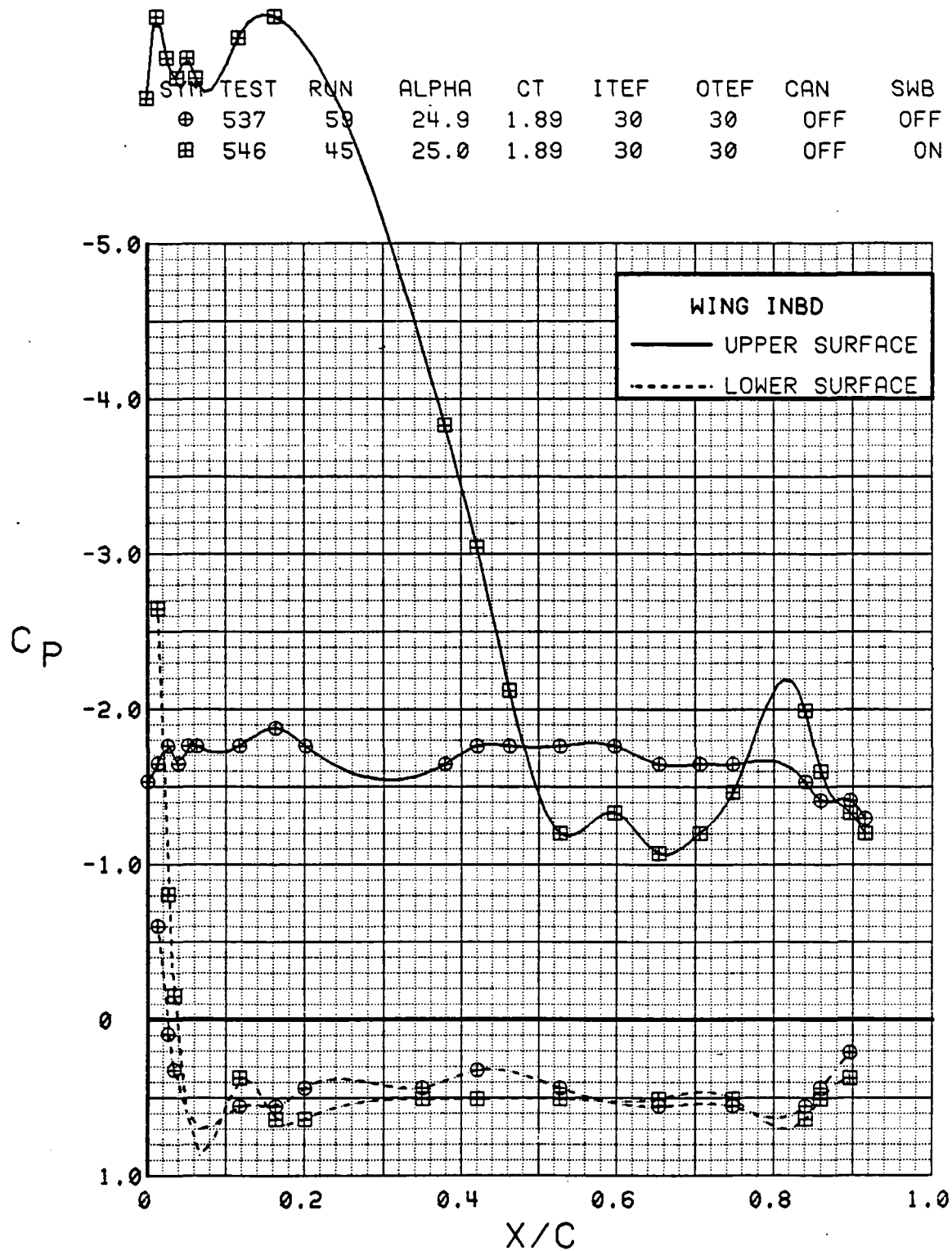


Figure 3.2.2-159 Spanwise Blowing Effects, Flaps Deflected,  
 $C_T = 1.8$ , Inboard, Alpha = 24 deg

SYM	TEST	RUN	ALPHA	CT	ITEF	OTEF	CAN	SWB
⊕	537	59	29.0	1.84	30	30	OFF	OFF
⊞	546	45	29.1	1.90	30	30	OFF	ON

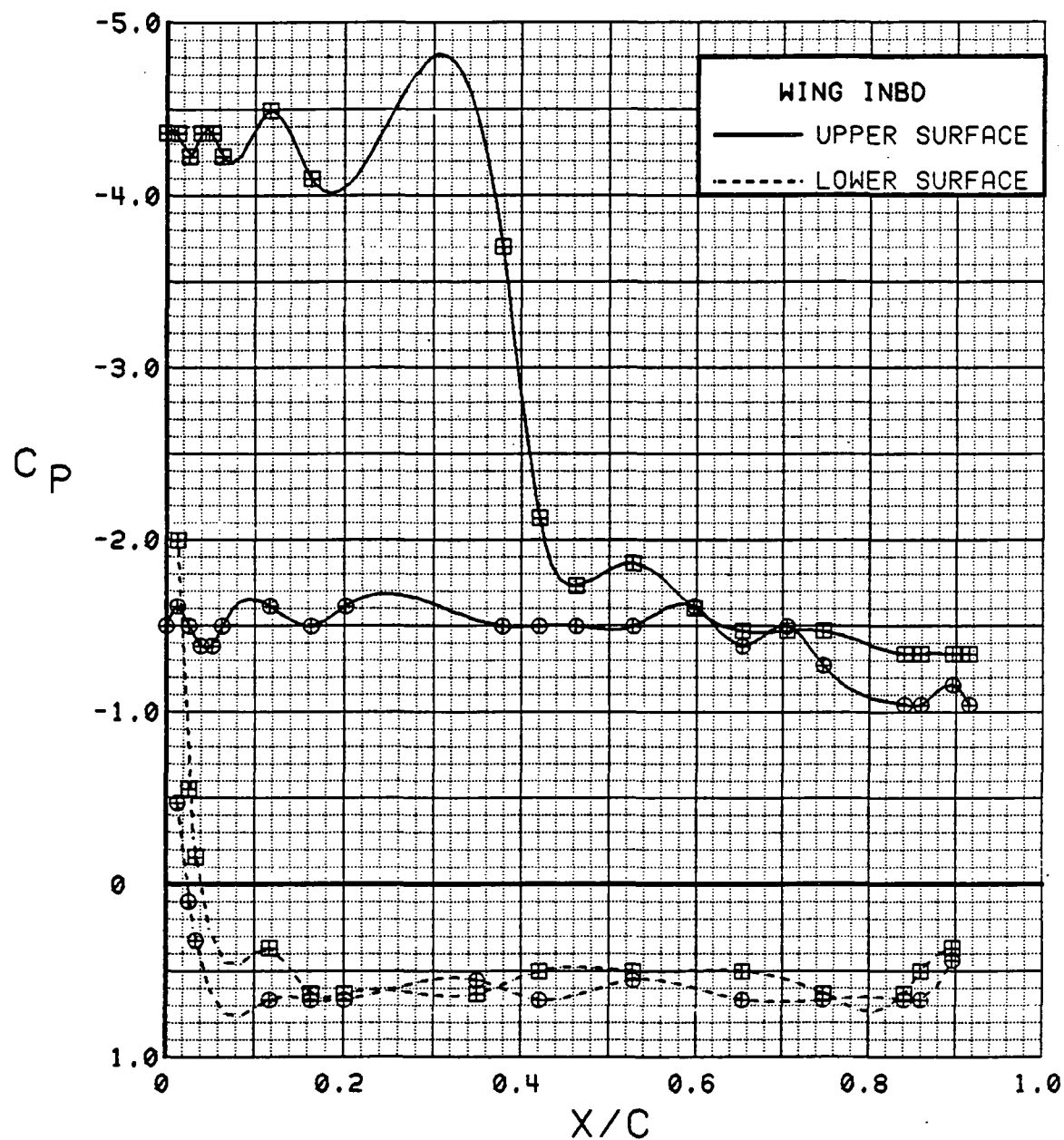


Figure 3.2.2-160 Spanwise Blowing Effects, Flaps Deflected,  $C_T = 1.8$ , Inboard, Alpha = 28 deg

SYM	TEST	RUN	ALPHA	CT	ITEF	OTEF	CAN	SWB
⊕	537	59	33.0	1.87	30	30	OFF	OFF
⊞	546	45	33.0	1.89	30	30	OFF	ON

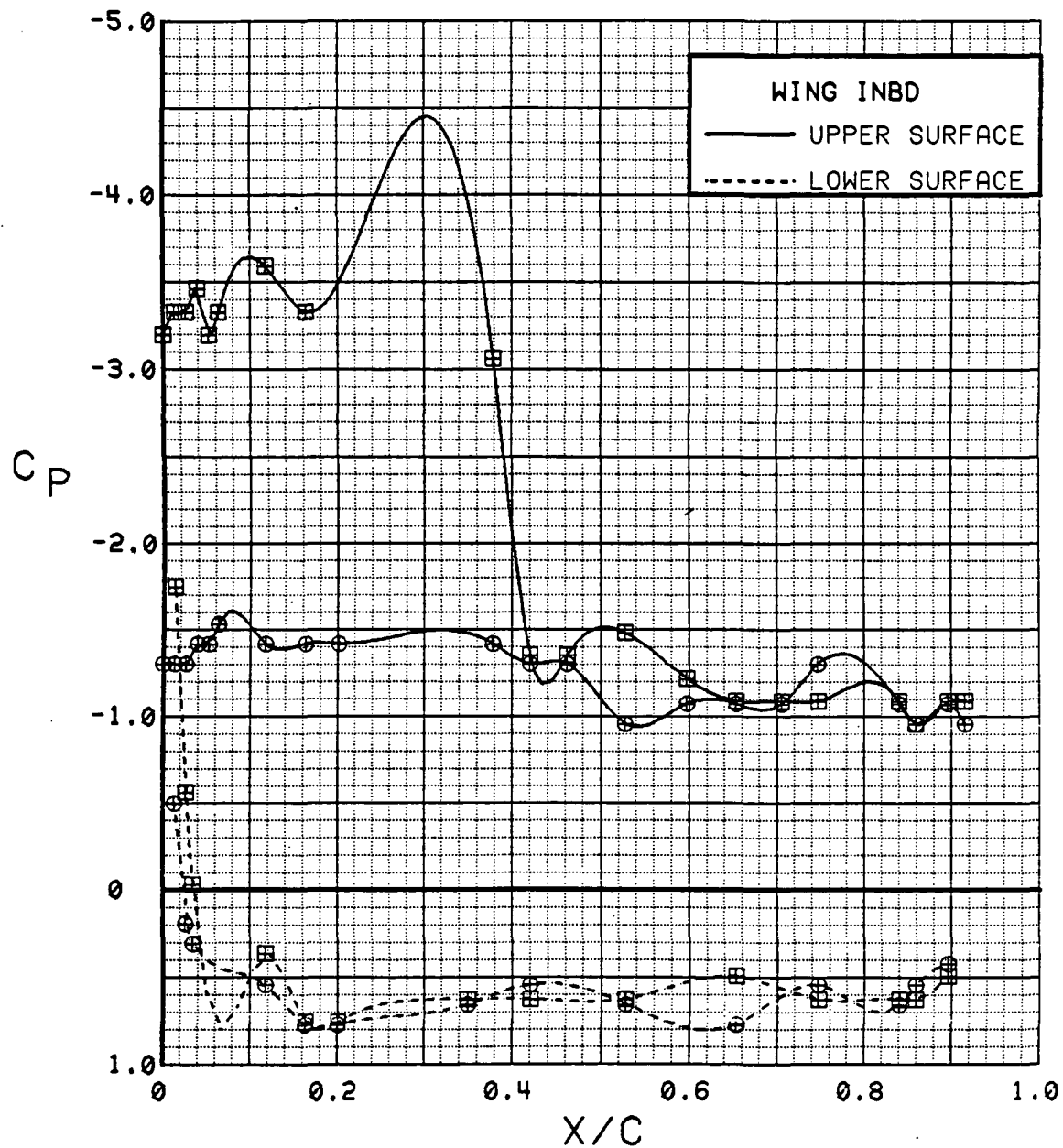


Figure 3.2.2-161 Spanwise Blowing Effects, Flaps Deflected,  
 $C_T = 1.8$ , Inboard, Alpha = 32 deg

SYM	TEST	RUN	ALPHA	CT	ITEF	OTEF	CAN	SWB
⊕	537	59	0.3	1.88	30	30	OFF	OFF
⊞	546	45	0.4	1.89	30	30	OFF	ON

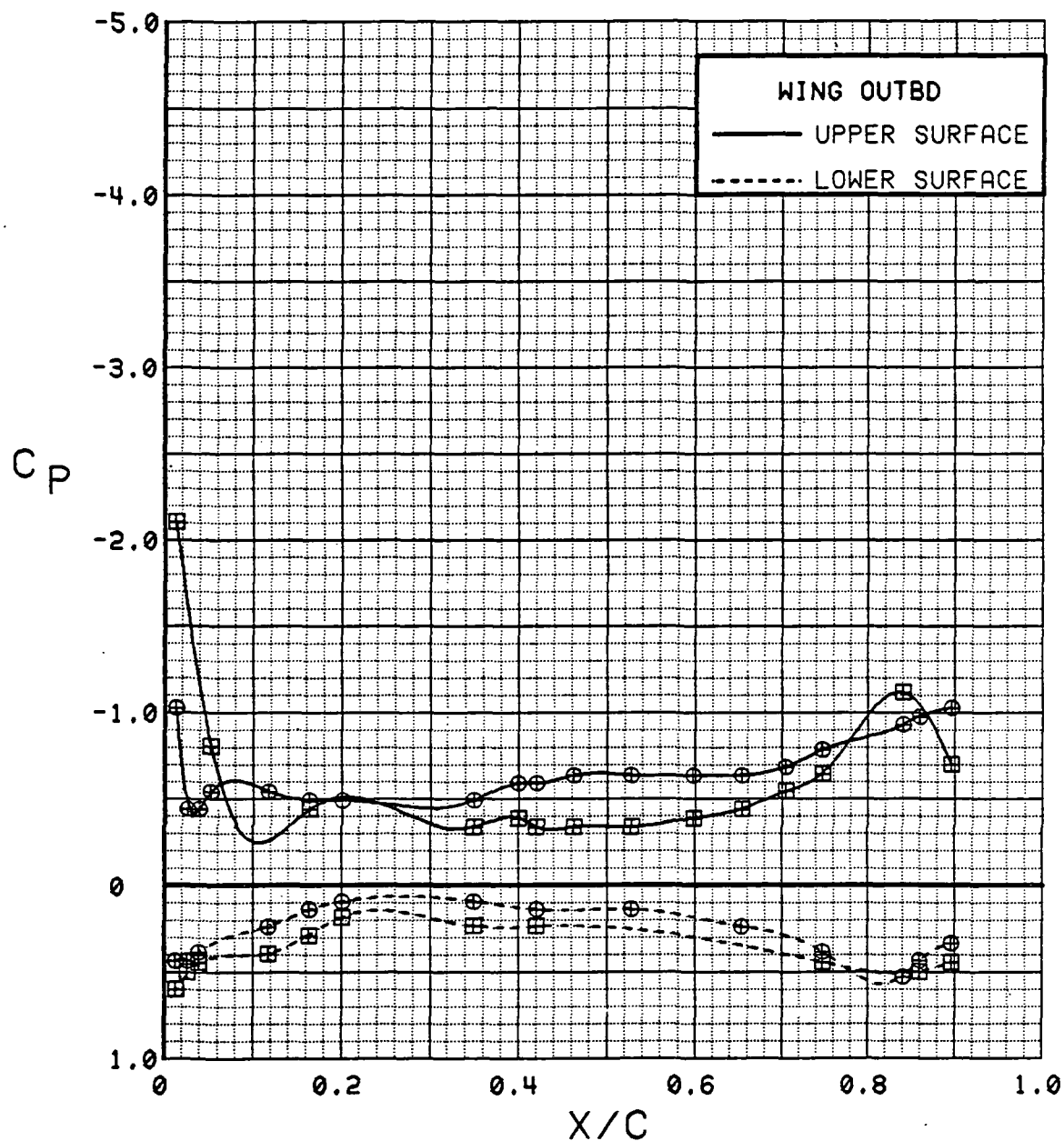


Figure 3.2.2-162 Spanwise Blowing Effects, Flaps Deflected,  
 $C_T = 1.8$ , Outboard, Alpha = 0 deg

SYM	TEST	RUN	ALPHA	CT	ITEF	OTEF	CAN	SWB
⊕	537	59	4.4	1.88	30	30	OFF	OFF
⊞	546	45	4.5	1.91	30	30	OFF	ON

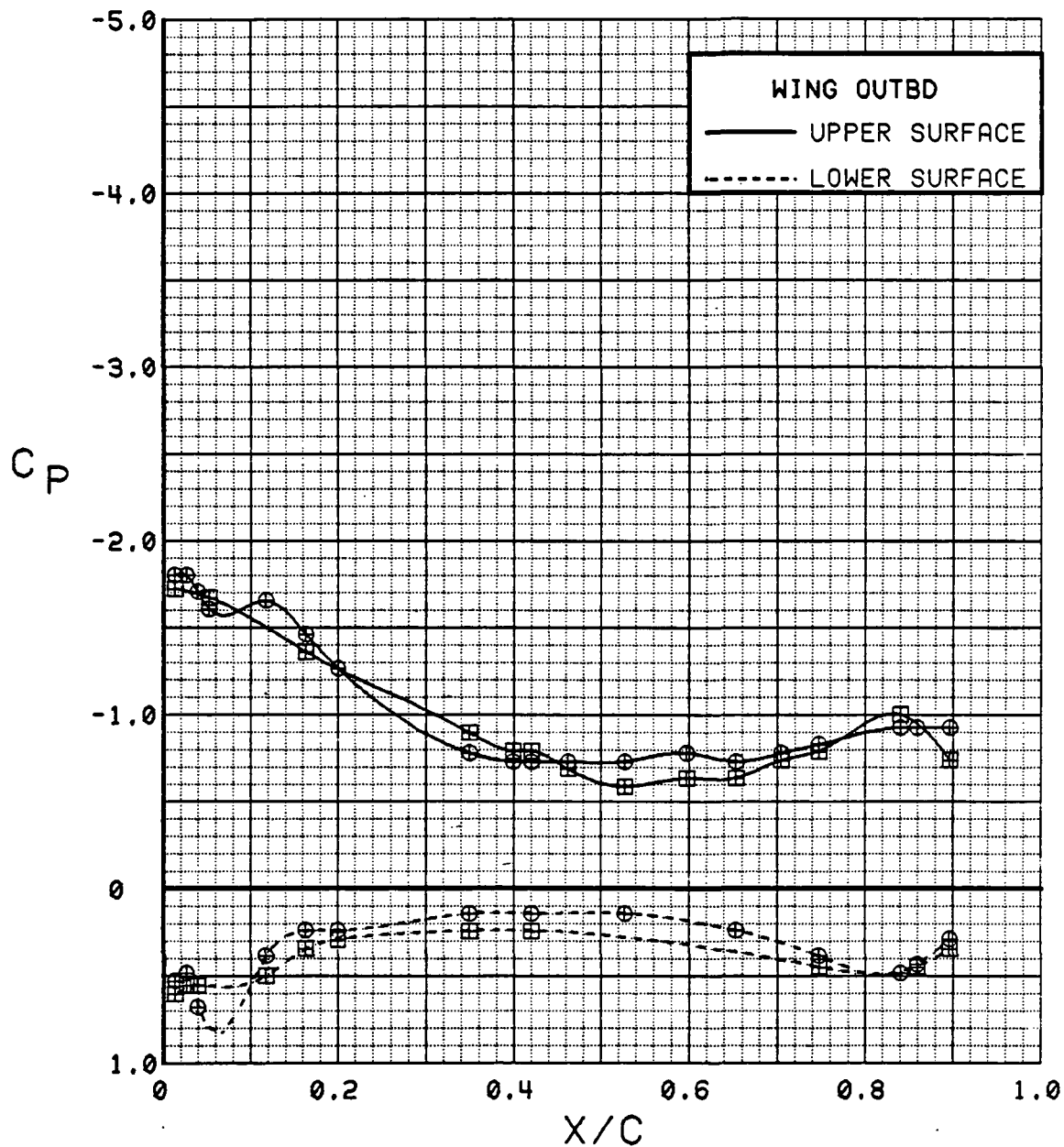


Figure 3.2.2-163 Spanwise Blowing Effects, Flaps Deflected,  
 $C_T = 1.8$ , Outboard, Alpha = 4 deg

SYM	TEST	RUN	ALPHA	CT	ITEF	OTEF	CAN	SWB
⊕	537	59	8.6	1.88	30	30	OFF	OFF
⊞	546	45	8.7	1.90	30	30	OFF	ON

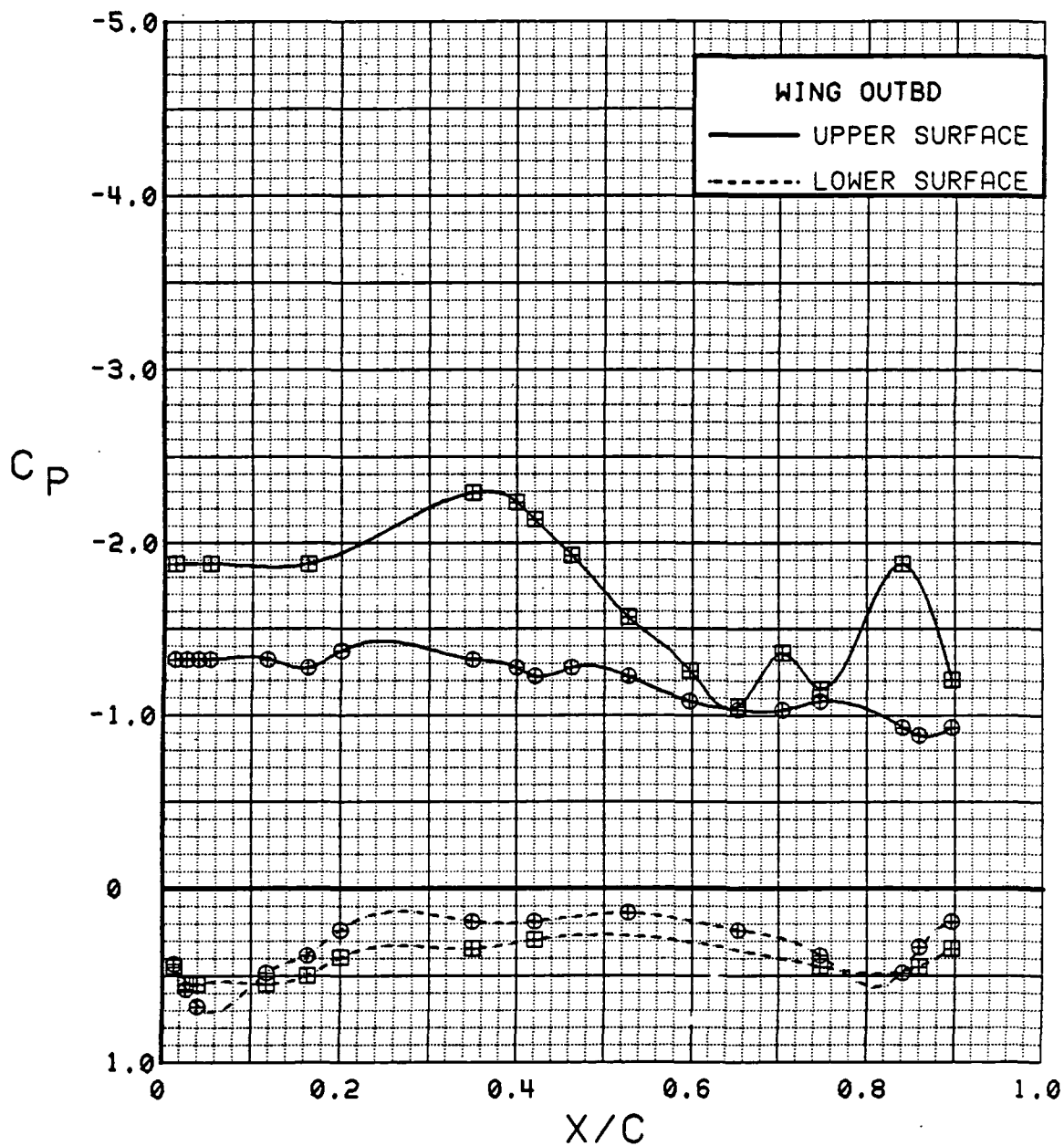


Figure 3.2.2-164 Spanwise Blowing Effects, Flaps Deflected,  
 $C_T = 1.8$ , Outboard, Alpha = 8 deg



SYM	TEST	RUN	ALPHA	CT	ITEF	OTEF	CAN	SWB
⊕	537	59	12.6	1.88	30	30	OFF	OFF
⊞	546	45	12.9	1.88	30	30	OFF	ON

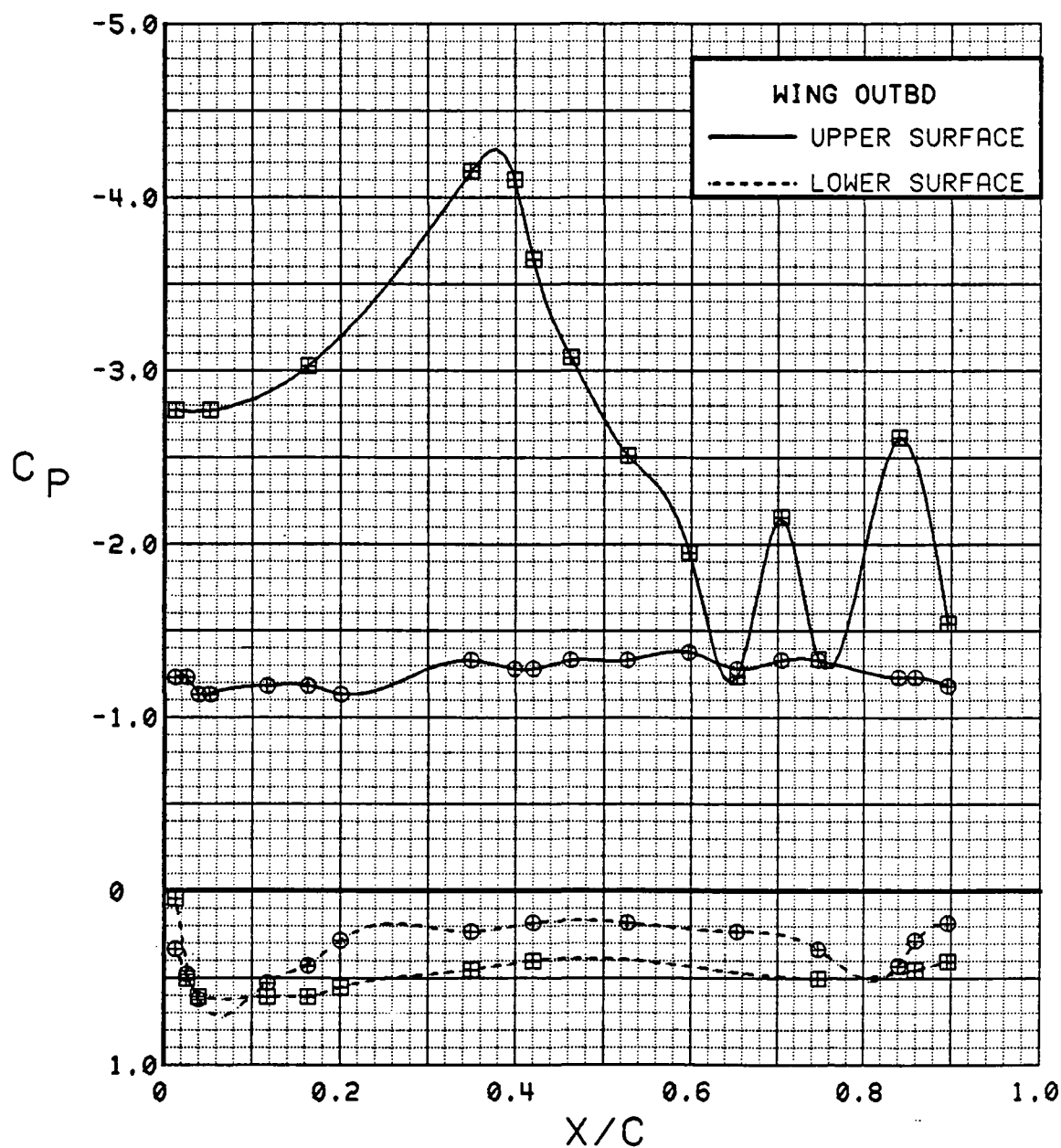


Figure 3.2.2-165 Spanwise Blowing Effects, Flaps Deflected,  
 $C_T = 1.8$ , Outboard, Alpha = 12 deg

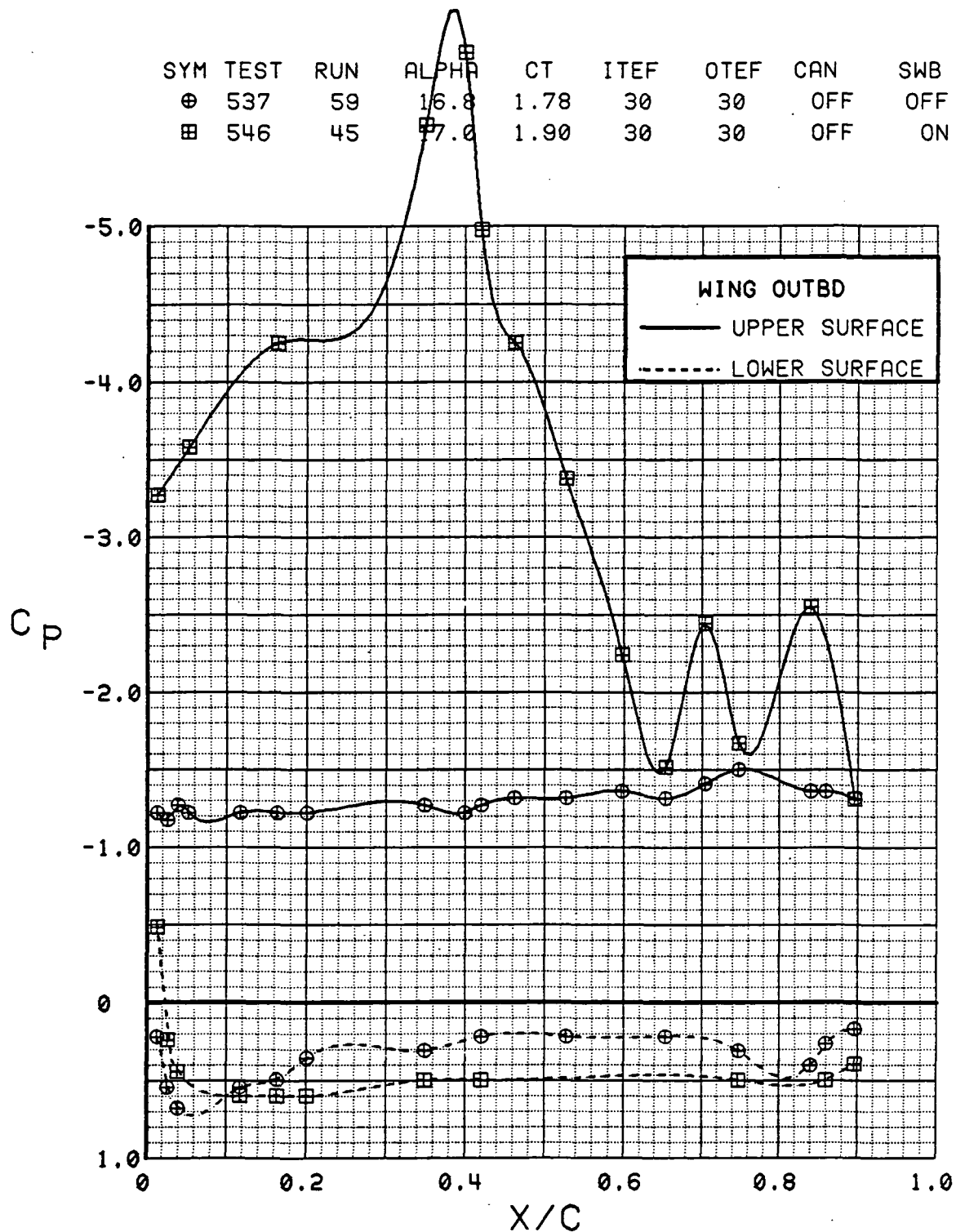


Figure 3.2.2-166 Spanwise Blowing Effects, Flaps Deflected,  
 $C_T = 1.8$ , Outboard, Alpha = 16 deg

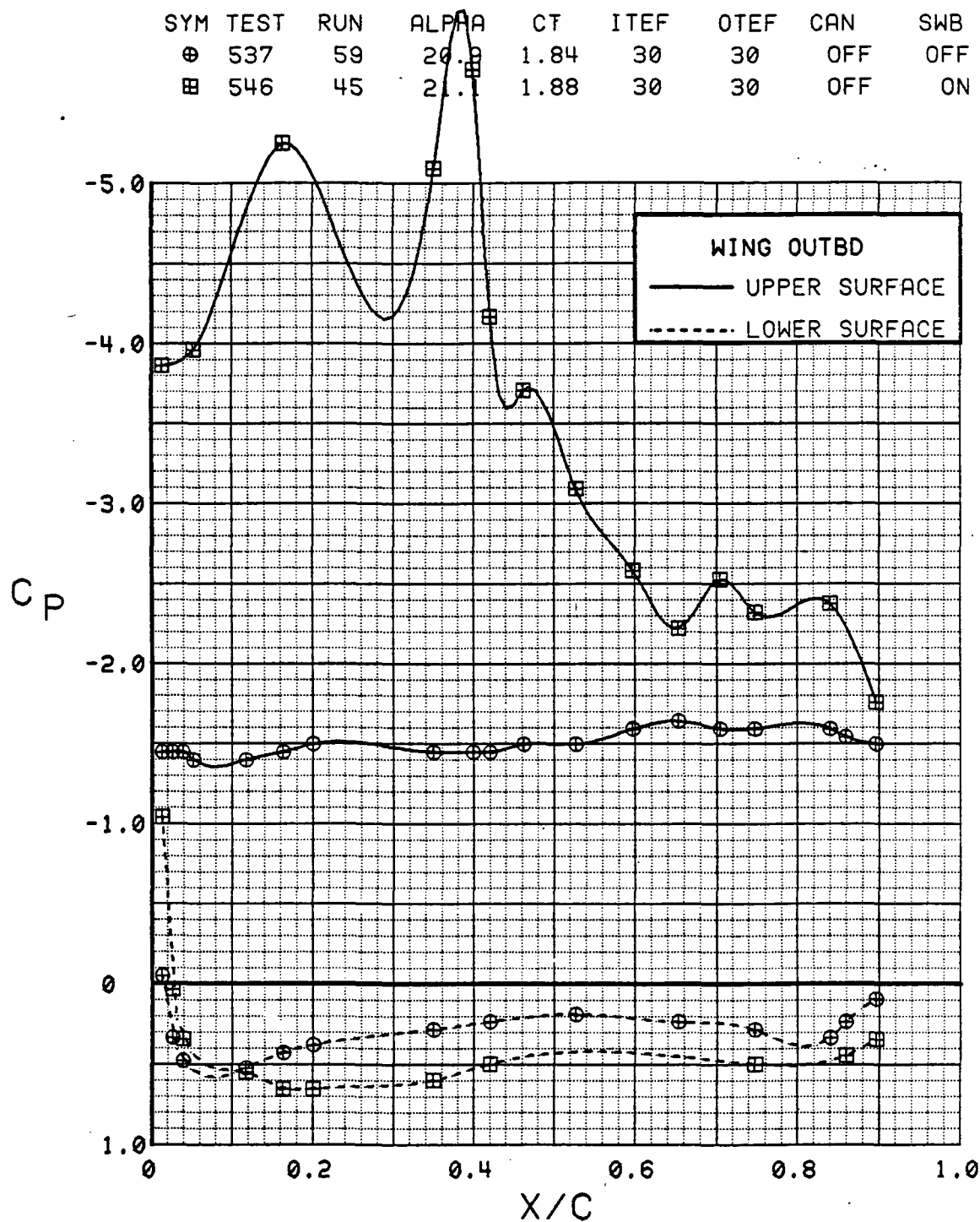


Figure 3.2.2-167 Spanwise Blowing Effects, Flaps Deflected,  
 $C_T = 1.8$ , Outboard, Alpha = 20 deg

SYM	TEST	RUN	ALPHA	CT	ITEF	OTEF	CAN	SWB
⊕	537	59	24.9	1.89	30	30	OFF	OFF
⊞	546	45	25.0	1.89	30	30	OFF	ON

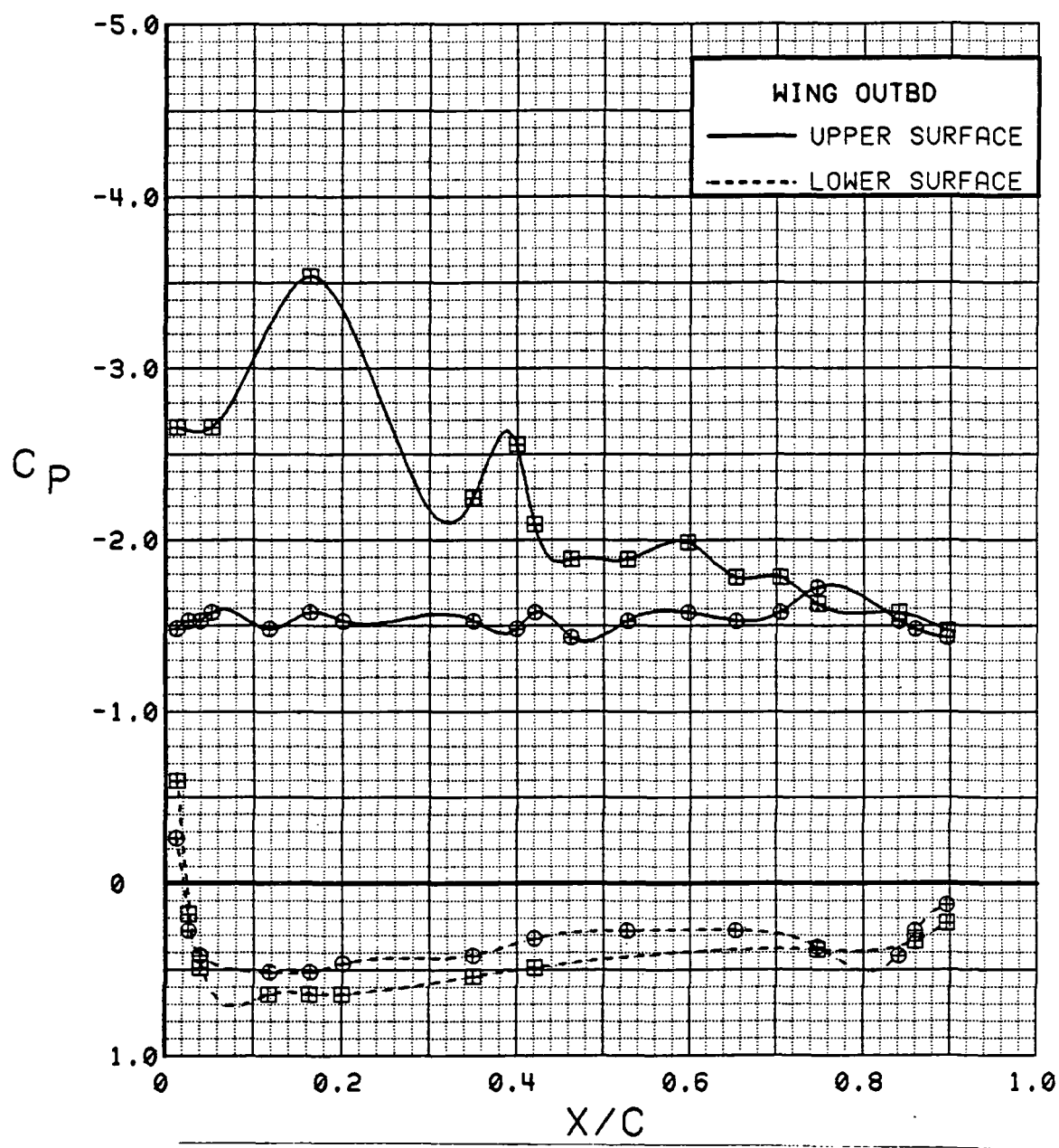


Figure 3.2.2-168 Spanwise Blowing Effects, Flaps Deflected,  $C_T = 1.8$ , Outboard, Alpha = 24 deg

SYM	TEST	RUN	ALPHA	CT	ITEF	OTEF	CAN	SWB
⊕	537	59	29.0	1.84	30	30	OFF	OFF
⊞	546	45	29.1	1.90	30	30	OFF	ON

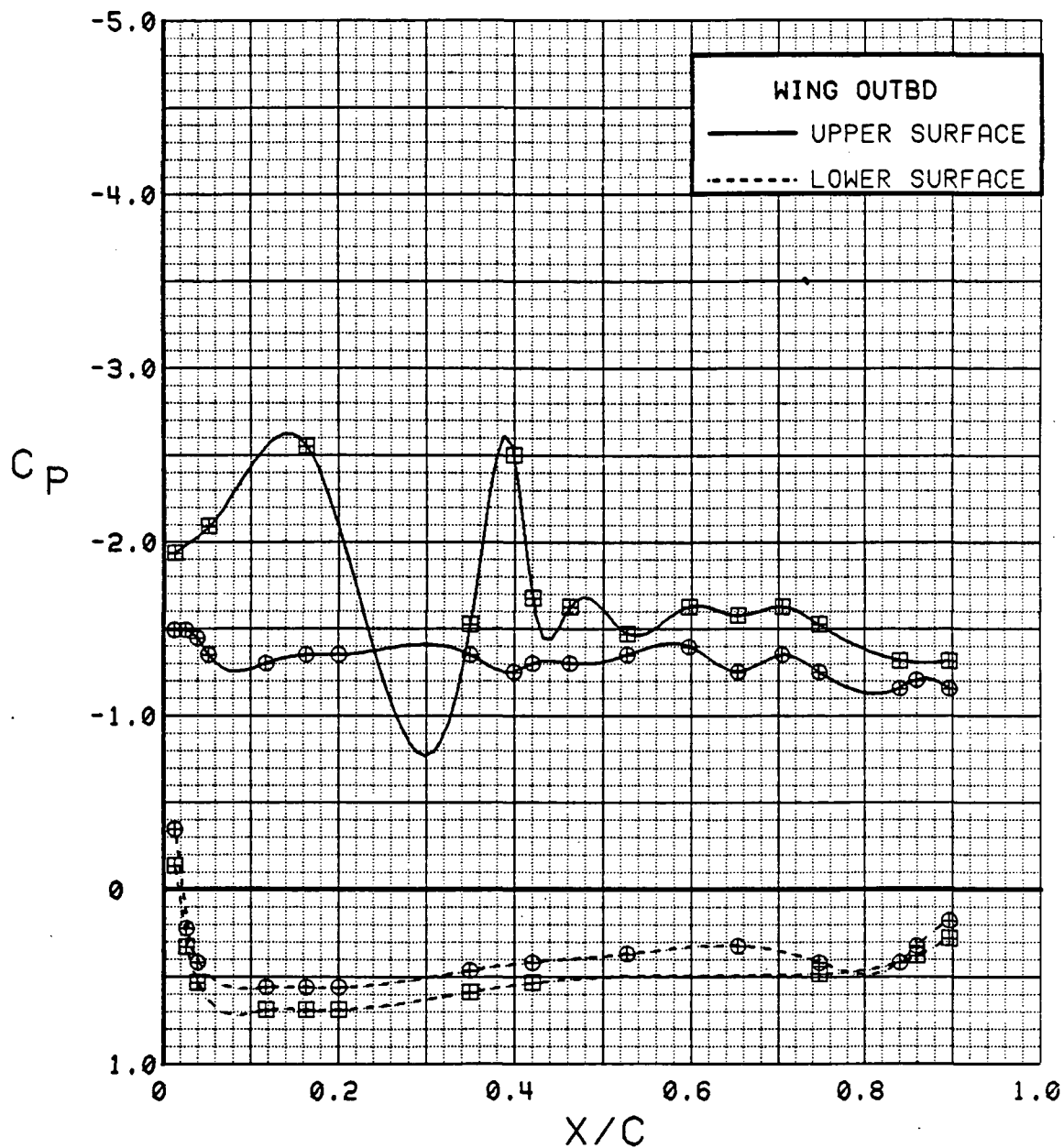


Figure 3.2.2-169 Spanwise Blowing Effects, Flaps Deflected,  
 $C_T = 1.8$ , Outboard, Alpha = 28 deg

SYM	TEST	RUN	ALPHA	CT	ITEF	OTEF	CAN	SWB
⊕	537	59	33.0	1.87	30	30	OFF	OFF
⊞	546	45	33.0	1.89	30	30	OFF	ON

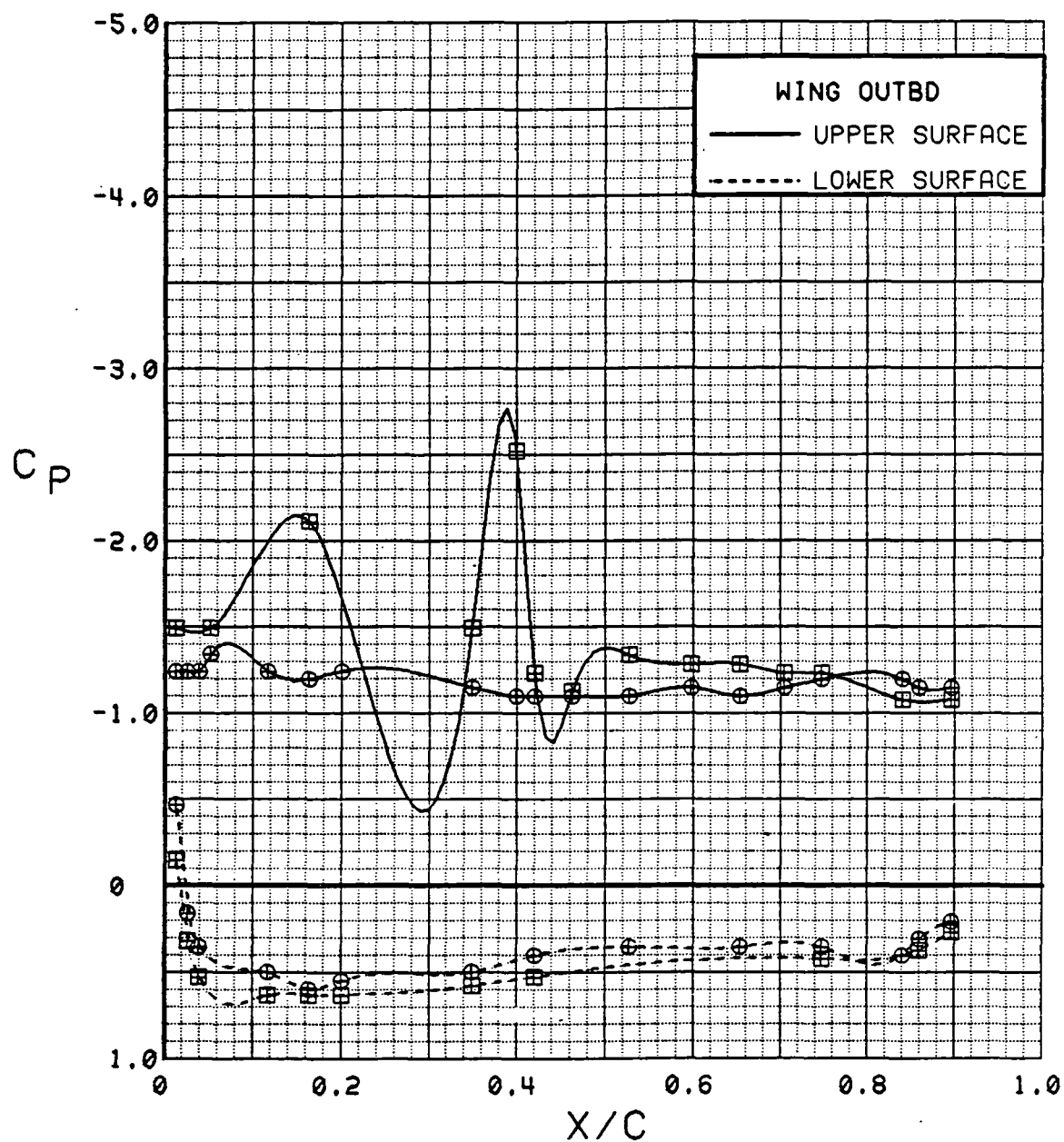


Figure 3.2.2-170 Spanwise Blowing Effects, Flaps Deflected,  $C_T = 1.8$ , Outboard, Alpha = 32 deg

SYM	TEST	RUN	ALPHA	CT	ITEF	OTEF	CAN	SWB
⊕	537	59	0.3	1.88	30	30	OFF	OFF
⊞	546	45	0.4	1.89	30	30	OFF	ON

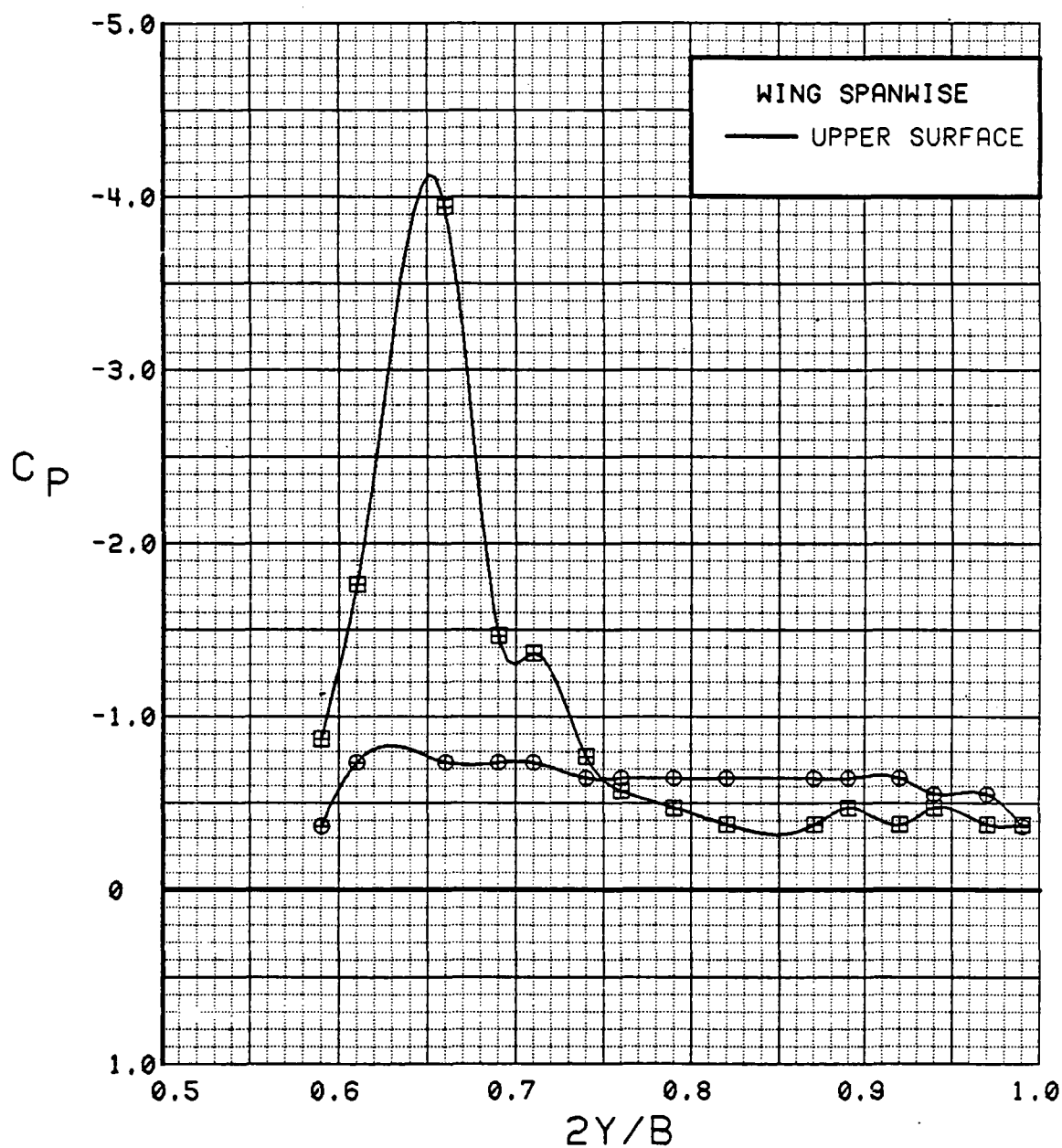


Figure 3.2.2-171 Spanwise Blowing Effects, Flaps Deflected,  
C<sub>T</sub> = 1.8, Spanwise, Alpha = 0 deg

SYM	TEST	RUN	ALPHA	CT	ITEF	QTEF	CAN	SWB
⊕	537	59	4.4	1.88	30	30	OFF	OFF
⊞	546	45	4.5	1.91	30	30	OFF	ON

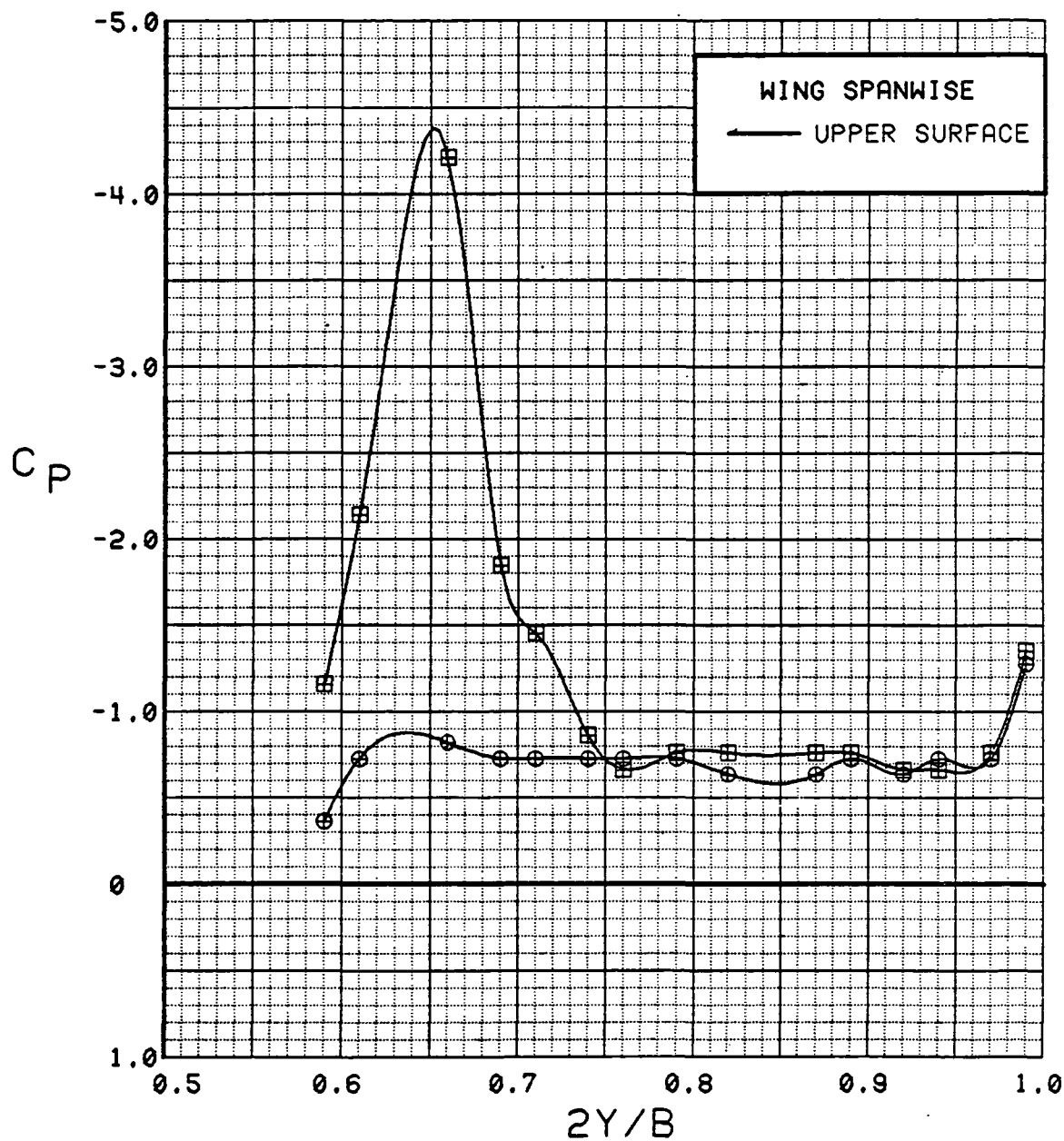


Figure 3.2.2-172 Spanwise Blowing Effects, Flaps Deflected,  
 $C_T = 1.8$ , Spanwise, Alpha = 4 deg



SYM	TEST	RUN	ALPHA	CT	ITEF	OTEF	CAN	SWB
●	537	59	8.6	1.88	30	30	OFF	OFF
■	546	45	8.7	1.90	30	30	OFF	ON

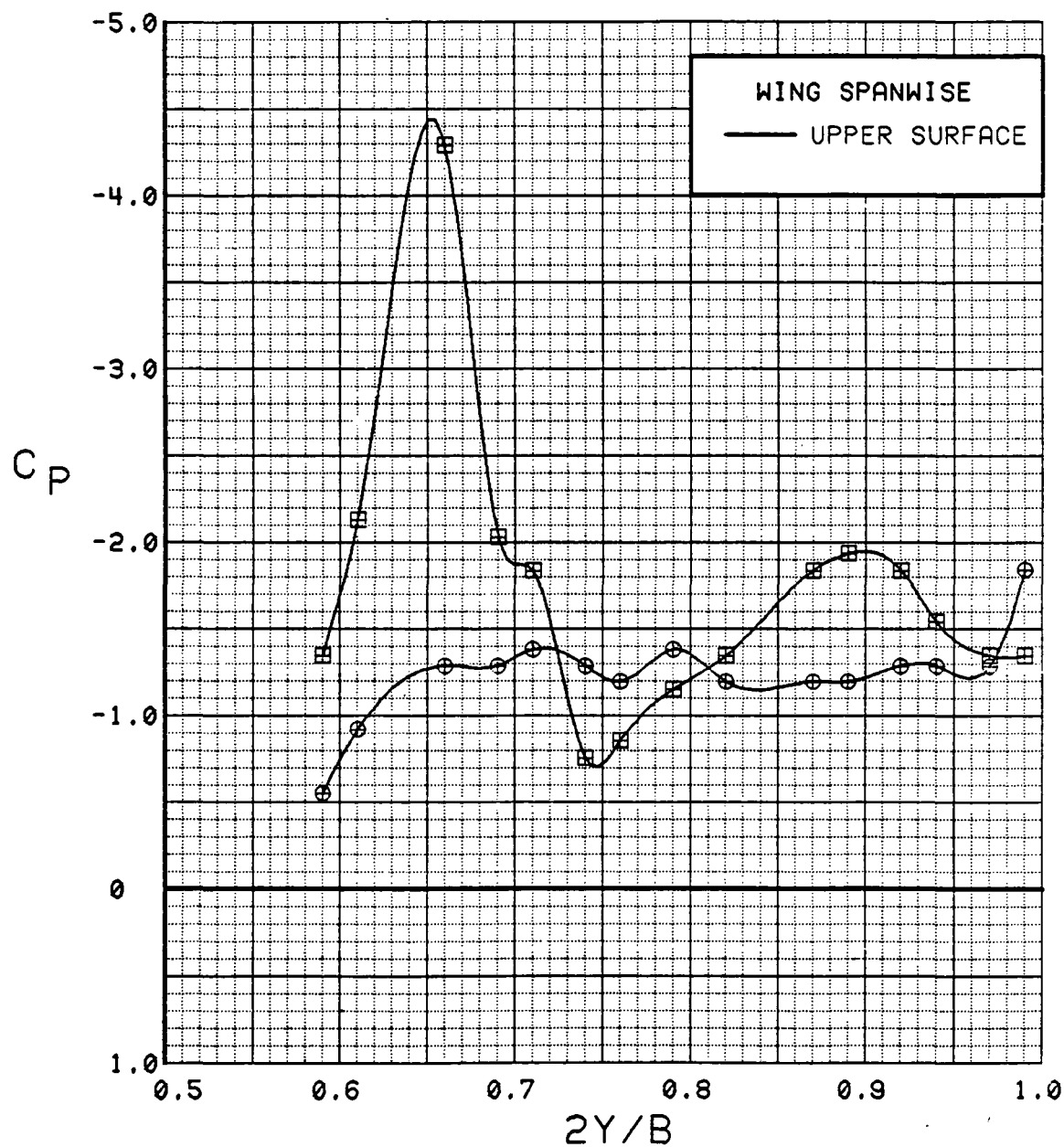


Figure 3.2.2-173 Spanwise Blowing Effects, Flaps Deflected,  
 $C_T = 1.8$ , Spanwise, Alpha = 8 deg

SYM	TEST	RUN	ALPHA	CT	ITEF	OTEF	CAN	SWB
⊙	537	59	12.6	1.88	30	30	OFF	OFF
⊠	546	45	12.9	1.88	30	30	OFF	ON

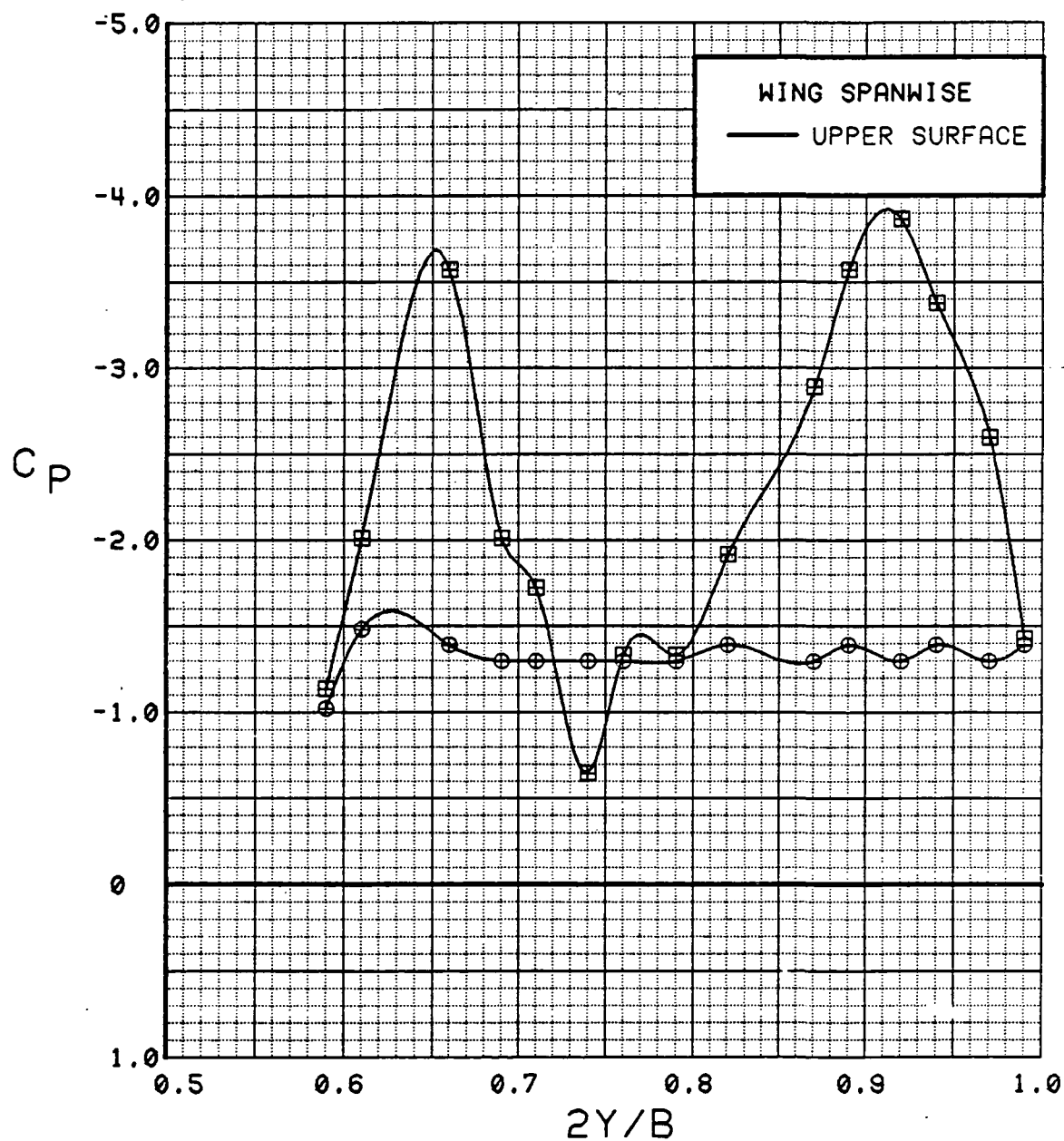


Figure 3.2.2-174 Spanwise Blowing Effects, Flaps Deflected,  
 $C_T = 1.8$ , Spanwise,  $\alpha = 12^\circ$

SYM	TEST	RUN	ALPHA	CT	ITEF	OTEF	CAN	SWB
⊙	537	59	16.8	1.78	30	30	OFF	OFF
⊠	546	45	17.0	1.90	30	30	OFF	ON

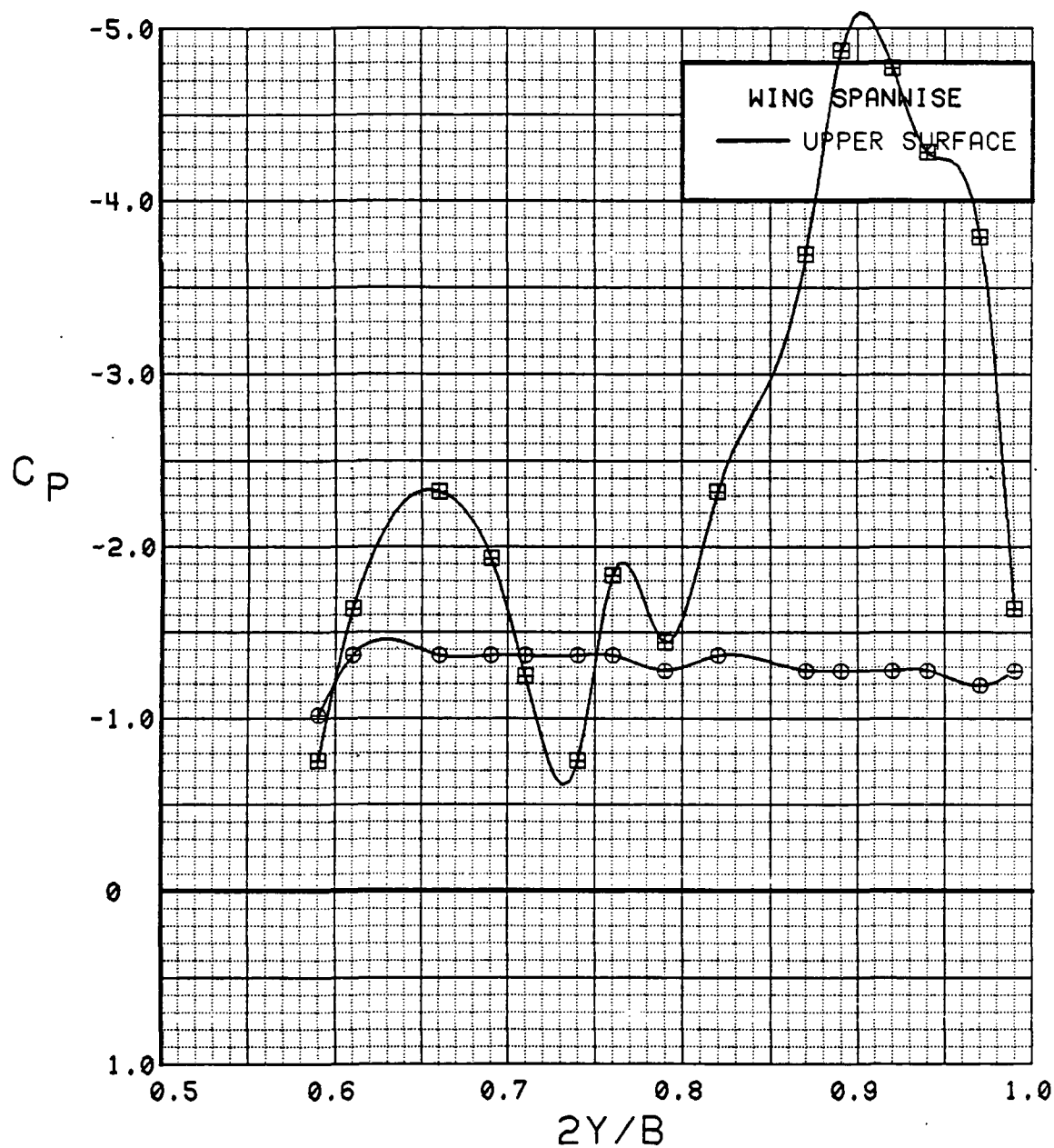


Figure 3.2.2-175 Spanwise Blowing Effects, Flaps Deflected,  $C_T = 1.8$ , Spanwise, Alpha = 16 deg

SYM	TEST	RUN	ALPHA	CT	ITEF	OTEF	CAN	SWB
⊕	537	59	20.9	1.84	30	30	OFF	OFF
⊞	546	45	21.1	1.88	30	30	OFF	ON

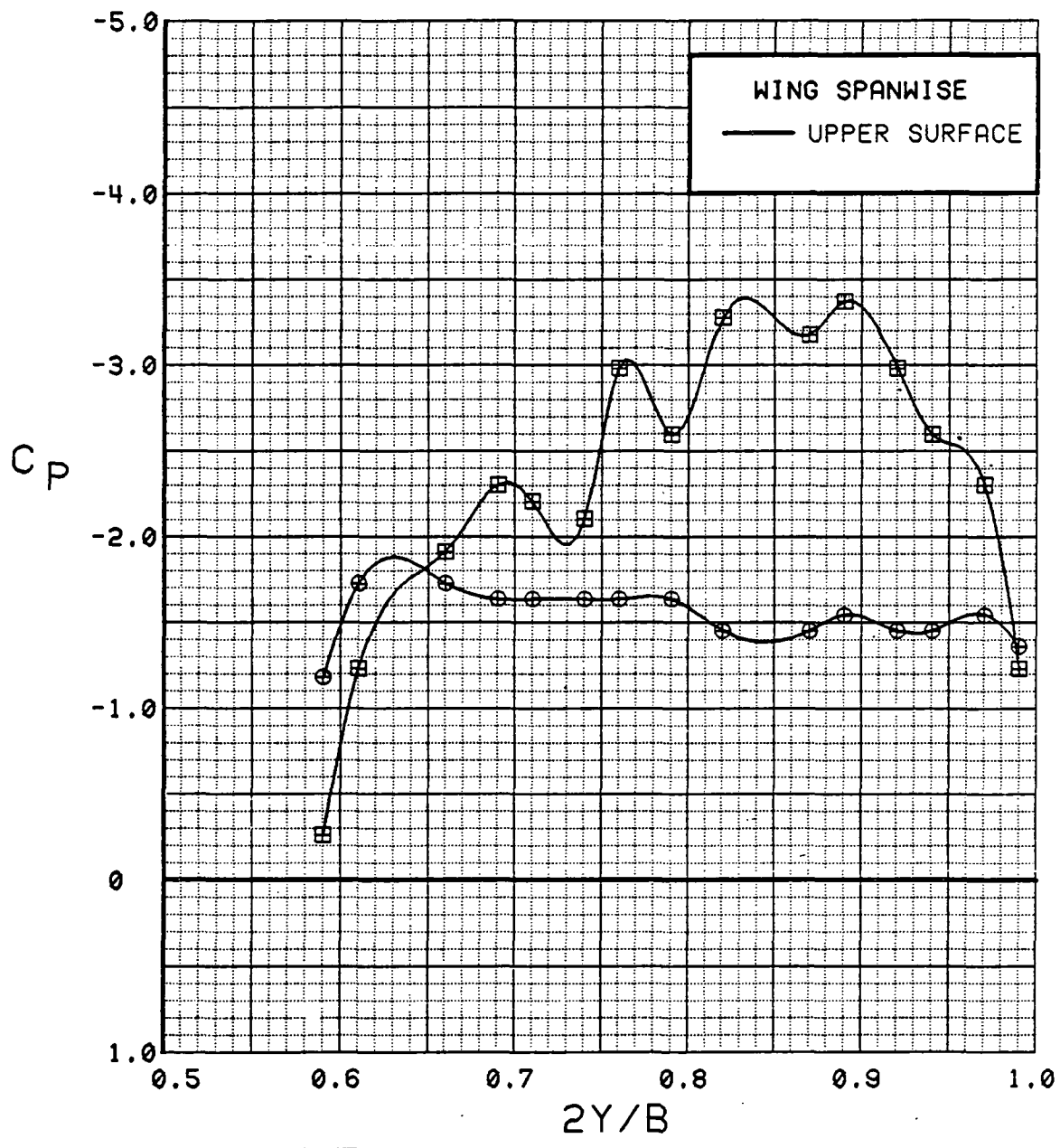


Figure 3.2.2-176 Spanwise Blowing Effects, Flaps Deflected,  $C_T = 1.8$ , Spanwise, Alpha = 20 deg

SYM	TEST	RUN	ALPHA	CT	ITEF	OTEF	CAN	SWB
●	537	59	24.9	1.89	30	30	OFF	OFF
■	546	45	25.0	1.89	30	30	OFF	ON

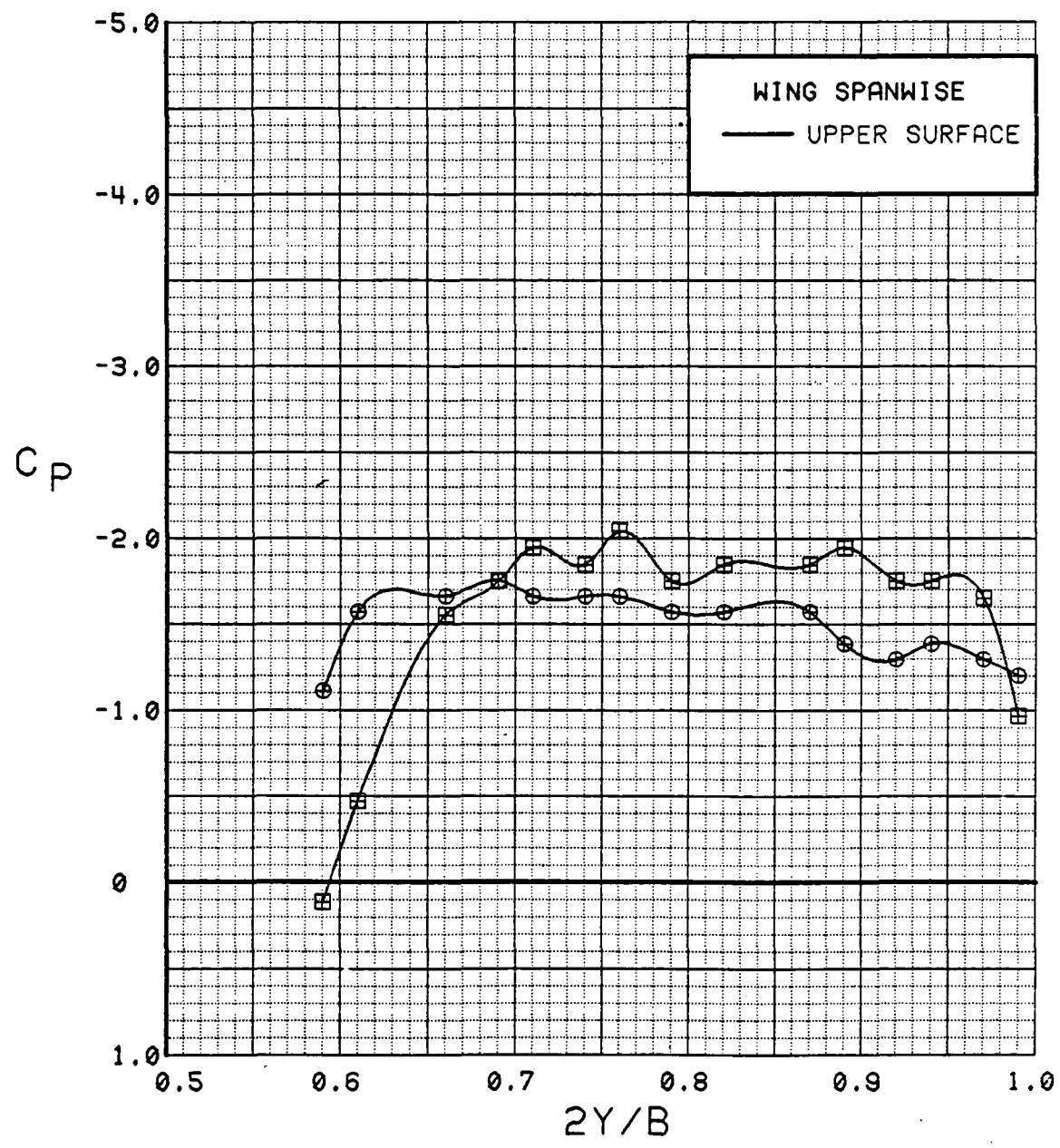


Figure 3.2.2-177 Spanwise Blowing Effects, Flaps Deflected,  $C_T = 1.8$ , Spanwise, Alpha = 24 deg

SYM	TEST	RUN	ALPHA	CT	ITEF	OTEF	CAN	SWB
⊙	537	59	29.0	1.84	30	30	OFF	OFF
⊠	546	45	29.1	1.90	30	30	OFF	ON

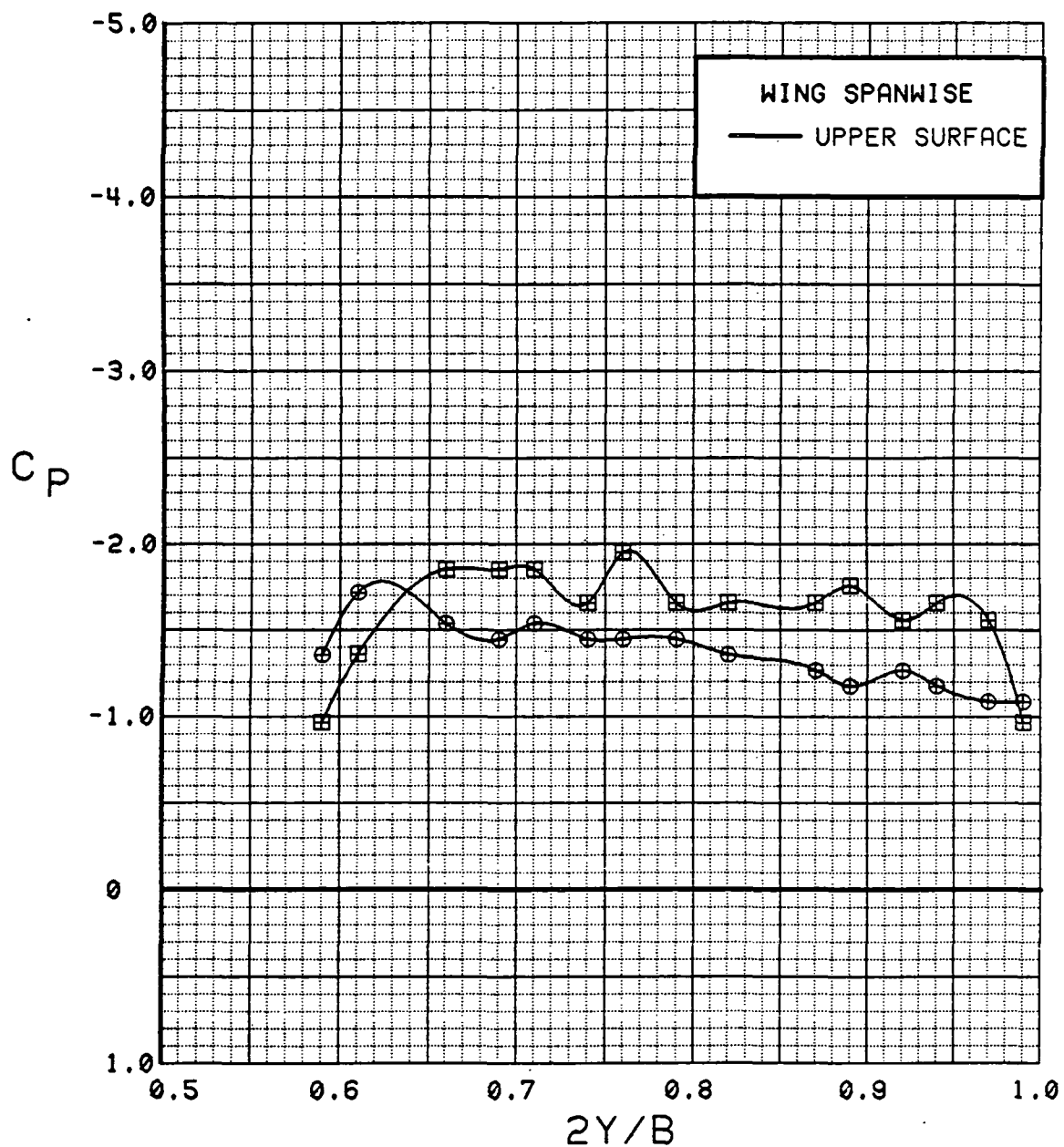


Figure 3.2.2-178 Spanwise Blowing Effects, Flaps Deflected,  
 $C_T = 1.8$ , Spanwise, Alpha = 28 deg

SYM	TEST	RUN	ALPHA	CT	ITEF	OTEF	CAN	SWB
●	537	59	33.0	1.87	30	30	OFF	OFF
■	546	45	33.0	1.89	30	30	OFF	ON

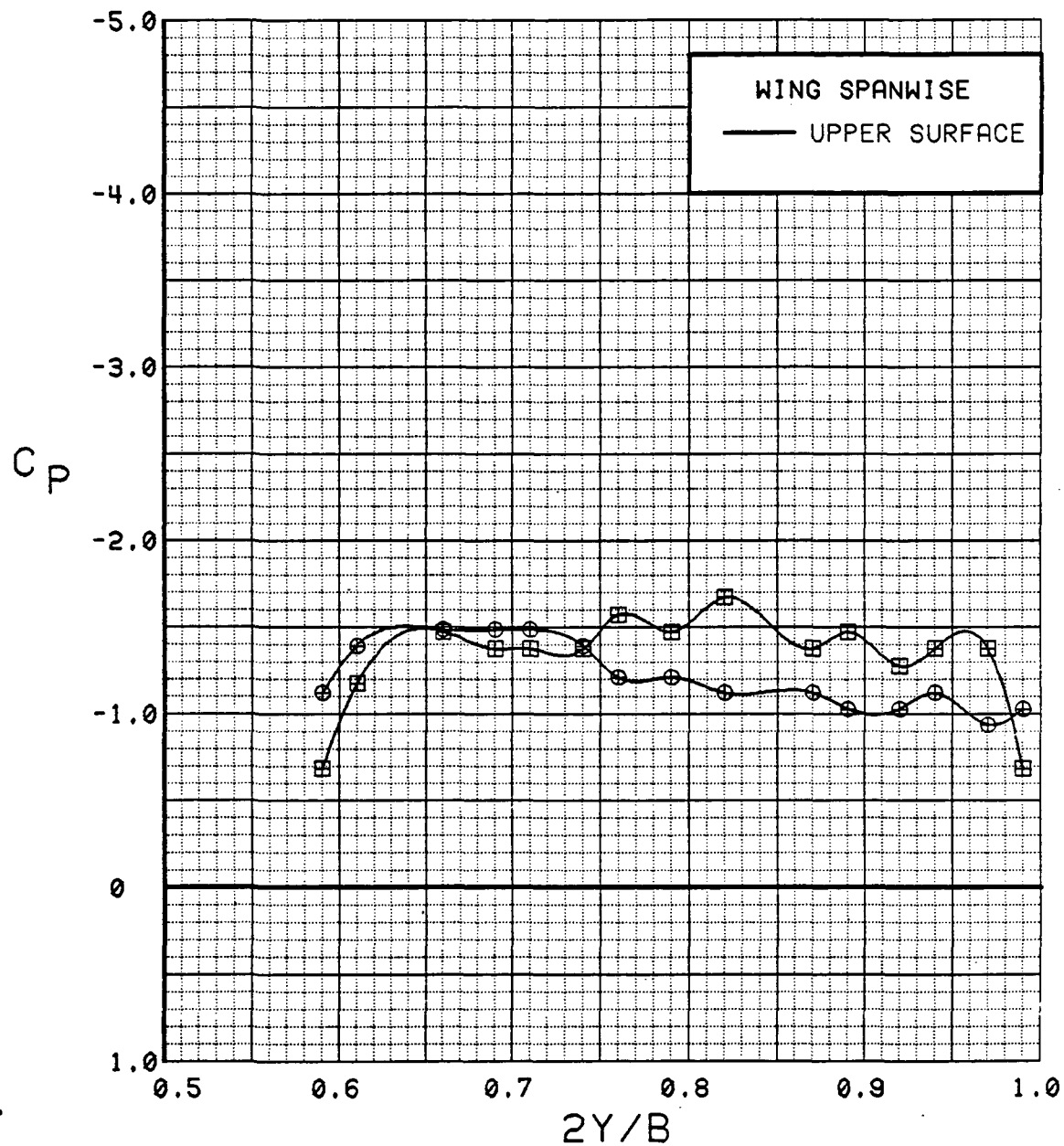


Figure 3.2.2-179 Spanwise Blowing Effects, Flaps Deflected,  
 $C_T = 1.8$ , Spanwise, Alpha = 32 deg

# WING INBOARD

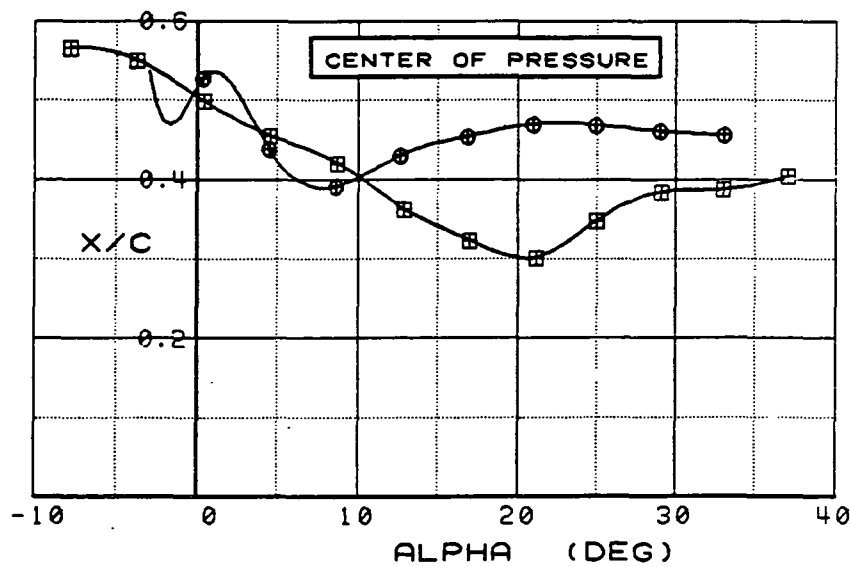
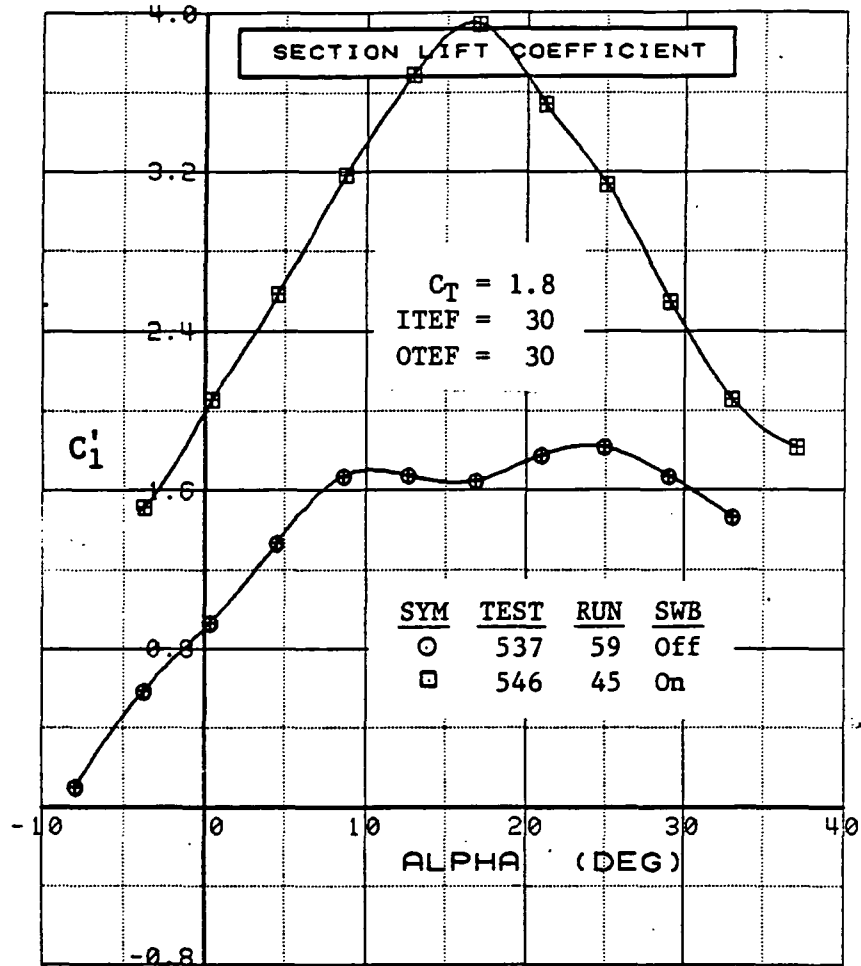


Figure 3.2.2-180 Spanwise Blowing Effects, Flaps Deflected,  $C_T = 1.8$ , Inboard, Integrated Section Properties



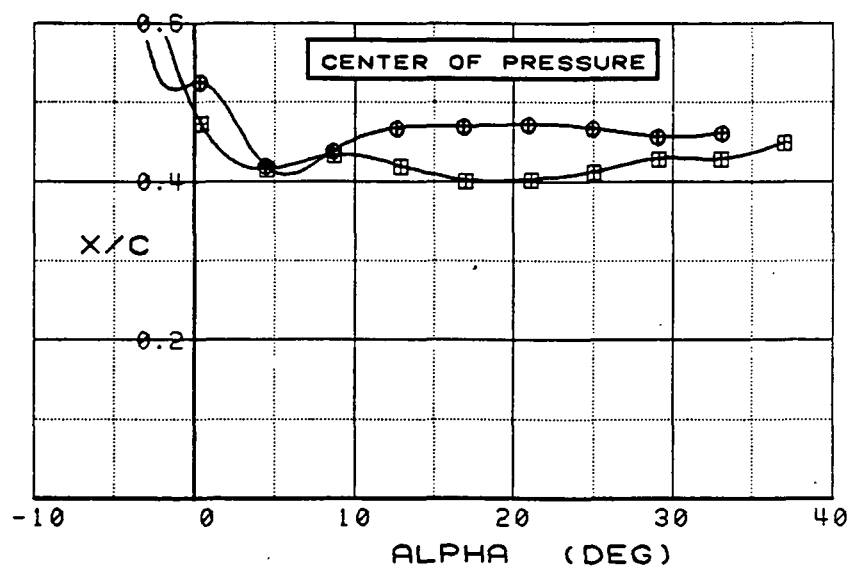
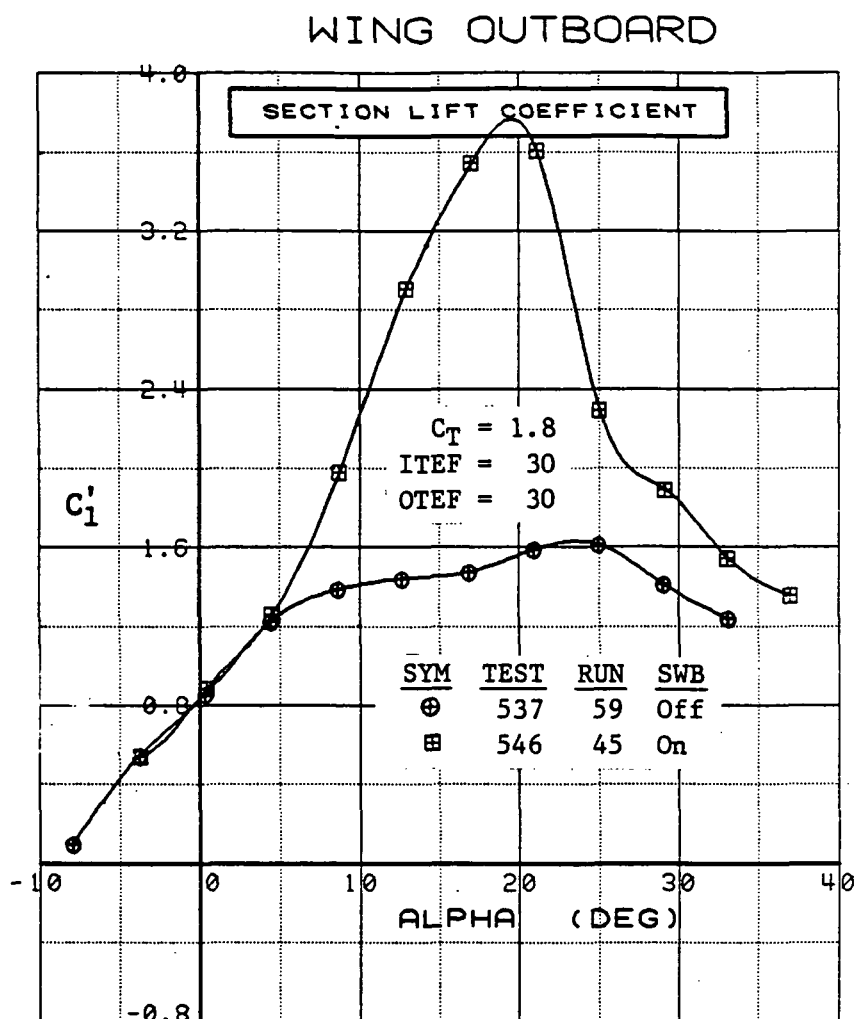


Figure 3.2.2-181 Spanwise Blowing Effects, Flaps Deflected,  
 $C_T = 1.8$ , Outboard, Integrated Section Properties

**(This page intentionally left blank.)**

### 3.2.3 Canard

#### 3.2.3.1 Basic Flowfield Characteristics and Flap Effects

**3.2.3.1.1 Canard Flaps Neutral.** The single chordwise row of pressure taps located near the midpoint of the canard exposed semispan provided a meager but useful insight into the canard flowfield features. Upper-surface pressures suggest the occurrence of leading-edge stall at low  $\alpha$ , but boundary layer reattachment preserved potential flow back to the trailing edge. At high  $\alpha$ s, a leading-edge vortex moved over the instrumented station and caused a significant modification to the flowfield. Typical section  $C_p$  data and integrated section characteristics are presented in Figures 3.2.3-1 through -6.

With the canard undeflected and its flaps neutral, leading-edge stall was not present at the pressure-instrumented span station when the local angle of attack was near zero (see Figure 3.2.3-1, for example). As pitch attitude was increased, a short-bubble-type separation presumably occurred at the leading edge near the tip and moved inboard; the outboard region of the canard became largely stalled. When separation reached the row of pressure taps, there was a reduction in the suction peak measured at the leading edge. With a little higher  $\alpha$  (e.g.,  $\alpha = 4$  deg), the pressure distribution near the leading edge was nearly flattened out, but sometimes lower pressure still occurred for a short distance aft of this stall region (e.g.,  $\alpha = 8$  deg). Finally, at high  $\alpha$ s,  $C_p$  became nearly constant along the entire upper surface at this span station, with pressures at the trailing edge considerably lower than ambient. These trends are similar to results found for the wing with canard off and, thus, suggest a stall pattern like that shown in Section 3.2.1. A superficial examination of Figures 3.2.3-1 through -4 suggests that the principal canard flow features were altered little by wing-flap deflection and less by power setting. However, they did have a measurable effect on section lift, particularly with power on, as Figures 3.2.3-5 and -6 indicate. Effects of more significance were produced by canard-geometry variations.

As was inferred for the wing, the canard stall boundary was the outboard edge or primary separation line of a weak, free vortex. The origin of this leading-edge vortex has been taken herein to be the innermost point on the leading edge where  $C_p$  ceased to reduce with increased  $\alpha$  or canard deflection,  $\delta_c$ . The precise angle at which this occurred on the canard leading-edge at its instrumented station  $\alpha^*$ , was difficult to pinpoint because data were obtained in 4-degree  $\alpha$  intervals. However, compared to the wing alone (canard off) near its midspan,  $\alpha^*$  for the canard seems to be three to four degrees lower because of wing-induced-circulation effects on the canard and the larger canard leading-edge sweep. It also appears that a change in canard deflection or flap setting at fixed  $\alpha$  affected  $\alpha^*$  in a manner inversely proportional to the canard lift. The obvious reason is that an increase in canard lift produced increased loading (increased local velocity) at the leading edge, thus precipitating earlier leading-edge separation. This phenomenon is illustrated in Figure 3.2.3-7. With canard deflection zero and canard flaps neutral, there was no stall evident at this angle of attack, which means that the separation boundary and leading-edge vortex (if either existed) were outboard of this span station. As canard deflection was introduced, stall barely set in at  $\delta_c = 5$  deg, with the weak vortex (low rotation rate) apparently crossing the chord near  $x/c = .10$ . With a 10-deg canard deflection, the vortex core moved a bit more aft (having originated further inboard) and was larger, thus affecting a longer region of the chord. The vortex moved progressively further inboard with increased deflection until it was lying entirely inboard of the instrumented station at  $\delta_c = 25$  deg, where the whole section appears to have been stalled. The fact that the suction peak below the vortex core did not continue to increase in magnitude for  $\delta_c > 10$  deg seems to indicate that the vortex grew weaker as it enlarged

and turned downstream and that perhaps it was displaced higher above the canard surface. (It is pertinent that the analysis of canard-on wing pressure data failed to pinpoint the presence of the canard leading-edge vortex, nevertheless, it was concluded that the wing vortex development was strongly influenced by the canard vortical wake in a confluent manner.)

**3.2.3.1.2 Canard Flaps Deflecting.** As one might expect, stall onset was delayed to higher alpha when the leading-edge flap was lowered. With  $\delta_c = 0$  deg and  $\delta_l = 10$  deg, Figure 3.2.3-8 shows that stall at  $\alpha = 8$  deg was almost eliminated. With  $\delta_l = 30$  deg, the suction peak at  $x/c = .14$  was caused by the expansion created by the contour corner at the hingeline, and the flow appears to have negotiated the turn without separation. When the trailing-edge flap was lowered,  $\alpha_1^*$  was slightly reduced. Although  $\delta_t = 30$  deg produced a significant change in upper- and lower-surface pressures, the typical distribution shown in Figures 3.2.3-9 indicates that upper-surface flow did not efficiently negotiate the contour discontinuity at the trailing-edge-flap hingeline, perhaps due to boundary-layer separation. Lesser canard trailing-edge flap deflections were not tested. With  $\delta_c = 20$  deg and  $\alpha = 4.5$  deg (Figure 3.2.3-10), a leading-edge deflection of 10 deg did not eliminate leading-edge stall. This was also true of  $\delta_l = 30$  deg, but the section was then only barely into a stall condition.

On the basis of these and other data with wing flaps at 30 deg,  $C_T = 0.9$ , and combined variations in canard deflection and geometry, the following approximate relationship was derived:

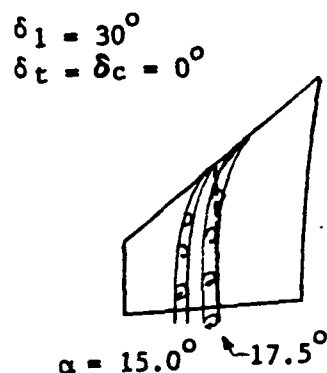
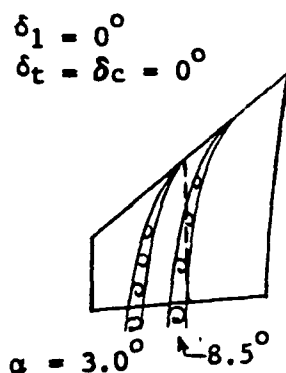
$$\alpha_1^* = 3.0 - 0.7 \delta_c + 0.4 \delta_l - 0.2 \delta_t \quad \text{Equation (3)}$$

where all angles are in degrees. The angle of attack at which the trailing-edge pressure began to reduce significantly,  $\alpha_t^*$ , was defined to be the instant when the inboard edge of the vortex signature first reached the trailing edge at the instrumented span station.

This occurred at an alpha about 1.0 to 5.5 degrees higher than  $\alpha_1^*$ . Approximately,

$$\alpha_t^* = 8.5 - 0.7 \delta_c + 0.3 \delta_l - 0.2 \delta_t \quad \text{Equation (4)}$$

The variable difference between  $\alpha_1^*$  and  $\alpha_t^*$  was brought about by leading-edge flap deflection. Whereas drooping the leading edge delayed separation by almost half the deflection angle, per Equation (3), it also caused the vortex sweep to increase so that at  $\delta_l = 30$  deg it began to cross the trailing edge only 2.5 degrees later than when the vortex origin was at the leading edge, as depicted below.



Values of  $\alpha_t^*$  defined by Equation 4 were deduced from the data with the wing flap and aileron deflected down 30 deg. Smaller deflections produced higher  $\alpha_t^*$  values and presumably induced less downstream curvature so that at  $\alpha_1^* \leq \alpha \leq \alpha_t^*$  less of the instrumented chord was under the vortex. Canard data with variations in wing flap/aileron deflection are presented in Subsection 3.2.3.2.2.

The local onset of leading-edge stall, at  $\alpha_1^*$ , did not mean the section lift at that span station ceased to increase with alpha. Although stall sharply reduced the leading-edge  $C_p$  to values well below the peak recorded negative value of about -4.4 deg, the reduction at  $\alpha > \alpha_1^*$  limited the loading for only a short distance downstream. It seems the vortex traversing the chord served to more than offset this loss in upper-surface section lift, particularly when the canard deflection and flap settings were not at their highest values (see Figure 3.2.3-7). Also, lower-surface  $C_p$  increased with alpha, undisturbed by leading-edge stall, so that section lift continued to increase beyond  $\alpha_1^*$ . This is illustrated in Figures 3.2.3-11 and 3.2.3-12 which present typical values of  $C_l$  based on Equation (1) with the term  $\cos(\alpha)$  replaced by  $\cos(\alpha + \delta_c)$ . Corresponding values of  $\alpha_1^*$  and  $\alpha_t^*$ , as defined by Equations 3 and 4, are noted for each curve. In general, section lift is shown to have continued to increase with alpha beyond  $\alpha_1^*$ . At approximately  $\alpha = \alpha_t^*$ , the rate of  $C_l$  increase became less rapid. Stall set in shortly thereafter, but lift was maintained fairly constant throughout the high-alpha range. It is believed that canard lift was preserved beyond stall onset in part due to the wing circulation flowfield. This wing-induced effect on the canard has been inferred from canard pressure changes observed as wing trailing-edge flap deflection and power setting were varied.

### 3.2.3.2 Wing-Induced Effects

**3.2.3.2.1 Wing Flap Settings Fixed.** The canard data presented in Figures 3.2.3-7 through -12 were with the canard in the aft position, with the wing flap and aileron each at 30 deg, and with power set nominally at  $C_T = 0.9$ . Canard flap setting variations were not tested with the wing trailing edge neutral. With the canard surfaces neutral, however, variations in canard fore/aft location, wing trailing-edge setting, and power show clear evidence of wing-induced effects on the canard. Before addressing the canard response caused by its relocation forward on the nacelle, it is instructive to examine the  $C_p$  results shown in Figure 3.2.3-13 for (a)  $\alpha = 20$  deg with  $\delta_c = 0$  deg, and (b)  $\alpha = 0$  deg with  $\delta_c = 20$  deg. If there was no wing-induced contribution to the canard flow field, the difference in  $C_p$  would have to be attributed to canard unporting or to nacelle/strake load carryover. The large changes in  $C_p$  magnitude and chordwise trend, however, suggest wing-induced effects were predominant.

Relocation of the canard at a more-forward longitudinal station resulted in significant changes in  $C_p$  and  $C_l$ , as may be noted at successively higher alpha in Figures 3.2.3-14 through -20 with  $C_T = 0.9$  and in Figures 3.2.3-21 through -27 with  $C_T = 0$ . With  $C_T = 0.90$ , lower-surface  $C_p$  differences, including those aft on the chord, indicate a slightly lower effective angle of attack for the forward canard station. Upper-surface changes near the leading-edge suggest a moderate reduction in local upwash, whereas aft on the chord the results were mixed. For example, the crossover in upper-surface  $C_p$  at  $\alpha = 4$  deg (Figure 3.2.3-15) was likely the consequence of a weaker leading-edge vortex with the canard forward. At  $\alpha = 16$  deg and especially 20 deg (Figures 3.2.3-18 and -19) there was a conspicuous reduction in section lift because canard-forward, upper-surface pressures were reduced very little with the increase in alpha. The breakdown in section lift is obvious in Figure 3.2.3-20. With  $C_T = 0$  (Figures 3.2.3-21 through -27) there were similar incremental trends at low alpha but notable exceptions elsewhere. In particular, moving the canard forward produced lower-surface  $C_p$  changes with power off that were

larger at  $\alpha = 12$  and  $20$  deg but were reversed in sign at  $\alpha = 16$  deg (Figures 3.2.3-25 vs. -18). Meanwhile, upper-surface  $C_p$  changes at  $\alpha = 16$  deg were almost the same as they were with power, but at  $\alpha = 20$  deg (Figure 3.2.3-26) the canard relocation did not cause as significant a loss in canard lift (Figure 3.2.3-27) because the canard-aft pressures changed little when  $\alpha$  was increased to  $20$  deg. The cause of this perplexing canard behavior is not clearly understood, but it was likely the consequence of wing-flowfield interactions with the canard wake, as discussed at the end of Subsection 3.2.4.2.2.

**3.2.3.2.2 Wing Flaps Deflecting.** Wing trailing-edge deflection also had an impact on canard  $C_p$ , as may be seen in Figures 3.2.3-28 through -33. At  $\alpha = 4.2$  deg (Figures 3.2.3-28) lowering the wing flap and aileron produced a systematic change in canard upper surface  $C_p$  except for  $\delta_{TE} = 20$  deg. Leading-edge stall was present at all deflections but appears to have been more acute with the trailing edge down. Also, the vortex was drawn inboard, crossed the instrumented chord further aft, and increased section lift. At  $\alpha = 8.5$  deg (Figure 3.2.3-29) the same trend is evident except that data for the  $20$ -deg setting were no longer unique. More of the chord lay underneath the vortex when the wing trailing edge was deflected. Canard trailing-edge pressure was lowered only slightly by wing flap deflection, but the inboard edge of the vortex appears to have approached the trailing edge of this canard station as deflection was increased to  $30$  deg. All trailing-edge pressures were lower at  $\alpha = 12$  deg (Figure 3.2.3-30). Thus, the data indicate that  $\alpha$  exceeded  $\alpha_i^*$  for all settings. However, of particular significance is the magnitude of the change in canard upper-and lower-surface pressures that was induced by the wing along most of the canard chord. Not understood is how the wing influence could be transmitted so far forward and improve canard lift despite the stall conditions that prevailed on the canard. This phenomenon, also manifested at  $\alpha = 16$  and  $20$  deg (Figures 3.2.3-31 and -32), seems to reflect an increase in canard lift that is in consonance with a change in wing lift. The integrated section properties  $C_l$  and  $(x/c)_{Cp}$ , summarized in Figure 3.2.3-33, confirm that wing-flap deflections at high  $\alpha$ s produced significant changes in canard lift but only small changes in center of pressure.

**3.2.3.2.3 Power Without Spanwise Blowing.** Power incremental effects on canard pressures are presented in this subsection. The results with only a  $C_T$  value of  $1.4$  are discussed first because of the following factors.

A cursory examination of both canard and wing pressure data, with variations in power setting, disclosed trends in leading-edge  $C_p$  that seemed to be somewhat inconsistent with the flowfield model envisioned from power-off data. (The subject canard data at all  $C_T$  values will be presented subsequently.) A degree of order was perceived, however, when it was recognized that tunnel  $q$  (and therefore  $Re$ ) also changed with power setting and that  $q$  was virtually the same at  $C_T = 0$  and  $C_T = 1.4$ . Fortunately, the test program included a series of runs in which only tunnel  $q$  was varied, with power off and inlets blocked. These results confirmed that  $q$  variations affected the canard pressures moderately and the wing pressures more significantly. (It has been further inferred from power-on data that  $q$  effects were magnified on both surfaces when power was applied.) Figures 3.2.3-34 through -37 present the canard data at three  $q$  values and at four angles of attack up to  $12$  deg. Although the effects of increased  $Re$  were not entirely consistent,  $C_p$  values at  $x/c = 0$  were generally reduced (the suction peak increased) when  $\alpha$  was below  $\alpha_i^*$  (Figure 3.2.3-34) and stall was slightly ameliorated at  $\alpha$  just above  $\alpha_i^*$  (Figure -35). (Note: The corresponding wing data, presented in Subsection 3.2.4.4, shows more distinct effects.) A puzzling phenomenon, however, was the effect of  $q$  variations on canard lower surface  $C_p$ . These trends were even more inconsistent but too large perhaps to be ascribed to random instrumentation inaccuracies, so at present they cannot be reasonably explained.

Effects of  $C_T$ , spanwise blowing off, are illustrated in the next sixteen figures for  $C_T = 0$  vs  $C_T = 1.4$  with the wing trailing edge both neutral (Figures 3.2.3-38 through -45) and at 30 deg (Figures 3.2.3-46 through -53). As discussed above, the reason for the presentation of the power off-on comparisons of  $C_T = 1.40$  is that tunnel  $q$  was the same (15 psf). At  $0 < \alpha < 16$  deg with zero flap setting (Figures 3.2.3-38 through -42)  $C_T$  appears to have induced a small increase in canard lift, with  $C_p$  trends suggesting that upwash was increased and the leading-edge vortex was moved inboard slightly. This is what also occurred due to wing trailing-edge deflection with power off, but to a greater degree then. Reason for the "blip" in upper-surface  $C_p$  that appears in Figure -40 at  $x/c = 0.65$  is unknown; it did not occur elsewhere. At high alpha, however, a strong influence of  $C_T$  on canard  $C_p$  distribution and  $C_l$ , which is evident in Figures 3.2.3-43 through -44, was quite unexpected. This facet is addressed again in the next paragraph. With flap and aileron at 30 deg and at low alpha (Figures 3.2.3-46 through -52),  $C_T$  produced slightly more  $C_p$  change aft on the chord than at zero deflection but less increase in lift. However, the high-alpha wing-influence phenomenon appeared sooner ( $\alpha = 12$  deg) than with flaps neutral ( $\alpha = 16$  deg) and the  $C_l$  increase was almost as much at the highest alpha settings (compare Figures 3.2.3-45 and -53).

Figures 3.2.3-54 through -59 contain canard-pressure data for the complete range of  $C_T$  values with wing flaps undeflected. These are the "problem" data alluded to in the second paragraph of this subsection. Figure 3.2.3-54 shows the data at low  $C_T$  that appeared to contradict the premise that wing flap deflection and  $C_T$  each induced an upwash increase at the canard. Note that the leading edge was stalled with power off and at thrust values greater than  $C_T = .93$ , so a presumed increase in upwash at  $C_T = 0.48$  should not have alleviated stall. However, the data in Figure 3.2.3-54 indicate that stall was eliminated at  $C_T = .27$  and at  $C_T = .48$ . The reason for this anomaly is found in the aforementioned variation in wind tunnel  $q$  that was made in order to alter  $C_T$ , as noted in Table 8.

Table 8 Tunnel Conditions With Power Variations

$C_T$	0	0.27	0.48	0.93	1.40	1.84
$q$ (psf)	15	63	37	23	15	11
$Re(10^6/\text{ft.})$	0.72	1.47	1.13	0.89	0.72	0.61

Note that  $Re$  was higher for the first three non-zero  $C_T$  values than it was at zero  $C_T$ . Also  $\alpha = 4$  deg (Figure 3.2.3-54) was just above  $\alpha_l^*$ , which was approximately 3 deg (as deduced from Equation (3) and data at  $C_T = 0.9$ ). The leading edge was barely into a stall condition at  $C_T = .93$ . At the lower  $C_T$  values, it appears that local separation was reduced and that the origin of the leading-edge vortex formation was nudged outboard of the instrumented span station because of the higher  $Re$  values. (The influence of  $Re$  is discussed in more detail in subsection 3.2.2.2.) Compared to the power-off data at  $\alpha = 8$  deg (Figure 3.2.3-55) the vortex appears to have crossed the instrumented chord further forward at  $C_T = 0.47$  and further aft at  $C_T = 1.90$ . The trend showing higher lift with power on persisted (in reduced magnitude) at  $\alpha = 12$  deg (Figure 3.2.3-57) despite the generally stalled conditions at this span station. The favorable effect of power reemerged dramatically at the highest alpha (Figures 3.2.3-59) over-shadowing any  $Re$  implications. Section lift, presented in Figure 3.2.3-60, illustrates this remarkable

phenomenon irrespective of  $R_e$  differences. As mentioned above, it is not understood just how the wing-jet exhaust could strongly influence the canard when it was deeply stalled. Perhaps a weak clue (Figure 3.2.3-58) is the  $C_p$  change induced on the lower surface, where pressures were reduced slightly with increased  $C_T$ . The inference is that the jet accelerated the overall canard flowfield. Since, according to potential flow theory,  $C_p$  is proportional to  $(V + \Delta V)^2$ , a change in  $C_p$  would result from an acceleration on both surfaces (as it did) but more so on the upper surface where local  $V$  was higher. The fact that changes in  $(x/c)_{C_p}$  (Figure 3.2.3-60) were small supports this thesis. Another explanation is that perhaps the wing load changes were extended inboard onto the nacelle, transmitted forward toward the inlet (while decreasing, of course) and then were spilled onto the canard as a spanwise carryover load. However, strake pressure changes did not support this thesis consistently (see Figures 3.1-6b and 3.1-7c, for example). Had there been some nacelle pressure measurements, they might have been more enlightening.

Canard pressure data for the complete power range with wing flaps deflected down 30 deg are presented in Figures 3.2.3-61 through -66. These results reveal the same anomaly at  $\alpha = 4$  deg (Figure 3.2.3-61) as did the flaps-neutral data (Figure 3.2.3-54) except that the canard section was now more-deeply in stall and, thus, less amenable to the benefits of increased  $R_e$ . However, the influence of power at high  $\alpha$  (Figure 3.2.3-66) was less than it was with zero flap deflection (Figure 3.2.3-59). It might be plausible to ascribe this change to the fact that the canard section stalled earlier (and thus more completely?) with flaps down, even though the chordwise data trends at  $C_T = 0$  with both flap settings indicate deep stall in each case. Nevertheless, the increased in  $C_l$  at high  $\alpha$  was still considerable, as shown in Figure 3.2.3-67.

**3.2.3.2.4 Spanwise Blowing.** Spanwise blowing (SWB) over the wing had an influence on canard  $C_p$  that was similar to the effect of the jet exhaust in magnitude and trend. One small difference was that SWB tended to reduce  $C_p$  on the lower surface, particularly near the leading edge, for reasons not known. Representative  $C_p$  results with SWB off and on are shown in Figures 3.2.3-68 through -74 at  $C_T = 0.9$  and in Figures 3.2.3-75 through -81 with  $C_T = 1.8$  for alphas ranging from zero to 30 deg and wing flaps deflected. As occurred with flap blowing alone, the induced effects on the canard caused by SWB were modest at low-and mid-alpha and remarkably strong at  $\alpha = 20$  deg (Figures 3.2.3-73 and -80). However, at the highest alphas the SWB influence waned (Figures 3.2.3-74 and -81) compared to that with flap blowing alone (Figures 3.2.3-59 and -66). Section-lift coefficient results, Figures 3.2.3-82 and -83, further highlight this difference in canard response (compare Figure 3.2.3-67). The reason SWB had less effect on the canard at 28 deg was that SWB did not increase wing circulation nearly as much as flap blowing alone in this alpha region. Hence, induced effects were less at the canard. The relative effect on wing characteristics caused by the two modes of power extraction are discussed in Subsections 3.2.4.4 and 3.2.4.5.



SYM	TEST	RUN	ALPHA	CT	ITEF	OTEF	CAN	SWB
⊕	543	63	0.1	0.00	0	0	0	OFF
⊞	543	63	4.2	0.00	0	0	0	OFF
△	543	63	8.3	0.00	0	0	0	OFF
⬠	543	63	12.5	0.00	0	0	0	OFF
*	543	63	16.6	0.00	0	0	0	OFF
+	543	63	20.7	0.00	0	0	0	OFF

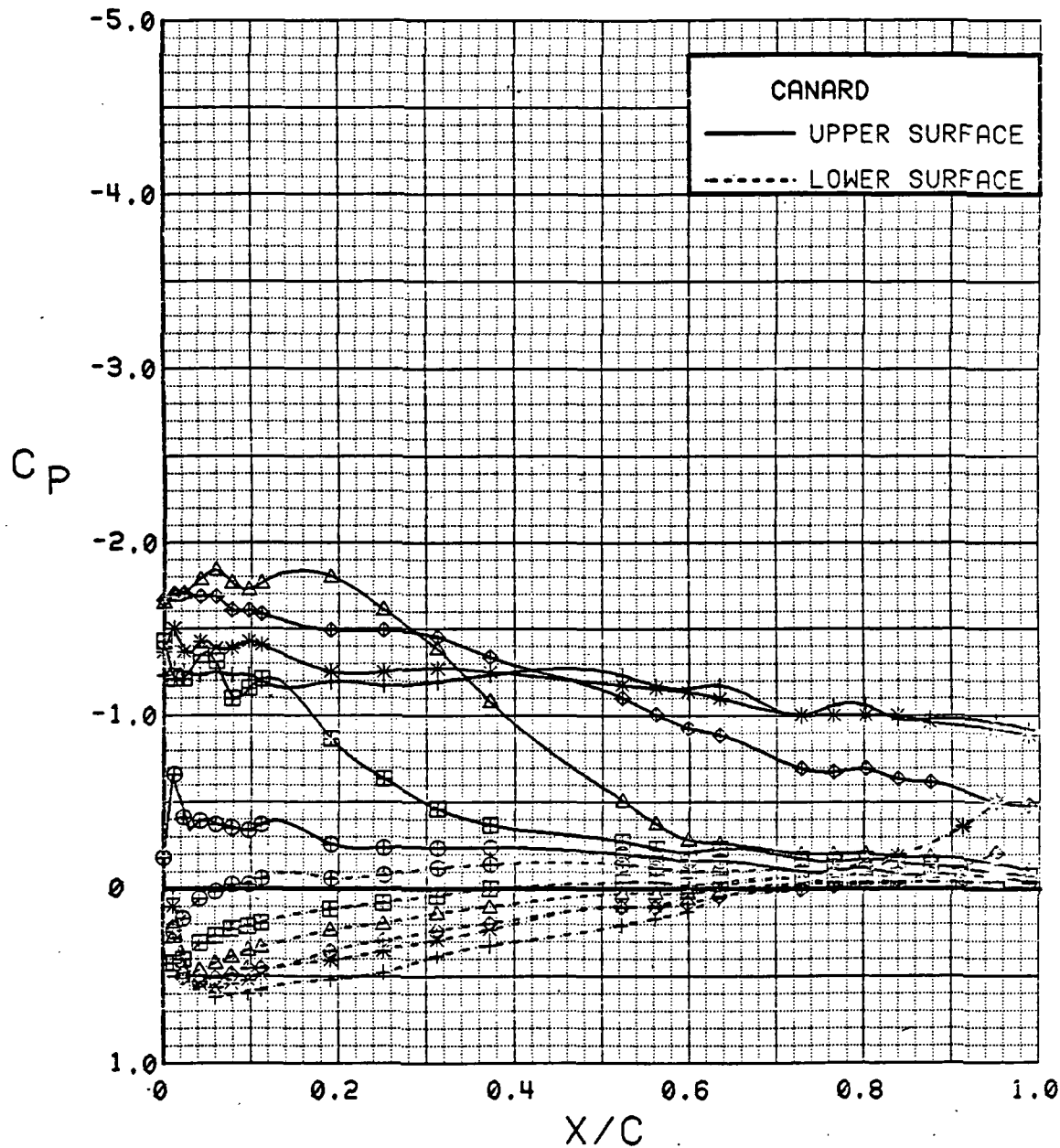


Figure 3.2.3-1 Angle of Attack Effects on Canard, Power Off, Flaps Neutral

SYM	TEST	RUN	ALPHA	CT	ITEF	OTEF	CAN	SWB
⊕	543	11	0.3	0.00	30	30	0	OFF
⊞	543	11	4.4	0.00	30	30	0	OFF
△	543	11	8.5	0.00	30	30	0	OFF
⊕	543	11	12.7	0.00	30	30	0	OFF
*	543	11	16.8	0.00	30	30	0	OFF
+	543	11	20.8	0.00	30	30	0	OFF

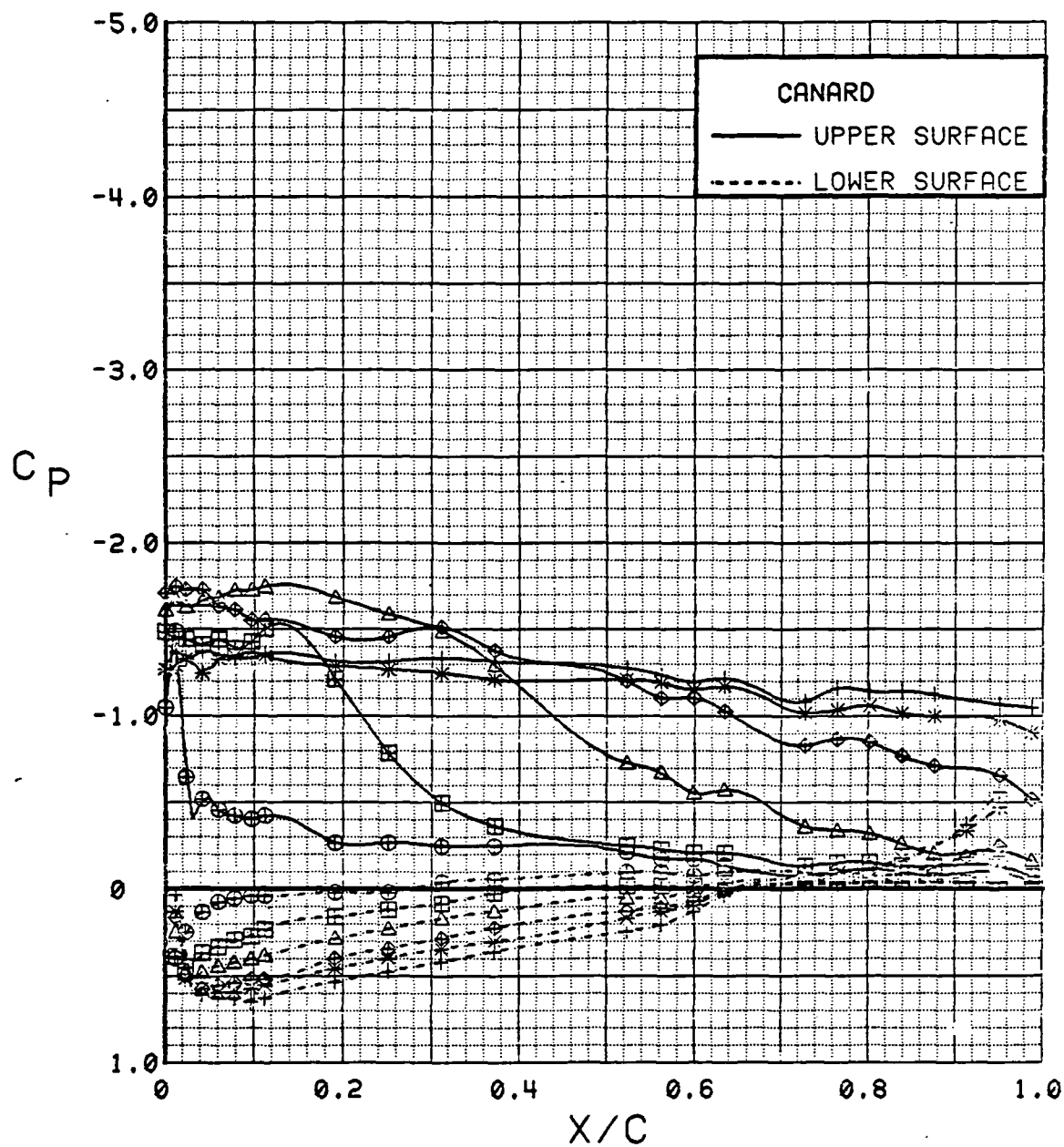


Figure 3.2.3-2 Angle of Attack Effects on Canard, Power Off, Flaps Deflected

SYM	TEST	RUN	ALPHA	CT	ITEF	OTEF	CAN	SWB
⊕	543	60	0.1	0.94	0	0	0	OFF
⊞	543	60	4.3	0.93	0	0	0	OFF
△	543	60	8.4	0.94	0	0	0	OFF
⊕	543	60	12.5	0.94	0	0	0	OFF
*	543	60	16.7	0.93	0	0	0	OFF
+	543	60	20.8	0.93	0	0	0	OFF

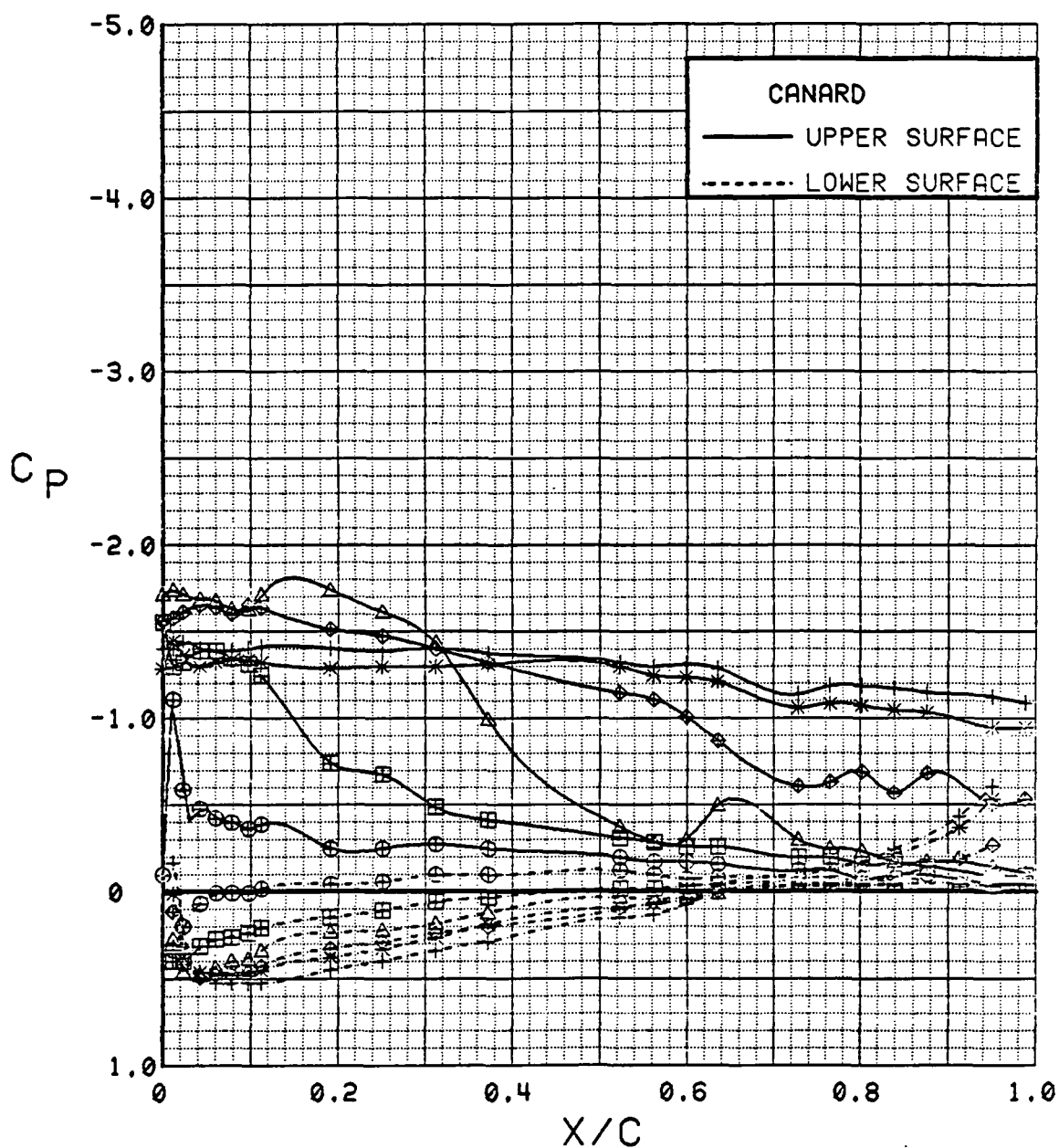


Figure 3.2.3-3 Angle of Attack Effects on Canard,  $C_T = 0.9$ , Flaps Neutral

SYM	TEST	RUN	ALPHA	CT	ITEF	OTEF	CAN	SWB
⊕	543	6	0.3	0.94	30	30	0	OFF
⊞	543	6	4.5	0.94	30	30	0	OFF
△	543	6	8.6	0.91	30	30	0	OFF
⬠	543	6	12.8	0.92	30	30	0	OFF
*	543	6	16.9	0.92	30	30	0	OFF
+	543	6	21.0	0.93	30	30	0	OFF

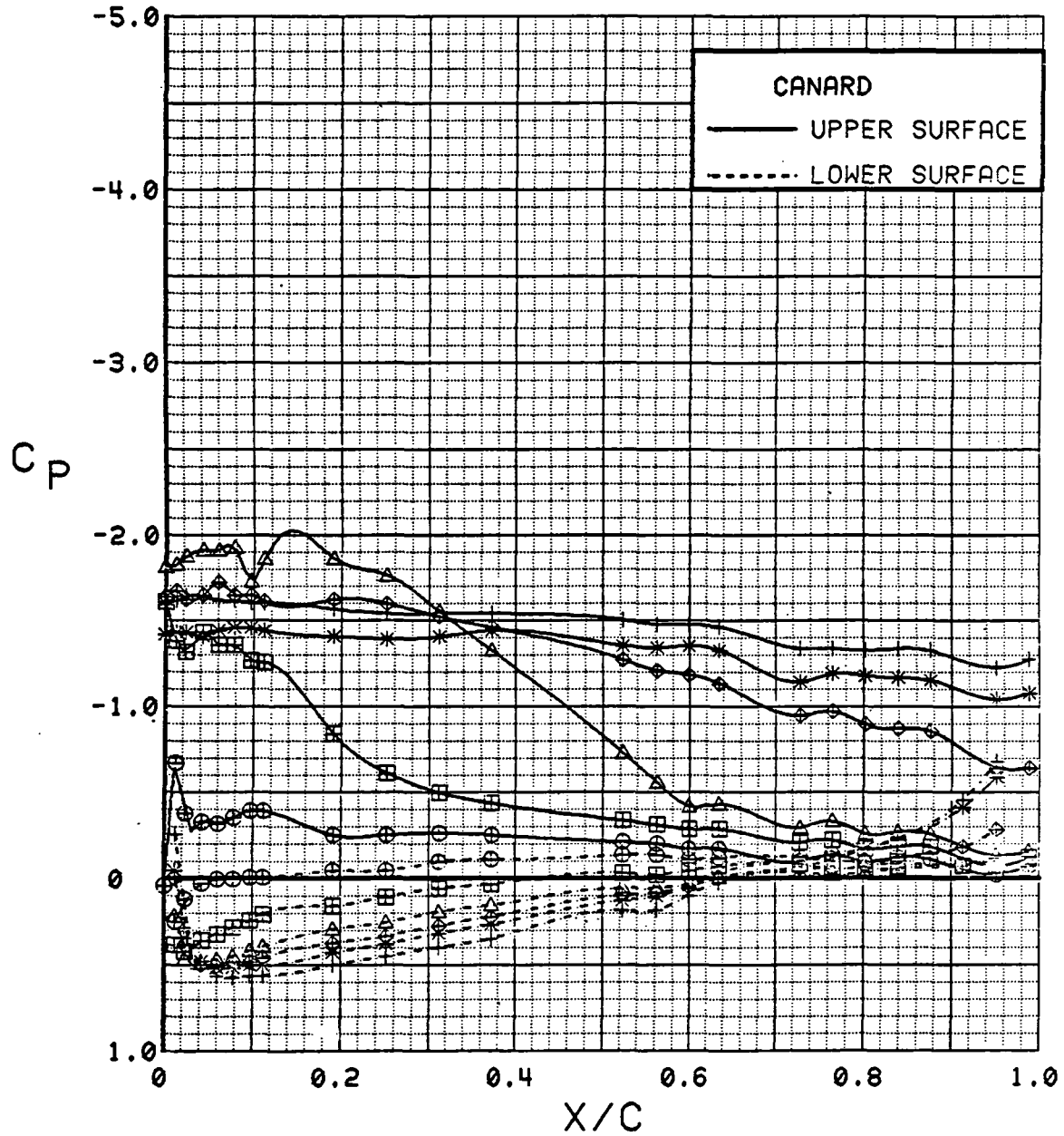


Figure 3.2.3-4 Angle of Attack Effects on Canard,  $C_T = 0.9$ , Flaps Deflected

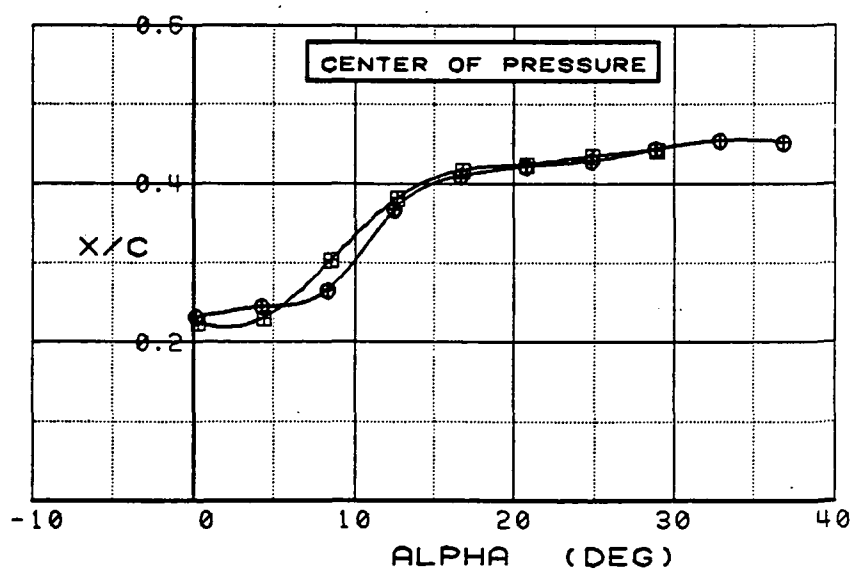
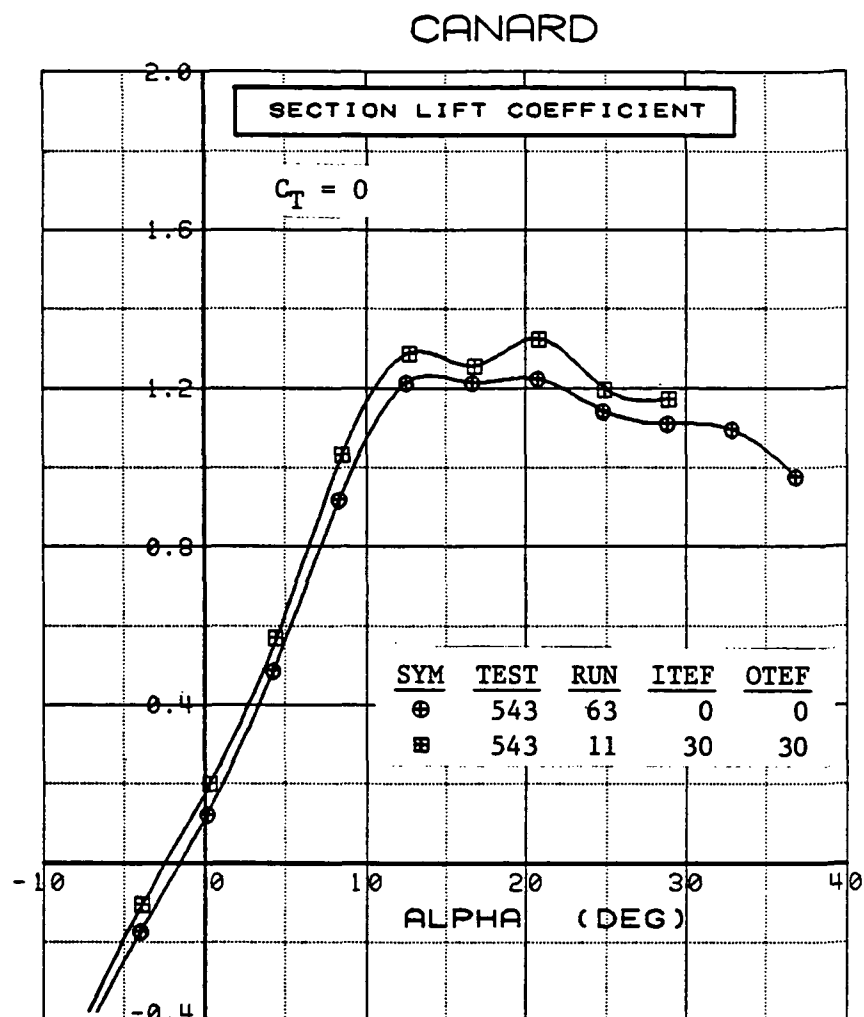


Figure 3.2.3-5 Wing Trailing-edge Flap Effects on Canard, Power Off, Integrated Section Properties

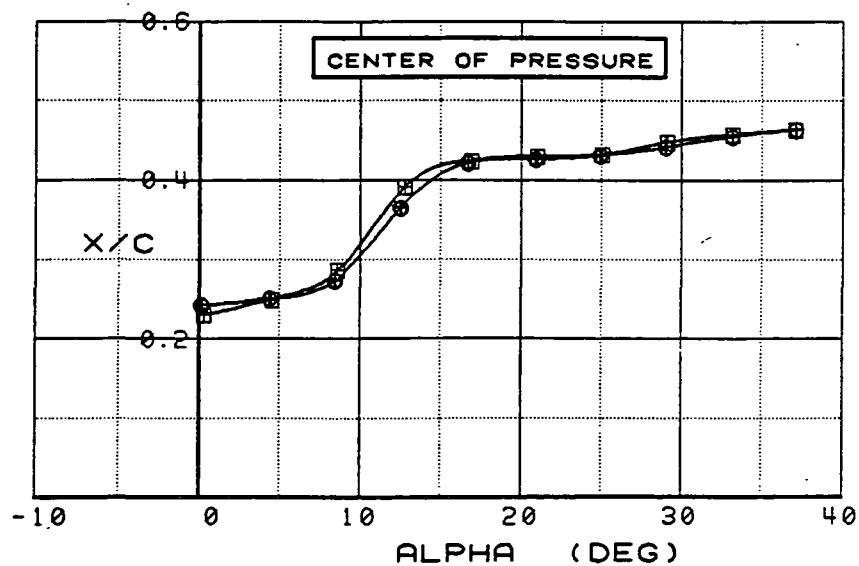
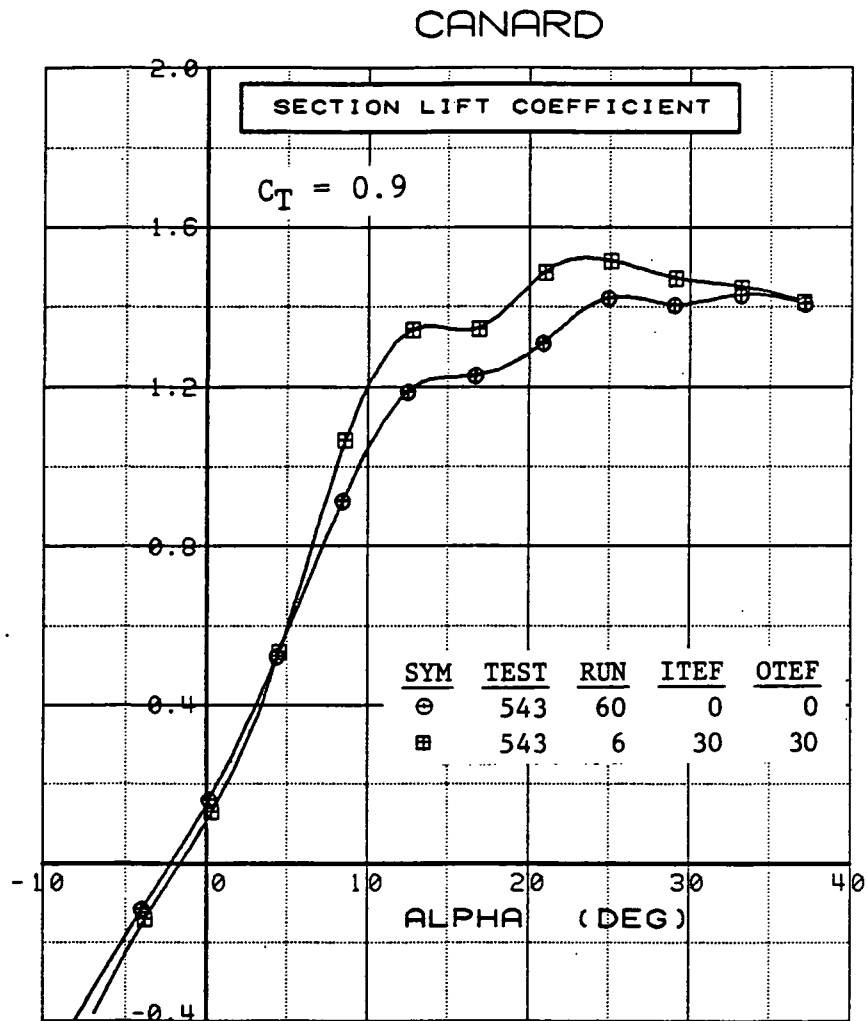


Figure 3.2.3-6 Wing Trailing-edge Flap Effects on Canard,  $C_T$  0.9, Integrated Section Properties

SYM	TEST	RUN	ALPHA	CT	ITEF	OTEF	CAN	SWB
⊕	543	23	0.3	0.94	30	30	0	OFF
⊞	543	23	0.3	0.94	30	30	5	OFF
△	543	23	0.4	0.94	30	30	10	OFF
⊕	543	23	0.4	0.94	30	30	15	OFF
*	543	23	0.4	0.95	30	30	20	OFF
+	543	23	0.4	0.94	30	30	25	OFF

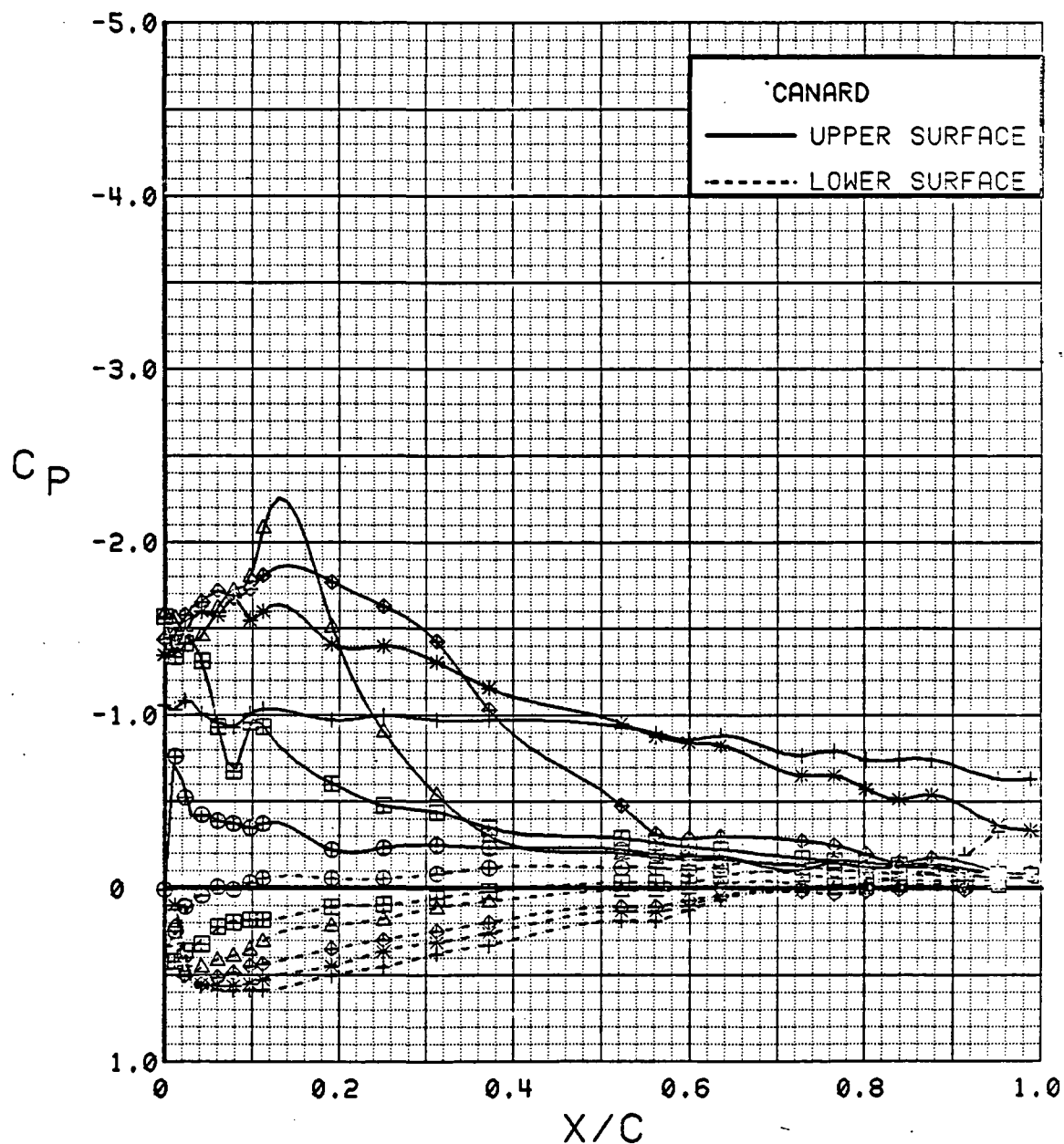


Figure 3.2.3-7 Canard Deflection Effects

SYM	TEST	RUN	ALPHA	CT	ITEF	OTEF	CAN	SWB	$\delta_l$	$\delta_t$
⊕	543	6	8.6	0.91	30	30	0	OFF	0	0
⊞	543	25	8.6	0.93	30	30	0	OFF	10	0
Δ	543	29	8.6	0.93	30	30	0	OFF	30	0

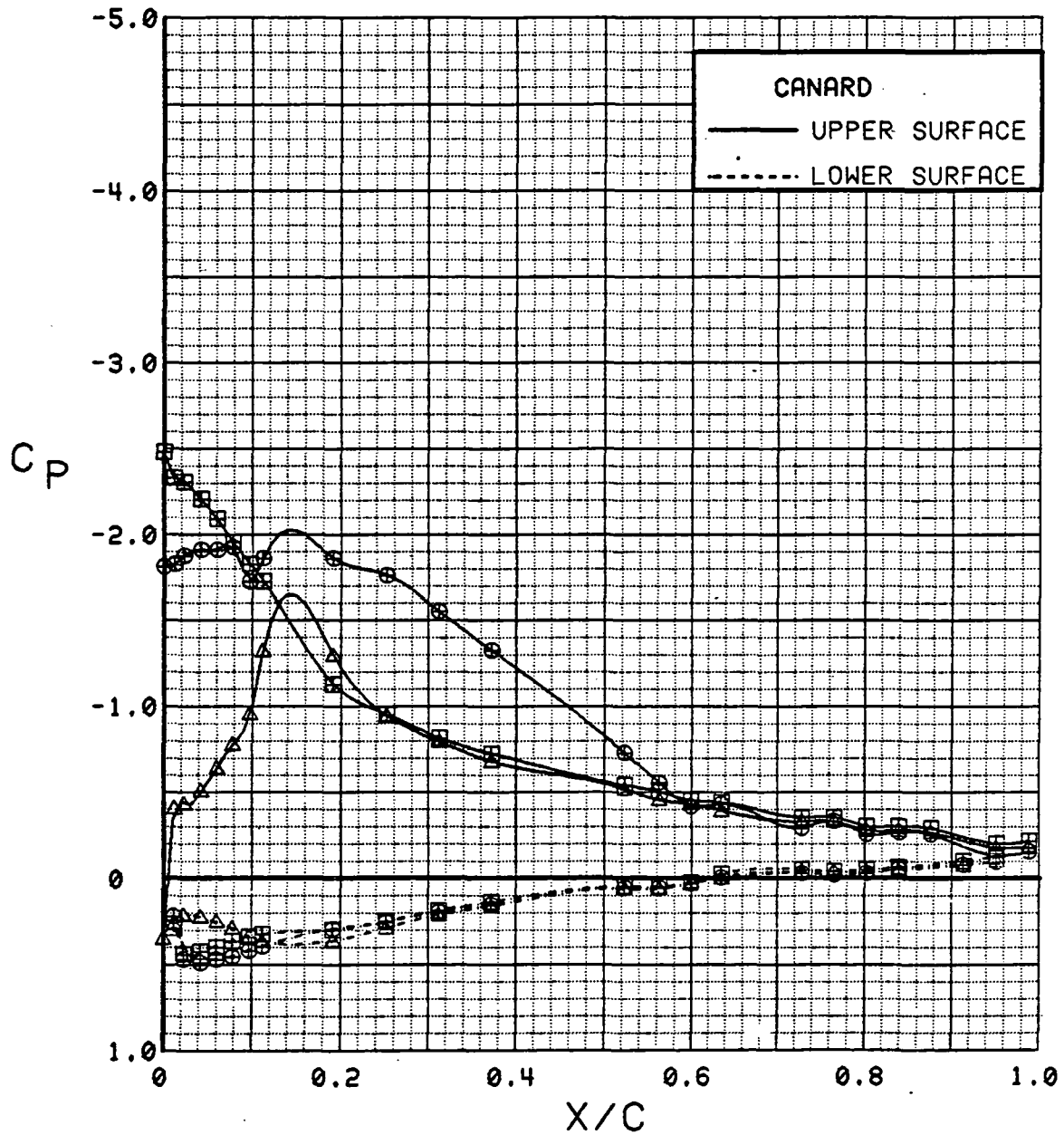


Figure 3.2.3-8 Canard Leading-Edge Deflection Effects



SYM	TEST	RUN	ALPHA	CT	ITEF	OTEF	CAN	SWB	$\delta_l$	$\delta_t$
⊕	543	6	8.6	0.91	30	30	0	OFF	0	0
⊞	543	29	8.6	0.93	30	30	0	OFF	30	0
Δ	543	34	8.7	0.93	30	30	0	OFF	30	30

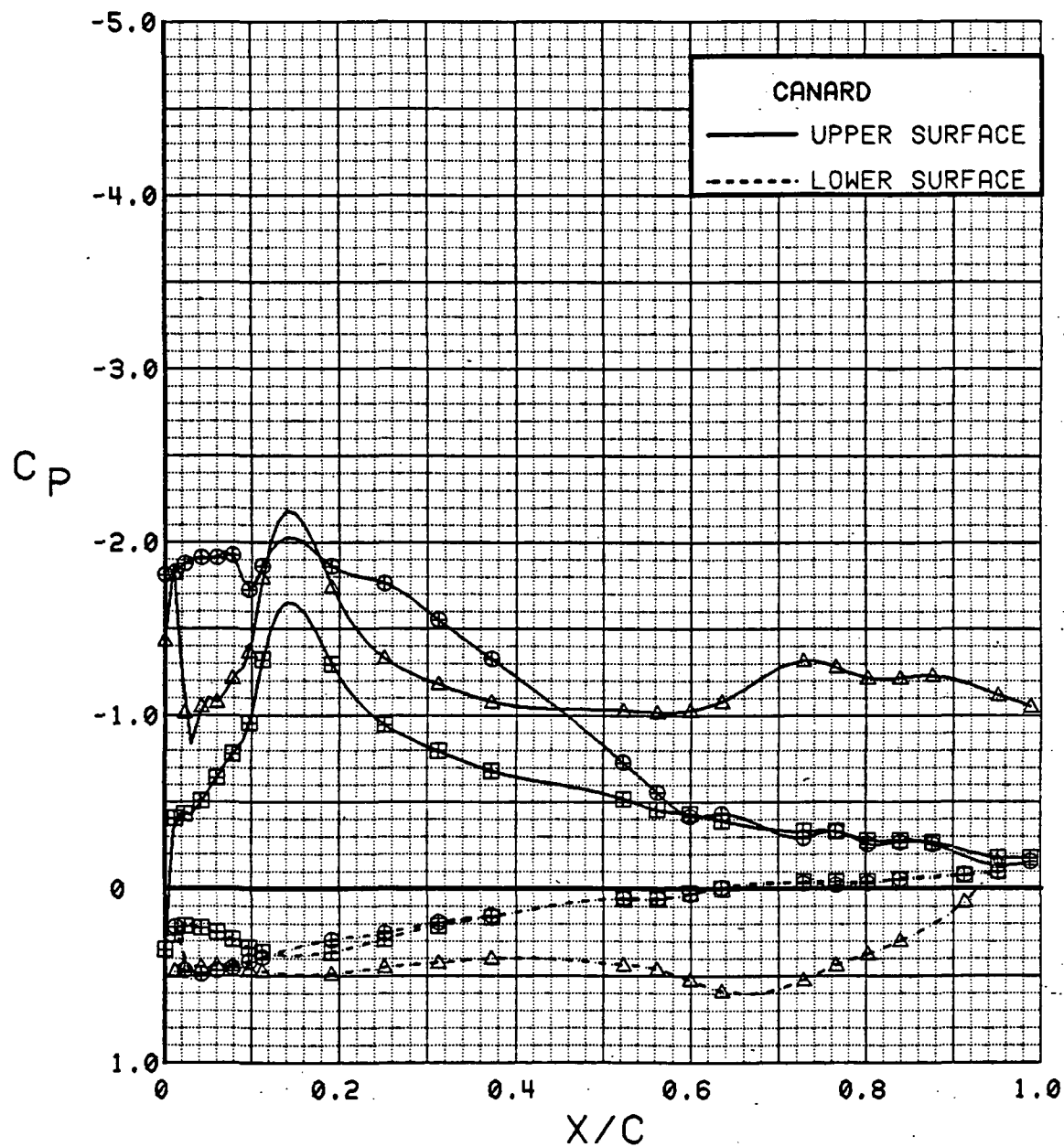


Figure 3.2.3-9

Canard Leading- and Trailing-Edge Deflection Effects

SYM	TEST	RUN	ALPHA	CT	ITEF	OTEF	CAN	SWB	$\delta_l$	$\delta_t$
⊕	543	21	4.5	0.94	30	30	20	OFF	0	0
⊞	543	26	4.5	0.93	30	30	20	OFF	10	0
Δ	543	31	4.5	0.94	30	30	20	OFF	30	0

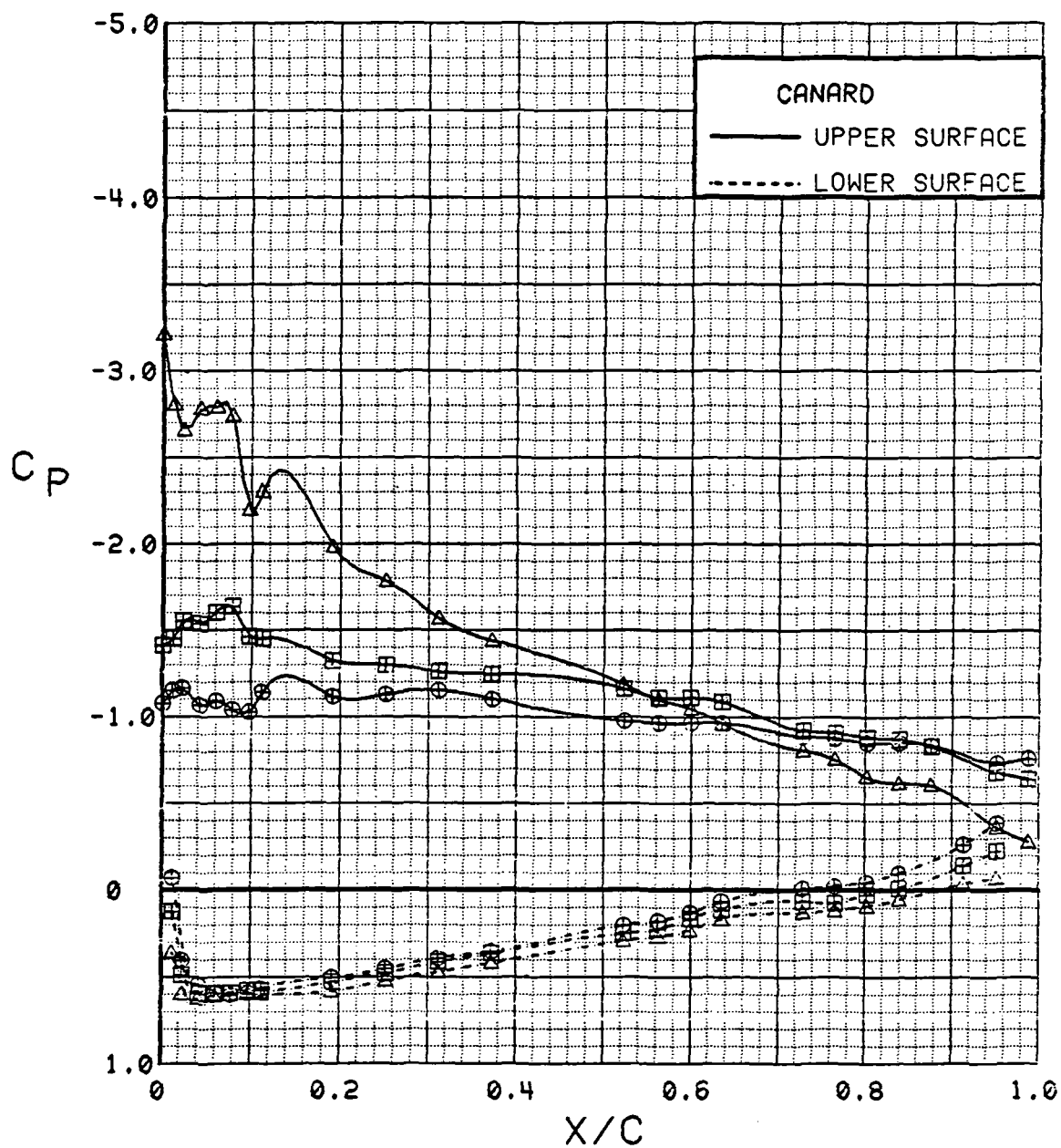


Figure 3.2.3-10 Canard Leading-Edge Deflection Effects, Canard Deflected

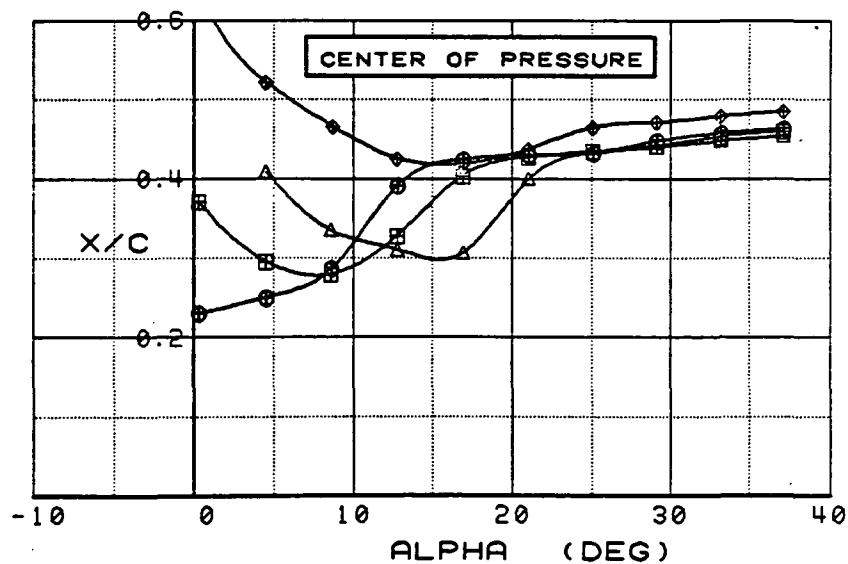
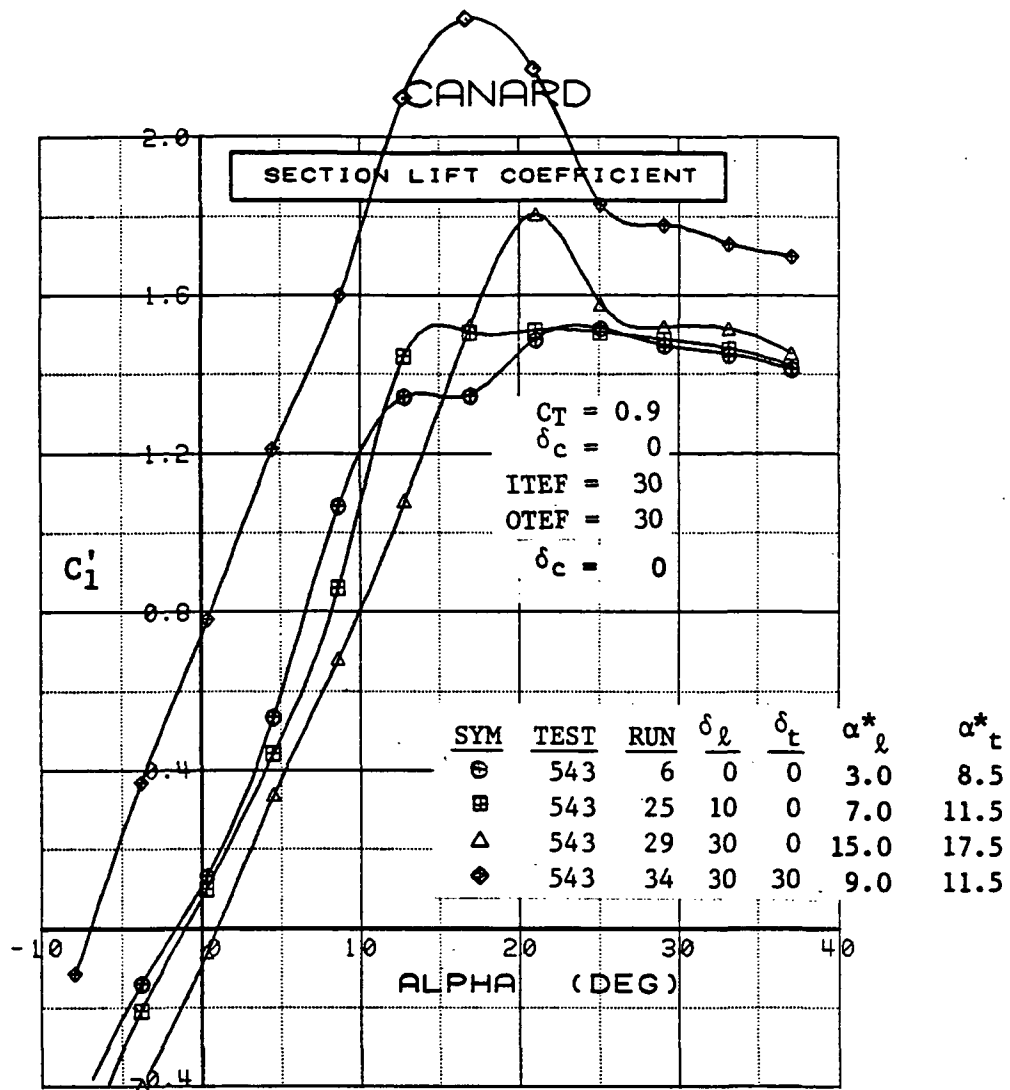


Figure 3.2.3-11 Canard Leading- and Trailing-Edge Deflection Effects, Integrated Section Properties

## CANARD

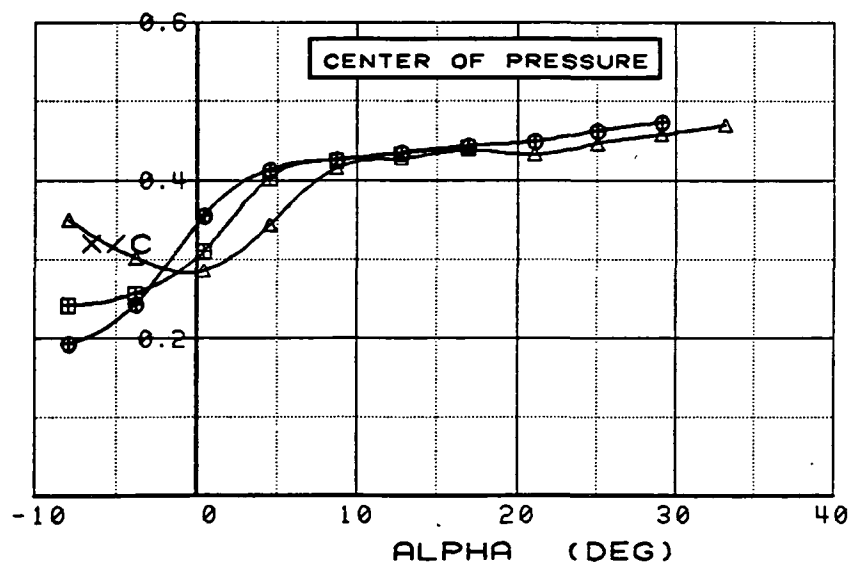
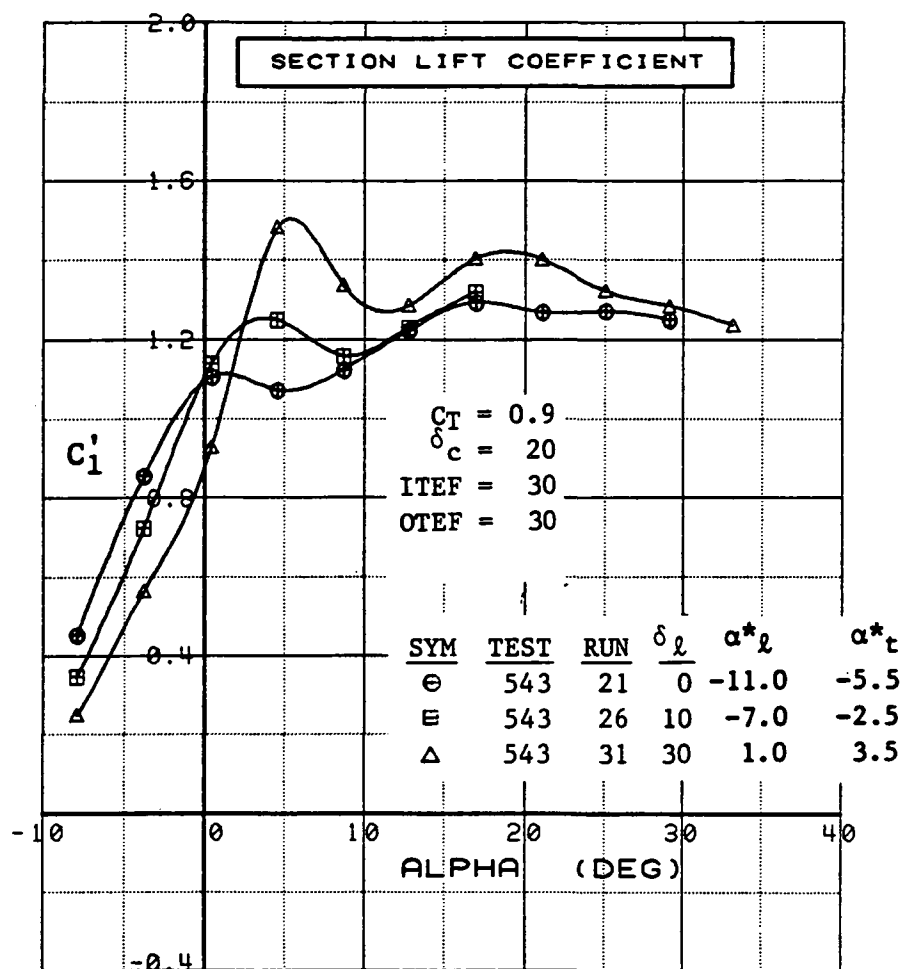


Figure 3.2.3-12 Canard Leading-Edge Deflection Effects, Integrated Section Properties

SYM	TEST	RUN	ALPHA	CT	ITEF	OTEF	CAN	SWB
⊕	543	6	21.0	0.93	30	30	0	OFF
⊞	543	21	0.4	0.94	30	30	20	OFF

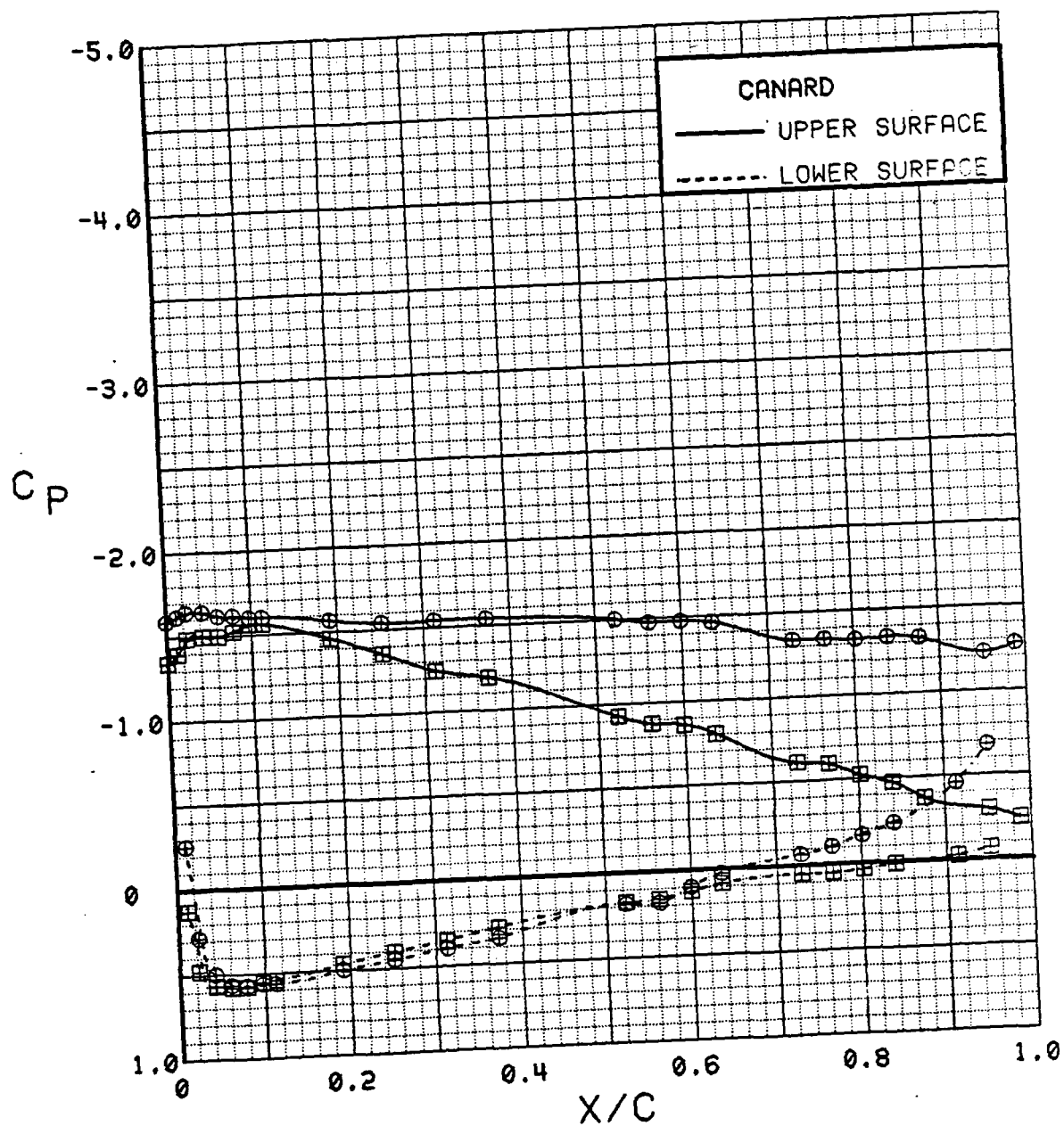


Figure 3.2.3-13 Effect of Fuselage/Nacelle Orientation on Canard Pressures

SYM	TEST	RUN	ALPHA	CT	ITEF	OTEF	CAN	SWB	CAN
⊕	537	32	0.3	0.91	30	30	0	OFF	FOR
⊞	543	6	0.3	0.94	30	30	0	OFF	AFT

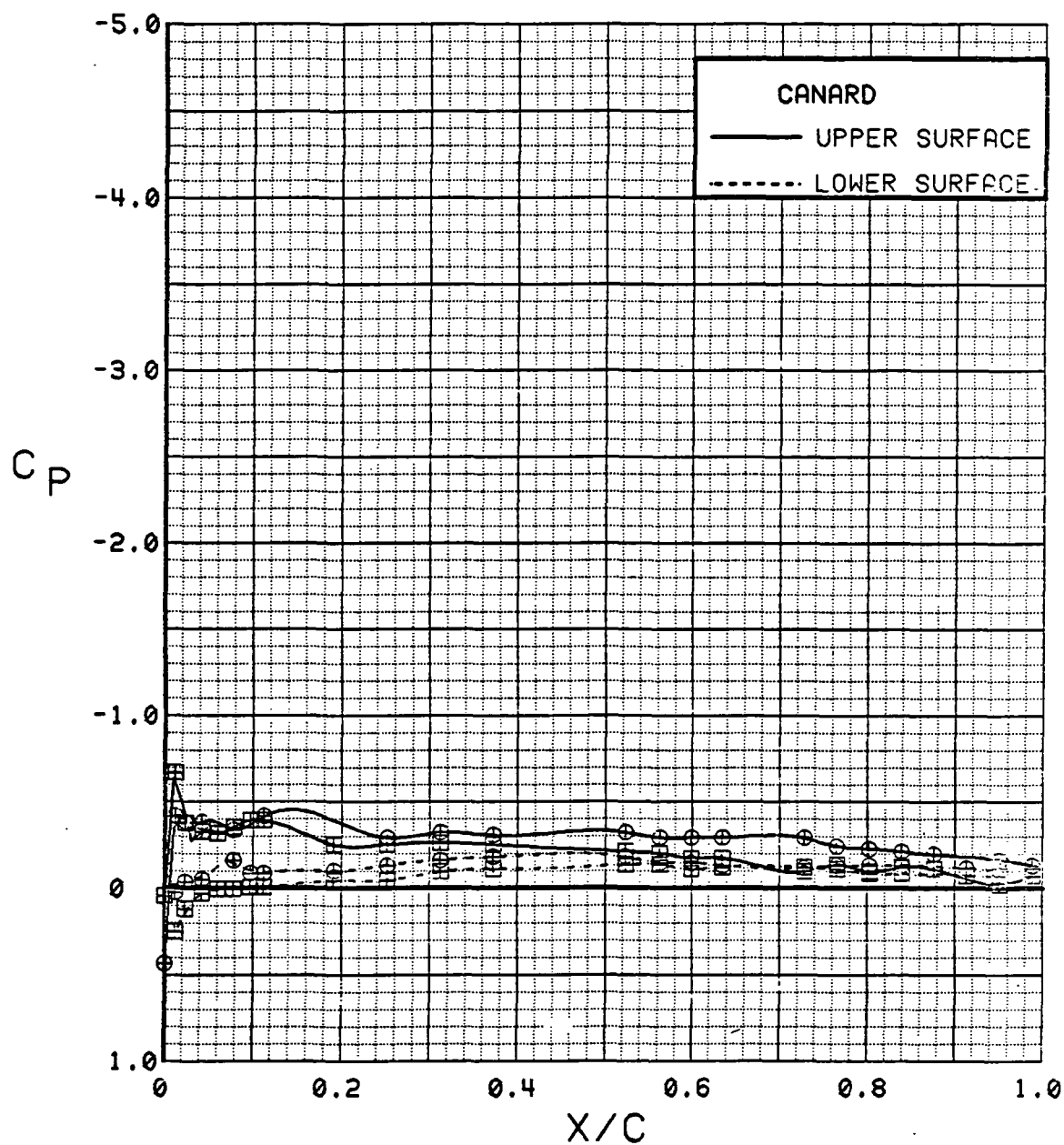


Figure 3.2.3-14 Canard Fore/Aft Comparison, Power on, Alpha = 0 deg

SYM	TEST	RUN	ALPHA	CT	ITEF	OTEF	CAN	SWB	CAN
⊕	537	32	4.5	0.91	30	30	0	OFF	FOR
⊞	543	6	4.5	0.94	30	30	0	OFF	AFT

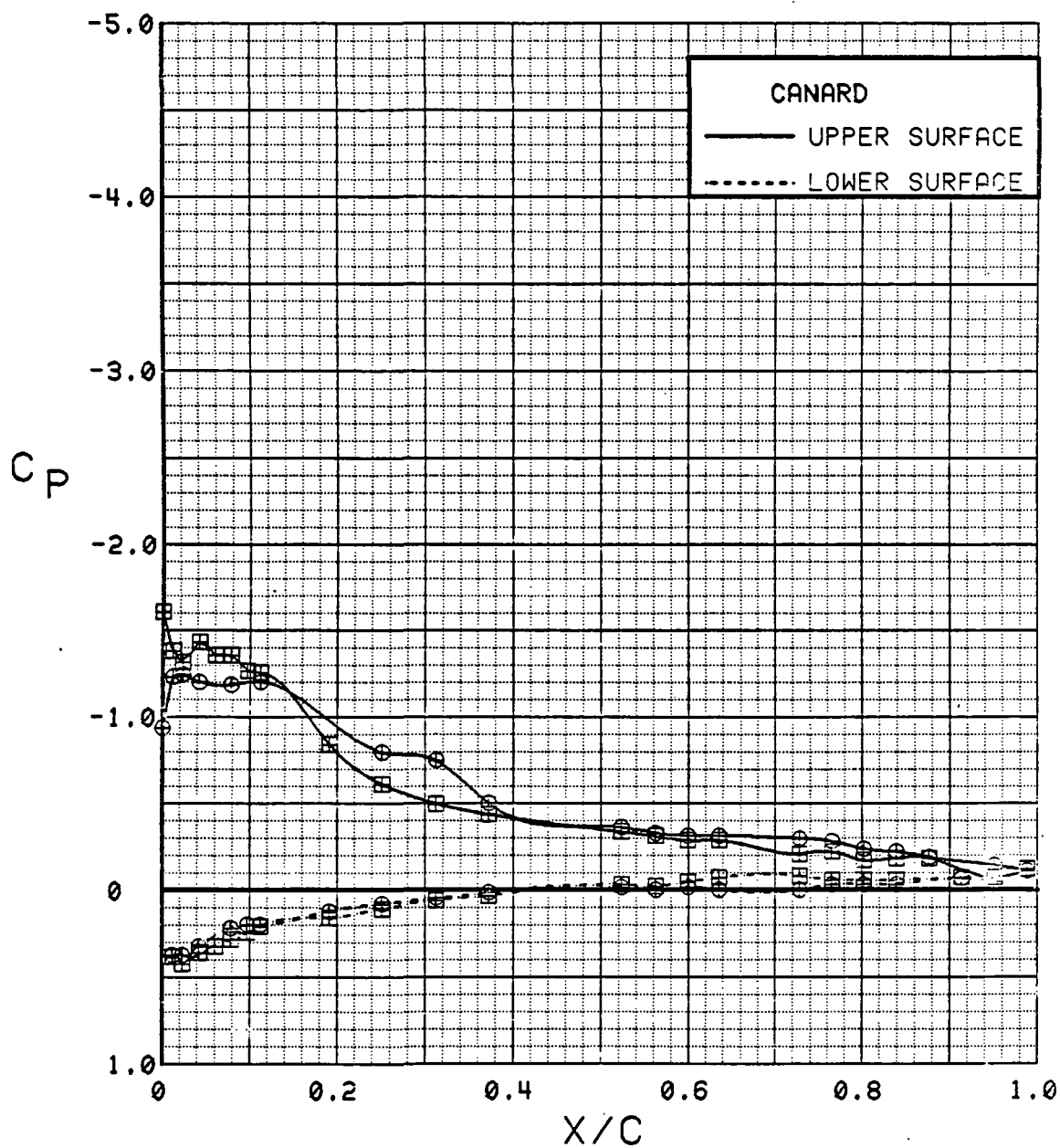


Figure 3.2.3-15 Canard Fore/Aft Comparison, Power on, Alpha = 4 deg

SYM	TEST	RUN	ALPHA	CT	ITEF	OTEF	CAN	SWB	CAN
⊕	537	32	8.6	0.90	30	30	0	OFF	FOR
⊞	543	6	8.6	0.91	30	30	0	OFF	AFT

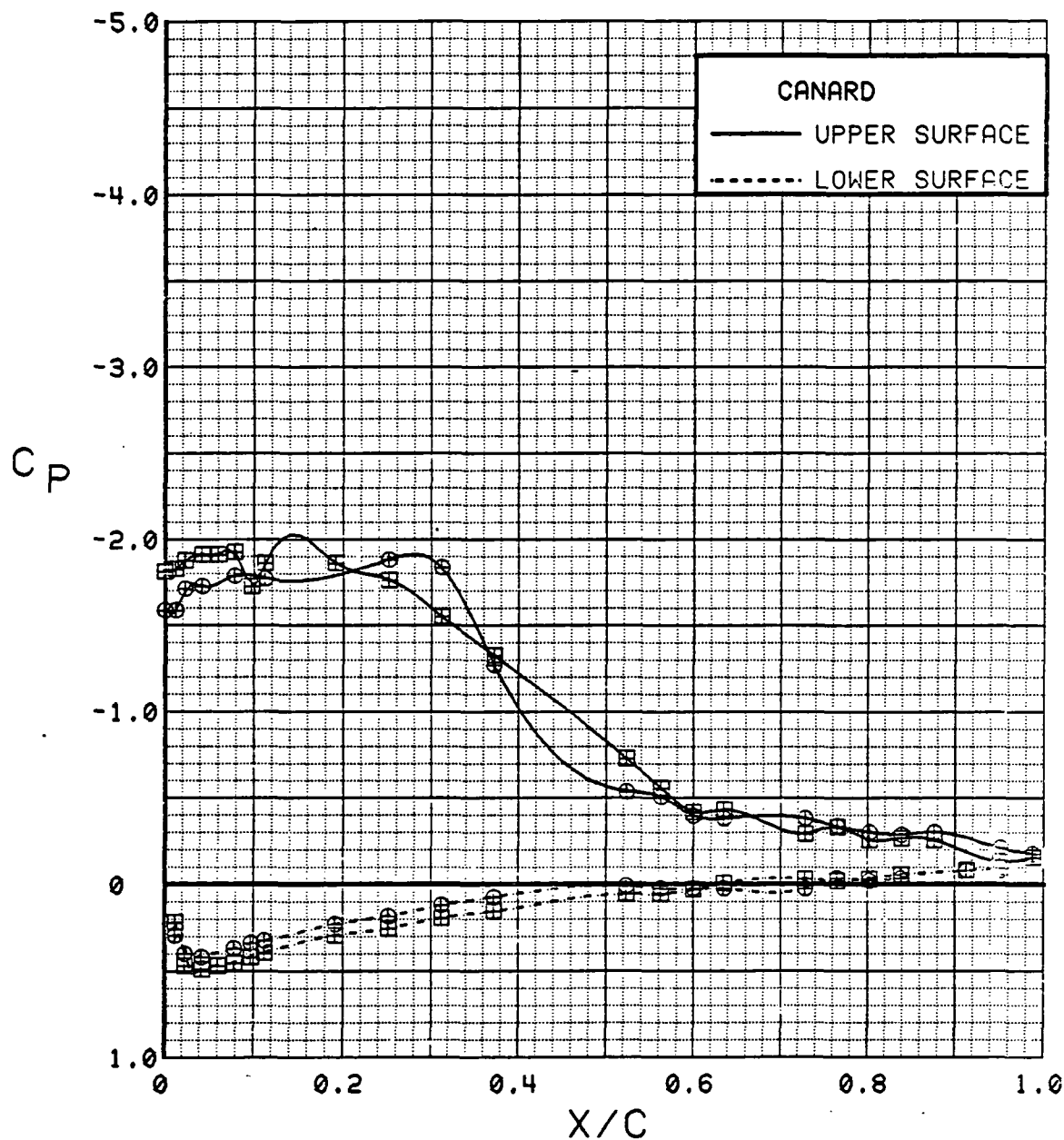


Figure 3.2.3-16 Canard Fore/Aft Comparison, Power on, Alpha = 8 deg



SYM	TEST	RUN	ALPHA	CT	ITEF	OTEF	CAN	SWB	CAN
⊕	537	32	12.8	0.92	30	30	0	OFF	FOR
⊞	543	6	12.8	0.92	30	30	0	OFF	AFT

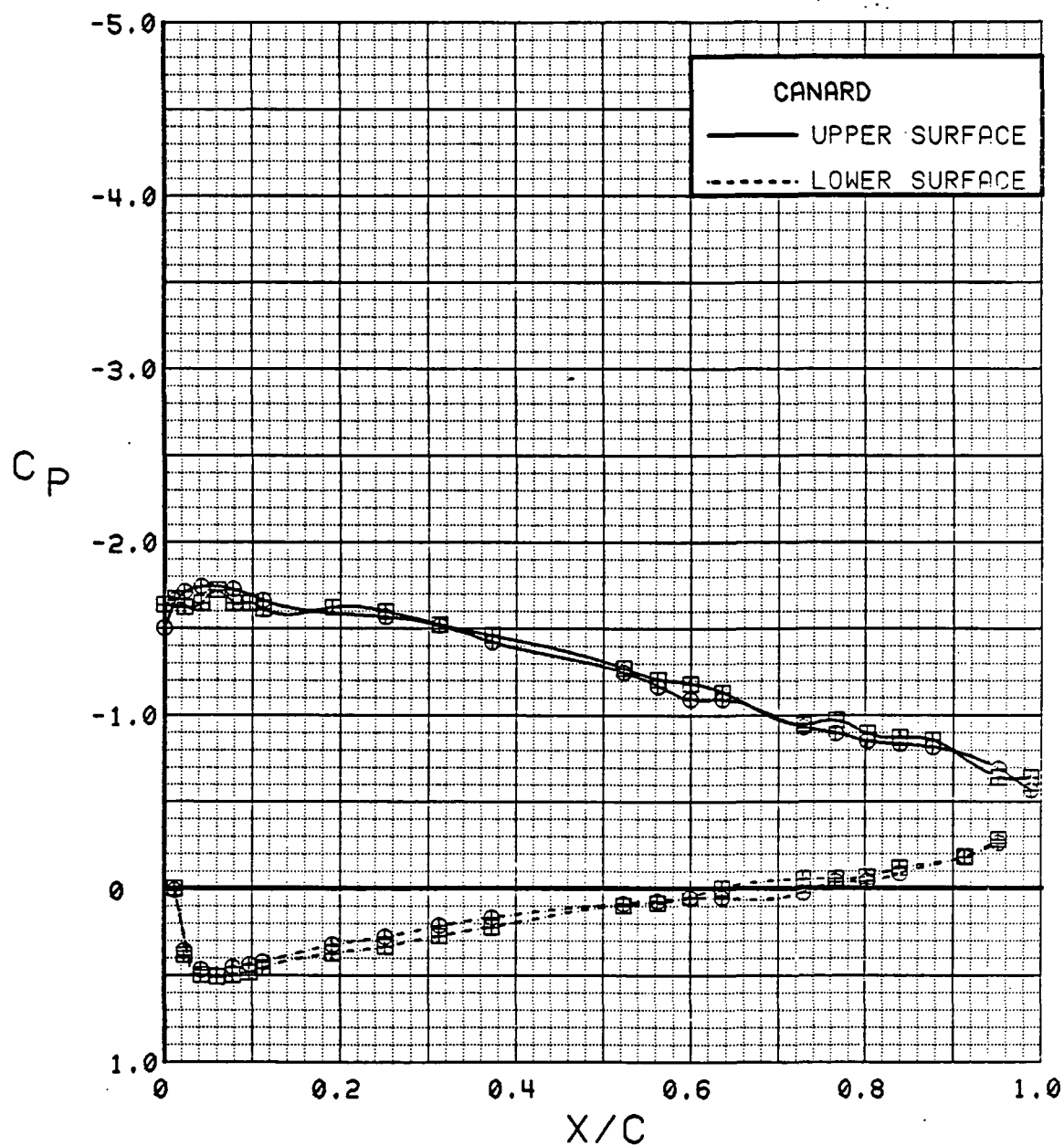


Figure 3.2.3-17 Canard Fore/Aft Comparison, Power on, Alpha = 12 deg

SYM	TEST	RUN	ALPHA	CT	ITEF	OTEF	CAN	SWB	CAN
⊕	537	32	16.8	0.92	30	30	0	OFF	FOR
⊞	543	6	16.9	0.92	30	30	0	OFF	AFT

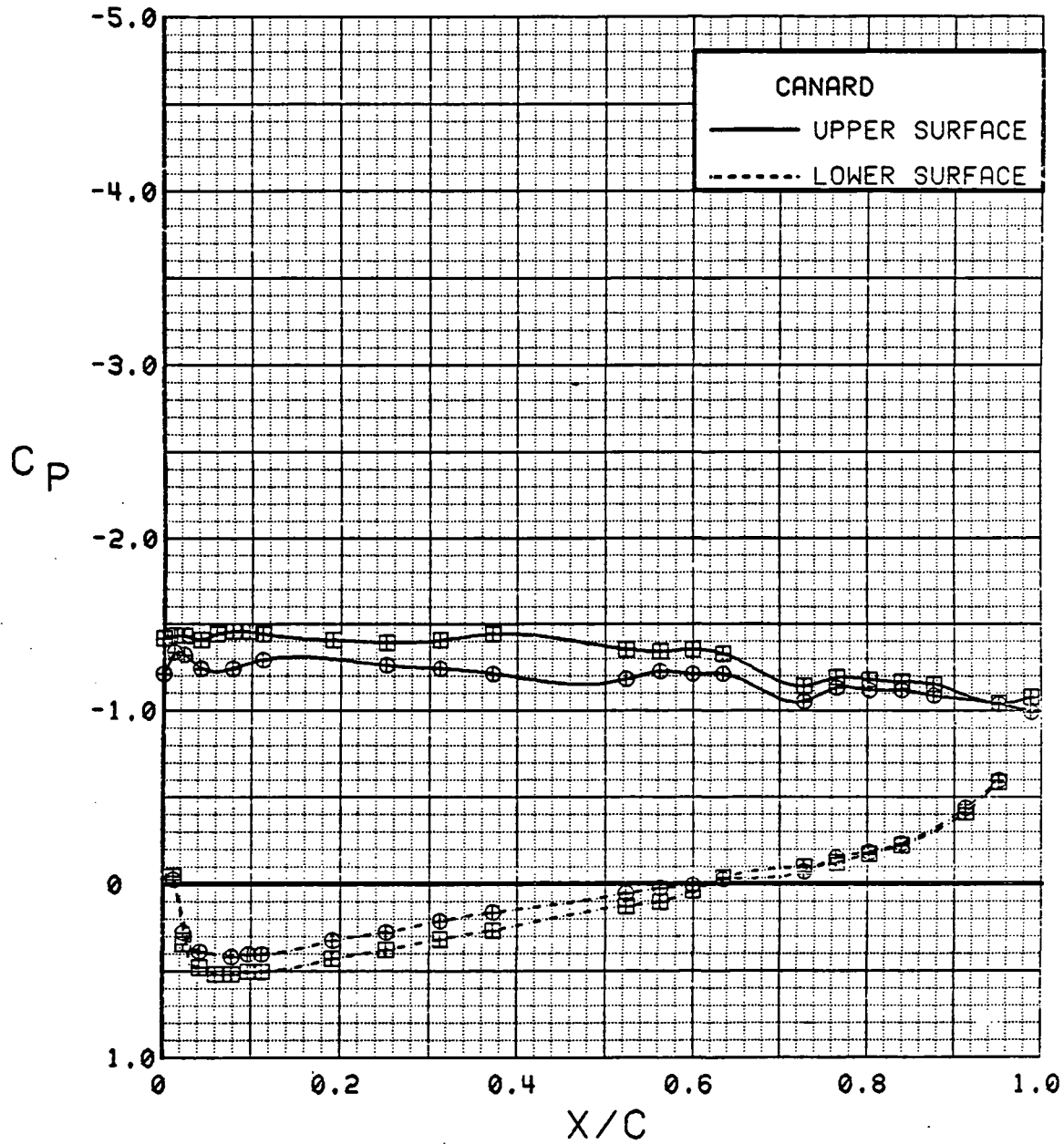


Figure 3.2.3-18 Canard Fore/Aft Comparison, Power on, Alpha = 16 deg

SYM	TEST	RUN	ALPHA	CT	ITEF	OTEF	CAN	SWB	CAN
⊕	537	32	20.9	0.90	30	30	0	OFF	FOR
⊞	543	6	21.0	0.93	30	30	0	OFF	AFT

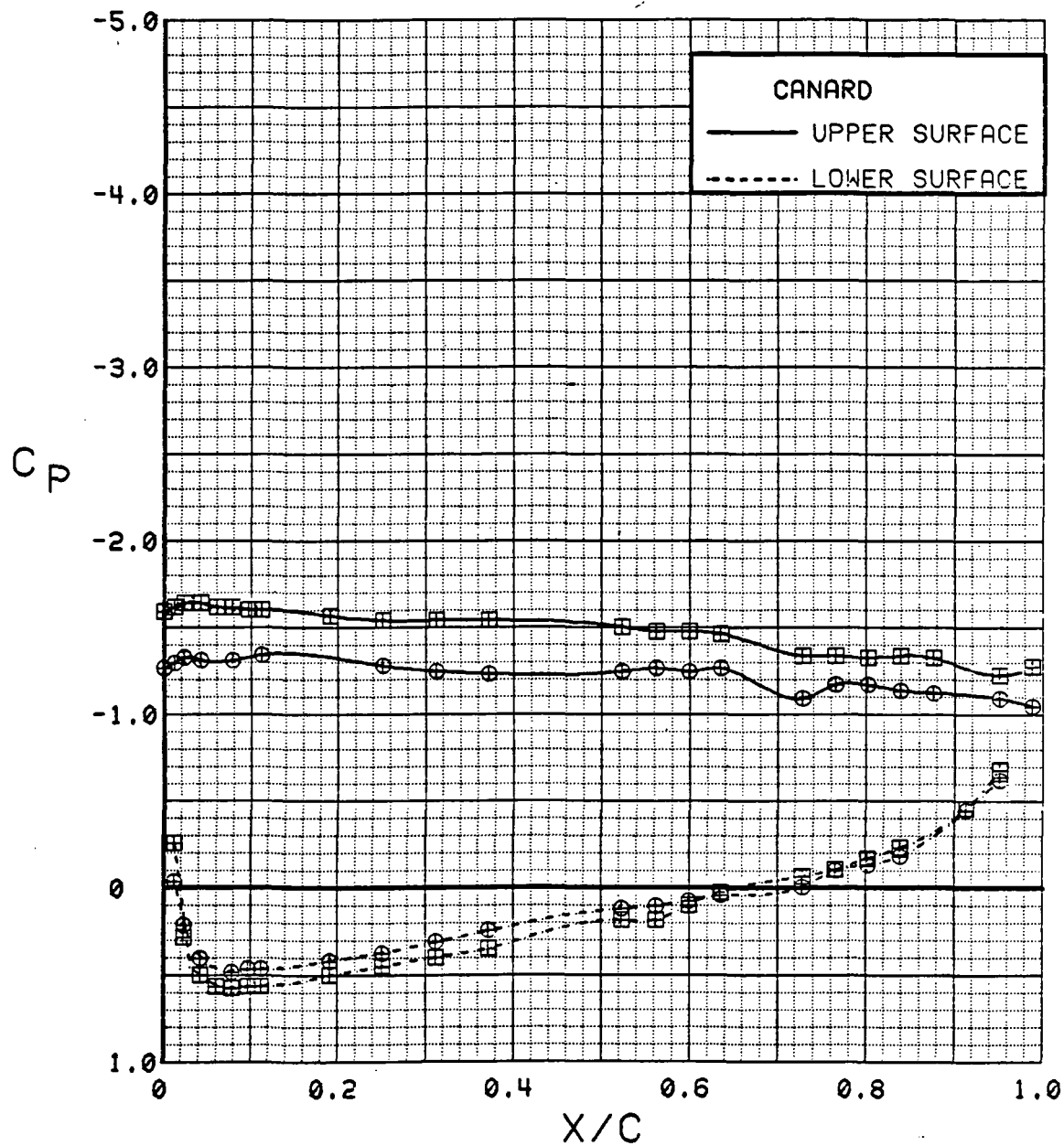
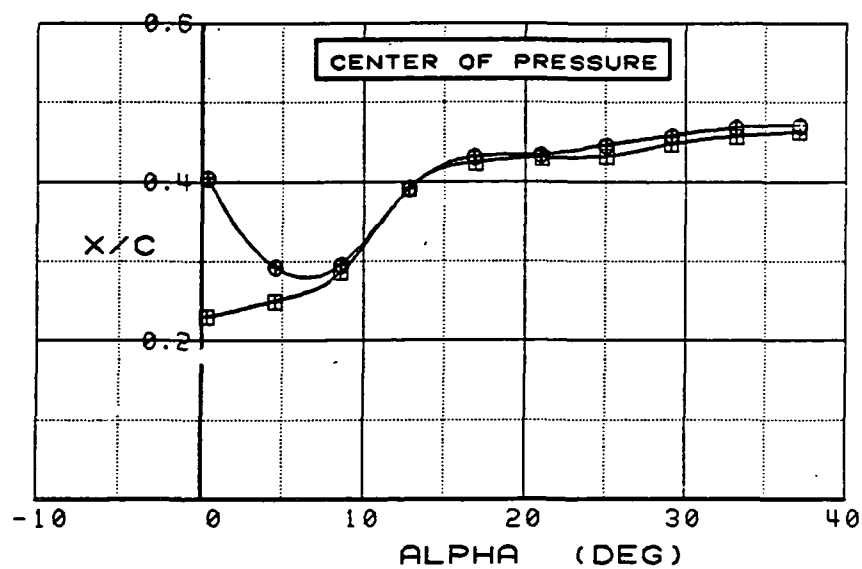
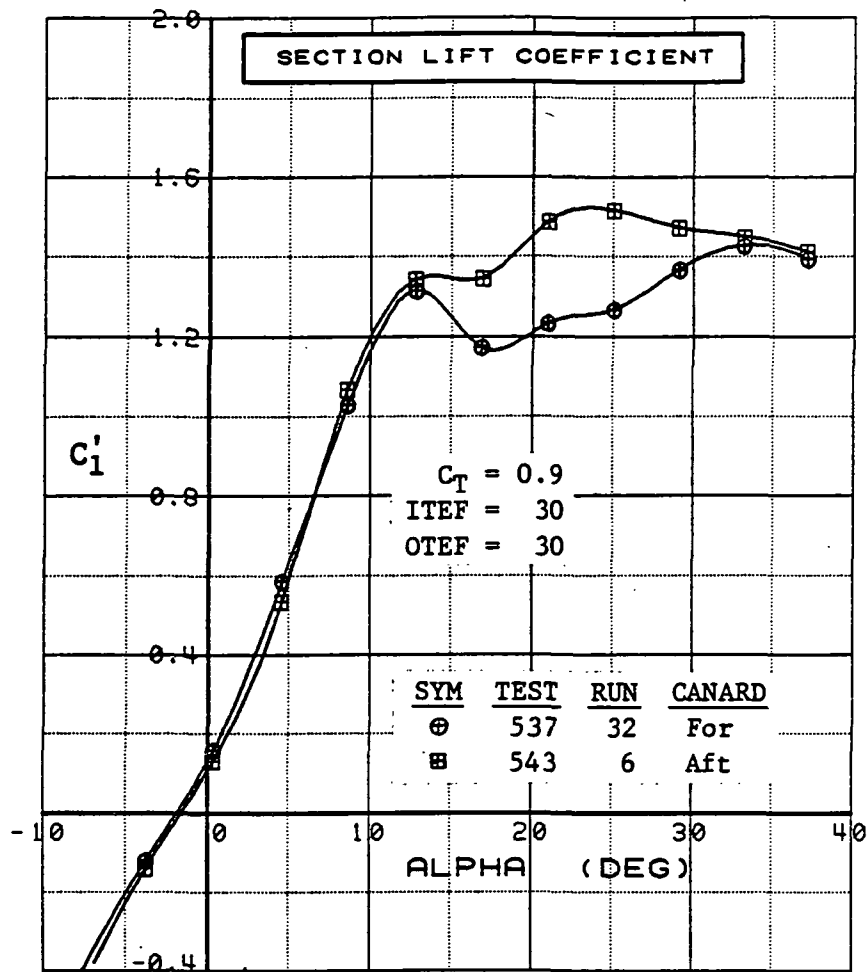


Figure 3.2.3-19 Canard Fore/Aft Comparison, Power on, Alpha = 20 deg

## CANARD



, Figure 3.2.3-20 Canard Fore/Aft Comparison, Integrated Section Properties

SYM	TEST	RUN	ALPHA	CT	ITEF	OTEF	CAN	SWB	CAN
⊕	537	12	0.3	0.00	30	30	0	OFF	FOR
⊞	543	11	0.3	0.00	30	30	0	OFF	AFT

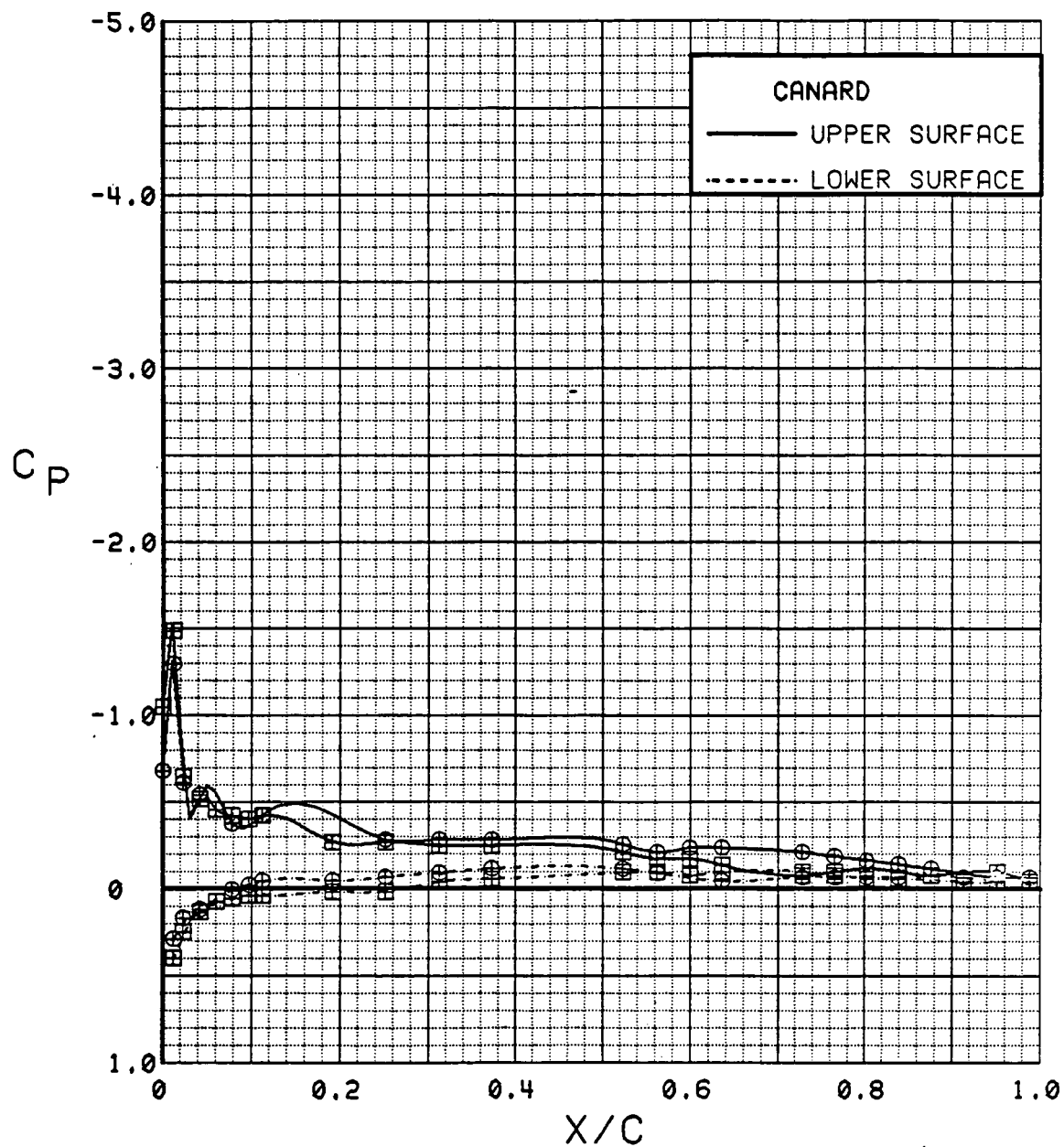


Figure 3.2.3-21 Canard Fore/Aft Comparison, Power off, Alpha = 0 deg

SYM	TEST	RUN	ALPHA	CT	ITEF	OTEF	CAN	SWB	CAN
⊕	537	12	4.4	0.00	30	30	0	OFF	FOR
⊞	543	11	4.4	0.00	30	30	0	OFF	AFT

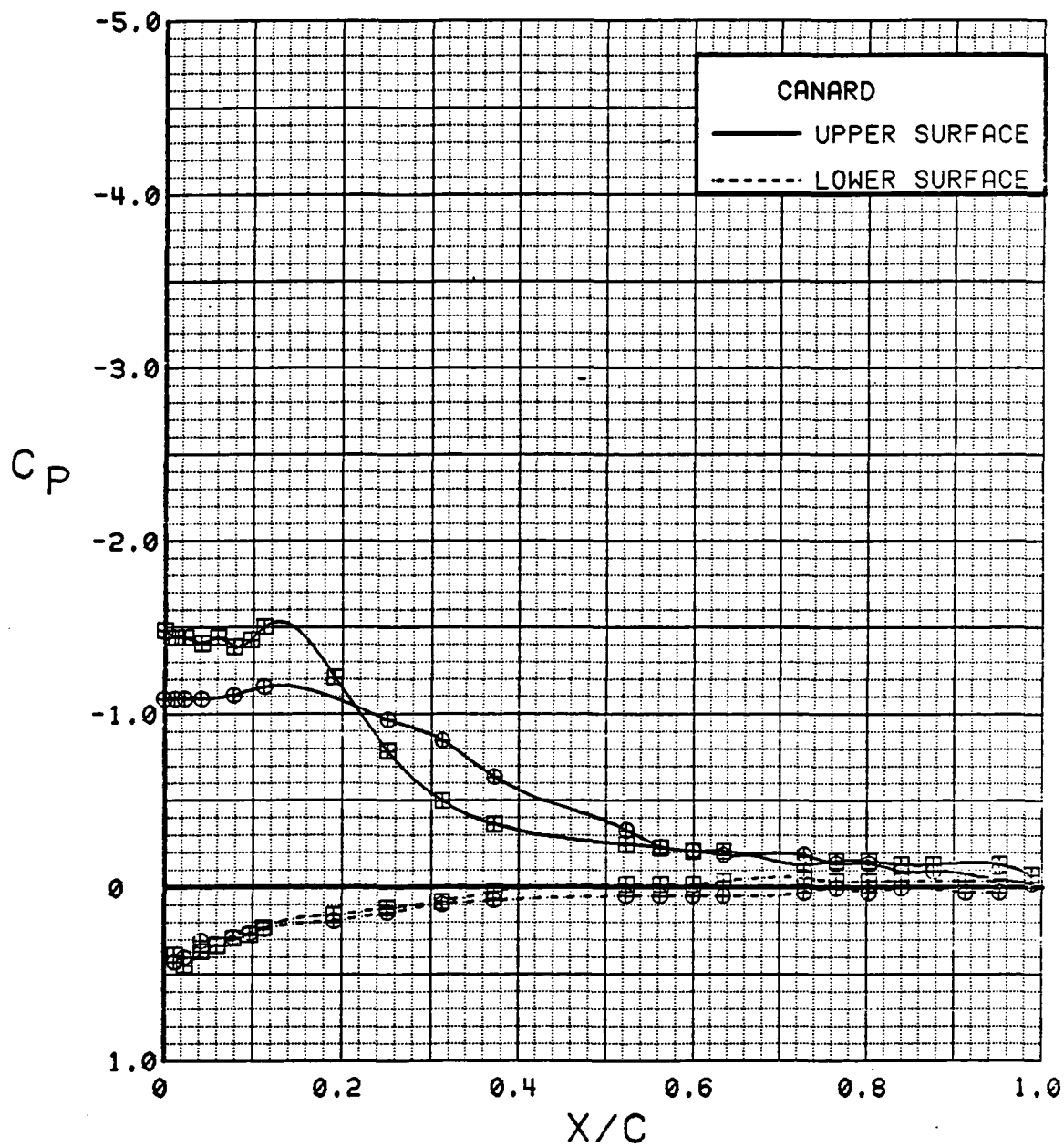


Figure 3.2.3-22 Canard Fore/Aft Comparison, Power off, Alpha = 4 deg

SYM	TEST	RUN	ALPHA	CT	ITEF	OTEF	CAN	SWB	CAN
⊕	537	12	8.5	0.00	30	30	0	OFF	FOR
⊞	543	11	8.5	0.00	30	30	0	OFF	AFT

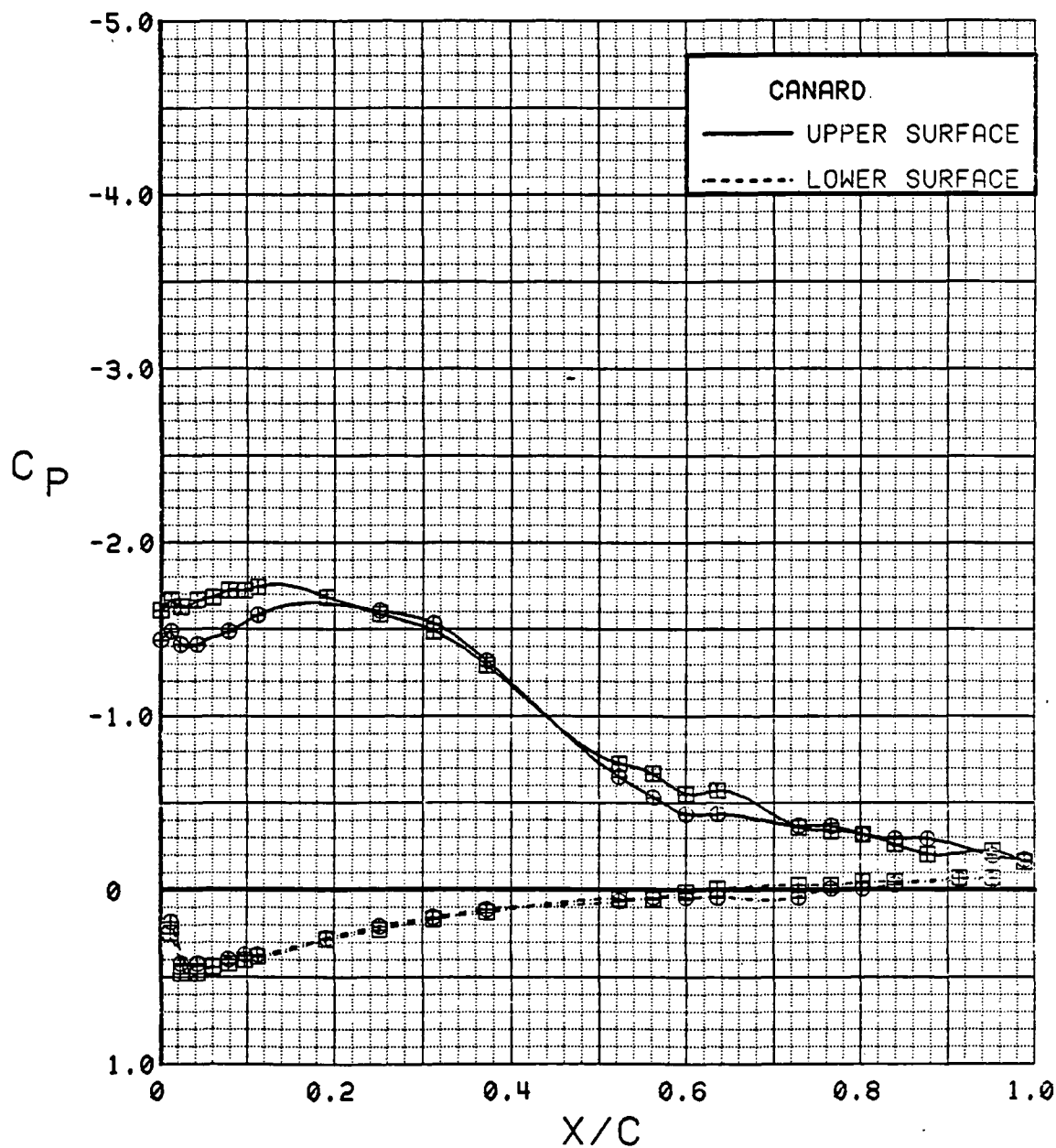


Figure 3.2.3-23 Canard Fore/Aft Comparison, Power off, Alpha = 8 deg

SYM	TEST	RUN	ALPHA	CT	ITEF	OTEF	CAN	SWB	CAN
⊕	537	12	12.7	0.00	30	30	0	OFF	FOR
⊞	543	11	12.7	0.00	30	30	0	OFF	AFT

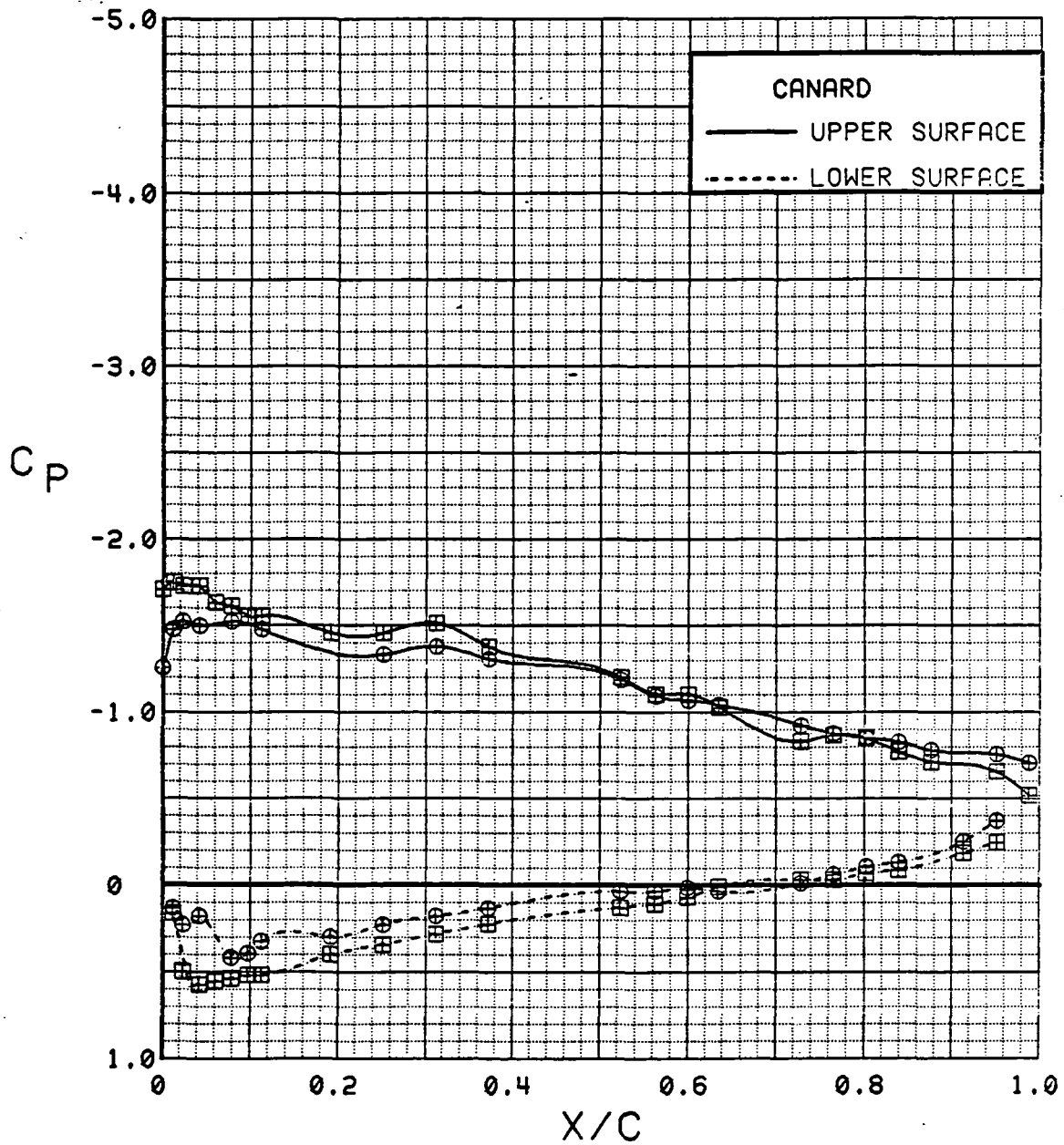


Figure 3.2.3-24 Canard Fore/Aft Comparison, Power off, Alpha = 12 deg



SYM	TEST	RUN	ALPHA	CT	ITEF	OTEF	CAN	SWB	CAN
⊕	537	12	16.7	0.00	30	30	0	OFF	FOR
⊞	543	11	16.8	0.00	30	30	0	OFF	AFT

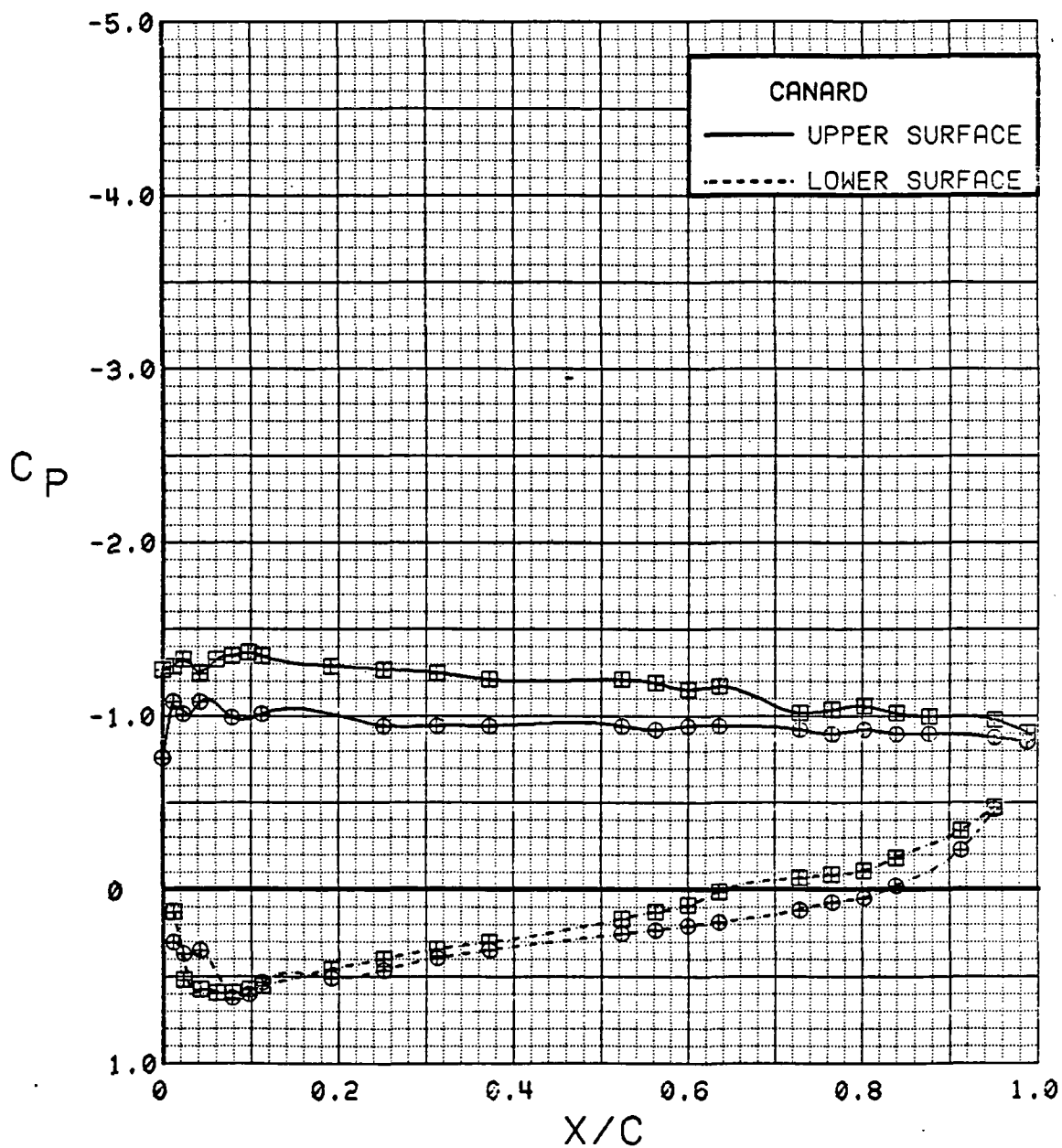


Figure 3.2.3-25 Canard Fore/Aft Comparison, Power off, Alpha = 16 deg

SYM	TEST	RUN	ALPHA	CT	ITEF	OTEF	CAN	SWB	CAN
⊕	537	12	20.8	0.00	30	30	0	OFF	FOR
⊞	543	11	20.8	0.00	30	30	0	OFF	AFT

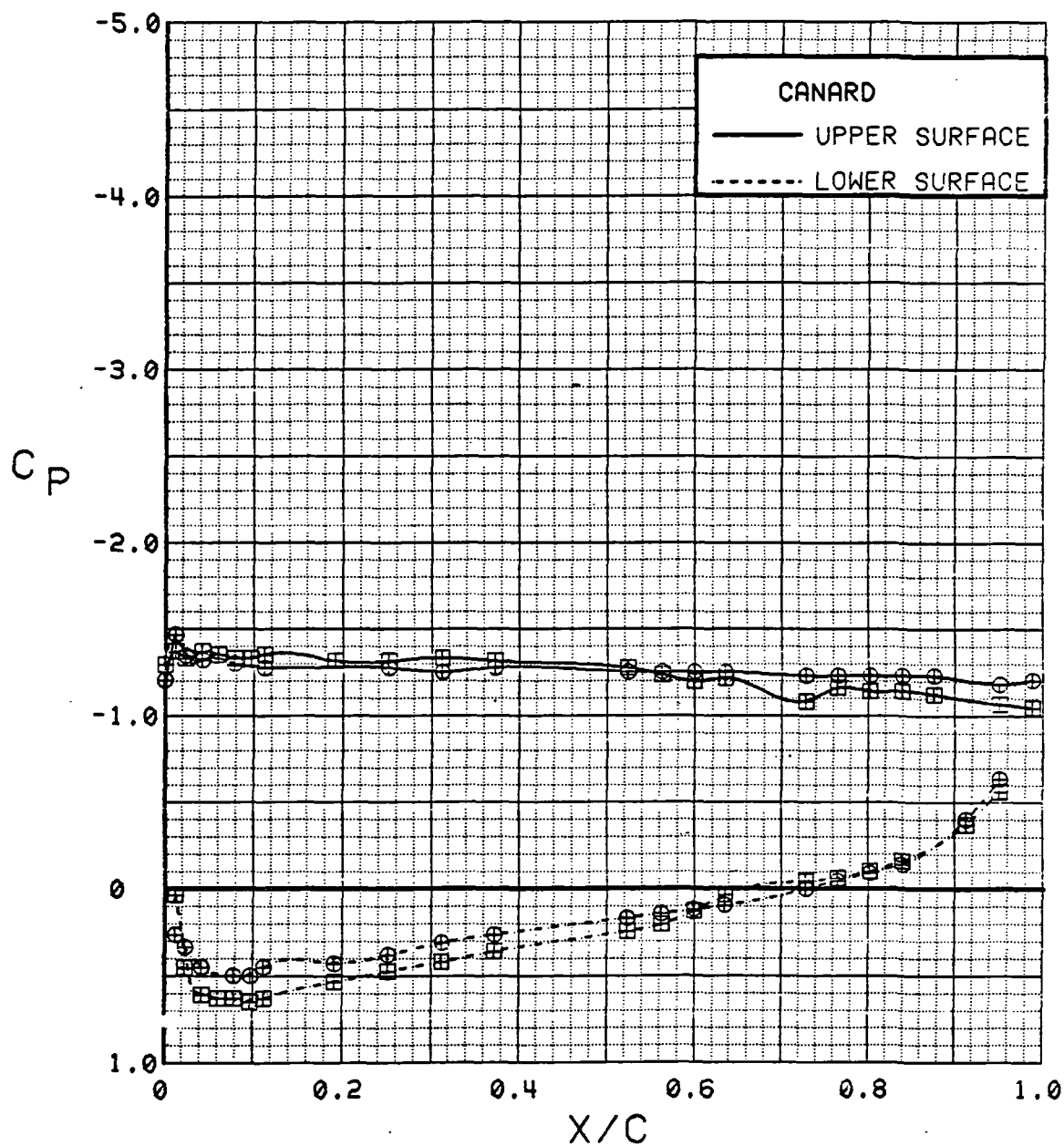


Figure 3.2.3-26 Canard Fore/Aft Comparison, Power off, Alpha = 20 deg

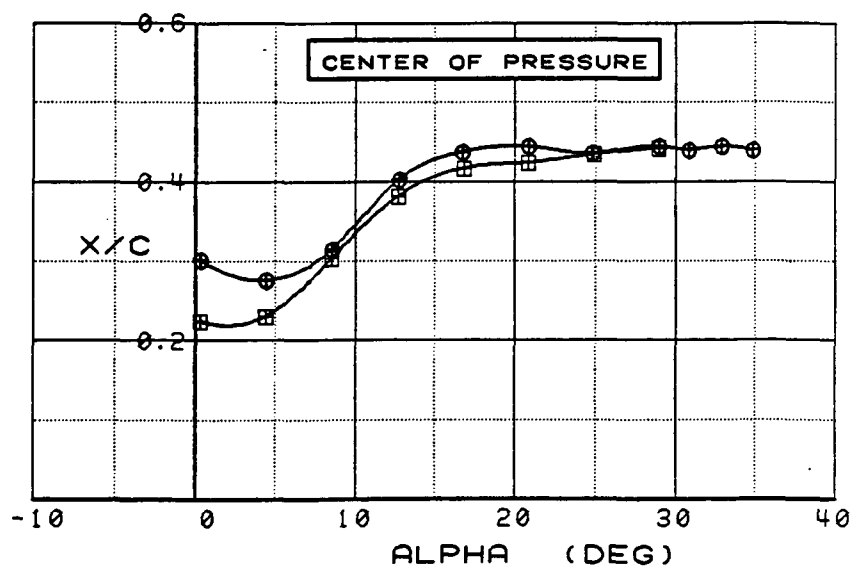
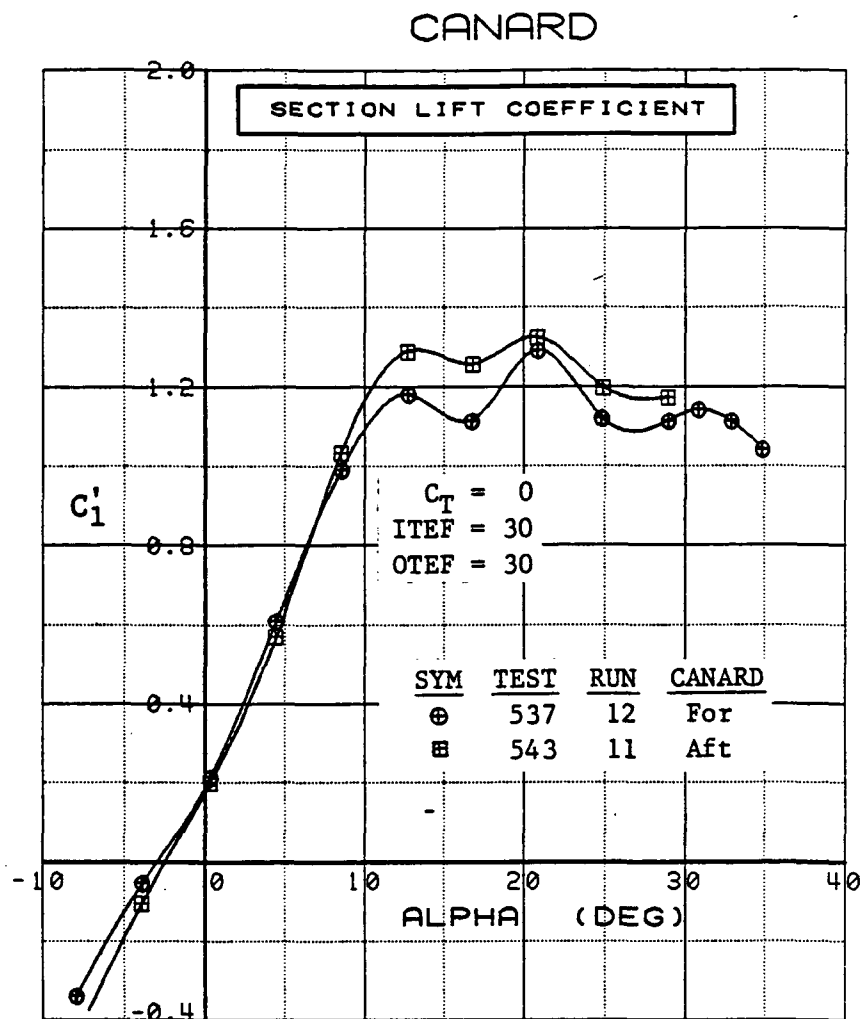


Figure 3.2.3-27 Canard Fore/Aft Comparison, Power off, Integrated Section Properties

SYM	TEST	RUN	ALPHA	CT	ITEF	OTEF	CAN	SWB
⊕	543	88	4.1	0.00	-20	-20	0	OFF
⊞	543	76	4.2	0.00	-10	0	0	OFF
△	543	63	4.2	0.00	0	0	0	OFF
◆	543	83	4.3	0.00	10	10	0	OFF
*	543	69	4.3	0.00	20	20	0	OFF
+	543	11	4.4	0.00	30	30	0	OFF

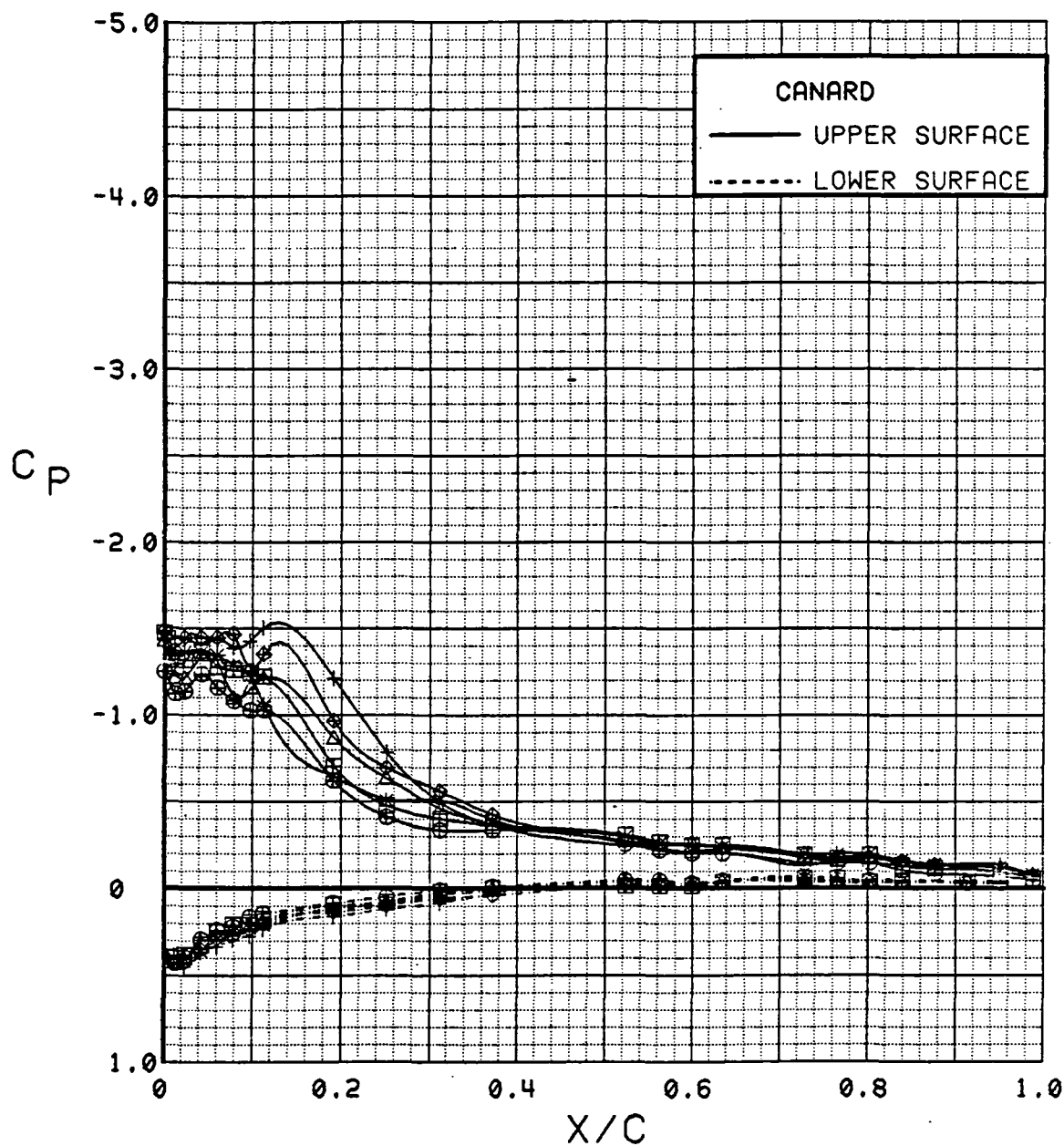


Figure 3.2.3-28 Wing Trailing-Edge Flap Effects on Canard,  
Alpha = 4 deg

SYM	TEST	RUN	ALPHA	CT	ITEF	OTEF	CAN	SWB
⊕	543	88	8.2	0.00	-20	-20	0	OFF
⊞	543	76	8.3	0.00	-10	0	0	OFF
△	543	63	8.3	0.00	0	0	0	OFF
⬠	543	83	8.4	0.00	10	10	0	OFF
*	543	69	8.5	0.00	20	20	0	OFF
+	543	11	8.5	0.00	30	30	0	OFF

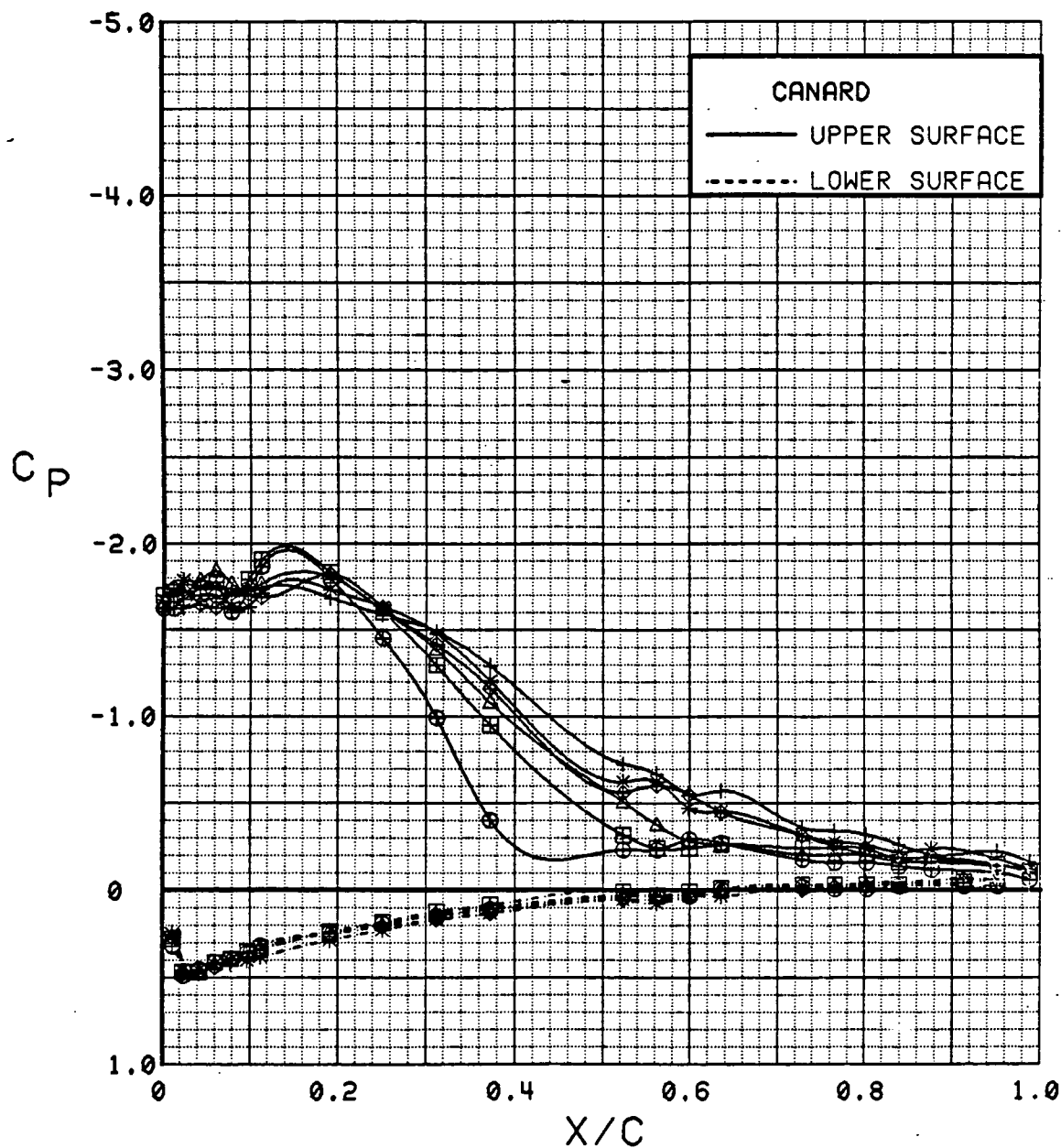


Figure 3.2.3-29

Wing Trailing-Edge Flap Effects on Canard,  
Alpha = 8 deg

SYM	TEST	RUN	ALPHA	CT	ITEF	OTEF	CAN	SWB
⊕	543	88	12.3	0.00	-20	-20	0	OFF
⊞	543	76	12.4	0.00	-10	0	0	OFF
△	543	63	12.5	0.00	0	0	0	OFF
⊕	543	69	12.6	0.00	20	20	0	OFF
*	543	11	12.7	0.00	30	30	0	OFF

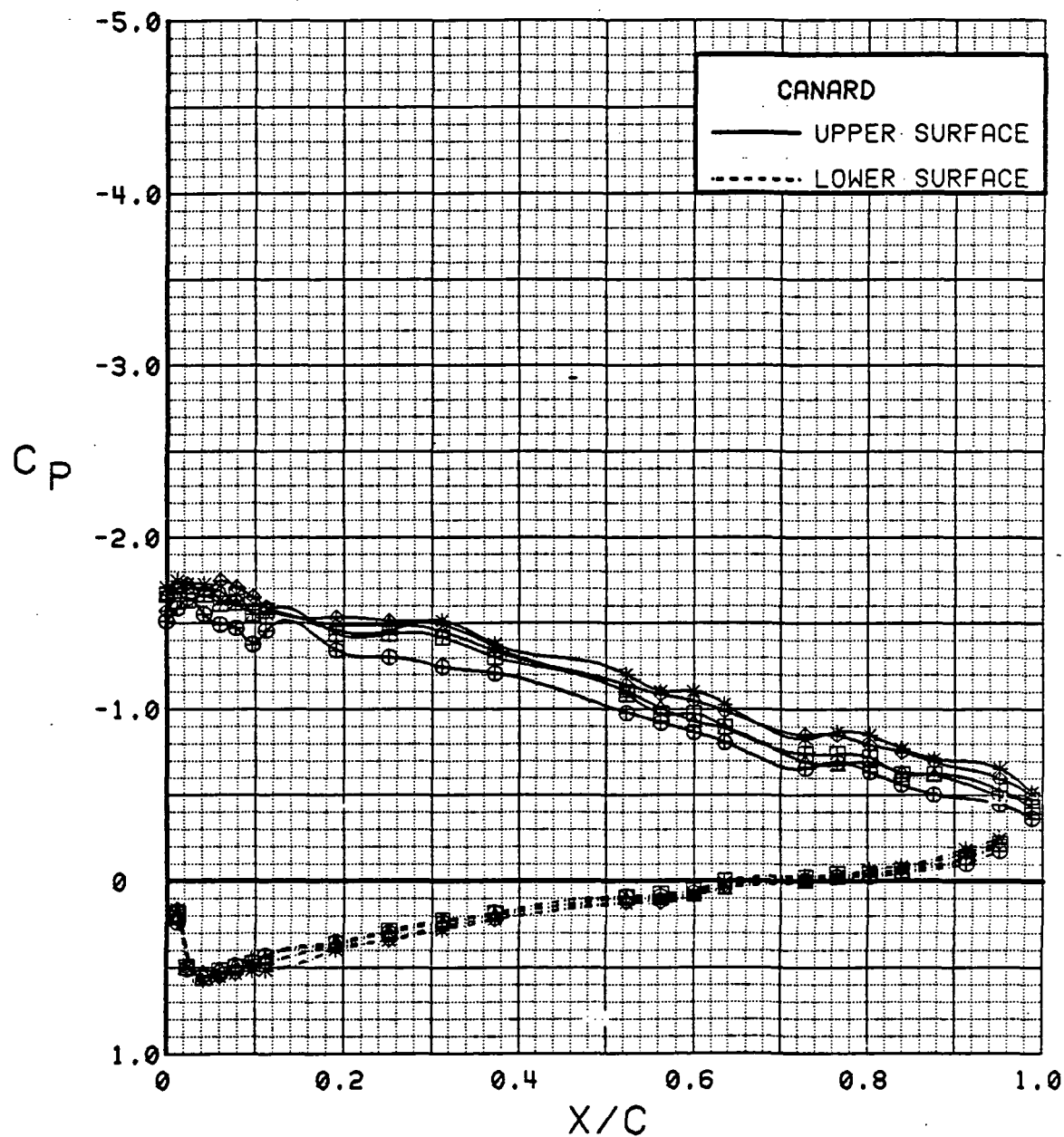


Figure 3.2.3-30 Wing Trailing-Edge Flap Effects on Canard,  
Alpha = 12 deg

SYM	TEST	RUN	ALPHA	CT	ITEF	OTEF	CAN	SWB
⊕	543	88	16.5	0.00	-20	-20	0	OFF
⊞	543	76	16.5	0.00	-10	0	0	OFF
△	543	63	16.6	0.00	0	0	0	OFF
◆	543	83	16.7	0.00	10	10	0	OFF
*	543	69	16.7	0.00	20	20	0	OFF
+	543	11	16.8	0.00	30	30	0	OFF

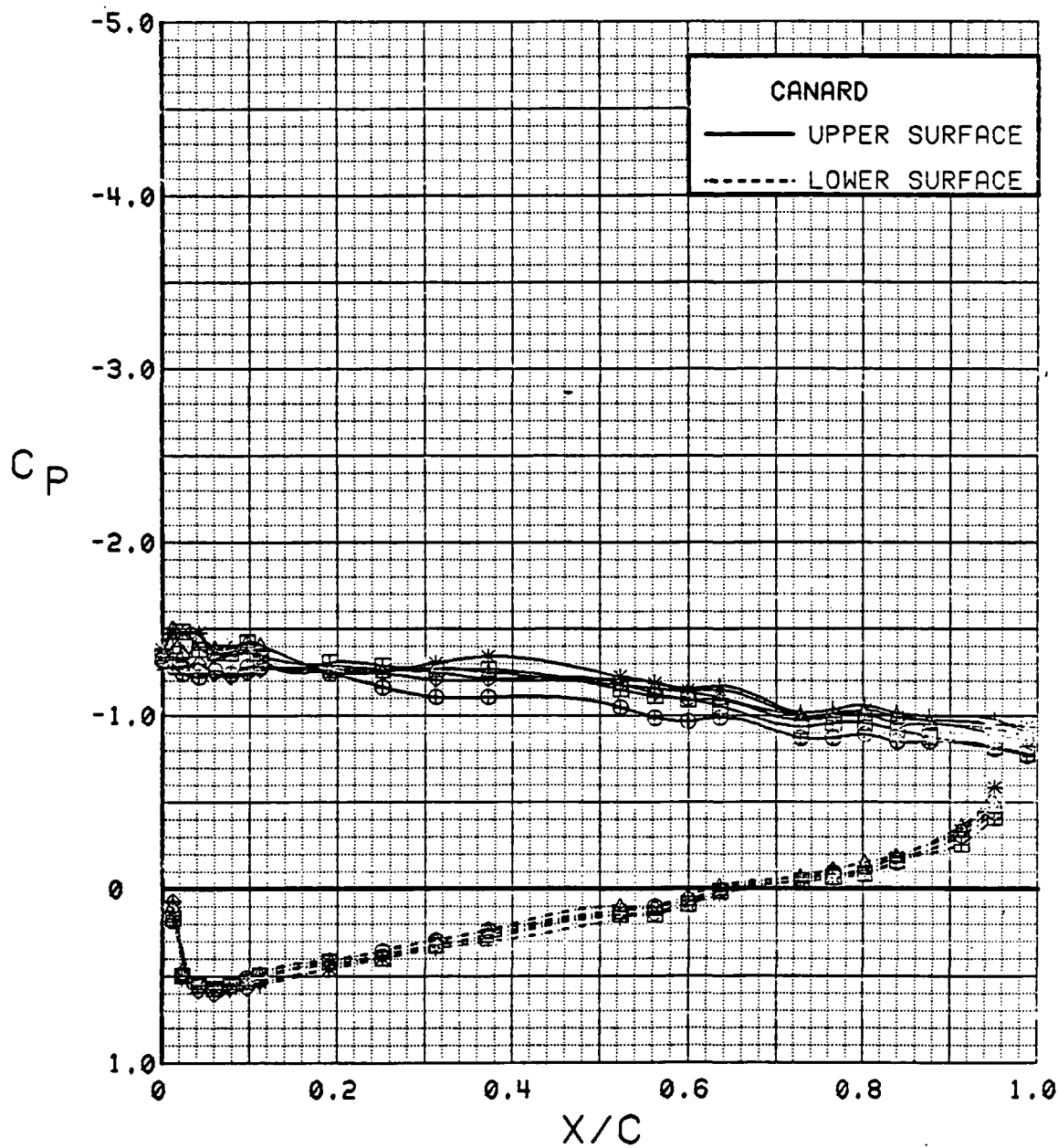


Figure 3.2.3-31 Wing Trailing-Edge Flap Effects on Canard,  
Alpha = 16 deg

SYM	TEST	RUN	ALPHA	CT	ITEF	OTEF	CAN	SWB
⊕	543	88	20.6	0.00	-20	-20	0	OFF
⊞	543	76	20.6	0.00	-10	0	0	OFF
△	543	63	20.7	0.00	0	0	0	OFF
◆	543	69	20.8	0.00	20	20	0	OFF
*	543	11	20.8	0.00	30	30	0	OFF

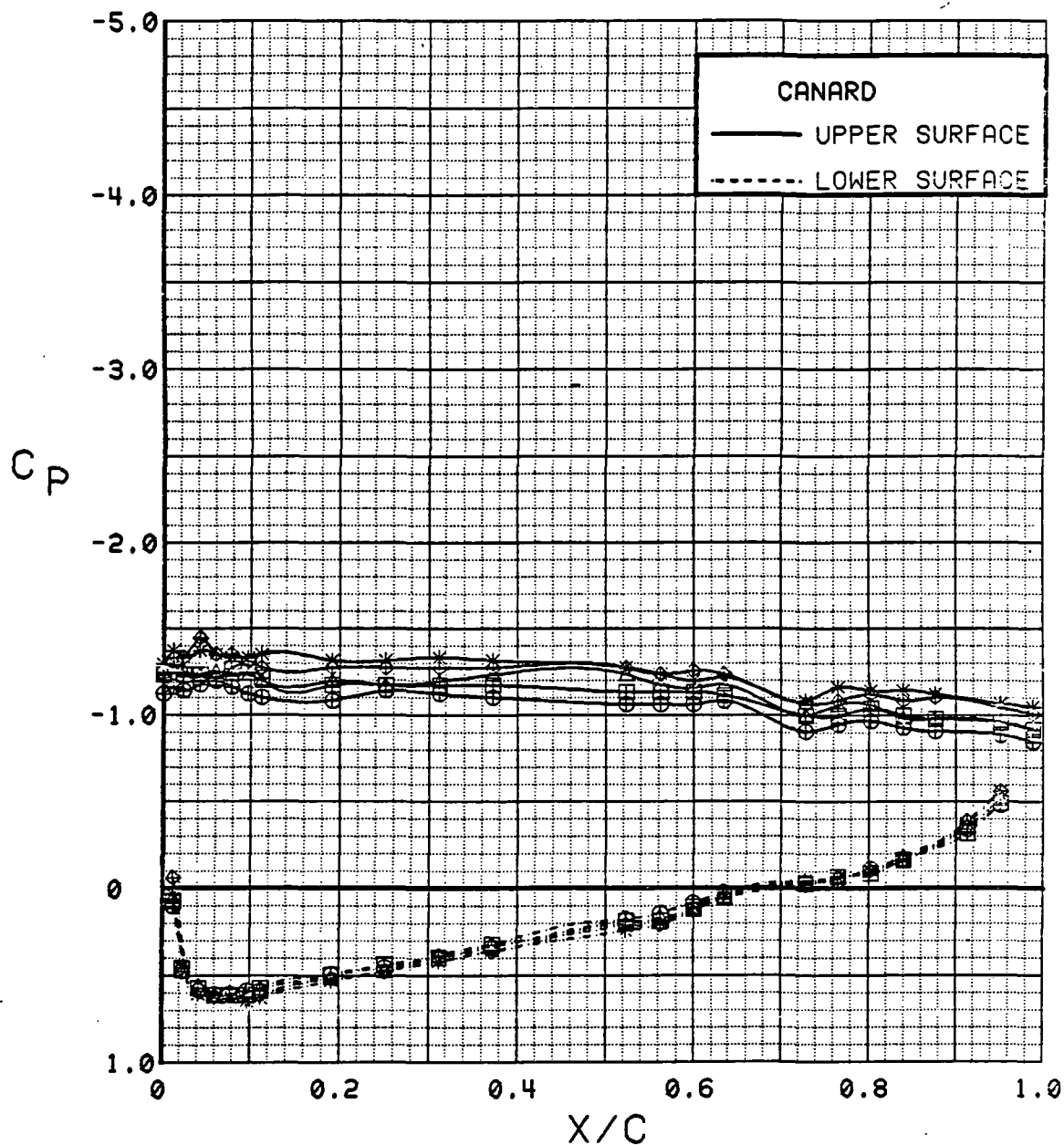


Figure 3.2.3-32 Wing Trailing-Edge Flap Effects on Canard,  
Alpha = 20 deg



## CANARD

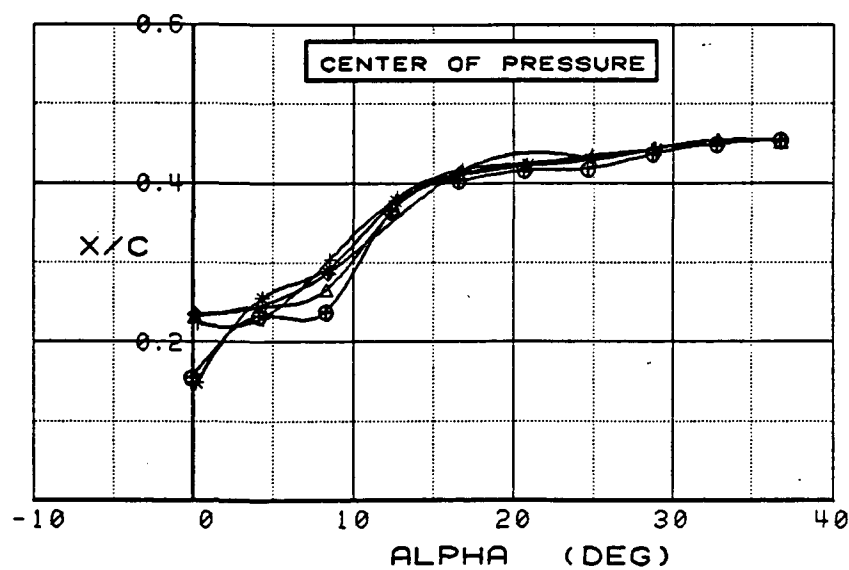
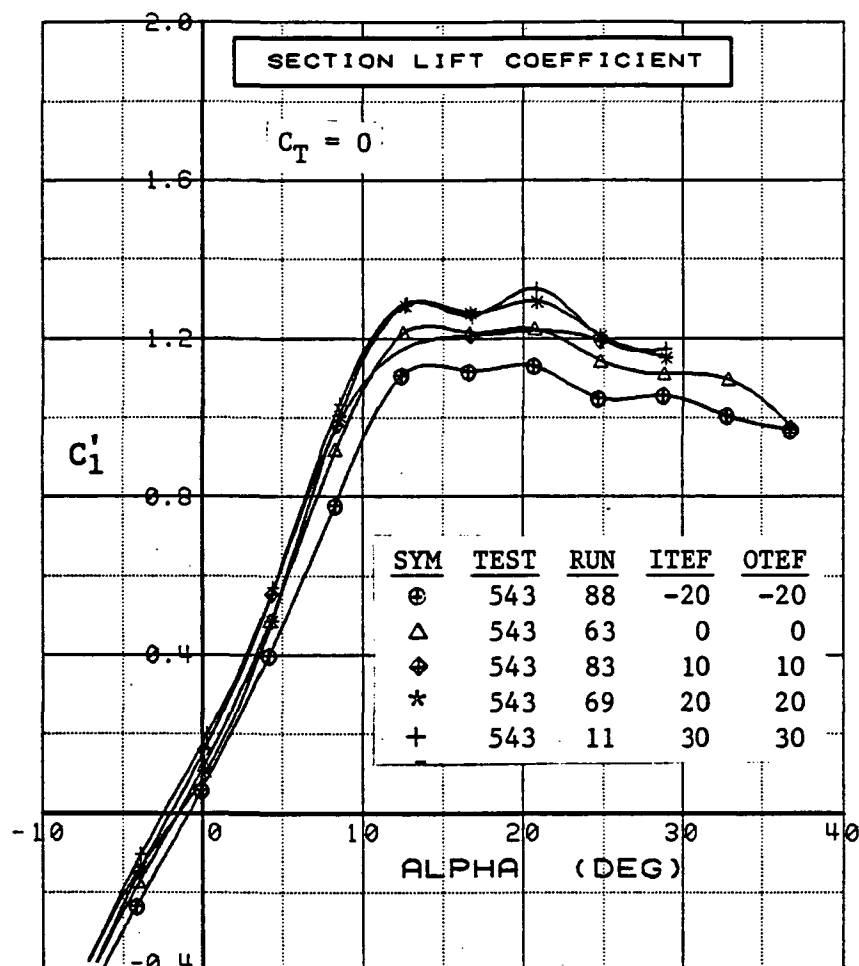


Figure 3.2.3-33 Wing Trailing-Edge Flap Effects on Canard, Integrated Section Properties

SYM	TEST	RUN	ALPHA	CT	ITEF	OTEF	CAN	SWB	q
⊕	537	17	0.2	0.00	30	30	0	OFF	7
⊞	537	12	0.3	0.00	30	30	0	OFF	15
Δ	537	18	0.3	0.00	30	30	0	OFF	40

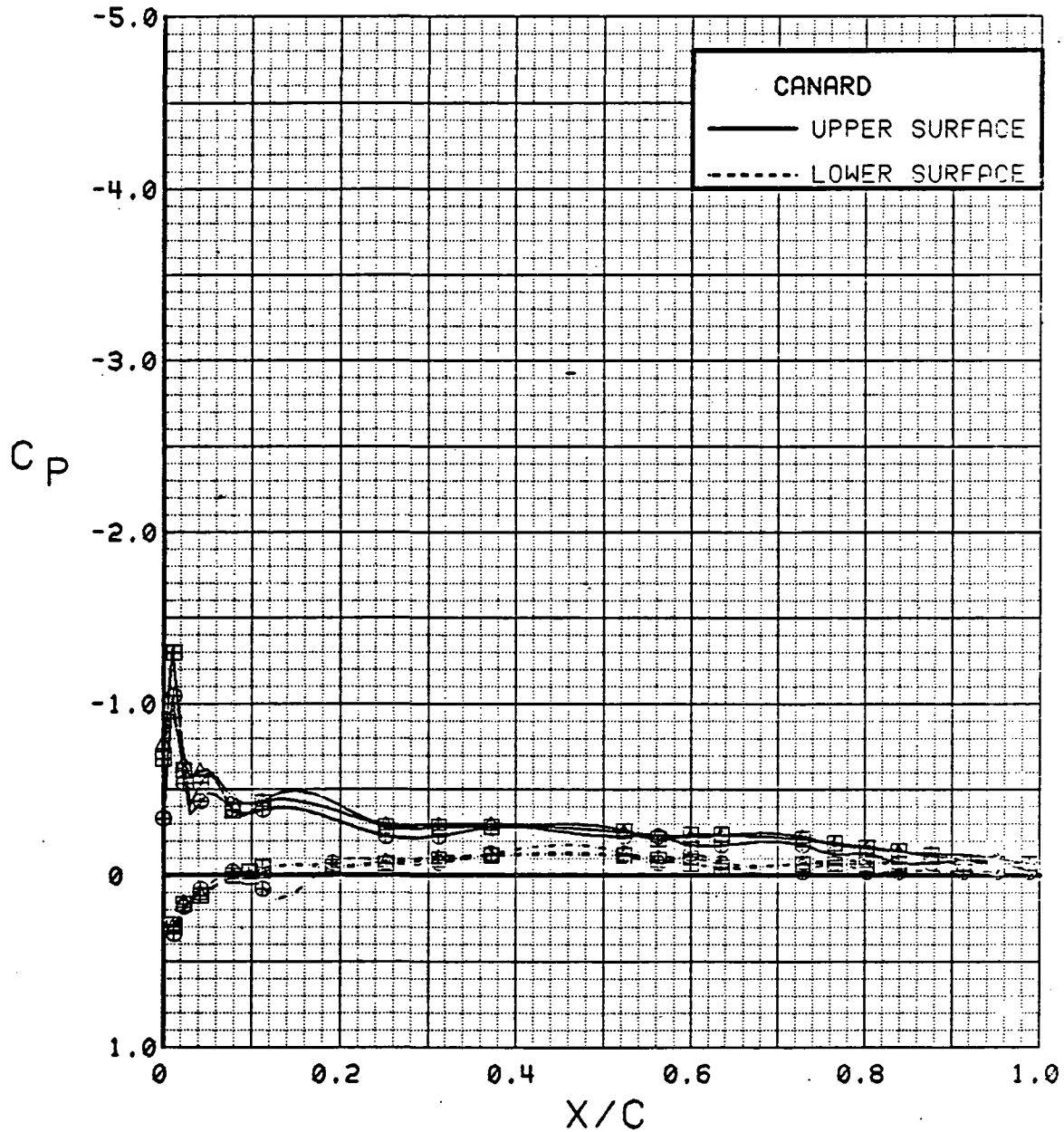


Figure 3.2.3-34 Dynamic Pressure Effects, Alpha = 0 deg

SYM	TEST	RUN	ALPHA	CT	ITEF	OTEF	CAN	SWB	q
⊕	537	17	4.4	0.00	30	30	0	OFF	7
⊞	537	12	4.4	0.00	30	30	0	OFF	15
Δ	537	18	4.4	0.00	30	30	0	OFF	40

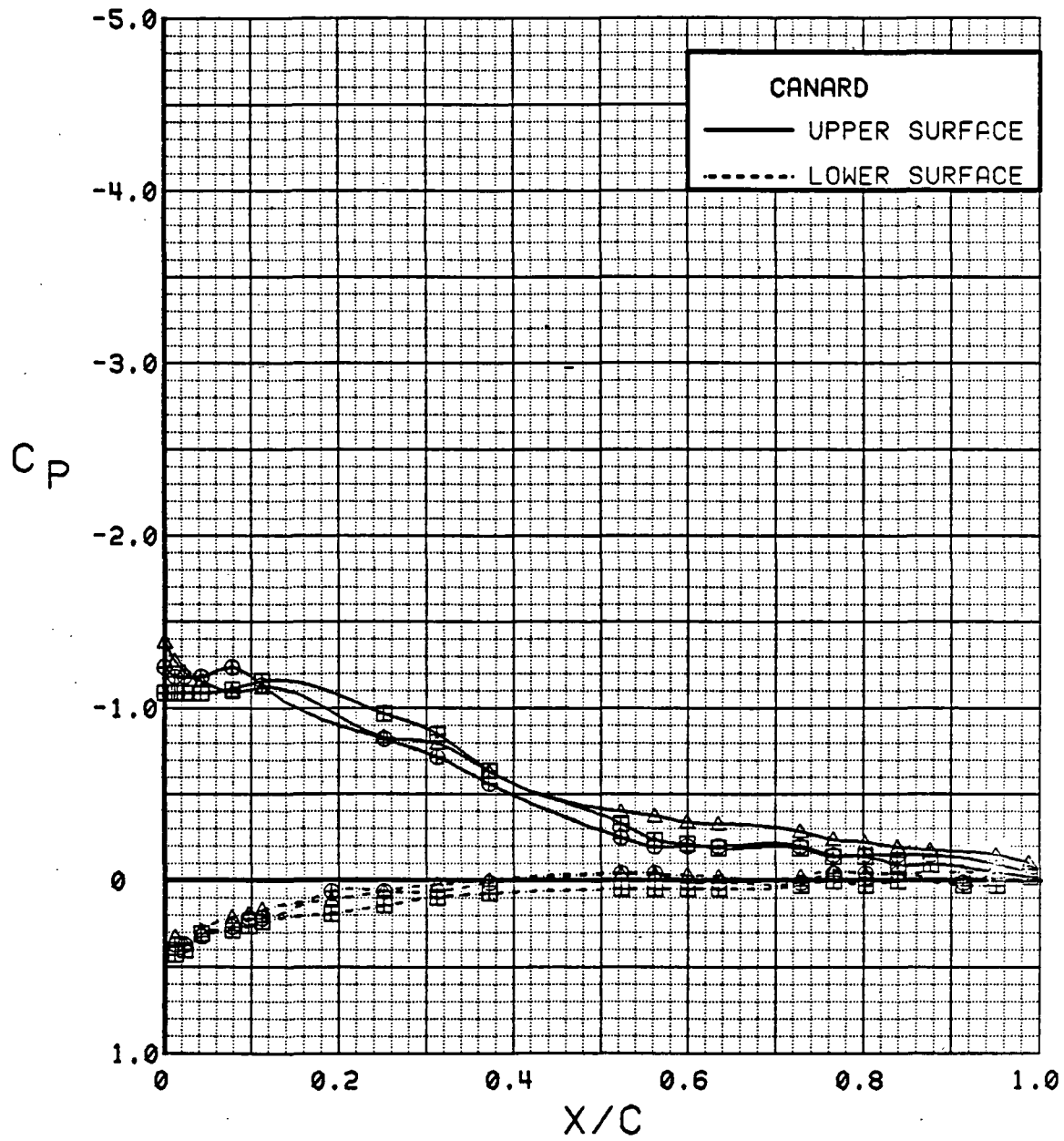


Figure 3.2.3-35 Dynamic Pressure Effects, Alpha = 4 deg

SYM	TEST	RUN	ALPHA	CT	ITEF	OTEF	CAN	SNB	q
⊕	537	17	8.5	0.00	30	30	0	OFF	7
⊞	537	12	8.5	0.00	30	30	0	OFF	15
Δ	537	18	8.5	0.00	30	30	0	OFF	40

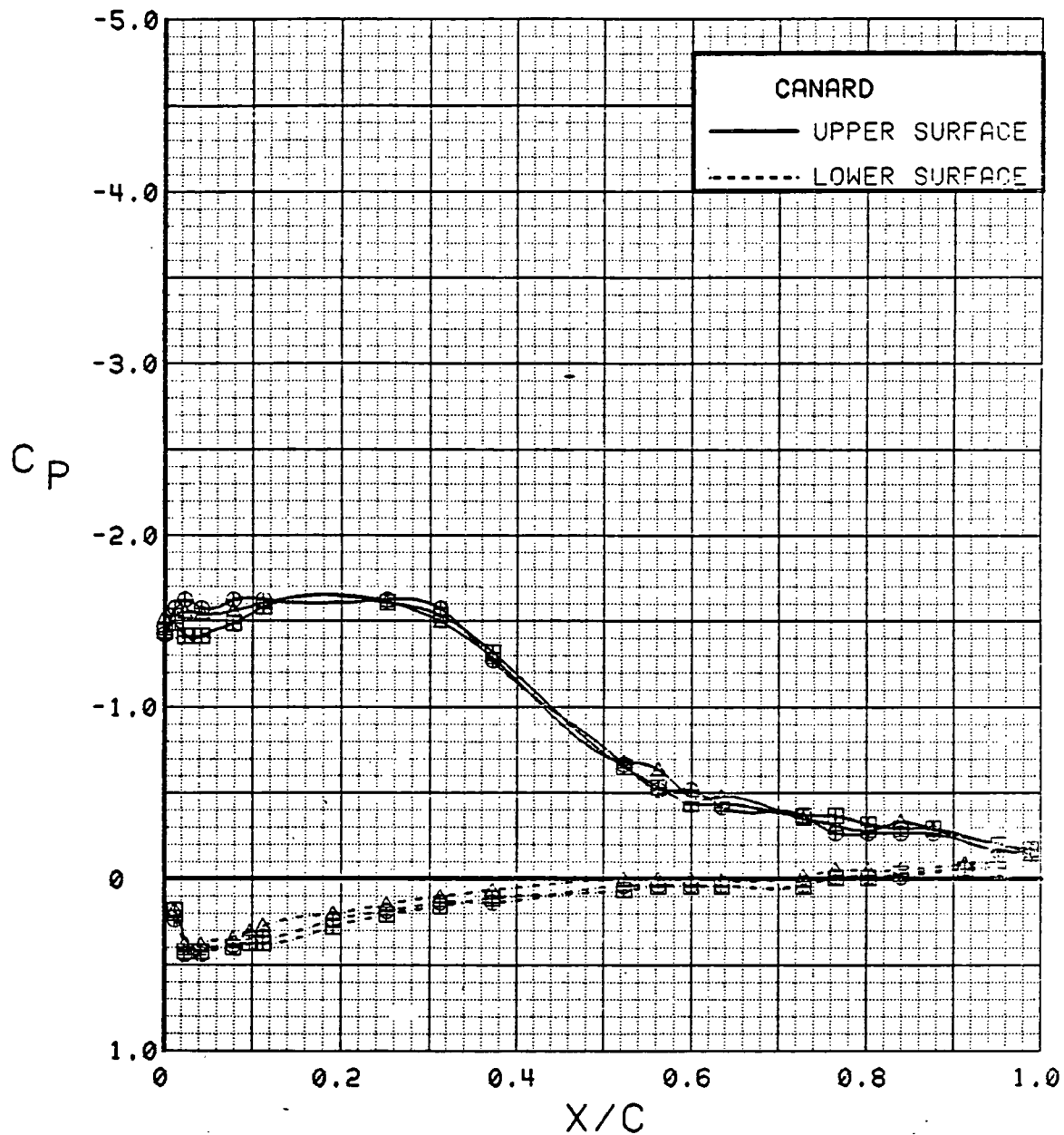


Figure 3.2.3-36 Dynamic Pressure Effects, Alpha = 8 deg

SYM	TEST	RUN	ALPHA	CT	ITEF	OTEF	CAN	SWB	q
⊕	537	17	12.7	0.00	30	30	0	OFF	7
⊞	537	12	12.7	0.00	30	30	0	OFF	15
Δ	537	18	12.7	0.00	30	30	0	OFF	40

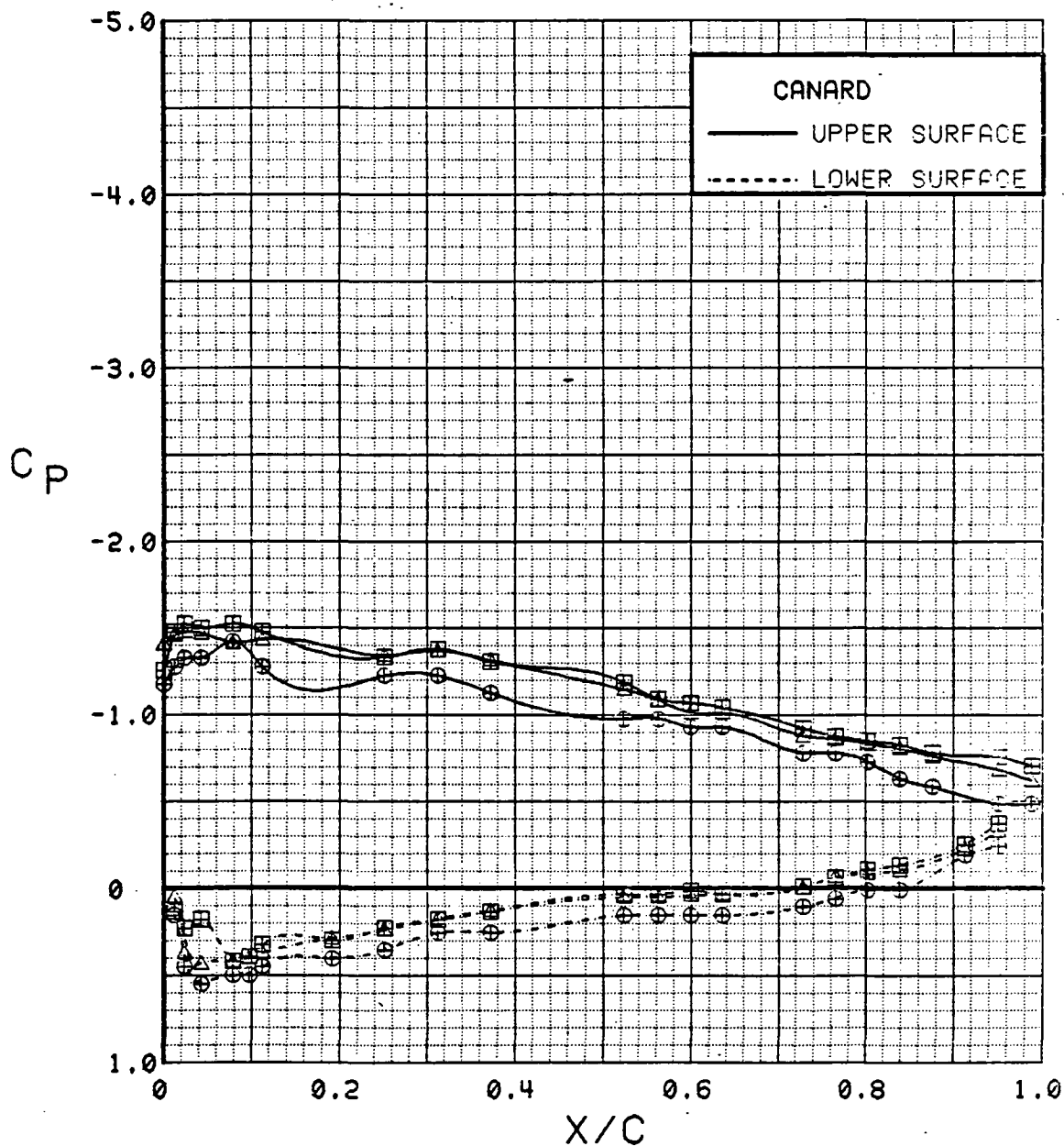


Figure 3.2.3-37 Dynamic Pressure Effects, Alpha = 12 deg

SYM	TEST	RUN	ALPHA	CT	ITEF	OTEF	CAN	SWB
⊕	543	63	0.1	0.00	0	0	0	OFF
⊞	543	59	0.1	1.42	0	0	0	OFF

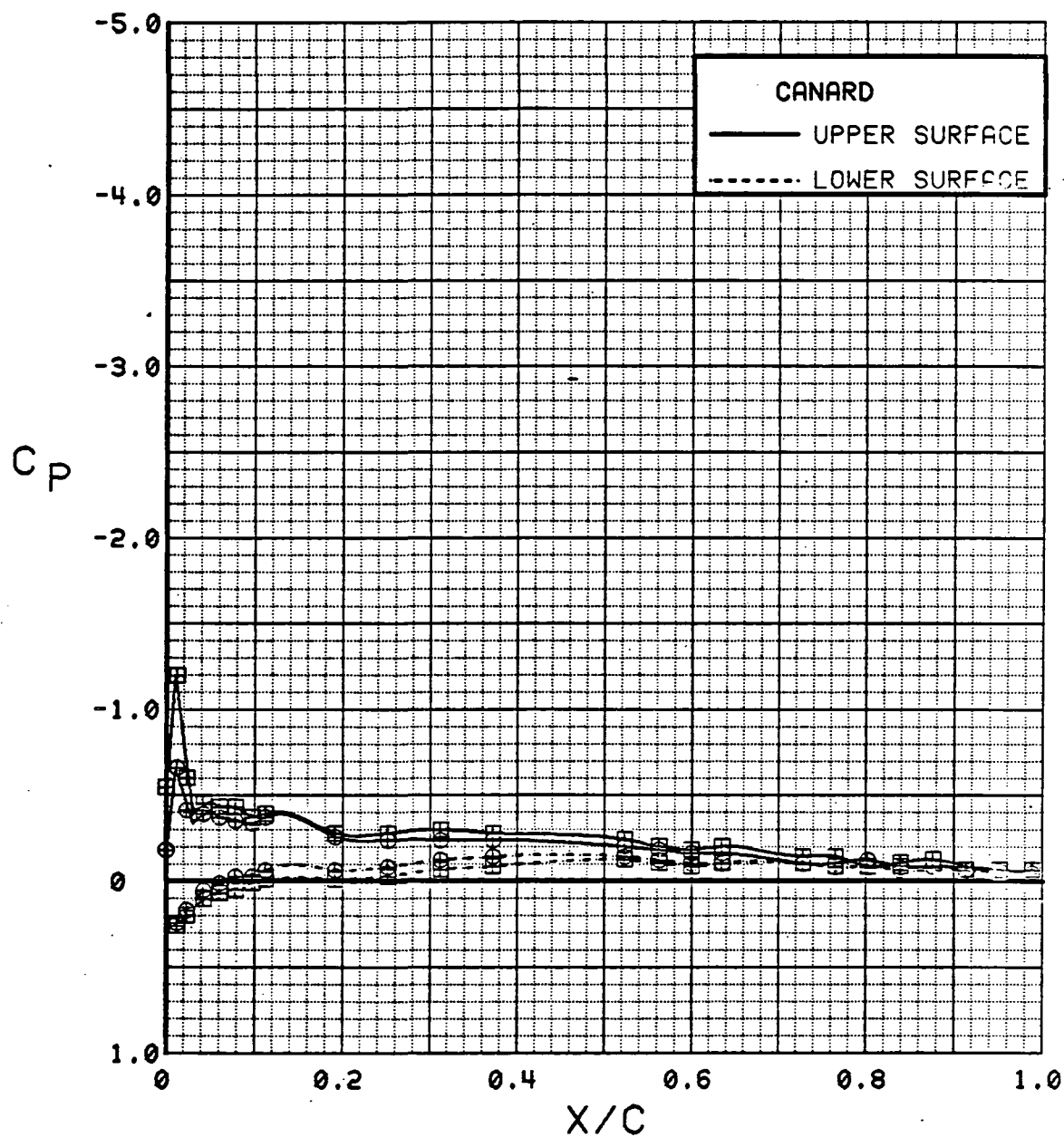


Figure 3.2.3-38 Power-off/Power-on Comparisons, Wing Flaps Neutral, Alpha = 0 deg

SYM	TEST	RUN	ALPHA	CT	ITEF	OTEF	CAN	SWB
⊕	543	63	4.2	0.00	0	0	0	OFF
⊞	543	59	4.3	1.40	0	0	0	OFF

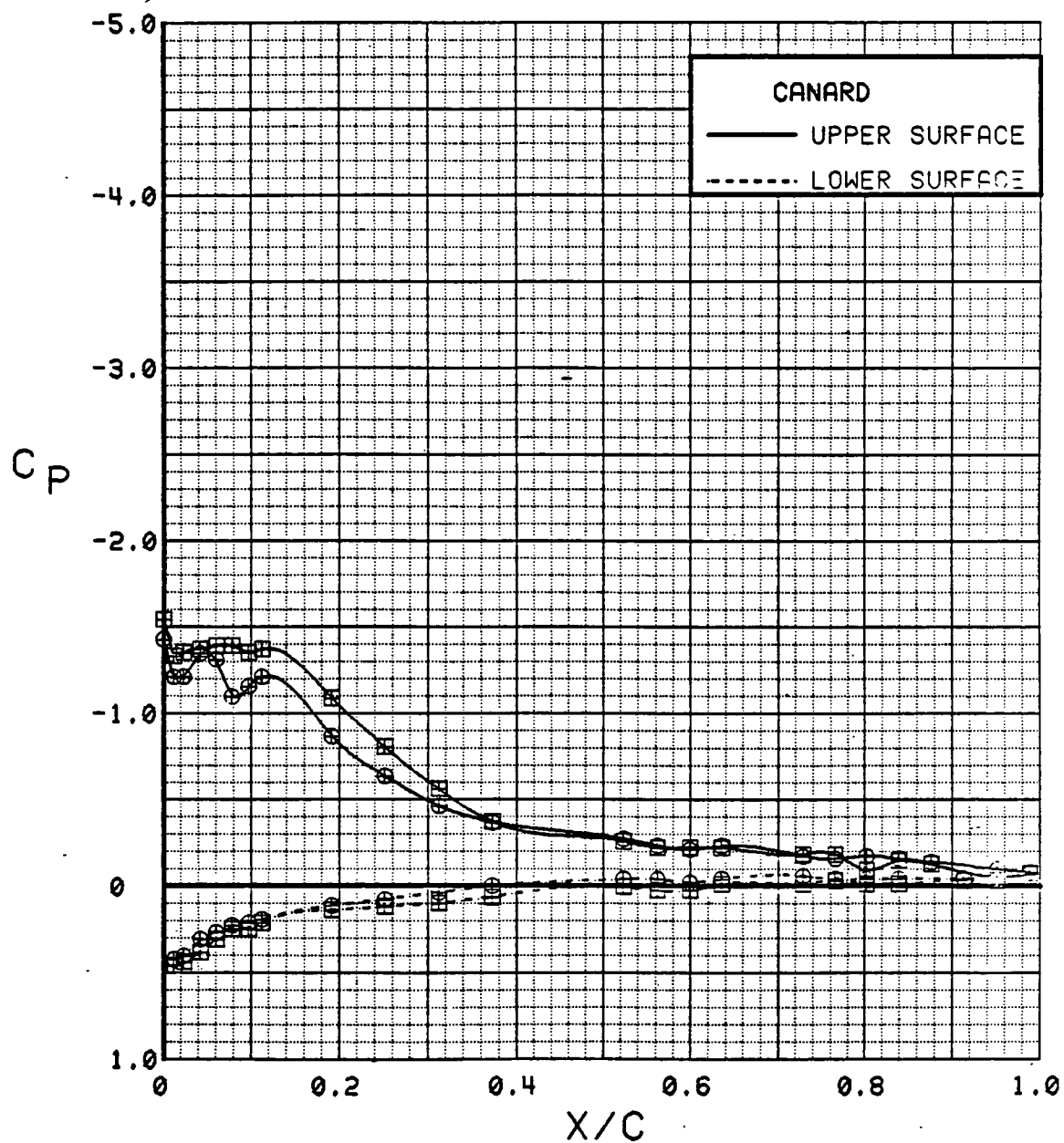


Figure 3.2.3-39 Power-off/Power-on Comparisons, Wing Flaps Neutral,  $\alpha = 4^\circ$

SYM	TEST	RUN	ALPHA	CT	ITEF	OTEF	CAN	SWB
⊕	543	63	8.3	0.00	0	0	0	OFF
⊞	543	59	8.4	1.41	0	0	0	OFF

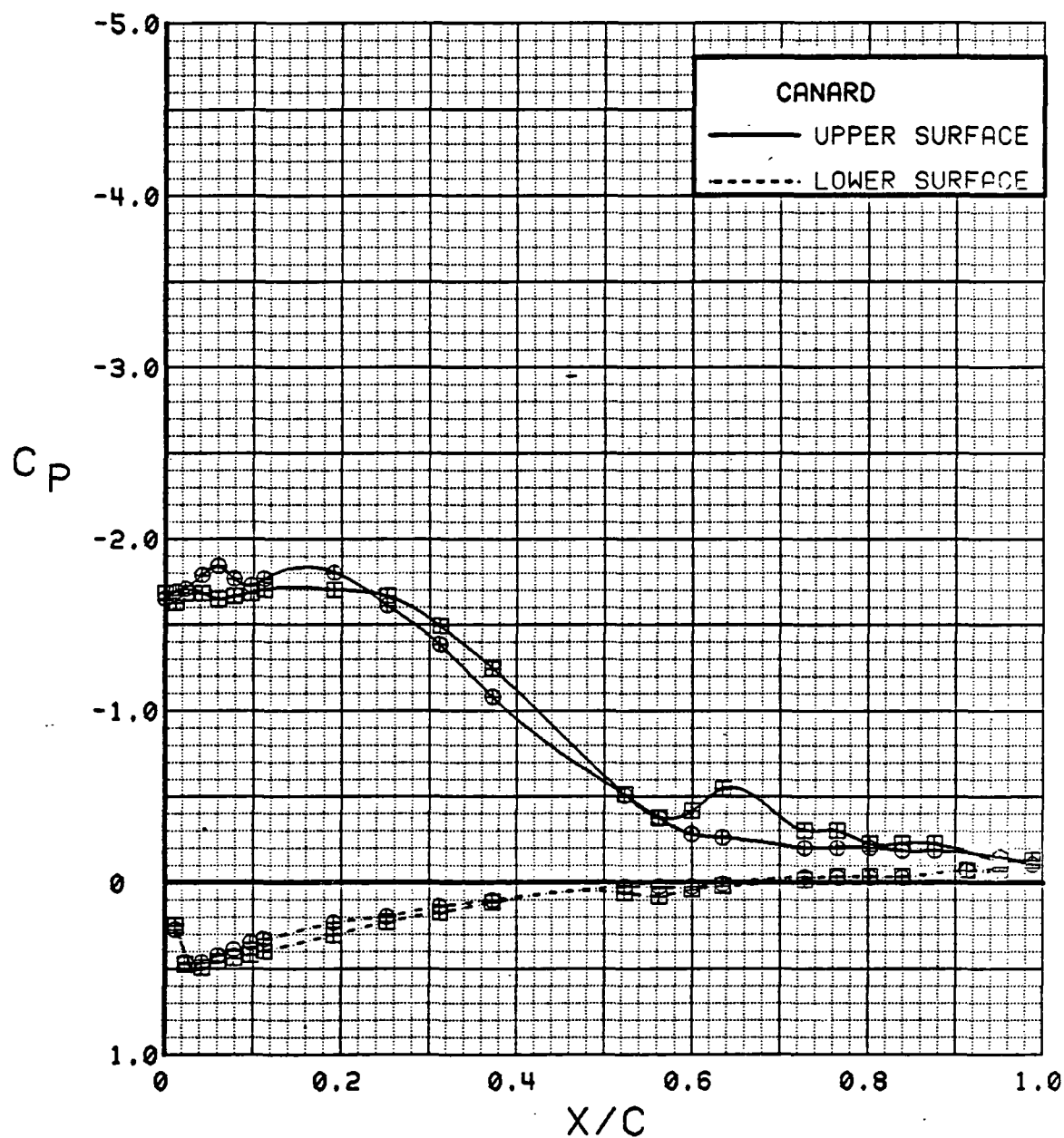


Figure 3.2.3-40 Power-off/Power-on Comparisons, Wing Flaps Neutral,  $\alpha = 8^\circ$



SYM	TEST	RUN	ALPHA	CT	ITEF	OTEF	CAN	SWB
⊕	543	63	12.5	0.00	0	0	0	OFF
⊞	543	59	12.6	1.42	0	0	0	OFF

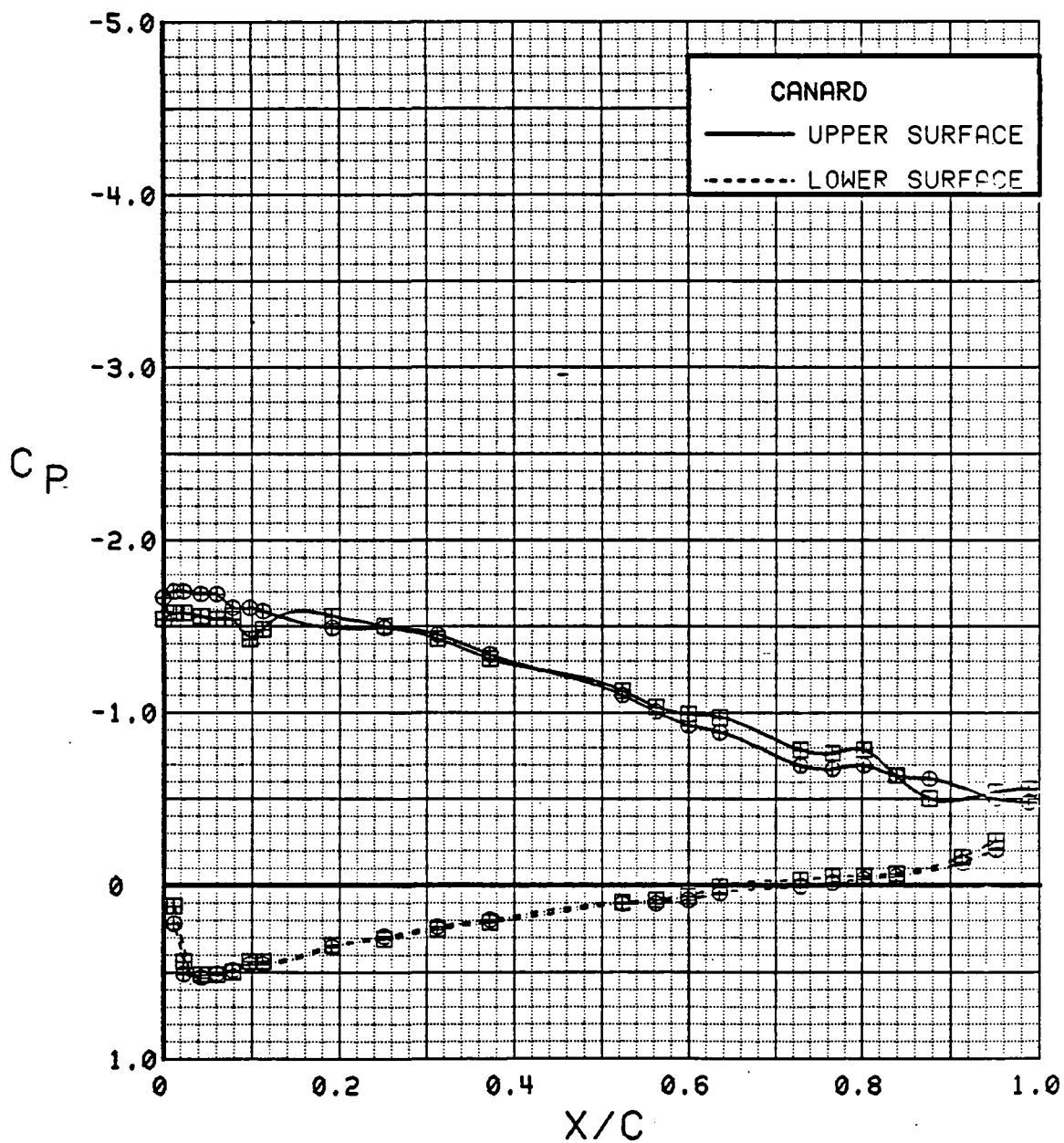


Figure 3.2.3-41 Power-off/Power-on Comparisons, Wing Flaps Neutral, Alpha = 12 deg

SYM	TEST	RUN	ALPHA	CT	ITEF	OTEF	CAN	SWB
⊕	543	63	16.6	0.00	0	0	0	OFF
⊞	543	59	16.7	1.42	0	0	0	OFF

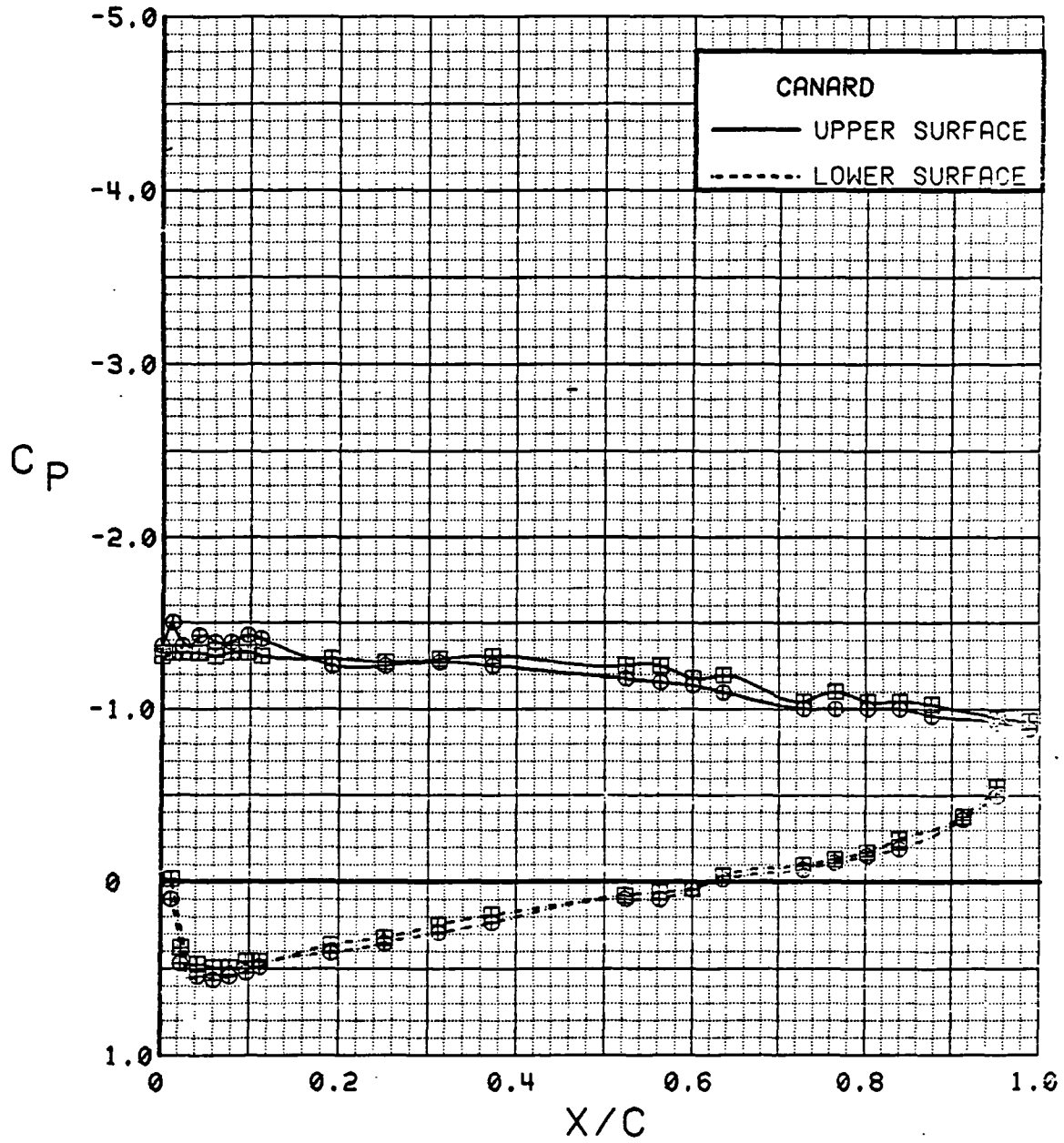


Figure 3.2.3-42 Power-off/Power-on Comparisons, Wing Flaps Neutral, Alpha = 16 deg

SYM	TEST	RUN	ALPHA	CT	ITEF	OTEF	CAN	SWB
⊕	543	63	20.7	0.00	0	0	0	OFF
⊞	543	59	20.8	1.41	0	0	0	OFF

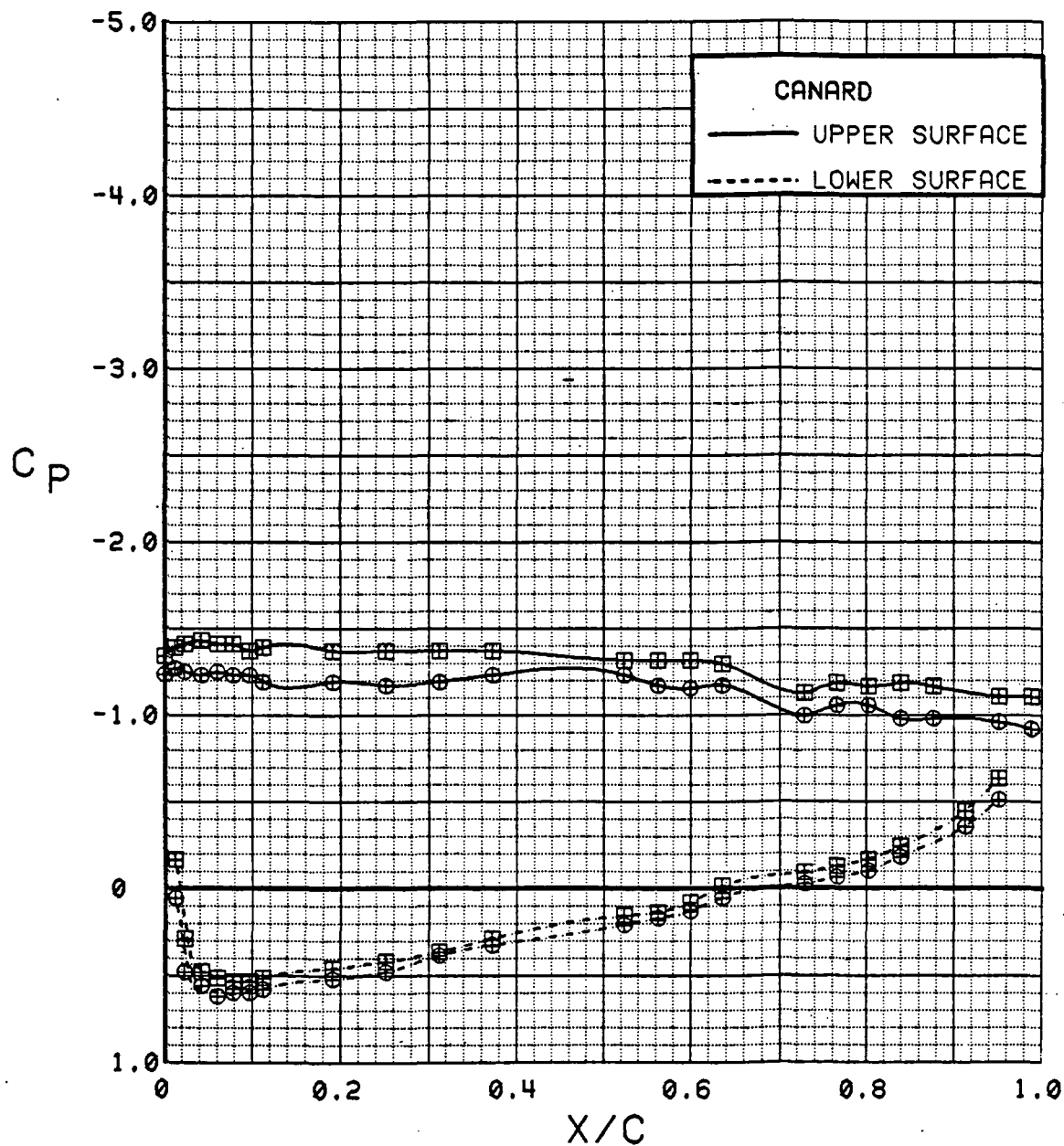


Figure 3.2.3-43 Power-off/Power-on Comparisons, Wing Flaps Neutral, Alpha = 20 deg

SYM	TEST	RUN	ALPHA	CT	ITEF	OJEF	CAN	SWB
⊕	543	63	36.8	0.00	0	0	0	OFF
⊞	543	59	37.2	1.41	0	0	0	OFF

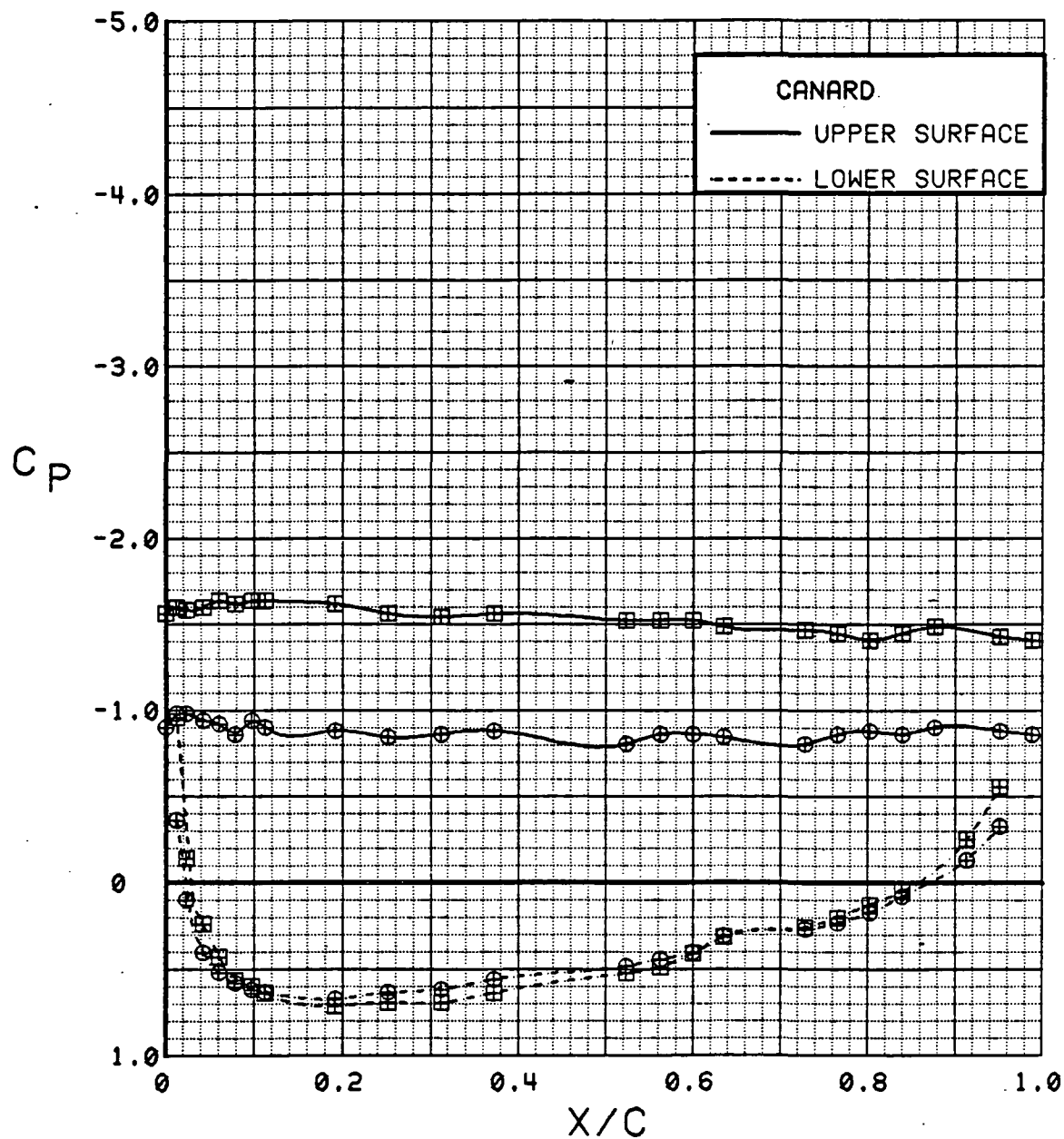


Figure 3.2.3-44 Power-off/Power-on Comparisons, Wing Flaps Neutral, Alpha = 36 deg

## CANARD

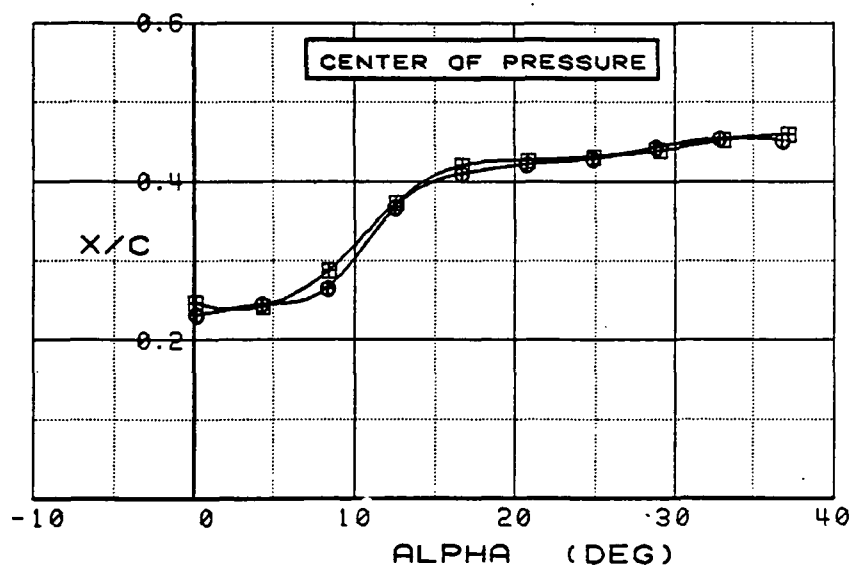
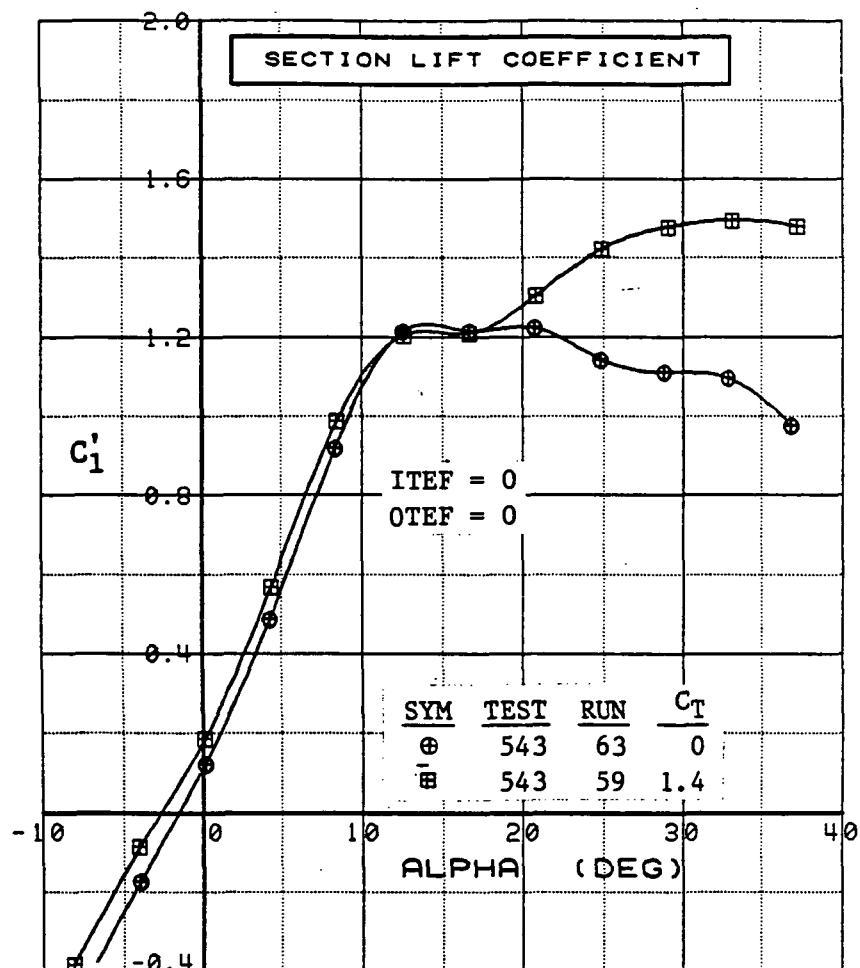


Figure 3.2.3-45 Power-off/Power-on Comparisons, Wing Flaps Neutral, Integrated Section Properties

SYM	TEST	RUN	ALPHA	CT	ITEF	OTEF	CAN	SWB
⊕	543	11	0.3	0.00	30	30	0	OFF
⊞	543	5	0.4	1.41	30	30	0	OFF

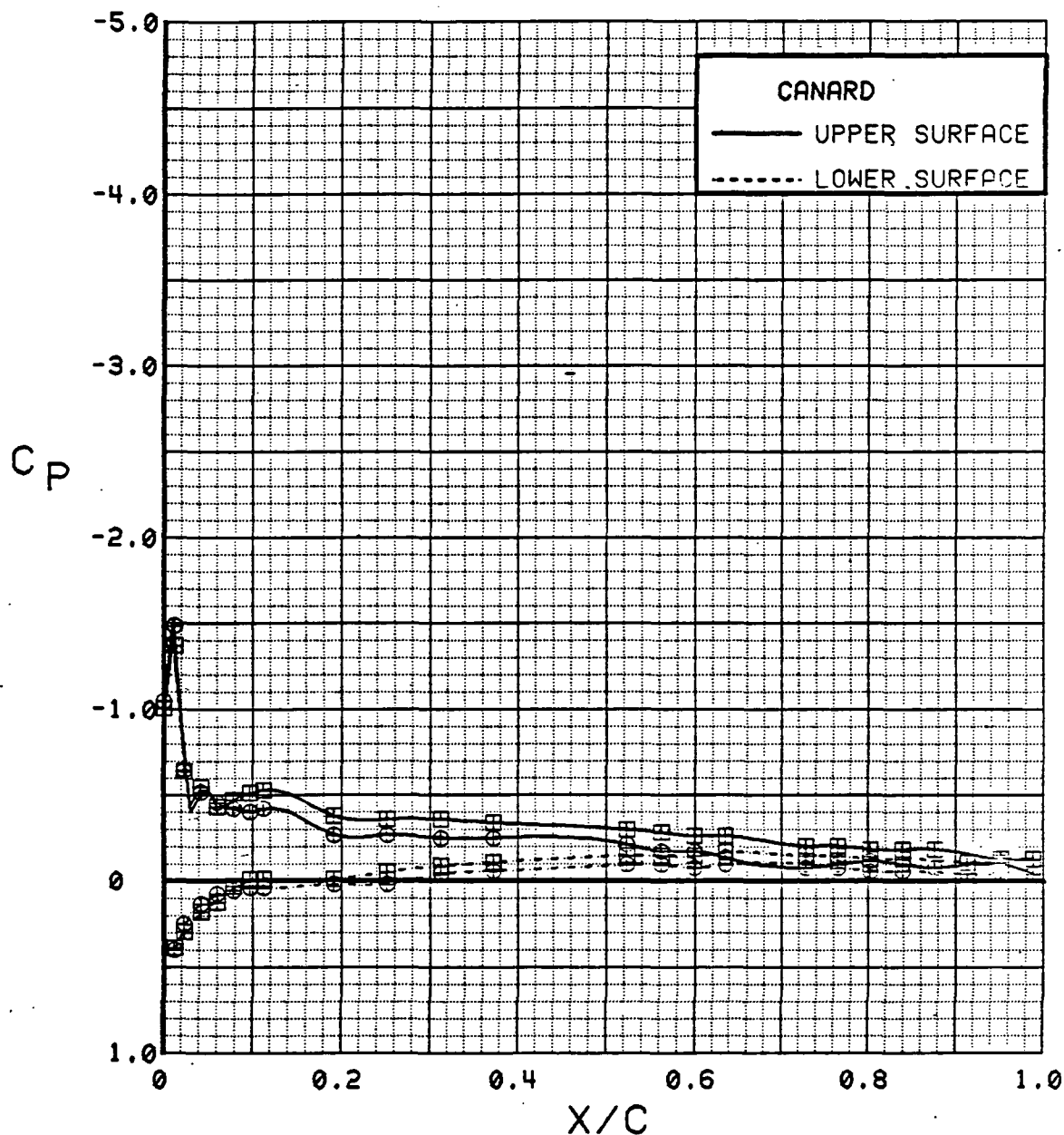


Figure 3.2.3-46 Power-off/Power-on Comparisons, Wing Flaps Deflected, Alpha = 0 deg

SYM	TEST	RUN	ALPHA	CT	ITEF	OTEF	CAN	SWB
⊕	543	11	4.4	0.00	30	30	0	OFF
⊞	543	5	4.5	1.40	30	30	0	OFF

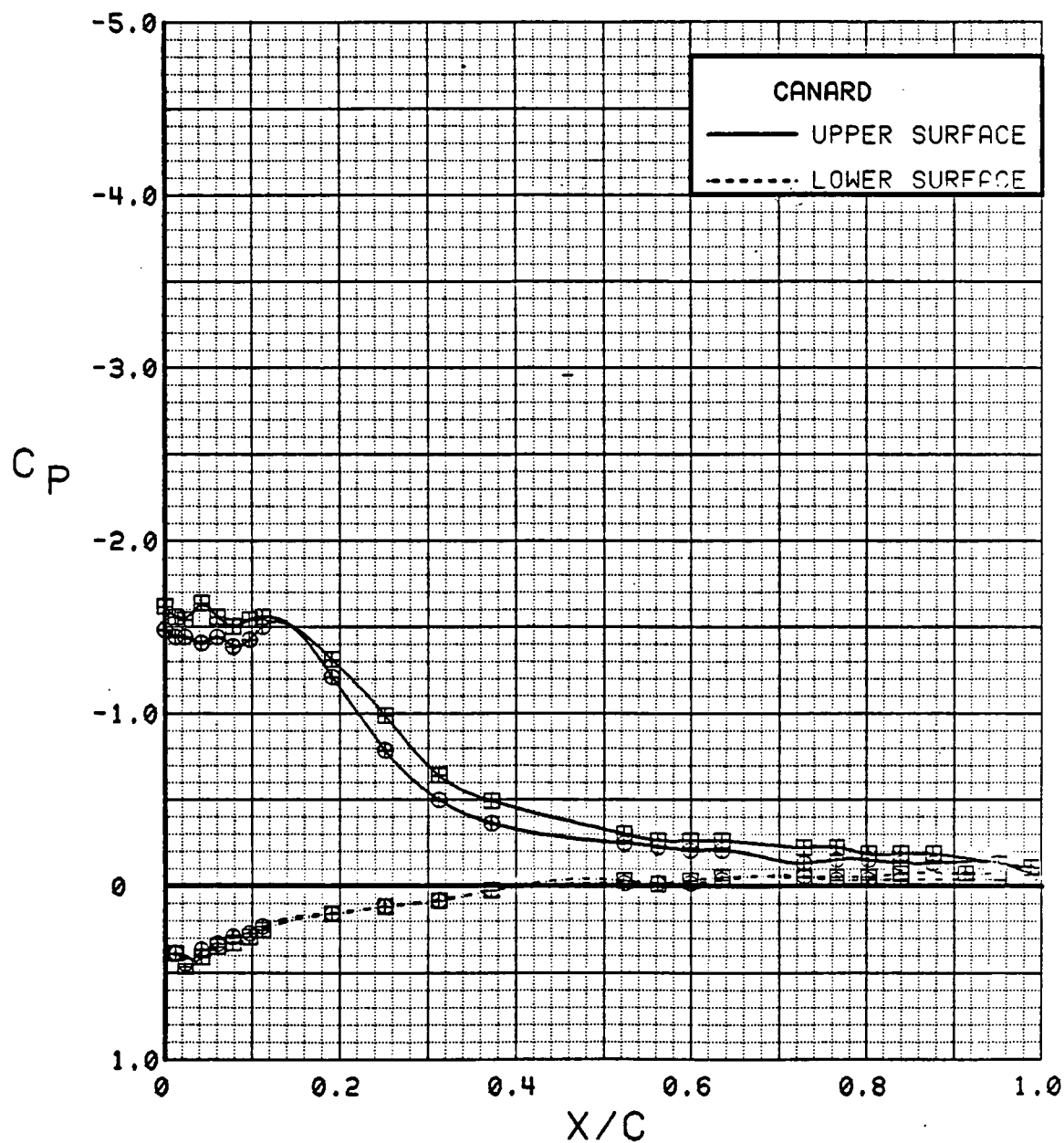


Figure 3.2.3-47 Power-off/Power-on Comparisons, Wing Flaps Deflected, Alpha = 4 deg

SYM	TEST	RUN	ALPHA	CT	ITEF	OTEF	CAN	SWB
⊕	543	11	8.5	0.00	30	30	0	OFF
⊞	543	5	8.7	1.40	30	30	0	OFF

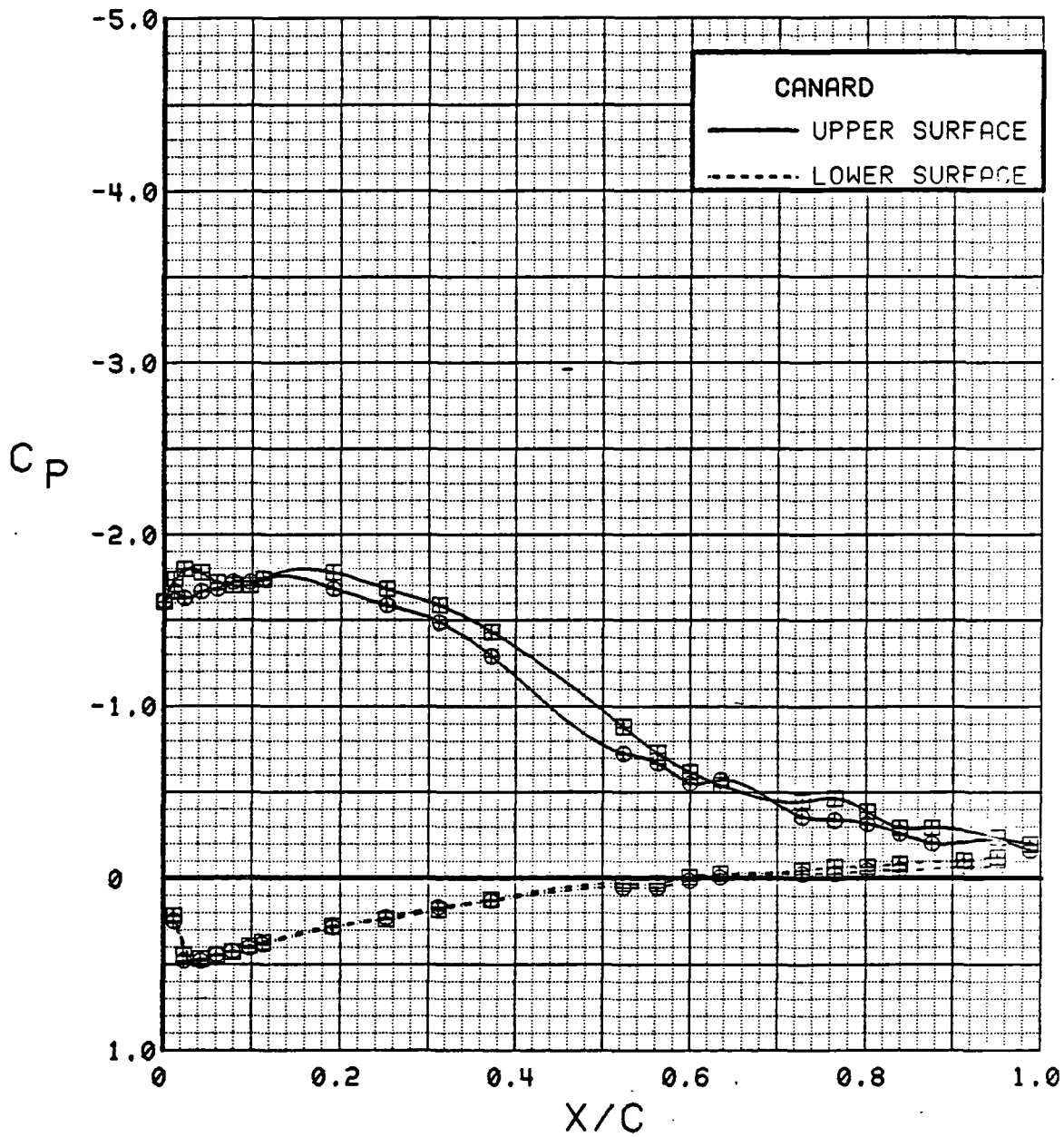


Figure 3.2.3-48 Power-off/Power-on Comparisons, Wing Flaps Deflected, Alpha = 8 deg



SYM	TEST	RUN	ALPHA	CT	ITEF	OTEF	CAN	SWB
⊕	543	11	12.7	0.00	30	30	0	OFF
⊞	543	5	12.8	1.39	30	30	0	OFF

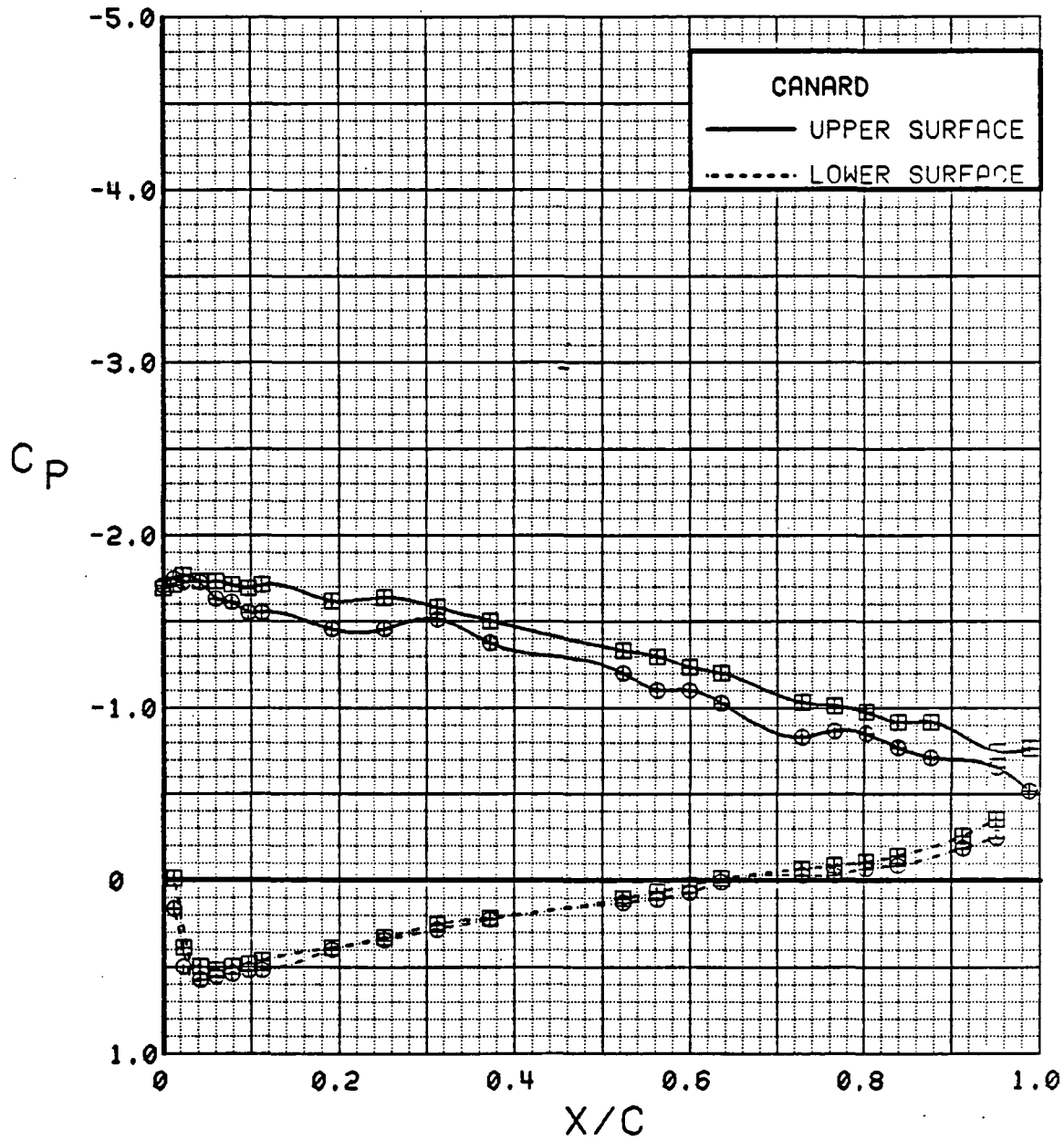


Figure 3.2.3-49 Power-off/Power-on Comparisons, Wing Flaps Deflected, Alpha = 12 deg

SYM	TEST	RUN	ALPHA	CT	ITEF	OTEF	CAN	SWB
⊕	543	11	16.8	0.00	30	30	0	OFF
⊞	543	5	16.9	1.40	30	30	0	OFF

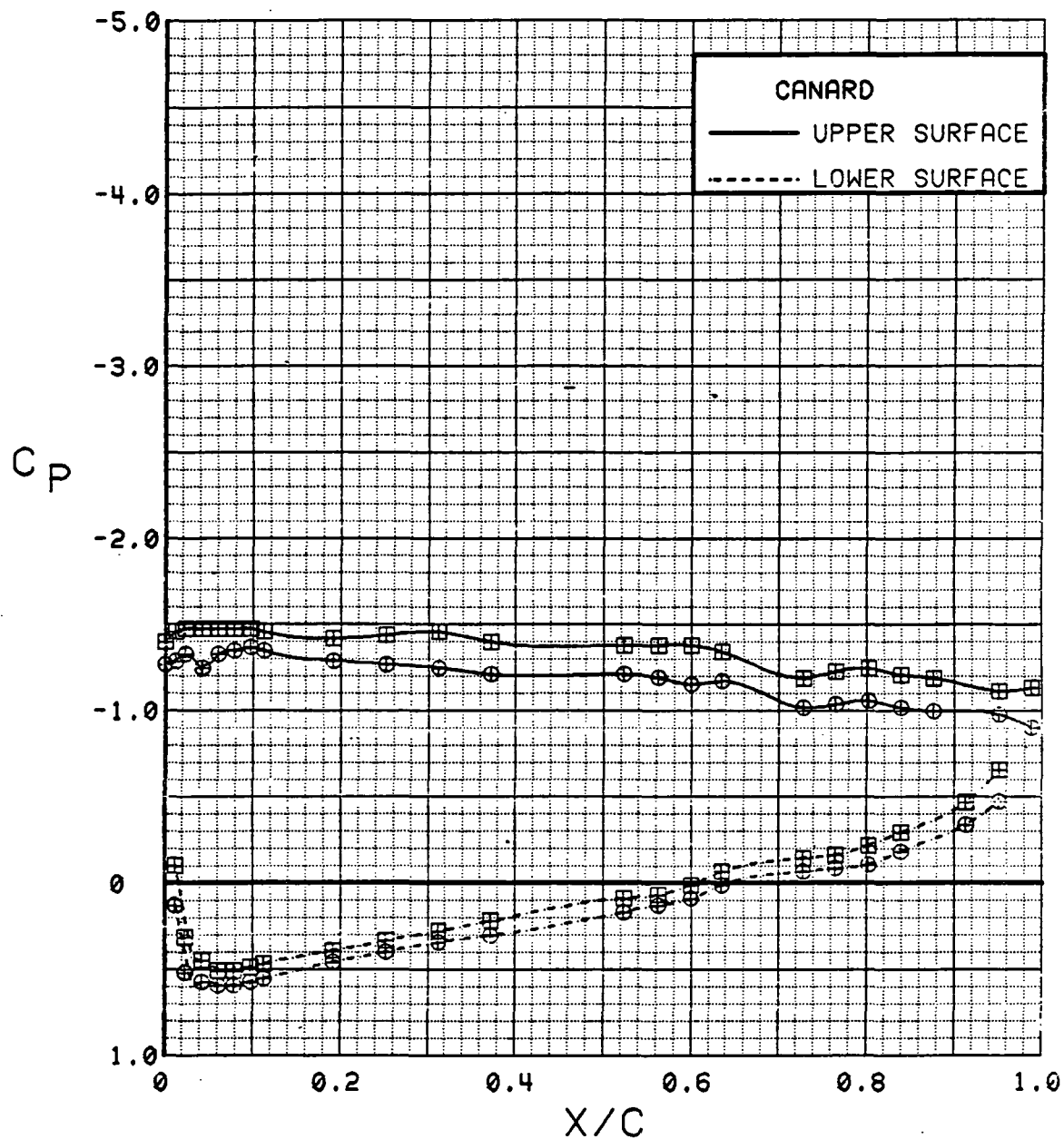


Figure 3.2.3-50 Power-off/Power-on Comparisons, Wing Flaps Deflected, Alpha = 16 deg

SYM	TEST	RUN	ALPHA	CT	ITEF	OTEF	CAN	SWB
⊕	543	11	20.8	0.00	30	30	0	OFF
⊞	543	5	21.0	1.42	30	30	0	OFF

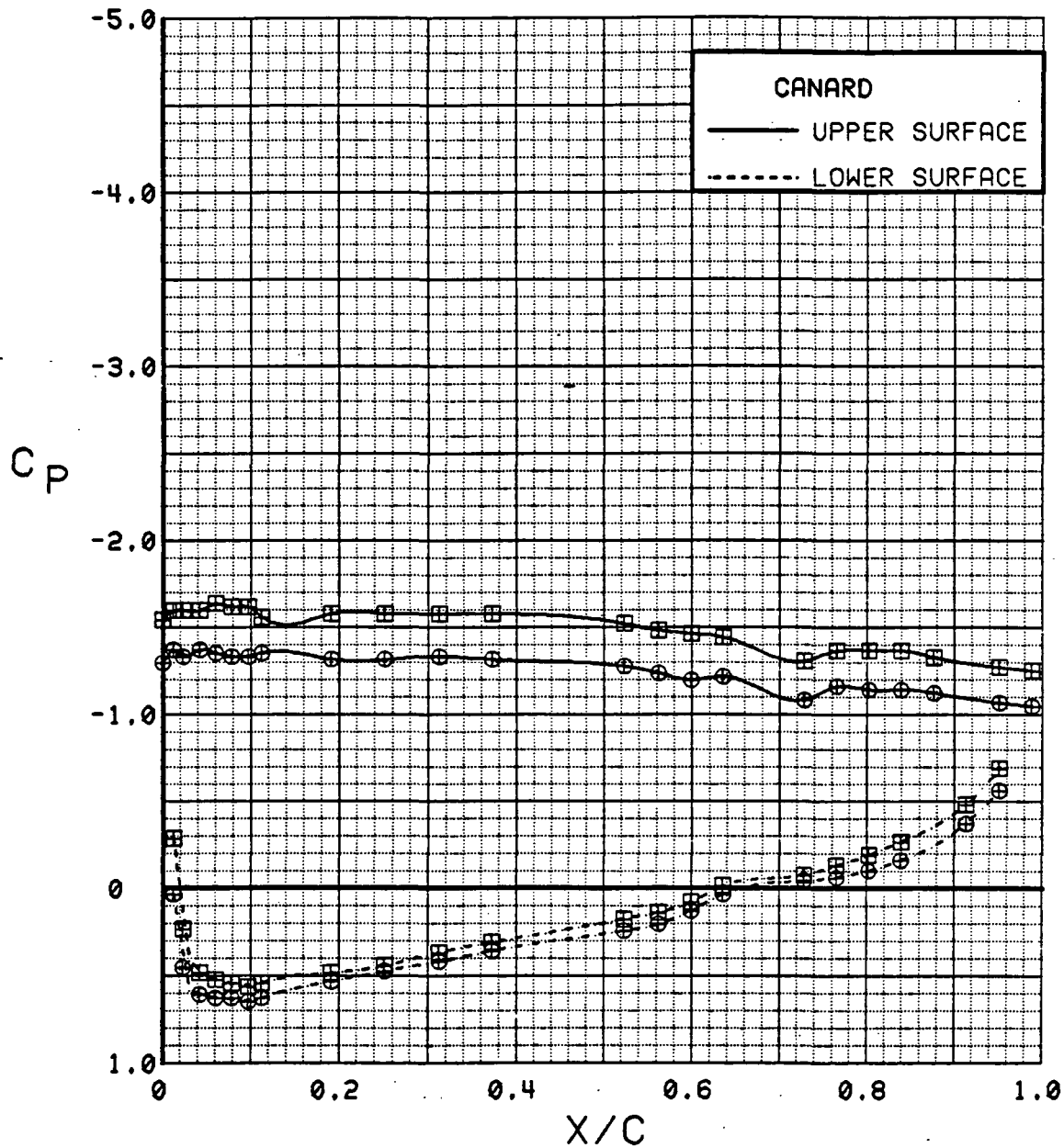


Figure 3.2.3-51 Power-off/Power-on Comparisons, Wing Flaps Deflected, Alpha = 20 deg

SYM	TEST	RUN	ALPHA	CT	ITEF	OTEF	CAN	SWB
⊕	543	11	28.9	0.00	30	30	0	OFF
⊞	543	5	29.2	1.39	30	30	0	OFF

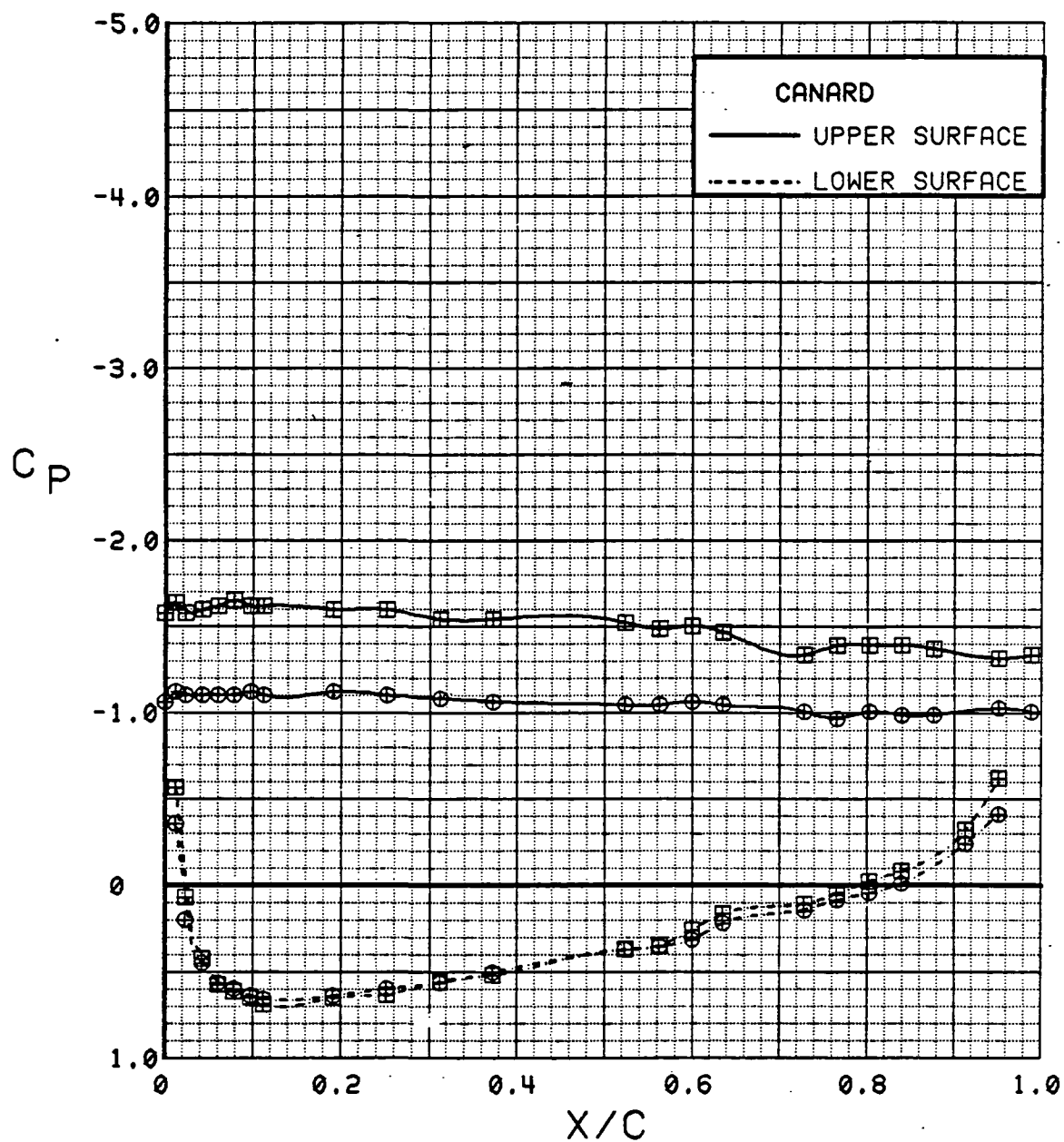


Figure 3.2.3-52 Power-off/Power-on Comparisons, Wing Flaps Deflected,  $\alpha = 28^\circ$

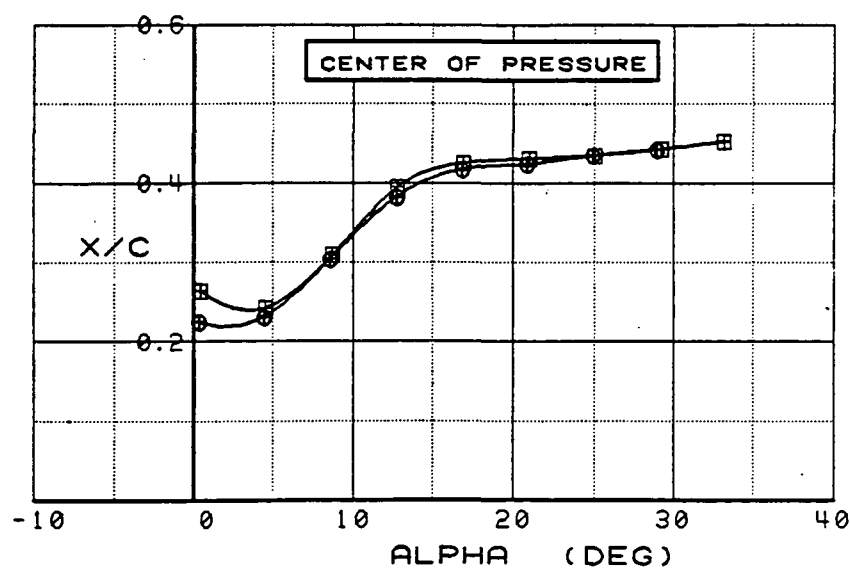
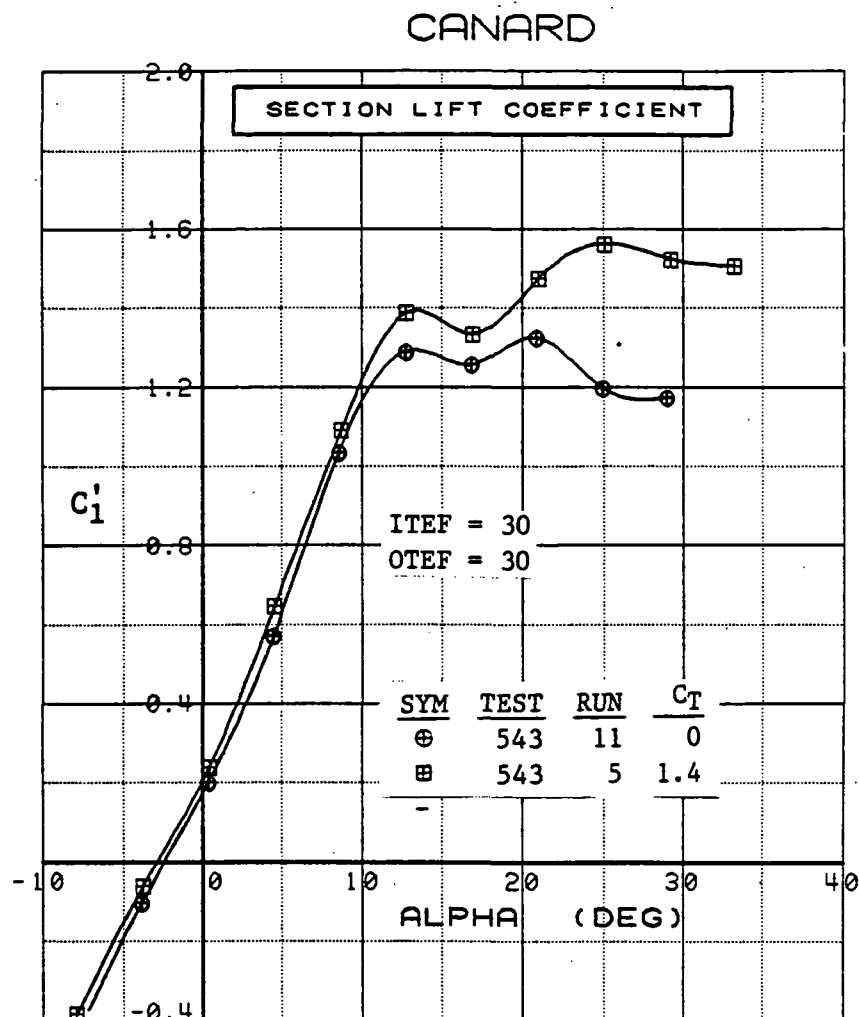


Figure 3.2.3-53 Power-off/Power-on Comparisons, Wing Flaps Deflected  
Integrated Section Properties

SYM	TEST	RUN	ALPHA	CT	ITEF	OTEF	CAN	SWB
⊕	543	63	4.2	0.00	0	0	0	OFF
⊞	543	64	4.2	0.27	0	0	0	OFF
△	543	62	4.2	0.48	0	0	0	OFF
⊕	543	60	4.3	0.93	0	0	0	OFF
*	543	59	4.3	1.40	0	0	0	OFF
+	543	58	4.3	1.84	0	0	0	OFF

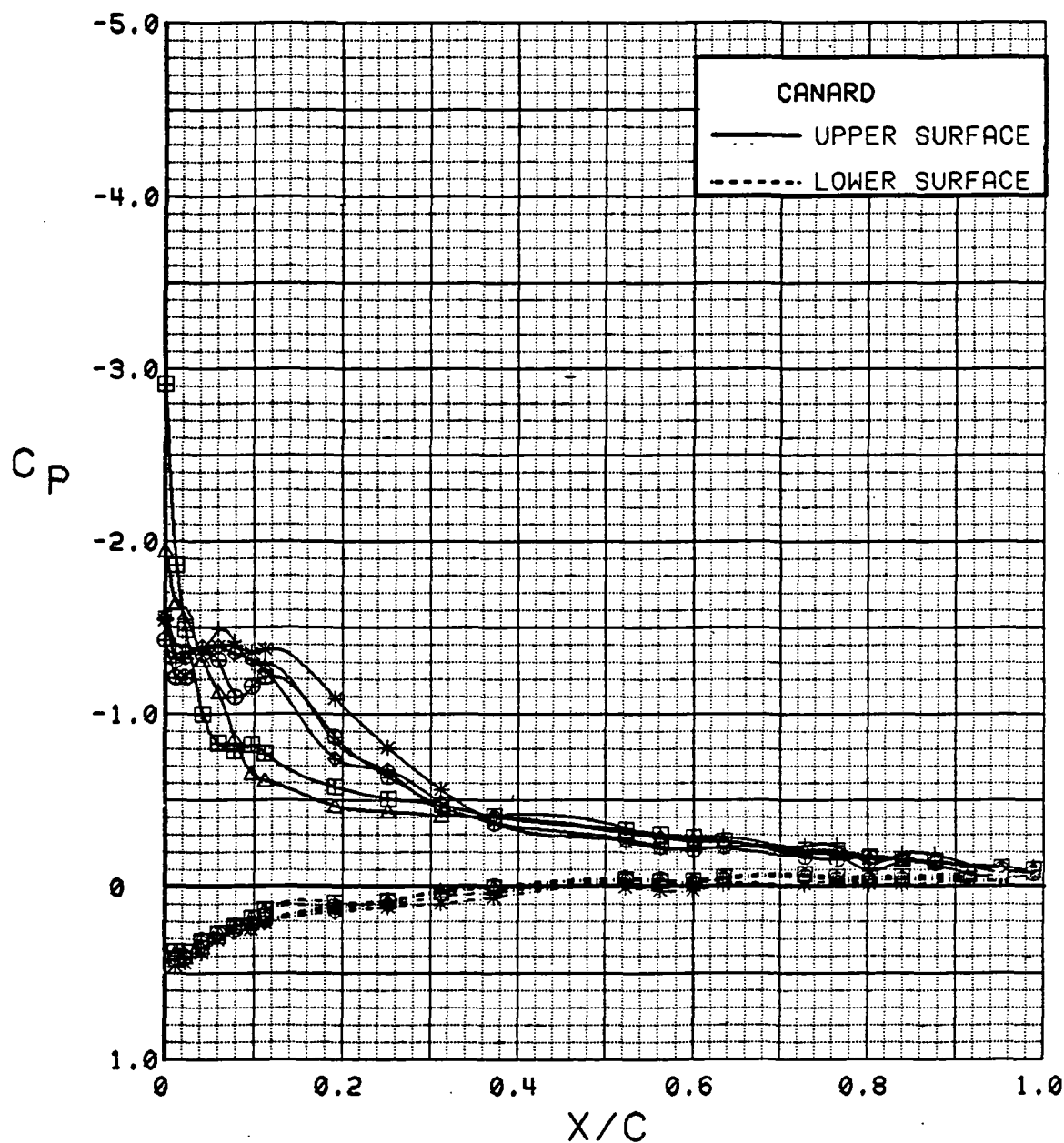


Figure 3.2.3-54 Power Effects, Wing Flaps Neutral, Alpha = 4 deg

SYM	TEST	RUN	ALPHA	CT	ITEF	OTEF	CAN	SWB
⊕	543	63	8.3	0.00	0	0	0	OFF
⊞	543	64	8.4	0.27	0	0	0	OFF
△	543	62	8.4	0.47	0	0	0	OFF
◆	543	60	8.4	0.94	0	0	0	OFF
*	543	59	8.4	1.41	0	0	0	OFF
+	543	58	8.4	1.90	0	0	0	OFF

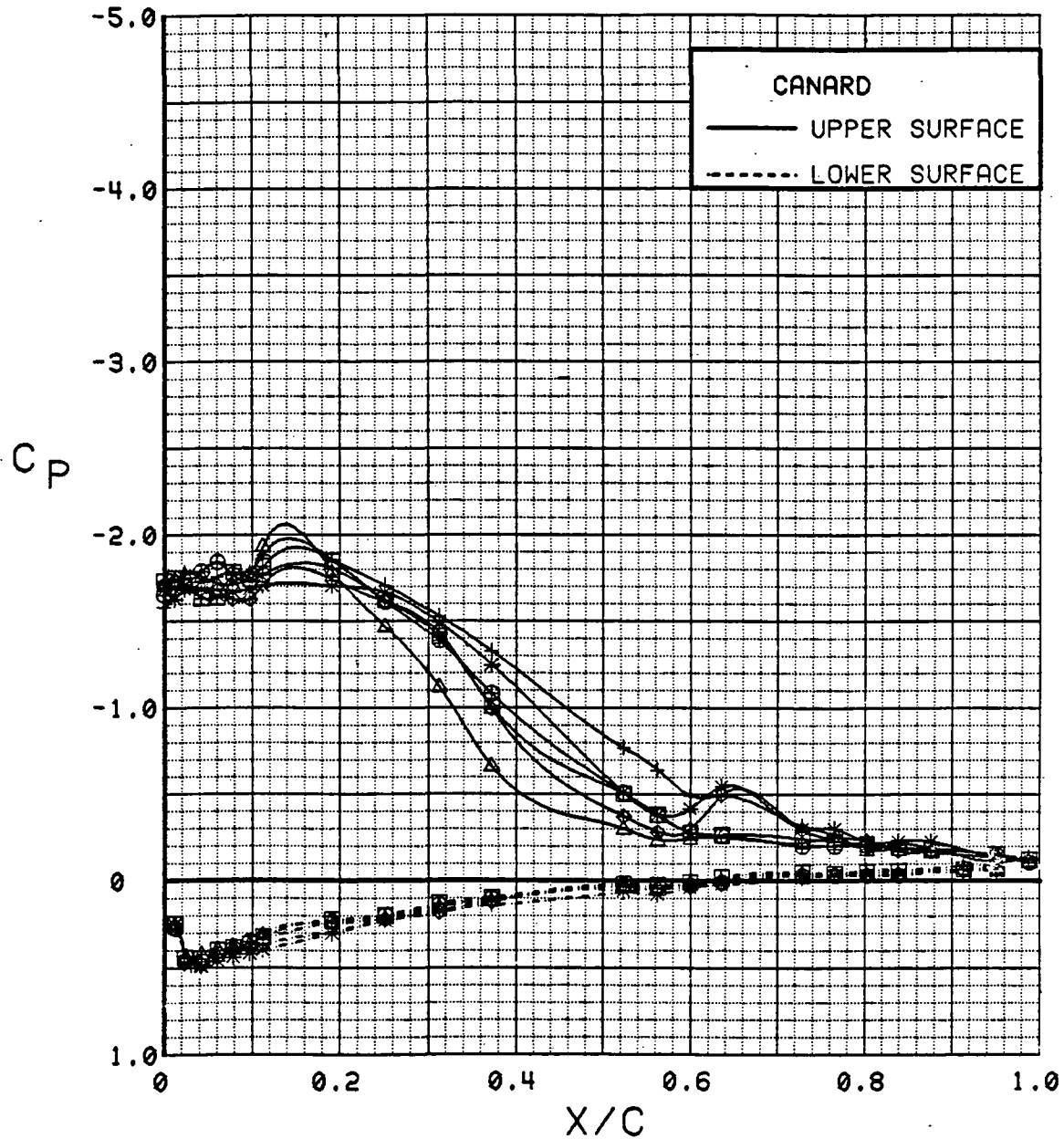


Figure 3.2.3-55 Power Effects, Wing Flaps Neutral, Alpha = 8 deg

SYM	TEST	RUN	ALPHA	CT	ITEF	OTEF	CAN	SWB
⊕	543	63	12.5	0.00	0	0	0	OFF
⊞	543	64	12.5	0.26	0	0	0	OFF
△	543	62	12.5	0.47	0	0	0	OFF
⊕	543	60	12.5	0.94	0	0	0	OFF
*	543	59	12.6	1.42	0	0	0	OFF
+	543	58	12.6	1.87	0	0	0	OFF

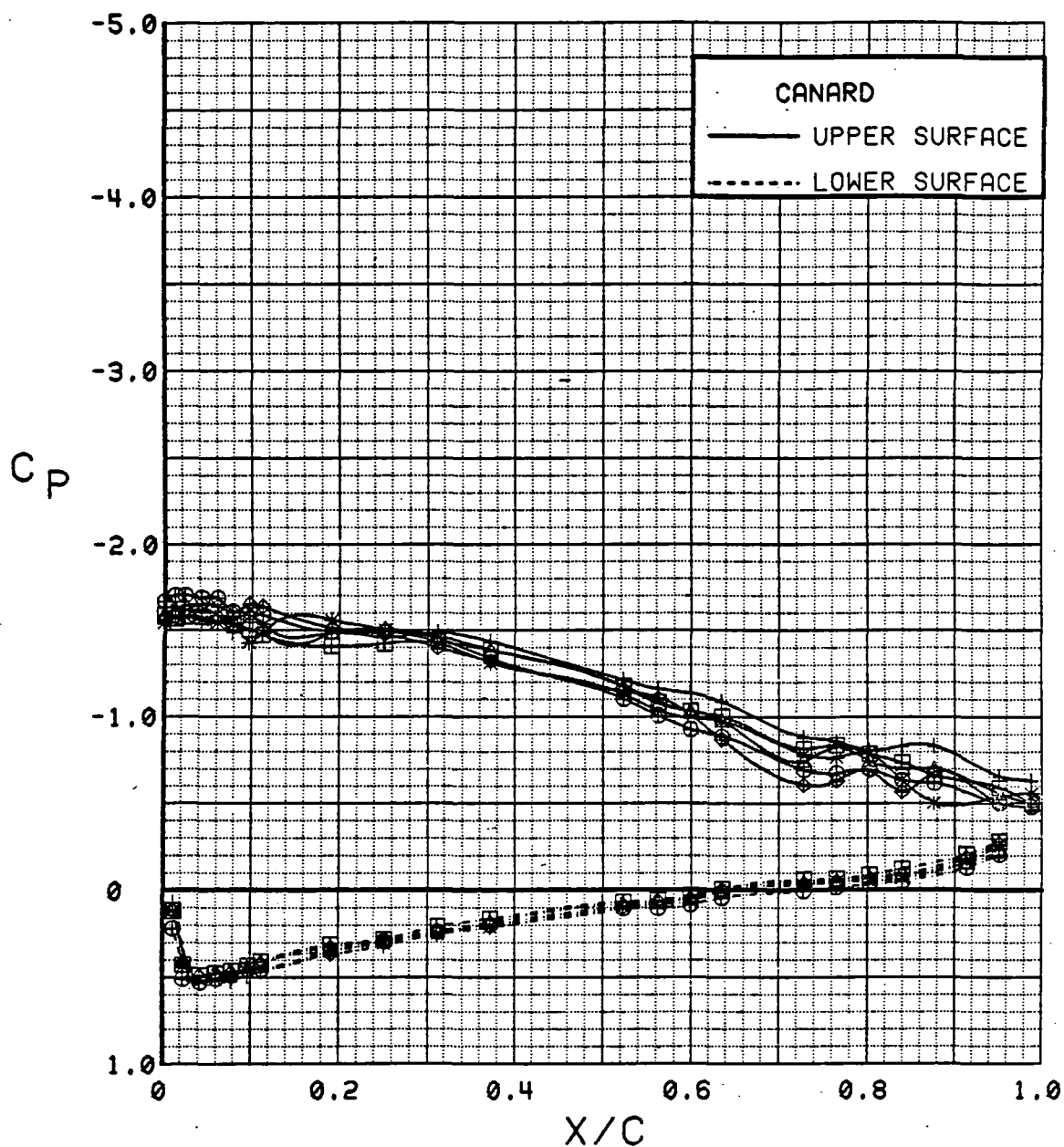


Figure 3.2.3-56 Power Effects, Wing Flaps Neutral, Alpha = 12 deg



SYM	TEST	RUN	ALPHA	CT	ITEF	OTEF	CAN	SWB
⊕	543	63	16.6	0.00	0	0	0	OFF
⊞	543	64	16.6	0.27	0	0	0	OFF
△	543	62	16.6	0.47	0	0	0	OFF
⊕	543	60	16.7	0.93	0	0	0	OFF
*	543	59	16.7	1.42	0	0	0	OFF
+	543	58	16.7	1.87	0	0	0	OFF

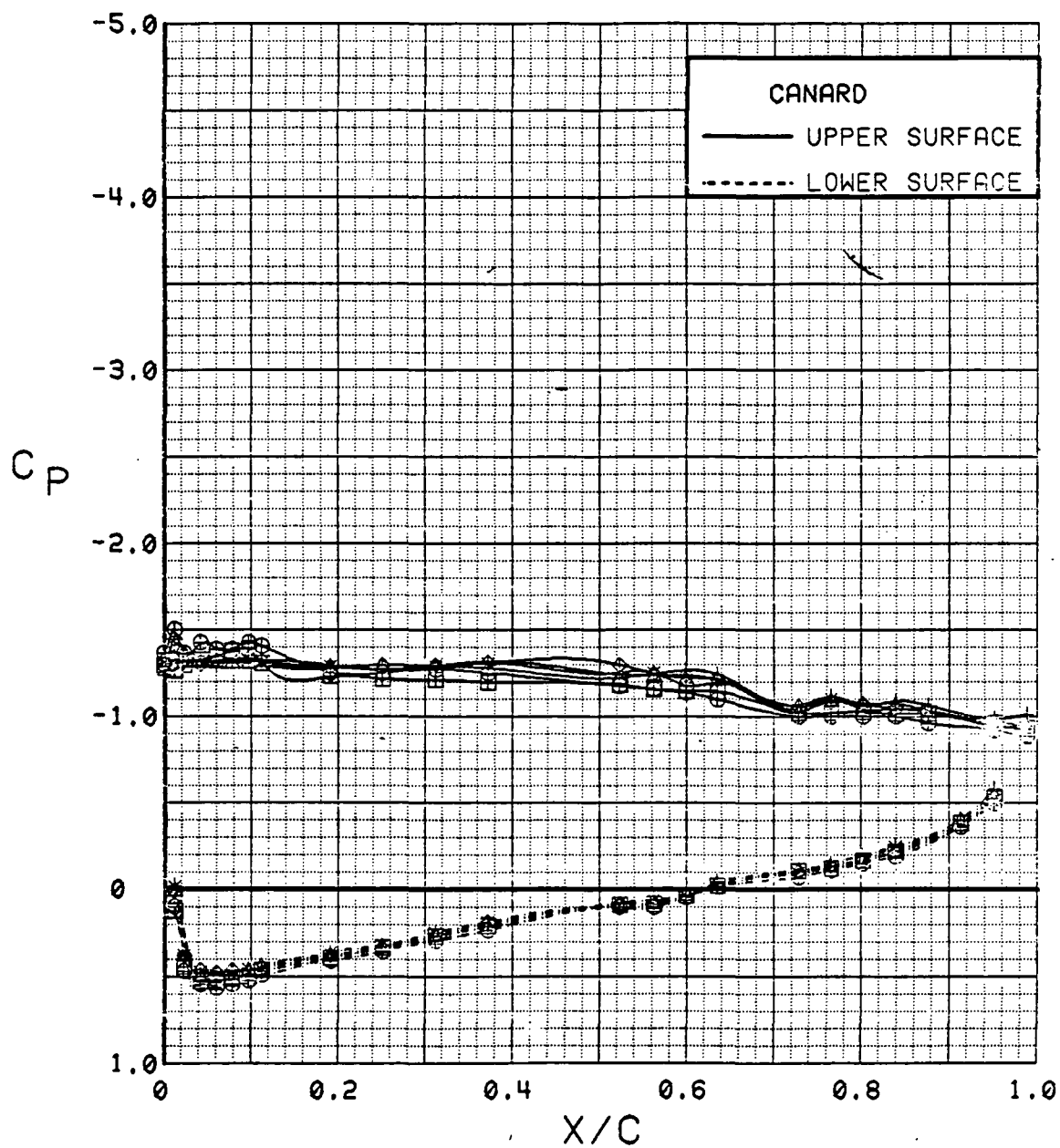


Figure 3.2.3-57 Power Effects, Wing Flaps Neutral, Alpha = 16 deg

SYM	TEST	RUN	ALPHA	CT	ITEF	OTEF	CAN	SWB
⊕	543	63	20.7	0.00	0	0	0	OFF
⊞	543	64	20.8	0.27	0	0	0	OFF
△	543	62	20.8	0.47	0	0	0	OFF
⊕	543	60	20.8	0.93	0	0	0	OFF
*	543	59	20.8	1.41	0	0	0	OFF
+	543	58	20.8	1.72	0	0	0	OFF

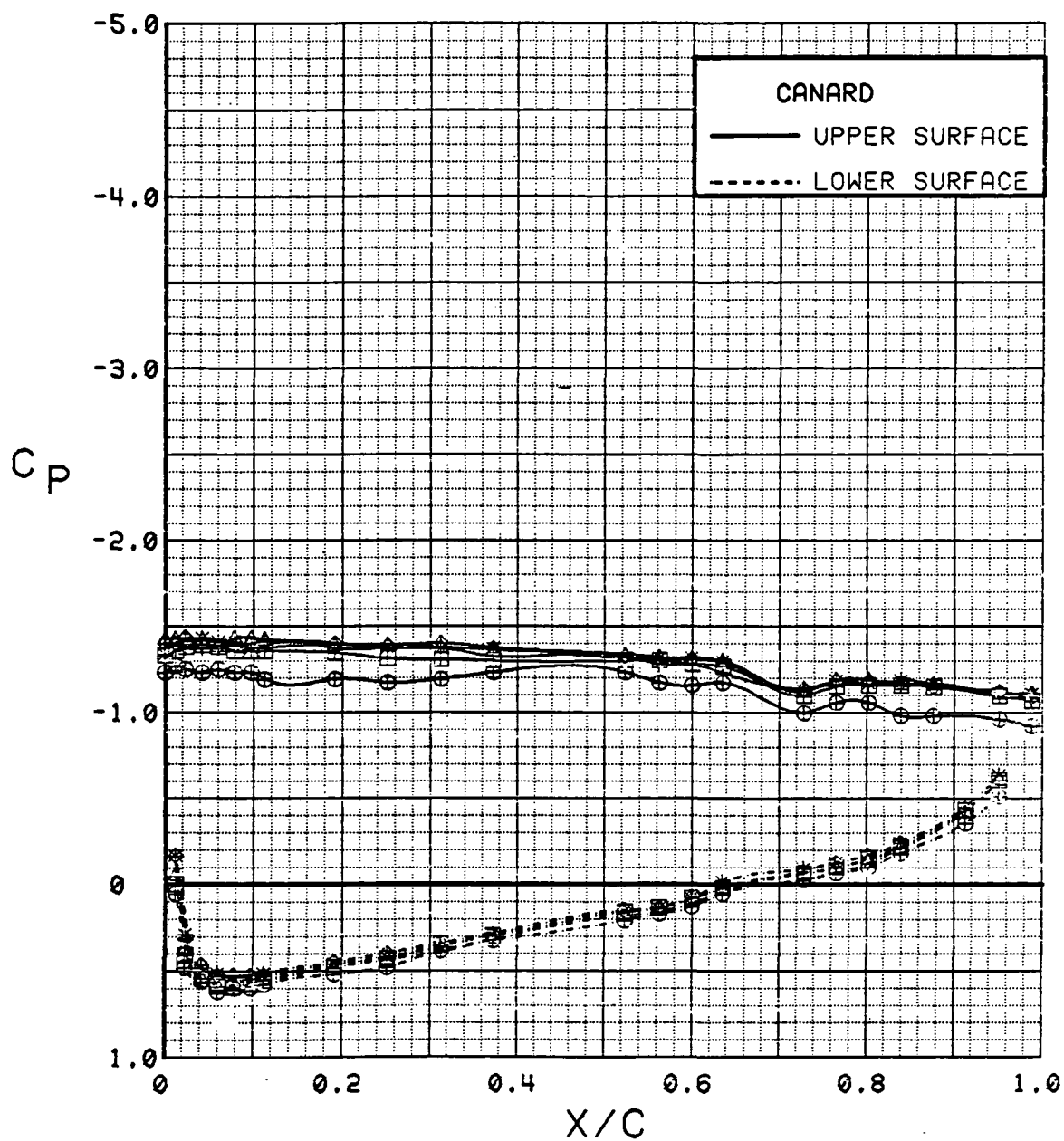


Figure 3.2.3-58 Power Effects, Wing Flaps Neutral, Alpha = 20 deg

SYM	TEST	RUN	ALPHA	CT	ITEF	OTEF	CAN	SWB
⊕	543	63	32.8	0.00	0	0	0	OFF
⊞	543	62	33.0	0.46	0	0	0	OFF
△	543	60	33.1	0.94	0	0	0	OFF
◆	543	59	33.1	1.43	0	0	0	OFF
*	543	58	33.2	1.89	0	0	0	OFF

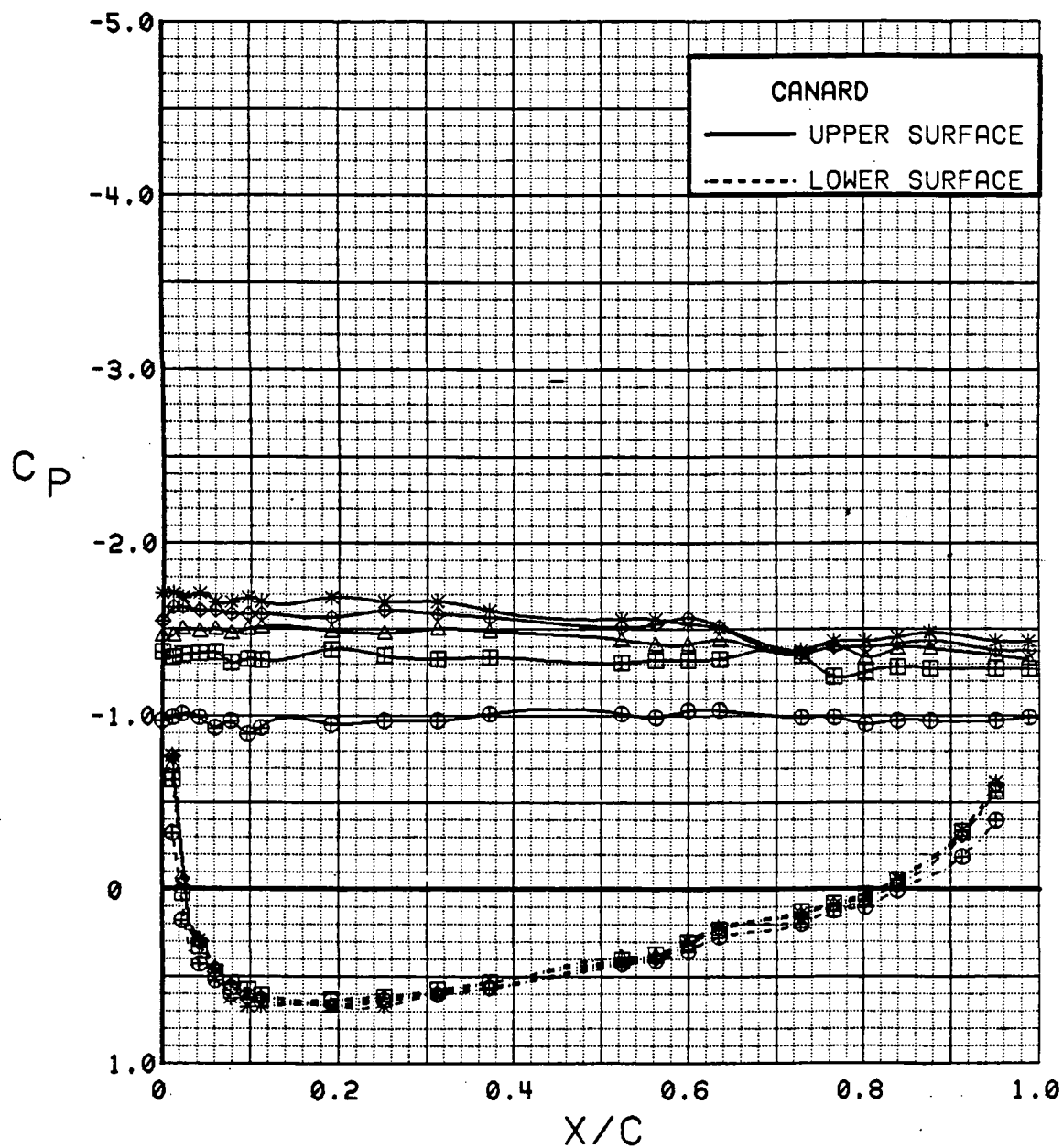


Figure 3.2.3-59 Power Effects, Wing Flaps Neutral, Alpha = 32 deg

## CANARD

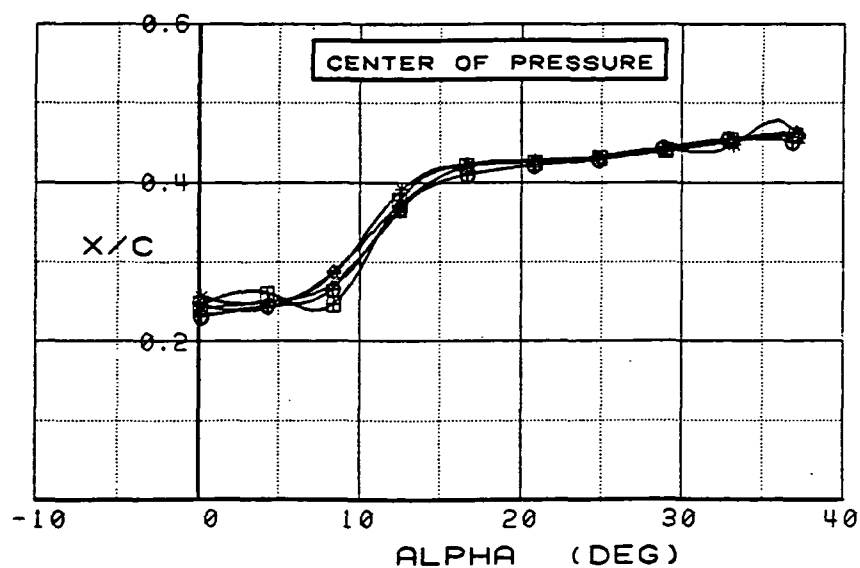
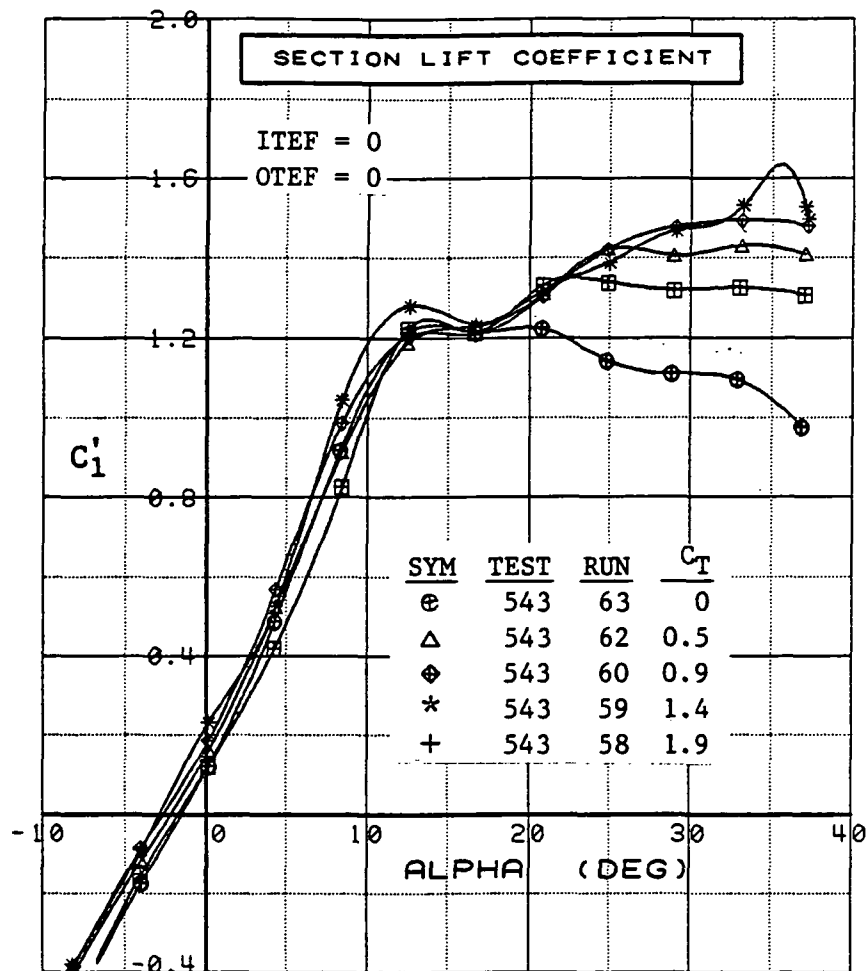


Figure 3.2.3-60 Power Effects, Wing Flaps Neutral,  
Integrated Section Properties

SYM	TEST	RUN	ALPHA	CT	ITEF	OTEF	CAN	SWB
⊕	543	11	4.4	0.00	30	30	0	OFF
⊞	543	10	4.5	0.27	30	30	0	OFF
△	543	8	4.5	0.47	30	30	0	OFF
⬠	543	6	4.5	0.94	30	30	0	OFF
*	543	5	4.5	1.40	30	30	0	OFF
+	543	4	4.5	1.90	30	30	0	OFF

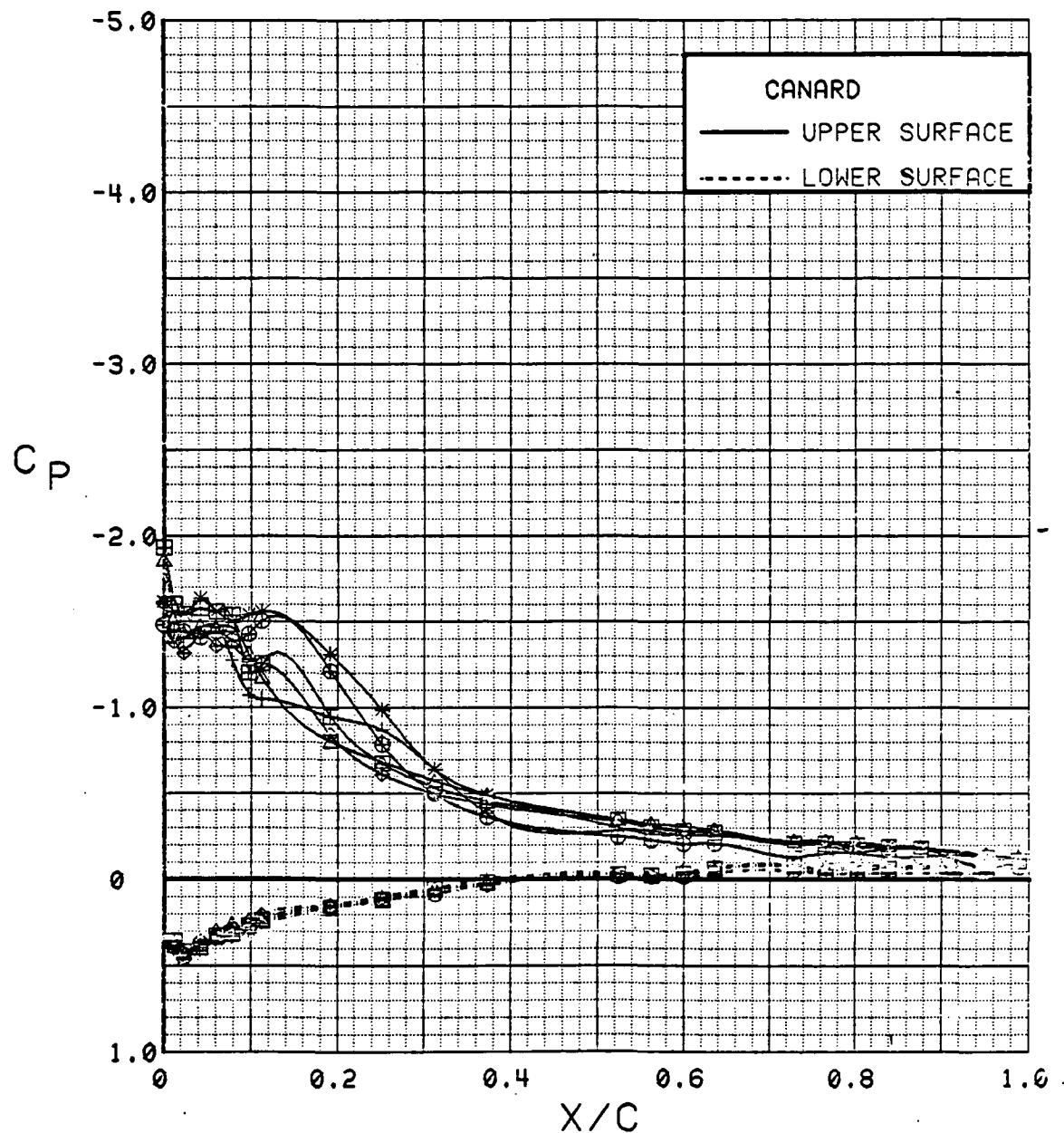


Figure 3.2.3-61 Power Effects, Wing Flaps Deflected, Alpha = 4 deg

SYM	TEST	RUN	ALPHA	CT	ITEF	OTEF	CAN	SWB
⊕	543	11	8.5	0.00	30	30	0	OFF
⊞	543	10	8.6	0.27	30	30	0	OFF
△	543	8	8.6	0.47	30	30	0	OFF
⬠	543	6	8.6	0.91	30	30	0	OFF
*	543	5	8.7	1.40	30	30	0	OFF
+	543	4	8.7	1.85	30	30	0	OFF

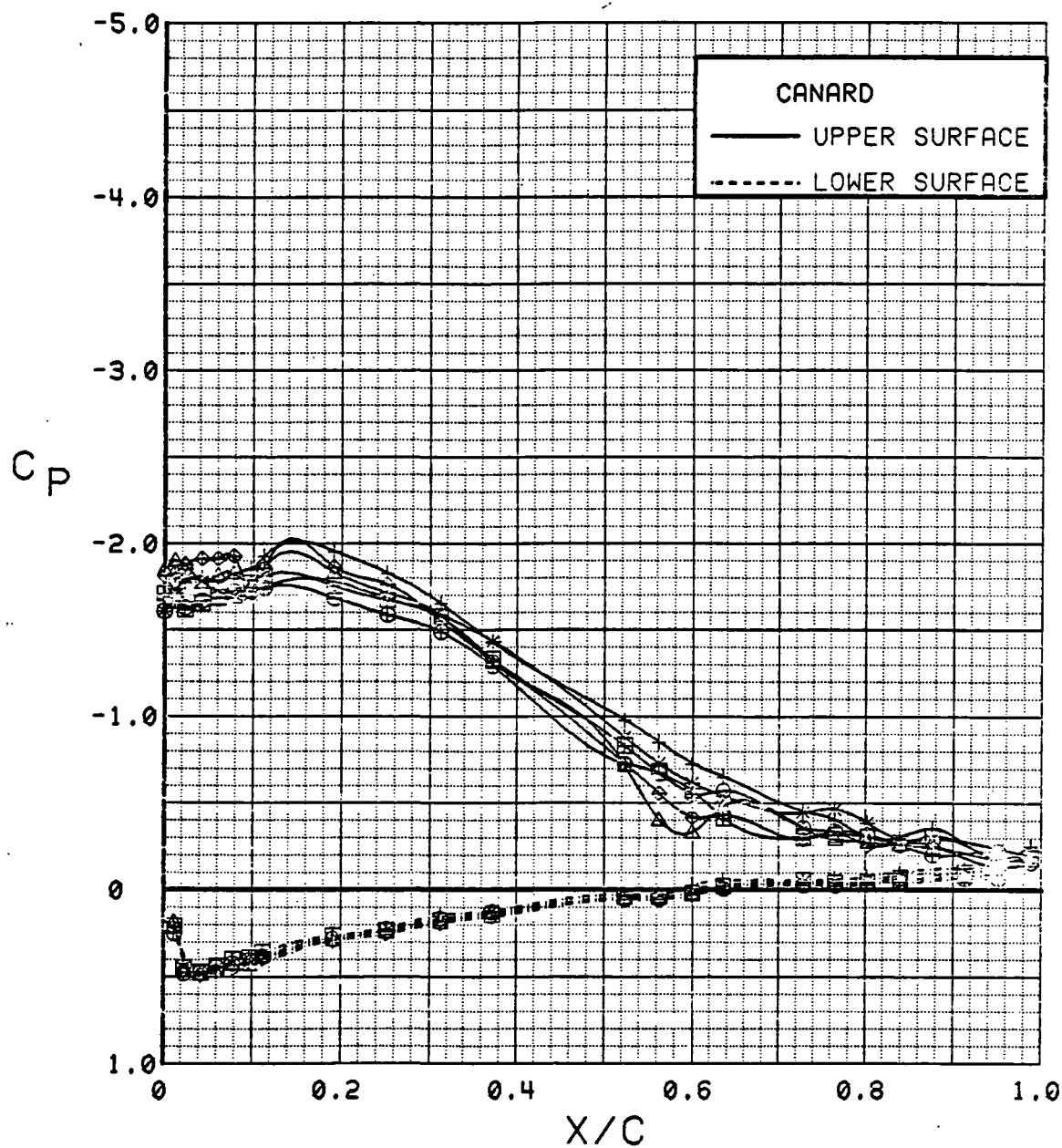


Figure 3.2.3-62 Power Effects, Wing Flaps Deflected, Alpha = 8 deg

SYM	TEST	RUN	ALPHA	CT	ITEF	OTEF	CAN	SWB
⊕	543	11	12.7	0.00	30	30	0	OFF
⊞	543	10	12.8	0.27	30	30	0	OFF
△	543	8	12.8	0.46	30	30	0	OFF
⊕	543	6	12.8	0.92	30	30	0	OFF
*	543	5	12.8	1.39	30	30	0	OFF
+	543	4	12.8	1.86	30	30	0	OFF

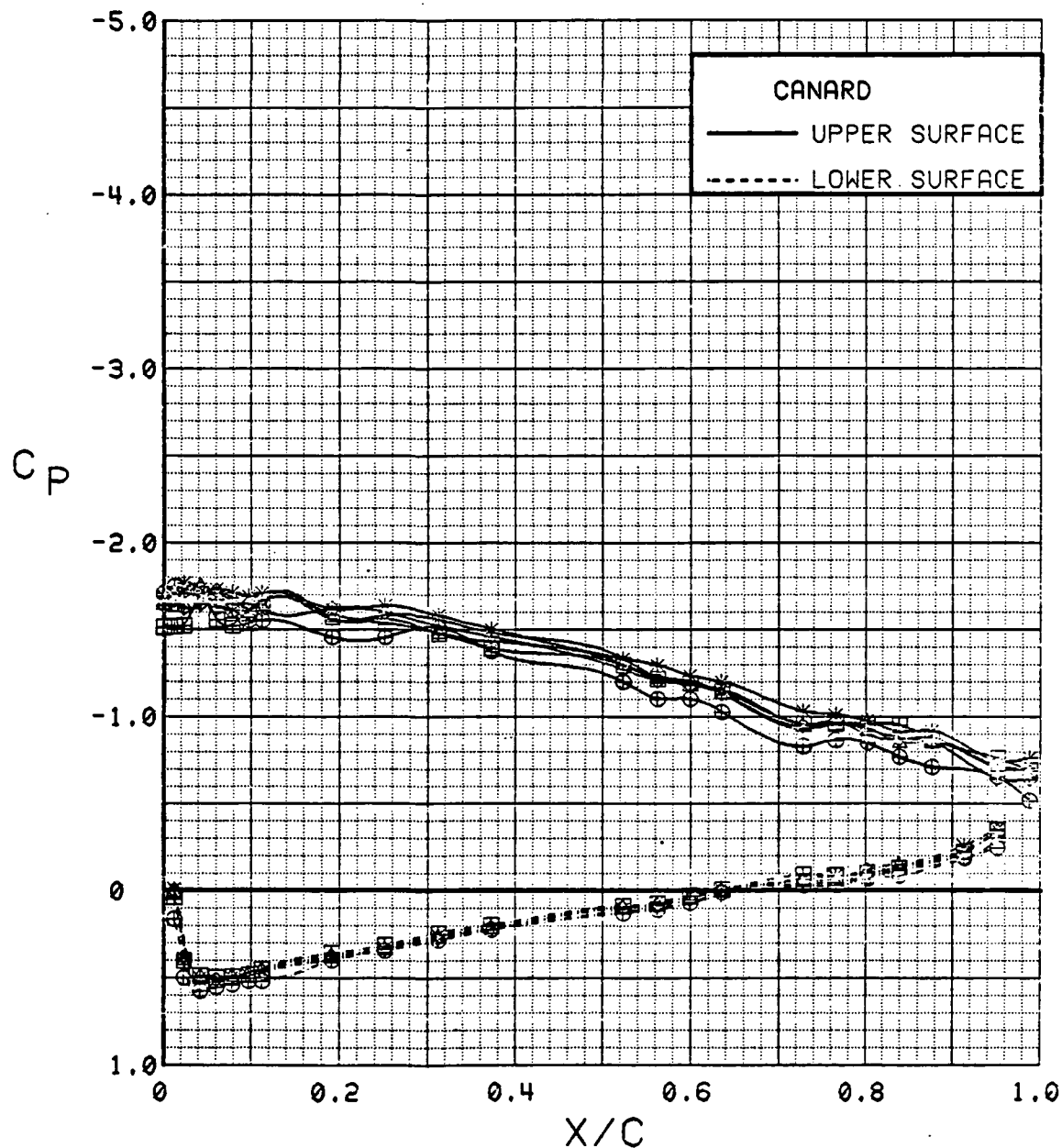


Figure 3.2.3-63 Power Effects, Wing Flaps Deflected, Alpha = 12 deg

SYM	TEST	RUN	ALPHA	CT	ITEF	OTEF	CAN	SWB
⊕	543	11	16.8	0.00	30	30	0	OFF
⊞	543	10	16.9	0.26	30	30	0	OFF
△	543	8	16.9	0.47	30	30	0	OFF
⊕	543	6	16.9	0.92	30	30	0	OFF
*	543	5	16.9	1.40	30	30	0	OFF
+	543	4	16.9	1.86	30	30	0	OFF

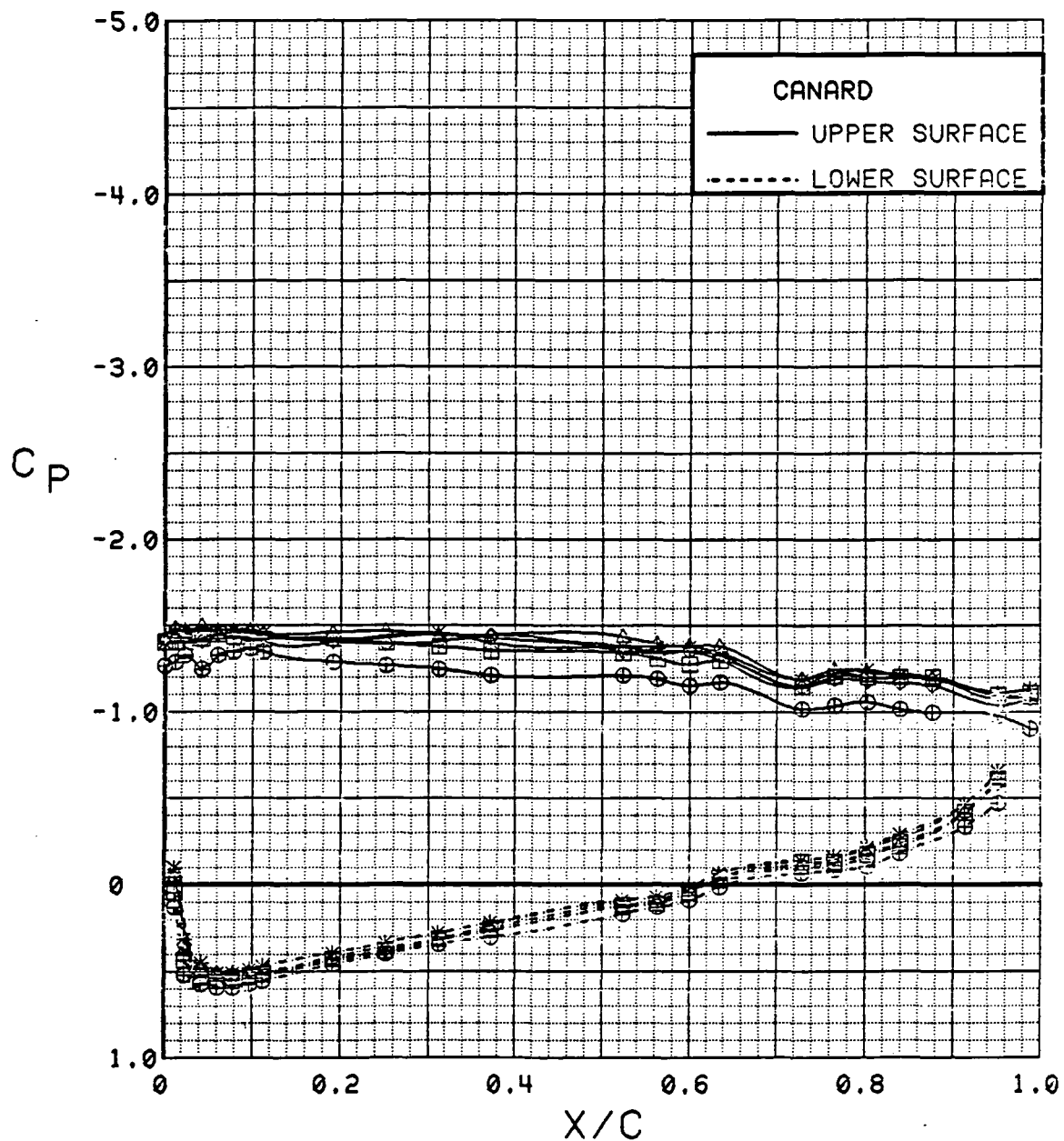


Figure 3.2.3-64 Power Effects, Wing Flaps Deflected, Alpha = 16 deg



SYM	TEST	RUN	ALPHA	CT	ITEF	OTEF	CAN	SWB
⊕	543	11	20.8	0.00	30	30	0	OFF
⊞	543	10	21.0	0.27	30	30	0	OFF
△	543	8	21.0	0.46	30	30	0	OFF
⬠	543	6	21.0	0.93	30	30	0	OFF
*	543	5	21.0	1.42	30	30	0	OFF
+	543	4	21.1	1.88	30	30	0	OFF

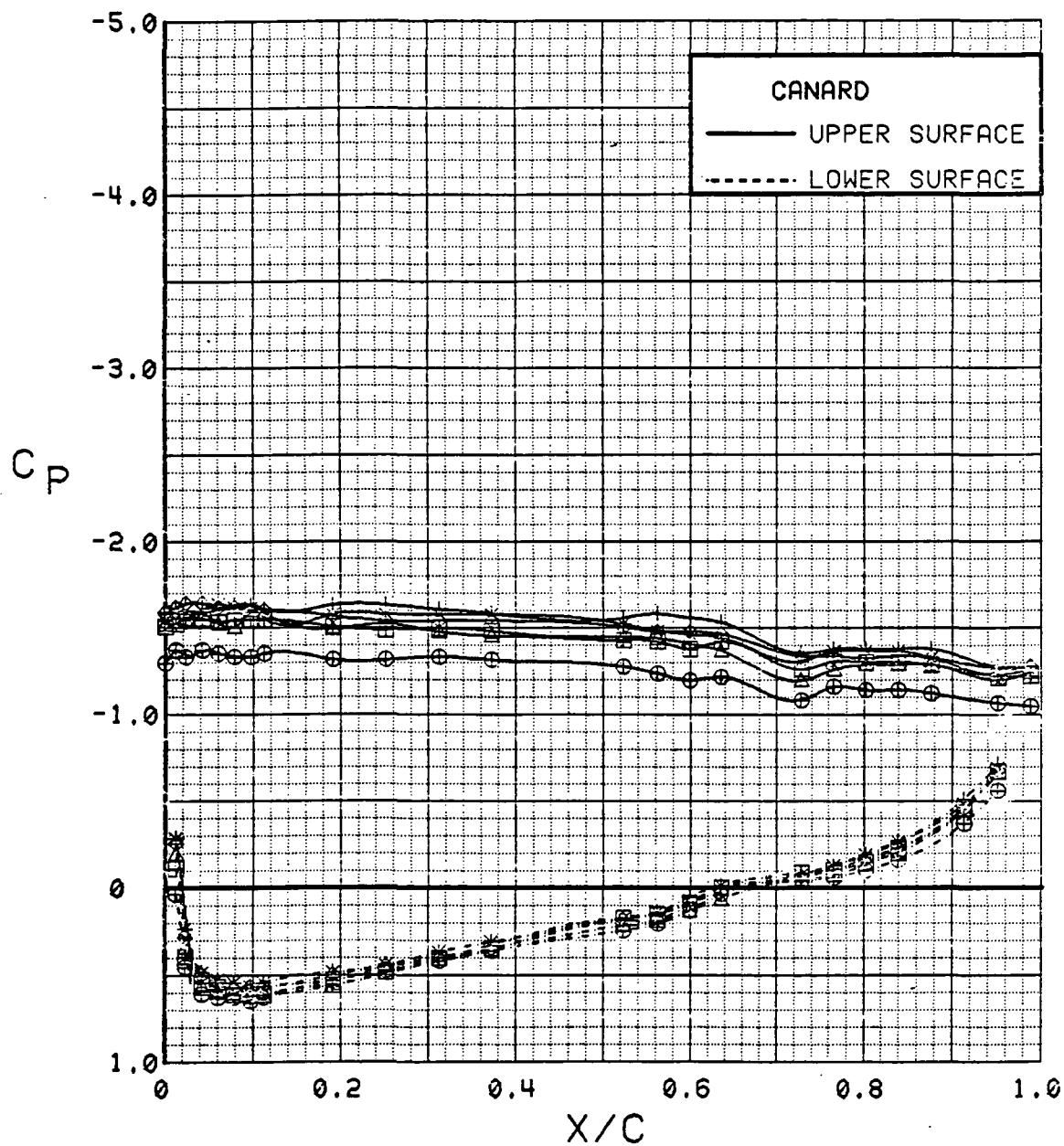


Figure 3.2.3-65 Power Effects, Wing Flaps Deflected, Alpha = 20 deg

SYM	TEST	RUN	ALPHA	CT	ITEF	OTEF	CAN	SWB
⊕	543	11	28.9	0.00	30	30	0	OFF
⊞	543	8	29.1	0.46	30	30	0	OFF
△	543	6	29.1	0.93	30	30	0	OFF
⊕	543	5	29.2	1.39	30	30	0	OFF
*	543	4	29.2	1.89	30	30	0	OFF

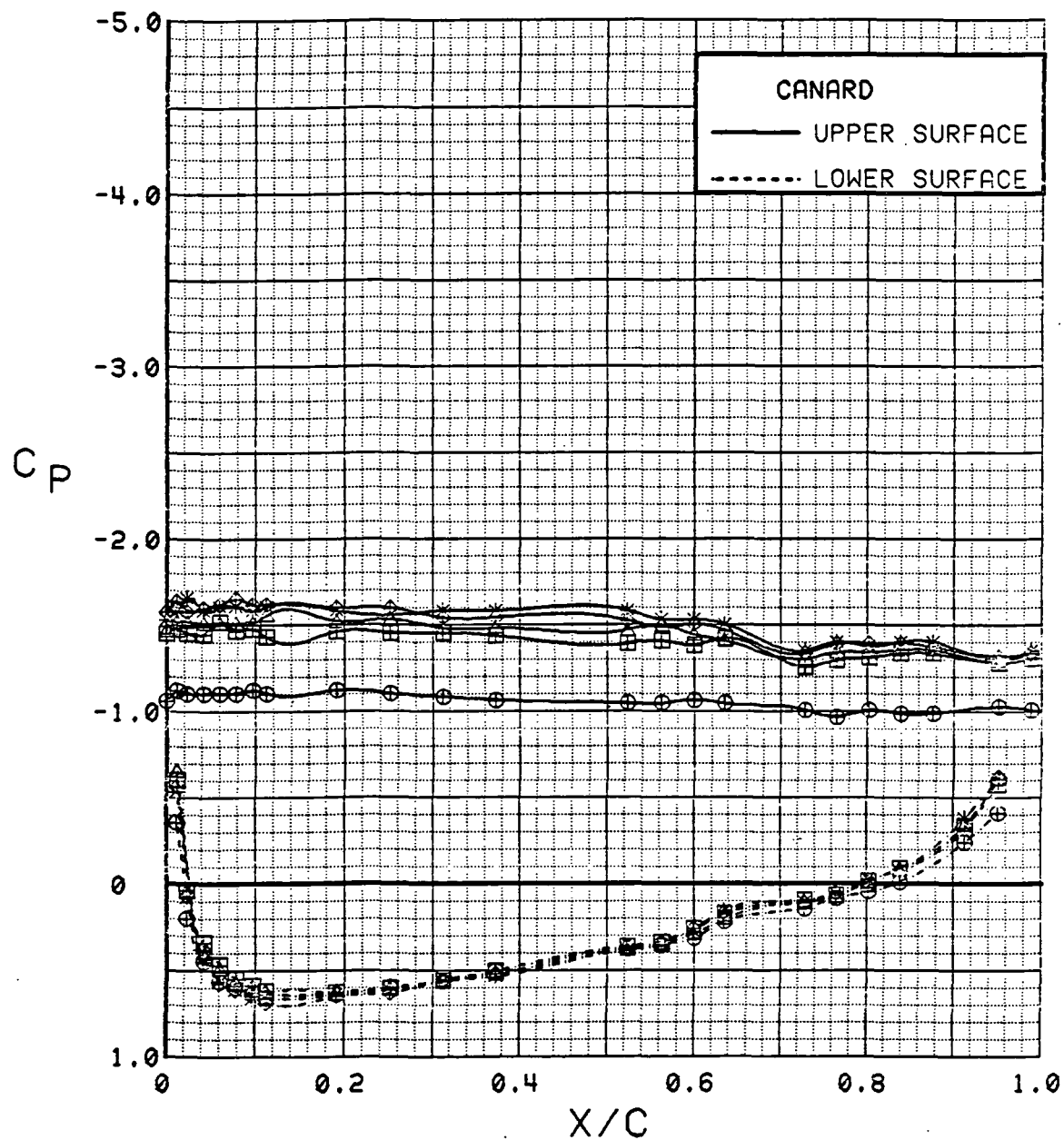


Figure 3.2.3-66 Power Effects, Wing Flaps Deflected, Alpha = 28 deg

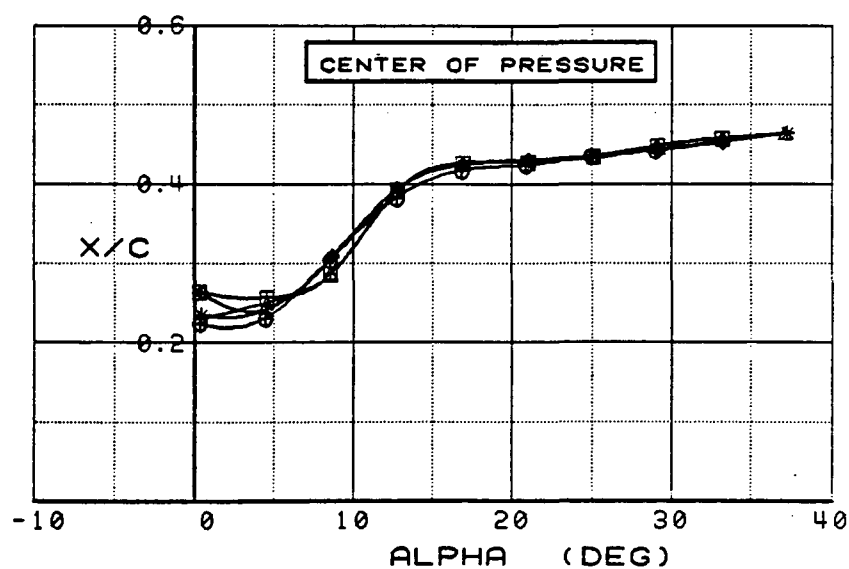
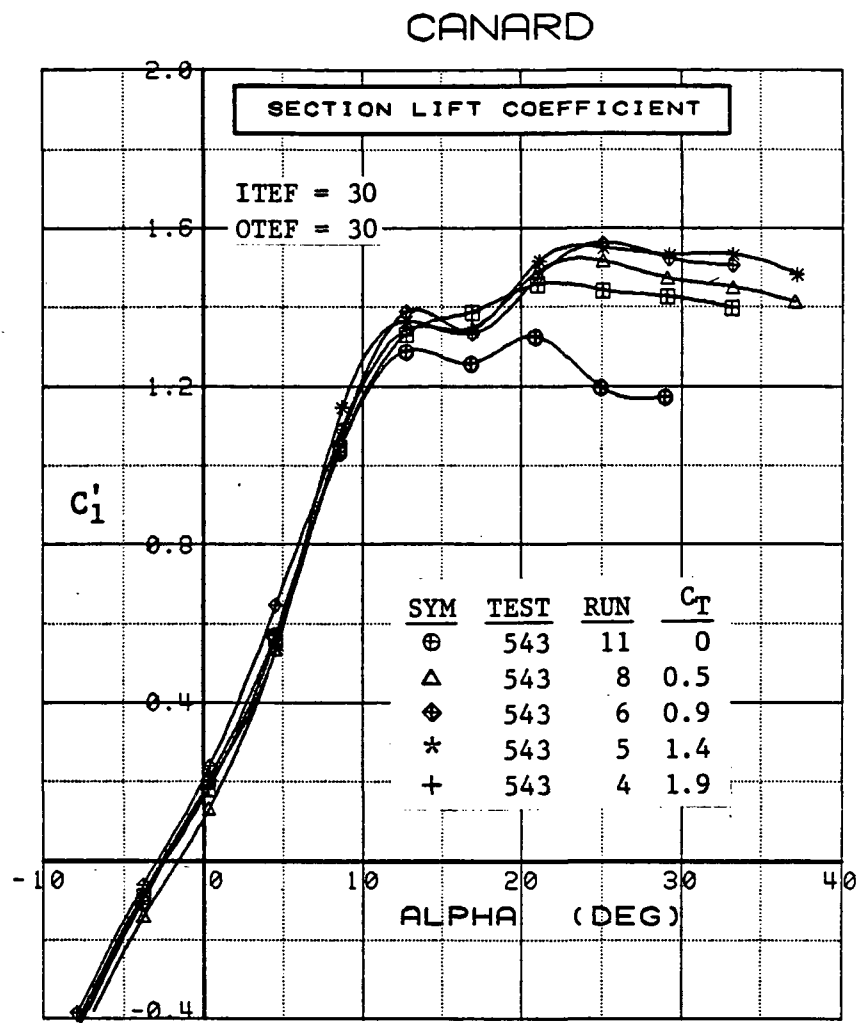


Figure 3.2.3-67 Power Effects, Wing Flaps Deflected, Integrated Section Properties

SYM	TEST	RUN	ALPHA	CT	ITEF	OTEF	CAN	SWB
⊕	537	32	0.3	0.91	30	30	0	OFF
⊞	537	49	0.4	0.90	30	30	0	ON

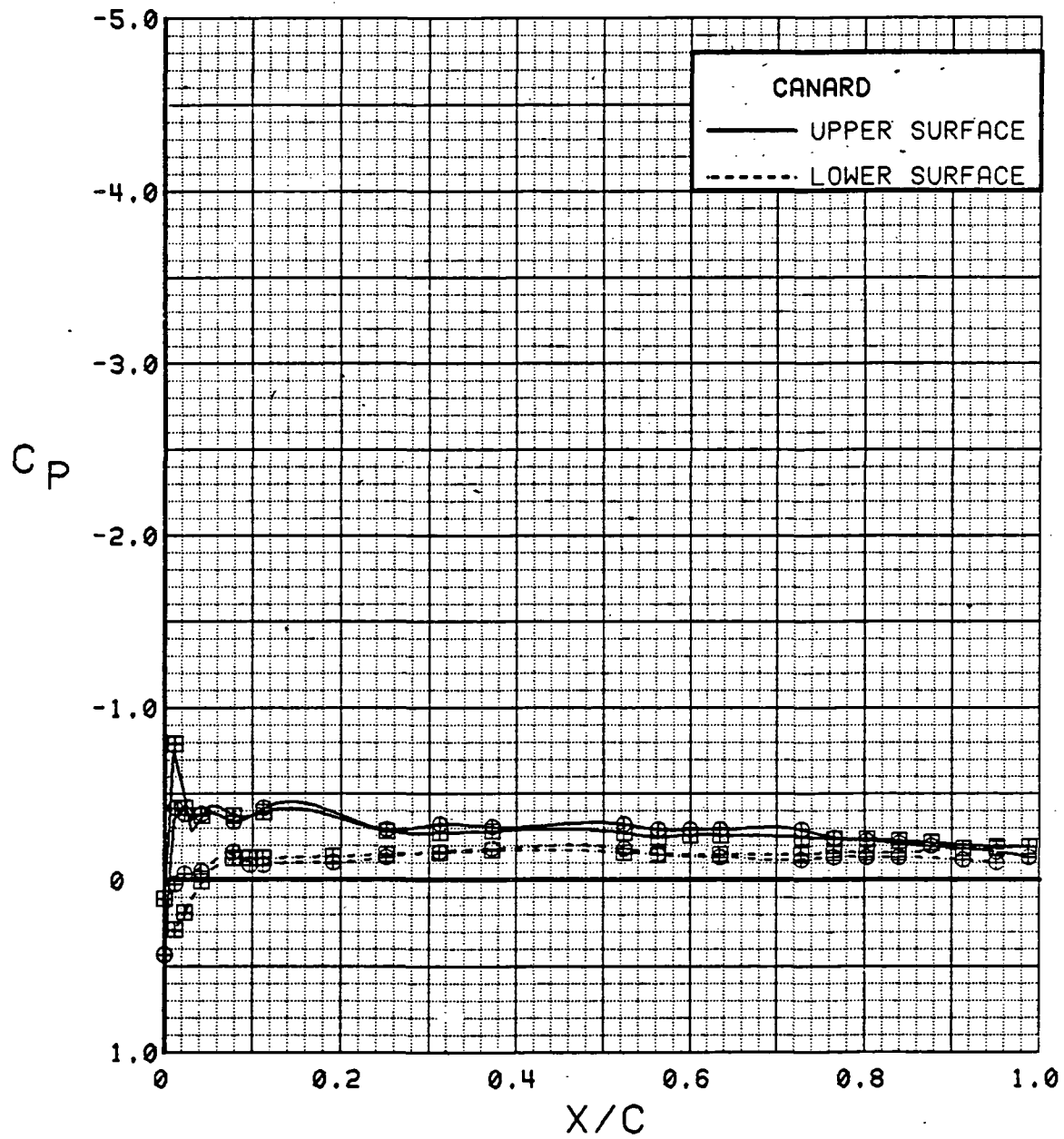


Figure 3.2.3-68 Spanwise Blowing Effects,  $C_T = 0.9$ ,  $\alpha = 0$  deg

SYM	TEST	RUN	ALPHA	CT	ITEF	OTEF	CAN	SWB
⊕	537	32	4.5	0.91	30	30	0	OFF
⊞	537	49	4.5	0.90	30	30	0	ON

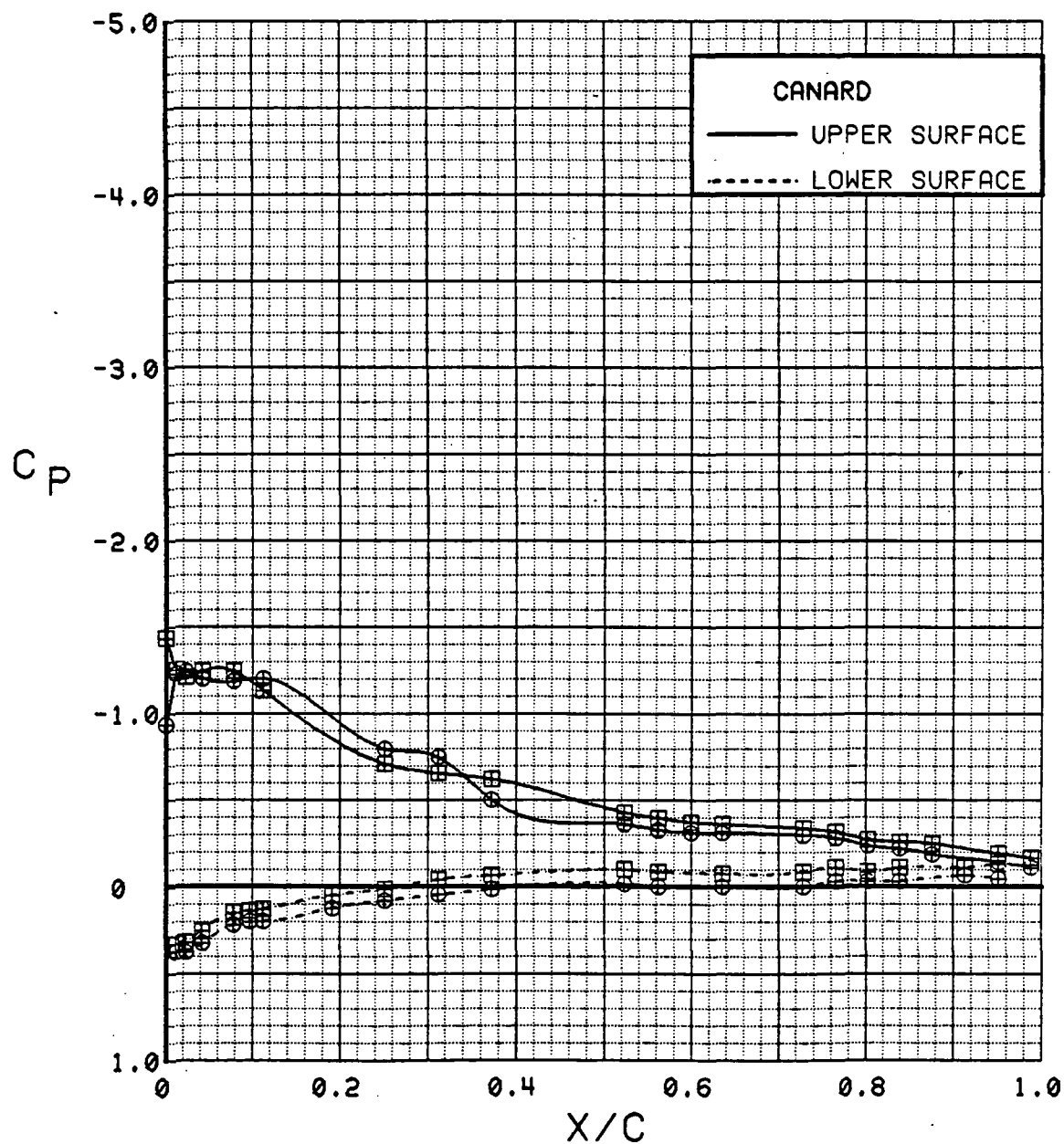


Figure 3.2.3-69 Spanwise Blowing Effects,  $C_T = 0.9$ ,  $\alpha = 4$  deg

SYM	TEST	RUN	ALPHA	CT	ITEF	OTEF	CAN	SWB
⊕	537	32	8.6	0.90	30	30	0	OFF
⊞	537	49	8.7	0.90	30	30	0	ON

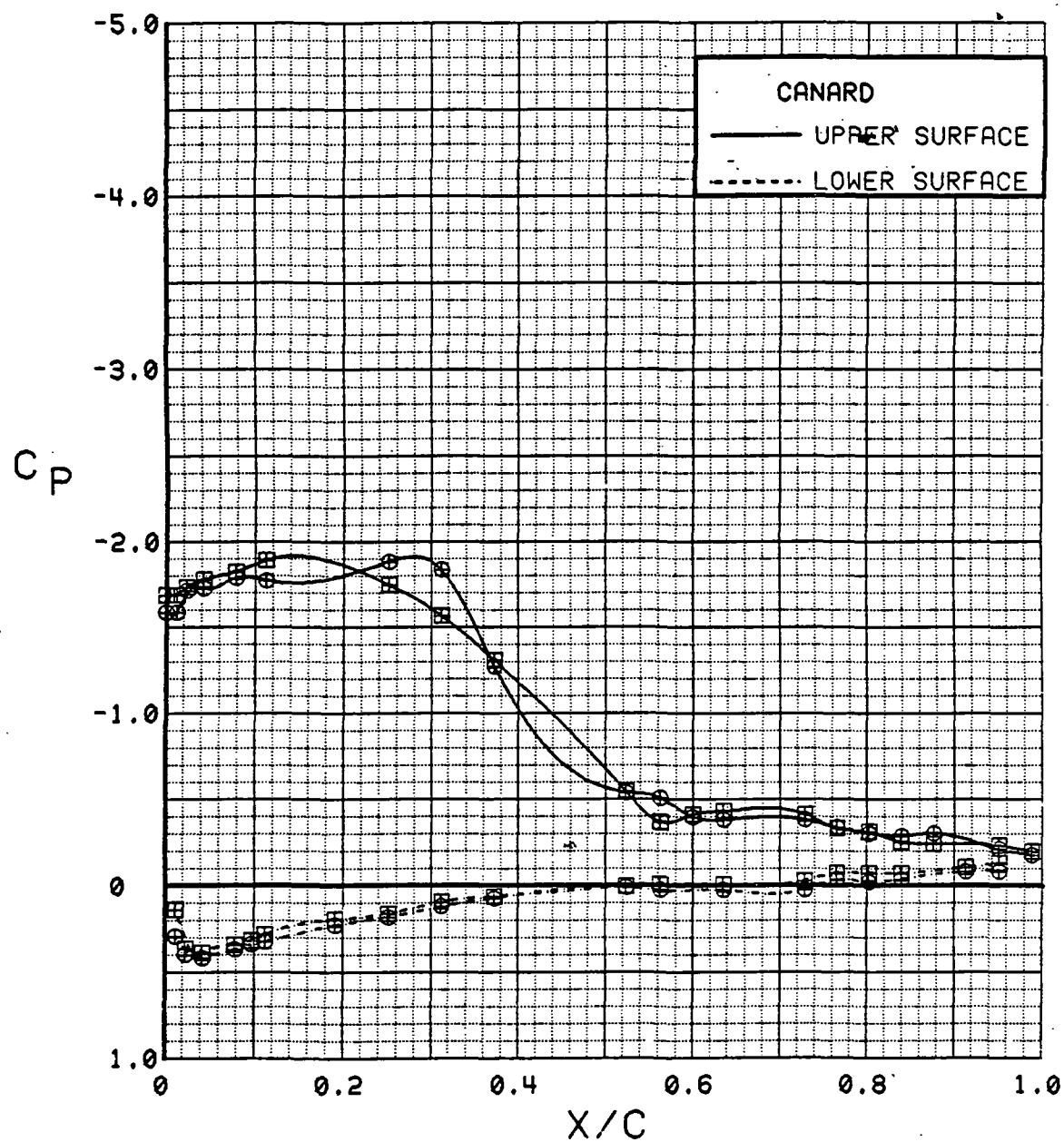


Figure 3.2.3-70 Spanwise Blowing Effects,  $C_T = 0.9$ ,  $\alpha = 8$  deg

SYM	TEST	RUN	ALPHA	CT	ITEF	OTEF	CAN	SWB
⊕	537	32	12.8	0.92	30	30	0	OFF
⊞	537	49	12.9	0.90	30	30	0	ON

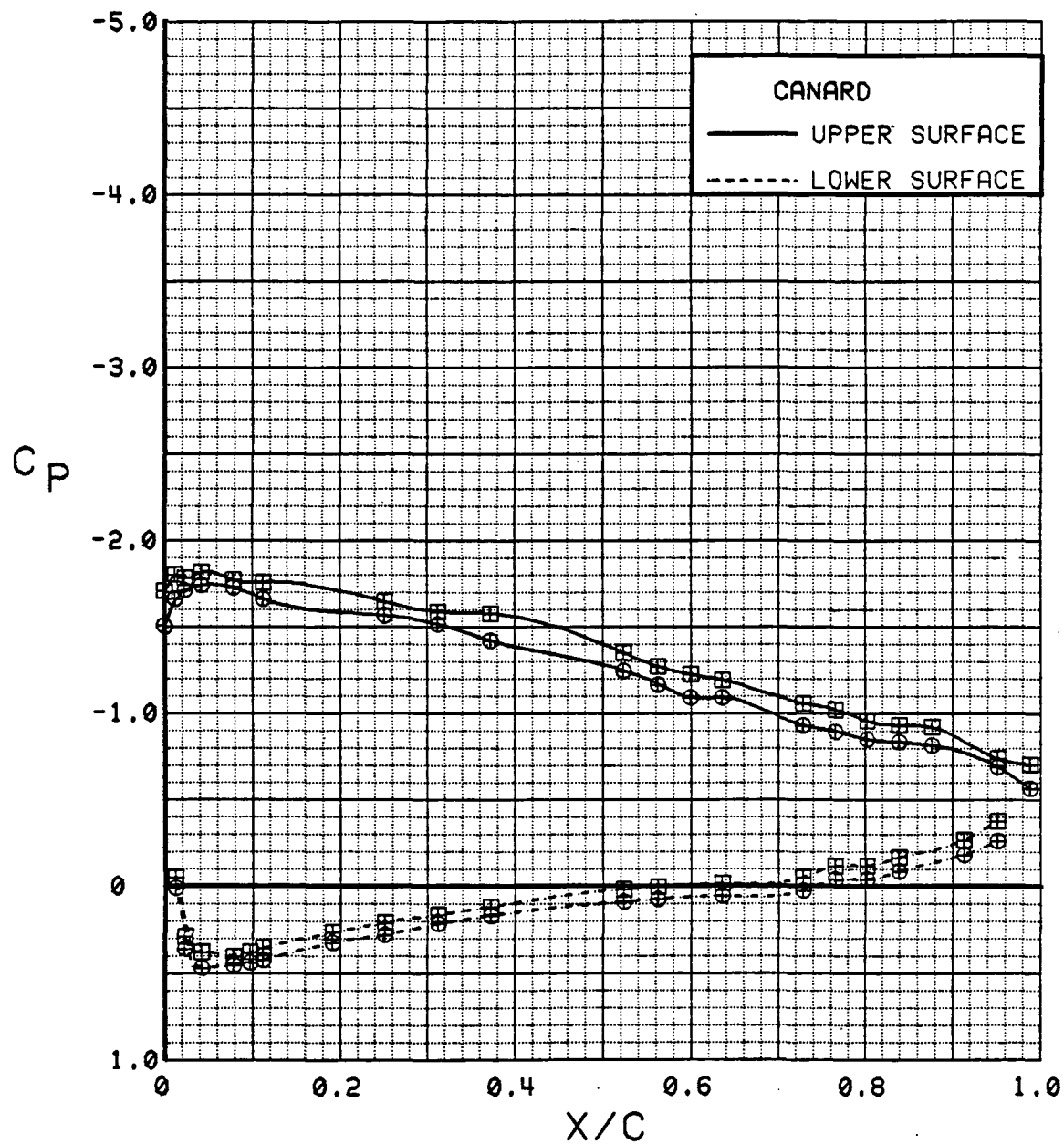


Figure 3.2.3-71 Spanwise Blowing Effects,  $C_T = 0.9$ ,  $\alpha = 12$  deg

SYM	TEST	RUN	ALPHA	CT	ITEF	OTEF	CAN	SWB
⊕	537	32	16.8	0.92	30	30	0	OFF
⊞	537	49	17.0	0.93	30	30	0	ON

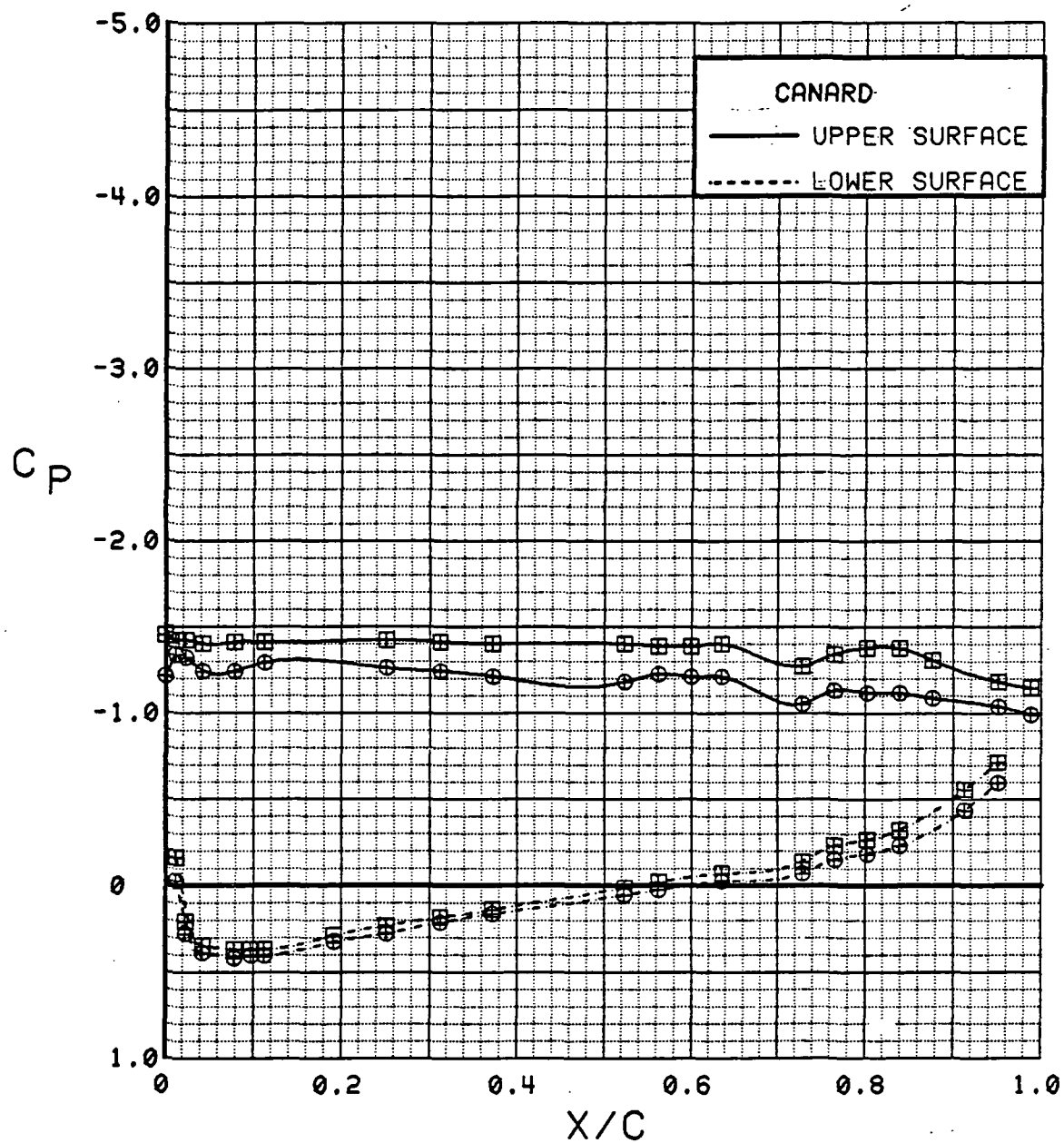


Figure 3.2.3-72 Spanwise Blowing Effects,  $C_T = 0.9$ ,  $\alpha = 16^\circ$



SYM	TEST	RUN	ALPHA	CT	ITEF	OTEF	CAN	SWB
⊕	537	32	20.9	0.90	30	30	0	OFF
⊞	537	49	21.1	0.93	30	30	0	ON

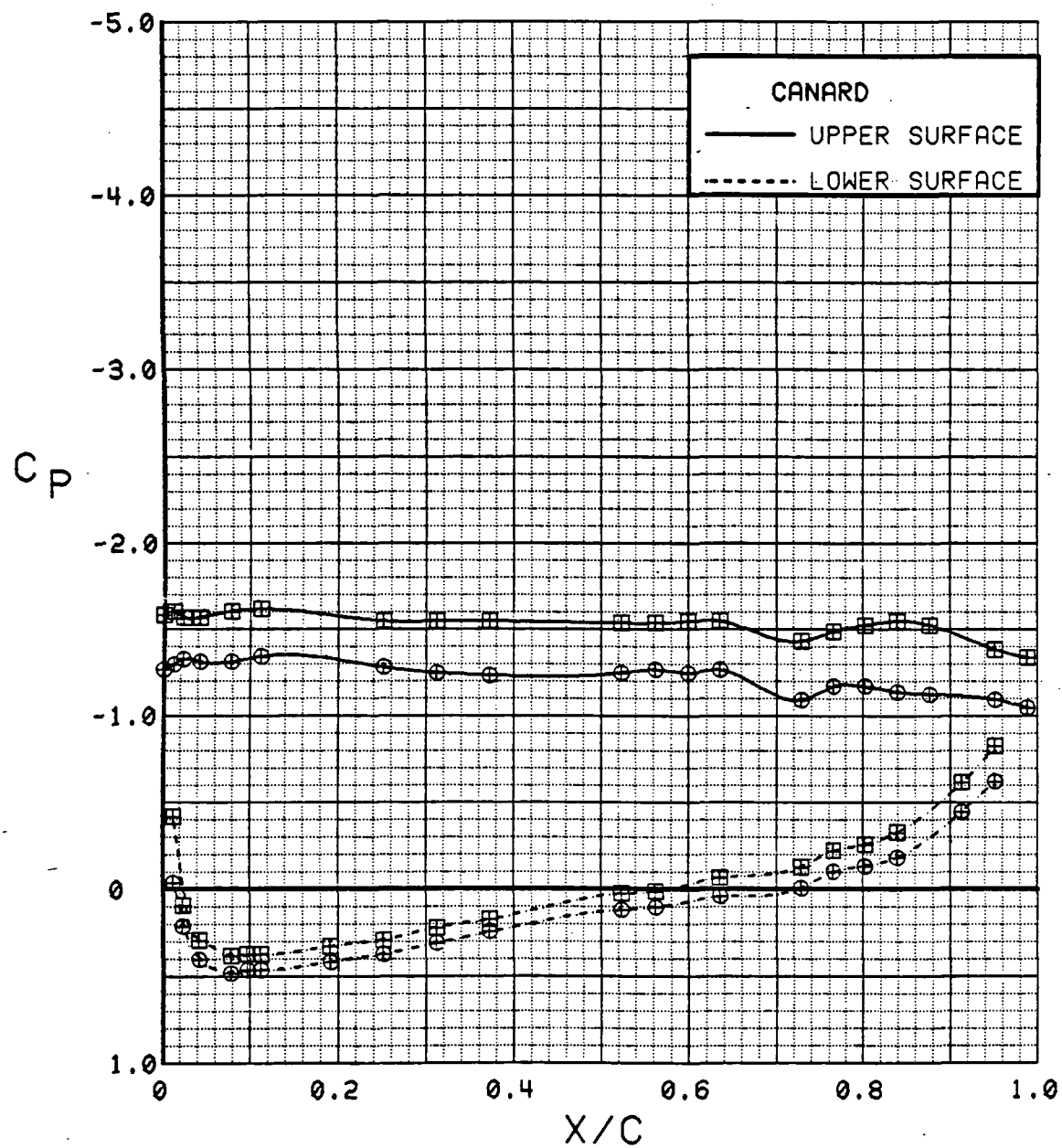


Figure 3.2.3-73 Spanwise Blowing Effects,  $C_T = 0.9$ ,  $\alpha = 20^\circ$

SYM	TEST	RUN	ALPHA	CT	ITEF	OTEF	CAN	SWB
⊕	537	32	37.1	0.93	30	30	0	OFF
⊞	537	49	37.1	0.92	30	30	0	ON

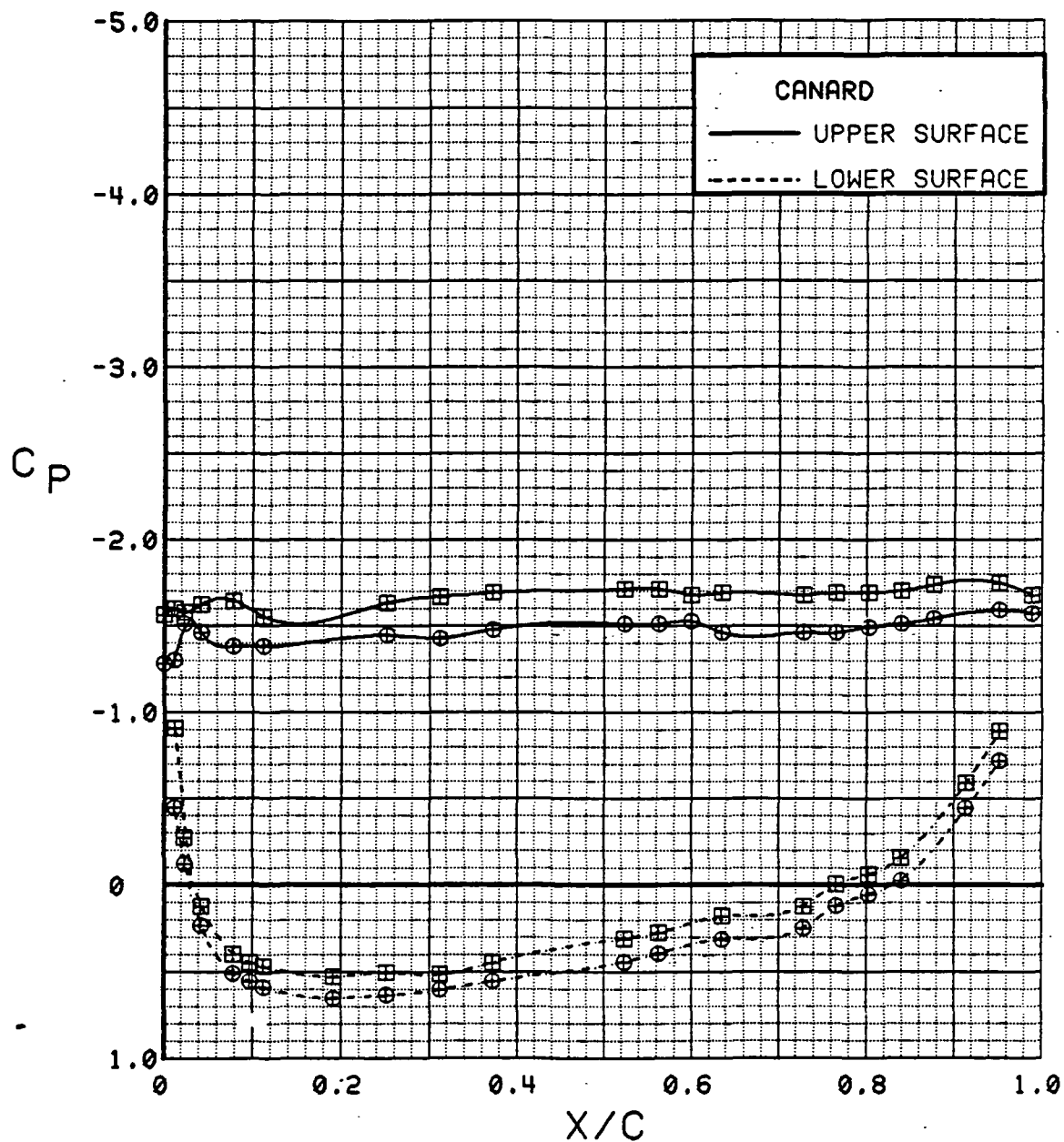


Figure 3.2.3-74 Spanwise Blowing Effects,  $C_T = 0.9$ ,  $\alpha = 36^\circ$

SYM	TEST	RUN	ALPHA	CT	ITEF	OTEF	CAN	SWB
⊕	537	28	0.3	1.89	30	30	0	OFF
⊞	537	53	0.4	1.81	30	30	0	ON

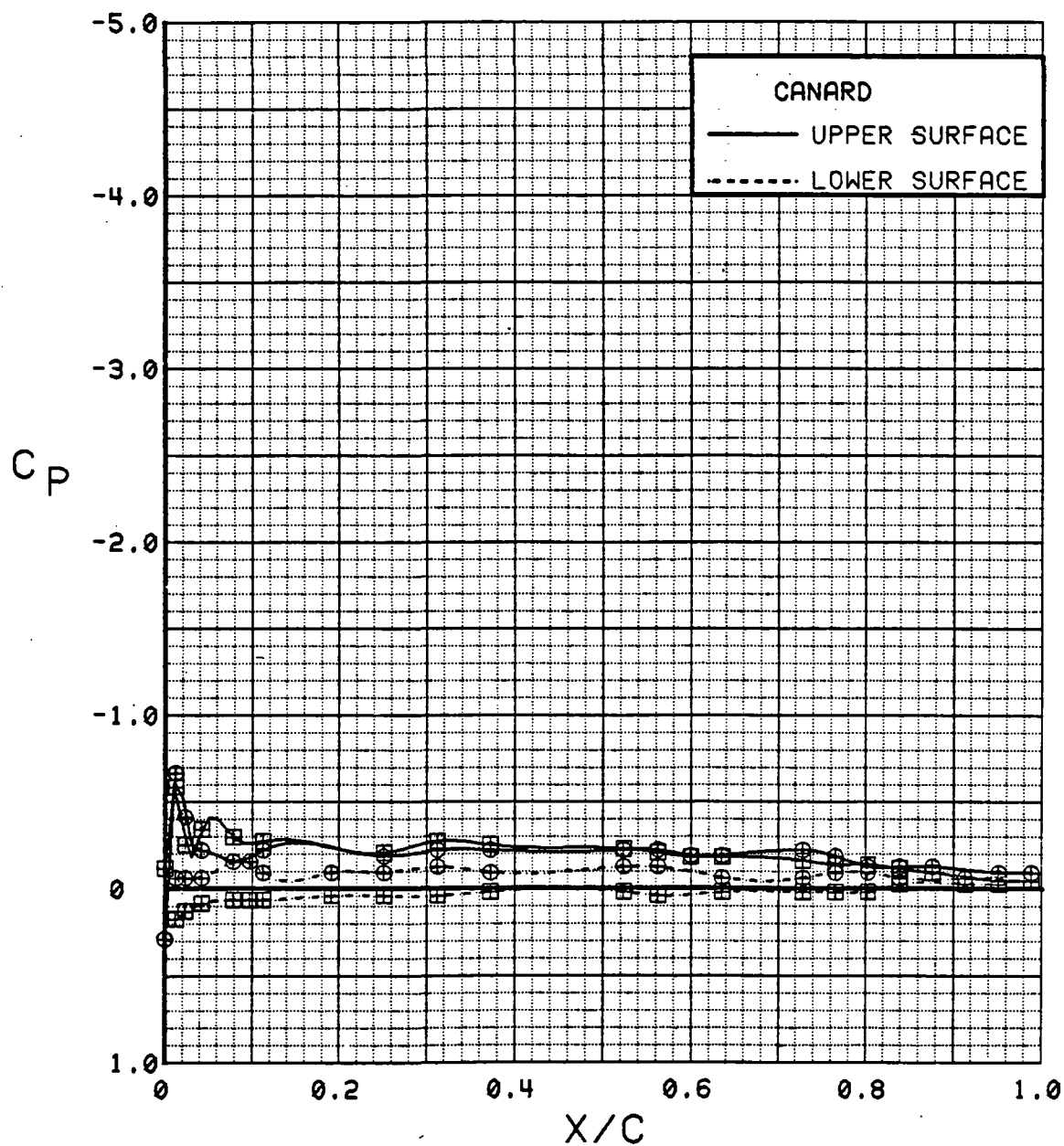


Figure 3.2.3-75 Spanwise Blowing Effects,  $C_T = 1.8$ ,  $\alpha = 0^\circ$

SYM	TEST	RUN	ALPHA	CT	ITEF	OTEF	CAN	SWB
⊕	537	28	4.5	1.87	30	30	0	OFF
⊞	537	53	4.5	1.81	30	30	0	ON

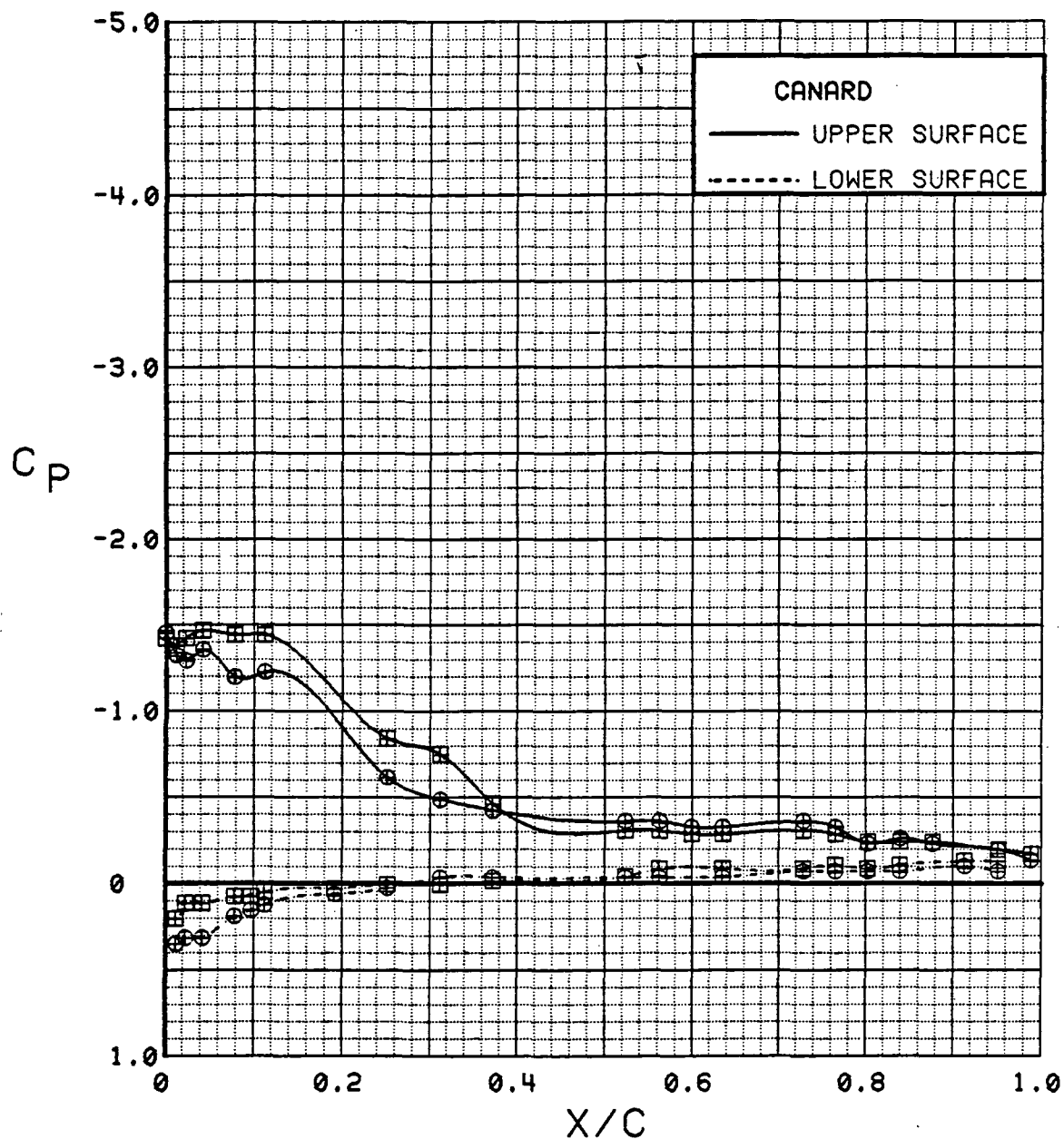


Figure 3.2.3-76 Spanwise Blowing Effects,  $C_T = 1.8$ ,  $\alpha = 4$  deg

SYM	TEST	RUN	ALPHA	CT	ITEF	OTEF	CAN	SWB
⊕	537	28	8.7	1.88	30	30	0	OFF
⊞	537	53	8.7	1.83	30	30	0	ON

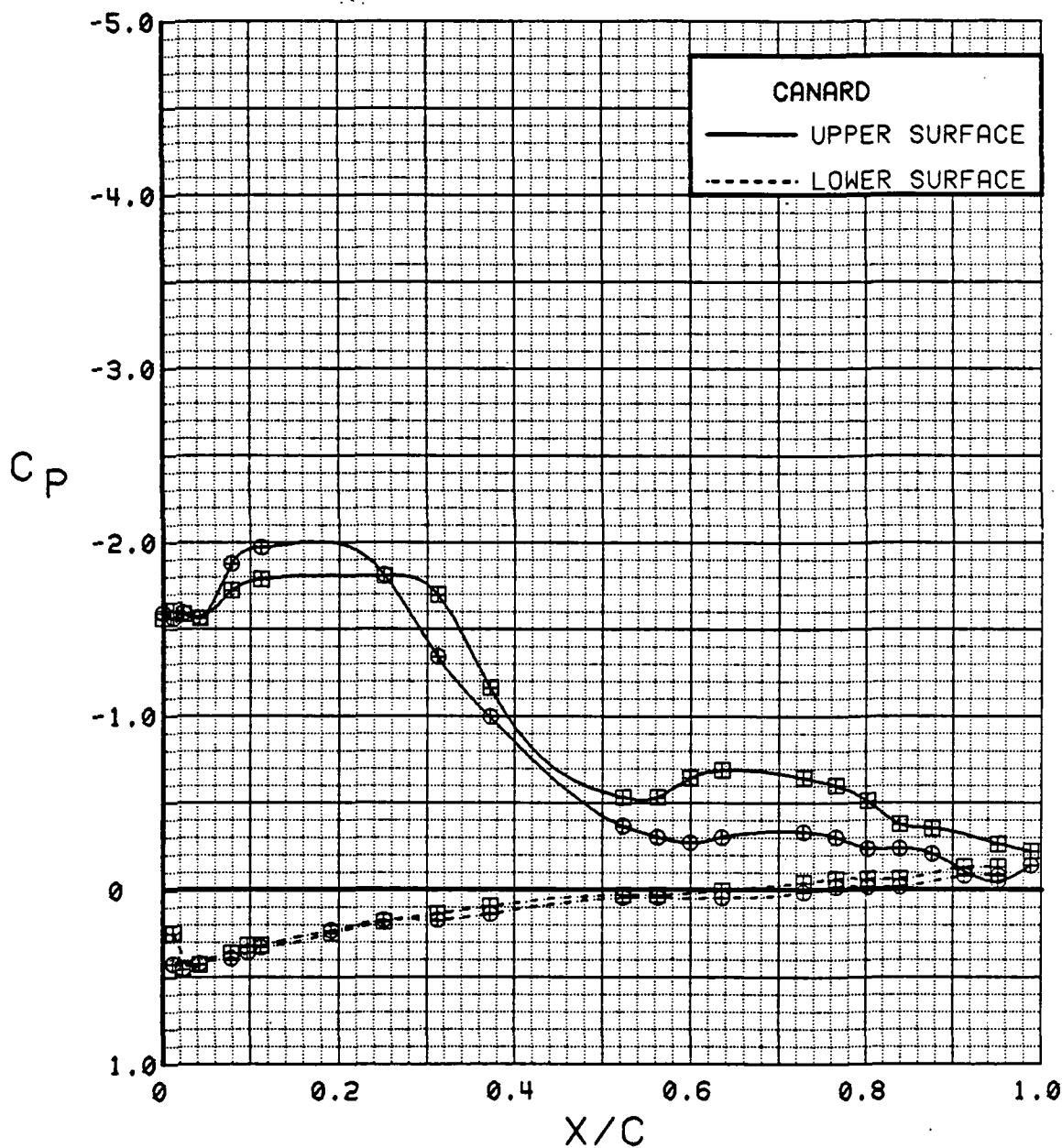


Figure 3.2.3-77 Spanwise Blowing Effects,  $C_T = 1.8$ ,  $\alpha = 8^\circ$

SYM	TEST	RUN	ALPHA	CT	ITEF	OTEF	CAN	SWB
⊕	537	28	12.8	1.82	30	30	0	OFF
⊞	537	53	12.9	1.82	30	30	0	ON

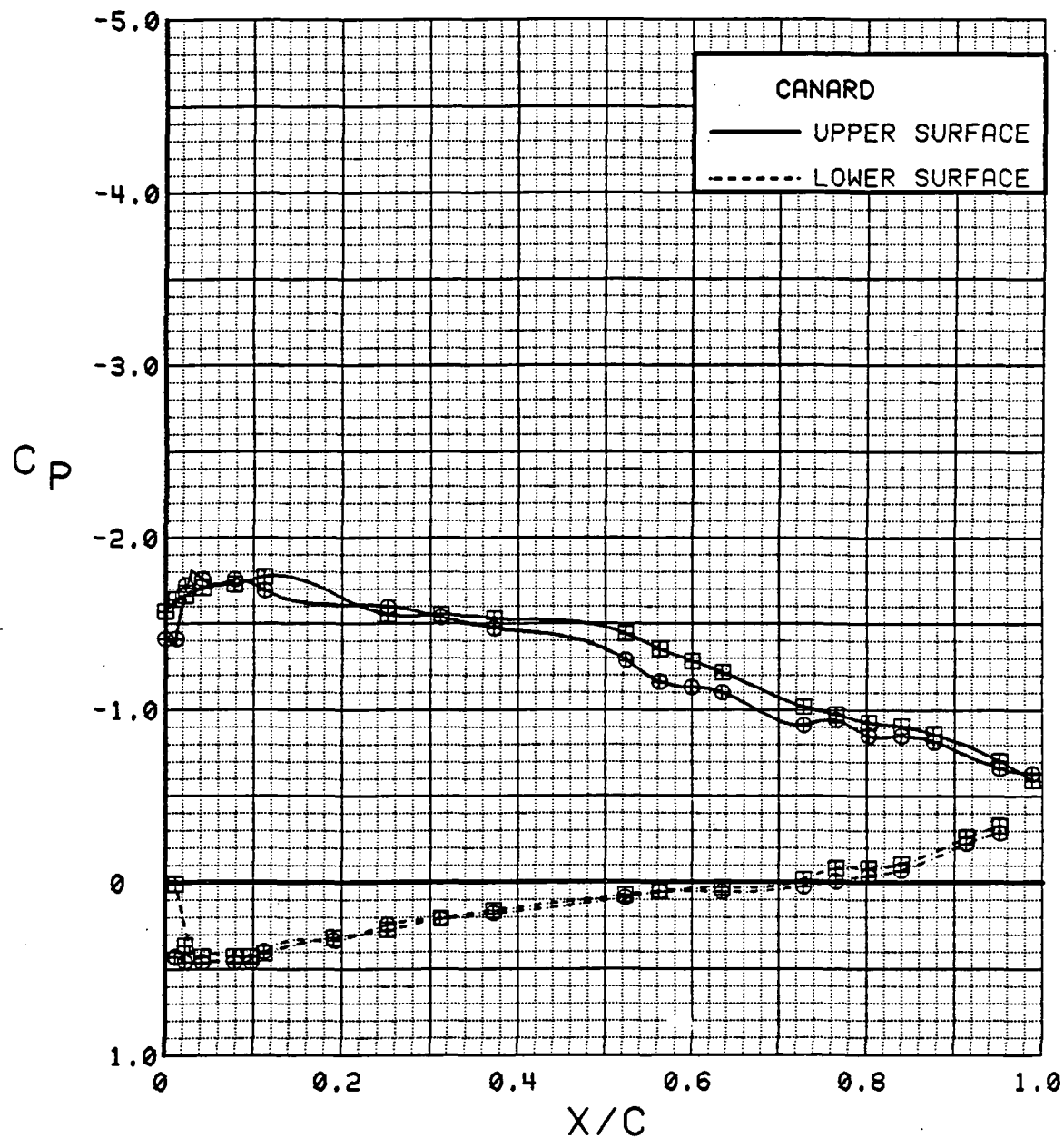


Figure 3.2.3-78 Spanwise Blowing Effects,  $C_T = 1.8$ ,  $\alpha = 12^\circ$

SYM	TEST	RUN	ALPHA	CT	ITEF	OTEF	CAN	SWB
⊕	537	28	16.9	1.84	30	30	0	OFF
⊞	537	53	17.1	1.79	30	30	0	ON

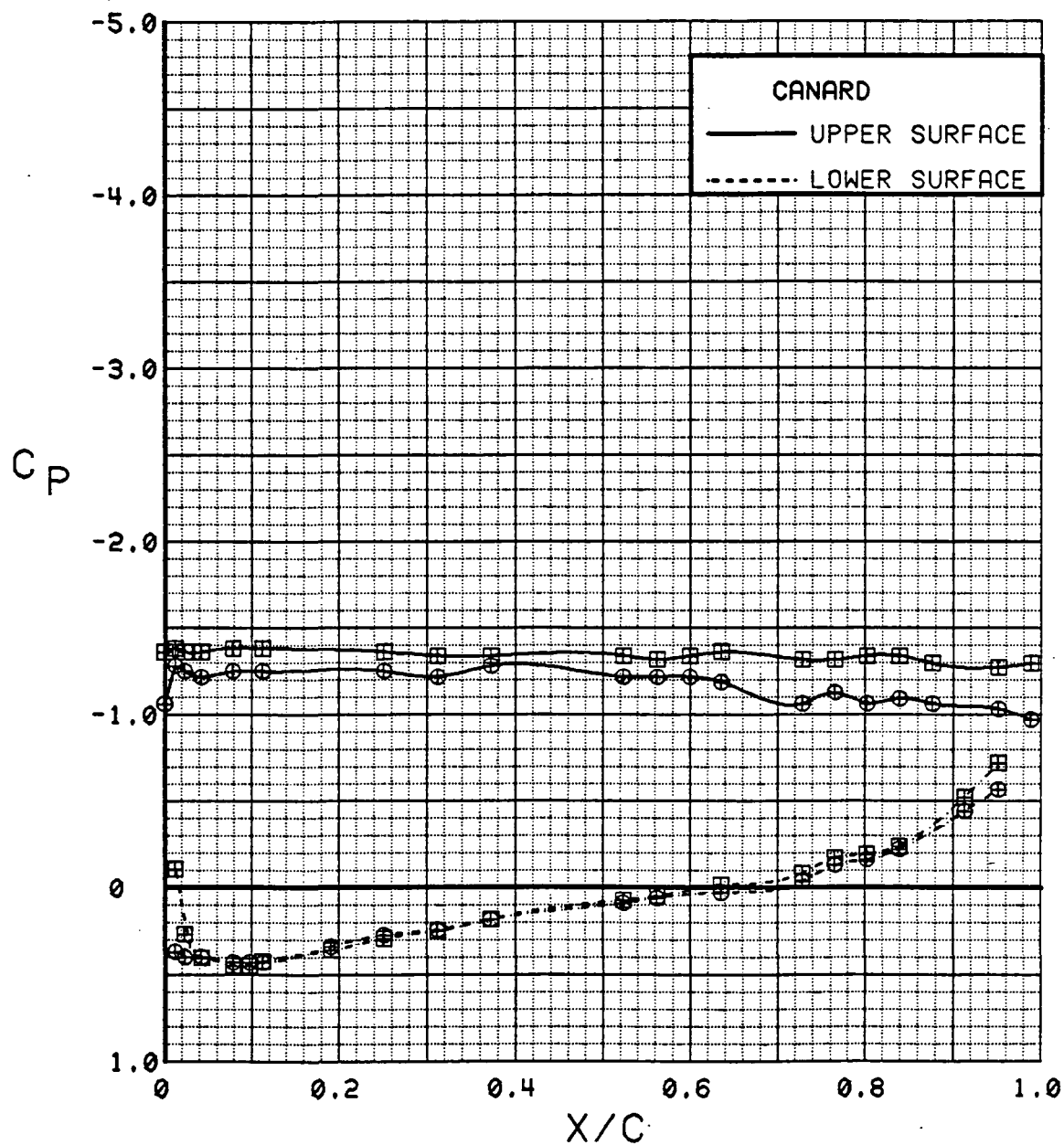


Figure 3.2.3-79 Spanwise Blowing Effects,  $C_T = 1.8$ ,  $\alpha = 16^\circ$

SYM	TEST	RUN	ALPHA	CT	ITEF	OTEF	CAN	SWB
⊕	537	28	21.0	1.83	30	30	0	OFF
⊞	537	53	21.2	1.83	30	30	0	ON

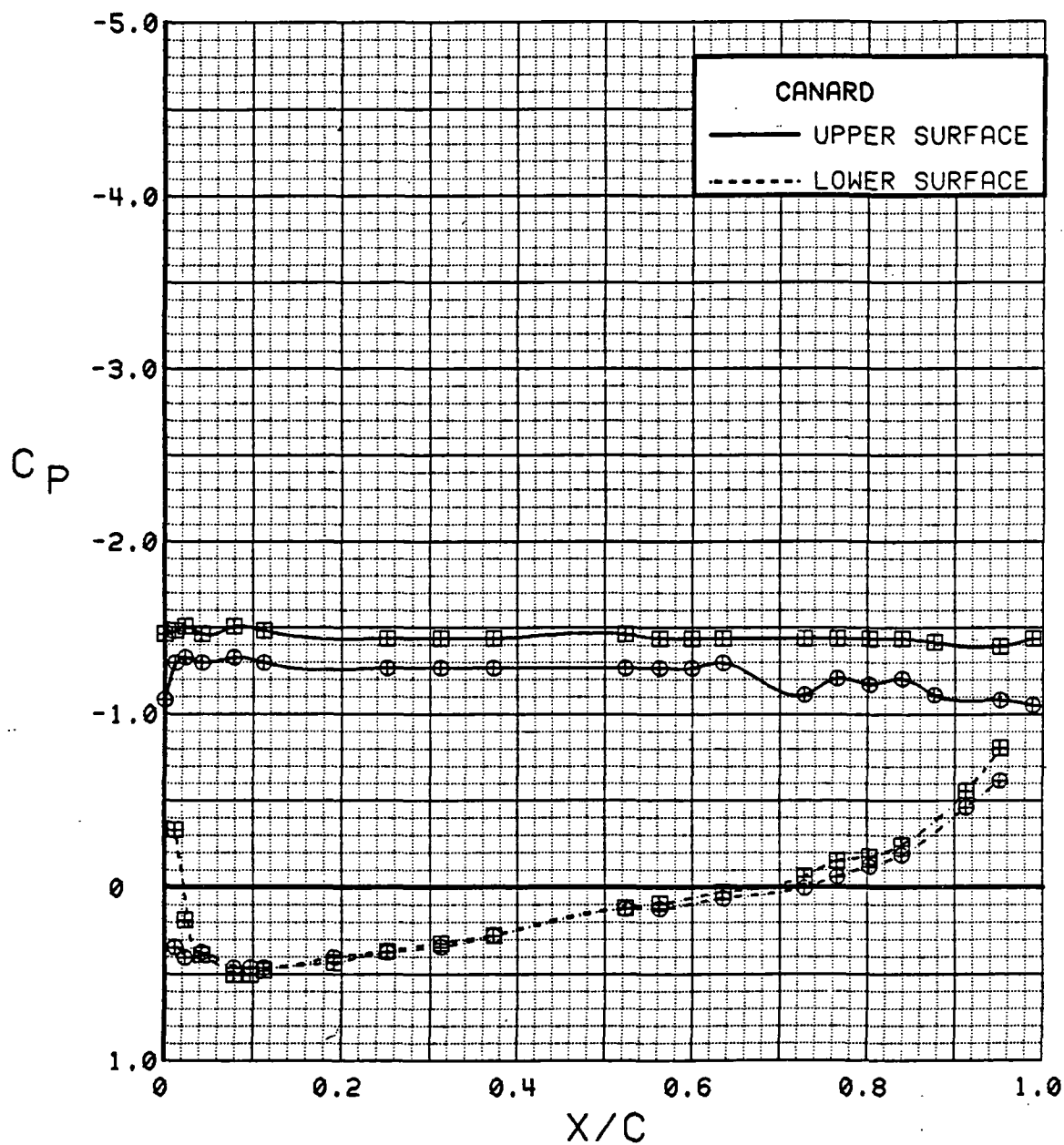


Figure 3.2.3-80 Spanwise Blowing Effects,  $C_T = 1.8$ ,  $\alpha = 20^\circ$



SYM	TEST	RUN	ALPHA	CT	ITEF	OTEF	CAN	SWB
⊕	537	28	29.1	1.83	30	30	0	OFF
⊞	537	53	29.3	1.81	30	30	0	ON

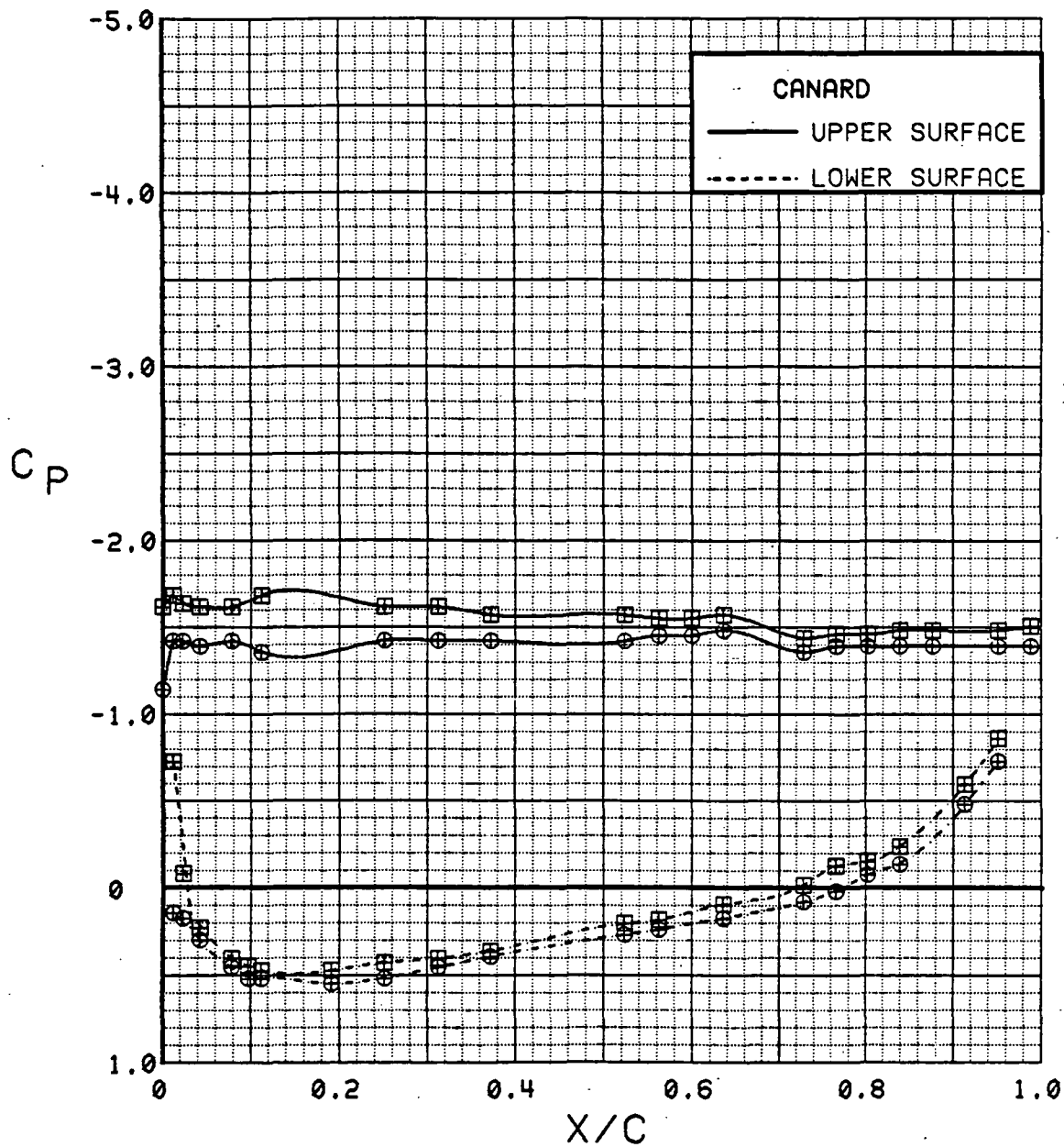


Figure 3.2.3-81 Spanwise Blowing Effects,  $C_T = 1.8$ ,  $\alpha = 28^\circ$

## CANARD

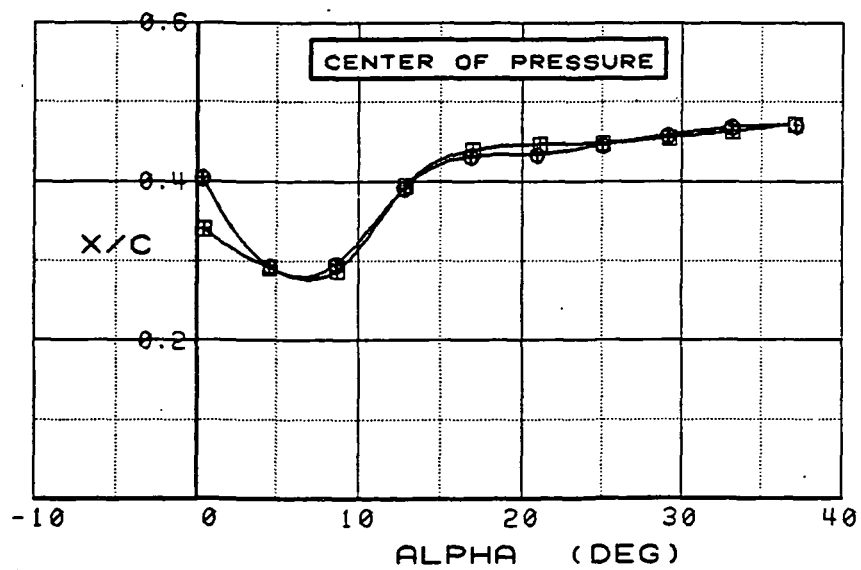
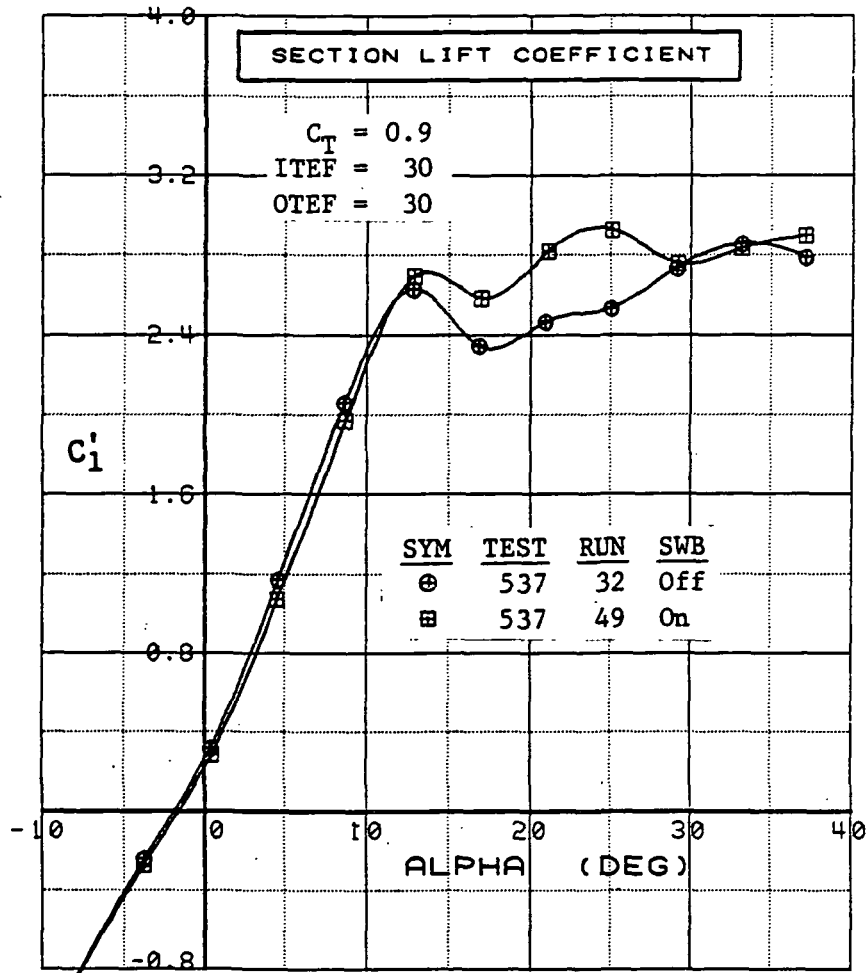


Figure 3.2.3-82 Spanwise Blowing Effects,  $C_T = 0.9$ , Integrated Section Properties

## CANARD

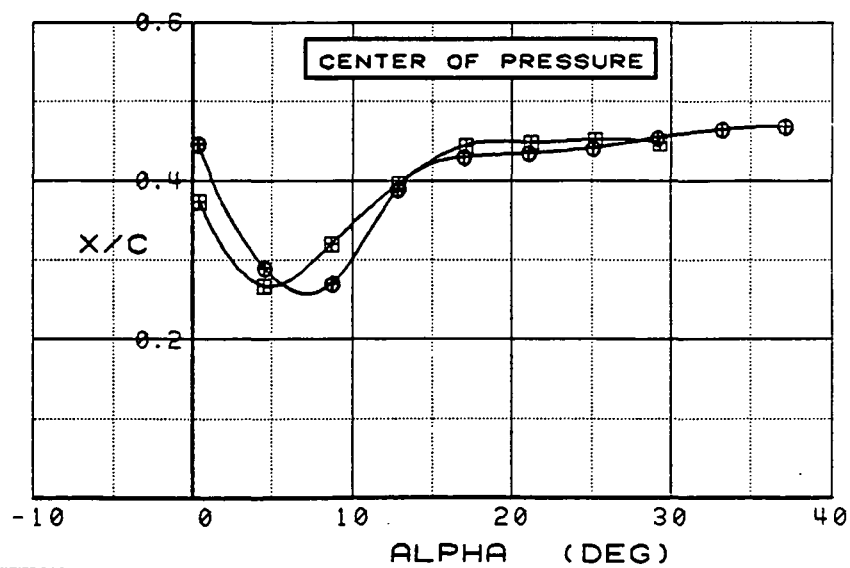
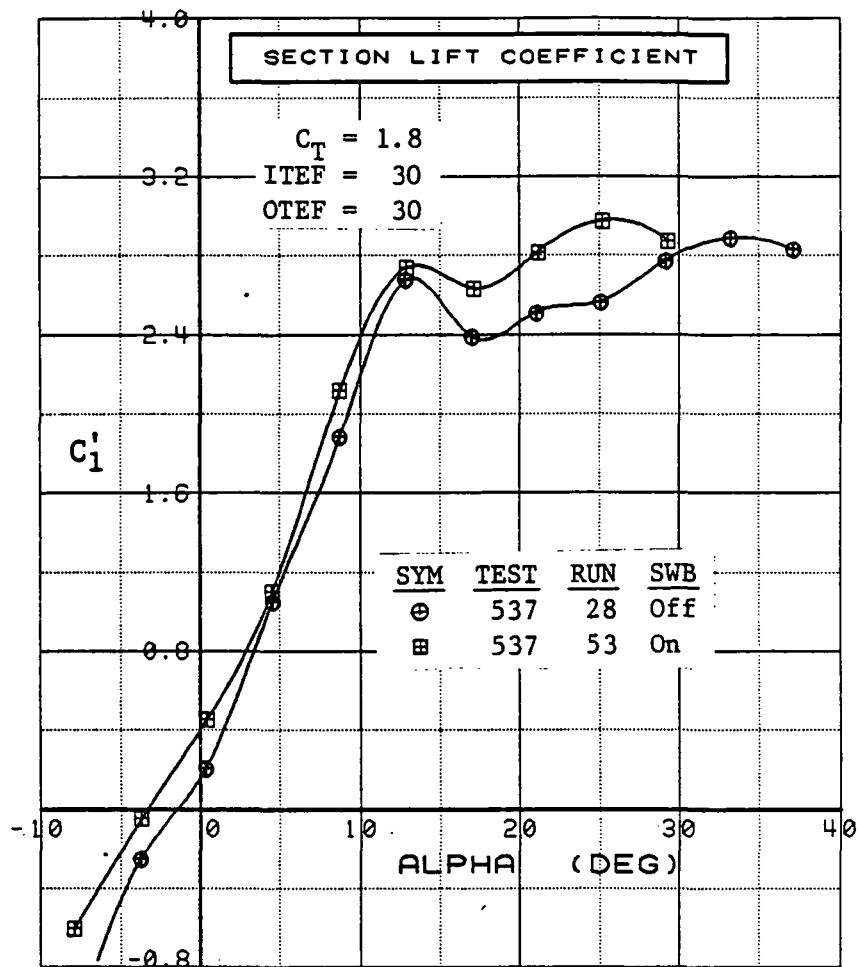


Figure 3.2.3-83 Spanwise Blowing Effects,  $C_T = 1.8$ , Integrated Section Properties

**(This page intentionally left blank.)**

### 3.2.4 Wing With Canard

#### 3.2.4.1 Basic Flowfield Characteristics and Data Preview

Wing pressure distributions inboard, outboard, and spanwise, in that order, are previewed in this subsection with the canard and the canard flaps neutral. Power-off data with variations in angle of attack are shown with wing flaps neutral in Figures 3.2.4-1 through -6, and with flaps down 30 deg in Figures 3.2.4-7 through -12. Corresponding data with a representative  $C_T$  value of 0.9 follow in Figures 3.2.4-14 through -25 to illustrate the overall similarity in trends. (Canard pressure data for these four configurations are presented in Subsection 3.2.3.) Effects of canard variables, other wing flap deflections, and the entire power spectrum are addressed in subsequent Subsections 3.2.4.2 through 3.2.4.5.

**3.2.4.1.1 Power Off.** With flaps neutral, pressure distributions at the inboard station at low to medium angles of attack (Figure 3.2.4-1) show the same trends as the wing alone and the canard (i.e., attached flow at low  $\alpha$  followed by the onset of leading-edge separation and a free vortex at increased  $\alpha$ ). Compared to the wing alone (Figure 3.2.2-1, for example), higher suction peaks followed by a recompression are more evident with the canard on. The flow appears to have remained undisturbed by vortex flow to higher  $\alpha$  than with the canard off. Obviously, the influence of the canard was significant, so this effect is later highlighted by canard on-off comparisons in Subsection 3.2.4.2. The wing inboard pressures at medium to high  $\alpha$  (Figure 3.2.4-2) show a sudden reduction at the upper-surface trailing edge at  $\alpha = 24$  deg, as the vortex first reached that region, and a flattening of the upper-surface  $C_p$ , eventually all the way forward to the leading edge, as stall deepened. The outboard station pressures (Figures 3.2.4-3 and -4) show an earlier onset of leading-edge separation than occurred inboard, and an earlier pressure diversion at the trailing edge. Like the wing alone, this transpired outboard at lower  $\alpha$  because the vortex originated near the wing tip and moved inboard with increased  $\alpha$ . The canard appears to have influenced the outboard stall onset to a lesser degree. The midchord spanwise data (Figures 3.2.4-5 and -6) provide some evidence of an inboard movement of the leading-edge vortex with increasing  $\alpha$ . At  $\alpha \geq 20$  deg, the vortex location is indiscernible, perhaps, because it was displaced well above the midchord region of the wing.

With the inboard flap and the aileron (outboard flap) down 30 deg, leading-edge stall at the inboard station (Figures 3.2.4-7 and -8) appears to have just set in at  $\alpha = 8$  deg. The suction peak achieved ( $C_p = -5.2$ ) was about half the magnitude of the highest level recorded in the entire test program. Eventually, stall onset occurred at an  $\alpha$  several degrees higher than with the canard off, but it was at a lower  $\alpha$  than with flaps neutral. Flap load was maintained fairly well up to an  $\alpha$  of about 16 deg. Outboard station data (Figures 3.2.4-9 and -10) also show earlier stall onset with flaps down and a stronger vortex effect at a fixed  $\alpha$ , because the vortex origin was now further inboard of that station. The spanwise data (Figures 3.2.4-11 and -12) at  $\alpha = 8$  deg indicate that the vortex traversing the tip region was a little stronger and, as at other angles, somewhat further inboard than with the trailing edge neutral.

A summary of approximate  $\alpha_{st}^*$  values, power off, is presented in Figure 3.2.4-13. Wing-alone values from Figure 3.2.2-7 are included for comparison.

**3.2.4.1.2 Power Without Spanwise Blowing.** The effects of angle of attack with power set at a nominal  $C_T$  of 0.9 (Figures 3.2.4-14 through -25) differed from those at  $C_T = 0$  in that upper-surface pressures were generally reduced by power. Thus, a higher leading-edge suction peak was measured whenever stall had not set in, but this in turn precipi-

tated a slightly lower stall-onset  $\alpha$ . Then, when stall was already present at  $C_T = 0$ , power tended to intensify the vortex and cause it to affect more of the chord. Other factors, such as differences in tunnel  $R_e$ , influenced the apparent impact of power. These considerations are presented in greater detail in Subsection 3.2.4.4.

**3.2.4.1.3 Data Peculiarities.** A curious phenomenon appeared in some of the wing power-off and power-on data at low and intermediate  $\alpha$ s: midchord regions of invariant upper-surface pressure. The results in question were prevalent at the inboard station and may be noted in Figures 3.2.4-1, -2, -7, and -15, for example. Some other "flat" regions, not necessarily strange, were those along the lower surface (e.g., Figure 3.2.4-1) and those along the upper surface in high- $\alpha$ -stall situations (e.g., Figure 3.2.4-2), which are not uncommon results under these circumstances. Unusual, however, were the constant- $C_p$  regions along much of the upper surface, such as those at  $\alpha = 4$  deg and 16 deg in Figure 3.2.4-1. Within some of the extensive nearly-flat regions, there sometimes were two or more plateaus that differed by a change in  $C_p$  of 0.1 or so (see Figure 3.2.4-14). Although some unrecognized flow mechanism may be responsible, it seems more likely that the pressure-instrumentation recording system simply filtered out (rounded off) pressure coefficient changes of less than, say,  $\pm .05$ , particularly when chordwise pressure gradients were small.

Another data feature of unknown cause is a high pressure that was consistently recorded at the innermost span station (see Figure 3.2.4-5, for example). The tap generally responded to geometry and power perturbations as did adjacent taps. The only clue to its cause, possibly inlet spillage, was that the pressure increased a large amount, at that tap only, when the inlets were blocked and tunnel  $q$  was reduced to the lowest test value.

### 3.2.4.2 Canard Effects

**3.2.4.2.1 Flowfield Interactions.** In general, the canard downwash increased the upper-surface pressures along most of the inboard wing chord. An important exception occurred when the downwash reduced or eliminated leading-edge stall, thus allowing greater suction to be realized at the leading edge and a short distance downstream. As a leading-edge vortex developed on the wing, the canard leading-edge vortex apparently interacted favorably, augmenting its strength and retarding the inboard stall progression. Canard flowfield interactions usually reduced the lower-surface pressures in the forward region and increased those in the aft region of the inboard wing chord. Outboard on the wing, it was difficult to discern the canard/wing interactions solely on the basis of the outboard row of pressure measurements. The canard-tip vortex evidently interacted with the wing leading-edge vortex, but only occasionally was the effect on  $C_p$  conspicuous because it seems the tip vortex trailed above the wing somewhere near the outboard station. At low  $\alpha$  there was a small increase in downwash caused by the canard, either because the tip vortex was outboard of the primary-canard downwash field or because the inboard perimeter of the tip vortex grazed the wing near that station. Thus, stall-onset  $\alpha$  at the outboard station was delayed about one degree by the canard with  $\delta_c = \delta_l = \delta_t = 0$  (see Figure 3.2.4-13). At moderate  $\alpha$ , the stronger canard-tip-vortex peripheral flow imparted a modest acceleration to the wing surface flow, slightly reducing both upper-surface and lower-surface pressures. However, when the canard-tip vortex encountered the wing leading-edge vortex near the outboard leading edge, the tip vortex augmented the leading-edge vortex and, thus, increased the suction on the wing. This interaction did not persist or grow with  $\alpha$  because as flow in the outboard region of the canard separated and a leading-edge vortex was formed, some of the canard vorticity was disbursed at the expense of the canard-tip vortex, thereby reducing the tip vortex strength and its influence on the wing. At higher  $\alpha$  as the wing leading-edge vortex moved inboard of the wing outboard station, the canard-tip vortex induced an increase in

velocity over the entire outboard chord and eventually (at the highest alpha tested) this influence virtually disappeared.

**3.2.4.2.2 Canard On/Off Comparisons.** Wing pressure distributions and section lift coefficients presented in Figures 3.2.4-26 through -51 show the influence of the canard wake on the wing flowfield for the model with the canard neutral, wing flaps neutral, and power off. Comparable results with flaps deflected 30 deg are presented in Figures 3.2.4-52 through -77. Then, because the canard influence was affected by power applied at the inboard flap, canard-on/off-data comparisons with a nominal  $C_T = 0.9$  are shown for each flap deflection in Figures 3.2.4-78 through -138. (The effects at all power levels with the canard on, are discussed in Subsections 3.2.4.4 and 3.2.4.5.) Finally, with the aid of Figures 3.2.4-139 through -152, unique results caused by a forward shift in the canard location are addressed.

With wing flaps undeflected and power off, Figures 3.2.4-26 through -33, 3.2.4-34 through -41, and 3.2.4-42 through -49 summarize wing pressure distributions inboard, outboard, and spanwise, respectively, at angles of attack from zero to 32 deg (nom). The inboard data at  $\alpha = 0$  (Figure 3.2.4-26) exhibit the results one might expect from a canard induced downwash: increased pressure along virtually all of the upper surface and decreased pressure near the leading edge on the lower surface. The canard, however, also produced an increase in lower-surface pressure aft along most of the chord, as though the canard had induced a pseudo increase in wing angle of attack. This result, not understood at present, occurred at most angles of attack and irrespective of wing flap or power settings. Canard-off data were unavailable at  $\alpha = 4$  deg. At  $\alpha = 8$  deg (Figure 3.2.4-27), the canard wake eliminated stall on the upper surface and, consequently, displaced the wing leading-edge vortex outboard. Wing leading-edge separation with the canard on (i.e., the leading-edge vortex) made its first appearance at the inboard wing station at an alpha between 8 and 12 deg, which was about three deg later than with the canard off. Because of this delay, the presence of the vortex at  $\alpha = 12$  to 24 deg (Figures 3.2.4-28 through -31) produced a sharp contrast in the upper-surface pressure distributions. The origin of the canard-on vortex was not as far inboard, thus the vortex influence was concentrated nearer the leading-edge of the inboard station. Also contributing to the contrast was the longer alpha span it took for the vortex to move inboard, i.e., to blanket the aft-chord region, showing no indication of having done so until  $\alpha = 24$  deg (Figure 3.2.4-31) when the first significant reduction in pressure at the last tap appeared. With the canard off, this transition took place within an alpha change of less than 4 deg (note the reduction in trailing-edge pressure between  $\alpha = 8$  deg and 12 deg, Figures 3.2.4-27 and -28). Thus, the canard wake evidently delayed both the onset and the inboard advance of the leading-edge separation.

Another significant difference inboard was the  $C_p$  distribution beneath the wing vortex, which appeared to be larger (more favorable) with the canard on. The cause may well have been the leading-edge vortex shed by the canard. Although its presence was not discernible in the wing pressure data as a separate entity, it could have merged with the wing leading-edge vortex, and thereby, increased its strength and stability. It seems unlikely that canard downwash was alone responsible for the larger vortex effects, for otherwise the upper-surface  $C_p$  distributions would have looked more like the canard-off data at an alpha 3 or 4 deg lower. The canard benefits persisted at even higher alpha values, although to a much lesser degree. At  $\alpha = 32$  deg (Figure 3.2.4-33), note that the incremental upper-surface pressures due to the canard were almost invariant along the chord. Neither downwash nor upwash effects on the forward lower surface are discernible, so one might again conclude that the canard wake was being energized locally by the canard leading-edge vortex.

In terms of inboard section lift, the canard downwash was detrimental until vortex flow set in significantly (the canard-off vortex having moved entirely inboard by then), after which the canard-on lift was greater. This result is more apparent when  $C_{l'}$  is examined (Figure 3.2.4-50).  $\alpha_1^*$  is estimated to have been 10.4 deg with the canard on and 7.2 deg with the canard off (see Figure 3.2.4-13). The more-gradual movement of the canard-on vortex resulted in a corresponding difference in the aft rate of movement of the center of pressure until a common value was achieved at  $\alpha = 28$  deg, at which point the vortex had evidently moved entirely inboard of the instrumented station in both cases (note the similarity in aft pressure distributions in Figure 3.2.4-32).

The outboard data at  $\alpha = 0$  (Figure 3.2.4-34) reflect a slight canard-induced downwash that increased static pressures in the fore and aft region of the lower surface. There was also an increase in pressures aft on the lower surface, similar to that which occurred persistently at the inboard station but dissimilar at the outboard station in its lack of consistency at other alpha, flap, and power settings. In fact, outboard lower-surface pressure changes caused by the canard may best be considered as having been insignificant, except for the aforementioned downwash response at low alpha. On the upper surface as alpha was increased, the canard-induced change in pressure distribution at first resembled that which formed inboard but about four degrees earlier. For example, the outboard data change at  $\alpha = 8$  deg (Figure 3.2.4-35) look more like the inboard data change at  $\alpha = 12$  deg (Figure 3.2.4-28) than at 8 deg (Figure 3.2.4-27). However, at successively higher alpha the similarities faded because the canard contribution outboard rapidly diminished amidst stall-like pressure distributions with the canard either on or off (See Figures 3.2.4-36 through -39), but the canard-on inboard pressures (Figures 3.2.4-28 through -31) did not flatten out because of the sustained vortex augmentation produced there by the canard, as previously discussed. Obviously, the canard influence was much less pronounced outboard. With downwash having delayed outboard stall onset by only about one deg (See Figure 3.2.4-13), the principal benefit induced by the canard was a tip vortex interaction that only modestly enhanced the wing leading-edge vortex and did little to retard its movement inboard. However, this was not necessarily detrimental to lift at that station. The vortex recompression that was evident in the midchord region at  $\alpha = 8$  deg (Figure 3.2.4-35) had virtually disappeared at  $\alpha = 12$  deg (Figure 3.2.4-36) since the wing vortex had moved well inboard. In its place, the canard-tip vortex evidently induced a significant flow acceleration (perhaps via entrainment) that reduced pressures in the region of closest proximity, i.e., forward on the upper surface. (Another factor might have been the emergence of a secondary leading-edge vortex, near the canard tip, that joined with and strengthened the tip vortex. Such a development was detected at  $\alpha = 13$  deg on a model simulating an F-4 wing without a leading-edge discontinuity (Reference 17), but the Ames Fighter model instrumentation was not sufficient to have detected a secondary vortex.) This influence persisted to  $\alpha = 24$  deg (Figure 3.2.4-39). At the highest alpha settings (Figures 3.2.4-40 and -41) the canard effects were nil or even a little adverse.

It may be somewhat surprising that canard tip vortex interactions were not stronger at the outboard station considering the planview alignment of the canard tip just inboard of wing  $2y/b = .84$ . Data at  $\alpha = 4$  deg with flaps deflected (to be discussed subsequently) did show a more direct tip-vortex influence, but two other factors had an important bearing at higher angles: (1) the elevated location of the canard (in sideview) and (2) a weakening of the tip vortex with the onset of canard leading-edge separation. The first factor meant that the tip vortex core passed well above the wing, rather than near the leading edge, since a tip vortex tends to trail a lifting surface in a path more nearly streamwise than in the extended plane of that surface. The second came about because the canard leading-edge vortex usurped vorticity that otherwise would have been concentrated at the canard tip.



Spanwise data (Figures 3.2.4-42 through -49) seem to confirm that downwash from the canard was dominant at  $\alpha = 8$  deg, that its influence inboard was sustained at 12 deg, and that as the wing leading-edge vortex moved inboard at  $\alpha > 8$  deg, the canard-induced augmentation overshadowed the downwash contribution in that vortex region. In examining the midchord pressures, however, it should be borne in mind that much of the canard wake interaction in the mid-alpha range occurred forward on the wing, and thus, cannot be fully recognized in these results.

The contrast in canard influence at the outboard and inboard wing stations is clearly reaffirmed in the section lift coefficient and center of pressure results, Figures 3.2.4-50 and -51.

With flaps set at 30 deg and power off, the same qualitative effects on wing  $C_p$  caused by the canard may be noted in Figures 3.2.4-52 through -75. However, since flap deflection had increased wing-alone upper-surface velocities and brought on stall at a lower alpha, the canard downwash influence was now manifestly greater (see the  $(V + \Delta V)^2$  analogy discussed in Subsection 3.2.2.1). Thus, before stall onset, the canard now produced more change in the inboard upper-surface pressures (compare Figures 3.2.4-52 and -26). Then, at an intermediate alpha where canard-off stall already existed, canard downwash either eliminated local stall (it barely did so at  $\alpha = 8$  deg, Figure 3.2.4-54), or it nudged outboard the stronger vortex that existed at that station because of flap deflection (note the steeper recompression when comparing Figures 3.2.4-55 and -28). At high alphas, the vortex appears to have been influenced less favorably by the canard when the flaps were down (compare Figures 3.2.4-57 and -30, for example). Reduced recompression aft of the vortex, however, actually resulted in more lift increment due to the canard at  $\alpha = 20$  deg and no significant difference at  $\alpha \geq 24$  deg. Outboard on the wing, canard interactions were again more pronounced with flaps down when vortex interactions first occurred (compare Figures 3.2.4-62 and -35). At higher alpha, the vortex again seems to have been curved downstream more by the flaps but with little net change in canard impact. Spanwise data suggest that the canard did more to produce a stronger vortex outboard at  $\alpha = 8$  deg (Figure 3.2.4-70 vs -43) and a broader vortex influence inwards at  $\alpha = 12$  and 16 deg (Figures 3.2.4-71 vs -44 and 3.2.4-72 vs -45) than it did when flaps were undeflected. Otherwise there was little difference of note. Section lift results, Figures 3.2.4-76 and -77, also show that when the wing flaps were deflected the canard produced (1) more loss in inboard lift at low- and mid-alpha and (2) a larger gain in outboard lift at high alpha than it did with flaps undeflected (compare Figures 3.2.4-50 and -51).

With wing flaps undeflected and power on ( $C_T = 0.9$ ), Figures 3.2.4-78 through -107, the canard influence on the wing was generally less than with flaps deflected and power off. The reason it was less is that the wing flowfield intensity was less with power alone than with flaps alone, so with power alone the canard-induced velocity perturbations had less effect on wing  $C_p$  levels. All relative changes in  $C_p$  can thus be reconciled from this viewpoint with one exception: the inboard lower surface responded more to the canard downwash at low and mid alpha only with power (see Figures 3.2.4-78 through -81 vs 3.2.4-52 through -55), for reasons unknown. Otherwise,  $C_p$ -distribution changes caused by the canard were very similar to those that occurred with zero power and zero flaps, especially when alpha was not near stall onset (compare Figures 3.2.4-78 and -26, -80 and -27, -82 and -29, for example). Near stall onset, the deeper degree of stall existing with power allowed a greater apparent suction and vortex displacement outboard to be realized from the downwash (see Figures 3.2.4-81 and -28). Section lift, Figures 3.2.4-108 and -109, mirrors the small differences in canard influence between power-on and power-off results (Figures 3.2.4-50 and -51).

With combined flap deflection and power ( $C_T = 0.9$ ), Figures 3.2.4-110 through -136, canard on/off results were particularly enlightening when compared with the results discussed above, which had only flaps deflected or only power, to discern if the individual contributions were simply additive. In some regions they were, but in others, the combined power/flap arrangement yielded canard interactions that were sometimes more favorable, other times unfavorable. Inboard at  $\alpha = 0$ , for example, some upper-surface contributions were additive: compare Figures 3.2.4-52, -78, and -110, which show increased response to downwash at the leading edge with flap deflection only, power only, and flaps plus power, respectively. Linear superposition of the first two canard-induced increments in  $C_p$  virtually equals the third. However, note that lower-surface pressures generally do not equate, especially near the leading edge, and that upper-surface pressures emphatically do not aft of  $x/c \approx .20$  since downwash effects there are indistinguishable in Figure 3.2.4-110. This upper-surface behavior suggests that the surface flow was so highly energized by combined flap deflection and power that aft on the chord the flow was impervious to the downwash, even though the downwash was moderate at zero alpha yet apparent in the  $C_p$  changes at the more-sensitive leading edge. The same result appeared at  $\alpha = 4$  deg (compare Figures 3.2.4-53, -79, and -111) despite the inception of leading-edge stall and its vortex. Again, lower-surface pressure increments were not cumulative and upper-surface seemingly did not respond to downwash. The high energy of the flowfield is presumed to have continued its influence at  $\alpha = 4$  deg. Further speculation on the cause of different lower-surface responses to the canard would be very conjectural, particularly when it is noted that the lower-surface data of Figures 3.2.4-110 through -118 show a more consistent response to induced downwash than any other canard on/off results. Regarding further the inboard upper-surface data, the "impervious to the downwash" trait cannot be identified at  $\alpha > 4$  deg, not necessarily because it was not there, but rather because it could have been obscured by the large  $C_p$  changes associated with different leading-edge vortex conditions. It might be pertinent, however, that when the vortex influence began to wane at higher alpha (say,  $\alpha = 16$  deg, Figure 3.2.4-114), the canard-induced  $C_p$  changes with power and flaps (Figures 3.2.4-114 through -118) resembled the flaps-only results (Figures 3.2.4-56 through -59) more than the power-only data (Figures 3.2.4-82 through -86). Outboard wing data plots, Figures 3.2.4-119 through -127, show that canard-induced  $C_p$  increments with both power and deflected flaps approximate the sum of power-only and flap-only increments more consistently. For example, compare Figures 3.2.4-89, -61, and -120 at  $\alpha = 4$  deg. When stronger vortex interactions took place the equivalence was reduced (Figures 3.2.4-62, -90, and -121 at  $\alpha = 8$  deg), but thereafter, the equivalence was dependent on alpha. Spanwise pressure measurements, Figures 3.2.4-128 through -136, provided no further clues as to why canard incremental effects with power and flap deflection were sometimes additive, sometimes not. The tendency for pressure distributions to have resembled those with flap deflection only is reflected in the section lift trends, Figures 3.2.4-137 and -138 (compare with Figures 3.2.4-76 and -77).

Regarding canard-wing interactions in general, and the above results in particular, it is surmised that the strength and orientation of the canard wake had a strong bearing on the degree to which it could accommodate, or be accommodated by, the wing flowfield. Considering the remarkable influence exhibited on the canard caused by changes in wing loading via power and flap deflection (see Subsection 3.2.3.2), it seems likely that significant flowfield interactions occurred in the canard near-field wake as well. Clearly, the canard downwash was contra-directional to the wing upwash field, and, intuitively, one might rate the wing flowfield as the more dominant in energy content. In their confrontation, the wing flowfield would have influenced the canard wake more than vice versa and in different degrees depending on the status of the wing (i.e., power setting, flap setting, angle of attack). This reasoning can lead to a scenario in which the wing circulatory flow was elevated to such a high-energy state that the canard wake was possibly overwhelmed

and made to simply skip over the wing without significantly affecting the wing surface pressure distribution. Such an event evidently transpired when the canard was placed further forward on the nacelle, as described below.

Previously presented results have been with the canard in the aft location. Attention is now focused on the unique results that occurred, at an  $\alpha$  near 16 deg and higher, when the canard was tested in the forward location (see Figure 2-3). Limited pressure data for the forward location are presented in Figures 3.2.4-139 through -150, all with the canard undeflected and wing flaps deflected 30 deg. Included are power-off data from the inboard station and the outboard station at  $\alpha = 12, 16$  and  $20$  deg, respectively, followed by corresponding data with power set at  $C_T = 0.9$ . These canard-on data are presented alongside the same canard-off data as previously shown in order to highlight the dissimilarity in canard-induced effects that occurred inboard with the forward canard location and power on. Beginning with the power-off results for contrast, a cursory comparison of inboard-wing-station data with the canard forward and the canard aft, Figures 3.2.4-139 vs -55 ( $\alpha = 12$  deg), 3.2.4-140 vs -56 ( $\alpha = 16$  deg), and 3.2.4-141 vs -57 ( $\alpha = 20$  deg), reveals that the canard-induced pressure changes were very similar. Outboard-station pressure changes caused by the canard with  $C_T = 0$  were also similar (Figures 3.2.4-142 vs -63, -143 vs -64, and -144 vs -65), and the same was virtually true with  $C_T = 0.9$  (Figures 3.2.4-148 through -150 vs 3.2.4-122 through -124). The feature point of interest is what happened inboard at  $\alpha = 16$  deg and above. At  $\alpha = 12$  deg (Figures 3.2.4-145 vs -113), the canard-forward and canard-aft effects were large and similar on the upper surface; at  $\alpha = 16$  deg (Figures 3.2.4-146 vs -114) the contrast in canard effects is startling, particularly forward of  $x/c = .46$ , and again at  $\alpha = 20$  deg (Figures 3.2.4-147 vs -115). Note that the lower-surface pressures nearest the leading edge at all three angles of attack indicate distinctly lesser induced downwash effects with the canard forward. It has been deduced, therefore, that the wake from the canard in the forward location, its energy having been dissipated more through the longer distance in transit to the wing, was displaced well above the wing by the wing flowfield, more so because the flowfield had been intensified by power and flap deflection. Power-off data with the canard forward exhibited a similar loss in canard-induced wing lift, but a small reduction first appeared at  $\alpha = 20$  deg, and the loss was total by  $\alpha = 24$  deg, or about four or five deg higher than with  $C_T = 0.9$  (i.e., power made it happen at lower  $\alpha$ ). There was also an inkling of this interaction in the canard-aft data but without the drastic consequences. Those data at  $\alpha = 16$  deg, showed that the canard influence forward on the inboard chord was less with combined power and deflected flaps (Figure 3.2.4-114) than with either flaps alone (Figure 3.2.4-56) or power alone (Figure 3.2.4-82). Yet, in that case, it appears the wake energy level, when approaching the wing, was sufficient to avert complete subjugation. The phenomenon persisted at high angles until the wake in either canard position was ineffectual, as was also reflected in section lift results, Figures 3.2.4-160 and -161 (compare with Figures 3.2.4-137 and -138).

Canard-on wing-pressure data comparisons in fore and aft locations are reviewed in Subsection 3.2.4.2.5, rather than immediately following, in order to more closely parallel the topic sequence followed in presenting canard results in Subsection 3.2.3.2.1. Therein, it is recalled, the canard pressures are shown to have also undergone a significant loss in lift as its wake was influenced at the conditions discussed above.

**3.2.4.2.3 Canard Deflection.** The effect of canard deflection,  $\delta_c$ , on wing pressure is illustrated in Figures 3.2.4-153 through -161 at nominal  $\alpha$  values of 4, 8 and 12 deg. As to be expected, the data for the inboard wing section (Figures -153 through -155) show the results of reduced canard downwash for negative canard deflections and increased canard downwash for positive deflections. Thus, at low  $\alpha$  (Figure 3.2.4-153),  $\delta_c = -10$  deg resulted in a higher suction peak since the section was not stalled, but  $\delta_c = -20$  deg

incurred stall and a leading-edge vortex origin positioned inboard of  $2y/b = .64$ . Conversely, positive deflections suppressed the upper-surface loadings and reduced lower surface pressure. Those phenomena persisted at  $\alpha = 8$  and  $12$  deg (Figures -154 and -155). Comparing inboard data for the wing without a canard (Figure 3.2.2-4) at  $\alpha = 4$  deg, it is of interest to note the similarity in upper- and lower-surface pressure distributions with  $\delta_c = -10$  deg. The only significant difference is that the canard appears to have enhanced the lifting load on the aileron (outboard trailing-edge flap). At  $\alpha = 8$  deg, the data for  $\delta_c = -20$  deg are more comparable to the canard-off trends but the aileron load is improved less, presumably because the vortex field of the wing alone had itself effected an improvement. At  $\alpha = 12$  deg, the data for  $\delta_c = -20$  deg are again most similar.

At the outboard wing station (Figures -156 through -158), the wing response to the varying strength of the canard tip vortex (or combined vortex system) is more difficult to perceive as an orderly trend. Nevertheless, at  $\alpha = 4$  deg (Figure -156), negative canard settings evidently increased the wing leading-edge vortex strength, as indicated by the longer chordwise extent of the reduced upper surface pressures, while the stronger canard vortices produced by positive deflections seem to have moved the wing vortex outboard. At  $\alpha = 8$  deg (Figure -157), where a vortex at  $\delta_c = 0$  deg already extended over the forward half of the chord, the weaker canard vortex at  $-10$  and  $-20$  deg deflection allowed the wing vortex origin to be further inboard (and the vortex to thus extend further aft over this section), whereas, at  $10$  deg deflection the wing vortex was evidently enhanced and then less so with  $20$  deg deflection. At  $\alpha = 12$  deg (Figure -158) there is less evidence of a direct interaction of the canard and wing vortex system, probably because the wing vortex origin was well inboard of this station at the outset ( $\delta_c = 0$ ). It is significant to note at all angles of attack and deflections, however, that lower-surface pressures at the outboard station were affected much less by canard deflection changes than transpired inboard, thus indicating that the canard tip wake region passed above and not below the wing. Compared with canard-off data (Figure 3.2.2-5), the same similarities prevail for  $\delta_c = -10$  deg and  $-20$  deg as occurred inboard, except that aileron load outboard was not materially enhanced by the canard.

The spanwise data at the midchord station (Figure 3.2.4-159 through -161) are of little diagnostic benefit. At  $\alpha = 4$  and  $8$  deg they suggest that the wing vortex moved inboard due to negative canard deflections and perhaps a bit outboard at positive deflections. At  $\alpha = 12$  deg this outboard movement appears to have been more pronounced, presumably because the stronger canard tip vortex was more dominant and drew the wing vortex outboard with it, even at zero canard deflection.

The effects of canard deflection on the wing section integrated properties are summarized in Figures -162 and -163. At low  $\alpha$  values, each plot shows that the trend in wing  $C_l'$  responded predictably to the presumed changes in canard downwash. At the outboard station, Figure -163, the orderly changes in  $C_l'$  and the small changes in  $(x/c)_{cp}$  suggest there were no strong, direct interactions between the wing and the canard tip vortex, although the vortex must have undergone significant variations in strength and vertical displacement with canard deflection. At high  $\alpha$ s, as the canard experienced different degrees of stall, the wing response was quite varied. An interesting consequence was that inboard maximum  $C_l'$  values thus occurred at widely different  $\alpha$ s, but the lift magnitudes were not a great deal different. In contrast, the outboard section peak  $C_l'$  values were more varied.

**3.2.4.2.4 Canard Flaps.** Wing pressure results with variations in canard leading-edge-flap deflection are presented in Figures 3.2.4-164 through -190, and with combined leading-edge and trailing-edge flap deflections in Figures -191 through -205. An interest-

ing though imperfect correlation is shown to exist between the qualitative changes in wing pressure distribution and canard section lift coefficient,  $C_{l'}$ , due to flap deflection. Values of wing  $C_{l'}$  and  $(x/c)_{cp}$  are then shown in Figures -206 and -207.

With the canard undeflected ( $\delta_c = 0$ ), wing section and spanwise pressure distributions are shown in Figures 3.2.4-164 through -178 for three canard leading-edge-flap deflections with zero canard trailing-edge-flap deflections. Corresponding values of canard section lift coefficient, previously summarized in Figure 3.2.2-11, are listed on each plot for convenience. At the wing inboard station it may be noted that the peak leading-edge pressure coefficient increased (negatively) as canard section lift was reduced by leading-edge flap deflection at  $\alpha = 0$  deg (Figure -164) and 4 deg (Figure -165). The higher peaks were the consequence of reduced downwash from the canard. The same trend is evident at  $\alpha = 8$  deg (Figure -166), where the  $C_p$  values annotated above the legend show that pressures again decreased. However, the changes were not in sequence since the  $C_p$  level with  $\delta_1 = 30$  deg was not quite as low as with  $\delta_1 = 10$  deg even though canard  $C_{l'}$  was lower. What happened was that stall had just set in (note the leading-edge vortex with both flap settings). At high alpha the results were not as consistent. At  $\alpha = 12$  deg (Figure -167), again because canard lift and downwash were less, there was a greater degree of stall and a stronger vortex with  $\delta_1 = 30$  deg as expected, but the opposite did not occur with a 10 deg deflection. Finally, at  $\alpha = 16$  deg (Figure -168),  $\delta_1 = 10$  deg produced the least wing stall and perhaps the weakest vortex, but  $\delta_1 = 30$  deg should have produced essentially the same result, according to the  $C_{l'}$  analogy, and did not. The analysis of canard on/off data comparisons concluded there was a strong interplay between the canard and wing leading-edge vortices (see Subsection 3.2.4.2.2). Therefore, a consistent trend with canard  $C_{l'}$  should not be expected when the canard vortex was located virtually entirely inboard of the canard pressure-measuring station, as it was at  $\alpha = 16$  deg with  $\delta_1 = 10$  deg (and nearly so with  $\delta_1 = 30$  deg), according to Equation (4). At the outboard wing station (Figures 3.2.4-169 through -173), pressure changes at low alpha also reflected the reduction in downwash due to canard flap deflection. At intermediate alpha, canard on/off comparisons (Subsection 3.2.4.2.2), led to the conclusion that the canard tip vortex enhanced the wing leading-edge vortex. This influence is difficult to correlate or even identify within the smaller changes produced by just canard leading-edge flap deflection. It can not even be presumed true that a change in tip vortex strength was directly proportional to canard  $C_{l'}$ , in magnitude or sign, since  $C_{l'}$  was evaluated well inboard on the canard and evidently there was a significant vorticity interchange with its leading-edge vortex. Consequently, trying to relate the changes in wing pressure to presumed changes in the tip vortex strength (keyed to  $C_{l'}$ ) is highly conjectural and perhaps not very significant anyway since the outboard wing pressure response seemed to largely be an extension of occurrences inboard. For example, at  $\alpha = 0$  deg (Figure 3.2.4-169) the pressure changes, though almost indiscernible, appear to reflect the reduction in canard downwash associated with reduced  $C_{l'}$ . The same is true on the lower surface at  $\alpha = 4$  deg (Figure -170), and stall was intensified and the vortex strengthened on the upper surface after having already set in (barely) at zero flap deflection (see Figure 3.2.4-13). Then, at  $\alpha = 8$  deg (Figure -171), the wing vortex was drawn inboard and thus crossed the chord slightly more downstream as downwash decreased. One could be inclined instead to interpret the pressure changes due to the 10-deg flap setting as being consistent with a reduction in tip vortex strength, and consequently, in wing vortex enhancement. The lowering of pressure at  $x/c = 0.90$  (particularly with  $\delta_1 = 30$  deg) and the downstream shift in the suction regions favor the former interpretation while yet recognizing that some tip vortex interaction was likely also present. At  $\alpha = 12$  and 16 deg (Figures 3.2.4-172 and -173) there was little to preferentially support either point of view since the wing vortex was well inboard of this station and  $C_{l'}$  changes were small. The spanwise data (Figures 3.2.4-174 through -178)

seem to lend further credence to the thesis that the wing leading-edge vortex moved inboard with reduced  $C_{l'}$  (see Figure -177, in particular).

With the canard deflected ( $\delta_c = 20$  deg), lowering the leading-edge flap decreased canard stall. Figures 3.2.4-179 through -190 present the wing pressure distributions and show once again that, in general, an increase in canard downwash reduced wing leading-edge stall and displaced the inboard wing vortex outwards slightly at low  $\alpha$ , and that it increased the suction under the outboard wing vortex at intermediate  $\alpha$ .

A combination of canard leading-edge and trailing-edge deflection with  $\delta_c = 0$  highlighted the impact of a strong increase in downwash due to  $\delta_t = 30$  deg. Figures 3.2.4-191 through -195 reveal a pronounced reduction in the inboard lower-surface pressures and a suppression of leading-edge stall that delayed the  $\alpha$  at which the vortex appeared there by about 5 deg (i.e., to about 13 deg). Outboard on the wing, Figures 3.2.4-196 through -200, the impact was again less dramatic except for tip-vortex-induced enhancement at  $\alpha = 8$  deg and above, whereas, the spanwise distributions, Figures 3.2.4-201 through -205, appear to show a delay in vortex inward movement with increased  $\alpha$ . Wing section values of  $C_{l'}$  and  $(x/c)_{cp}$  are presented in Figures 3.2.4-206 and -207. Each shows the results with canard flaps neutral, with only the leading edge deflected, and with both leading-edge and trailing-edge flaps deflected down 30 deg. The most noteworthy features were: (1) canard leading-edge deflection had little net impact on the wing, inboard or outboard; (2) inboard lift at low and mid  $\alpha$  was greatly reduced and  $(x/c)_{cp}$  was shifted aft by canard trailing-edge flap deflection, due to increased downwash, but the changes decreased after the wing leading-edge vortex finally appeared (near  $\alpha = 13$  deg); and (3) outboard lift was a little less with  $\delta_t = 30$  deg until the canard tip vortex interaction began at  $\alpha = 8$  deg, with the added loading occurring forward on the section.

**3.2.4.2.5 Canard Location.** The effect on canard pressure data caused by relocating the canard further forward on the nacelle, approximately doubling the longitudinal separation distance from the wing (see Figure 2-3), is discussed in Subsection 3.2.3.2.1. The change in wing pressure this produced, in terms of gross canard on/off effects, is addressed in Subsection 3.2.4.2.2, but for only a narrow  $\alpha$  region. To conclude the coverage of this subject, direct fore/aft comparisons of wing pressure and section lift are herein presented with wing flaps deflected 30 deg and power off (Figures 3.2.4-208 through -225) and with power set at  $C_T = 0.9$  (Figures 3.2.4-226 through -247).

Inboard-wing-section pressure comparisons with  $C_T = 0$ , Figures 3.2.4-208 through -213, show that the canard relocation forward produced an increase in local flow velocity at the wing, rather than predominantly a reduction in downwash, which one might perhaps be inclined to expect. For example, at  $\alpha = 0$  (Figure -208) an increase in local  $q$  was indicated because pressures were lowered along the entire upper surface. Reduced upper-surface pressures could also be caused by reduced downwash, but pressures were also reduced forward on the lower surface, which a relative decrease in downwash would not cause. Essentially the same was true at  $\alpha = 4$  deg, whereas at 8 deg the small local change was enough to transform the leading-edge status from "not quite" to "barely" into stall. Higher angles of attack consistently produced a slightly stronger leading-edge vortex with the canard forward because of the earlier separation. Along the lower surface, the only conspicuous change in trend appeared at  $\alpha = 20$  deg, where pressures in the midchord region were increased due to the forward movement. (Note: A similar trend digression also occurred on the canard, but at  $\alpha = 16$  deg. See Figure 3.2.3-25.) Outboard data, Figures 3.2.4-214 through -219, showed trends similar to those at the inboard station. The incremental changes were less pronounced except at  $\alpha = 8$  deg, where the canard tip vortex interaction with the wing flowfield was greatly reduced by the forward relocation.

This suggests that the tip vortex trailed further above the wing, as should be expected for the forward location since a lifting-surface tip vortex trails downstream along a path more nearly streamwise than in the extended chordplane. Spanwise data, Figures 3.2.4-220 through -225, provided little more than an imprecise indication that the wing vortex path was not greatly altered by the canard relocation. Section lift results also revealed little net impact.

Inboard wing pressures with  $C_T = 0.90$ , Figures 3.2.4-226 through -231, indicate that reduced downwash was the predominant result of the canard relocation forward on the nacelle. The clues are that lower-surface pressures were more often increased than decreased, especially near the leading edge, and that the wing leading-edge vortex was moved inboard (see Figures 3.2.4-226 and -227). Dramatic changes took place at  $\alpha = 16$  deg and 20 deg; the canard-forward wake influenced the wing upper-surface flow less (see canard on/off comparisons, Figures 3.2.4-146 and -147), and it accelerated the lower-surface flow aft of  $x/c = .30$ . A precursor of the large changes to follow was the nature of the wing response to canard relocation with power on at  $\alpha = 12$  deg (Figure -229) compared to that with  $C_T = 0$  (Figure -211). With  $C_T = 0$ , the canard shift resulted mainly in slightly accelerated wing flow; with  $C_T = 0.90$ , the wing vortex was displaced inwards and lower-surface pressures were increased. This can be interpreted as a lessening of the favorable canard-downwash influence on the wing vortex development (see the related discussion in Subsection 3.2.4.2.1). These results strongly indicate that the canard-forward wake underwent a change in its vertical velocity component when power was applied, as though the wake was beginning to be turned or diverted upwards by the stronger wing flowfield with power on. By  $\alpha = 16$  deg (Figure 3.2.4-230) the turning was virtually complete and the canard wake was thus accommodated differently by the wing, as indicated by change in upper- and lower-surface  $C_p$ . Outboard wing pressure changes, Figures 3.2.4-232 through -237, provide strong evidence that the canard forward movement reduced the downwash intensity and caused the wing vortex to move inward more rapidly with  $C_T = 0.90$  than without power. Spanwise data, Figures 3.2.4-238 through -243, suggest the same thing. Section lift coefficients reveal the severe loss in wing inboard lift that occurred at  $\alpha \geq 16$  deg when the canard was moved forward with  $C_T = 0.90$ . Compare inboard Figures 3.2.4-151 with canard forward and -137 with canard aft. Comparison of the outboard Figures 3.2.4-152 and -138 shows little net effect.

A closing comment on the canard fore/aft results is a rhetorical cause-and-effect question: When the canard was moved forward and power was applied, did the wing itself first induce a premature reduction in canard lift that resulted in a degenerated wake, or instead did the wing affect the wake first? A clue to the correct answer may be sought in the canard pressure distribution trends, Figures 3.2.3-17 through -19, and  $C_l'$  results, Figure 3.2.3-20. The search is inconclusive, however, because a change in the canard wake, once stabilized, had to be manifested in a change in canard lift. Hence, the canard data reflected the end result of whatever induced that change. Only a time-dependent cross-correlation could have established the initial source of what caused the loss in lift. Instrumentation of this type was not used.

### 3.2.4.3 Wing Flap Effects

Test results obtained with flap deflections ranging from -20 deg (trailing edge up) to 30 deg (down) are presented in Figures 3.2.4-244 through -260 with  $C_T = 0$ , Figures -261 through -277 with  $C_T = 0.9$ , and Figures -278 through -294 with  $C_T = 1.9$ . Included are data with the inboard (powered) flap deflected -10 deg and the outboard flap (aileron) neutral. Pressure data only in the  $\alpha$  range from 4 deg to 20 deg are presented here, in the interest of brevity, because the most significant flap trends are recognizable there. The pressure distribution features were generally compatible with the flow model

described in previous subsections of this report. Therefore, more attention is directed to the evidence regarding flap performance itself than to the impact the flap deflection variations may have had on the wing flowfield.

**3.2.4.3.1 Power Off.** The upper-surface pressure distributions at the inboard span station, Figures 3.2.4-244 through -248, show that the 30/30 flap setting was excessive. This is evident in the delayed recompression aft of the hingeline ( $x/c \approx .80$ ) at  $\alpha = 4$  deg (Figure -244) and in the equal or higher pressures (less-negative  $C_p$ ) along most of the chord compared with 10/10 and 20/20 results, particularly at  $\alpha = 8$  deg (Figure -245). Flap-induced increases in circulation are reflected in the leading edge pressures at  $\alpha = 8$  deg, where separation had not quite set in with the 30/30 setting or with the lower deflections. (Note: The upper-surface pressure trend forward of  $x/c = 0.04$  suggests that stall had occurred, but this result is deemed to have been unique to this run. Statistically, stall-onset occurred at  $\alpha = \alpha_1^* = 8.8$  deg, see Figure 3.2.4-13.) With a leading-edge vortex present at  $\alpha = 12$  deg (Figure -246), the subsequent changes in its intensity are clearly evident in the pressure distributions back to  $x/c = 0.32$ . At  $\alpha \geq 12$  deg the load distribution on the flap itself with a 30/30 setting is now more similar to that with a 20/20 setting, presumably because both are being directly influenced by the leading-edge vortex. Lower-surface pressures appear to be reasonably well ordered with flap deflection at all angles of attack. Outboard pressure distributions, Figures 3.2.4-249 through -253, add little to the above conclusions regarding the relative merits of the 30/30 flap setting. However, with flap settings greater than zero and  $\alpha = 12$  deg (Figure -251), the disparity in pressure levels, upper vs lower, near the trailing edge is evidence of vortex-induced suction. At  $\alpha = 16$  deg (Figure -252), all flap settings but -20/-20 appear stalled, which is not surprising since leading-edge separation had advanced well inboard at all deflections (see Figure 3.2.4-13), and by  $\alpha = 20$  deg (Figure -253), the entire outer wing panel was likely stalled. Spanwise data, Figures 3.2.4-254 through -258, suggest that the leading-edge vortex moved inboard with increased flap deflection and was well inside of the outboard pressure-measuring station ( $2y/b = 0.84$ ) by  $\alpha = 20$  deg. Unpowered section lift and center-of-pressure variations with flap deflection, Figures 3.2.4-259 and -260, are not unusual in the trends displayed. The 30/30 setting generally provided the most  $C_{l'}$ , both inboard and outboard, in spite of the inefficient flap loading alluded to above.  $\alpha_1^*$  values from Figure 3.2.4-13 are noted on each figure. The increment in maximum  $C_{l'}$  each positive deflection achieved was on the order of two-thirds the value at  $\alpha = 0$ , while the  $\alpha$  at that lift decreased only moderately.

**3.2.4.3.2 Power Without Spanwise Blowing.** With thrust settings of  $C_T = 0.9$  and 1.9, the inboard chordwise data presented in Figures 3.2.4-261 through -265 and -278 through -282, respectively, show that pressure levels were generally similar to those at  $C_T = 0$ . Except for the -20/-20 setting, all upper-surface pressures were lowered aft of about  $x/c = 0.30$ , but loads on the flap itself indicate that the flow was still separated with the 30/30 flap setting. A point of some interest is the change in pressure at the leading edge and just aft when power was applied at  $\alpha = 12$  deg with the -20/-20 flap (Figure -263 vs -246). In this case, power reduced or eliminated stall, which seems to be contrary to previous interpretations of power effects that depict an inboard shift of the leading-edge vortex due to an increase in circulation. There is no contradiction, however, because doubtlessly, circulation was reduced by power when applied with the flap deflected up 20 deg (note that lower-surface pressures were reduced). Another trend, not necessarily related to a power effect on flaps, is trailing-edge flow separation. Note in Figure 3.2.4-267, for example, that upper-surface and lower-surface pressure distributions with the 30/30 setting flattened out and became parallel in the neighborhood of  $x/c = .90$  (in Figure -285 they even diverged). It seems unlikely that instrumentation aft of that station would have shown the two levels to have merged at the trailing edge and thus satisfy the Kutta condition for attached flow. More likely the Kutta condition was not



met because the upper-surface flow separated. This phenomenon in regards to leading-edge vortex flow on a canard/wing model has also been reported in Reference 16. Outboard and spanwise data plots (Figures 3.2.4-266 through -275 and -283 through -292) also show that power did not significantly alter the relative effects of flap deflection, since power essentially changed the wing circulation intensity in amounts that were less proportionally responsive to  $C_T$  than to flap setting in the low- and mid-alpha range.  $C_l'$  and  $(x/c)_{cp}$  results, Figures 3.2.4-276 and -277 with  $C_T = 0.9$  plus -293 and -294 with  $C_T = 1.9$ , bear out the above inference, with some exceptions. The lift curves were somewhat smoother with  $C_T = 0.9$ , but at  $C_T = 1.9$  they were more undulated at settings other than -20/-20. (Note: When comparing Figures 3.2.4-276 and -277 with the others, observe that these two plots include data with the -10/0 setting instead of the 10/10 results.) The relative performance merits of the 20/20 and 30/30 settings were mixed.

#### 3.2.4.4 Power Effects Without Spanwise Blowing

**3.2.4.4.1 Power at Constant  $q$ .** The presentation of power effects on the wing alone (Subsection 3.2.2.2) and on the canard (Subsection 3.2.3.2.3) included detailed discussions of the significance of tunnel  $q$ . As noted there, thrust coefficient variations were attained by varying  $q$ , and thus  $Re$ , with only  $C_T = 1.40$  having the same values as at  $C_T = 0$  (see Table 8 in Subsection 3.2.3.2.3). The change accompanying other power settings affected the leading-edge pressure at low alpha and, subsequently, the leading-edge vortex development at higher alpha. A series of runs conducted with the inlets blocked ( $C_T = 0$ ) and  $q$  varying provided independent evidence of the  $Re$  impact. Those wing pressure measurements are presented in Figures 3.2.4-295 through -306. The data with  $C_T = 0$  and  $C_T = 1.4$  are then compared in Figures 3.2.4-307 through -358.

Inboard wing chordwise pressures obtained with  $q$  varying from 15 to 40 psf, Figures 3.2.4-295 through -298, show that the levels at  $x/c = 0$  increased negatively. Of particular interest is the accompanying leading-edge vortex development at  $\alpha = 8$  deg (Figure -297), where increasing  $Re$  progressively reduced the strength of the vortex. Actually, it reduced separation along the entire leading edge and thereby moved the vortex origin outboard. Consequently, the vortex no longer crossed this chord at the highest  $q$ . At the outboard station, Figures 3.2.4-299 through -302, the same thing took place but at an alpha four deg lower (Figure -300). By  $\alpha = 8$  deg, clearly the vortex blanketed less of the chord as  $q$  increased. The spanwise data, Figures 3.2.4-303 through -306, provide some indication that the vortex moved outboard with increased  $q$ , such as at  $\alpha = 8$  deg (Figure -305).

Pressure comparisons at power settings that exclude  $Re$  differences, i.e.,  $C_T = 0$  vs  $C_T = 1.4$ , are presented in Figures 3.2.4-307 through -330 with flaps undeflected, and in Figures 3.2.4-333 through -356 with flaps deflected 30 deg. In each case, alpha ranges from 0 deg to 28 deg. Corresponding section lift coefficient results are shown in Figures 3.2.4-331, -332 and -357, -358.

With zero flap deflection, pressures at the inboard station reveal that power generally increased local velocity at the leading edge and along most of the upper and lower surfaces. At  $\alpha = 0$  and 4 deg, there also was a slight increase in upwash, but by  $\alpha = 8$  deg the induced velocity overshadowed any upwash change (note in Figure 3.2.4-309 the overall decrease in lower-surface pressures). The significant change at  $\alpha = 8$  deg was the reduced upper-surface pressure aft of  $x/c = 0.6$ . The reasons for this occurrence are not clear. The same trend occurred on the wing alone (see Figure 3.2.2-77), but there the section was also being influenced by a leading-edge vortex that was enhanced by power. With the canard on, the vortex had not appeared at this alpha, but even when it had, at  $\alpha = 12$  deg (Figure 3.2.4-310), the aft load increase was still large (and it was compar-

able to that generated at  $\alpha = 8$  deg without the canard). Significant power-induced changes persisted at higher angles of attack, on the upper-surface in particular. At  $\alpha = 28$  deg (Figure 3.2.4-314), the peculiar spike just aft of the leading edge is believed to have been an erroneous data point. Outboard pressures, Figures 3.2.4-315 through -322, show much lower power benefits in the region of the aileron but stronger induced upwash, with its consequences evident forward on the chord, that persisted to  $\alpha = 8$  deg. The absence of a large change in upper-surface loading at  $\alpha = 0$  to 12 deg, except for that which was due to vortex enhancement, changed markedly at  $\alpha = 20$  deg and above (compare Figures 3.2.4-319 and -320). Canard on/off comparisons offered no indication of exceptional interactions that might explain this phenomenon. The fact that the outboard wing panel benefited significantly from power, even though it was severely stalled, suggests that the load change was simply a carryover from the large load enhancement inboard. The spanwise pressure distributions, Figures 3.2.4-323 through -330, provide little detail, indicating there was an almost uniform reduction in pressure across the span except when the leading-edge vortex was enhanced by power (Figure 3.2.4-326). Section lift and center of pressure results, Figures 3.2.4-331 and -332, show that the benefits of power were indeed remarkable in two respects: (1) the large magnitude of lift produced beyond power-off stall alpha, with almost as much gain outboard as inboard; and (2), the fairly small aft shift in  $(x/c)_{cp}$ .

With flaps deflected 30 deg, Figures 3.2.4-333 through -358, power-induced flow accelerations were perhaps no greater in magnitude than they were with flaps neutral (inboard lower-surface  $C_p$  changes were comparable). When superimposed on the higher upper-surface velocity levels brought on by the flaps, however, the changes in  $C_p$  were much greater, because of the proportionality of  $C_p$  with  $(V + \Delta V)^2$ . A feature of note inboard is that loads were not enhanced more on the flap than further forward (see Figures 3.2.4-333 and -336, for example). Outboard, the larger power-induced flow acceleration with flaps deflected had a remarkable impact on canard tip vortex interactions with the wing leading-edge vortex at  $\alpha = 8$  deg (Figure -343). Evidently, the wing vortex was moved inboard by power and blanketed more of the chord, so the region of interaction with the canard tip vortex was not as narrowly confined as it was with  $C_T = 0$ . Spanwise data at the same alpha (Figure -351), seem to confirm this inward displacement of the vortex. Section integrated parameters, shown in Figures 3.2.4-357 and -358, reveal that more lift gain due to power was realized with flaps deflected 30 deg than when neutral (compare Figures 3.2.4-331 and -332). Equally noteworthy was the even smaller aft shift in  $(x/c)_{cp}$ , which further denotes that the principal flowfield change due to power was a global increase in velocity rather than a localized increase near the nozzle.

**3.2.4.4.2 Power Buildup.** Test results for the entire range of  $C_T$  values are presented in Figures 3.2.4-359 through -384 with zero flap setting, and in Figures 3.2.4-385 through -407 with a 30-deg setting. There were no unusual trends at the other power settings that have not been addressed elsewhere. For example, the high-suction peaks at the inboard station with  $0 < C_T < 1.4$  at  $\alpha = 12$  deg (Figure 3.2.4-361), achieved, despite the presence of separation at  $C_T = 0$  and 1.4, were due to an increase in  $Re$  (see Subsection 3.2.2.2). Also, as occurred on the wing alone, the effects of power at all alpha values were generally progressive, as when loading was increased aft at low alpha (Figures 3.2.4-360 and -367) and along the entire chord at high alpha (Figures 3.2.4-365 and -373). An occasional exception occurred at the highest power setting, which did not always exceed  $C_T = 1.4$  in its effect on pressures. This is quite evident in the lift coefficient summaries, Figures 3.2.4-383, -384, -406 and -407.

### 3.2.4.5, Spanwise Blowing Effects

Spanwise blowing (SWB) data were available with the canard at the forward station and also at the aft station. There were instrumentation problems during both series of runs, particularly so with the canard aft. For this reason, the wing pressure data reported herein are with the canard forward and wing flaps deflected 30 deg. Data comparisons with the canard at both stations indicated that wing pressure differences, once canard downwash changes were accounted for, were not significant relative to the large SWB effect itself.

**3.2.4.5.1 SWB Off/On Comparisons.** Pressure data comparisons covering the entire alpha range with  $C_T = 0.9$  are presented in Figures 3.2.4-408 through -434, and corresponding section lift and center-of-pressure values are shown in Figures 3.2.4-435 and -436. Similar results with  $C_T = 1.8$  are presented in Figures 3.2.4-437 through -462. These are the same conditions for which wing-alone SWB results are presented in Subsection 3.2.2.3.

With  $C_T = 0.9$ , the inboard chordwise pressures in Figures 3.2.4-408 through -416 reveal an induced upwash due to SWB at low alpha and a large increase in liftwise loading along the aft two-thirds of the upper surface. At  $\alpha = 8$  deg (Figure -410), where leading-edge separation had been imminent, SWB caused the leading-edge vortex to originate further inboard so that a strong, well-established vortex crossed the forward portion of the instrumented chord. Note that the aft loading buildup changed little from what it was at lower alpha settings. As alpha was increased further, however, the character of the flowfield was altered substantially. As is noted elsewhere in this report, applying power at the inboard flap without SWB caused the wing leading-edge vortex to move inboard slightly. Thus, at  $\alpha = 8$  deg, it affected more of this inboard chord as the weak vortex turned downstream. Figures 3.2.4-411 through -416 show that SWB caused the vortex to become much stronger and to blanket less of the chord with increased alpha. The contrast is particularly graphic at  $\alpha = 16$  deg (Figure -412) because with no SWB, as discussed in Subsection 3.2.4.2.5, the wake from the forward canard ceased to postpone stall and the presence of the leading-edge vortex, thus its origin was well inboard of this span station. SWB may not have moved the origin much further, but it enhanced the vortex strength, and hence, reduced its sweepback so that it now crossed  $2y/b = .64$  well forward on the chord. The low-pressure region beneath the SWB jet, that went unchanged at  $\alpha \leq 8$  deg, now had shifted forward at  $\alpha = 16$  deg as though drawn by the leading-edge vortex. At higher alphas the shape of the forward and aft loadings suggests that the SWB jet became vortical, with a typical trailing recompression. But a recompression is no longer evident immediately aft of the leading-edge vortex, as though there were two parallel vortices supplementing each other (see Figure 3.2.4-414). By maximum alpha they were totally indistinguishable. Since enhancement of the leading-edge vortex did not become significant until  $\alpha = 12$  deg, it can be inferred that more lift benefit might have been realized if (1) the SWB jet had been positioned a little further forward and (2) a stronger leading-edge vortex had been induced to set in at a lower alpha, as with a sharper airfoil leading-edge, less camber, or an inboard wing-nacelle strake. The outboard data with  $C_T = 0.9$ , Figures 3.2.4-417 through -425, also show a small increase in upwash at low alpha caused by SWB, resulting in higher pressure on the lower surface and an inboard shift of the leading-edge vortex at  $\alpha = 4$  deg (Figure -418). Also, a slight increase in flap load is a hint that the vortex energy content was raised. Vortex enhancement was conspicuous at  $\alpha = 12$  deg (Figure 3.2.4-420), and at yet higher alpha settings, a distinct suction peak was remarkably "locked in" at  $x/c = 0.4$ , probably because the leading-edge vortex was stabilized by SWB. Increases in lower-surface pressure were consistent with an increase in effective angle of attack associated with a large increase in lift (inboard section pressures did likewise). There appears to be more distinction between the leading-edge vortex and the SWB

jet at  $\alpha = 25$  deg (Figure 3.2.4-423) and above than there was at the inboard station, suggesting that the two vortices (if there were two) did not actually meld into one, yet did not separate much either. The spanwise midchord pressures, Figures 3.2.4-426 through -434, seem to show (1) a SWB jet influence that is dominant inboard at low  $\alpha$ , with early leading-edge vortex enhancement effects outboard (Figure -427), (2) strong enhancement beginning at  $\alpha = 12$  deg (Figure -429), and (3) near-coincidence of the jet and leading-edge vortex at  $\alpha = 20$  deg (Figure -431) and above. Section integrated results, Figures 3.2.4-435 and -436, are significant in depicting both the large lift increments afforded by SWB and the forward shift in the centroid of those lift increments as  $\alpha$  was increased.

With  $C_T = 1.8$ , Figures 3.2.4-437 through -460 show the inboard  $C_p$  trends to have been affected by SWB in much the same manner but to a larger degree than they were with  $C_T = 0.9$ . In fact, once the leading-edge vortex had appeared at  $2y/b = 0.64$ , the upper-surface patterns look similar to those with  $C_T = 0.9$  but at an  $\alpha$  four degrees lower (compare Figures 3.2.4-440 and -412, or -441 and -413, for example). Clearly, the leading-edge vortex was now more enhanced at a fixed  $\alpha$ , and this benefit persisted at high  $\alpha$  (compare Figures 3.2.4-444 and -415). There were more distinguishing features in the outboard data at  $C_T = 1.8$ , such as more induced upwash and higher loads near the trailing edge ( $\alpha = 12$  deg, Figures 3.2.4-448 vs -420), the latter indicative that confluence of the SWB jet and the leading-edge vortex was less likely. Spanwise trends at  $\alpha = 12$  deg, (Figure -456) and above also suggest that the leading-edge vortex was enhanced more by the higher  $C_T$ , and that there was little increase in suction generated under the SWB jet. Center of pressure results, Figures 3.2.4-461 and -462, show the aft shift in loading more clearly when compared with the  $C_T = 0.9$  results (Figures 3.2.4-435 and -436).

An analysis of temperature measurements that were acquired on the wing provided a good insight into the behavior of the SWB jet. Furthermore, when the isotherm patterns were compared with isobar distributions gleaned from the pressure measurement, the composite picture complemented the flowfield model described herein and added some important new clues regarding the interplay between the vortex and the SWB jet. These results are presented in Section 3.2.6.

**3.2.4.5.2 Power Buildup.** The results of a sequential power increase with SWB are presented in Figures 3.2.4-463 through -476. The pressure data plots are limited to angles of attack of 4, 12, 20 and 28 deg in the interest of brevity while still illustrating the principal trends. They include the results with  $C_T = 0$  in order to highlight the gross effects of power rather than just the incremental changes between  $C_T$  levels. The section integrated properties cover the entire  $\alpha$  range.

The inboard  $C_p$  trends (Figures 3.2.4-463 through -466) show a progressive increase in induced upper-surface loading with power buildup, as to be expected. At  $\alpha = 4$  and 12 deg the centroid of this loading change moved forward markedly. Presumably, this movement reflects the increased resistance to the downstream impetus the wing flowfield imparted to the SWB jet. The lower-surface pressures were rather mixed, but generally they indicate an increase in induced upwash with power, as does the successive increase in leading-edge loading and vortex strength at  $\alpha = 12$  deg. At  $\alpha = 20$  and 28 deg the loading aft of the midchord was nearly insensitive to power compared to the large effects forward. The general stall condition at this station was entirely subordinated (note that zero-power data were not available at  $\alpha = 28$  deg, Figure -466). At these high  $\alpha$  settings the SWB jet appears to have been at its most forward position on the chord, since the low-pressure peaks shifted little with  $\alpha$  or power setting. The "humpy"  $C_p$  distributions suggest that the vortex and jet remained distinct entities irrespective of  $C_T$ .

Outboard  $C_p$  trends (Figures 3.2.4-467 through -470) were generally "stacked" proportionately with power setting except for  $C_T = 0.9$  (see Figure -467) and except for a region near  $x/c = 0.7$  (see Figure -468). The latter result indicates that at the higher powers the jet extended its influence further outboard, enough to enhance the leading-edge vortex and push it back across the chord. This created a typical expansion-compression pattern (see the "vortex region" sketch in Subsection 3.2.1). No reason is known for the  $C_T = 0.9$  power level to have been unique. Spanwise data trends (Figures 3.2.4-472 through -474) presented few anomalies as regards the orderliness of power/SWB effects.

$C_l'$  and  $(x/c)_{cp}$  results were quite impressive. Figures 3.2.4-475 and -476 reveal that power, when applied with SWB, increased  $C_l'$  at the inboard station at all alphas, with the peak values occurring at high alphas. Maximum lift was doubled with  $C_T = 1.8$ . Note in Figure 3.2.4-475 that power induced an aft  $(x/c)_{cp}$  shift at low and mid alphas because, at the inboard chord, the jet loading was localized near and aft of the midpoint and the leading-edge vortex was too remote from the jet to be strongly influenced. The  $(x/c)_{cp}$  shift due to power was reversed at high alphas because the leading-edge vortex (now further inboard) was enhanced and unswept (along with the jet), thus inducing a load increase further forward.  $C_l'$  at the outboard station (Figure 3.2.4-476) was increased little by power near zero alpha, but the peak value was increased by a factor of 2.5. The  $(x/c)_{cp}$  changes were smaller than occurred inboard, but a reversal in trend with power began when SWB augmented the leading-edge vortex contribution. The large increase in loading outboard (see Figure 3.2.4-473) suggests that SWB could be a powerful roll-control device if applied unilaterally.

SYM	TEST	RUN	ALPHA	CT	ITEF	OTEF	CAN	SWB
⊕	543	63	0.1	0.00	0	0	0	OFF
⊞	543	63	4.2	0.00	0	0	0	OFF
△	543	63	8.3	0.00	0	0	0	OFF
⬢	543	63	12.5	0.00	0	0	0	OFF
*	543	63	16.6	0.00	0	0	0	OFF

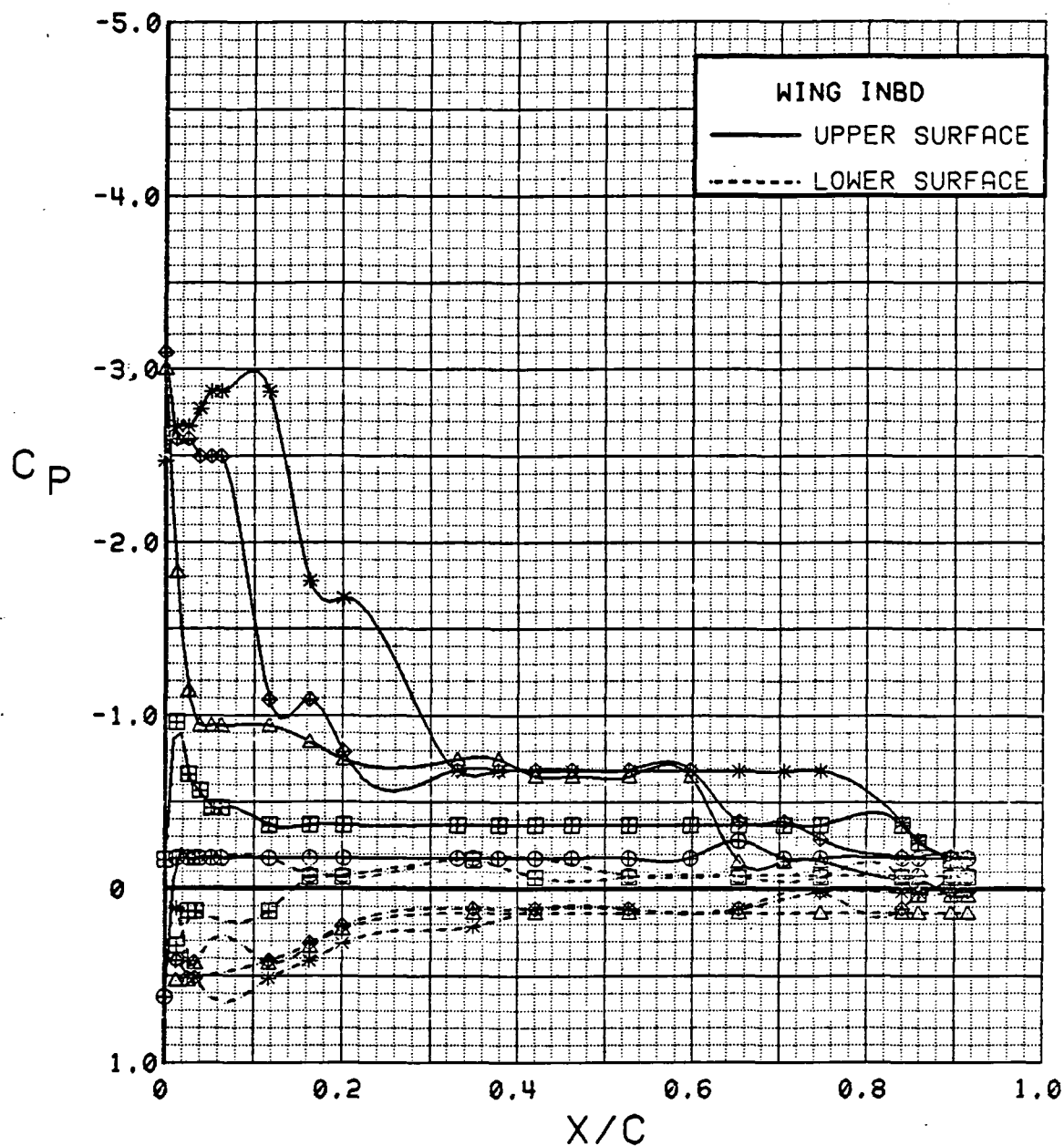


Figure 3.2.4-1

Angle of Attack Effects, Power off, Inboard,  
Flaps Neutral, Low Alpha

SYM	TEST	RUN	ALPHA	CT	ITEF	OTEF	CAN	SWB
⊕	543	63	16.6	0.00	0	0	0	OFF
⊞	543	63	20.7	0.00	0	0	0	OFF
△	543	63	24.8	0.00	0	0	0	OFF
⊕	543	63	28.8	0.00	0	0	0	OFF
*	543	63	32.8	0.00	0	0	0	OFF

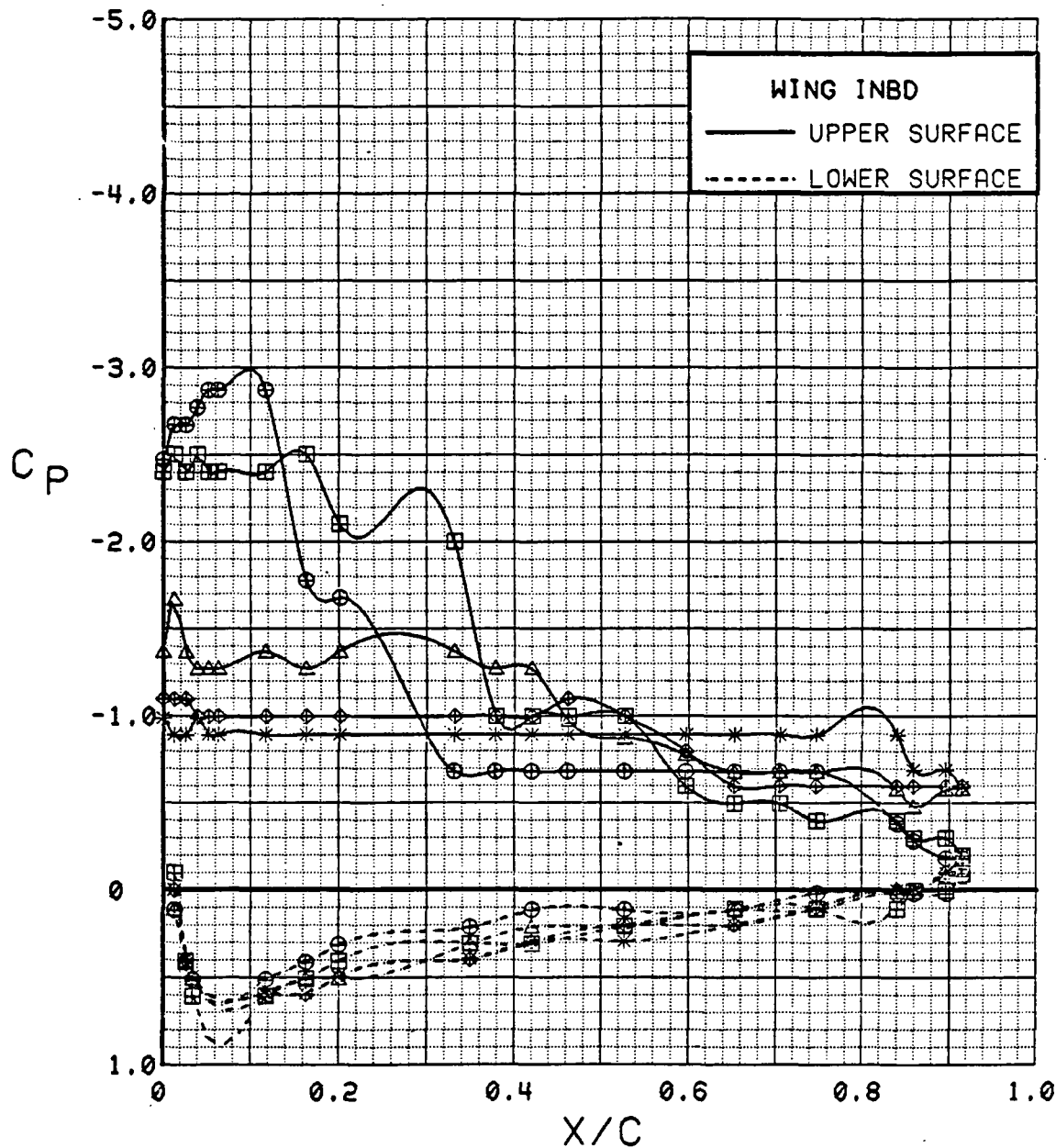


Figure 3.2.4-2

Angle of Attack Effects, Power off, Inboard,  
Flaps Neutral, High Alpha

SYM	TEST	RUN	ALPHA	CT	ITEF	OTEF	CAN	SWB
⊕	543	63	0.1	0.00	0	0	0	OFF
⊞	543	63	4.2	0.00	0	0	0	OFF
△	543	63	8.3	0.00	0	0	0	OFF
⬠	543	63	12.5	0.00	0	0	0	OFF
*	543	63	16.6	0.00	0	0	0	OFF

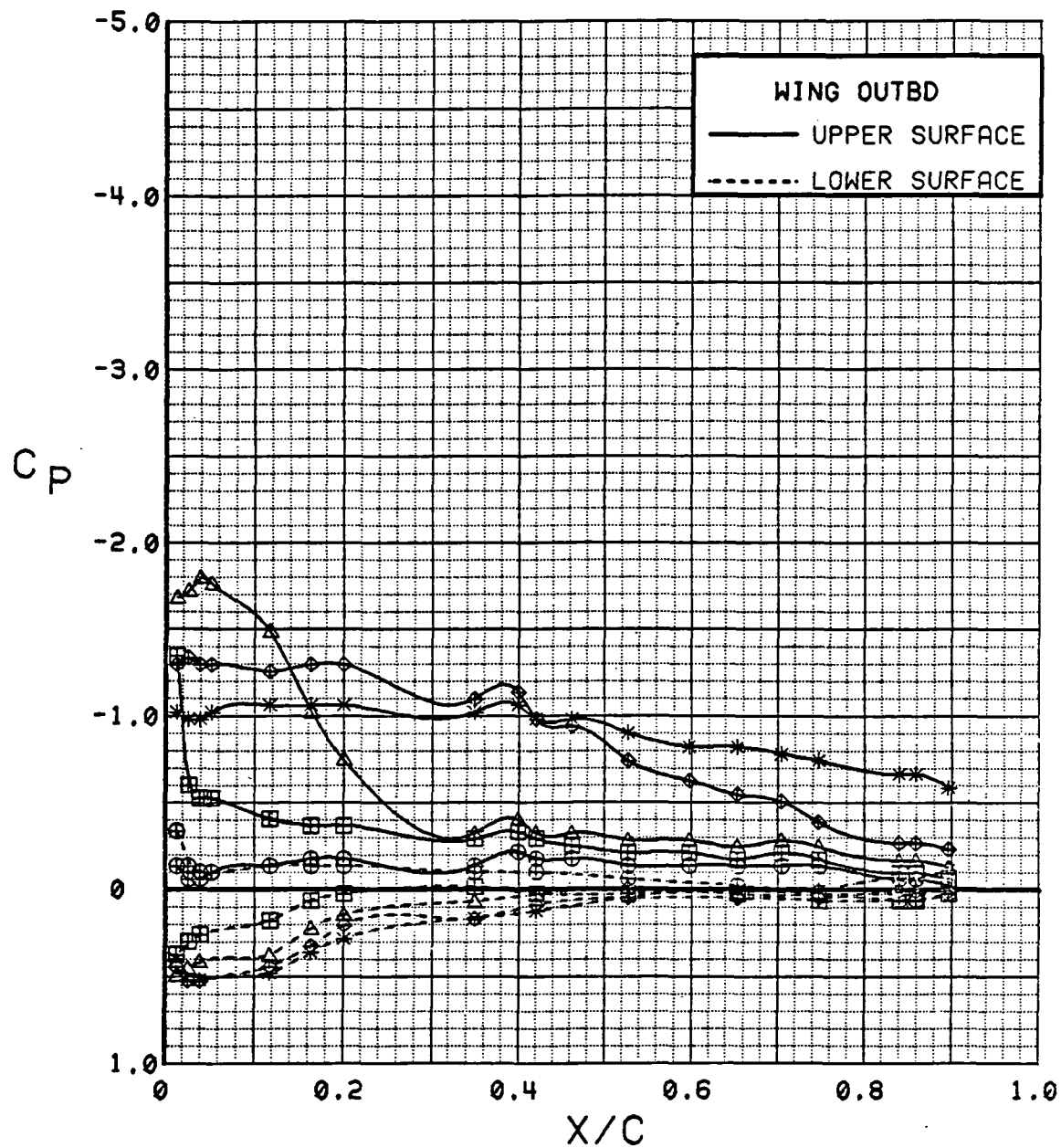


Figure 3.2.4-3

Angle of Attack Effects, Power off, Outboard,  
Flaps Neutral, Low Alpha



4

SYM	TEST	RUN	ALPHA	CT	ITEF	OTEF	CAN	SWB
⊕	543	63	16.6	0.00	0	0	0	OFF
⊞	543	63	20.7	0.00	0	0	0	OFF
△	543	63	24.8	0.00	0	0	0	OFF
◆	543	63	28.8	0.00	0	0	0	OFF
*	543	63	32.8	0.00	0	0	0	OFF

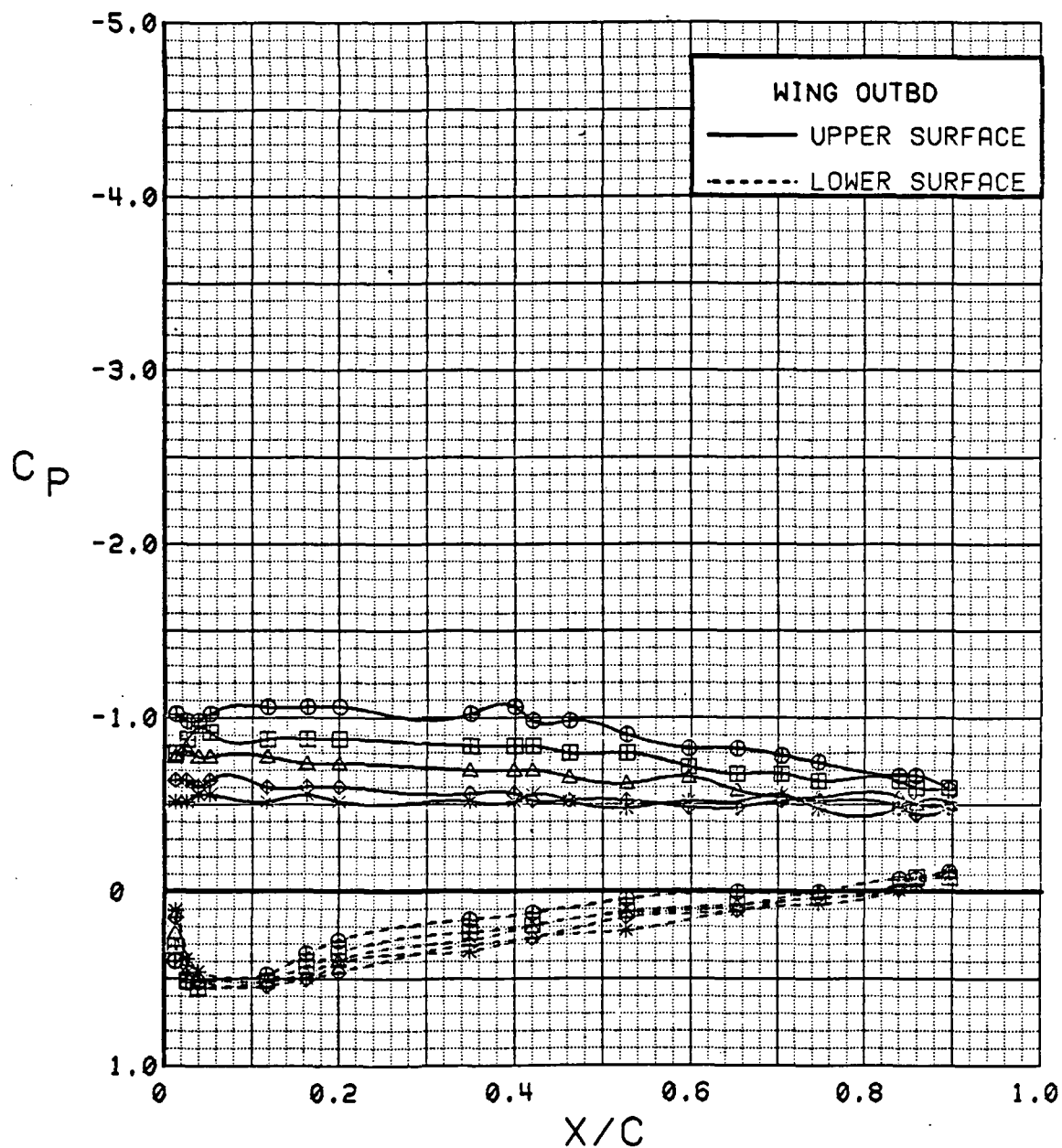


Figure 3.2.4-4

Angle of Attack Effects, Power off, Outboard,  
Flaps Neutral, High Alpha

SYM	TEST	RUN	ALPHA	CT	ITEF	OTEF	CAN	SWB
⊗	543	63	0.1	0.00	0	0	0	OFF
⊠	543	63	4.2	0.00	0	0	0	OFF
△	543	63	8.3	0.00	0	0	0	OFF
◆	543	63	12.5	0.00	0	0	0	OFF
*	543	63	16.6	0.00	0	0	0	OFF

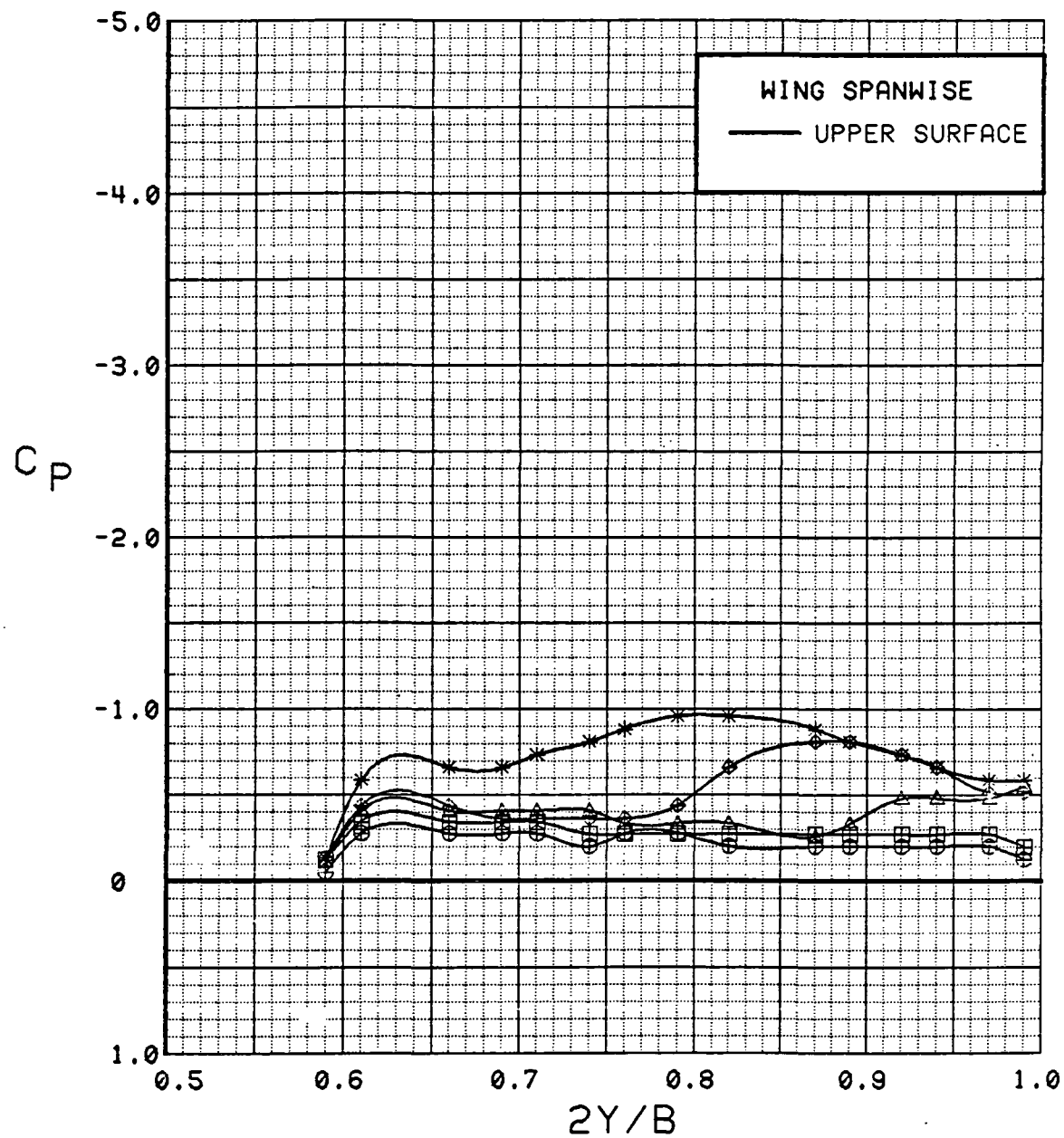


Figure 3.2.4-5

Angle of Attack Effects, Power off, Spanwise,  
Flaps Neutral, Low Alpha

SYM	TEST	RUN	ALPHA	CT	ITEF	OTEF	CAN	SWB
⊕	543	63	16.6	0.00	0	0	0	OFF
⊞	543	63	20.7	0.00	0	0	0	OFF
△	543	63	24.8	0.00	0	0	0	OFF
◆	543	63	28.8	0.00	0	0	0	OFF
*	543	63	32.8	0.00	0	0	0	OFF

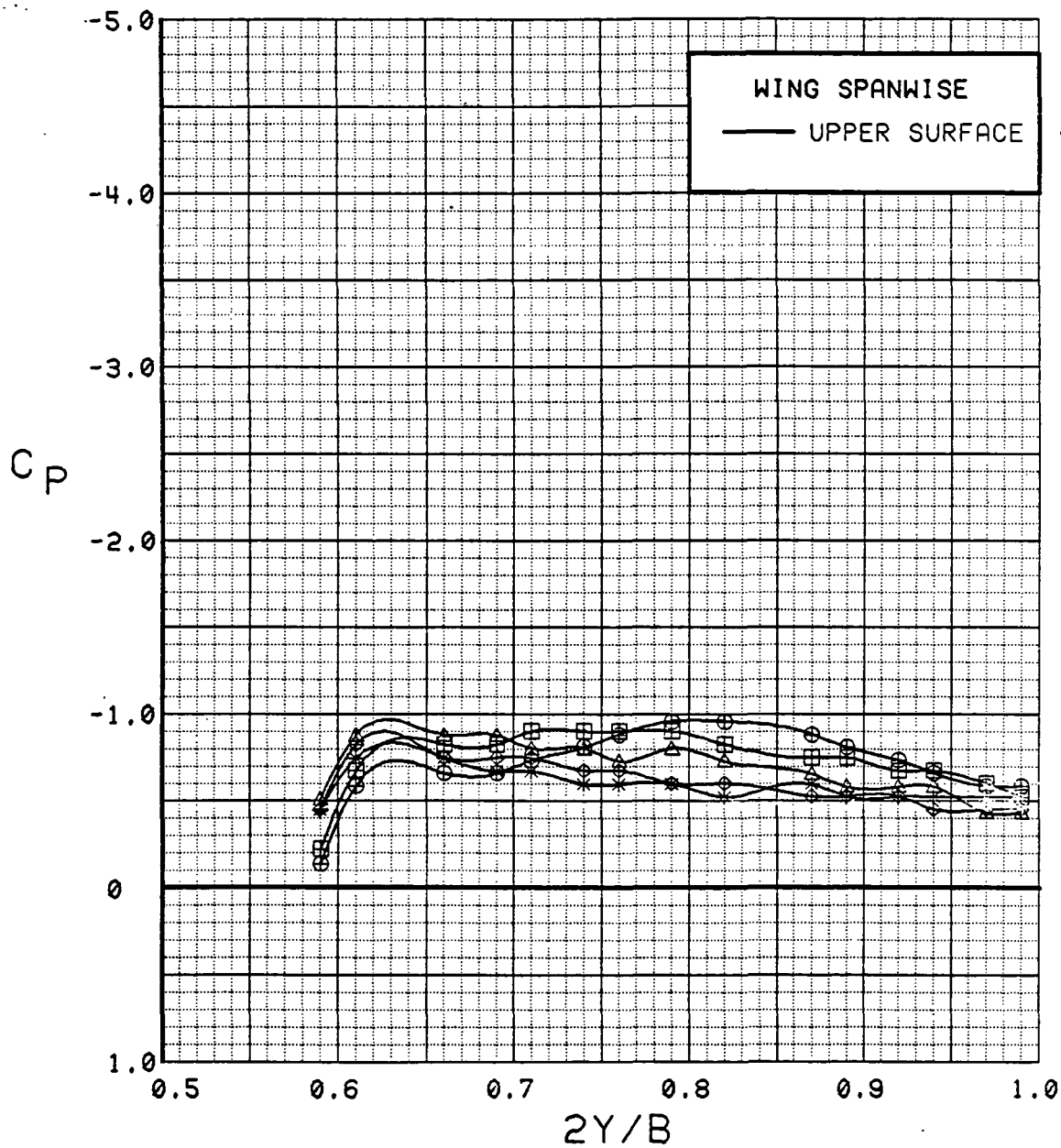


Figure 3.2.4-6

Angle of Attack Effects, Power off, Spanwise,  
Flaps Neutral, High Alpha

SYM	TEST	RUN	ALPHA	CT	ITEF	OTEF	CAN	SWB
⊕	543	11	0.3	0.00	30	30	0	OFF
⊞	543	11	4.4	0.00	30	30	0	OFF
△	543	11	8.5	0.00	30	30	0	OFF
⬠	543	11	12.7	0.00	30	30	0	OFF
*	543	11	16.8	0.00	30	30	0	OFF

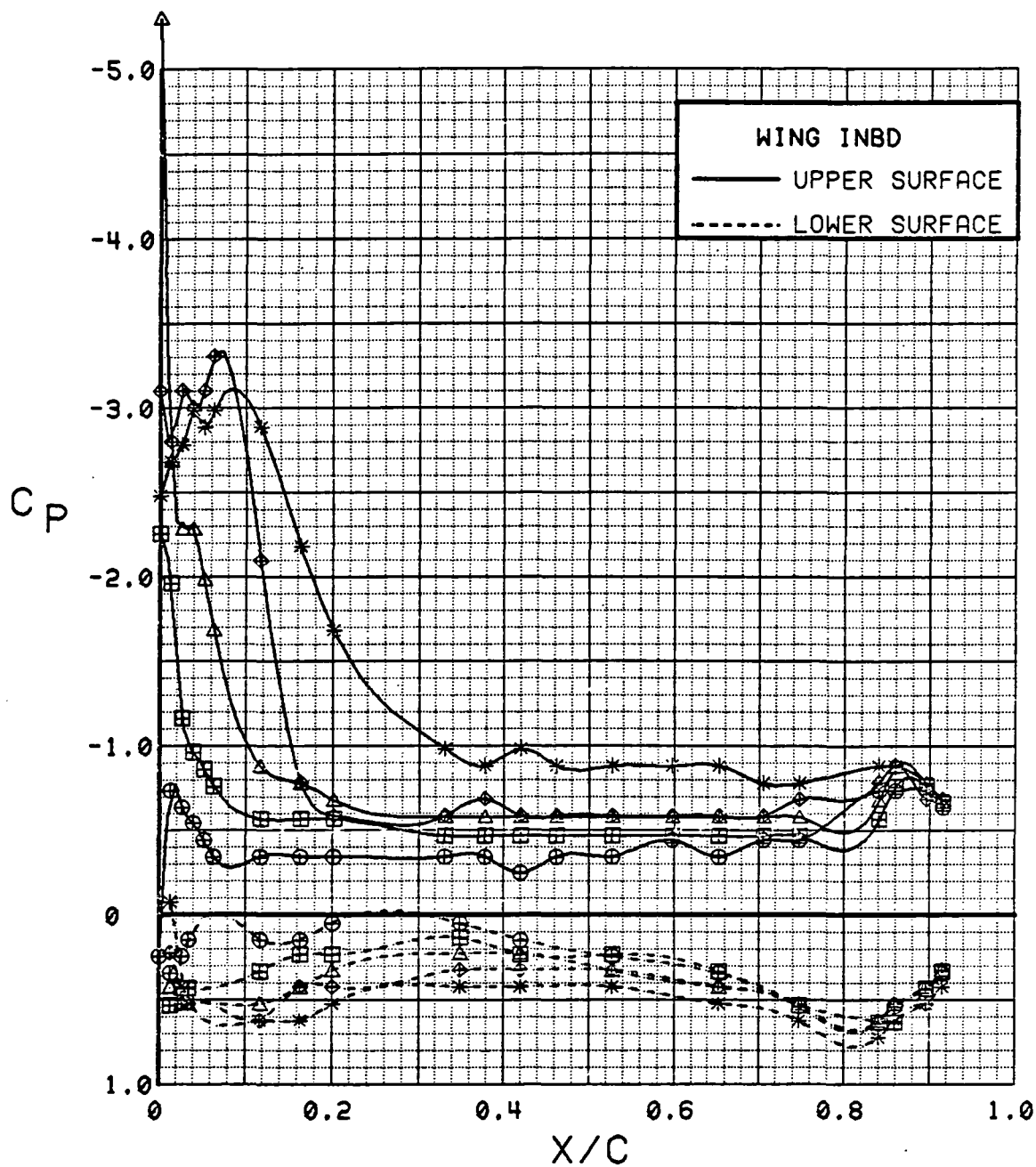


Figure 3.2.4-7 Angle of Attack Effects, Power off, Inboard, Flaps Deflected, Low Alpha

SYM	TEST	RUN	ALPHA	CT	ITEF	OTEF	CAN	SWB
⊕	543	11	16.8	0.00	30	30	0	OFF
⊞	543	11	20.8	0.00	30	30	0	OFF
△	543	11	24.9	0.00	30	30	0	OFF
⊕	543	11	28.9	0.00	30	30	0	OFF

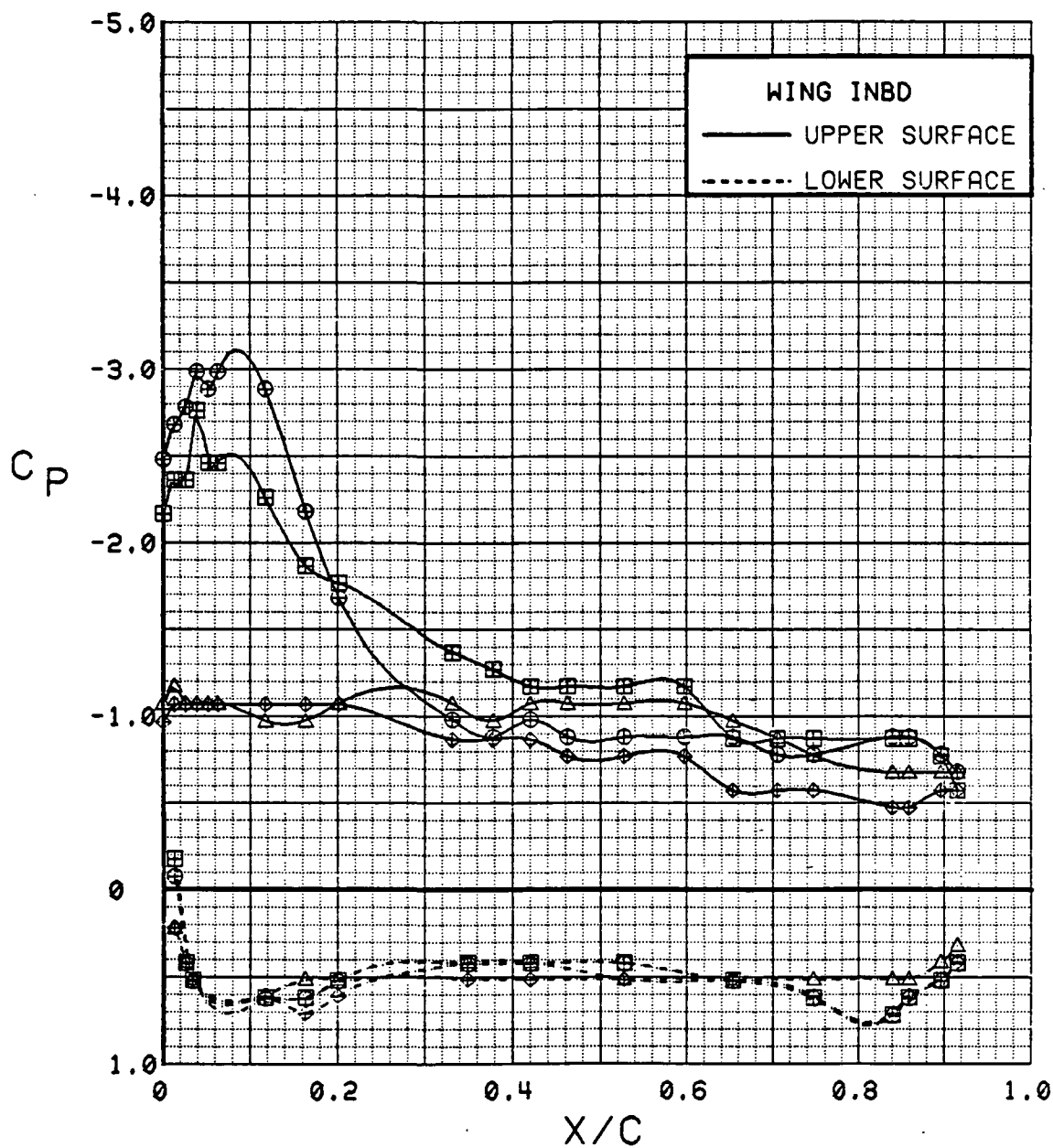


Figure 3.2.4-8 Angle of Attack Effects, Power off, Inboard, Flaps Deflected, High Alpha

SYM	TEST	RUN	ALPHA	CT	ITEF	OTEF	CAN	SWB
⊕	543	11	0.3	0.00	30	30	0	OFF
⊞	543	11	4.4	0.00	30	30	0	OFF
△	543	11	8.5	0.00	30	30	0	OFF
⊕	543	11	12.7	0.00	30	30	0	OFF
*	543	11	16.8	0.00	30	30	0	OFF

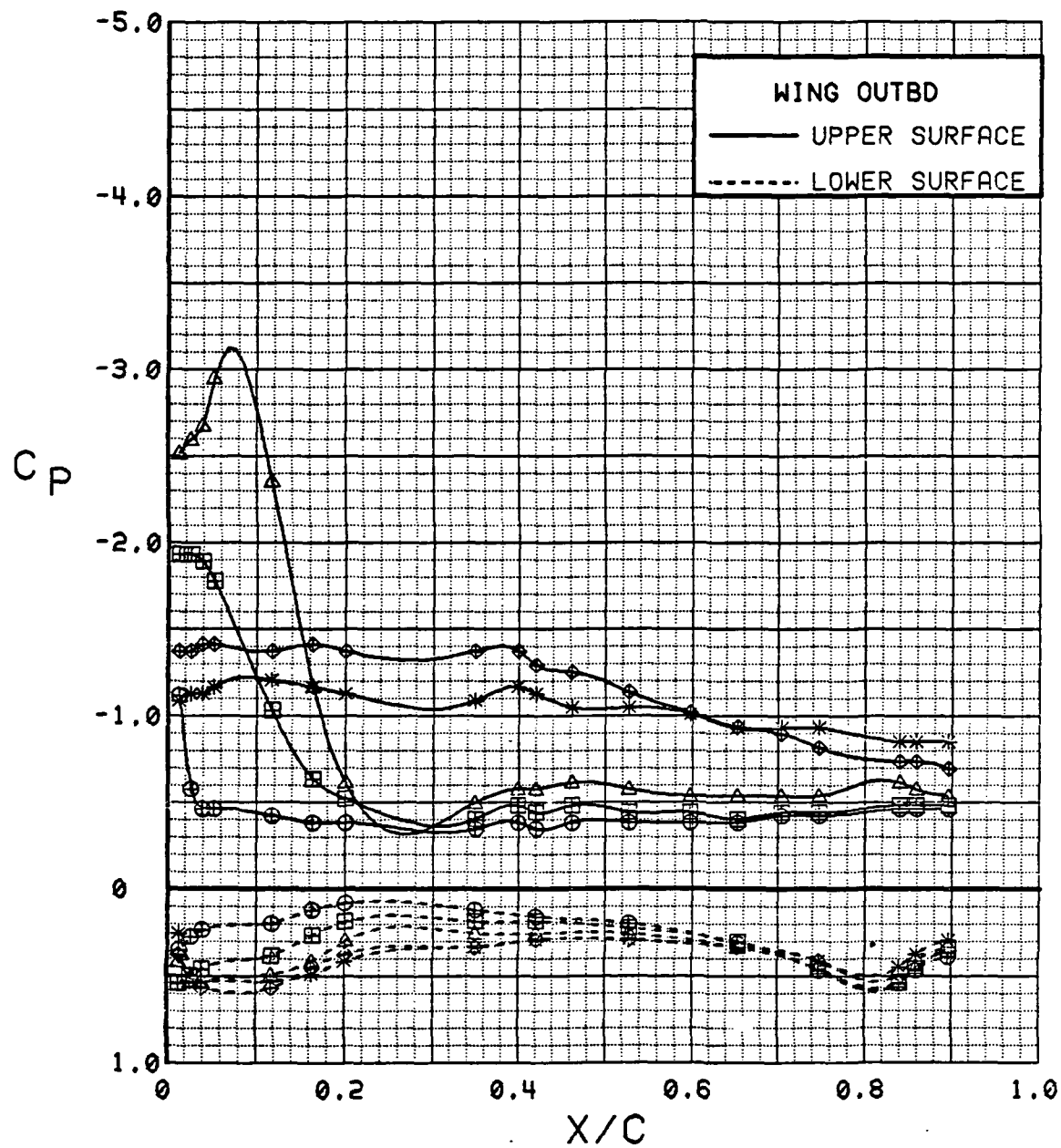


Figure 3.2.4-9

Angle of Attack Effects, Power off, Outboard,  
Flaps Deflected, Low Alpha

SYM	TEST	RUN	ALPHA	CT	ITEF	OTEF	CAN	SWB
⊕	543	11	16.8	0.00	30	30	0	OFF
⊞	543	11	20.8	0.00	30	30	0	OFF
△	543	11	24.9	0.00	30	30	0	OFF
◆	543	11	28.9	0.00	30	30	0	OFF

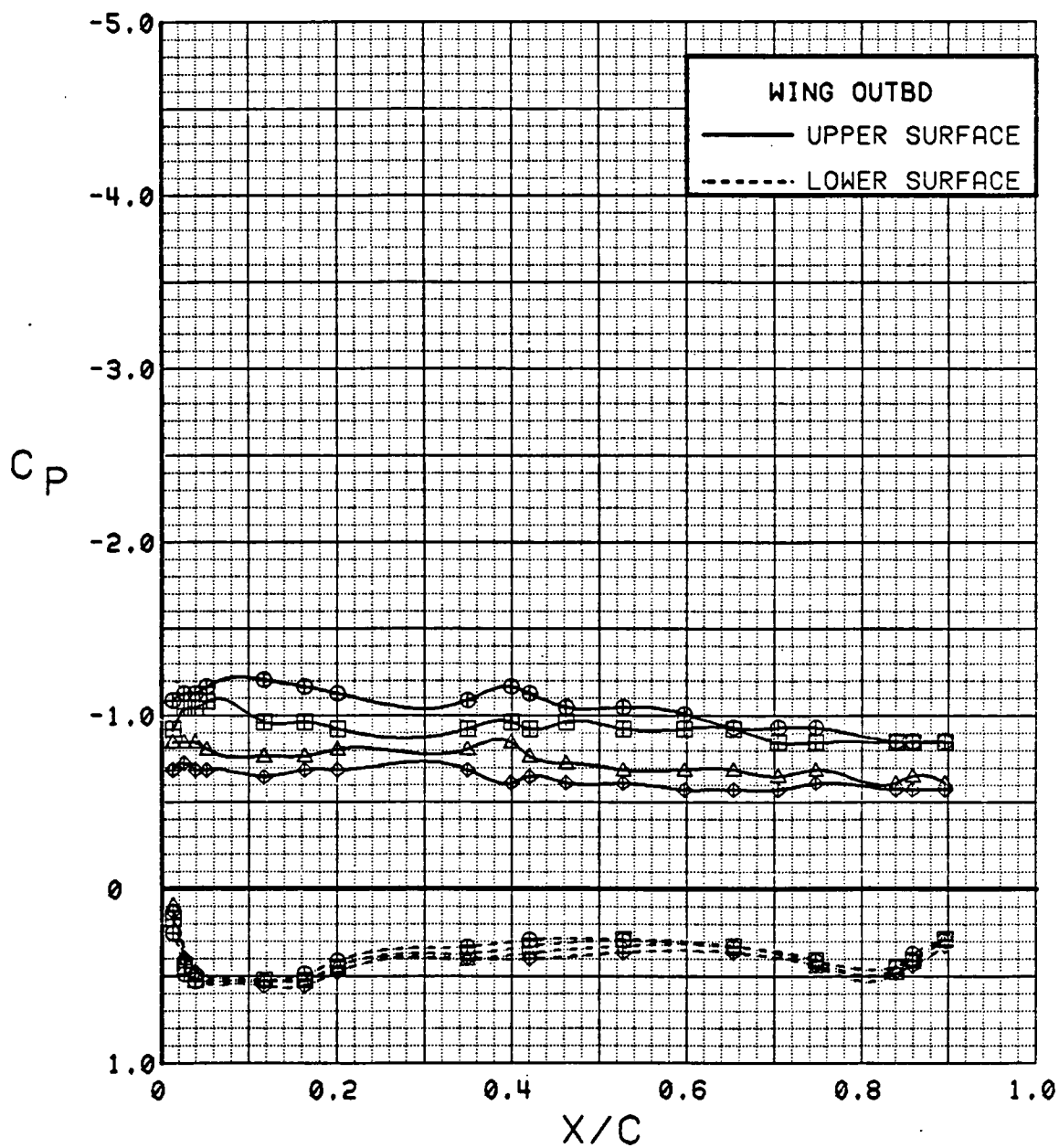


Figure 3.2.4-10 Angle of Attack Effects, Power off, Outboard, Flaps Deflected, High Alpha

SYM	TEST	RUN	ALPHA	CT	ITEF	OTEF	CAN	SWB
⊕	543	11	0.3	0.00	30	30	0	OFF
⊞	543	11	4.4	0.00	30	30	0	OFF
△	543	11	8.5	0.00	30	30	0	OFF
◆	543	11	12.7	0.00	30	30	0	OFF
*	543	11	16.8	0.00	30	30	0	OFF

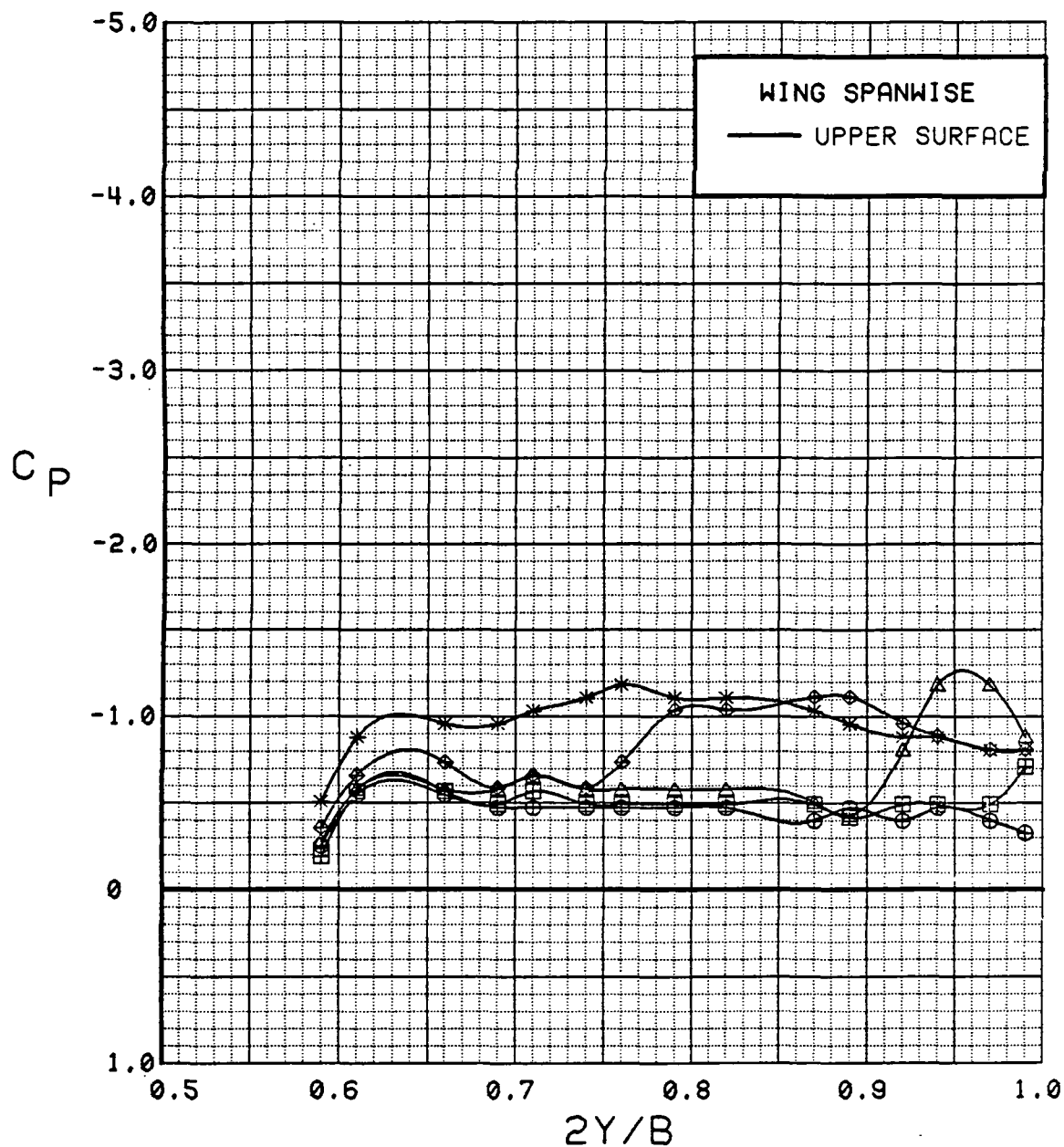


Figure 3.2.4-11 Angle of Attack Effects, Power off, Spanwise, Flaps Deflected, Low Alpha



SYM	TEST	RUN	ALPHA	CT	ITEF	OTEF	CAN	SWB
⊕	543	11	16.8	0.00	30	30	0	OFF
⊞	543	11	20.8	0.00	30	30	0	OFF
△	543	11	24.9	0.00	30	30	0	OFF
◆	543	11	28.9	0.00	30	30	0	OFF

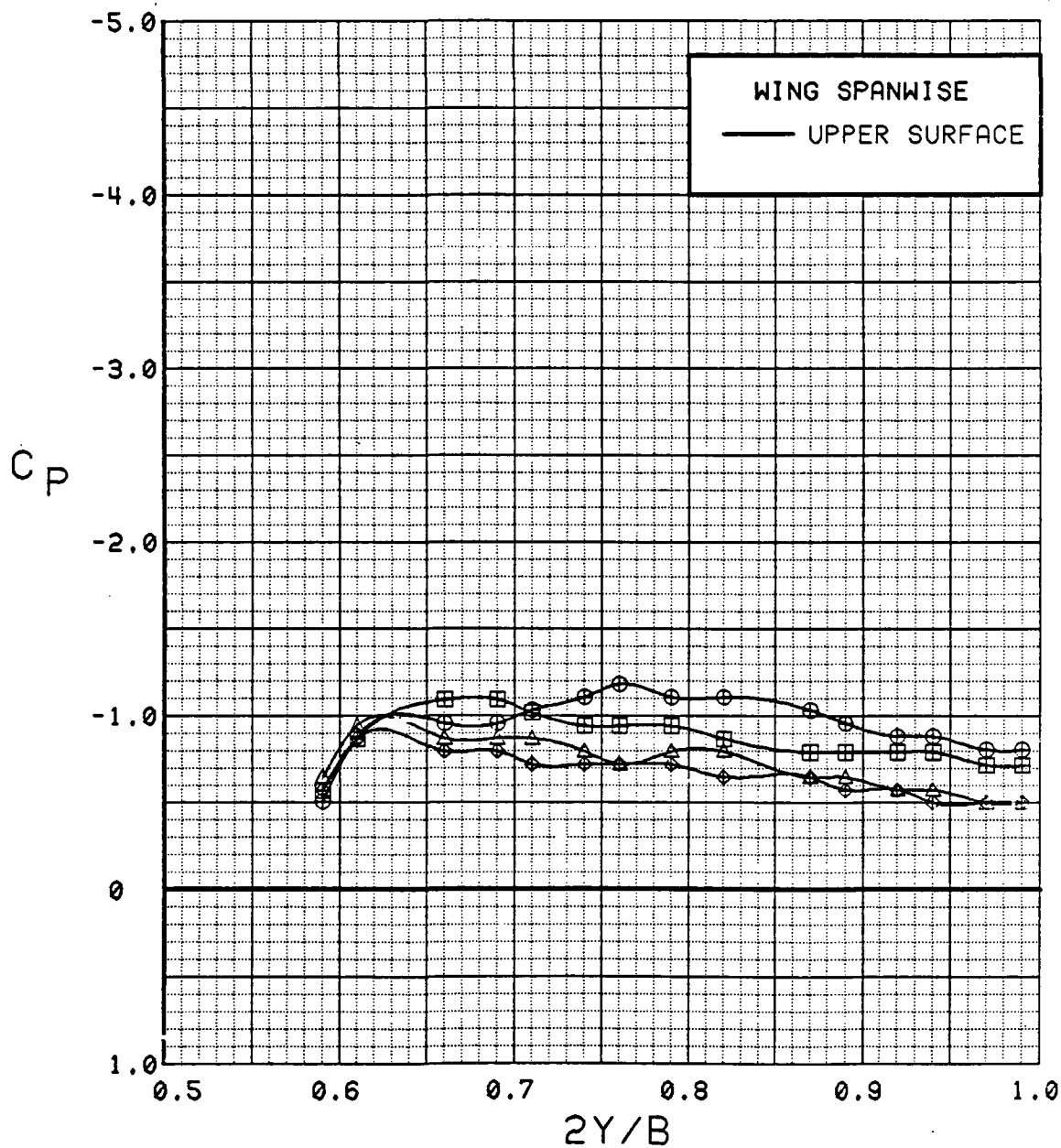


Figure 3.2.4-12 Angle of Attack Effects, Power off, Spanwise, Flaps Deflected, High Alpha

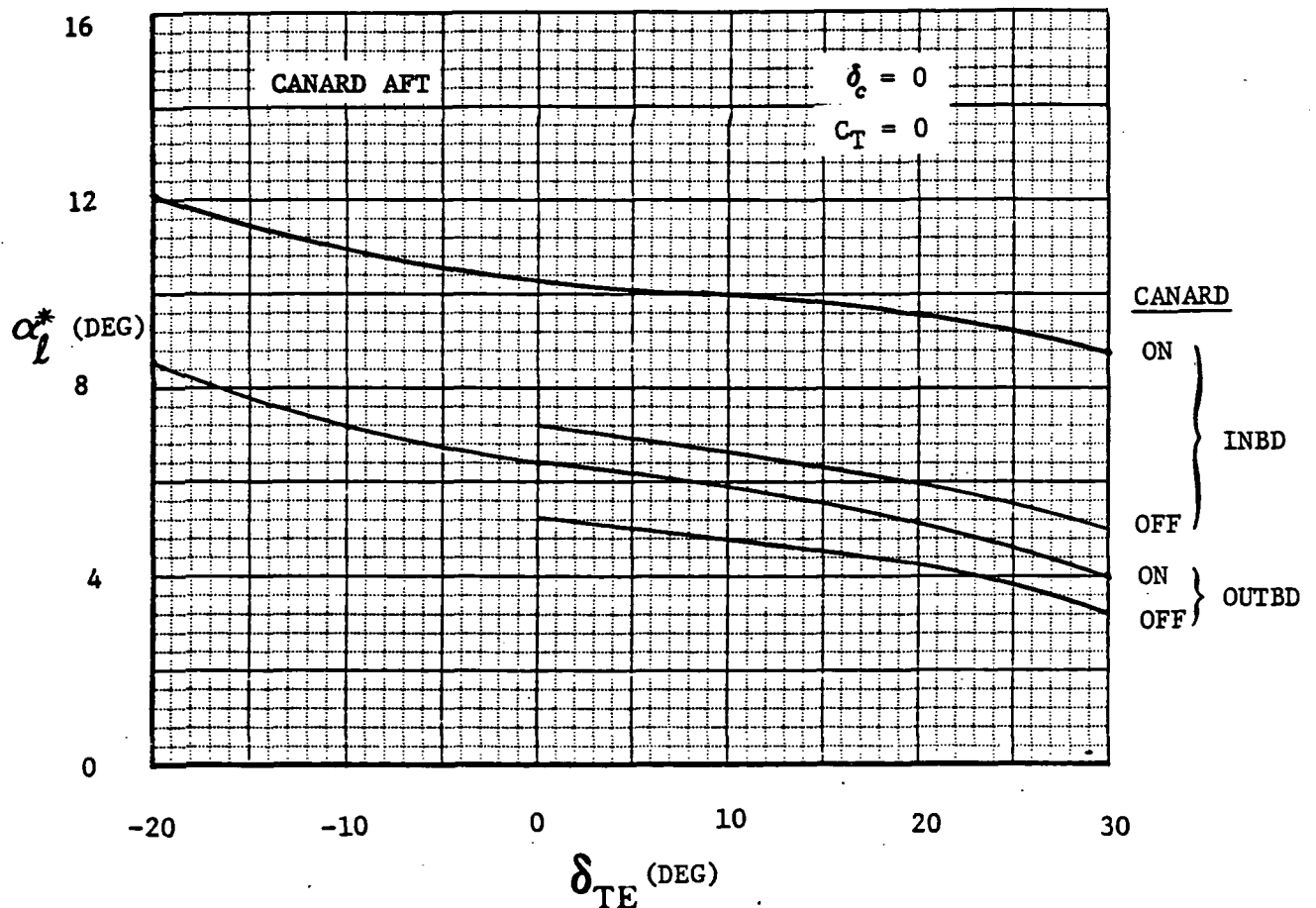
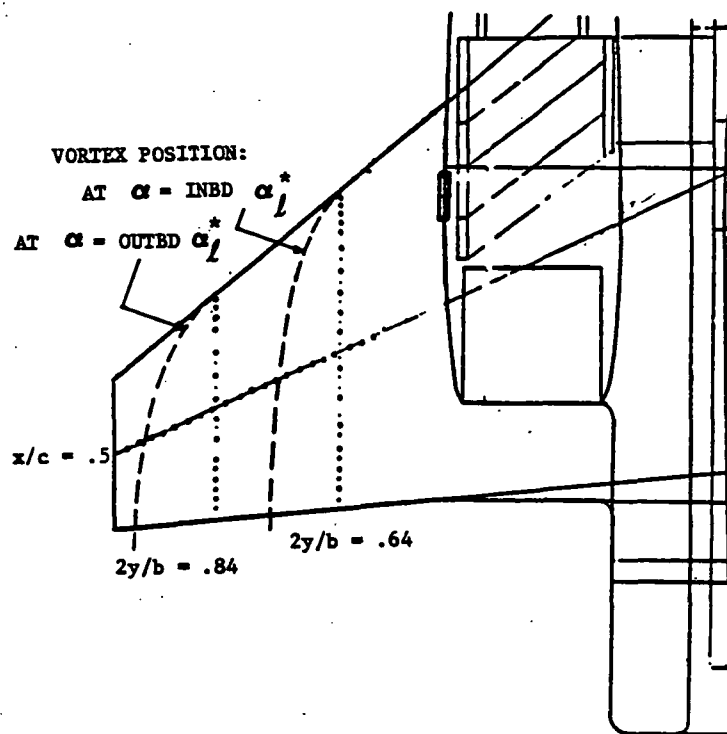


Figure 3.2.4-13 Origin of Leading-Edge Vortex, Canard On

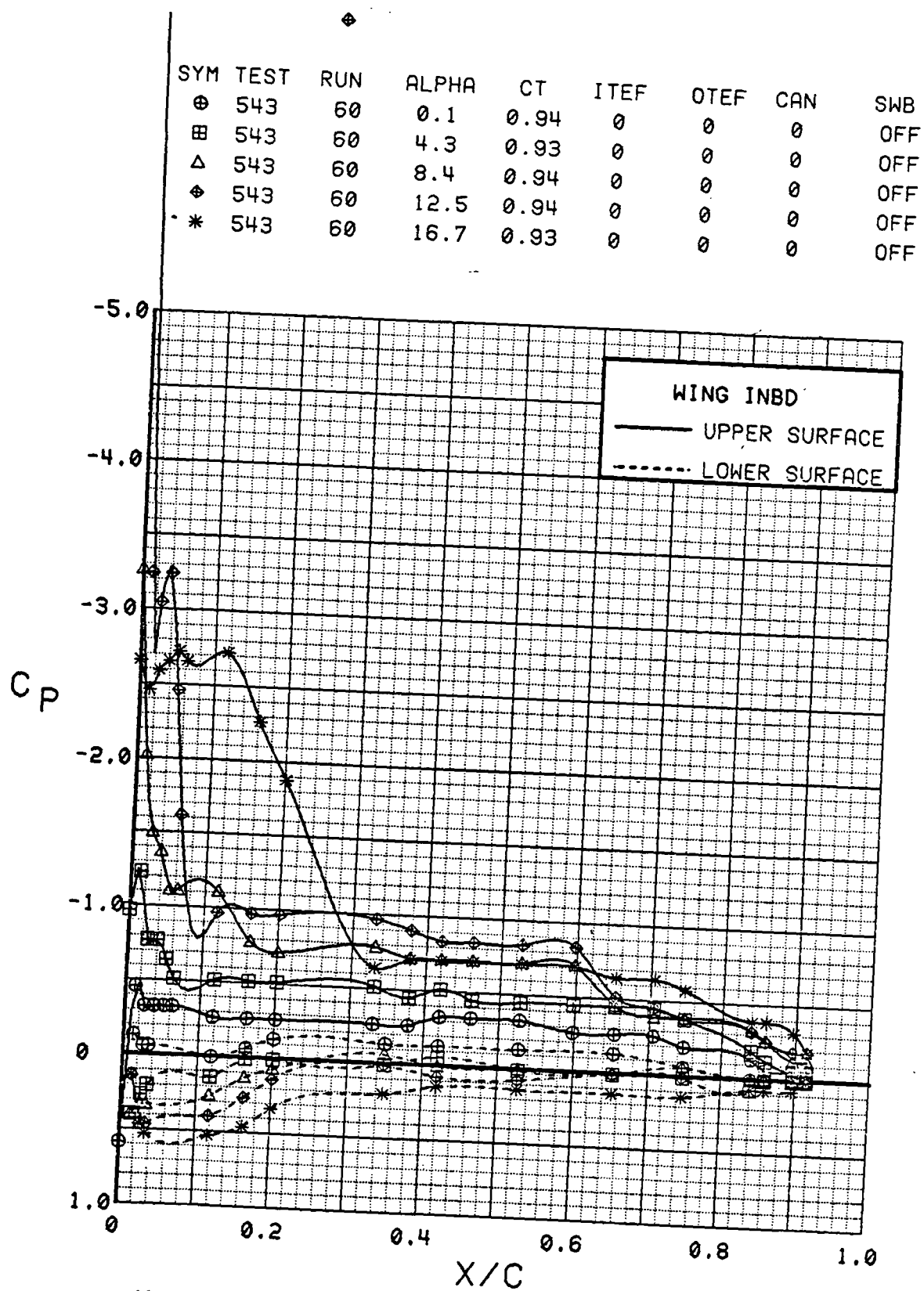


Figure 3.2.4-14 Angle of Attack Effects,  $C_T = 0.9$ , Inboard, Flaps Neutral, Low Alpha

SYM	TEST	RUN	ALPHA	CT	ITEF	OTEF	CAN	SWB
⊕	543	60	16.7	0.93	0	0	0	OFF
⊞	543	60	20.8	0.93	0	0	0	OFF
△	543	60	24.9	0.93	0	0	0	OFF
⊕	543	60	29.0	0.93	0	0	0	OFF
*	543	60	33.1	0.94	0	0	0	OFF

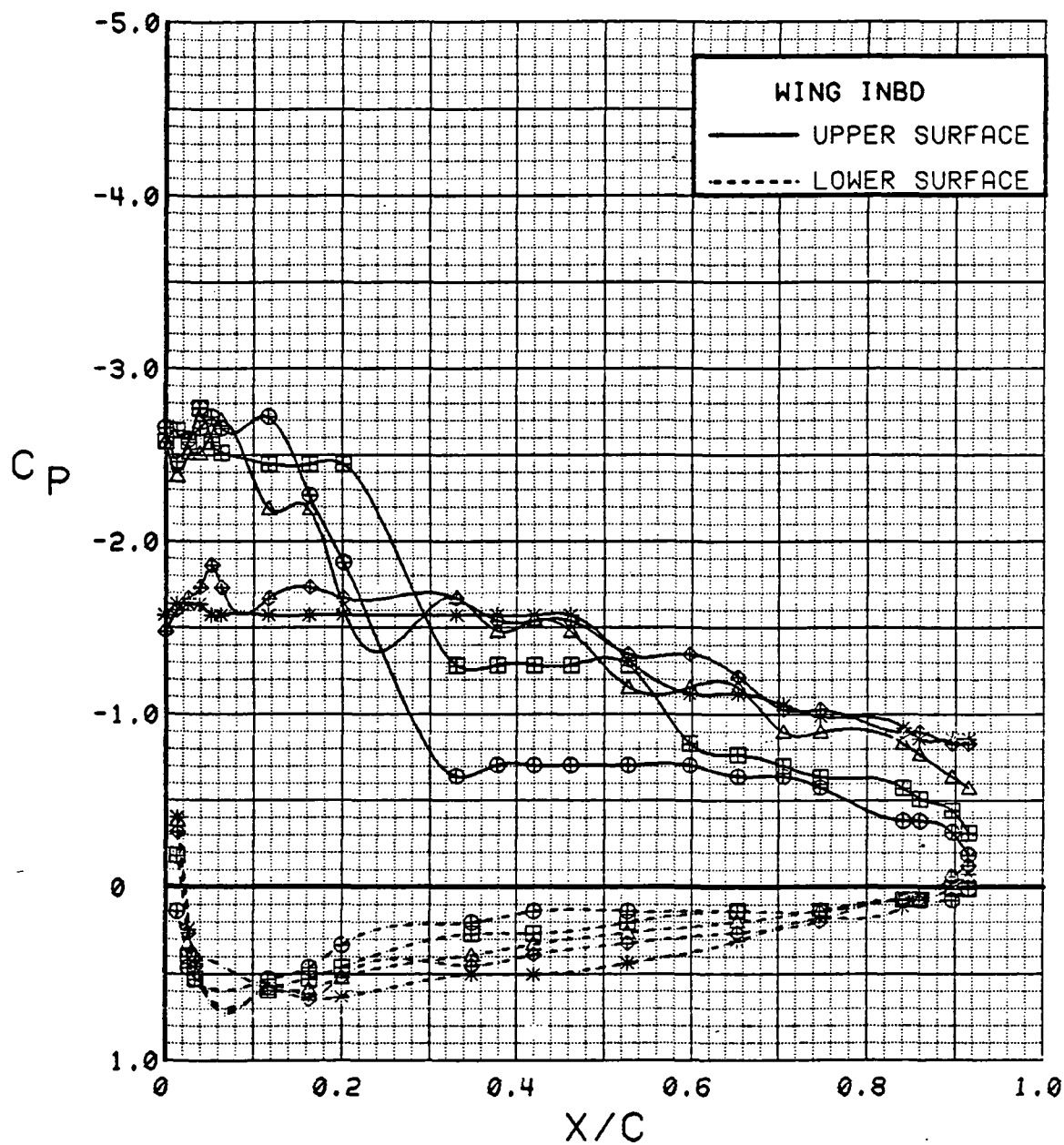


Figure 3.2.4-15 Angle of Attack Effects,  $C_T = 0.9$ , Inboard, Flaps Neutral, High Alpha

SYM	TEST	RUN	ALPHA	CT	ITEF	OTEF	CAN	SWB
⊕	543	60	0.1	0.94	0	0	0	OFF
⊞	543	60	4.3	0.93	0	0	0	OFF
△	543	60	8.4	0.94	0	0	0	OFF
⬠	543	60	12.5	0.94	0	0	0	OFF
*	543	60	16.7	0.93	0	0	0	OFF

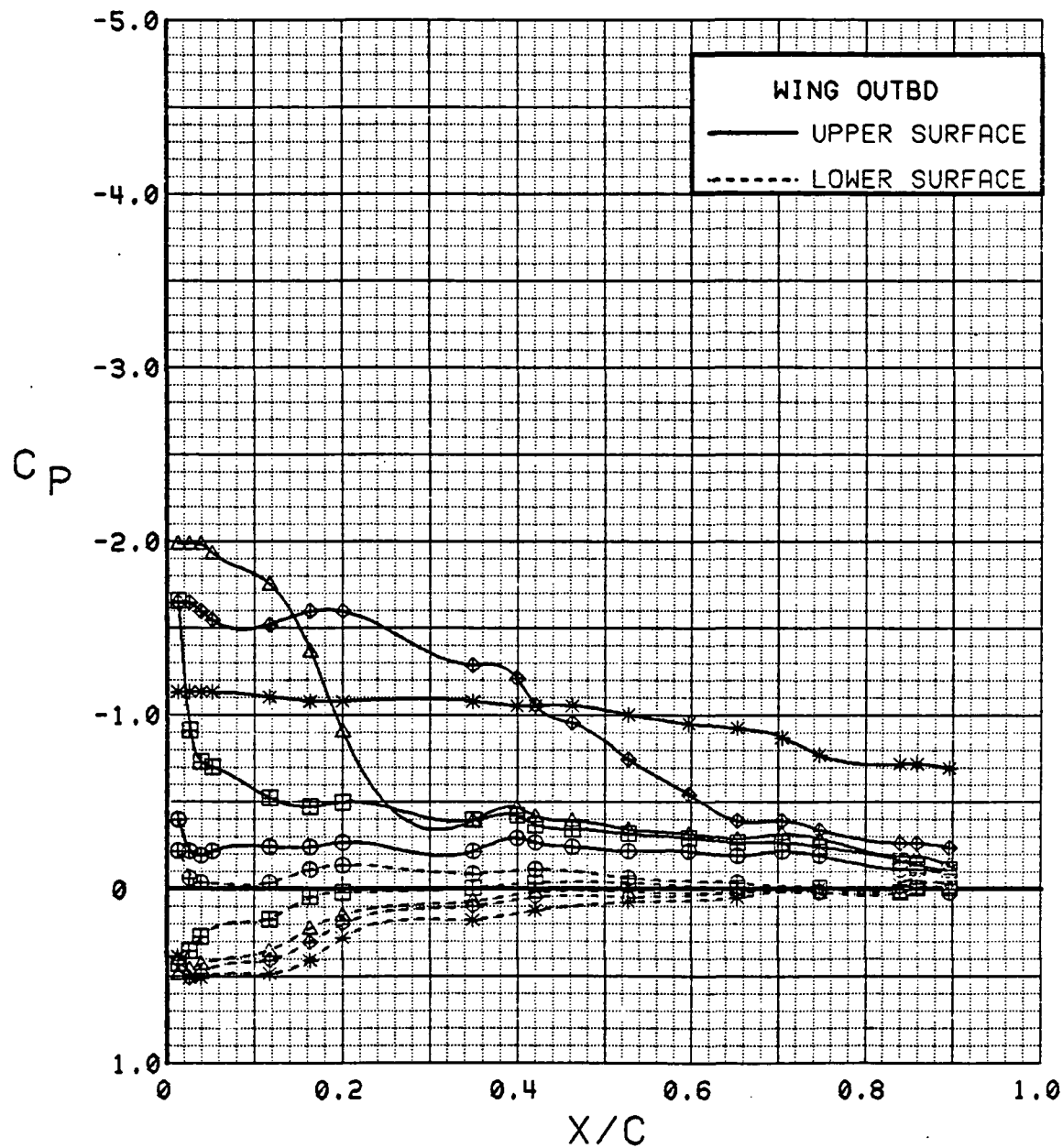


Figure 3.2.4-16

Angle of Attack Effects,  $C_T = 0.9$ , Outboard,  
Flaps Neutral, Low Alpha

SYM	TEST	RUN	ALPHA	CT	ITEF	OTEF	CAN	SWB
⊕	543	60	16.7	0.93	0	0	0	OFF
⊞	543	60	20.8	0.93	0	0	0	OFF
△	543	60	24.9	0.93	0	0	0	OFF
⊕	543	60	29.0	0.93	0	0	0	OFF
*	543	60	33.1	0.94	0	0	0	OFF

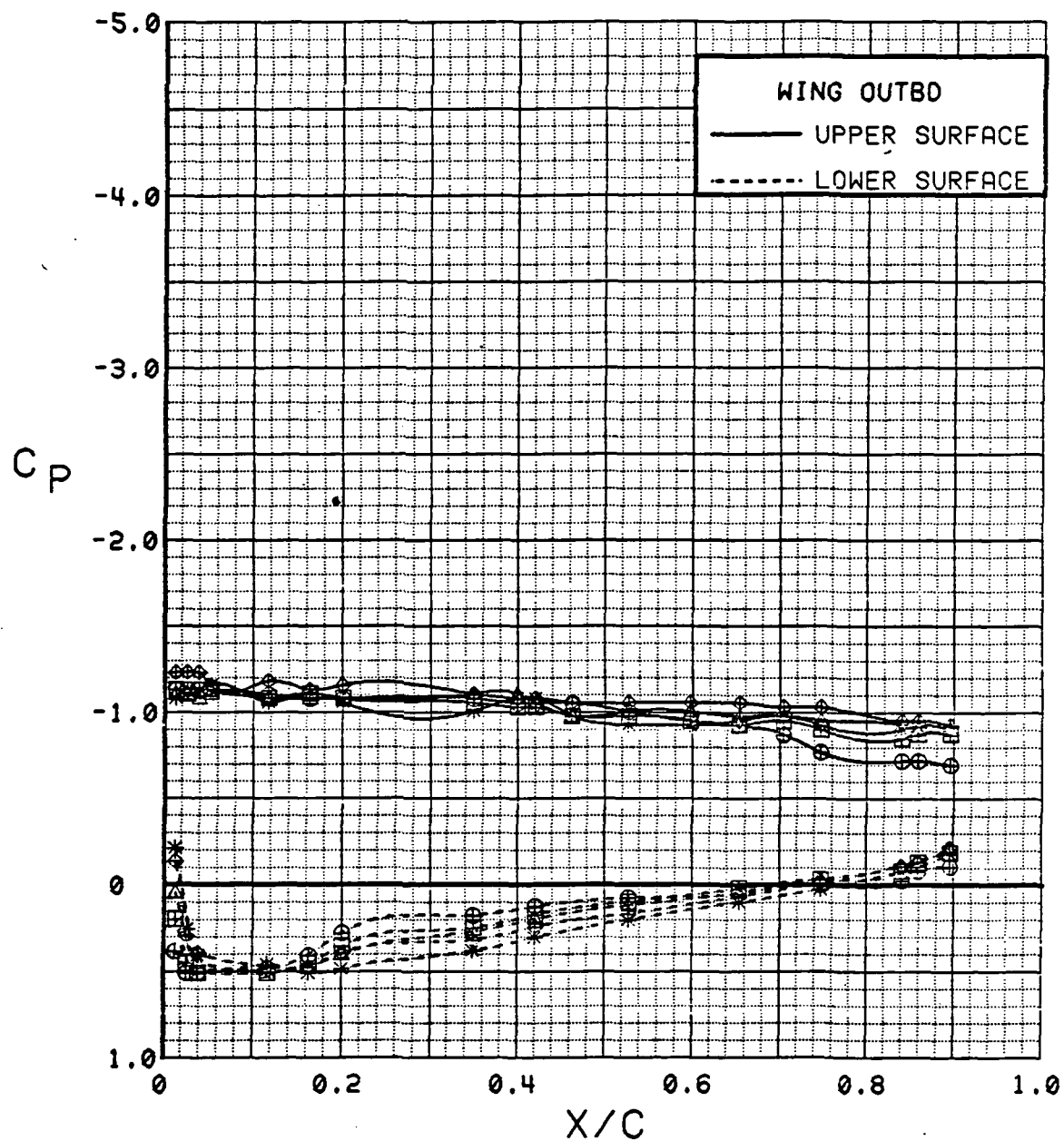


Figure 3.2.4-17 Angle of Attack Effects,  $C_T = 0.9$ , Outboard, Flaps Neutral, High Alpha

SYM	TEST	RUN	ALPHA	CT	ITEF	OTEF	CAN	SWB
⊕	543	60	0.1	0.94	0	0	0	OFF
⊞	543	60	4.3	0.93	0	0	0	OFF
△	543	60	8.4	0.94	0	0	0	OFF
◆	543	60	12.5	0.94	0	0	0	OFF
*	543	60	16.7	0.93	0	0	0	OFF

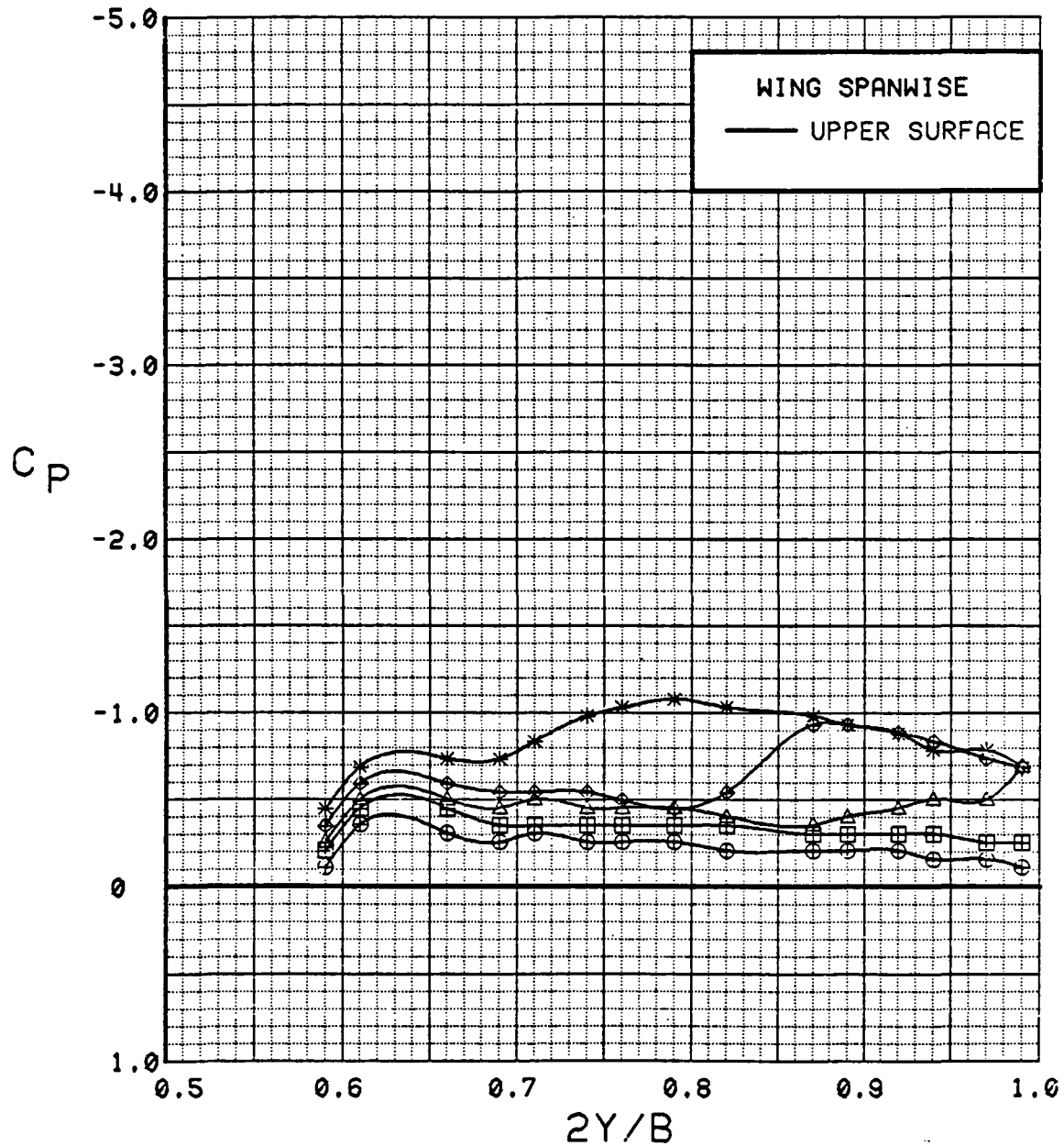


Figure 3.2.4-18

Angle of Attack Effects,  $C_T = 0.9$ , Spanwise,  
Flaps Neutral, Low Alpha

SYM	TEST	RUN	ALPHA	CT	ITEF	OTEF	CAN	SWB
⊙	543	60	16.7	0.93	0	0	0	OFF
⊠	543	60	20.8	0.93	0	0	0	OFF
△	543	60	24.9	0.93	0	0	0	OFF
◆	543	60	29.0	0.93	0	0	0	OFF
*	543	60	33.1	0.94	0	0	0	OFF

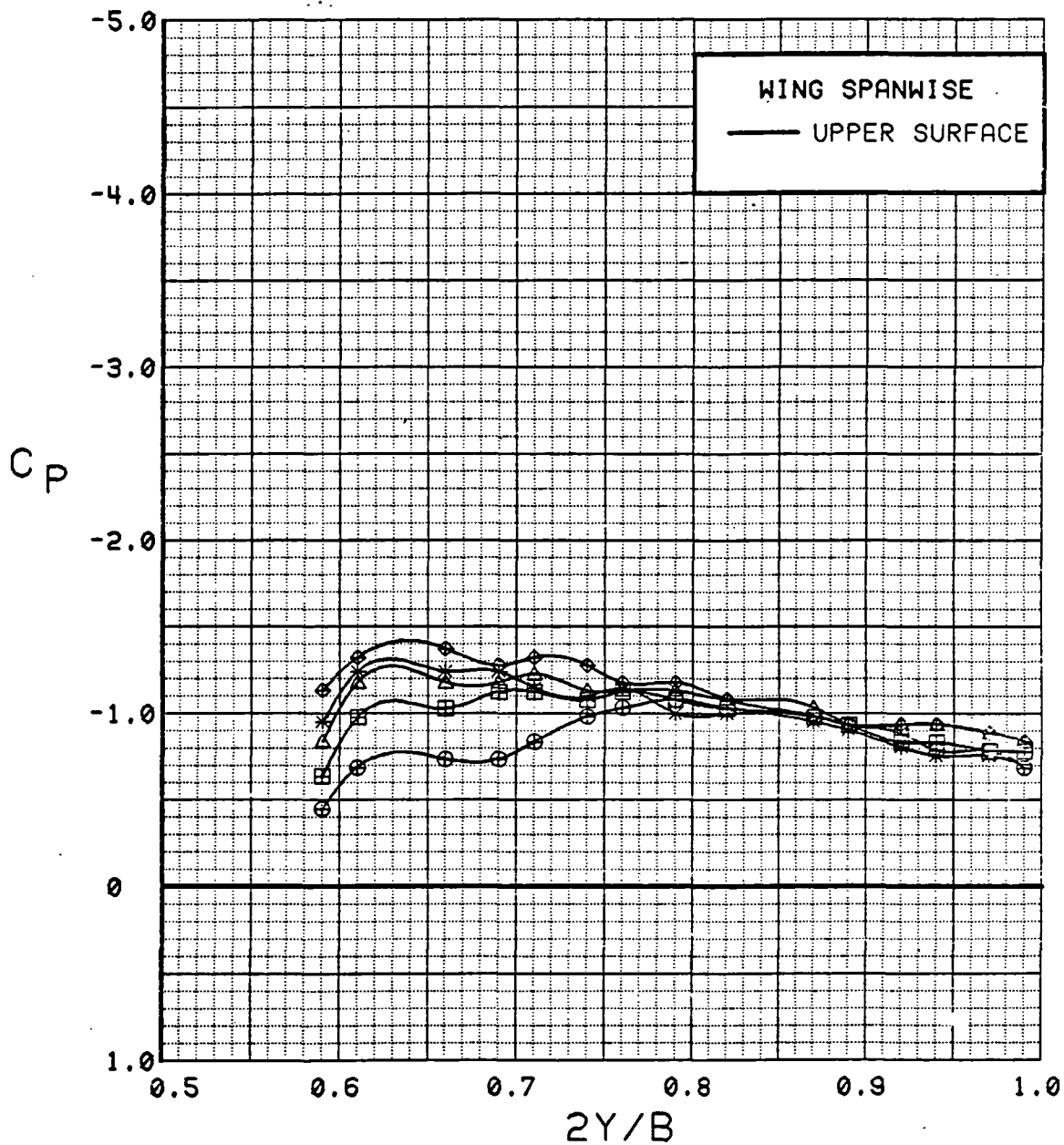


Figure 3.2.4-19 Angle of Attack Effects,  $C_T = 0.9$ , Spanwise, Flaps Neutral, High Alpha



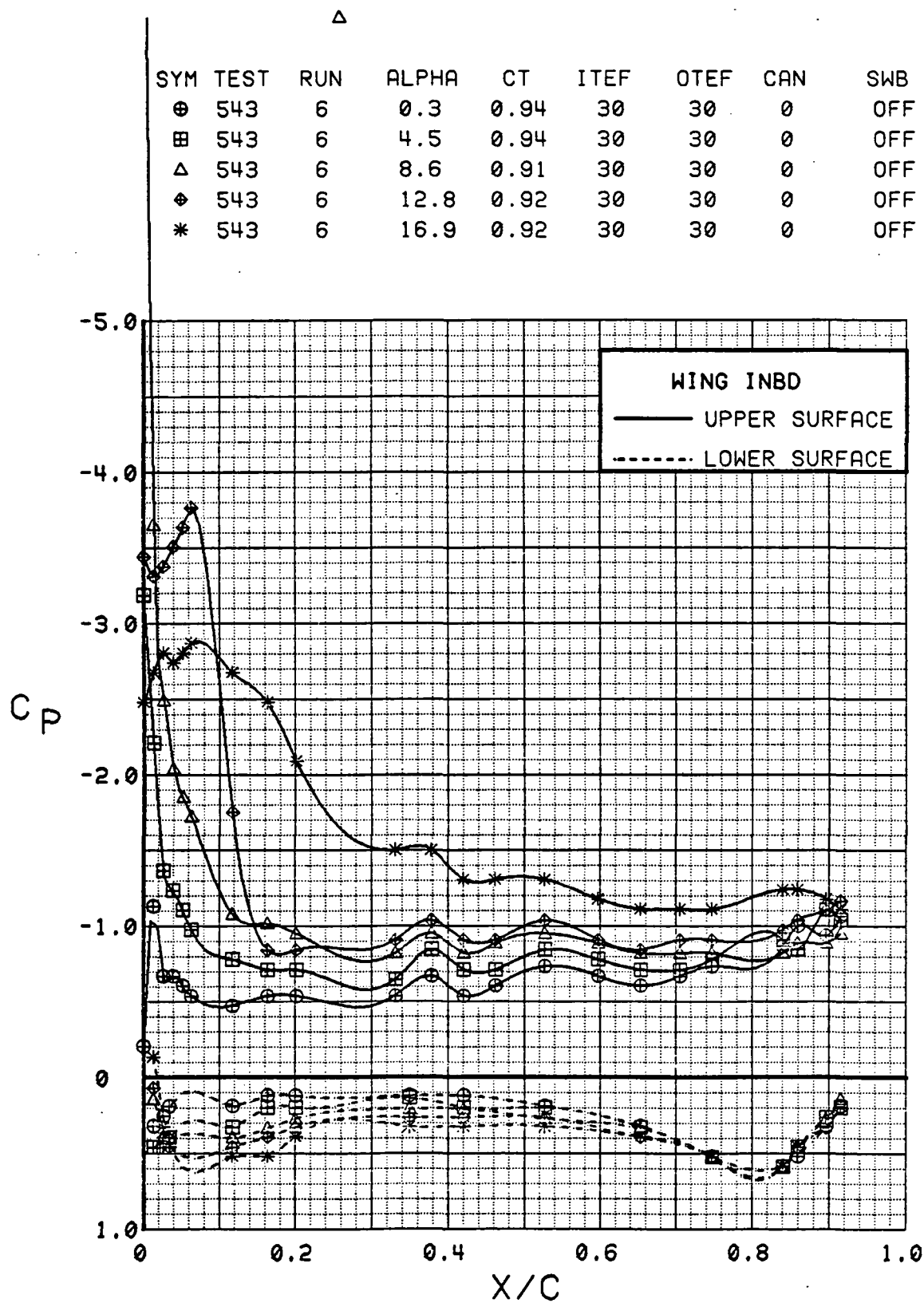


Figure 3.2.4-20 Angle of Attack Effects,  $C_T = 0.9$ , Inboard, Flaps Deflected, Low Alpha

SYM	TEST	RUN	ALPHA	CT	ITEF	OTEF	CAN	SWB
⊕	543	6	16.9	0.92	30	30	0	OFF
⊞	543	6	21.0	0.93	30	30	0	OFF
△	543	6	25.1	0.93	30	30	0	OFF
◆	543	6	29.1	0.93	30	30	0	OFF
*	543	6	33.2	0.92	30	30	0	OFF

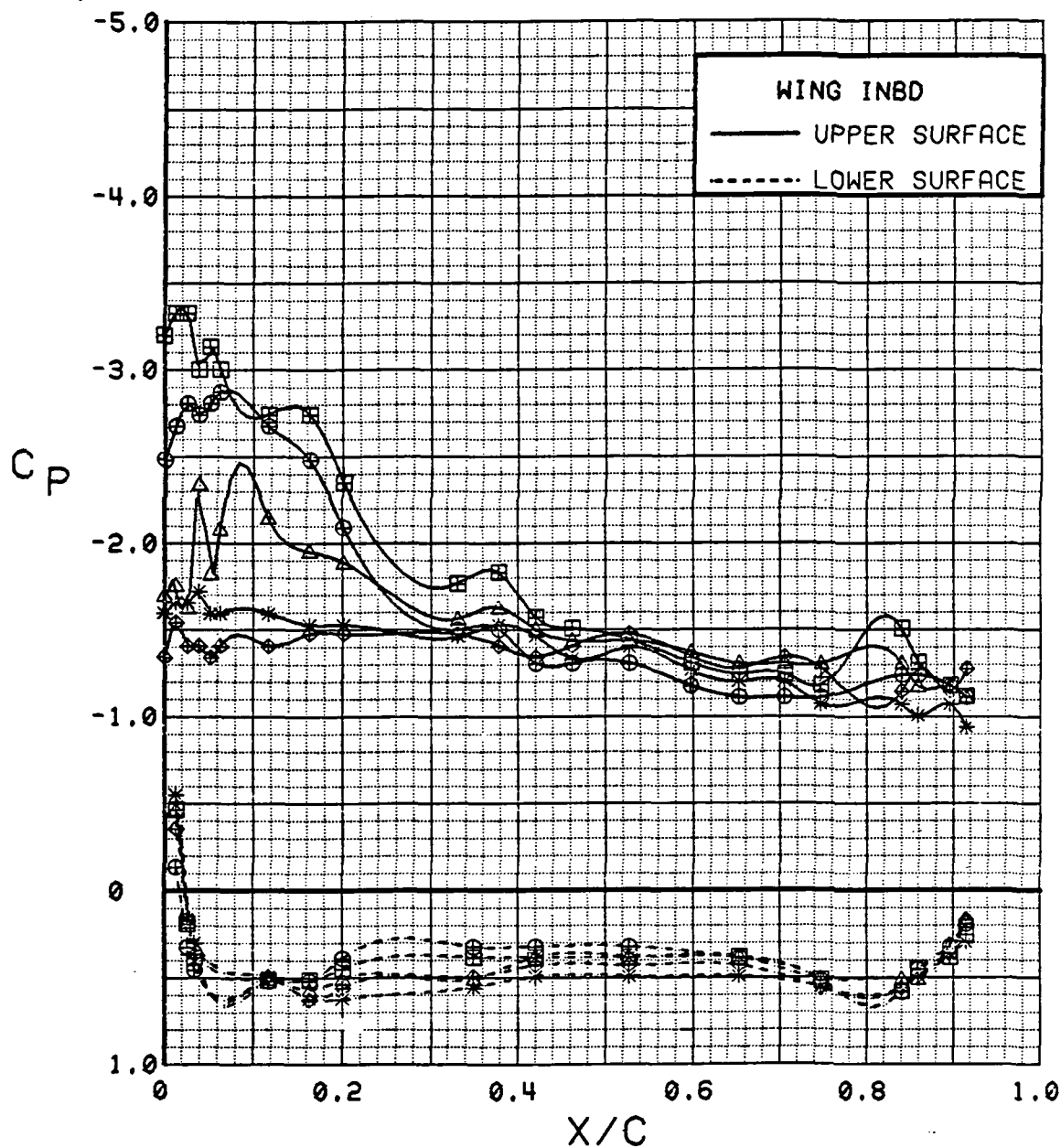


Figure 3.2.4-21 Angle of Attack Effects,  $C_T = 0.9$ , Inboard, Flaps Deflected, High Alpha

SYM	TEST	RUN	ALPHA	CT	ITEF	OTEF	CAN	SWB
⊕	543	6	0.3	0.94	30	30	0	OFF
⊞	543	6	4.5	0.94	30	30	0	OFF
△	543	6	8.6	0.91	30	30	0	OFF
⬠	543	6	12.8	0.92	30	30	0	OFF
*	543	6	16.9	0.92	30	30	0	OFF

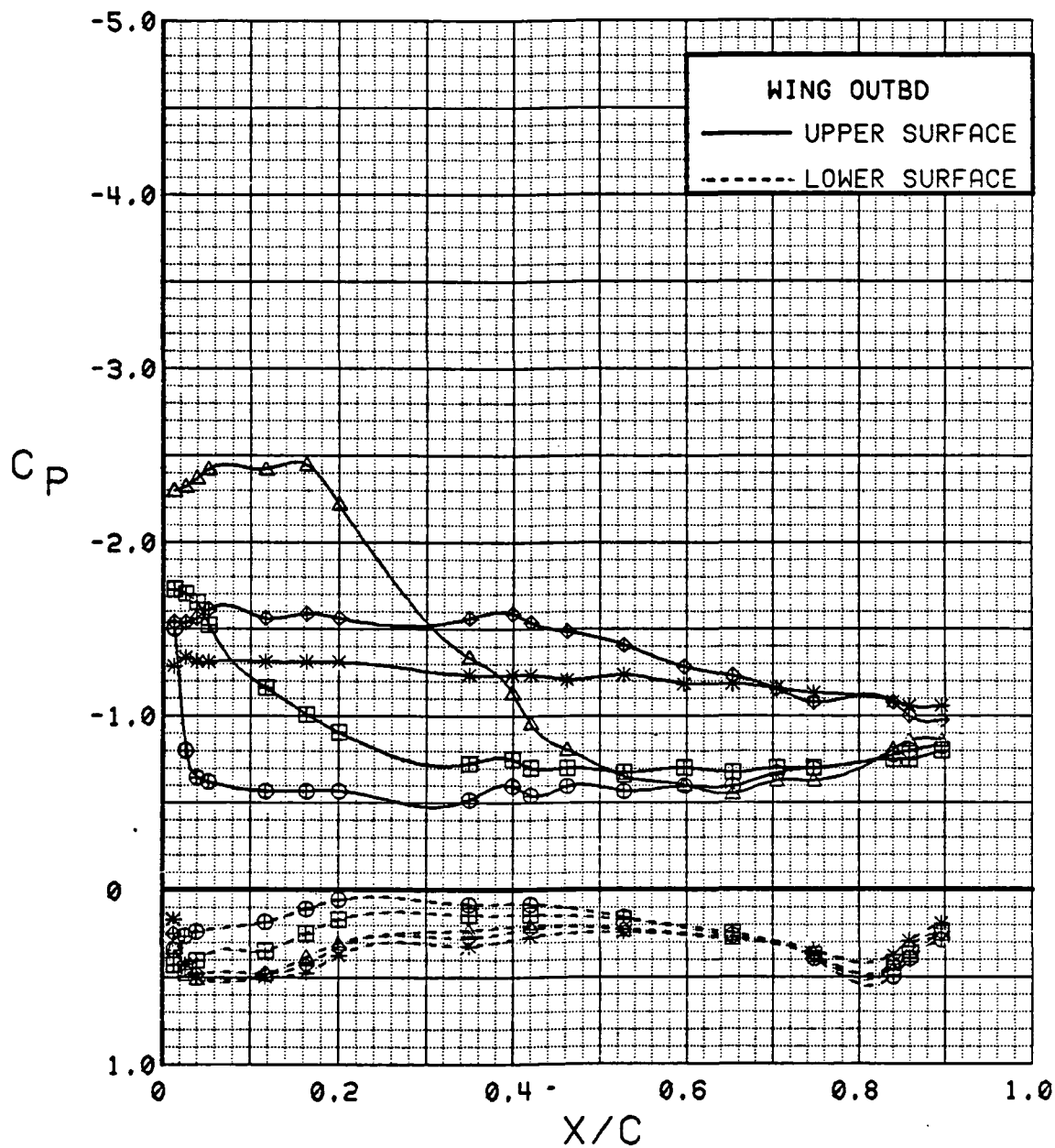


Figure 3.2.4-22 Angle of Attack Effects,  $C_T = 0.9$ , Outboard, Flaps Deflected, Low Alpha

SYM	TEST	RUN	ALPHA	CT	ITEF	OTEF	CAN	SWB
⊕	543	6	16.9	0.92	30	30	0	OFF
⊞	543	6	21.0	0.93	30	30	0	OFF
△	543	6	25.1	0.93	30	30	0	OFF
⊕	543	6	29.1	0.93	30	30	0	OFF
*	543	6	33.2	0.92	30	30	0	OFF

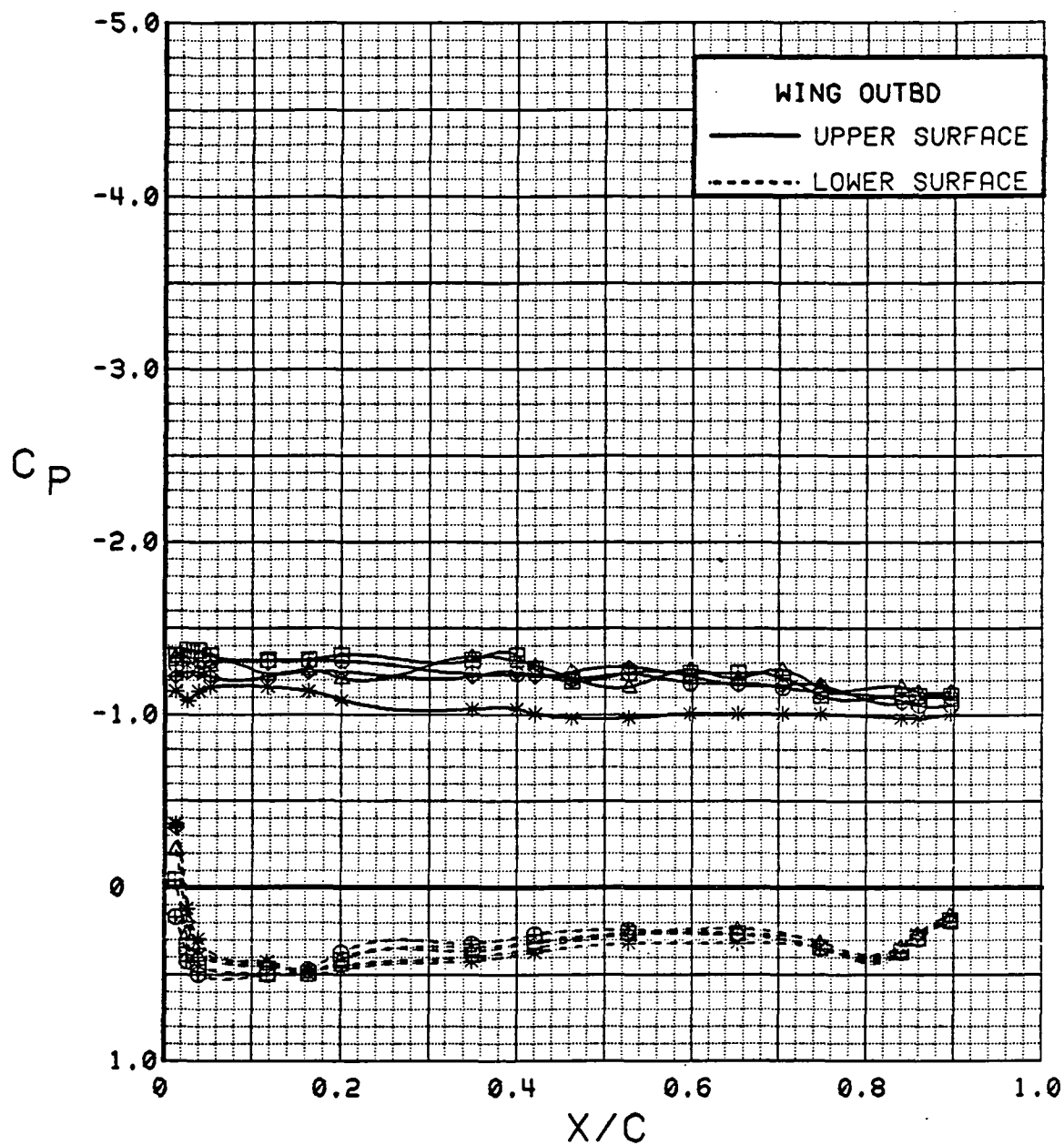


Figure 3.2.4-23 Angle of Attack Effects,  $C_T = 0.9$ , Outboard, Flaps Deflected, High Alpha

SYM	TEST	RUN	ALPHA	CT	ITEF	OTEF	CAN	SWB
⊕	543	6	0.3	0.94	30	30	0	OFF
⊞	543	6	4.5	0.94	30	30	0	OFF
△	543	6	8.6	0.91	30	30	0	OFF
◆	543	6	12.8	0.92	30	30	0	OFF
*	543	6	16.9	0.92	30	30	0	OFF

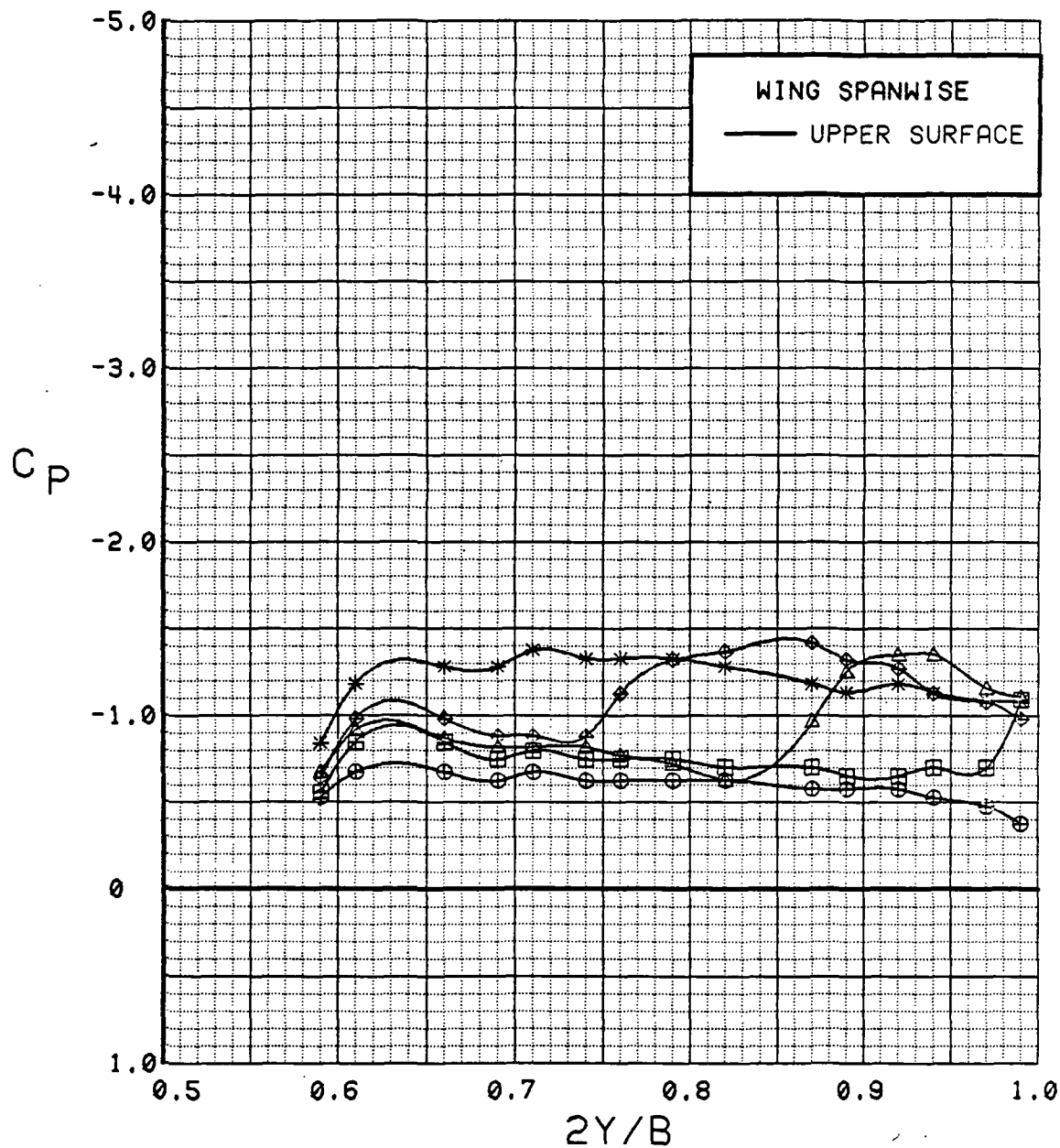


Figure 3.2.4-24 Angle of Attack Effects,  $C_T = 0.9$ , Spanwise, Flaps Deflected, Low Alpha

SYM	TEST	RUN	ALPHA	CT	ITEF	OTEF	CAN	SWB
⊙	543	6	16.9	0.92	30	30	0	OFF
⊠	543	6	21.0	0.93	30	30	0	OFF
△	543	6	25.1	0.93	30	30	0	OFF
◆	543	6	29.1	0.93	30	30	0	OFF
*	543	6	33.2	0.92	30	30	0	OFF

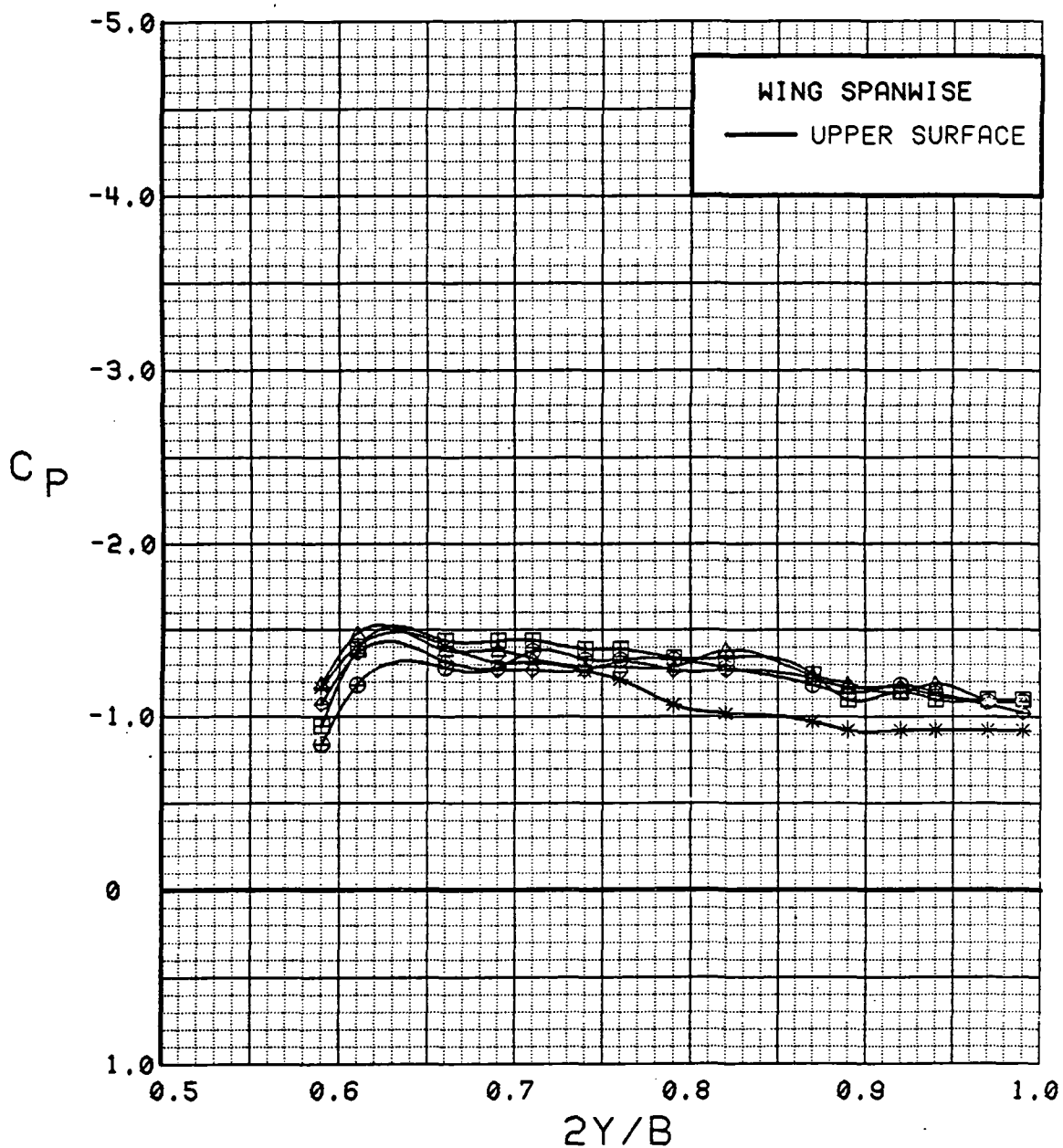


Figure 3.2.4-25 Angle of Attack Effects,  $C_T = 0.9$ , Spanwise, Flaps Deflected, High Alpha

SYM	TEST	RUN	ALPHA	CT	ITEF.	OTEF	CAN	SWB
⊕	543	63	0.1	0.00	0	0	0	OFF
⊞	537	74	0.1	0.00	0	0	OFF	OFF

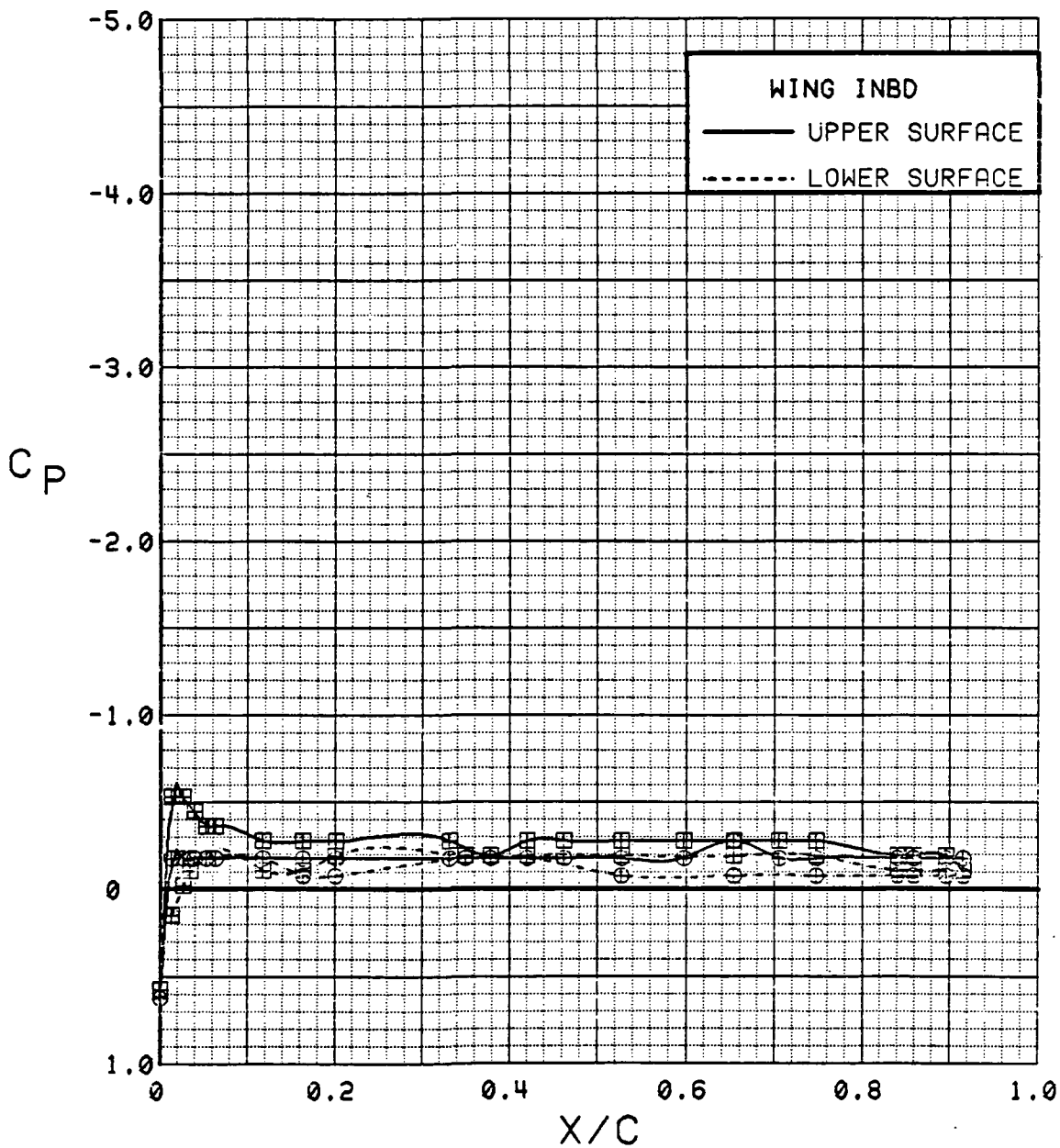


Figure 3.2.4-26

Canard On/Off Effects, Inboard, Power Off,  
Flaps Neutral, Alpha = 0 deg

C-5

SYM	TEST	RUN	ALPHA	CT	ITEF	OTEF	CAN	SWB
⊕	543	63	8.3	0.00	0	0	0	OFF
⊞	537	74	8.3	0.00	0	0	OFF	OFF

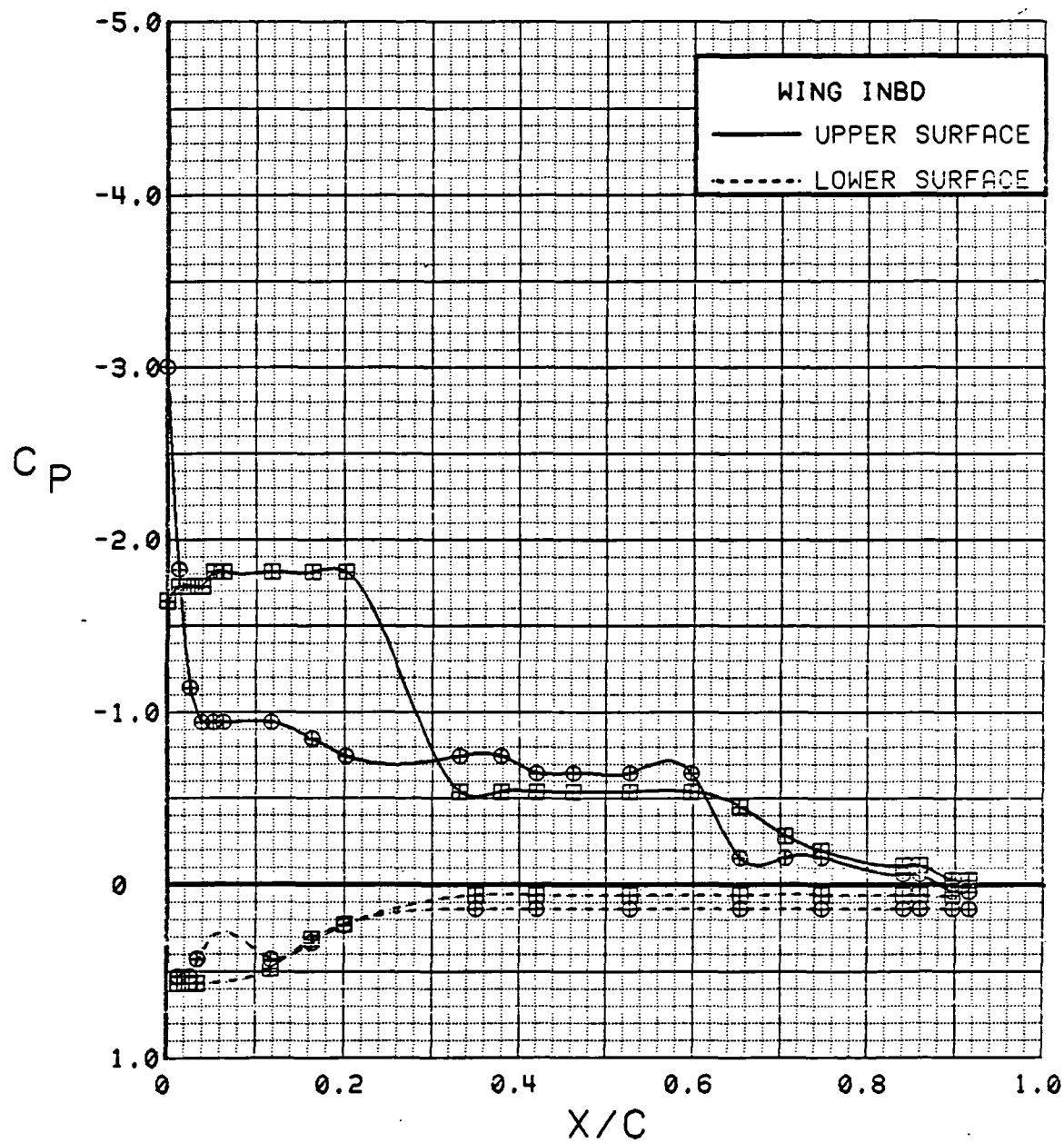


Figure 3.2.4-27

Canard On/Off Effects, Inboard, Power Off,  
Flaps Neutral, Alpha = 8 deg



SYM	TEST	RUN	ALPHA	CT	ITEF	OTEF	CAN	SWB
⊕	543	63	12.5	0.00	0	0	0	OFF
⊞	537	74	12.4	0.00	0	0	OFF	OFF

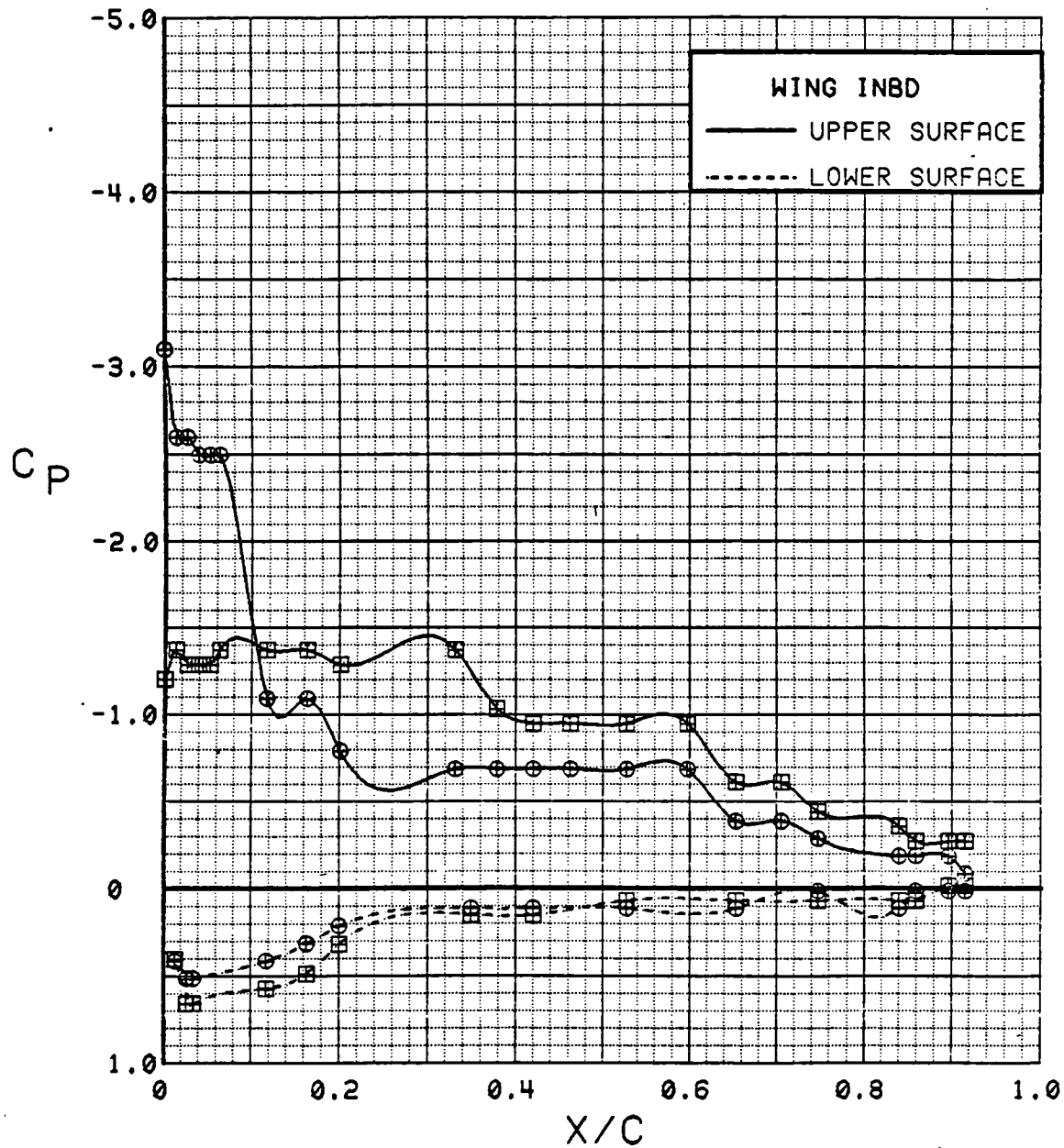


Figure 3.2.4-28

Canard On/Off Effects, Inboard, Power Off,  
Flaps Neutral, Alpha = 12 deg

SYM	TEST	RUN	ALPHA	CT	ITEF	OTEF	CAN	SWB
⊕	543	63	16.6	0.00	0	0	0	OFF
⊞	537	74	16.5	0.00	0	0	OFF	OFF

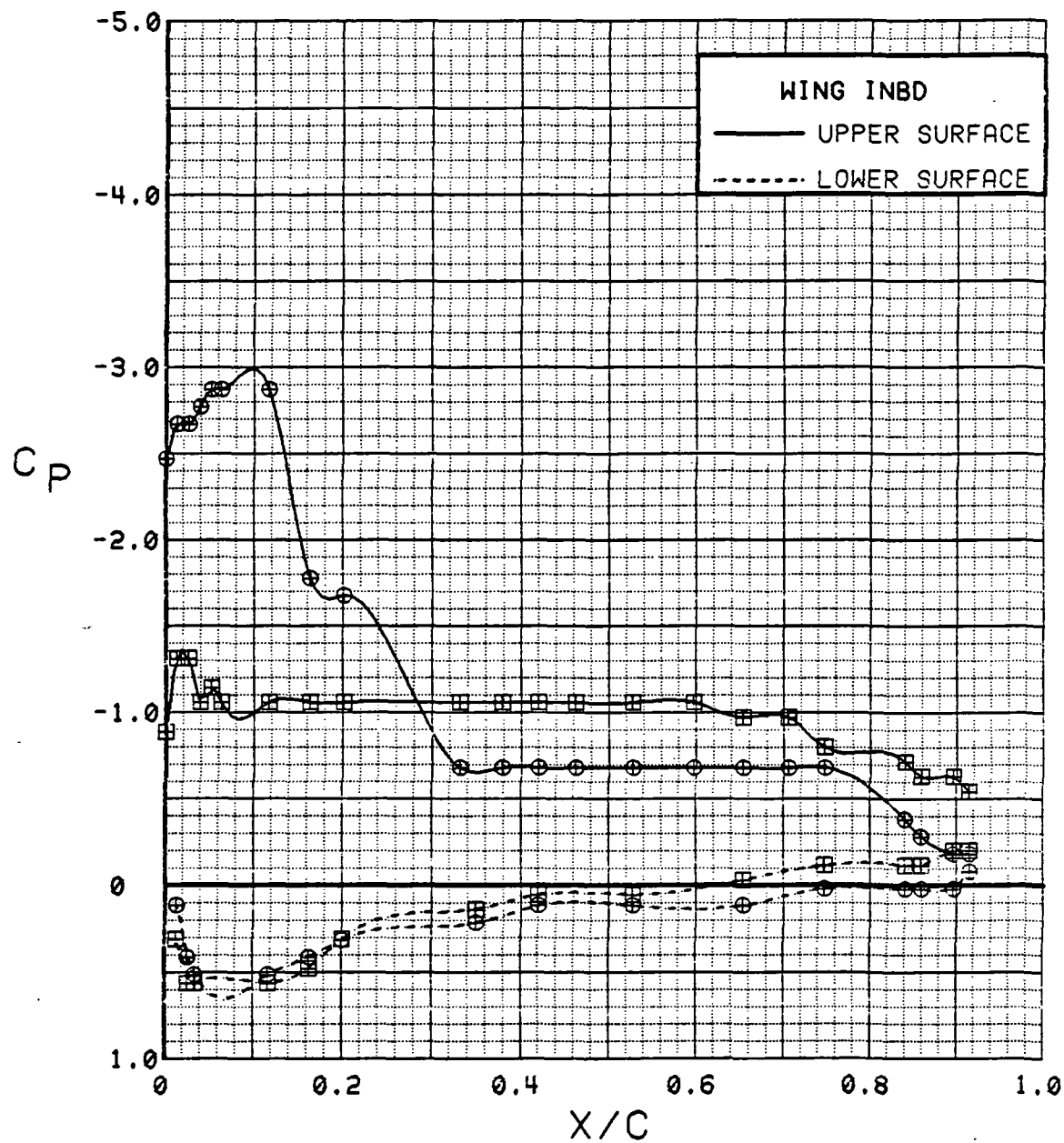


Figure 3.2.4-29 Canard On/Off Effects, Inboard, Power Off, Flaps Neutral, Alpha = 16 deg

SYM	TEST	RUN	ALPHA	CT	ITEF	OTEF	CAN	SWB
⊕	543	63	20.7	0.00	0	0	0	OFF
⊞	537	74	20.5	0.00	0	0	OFF	OFF

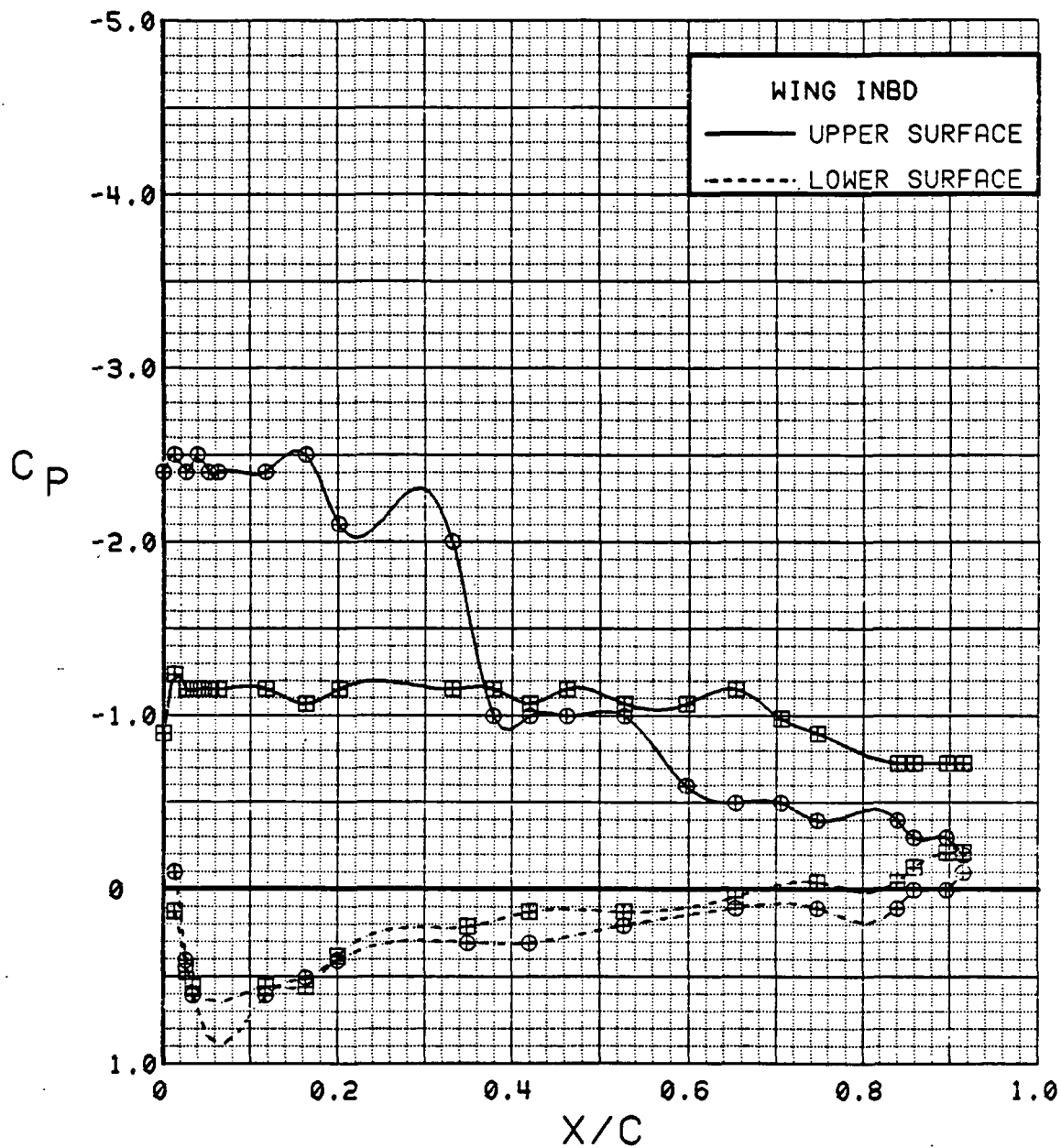


Figure 3.2.4-30

Canard On/Off Effects, Inboard, Power Off,  
Flaps Neutral, Alpha = 20 deg

SYM	TEST	RUN	ALPHA	CT	ITEF	OTEF	CAN	SWB
⊕	543	63	24.8	0.00	0	0	0	OFF
⊞	537	74	24.6	0.00	0	0	OFF	OFF

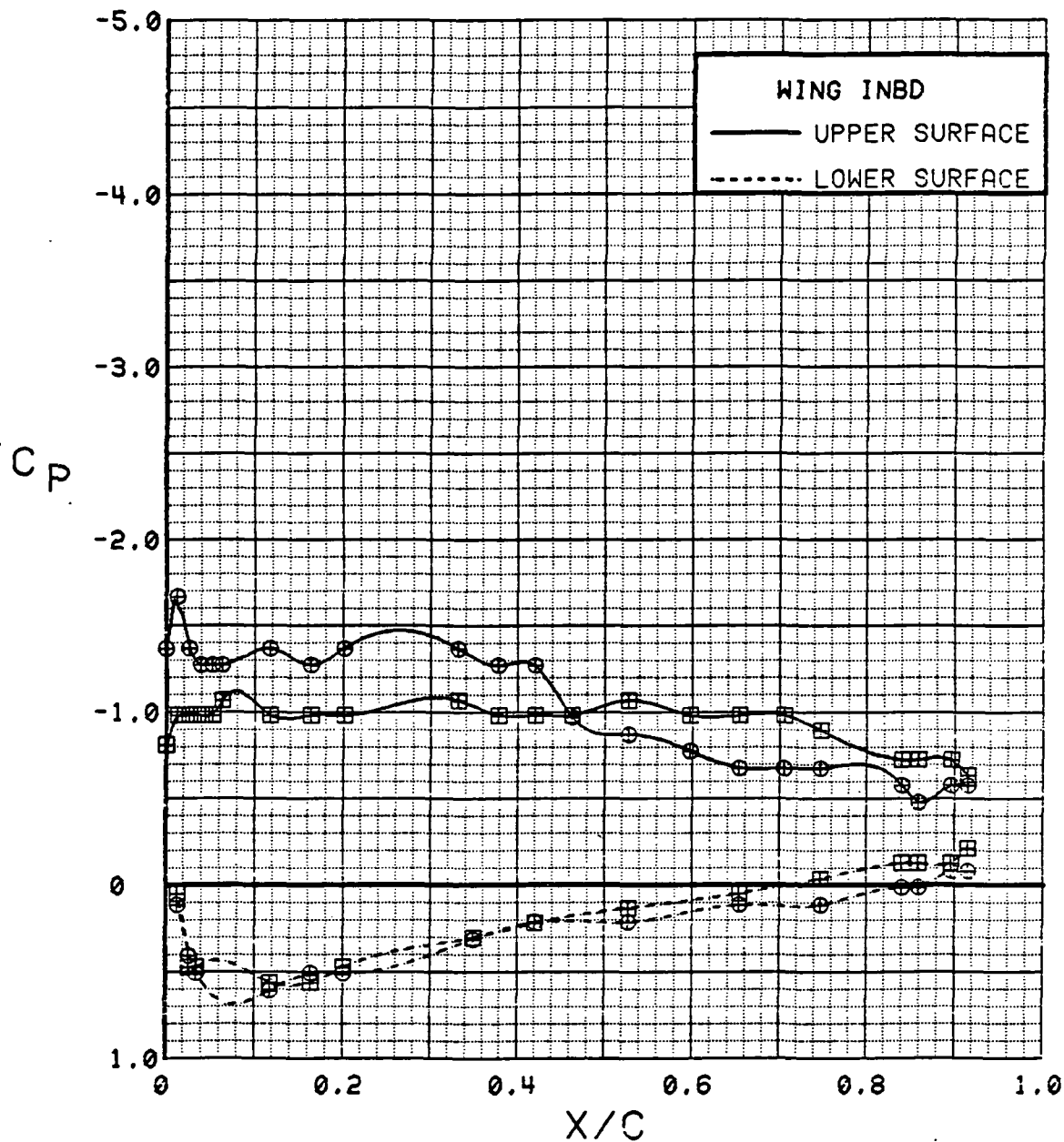


Figure 3.2.4-31 Canard On/Off Effects, Inboard, Power Off, Flaps Neutral, Alpha = 24 deg

SYM	TEST	RUN	ALPHA	CT	ITEF	OTEF	CAN	SWB
⊕	543	63	28.8	0.00	0	0	0	OFF
⊞	537	74	28.6	0.00	0	0	OFF	OFF

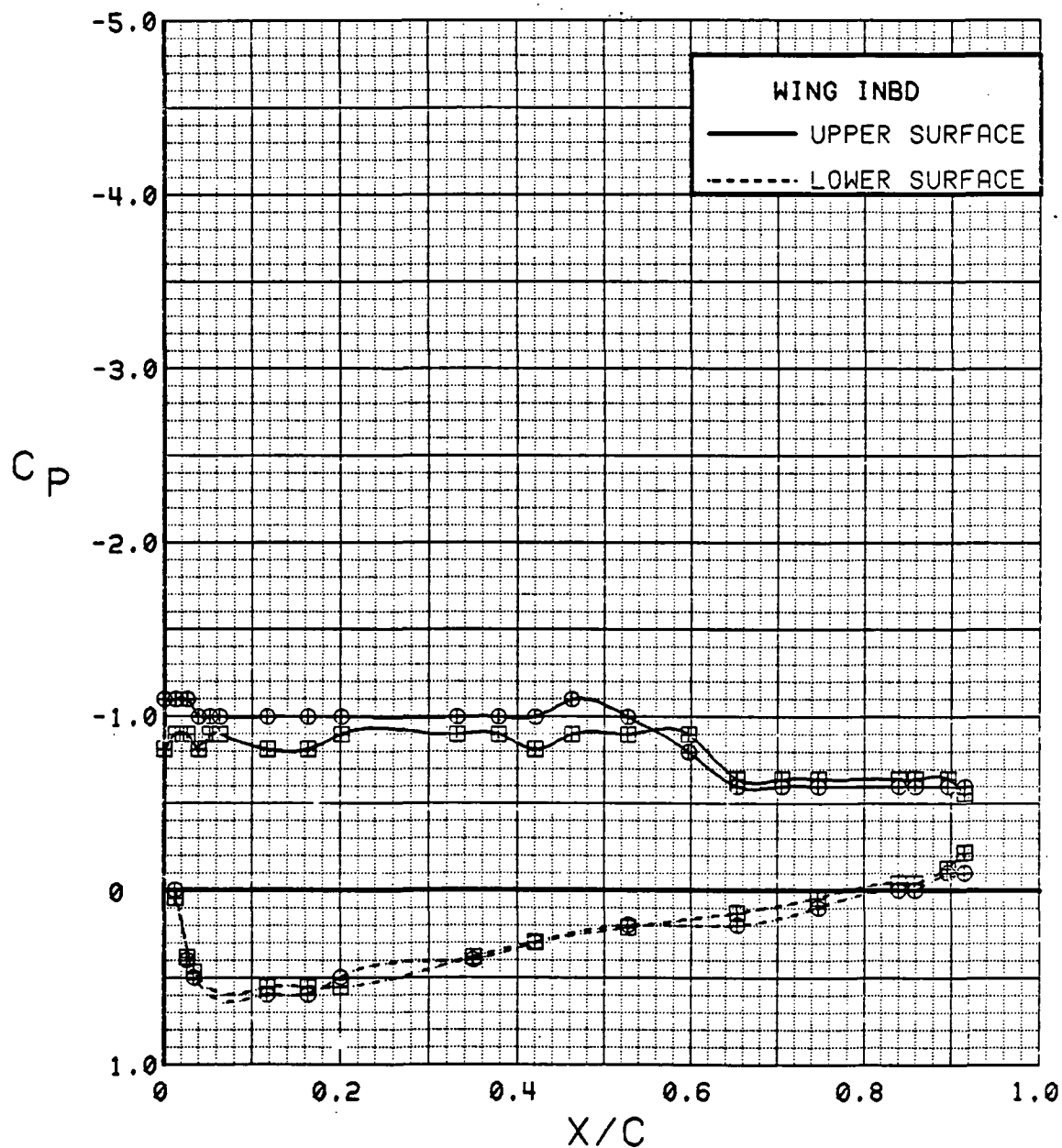


Figure 3.2.4-32

Canard On/Off Effects, Inboard, Power Off,  
Flaps Neutral, Alpha = 28 deg

SYM	TEST	RUN	ALPHA	CT	ITEF	OTEF	CAN	SWB
⊕	543	63	32.8	0.00	0	0	0	OFF
⊞	537	74	32.6	0.00	0	0	OFF	OFF

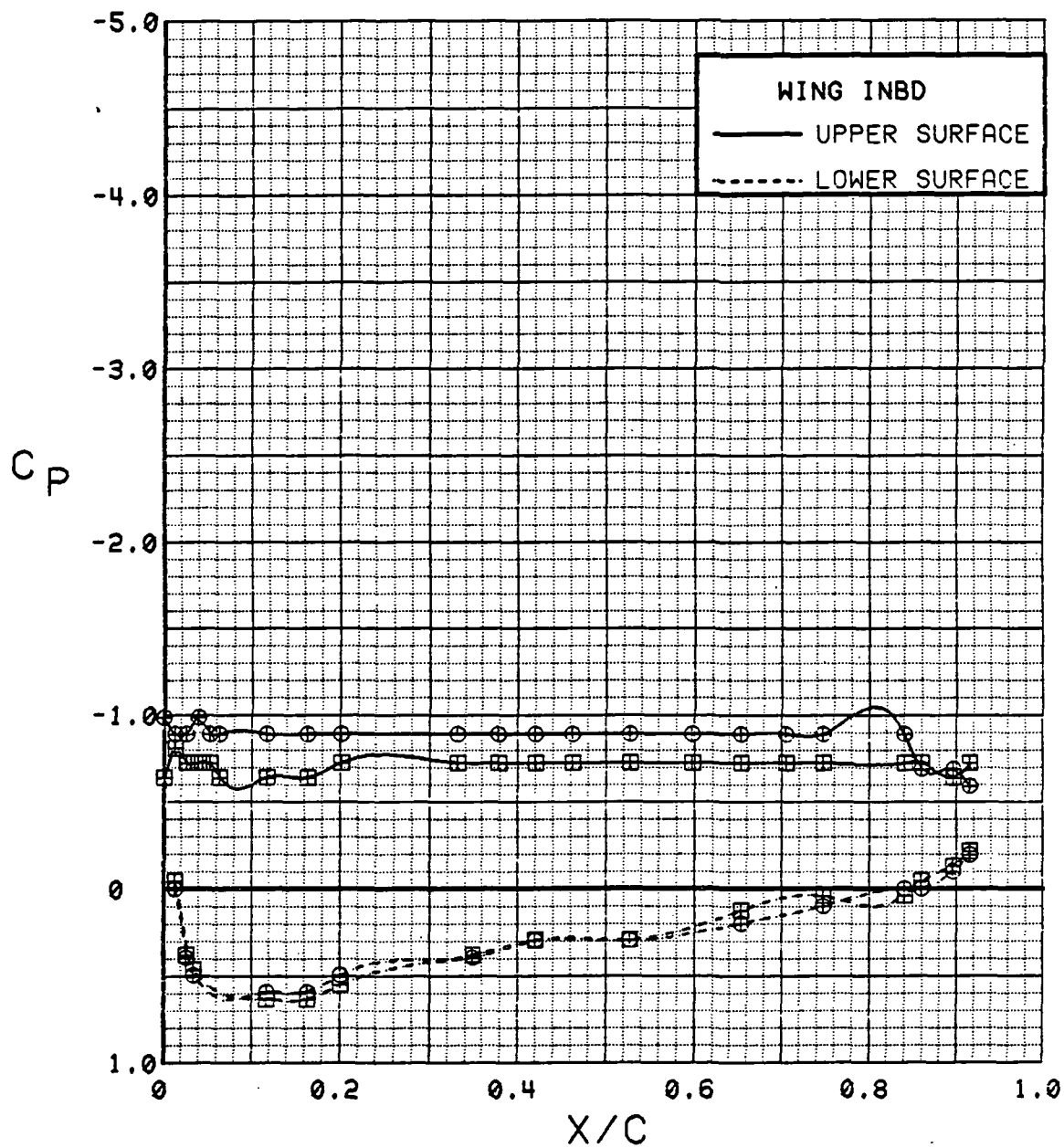


Figure 3.2.4-33 Canard On/Off Effects, Inboard, Power Off,  
Flaps Neutral, Alpha = 32 deg

SYM	TEST	RUN	ALPHA	CT	ITEF	OTEF	CAN	SWB
⊕	543	63	0.1	0.00	0	0	0	OFF
⊞	537	74	0.1	0.00	0	0	OFF	OFF

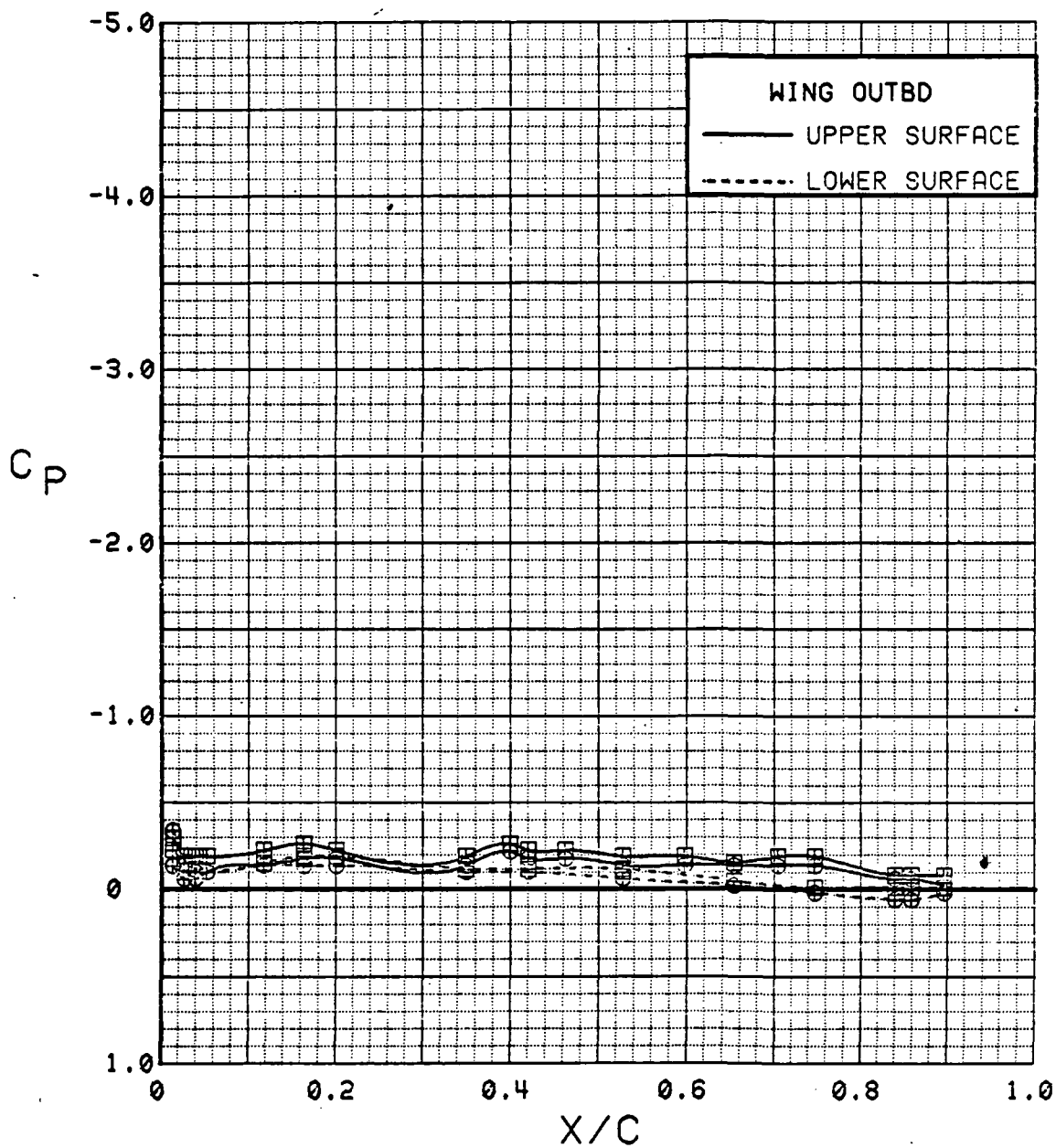


Figure 3.2.4-34 Canard On/Off Effects, Outboard, Power Off, Flaps Neutral, Alpha = 0 deg

SYM	TEST	RUN	ALPHA	CT	ITEF	OTEF	CAN	SWB
⊕	543	63	8.3	0.00	0	0	0	OFF
⊞	537	74	8.3	0.00	0	0	OFF	OFF

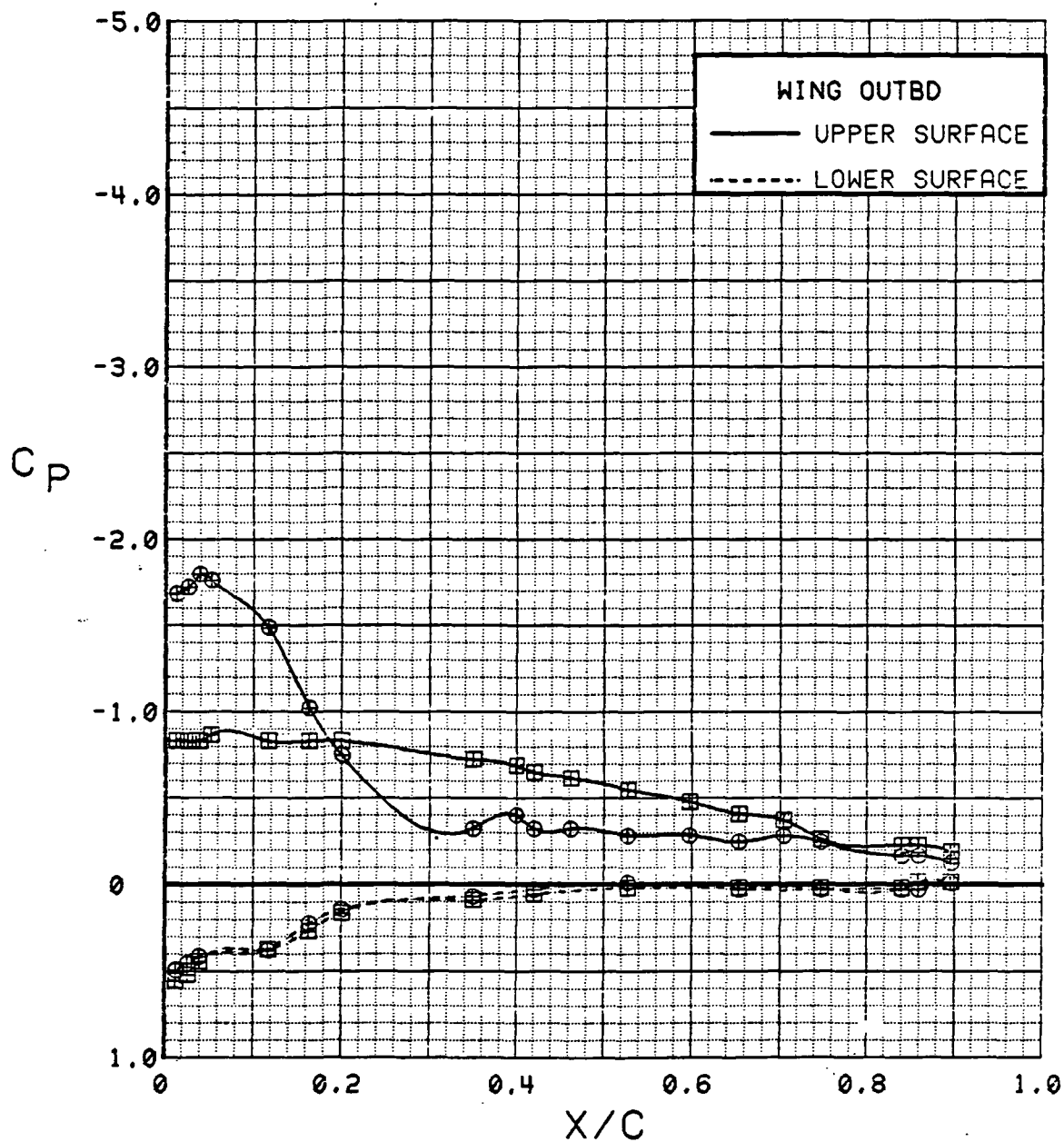


Figure 3.2.4-35 Canard On/Off Effects, Outboard, Power Off, Flaps Neutral, Alpha = 8 deg



SYM	TEST	RUN	ALPHA	CT	ITEF	OTEF	CAN	SWB
⊕	543	63	12.5	0.00	0	0	0	OFF
⊞	537	74	12.4	0.00	0	0	OFF	OFF

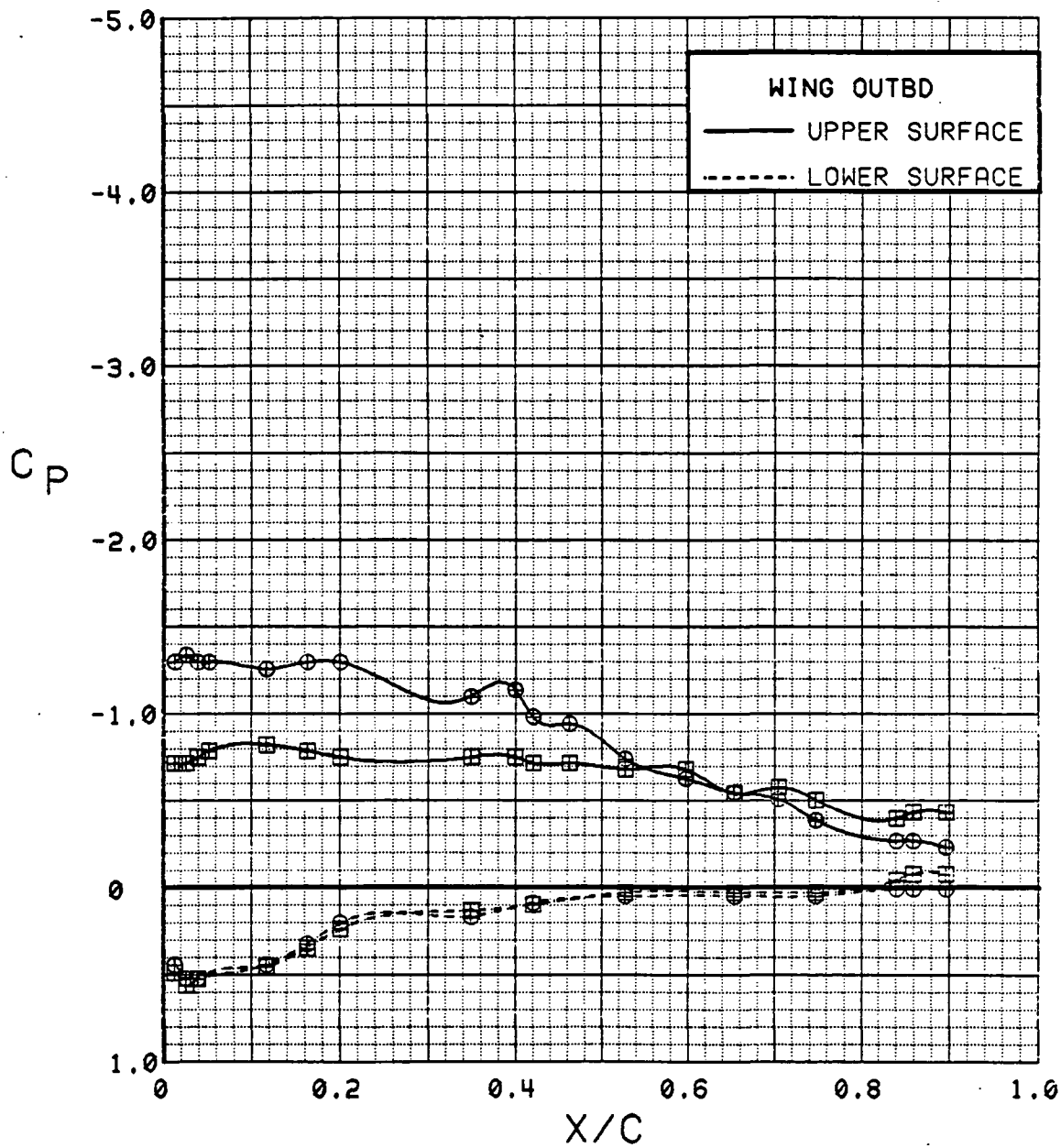


Figure 3.2.4-36 Canard On/Off Effects, Outboard, Power Off, Flaps Neutral, Alpha = 12 deg

SYM	TEST	RUN	ALPHA	CT	ITEF	OTEF	CAN	SWB
⊕	543	63	16.6	0.00	0	0	0	OFF
⊞	537	74	16.5	0.00	0	0	OFF	OFF

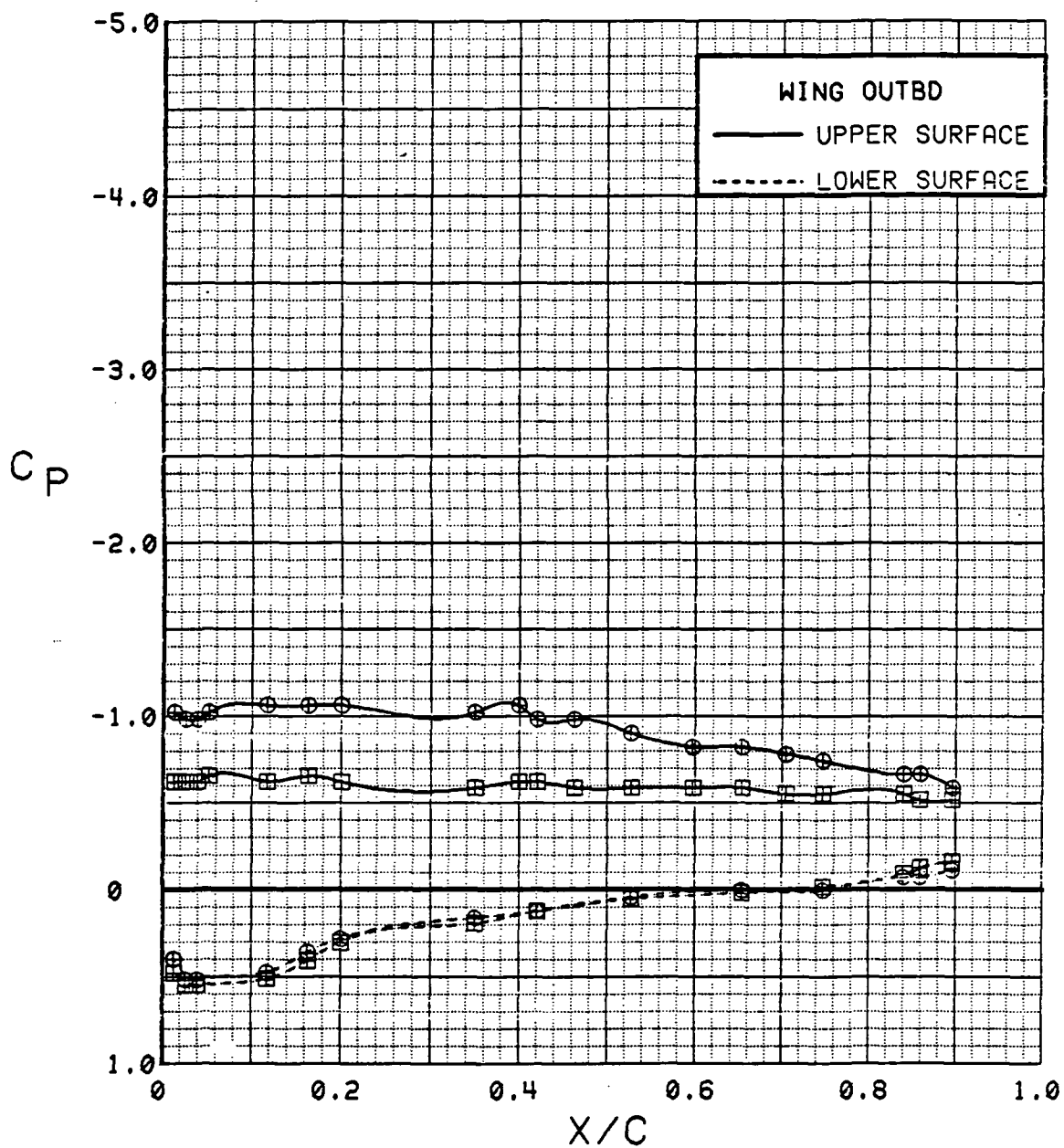


Figure 3.2.4-37 Canard On/Off Effects, Outboard, Power Off, Flaps Neutral, Alpha = 16 deg

SYM	TEST	RUN	ALPHA	CT	ITEF	OTEF	CAN	SWB
⊕	543	63	20.7	0.00	0	0	0	OFF
⊞	537	74	20.5	0.00	0	0	OFF	OFF

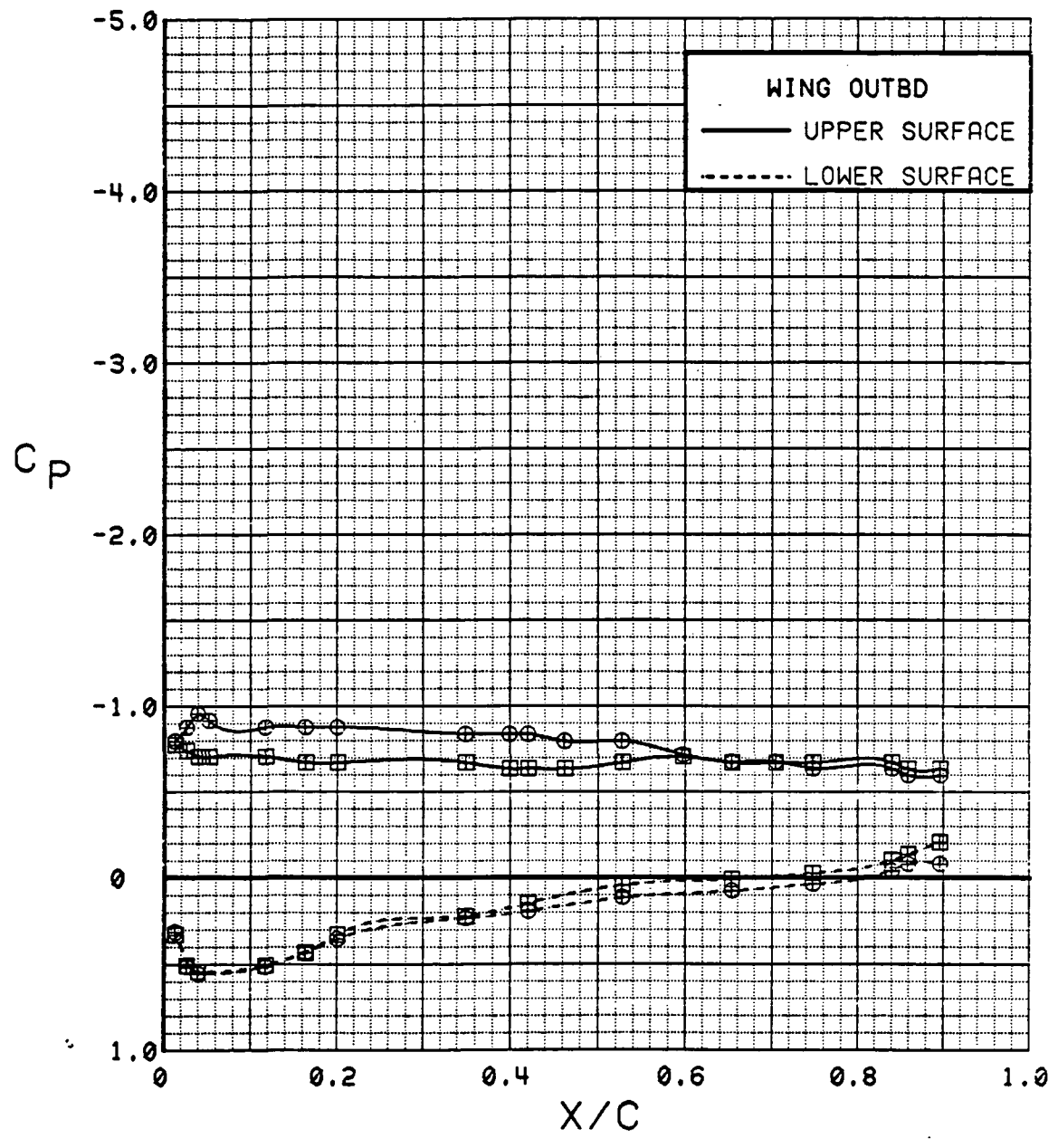


Figure 3.2.4-38 Canard On/Off Effects, Outboard, Power Off, Flaps Neutral, Alpha = 20 deg

SYM	TEST	RUN	ALPHA	CT	ITEF	OTEF	CAN	SWB
⊕	543	63	24.8	0.00	0	0	0	OFF
⊞	537	74	24.6	0.00	0	0	OFF	OFF

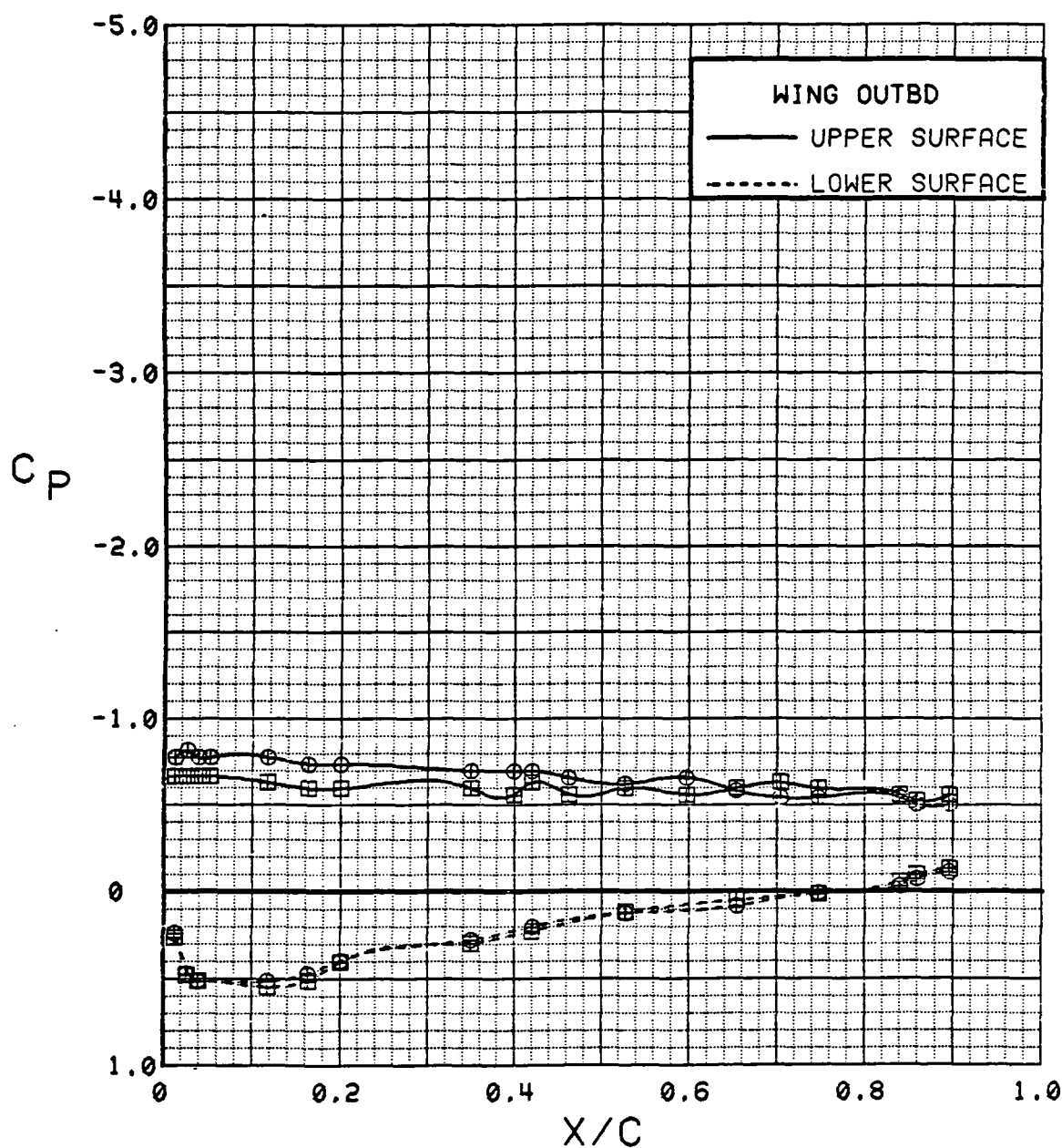


Figure 3.2.4-39 Canard On/Off Effects, Outboard, Power Off, Flaps Neutral, Alpha = 24 deg

SYM	TEST	RUN	ALPHA	CT	ITEF	OTEF	CAN	SWB
⊕	543	63	28.8	0.00	0	0	0	OFF
⊞	537	74	28.6	0.00	0	0	OFF	OFF

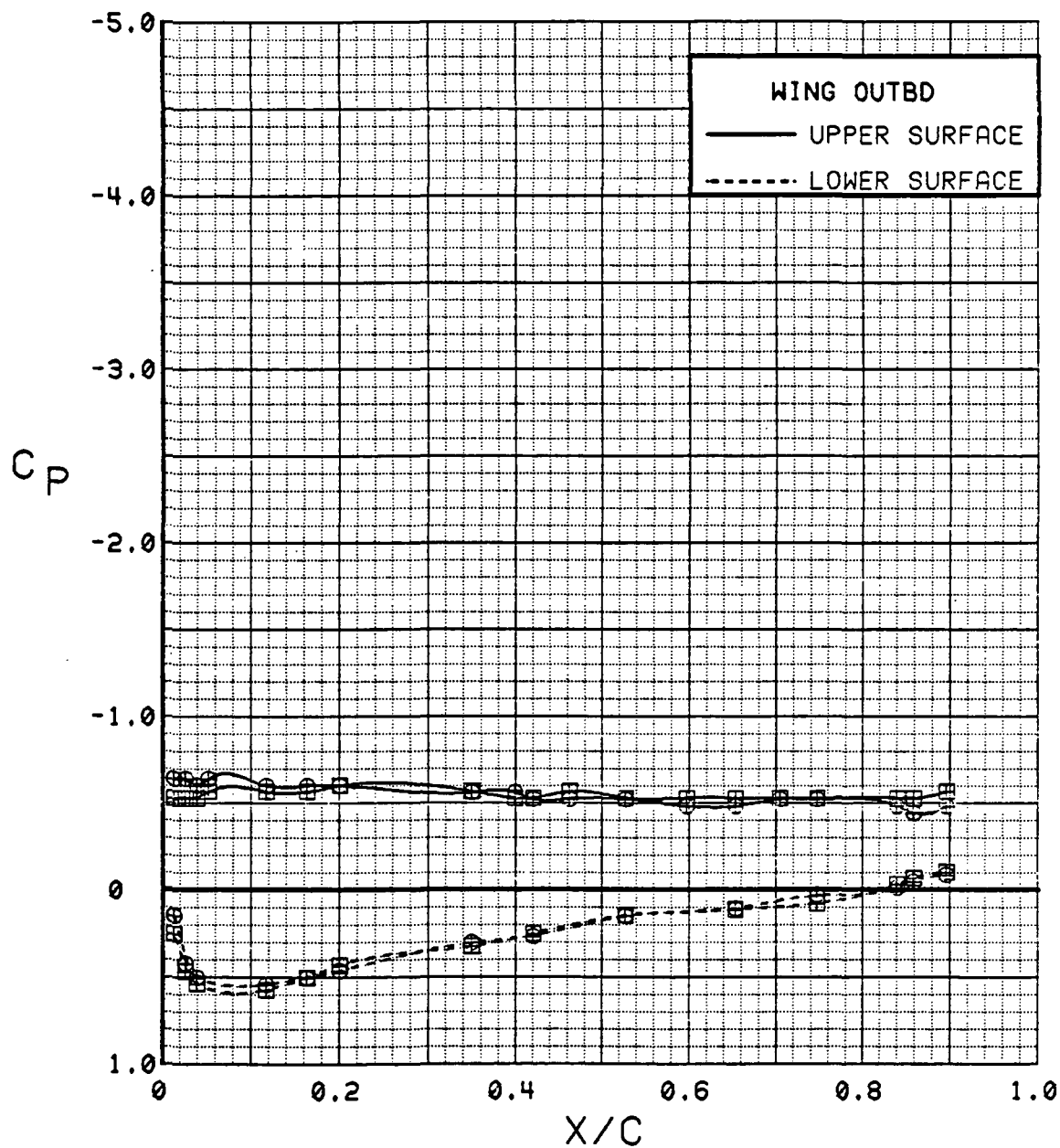


Figure 3.2.4-40 Canard On/Off Effects, Outboard, Power Off, Flaps Neutral, Alpha = 28 deg

SYM	TEST	RUN	ALPHA	CT	ITEF	OTEF	CAN	SWB
⊕	543	63	32.8	0.00	0	0	0	OFF
⊞	537	74	32.6	0.00	0	0	OFF	OFF

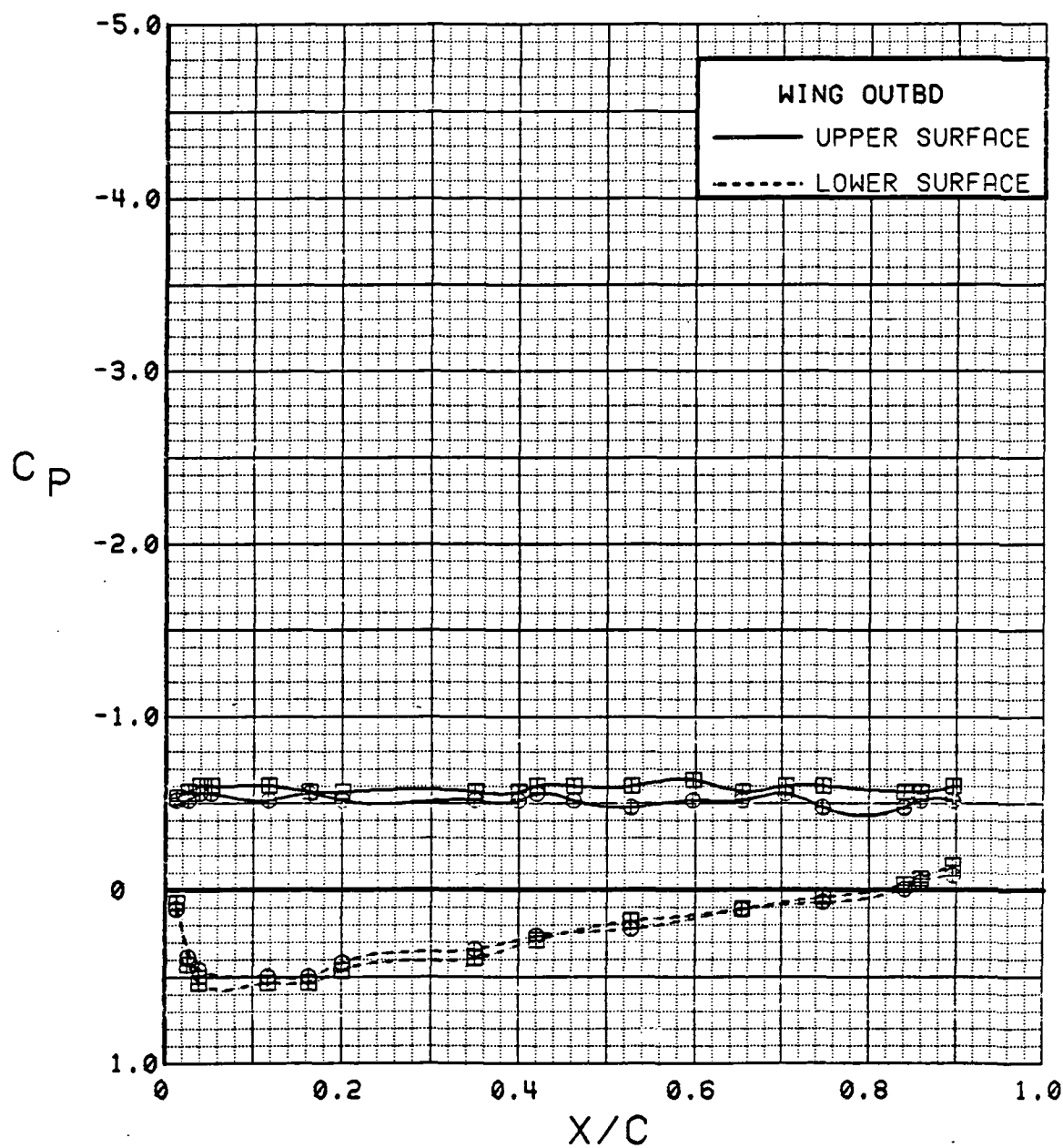


Figure 3.2.4-41 Canard On/Off Effects, Outboard, Power Off, Flaps Neutral, Alpha = 32 deg

SYM	TEST	RUN	ALPHA	CT	ITEF	OTEF	CAN	SWB
●	543	63	0.1	0.00	0	0	0	OFF
■	537	74	0.1	0.00	0	0	OFF	OFF

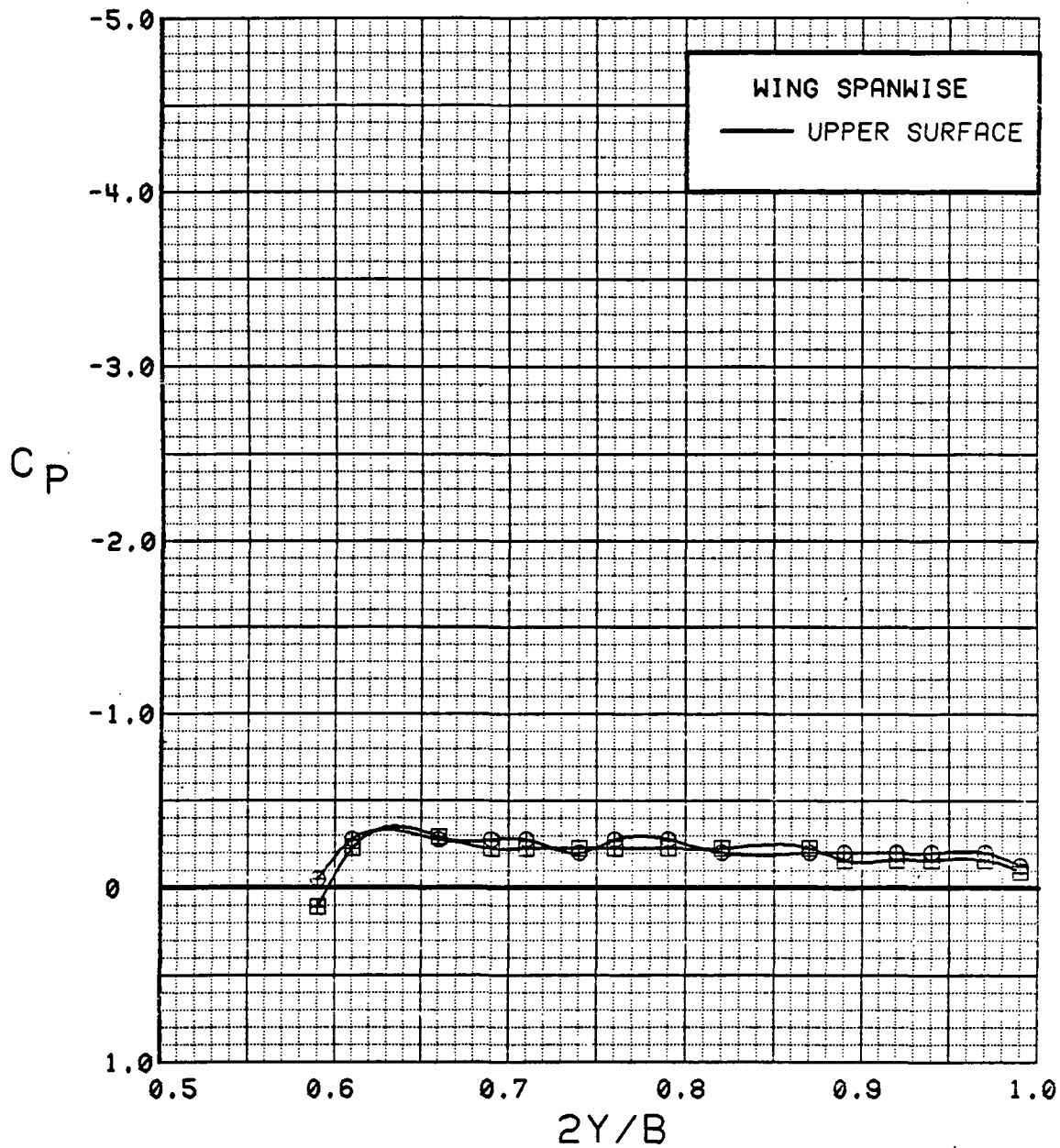


Figure 3.2.4-42 Canard On/Off Effects, Spanwise, Power Off, Flaps Neutral, Alpha = 0 deg

SYM	TEST	RUN	ALPHA	CT	ITEF	OTEF	CAN	SWB
⊙	543	63	8.3	0.00	0	0	0	OFF
⊠	537	74	8.3	0.00	0	0	OFF	OFF

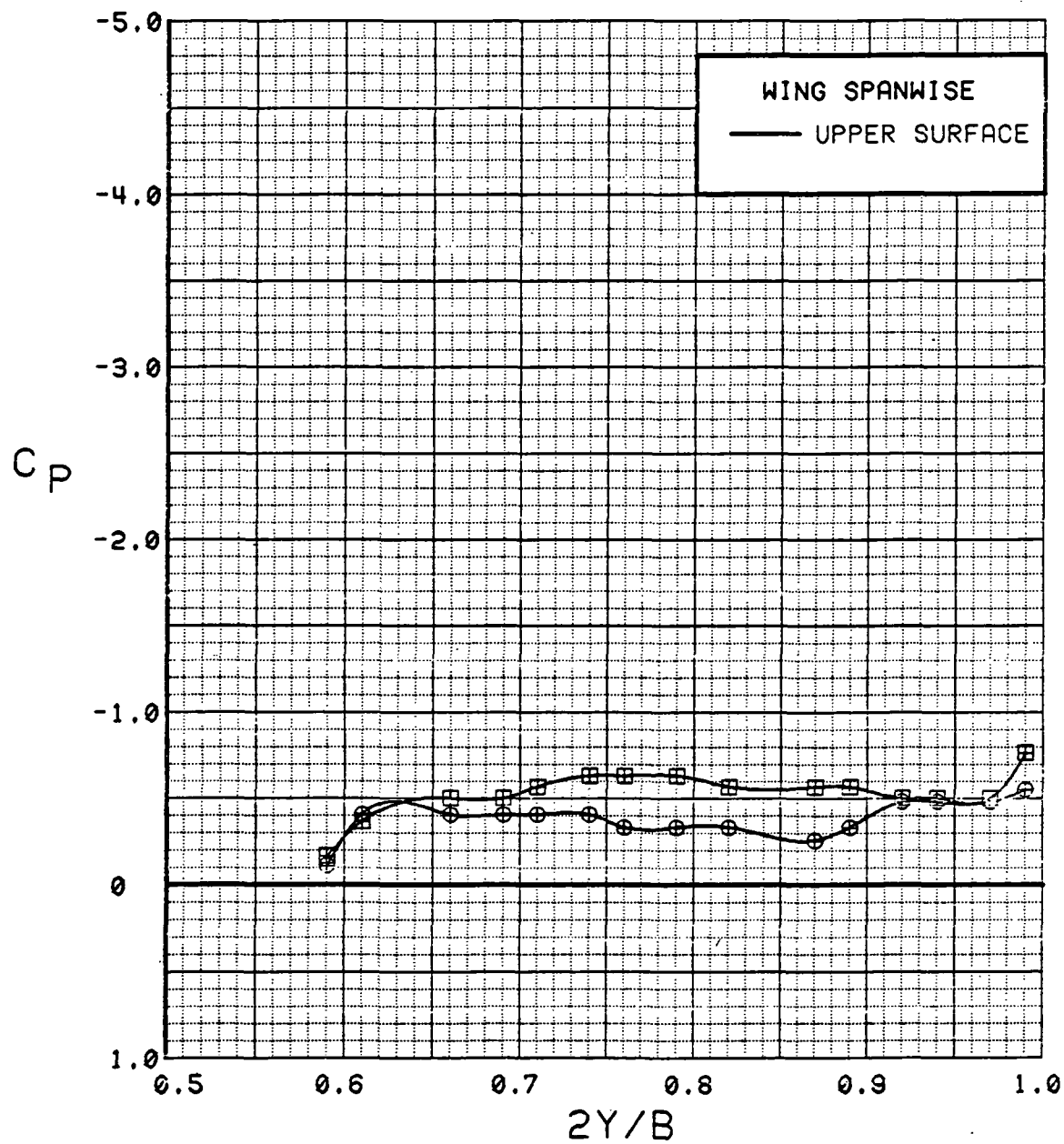


Figure 3.2.4-43

Canard On/Off Effects, Spanwise, Power Off,  
Flaps Neutral, Alpha = 8 deg



SYM	TEST	RUN	ALPHA	CT	ITEF	OTEF	CAN	SWB
⊕	543	63	12.5	0.00	0	0	0	OFF
⊞	537	74	12.4	0.00	0	0	OFF	OFF

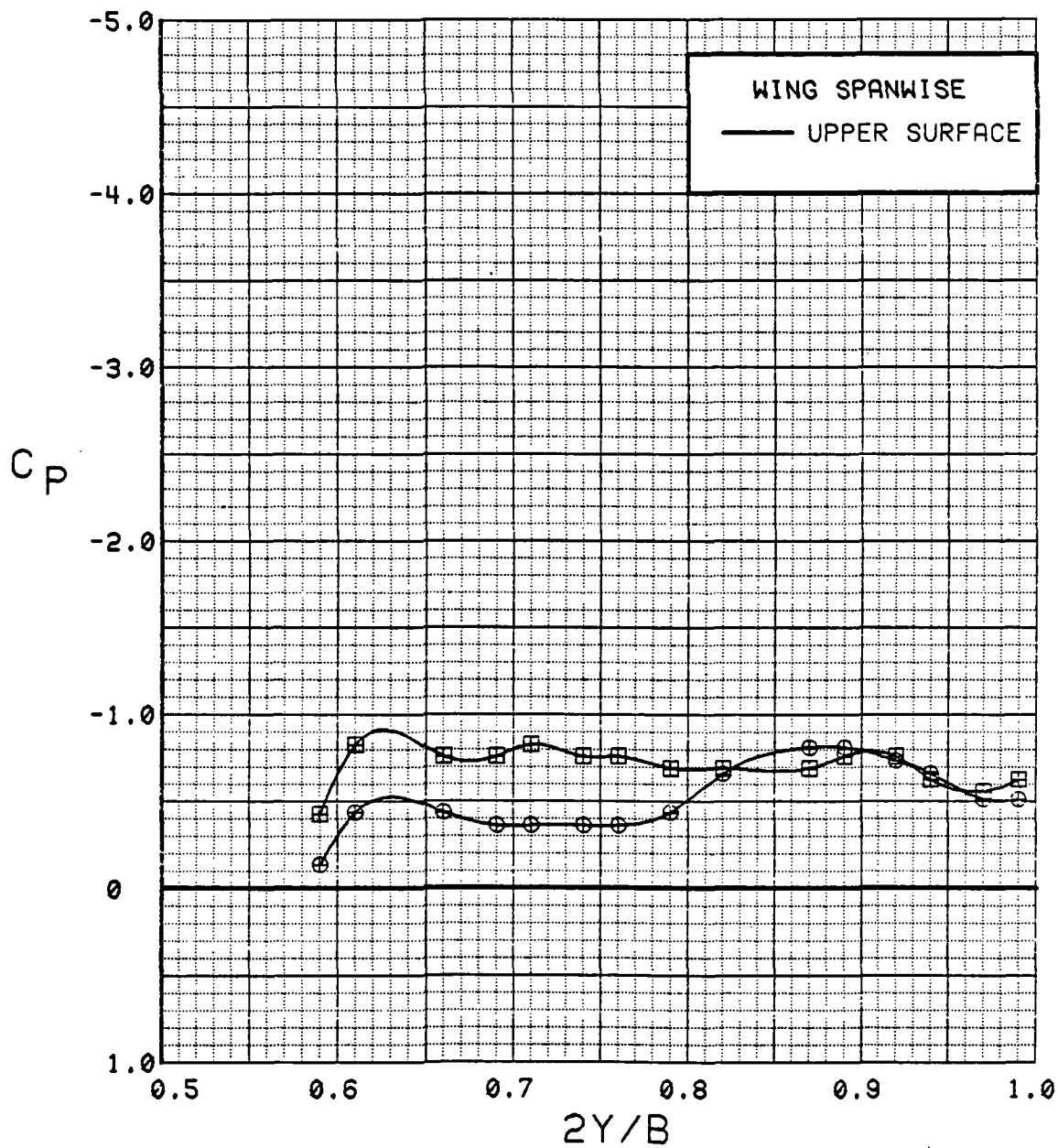


Figure 3.2.4-44 Canard On/Off Effects, Spanwise, Power Off, Flaps Neutral, Alpha = 12 deg

SYM	TEST	RUN	ALPHA	CT	ITEF	OTEF	CAN	SWB
⊕	543	63	16.6	0.00	0	0	0	OFF
⊞	537	74	16.5	0.00	0	0	OFF	OFF

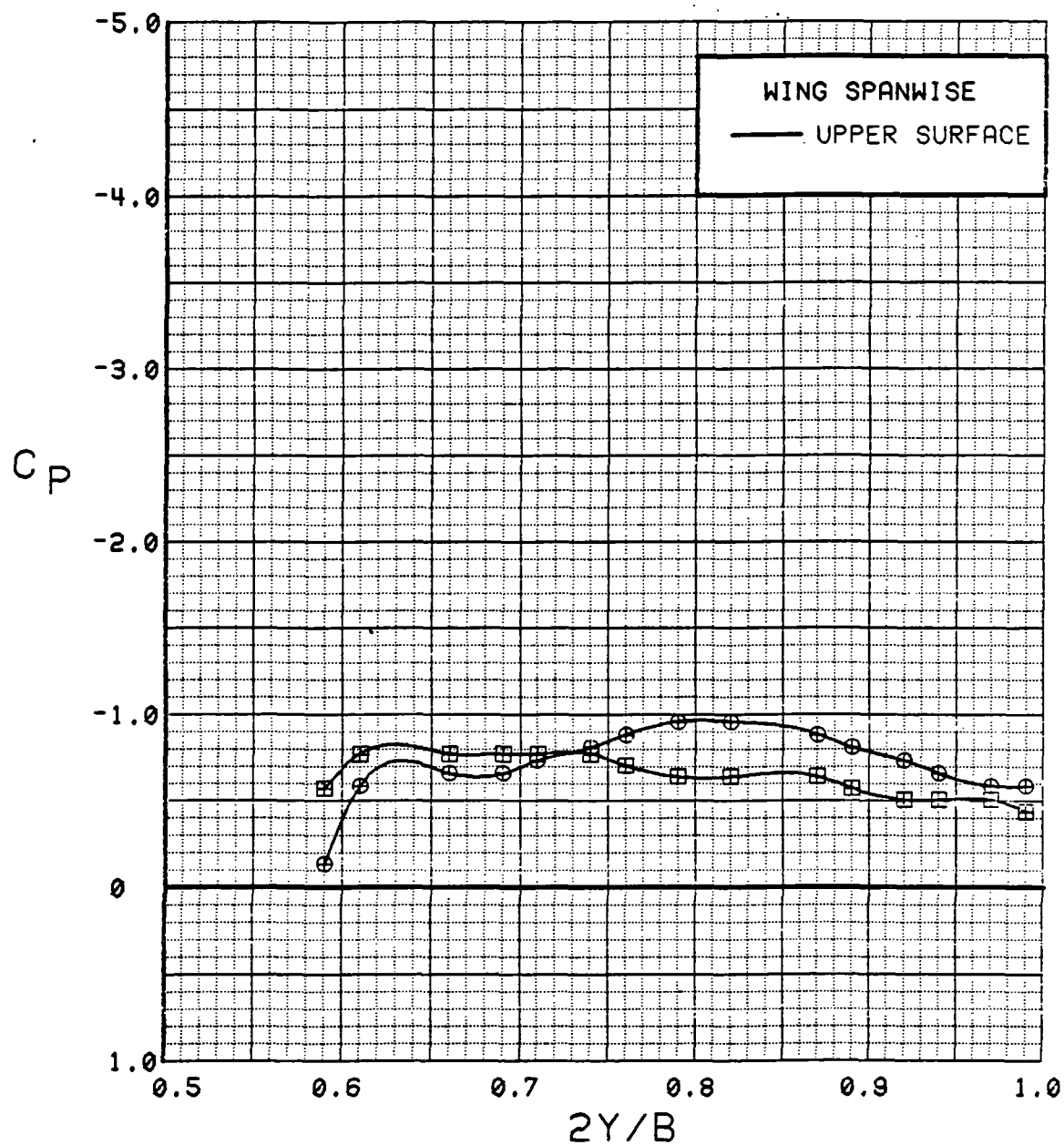


Figure 3.2.4-45 Canard On/Off Effects, Spanwise, Power Off, Flaps Neutral, Alpha = 16 deg

SYM	TEST	RUN	ALPHA	CT	ITEF	OTEF	CAN	SWB
⊕	543	63	20.7	0.00	0	0	0	OFF
⊞	537	74	20.5	0.00	0	0	OFF	OFF

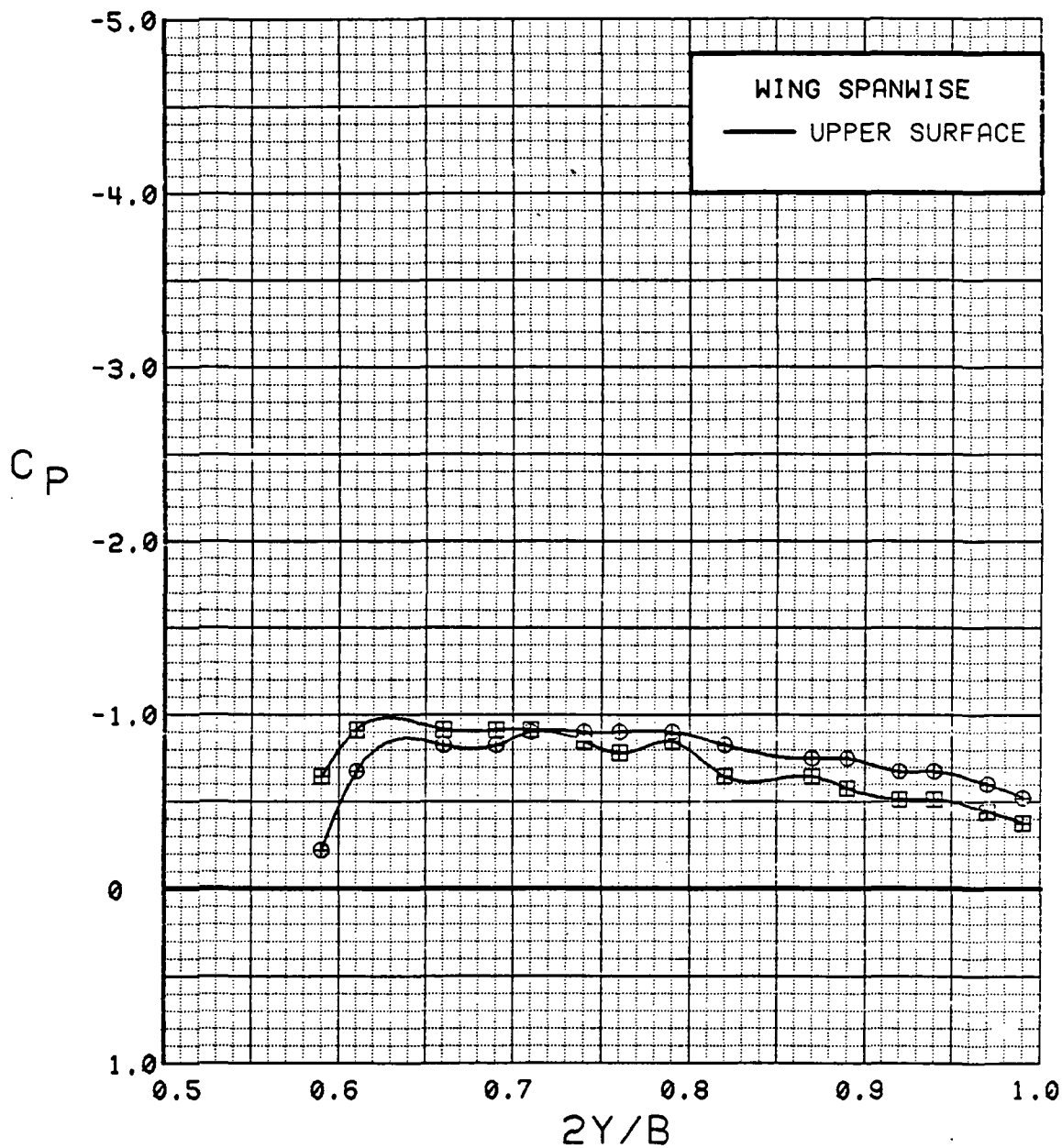


Figure 3.2.4-46 Canard On/Off Effects, Spanwise, Power Off, Flaps Neutral, Alpha = 20 deg

SYM	TEST	RUN	ALPHA	CT	ITEF	OTEF	CAN	SWB
⊕	543	63	24.8	0.00	0	0	0	OFF
⊞	537	74	24.6	0.00	0	0	OFF	OFF

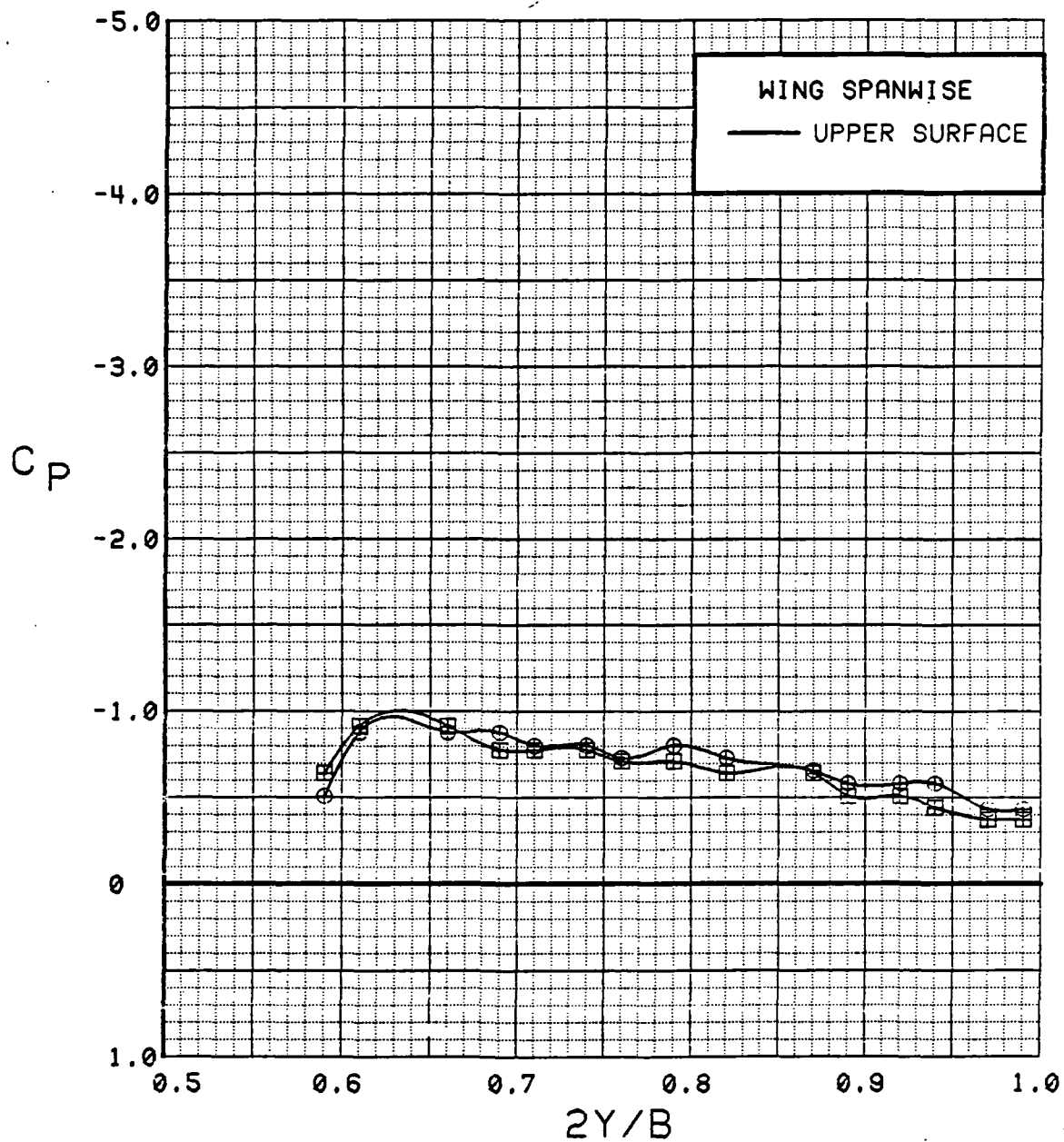


Figure 3.2.4-47

Canard On/Off Effects, Spanwise, Power Off,  
Flaps Neutral, Alpha = 24 deg

SYM	TEST	RUN	ALPHA	CT	ITEF	OTEF	CAN	SWB
⊕	543	63	28.8	0.00	0	0	0	OFF
⊞	537	74	28.6	0.00	0	0	OFF	OFF

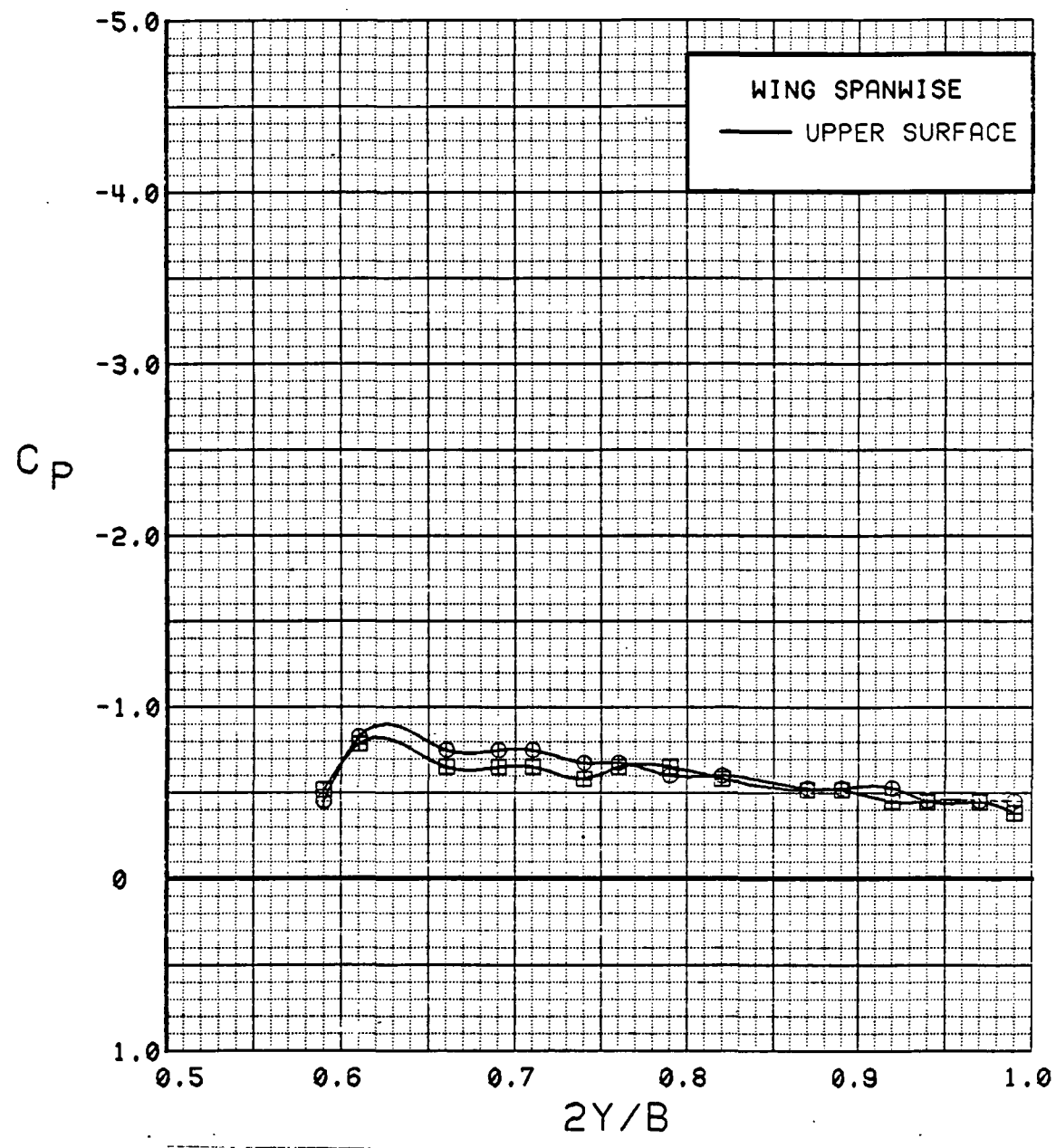


Figure 3.2.4-48 Canard On/Off Effects, Spanwise, Power Off, Flaps Neutral, Alpha = 28 deg

SYM	TEST	RUN	ALPHA	CT	ITEF	OTEF	CAN	SWB
⊕	543	63	32.8	0.00	0	0	0	OFF
⊞	537	74	32.6	0.00	0	0	OFF	OFF

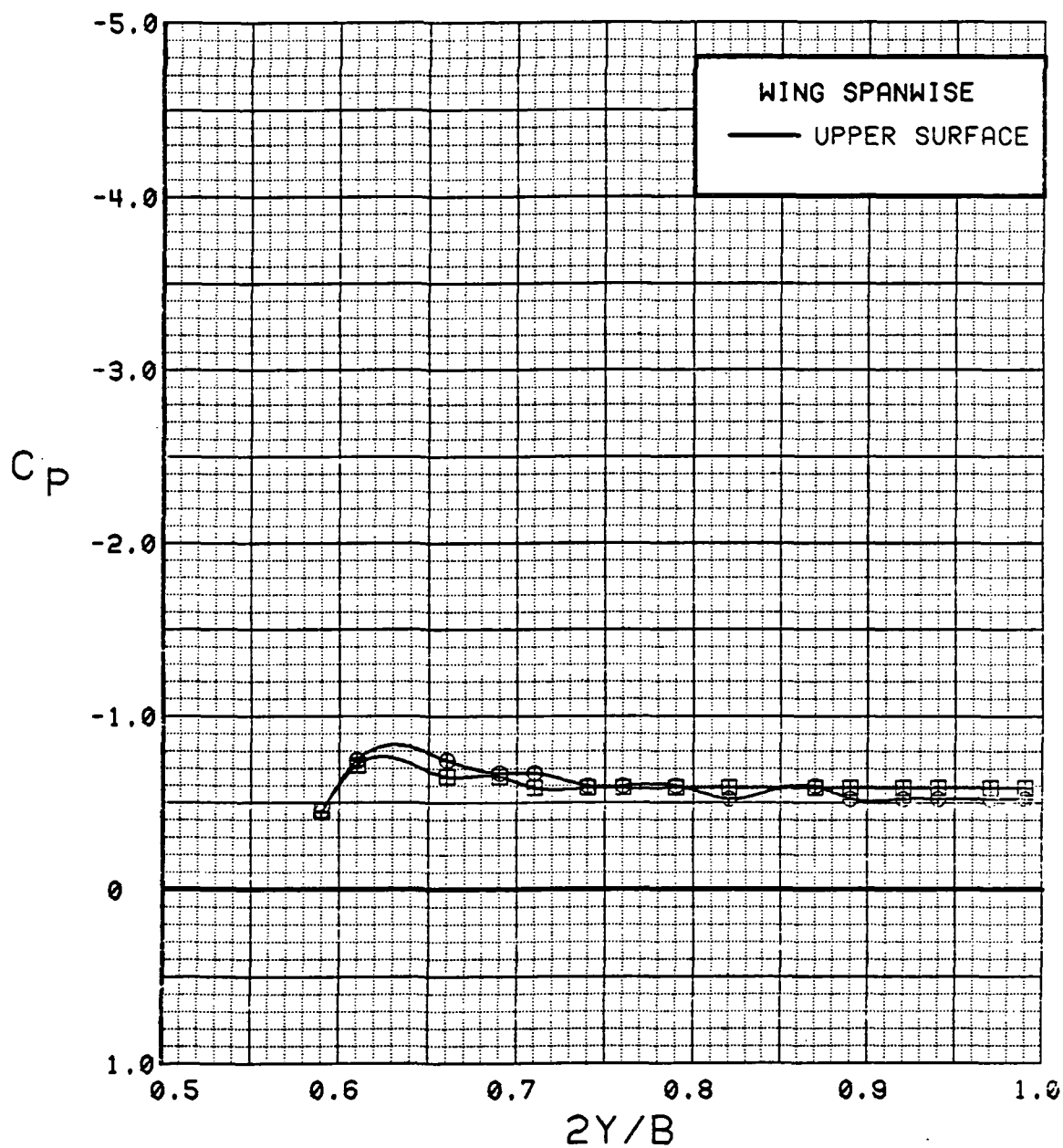


Figure 3.2.4-49

Canard On/Off Effects, Spanwise, Power Off,  
Flaps Neutral, Alpha = 32 deg

## WING INBOARD

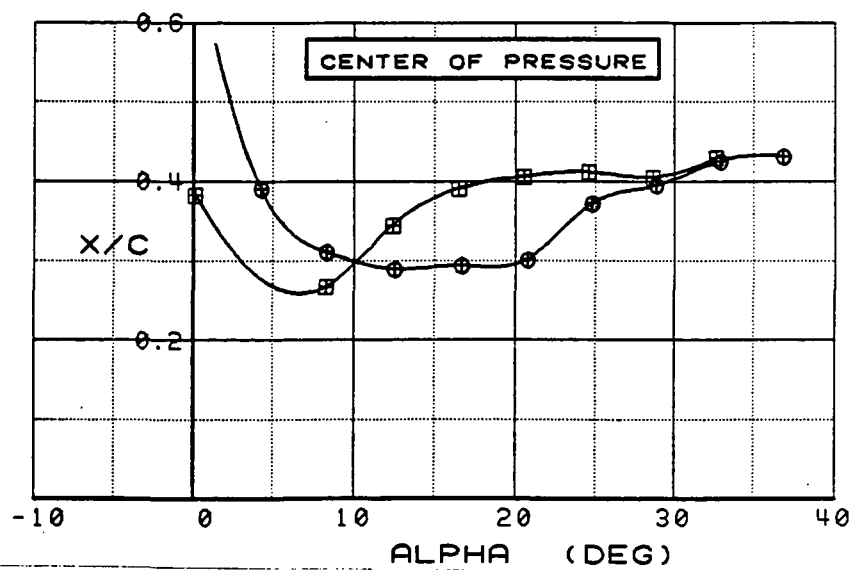
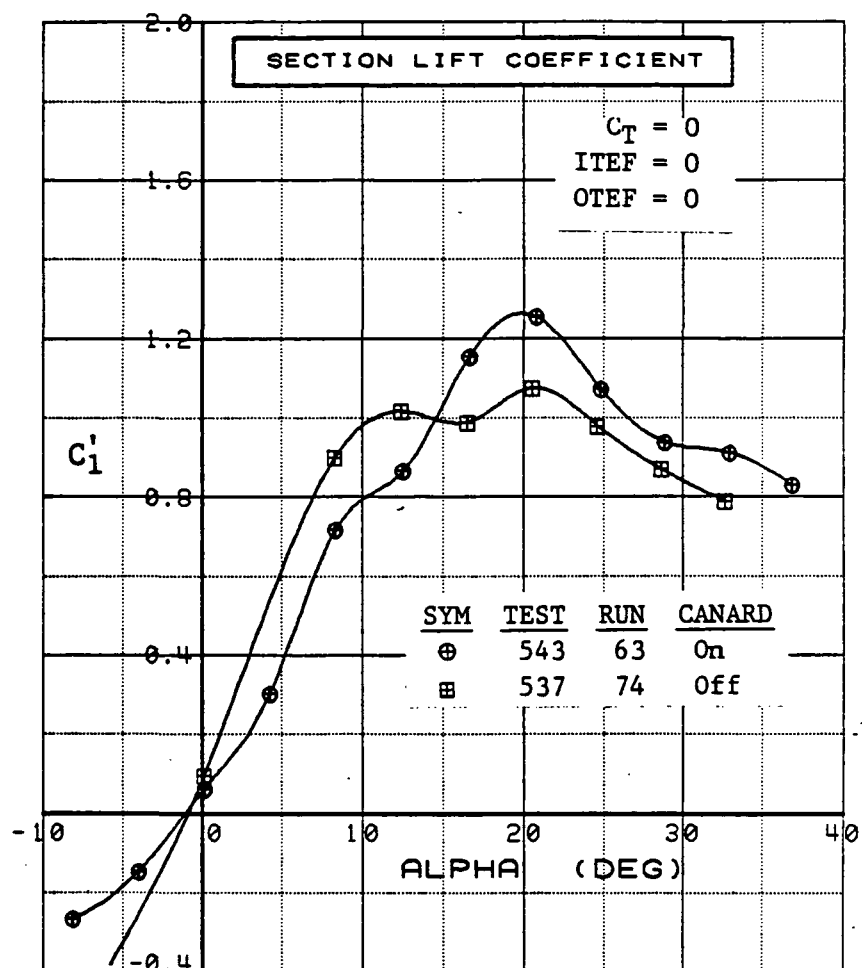


Figure 3.2.4-50

Canard On/Off Effects, Inboard, Power Off,  
Flaps Neutral, Integrated Section Properties

# WING OUTBOARD

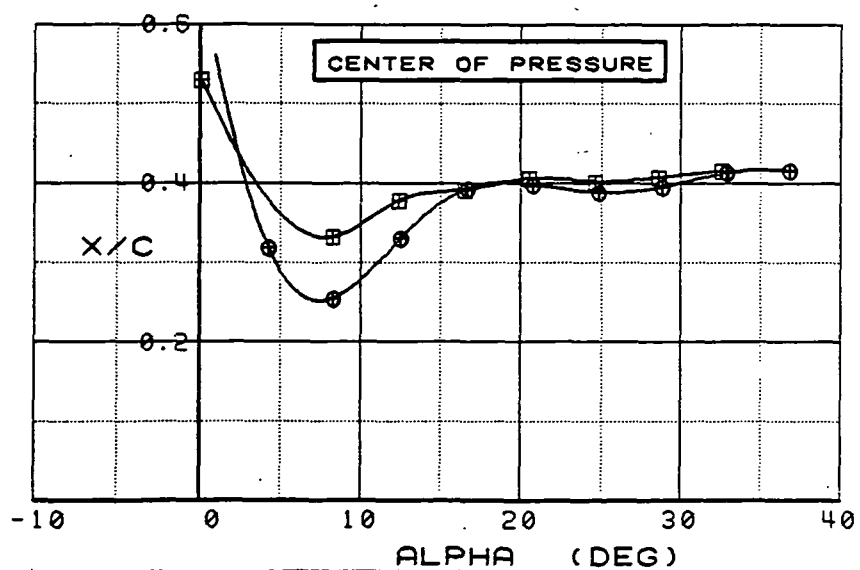
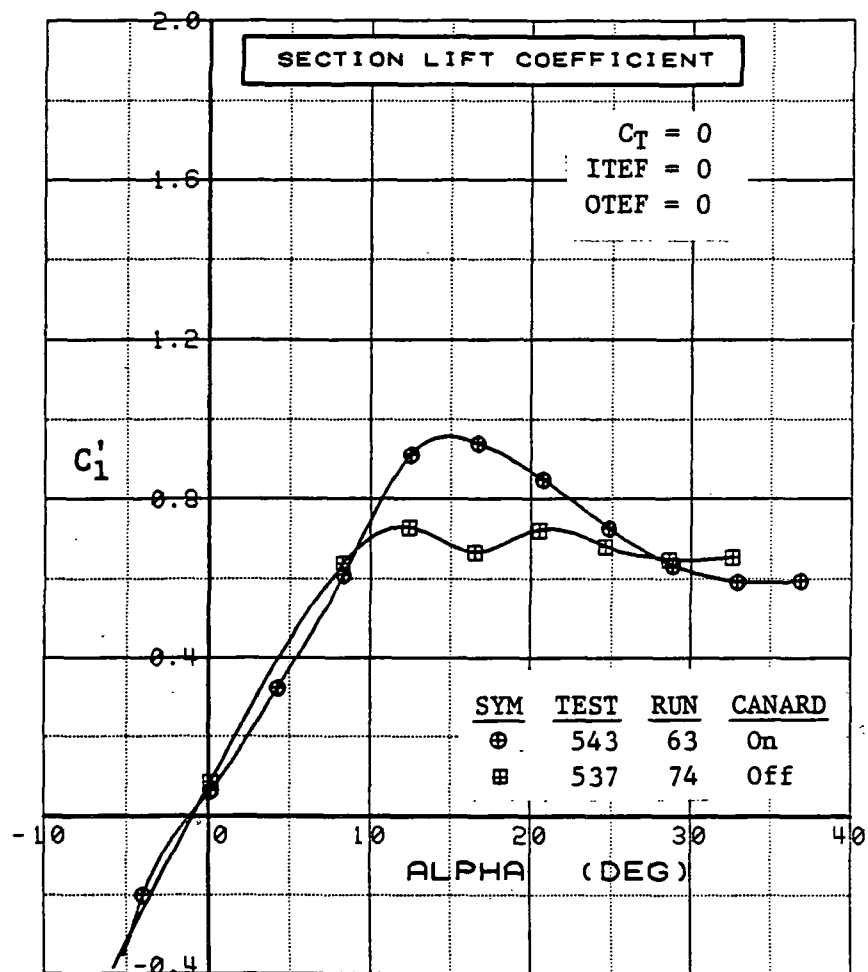


Figure 3.2.4-51

Canard On/Off Effects, Outboard, Power Off,  
 Flaps Neutral, Integrated Section Properties



SYM	TEST	RUN	ALPHA	CT	ITEF	OTEF	CAN	SWB
⊕	543	11	0.3	0.00	30	30	0	OFF
⊞	537	69	0.2	0.00	30	30	OFF	OFF

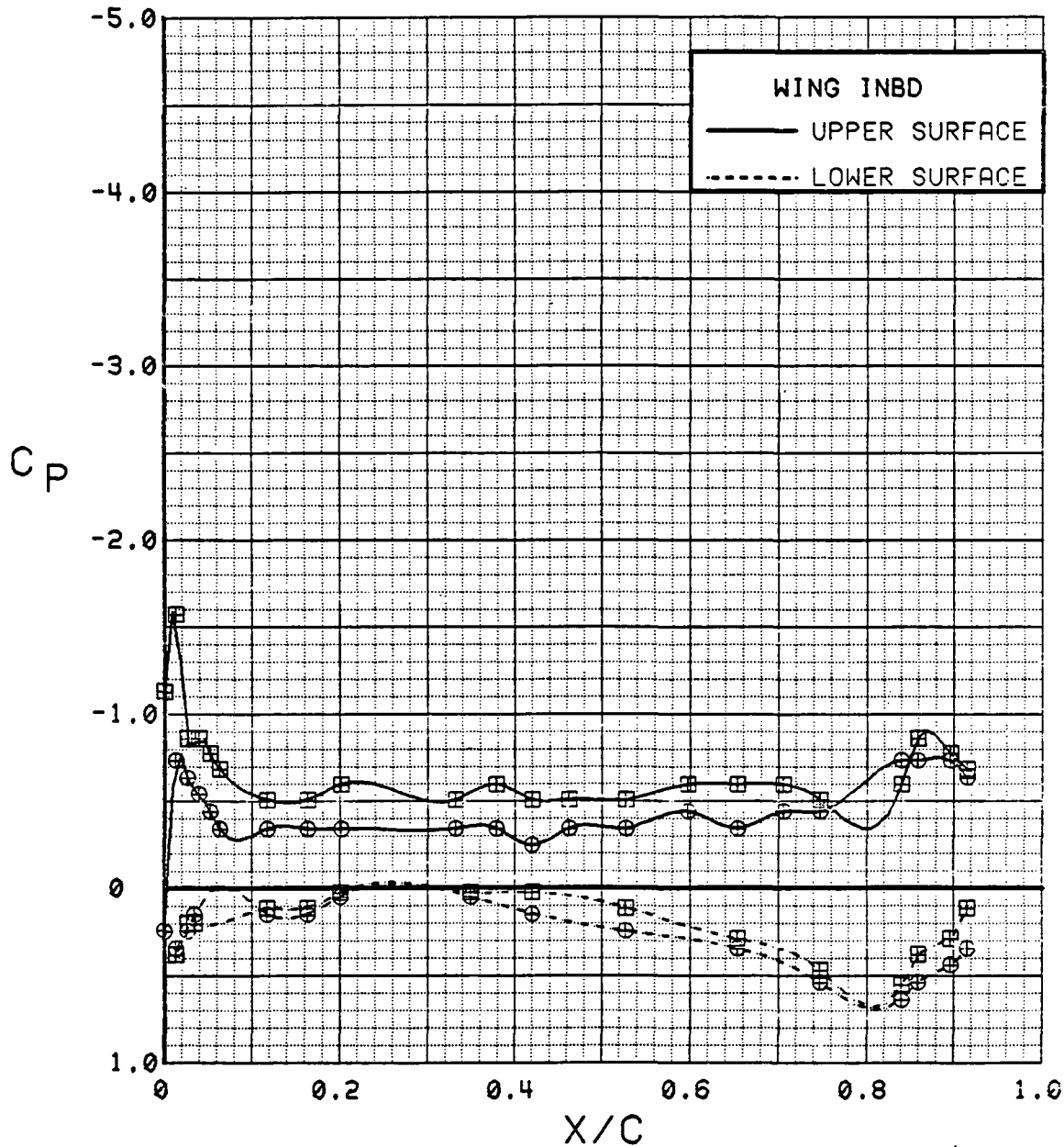


Figure 3.2.4-52 Canard On/Off Effects, Inboard, Power Off,  
Flaps Deflected, Alpha = 0 deg

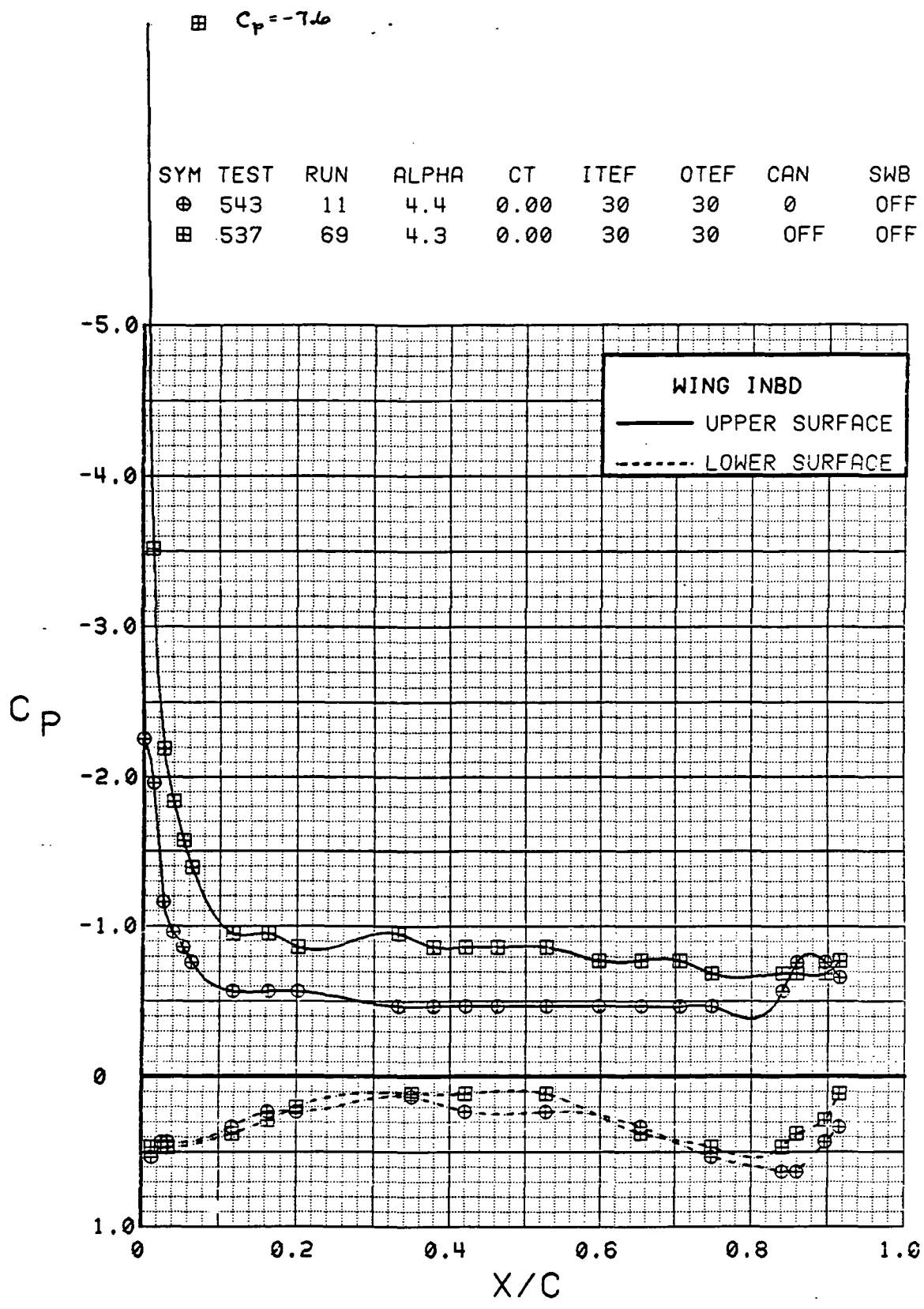


Figure 3.2.4-53 Canard On/Off Effects, Inboard, Power Off, Flaps Deflected, Alpha = 4 deg

SYM	TEST	RUN	ALPHA	CT	ITEF	OTEF	CAN	SWB
⊕	543	11	8.5	0.00	30	30	0	OFF
⊞	537	69	8.5	0.00	30	30	OFF	OFF

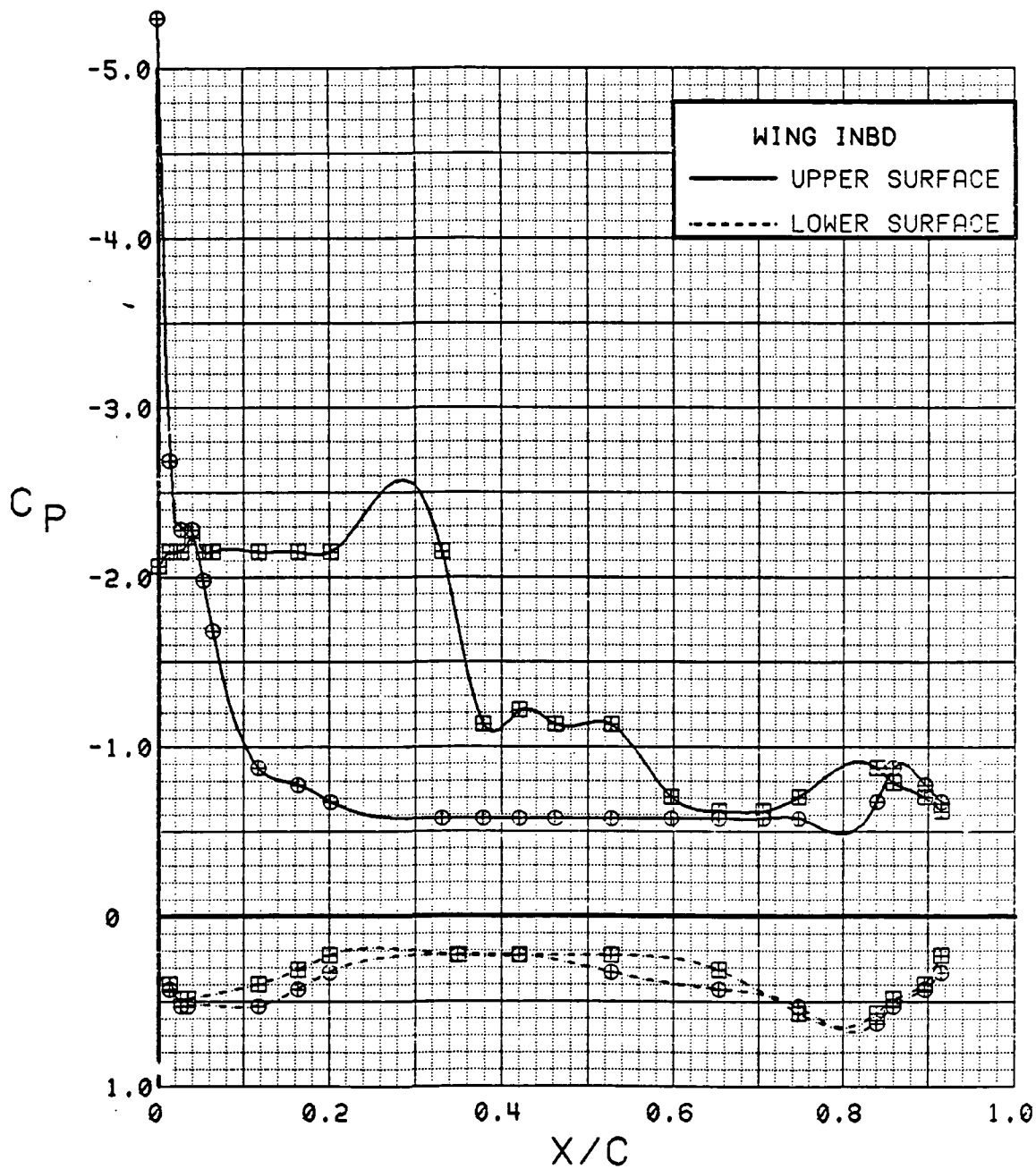


Figure 3.2.4-54 Canard On/Off Effects, Inboard, Power Off, Flaps Deflected, Alpha = 8 deg

SYM	TEST	RUN	ALPHA	CT	ITEF	OTEF	CAN	SWB
⊕	543	11	12.7	0.00	30	30	0	OFF
⊞	537	69	12.5	0.00	30	30	OFF	OFF

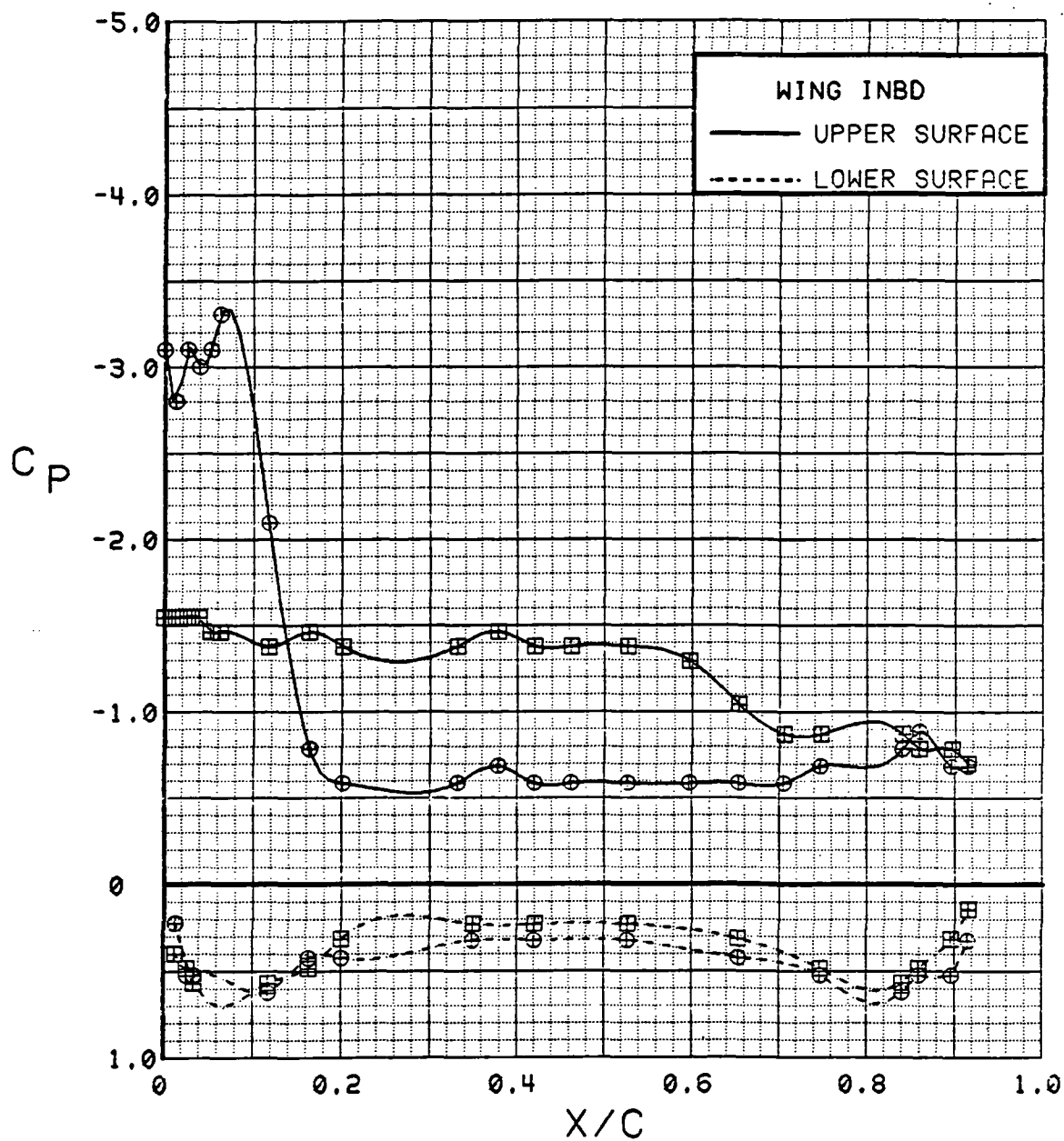


Figure 3.2.4-55 Canard On/Off Effects, Inboard, Power Off, Flaps Deflected, Alpha = 12 deg

SYM	TEST	RUN	ALPHA	CT	ITEF	OTEF	CAN	SWB
⊕	543	11	16.8	0.00	30	30	0	OFF
⊞	537	69	16.6	0.00	30	30	OFF	OFF

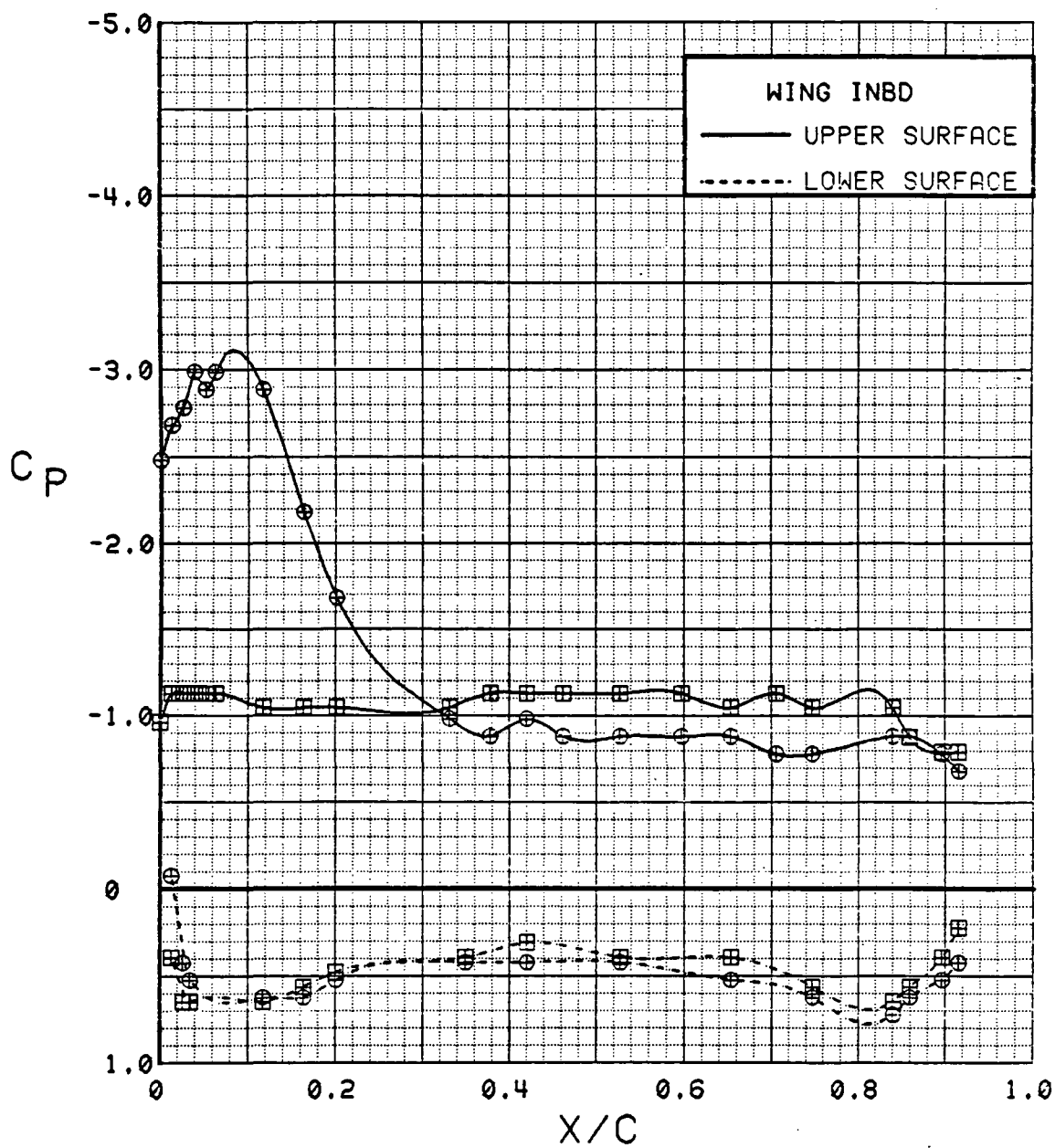


Figure 3.2.4-56 Canard On/Off Effects, Inboard, Power Off, Flaps Deflected, Alpha = 16 deg

SYM	TEST	RUN	ALPHA	CT	ITEF	OTEF	CAN	SWB
⊕	543	11	20.8	0.00	30	30	0	OFF
⊞	537	69	20.6	0.00	30	30	OFF	OFF

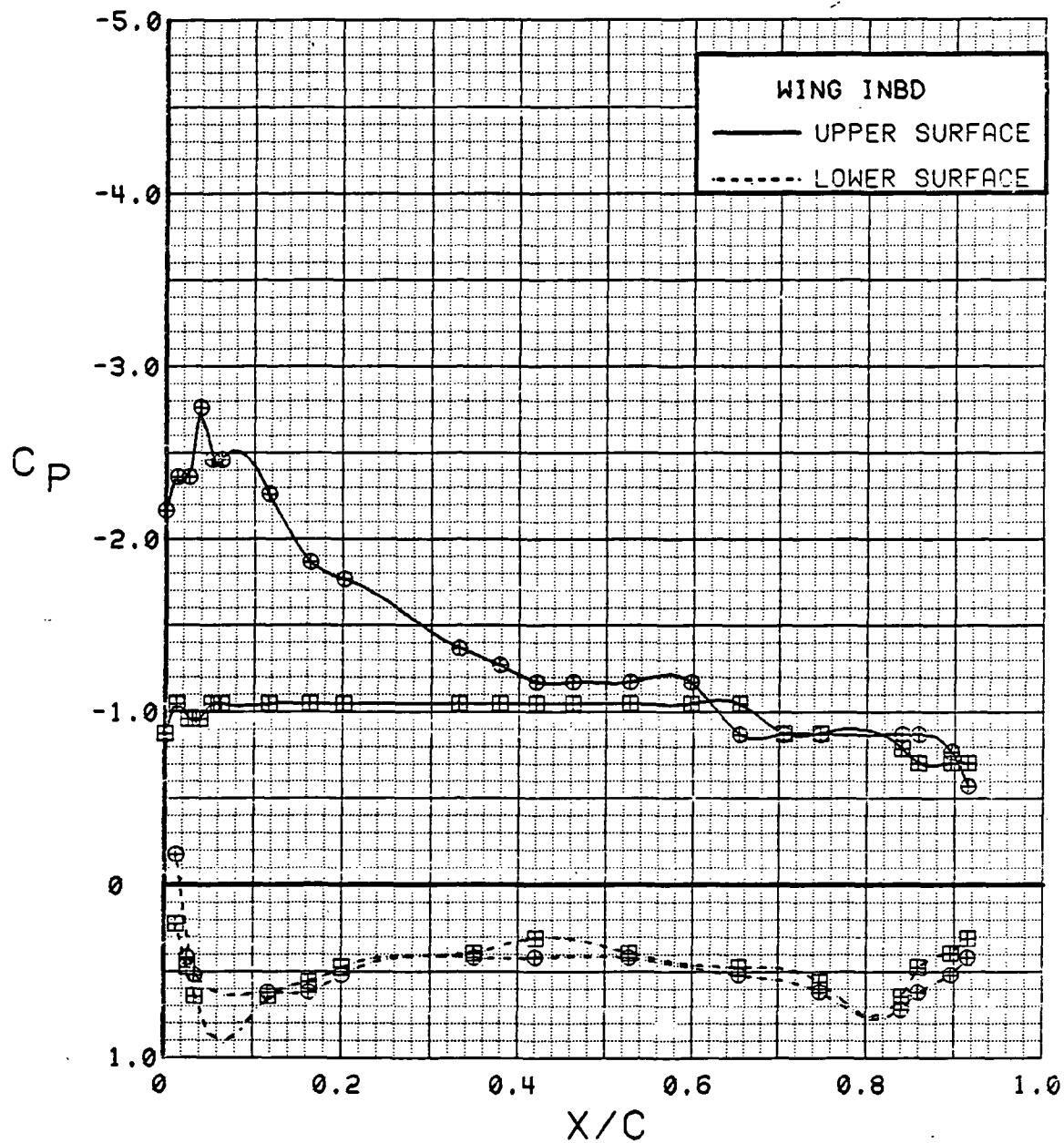


Figure 3.2.4-57 Canard On/Off Effects, Inboard, Power Off, Flaps Deflected, Alpha = 20 deg

SYM	TEST	RUN	ALPHA	CT	ITEF	OTEF	CAN	SWB
⊕	543	11	24.9	0.00	30	30	0	OFF
⊞	537	69	24.7	0.00	30	30	OFF	OFF

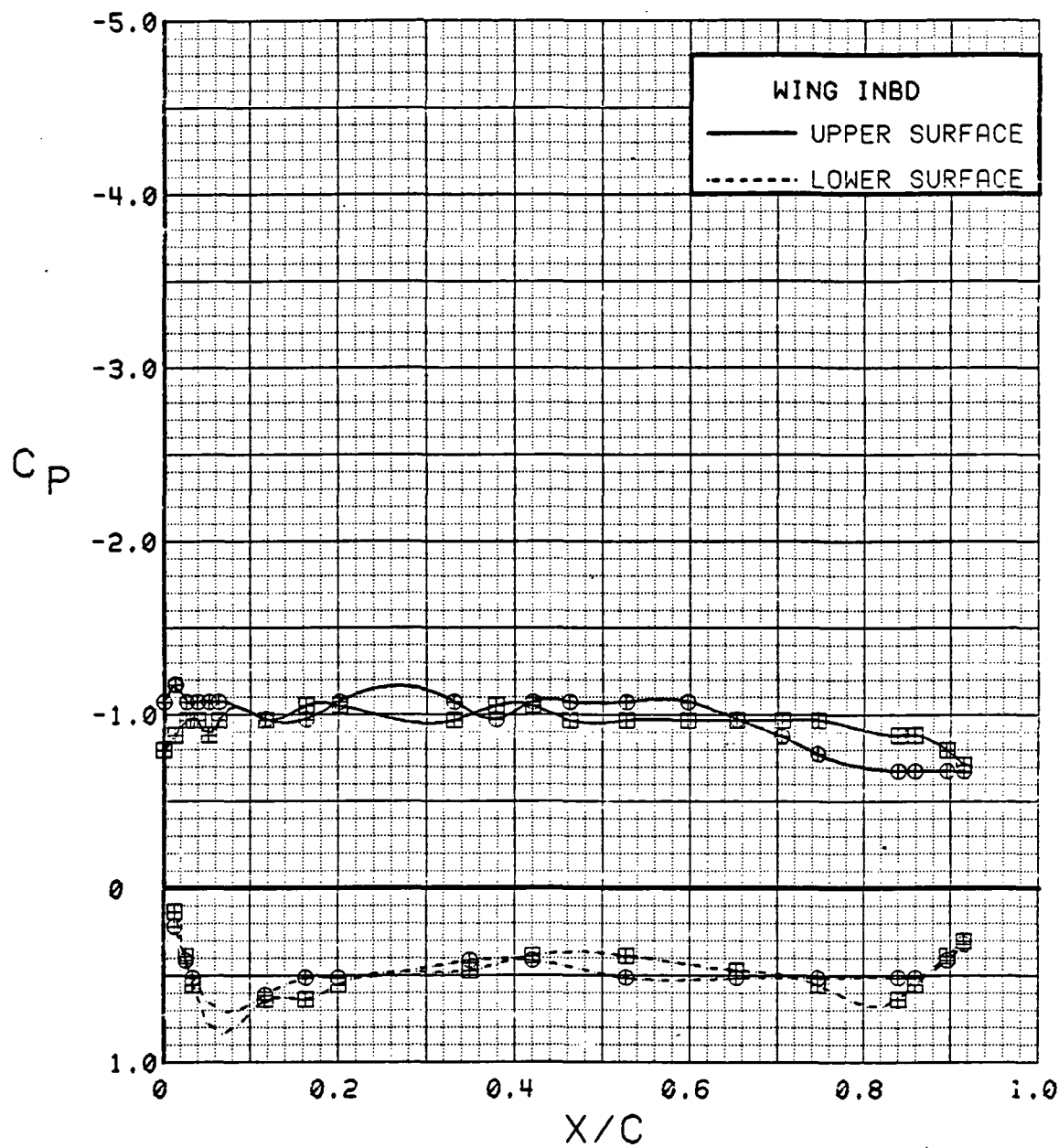


Figure 3.2.4-58 Canard On/Off Effects, Inboard, Power Off, Flaps Deflected, Alpha = 24 deg

SYM	TEST	RUN	ALPHA	CT	ITEF	OTEF	CAN	SWB
⊕	543	11	28.9	0.00	30	30	0	OFF
⊞	537	69	28.7	0.00	30	30	OFF	OFF

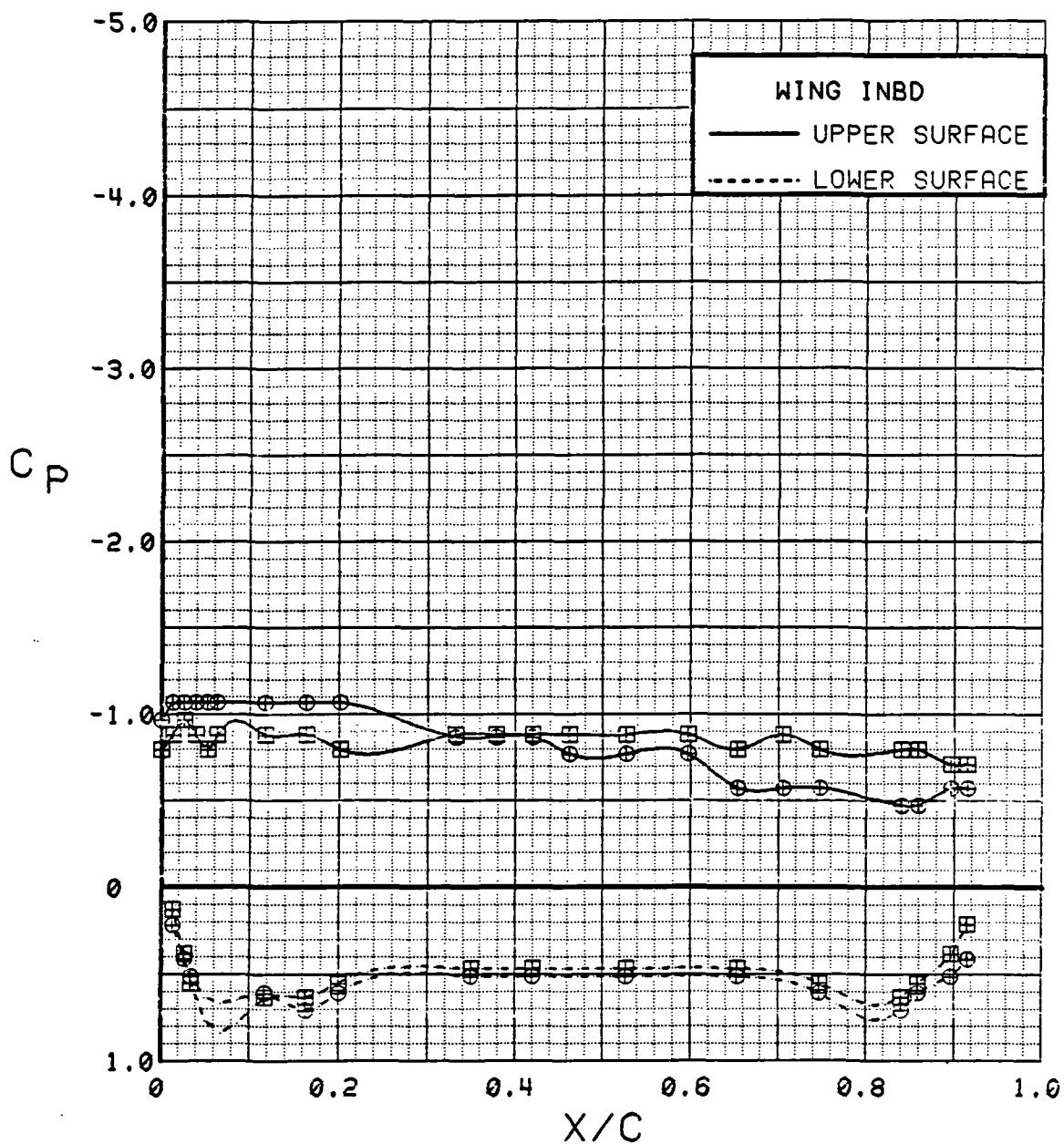


Figure 3.2.4-59

Canard On/Off Effects, Inboard, Power Off,  
Flaps Deflected, Alpha = 28 deg



SYM	TEST	RUN	ALPHA	CT	ITEF	OTEF	CAN	SWB
⊕	543	11	0.3	0.00	30	30	0	OFF
⊞	537	69	0.2	0.00	30	30	OFF	OFF

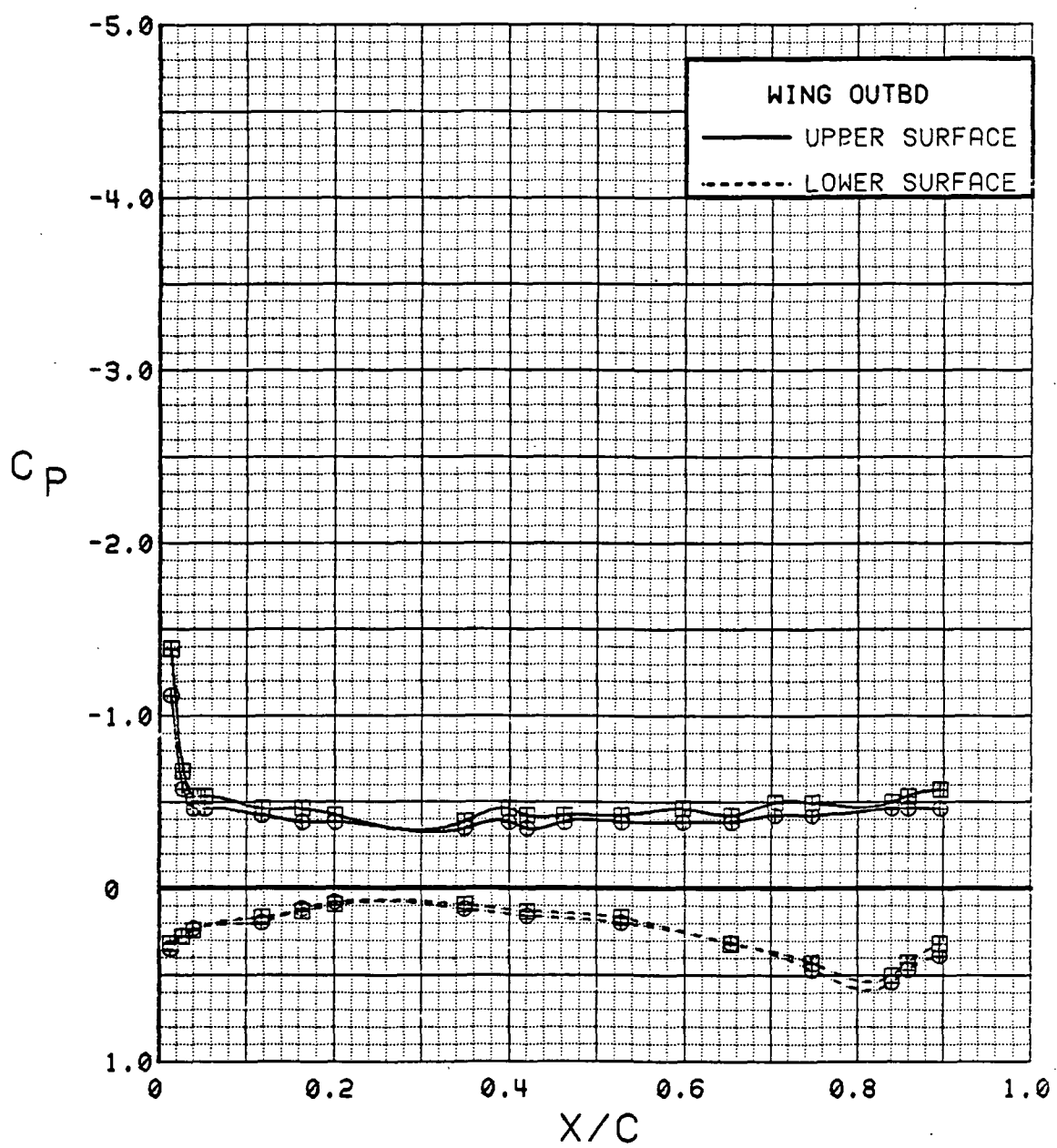


Figure 3.2.4-60 Canard On/Off Effects, Outboard, Power Off, Flaps Deflected, Alpha = 0 deg

SYM	TEST	RUN	ALPHA	CT	ITEF	OTEF	CAN	SWB
⊕	543	11	4.4	0.00	30	30	0	OFF
⊞	537	69	4.3	0.00	30	30	OFF	OFF

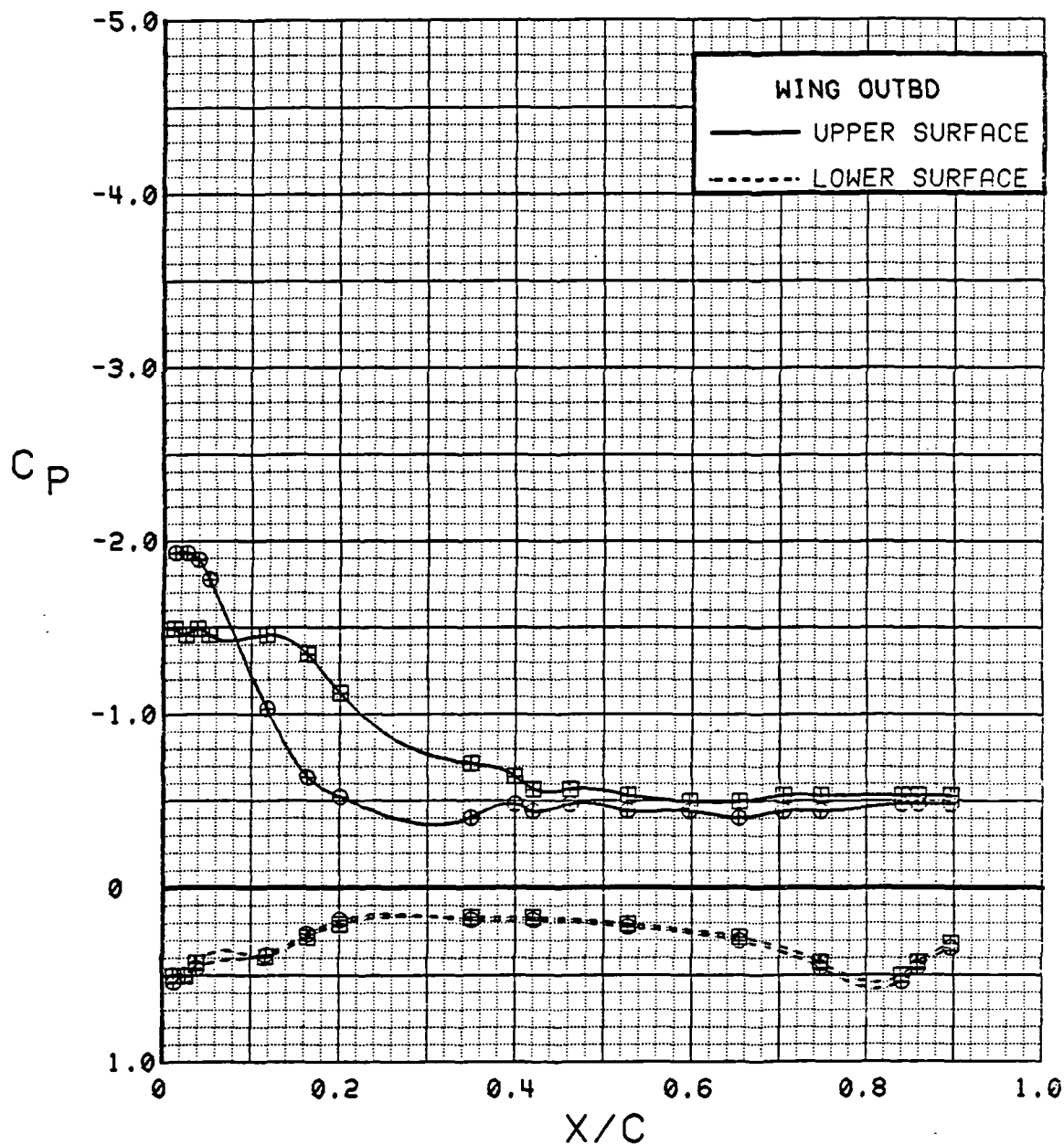


Figure 3.2.4-61 Canard On/Off Effects, Outboard, Power Off, Flaps Deflected, Alpha = 4 deg

SYM	TEST	RUN	ALPHA	CT	ITEF	OTEF	CAN	SWB
⊕	543	11	8.5	0.00	30	30	0	OFF
⊞	537	69	8.5	0.00	30	30	OFF	OFF

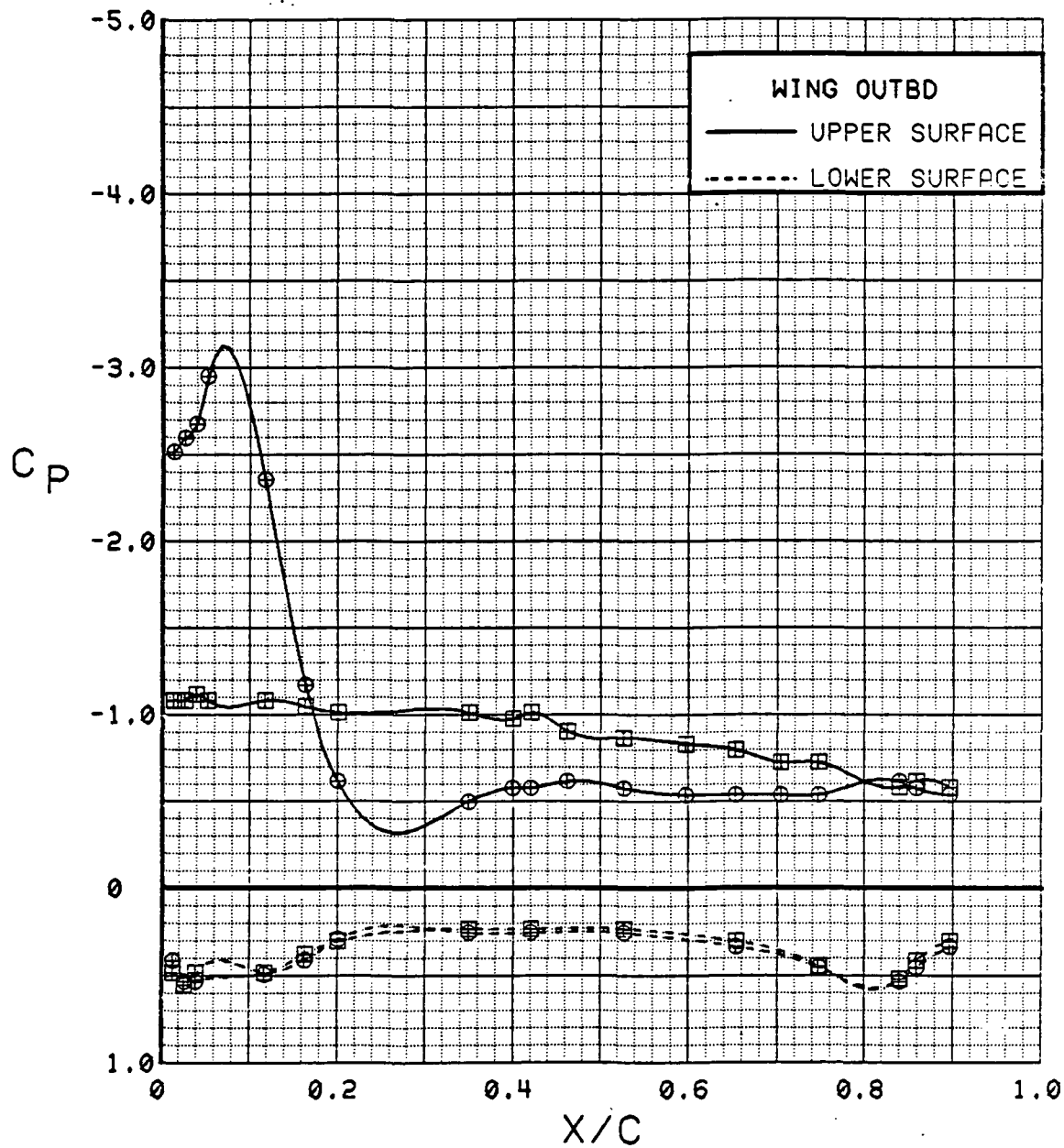


Figure 3.2.4-62 Canard On/Off Effects, Outboard, Power Off, Flaps Deflected, Alpha = 8 deg

SYM	TEST	RUN	ALPHA	CT	ITEF	OTEF	CAN	SWB
⊕	543	11	12.7	0.00	30	30	0	OFF
⊞	537	69	12.5	0.00	30	30	OFF	OFF

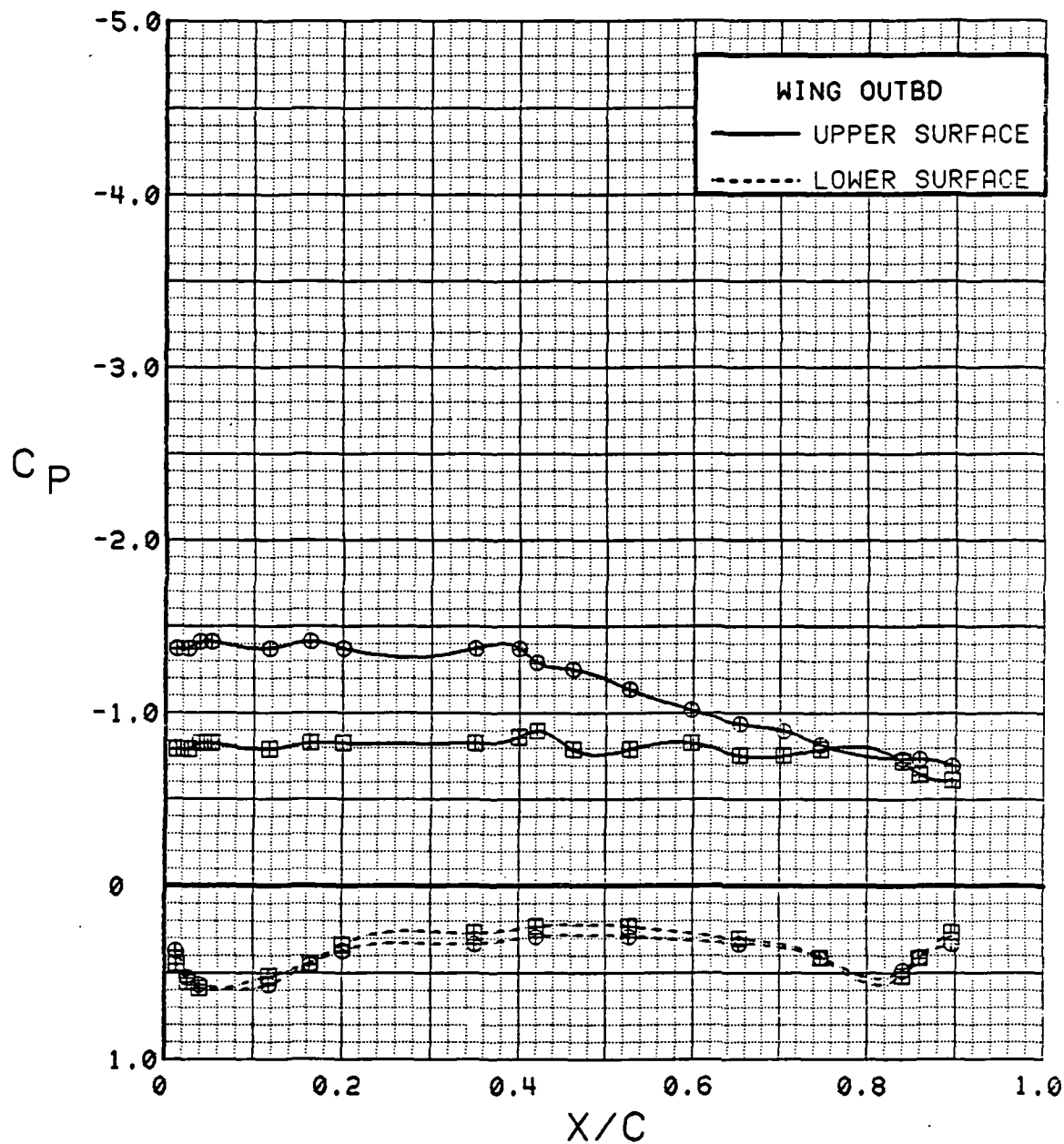


Figure 3.2.4-63

Canard On/Off Effects, Outboard, Power Off,  
Flaps Deflected, Alpha = 12 deg

SYM	TEST	RUN	ALPHA	CT	ITEF	OTEF	CAN	SWB
⊕	543	11	16.8	0.00	30	30	0	OFF
⊞	537	69	16.6	0.00	30	30	OFF	OFF

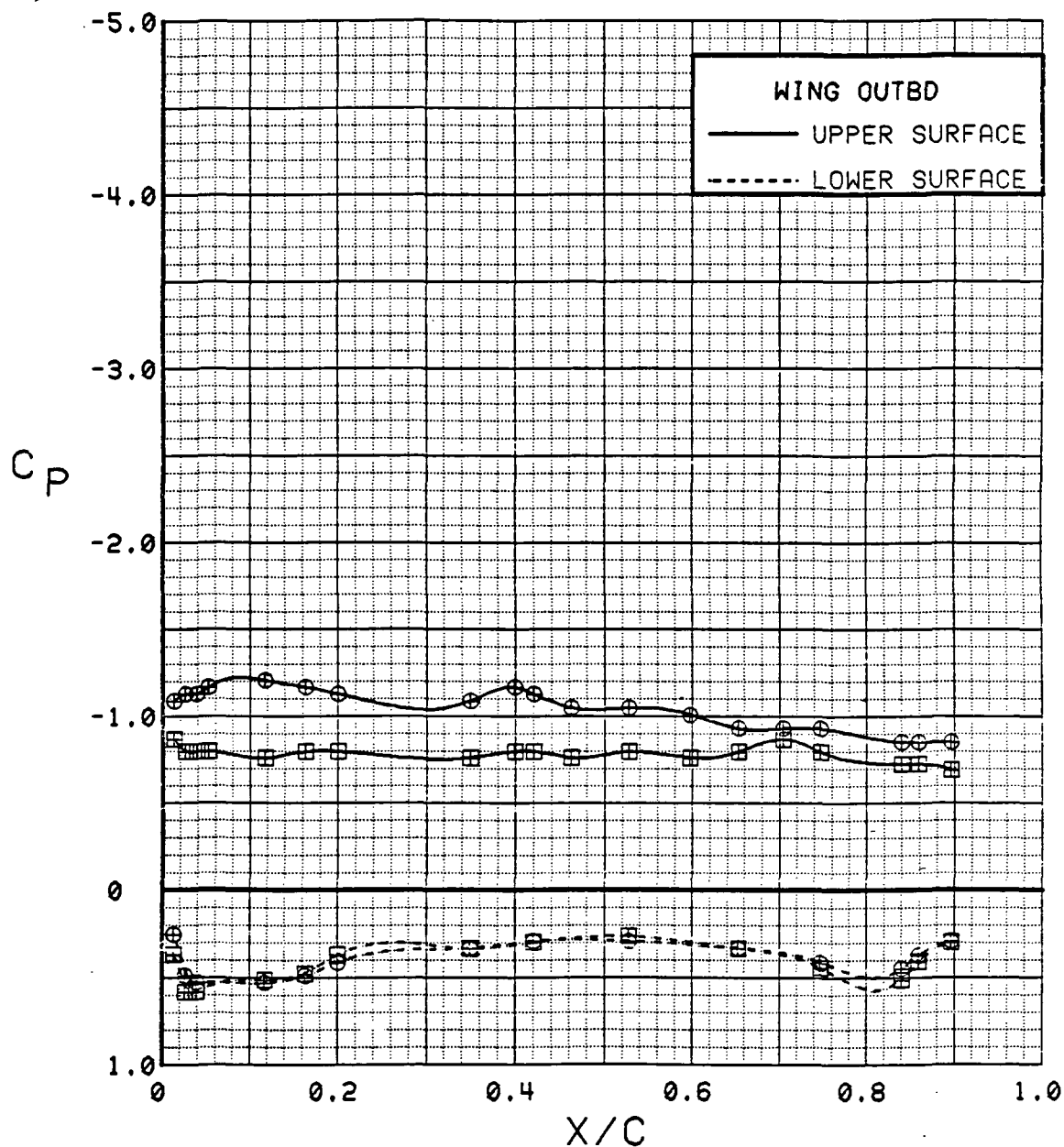


Figure 3.2.4-64 Canard On/Off Effects, Outboard, Power Off, Flaps Deflected, Alpha = 16 deg

SYM	TEST	RUN	ALPHA	CT	ITEF	OTEF	CAN	SWB
⊕	543	11	20.8	0.00	30	30	0	OFF
⊞	537	69	20.6	0.00	30	30	OFF	OFF

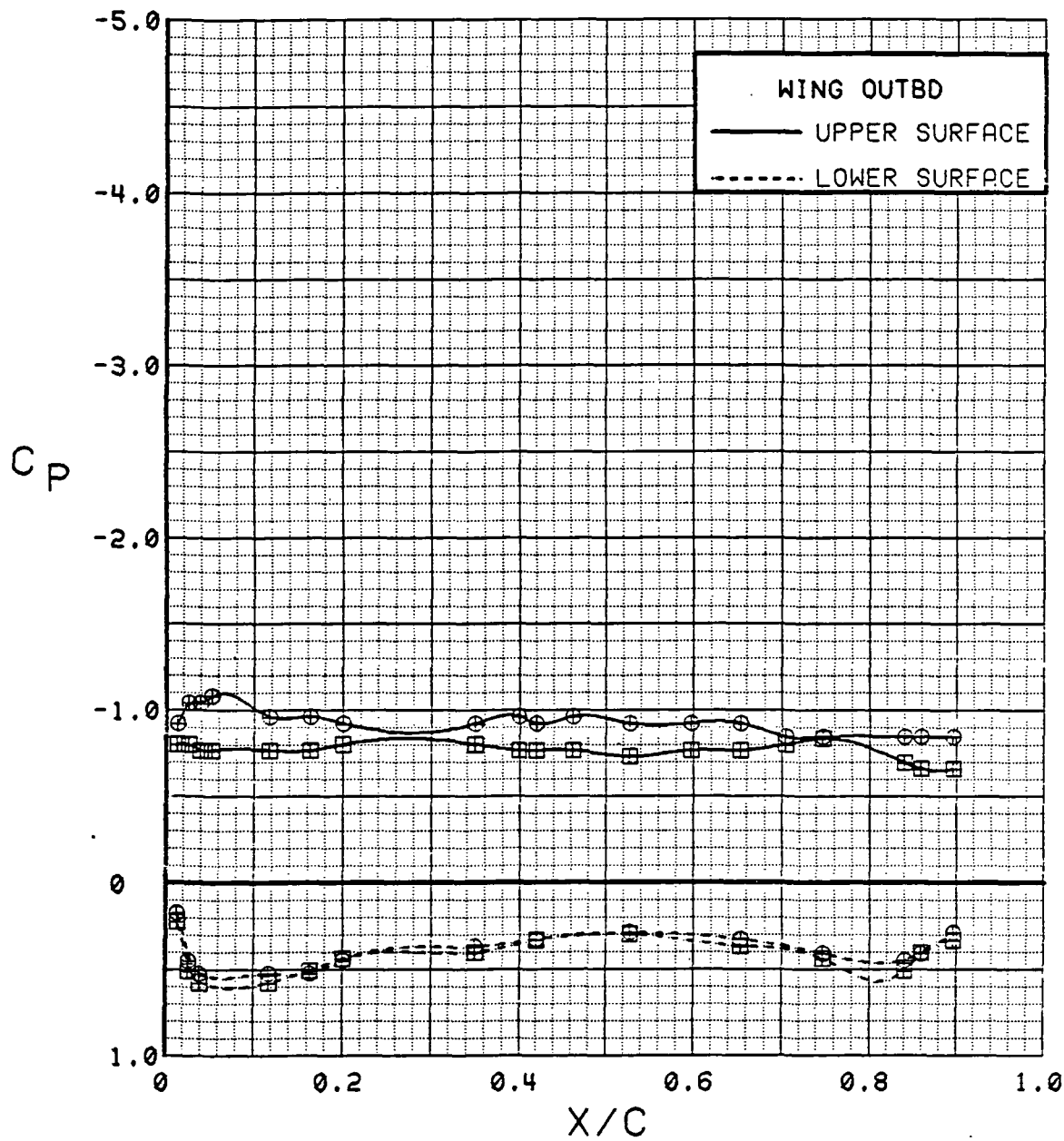


Figure 3.2.4-65 Canard On/Off Effects, Outboard, Power Off, Flaps Deflected, Alpha = 20 deg

SYM	TEST	RUN	ALPHA	CT	ITEF	OTEF	CAN	SWB
⊕	543	11	24.9	0.00	30	30	0	OFF
⊞	537	69	24.7	0.00	30	30	OFF	OFF

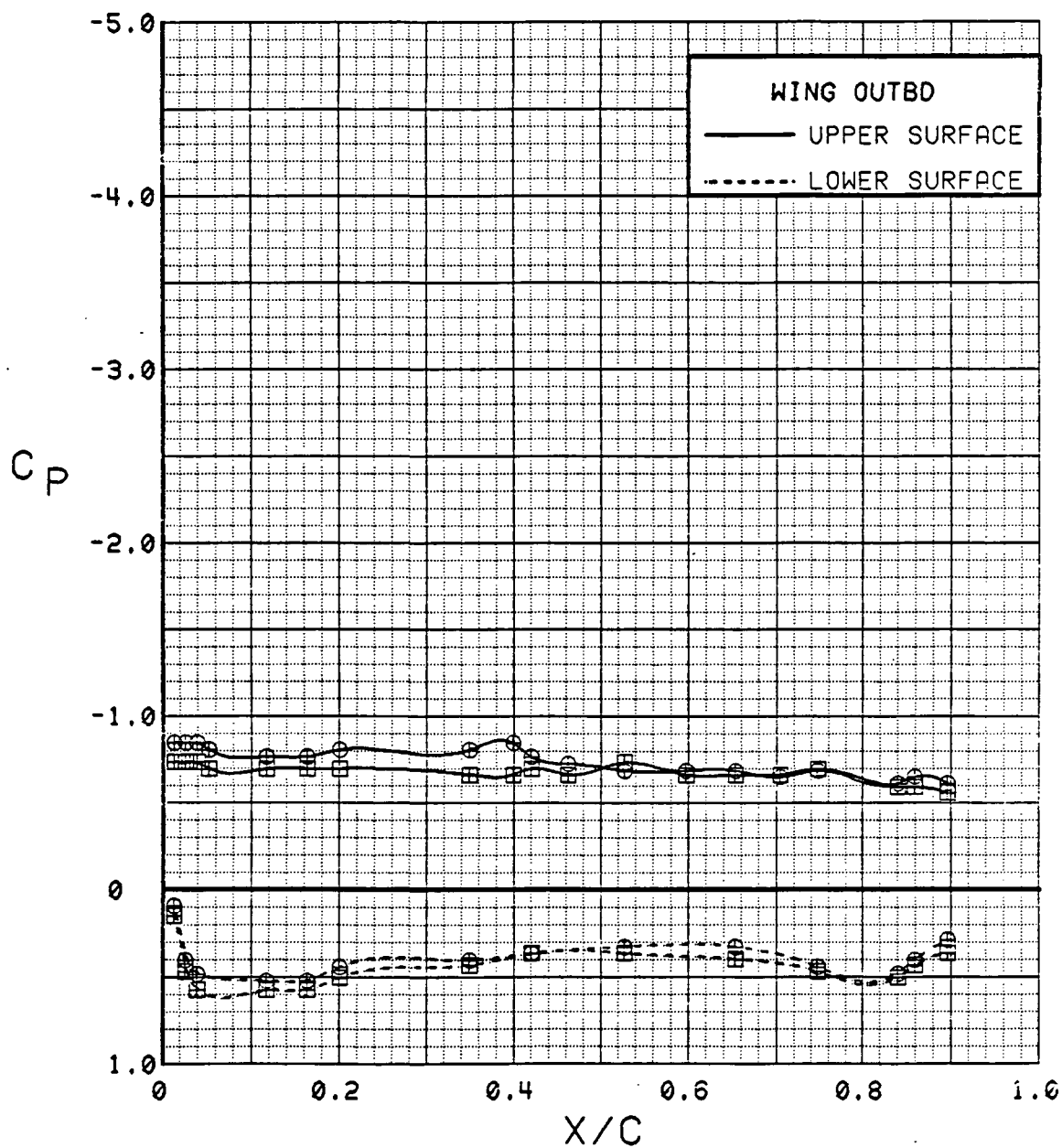


Figure 3.2.4-66 Canard On/Off Effects, Outboard, Power Off, Flaps Deflected, Alpha = 24 deg

SYM	TEST	RUN	ALPHA	CT	ITEF	OTEF	CAN	SWB
⊕	543	11	28.9	0.00	30	30	0	OFF
⊞	537	69	28.7	0.00	30	30	OFF	OFF

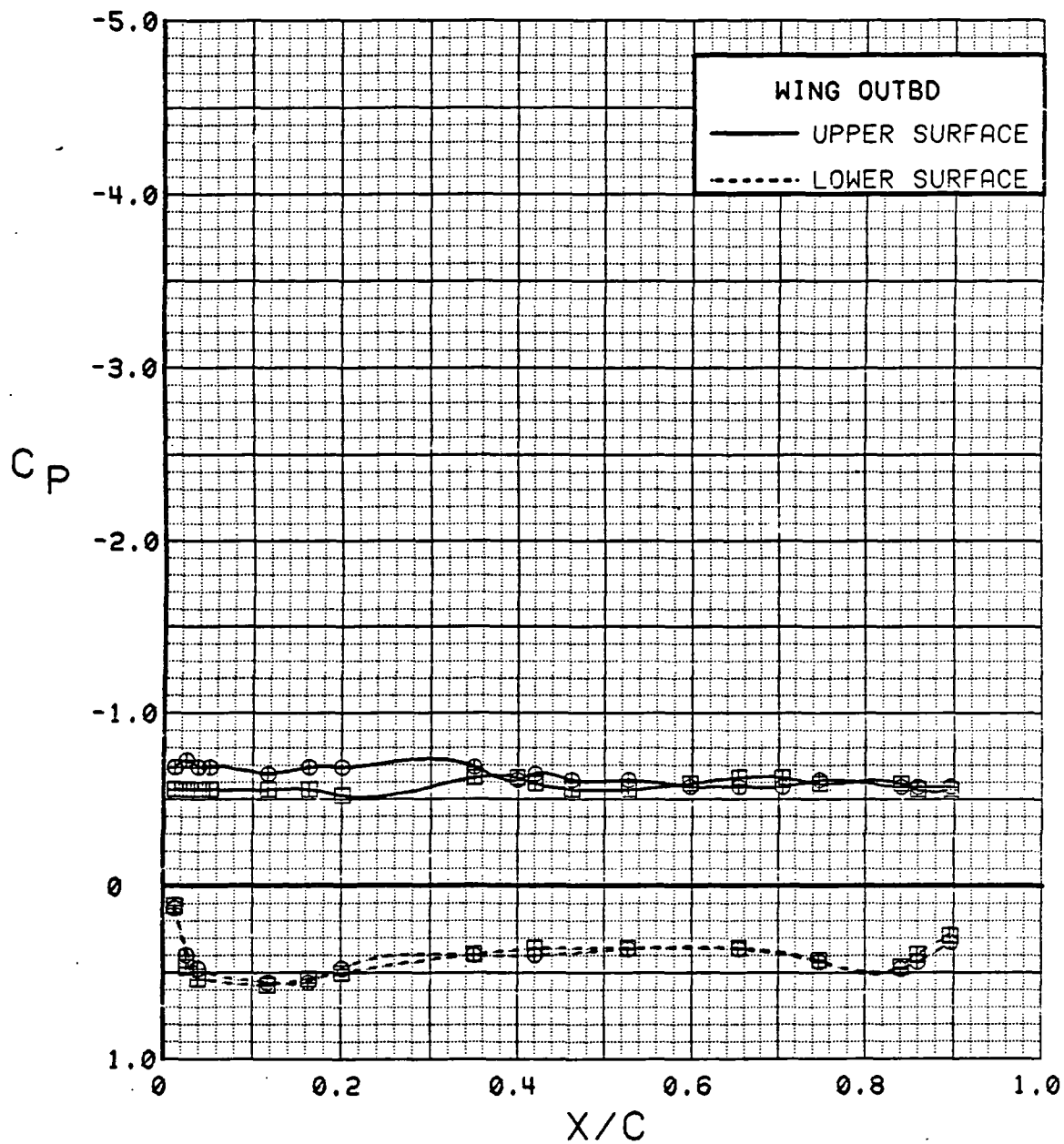


Figure 3.2.4-67 Canard On/Off Effects, Outboard, Power Off, Flaps Deflected, Alpha = 28 deg



SYM	TEST	RUN	ALPHA	CT	ITEF	OTEF	CAN	SWB
⊕	543	11	0.3	0.00	30	30	0	OFF
⊞	537	69	0.2	0.00	30	30	OFF	OFF

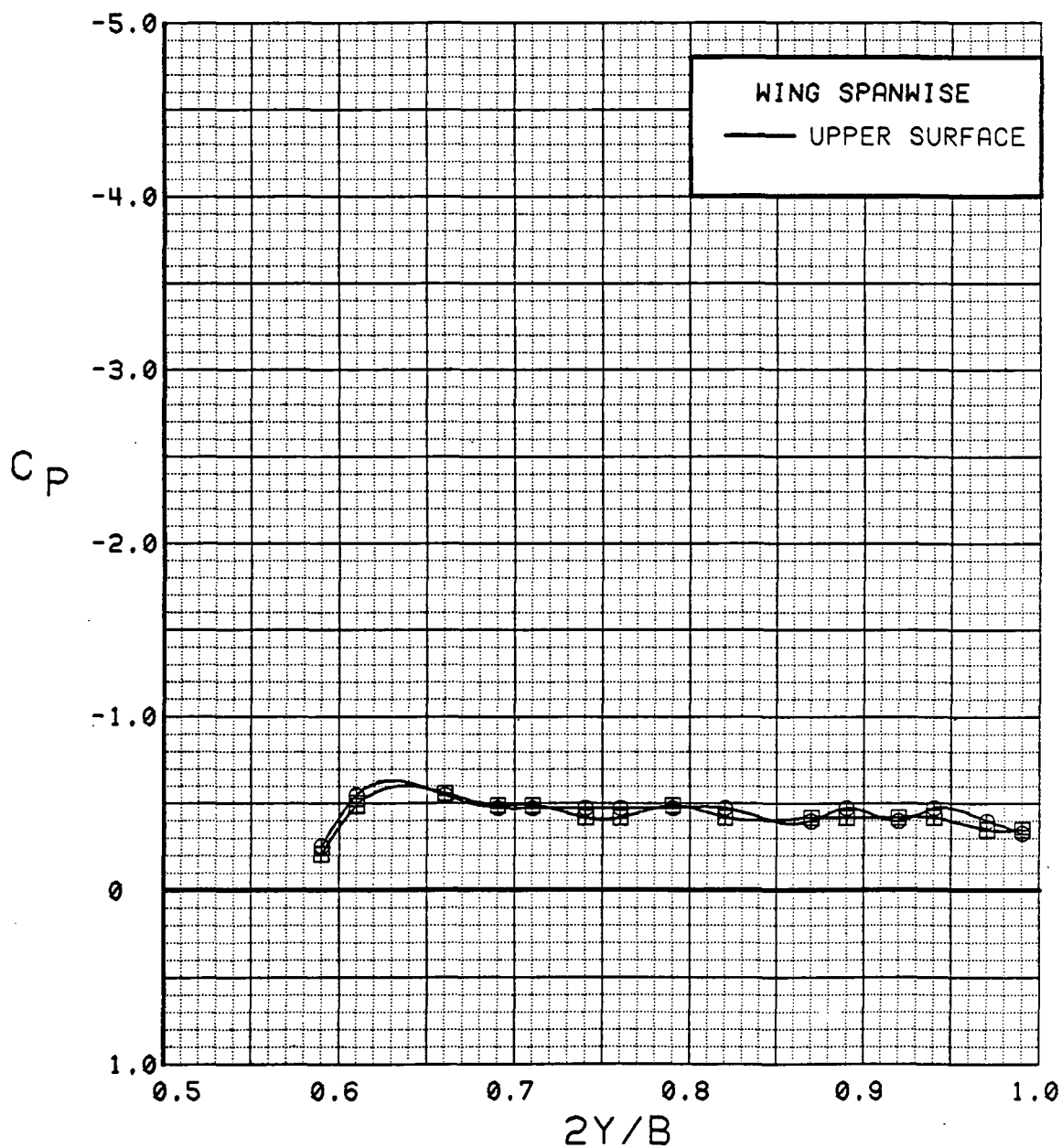


Figure 3.2.4-68

Canard On/Off Effects, Spanwise, Power Off,  
Flaps Deflected, Alpha = 0 deg

SYM	TEST	RUN	ALPHA	CT	ITEF	OTEF	CAN	SWB
⊕	543	11	4.4	0.00	30	30	0	OFF
⊞	537	69	4.3	0.00	30	30	OFF	OFF

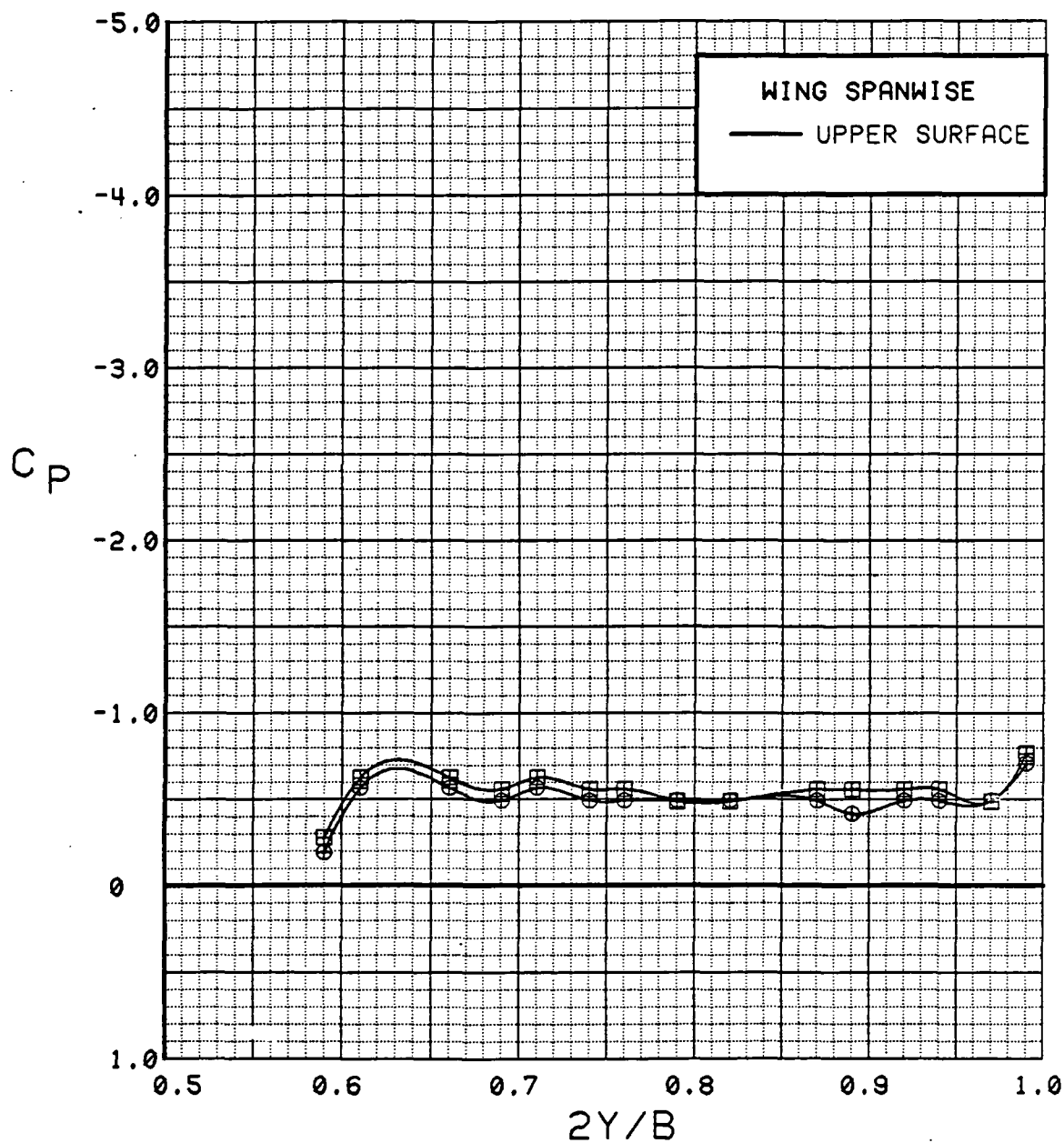


Figure 3.2.4-69 Canard On/Off Effects, Spanwise, Power Off, Flaps Deflected, Alpha = 4 deg

SYM	TEST	RUN	ALPHA	CT	ITEF	OTEF	CAN	SWB
⊕	543	11	8.5	0.00	30	30	0	OFF
⊞	537	69	8.5	0.00	30	30	OFF	OFF

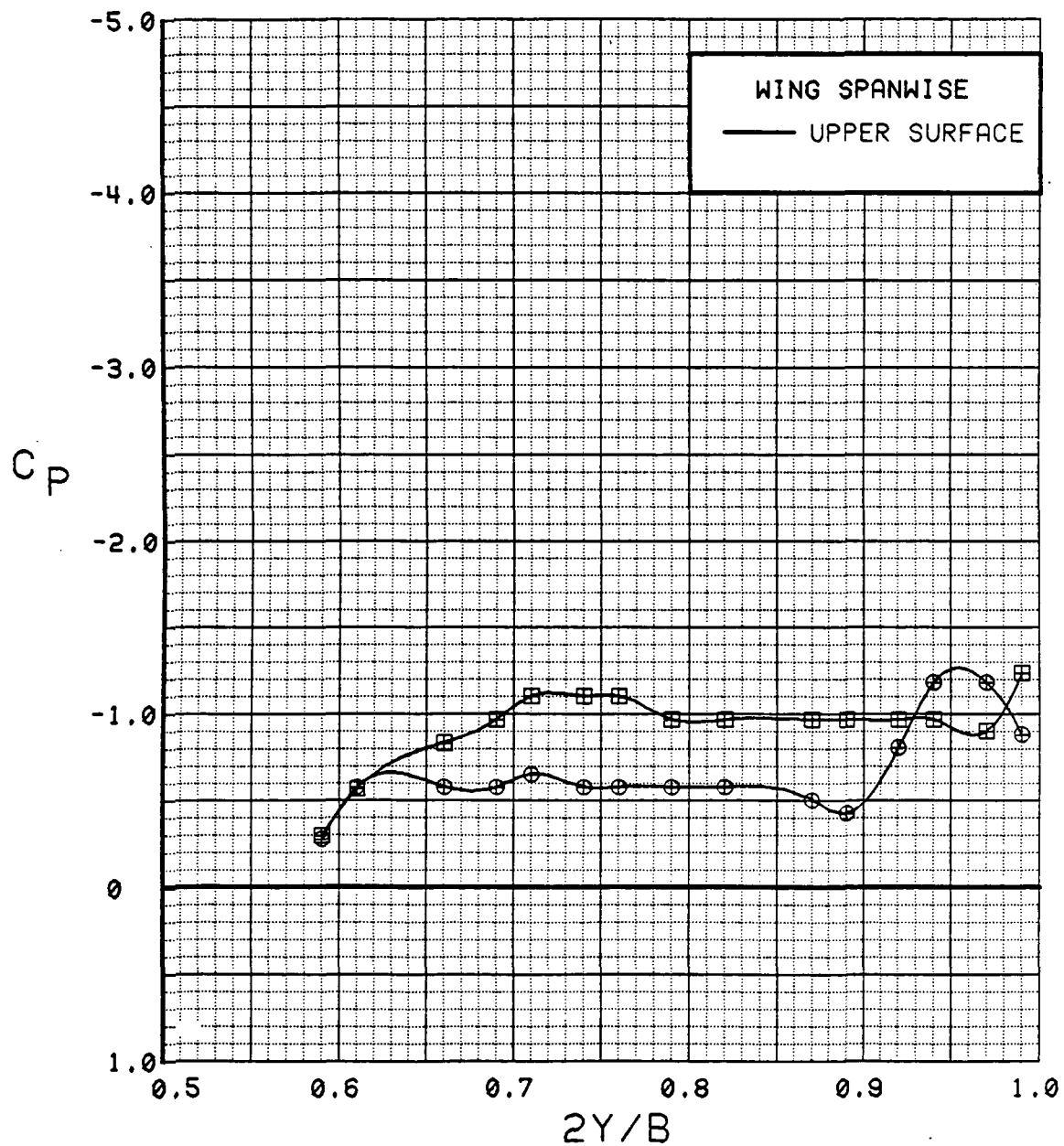


Figure 3.2.4-70

Canard On/Off Effects, Spanwise, Power Off,  
Flaps Deflected, Alpha = 8 deg

SYM	TEST	RUN	ALPHA	CT	ITEF	OTEF	CAN	SWB
⊕	543	11	12.7	0.00	30	30	0	OFF
⊞	537	69	12.5	0.00	30	30	OFF	OFF

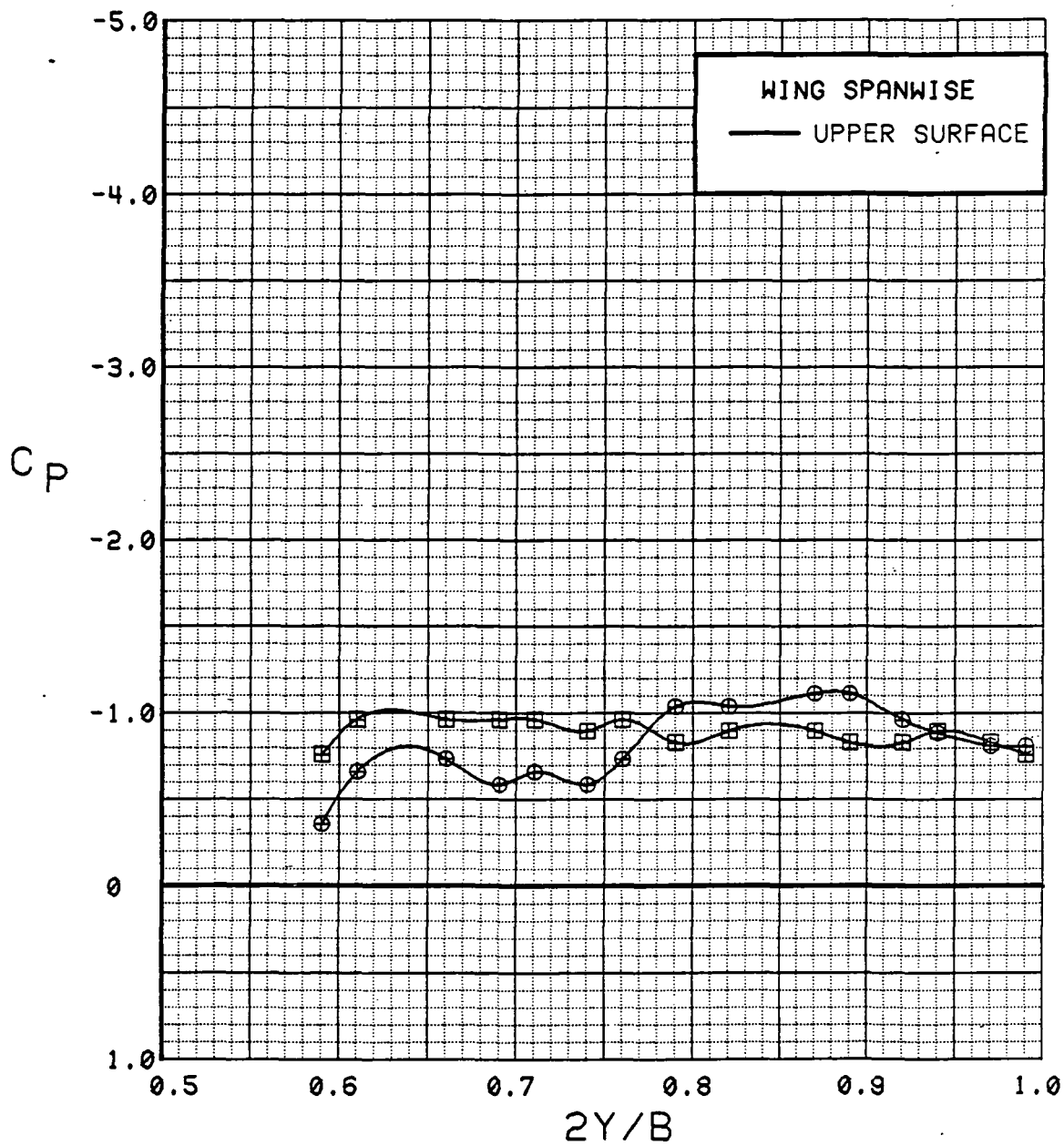


Figure 3.2.4-71 Canard On/Off Effects, Spanwise, Power Off, Flaps Deflected, Alpha = 12 deg

SYM	TEST	RUN	ALPHA	CT	ITEF	OTEF	CAN	SWB
●	543	11	16.8	0.00	30	30	0	OFF
■	537	69	16.6	0.00	30	30	OFF	OFF

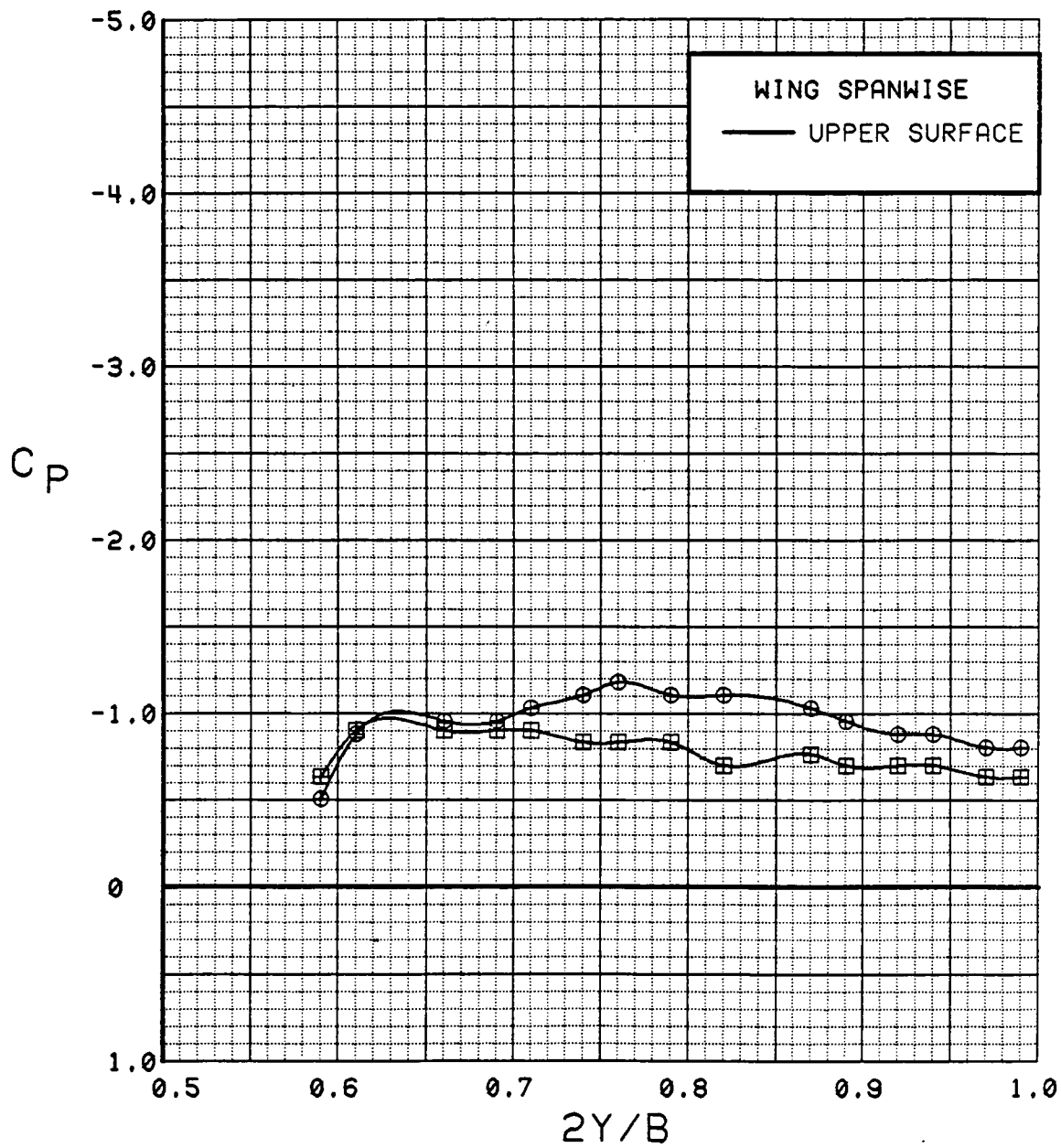


Figure 3.2.4-72 Canard On/Off Effects, Spanwise, Power Off, Flaps Deflected, Alpha = 16 deg

SYM	TEST	RUN	ALPHA	CT	ITEF	OTEF	CAN	SWB
●	543	11	20.8	0.00	30	30	0	OFF
■	537	69	20.6	0.00	30	30	OFF	OFF

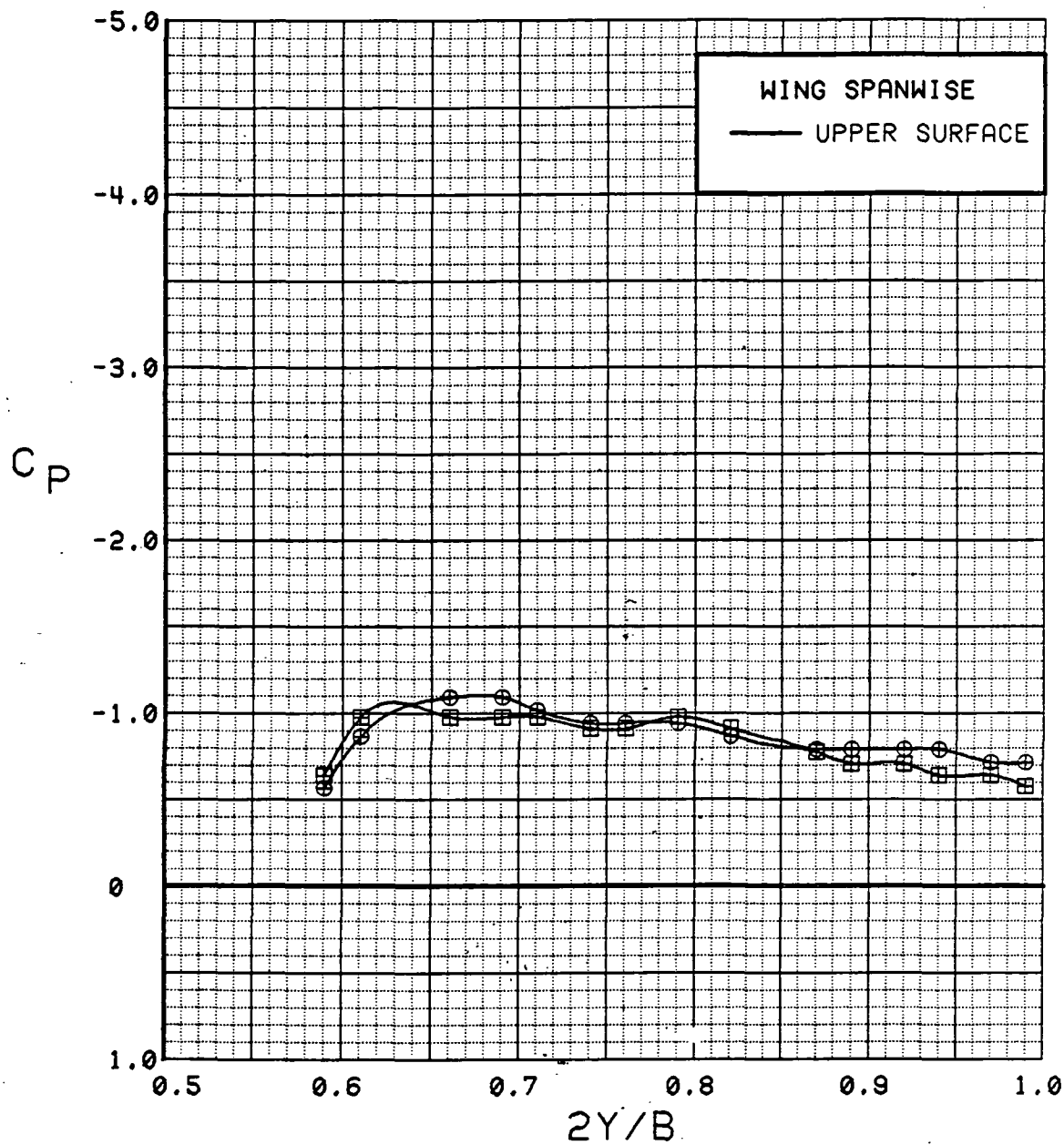


Figure 3.2.4-73 Canard On/Off Effects, Spanwise, Power Off, Flaps Deflected, Alpha = 20 deg

SYM	TEST	RUN	ALPHA	CT	ITEF	OTEF	CAN	SWB
●	543	11	24.9	0.00	30	30	0	OFF
■	537	69	24.7	0.00	30	30	OFF	OFF

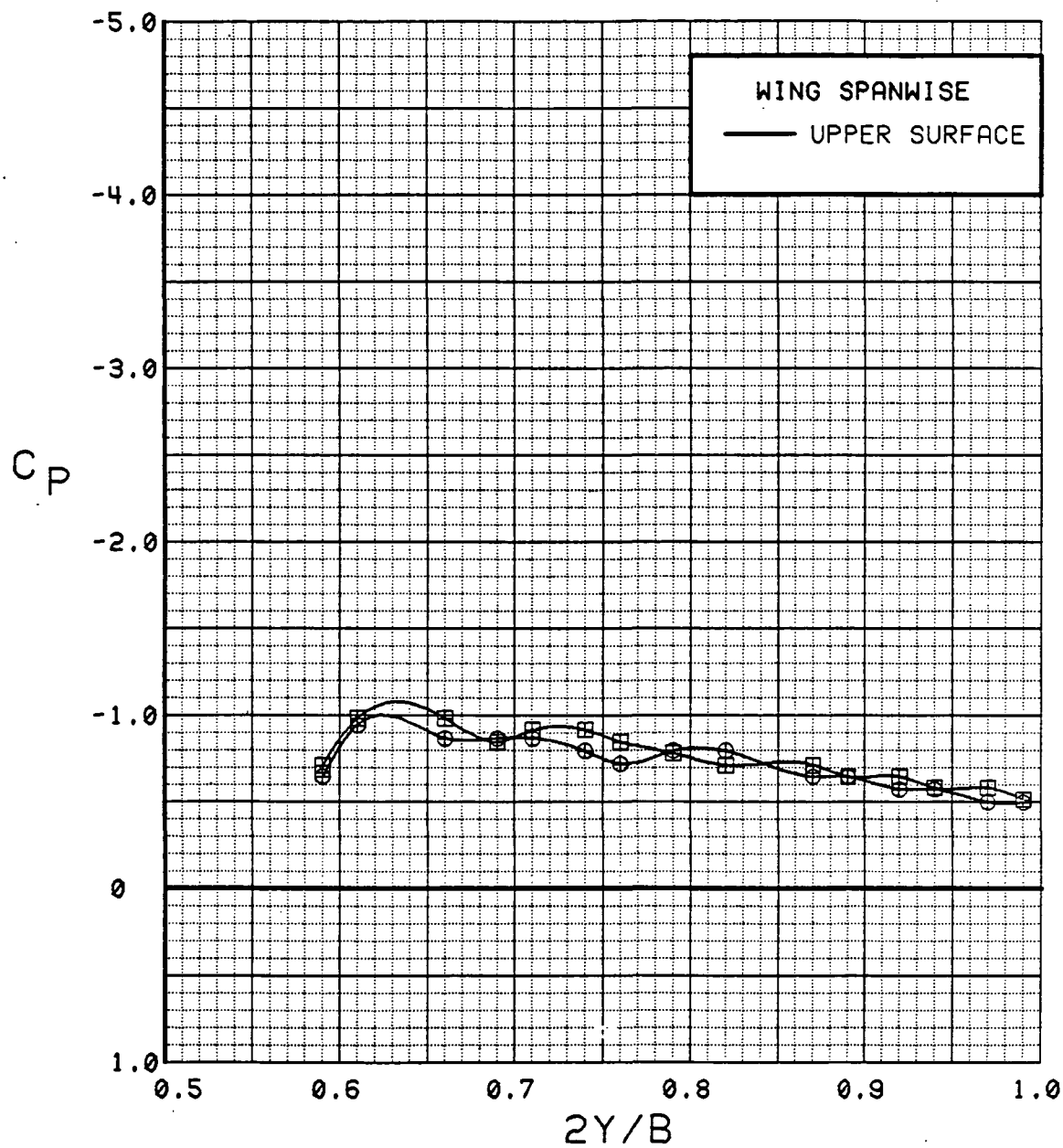


Figure 3.2.4-74 Canard On/Off Effects, Spanwise, Power Off, Flaps Deflected, Alpha = 24 deg

SYM	TEST	RUN	ALPHA	CT	ITEF	OTEF	CAN	SWB
●	543	11	28.9	0.00	30	30	0	OFF
■	537	69	28.7	0.00	30	30	OFF	OFF

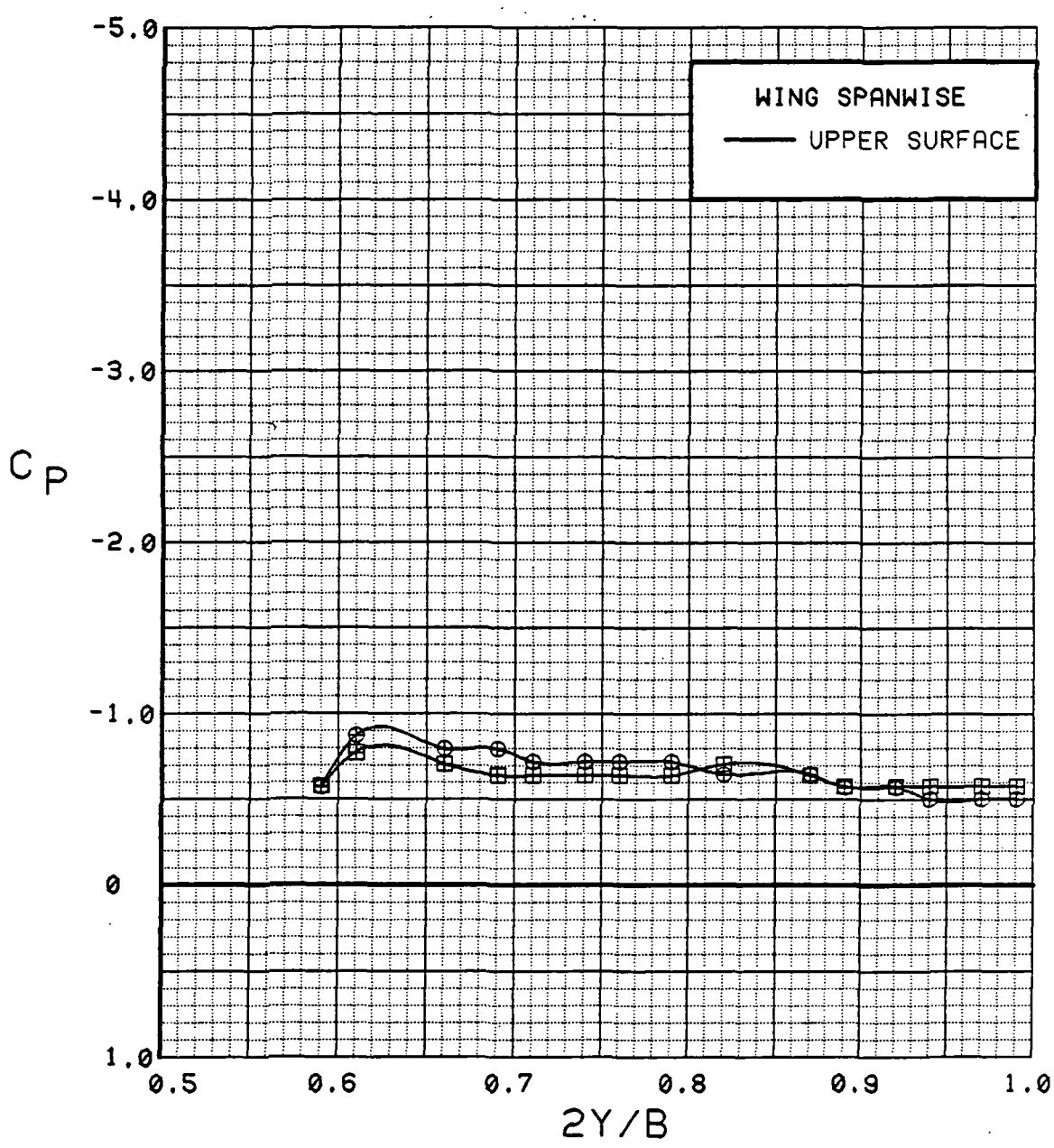


Figure 3.2.4-75 Canard On/Off Effects, Spanwise, Power Off, Flaps Deflected, Alpha = 28 deg



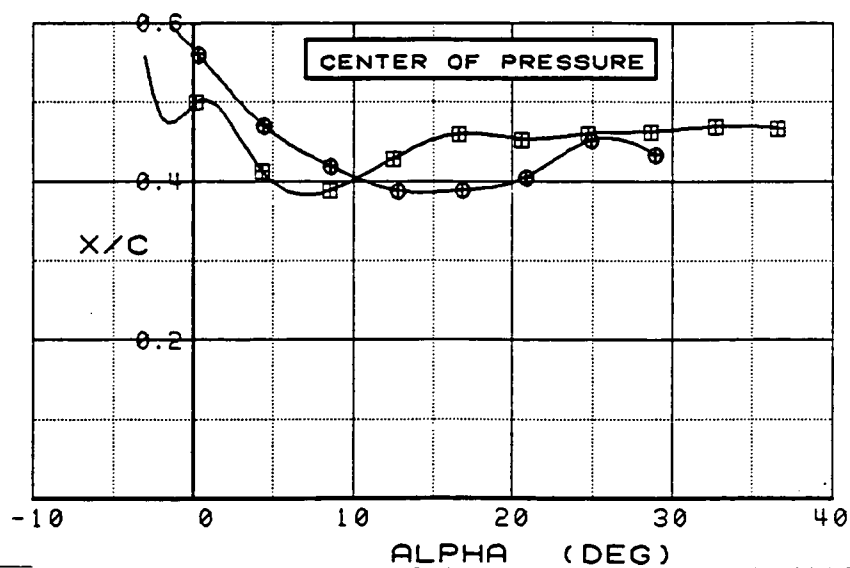
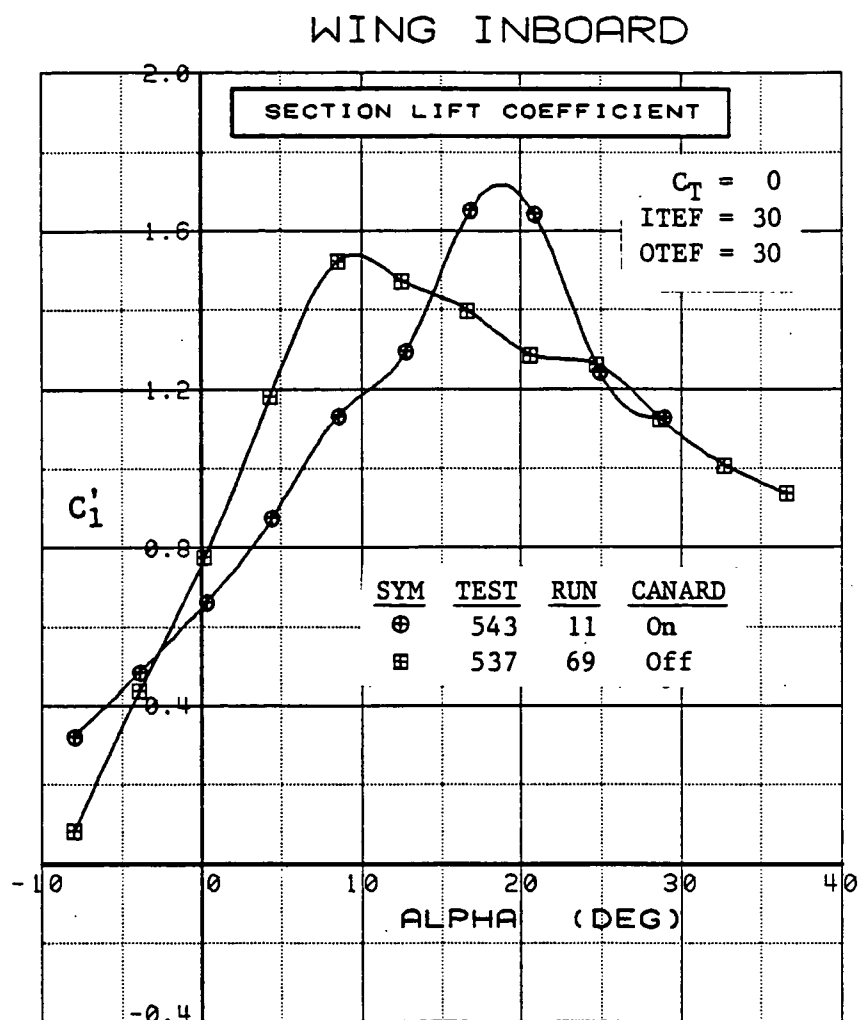


Figure 3.2.4-76

Canard On/Off Effects, Inboard, Power Off,  
Flaps Deflected, Integrated Section Properties

# WING OUTBOARD

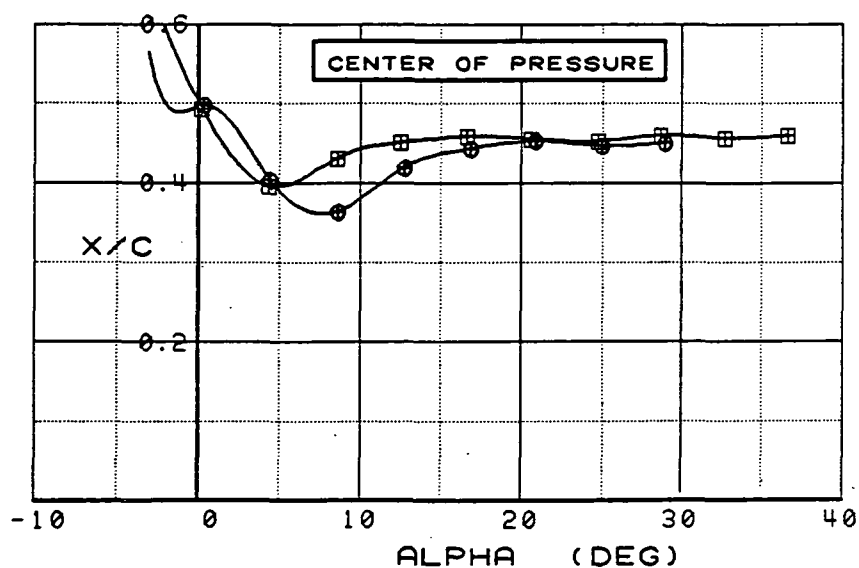
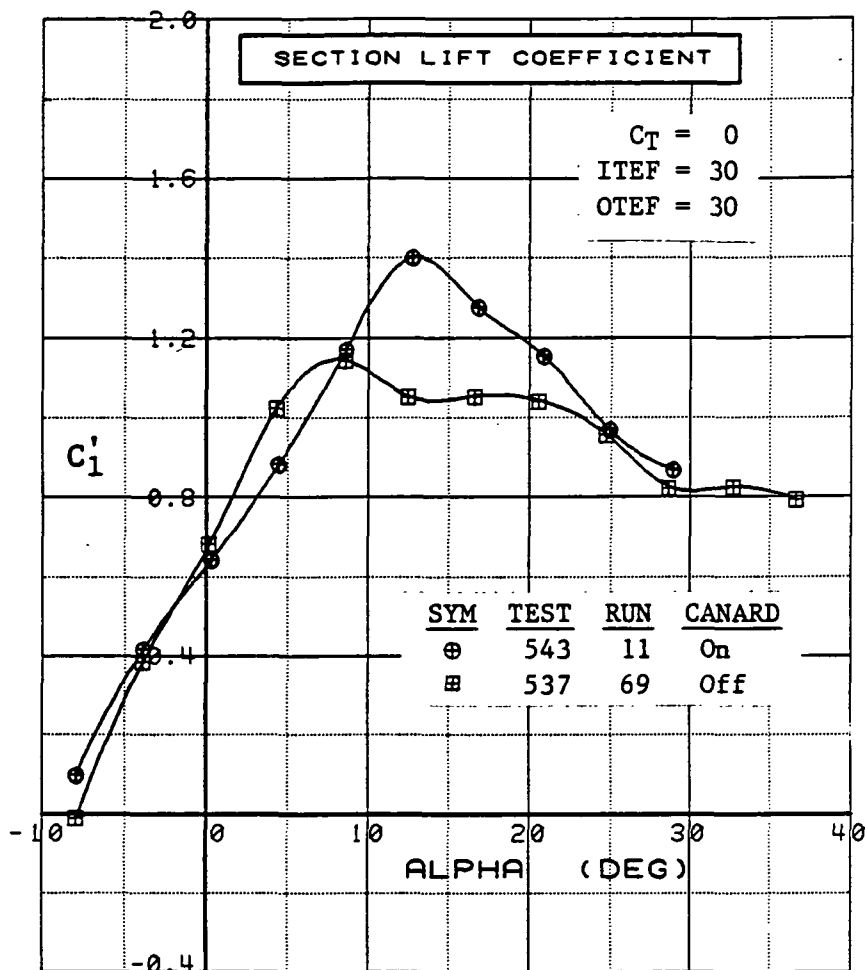


Figure 3.2.4-77 Canard On/Off Effects, Outboard, Power Off, Flaps Deflected, Integrated Section Properties

SYM	TEST	RUN	ALPHA	CT	ITEF	OTEF	CAN	SWB
⊕	543	60	0.1	0.94	0	0	0	OFF
⊞	537	72	0.1	0.89	0	0	OFF	OFF

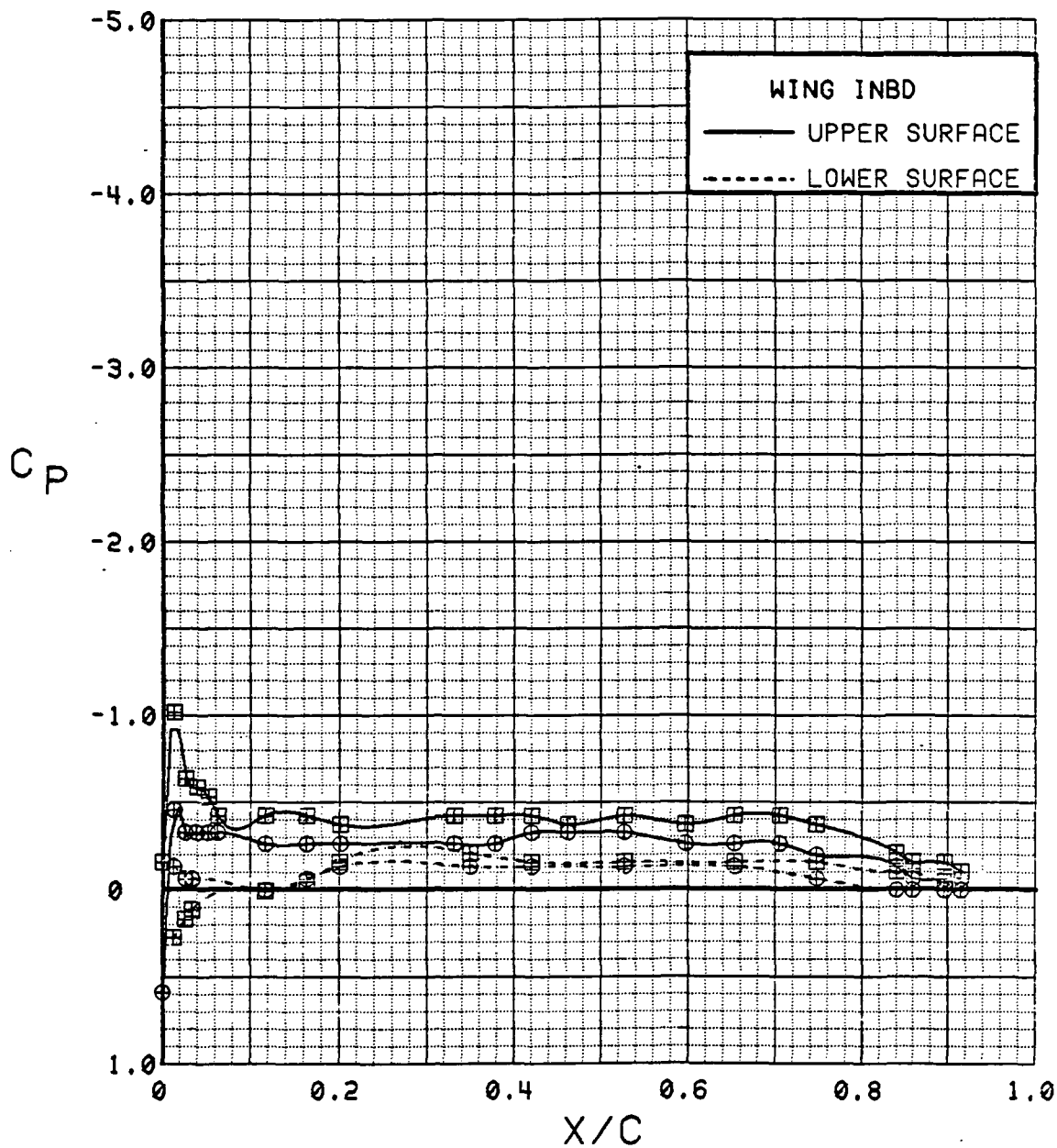


Figure 3.2.4-78 Canard On/Off Effects, Inboard,  $C_T = 0.9$ ,  
Flaps Neutral, Alpha = 0 deg

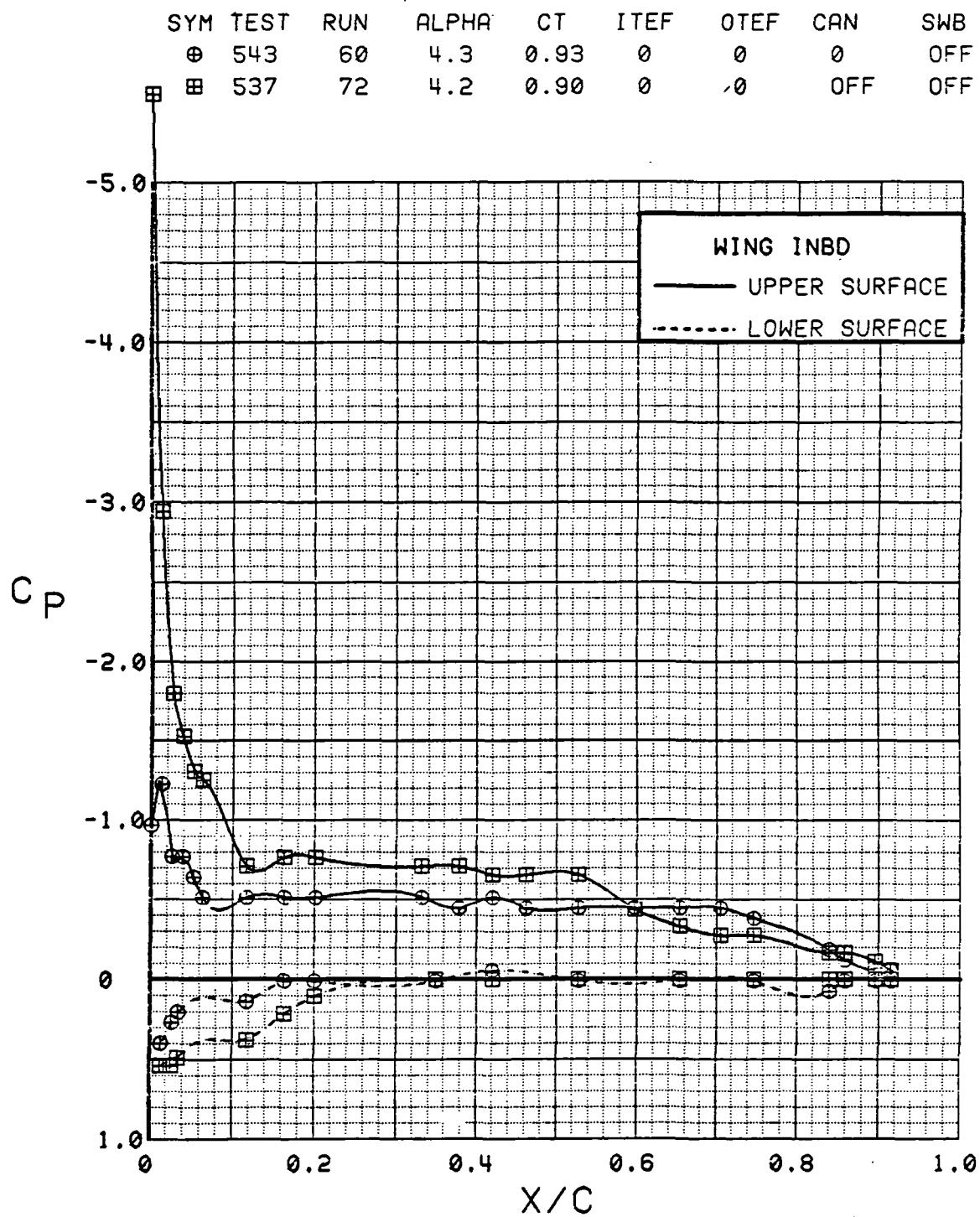


Figure 3.2.4-79

Canard On/Off Effects, Inboard,  $C_T = 0.9$ ,  
Flaps Neutral, Alpha = 4 deg

SYM	TEST	RUN	ALPHA	CT	ITEF	OTEF	CAN	SWB
⊕	543	60	8.4	0.94	0	0	0	OFF
⊞	537	72	8.3	0.92	0	0	OFF	OFF

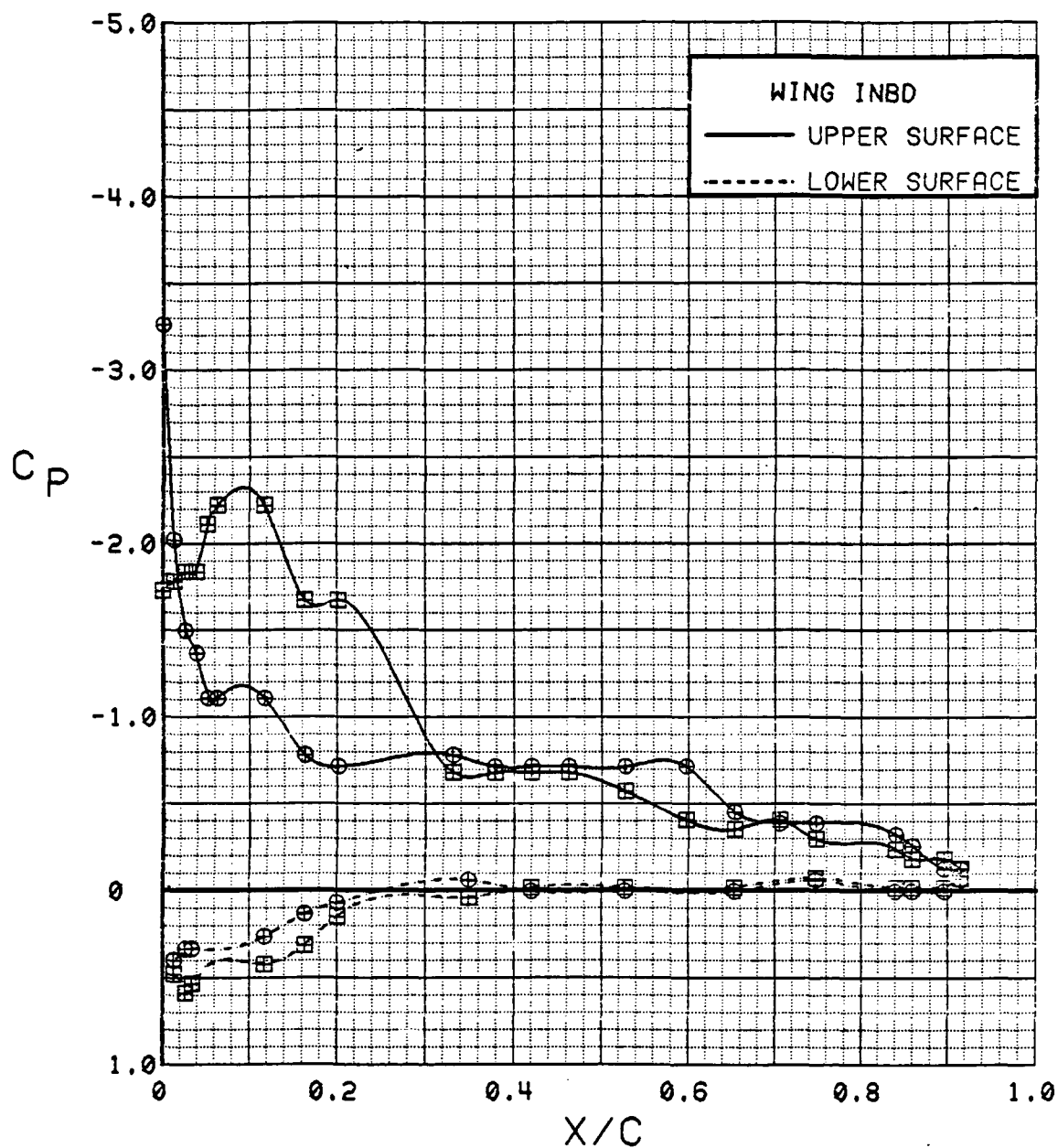


Figure 3.2.4-80

Canard On/Off Effects, Inboard,  $C_T = 0.9$ ,  
Flaps Neutral, Alpha = 8 deg

$$\oplus C_p = -9.48$$

SYM	TEST	RUN	ALPHA	CT	ITEF	OTEF	CAN	SWB
$\oplus$	543	60	12.5	0.94	0	0	0	OFF
$\boxplus$	537	72	12.4	0.91	0	0	OFF	OFF

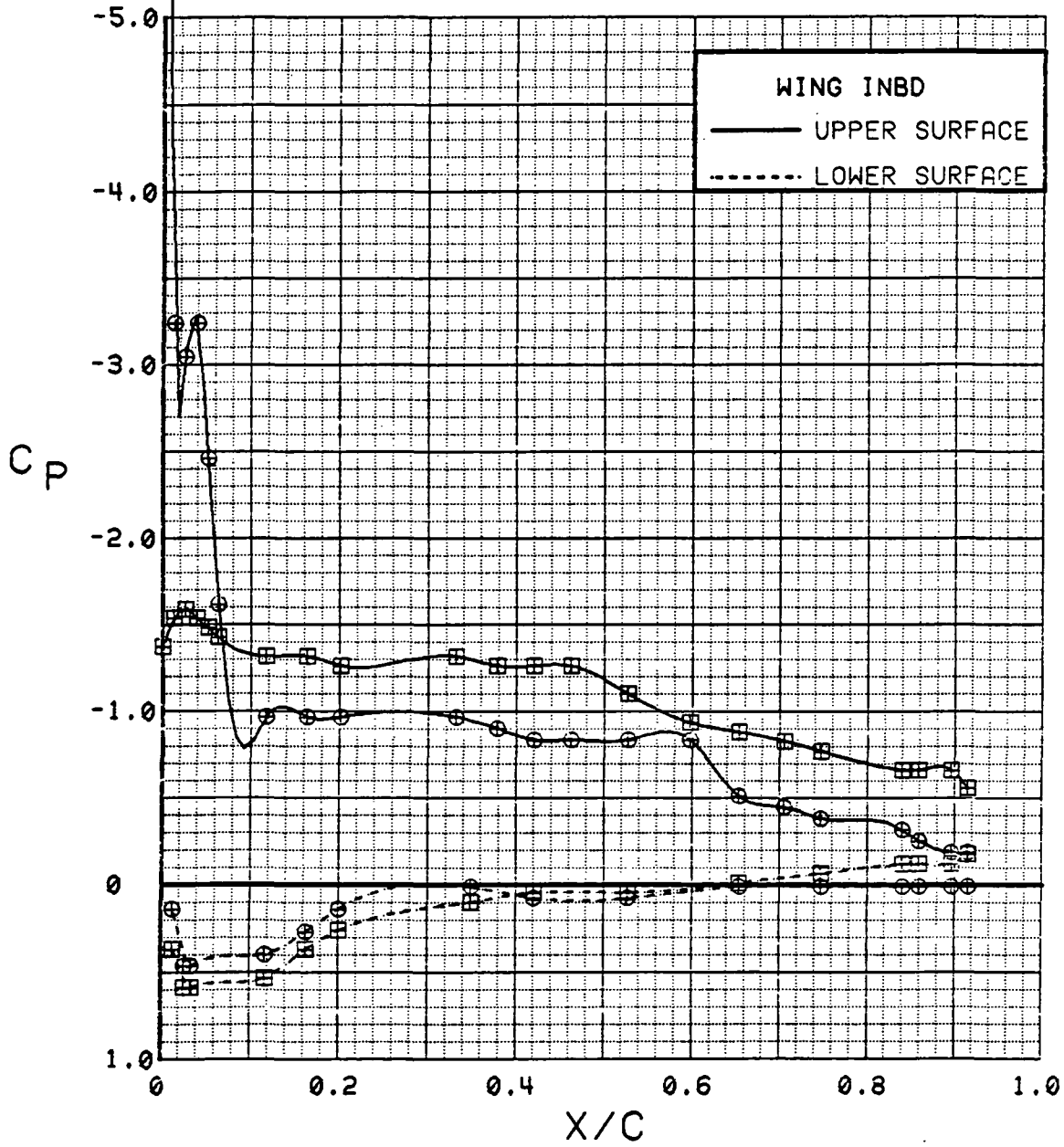


Figure 3.2.4-81 Canard On/Off Effects, Inboard,  $C_T = 0.9$ , Flaps Neutral,  $\alpha = 12$  deg

SYM	TEST	RUN	ALPHA	CT	ITEF	OTEF	CAN	SWB
⊕	543	60	16.7	0.93	0	0	0	OFF
⊞	537	72	16.5	0.91	0	0	OFF	OFF

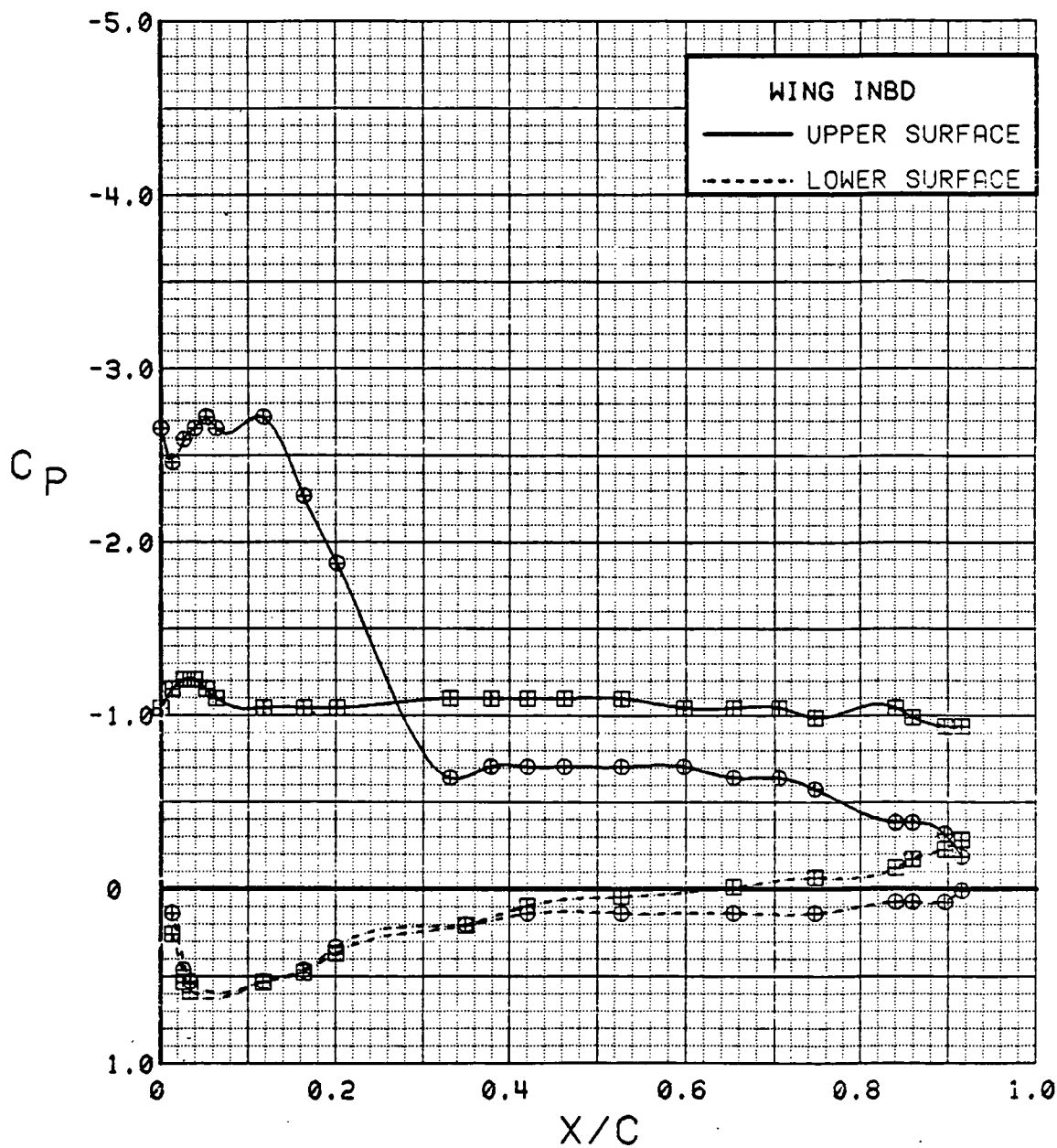


Figure 3.2.4-82 Canard On/Off Effects, Inboard,  $C_T = 0.9$ , Flaps Neutral, Alpha = 16 deg

SYM	TEST	RUN	ALPHA	CT	ITEF	OTEF	CAN	SWB
⊕	543	60	20.8	0.93	0	0	0	OFF
⊞	537	72	20.6	0.93	0	0	OFF	OFF

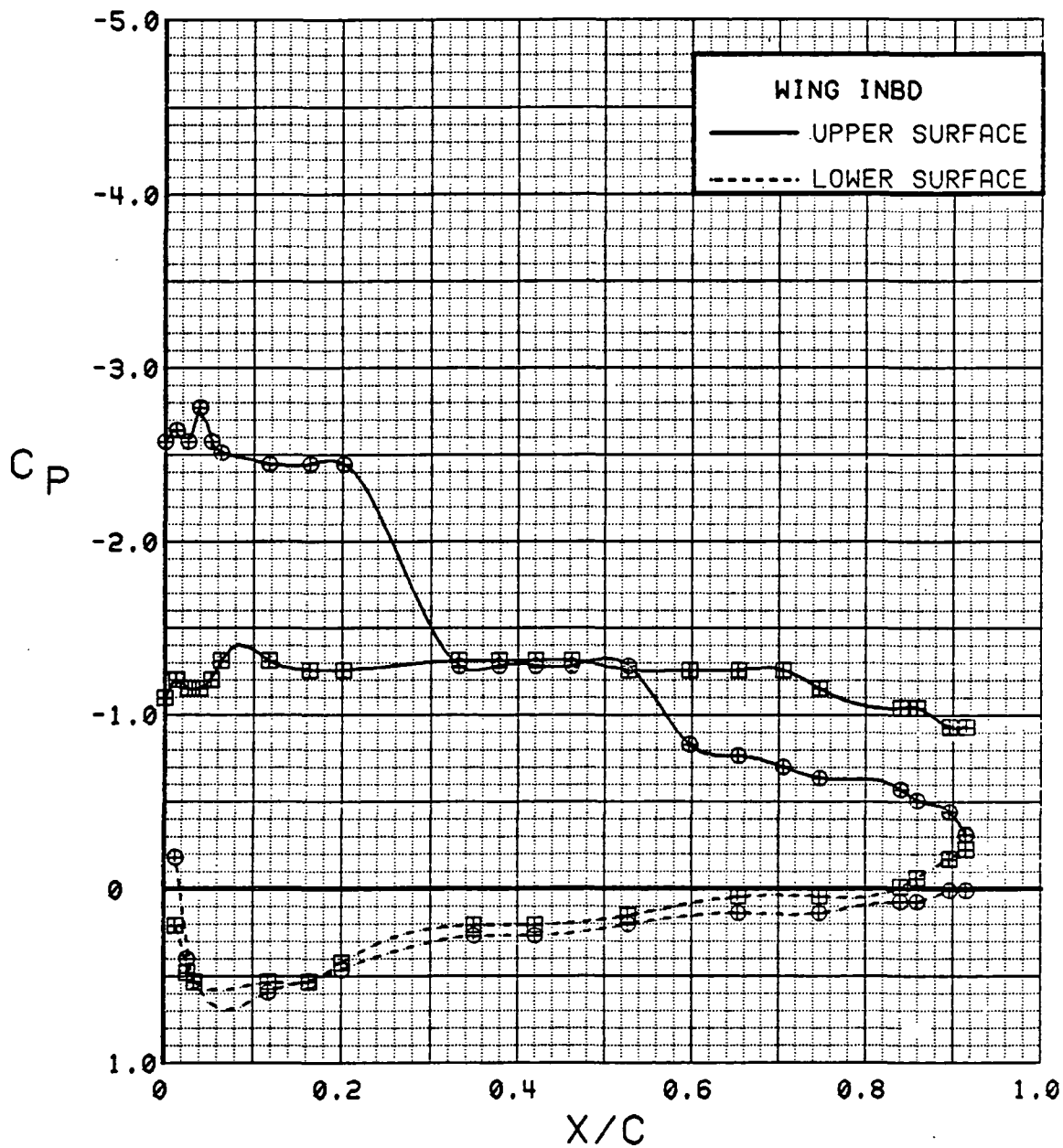


Figure 3.2.4-83

Canard On/Off Effects, Inboard,  $C_T = 0.9$ ,  
Flaps Neutral, Alpha = 20 deg



SYM	TEST	RUN	ALPHA	CT	ITEF	OTEF	CAN	SWB
⊕	543	60	24.9	0.93	0	0	0	OFF
⊞	537	72	24.7	0.91	0	0	OFF	OFF

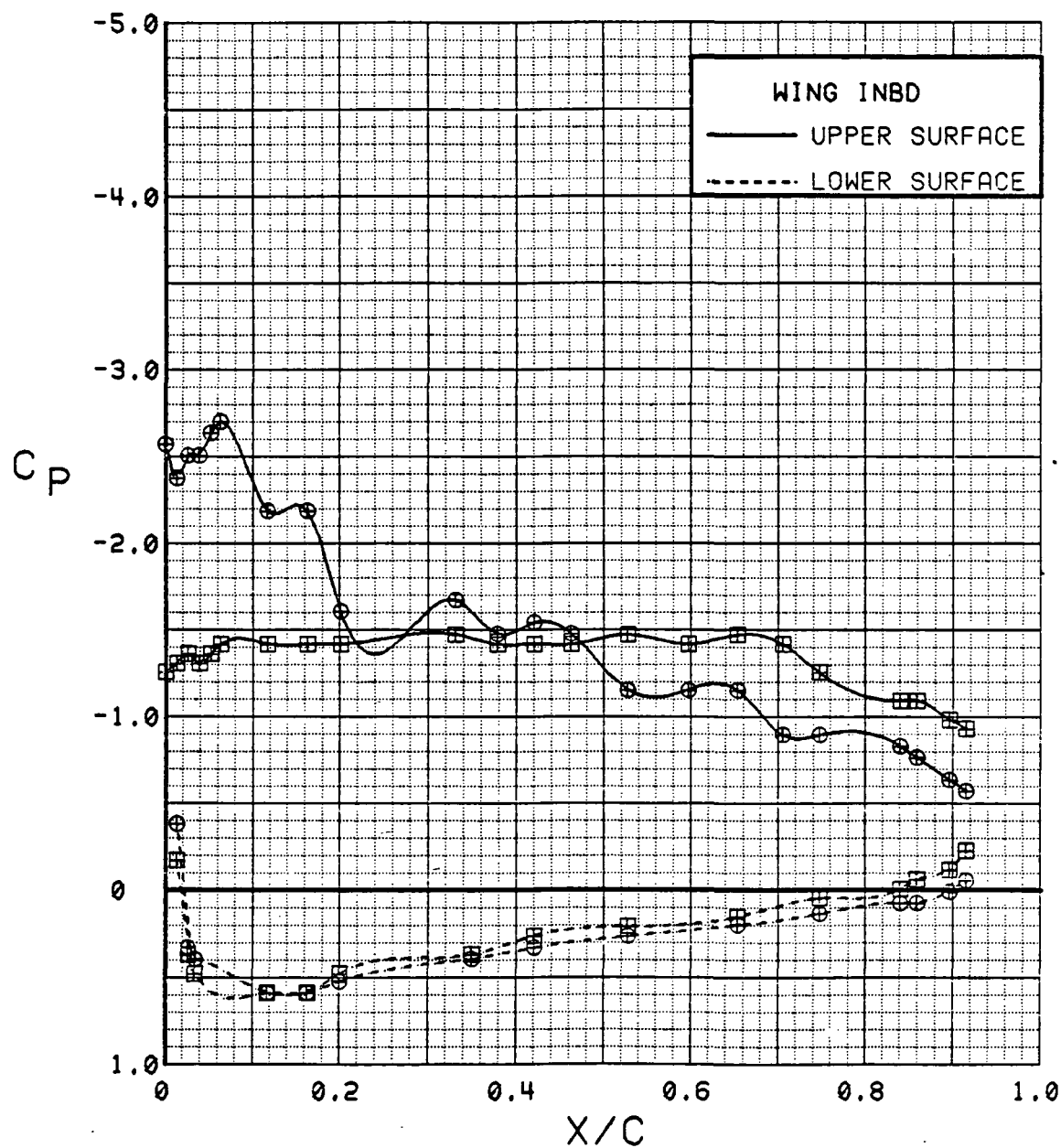


Figure 3.2.4-84 Canard On/Off Effects, Inboard,  $C_T = 0.9$ , Flaps Neutral, Alpha = 24 deg

SYM	TEST	RUN	ALPHA	CT	ITEF	OTEF	CAN	SWB
⊕	543	60	29.0	0.93	0	0	0	OFF
⊞	537	72	28.8	0.91	0	0	OFF	OFF

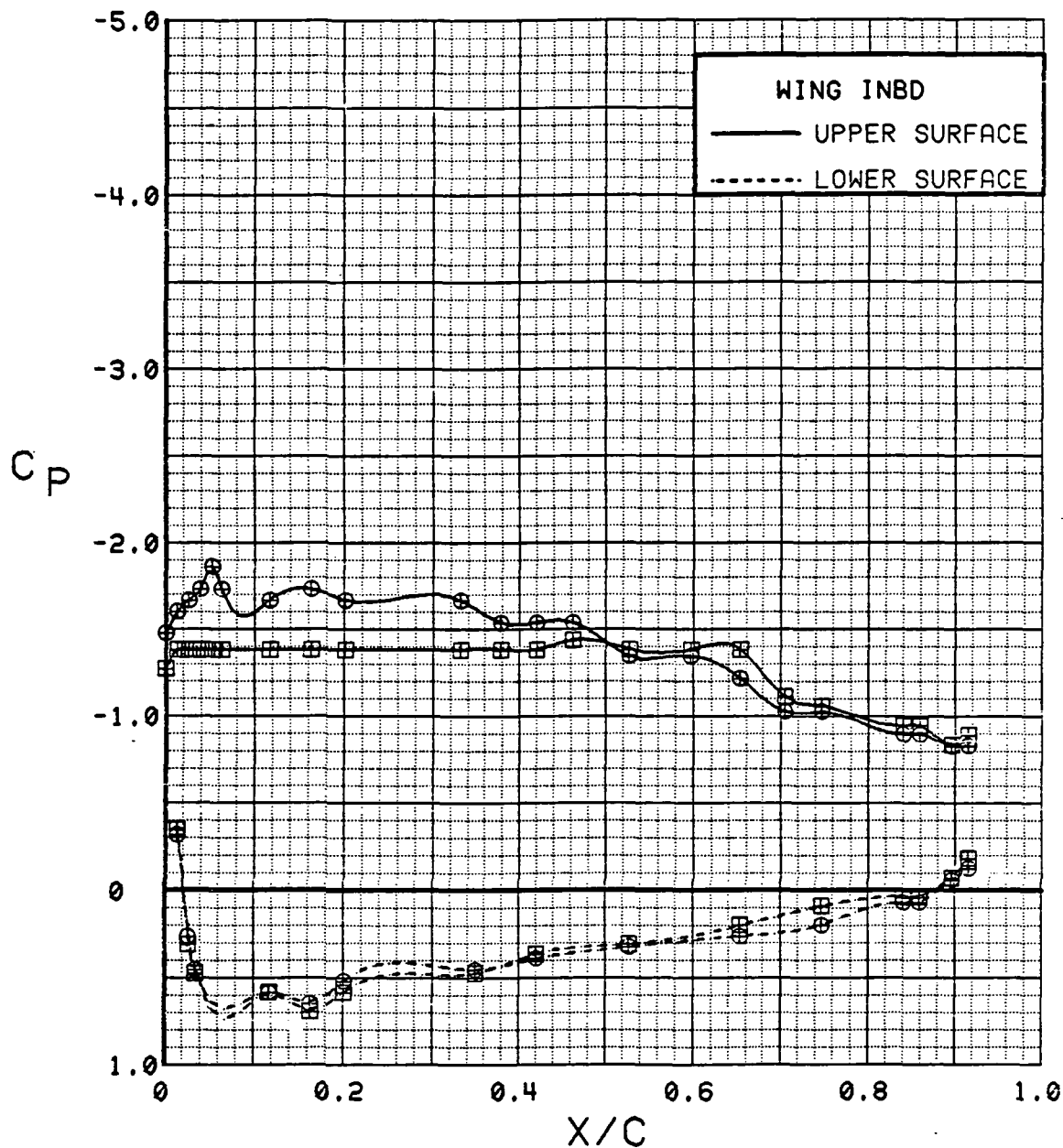


Figure 3.2.4-85 Canard On/Off Effects, Inboard,  $C_T = 0.9$ , Flaps Neutral,  $\alpha = 28$  deg

SYM	TEST	RUN	ALPHA	CT	ITEF	OTEF	CAN	SWB
⊕	543	60	33.1	0.94	0	0	0	OFF
⊞	537	72	32.9	0.92	0	0	OFF	OFF

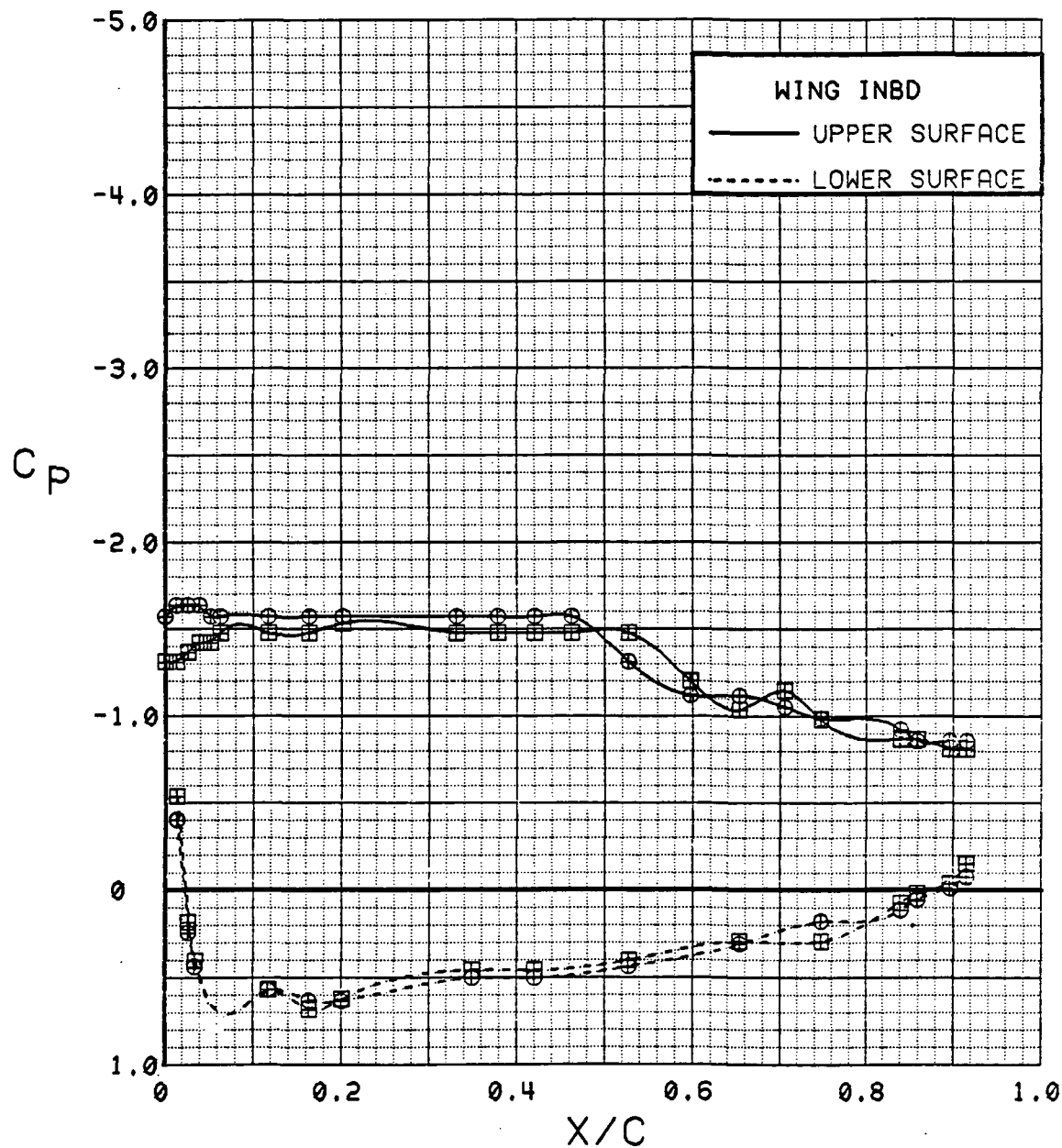


Figure 3.2.4-86 Canard On/Off Effects, Inboard,  $C_T = 0.9$ , Flaps Neutral, Alpha = 32 deg

SYM	TEST	RUN	ALPHA	CT	ITEF	OTEF	CAN	SWB
⊕	543	60	37.1	0.93	0	0	0	OFF
⊞	537	72	36.9	0.92	0	0	OFF	OFF

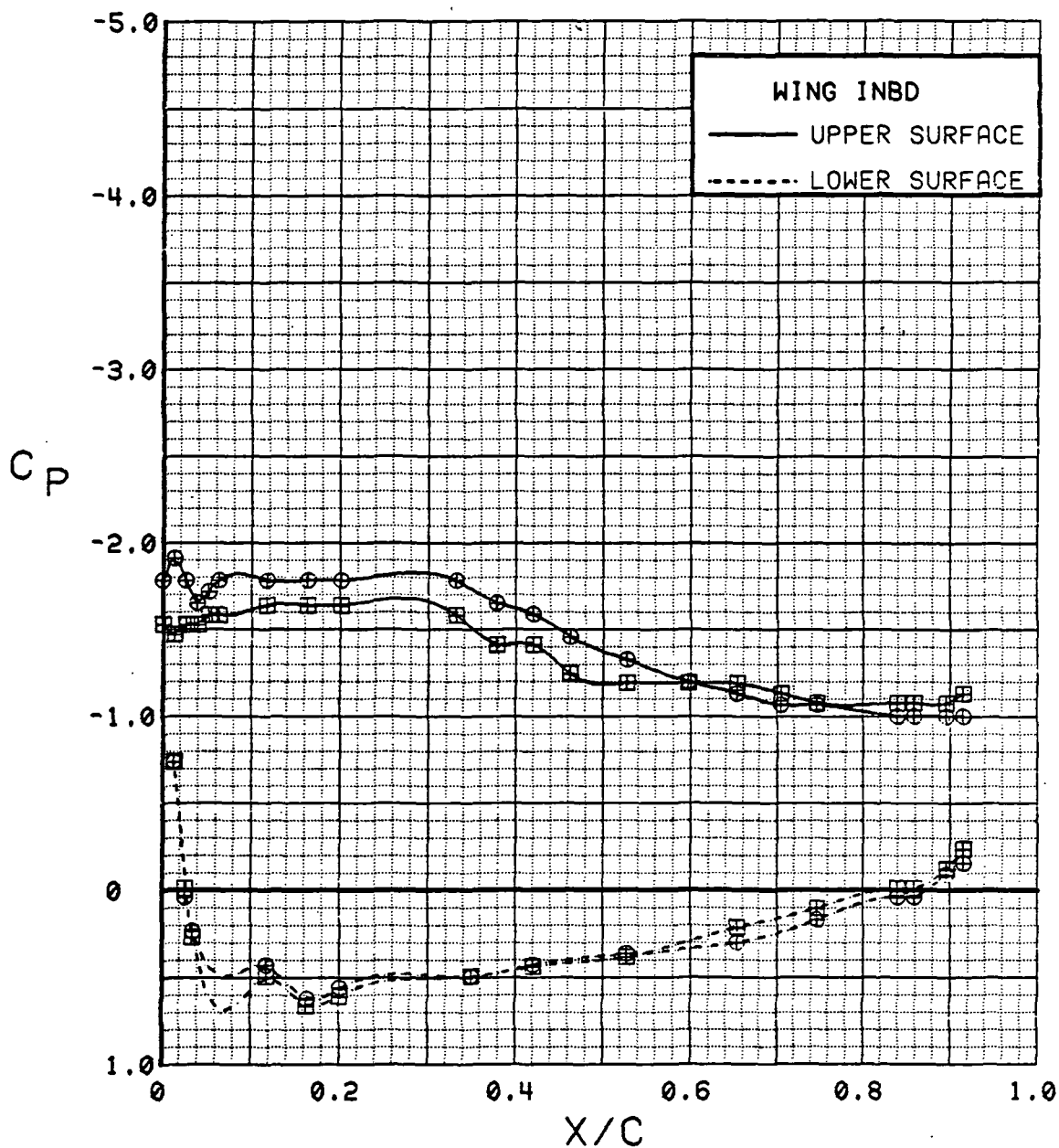


Figure 3.2.4-87

Canard On/Off Effects, Inboard,  $CT = 0.9$ ,  
Flaps Neutral,  $\alpha = 36$  deg

SYM	TEST	RUN	ALPHA	CT	ITEF	OTEF	CAN	SWB
⊕	543	60	0.1	0.94	0	0	0	OFF
⊞	537	72	0.1	0.89	0	0	OFF	OFF

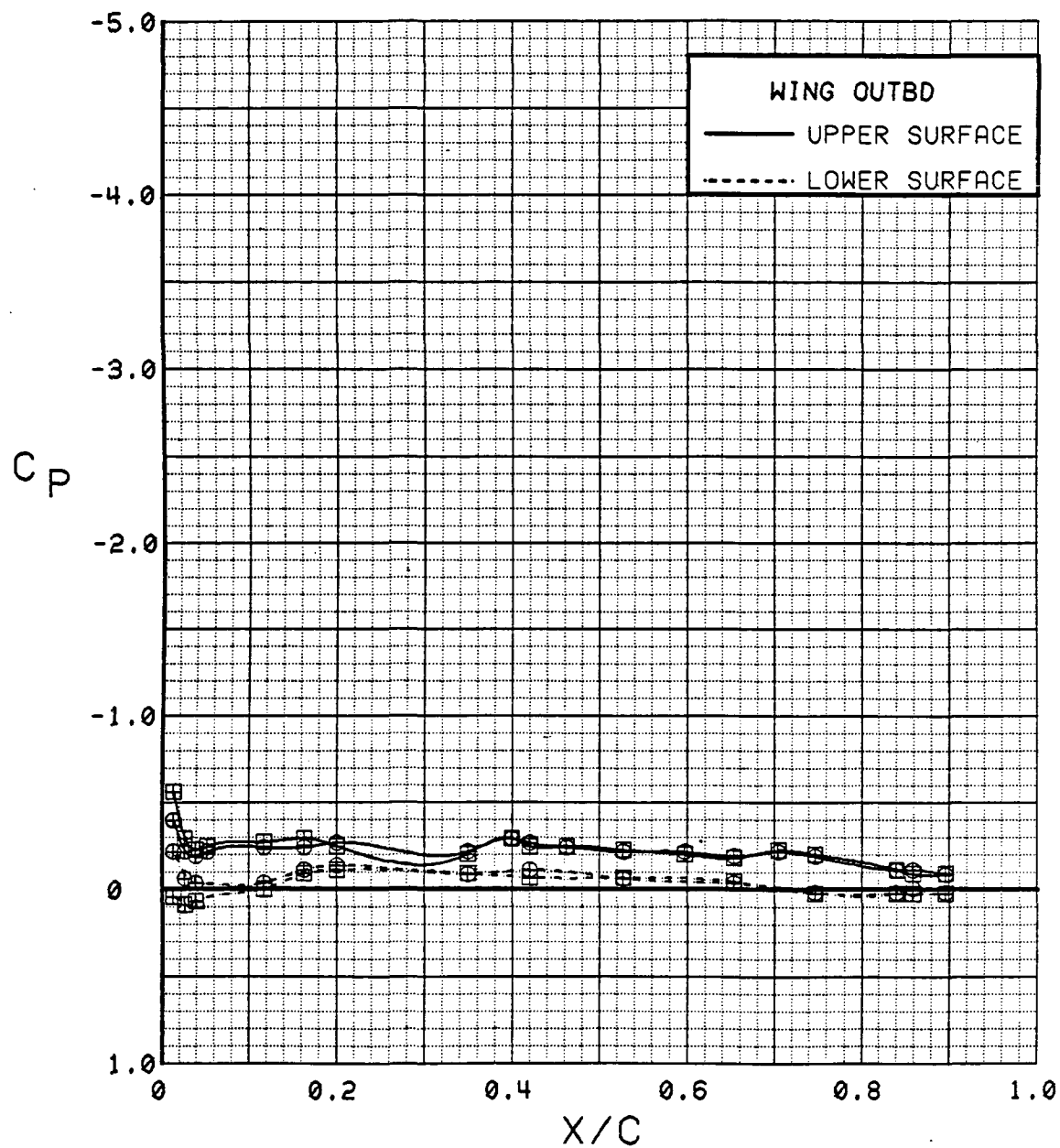


Figure 3.2.4-88 Canard On/Off Effects, Outboard,  $C_T = 0.9$ , Flaps Neutral, Alpha = 0 deg

SYM	TEST	RUN	ALPHA	CT	ITEF	OTEF	CAN	SWB
⊕	543	60	4.3	0.93	0	0	0	OFF
⊞	537	72	4.2	0.90	0	0	OFF	OFF

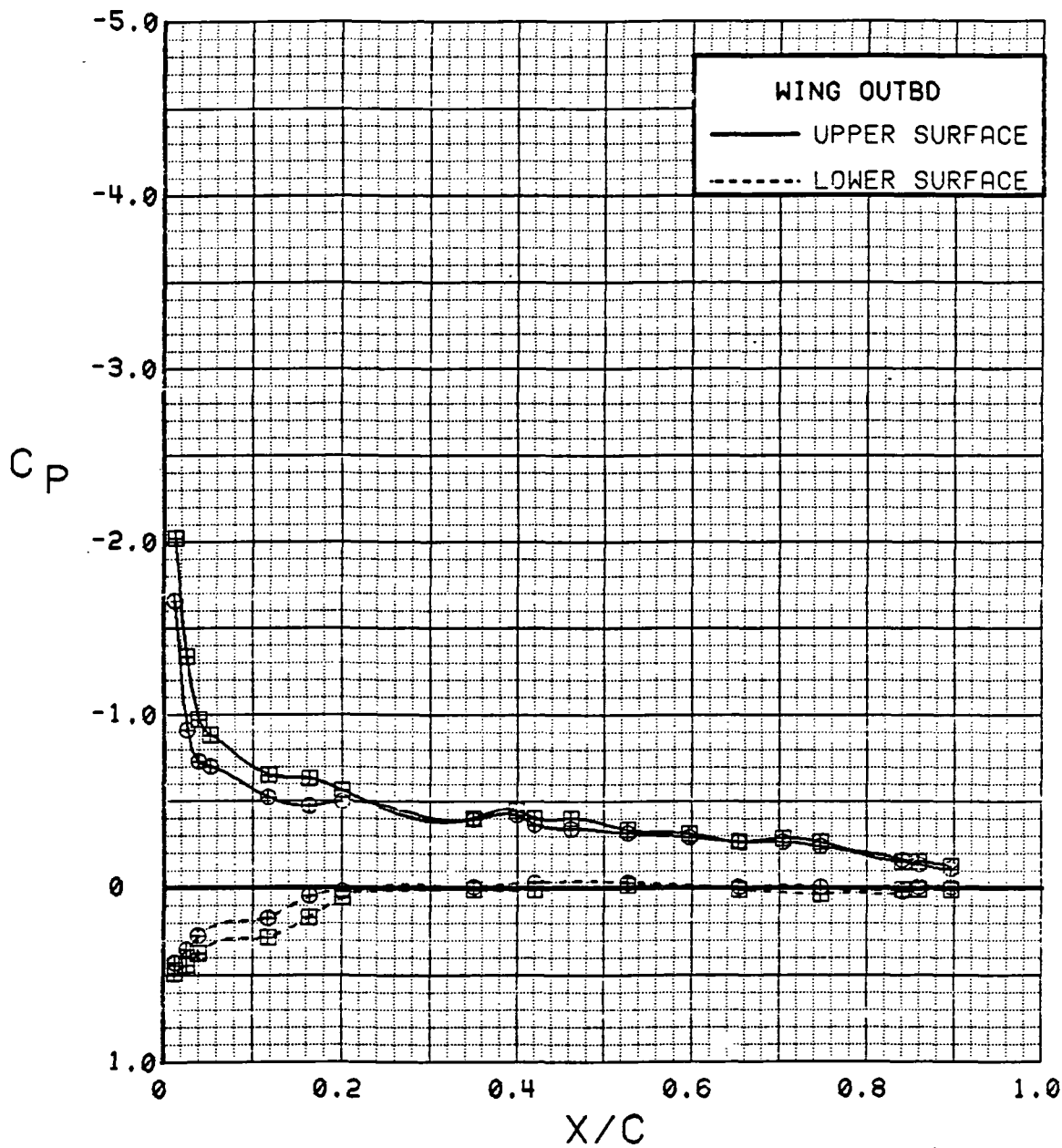


Figure 3.2.4-89 Canard On/Off Effects, Outboard,  $C_T = 0.9$ , Flaps Neutral, Alpha = 4 deg

SYM	TEST	RUN	ALPHA	CT	ITEF	OTEF	CAN	SWB
⊕	543	60	8.4	0.94	0	0	0	OFF
⊞	537	72	8.3	0.92	0	0	OFF	OFF

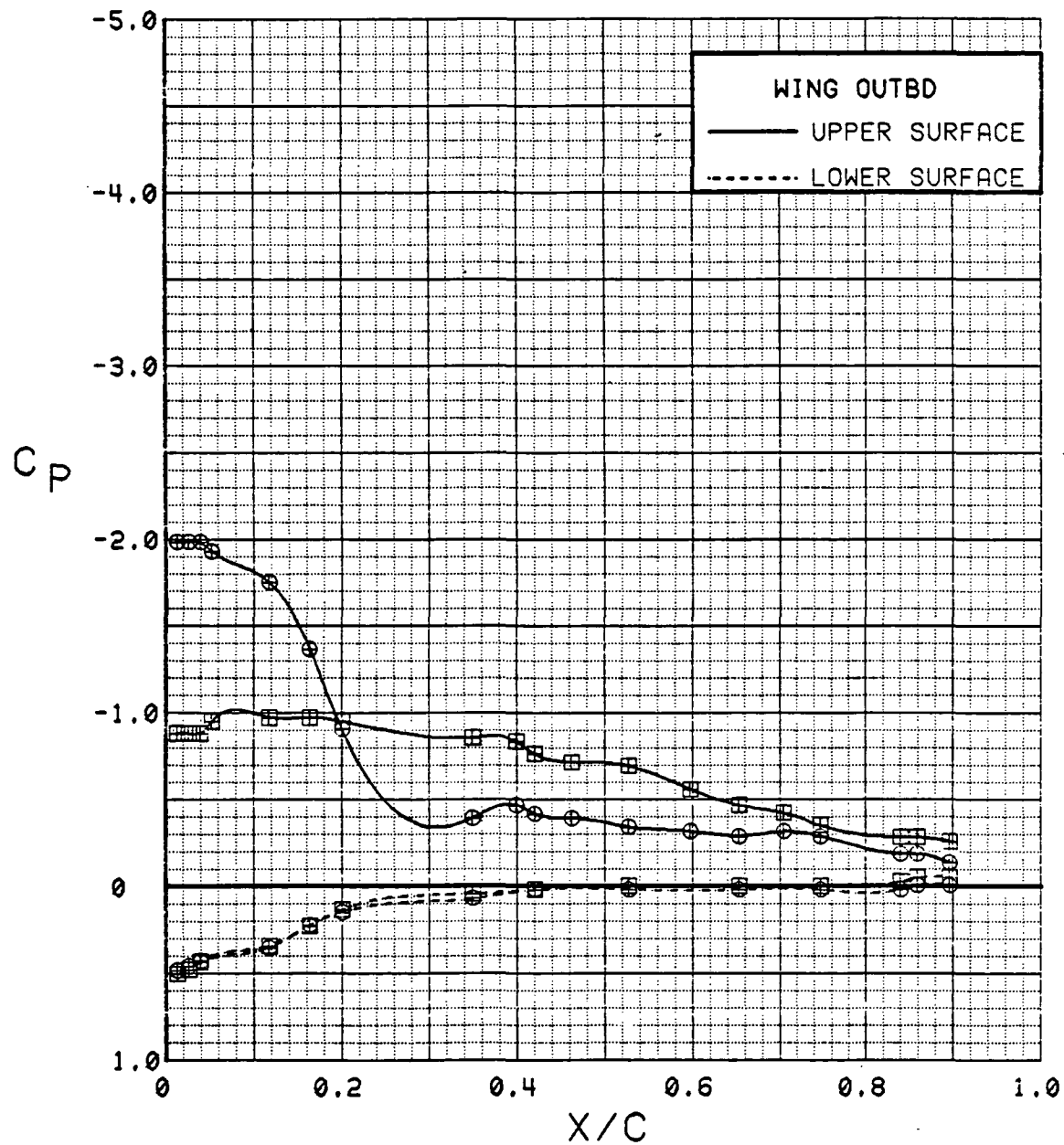


Figure 3.2.4-90 Canard On/Off Effects, Outboard,  $C_T = 0.9$ , Flaps Neutral, Alpha = 8 deg

SYM	TEST	RUN	ALPHA	CT	ITEF	OTEF	CAN	SWB
⊕	543	60	12.5	0.94	0	0	0	OFF
⊞	537	72	12.4	0.91	0	0	OFF	OFF

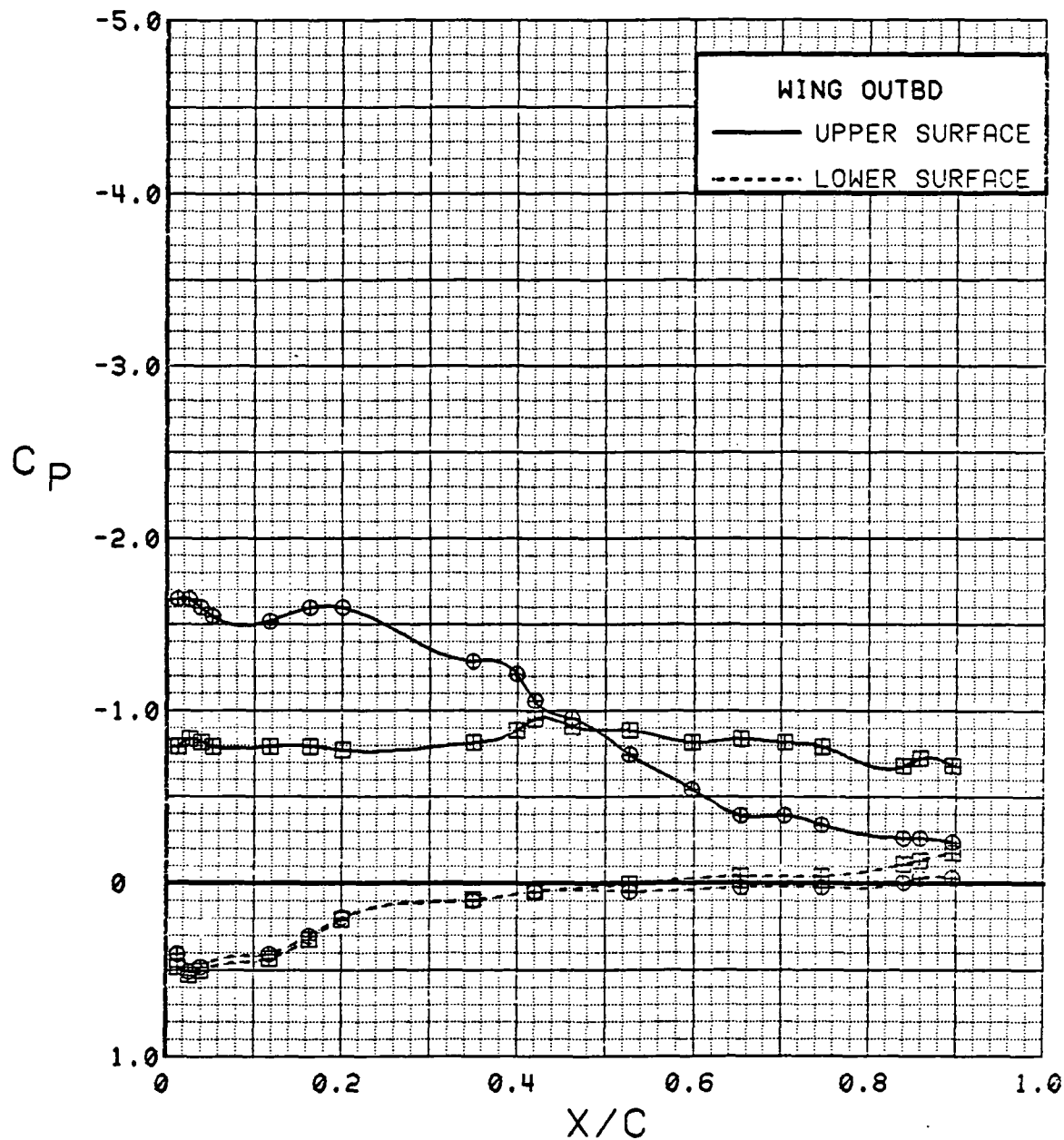


Figure 3.2.4-91

Canard On/Off Effects, Outboard,  $C_T = 0.9$ ,  
Flaps Neutral, Alpha = 12 deg



SYM	TEST	RUN	ALPHA	CT	ITEF	OTEF	CAN	SWB
⊕	543	60	16.7	0.93	0	0	0	OFF
⊞	537	72	16.5	0.91	0	0	OFF	OFF

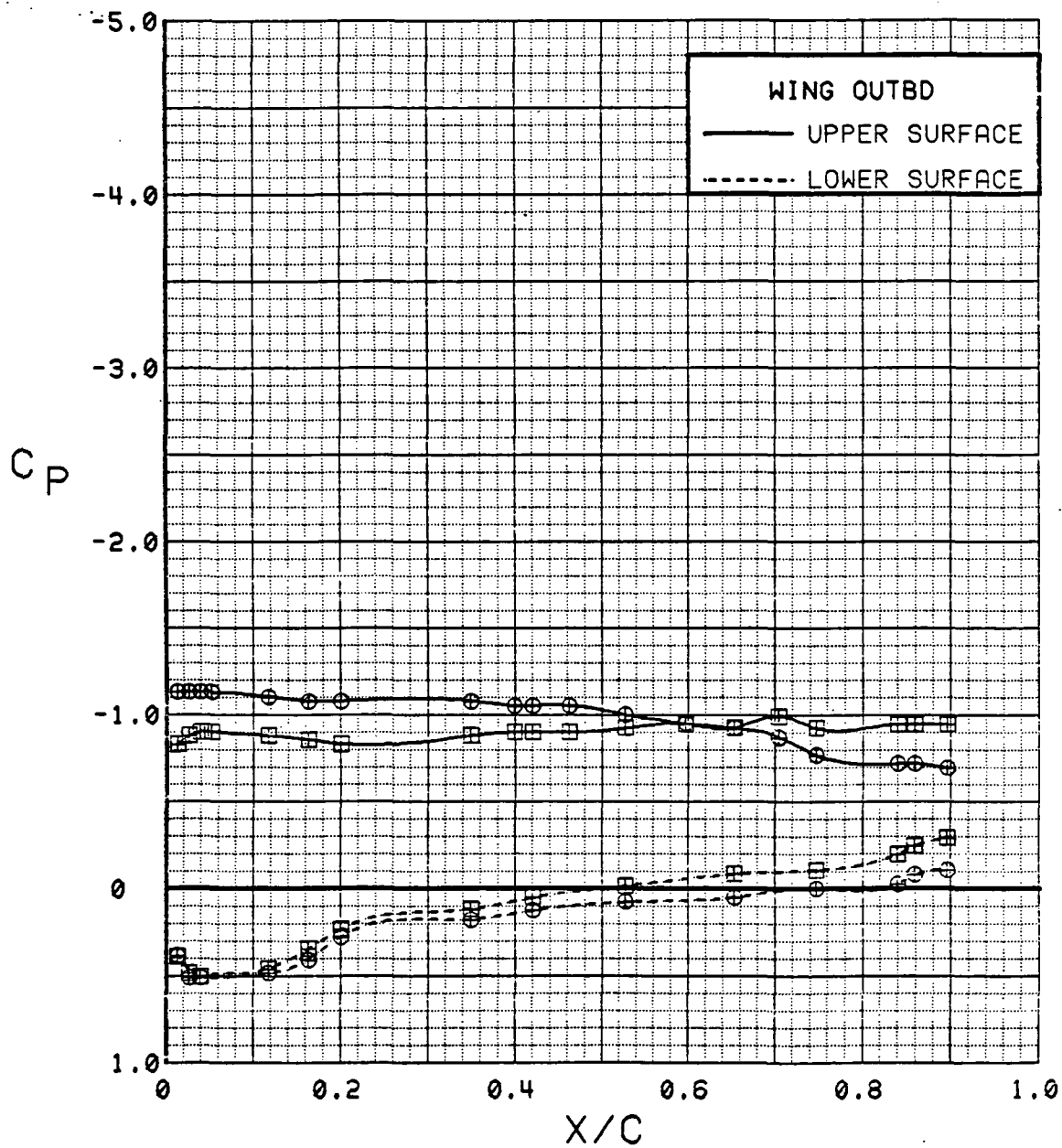


Figure 3.2.4-92 Canard On/Off Effects, Outboard,  $C_T = 0.9$ ,  
Flaps Neutral, Alpha = 16 deg

SYM	TEST	RUN	ALPHA	CT	ITEF	OTEF	CAN	SWB
⊕	543	60	20.8	0.93	0	0	0	OFF
⊞	537	72	20.6	0.93	0	0	OFF	OFF

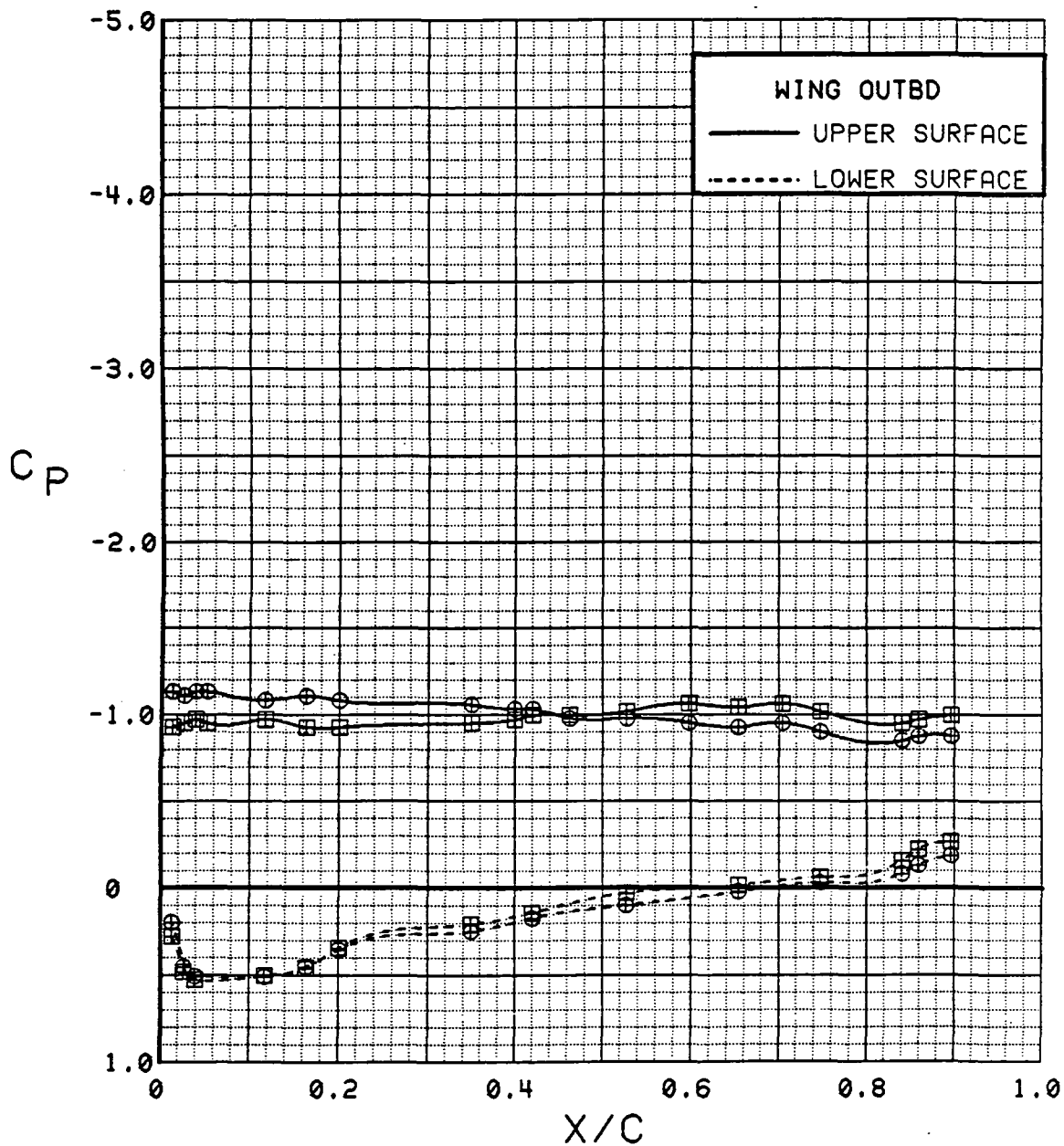


Figure 3.2.4-93 Canard On/Off Effects, Outboard,  $C_T = 0.9$ , Flaps Neutral, Alpha = 20 deg

SYM	TEST	RUN	ALPHA	CT	ITEF	OTEF	CAN	SWB
⊕	543	60	24.9	0.93	0	0	0	OFF
⊞	537	72	24.7	0.91	0	0	OFF	OFF

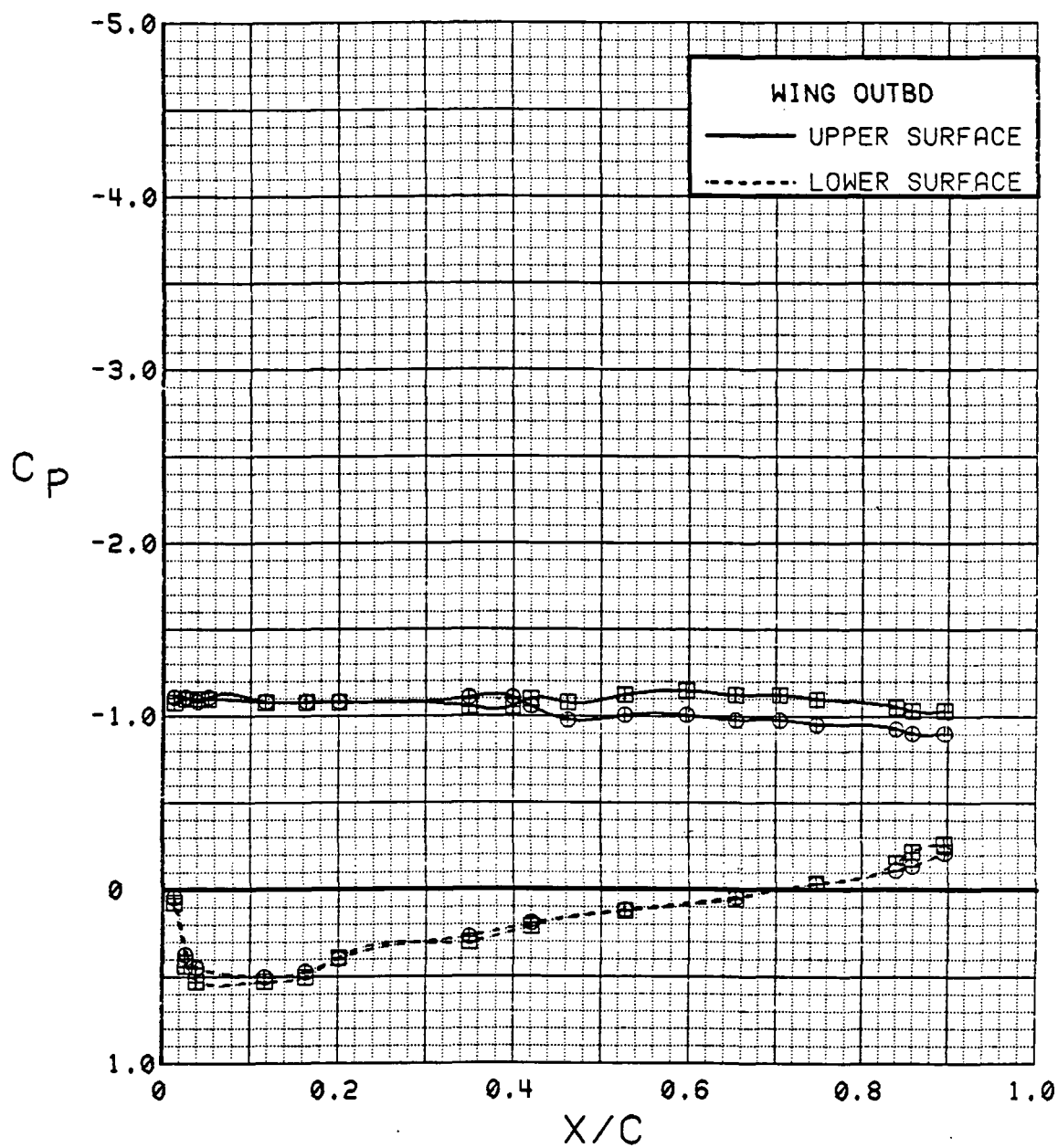


Figure 3.2.4-94 Canard On/Off Effects, Outboard,  $C_T = 0.9$ , Flaps Neutral, Alpha = 24 deg

SYM	TEST	RUN	ALPHA	CT	ITEF	OTEF	CAN	SWB
⊕	543	60	29.0	0.93	0	0	0	OFF
⊞	537	72	28.8	0.91	0	0	OFF	OFF

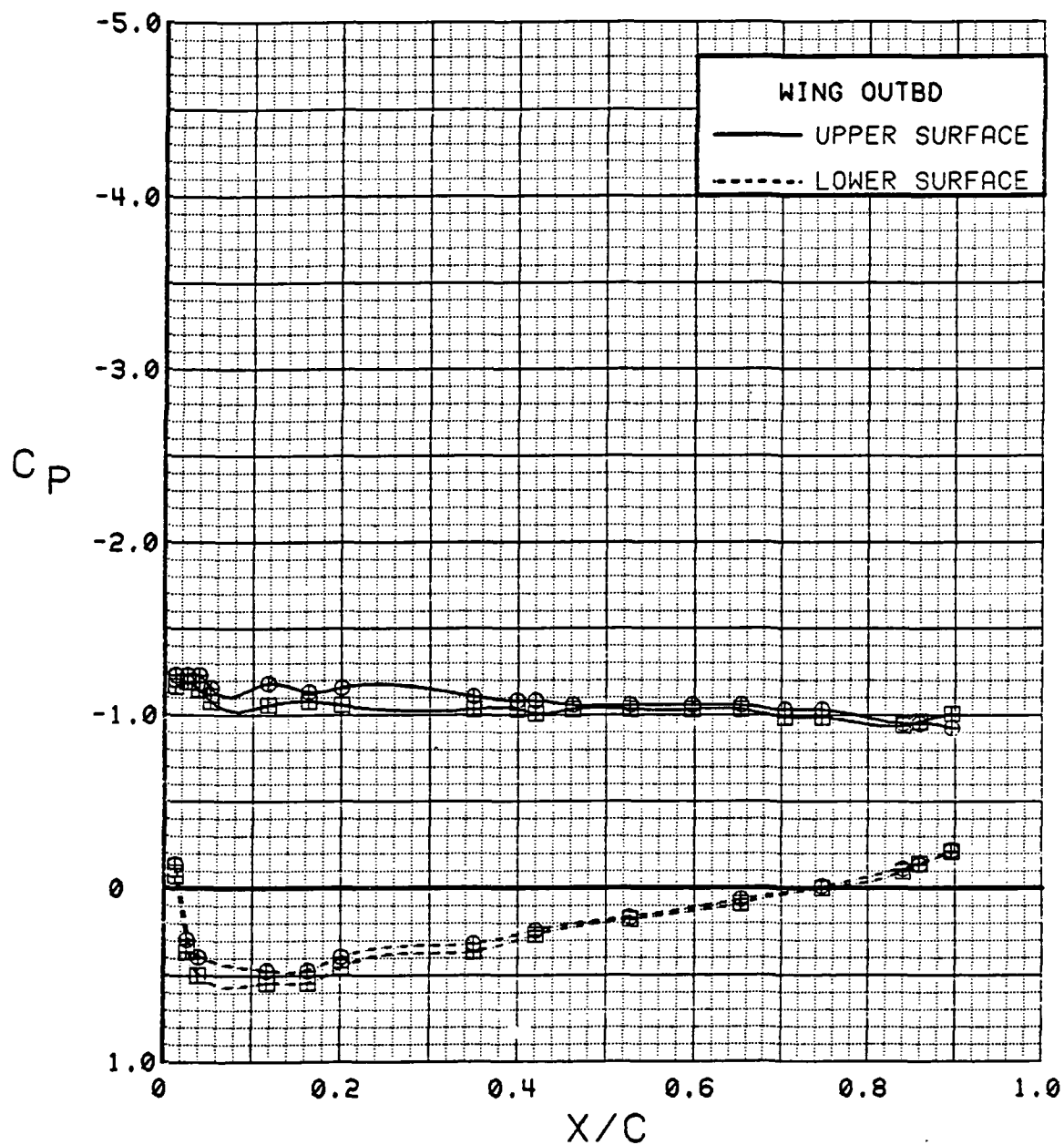


Figure 3.2.4-95

Canard On/Off Effects, Outboard,  $C_T = 0.9$ ,  
Flaps Neutral, Alpha = 28 deg

SYM	TEST	RUN	ALPHA	CT	ITEF	OTEF	CAN	SWB
⊕	543	60	33.1	0.94	0	0	0	OFF
⊞	537	72	32.9	0.92	0	0	OFF	OFF

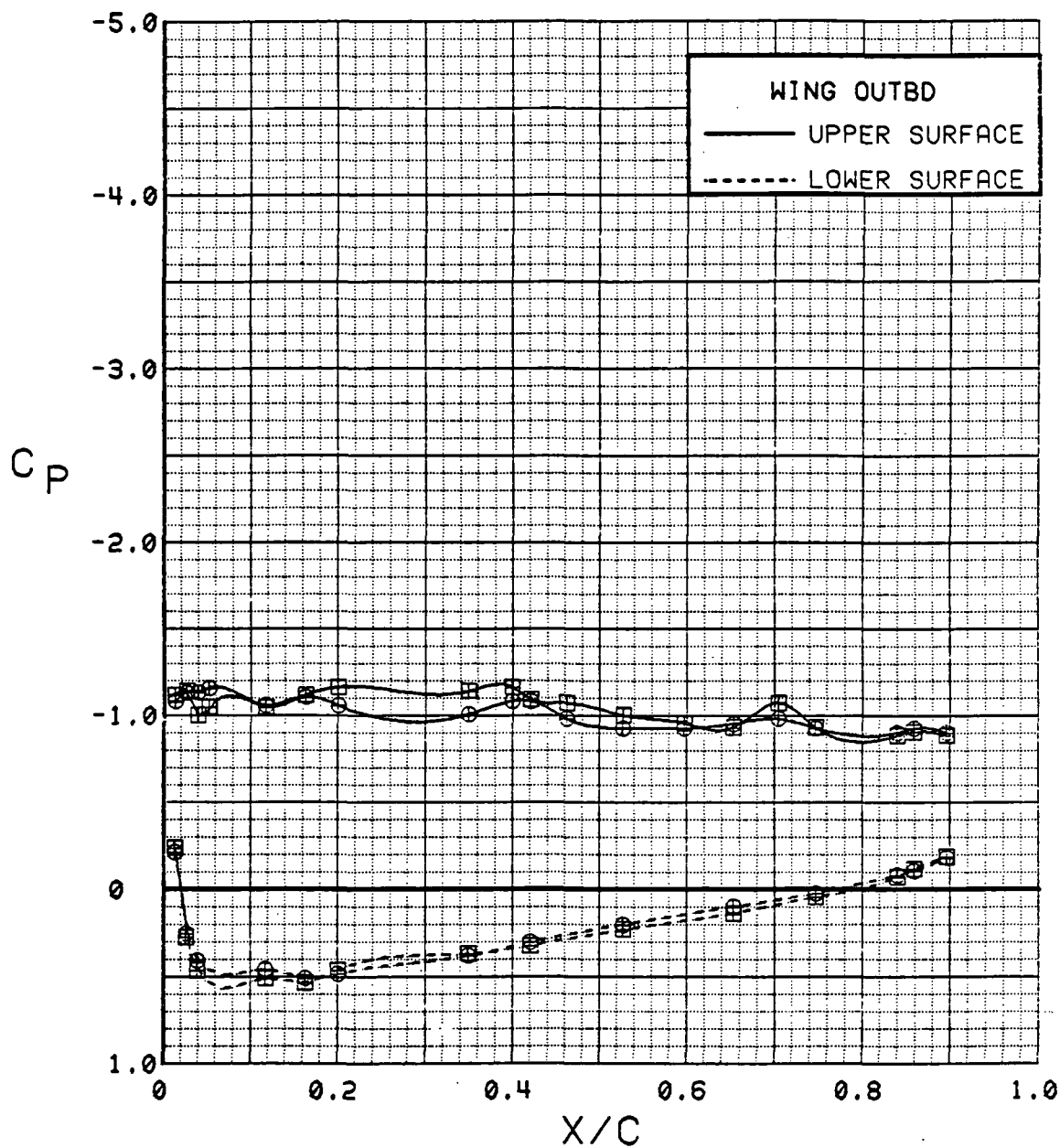


Figure 3.2.4-96 Canard On/Off Effects, Outboard,  $C_T = 0.9$ , Flaps Neutral, Alpha = 32 deg

SYM	TEST	RUN	ALPHA	CT	ITEF	OTEF	CAN	SWB
⊕	543	60	37.1	0.93	0	0	0	OFF
⊞	537	72	36.9	0.92	0	0	OFF	OFF

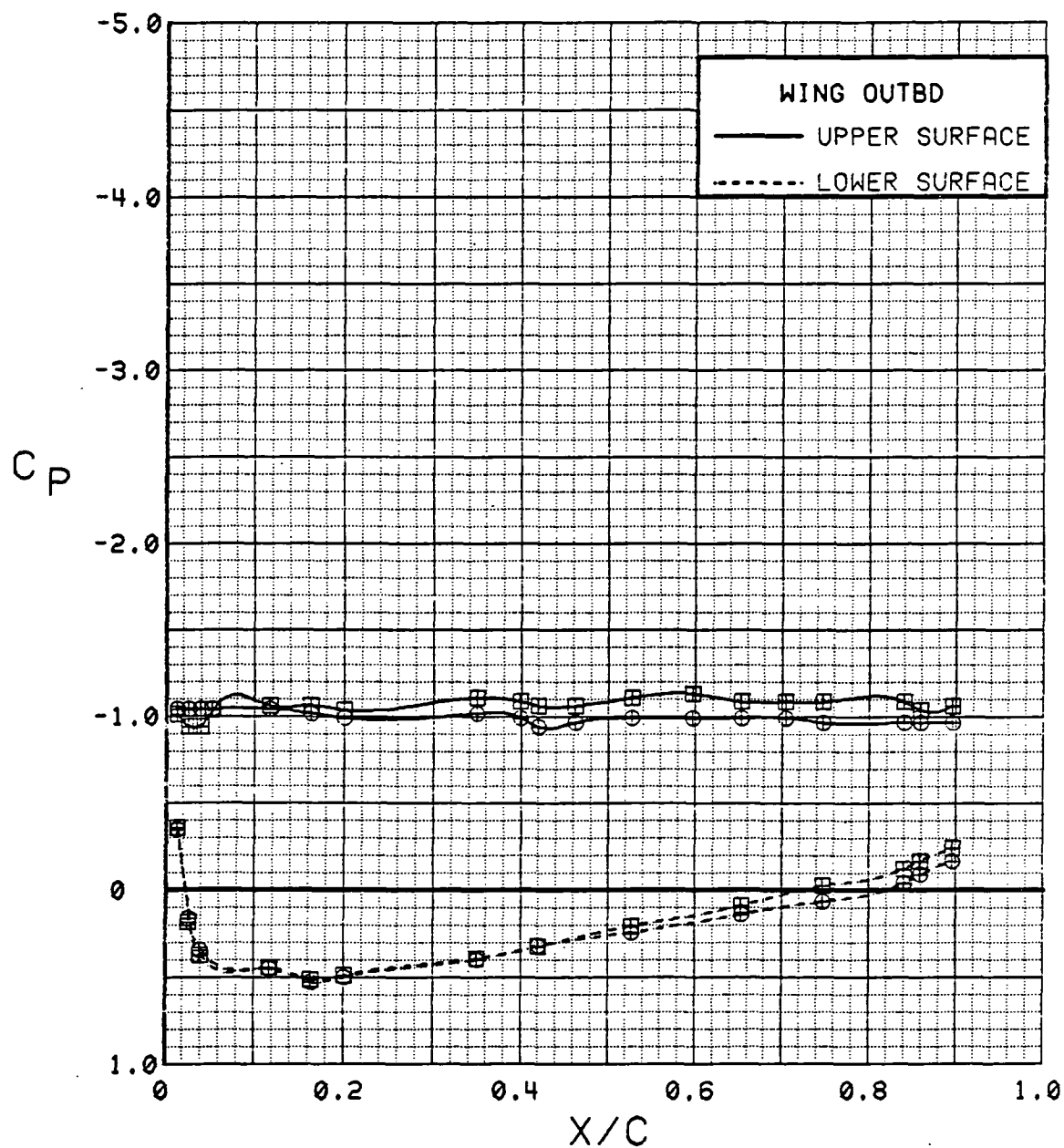


Figure 3.2.4-97 Canard On/Off Effects, Outboard,  $C_T = 0.9$ , Flaps Neutral, Alpha = 36 deg

SYM	TEST	RUN	ALPHA	CT	ITEF	OTEF	CAN	SWB
⊙	543	60	0.1	0.94	0	0	0	OFF
⊠	537	72	0.1	0.89	0	0	OFF	OFF

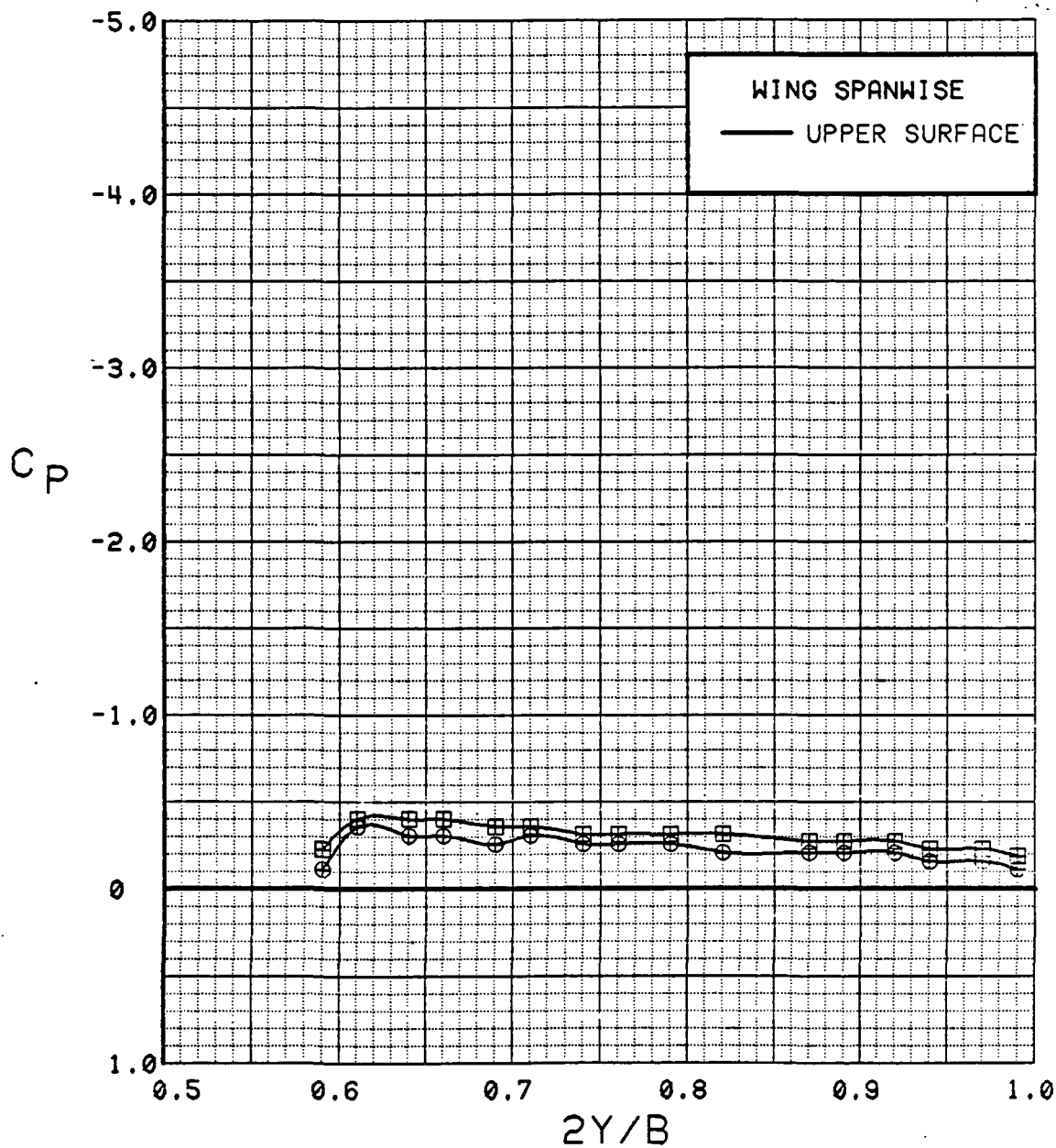


Figure 3.2.4-98 Canard On/Off Effects, Spanwise,  $C_T = 0.9$ , Flaps Neutral, Alpha = 0 deg

SYM	TEST	RUN	ALPHA	CT	ITEF	OTEF	CAN	SWB
⊕	543	60	4.3	0.93	0	0	0	OFF
⊞	537	72	4.2	0.90	0	0	OFF	OFF

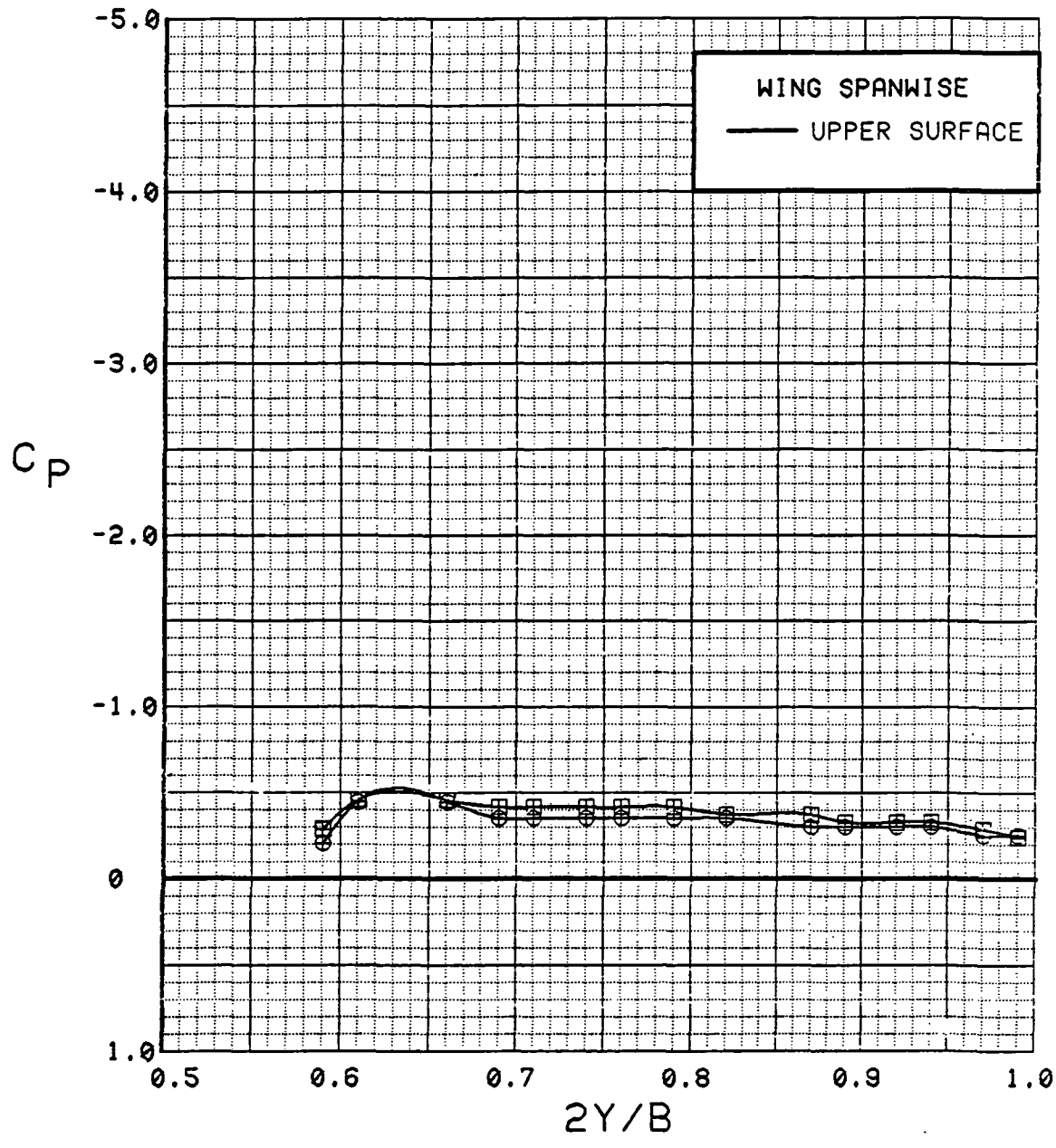


Figure 3.2.4-99 Canard On/Off Effects, Spanwise,  $C_T = 0.9$ , Flaps Neutral, Alpha = 4 deg



SYM	TEST	RUN	ALPHA	CT	ITEF	OTEF	CAN	SWB
⊙	543	60	8.4	0.94	0	0	0	OFF
⊠	537	72	8.3	0.92	0	0	OFF	OFF

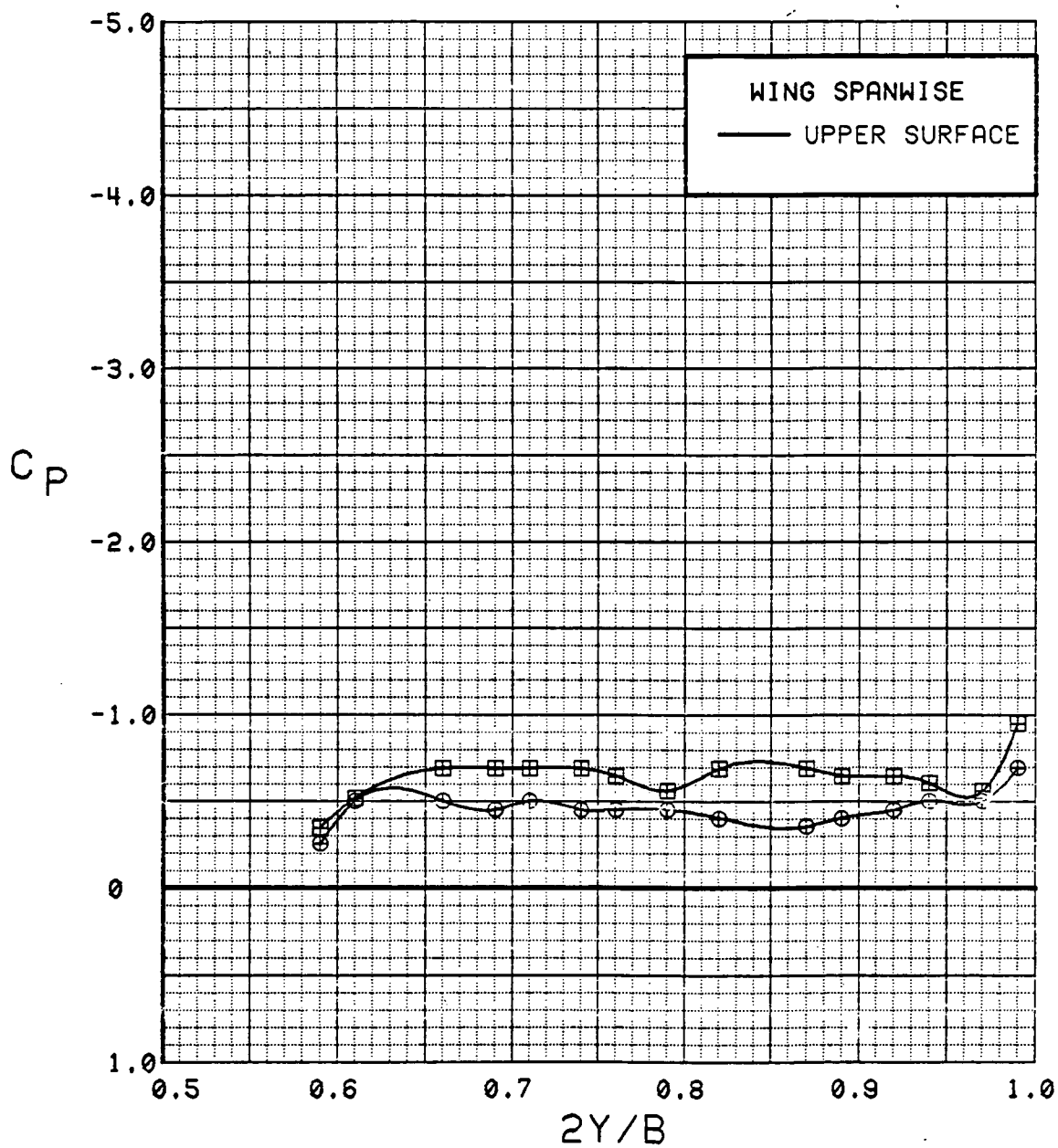


Figure 3.2.4-100 Canard On/Off Effects, Spanwise,  $C_T = 0.9$ , Flaps Neutral, Alpha = 8 deg

SYM	TEST	RUN	ALPHA	CT	ITEF	OTEF	CAN	SWB
⊙	543	60	12.5	0.94	0	0	0	OFF
⊠	537	72	12.4	0.91	0	0	OFF	OFF

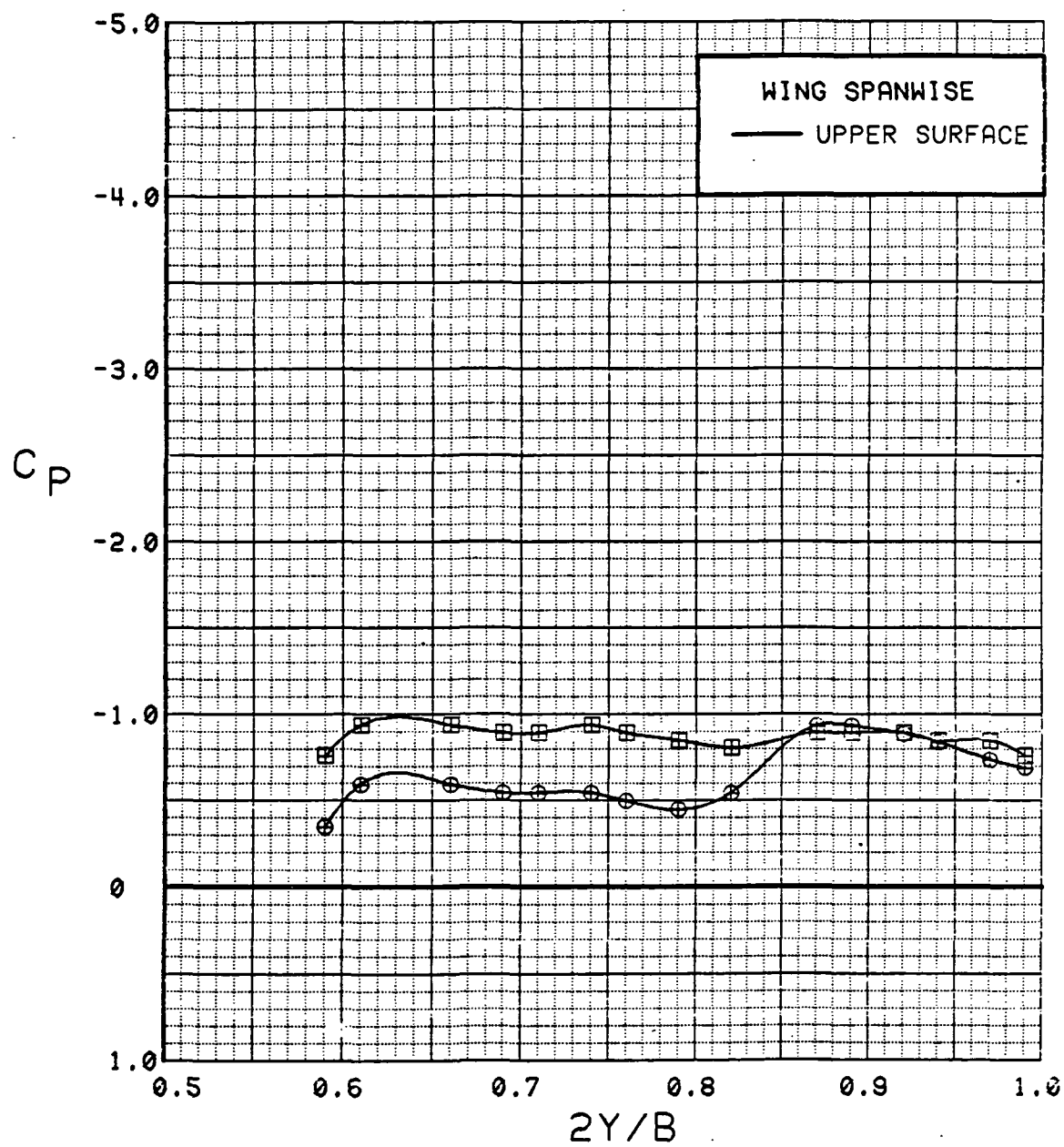


Figure 3.2.4-101 Canard On/Off Effects, Spanwise,  $C_T = 0.9$ , Flaps Neutral, Alpha = 12 deg

SYM	TEST	RUN	ALPHA	CT	ITEF	OTEF	CAN	SWB
⊕	543	60	16.7	0.93	0	0	0	OFF
⊞	537	72	16.5	0.91	0	0	OFF	OFF

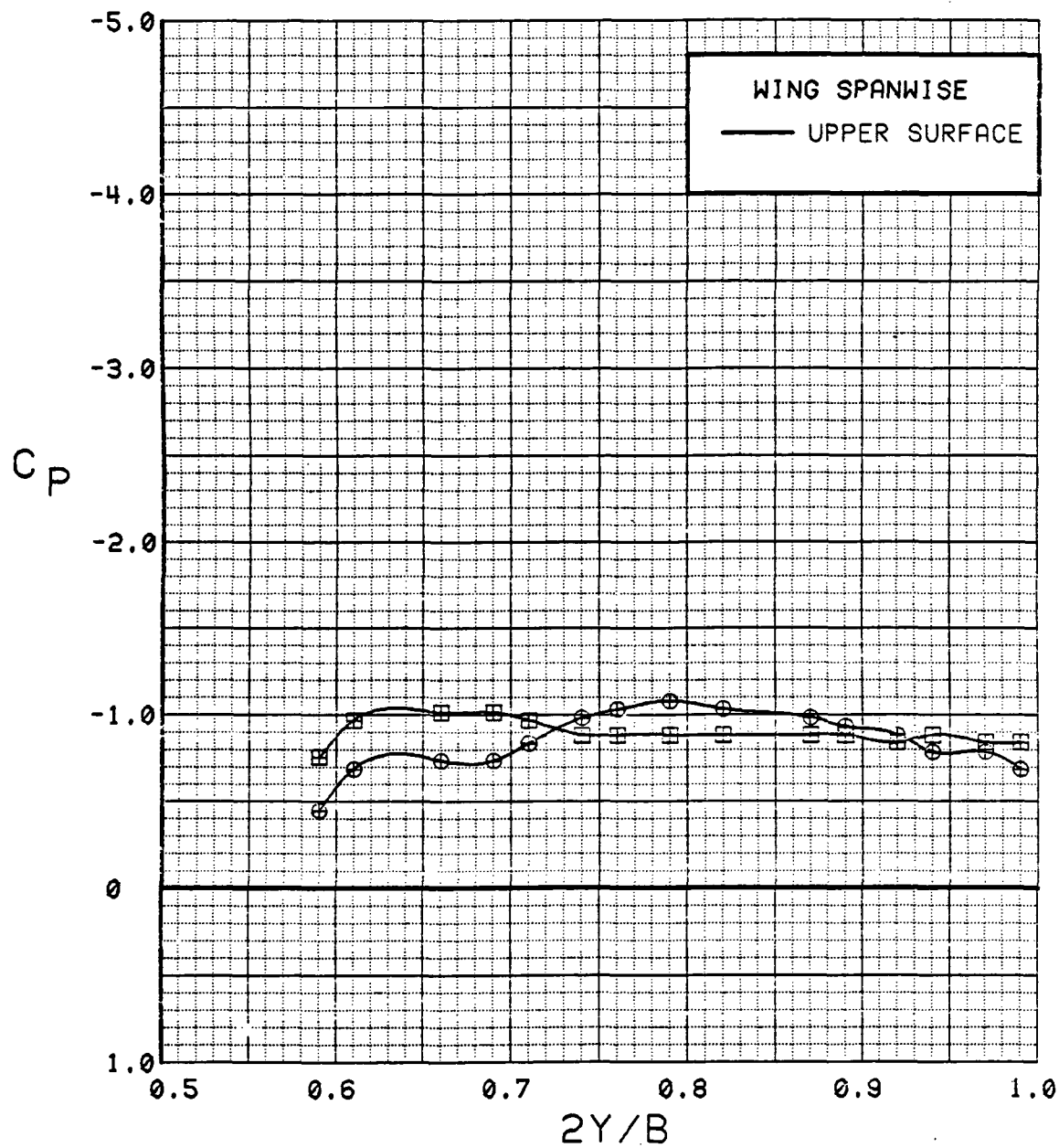


Figure 3.2.4-102 Canard On/Off Effects, Spanwise,  $C_T = 0.9$ , Flaps Neutral, Alpha = 16 deg

SYM	TEST	RUN	ALPHA	CT	ITEF	OTEF	CAN	SWB
●	543	60	20.8	0.93	0	0	0	OFF
■	537	72	20.6	0.93	0	0	OFF	OFF

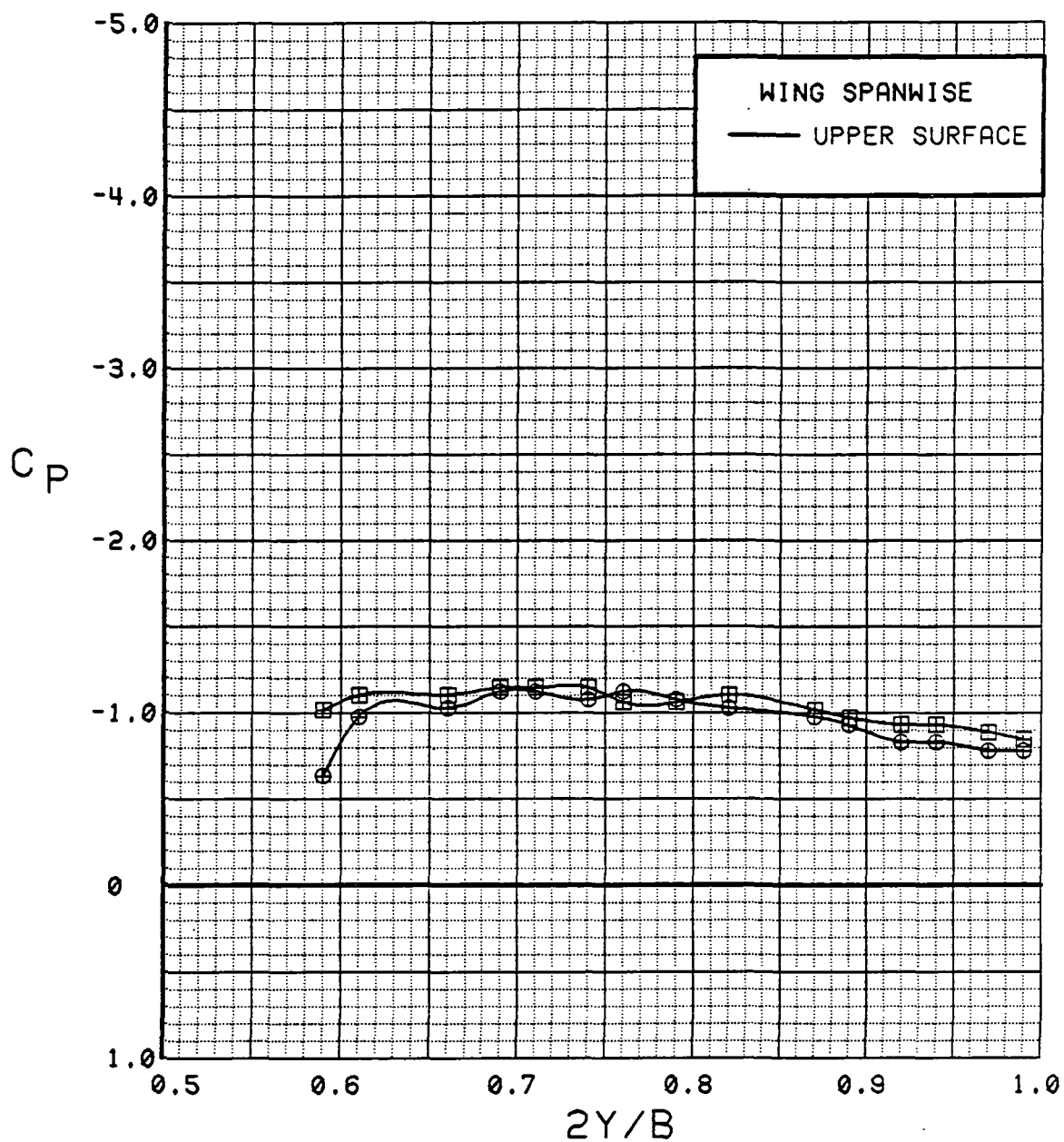


Figure 3.2.4-103 Canard On/Off Effects, Spanwise,  $C_T = 0.9$ , Flaps Neutral,  $\alpha = 20$  deg

SYM	TEST	RUN	ALPHA	CT	ITEF	OTEF	CAN	SWB
●	543	60	24.9	0.93	0	0	0	OFF
■	537	72	24.7	0.91	0	0	OFF	OFF

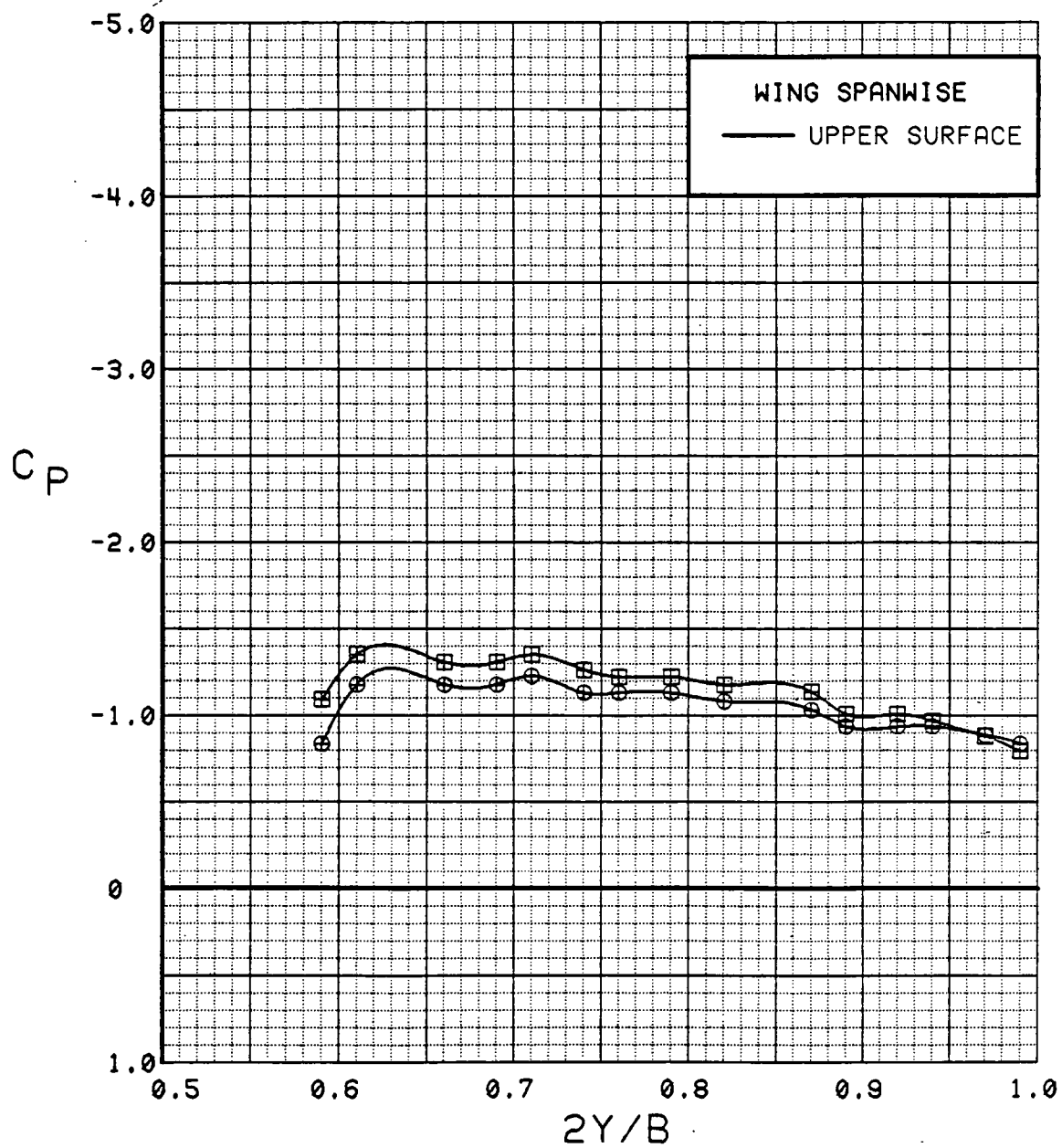


Figure 3.2.4-104 Canard On/Off Effects, Spanwise,  $C_T = 0.9$ , Flaps Neutral, Alpha = 24 deg

SYM	TEST	RUN	ALPHA	CT	ITEF	OTEF	CAN	SWB
⊙	543	60	29.0	0.93	0	0	0	OFF
⊠	537	72	28.8	0.91	0	0	OFF	OFF

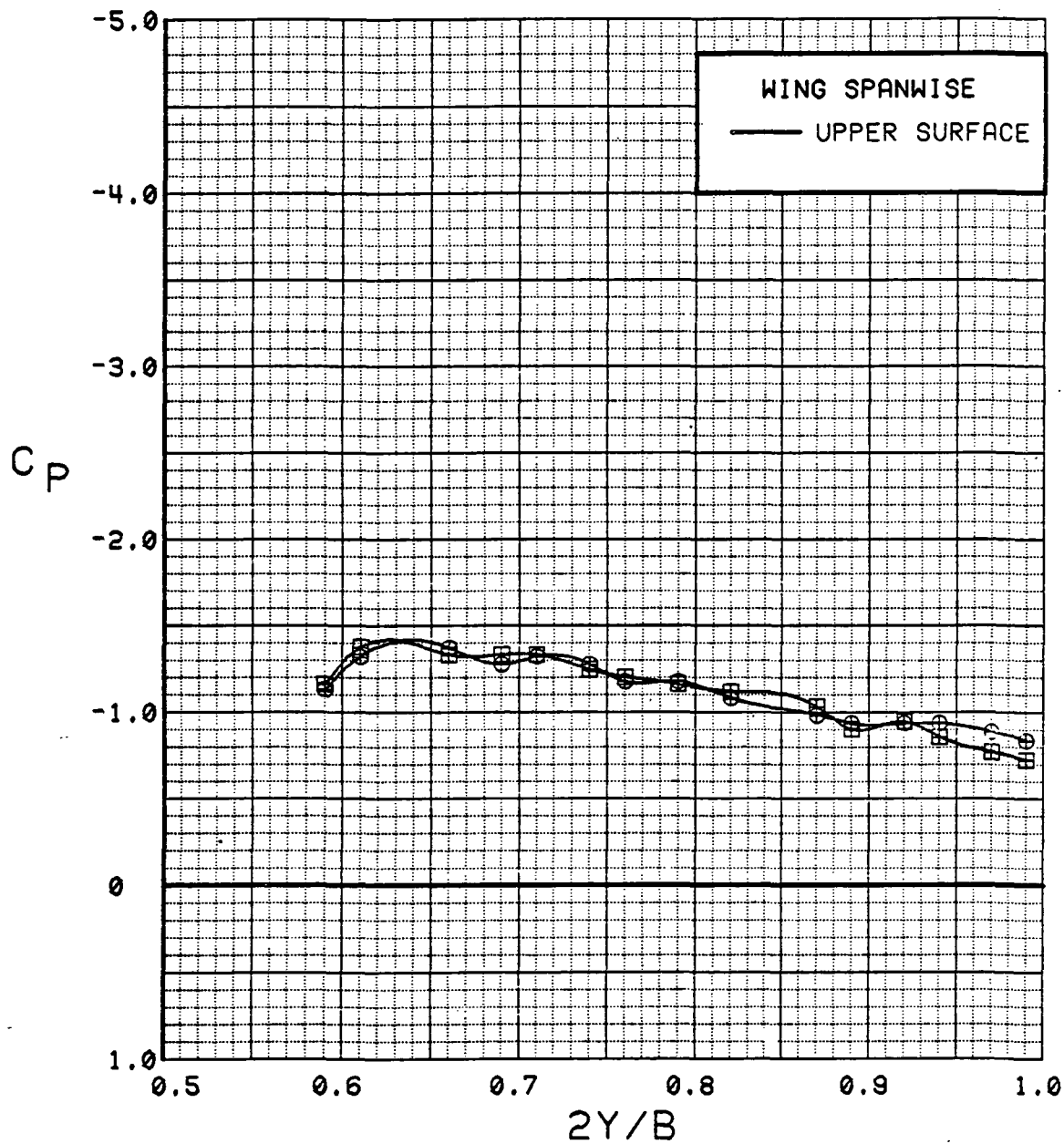


Figure 3.2.4-105 Canard On/Off Effects, Spanwise,  $C_T = 0.9$ , Flaps Neutral, Alpha = 28 deg

SYM	TEST	RUN	ALPHA	CT	ITEF	OTEF	CAN	SWB
●	543	60	33.1	0.94	0	0	0	OFF
■	537	72	32.9	0.92	0	0	OFF	OFF

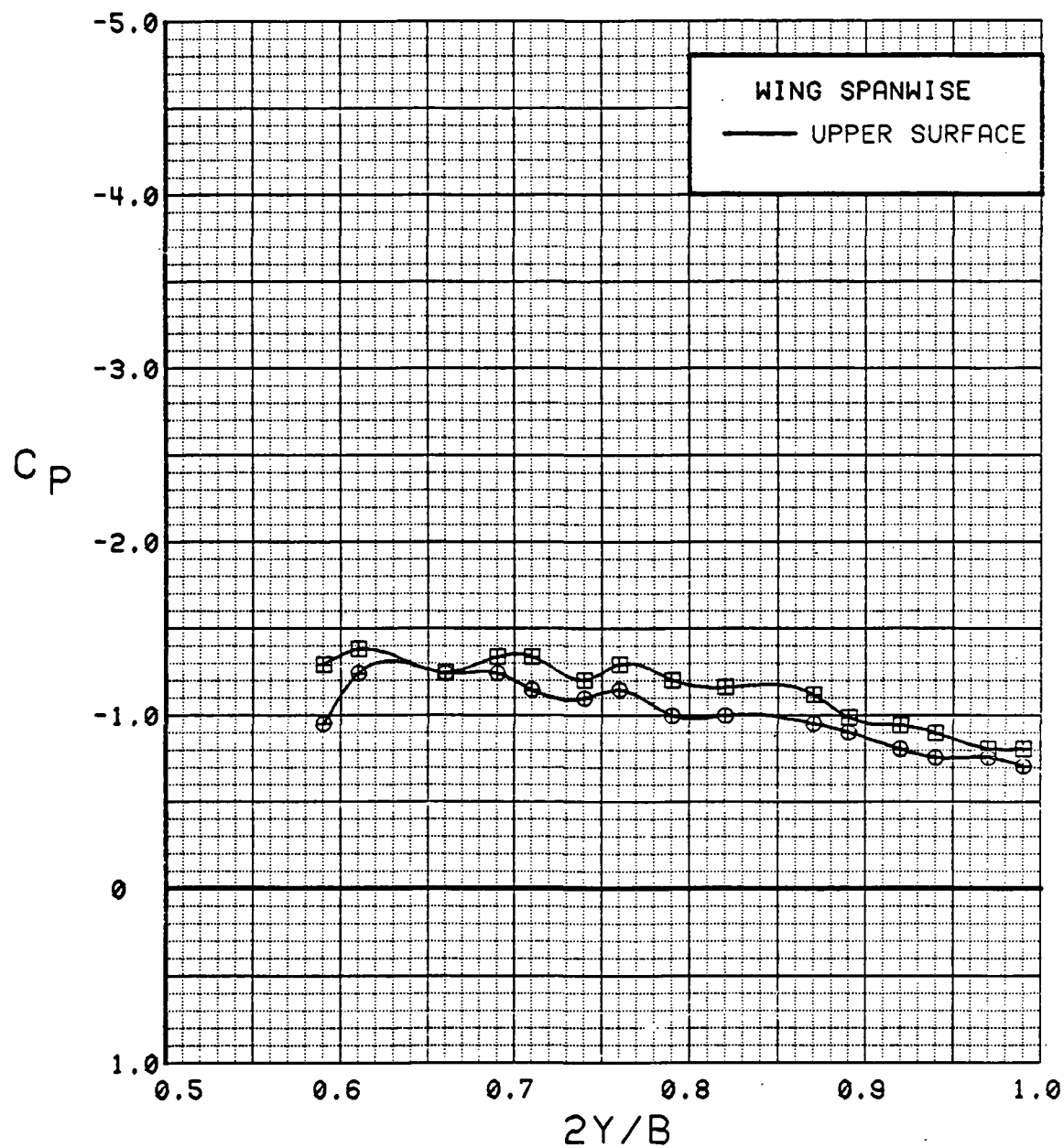


Figure 3.2.4-106 Canard On/Off Effects, Spanwise,  $C_T = 0.9$ , Flaps Neutral, Alpha = 32 deg

SYM	TEST	RUN	ALPHA	CT	ITEF	OTEF	CAN	SWB
●	543	60	37.1	0.93	0	0	0	OFF
■	537	72	36.9	0.92	0	0	OFF	OFF

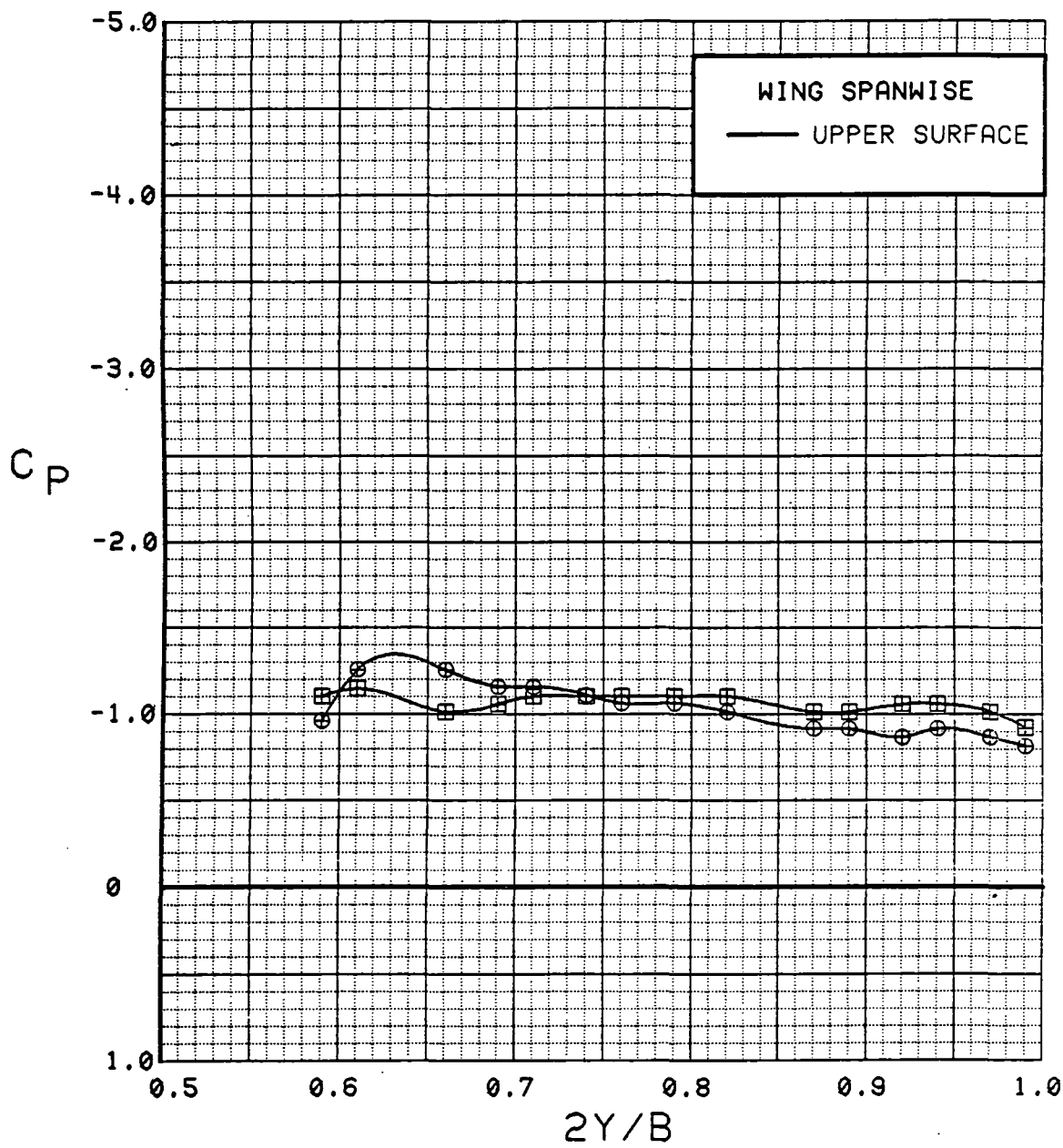


Figure 3.2.4-107 Canard On/Off Effects, Spanwise,  $C_T = 0.9$ , Flaps Neutral, Alpha = 36 deg



## WING INBOARD

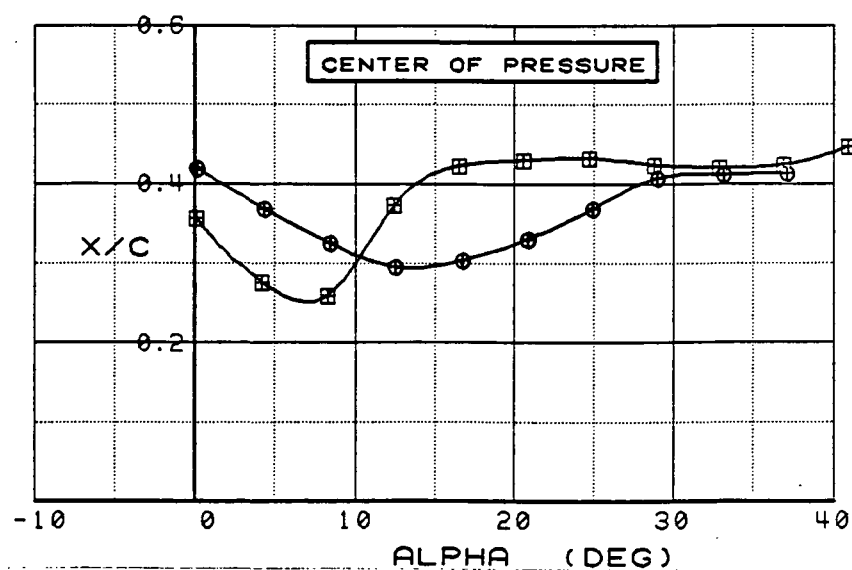
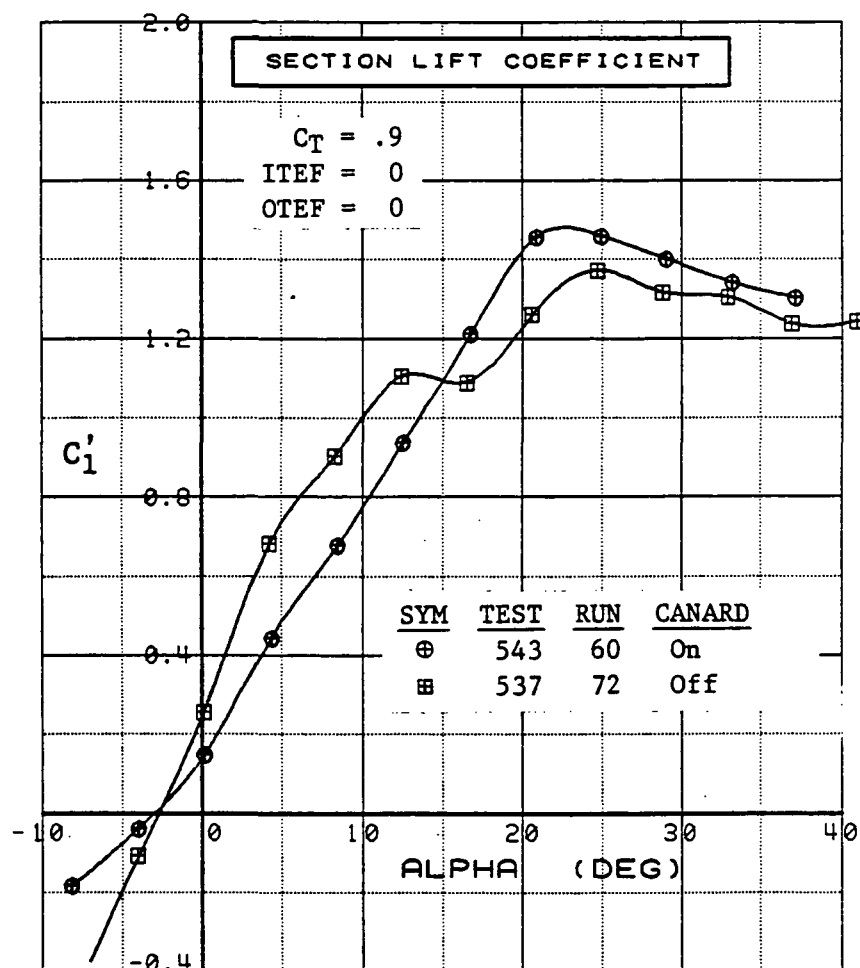


Figure 3.2.4-108 Canard On/Off Effects, Inboard,  $C_T = 0.9$ , Flaps Neutral, Integrated Section Properties

## WING OUTBOARD

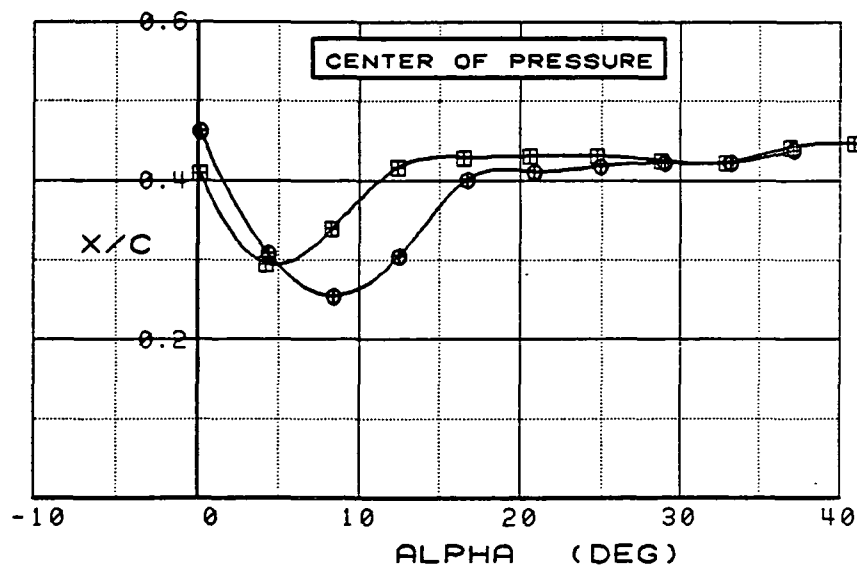
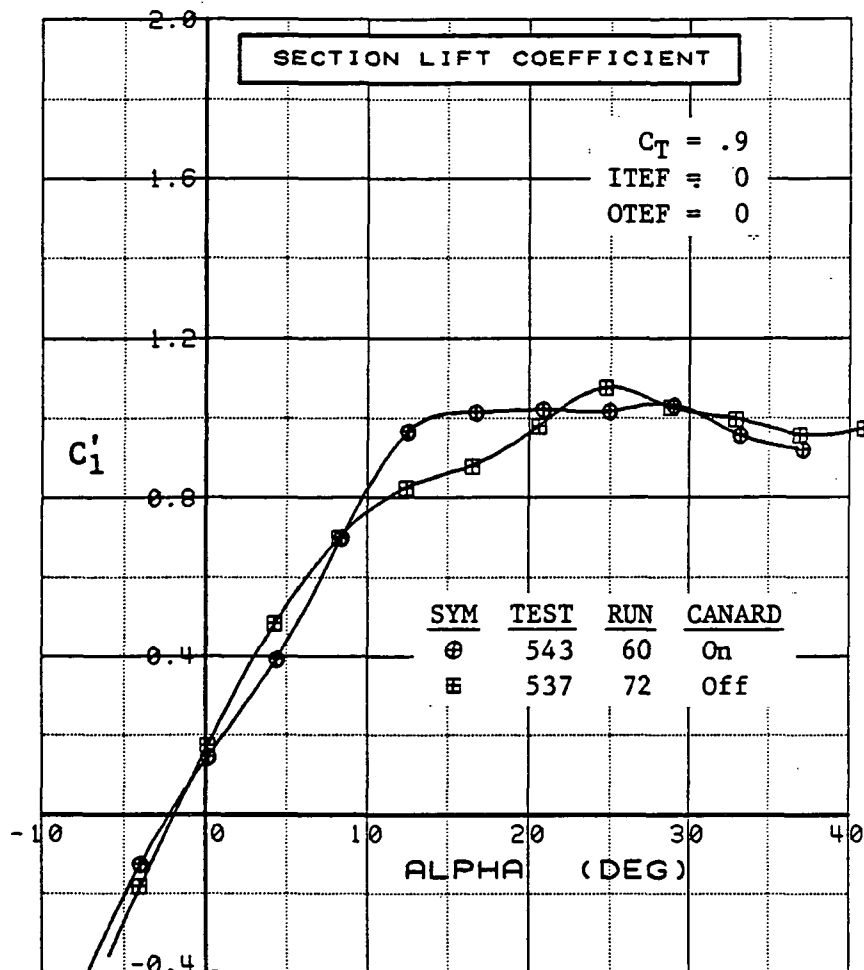


Figure 3.2.4-109 Canard On/Off Effects, Outboard,  $C_T = 0.9$ , Flaps Neutral, Integrated Section Properties

SYM	TEST	RUN	ALPHA	CT	ITEF	OTEF	CAN	SWB
⊕	543	6	0.3	0.94	30	30	0	OFF
⊞	537	61	0.4	0.94	30	30	OFF	OFF

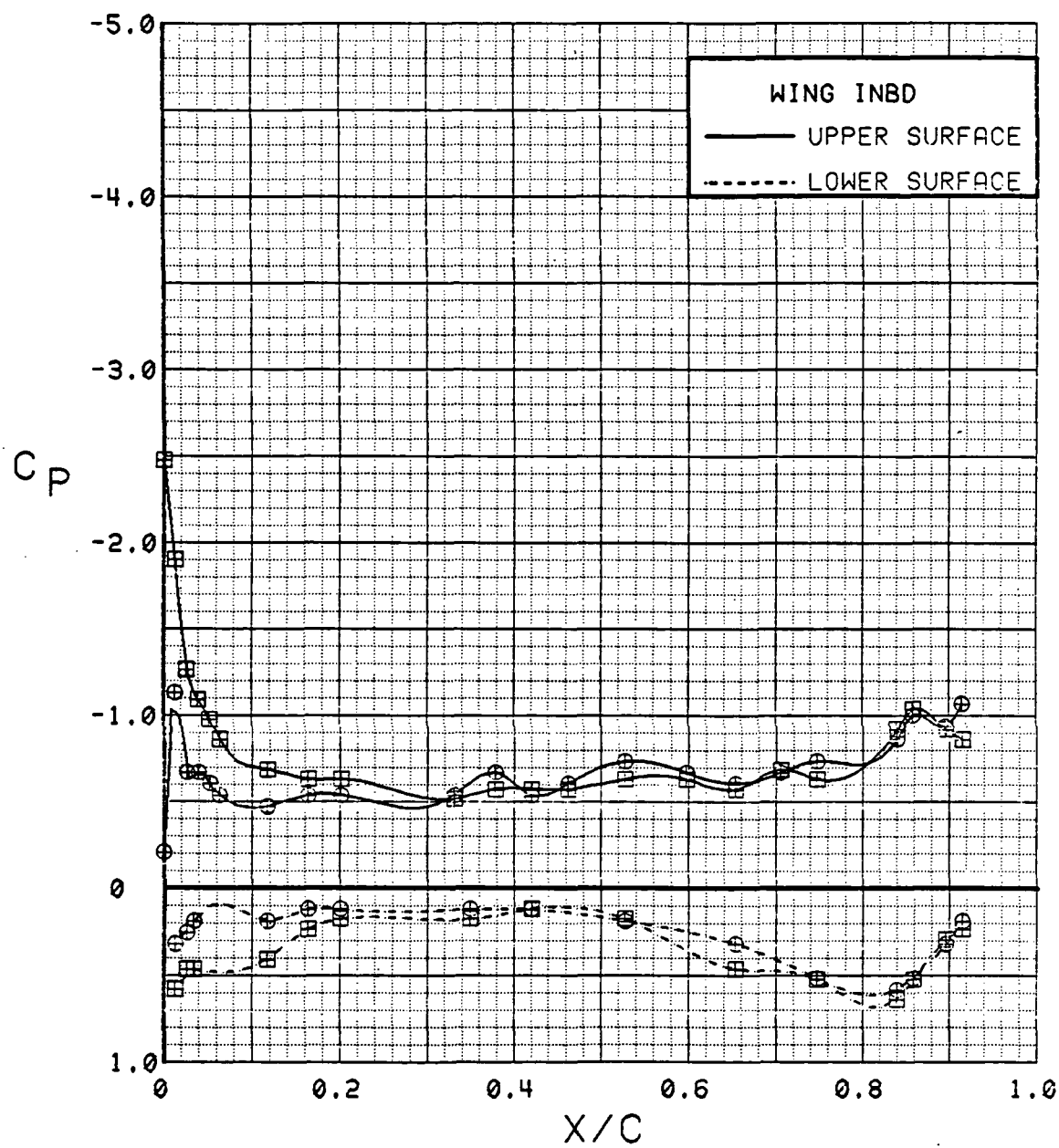


Figure 3.2.4-110 Canard On/Off Effects, Inboard,  $C_T = 0.9$ , Flaps Deflected, Alpha = 0 deg

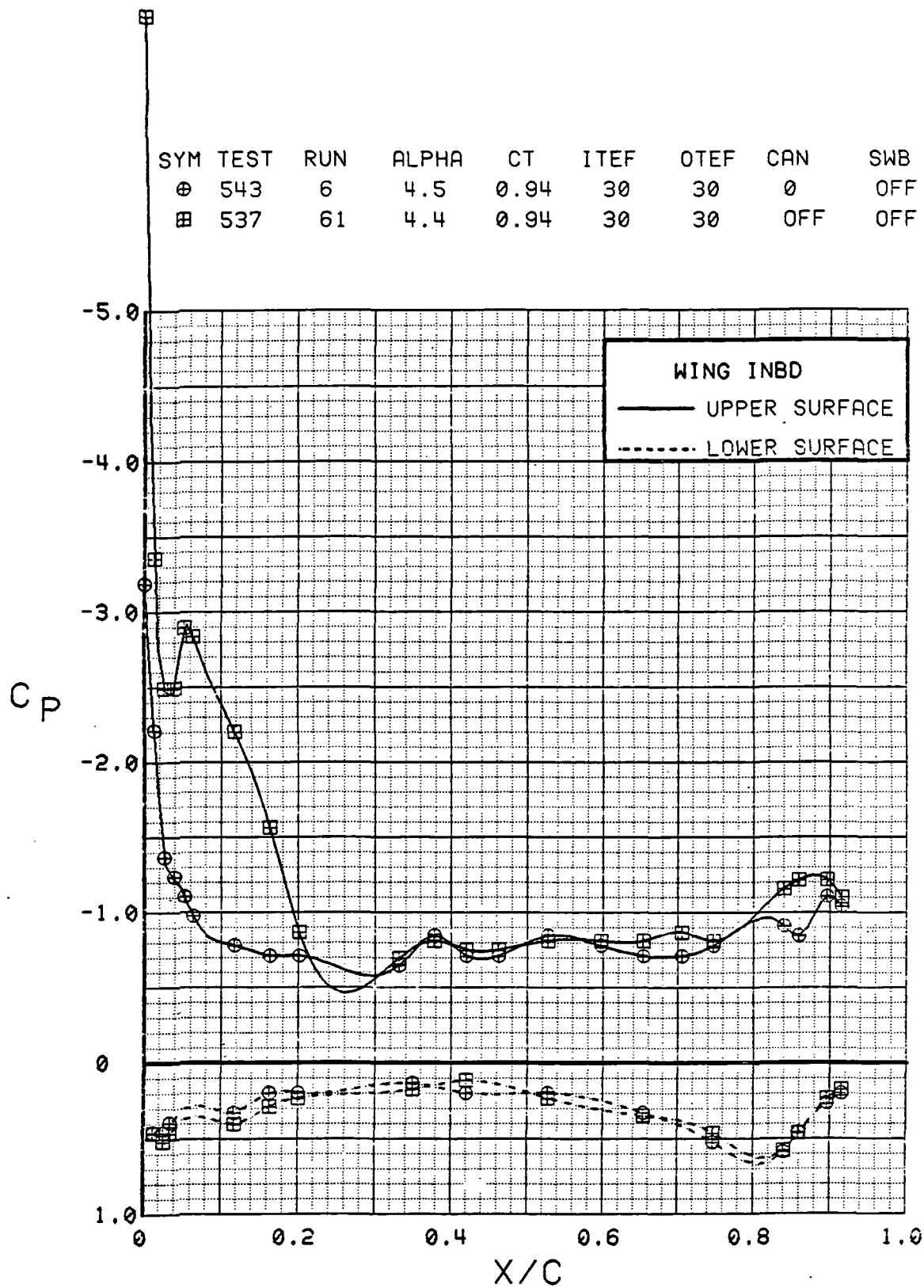


Figure 3.2.4-111 Canard On/Off Effects, Inboard,  $C_T = 0.9$ , Flaps Deflected,  $\alpha = 4^\circ$

$$\oplus C_p = -9.82$$

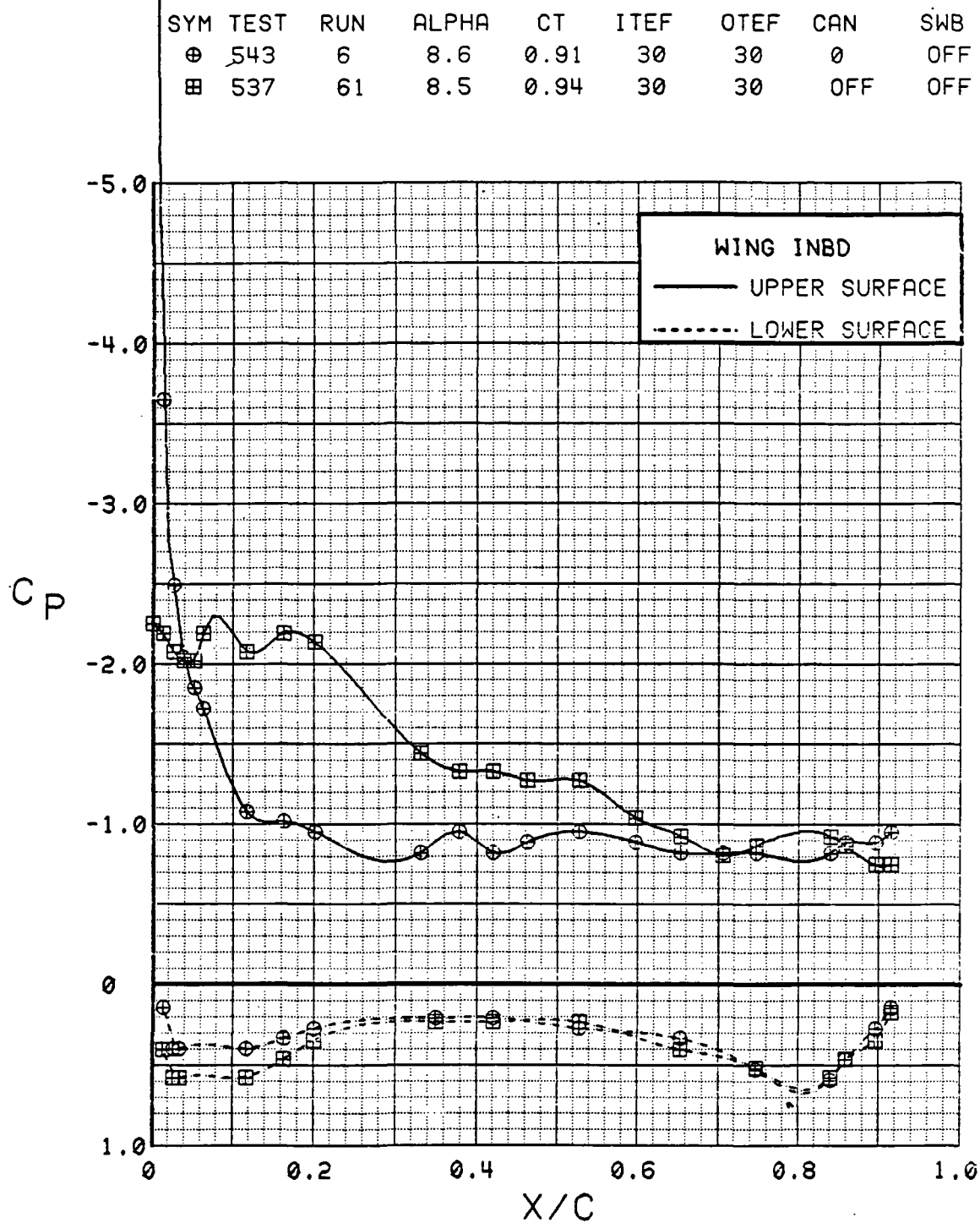


Figure 3.2.4-112 Canard On/Off Effects, Inboard,  $C_T = 0.9$ , Flaps Deflected,  $\alpha = 8$  deg

SYM	TEST	RUN	ALPHA	CT	ITEF	OTEF	CAN	SWB
⊕	543	6	12.8	0.92	30	30	0	OFF
⊞	537	61	12.6	0.92	30	30	OFF	OFF

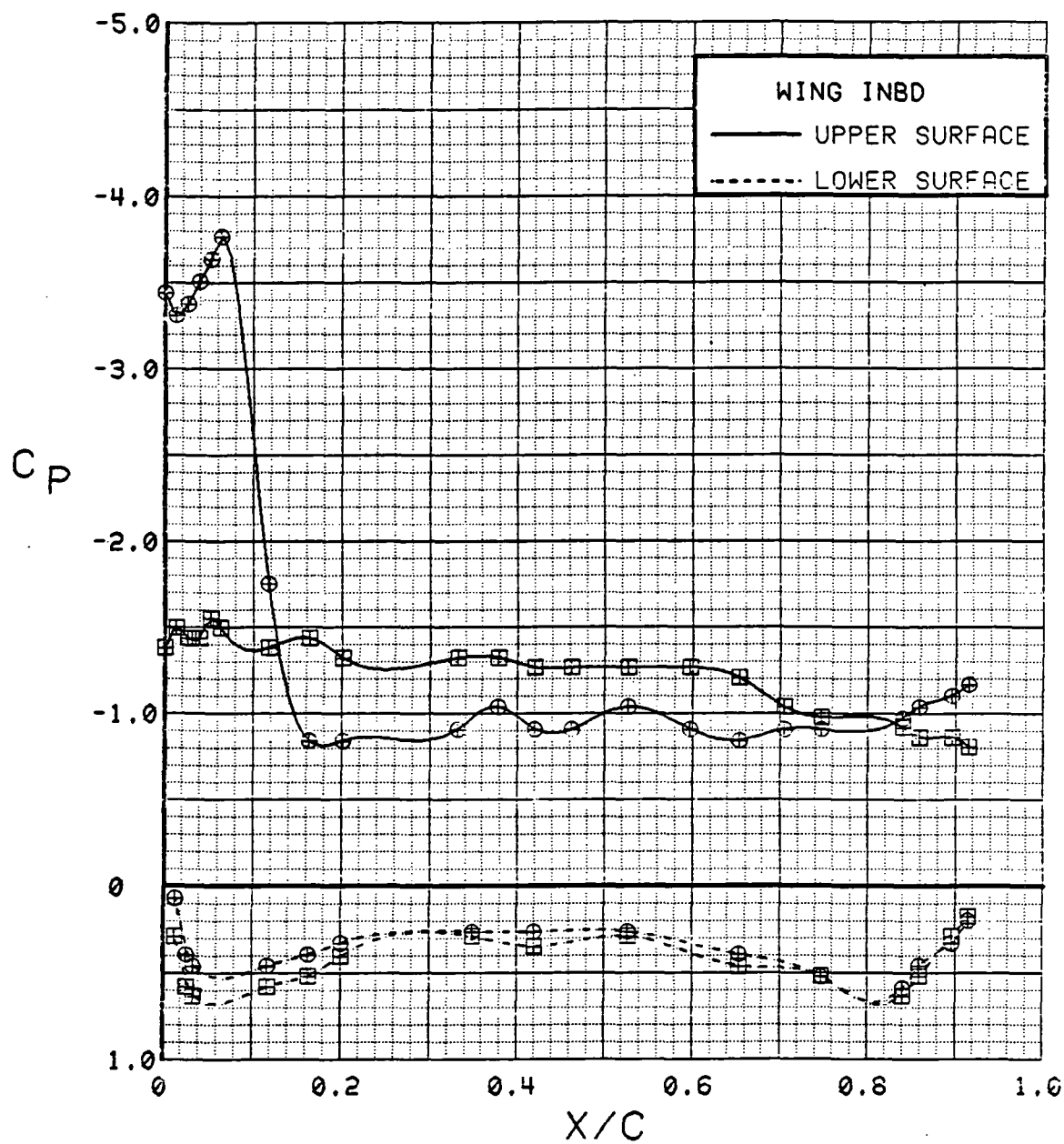


Figure 3.2.4-113 Canard On/Off Effects, Inboard,  $C_T = 0.9$ , Flaps Deflected, Alpha = 12 deg

SYM	TEST	RUN	ALPHA	CT	ITEF	OTEF	CAN	SWB
⊕	543	6	16.9	0.92	30	30	0	OFF
⊞	537	61	16.7	0.94	30	30	OFF	OFF

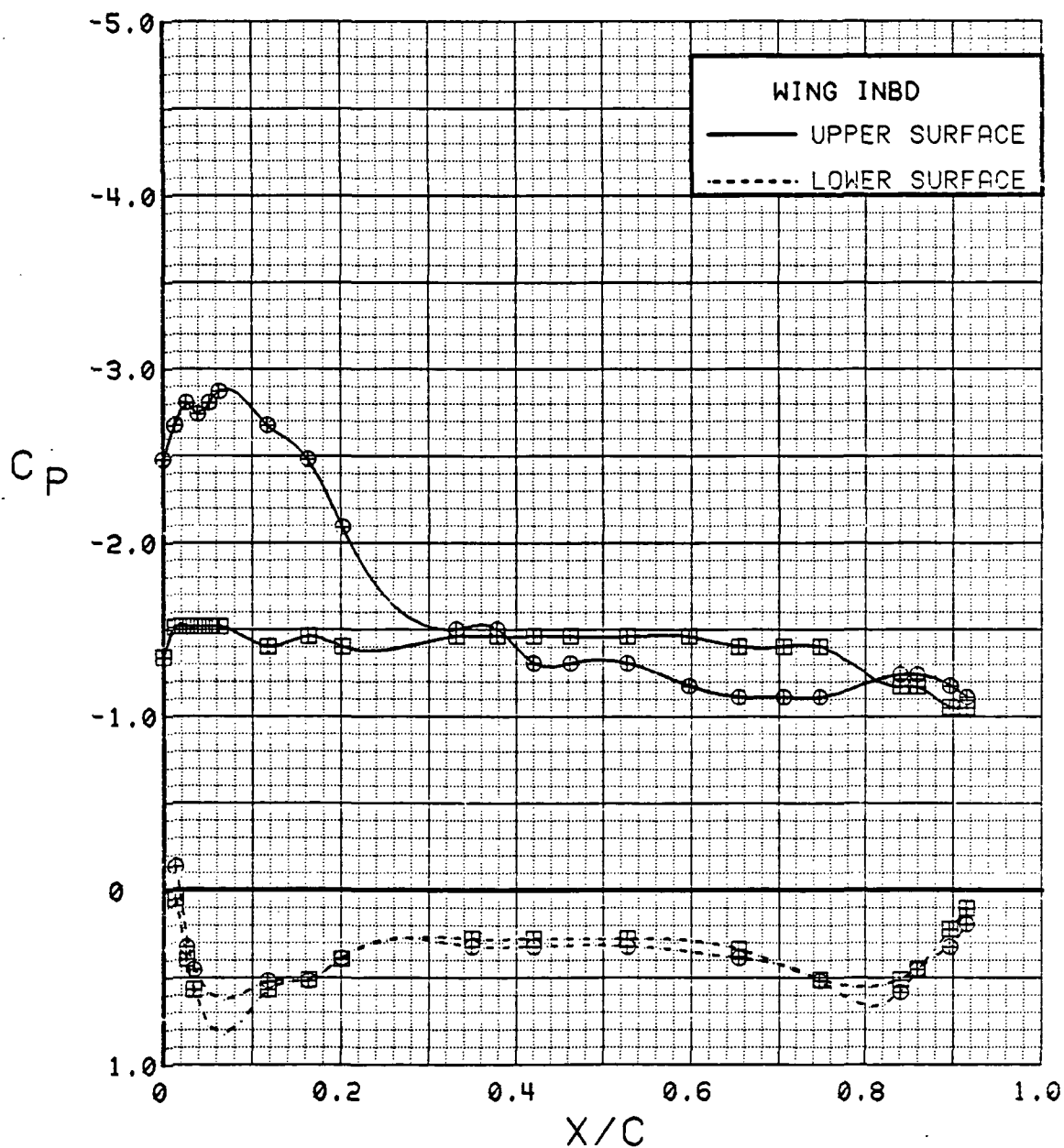


Figure 3.2.4-114 Canard On/Off Effects, Inboard,  $C_T = 0.9$ , Flaps Deflected,  $\alpha = 16$  deg

SYM	TEST	RUN	ALPHA	CT	ITEF	OTEF	CAN	SWB
⊕	543	6	21.0	0.93	30	30	0	OFF
⊞	537	61	20.8	0.92	30	30	OFF	OFF

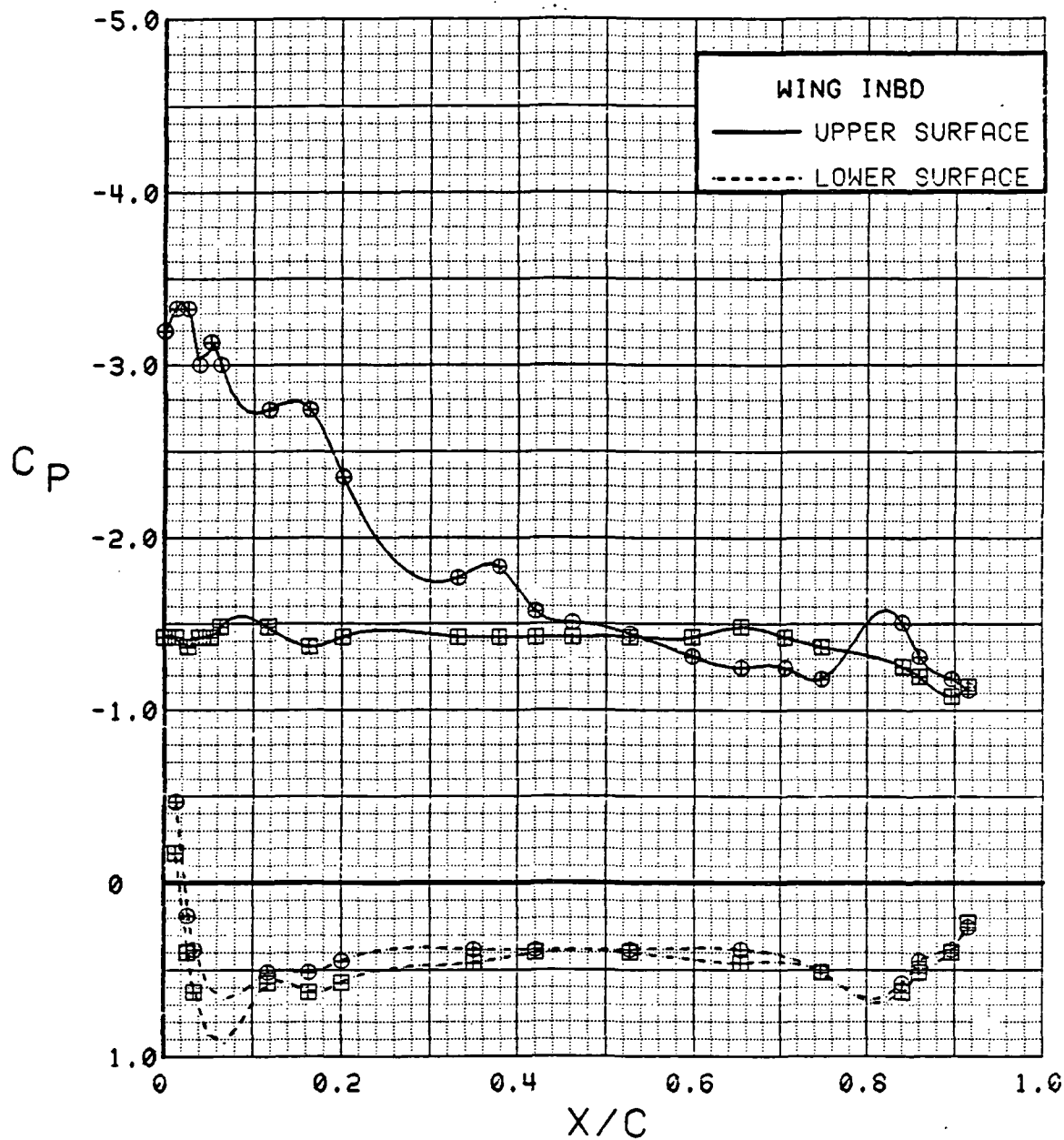


Figure 3.2.4-115 Canard On/Off Effects, Inboard,  $C_T = 0.9$ ,  
Flaps Deflected,  $\alpha = 20^\circ$



SYM	TEST	RUN	ALPHA	CT	ITEF	OTEF	CAN	SWB
⊕	543	6	25.1	0.93	30	30	0	OFF
⊞	537	61	24.9	0.92	30	30	OFF	OFF

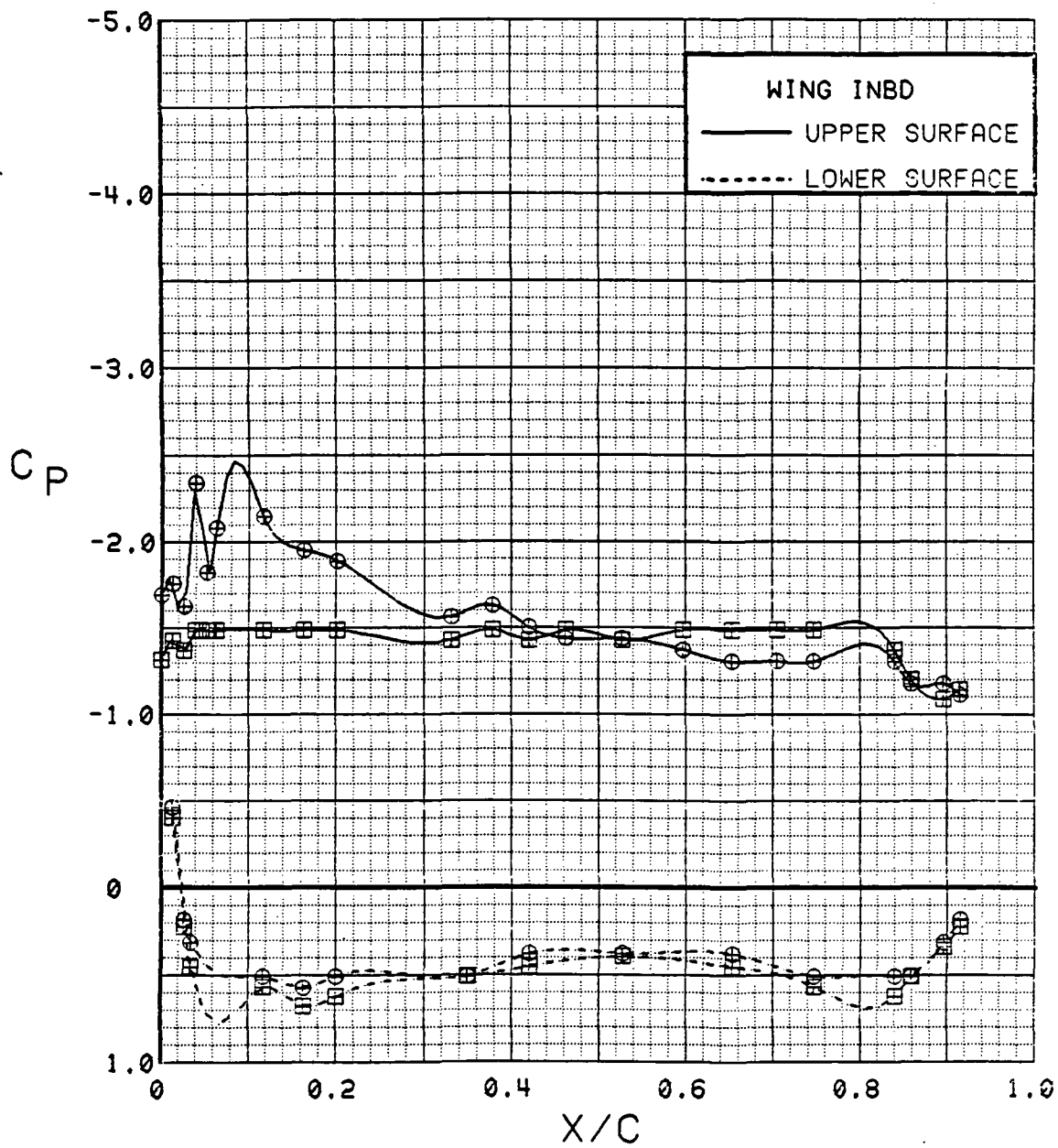


Figure 3.2.4-116 Canard On/Off Effects, Inboard,  $C_T = 0.9$ , Flaps Deflected, Alpha = 24 deg

117

SYM	TEST	RUN	ALPHA	CT	ITEF	OTEF	CAN	SWB
⊕	543	6	29.1	0.93	30	30	0	OFF
⊞	537	61	28.9	0.93	30	30	OFF	OFF

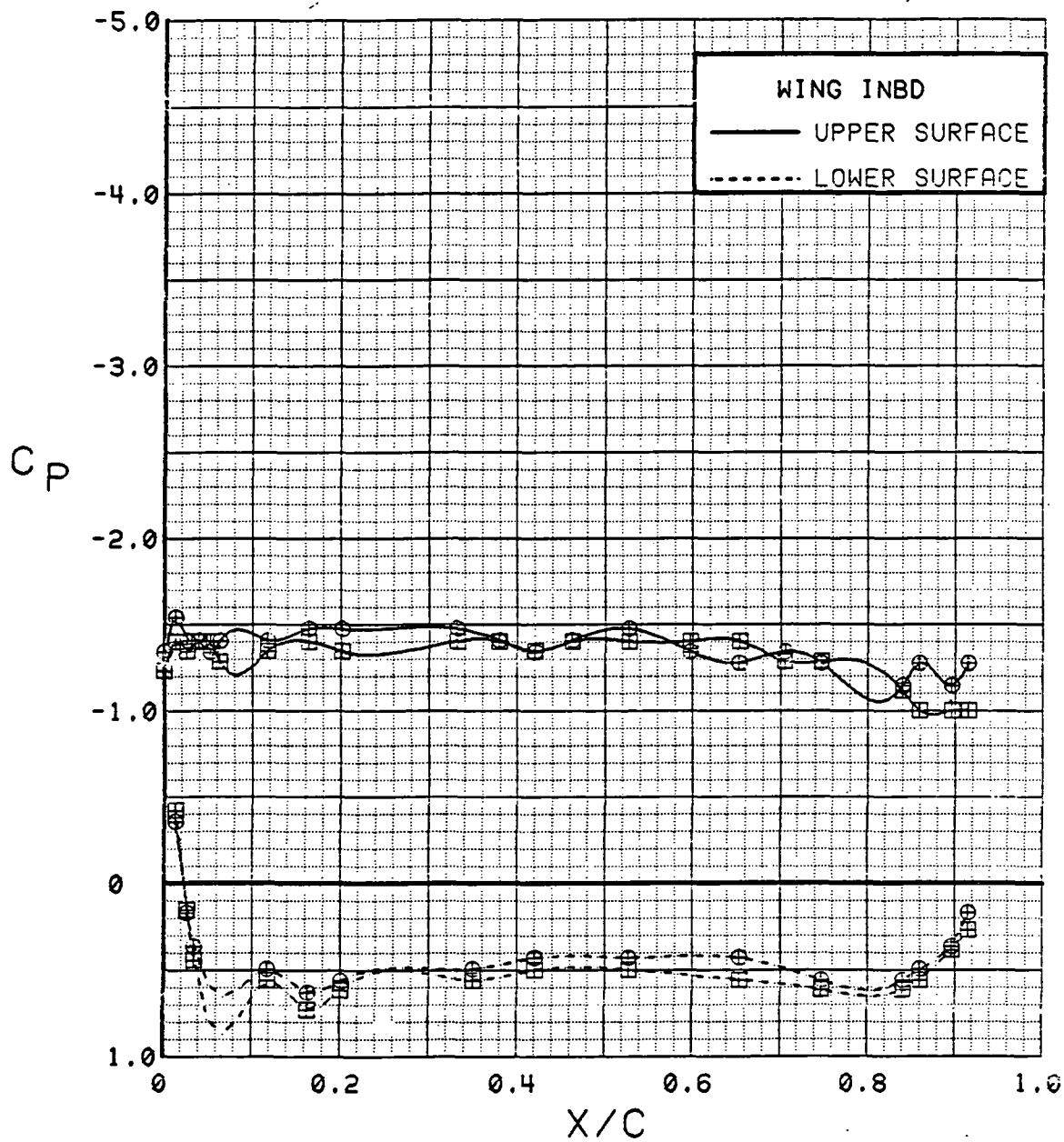


Figure 3.2.4-117 Canard On/Off Effects, Inboard,  $C_T = 0.9$ , Flaps Deflected,  $\alpha = 28^\circ$

SYM	TEST	RUN	ALPHA	CT	ITEF	OTEF	CAN	SWB
⊕	543	6	33.2	0.92	30	30	0	OFF
⊞	537	61	32.9	0.93	30	30	OFF	OFF

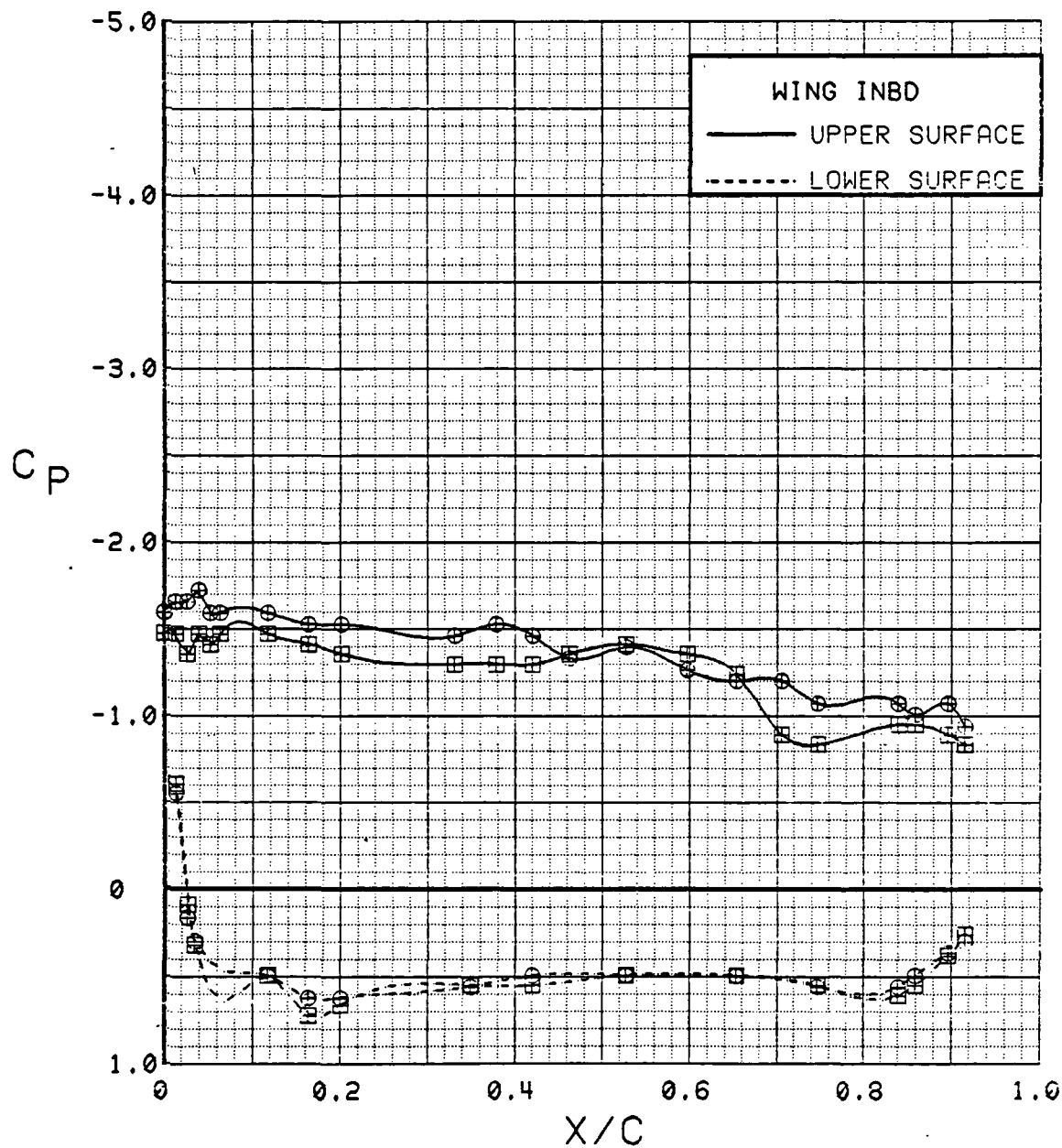


Figure 3.2.4-118 Canard On/Off Effects, Inboard,  $C_T = 0.9$ , Flaps Deflected,  $\alpha = 32^\circ$

SYM	TEST	RUN	ALPHA	CT	ITEF	OTEF	CAN	SWB
⊕	543	6	0.3	0.94	30	30	0	OFF
⊞	537	61	0.4	0.94	30	30	OFF	OFF

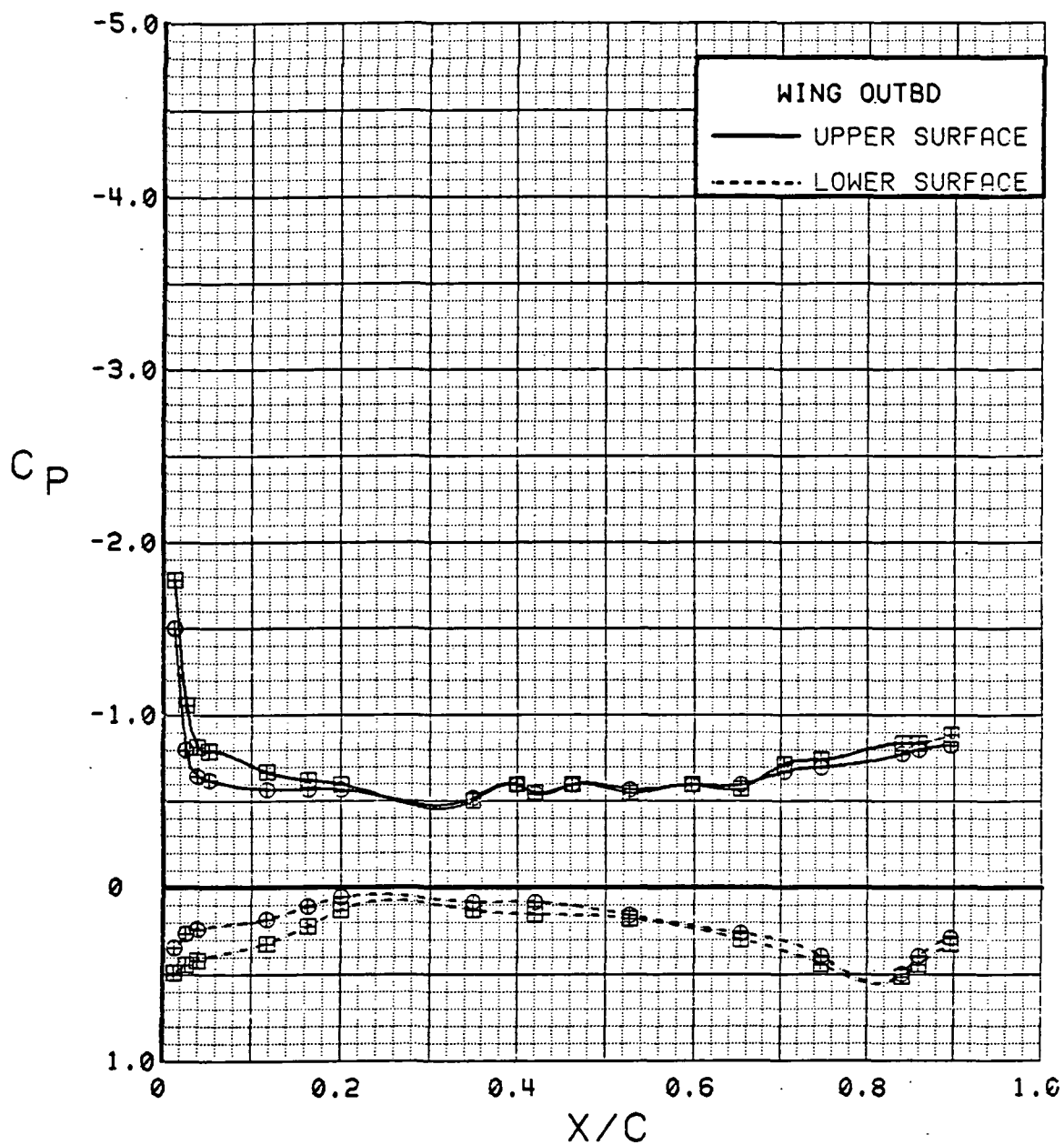


Figure 3.2.4-119 Canard On/Off Effects, Outboard,  $C_T = 0.9$ , Flaps Deflected, Alpha = 0 deg

SYM	TEST	RUN	ALPHA	CT	ITEF	OTEF	CAN	SWB
⊕	543	6	4.5	0.94	30	30	0	OFF
⊞	537	61	4.4	0.94	30	30	OFF	OFF

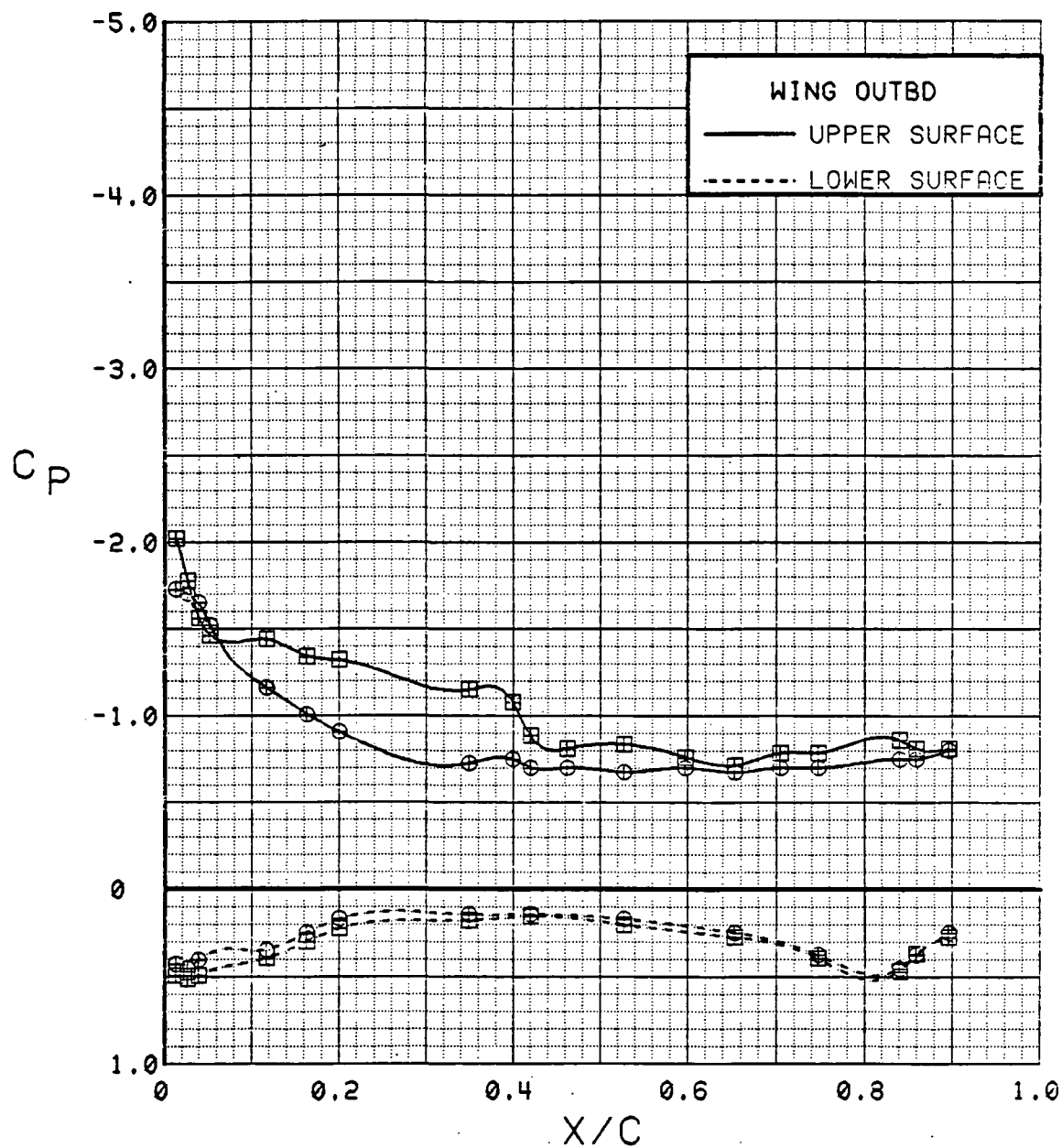


Figure 3.2.4-120 Canard On/Off Effects, Outboard,  $C_T = 0.9$ , Flaps Deflected,  $\alpha = 4$  deg

SYM	TEST	RUN	ALPHA	CT	ITEF	OTEF	CAN	SWB
⊕	543	6	8.6	0.91	30	30	0	OFF
⊞	537	61	8.5	0.94	30	30	OFF	OFF

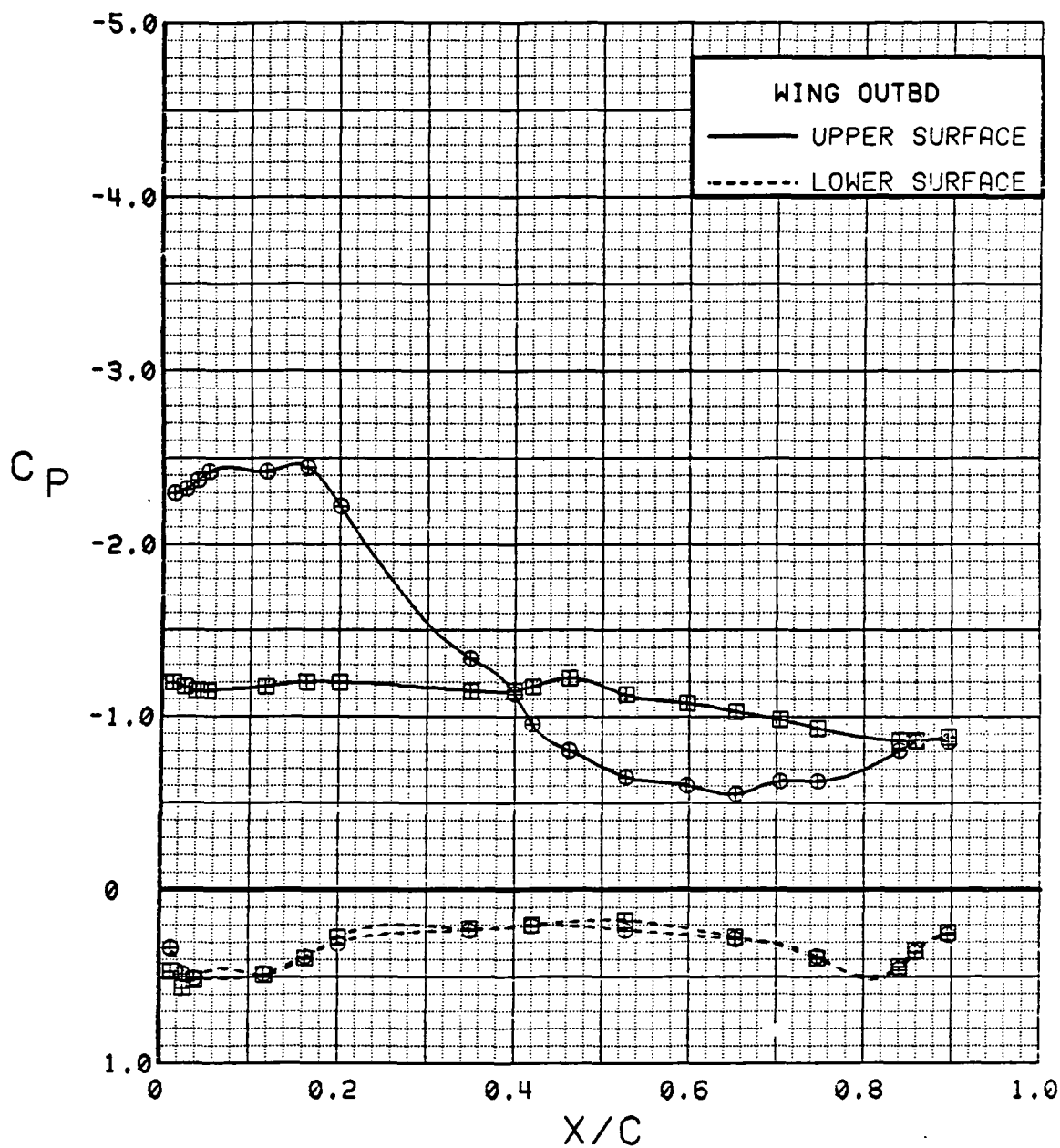


Figure 3.2.4-121 Canard On/Off Effects, Outboard,  $C_T = 0.9$ , Flaps Deflected, Alpha = 8 deg

SYM	TEST	RUN	ALPHA	CT	ITEF	OTEF	CAN	SWB
⊕	543	6	12.8	0.92	30	30	0	OFF
⊞	537	61	12.6	0.92	30	30	OFF	OFF

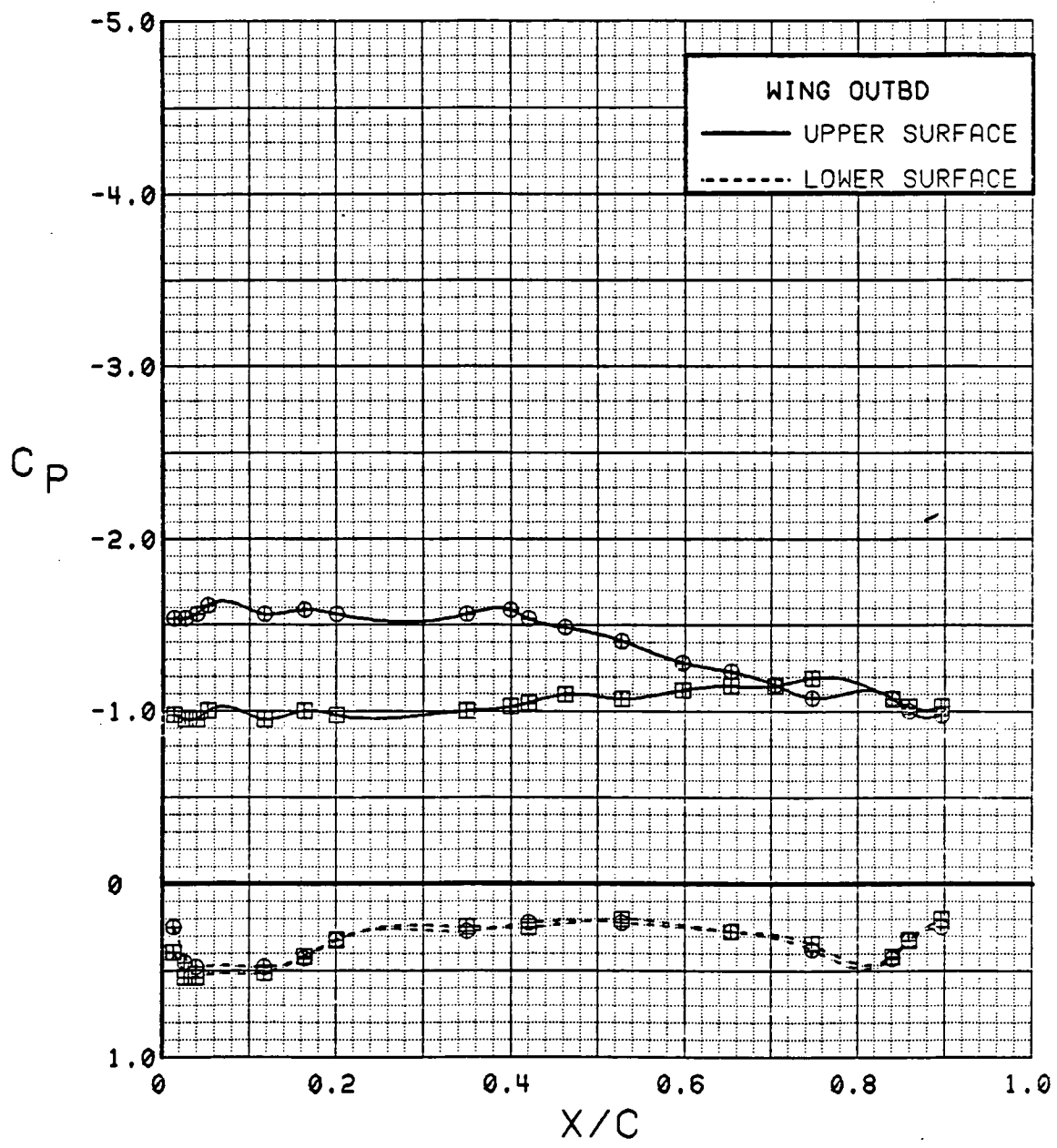


Figure 3.2.4-122 Canard On/Off Effects, Outboard,  $C_T = 0.9$ , Flaps Deflected, Alpha = 12 deg

SYM	TEST	RUN	ALPHA	CT	ITEF	OTEF	CAN	SWB
⊕	543	6	16.9	0.92	30	30	0	OFF
⊞	537	61	16.7	0.94	30	30	OFF	OFF

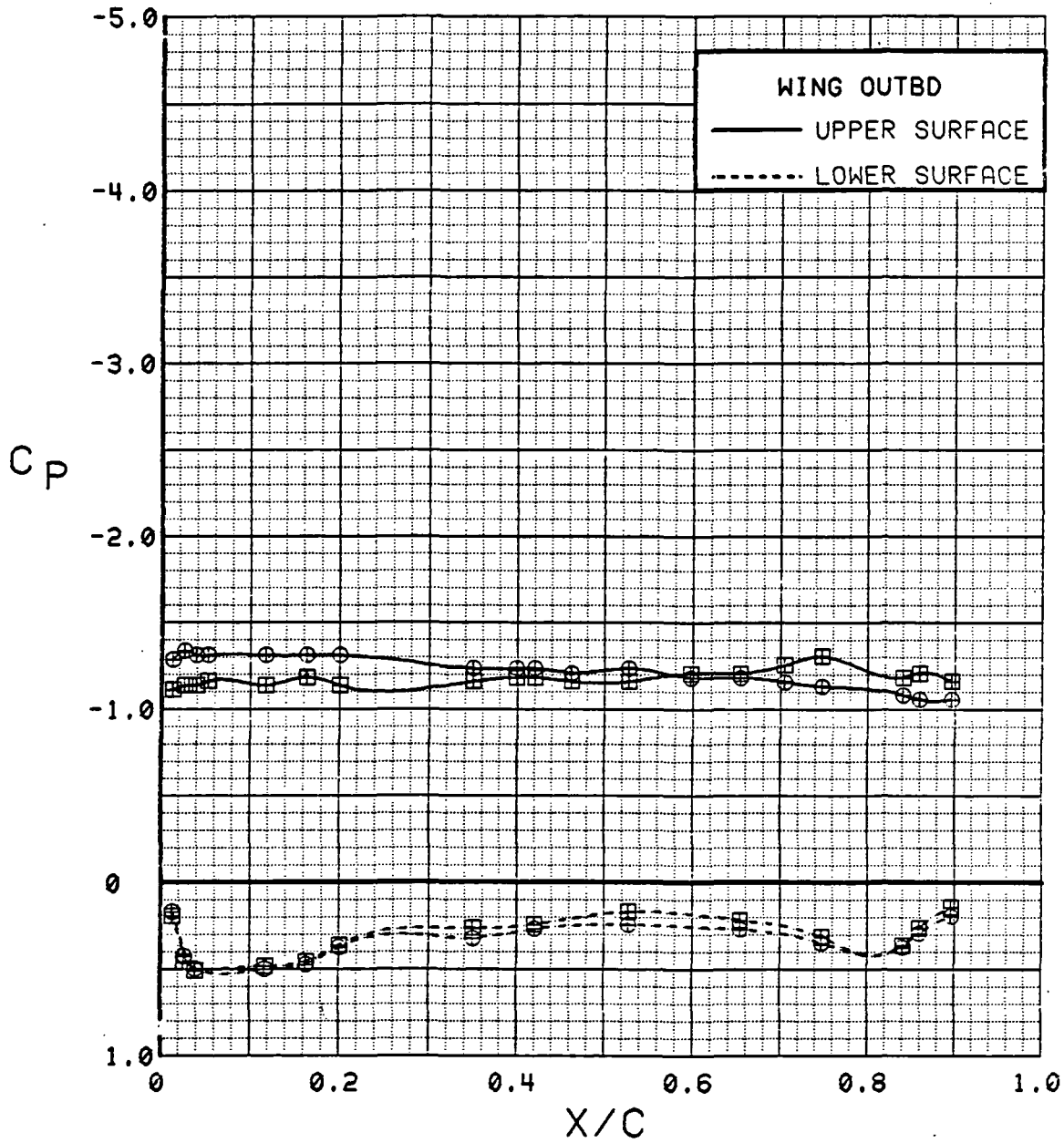


Figure 3.2.4-123 Canard On/Off Effects, Outboard,  $C_T = 0.9$ , Flaps Deflected,  $\alpha = 16^\circ$



SYM	TEST	RUN	ALPHA	CT	ITEF	OTEF	CAN	SWB
⊕	543	6	21.0	0.93	30	30	0	OFF
⊞	537	61	20.8	0.92	30	30	OFF	OFF

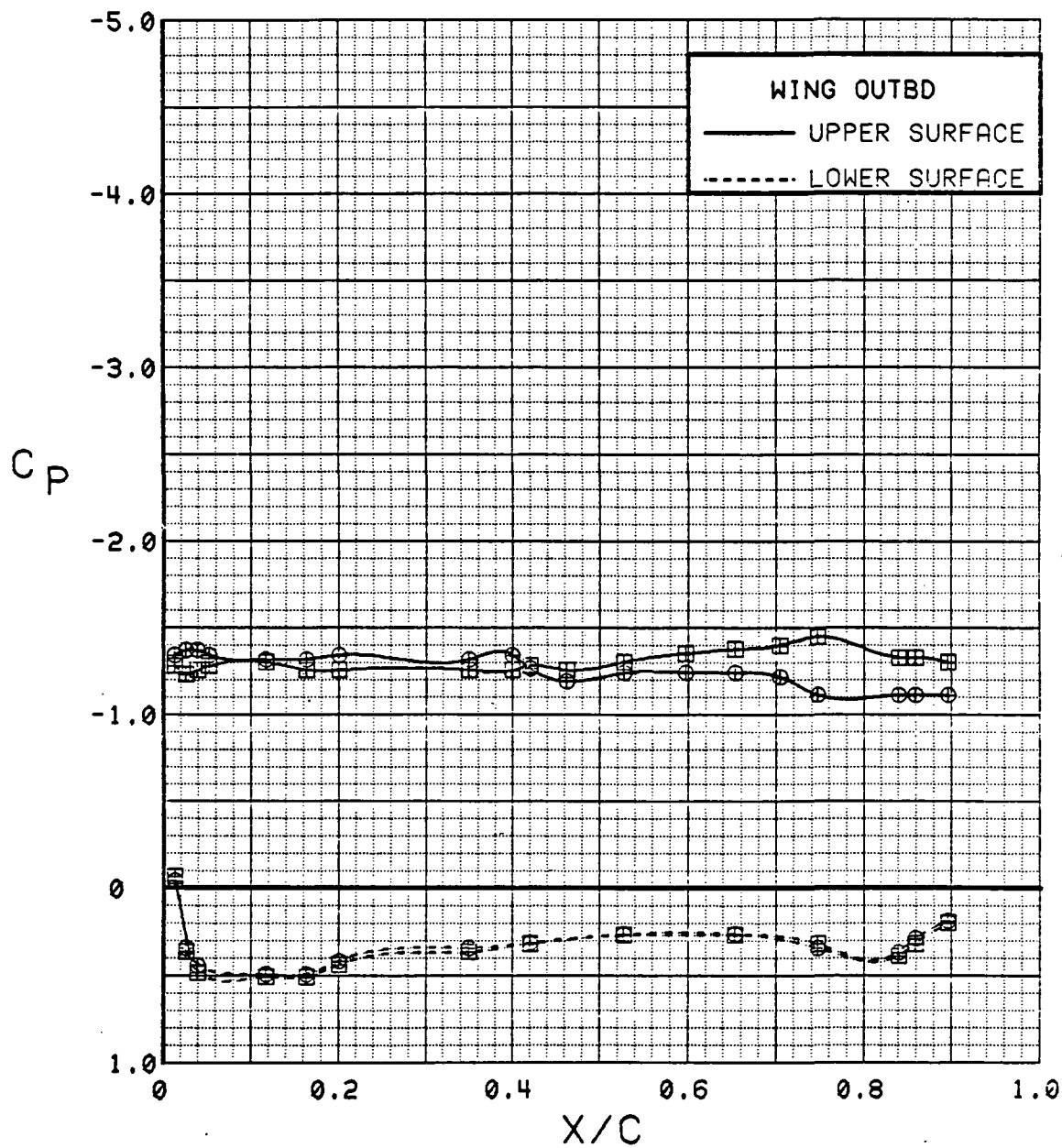


Figure 3.2.4-124 Canard On/Off Effects, Outboard,  $C_T = 0.9$ , Flaps Deflected, Alpha = 20 deg

SYM	TEST	RUN	ALPHA	CT	ITEF	OTEF	CAN	SWB
⊕	543	6	25.1	0.93	30	30	0	OFF
⊞	537	61	24.9	0.92	30	30	OFF	OFF

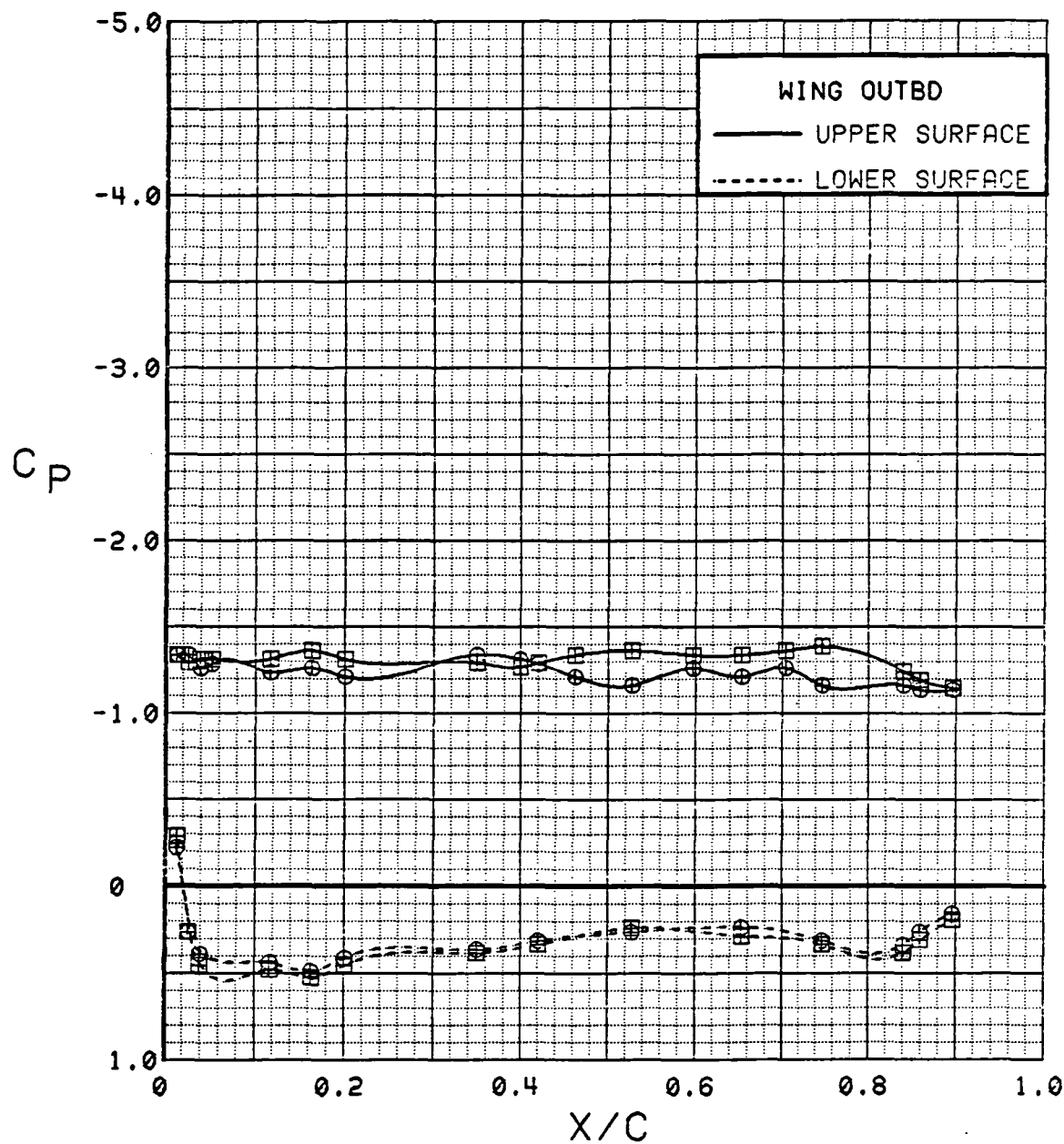


Figure 3.2.4-125 Canard On/Off Effects, Outboard,  $C_T = 0.9$ , Flaps Deflected, Alpha = 24 deg

SYM	TEST	RUN	ALPHA	CT	ITEF	OTEF	CAN	SWB
⊕	543	6	29.1	0.93	30	30	0	OFF
⊞	537	61	28.9	0.93	30	30	OFF	OFF

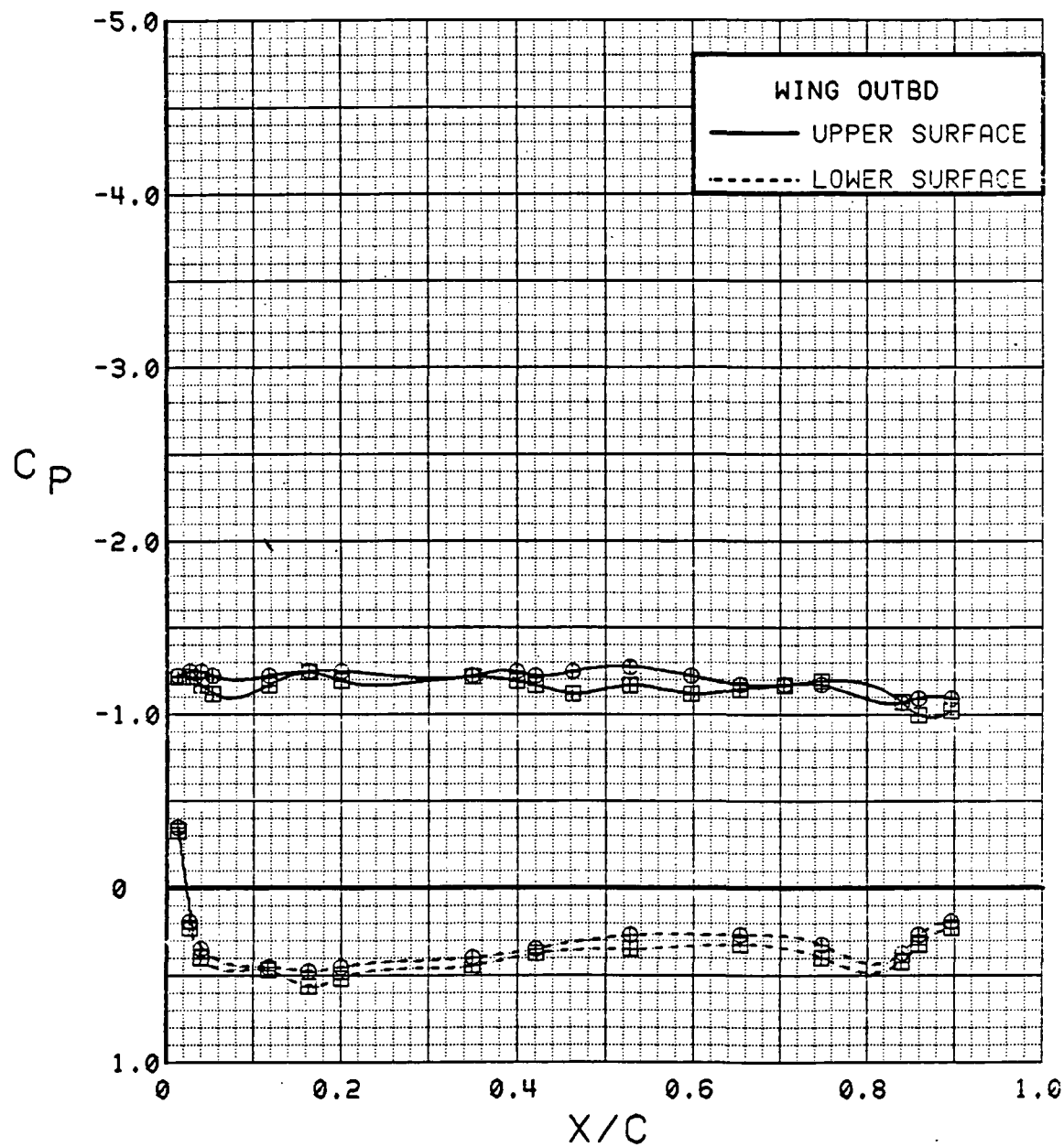


Figure 3.2.4-126 Canard On/Off Effects, Outboard,  $C_T = 0.9$ , Flaps Deflected, Alpha = 28 deg

SYM	TEST	RUN	ALPHA	CT	ITEF	OTEF	CAN	SWB
⊕	543	6	33.2	0.92	30	30	0	OFF
⊞	537	61	32.9	0.93	30	30	OFF	OFF

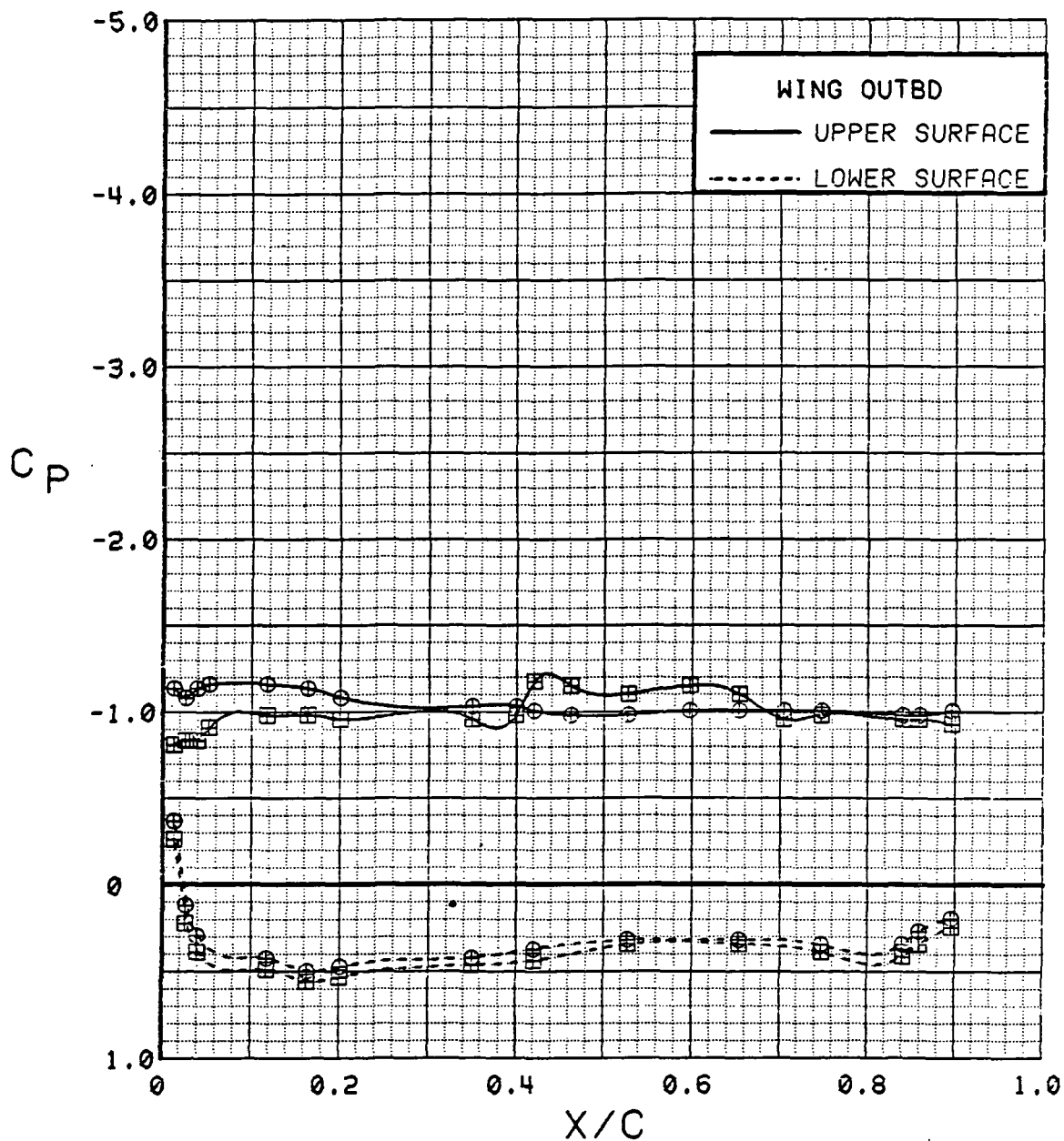


Figure 3.2.4-127

Canard On/Off Effects, Outboard,  $C_T = 0.9$ ,  
Flaps Deflected, Alpha = 32 deg

SYM	TEST	RUN	ALPHA	CT	ITEF	OTEF	CAN	SWB
⊕	543	6	0.3	0.94	30	30	0	OFF
⊞	537	61	0.4	0.94	30	30	OFF	OFF

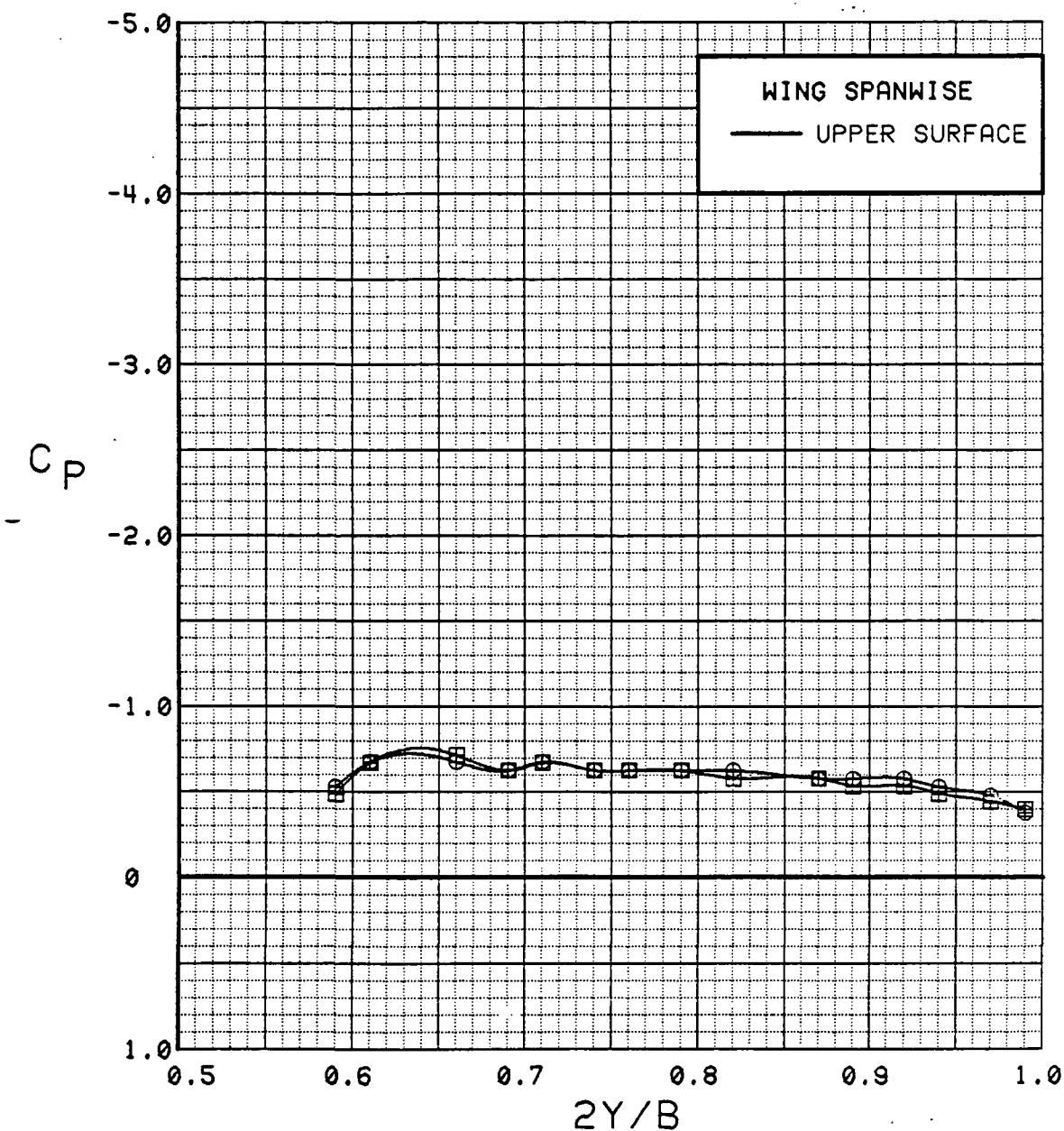


Figure 3.2.4-128 Canard On/Off Effects, Spanwise,  $C_T = 0.9$ , Flaps Deflected,  $\alpha = 0$  deg

SYM	TEST	RUN	ALPHA	CT	ITEF	OTEF	CAN	SWB
⊙	543	6	4.5	0.94	30	30	0	OFF
⊠	537	61	4.4	0.94	30	30	OFF	OFF

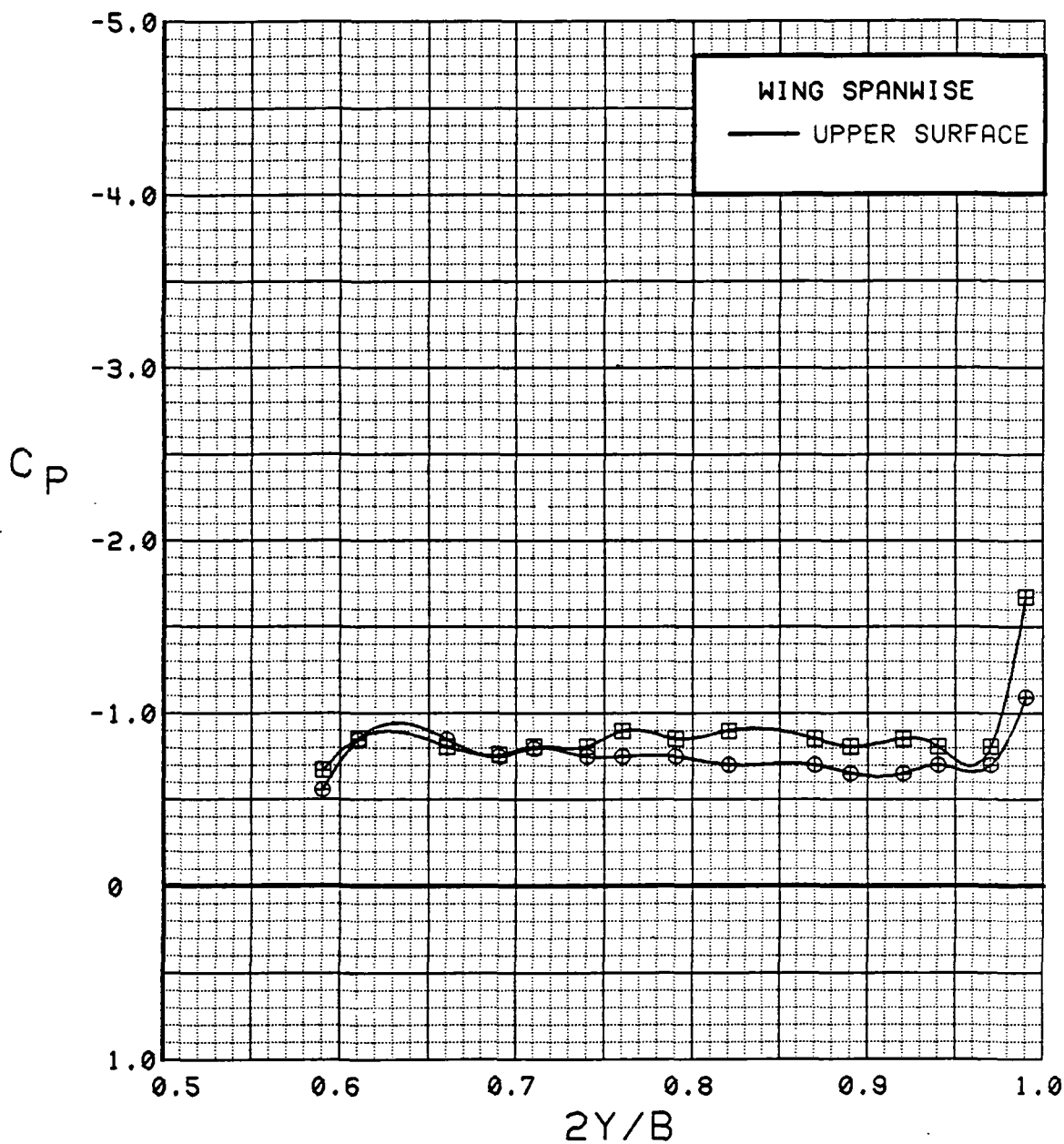


Figure 3.2.4-129 Canard On/Off Effects, Spanwise,  $C_T = 0.9$ , Flaps Deflected,  $\alpha = 4$  deg

SYM	TEST	RUN	ALPHA	CT	ITEF	OTEF	CAN	SWB
•	543	6	8.6	0.91	30	30	0	OFF
■	537	61	8.5	0.94	30	30	OFF	OFF

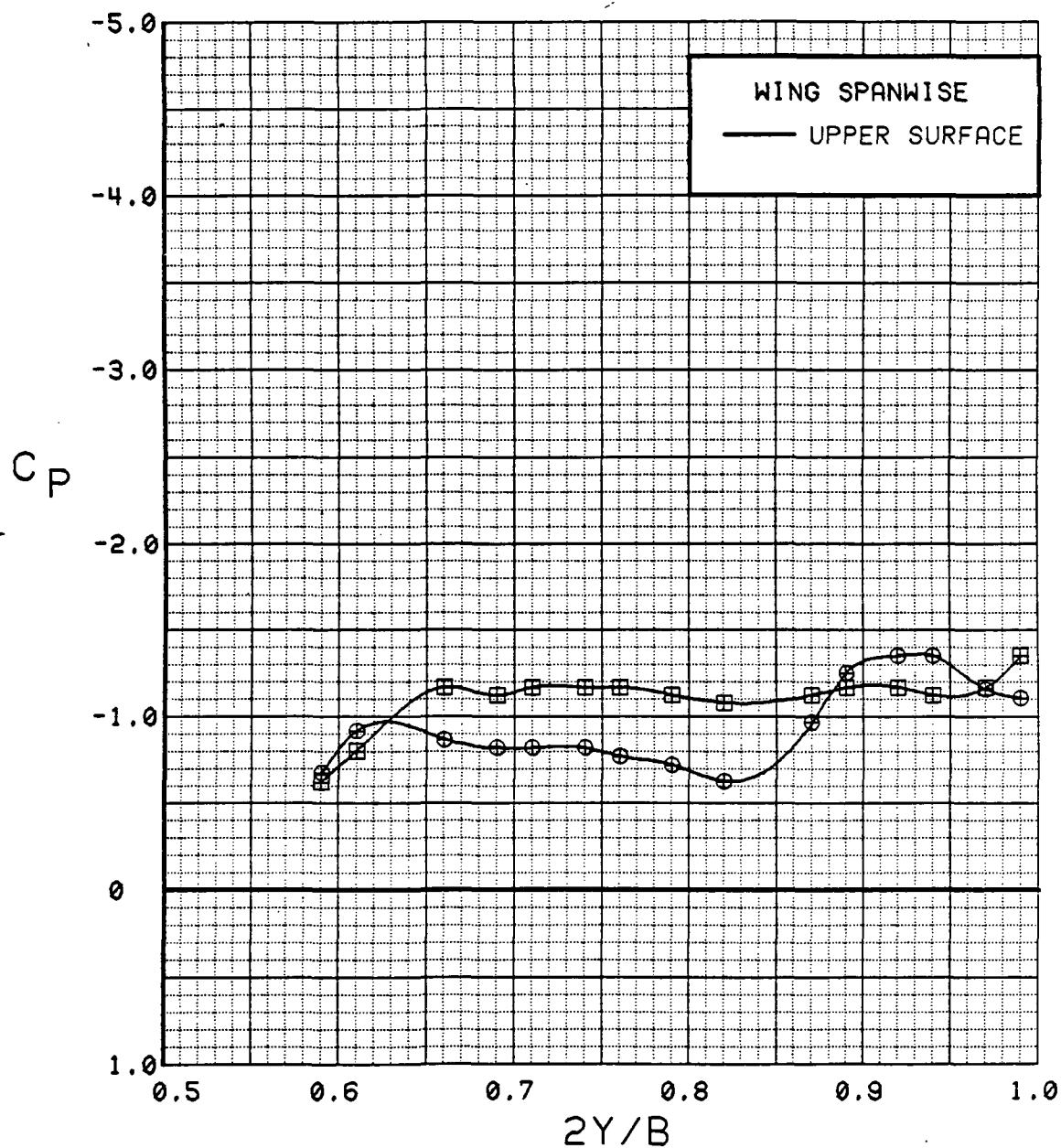


Figure 3.2.4-130 Canard On/Off Effects, Spanwise,  $C_T = 0.9$ , Flaps Deflected,  $\alpha = 8$  deg

SYM	TEST	RUN	ALPHA	CT	ITEF	OTEF	CAN	SWB
⊕	543	6	12.8	0.92	30	30	0	OFF
⊞	537	61	12.6	0.92	30	30	OFF	OFF

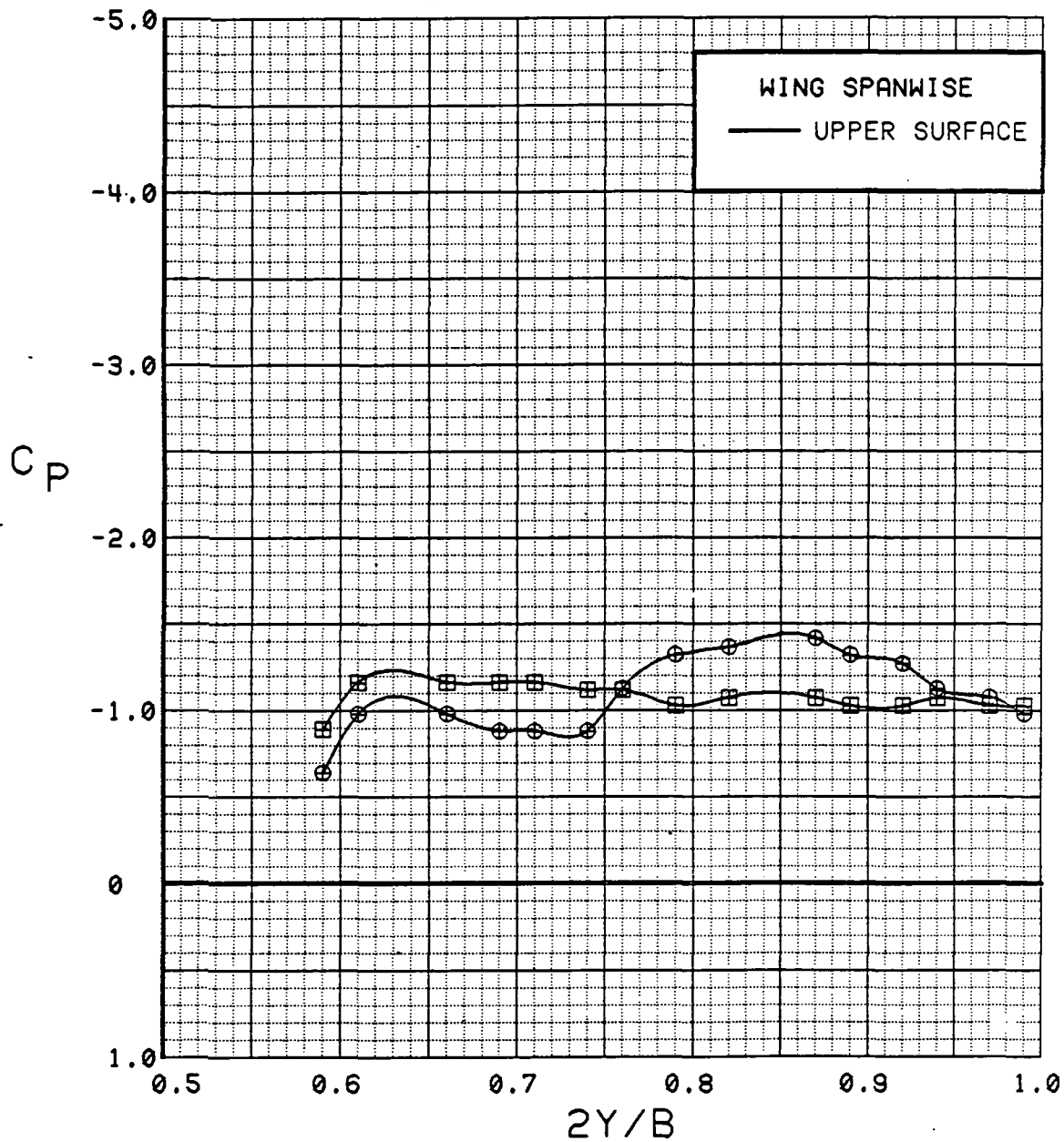


Figure 3.2.4-131 Canard On/Off Effects, Spanwise,  $C_T = 0.9$ , Flaps Deflected, Alpha = 12 deg



SYM	TEST	RUN	ALPHA	CT	ITEF	OTEF	CAN	SWB
⊕	543	6	16.9	0.92	30	30	0	OFF
⊞	537	61	16.7	0.94	30	30	OFF	OFF

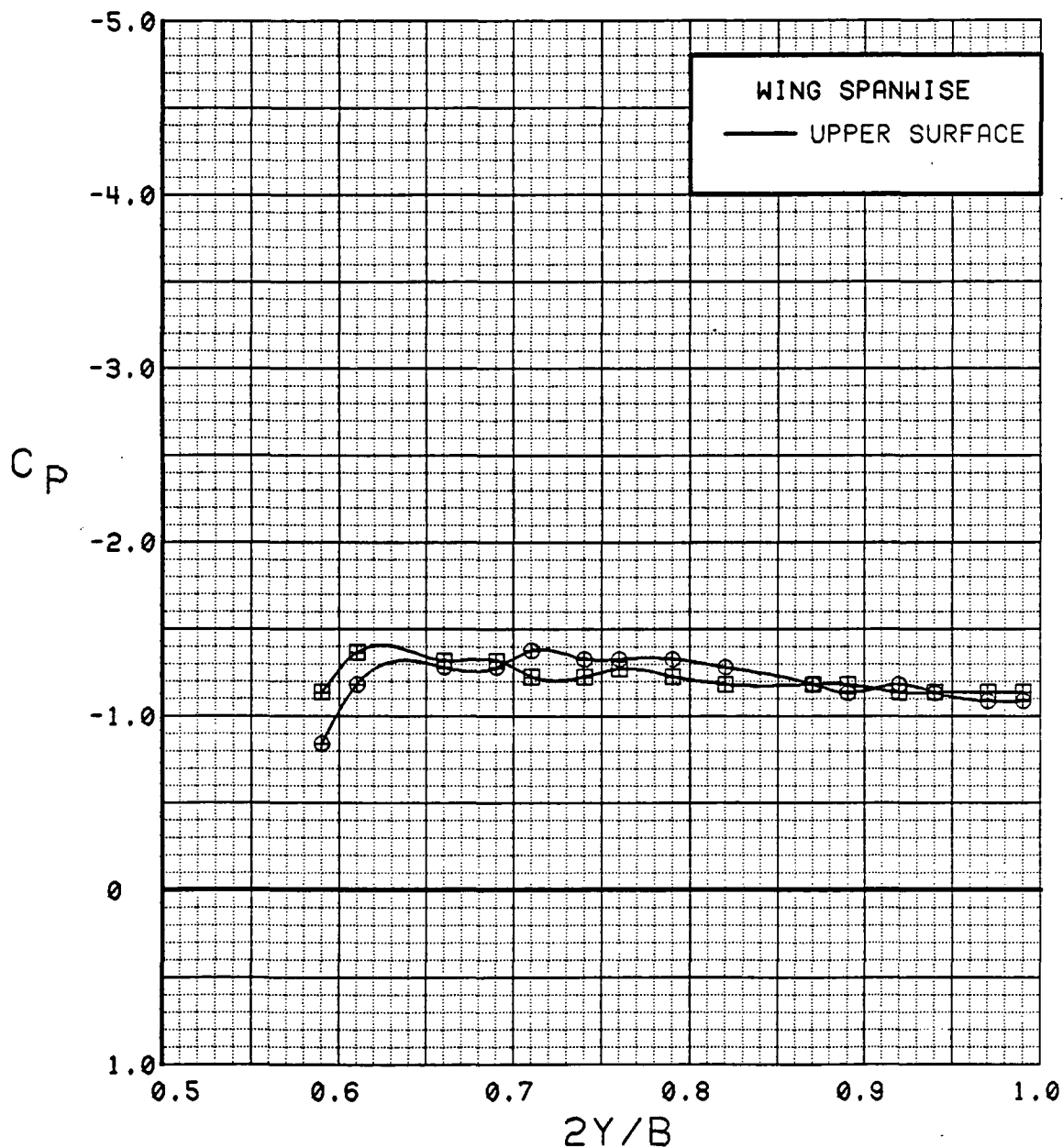


Figure 3.2.4-132 Canard On/Off Effects, Spanwise,  $C_T = 0.9$ , Flaps Deflected, Alpha = 16 deg

SYM	TEST	RUN	ALPHA	CT	ITEF	OTEF	CAN	SWB
⊕	543	6	21.0	0.93	30	30	0	OFF
⊞	537	61	20.8	0.92	30	30	OFF	OFF

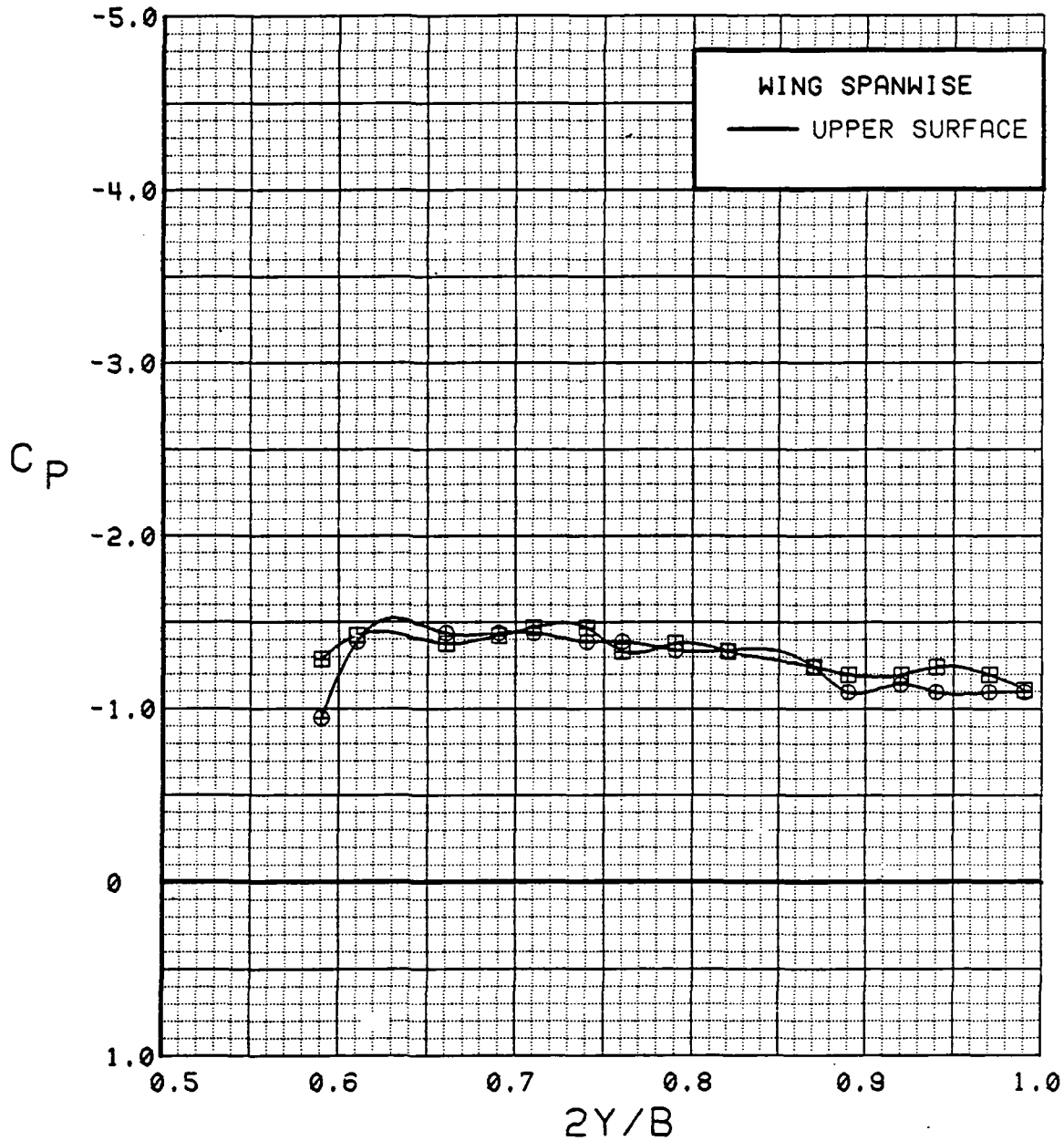


Figure 3.2.4-133 Canard On/Off Effects, Spanwise,  $C_T = 0.9$ , Flaps Deflected, Alpha = 20 deg

SYM	TEST	RUN	ALPHA	CT	ITEF	OTEF	CAN	SWB
⊕	543	6	25.1	0.93	30	30	0	OFF
⊞	537	61	24.9	0.92	30	30	OFF	OFF

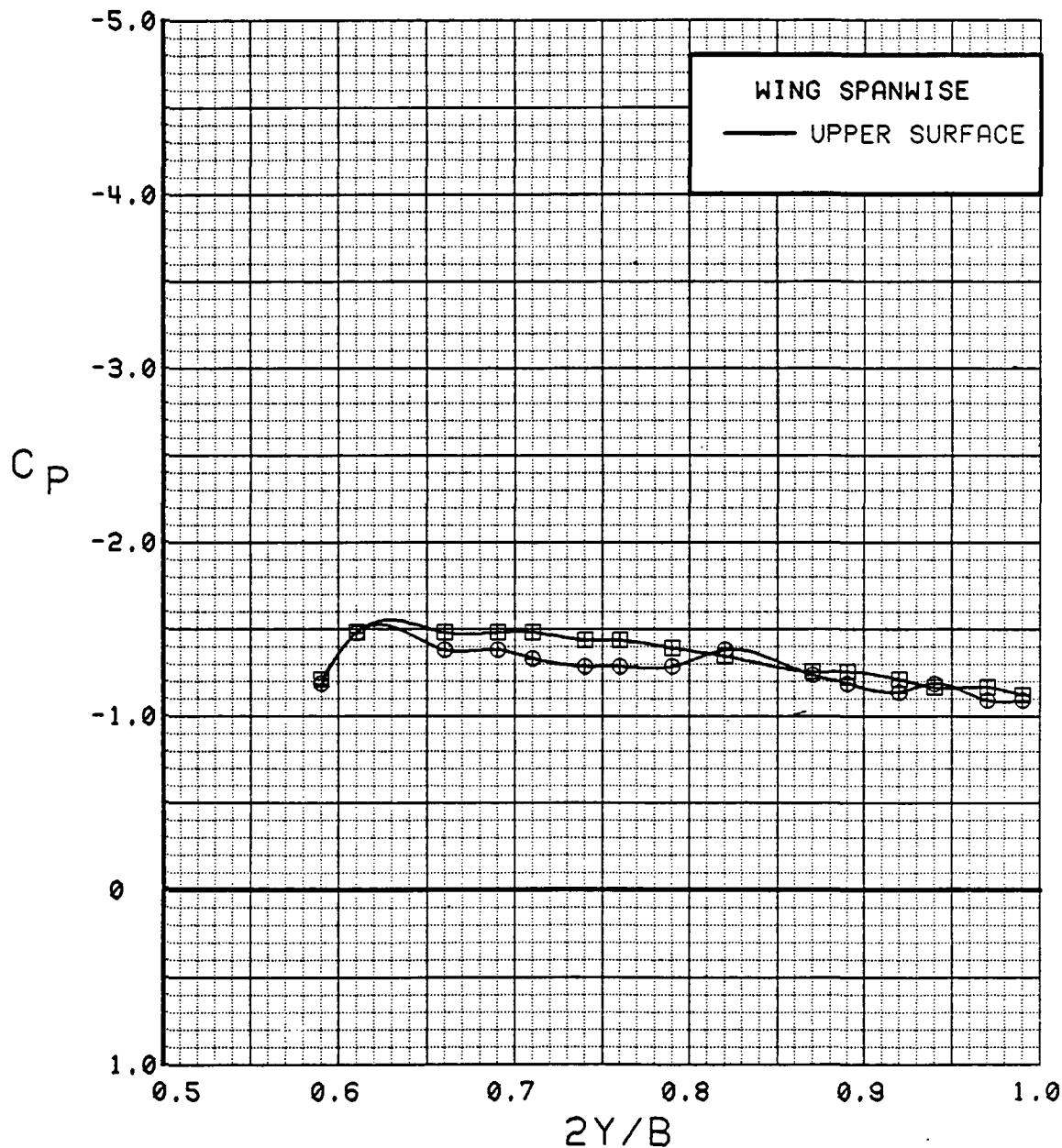


Figure 3.2.4-134 Canard On/Off Effects, Spanwise,  $C_T = 0.9$ , Flaps Deflected,  $\alpha = 24$  deg

SYM	TEST	RUN	ALPHA	CT	ITEF	OTEF	CAN	SWB
⊙	543	6	29.1	0.93	30	30	0	OFF
⊠	537	61	28.9	0.93	30	30	OFF	OFF

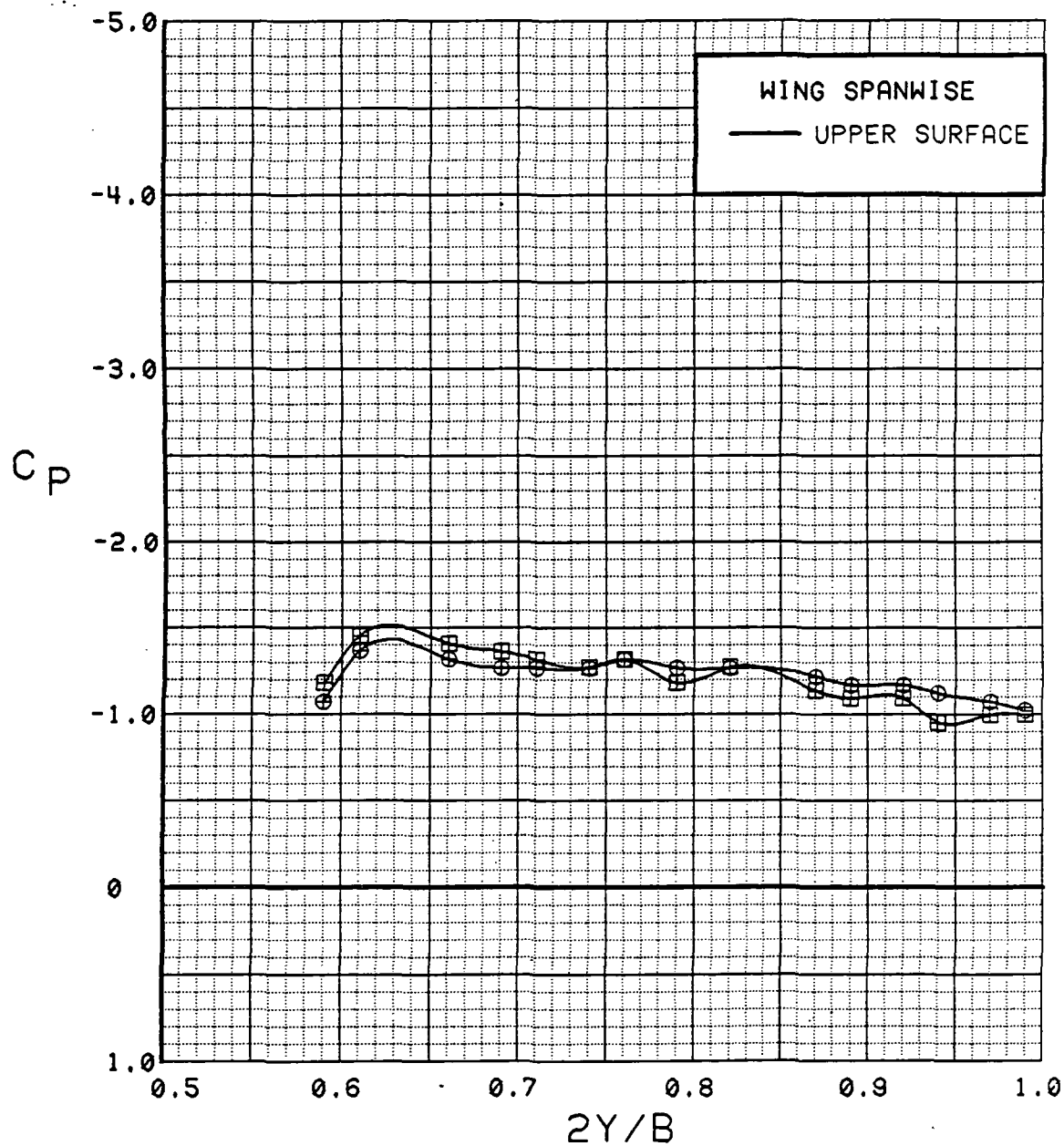


Figure 3.2.4-135 Canard On/Off Effects, Spanwise,  $C_T = 0.9$ , Flaps Deflected, Alpha = 28 deg

SYM	TEST	RUN	ALPHA	CT	ITEF	OTEF	CAN	SWB
⊕	543	6	33.2	0.92	30	30	0	OFF
⊞	537	61	32.9	0.93	30	30	OFF	OFF

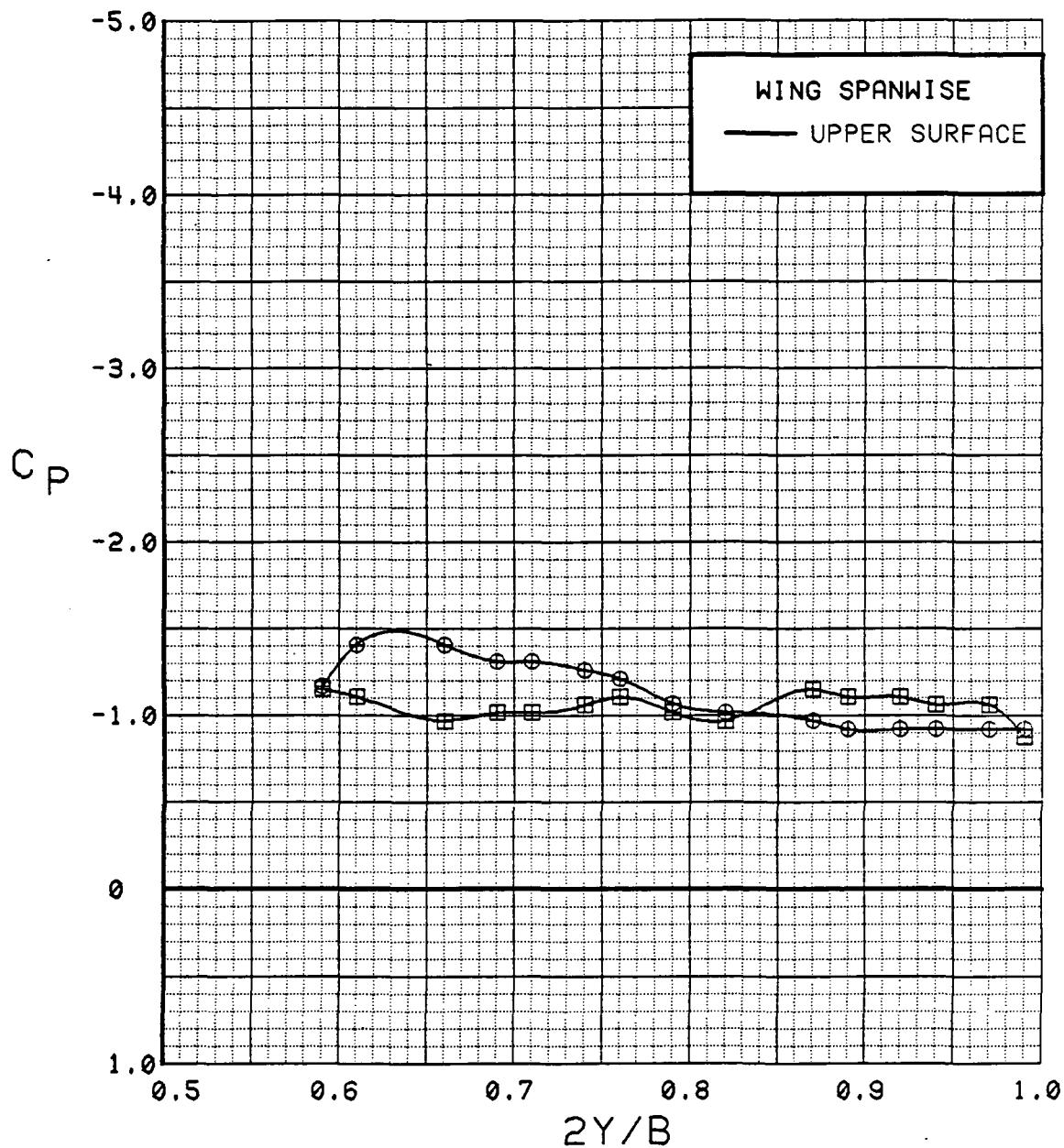


Figure 3.2.4-136 Canard On/Off Effects, Spanwise,  $C_T = 0.9$ , Flaps Deflected, Alpha = 32 deg

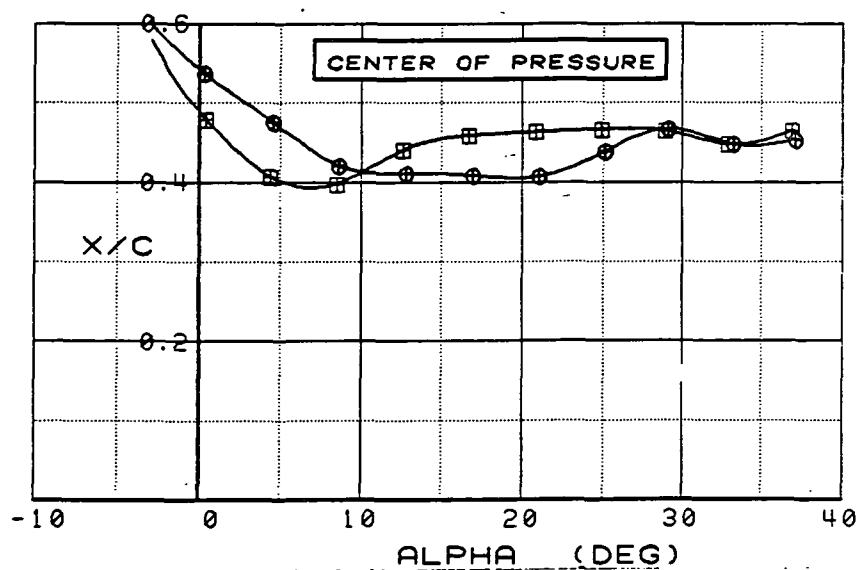
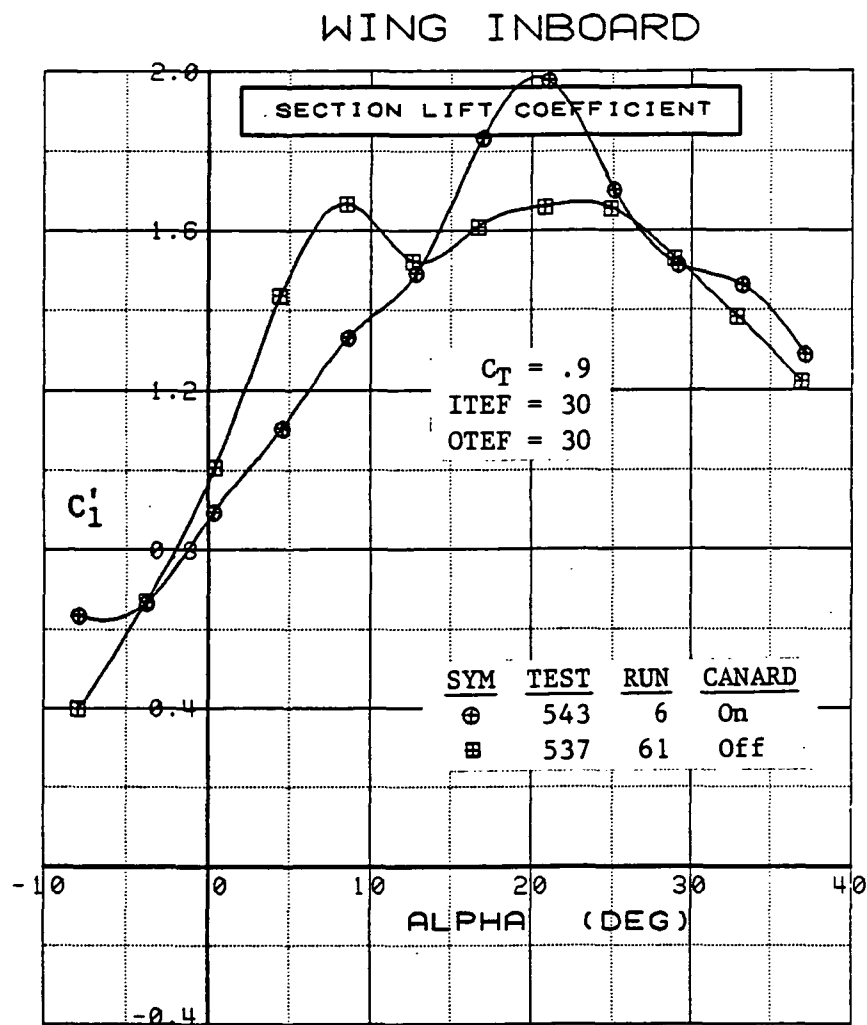


Figure 3.2.4-137 Canard On/Off Effects, Inboard,  $C_T = 0.9$ , Flaps Deflected, Integrated Section Properties

## WING OUTBOARD

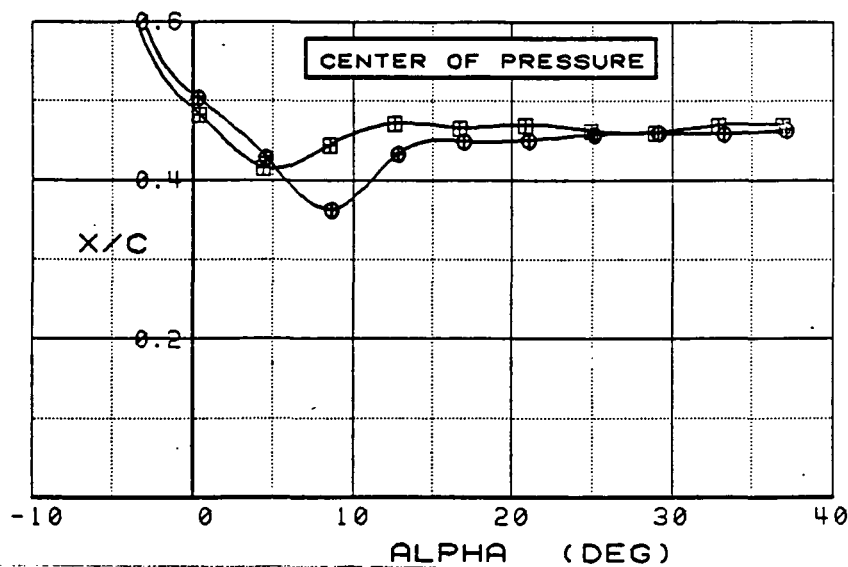
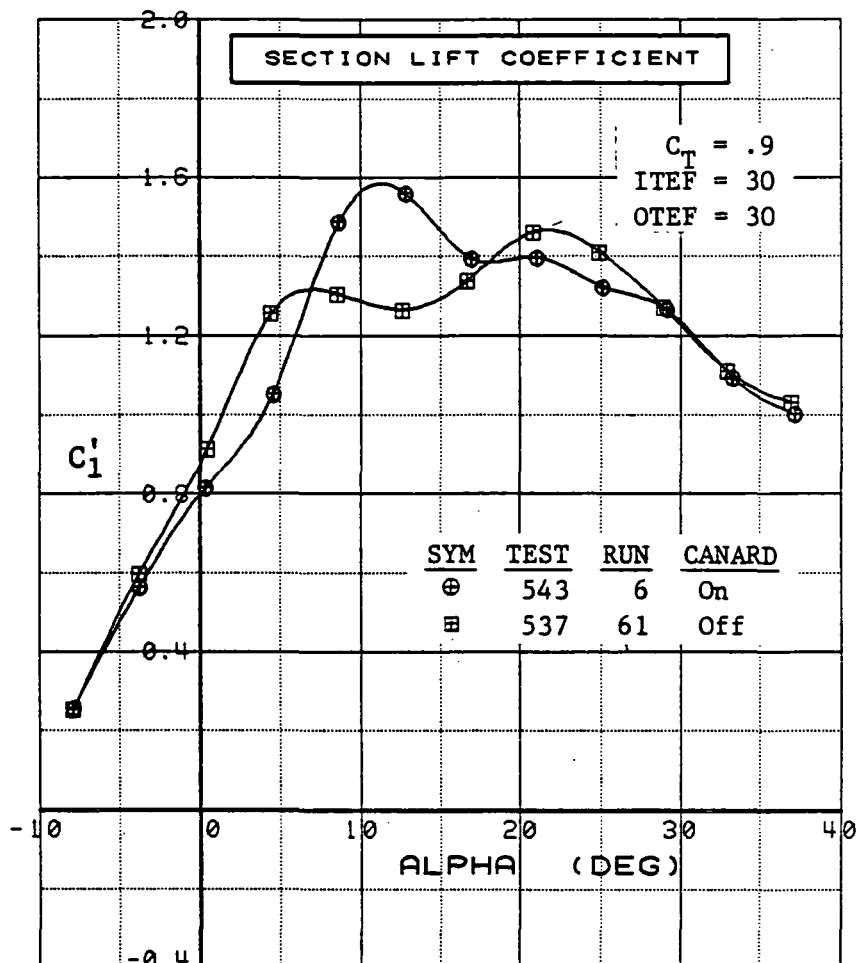


Figure 3.2.4-138

Canard On/Off Effects, Outboard,  $C_T = 0.9$ ,  
 Flaps Deflected, Integrated Section Properties

SYM	TEST	RUN	ALPHA	CT	ITEF	OTEF	CAN	SWB
⊕	537	12	12.7	0.00	30	30	0	OFF
⊞	537	69	12.5	0.00	30	30	OFF	OFF

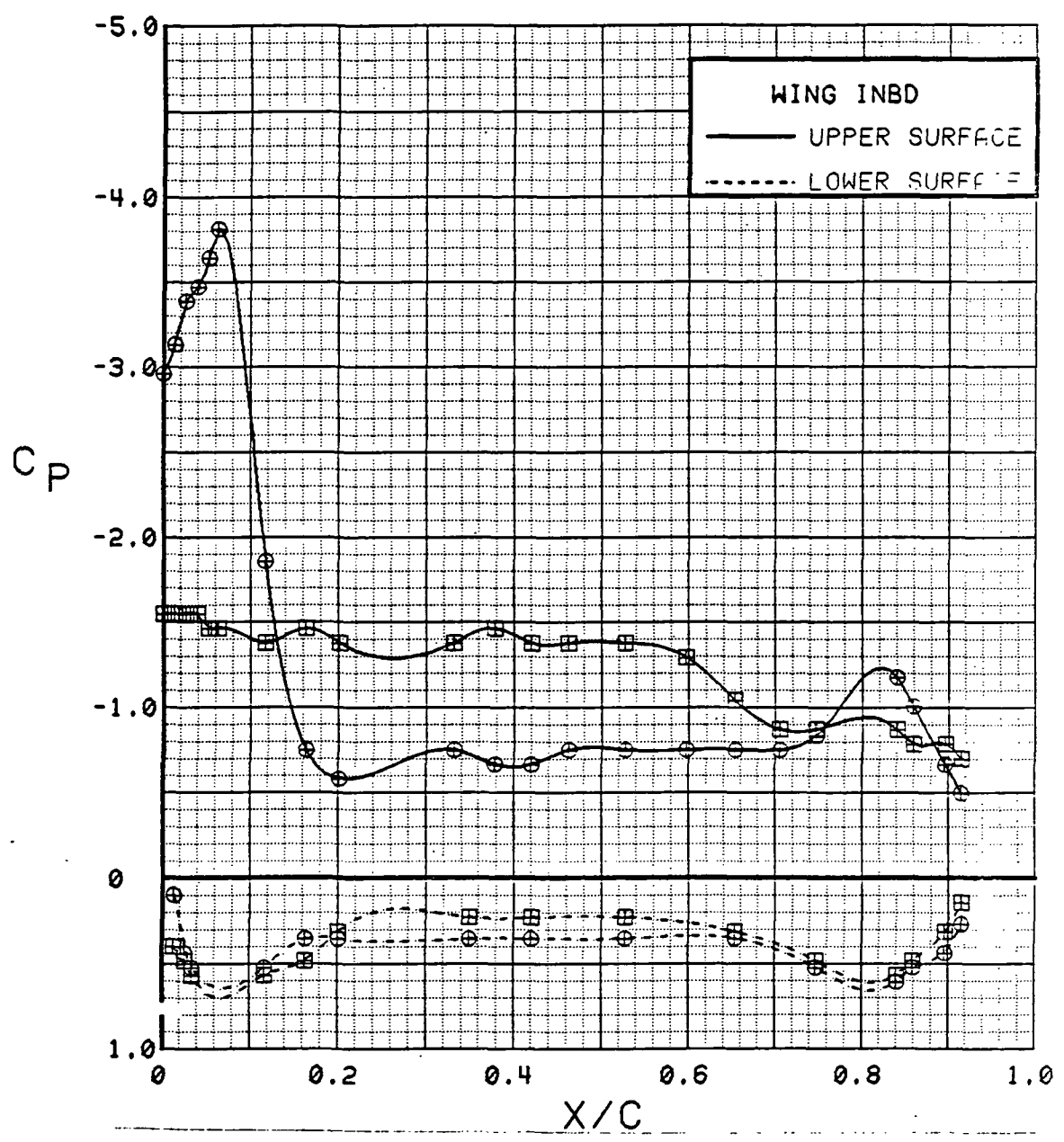


Figure 3.2.4-139 Canard On/Off Effects, Forward Position, Inboard, Power Off, Alpha = 12 deg



SYM	TEST	RUN	ALPHA	CT	ITEF	OTEF	CAN	SWB
⊕	537	12	16.7	0.00	30	30	0	OFF
⊞	537	69	16.6	0.00	30	30	OFF	OFF

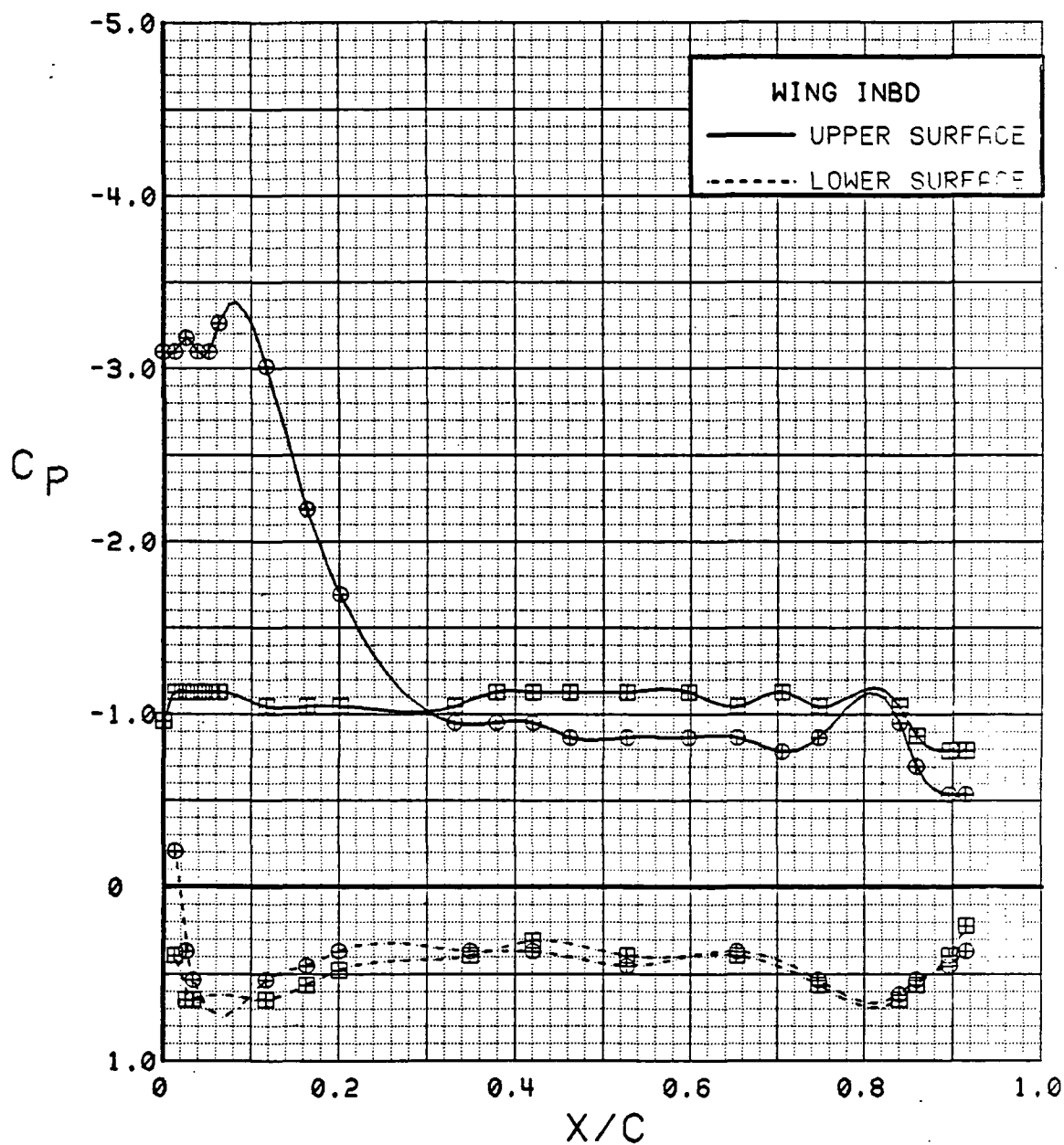


Figure 3.2.4-140 Canard On/Off Effects, Forward Position, Inboard, Power Off, Alpha = 16 deg

SYM	TEST	RUN	ALPHA	CT	ITEF	OTEF	CAN	SWB
⊕	537	12	20.8	0.00	30	30	0	OFF
⊞	537	69	20.6	0.00	30	30	OFF	OFF

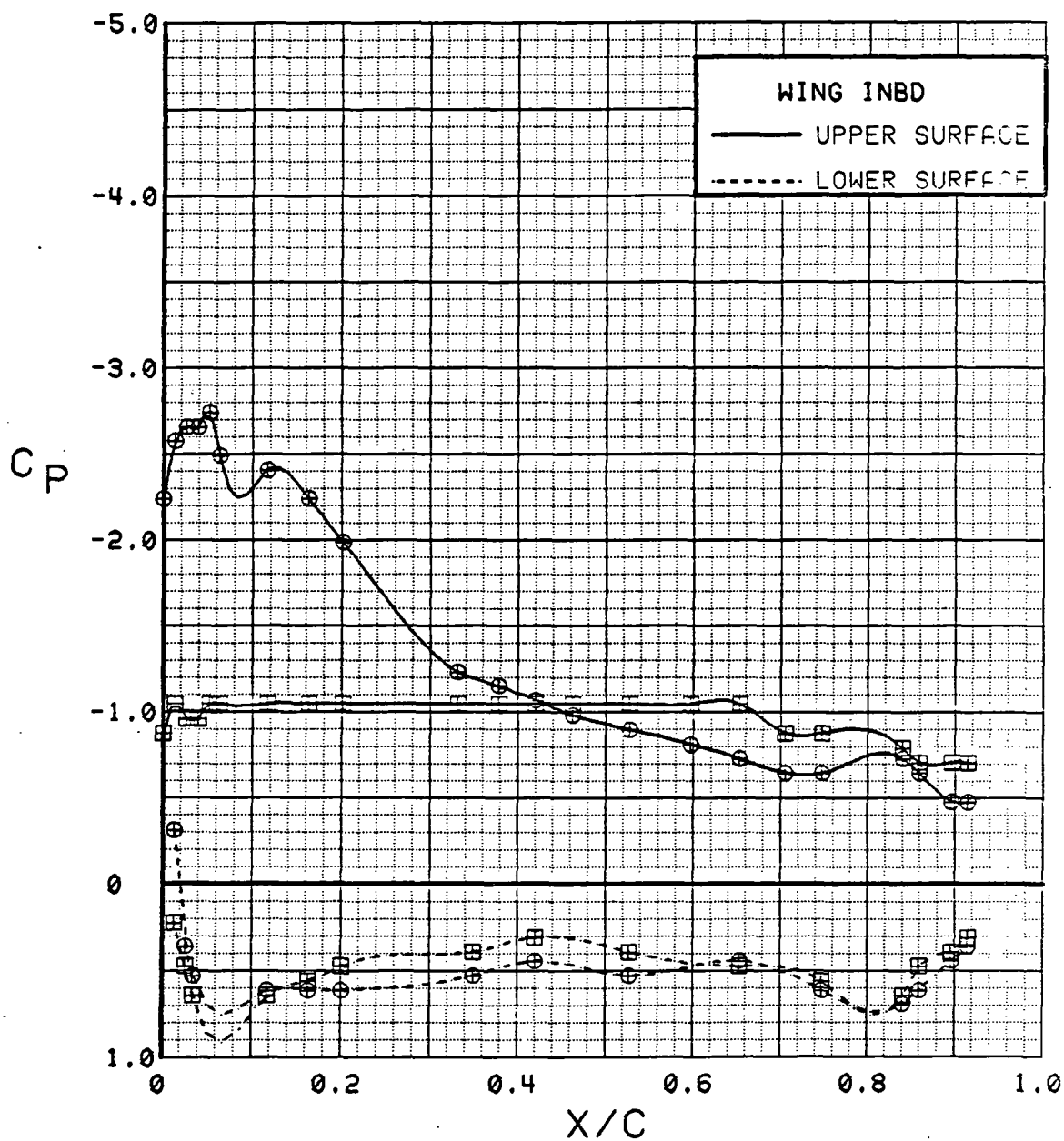


Figure 3.2.4-141 Canard On/Off Effects, Forward Position, Inboard, Power Off, Alpha = 20 deg

SYM	TEST	RUN	ALPHA	CT.	ITEF	OTEF	CAN	SWB
⊕	537	12	12.7	0.00	30	30	0	OFF
⊞	537	69	12.5	0.00	30	30	OFF	OFF

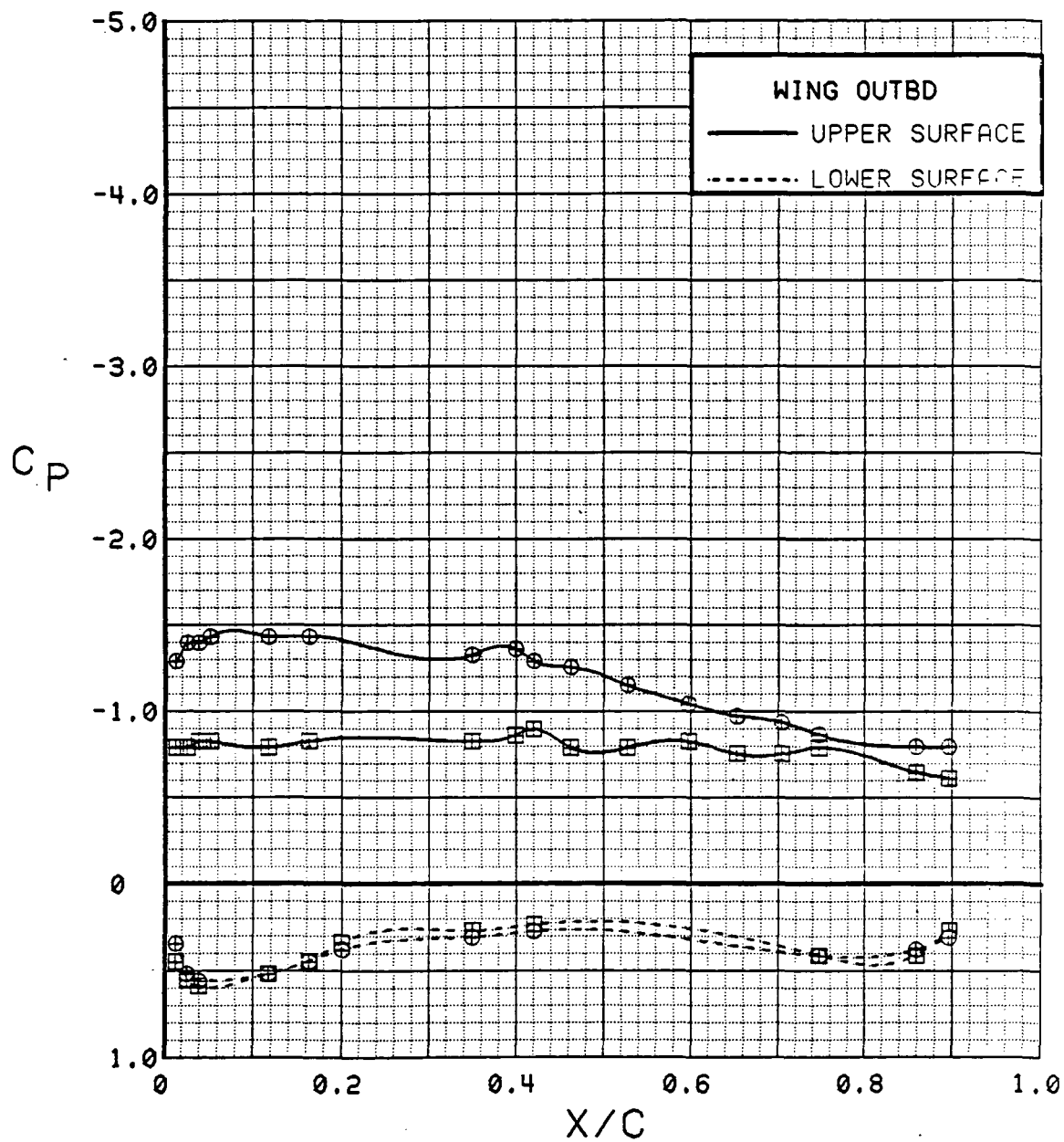


Figure 3.2.4-142 Canard On/Off Effects, Forward Position, Outboard, Power Off, Alpha = 12 deg

SYM	TEST	RUN	ALPHA	CT	ITEF	OTEF	CAN	SWB
⊕	537	12	16.7	0.00	30	30	0	OFF
⊞	537	69	16.6	0.00	30	30	OFF	OFF

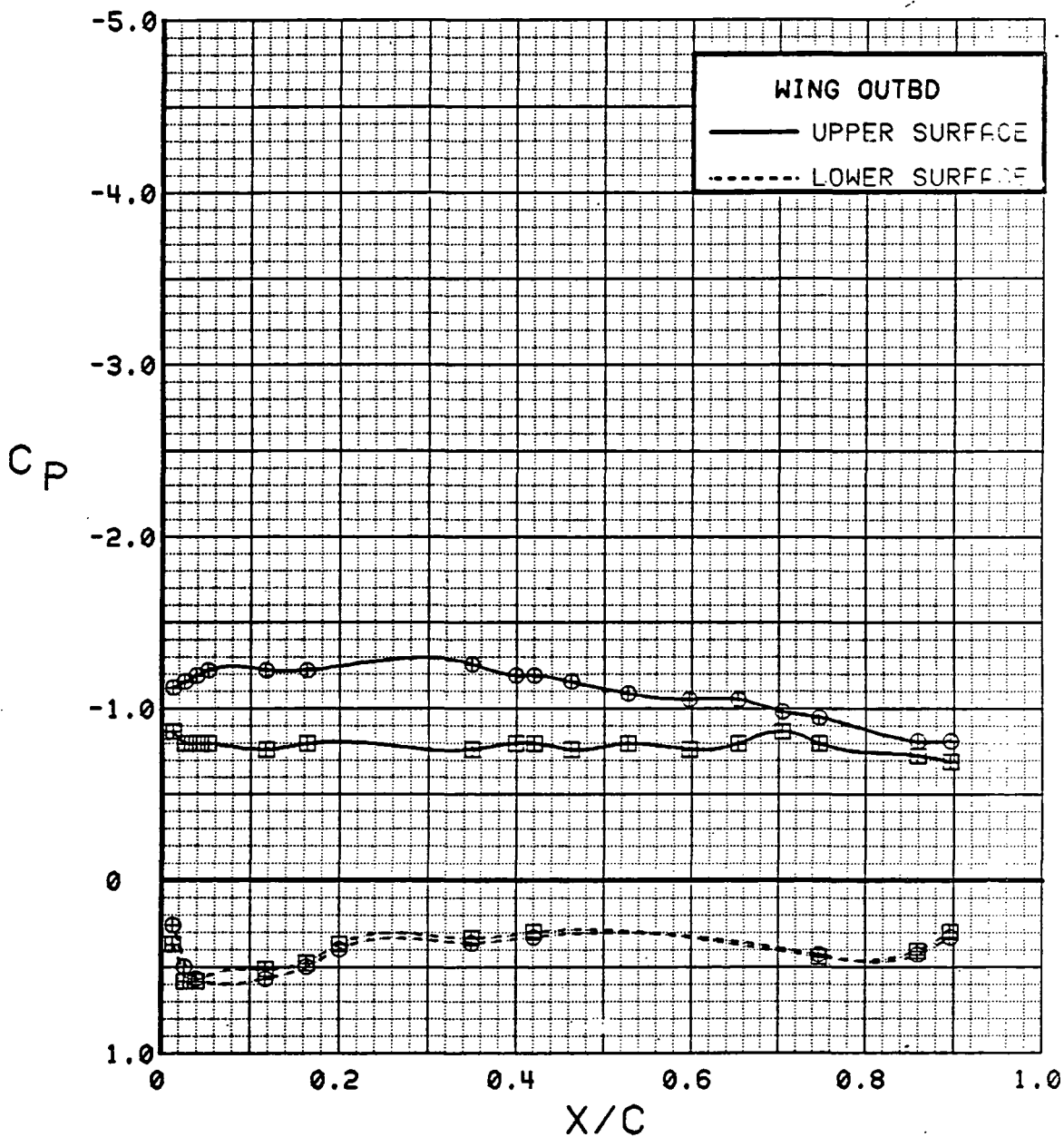


Figure 3.2.4-143 Canard On/Off Effects, Forward Position, Outboard, Power Off, Alpha = 16 deg

SYM	TEST	RUN	ALPHA	CT	ITEF	OTEF	CAN	SWB
⊕	537	12	20.8	0.00	30	30	0	OFF
⊞	537	69	20.6	0.00	30	30	OFF	OFF

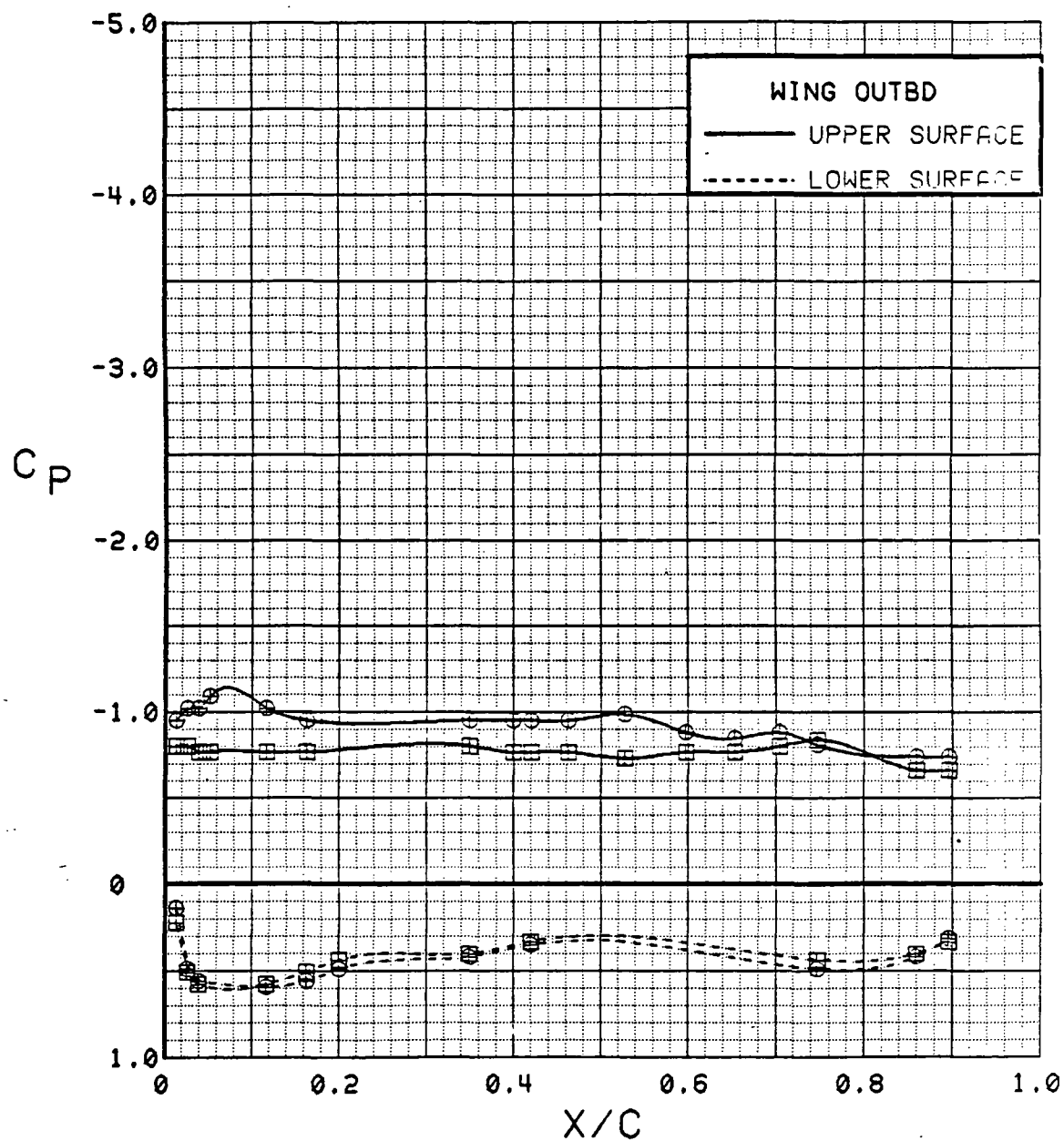


Figure 3.2.4-144 Canard On/Off Effects, Forward Position, Outboard, Power Off, Alpha = 20 deg

220

SYM	TEST	RUN	ALPHA	CT	ITEF	OTEF	CAN	SWB
⊕	537	32	12.8	0.92	30	30	0	OFF
⊞	537	61	12.6	0.92	30	30	OFF	OFF

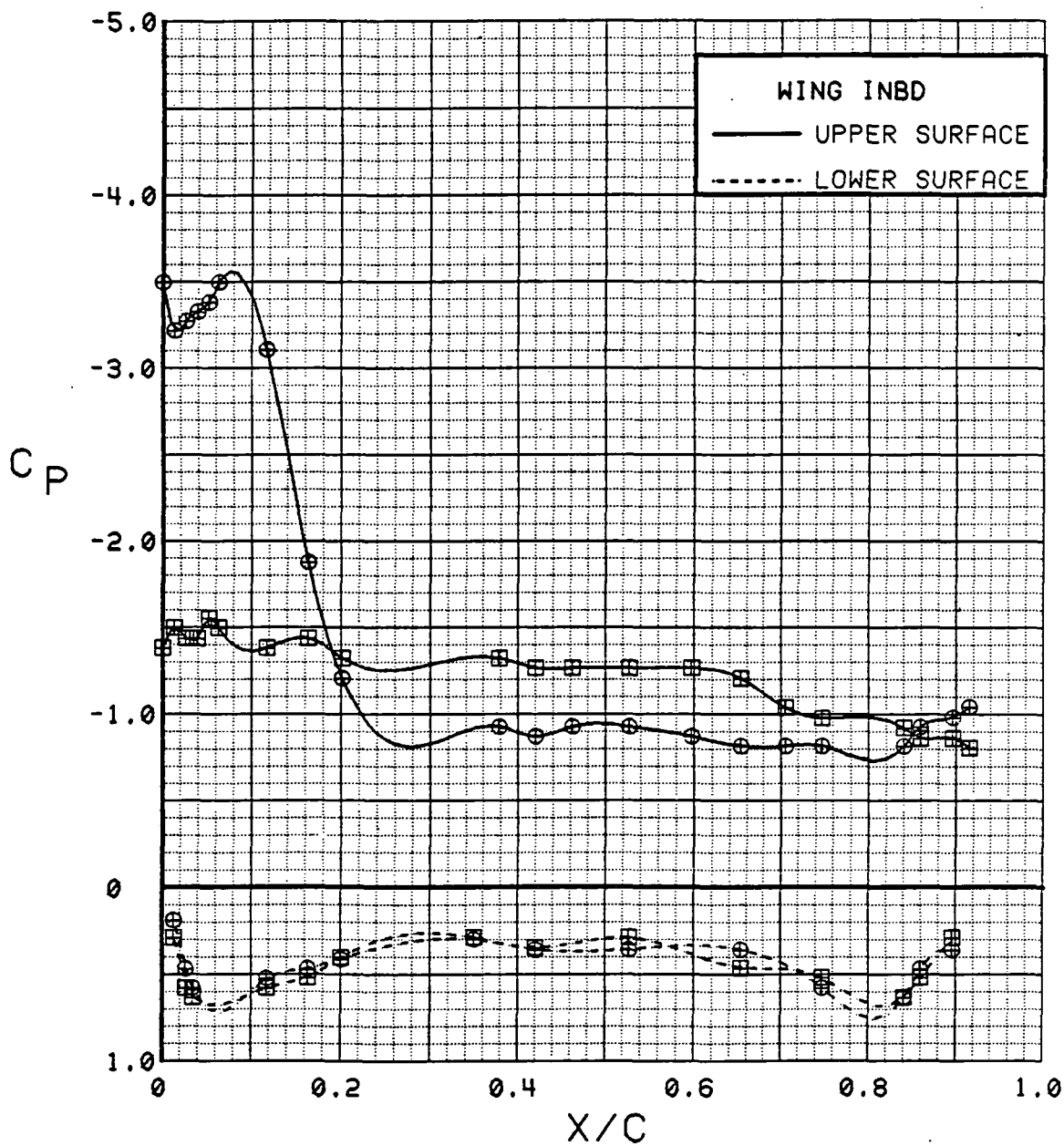


Figure 3.2.4-145 Canard On/Off Effects, Forward Position, Inboard,  $C_T = 0.9$ ,  $\alpha = 12$  deg

SYM	TEST	RUN	ALPHA	CT	ITEF	OTEF	CAN	SWB
⊕	537	32	16.8	0.92	30	30	0	OFF
⊞	537	61	16.7	0.94	30	30	OFF	OFF

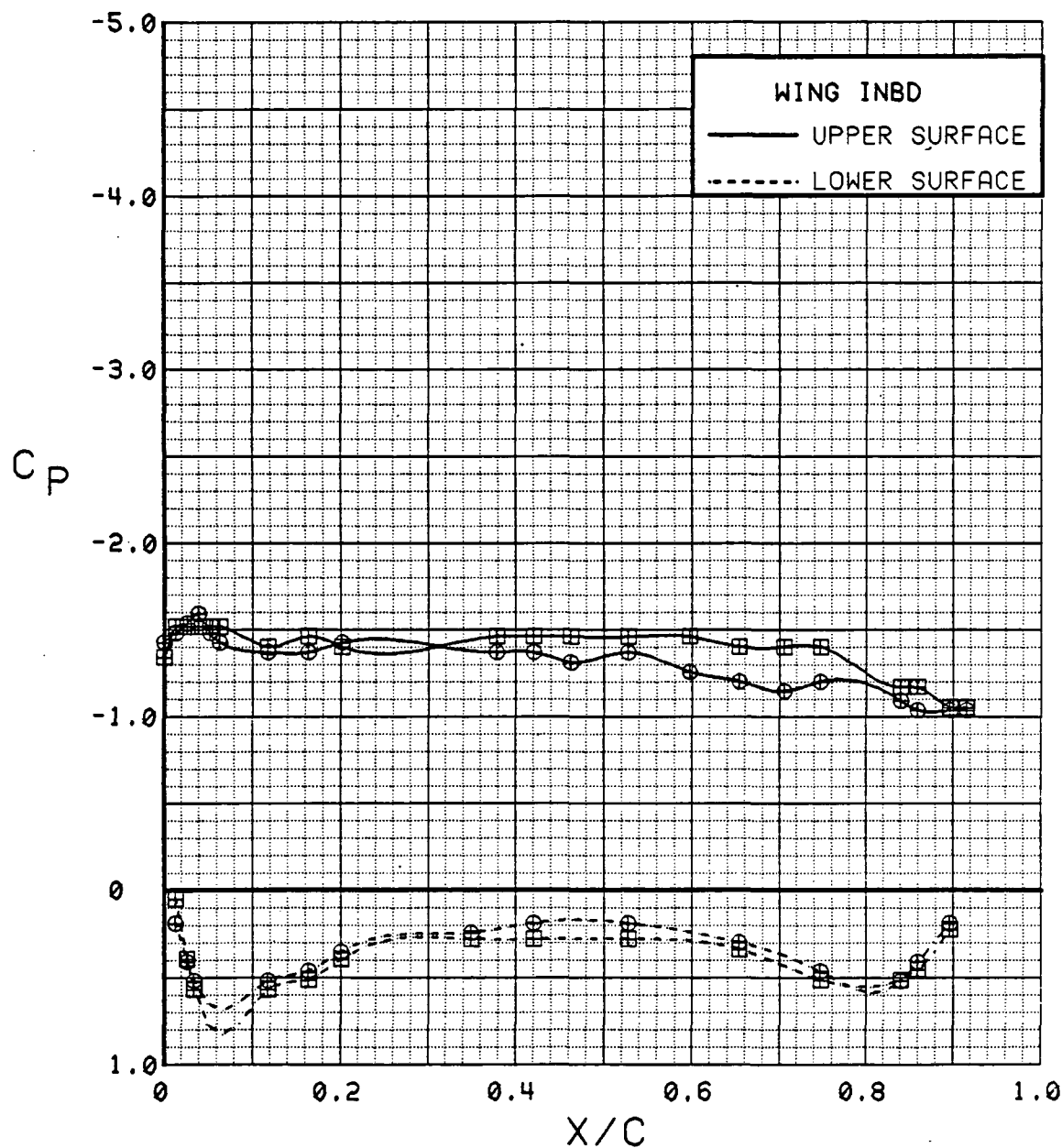


Figure 3.2.4-146 Canard On/Off Effects, Forward Position, Inboard,  
 $C_T = 0.9$ ,  $\alpha = 16$  deg

SYM	TEST	RUN	ALPHA	CT	ITEF	OTEF	CAN	SWB
⊕	537	32	20.9	0.90	30	30	0	OFF
⊞	537	61	20.8	0.92	30	30	OFF	OFF

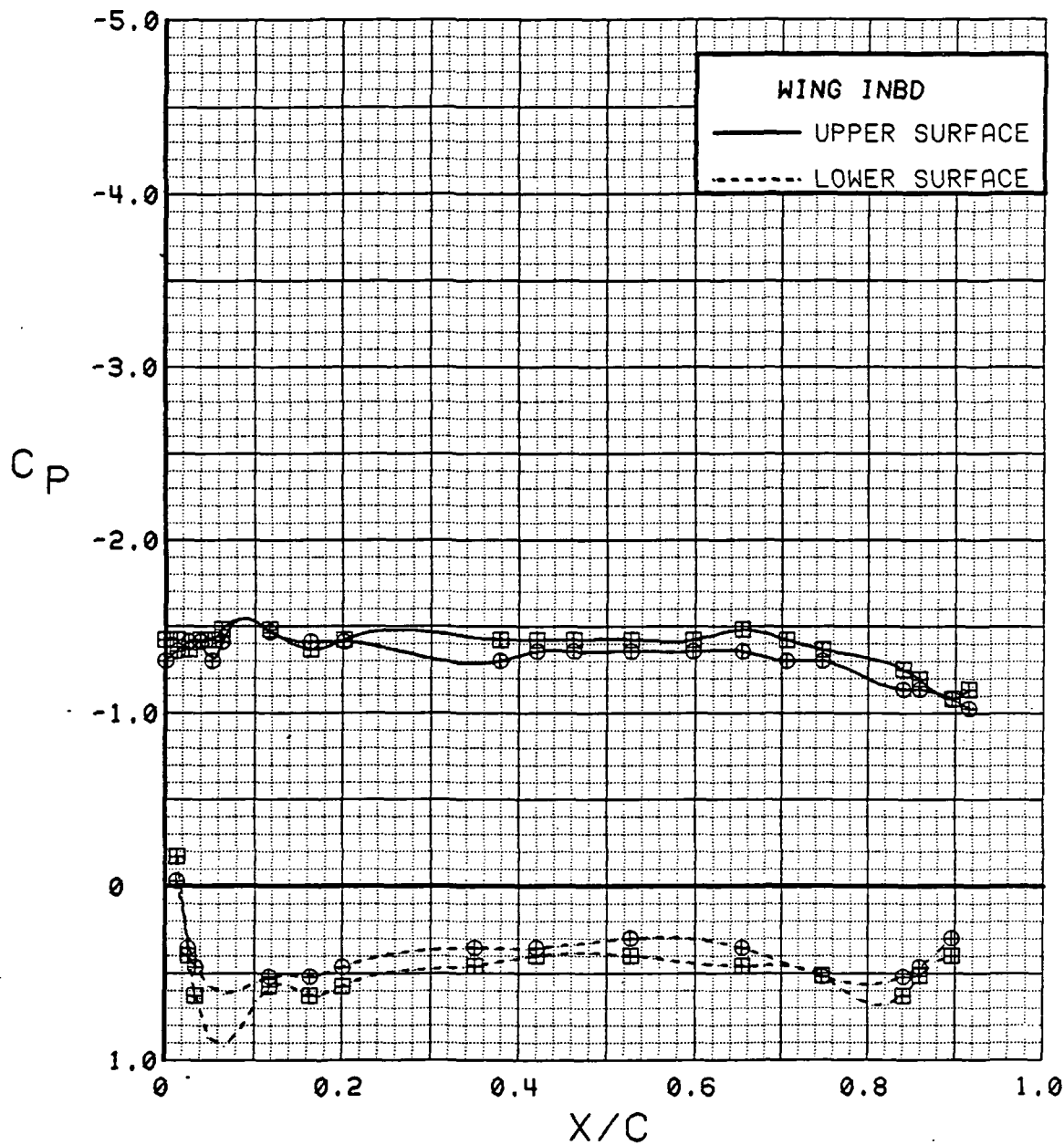


Figure 3.2.4-147 Canard On/Off Effects, Forward Position, Inboard,  $C_T = 0.9$ ,  $\alpha = 20$  deg



SYM	TEST	RUN	ALPHA	CT	ITEF	OTEF	CAN	SWB
⊕	537	32	12.8	0.92	30	30	0	OFF
⊞	537	61	12.6	0.92	30	30	OFF	OFF

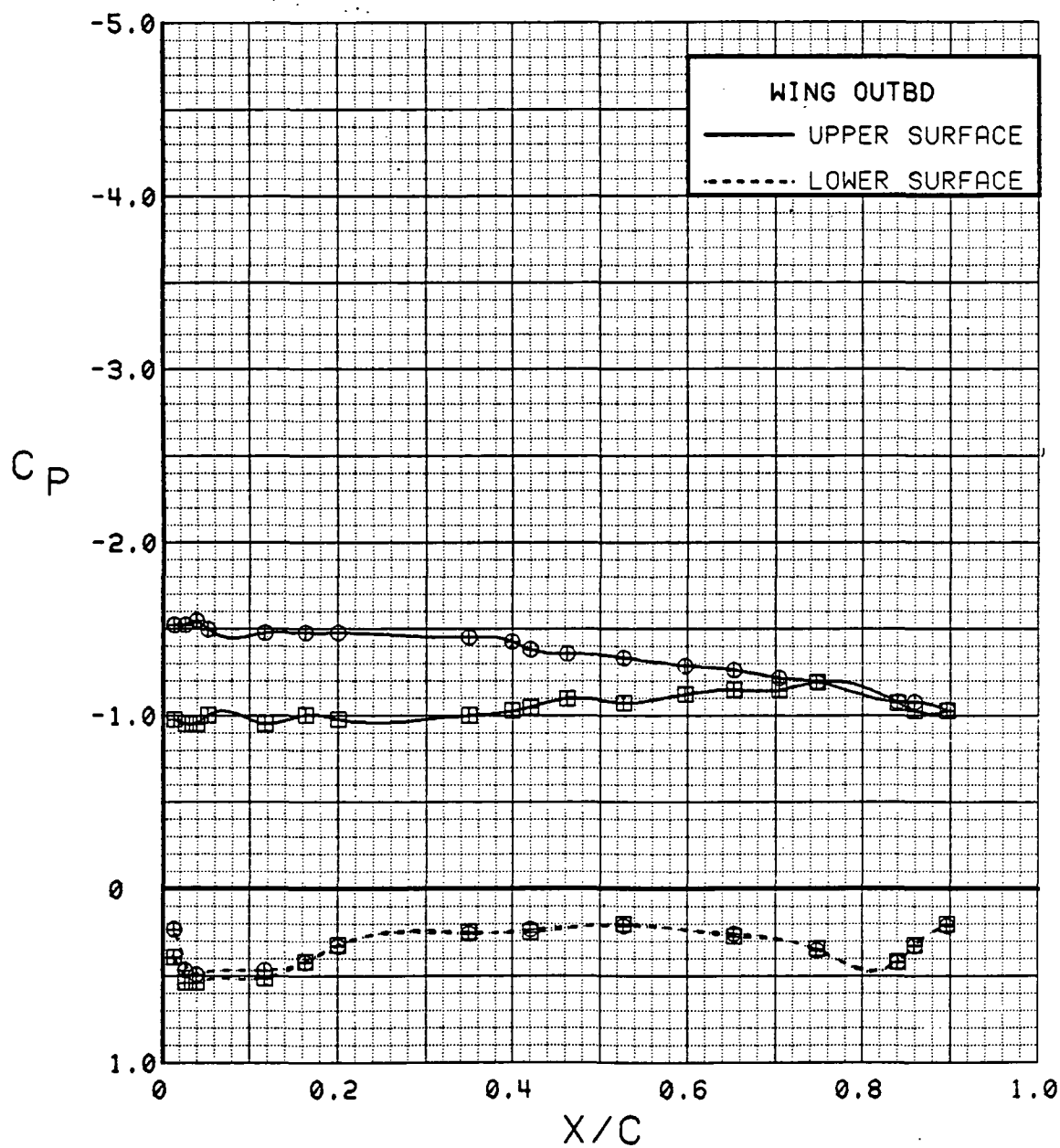


Figure 3.2.4-148 Canard On/Off Effects, Forward Position, Outboard,  
 $C_T = 0.9$ ,  $\alpha = 12$  deg

SYM	TEST	RUN	ALPHA	CT	ITEF	OTEF	CAN	SWB
⊕	537	32	16.8	0.92	30	30	0	OFF
⊞	537	61	16.7	0.94	30	30	OFF	OFF

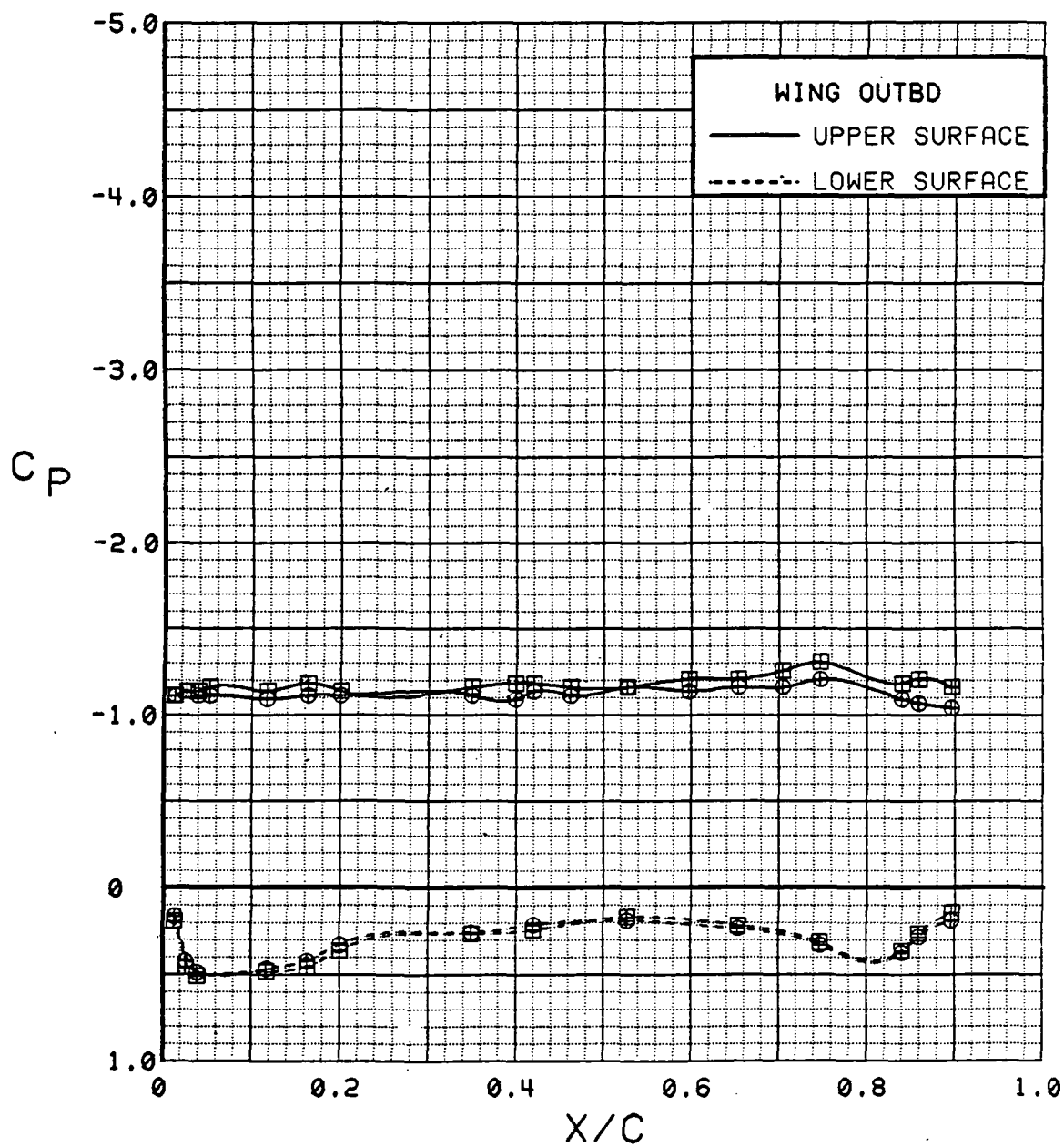


Figure 3.2.4-149 Canard On/Off Effects, Forward Position, Outboard,  $C_T = 0.9$ ,  $\alpha = 16$  deg

SYM	TEST	RUN	ALPHA	CT	ITEF	OTEF	CAN	SWB
⊕	537	32	20.9	0.90	30	30	0	OFF
⊞	537	61	20.8	0.92	30	30	OFF	OFF

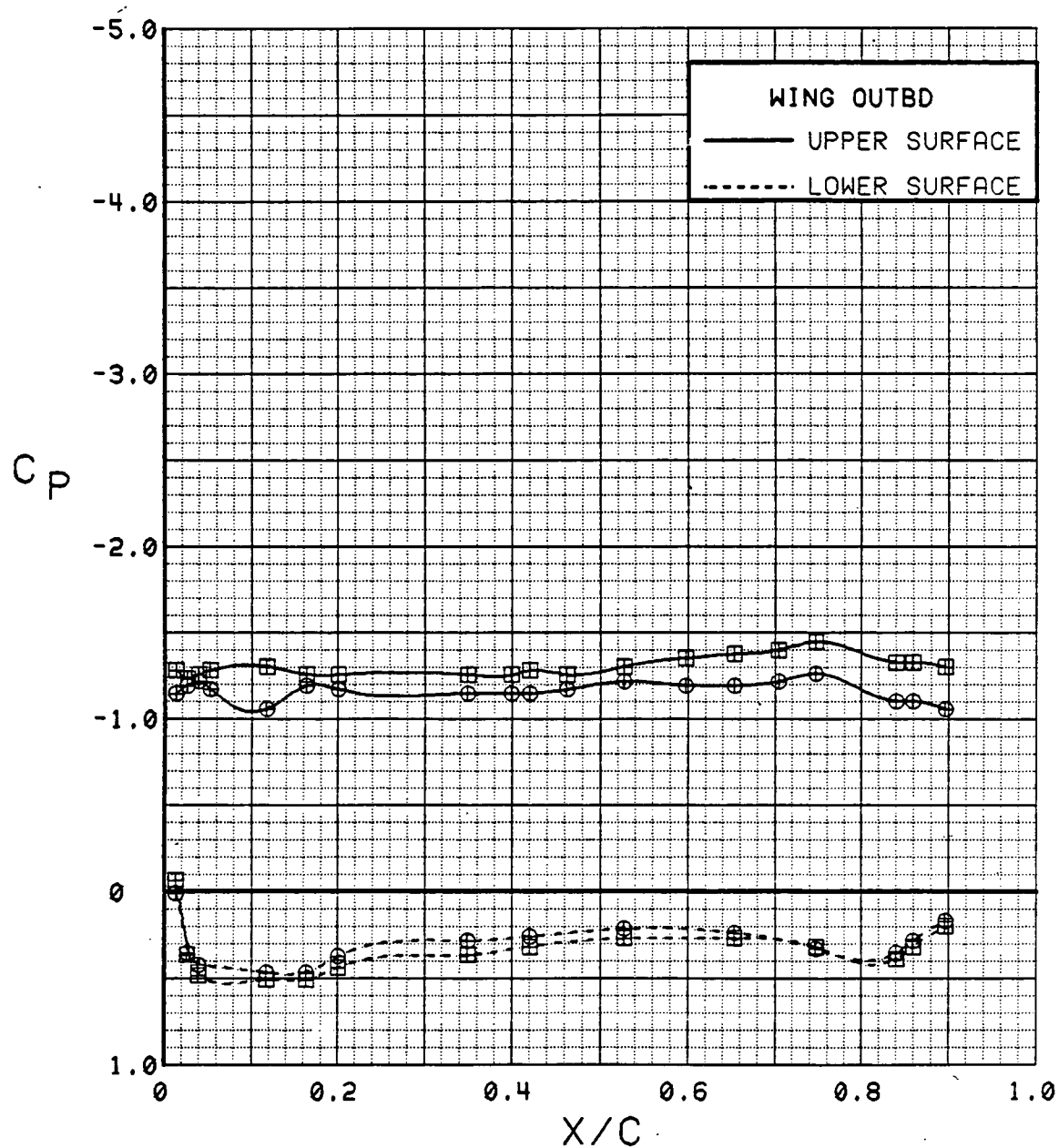


Figure 3.2.4-150 Canard On/Off Effects, Forward Position, Outboard,  $C_T = 0.9$ ,  $\alpha = 20^\circ$

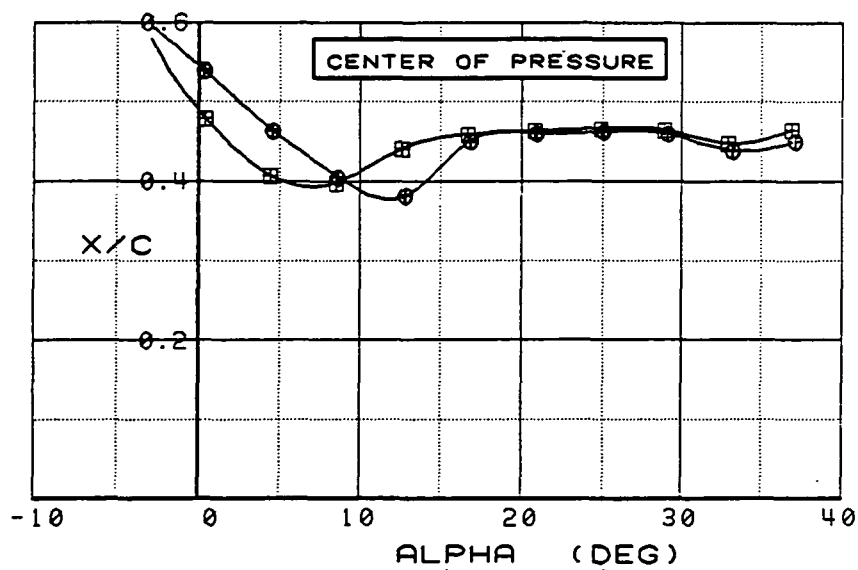
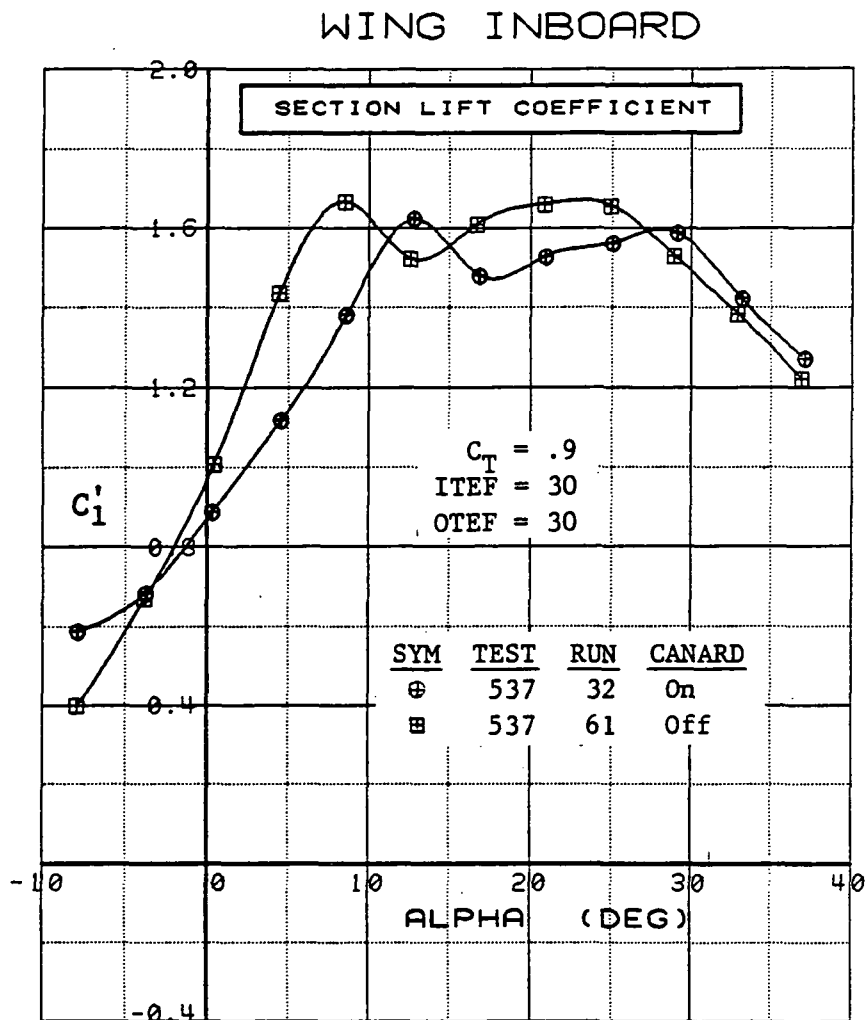


Figure 3.2.4-151 Canard On/Off Effects, Forward Position, Inboard,  $C_T = 0.9$ , Integrated Section Properties

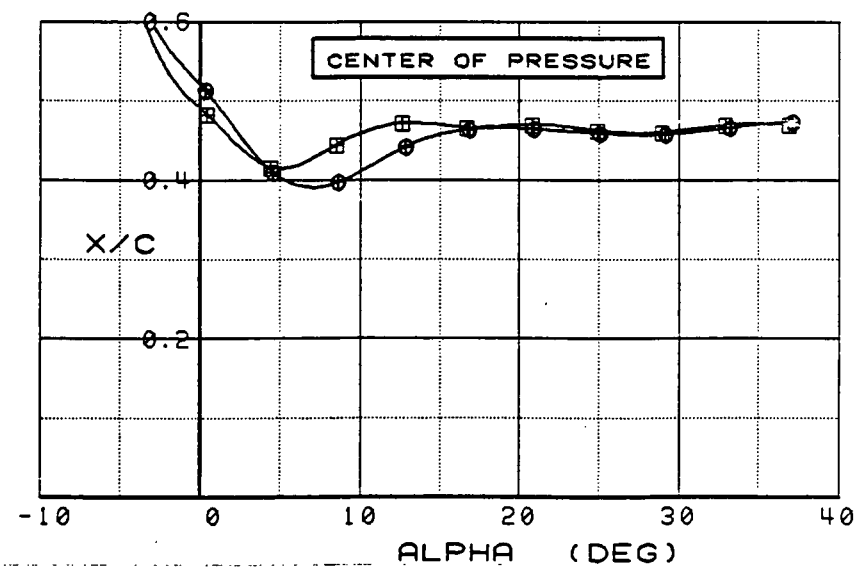
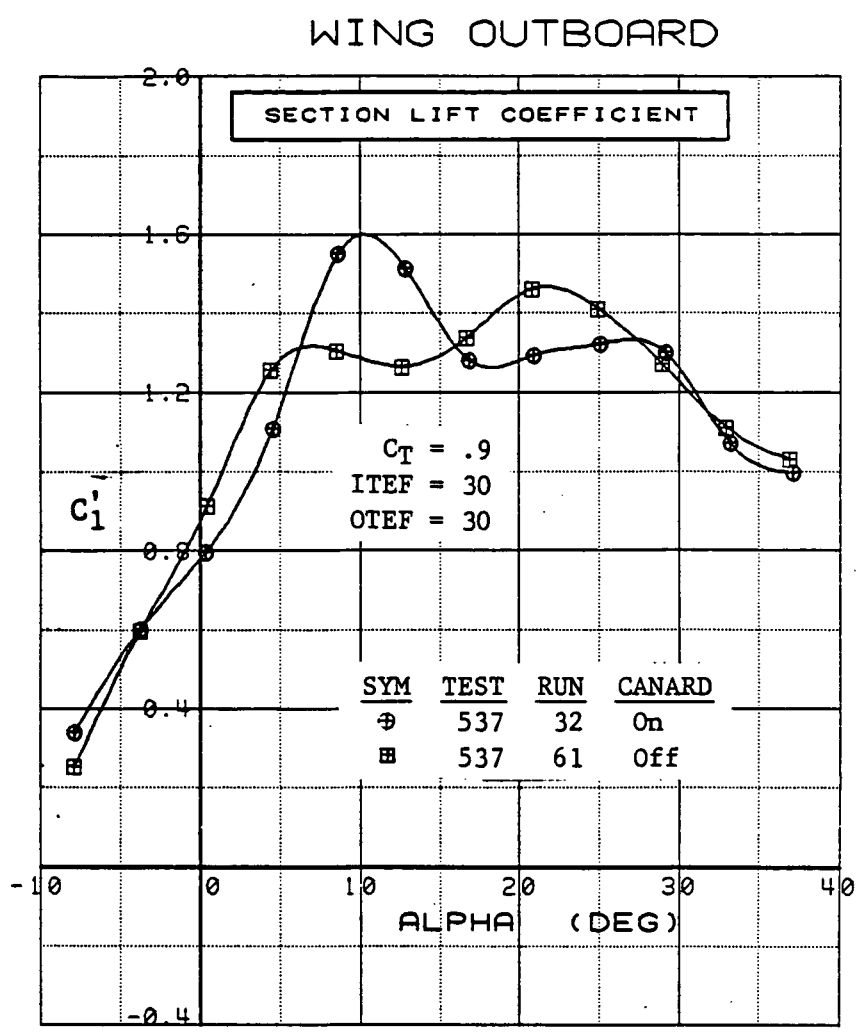


Figure 3.2.4-152 Canard On/Off Effects, Forward Position, Outboard,  $C_T = 0.9$ , Integrated Section Properties

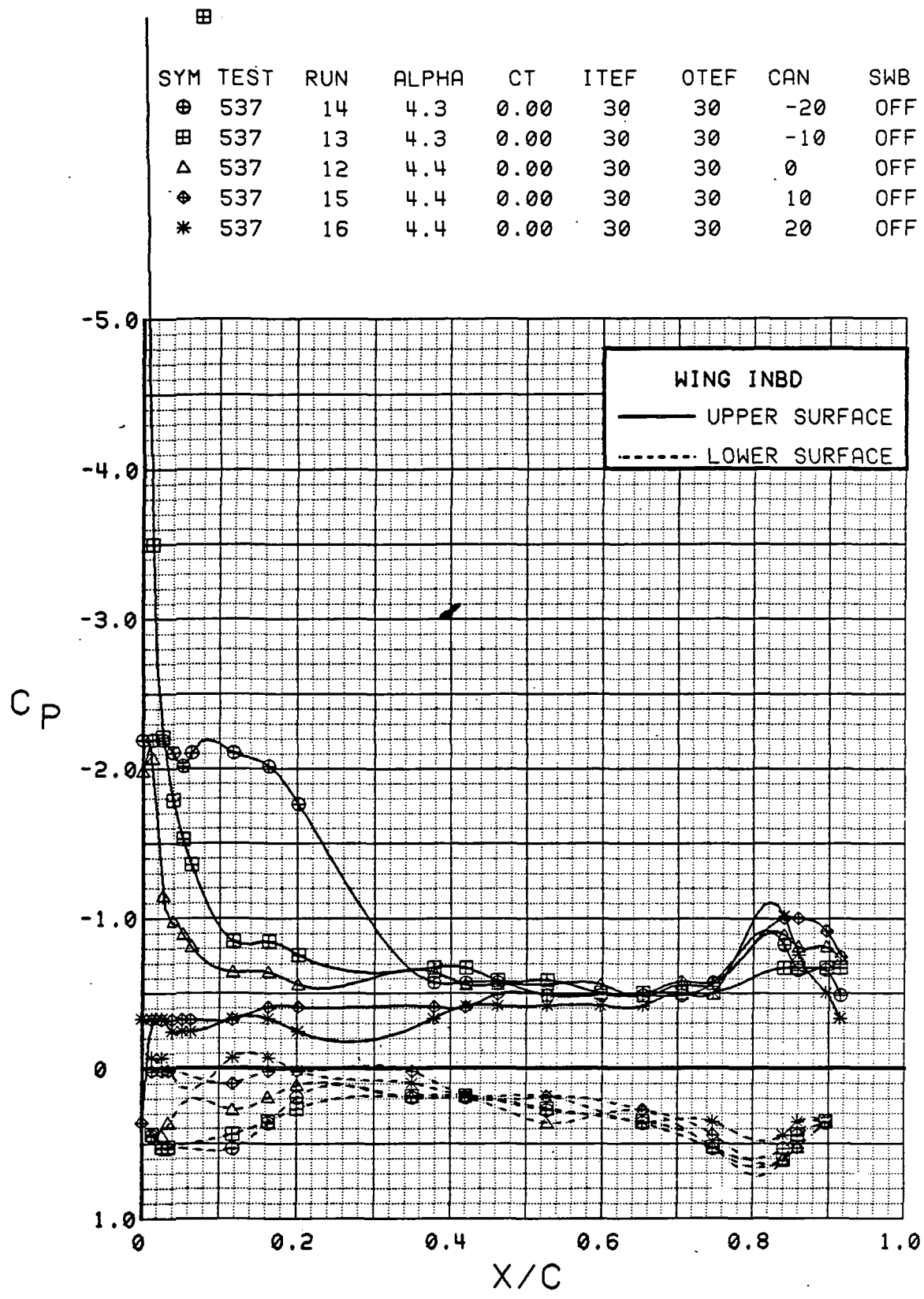


Figure 3.2.4-153 Canard Deflection Effects, Wing Inboard, Alpha = 4 deg

SYM	TEST	RUN	ALPHA	CT	ITEF	OTEF	CAN	SWB
⊕	537	14	8.4	0.00	30	30	-20	OFF
⊞	537	13	8.5	0.00	30	30	-10	OFF
△	537	12	8.5	0.00	30	30	0	OFF
⊕	537	15	8.6	0.00	30	30	10	OFF
*	537	16	8.5	0.00	30	30	20	OFF

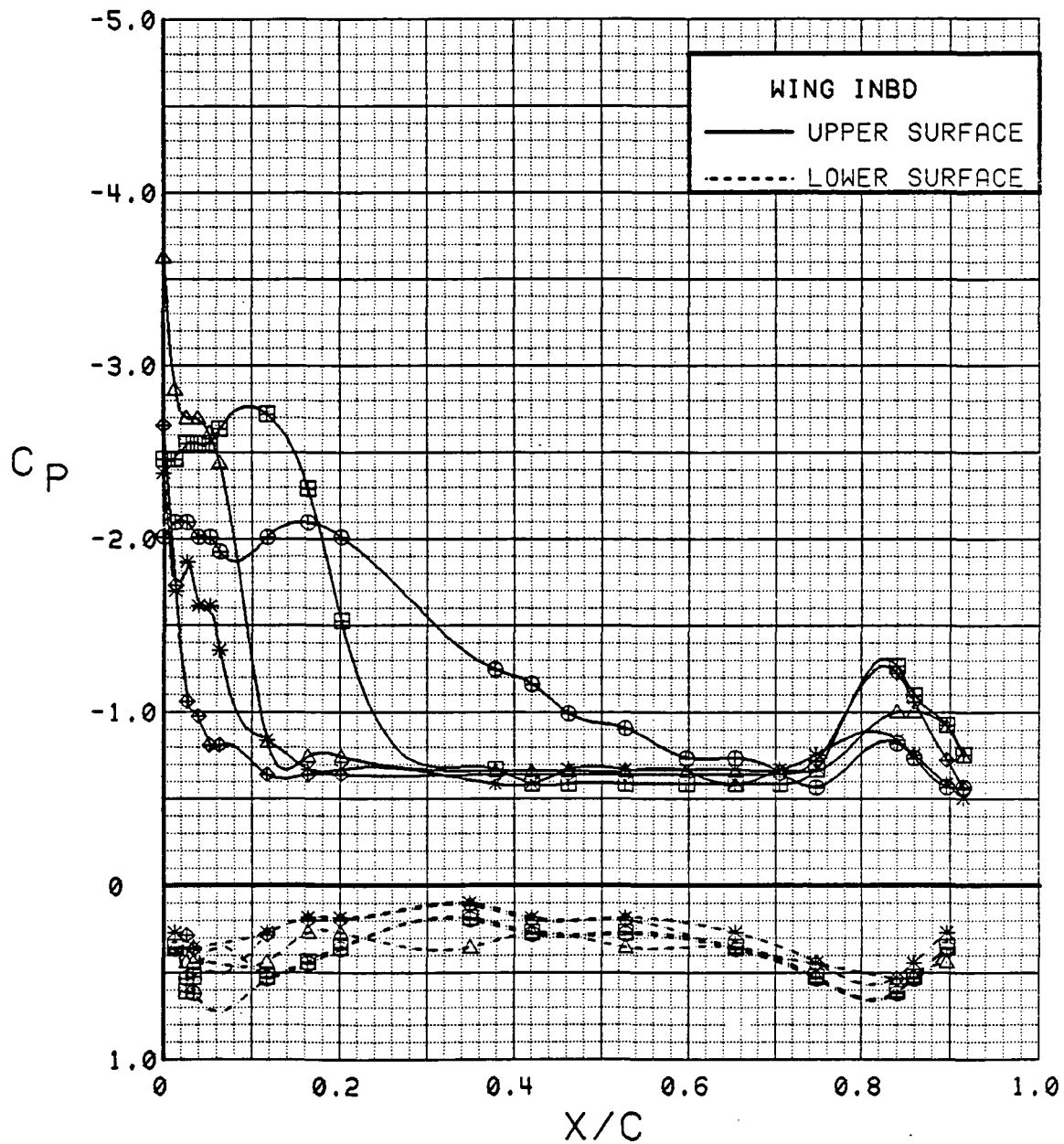


Figure 3.2.4-154 Canard Deflection Effects, Wing Inboard, Alpha = 8 deg

SYM	TEST	RUN	ALPHA	CT	ITEF	OTEF	CAN	SWB
⊕	537	14	12.5	0.00	30	30	-20	OFF
⊞	537	13	12.6	0.00	30	30	-10	OFF
△	537	12	12.7	0.00	30	30	0	OFF
◆	537	15	12.7	0.00	30	30	10	OFF
*	537	16	12.6	0.00	30	30	20	OFF

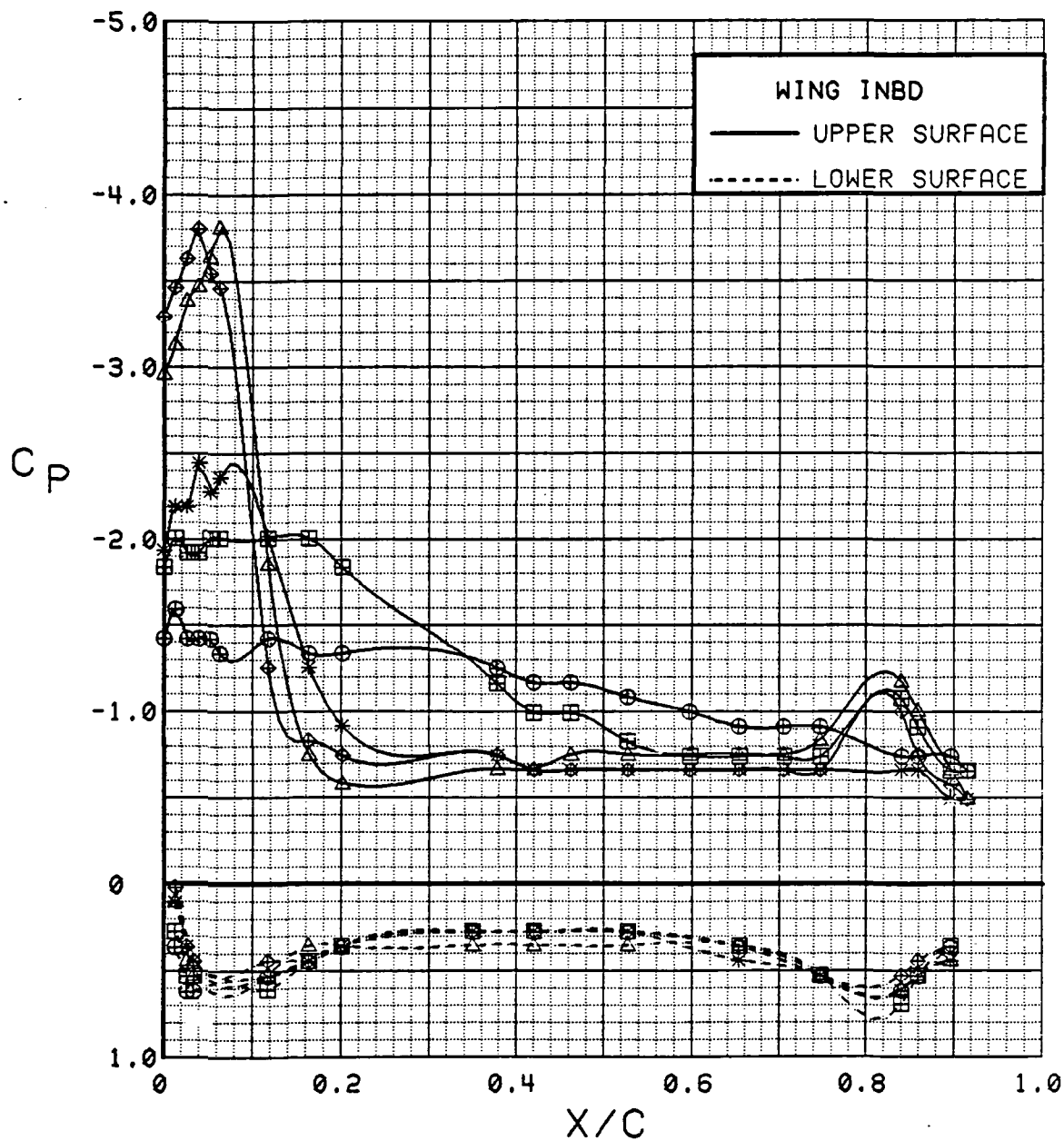


Figure 3.2.4-155 Canard Deflection Effects, Wing Inboard, Alpha = 12 deg



SYM	TEST	RUN	ALPHA	CT	ITEF	OTEF	CAN	SWB
⊕	537	14	4.3	0.00	30	30	-20	OFF
⊞	537	13	4.3	0.00	30	30	-10	OFF
△	537	12	4.4	0.00	30	30	0	OFF
⊕	537	15	4.4	0.00	30	30	10	OFF
*	537	16	4.4	0.00	30	30	20	OFF

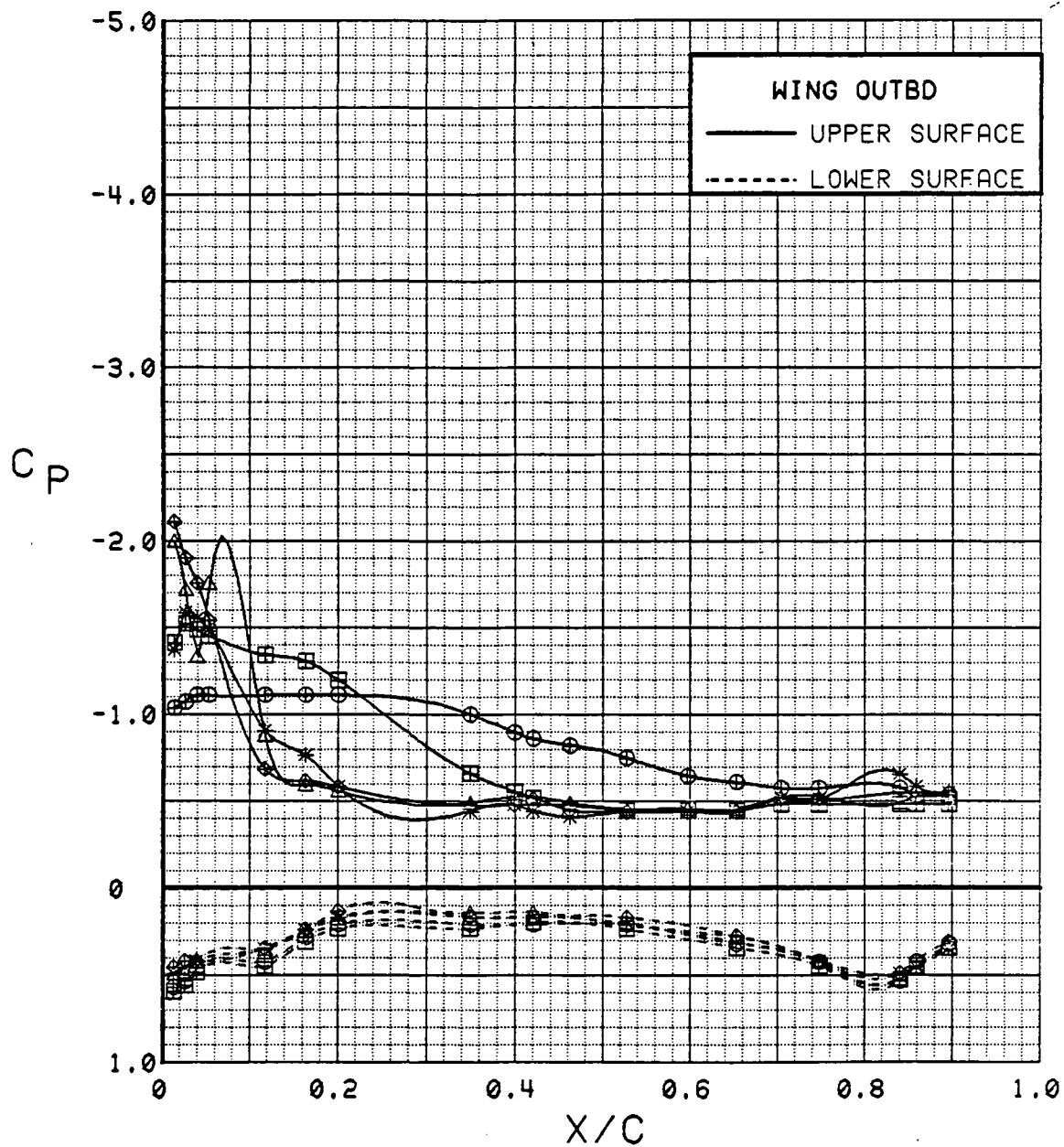


Figure 3.2.4-156 Canard Deflection Effects, Wing Outboard, Alpha = 4 deg

SYM	TEST	RUN	ALPHA	CT	ITEF	OTEF	CAN	SWB
⊕	537	14	8.4	0.00	30	30	-20	OFF
⊞	537	13	8.5	0.00	30	30	-10	OFF
△	537	12	8.5	0.00	30	30	0	OFF
⊕	537	15	8.6	0.00	30	30	10	OFF
*	537	16	8.5	0.00	30	30	20	OFF

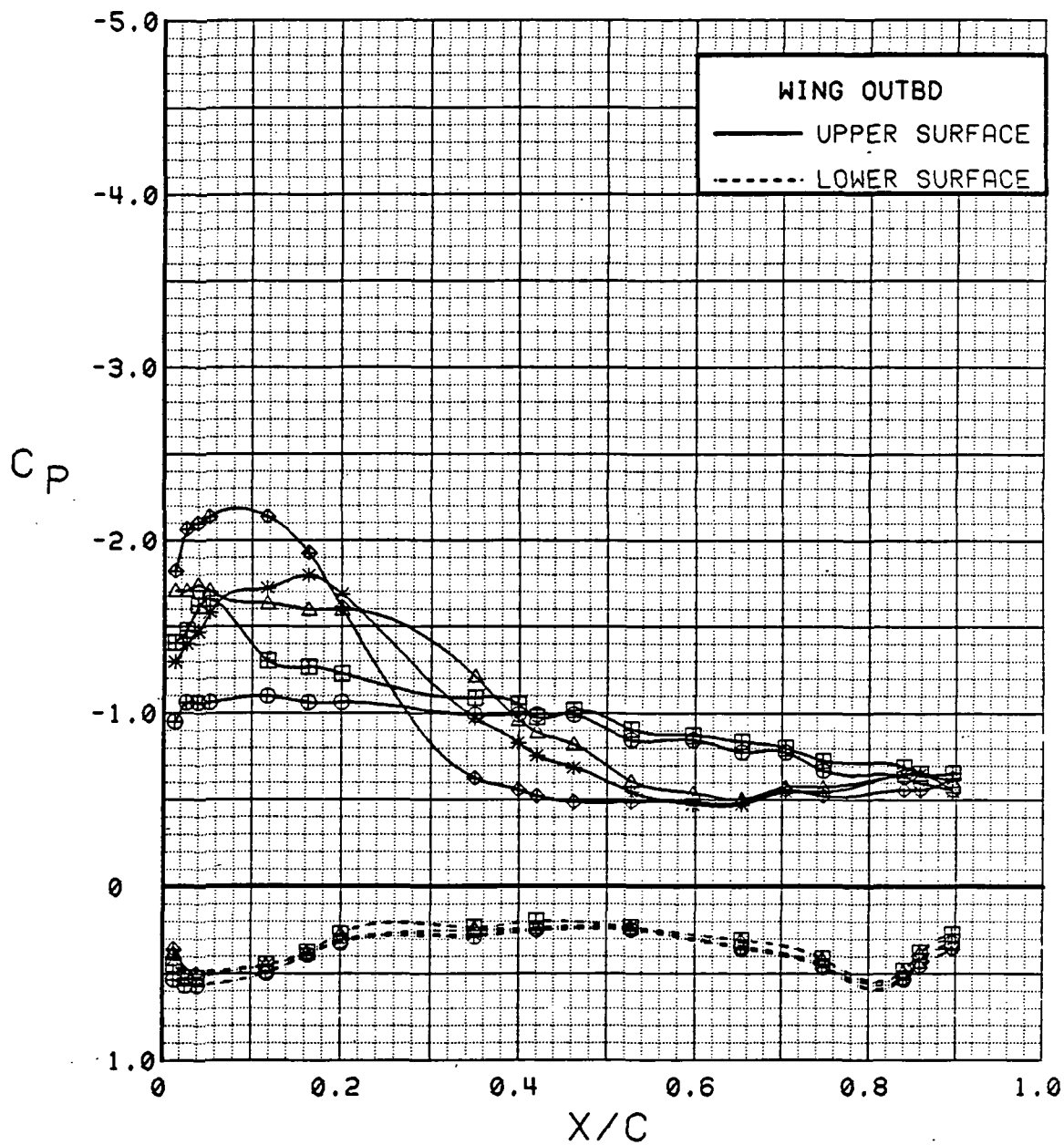


Figure 3.2.4-157 Canard Deflection Effects, Wing Outboard, Alpha = 8 deg

SYM	TEST	RUN	ALPHA	CT	ITEF	OTEF	CAN	SWB
⊕	537	14	12.5	0.00	30	30	-20	OFF
⊞	537	13	12.6	0.00	30	30	-10	OFF
△	537	12	12.7	0.00	30	30	0	OFF
◆	537	15	12.7	0.00	30	30	10	OFF
*	537	16	12.6	0.00	30	30	20	OFF

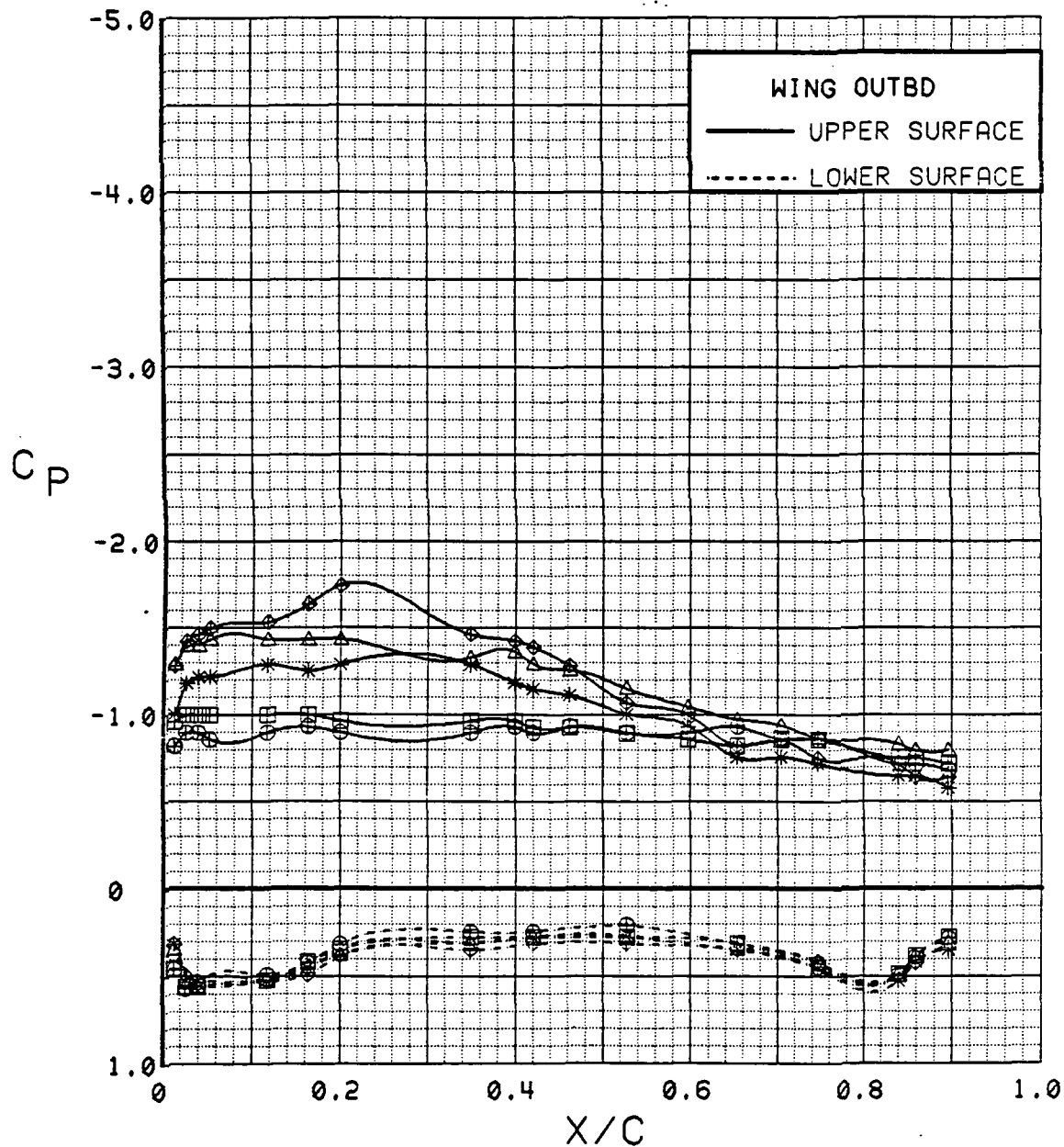


Figure 3.2.4-158 Canard Deflection Effects, Wing Outboard, Alpha = 12 deg

SYM	TEST	RUN	ALPHA	CT	ITEF	OTEF	CAN	SWB
⊕	537	14	4.3	0.00	30	30	-20	OFF
⊞	537	13	4.3	0.00	30	30	-10	OFF
△	537	12	4.4	0.00	30	30	0	OFF
◆	537	15	4.4	0.00	30	30	10	OFF
*	537	16	4.4	0.00	30	30	20	OFF

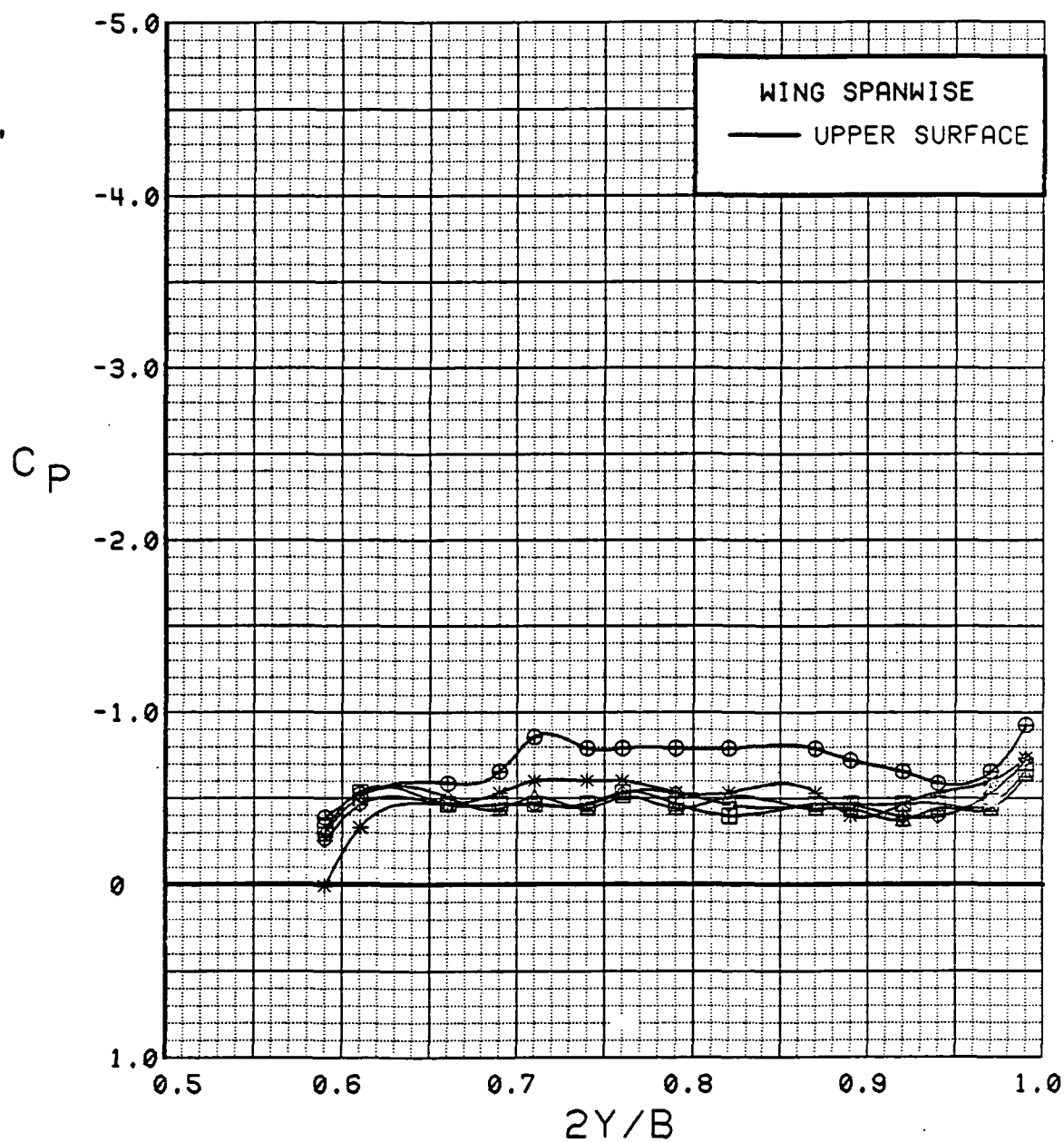


Figure 3.2.4-159 Canard Deflection Effects, Wing Spanwise, Alpha = 4 deg

SYM	TEST	RUN	ALPHA	CT	ITEF	OTEF	CAN	SWB
⊕	537	14	8.4	0.00	30	30	-20	OFF
⊞	537	13	8.5	0.00	30	30	-10	OFF
△	537	12	8.5	0.00	30	30	0	OFF
◆	537	15	8.6	0.00	30	30	10	OFF
*	537	16	8.5	0.00	30	30	20	OFF

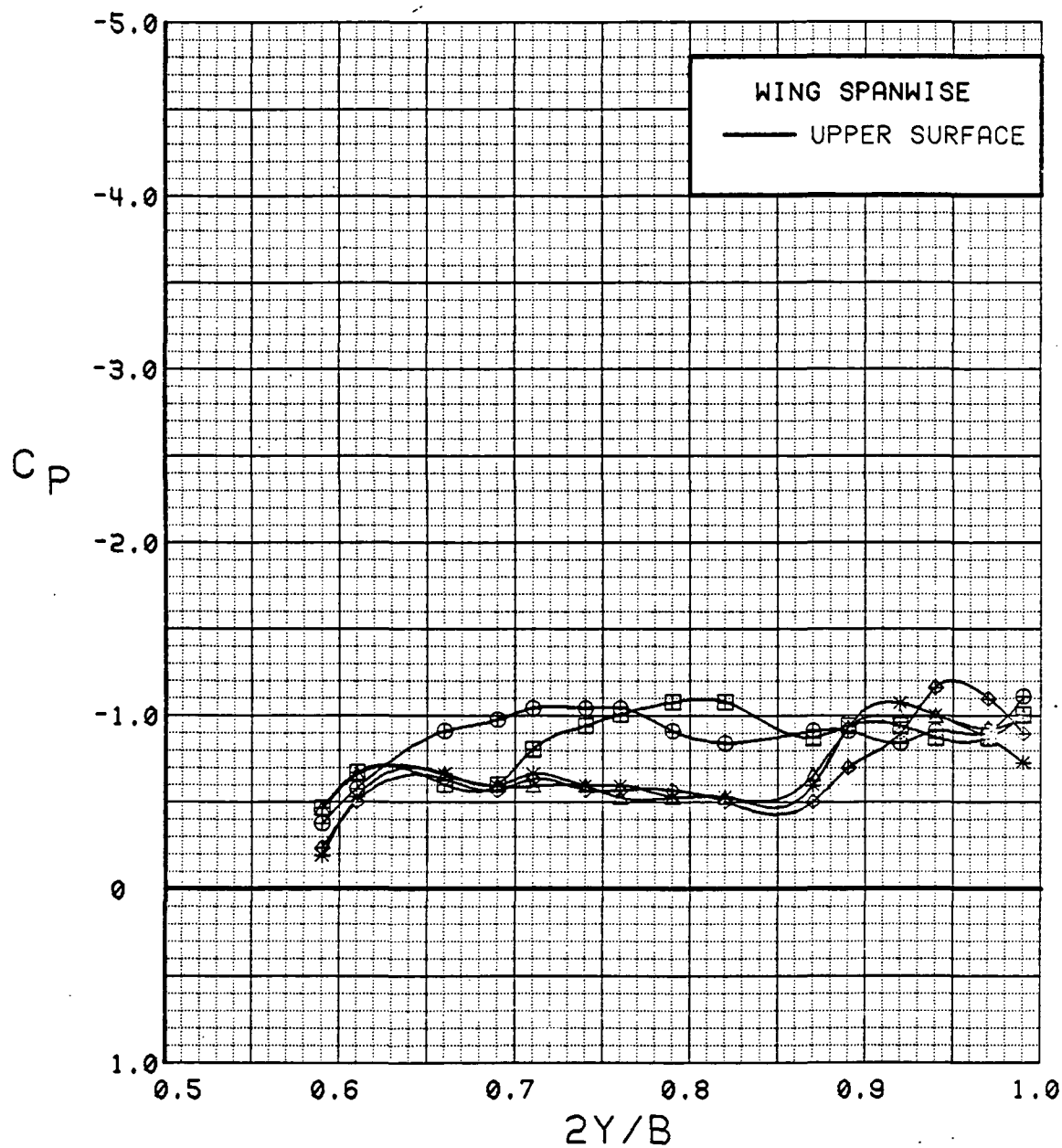


Figure 3.2.4-160 Canard Deflection Effects, Wing Spanwise, Alpha = 8 deg

SYM	TEST	RUN	ALPHA	CT	ITEF	OTEF	CAN	SWB
⊕	537	14	12.5	0.00	30	30	-20	OFF
⊞	537	13	12.6	0.00	30	30	-10	OFF
△	537	12	12.7	0.00	30	30	0	OFF
◆	537	15	12.7	0.00	30	30	10	OFF
*	537	16	12.6	0.00	30	30	20	OFF

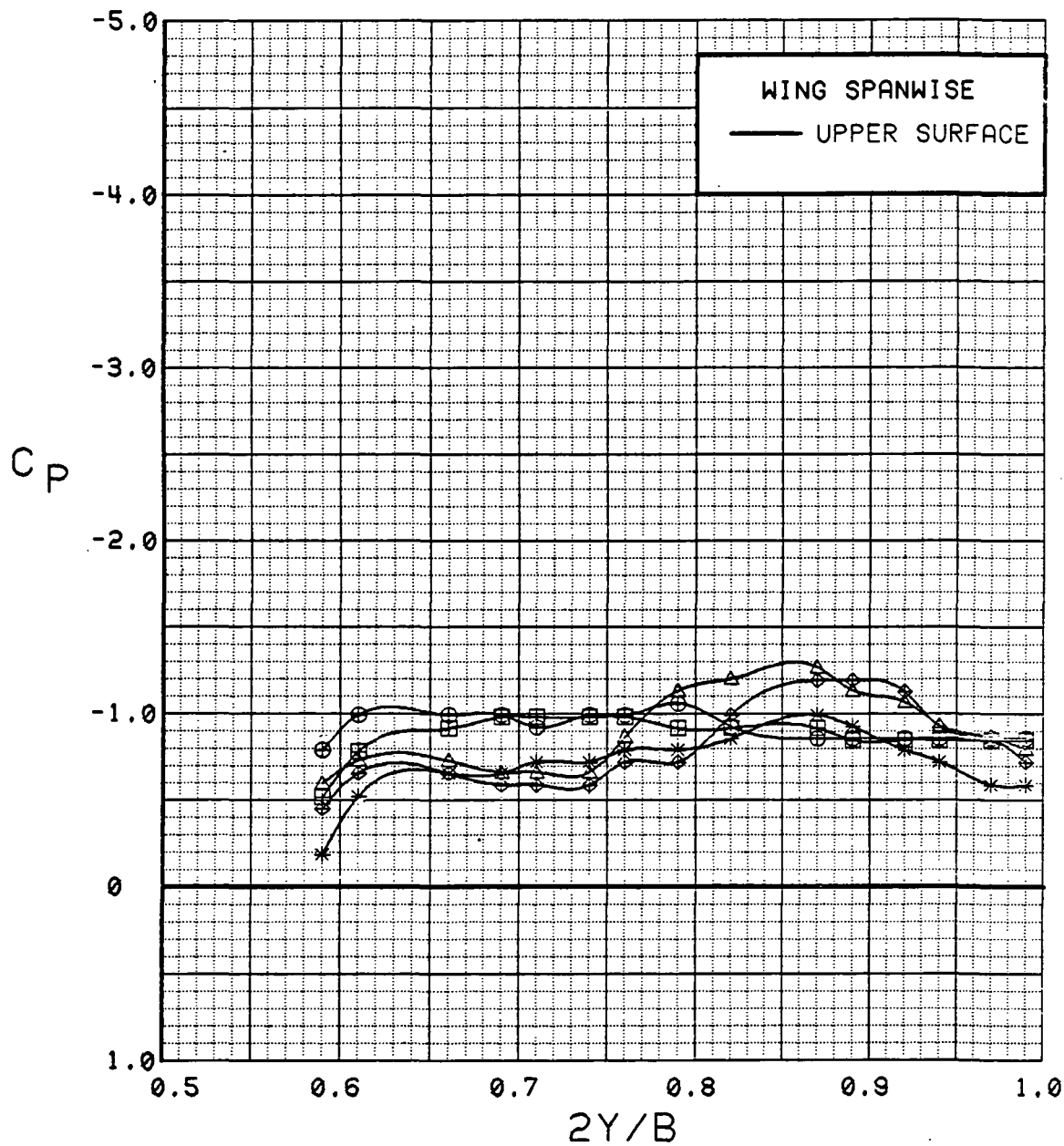


Figure 3.2.4-161 Canard Deflection Effects, Wing Spanwise, Alpha = 12 deg

# WING INBOARD

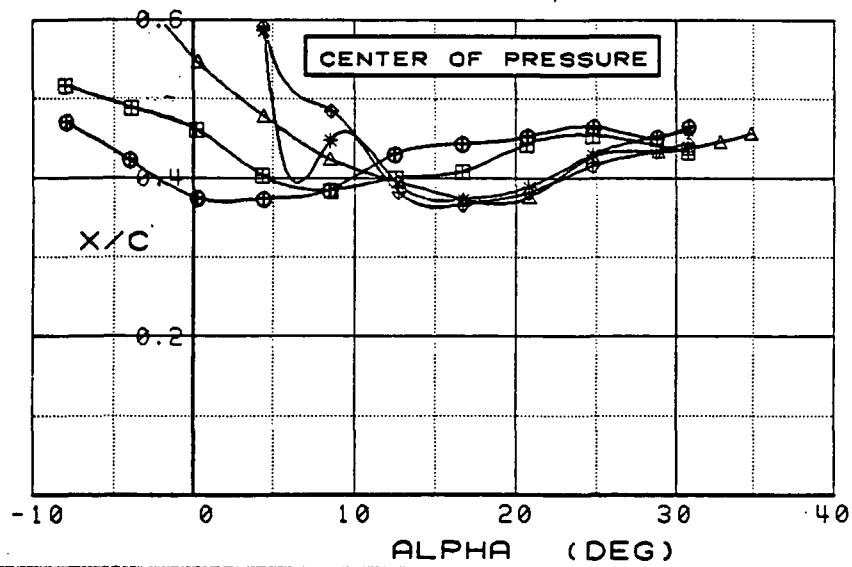
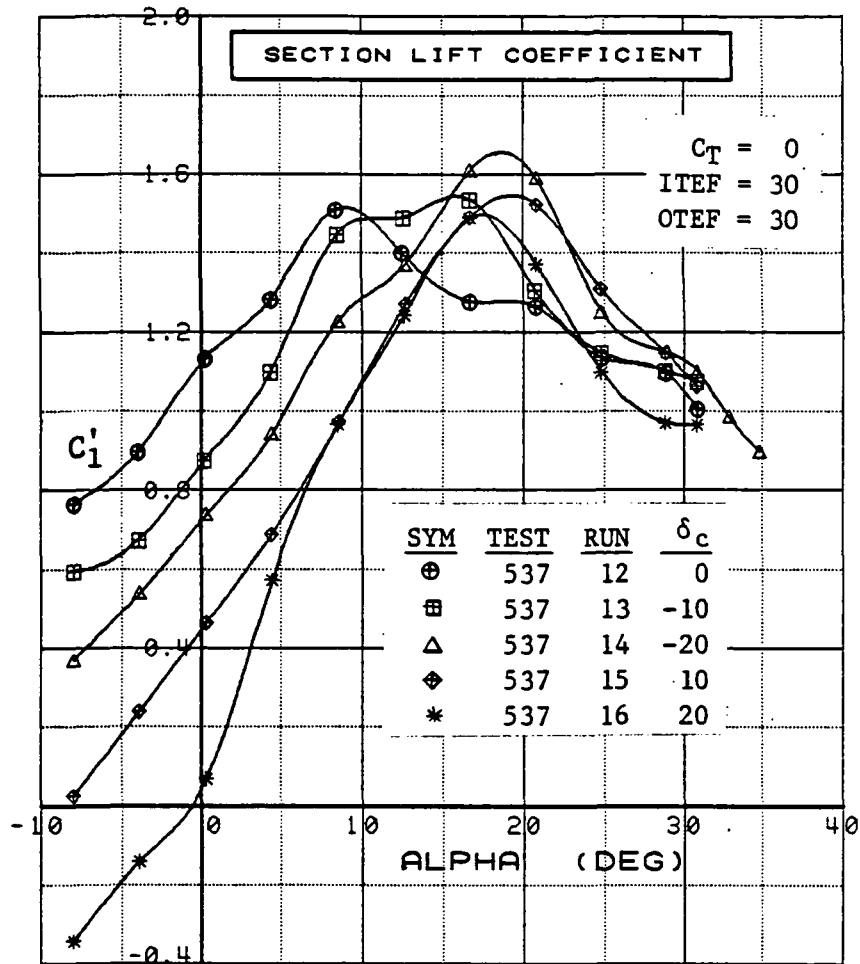


Figure 3.2.4-162 Canard Deflection Effects, Inboard, Flaps Deflected, Integrated Section Properties

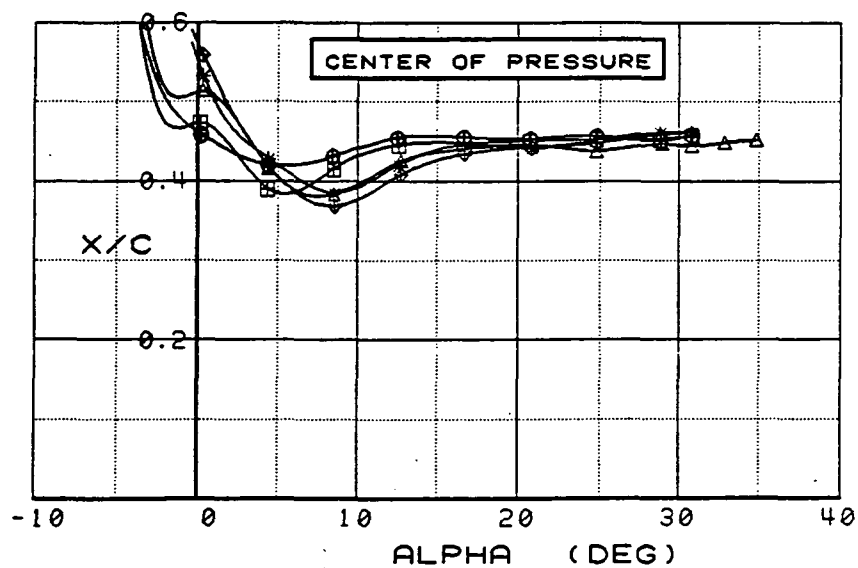
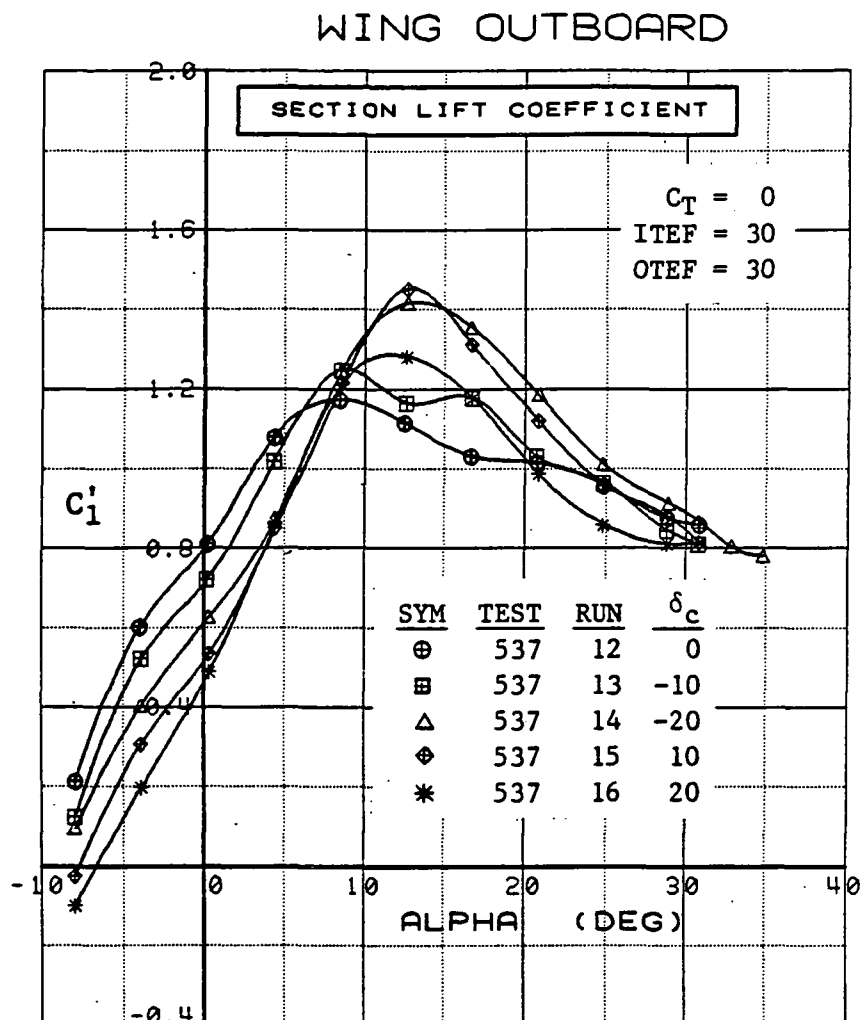


Figure 3.2.4-163 Canard Deflection Effects, Outboard, Flaps Deflected, Integrated Section Properties



SYM	TEST	RUN	ALPHA	CT	ITEF	OTEF	CAN	SWB
⊕	543	6	0.3	0.94	30	30	0	OFF
⊞	543	25	0.3	0.93	30	30	0	OFF
Δ	543	29	0.3	0.93	30	30	0	OFF

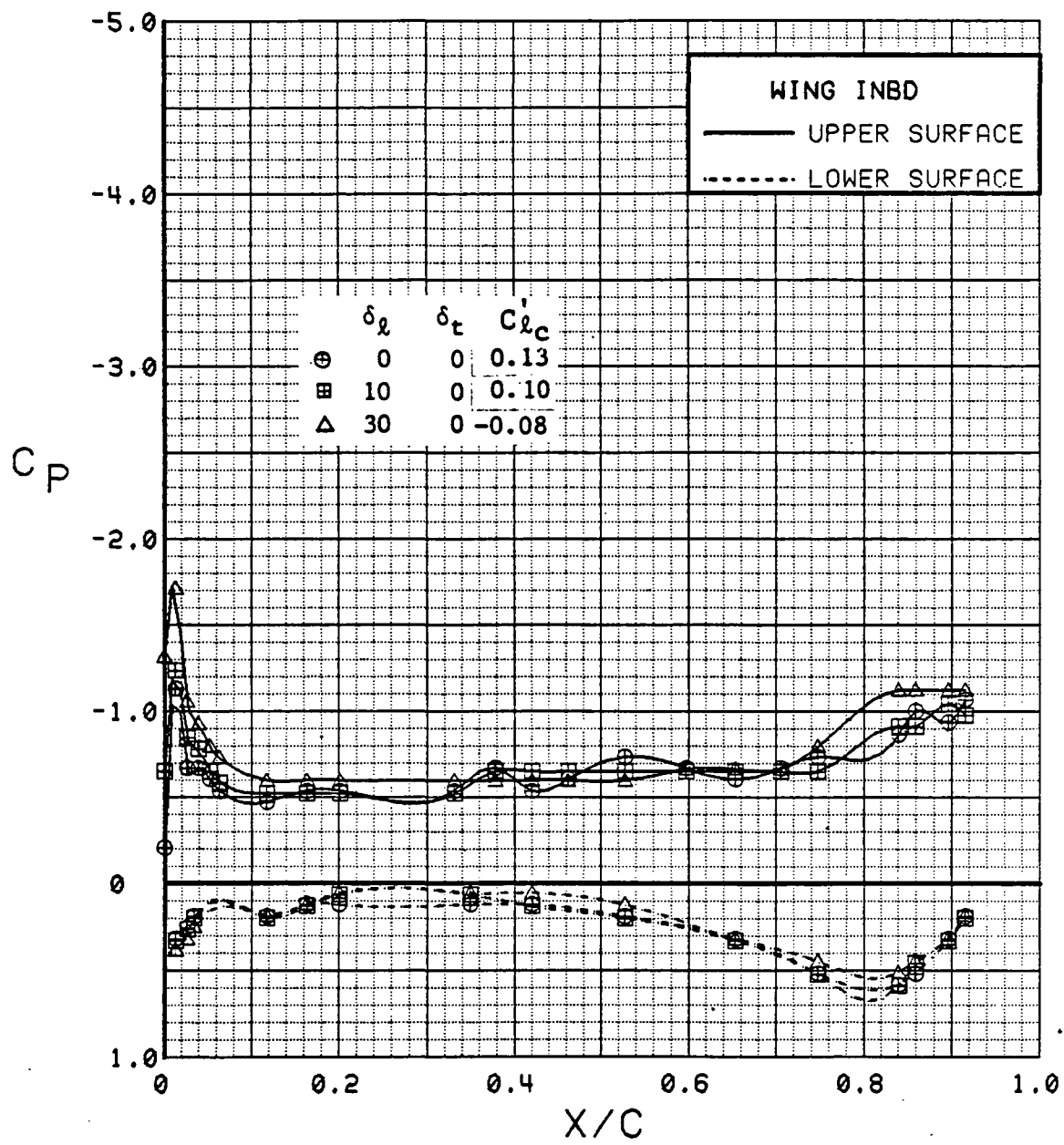


Figure 3.2.4-164 Canard Leading-Edge Flap Deflection Effects, Inboard,  $C_T = 0.9$ , Canard Neutral, Alpha = 0 deg

SYM	TEST	RUN	ALPHA	CT	ITEF	OTEF	CAN	SWB
⊕	543	6	4.5	0.94	30	30	0	OFF
⊞	543	25	4.5	0.94	30	30	0	OFF
Δ	543	29	4.5	0.93	30	30	0	OFF

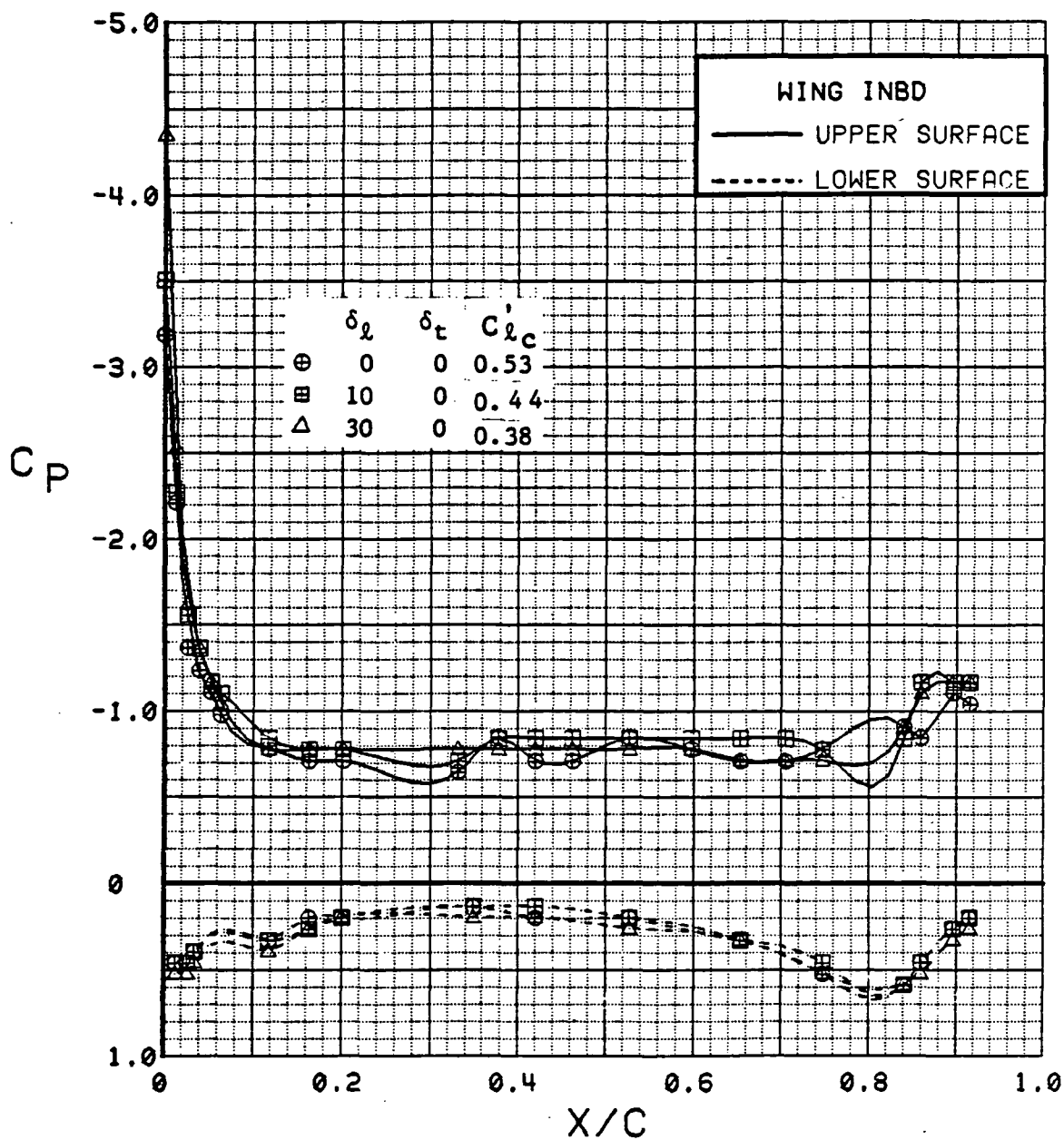


Figure 3.2.4-165 Canard Leading-Edge Flap Deflection Effects, Inboard,  $C_T = 0.9$ , Canard Neutral, Alpha = 4 deg

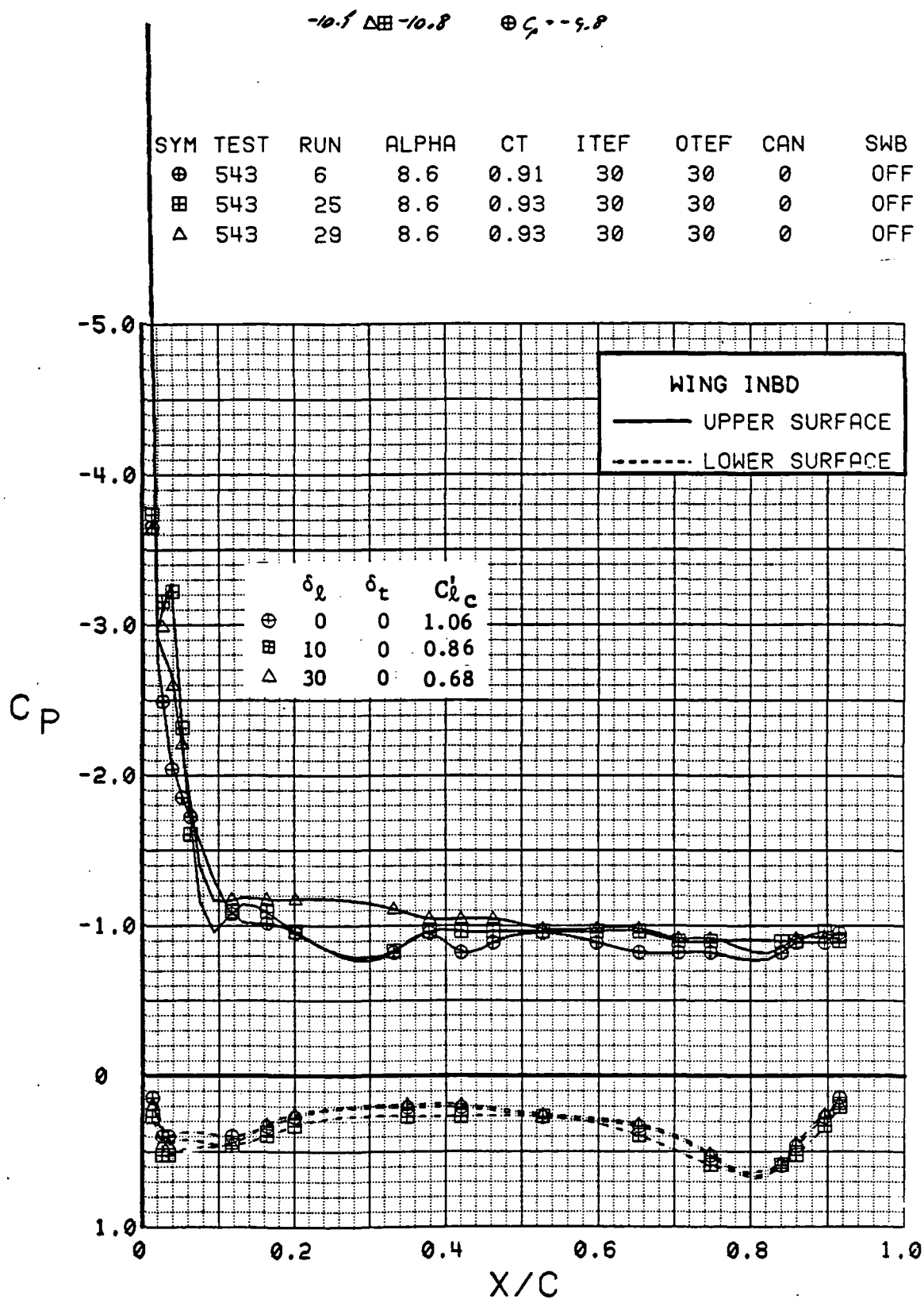


Figure 3.2.4-166 Canard Leading-Edge Flap Deflection Effects, Inboard,  $C_T = 0.9$ , Canard Neutral,  $\alpha = 8$  deg

SYM	TEST	RUN	ALPHA	CT	ITEF	OTEF	CAN	SWB
⊕	543	6	12.8	0.92	30	30	0	OFF
⊞	543	25	12.8	0.92	30	30	0	OFF
Δ	543	29	12.8	0.92	30	30	0	OFF

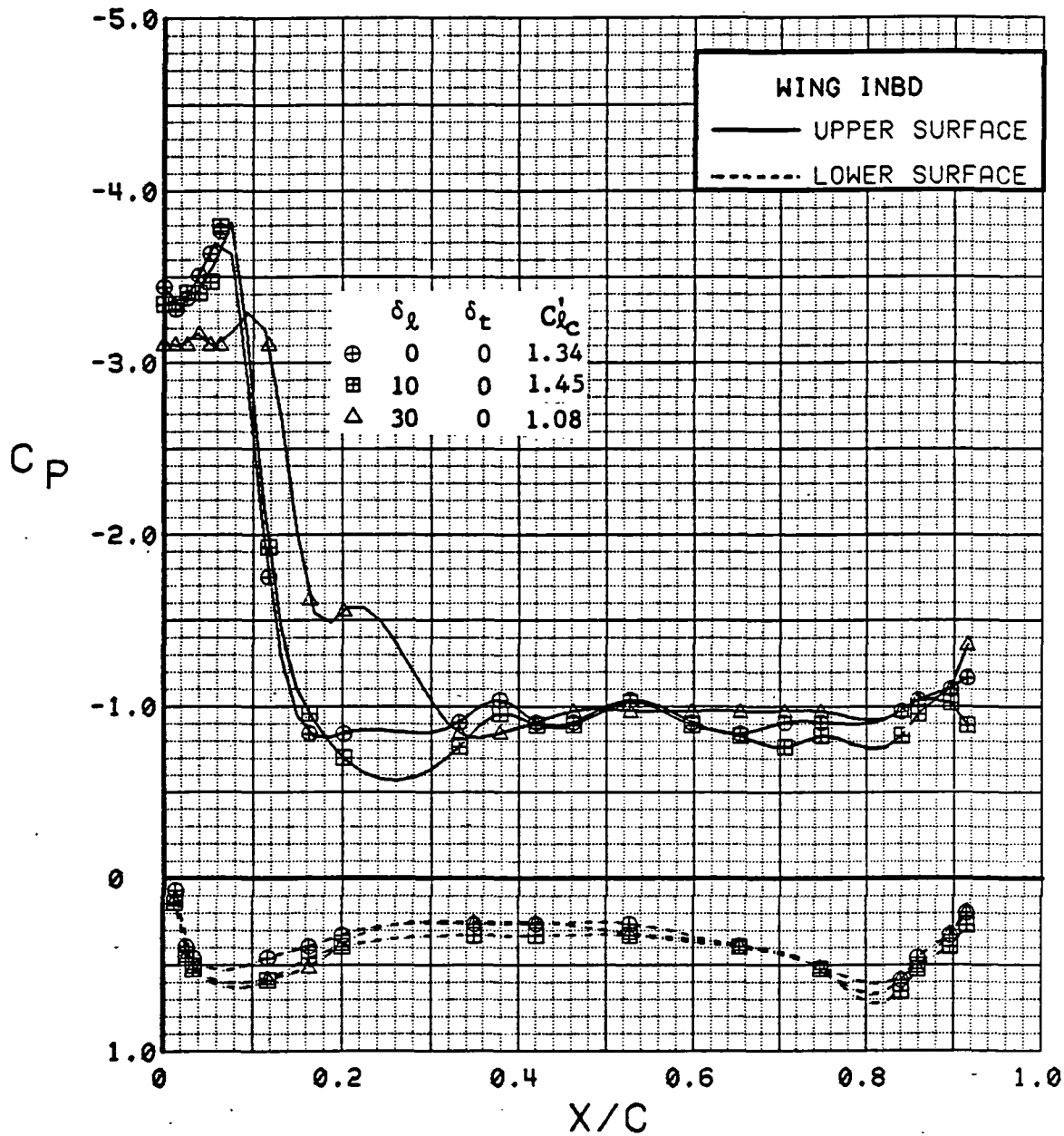


Figure 3.2.4-167 Canard Leading-Edge Flap Deflection Effects, Inboard,  $C_T = 0.9$ , Canard Neutral, Alpha = 12 deg

SYM	TEST	RUN	ALPHA	CT	ITEF	OTEF	CAN	SWB
⊕	543	6	16.9	0.92	30	30	0	OFF
⊞	543	25	16.9	0.93	30	30	0	OFF
Δ	543	29	16.9	0.93	30	30	0	OFF

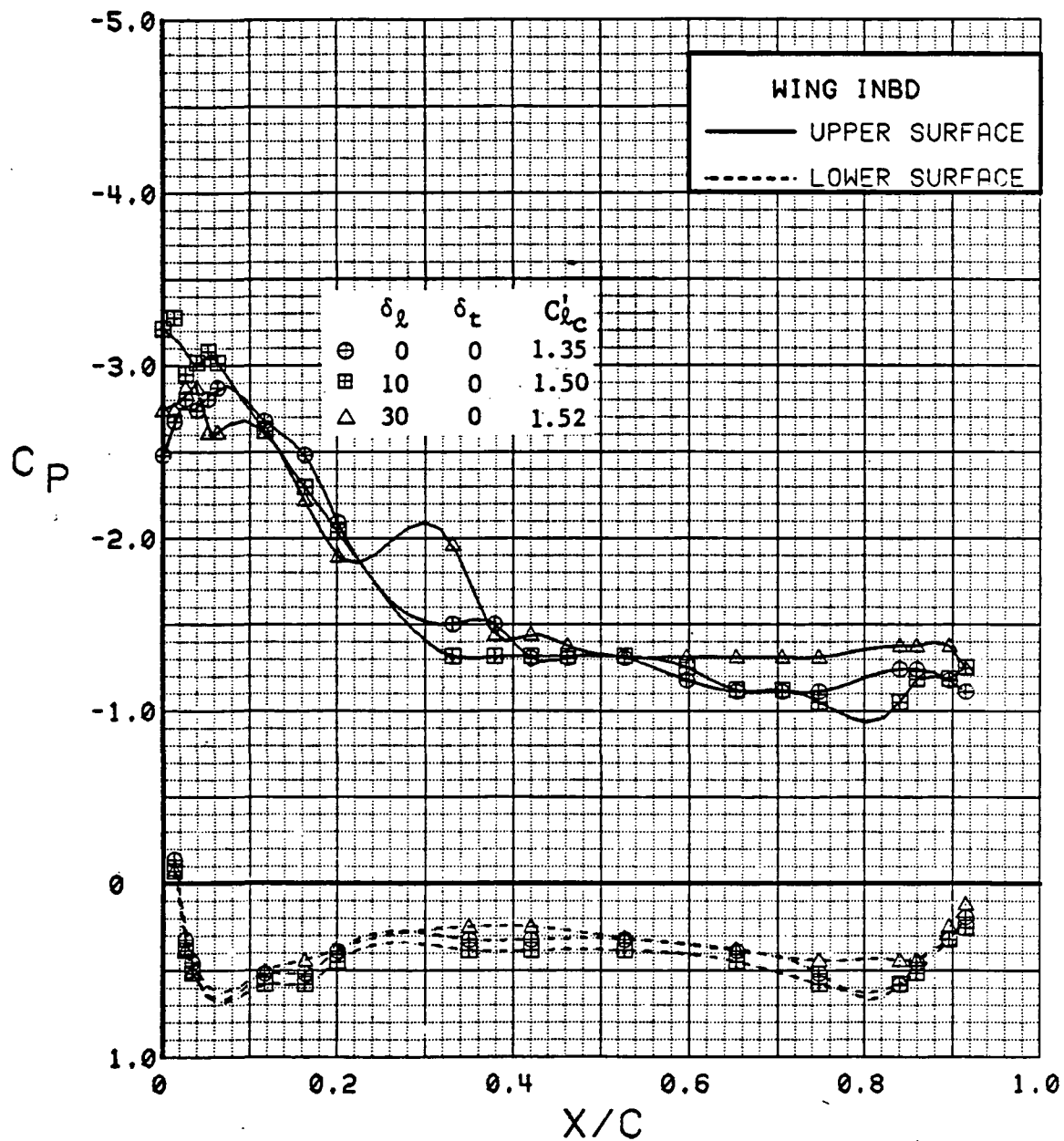


Figure 3.2.4-168 Canard Leading-Edge Flap Deflection Effects, Inboard,  $C_T = 0.9$ , Canard Neutral, Alpha = 16 deg

SYM	TEST	RUN	ALPHA	CT	ITEF	OTEF	CAN	SWB
⊕	543	6	0.3	0.94	30	30	0	OFF
⊞	543	25	0.3	0.93	30	30	0	OFF
Δ	543	29	0.3	0.93	30	30	0	OFF

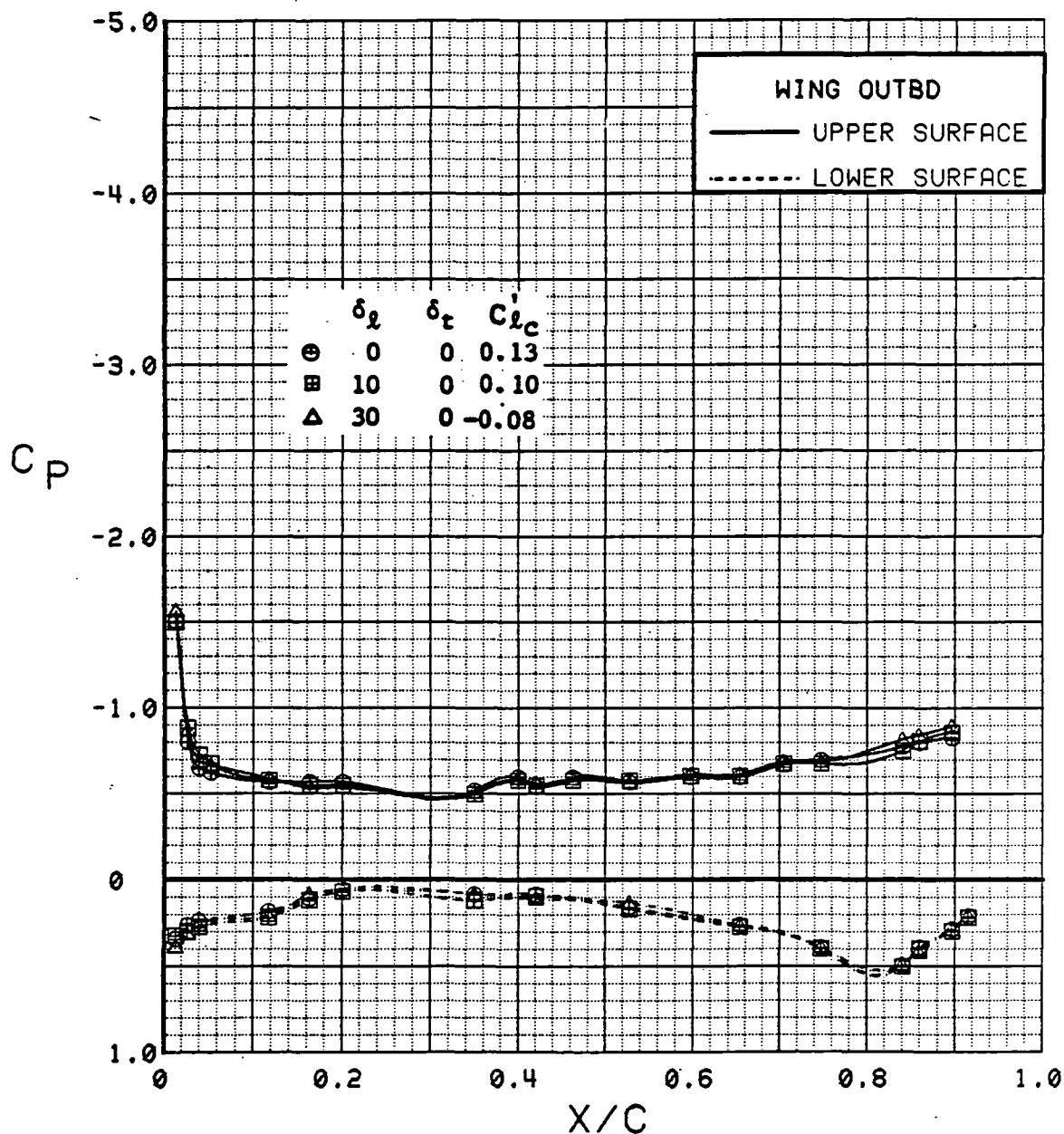


Figure 3.2.4-169 Canard Leading-Edge Flap Deflection Effects, Outboard,  $C_T$  0.9, Canard Neutral,  $\alpha = 0^\circ$

SYM	TEST	RUN	ALPHA	CT	ITEF	OTEF	CAN	SWB
⊕	543	6	4.5	0.94	30	30	0	OFF
⊞	543	25	4.5	0.94	30	30	0	OFF
Δ	543	29	4.5	0.93	30	30	0	OFF

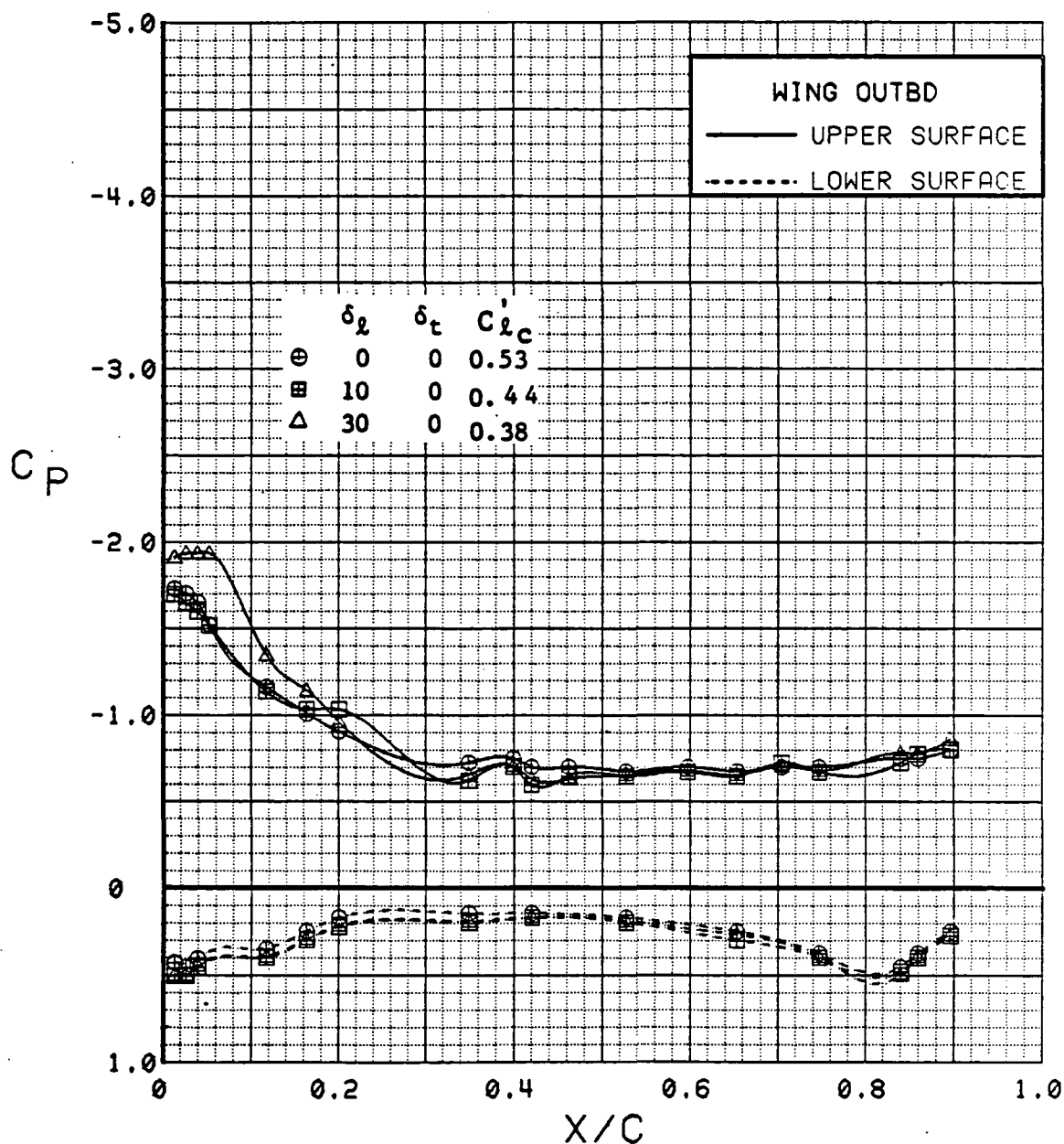


Figure 3.2.4-170 Canard Leading-Edge Flap Deflection Effects, Outboard,  $C_T$  0.9, Canard Neutral, Alpha = 4 deg

SYM	TEST	RUN	ALPHA	CT	ITEF	OTEF	CAN	SWB
⊕	543	6	8.6	0.91	30	30	0	OFF
⊞	543	25	8.6	0.93	30	30	0	OFF
△	543	29	8.6	0.93	30	30	0	OFF

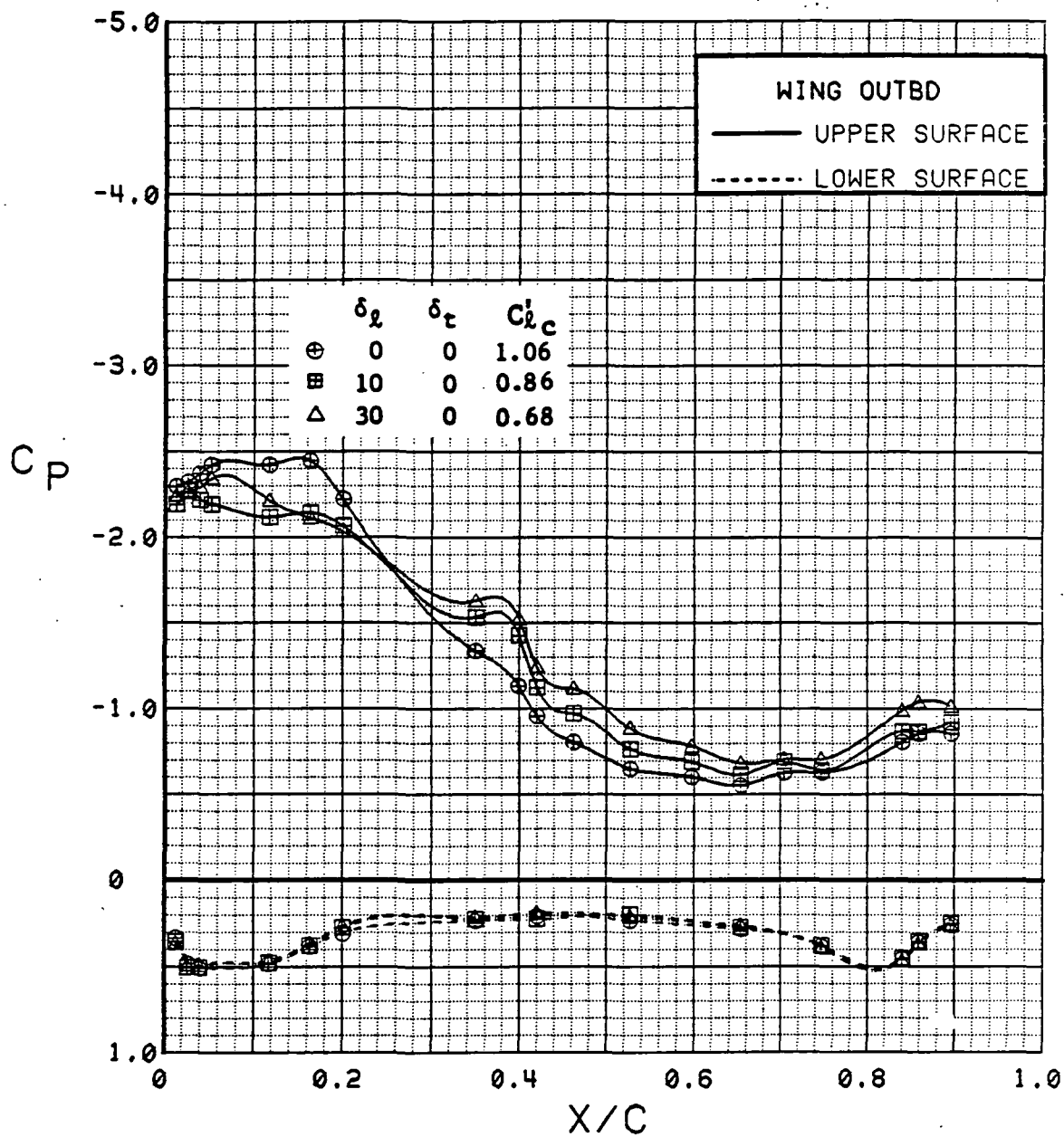


Figure 3.2.4-171 Canard Leading-Edge Flap Deflection Effects, Outboard,  $C_T$  0.9, Canard Neutral,  $\alpha = 8$  deg



SYM	TEST	RUN	ALPHA	CT	ITEF	OTEF	CAN	SWB
⊕	543	6	12.8	0.92	30	30	0	OFF
⊞	543	25	12.8	0.92	30	30	0	OFF
Δ	543	29	12.8	0.92	30	30	0	OFF

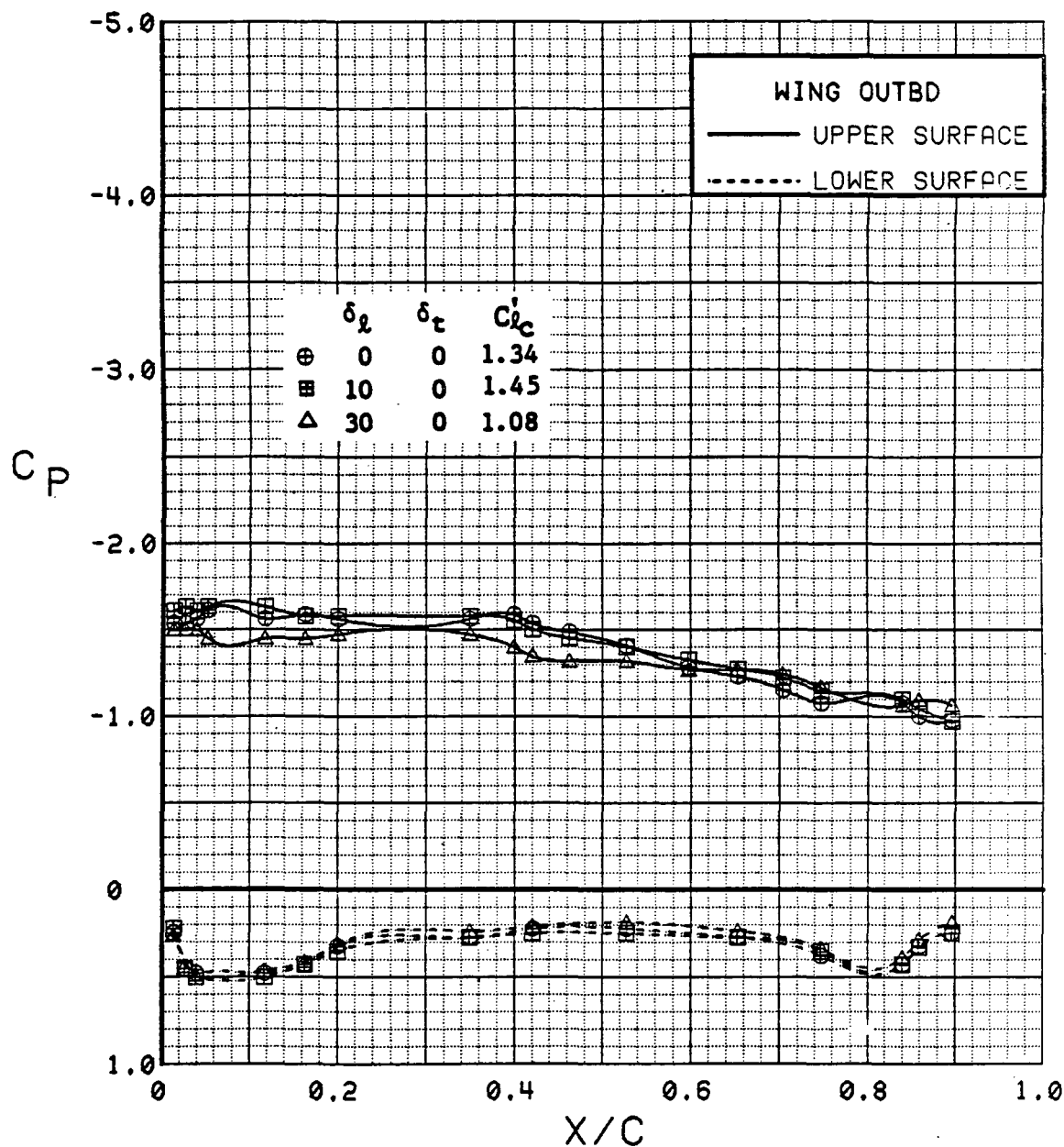


Figure 3.2.4-172 Canard Leading-Edge Flap Deflection Effects, Outboard,  $C_T$  0.9, Canard Neutral, Alpha = 12 deg

SYM	TEST	RUN	ALPHA	CT	ITEF	OTEF	CAN	SWB
⊕	543	6	16.9	0.92	30	30	0	OFF
⊞	543	25	16.9	0.93	30	30	0	OFF
Δ	543	29	16.9	0.93	30	30	0	OFF

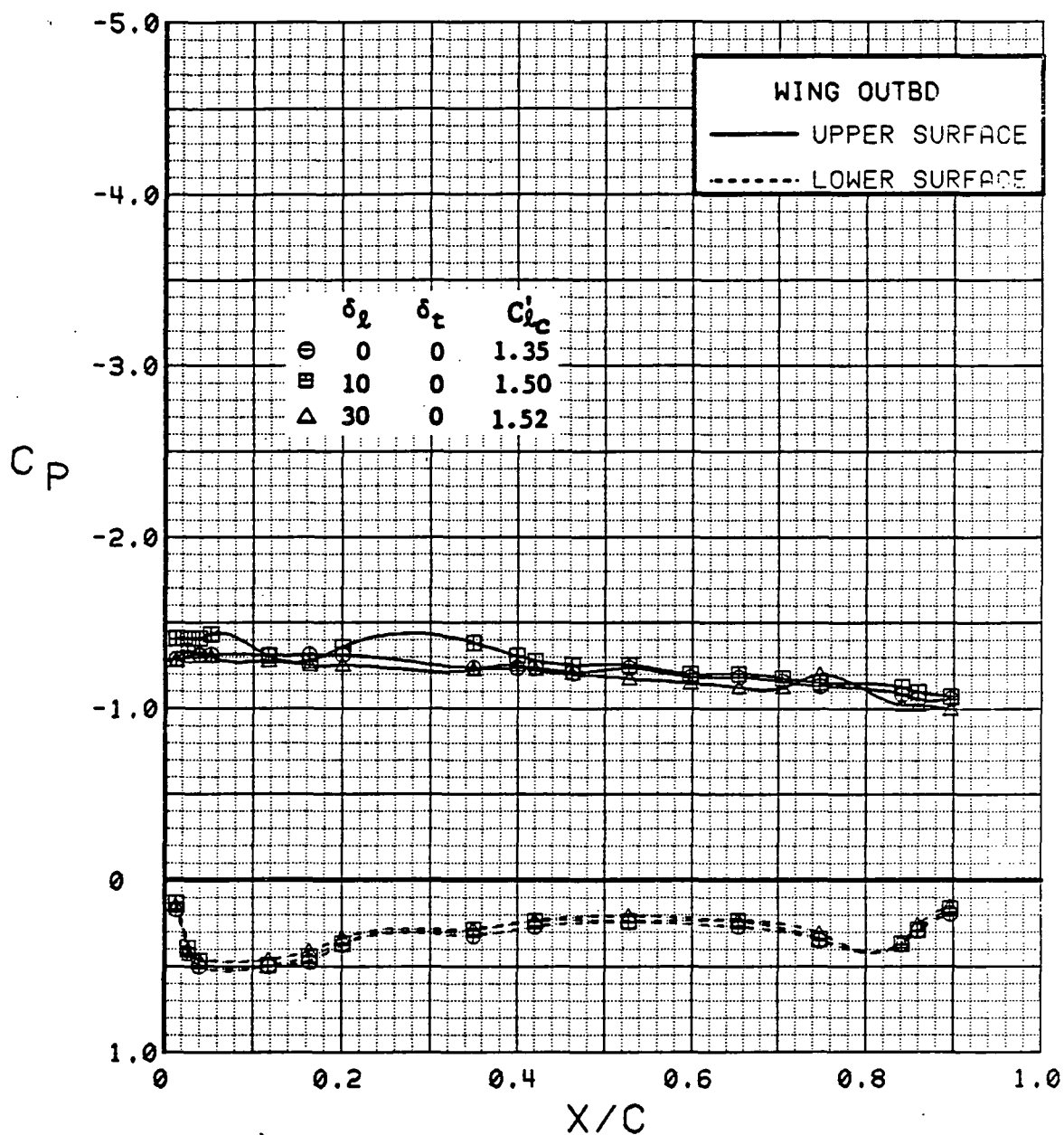


Figure 3.2.4-173 Canard Leading-Edge Flap Deflection Effects, Outboard,  $C_T$  0.9, Canard Neutral, Alpha = 16 deg

SYM	TEST	RUN	ALPHA	CT	ITEF	OTEF	CAN	SWB
⊕	543	6	0.3	0.94	30	30	0	OFF
⊞	543	25	0.3	0.93	30	30	0	OFF
△	543	29	0.3	0.93	30	30	0	OFF

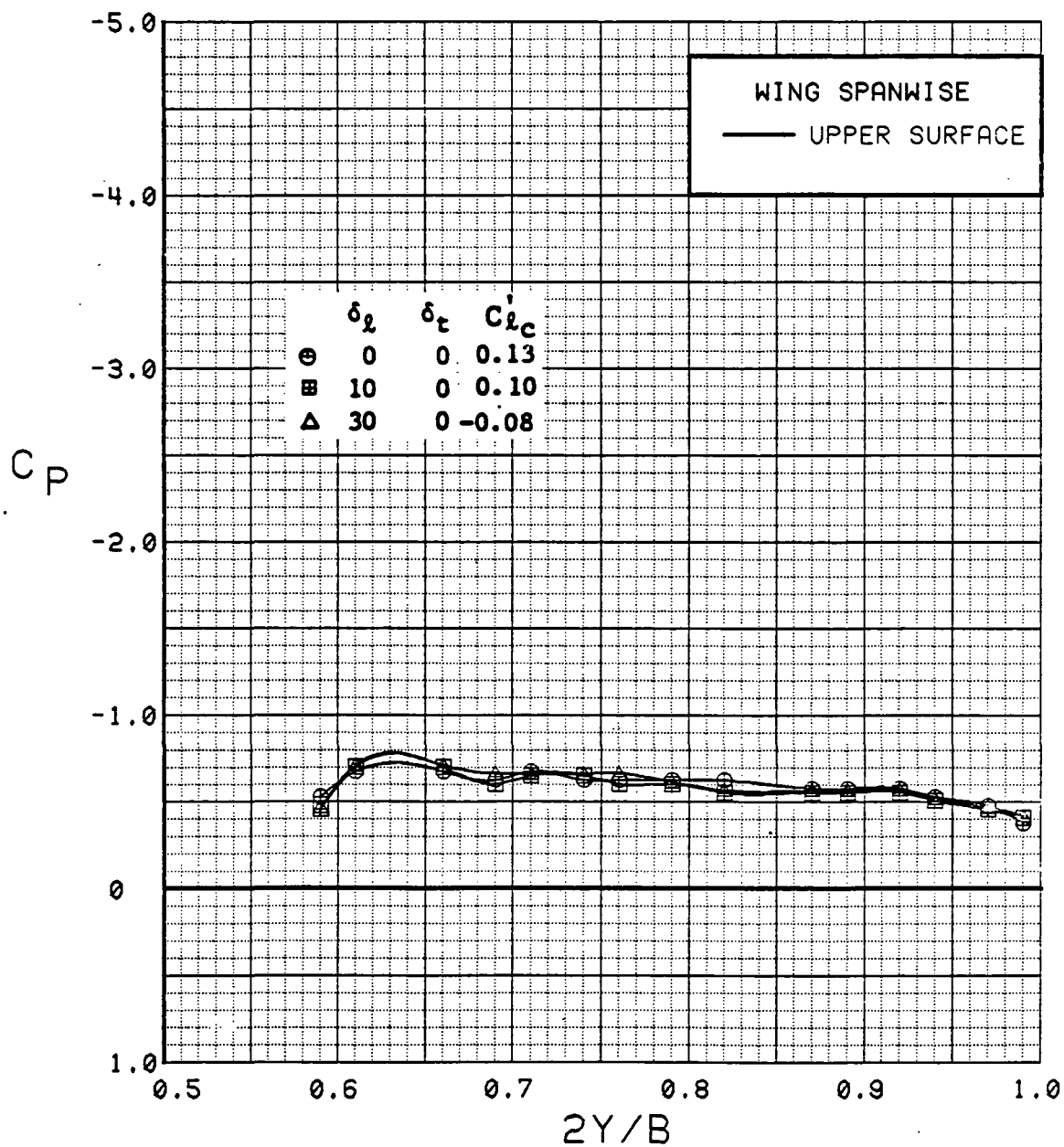


Figure 3.2.4-174 Canard Leading-Edge Flap Deflection Effects, Spanwise,  $C_T = 0.9$ , Canard Neutral, Alpha = 0 deg

SYM	TEST	RUN	ALPHA	CT	ITEF	OTEF	CAN	SWB
⊕	543	6	4.5	0.94	30	30	0	OFF
⊞	543	25	4.5	0.94	30	30	0	OFF
Δ	543	29	4.5	0.93	30	30	0	OFF

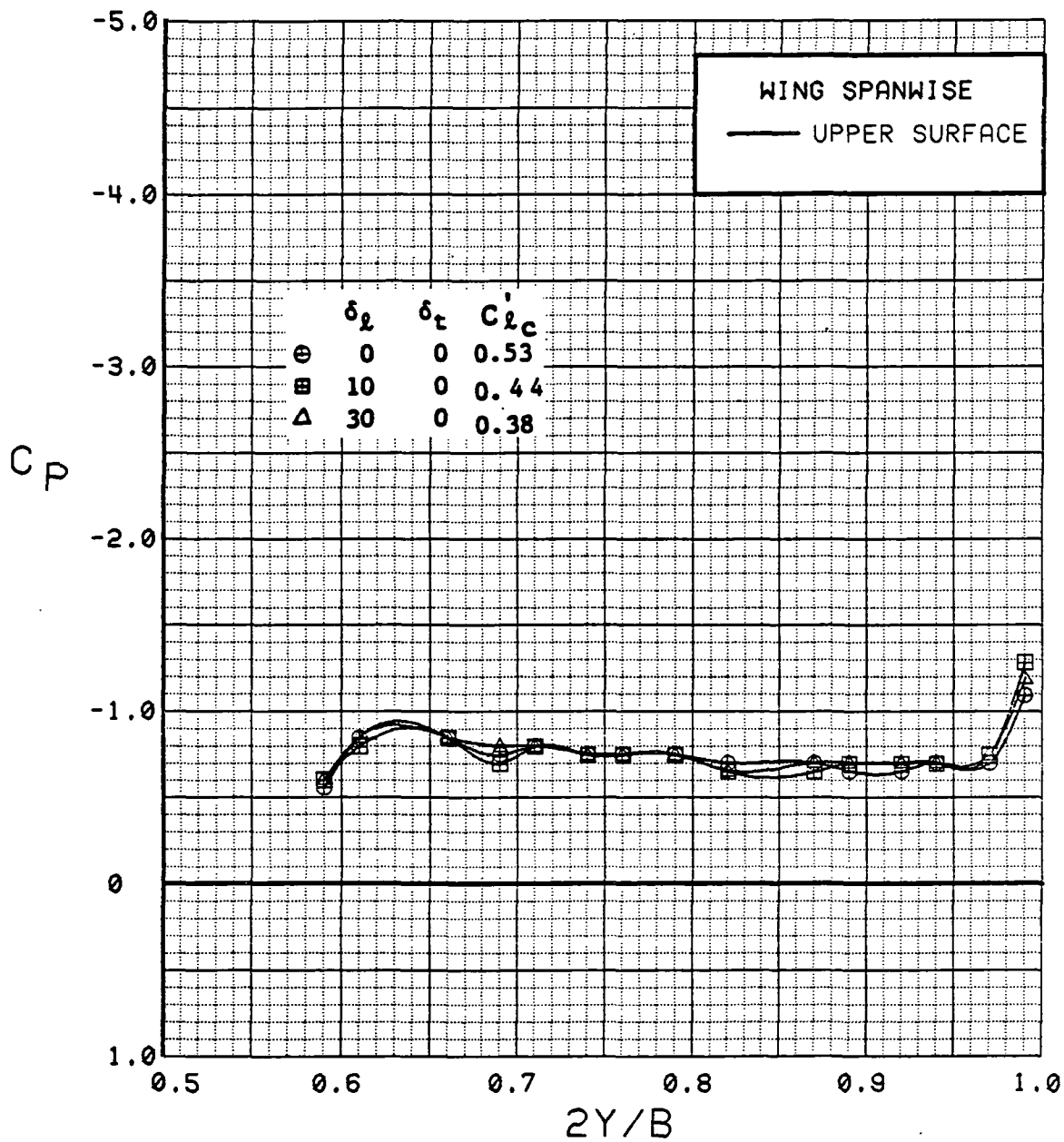


Figure 3.2.4-175 Canard Leading-Edge Flap Deflection Effects, Spanwise,  $C_T = 0.9$ , Canard Neutral,  $\alpha = 4$  deg

SYM	TEST	RUN	ALPHA	CT	ITEF	OTEF	CAN	SWB
⊕	543	6	8.6	0.91	30	30	0	OFF
⊞	543	25	8.6	0.93	30	30	0	OFF
△	543	29	8.6	0.93	30	30	0	OFF

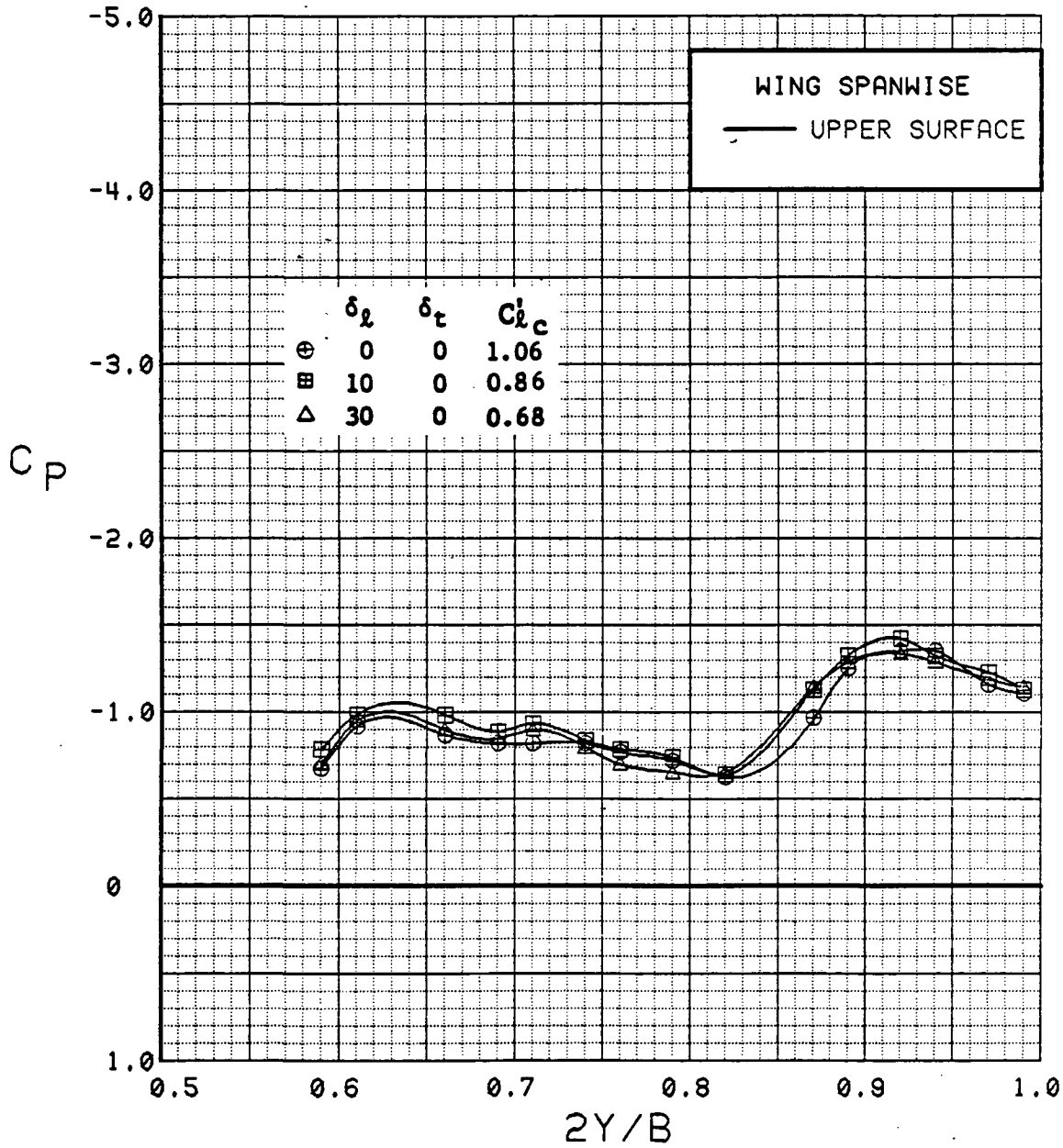


Figure 3.2.4-176 Canard Leading-Edge Flap Deflection Effects,  
Spanwise,  $C_T = 0.9$ , Canard Neutral, Alpha = 8 deg

SYM	TEST	RUN	ALPHA	CT	ITEF	OTEF	CAN	SWB
⊕	543	6	12.8	0.92	30	30	0	OFF
⊞	543	25	12.8	0.92	30	30	0	OFF
△	543	29	12.8	0.92	30	30	0	OFF

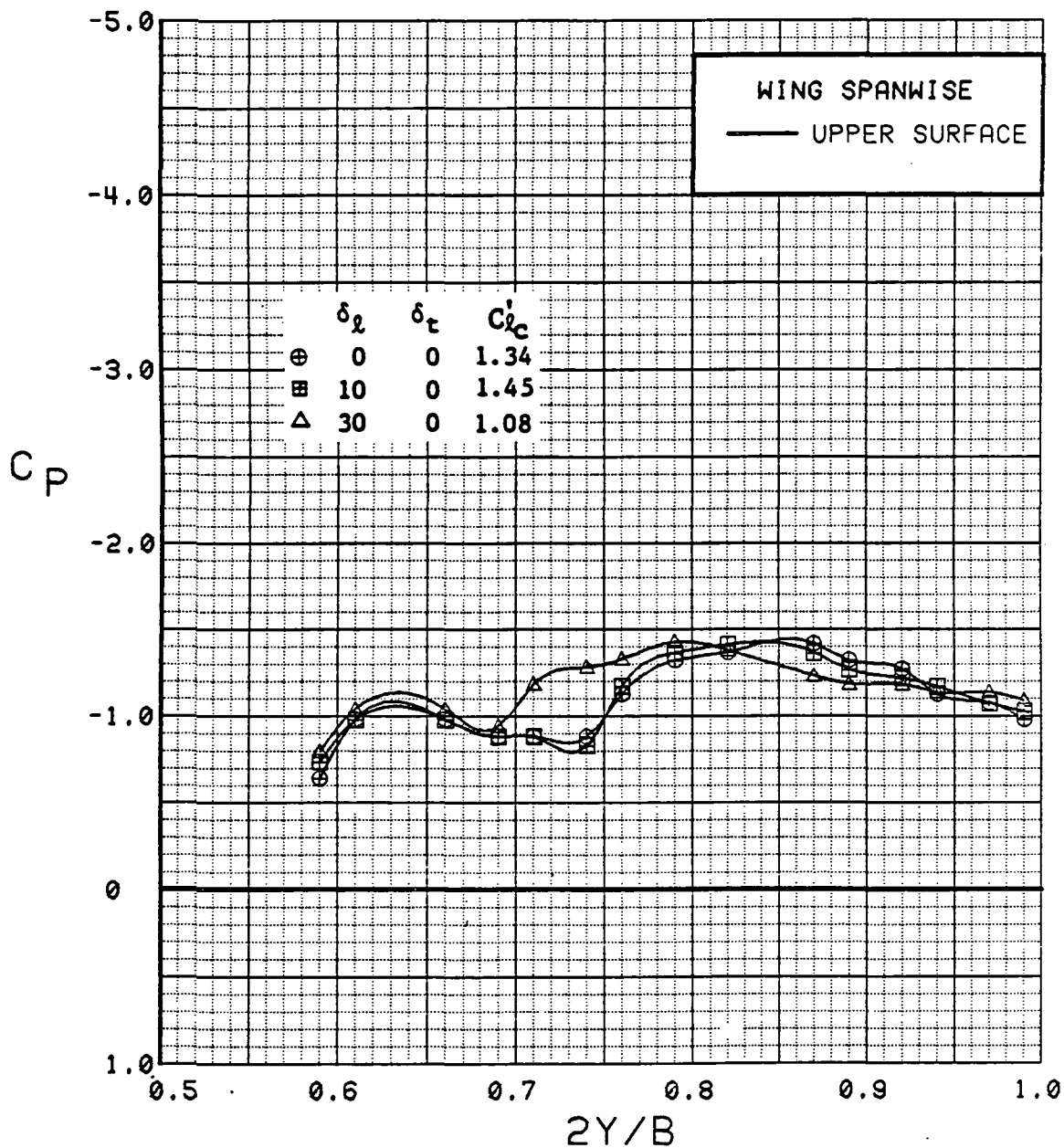


Figure 3.2.4-177 Canard Leading-Edge Flap Deflection Effects,  
Spanwise,  $C_T = 0.9$ , Canard Neutral, Alpha = 12 deg

SYM	TEST	RUN	ALPHA	CT	ITEF	OTEF	CAN	SWB
⊙	543	6	16.9	0.92	30	30	0	OFF
⊠	543	25	16.9	0.93	30	30	0	OFF
△	543	29	16.9	0.93	30	30	0	OFF

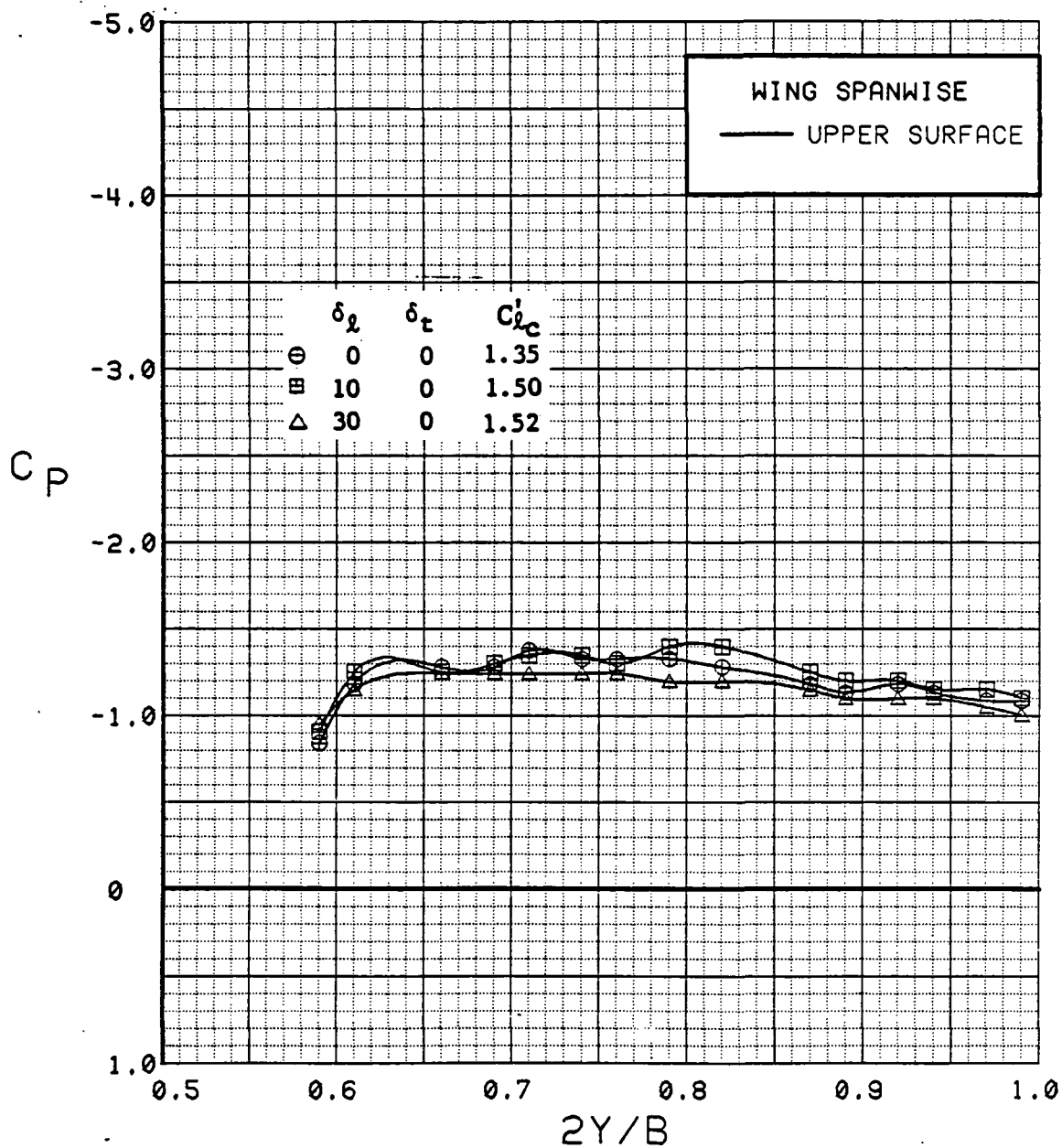


Figure 3.2.4-178 Canard Leading-Edge Flap Deflection Effects, Spanwise,  $C_T = 0.9$ , Canard Neutral, Alpha = 16 deg

SYM	TEST	RUN	ALPHA	CT	ITEF	OTEF	CAN	SWB
⊕	543	21	4.5	0.94	30	30	20	OFF
⊞	543	26	4.5	0.93	30	30	20	OFF
Δ	543	31	4.5	0.94	30	30	20	OFF

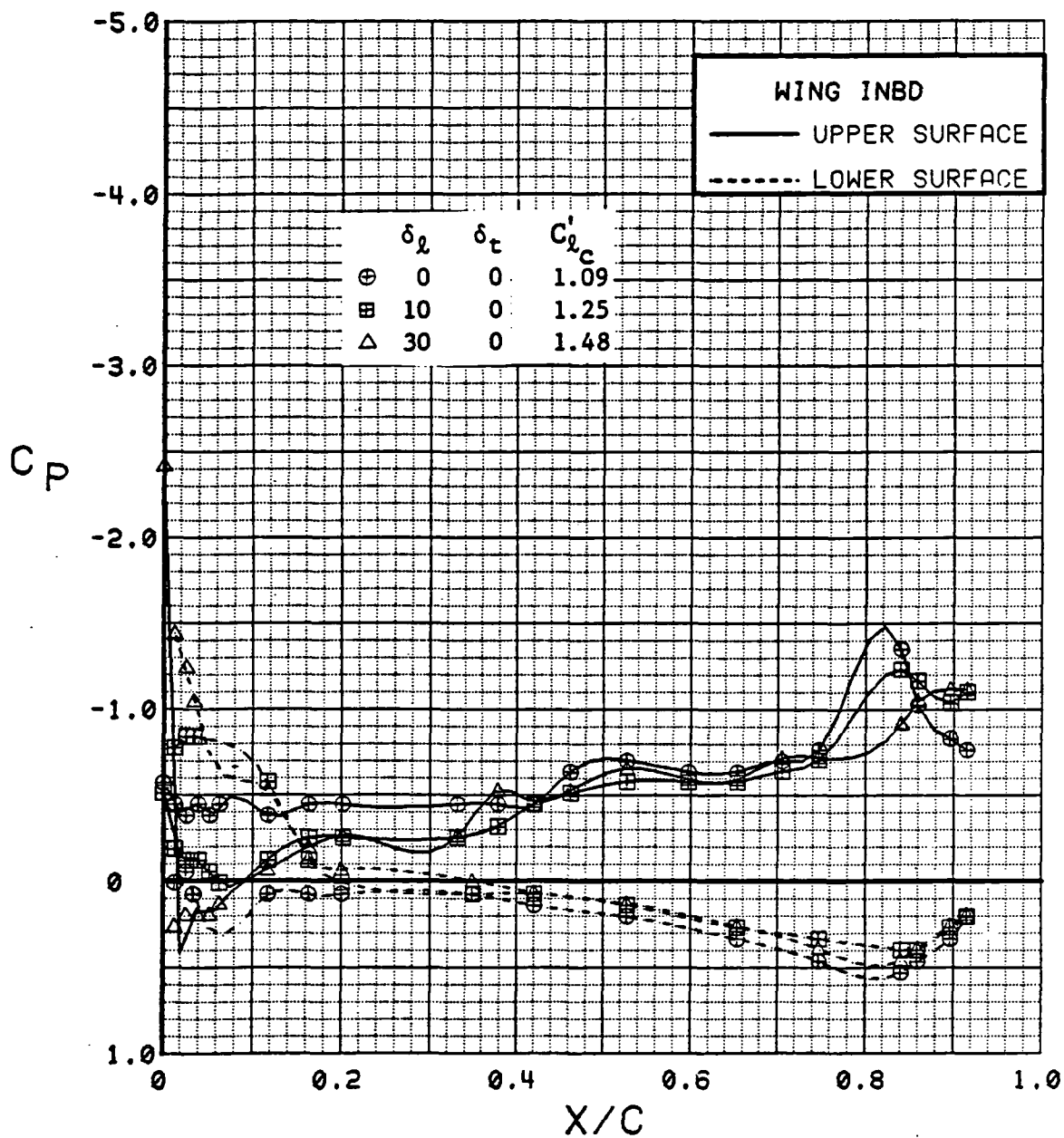


Figure 3.2.4-179 Canard Leading-Edge Flap Deflection Effects, Inboard,  $C_T$  0.9, Canard Deflected,  $\alpha = 4$  deg



SYM	TEST	RUN	ALPHA	CT	ITEF	OTEF	CAN	SWB
⊕	543	21	8.7	0.93	30	30	20	OFF
⊞	543	26	8.7	0.93	30	30	20	OFF
Δ	543	31	8.7	0.93	30	30	20	OFF

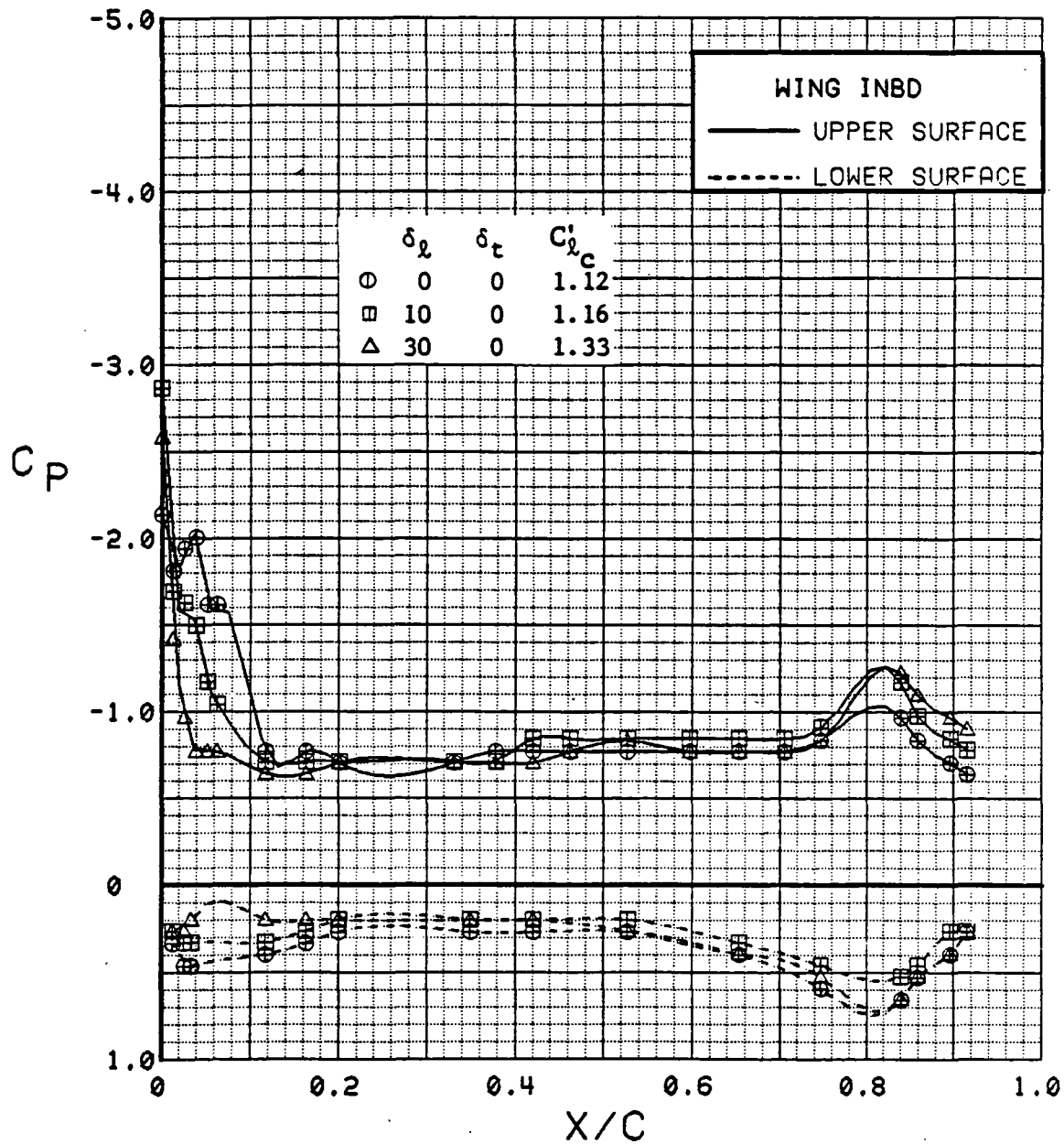


Figure 3.2.4-180 Canard Leading-Edge Flap Deflection Effects, Inboard,  $C_T$  0.9, Canard Deflected, Alpha = 8 deg

SYM	TEST	RUN	ALPHA	CT	ITEF	OTEF	CAN	SWB
⊕	543	21	12.8	0.93	30	30	20	OFF
⊞	543	26	12.8	0.95	30	30	20	OFF
Δ	543	31	12.8	0.94	30	30	20	OFF

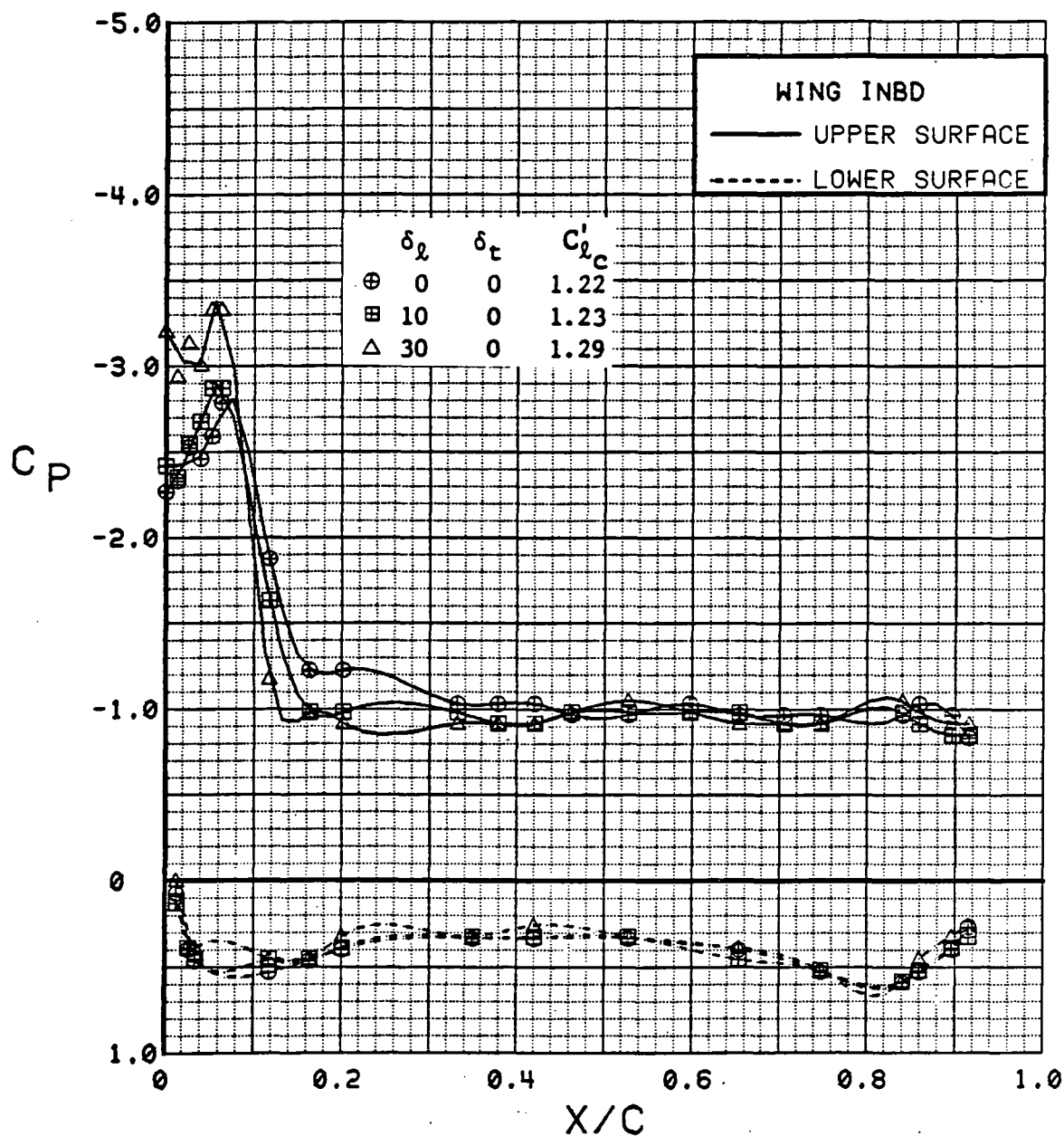


Figure 3.2.4-181 Canard Leading-Edge Flap Deflection Effects, Inboard,  $C_T$  0.9, Canard Deflected, Alpha = 12 deg

SYM	TEST	RUN	ALPHA	CT	ITEF	OTEF	CAN	SWB
⊕	543	21	16.9	0.94	30	30	20	OFF
⊞	543	26	16.9	0.93	30	30	20	OFF
Δ	543	31	16.9	0.92	30	30	20	OFF

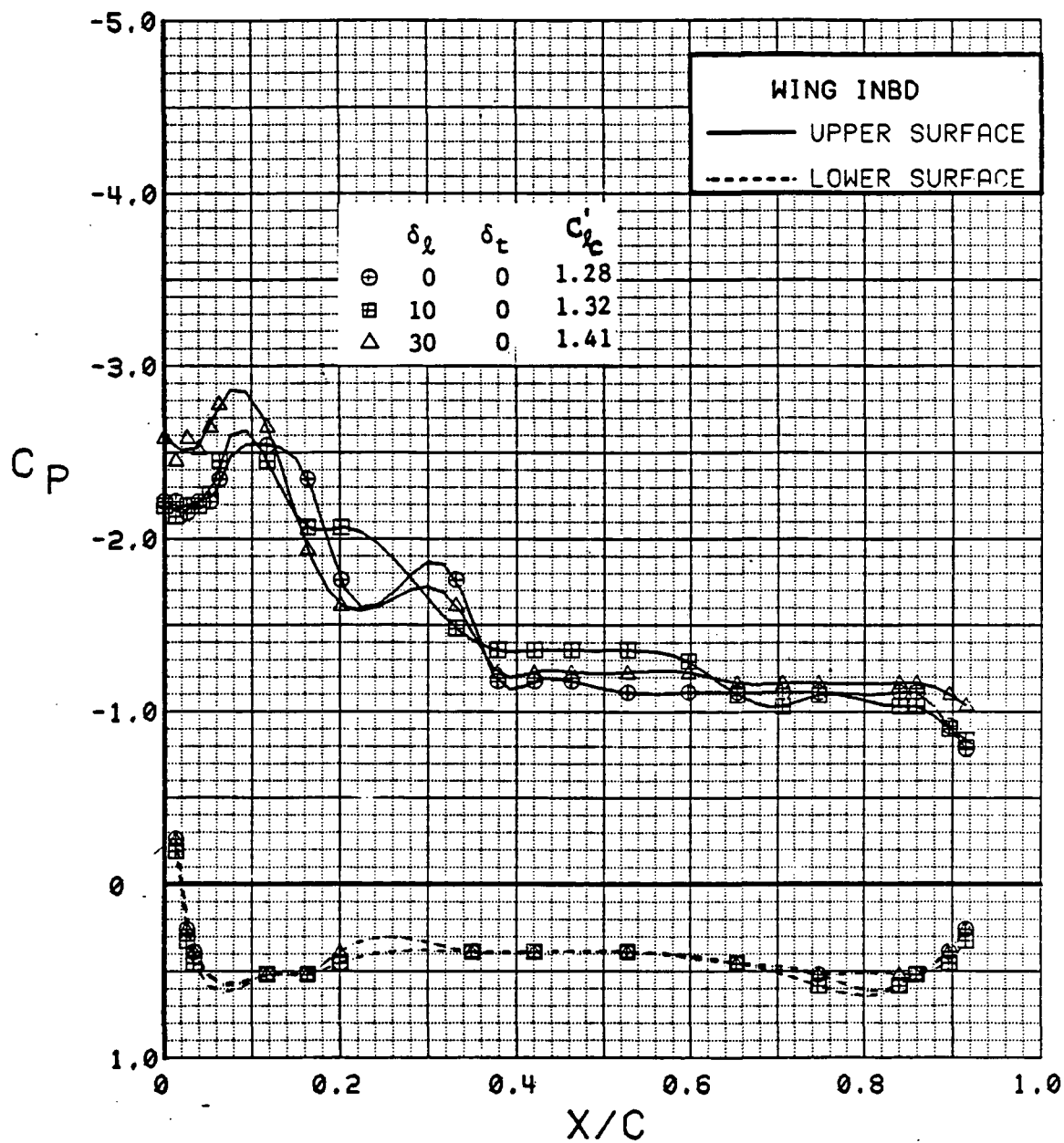


Figure 3.2.4-182 Canard Leading-Edge Flap Deflection Effects, Inboard,  $C_T$  0.9, Canard Deflected,  $\alpha = 16$  deg

SYM	TEST	RUN	ALPHA	CT	ITEF	OTEF	CAN	SWB
⊕	543	21	4.5	0.94	30	30	20	OFF
⊞	543	26	4.5	0.93	30	30	20	OFF
Δ	543	31	4.5	0.94	30	30	20	OFF

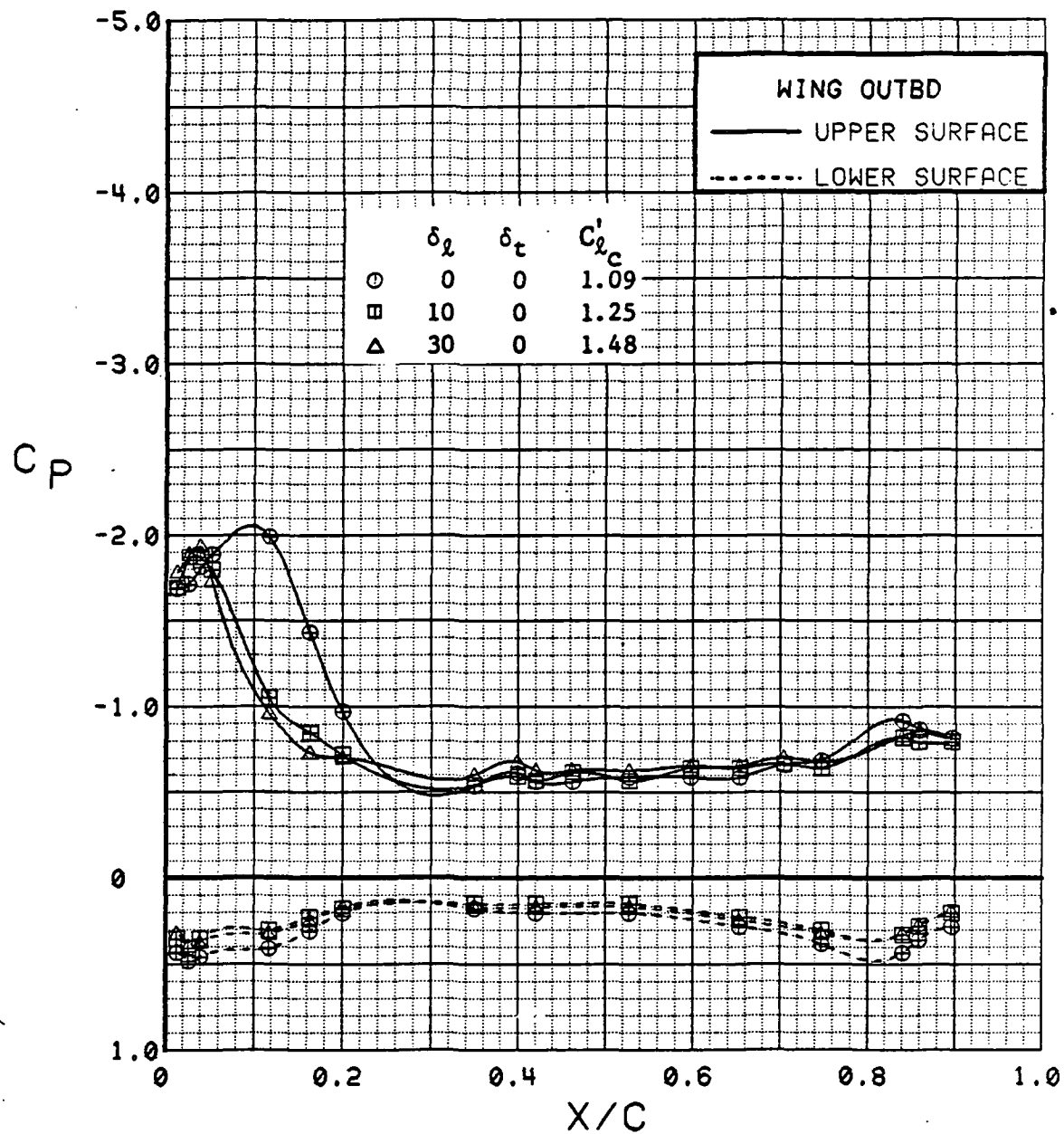


Figure 3.2.4-183 Canard Leading-Edge Flap Deflection Effects, Outboard,  $C_T = 0.9$ , Canard Deflected, Alpha = 4 deg

SYM	TEST	RUN	ALPHA	CT	ITEF	OTEF	CAN	SWB
⊕	543	21	8.7	0.93	30	30	20	OFF
⊞	543	26	8.7	0.93	30	30	20	OFF
Δ	543	31	8.7	0.93	30	30	20	OFF

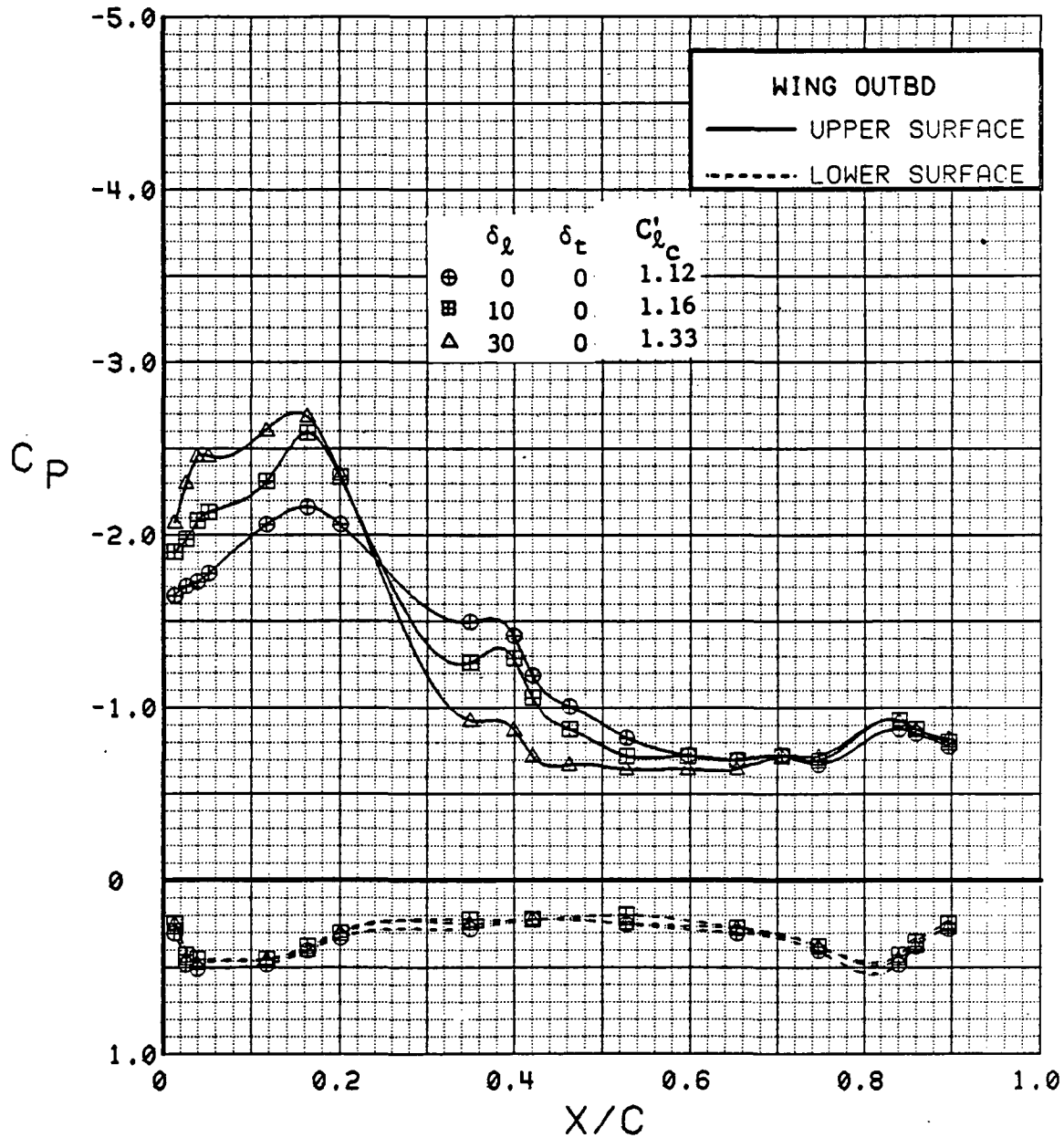


Figure 3.2.4-184 Canard Leading-Edge Flap Deflection Effects, Outboard,  $C_T = 0.9$ , Canard Deflected, Alpha = 8 deg

SYM	TEST	RUN	ALPHA	CT	ITEF	OTEF	CAN	SWB
⊕	543	21	12.8	0.93	30	30	20	OFF
⊞	543	26	12.8	0.95	30	30	20	OFF
Δ	543	31	12.8	0.94	30	30	20	OFF

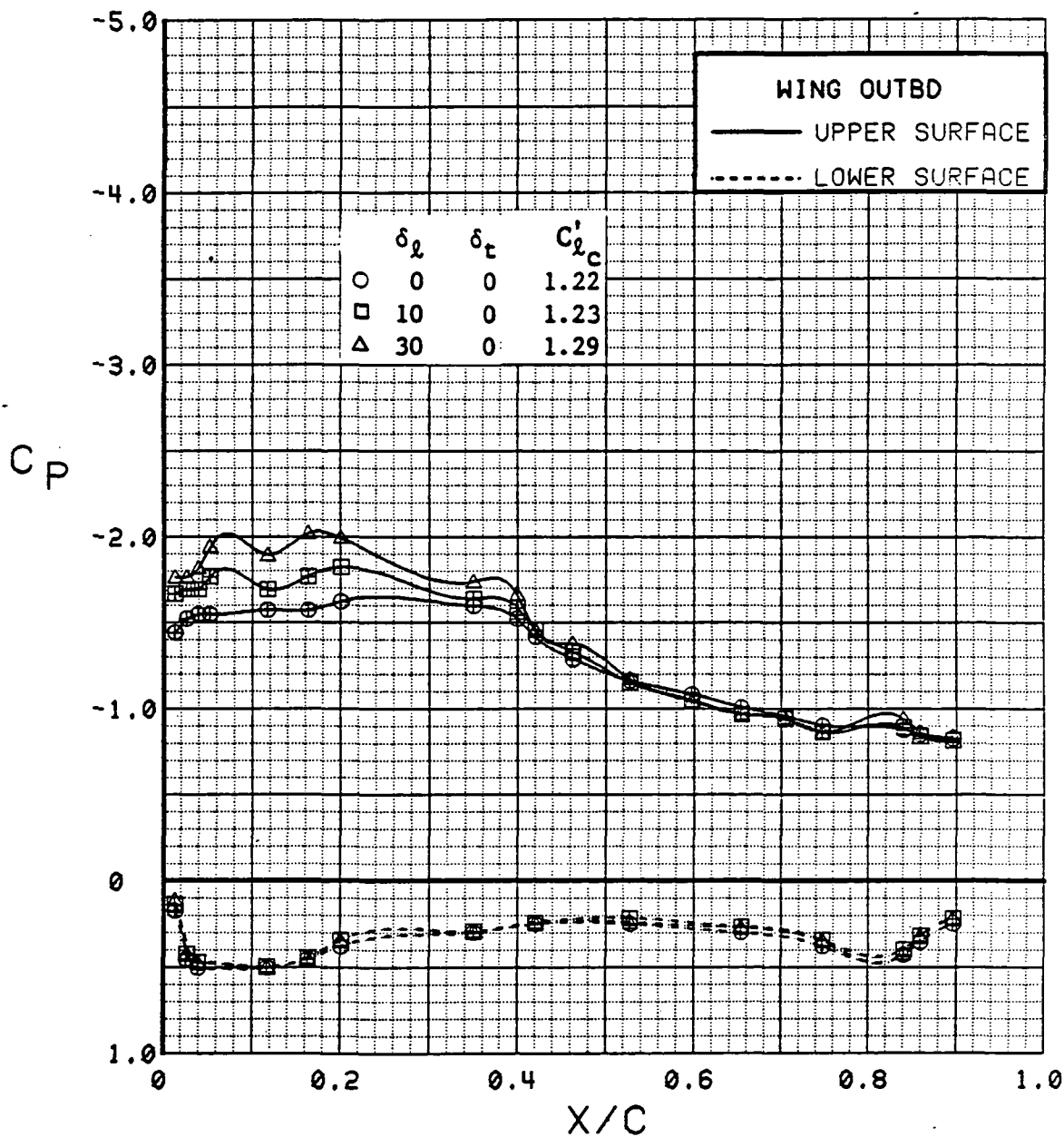


Figure 3.2.4-185 Canard Leading-Edge Flap Deflection Effects, Outboard,  $C_T = 0.9$ , Canard Deflected,  $\alpha = 12$  deg

SYM	TEST	RUN	ALPHA	CT	ITEF	OTEF	CAN	SWB
⊕	543	21	16.9	0.94	30	30	20	OFF
⊞	543	26	16.9	0.93	30	30	20	OFF
Δ	543	31	16.9	0.92	30	30	20	OFF

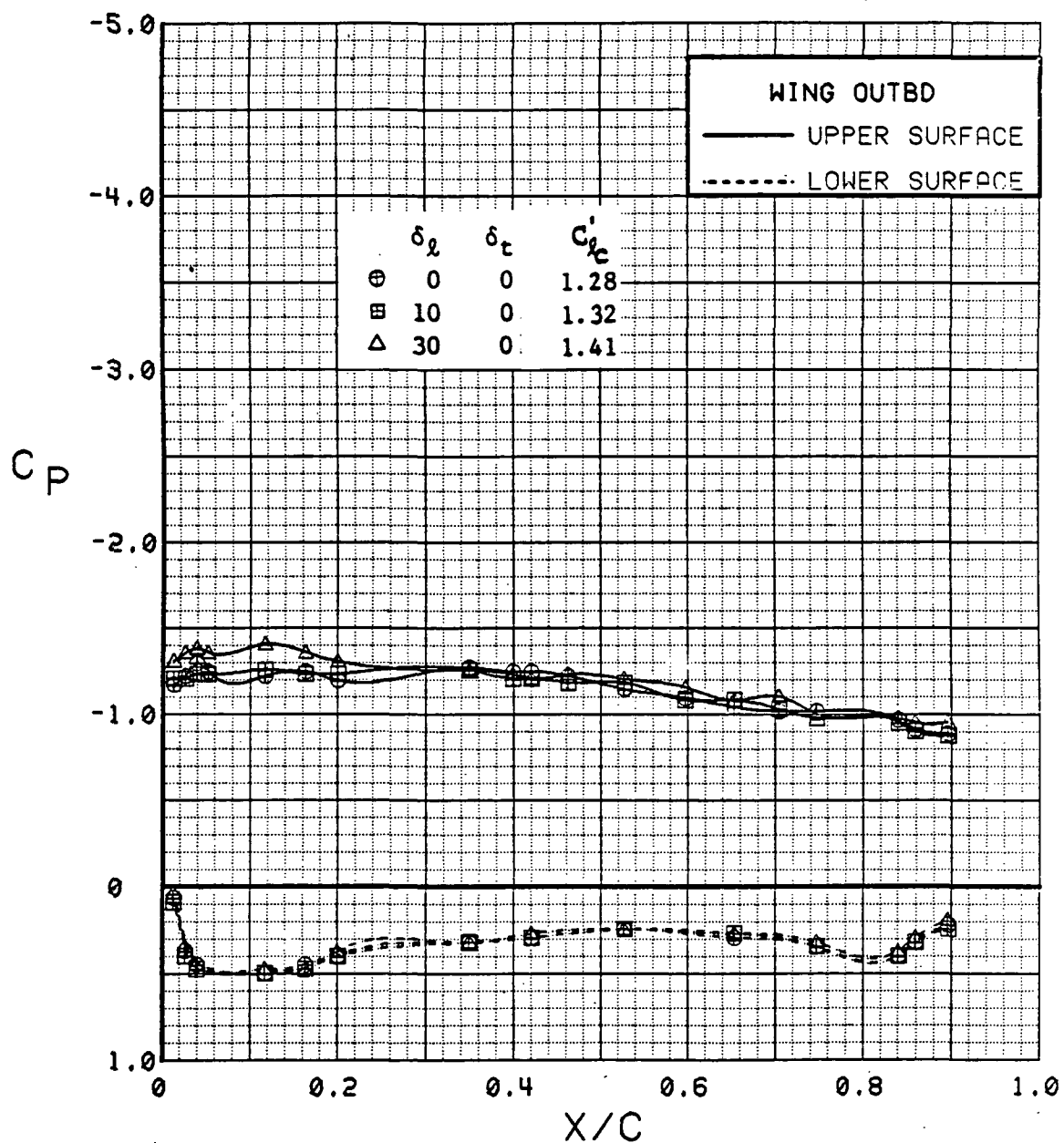


Figure 3.2.4-186 Canard Leading-Edge Flap Deflection Effects, Outboard,  $C_T = 0.9$ , Canard Deflected, Alpha = 16 deg

SYM	TEST	RUN	ALPHA	CT	ITEF	OTEF	CAN	SWB
⊙	543	21	4.5	0.94	30	30	20	OFF
⊞	543	26	4.5	0.93	30	30	20	OFF
△	543	31	4.5	0.94	30	30	20	OFF

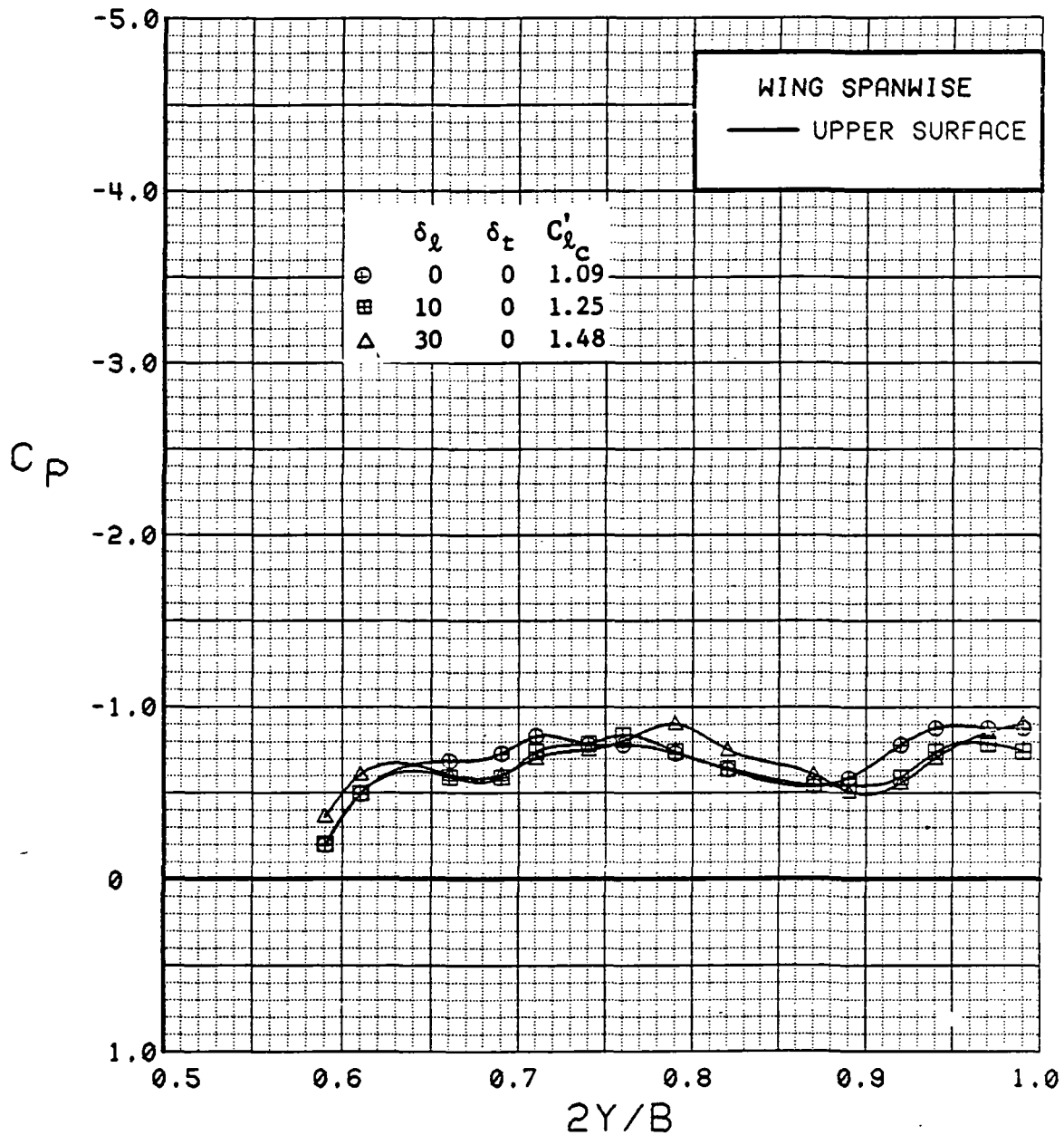


Figure 3.2.4-187 Canard Leading-Edge Flap Deflection Effects,  
Spanwise,  $C_T = 0.9$ , Canard Deflected, Alpha = 4 deg



SYM	TEST	RUN	ALPHA	CT	ITEF	OTEF	CAN	SWB
⊕	543	21	8.7	0.93	30	30	20	OFF
⊞	543	26	8.7	0.93	30	30	20	OFF
Δ	543	31	8.7	0.93	30	30	20	OFF

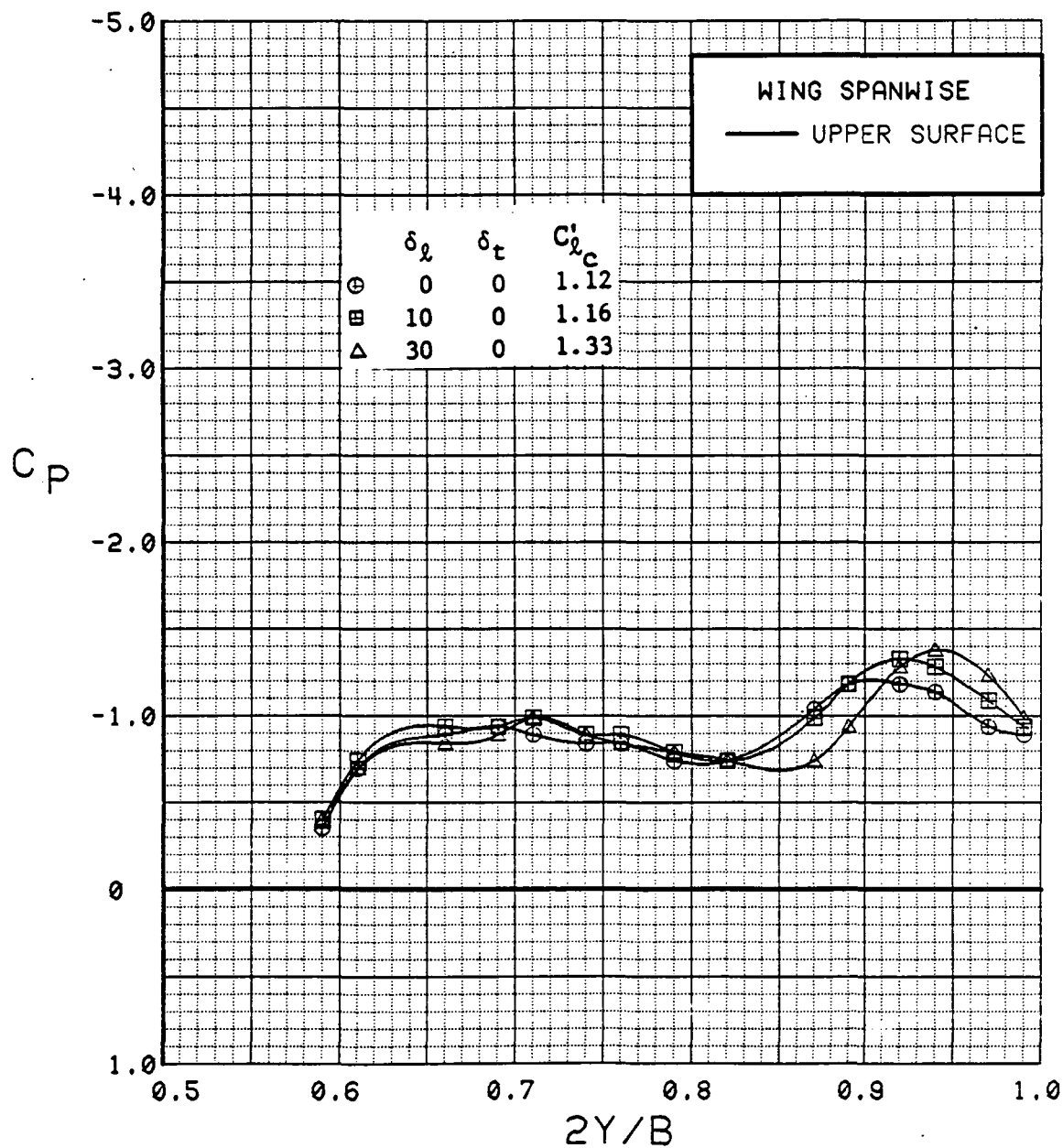


Figure 3.2.4-188 Canard Leading-Edge Flap Deflection Effects,  
Spanwise,  $C_T = 0.9$ , Canard Deflected, Alpha = 8 deg

SYM	TEST	RUN	ALPHA	CT	ITEF	OTEF	CAN	SWB
⊕	543	21	12.8	0.93	30	30	20	OFF
⊞	543	26	12.8	0.95	30	30	20	OFF
Δ	543	31	12.8	0.94	30	30	20	OFF

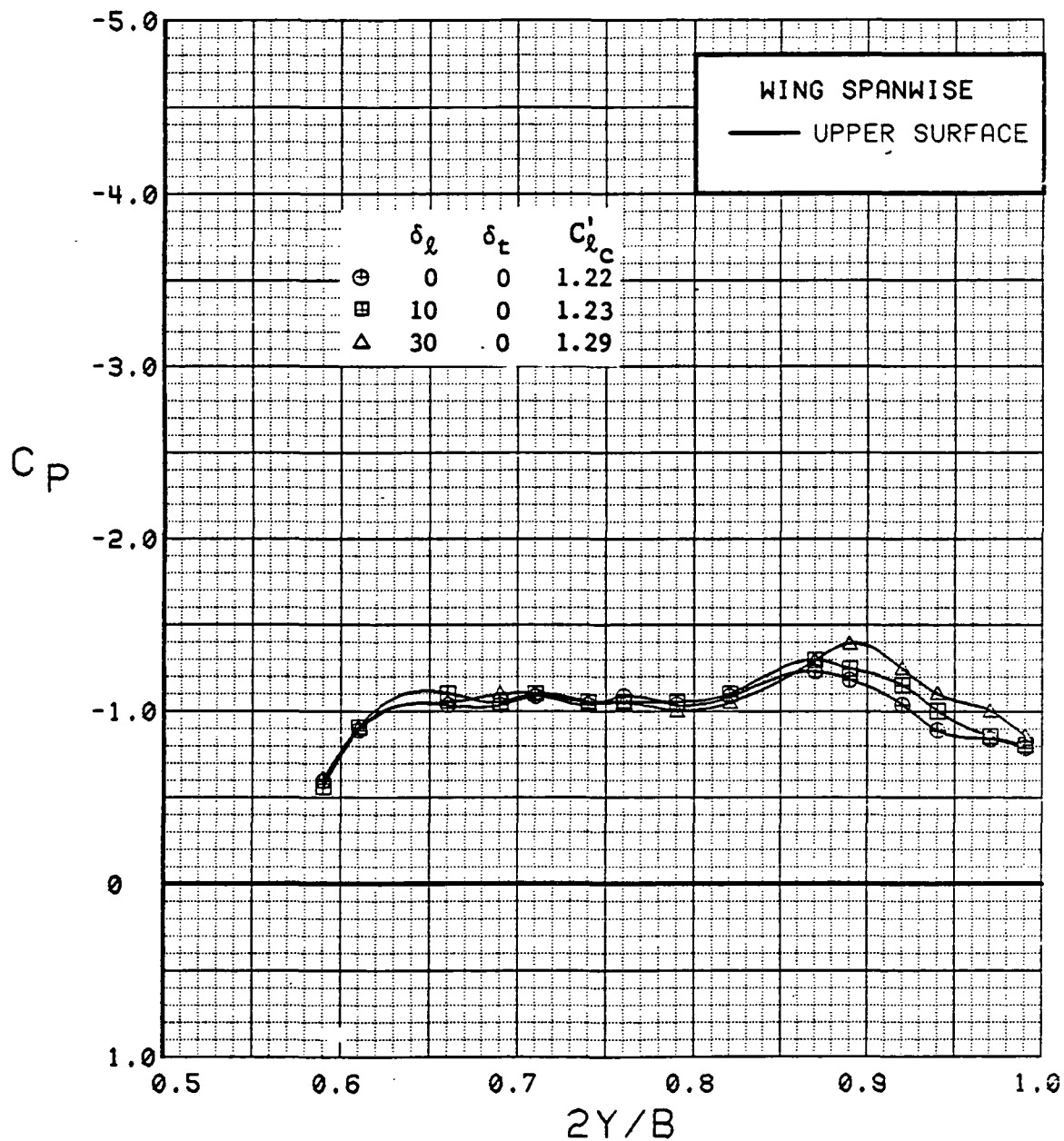


Figure 3.2.4-189 Canard Leading-Edge Flap Deflection Effects,  
Spanwise,  $C_T = 0.9$ , Canard Deflected, Alpha = 12 deg

SYM	TEST	RUN	ALPHA	CT	ITEF	OTEF	CAN	SWB
⊕	543	21	16.9	0.94	30	30	20	OFF
⊞	543	26	16.9	0.93	30	30	20	OFF
Δ	543	31	16.9	0.92	30	30	20	OFF

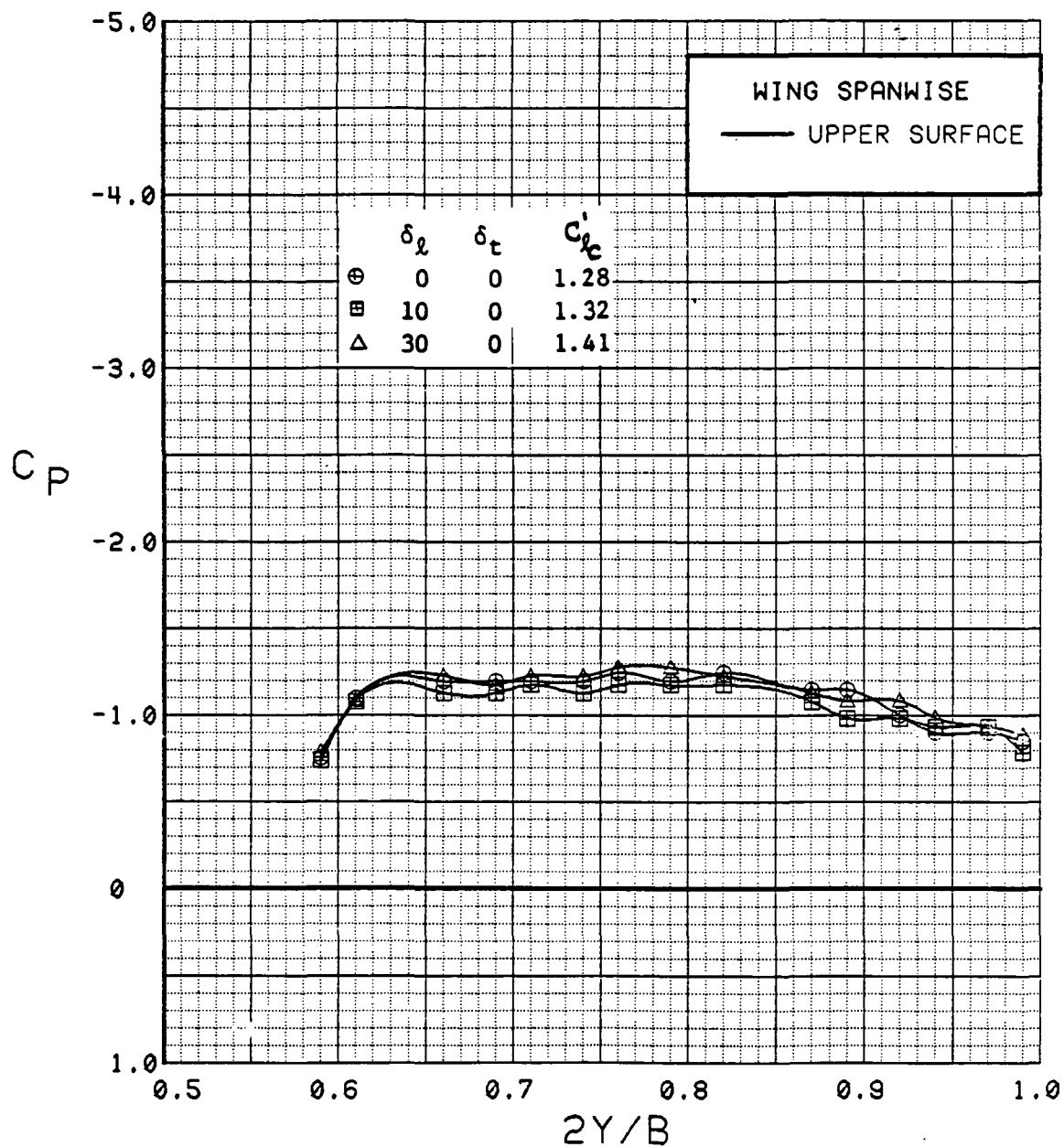


Figure 3.2.4-190 Canard Leading-Edge Flap Deflection Effects,  
Spanwise,  $C_T = 0.9$ , Canard Deflected, Alpha = 16 deg

SYM	TEST	RUN	ALPHA	CT	ITEF	OTEF	CAN	SWB
⊕	543	6	0.3	0.94	30	30	0	OFF
⊞	543	29	0.3	0.93	30	30	0	OFF
Δ	543	34	0.4	0.93	30	30	0	OFF

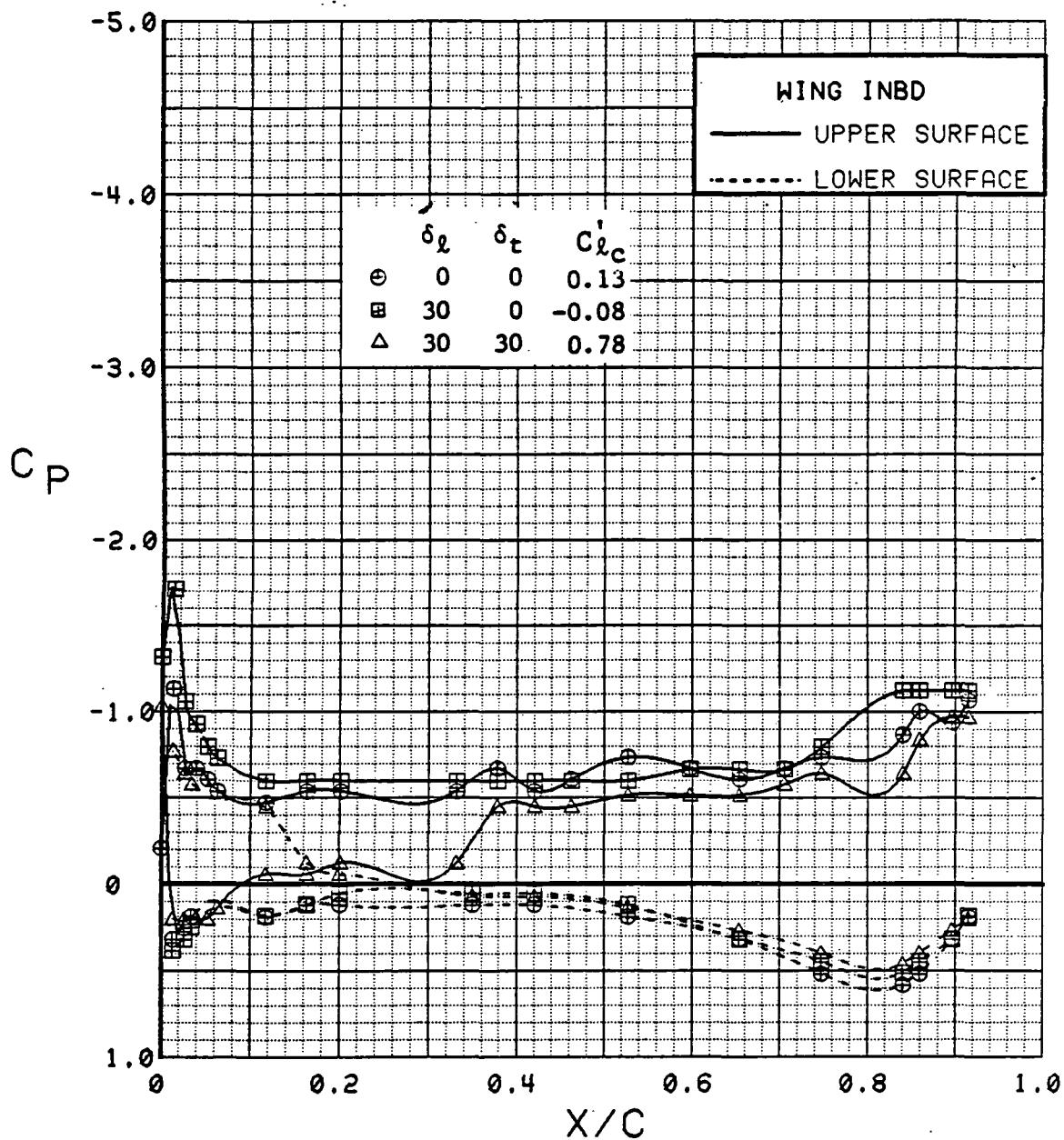


Figure 3.2.4-191 Combined Canard Flap Deflection Effects, Inboard, Alpha = 0 deg

SYM	TEST	RUN	ALPHA	CT	ITEF	OTEF	CAN	SWB
⊕	543	6	4.5	0.94	30	30	0	OFF
⊞	543	29	4.5	0.93	30	30	0	OFF
Δ	543	34	4.5	0.91	30	30	0	OFF

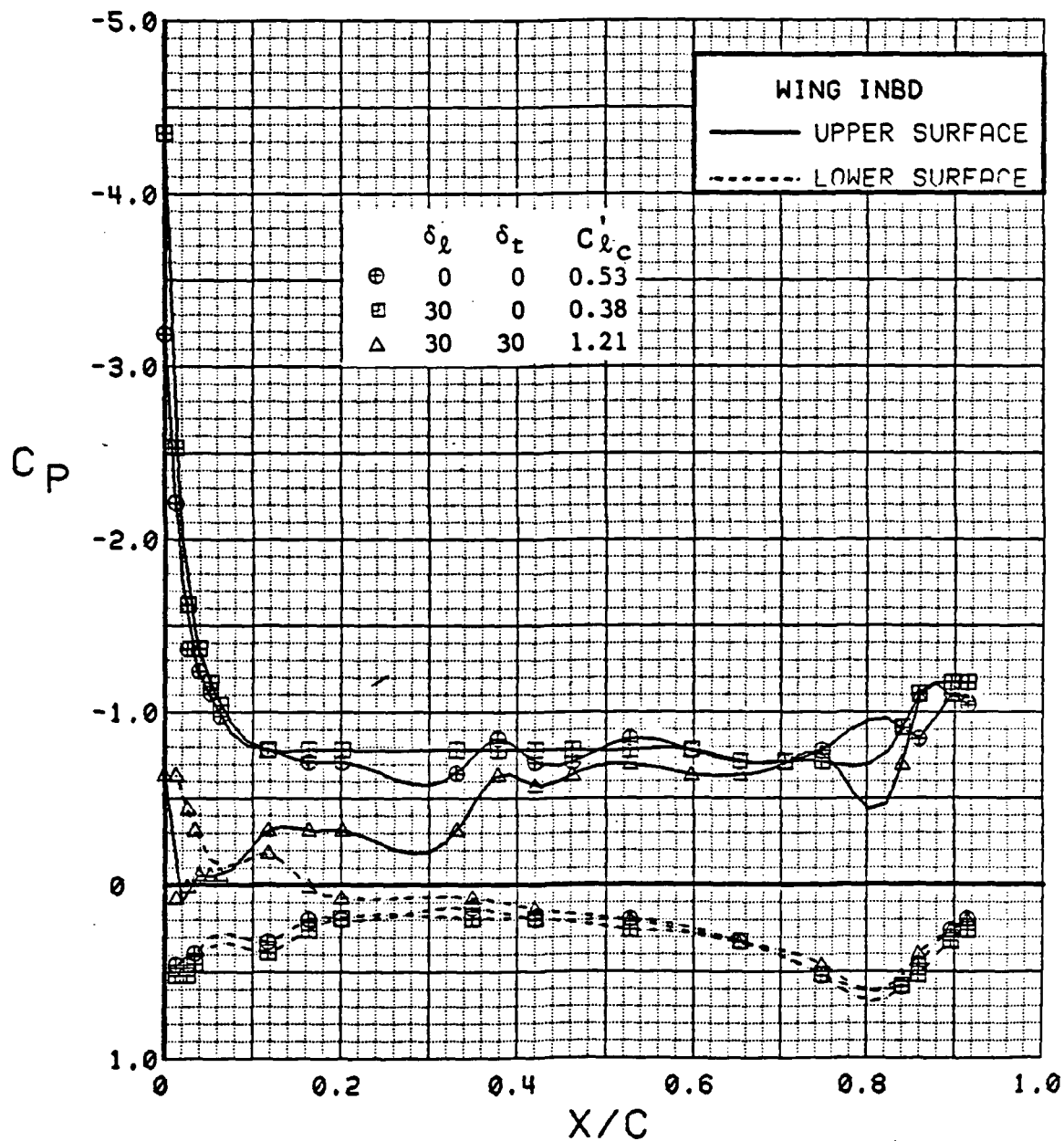


Figure 3.2.4-192 Combined Canard Flap Deflection Effects, Inboard, Alpha = 4 deg

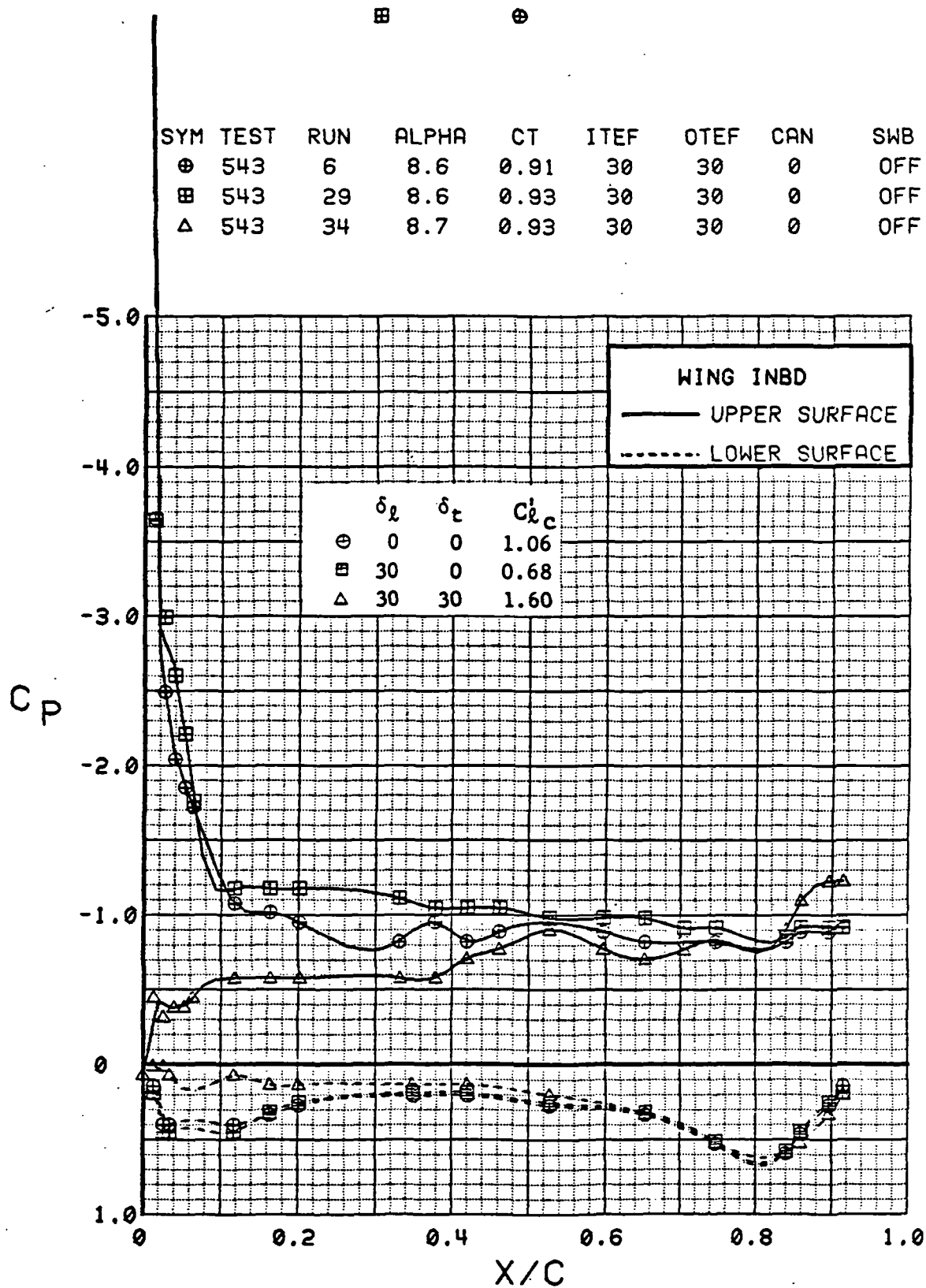


Figure 3.2.4-193 Combined Canard Flap Deflection Effects, Inboard, Alpha = 8 deg

SYM	TEST	RUN	ALPHA	CT	ITEF	OTEF	CAN	SWB
⊕	543	6	12.8	0.92	30	30	0	OFF
⊞	543	29	12.8	0.92	30	30	0	OFF
Δ	543	34	12.8	0.92	30	30	0	OFF

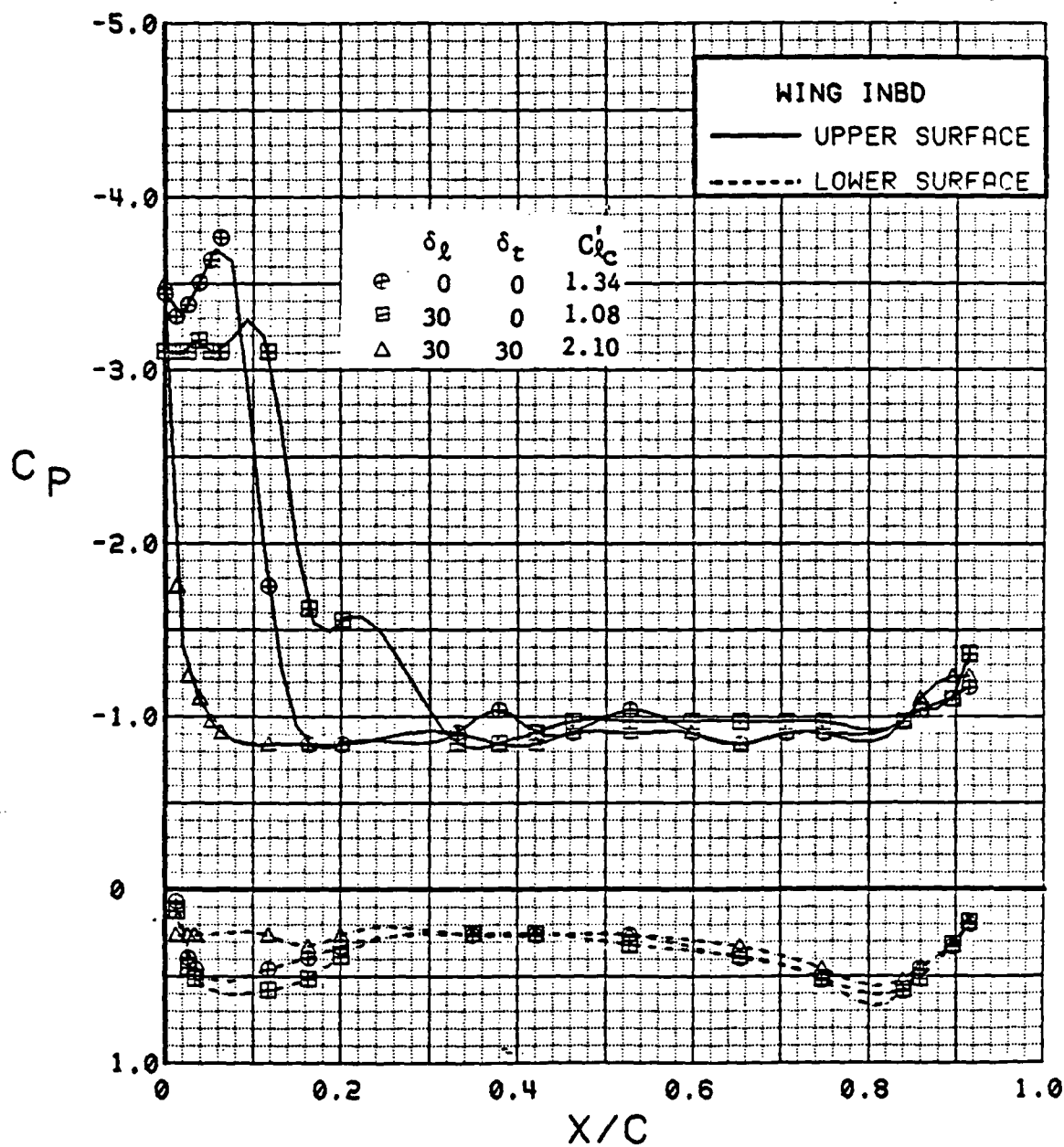


Figure 3.2.4-194 Combined Canard Flap Deflection Effects, Inboard, Alpha = 12 deg

SYM	TEST	RUN	ALPHA	CT	ITEF	OTEF	CAN	SWB
⊕	543	6	16.9	0.92	30	30	0	OFF
⊞	543	29	16.9	0.93	30	30	0	OFF
Δ	543	34	16.9	0.93	30	30	0	OFF

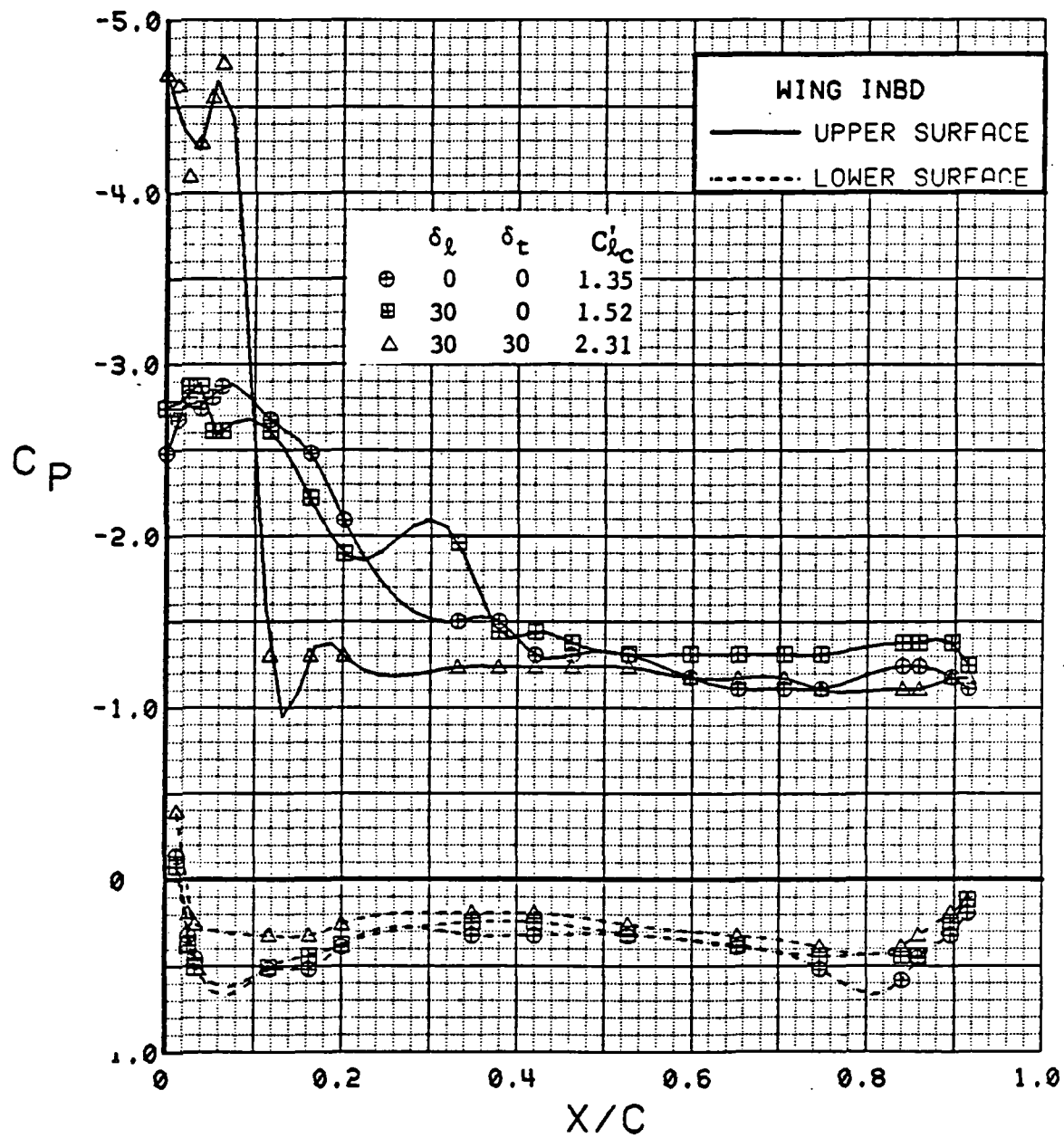


Figure 3.2.4-195 Combined Canard Flap Deflection Effects, Inboard, Alpha = 16 deg



SYM	TEST	RUN	ALPHA	CT	ITEF	OTEF	CAN	SWB
⊕	543	6	0.3	0.94	30	30	0	OFF
⊞	543	29	0.3	0.93	30	30	0	OFF
Δ	543	34	0.4	0.93	30	30	0	OFF

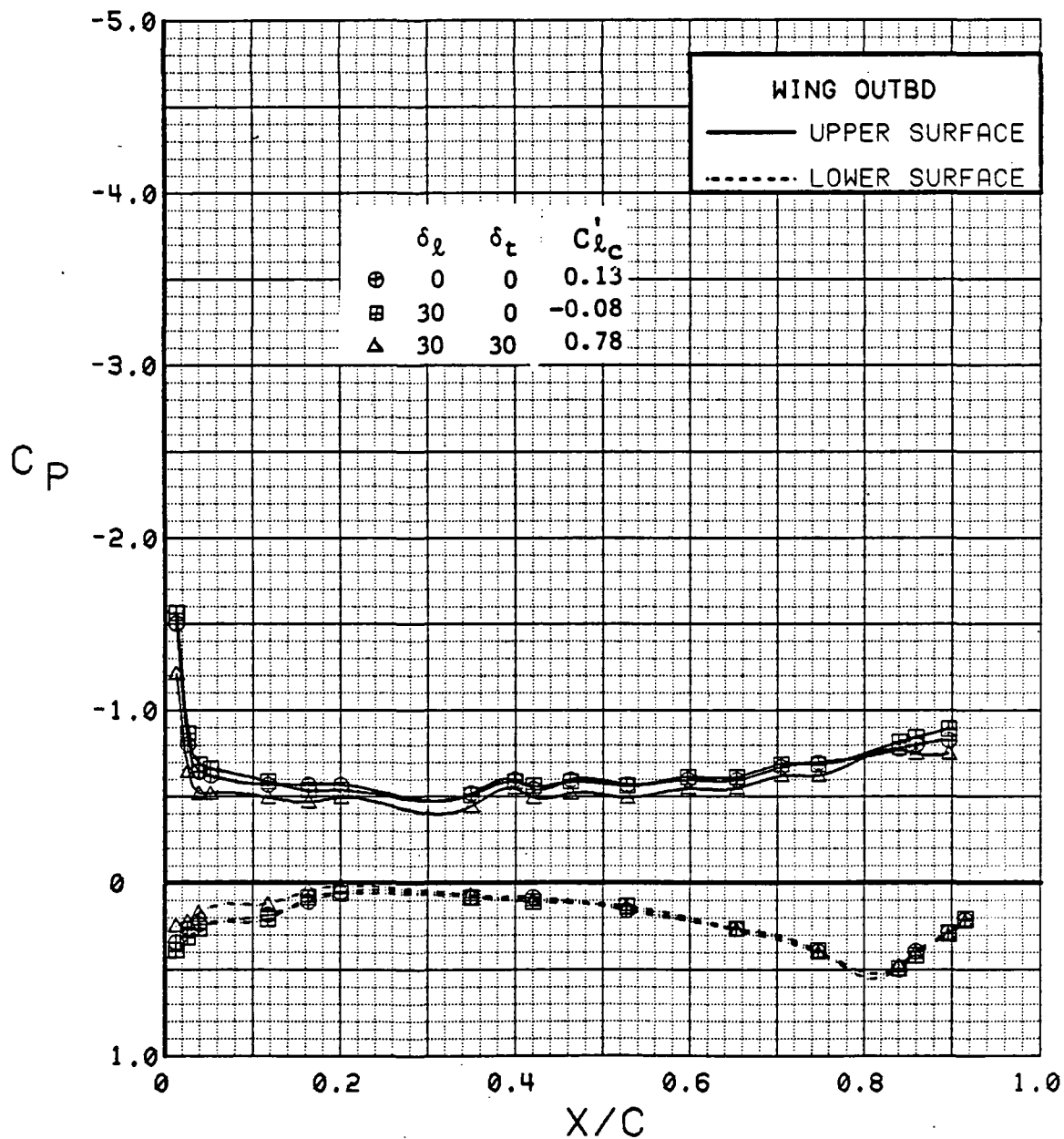


Figure 3.2.4-196 Combined Canard Flap Deflection Effects, Outboard, Alpha = 0 deg

SYM	TEST	RUN	ALPHA	CT	ITEF	OTEF	CAN	SWB
⊕	543	6	4.5	0.94	30	30	0	OFF
⊞	543	29	4.5	0.93	30	30	0	OFF
Δ	543	34	4.5	0.91	30	30	0	OFF

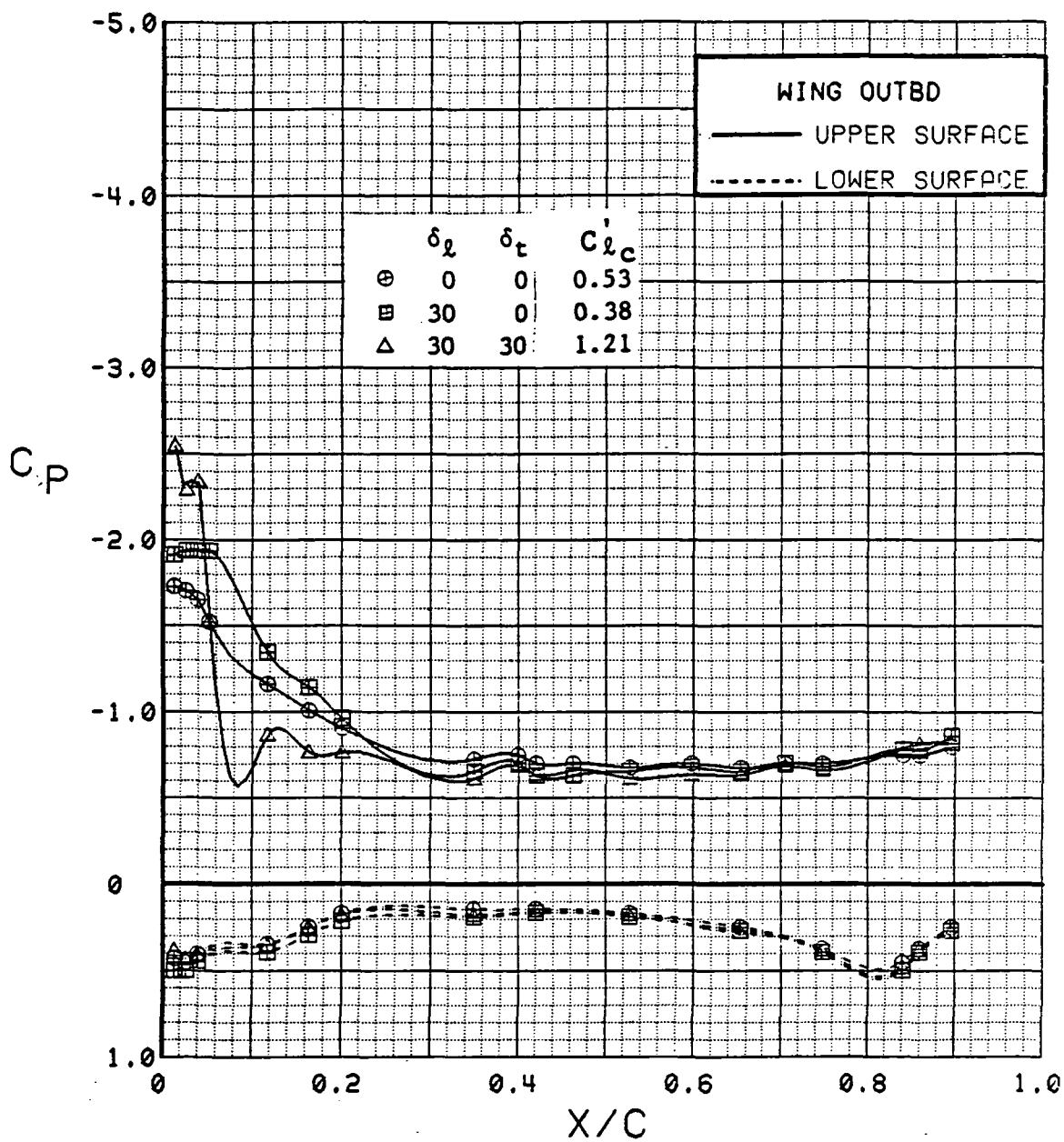


Figure 3.2.4-197 Combined Canard Flap Deflection Effects, Outboard, Alpha = 4 deg

SYM	TEST	RUN	ALPHA	CT	ITEF	OTEF	CAN	SWB
⊕	543	6	8.6	0.91	30	30	0	OFF
⊞	543	29	8.6	0.93	30	30	0	OFF
Δ	543	34	8.7	0.93	30	30	0	OFF

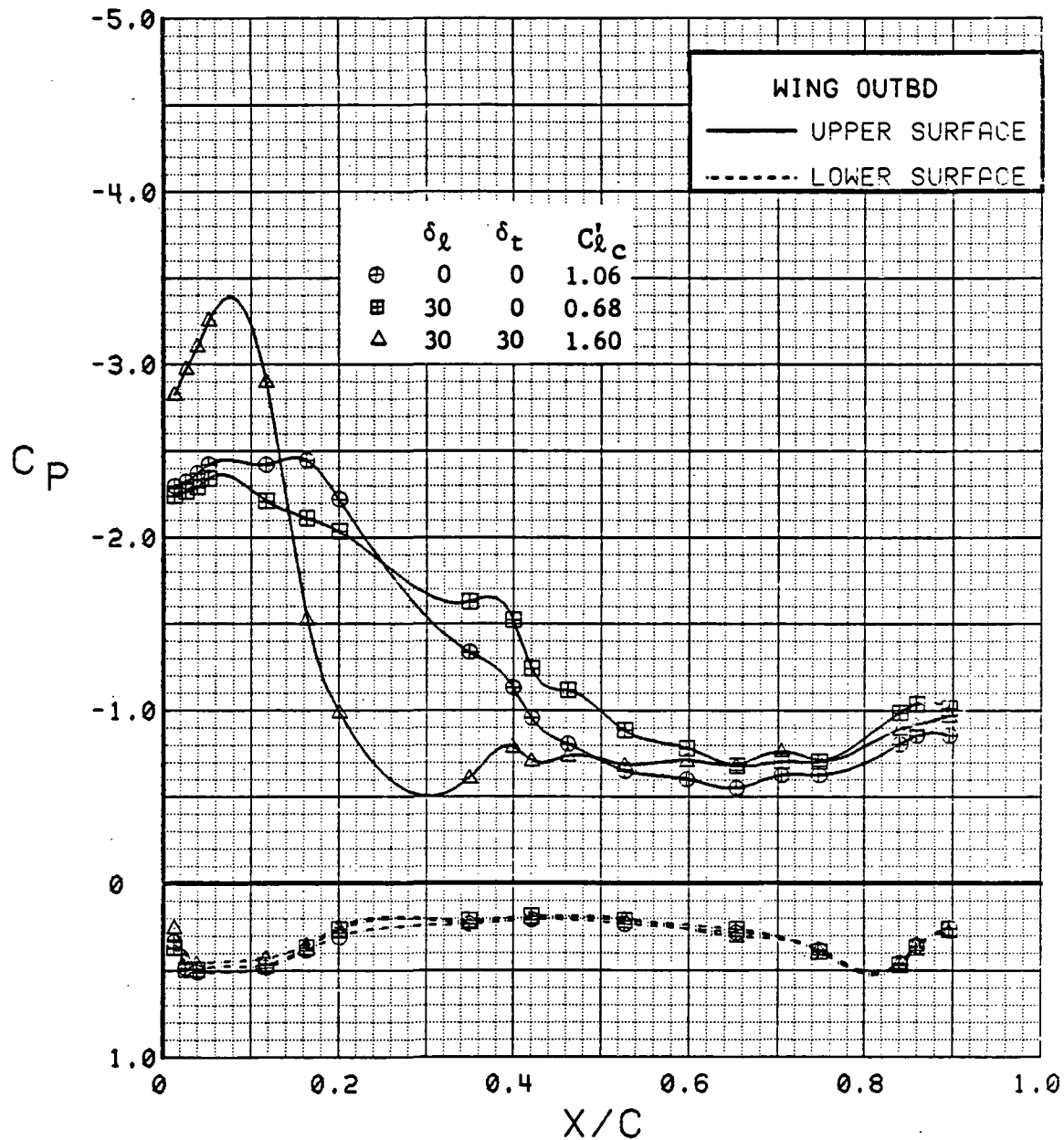


Figure 3.2.4-198 Combined Canard Flap Deflection Effects, Outboard, Alpha = 8 deg

SYM	TEST	RUN	ALPHA	CT	ITEF	OTEF	CAN	SWB
⊕	543	6	12.8	0.92	30	30	0	OFF
⊞	543	29	12.8	0.92	30	30	0	OFF
Δ	543	34	12.8	0.92	30	30	0	OFF

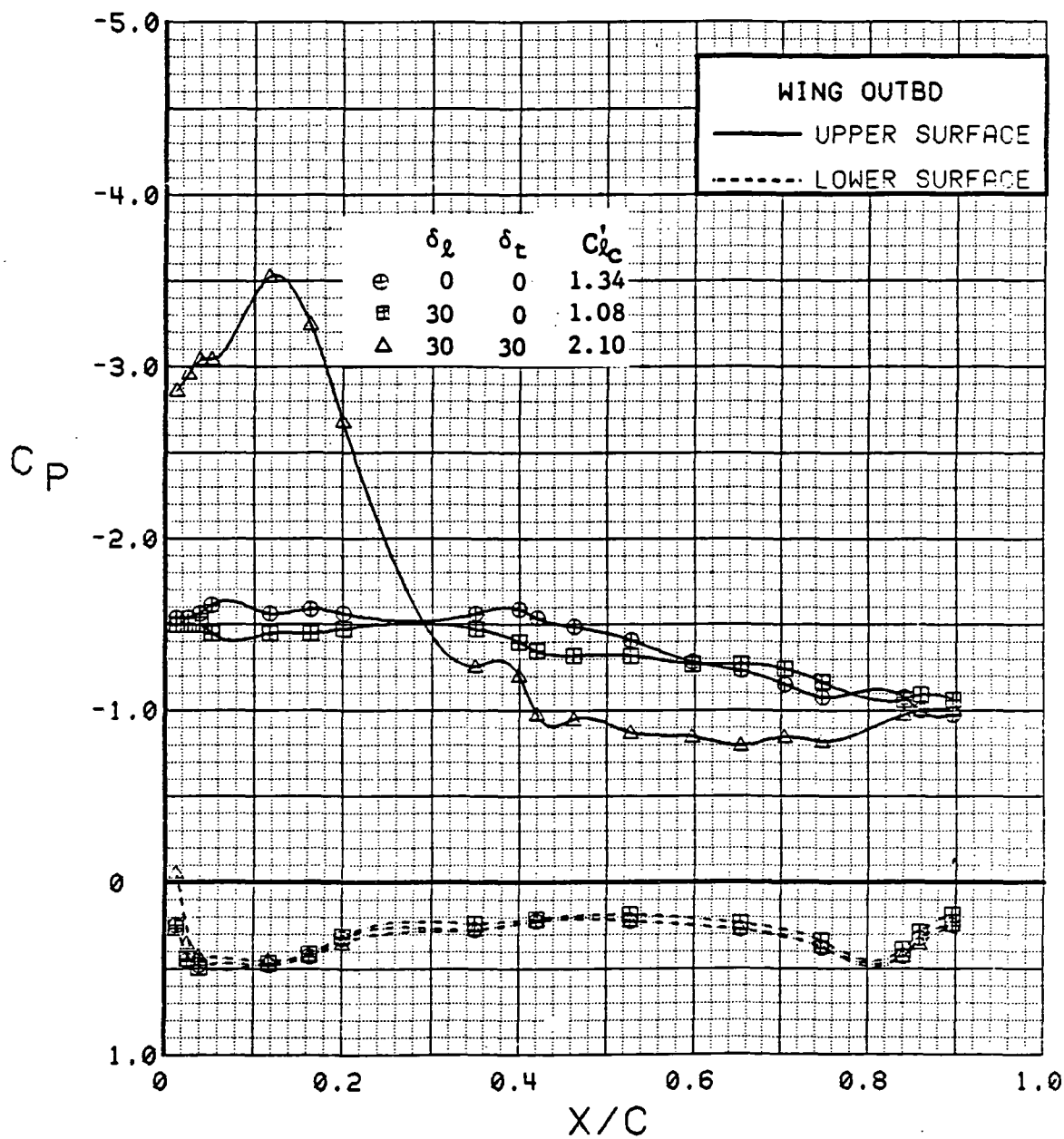


Figure 3.2.4-199 Combined Canard Flap Deflection Effects, Outboard, Alpha = 12 deg

SYM	TEST	RUN	ALPHA	CT	ITEF	OTEF	CAN	SWB
⊕	543	6	16.9	0.92	30	30	0	OFF
⊞	543	29	16.9	0.93	30	30	0	OFF
Δ	543	34	16.9	0.93	30	30	0	OFF

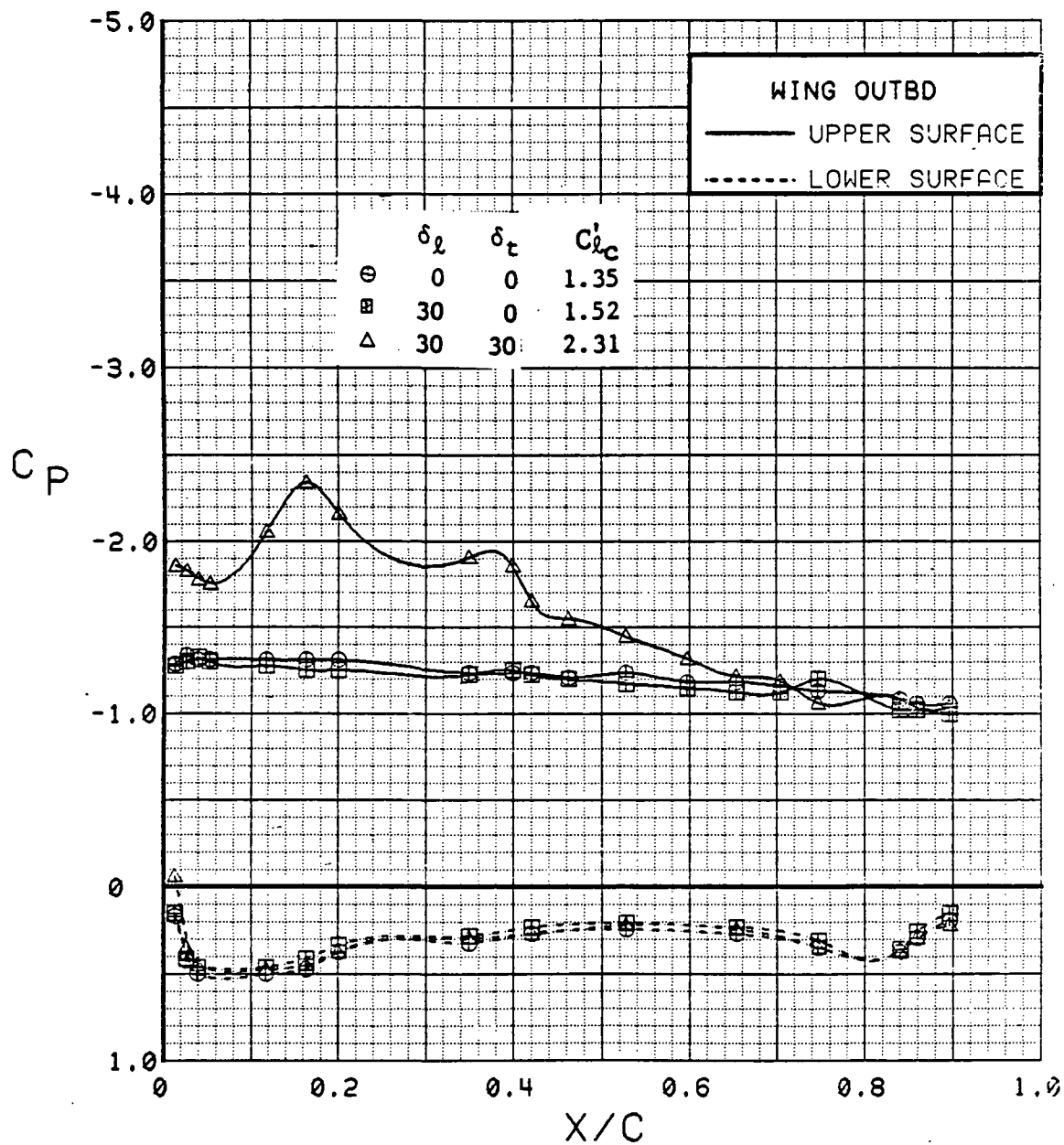


Figure 3.2.4-200 Combined Canard Flap Deflection Effects, Outboard, Alpha = 16 deg

SYM	TEST	RUN	ALPHA	CT	ITEF	OTEF	CAN	SWB
⊕	543	6	0.3	0.94	30	30	0	OFF
⊞	543	29	0.3	0.93	30	30	0	OFF
Δ	543	34	0.4	0.93	30	30	0	OFF

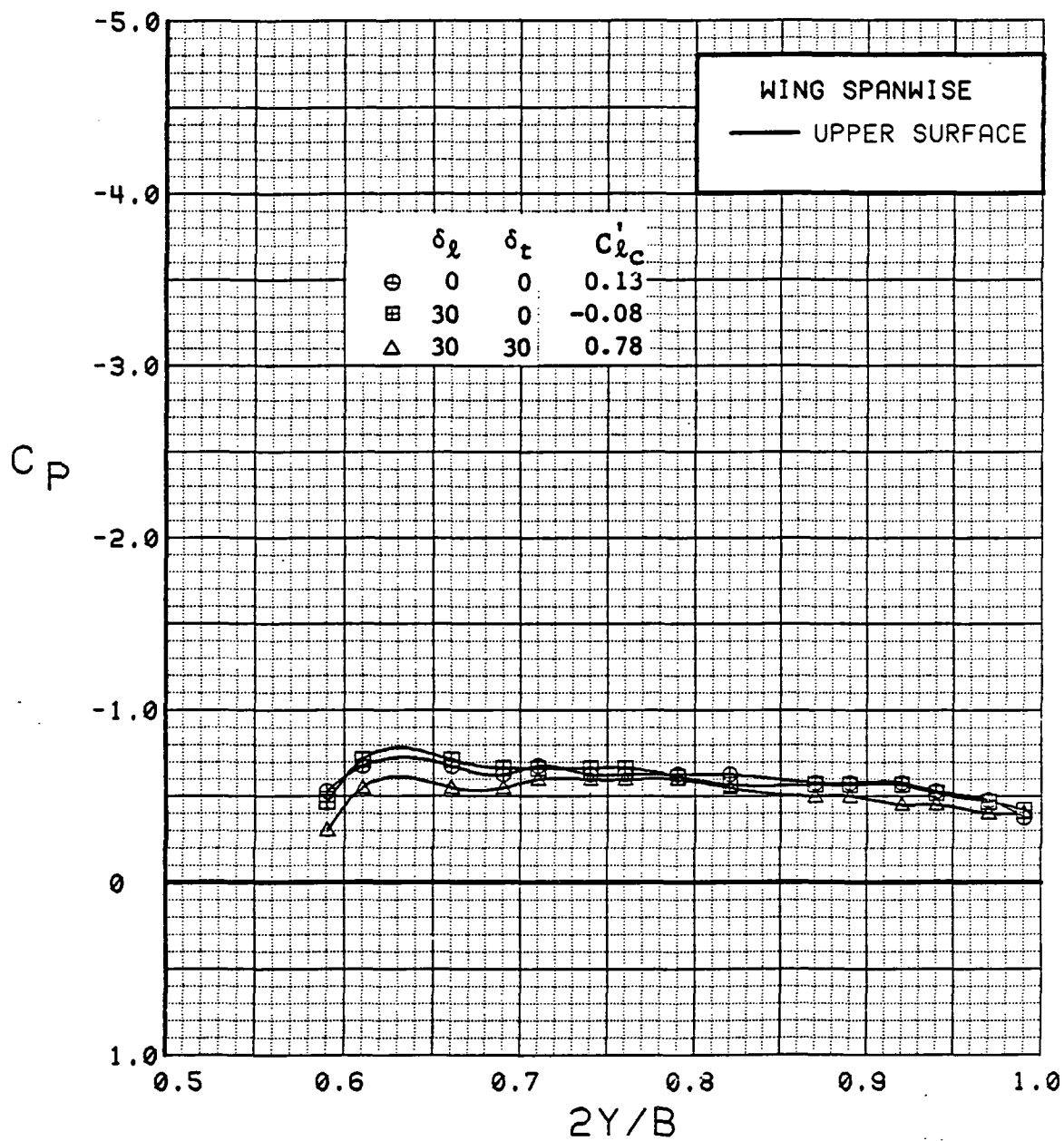


Figure 3.2.4-201 Combined Canard Flap Deflection Effects, Spanwise, Alpha = 0 deg

SYM	TEST	RUN	ALPHA	CT	ITEF	OTEF	CAN	SWB
⊕	543	6	4.5	0.94	30	30	0	OFF
⊞	543	29	4.5	0.93	30	30	0	OFF
Δ	543	34	4.5	0.91	30	30	0	OFF

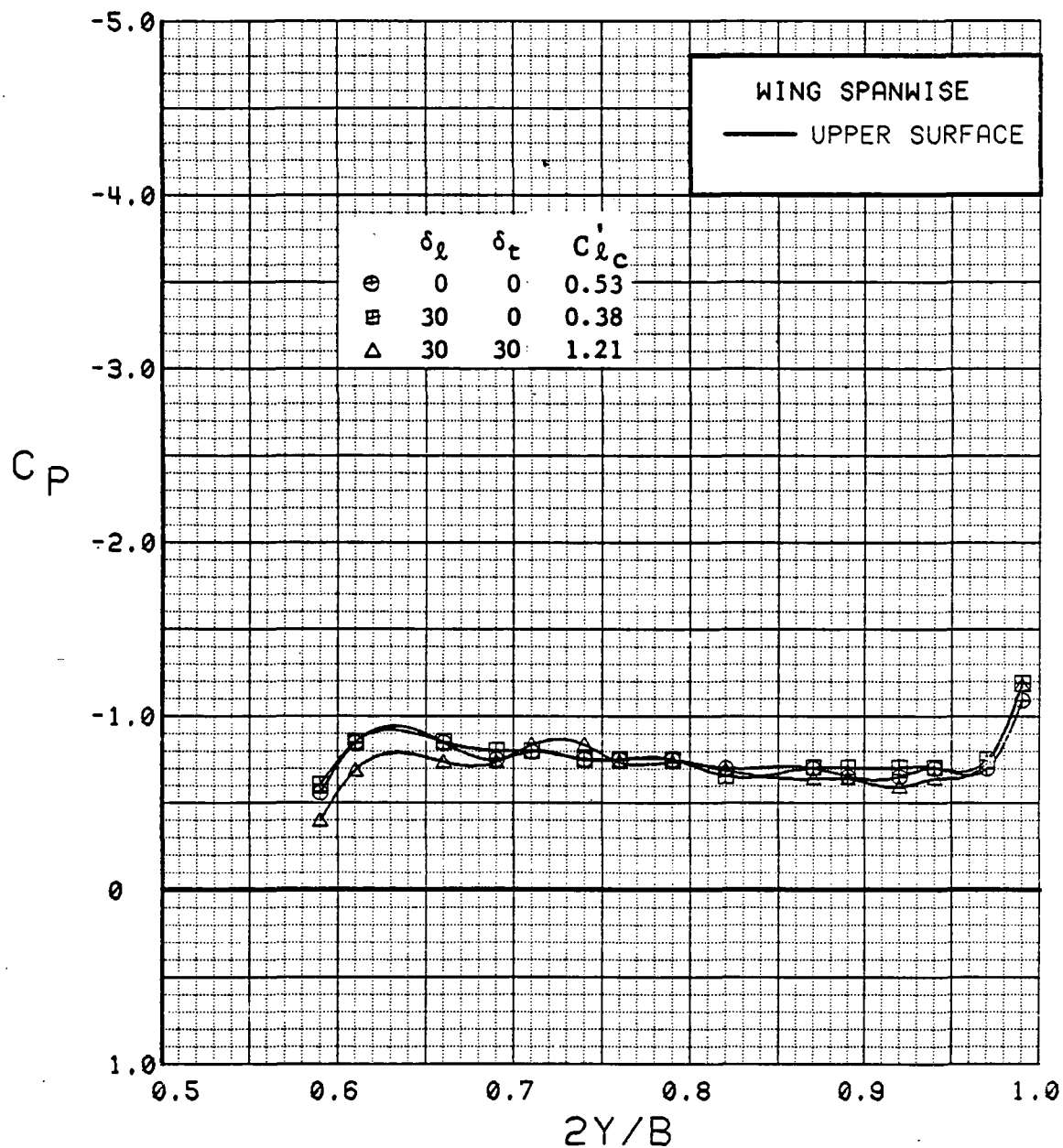


Figure 3.2.4-202 Combined Canard Flap Deflection Effects, Spanwise, Alpha = 4 deg

SYM	TEST	RUN	ALPHA	CT	ITEF	OTEF	CAN	SWB
⊕	543	6	8.6	0.91	30	30	0	OFF
⊞	543	29	8.6	0.93	30	30	0	OFF
Δ	543	34	8.7	0.93	30	30	0	OFF

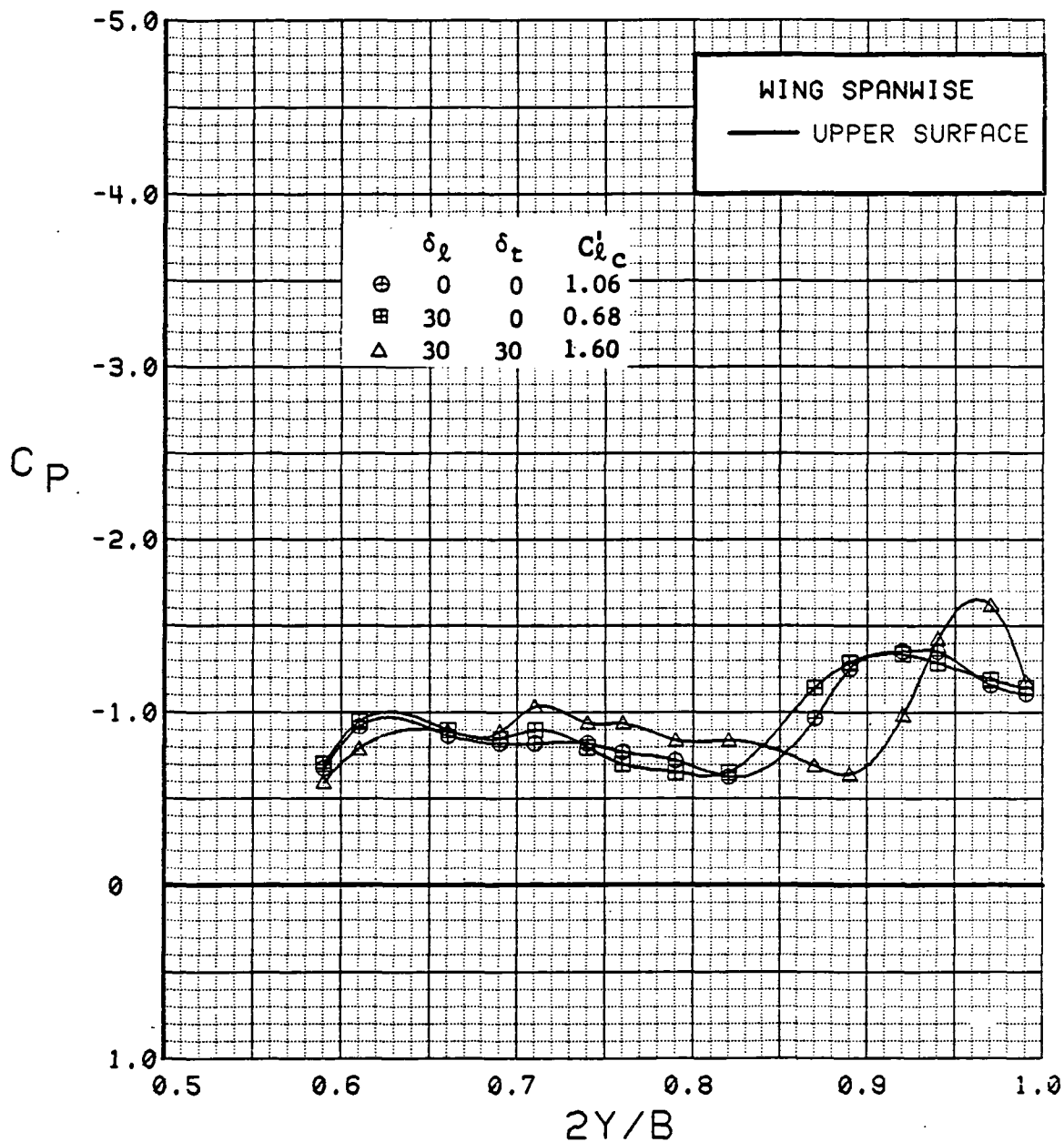


Figure 3.2.4-203 Combined Canard Flap Deflection Effects, Spanwise, Alpha = 8 deg



SYM	TEST	RUN	ALPHA	CT	ITEF	OTEF	CAN	SWB
⊕	543	6	12.8	0.92	30	30	0	OFF
⊞	543	29	12.8	0.92	30	30	0	OFF
Δ	543	34	12.8	0.92	30	30	0	OFF

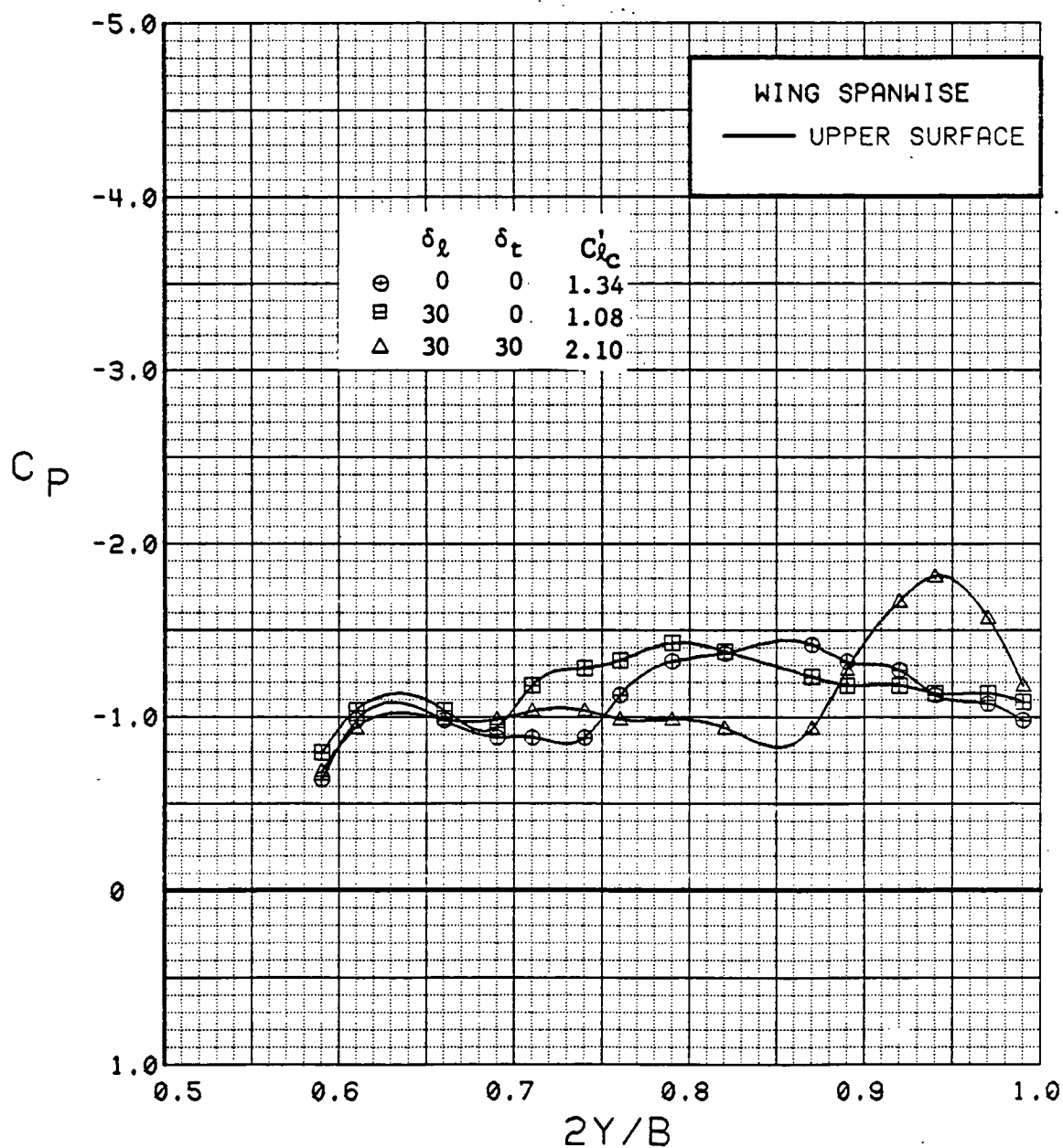


Figure 3.2.4-204 Combined Canard Flap Deflection Effects, Spanwise, Alpha = 12 deg

SYM	TEST	RUN	ALPHA	CT	ITEF	OTEF	CAN	SWB
⊕	543	6	16.9	0.92	30	30	0	OFF
⊞	543	29	16.9	0.93	30	30	0	OFF
Δ	543	34	16.9	0.93	30	30	0	OFF

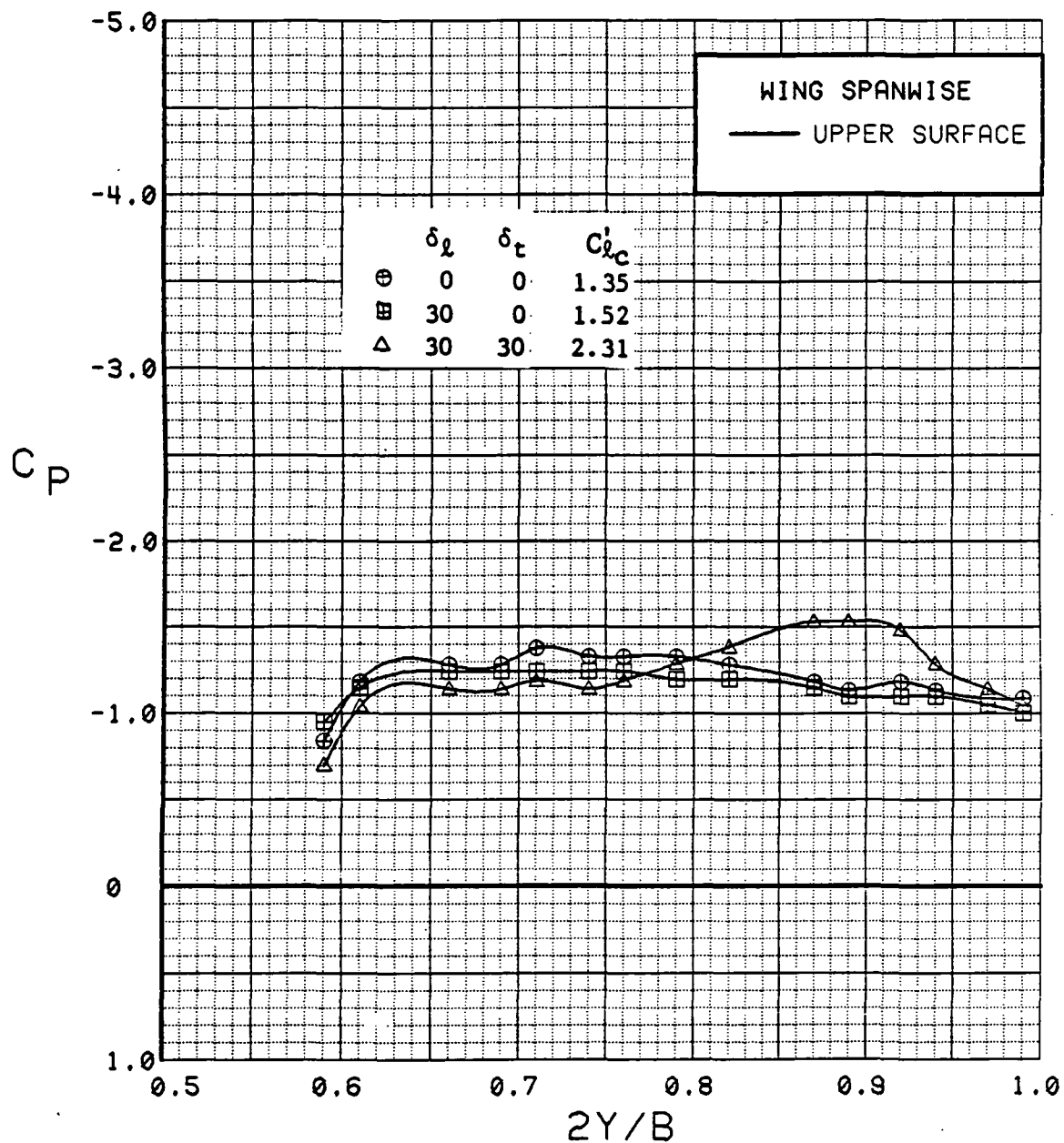


Figure 3.2.4-205 Combined Canard Flap Deflection Effects, Spanwise,  
Alpha = 16 deg

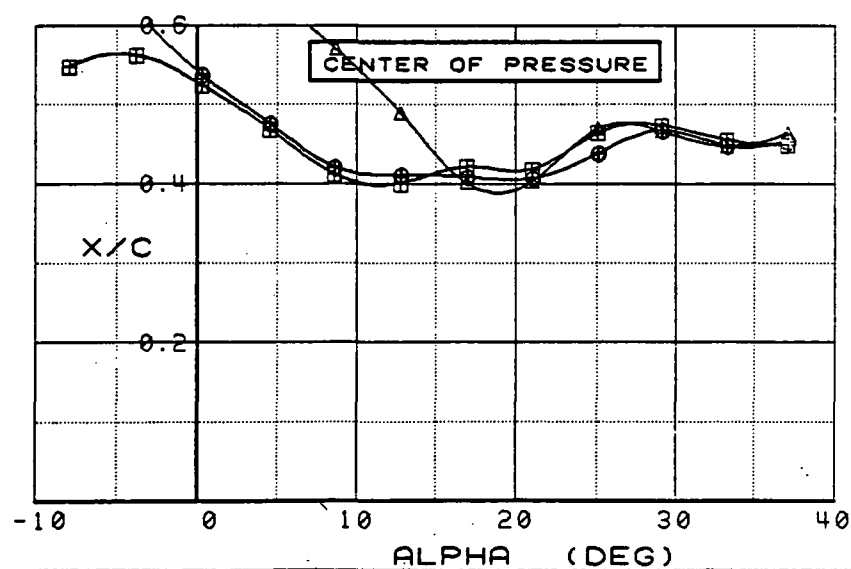
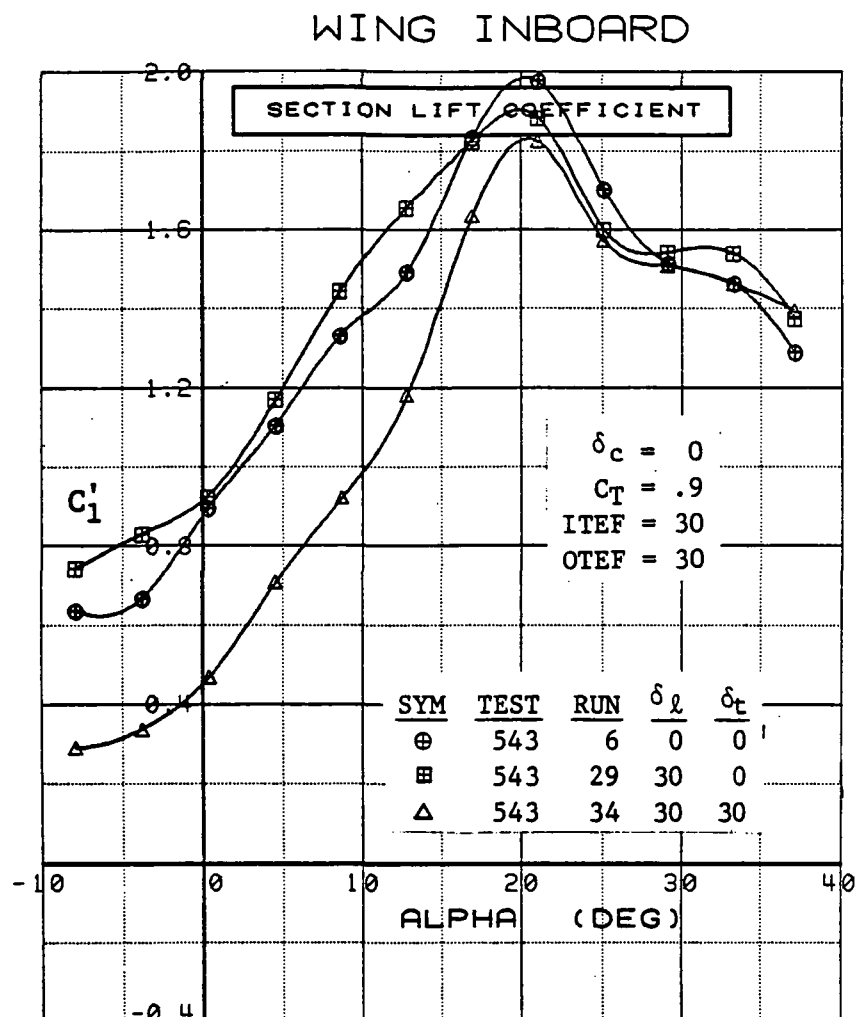


Figure 3.2.4-206 Combined Canard Flap Deflection Effects, Inboard, Integrated Section Properties

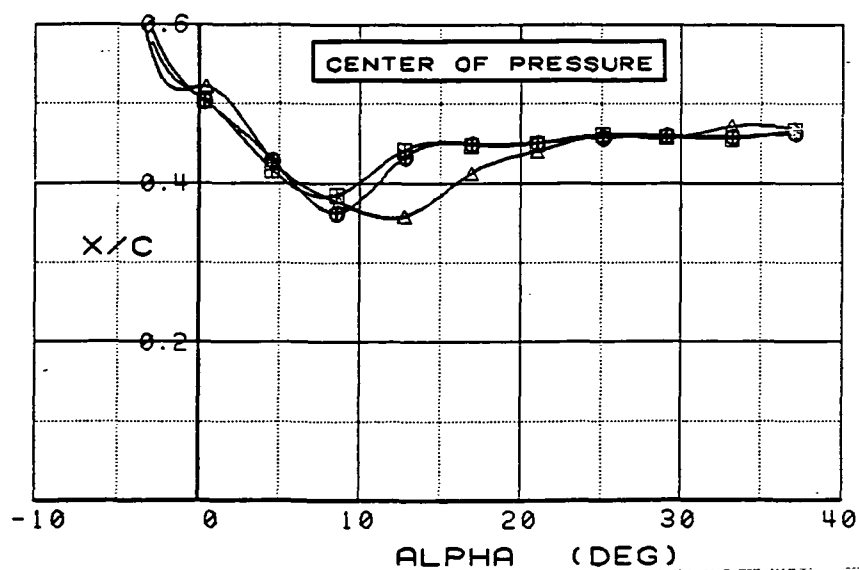
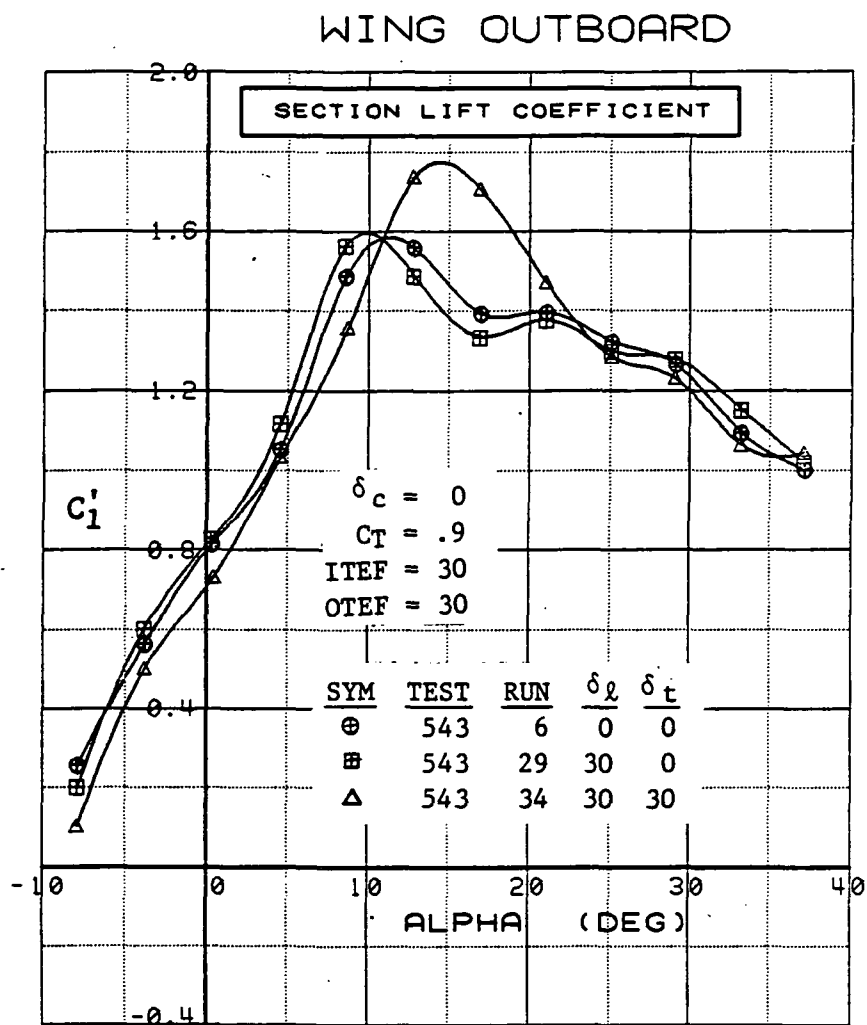


Figure 3.2.4-207 Combined Canard Flap Deflection Effects, Outboard, Integrated Section Properties

SYM	TEST	RUN	ALPHA	CT	ITEF	OTEF	CAN	SWB	CAN
⊕	537	12	0.3	0.00	30	30	0	OFF	FOR
⊞	543	11	0.3	0.00	30	30	0	OFF	AFT

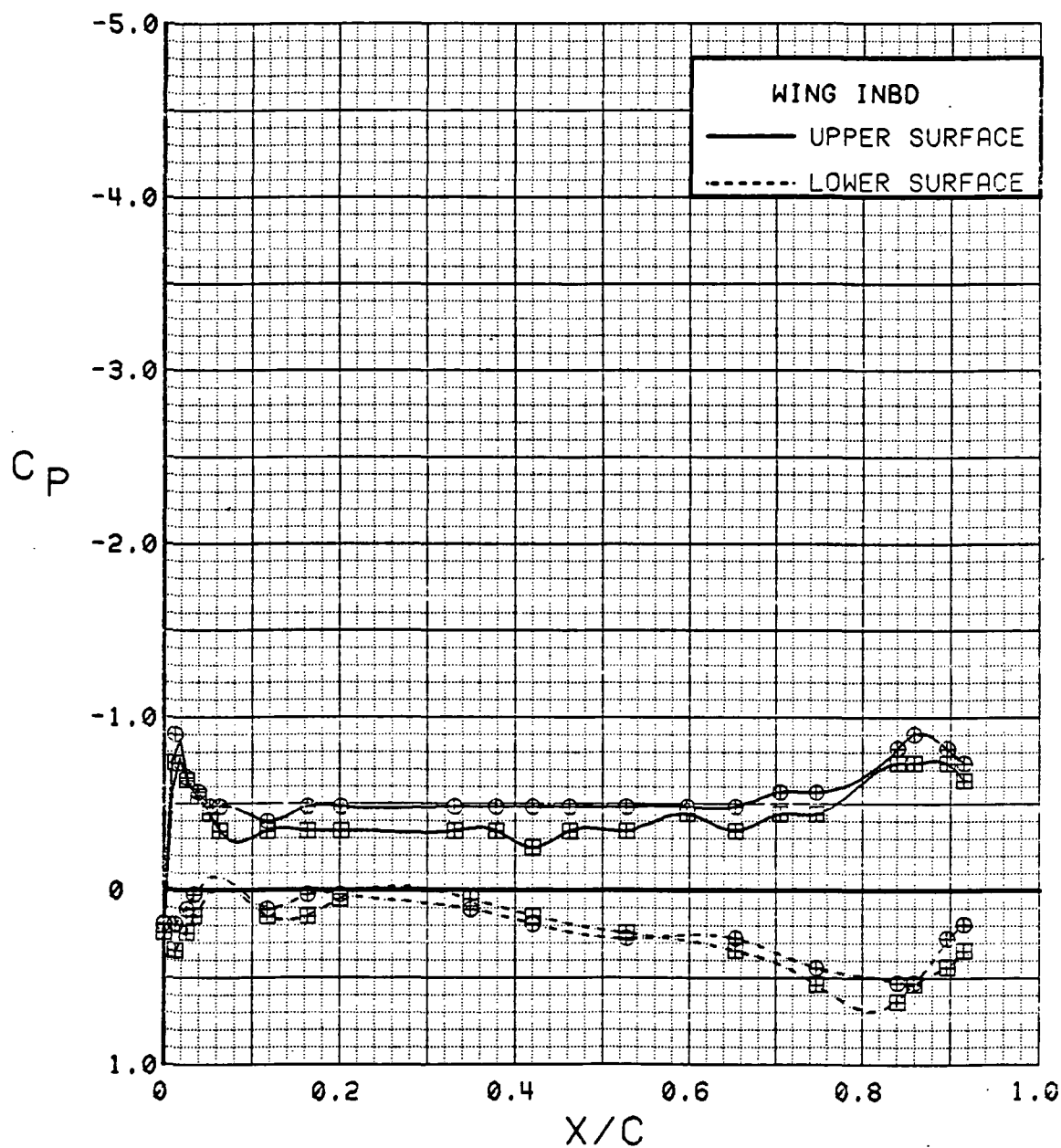


Figure 3.2.4-208 Canard Position Effects, Inboard, Power Off, Alpha = 0 deg

SYM	TEST	RUN	ALPHA	CT	ITEF	OTEF	CAN	SWB	CAN
⊕	537	12	4.4	0.00	30	30	0	OFF	FOR
⊞	543	11	4.4	0.00	30	30	0	OFF	AFT

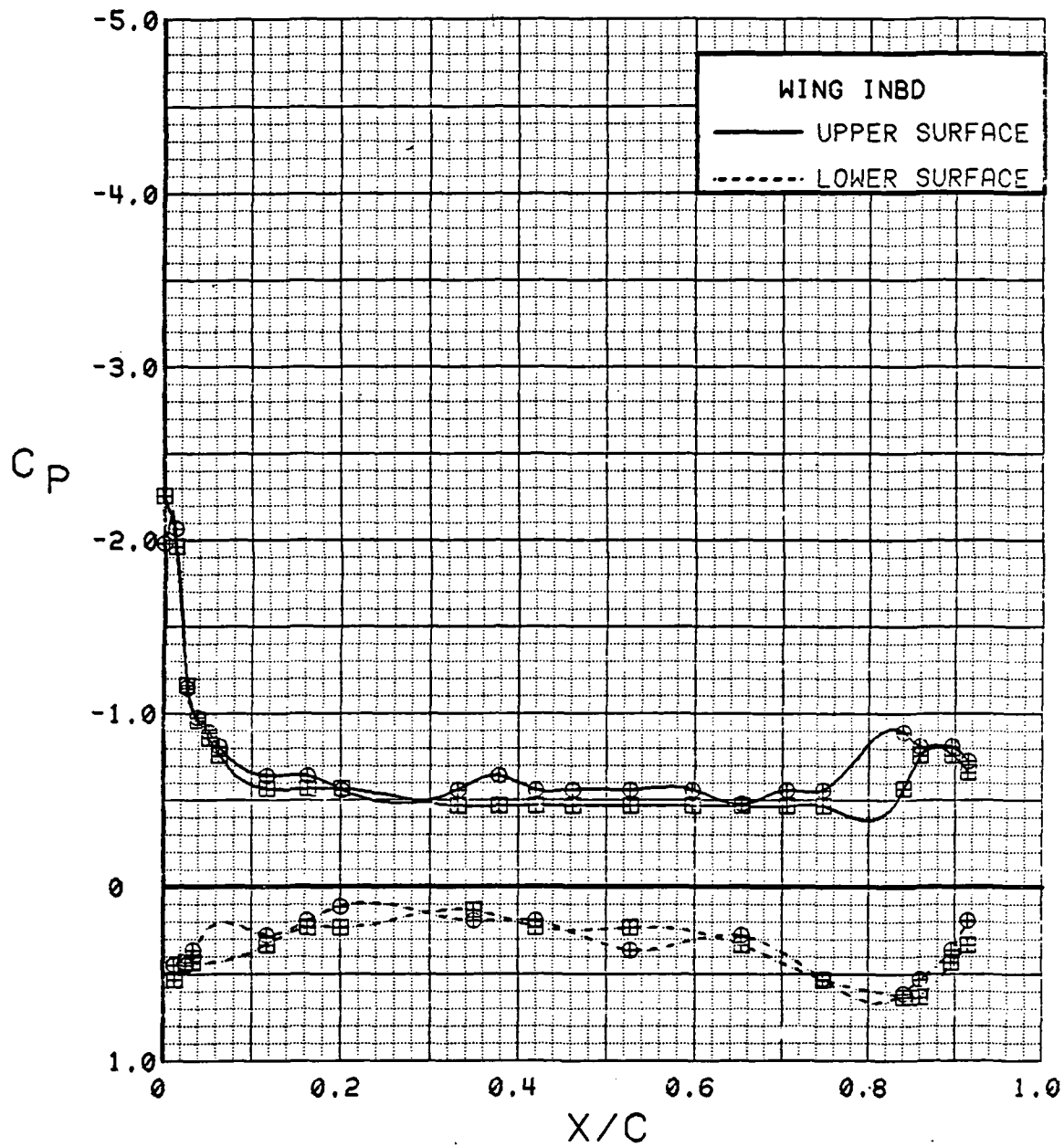


Figure 3.2.4-209 Canard Position Effects, Inboard, Power Off, Alpha = 4 deg

SYM	TEST	RUN	ALPHA	CT	ITEF	OTEF	CAN	SWB	CAN
⊕	537	12	8.5	0.00	30	30	0	OFF	FOR
⊞	543	11	8.5	0.00	30	30	0	OFF	AFT

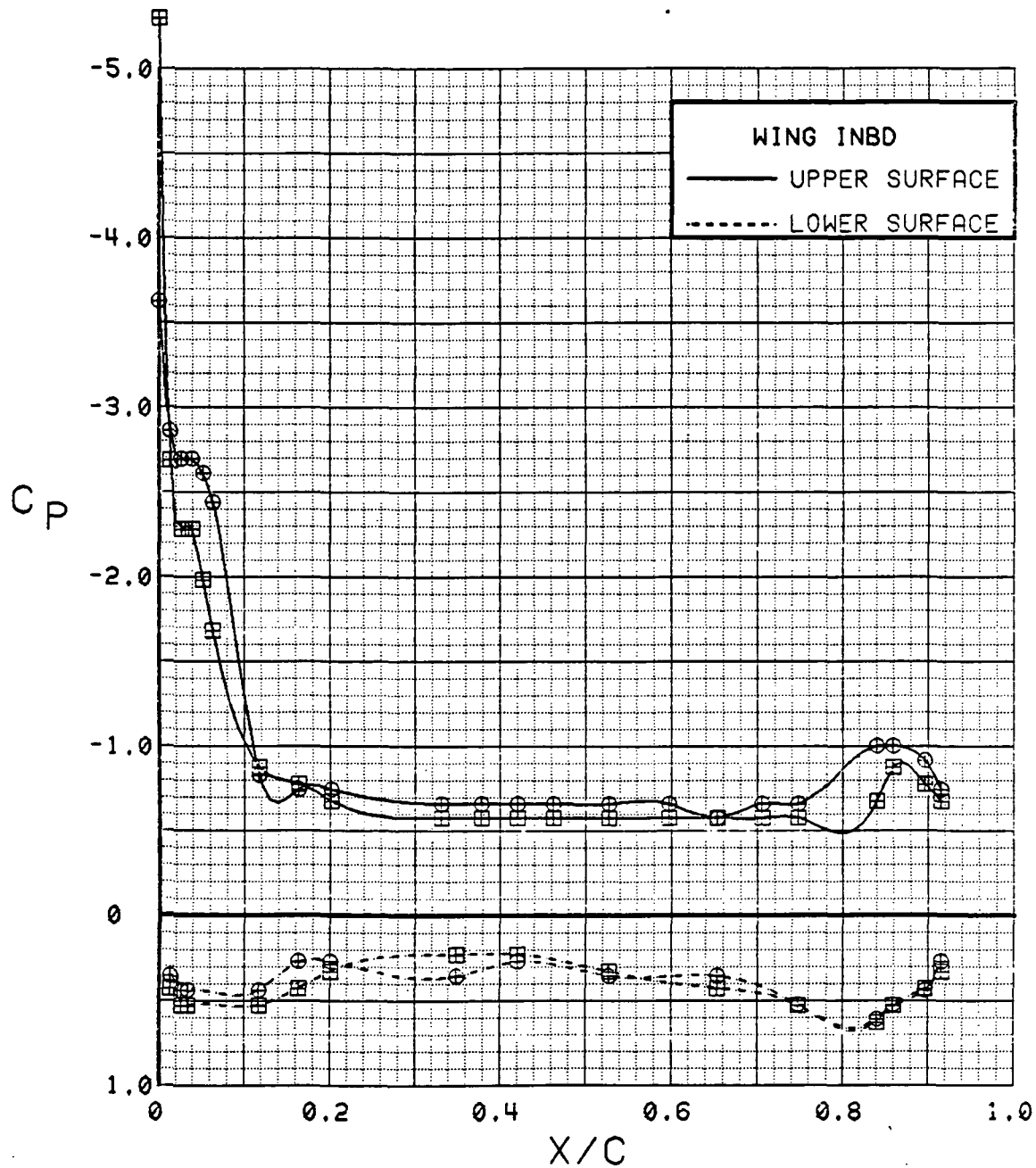


Figure 3.2.4-210 Canard Position Effects, Inboard, Power Off, Alpha = 8 deg

SYM	TEST	RUN	ALPHA	CT	ITEF	OTEF	CAN	SWB	CAN
⊕	537	12	12.7	0.00	30	30	0	OFF	FOR
⊞	543	11	12.7	0.00	30	30	0	OFF	AFT

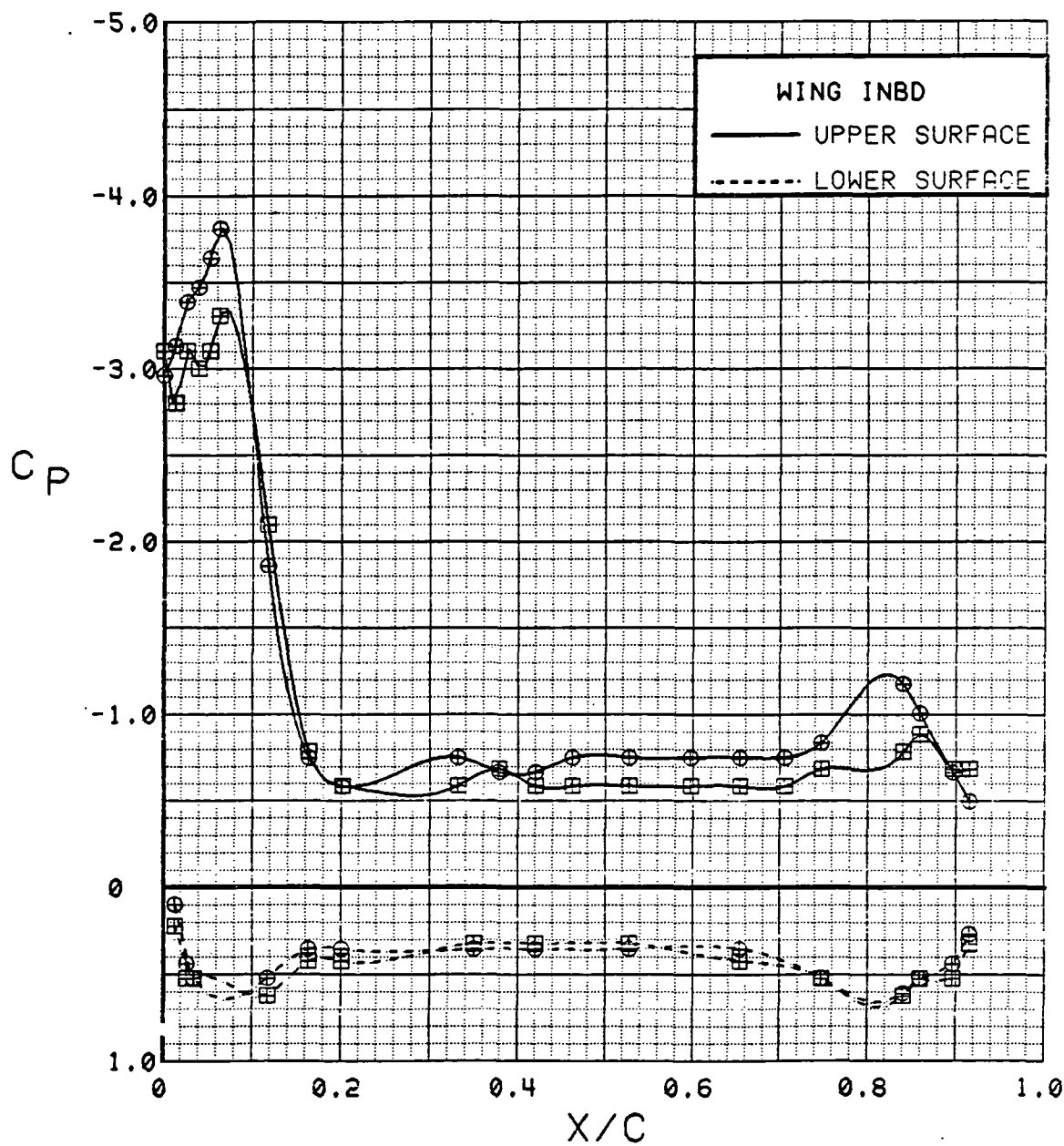


Figure 3.2.4-211 Canard Position Effects, Inboard, Power Off, Alpha = 12 deg



SYM	TEST	RUN	ALPHA	CT	ITEF	OTEF	CAN	SWB	CAN
⊕	537	12	16.7	0.00	30	30	0	OFF	FOR
⊞	543	11	16.8	0.00	30	30	0	OFF	AFT

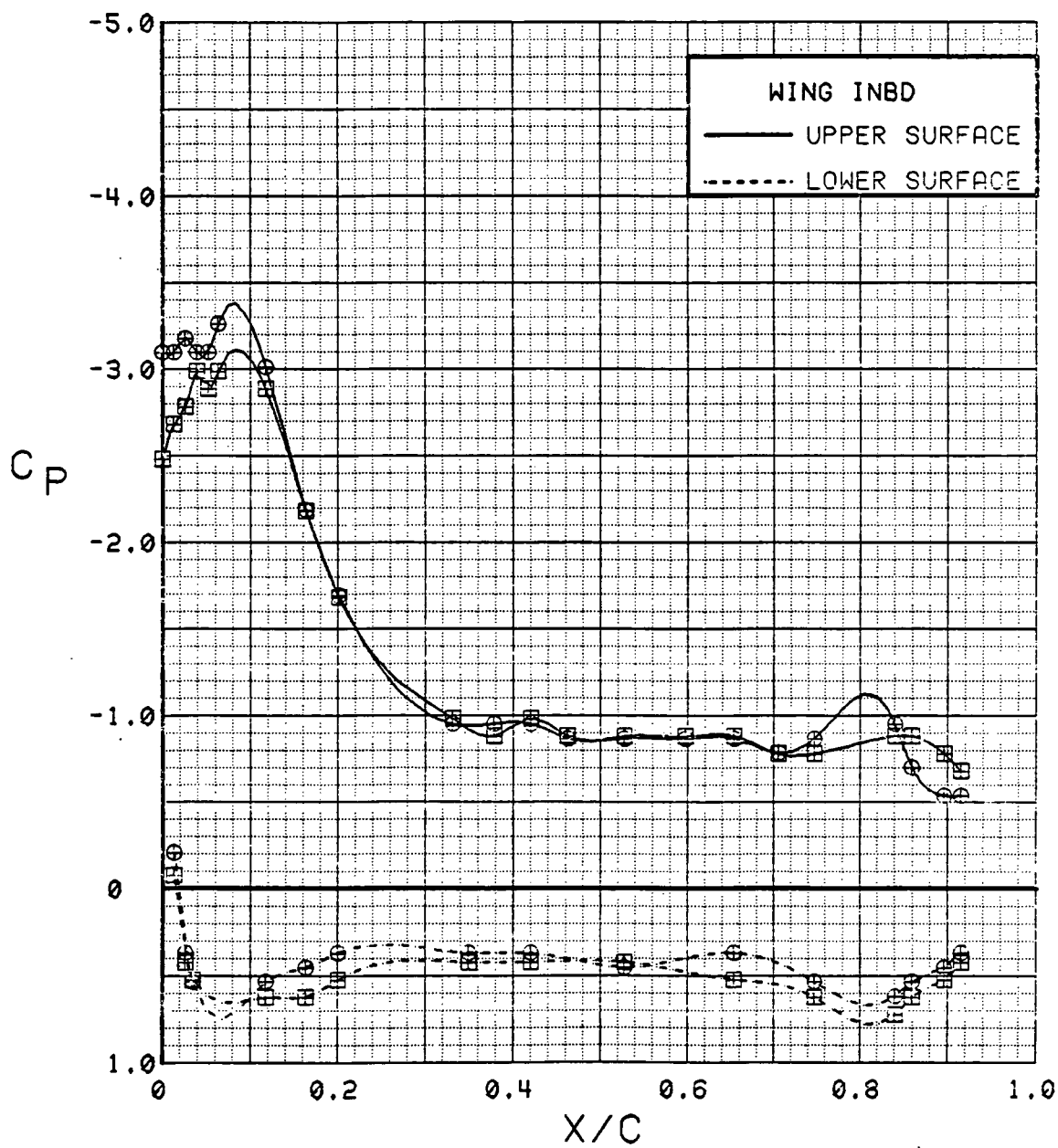


Figure 3.2.4-212 Canard Position Effects, Inboard, Power Off, Alpha = 16 deg

SYM	TEST	RUN	ALPHA	CT	ITEF	OTEF	CAN	SWB	CAN
⊕	537	12	20.8	0.00	30	30	0	OFF	FOR
⊞	543	11	20.8	0.00	30	30	0	OFF	AFT

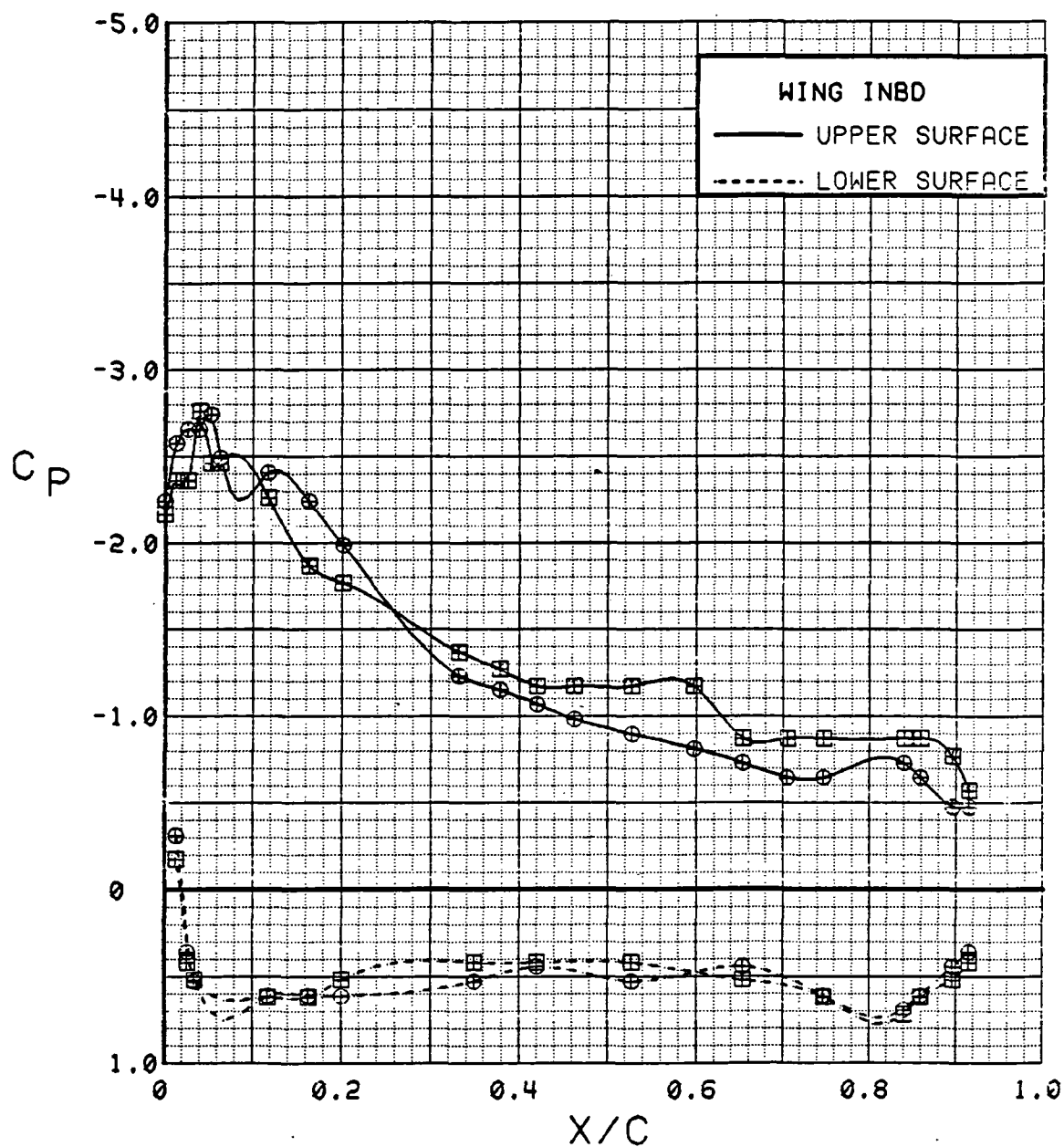


Figure 3.2.4-213 Canard Position Effects, Inboard, Power Off, Alpha = 20 deg

SYM	TEST	RUN	ALPHA	CT	ITEF	OTEF	CAN	SWB	CAN
⊕	537	12	0.3	0.00	30	30	0	OFF	FOR
⊞	543	11	0.3	0.00	30	30	0	OFF	AFT

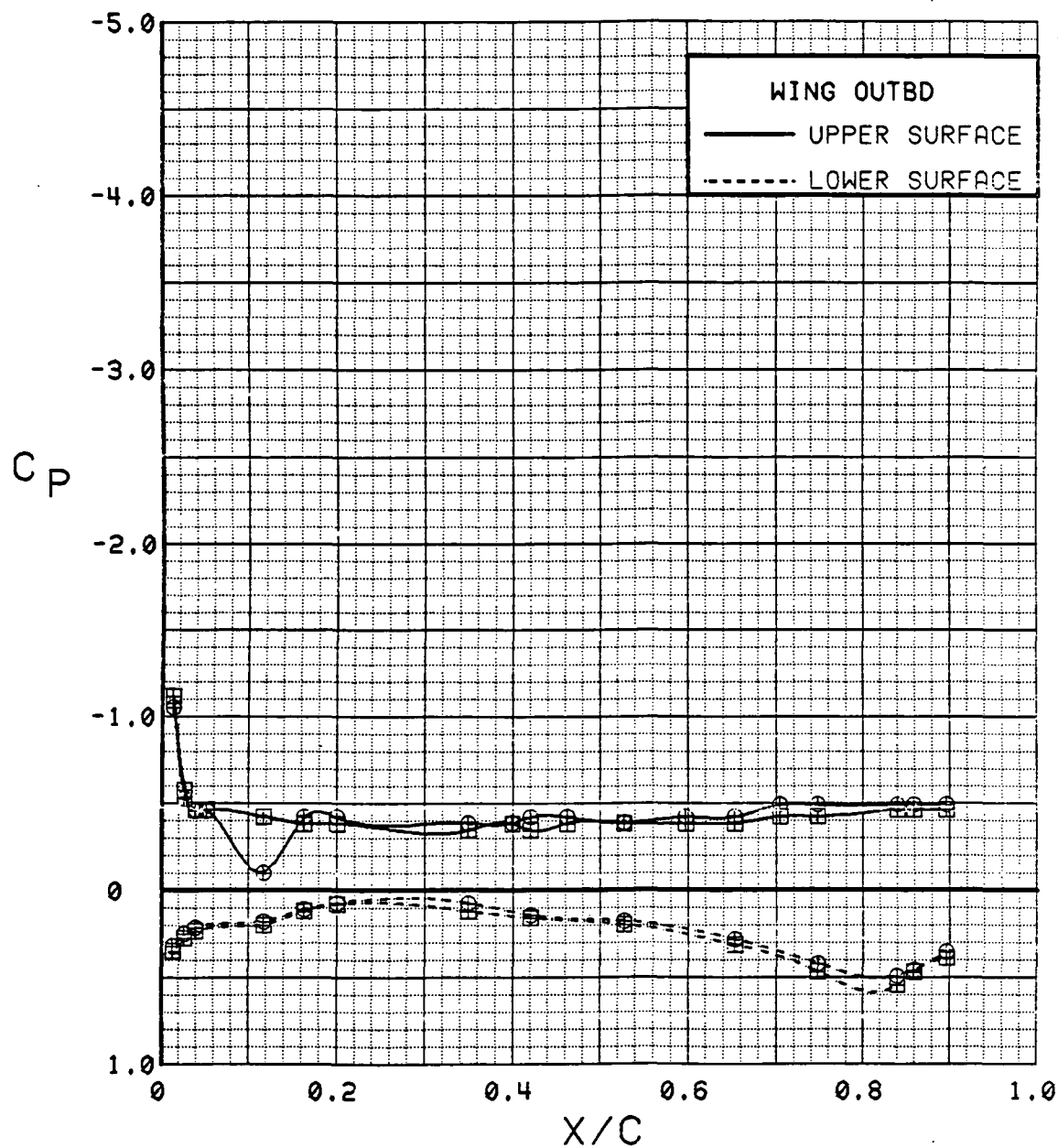


Figure 3.2.4-214 Canard Position Effects, Outboard, Power Off, Alpha = 0 deg

SYM	TEST	RUN	ALPHA	CT	ITEF	OTEF	CAN	SWB	CAN
⊕	537	12	4.4	0.00	30	30	0	OFF	FOR
⊞	543	11	4.4	0.00	30	30	0	OFF	AFT

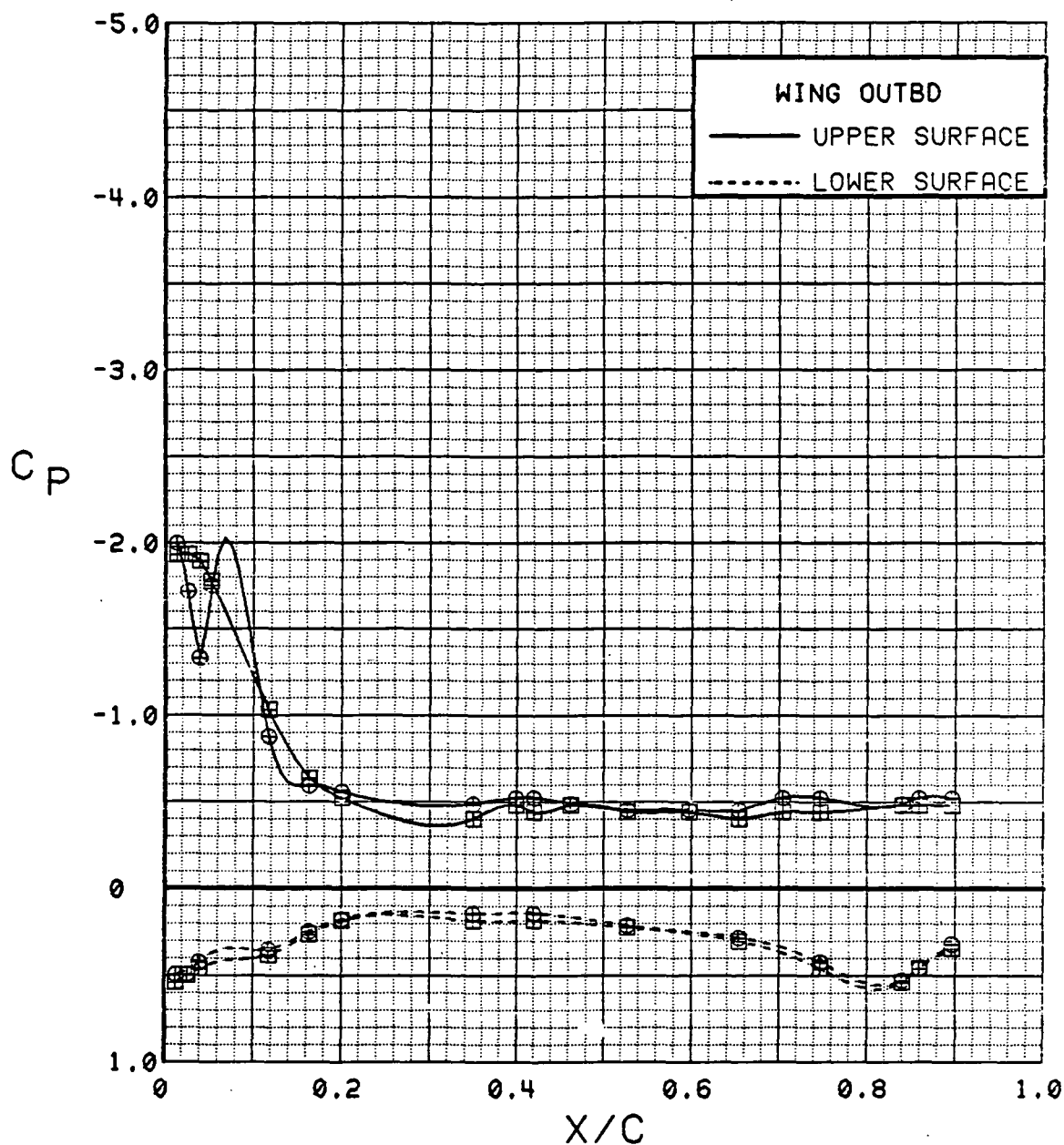


Figure 3.2.4-215 Canard Position Effects, Outboard, Power Off, Alpha = 4 deg

SYM	TEST	RUN	ALPHA	CT	ITEF	OTEF	CAN	SWB	CAN
⊕	537	12	8.5	0.00	30	30	0	OFF	FOR
⊞	543	11	8.5	0.00	30	30	0	OFF	AFT

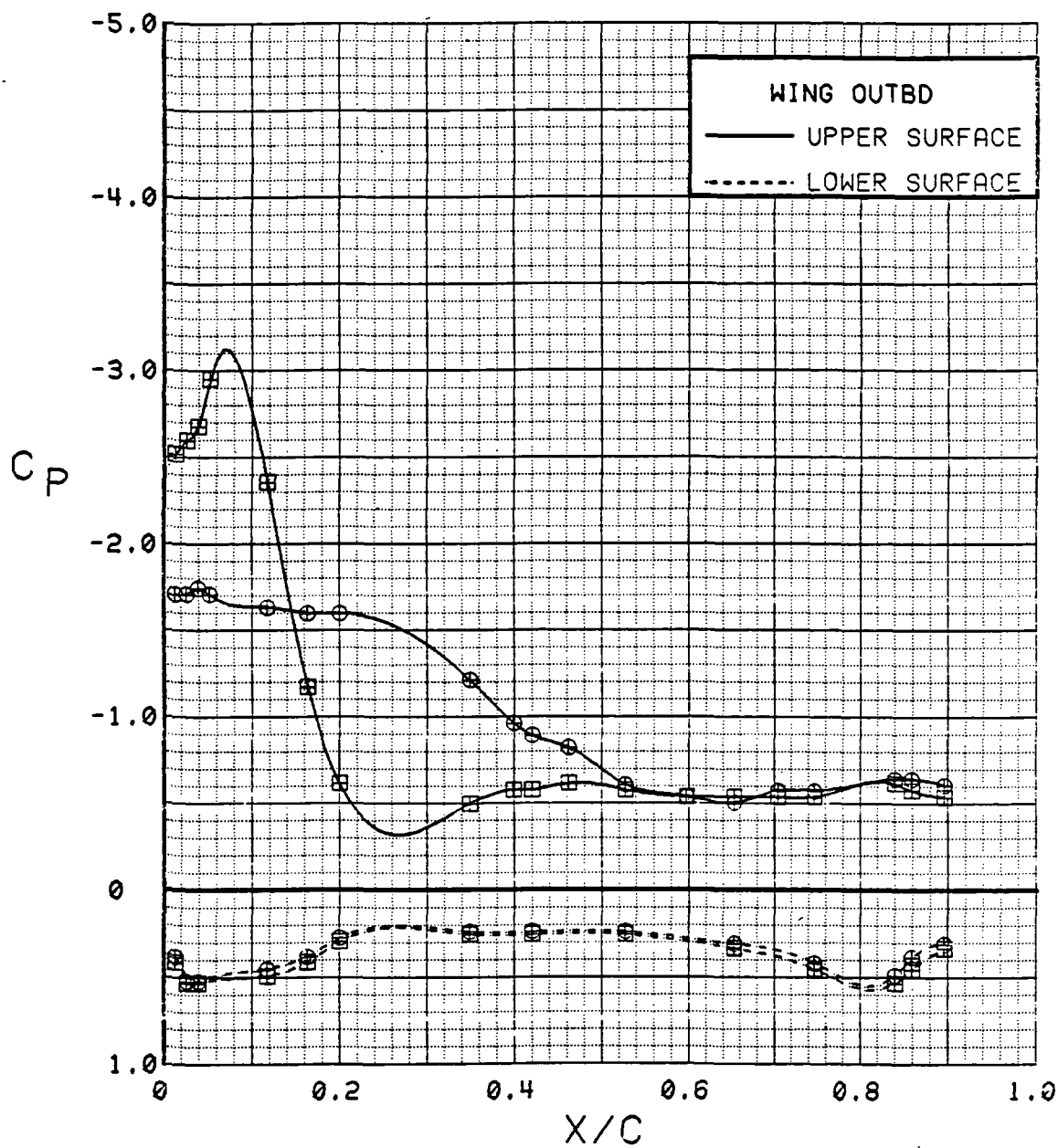


Figure 3.2.4-216 Canard Position Effects, Outboard, Power Off, Alpha = 8 deg

SYM	TEST	RUN	ALPHA	CT	ITEF	OTEF	CAN	SWB	CAN
⊕	537	12	12.7	0.00	30	30	0	OFF	FOR
⊞	543	11	12.7	0.00	30	30	0	OFF	AFT

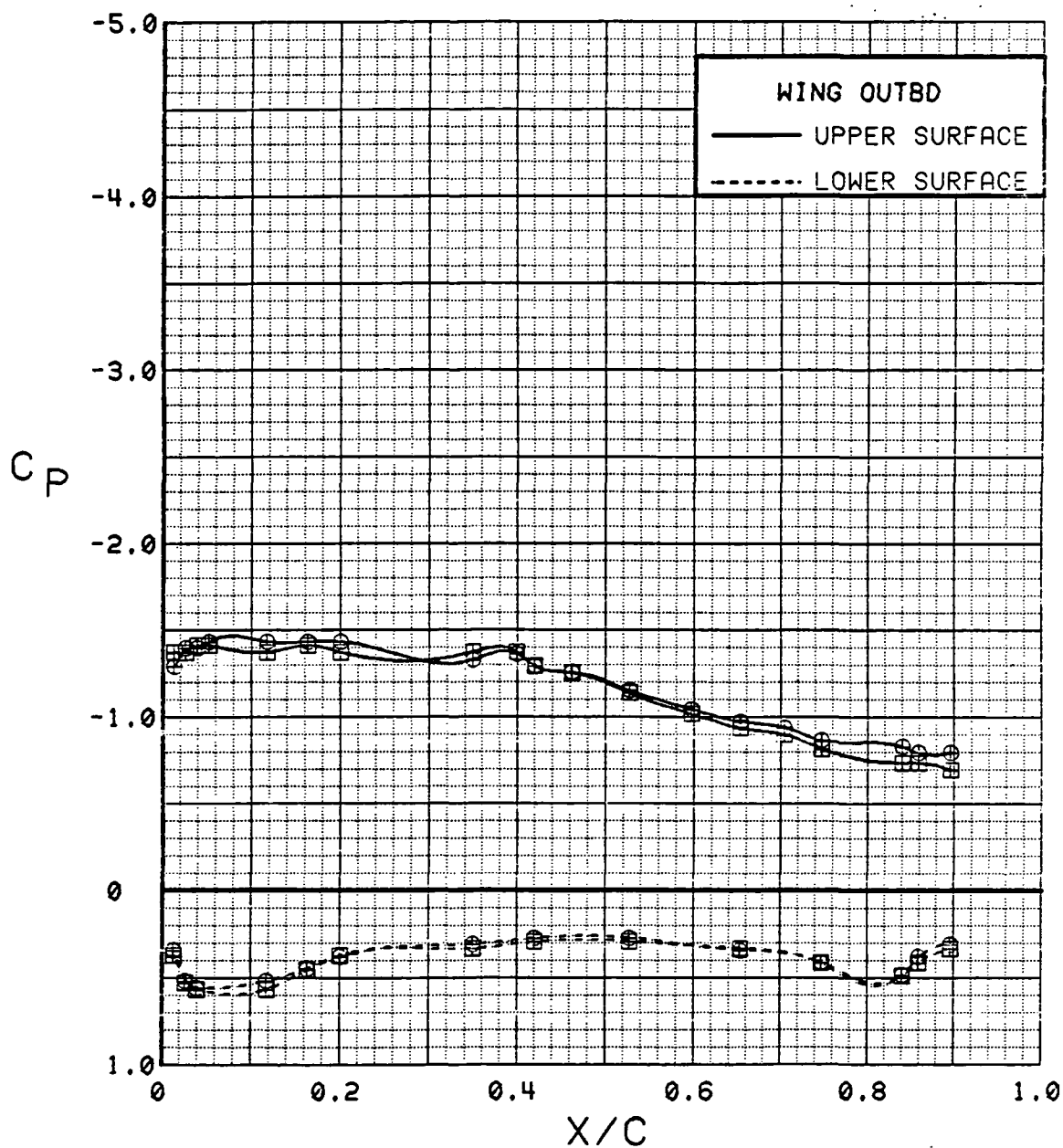


Figure 3.2.4-217 Canard Position Effects, Outboard, Power Off, Alpha = 12 deg

SYM	TEST	RUN	ALPHA	CT	ITEF	OTEF	CAN	SWB	CAN
⊕	537	12	16.7	0.00	30	30	0	OFF	FOR
⊞	543	11	16.8	0.00	30	30	0	OFF	AFT

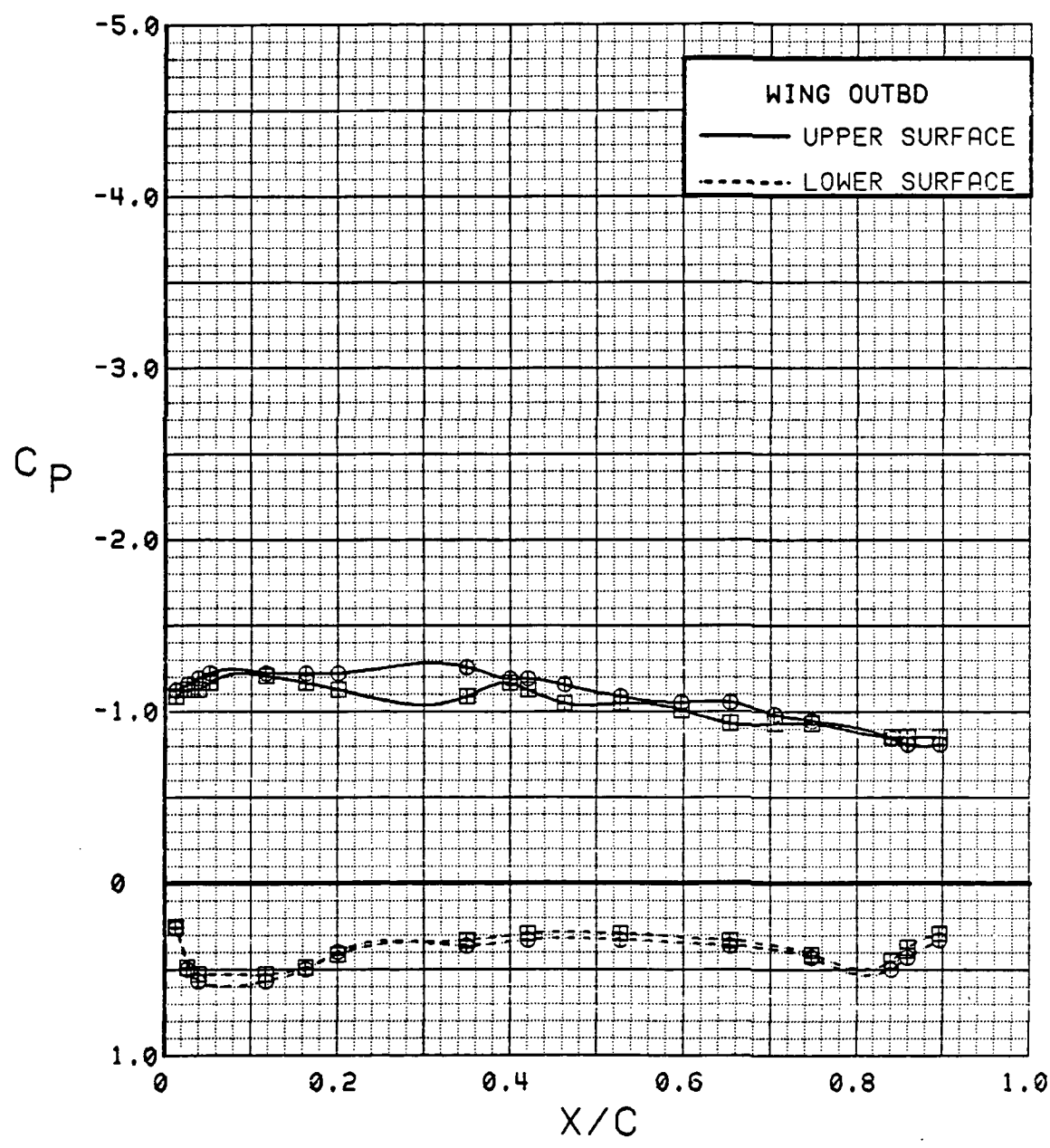


Figure 3.2.4-218 Canard Position Effects, Outboard, Power Off, Alpha = 16 deg

SYM	TEST	RUN	ALPHA	CT	ITEF	OTEF	CAN	SWB	CAN
⊕	537	12	20.8	0.00	30	30	0	OFF	FOR
⊞	543	11	20.8	0.00	30	30	0	OFF	AFT

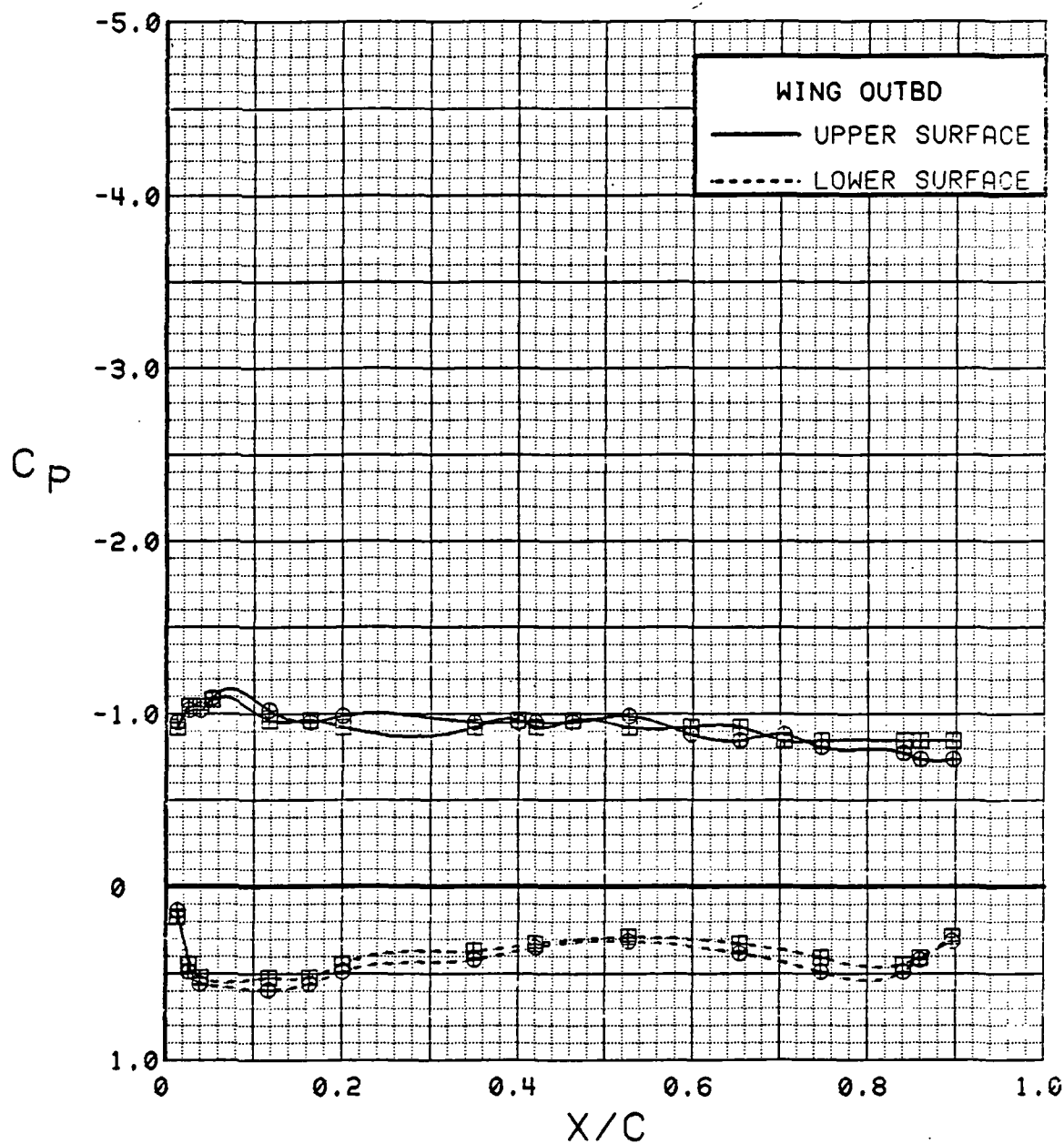


Figure 3.2.4-219 Canard Position Effects, Outboard, Power Off, Alpha = 20 deg



SYM	TEST	RUN	ALPHA	CT	ITEF	OTEF	CAN	SWB	CAN
⊕	537	12	0.3	0.00	30	30	0	OFF	FOR
⊞	543	11	0.3	0.00	30	30	0	OFF	AFT

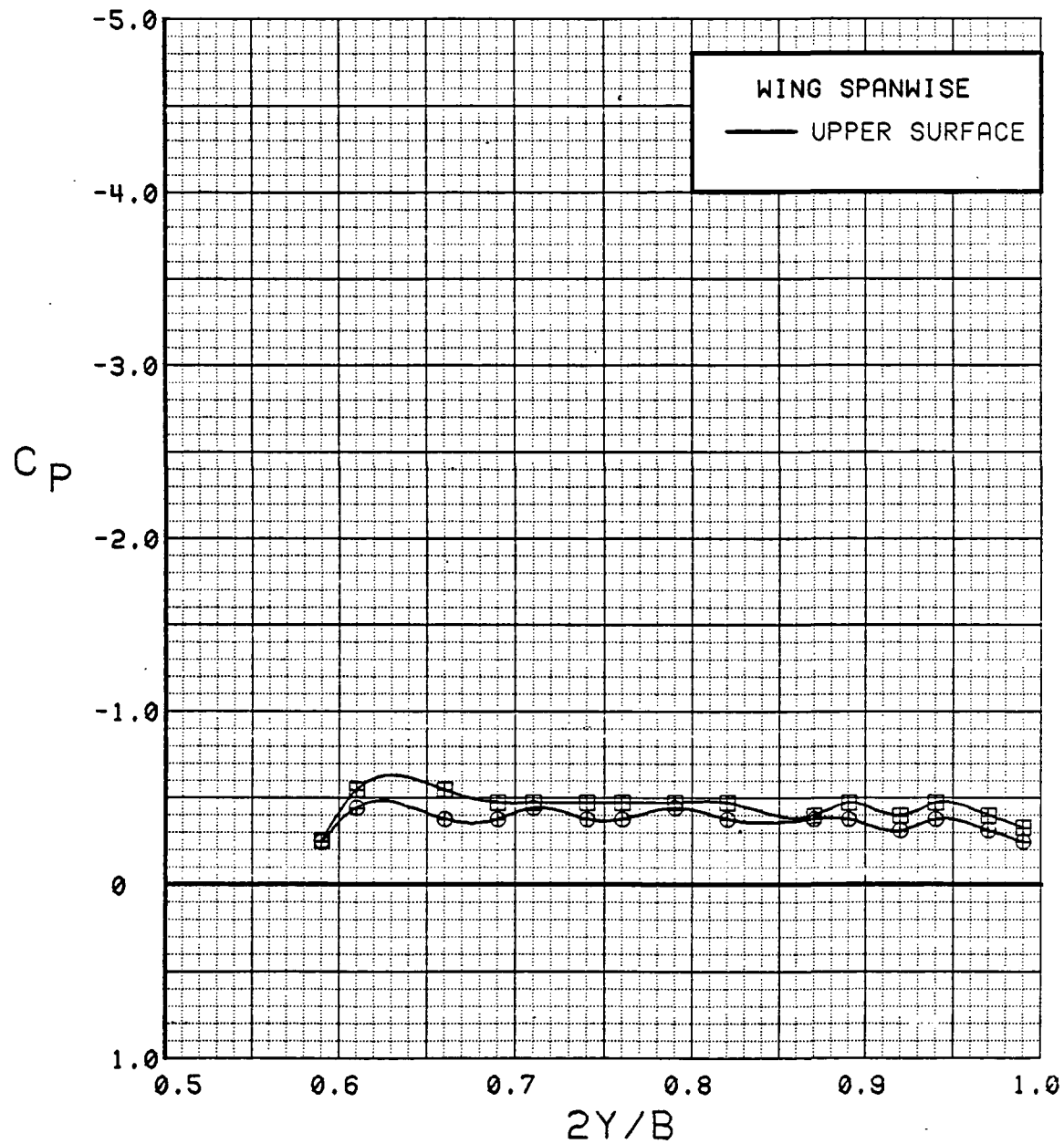


Figure 3.2.4-220 Canard Position Effects, Spanwise, Power Off, Alpha = 0 deg

C-7

SYM	TEST	RUN	ALPHA	CT	ITEF	OTEF	CAN	SWB	CAN
⊕	537	12	4.4	0.00	30	30	0	OFF	FOR
⊞	543	11	4.4	0.00	30	30	0	OFF	AFT

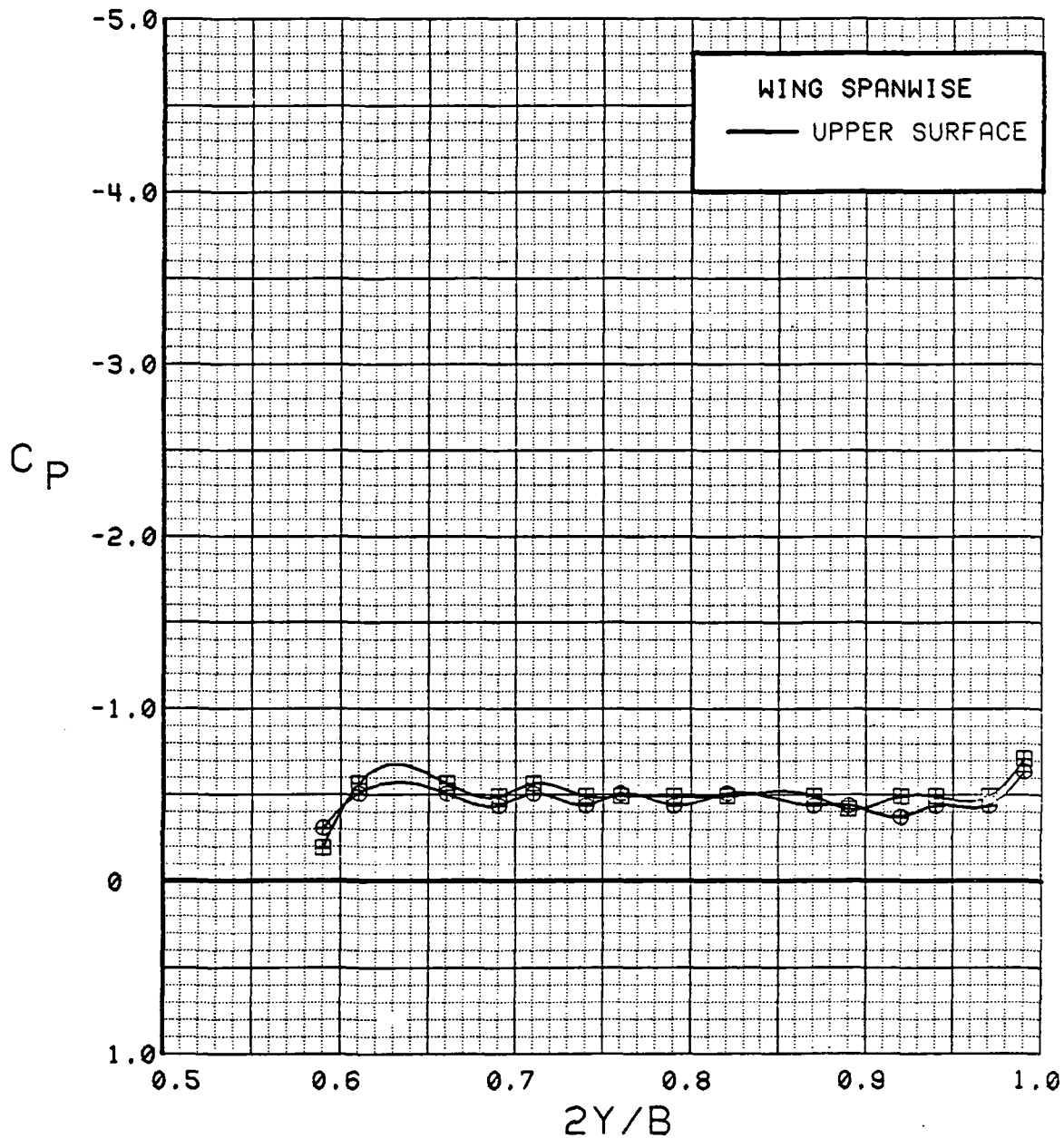


Figure 3.2.4-221 Canard Position Effects, Spanwise, Power Off, Alpha = 4 deg

SYM	TEST	RUN	ALPHA	CT	ITEF	OTEF	CAN	SWB	CAN
⊙	537	12	8.5	0.00	30	30	0	OFF	FOR
⊠	543	11	8.5	0.00	30	30	0	OFF	AFT

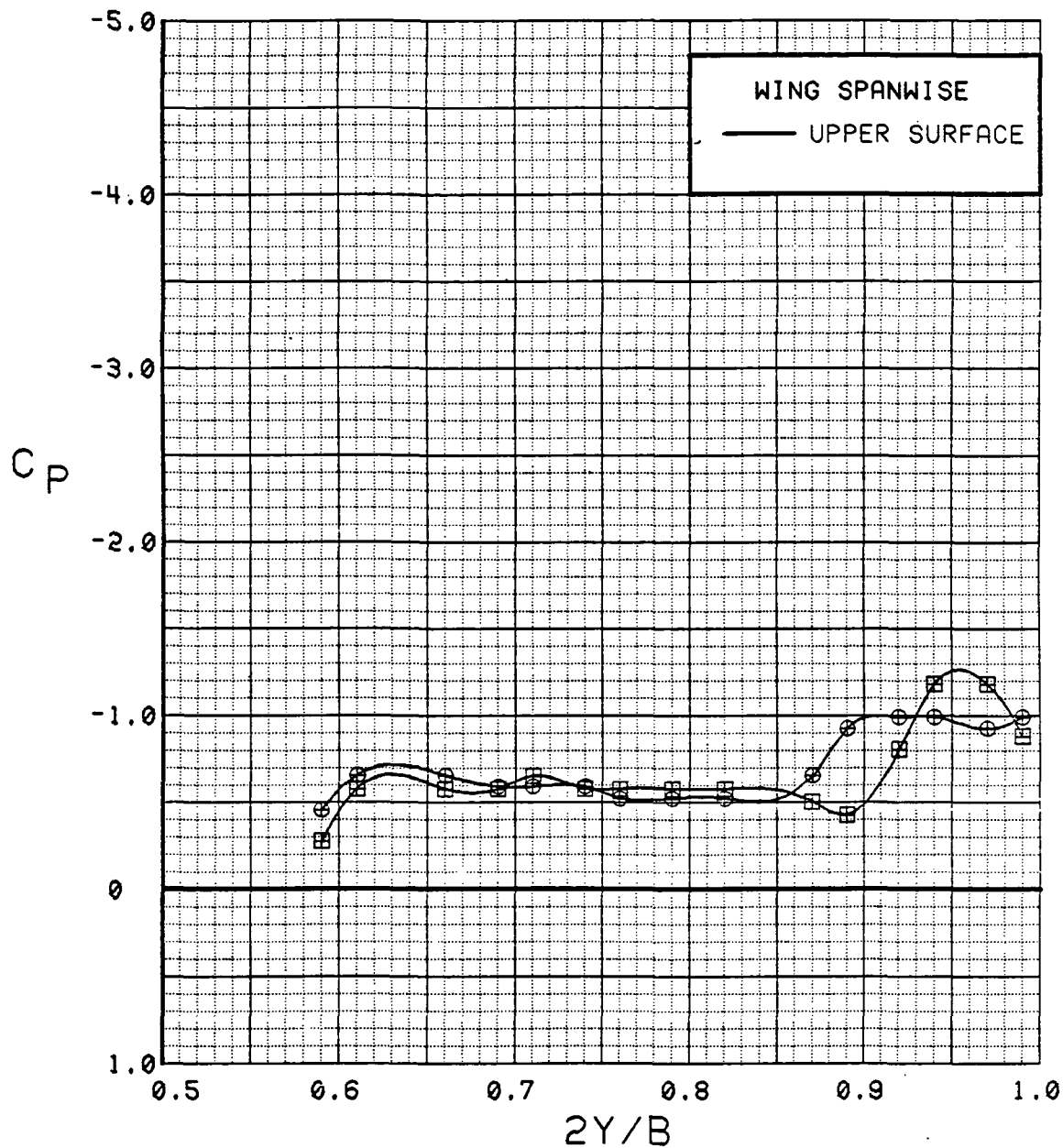


Figure 3.2.4-222 Canard Position Effects, Spanwise, Power Off, Alpha = 8 deg

SYM	TEST	RUN	ALPHA	CT	ITEF	OTEF	CAN	SWB	CAN
⊕	537	12	12.7	0.00	30	30	0	OFF	FOR
⊞	543	11	12.7	0.00	30	30	0	OFF	AFT

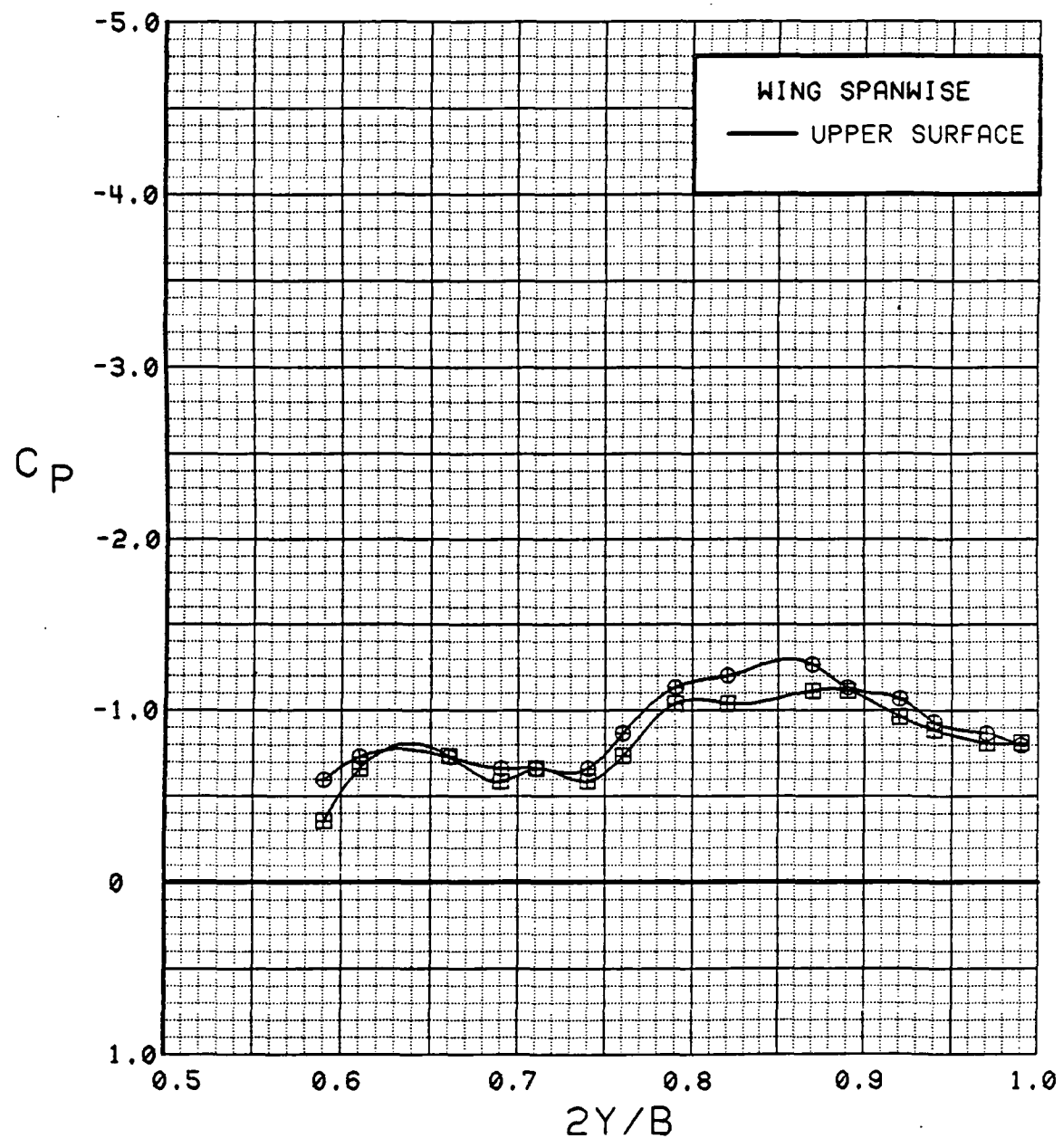


Figure 3.2.4-223 Canard Position Effects, Spanwise, Power Off, Alpha = 12 deg

SYM	TEST	RUN	ALPHA	CT	ITEF	OTEF	CAN	SWB	CAN
⊕	537	12	16.7	0.00	30	30	0	OFF	FOR
⊞	543	11	16.8	0.00	30	30	0	OFF	AFT

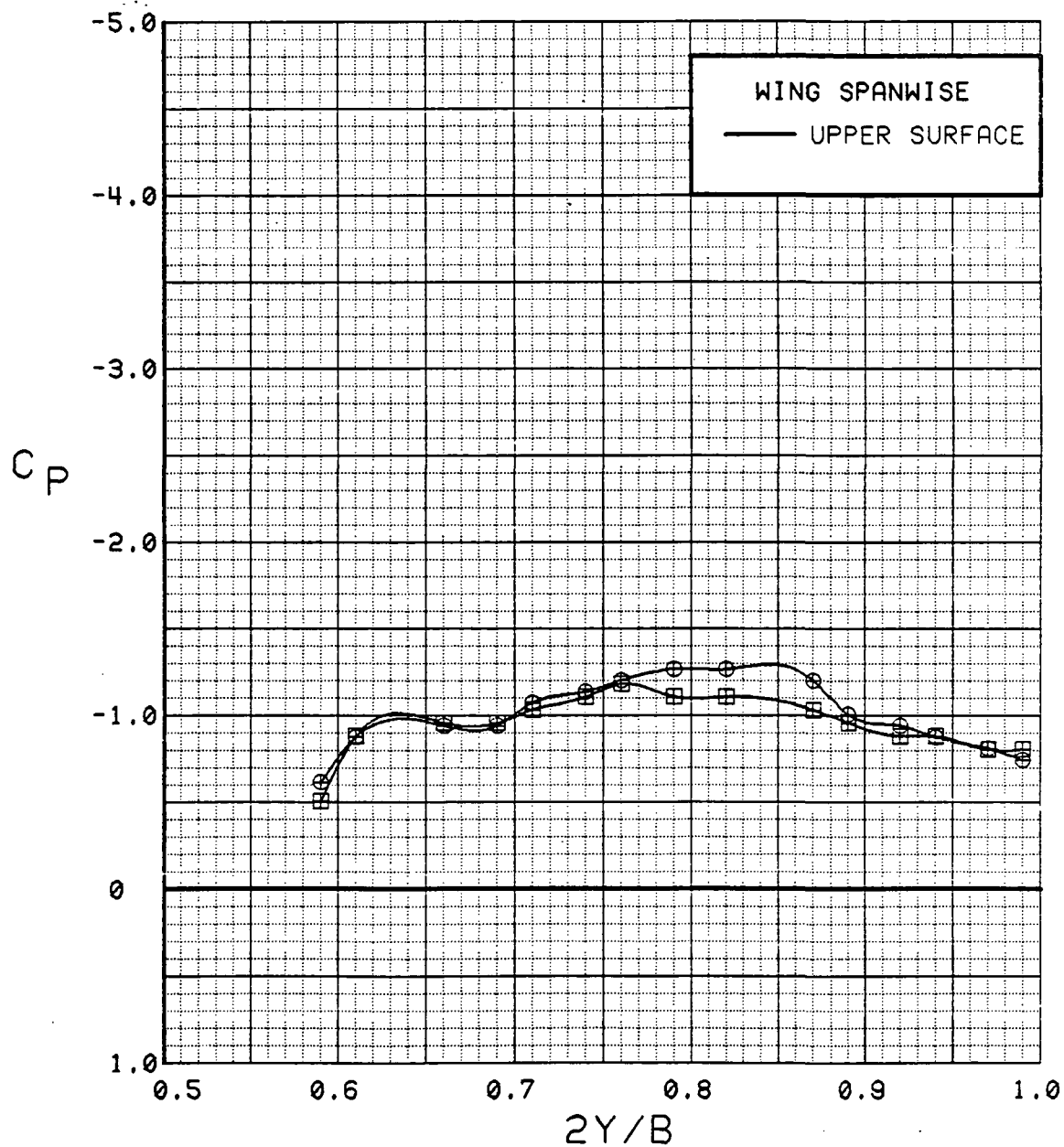


Figure 3.2.4-224 Canard Position Effects, Spanwise, Power Off, Alpha = 16 deg

SYM	TEST	RUN	ALPHA	CT	ITEF	OTEF	CAN	SWB	CAN.
⊕	537	12	20.8	0.00	30	30	0	OFF	FOR
⊞	543	11	20.8	0.00	30	30	0	OFF	AFT

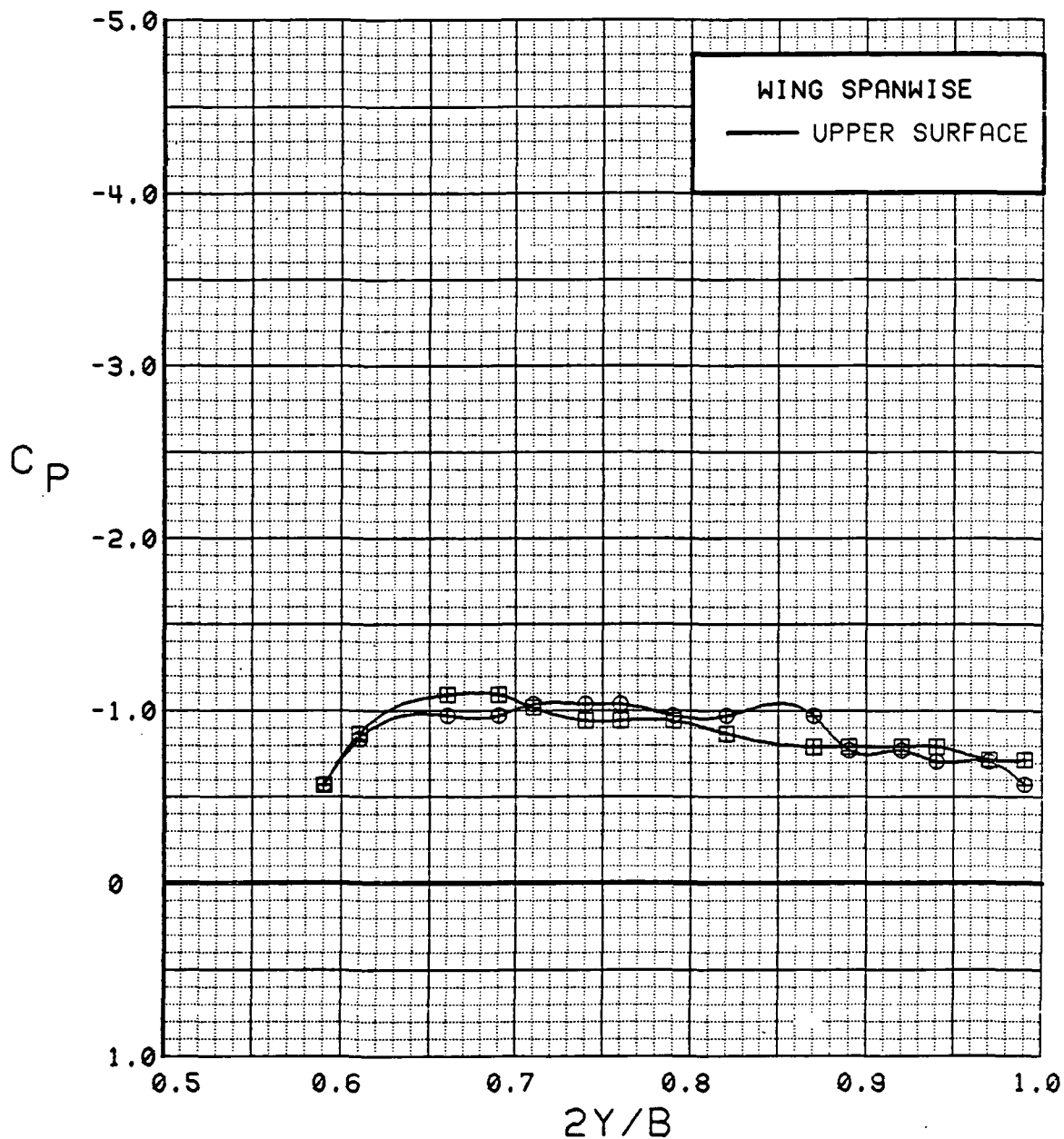


Figure 3.2.4-225 Canard Position Effects, Spanwise, Power Off, Alpha = 20 deg

SYM	TEST	RUN	ALPHA	CT	ITEF	OTEF	CAN	SWB	CAN
⊕	537	32	0.3	0.91	30	30	0	OFF	FOR
⊞	543	6	0.3	0.94	30	30	0	OFF	AFT

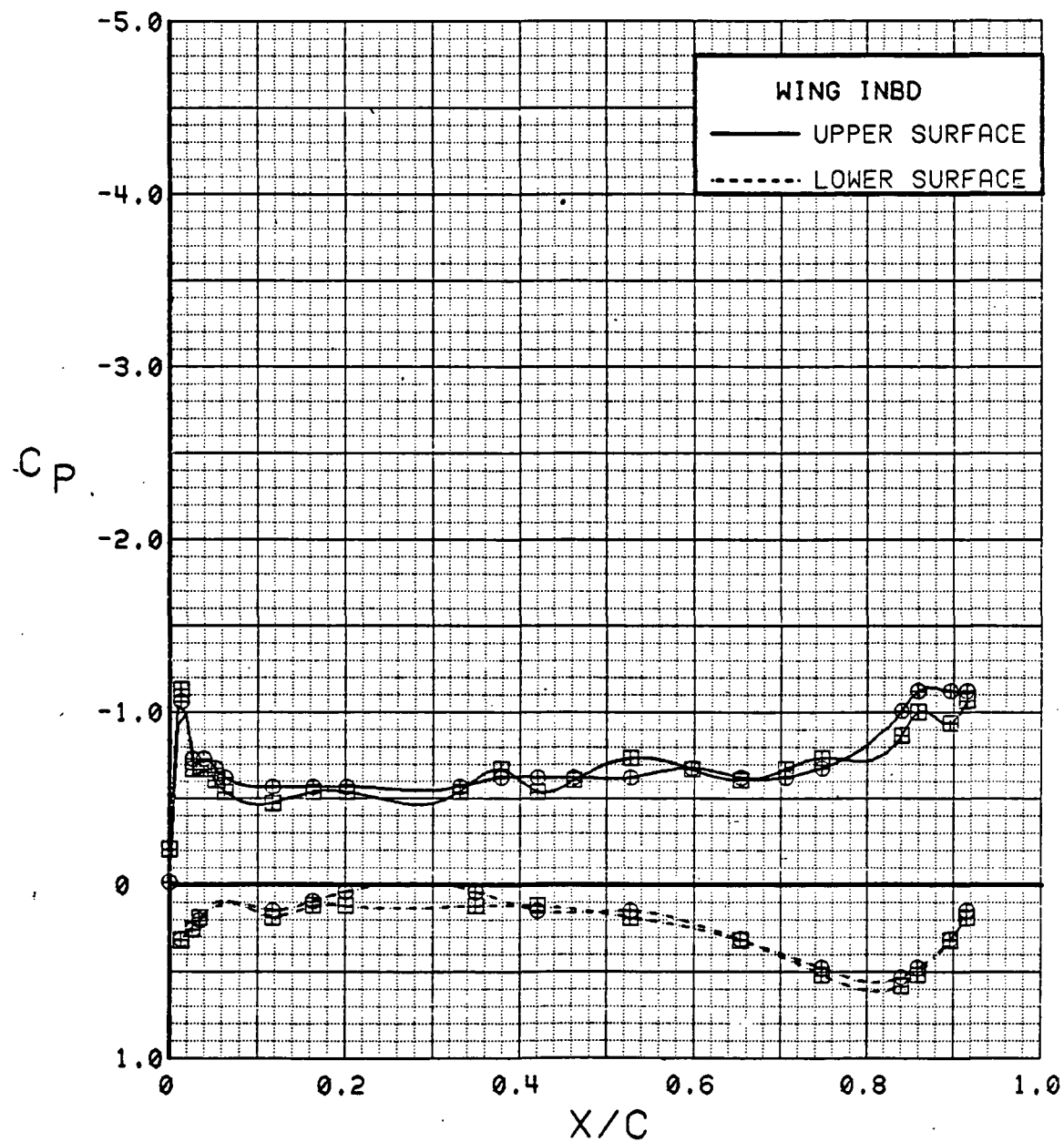


Figure 3.2.4-226 Canard Position Effects, Inboard,  $C_T = 0.9$ ,  $\alpha = 0$  deg

SYM	TEST	RUN	ALPHA	CT	ITEF	OTEF	CAN	SWB	CAN
⊕	537	32	4.5	0.91	30	30	0	OFF	FOR
⊞	543	6	4.5	0.94	30	30	0	OFF	AFT

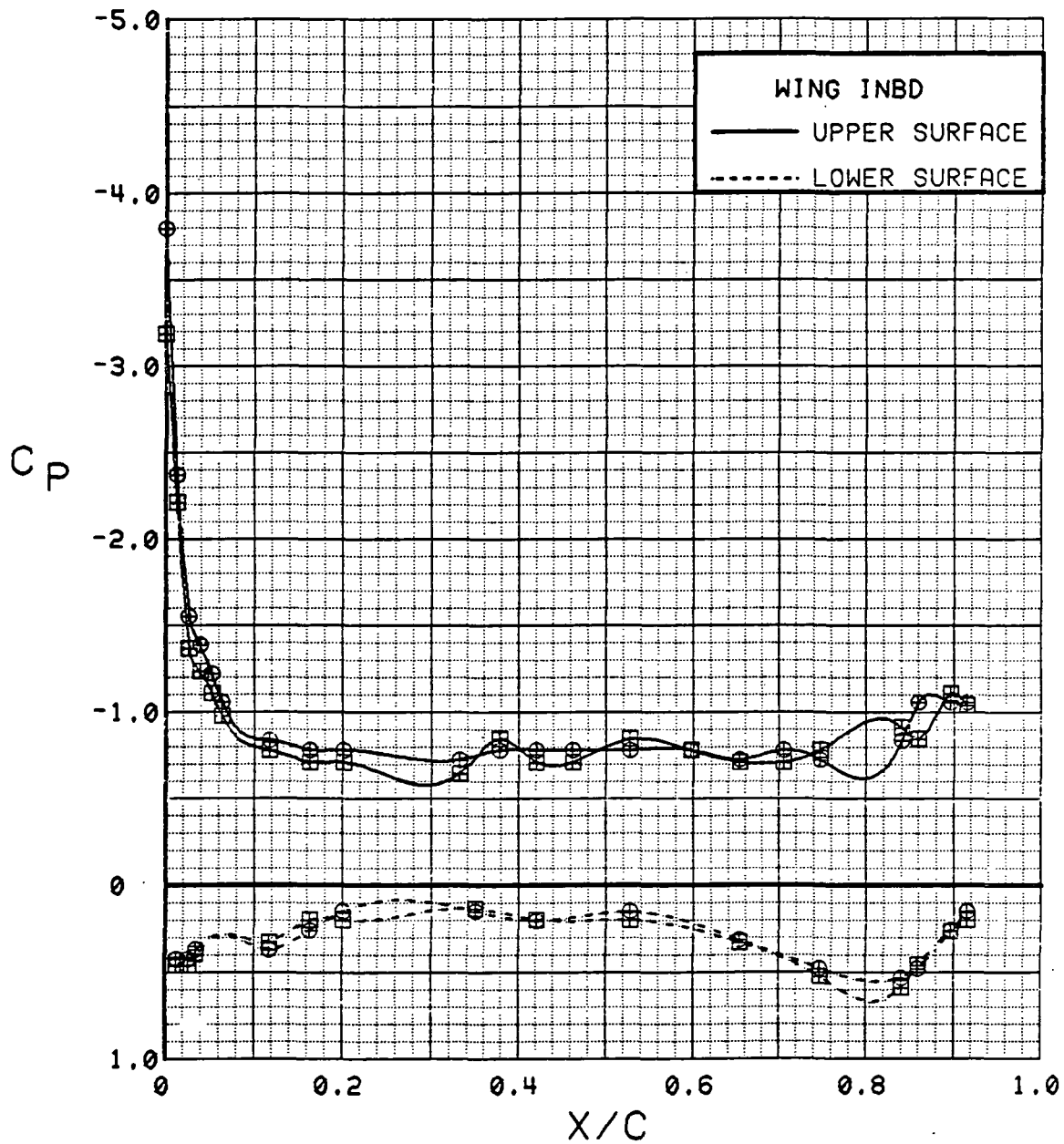


Figure 3.2.4-227 Canard Position Effects, Inboard,  $C_T = 0.9$ ,  $\alpha = 4$  deg



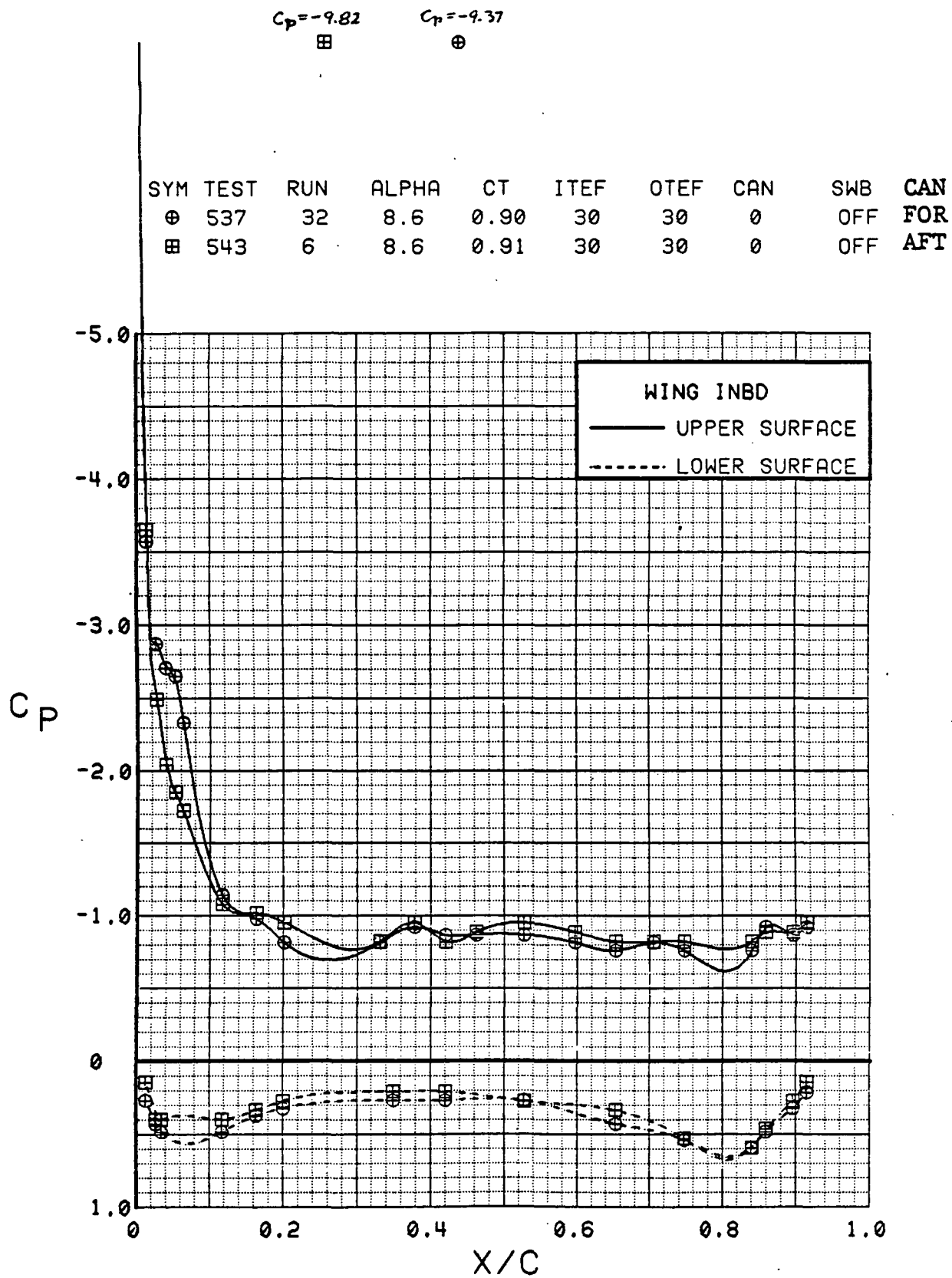


Figure 3.2.4-228 Canard Position Effects, Inboard,  $C_T = 0.9$ ,  $\alpha = 8^\circ$

SYM	TEST	RUN	ALPHA	CT	ITEF	OTEF	CAN	SWB	CAN
⊕	537	32	12.8	0.92	30	30	0	OFF	FOR
⊞	543	6	12.8	0.92	30	30	0	OFF	AFT

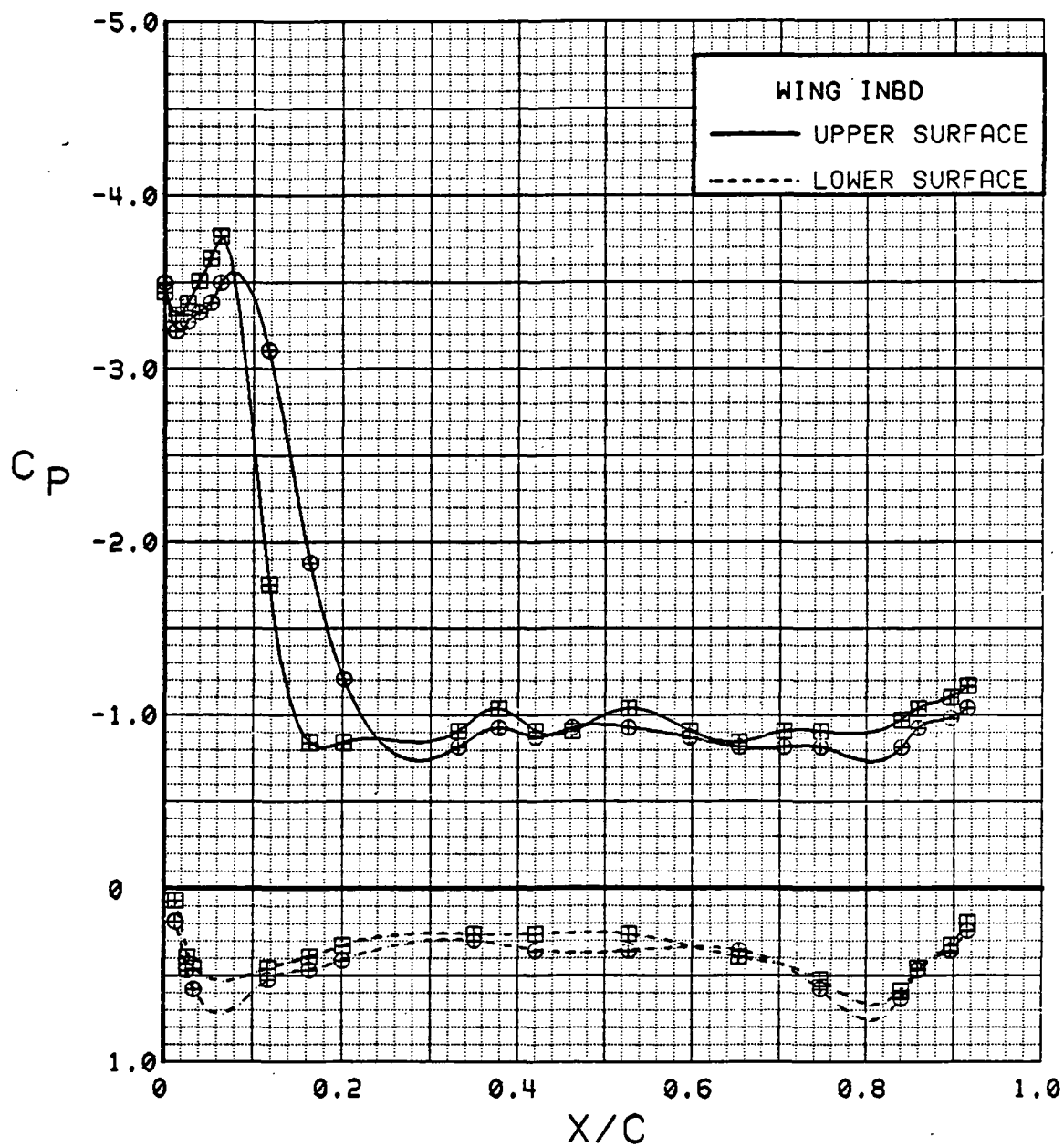


Figure 3.2.4-229 Canard Position Effects, Inboard,  $C_T = 0.9$ ,  $\alpha = 12$  deg

SYM	TEST	RUN	ALPHA	CT	ITEF	OTEF	CAN	SWB	CAN
⊕	537	32	16.8	0.92	30	30	0	OFF	FOR
⊞	543	6	16.9	0.92	30	30	0	OFF	AFT

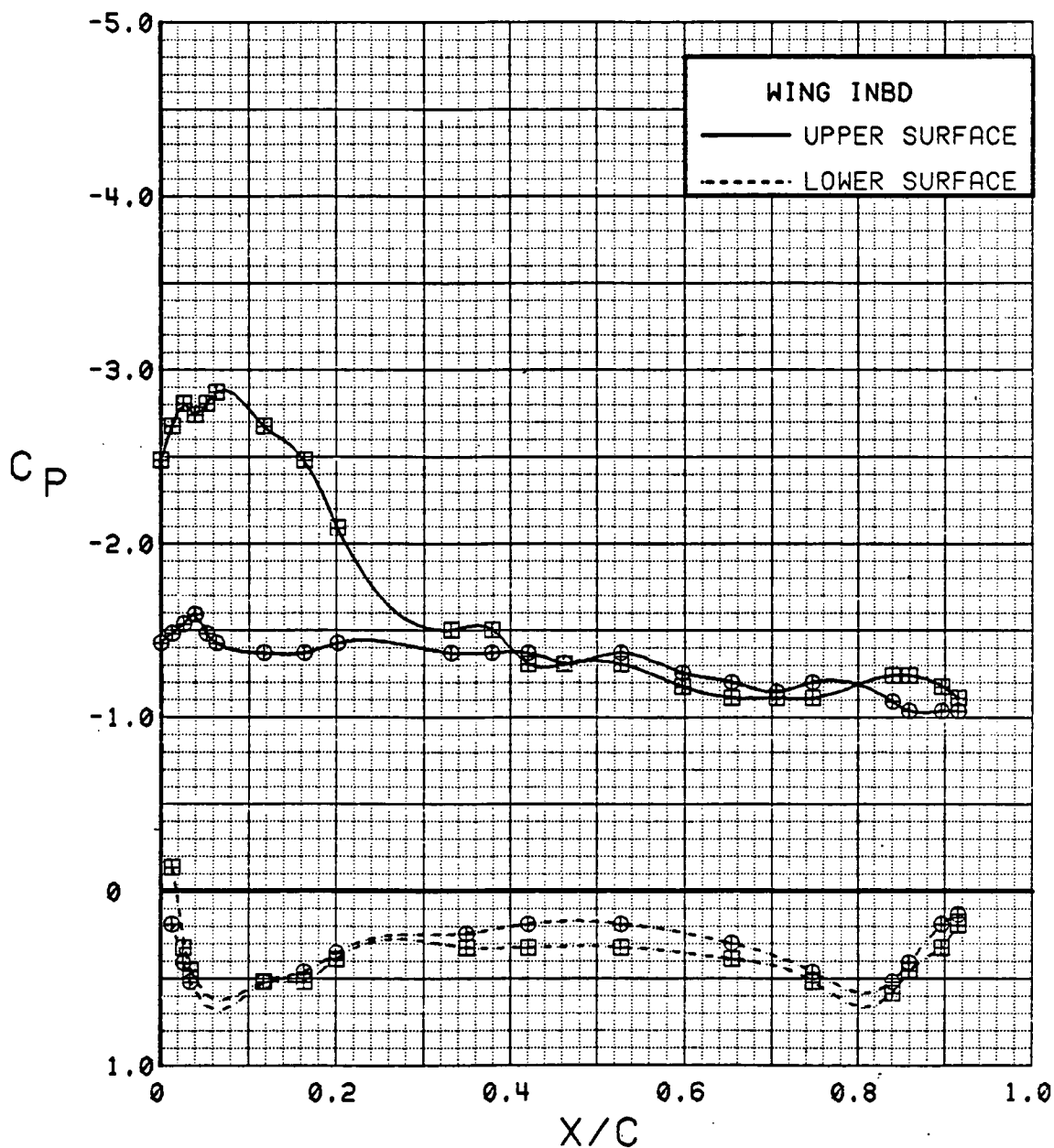


Figure 3.2.4-230 Canard Position Effects, Inboard,  $C_T = 0.9$ ,  $\alpha = 16^\circ$

SYM	TEST	RUN	ALPHA	CT	ITEF	OTEF	CAN	SWB	CAN
⊕	537	32	20.9	0.90	30	30	0	OFF	FOR
⊞	543	6	21.0	0.93	30	30	0	OFF	AFT

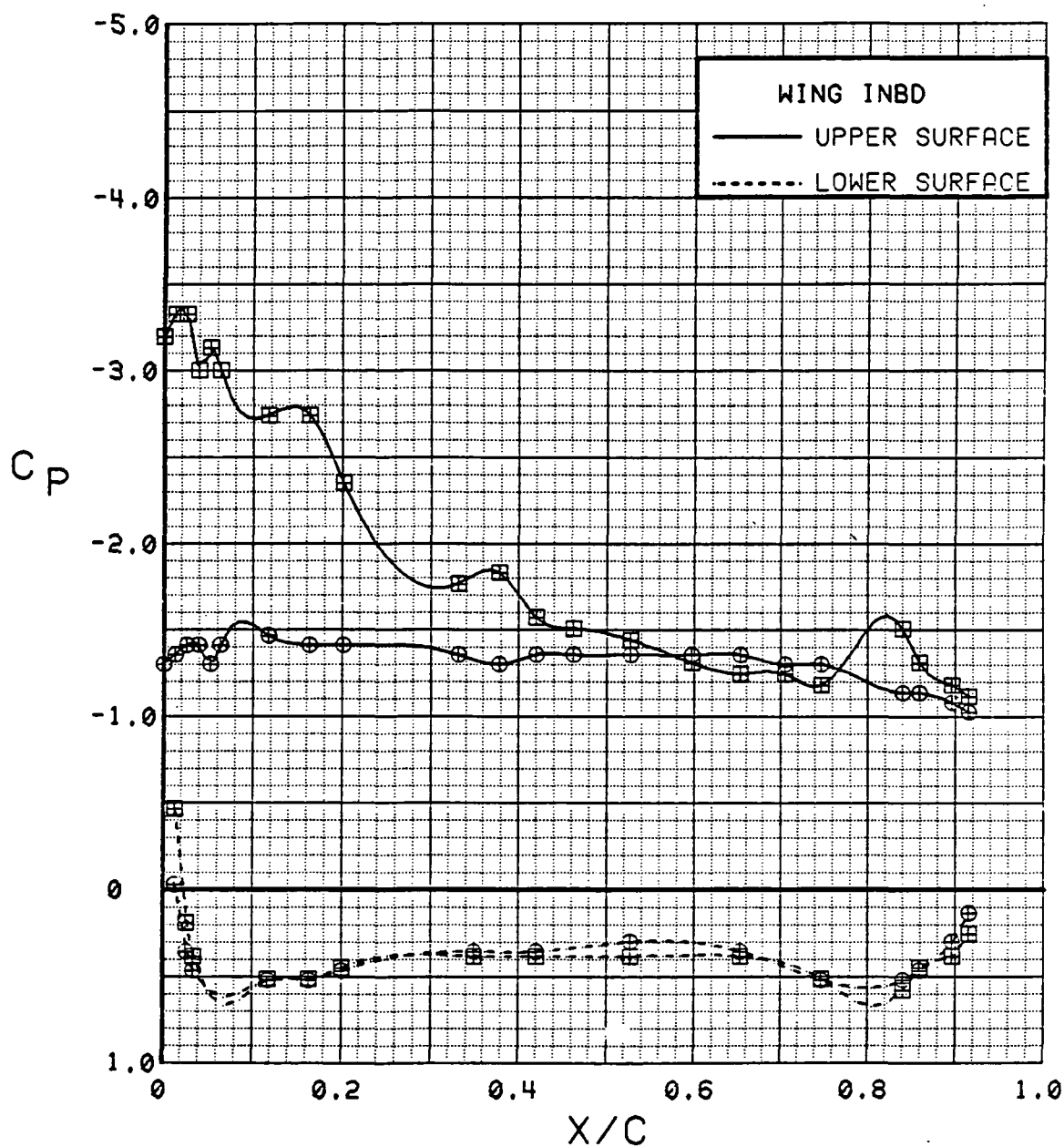


Figure 3.2.4-231 Canard Position Effects, Inboard,  $C_T = 0.9$ ,  $\alpha = 20$  deg

SYM	TEST	RUN	ALPHA	CT	ITEF	OTEF	CAN	SWB	CAN
⊕	537	32	0.3	0.91	30	30	0	OFF	FOR
⊞	543	6	0.3	0.94	30	30	0	OFF	AFT

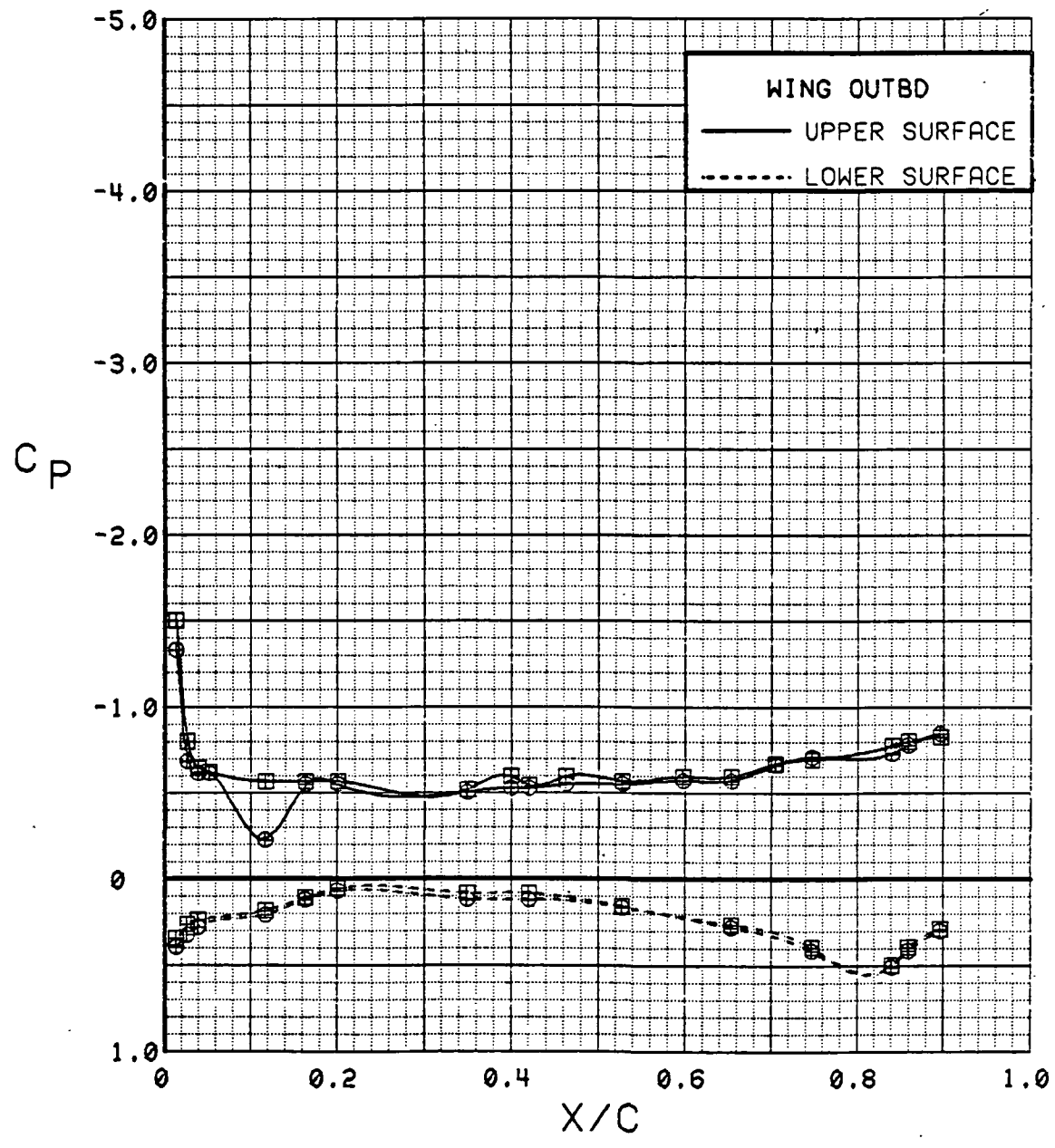


Figure 3.2.4-232 Canard Position Effects, Outboard,  $C_T = 0.9$ ,  $\alpha = 0^\circ$

SYM	TEST	RUN	ALPHA	CT	ITEF	OTEF	CAN	SWB	CAN
⊕	537	32	4.5	0.91	30	30	0	OFF	FOR
⊞	543	6	4.5	0.94	30	30	0	OFF	AFT

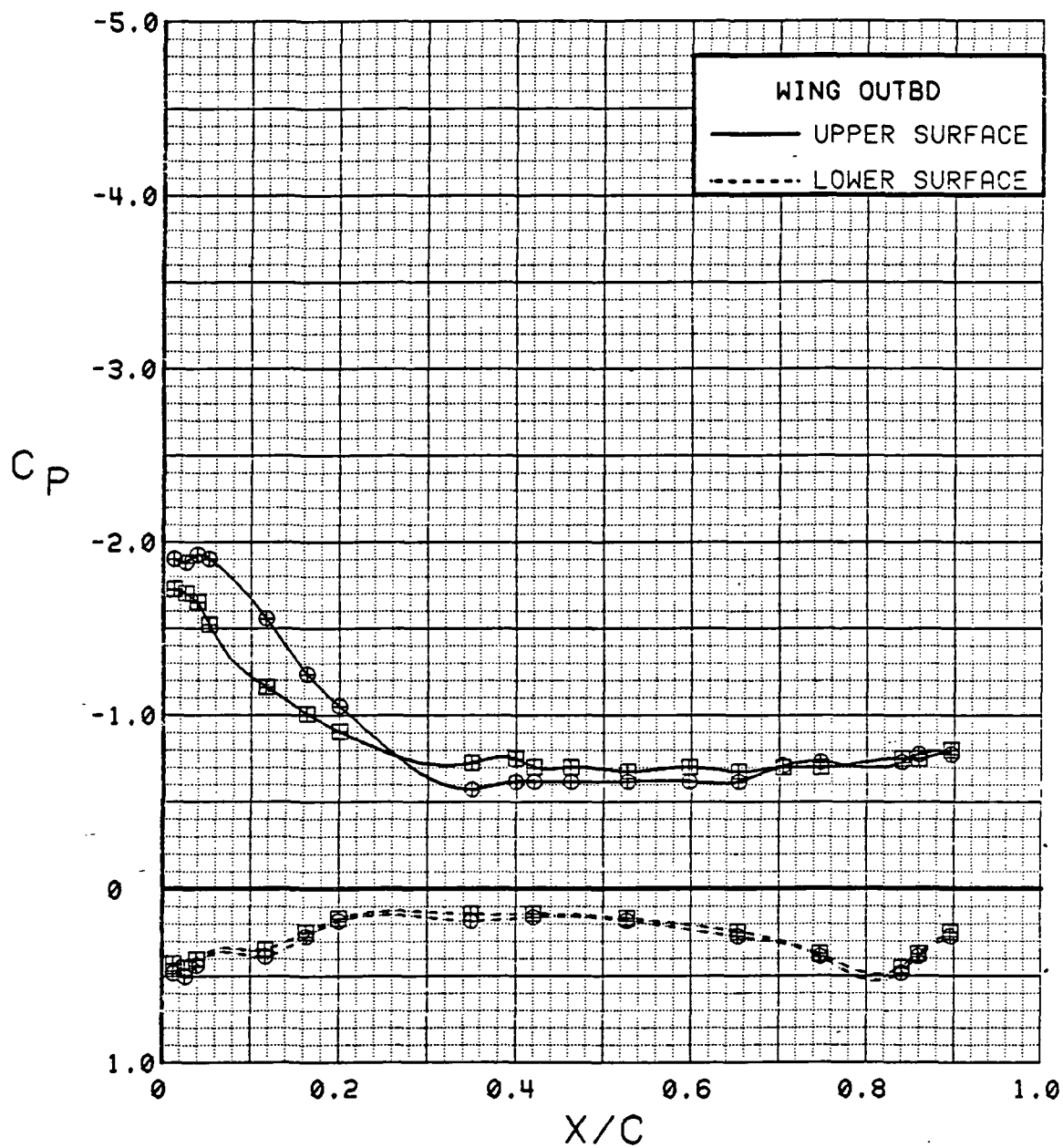


Figure 3.2.4-233 Canard Position Effects, Outboard,  $C_T = 0.9$ ,  $\alpha = 4$  deg

SYM	TEST	RUN	ALPHA	CT	ITEF	OTEF	CAN	SWB	CAN
⊕	537	32	8.6	0.90	30	30	0	OFF	FOR
⊞	543	6	8.6	0.91	30	30	0	OFF	AFT

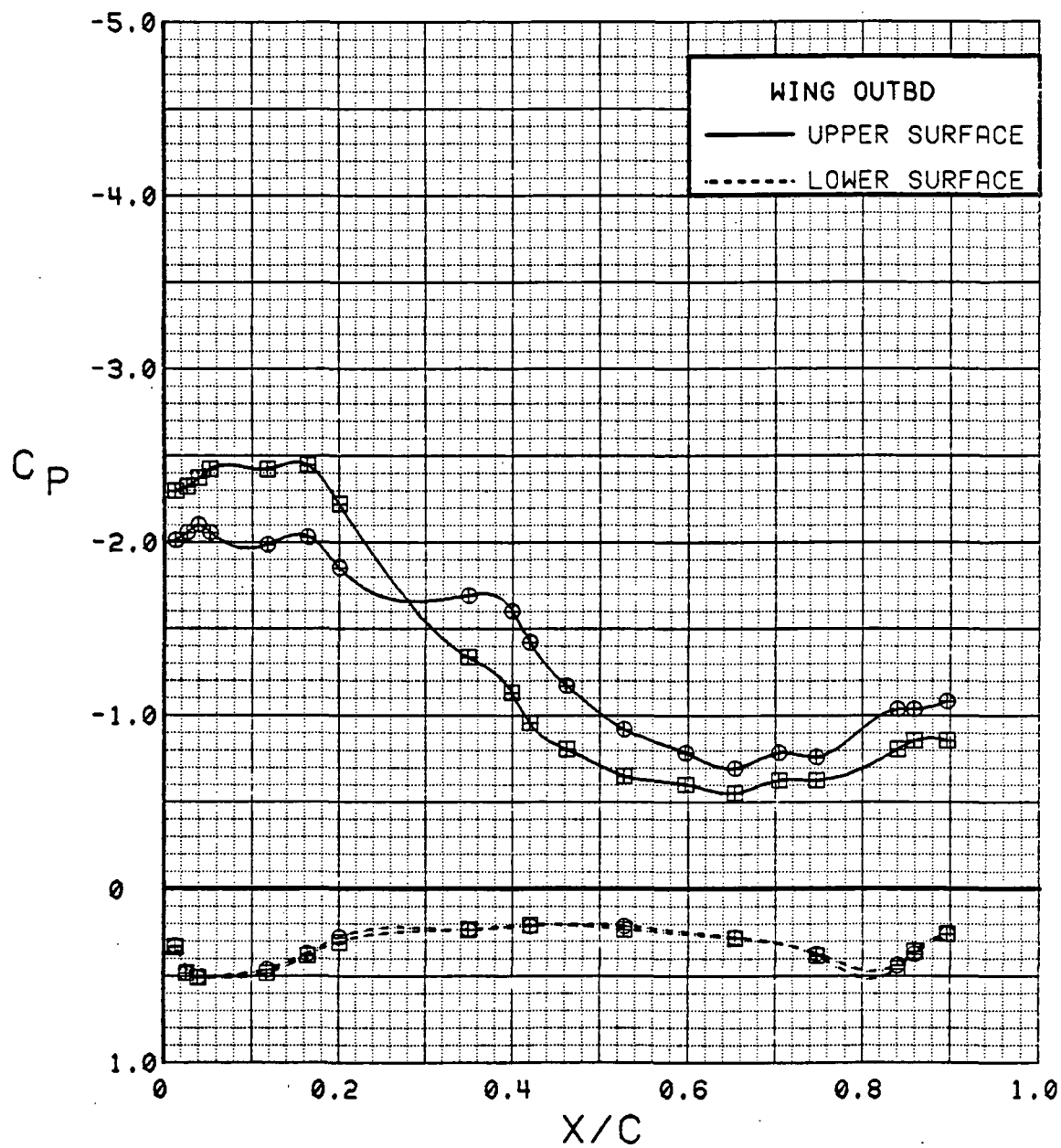


Figure 3.2.4-234 Canard Position Effects, Outboard,  $C_T = 0.9$ ,  $\alpha = 8$  deg

SYM	TEST	RUN	ALPHA	CT	ITEF	OTEF	CAN	SWB	CAN
⊕	537	32	12.8	0.92	30	30	0	OFF	FOR
⊞	543	6	12.8	0.92	30	30	0	OFF	AFT

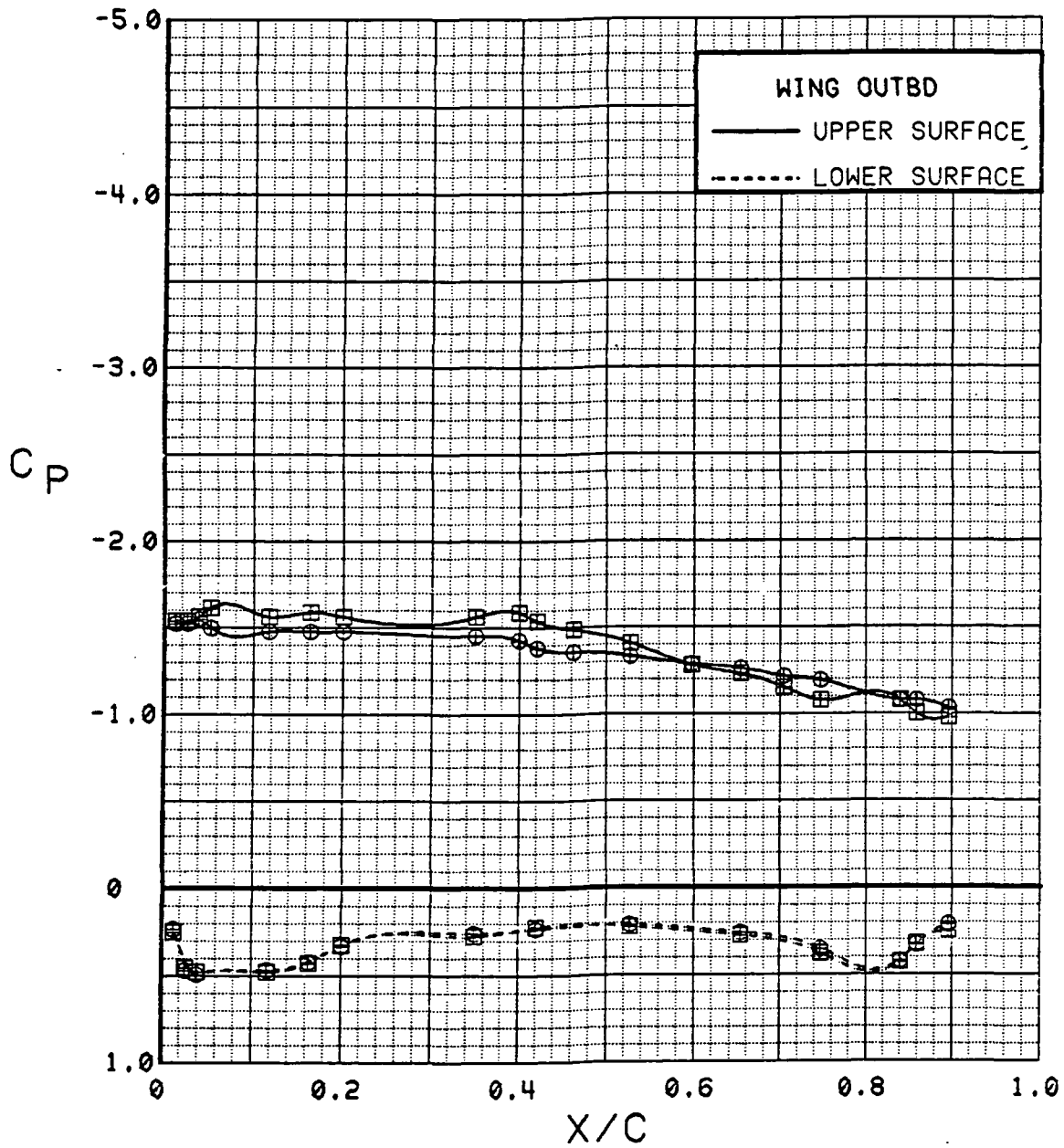


Figure 3.2.4-235 Canard Position Effects, Outboard,  $C_T = 0.9$ ,  $\alpha = 12^\circ$



SYM	TEST	RUN	ALPHA	CT	ITEF	OTEF	CAN	SWB	CAN
⊕	537	32	16.8	0.92	30	30	0	OFF	FOR
⊞	543	6	16.9	0.92	30	30	0	OFF	AFT

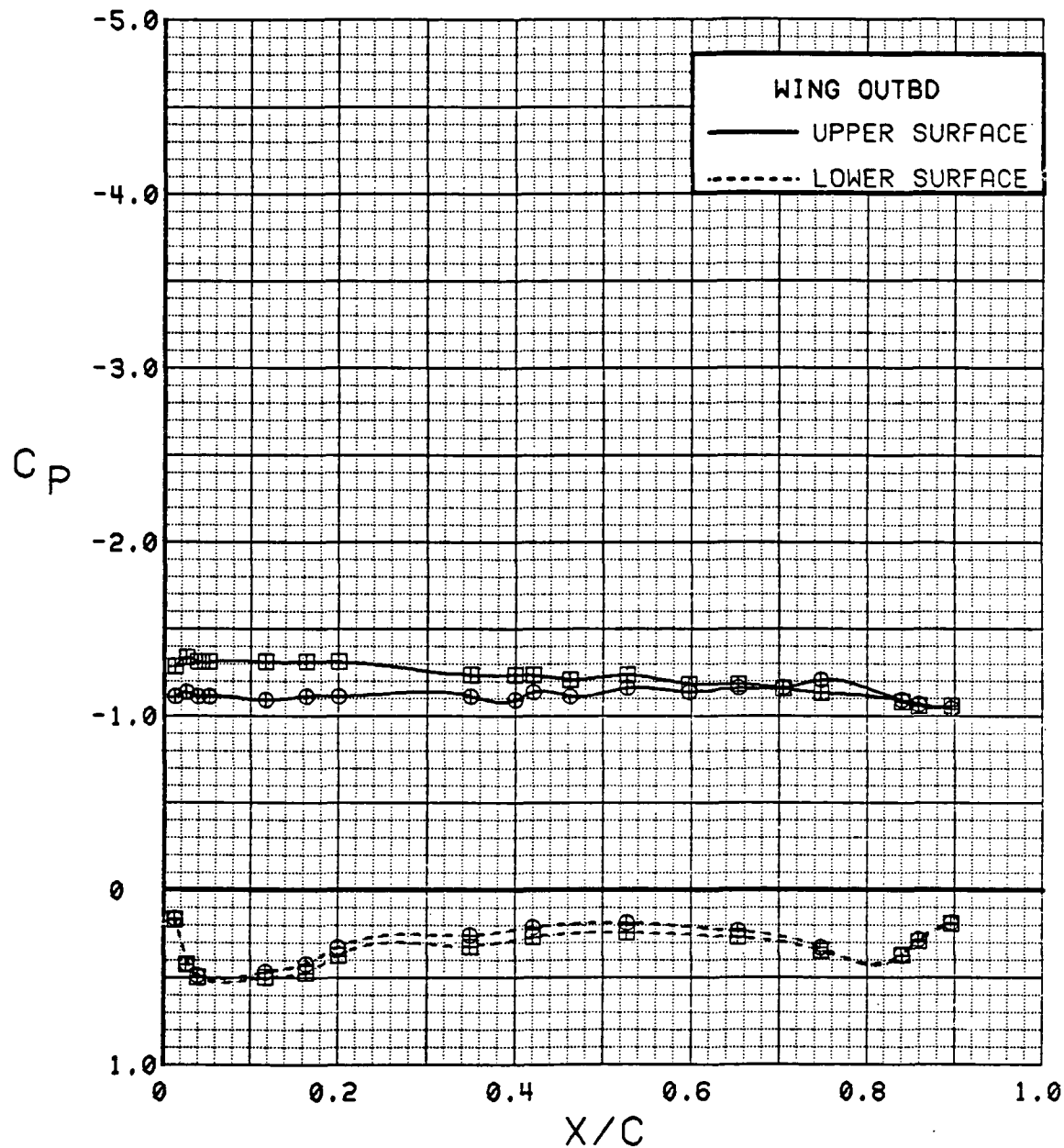


Figure 3.2.4-236 Canard Position Effects, Outboard,  $C_T = 0.9$ , Alpha = 16 deg

SYM	TEST	RUN	ALPHA	CT	ITEF	OTEF	CAN	SWB	CAN
⊕	537	32	20.9	0.90	30	30	0	OFF	FOR
⊞	543	6	21.0	0.93	30	30	0	OFF	AFT

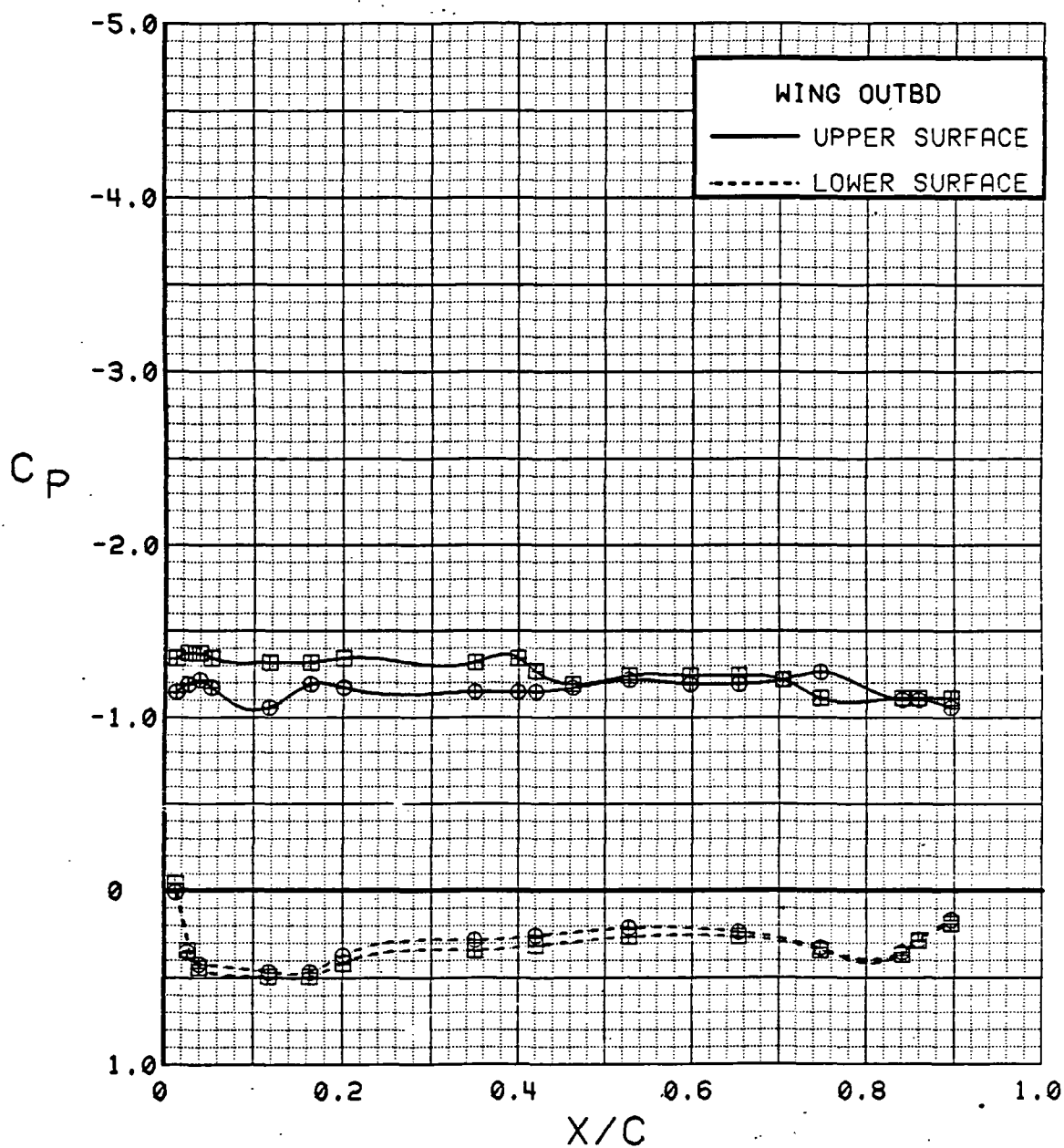


Figure 3.2.4-237 Canard Position Effects, Outboard,  $C_T = 0.9$ ,  $\alpha = 20^\circ$

SYM	TEST	RUN	ALPHA	CT	ITEF	OTEF	CAN	SWB	CAN
⊕	537	32	0.3	0.91	30	30	0	OFF	FOR
⊞	543	6	0.3	0.94	30	30	0	OFF	AFT

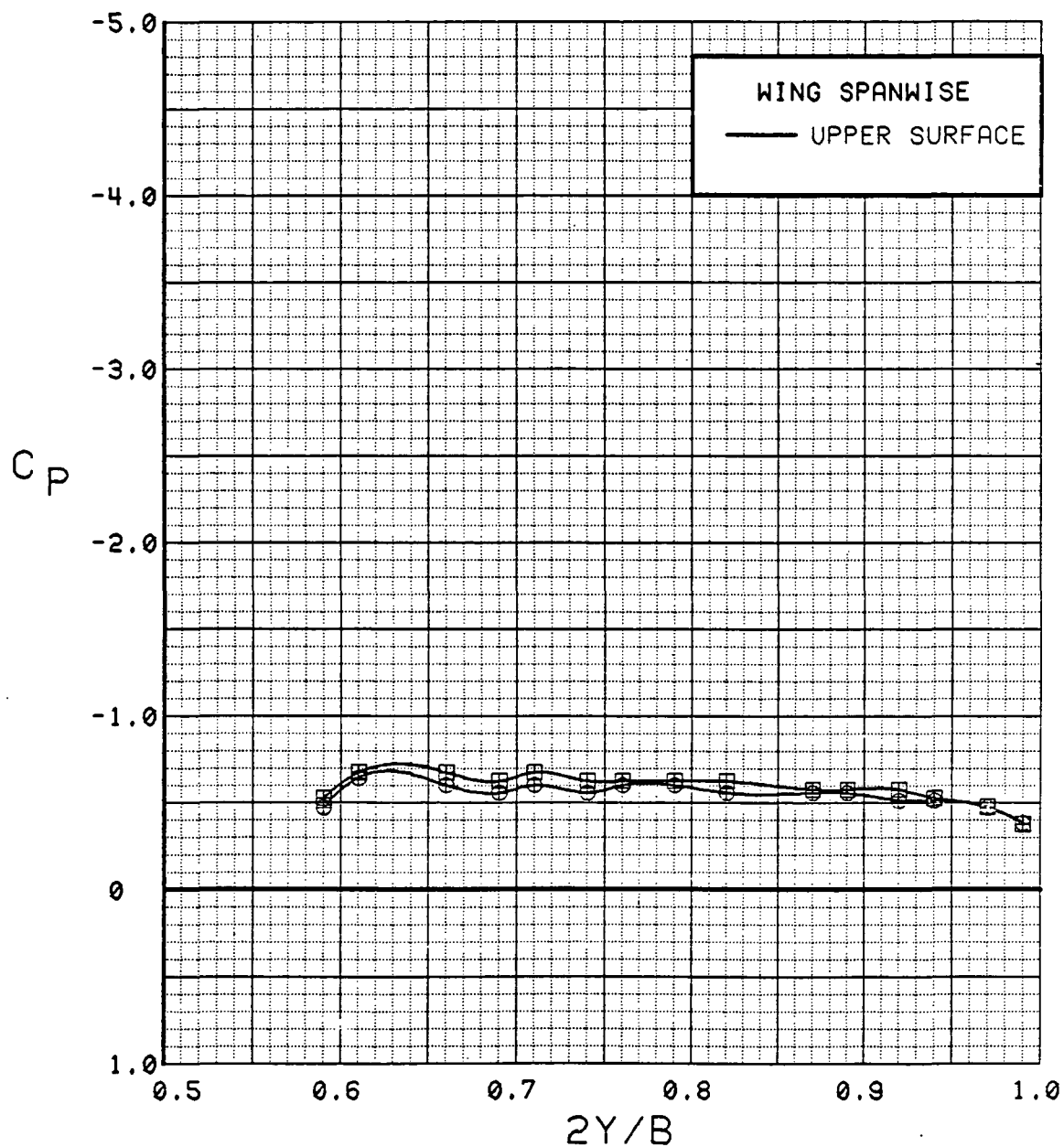


Figure 3.2.4-238 Canard Position Effects, Spanwise,  $C_T = 0.9$ ,  $\alpha = 0^\circ$

SYM	TEST	RUN	ALPHA	CT	ITEF	OTEF	CAN	SWB	CAN
⊕	537	32	4.5	0.91	30	30	0	OFF	FOR
⊗	543	6	4.5	0.94	30	30	0	OFF	AFT

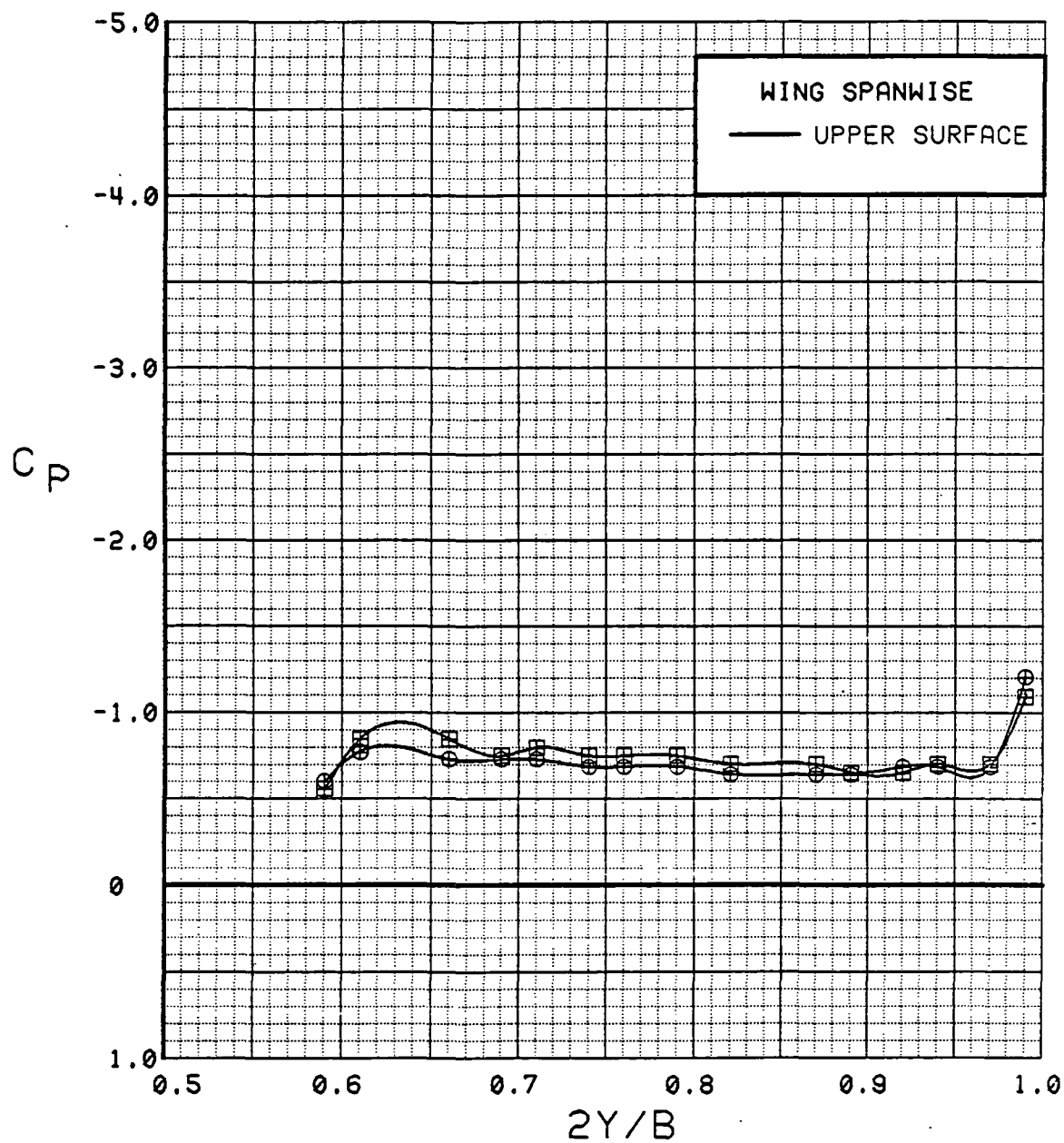


Figure 3.2.4-239 Canard Position Effects, Spanwise,  $C_T = 0.9$ ,  $\alpha = 4$  deg

SYM	TEST	RUN	ALPHA	CT	ITEF	OTEF	CAN	SWB	CAN
⊕	537	32	8.6	0.90	30	30	0	OFF	FOR
⊞	543	6	8.6	0.91	30	30	0	OFF	AFT

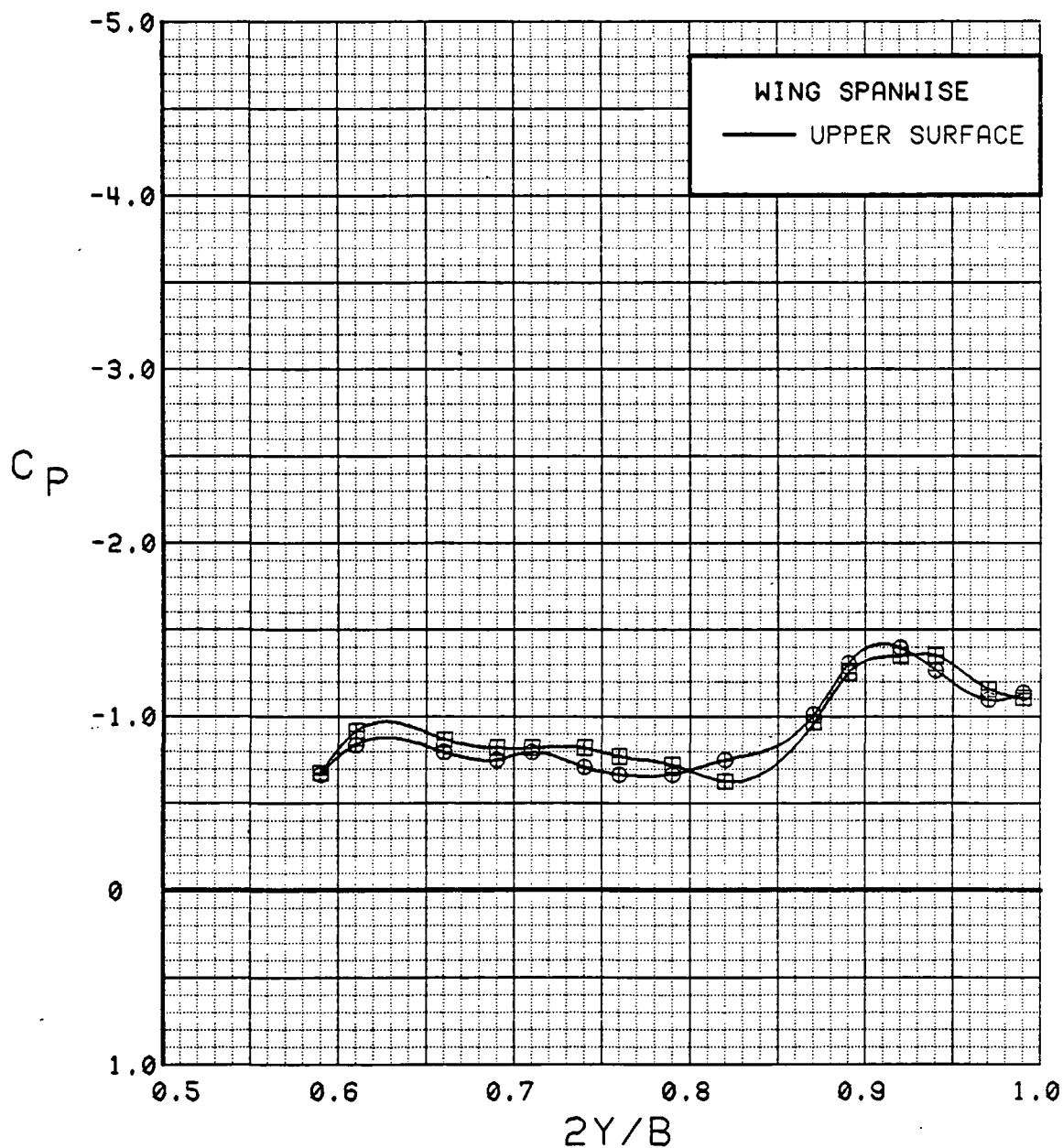


Figure 3.2.4-240 Canard Position Effects, Spanwise,  $C_T = 0.9$ ,  $\alpha = 8^\circ$

SYM	TEST	RUN	ALPHA	CT	ITEF	OTEF	CAN	SWB	CAN
●	537	32	12.8	0.92	30	30	0	OFF	FOR
■	543	6	12.8	0.92	30	30	0	OFF	AFT

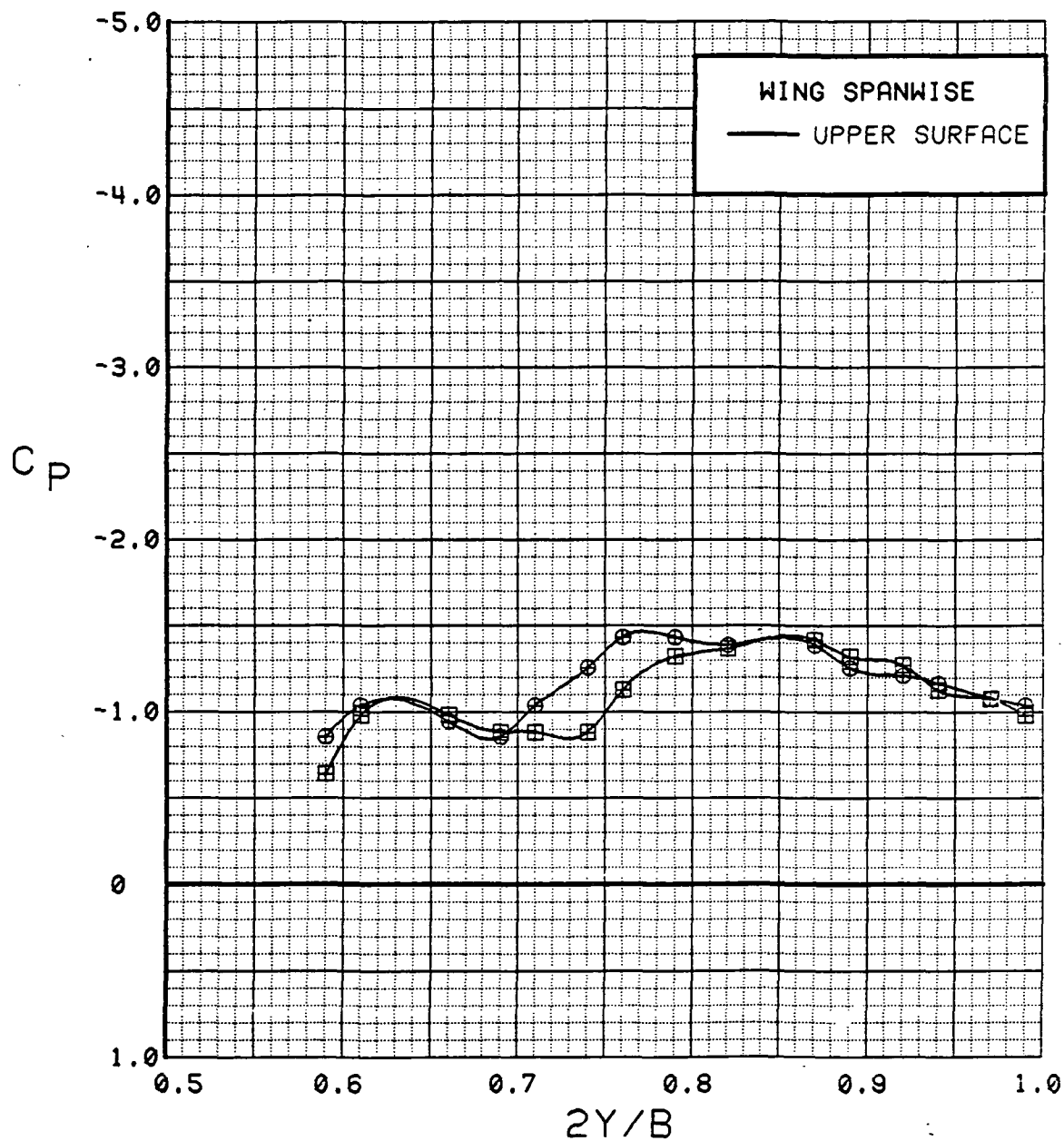


Figure 3.2.4-241 Canard Position Effects, Spanwise,  $C_T = 0.9$ ,  $\alpha = 12$  deg

SYM	TEST	RUN	ALPHA	CT	ITEF	OTEF	CAN	SWB	CAN
⊕	537	32	16.8	0.92	30	30	0	OFF	FOR
⊞	543	6	16.9	0.92	30	30	0	OFF	AFT

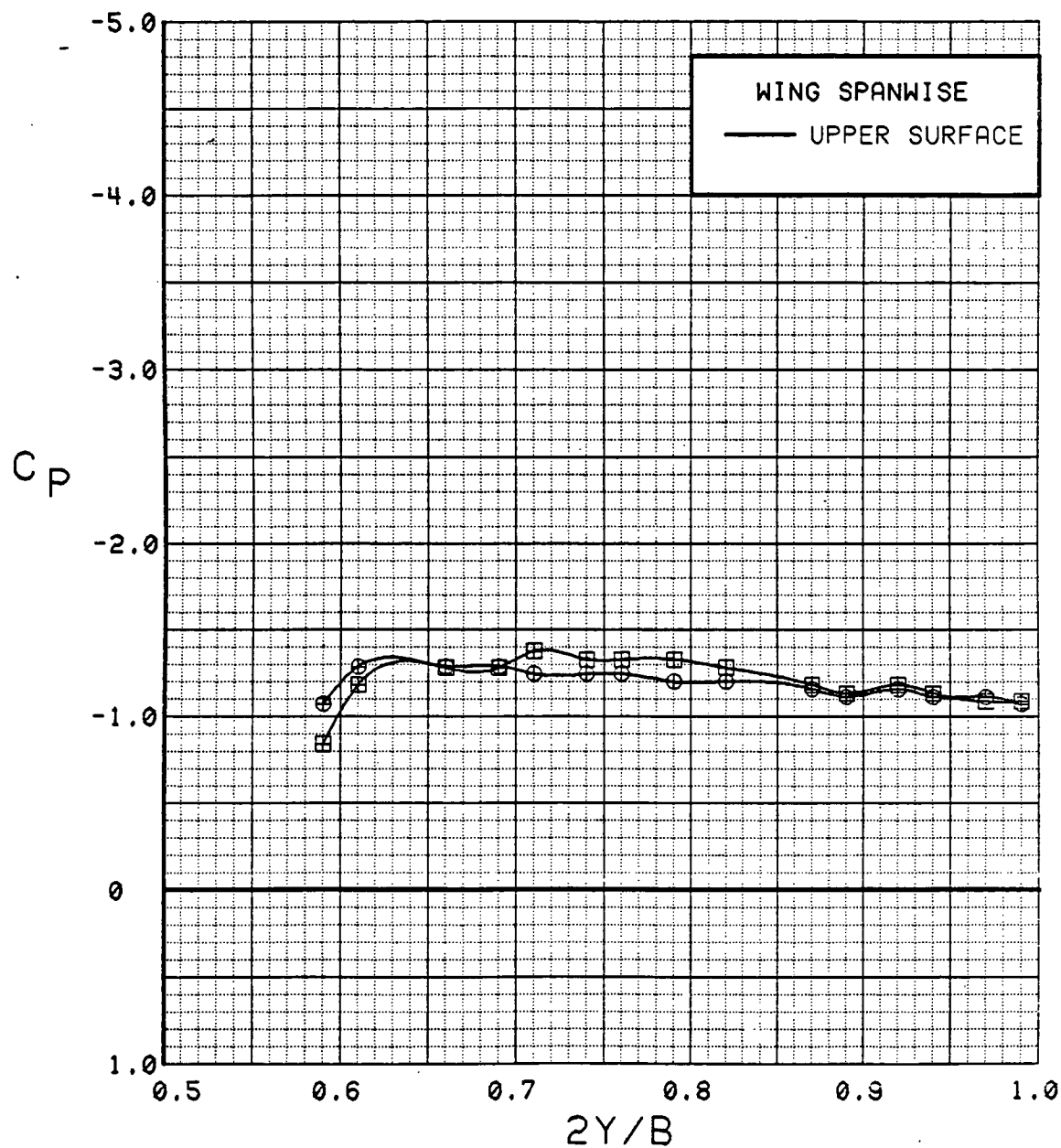


Figure 3.2.4-242 Canard Position Effects, Spanwise,  $C_T = 0.9$ ,  $\alpha = 16^\circ$

SYM	TEST	RUN	ALPHA	CT	ITEF	OTEF	CAN	SWB	CAN
⊙	537	32	20.9	0.90	30	30	0	OFF	FOR
⊠	543	6	21.0	0.93	30	30	0	OFF	AFT

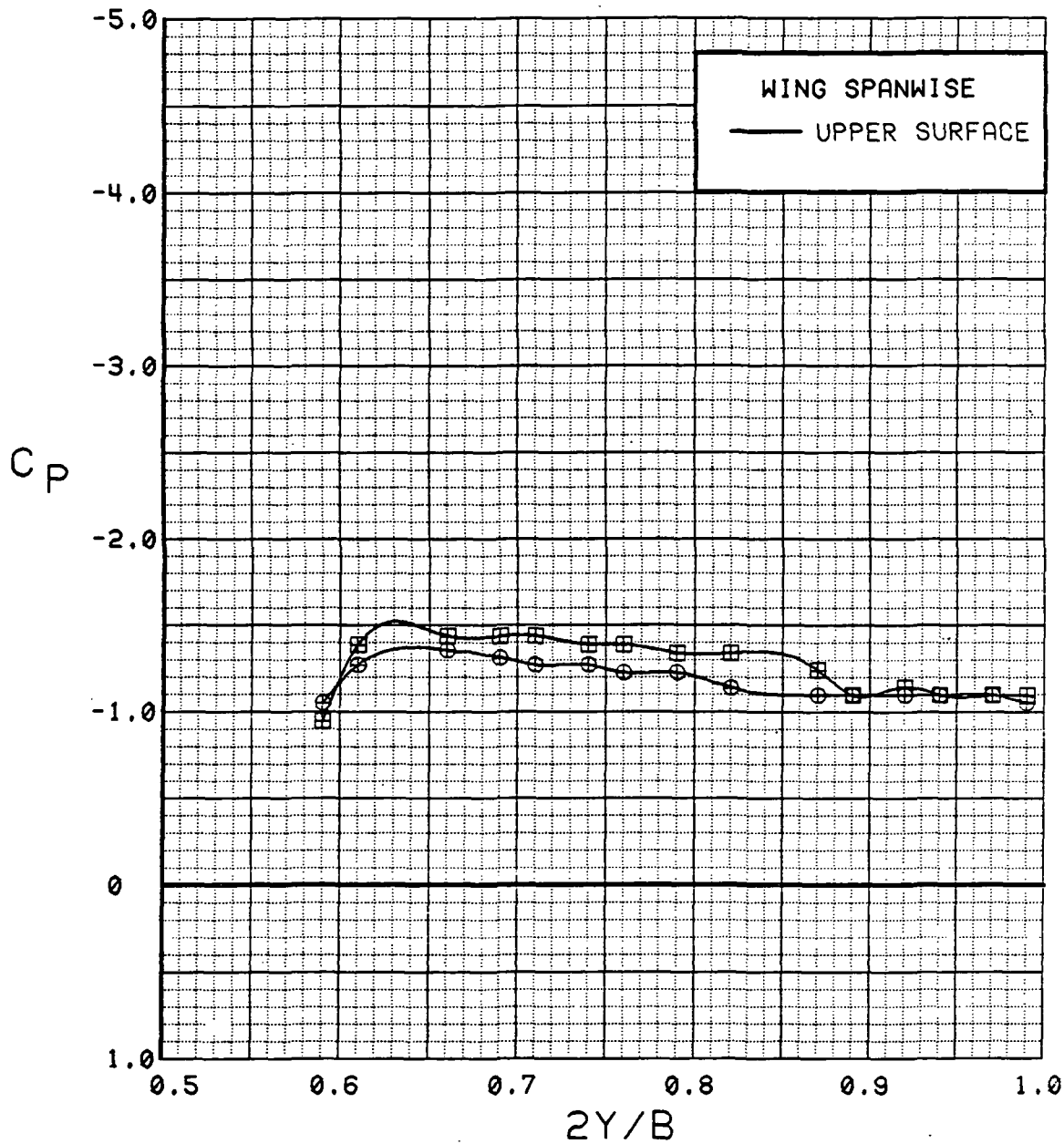


Figure 3.2.4-243 Canard Position Effects, Spanwise,  $C_T = 0.9$ ,  $\alpha = 20$  deg

ORIGINAL PAGE IS  
OF POOR QUALITY



SYM	TEST	RUN	ALPHA	CT	ITEF	OTEF	CAN	SWB
⊕	543	88	4.1	0.00	-20	-20	0	OFF
⊞	543	76	4.2	0.00	-10	0	0	OFF
△	543	63	4.2	0.00	0	0	0	OFF
◆	543	83	4.3	0.00	10	10	0	OFF
*	543	69	4.3	0.00	20	20	0	OFF
+	543	11	4.4	0.00	30	30	0	OFF

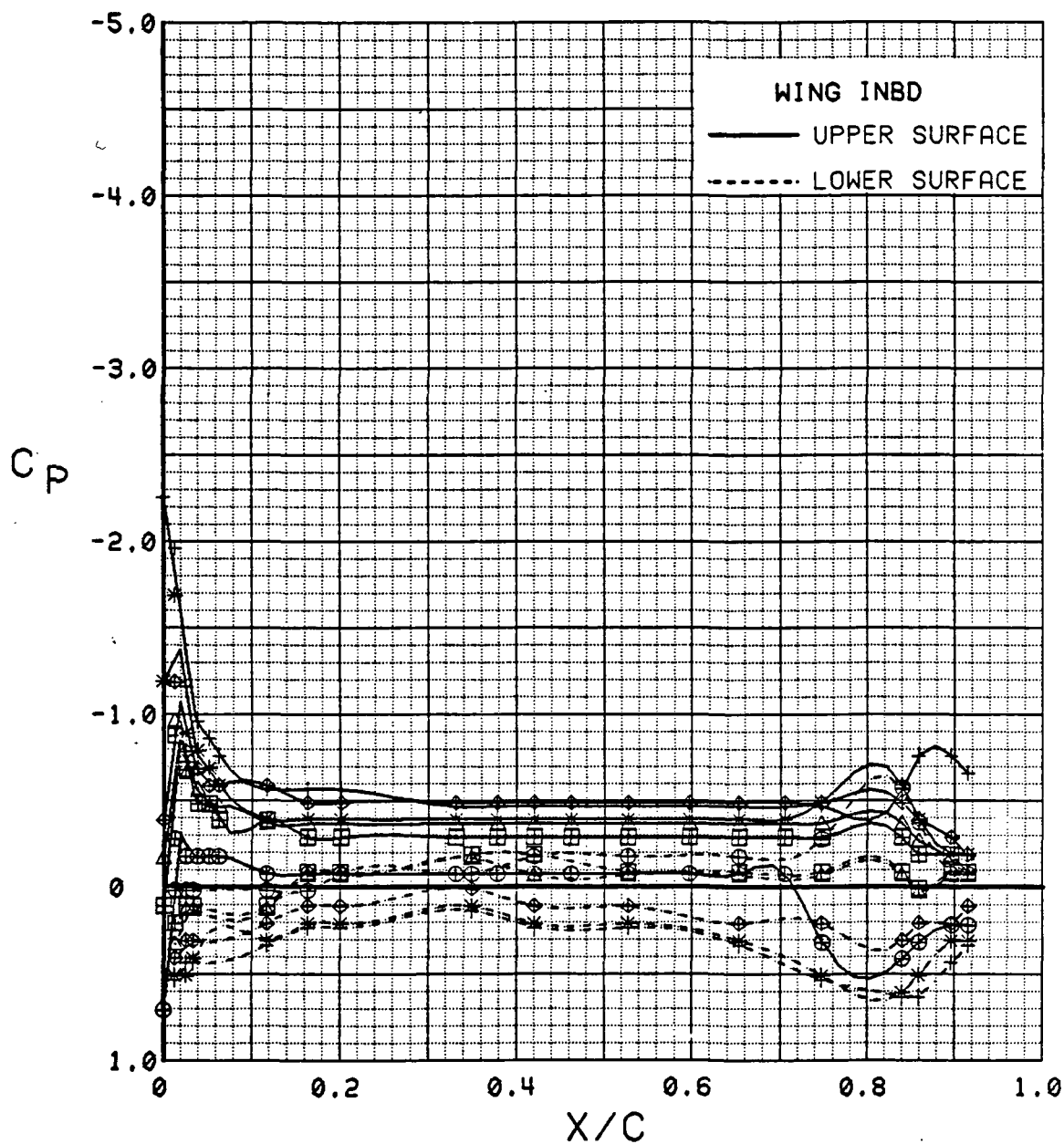


Figure 3.2.4-244 Wing Flap Effects, Inboard, Power Off, Alpha = 4 deg

SYM	TEST	RUN	ALPHA	CT	ITEF	OTEF	CAN	SWB
⊕	543	88	8.2	0.00	-20	-20	0	OFF
⊞	543	76	8.3	0.00	-10	0	0	OFF
△	543	63	8.3	0.00	0	0	0	OFF
⬠	543	83	8.4	0.00	10	10	0	OFF
*	543	69	8.5	0.00	20	20	0	OFF
+	543	11	8.5	0.00	30	30	0	OFF

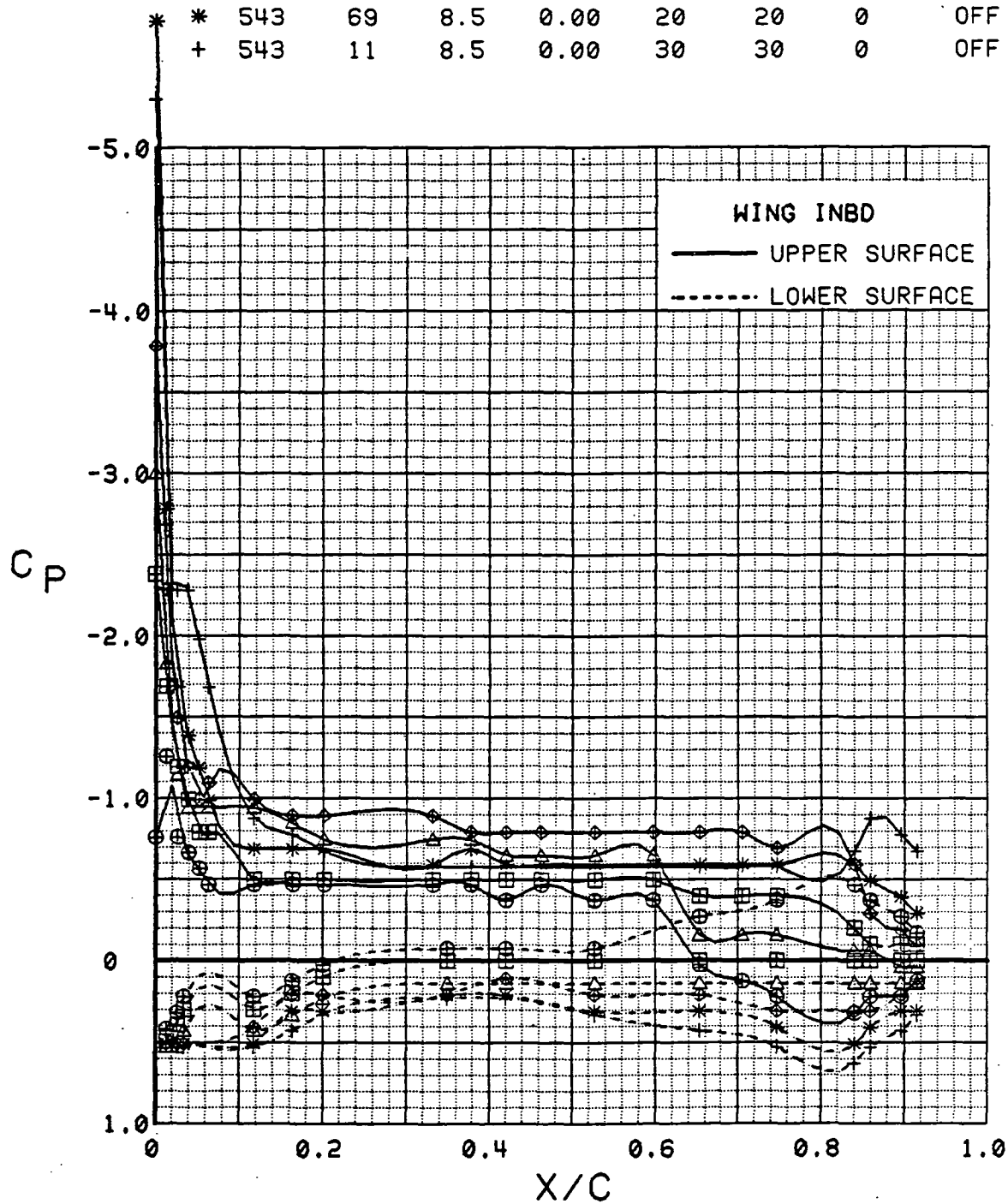


Figure 3.2.4-245 Wing Flap Effects, Inboard, Power Off, Alpha = 8 deg

SYM	TEST	RUN	ALPHA	CT	ITEF	OTEF	CAN	SWB
⊕	543	88	12.3	0.00	-20	-20	0	OFF
⊞	543	76	12.4	0.00	-10	0	0	OFF
△	543	63	12.5	0.00	0	0	0	OFF
◆	543	69	12.6	0.00	20	20	0	OFF
*	543	11	12.7	0.00	30	30	0	OFF

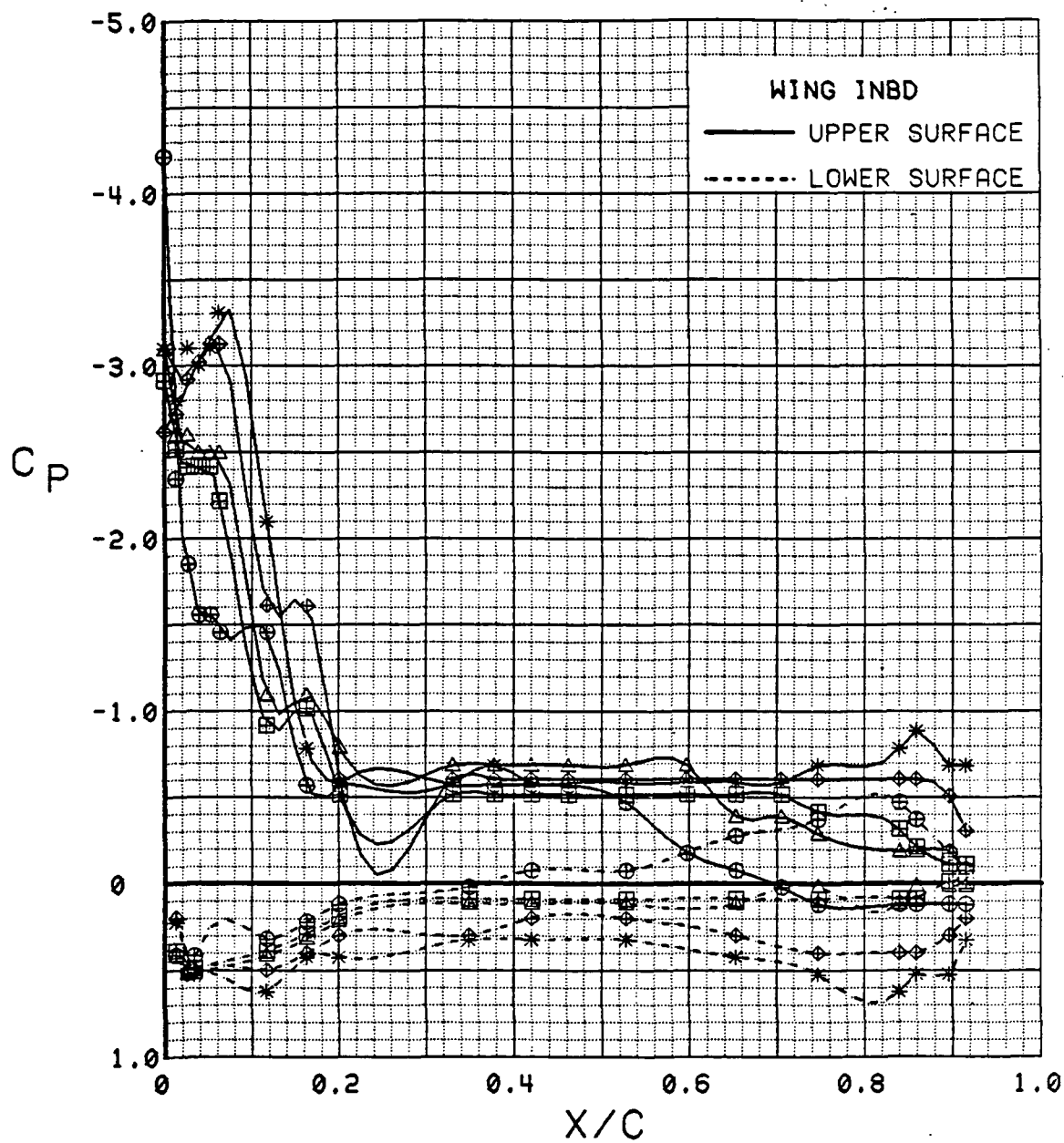


Figure 3.2.4-246 Wing Flap Effects, Inboard, Power Off, Alpha = 12 deg

SYM	TEST	RUN	ALPHA	CT	ITEF	OTEF	CAN	SWB
⊕	543	88	16.5	0.00	-20	-20	0	OFF
⊞	543	76	16.5	0.00	-10	0	0	OFF
△	543	63	16.6	0.00	0	0	0	OFF
⊕	543	83	16.7	0.00	10	10	0	OFF
*	543	69	16.7	0.00	20	20	0	OFF
+	543	11	16.8	0.00	30	30	0	OFF

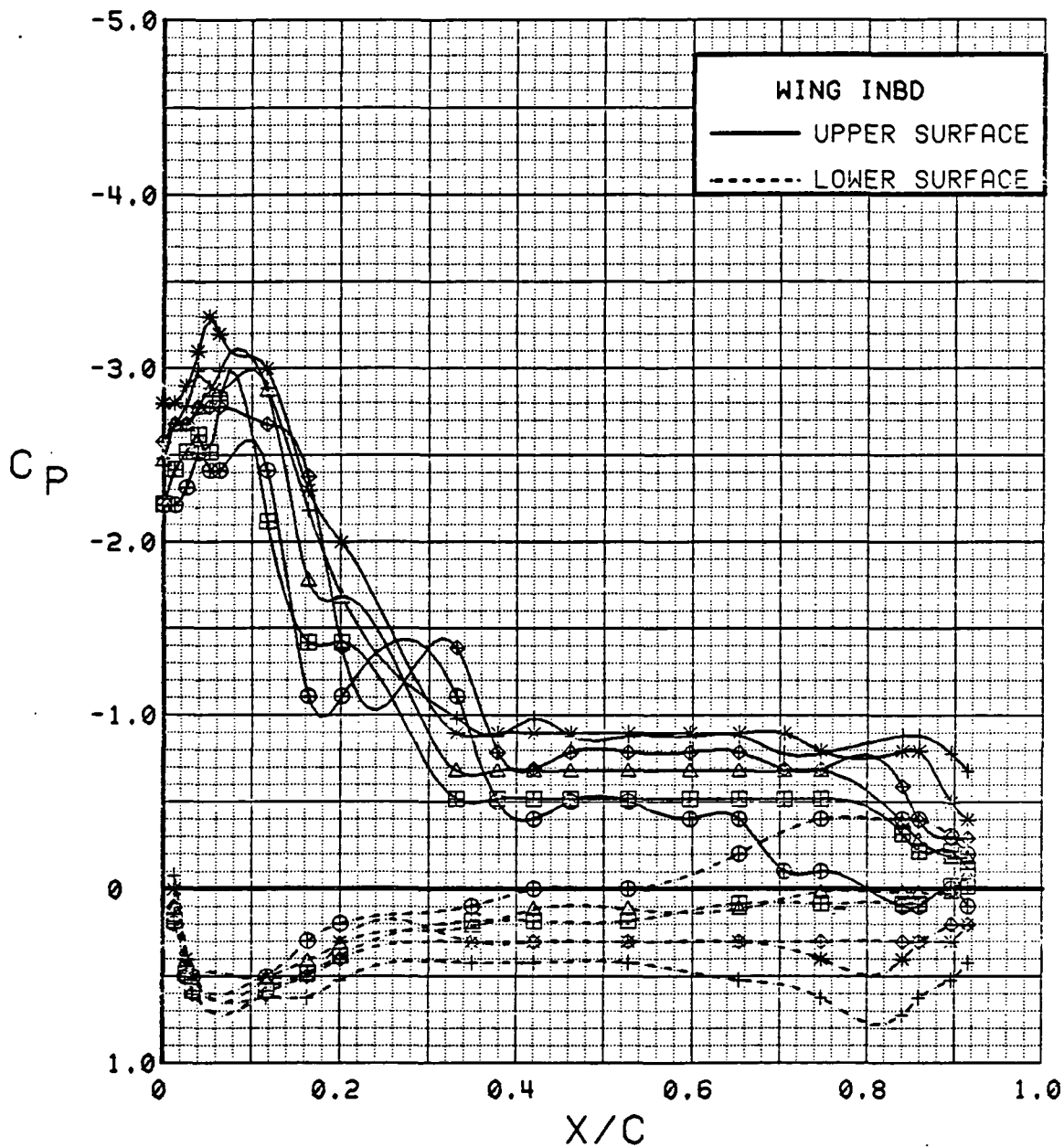


Figure 3.2.4-247 Wing Flap Effects, Inboard, Power Off, Alpha = 16 deg

SYM	TEST	RUN	ALPHA	CT	ITEF	OTEF	CAN	SWB
⊕	543	88	20.6	0.00	-20	-20	0	OFF
⊞	543	76	20.6	0.00	-10	0	0	OFF
△	543	63	20.7	0.00	0	0	0	OFF
⊕	543	69	20.8	0.00	20	20	0	OFF
*	543	11	20.8	0.00	30	30	0	OFF

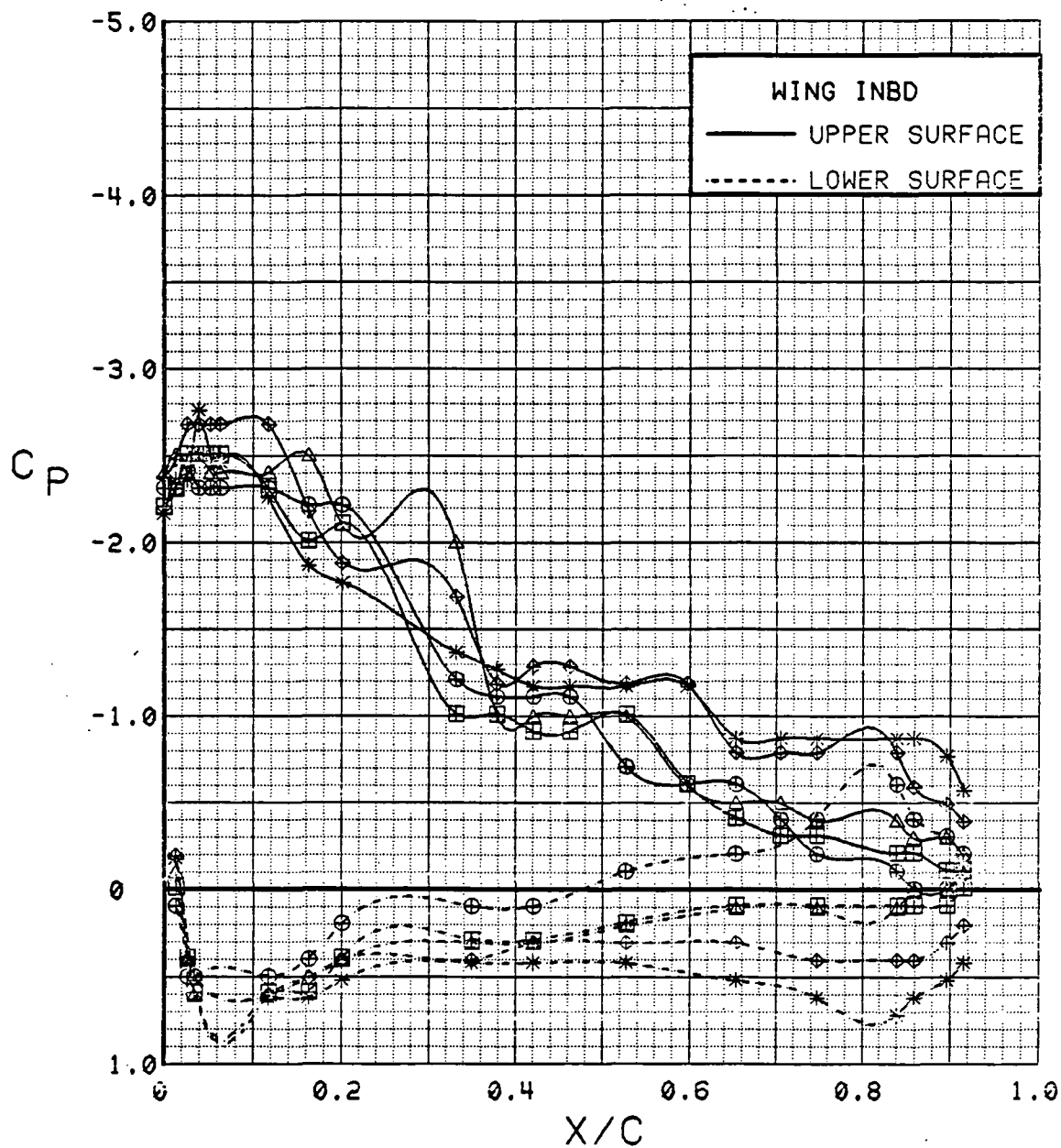


Figure 3.2.4-248 Wing Flap Effects, Inboard, Power Off, Alpha = 20 deg

SYM	TEST	RUN	ALPHA	CT	ITEF	OTEF	CAN	SWB
⊕	543	88	4.1	0.00	-20	-20	0	OFF
⊞	543	76	4.2	0.00	-10	0	0	OFF
△	543	63	4.2	0.00	0	0	0	OFF
⬠	543	83	4.3	0.00	10	10	0	OFF
*	543	69	4.3	0.00	20	20	0	OFF
+	543	11	4.4	0.00	30	30	0	OFF

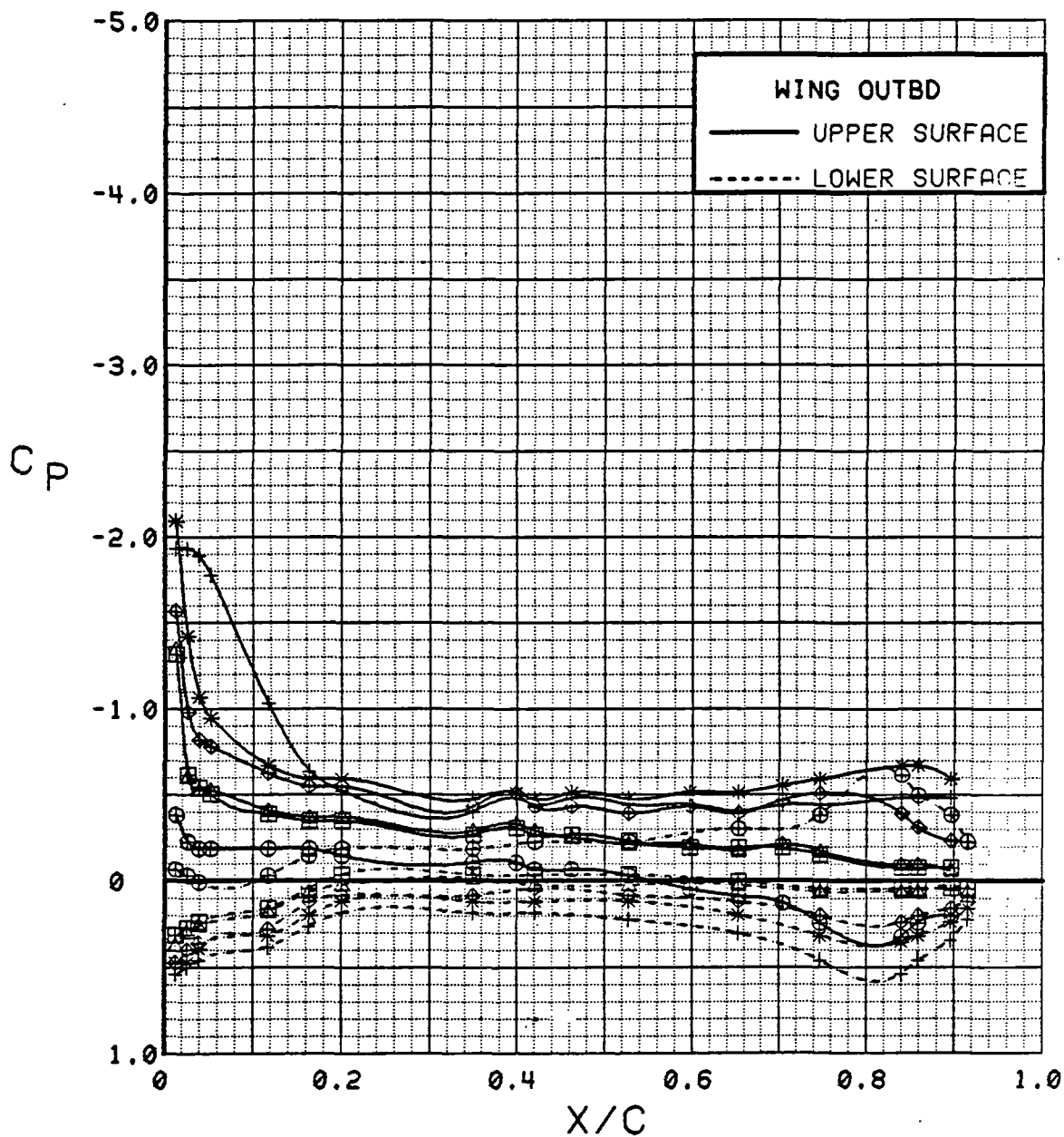


Figure 3.2.4-249 Wing Flap Effects, Outboard, Power Off, Alpha = 4 deg

SYM	TEST	RUN	ALPHA	CT	ITEF	OTEF	CAN	SWB
⊕	543	88	8.2	0.00	-20	-20	0	OFF
⊞	543	76	8.3	0.00	-10	0	0	OFF
△	543	63	8.3	0.00	0	0	0	OFF
⬢	543	83	8.4	0.00	10	10	0	OFF
*	543	69	8.5	0.00	20	20	0	OFF
+	543	11	8.5	0.00	30	30	0	OFF

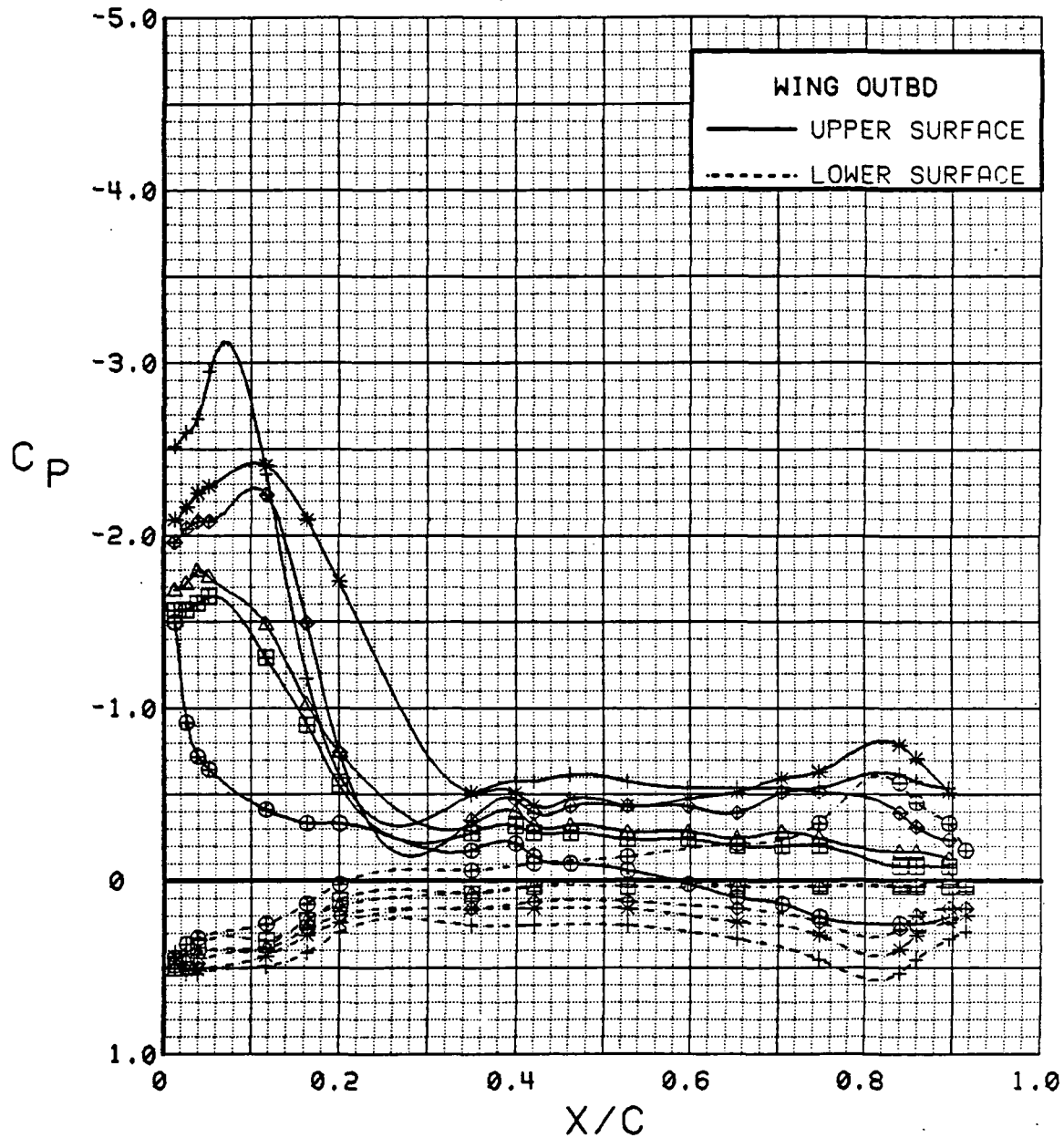


Figure 3.2.4-250 Wing Flap Effects, Outboard, Power Off, Alpha = 8 deg

SYM	TEST	RUN	ALPHA	CT	ITEF	OTEF	CAN	SWB
⊕	543	88	12.3	0.00	-20	-20	0	OFF
⊞	543	76	12.4	0.00	-10	0	0	OFF
△	543	63	12.5	0.00	0	0	0	OFF
⊕	543	69	12.6	0.00	20	20	0	OFF
*	543	11	12.7	0.00	30	30	0	OFF

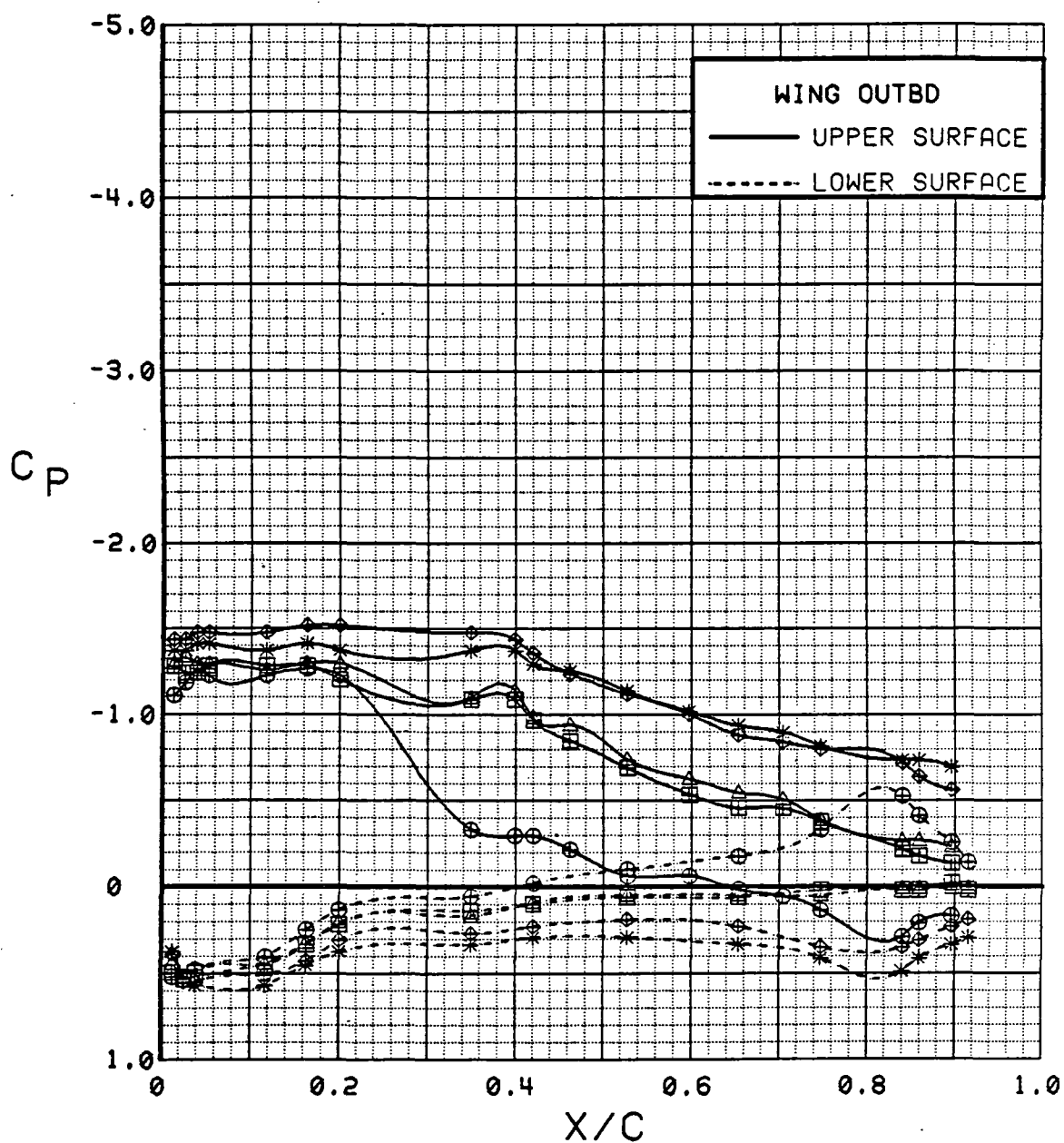


Figure 3.2.4-251 Wing Flap Effects, Outboard, Power Off, Alpha = 12 deg



SYM	TEST	RUN	ALPHA	CT	ITEF	OTEF	CAN	SWB
⊕	543	88	16.5	0.00	-20	-20	0	OFF
⊞	543	76	16.5	0.00	-10	0	0	OFF
△	543	63	16.6	0.00	0	0	0	OFF
⊕	543	83	16.7	0.00	10	10	0	OFF
*	543	69	16.7	0.00	20	20	0	OFF
+	543	11	16.8	0.00	30	30	0	OFF

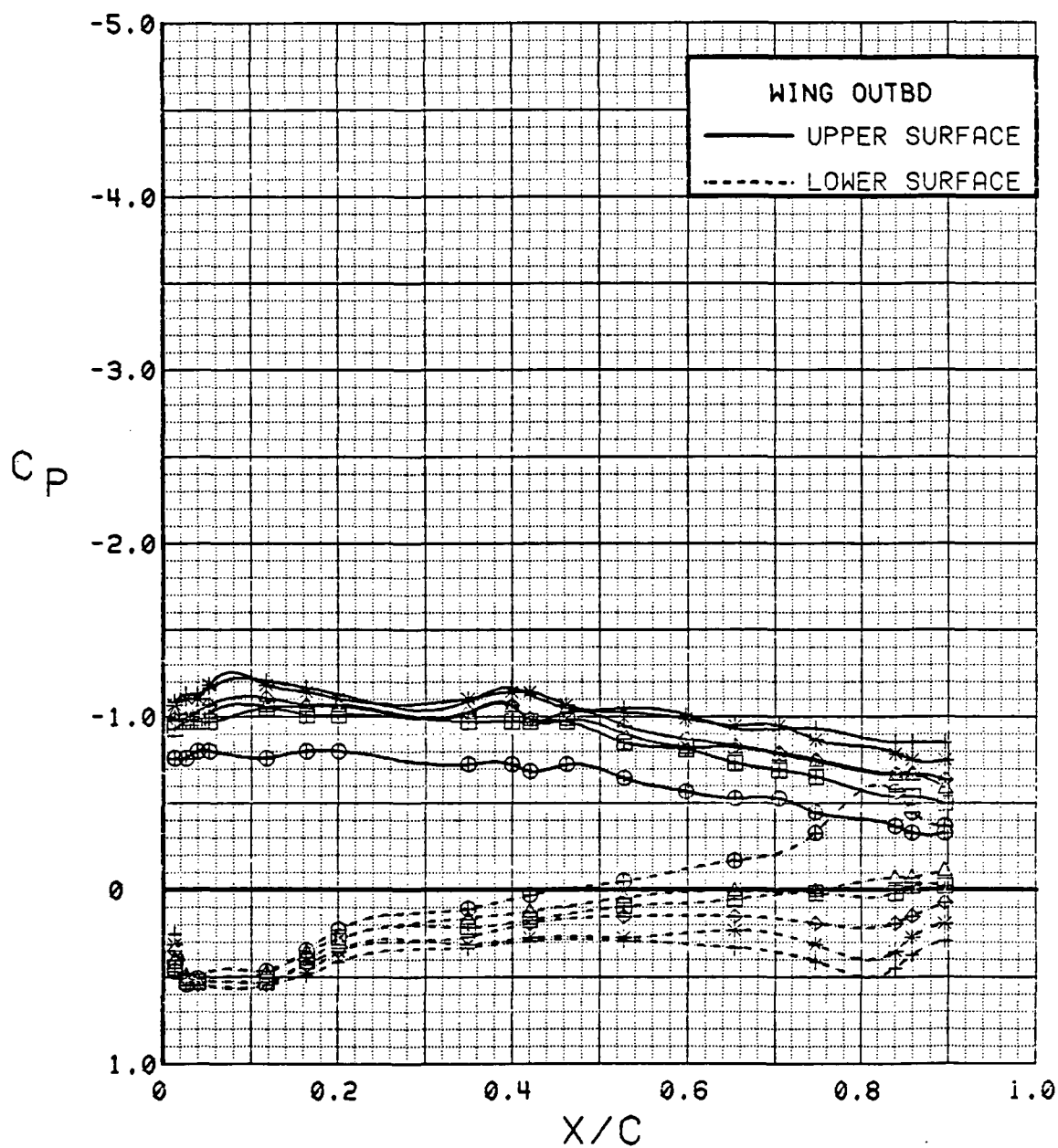


Figure 3.2.4-252 Wing Flap Effects, Outboard, Power Off, Alpha = 16 deg

SYM	TEST	RUN	ALPHA	CT	ITEF	OTEF	CAN	SWB
⊕	543	88	20.6	0.00	-20	-20	0	OFF
⊞	543	76	20.6	0.00	-10	0	0	OFF
△	543	63	20.7	0.00	0	0	0	OFF
⊕	543	69	20.8	0.00	20	20	0	OFF
*	543	11	20.8	0.00	30	30	0	OFF

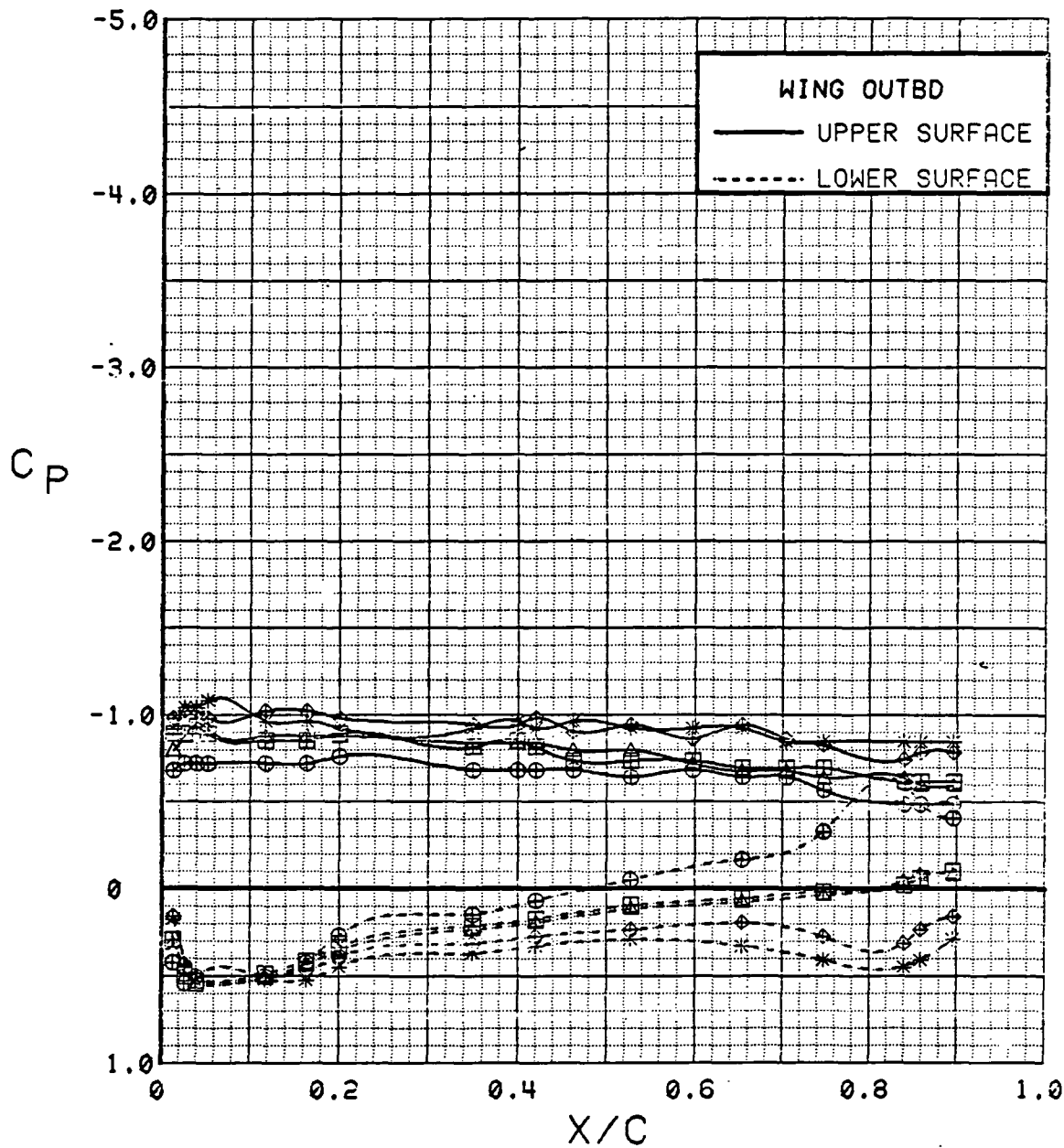


Figure 3.2.4-253 Wing Flap Effects, Outboard, Power Off, Alpha = 20 deg

SYM	TEST	RUN	ALPHA	CT	ITEF	OTEF	CAN	SWB
⊕	543	88	4.1	0.00	-20	-20	0	OFF
⊞	543	76	4.2	0.00	-10	0	0	OFF
△	543	63	4.2	0.00	0	0	0	OFF
◆	543	83	4.3	0.00	10	10	0	OFF
*	543	69	4.3	0.00	20	20	0	OFF
+	543	11	4.4	0.00	30	30	0	OFF

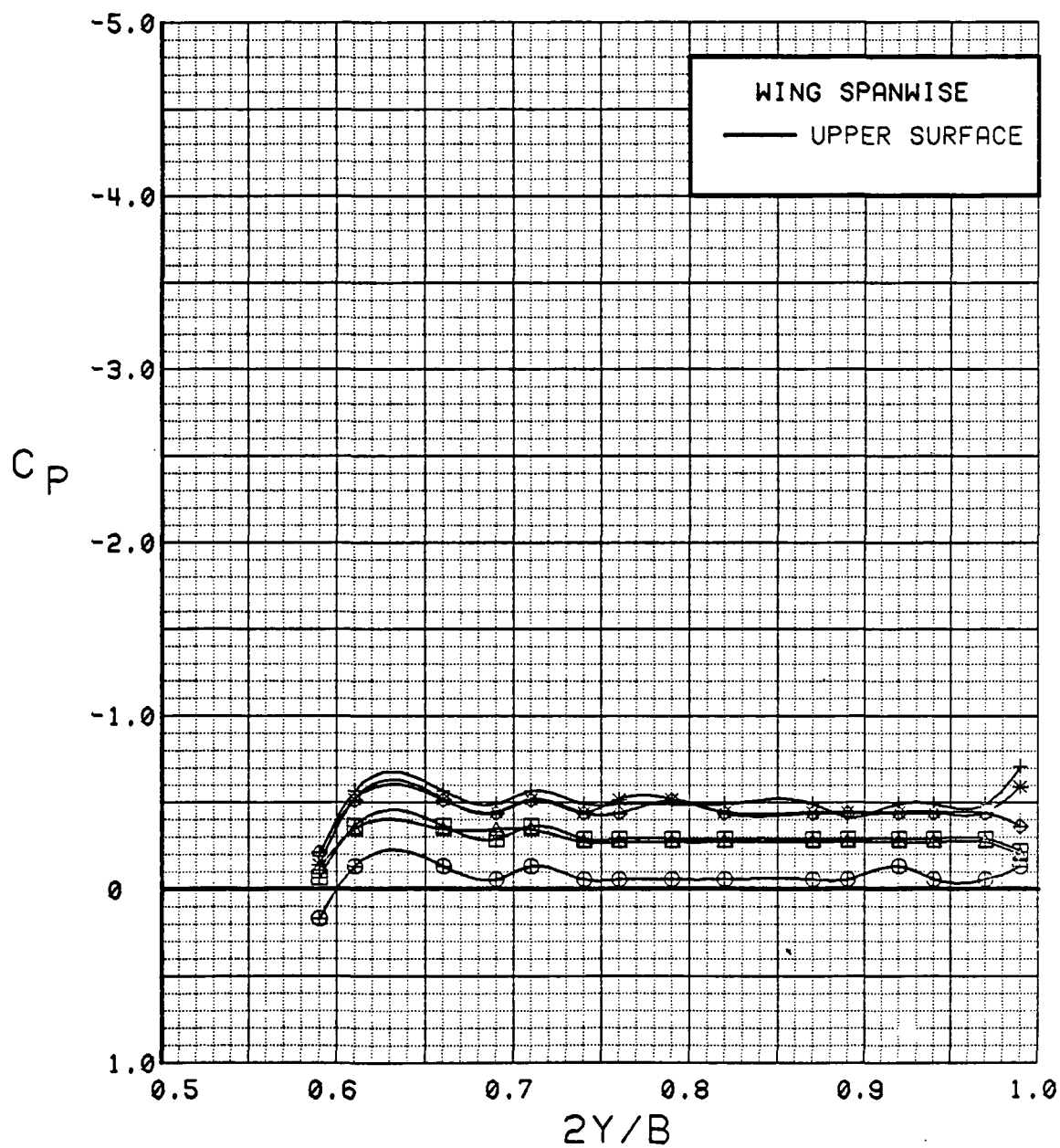


Figure 3.2.4-254 Wing Flap Effects, Spanwise, Power Off, Alpha = 4 deg

SYM	TEST	RUN	ALPHA	CT	ITEF	OTEF	CAN	SWB
⊕	543	88	8.2	0.00	-20	-20	0	OFF
⊞	543	76	8.3	0.00	-10	0	0	OFF
△	543	63	8.3	0.00	0	0	0	OFF
◆	543	83	8.4	0.00	10	10	0	OFF
*	543	69	8.5	0.00	20	20	0	OFF
+	543	11	8.5	0.00	30	30	0	OFF

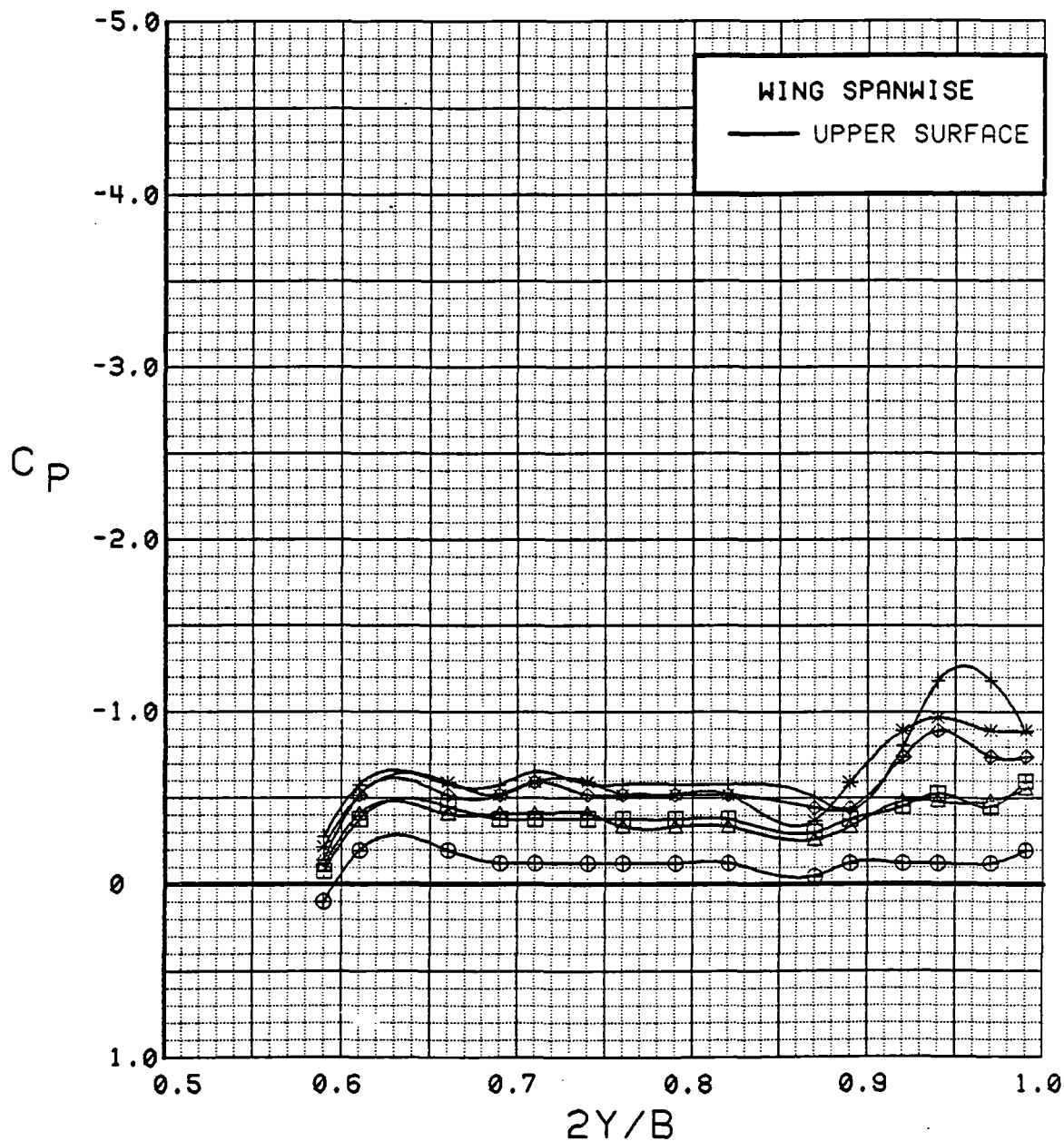


Figure 3.2.4-255 Wing Flap Effects, Spanwise, Power Off, Alpha = 8 deg

SYM	TEST	RUN	ALPHA	CT	ITEF	OTEF	CAN	SWB
⊕	543	88	12.3	0.00	-20	-20	0	OFF
⊞	543	76	12.4	0.00	-10	0	0	OFF
△	543	63	12.5	0.00	0	0	0	OFF
◆	543	69	12.6	0.00	20	20	0	OFF
*	543	11	12.7	0.00	30	30	0	OFF

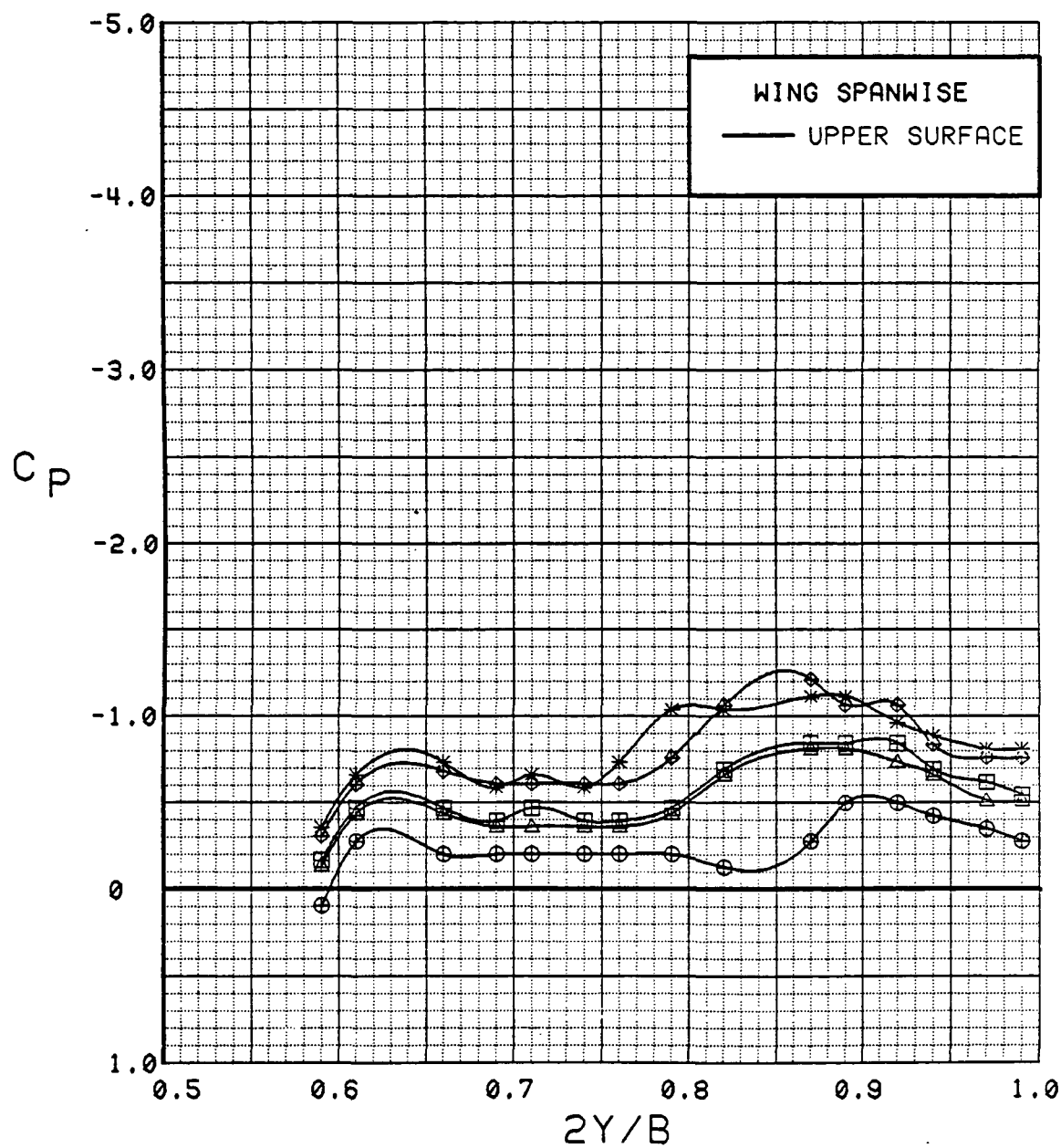


Figure 3.2.4-256 Wing Flap Effects, Spanwise, Power Off, Alpha = 12 deg

SYM	TEST	RUN	ALPHA	CT	ITEF	OTEF	CAN	SWB
⊗	543	88	16.5	0.00	-20	-20	0	OFF
⊠	543	76	16.5	0.00	-10	0	0	OFF
△	543	63	16.6	0.00	0	0	0	OFF
◆	543	83	16.7	0.00	10	10	0	OFF
*	543	69	16.7	0.00	20	20	0	OFF
+	543	11	16.8	0.00	30	30	0	OFF

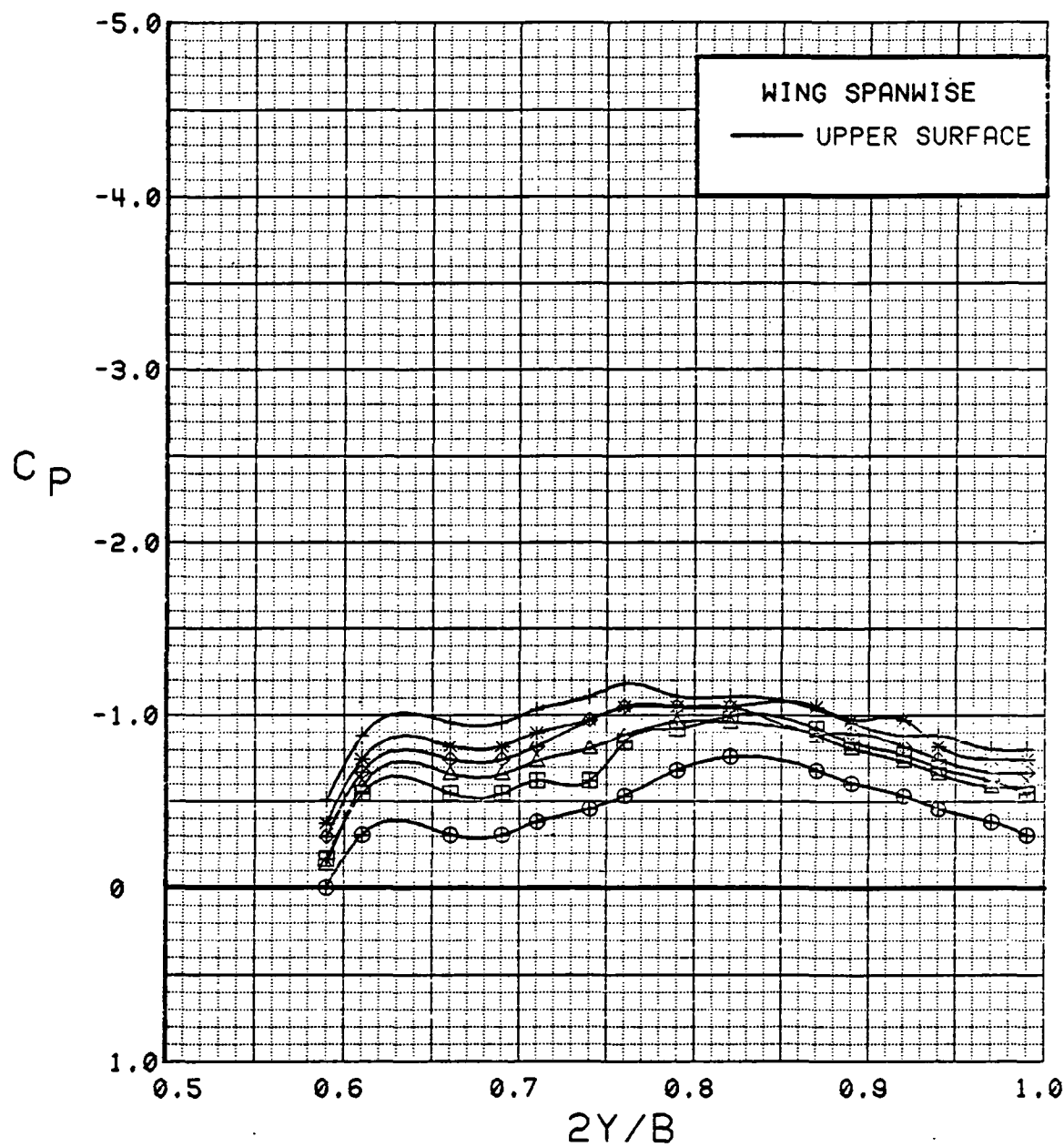


Figure 3.2.4-257 Wing Flap Effects, Spanwise, Power Off, Alpha = 16 deg

SYM	TEST	RUN	ALPHA	CT	ITEF	OTEF	CAN	SWB
⊕	543	88	20.6	0.00	-20	-20	0	OFF
⊞	543	76	20.6	0.00	-10	0	0	OFF
△	543	63	20.7	0.00	0	0	0	OFF
◆	543	69	20.8	0.00	20	20	0	OFF
*	543	11	20.8	0.00	30	30	0	OFF

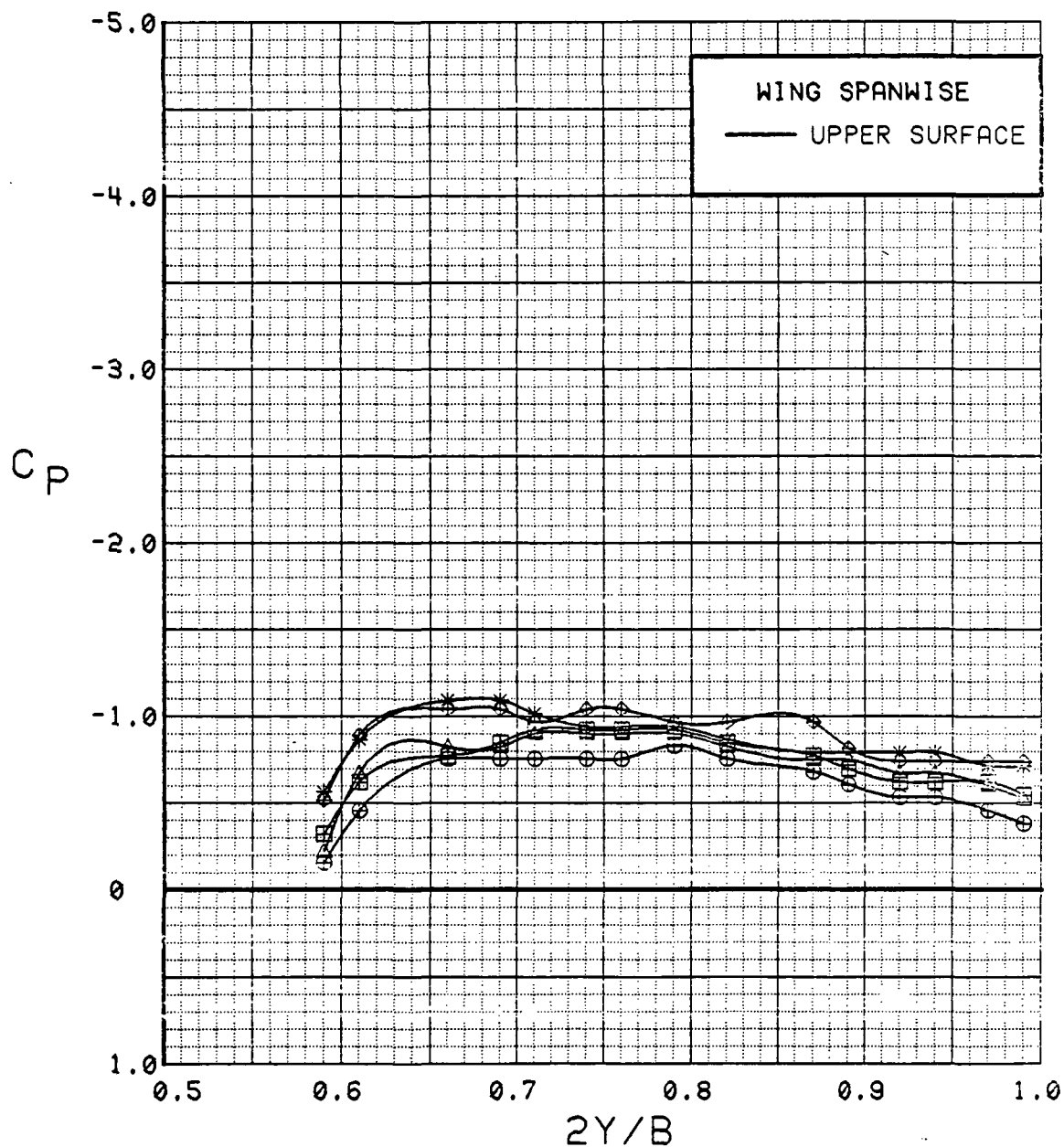


Figure 3.2.4-258 Wing Flap Effects, Spanwise, Power Off, Alpha = 20 deg

# WING INBOARD

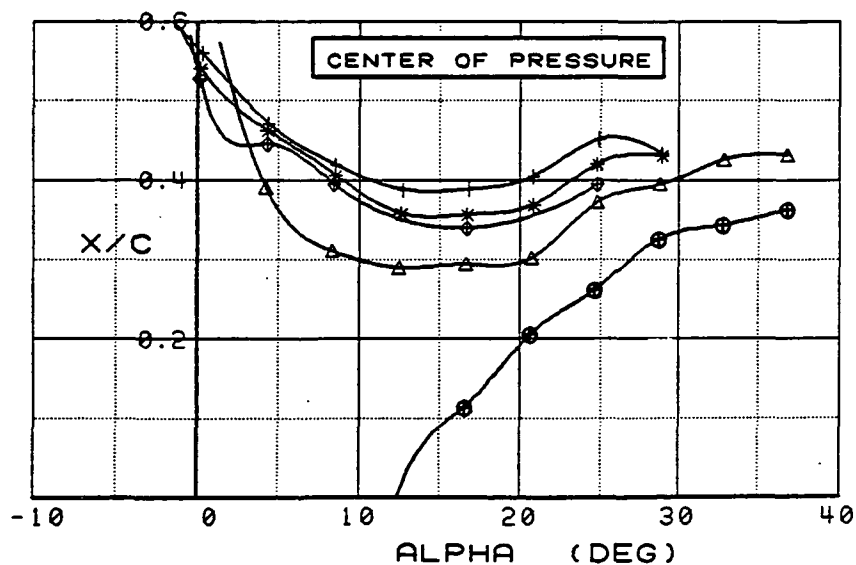
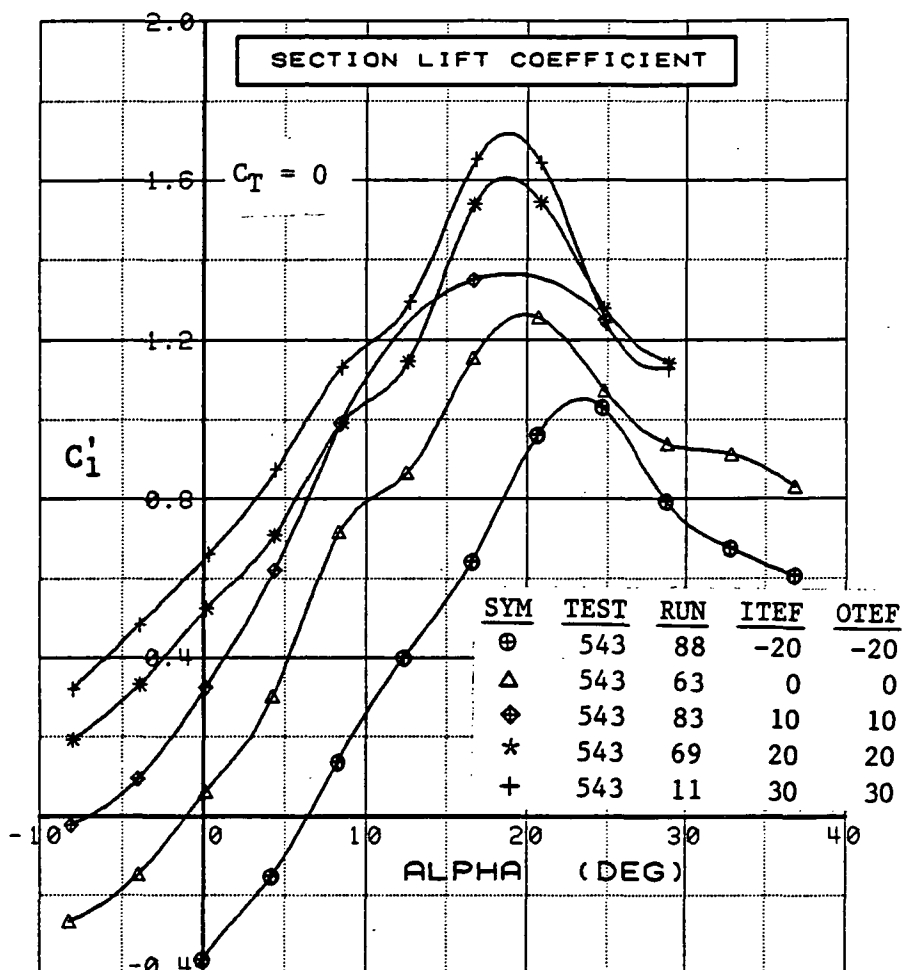


Figure 3.2.4-259 Wing Flap Effects, Inboard, Power Off,  
Integrated Section Properties



## WING OUTBOARD

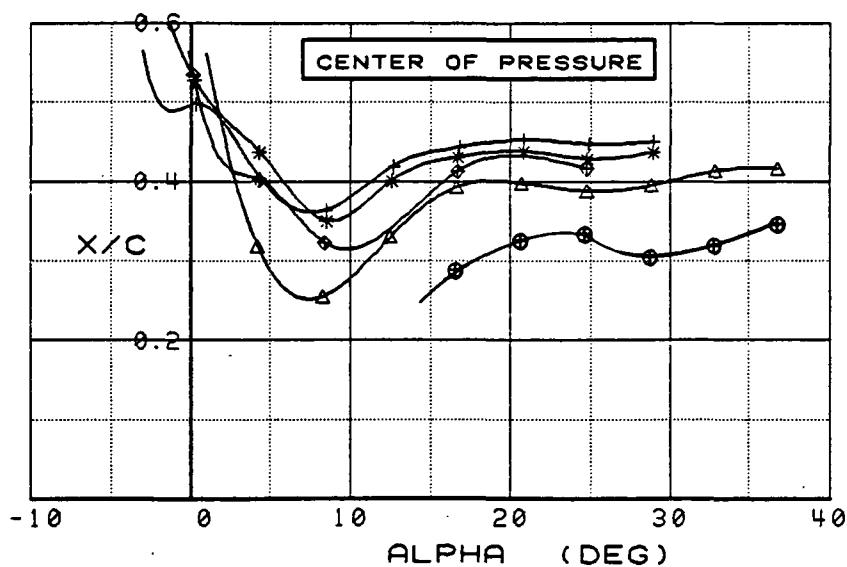
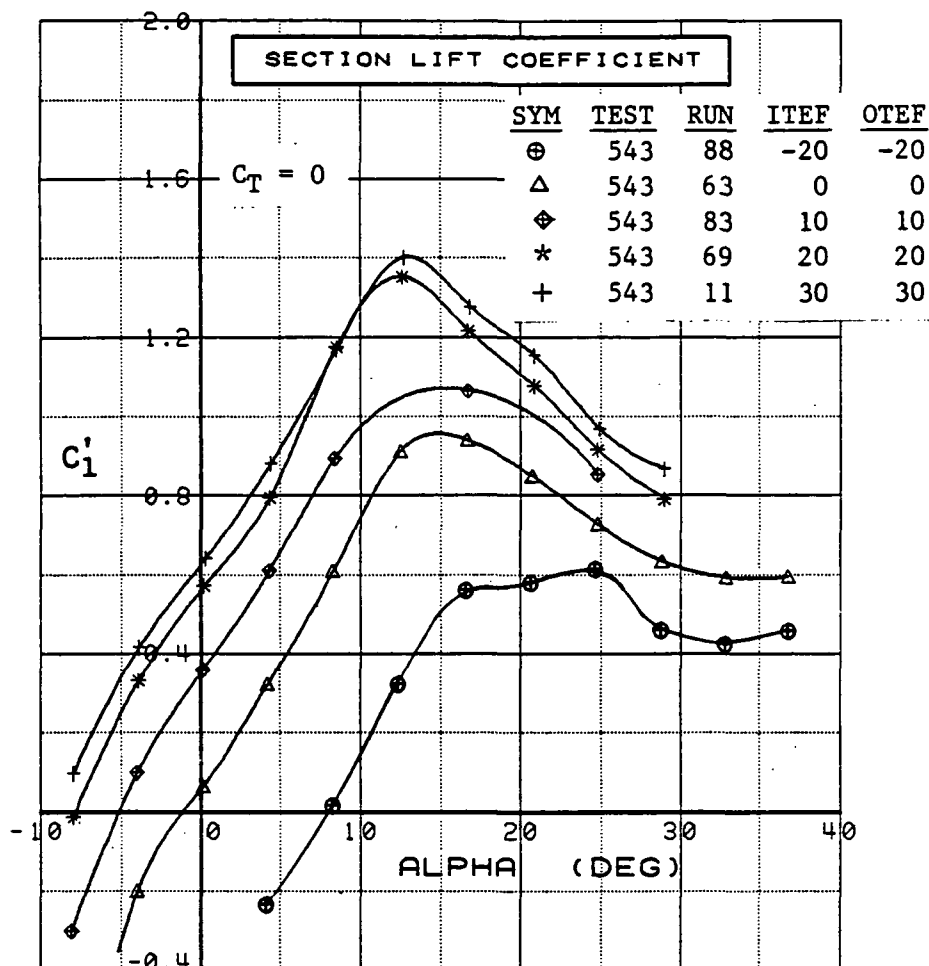


Figure 3.2.4-260 Wing Flap Effects, Outboard, Power Off,  
Integrated Section Properties

SYM	TEST	RUN	ALPHA	CT	ITEF	OTEF	CAN	SWB
⊕	543	86	4.0	0.92	-20	-20	0	OFF
⊞	543	74	4.2	0.93	-10	0	0	OFF
△	543	60	4.3	0.93	0	0	0	OFF
◆	543	68	4.4	0.94	20	20	0	OFF
*	543	6	4.5	0.94	30	30	0	OFF

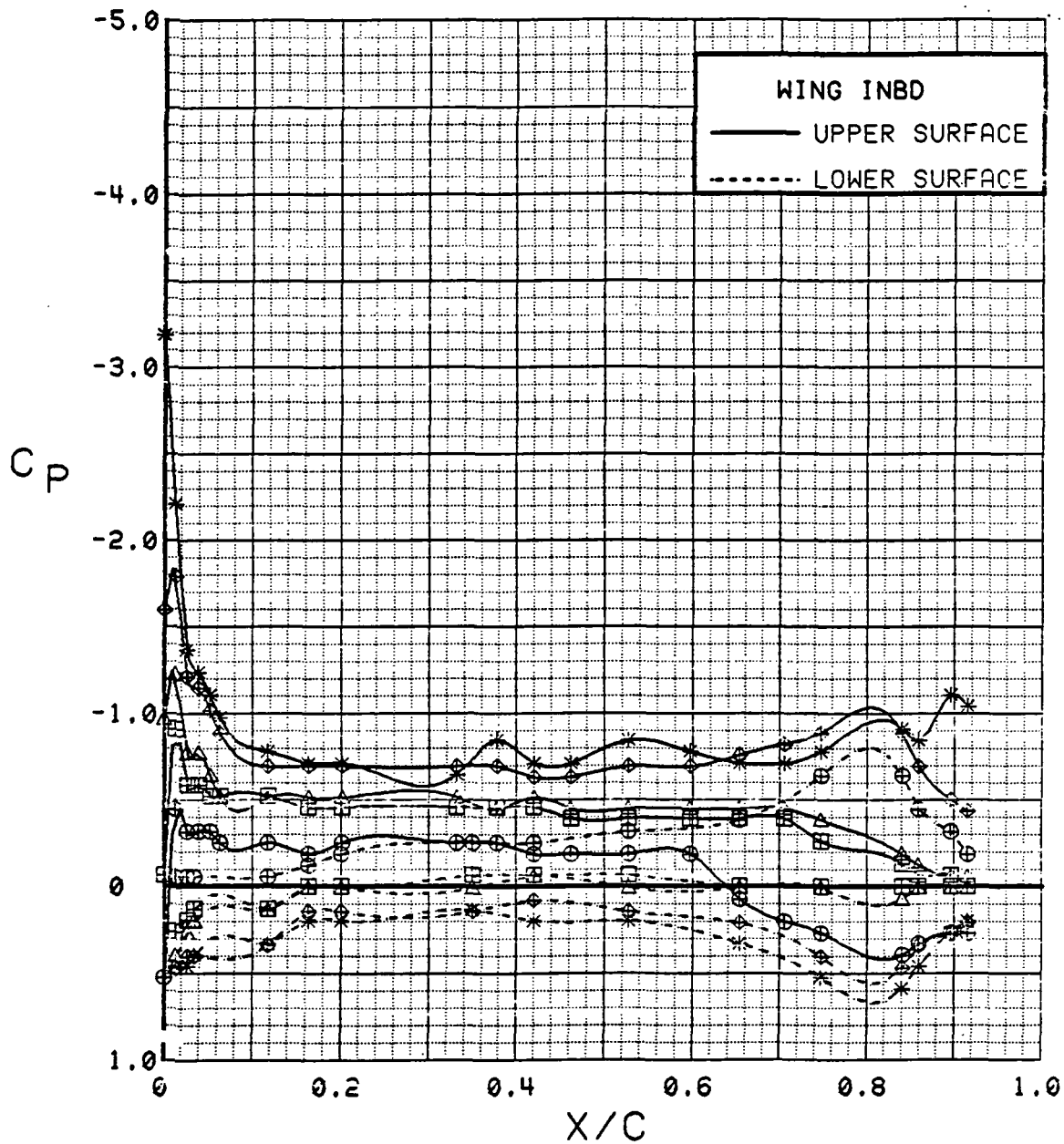


Figure 3.2.4-261 Wing Flap Effects, Inboard,  $C_T = 0.9$ ,  $\alpha = 4$  deg

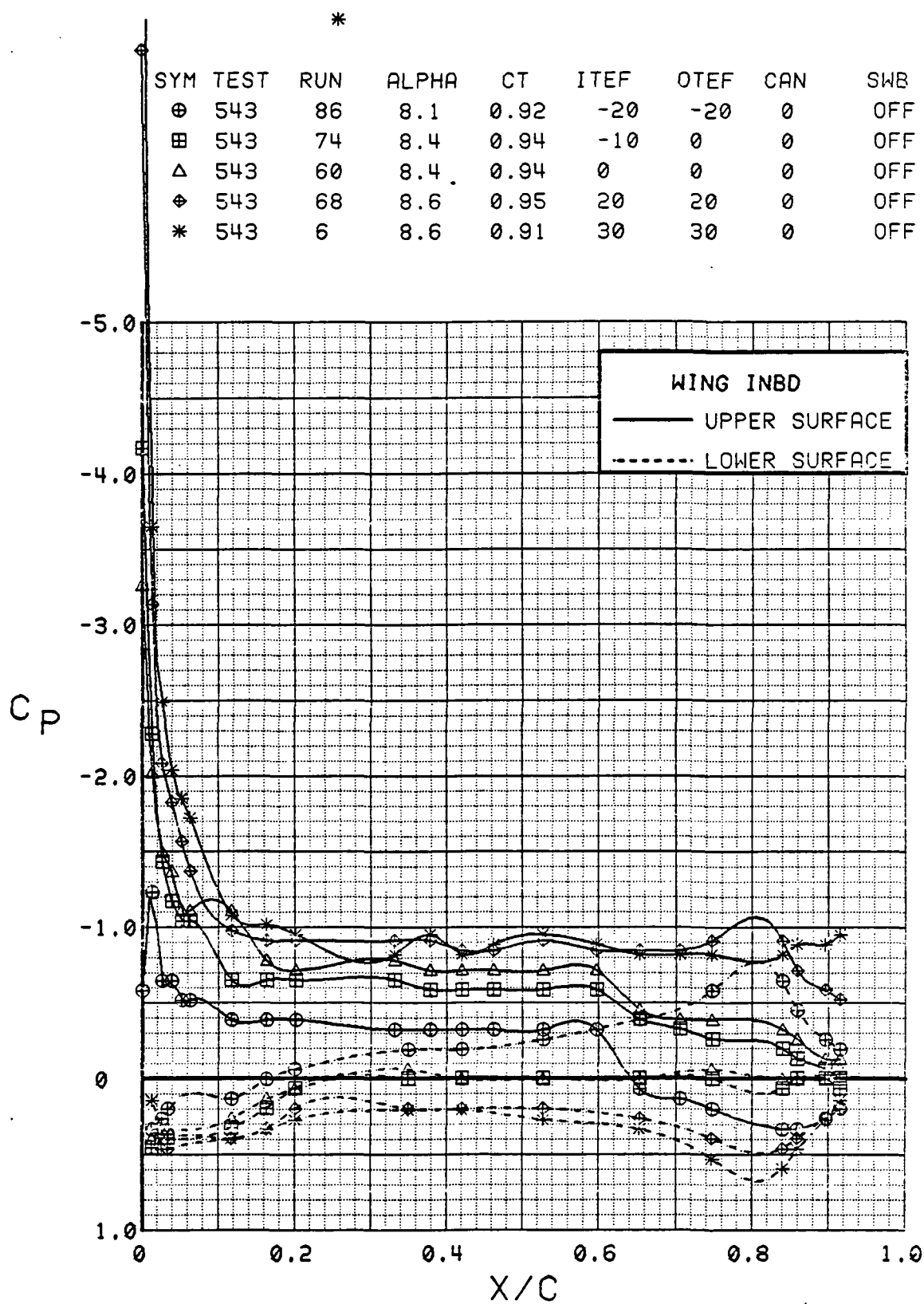


Figure 3.2.4-262 Wing Flap Effects, Inboard,  $C_T = 0.9$ ,  $\alpha = 8$  deg

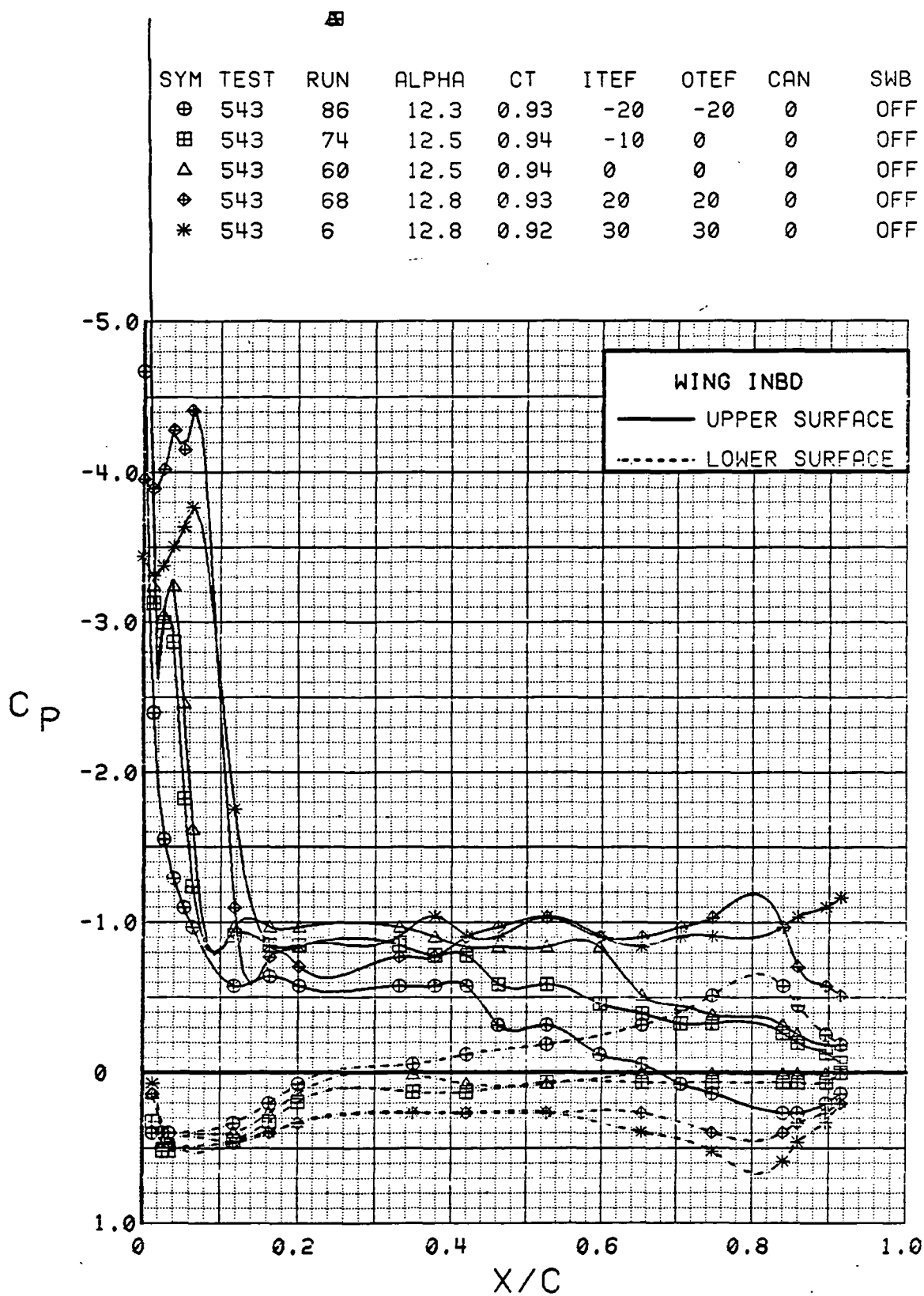


Figure 3.2.4-263 Wing Flap Effects, Inboard,  $C_T = 0.9$ ,  $\alpha = 12$  deg

SYM	TEST	RUN	ALPHA	CT	ITEF	OTEF	CAN	SWB
⊕	543	86	16.5	0.92	-20	-20	0	OFF
⊞	543	74	16.6	0.94	-10	0	0	OFF
△	543	60	16.7	0.93	0	0	0	OFF
⊕	543	68	16.9	0.94	20	20	0	OFF
*	543	6	16.9	0.92	30	30	0	OFF

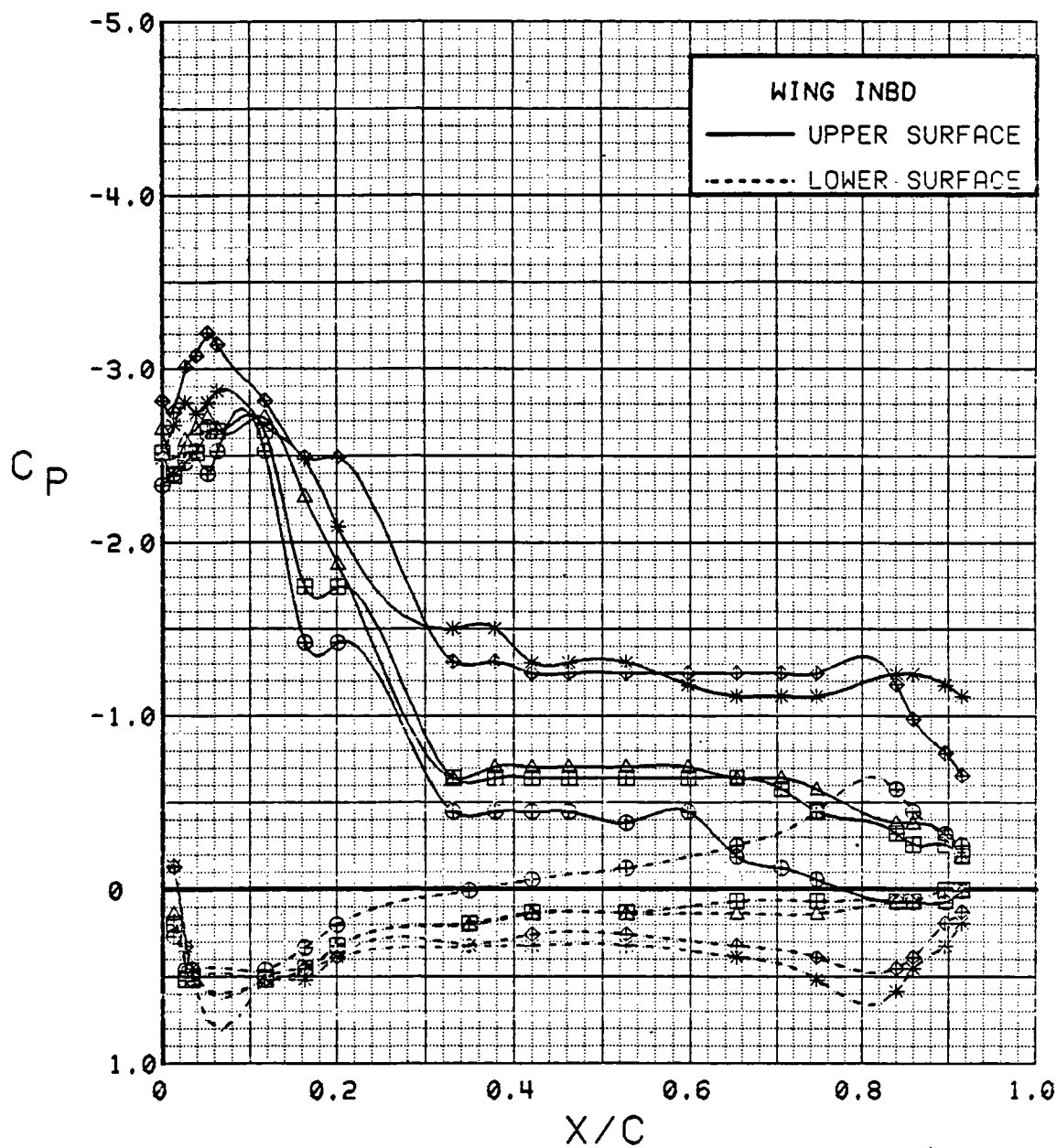


Figure 3.2.4-264 Wing Flap Effects, Inboard,  $C_T = 0.9$ ,  $\alpha = 16$  deg

SYM	TEST	RUN	ALPHA	CT	ITEF	OTEF	CAN	SWB
⊕	543	86	20.6	0.93	-20	-20	0	OFF
⊞	543	74	20.8	0.94	-10	0	0	OFF
△	543	60	20.8	0.93	0	0	0	OFF
⊕	543	68	21.0	0.92	20	20	0	OFF
*	543	6	21.0	0.93	30	30	0	OFF

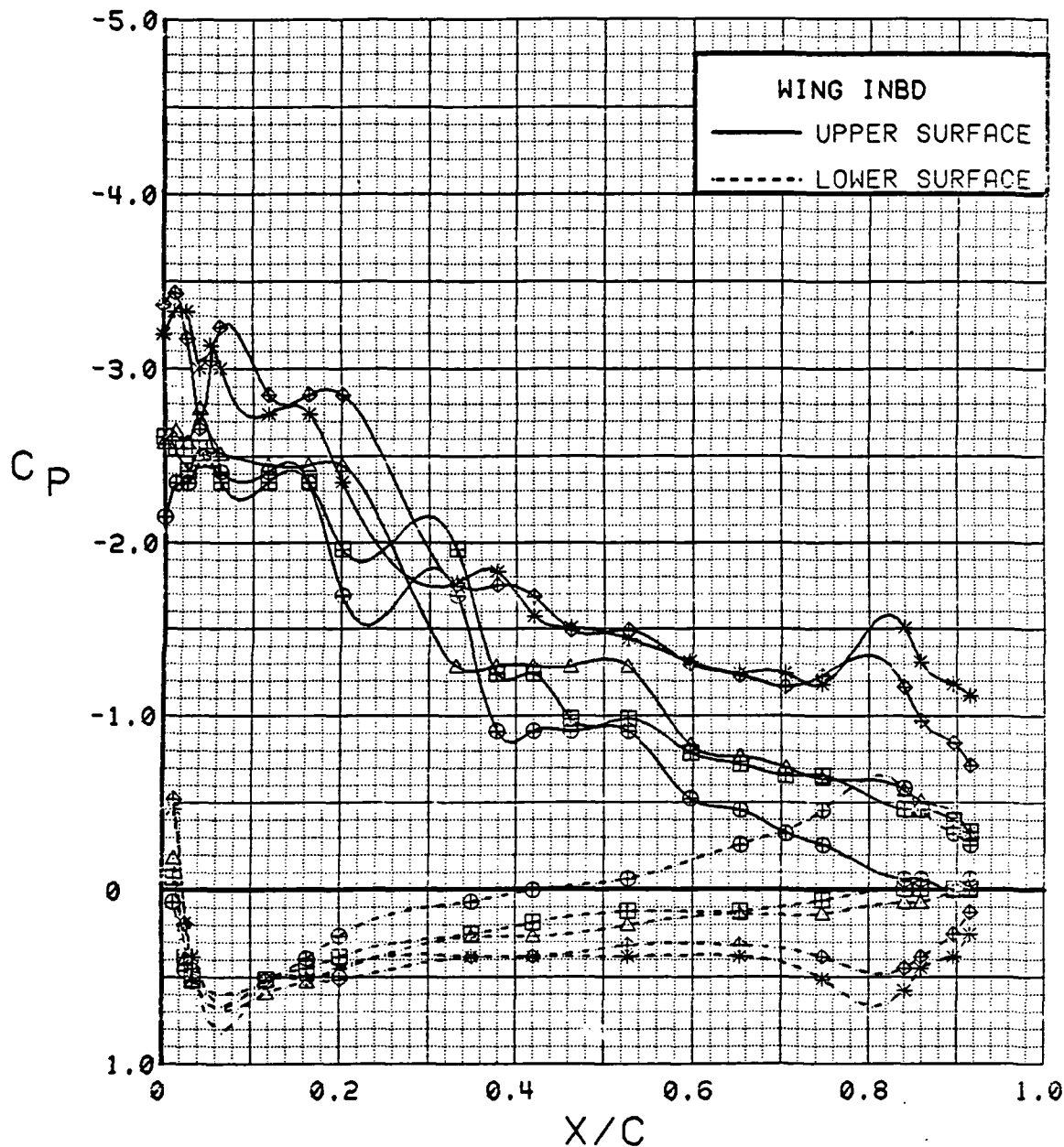


Figure 3.2.4-265 Wing Flap Effects, Inboard,  $C_T = 0.9$ ,  $\alpha = 20^\circ$

SYM	TEST	RUN	ALPHA	CT	ITEF	OTEF	CAN	SWB
⊕	543	86	4.0	0.92	-20	-20	0	OFF
⊞	543	74	4.2	0.93	-10	0	0	OFF
△	543	60	4.3	0.93	0	0	0	OFF
⊕	543	68	4.4	0.94	20	20	0	OFF
*	543	6	4.5	0.94	30	30	0	OFF

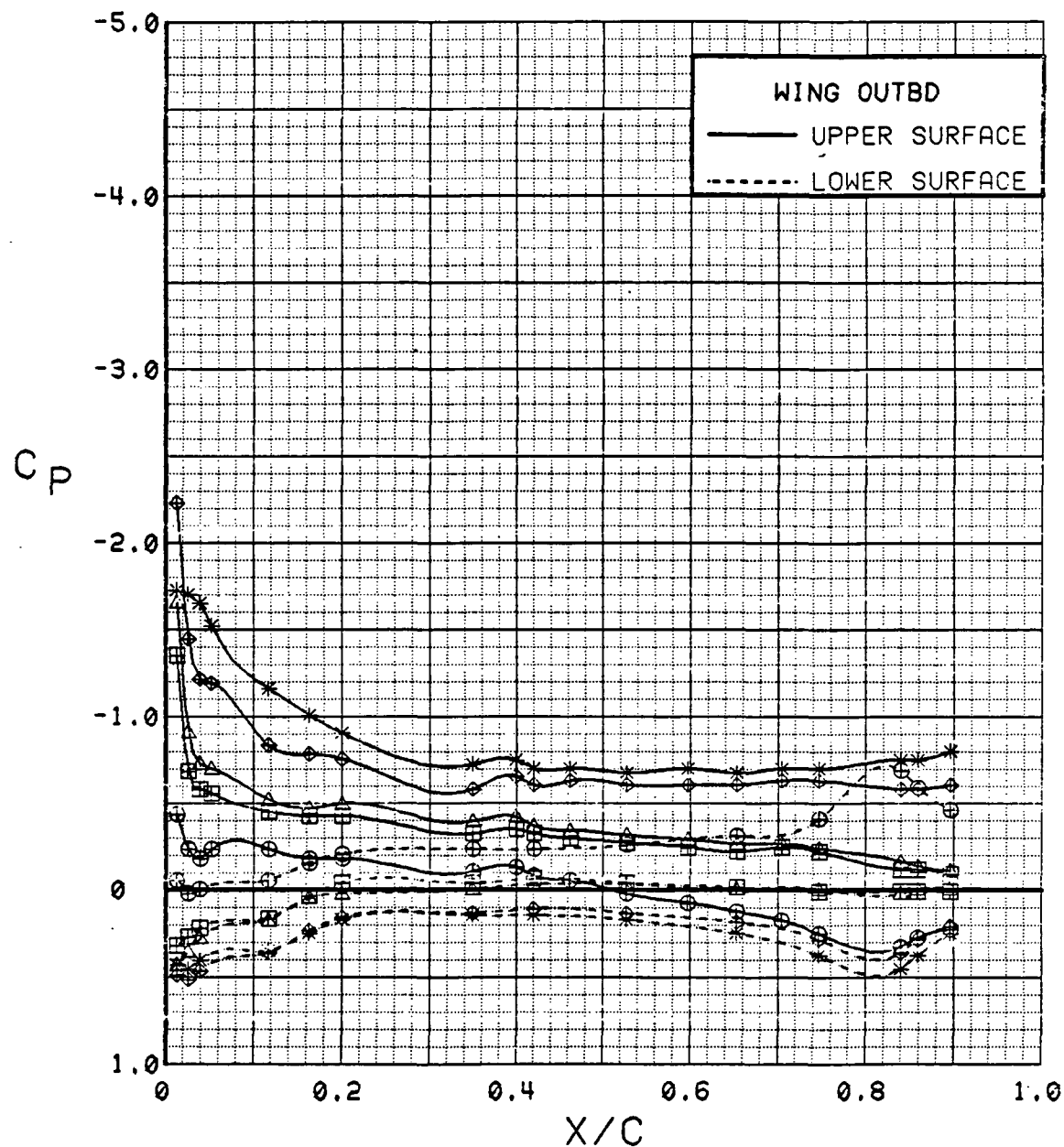


Figure 3.2.4-266 Wing Flap Effects, Outboard,  $C_T = 0.9$ ,  $\alpha = 4$  deg

SYM	TEST	RUN	ALPHA	CT	ITEF	OTEF	CAN	SWB
⊕	543	86	8.1	0.92	-20	-20	0	OFF
⊞	543	74	8.4	0.94	-10	0	0	OFF
△	543	60	8.4	0.94	0	0	0	OFF
⊕	543	68	8.6	0.95	20	20	0	OFF
*	543	6	8.6	0.91	30	30	0	OFF

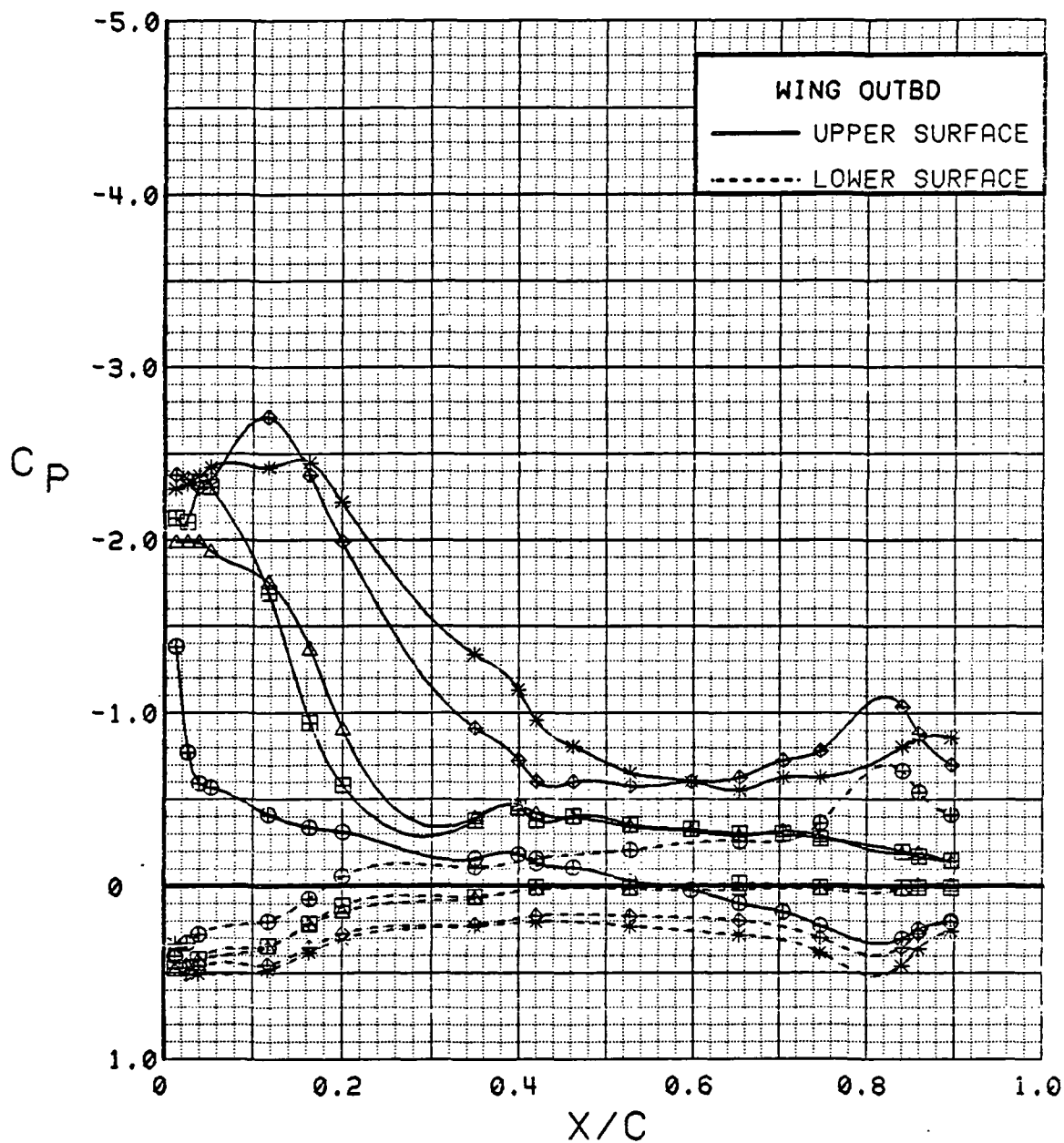


Figure 3.2.4-267 Wing Flap Effects, Outboard,  $C_T = 0.9$ ,  $\alpha = 8$  deg



SYM	TEST	RUN	ALPHA	CT	ITEF	OTEF	CAN	SWB
⊕	543	86	12.3	0.93	-20	-20	0	OFF
⊞	543	74	12.5	0.94	-10	0	0	OFF
△	543	60	12.5	0.94	0	0	0	OFF
⊕	543	68	12.8	0.93	20	20	0	OFF
*	543	6	12.8	0.92	30	30	0	OFF

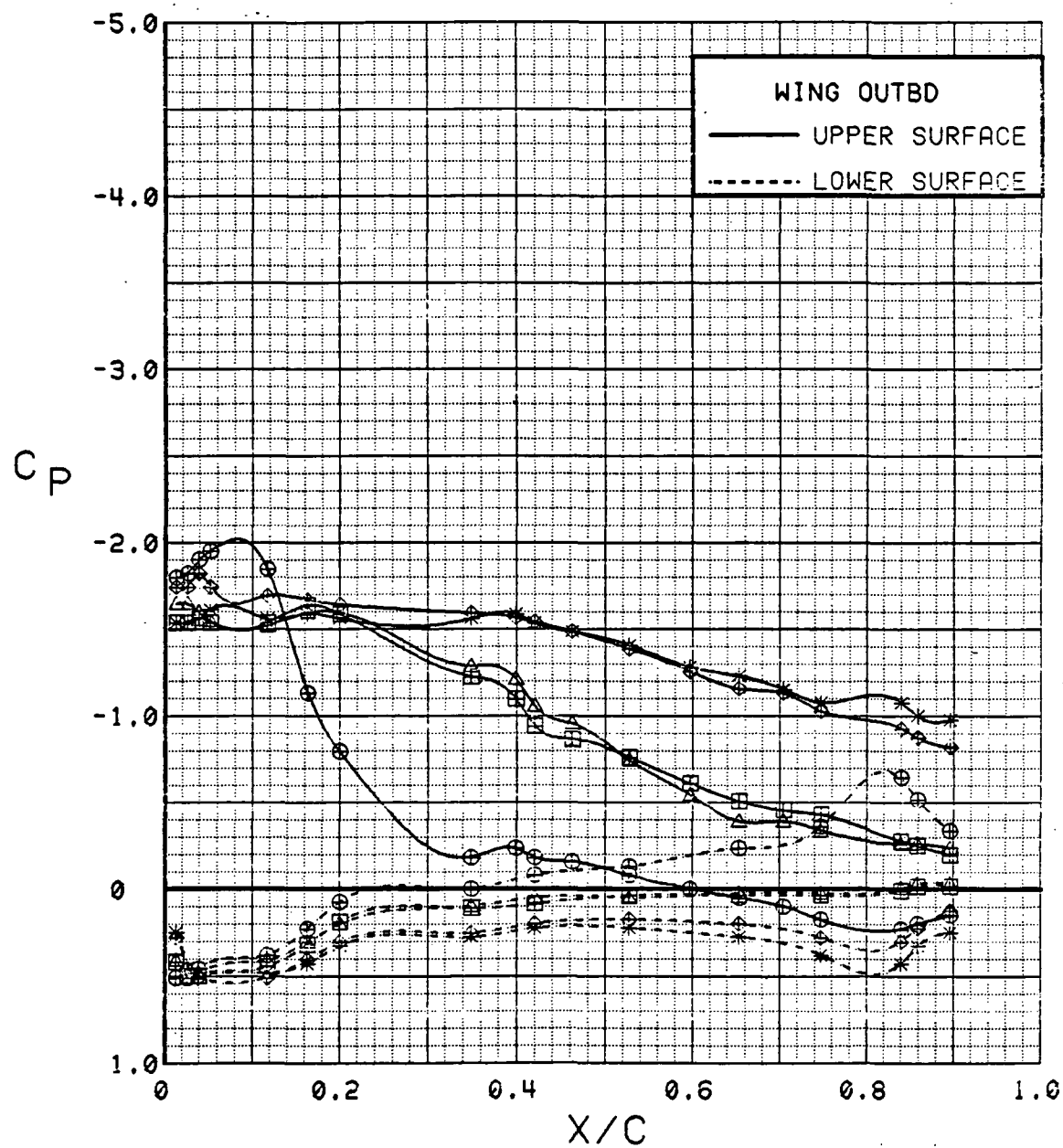


Figure 3.2.4-268 Wing Flap Effects, Outboard,  $C_T = 0.9$ ,  $\alpha = 12$  deg

SYM	TEST	RUN	ALPHA	CT	ITEF	OTEF	CAN	SWB
⊕	543	86	16.5	0.92	-20	-20	0	OFF
⊞	543	74	16.6	0.94	-10	0	0	OFF
△	543	60	16.7	0.93	0	0	0	OFF
⊕	543	68	16.9	0.94	20	20	0	OFF
*	543	6	16.9	0.92	30	30	0	OFF

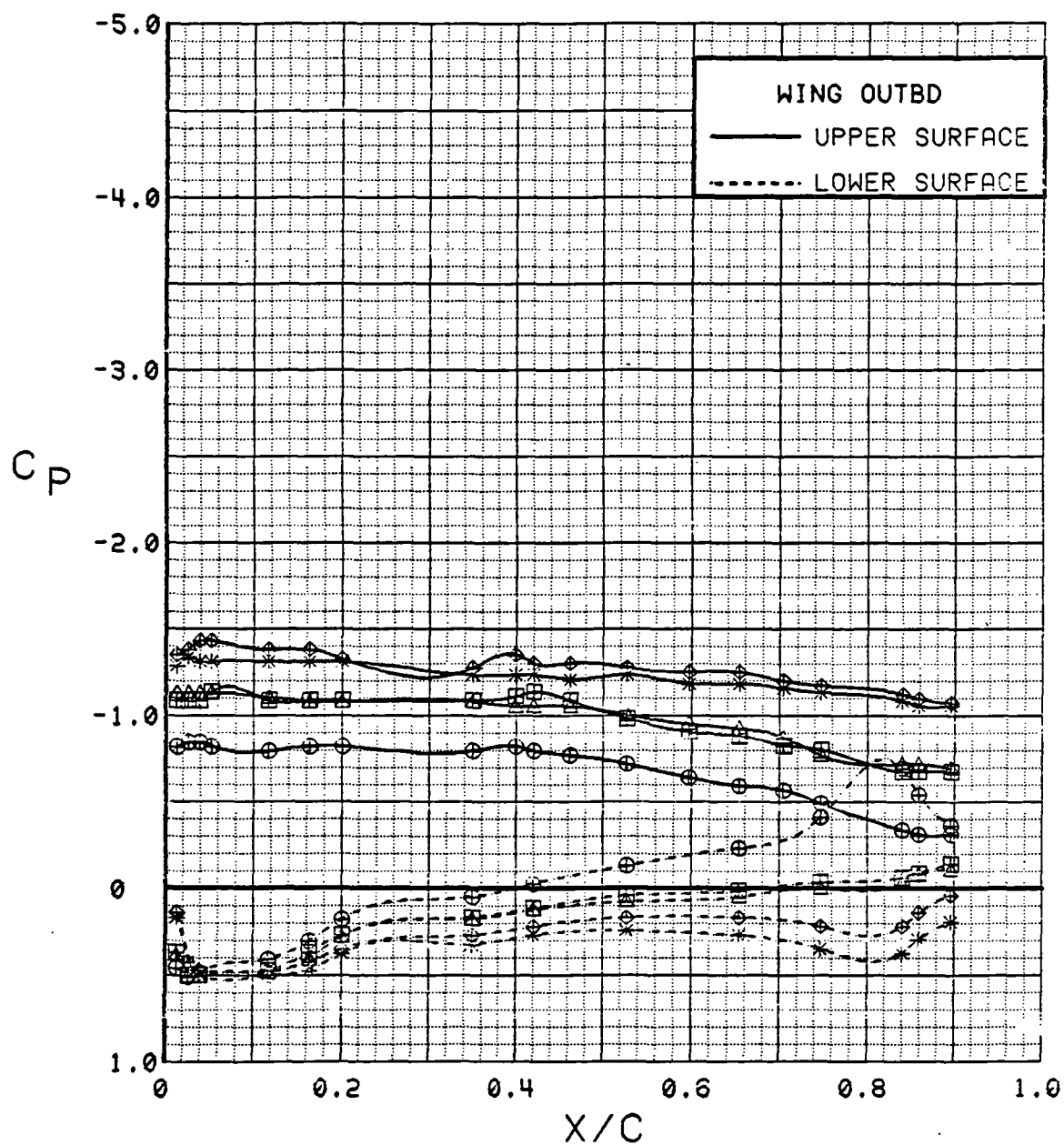


Figure 3.2.4-269 Wing Flap Effects, Outboard,  $C_T = 0.9$ ,  $\alpha = 16^\circ$

SYM	TEST	RUN	ALPHA	CT	ITEF	OTEF	CAN	SWB
⊕	543	86	20.6	0.93	-20	-20	0	OFF
⊞	543	74	20.8	0.94	-10	0	0	OFF
△	543	60	20.8	0.93	0	0	0	OFF
⊕	543	68	21.0	0.92	20	20	0	OFF
*	543	6	21.0	0.93	30	30	0	OFF

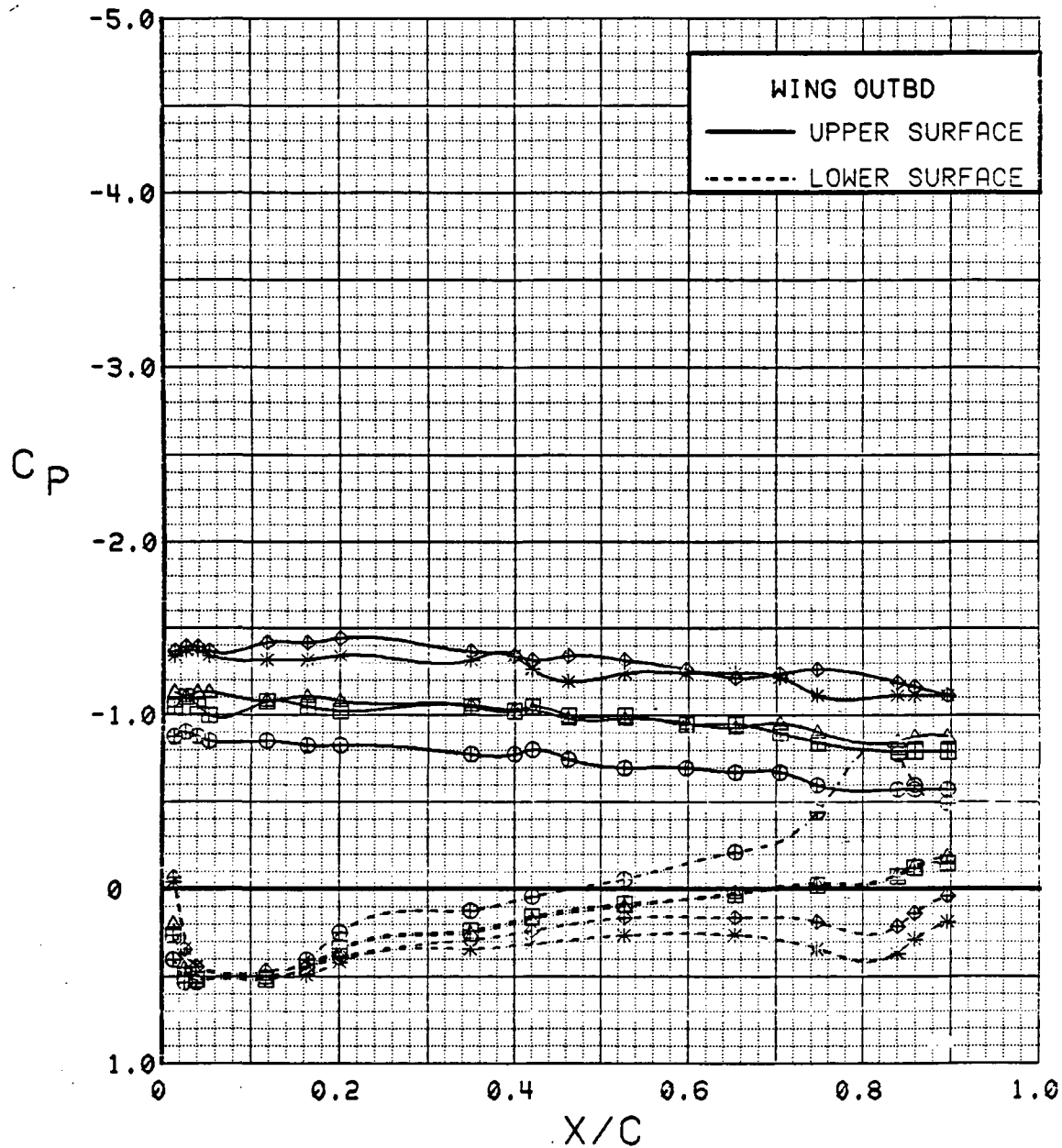


Figure 3.2.4-270 Wing Flap Effects, Outboard,  $C_T = 0.9$ ,  $\alpha = 20$  deg

SYM	TEST	RUN	ALPHA	CT	ITEF	OTEF	CAN	SWB
⊕	543	86	4.0	0.92	-20	-20	0	OFF
⊞	543	74	4.2	0.93	-10	0	0	OFF
△	543	60	4.3	0.93	0	0	0	OFF
◆	543	68	4.4	0.94	20	20	0	OFF
*	543	6	4.5	0.94	30	30	0	OFF

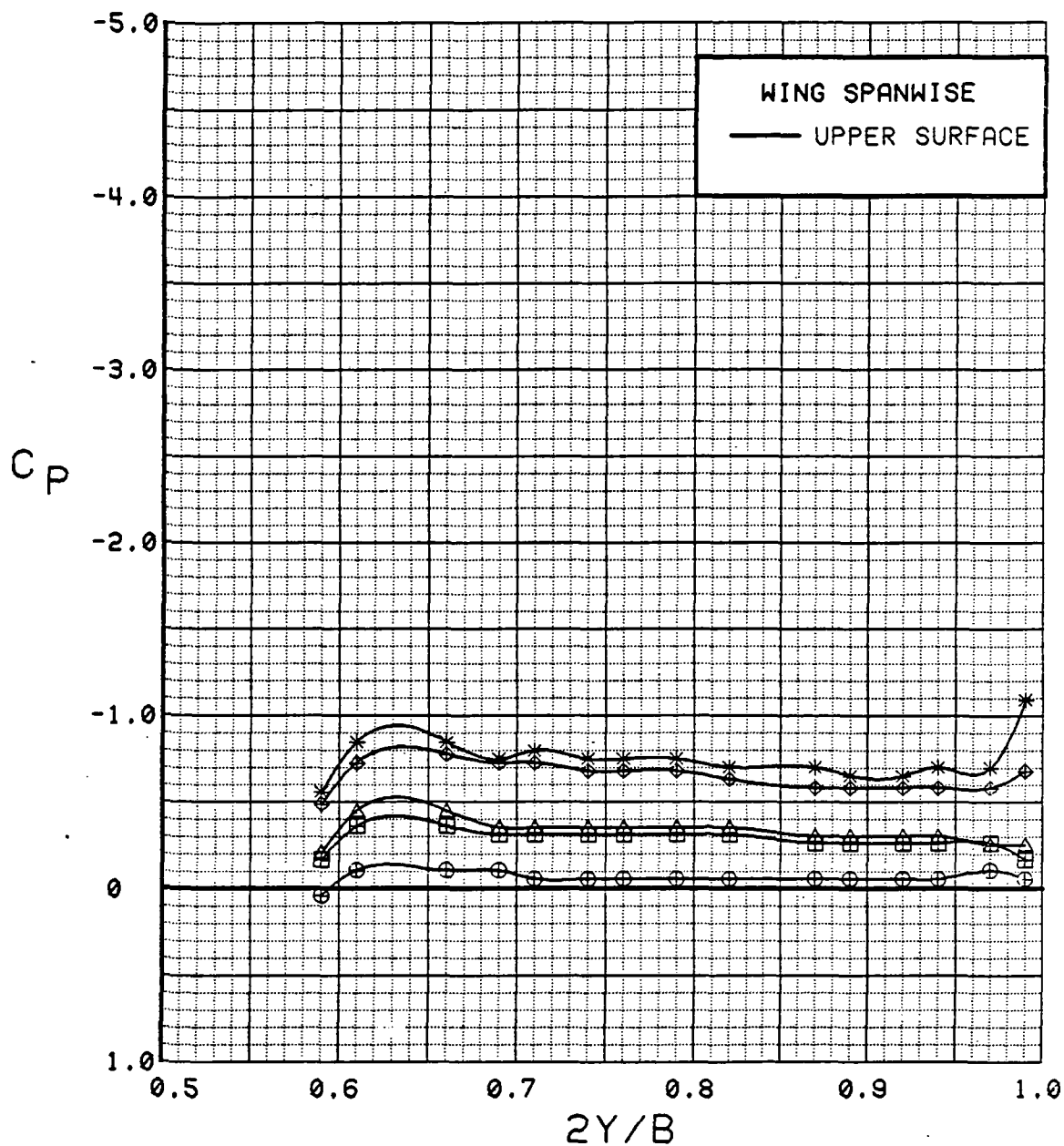


Figure 3.2.4-271 Wing Flap Effects, Spanwise,  $C_T = 0.9$ ,  $\alpha = 4$  deg

SYM	TEST	RUN	ALPHA	CT	ITEF	OTEF	CAN	SWB
⊕	543	86	8.1	0.92	-20	-20	0	OFF
⊞	543	74	8.4	0.94	-10	0	0	OFF
△	543	60	8.4	0.94	0	0	0	OFF
◆	543	68	8.6	0.95	20	20	0	OFF
*	543	6	8.6	0.91	30	30	0	OFF

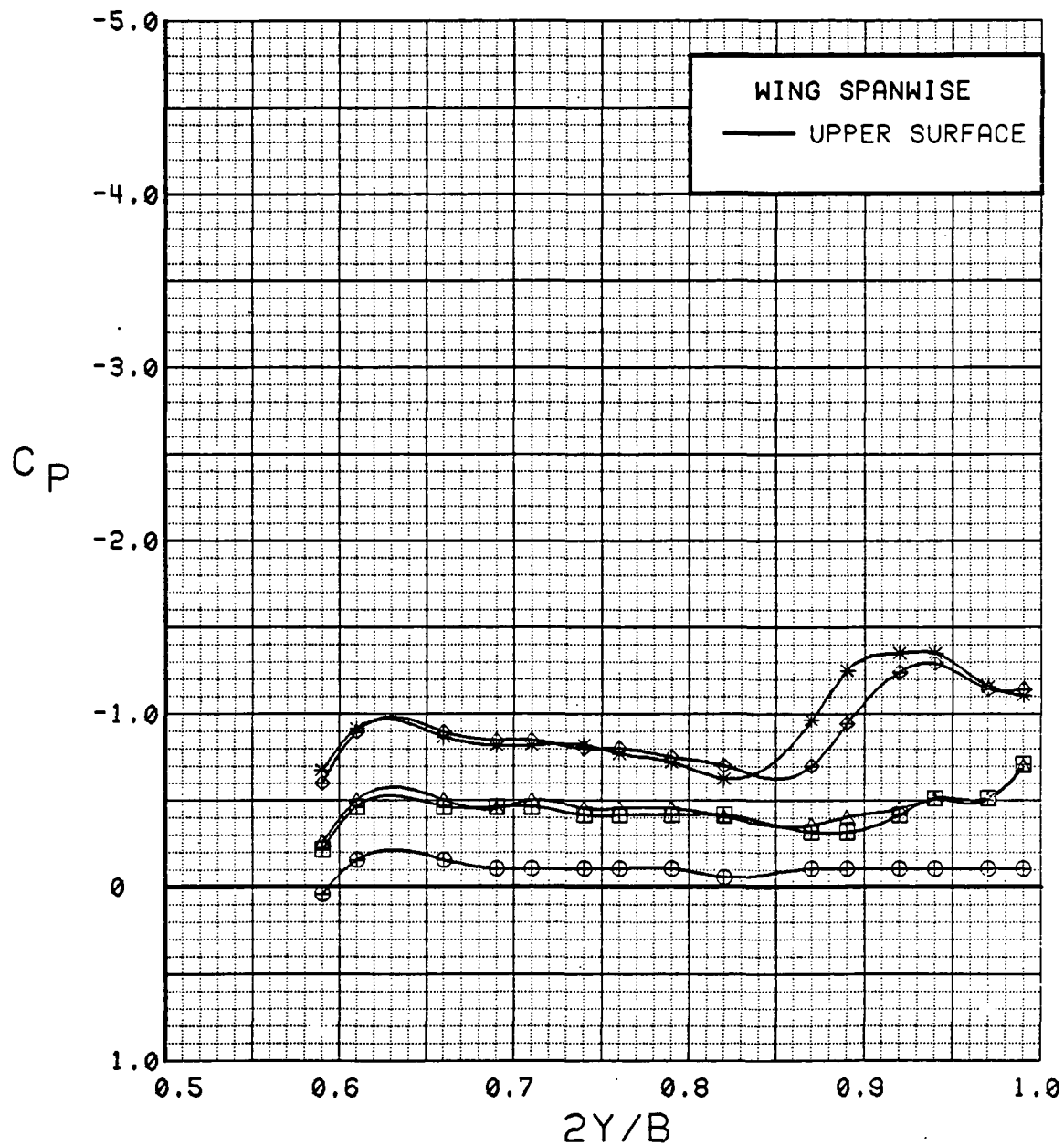


Figure 3.2.4-272 Wing Flap Effects, Spanwise,  $C_T = 0.9$ ,  $\alpha = 8$  deg

SYM	TEST	RUN	ALPHA	CT	ITEF	OTEF	CAN	SWB
⊕	543	86	12.3	0.93	-20	-20	0	OFF
⊞	543	74	12.5	0.94	-10	0	0	OFF
△	543	60	12.5	0.94	0	0	0	OFF
◆	543	68	12.8	0.93	20	20	0	OFF
*	543	6	12.8	0.92	30	30	0	OFF

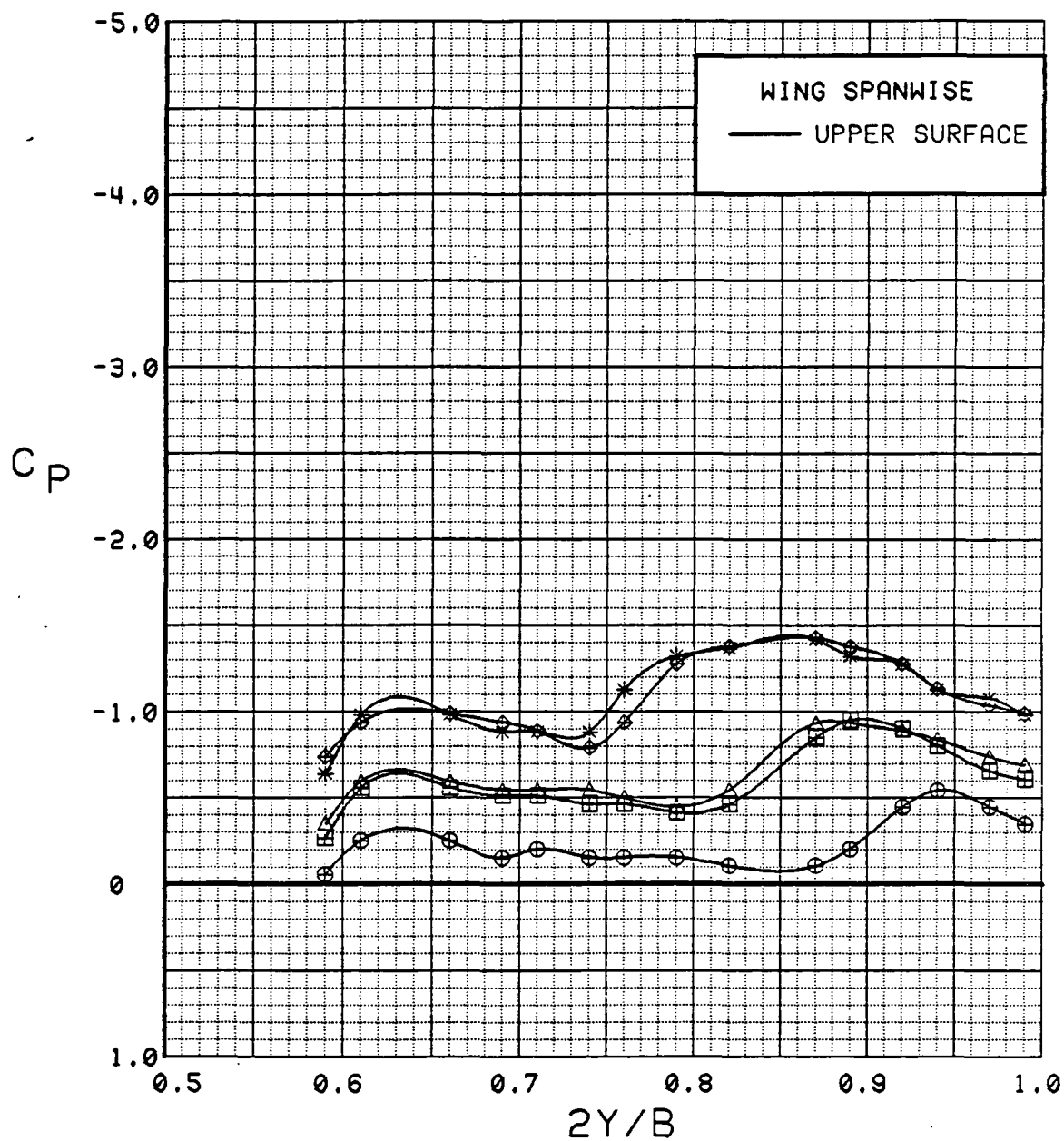


Figure 3.2.4-273 Wing Flap Effects, Spanwise,  $C_T = 0.9$ , Alpha = 12 deg

SYM	TEST	RUN	ALPHA	CT	ITEF	OTEF	CAN	SWB
⊕	543	86	16.5	0.92	-20	-20	0	OFF
⊞	543	74	16.6	0.94	-10	0	0	OFF
△	543	60	16.7	0.93	0	0	0	OFF
◆	543	68	16.9	0.94	20	20	0	OFF
*	543	6	16.9	0.92	30	30	0	OFF

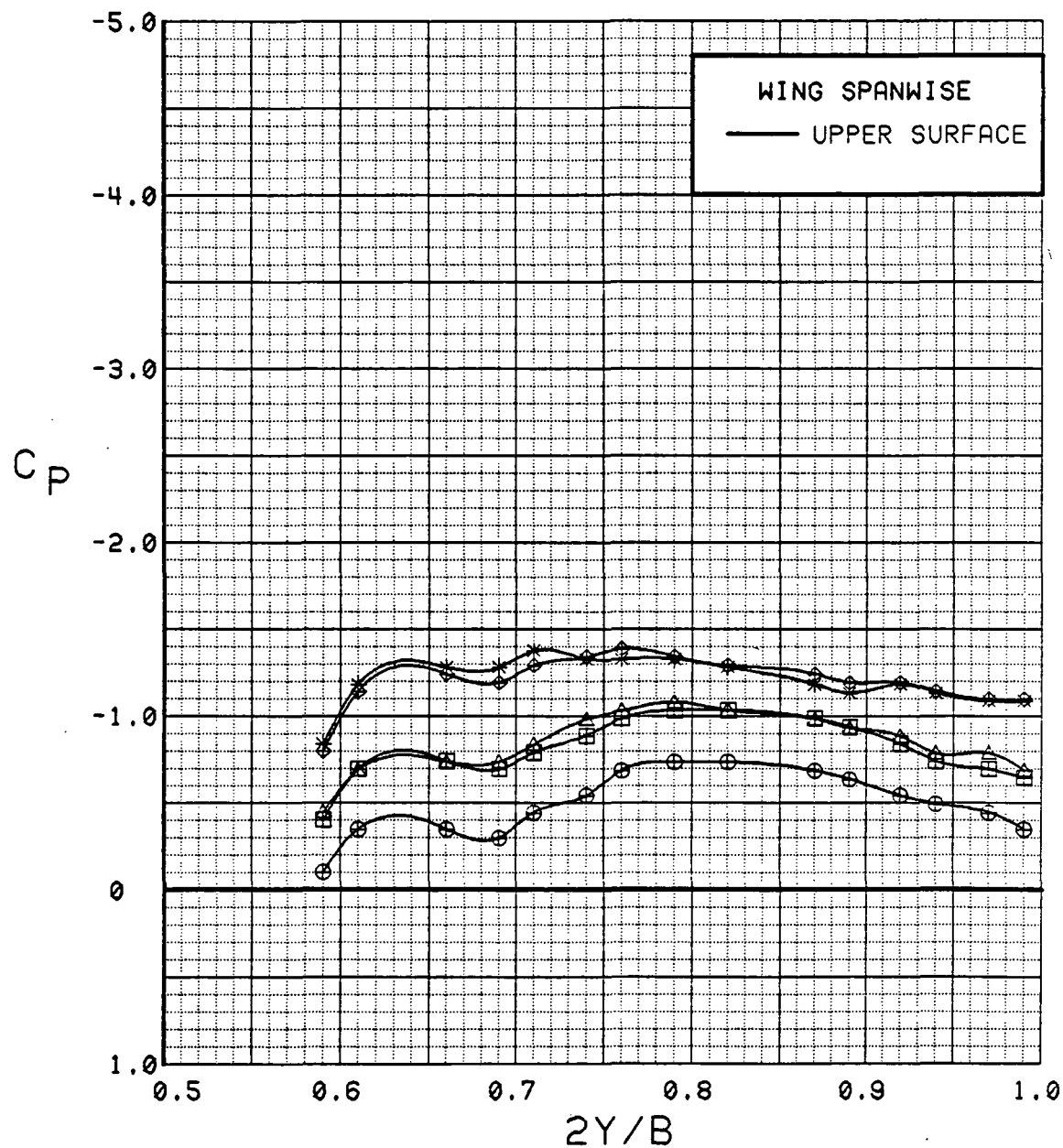


Figure 3.2.4-274 Wing Flap Effects, Spanwise,  $C_T = 0.9$ , Alpha = 16 deg

SYM	TEST	RUN	ALPHA	CT	ITEF	OTEF	CAN	SWB
⊕	543	86	20.6	0.93	-20	-20	0	OFF
⊞	543	74	20.8	0.94	-10	0	0	OFF
△	543	60	20.8	0.93	0	0	0	OFF
◆	543	68	21.0	0.92	20	20	0	OFF
*	543	6	21.0	0.93	30	30	0	OFF

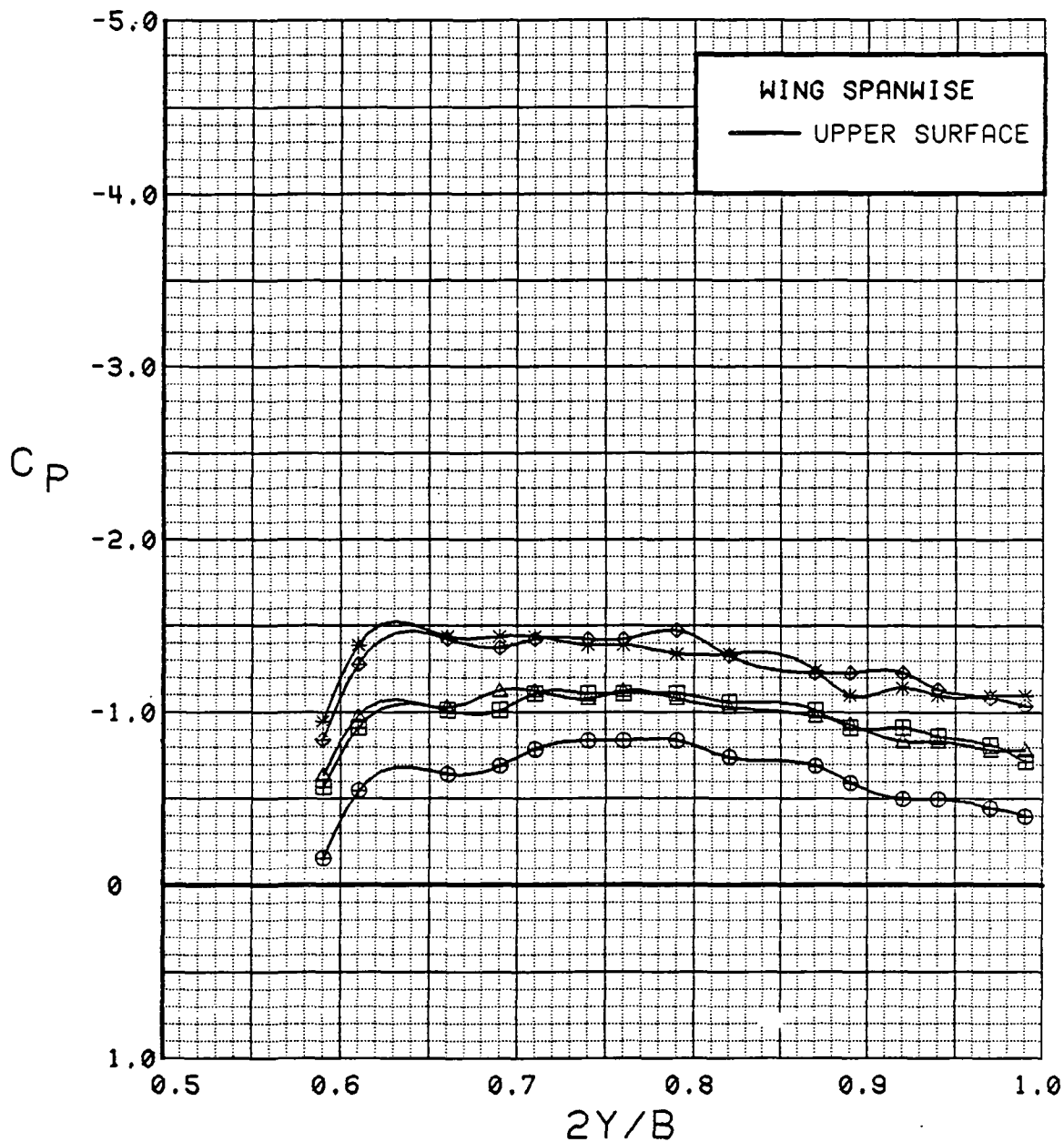


Figure 3.2.4-275 Wing Flap Effects, Spanwise,  $C_T = 0.9$ ,  $\alpha = 20^\circ$



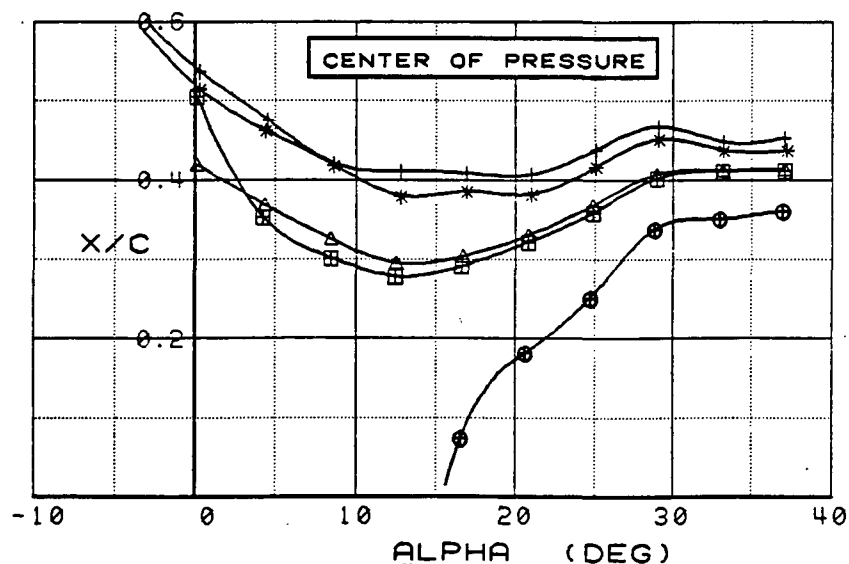
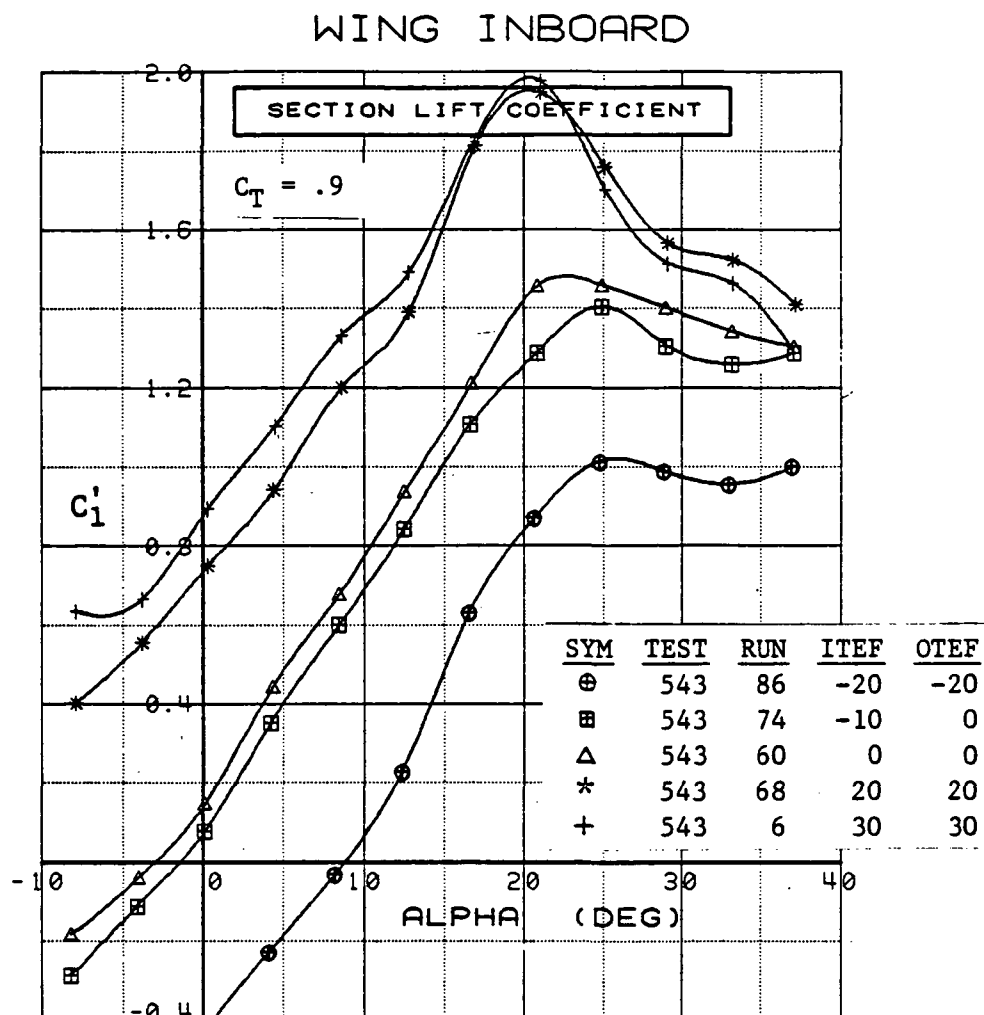


Figure 3.2.4-276 Wing Flap Effects, Inboard,  $C_T = 0.9$ , Integrated Section Properties

## WING OUTBOARD

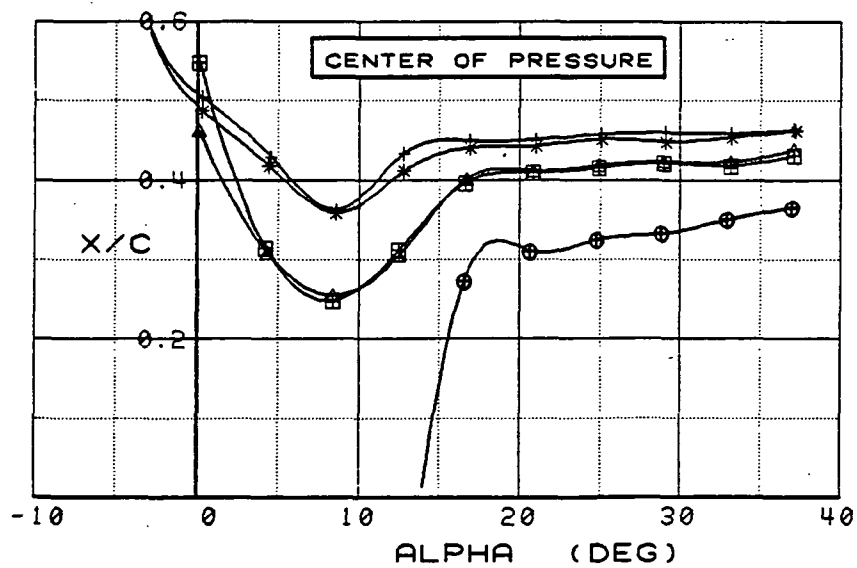
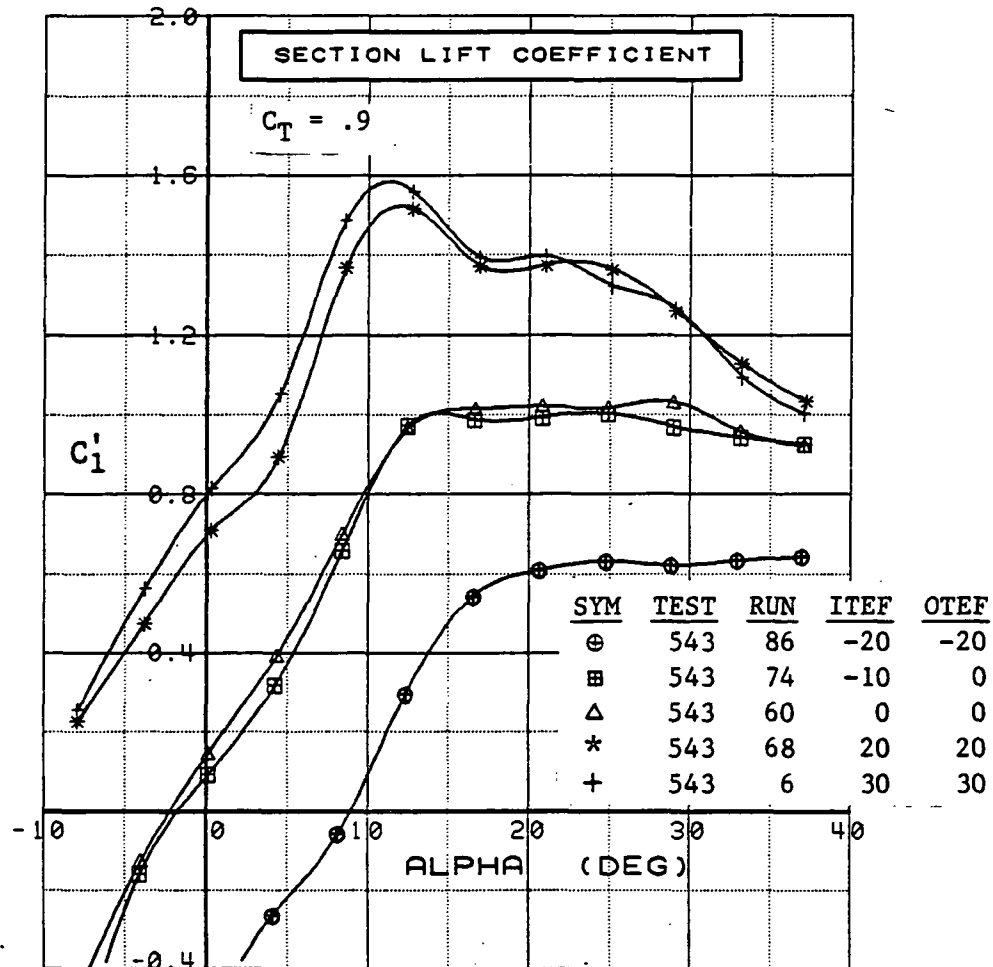


Figure 3.2.4-277 Wing Flap Effects, Outboard,  $C_T = 0.9$ , Integrated Section Properties

SYM	TEST	RUN	ALPHA	CT	ITEF	OTEF	CAN	SWB
⊕	543	85	4.0	1.89	-20	-20	0	OFF
⊞	543	72	4.2	1.96	-10	0	0	OFF
△	543	58	4.3	1.84	0	0	0	OFF
⊕	543	81	4.4	1.87	10	10	0	OFF
*	543	67	4.5	1.89	20	20	0	OFF
+	543	4	4.5	1.90	30	30	0	OFF

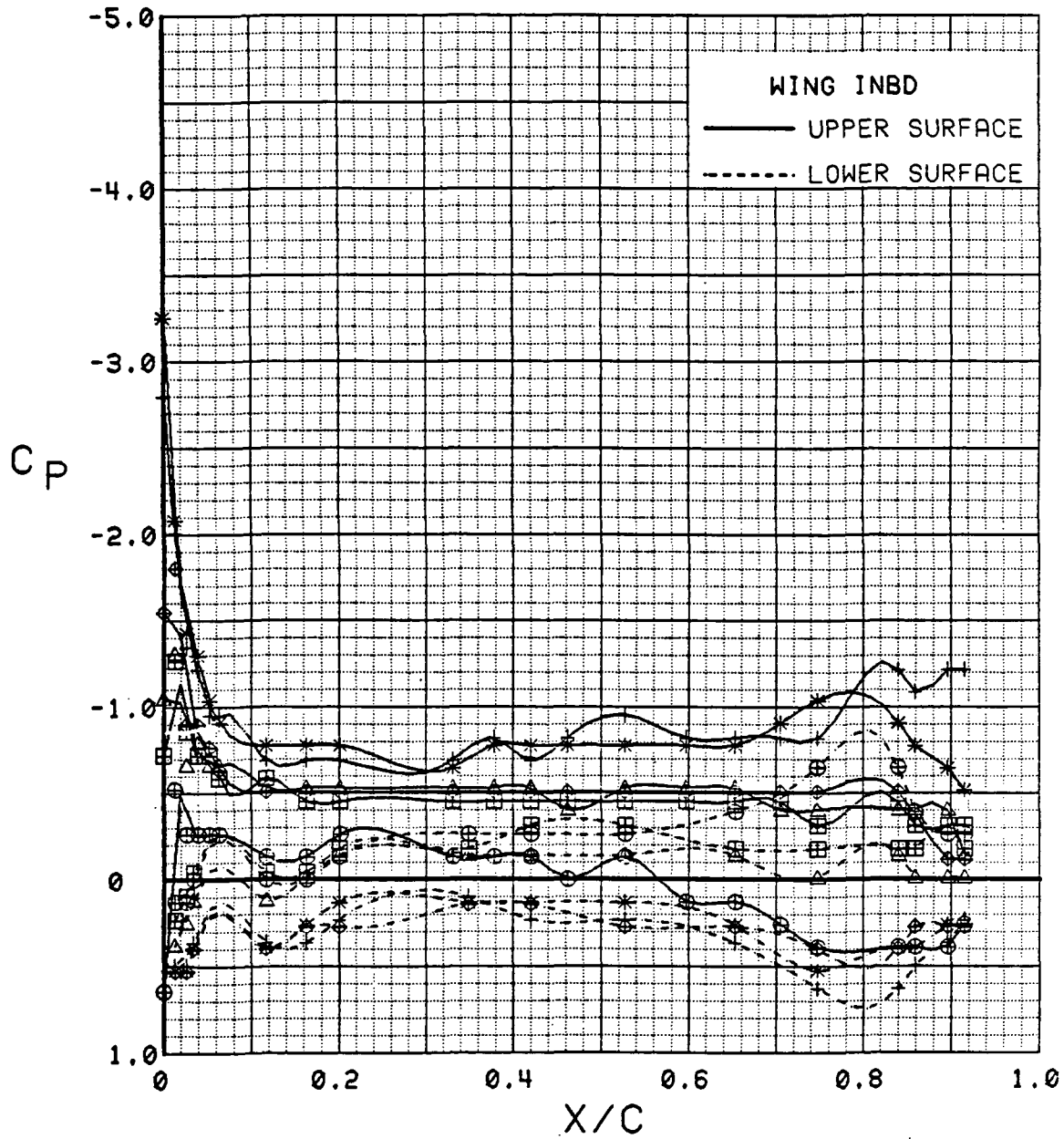


Figure 3.2.4-278 Wing Flap Effects, Inboard,  $C_T = 1.9$ ,  $\alpha = 4$  deg

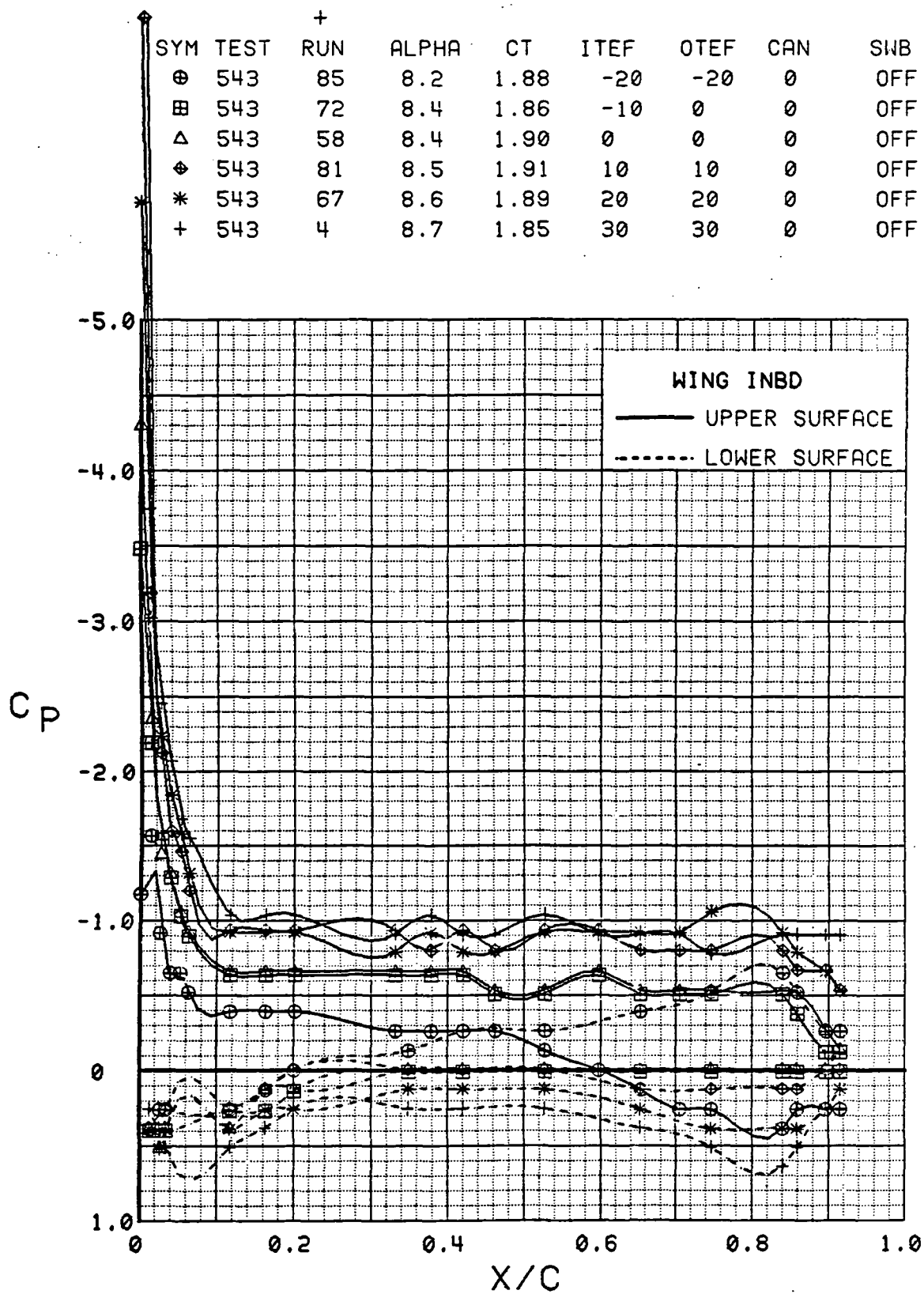


Figure 3.2.4-279 Wing Flap Effects, Inboard,  $C_T = 1.9$ ,  $\alpha = 8$  deg

SYM	TEST	RUN	ALPHA	CT	ITEF	OTEF	CAN	SWB
⊕	543	85	12.3	1.84	-20	-20	0	OFF
⊞	543	72	12.6	1.87	-10	0	0	OFF
△	543	58	12.6	1.87	0	0	0	OFF
⬢	543	81	12.7	1.87	10	10	0	OFF
*	543	67	12.8	1.90	20	20	0	OFF
+	543	4	12.8	1.86	30	30	0	OFF

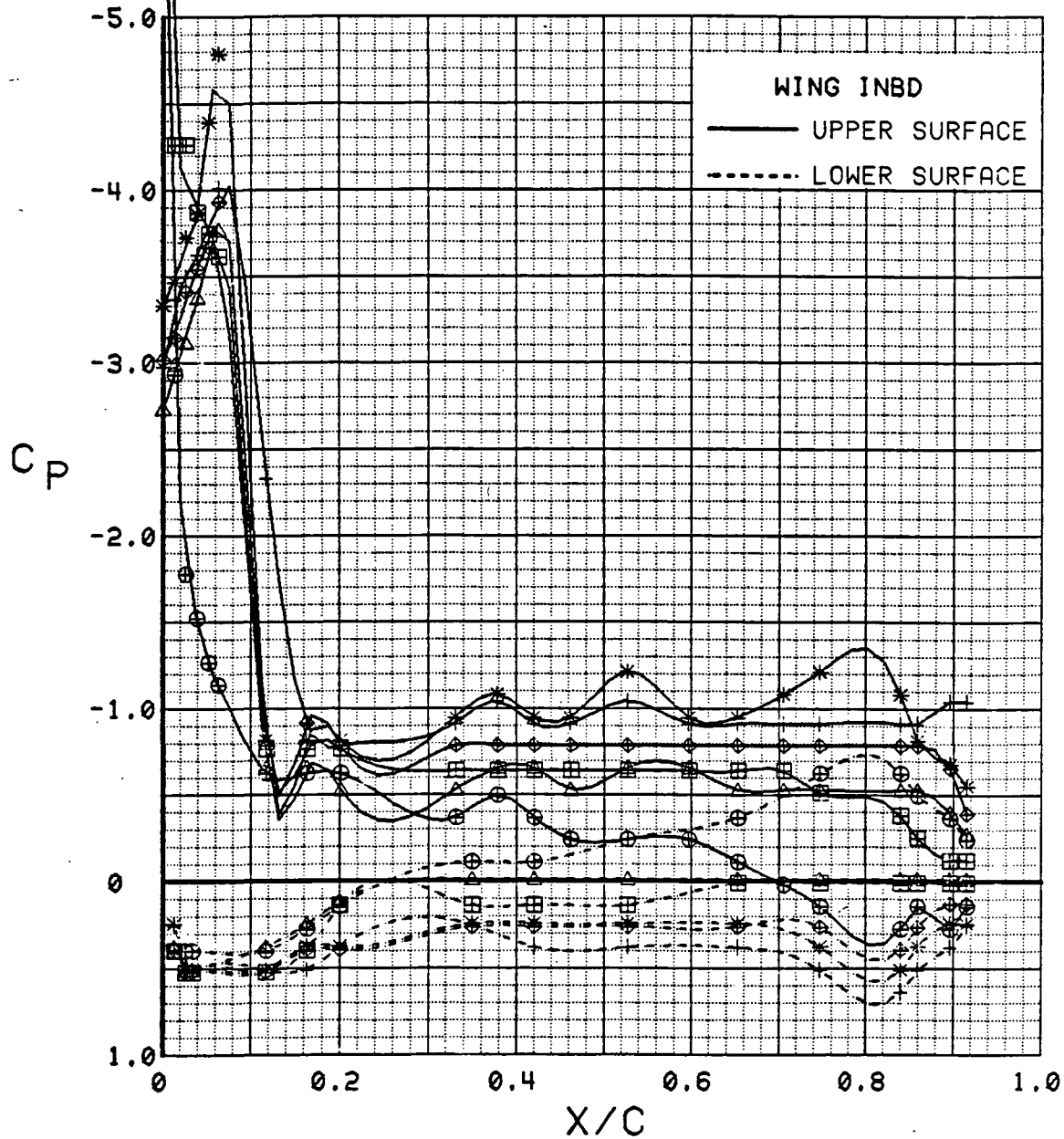


Figure 3.2.4-280 Wing Flap Effects, Inboard,  $C_T = 1.9$ ,  $\alpha = 12$  deg

SYM	TEST	RUN	ALPHA	CT	ITEF	OTEF	CAN	SWB
⊕	543	85	16.5	1.86	-20	-20	0	OFF
⊞	543	72	16.7	1.86	-10	0	0	OFF
△	543	58	16.7	1.87	0	0	0	OFF
◆	543	81	16.8	1.91	10	10	0	OFF
*	543	67	16.9	1.90	20	20	0	OFF
+	543	4	16.9	1.86	30	30	0	OFF

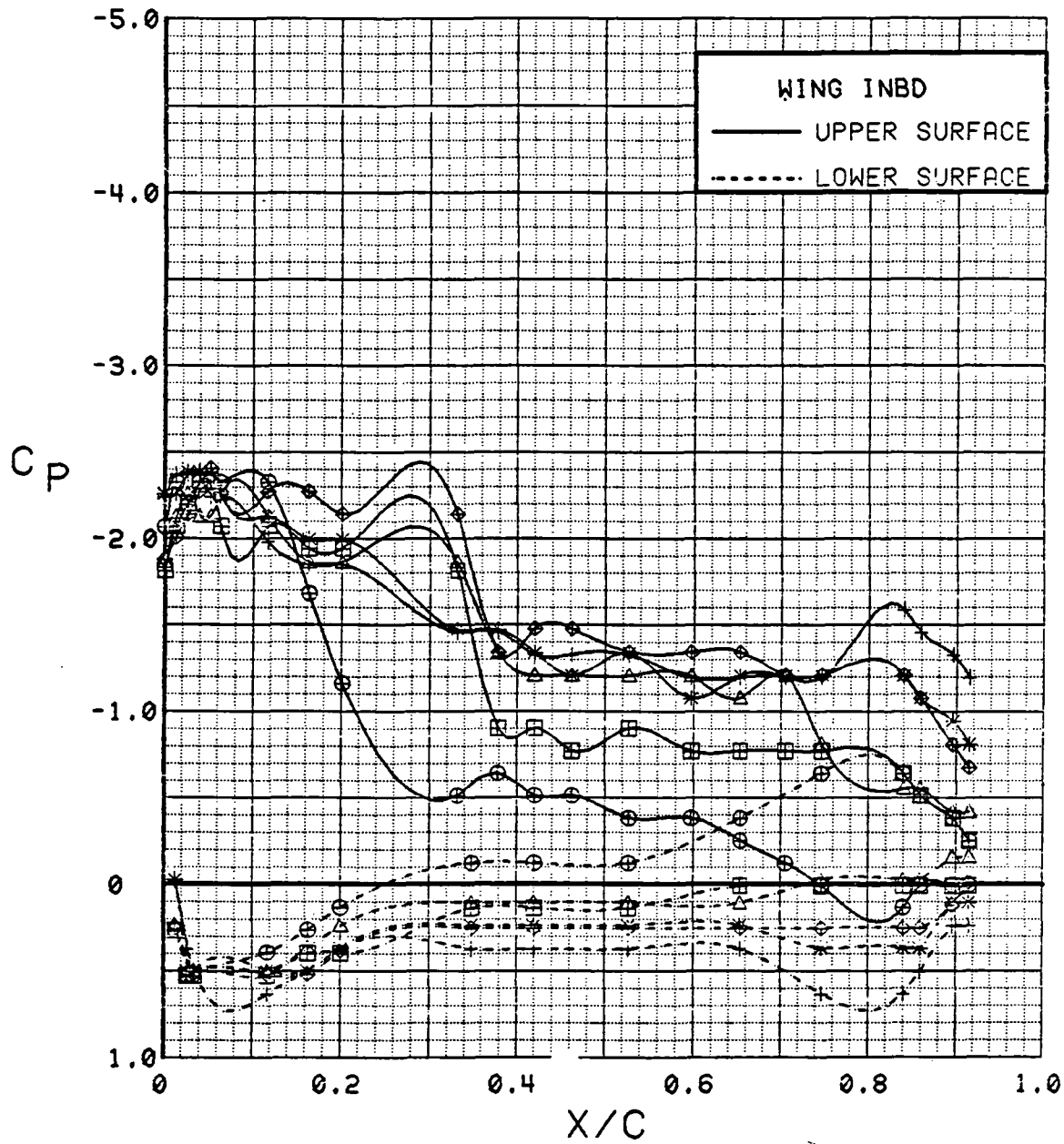


Figure 3.2.4-281 Wing Flap Effects, Inboard,  $C_T = 1.9$ ,  $\alpha = 16$  deg

SYM	TEST	RUN	ALPHA	CT	ITEF	OTEF	CAN	SWB
⊕	543	85	20.6	1.85	-20	-20	0	OFF
⊞	543	72	20.8	1.86	-10	0	0	OFF
△	543	58	20.8	1.72	0	0	0	OFF
⊕	543	81	21.0	1.84	10	10	0	OFF
*	543	67	21.0	1.86	20	20	0	OFF
+	543	4	21.1	1.88	30	30	0	OFF

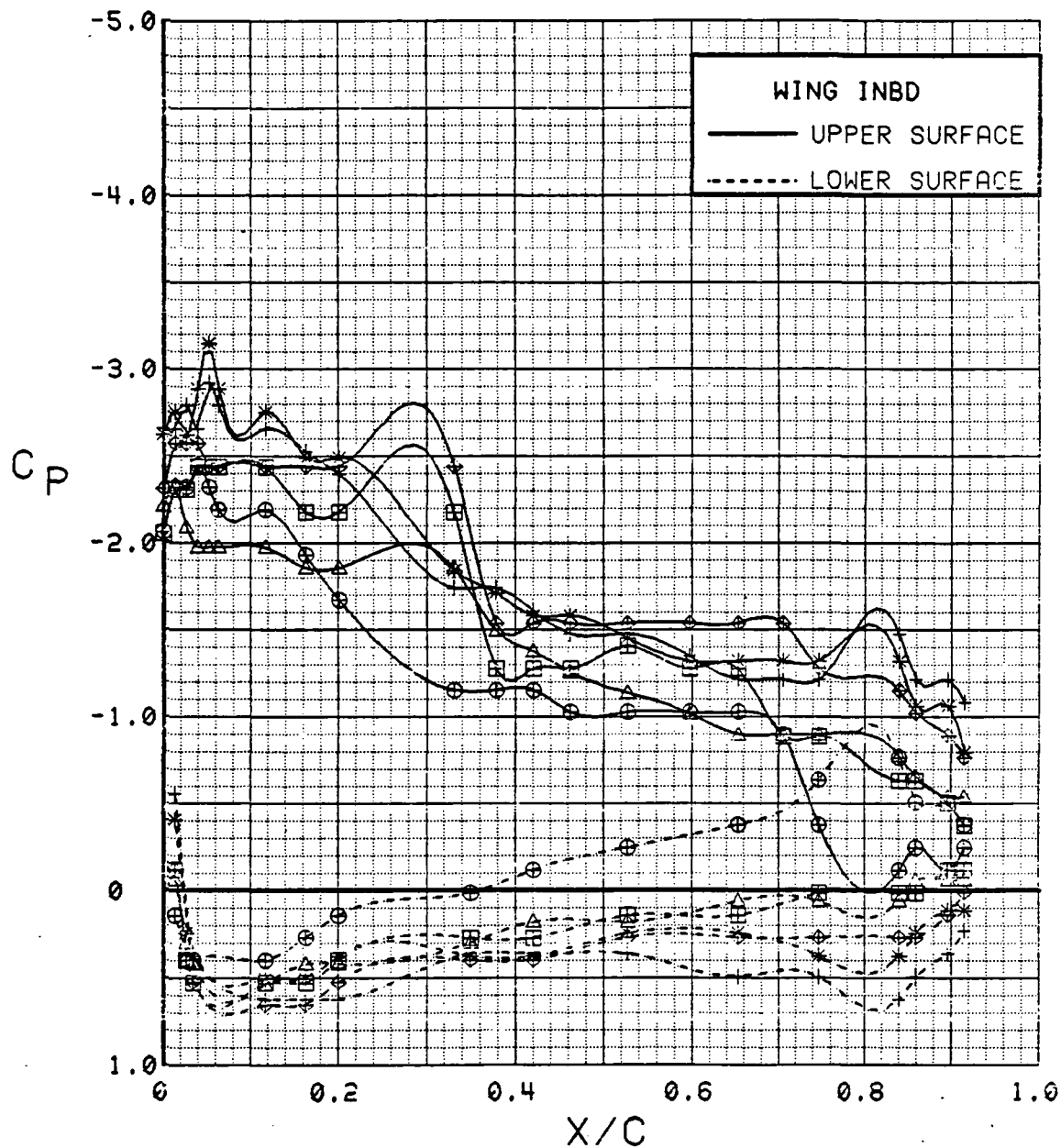


Figure 3.2.4-282 Wing Flap Effects, Inboard,  $C_T = 1.9$ ,  $\alpha = 20$  deg

SYM	TEST	RUN	ALPHA	CT	ITEF	OTEF	CAN	SWB
⊕	543	85	4.0	1.89	-20	-20	0	OFF
⊞	543	72	4.2	1.96	-10	0	0	OFF
△	543	58	4.3	1.84	0	0	0	OFF
⊕	543	81	4.4	1.87	10	10	0	OFF
*	543	67	4.5	1.89	20	20	0	OFF
+	543	4	4.5	1.90	30	30	0	OFF

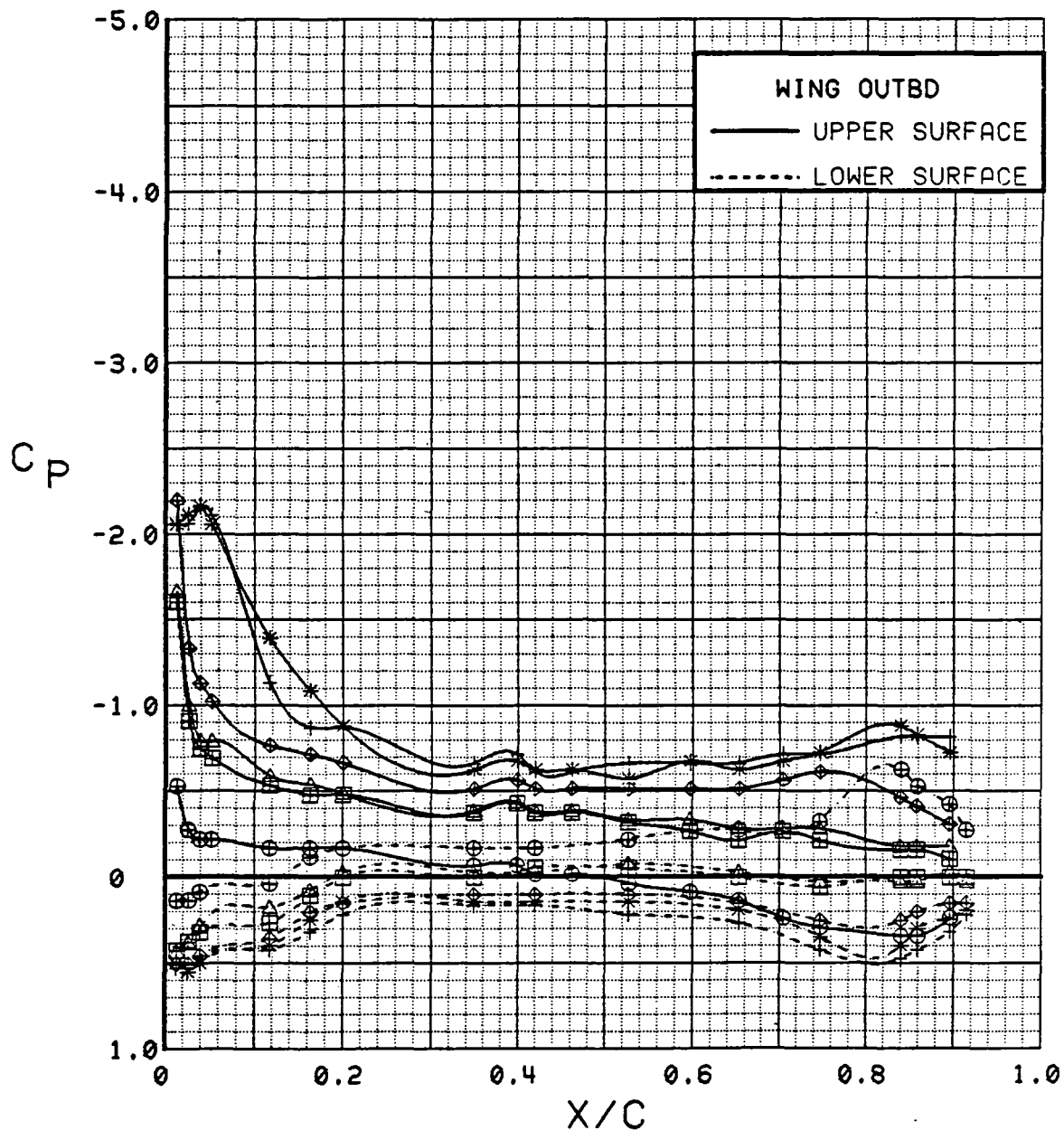


Figure 3.2.4-283 Wing Flap Effects, Outboard,  $C_T = 1.9$ ,  $\alpha = 4$  deg



SYM	TEST	RUN	ALPHA	CT	ITEF	OTEF	CAN	SWB
⊕	543	85	8.2	1.88	-20	-20	0	OFF
⊞	543	72	8.4	1.86	-10	0	0	OFF
△	543	58	8.4	1.90	0	0	0	OFF
⊕	543	81	8.5	1.91	10	10	0	OFF
*	543	67	8.6	1.89	20	20	0	OFF
+	543	4	8.7	1.85	30	30	0	OFF

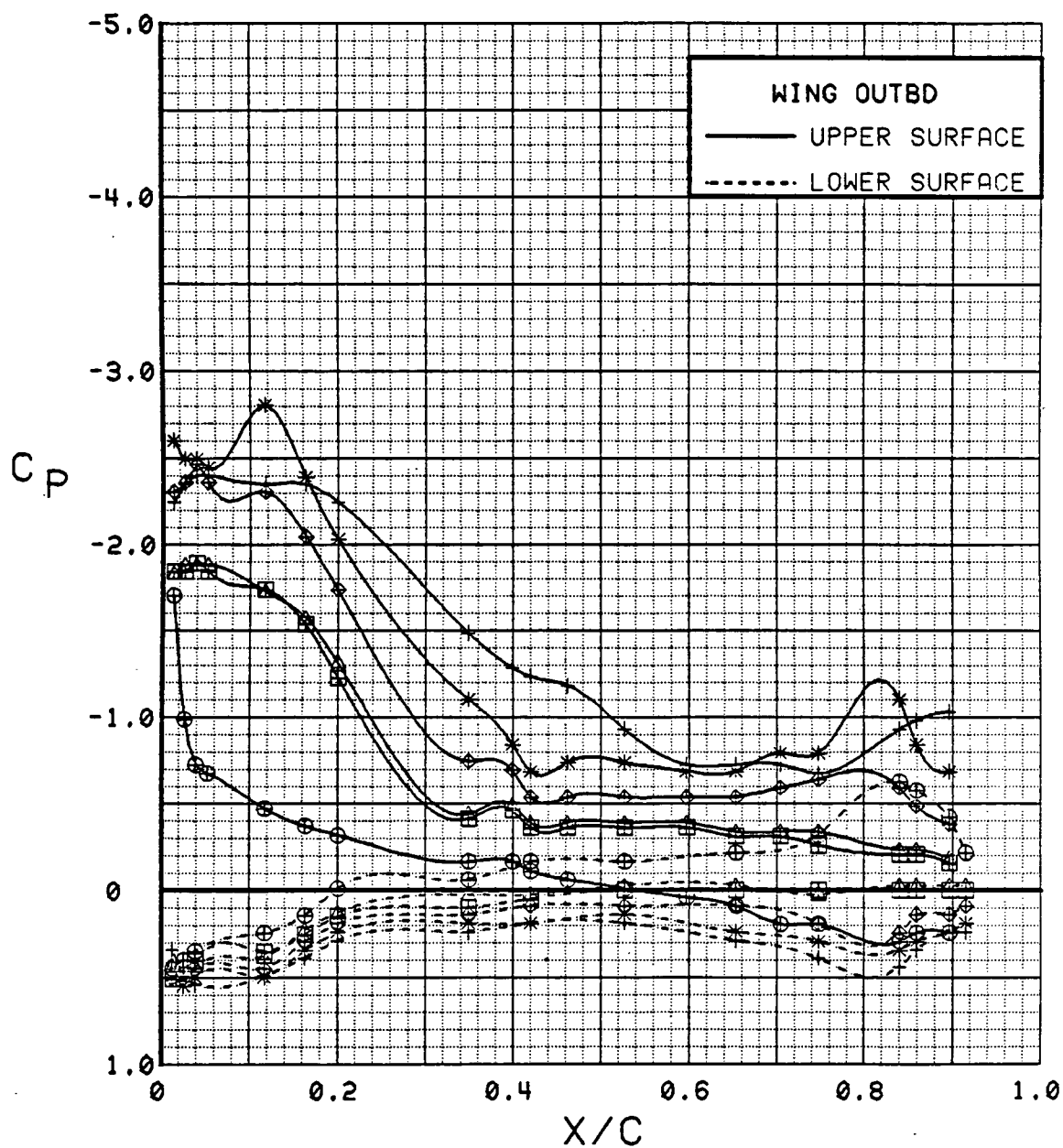


Figure 3.2.4-284 Wing Flap Effects, Outboard,  $C_T = 1.9$ ,  $\alpha = 8^\circ$

SYM	TEST	RUN	ALPHA	CT	ITEF	OTEF	CAN	SWB
⊕	543	85	12.3	1.84	-20	-20	0	OFF
⊞	543	72	12.6	1.87	-10	0	0	OFF
△	543	58	12.6	1.87	0	0	0	OFF
⊕	543	81	12.7	1.87	10	10	0	OFF
*	543	67	12.8	1.90	20	20	0	OFF
+	543	4	12.8	1.86	30	30	0	OFF

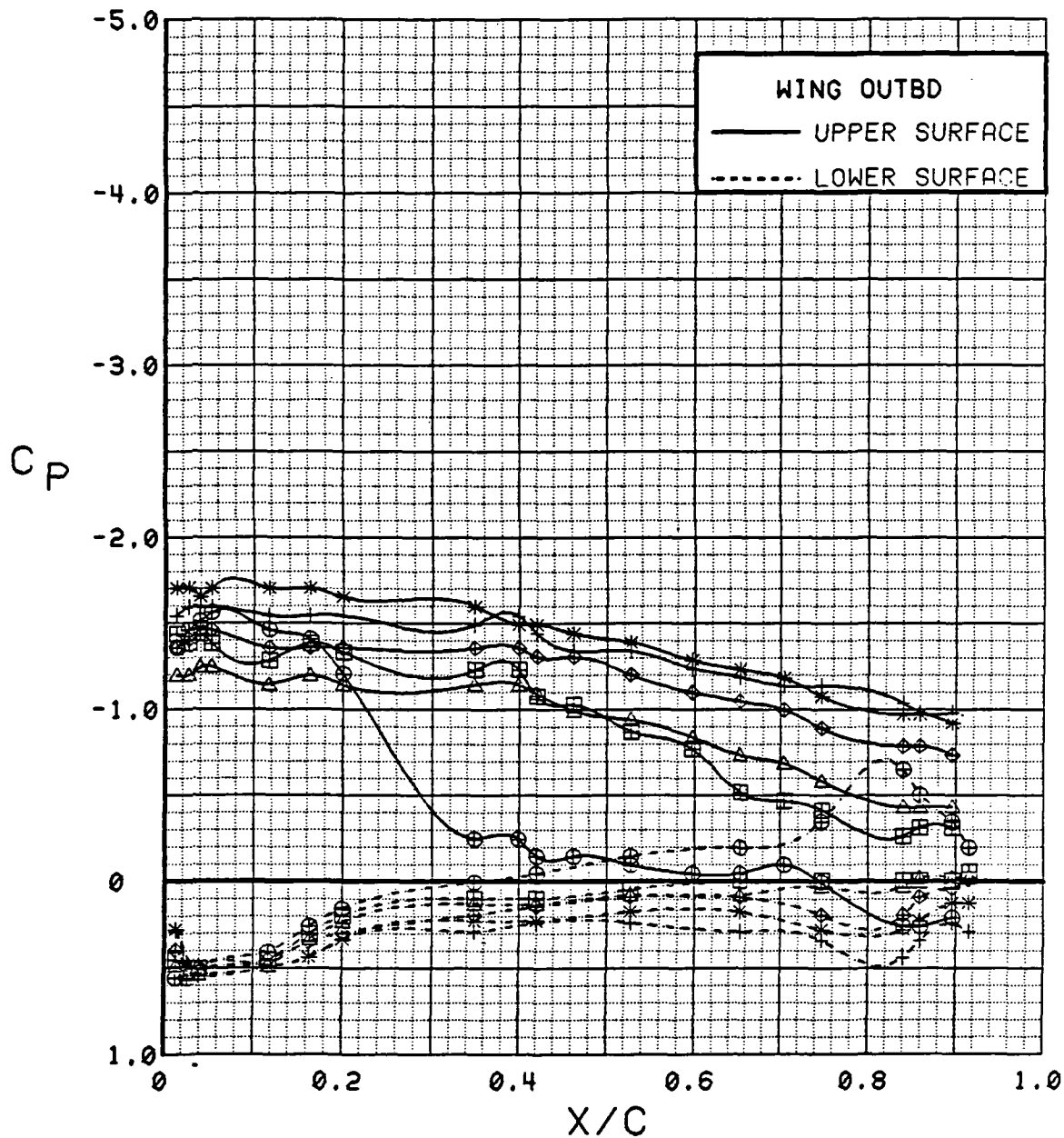


Figure 3.2.4-285 Wing Flap Effects, Outboard,  $C_T = 1.9$ ,  $\alpha = 12$  deg

SYM	TEST	RUN	ALPHA	CT	ITEF	OTEF	CAN	SWB
⊕	543	85	16.5	1.86	-20	-20	0	OFF
⊞	543	72	16.7	1.86	-10	0	0	OFF
△	543	58	16.7	1.87	0	0	0	OFF
⊕	543	81	16.8	1.91	10	10	0	OFF
*	543	67	16.9	1.90	20	20	0	OFF
+	543	4	16.9	1.86	30	30	0	OFF

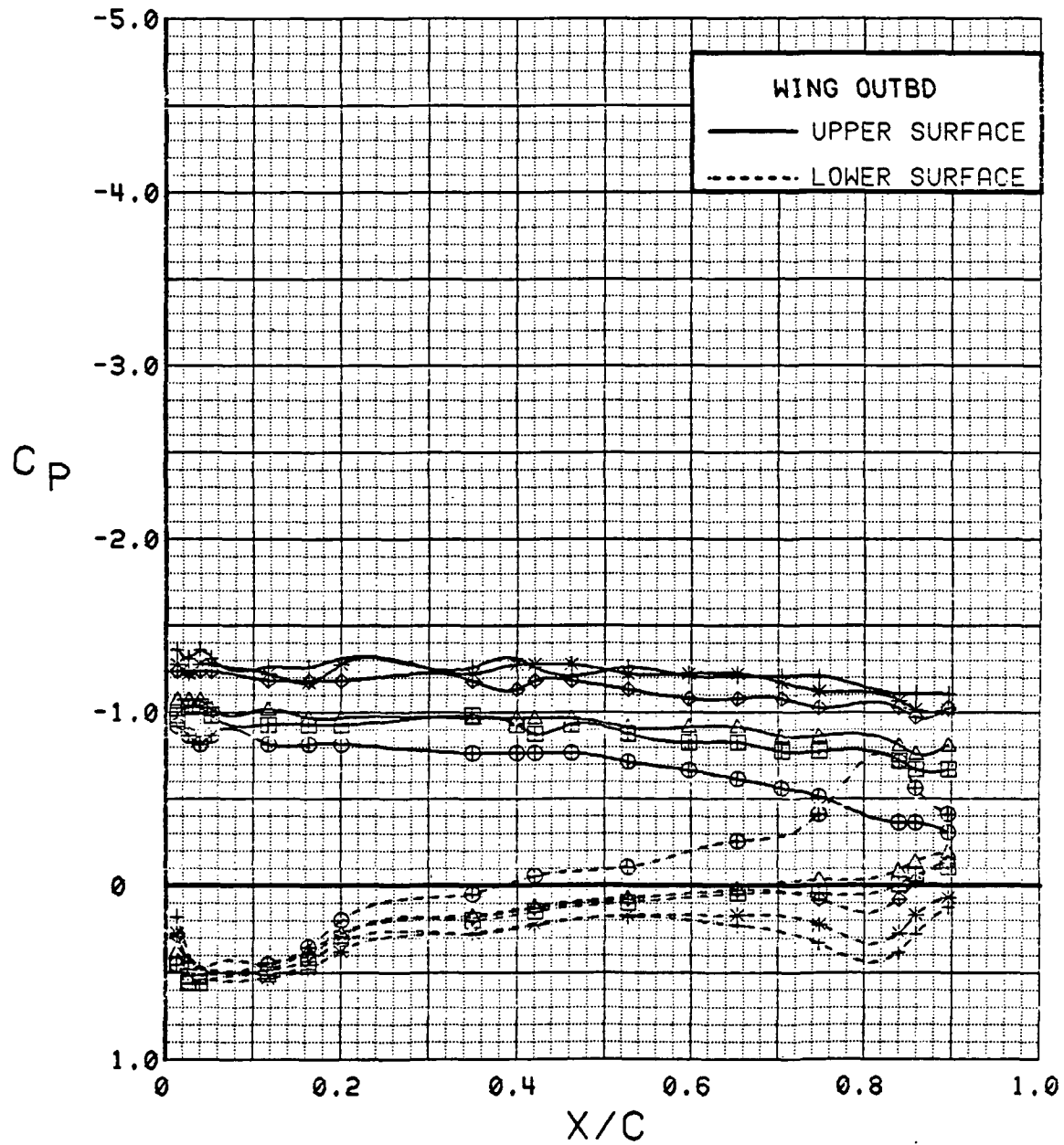


Figure 3.2.4-286 Wing Flap Effects, Outboard,  $C_T = 1.9$ ,  $\alpha = 16^\circ$

SYM	TEST	RUN	ALPHA	CT	ITEF	OTEF	CAN	SWB
⊕	543	85	20.6	1.85	-20	-20	0	OFF
⊞	543	72	20.8	1.86	-10	0	0	OFF
△	543	58	20.8	1.72	0	0	0	OFF
⊕	543	81	21.0	1.84	10	10	0	OFF
*	543	67	21.0	1.86	20	20	0	OFF
+	543	4	21.1	1.88	30	30	0	OFF

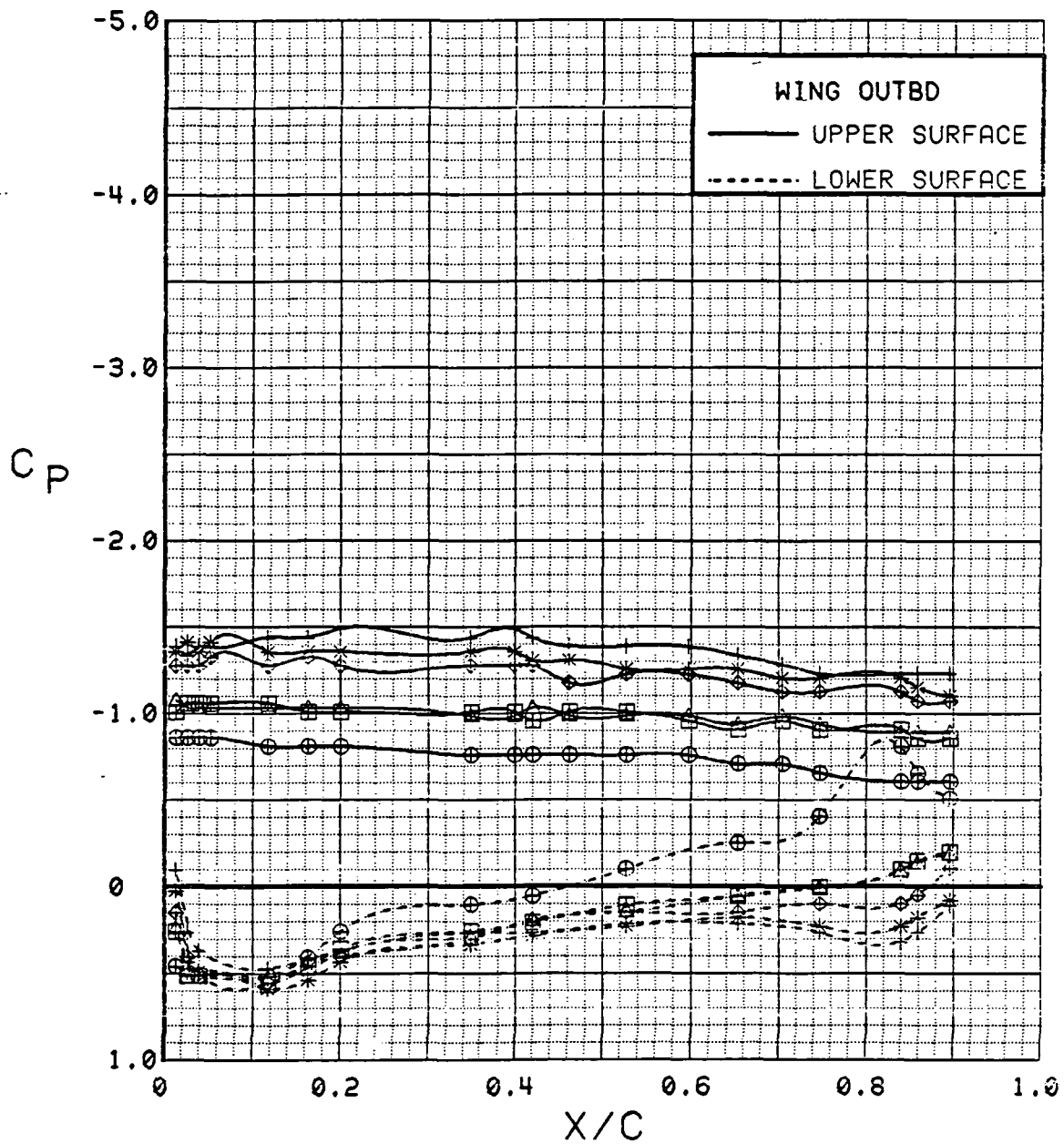


Figure 3.2.4-287 Wing Flap Effects, Outboard,  $C_T = 1.9$ ,  $\alpha = 20^\circ$

SYM	TEST	RUN	ALPHA	CT	ITEF	OTEF	CAN	SWB
⊕	543	85	4.0	1.89	-20	-20	0	OFF
⊞	543	72	4.2	1.96	-10	0	0	OFF
△	543	58	4.3	1.84	0	0	0	OFF
◆	543	81	4.4	1.87	10	10	0	OFF
*	543	67	4.5	1.89	20	20	0	OFF
+	543	4	4.5	1.90	30	30	0	OFF

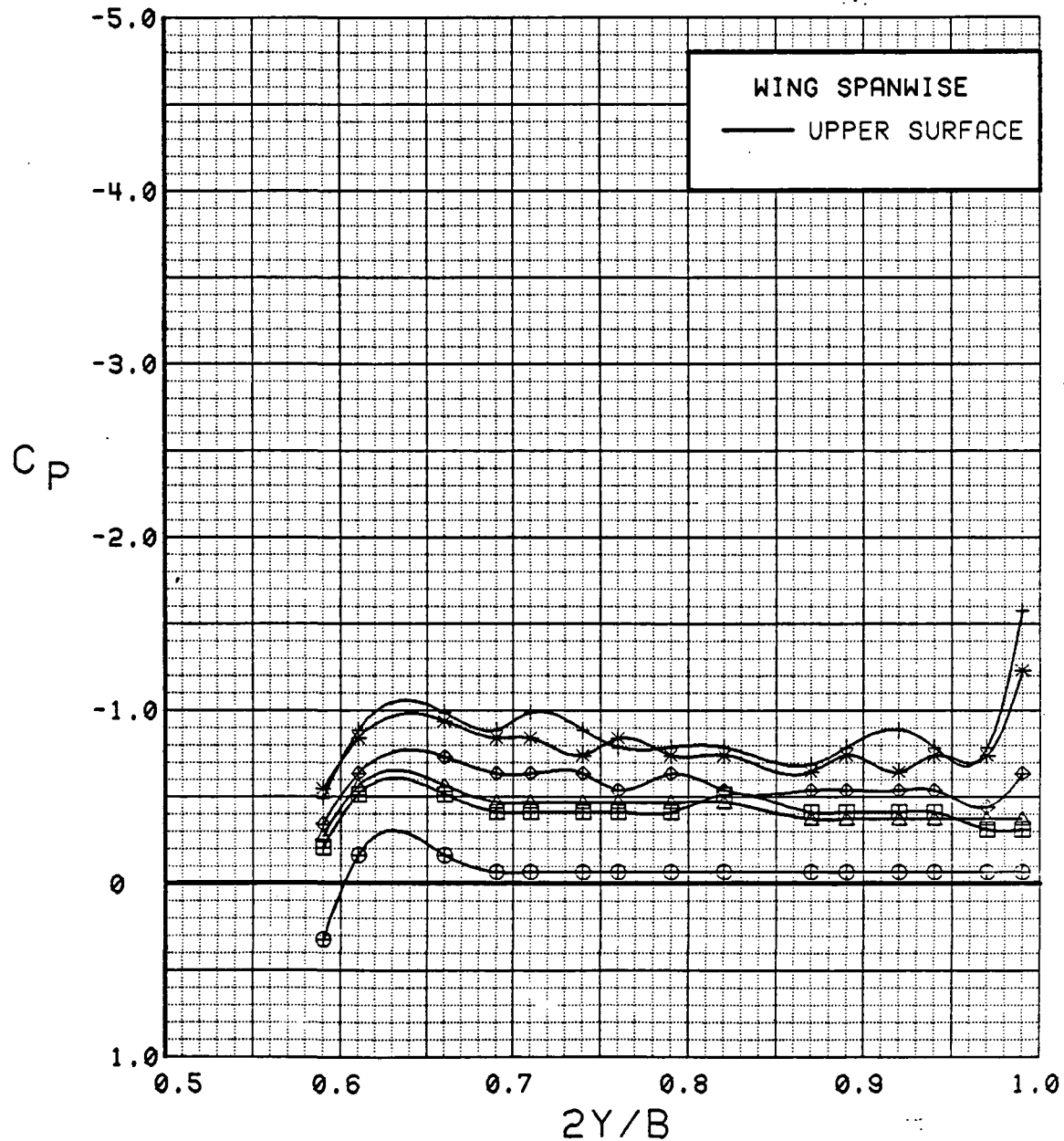


Figure 3.2.4-288 Wing Flap Effects, Spanwise,  $C_T = 1.9$ ,  $\alpha = 4^\circ$

SYM	TEST	RUN	ALPHA	CT	ITEF	OTEF	CAN	SWB
⊕	543	85	8.2	1.88	-20	-20	0	OFF
⊞	543	72	8.4	1.86	-10	0	0	OFF
△	543	58	8.4	1.90	0	0	0	OFF
◆	543	81	8.5	1.91	10	10	0	OFF
*	543	67	8.6	1.89	20	20	0	OFF
+	543	4	8.7	1.85	30	30	0	OFF

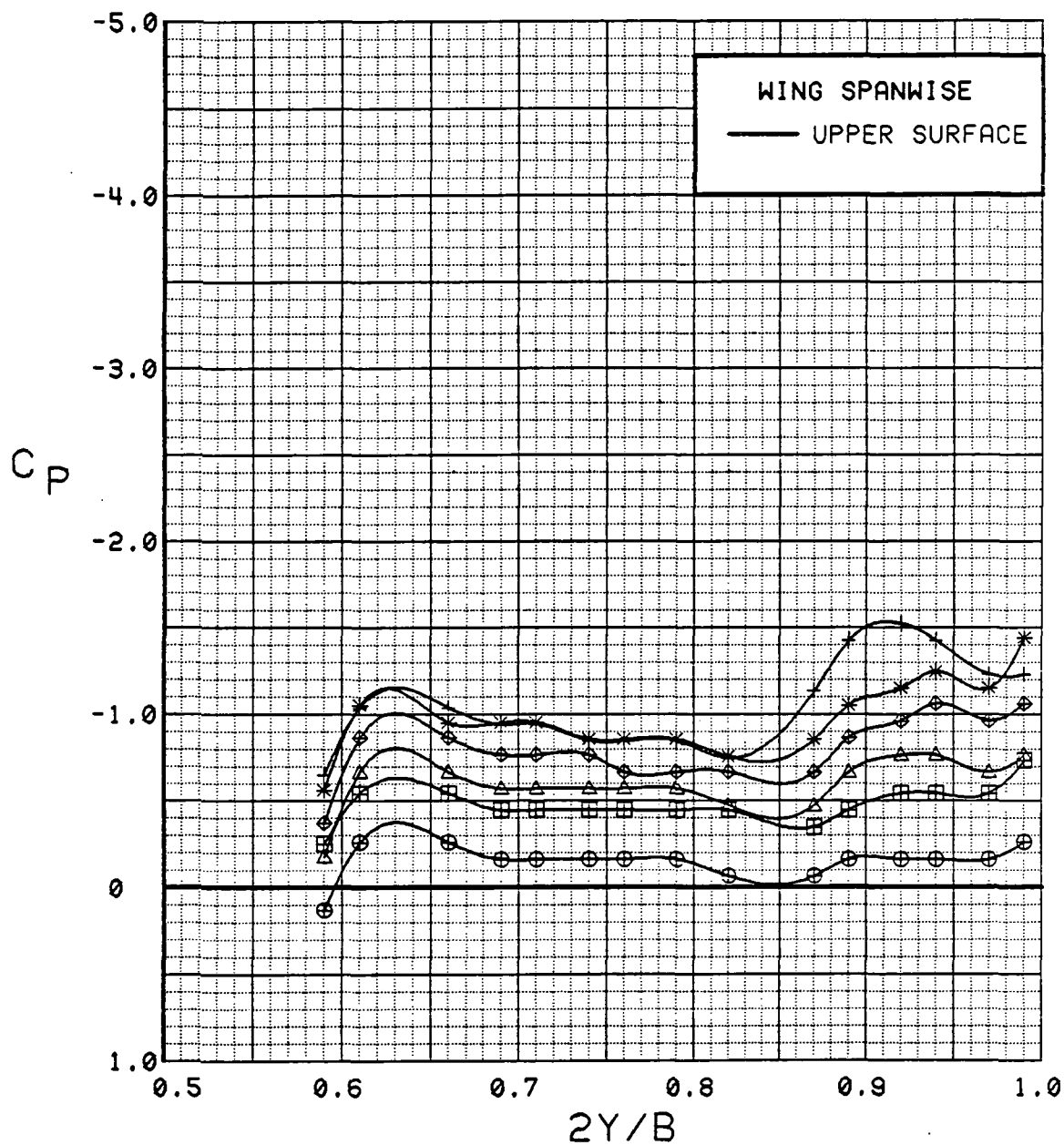


Figure 3.2.4-289 Wing Flap Effects, Spanwise,  $C_T = 1.9$ ,  $\alpha = 8^\circ$

SYM	TEST	RUN	ALPHA	CT	ITEF	OTEF	CAN	SWB
⊕	543	85	12.3	1.84	-20	-20	0	OFF
⊞	543	72	12.6	1.87	-10	0	0	OFF
△	543	58	12.6	1.87	0	0	0	OFF
◆	543	81	12.7	1.87	10	10	0	OFF
*	543	67	12.8	1.90	20	20	0	OFF
+	543	4	12.8	1.86	30	30	0	OFF

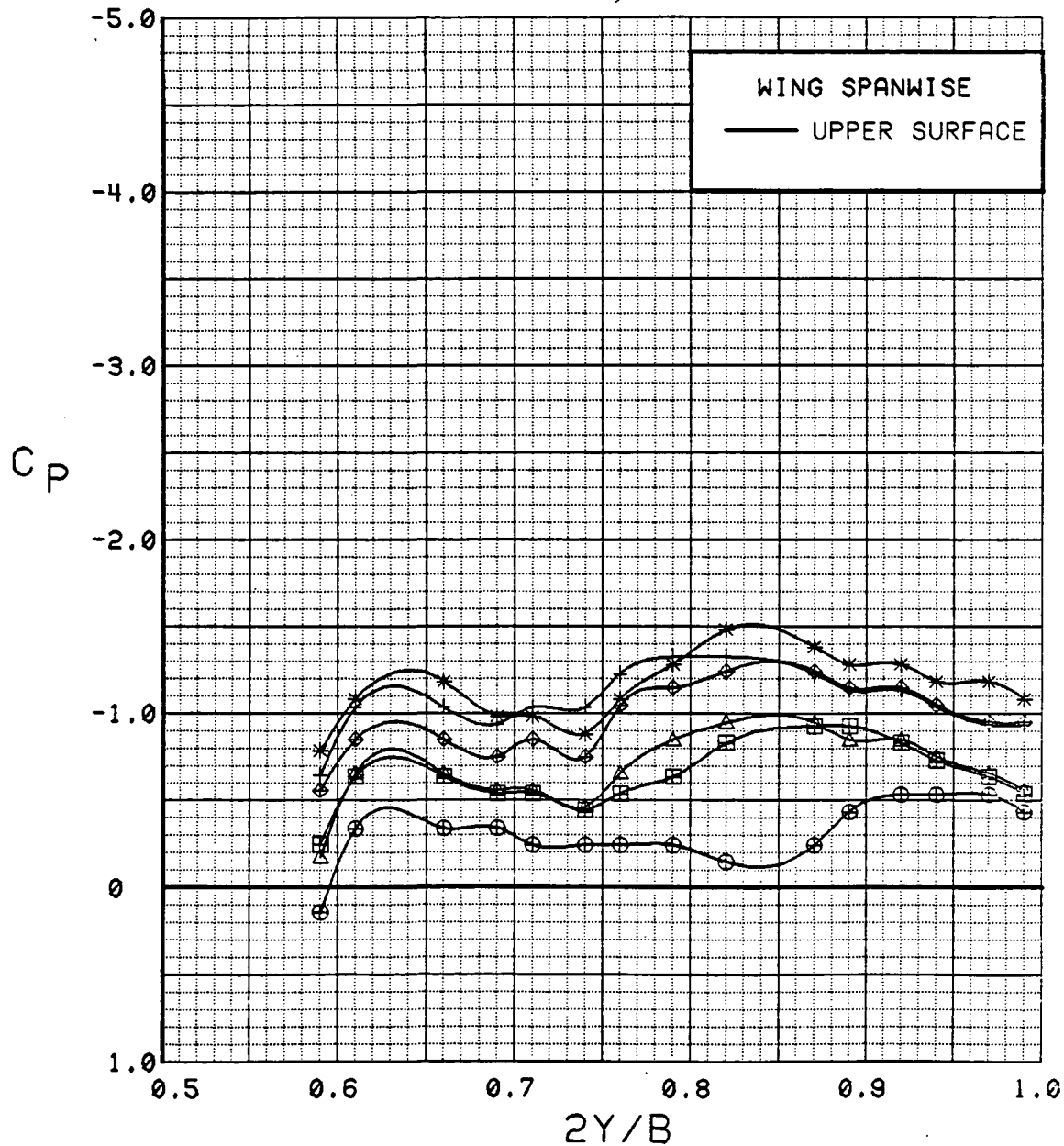


Figure 3.2.4-290 Wing Flap Effects, Spanwise,  $C_T = 1.9$ ,  $\alpha = 12^\circ$

SYM	TEST	RUN	ALPHA	CT	ITEF	OTEF	CAN	SWB
⊕	543	85	16.5	1.86	-20	-20	0	OFF
⊞	543	72	16.7	1.86	-10	0	0	OFF
△	543	58	16.7	1.87	0	0	0	OFF
◆	543	81	16.8	1.91	10	10	0	OFF
*	543	67	16.9	1.90	20	20	0	OFF
+	543	4	16.9	1.86	30	30	0	OFF

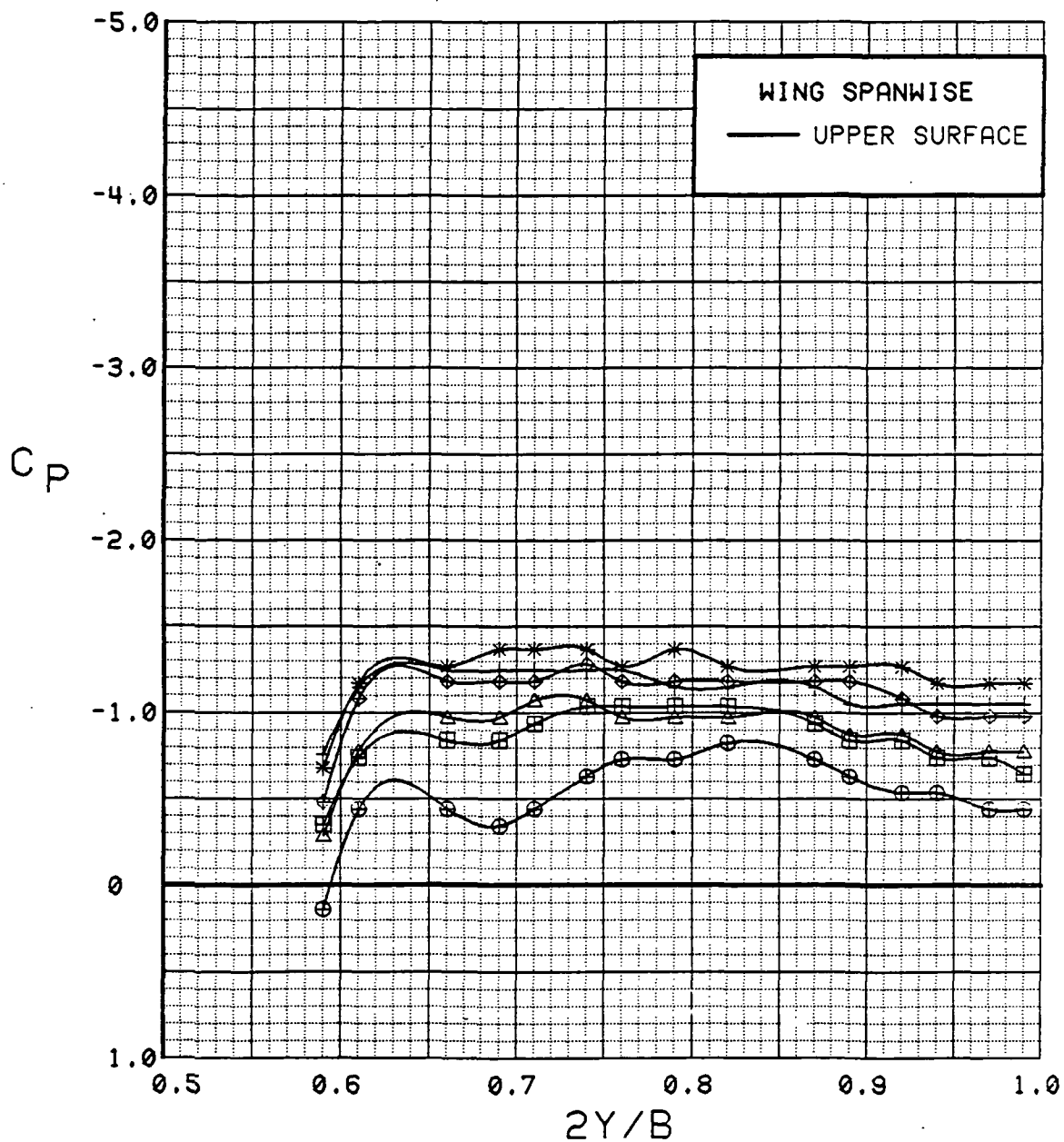


Figure 3.2.4-291 Wing Flap Effects, Spanwise,  $C_T = 1.9$ ,  $\alpha = 16^\circ$



SYM	TEST	RUN	ALPHA	CT	ITEF	OTEF	CAN	SWB
⊕	543	85	20.6	1.85	-20	-20	0	OFF
⊞	543	72	20.8	1.86	-10	0	0	OFF
△	543	58	20.8	1.72	0	0	0	OFF
◆	543	81	21.0	1.84	10	10	0	OFF
*	543	67	21.0	1.86	20	20	0	OFF
+	543	4	21.1	1.88	30	30	0	OFF

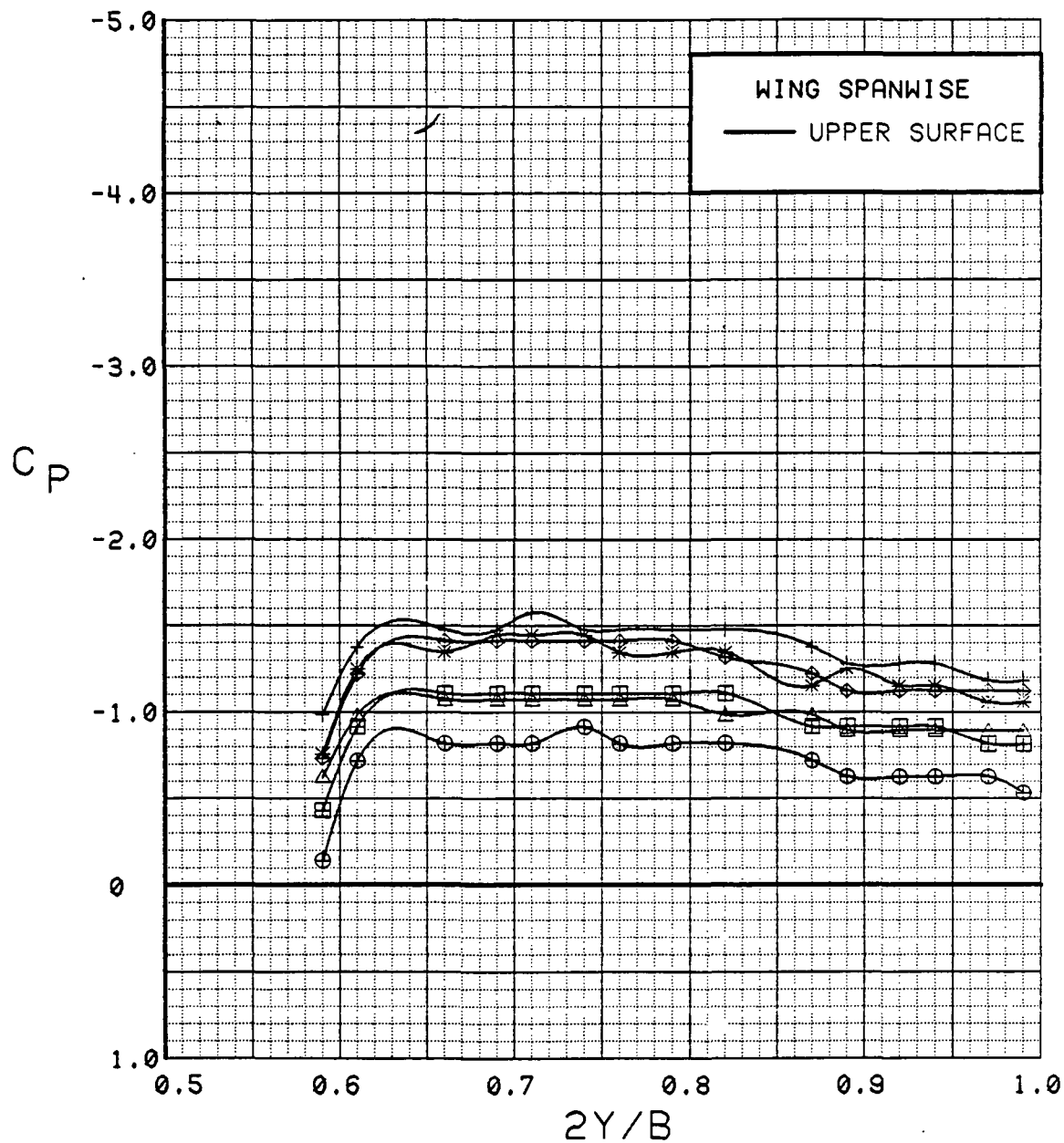


Figure 3.2.4-292 Wing Flap Effects, Spanwise,  $C_T = 1.9$ , Alpha = 20 deg

# WING INBOARD

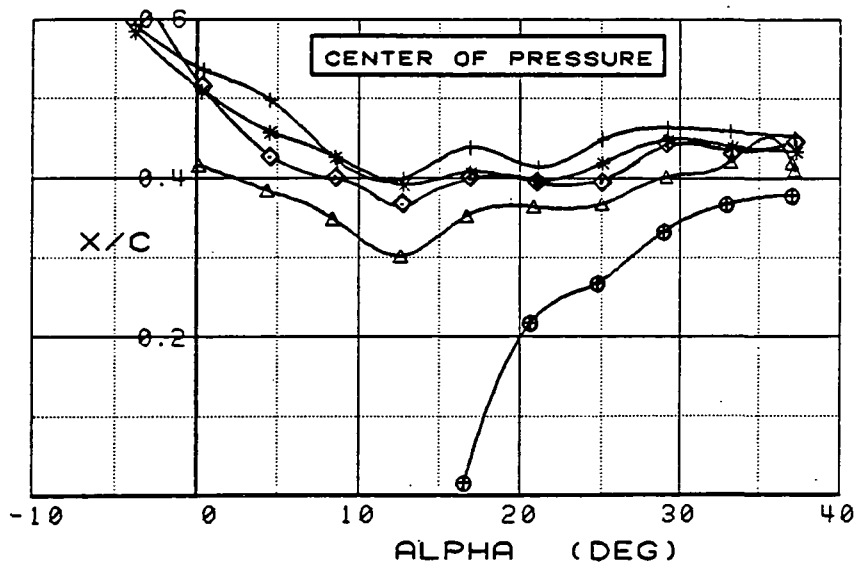
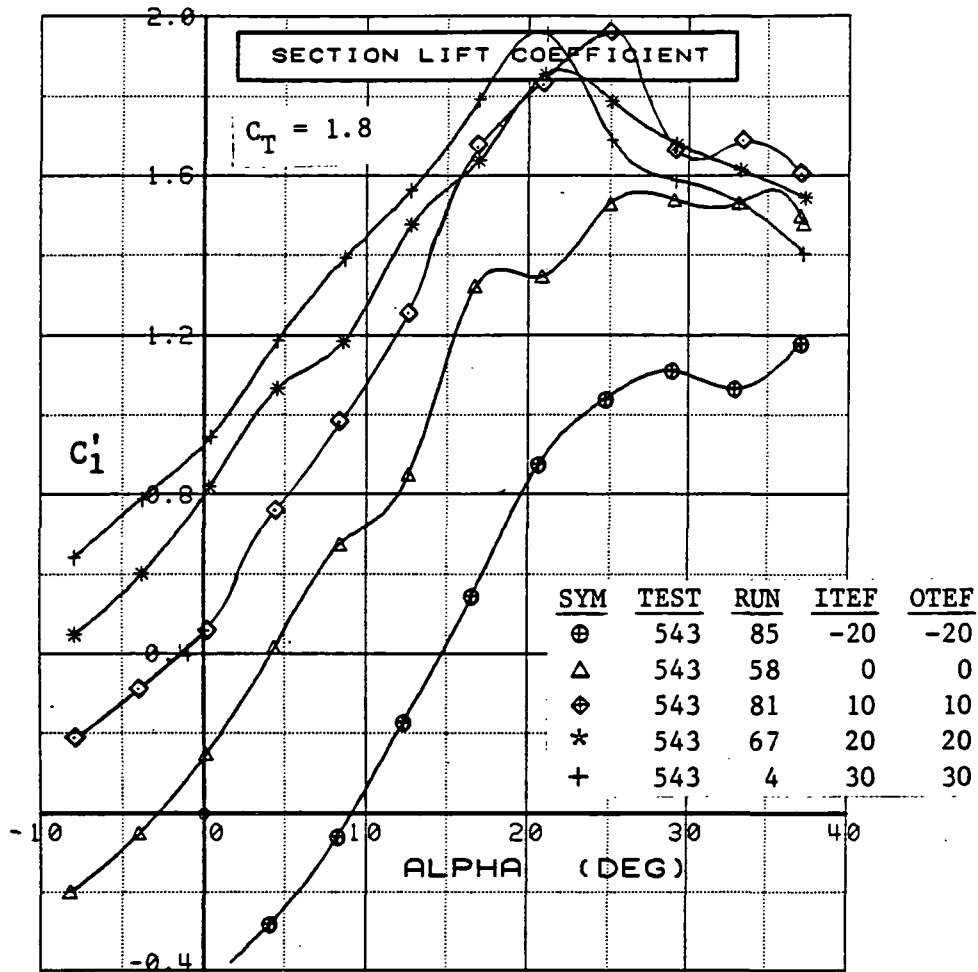


Figure 3.2.4-293 Wing Flap Effects, Inboard,  $C_T = 1.9$ , Integrated Section Properties

## WING OUTBOARD

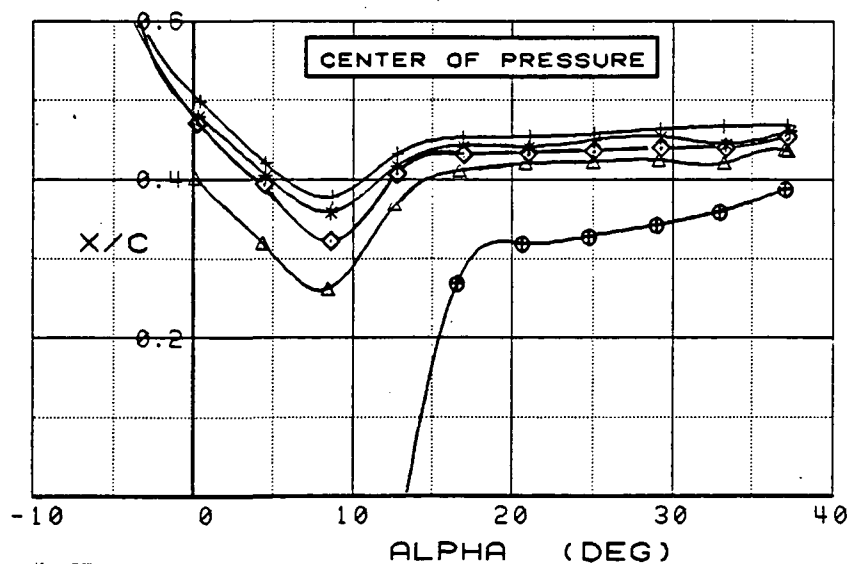
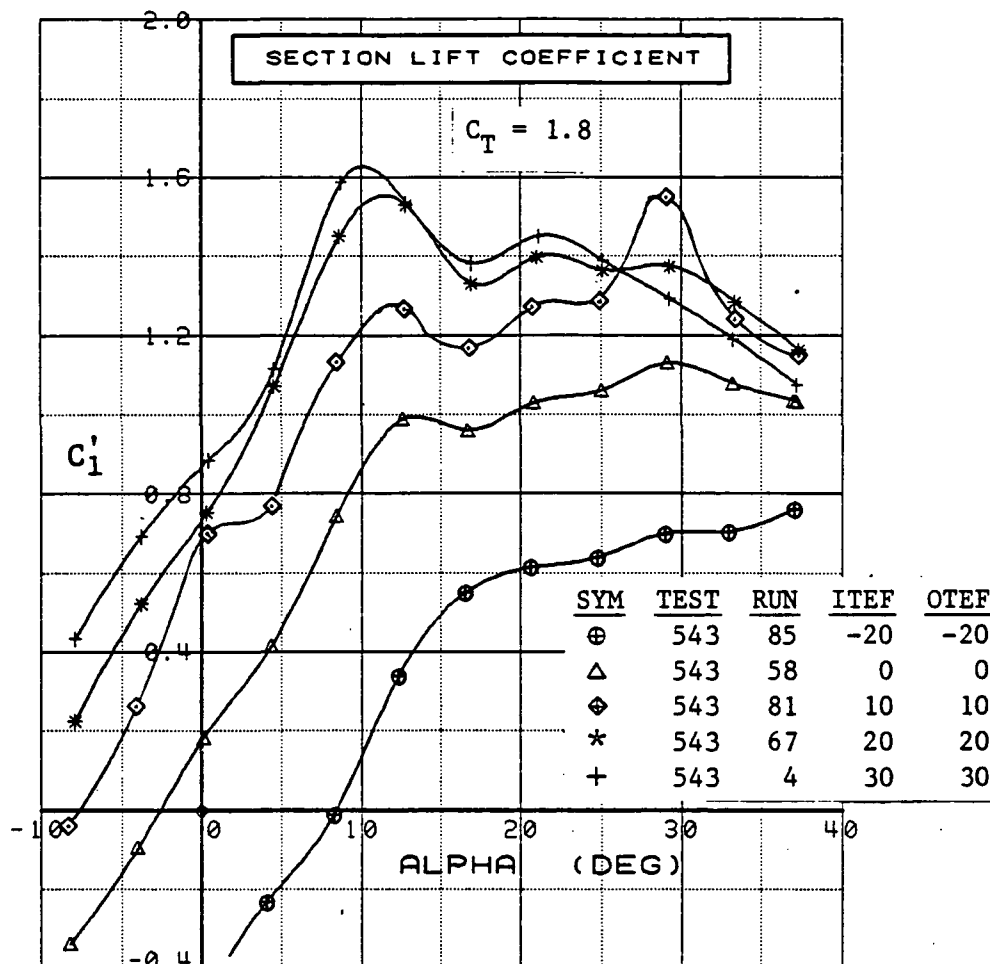


Figure 3.2.4-294 Wing Flap Effects, Outboard,  $C_T = 1.9$ , Integrated Section Properties

SYM	TEST	RUN	ALPHA	CT	ITEF	OTEF	CAN	SWB	q
⊕	537	17	0.2	0.00	30	30	0	OFF	7
⊞	537	12	0.3	0.00	30	30	0	OFF	15
Δ	537	18	0.3	0.00	30	30	0	OFF	40

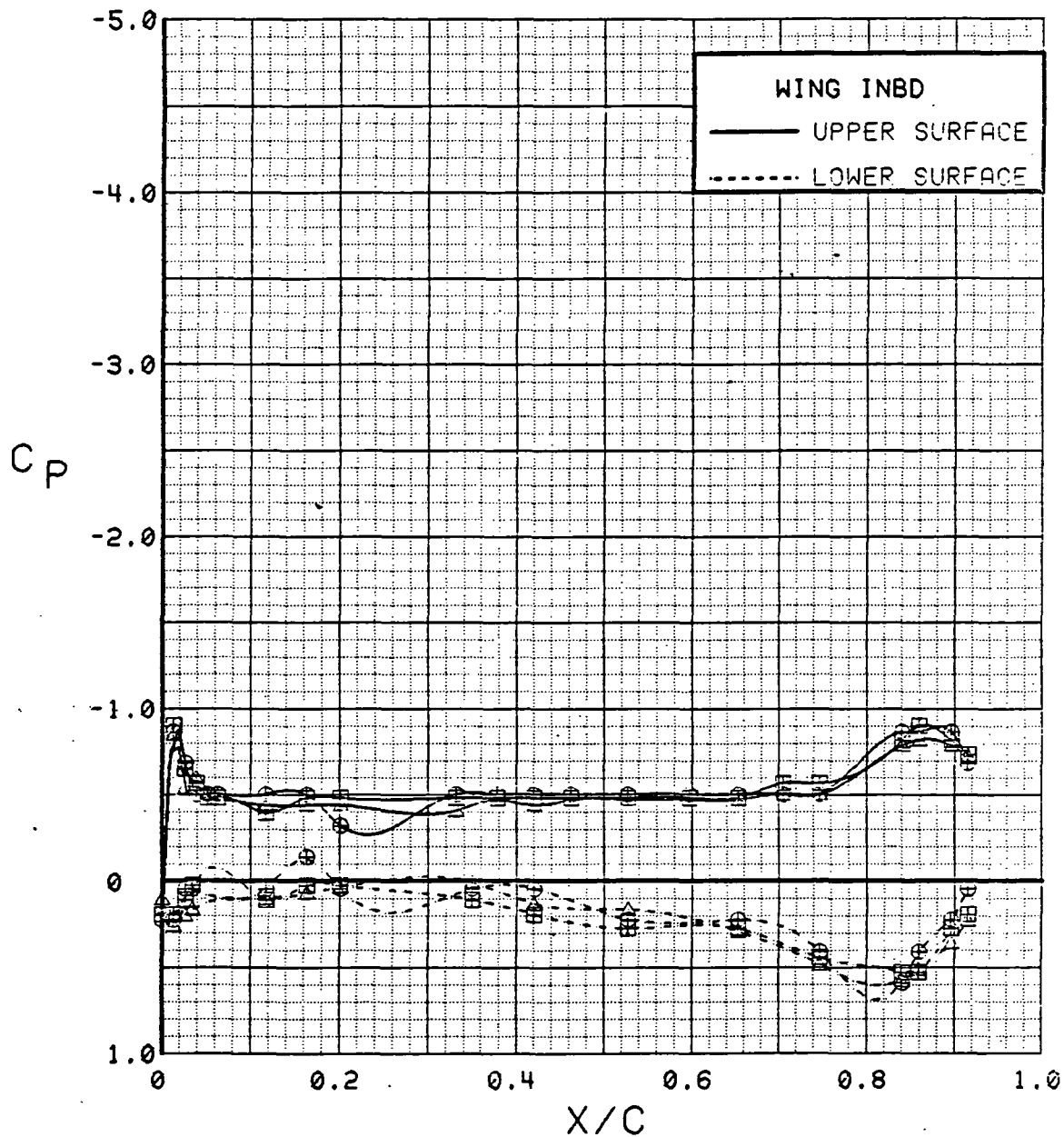


Figure 3.2.4-295 Dynamic Pressure Effects, Flaps Deflected, Power off, Inboard, Alpha = 0 deg

SYM	TEST	RUN	ALPHA	CT	ITEF	OTEF	CAN	SWB	q
⊕	537	17	4.4	0.00	30	30	0	OFF	7
⊞	537	12	4.4	0.00	30	30	0	OFF	15
Δ	537	18	4.4	0.00	30	30	0	OFF	40

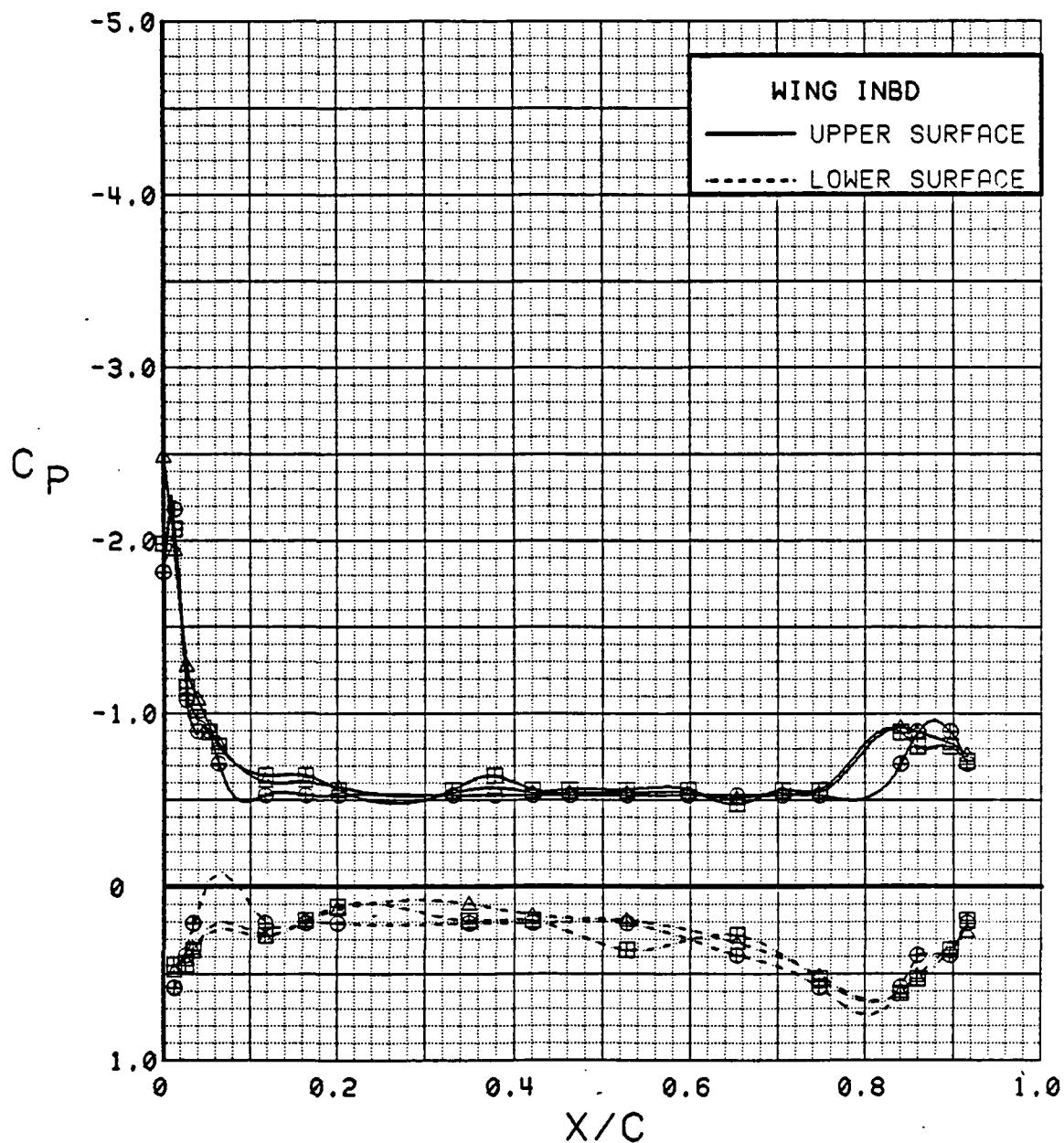


Figure 3.2.4-296 Dynamic Pressure Effects, Flaps Deflected, Power off, Inboard, Alpha = 4 deg

SYM	TEST	RUN	ALPHA	CT	ITEF	OTEF	CAN	SWB	q
⊕	537	17	8.5	0.00	30	30	0	OFF	7
⊞	537	12	8.5	0.00	30	30	0	OFF	15
Δ	537	18	8.5	0.00	30	30	0	OFF	40

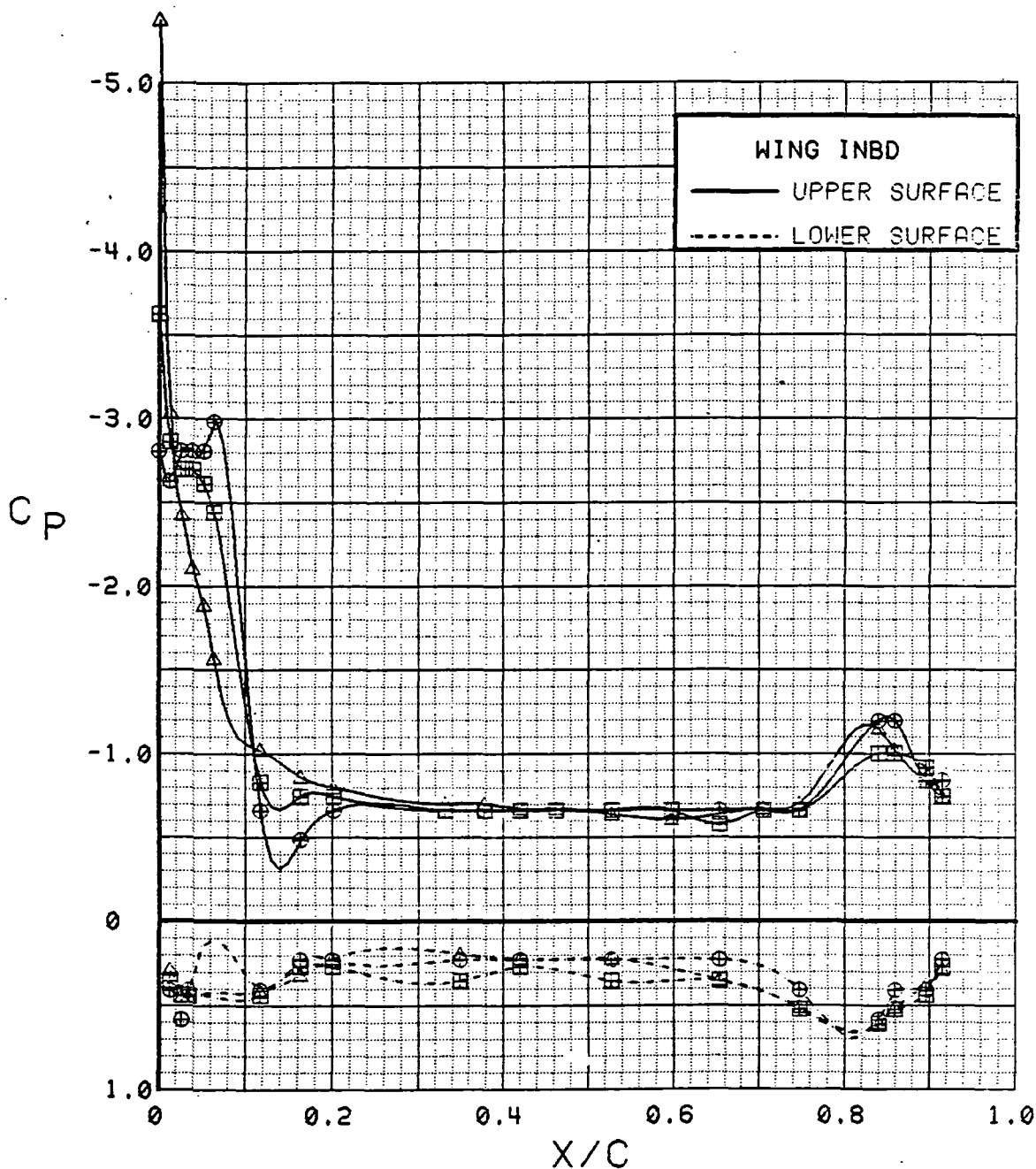


Figure 3.2.4-297 Dynamic Pressure Effects, Flaps Deflected, Power off, Inboard, Alpha = 8 deg

SYM	TEST	RUN	ALPHA	CT	ITEF	OTEF	CAN	SWB	q
⊕	537	17	12.7	0.00	30	30	0	OFF	7
⊞	537	12	12.7	0.00	30	30	0	OFF	15
Δ	537	18	12.7	0.00	30	30	0	OFF	40

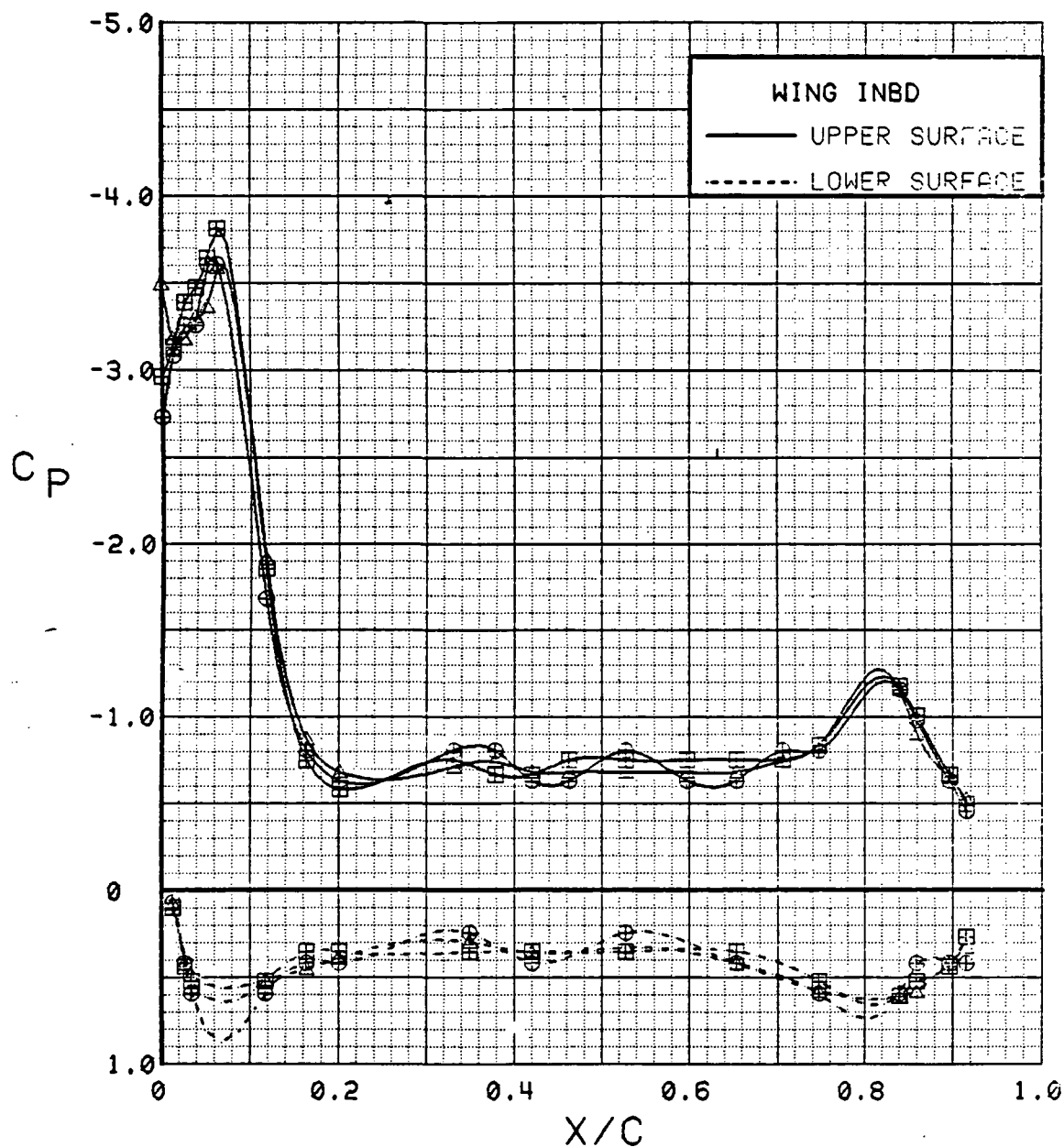


Figure 3.2.4-298 Dynamic Pressure Effects, Flaps Deflected,  
Power off, Inboard, Alpha = 12 deg

SYM	TEST	RUN	ALPHA	CT	ITEF	OTEF	CAN	SWB	q
⊕	537	17	0.2	0.00	30	30	0	OFF	7
⊞	537	12	0.3	0.00	30	30	0	OFF	15
Δ	537	18	0.3	0.00	30	30	0	OFF	40

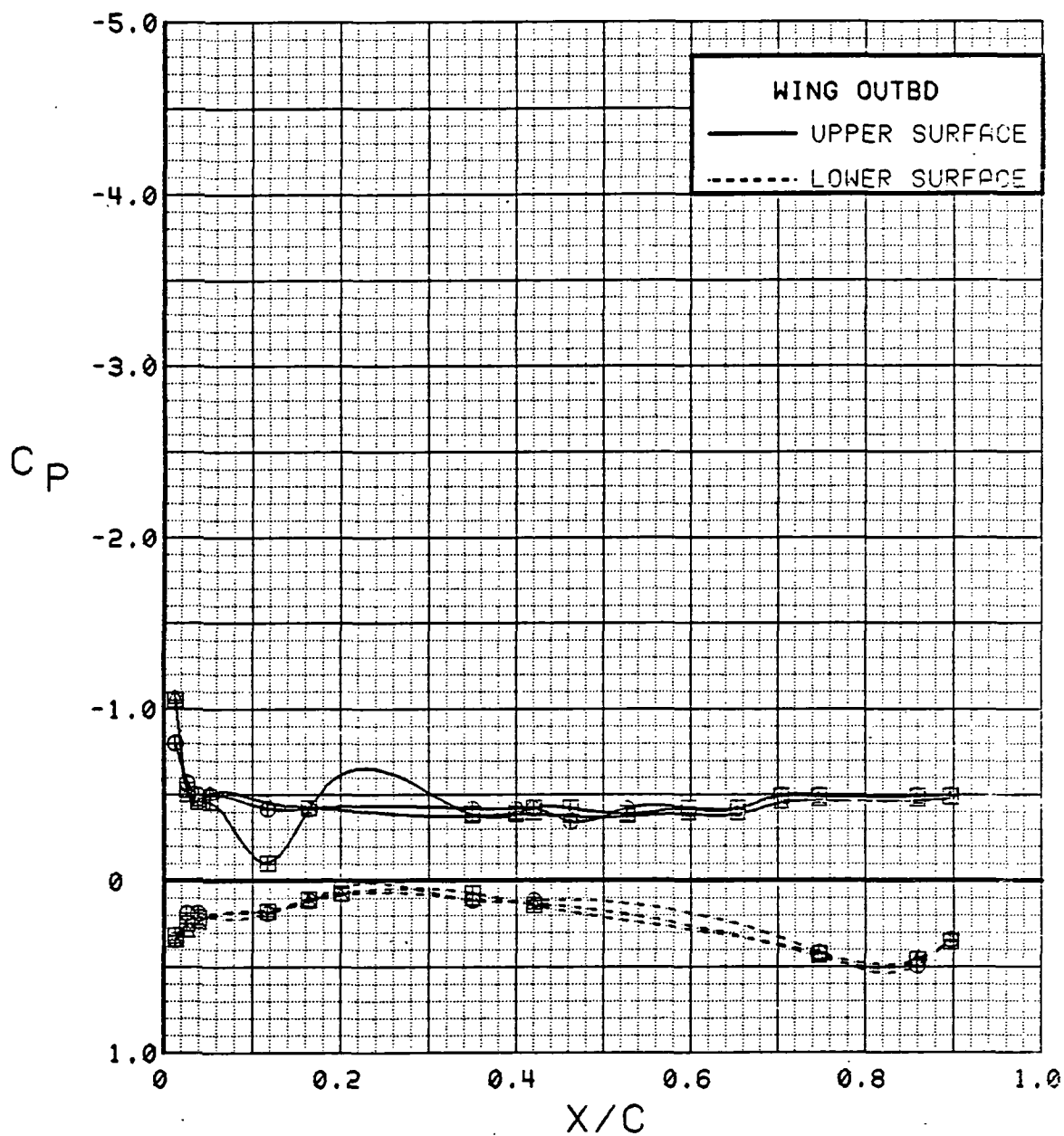


Figure 3.2.4-299 Dynamic Pressure Effects, Flaps Deflected, Power off, Outboard, Alpha = 0 deg



SYM	TEST	RUN	ALPHA	CT	ITEF	OTEF	CAN	SWB	q
⊕	537	17	4.4	0.00	30	30	0	OFF	7
⊞	537	12	4.4	0.00	30	30	0	OFF	15
△	537	18	4.4	0.00	30	30	0	OFF	40

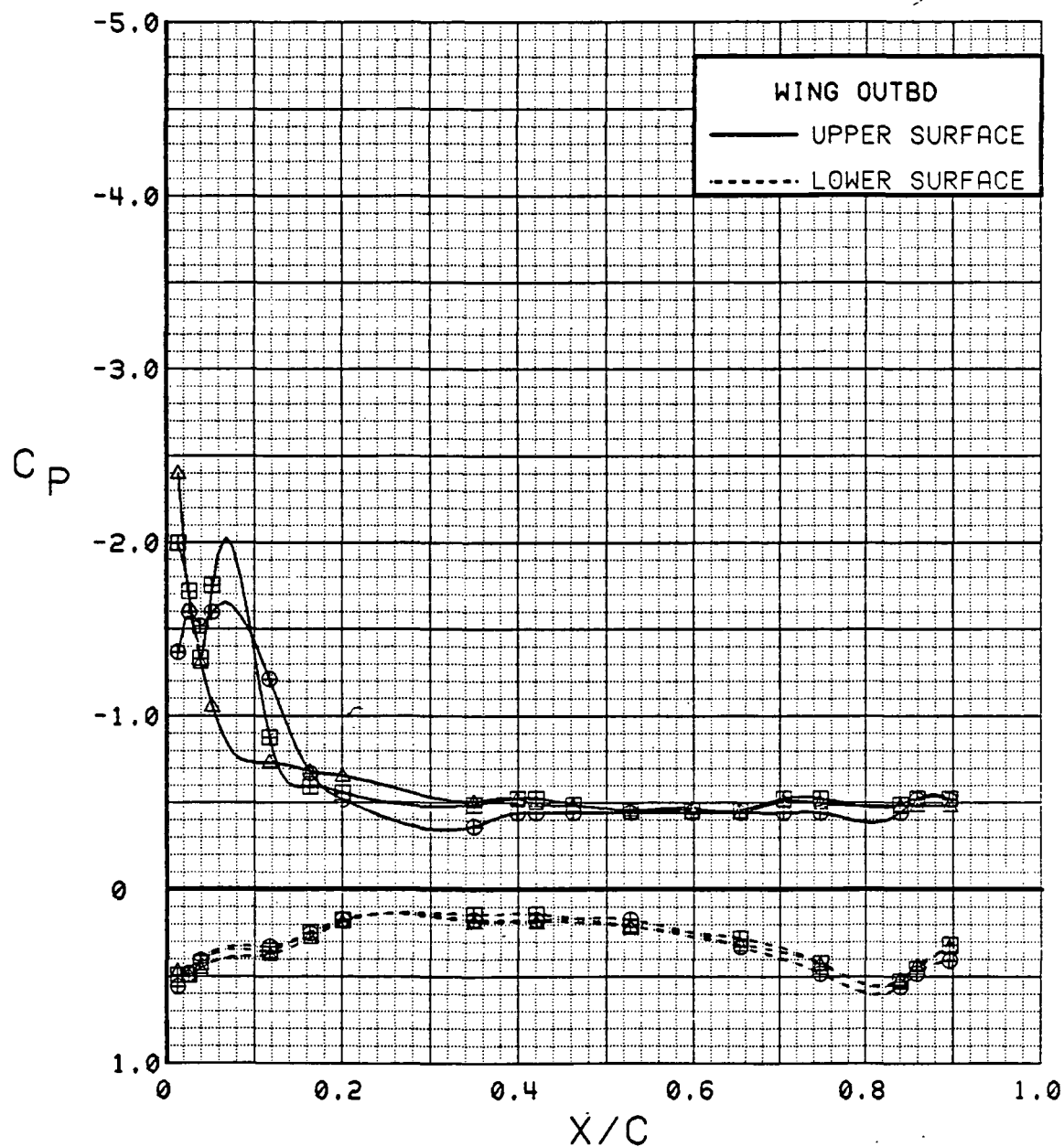


Figure 3.2.4-300 Dynamic Pressure Effects, Flaps Deflected, Power off, Outboard, Alpha = 4 deg

SYM	TEST	RUN	ALPHA	CT	ITEF	OTEF	CAN	SWB	q
⊕	537	17	8.5	0.00	30	30	0	OFF	7
⊞	537	12	8.5	0.00	30	30	0	OFF	15
△	537	18	8.5	0.00	30	30	0	OFF	40

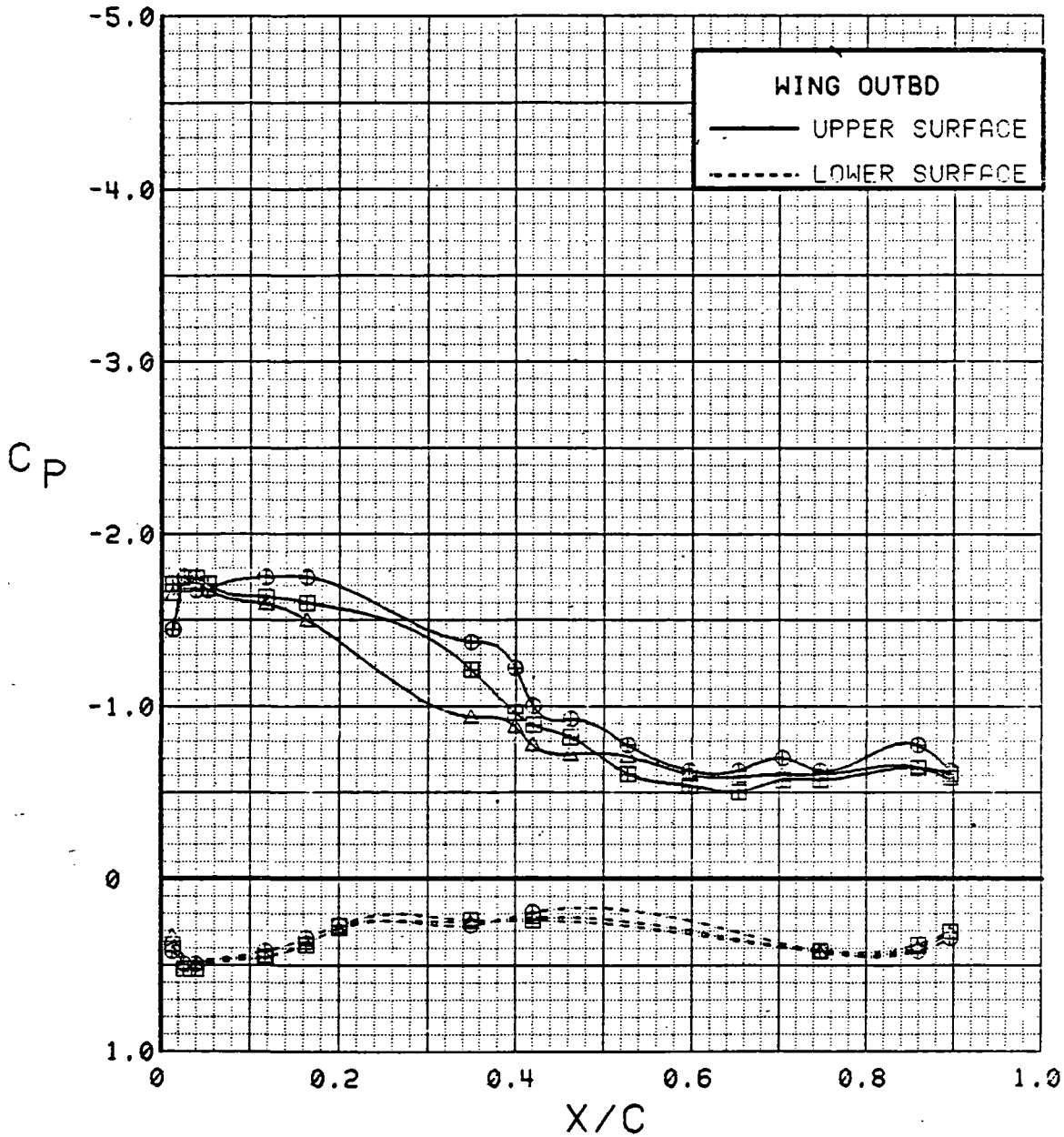


Figure 3.2.4-301 Dynamic Pressure Effects, Flaps Deflected, Power off, Outboard, Alpha = 8 deg

SYM	TEST	RUN	ALPHA	CT	ITEF	OTEF	CAN	SWB	q
⊕	537	17	12.7	0.00	30	30	0	OFF	7
⊞	537	12	12.7	0.00	30	30	0	OFF	15
Δ	537	18	12.7	0.00	30	30	0	OFF	40

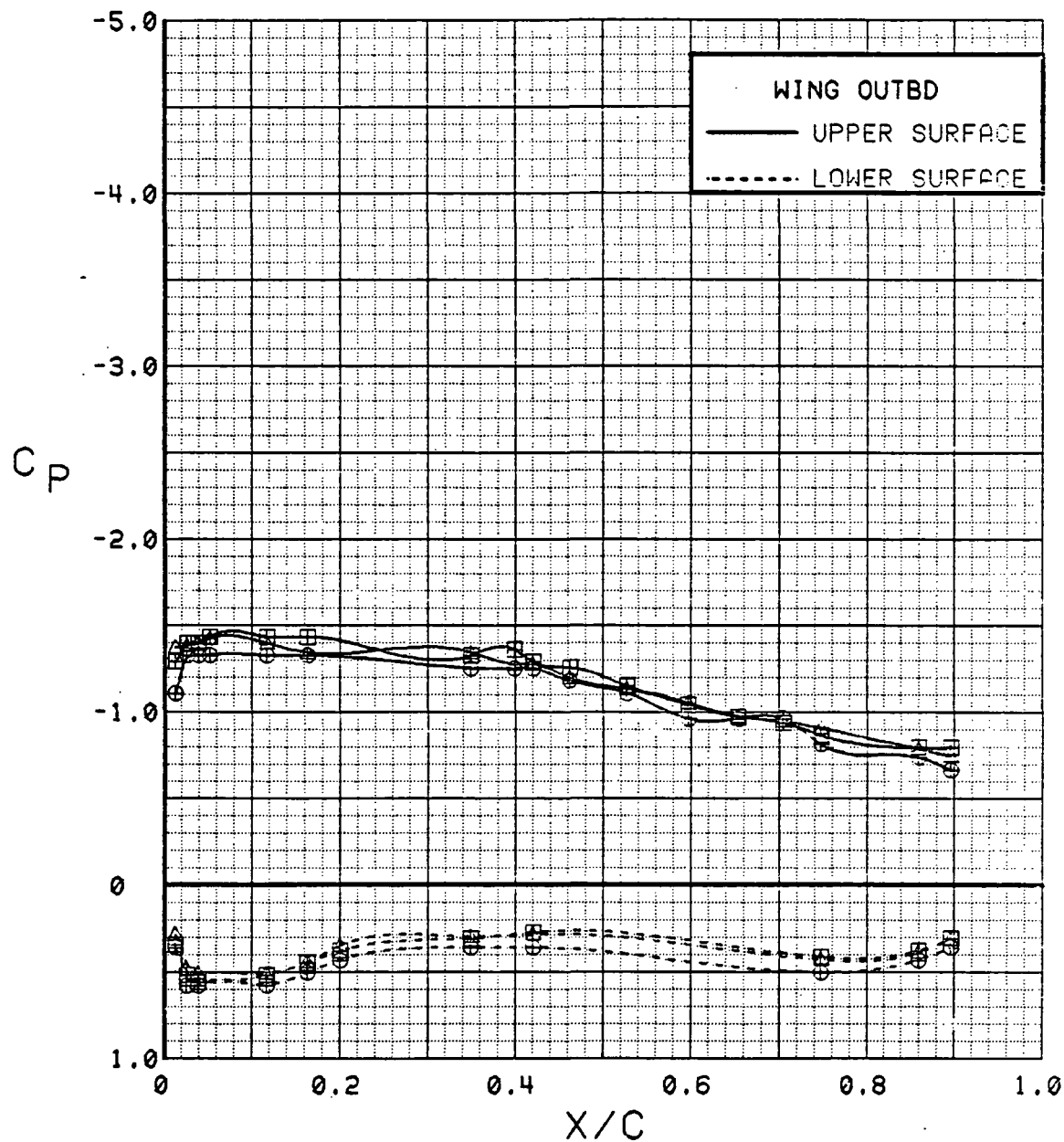


Figure 3.2.4-302 Dynamic Pressure Effects, Flaps Deflected, Power off, Outboard, Alpha = 12 deg

SYM	TEST	RUN	ALPHA	CT	ITEF	OTEF	CAN	SWB	q
⊕	537	17	0.2	0.00	30	30	0	OFF	7
⊞	537	12	0.3	0.00	30	30	0	OFF	15
△	537	18	0.3	0.00	30	30	0	OFF	40

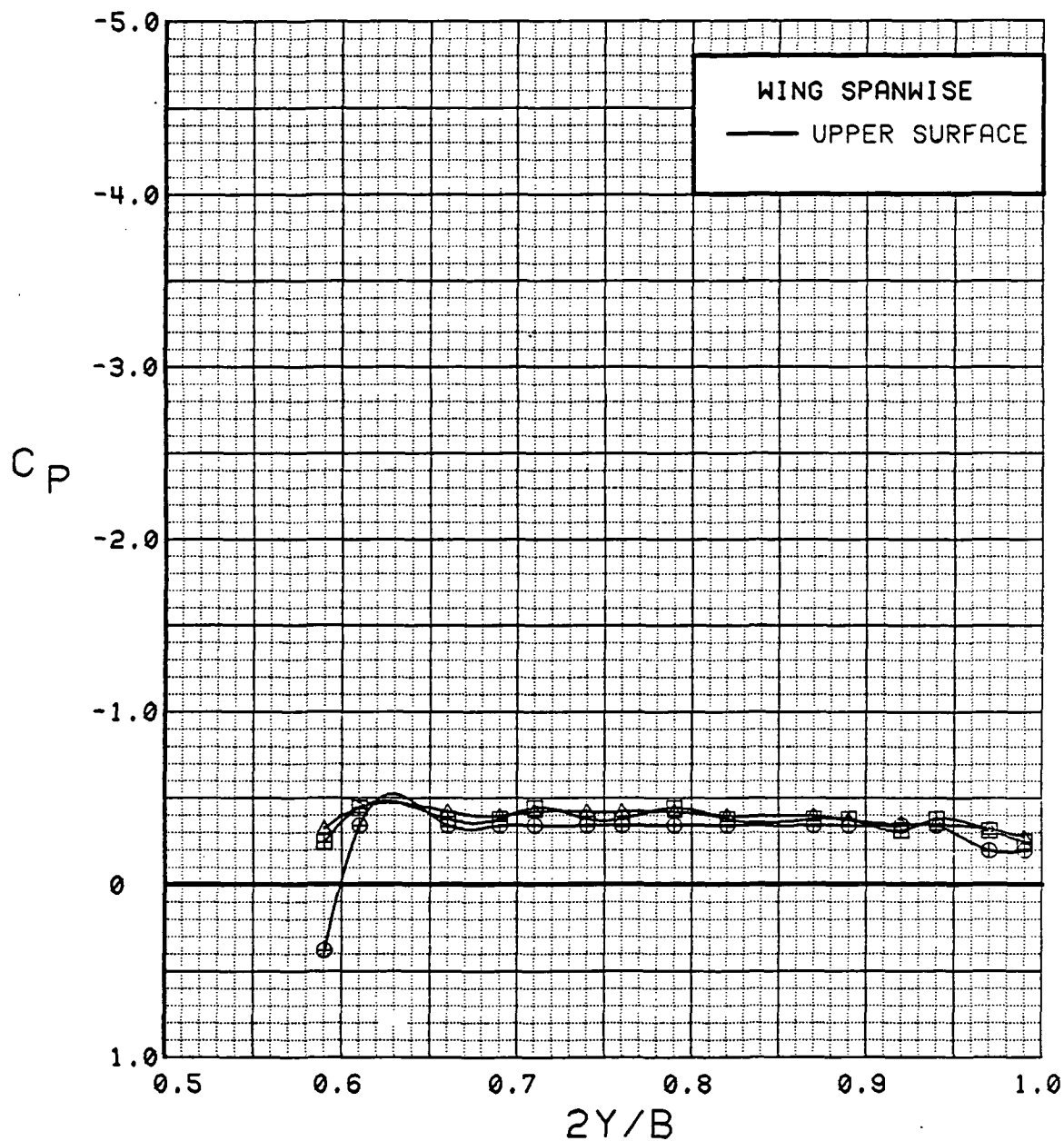


Figure 3.2.4-303 Dynamic Pressure Effects, Flaps Deflected,  
Power off, Spanwise, Alpha = 0 deg

SYM	TEST	RUN	ALPHA	CT	ITEF	OTEF	CAN	SWB	q
⊕	537	17	4.4	0.00	30	30	0	OFF	7
⊞	537	12	4.4	0.00	30	30	0	OFF	15
△	537	18	4.4	0.00	30	30	0	OFF	40

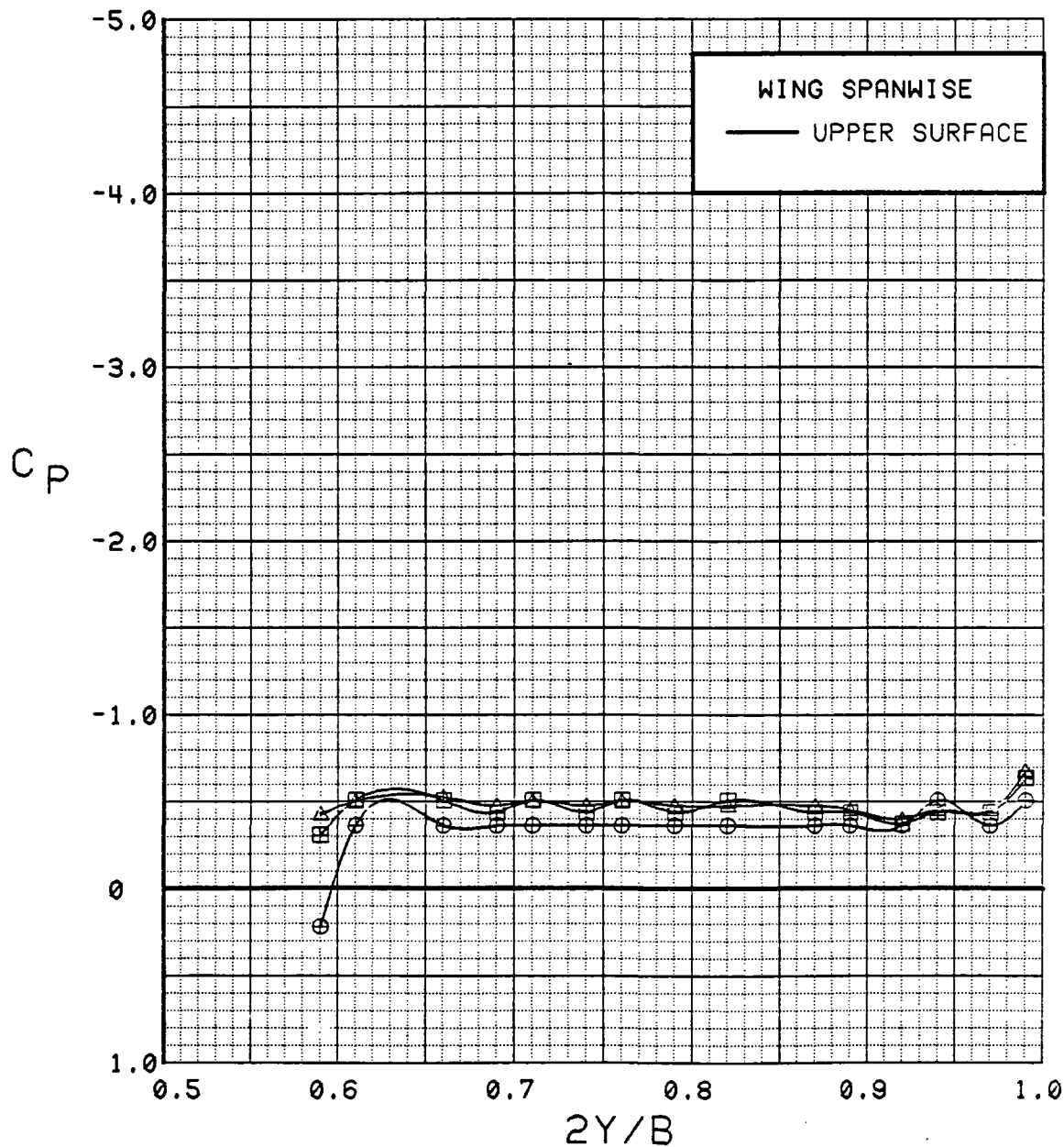


Figure 3.2.4-304 Dynamic Pressure Effects, Flaps Deflected,  
Power off, Spanwise, Alpha = 4 deg

SYM	TEST	RUN	ALPHA	CT	ITEF	OTEF	CAN	SWB	q
⊕	537	17	8.5	0.00	30	30	0	OFF	7
⊞	537	12	8.5	0.00	30	30	0	OFF	15
△	537	18	8.5	0.00	30	30	0	OFF	40

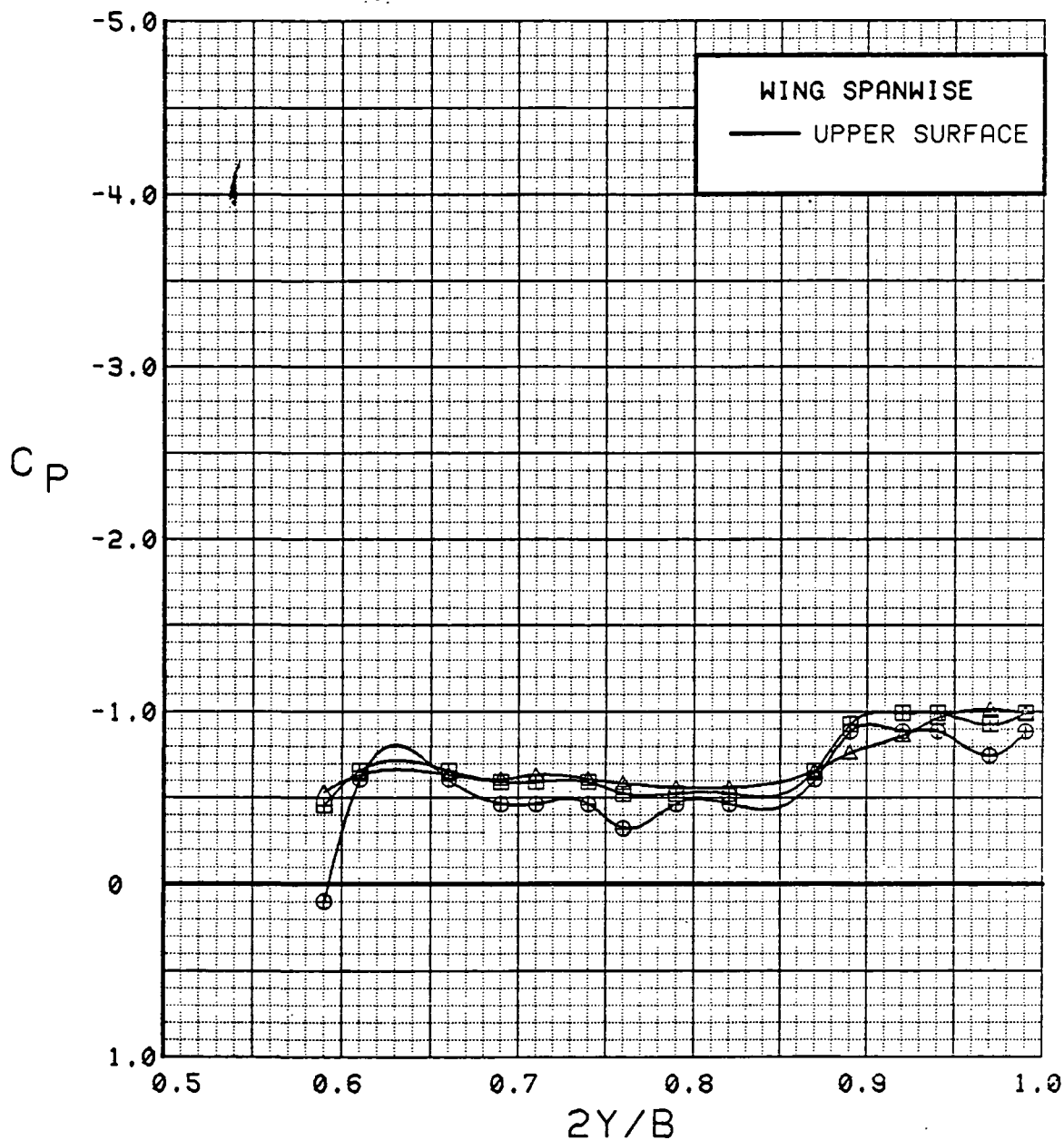


Figure 3.2.4-305 Dynamic Pressure Effects, Flaps Deflected, Power off, Spanwise, Alpha = 8 deg

SYM	TEST	RUN	ALPHA	CT	ITEF	OTEF	CAN	SWB	q
⊕	537	17	12.7	0.00	30	30	0	OFF	7
⊞	537	12	12.7	0.00	30	30	0	OFF	15
△	537	18	12.7	0.00	30	30	0	OFF	40

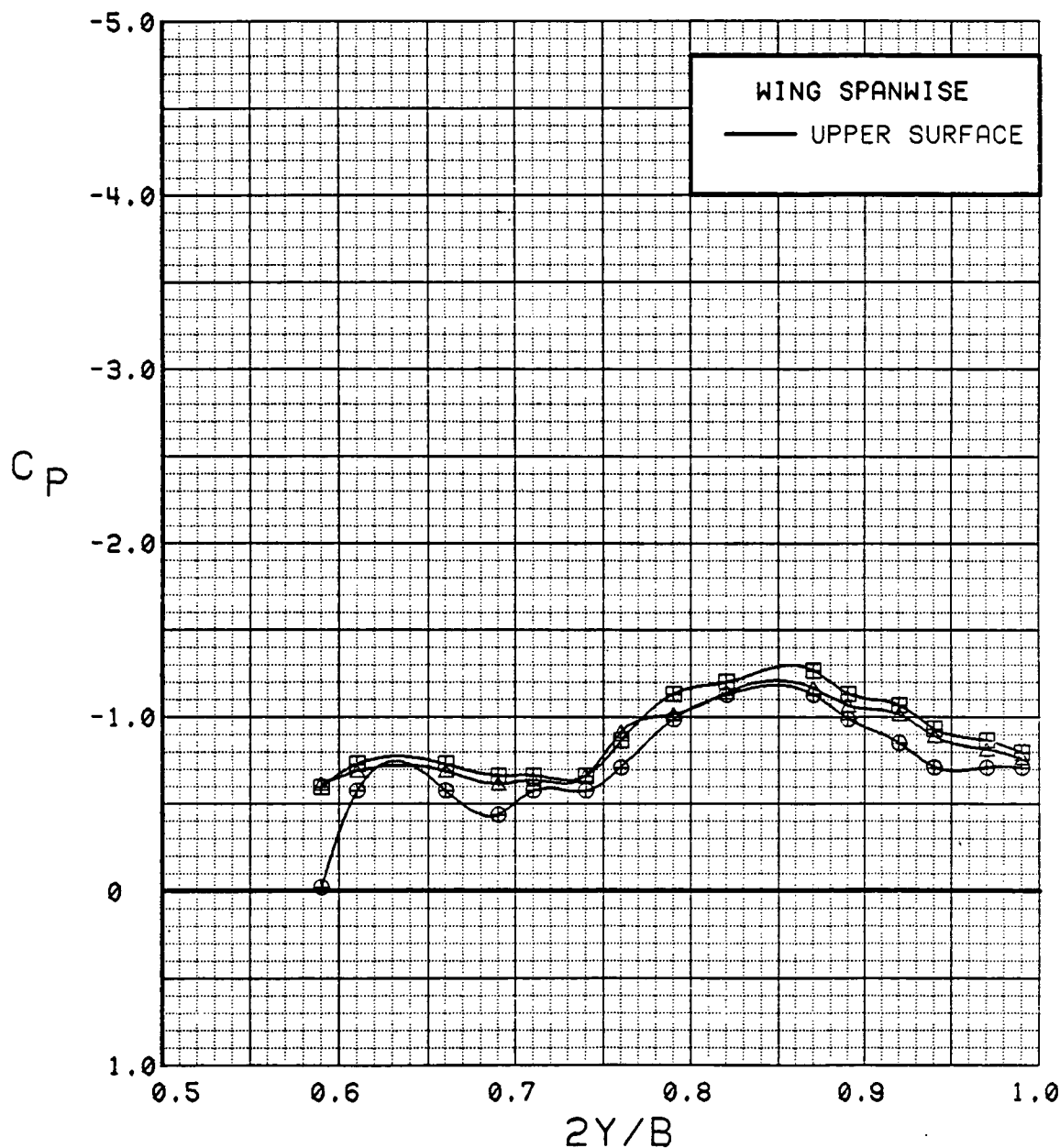


Figure 3.2.4-306 Dynamic Pressure Effects, Flaps Deflected, Power off, Spanwise, Alpha = 12 deg

SYM	TEST	RUN	ALPHA	CT	ITEF	OTEF	CAN	SWB
⊕	543	63	0.1	0.00	0	0	0	OFF
⊞	543	59	0.1	1.42	0	0	0	OFF

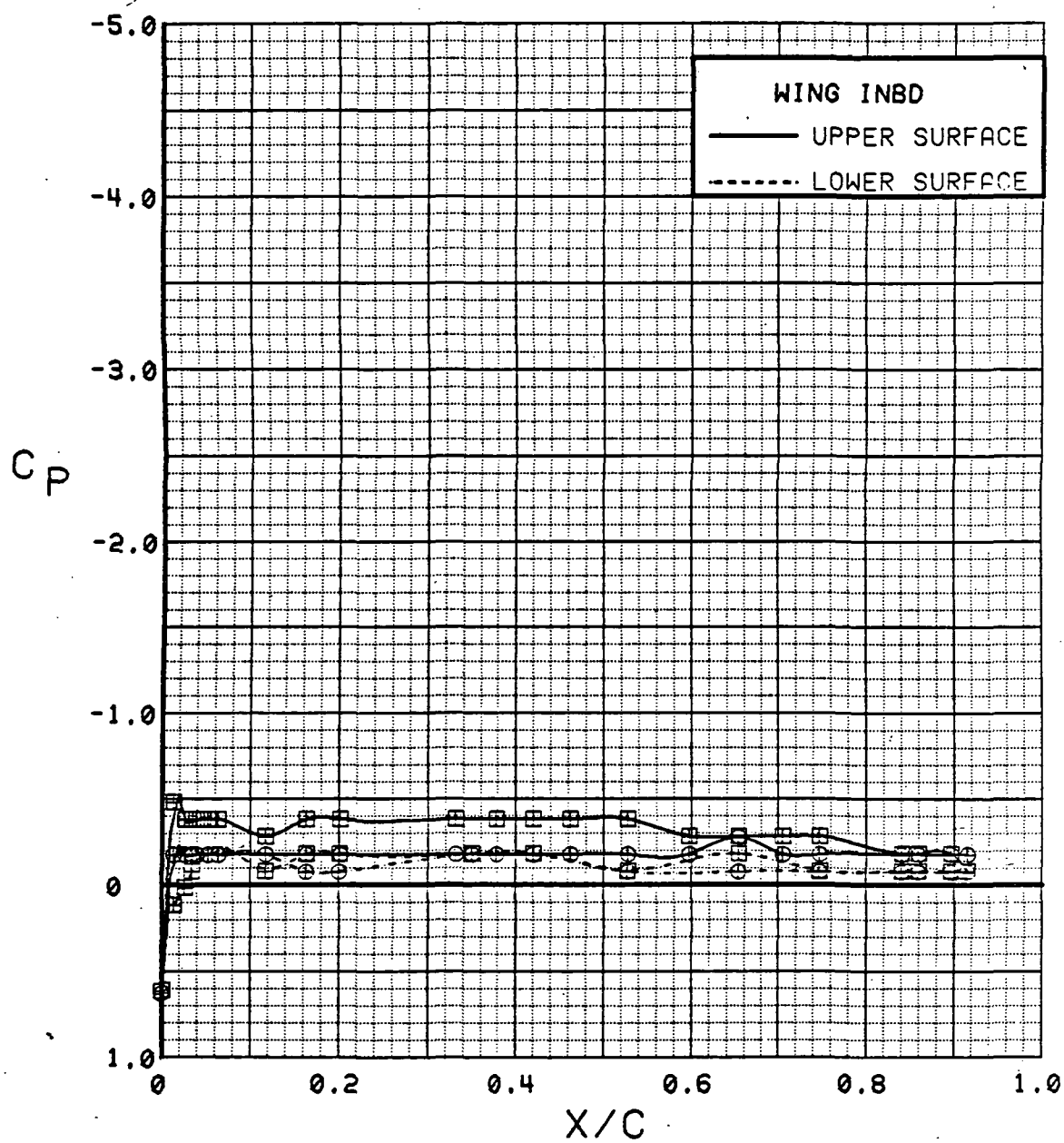


Figure 3.2.4-307 Power Effects, Flaps Neutral, Inboard, Alpha = 0 deg



SYM	TEST	RUN	ALPHA	CT	ITEF	OTEF	CAN	SWB
⊕	543	63	4.2	0.00	0	0	0	OFF
⊞	543	59	4.3	1.40	0	0	0	OFF

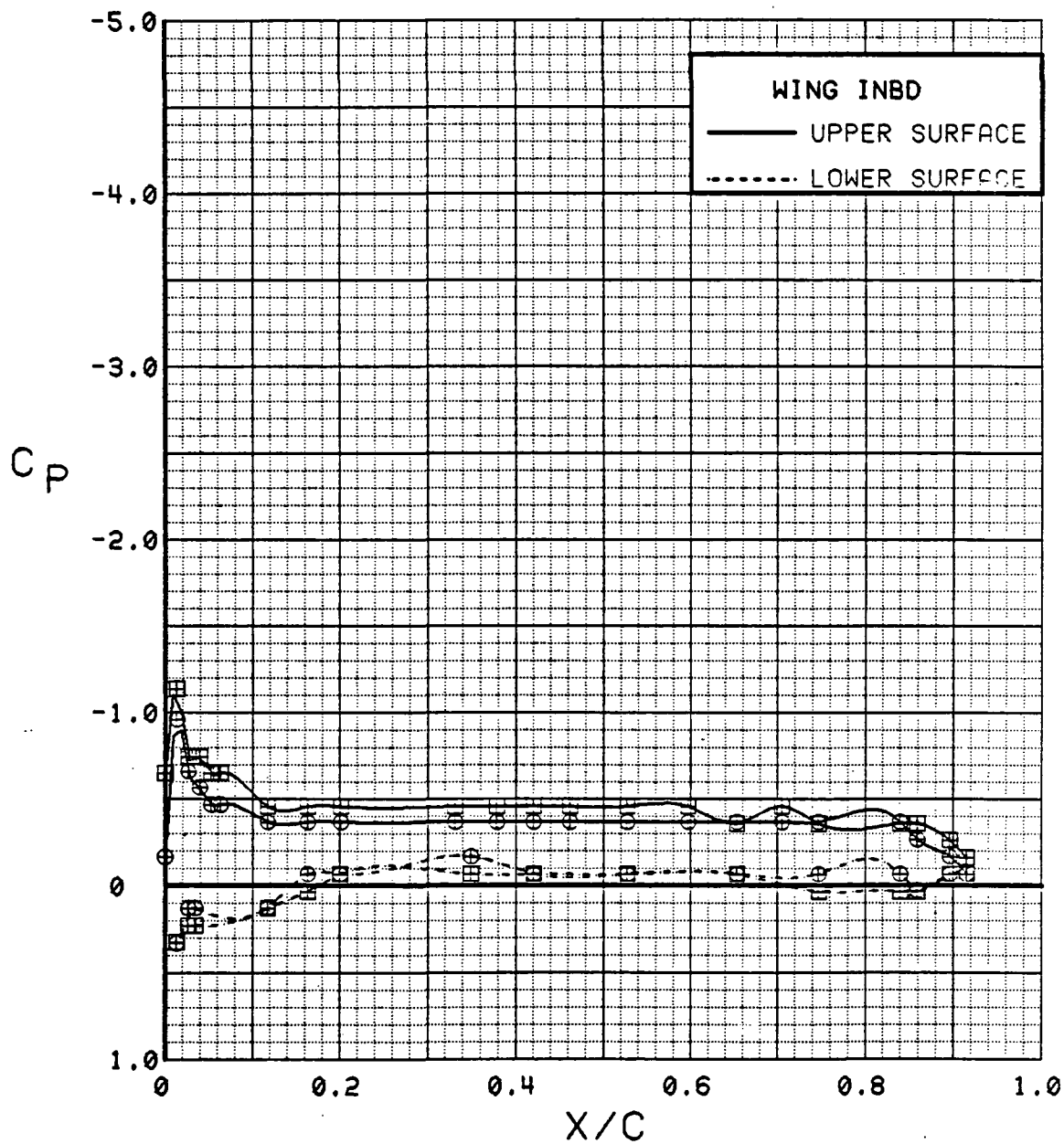


Figure 3.2.4-308 Power Effects, Flaps Neutral, Inboard, Alpha = 4 deg

SYM	TEST	RUN	ALPHA	CT	ITEF	OTEF	CAN-	SWB
⊕	543	63	8.3	0.00	0	0	0	OFF
⊞	543	59	8.4	1.41	0	0	0	OFF

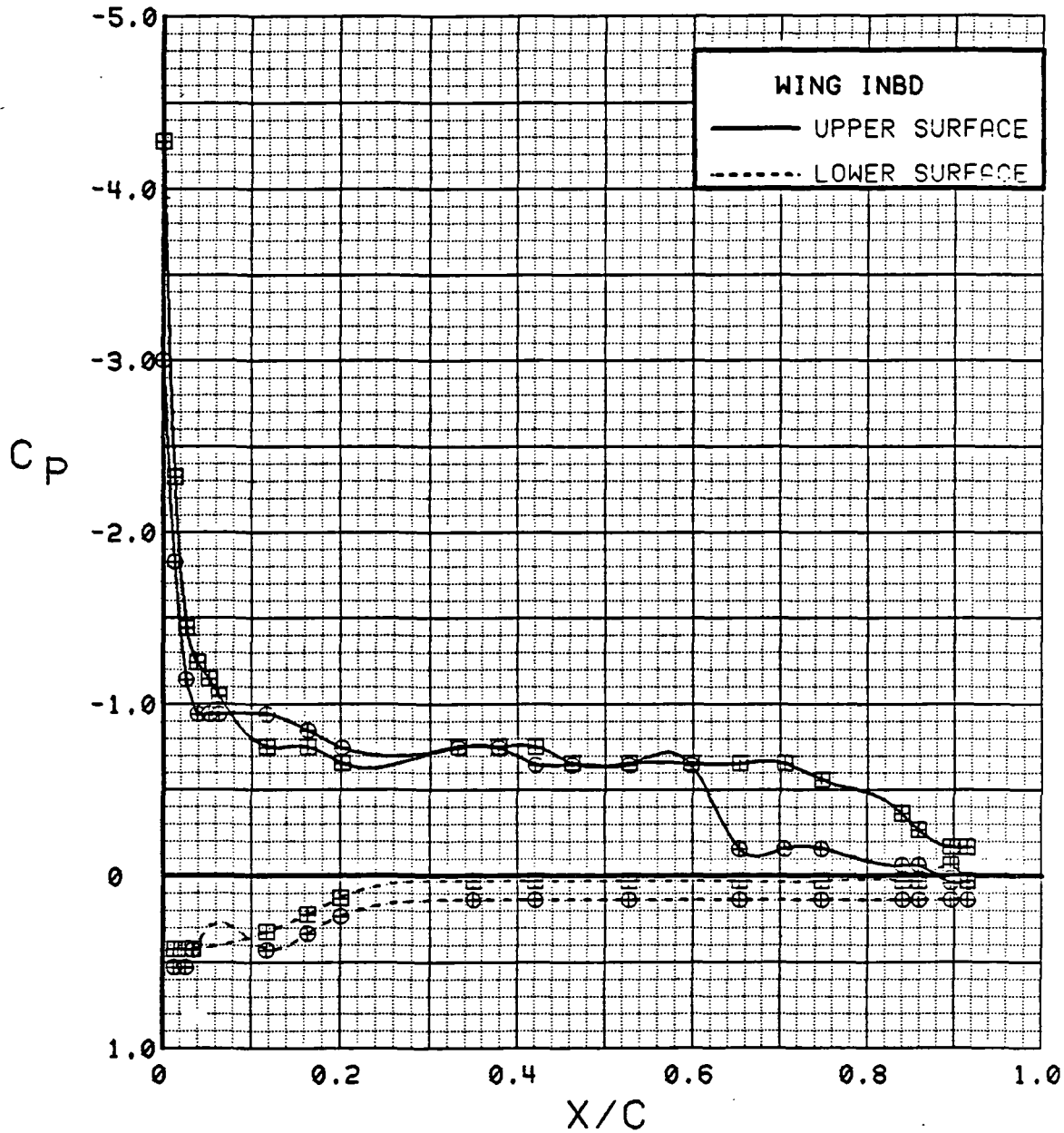


Figure 3.2.4-309 Power Effects, Flaps Neutral, Inboard, Alpha = 8 deg

SYM	TEST	RUN	ALPHA	CT	ITEF	OTEF	CAN	SWB
⊕	543	63	12.5	0.00	0	0	0	OFF
⊞	543	59	12.6	1.42	0	0	0	OFF

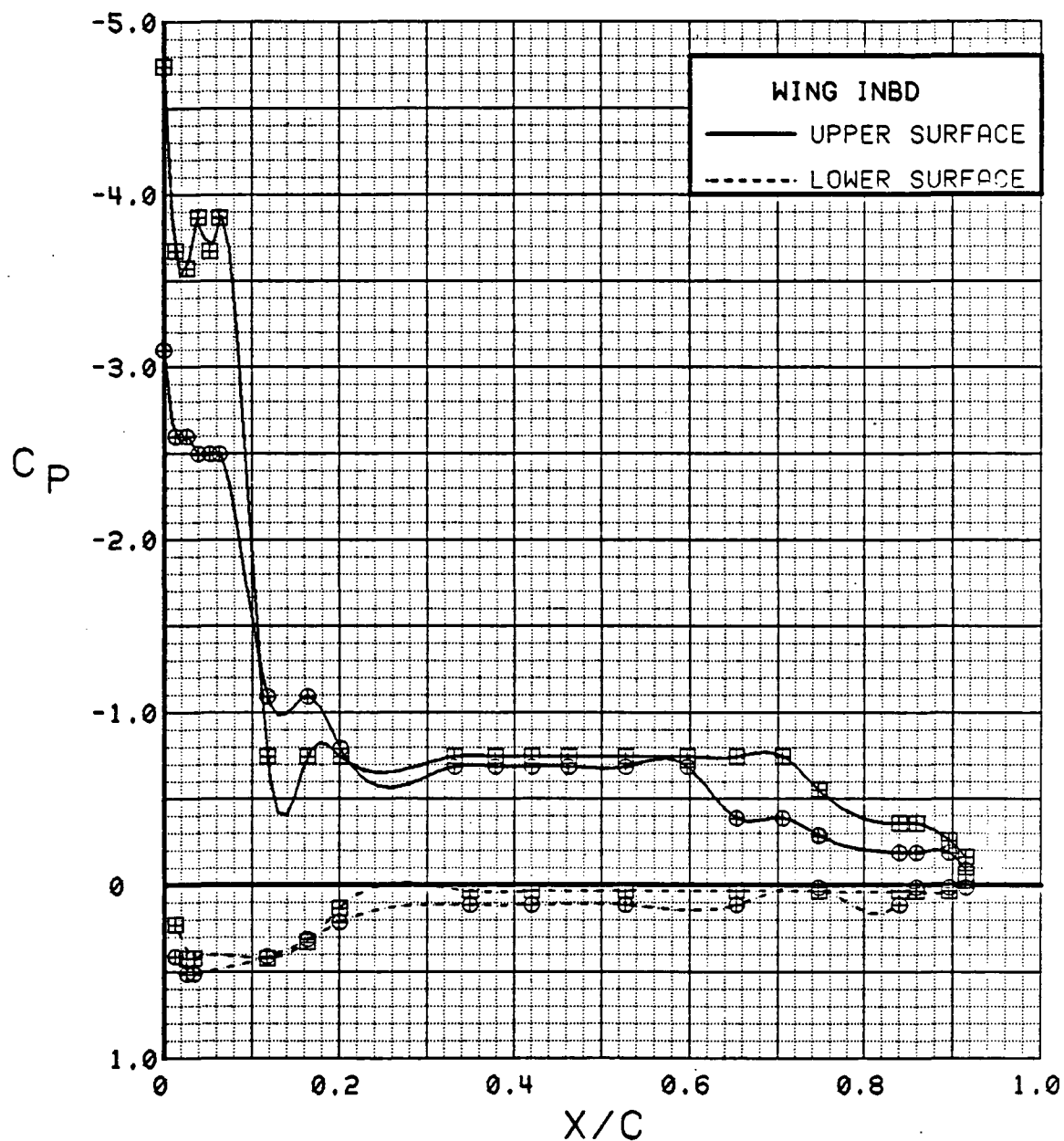


Figure 3.2.4-310 Power Effects, Flaps Neutral, Inboard, Alpha = 12 deg

SYM	TEST	RUN	ALPHA	CT	ITEF	OTEF	CAN	SWB
⊕	543	63	16.6	0.00	0	0	0	OFF
⊞	543	59	16.7	1.42	0	0	0	OFF

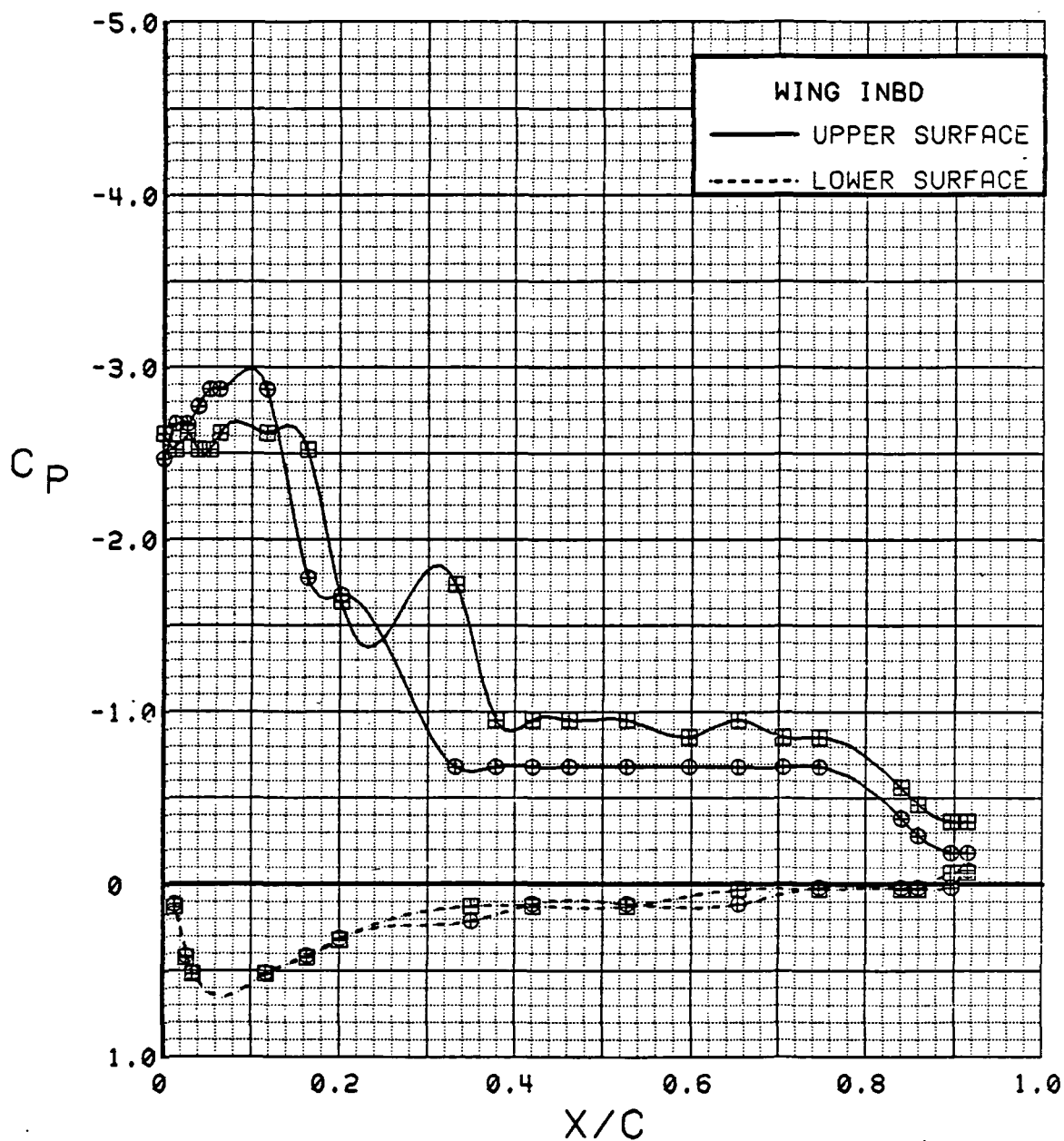


Figure 3.2.4-311 Power Effects, Flaps Neutral, Inboard, Alpha = 16 deg

SYM	TEST	RUN	ALPHA	CT	ITEF	OTEF	CAN	SWB
⊕	543	63	20.7	0.00	0	0	0	OFF
⊞	543	59	20.8	1.41	0	0	0	OFF

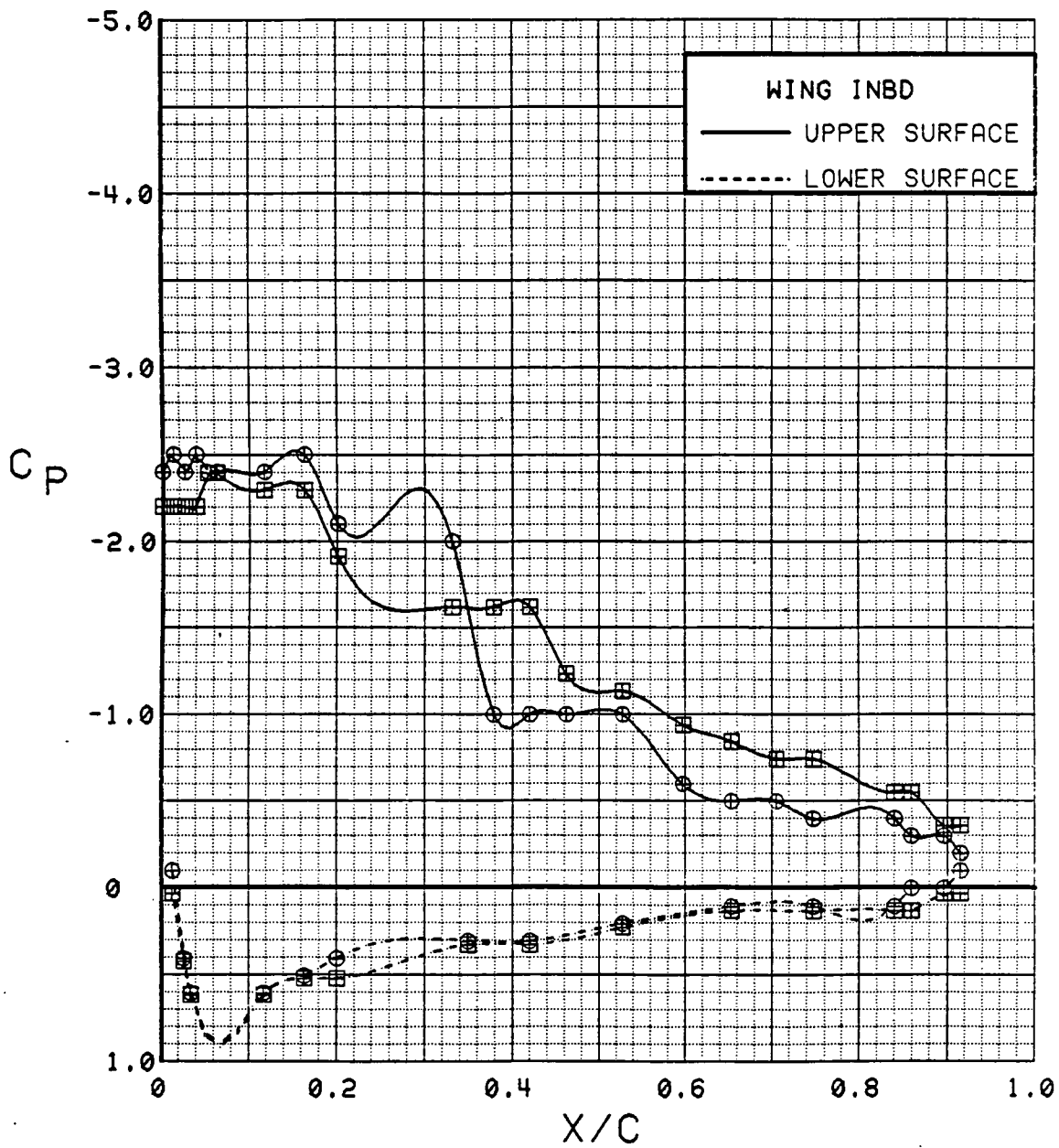


Figure 3.2.4-312 Power Effects, Flaps Neutral, Inboard, Alpha = 20 deg

SYM	TEST	RUN	ALPHA	CT	ITEF	OTEF	CAN	SWB
⊕	543	63	24.8	0.00	0	0	0	OFF
⊞	543	59	24.9	1.43	0	0	0	OFF

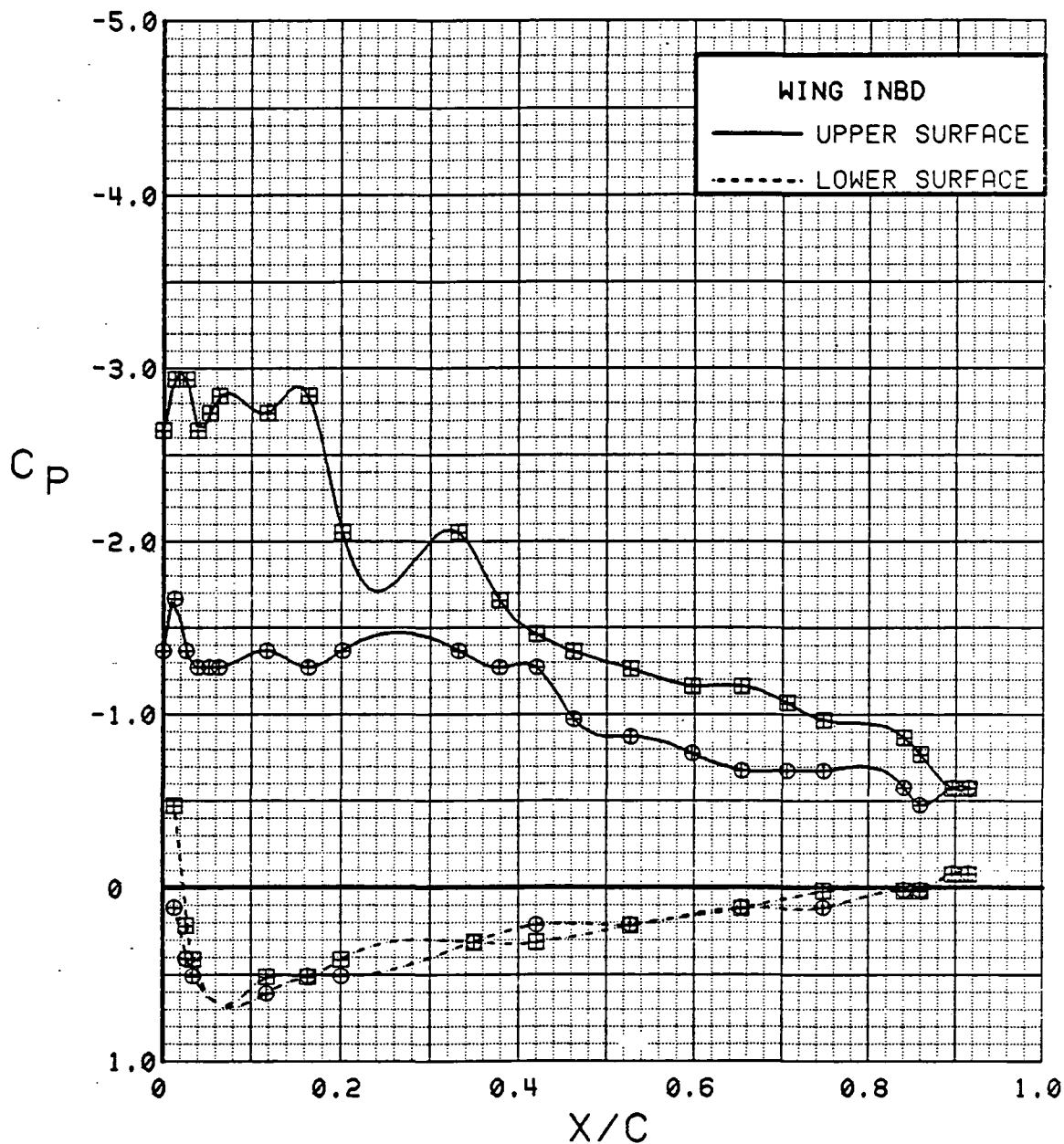


Figure 3.2.4-313 Power Effects, Flaps Neutral, Inboard, Alpha = 24 deg

SYM	TEST	RUN	ALPHA	CT	ITEF	OTEF	CAN	SWB
⊕	543	63	28.8	0.00	0	0	0	OFF
⊞	543	59	29.1	1.41	0	0	0	OFF

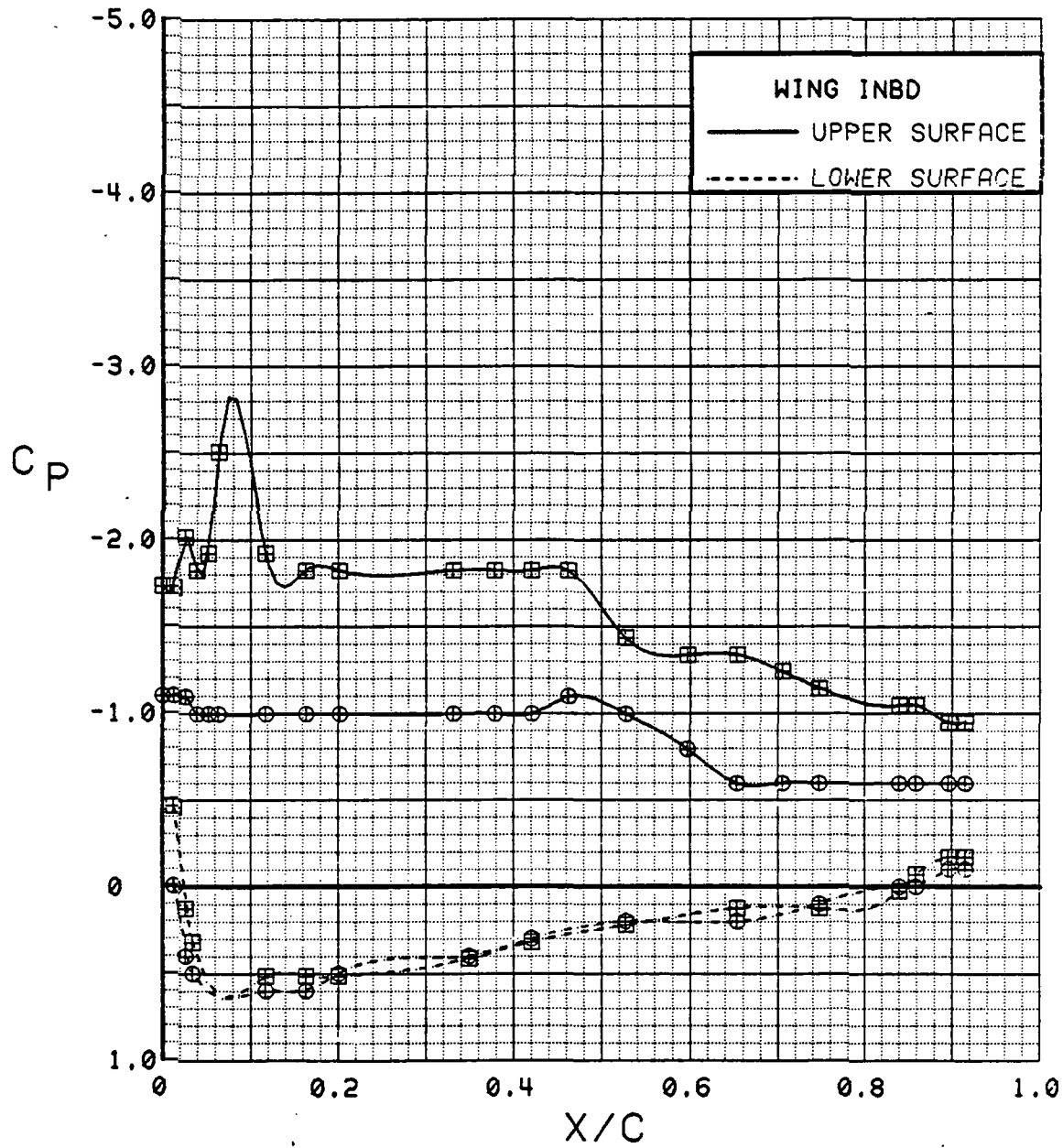


Figure 3.2.4-314 Power Effects, Flaps Neutral, Inboard, Alpha = 28 deg

SYM	TEST	RUN	ALPHA	CT	ITEF	OTEF	CAN	SWB
⊕	543	63	0.1	0.00	0	0	0	OFF
⊞	543	59	0.1	1.42	0	0	0	OFF

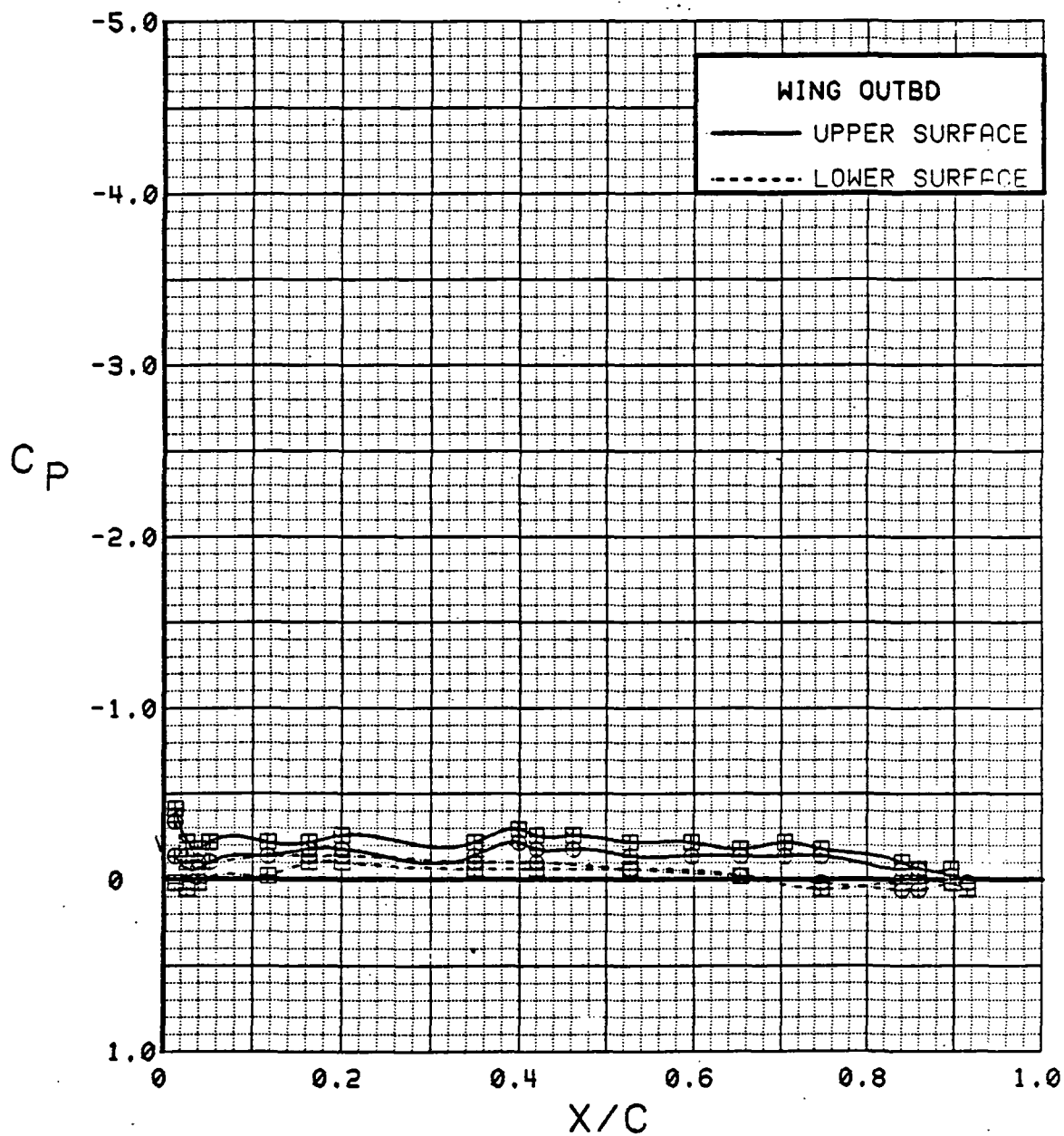


Figure 3.2.4-315 Power Effects, Flaps Neutral, Outboard, Alpha = 0 deg



SYM	TEST	RUN	ALPHA	CT	ITEF	OTEF	CAN	SWB
⊕	543	63	4.2	0.00	0	0	0	OFF
⊞	543	59	4.3	1.40	0	0	0	OFF

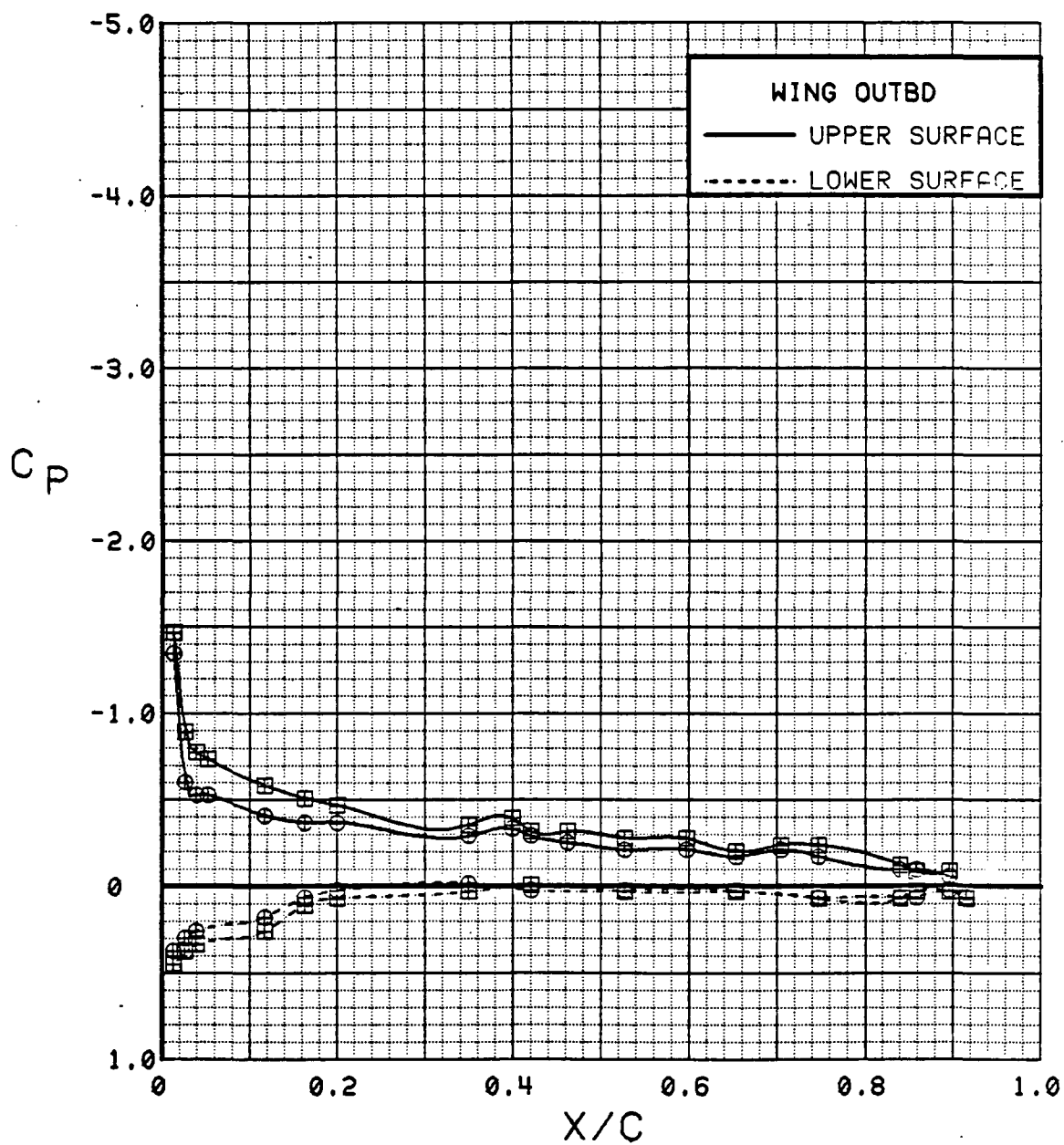


Figure 3.2.4-316 Power Effects, Flaps Neutral, Outboard, Alpha = 4 deg

SYM	TEST	RUN	ALPHA	CT	ITEF	OTEF	CAN	SWB
⊕	543	63	8.3	0.00	0	0	0	OFF
⊞	543	59	8.4	1.41	0	0	0	OFF

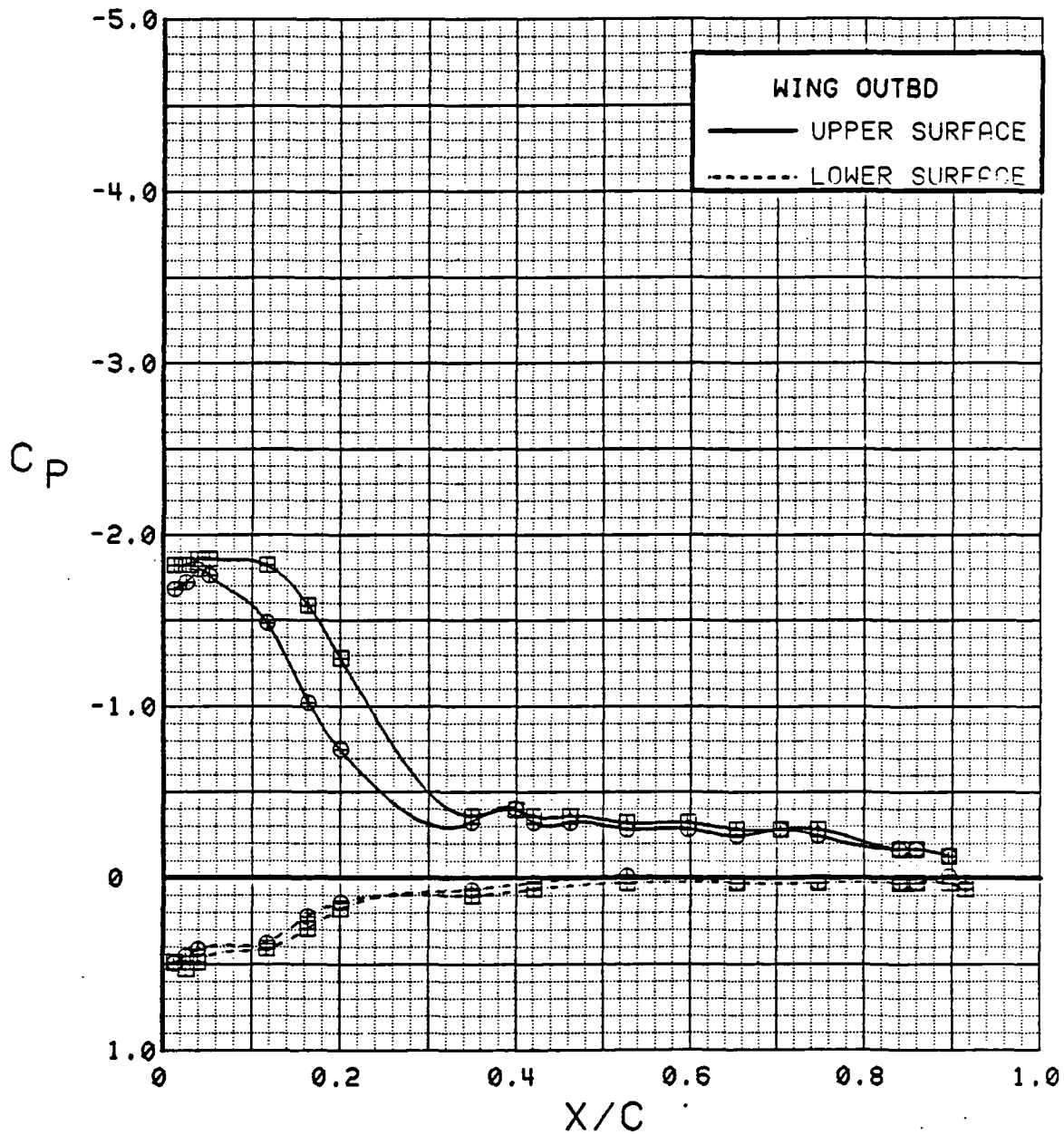


Figure 3.2.4-317 Power Effects, Flaps Neutral, Outboard, Alpha = 8 deg

ORIGINAL PAGE IS  
OF POOR QUALITY

SYM	TEST	RUN	ALPHA	CT	ITEF	OTEF	CAN	SWB
⊕	543	63	12.5	0.00	0	0	0	OFF
⊞	543	59	12.6	1.42	0	0	0	OFF

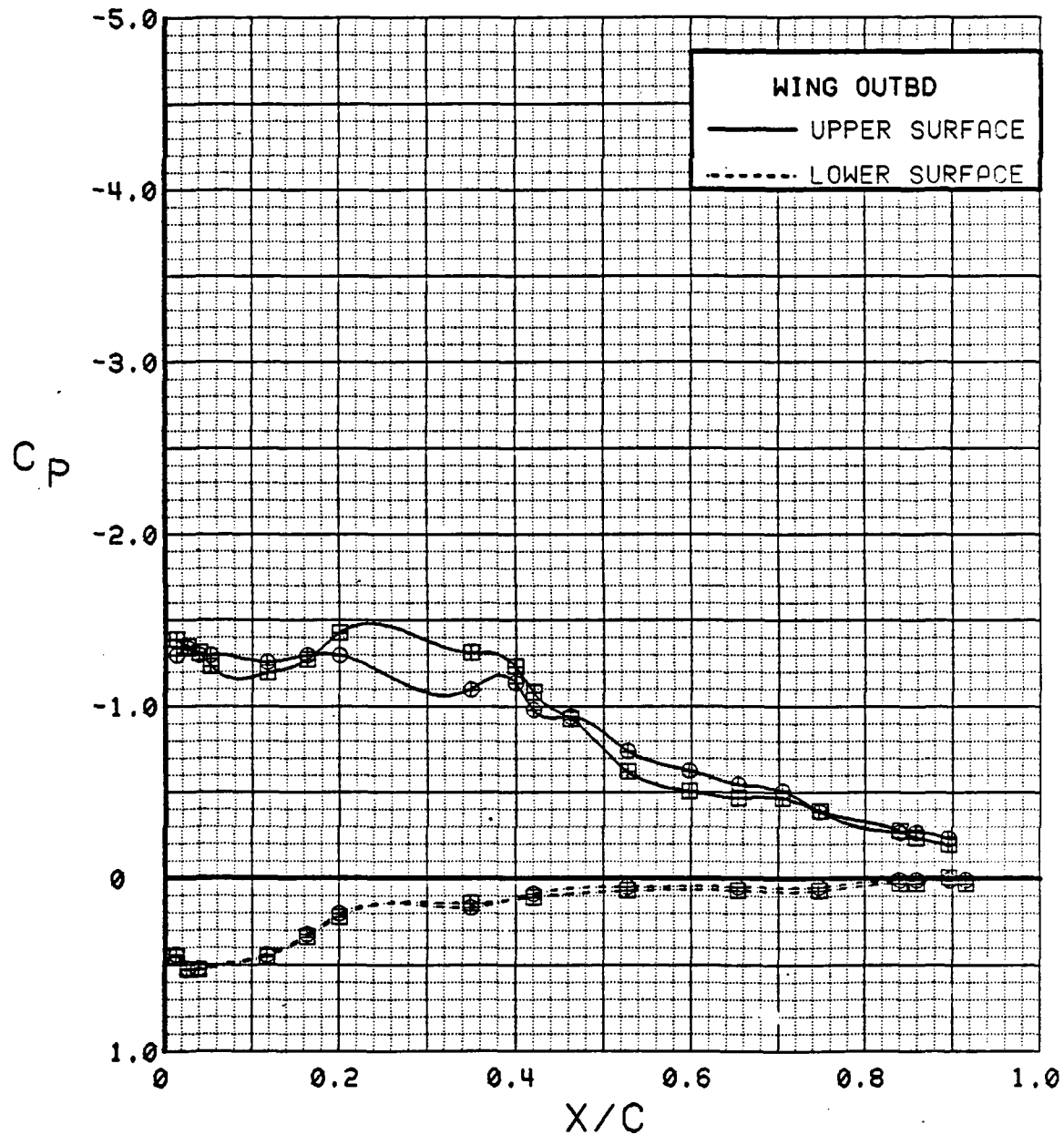


Figure 3.2.4-318 Power Effects, Flaps Neutral, Outboard, Alpha = 12 deg

SYM	TEST	RUN	ALPHA	CT	ITEF	OTEF	CAN	SWB
⊕	543	63	16.6	0.00	0	0	0	OFF
⊞	543	59	16.7	1.42	0	0	0	OFF

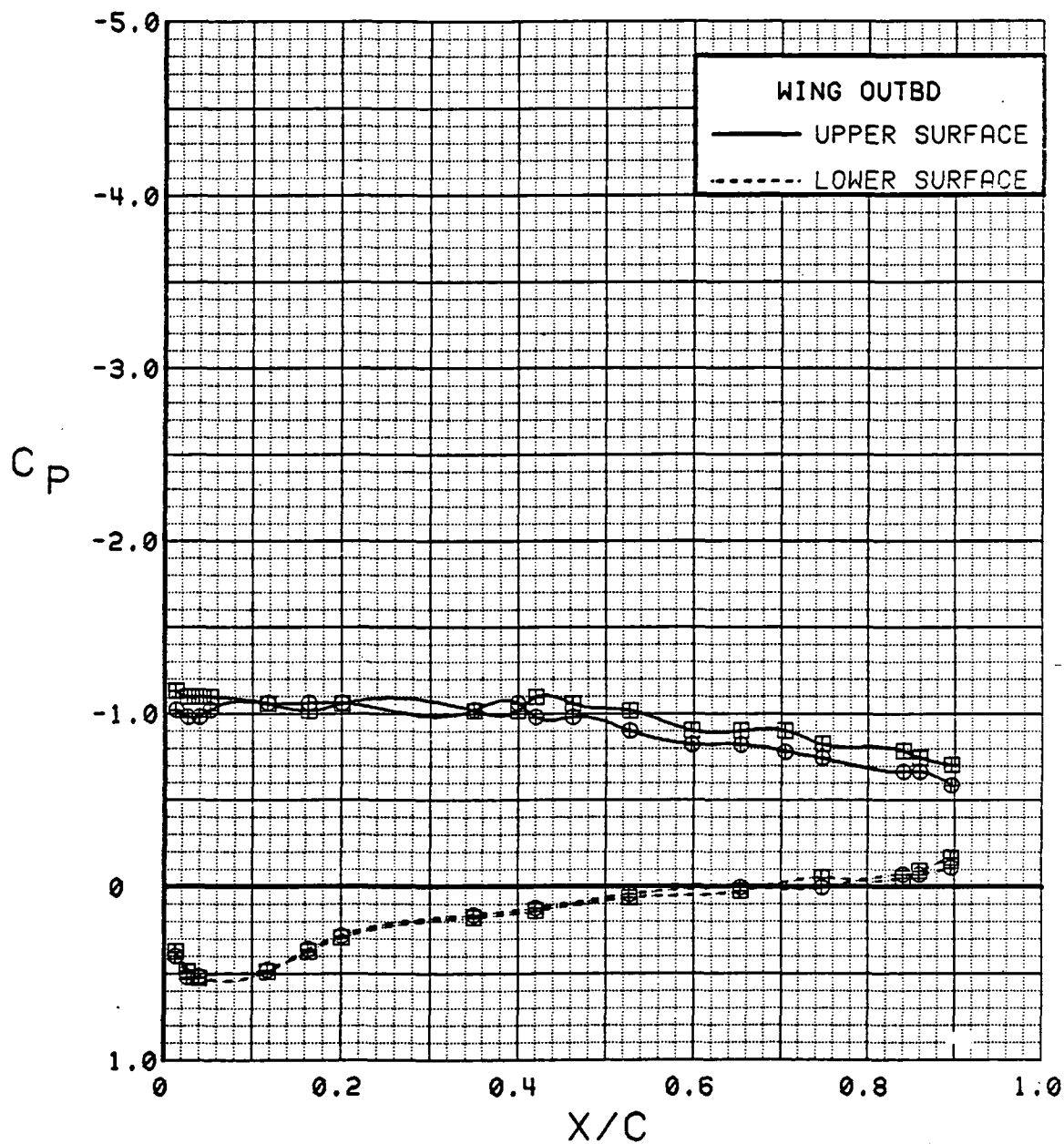


Figure 3.2.4-319 Power Effects, Flaps Neutral, Outboard, Alpha = 16 deg

SYM	TEST	RUN	ALPHA	CT	ITEF	OTEF	CAN	SWB
⊕	543	63	20.7	0.00	0	0	0	OFF
⊞	543	59	20.8	1.41	0	0	0	OFF

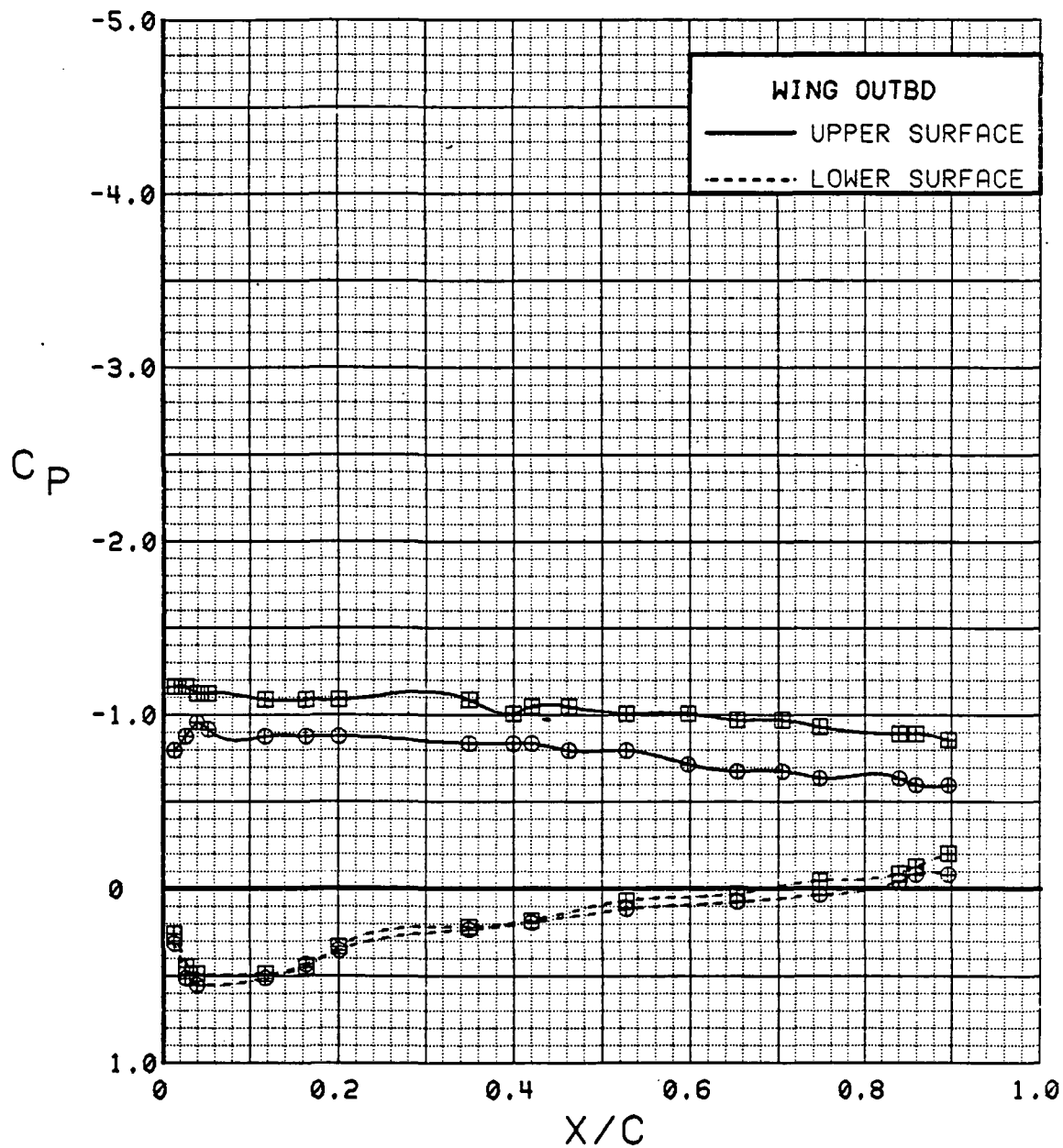


Figure 3.2.4-320 Power Effects, Flaps Neutral, Outboard, Alpha = 20 deg

SYM	TEST	RUN	ALPHA	CT	ITEF	OTEF	CAN	SWB
⊕	543	63	24.8	0.00	0	0	0	OFF
⊞	543	59	24.9	1.43	0	0	0	OFF

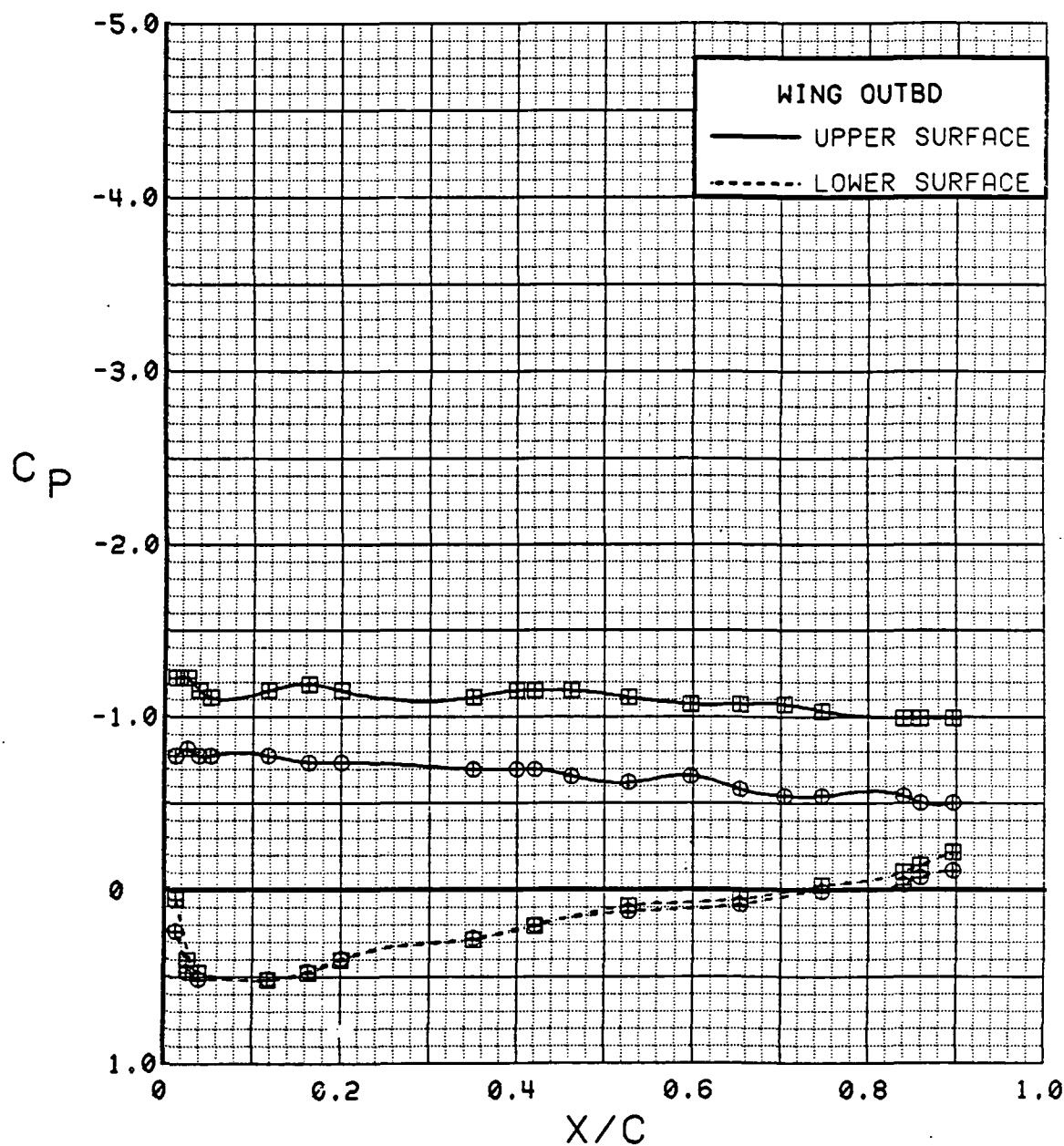


Figure 3.2.4-321 Power Effects, Flaps Neutral, Outboard, Alpha = 24 deg

SYM	TEST	RUN	ALPHA	CT	ITEF	OTEF	CAN	SWB
⊕	543	63	28.8	0.00	0	0	0	OFF
⊞	543	59	29.1	1.41	0	0	0	OFF

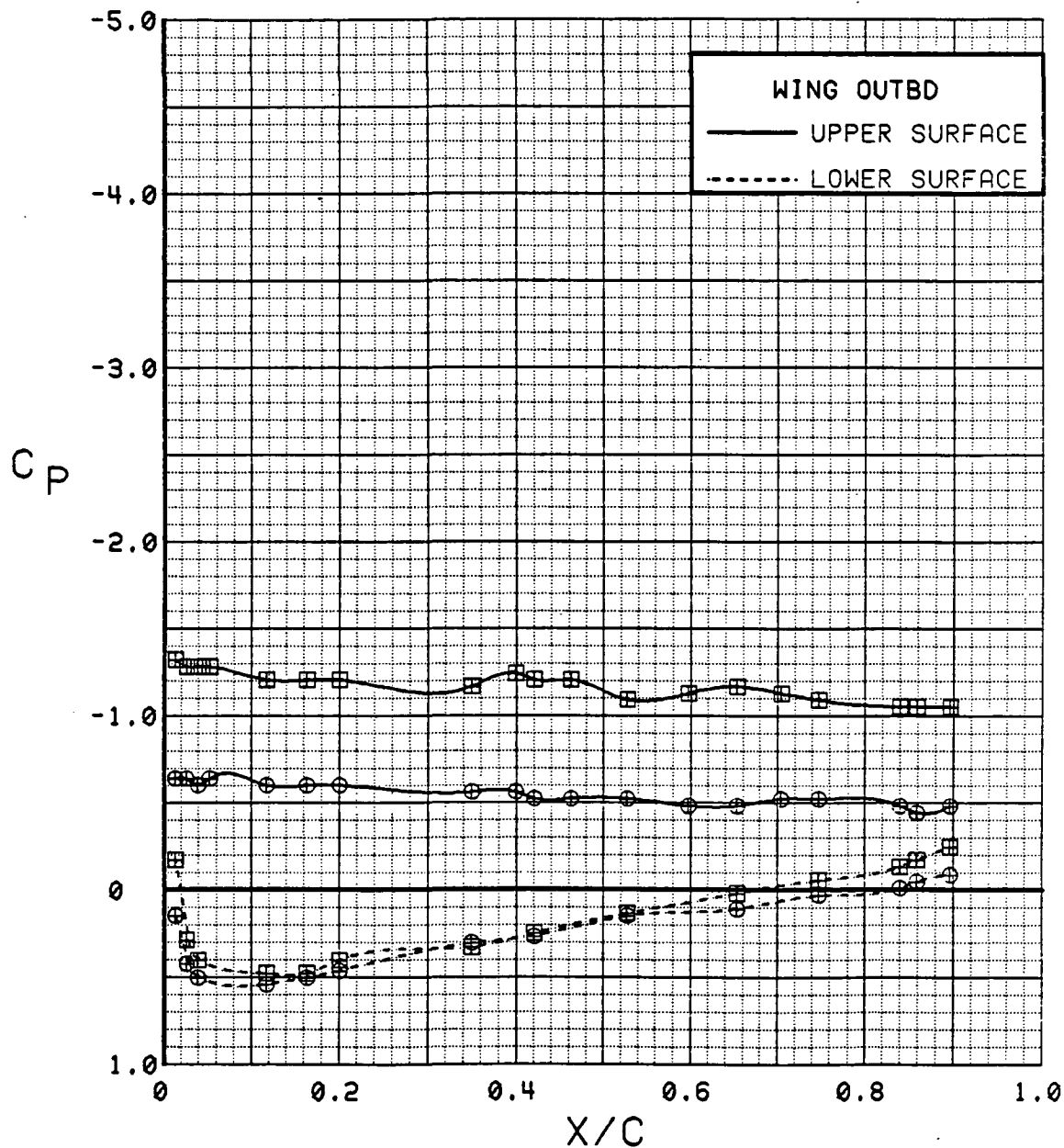


Figure 3.2.4-322 Power Effects, Flaps Neutral, Outboard, Alpha = 28 deg

SYM	TEST	RUN	ALPHA	CT	ITEF	OTEF	CAN	SWB
⊕	543	63	0.1	0.00	0	0	0	OFF
⊞	543	59	0.1	1.42	0	0	0	OFF

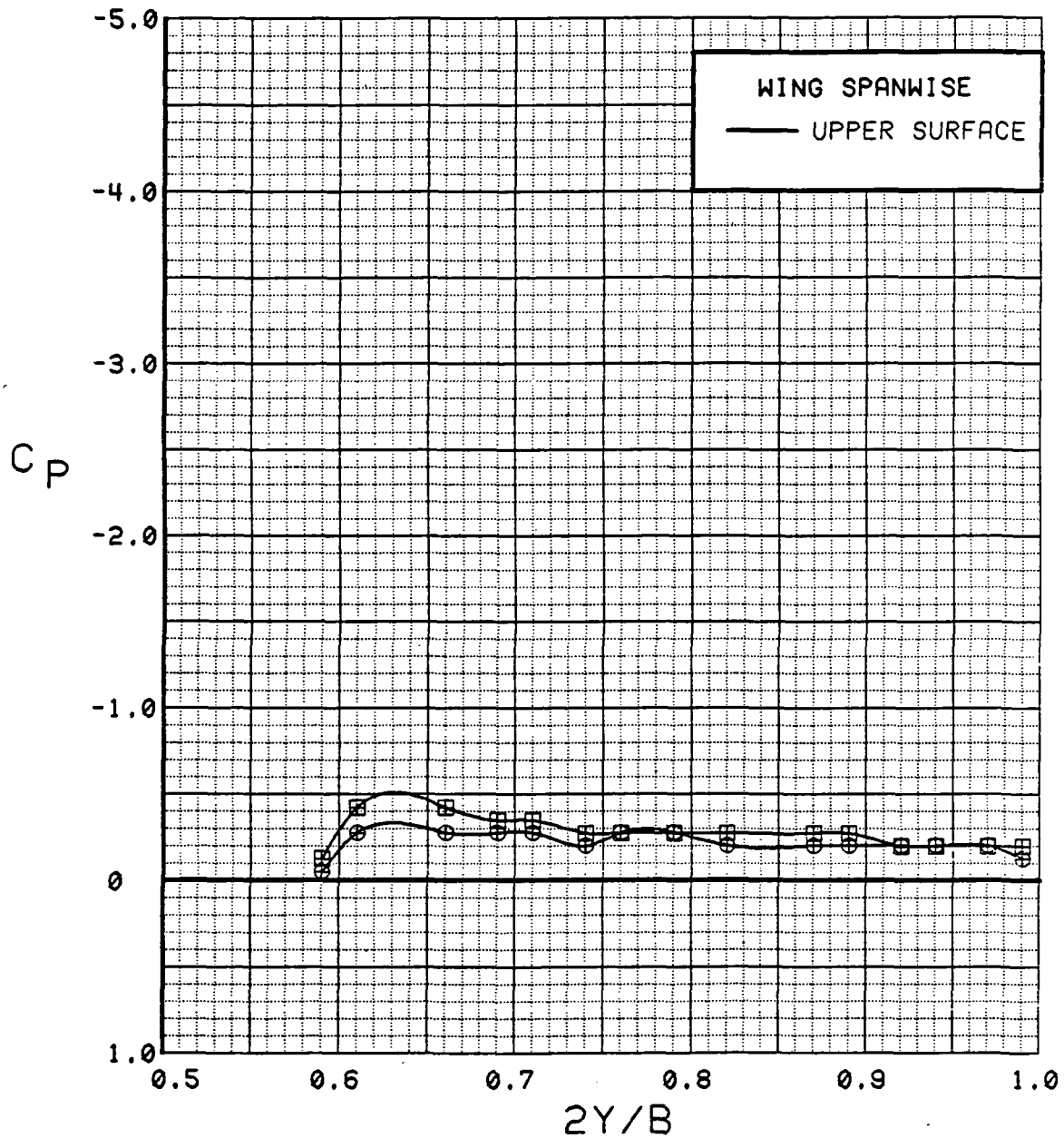


Figure 3.2.4-323 Power Effects, Flaps Neutral, Spanwise, Alpha = 0 deg



SYM	TEST	RUN	ALPHA	CT	ITEF	OTEF	CAN	SWB
⊕	543	63	4.2	0.00	0	0	0	OFF
⊞	543	59	4.3	1.40	0	0	0	OFF

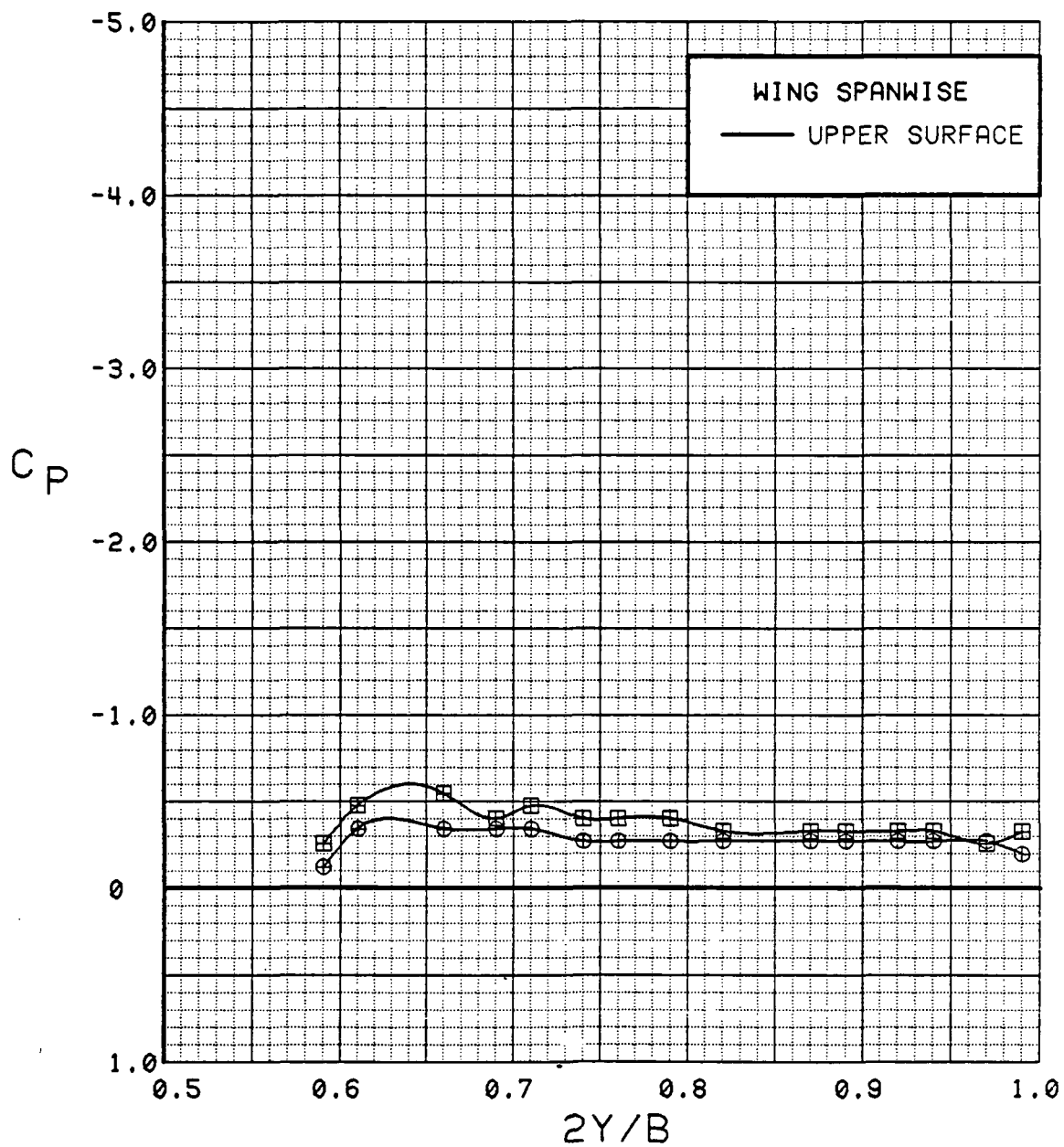


Figure 3.2.4-324 Power Effects, Flaps Neutral, Spanwise, Alpha = 4 deg

SYM	TEST	RUN	ALPHA	CT	ITEF	OTEF	CAN	SWB
⊙	543	63	8.3	0.00	0	0	0	OFF
⊠	543	59	8.4	1.41	0	0	0	OFF

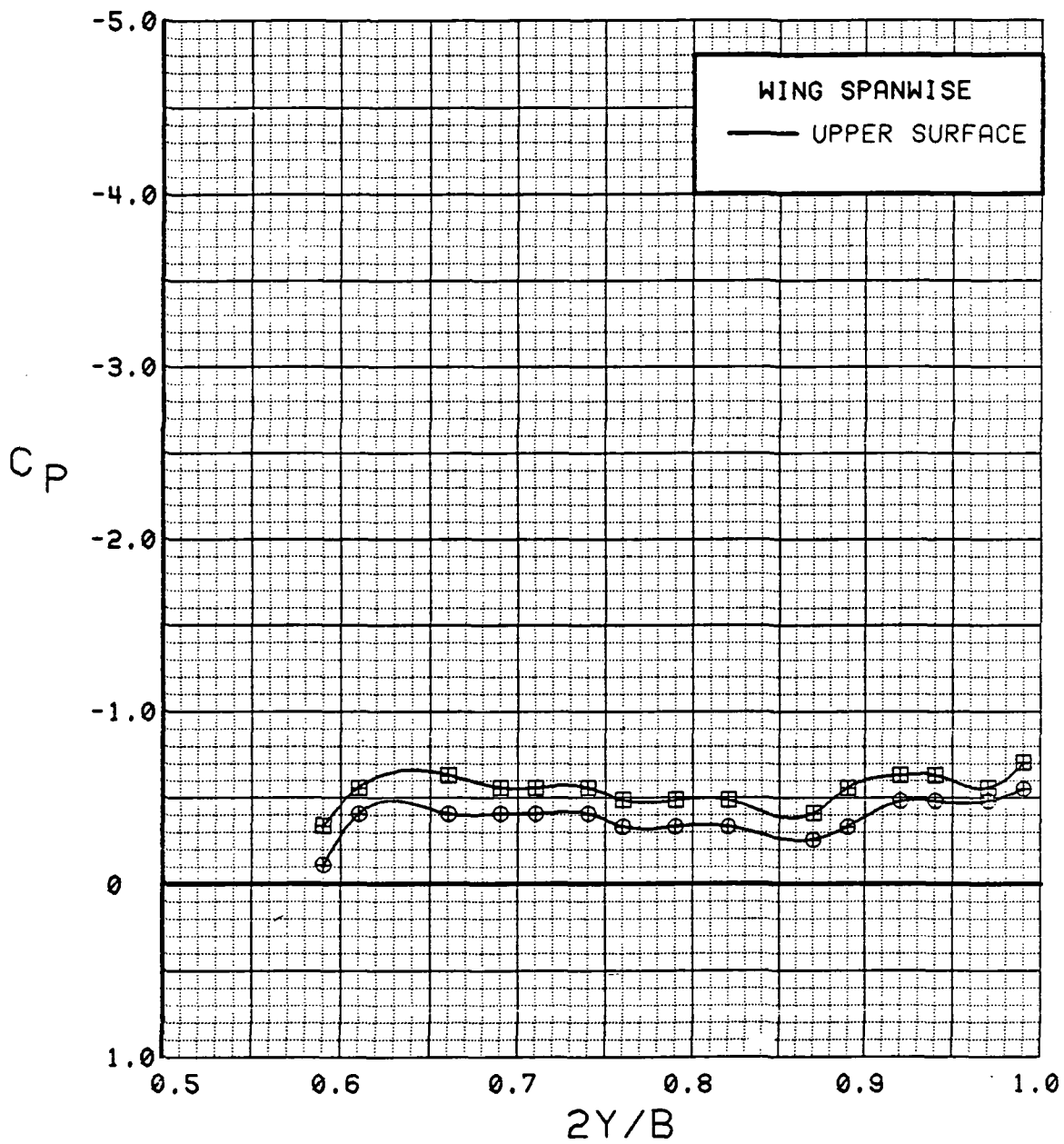


Figure 3.2.4-325 Power Effects, Flaps Neutral, Spanwise, Alpha = 8 deg

SYM	TEST	RUN	ALPHA	CT	ITEF	OTEF	CAN	SWB
⊕	543	63	12.5	0.00	0	0	0	OFF
⊞	543	59	12.6	1.42	0	0	0	OFF

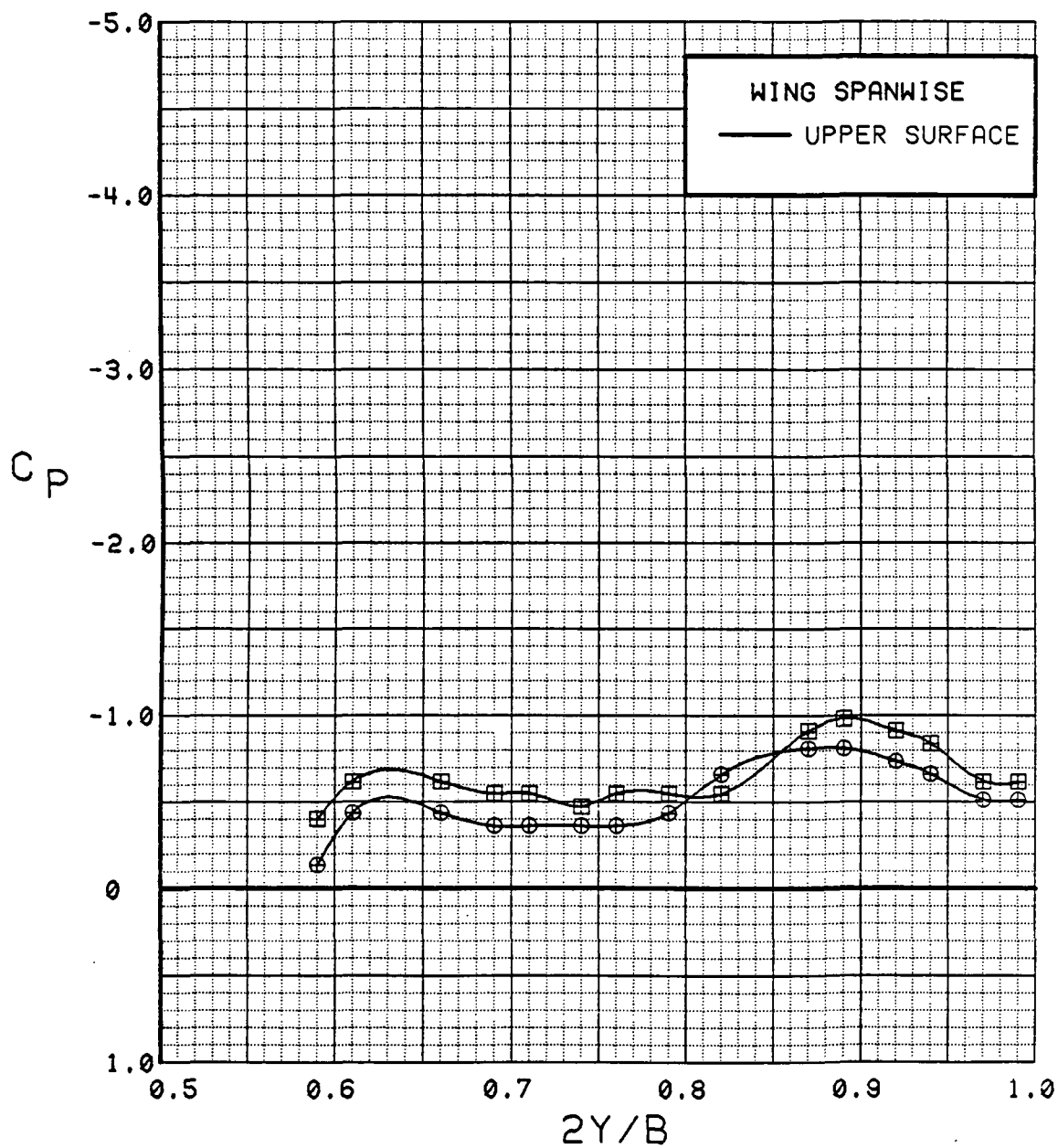


Figure 3.2.4-326 Power Effects, Flaps Neutral, Spanwise, Alpha = 12 deg

SYM	TEST	RUN	ALPHA	CT	ITEF	OTEF	CAN	SWB
⊕	543	63	16.6	0.00	0	0	0	OFF
⊞	543	59	16.7	1.42	0	0	0	OFF

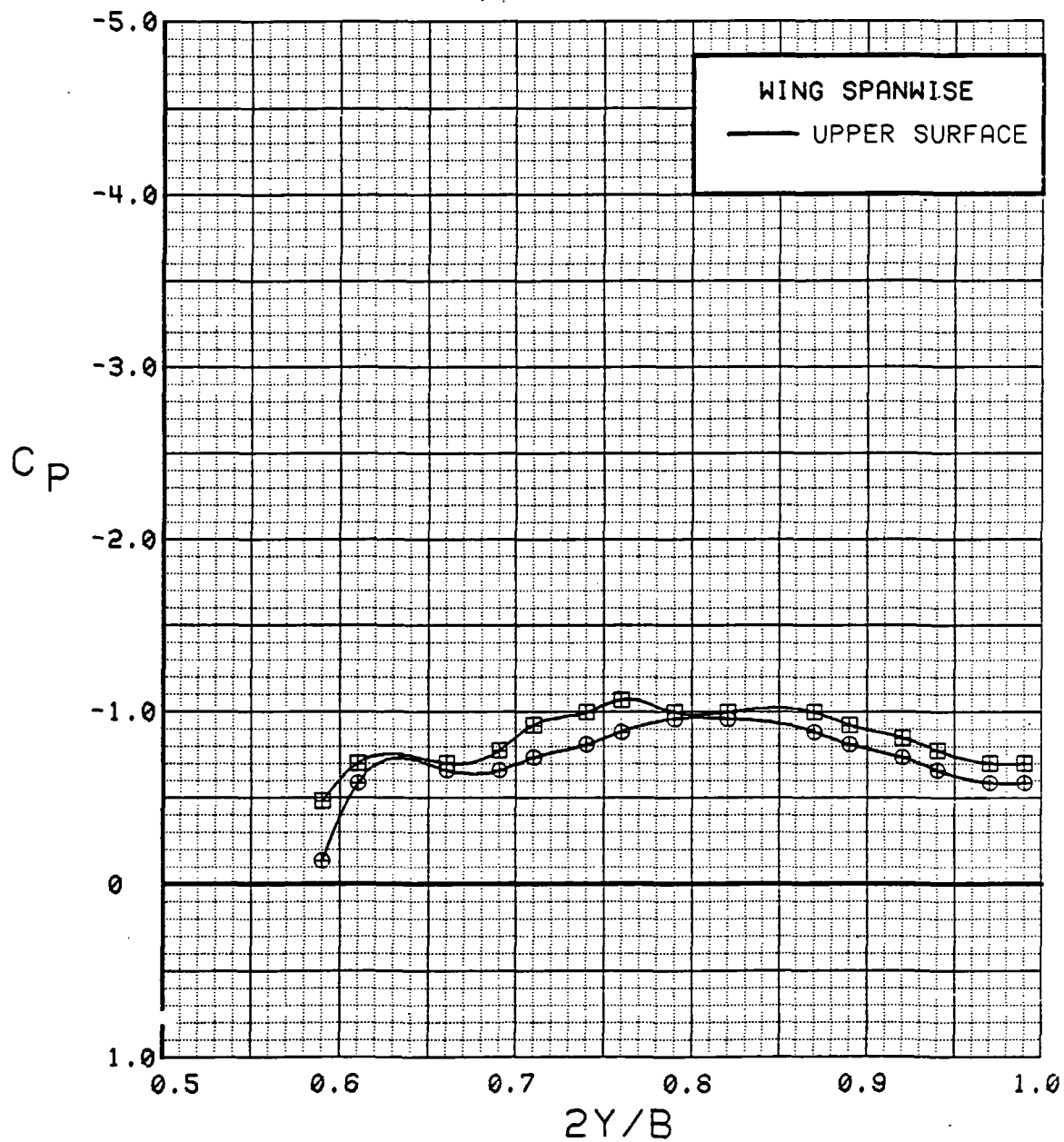


Figure 3.2.4-327 Power Effects, Flaps Neutral, Spanwise, Alpha = 16 deg

SYM	TEST	RUN	ALPHA	CT	ITEF	OTEF	CAN	SWB
⊕	543	63	20.7	0.00	0	0	0	OFF
⊞	543	59	20.8	1.41	0	0	0	OFF

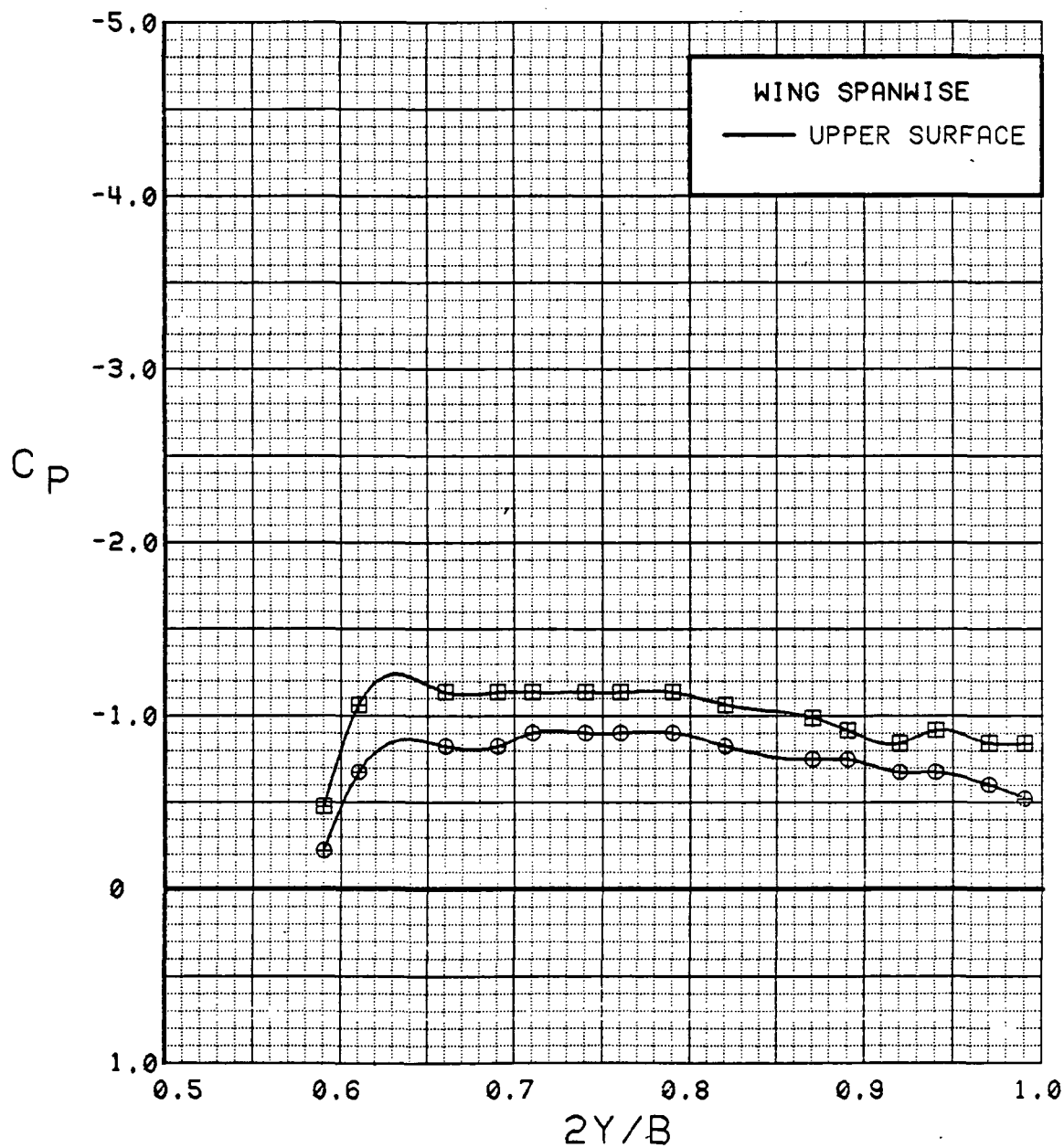


Figure 3.2.4-328 Power Effects, Flaps Neutral, Spanwise, Alpha = 20 deg

SYM	TEST	RUN	ALPHA	CT	ITEF	OTEF	CAN	SWB
⊙	543	63	24.8	0.00	0	0	0	OFF
⊠	543	59	24.9	1.43	0	0	0	OFF

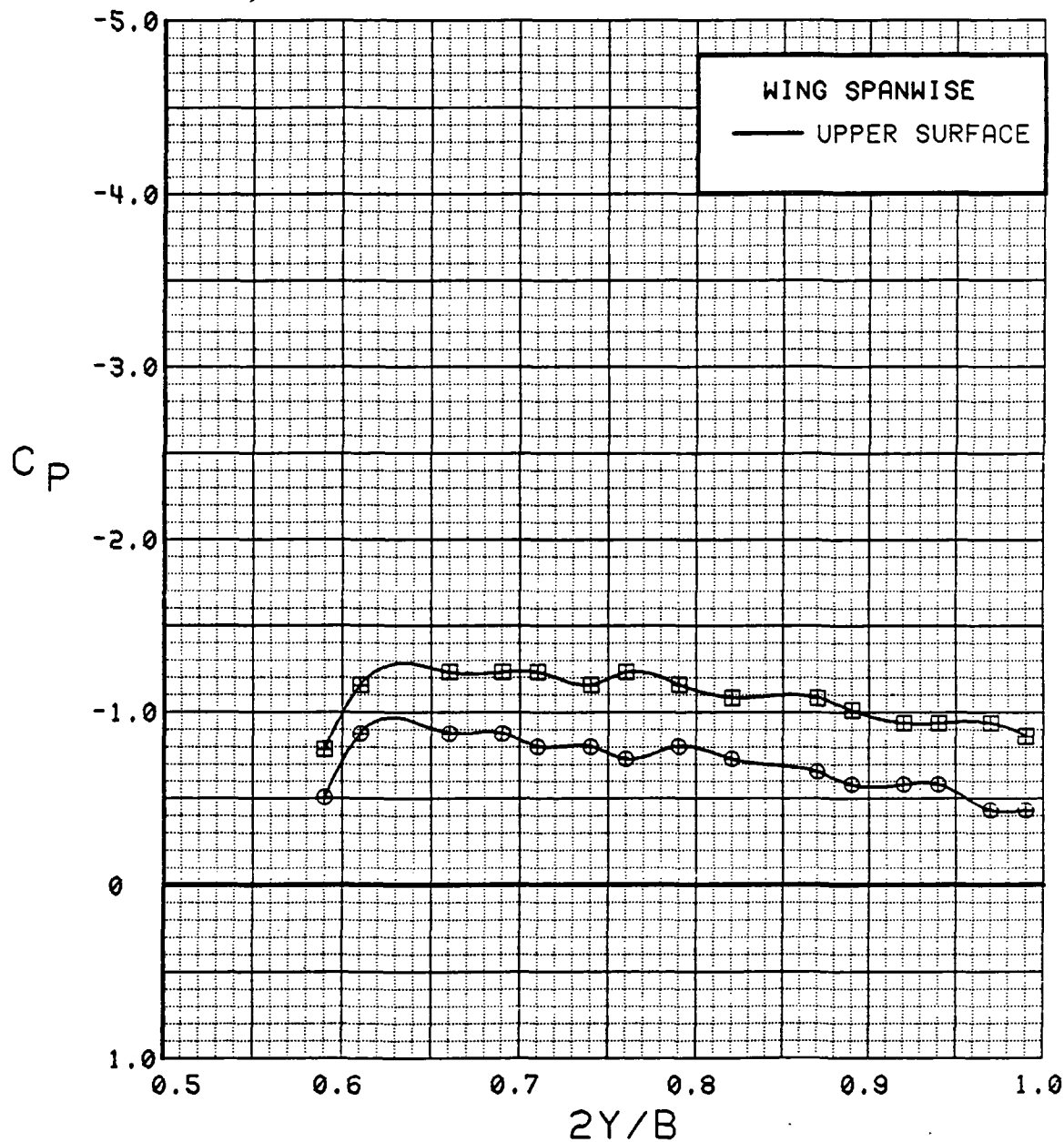


Figure 3.2.4-329 Power Effects, Flaps Neutral, Spanwise, Alpha = 24 deg

SYM	TEST	RUN	ALPHA	CT	ITEF	OTEF	CAN	SWB
⊕	543	63	28.8	0.00	0	0	0	OFF
⊞	543	59	29.1	1.41	0	0	0	OFF

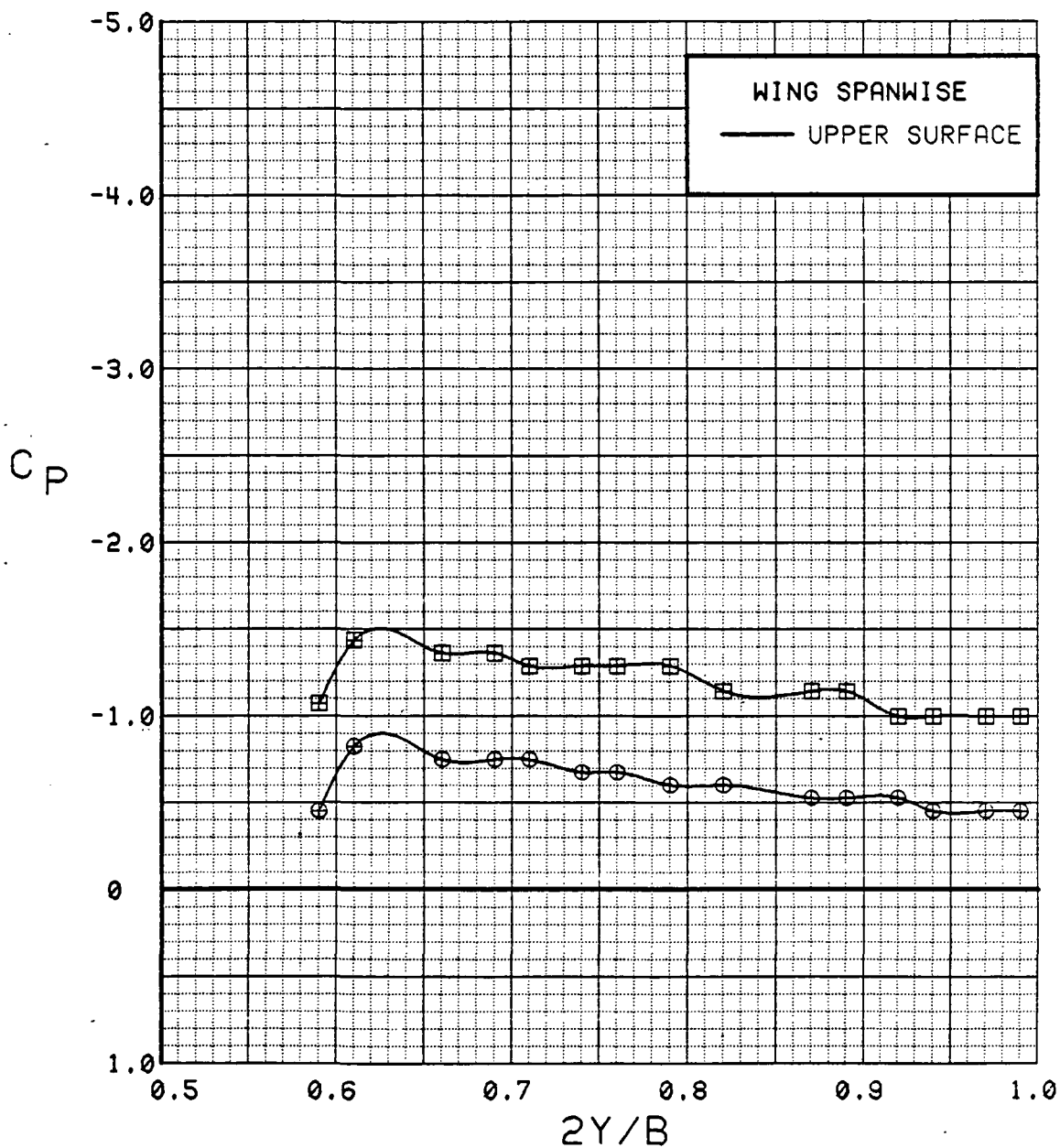


Figure 3.2.4-330 Power Effects, Flaps Neutral, Spanwise, Alpha = 28 deg

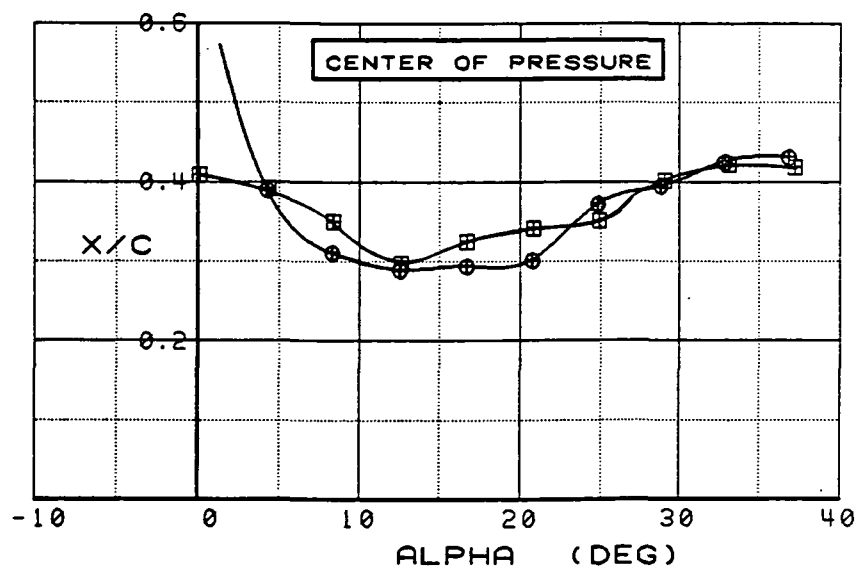
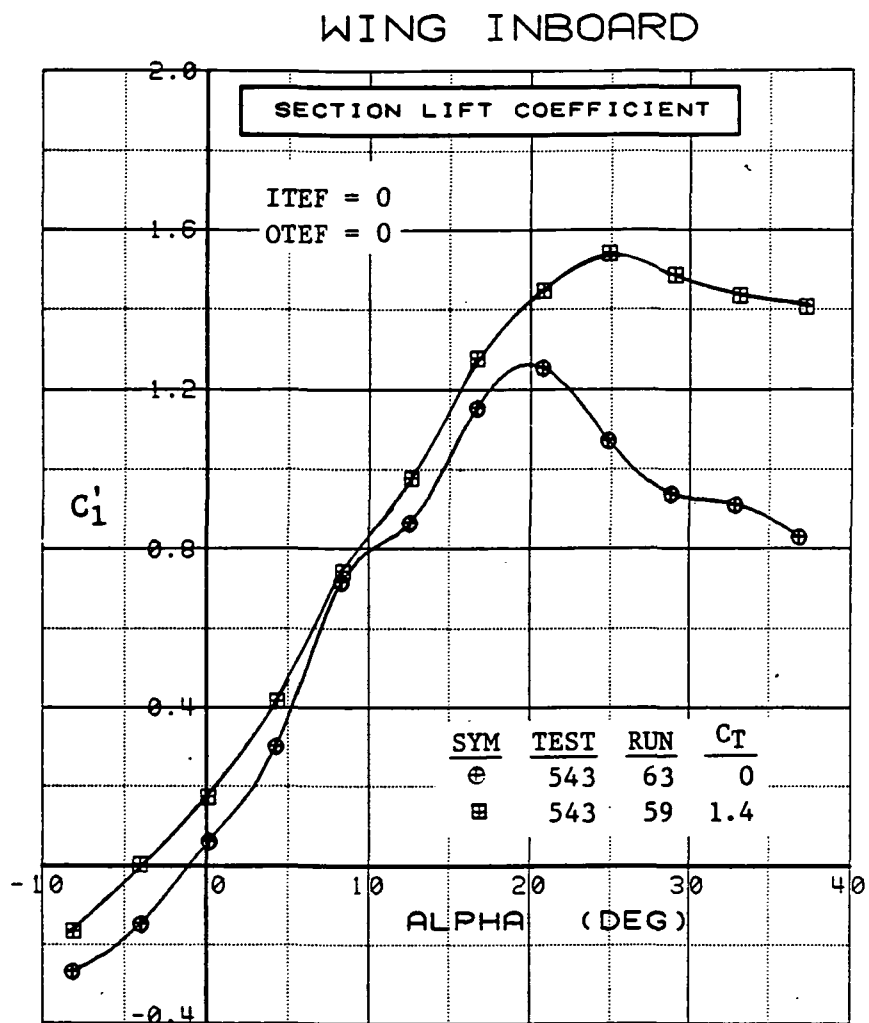


Figure 3.2.4-331 Power Effects, Inboard, Integrated Section Properties



## WING OUTBOARD

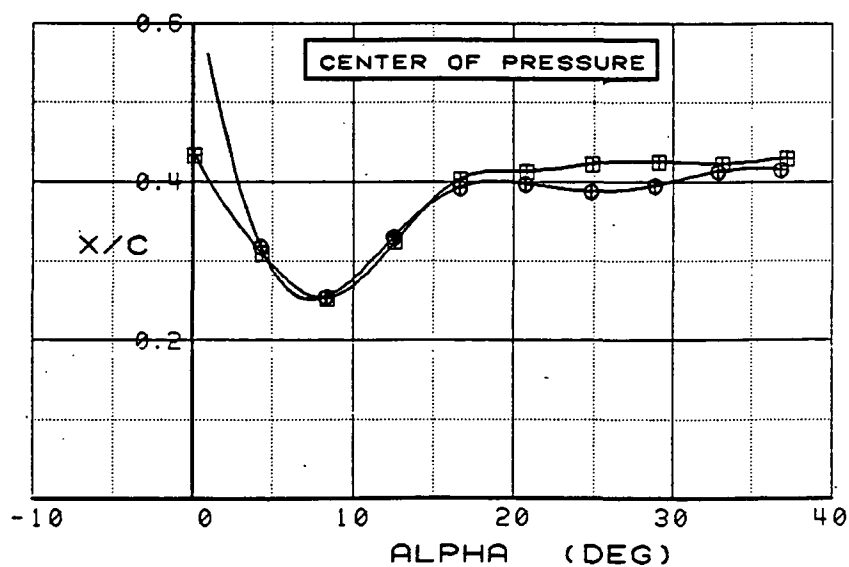
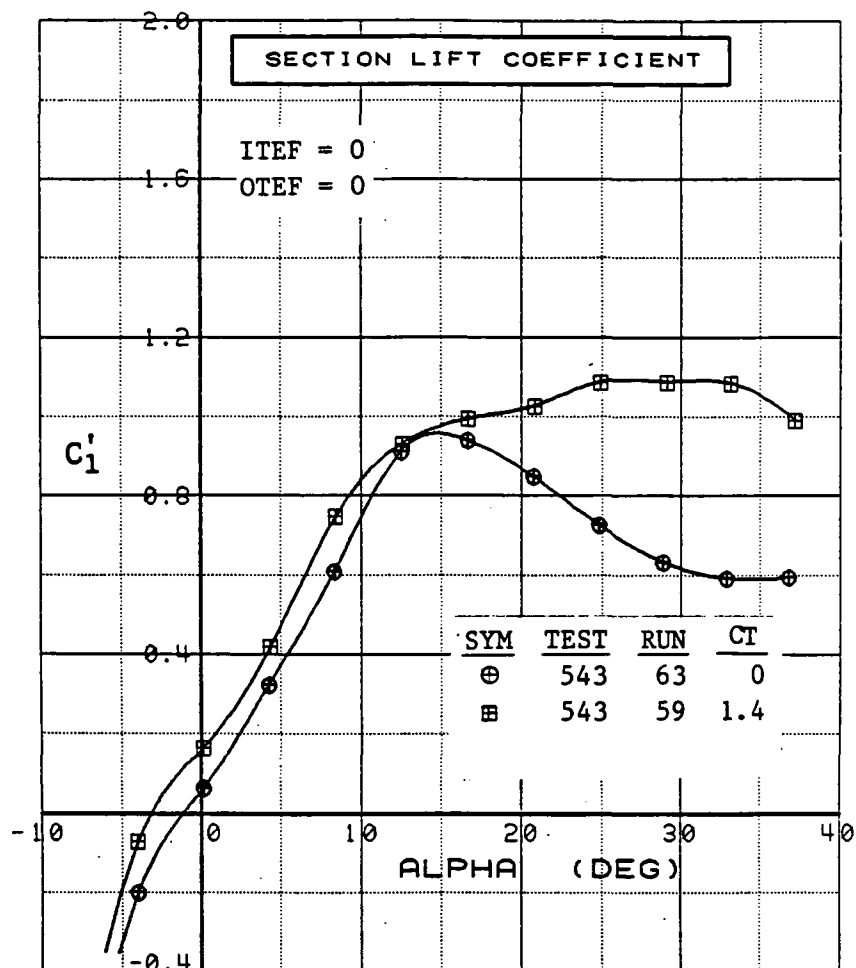


Figure 3.2.4-332 Power Effects, Outboard, Integrated Section Properties

SYM	TEST	RUN	ALPHA	CT	ITEF	OTEF	CAN	SWB
⊕	543	11	0.3	0.00	30	30	0	OFF
⊞	543	5	0.4	1.41	30	30	0	OFF

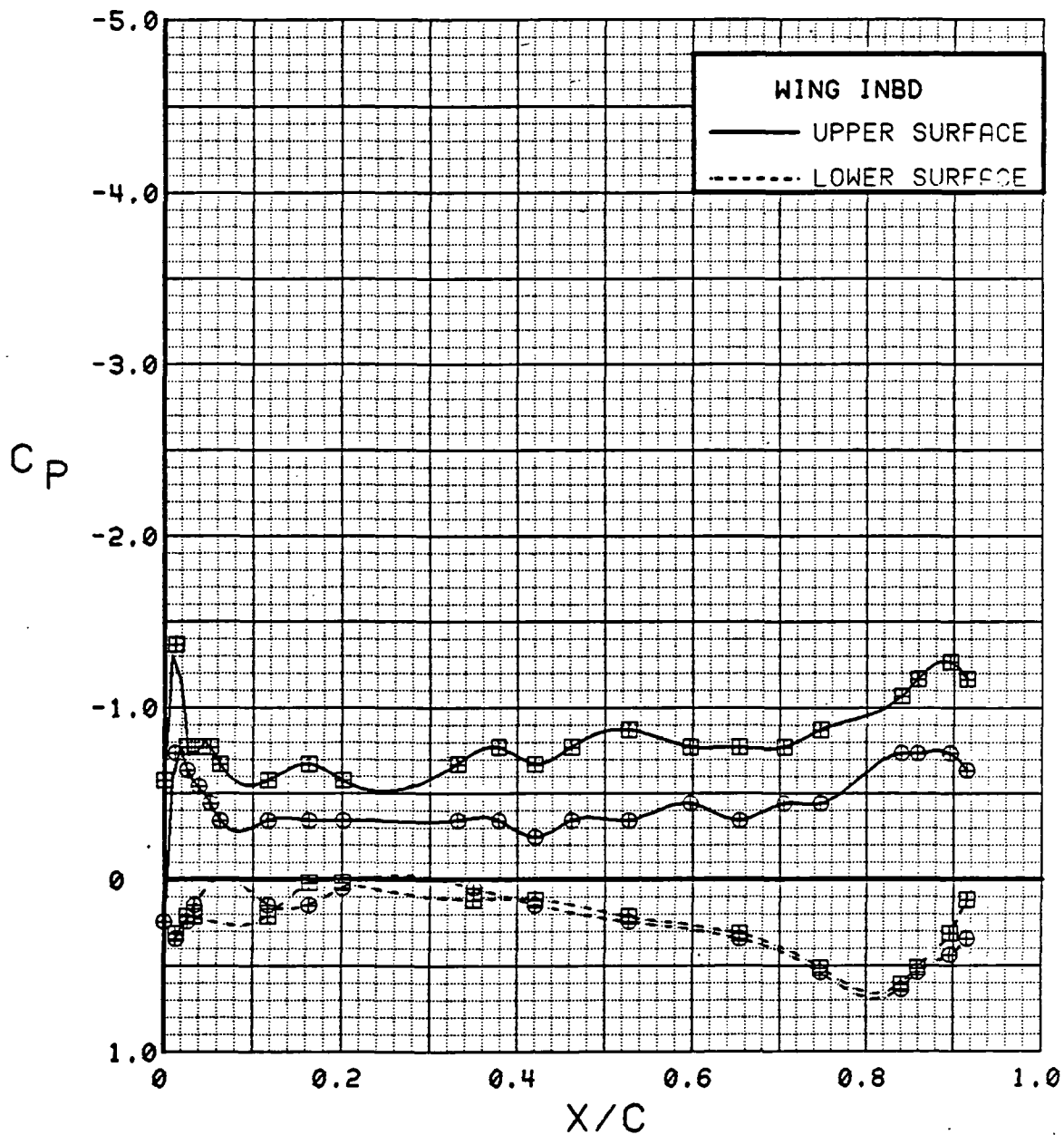


Figure 3.2.4-333 Power Effects, Flaps Deflected, Inboard, Alpha = 0 deg

SYM	TEST	RUN	ALPHA	CT	ITEF	OTEF	CAN	SWB
⊕	543	11	4.4	0.00	30	30	0	OFF
⊞	543	5	4.5	1.40	30	30	0	OFF

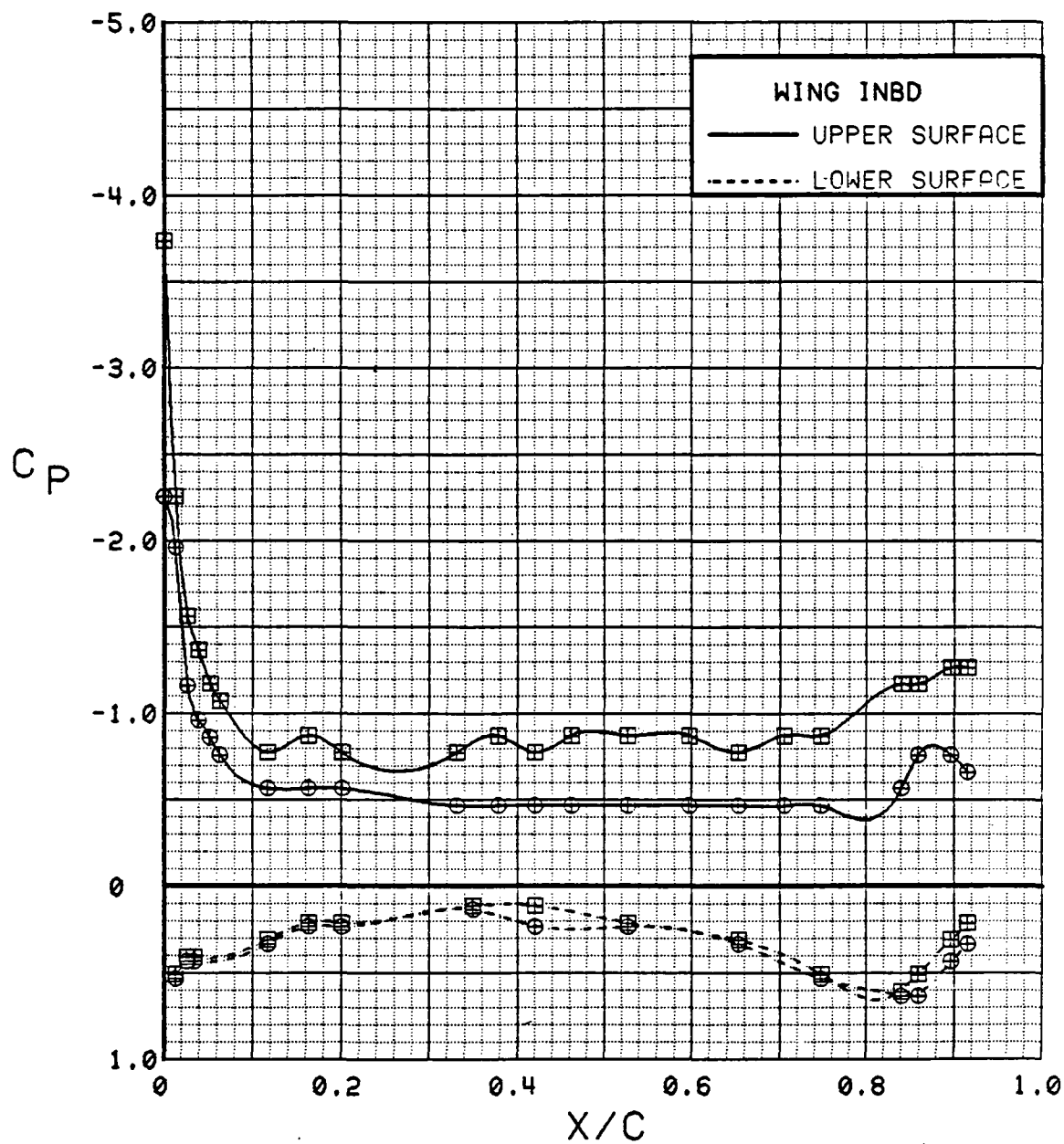


Figure 3.2.4-334 Power Effects, Flaps Deflected, Inboard, Alpha = 4 deg

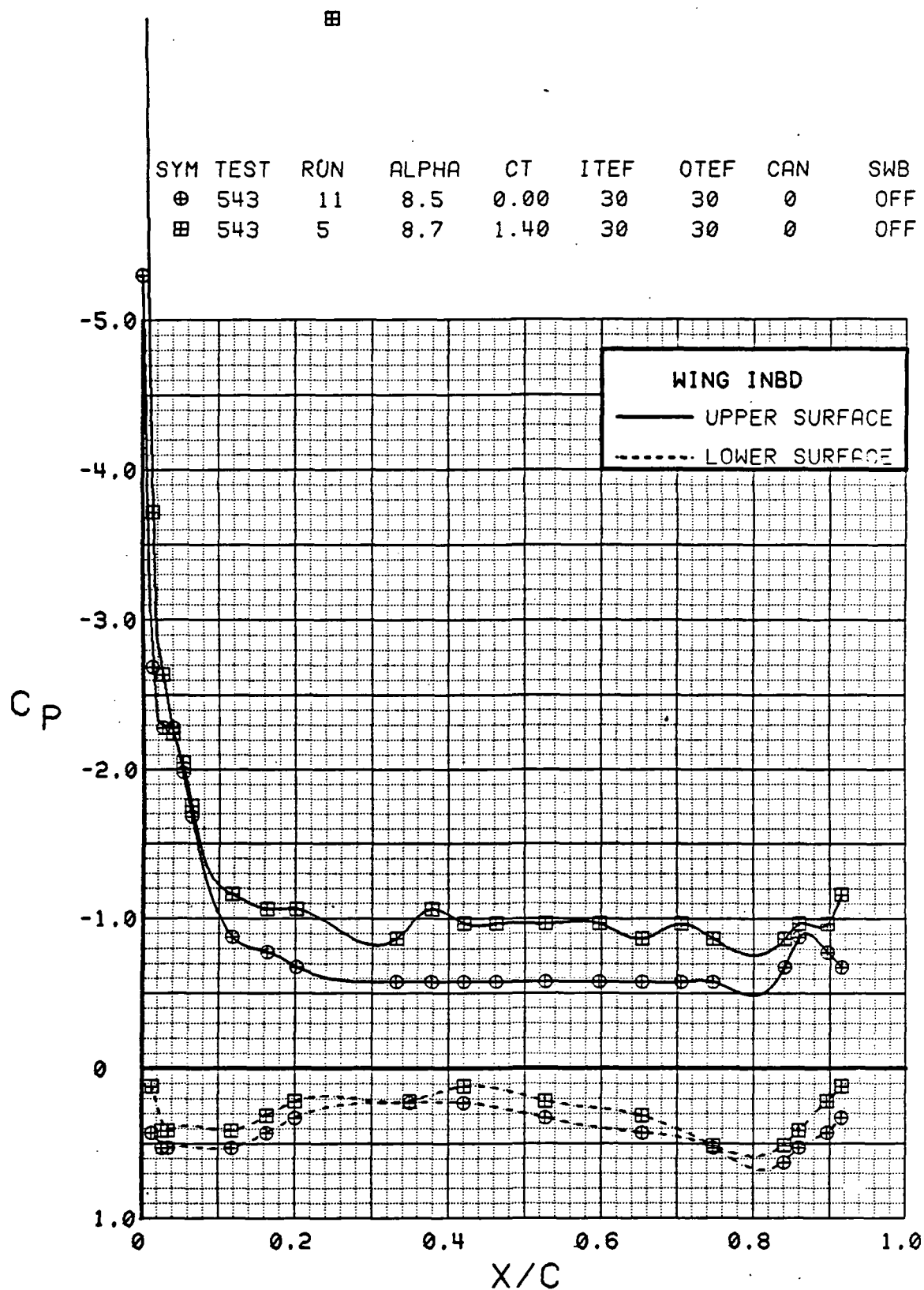


Figure 3.2.4-335 Power Effects, Flaps Deflected, Inboard, Alpha = 8 deg

SYM	TEST	RUN	ALPHA	CT	ITEF	OTEF	CAN	SWB
⊕	543	11	12.7	0.00	30	30	0	OFF
⊞	543	5	12.8	1.39	30	30	0	OFF

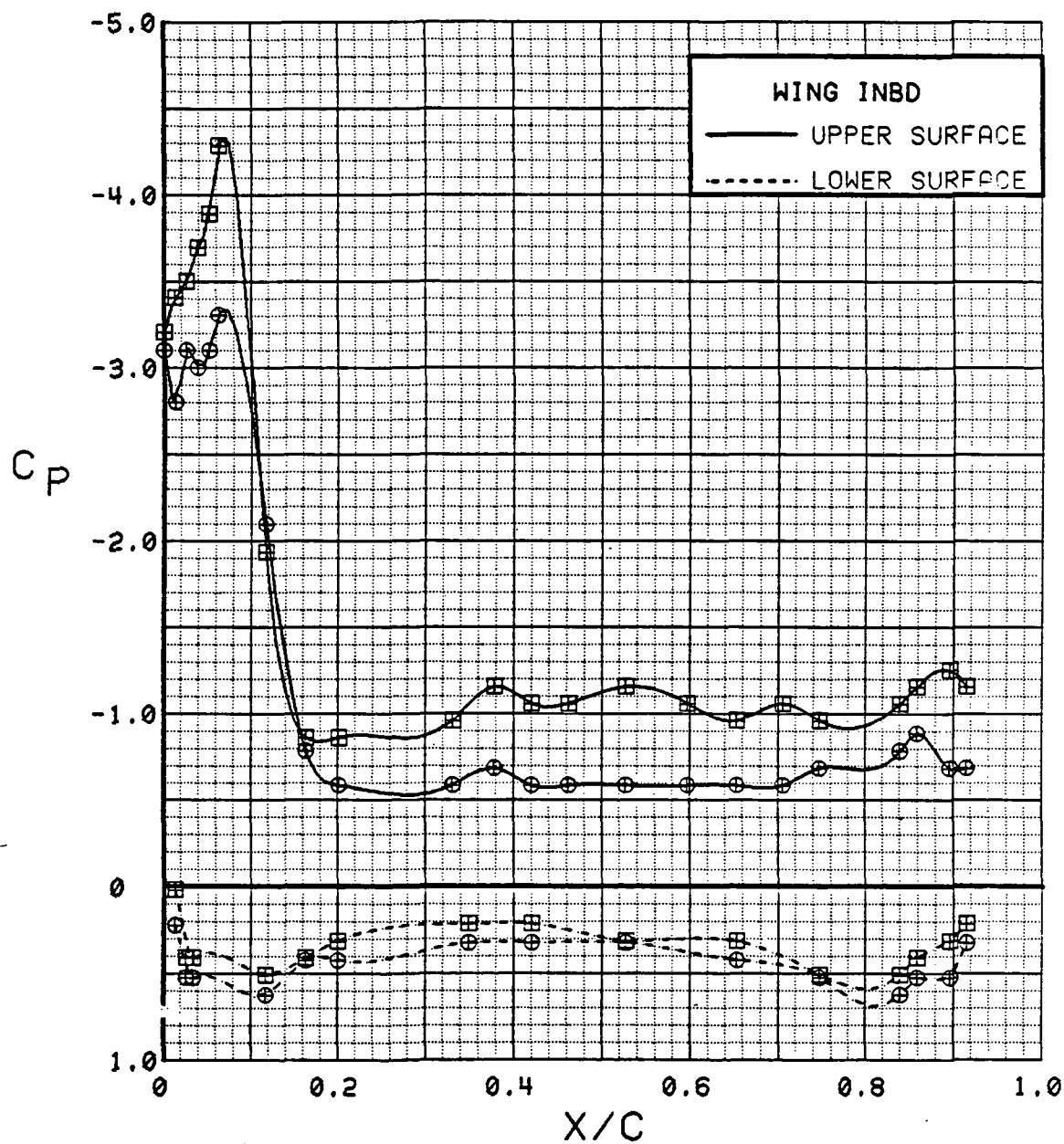


Figure 3.2.4-336 Power Effects, Flaps Deflected, Inboard, Alpha = 12 deg

SYM	TEST	RUN	ALPHA	CT	ITEF	OTEF	CAN	SWB
⊕	543	11	16.8	0.00	30	30	0	OFF
⊞	543	5	16.9	1.40	30	30	0	OFF

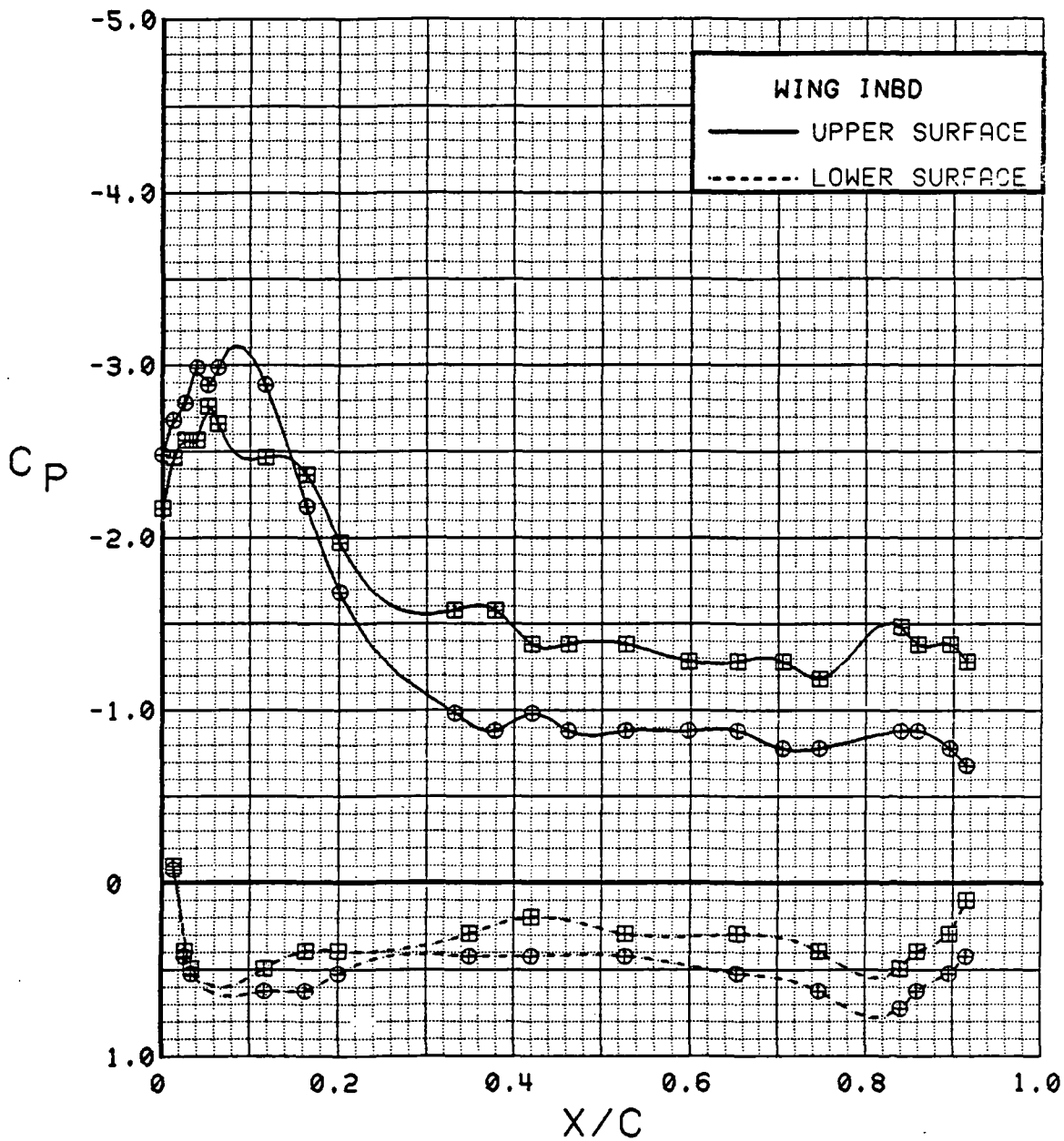


Figure 3.2.4-337 Power Effects, Flaps Deflected, Inboard, Alpha = 16 deg

SYM	TEST	RUN	ALPHA	CT	ITEF	OTEF	CAN	SWB
⊕	543	11	20.8	0.00	30	30	0	OFF
⊞	543	5	21.0	1.42	30	30	0	OFF

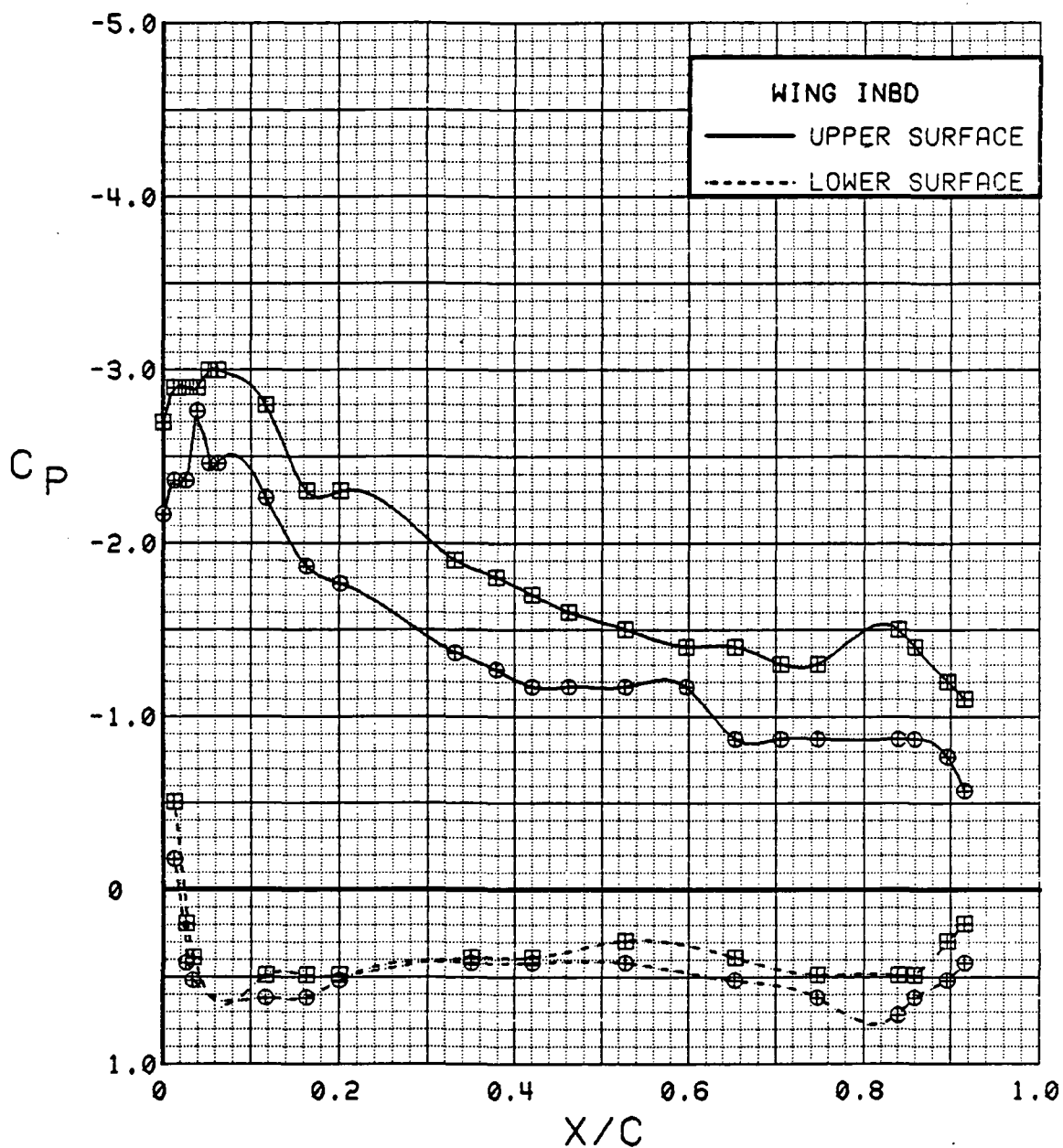


Figure 3.2.4-338 Power Effects, Flaps Deflected, Inboard, Alpha = 20 deg

SYM	TEST	RUN	ALPHA	CT	ITEF	OTEF	CAN	SWB
⊕	543	11	24.9	0.00	30	30	0	OFF
⊞	543	5	25.1	1.42	30	30	0	OFF

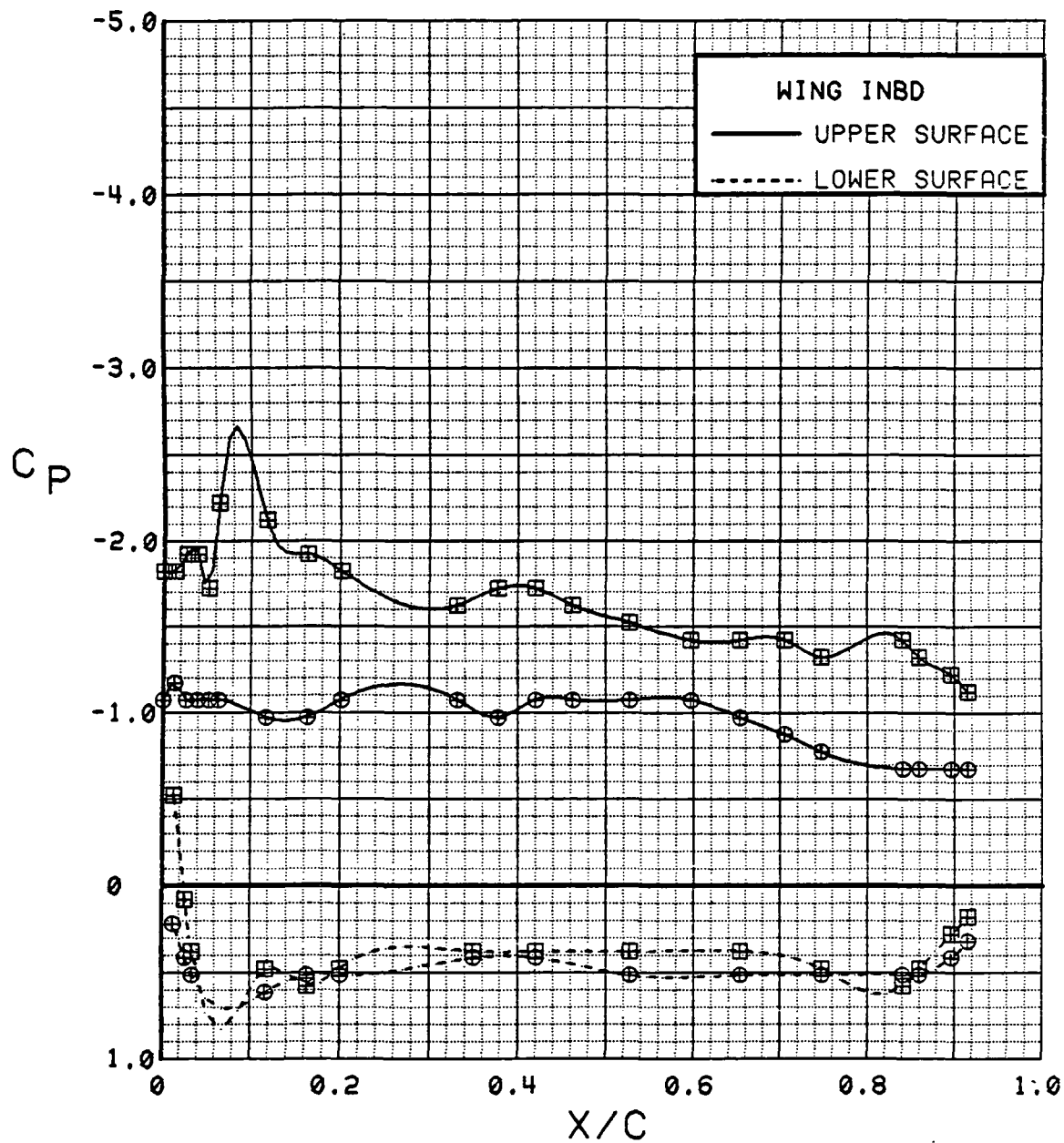


Figure 3.2.4-339 Power Effects, Flaps Deflected, Inboard, Alpha = 24 deg



SYM	TEST	RUN	ALPHA	CT	ITEF	OTEF	CAN	SWB
⊕	543	11	28.9	0.00	30	30	0	OFF
⊞	543	5	29.2	1.39	30	30	0	OFF

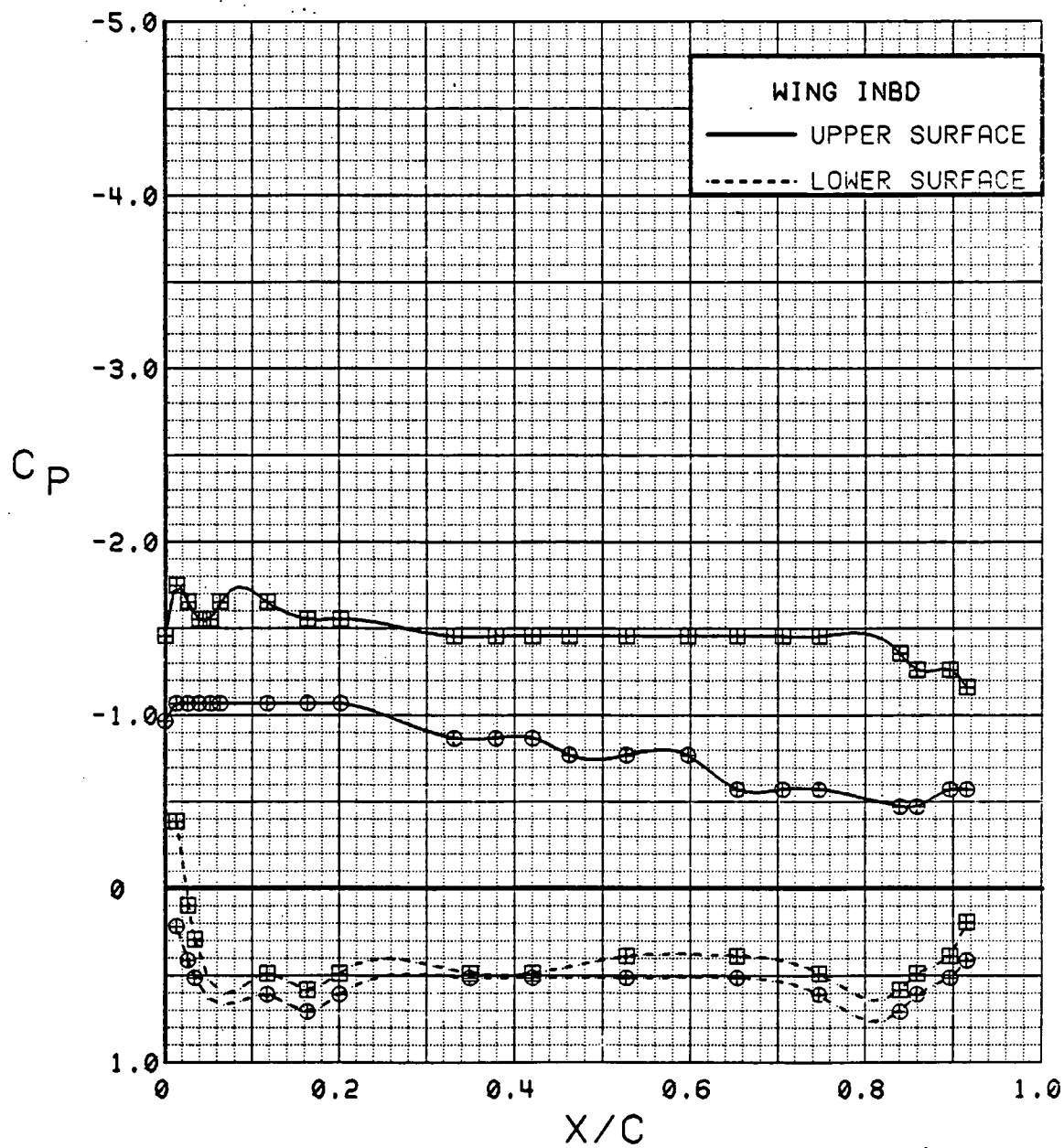


Figure 3.2.4-340 Power Effects, Flaps Deflected, Inboard, Alpha = 28 deg

SYM	TEST	RUN	ALPHA	CT	ITEF	OTEF	CAN	SWB
⊕	543	11	0.3	0.00	30	30	0	OFF
⊞	543	5	0.4	1.41	30	30	0	OFF

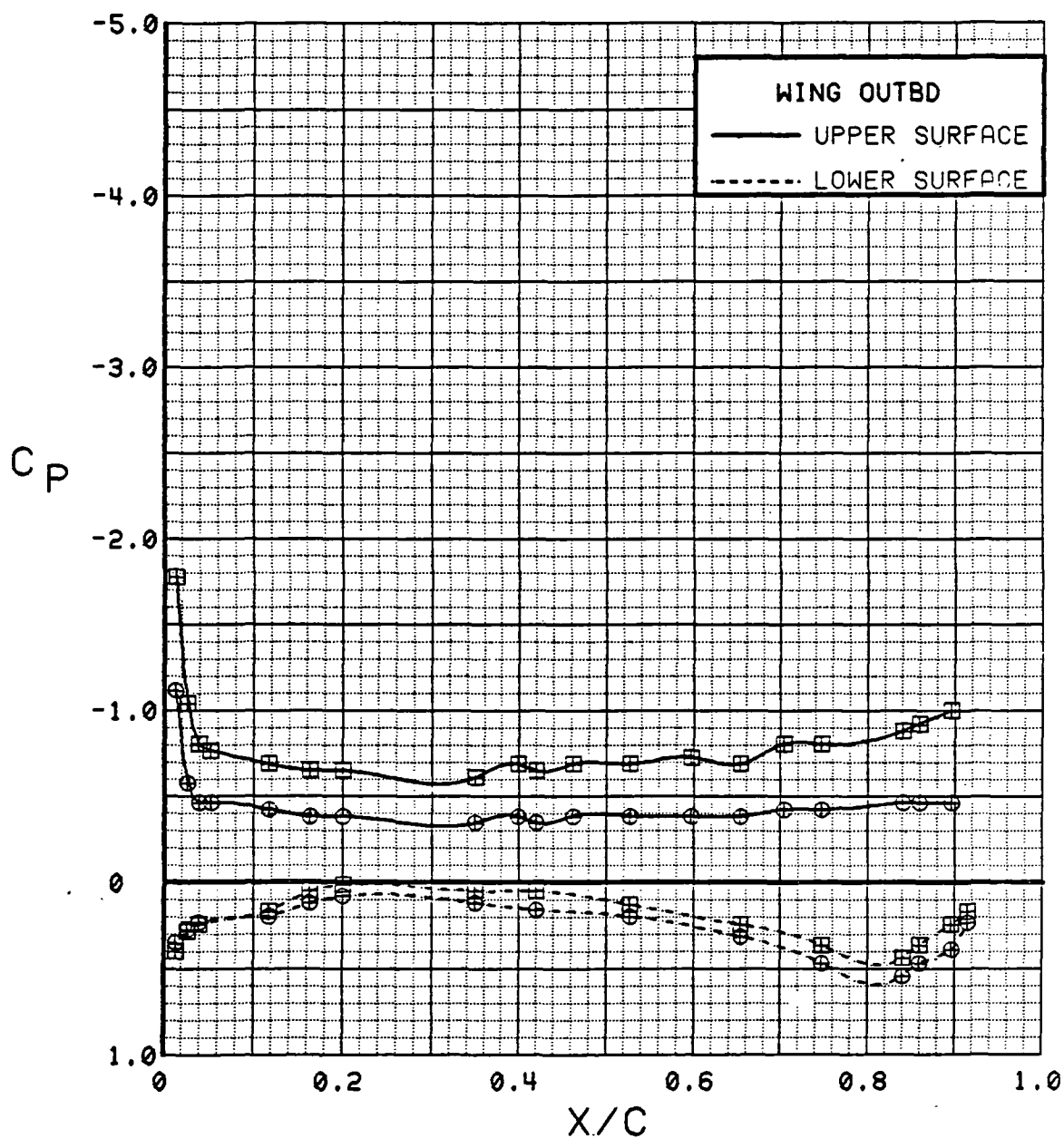


Figure 3.2.4-341 Power Effects, Flaps Deflected, Outboard, Alpha = 0 deg

SYM	TEST	RUN	ALPHA	CT	ITEF	OTEF	CAN	SWB
⊕	543	11	4.4	0.00	30	30	0	OFF
⊞	543	5	4.5	1.40	30	30	0	OFF

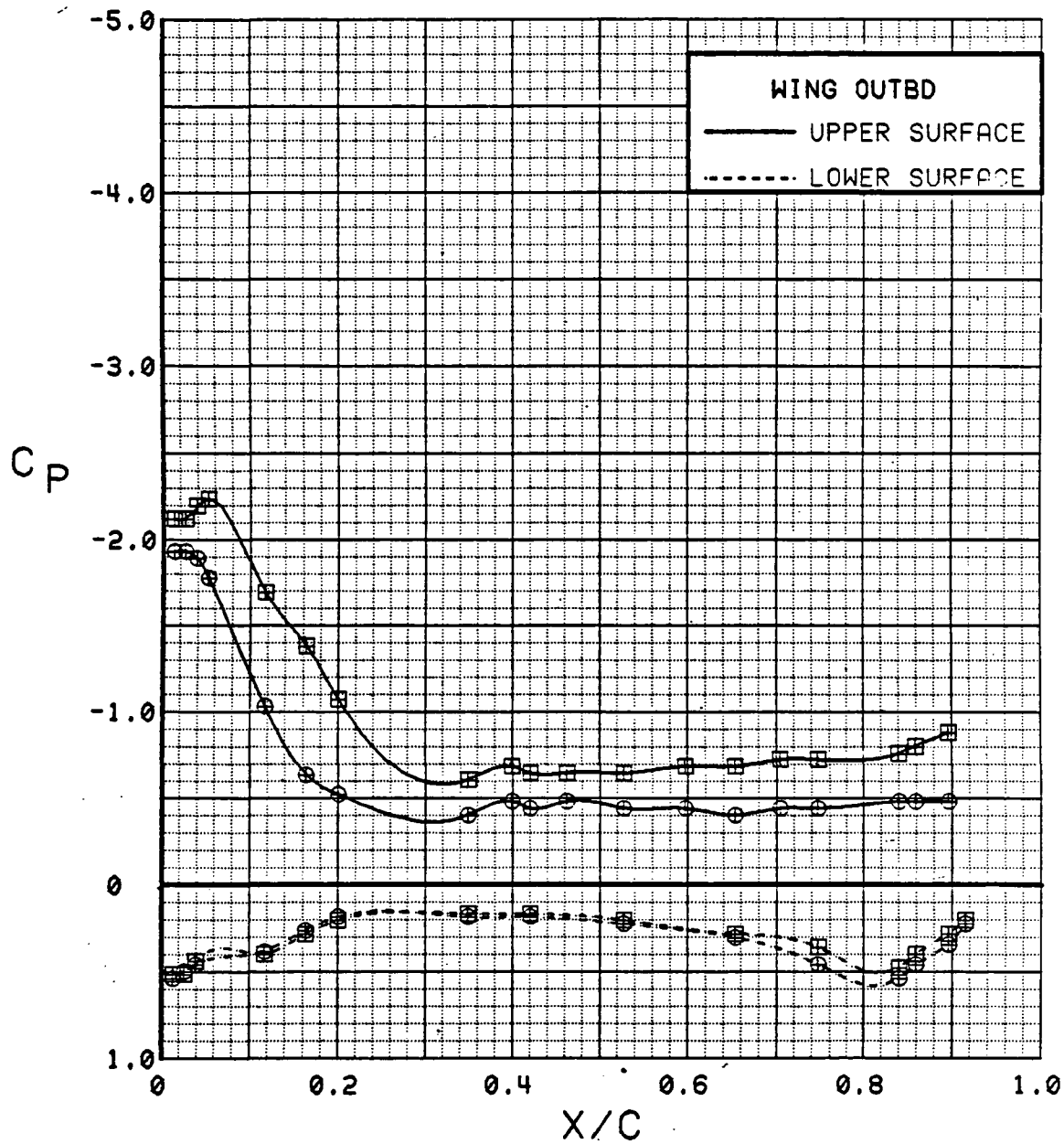


Figure 3.2.4-342 Power Effects, Flaps Deflected, Outboard, Alpha = 4 deg

SYM	TEST	RUN	ALPHA	CT	ITEF	OTEF	CAN	SWB
⊕	543	11	8.5	0.00	30	30	0	OFF
⊞	543	5	8.7	1.40	30	30	0	OFF

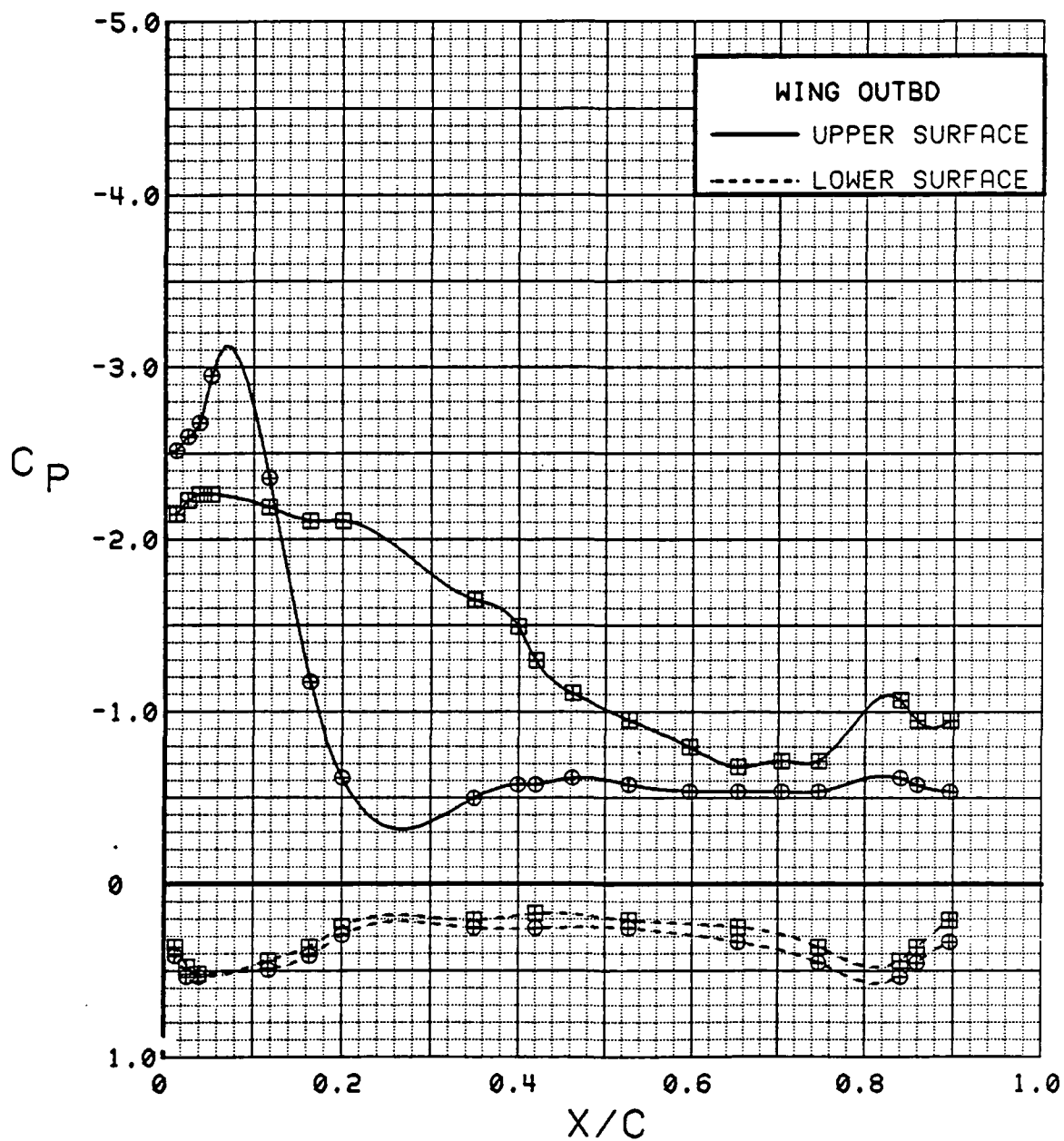


Figure 3.2.4-343 Power Effects, Flaps Deflected, Outboard, Alpha = 8 deg

SYM	TEST	RUN	ALPHA	CT	ITEF	OTEF	CAN	SWB
⊕	543	11	12.7	0.00	30	30	0	OFF
⊞	543	5	12.8	1.39	30	30	0	OFF

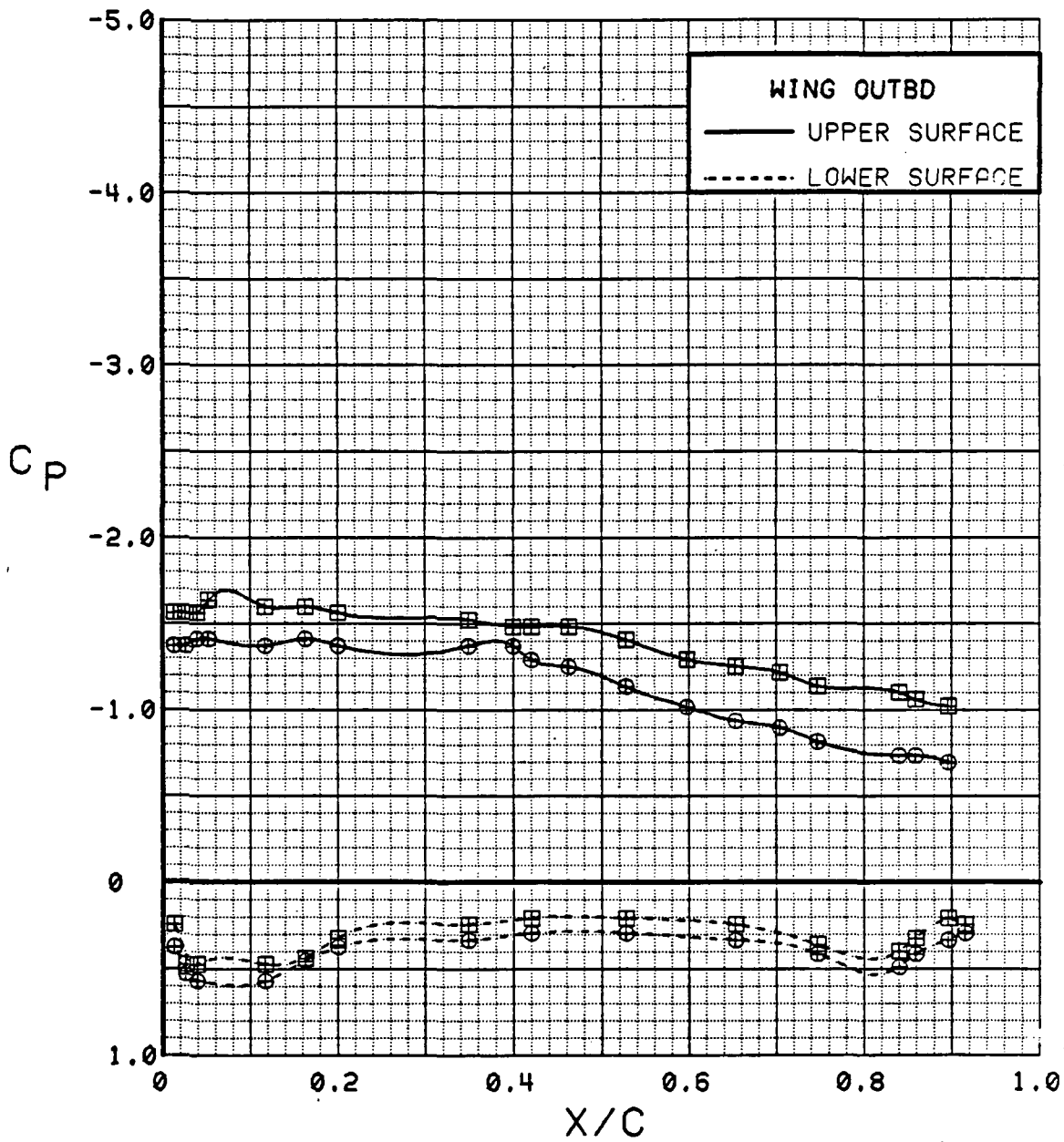


Figure 3.2.4-344 Power Effects, Flaps Deflected, Outboard, Alpha = 12 deg

SYM	TEST	RUN	ALPHA	CT	ITEF	OTEF	CAN	SWB
⊕	543	11	16.8	0.00	30	30	0	OFF
⊞	543	5	16.9	1.40	30	30	0	OFF

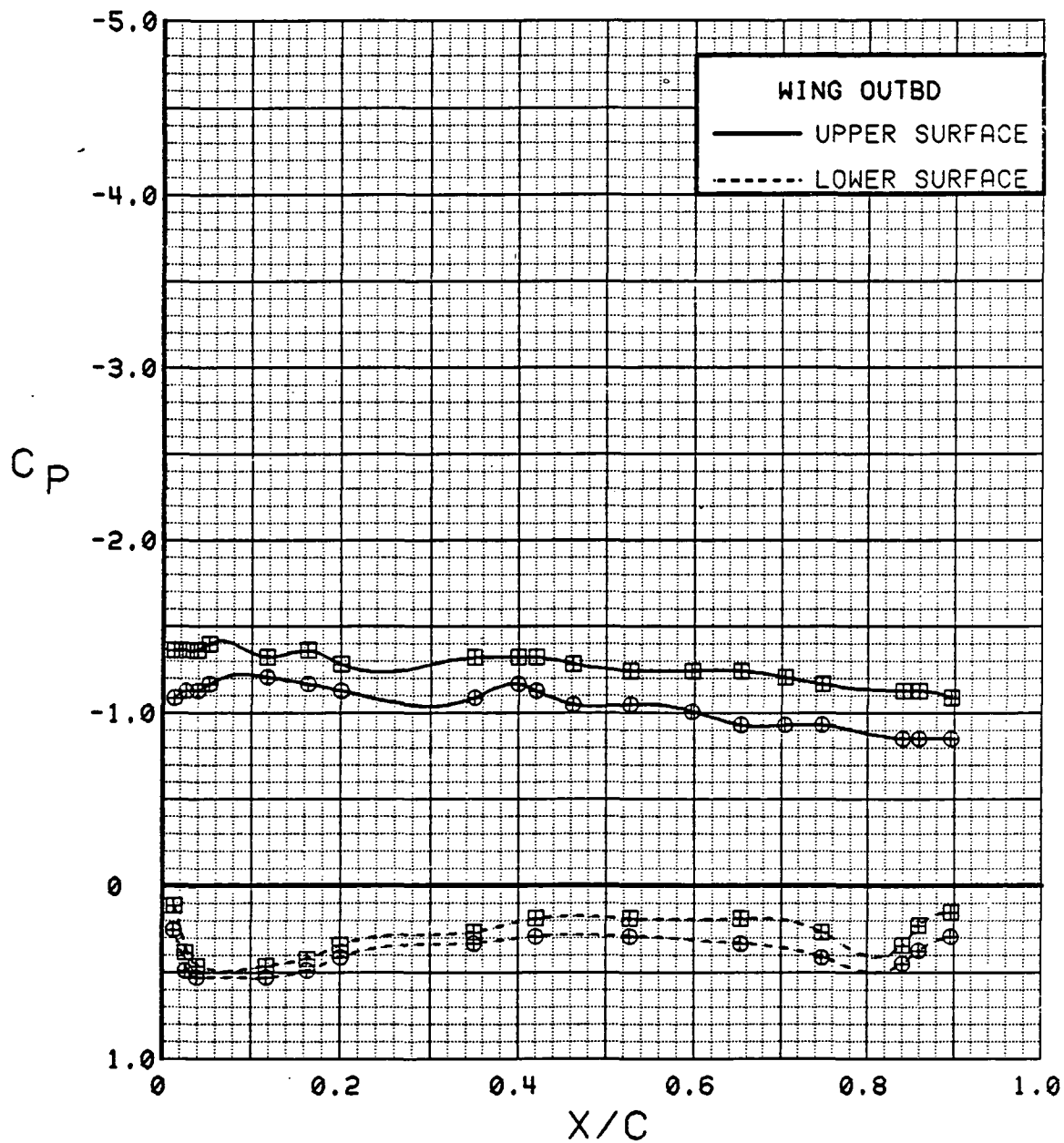


Figure 3.2.4-345 Power Effects, Flaps Deflected, Outboard, Alpha = 16 deg

SYM	TEST	RUN	ALPHA	CT	ITEF	OTEF	CAN	SWB
⊕	543	11	20.8	0.00	30	30	0	OFF
⊞	543	5	21.0	1.42	30	30	0	OFF

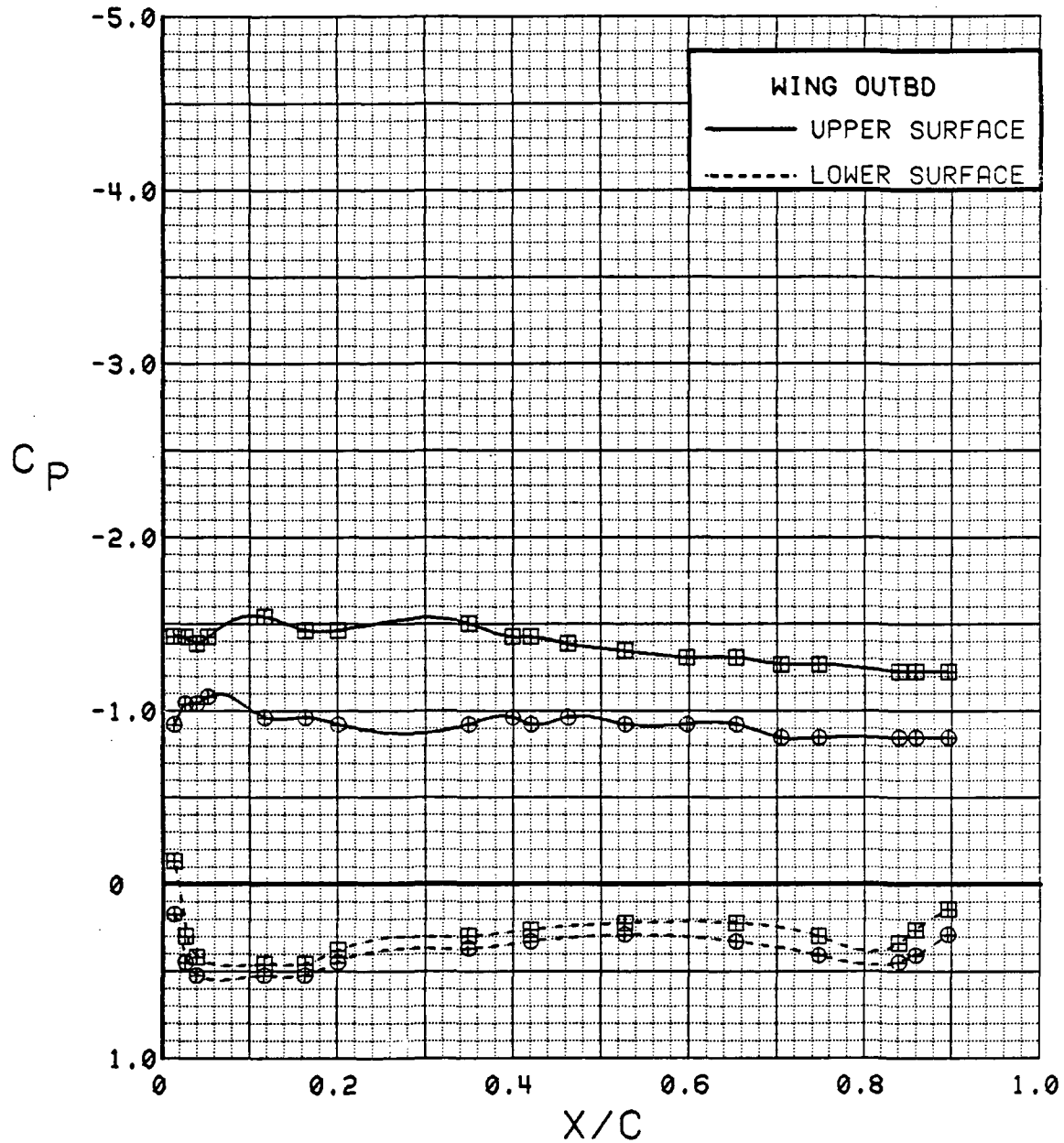


Figure 3.2.4-346 Power Effects, Flaps Deflected, Outboard, Alpha = 20 deg

SYM	TEST	RUN	ALPHA	CT	ITEF	OTEF	CAN	SWB
⊕	543	11	24.9	0.00	30	30	0	OFF
⊞	543	5	25.1	1.42	30	30	0	OFF

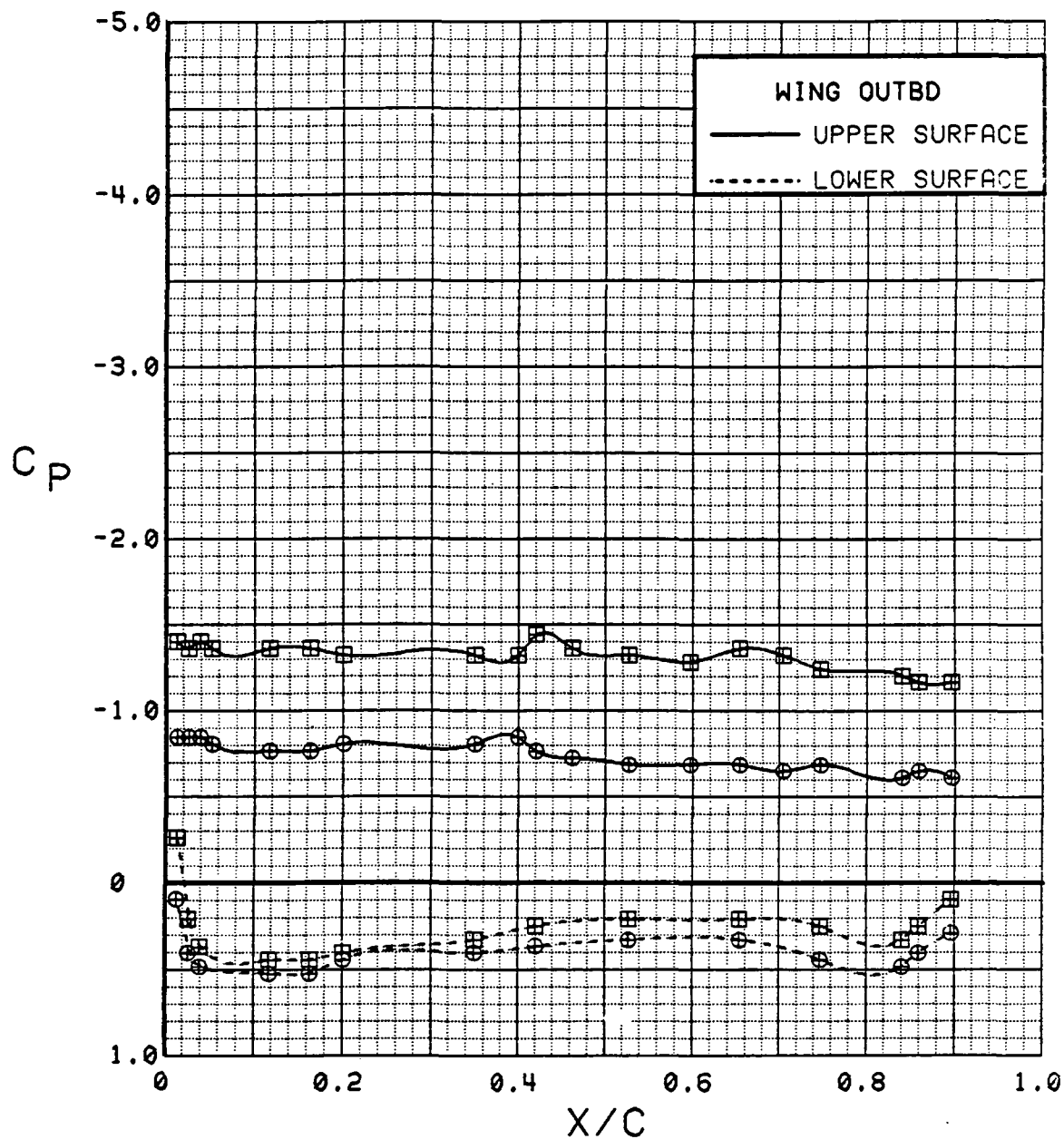


Figure 3.2.4-347 Power Effects, Flaps Deflected, Outboard, Alpha = 24 deg



SYM	TEST	RUN	ALPHA	CT	ITEF	OTEF	CAN	SWB
⊕	543	11	28.9	0.00	30	30	0	OFF
⊞	543	5	29.2	1.39	30	30	0	OFF

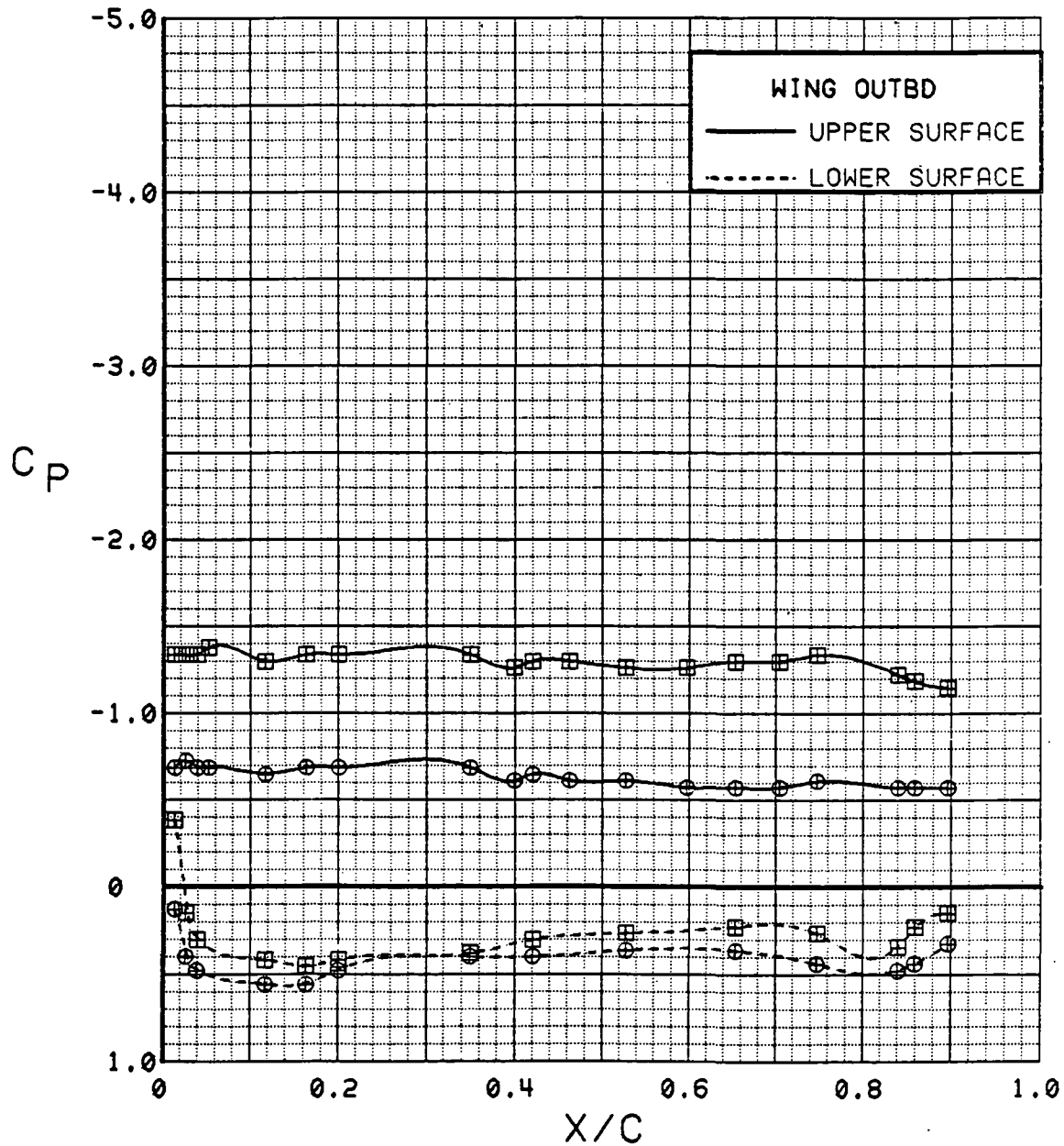


Figure 3.2.4-348 Power Effects, Flaps Deflected, Outboard, Alpha = 28 deg

SYM	TEST	RUN	ALPHA	CT	ITEF	OTEF	CAN	SWB
⊕	543	11	0.3	0.00	30	30	0	OFF
⊞	543	5	0.4	1.41	30	30	0	OFF

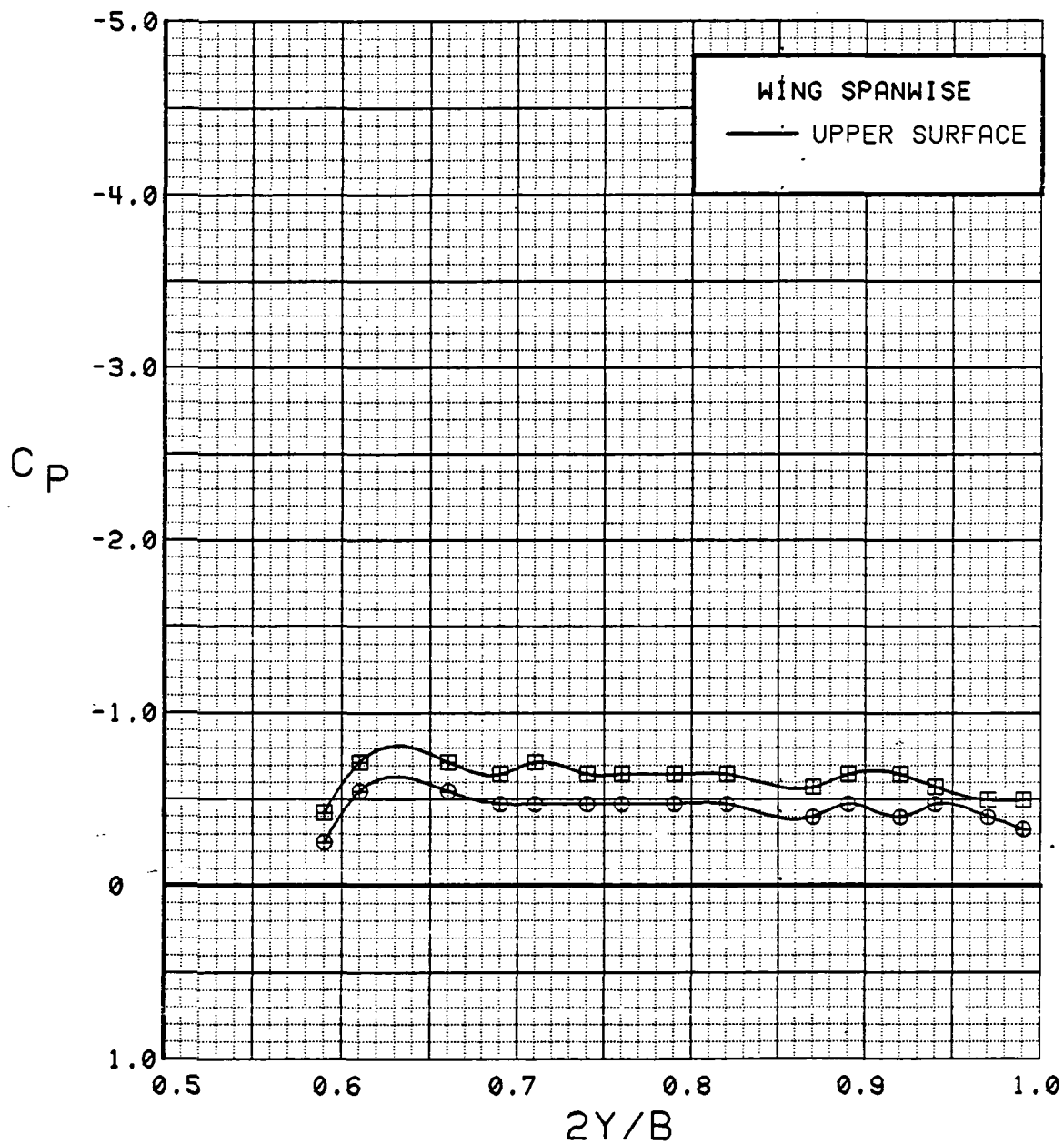


Figure 3.2.4-349 Power Effects, Flaps Deflected, Spanwise, Alpha = 0 deg

SYM	TEST	RUN	ALPHA	CT	ITEF	OTEF	CAN	SWB
⊙	543	11	4.4	0.00	30	30	0	OFF
⊠	543	5	4.5	1.40	30	30	0	OFF

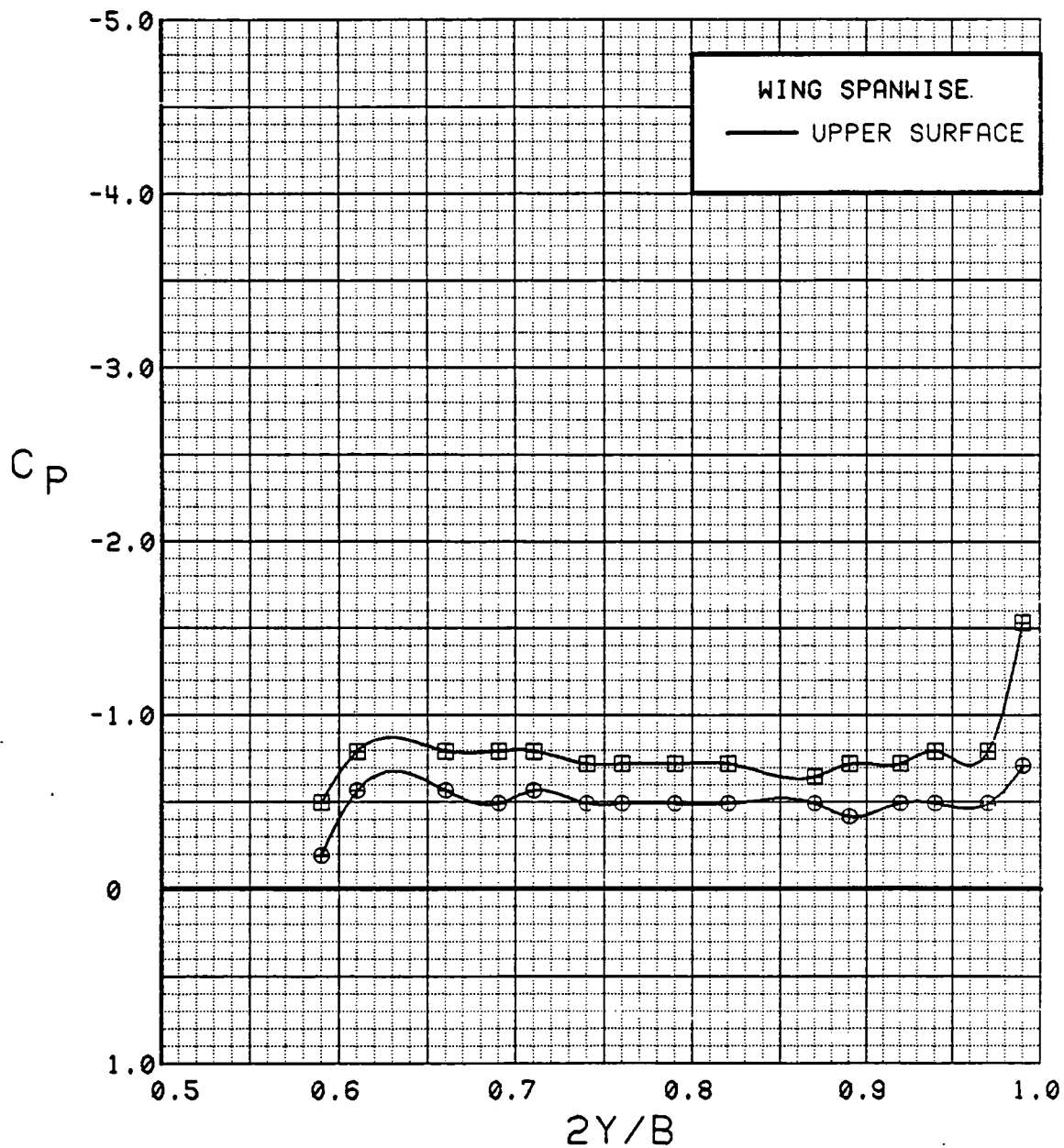


Figure 3.2.4-350 Power Effects, Flaps Deflected, Spanwise, Alpha = 4 deg

SYM	TEST	RUN	ALPHA	CT	ITEF	OTEF	CAN	SWB
⊕	543	11	8.5	0.00	30	30	0	OFF
⊞	543	5	8.7	1.40	30	30	0	OFF

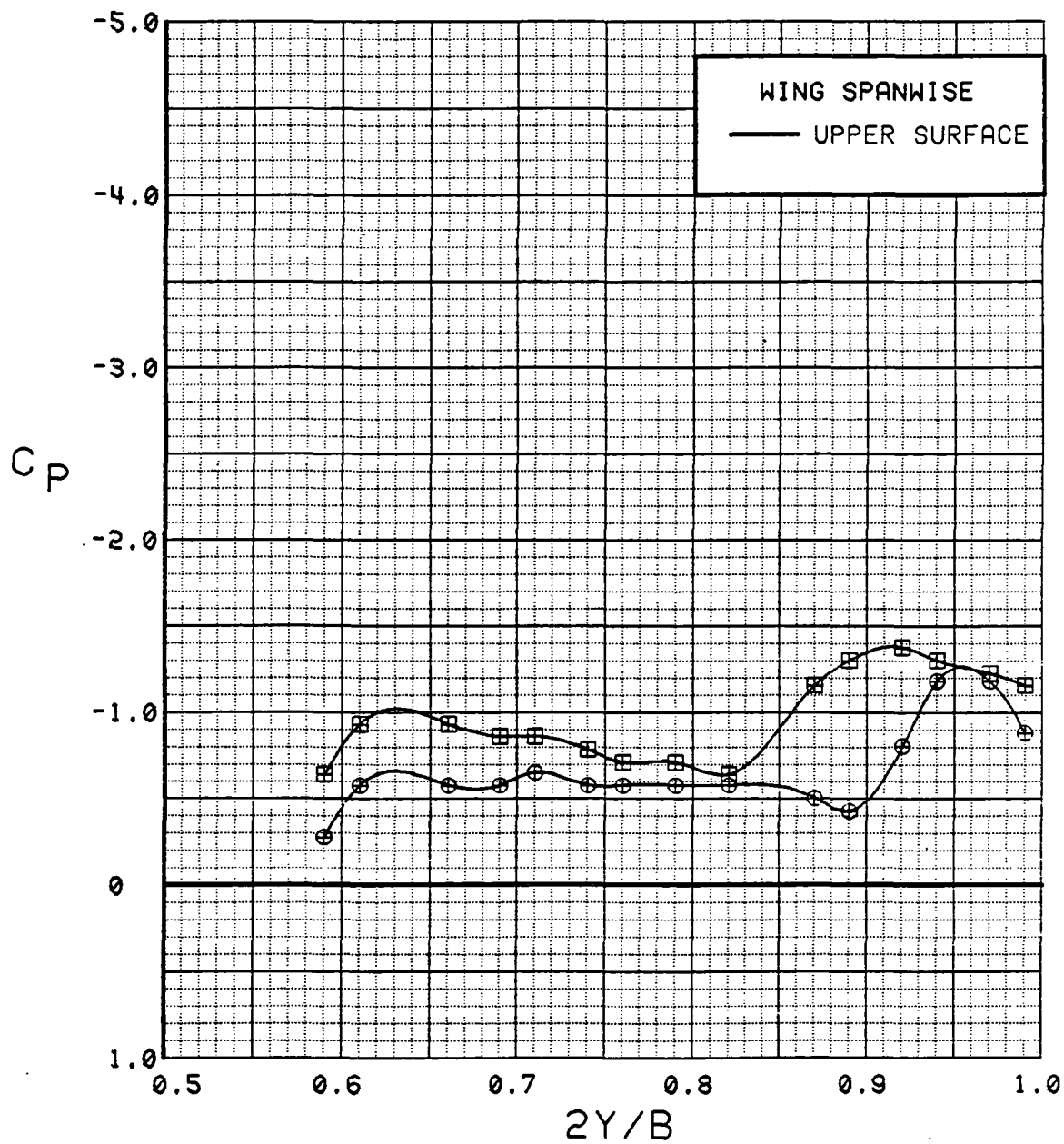


Figure 3.2.4-351 Power Effects, Flaps Deflected, Spanwise, Alpha = 8 deg

SYM	TEST	RUN	ALPHA	CT	ITEF	OTEF	CAN	SWB
⊗	543	11	12.7	0.00	30	30	0	OFF
⊗	543	5	12.8	1.39	30	30	0	OFF

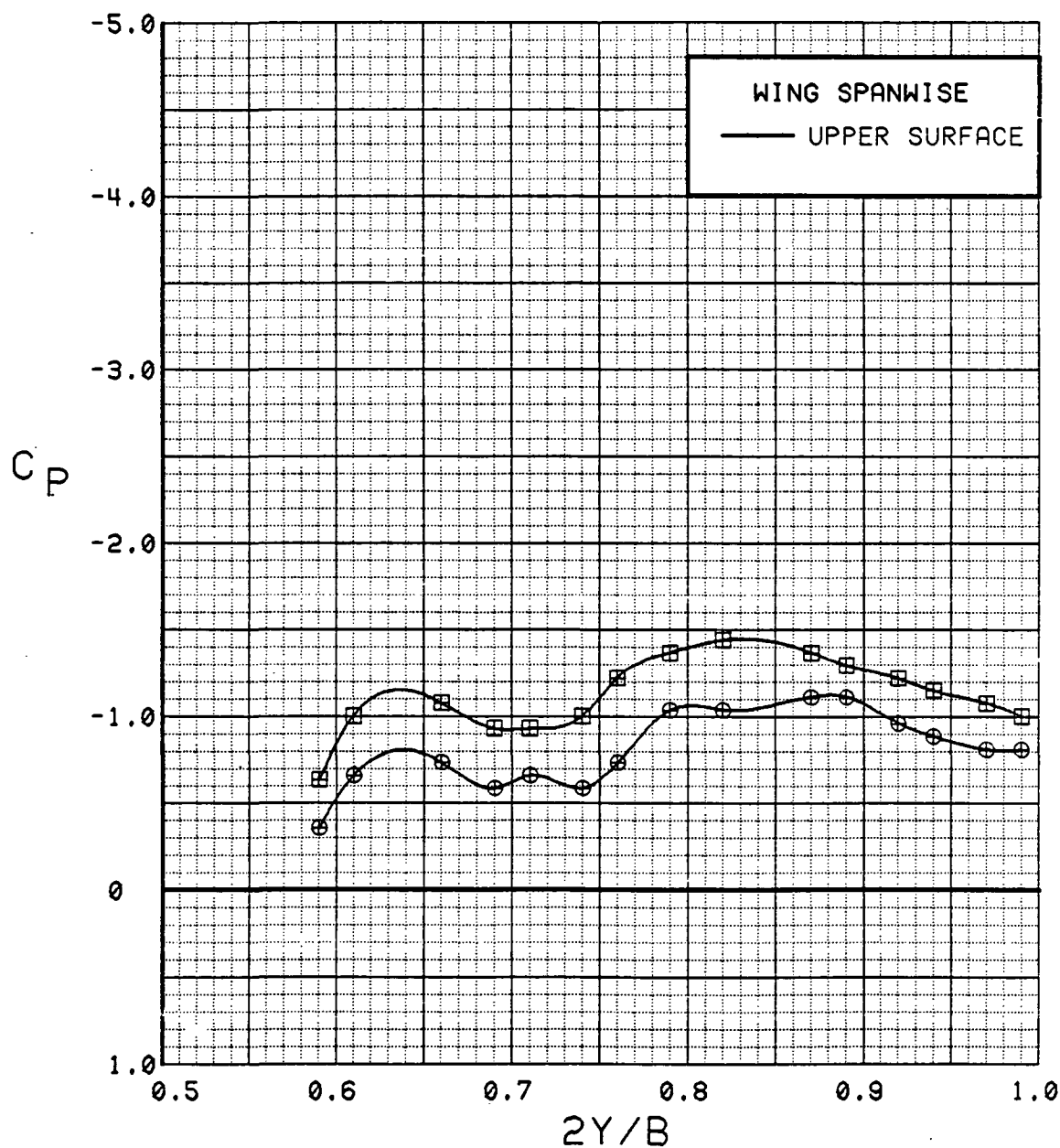


Figure 3.2.4-352 Power Effects, Flaps Deflected, Spanwise, Alpha = 12 deg

SYM	TEST	RUN	ALPHA	CT	ITEF	OTEF	CAN	SWB
⊙	543	11	16.8	0.00	30	30	0	OFF
⊠	543	5	16.9	1.40	30	30	0	OFF

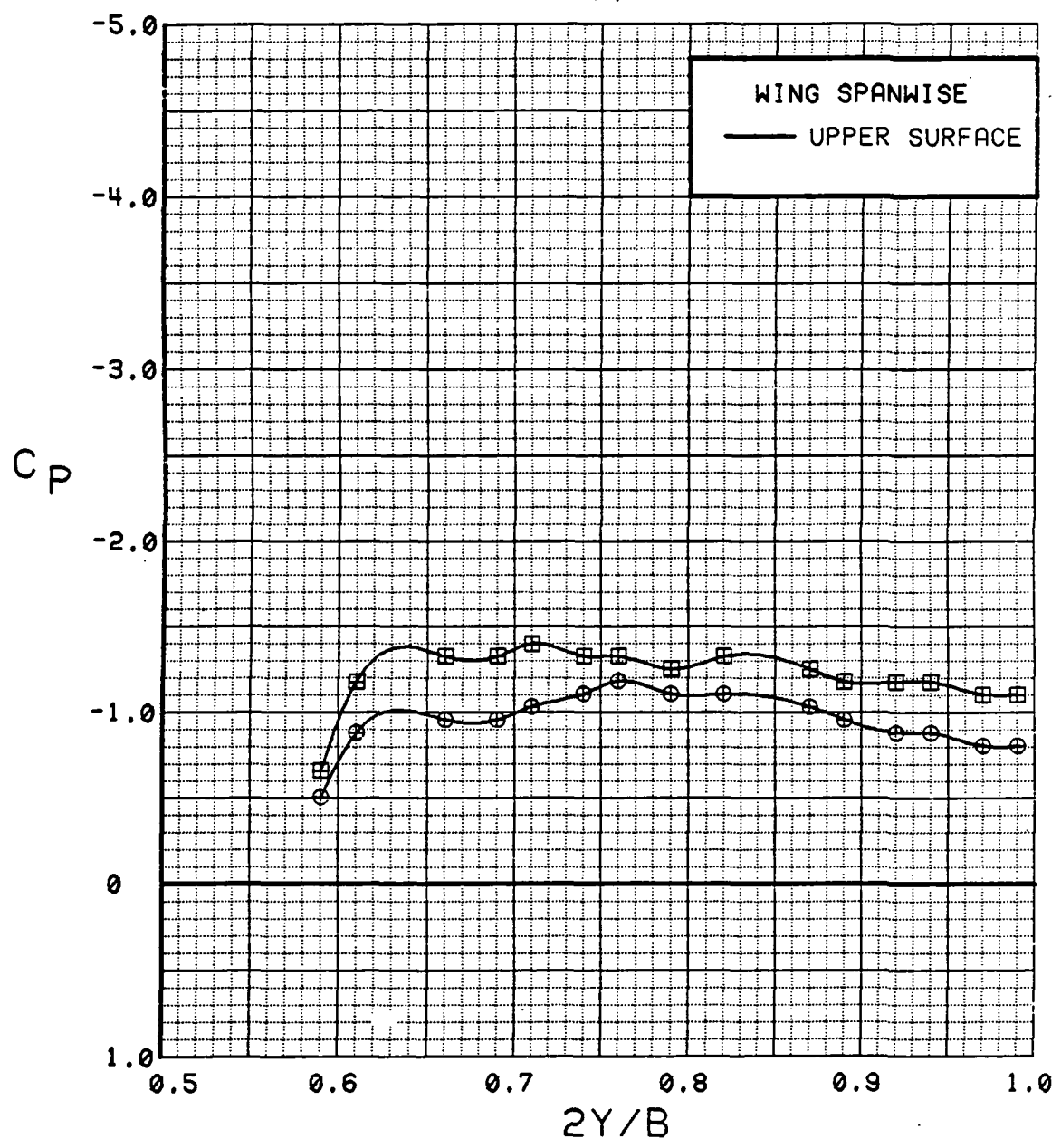


Figure 3.2.4-353 Power Effects, Flaps Deflected, Spanwise, Alpha = 16 deg

SYM	TEST	RUN	ALPHA	CT	ITEF	OTEF	CAN	SWB
⊕	543	11	20.8	0.00	30	30	0	OFF
⊞	543	5	21.0	1.42	30	30	0	OFF

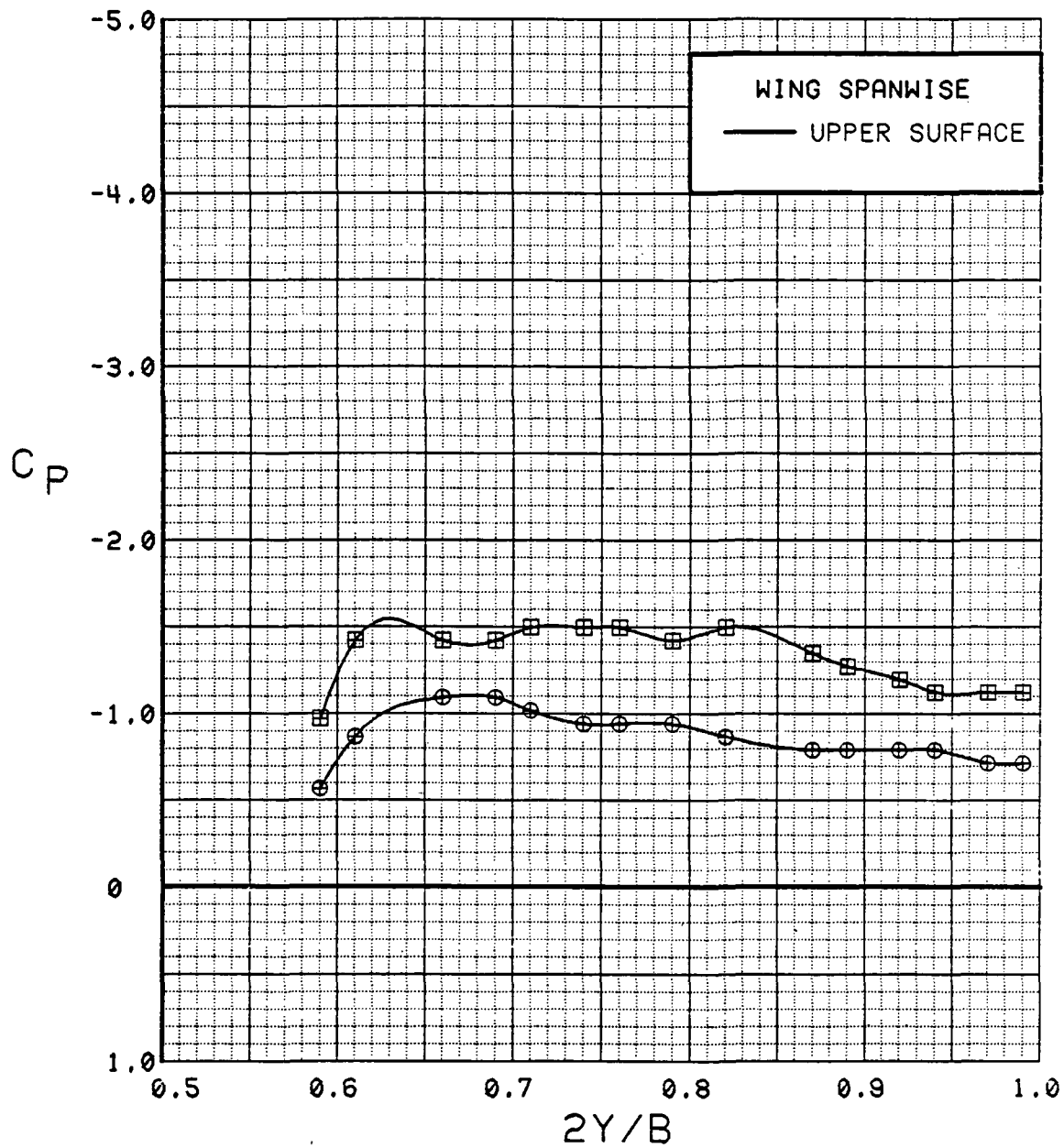


Figure 3.2.4-354 Power Effects, Flaps Deflected, Spanwise, Alpha = 20 deg

SYM	TEST	RUN	ALPHA	CT	ITEF	OTEF	CAN	SWB
⊙	543	11	24.9	0.00	30	30	0	OFF
⊠	543	5	25.1	1.42	30	30	0	OFF

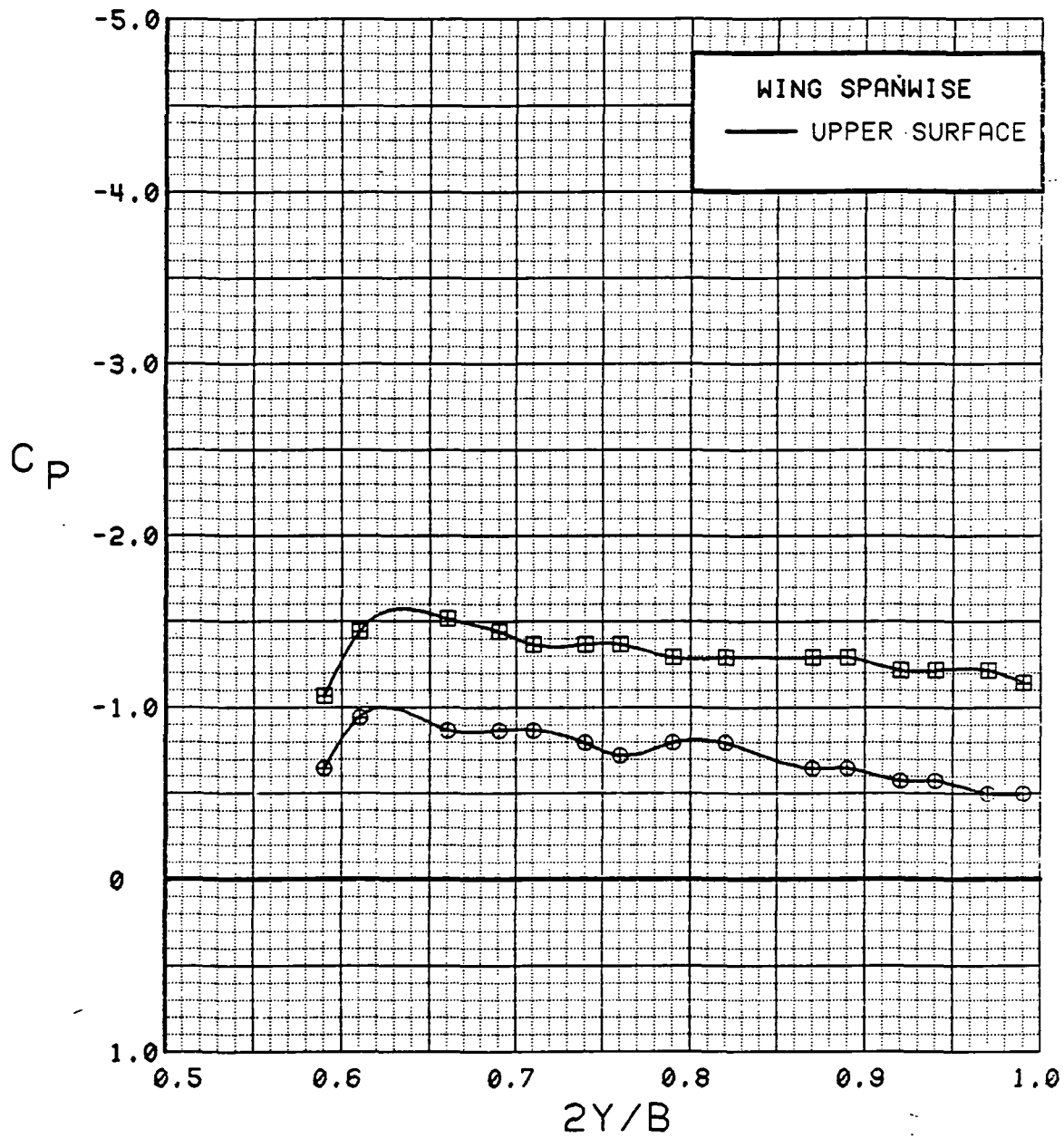


Figure 3.2.4-355 Power Effects, Flaps Deflected, Spanwise, Alpha = 24 deg



SYM	TEST	RUN	ALPHA	CT	ITEF	OTEF	CAN	SWB
⊕	543	11	28.9	0.00	30	30	0	OFF
⊞	543	5	29.2	1.39	30	30	0	OFF

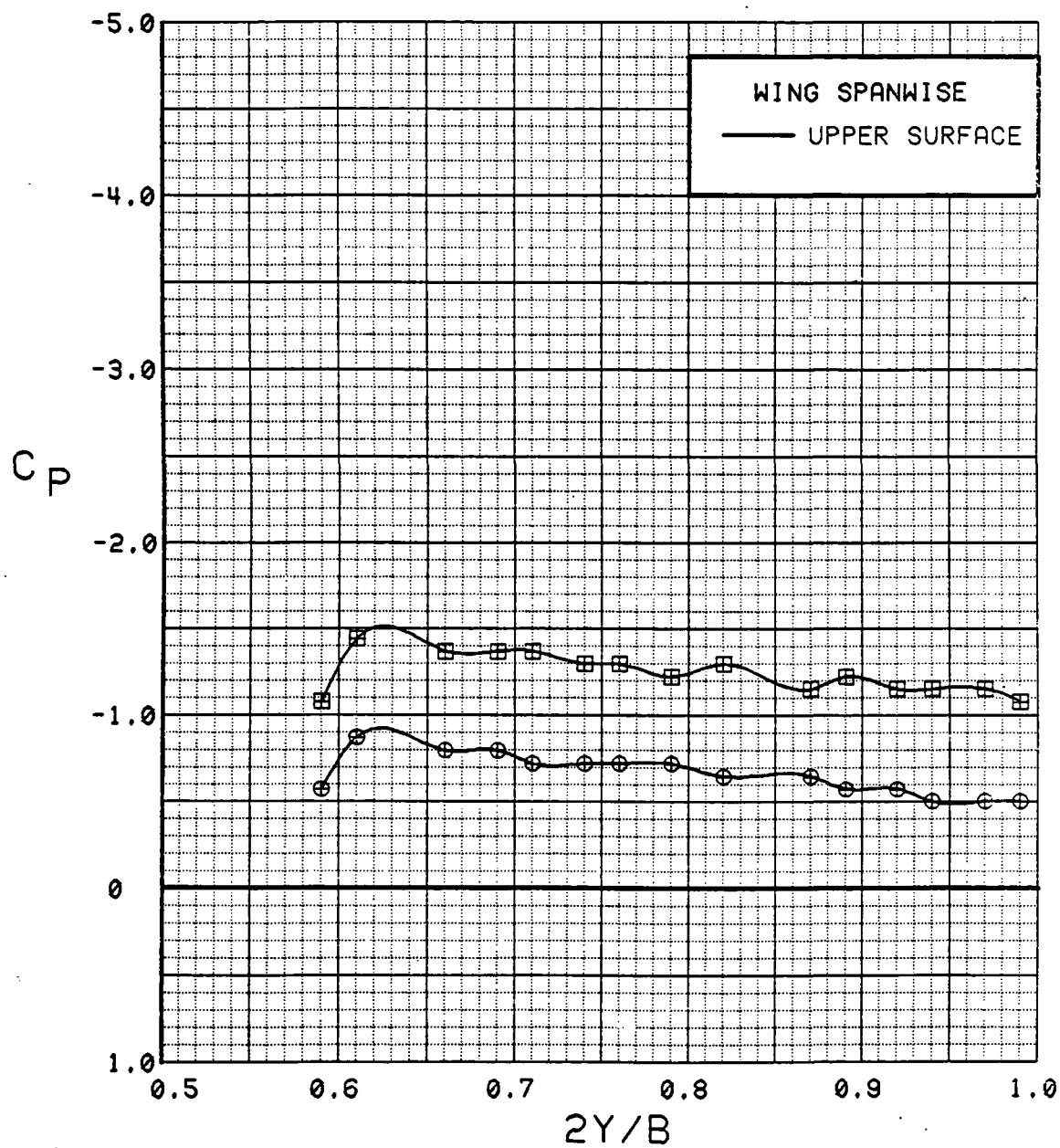


Figure 3.2.4-356 Power Effects, Flaps Deflected, Spanwise, Alpha = 28 deg

# WING INBOARD

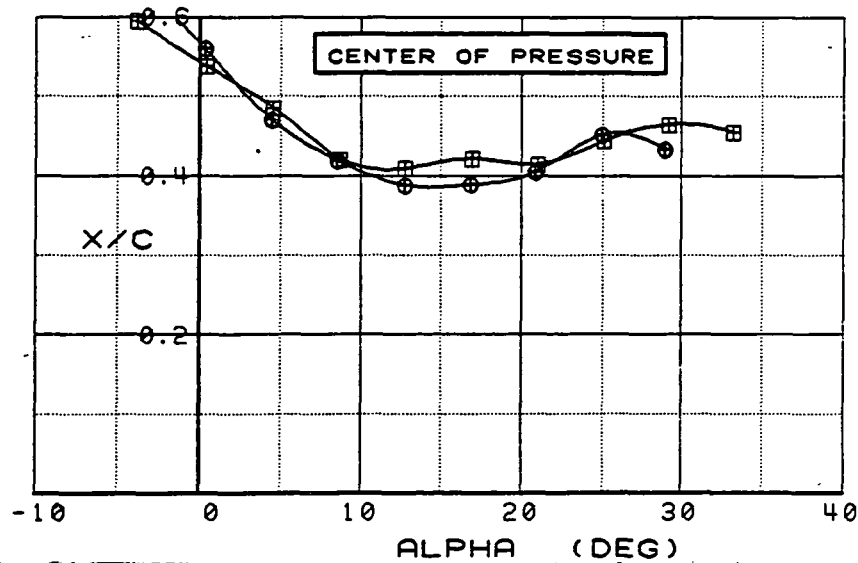
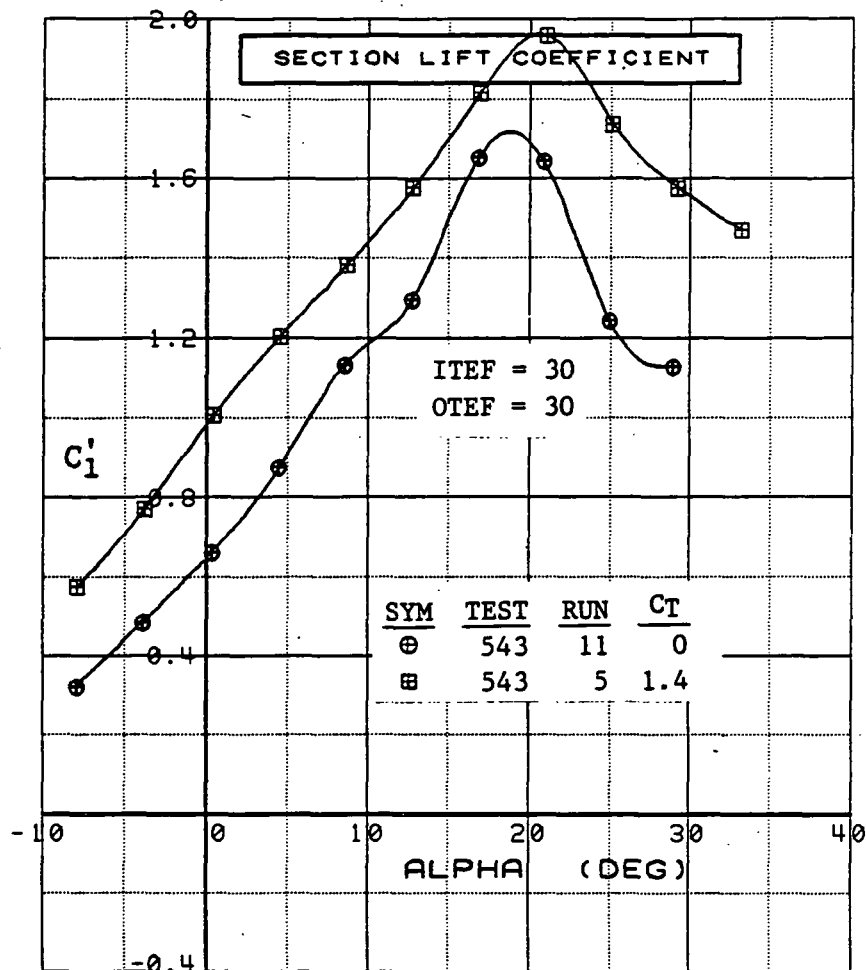


Figure 3.2.4-357 Power Effects, Inboard, Flaps Deflected, Integrated Section Properties

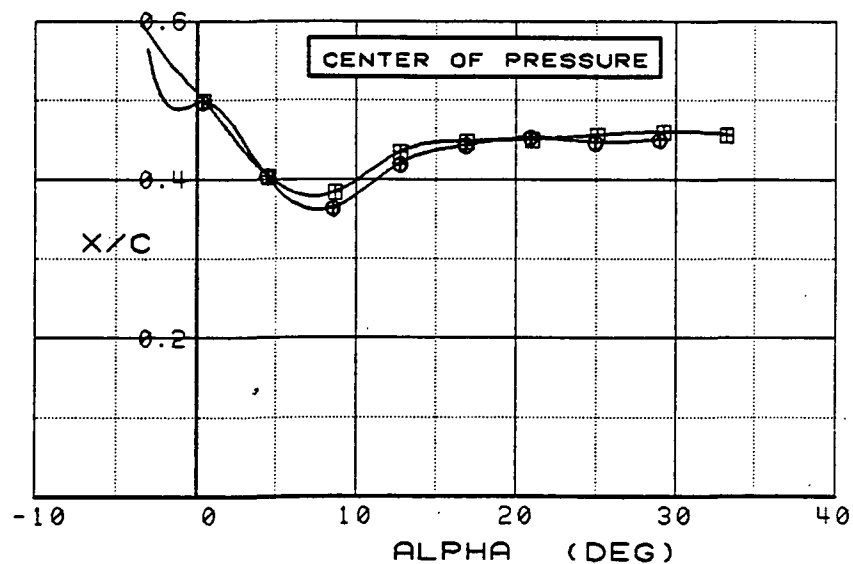
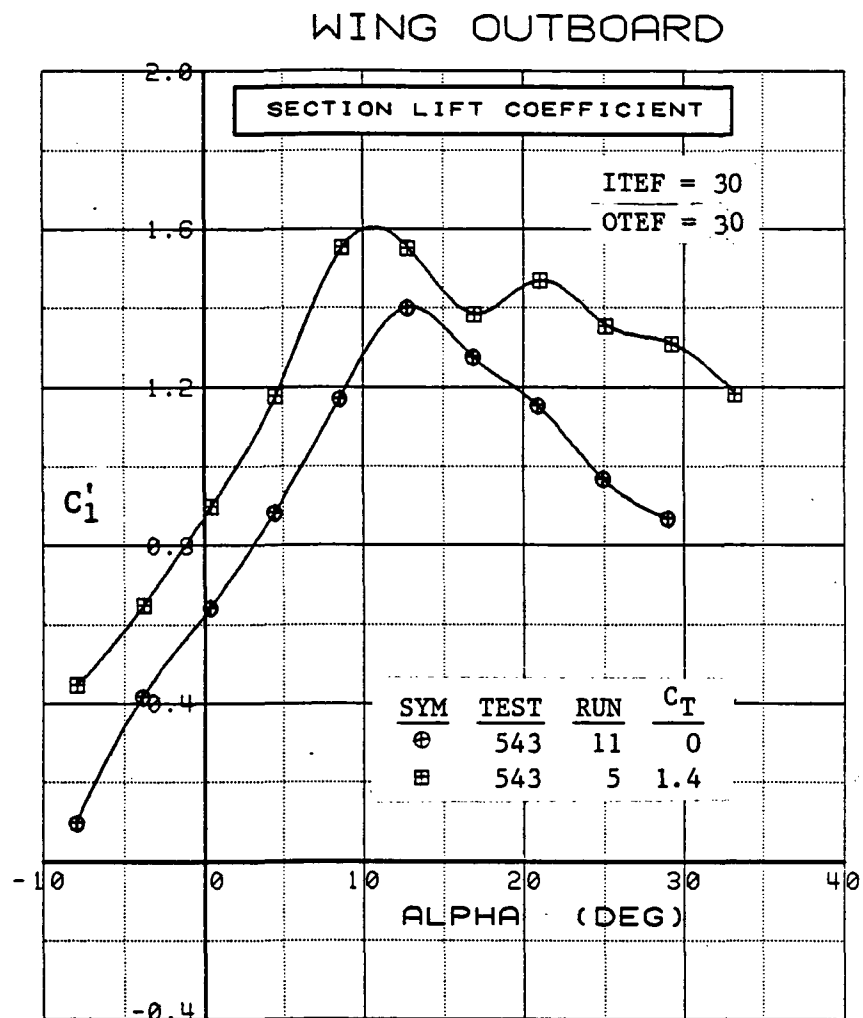


Figure 3.2.4-358 Power Effects, Outboard, Flaps Deflected, Integrated Section Properties

SYM	TEST	RUN	ALPHA	CT	ITEF	OTEF	CAN	SWB
⊕	543	63	4.2	0.00	0	0	0	OFF
⊞	543	64	4.2	0.27	0	0	0	OFF
△	543	62	4.2	0.48	0	0	0	OFF
◆	543	60	4.3	0.93	0	0	0	OFF
*	543	59	4.3	1.40	0	0	0	OFF
+	543	58	4.3	1.84	0	0	0	OFF

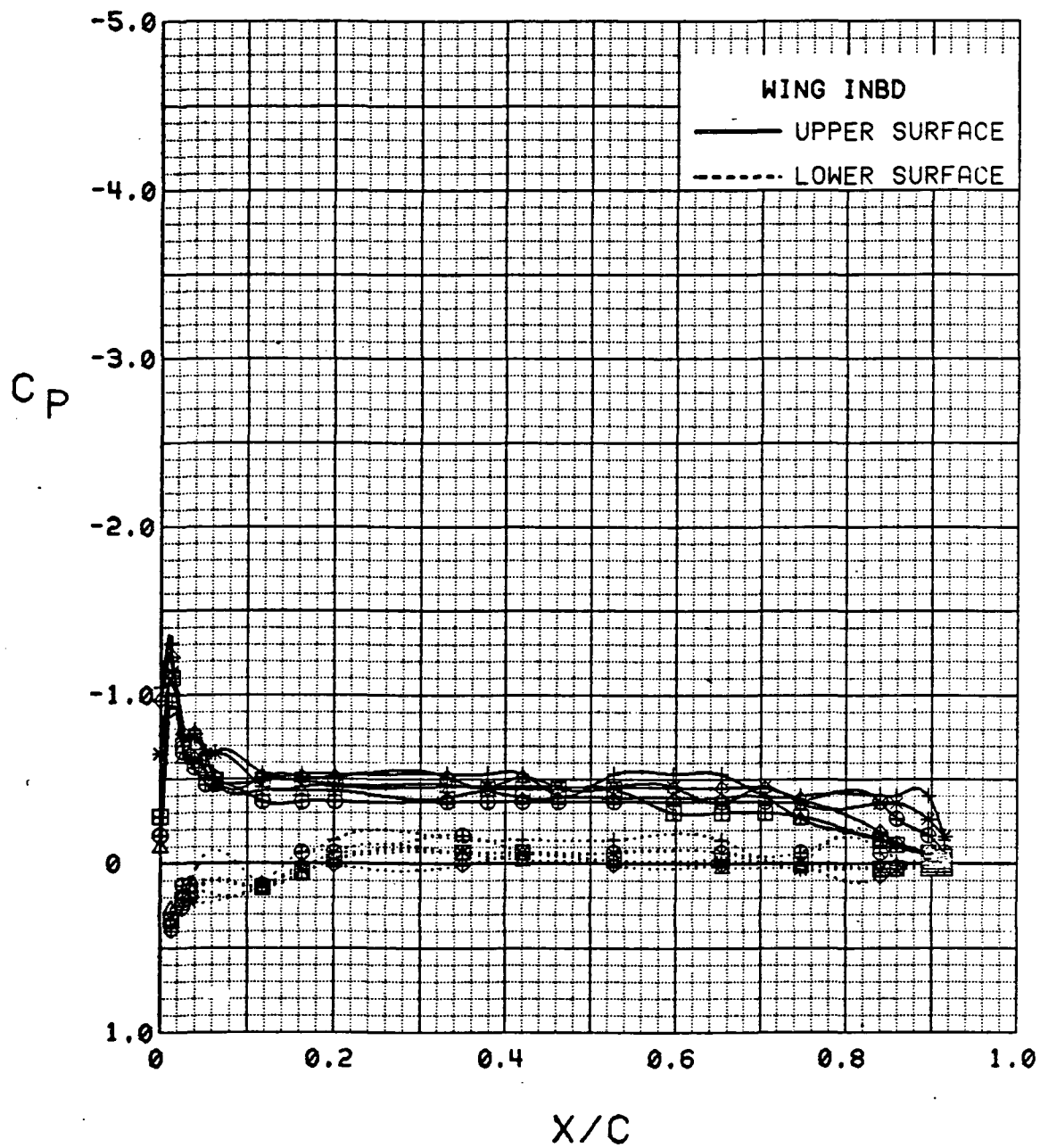


Figure 3.2.4-359 Power Buildup, Flaps Neutral, Inboard, Alpha = 4 deg

SYM	TEST	RUN	ALPHA	CT	ITEF	OTEF	CAN	SWB
⊕	543	63	8.3	0.00	0	0	0	OFF
⊞	543	64	8.4	0.27	0	0	0	OFF
△	543	62	8.4	0.47	0	0	0	OFF
◆	543	60	8.4	0.94	0	0	0	OFF
*	543	59	8.4	1.41	0	0	0	OFF
+	543	58	8.4	1.90	0	0	0	OFF

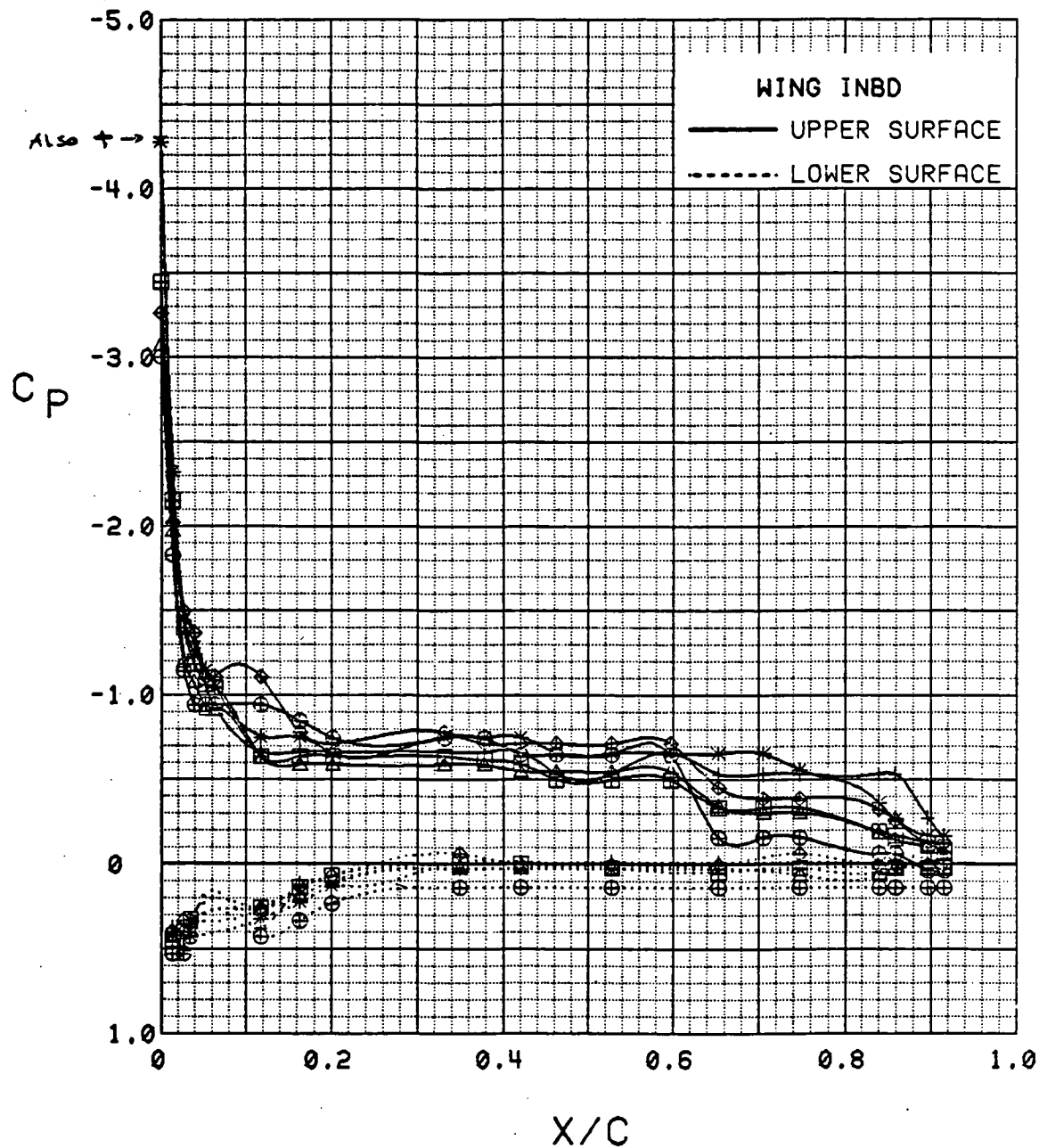


Figure 3.2.4-360 Power Buildup, Flaps Neutral, Inboard, Alpha = 8 deg

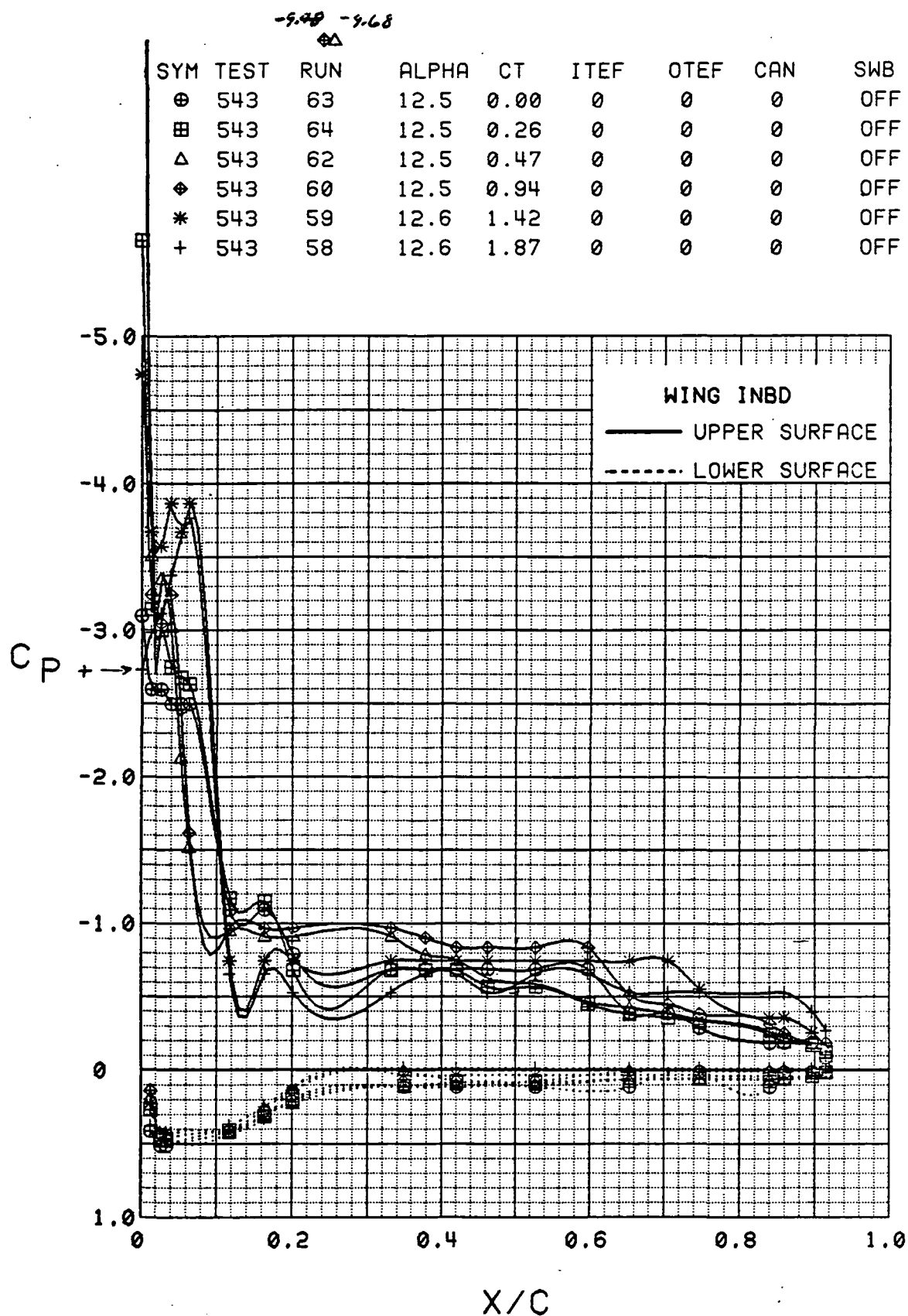


Figure 3.2.4-361 Power Buildup, Flaps Neutral, Inboard, Alpha = 12 deg

SYM	TEST	RUN	ALPHA	CT	ITEF	OTEF	CAN	SWB
⊕	543	63	16.6	0.00	0	0	0	OFF
⊞	543	64	16.6	0.27	0	0	0	OFF
△	543	62	16.6	0.47	0	0	0	OFF
◆	543	60	16.7	0.93	0	0	0	OFF
*	543	59	16.7	1.42	0	0	0	OFF
+	543	58	16.7	1.87	0	0	0	OFF

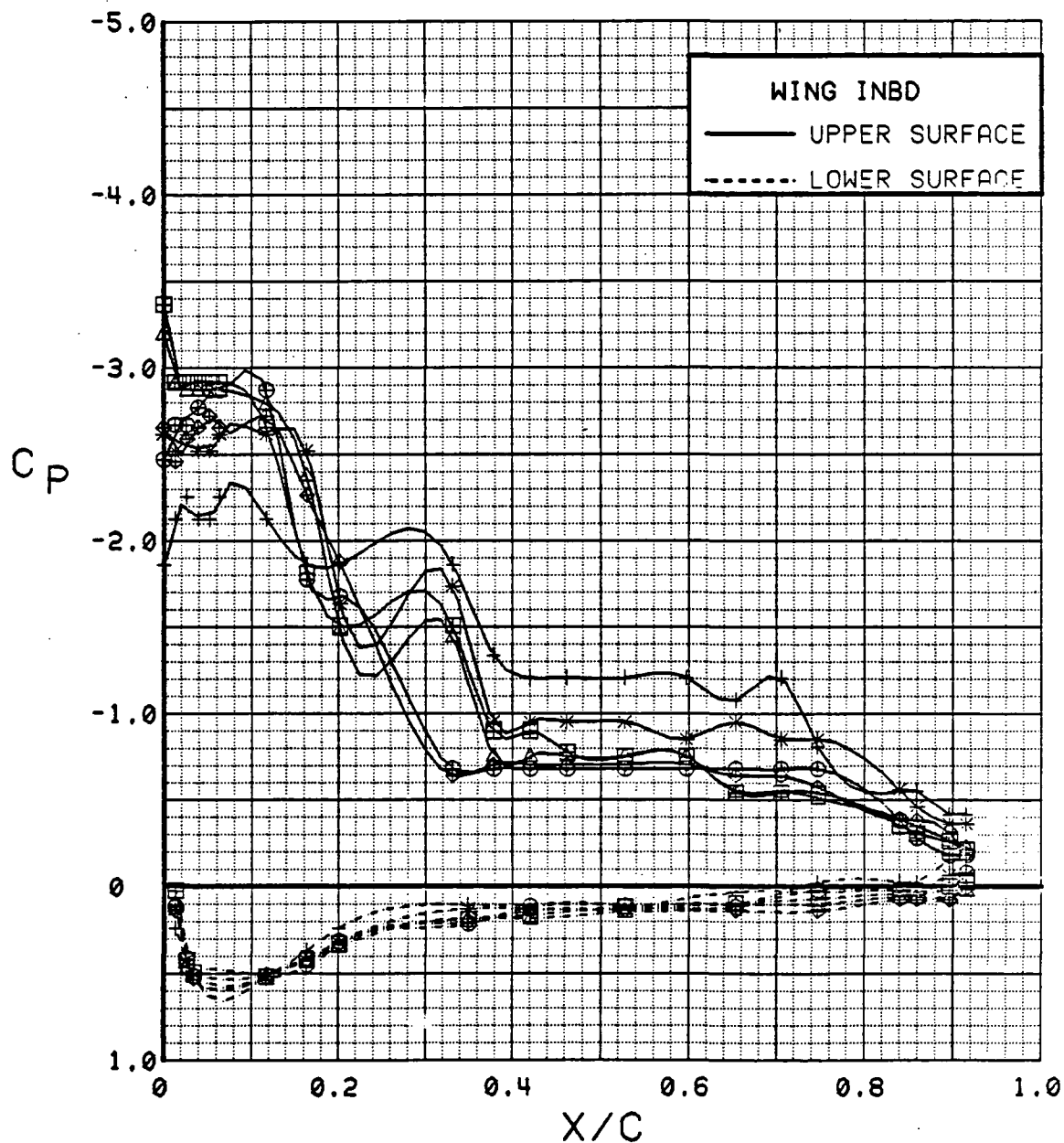


Figure 3.2.4-362 Power Buildup, Flaps Neutral, Inboard, Alpha = 16 deg

SYM	TEST	RUN	ALPHA	CT	ITEF	OTEF	CAN	SWB
⊕	543	63	20.7	0.00	0	0	0	OFF
⊞	543	64	20.8	0.27	0	0	0	OFF
△	543	62	20.8	0.47	0	0	0	OFF
⊕	543	60	20.8	0.93	0	0	0	OFF
*	543	59	20.8	1.41	0	0	0	OFF
+	543	58	20.8	1.72	0	0	0	OFF

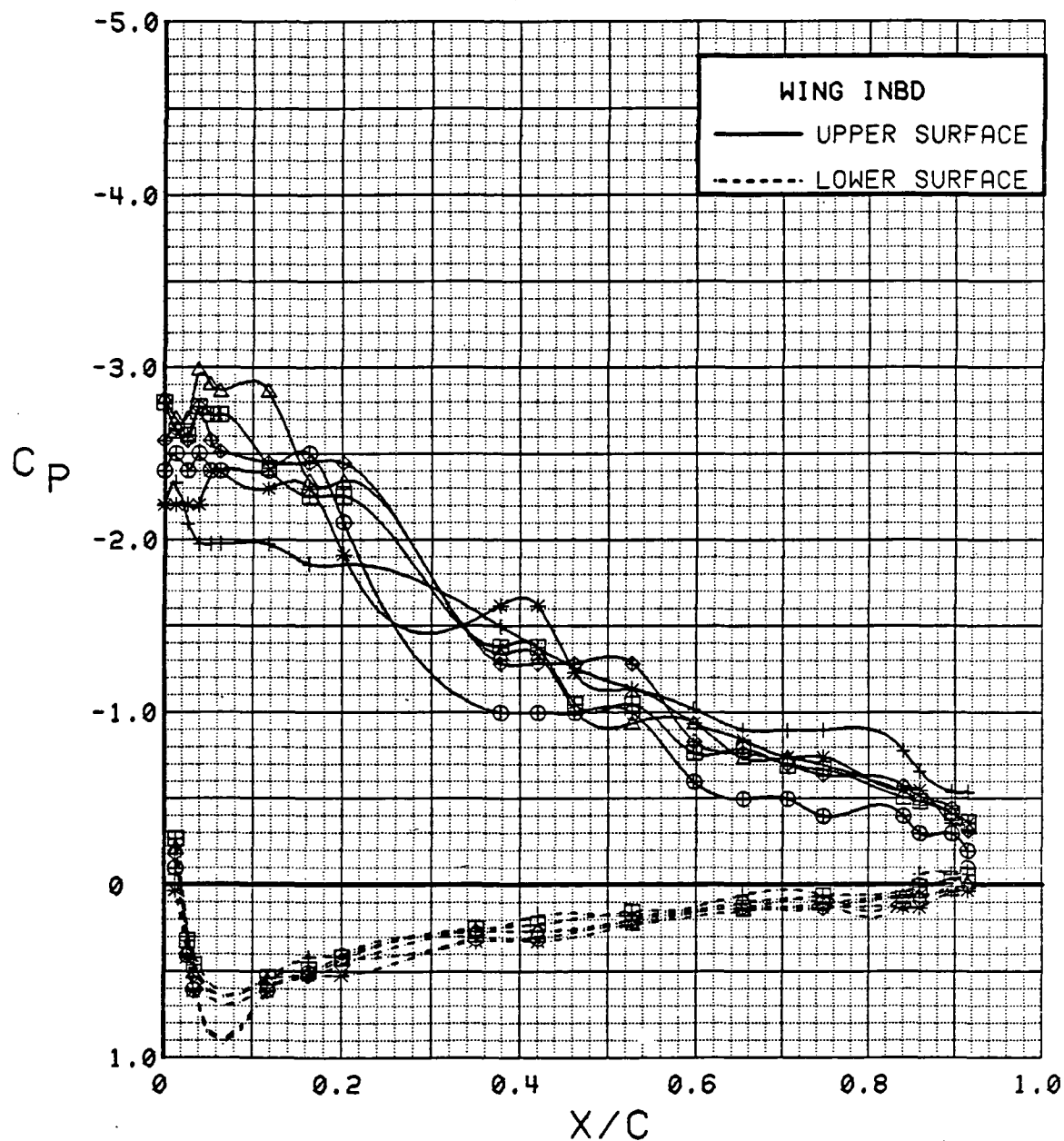


Figure 3.2.4-363 Power Buildup, Flaps Neutral, Inboard, Alpha = 20 deg



SYM	TEST	RUN	ALPHA	CT	ITEF	OTEF	CAN	SWB
⊕	543	63	24.8	0.00	0	0	0	OFF
⊞	543	64	24.9	0.26	0	0	0	OFF
△	543	62	24.9	0.47	0	0	0	OFF
⬠	543	60	24.9	0.93	0	0	0	OFF
*	543	59	24.9	1.43	0	0	0	OFF
+	543	58	25.0	1.86	0	0	0	OFF

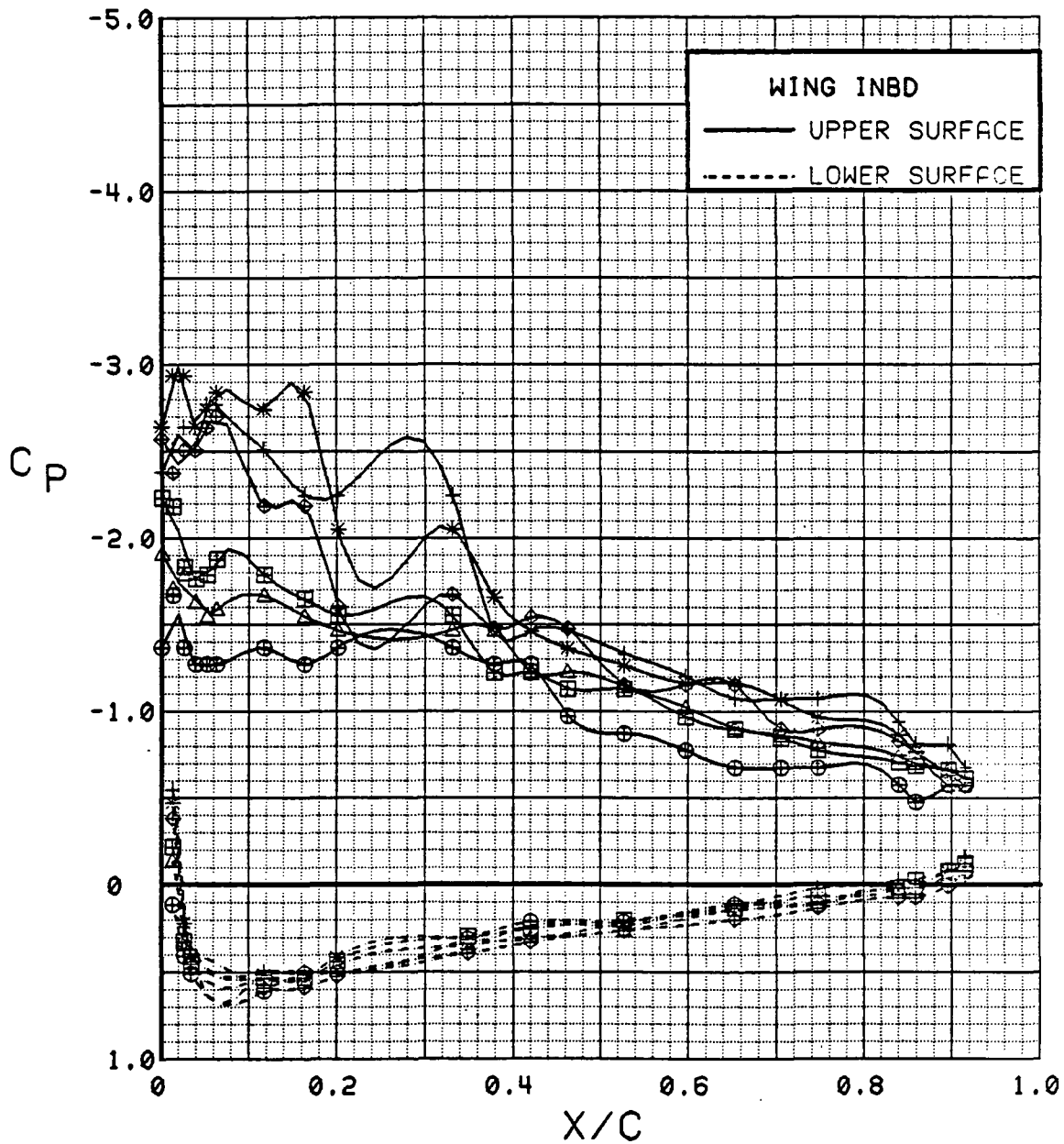


Figure 3.2.4-364 Power Buildup, Flaps Neutral, Inboard, Alpha = 24 deg

SYM	TEST	RUN	ALPHA	CT	ITEF	OTEF	CAN	SWB
⊕	543	63	28.8	0.00	0	0	0	OFF
⊞	543	64	28.9	0.27	0	0	0	OFF
△	543	62	29.0	0.47	0	0	0	OFF
⬢	543	60	29.0	0.93	0	0	0	OFF
*	543	59	29.1	1.41	0	0	0	OFF
+	543	58	29.1	1.83	0	0	0	OFF

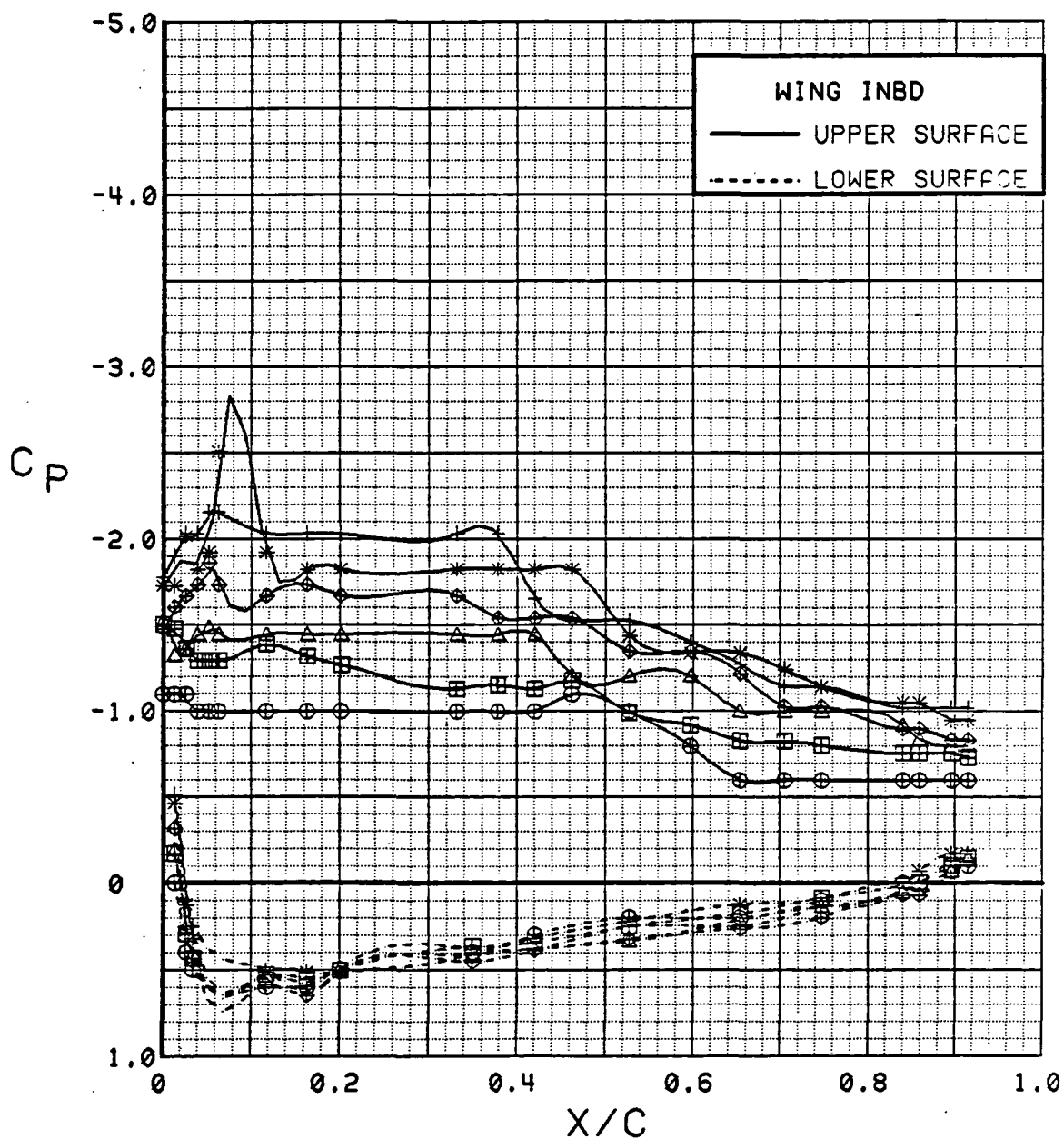


Figure 3.2.4-365 Power Buildup, Flaps Neutral, Inboard, Alpha = 28 deg

SYM	TEST	RUN	ALPHA	CT	ITEF	OTEF	CAN	SWB
⊕	543	63	32.8	0.00	0	0	0	OFF
⊞	543	62	33.0	0.46	0	0	0	OFF
△	543	60	33.1	0.94	0	0	0	OFF
⬢	543	59	33.1	1.43	0	0	0	OFF
*	543	58	33.2	1.89	0	0	0	OFF

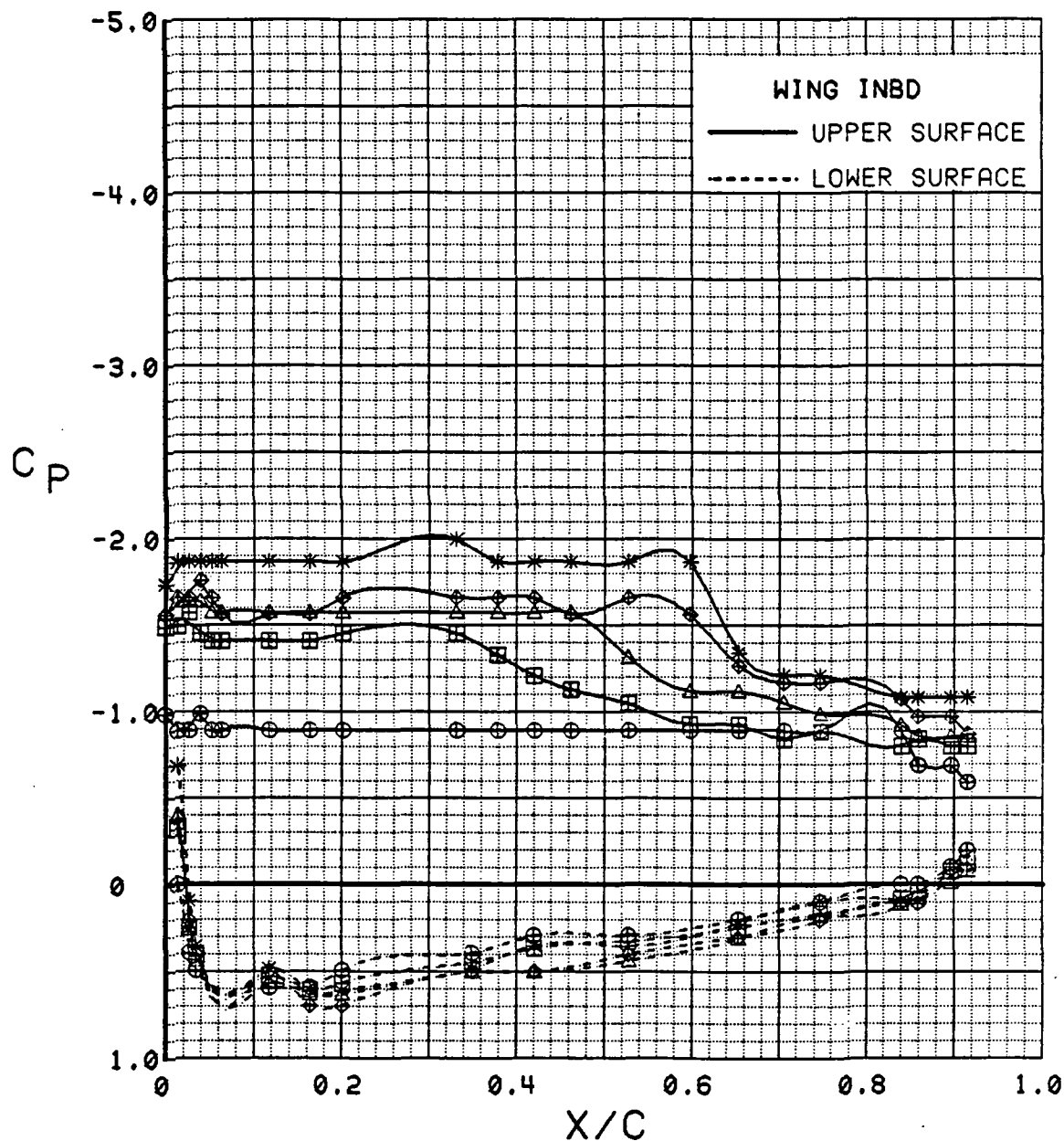


Figure 3.2.4-366 Power Buildup, Flaps Neutral, Inboard, Alpha = 32 deg

SYM	TEST	RUN	ALPHA	CT	ITEF	OTEF	CAN	SWB
⊕	543	63	4.2	0.00	0	0	0	OFF
⊞	543	64	4.2	0.27	0	0	0	OFF
△	543	62	4.2	0.48	0	0	0	OFF
⊕	543	60	4.3	0.93	0	0	0	OFF
*	543	59	4.3	1.40	0	0	0	OFF
+	543	58	4.3	1.84	0	0	0	OFF

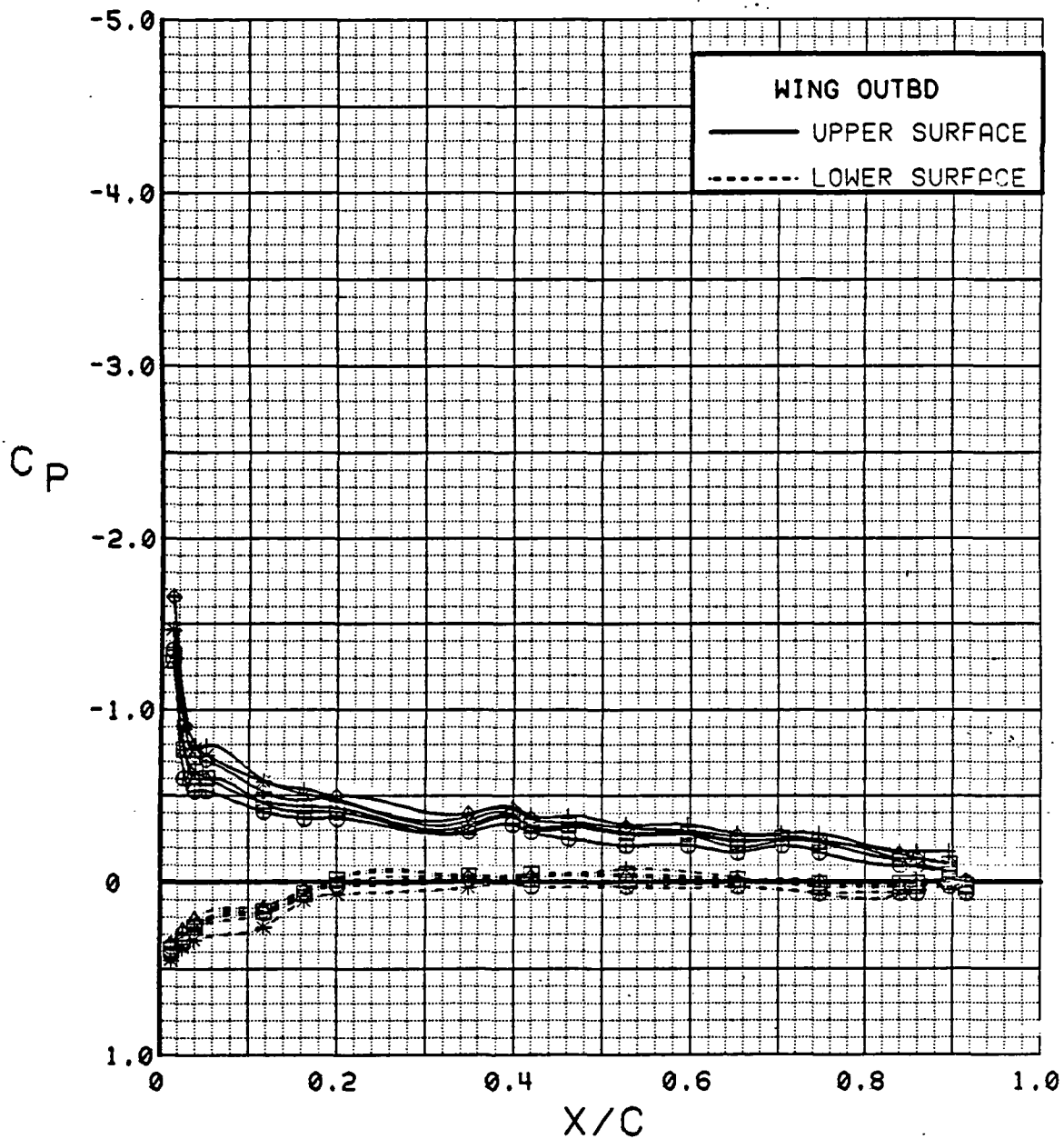


Figure 3.2.4-367 Power Buildup, Flaps Neutral, Outboard, Alpha = 4 deg

SYM	TEST	RUN	ALPHA	CT	ITEF	OTEF	CAN	SWB
⊕	543	63	8.3	0.00	0	0	0	OFF
⊞	543	64	8.4	0.27	0	0	0	OFF
△	543	62	8.4	0.47	0	0	0	OFF
⊕	543	60	8.4	0.94	0	0	0	OFF
*	543	59	8.4	1.41	0	0	0	OFF
+	543	58	8.4	1.90	0	0	0	OFF

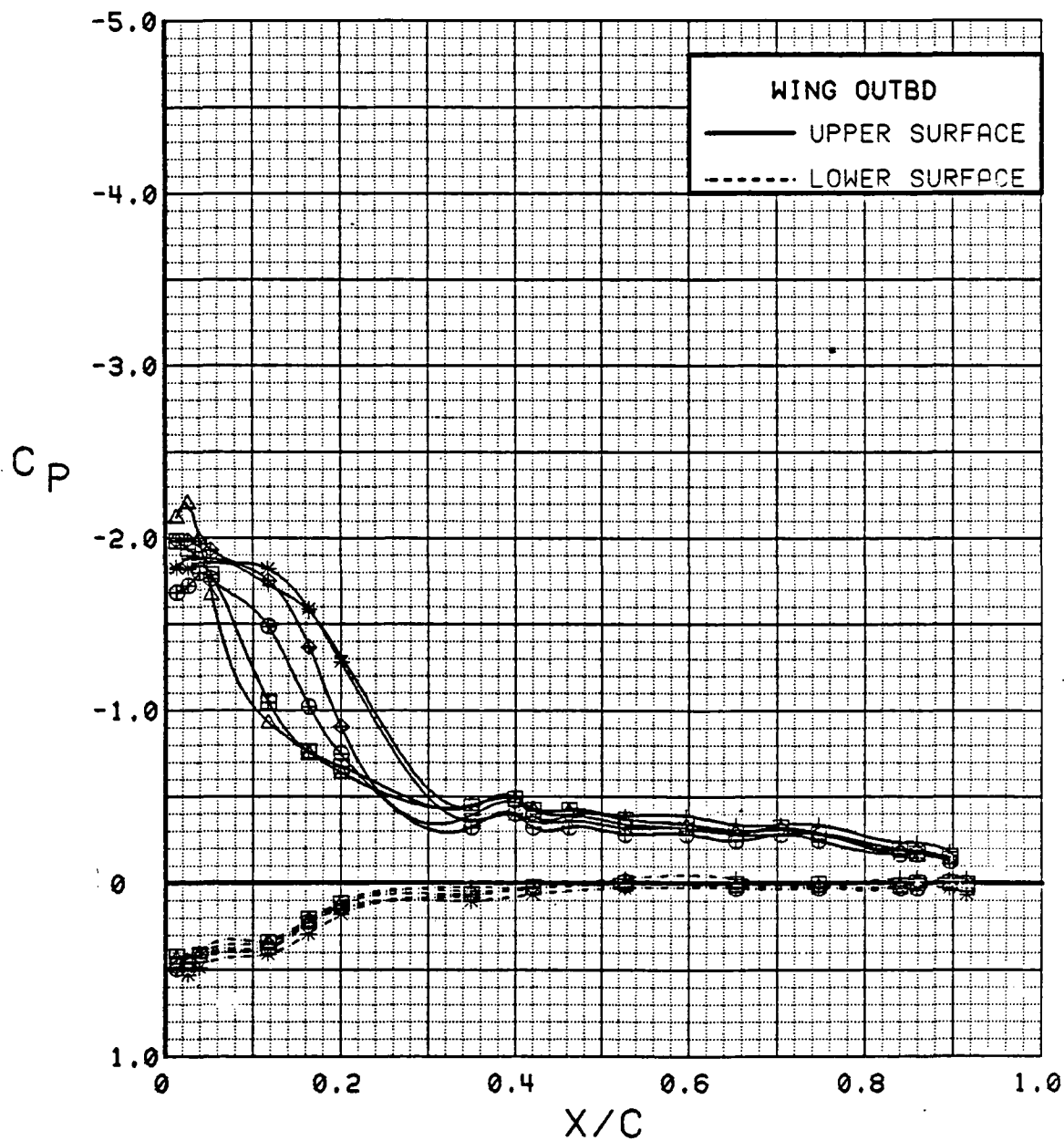


Figure 3.2.4-368 Power Buildup, Flaps Neutral, Outboard, Alpha = 8 deg

SYM	TEST	RUN	ALPHA	CT	ITEF	OTEF	CAN	SWB
⊕	543	63	12.5	0.00	0	0	0	OFF
⊞	543	64	12.5	0.26	0	0	0	OFF
△	543	62	12.5	0.47	0	0	0	OFF
◆	543	60	12.5	0.94	0	0	0	OFF
*	543	59	12.6	1.42	0	0	0	OFF
+	543	58	12.6	1.87	0	0	0	OFF

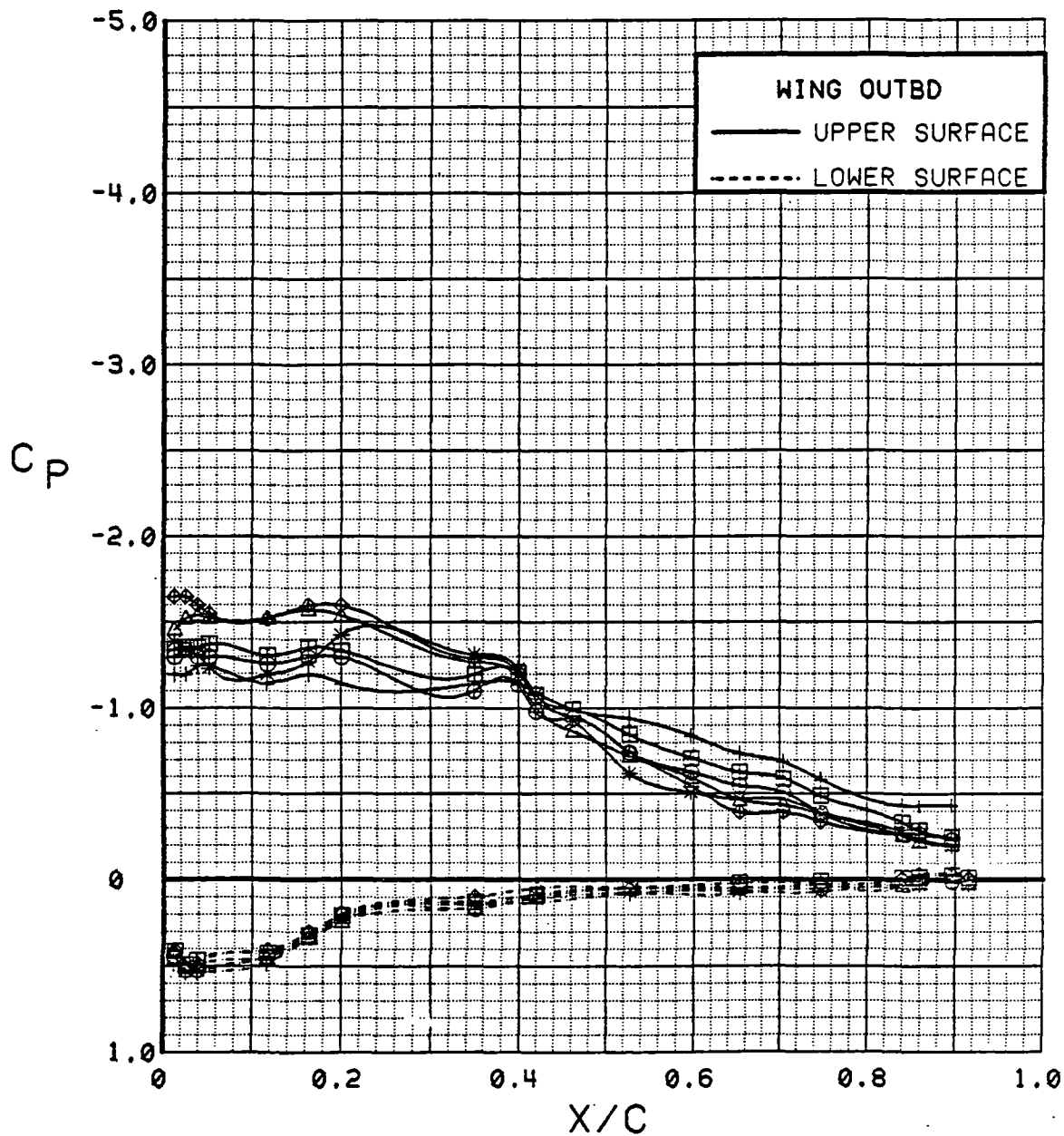


Figure 3.2.4-369 Power Buildup, Flaps Neutral, Outboard, Alpha = 12 deg

SYM	TEST	RUN	ALPHA	CT	ITEF	OTEF	CAN	SWB
⊕	543	63	16.6	0.00	0	0	0	OFF
⊞	543	64	16.6	0.27	0	0	0	OFF
△	543	62	16.6	0.47	0	0	0	OFF
⊕	543	60	16.7	0.93	0	0	0	OFF
*	543	59	16.7	1.42	0	0	0	OFF
+	543	58	16.7	1.87	0	0	0	OFF

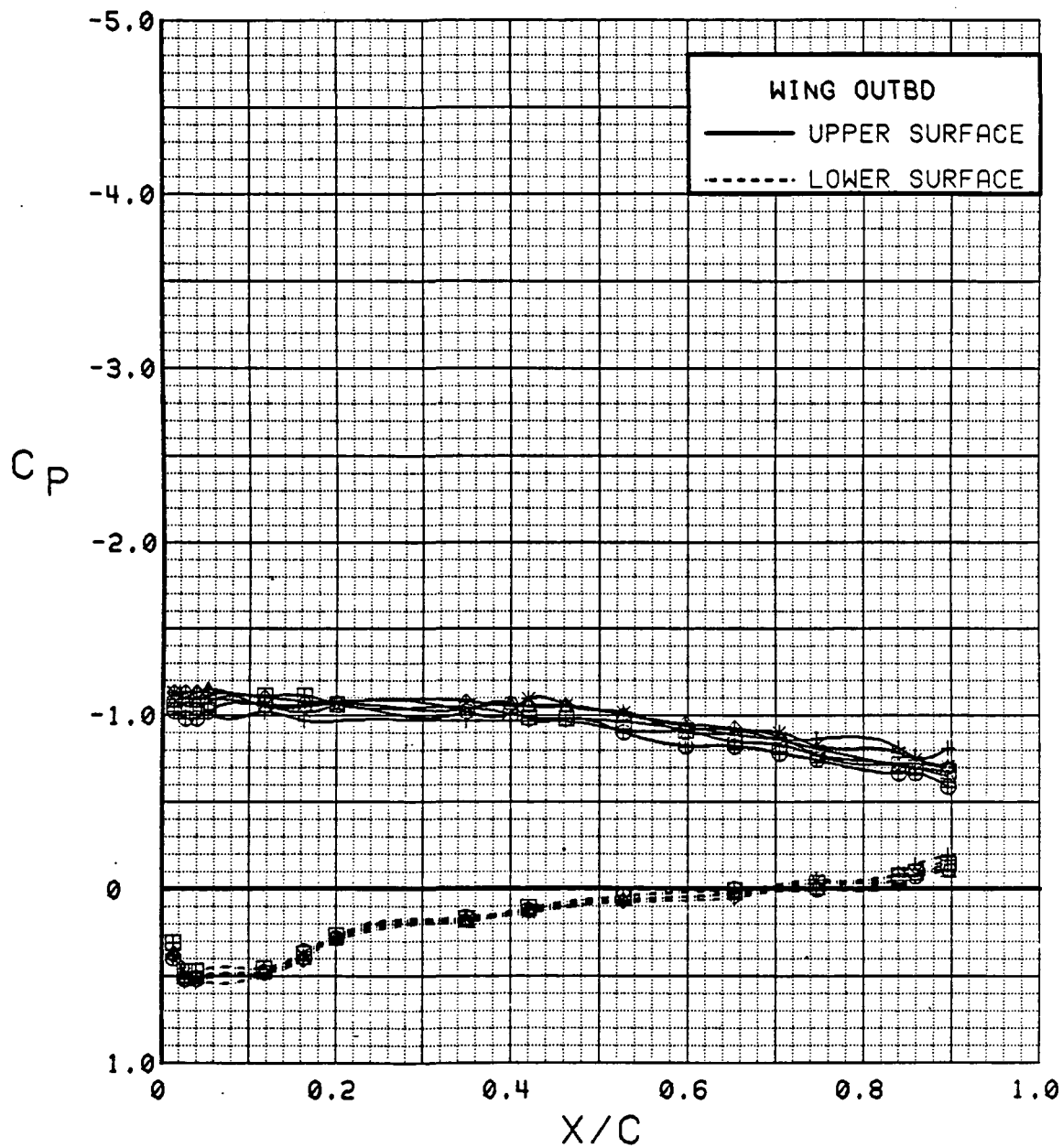


Figure 3.2.4-370 Power Buildup, Flaps Neutral, Outboard, Alpha = 16 deg

SYM	TEST	RUN	ALPHA	CT	ITEF	OTEF	CAN	SWB
⊕	543	63	20.7	0.00	0	0	0	OFF
⊞	543	64	20.8	0.27	0	0	0	OFF
△	543	62	20.8	0.47	0	0	0	OFF
⊕	543	60	20.8	0.93	0	0	0	OFF
*	543	59	20.8	1.41	0	0	0	OFF
+	543	58	20.8	1.72	0	0	0	OFF

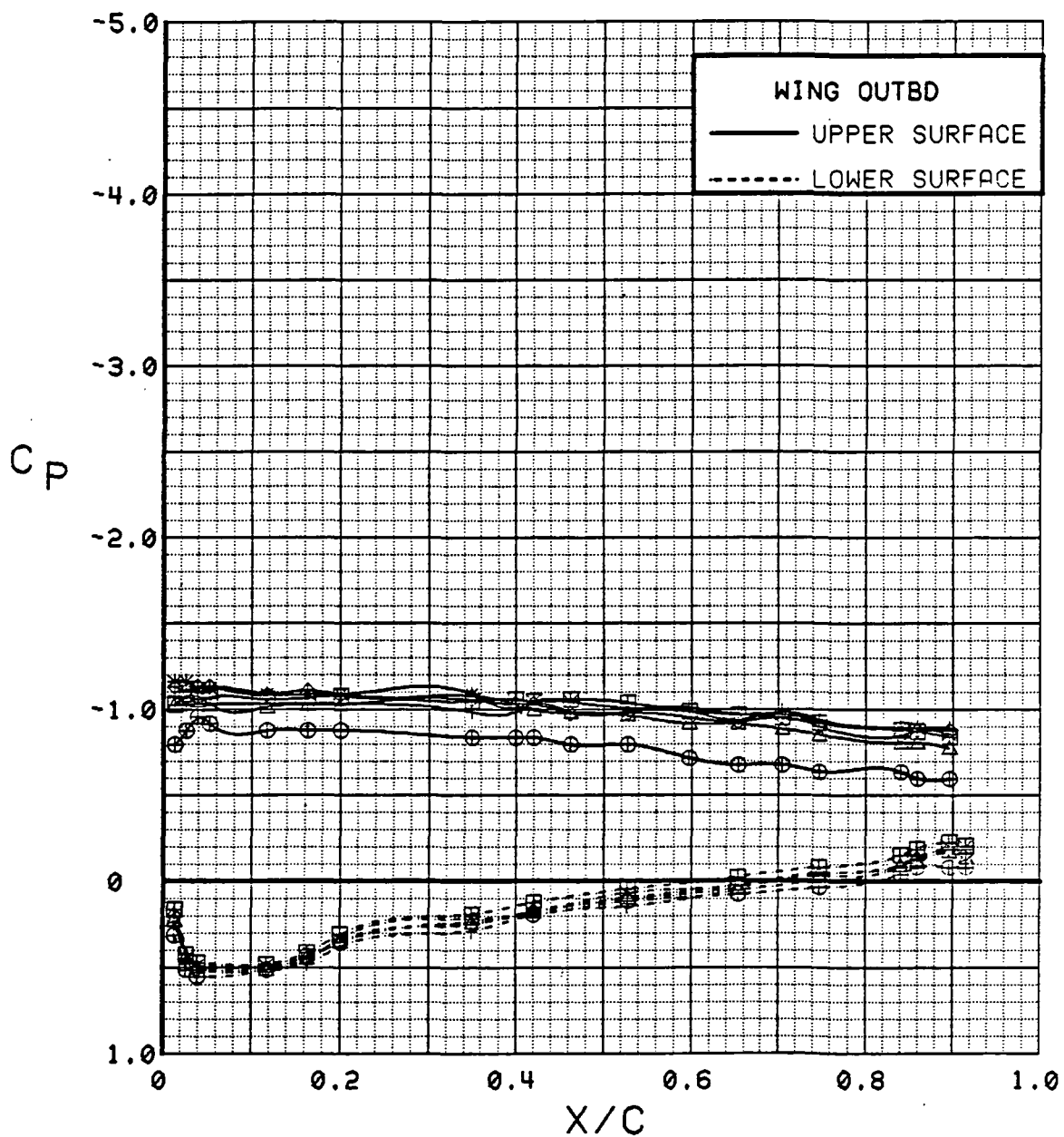


Figure 3.2.4-371 Power Buildup, Flaps Neutral, Outboard, Alpha = 20 deg



SYM	TEST	RUN	ALPHA	CT	ITEF	OTEF	CAN	SWB
⊕	543	63	24.8	0.00	0	0	0	OFF
⊞	543	64	24.9	0.26	0	0	0	OFF
△	543	62	24.9	0.47	0	0	0	OFF
⬠	543	60	24.9	0.93	0	0	0	OFF
*	543	59	24.9	1.43	0	0	0	OFF
+	543	58	25.0	1.86	0	0	0	OFF

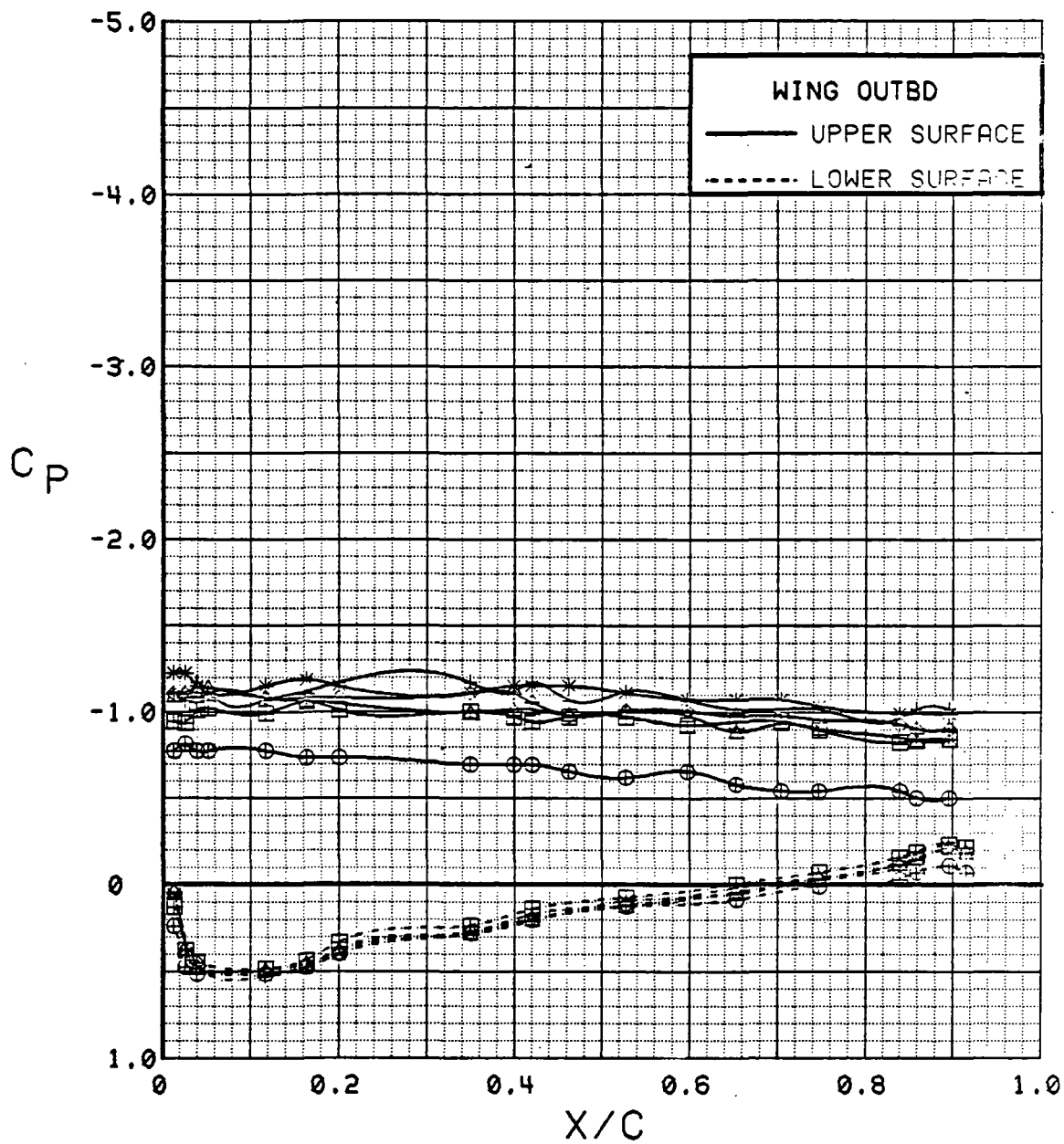


Figure 3.2.4-372 Power Buildup, Flaps Neutral, Outboard, Alpha = 24 deg

SYM	TEST	RUN	ALPHA	CT	ITEF	OTEF	CAN	SHIB
⊕	543	63	28.8	0.00	0	0	0	OFF
⊞	543	64	28.9	0.27	0	0	0	OFF
△	543	62	29.0	0.47	0	0	0	OFF
⊕	543	60	29.0	0.93	0	0	0	OFF
*	543	59	29.1	1.41	0	0	0	OFF
+	543	58	29.1	1.83	0	0	0	OFF

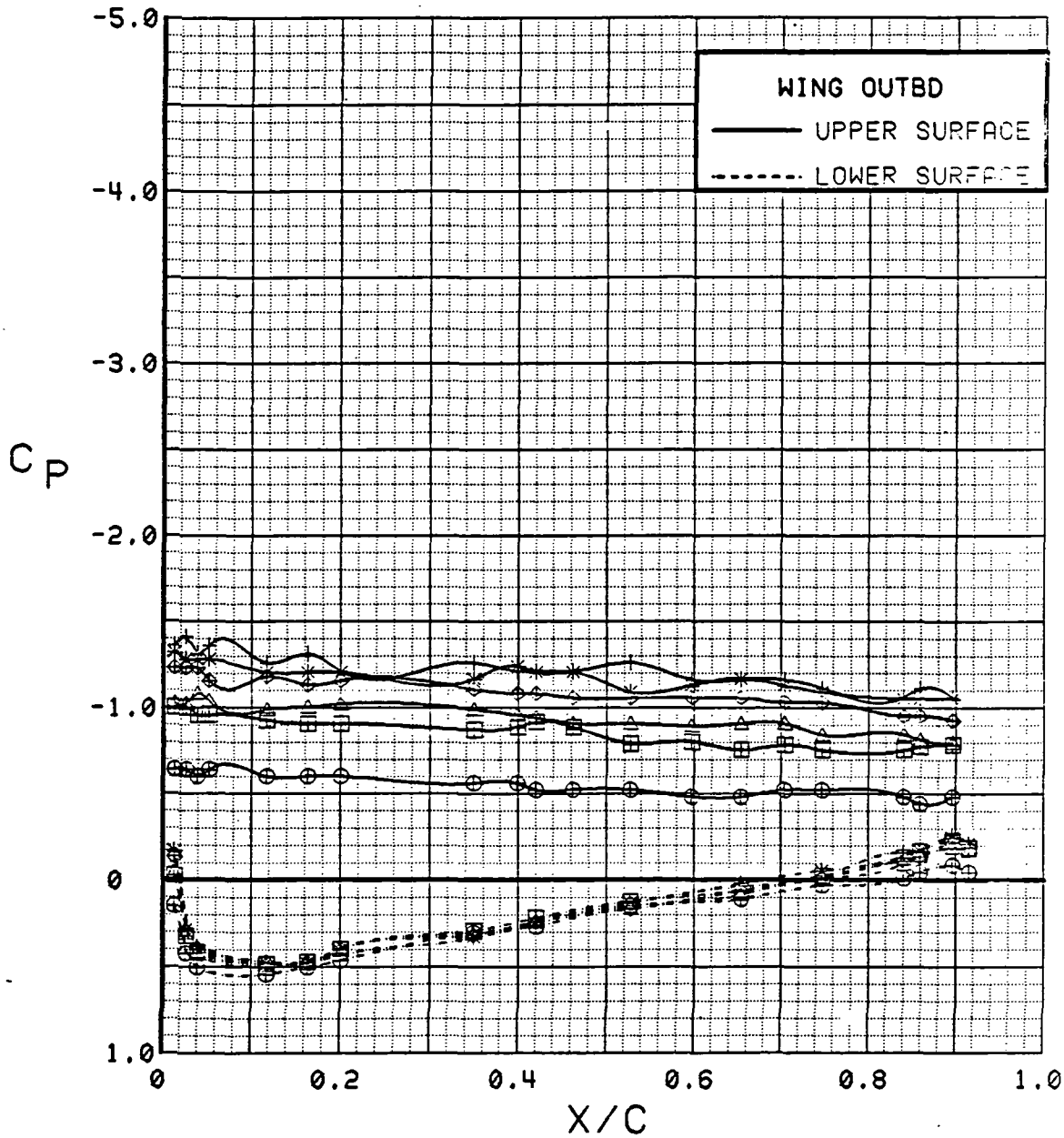


Figure 3.2.4-373 Power Buildup, Flaps Neutral, Outboard, Alpha = 28 deg

SYM	TEST	RUN	ALPHA	CT	ITEF	OTEF	CAN	SWB
⊕	543	63	32.8	0.00	0	0	0	OFF
⊞	543	62	33.0	0.46	0	0	0	OFF
△	543	60	33.1	0.94	0	0	0	OFF
⬠	543	59	33.1	1.43	0	0	0	OFF
*	543	58	33.2	1.89	0	0	0	OFF

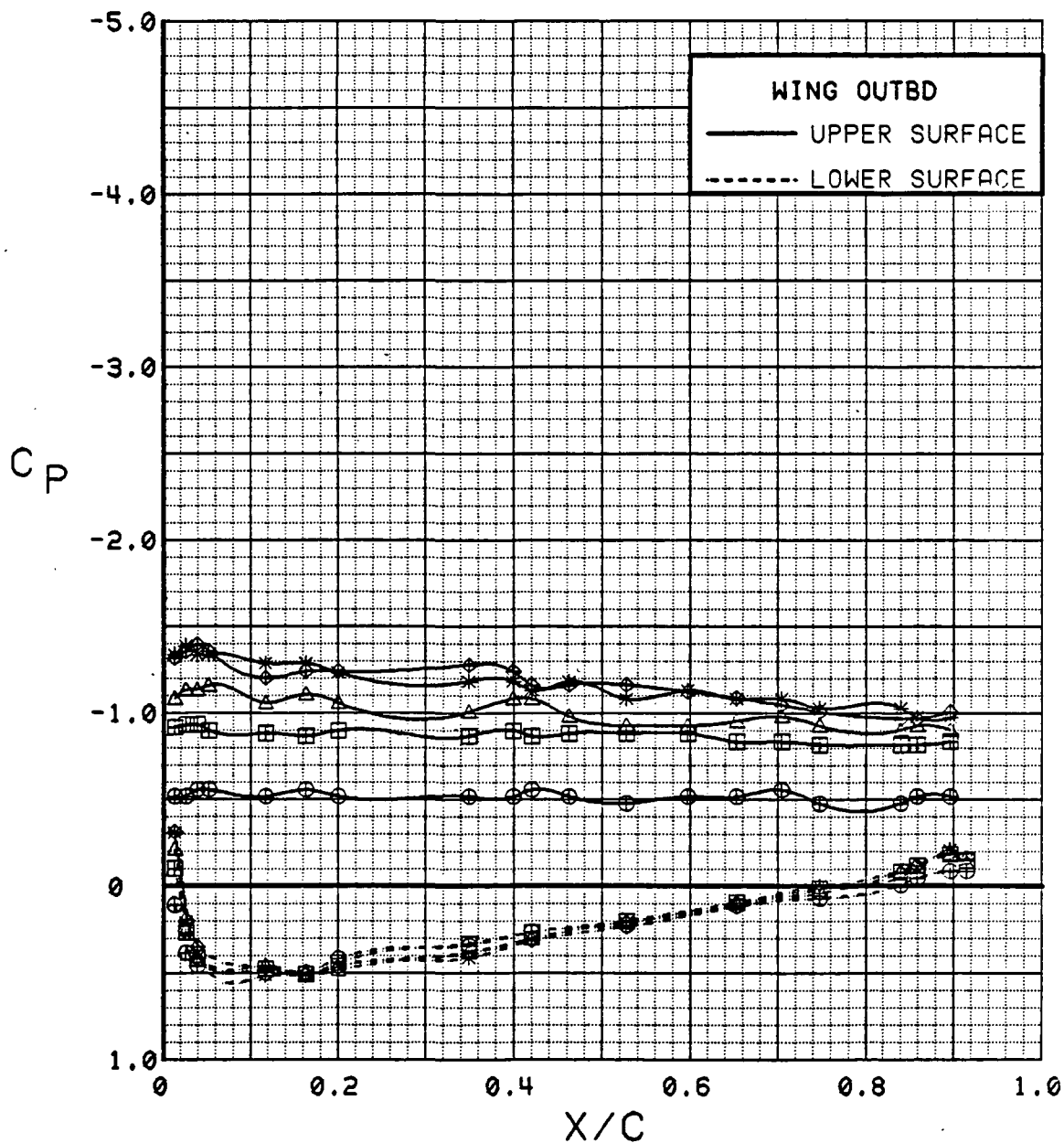


Figure 3.2.4-374 Power Buildup, Flaps Neutral, Outboard, Alpha = 32 deg

SYM	TEST	RUN	ALPHA	CT	ITEF	OTEF	CAN	SWB
⊕	543	63	4.2	0.00	0	0	0	OFF
⊞	543	64	4.2	0.27	0	0	0	OFF
△	543	62	4.2	0.48	0	0	0	OFF
◆	543	60	4.3	0.93	0	0	0	OFF
*	543	59	4.3	1.40	0	0	0	OFF
+	543	58	4.3	1.84	0	0	0	OFF

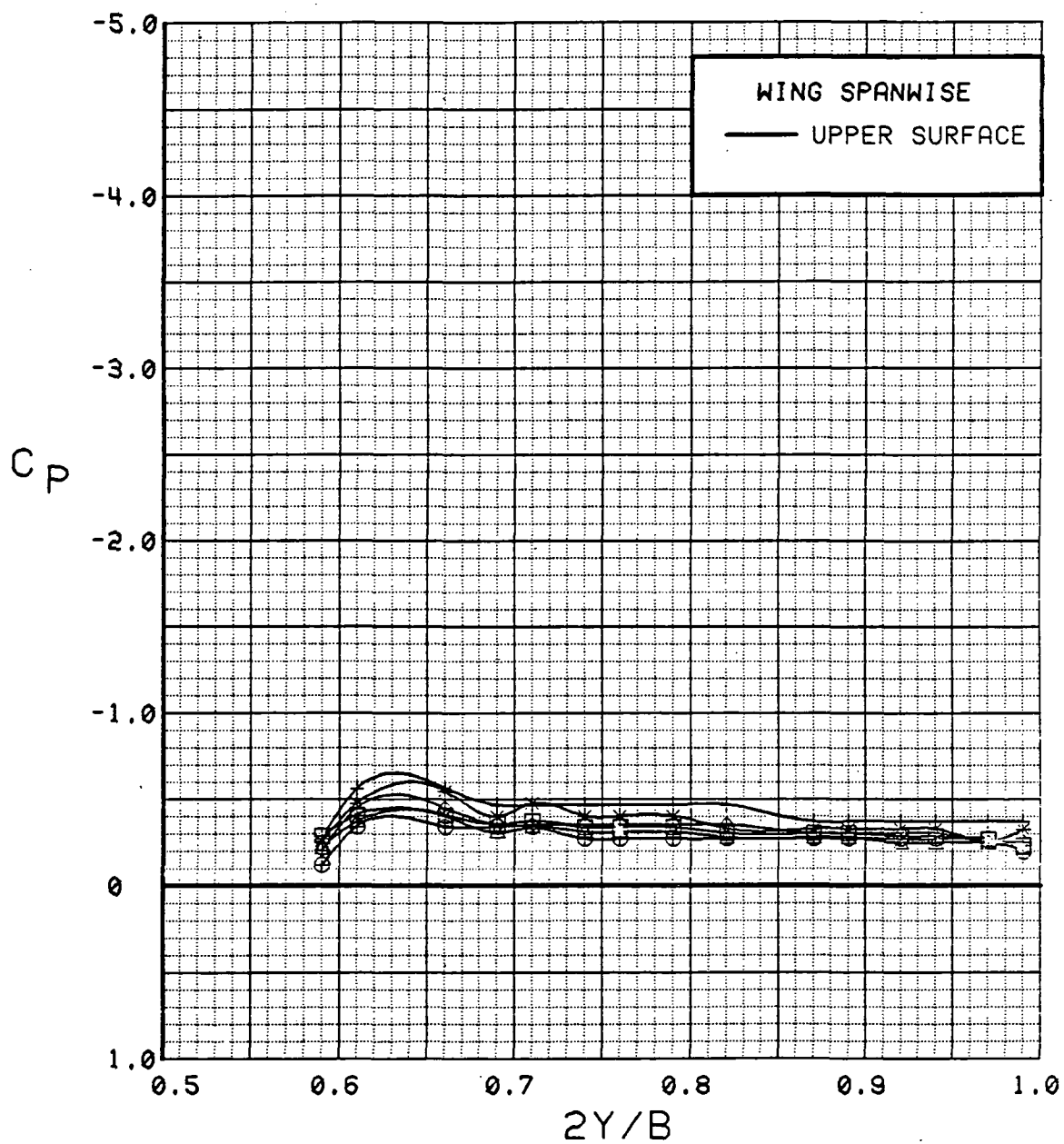


Figure 3.2.4-375 Power Buildup, Flaps Neutral, Spanwise, Alpha = 4 deg

SYM	TEST	RUN	ALPHA	CT	ITEF	OTEF	CAN	SWB
⊕	543	63	8.3	0.00	0	0	0	OFF
⊞	543	64	8.4	0.27	0	0	0	OFF
△	543	62	8.4	0.47	0	0	0	OFF
◆	543	60	8.4	0.94	0	0	0	OFF
*	543	59	8.4	1.41	0	0	0	OFF
+	543	58	8.4	1.90	0	0	0	OFF

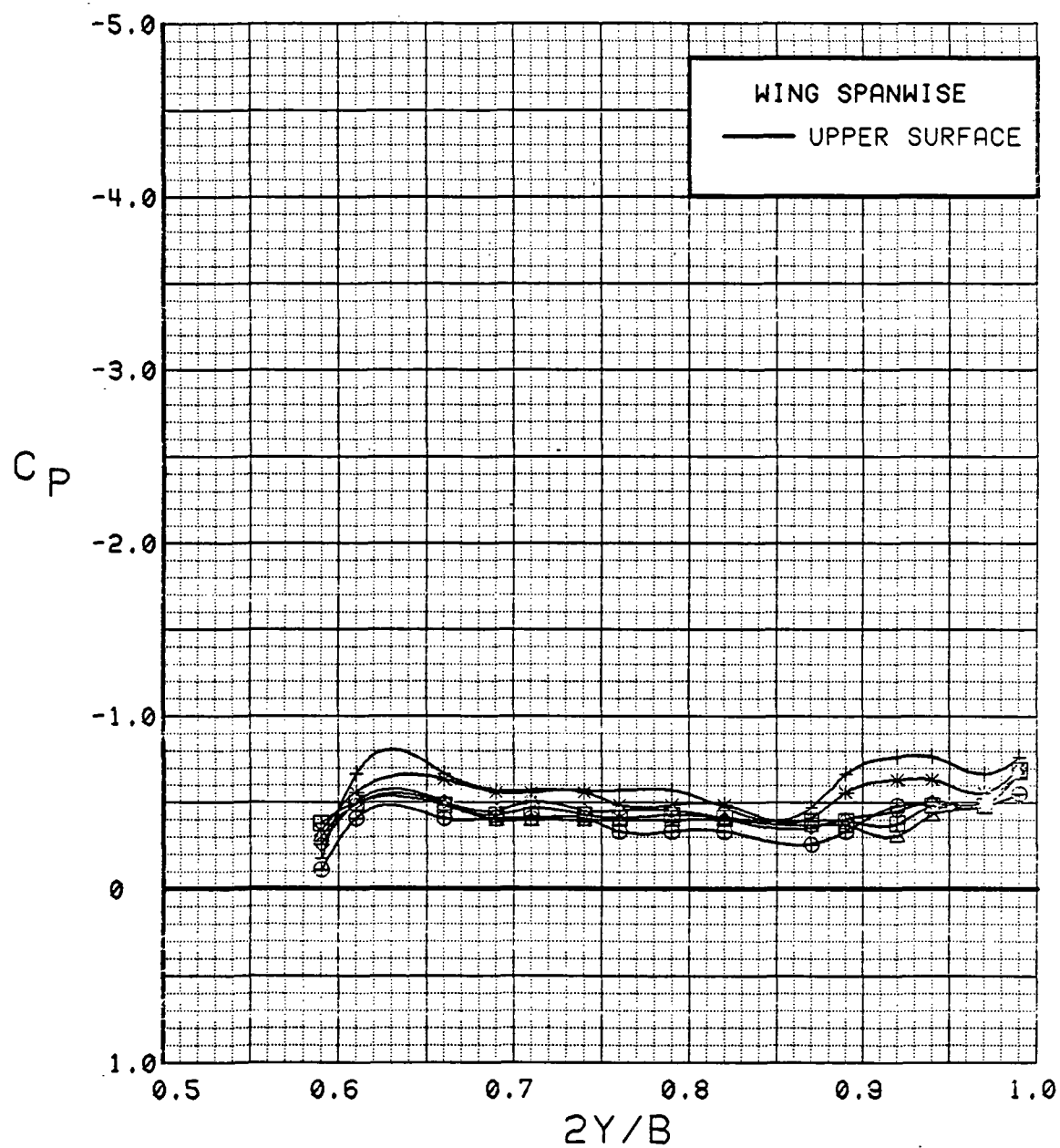


Figure 3.2.4-376 Power Buildup, Flaps Neutral, Spanwise, Alpha = 8 deg

SYM	TEST	RUN	ALPHA	CT	ITEF	OTEF	CAN	SWB
⊕	543	63	12.5	0.00	0	0	0	OFF
⊞	543	64	12.5	0.26	0	0	0	OFF
△	543	62	12.5	0.47	0	0	0	OFF
◆	543	60	12.5	0.94	0	0	0	OFF
*	543	59	12.6	1.42	0	0	0	OFF
+	543	58	12.6	1.87	0	0	0	OFF

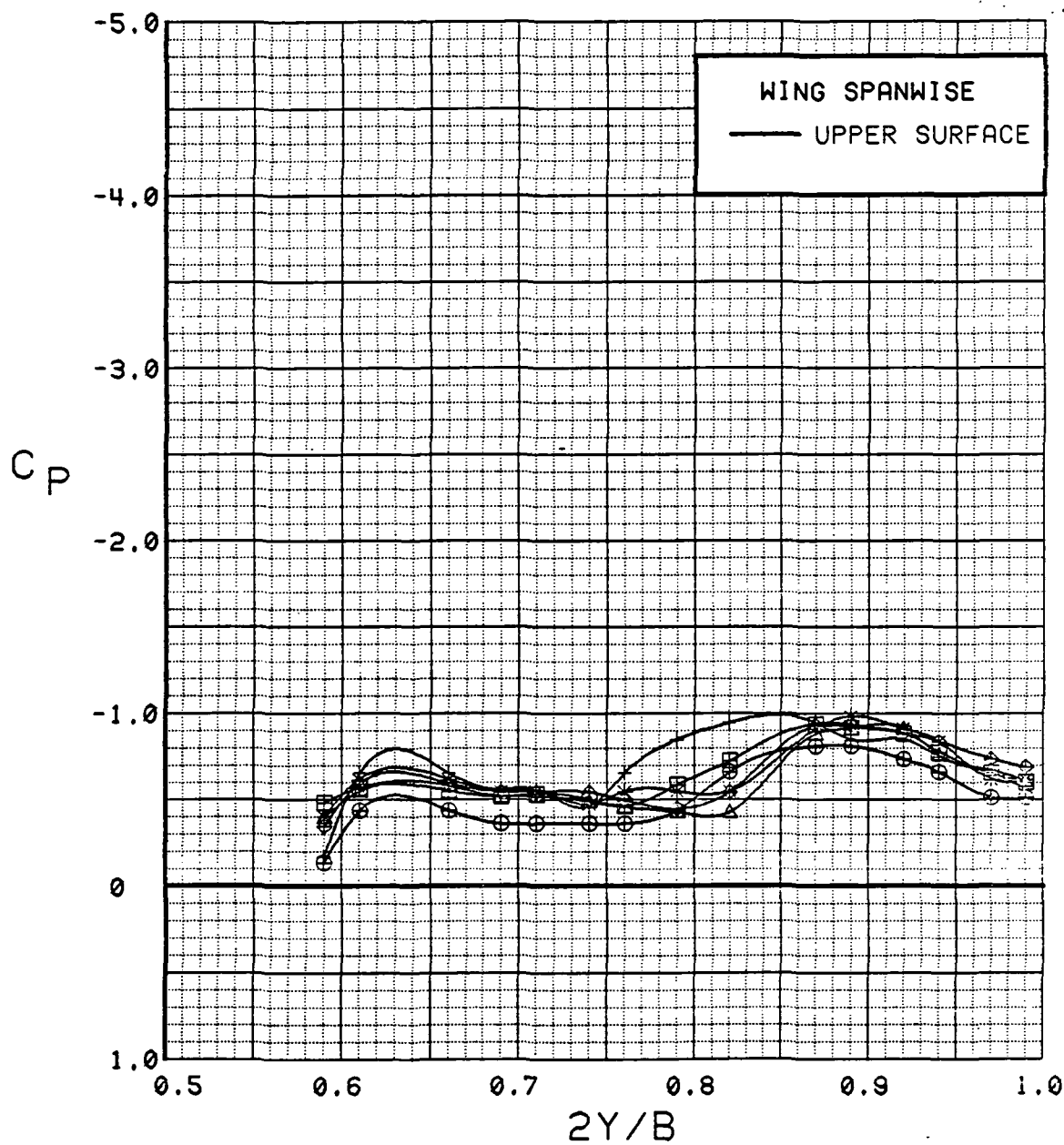


Figure 3.2.4-377 Power Buildup, Flaps Neutral, Spanwise, Alpha = 12 deg

SYM	TEST	RUN	ALPHA	CT	ITEF	OTEF	CAN	SWB
⊕	543	63	16.6	0.00	0	0	0	OFF
⊞	543	64	16.6	0.27	0	0	0	OFF
△	543	62	16.6	0.47	0	0	0	OFF
◆	543	60	16.7	0.93	0	0	0	OFF
*	543	59	16.7	1.42	0	0	0	OFF
+	543	58	16.7	1.87	0	0	0	OFF

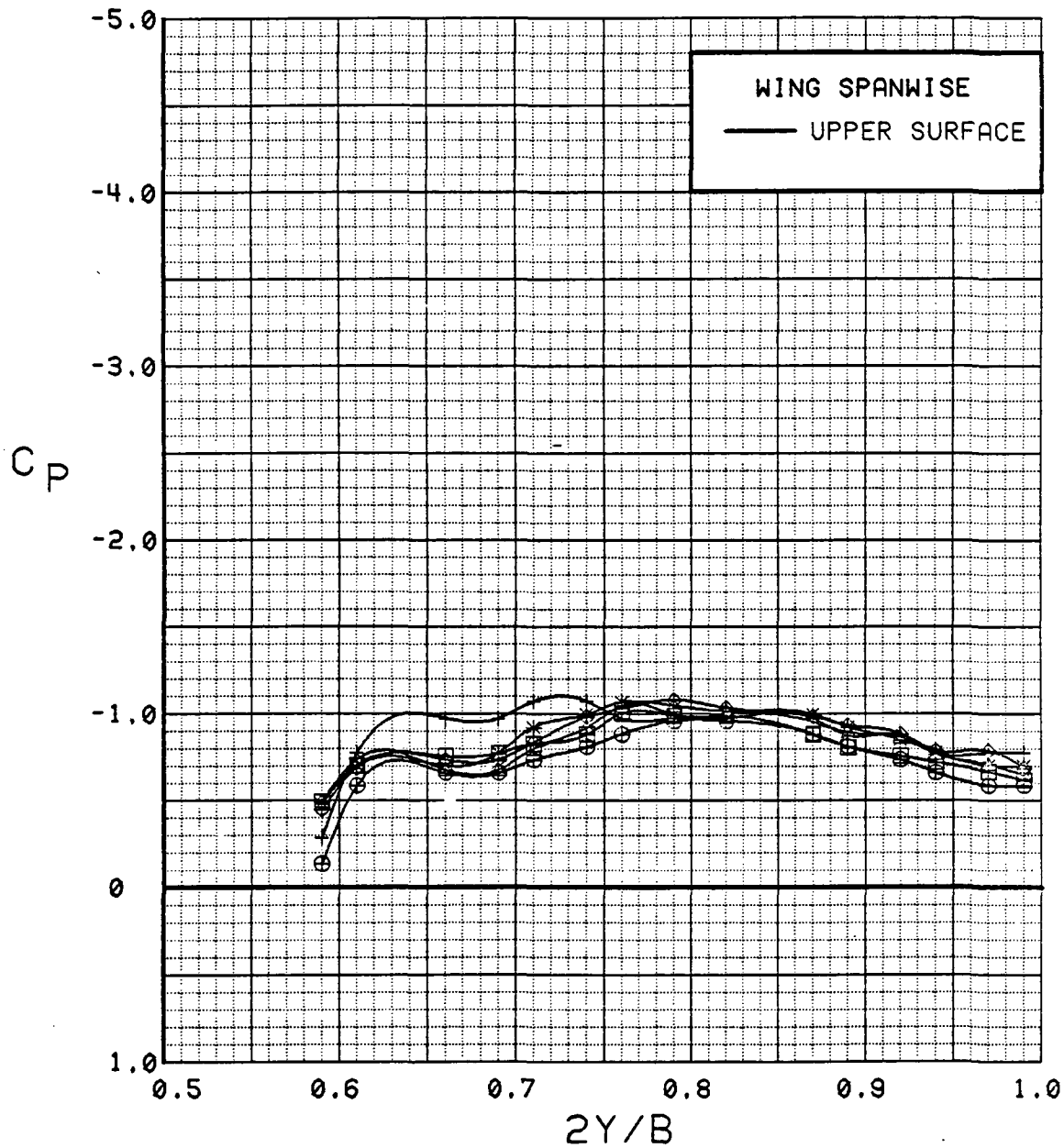


Figure 3.2.4-378 Power Buildup, Flaps Neutral, Spanwise, Alpha = 16 deg

SYM	TEST	RUN	ALPHA	CT	ITEF	OTEF	CAN	SWB
⊕	543	63	20.7	0.00	0	0	0	OFF
⊞	543	64	20.8	0.27	0	0	0	OFF
△	543	62	20.8	0.47	0	0	0	OFF
◆	543	60	20.8	0.93	0	0	0	OFF
*	543	59	20.8	1.41	0	0	0	OFF
+	543	58	20.8	1.72	0	0	0	OFF

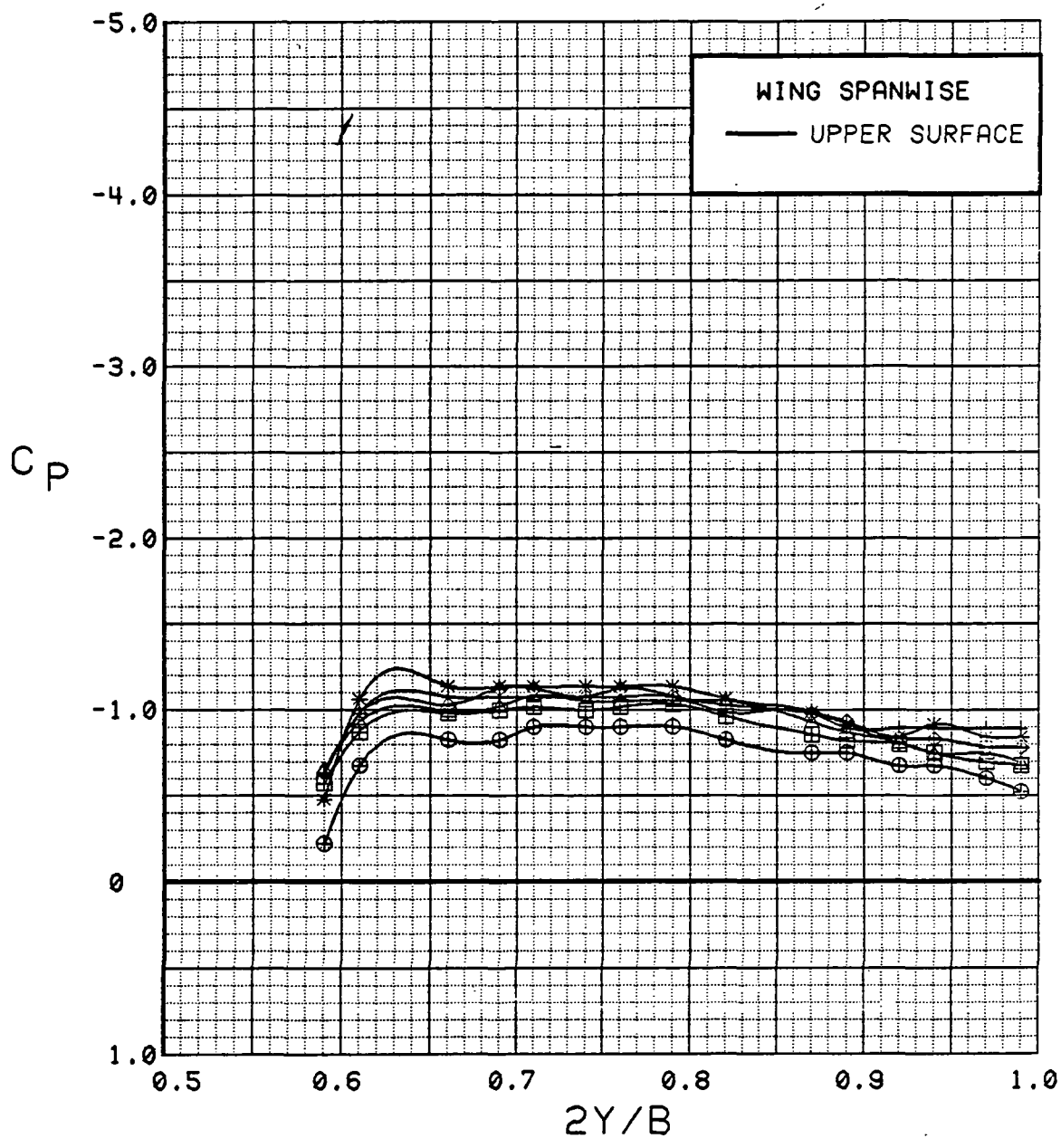


Figure 3.2.4-379 Power Buildup, Flaps Neutral, Spanwise, Alpha = 20 deg



SYM	TEST	RUN	ALPHA	CT	ITEF	OTEF	CAN	SWB
⊕	543	63	24.8	0.00	0	0	0	OFF
⊞	543	64	24.9	0.26	0	0	0	OFF
△	543	62	24.9	0.47	0	0	0	OFF
◆	543	60	24.9	0.93	0	0	0	OFF
*	543	59	24.9	1.43	0	0	0	OFF
+	543	58	25.0	1.86	0	0	0	OFF

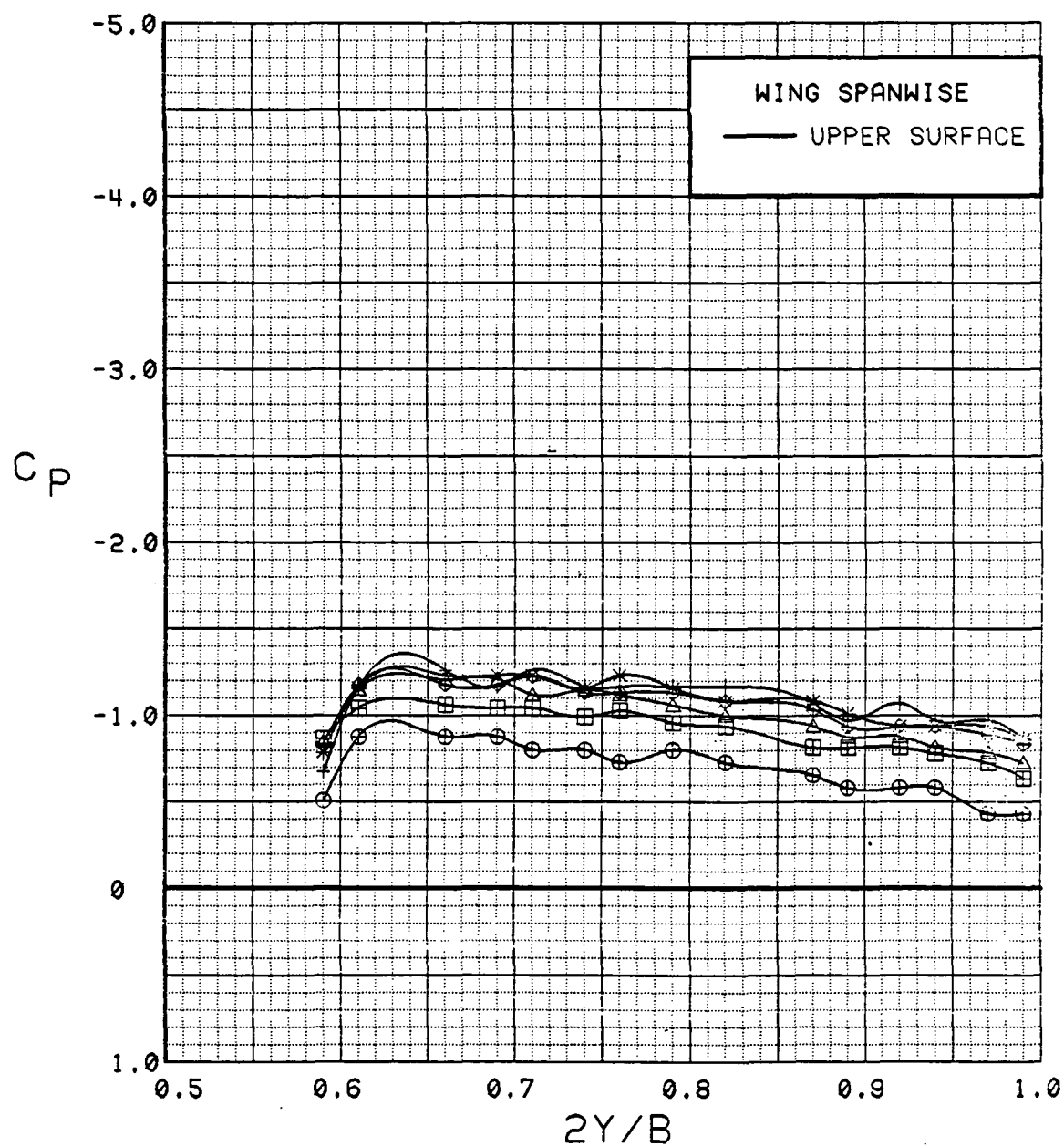


Figure 3.2.4-380 Power Buildup, Flaps Neutral, Spanwise, Alpha = 24 deg

SYM	TEST	RUN	ALPHA	CT	ITEF	OTEF	CAN	SWB
⊙	543	63	28.8	0.00	0	0	0	OFF
⊠	543	64	28.9	0.27	0	0	0	OFF
△	543	62	29.0	0.47	0	0	0	OFF
◆	543	60	29.0	0.93	0	0	0	OFF
*	543	59	29.1	1.41	0	0	0	OFF
+	543	58	29.1	1.83	0	0	0	OFF

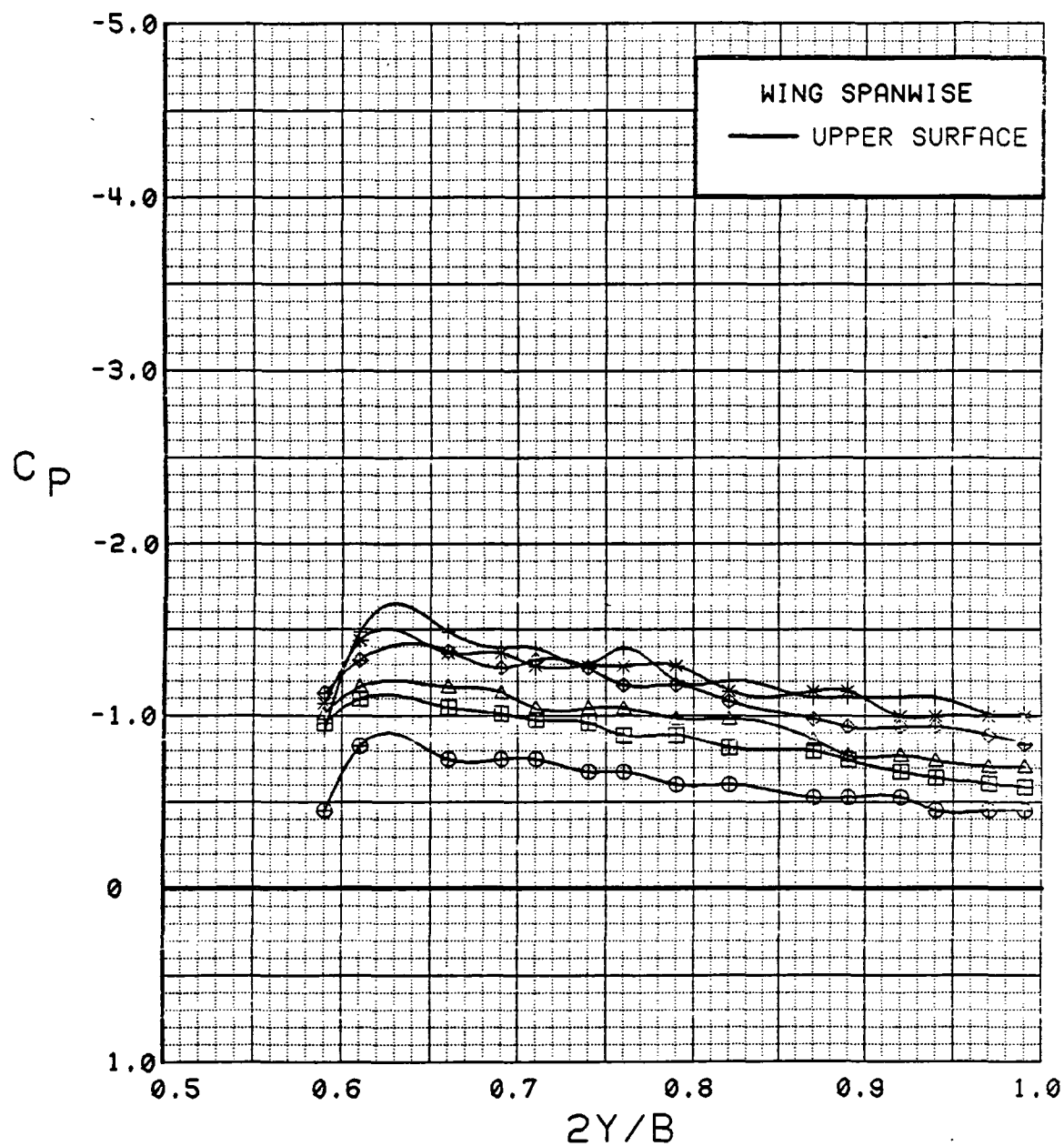


Figure 3.2.4-381 Power Buildup, Flaps Neutral, Spanwise, Alpha = 28 deg

SYM	TEST	RUN	ALPHA	CT	ITEF	OTEF	CAN	SWB
⊕	543	63	32.8	0.00	0	0	0	OFF
⊞	543	62	33.0	0.46	0	0	0	OFF
△	543	60	33.1	0.94	0	0	0	OFF
◆	543	59	33.1	1.43	0	0	0	OFF
*	543	58	33.2	1.89	0	0	0	OFF

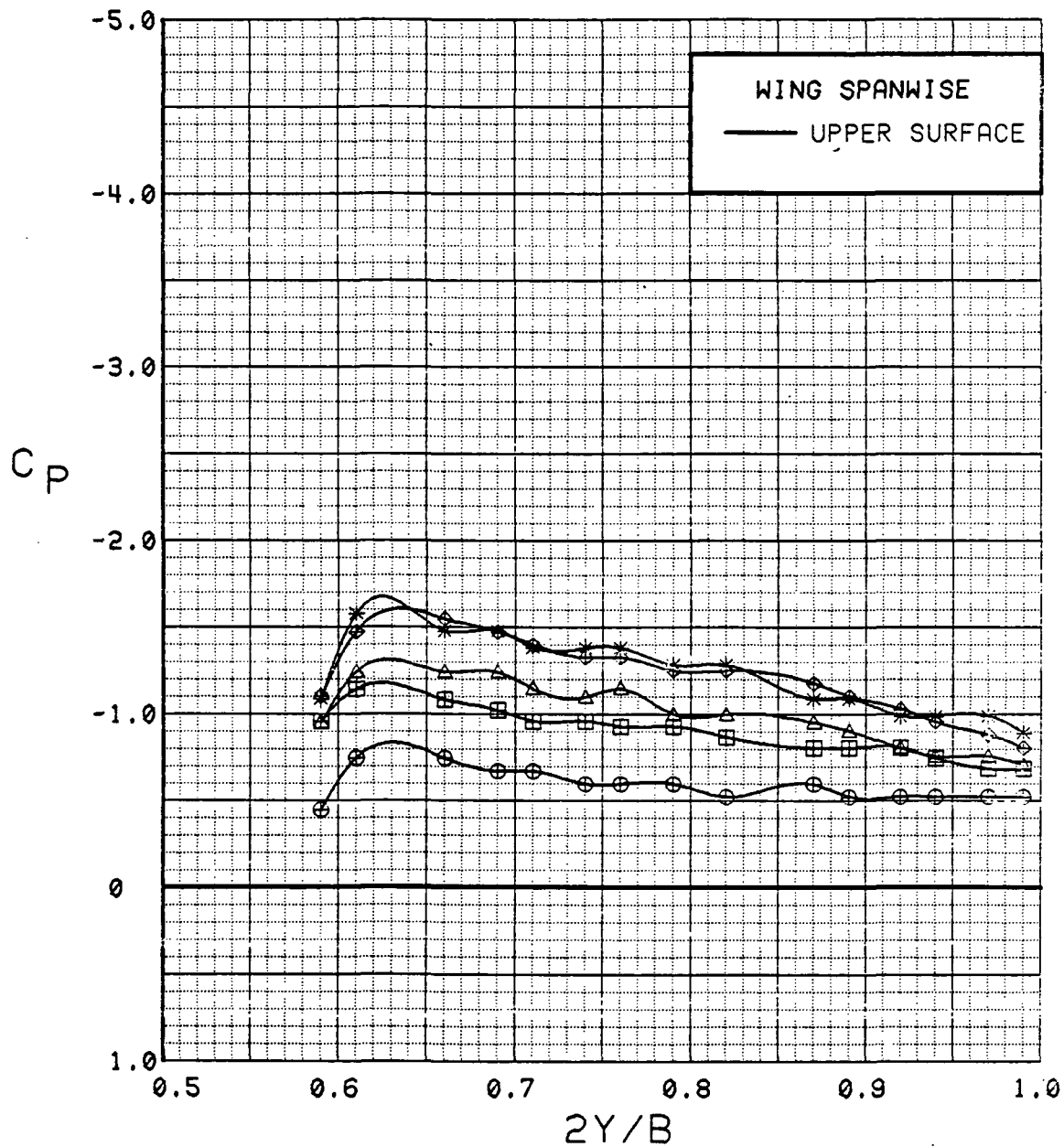


Figure 3.2.4-382 Power Buildup, Flaps Neutral, Spanwise, Alpha = 32 deg

# WING INBOARD

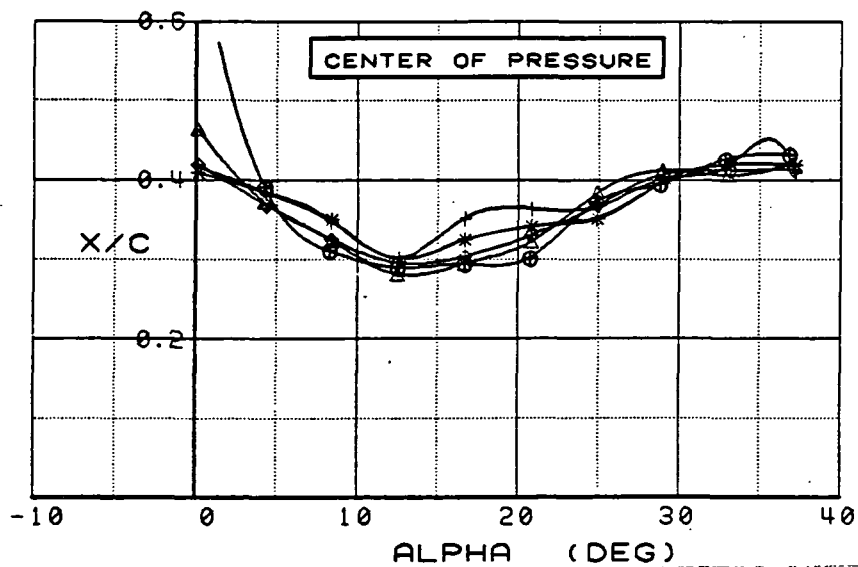
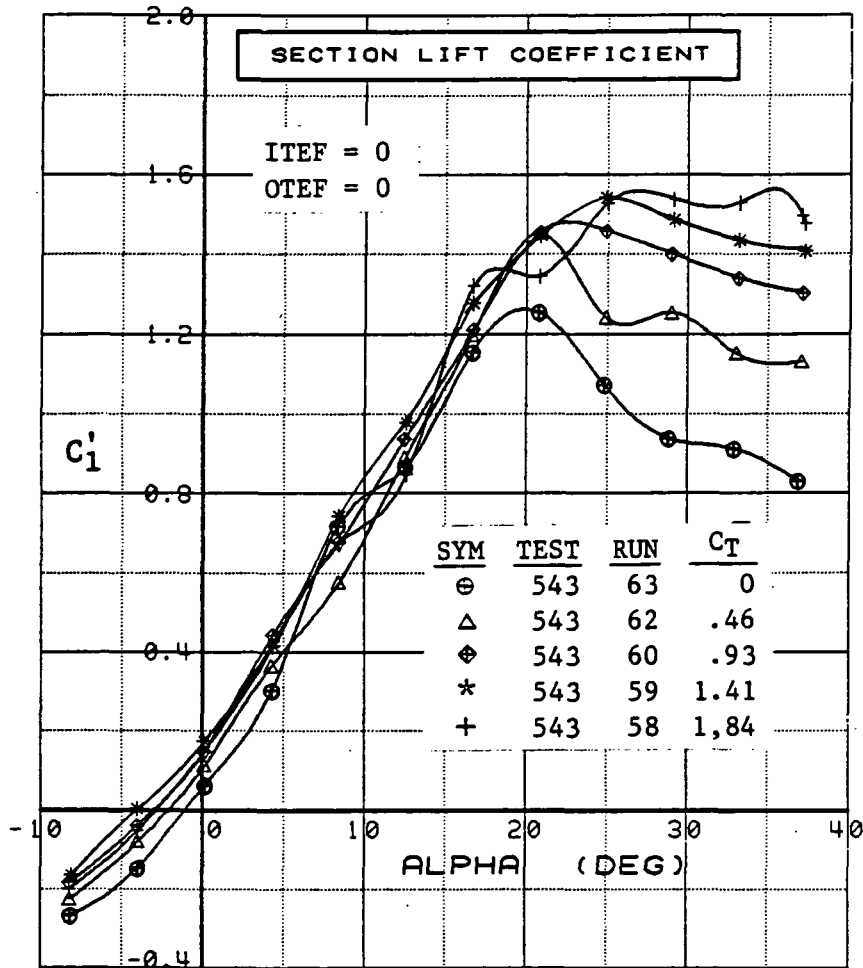


Figure 3.2.4-383 Power Buildup, Inboard, Flaps Neutral, Integrated Section Properties

# WING OUTBOARD

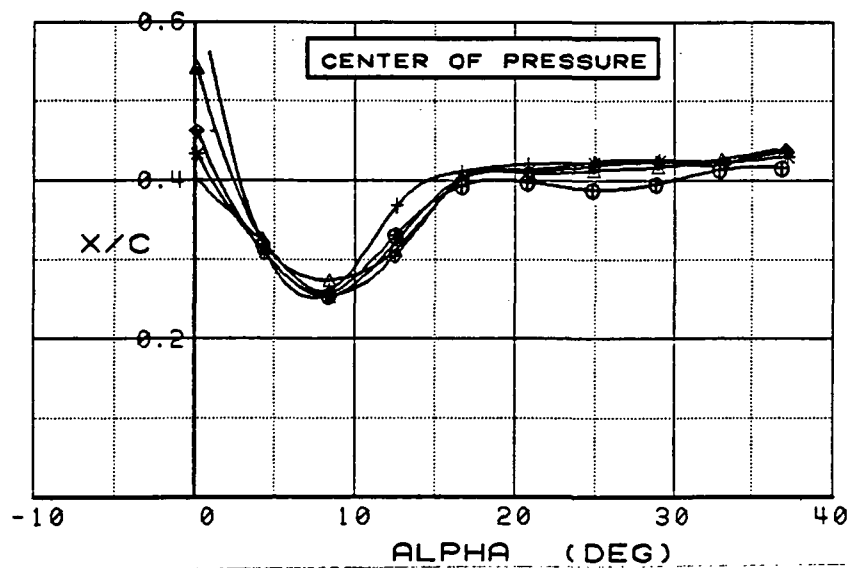
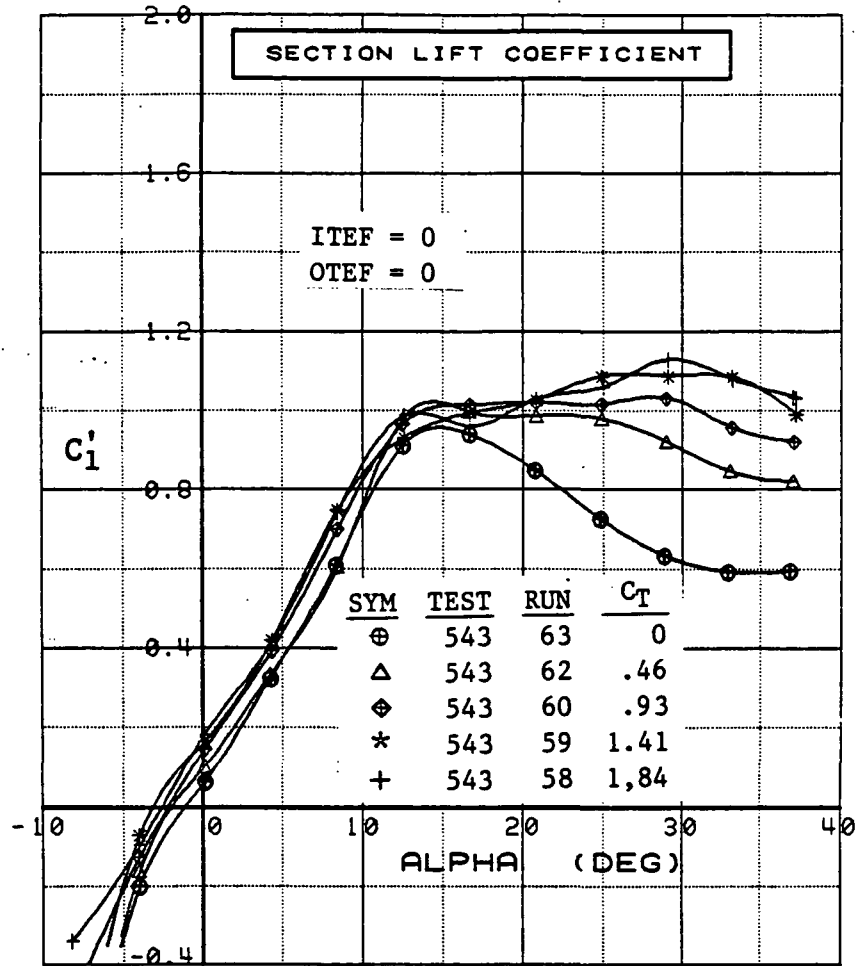


Figure 3.2.4-384 Power Buildup, Outboard, Flaps Neutral, Integrated Section Properties

SYM	TEST	RUN	ALPHA	CT	ITEF	OTEF	CAN	SWB
⊕	543	11	4.4	0.00	30	30	0	OFF
⊞	543	8	4.5	0.47	30	30	0	OFF
△	543	6	4.5	0.94	30	30	0	OFF
⊕	543	5	4.5	1.40	30	30	0	OFF
*	543	4	4.5	1.90	30	30	0	OFF

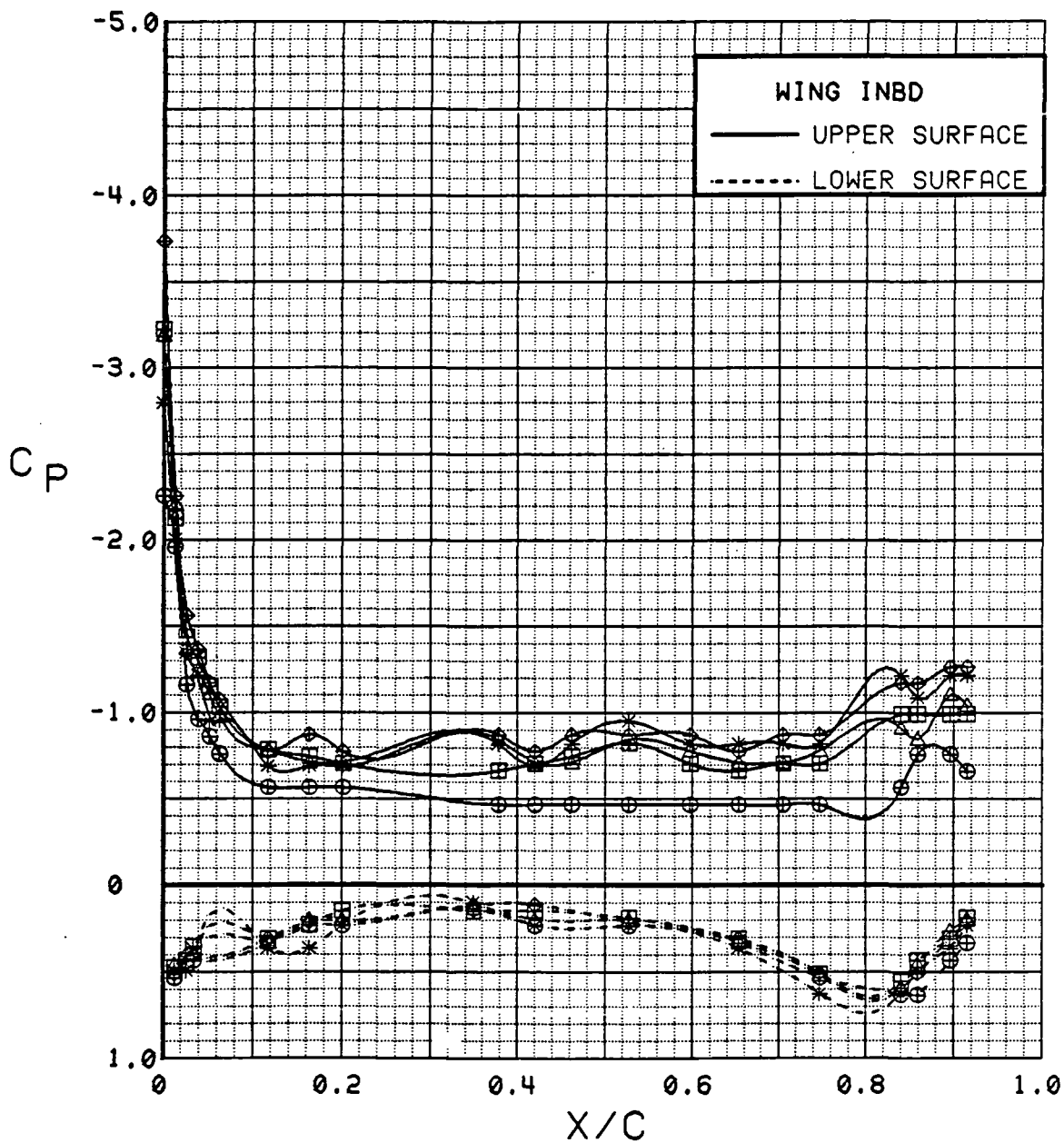


Figure 3.2.4-385 Power Buildup, Flaps Deflected, Inboard, Alpha = 4 deg

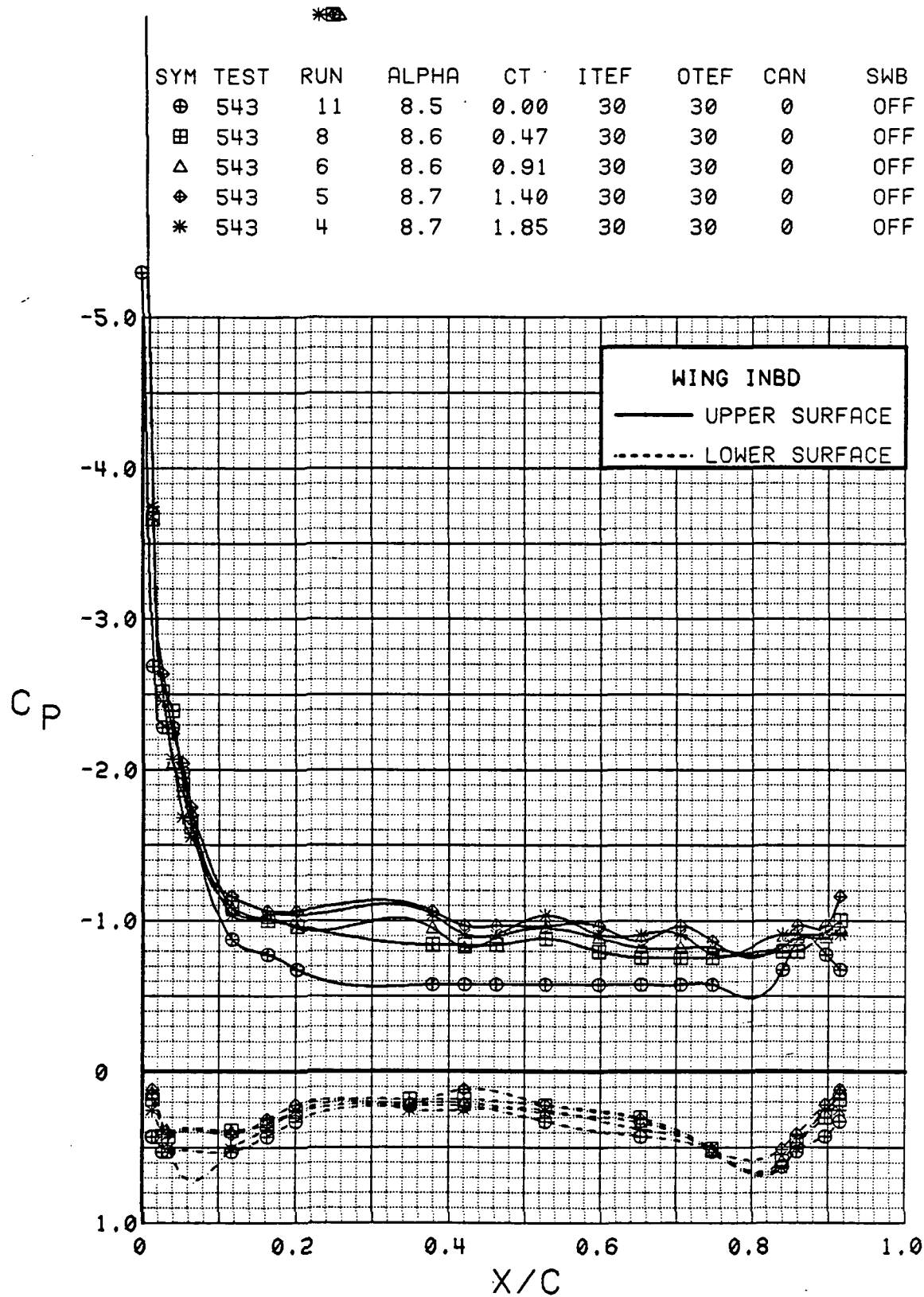


Figure 3.2.4-386 Power Buildup, Flaps Deflected, Inboard, Alpha = 8 deg

SYM	TEST	RUN	ALPHA	CT	ITEF	OTEF	CAN	SWB
⊕	543	11	12.7	0.00	30	30	0	OFF
⊞	543	8	12.8	0.46	30	30	0	OFF
△	543	6	12.8	0.92	30	30	0	OFF
⊕	543	5	12.8	1.39	30	30	0	OFF
*	543	4	12.8	1.86	30	30	0	OFF

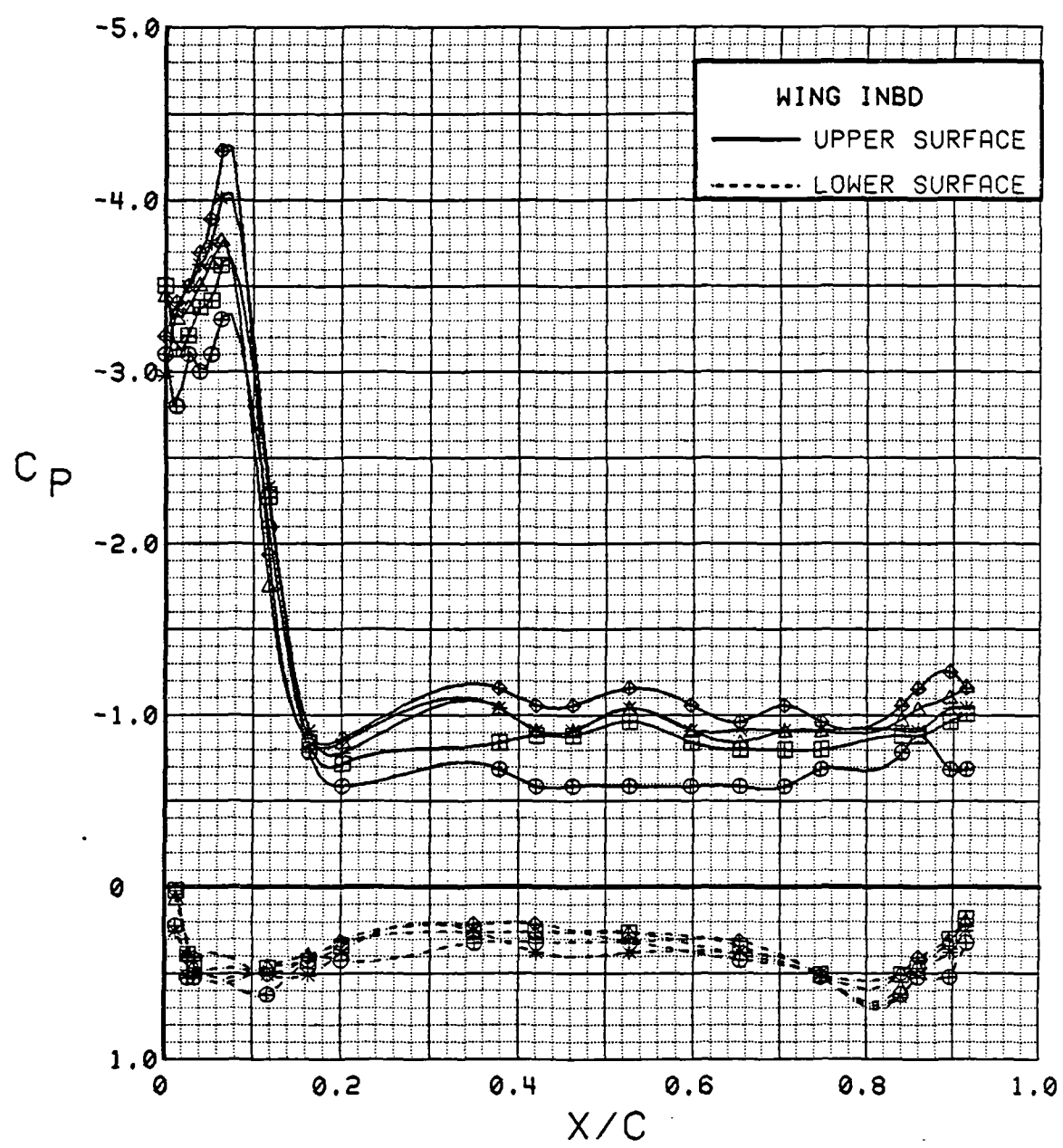


Figure 3.2.4-387 Power Buildup, Flaps Deflected, Inboard, Alpha = 12 deg



SYM	TEST	RUN	ALPHA	CT	ITEF	OTEF	CAN	SWB
⊕	543	11	16.8	0.00	30	30	0	OFF
⊞	543	8	16.9	0.47	30	30	0	OFF
△	543	6	16.9	0.92	30	30	0	OFF
⊕	543	5	16.9	1.40	30	30	0	OFF
*	543	4	16.9	1.86	30	30	0	OFF

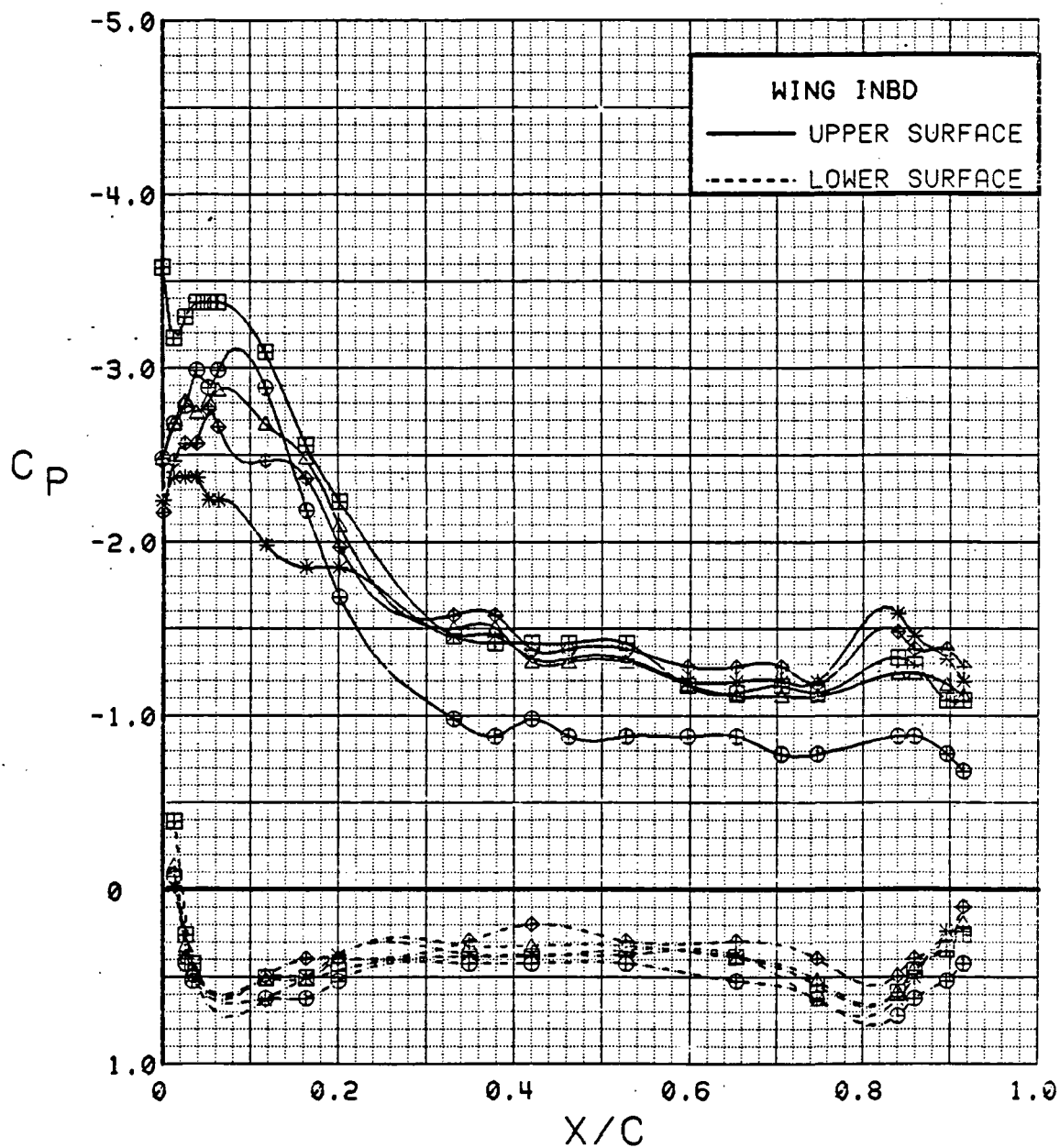


Figure 3.2.4-388 Power Buildup, Flaps Deflected, Inboard, Alpha = 16 deg

SYM	TEST	RUN	ALPHA	CT	ITEF	OTEF	CAN	SWB
⊕	543	11	20.8	0.00	30	30	0	OFF
⊞	543	8	21.0	0.46	30	30	0	OFF
△	543	6	21.0	0.93	30	30	0	OFF
◆	543	5	21.0	1.42	30	30	0	OFF
*	543	4	21.1	1.88	30	30	0	OFF

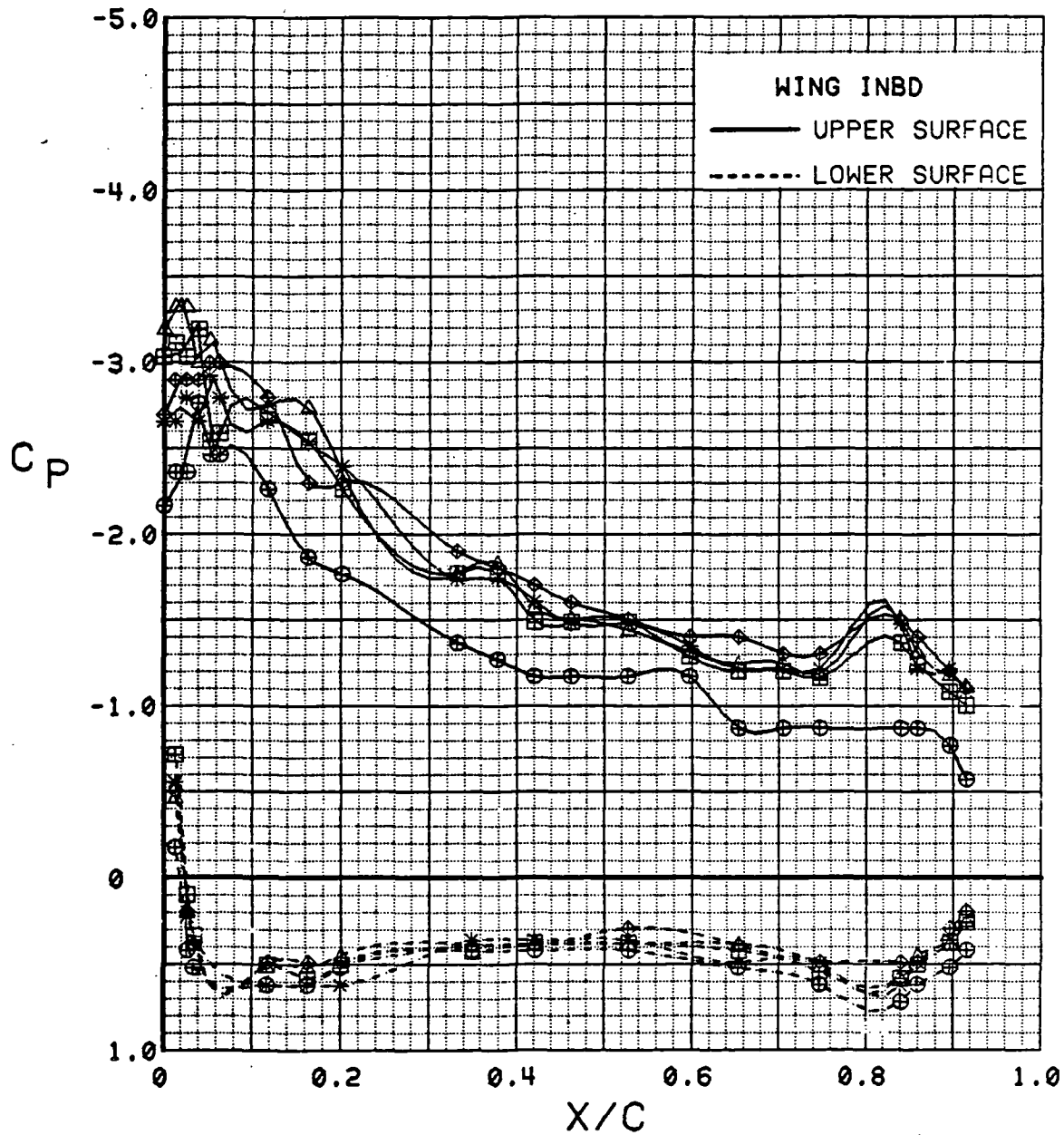


Figure 3.2.4-389 Power Buildup, Flaps Deflected, Inboard, Alpha = 20 deg

SYM	TEST	RUN	ALPHA	CT	ITEF	OTEF	CAN	SWB
⊕	543	11	24.9	0.00	30	30	0	OFF
⊞	543	8	25.1	0.47	30	30	0	OFF
△	543	6	25.1	0.93	30	30	0	OFF
⬢	543	5	25.1	1.42	30	30	0	OFF
*	543	4	25.1	1.89	30	30	0	OFF

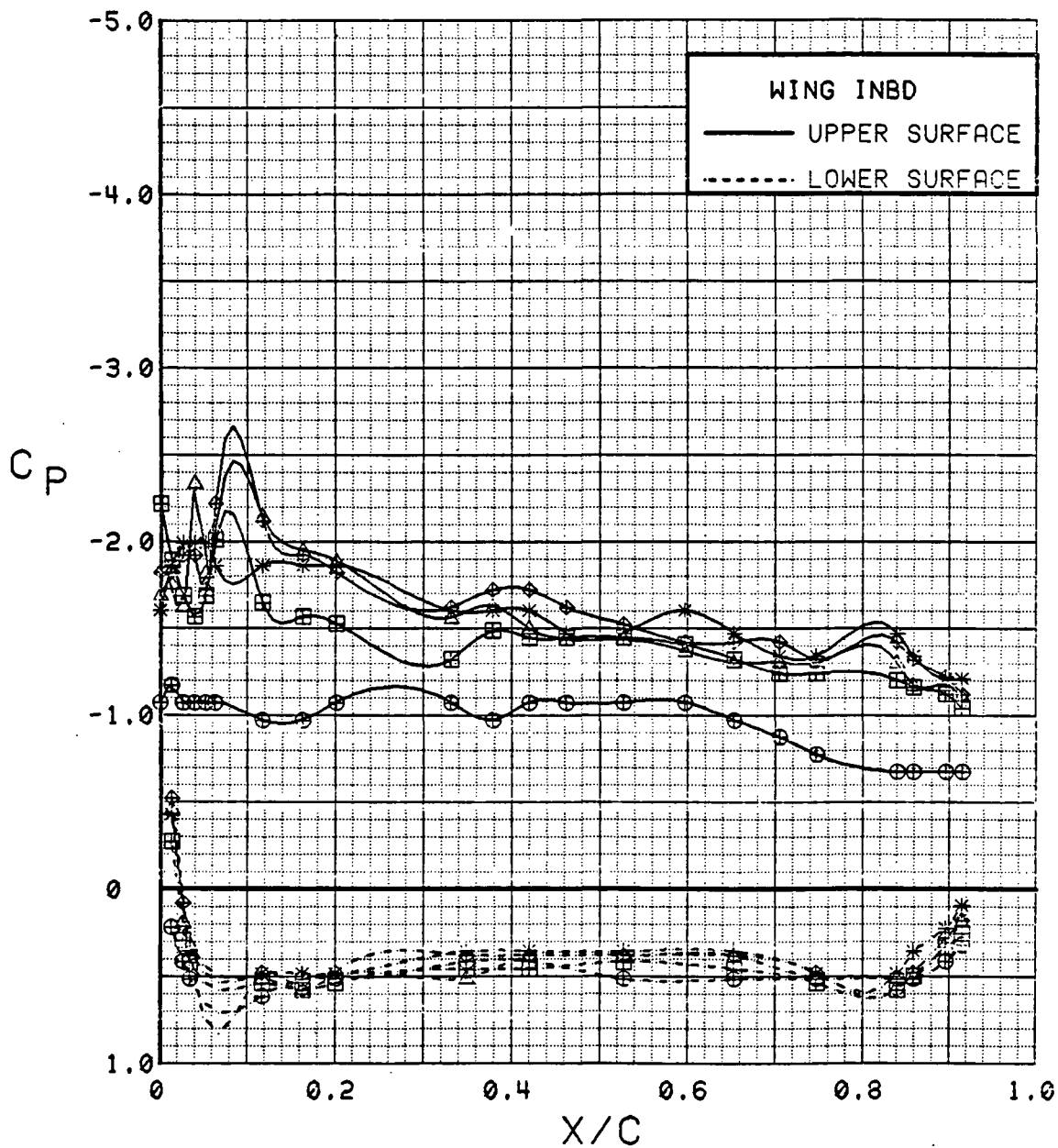


Figure 3.2.4-390 Power Buildup, Flaps Deflected, Inboard, Alpha = 24 deg

SYM	TEST	RUN	ALPHA	CT	ITEF	OTEF	CAN	SWB
⊕	543	11	28.9	0.00	30	30	0	OFF
⊞	543	8	29.1	0.46	30	30	0	OFF
△	543	6	29.1	0.93	30	30	0	OFF
◆	543	5	29.2	1.39	30	30	0	OFF
*	543	4	29.2	1.89	30	30	0	OFF

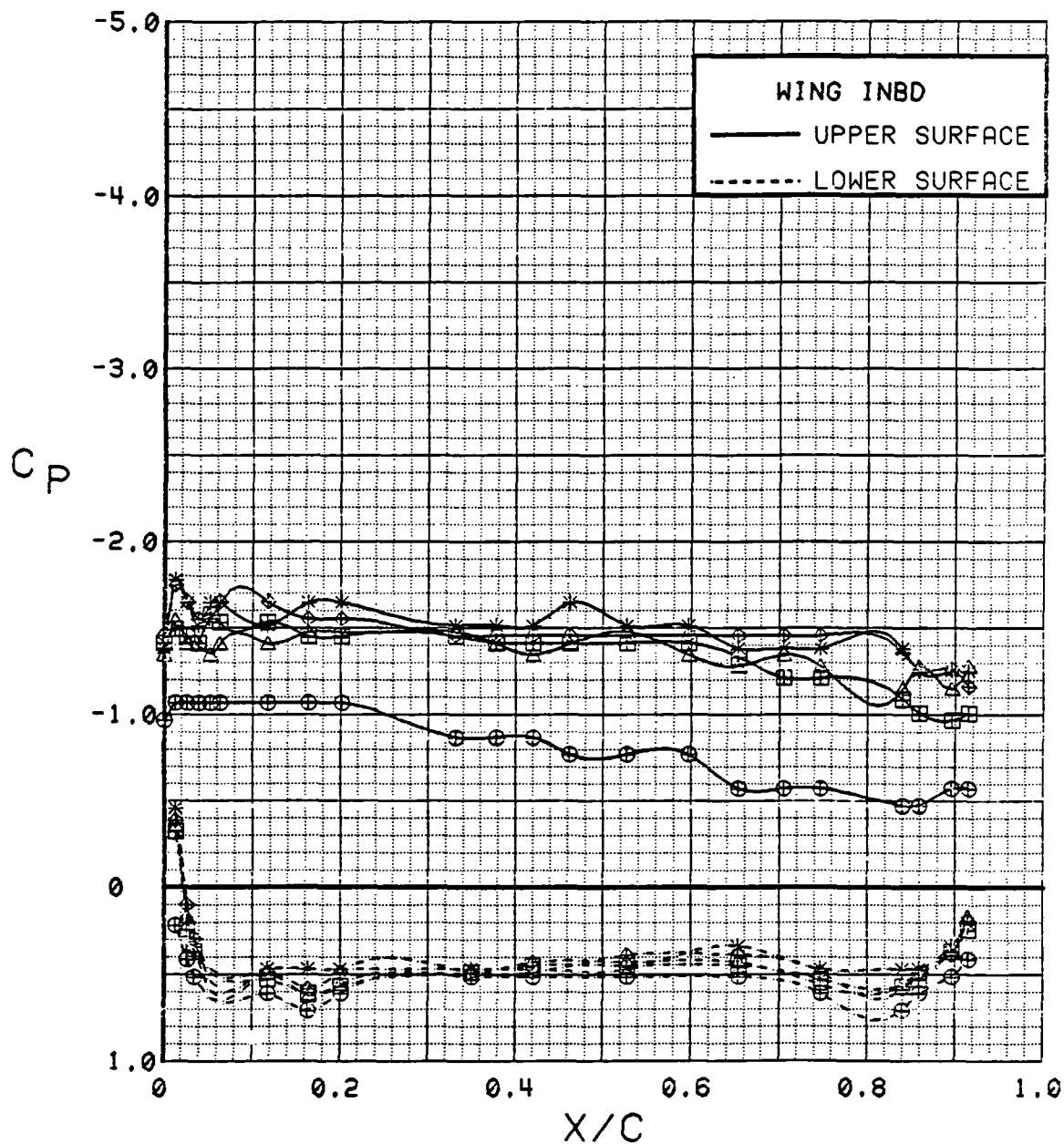


Figure 3.2.4-391 Power Buildup, Flaps Deflected, Inboard, Alpha = 28 deg

SYM	TEST	RUN	ALPHA	CT	ITEF	OTEF	CAN	SWB
⊕	543	11	4.4	0.00	30	30	0	OFF
⊞	543	8	4.5	0.47	30	30	0	OFF
△	543	6	4.5	0.94	30	30	0	OFF
⊕	543	5	4.5	1.40	30	30	0	OFF
*	543	4	4.5	1.90	30	30	0	OFF

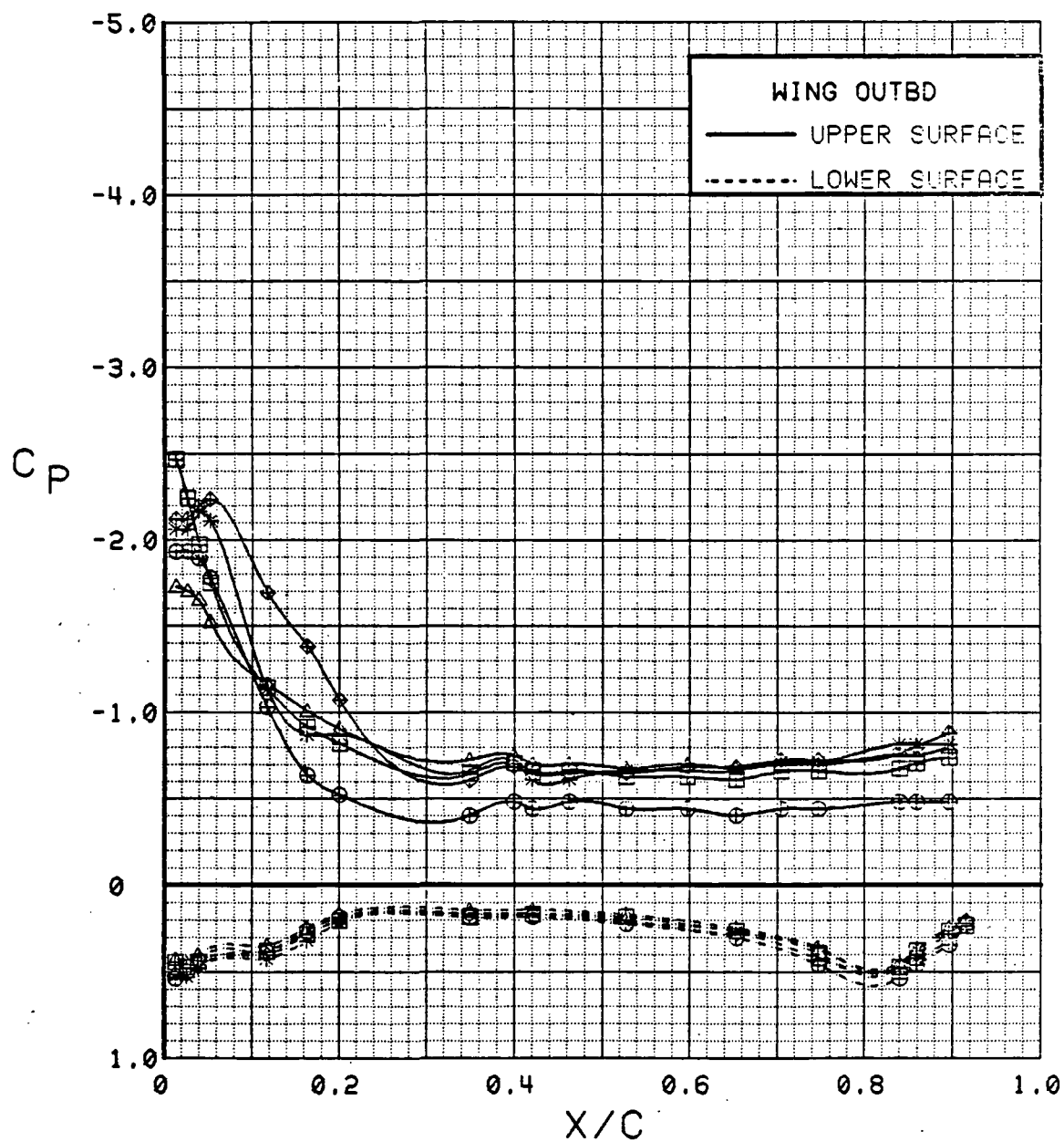


Figure 3.2.4-392 Power Buildup, Flaps Deflected, Outboard, Alpha = 4 deg

SYM	TEST	RUN	ALPHA	CT	ITEF	OTEF	CAN	SWB
⊕	543	11	8.5	0.00	30	30	0	OFF
⊞	543	8	8.6	0.47	30	30	0	OFF
△	543	6	8.6	0.91	30	30	0	OFF
⬠	543	5	8.7	1.40	30	30	0	OFF
*	543	4	8.7	1.85	30	30	0	OFF

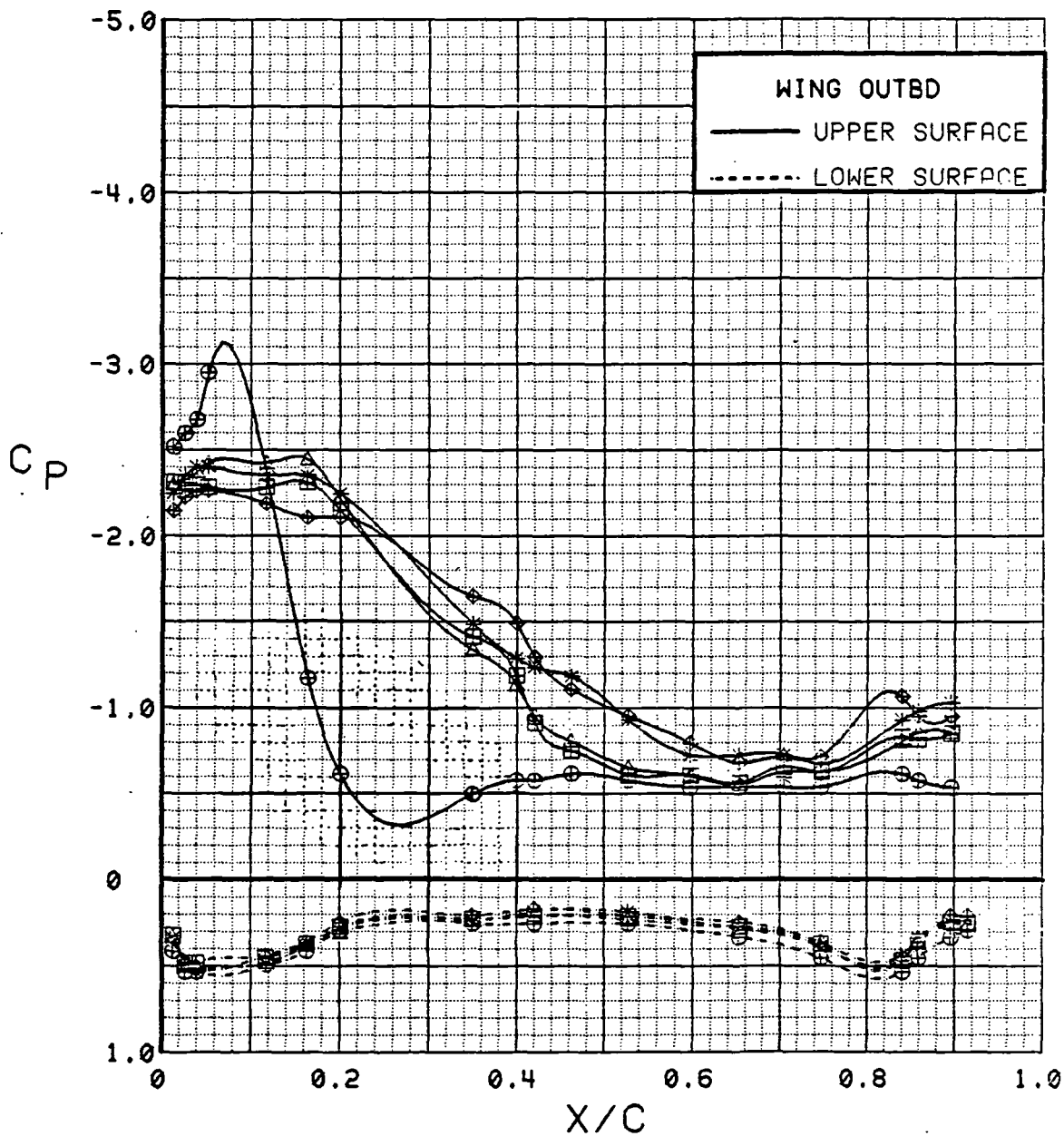


Figure 3.2.4-393 Power Buildup, Flaps Deflected, Outboard, Alpha = 8 deg

SYM	TEST	RUN	ALPHA	CT	ITEF	OTEF	CAN	SNB
⊕	543	11	12.7	0.00	30	30	0	OFF
⊞	543	8	12.8	0.46	30	30	0	OFF
△	543	6	12.8	0.92	30	30	0	OFF
◆	543	5	12.8	1.39	30	30	0	OFF
*	543	4	12.8	1.86	30	30	0	OFF

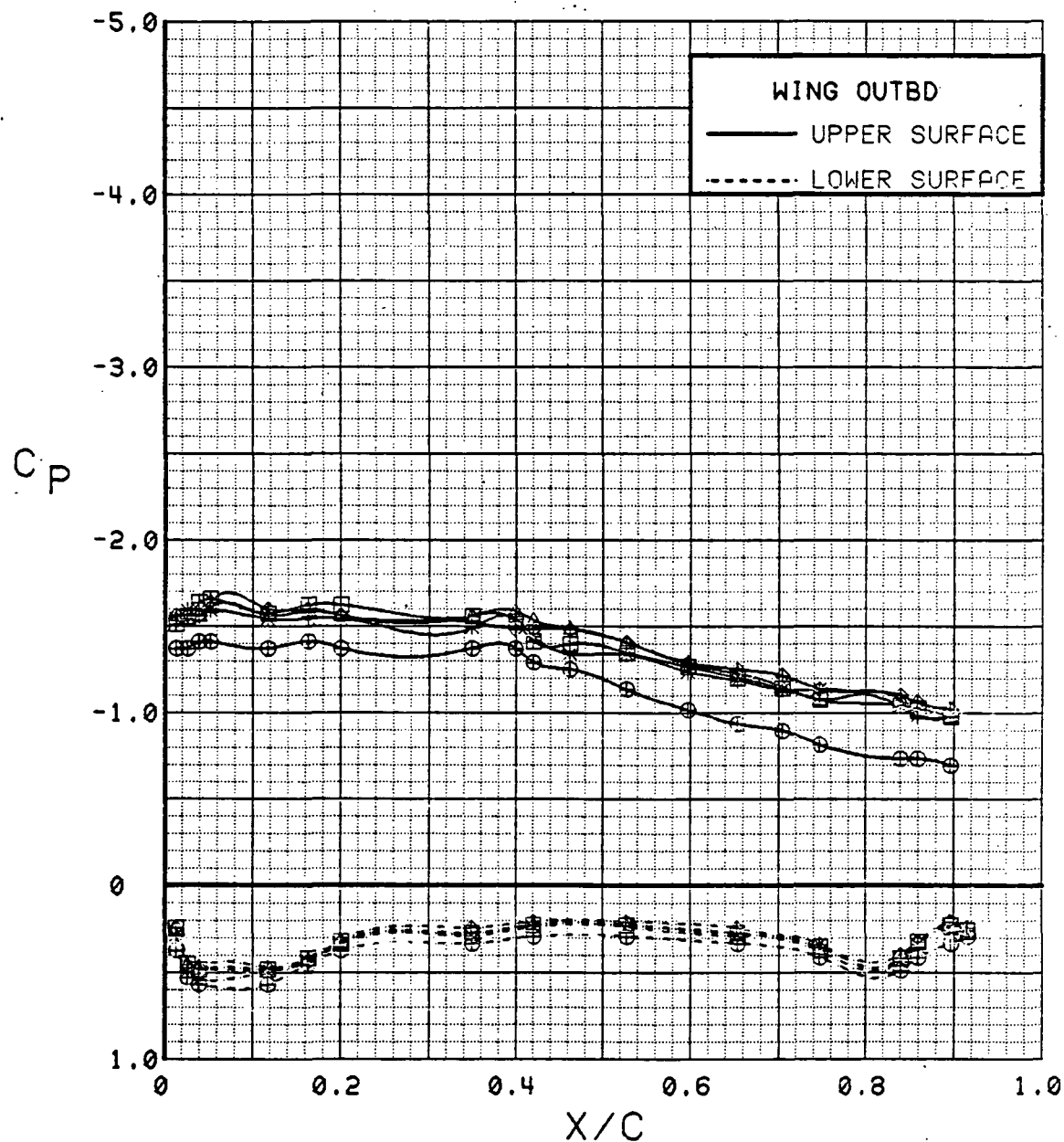


Figure 3.2.4-394 Power Buildup, Flaps Deflected, Outboard, Alpha = 12 deg

SYM	TEST	RUN	ALPHA	CT	ITEF	OTEF	CAN	SWB
⊕	543	11	16.8	0.00	30	30	0	OFF
⊞	543	8	16.9	0.47	30	30	0	OFF
△	543	6	16.9	0.92	30	30	0	OFF
⊕	543	5	16.9	1.40	30	30	0	OFF
*	543	4	16.9	1.86	30	30	0	OFF

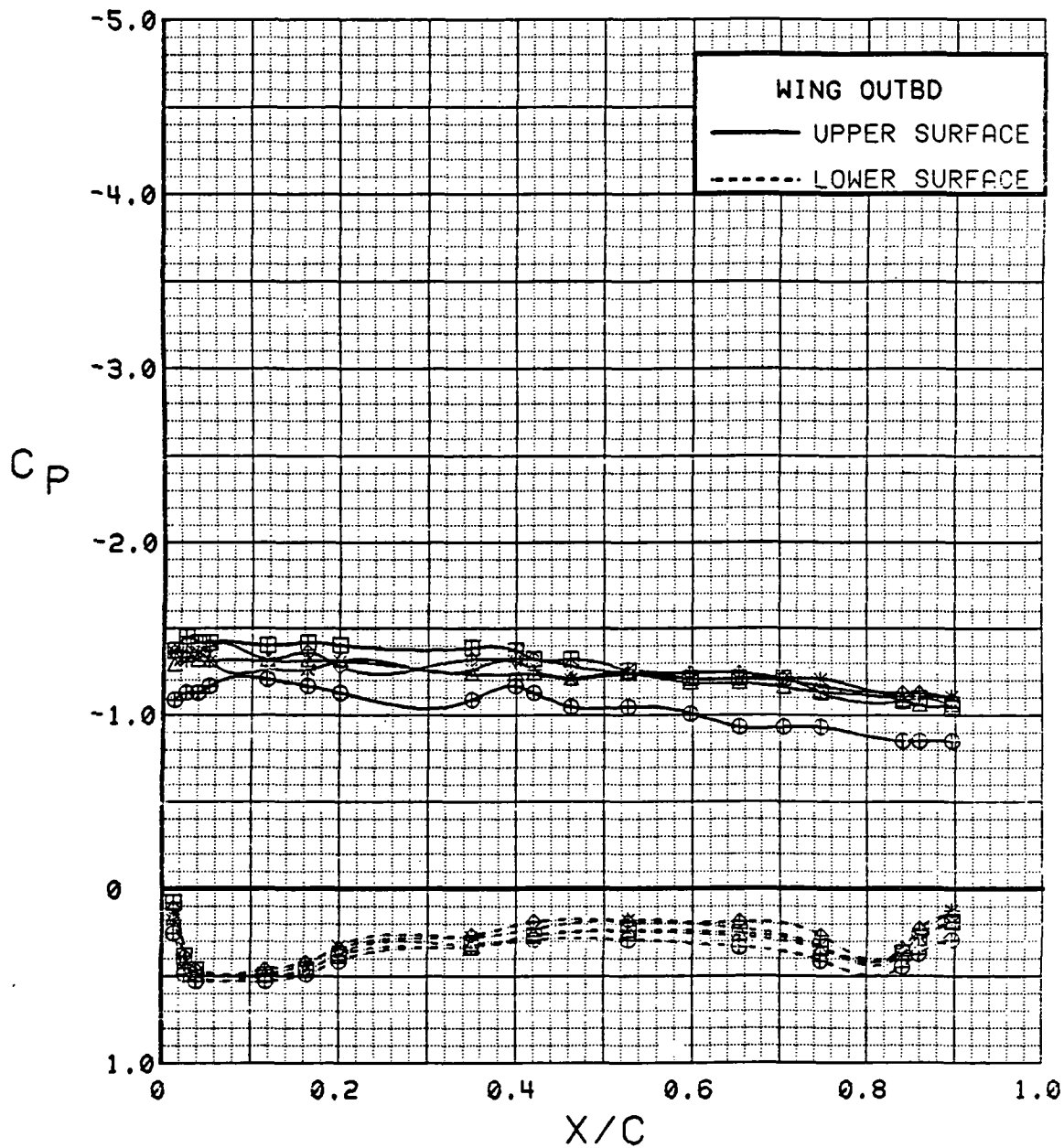


Figure 3.2.4-395 Power Buildup, Flaps Deflected, Outboard, Alpha = 16 deg



SYM	TEST	RUN	ALPHA	CT	ITEF	OTEF	CAN	SNB
⊕	543	11	20.8	0.00	30	30	0	OFF
⊞	543	8	21.0	0.46	30	30	0	OFF
△	543	6	21.0	0.93	30	30	0	OFF
⊕	543	5	21.0	1.42	30	30	0	OFF
*	543	4	21.1	1.88	30	30	0	OFF

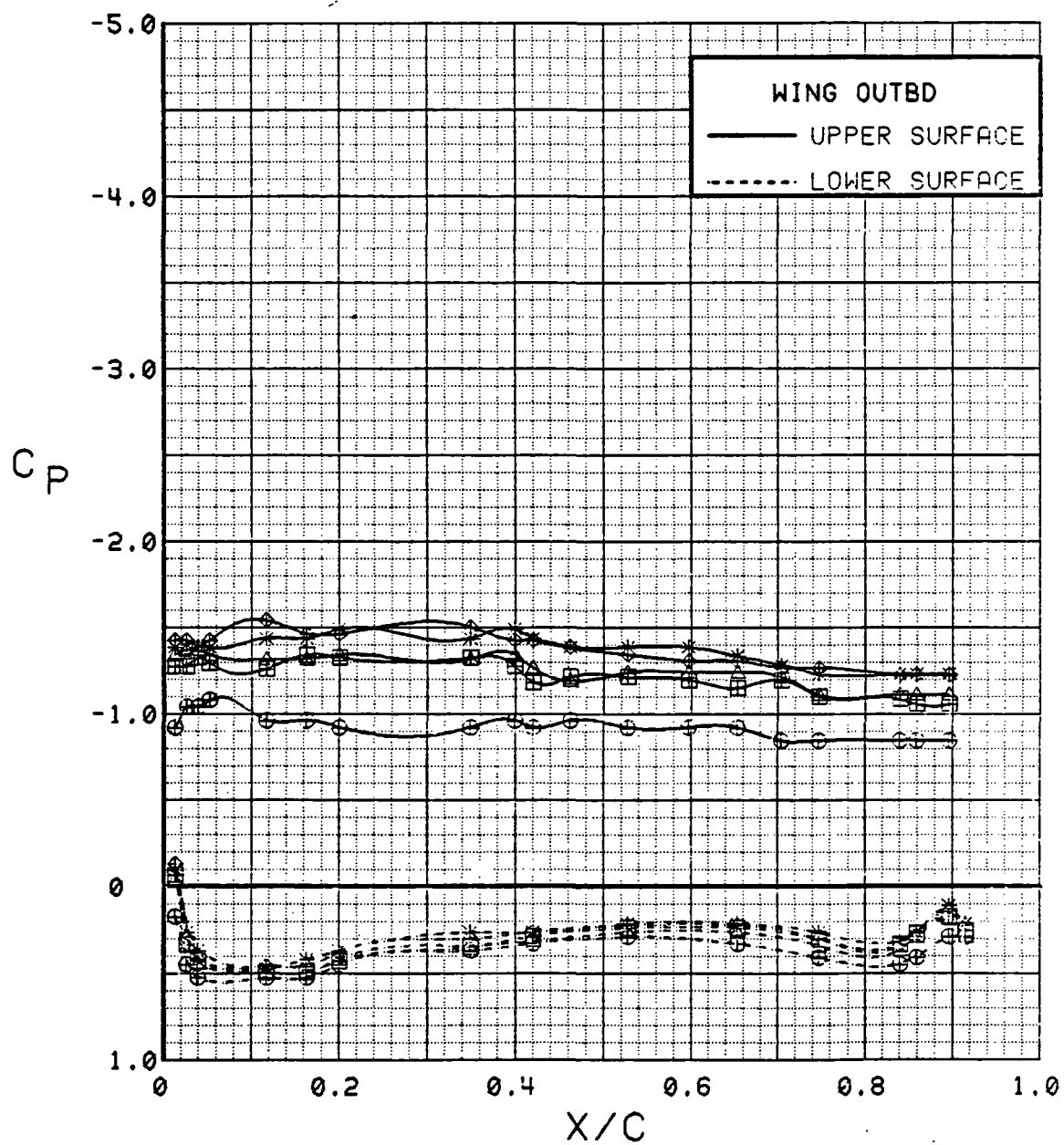


Figure 3.2.4-396 Power Buildup, Flaps Deflected, Outboard, Alpha = 20 deg

SYM	TEST	RUN	ALPHA	CT	ITEF	OTEF	CAN	SWB
⊕	543	11	24.9	0.00	30	30	0	OFF
⊞	543	8	25.1	0.47	30	30	0	OFF
△	543	6	25.1	0.93	30	30	0	OFF
⊕	543	5	25.1	1.42	30	30	0	OFF
*	543	4	25.1	1.89	30	30	0	OFF

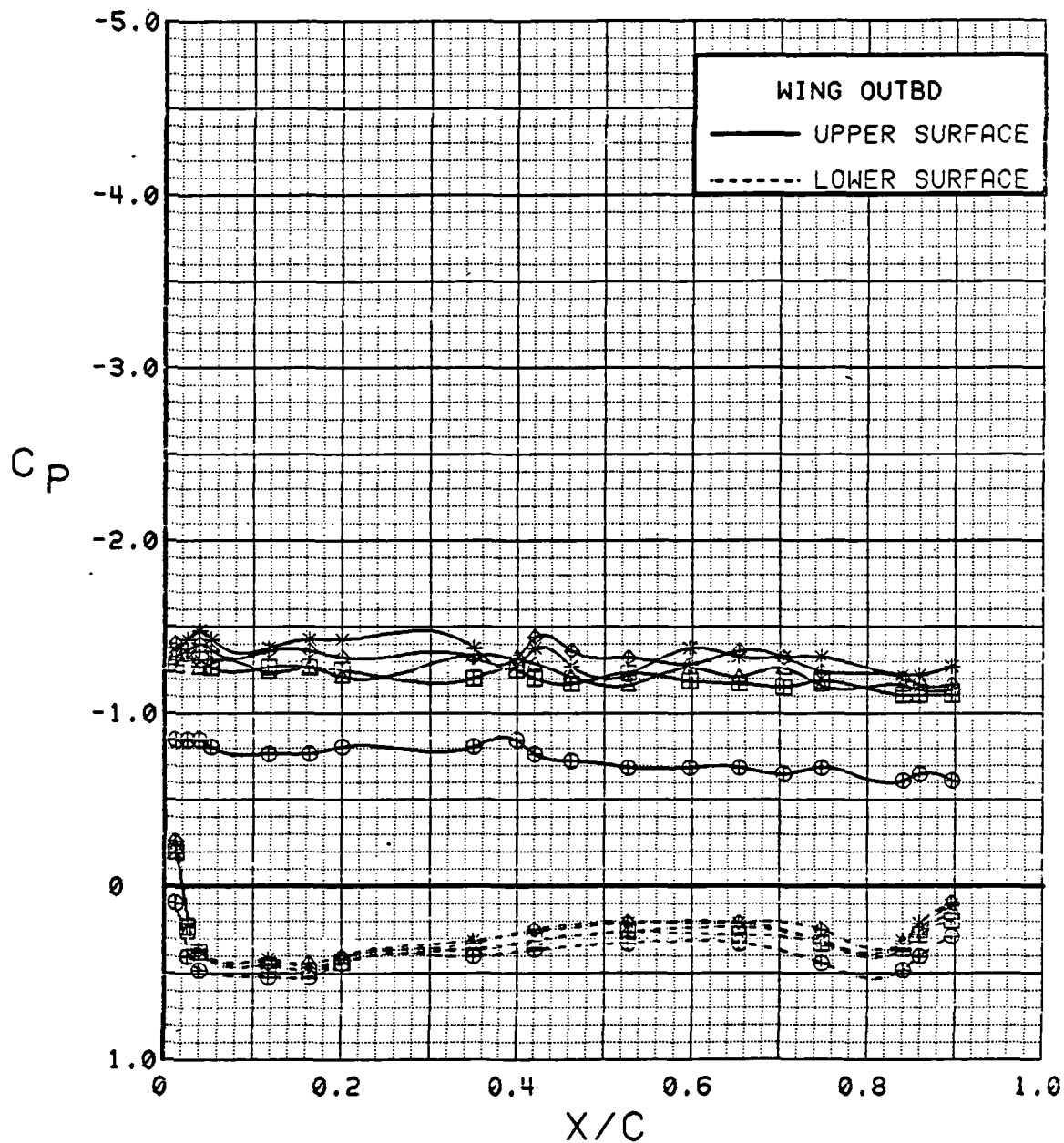


Figure 3.2.4-397 Power Buildup, Flaps Deflected, Outboard, Alpha = 24 deg

SYM	TEST	RUN	ALPHA	CT	ITEF	OTEF	CAN	SWB
⊕	543	11	28.9	0.00	30	30	0	OFF
⊞	543	8	29.1	0.46	30	30	0	OFF
△	543	6	29.1	0.93	30	30	0	OFF
⬠	543	5	29.2	1.39	30	30	0	OFF
*	543	4	29.2	1.89	30	30	0	OFF

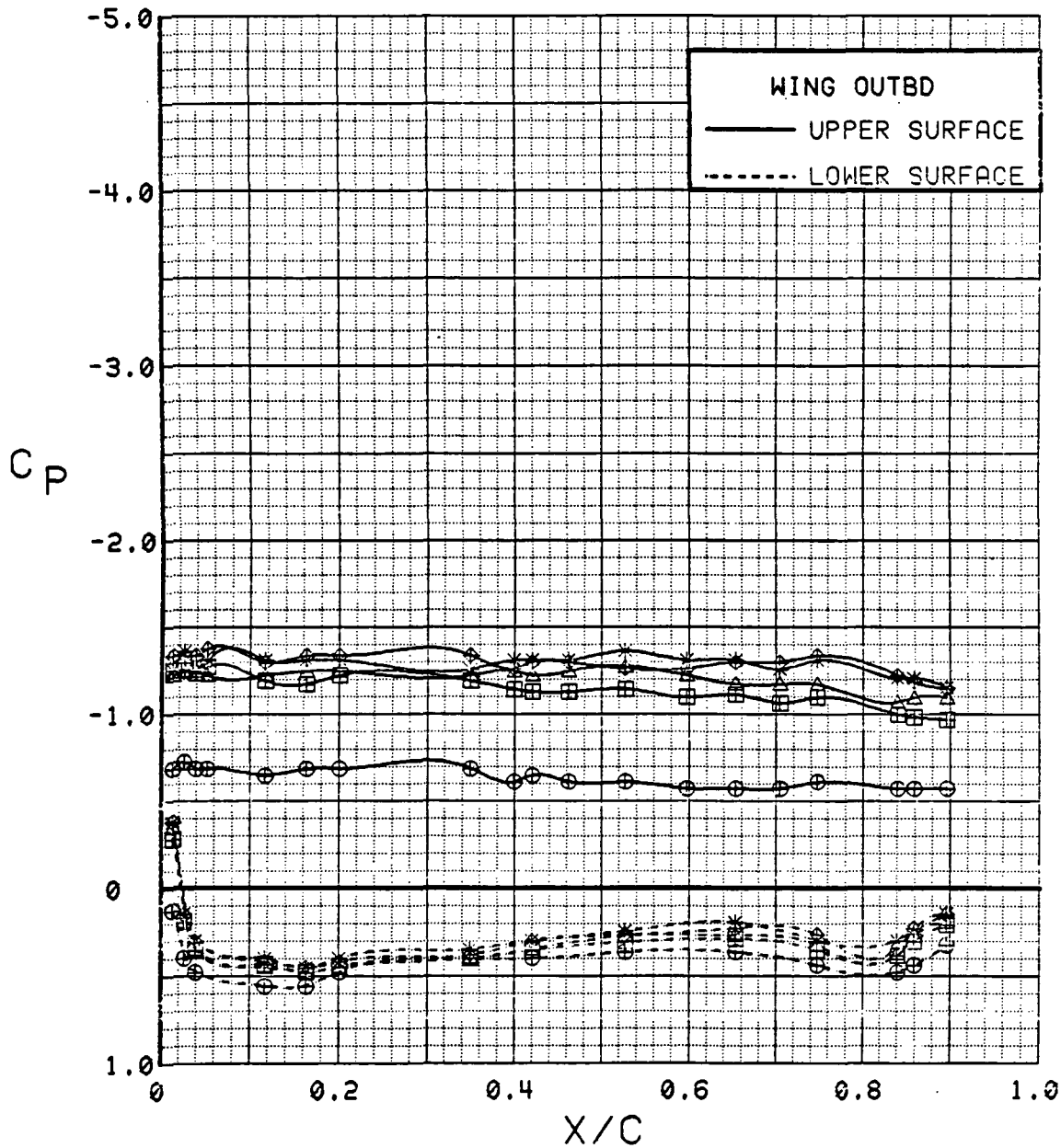


Figure 3.2.4-398 Power Buildup, Flaps Deflected, Outboard, Alpha = 28 deg

SYM	TEST	RUN	ALPHA	CT	ITEF	OTEF	CAN	SWB
⊕	543	11	4.4	0.00	30	30	0	OFF
⊞	543	8	4.5	0.47	30	30	0	OFF
△	543	6	4.5	0.94	30	30	0	OFF
◆	543	5	4.5	1.40	30	30	0	OFF
*	543	4	4.5	1.90	30	30	0	OFF

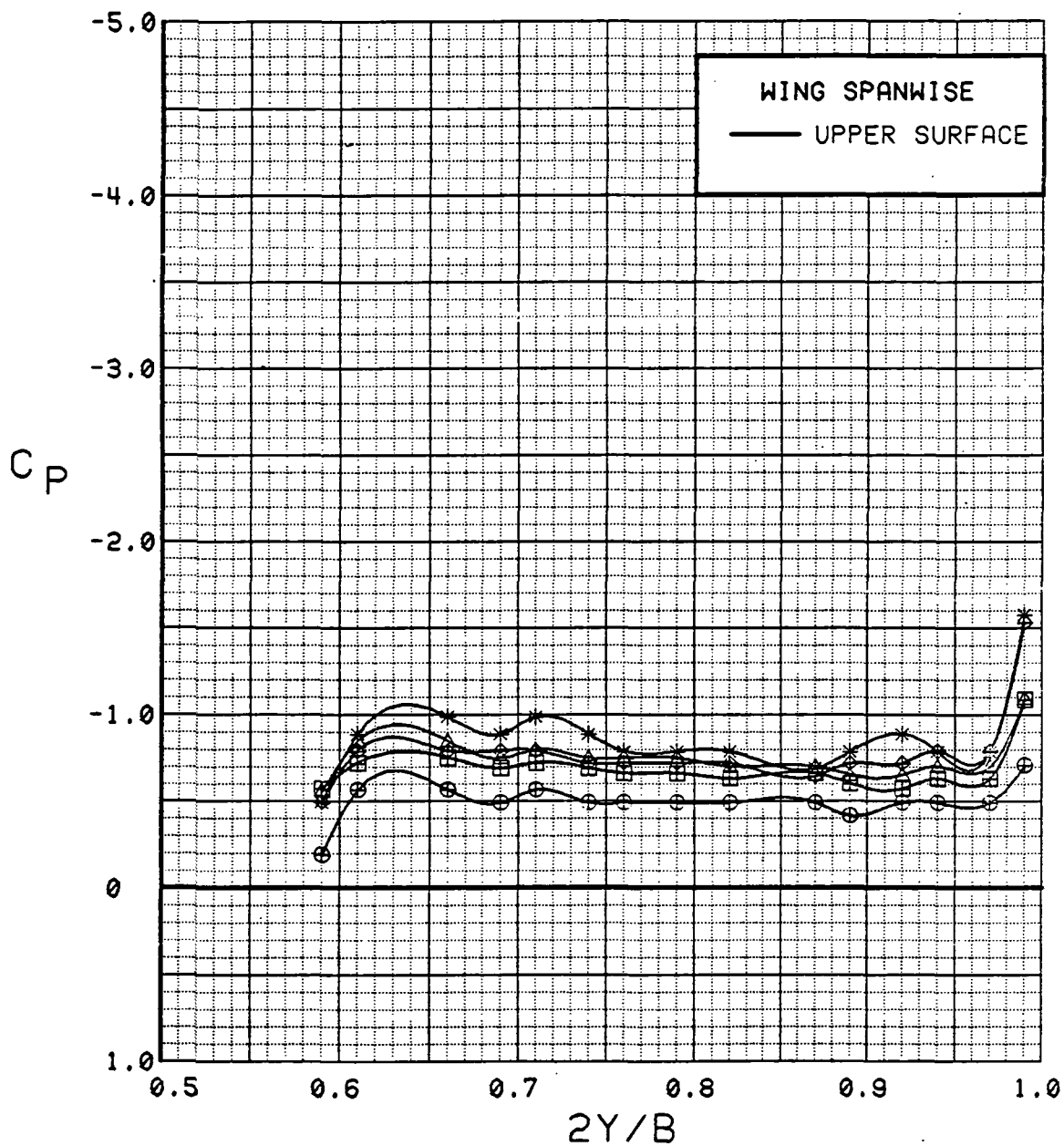


Figure 3.2.4-399 Power Buildup, Flaps Deflected, Spanwise, Alpha = 4 deg

SYM	TEST	RUN	ALPHA	CT	ITEF	OTEF	CAN	SWB
⊕	543	11	8.5	0.00	30	30	0	OFF
⊞	543	8	8.6	0.47	30	30	0	OFF
△	543	6	8.6	0.91	30	30	0	OFF
◆	543	5	8.7	1.40	30	30	0	OFF
*	543	4	8.7	1.85	30	30	0	OFF

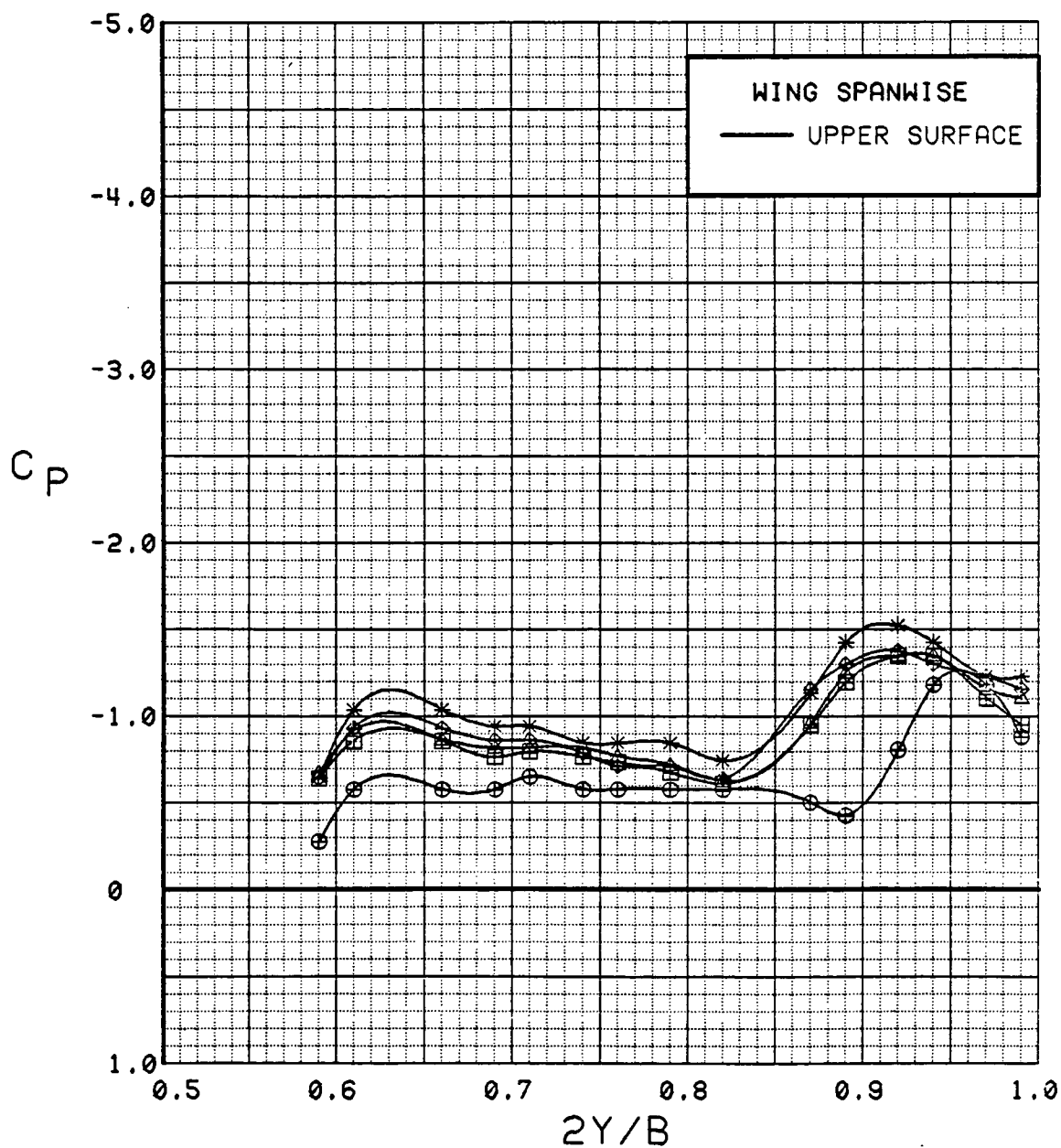


Figure 3.2.4-400 Power Buildup, Flaps Deflected, Spanwise, Alpha = 8 deg

SYM	TEST	RUN	ALPHA	CT	ITEF	OTEF	CAN	SWB
⊕	543	11	12.7	0.00	30	30	0	OFF
⊞	543	8	12.8	0.46	30	30	0	OFF
△	543	6	12.8	0.92	30	30	0	OFF
◆	543	5	12.8	1.39	30	30	0	OFF
*	543	4	12.8	1.86	30	30	0	OFF

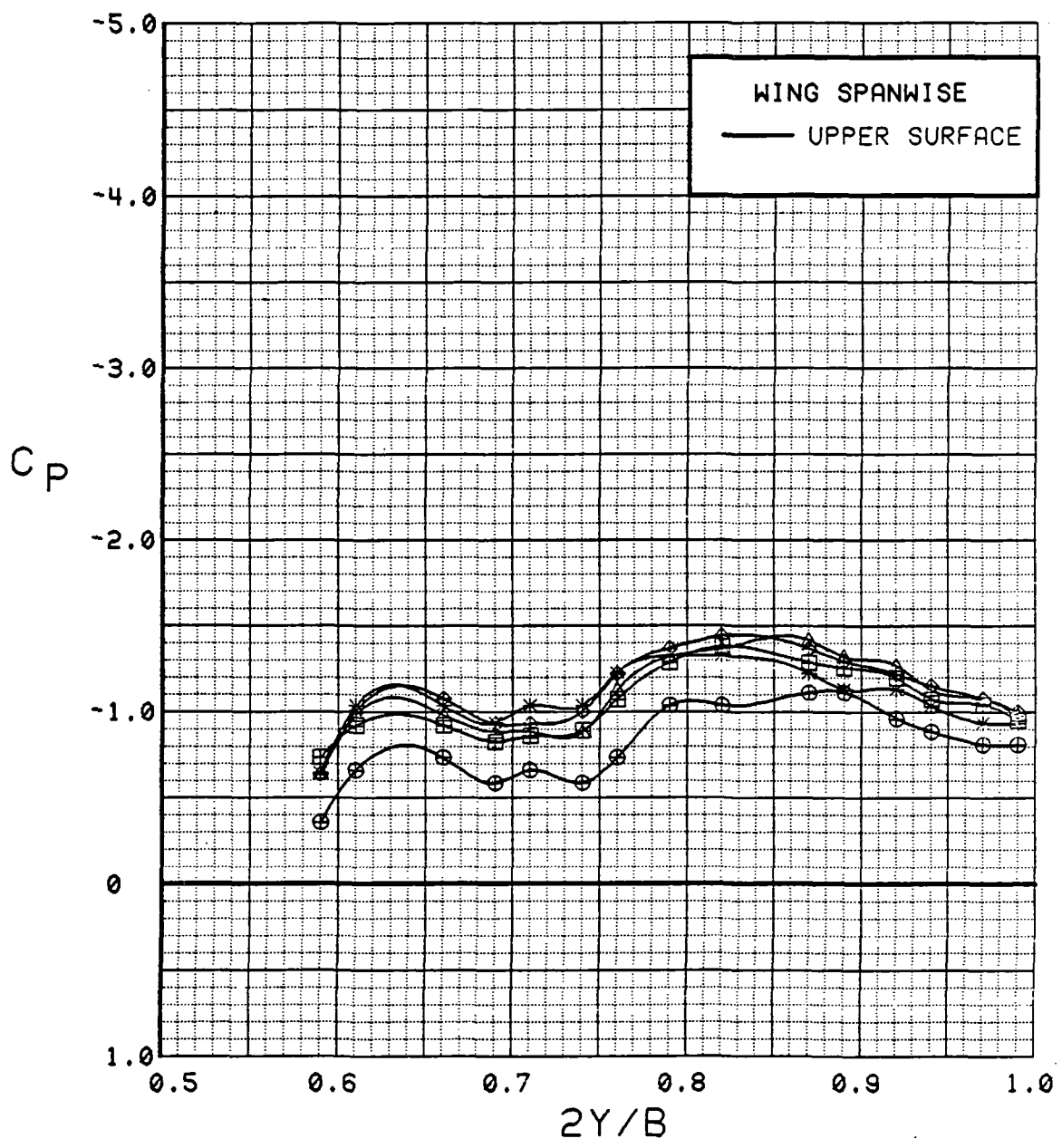


Figure 3.2.4-401 Power Buildup, Flaps Deflected, Spanwise, Alpha = 12 deg

SYM	TEST	RUN	ALPHA	CT	ITEF	OTEF	CAN	SWB
⊕	543	11	16.8	0.00	30	30	0	OFF
⊞	543	8	16.9	0.47	30	30	0	OFF
△	543	6	16.9	0.92	30	30	0	OFF
◆	543	5	16.9	1.40	30	30	0	OFF
*	543	4	16.9	1.86	30	30	0	OFF

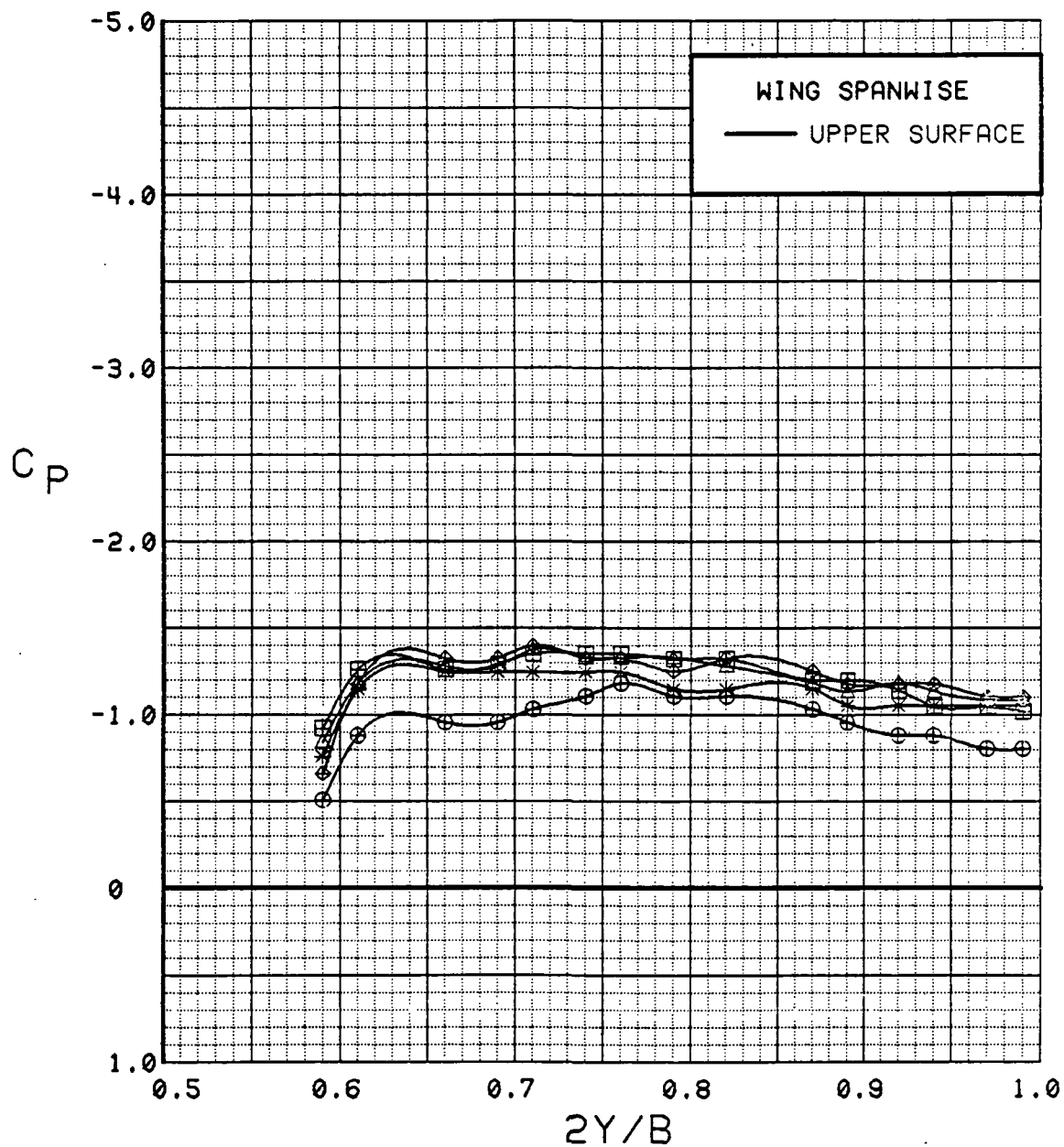


Figure 3.2.4-402 Power Buildup, Flaps Deflected, Spanwise, Alpha = 16 deg

SYM	TEST	RUN	ALPHA	CT	ITEF	OTEF	CAN	SWB
⊕	543	11	20.8	0.00	30	30	0	OFF
⊞	543	8	21.0	0.46	30	30	0	OFF
△	543	6	21.0	0.93	30	30	0	OFF
◆	543	5	21.0	1.42	30	30	0	OFF
*	543	4	21.1	1.88	30	30	0	OFF

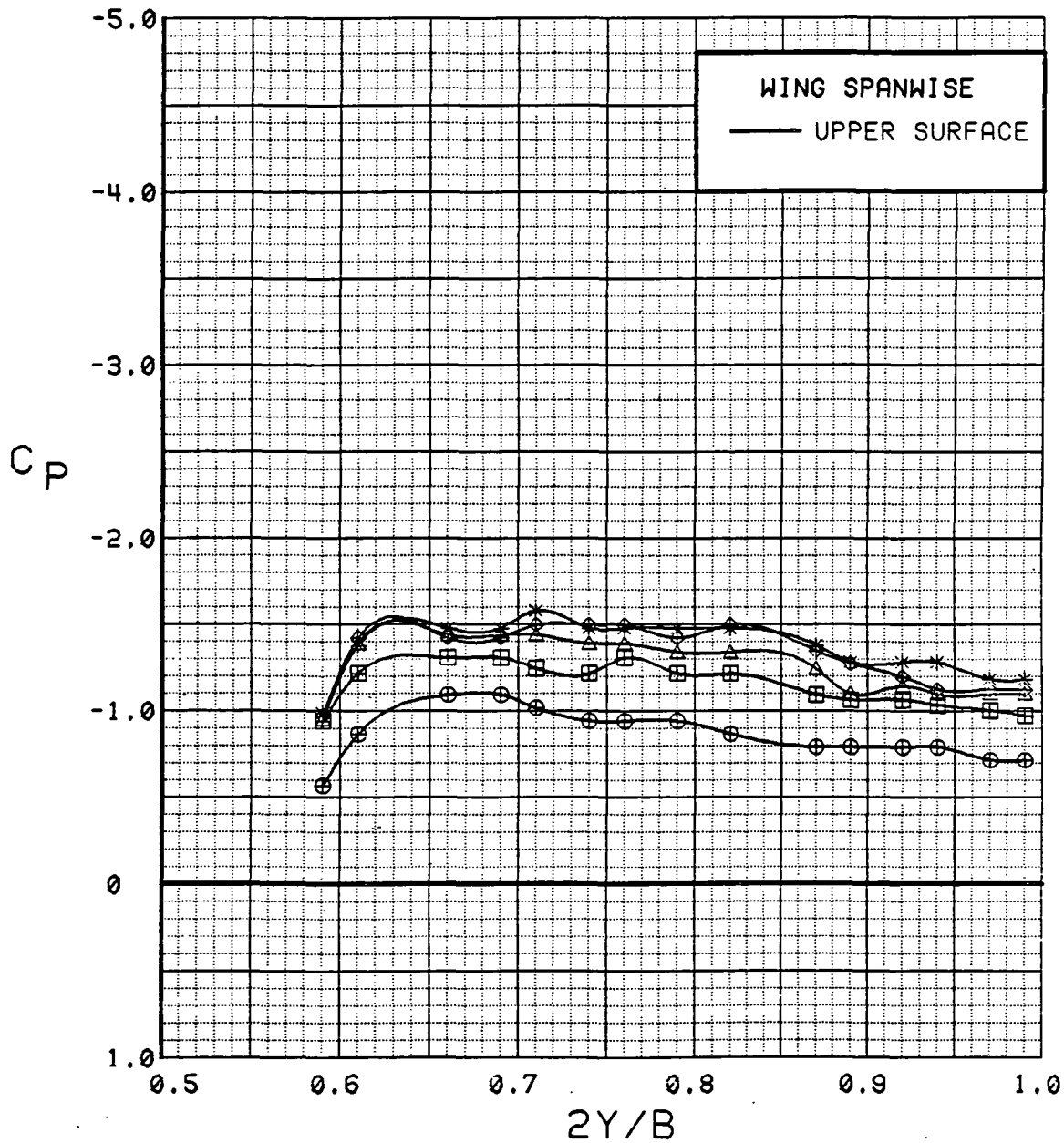


Figure 3.2.4-403 Power Buildup, Flaps Deflected, Spanwise, Alpha = 20 deg



SYM	TEST	RUN	ALPHA	CT	ITEF	OTEF	CAN	SWB
⊕	543	11	24.9	0.00	30	30	0	OFF
⊞	543	8	25.1	0.47	30	30	0	OFF
△	543	6	25.1	0.93	30	30	0	OFF
◆	543	5	25.1	1.42	30	30	0	OFF
*	543	4	25.1	1.89	30	30	0	OFF

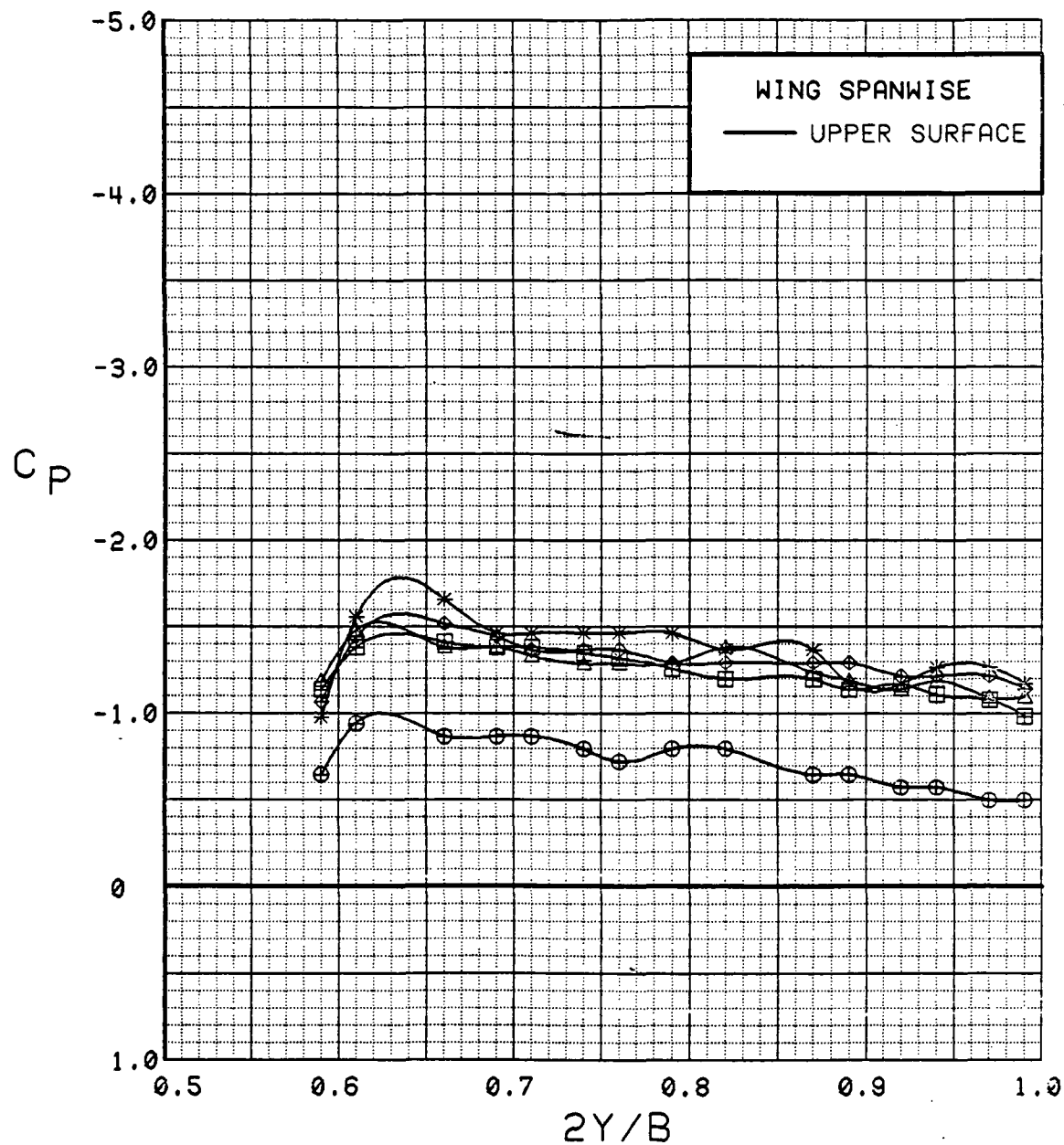


Figure 3.2.4-404 Power Buildup, Flaps Deflected, Spanwise, Alpha = 24 deg

SYM	TEST	RUN	ALPHA	CT	ITEF	OTEF	CAN	SWB
⊕	543	11	28.9	0.00	30	30	0	OFF
⊞	543	8	29.1	0.46	30	30	0	OFF
△	543	6	29.1	0.93	30	30	0	OFF
◆	543	5	29.2	1.39	30	30	0	OFF
*	543	4	29.2	1.89	30	30	0	OFF

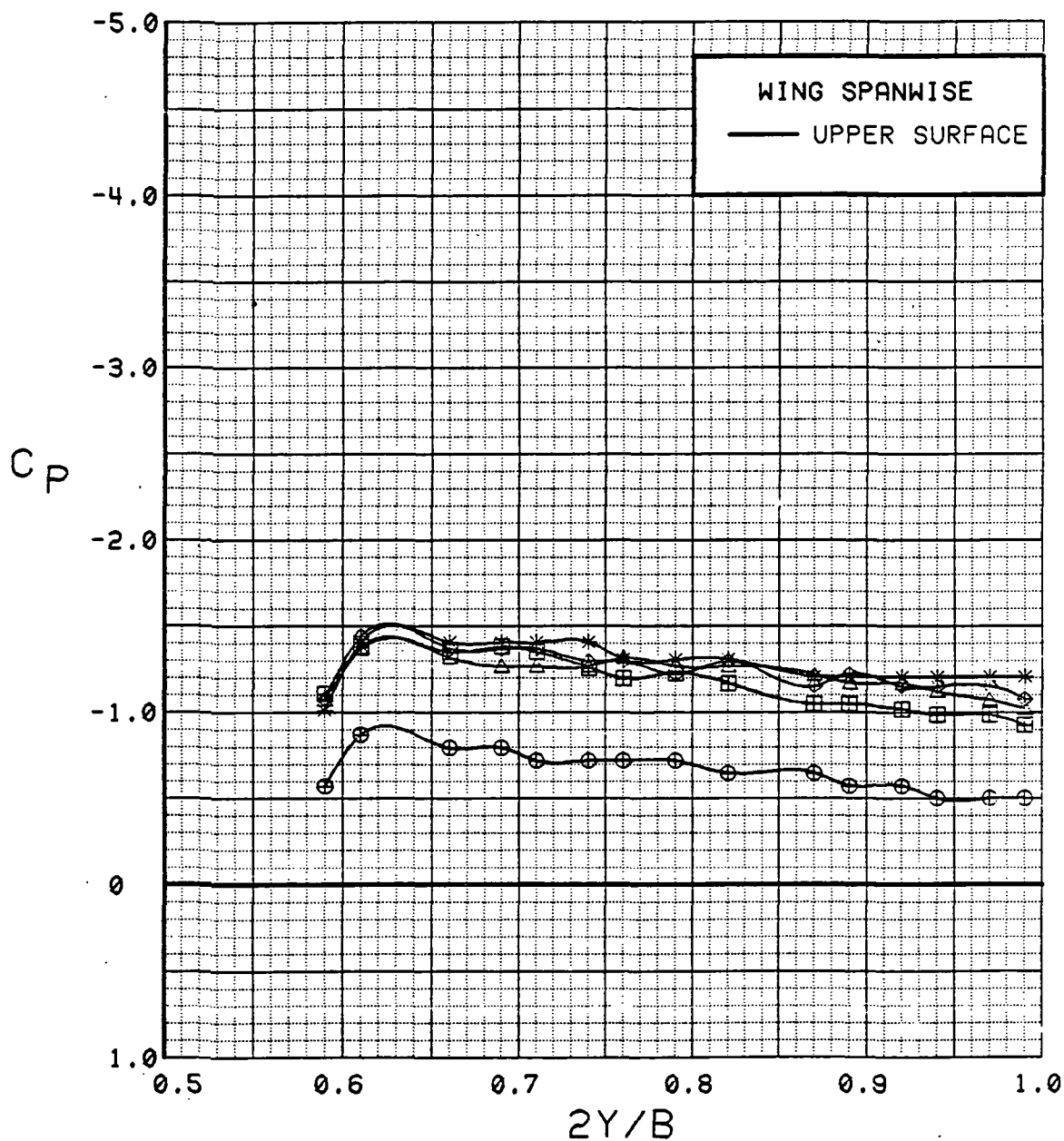


Figure 3.2.4-405 Power Buildup, Flaps Deflected, Spanwise, Alpha = 28 deg

# WING INBOARD

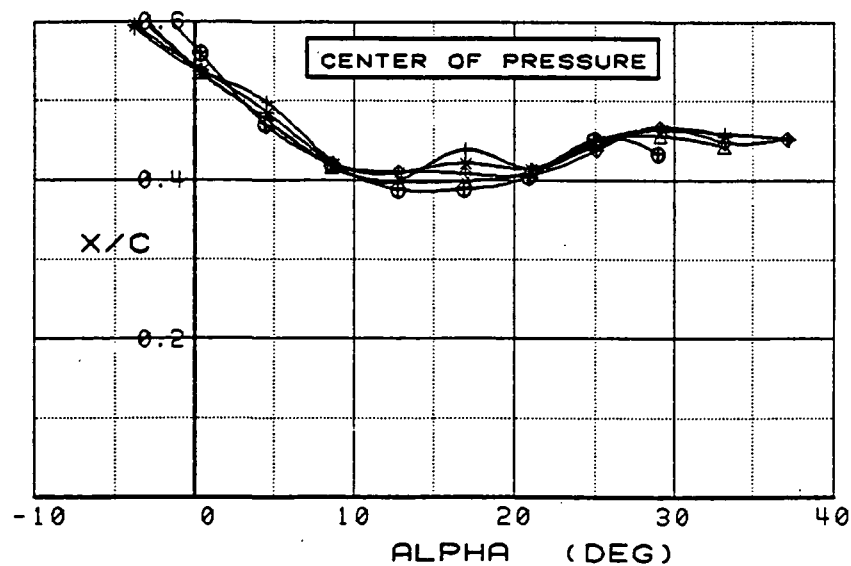
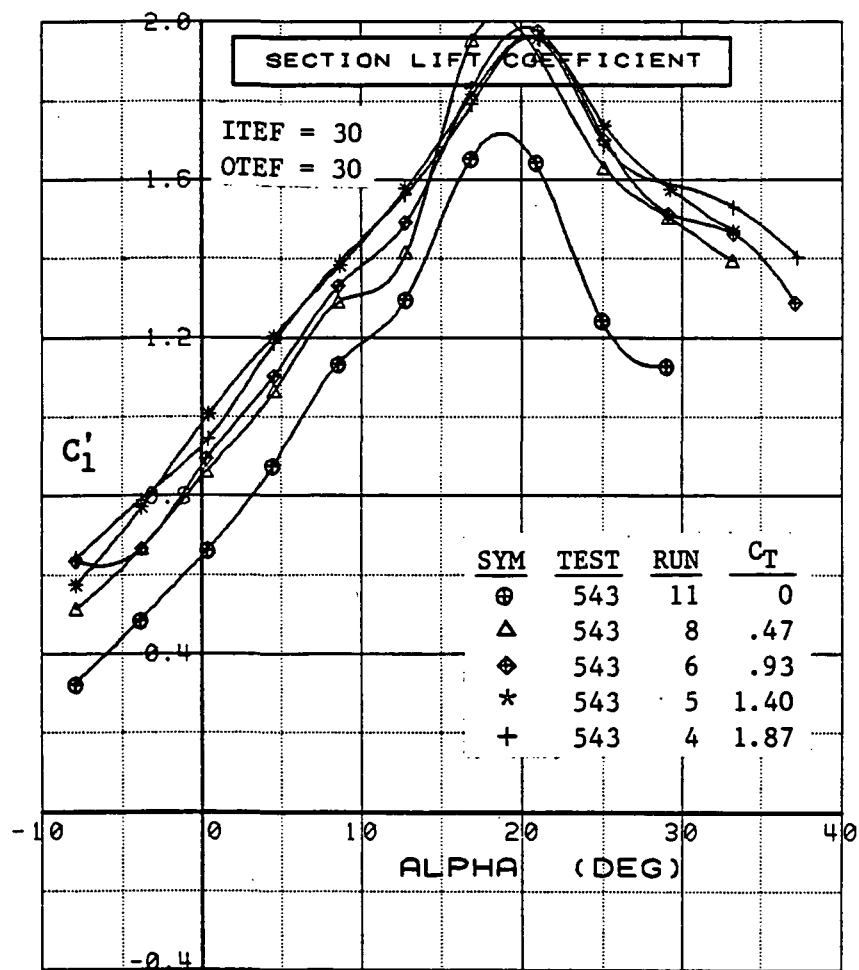


Figure 3.2.4-406 Power Buildup, Inboard, Flaps Deflected, Integrated Section Properties

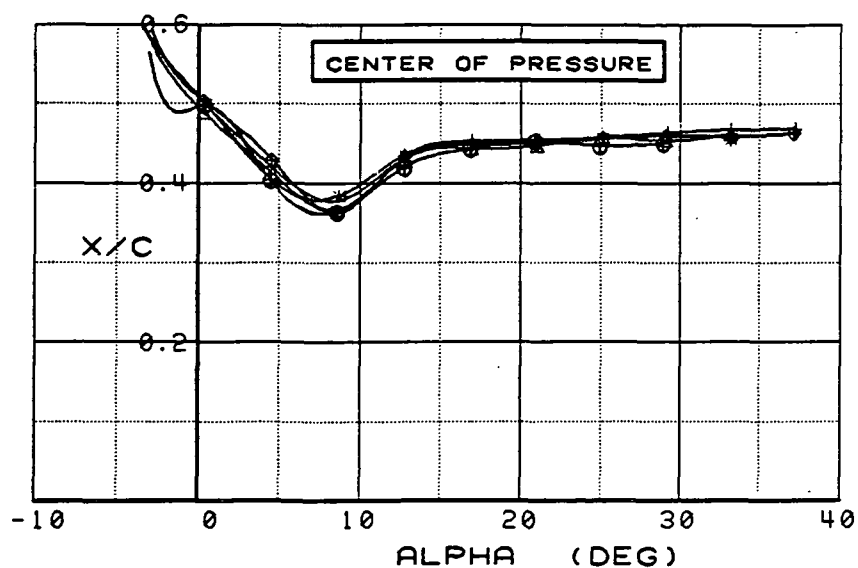
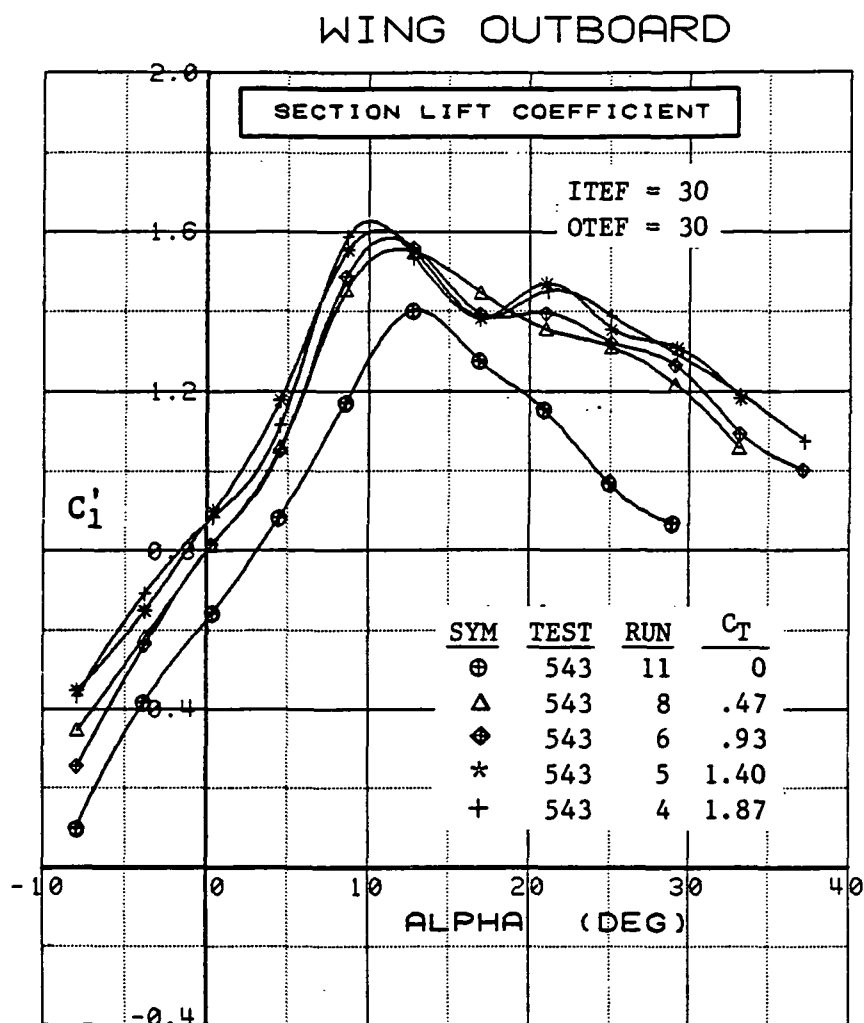


Figure 3.2.4-407 Power Buildup, Outboard, Flaps Deflected, Integrated Section Properties

SYM	TEST	RUN	ALPHA	CT	ITEF	OTEF	CAN	SWB
⊕	537	32	0.3	0.91	30	30	0	OFF
⊞	537	49	0.4	0.90	30	30	0	ON

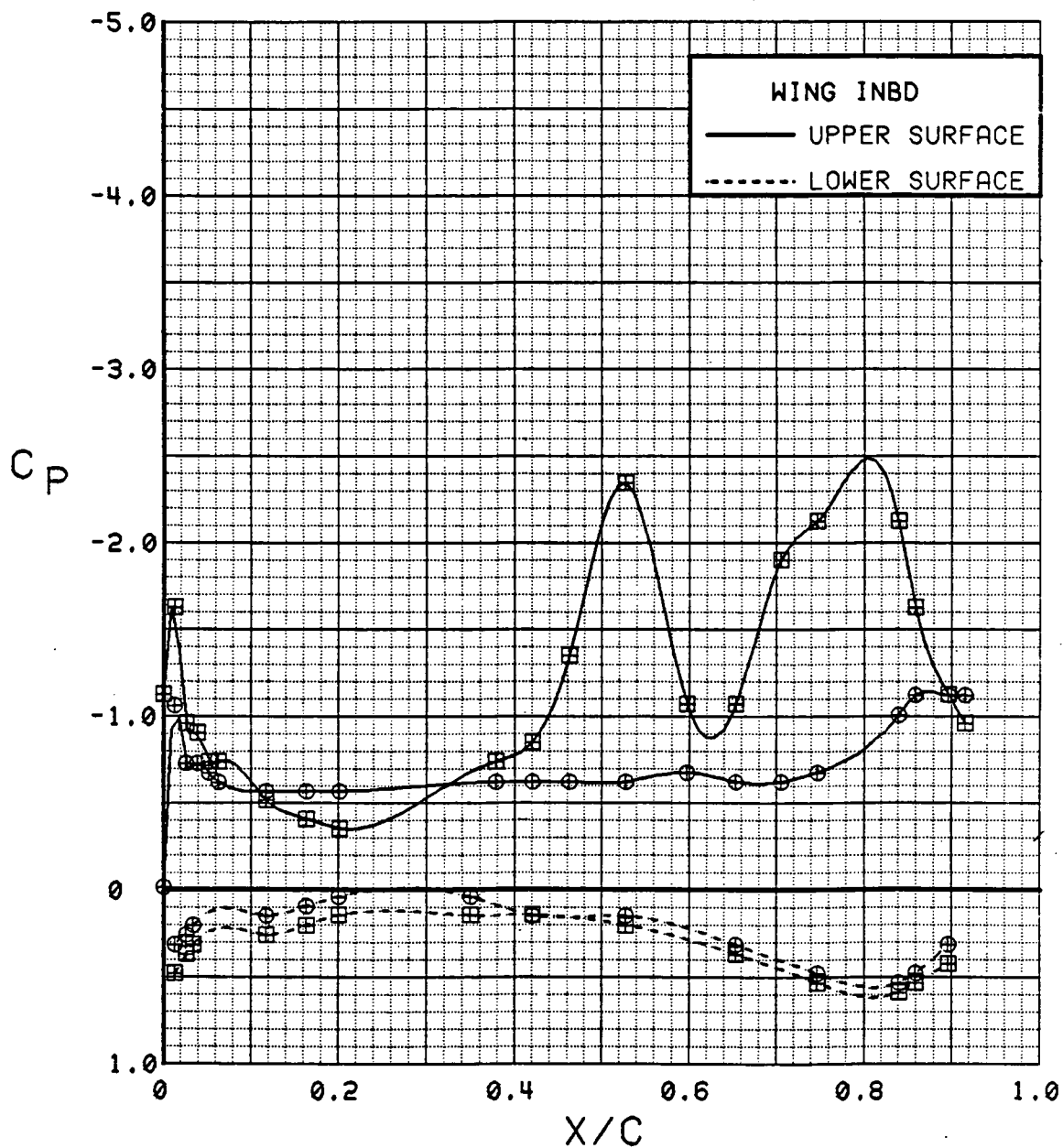


Figure 3.2.4-408 Spanwise Blowing Effects, Inboard,  $C_T = 0.9$ ,  $\alpha = 0$  deg

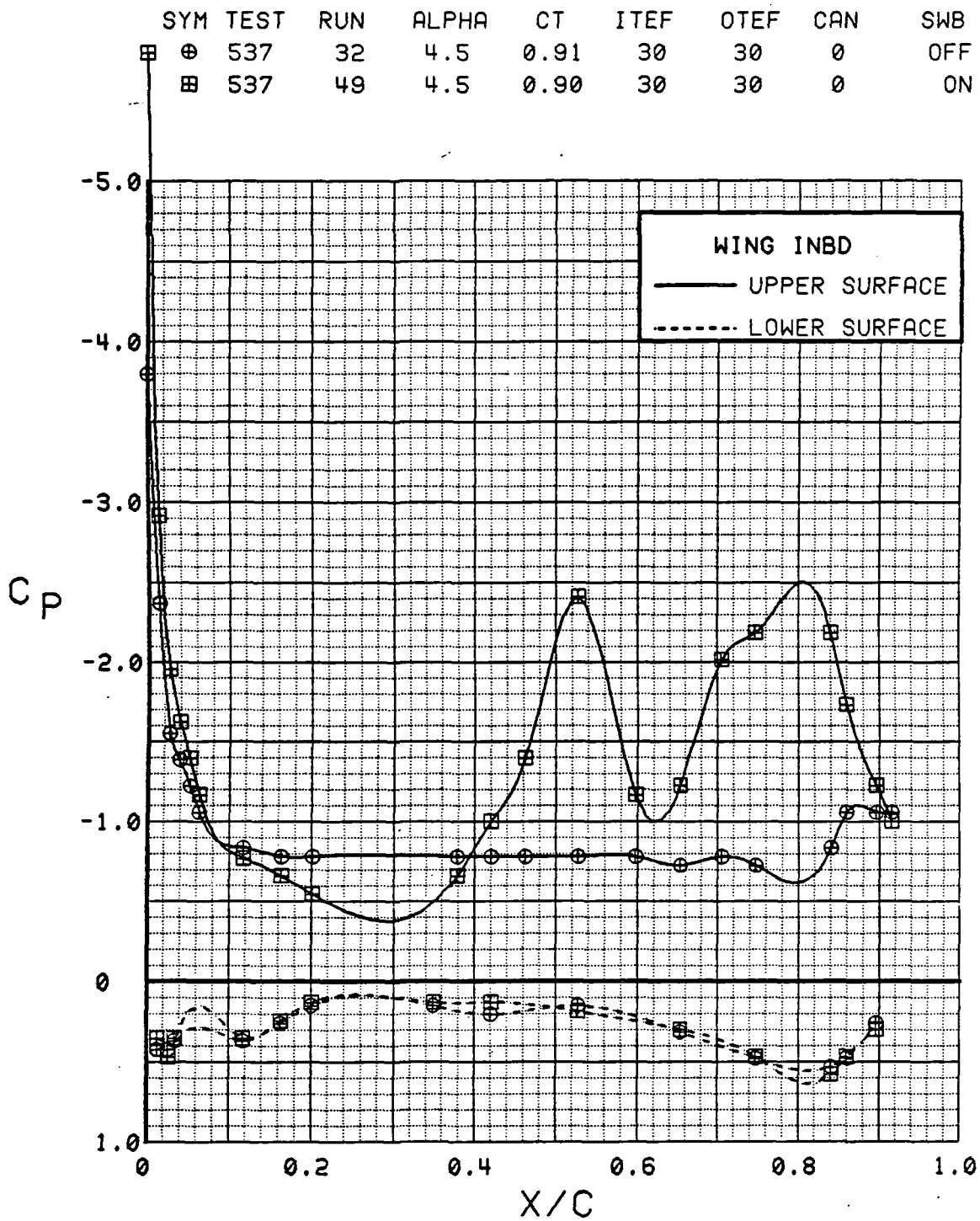


Figure 3.2.4-409 Spanwise Blowing Effects, Inboard,  $C_T = 0.9$ ,  $\alpha = 4$  deg

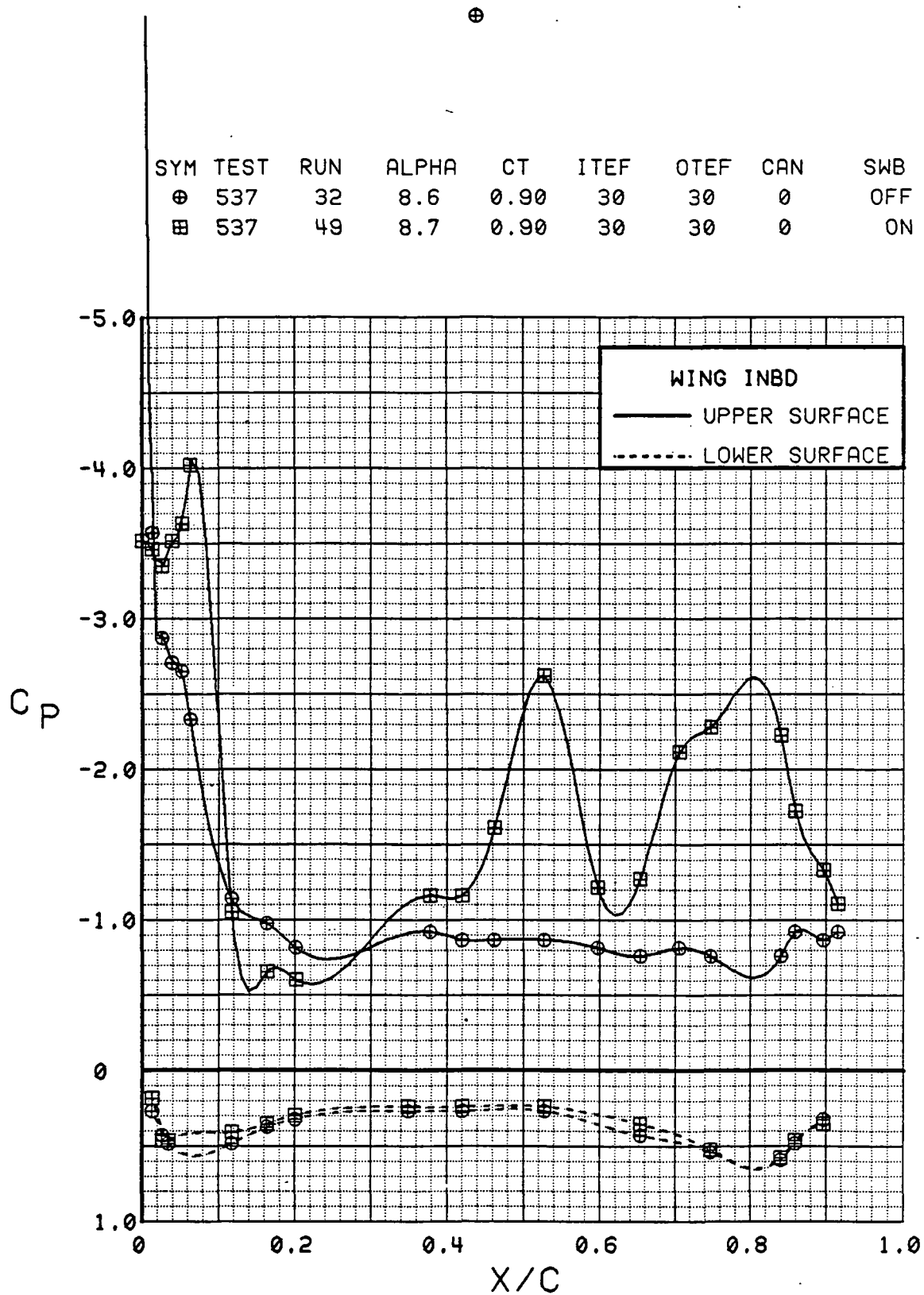


Figure 3.2.4-410 Spanwise Blowing Effects, Inboard,  $C_T = 0.9$ ,  $\alpha = 8$  deg

SYM	TEST	RUN	ALPHA	CT	ITEF	OTEF	CAN	SWB
⊕	537	32	12.8	0.92	30	30	0	OFF
⊞	537	49	12.9	0.90	30	30	0	ON

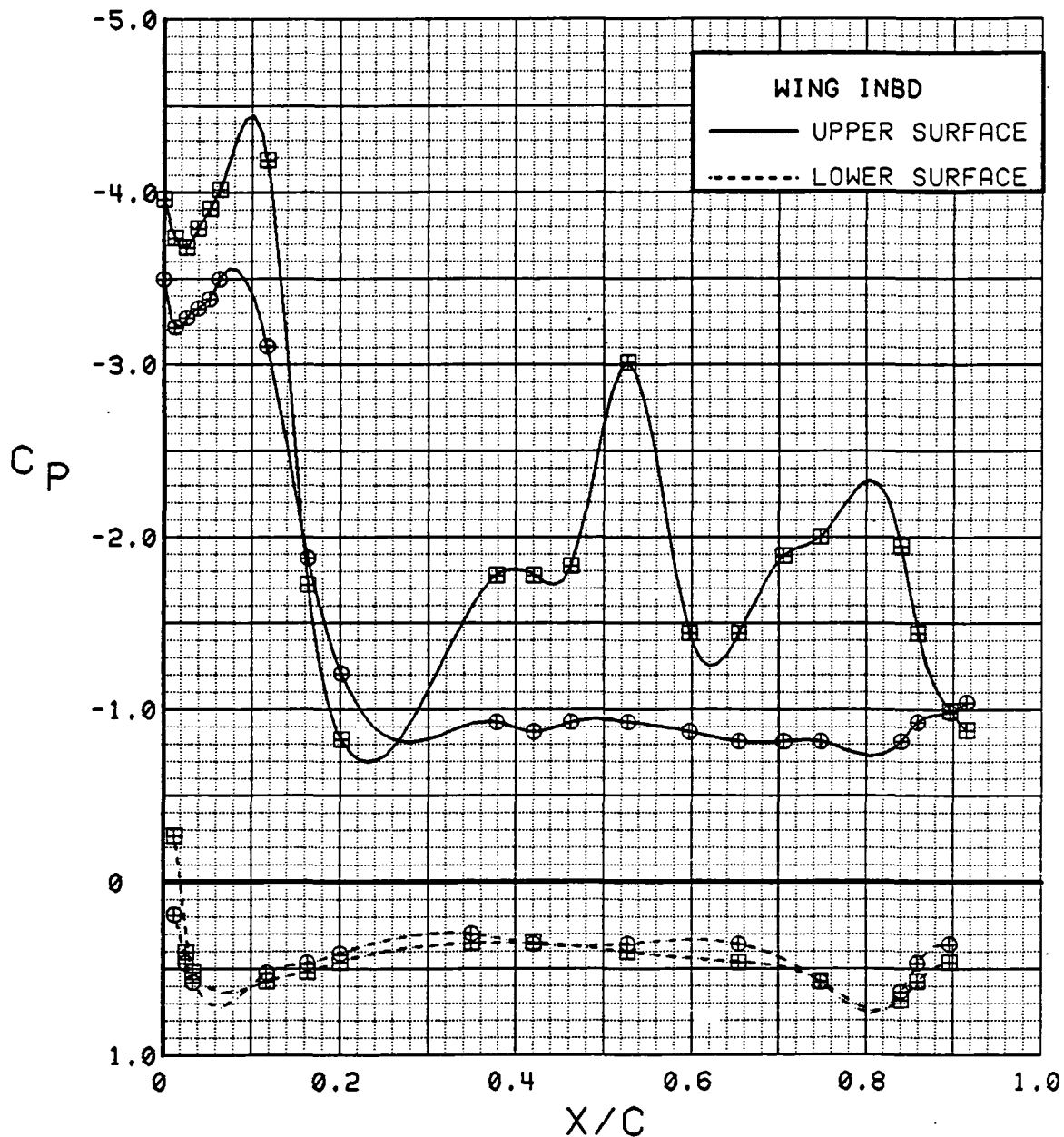


Figure 3.2.4-111 Spanwise Blowing Effects, Inboard,  $C_T = 0.9$ ,  $\alpha = 12$  deg



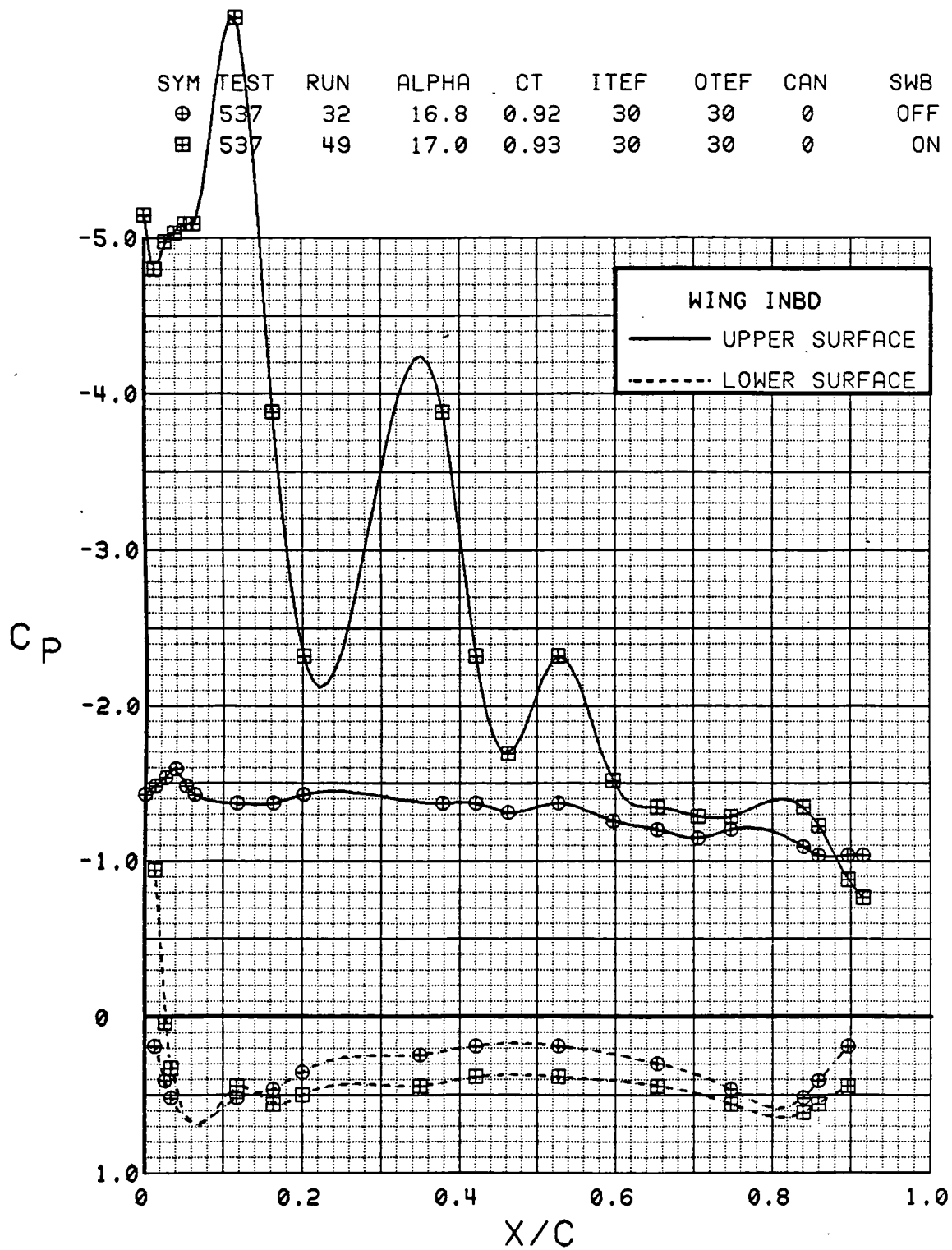


Figure 3.2.4-412 Spanwise Blowing Effects, Inboard,  $C_T = 0.9$ ,  $\alpha = 16^\circ$

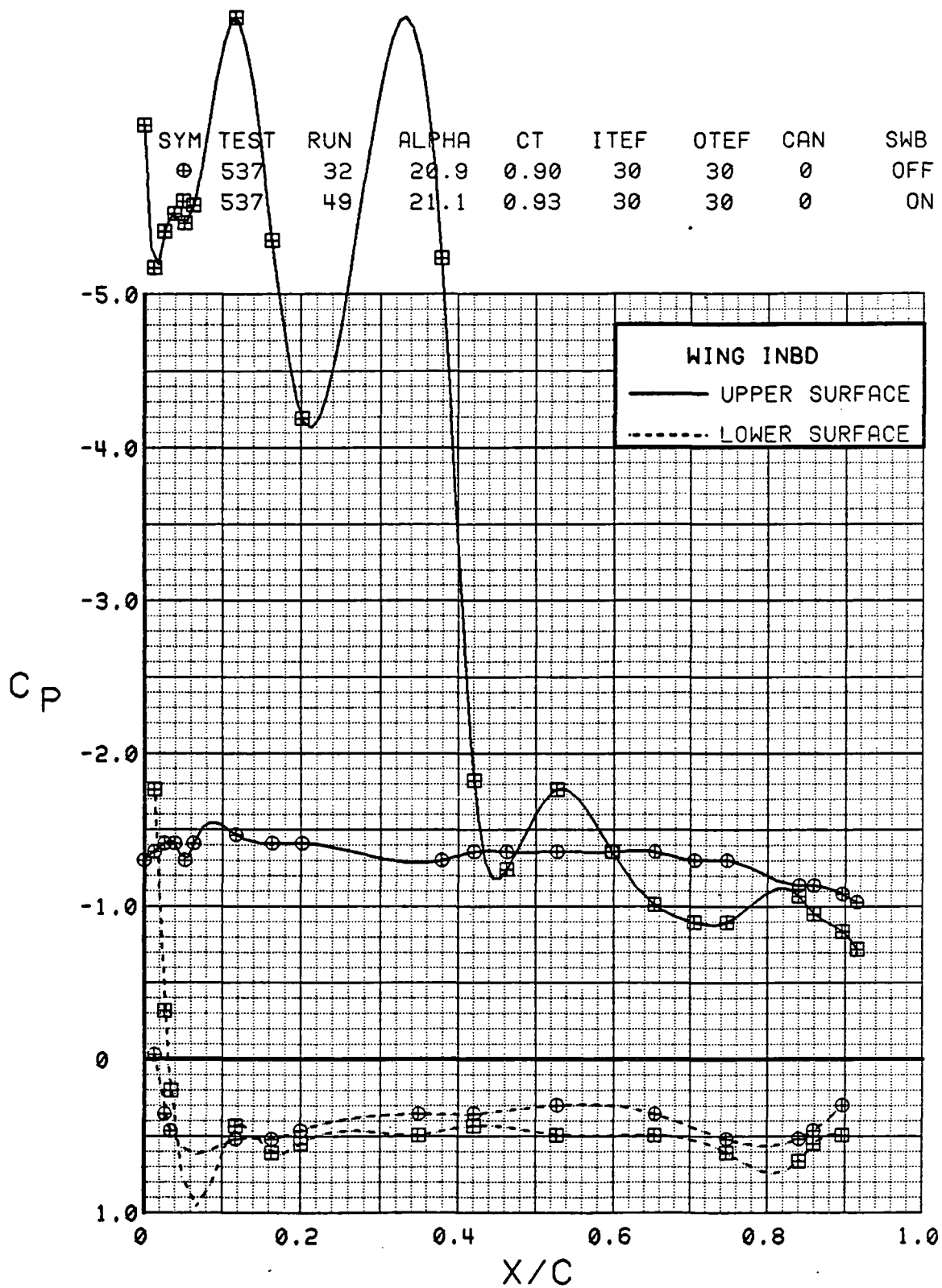


Figure 3.2.4-413 Spanwise Blowing Effects, Inboard,  $C_T = 0.9$ ,  $\alpha = 20^\circ$

SYM	TEST	RUN	ALPHA	CT	ITEF	OTEF	CAN	SWB
⊕	537	32	25.0	0.91	30	30	0	OFF
⊞	537	49	25.1	0.93	30	30	0	ON

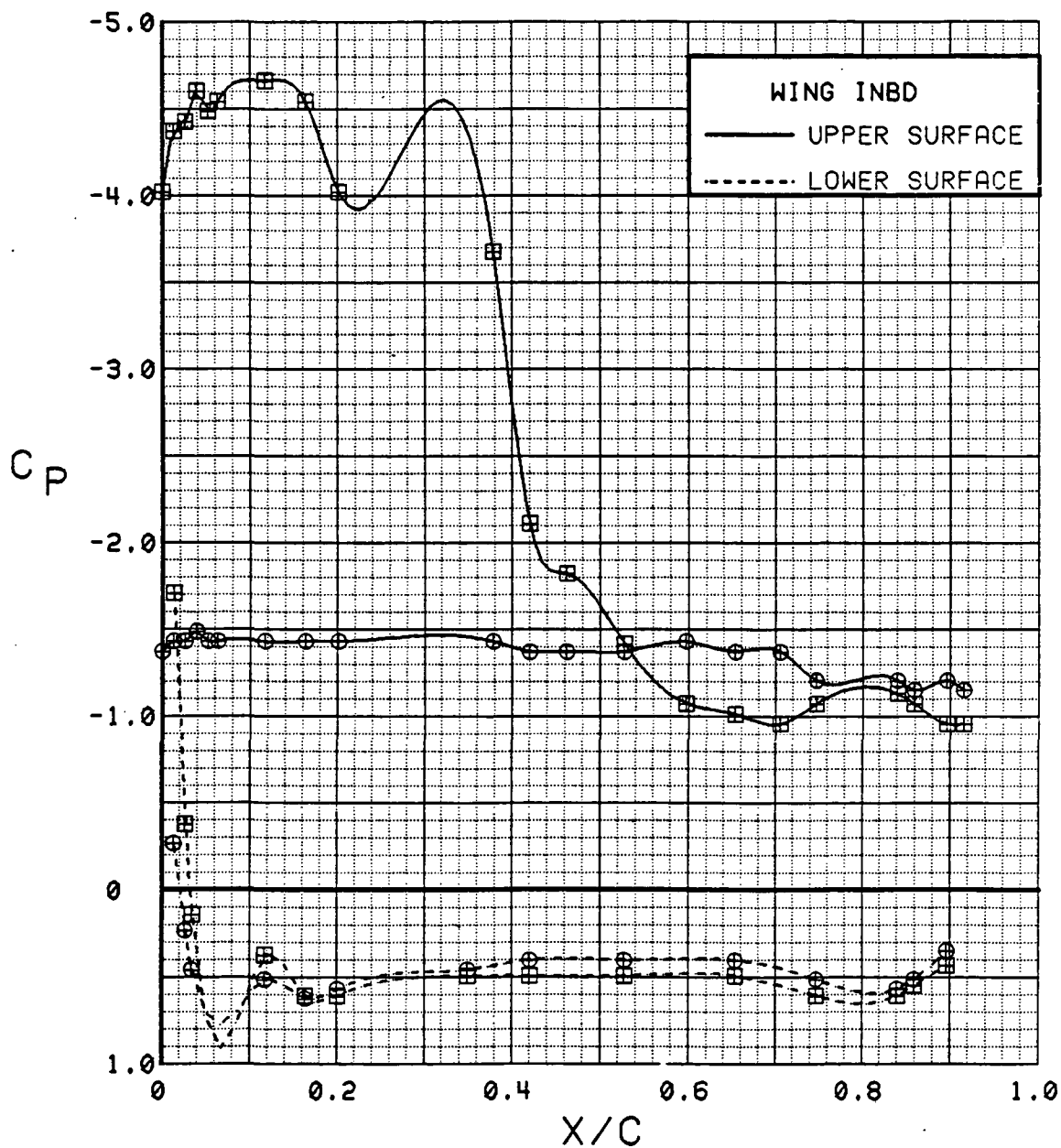


Figure 3.2.4-414 Spanwise Blowing Effects, Inboard,  $C_T = 0.9$ ,  $\alpha = 24^\circ$

C-9

SYM	TEST	RUN	ALPHA	CT	ITEF	OTEF	CAN	SWB
⊕	537	32	29.1	0.93	30	30	0	OFF
⊞	537	49	29.2	0.94	30	30	0	ON

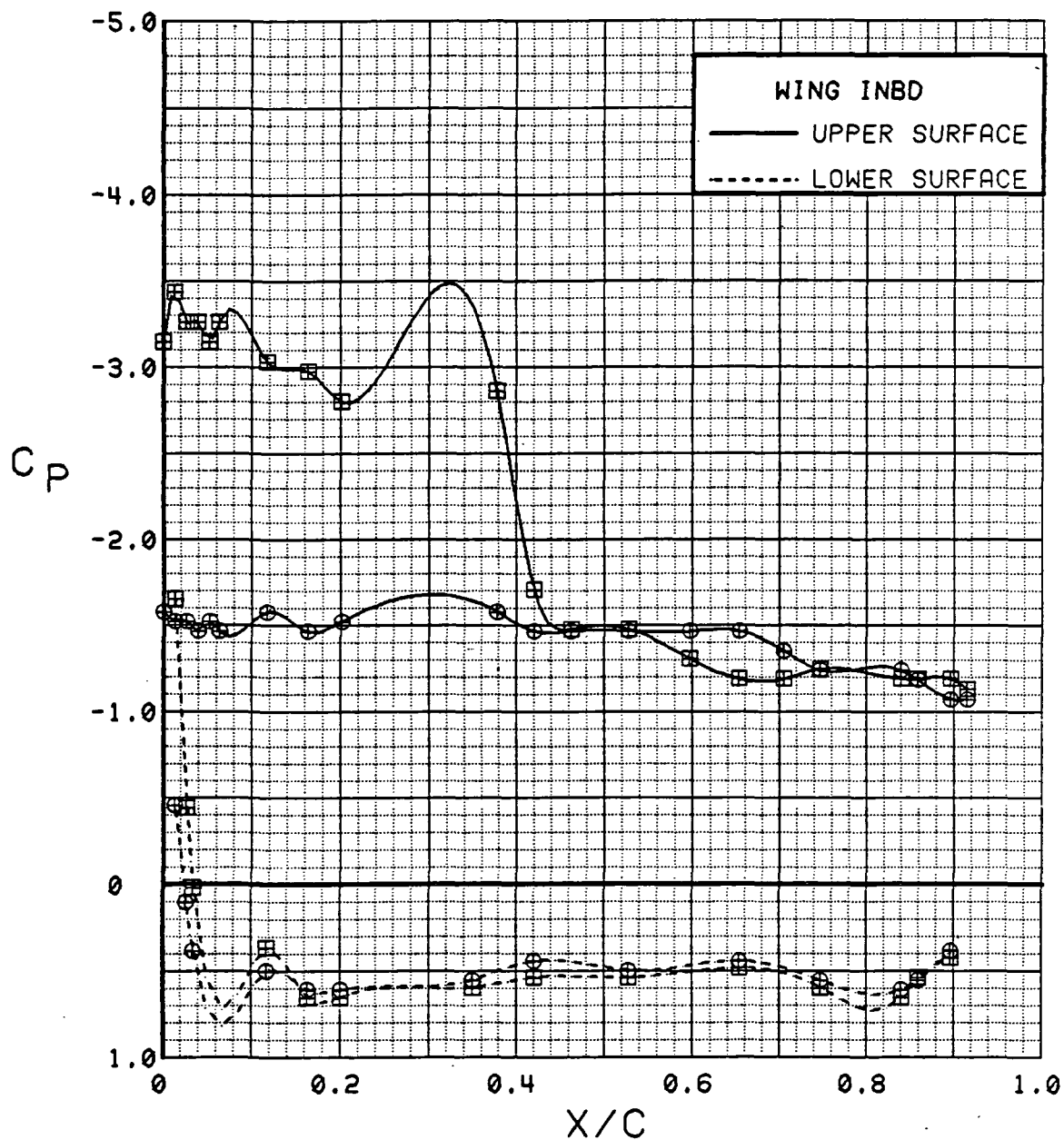


Figure 3.2.4-415 Spanwise Blowing Effects, Inboard,  $C_T = 0.9$ ,  $\alpha = 28$  deg

SYM	TEST	RUN	ALPHA	CT	ITEF	OTEF	CAN	SWB
⊕	537	32	33.1	0.91	30	30	0	OFF
⊞	537	49	33.2	0.91	30	30	0	ON

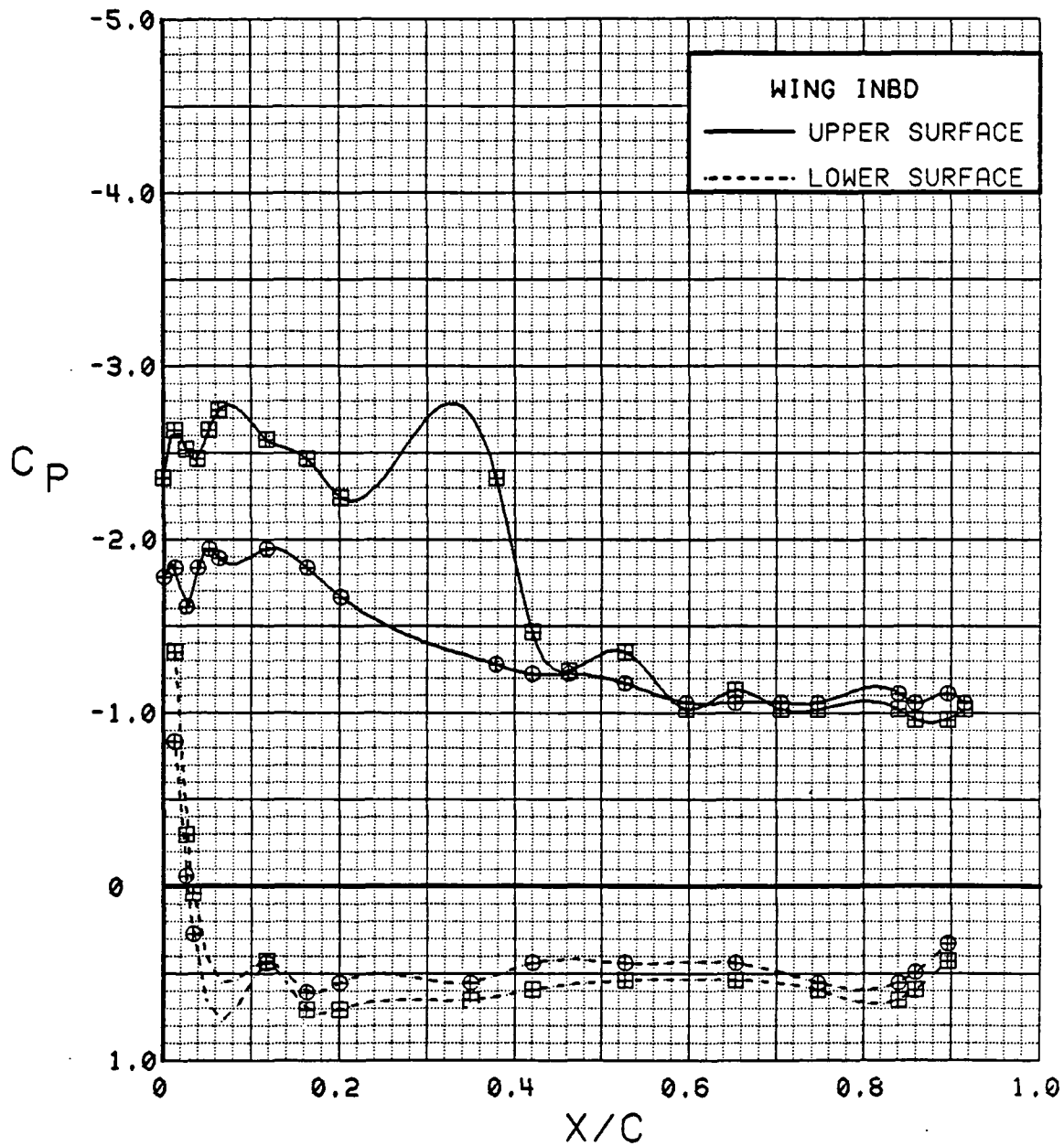


Figure 3.2.4-416 Spanwise Blowing Effects, Inboard,  $C_T = 0.9$ ,  $\alpha = 32$  deg

SYM	TEST	RUN	ALPHA	CT	ITEF	OTEF	CAN	SWB
⊕	537	32	0.3	0.91	30	30	0	OFF
⊞	537	49	0.4	0.90	30	30	0	ON

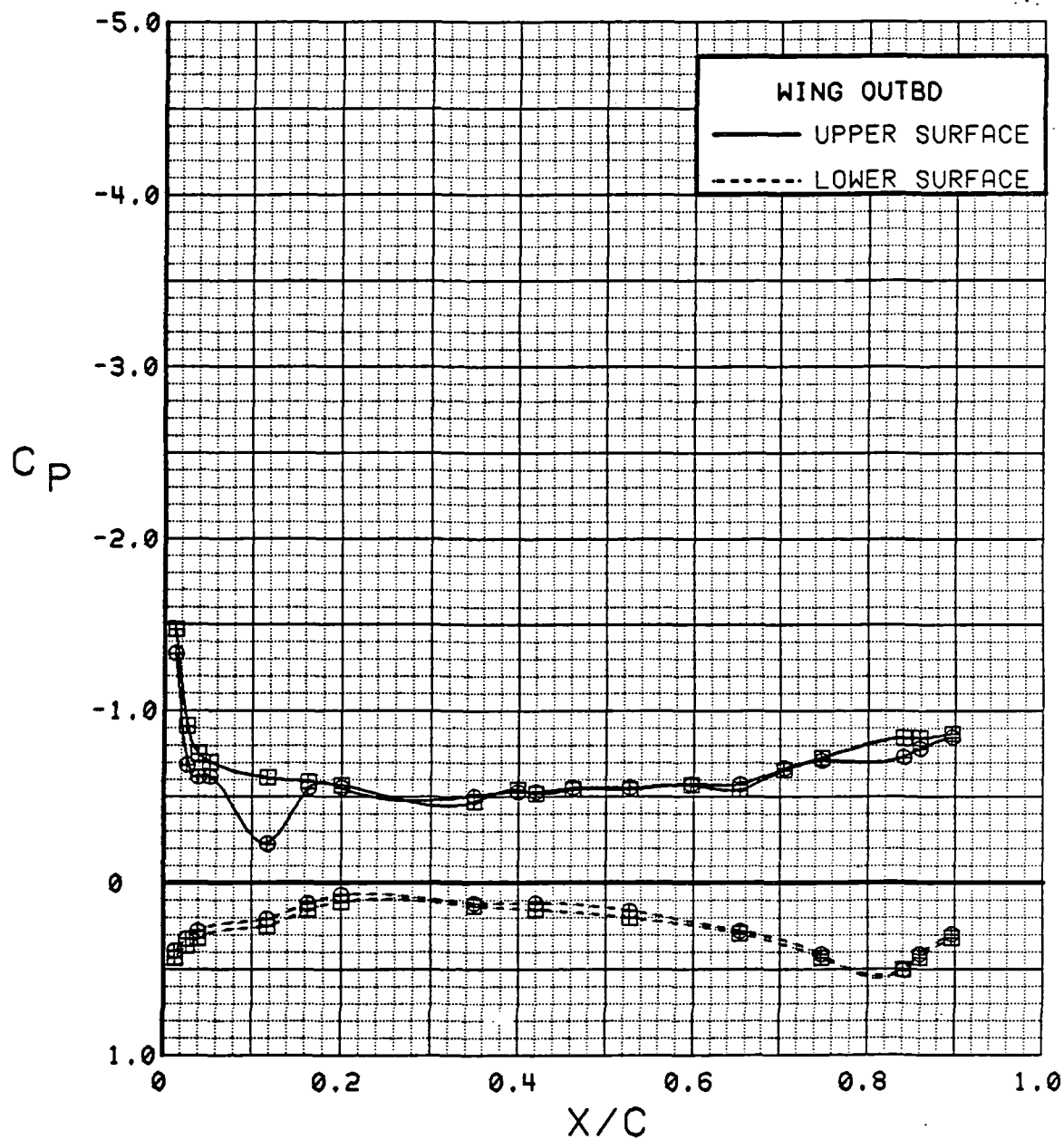


Figure 3.2.4-417 Spanwise Blowing Effects, Outboard,  $C_T = 0.9$ ,  $\alpha = 0$  deg

SYM	TEST	RUN	ALPHA	CT	ITEF	OTEF	CAN	SWB
⊕	537	32	4.5	0.91	30	30	0	OFF
⊞	537	49	4.5	0.90	30	30	0	ON

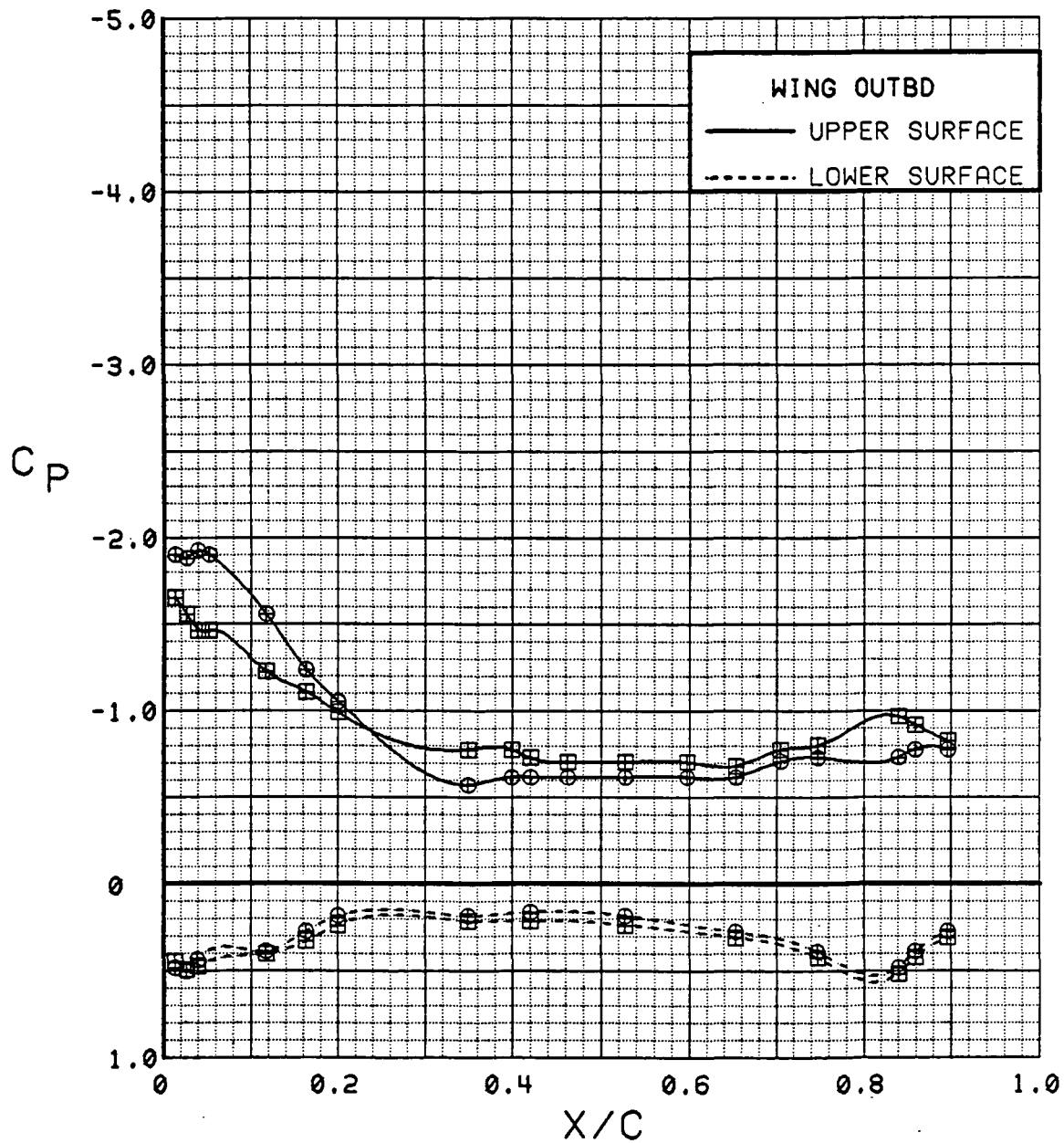


Figure 3.2.4-418 Spanwise Blowing Effects, Outboard,  $C_T = 0.9$ ,  $\alpha = 4$  deg

SYM	TEST	RUN	ALPHA	CT	ITEF	OTEF	CAN	SWB
⊕	537	32	8.6	0.90	30	30	0	OFF
⊞	537	49	8.7	0.90	30	30	0	ON

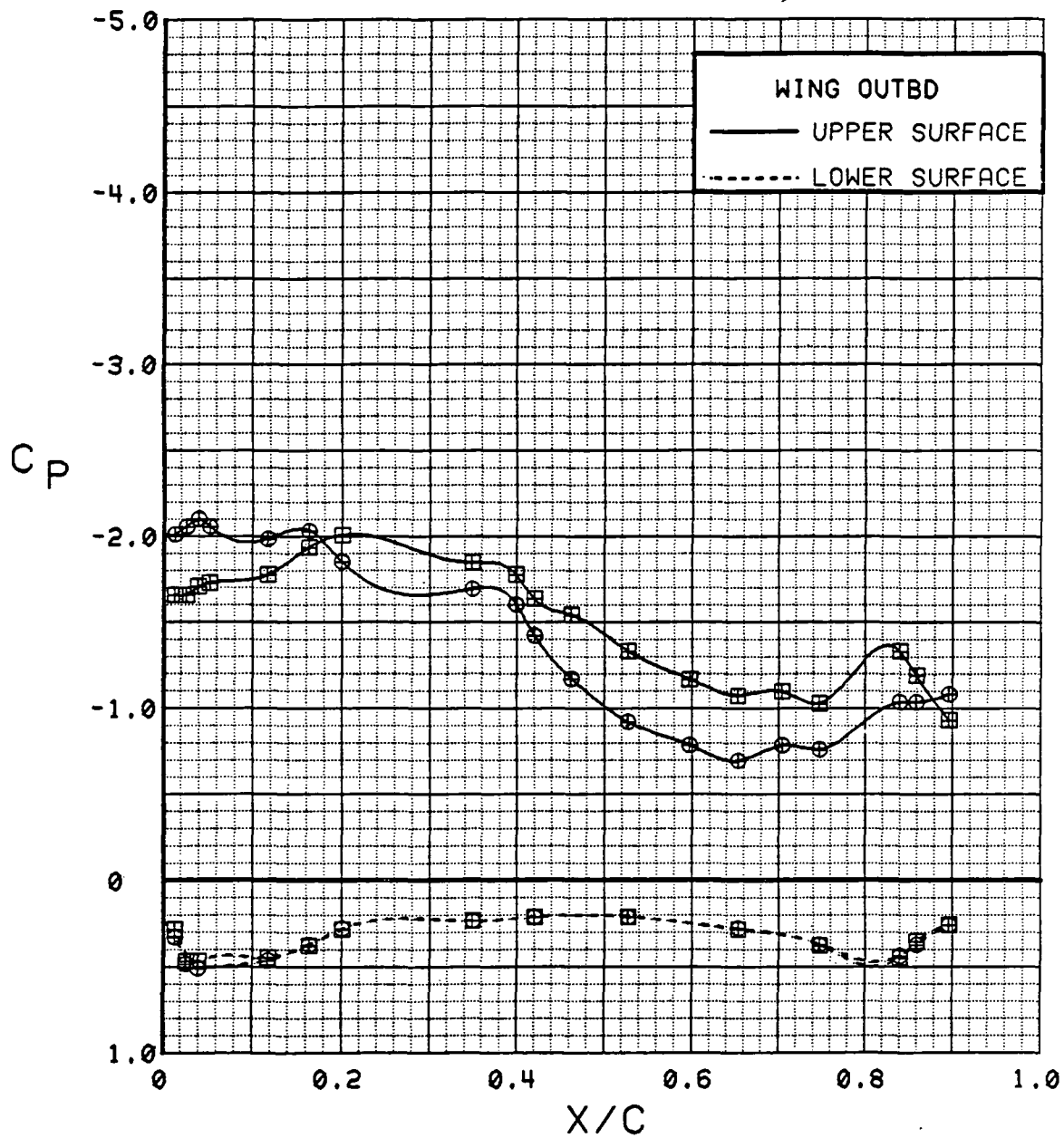


Figure 3.2.4-419 Spanwise Blowing Effects, Outboard,  $C_T = 0.9$ ,  $\alpha = 8$  deg



SYM	TEST	RUN	ALPHA	CT	ITEF	OTEF	CAN	SWB
⊕	537	32	12.8	0.92	30	30	0	OFF
⊞	537	49	12.9	0.90	30	30	0	ON

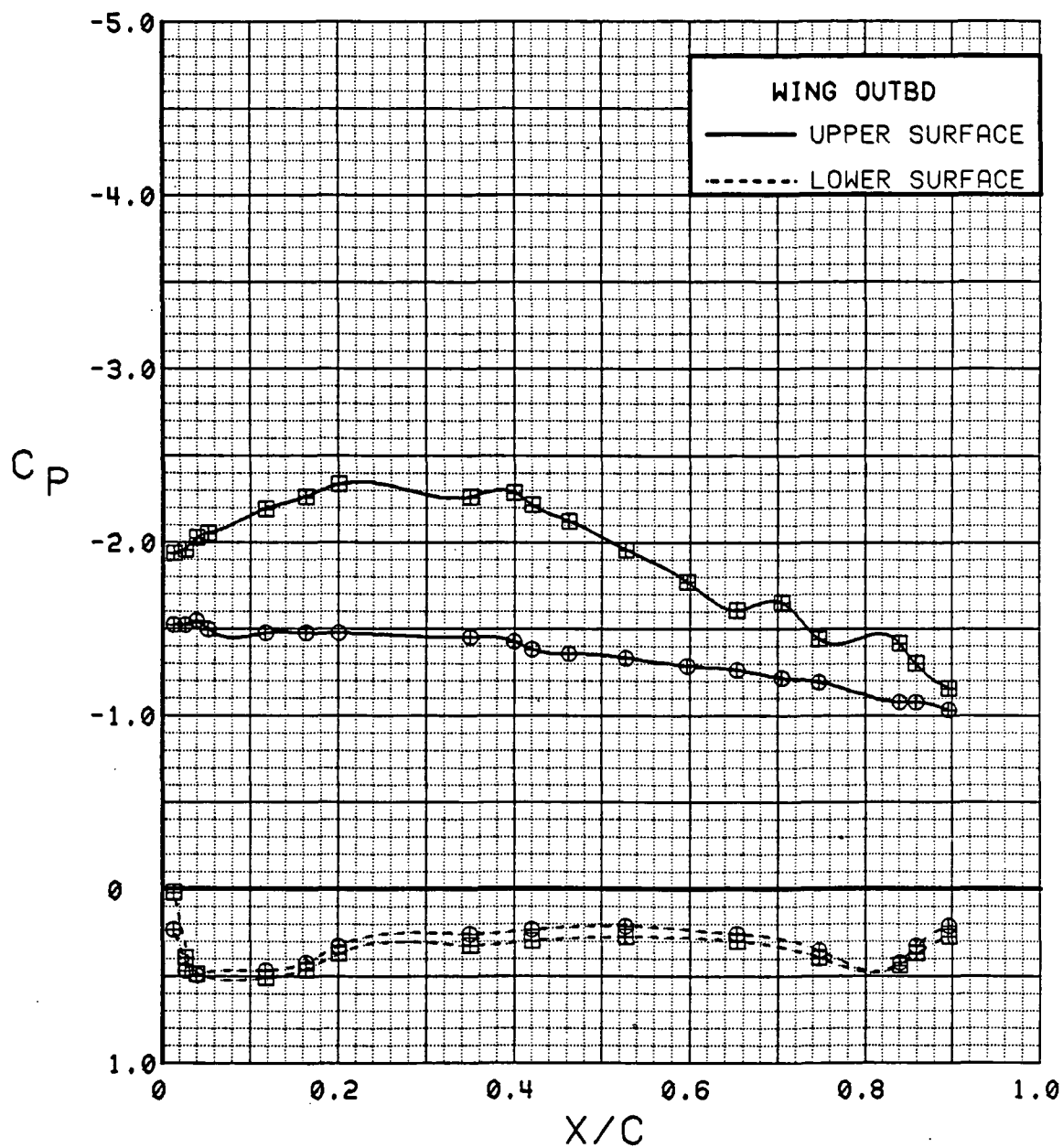


Figure 3.2.4-420 Spanwise Blowing Effects, Outboard,  $C_T = 0.9$ ,  $\alpha = 12$  deg

SYM	TEST	RUN	ALPHA	CT	ITEF	OTEF	CAN	SWB
⊕	537	32	16.8	0.92	30	30	0	OFF
⊞	537	49	17.0	0.93	30	30	0	ON

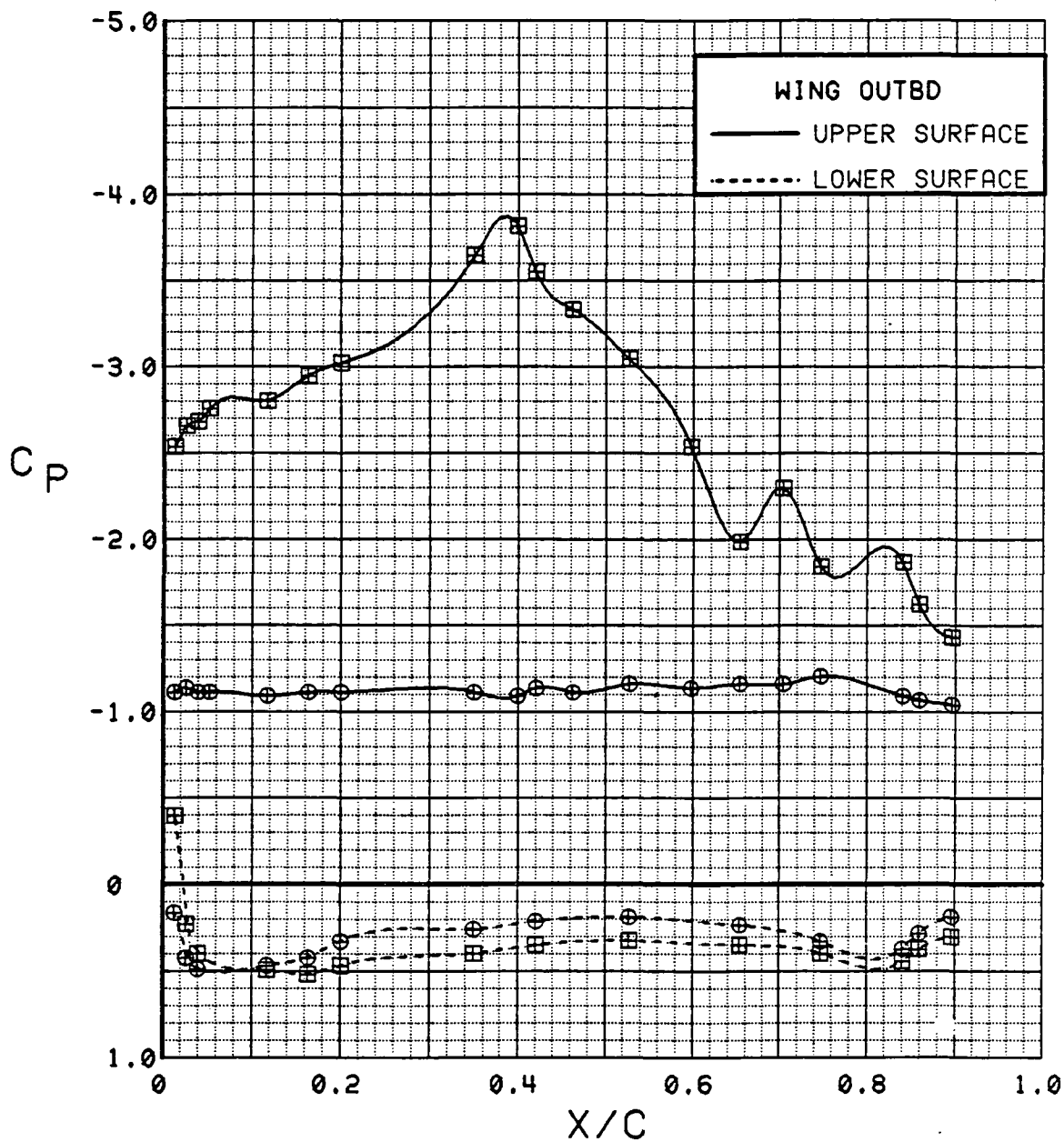


Figure 3.2.4-21 Spanwise Blowing Effects, Outboard,  $C_T = 0.9$ ,  $\alpha = 16$  deg

SYM	TEST	RUN	ALPHA	CT	ITEF	OTEF	CAN	SWB
⊕	537	32	20.9	0.90	30	30	0	OFF
⊞	537	49	21.1	0.93	30	30	0	ON

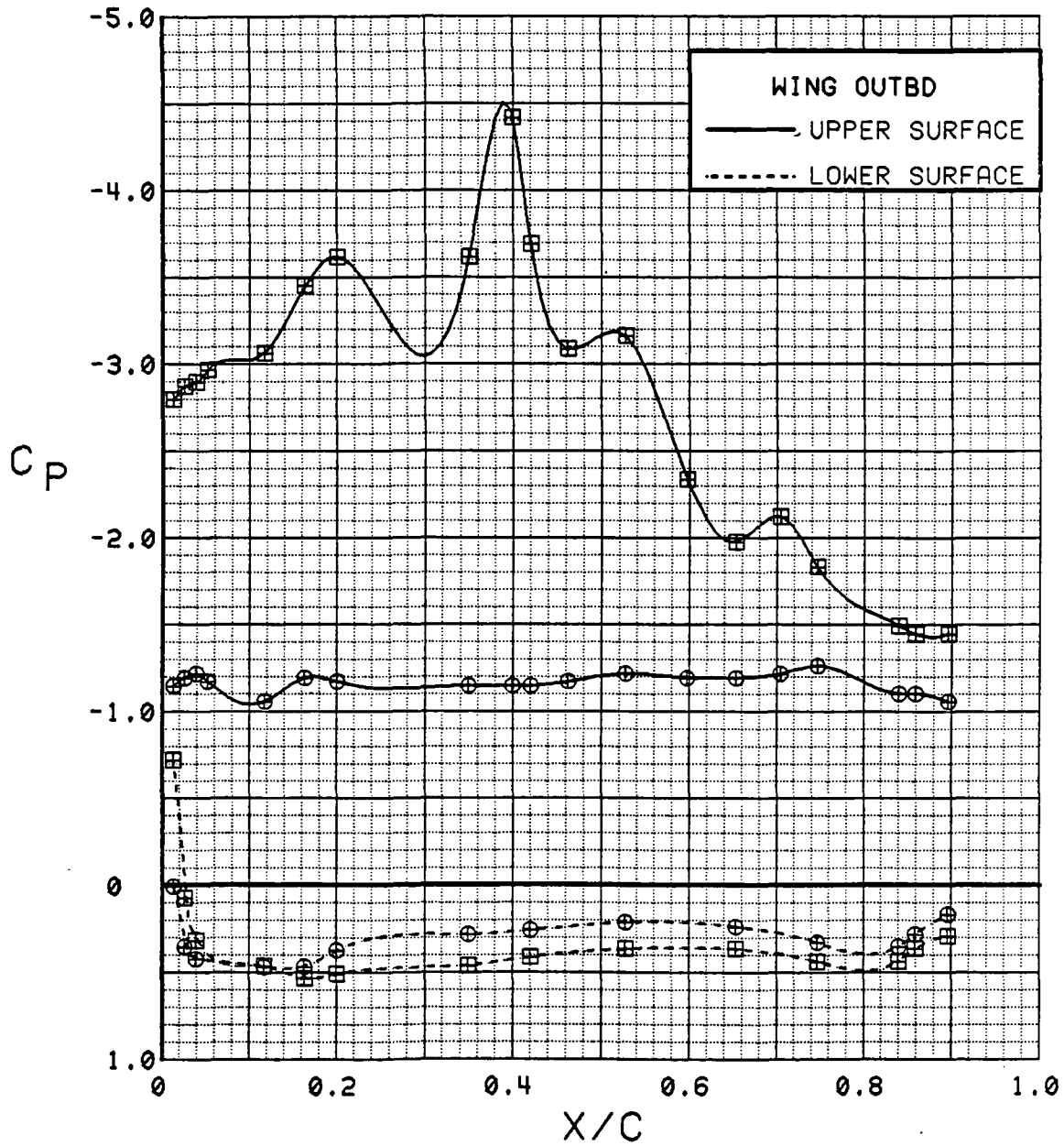


Figure 3.2.4-422 Spanwise Blowing Effects, Outboard,  $C_T = 0.9$ ,  $\alpha = 20$  deg

SYM	TEST	RUN	ALPHA	CT	ITEF	OTEF	CAN	SWB
⊕	537	32	25.0	0.91	30	30	0	OFF
⊞	537	49	25.1	0.93	30	30	0	ON

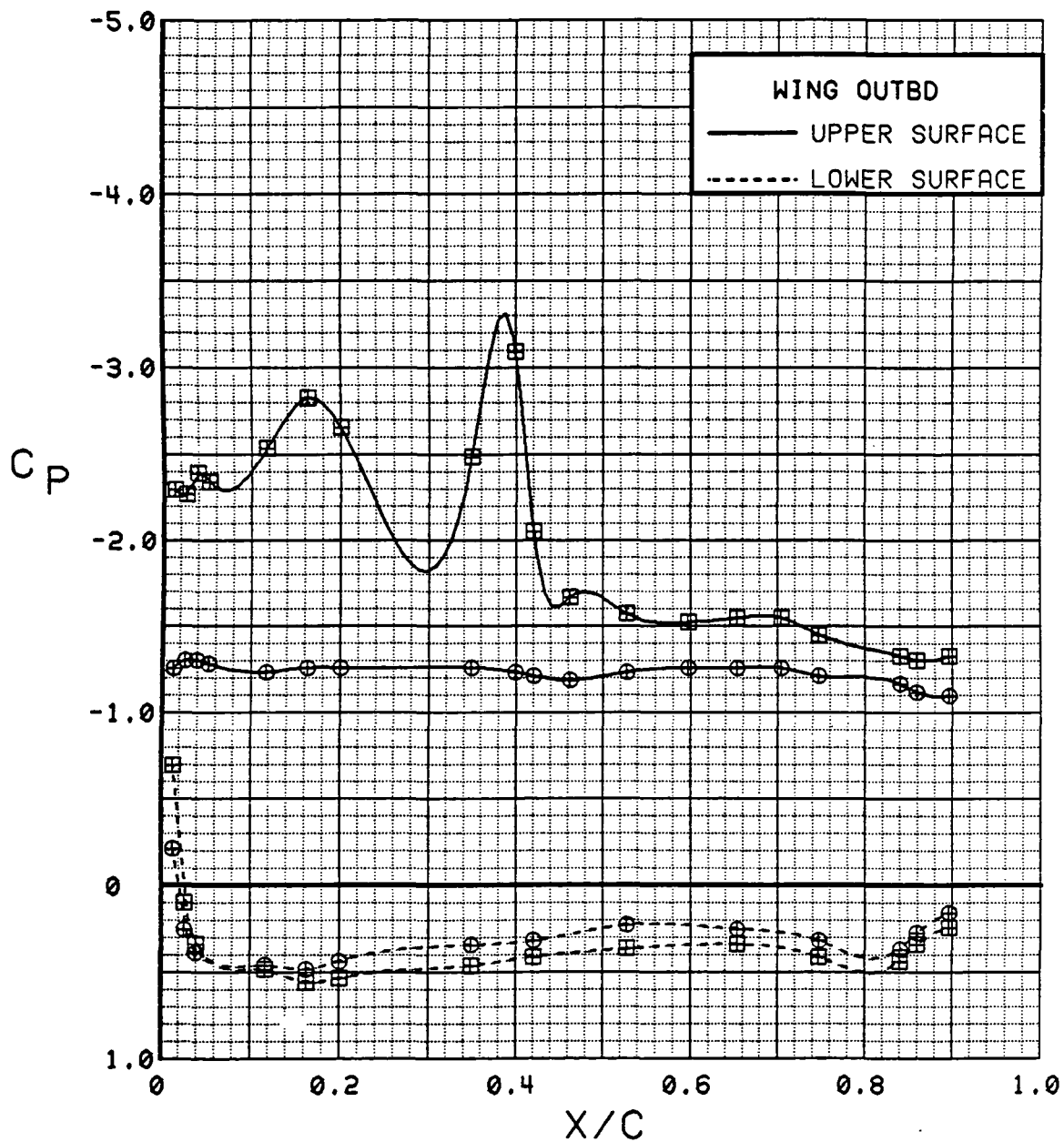


Figure 3.2.4-23 Spanwise Blowing Effects, Outboard,  $C_T = 0.9$ ,  $\alpha = 24$  deg

SYM	TEST	RUN	ALPHA	CT	ITEF	OTEF	CAN	SWB
⊕	537	32	29.1	0.93	30	30	0	OFF
⊞	537	49	29.2	0.94	30	30	0	ON

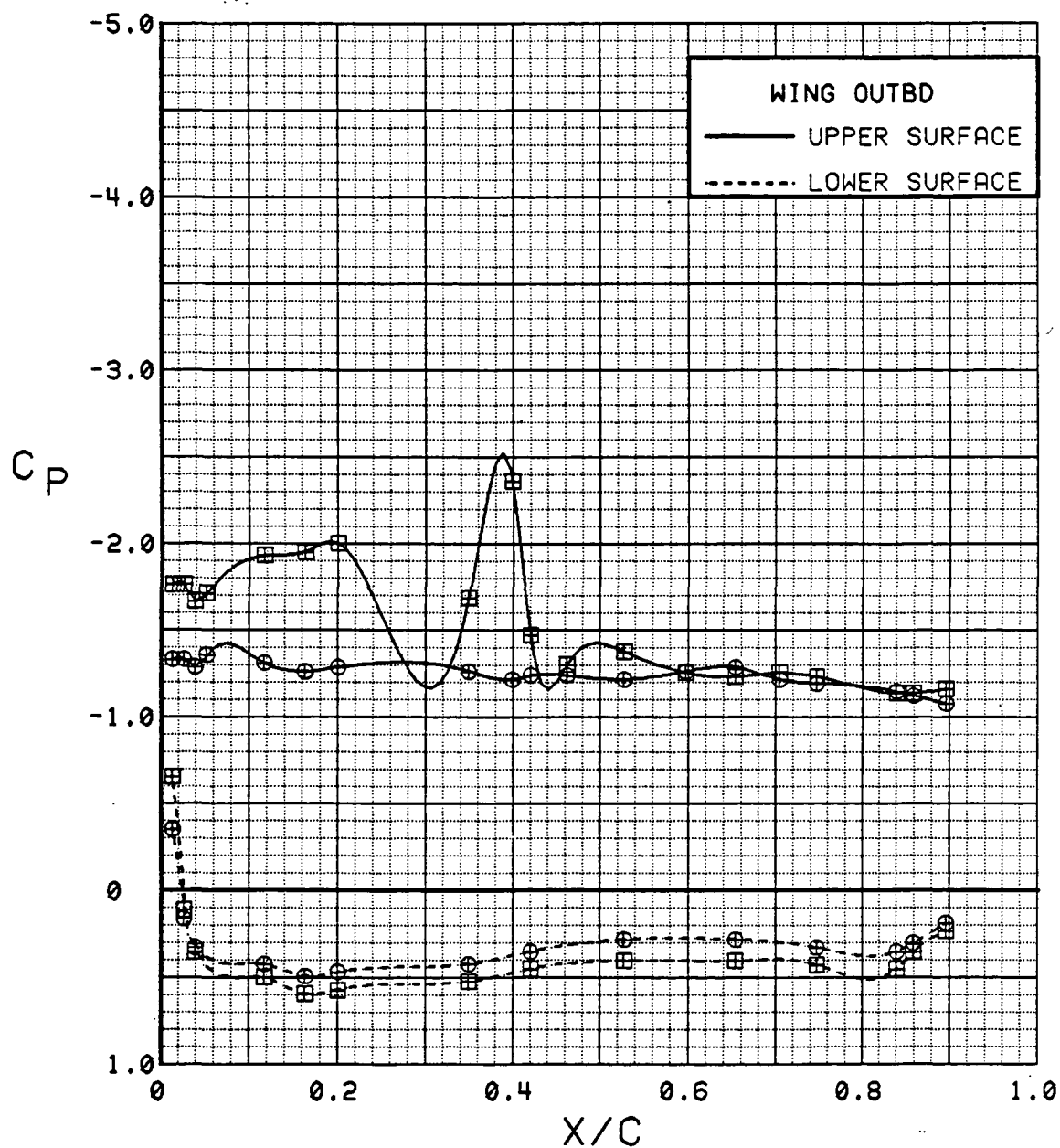


Figure 3.2.4-424 Spanwise Blowing Effects, Outboard,  $C_T = 0.9$ ,  $\alpha = 28^\circ$

SYM	TEST	RUN	ALPHA	CT	ITEF	OTEF	CAN	SWB
⊕	537	32	33.1	0.91	30	30	0	OFF
⊞	537	49	33.2	0.91	30	30	0	ON

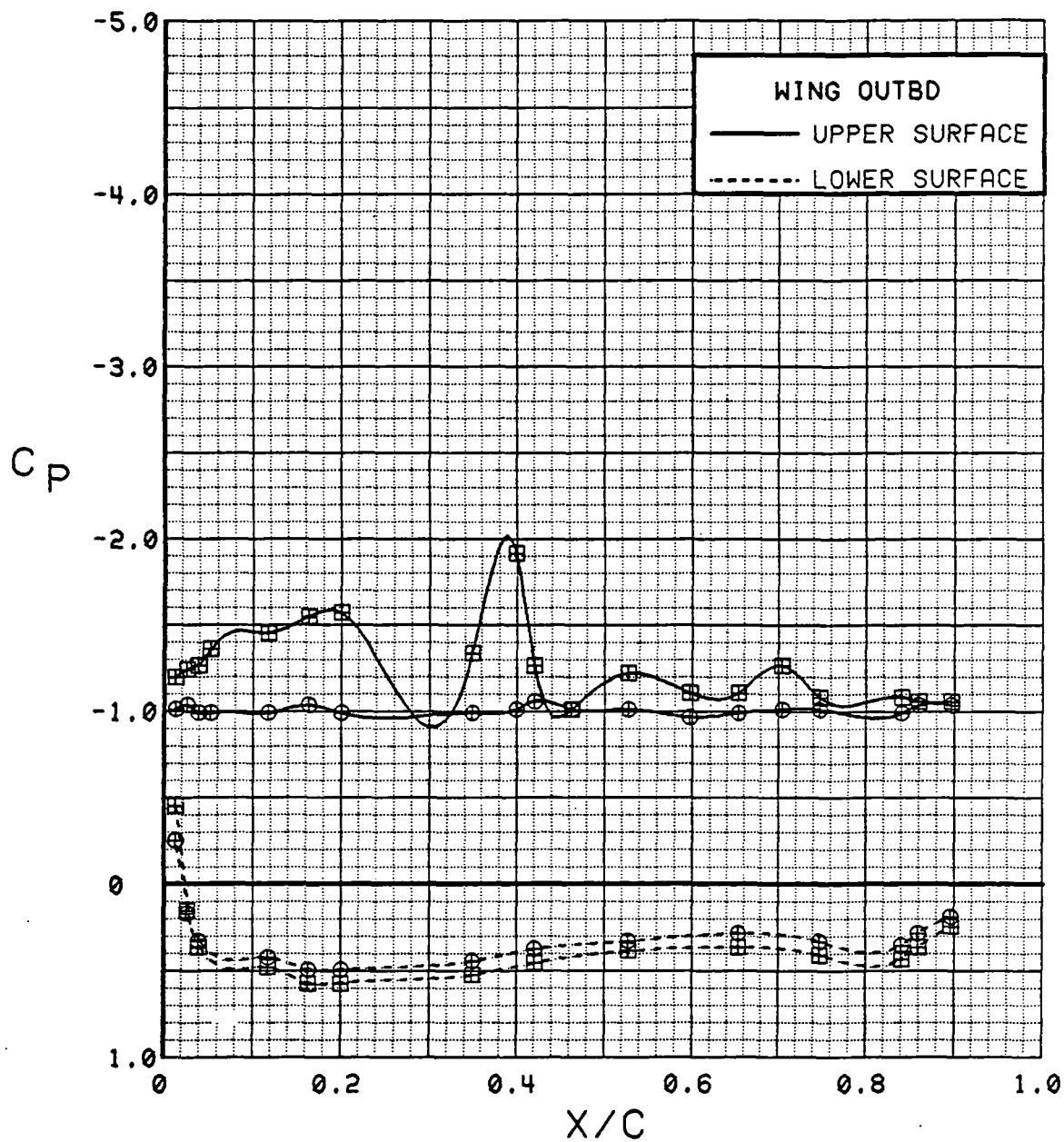


Figure 3.2.4-425 Spanwise Blowing Effects, Outboard,  $C_T = 0.9$ ,  $\alpha = 32$  deg

SYM	TEST	RUN	ALPHA	CT	ITEF	OTEF	CAN	SWB
⊕	537	32	0.3	0.91	30	30	0	OFF
⊞	537	49	0.4	0.90	30	30	0	ON

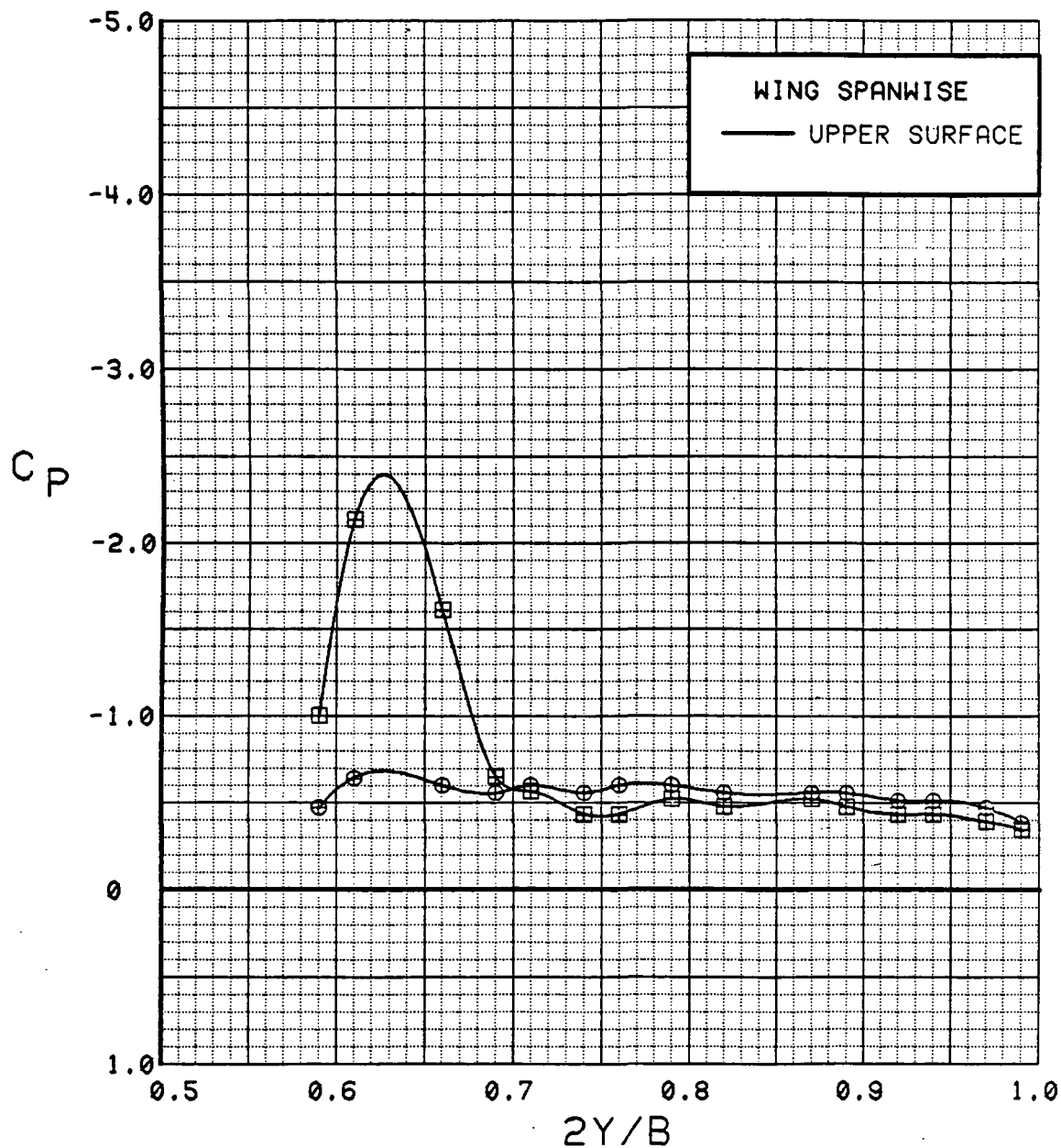


Figure 3.2.4-426 Spanwise Blowing Effects, Spanwise,  $C_T = 0.9$ ,  $\alpha = 0$  deg

SYM	TEST	RUN	ALPHA	CT	ITEF	OTEF	CAN	SWB
⊕	537	32	4.5	0.91	30	30	0	OFF
⊞	537	49	4.5	0.90	30	30	0	ON

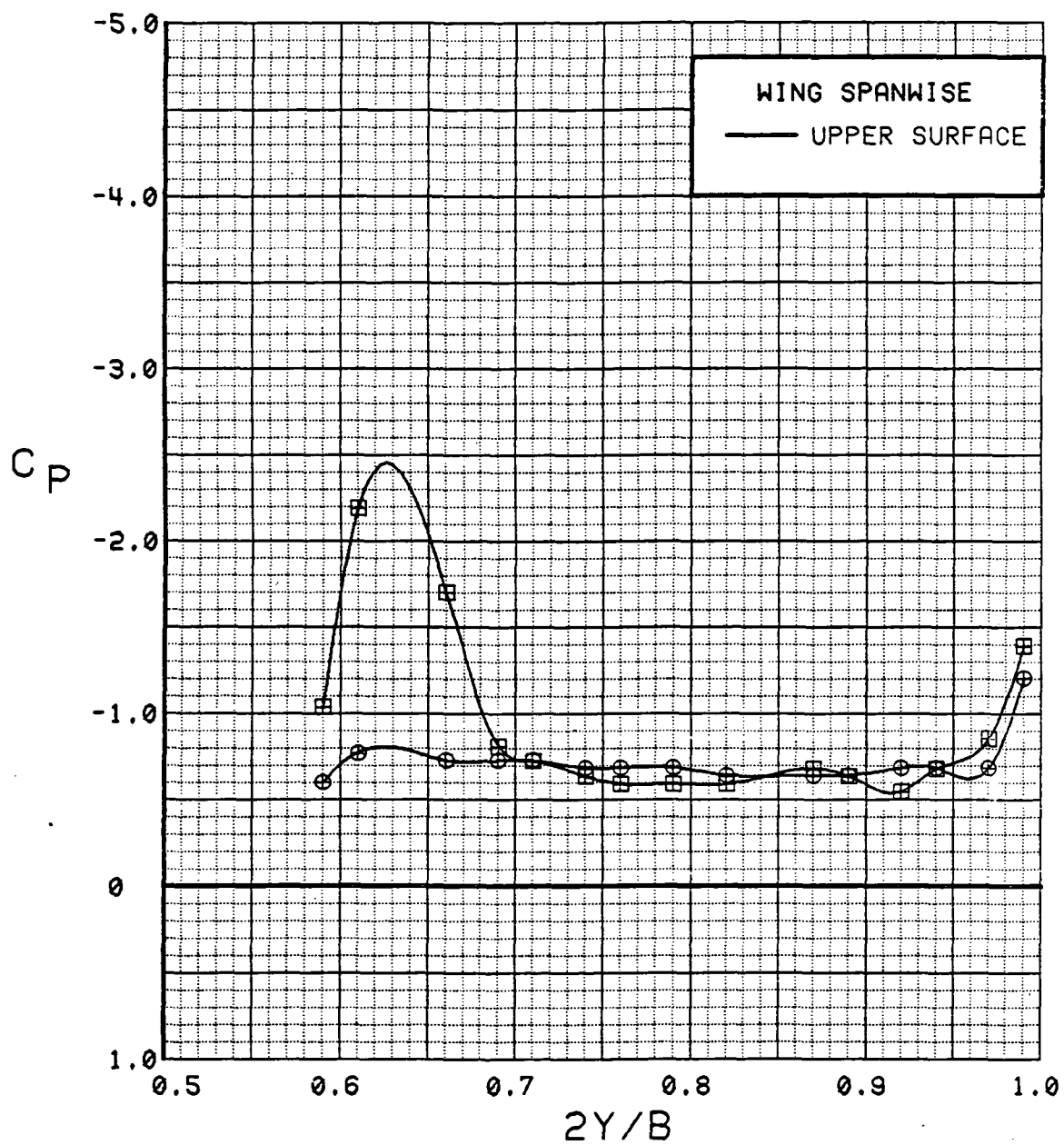


Figure 3.2.4-27 Spanwise Blowing Effects, Spanwise,  $C_T = 0.9$ ,  $\alpha = 4$  deg



SYM	TEST	RUN	ALPHA	CT	ITEF	OTEF	CAN	SWB
⊙	537	32	8.6	0.90	30	30	0	OFF
⊠	537	49	8.7	0.90	30	30	0	ON

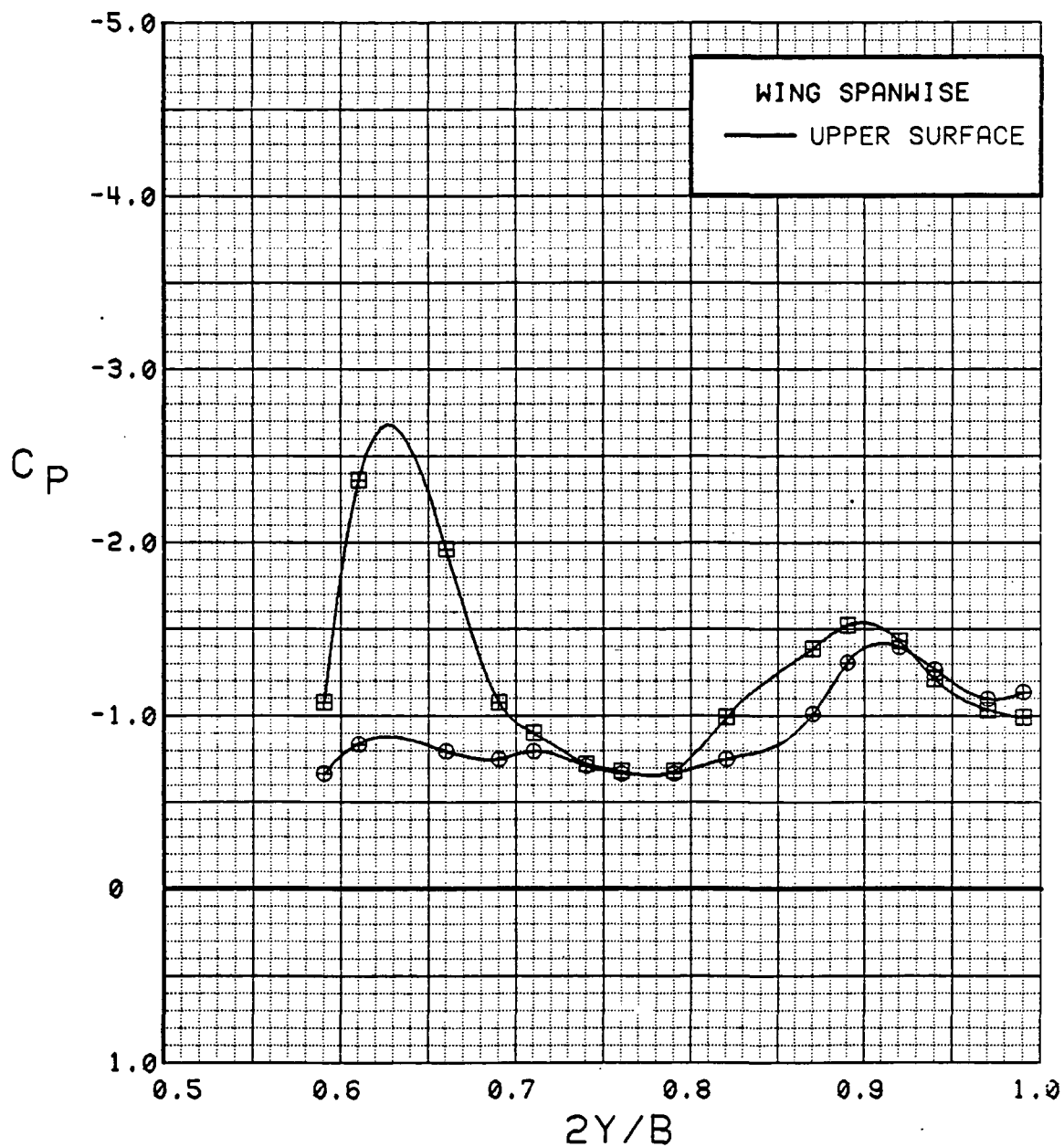


Figure 3.2.4-428 Spanwise Blowing Effects, Spanwise,  $C_T = 0.9$ ,  $\alpha = 8$  deg

SYM	TEST	RUN	ALPHA	CT	ITEF	OTEF	CAN	SWB
●	537	32	12.8	0.92	30	30	0	OFF
■	537	49	12.9	0.90	30	30	0	ON

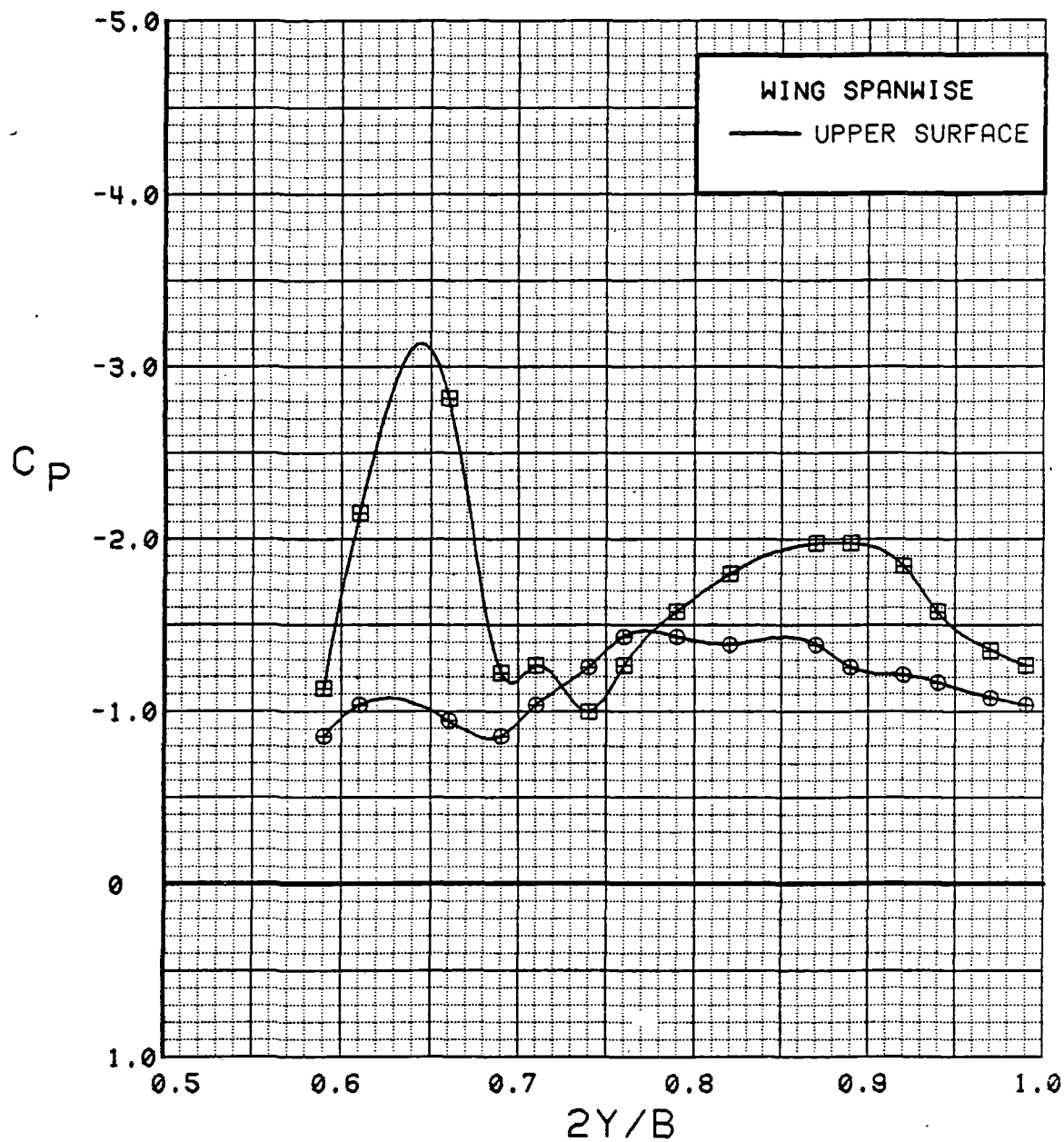


Figure 3.2.4-429 Spanwise Blowing Effects, Spanwise,  $C_T = 0.9$ ,  $\alpha = 12$  deg

SYM	TEST	RUN	ALPHA	CT	ITEF	OTEF	CAN	SWB
●	537	32	16.8	0.92	30	30	0	OFF
■	537	49	17.0	0.93	30	30	0	ON

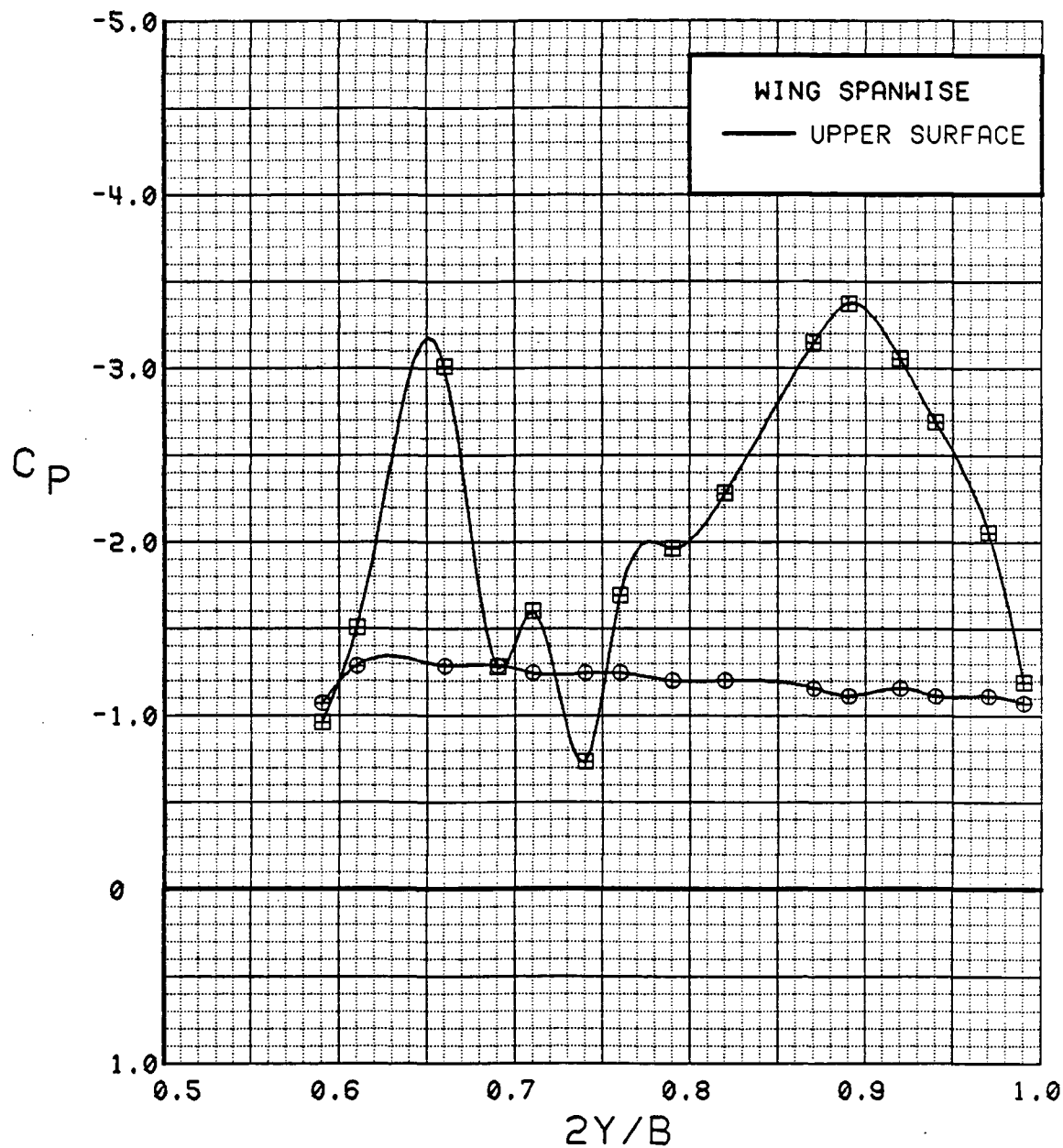


Figure 3.2.4-430 Spanwise Blowing Effects, Spanwise,  $C_T = 0.9$ ,  $\alpha = 16$  deg

SYM	TEST	RUN	ALPHA	CT	ITEF	OTEF	CAN	SWB
⊕	537	32	20.9	0.90	30	30	0	OFF
⊞	537	49	21.1	0.93	30	30	0	ON

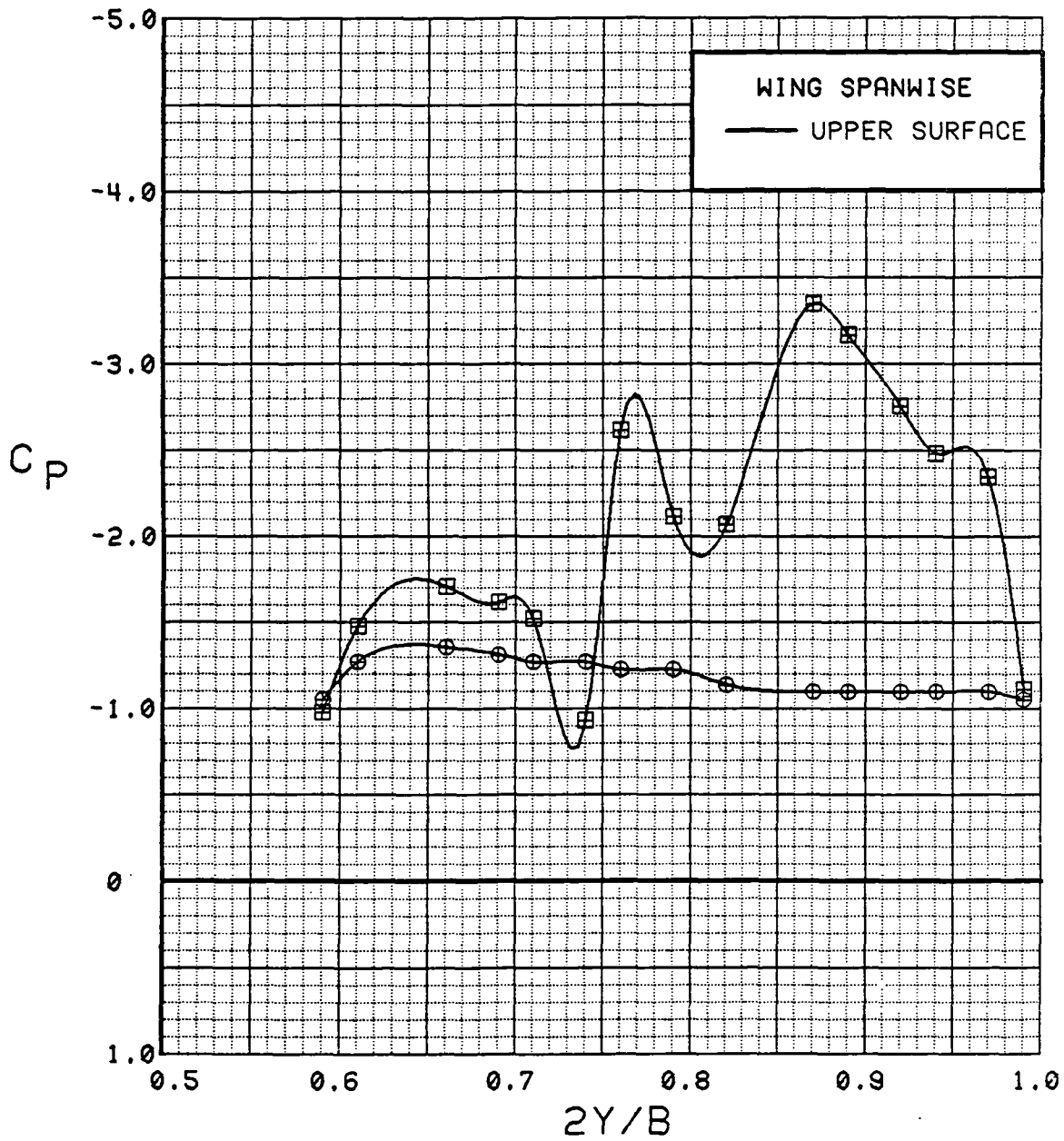


Figure 3.2.4-431 Spanwise Blowing Effects, Spanwise,  $C_T = 0.9$ ,  $\alpha = 20$  deg

SYM	TEST	RUN	ALPHA	CT	ITEF	OTEF	CAN	SWB
⊙	537	32	25.0	0.91	30	30	0	OFF
⊠	537	49	25.1	0.93	30	30	0	ON

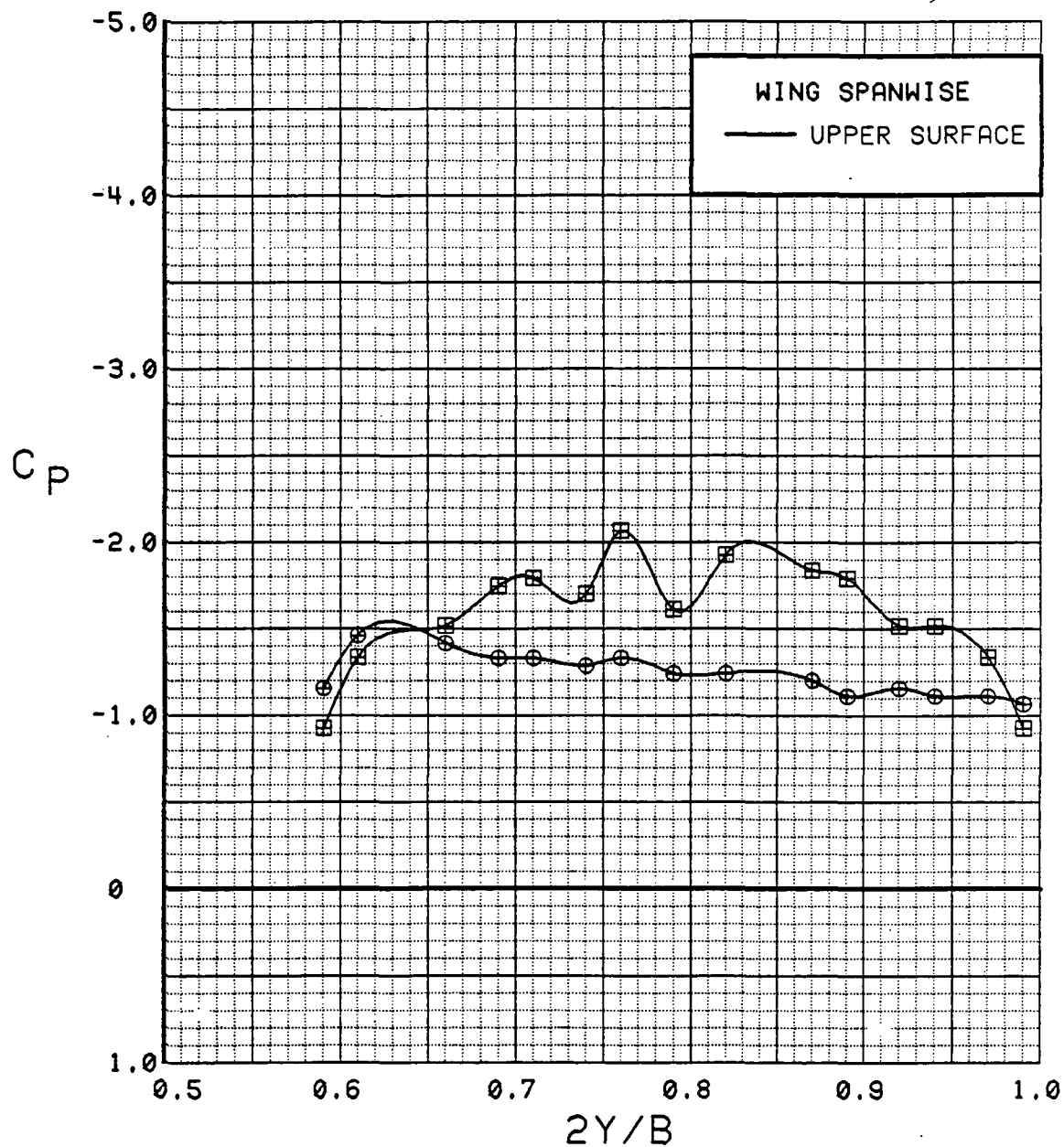


Figure 3.2.4-432 Spanwise Blowing Effects, Spanwise,  $C_T = 0.9$ ,  $\alpha = 24$  deg

SYM	TEST	RUN	ALPHA	CT	ITEF	OTEF	CAN	SWB
⊙	537	32	29.1	0.93	30	30	0	OFF
⊠	537	49	29.2	0.94	30	30	0	ON

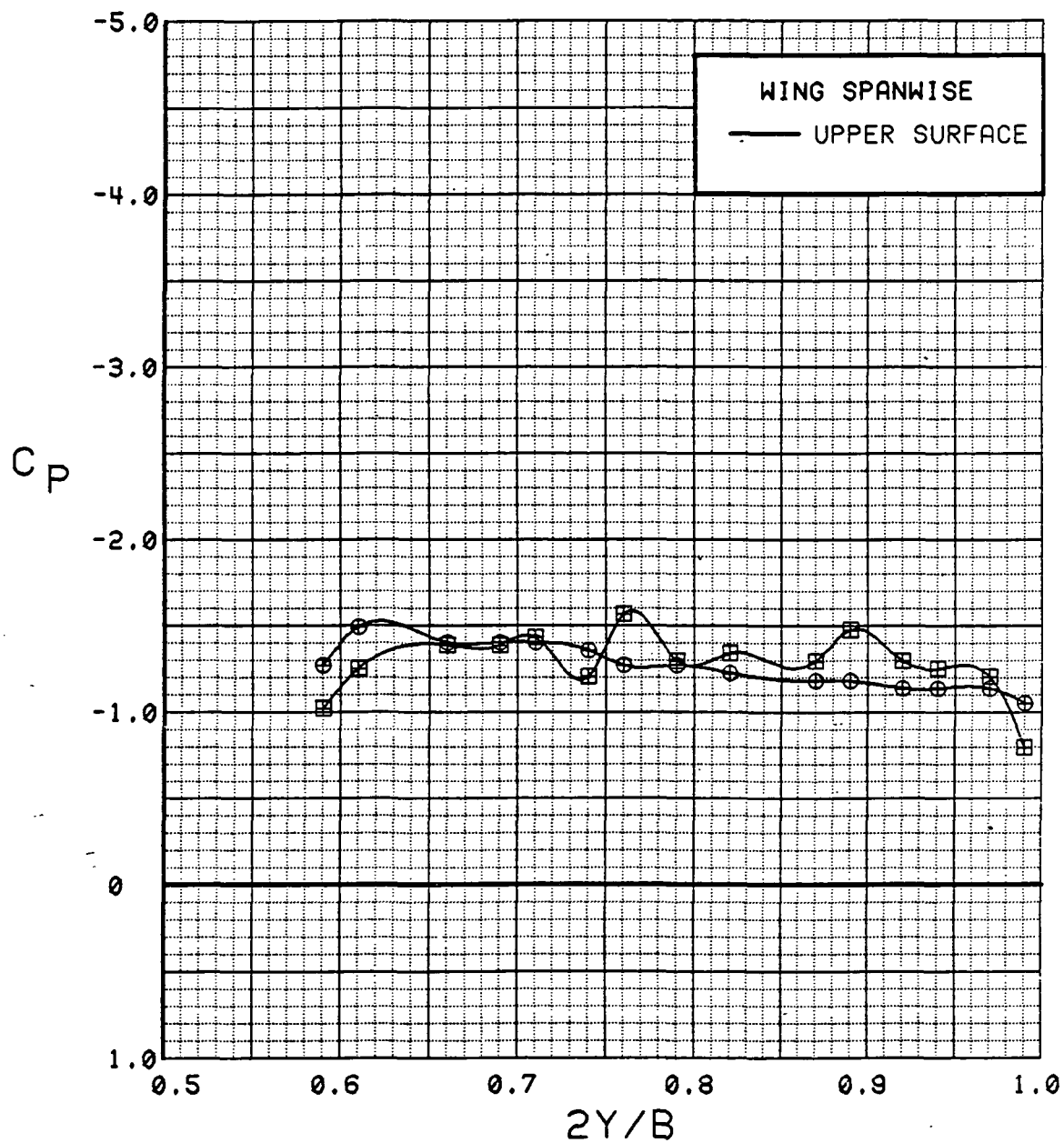


Figure 3.2.4-433 Spanwise Blowing Effects, Spanwise,  $C_T = 0.9$ ,  $\alpha = 28^\circ$

SYM	TEST	RUN	ALPHA	CT	ITEF	OTEF	CAN	SWB
⊕	537	32	33.1	0.91	30	30	0	OFF
⊞	537	49	33.2	0.91	30	30	0	ON

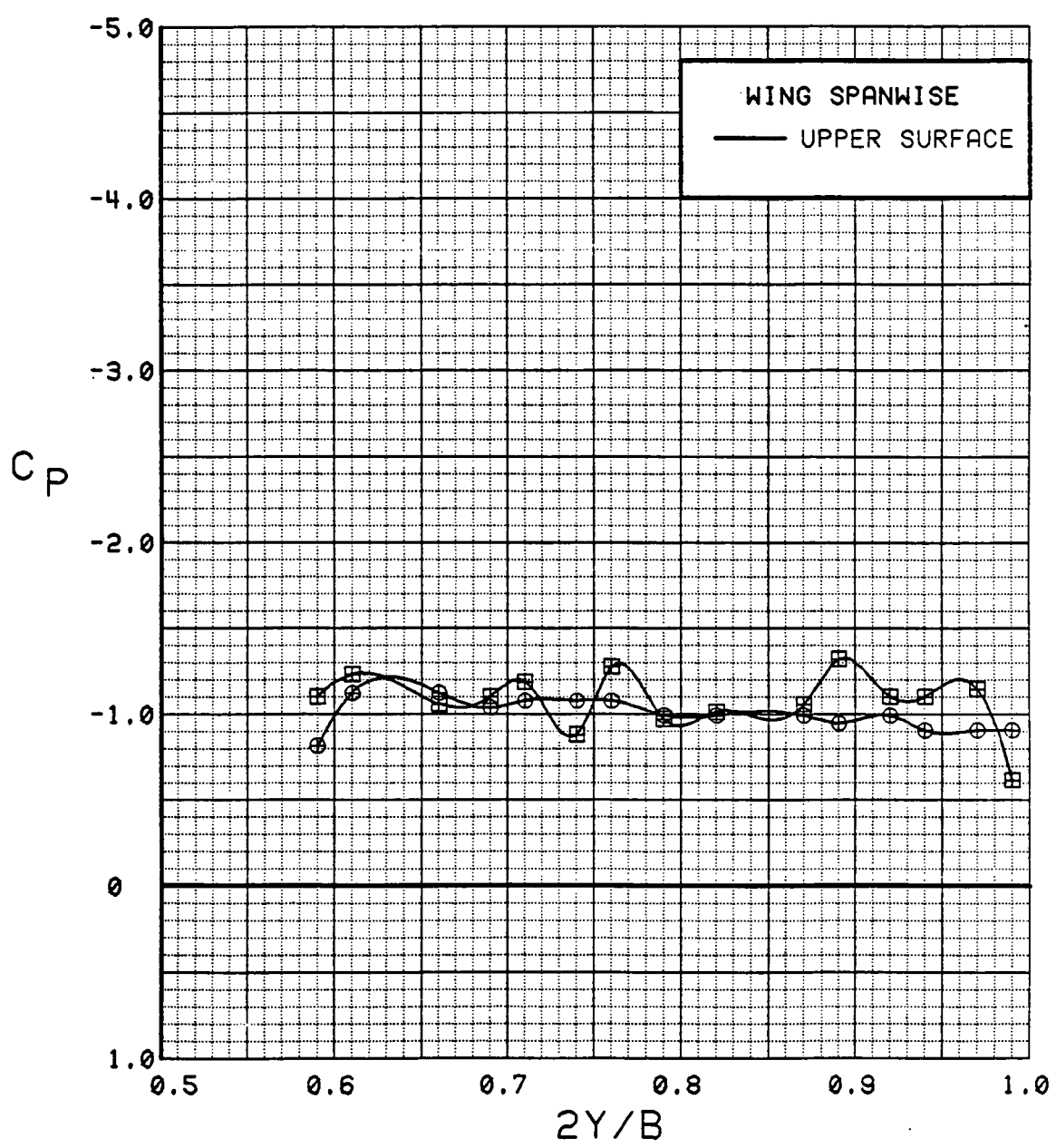


Figure 3.2.4-434 Spanwise Blowing Effects, Spanwise,  $C_T = 0.9$ ,  $\alpha = 32$  deg

## WING INBOARD

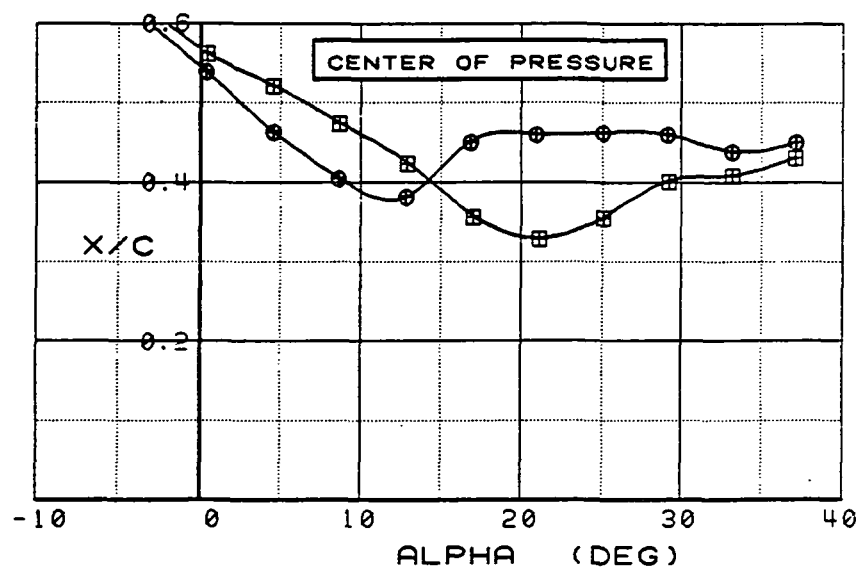
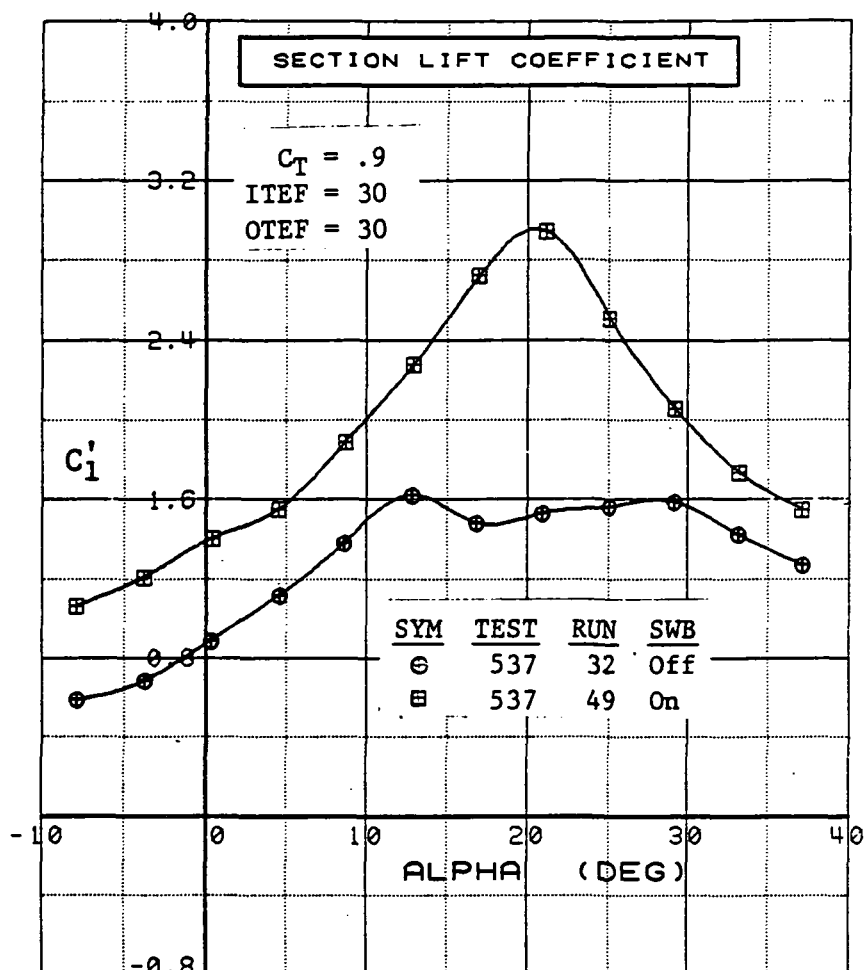


Figure 3.2.4-435 Spanwise Blowing Effects, Inboard,  $C_T = 0.9$ , Integrated Section Properties



## WING OUTBOARD

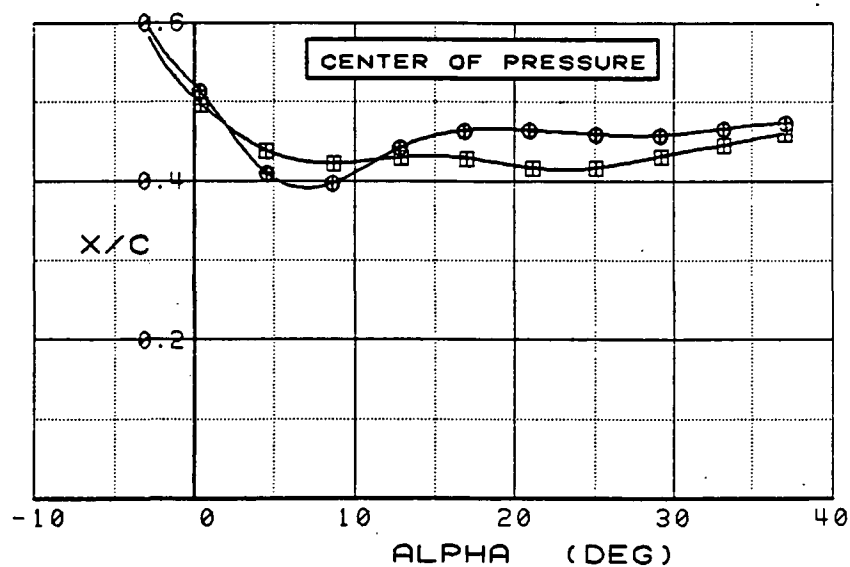
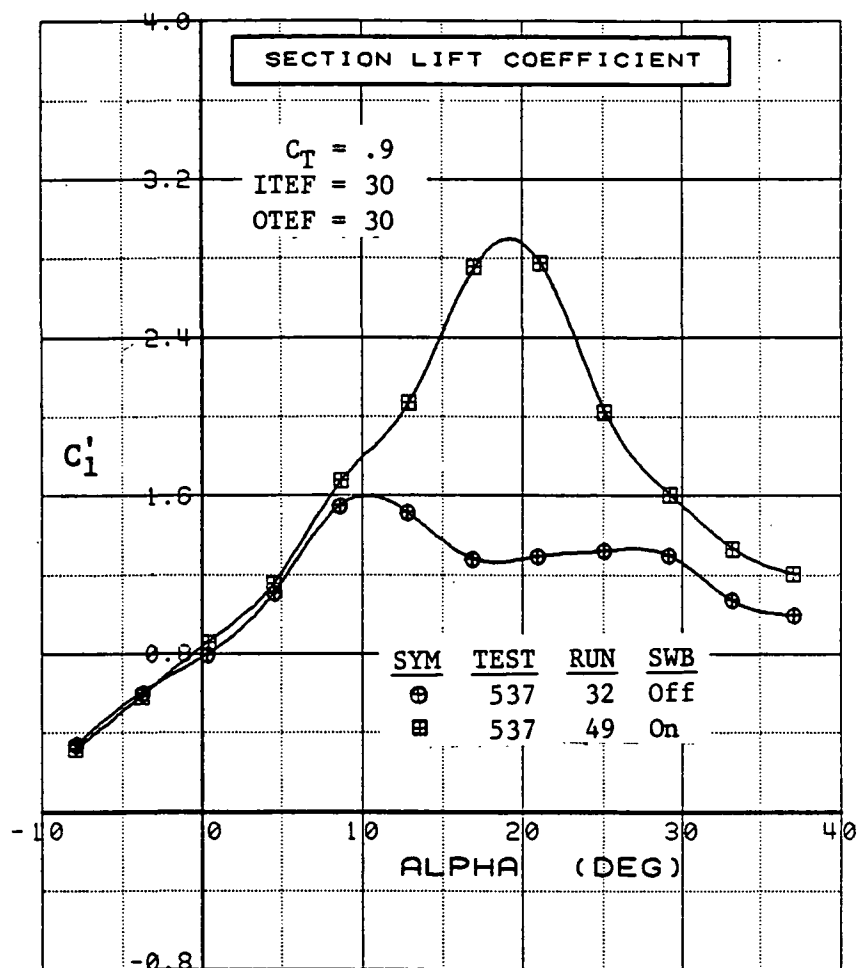


Figure 3.2.4-436 Spanwise Blowing Effects, Outboard,  $C_T = 0.9$ , Integrated Section Properties

SYM	TEST	RUN	ALPHA	CT	ITEF	OTEF	CAN	SWB
⊕	537	28	0.3	1.89	30	30	0	OFF
⊞	537	53	0.4	1.81	30	30	0	ON

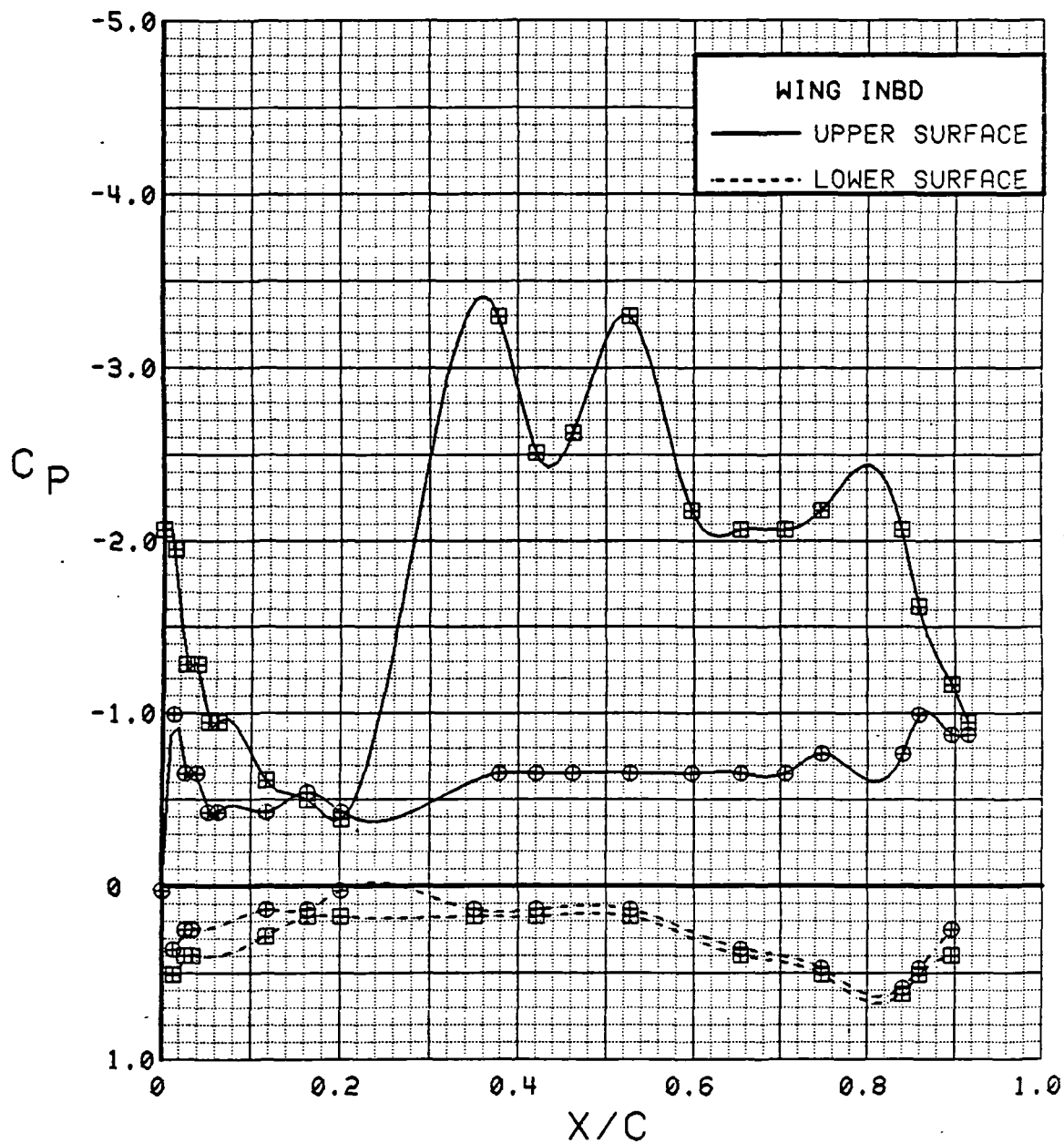


Figure 3.2.4-437 Spanwise Blowing Effects, Inboard,  $C_T = 1.9$ ,  $\alpha = 0^\circ$

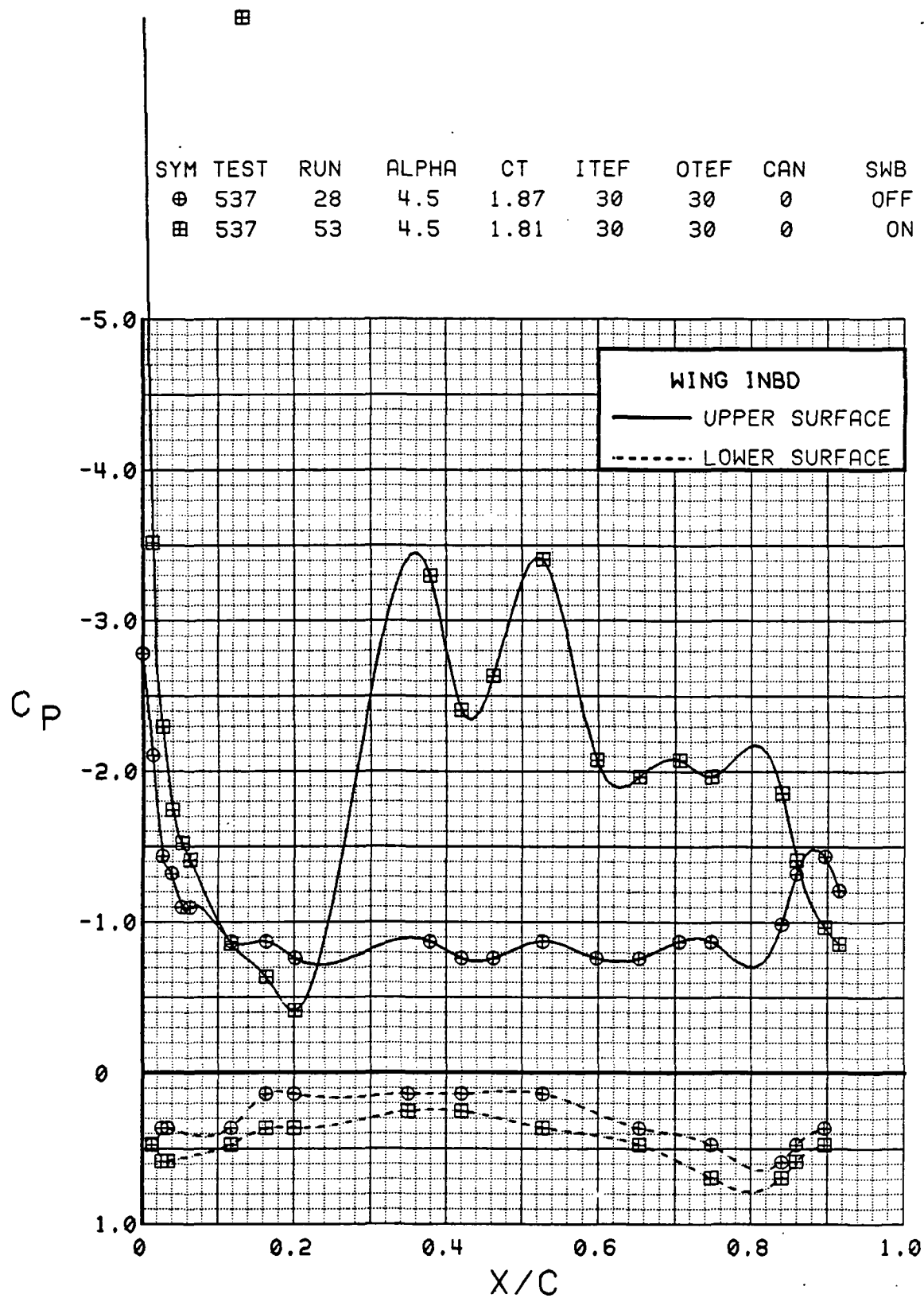


Figure 3.2.4-438 Spanwise Blowing Effects, Inboard,  $C_T = 1.9$ ,  $\alpha = 4^\circ$

SYM	TEST	RUN	ALPHA	CT	ITEF	OTEF	CAN	SWB
⊕	537	28	8.7	1.88	30	30	0	OFF
⊞	537	53	8.7	1.83	30	30	0	ON

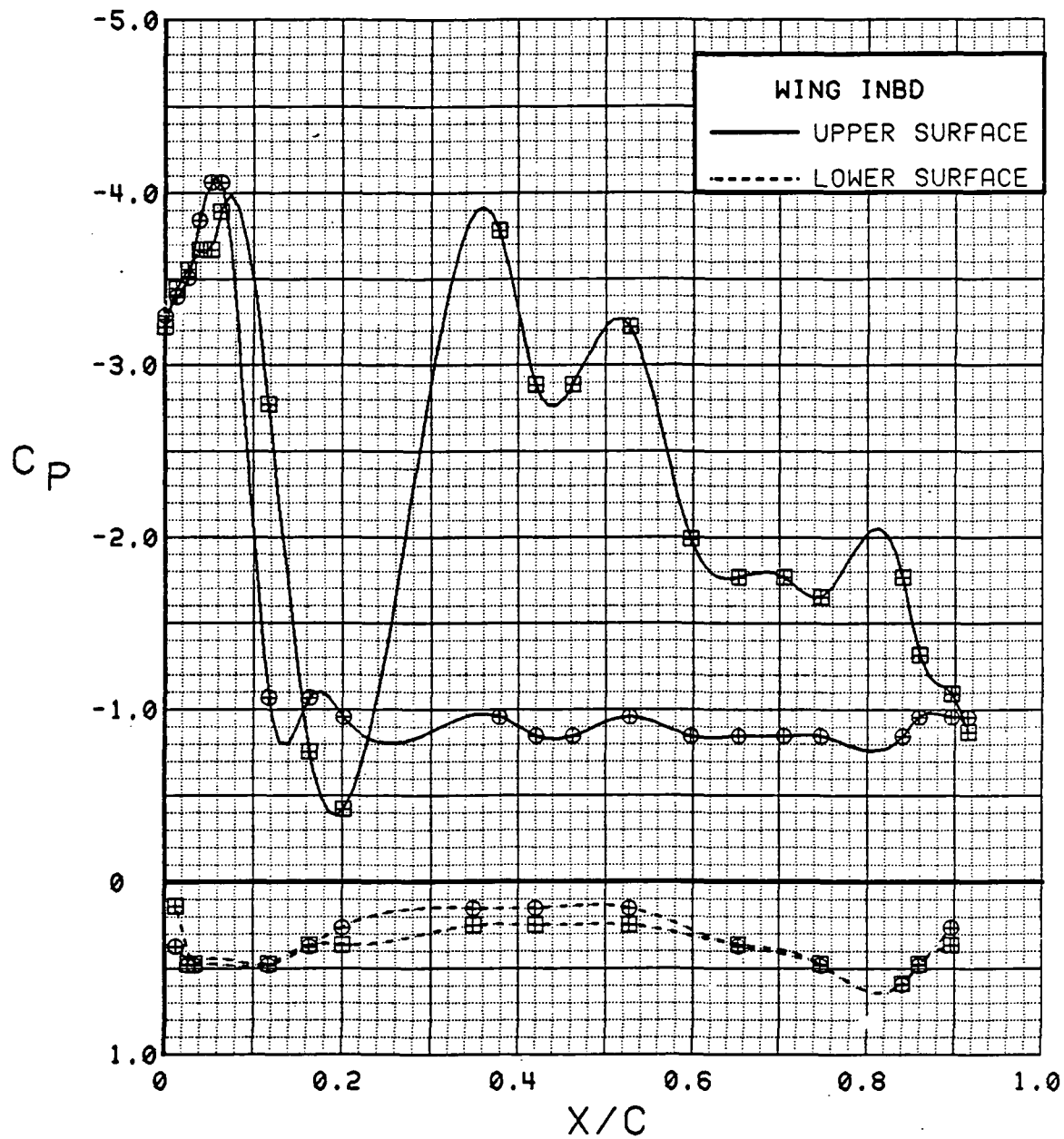


Figure 3.2.4-439 Spanwise Blowing Effects, Inboard,  $C_T = 1.9$ ,  $\alpha = 8^\circ$

SYM	TEST	RUN	ALPHA	CT	ITEF	OTEF	CAN	SWB
⊕	537	28	12.8	1.82	30	30	0	OFF
⊞	537	53	12.9	1.82	30	30	0	ON

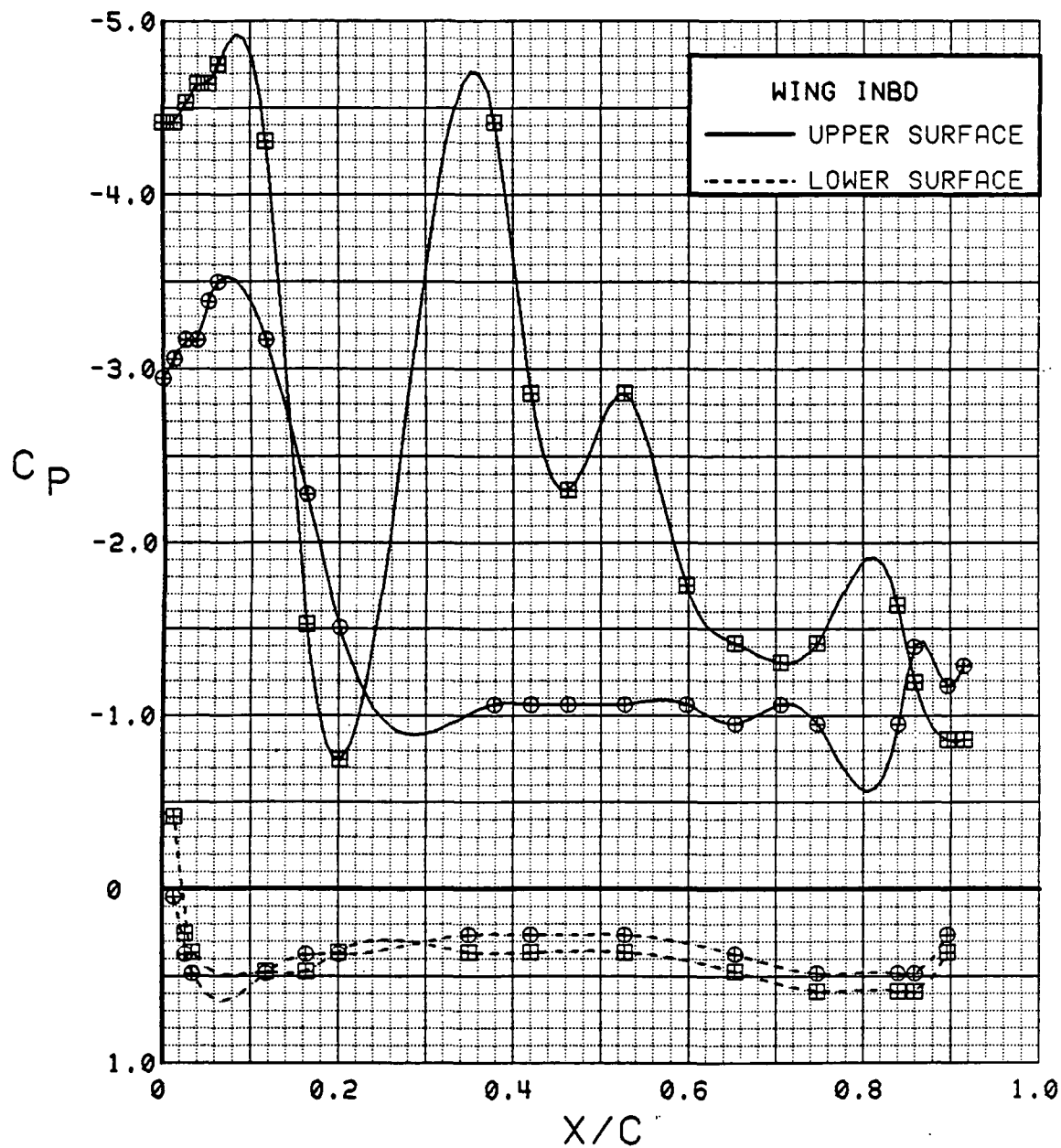


Figure 3.2.4-440 Spanwise Blowing Effects, Inboard,  $C_T = 1.9$ ,  $\alpha = 12$  deg

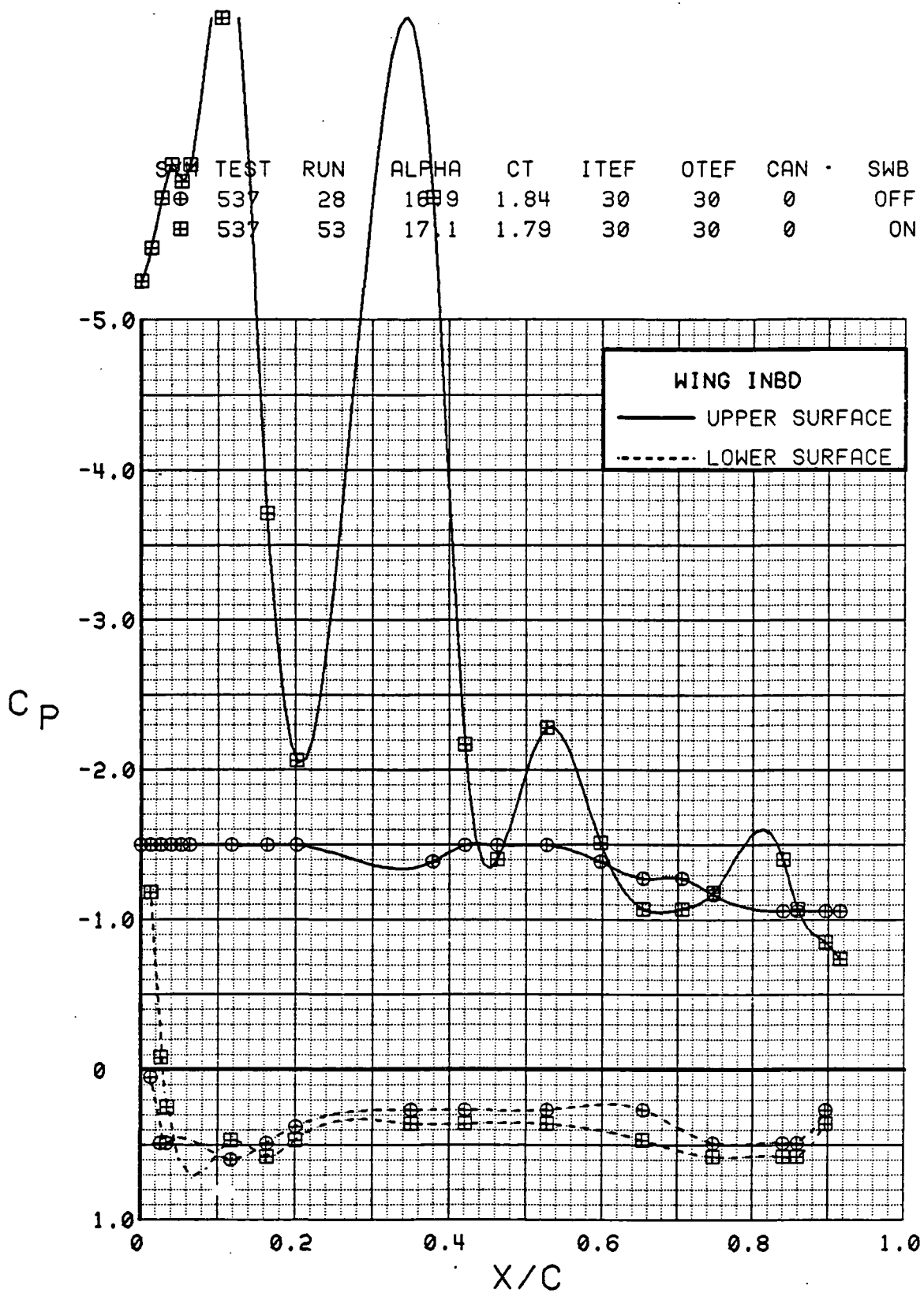


Figure 3.2.4-441 Spanwise Blowing Effects, Inboard,  $C_T = 1.9$ ,  $\alpha = 16^\circ$

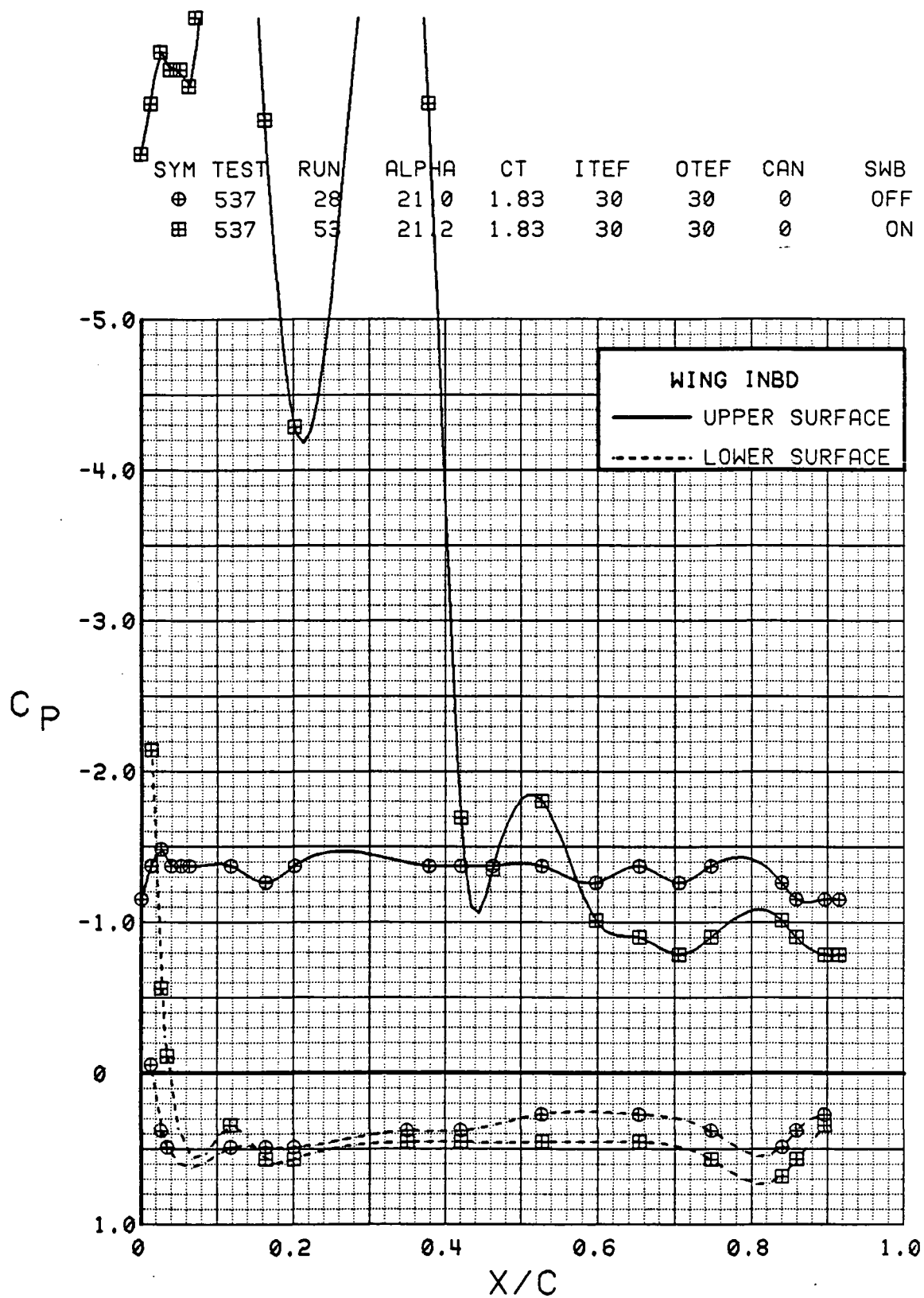


Figure 3.2.4-442 Spanwise Blowing Effects, Inboard,  $C_T = 1.9$ ,  $\alpha = 20^\circ$

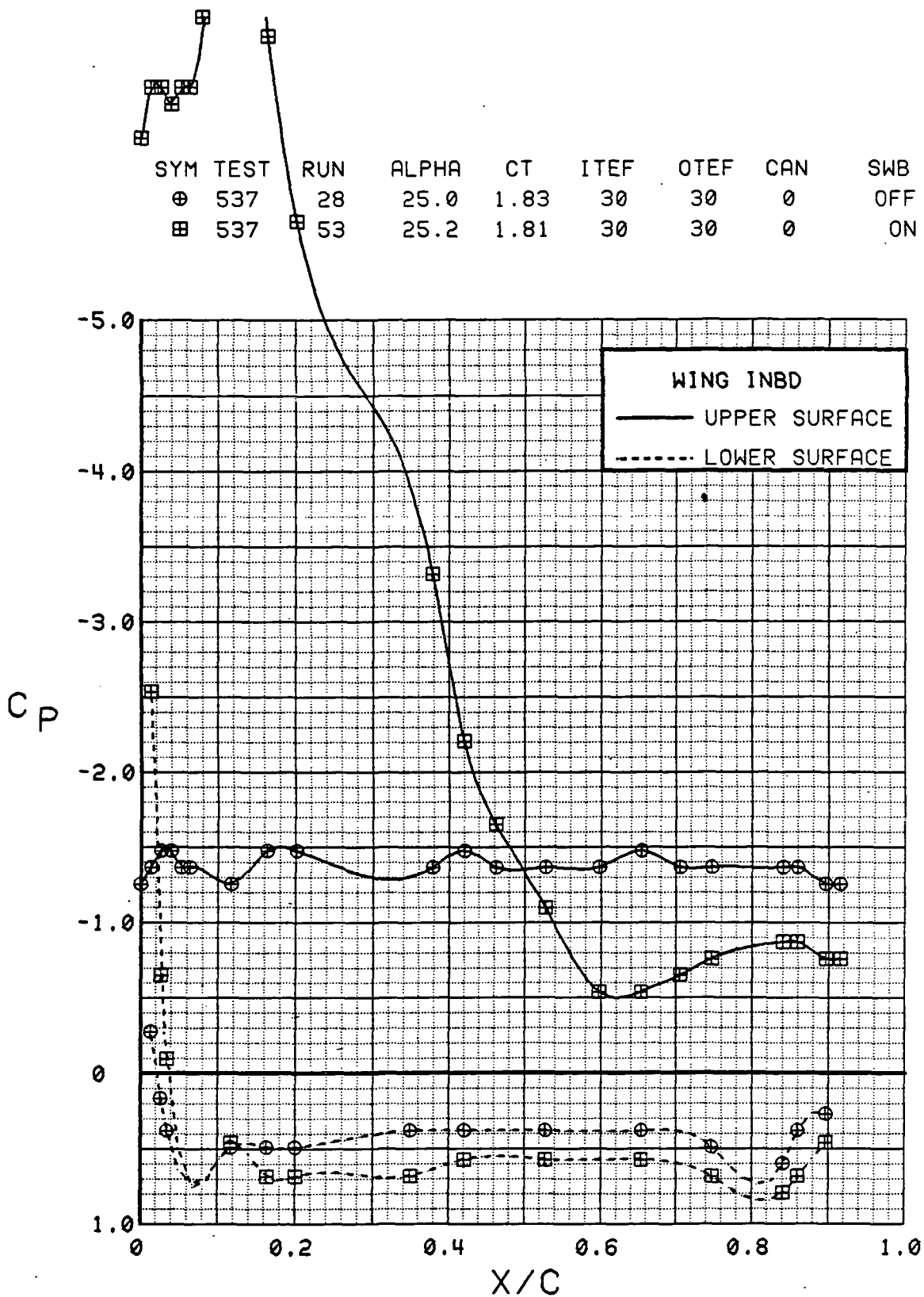


Figure 3.2.4-443 Spanwise Blowing Effects, Inboard,  $C_T = 1.9$ ,  $\alpha = 24$  deg



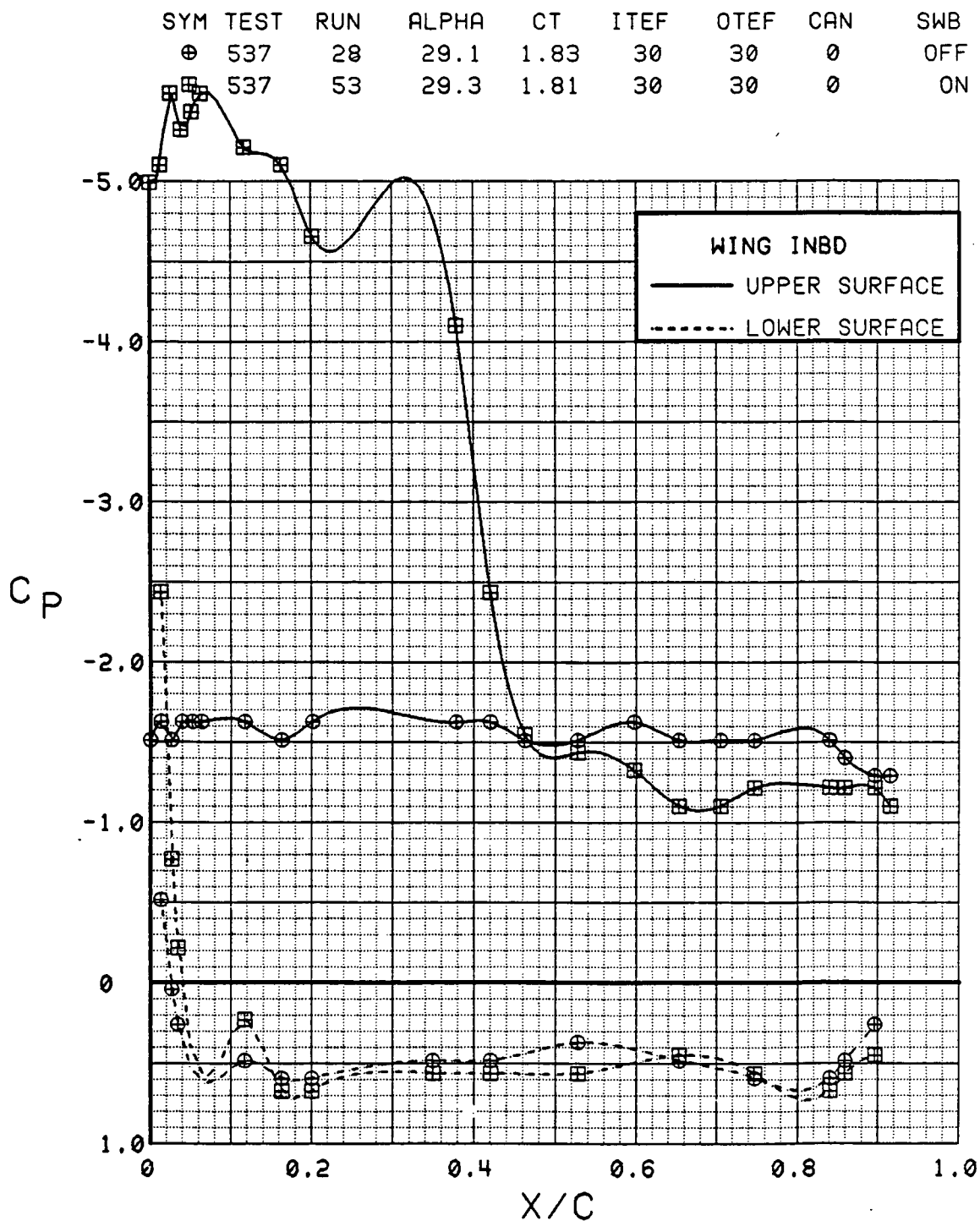


Figure 3.2.4-444 Spanwise Blowing Effects, Inboard,  $C_T = 1.9$ ,  $\alpha = 28$  deg

SYM	TEST	RUN	ALPHA	CT	ITEF	OTEF	CAN	SWB
⊕	537	28	0.3	1.89	30	30	0	OFF
⊞	537	53	0.4	1.81	30	30	0	ON

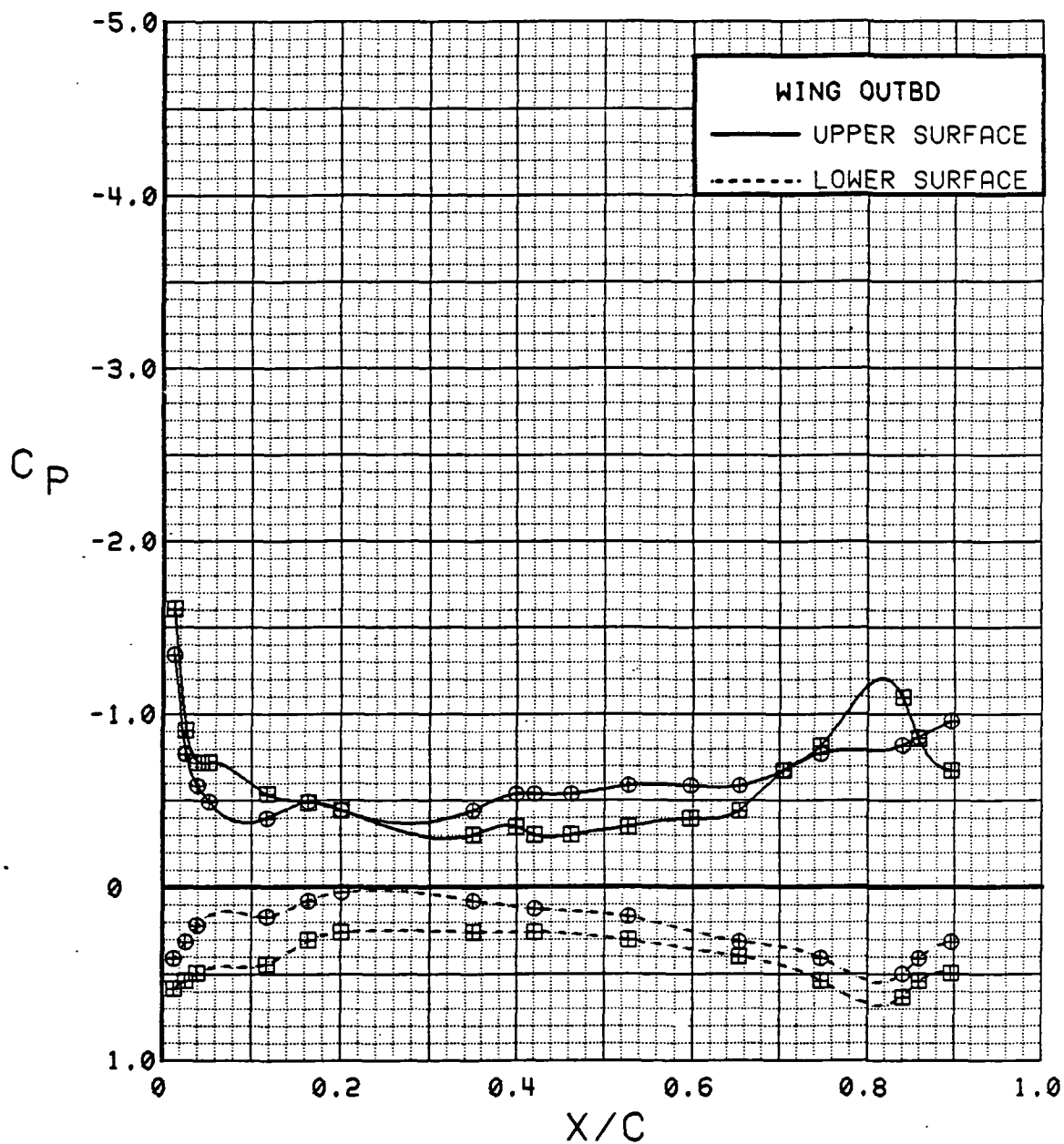


Figure 3.2.4-445 Spanwise Blowing Effects, Outboard,  $C_T \approx 1.9$ ,  $\alpha = 0^\circ$

SYM	TEST	RUN	ALPHA	CT	ITEF	OTEF	CAN	SWB
⊕	537	28	4.5	1.87	30	30	0	OFF
⊞	537	53	4.5	1.81	30	30	0	ON

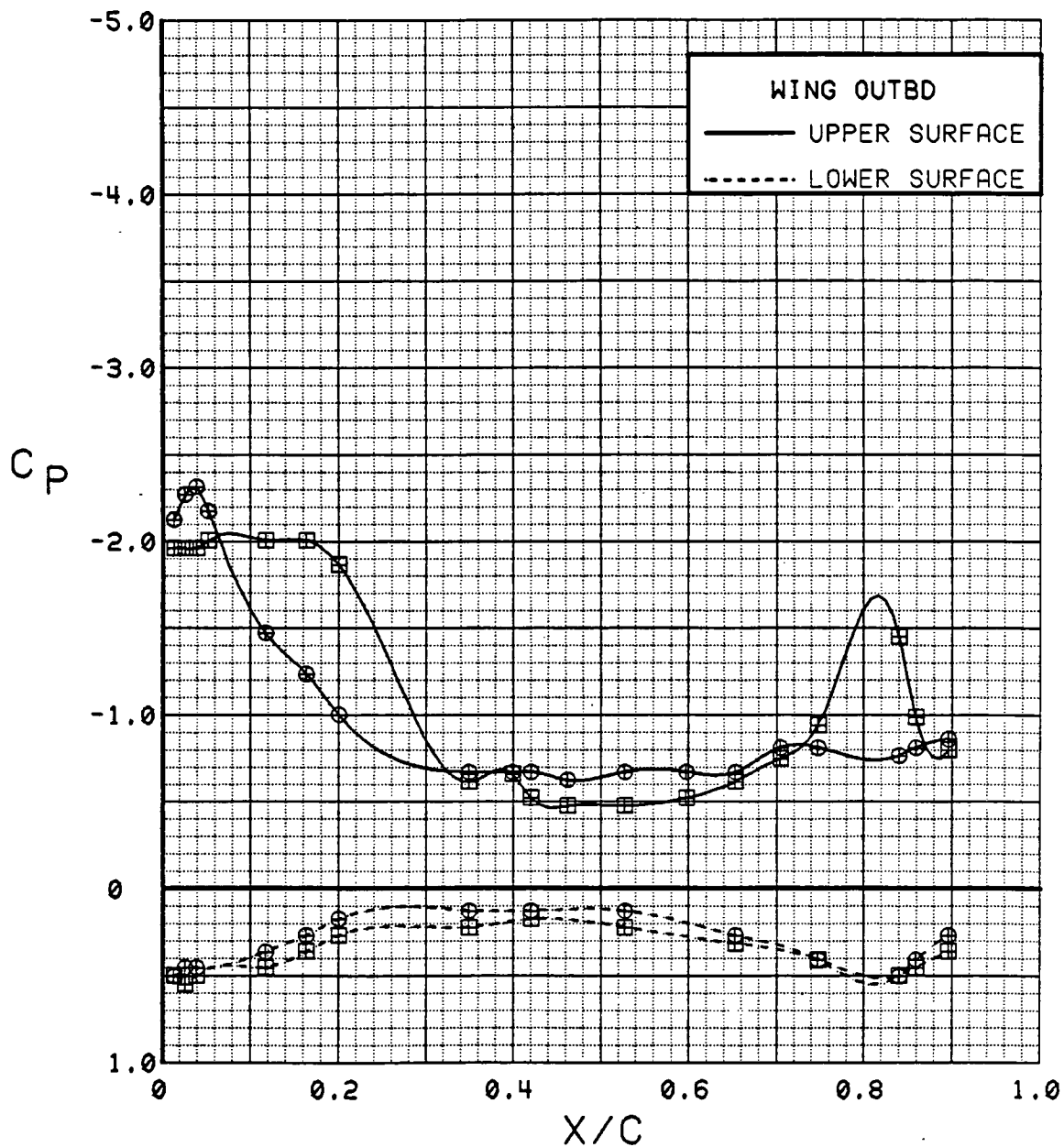


Figure 3.2.4-446 Spanwise Blowing Effects, Outboard,  $C_T = 1.9$ ,  $\alpha = 4$  deg

SYM	TEST	RUN	ALPHA	CT	ITEF	OTEF	CAN	SWB
⊕	537	28	8.7	1.88	30	30	0	OFF
⊞	537	53	8.7	1.83	30	30	0	ON

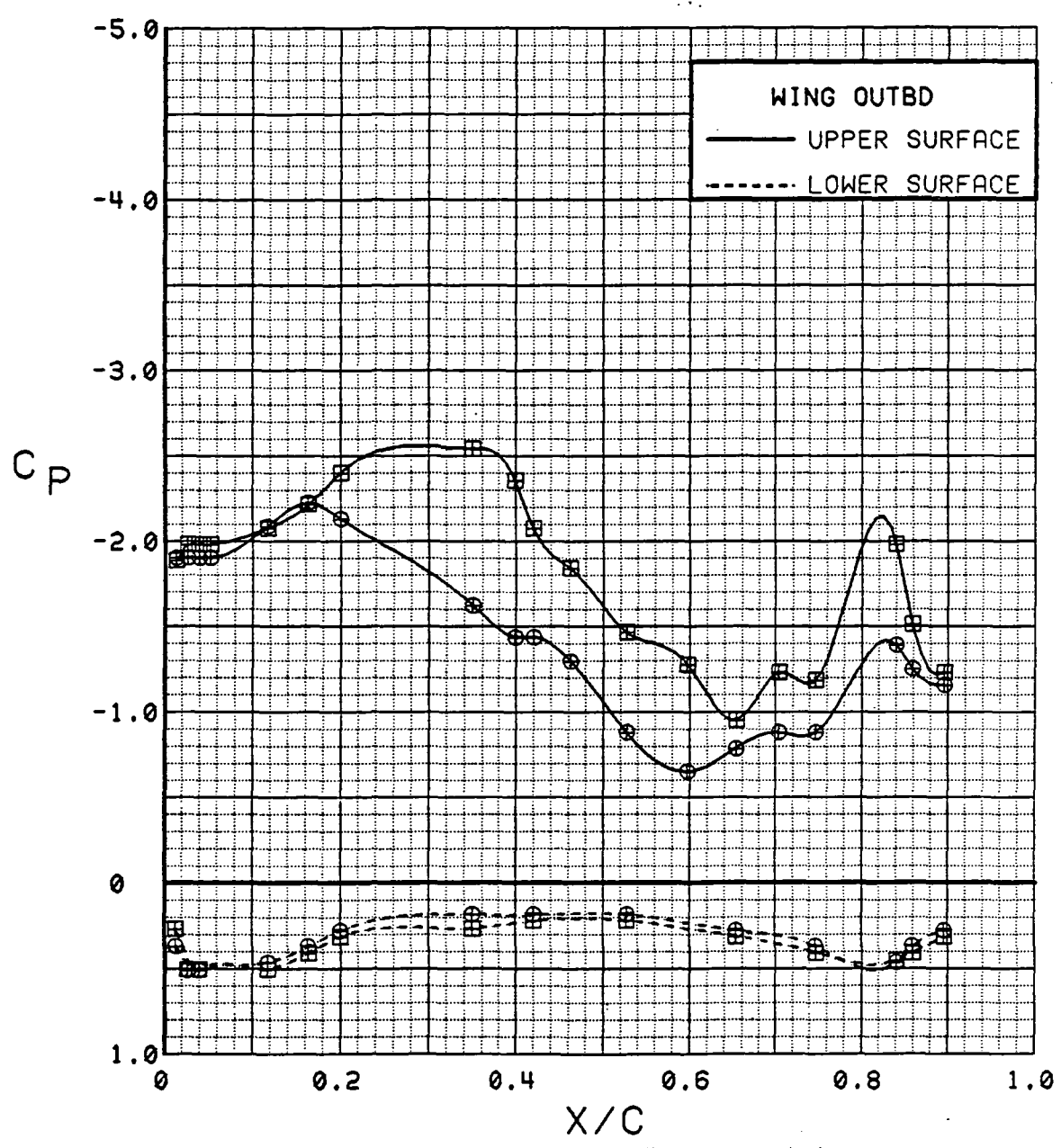


Figure 3.2.4-447 Spanwise Blowing Effects, Outboard,  $C_T = 1.9$ ,  $\alpha = 8$  deg

SYM	TEST	RUN	ALPHA	CT	ITEF	OTEF	CAN	SWB
⊕	537	28	12.8	1.82	30	30	0	OFF
⊞	537	53	12.9	1.82	30	30	0	ON

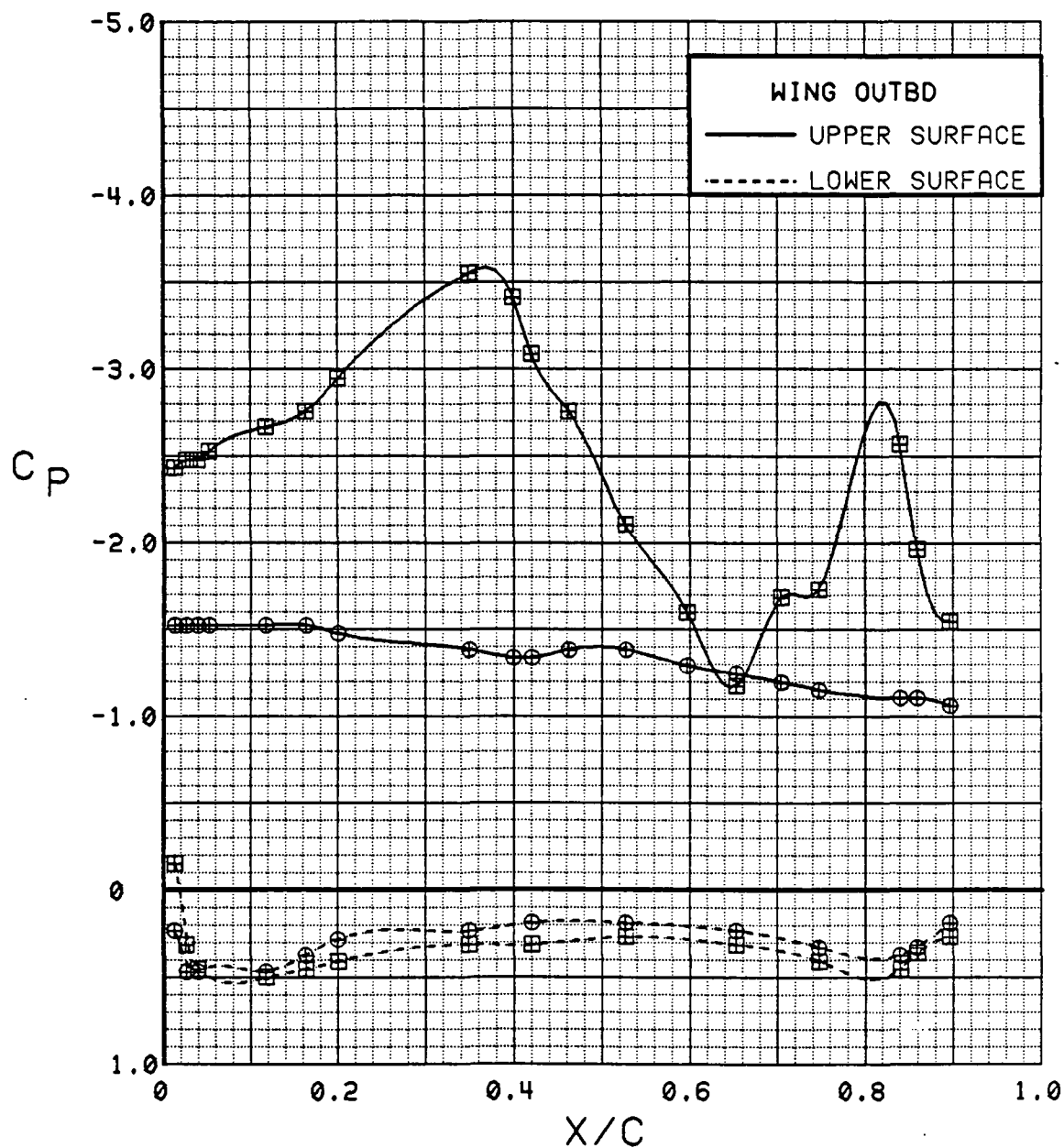


Figure 3.2.4-448 Spanwise Blowing Effects, Outboard,  $C_T = 1.9$ ,  $\alpha = 12^\circ$

201

SYM	TEST	RUN	ALPHA	CT	ITEF	OTEF	CAN	SWB
⊕	537	28	16.9	1.84	30	30	0	OFF
⊞	537	53	17.1	1.79	30	30	0	ON

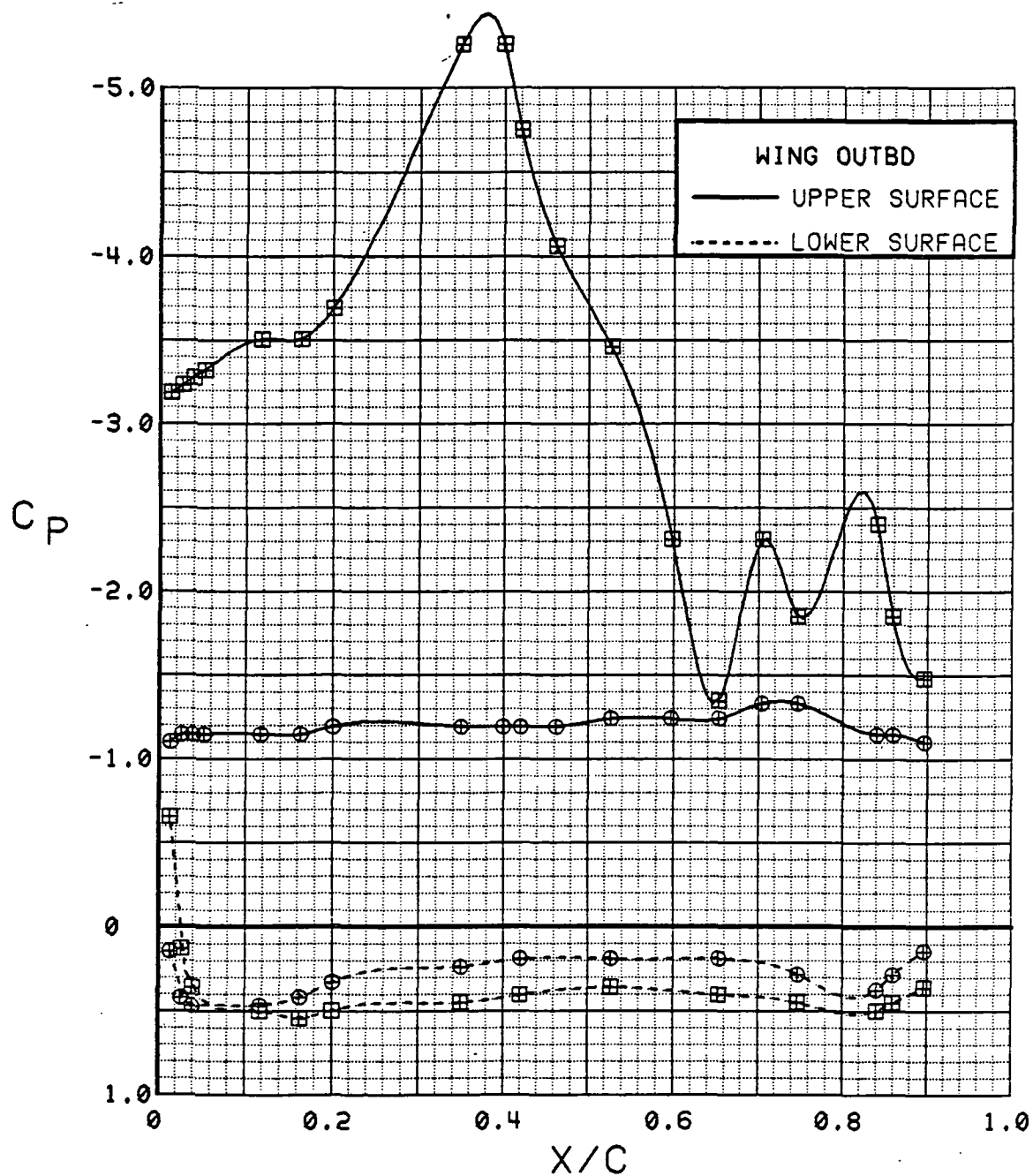


Figure 3.2.4-449 Spanwise Blowing Effects, Outboard,  $C_T = 1.9$ ,  $\alpha = 16$  deg

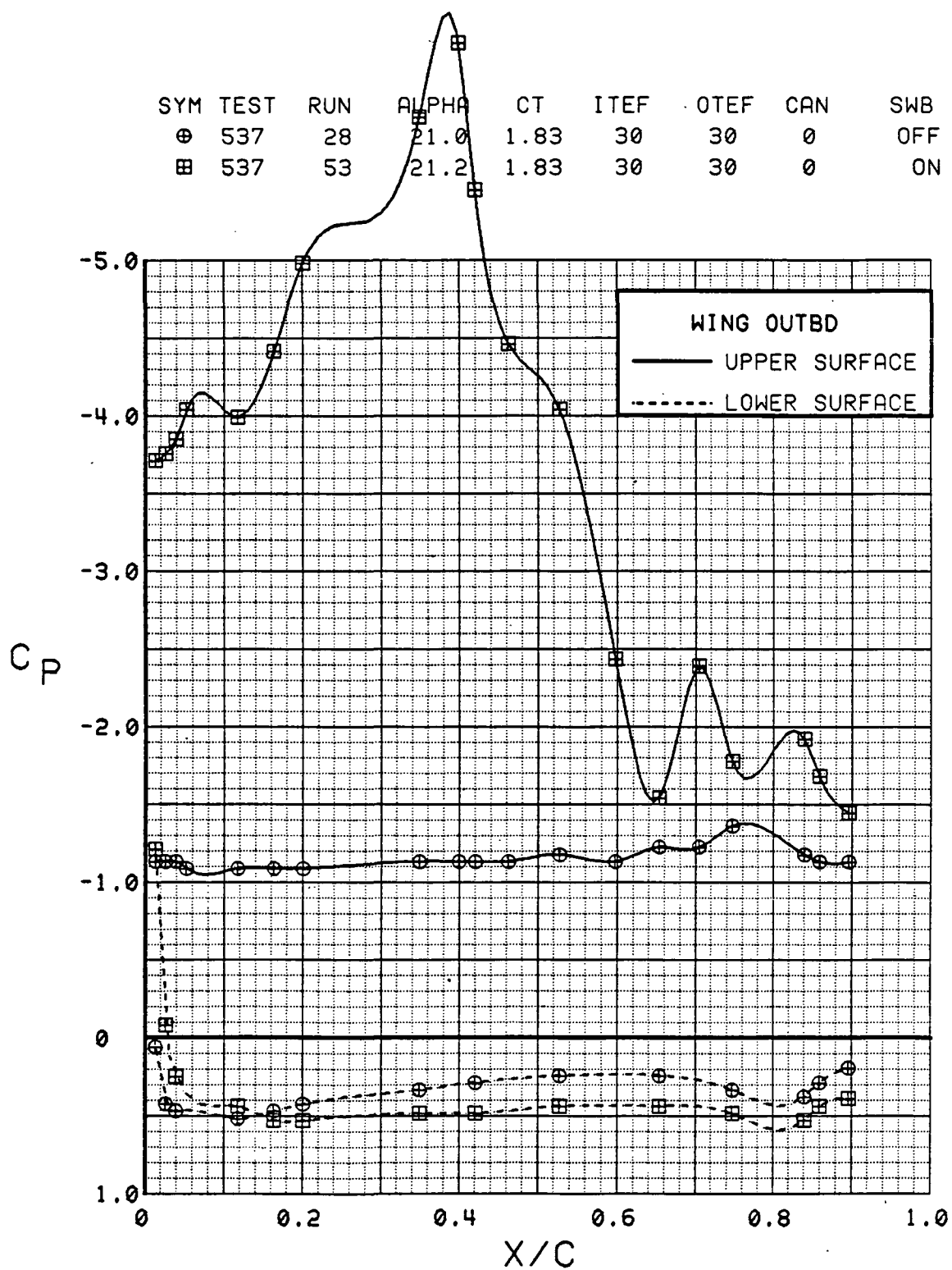


Figure 3.2.4-450 Spanwise Blowing Effects, Outboard,  $C_T = 1.9$ ,  $\alpha = 20^\circ$

SYM	TEST	RUN	ALPHA	CT	ITEF	OTEF	CAN	SWB
⊕	537	28	25.0	1.83	30	30	0	OFF
⊞	537	53	25.2	1.81	30	30	0	ON

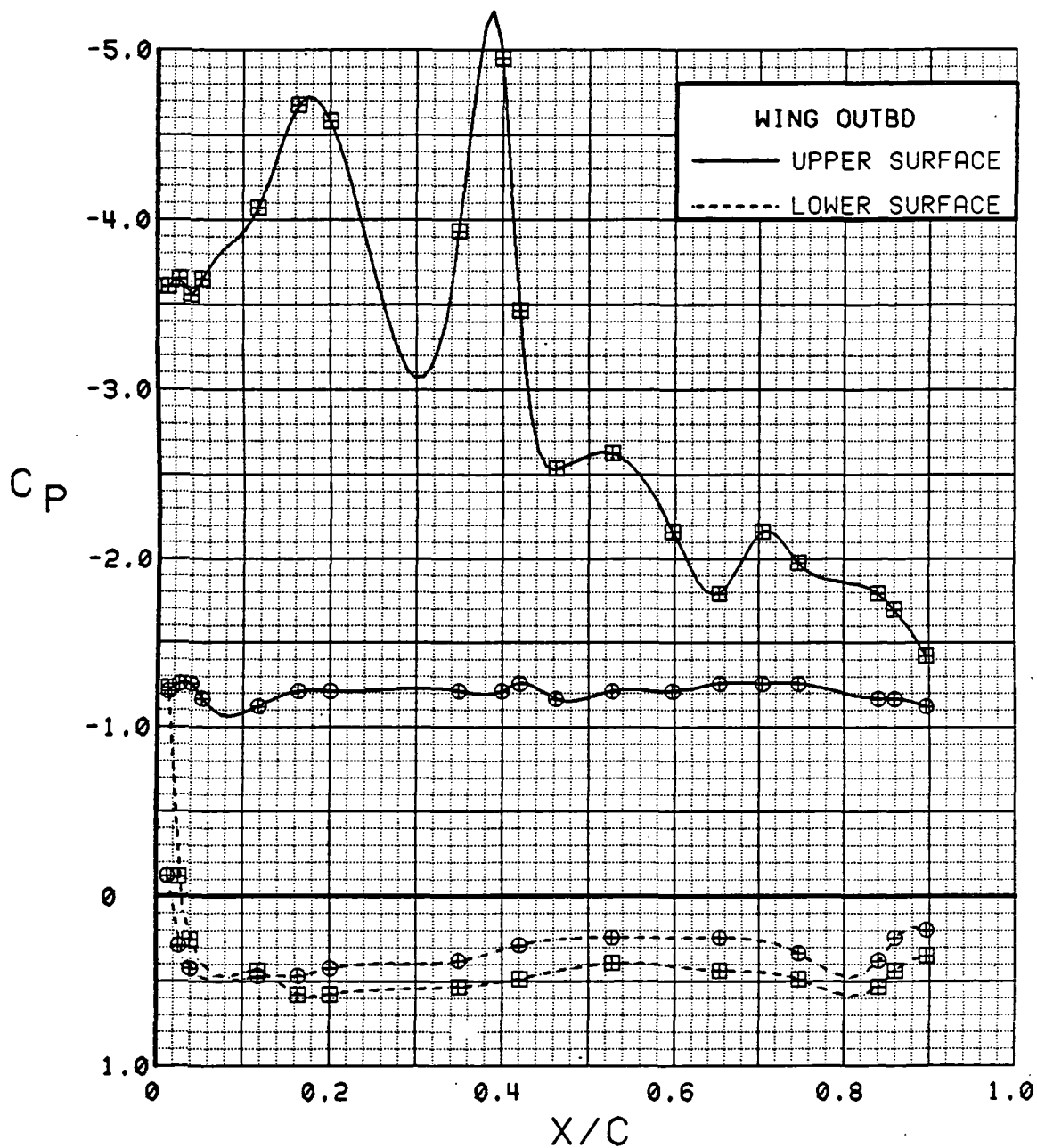


Figure 3.2.4-451 Spanwise Blowing Effects, Outboard,  $C_T = 1.9$ ,  $\alpha = 24^\circ$



SYM	TEST	RUN	ALPHA	CT	ITEF	OTEF	CAN	SWB
⊕	537	28	29.1	1.83	30	30	0	OFF
⊞	537	53	29.3	1.81	30	30	0	ON

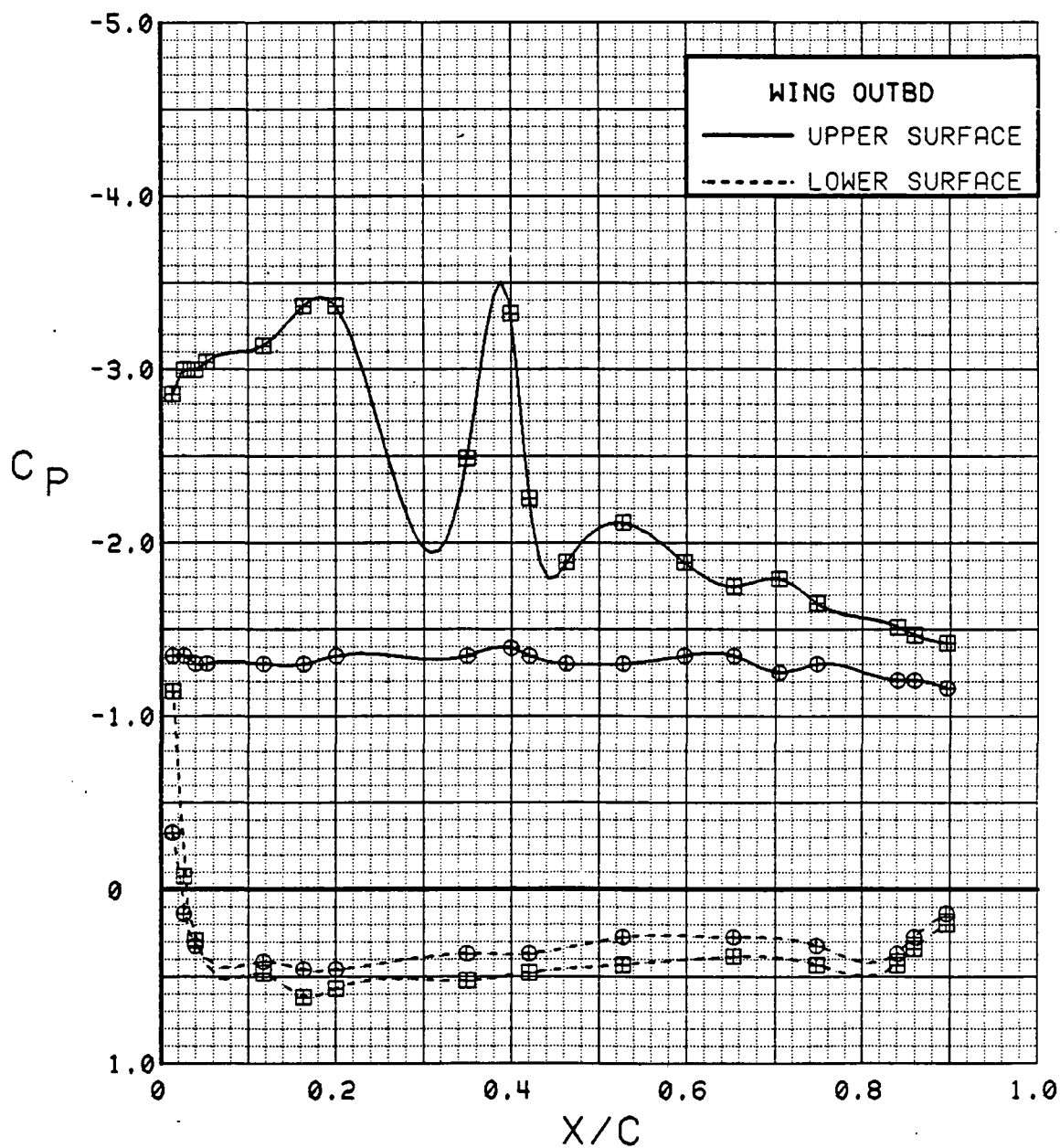


Figure 3.2.4-452 Spanwise Blowing Effects, Outboard,  $C_T = 1.9$ ,  $\alpha = 28$  deg

SYM	TEST	RUN	ALPHA	CT	ITEF	OTEF	CAN	SWB
⊙	537	28	0.3	1.89	30	30	0	OFF
⊠	537	53	0.4	1.81	30	30	0	ON

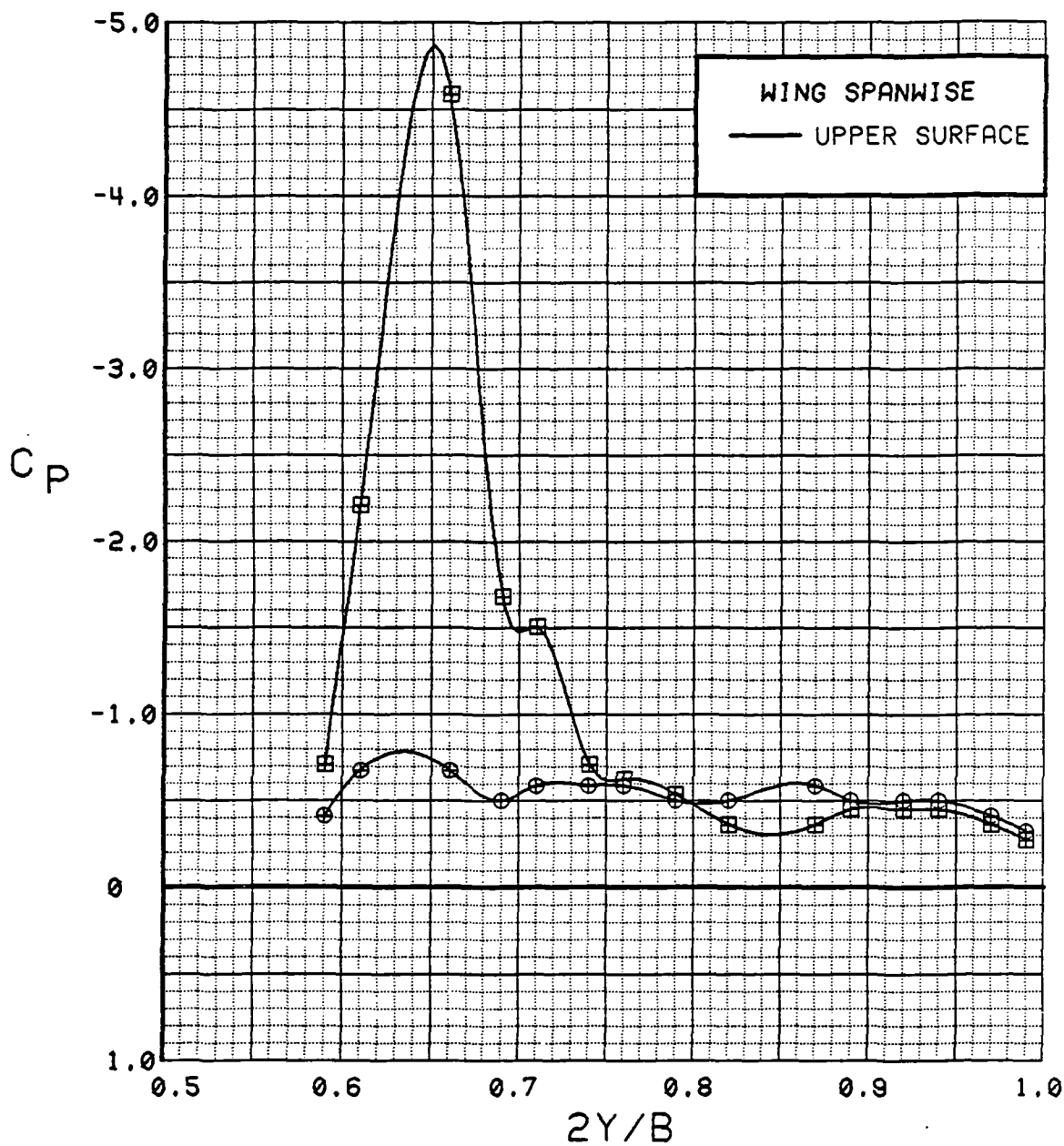


Figure 3.2.4-453 Spanwise Blowing Effects, Spanwise,  $C_T = 1.9$ ,  $\alpha = 0$  deg

SYM	TEST	RUN	ALPHA	CT	ITEF	OTEF	CAN	SWB
●	537	28	4.5	1.87	30	30	0	OFF
■	537	53	4.5	1.81	30	30	0	ON

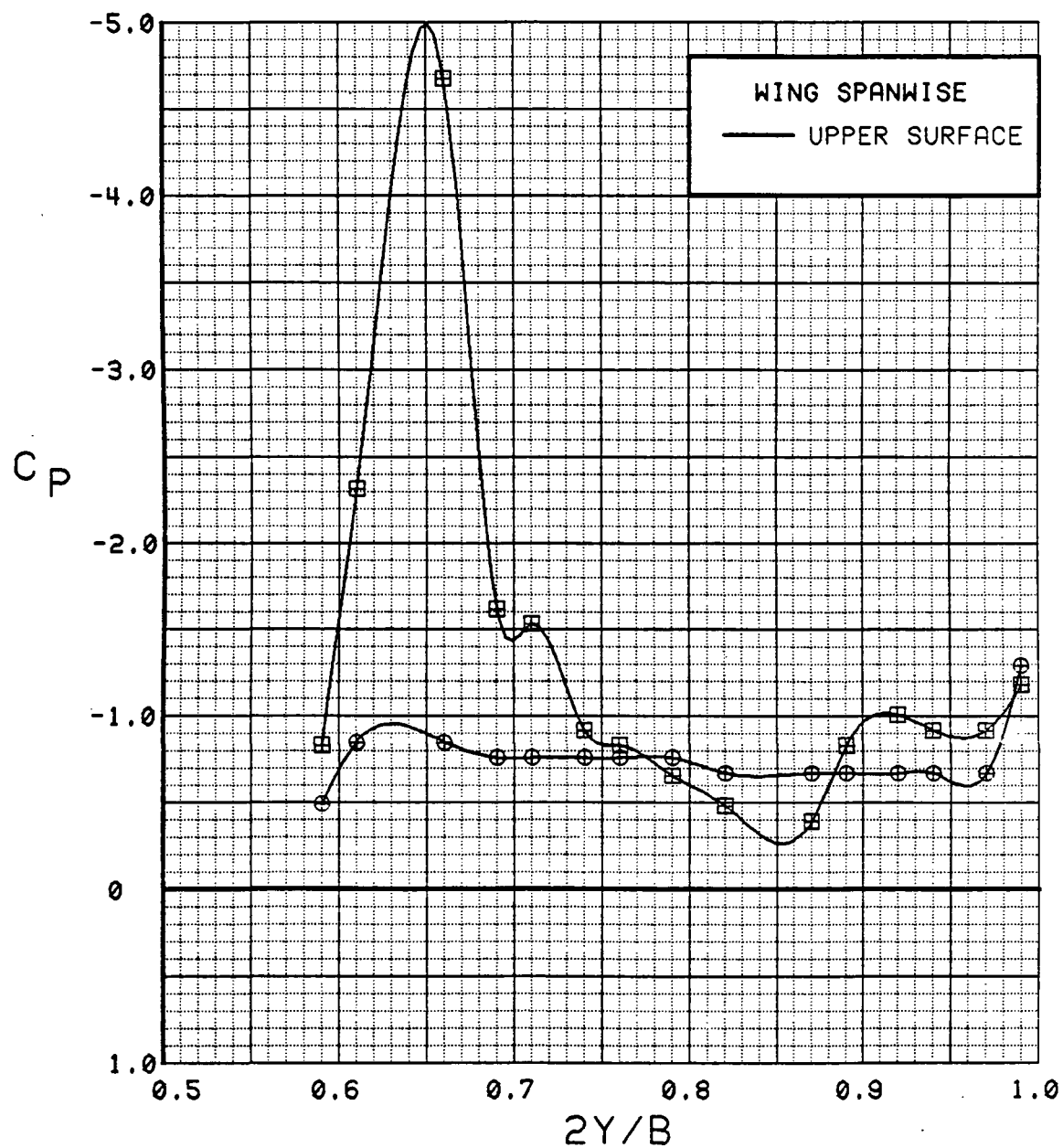


Figure 3.2.4-454 Spanwise Blowing Effects, Spanwise,  $C_T = 1.9$ ,  $\alpha = 4$  deg

SYM	TEST	RUN	ALPHA	CT	ITEF	OTEF	CAN	SWB
●	537	28	8.7	1.88	30	30	0	OFF
■	537	53	8.7	1.83	30	30	0	ON

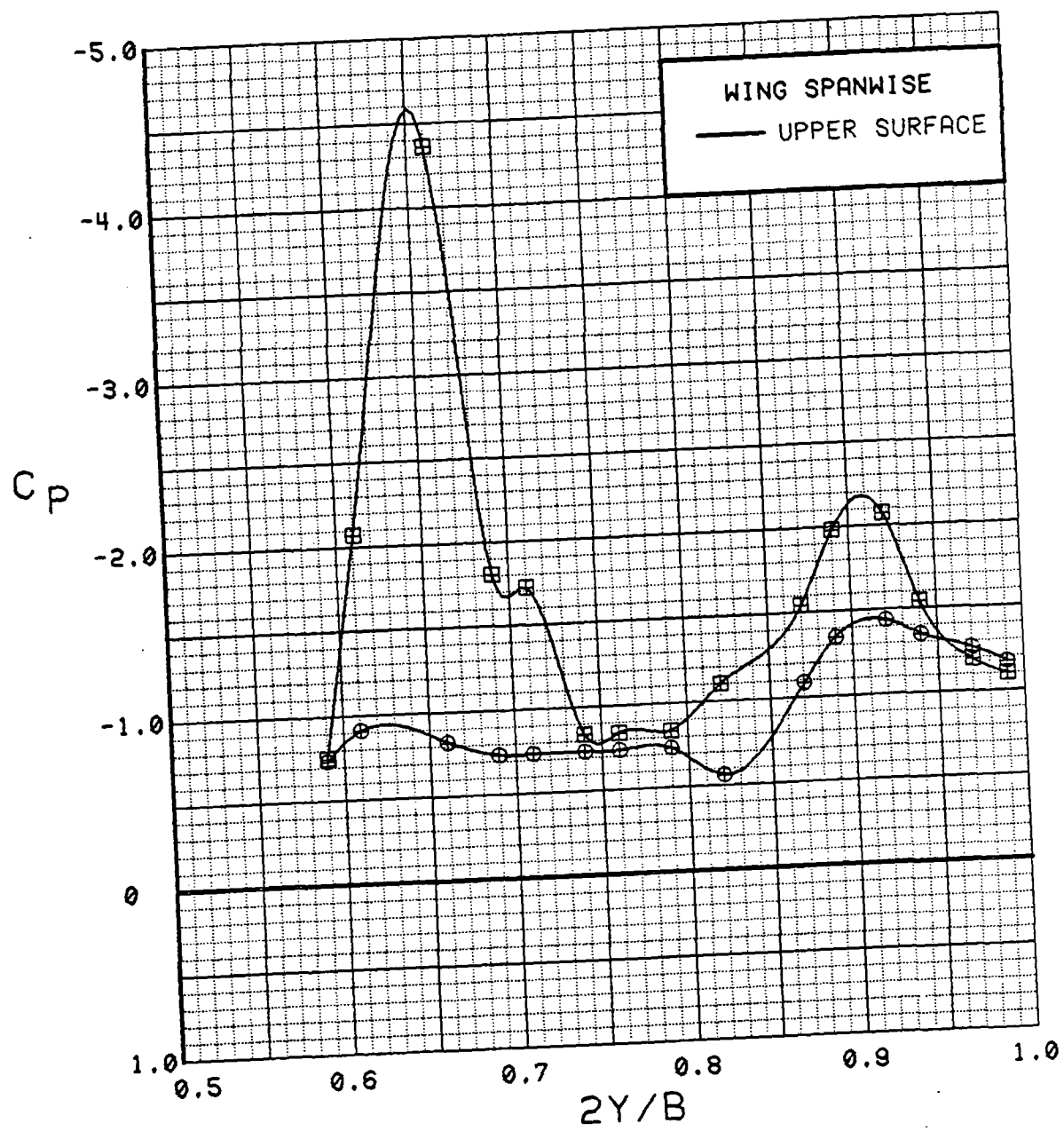


Figure 3.2.4-455 Spanwise Blowing Effects, Spanwise,  $C_T = 1.9$ ,  $\alpha = 8^\circ$

SYM	TEST	RUN	ALPHA	CT	ITEF	OTEF	CAN	SWB
⊕	537	28	12.8	1.82	30	30	0	OFF
⊞	537	53	12.9	1.82	30	30	0	ON

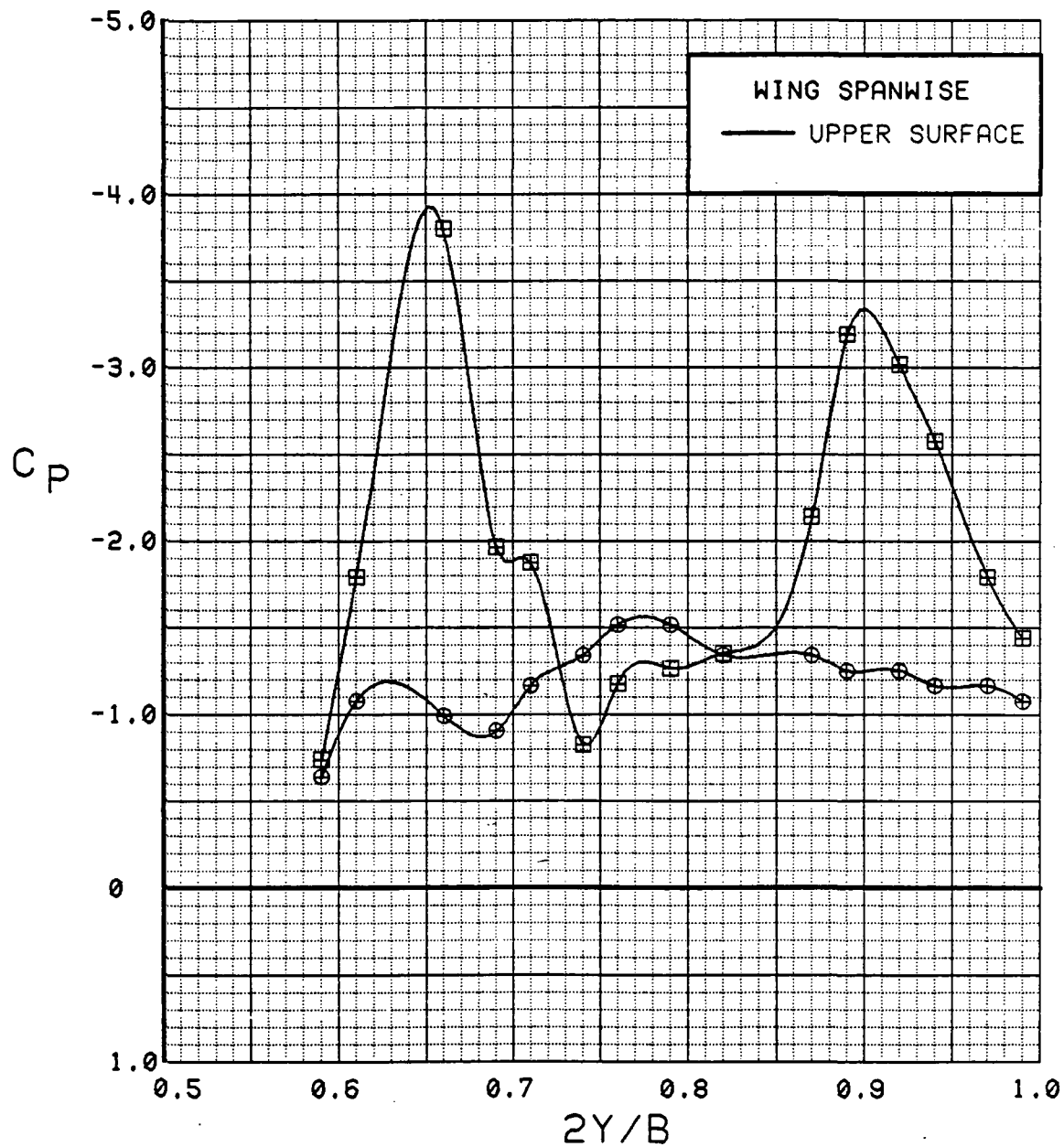


Figure 3.2.4-456 Spanwise Blowing Effects, Spanwise,  $C_T = 1.9$ ,  $\alpha = 12^\circ$

SYM	TEST	RUN	ALPHA	CT	ITEF	OTEF	CAN	SWB
⊙	537	28	16.9	1.84	30	30	0	OFF
⊠	537	53	17.1	1.79	30	30	0	ON

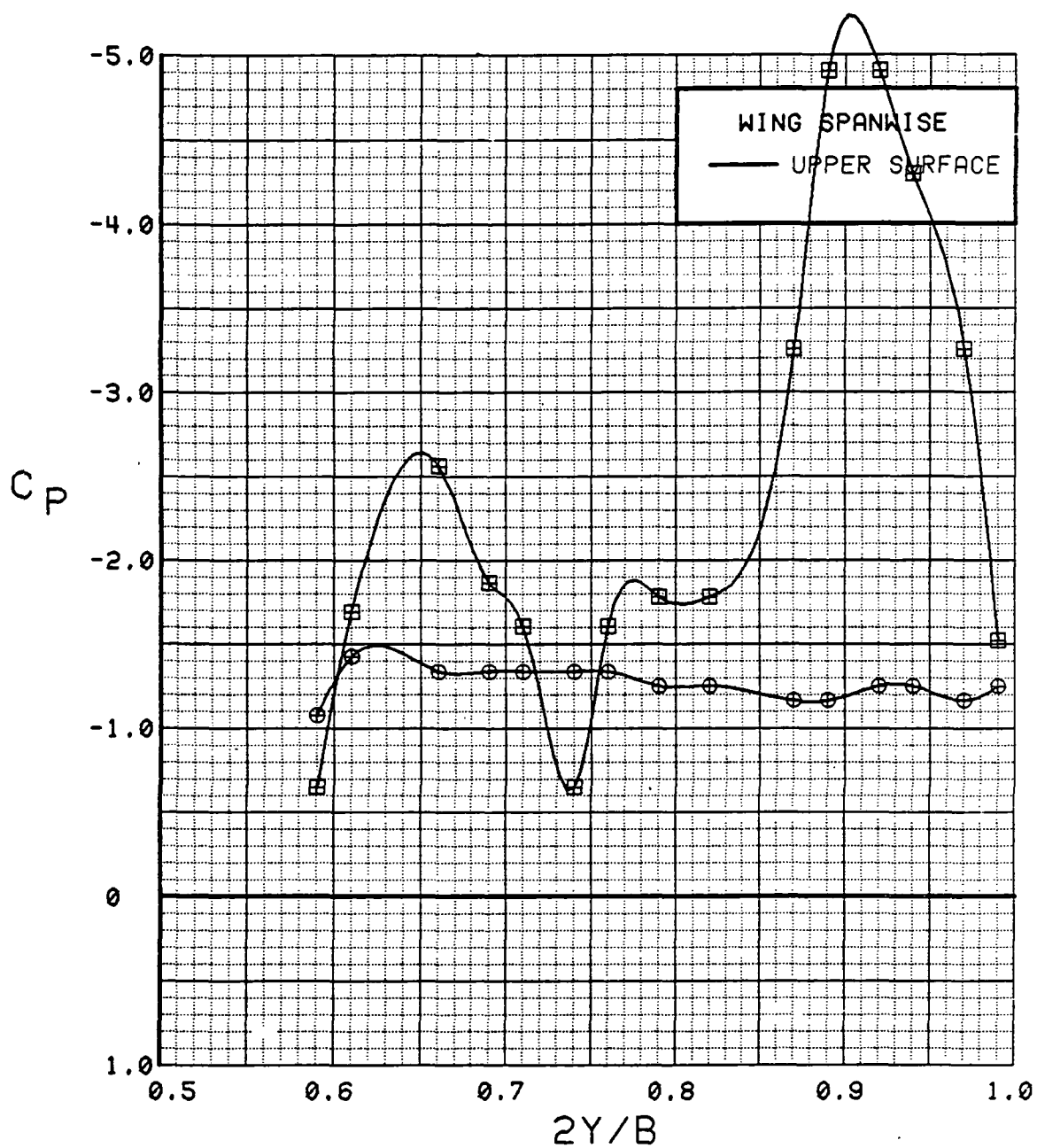


Figure 3.2.4-457 Spanwise Blowing Effects, Spanwise,  $C_T = 1.9$ ,  $\alpha = 16$  deg

SYM	TEST	RUN	ALPHA	CT	ITEF	OTEF	CAN	SWB
⊕	537	28	21.0	1.83	30	30	0	OFF
⊞	537	53	21.2	1.83	30	30	0	ON

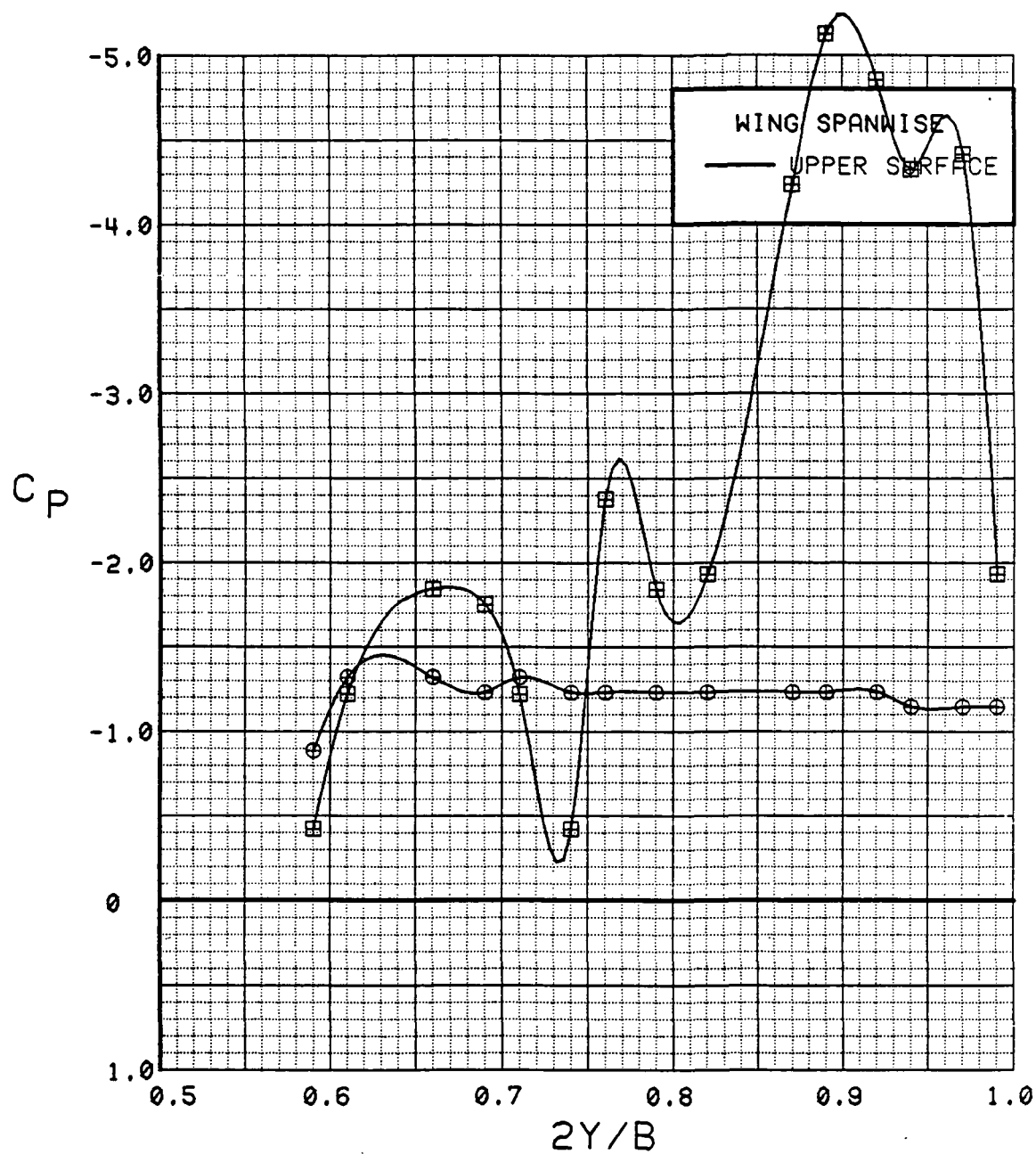


Figure 3.2.4-458 Spanwise Blowing Effects, Spanwise,  $C_T = 1.9$ ,  $\alpha = 20^\circ$

SYM	TEST	RUN	ALPHA	CT	ITEF	OTEF	CAN	SWB
⊕	537	28	25.0	1.83	30	30	0	OFF
⊗	537	53	25.2	1.81	30	30	0	ON

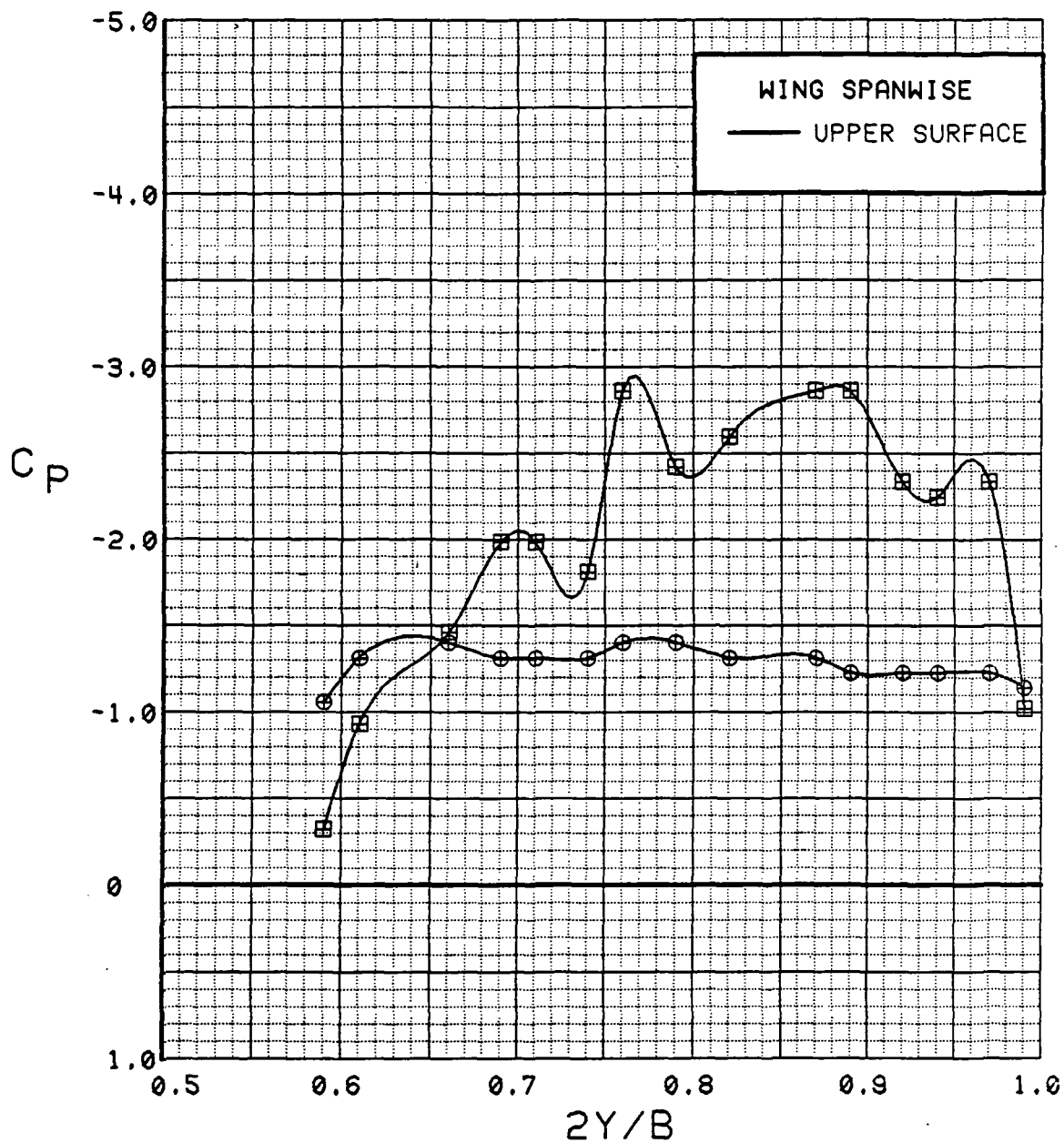


Figure 3.2.4-459 Spanwise Blowing Effects, Spanwise,  $C_T = 1.9$ ,  $\alpha = 24^\circ$



SYM	TEST	RUN	ALPHA	CT	ITEF	OTEF	CAN	SWB
⊕	537	28	29.1	1.83	30	30	0	OFF
⊞	537	53	29.3	1.81	30	30	0	ON

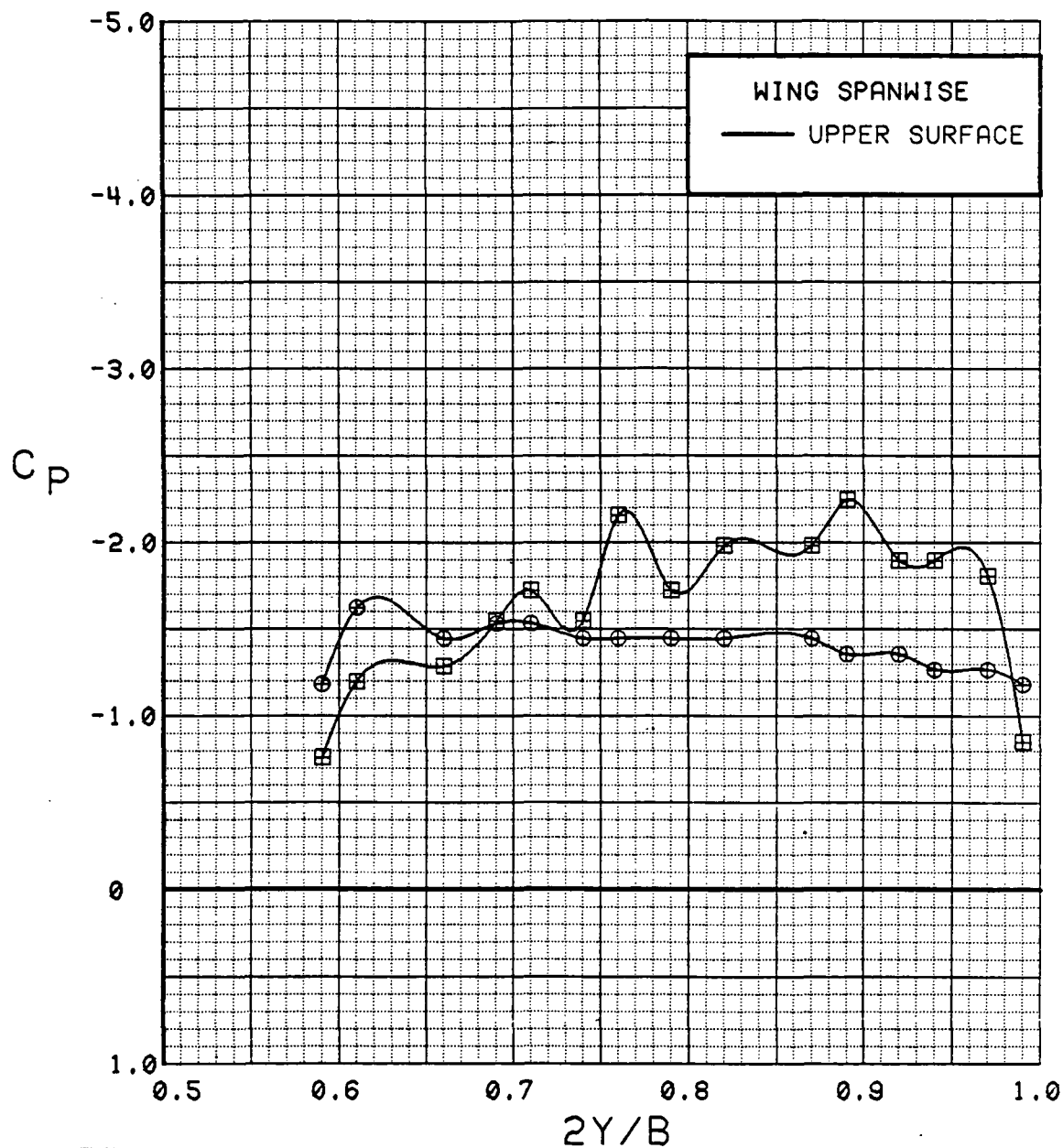


Figure 3.2.4-460 Spanwise Blowing Effects, Spanwise,  $C_T = 1.9$ ,  $\alpha = 28^\circ$

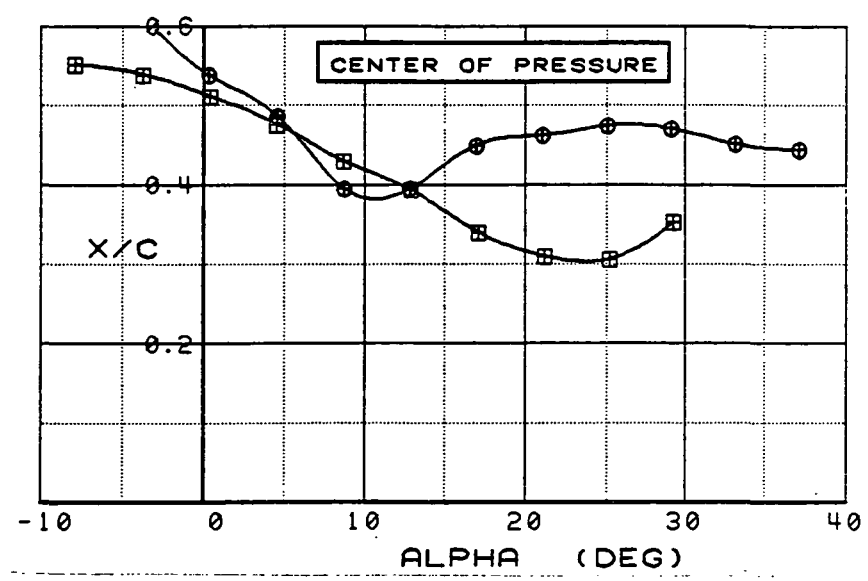
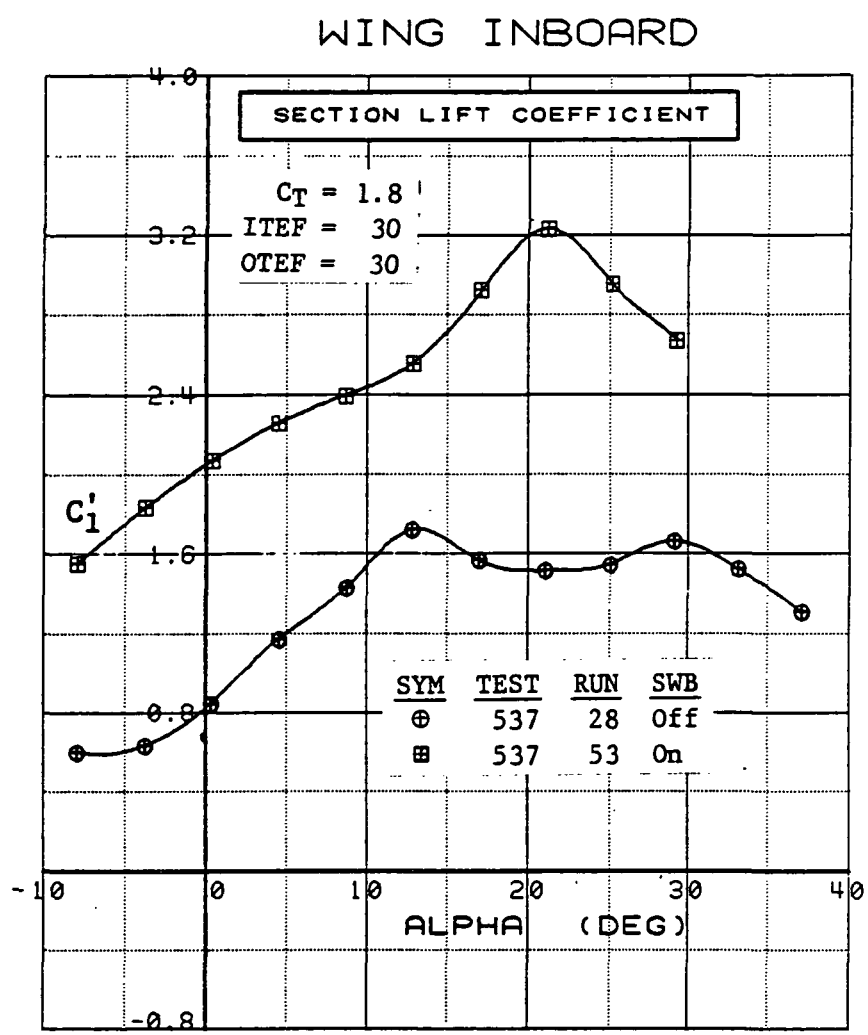


Figure 3.2.4-461 Spanwise Blowing Effects, Inboard,  $C_T = 1.9$ , Integrated Section Properties

## WING OUTBOARD

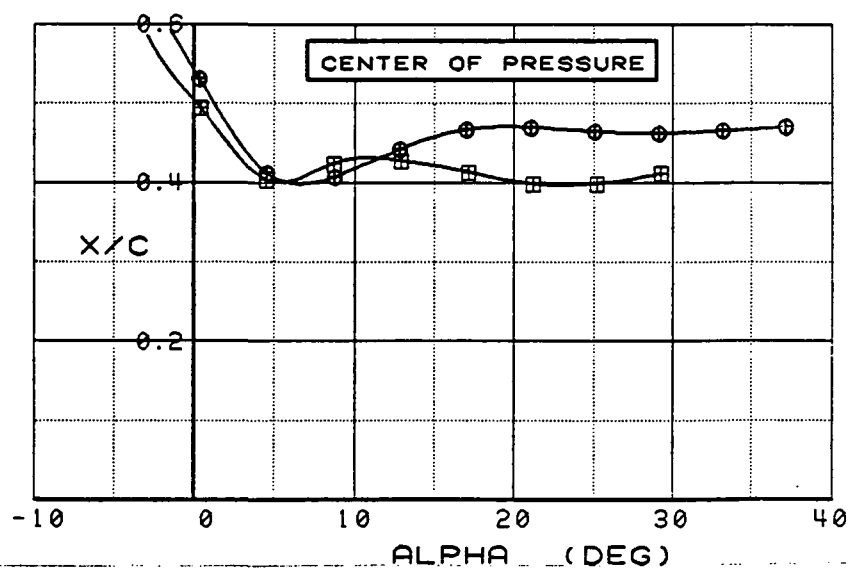
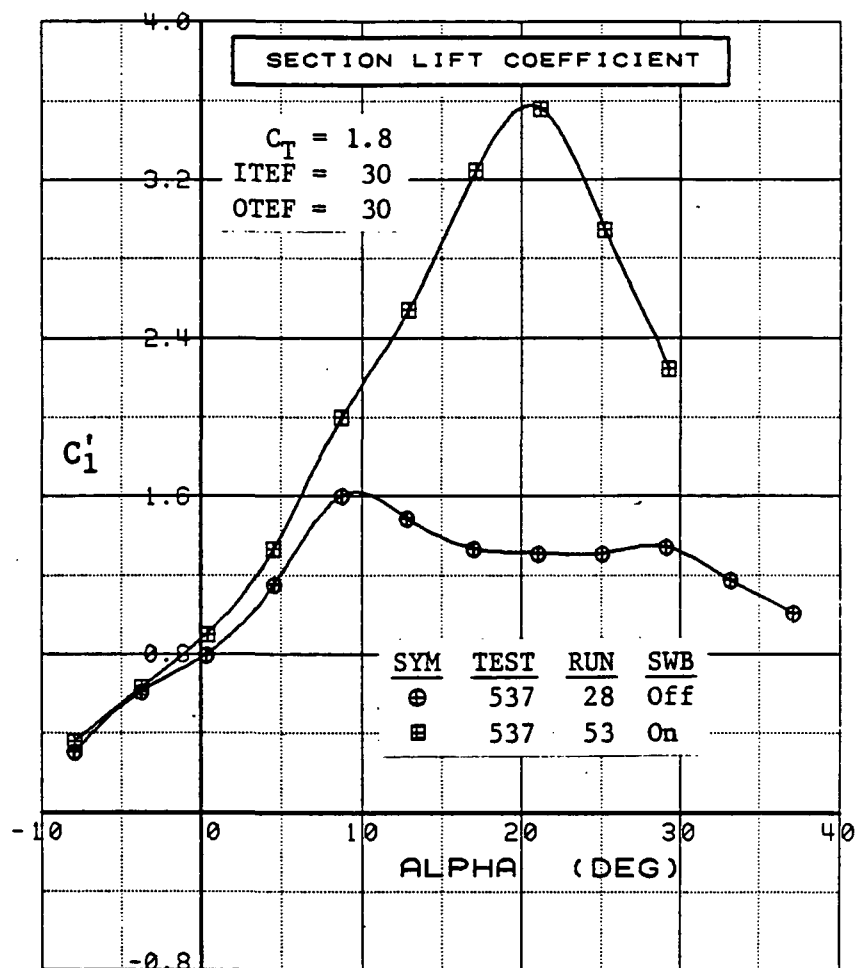


Figure 3.2.4-462 Spanwise Blowing Effects, Outboard,  $C_T = 1.9$ , Integrated Section Properties

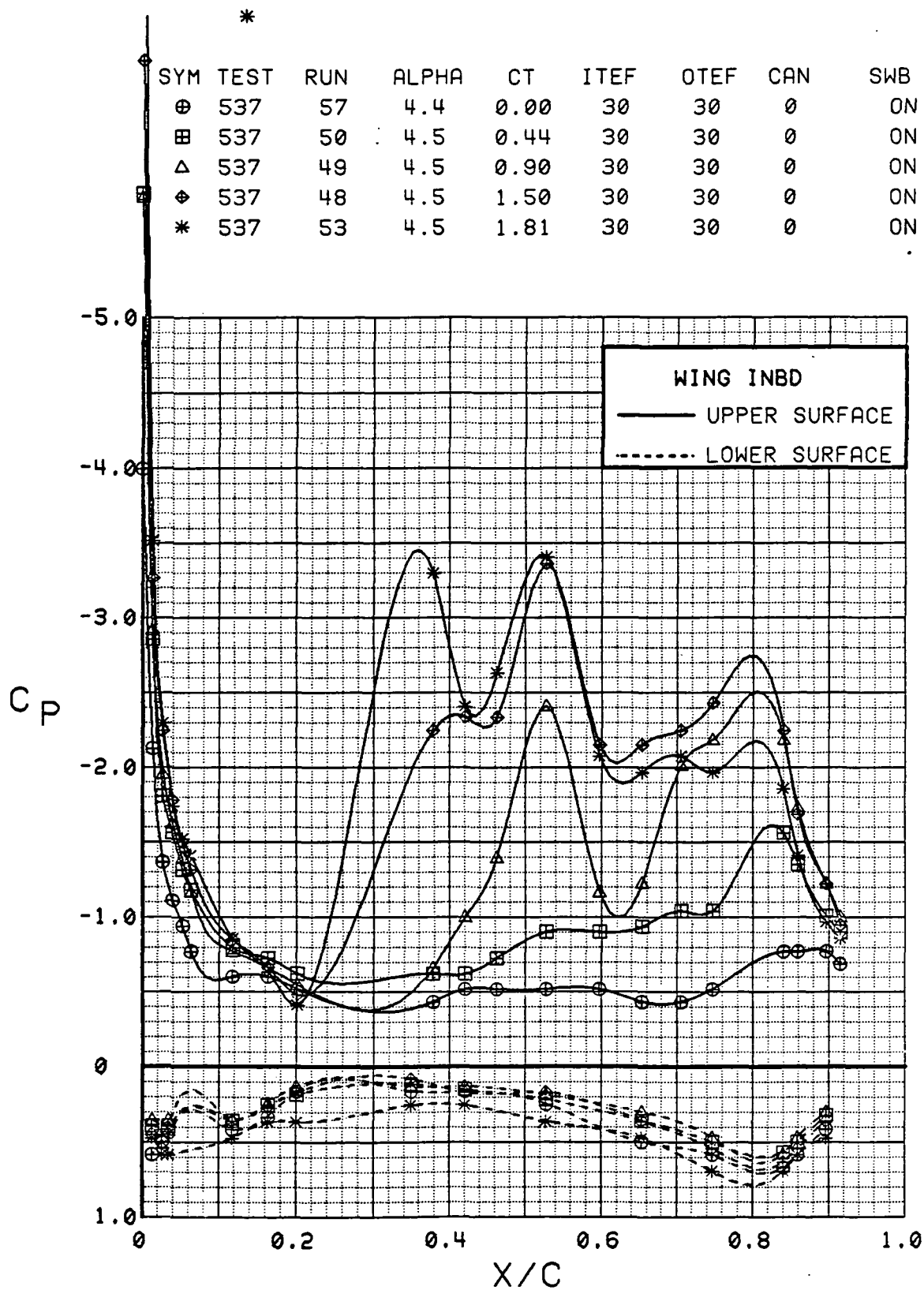


Figure 3.2.4-463 Power Buildup, Spanwise Blowing On, Inboard, Alpha = 4 deg

SYM	TEST	RUN	ALPHA	CT	ITEF	OTEF	CAN	SWB
⊕	537	57	12.7	0.00	30	30	0	ON
⊞	537	50	12.8	0.45	30	30	0	ON
△	537	49	12.9	0.90	30	30	0	ON
◆	537	48	12.9	1.51	30	30	0	ON
*	537	53	12.9	1.82	30	30	0	ON

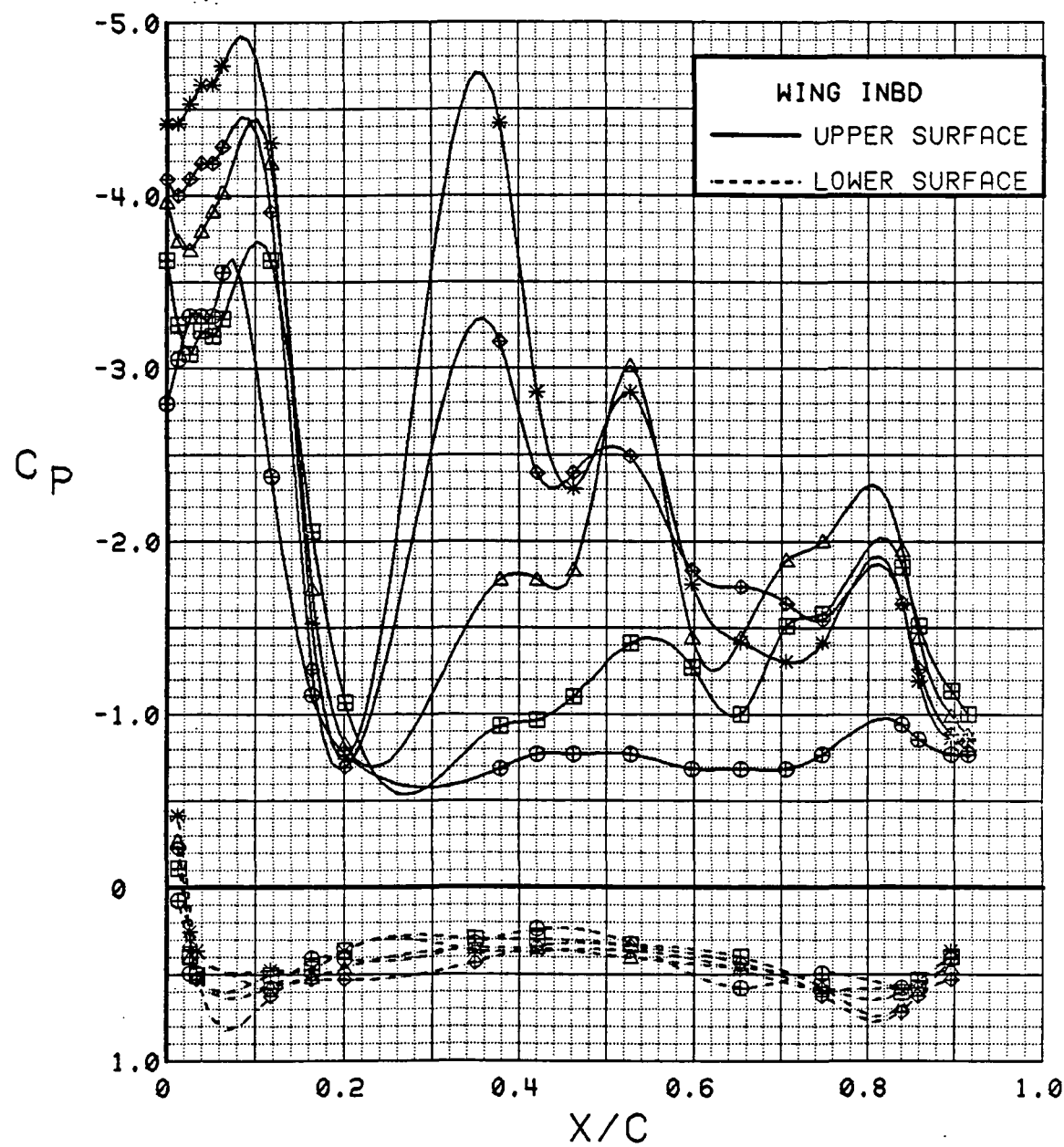


Figure 3.2.4-464 Power Buildup, Spanwise Blowing On, Inboard, Alpha = 12 deg

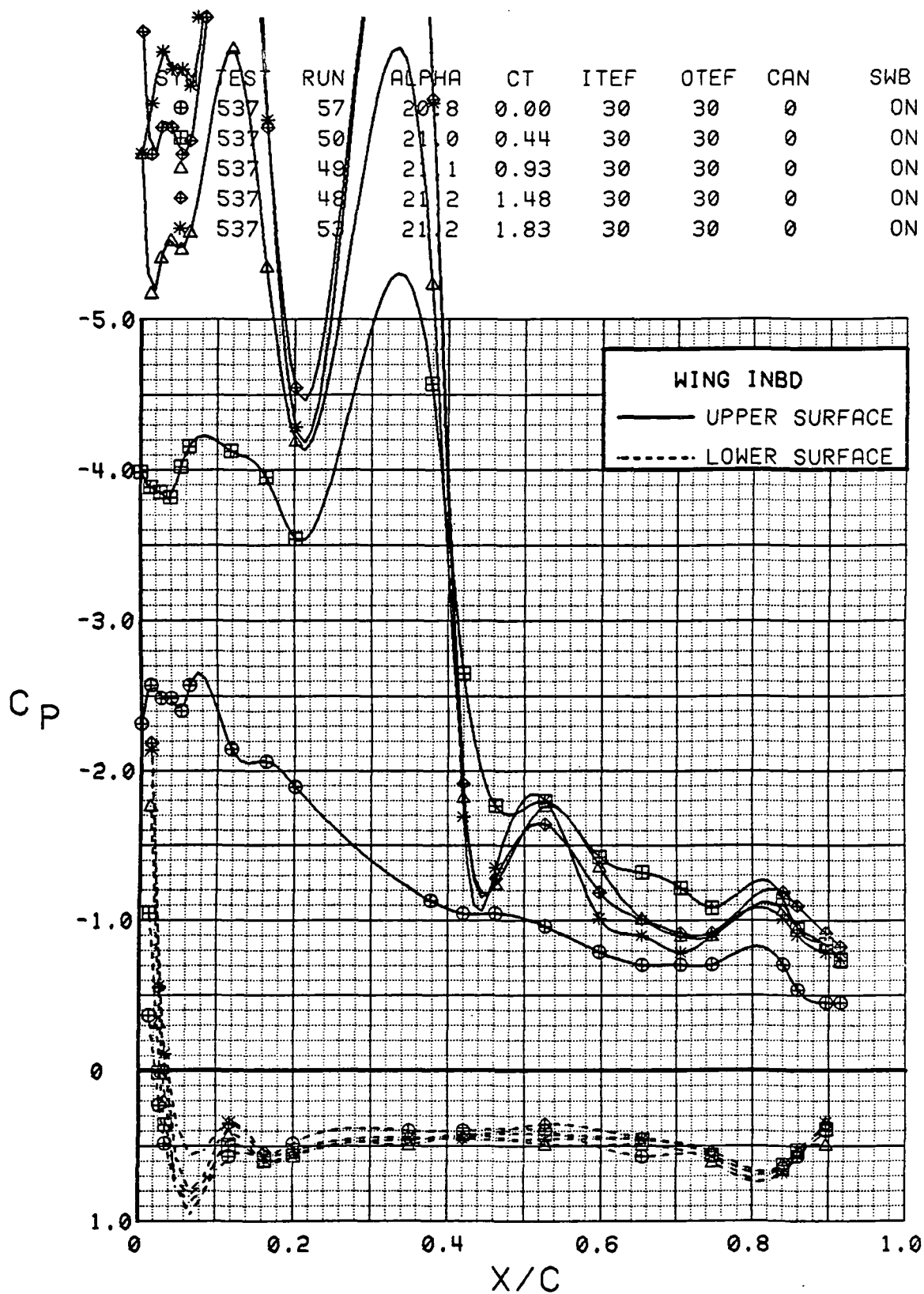


Figure 3.2.4-465 Power Buildup, Spanwise Blowing On, Inboard, Alpha = 20 deg

SYM	TEST	RUN	ALPHA	CT	ITEF	OTEF	CAN	SWB
⊕	537	50	29.1	0.45	30	30	0	ON
⊞	537	49	29.2	0.94	30	30	0	ON
△	537	48	29.2	1.49	30	30	0	ON
◇	537	53	29.3	1.81	30	30	0	ON

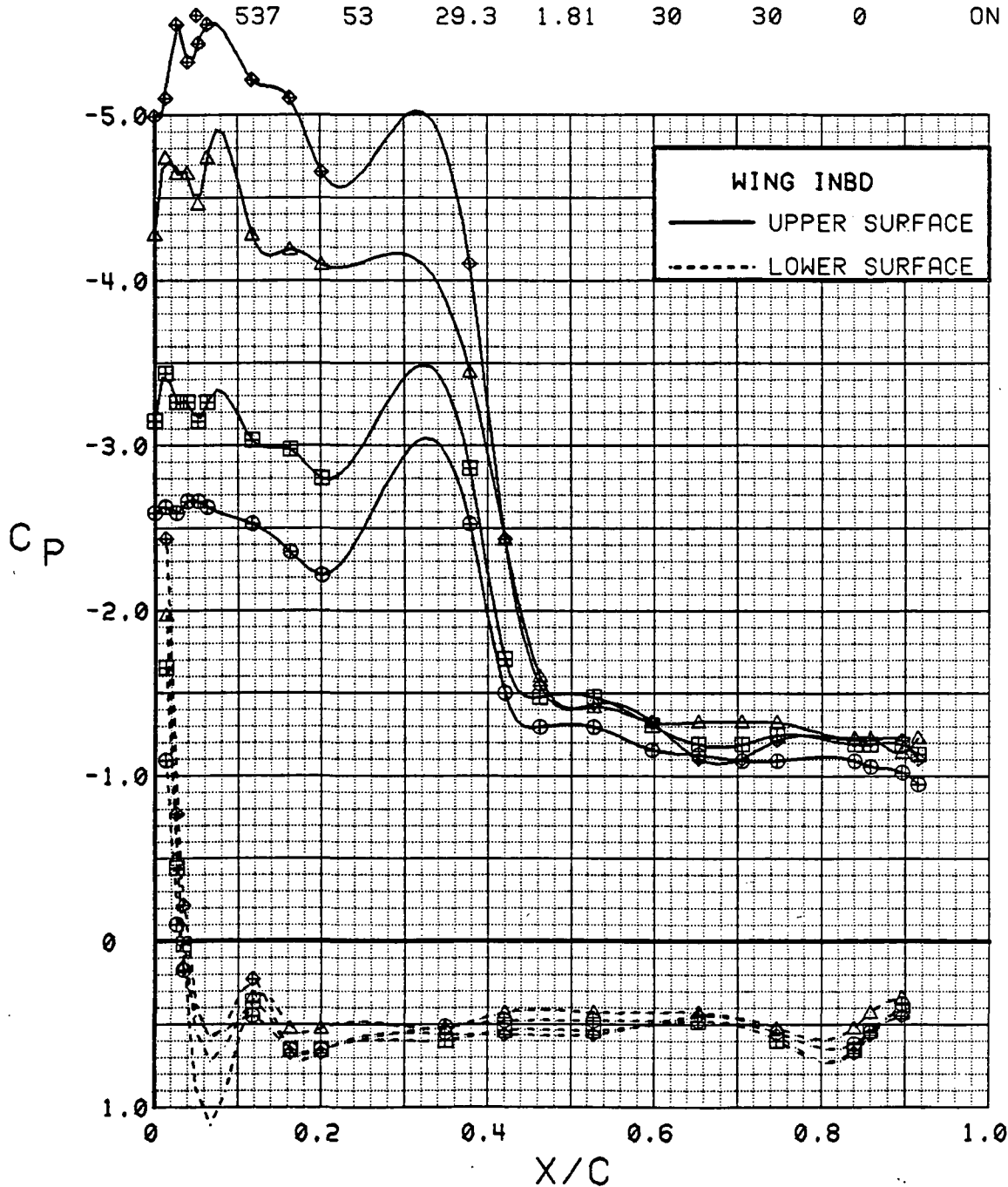


Figure 3.2.4-466 Power Buildup, Spanwise Blowing On, Inboard, Alpha = 28 deg

SYM	TEST	RUN	ALPHA	CT	ITEF	OTEF	CAN	SWB
⊕	537	57	4.4	0.00	30	30	0	ON
⊞	537	50	4.5	0.44	30	30	0	ON
△	537	49	4.5	0.90	30	30	0	ON
⊕	537	48	4.5	1.50	30	30	0	ON
*	537	53	4.5	1.81	30	30	0	ON

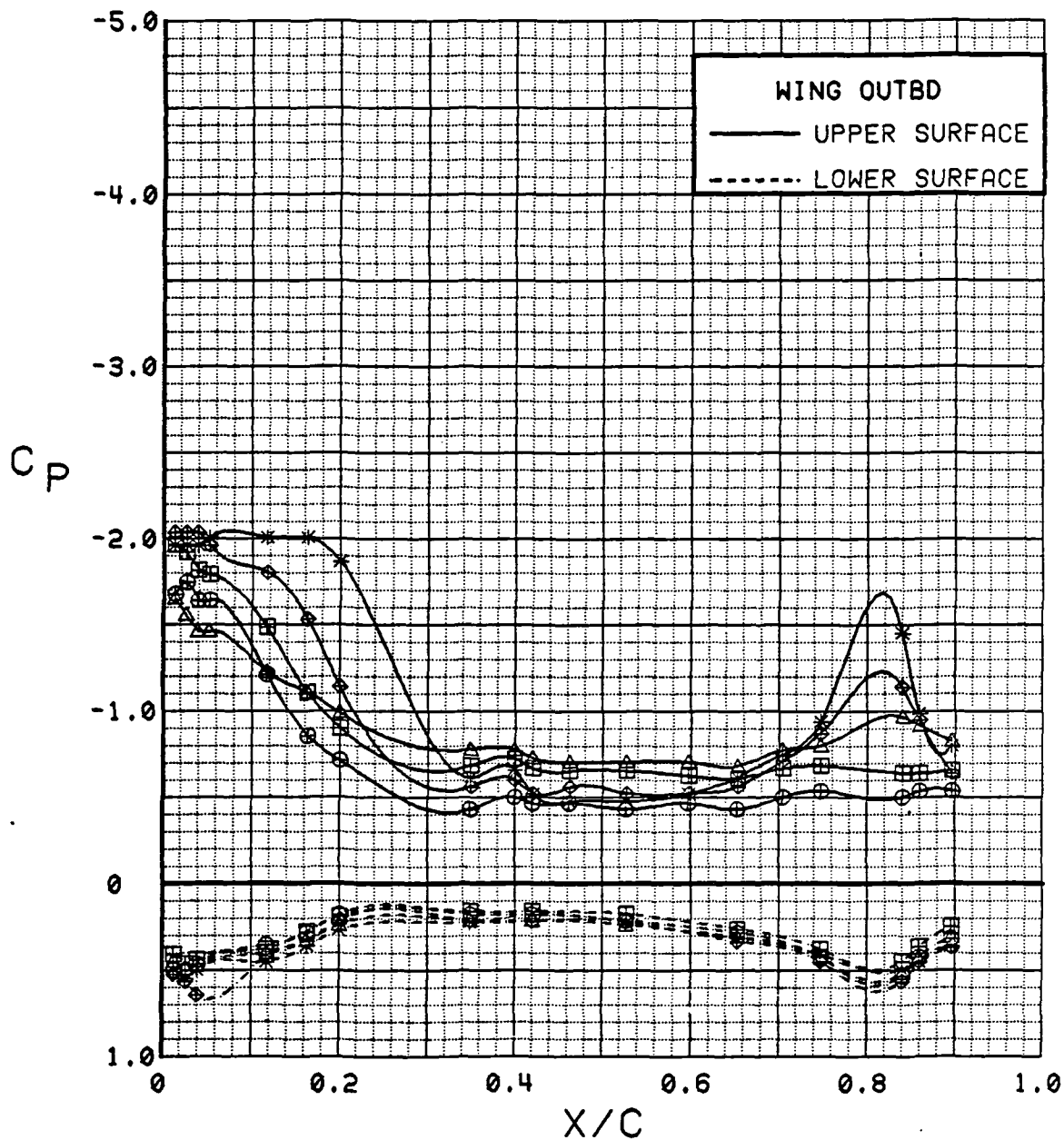


Figure 3.2.4-467 Power Buildup, Spanwise Blowing On, Outboard, Alpha = 4 deg



SYM	TEST	RUN	ALPHA	CT	ITEF	OTEF	CAN	SWB
⊕	537	57	12.7	0.00	30	30	0	ON
⊞	537	50	12.8	0.45	30	30	0	ON
△	537	49	12.9	0.90	30	30	0	ON
⊕	537	48	12.9	1.51	30	30	0	ON
*	537	53	12.9	1.82	30	30	0	ON

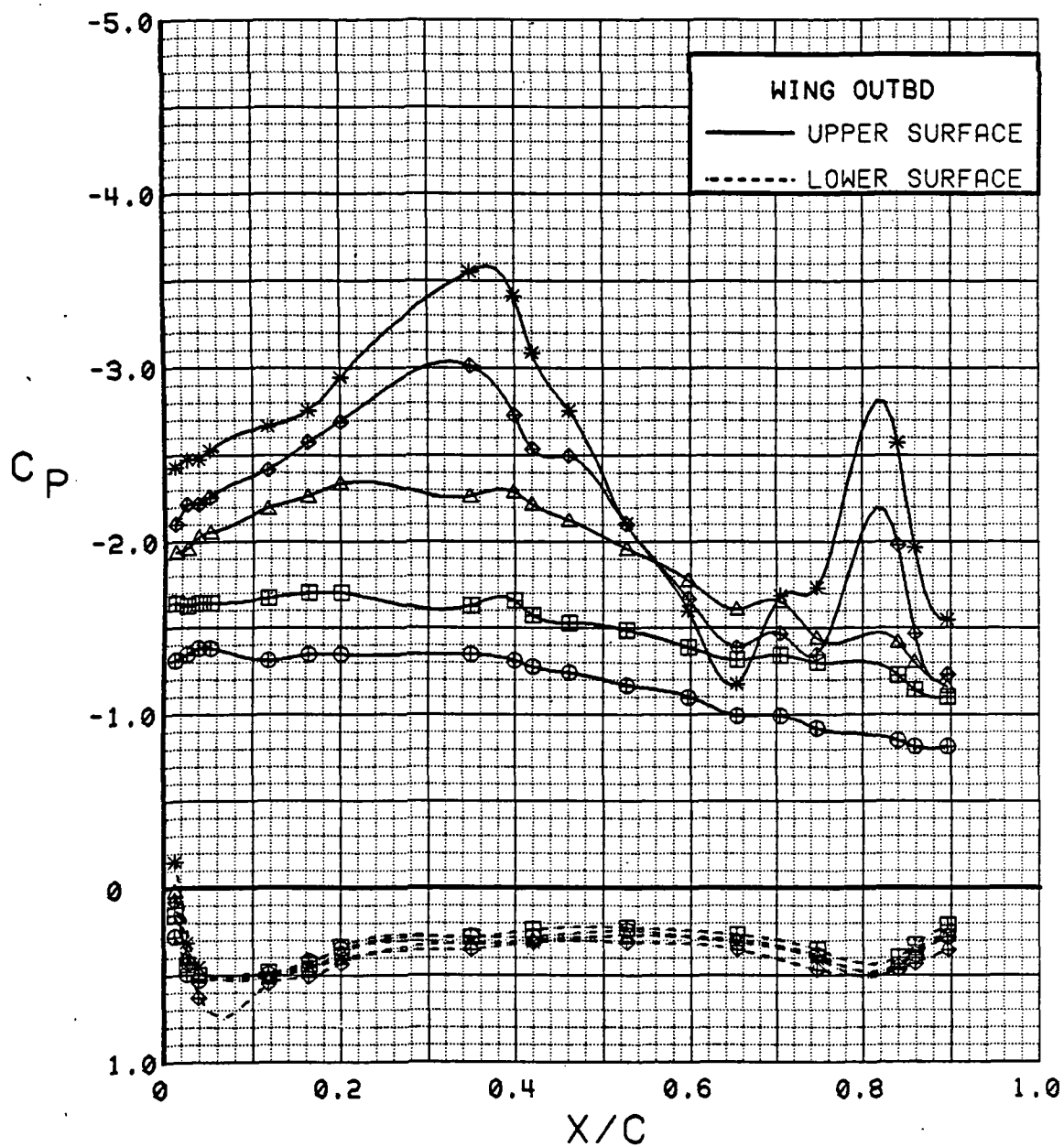


Figure 3.2.4-468 Power Buildup, Spanwise Blowing On, Outboard, Alpha = 12 deg

SYM	TEST	RUN	ALPHA	CT	ITEF	OTEF	CAN	SWB
⊕	537	57	20.3	0.00	30	30	0	ON
⊞	537	50	21.0	0.44	30	30	0	ON
△	537	49	21.1	0.93	30	30	0	ON
⬠	537	48	21.2	1.48	30	30	0	ON
*	537	53	21.2	1.83	30	30	0	ON

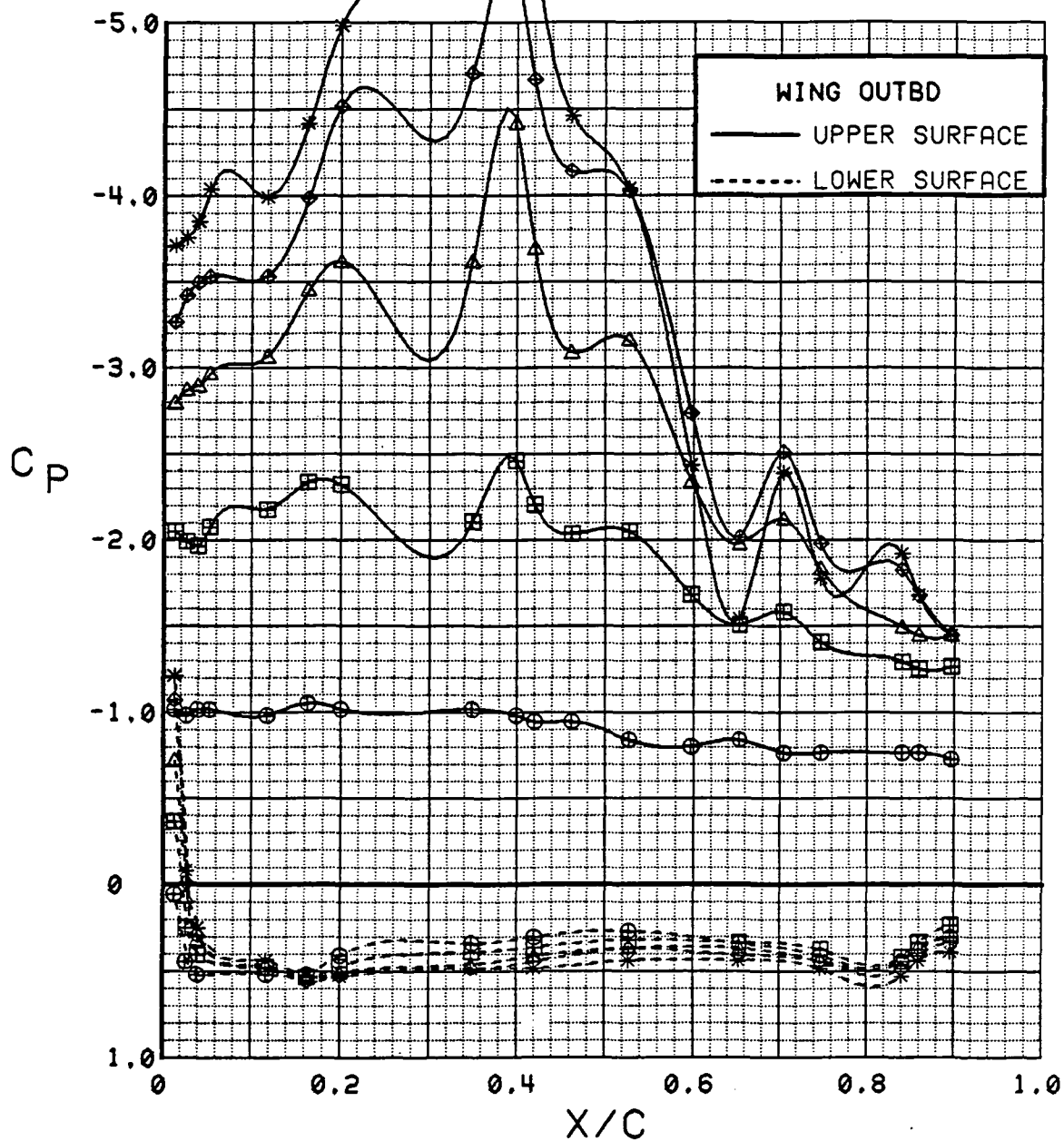


Figure 3.2.4-469 Power Buildup, Spanwise Blowing On, Outboard, Alpha = 20 deg

SYM	TEST	RUN	ALPHA	CT	ITEF	OTEF	CAN	SWB
⊕	537	50	29.1	0.45	30	30	0	ON
⊞	537	49	29.2	0.94	30	30	0	ON
△	537	48	29.2	1.49	30	30	0	ON
⬠	537	53	29.3	1.81	30	30	0	ON

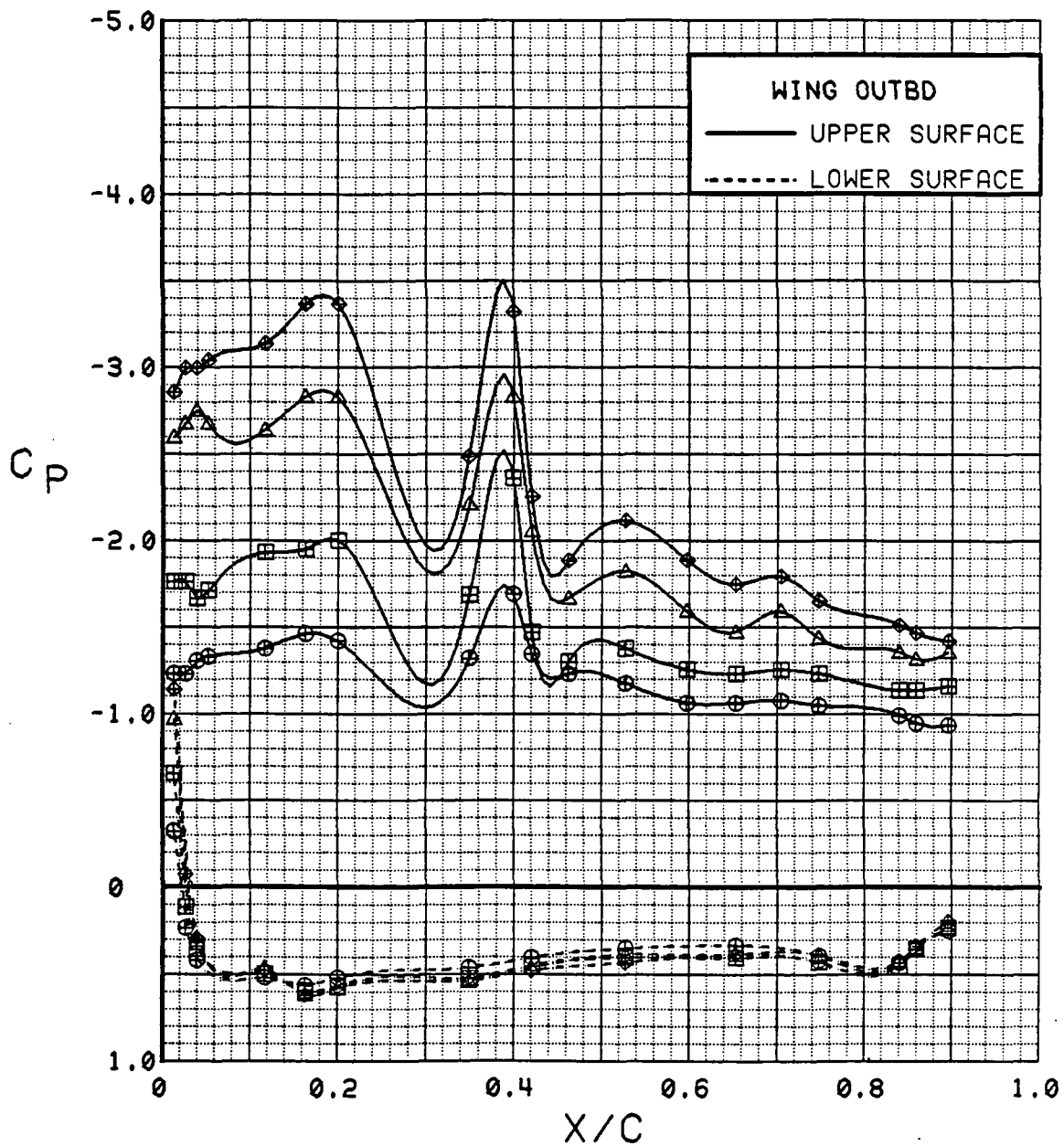


Figure 3.2.4-470 Power Buildup, Spanwise Blowing On, Outboard, Alpha = 28 deg

SYM	TEST	RUN	ALPHA	CT	ITEF	OTEF	CAN	SWB
⊕	537	57	4.4	0.00	30	30	0	ON
⊞	537	50	4.5	0.44	30	30	0	ON
△	537	49	4.5	0.90	30	30	0	ON
◆	537	48	4.5	1.50	30	30	0	ON
*	537	53	4.5	1.81	30	30	0	ON

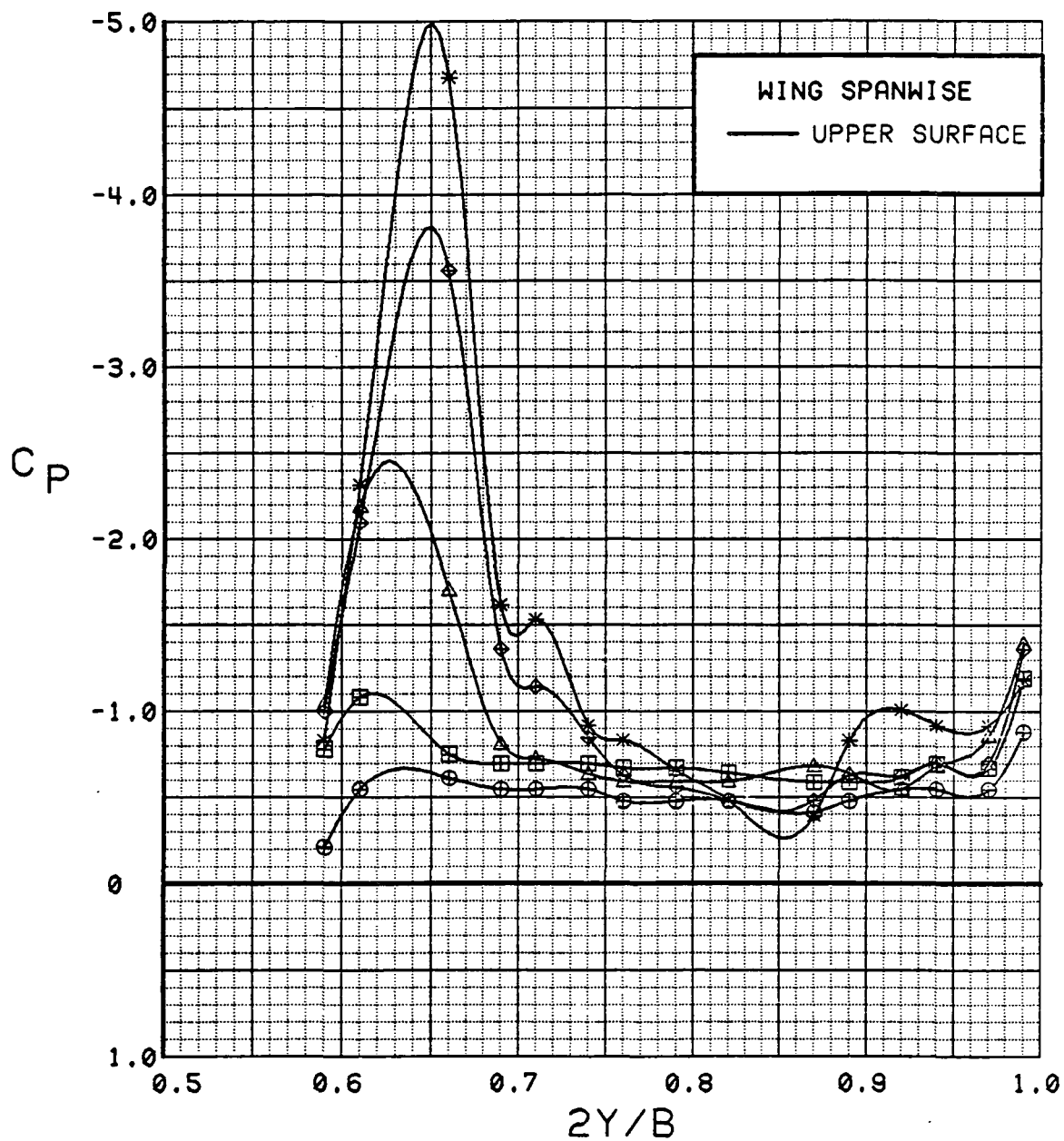


Figure 3.2.4-471 Power Buildup, Spanwise Blowing On, Spanwise, Alpha = 4 deg

SYM	TEST	RUN	ALPHA	CT	ITEF	OTEF	CAN	SWB
⊕	537	57	12.7	0.00	30	30	0	ON
⊞	537	50	12.8	0.45	30	30	0	ON
△	537	49	12.9	0.90	30	30	0	ON
◆	537	48	12.9	1.51	30	30	0	ON
*	537	53	12.9	1.82	30	30	0	ON

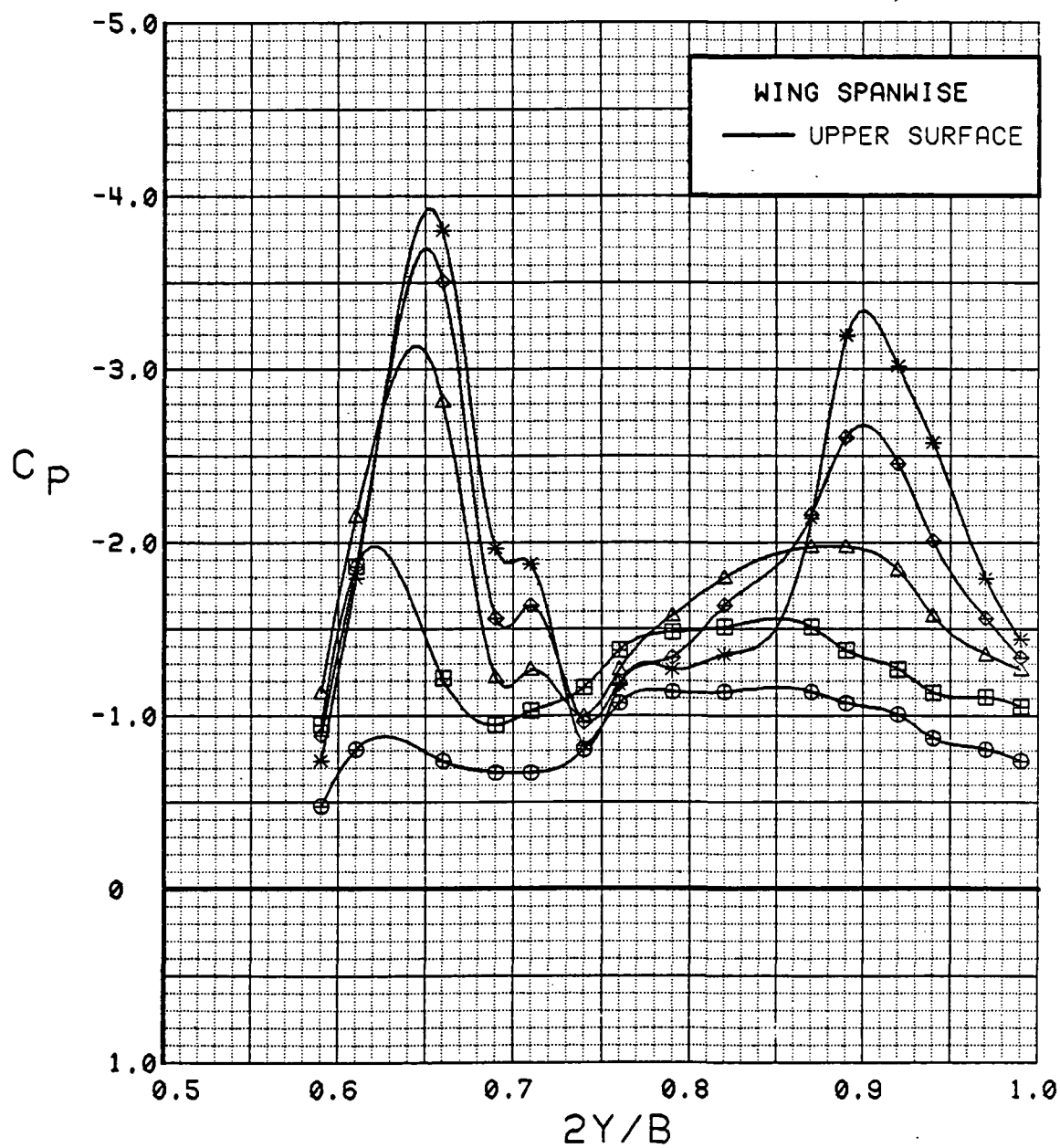


Figure 3.2.4-472 Power Buildup, Spanwise Blowing On, Spanwise, Alpha = 12 deg

SYM	TEST	RUN	ALPHA	CT	ITEF	OTEF	CAN	SWB
⊕	537	57	20.8	0.00	30	30	0	ON
⊗	537	50	21.0	0.44	30	30	0	ON
△	537	49	21.1	0.93	30	30	0	ON
◆	537	48	21.2	1.48	30	30	0	ON
*	537	53	21.2	1.83	30	30	0	ON

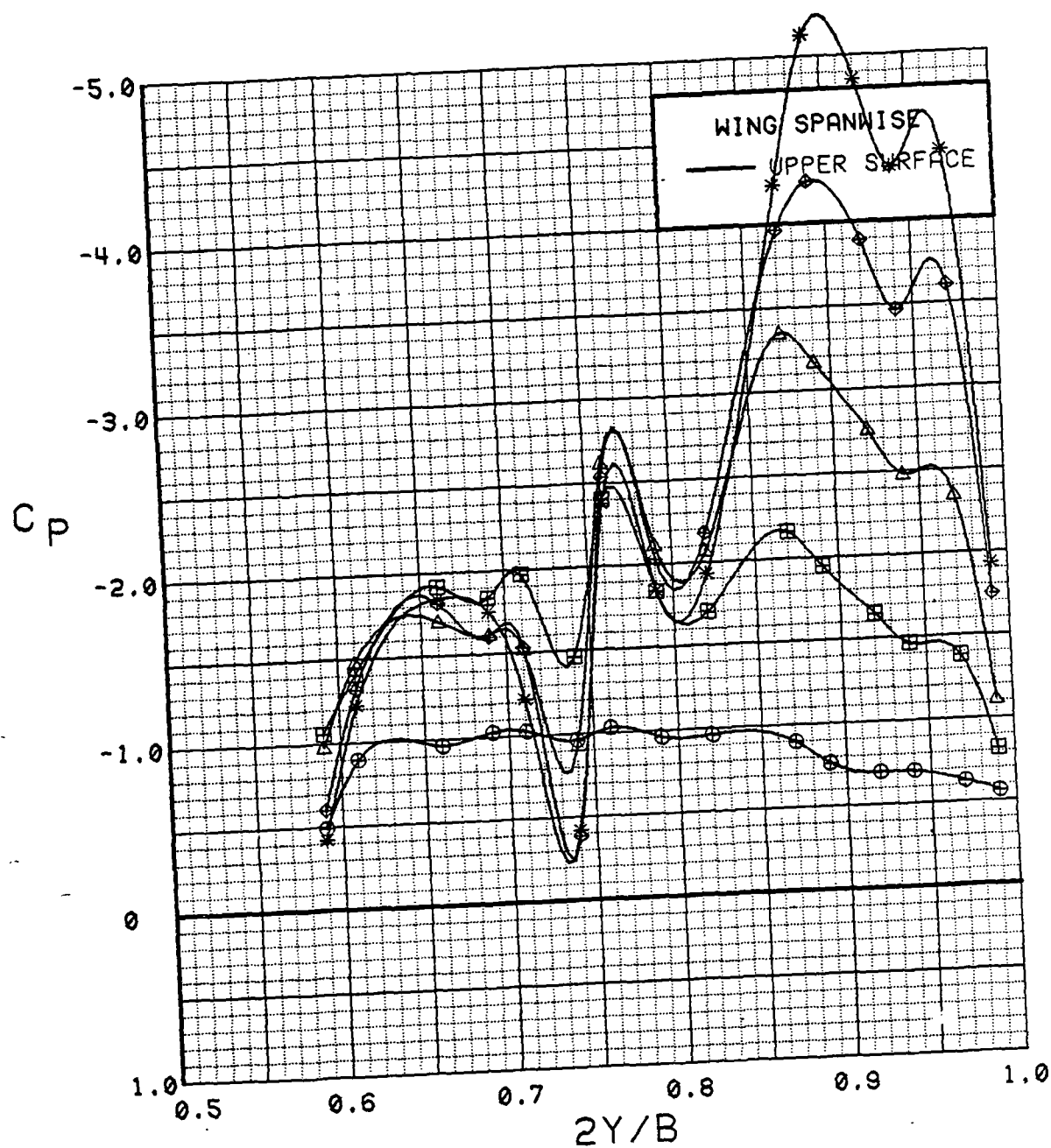


Figure 3.2.4-473 Power Buildup, Spanwise Blowing On, Spanwise, Alpha = 20 deg

SYM	TEST	RUN	ALPHA	CT	ITEF	OTEF	CAN	SWB
●	537	50	29.1	0.45	30	30	0	ON
■	537	49	29.2	0.94	30	30	0	ON
△	537	48	29.2	1.49	30	30	0	ON
◆	537	53	29.3	1.81	30	30	0	ON

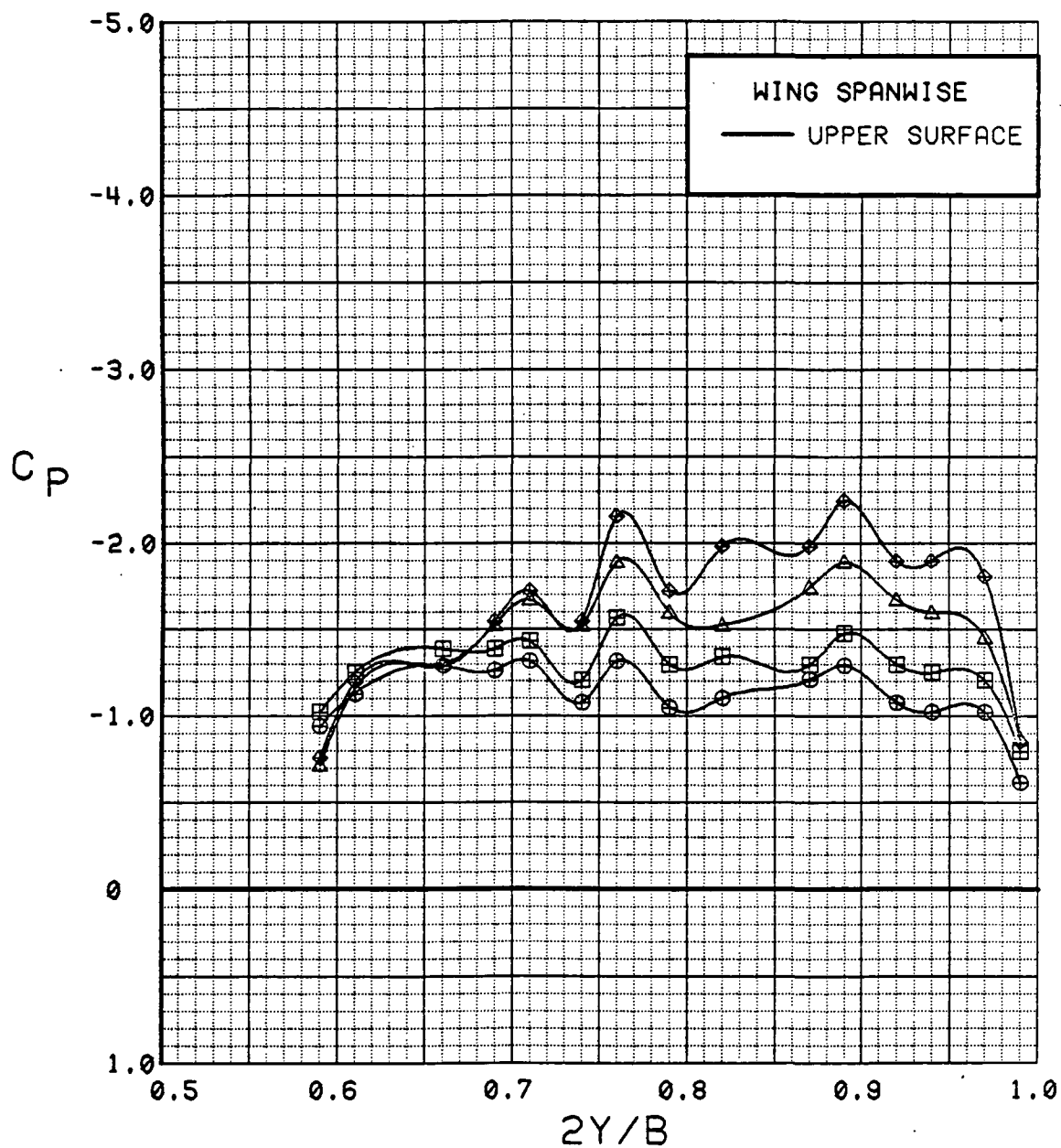


Figure 3.2.4-474 Power Buildup, Spanwise Blowing On, Spanwise, Alpha = 28 deg

# WING INBOARD

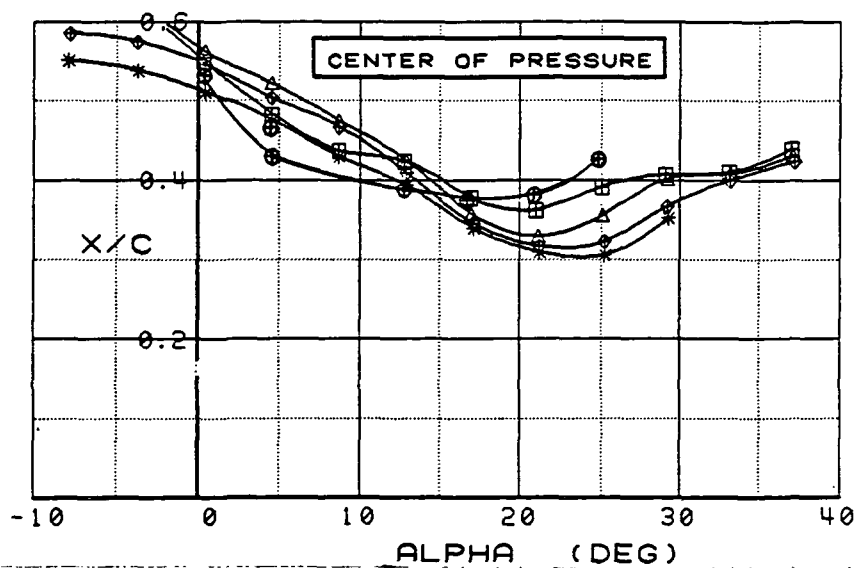
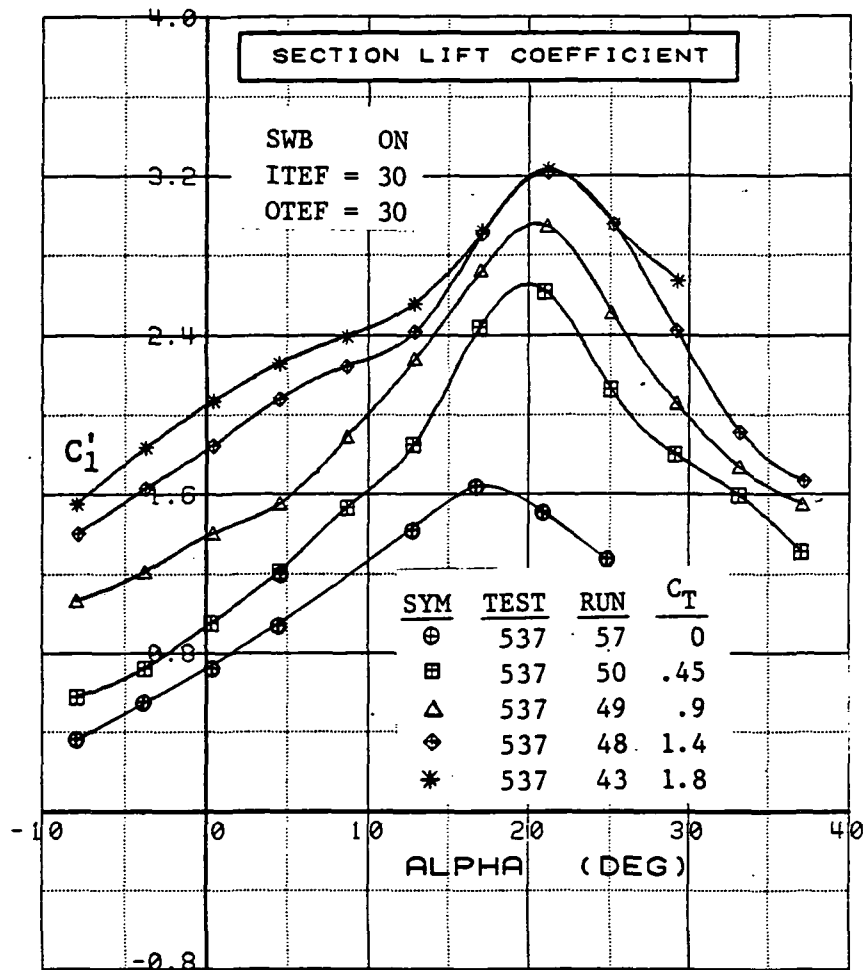


Figure 3.2.4-475 Power Buildup, Spanwise Blowing On, Inboard, Integrated Section Properties



## WING OUTBOARD

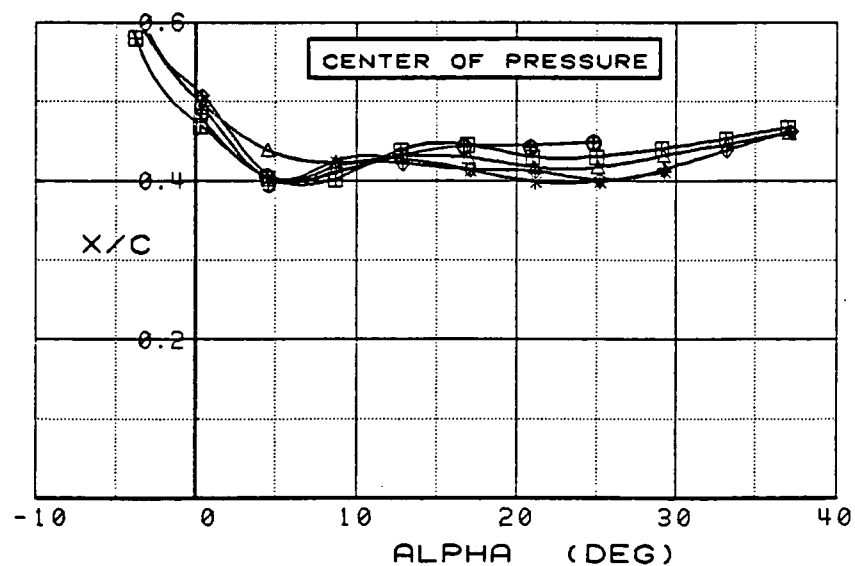
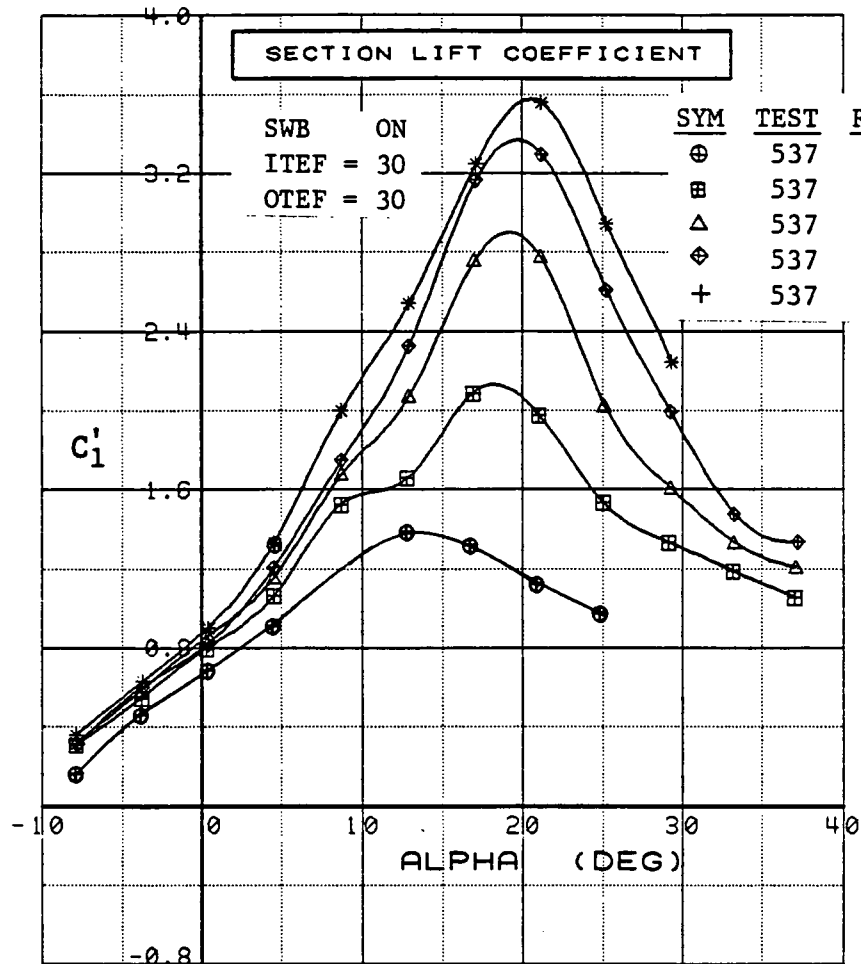


Figure 3.2.4-476 Power Buildup, Spanwise Blowing On, Outboard, Integrated Section Properties

**(This page intentionally left blank.)**

### 3.2.5 Correlation with Small-Scale Model

The General Dynamics Vectored-Engine-Over Wing (VEO-Wing) concept was developed and tested, as discussed in Section 2, in cooperation with the Air Force and NASA. During this development, several small-scale wind-tunnel models of both powered and unpowered configurations were tested. The latest of these tests was on the .108-scale VEO-Wing Research Model, which is a wing/canard configuration with podded nacelles. The planform of this model, which is very similar to that of the Ames Fighter Model, is shown installed in the Langley V/STOL Tunnel in Figure 3.2.5-1.

A comparison of the planform shapes of the large- and small-scale models, with the locations of the pressure taps that were used in the following data presentation, is shown in Figure 3.2.5-2. The small-scale model was instrumented to obtain pressure data on the nacelle, ramp, and wing. Table 9 lists the locations of the pressure taps on the wing, which are arranged in one row on the upper surface and one row on the lower surface. Upper surface taps are located on the left-hand wing; lower-surface taps were located at the

TABLE 9  
PRESSURE TAP LOCATIONS ON  
THE SMALL-SCALE VEO-WING MODEL

Percent Chord	Orifice distance From L.E. cm(in)	
5	1.407	(.554)
15	4.219	(1.661)
25	7.033	(2.769)
31	8.722	(3.434)
40	11.252	(4.430)
50	14.067	(5.538)
60	16.881	(6.646)
70	19.693	(7.753)
78	21.943	(8.639)
90	25.319	(9.968)

100% chord = 28.118 cm (11.070 in)

same span station but on the right-hand wing. It is noted that the local  $\alpha$  at the pressure taps was almost identical for the two models. Both of the models have 4 deg of twist and no incidence in the wing. A complete description of the small-scale model is presented in Reference 18. Primary considerations in the comparison of data from these two models are (1) the relative spanwise locations of the rows of pressure taps, and (2) the percentage of primary nozzle mass flux that is diverted to the spanwise nozzle when SWB is on. In addressing the first consideration, it can be seen in Figure 3.2.5-2 that the non-dimensionalized distance between the SWB nozzle and pressure taps is somewhat greater on the large-scale model than on the small-scale model. The distance from the side of the nacelle to the chordwise row of pressure taps (non-dimensionalized by wing semi-span) for the small-scale model is  $\delta 2y/b = 0.12$  and a similar dimension on the large-scale model is  $\delta 2y/b = 0.16$ .

The second item due consideration is the percentage of mass flux that was diverted to the SWB nozzles. SWB nozzle variations were tested on the small-scale model to deter-

mine the effects of nozzle shape, size, and sweep. The nozzle that most closely matched the large-scale SWB nozzle was also flush, rectangular, and aft swept at a 40-deg angle. (The model-part designation is N1AA for this SWB nozzle). The small-scale model SWB nozzle had an exit area that was 30% of the total exit area of the primary and SWB nozzles. In contrast, the SWB nozzle exit area for the large-scale model was only 14% of the total. Thus, the percentage of mass flux through the SWB nozzle on the small-scale model was approximately twice that on the large-scale model, and this mismatch should be kept in mind when making a comparison of the models with SWB on.

Small-scale model data presented in this section were acquired in the NASA/Langley V/STOL Wind Tunnel Facility (Test No. 204). Both this tunnel and the Ames 40 x 80 foot Wing Tunnel are atmospheric, which lends a degree of similarity to the test conditions. However, it should be noted that the techniques for varying the thrust coefficient were quite different. On the large-scale model,  $C_T$  was varied by changing  $q$ , as discussed in Section 2.2. For the small-scale model, which had a faired-over inlet,  $C_T$  was varied by changing the nozzle-pressure ratio with the external air supply while holding tunnel  $q$  constant. The local Reynolds number ( $Re$ ) along the chordwise rows of pressure taps varied quite significantly between the two models. Based on the local chord at the span station of the pressure taps, the small-scale model  $Re$  was  $1.1 \times 10^6$ . A similar  $Re$  for the large-scale model varied from  $4.2 \times 10^6$  to  $7.7 \times 10^6$ , dependent upon the tunnel conditions that were required to obtain the desired values of  $C_T$ . (Further discussions of these conditions are given in Sections 3.2.2.2.1 and 3.2.3.2.3, and the  $Re$  values are delineated in Table 8.)

The following comparisons of pressure data reveal that the small-scale data are much smoother and appear more well-behaved than the large-scale data. Reasons for this dissimilarity are not known. It was at first conjectured that the flow might be laminar on one model and turbulent on the other. This, however, was not supported by other facts. The small-scale model was tested with a strip of grit located 1.8 cm (0.72 in) from the wing leading edge, ensuring a fully turbulent flow on the wing. The large-scale model, on the other hand, had local values of  $Re$  that were high because of the size of the model and that, when coupled with the sweep and thickness, should have tripped the boundary layer very near the leading edge. In addition to being generally smoother, it will probably be noticed that the small-scale model data does not exhibit a compression in the fairing of the lower surface data near the hinge-line of the deflecting trailing-edge flap. This can be credited to the malfunction of several of the pressure taps in this area and to the curve-fit routine, which faired smooth curves through the data with no allowance for the compression that typically occurs on the lower surface near the hinge line.

Wing pressure distributions comparing the effects of  $\alpha$  with the canards off are shown in Figure 3.2.5-3 and -4 for power on and power off. These data are for a trailing-edge flap deflection of 30 deg (the only condition available for comparison with the canards off). For the power-off case, Figure 3.2.5-3, the small-scale model was well into stall at  $\alpha = 12$  deg (as indicated by the almost-flat shape of the curve). The large-scale model was also separated at the leading edge at  $\alpha = 12$  deg, but the presence of the leading-edge vortex (discussed in Section 3.2.1) held the pressures near the leading edge at relatively high negative values up to  $\alpha = 20$  deg. This phenomena had given way by  $\alpha = 24$  deg; the large-scale model then exhibited the flat shape of a stalled section.

For the power-on comparison with canards off (Figure 3.2.5-4), the data were unavailable at  $\alpha = 8$  deg but show similar trends at  $\alpha = 0$  deg. At  $\alpha = 12$  deg, the small-scale model was obviously stalled, and the large-scale model was again influenced by the vortex, as indicated by the high negative pressures near the leading edge. At higher angles, both models were stalled and displayed about the same levels of pressure. Regardless of the power setting, the pressure levels are approximately the same for these two models both

before and after leading-edge stall. However, near the angles of attack where stall was beginning, the large-scale model developed more sectional lift because of the presence of the vortex.

Angle-of-attack effects with the canards installed are presented (Figures 3.2.5-5 through -8) for two power settings and two trailing-edge flap settings. The outstanding feature compared with power off and flaps neutral (Figure 3.2.5-5) is that the small-scale model leading-edge seems to remain attached to very high angles of attack. The large-scale model, in contrast, encountered favorable effects from the vortex at  $\alpha = 12$  deg and 16 deg, but it was deeply stalled at  $\alpha = 24$  deg. There is some evidence in this plot of a vortex on the small-scale model (similar to that on the large-scale model) that influenced the pressures. Note that a compression occurred at  $x/c = .25$  at  $\alpha = 16$  deg. This resembles the trends indicated by the taps located beneath the leading-edge vortex in the large-scale data.

Figure 3.2.5-6 shows the comparison of the models with trailing-edge flaps undeflected but power on. The application of power created more negative pressures near the leading edge of the small-scale model but did not bring on separation. The addition of power to the large-scale model strengthen the vortex at this location at  $\alpha = 12$  deg and significantly improved the sectional lift developed on the stalled section at  $\alpha = 25$  deg. Incidentally, the large-scale model at this condition dramatically shows the differences between attached flow, vortex-influenced flow, and stalled flow in the data curves for  $\alpha = 8, 12$ , and 16 deg, respectively.

Deflection of the trailing-edge flaps (Figure 3.2.5-7) increased circulation about the wing and "tended" to decrease the leading-edge pressures. The small-scale model flow, which had remained attached up to  $\alpha = 24$  deg without flap deflection, continued to be attached up to  $\alpha = 16$  deg when the flaps were deflected. At  $\alpha = 24$  deg, however, the increase in circulation caused the leading-edge flow to separate and the leading-edge pressures to increase, thus reversing the trend of more negative pressures with higher values of  $C_T$ . Trailing-edge flap deflection on the large-scale model also "tended" to decrease leading-edge pressures, which caused an earlier onset of the influence of the vortex and an earlier stall. The effects of  $\alpha$  with both power on and flaps deflected are shown in Figure 3.2.5-8. The trends in these data are similar to those in the power-off data (Figure 3.2.5.7) except that the overall upper surface pressures are decreased by the thrust-induced circulation.

The influence of the canards on each of the models is illustrated by a series of canard on/off comparisons at  $\alpha = 4, 12$ , and 20 deg. These plots are presented for power off (Figures 3.2.5-9 through -11) and for power on (Figures 3.2.5-12 through -14). The wing pressures on each model are directly influenced by the downwash of the canard, which in effect, reduced the local angle of attack. On the small-scale model, the canard downwash reduced the leading-edge suction at  $\alpha = 4$  deg (Figure 3.2.5-9), and at  $\alpha = 12$  deg (Figure 3.2.5-10) it caused the flow, which was barely stalled with the canard off, to reattach but remain under the influence of an apparent leading-edge vortex. The canard effect on the small-scale model at  $\alpha = 20$  deg (Figure 3.2.5-11) was very similar to the effect at  $\alpha = 12$  deg. The effects of the canard on the small-scale model with power on were almost the same as with power off as may be seen by a comparison of the small-scale data in Figures 3.2.5-9 through -11 with the small-scale data in Figures 3.2.5-12 through -14.

The effects of the canard on the wing pressures of the large-scale model were very similar to those of the small-scale model. A better definition of the pressure, however, is provided near the leading edge where the canard effects were greatest. Removal of the canard at  $\alpha = 4$  deg and  $C_T = 0$  (Figure 3.2.5-9) eliminated the downwash and caused a

change much like increasing  $\alpha$  from 4 deg to 8 deg, (compare with Figure 3.2.5-5). At  $\alpha = 12$  deg, removal of the canard on the large-scale model caused the wing to stall (Figure 3.2.5-10). At  $\alpha = 20$  deg (Figure 3.2.5-11) removal of the canard caused the distribution to be changed from partially stalled (sloped distribution) to completely stalled (flat distribution). Canard on/off effects with power on are almost the same at  $\alpha = 4$  and 12 deg (Figures 3.2.5-12 and -13). At  $\alpha = 20$  deg with power on, the wing was completely stalled with the canard off (Figure 3.2.5-14) and when the canard was installed, the downwash was not sufficient enough to cause reattachment on the wing as it had with power off.

In conclusion, the effects of the canards are almost identical between the large-scale and small-scale models in that the canard downwash delayed separation and retarded the inboard movement of the vortex. Where the effects of the canard appear drastically different between the two models, as in Figure 3.2.5-14, the reason lies in the basic differences in the wing flow patterns as illustrated by the  $\alpha$ -sweeps in Figures 3.2.5-3 through -8 and not in the relative effectiveness of the two canards or their downwash intensities.

Trailing-edge flap deflections are compared at  $\alpha = 4$  and 12 deg with power off and power on in Figures 3.2.5-15 through -18. For the power-off data at  $\alpha = 4$  deg, which are shown in Figure 3.2.5-15, flap deflections decreased the upper-surface pressures and increased the lower surface pressures over the entire wing chord on each model. Although the trends are similar, the small-scale model flap appears to have had slightly more effect. At  $\alpha = 12$  deg (Figure 3.2.5-16) the flap effects on the small-scale model were very similar to those at  $\alpha = 4$  deg. Deflection of the large-scale model flap at  $\alpha = 12$  deg uniformly increased the pressure on the lower surface, but the upper surface was complicated by a movement of the vortex from a position where it was only barely affecting the inboard row of pressure taps to a position further inboard where it had a strong influence on the entire row of taps. The aft portion of the chord was presumably near the vortex recompression since some of the pressures were higher with flap deflected. Consequently, the data for the large-scale model in Figure 3.2.5-16 are not indicative of the pressure changes due to flap deflection over the remainder of the wing. Data in Figures 3.2.5-17 and -18 show that the addition of power had little effect on the flap increment of either model, except for the large-scale model at  $\alpha = 12^\circ$ . (Compare Figures 3.2.5-16 and 3.2.5-18). In this case, the vortex did not adversely affect the flap incremental upper-surface loading as it had with poweroff.

Comparisons of the power effects on the large- and small-scale models are presented in Figures 3.2.5-19 through -26 for four angles of attack at flap deflection angles of 0 and 30 deg. Power-on data are shown exclusively for  $C_T \approx 1.4$  so that the tunnel  $q$  variations that influenced the large-scale model data would not distort this comparison. For the  $\alpha = 4$ -deg case (Figure 3.2.5-19) the flow was attached, and application of power decreased the upper surface pressures across the entire chord of both models. At  $\alpha = 8$  deg (Figure -20) the small-scale model pressures decreased across the entire chord as they did at  $\alpha = 4$  deg. The large-scale model data at  $\alpha = 8$  deg are less conclusive: the power caused a decrease in pressure at the leading edge, but aft of the leading edge, the power-on data fluctuated about the power-off data. The reason for this is somewhat unclear (as addressed in Subsection 3.2.4.3.1). At  $\alpha = 12$  deg (Figure 3.2.5-21) the small-scale model flow was still attached with power on and with power off, while the large-scale model flow, which was beginning to separate with power off, came under the strong influence of the vortex as it moved inboard with the application of power.

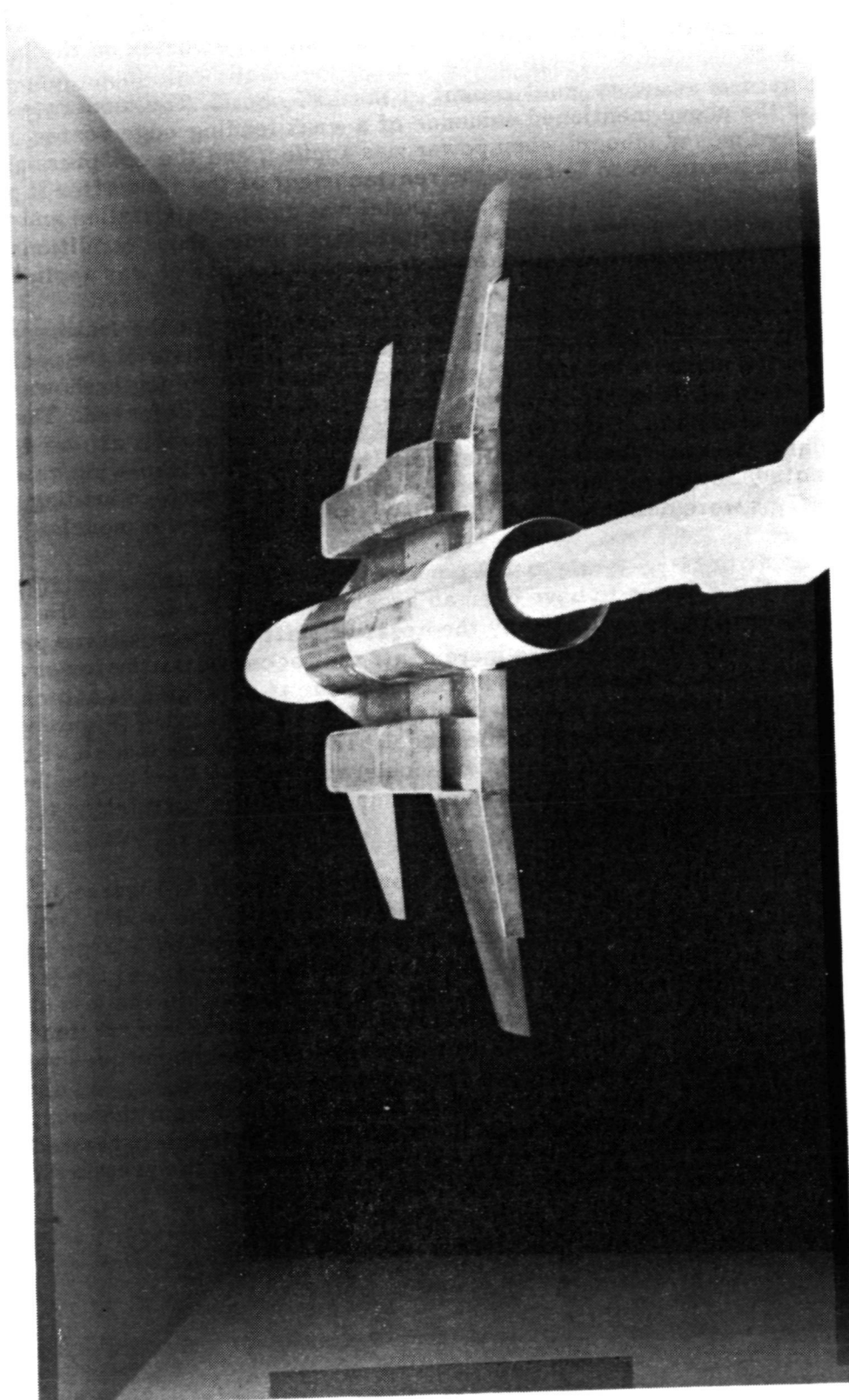
Power on the small-scale model at  $\alpha = 24$  deg produced faint evidence of a wing leading-edge vortex similar to the one on the large-scale model. Because of the wide spacing between pressure taps, this conclusion could not have been drawn solely from the small-scale model data. This vortex was identified only because of the authors' prior

exposure to the more well-defined trends of the leading-edge vortex on the large-scale model. Note in Figure 3.2.5-22 that power caused the small-scale model upper surface pressures to decrease at every point except at the 15% chord. The moderate compression at this point is the above mentioned evidence of a weak leading-edge vortex, which is presumed to have moved inboard when power was applied, and the compression near the 15% chord is also presumed to be from the reattachment of the flow after it passed over the vortex. At  $\alpha = 24$  deg, the large-scale model was completely stalled and the power effects, as discussed in earlier sections, are quite large under these conditions. This was demonstrated by the substantial decrease in pressures when power was applied.

The effects of power on the two models are compared with the trailing-edge flaps deflected in Figures 3.2.5-23 through -26. The same angles of attack are presented that were shown for the undeflected trailing edge except that  $\alpha = 16$  deg is shown instead of  $\alpha = 24$  deg because of the absence of data at  $\alpha = 24$  deg, flaps deflected. The relationship between the power effects of the large-scale and small-scale models at  $\alpha = 4, 8$ , and  $12$  deg is essentially the same for the flap-deflected case and the clean-wing case discussed above. It is noted, however, that power produced more upper surface loading when the trailing-edge flaps were deflected, but this similarly applied to both models.

Discussion of the large-scale model power effects in Subsections 3.2.3.2.3 and 3.2.4.4.1 pointed out that there seems to have been an acceleration of the flow on the lower surface when power was applied, as indicated by the negative shift in lower surface pressures. This is in contrast to positive pressure increments that occurred on the lower surface from increased upwash. This phenomenon did not occur at all angles of attack and flap settings, but it is noted that the clean-wing data at  $\alpha = 8$  and  $12$  deg (Figures 3.2.5-20 and -21) show it clearly on the large-scale model. The small-scale model, at these conditions, also shows that power caused an acceleration of the flow on the lower surface, but the decrease in pressure was smaller on this model, and the postulation of accelerated flow, although there, is less conclusive.

Comparisons of the effects of spanwise blowing are shown in Figures 3.2.5-27 through -30 for  $\alpha = 4$  and  $12$  deg at  $C_T \approx 0.9$  and  $1.9$ . Both of the models are generally affected by SWB with a compression nearing mid-chord, followed by a large suction peak. The compressions are caused by the wing flowfields as they approached the jets, and the areas of suction are the direct result of the high-velocity air within the jets passing over those portions of the wing chords. These patterns of compression and suction persisted at both of these alphas and power settings, although their relative magnitudes vary considerably. The small-scale model data are too sparse to develop a good understanding of the wing flowfield. Consequently, not much can be surmised from the comparisons of SWB except that general trends exist near the locations where the jets crossed the instrumented chords and that there was generally a reduction in the pressures near the leading edge.



General Dynamics Small-Scale VEO-Wing Model  
Installed in the NASA/Langley V/STOL Tunnel

Figure 3.2.5-1

ORIGINAL PAGE IS  
OF POOR QUALITY



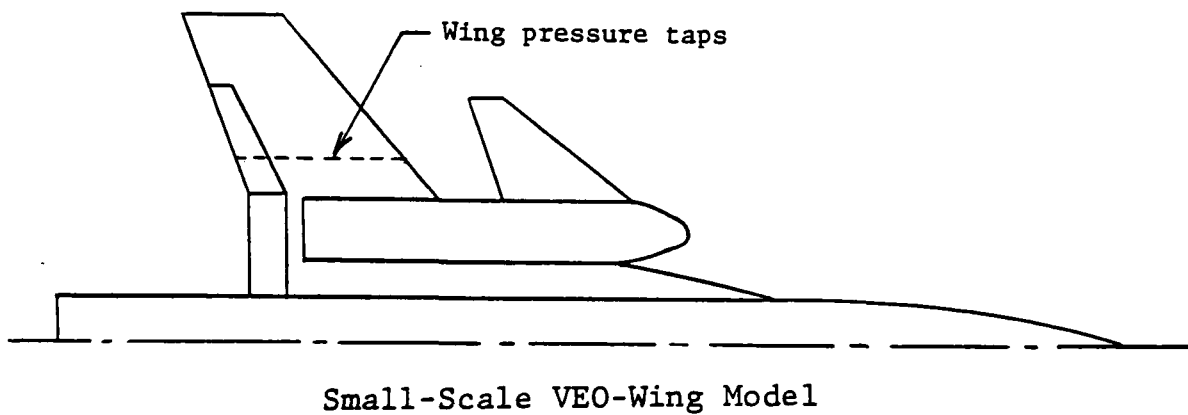
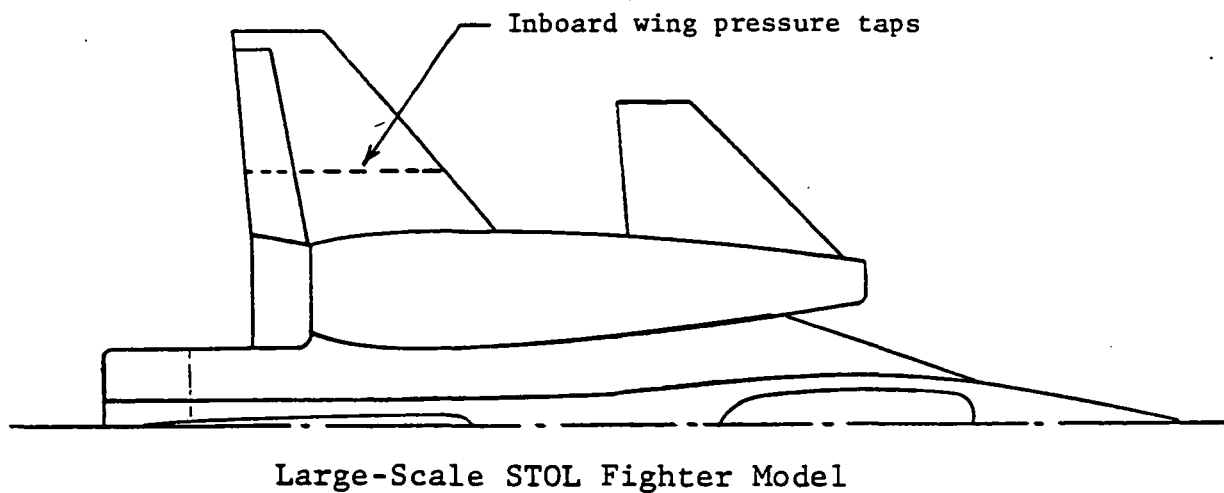
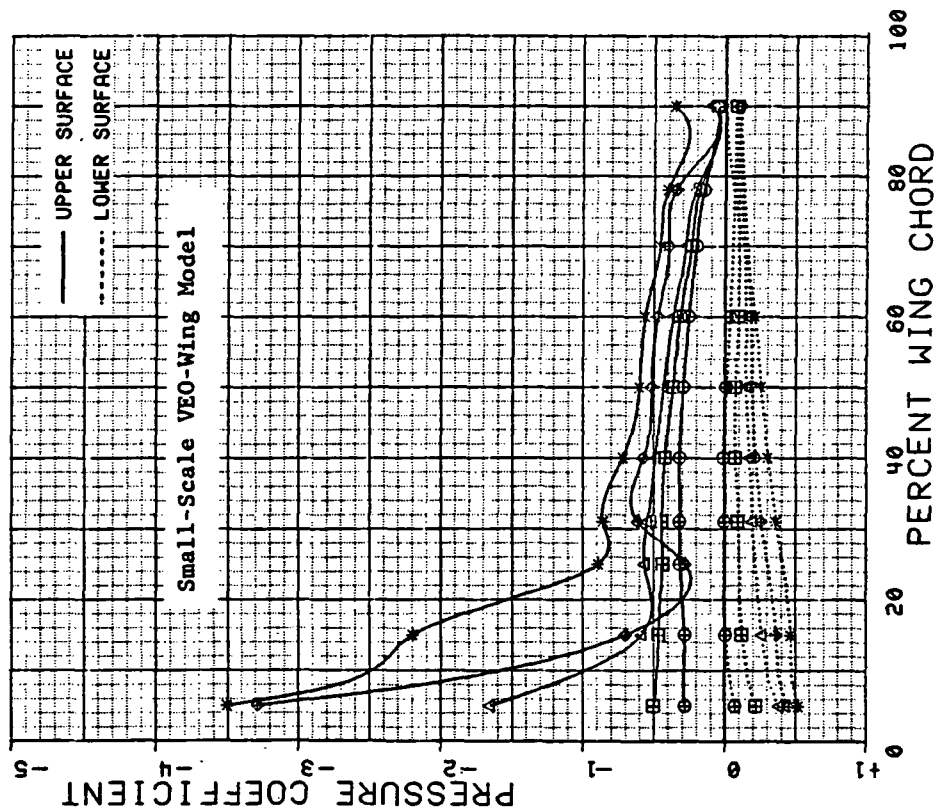


Figure 3.2.5-2 STOL Fighter Model and VEO-Wing Research Model  
Planform Comparison

SYM	TEST	RUN	ALPHA	CT	ITEF	OTEF	CAN	NOZ	SWB
⊕	204	153	4.02	0	0	0	0	N1AA	OFF
⊗	204	153	8.01	0	0	0	0	N1AA	OFF
Δ	204	153	12.01	0	0	0	0	N1AA	OFF
◆	204	257	16.09	0	0	0	0	N1AA	OFF
*	204	153	24.05	0	0	0	0	N1AA	OFF



SYM	TEST	RUN	ALPHA	CT	ITEF	OTEF	CAN	SWB
⊕	543	63	4.2	0.00	0	0	0	OFF
⊗	543	63	8.3	0.00	0	0	0	OFF
Δ	543	63	12.5	0.00	0	0	0	OFF
◆	543	63	16.6	0.00	0	0	0	OFF
*	543	63	24.8	0.00	0	0	0	OFF

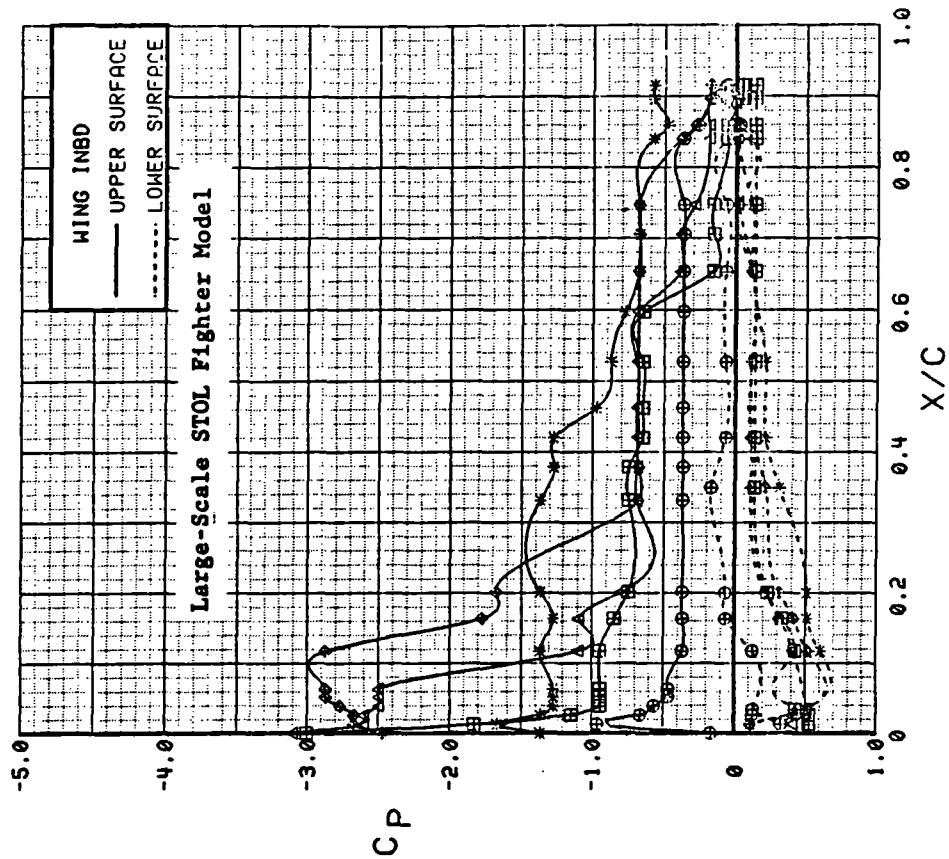
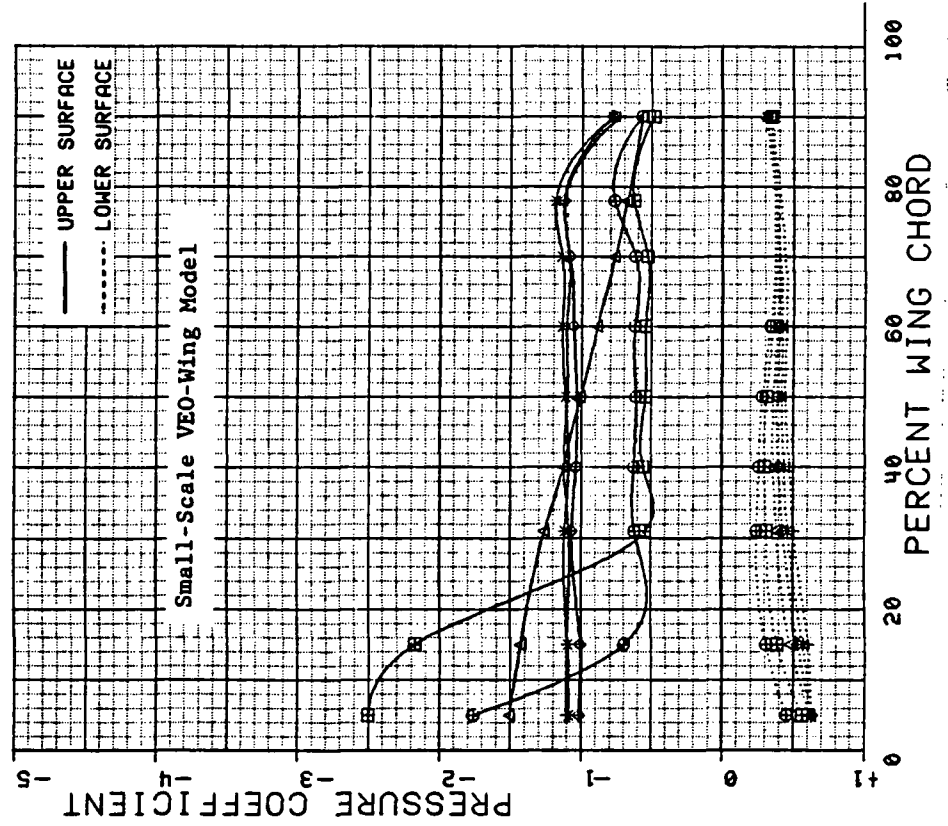


Figure 3.2.5-3 Comparison of Alpha Effects, Canards off, Flaps Undelected, Power Off

SYM	TEST	RUN	ALPHA	CT	ITEF	OTEF	CAN	NOZ	SWB
⊕	204	234	4.03	0	30	30	OFF	N1FA	OFF
⊞	204	234	8.01	0	30	30	OFF	N1FA	OFF
Δ	204	234	12.04	0	30	30	OFF	N1FA	OFF
◆	204	234	16.01	0	30	30	OFF	N1FA	OFF
✱	204	234	20.07	0	30	30	OFF	N1FA	OFF
+	204	234	24.07	0	30	30	OFF	N1FA	OFF



SYM	TEST	RUN	ALPHA	CT	ITEF	OTEF	CAN	SWB
⊕	537	12	4.4	0.00	30	30	OFF	OFF
⊞	537	12	8.5	0.00	30	30	OFF	OFF
Δ	537	12	12.7	0.00	30	30	OFF	OFF
◆	537	12	16.7	0.00	30	30	OFF	OFF
✱	537	12	20.8	0.00	30	30	OFF	OFF
+	537	12	24.8	0.00	30	30	OFF	OFF

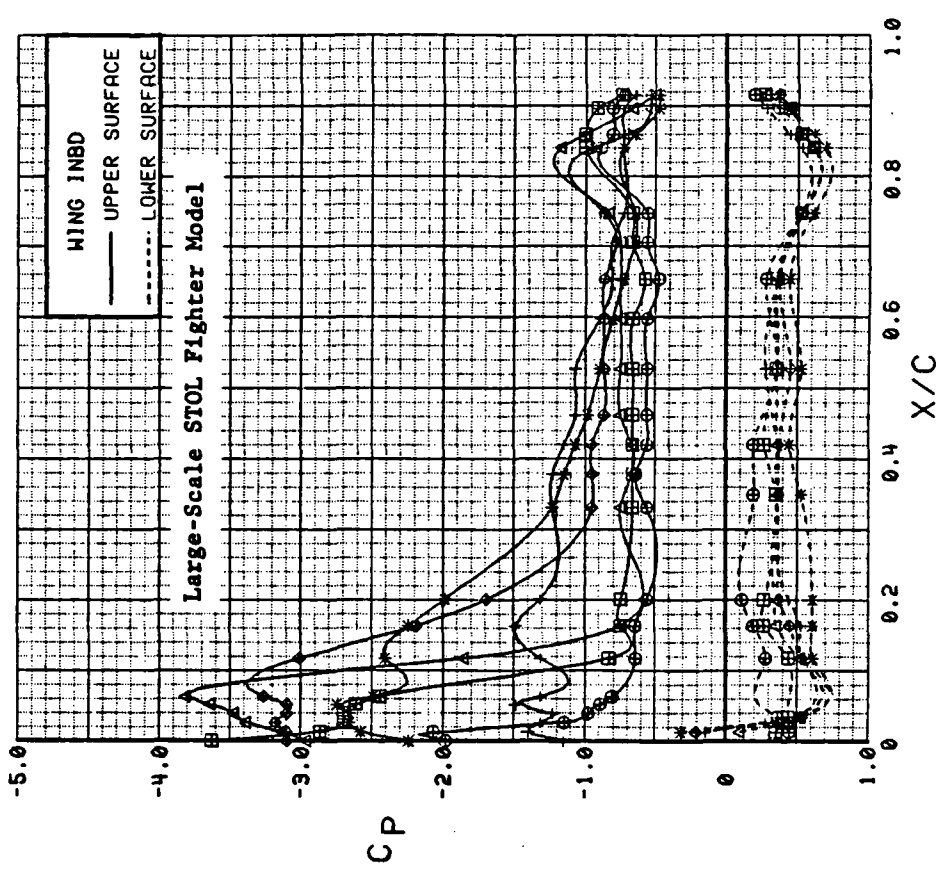
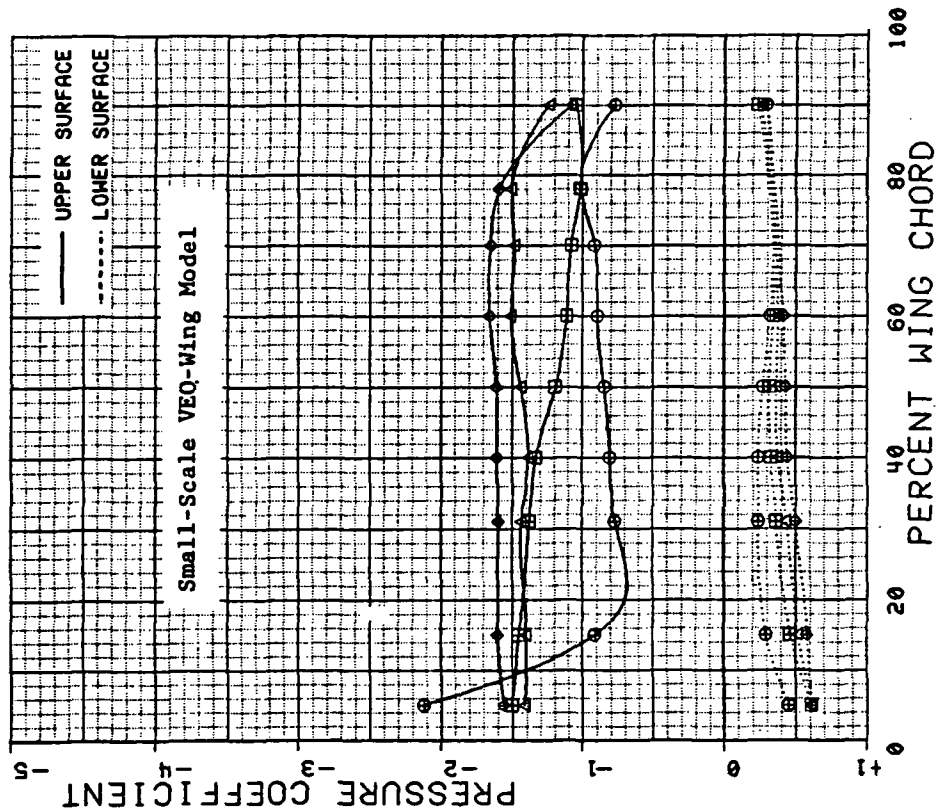


Figure 3.2.5-4 Comparison of Alpha Effects, Canards off, Flaps Undelected, Power On

SYM	TEST	RUN	ALPHA	CT	ITEF	OTEF	CAN	NOZ	SWB
⊕	204	238	4.01	2.0	30	30	OFF	N1FA	OFF
⊞	204	238	12.03	2.0	30	30	OFF	N1FA	OFF
△	204	238	16.02	2.0	30	30	OFF	N1FA	OFF
◆	204	238	20.11	2.0	30	30	OFF	N1FA	OFF



SYM	TEST	RUN	ALPHA	CT	ITEF	OTEF	CAN	SWB
⊕	537	28	4.5	1.87	30	30	OFF	OFF
⊞	537	28	12.8	1.82	30	30	OFF	OFF
△	537	28	16.9	1.84	30	30	OFF	OFF
◆	537	28	21.0	1.83	30	30	OFF	OFF

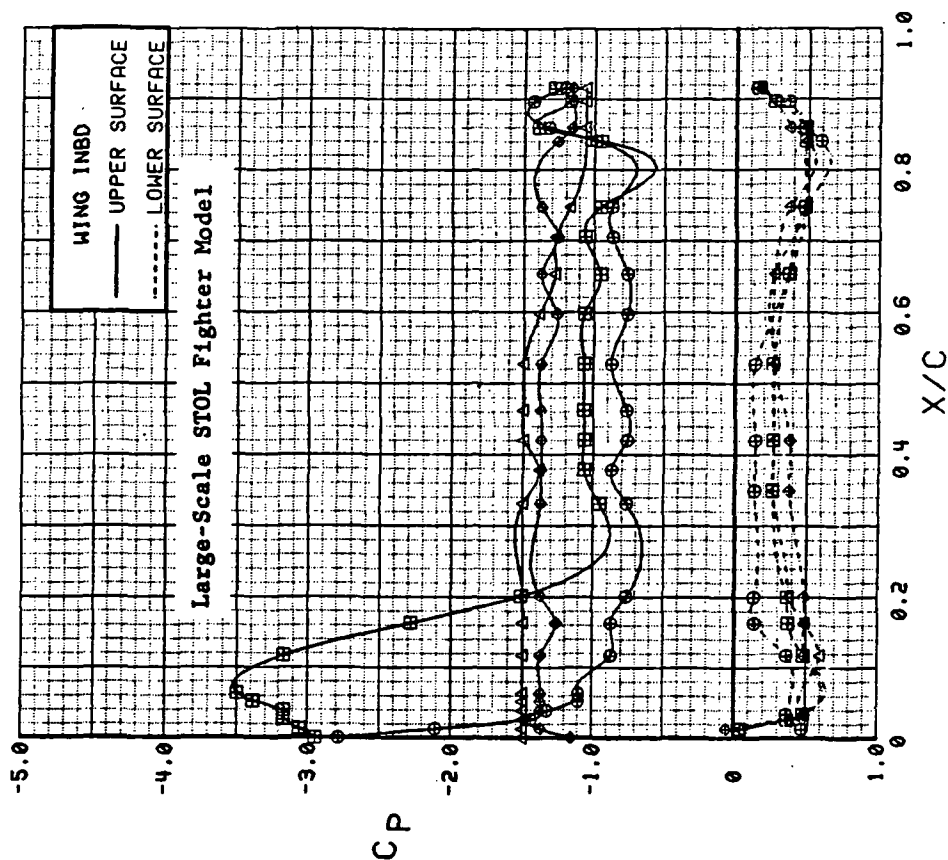
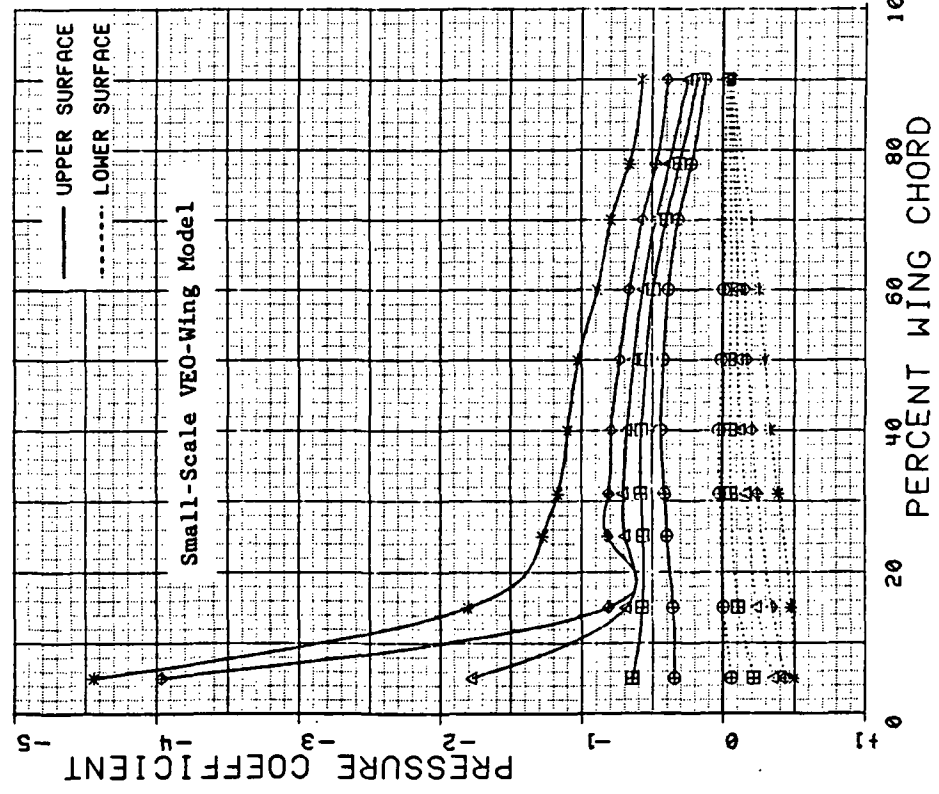


Figure 3.2.5-5 Comparison of Alpha Effects, Canards on, Flaps Undelected, Power Off

SYM	TEST	RUN	ALPHA	CT	ITEF	OTEF	CAN	NOZ	SWB
⊕	204	159	3.99	2.0	0	0	0	N1AA	OFF
⊗	204	159	7.97	2.0	0	0	0	N1AA	OFF
△	204	159	12.00	2.0	0	0	0	N1AA	OFF
◆	204	159	15.99	2.0	0	0	0	N1AA	OFF
*	204	159	23.98	2.0	0	0	0	N1AA	OFF



SYM	TEST	RUN	ALPHA	CT	ITEF	OTEF	CAN	SWB
⊕	543	58	4.3	1.84	0	0	0	OFF
⊗	543	58	8.4	1.90	0	0	0	OFF
△	543	58	12.6	1.87	0	0	0	OFF
◆	543	58	16.7	1.87	0	0	0	OFF
*	543	58	25.0	1.86	0	0	0	OFF

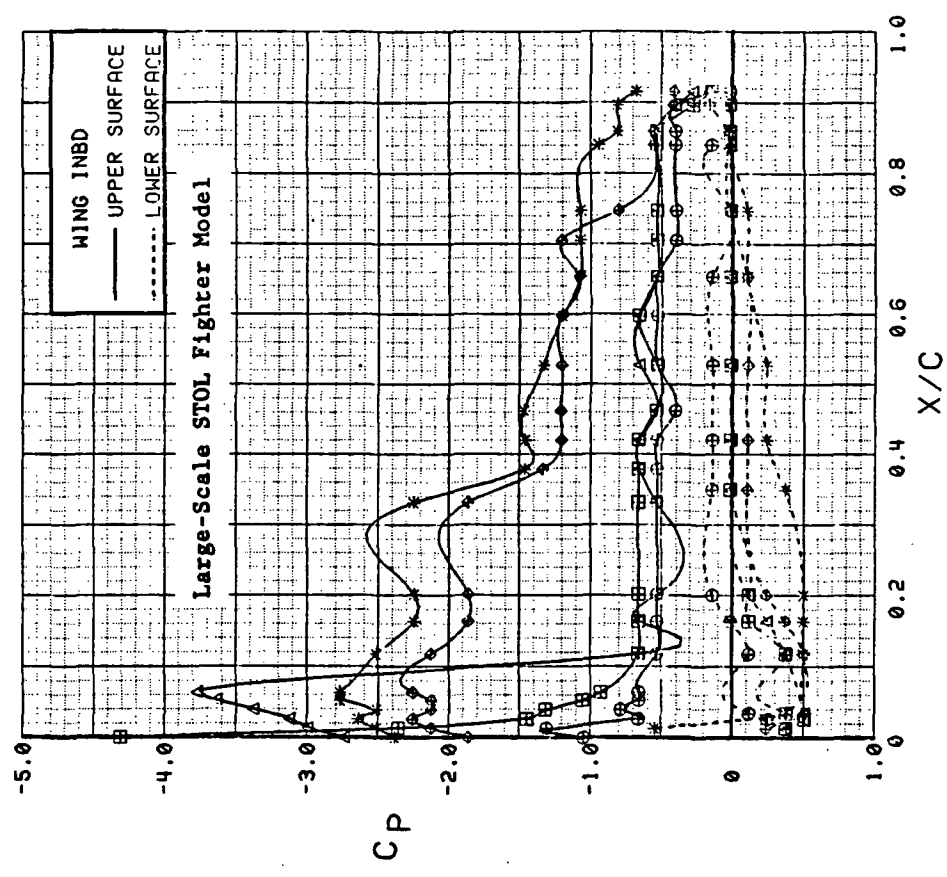
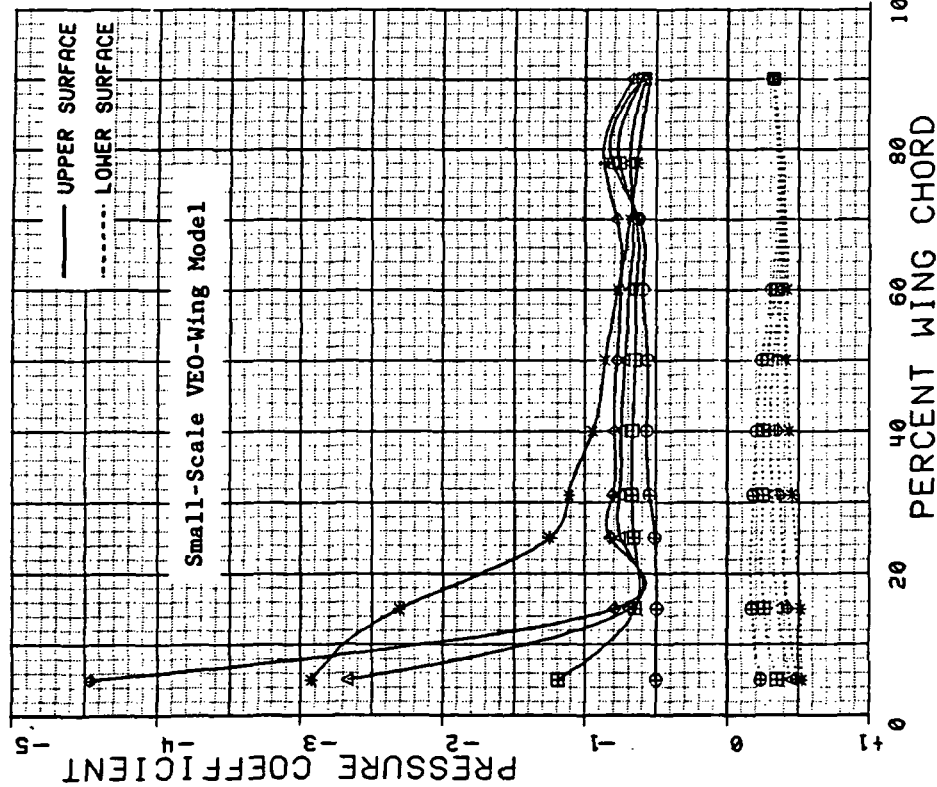


Figure 3.2.5-6 Comparison of Alpha Effects, Canards on, Flaps Undelected, Power On

SYM	TEST	RUN	ALPHA	CT	ITEF	OTEF	CAN	NOZ	SWB
⊕	204	168	3.98	0	30	30	0	NIFA	OFF
⊗	204	168	8.01	0	30	30	0	NIFA	OFF
△	204	168	11.99	0	30	30	0	NIFA	OFF
◆	204	168	16.00	0	30	30	0	NIFA	OFF
*	204	185	24.02	0	30	30	0	NIFA	OFF



SYM	TEST	RUN	ALPHA	CT	ITEF	OTEF	CAN	SWB
⊕	543	11	4.4	0.00	30	30	0	OFF
⊗	543	11	8.5	0.00	30	30	0	OFF
△	543	11	12.7	0.00	30	30	0	OFF
◆	543	11	16.8	0.00	30	30	0	OFF
*	543	11	24.9	0.00	30	30	0	OFF

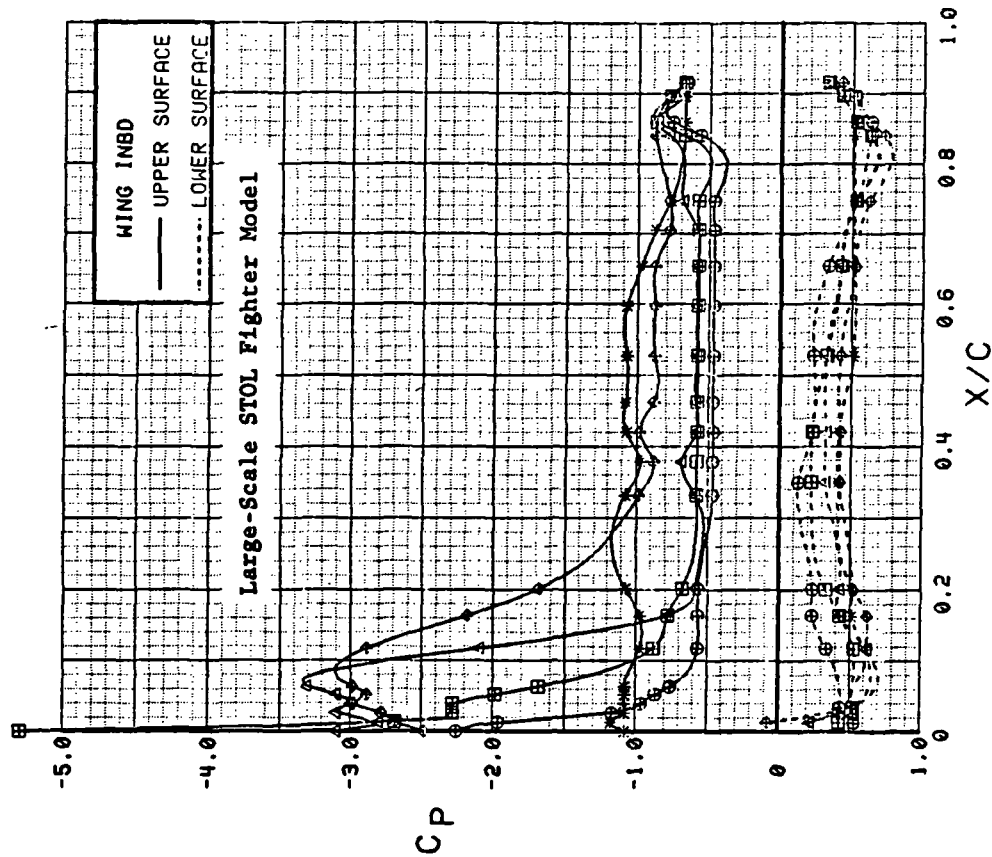
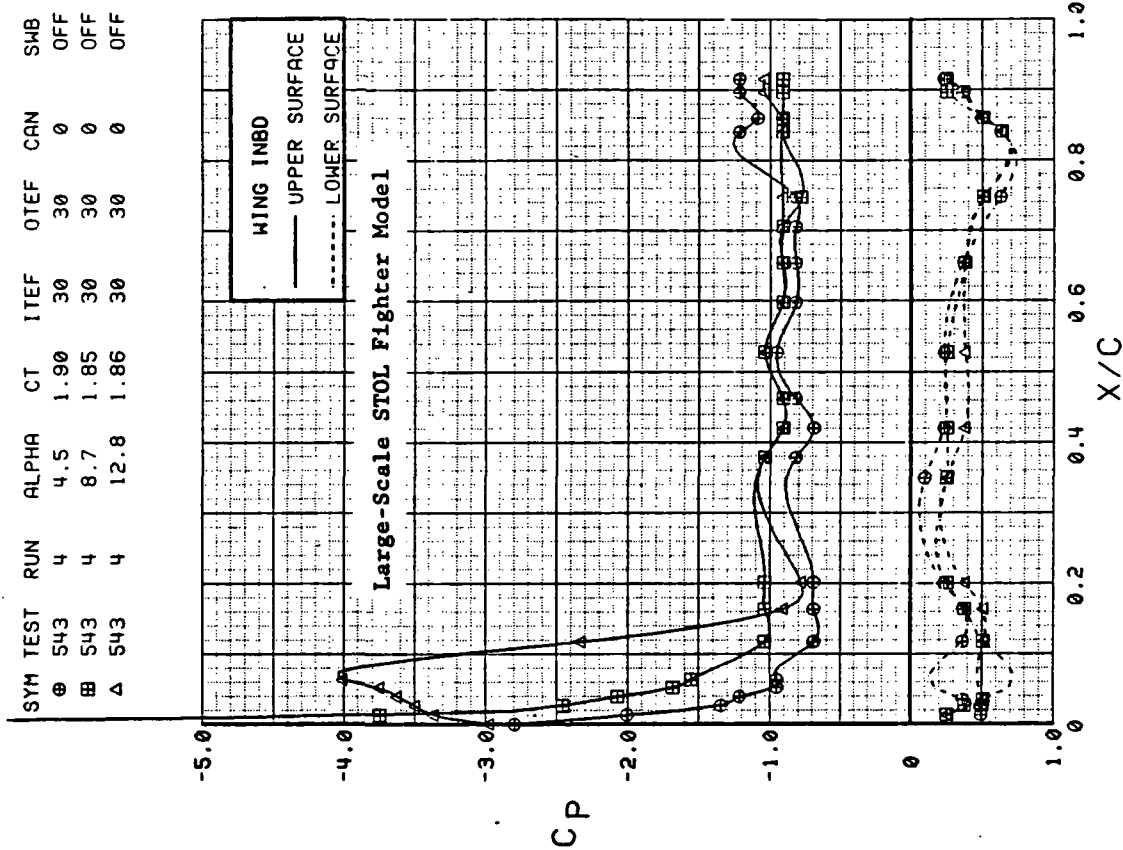
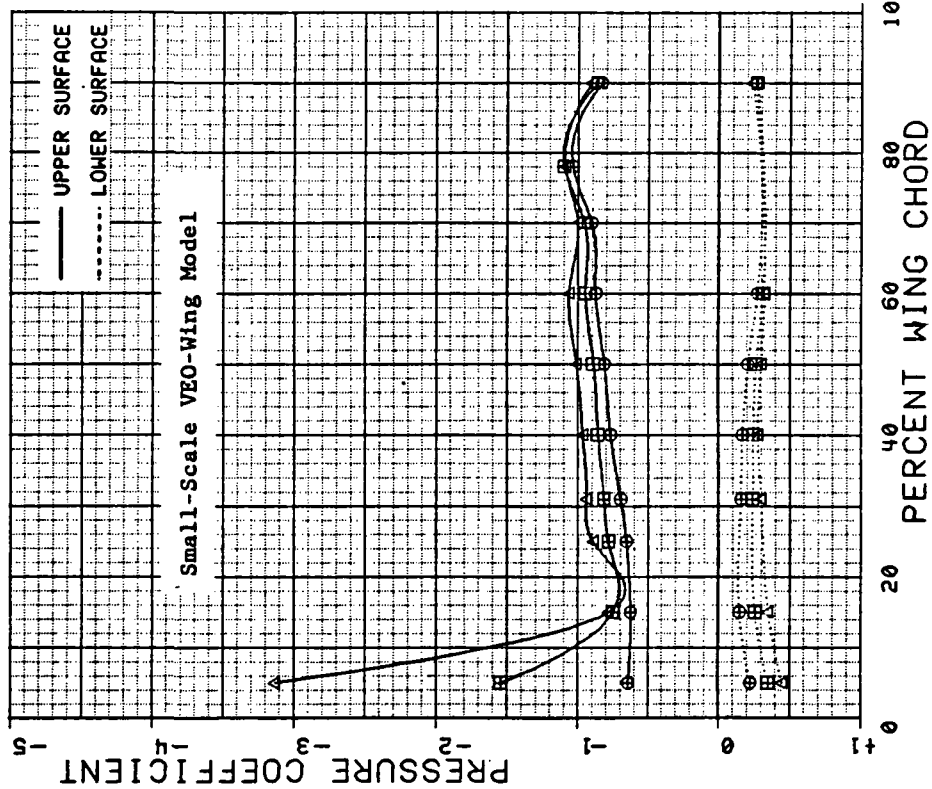


Figure 3.2.5-7 Comparison of Alpha Effects, Canards on, Flaps 30 deg, Power Off

SYM	TEST	RUN	ALPHA	CT	ITEF	OTEF	CAN	NOZ	SWB
⊙	204	171	3.97	2.0	30	30	0	NIFA	OFF
⊞	204	171	8.01	2.0	30	30	0	NIFA	OFF
Δ	204	171	11.98	2.0	30	30	0	NIFA	OFF



SYM	TEST	RUN	ALPHA	CT	ITEF	OTEF	CAN	SWB
⊙	543	4	4.5	1.90	30	30	0	OFF
⊞	543	4	8.7	1.85	30	30	0	OFF
Δ	543	4	12.8	1.86	30	30	0	OFF

Figure 3.2.5-8 Comparison of Alpha Effects, Canards on, Flaps 30 deg, Power On

SYM	TEST	RUN	ALPHA	CT	ITEF	OTEF	CAN	NOZ	SWB
⊕	204	168	3.98	0	30	30	0	NIFA	OFF
⊗	204	234	4.03	0	30	30	OFF	NIFA	OFF

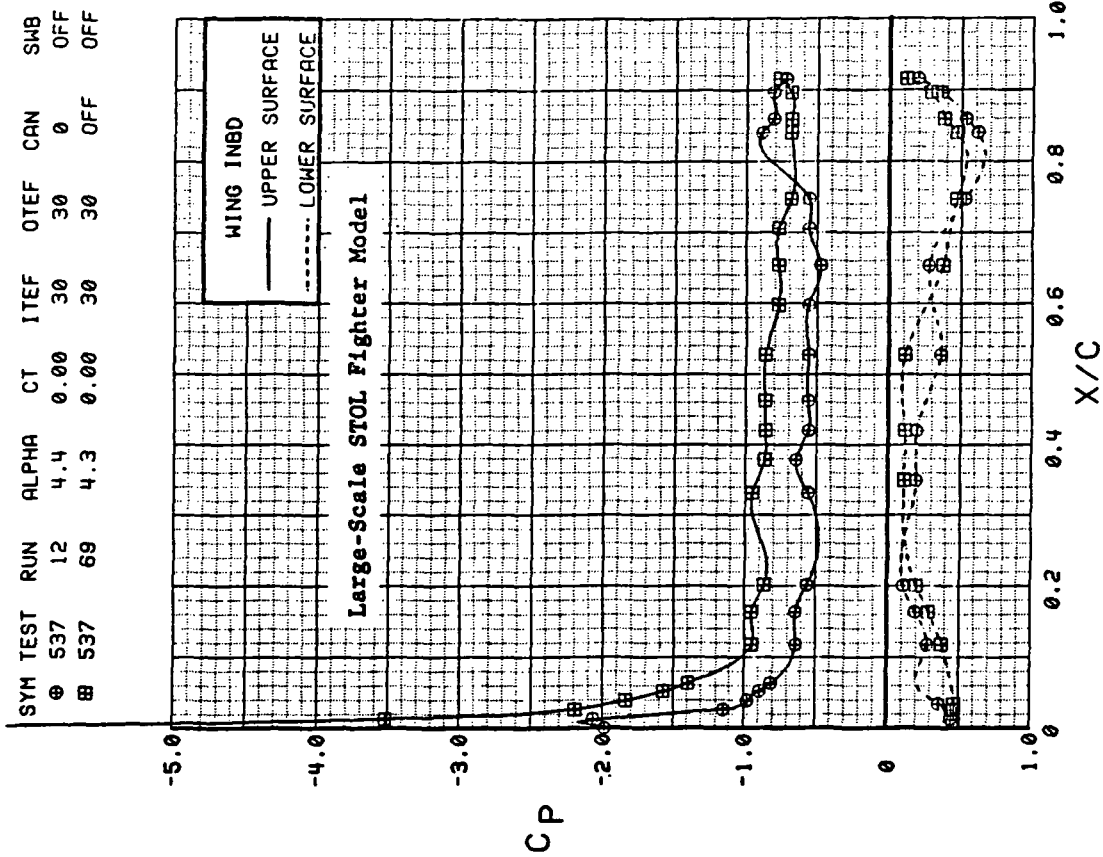
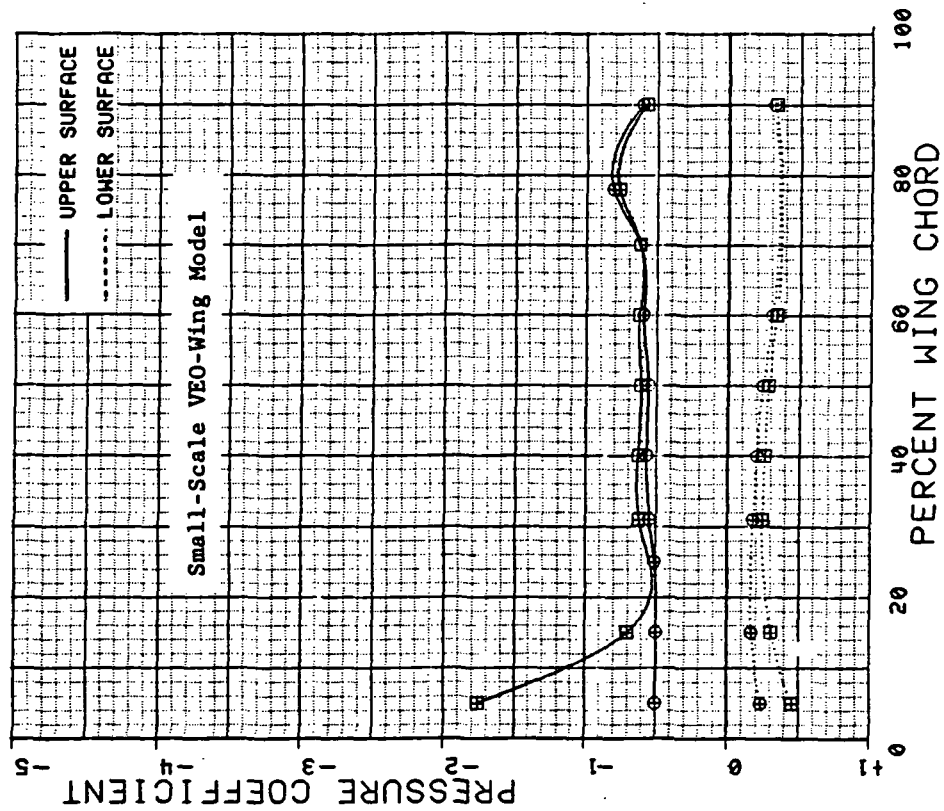


Figure 3.2.5-9 Comparison of Canard On/Off Effects, Power Off, Alpha = 4 deg



SYM	TEST	RUN	ALPHA	CT	ITEF	OTEF	CAN	NOZ	SMB
⊕	204	168	11.99	0	30	30	0	NIFA	OFF
⊕	204	234	12.04	0	30	30	OFF	NIFA	OFF

SYM	TEST	RUN	ALPHA	CT	ITEF	OTEF	CAN	SMB
⊕	537	12	12.7	0.00	30	30	0	OFF
⊕	537	69	12.5	0.00	30	30	OFF	OFF

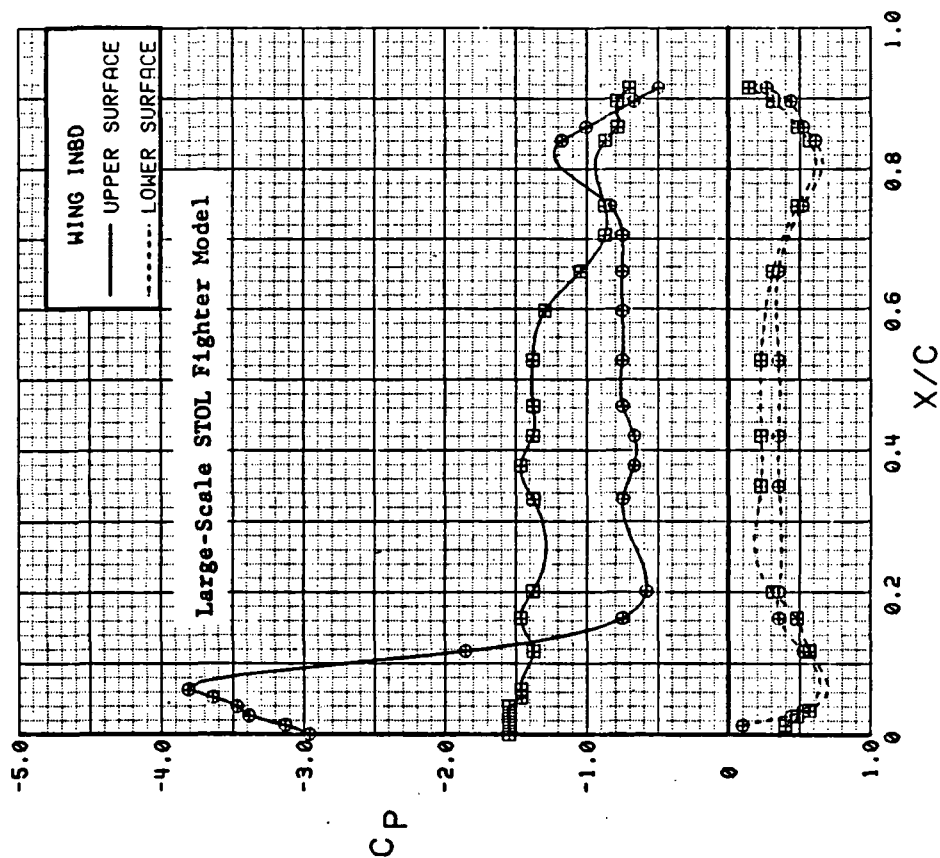
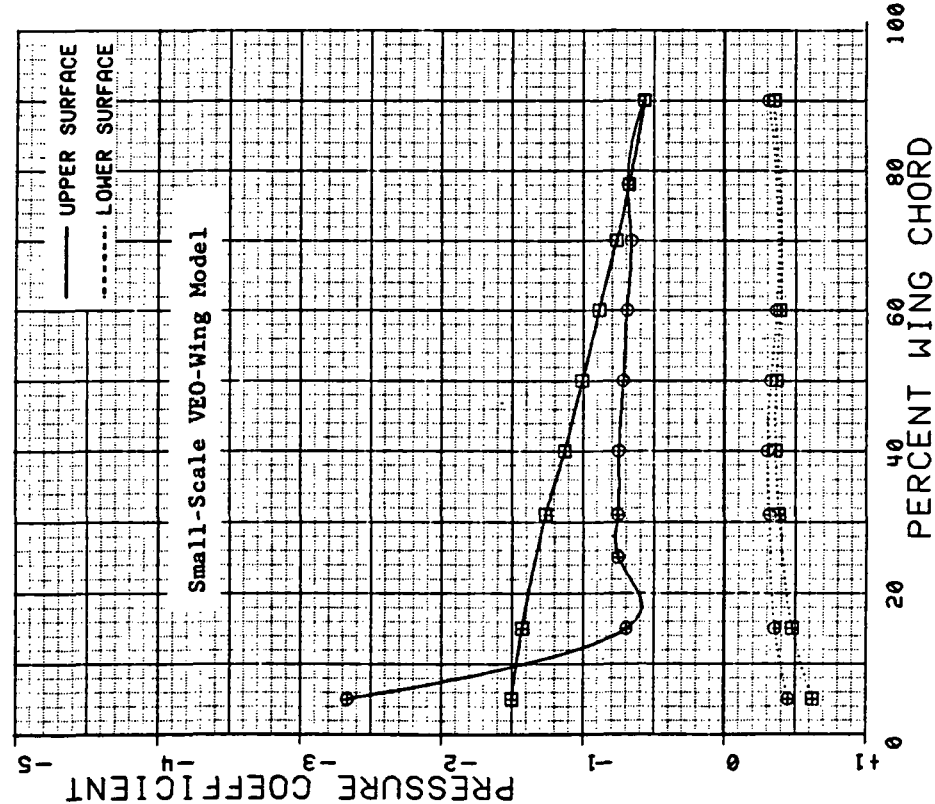


Figure 3.2.5-10 Comparison of Canard On/Off Effects, Power Off, Alpha = 12 deg

SYM	TEST	RUN	ALPHA	CT	ITEF	OTEF	CAN	NOZ	SWB
⊕	204	168	20.00	0	30	30	0	NIFA	OFF
⊕	204	234	20.07	0	30	30	0	OFF NIFA	OFF

SYM	TEST	RUN	ALPHA	CT	ITEF	OTEF	CAN	SWB
⊕	537	12	20.8	0.00	30	30	0	OFF
⊕	537	69	20.6	0.00	30	30	0	OFF

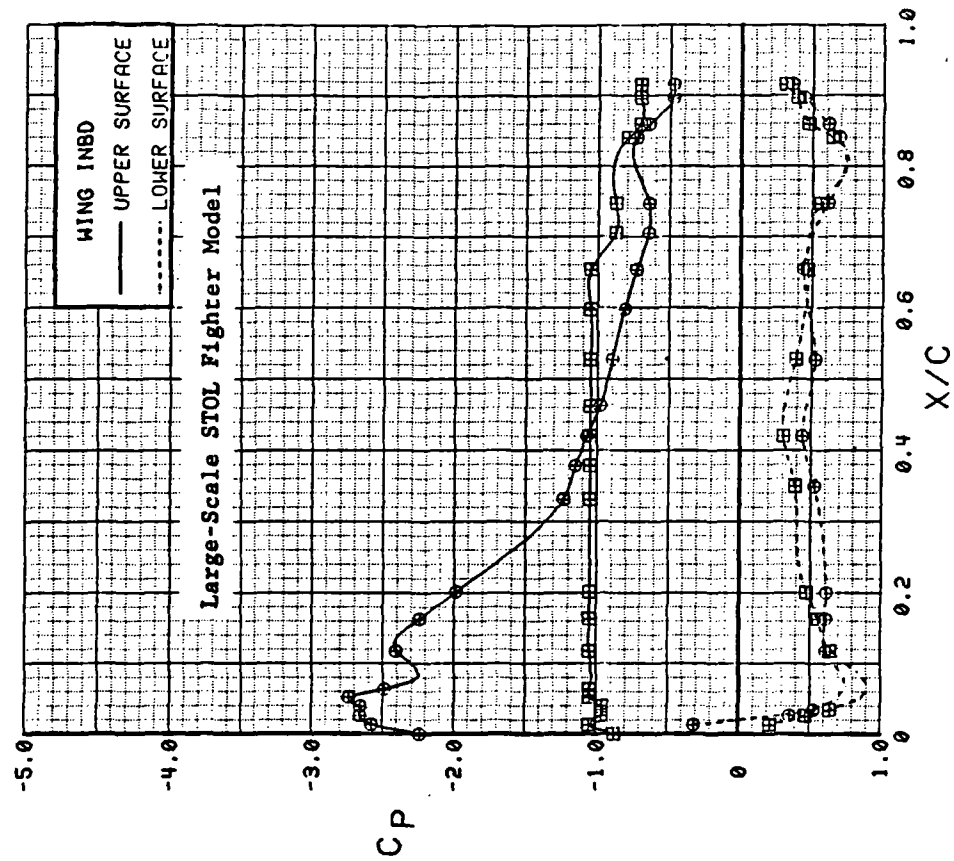
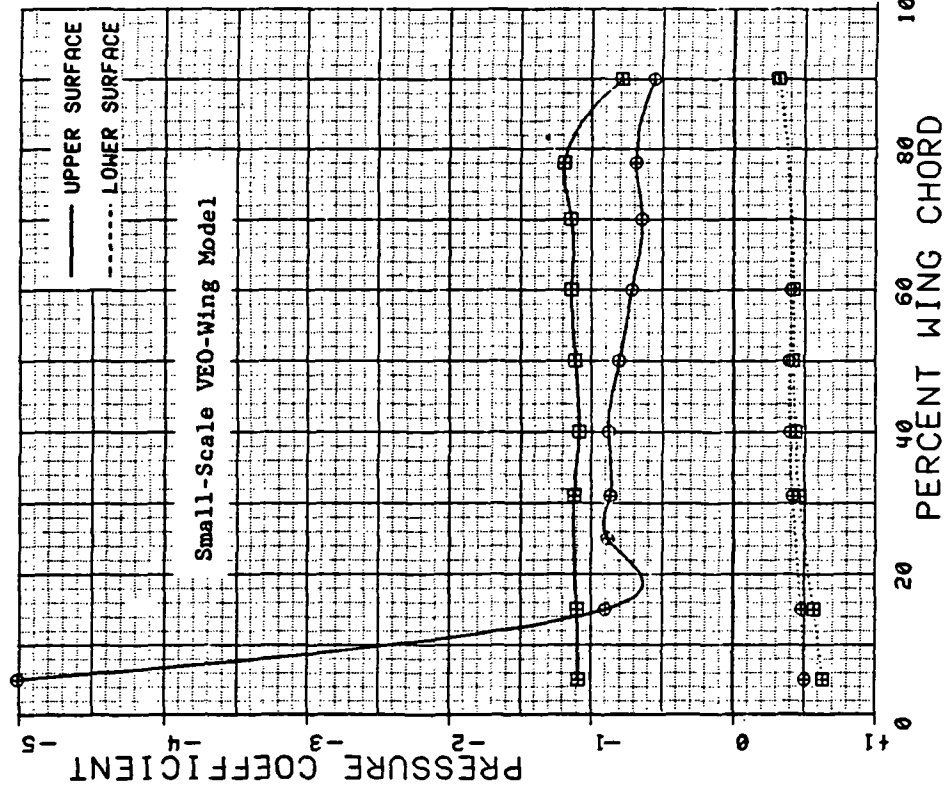


Figure 3.2.5-11 Comparison of Canard On/Off Effects, Power Off,  
Alpha = 20 deg

SYM	TEST	RUN	ALPHA	CT	ITEF	OTEF	CAN	NOZ	SMB
⊕	204	171	3.97	2.0	30	30	0	NIFA	OFF
⊕	204	238	4.01	2.0	30	30	0	OFF NIFA	OFF

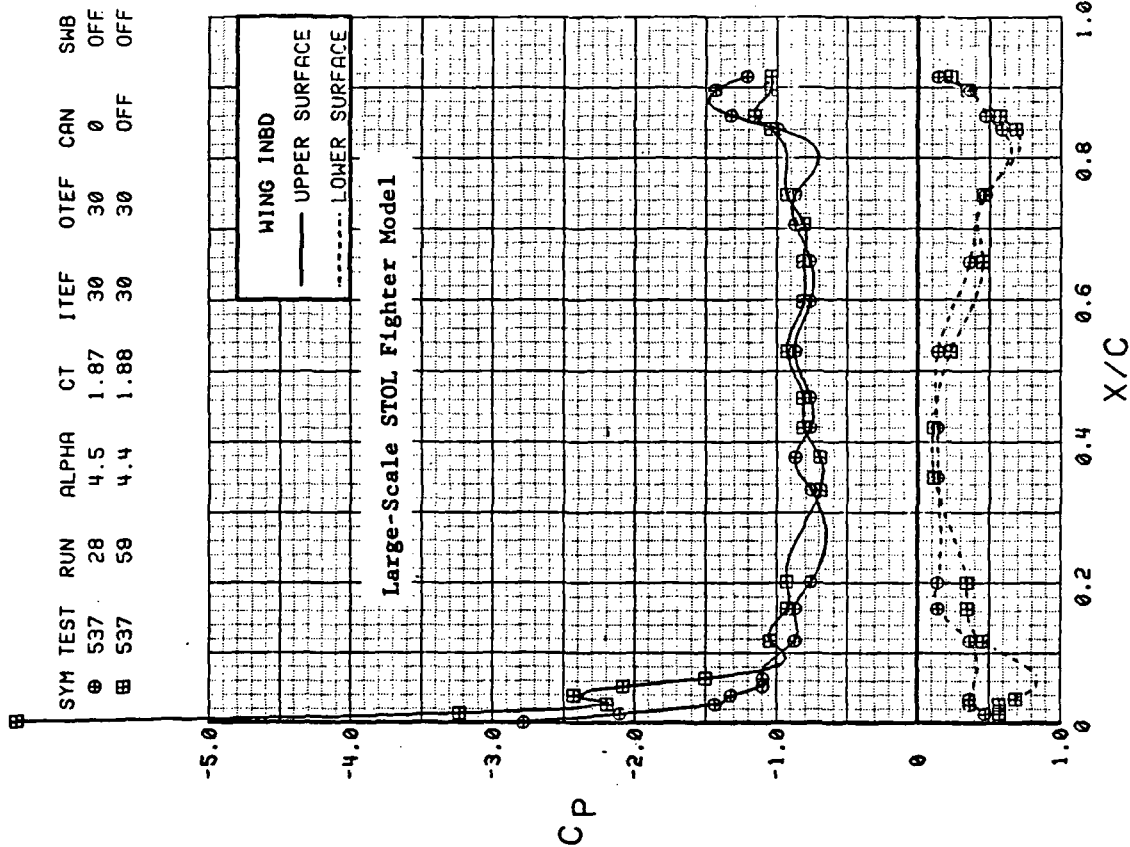
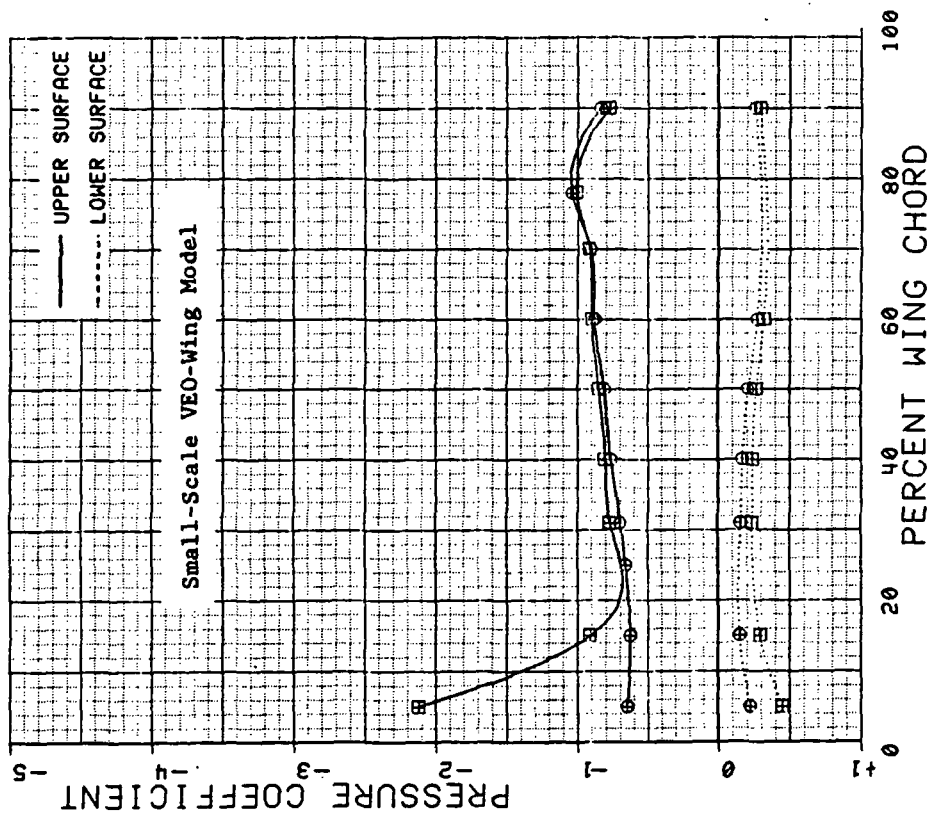


Figure 3.2.5-12 Comparison of Canard On/Off Effects, Power On,  
Alpha = 4 deg

SYM	TEST	RUN	ALPHA	CT	ITEF	OTEF	CAN	NOZ	SWB
⊕	204	171	11.98	2.0	30	30	0	NIFA	OFF
⊕	204	238	12.03	2.0	30	30	0	OFF	NIFA

SYM	TEST	RUN	ALPHA	CT	ITEF	OTEF	CAN	SWB
⊕	S37	28	12.8	1.82	30	30	0	OFF
⊕	S37	59	12.6	1.88	30	30	0	OFF

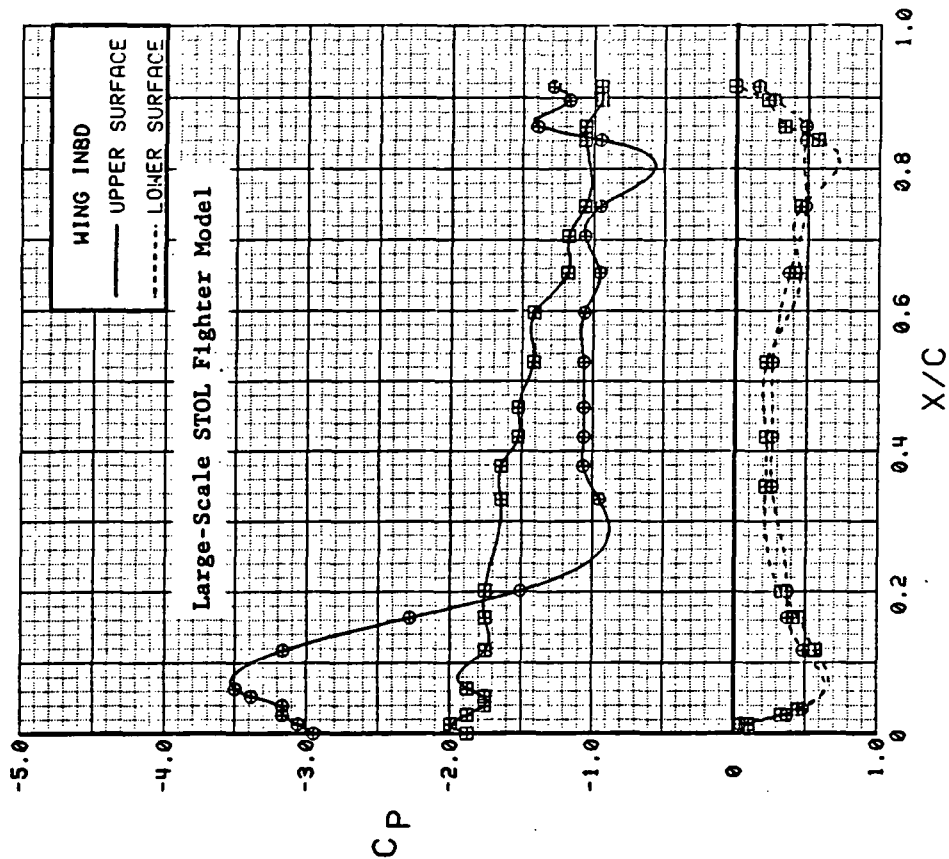
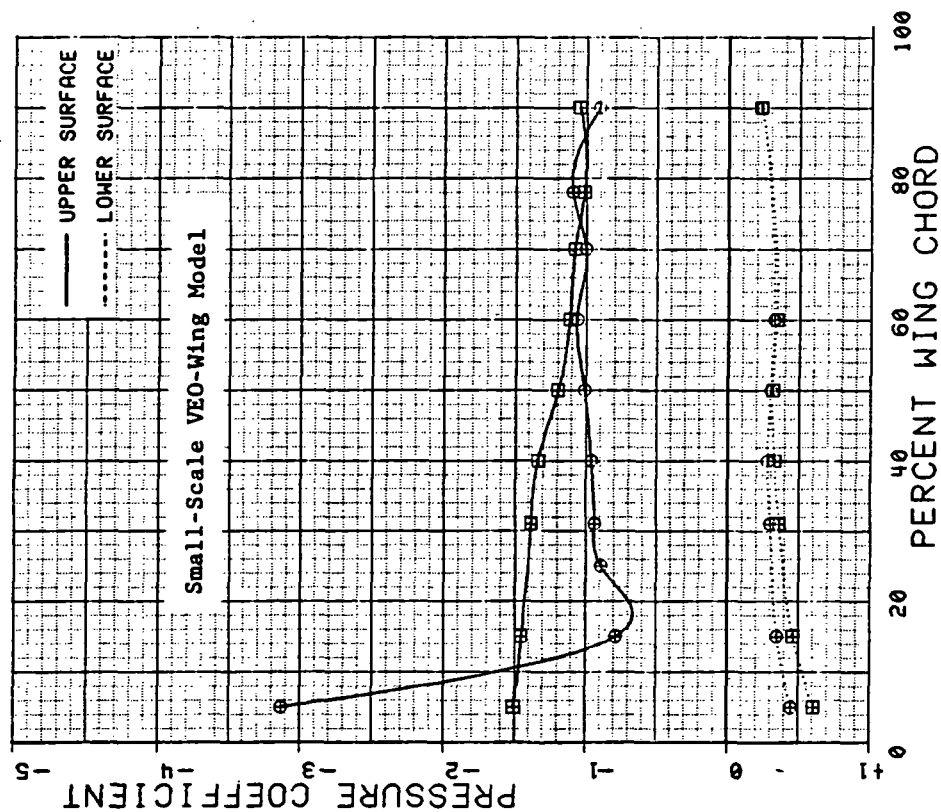
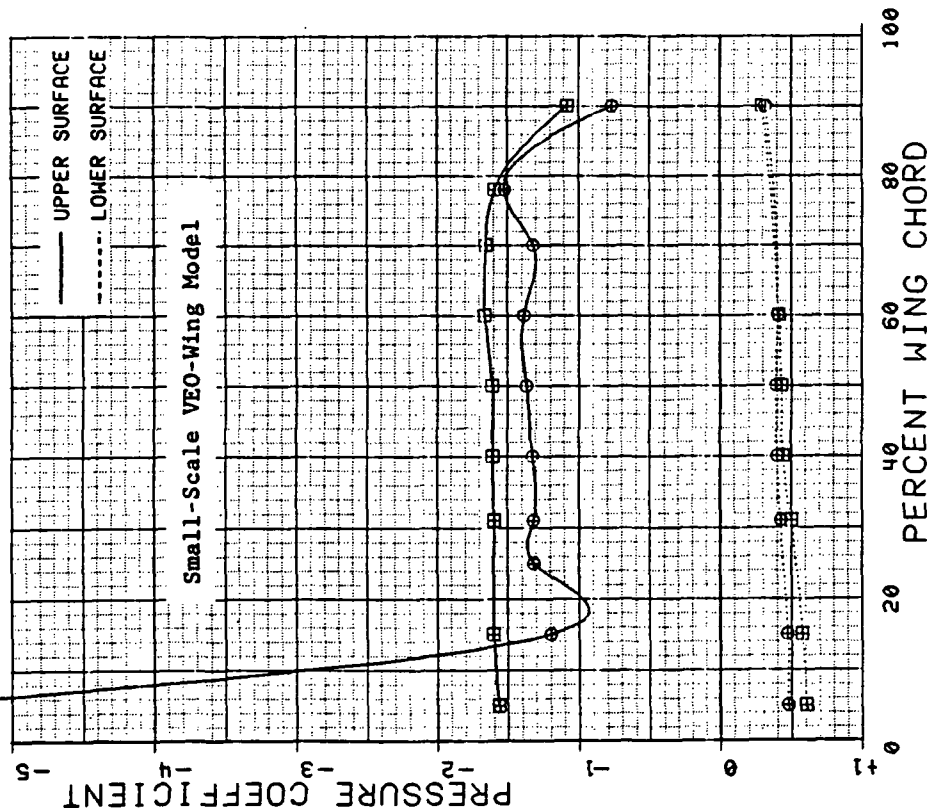


Figure 3.2.5-13 Comparison of Canard On/Off Effects, Power On,  
Alpha = 12 deg

SYM	TEST	RUN	ALPHA	CT	ITEF	OTEF	CAN	NOZ	SWB
⊕	204	171	19.96	2.0	30	30	0	N1FA	OFF
⊕	204	238	20.11	2.0	30	30	OFF	N1FA	OFF



SYM	TEST	RUN	ALPHA	CT	ITEF	OTEF	CAN	SWB
⊕	537	28	21.0	1.83	30	30	0	OFF
⊕	537	59	20.9	1.84	30	30	OFF	OFF

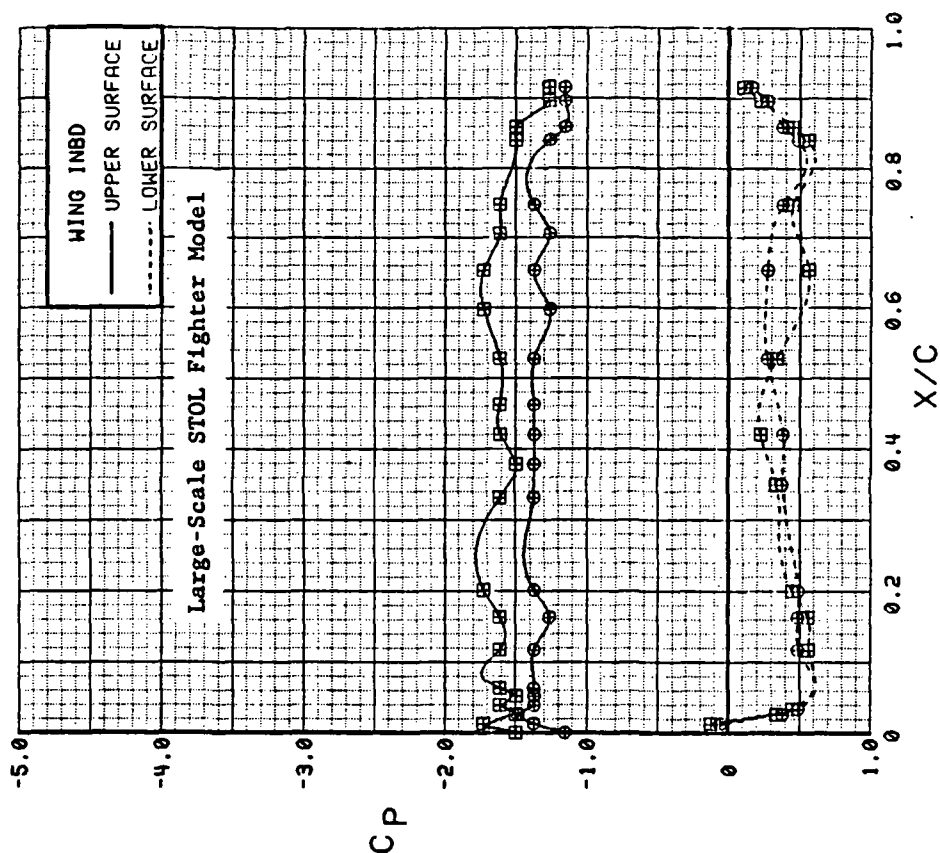


Figure 3.2.5-14 Comparison of Canard On/Off Effects, Power On, Alpha = 20 deg

SYM	TEST	RUN	ALPHA	CT	ITEF	OTEF	CAN	NOZ	SMB
⊕	204	153	4.02	0	0	0	0	0	NIAA OFF
⊕	204	168	3.98	0	30	30	0	0	NIFA OFF

SYM	TEST	RUN	ALPHA	CT	ITEF	OTEF	CAN	SMB
⊕	543	63	4.2	0.00	0	0	0	OFF
⊕	543	11	4.4	0.00	30	30	0	OFF

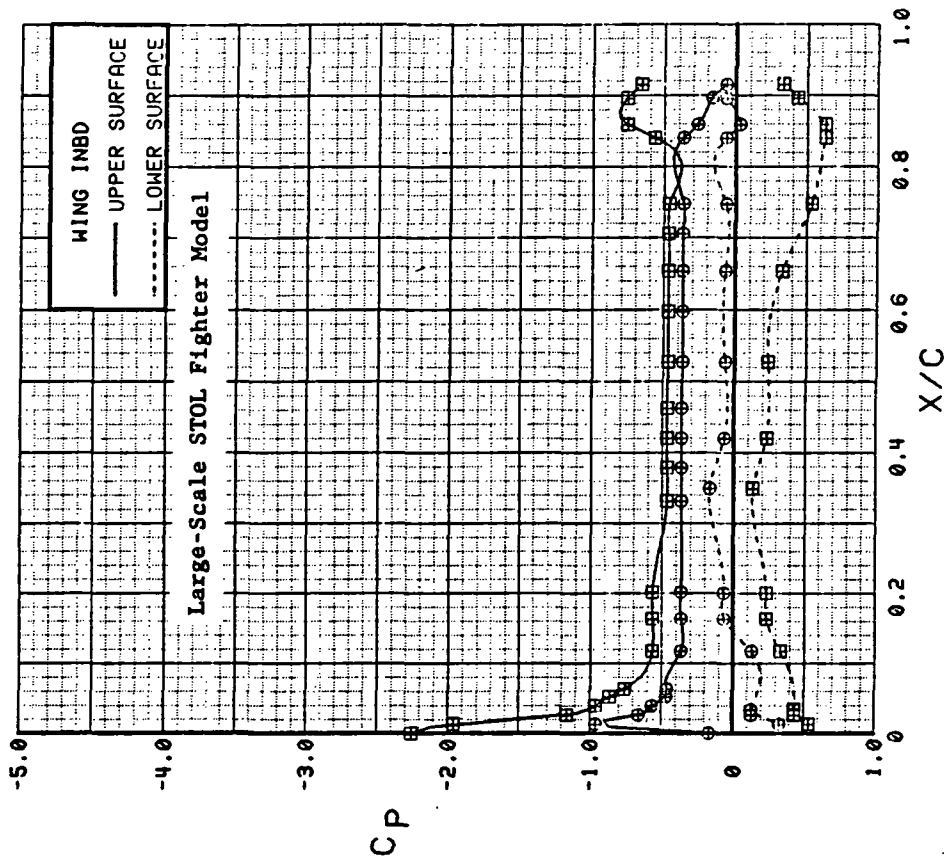
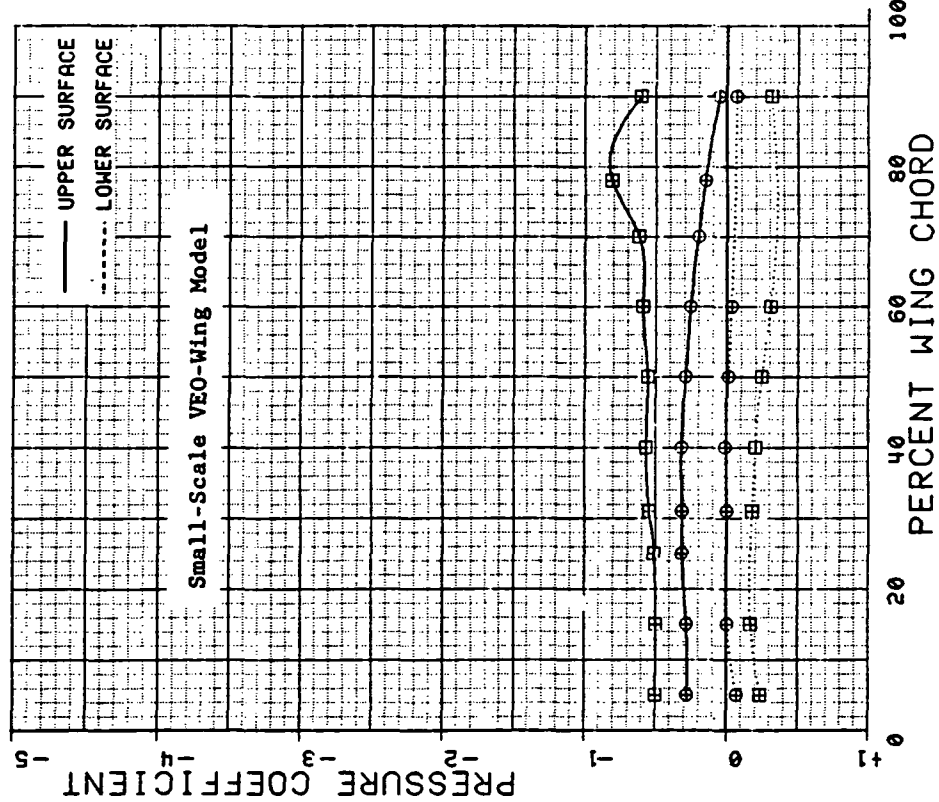


Figure 3.2.5-15 Comparison of Trailing-Edge Flap Effects, Power Off, Alpha = 4 deg

SYM	TEST	RUN	ALPHA	CT	ITEF	OTEF	CAN	NOZ	SMB
⊕	204	153	12.01	0	0	0	0	0	NIAR OFF
⊕	204	168	11.99	0	30	30	0	0	NIFA OFF

SYM	TEST	RUN	ALPHA	CT	ITEF	OTEF	CAN	SMB
⊕	543	63	12.5	0.00	0	0	0	OFF
⊕	543	11	12.7	0.00	30	30	0	OFF

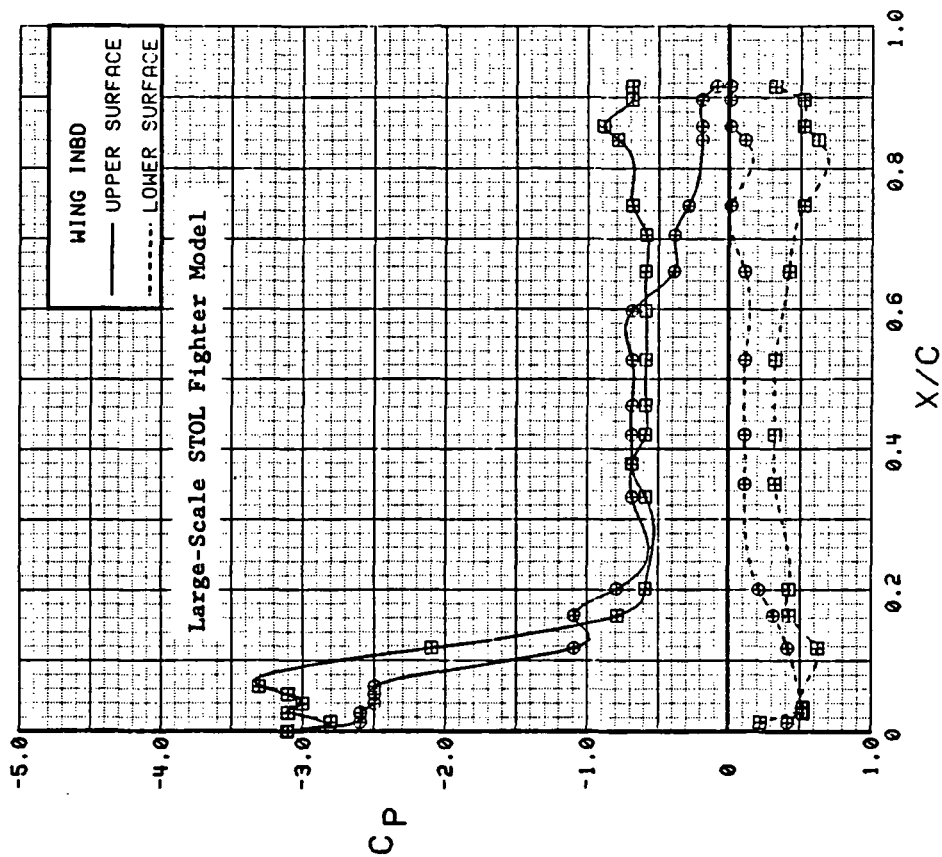
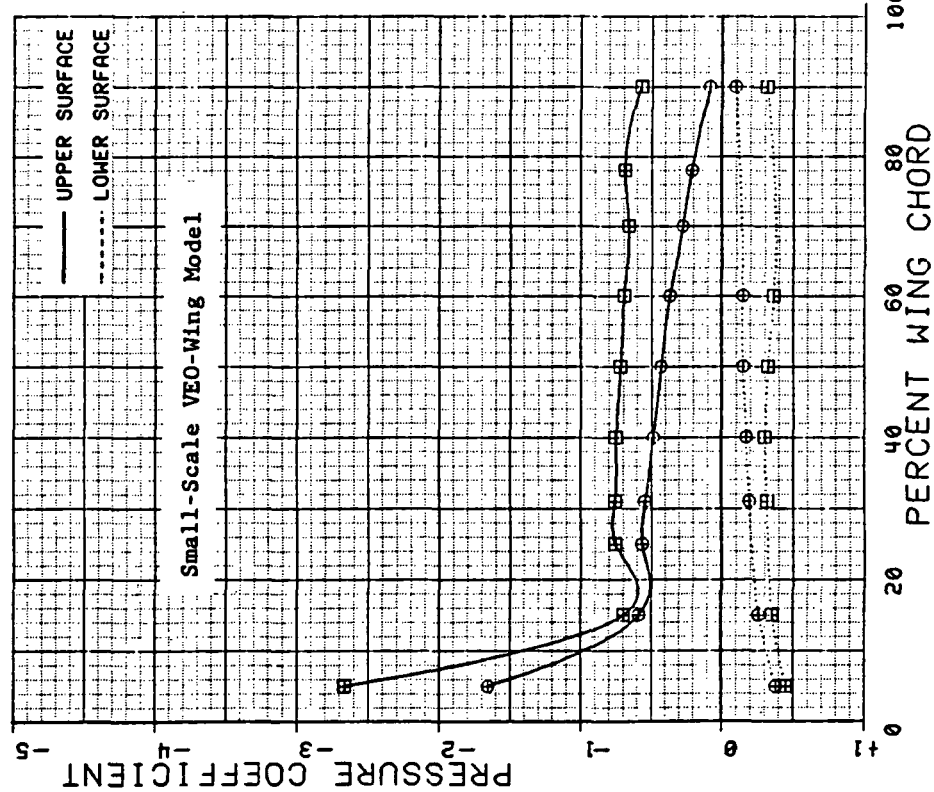


Figure 3.2.5-16 Comparison of Trailing-Edge Flap Effects,  
Power Off, Alpha = 12 deg

SYM	TEST	RUN	ALPHA	CT	ITEF	OFEF	CAN	NOZ	SWB
⊕	204	158	4.02	2.0	0	0	0	NIAA	OFF
⊕	204	172	3.99	2.0	30	30	0	NIFA	OFF

SYM	TEST	RUN	ALPHA	CT	ITEF	OFEF	CAN	SWB
⊕	543	58	4.3	1.84	0	0	0	OFF
⊕	543	4	4.5	1.90	30	30	0	OFF

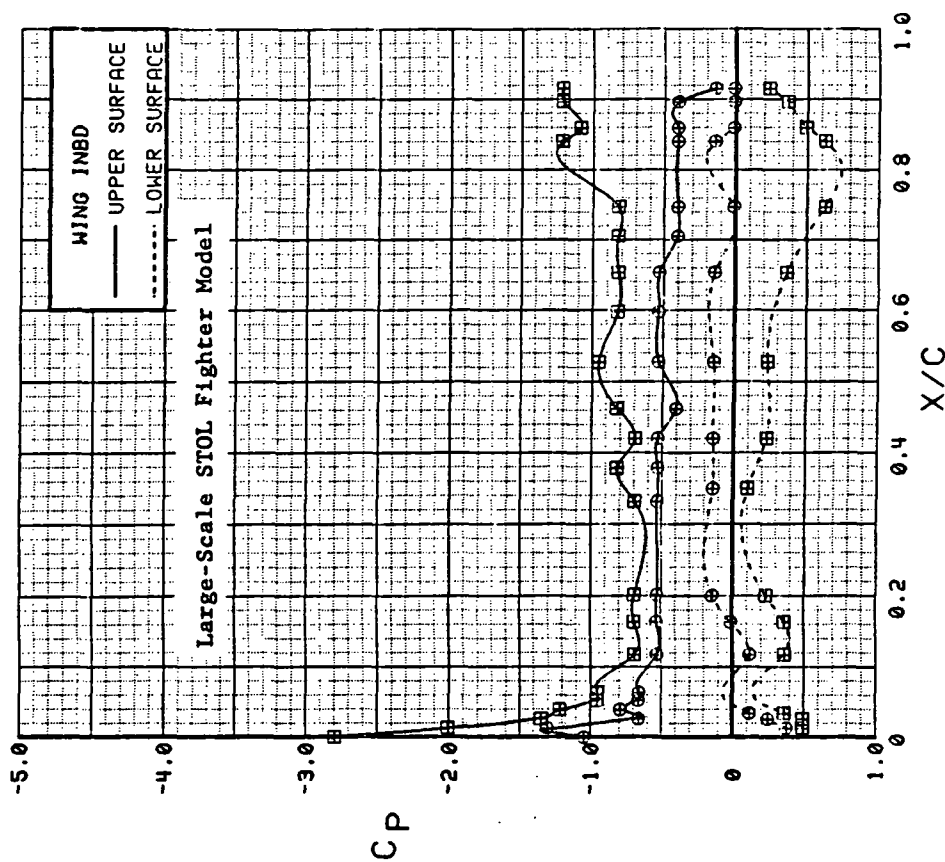
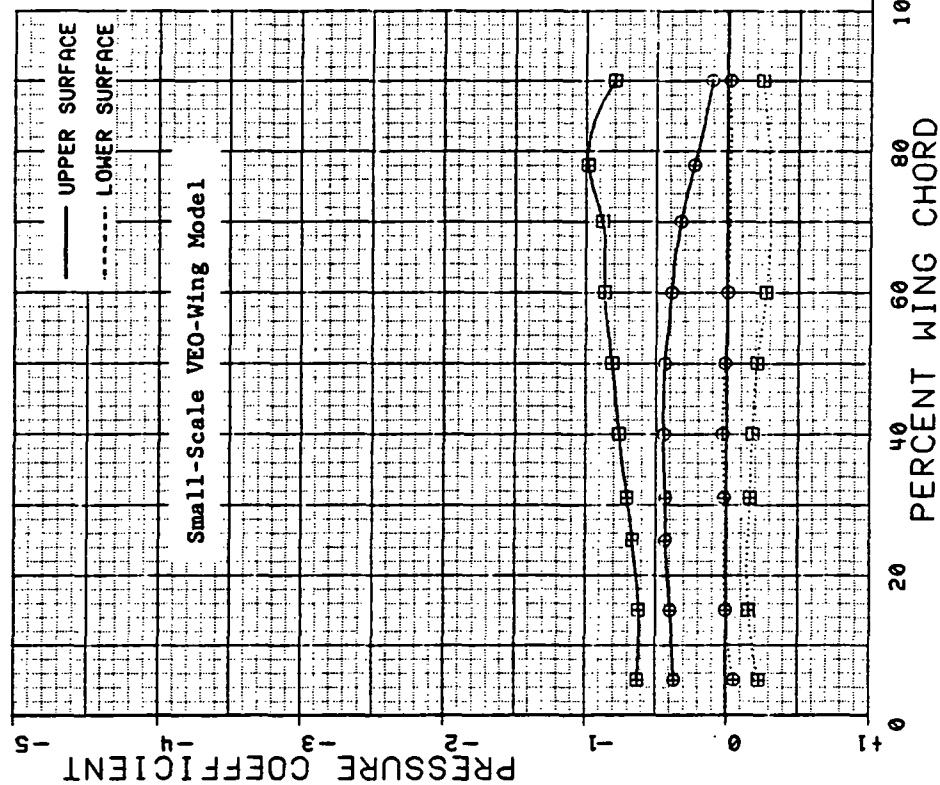


Figure 3.2.5-17 Comparison of Trailing-Edge Flap Effects, Power On, Alpha = 4 deg



SYM	TEST	RUN	ALPHA	CT	ITEF	OTEF	CAN	NOZ	SWB
⊕	204	158	11.96	2.0	0	0	0	0	NIAA OFF
⊕	204	172	11.97	2.0	30	30	0	0	NIFA OFF

SYM	TEST	RUN	ALPHA	CT	ITEF	OTEF	CAN	SWB
⊕	543	58	12.6	1.87	0	0	0	OFF
⊕	543	4	12.8	1.86	30	30	0	OFF

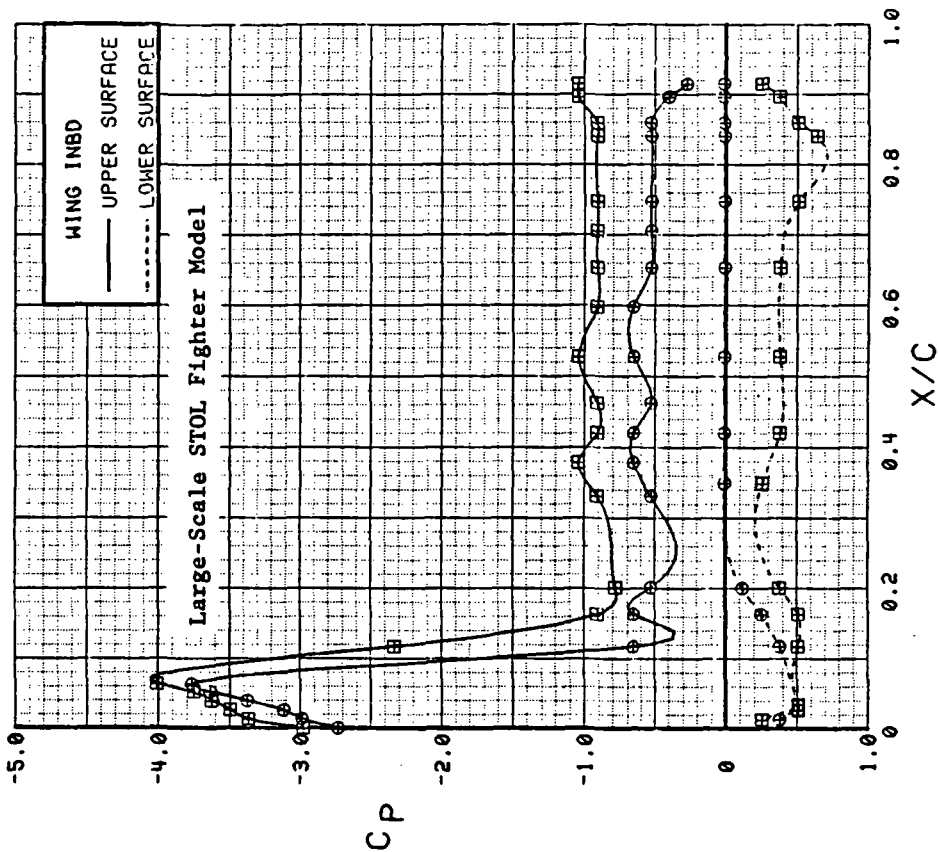
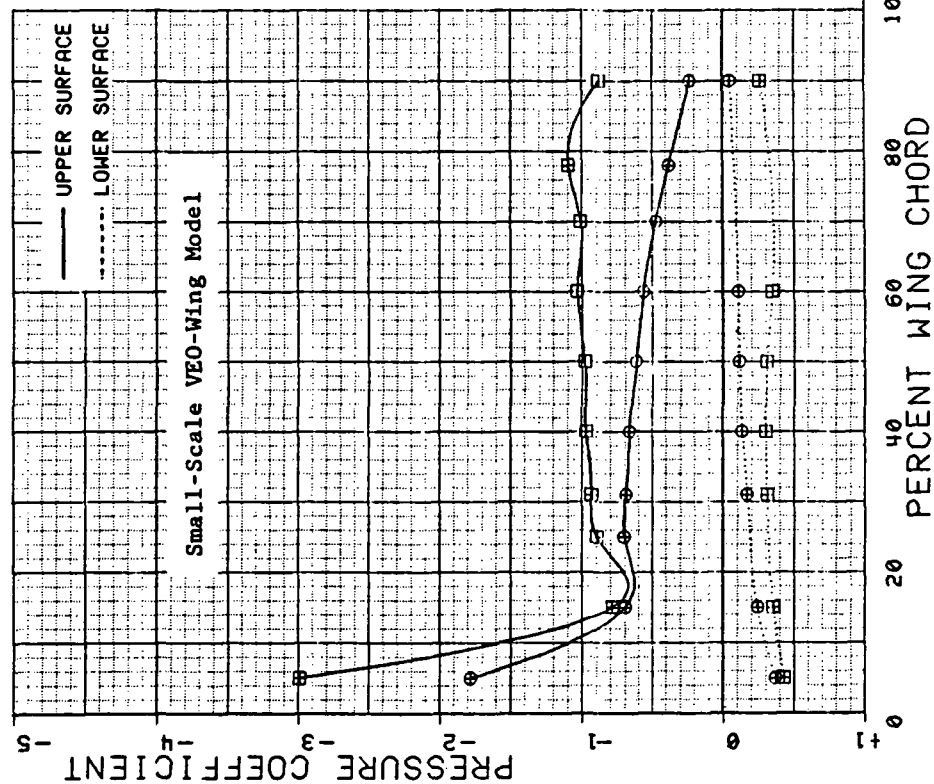


Figure 3.2.5-18 Comparison of Trailing-Edge Flap Effects, Power On, Alpha = 12 deg

SYM	TEST	RUN	ALPHA	CT	ITEF	OTEF	CAN	NOZ	SNB
⊕	204	153	4.02	0	0	0	0	0	OFF
⊕	204	158	4.02	1.5	0	0	0	0	OFF

SYM	TEST	RUN	ALPHA	CT	ITEF	OTEF	CAN	SNB
⊕	543	63	4.2	0.00	0	0	0	OFF
⊕	543	59	4.3	1.40	0	0	0	OFF

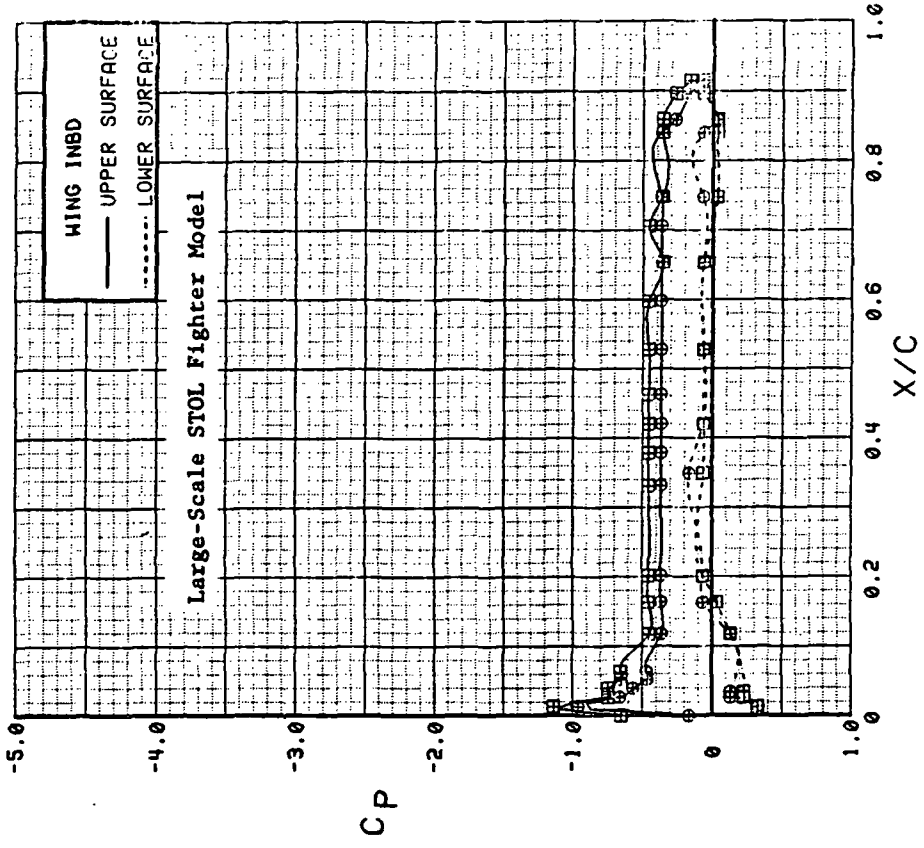
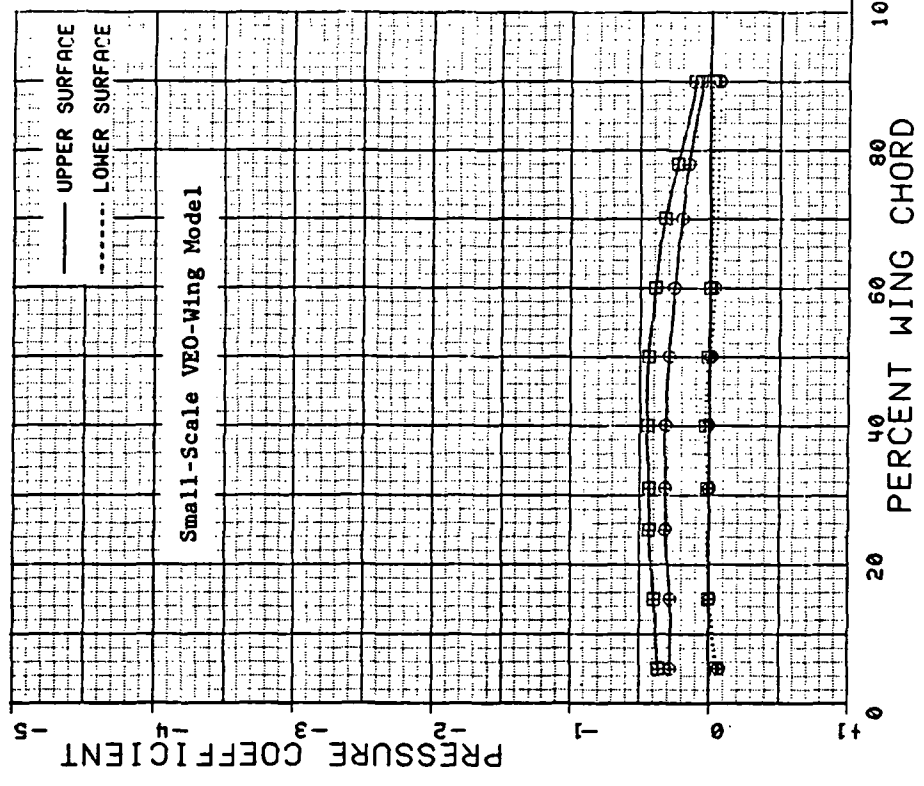


Figure 3.2.5-19 Comparison of Power Effects, Flaps Undelected, Alpha = 4 deg

SYM	TEST	RUN	ALPHA	CT	ITEF	OTEF	CAN	NOZ	SW6
⊕	204	153	8.01	0	0	0	0	N1AA	OFF
⊕	204	158	8.01	1.5	0	0	0	N1AA	OFF

SYM	TEST	RUN	ALPHA	CT	ITEF	OTEF	CAN	SW6
⊕	543	63	8.3	0.00	0	0	0	OFF
⊕	543	59	8.4	1.41	0	0	0	OFF

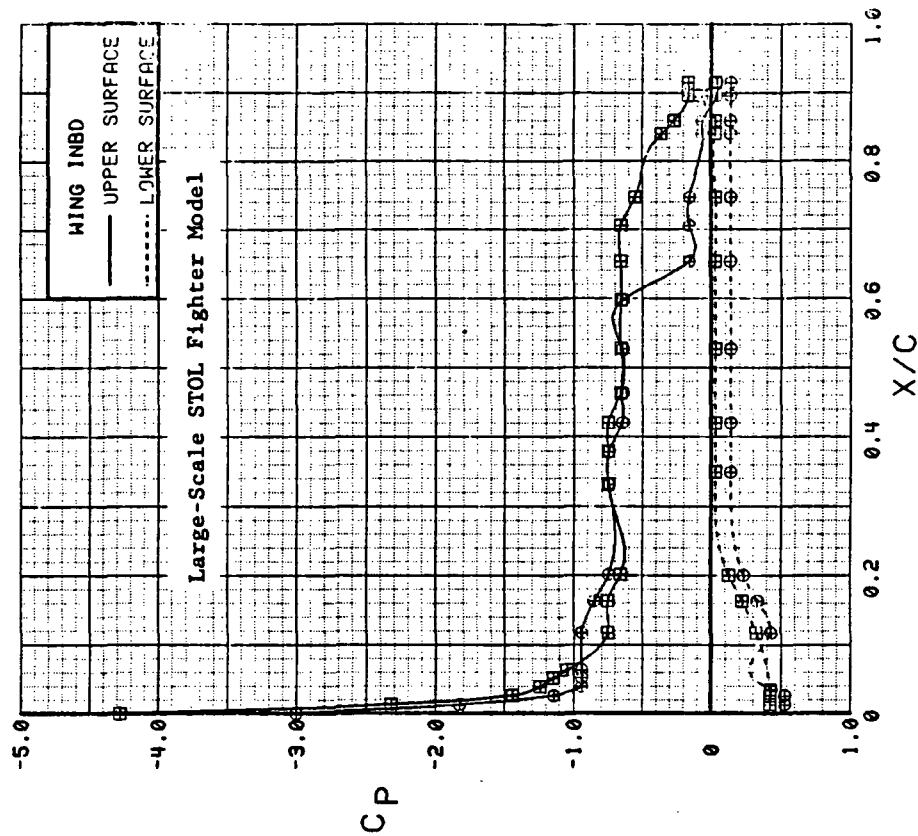
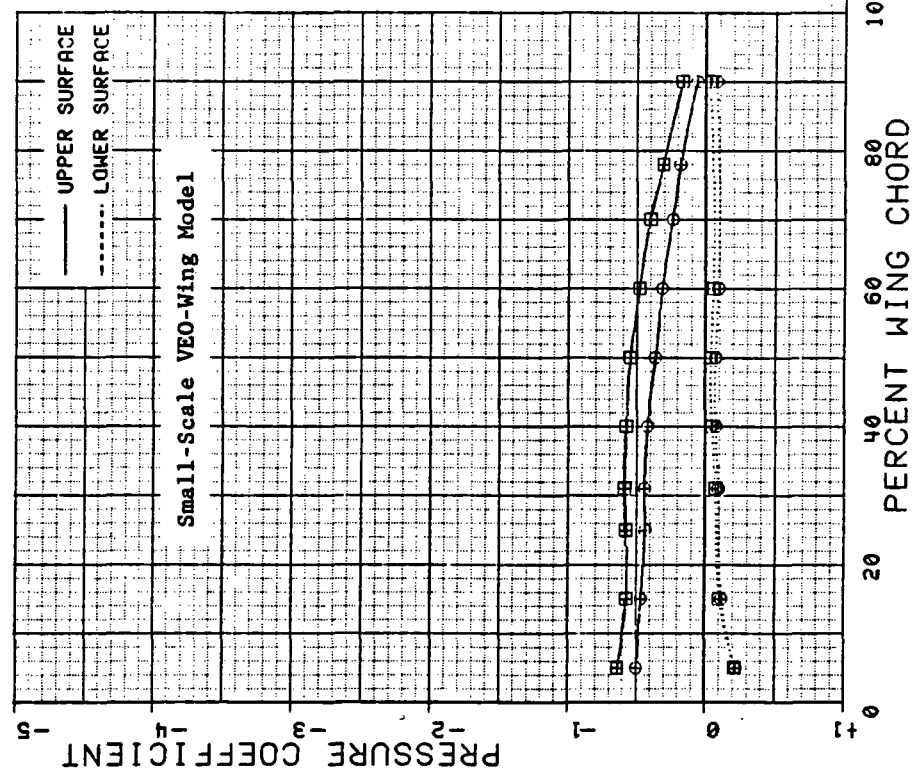


Figure 3.2.5-20 Comparison of Power Effects, Flaps Undelected,  
Alpha = 8 deg

SYM	TEST	RUN	ALPHA	CT	ITEF	OIEF	CAN	NOZ	SNB
⊕	204	153	12.01	0	0	0	0	0	NIAA OFF
⊕	204	158	11.96	1.5	0	0	0	0	NIAA OFF

SYM	TEST	RUN	ALPHA	CT	ITEF	OIEF	CAN	SNB
⊕	543	63	12.5	0.00	0	0	0	OFF
⊕	543	59	12.6	1.42	0	0	0	OFF

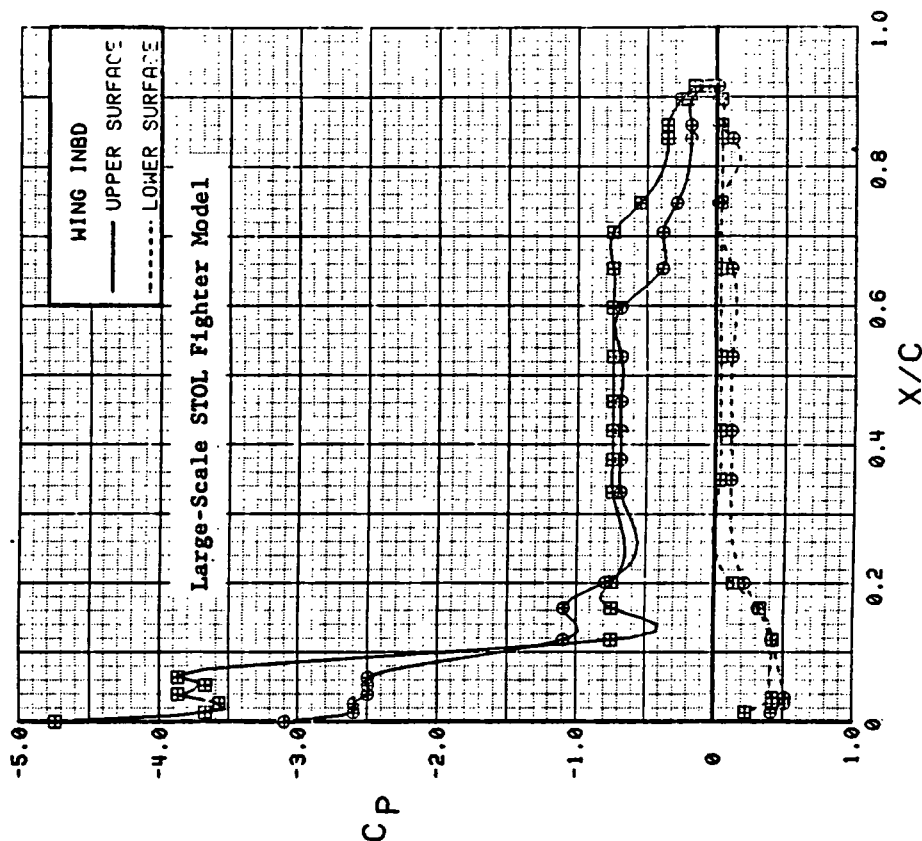
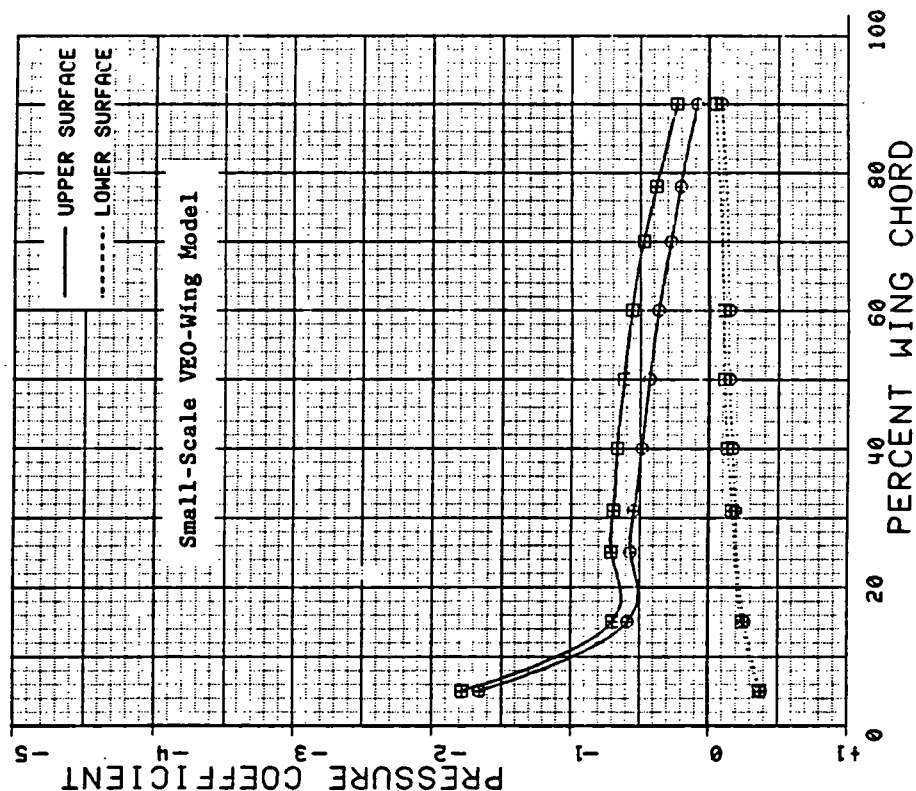


Figure 3.2.5-21 Comparison of Power Effects, Flaps Undelected, Alpha = 12 deg

SYM	TEST	RUN	ALPHA	CT	ITEF	QTEF	CAN	NOZ	SUB
⊕	204	153	24.05	0	0	0	0	0	NIAA OFF
⊕	204	158	23.99	1.5	0	0	0	0	NIAA OFF

SYM	TEST	RUN	ALPHA	CT	ITEF	QTEF	CAN	SUB
⊕	543	63	24.8	0.00	0	0	0	OFF
⊕	543	59	24.9	1.43	0	0	0	OFF

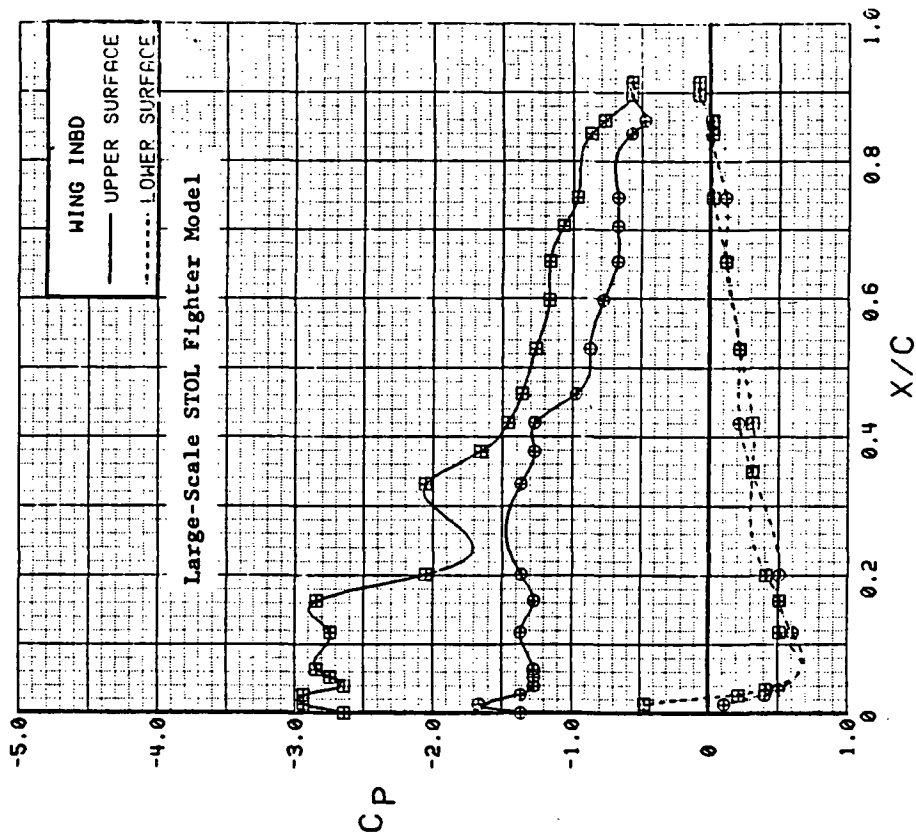
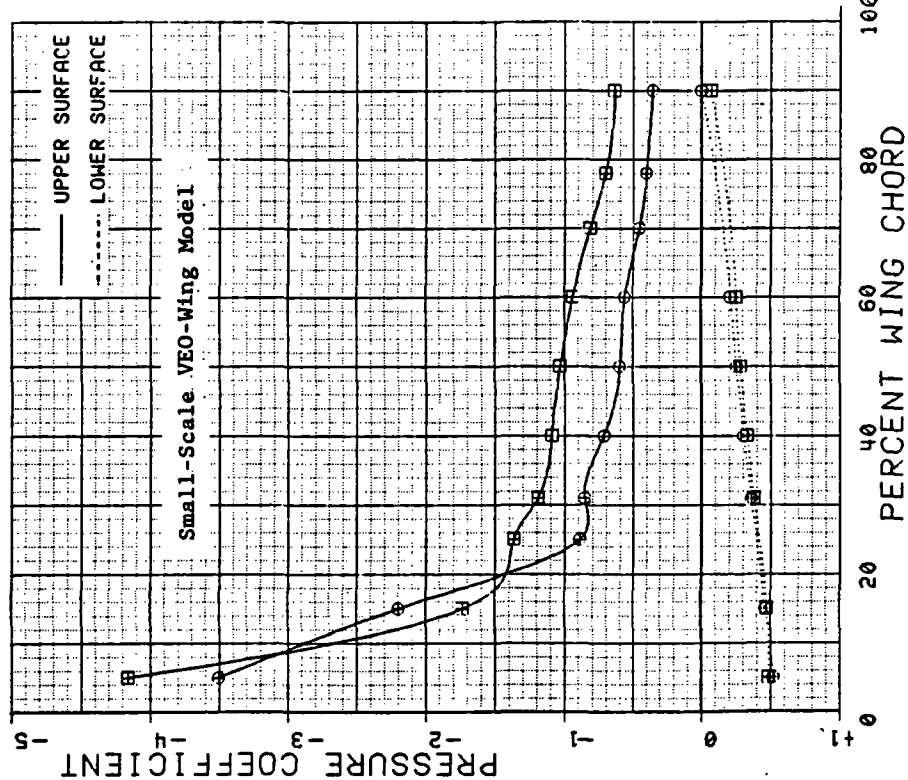
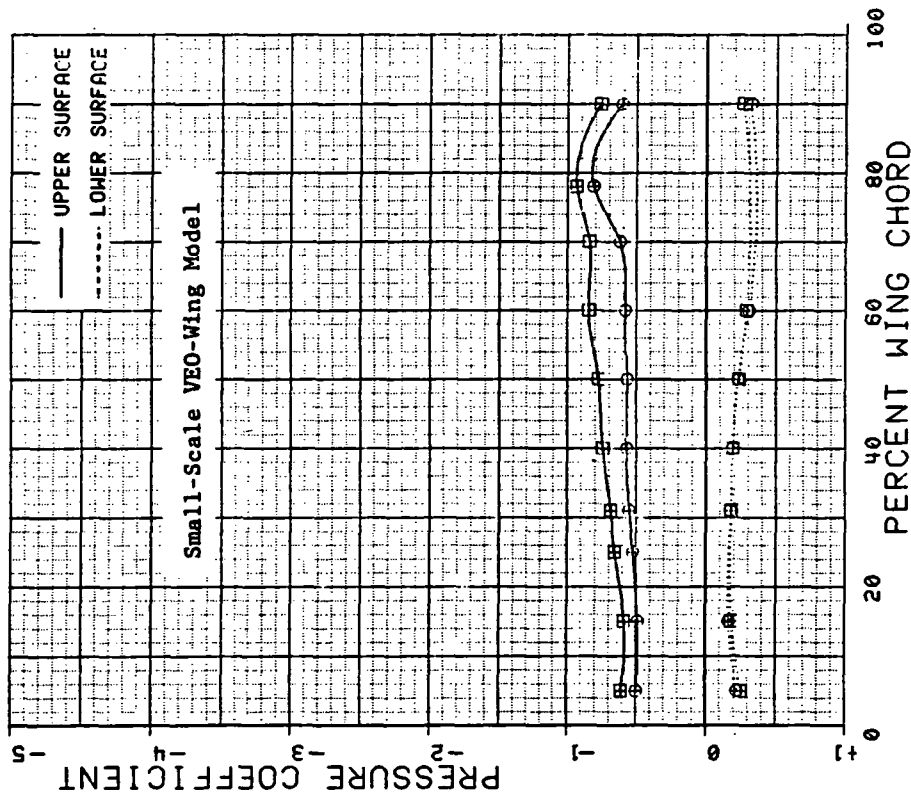


Figure 3.2.5-22 Comparison of Power Effects, Flaps Undelected,  
Alpha = 24 deg

SYM	TEST	RUN	ALPHA	CT	ITEF	OTEF	CAN	NOZ	SNB
⊕	204	185	4.02	0	30	30	0	NIFA	OFF
⊕	204	189	4.01	1.5	30	30	0	NIFA	OFF



SYM	TEST	RUN	ALPHA	CT	ITEF	OTEF	CAN	SNB
⊕	S43	11	4.4	0.00	30	30	0	OFF
⊕	S43	5	4.5	1.40	30	30	0	OFF

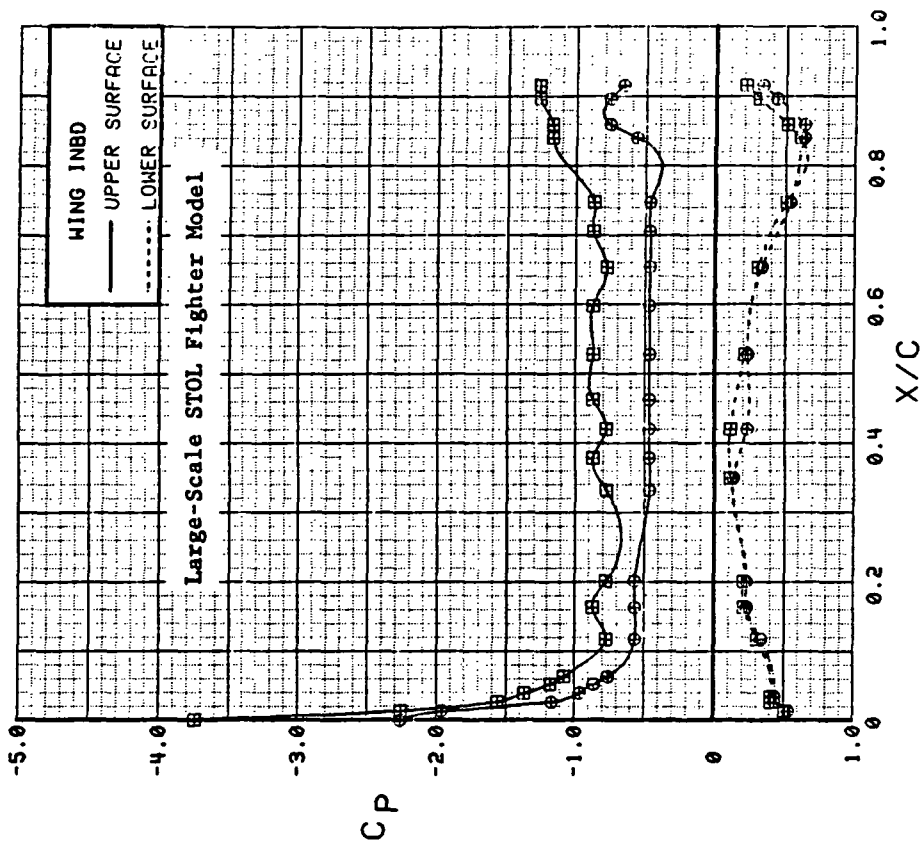


Figure 3.2.5-23 Comparison of Power Effects, Flaps 30 deg, Alpha = 4 deg

SYM	TEST	RUN	ALPHA	CT	ITEF	OTEF	CAN	NOZ	SIIB
⊕	204	185	8.00	0	30	30	0	NIFA	OFF
⊕	204	189	8.01	1.5	30	30	0	NIFA	OFF

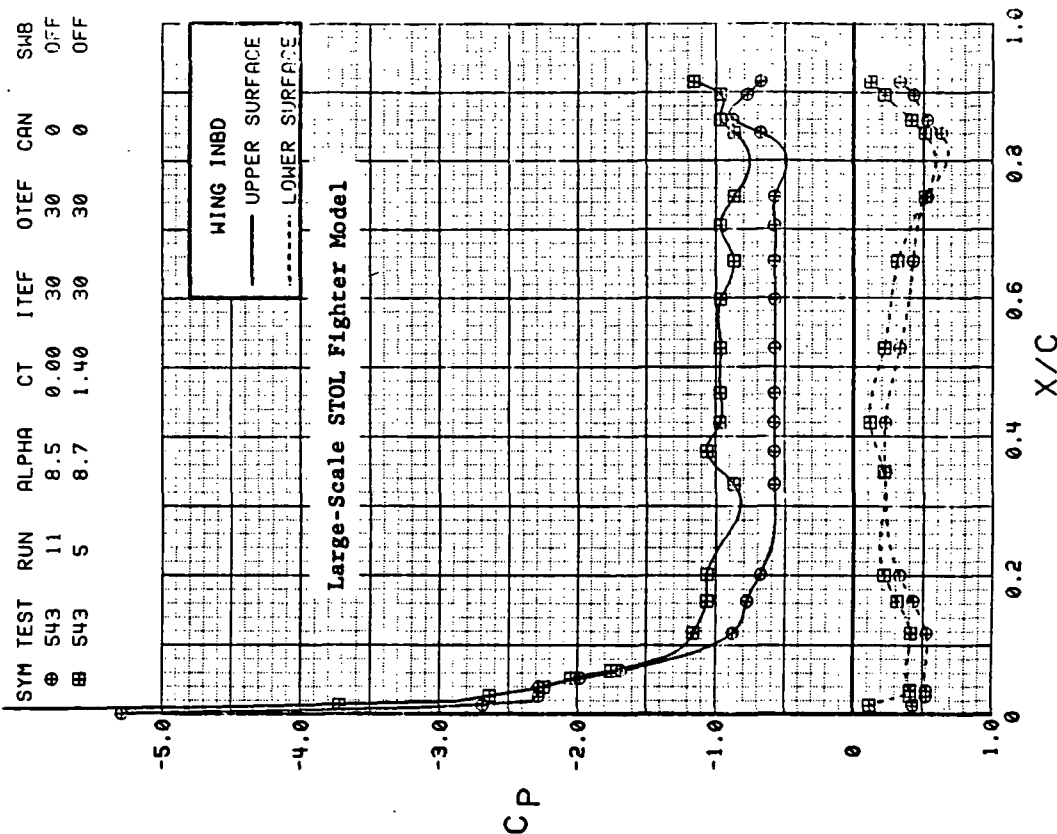
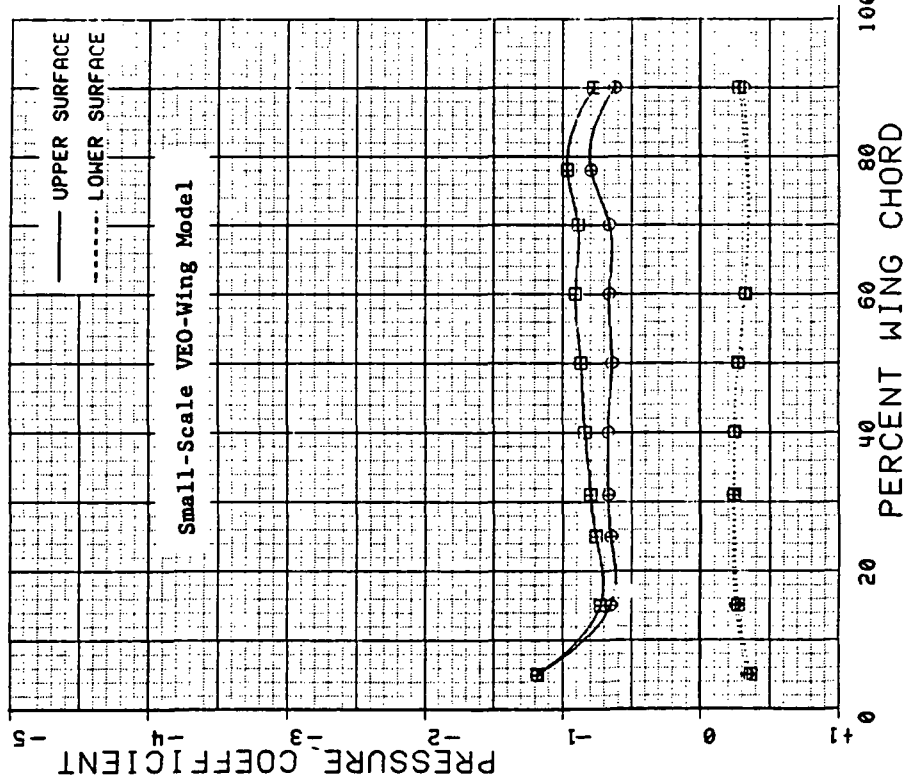


Figure 3.2.5-24 Comparison of Power Effects, Flaps 30 deg, Alpha = 8 deg

SYM	TEST	RUN	ALPHA	CT	ITEF	OTEF	CAN	NOZ	SMB
⊕	204	185	12.04	0	30	30	0	NIFA	OFF
⊕	204	189	11.98	1.5	30	30	0	NIFA	OFF

SYM	TEST	RUN	ALPHA	CT	ITEF	OTEF	CAN	SMB
⊕	543	11	12.7	0.00	30	30	0	OFF
⊕	543	5	12.8	1.39	30	30	0	OFF

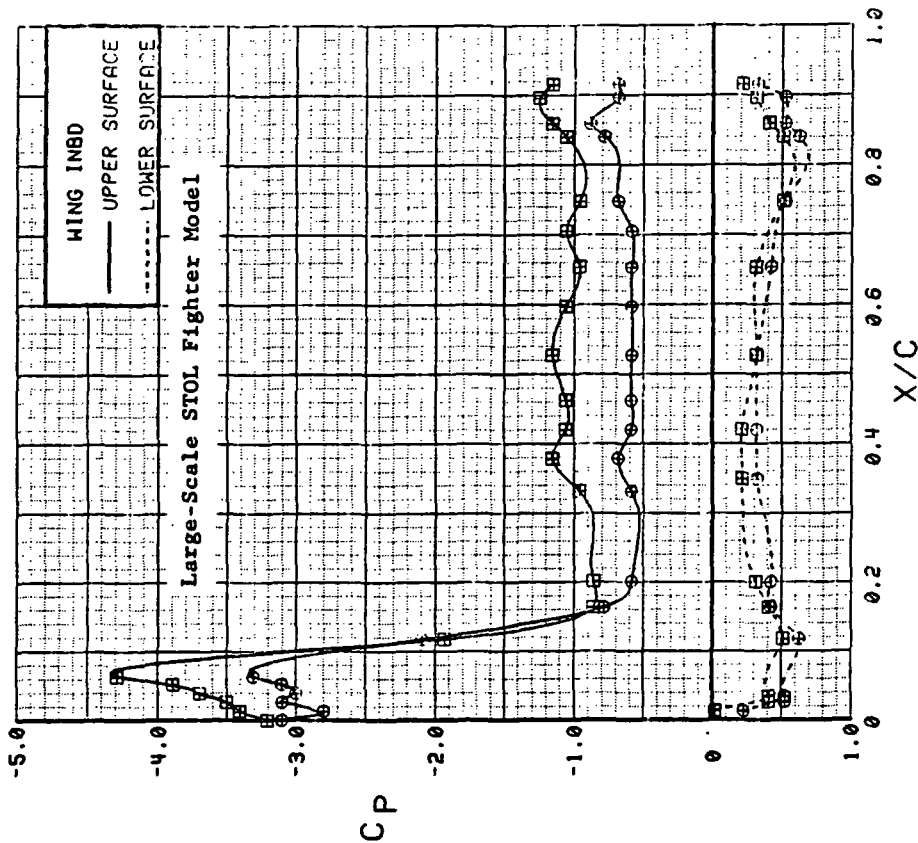
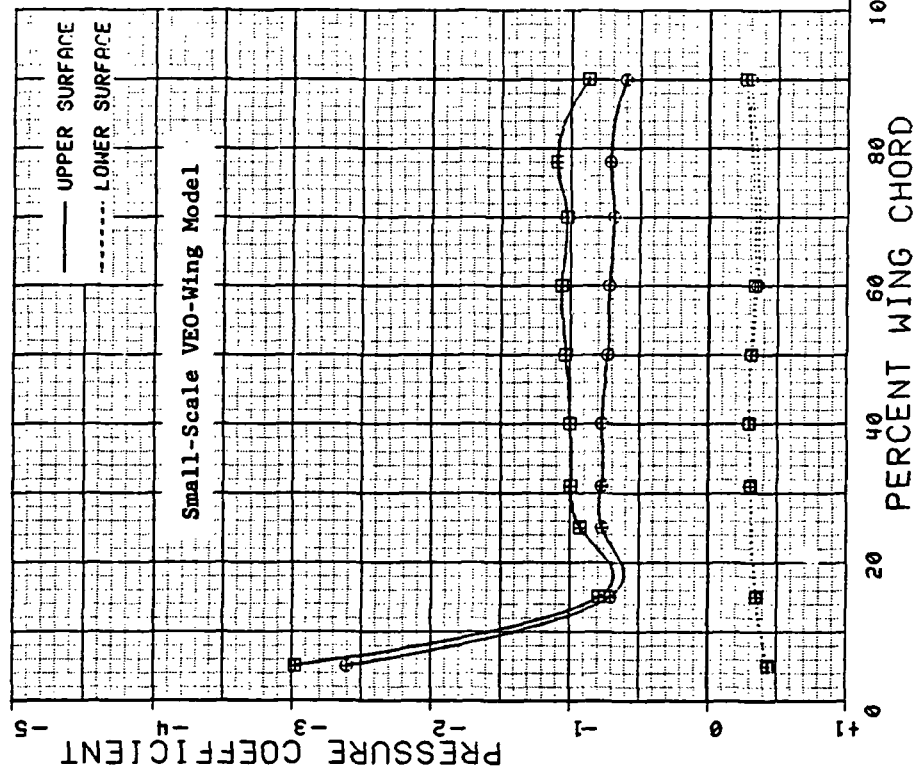
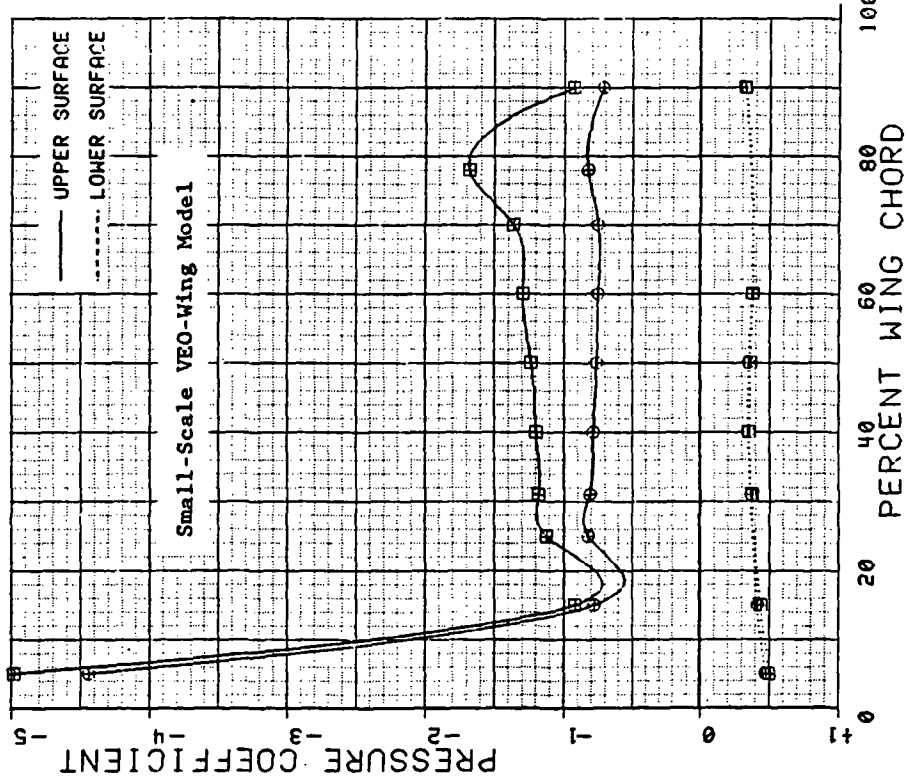


Figure 3.2.5-25 Comparison of Power Effects, Flaps 30 deg,  
Alpha = 12 deg



SYM	TEST	RUN	ALPHA	CT	ITEF	OTEF	CAN	NOZ	SHB
⊕	204	185	16.01	0	30	30	0	NIFA	OFF
⊕	204	189	16.00	1.5	30	30	0	NIFA	OFF



SYM	TEST	RUN	ALPHA	CT	ITEF	OTEF	CAN	SHB
⊕	543	11	16.8	0.00	30	30	0	OFF
⊕	543	5	16.9	1.40	30	30	0	OFF

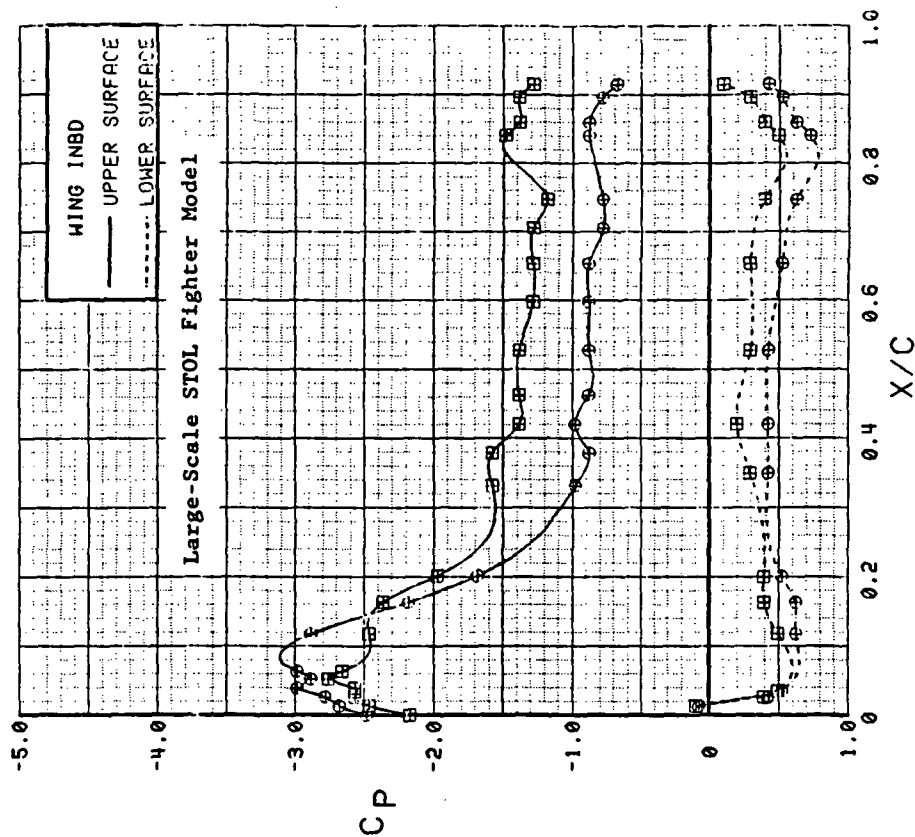


Figure 3.2.5-26 Comparison of Power Effects, Flaps 30 deg, Alpha = 16 deg

SYM	TEST	RUN	ALPHA	CT	ITEF	OTEF	CAN	NOZ	SWB
⊕	204	188	4.01	.9	30	30	0	NIFA	OFF
⊕	204	311	4.01	.9	30	30	0	NIEA	NII

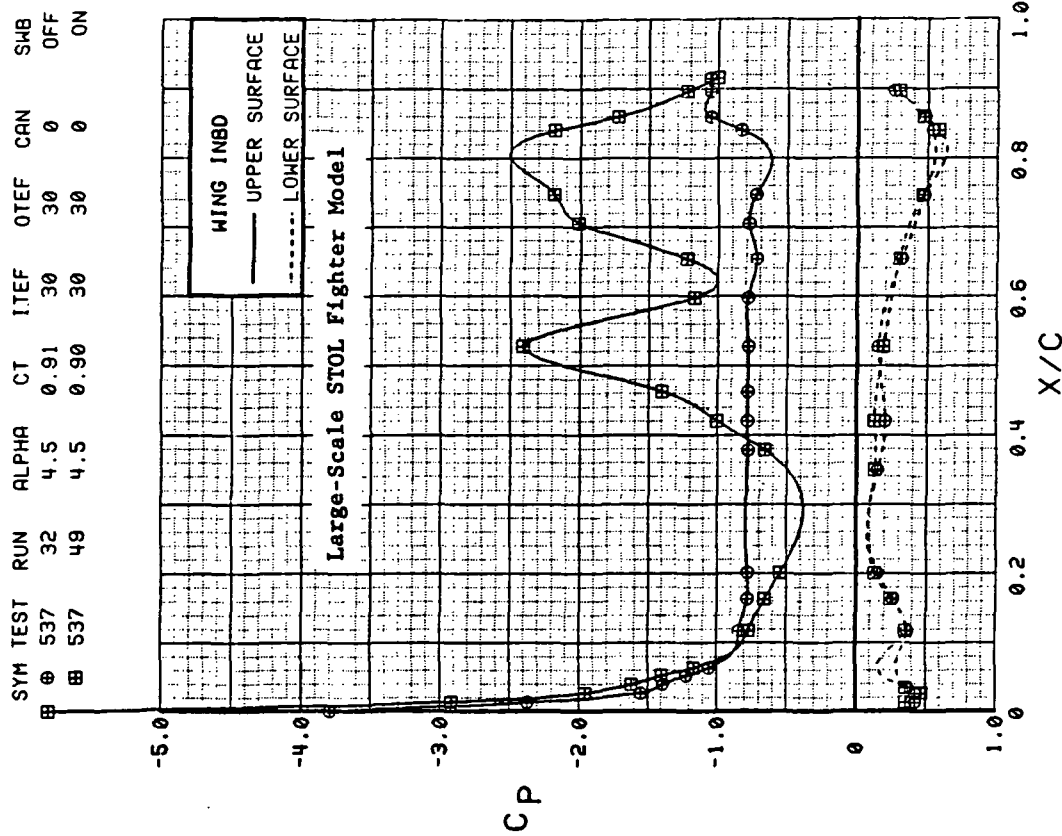
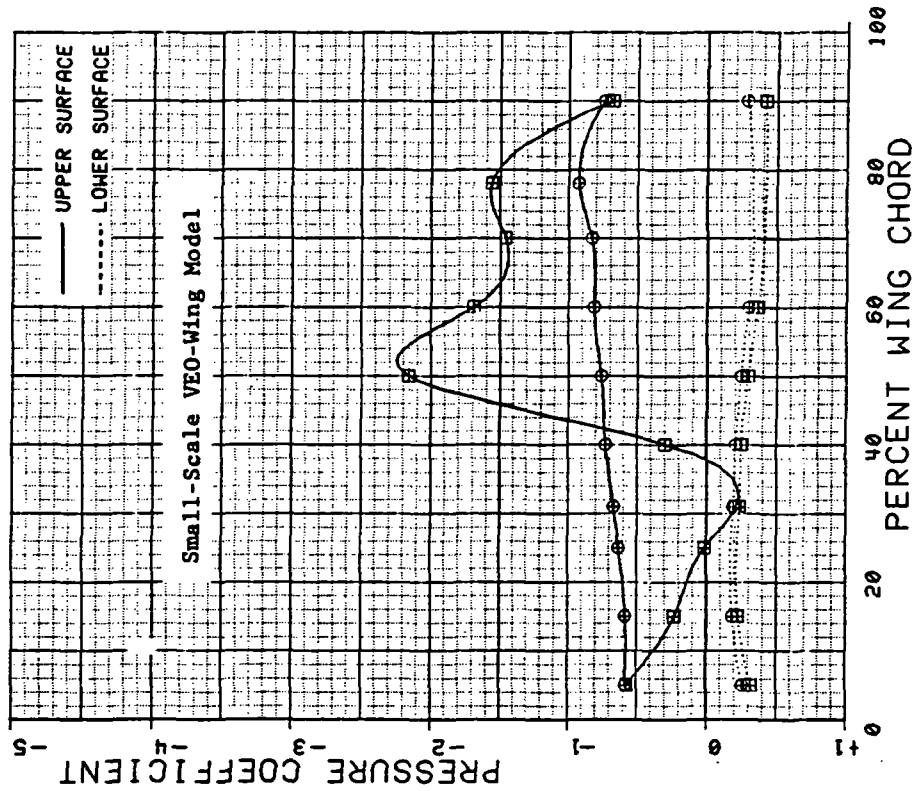


Figure 3.2.5-27 Comparison of Spanwise Blowing Effects,  
 $C_T = 0.9$ ,  $\alpha = 4^\circ$

SYM	TEST	RUN	ALPHA	CT	ITEF	OIEF	CAN	NOZ	SWB
⊕	204	188	12.04	.9	30	30	0	NIFA	OFF
⊕	204	311	11.98	.9	30	30	0	NIER	N11

SYM	TEST	RUN	ALPHA	CT	ITEF	OIEF	CAN	SWB
⊕	537	32	12.8	0.92	30	30	0	OFF
⊕	537	49	12.9	0.90	30	30	0	ON

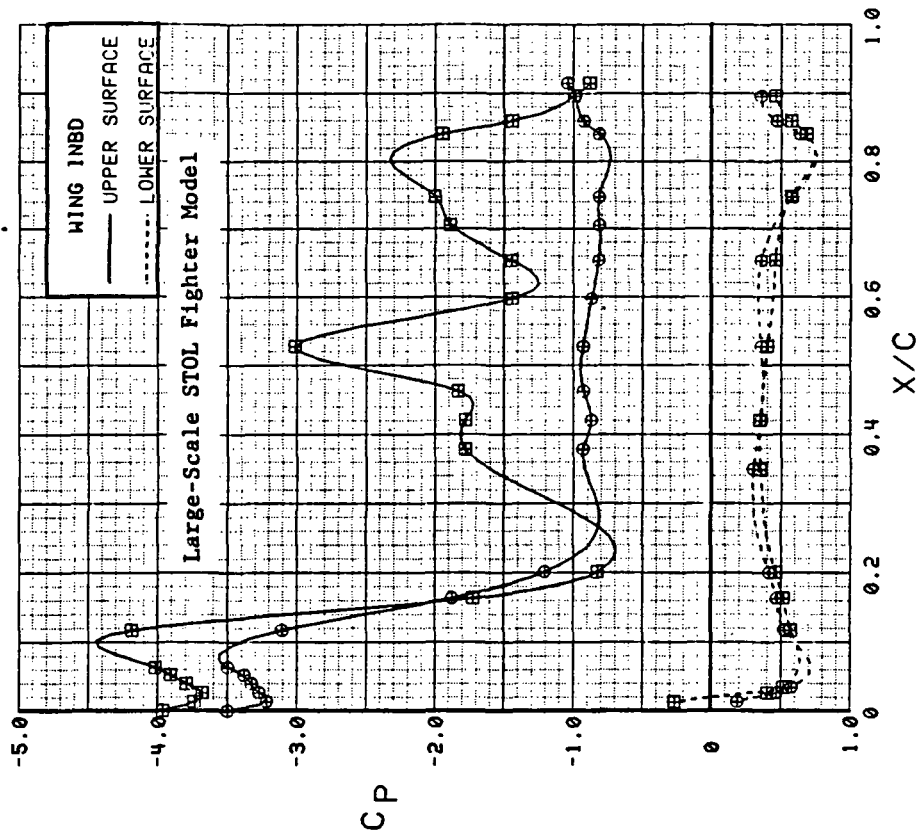
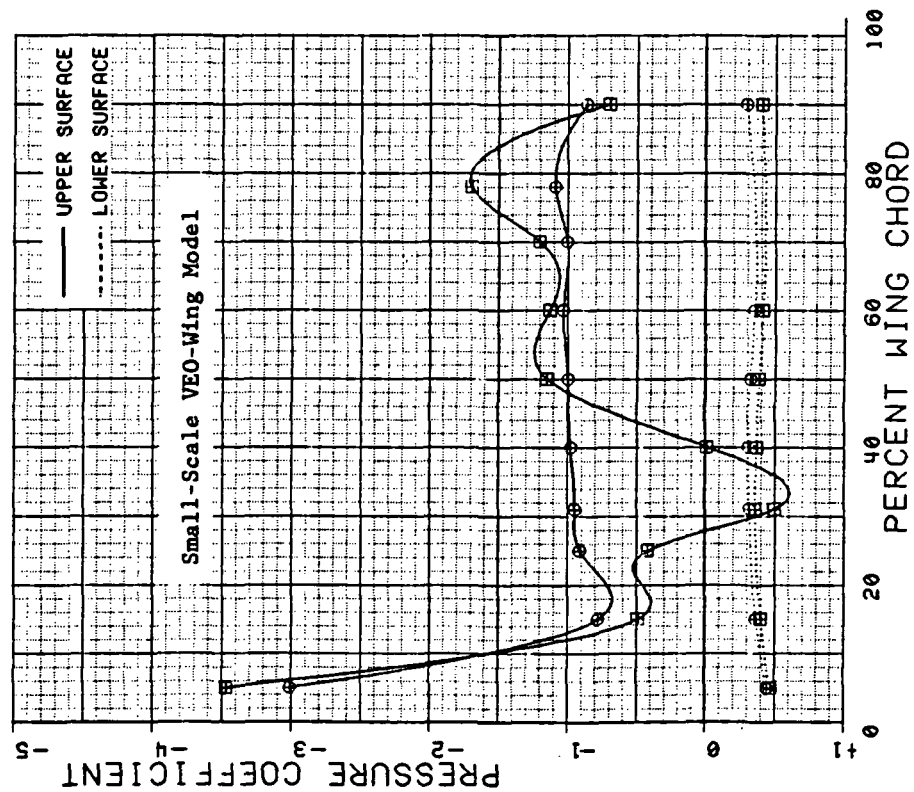


Figure 3.2.5-28 Comparison of Spanwise Blowing Effects,  
 $C_T = 0.9$ ,  $\alpha = 12^\circ$

SYM	TEST	RUN	ALPHA	CT	ITEF	OTEF	CAN	NOZ	SWB
0	204	190	4.00	2.0	30	30	0	NIFA	OFF
0	204	313	4.03	2.0	30	30	0	NIER	N11

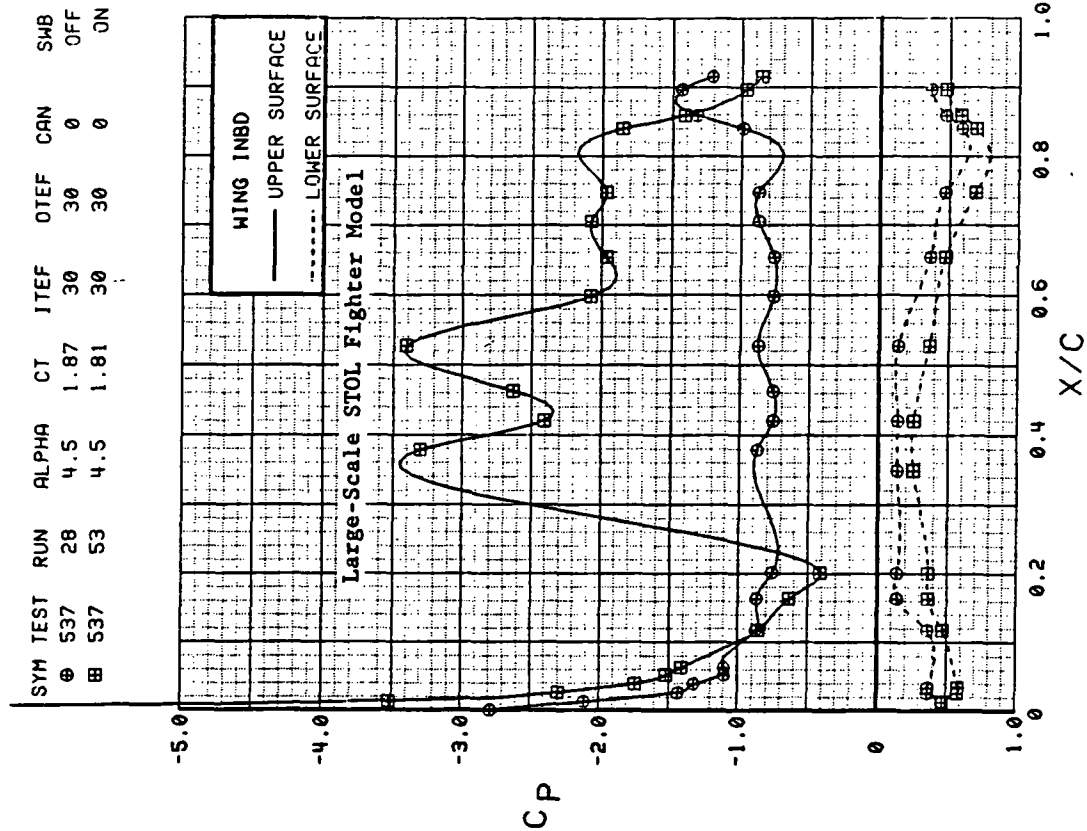
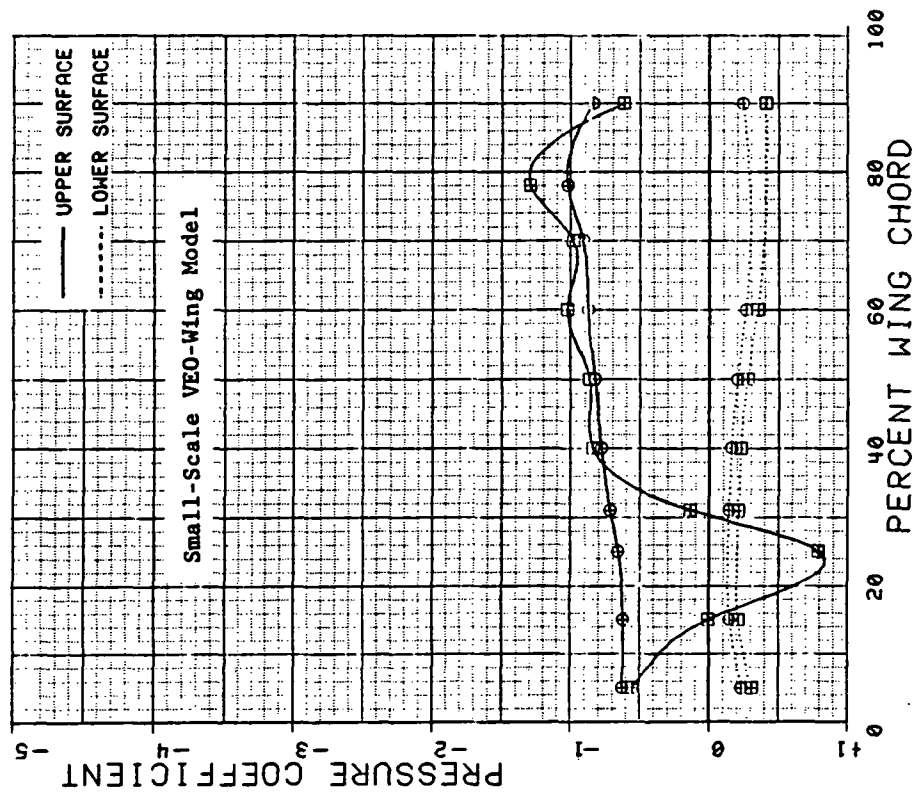


Figure 3.2.5-29 Comparison of Spanwise Blowing Effects,  
 $C_T = 1.9$ ,  $\alpha = 4^\circ$

SYM	TEST	RUN	ALPHA	CT	ITEF	OTEF	CAN	NOZ	SWB
⊕	204	190	12.02	2.0	30	30	0	N1FA	OFF
⊕	204	313	12.03	2.0	30	30	0	N1EA	N11

SYM	TEST	RUN	ALPHA	CT	ITEF	OTEF	CAN	SWB
⊕	537	28	12.8	1.82	30	30	0	OFF
⊕	537	53	12.9	1.82	30	30	0	ON

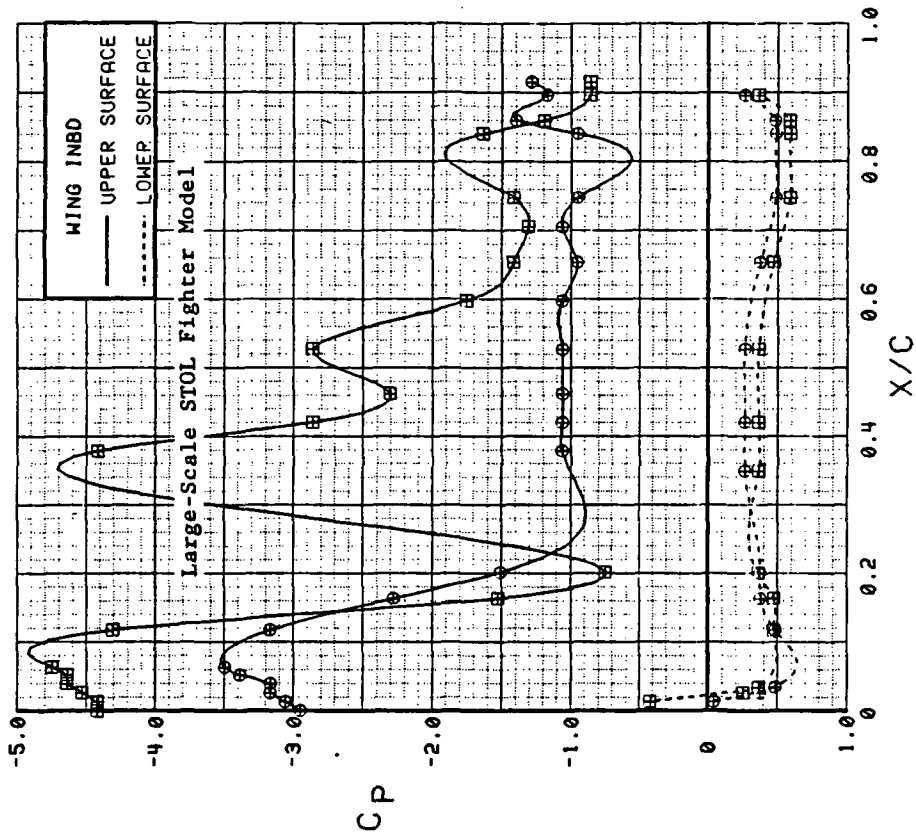
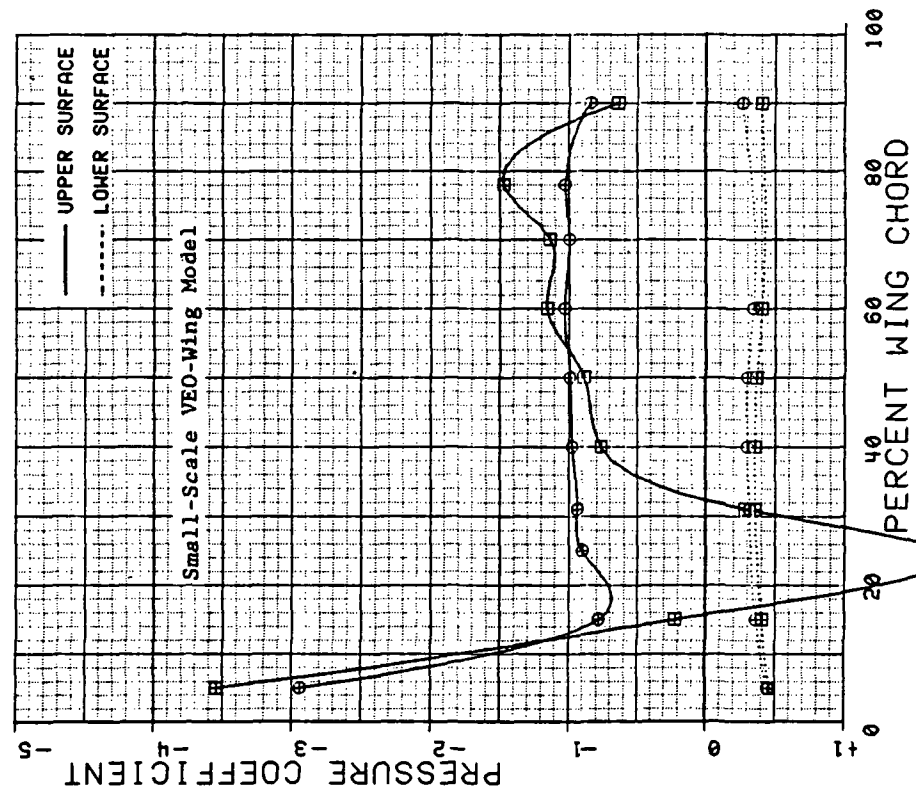


Figure 3.2.5-30 Comparison of Spanwise Blowing Effects,  
 $C_T = 1.9$ ,  $\alpha = 12^\circ$

**(This page intentionally left blank.)**

### 3.3 STRAKE RESULTS

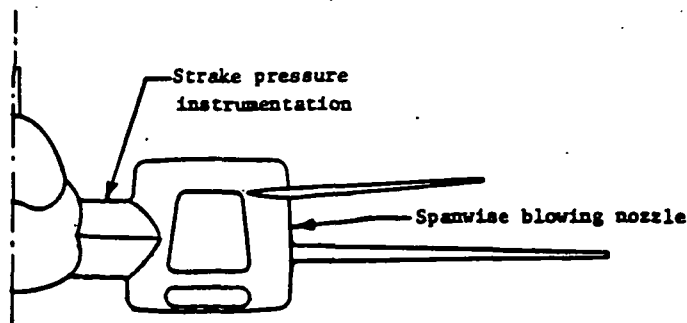
Data from the strake pressure taps discussed in Section 2.2 provide a good indication of the aerodynamic loading on the strake. These pressures, in general, behaved quite logically, responding to configuration changes in a manner that was generally anticipated. Power variations on the baseline model with no control surface deflections are shown in Figures 3.3-1 through -5 for several angles of attack. There is evidence in these plots of a small, local vortex on the sharp, highly-swept leading edge of the strake. At  $\alpha = 4$  deg, the second pressure tape (at 3% chord) was under the suction influence of the vortex as indicated by the spike in the pressure distributions (Figure 3.3-1). The strake leading-edge vortex was much stronger than the wing and canard leading-edge vortices because of the sharpness and the 72-deg sweep of the strake leading edge; this strength caused a more intense pressure fluctuation than was observed in either the wing or canard pressure data. Following the suction peak, a compression is indicated by the pressure tap at the 7% chord station. As explained in the discussion of the wing pressures, this was caused by the vortex impinging on the surface as it rotated and the flow reattached. Figures 3.3-2 through -5 show the development of the vortex as angle of attack was increased. The suction peak became even more pronounced, but the compression disappeared above  $\alpha = 8$  deg. Stall characteristics began to appear at  $\alpha = 20$  deg, and the strake was well into stall at  $\alpha \leq 29$  deg.

Power variations on the model with the trailing-edge flaps deflected 30 deg are shown for several angles of attack in Figures 3.3-6 through -10. The presence of a leading-edge vortex is also shown in these figures, and clearer depiction of the vortex development is presented in Figure 3.3-11, which shows concurrently the effects of angle of attack and power. Thrust coefficients of 0 and 1.4 only are shown in Figure 3.3-11 since both were tested at the same Reynolds number. It is interesting to note that the suction peak decreased with increasing thrust at  $\alpha = 8$  deg and below while higher angles of attack experienced a suction peak increase with increasing thrust.

The exhaust jet affected the pressures on the center portion of the strake at all trailing-edge flap settings. This effect is typical of that shown for 0- and 30-deg flap settings in Figures 3.3-1 through -10. As the flow accelerated along the boattail slopes approaching the nozzle exit on the inboard side of the nacelle, a small suction peak occurred on the strake upper surface just forward of the nozzle exit (75% chord). This modest suction extended forward to about the 30% chord. The data shown in Figure 3.3-7, which is for a trailing-edge flap setting of 30 deg and an angle of attack of 8 deg, represents a set of conditions between the 30% and 75% chord stations at which the effects of the exhaust jet were near maximum, except for negative flap deflections.

Power effects on the trailing-edge of the strake indicate that it was not subjected to a direct impact from the exhaust jet. The incremental loading caused by power was essentially independent of angle of attack and was small when the trailing-edge flaps were undeflected (Figures 3.3-1 through -5). For the flap-deflected case (Figures 3.3-6 through -10) the loading change on the aft part of the strake was primarily caused by a jet-induced suction on the lower surface. With power off, wing trailing-edge flap deflection had only a modest effect on the strake pressures, as shown by the flap variations in Figure 3.3-12. On the other hand, the flap variation with power-on (Figure 3.3-13) significantly impacted the upper surface pressures just aft of the nozzle exit, especially when the flap was set at negative deflections.

The spanwise blowing exhaust nozzle was on the outboard side of the nacelle and was physically separated from the strake upper surface by the nacelle, as illustrated by the sketch below. It appears from this geometry that spanwise blowing (SWB) would have



a minimal effect on the strake pressures. However, this was not the case, SWB increased strake loading, presumably by an increase in the circulation around the entire model. Figure 3.3-14 shows increased loading on both surfaces that is typical of a small increase in the angle of onset flow. Clear evidence of the circulation increase caused by SWB is shown by the data in Figure 3.3-15. With SWB off, the leading-edge pressures indicate that the flow was attached at  $\alpha = 4$  deg, but with SWB on, a vortex formed at the leading edge of the strake. The situation here was similar to that previously discussed for the canard and wing: when the flow was still attached but near separation, a leading-edge vortex moved inboard if either the angle-of-attack was increased or if there was an increase in circulation from another source. In this case, SWB increased the upwash at the strake leading-edge, caused separation, and hence, the inboard movement of the vortex. Data showing the effects at other angles of attack are shown in Figures 3.3-16 through -19.

Consideration must also be given to the fact that the primary-nozzle mass flux was reduced by 16% when the SWB nozzle was installed on the model and potentially had some influence on the strake pressures. Thus, the question arises as to how to uncouple the effect of the reduced mass flux of the primary nozzle from the direct effects of the SWB nozzle. The effects of the reduction in primary-nozzle mass flux are shown to be very small by an examination of the data in Figure 3.3-20. One curve has a thrust coefficient ( $C_T = 1.45$ ) that is approximately 20% less than that of the other curve ( $C_T = 1.80$ ). The change in thrust coefficients between these two curves was obtained by a change in dynamic pressure ( $q$ ) as opposed to a change in mass flux as occurred when SWB was turned on. Regardless of whether the  $C_T$  was changed by mass flux or  $q$ , the effect on the strake pressure distribution should have been approximately the same, which they were with the exception of the leading-edge pressures that were previously shown to be sensitive to  $q$  variations. Hence, it follows that the 16 % reduction in mass flow that occurred at the primary nozzle when SWB was turned on was not responsible for the changes in strake pressures. This discussion establishes, in conclusion, that the differences in the strake pressure distributions shown in Figures 3.3-1 through -10 result mostly from the exhaust jet of the spanwise nozzle and not from the reduced mass flow from the primary nozzle.



SYM	TEST	RUN	ALPHA	CT	ITEF	OTEF	CAN	SWB
⊕	543	63	4.2	0.00	0	0	0	OFF
⊞	543	62	4.2	0.48	0	0	0	OFF
△	543	60	4.3	0.93	0	0	0	OFF
⬠	543	59	4.3	1.40	0	0	0	OFF
*	543	58	4.3	1.84	0	0	0	OFF

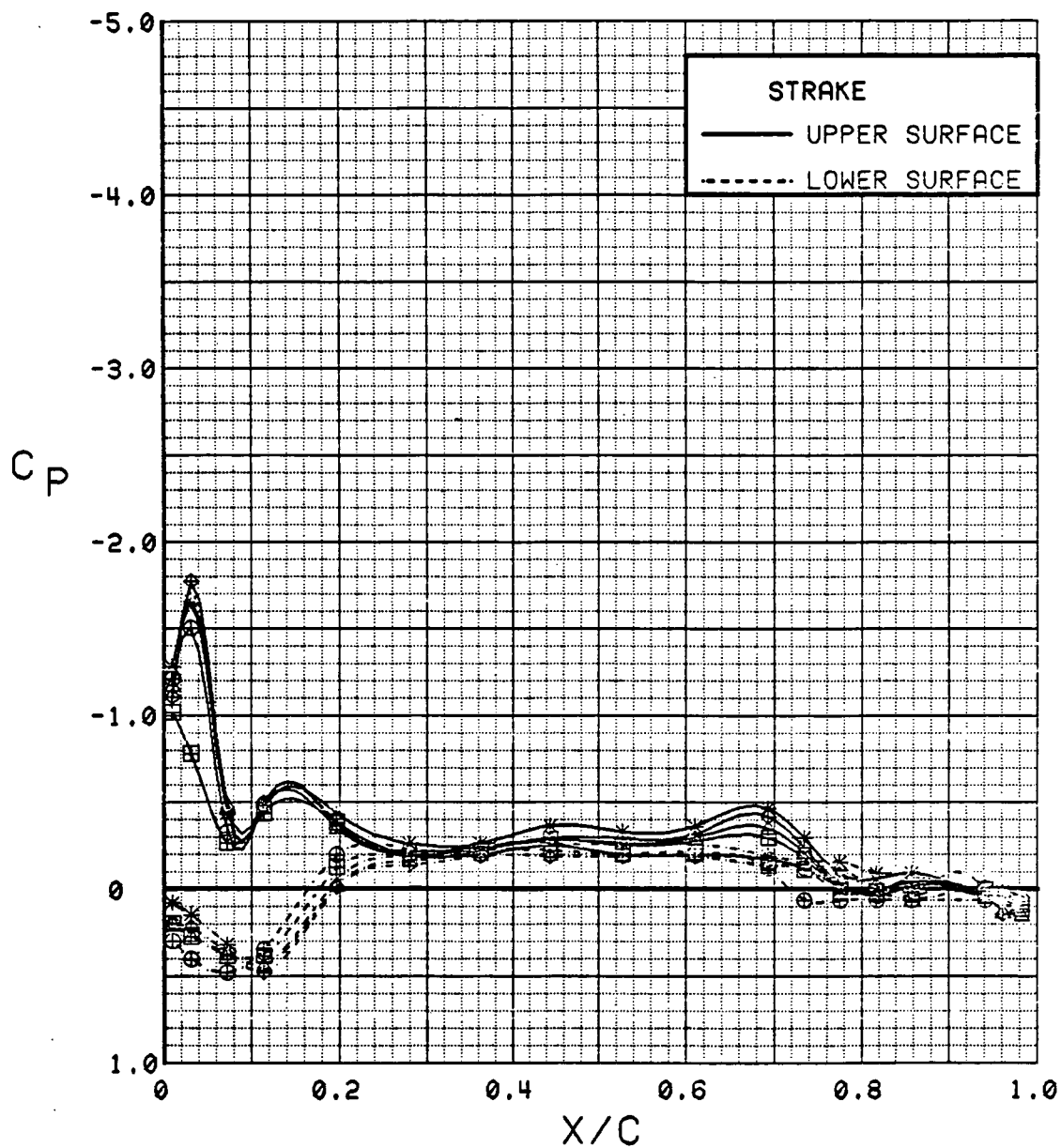


Figure 3.3-1 Power Effects on Strake Pressures, Wing Flaps Neutral  
Alpha = 4 deg

SYM	TEST	RUN	ALPHA	CT	ITEF	OTEF	CAN	SWB
⊕	543	63	8.3	0.00	0	0	0	OFF
⊞	543	62	8.4	0.47	0	0	0	OFF
△	543	60	8.4	0.94	0	0	0	OFF
⊕	543	59	8.4	1.41	0	0	0	OFF
*	543	58	8.4	1.90	0	0	0	OFF

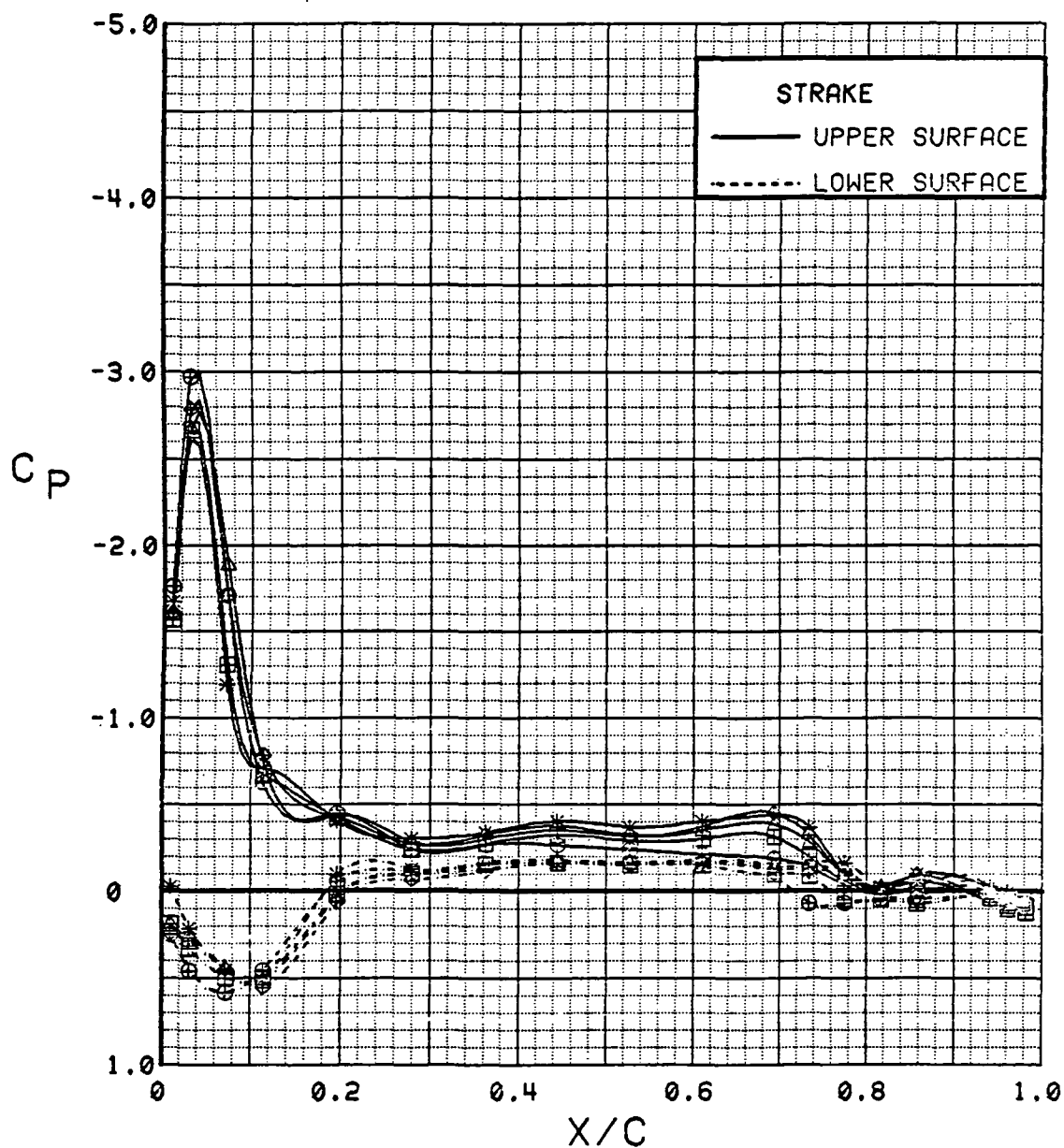


Figure 3.3-2

Power Effects on Strake Pressures, Wing Flaps Neutral  
Alpha = 8 deg

SYM	TEST	RUN	ALPHA	CT	ITEF	OTEF	CAN	SWB
⊕	543	63	12.5	0.00	0	0	0	OFF
⊞	543	62	12.5	0.47	0	0	0	OFF
△	543	60	12.5	0.94	0	0	0	OFF
⊕	543	59	12.6	1.42	0	0	0	OFF
*	543	58	12.6	1.87	0	0	0	OFF

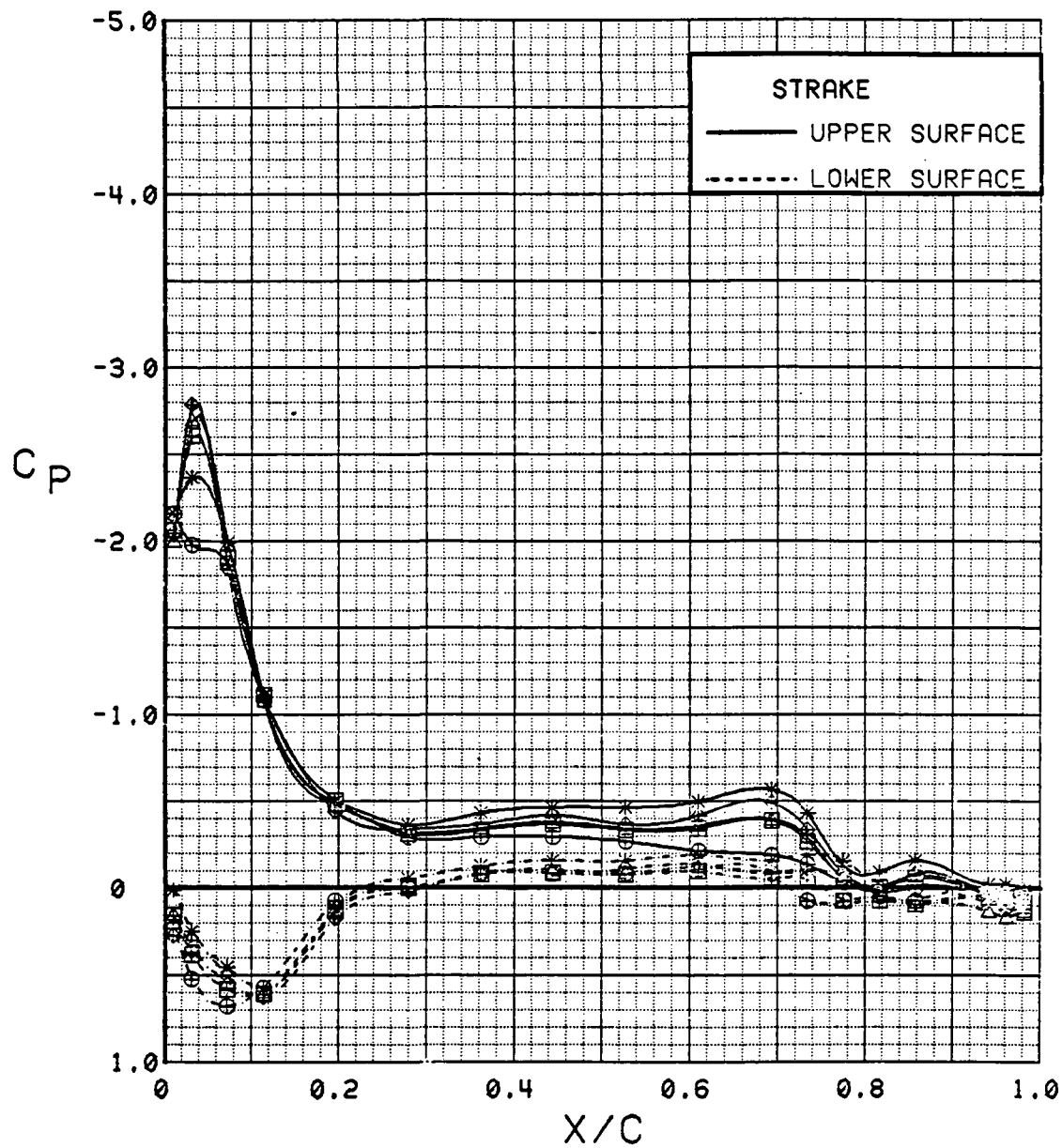


Figure 3.3-3

Power Effects on Strake Pressures, Wing Flaps Neutral  
Alpha = 12 deg

SYM	TEST	RUN	ALPHA	CT	ITEF	OTEF	CAN	SWB
⊕	543	63	20.7	0.00	0	0	0	OFF
⊞	543	62	20.8	0.47	0	0	0	OFF
△	543	60	20.8	0.93	0	0	0	OFF
⊕	543	59	20.8	1.41	0	0	0	OFF
*	543	58	20.8	1.72	0	0	0	OFF

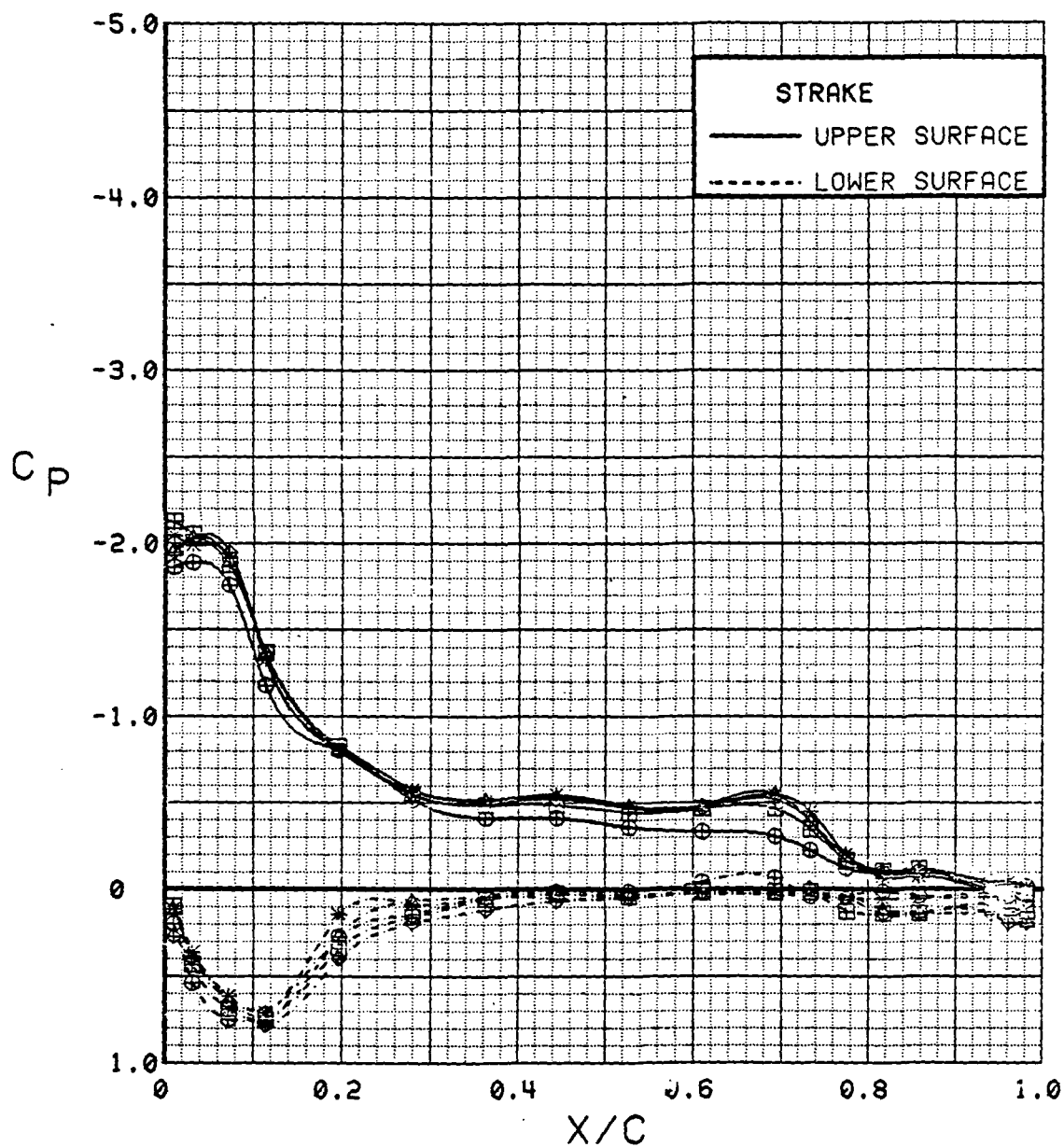


Figure 3.3-4

Power Effects on Strake Pressures, Wing Flaps Neutral  
Alpha = 21 deg

SYM	TEST	RUN	ALPHA	CT	ITEF	OTEF	CAN	SWB
⊕	543	63	28.8	0.00	0	0	0	OFF
⊞	543	62	29.0	0.47	0	0	0	OFF
△	543	60	29.0	0.93	0	0	0	OFF
⊕	543	59	29.1	1.41	0	0	0	OFF
*	543	58	29.1	1.83	0	0	0	OFF

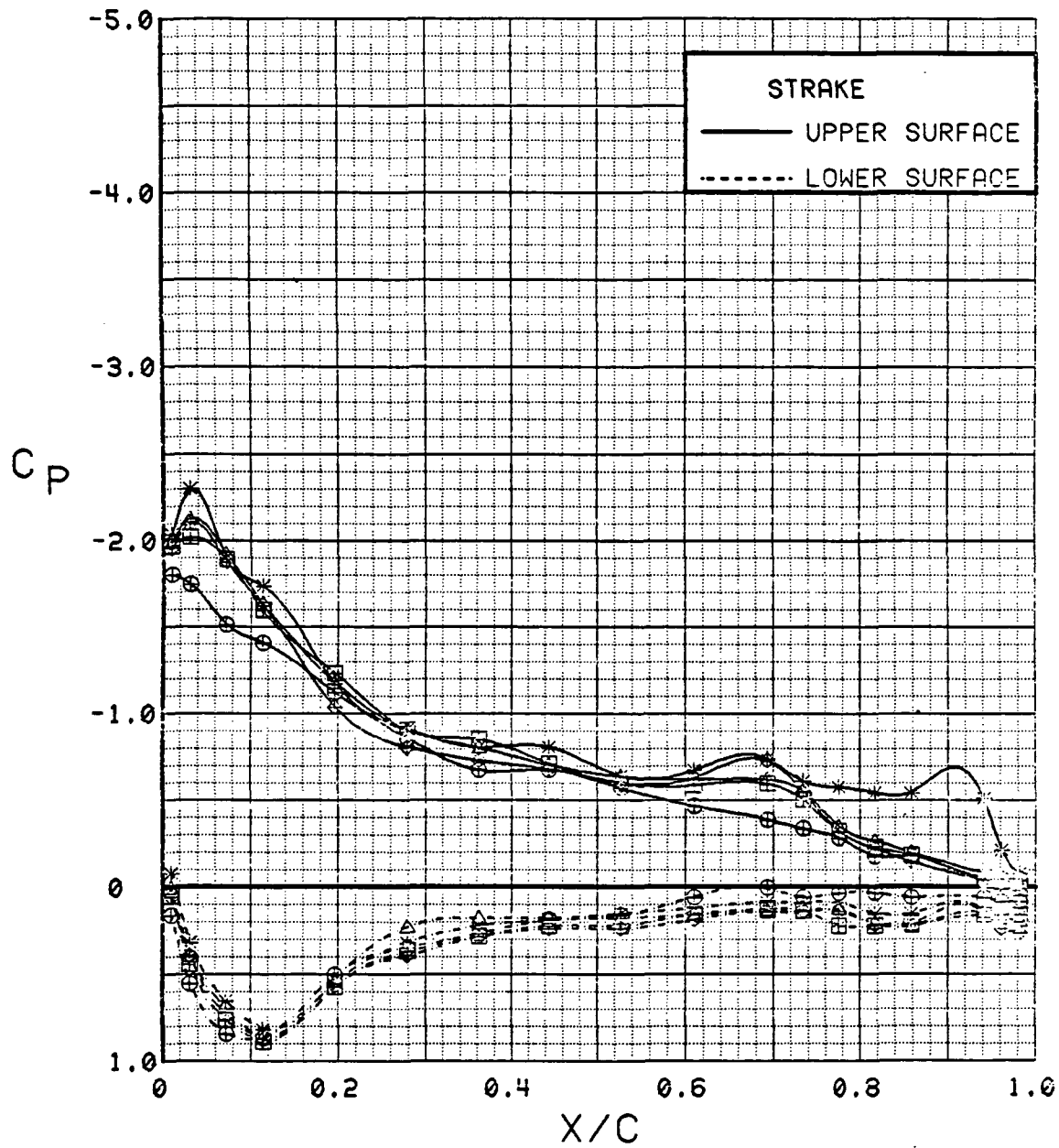


Figure 3.3-5

Power Effects on Strake Pressures, Wing Flaps Neutral  
Alpha = 29 deg

SYM	TEST	RUN	ALPHA	CT	ITEF	OTEF	CAN	SWB
⊕	543	11	4.4	0.00	30	30	0	OFF
⊞	543	8	4.5	0.47	30	30	0	OFF
△	543	6	4.5	0.94	30	30	0	OFF
⊕	543	5	4.5	1.40	30	30	0	OFF
*	543	4	4.5	1.90	30	30	0	OFF

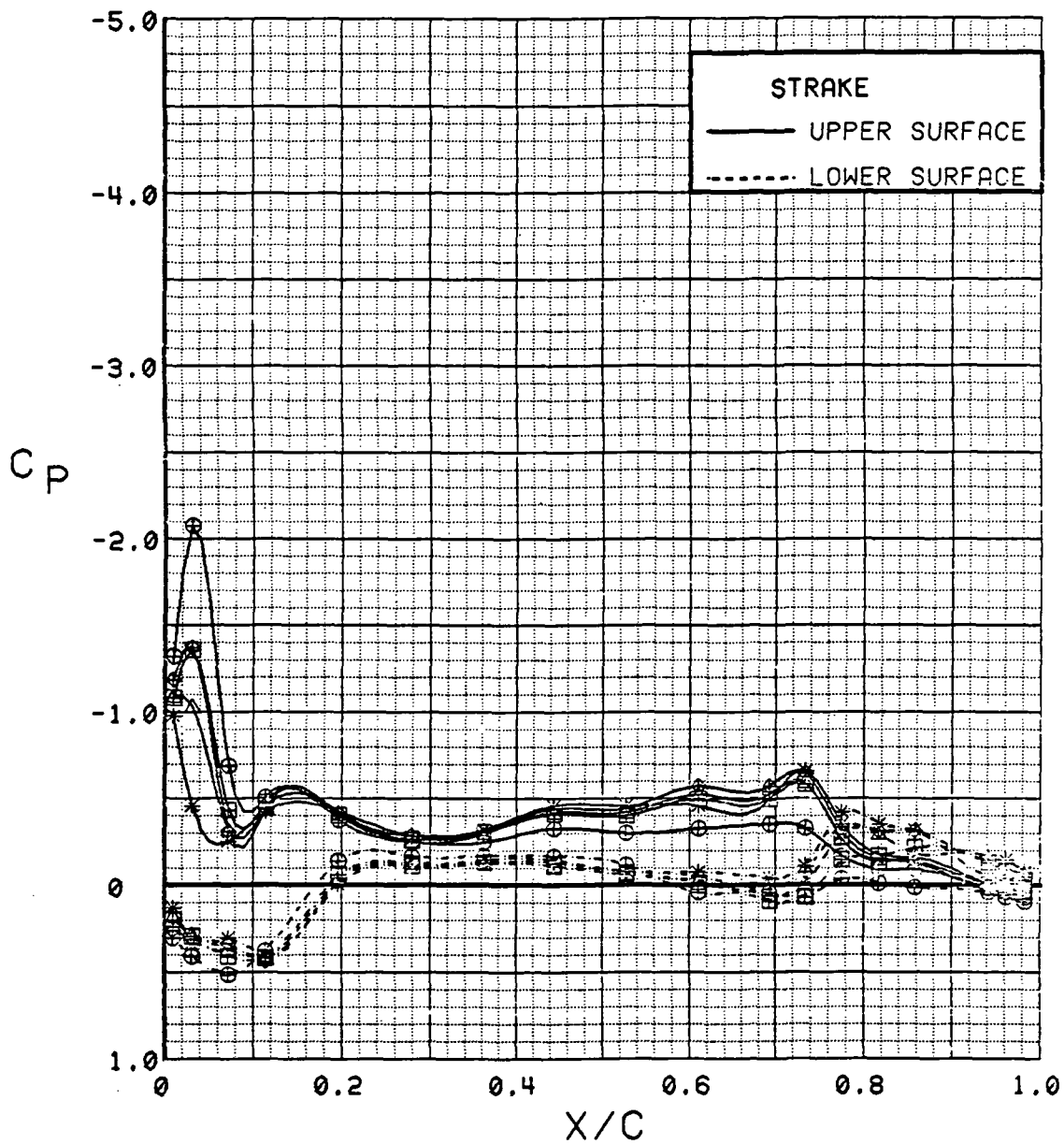


Figure 3.3-6

Power Effects on Strake Pressures, Wing Flaps Deflected  
Alpha = 4 deg

SYM	TEST	RUN	ALPHA	CT	ITEF	OTEF	CAN	SWB
⊕	543	11	8.5	0.00	30	30	0	OFF
⊞	543	8	8.6	0.47	30	30	0	OFF
△	543	6	8.6	0.91	30	30	0	OFF
⊕	543	5	8.7	1.40	30	30	0	OFF
*	543	4	8.7	1.85	30	30	0	OFF

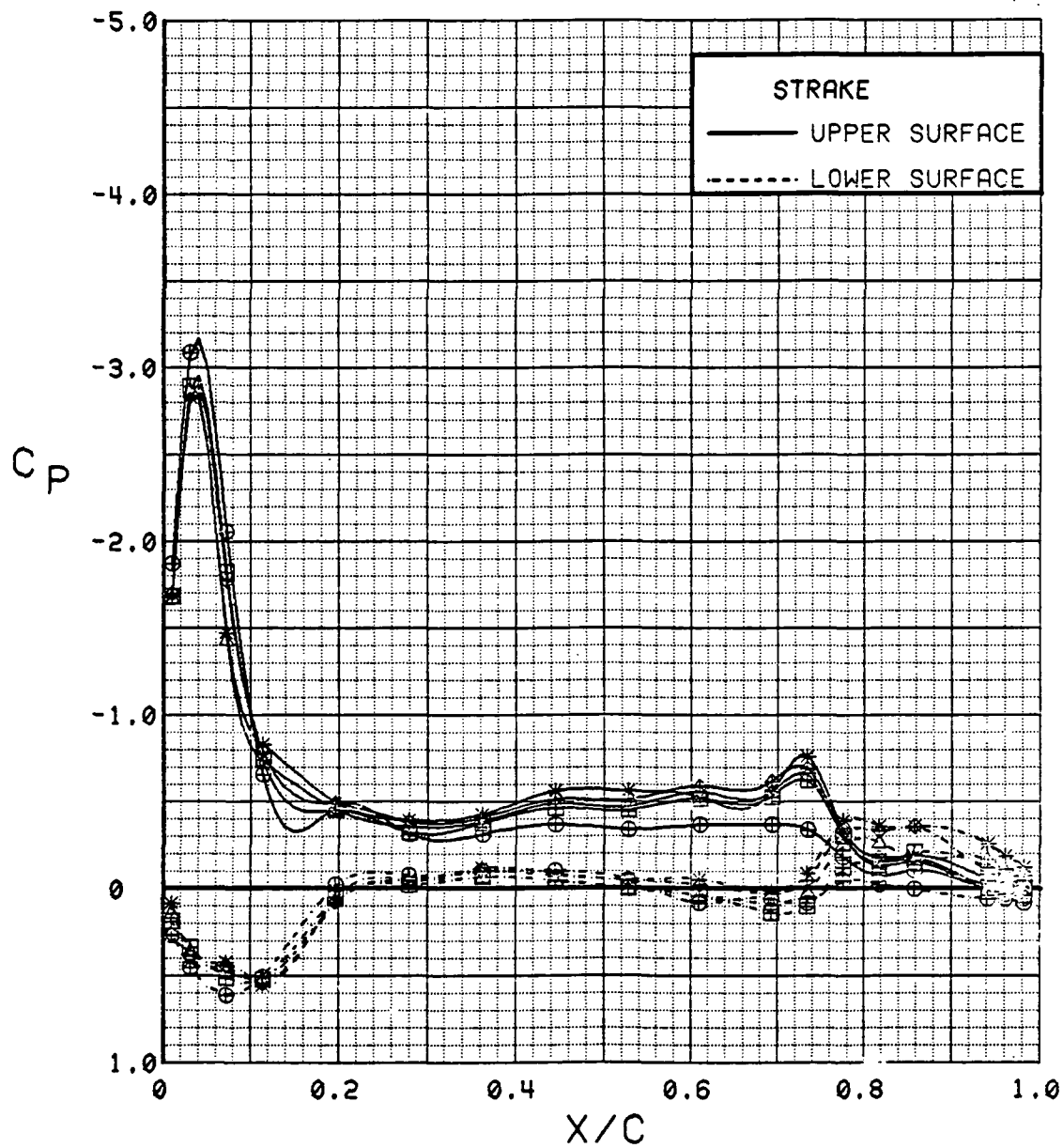


Figure 3.3-7 Power Effects on Strake Pressures, Wing Flaps Deflected  
Alpha = 8 deg

SYM	TEST	RUN	ALPHA	CT	ITEF	OTEF	CAN	SWB
⊕	543	11	12.7	0.00	30	30	0	OFF
⊞	543	8	12.8	0.46	30	30	0	OFF
△	543	6	12.8	-0.92	30	30	0	OFF
⬠	543	5	12.8	1.39	30	30	0	OFF
*	543	4	12.8	1.86	30	30	0	OFF

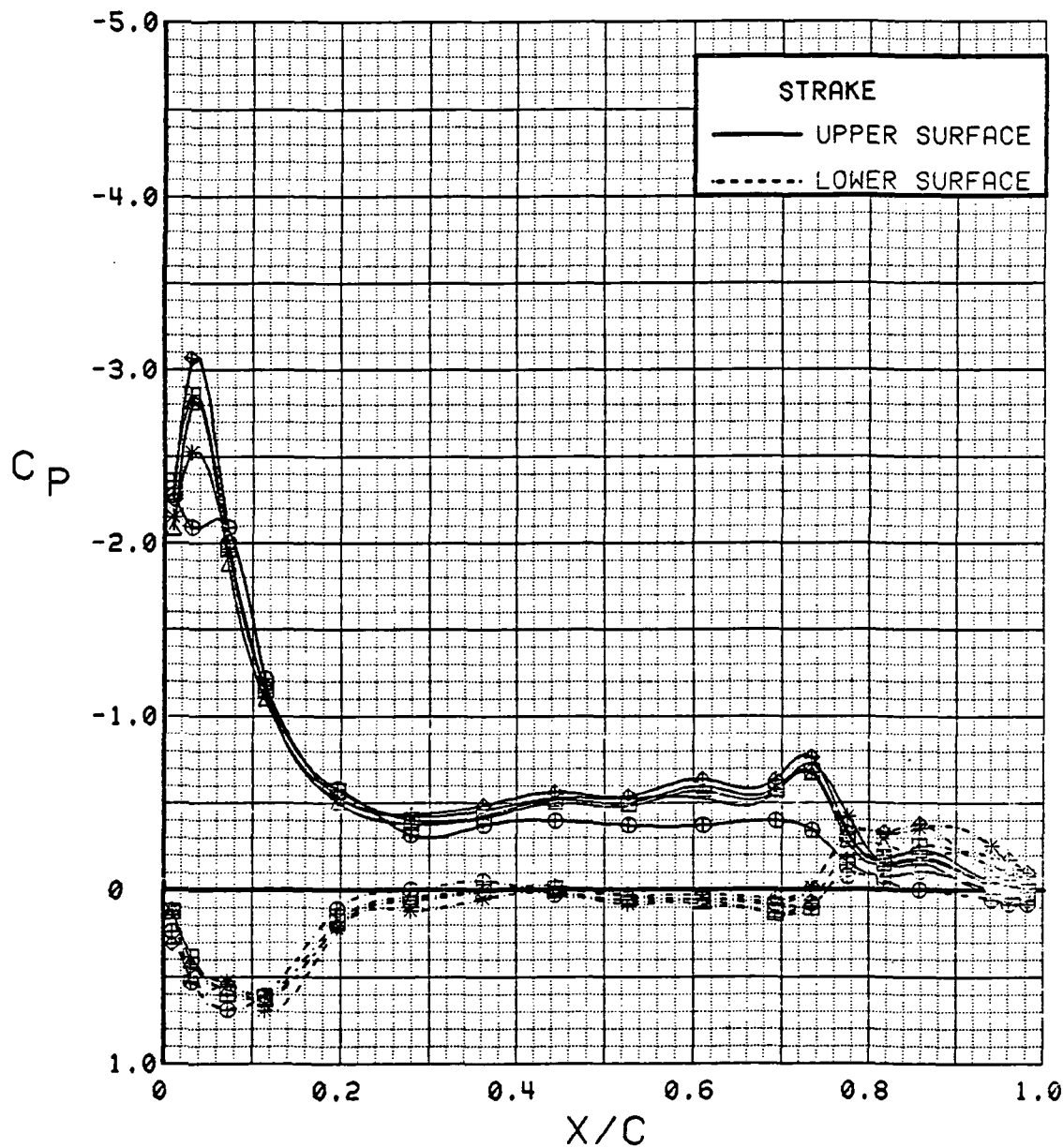


Figure 3.3-8

Power Effects on Strake Pressures, Wing Flaps Deflected  
Alpha = 12 deg



SYM	TEST	RUN	ALPHA	CT	ITEF	OTEF	CAN	SWB
⊕	543	11	20.8	0.00	30	30	0	OFF
⊞	543	8	21.0	0.46	30	30	0	OFF
△	543	6	21.0	0.93	30	30	0	OFF
◆	543	5	21.0	1.42	30	30	0	OFF
*	543	4	21.1	1.88	30	30	0	OFF

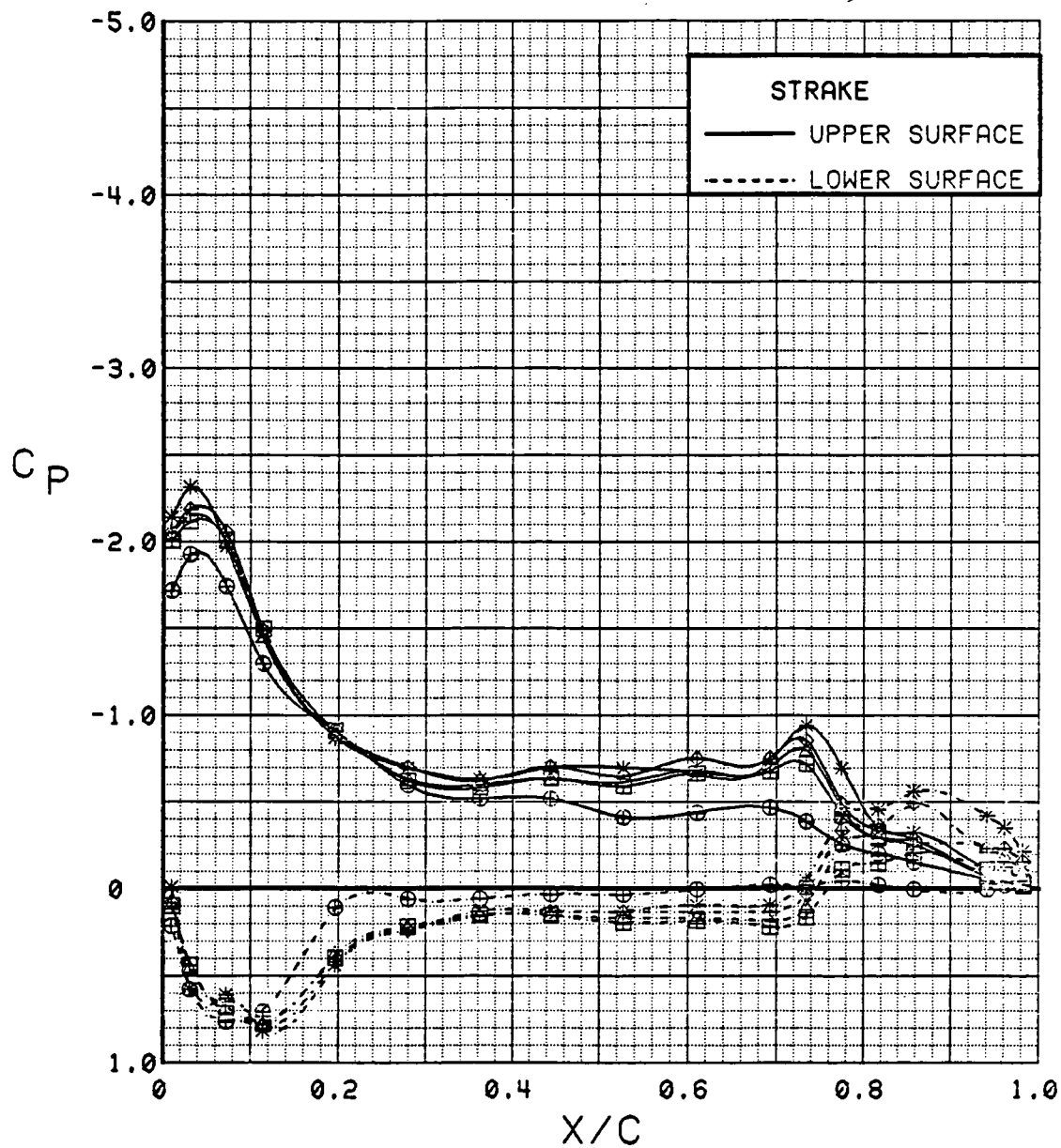


Figure 3.3-9

Power Effects on Strake Pressures, Wing Flaps Deflected  
Alpha = 21 deg

SYM	TEST	RUN	ALPHA	CT	ITEF	OTEF	CAN	SWB
⊕	543	11	28.9	0.00	30	30	0	OFF
⊞	543	8	29.1	0.46	30	30	0	OFF
△	543	6	29.1	0.93	30	30	0	OFF
◆	543	5	29.2	1.39	30	30	0	OFF
*	543	4	29.2	1.89	30	30	0	OFF

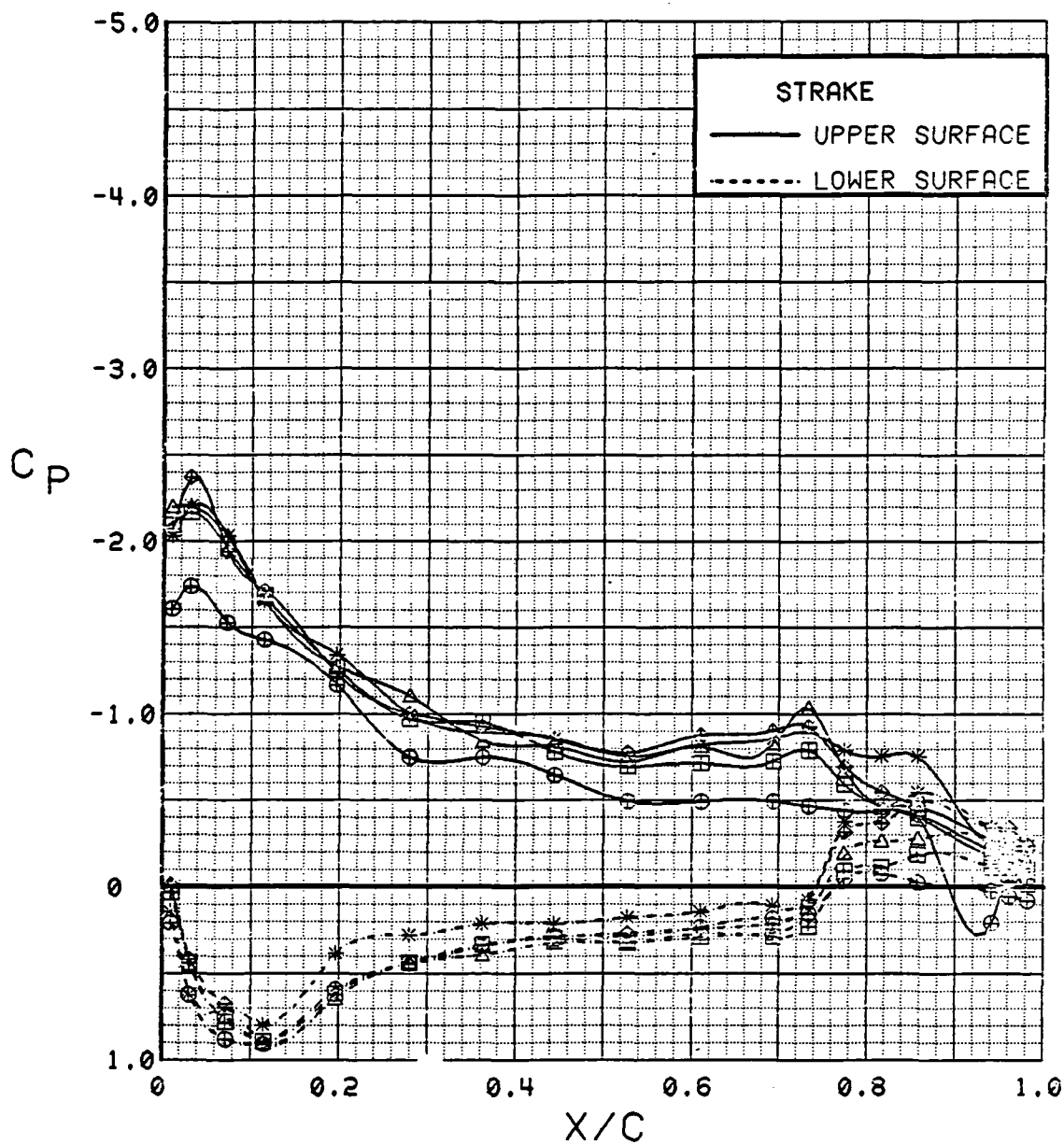


Figure 3.3-10

Power Effects on Strake Pressures, Wing Flaps Deflected  
Alpha = 29 deg

SYM	TEST	RUN	CT	ITEF	OTEF	CAN	SWB
⊕	543	11	0.00	30	30	0	OFF
⊞	543	5	1.39	30	30	0	OFF

STRAKE
— UPPER SURFACE
- - - - - LOWER SURFACE

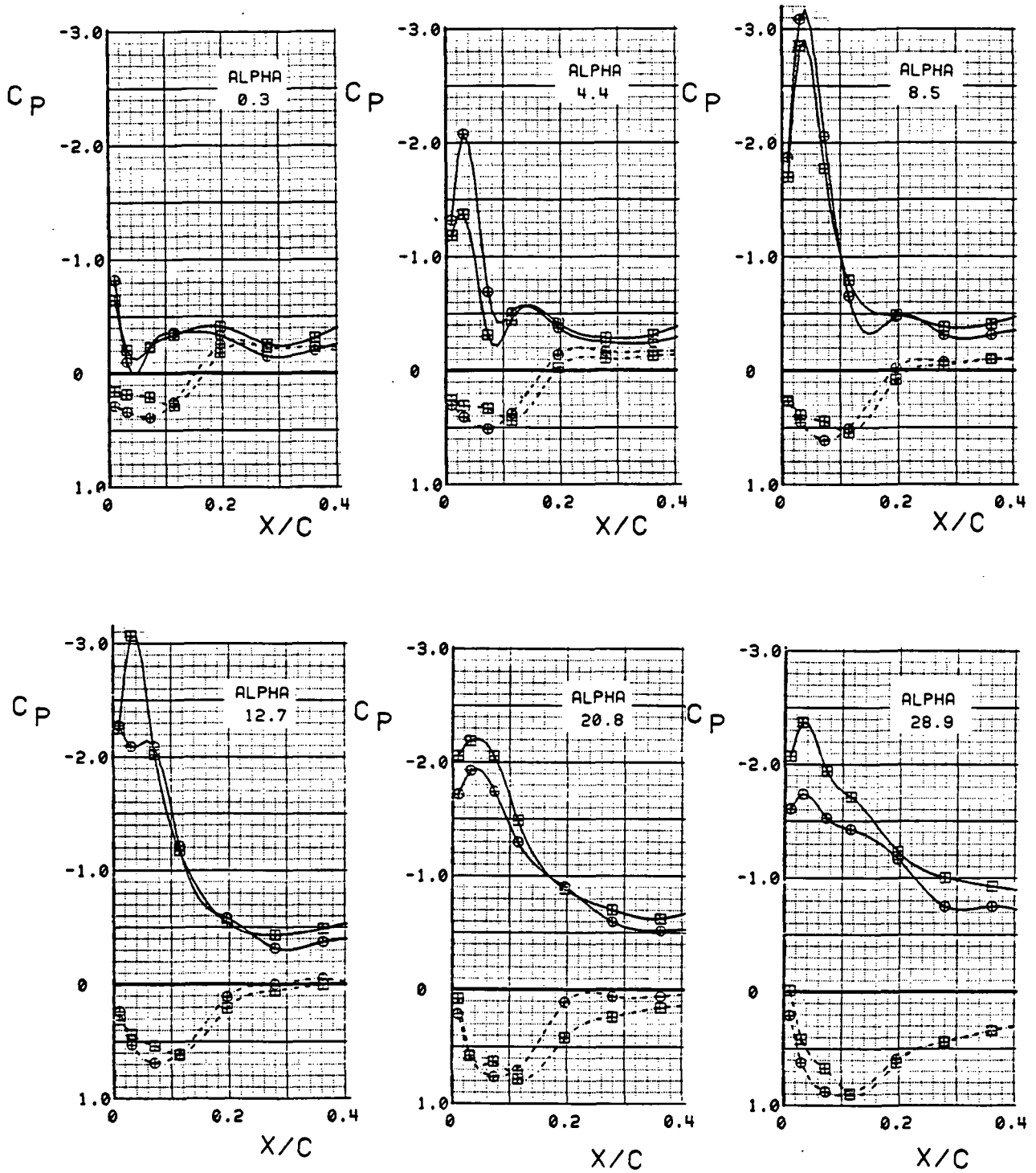


Figure 3.3-11 Strake Vortex Development

SYM	TEST	RUN	ALPHA	CT	ITEF	OTEF	CAN	SWB
⊕	543	88	8.2	0.00	-20	-20	0	OFF
⊞	543	76	8.3	0.00	-10	0	0	OFF
△	543	63	8.3	0.00	0	0	0	OFF
⊕	543	83	8.4	0.00	10	10	0	OFF
*	543	69	8.5	0.00	20	20	0	OFF
+	543	11	8.5	0.00	30	30	0	OFF

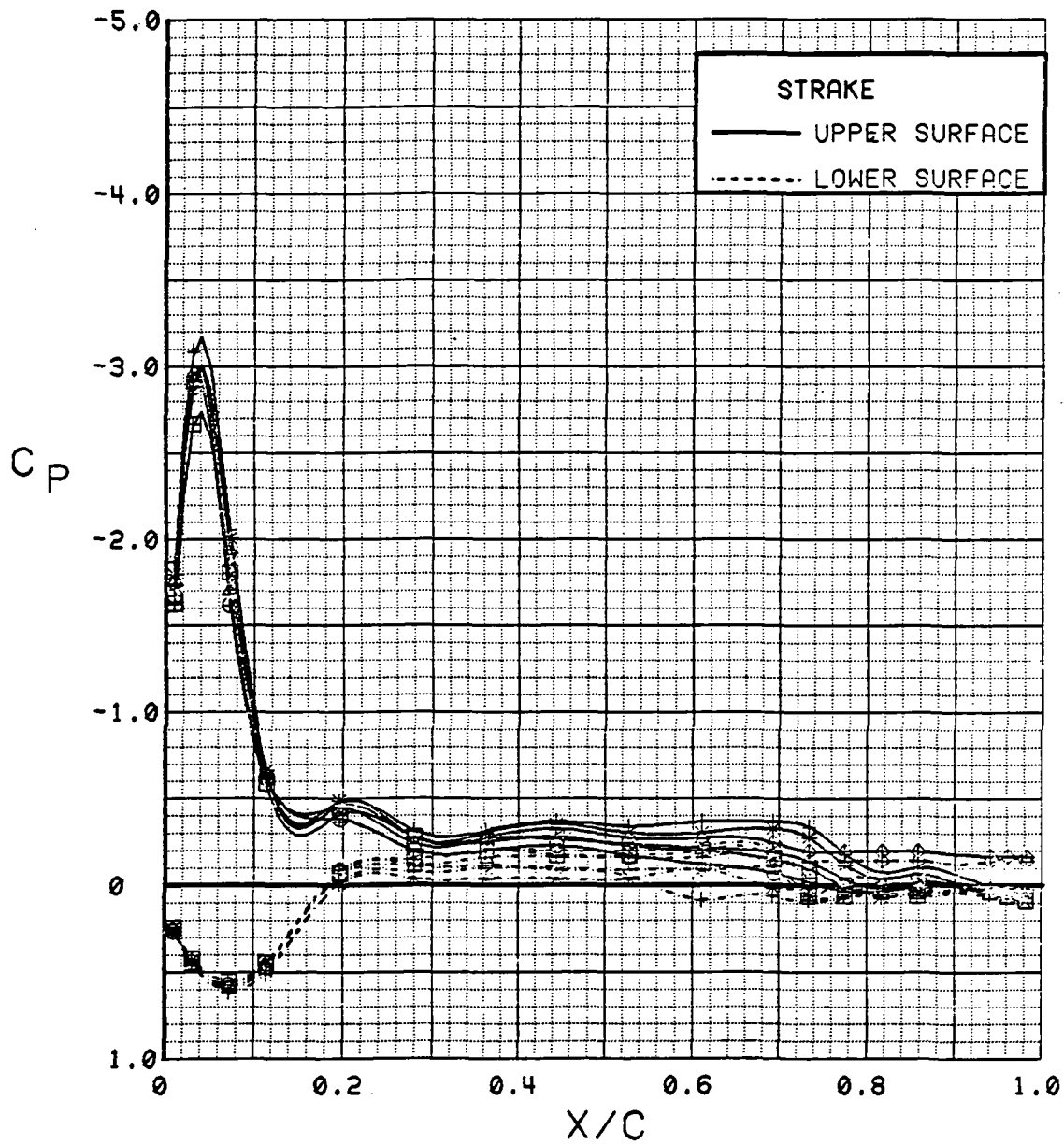


Figure 3.3-12 Wing Flap Effects on Strake Pressures, Power Off

SYM	TEST	RUN	ALPHA	CT	ITEF	OTEF	CAN	SWB
⊕	543	85	8.2	1.88	-20	-20	0	OFF
⊞	543	72	8.4	1.86	-10	0	0	OFF
△	543	58	8.4	1.90	0	0	0	OFF
⊕	543	81	8.5	1.91	10	10	0	OFF
*	543	67	8.6	1.89	20	20	0	OFF
+	543	4	8.7	1.85	30	30	0	OFF

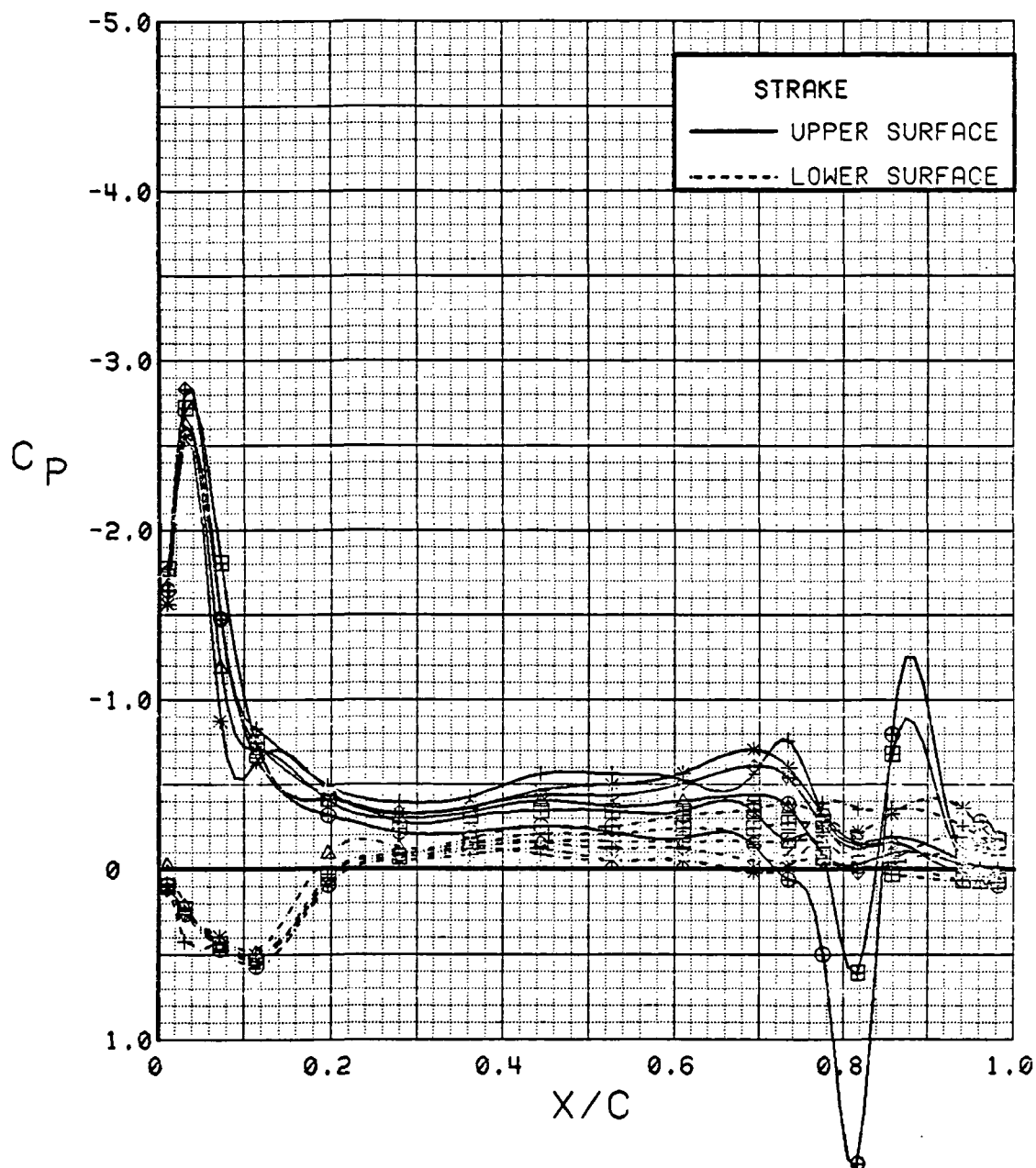


Figure 3.3-13 Wing Flap Effects on Strake Pressures, Power On

SYM	TEST	RUN	ALPHA	CT	ITEF	OTEF	CAN	SWB
⊕	537	28	0.3	1.89	30	30	0	OFF
⊞	537	53	0.4	1.81	30	30	0	ON

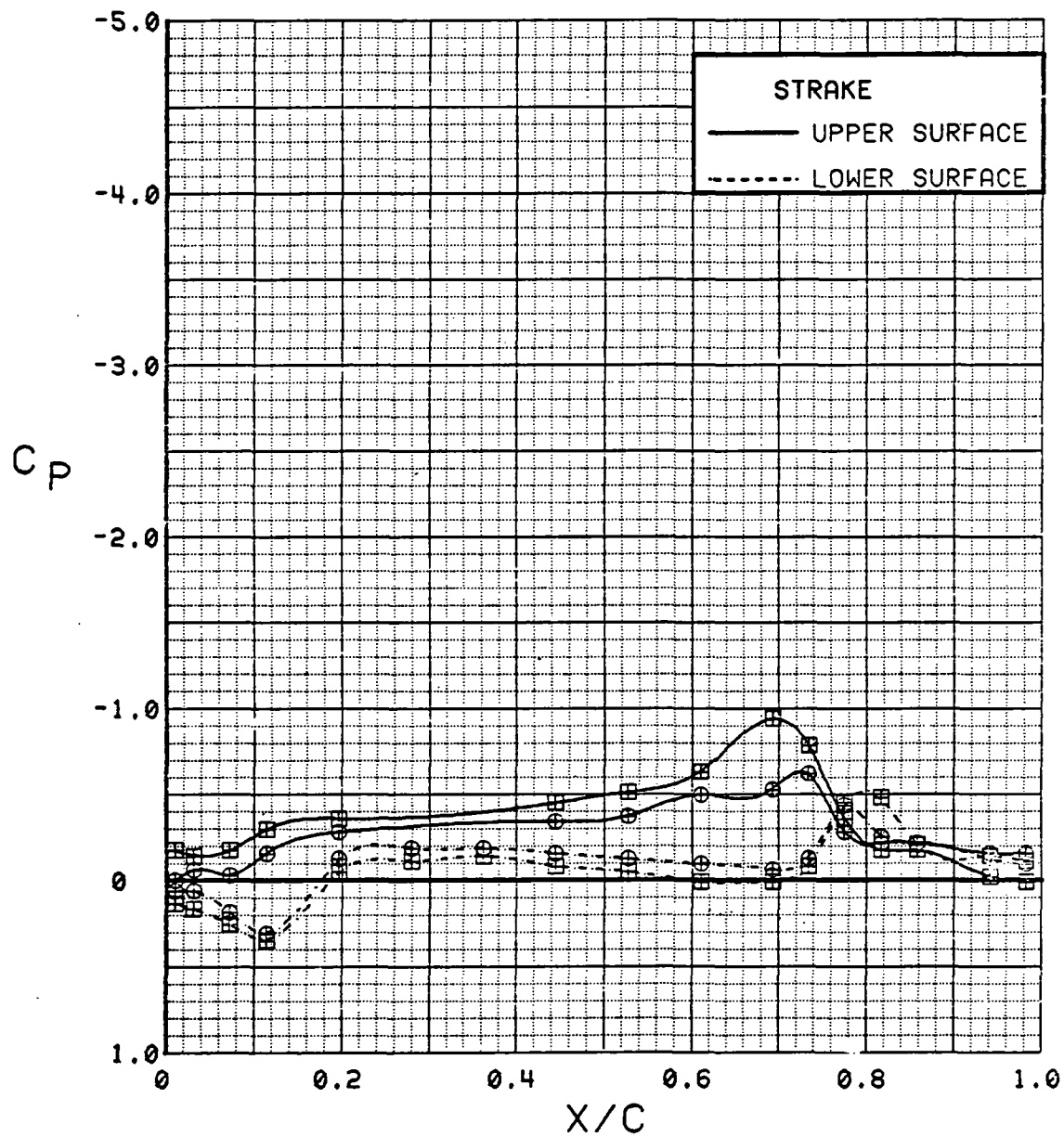


Figure 3.3-14

Spanwise Blowing Effect on Strake Pressures  
Alpha = 0 deg

SYM	TEST	RUN	ALPHA	CT	ITEF	OTEF	CAN	SWB
⊕	537	28	4.5	1.87	30	30	0	OFF
⊞	537	53	4.5	1.81	30	30	0	ON

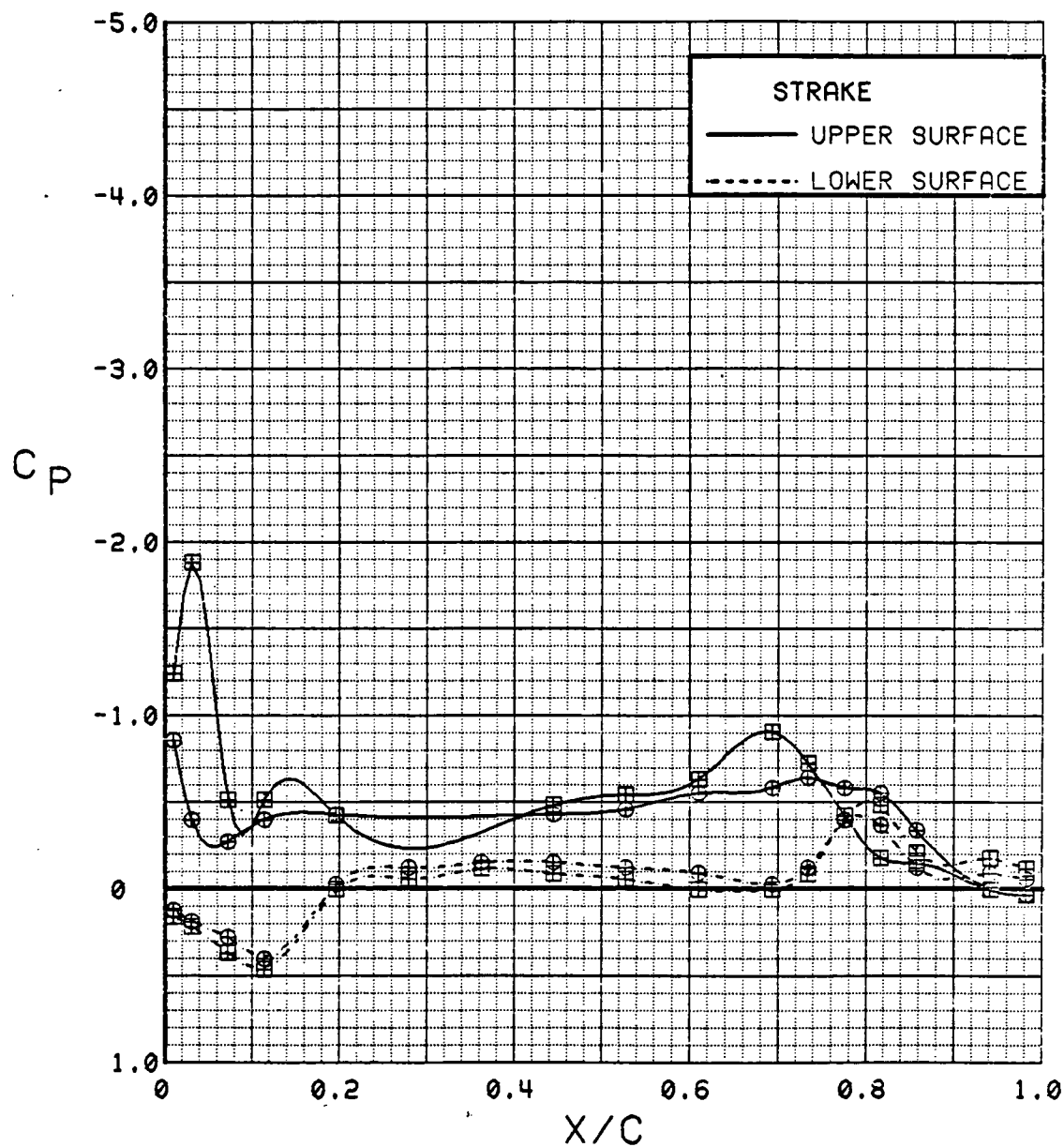


Figure 3.3-15

Spanwise Blowing Effect on Strake Pressures  
Alpha = 4 deg

SYM	TEST	RUN	ALPHA	CT	ITEF	OTEF	CAN	SWB
⊕	537	28	8.7	1.88	30	30	0	OFF
⊞	537	53	8.7	1.83	30	30	0	ON

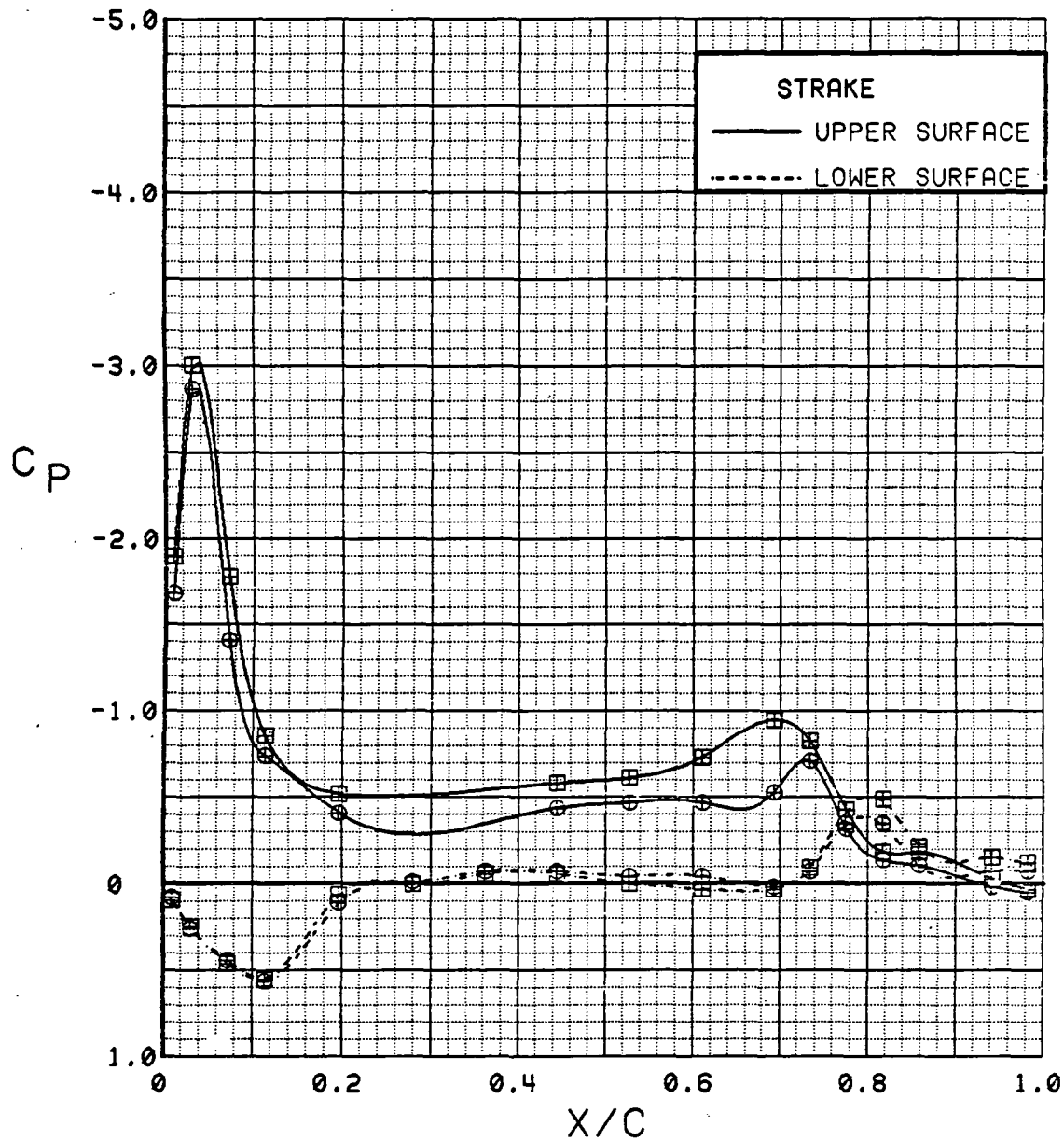


Figure 3.3-16 Spanwise Blowing Effect on Strake Pressures  
 $\alpha = 8^\circ$



SYM	TEST	RUN	ALPHA	CT	ITEF	OTEF	CAN	SWB
⊕	537	28	12.8	1.82	30	30	0	OFF
⊞	537	53	12.9	1.82	30	30	0	ON

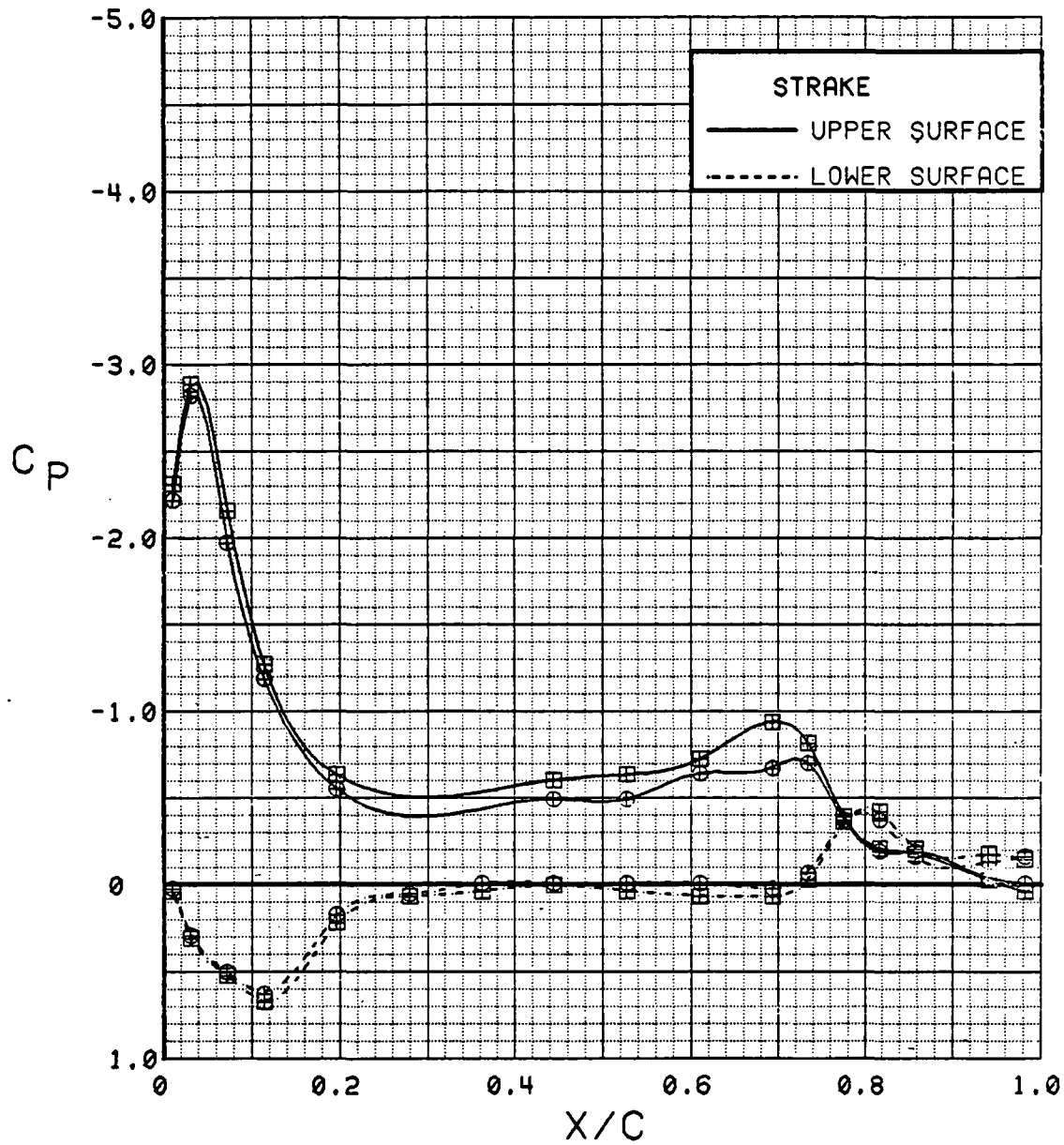


Figure 3.3-17 Spanwise Blowing Effect on Strake Pressures  
Alpha = 12 deg

SYM	TEST	RUN	ALPHA	CT	ITEF	OTEF	CAN	SWB
⊕	537	28	21.0	1.83	30	30	0	OFF
⊞	537	53	21.2	1.83	30	30	0	ON

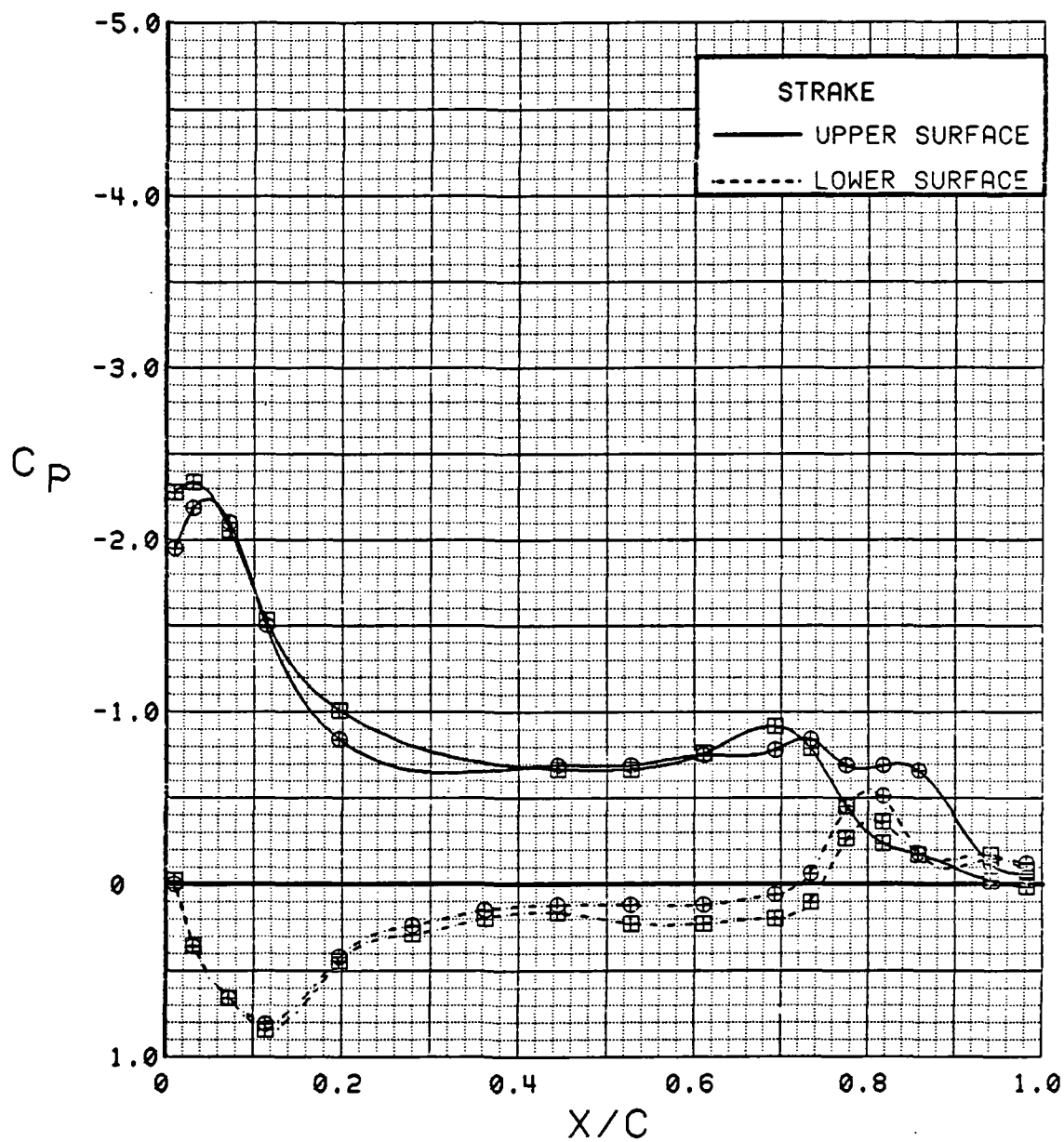


Figure 3.3-18 Spanwise Blowing Effect on Strake Pressures  
Alpha = 21 deg

SYM	TEST	RUN	ALPHA	CT	ITEF	OTEF	CAN	SWB
⊕	537	28	29.1	1.83	30	30	0	OFF
⊗	537	53	29.3	1.81	30	30	0	ON

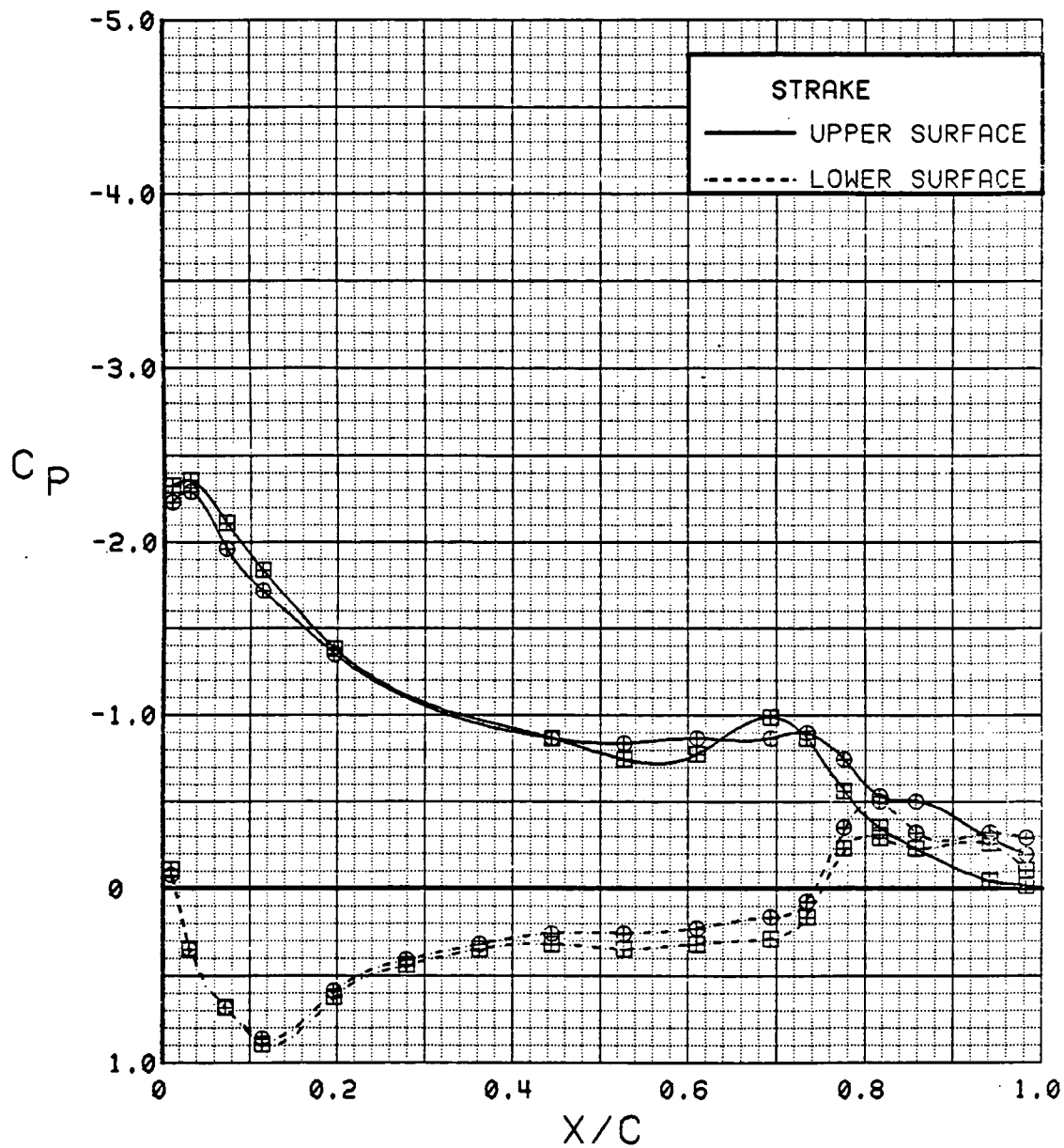


Figure 3.3-19

Spanwise Blowing Effect on Strake Pressures  
 $\alpha = 29^\circ$

SYM	TEST	RUN	ALPHA	CT	ITEF	OTEF	CAN	SWB
⊕	543	5	4.5	1.40	30	30	0	OFF
⊞	543	4	4.5	1.90	30	30	0	OFF

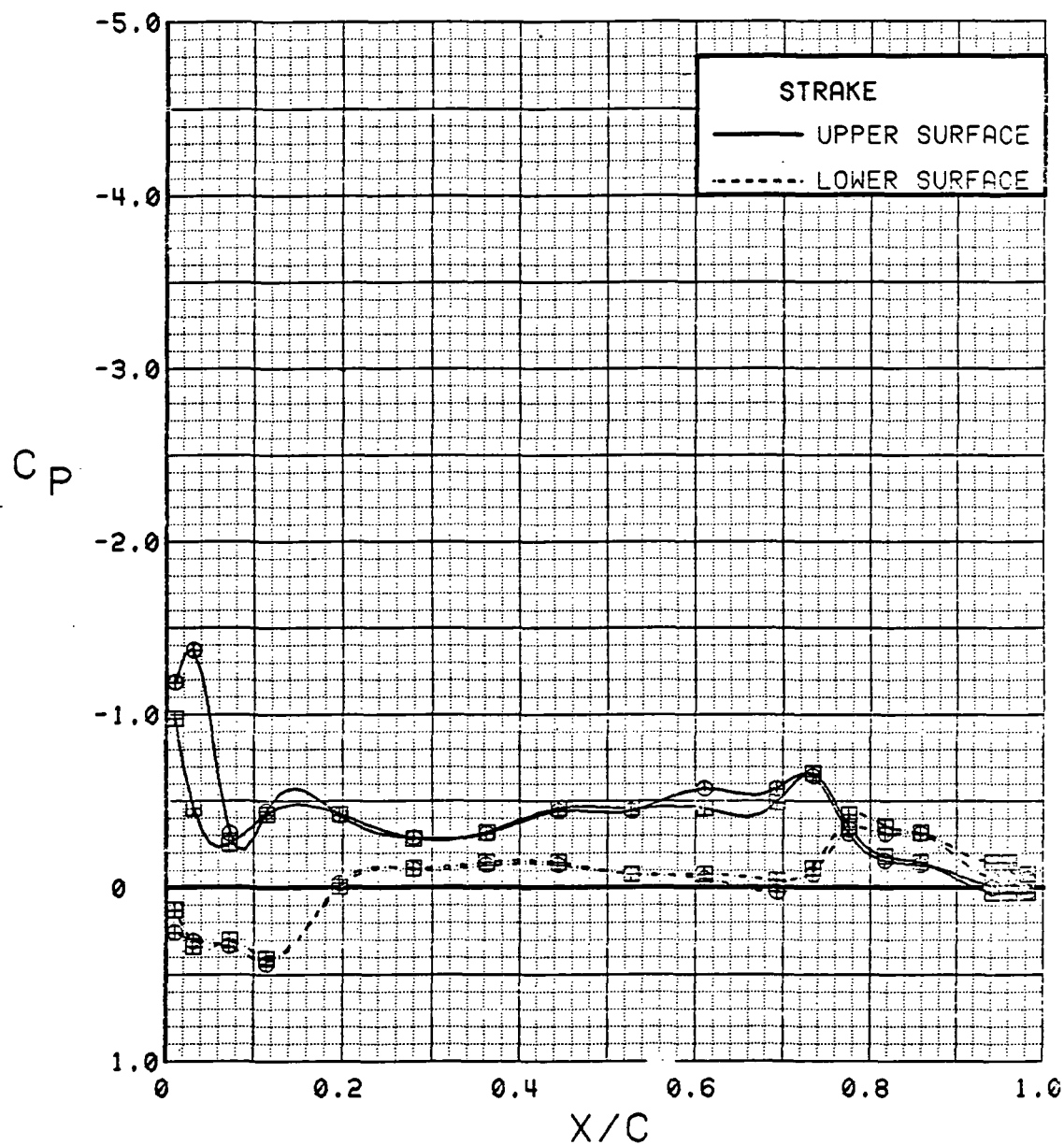


Figure 3.3-20

Power Effect on Strake Pressures

### 3.4 BEAVER TAIL

The STOL Fighter Model was designed with a deflectable beaver tail as a means of providing a nose-up moment for trim. Pressure orifices were placed on this surface to provide an insight to the local flowfield and the exhaust jet effects. The upper and lower surfaces were instrumented with three rows of pressure taps, the primary row was oriented spanwise at 60% of the beaver tail chord. The other rows were chordwise at 11% and 65% of the beaver-tail semi-span. The outboard chordwise row was a continuation of the strake instrumentation, which terminated at the trailing-edge of the beaver-tail. Further information concerning orifice and thermocouple locations is presented in Section 2.2.

Most of the configuration and test variables produced little or no change in the beaver tail pressure distributions; for instance, the power-off angle of attack variation (Figure 3.4-1) for a neutral trailing-edge flap (Figure 3.4-1) shows essentially no change in pressure. The boundary layer on the fuselage should have been relatively thick at this location, and apparently, the flow was aligned with both the upper and lower surfaces when it reached the beaver tail, regardless of the original onset flow angle. Figure 3.4-2 shows a similar alpha variation with the trailing-edge flap deflected 30 deg. The pressure distribution shows small changes with angle of attack; however, they are not significant. Since angle of attack seems relatively unimportant, other configuration variations (with the exception of beaver tail deflection) are presented at a representative alpha of 8 deg.

Figure 3.4-3 shows that trailing-edge-flap deflection with power off had little influence upon the beaver-tail pressure distribution. Such was not the case, however, with power on, in which case the engine exhaust jet was vectored in an upward or downward direction by the inboard trailing-edge flap, thus changing the exhaust position relative to the beaver tail. Figure 3.4-4 shows the effects of the jet deflection angle on the beaver-tail pressures. As indicated by the high-negative pressures at a few of the pressure taps near the edge of the beaver tail, the exhaust jet swept in a vertical plane beside the outboard edge of the undeflected beaver tail when the trailing-edge flap was deflected in the range of +10 to -10 deg. These pressures indicate that the jet was in close proximity to the beaver tail, but it was not significant in the generation of the overall forces and moments on that surface when the beaver tail was undeflected. Further information regarding the engine-exhaust jet effects on the beaver tail is presented in the beaver tail thermal analysis (Subsection 3.6.2).

With all other surfaces being neutral, the effects of beaver-tail deflection with power off are presented in Figure 3.4-5. The peak suction ( $C_p \approx -1.0$ ) produced on the lower surface seems appropriate considering the pressures that were developed near the hinge line of the deflected-wing-trailing-edge flap. More important than the level of these pressures, however, was the spanwise distribution (Figure 3.4-5) which shows that there was a large high-pressure area near the center of the lower surface where the beaver tail developed little load. The chordwise data, likewise, confirm that the low pressures observed near the tip of the lower surface did not carry over to the center of the beaver tail.

The effects of configuration variables, as mentioned earlier, are presented at  $\alpha = 8$  deg with the exception of beaver tail deflection. If one can envision the integrated forces developed by the upper and lower surfaces in Figure 3.4-6 at the different angles of attack, it can be seen that the section loads along the chordwise and spanwise rows of data progressively diminish as alpha is increased. Thus, the deflected beaver tail was more effective at the lower angles of attack.

When power was applied with the trailing-edge flaps undeflected (Figure 3.4-7), the beaver tail became somewhat more effective, but the "dead" area near the center remained ineffective, as it had with power off. One beneficial effect of power was that it almost nullified the loss in effectiveness that came with increasing angle of attack. (Again, envision the load represented by the area between the curves in Figure 3.4-8.)

The effects of power with the beaver tail at three different deflections can be compared in Figure 3.4-5 and -7 for the wing flap undeflected. Power increased the effectiveness, more so at the larger deflection. Power effects are more explicitly illustrated in Figure 3.4-9 with the beaver tail at its maximum deflection of 40 degrees and the wing trailing-edge again flap undeflected. As can be seen, the upper surface pressures were barely affected, but the jet created a significant amount of suction near the outboard edge of the lower surface. A similar power variation is shown in Figure 3.4-10 for the beaver tail still deflected to 40 deg but with the wing flap now deflected to 30 deg. Only with the combined deflections of the beaver tail and flap did the pressure loading across the span of the beaver tail become somewhat uniform. The spanwise data show some inconsistencies with power off, but the inboard-chordwise data clearly show that power caused the flow on the lower surface to separate. Note in Figure 3.4-10 that the power-off curve shows that the inboard-chordwise flow had reattached at  $x/c \approx 0.5$ . As power was increased, the reattachment point moved rearward until, at  $C_T = 1.8$ , the flow did not reattach. Although power caused separation on the lower surface, in this case it increased suction, thereby enhancing the beaver tail effectiveness.

SYM	TEST	RUN	ALPHA	CT	ITEF	OTEF	CAN	SWE	$\delta_{BT}$
●	543	63	0.1	0.00	0	0	0	OFF	0
■	543	63	8.3	0.00	0	0	0	OFF	0
▲	543	63	16.6	0.00	0	0	0	OFF	0
◆	543	63	28.8	0.00	0	0	0	OFF	0

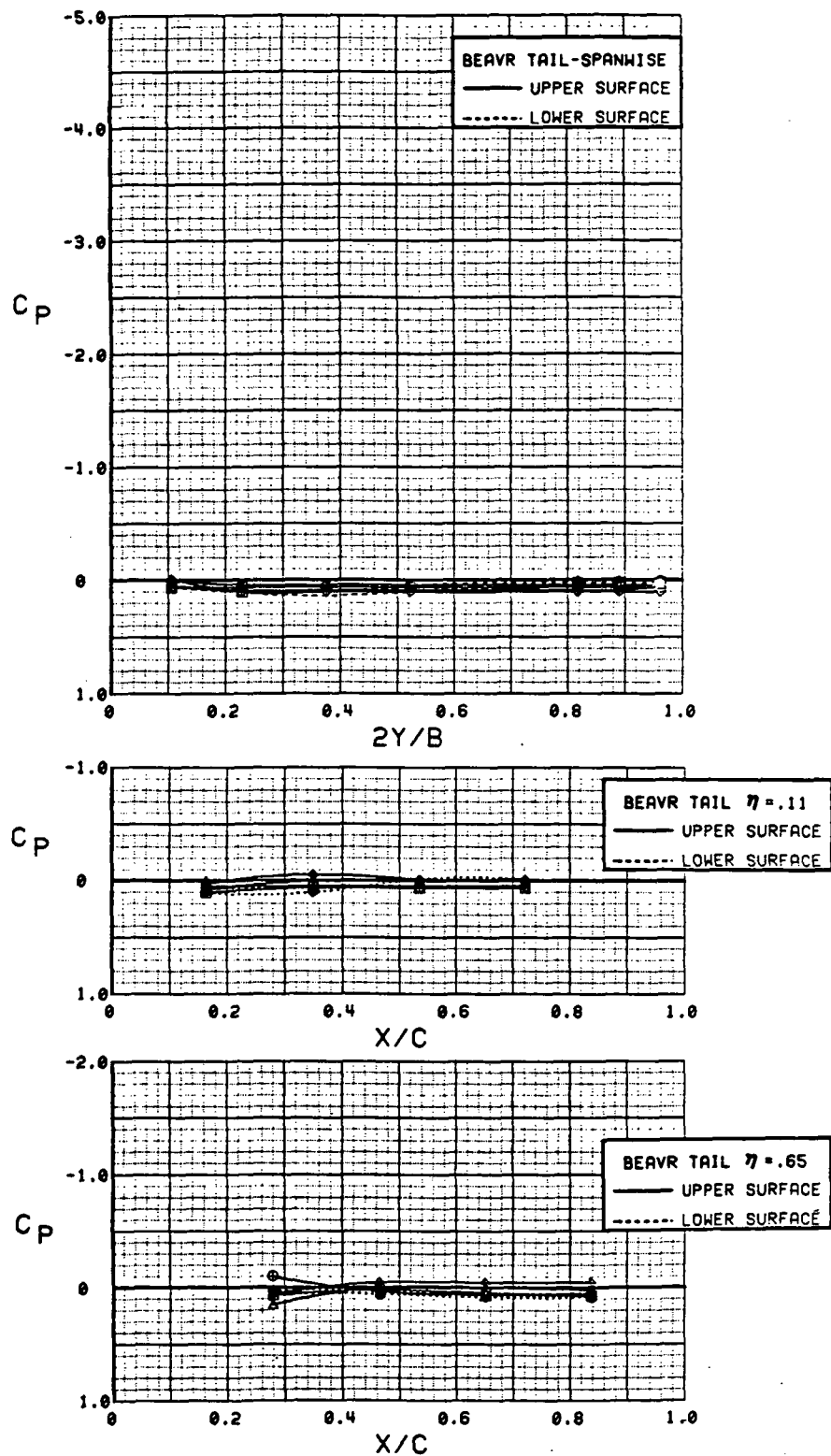


Figure 3.4-1 Angle of Attack Effects, Power Off, Beaver Tail Neutral Wing Flaps Neutral

SYM	TEST	RUN	ALPHA	CT	ITEF	OTEF	CAN	SWB	$\delta_{BT}$
●	537	12	0.3	0.00	30	30	0	OFF	0
■	537	12	8.5	0.00	30	30	0	OFF	0
△	537	12	16.7	0.00	30	30	0	OFF	0
◆	537	12	28.8	0.00	30	30	0	OFF	0

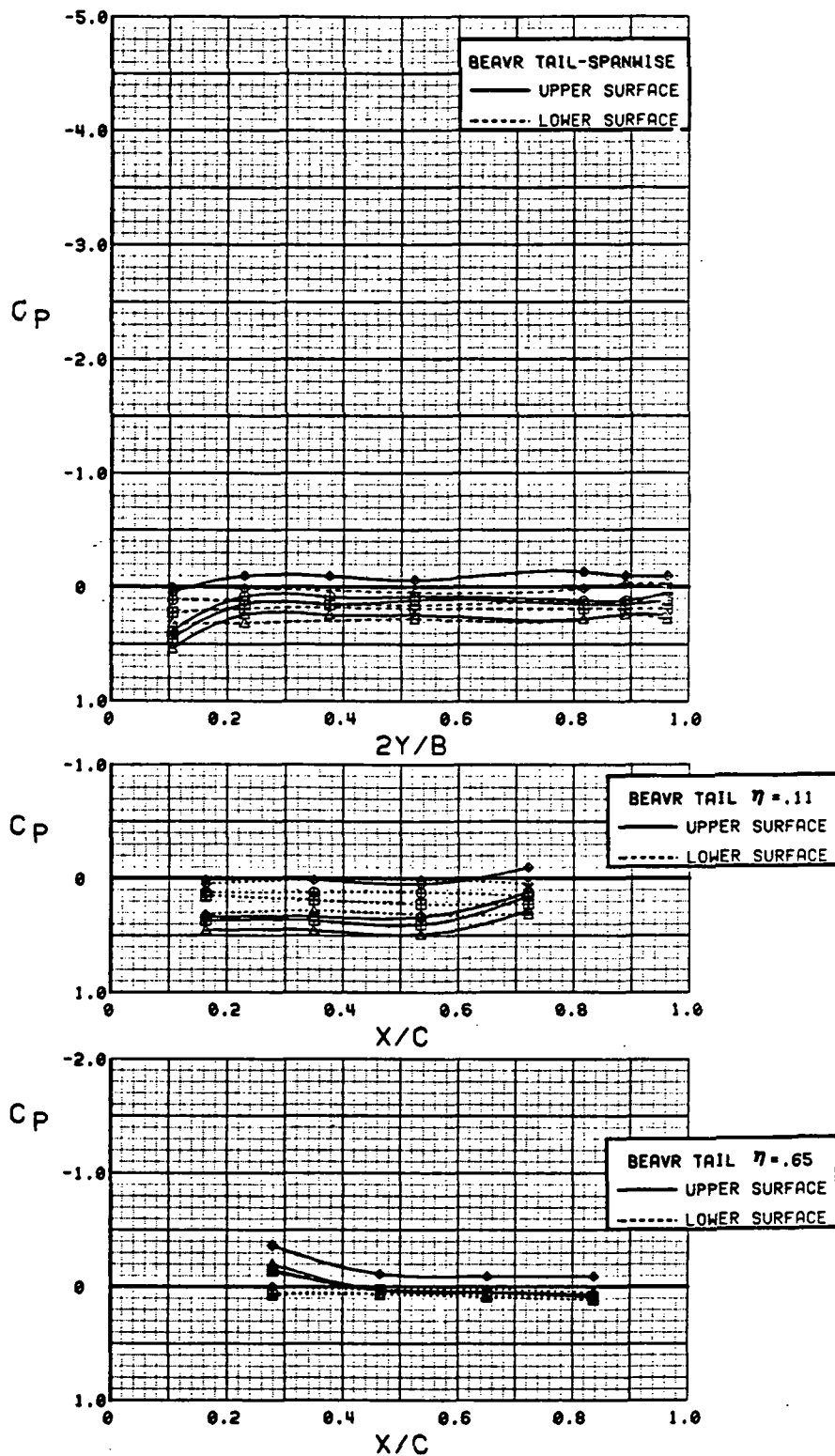


Figure 3.4-2

Angle of Attack Effects, Power Off, Beaver Tail Neutral  
Wing Flaps Deflected



SYM	TEST	RUN	ALPHA	CT	ITEF	OTEF	CAN	SWB	$\delta_{BT}$
⊙	543	88	8.2	0.00	-20	-20	0	OFF	0
⊗	543	76	8.3	0.00	-10	0	0	OFF	0
△	543	63	8.3	0.00	0	0	0	OFF	0
◆	543	83	8.4	0.00	10	10	0	OFF	0
*	543	69	8.5	0.00	20	20	0	OFF	0
+	537	12	8.5	0.00	30	30	0	OFF	0

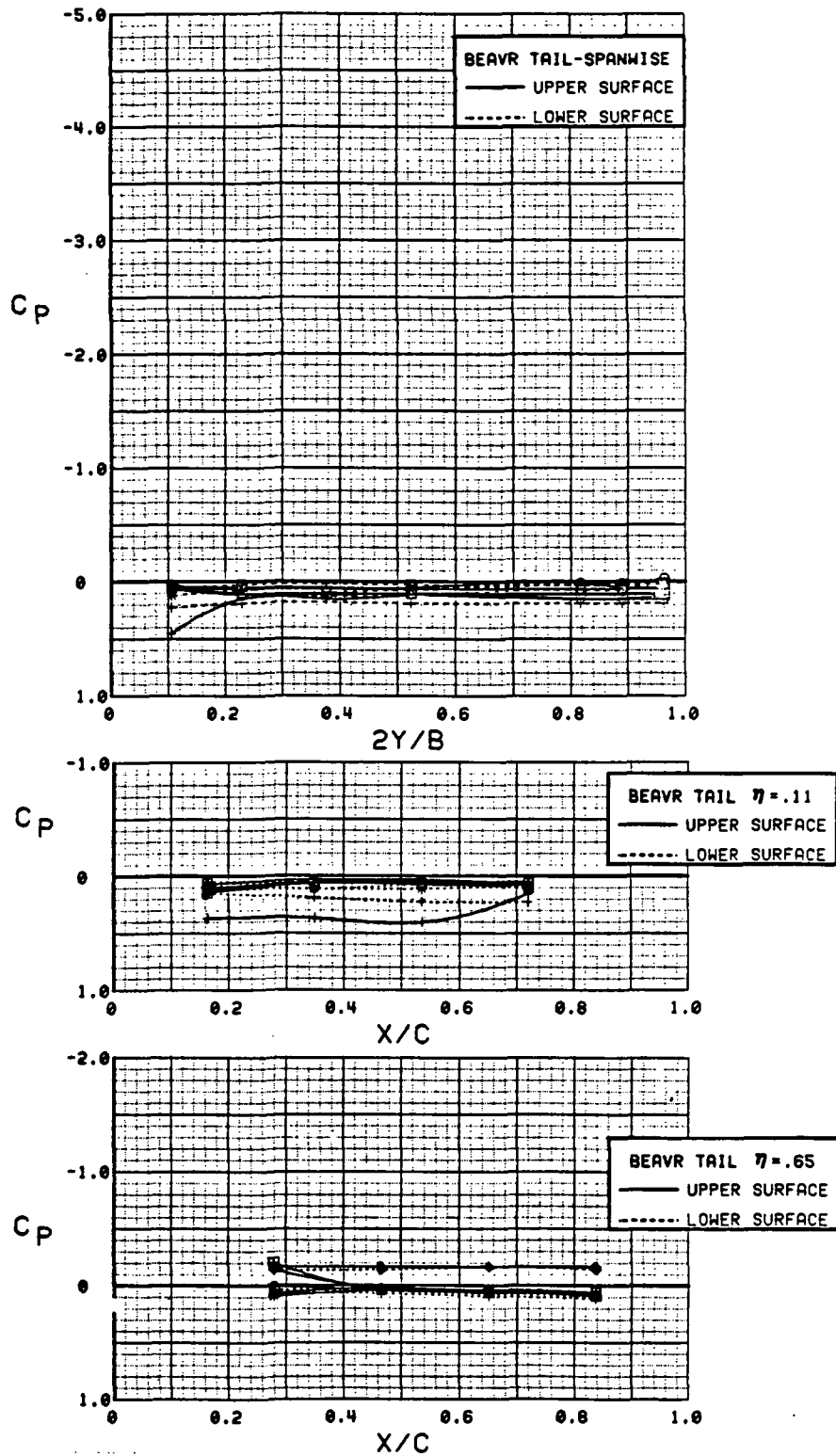


Figure 3.4-3 Wing Flap Deflection Effects, Power Off

SYM	TEST	RUN	ALPHA	CT	ITEF	OTEF	CAN	SWB	$\delta_{BT}$
⊙	543	85	8.2	1.88	-20	-20	0	OFF	0
⊠	543	72	8.4	1.86	-10	0	0	OFF	0
△	543	58	8.4	1.90	0	0	0	OFF	0
◆	543	81	8.5	1.91	10	10	0	OFF	0
*	543	67	8.6	1.89	20	20	0	OFF	0
+	537	28	8.7	1.88	30	30	0	OFF	0

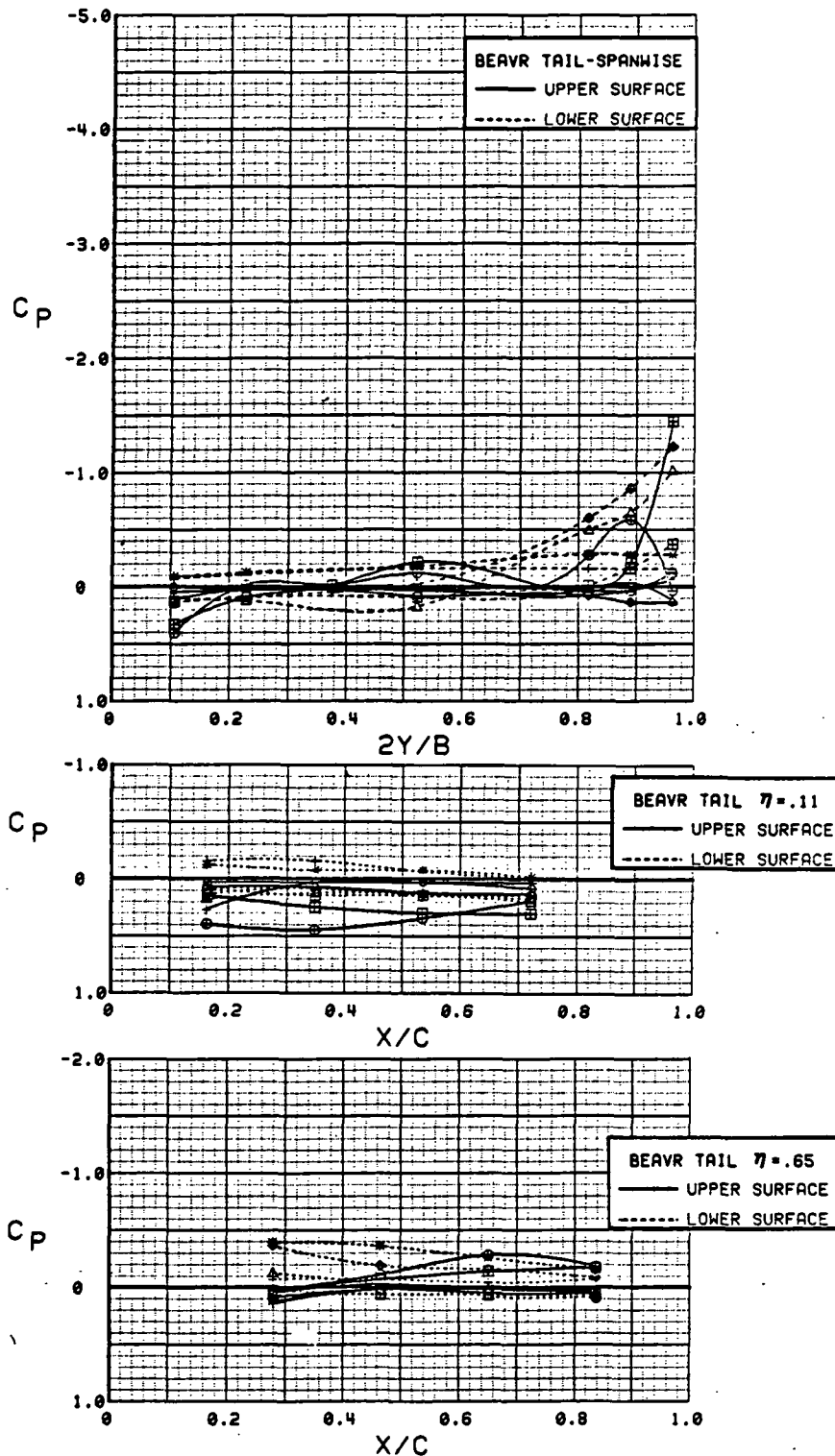


Figure 3.4-4 Wing Flap Deflection Effects, Power On

SYM	TEST	RUN	ALPHA	CT	ITEF	OTEF	CAN	SWB	$\delta_{BT}$
●	543	63	8.3	0.00	0	0	0	OFF	0
■	543	54	8.3	0.00	0	0	0	OFF	20
△	543	57	8.3	0.00	0	0	0	OFF	40

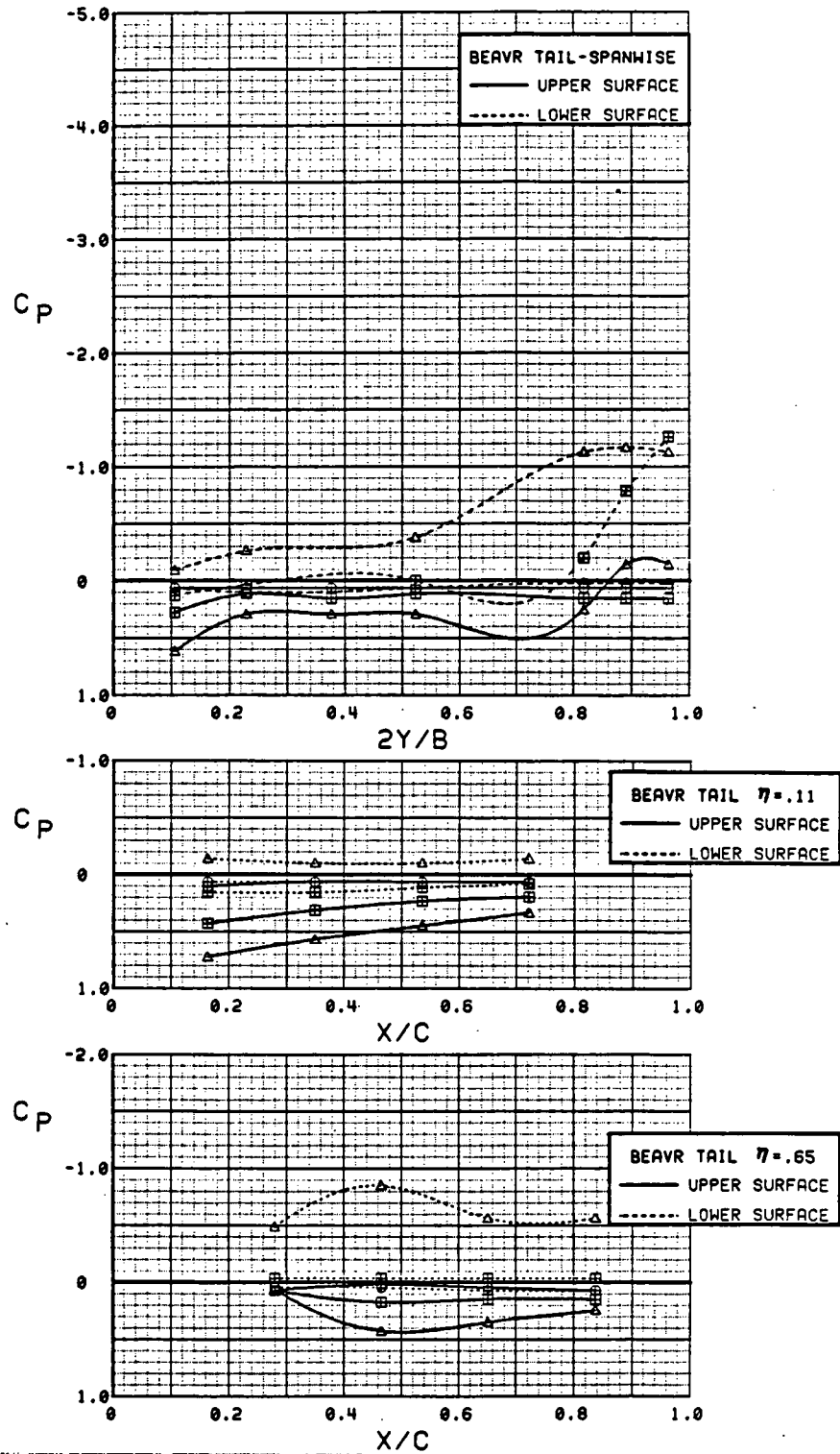


Figure 3.4-5 Beaver Tail Deflection Effects, Power Off

SYM	TEST	RUN	ALPHA	CT	ITEF	OTEF	CAN	SWB	$\delta_{BT}$
⊙	543	57	0.0	0.00	0	0	0	OFF	40
⊠	543	57	8.3	0.00	0	0	0	OFF	40
△	543	57	16.5	0.00	0	0	0	OFF	40
◆	543	57	28.7	0.00	0	0	0	OFF	40

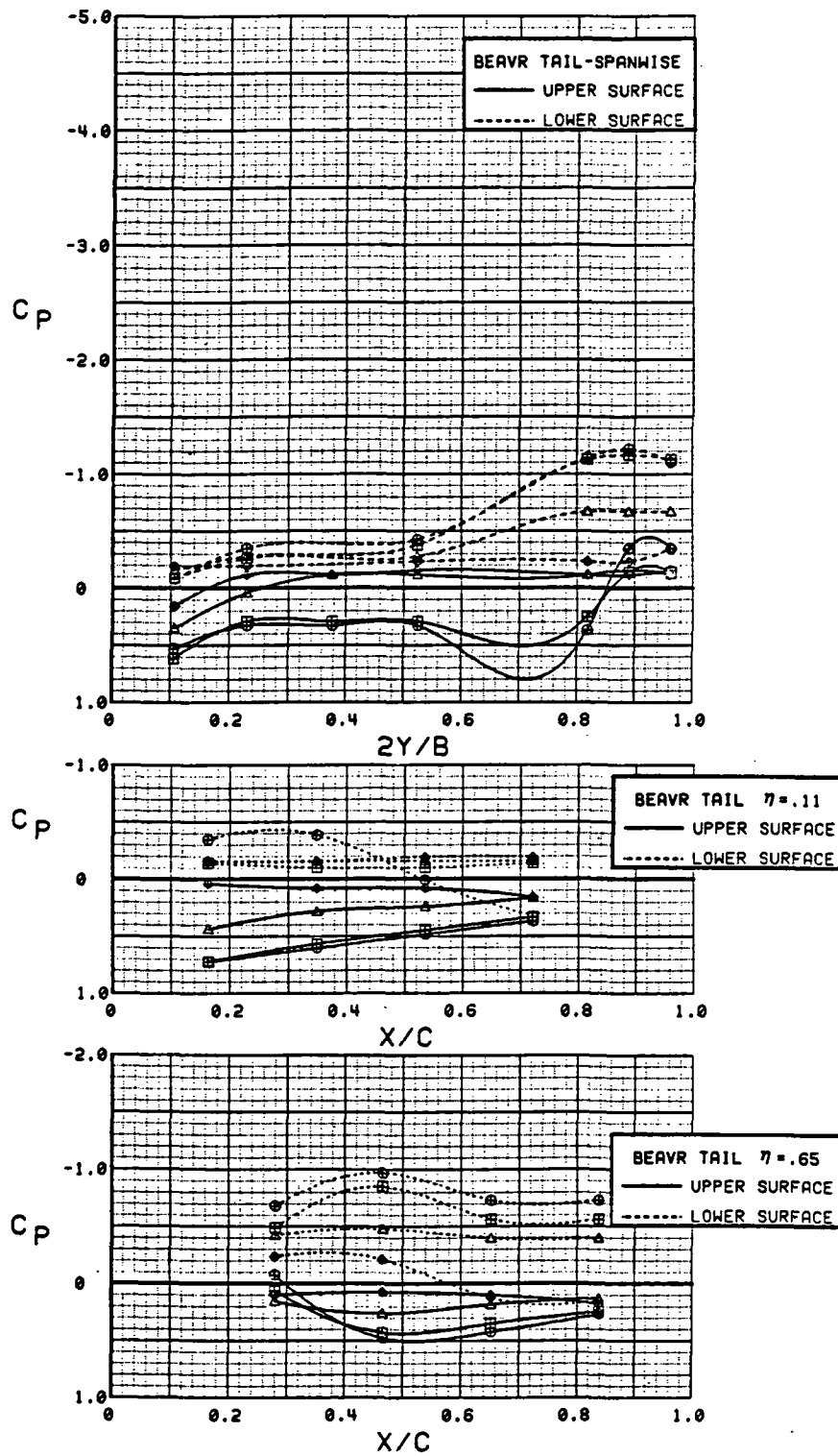


Figure 3.4-6 Angle of Attack Effects, Power Off, Beaver Tail Deflected

SYM	TEST	RUN	ALPHA	CT	ITEF	OTEF	CAN	SWB	$\delta_{BT}$
⊕	543	58	8.4	1.90	0	0	0	OFF	0
⊞	543	52	8.4	1.84	0	0	0	OFF	20
Δ	543	55	8.3	1.88	0	0	0	OFF	40

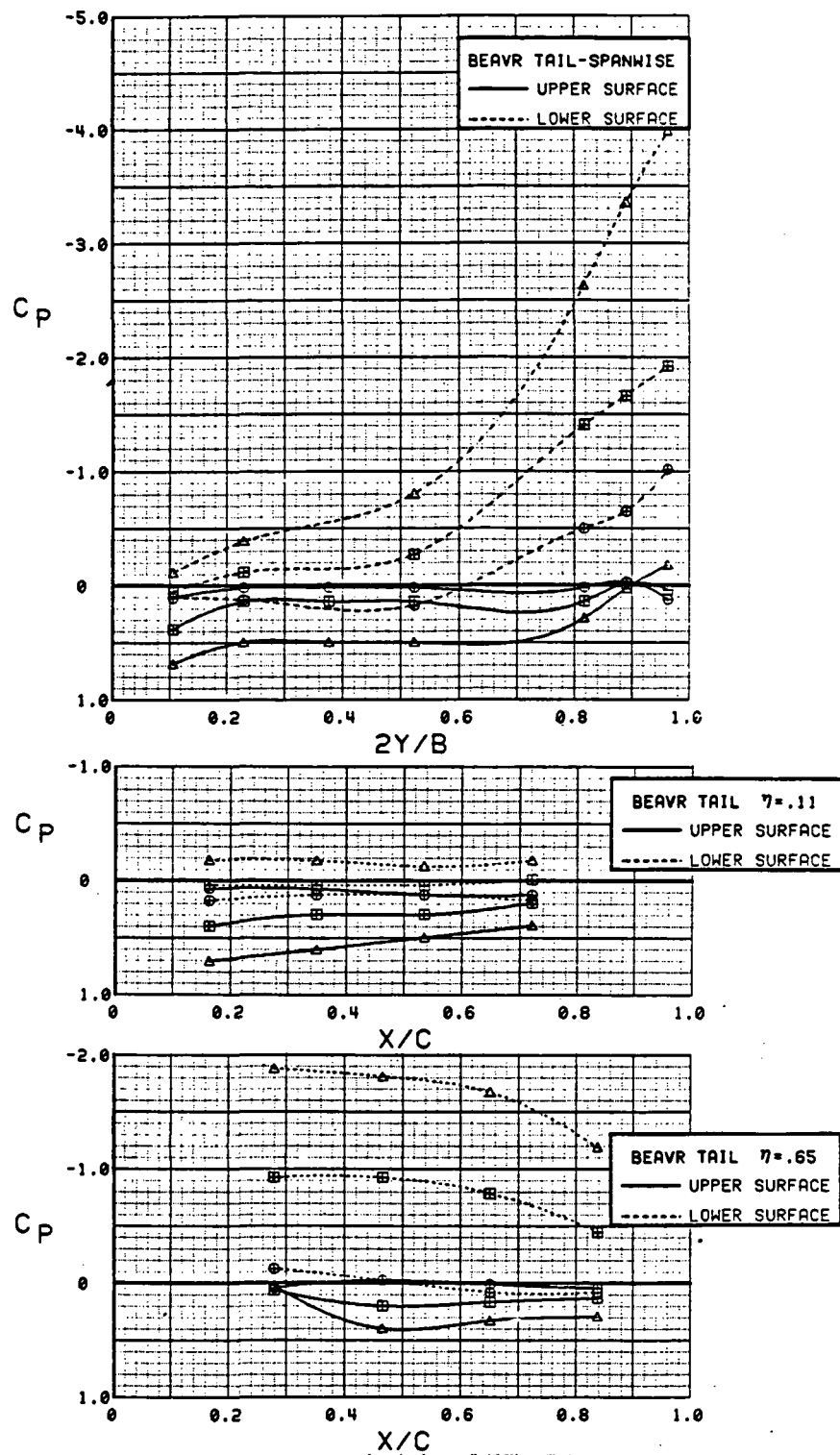


Figure 3.4-7 Beaver Tail Deflection Effects, Power On

SYM	TEST	RUN	ALPHA	CT	ITEF	OTEF	CAN	SWB	$\delta_{BT}$
●	543	55	0.0	1.88	0	0	0	OFF	40
■	543	55	8.3	1.88	0	0	0	OFF	40
▲	543	55	16.6	1.89	0	0	0	OFF	40
◆	543	55	28.9	1.89	0	0	0	OFF	40

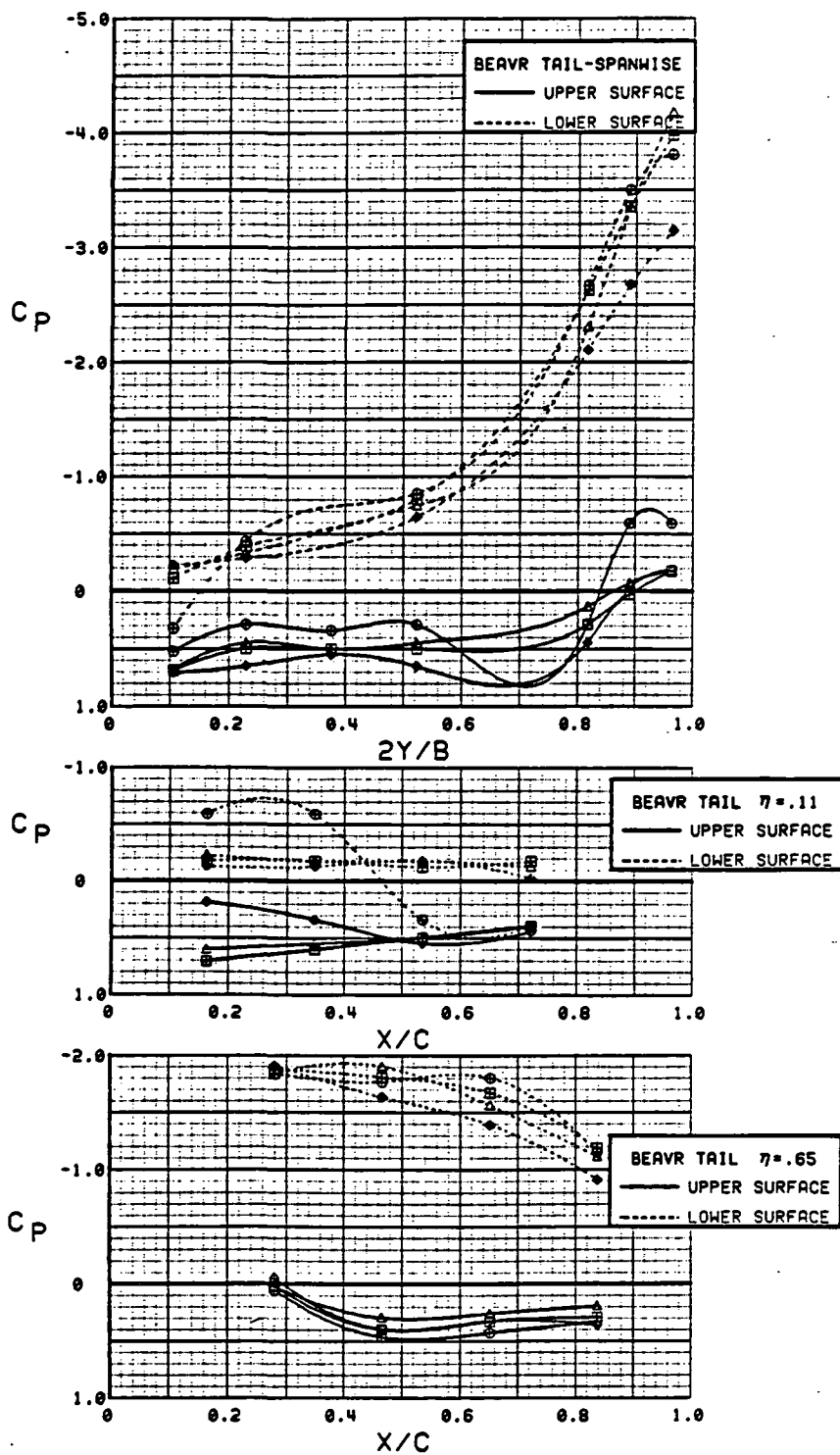


Figure 3.4-8 Alpha Effects, Power On, Beaver Tail Deflected

SYM	TEST	RUN	ALPHA	CT	ITEF	OTEF	CAN	SWB	6BT
●	543	57	8.3	0.00	0	0	0	OFF	40
■	543	56	8.3	0.93	0	0	0	OFF	40
△	543	55	8.3	1.88	0	0	0	OFF	40

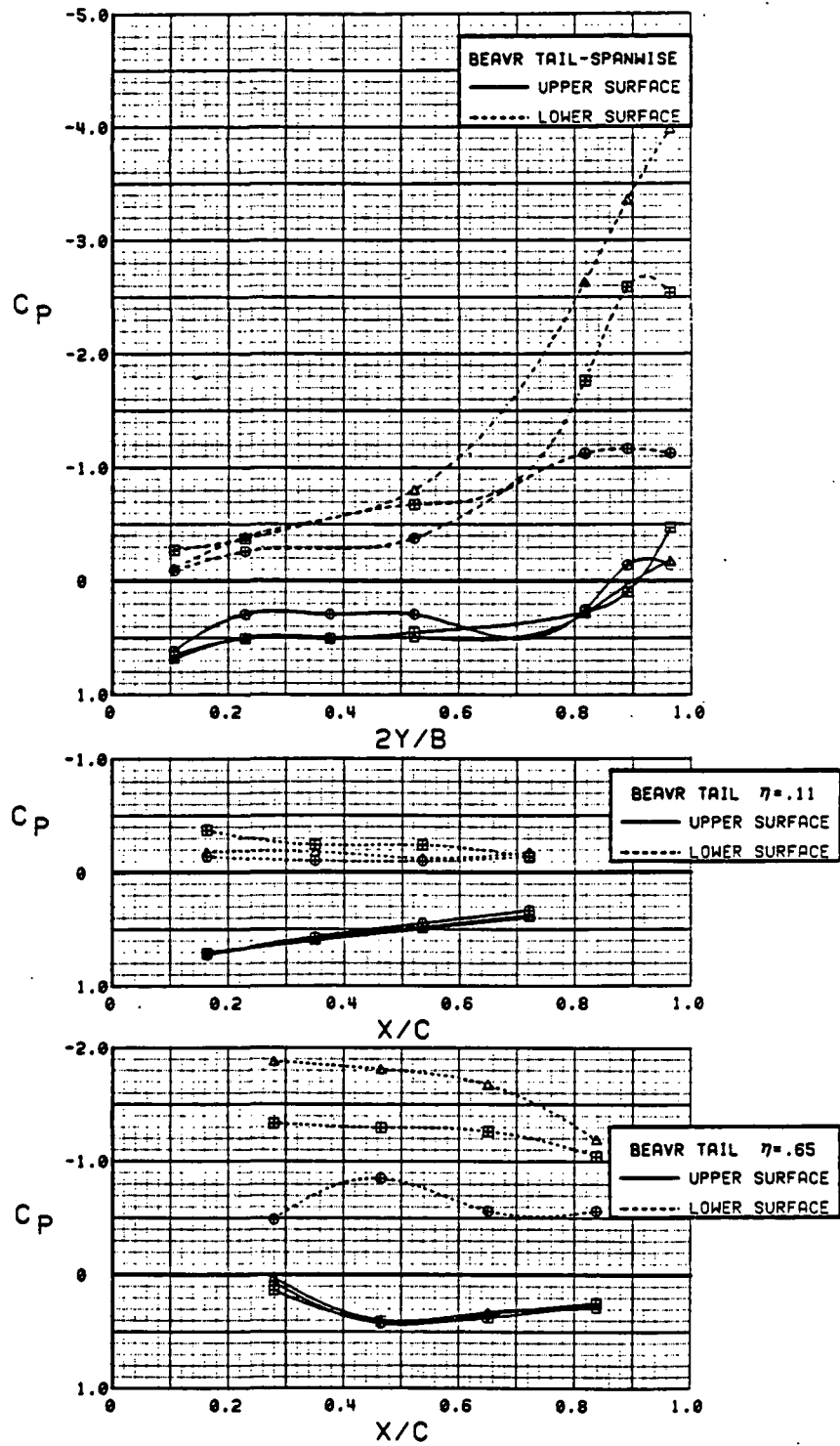


Figure 3.4-9 Power Effects, Wing Flaps Neutral

SYM	TEST	RUN	ALPHA	CT	ITEF	OTEF	CAN	SWB	$\delta_{BT}$
⊙	543	48	8.5	0.00	30	30	0	OFF	40
⊠	543	47	8.6	0.95	30	30	0	OFF	40
△	543	46	8.6	1.89	30	30	0	OFF	40

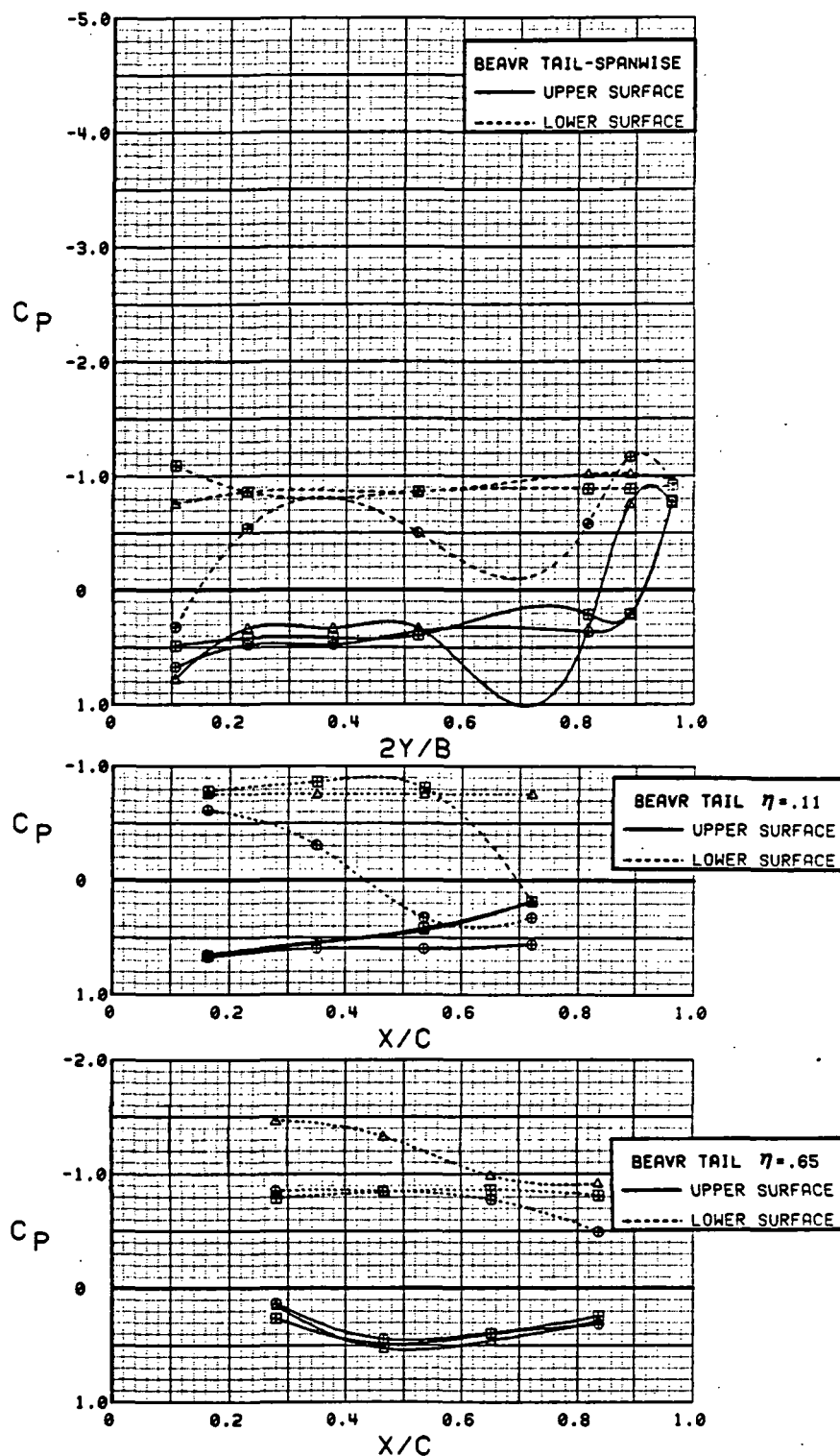


Figure 3.4-10 Power Effects, Wing Flaps Deflected



### 3.5 NOZZLE FLAP RESULTS

The nozzle flap, which is also referred to as the wing inboard-trailing-edge flap, was instrumented with pressure taps to measure the static pressure in the jet exhaust of the port engine. The following discussion presents the findings of a cursory analysis of the pressure data from this source. Table 2 lists the locations of the flap pressure taps.

Figure 3.5-1 shows the flap static pressure distribution during an alpha variation with power off and flaps neutral. It is noted that the hingeline of the flap was at the nozzle exit plane and corresponded with  $x/c = 0$ , whereas the flap trailing edge was at  $x/c = 1.0$ . The flatness of these curves shows that the flow was separated, as it should have been with power off since the flap was directly behind the nozzle. The trend of decreasing pressure with increasing alpha is presumably caused by an influence from the wing that carried over onto the flap. The stalled nature of the flowfield on the flap persisted at all combinations of alpha and flap deflection when the power was off with one exception - the -30 deg deflection (Figure 3.5-2) had a minor reduction in pressure near the trailing edge as if the flow had separated from the surface at that station.

When power was applied, the flowfield on the flap experienced a series of expansions and compressions as shown in Figure 3.5-3. The positions of the expansions and compressions remained unchanged with thrust coefficient changes, but the amplitude of the oscillations increased. EPR was almost constant; whereas,  $q$  was the primary variable; therefore, it is evident that the flowfield had a significant effect on the shock system of the exhaust jet, increasing the compression/expansion oscillations as  $q$  decreased. The pressure distributions on the flap (Figure 3.5-4) were essentially independent of angle of attack, but flap deflection had a significant influence, as one would expect. The expansion at  $x/c \approx 0.5$  was intensified when the flap was deflected downward. It is somewhat surprising, however, that the expansion and compression pattern remained so similar, even when the flaps were deflected upwards. Figure 3.5-4 shows extremely low pressures near the trailing edge of the flap when it was deflected to 30 deg. These pressures at first appeared to be caused by extraneous data points; however, Figure 3.5-5, shows additional data that confirm this trend, which presumably results from a separation of the upper-surface flow and an accompanying expansion of the high-pressure air from the lower surface of the flap around the flap trailing edge to the upper surface.

The power-on flap pressure distributions shown in Figure 3.5-5 were obtained with  $EPR \approx 2.0$ . The convergent-divergent nozzle at this EPR, with an area ratio of 1.09, should have issued the flow in an overexpanded state at a discharge Mach number of 1.35 with oblique shock waves then reducing the flow to subsonic speeds. Had the supersonic flow been sustained over the length of the flap, the static pressure distribution on the flap would have been constant. But such was not the case. The static-pressure profiles on the flap indicate that the transition to subsonic flow occurred upstream of the first pressure tap. It is felt that the presence of the nozzle rake may have initiated shock waves in the nozzle that hastened the transition of the flow to subsonic speeds.

The conclusions drawn from the flap pressure data are (1) the flow was subsonic as it flowed over the flap even though the nozzle discharge Mach number was supersonic and (2) the flow tended to separate near the trailing edge when the flap was deflected 30 deg.

SYM	TEST	RUN	ALPHA	CT	ITEF	OTEF	CAN	SWB
⊕	543	63	0.1	0.00	0	0	0	OFF
⊞	543	63	8.3	0.00	0	0	0	OFF
△	543	63	16.6	0.00	0	0	0	OFF
◆	543	63	24.8	0.00	0	0	0	OFF
*	543	63	32.8	0.00	0	0	0	OFF

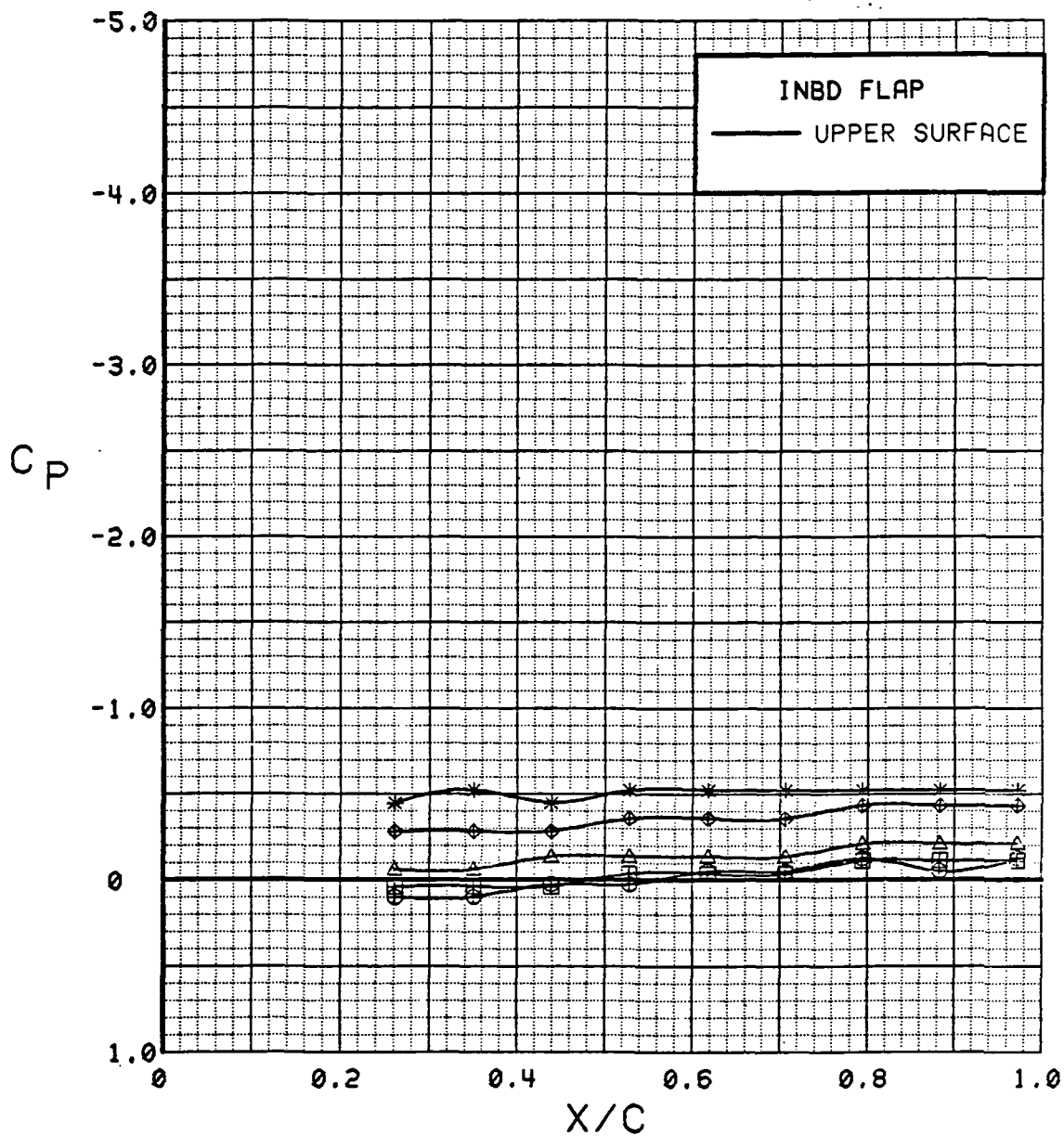


Figure 3.5-1 Angle of Attack Effects on Nozzle Flap, Power Off

SYM	TEST	RUN	ALPHA	CT	ITEF	OTEF	CAN	SWB
⊙	543	88	4.1	0.00	-20	-20	0	OFF
⊠	543	76	4.2	0.00	-10	0	0	OFF
△	543	63	4.2	0.00	0	0	0	OFF
◆	543	83	4.3	0.00	10	10	0	OFF
*	543	69	4.3	0.00	20	20	0	OFF
+	543	11	4.4	0.00	30	30	0	OFF

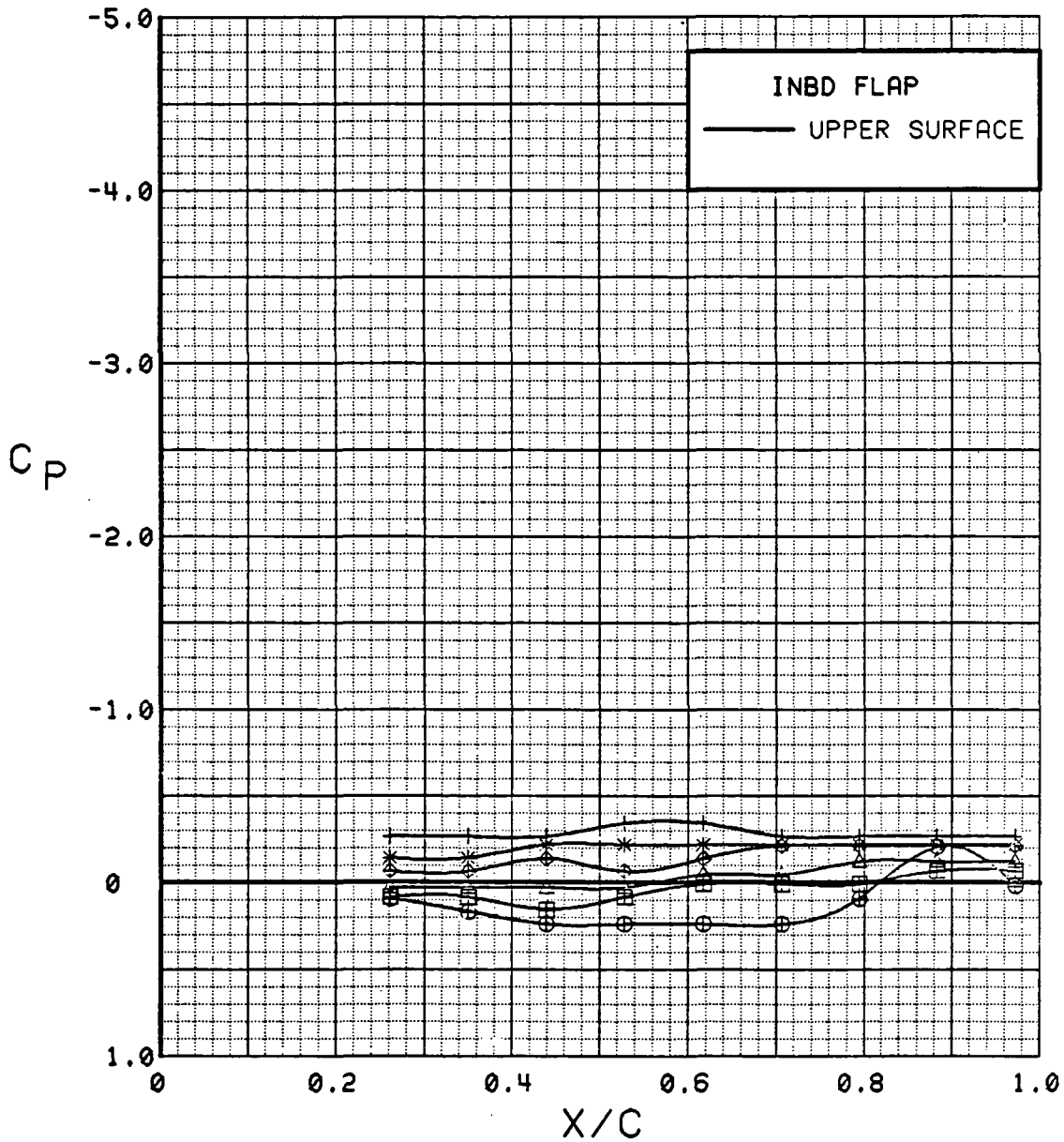


Figure 3.5-2

Nozzle Flap Deflection Effects, Power Off

SYM	TEST	RUN	ALPHA	CT	ITEF	OTEF	CAN	EPR	q
⊙	543	63	4.2	0.00	0	0	0	1.0	15
⊠	543	64	4.2	0.27	0	0	0	1.8	61
△	543	62	4.2	0.48	0	0	0	1.8	37
◆	543	60	4.3	0.93	0	0	0	2.1	23
*	543	59	4.3	1.40	0	0	0	2.1	15
+	543	58	4.3	1.84	0	0	0	2.1	11

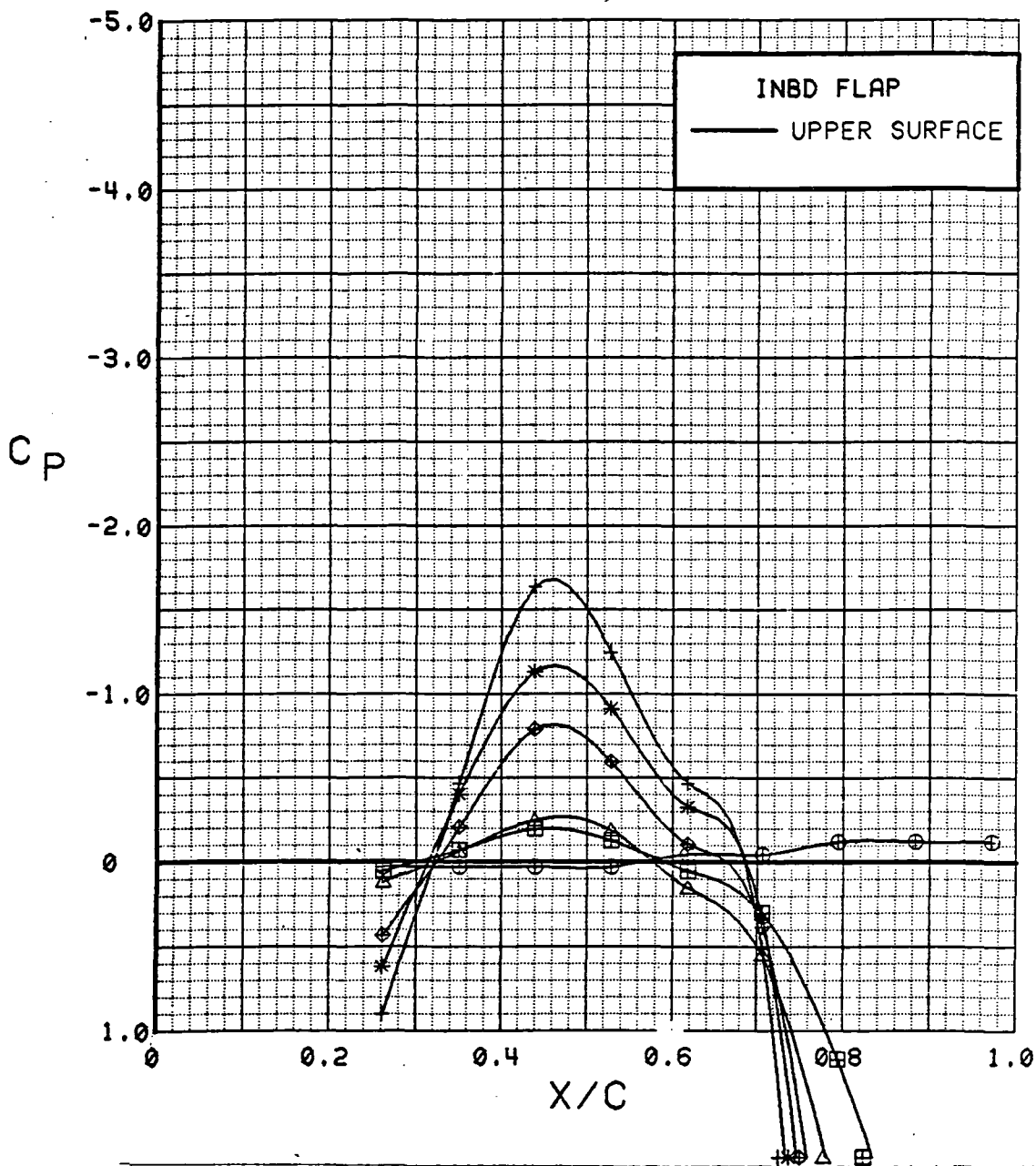


Figure 3.5-3

Dynamic Pressure Effects on Nozzle Flap, Power On

SYM	TEST	RUN	ALPHA	CT	ITEF	OTEF	CAN	SWB
⊕	543	85	4.0	1.89	-20	-20	0	OFF
⊞	543	72	4.2	1.96	-10	0	0	OFF
△	543	58	4.3	1.84	0	0	0	OFF
◆	543	81	4.4	1.87	10	10	0	OFF
*	543	67	4.5	1.89	20	20	0	OFF
+	543	4	4.5	1.90	30	30	0	OFF

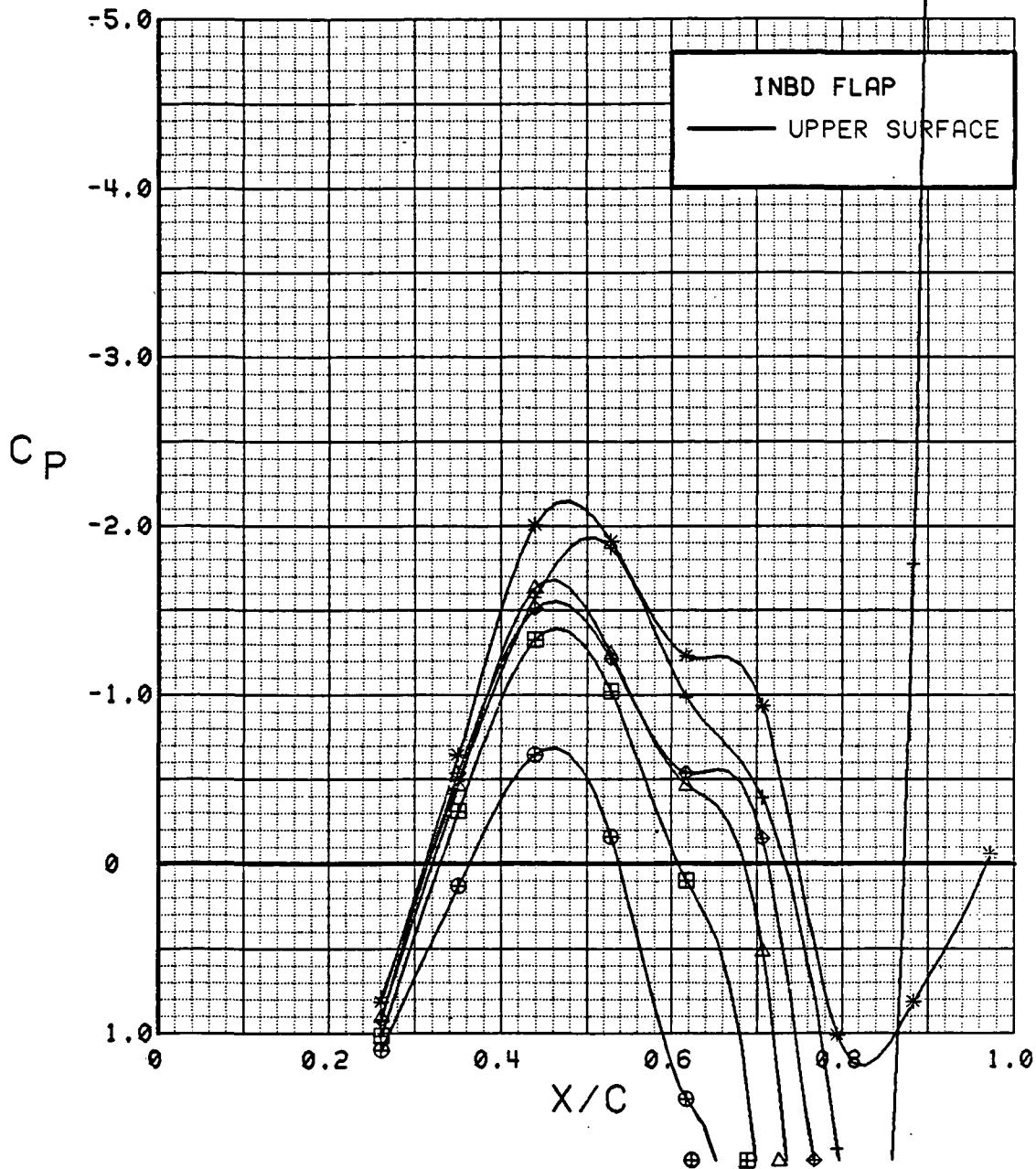


Figure 3.5-4 Nozzle Flap Deflection Effects, Power On

SYM	TEST	RUN	ALPHA	CT	ITEF	OTEF	CAN	SWB
⊕	543	4	0.4	1.89	30	30	0	OFF
⊞	543	4	8.7	1.85	30	30	0	OFF
△	543	4	16.9	1.86	30	30	0	OFF
◆	543	4	25.1	1.89	30	30	0	OFF
*	543	4	33.2	1.85	30	30	0	OFF

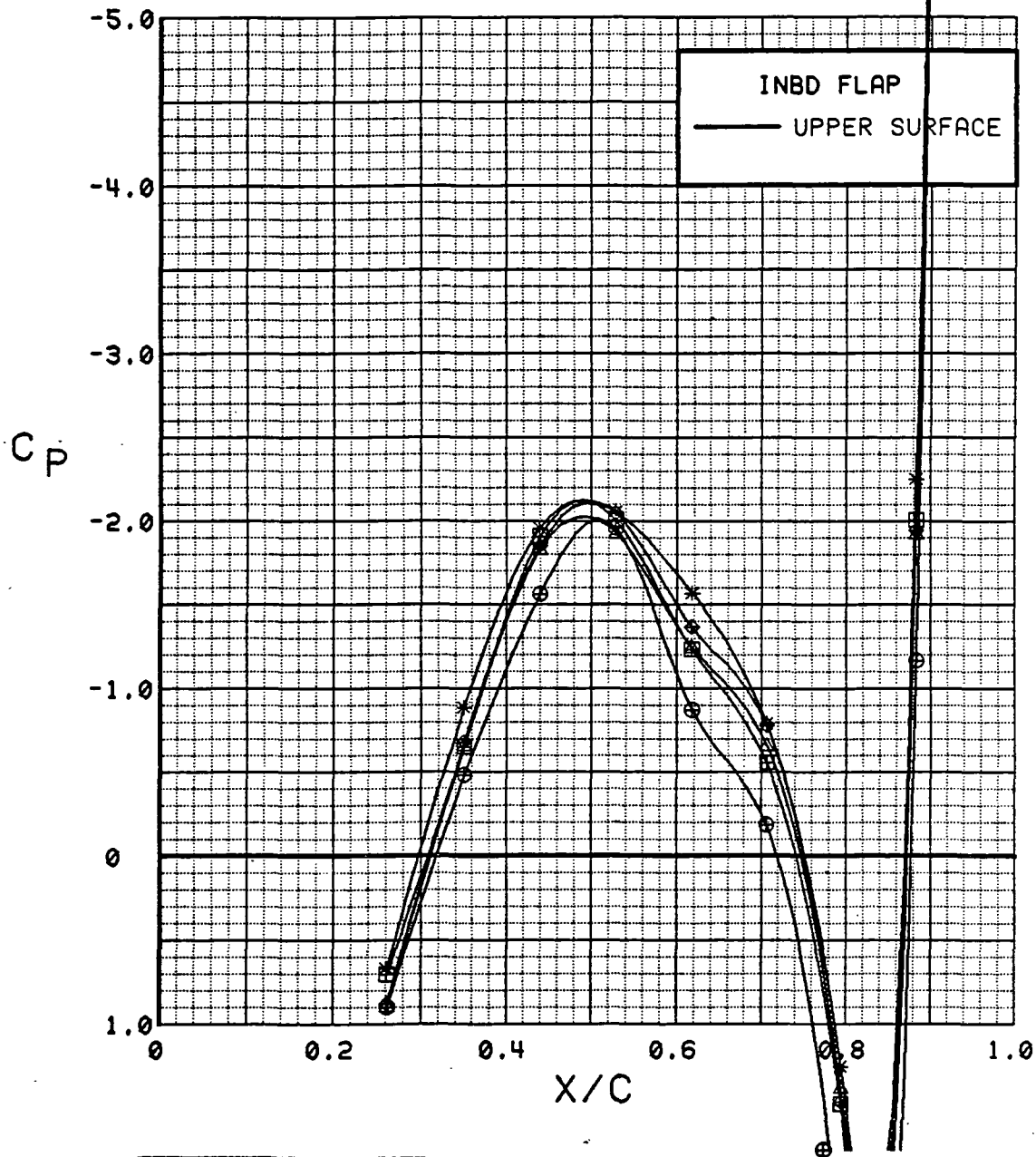


Figure 3.5-5 Angle of Attack Effects on Nozzle Flap, Power On

### 3.6 THERMAL ANALYSIS AND CORRELATION WITH PRESSURE DATA

#### 3.6.1 Wing Upper Surface

Thermocouples were installed on the port wing, as discussed in Section 2.2, to measure the temperature of the SWB nozzle exhaust at several locations on the upper surface. The spanwise flow was initially employed in Test 537 at static and  $C_T = 1.9$  conditions (Runs 45 and 47). The thermocouples began failing early in these runs, and only a few were functioning properly at the end of Run 47. The flow patterns of the spanwise jet could not be established from these runs alone due to the paucity of accurate readings.

All of the thermocouples were repaired prior to Test 546, but again they failed relatively early in the test. Runs 1 and 3 were at static and  $C_T = 1.9$  conditions and matched the configuration and test conditions for the first two SWB on runs in Test 537. It was fortunate that the same configuration was tested initially in both tests because it was this test procedure that provided two sets of data that could be used jointly to establish the thermal characteristics of the SWB nozzle exhaust - a task that could not have been otherwise accomplished. Despite the early failure of the thermocouples, which led to the lack of data to evaluate configuration variables, the data on the basic configuration at static and maximum power conditions provided a valuable insight into the potential temperature effects and the basic flow patterns of the SWB exhaust jet.

Wing temperature data at static tunnel conditions are shown in Figures 3.6-1 through -4 for various engine pressure ratios (EPR). Because of the variation in tunnel freestream temperature between runs, the incremental temperature rise above freestream ( $\Delta T$ ) was found to be the best parameter for comparison. The fairings that are shown in these plots were established not only from the data shown in each figure but also by relationship of these data to the family of EPR curves shown in Figure 3.6-5. It is also noted that the spanwise data set was more consistent than the chordwise data and was relied upon heavily in the establishment of the fairing of the chordwise data. Accordingly, a symbol is shown on each chordwise plot that was taken from the fairing of the spanwise data.

The data in Figure 3.6-5 establish points of constant temperature at each row of thermocouples. From these points, approximations were made of the isotherms on the wing upper surface at the various EPR's (Figures 3.6-6 and -7). Since the tunnel conditions were static for these data, the EPR variations were, of course, obtained by changing the engine RPM. Consequently, higher exhaust temperatures were inherent in the data at the higher EPR's. The engine duct total temperature (TEDFTP) that was measured at each EPR condition is noted on the figures.

Following the previously described procedure, temperature distributions and isotherms were developed for an  $\alpha$ -sweep with  $C_T = 1.9$ . The chordwise and spanwise temperature distributions and the data points are shown in Figures 3.6-8 through -15 for individual angles of attack, and Figure 3.6-16 illustrates that they form a consistent family of curves. The isotherms that were developed from these data are shown in Figures 3.6-17 through -24. Also shown in these plots, are a set of isobars that were developed from the same runs used for the thermal data (T537, Run 47, and T546, Run 3). The thermal trends, as mentioned earlier, were established by the joint use of these two runs. Therefore, the pressure distributions from these runs were also averaged before the isobars were developed; so the isotherm and isobar patterns would be on a consistent basis. Pressure data for this configuration, but with  $C_T = 1.8$ , are presented in Subsection 3.2.4.5.1 (Test 537, Run 53), should the reader desire to relate the pressure distributions with the isobars. Since the isobars were developed from a different run, small discrepancies between them are apparent upon close examination, but these discrepancies are not significant.

The Ames STOL Fighter Model was designed with the objective that the leading-edge vortex would be enhanced by the SWB jet; the force and pressure data indicate that this occurred. The following discussion addresses this point and other conclusions, drawn from a simultaneous examination of the isotherms, isobars, and previously-presented pressure distributions. It is worthy of note that construction of the isotherms and isobars required an extensive amount of imagination and judgment since some curves were based on as few as one or two data points. No effort was made to reconcile the patterns of the isobars and isotherms; it was, therefore, gratifying that they complemented each other in the establishment of the characteristics of the flow field. The following discussion identifies three somewhat different flow patterns that appear to exist in the low-, mid-, and high-alpha ranges.

For the low-alpha range ( $\alpha = 0, 4, \text{ and } 8 \text{ deg}$ ), the isotherms and isobars are shown jointly in Figures 3.6-17, -18, and -19. The SWB jet is characterized by a relatively narrow isotherm pattern that turns sharply downstream. When SWB was not employed, the airflow over the wing was generally attached in the region bounded by the isotherm pattern. It is presumed that it was the unidirectional characteristics of the attached flow that made it so forceful in turning the SWB jet. The peak-isotherm traces, which are transposed to the isobar patterns at each alpha, nearly coincide with the location of a minimum-pressure peak at the inboard row of pressure taps, thus establishing a firm relationship between the isotherms and isobars. Traces of the presumed path of the leading-edge vortex core are also shown on the isobar patterns. These traces, which were established through a thorough scrutiny of the chordwise- and spanwise-pressure distributions, fall characteristically along minimum-pressure peaks in the isobar patterns. As the vortex moved progressively inboard at  $\alpha = 0, 4, \text{ and } 8 \text{ deg}$ , it is noteworthy that in each case the traces of the vortex and jet are separated by a high-pressure region. At  $\alpha = 0 \text{ deg}$ , it is possibly caused by the compression that ordinarily follows a leading-edge-suction peak. At  $\alpha = 8 \text{ deg}$ , it is possibly caused by the reattachment of the freestream flow after it passed over the well-developed leading-edge vortex core, and for the intermediate angle of attack ( $\alpha = 4 \text{ deg}$ ) it is probably caused by effects from both of these phenomenon. At  $\alpha = 0, 4, \text{ and } 8 \text{ deg}$ , it is quite clear that the SWB jet was only slightly influenced by alpha and the position of the vortex. Conversely, at this stage SWB had a modest effect on the leading-edge vortex, inducing lower leading-edge pressures (hence earlier vortex development) through an indirect process, since the two flows did not come close together in this alpha range. Incidentally, the spanwise isobars near the hingeline of the flap are caused by a flow expansion because these data are for 30-deg flap deflection.

For the mid-alpha range ( $\alpha = 12 \text{ and } 17 \text{ deg}$ ) the isotherms and isobars are shown in Figures 3.6-20 and -21. At these conditions, the SWB jet was not forced downstream as sharply as it was in the low-alpha range, and a spreading of the jet occurred. This was the first indication that the vortex and jet came in contact, the vortex peripheral flow having drawn the jet boundary outboard. At  $\alpha = 12 \text{ deg}$ , the leading-edge vortex continued to be identifiable with a low-pressure crest; the high pressure region between the jet and vortex core was still intact. The high-suction regions at the leading edge were manifestations of a leading-edge vortex that was being strongly enhanced indirectly by SWB, as discussed in Subsection 3.2.4.5.1. At  $\alpha = 17 \text{ deg}$  (Figure 3.6-21) the definition of the vortex path was not so clear-cut. The track, as drawn, follows one low-pressure ridge as it emanates from the leading edge. As it approaches the trailing edge, it follows another low-pressure ridge; however, between the leading edge and the trailing edge, the vortex track traverses a region of increasing, then decreasing, pressure. It would have, perhaps, been more logical to have followed a continuous locus of monotonically-increasing pressure, but such as not possible except along the leading edge and nearer the tip. For the path shown at  $\alpha = 17 \text{ deg}$  to be wholly acceptable, one need only acknowledge that there was a "close encounter"



near the outboard station, where the jet augmented the vortex (or/and vice versa). The vortex-jet peripheral interactions occurred first in the mid-alpha range because the power-off vortex reattachment line was far enough inboard by that time to encounter the SWB jet when it was turned on. Then, since the vortex imposed a spanwise flow gradient on the wing surface, it spread the jet in that direction. At the same time, the jet was energizing the vortex and moving it outboard. Eventually, an equilibrium state was achieved as denoted by the vortex and jet positions in Figure 3.6-21. But the two flows remain distinct, with the isotherms (and hence the jet) remaining surprisingly uniform compared to the isobars.

For the high-alpha range ( $\alpha = 21, 25, \text{ and } 29 \text{ deg}$ ) the isotherms and isobars are shown in Figures 3.6-22, -23, and -24. At these conditions, the isotherms indicate that the SWB jet was not turned downstream at all by the wing flowfield. This can be verified by a comparison of the peak isotherm traces in these figures with the trace for the static condition (tunnel flow off) in Figure 3.6-7b. At  $\alpha = 25 \text{ deg}$ , the peak isotherm trace moved slightly forward of its static position. At  $\alpha = 29 \text{ deg}$ , the jet was unswept forward of its static sweep angle of  $41 \text{ deg}$  to a revised sweep angle of  $33 \text{ deg}$  near the wing tip. This was additional evidence that the leading-edge vortex drew the jet outboard and forward. Tracing the vortex path at  $\alpha = 21$  and  $25 \text{ deg}$  still presented the same problems as it did at  $\alpha = 17 \text{ deg}$ , and similar interactions evidently occurred. At  $\alpha = 29 \text{ deg}$ , the data used to construct the isobars were more sparse; therefore, the isobar patterns along the perceived paths of the vortex at lower angles were used to supplement the data and establish the low pressure ridges that are shown in Figure 3.6-24. Since the vortex paths in the high-alpha range curved downstream and the jet paths unswept, the surprising conclusion is that the two paths crossed. This occurred in planview only, because the vortex was positioned well above the wing with the jet beneath it, still interacting peripherally but not confluent. The intervention of the jet flow was responsible for the vortex pressure signature being less conspicuous at the higher alphas.

In conclusion, the correlation of pressure and temperature measurements revealed that

- (1) SWB produced a static temperature distribution that was moderately altered by the wing flowfield and least altered at  $\alpha \geq 21 \text{ deg}$ ;
- (2) The jet path over the wing, as indicated by the locus of peak isotherms, turned downstream at low alpha and then showed little change until  $\alpha \geq 21 \text{ deg}$ , where it unswept significantly;
- (3) The static pressure field beneath the jet produced significant lift, but downstream of the jet, the pressures changed little until the jet path unswept. In the region bounded by the jet centerline, the wing leading edge, and the wing tip, there were large changes caused by interactions with the lead-edge vortex. The jet first enhanced the vortex through induced upwash, then through peripheral interactions at higher alpha.

### 3.6.2 Beaver Tail

The upper surface of the beaver tail was instrumented with six thermocouples along a spanwise row to measure the thermal effects of the primary nozzle exhaust. At this instrumented station, which coincided with the station for the pressure instrumentation, the thermocouples and pressure taps were alternately installed, as described in Subsection 2.2. The thermal data are presented as an increment above the tunnel freestream temperature, as was done for the wing thermal data.

There were only three variables that significantly influenced the beaver tail temperature: (1) thrust coefficient, (2) trailing-edge flap deflection, and (3) beaver tail deflection. Figure 3.6-25 shows that with all surfaces neutral, the temperature increased near the edge of the beaver tail as power was increased. This temperature increase of nominally 100°F is relatively small when compared to the total temperature of the engine exhaust, which was about 1000°F above the tunnel temperature. Thus, it can be surmised that the beaver tail was heated only by the periphery of the exhaust jet and that the jet had experienced a substantial amount of mixing (hence, cooling) before it contacted the beaver tail instrumentation. The spanwise pressure data on the beaver tail at these conditions (Figure 3.6-25) do not show these effects.

Trailing-edge flap variations caused the greatest impact on the beaver tail temperature as shown by the profiles in Figure 3.6-26. Negative deflections of -10 and -20 deg on the inboard flap apparently deflected the exhaust, thereby, causing a portion of the exhaust jet to flow inboard over the beaver tail and, presumably, onto the area of the strake between the flap and the beaver tail. The -10 and -20 deg curves show a trend that indicates that the -20 deg deflection had less impact near the edge of the beaver tail but more impact near the centerline. The other flap settings show none of the spillage effects caused by the negative deflections. When the trailing-edge flap was undeflected, there remained a significant amount of heating near the edge. However, when the wing flap was lowered beyond 10 deg, the exhaust jet was apparently deflected beneath the beaver tail and caused no heating. The corresponding beaver tail pressure data on the upper surface (Figure 3.6-26) do not show any of the trends indicated by the thermal data. The strake pressure in Subsection 3.3, however, confirm that the negative wing-trailing-edge-flap deflections caused the exhaust to spill onto the strake area just inboard of the flap.

The effects of beaver tail deflection (at maximum power and with wing flaps undeflected) are shown in Figure 3.6-27. As the beaver tail was deflected, the instrumented chord was elevated with respect to the exhaust jet and, thus, somewhat removed from its influence. The upper surface pressures at these conditions are also shown in Figure 3.6-27, but the effects of the exhaust on the pressures were small. (Compare with power-off data in Figure 3.4-5.)

It is evident from these comparisons that the thermal data provide an insight to the flowfield not afforded by the pressure data. The negative wing-flap deflection in Figure 3.6-26, is a good example. The thermal data show that the jet was heating the inboard portion of the beaver tail, while the pressure data was not even registering the pressure of the jet.

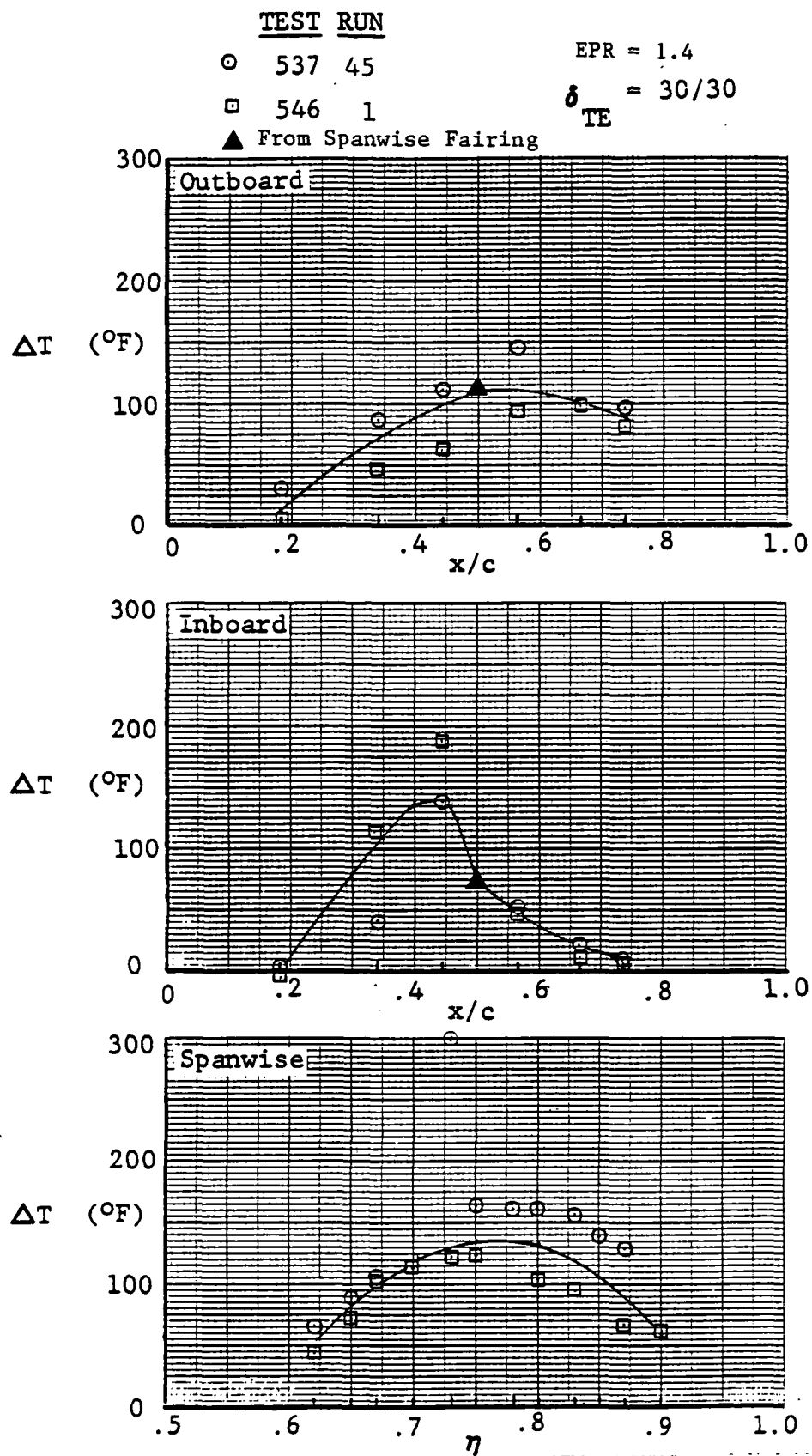


Figure 3.6-1

Wing Temperature Profiles at Static Conditions,  
 EPR = 1.4

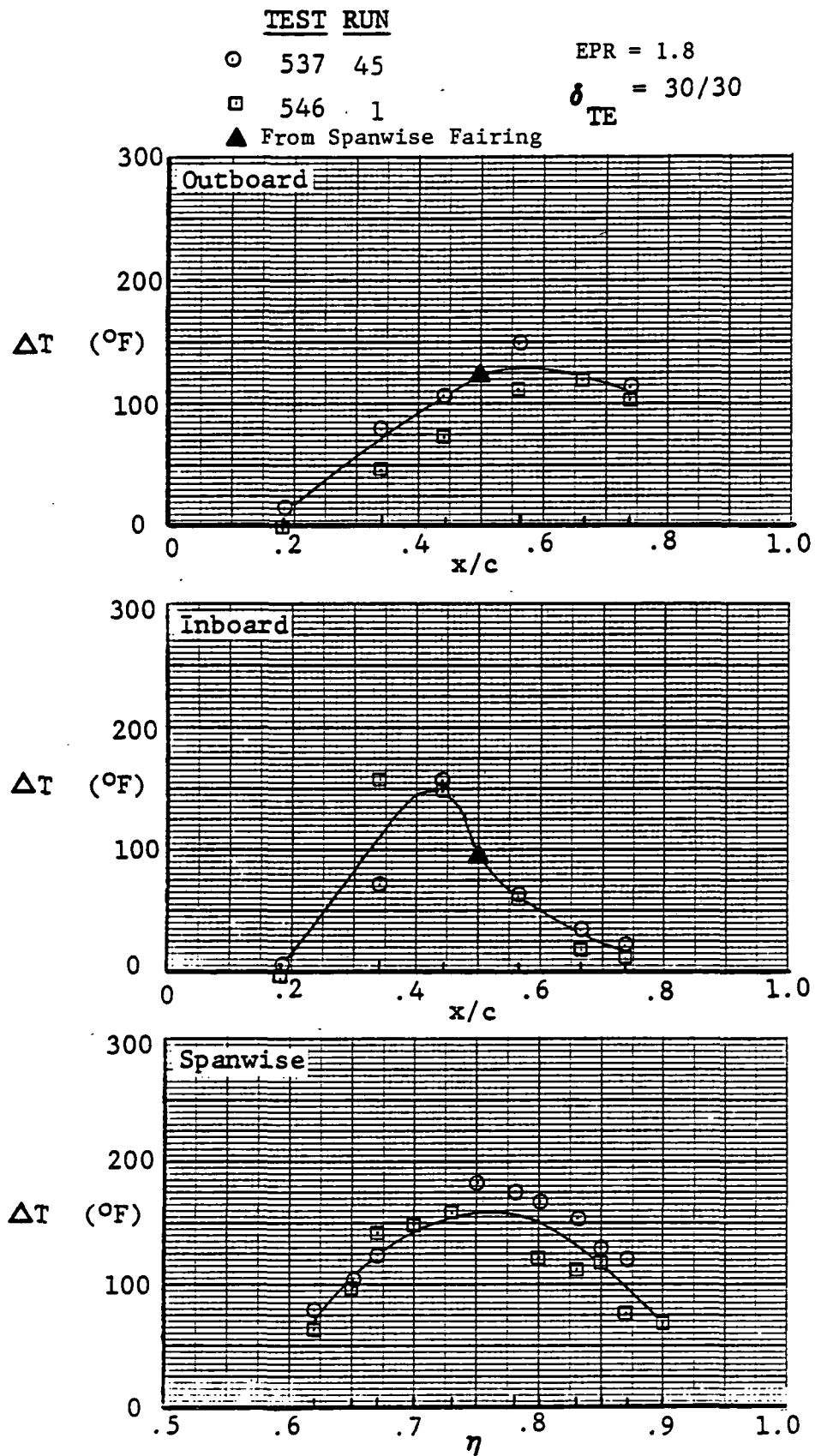


Figure 3.6-2 Wing Temperature Profiles at Static Conditions, EPR = 1.8

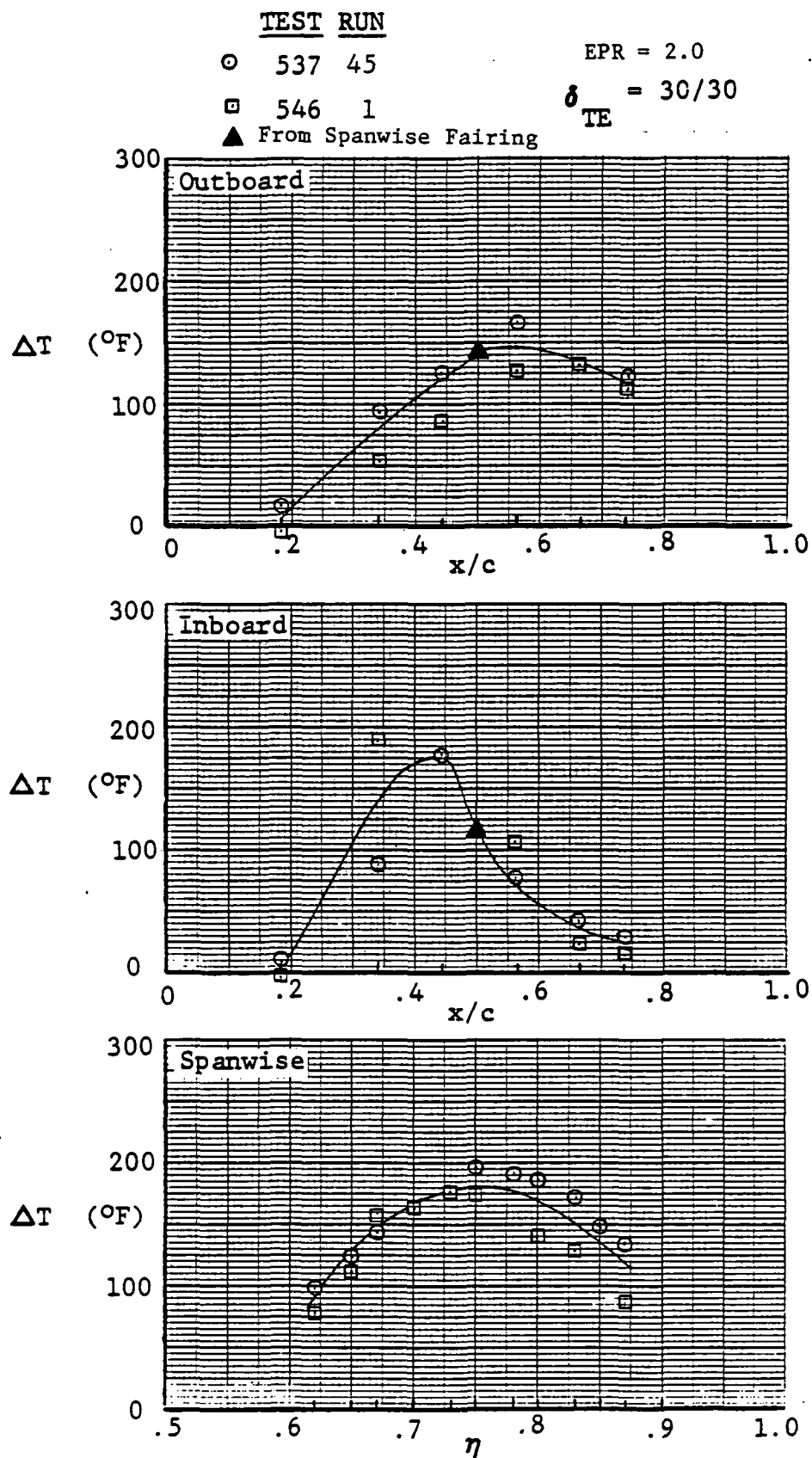


Figure 3.6-3

Wing Temperature Profiles at Static Conditions,  
 $EPR = 2.0$

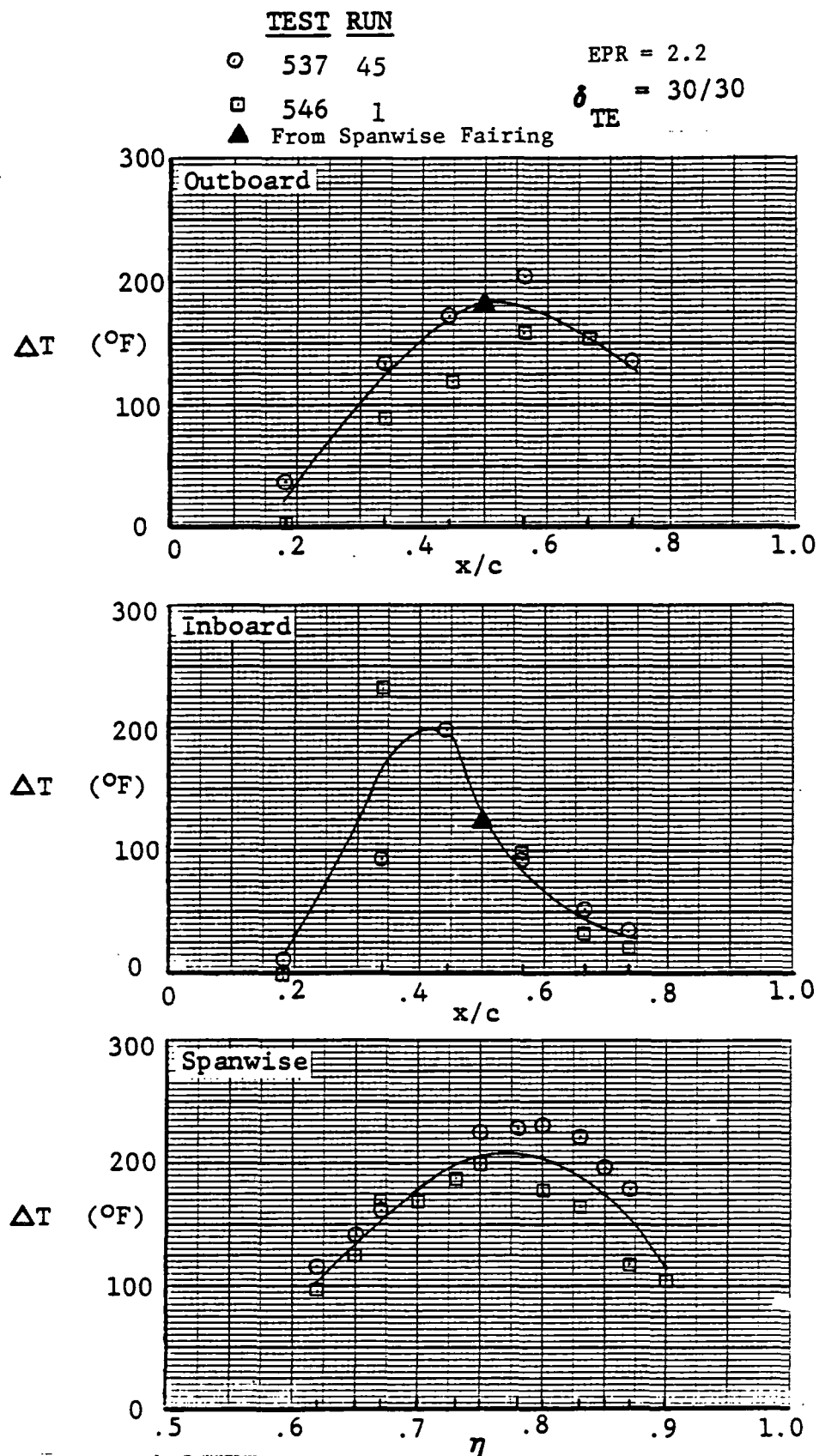


Figure 3.6-4 Wing Temperature Profiles at Static Conditions, EPR = 2.2

$$\delta_{TE} = 30/30$$

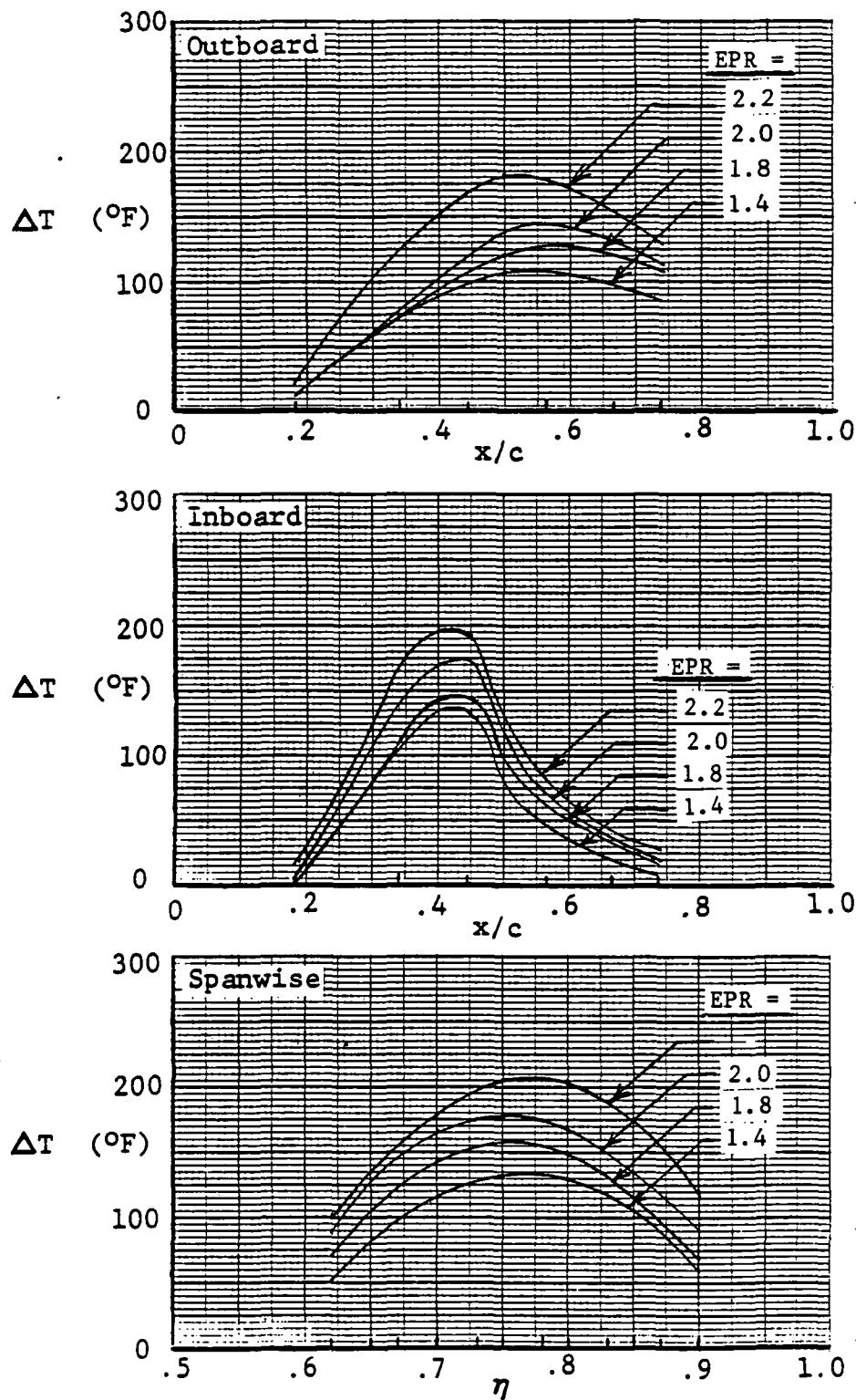


Figure 3.6-5 Family of Wing Temperature Profiles at Static Conditions

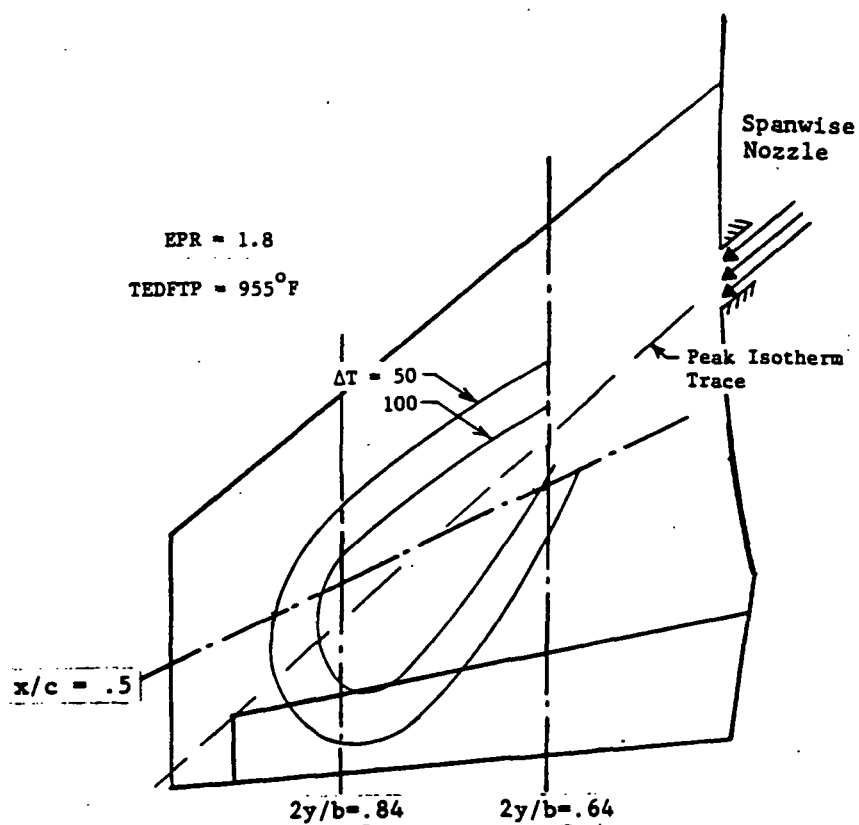
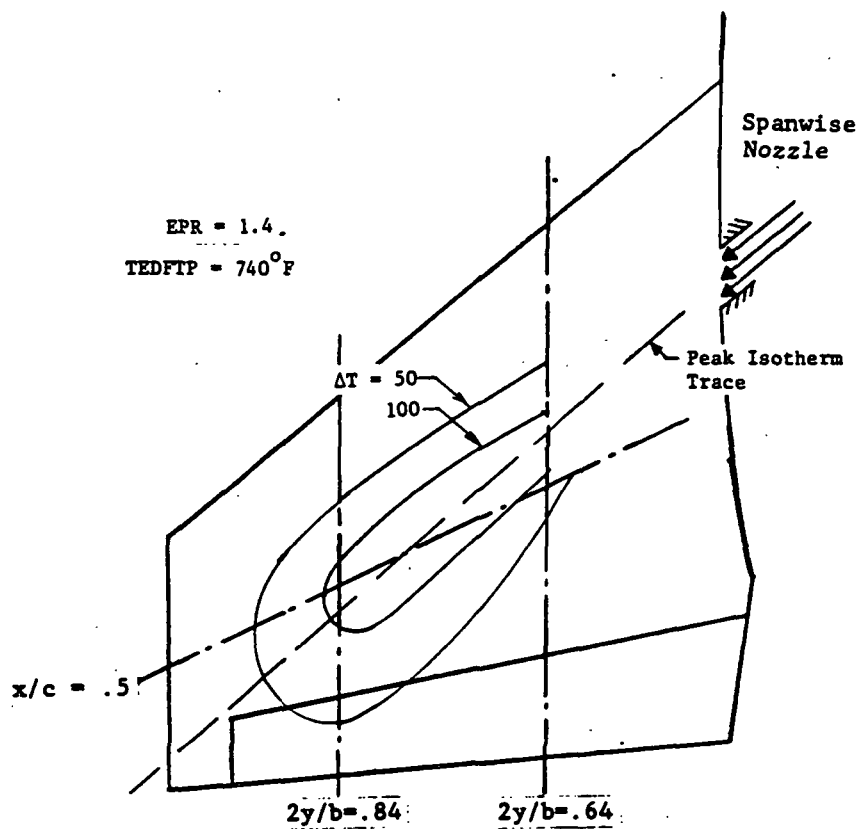


Figure 3.6-6 Isotherms at Static Conditions  
EPR = 1.4 and 1.8



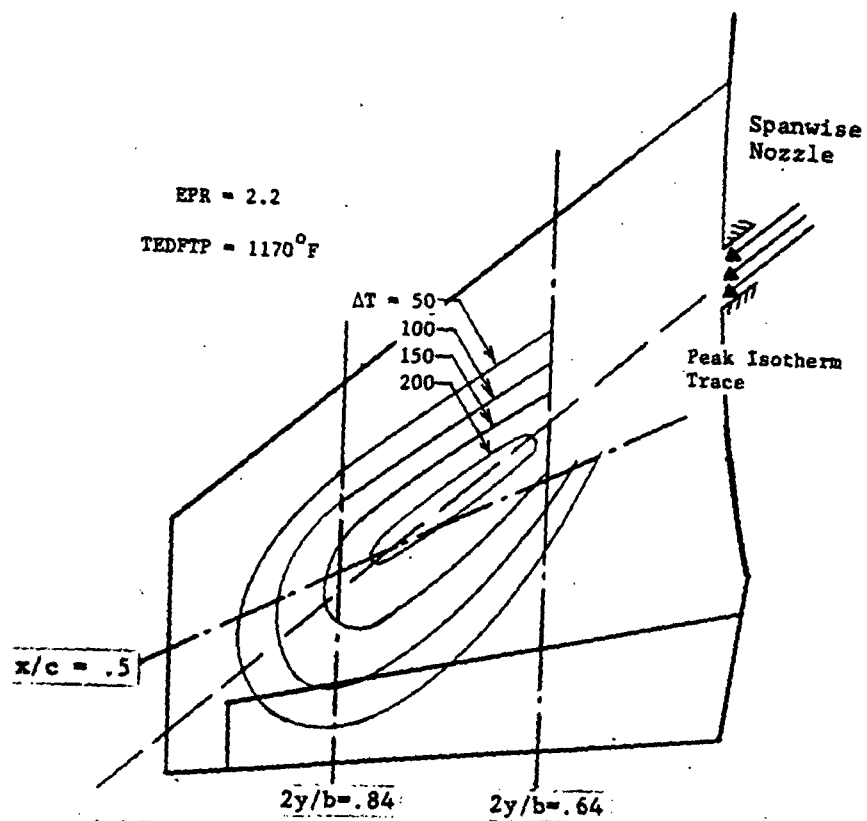
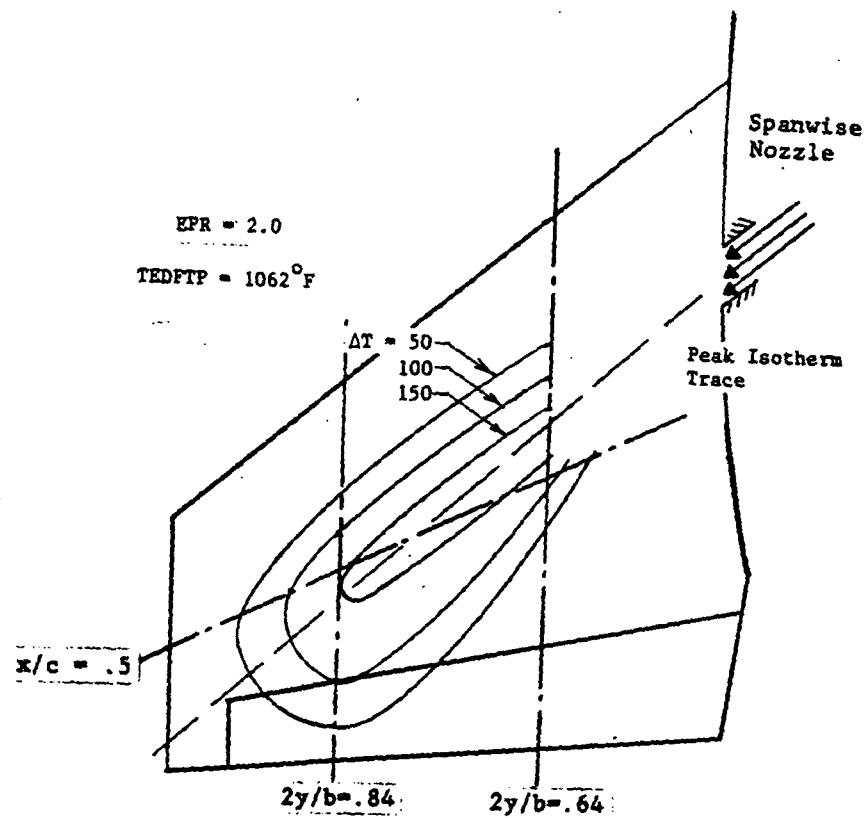


Figure 3.6-7 Isotherms at Static Conditions  
 EPR = 2.0 and 2.2

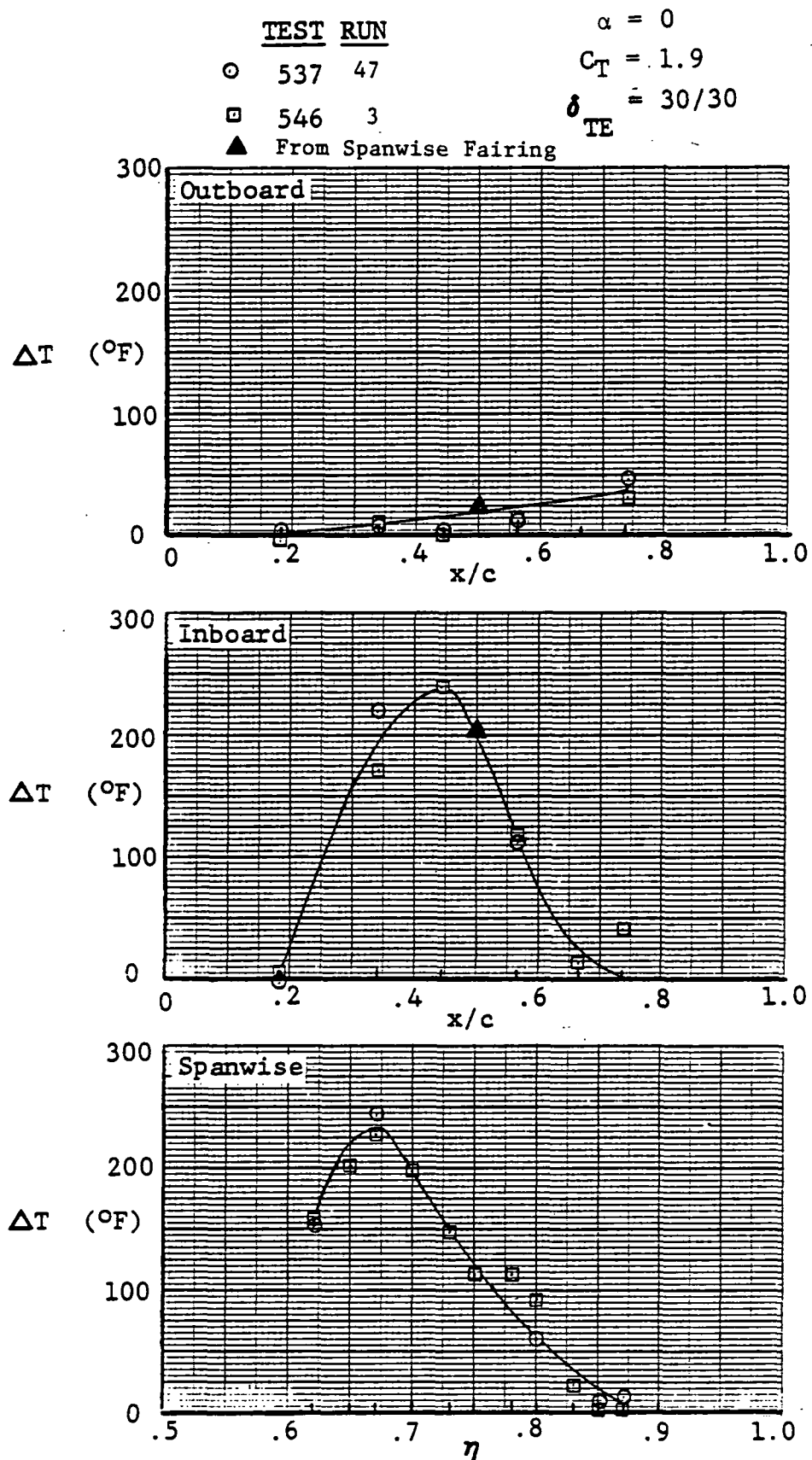
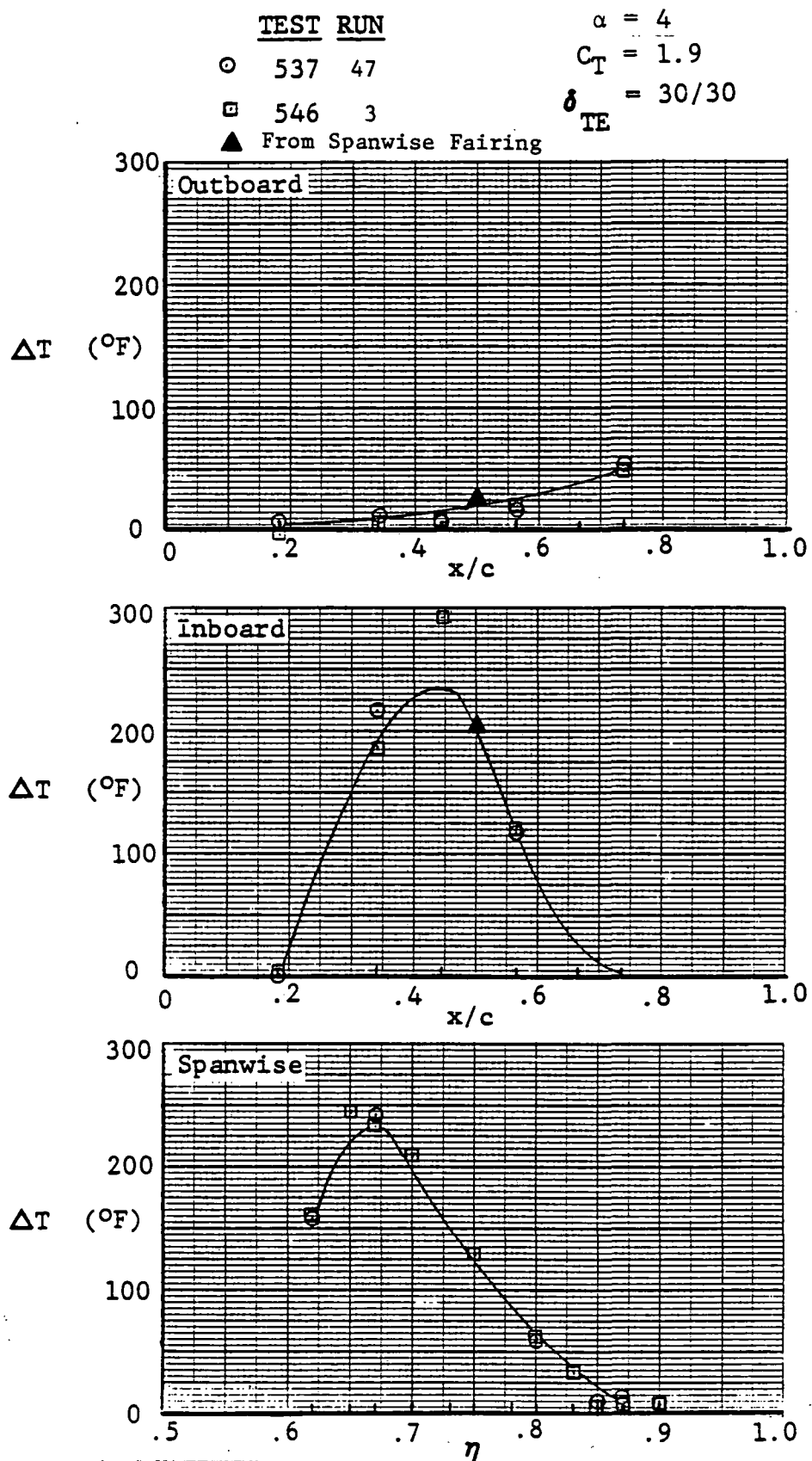


Figure 3.6-8 Wing Temperature Profiles, Alpha = 0 deg

ORIGINAL PAGE IS  
OF POOR QUALITY



ORIGINAL PAGE IS  
OF POOR QUALITY

Figure 3.6-9 Wing Temperature Profiles, Alpha = 4 deg

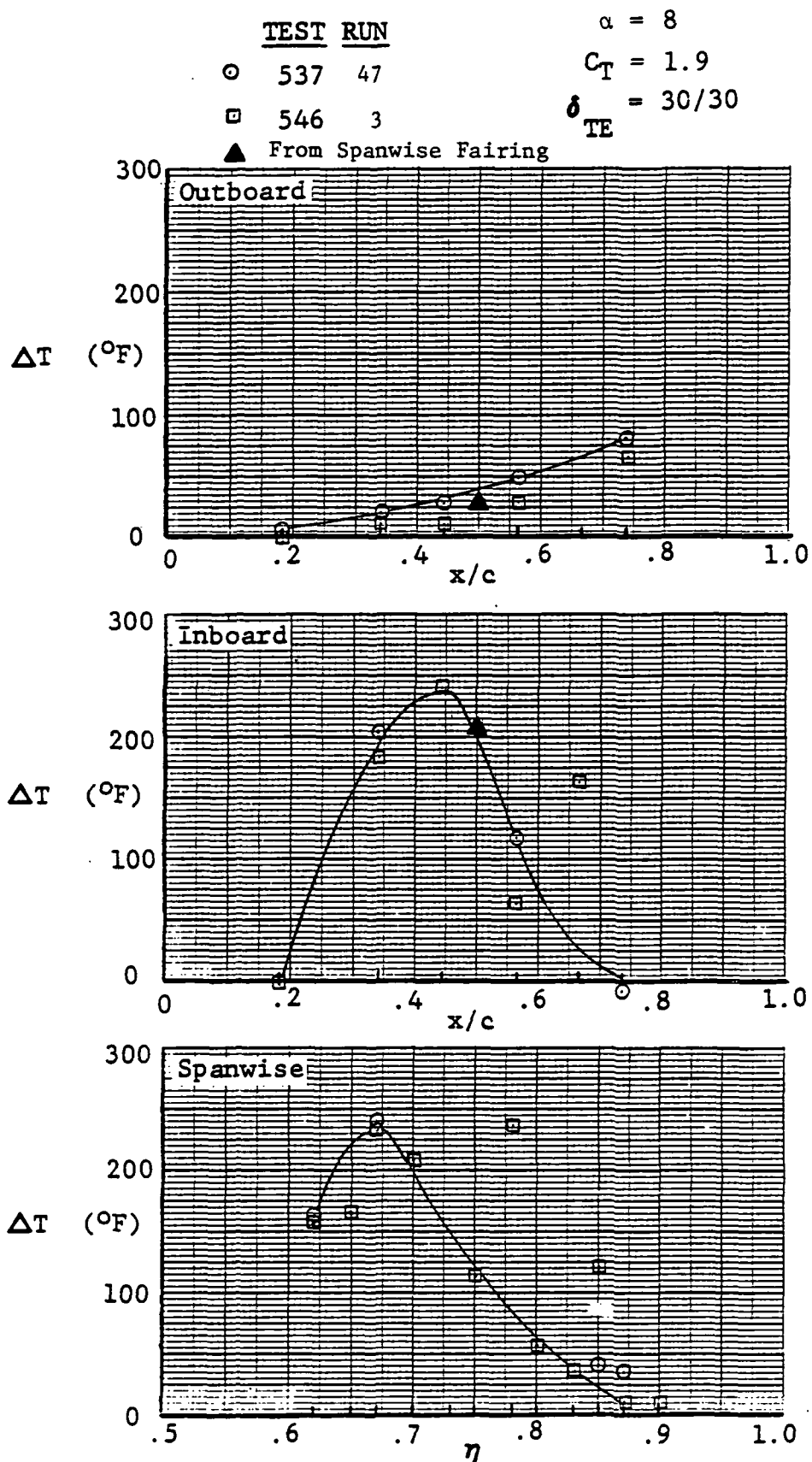


Figure 3.6-10 Wing Temperature Profiles, Alpha = 8 deg

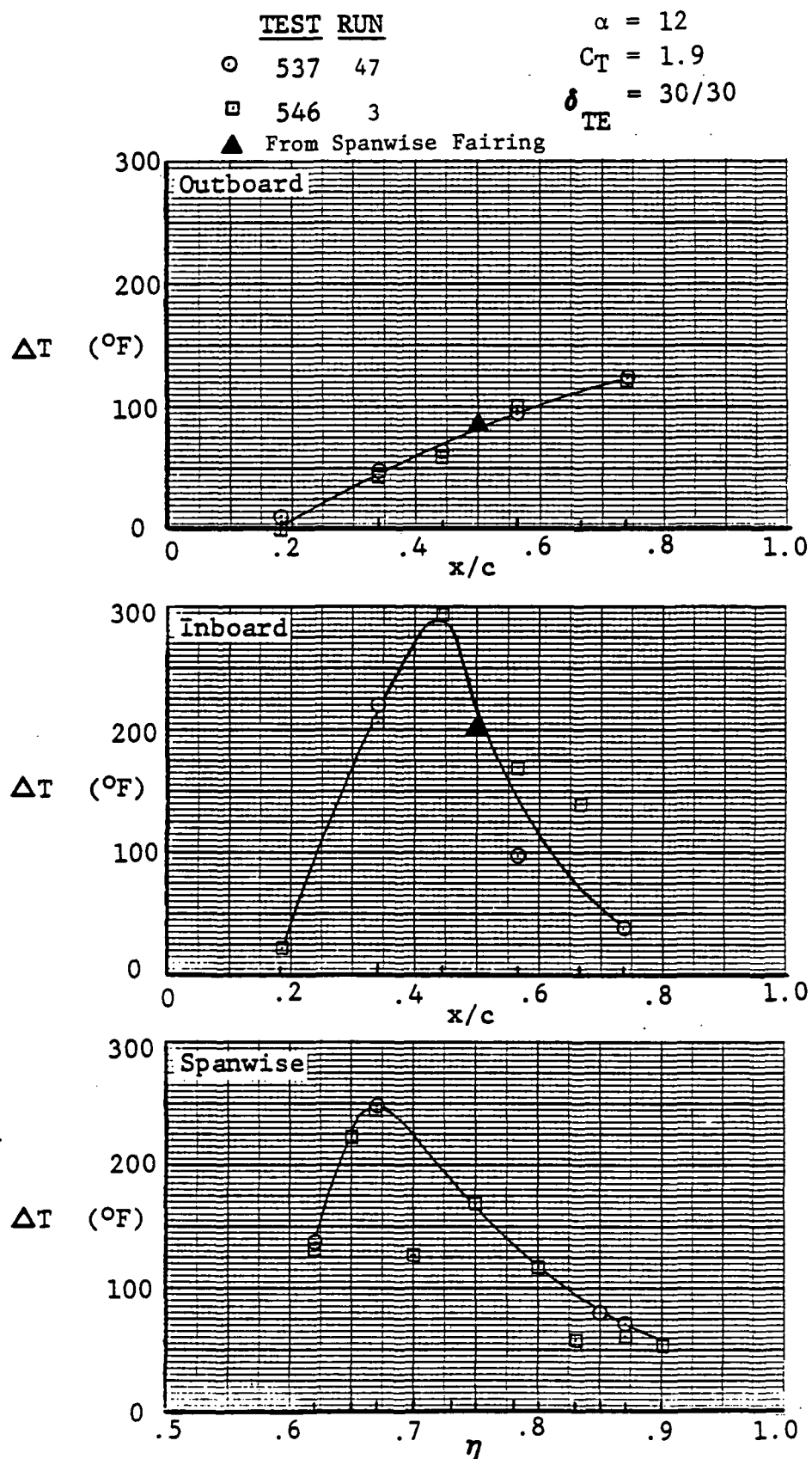


Figure 3.6-11 Wing Temperature Profiles, Alpha = 12 deg

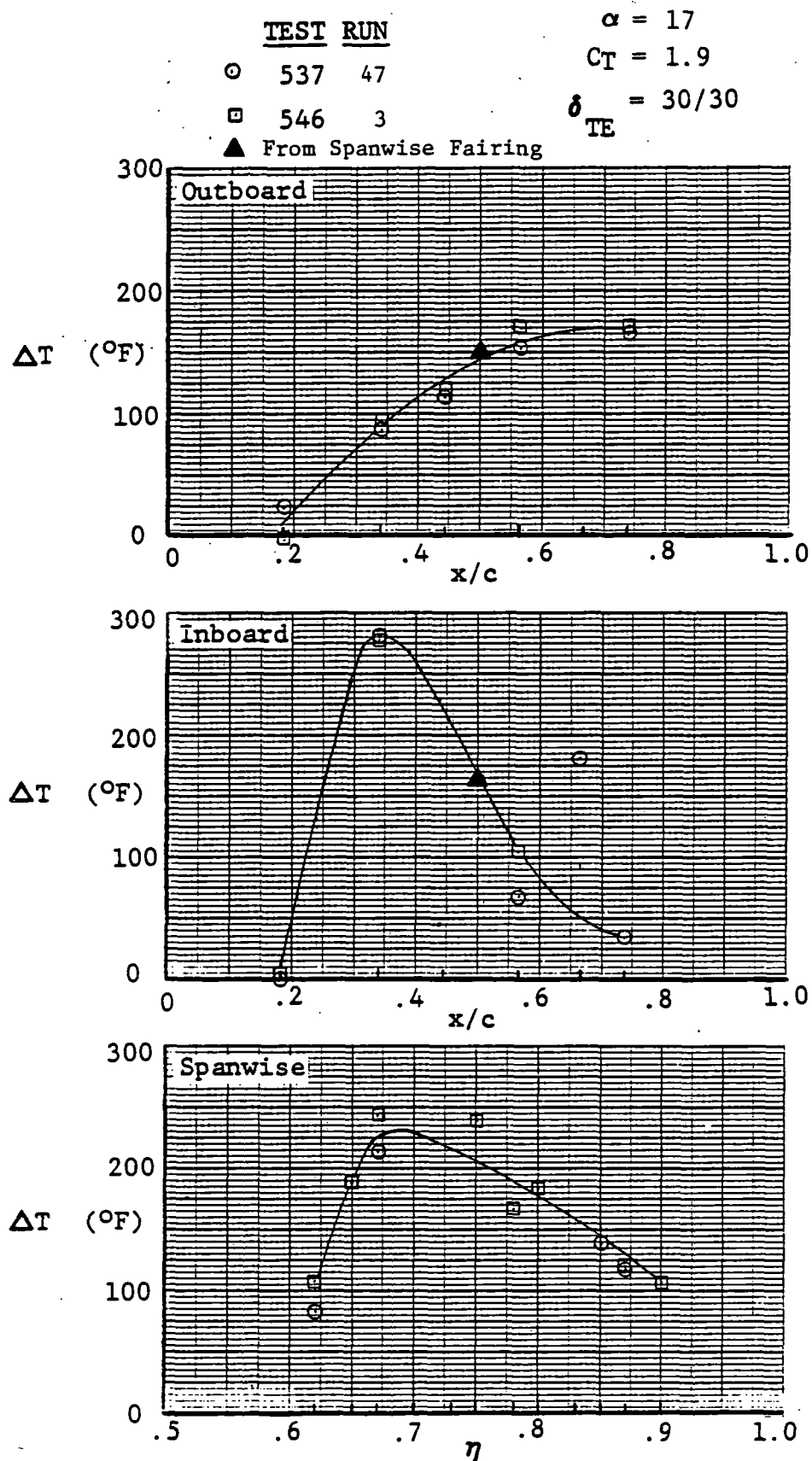


Figure 3.6-12 Wing Temperature Profiles, Alpha = 17 deg

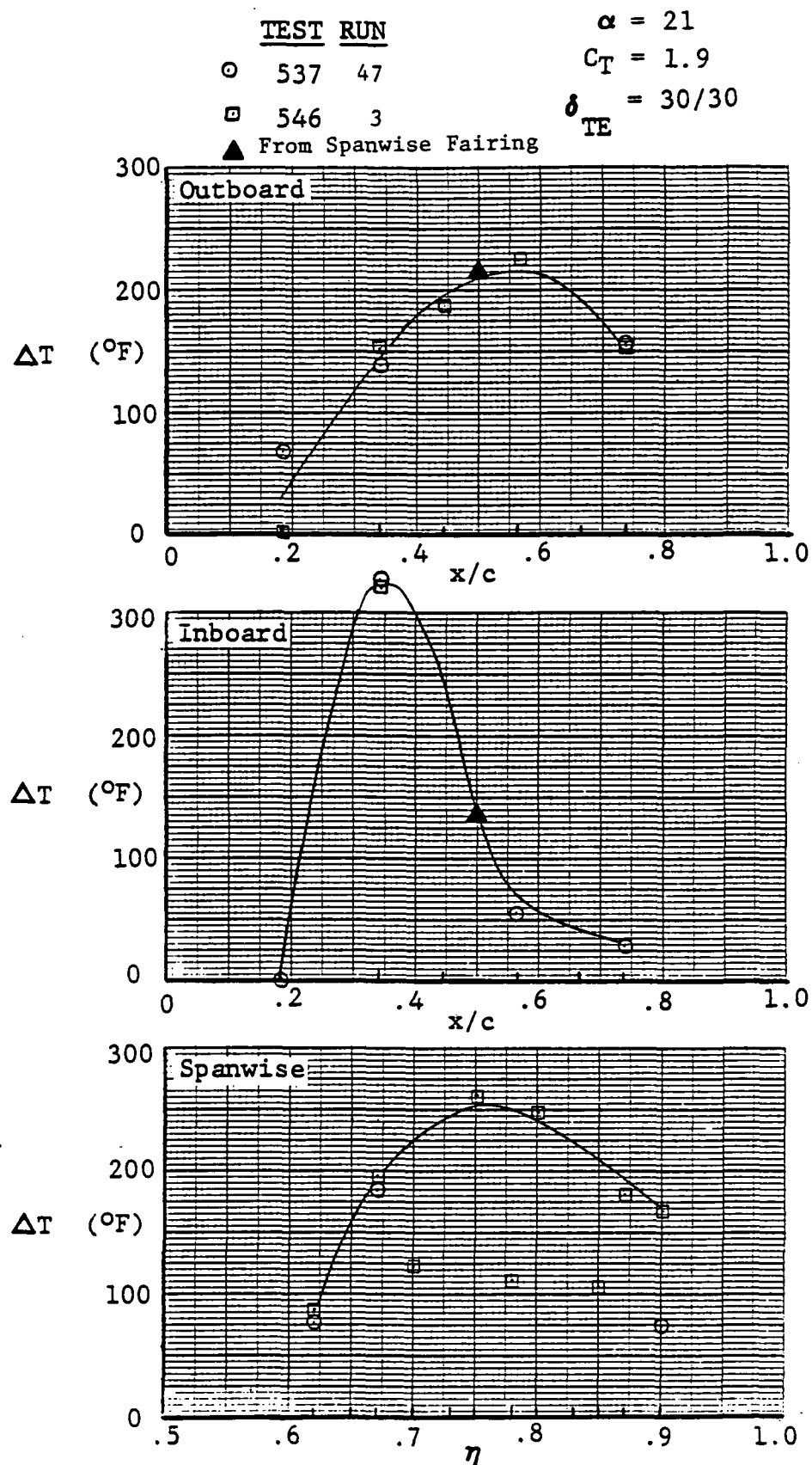


Figure 3.6-13 Wing Temperature Profiles, Alpha = 21 deg

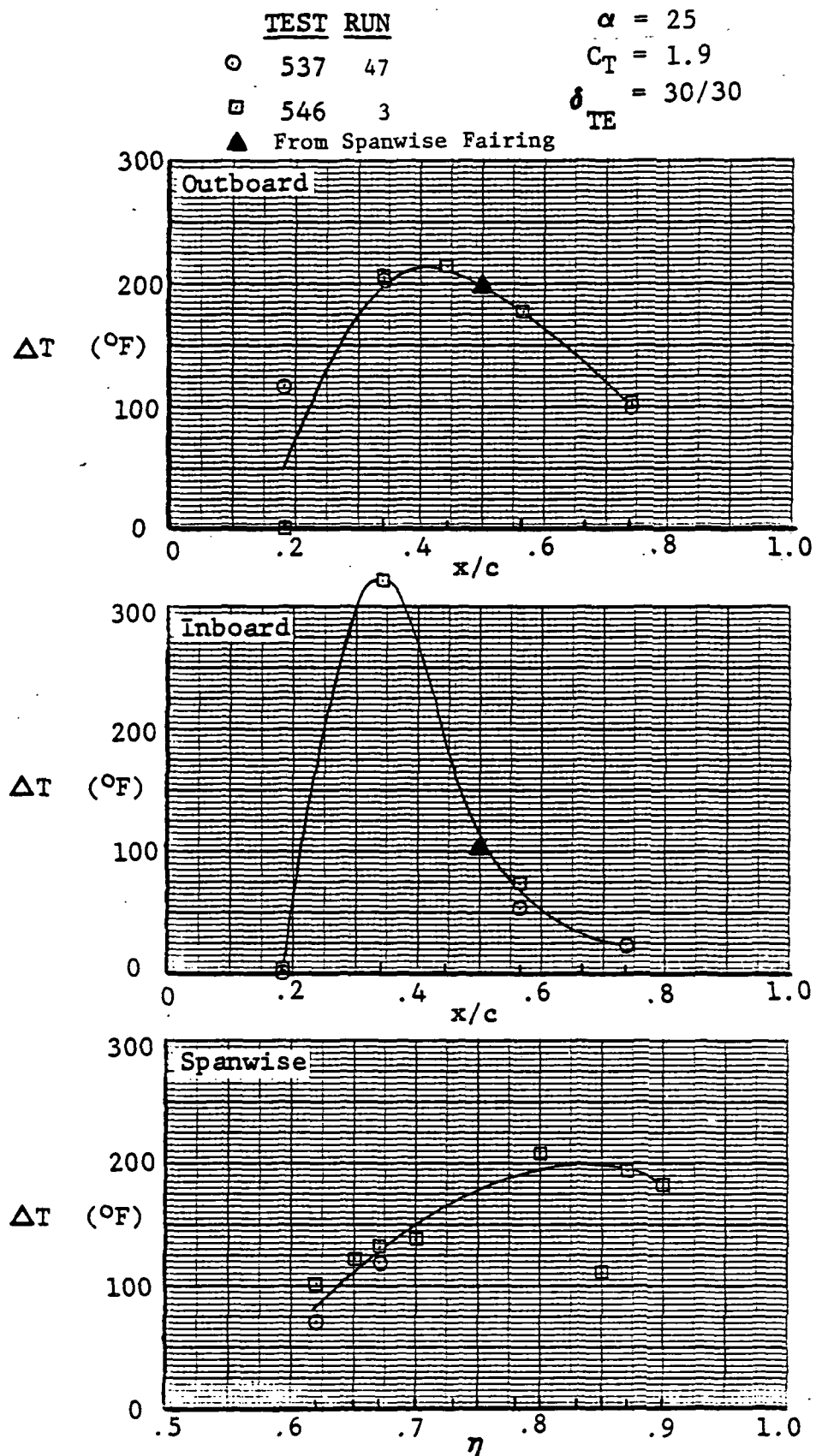


Figure 3.6-14 Wing Temperature Profiles, Alpha = 25 deg



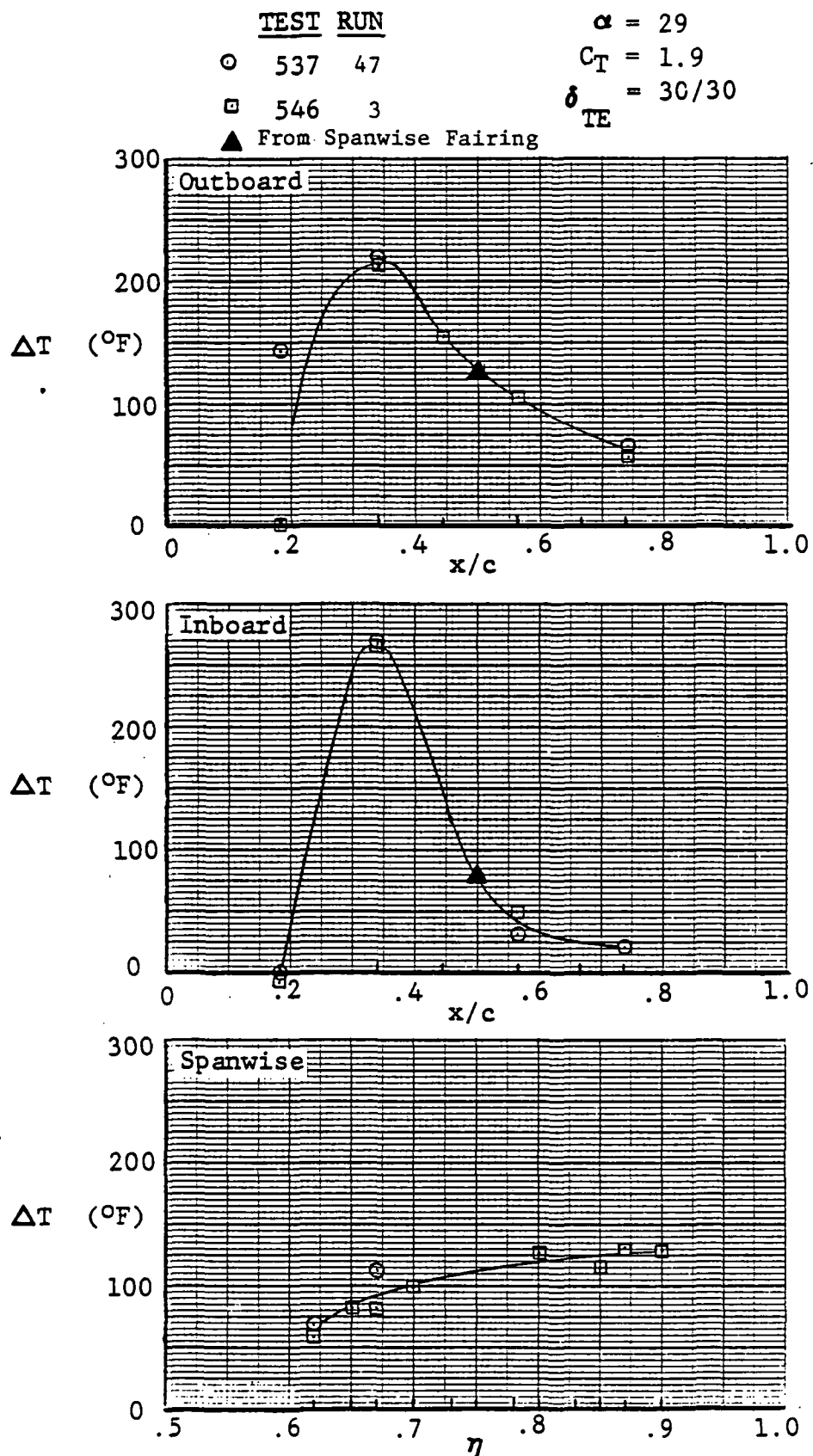


Figure 3.6-15 Wing Temperature Profiles, Alpha = 29 deg

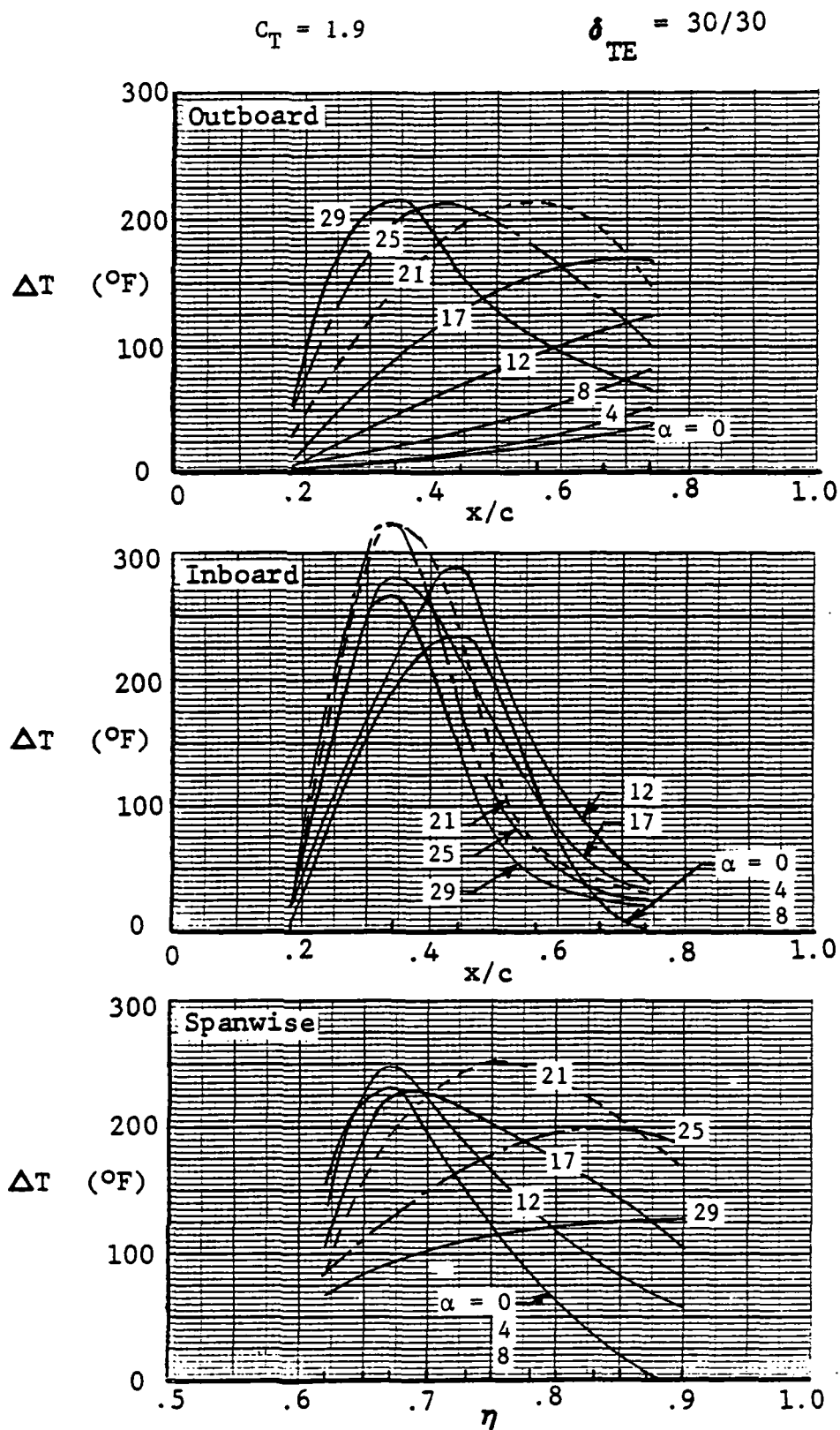
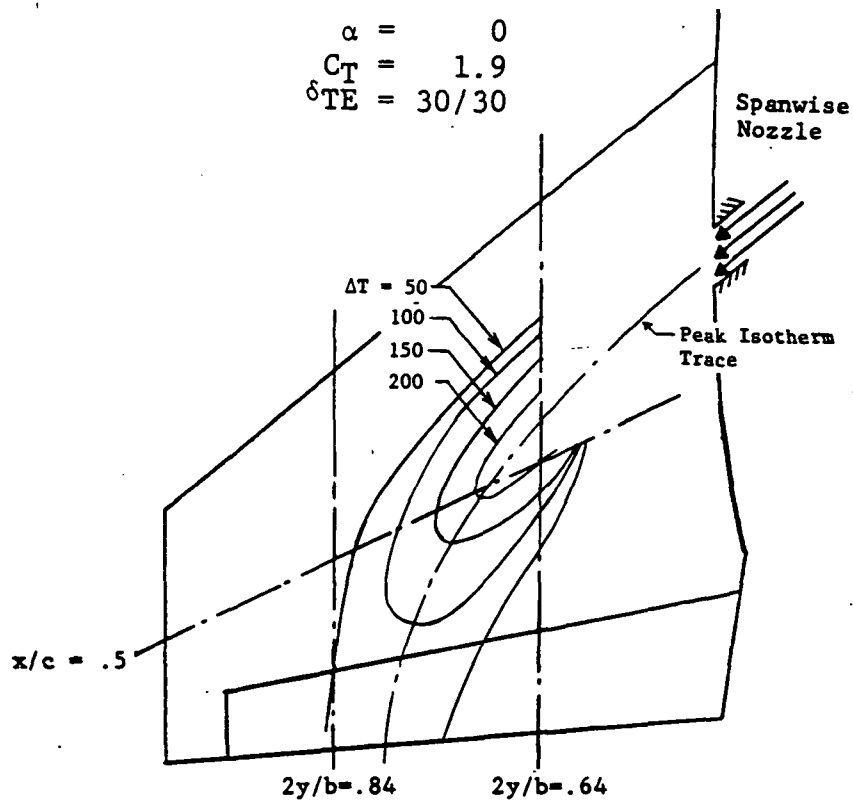


Figure 3.6-16 Family of Wing Temperature Profiles



Code	$C_p$ Range
0	0 to -1
1	-1 to -2
2	-2 to -3
3	-3 to -4
4	-4 to -5
5	-5 to -6
6	less than -6

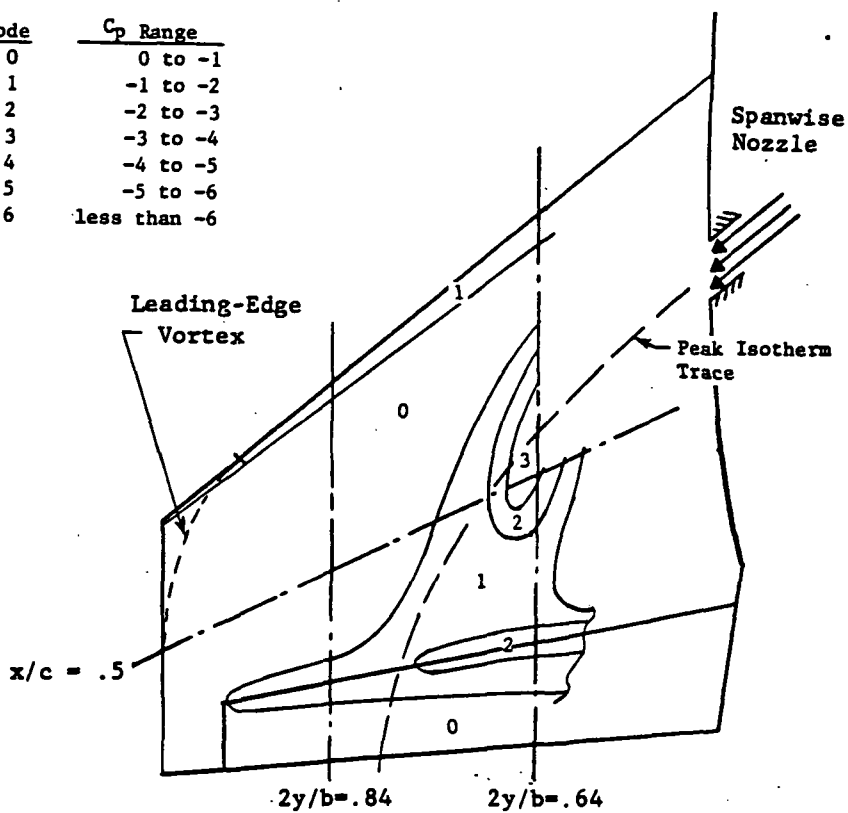


Figure 3.6-17 Comparison of Wing Isotherm and Isobar Patterns,  $\alpha = 0$  deg

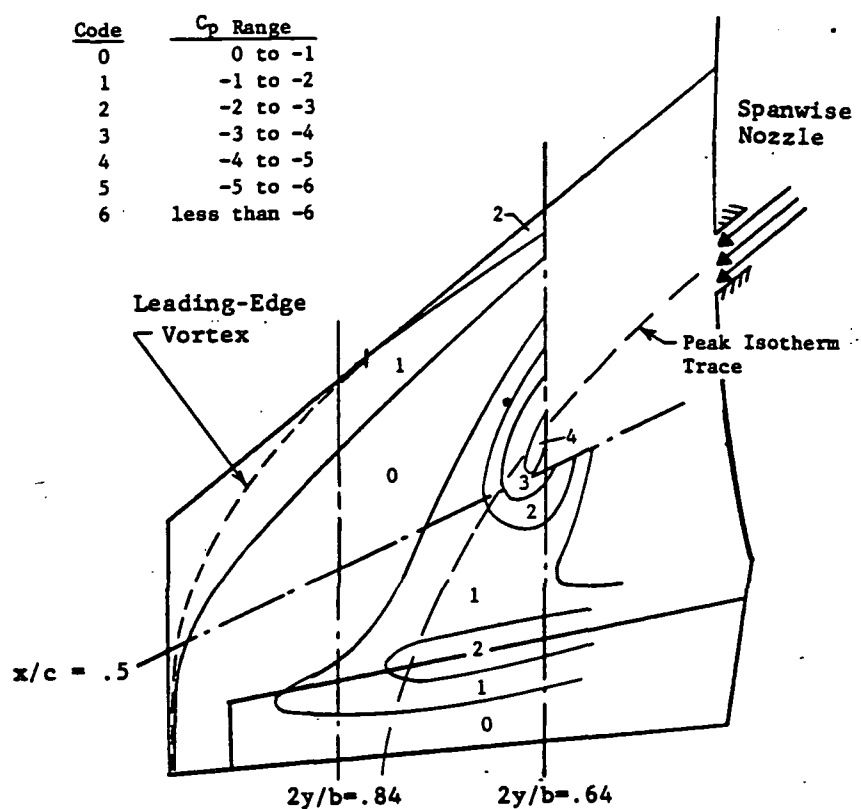
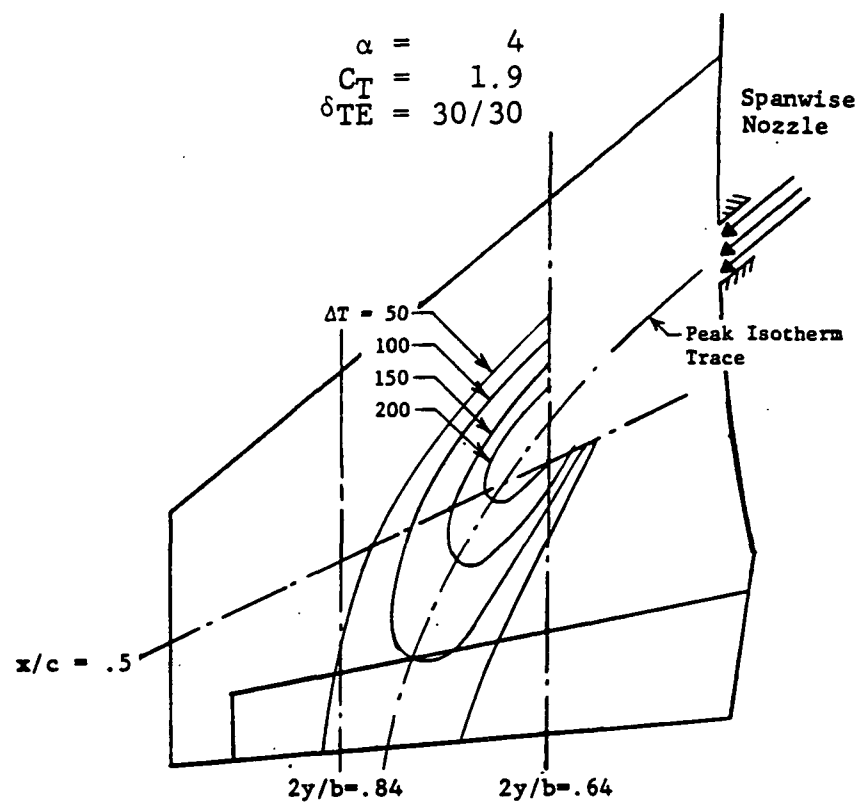


Figure 3.6-18 Comparison of Wing Isotherm and Isobar Patterns, Alpha = 4 deg

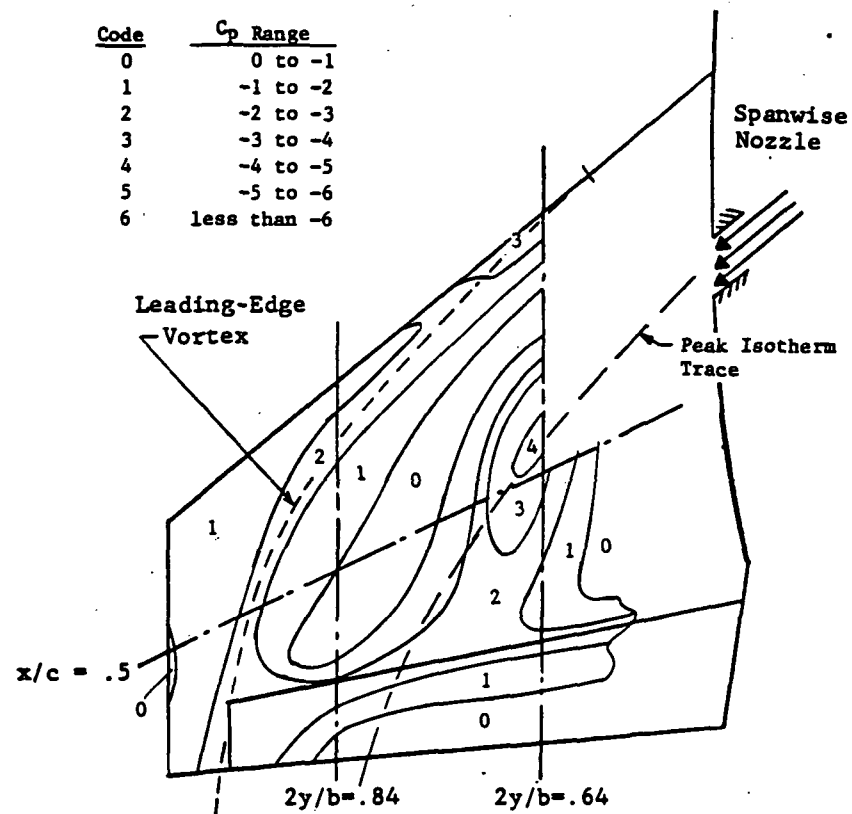
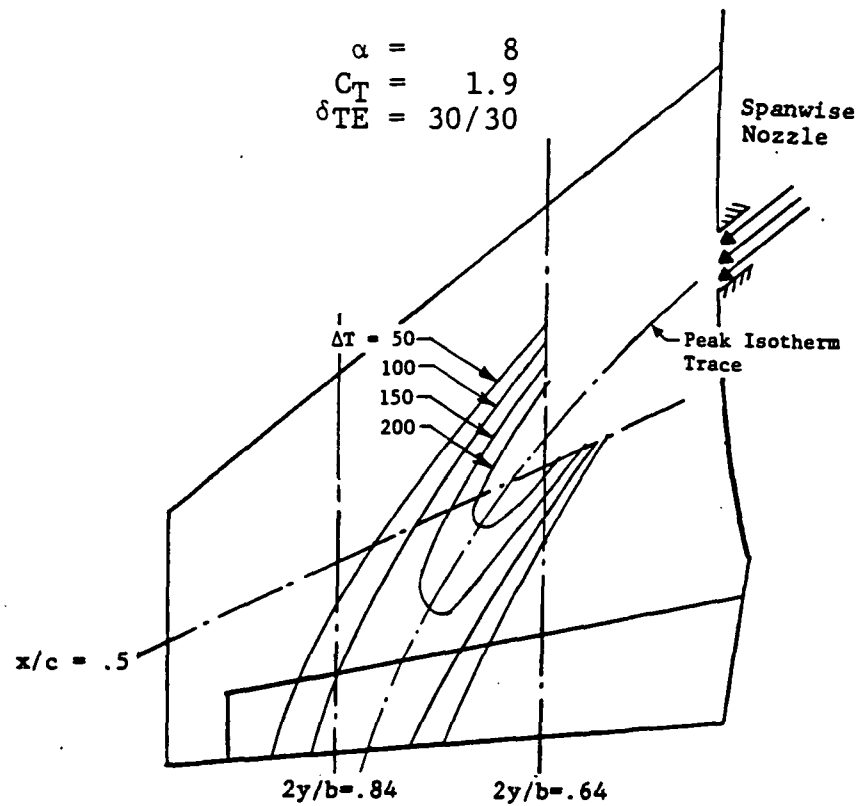


Figure 3.6-19 Comparison of Wing Isotherm and Isobar Patterns, Alpha = 8 deg

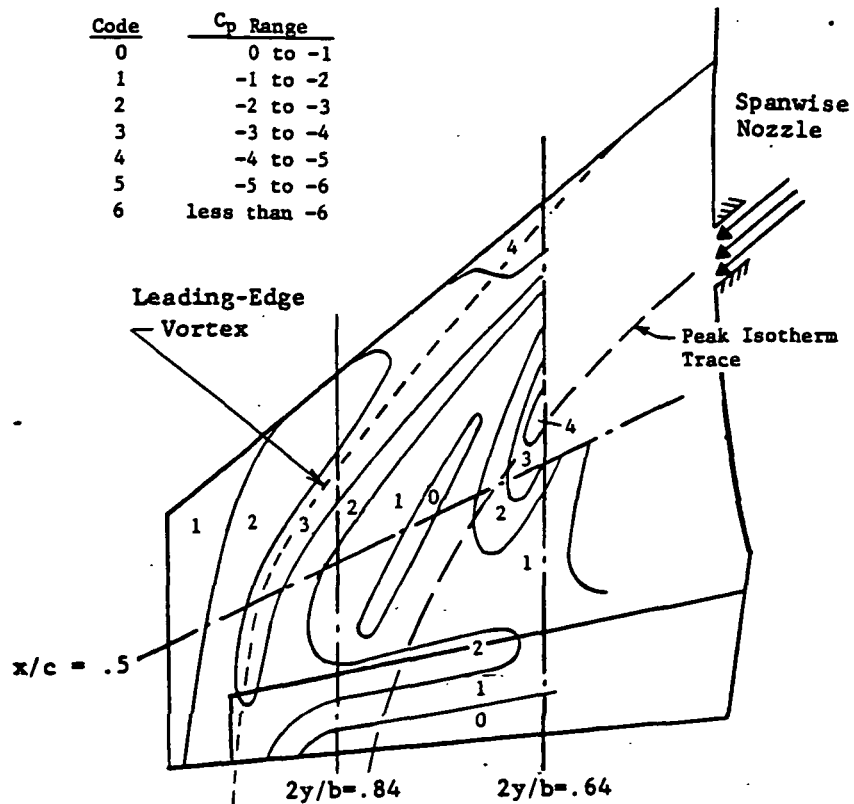
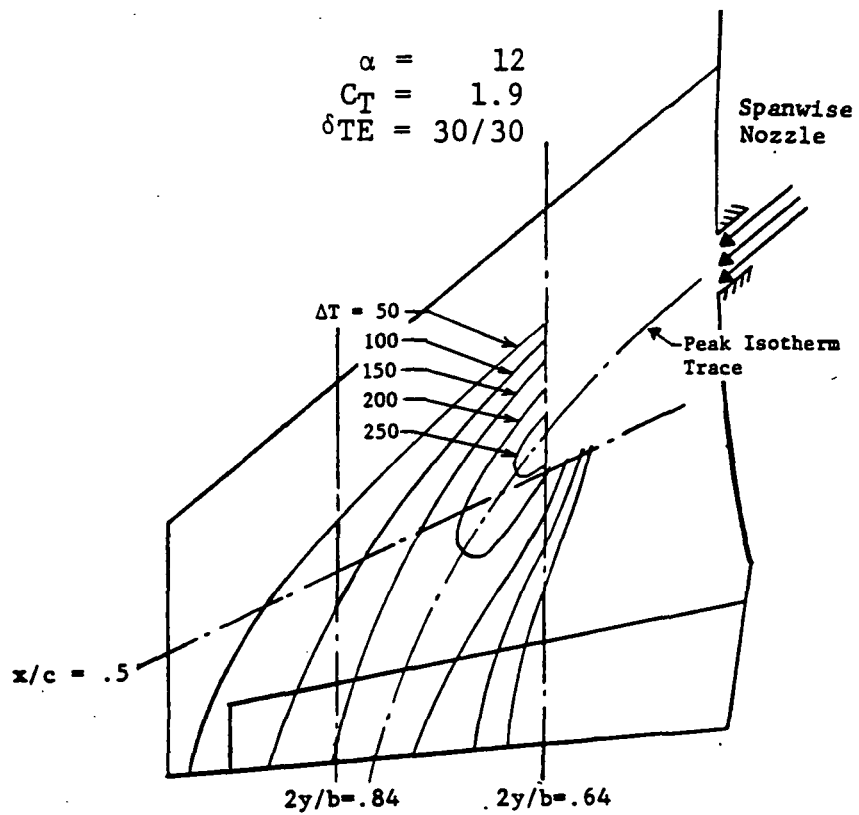


Figure 3.6-20

Comparison of Wing Isotherm and Isobar Patterns,  
Alpha = 12 deg

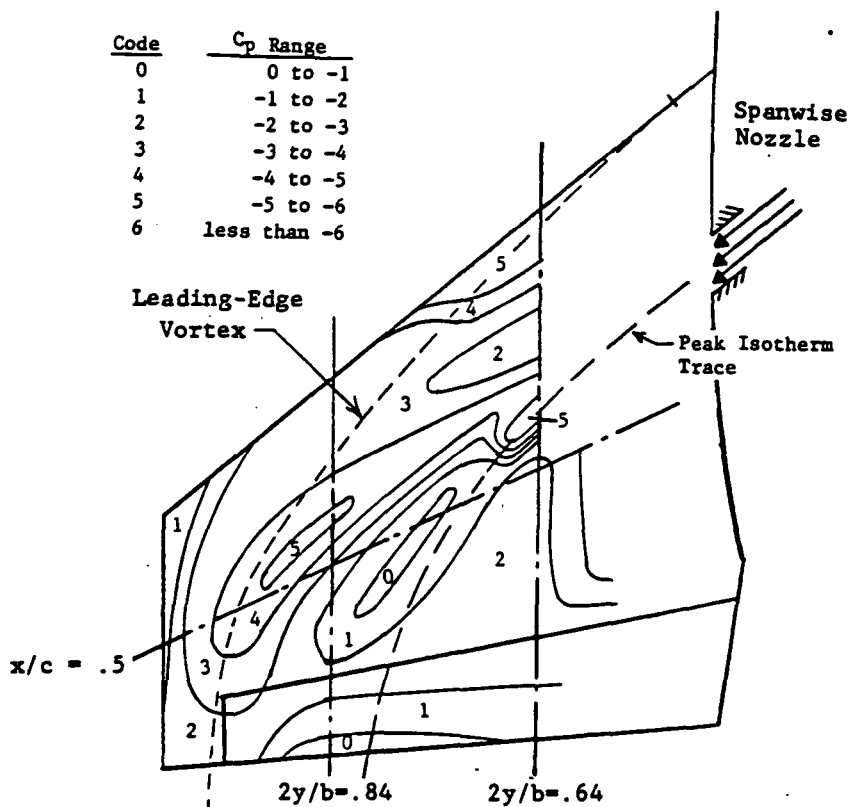
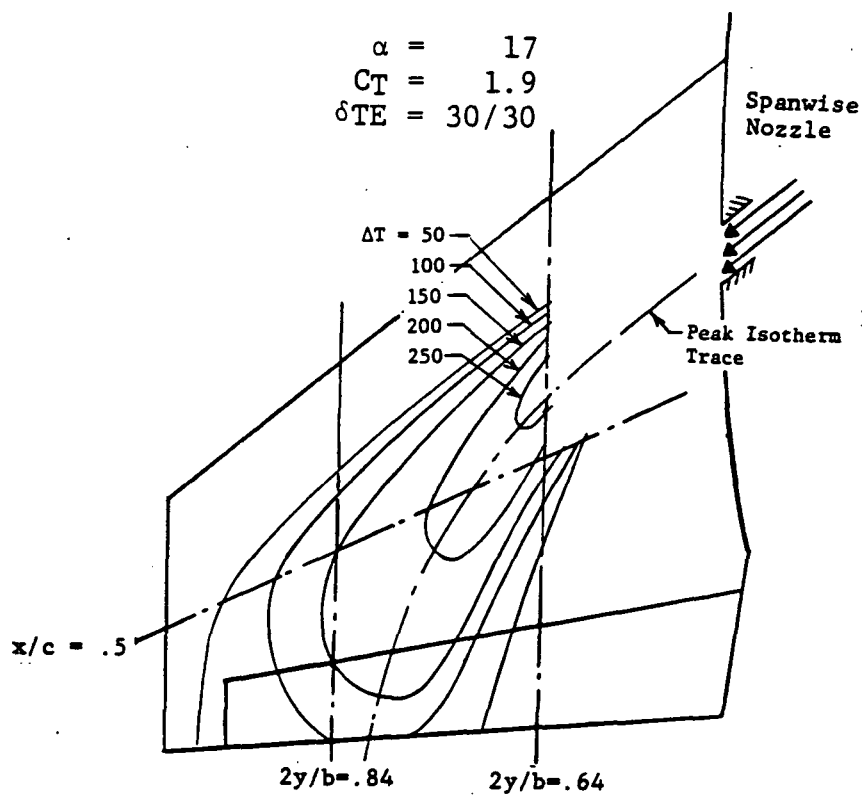


Figure 3.6-21 Comparison of Wing Isotherm and Isobar Patterns, Alpha = 17 deg

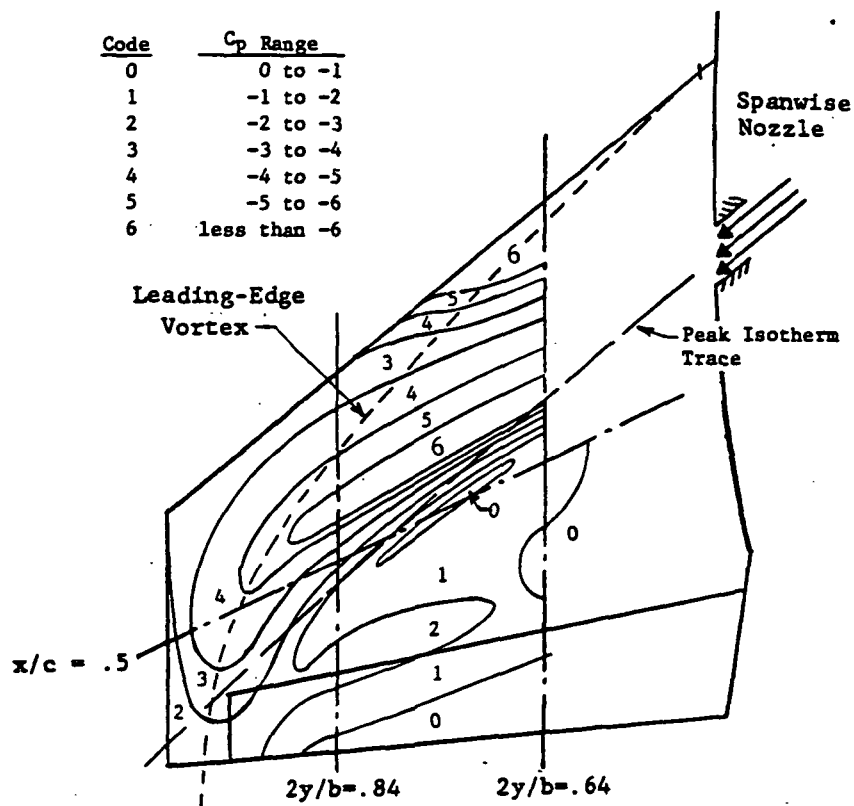
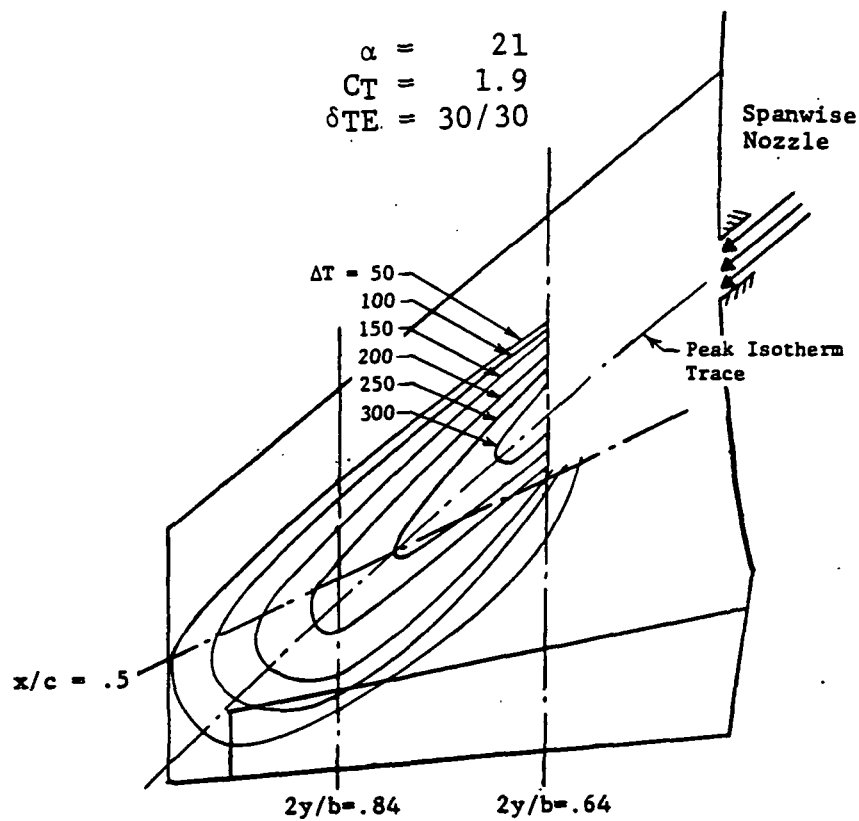


Figure 3.6-22 Comparison of Wing Isotherm and Isobar Patterns, Alpha = 21 deg



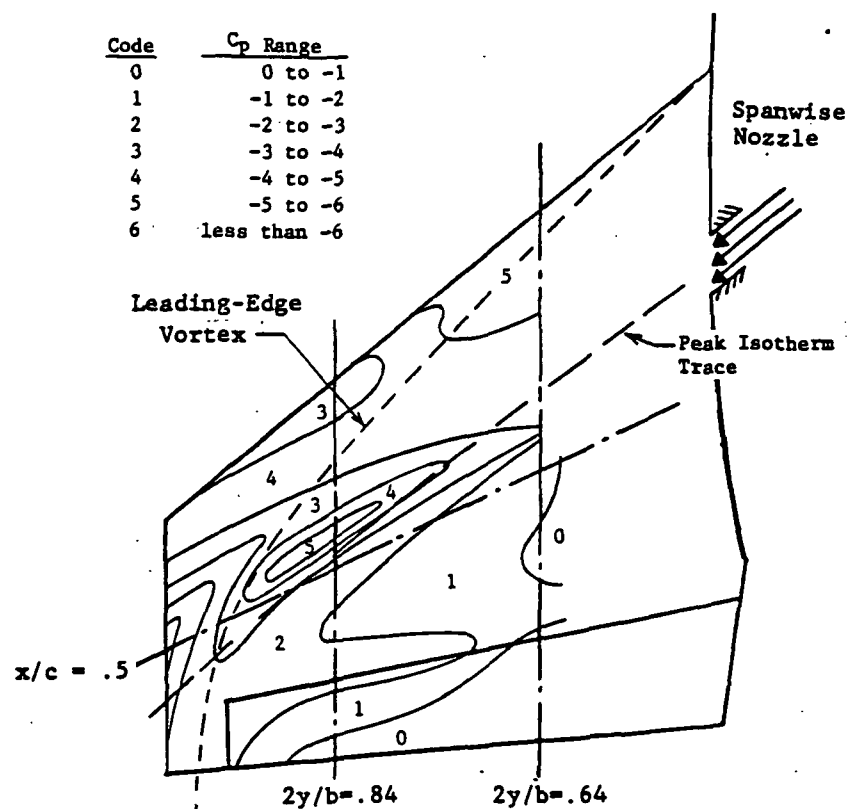
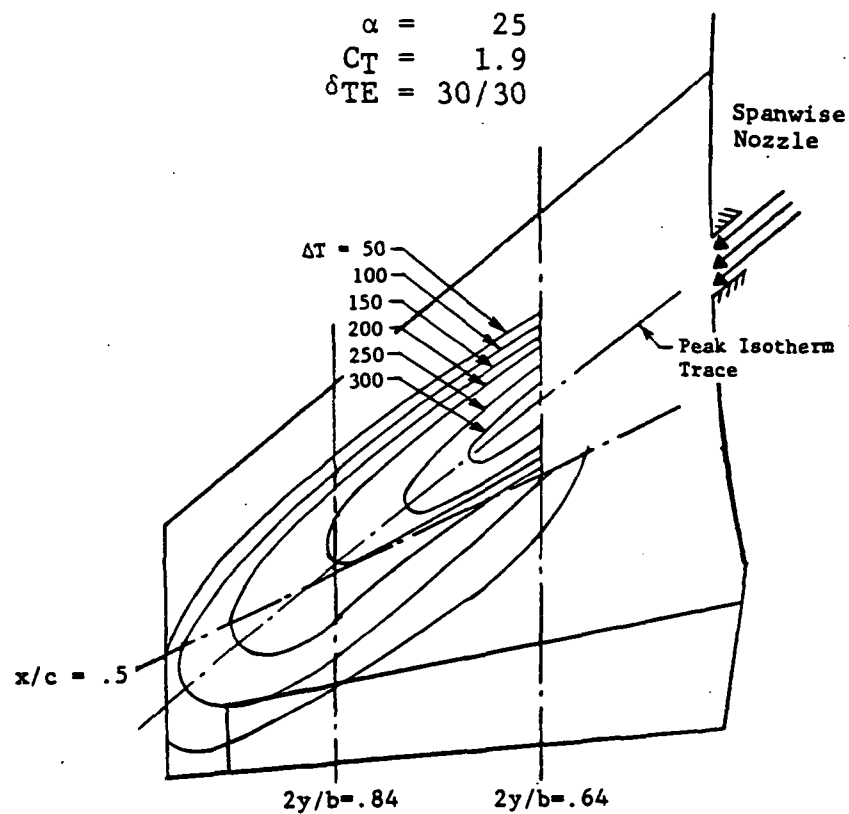
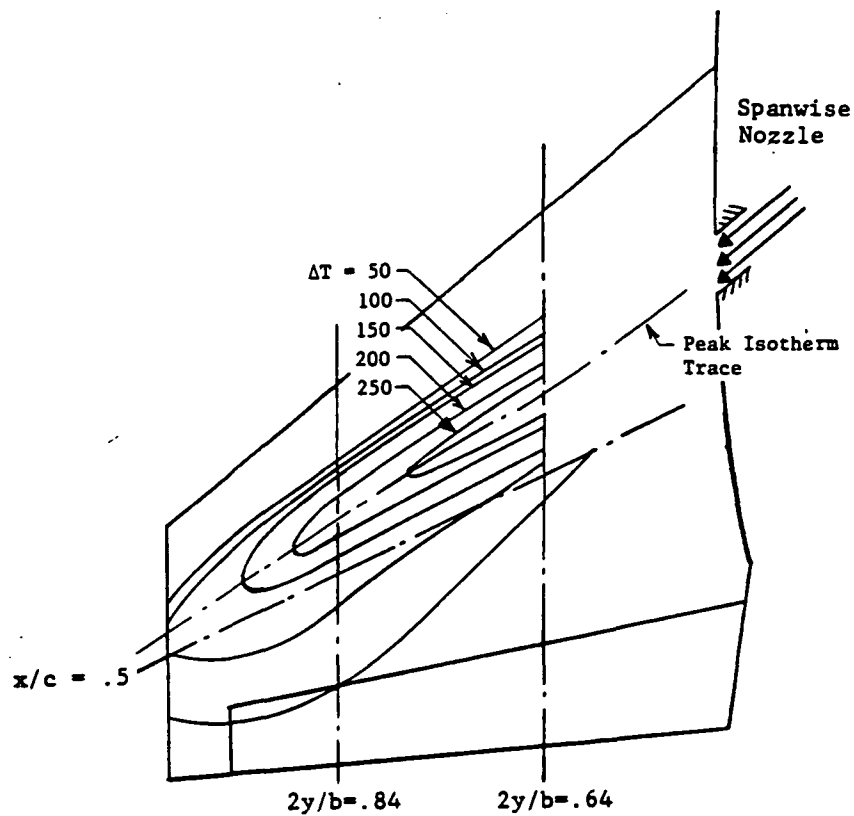


Figure 3.6-23      Comparison of Wing Isotherm and Isobar Patterns,  
 $\alpha = 25$  deg



Code	$C_p$ Range
0	0 to -1
1	-1 to -2
2	-2 to -3
3	-3 to -4
4	-4 to -5
5	-5 to -6
6	less than -6

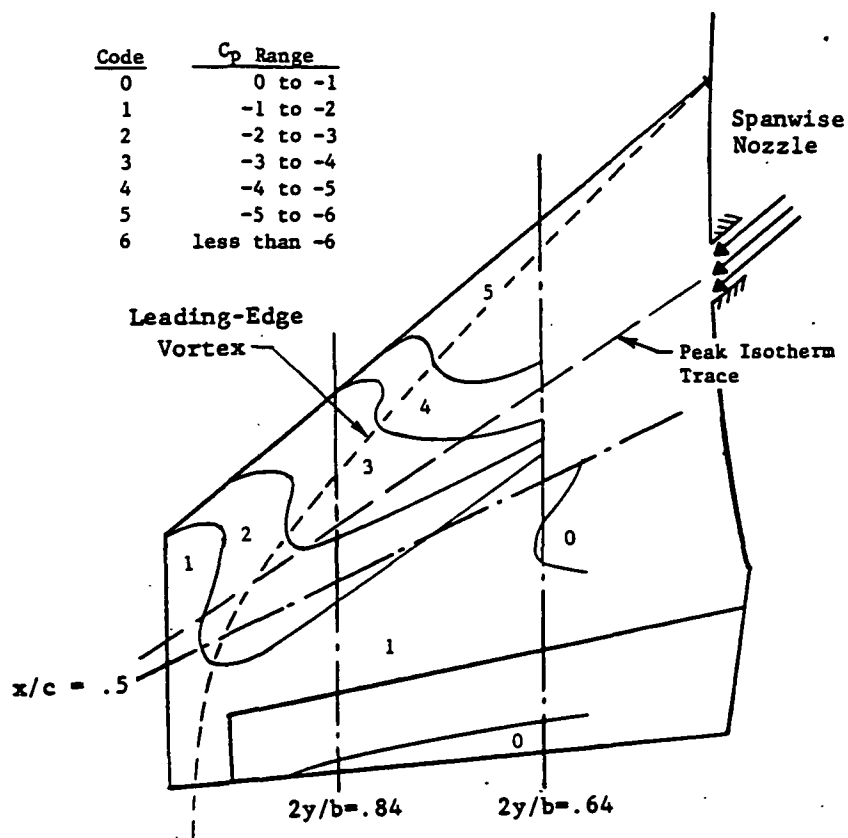


Figure 3.6-24

Comparison of Wing Isotherm and Isobar Patterns,  
 $\alpha = 29^\circ$

SYM	TEST	RUN	ALPHA	CT	ITEF	OTEF	CAN	SWB	$\delta_{BT}$
⊕	543	63	8.3	0.00	0	0	0	OFF	0
⊗	543	60	8.4	0.94	0	0	0	OFF	0
Δ	543	58	8.4	1.90	0	0	0	OFF	0

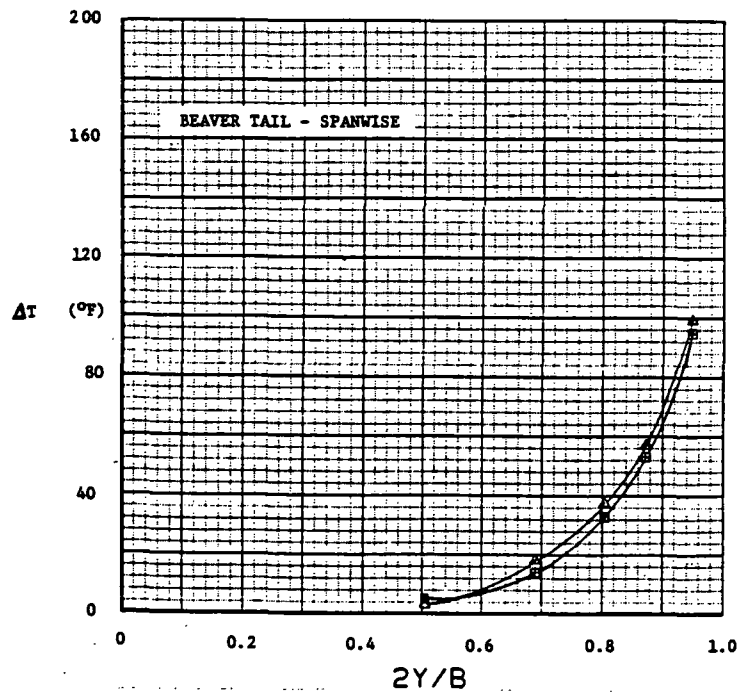
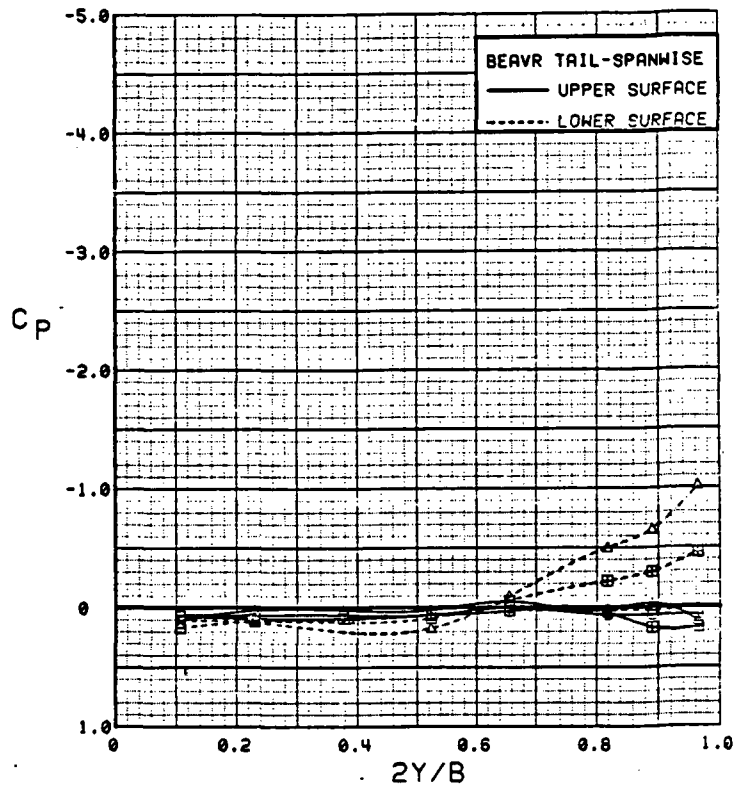


Figure 3.6-25

Power Effects on Beaver Tail Pressures and Temperatures

SYM	TEST	RUN	ALPHA	CT	ITEF	OTEF	CAN	SWB	$\delta_{BT}$
○	543	85	8.2	1.88	-20	-20	0	OFF	0
⊗	543	72	8.4	1.86	-10	0	0	OFF	0
△	543	58	8.4	1.90	0	0	0	OFF	0
◆	543	81	8.5	1.91	10	10	0	OFF	0
*	543	67	8.6	1.89	20	20	0	OFF	0
+	537	28	8.7	1.88	30	30	0	OFF	0

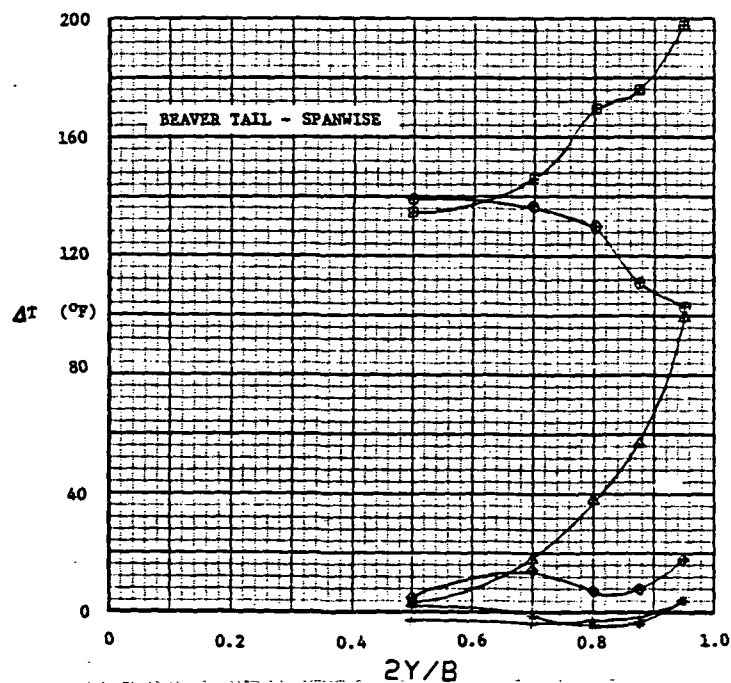
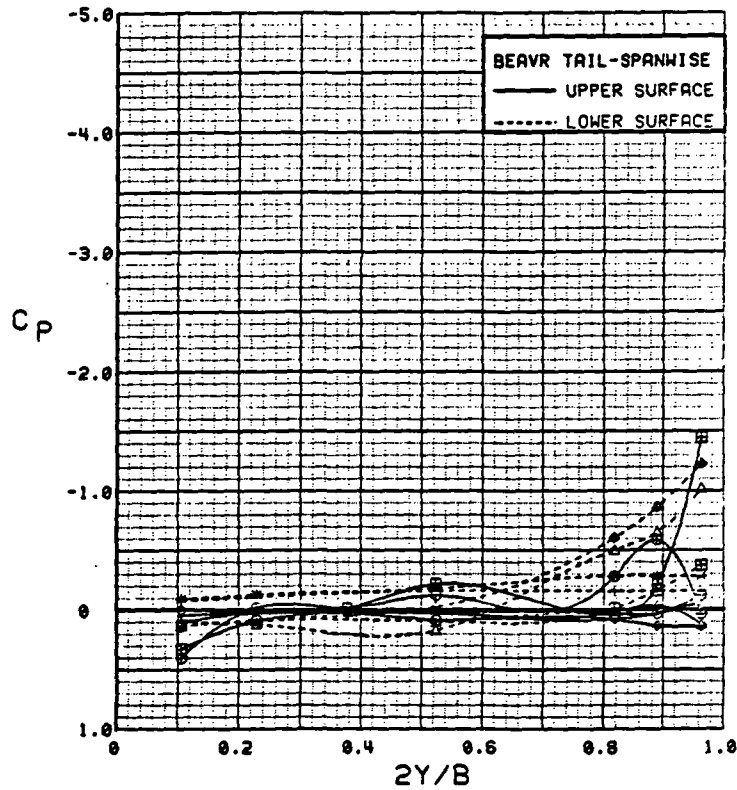


Figure 3.6-26 Wing Trailing-Edge Flap Effects on Beaver Tail Pressures and Temperatures

SYM	TEST	RUN	ALPHA	CT	ITEF	OTEF	CAN	SWB	$\delta_{BT}$
⊙	543	58	8.4	1.90	0	0	0	OFF	0
⊠	543	52	8.4	1.84	0	0	0	OFF	20
Δ	543	55	8.3	1.88	0	0	0	OFF	40

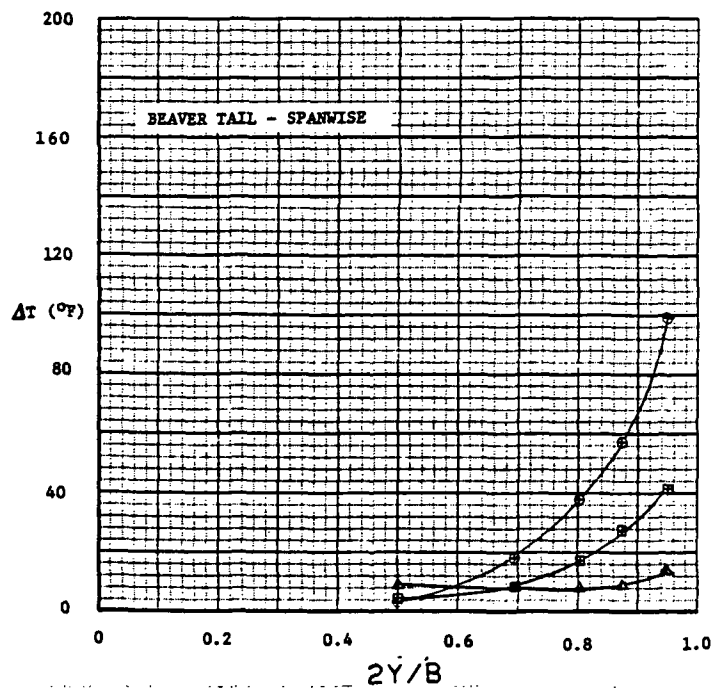
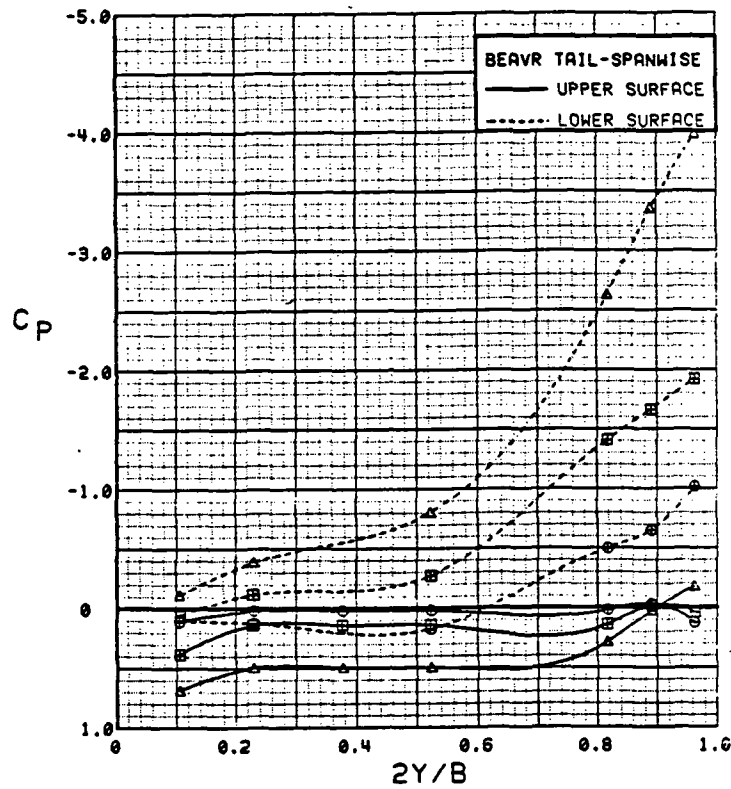


Figure 3.6-27 Beaver Tail Deflection Effects on Pressures and Temperatures

**(This page intentionally left blank.)**

## 4. ANALYTICAL EVALUATION

Integrated airframe/propulsion systems, such as those employed in the NASA/Ames STOL Fighter Model, are based on emerging technologies that need verification by test and analytical evaluation. The wind tunnel tests that were conducted on the Fighter Model have provided the data base for a thorough low-speed evaluation of this particular concept. In addition, these tests provided data that were used to evaluate the capability of two analytical methods for the estimation of the low-speed aerodynamic characteristics of powered-lift configurations. The following paragraphs present a discussion of the results obtained in analytical evaluations of the Ames Fighter Model with the Elementary Vortex Distribution Method and the General Dynamics Semi-Empirical Powered-Lift Prediction Method.

### 4.1 ELEMENTARY VORTEX DISTRIBUTION METHOD

The Elementary Vortex Distribution (EVD) Method presented in References 19 through 21 was selected to estimate the aerodynamic characteristics of the Ames Fighter Model because it contains the necessary elements for a general wing-design prediction method and the capability to handle powered-lift concepts. It was originally intended for use in the analysis of transport type configurations employing sophisticated high-lift systems at low-speeds. General Dynamics produced a modified version of this program for in-house use on transonic, high-performance aircraft by the application of scaling parameters to account for the effects of compressibility.

The EVD method employs a finite-element paneling technique to represent the wing and the jet sheet, each of which are typically divided into chordwise strips parallel to the freestream. Each strip is subdivided into rectangular panels. The vortex model uses a continuous linear vortex distribution in the chordwise direction, except for singularities at the leading edge, the flap hinge, and the trailing edge when there is a deflected jet. In the latter case, the real vortex distribution approaches infinity. The vortex model also uses a vortex distribution for the last element on the downstream end of the jet that prescribes the appropriate decay property (e.g., the vorticity intensity goes to zero as the distance behind the wing approaches infinity). The vortex model and its real counterpart for both a blown and an unblown section are illustrated in Figure 4-1, in which it is apparent that all the linear distributions are actually equivalent to a set of overlapping triangular distributions, with each of them straddling on two successive elements. In fact, the vortex model that has been adopted is now represented equivalently by a set of composite elementary vortex distributions (abbreviated as EVD's) consisting of the following four types:

- o Regular EVD: Triangular in shape and distributed over two successive elements.
- o Leading edge EVD: Distributed over the leading edge element. It is square root singular when approaching the leading edge and becomes zero at the other end of the element.
- o Hinge EVD: Consisting of two parts. One is the Regular EVD, the other is the additional hinge with its strength directly proportional to the deflection angle of the flap or the jet. It is distributed over the two elements adjacent to the flap hinge line or to the trailing edge with a deflected jet.

PRECEDING PAGE BLANK NOT FILMED

- o Infinity (Far-Jet) EVD: Distributed over the last two elements of the jet at the downstream end. The front half is linear, whereas the other half gradually decays to zero (proportional to  $x^{-2}$ ) on approaching infinity.

Several assumptions that are incorporated in the basic EVD jet-wing lifting-surface theory are summarized below:

- (1) Inviscid, incompressible, and irrotational.
- (2) No mixing between the external flow and the jet (i.e., no entrainment into the jet).
- (3) There is no spanwise component of velocity or jet momentum.
- (4) Roll up of the jet sheet and wing trailing vortex system is neglected.
- (5) The wing is assumed to be thin and is represented by a mean camber line.
- (6) All incidences on the wing-surface elements are small.
- (7) The jet sheet is thin.
- (8) The jet sheet deflection is small.

The EVD method has been verified numerous times through comparisons with model force data on powered configurations, several of which are presented in the original documentation of the method (Reference 21). Other comparisons on powered configuration, including a modified F-111 with a jet flap and the General Dynamics Vected-Engine-Over-Wing Research Model, are presented in Reference 22. These comparisons show that in most cases the method is reasonably accurate for the estimation of the overall force and moment data. Application of the EVD theory to the Ames Fighter Model was primarily to determine the capability of the method to predict the influence of the exhaust jet on wing surface pressures. This was done with full awareness that the assumption of a thin jet sheet was not satisfied by the over-wing-mounted engine exhaust of the Fighter Model.

The EVD method was originally developed for STOL transport-type configurations and can handle horizontal tail surfaces that are conventional, mid-tail, or T-tail. Flexibility does not exist, however, to analyze configurations with canards. Therefore, the only test data that were available for comparison with predictions were for the canard-off configuration. A further restriction was that canard-off data were acquired at only two trailing-edge flap deflections — 0 and 30 deg. Because of these restrictions, there were data from only two power sweeps that are directly comparable with predictions.

The EVD method was evaluated to determine its applicability as a pre-design tool for the estimation of the induced aerodynamic effects caused by the exhaust jet of the over-wing mounted engines. As a pre-design tool, its use should be relatively easy. Therefore, an all-wing representation of the model was chosen for this analysis. The paneling scheme, which is shown in Figure 4-2, consists of 22 chordwise strips. Each of these were subdivided into approximately 12 rectangular elements for a total of 260 elements to represent the configuration.

The EVD method is used to predict aerodynamic characteristics by determining the effects of certain fundamental cases and then combining these into composite cases. The fundamental cases are

- o Angles of attack
- o Twist
- o Camber
- o Dihedral
- o Jet deflection



- o Leading-edge flap deflection
- o Trailing-edge flap deflection

Once these fundamental cases were determined for unit values, composite cases were formed very easily to represent configurations at specified conditions. Since the effects of the fundamental cases were additive, a better understanding of the capability of the program was realized by an examination of these effects individually, rather than added together in a composite case. Fundamental case data for camber and twist, angle of attack, and trailing-edge flap deflection were determined with the EVD method and compared with the spanwise and chordwise pressure data on the wing to establish the method accuracy for the power-off configuration. A wing at zero angle of attack experiences a differential pressure distribution only because of the camber and twist. A test-to-theory comparison of the loading caused by camber and twist, only, is shown in Figure 4-3 for the three locations where wing pressure taps were installed on the model. The model spanwise taps on the wing were installed only on the upper surface, therefore, it should be noted that the spanwise distribution determined from the data includes only the effects on the upper surface, whereas the theoretical estimate includes differential upper and lower surface pressure effects. Since a mean camber line is used to represent the wing surface in the theoretical method, it was not possible to separate upper-surface from lower-surface effects. As a result of the differences between the manner in which the pressure loading is defined for data and theory, the spanwise plot must be viewed only as an indication of the relative trends. Chordwise plots in Figure 4-3 show that the loading caused by camber and twist are almost the same except near the leading edge. Outboard leading-edge pressure-loading differences are smaller than those inboard. These differences may be caused by an upwash, generated by the fuselage and nacelle, that is not predicted on the all-wing representation used in the EVD method.

Figure 4-4 shows the effects of increasing the angle of attack from 0 to 8 deg in data plots that are the same type as were discussed in the previous figure. The EVD method is linear with angle of attack and is appropriately compared to wind-tunnel data in the low angle of attack range that has near-linear aerodynamic characteristics. The 4-deg angle-of-attack data point was not available; therefore, it was necessary to obtain the effect of angle of attack between runs of 0 and 8 deg. This range of angle of attack is generally considered to be linear in overall force and moment coefficients. However, the leading-edge vortex that was described in Subsection 3.2.1 was evident at the inboard span station and was the cause of the large difference between the wind tunnel data and the EVD method prediction. The prediction method is a potential flow solution and does not have the capability to model separated flow, such as that which occurs when a vortex forms. Therefore, discrepancies of this type are explainable but cannot be overcome with the EVD Method.

Chordwise and spanwise pressure loading effects caused by a 30-deg deflection of the trailing-edge flaps are shown in Figure 4-5. This flap deflection is outside the range of potential-flow theory and was used only because data were not acquired at lower flap settings with the canard off. The EVD theory overpredicted the magnitude of the pressure spike at the point where the flow tried to negotiate the sharp turn at the flap hinge. Application of the EVD method to a more moderate deflection of 10 deg or less would be more appropriate. Wind tunnel data with the canard off were only acquired with trailing-edge flap deflections of 0 and 30 deg. The comparison shown in Figure 4-5 was made with full expectations of obtaining a false pressure spike in the prediction. Except in the region of the hinge, the EVD method shows a pressure loading similar to the data but slightly greater in magnitude. The trailing-edge-flap deflection increased the circulation about the entire wing and, consequently, increased the local angle of attack at the wing

leading edge. The EVD method was used to estimate this effect quite accurately, as evidenced by the comparison of the sharp increase in pressure loading at the wing leading edge. The spanwise plot shows a large overprediction of the mid-chord loading caused by the trailing-edge flap. Again, it is mentioned that the theoretical prediction includes differential upper- and lower-surface effects, whereas the spanwise data are only for the upper surface. Lower surface pressures at mid-chord are increased by trailing-edge flap deflections, as previously shown by the data in Figure 3.2.2-8 through -15. An adjustment to account for the change in the lower surface pressure would increase the loading indicated by the tunnel data and bring it closer to the predicted level.

The primary objective of the analysis of the Ames Fighter Model with the Elementary Vortex Distribution Method was to determine the capability of the method, to predict the effects of the exhaust jet on the wing pressure distribution. The results are shown in Figures 4-6 through 4-11, where the incremental pressure changes caused by power are shown for each of the locations where pressure data were acquired during the tests. As previously discussed in Subsection 3.2.2.1, the changes in dynamic pressure that were made in the tunnel operating conditions to vary the thrust coefficient ( $C_T$ ) also caused changes in the wing pressure distribution. Therefore, the only valid comparisons that could be made between runs with different power settings were at  $C_T = 0$  and  $C_T = 1.5$  since both runs were acquired at the same dynamic pressure condition. These were, in fact, the power settings that were used in the following discussion on the effects of power. Figure 4-6 shows the pressure loading at the inboard span station (64% semi-span) with trailing-edge-flap neutral. Predictions are shown for angles of attack of 0, 4, 8, and 12 deg. Comparative tunnel data are shown except at 4 deg where the data were not available. These plots show that the predictions for power effects on the chordwise pressure distributions were essentially invariant with angle of attack; whereas, the data indicate significantly different effects caused by power at the various angles of attack. Similar data for the outboard row of pressure taps (84% semi-span) are shown in Figure 4-7, and the spanwise comparisons at the 50% chordwise location are shown in Figure 4-8. All of these data show that the effect of the exhaust jet is relatively small when the trailing-edge flap is not deflected. Pressure data for the inboard, outboard, and spanwise locations (Figures 4-9 through 4-11) show that the power effects increase significantly when the trailing-edge flap is deflected to 30 deg. Chordwise plots in Figures 4-9 and 4-10 show little correlation between the actual and predicted incremental pressures caused by power. Even though the shapes do not match, the areas beneath the actual and predicted curves are roughly the same, indicating approximately the same sectional lift increment from the power effects. The incremental spanwise pressure load is shown in Figure 4-11 for the trailing-edge flaps deflected 30 deg. For this location, the results from EVD method were used to predict approximately the same load as that indicated by the data. Again, it is mentioned that the data curve represents only the change in upper surface pressures; whereas, the prediction is based on both upper and lower surfaces.

In summary, the EVD method has been evaluated as a means of estimating the power-off wing pressures and the effects of the exhaust jet on the Ames Fighter Model. Results show that the power-off estimates for the effects of camber, twist, and angle of attack match the wind tunnel data reasonably well. Effects of trailing-edge-flap deflection could only be correlated for a 30-deg deflection, which is somewhat beyond the range of a potential flow theory. Nevertheless, the trends appear to be correct except in the region of the trailing-edge-flap hingeline where the theory overpredicts the pressure spikes. It is believed that the procedure would provide accurate estimates for small deflections. The effects of power were strongly influenced during the tests by regions of non-attached flow (not handled by the potential flow theory) that caused large fluctuations in the shape of the incremental pressure distribution. Even though the shape is not accurately predicted, the overall-section normal forces obtained by pressure integrations

are reasonably well estimated by the method. The EVD method has an application as an easy-to-use, pre-design tool for estimating the power-induced wing loading for configurations with over-wing-mounted engines. As with most analytical methods, the user must use some judgment in applying the results of the theory, especially when the study model is expected to have areas of separated flow.

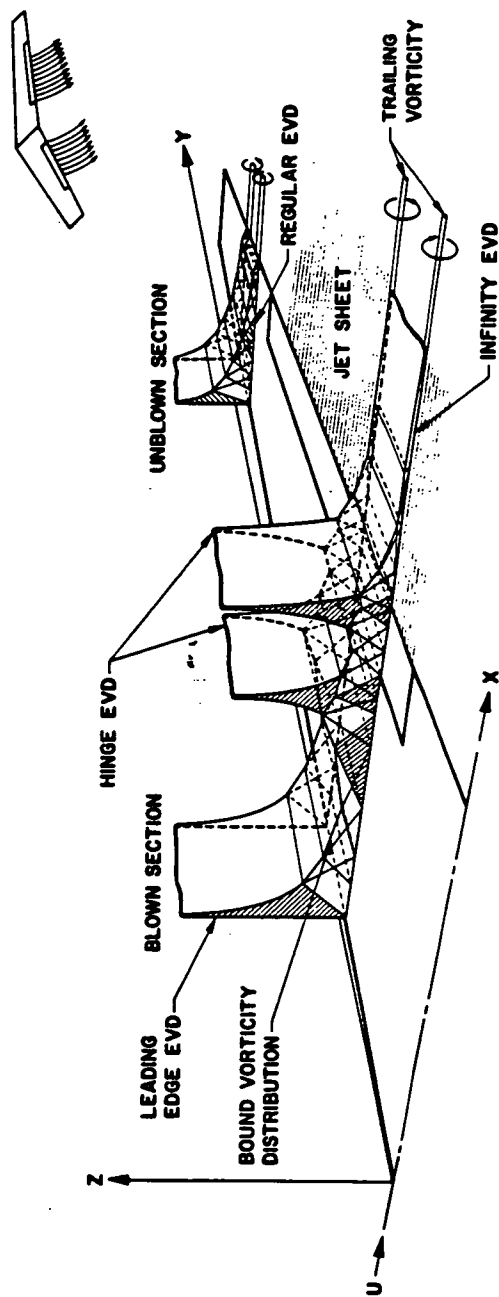


Figure 4-1 Illustration of the EVD Jet-Wing Method

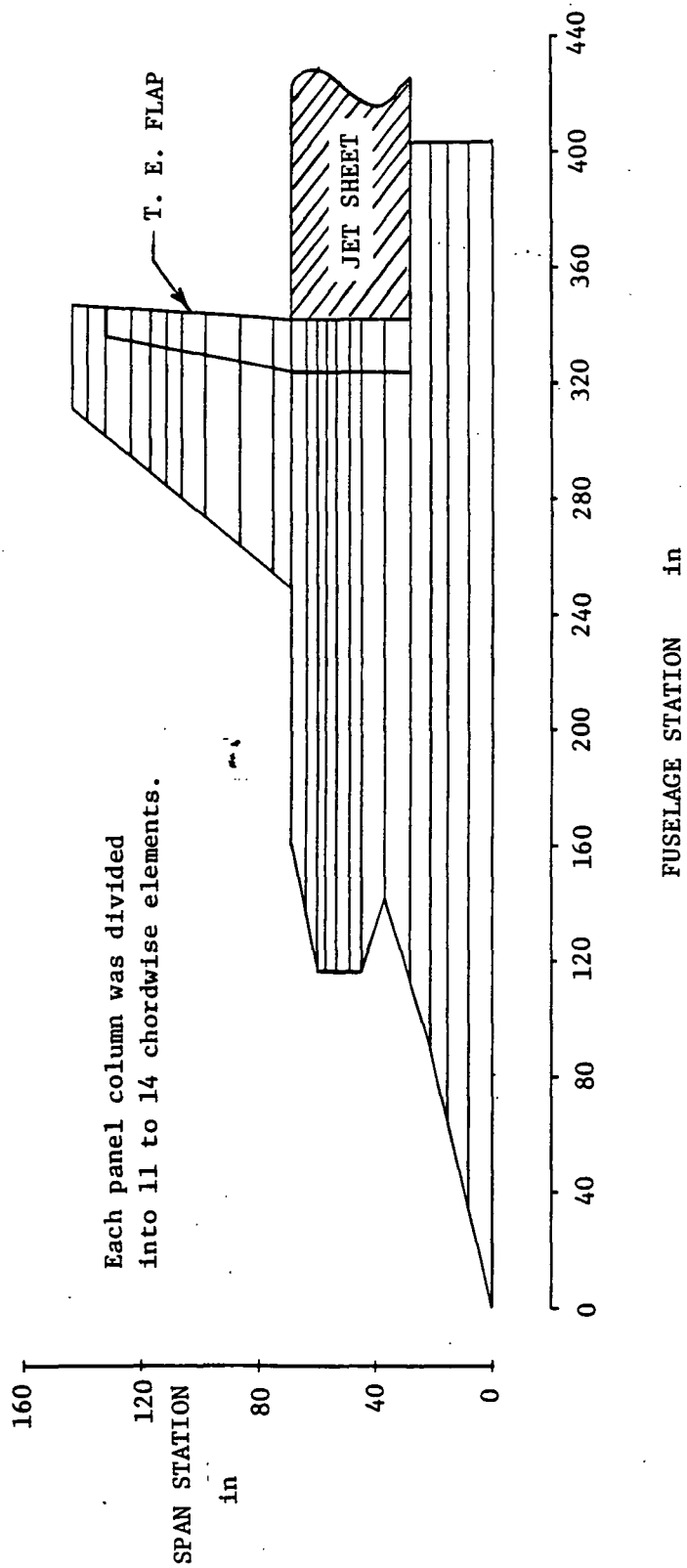


Figure 4-2 Paneling Scheme for STOL Fighter Model

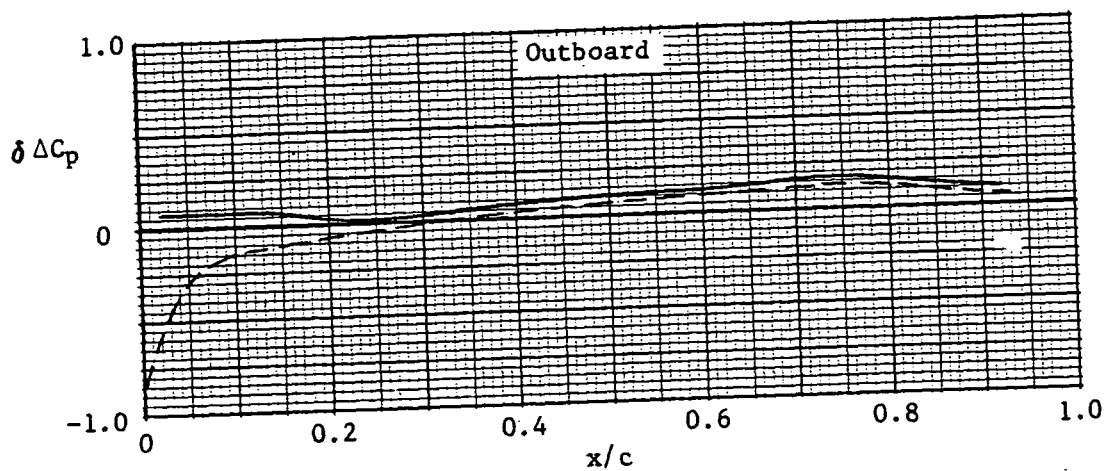
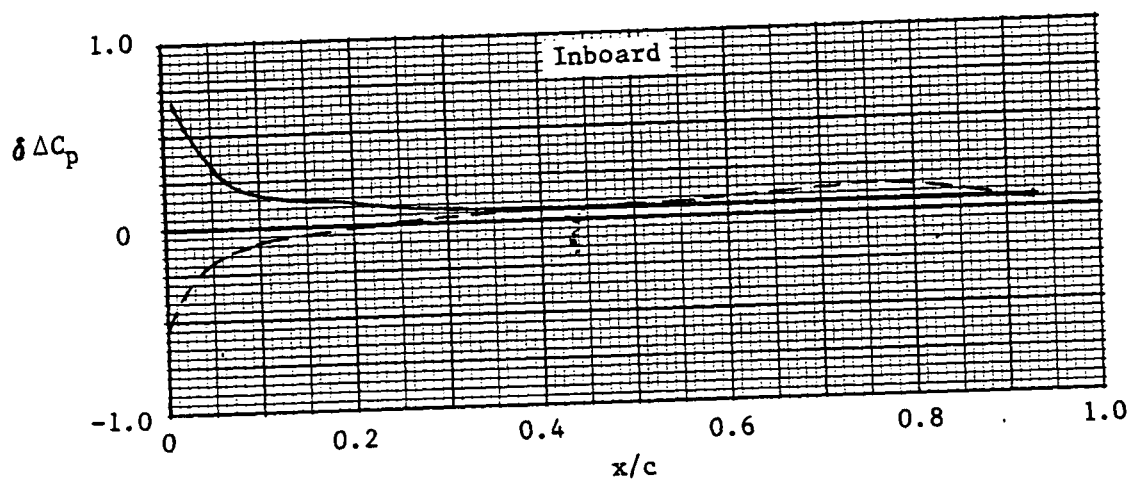
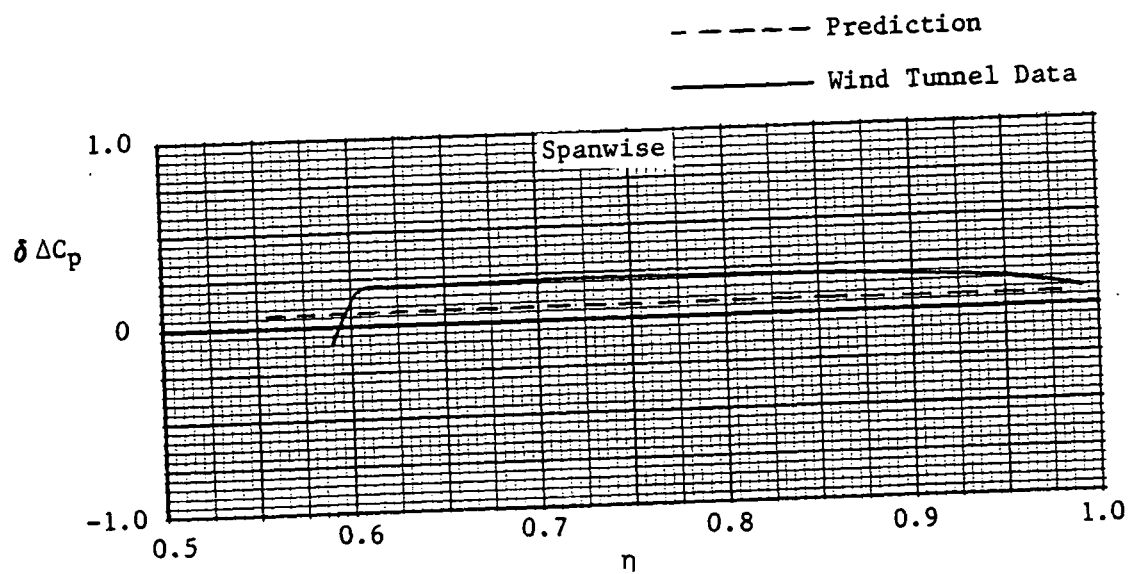
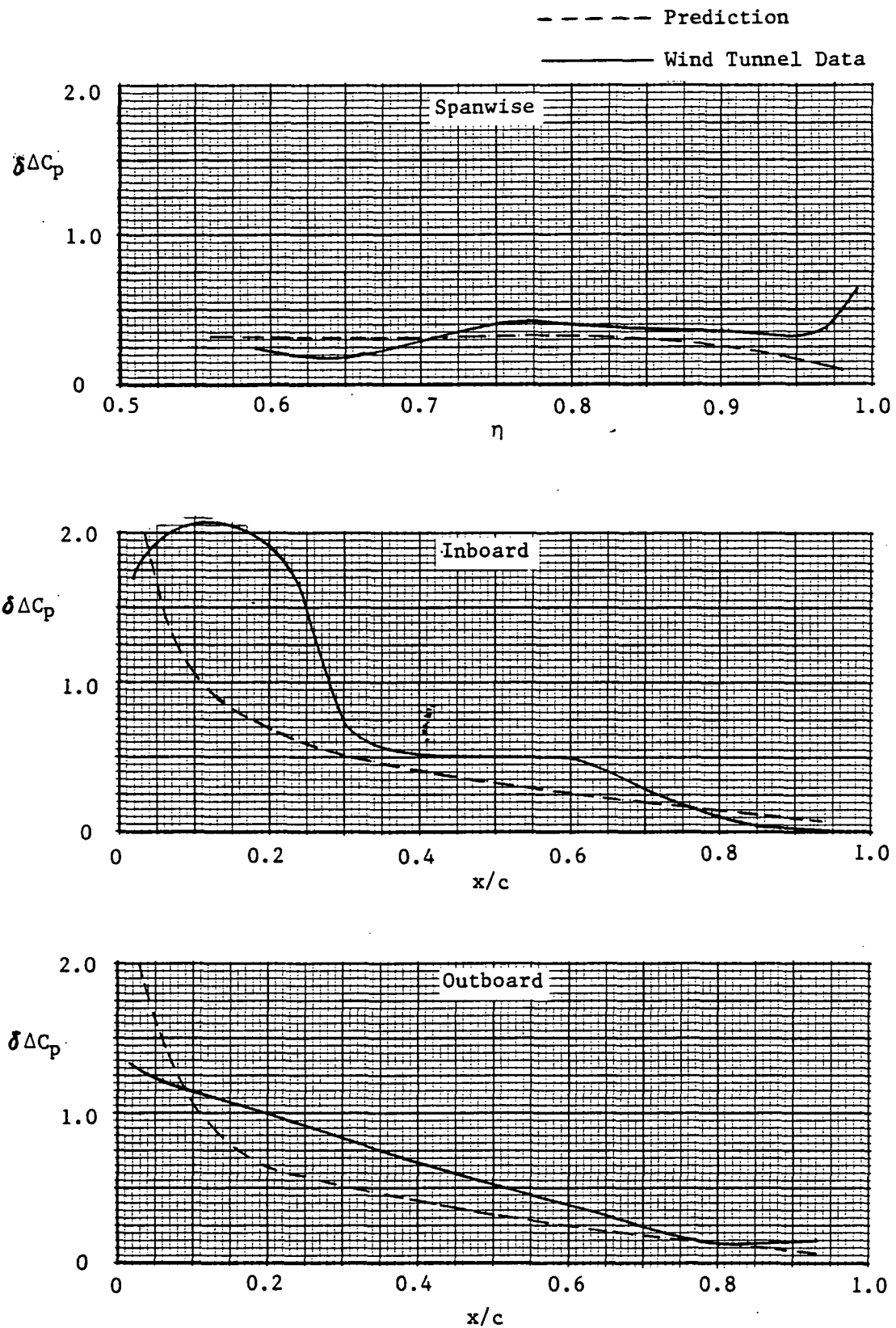


Figure 4-3

Comparisons of Data and EVD Method Predictions For  
Camber and Twist



**Figure 4-4** Comparisons of Data and EVD Method Predictions For 8 deg Angle of Attack

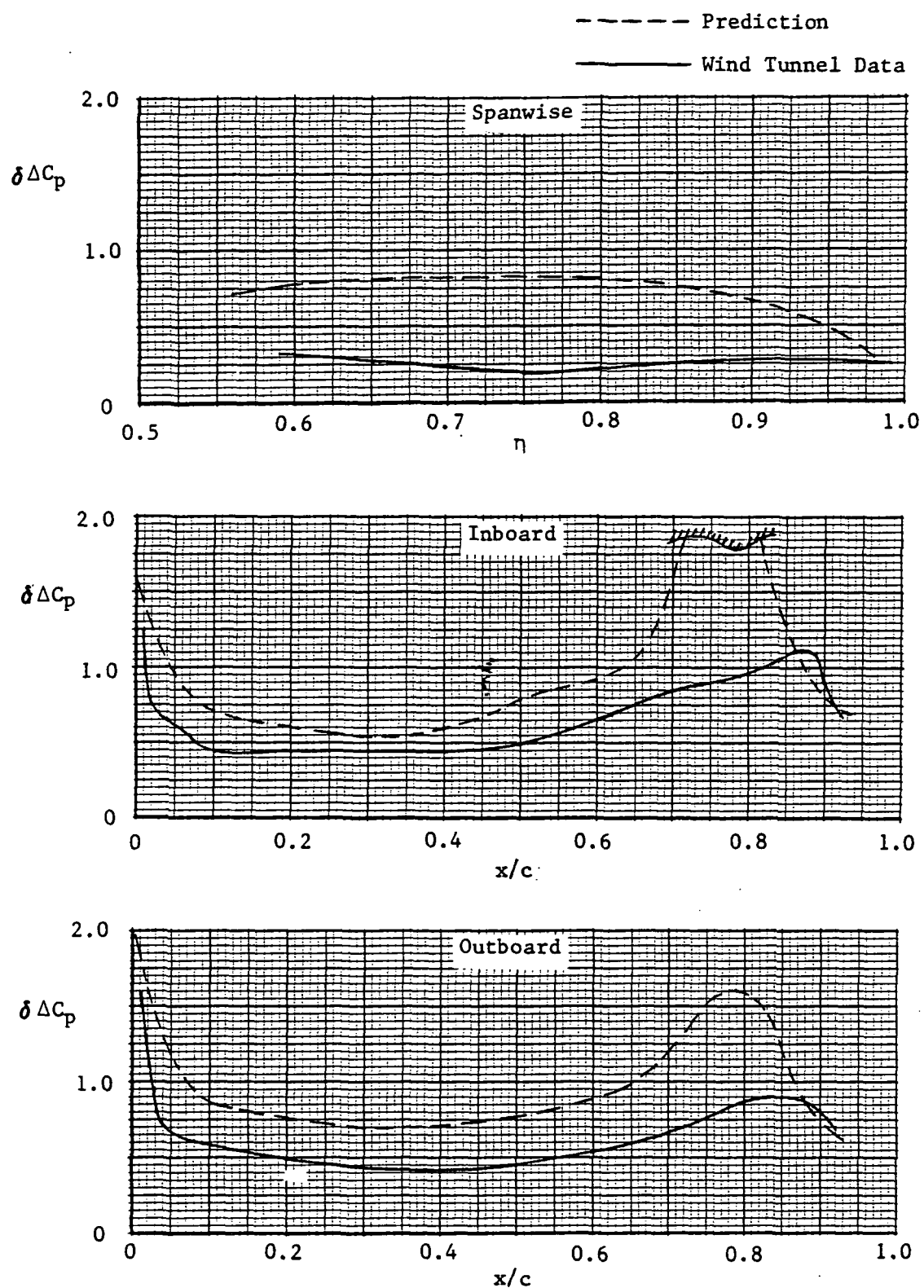


Figure 4-5

Comparisons of Data and EVD Method Predictions For  
30 deg Trailing-Edge Flap Deflection



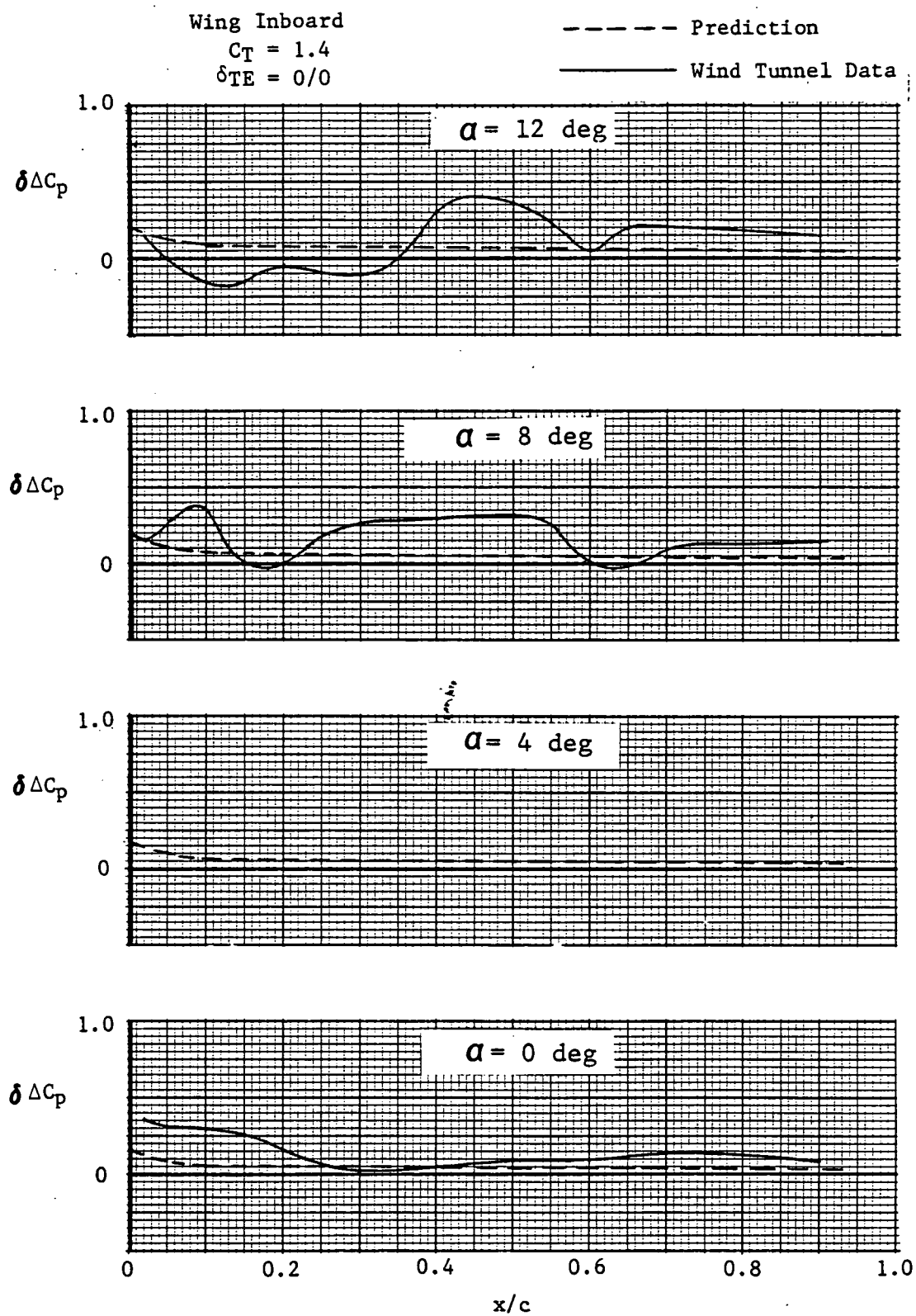


Figure 4-6

Comparisons of Data and EVD Method Predictions For  
 Power Effects, Wing Inboard, Flaps Neutral

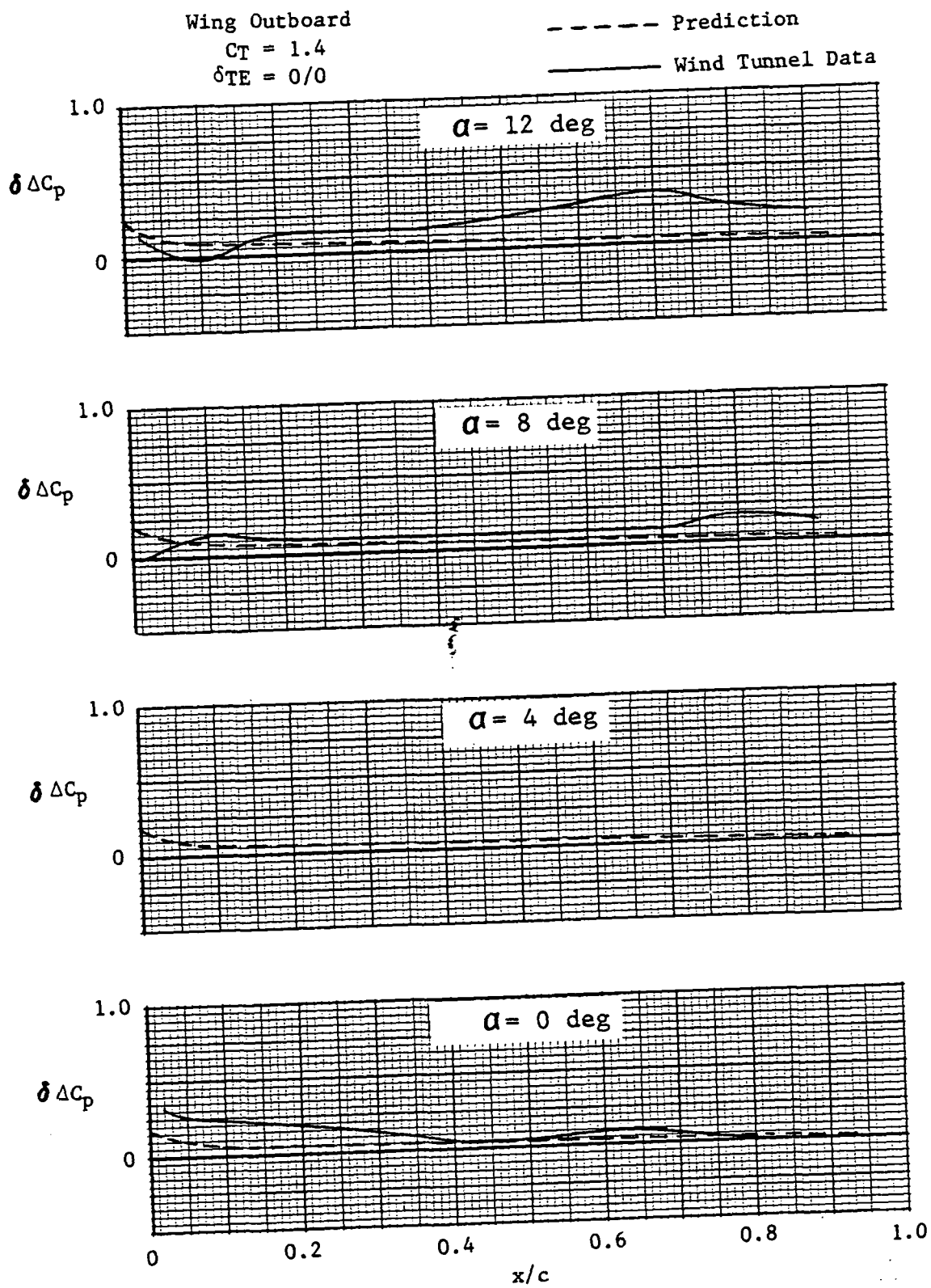


Figure 4-7

Comparisons of Data and EVD Method Predictions For  
 Power Effects, Wing Outboard, Flaps Neutral

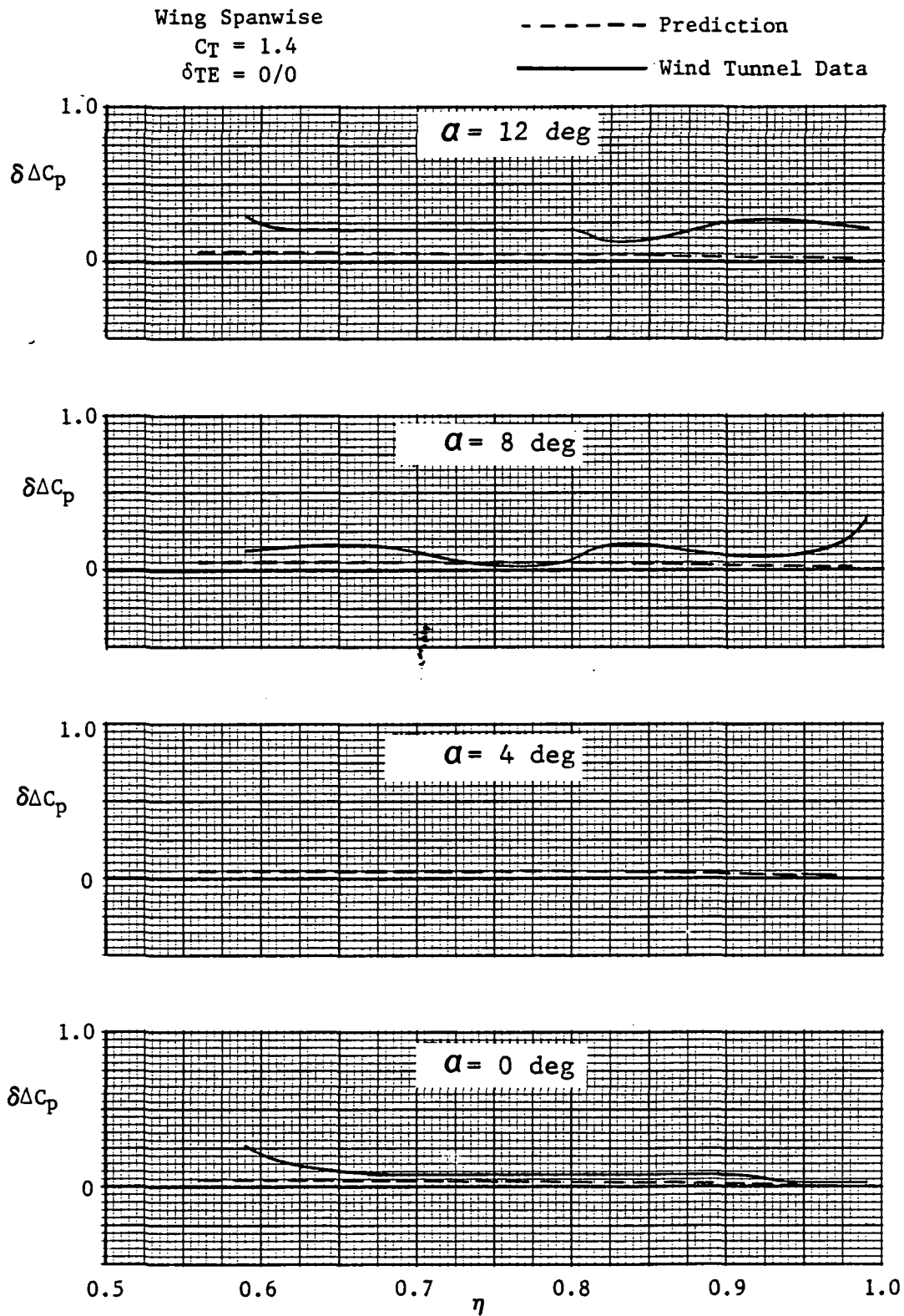


Figure 4-8

Comparisons of Data and EVD Method Predictions For  
 Power Effects, Wing Spanwise, Flaps Neutral

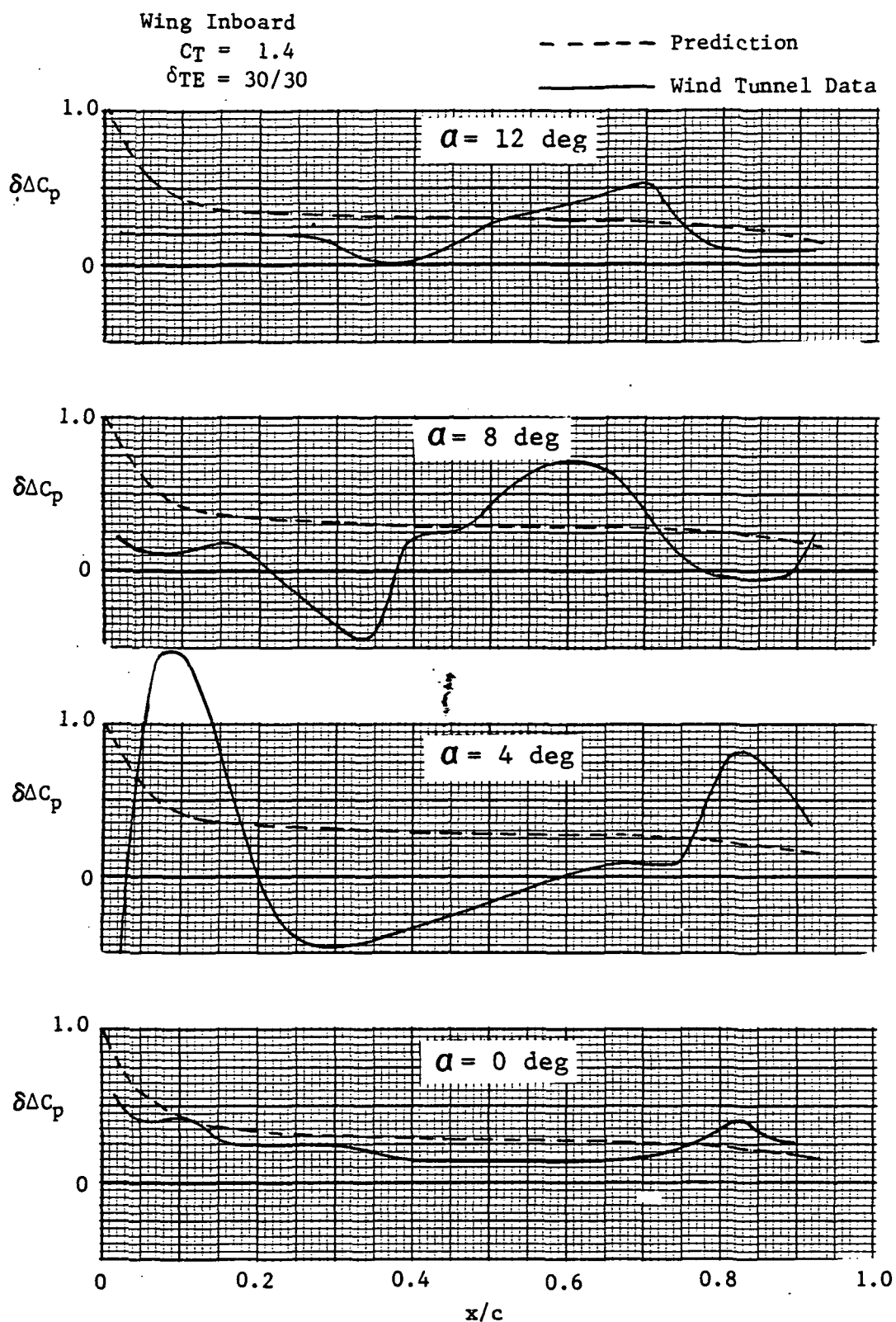


Figure 4-9

Comparisons of Data and EVD Method Predictions For  
 Power Effects, Wing Inboard, Flaps Deflected

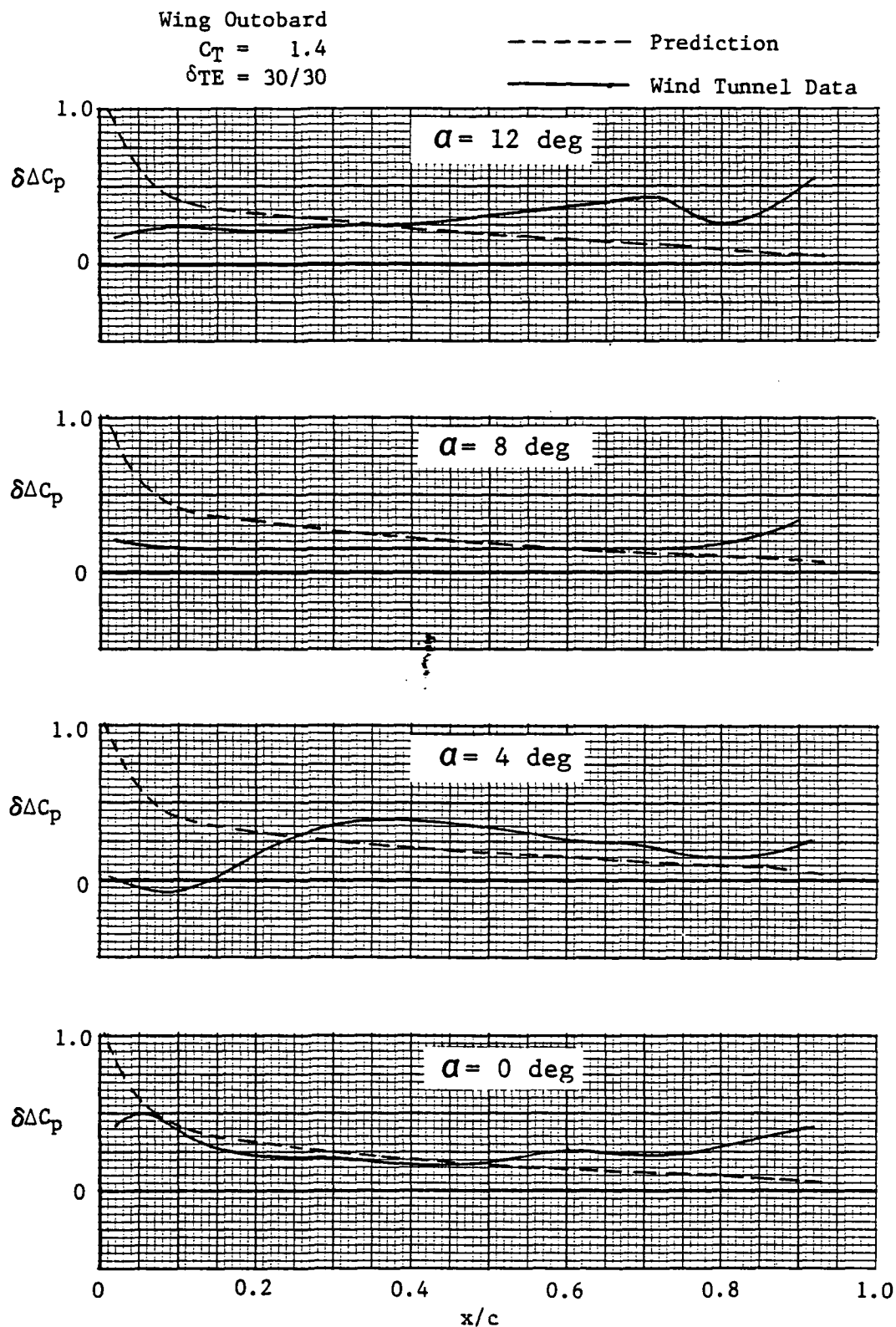


Figure 4-10

Comparisons of Data and EVD Method Predictions For  
 Power Effects, Wing Outboard, Flaps Deflected

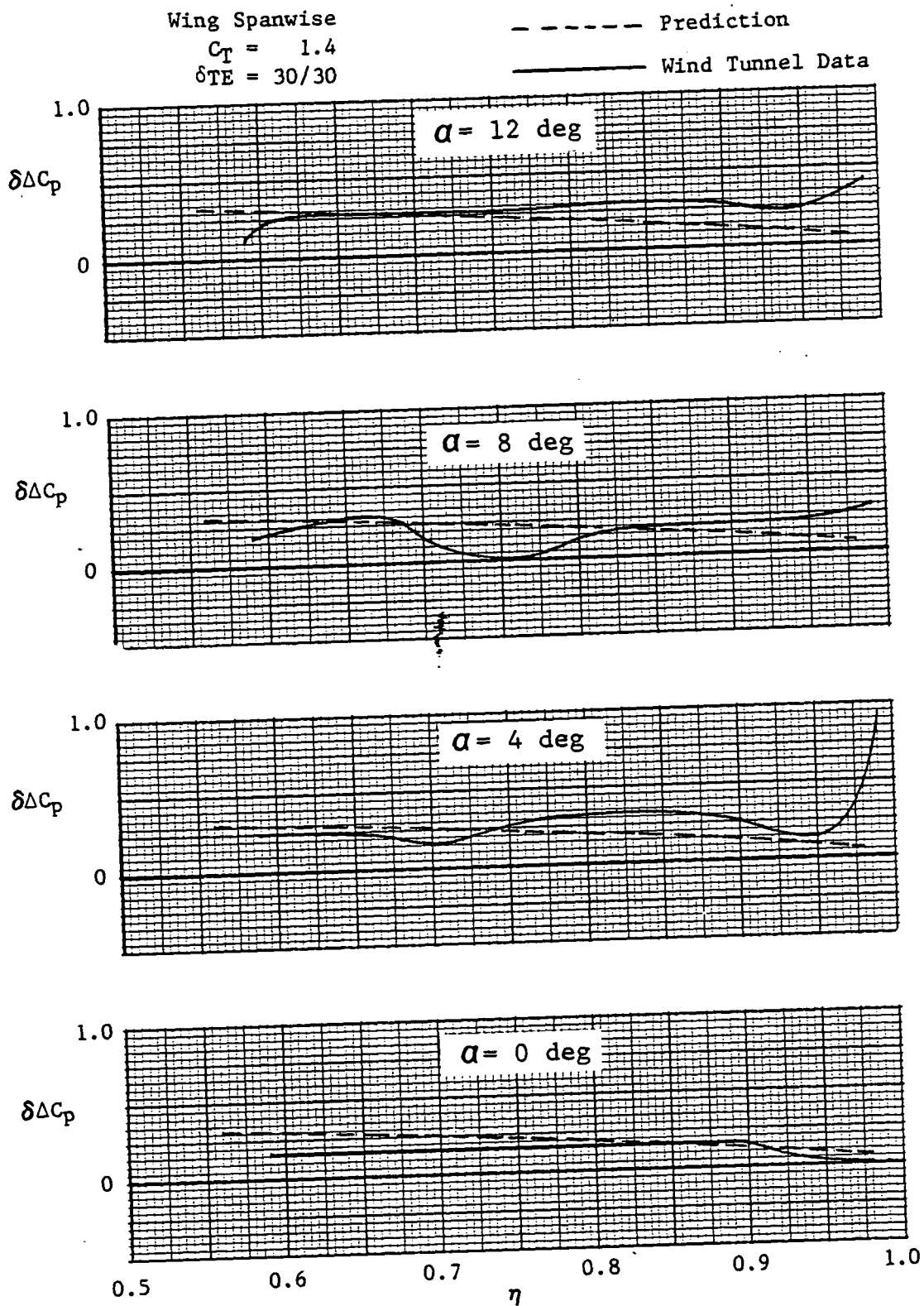


Figure 4-11

Comparisons of Data and EVD Method Predictions For  
 Power Effects, Wing Spanwise, Flaps Deflected

## 4.2 SEMI-EMPIRICAL POWERED-LIFT PREDICTION METHOD

The General Dynamics Powered-Lift Prediction Method was used to estimate the effects of power on the total force and moment coefficients. This method (Reference 23) was developed and programmed into a computer code under Air Force sponsorship and is available at General Dynamics and at the Air Force Flight Dynamics Lab. Power-off force and moment characteristics and descriptors for the geometry and propulsion system are required input. The method calculates thrust-included lift, drag, and pitching moment coefficients for different types of powered-lift aircraft. A very useful aspect of the program is the diagnostic information, e.g., lift augmentation, thrust recovery, downwash, and upwash, that can be used to help optimize a configuration. This method is applicable to high-performance fighters at conditions ranging from STOL to transonic maneuvers. The semi-empirical methods in this procedure are based on the two-dimensional jet-flap theories of Spence (Reference 24) and Erickson (Reference 25) correlated to various classes of powered-lift concepts (jet-flaps, externally blown flaps, and upper-surface blowing).

Predictions made with this method were compared with force data acquired on the STOL Fighter Model during Test 543. These comparisons were made for the baseline configuration (canards on, SWB off) with trailing-edge flap deflections of 0 and 30 deg. There was one anomaly in the data that required special consideration in order to make these comparisons possible. The force data from the static test stand did not match the force data that were obtained in the tunnel with the tunnel air flow off and the engines operating at an engine nozzle pressure ratio (EPR) of 2.1. When the flaps were deflected 30 deg and this EPR was maintained, the forces measured in the tunnel exceeded those measured on the static test stand by approximately 320 lb in axial force ( $\Delta A$ ) and 130 lb in normal force ( $\Delta N$ ). For the in-tunnel runs, the engines induced a small flow ( $q \approx 1$ ) in the closed circuit of the tunnel, which caused a low level of aerodynamic forces on the model. These forces, which are small in comparison to the mismatches, were estimated and were used to adjust the in-tunnel force data so that the values quoted above for  $\Delta A$  and  $\Delta N$  are representative of a zero-flow condition. The severity of the mismatches, which were embedded in the thrust-removed data, were determined by computing their impact on lift and drag. The incremental lift and drag coefficients that result from  $\Delta N$  and  $\Delta A$  were determined from the following equations.

$$\begin{aligned}\Delta C_L &= (\Delta N \cos \alpha - \Delta A \sin \alpha) + qS \\ \Delta C_D &= (\Delta A \cos \alpha + \Delta N \sin \alpha) + qS\end{aligned}$$

The resulting increments in lift and drag coefficients at a low angle of attack and at a moderate angle of attack are:

$\alpha$	$\Delta C_L$	$\Delta C_D$
0	.062	.153
12	.029	.163

It should be noted that the negative sign in the lift equation causes the axial and normal force errors to partially cancel. On the other hand, the positive sign in the drag equation causes the errors to be additive. These computations show that the error in the lift coefficient diminishes as angle of attack is increased and becomes small in relationship to the power-on lift coefficient. For instance,  $C_L \approx 2.0$  is obtained at  $\alpha = 12$  deg, even with the flaps in the neutral position. The error in the drag coefficient is quite large and

fairly constant with angle of attack, which causes an unacceptable error in the thrust-included minimum drag. The impact on the polar shape, however, is shown to be fairly small since the drag error is almost the same at both angles of attack. This discussion of the effects of the normal and axial force errors is presented to verify that, with the exception of minimum drag, the force data are acceptable for comparison with the Powered-Lift Prediction Method. Errors that are present have little or no bearing on the overall test-to-theory comparisons.

Predicted lift, moment, and drag coefficients are compared with wind-tunnel data in Figures 4-12 through 4-14 for the model with the canards and trailing-edge flaps undeflected. Since the clean-wing, power-off data are used as the input to the method, there are no predicted curves for these conditions. It can be observed in these curves that lift and moment data are estimated reasonably well. The method is correlated with experimental data for values of  $C_T \leq 1.0$ , with extrapolations of these correlations for higher values of  $C_T$ . Therefore, the minor discrepancies at  $C_T = 1.8$  are not surprising. The clean-wing drag predictions are shown in Figure 4-14. It should be noted that these predictions have been forced to match the data at the point of minimum drag. The comparisons, therefore, indicate only the accuracy of the procedure to estimate the polar shape.

Figures 4-15 through 4-17 show a similar set of comparisons for the trailing-edge flap deflected 30 deg. The overall levels of the lift and moment data are slightly under-predicted. It is noted, however, that the increments caused by power match those of the data very closely. The effects of power on the lift and moment increments are shown in Figure 4-18 for several combinations of angle of attack and trailing-edge flap deflection. This plot clearly illustrates that the method is very accurate for the estimation of lift and moment coefficients for the Fighter Model.

The capability to include induced aerodynamic effects from the jet exhaust is very important during aircraft sizing studies in which critical parameters, such as turn rates and take-off distances, determine the wing size, and hence, are driving functions in the overall aircraft weight and cost. The test-to-theory comparisons presented in this section demonstrate the capability of the Powered-Lift Prediction Method to predict the induced effects for engine-over-wing type configurations at takeoff and landing conditions. It is thus shown to be a useful preliminary design tool for sizing STOL aircraft to meet low-speed requirements. The capability of the Powered-Lift Prediction Method is not limited to STOL conditions; application has also been verified at transonic conditions (Reference 26).



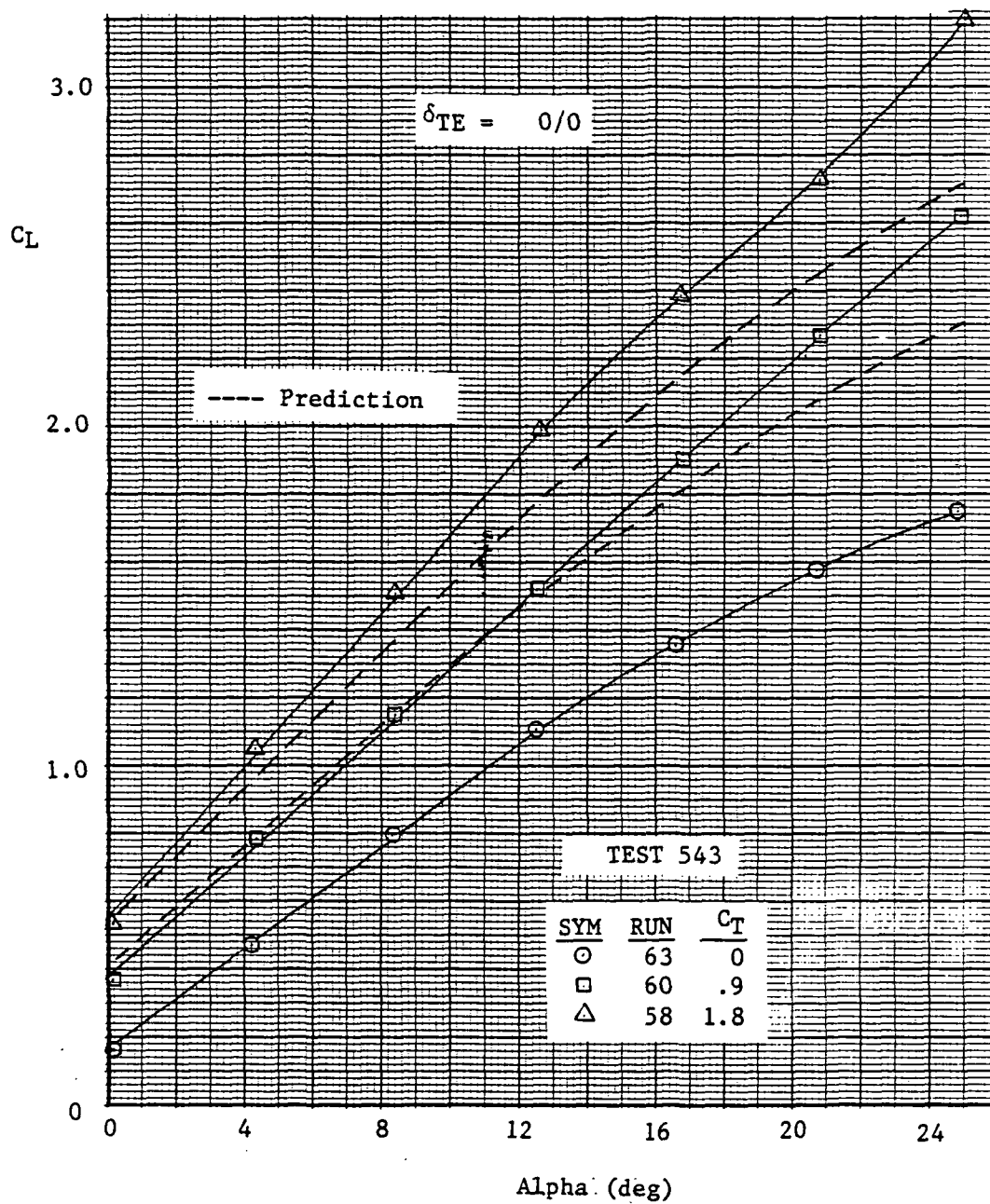


Figure 4-12

Comparison of Data and General Dynamics Prediction Method For Lift, Flaps Neutral

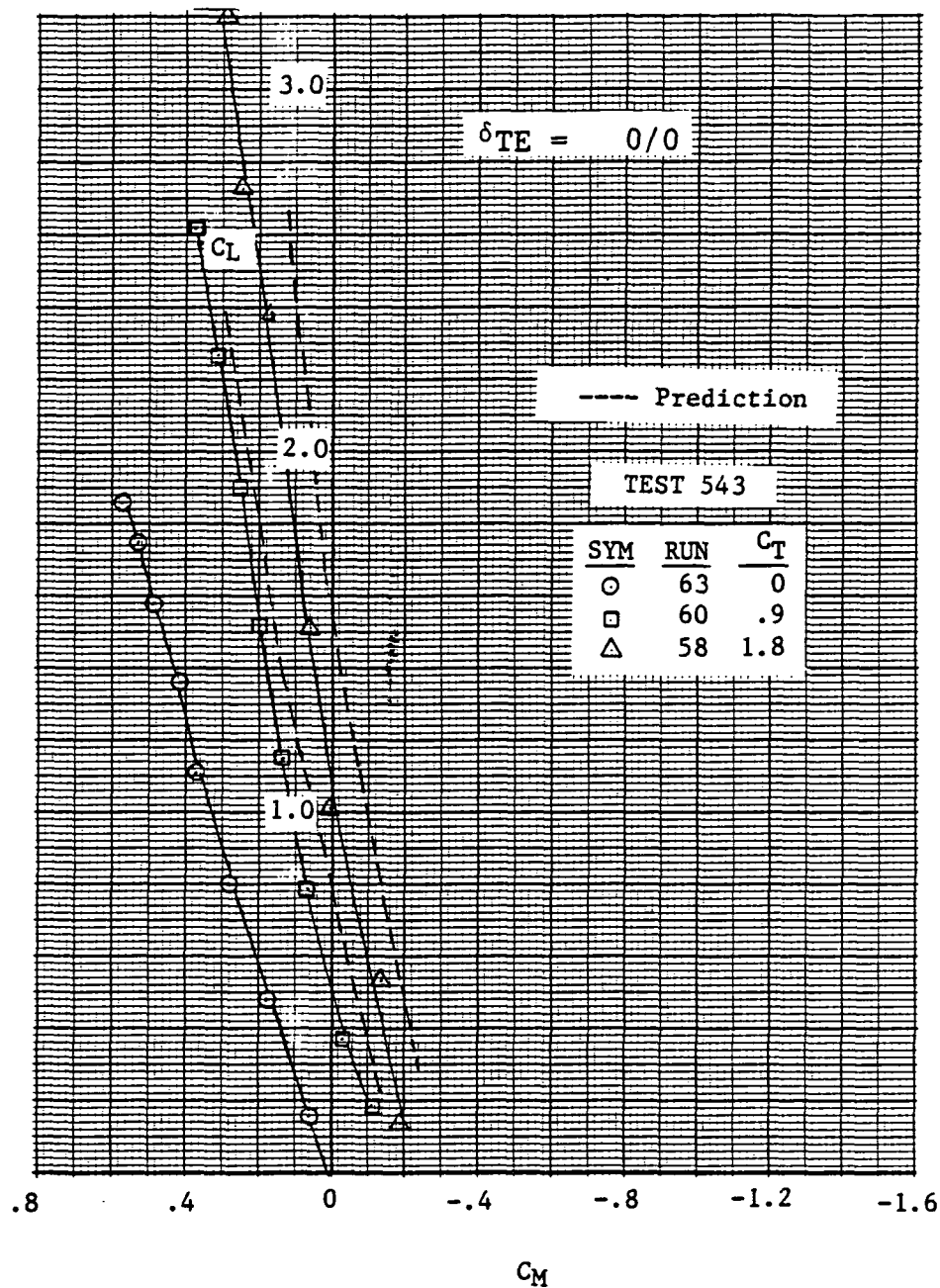


Figure 4-13

Comparison of Data and General Dynamics Prediction Method For Pitching Moment, Flaps Neutral

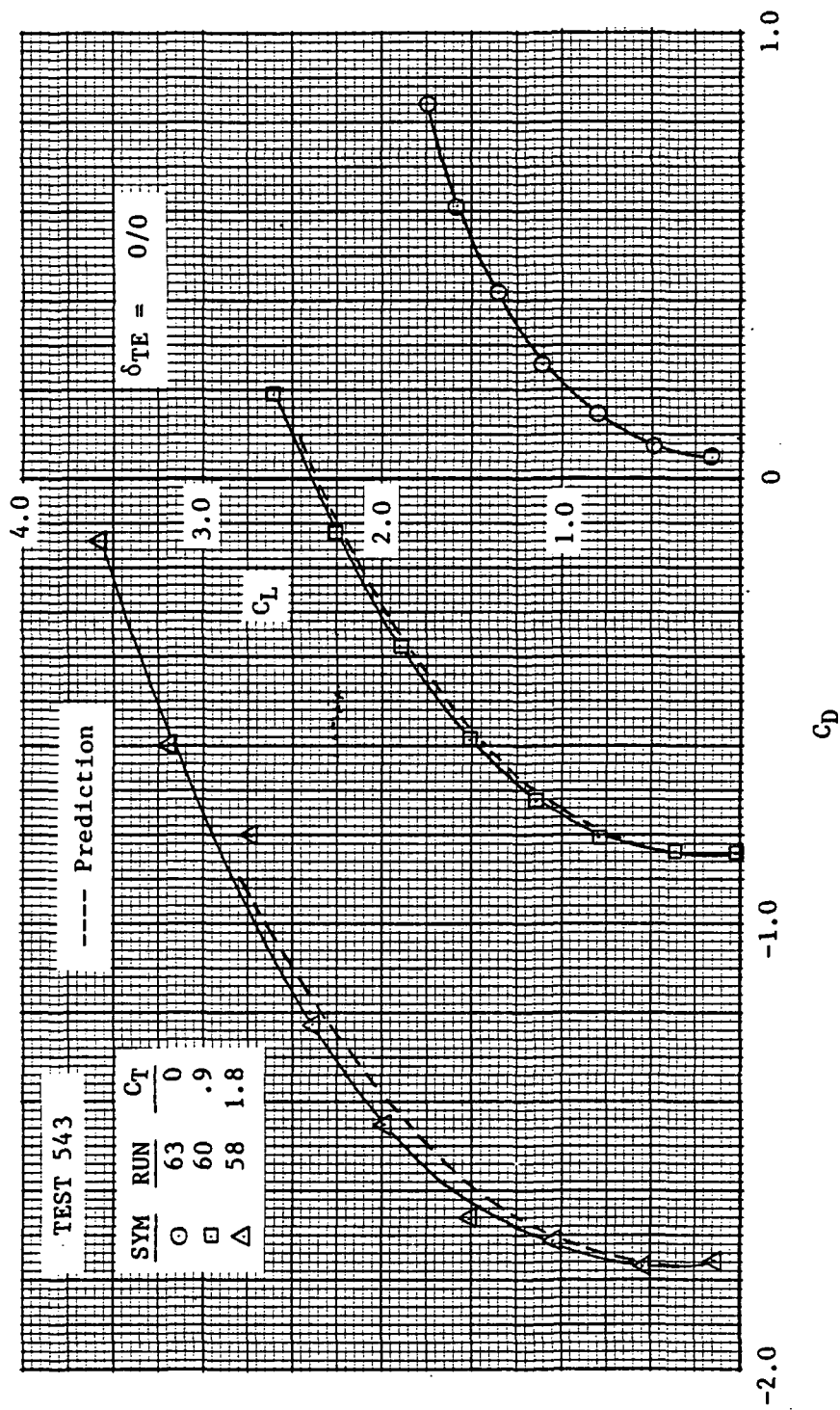


Figure 4-14 Comparison of Data and General Dynamics Prediction Method For Polar Shape, Flaps Neutral

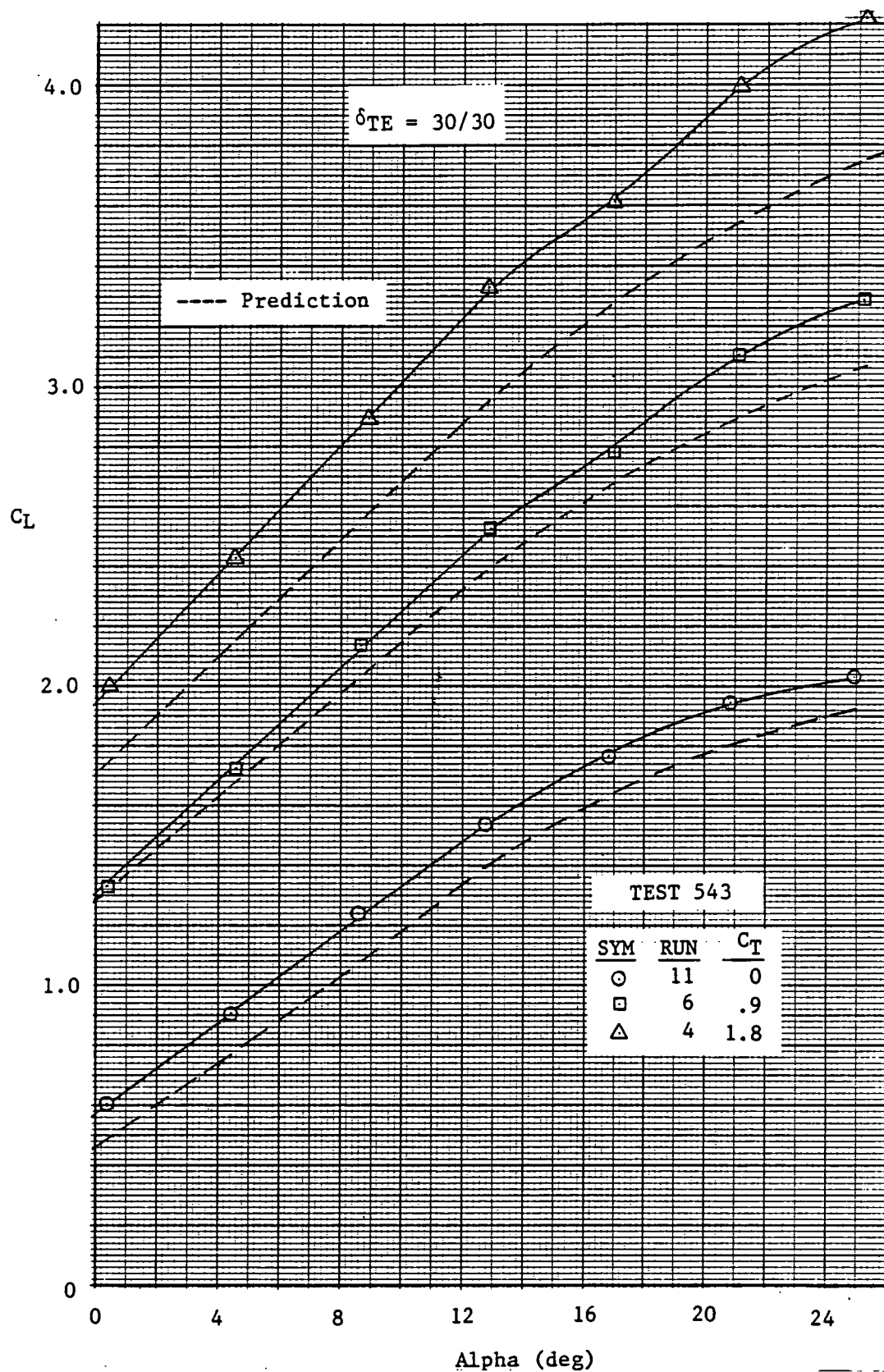


Figure 4-15

Comparison of Data and General Dynamics Prediction Method For Lift, Flaps Deflected

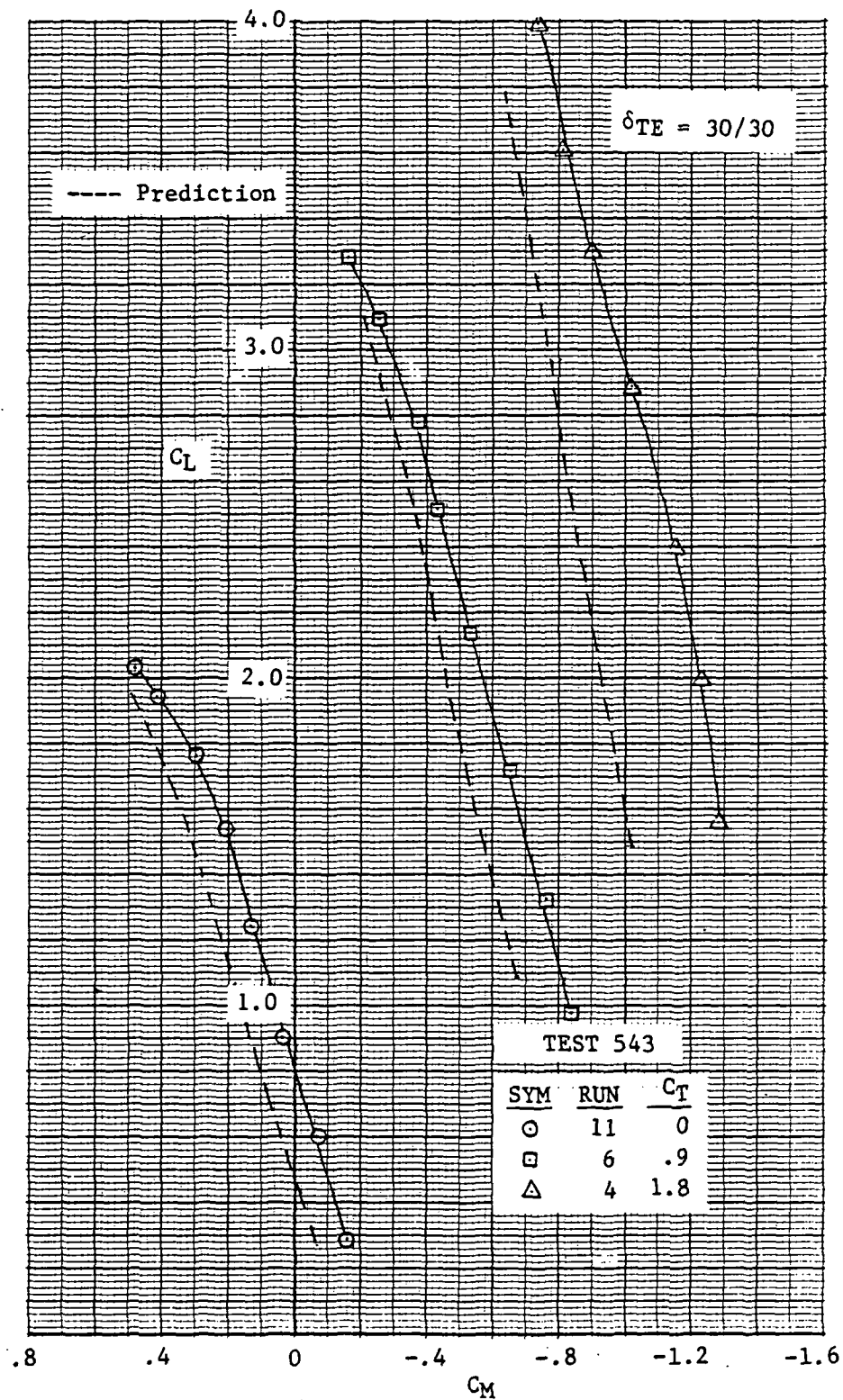


Figure 4-16

Comparison of Data and General Dynamics Prediction Method For Pitching Moment, Flaps Deflected

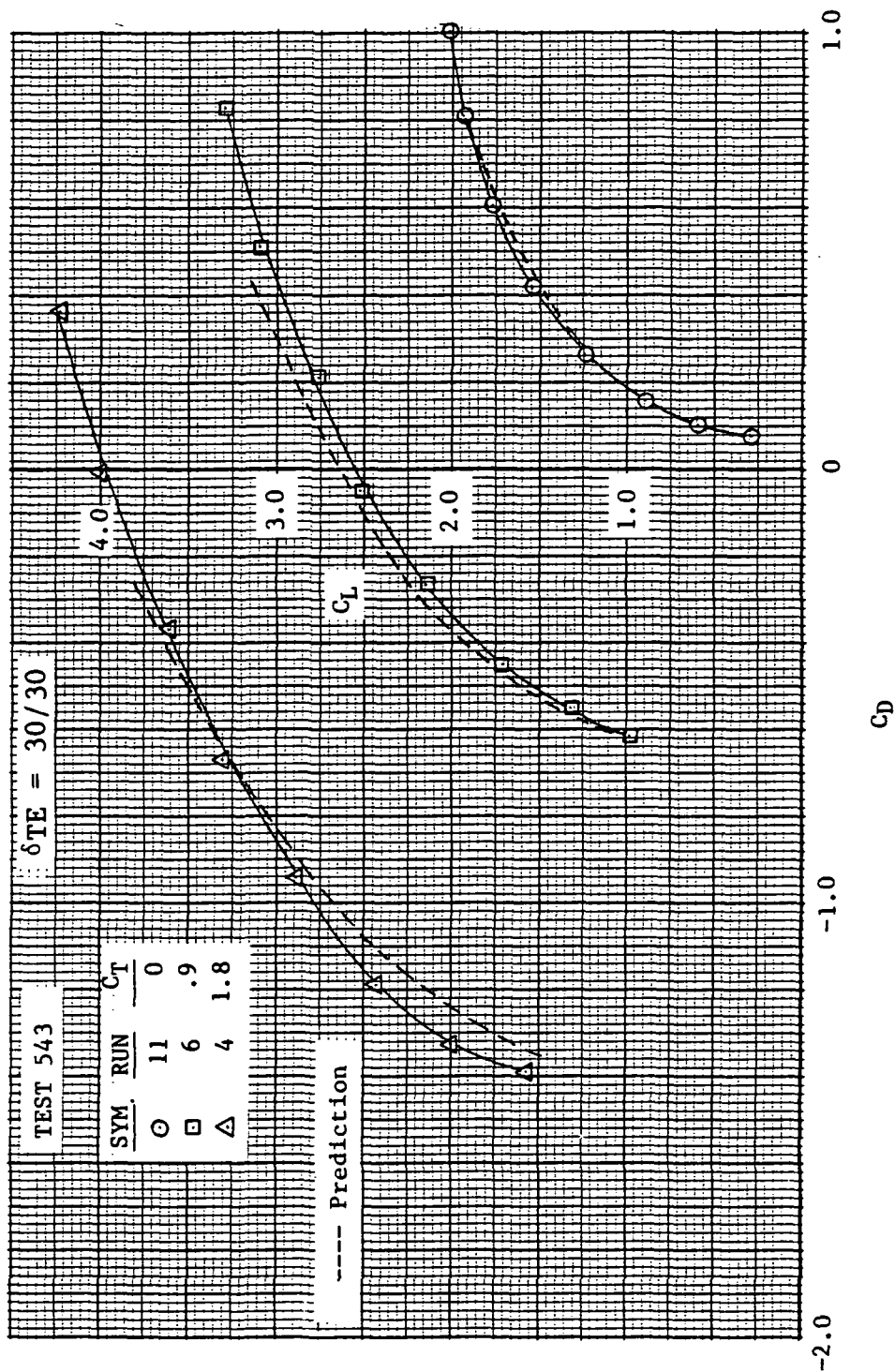


Figure 4-17 Comparison of Data and General Dynamics Prediction Method For Polar Shape, Flaps Deflected

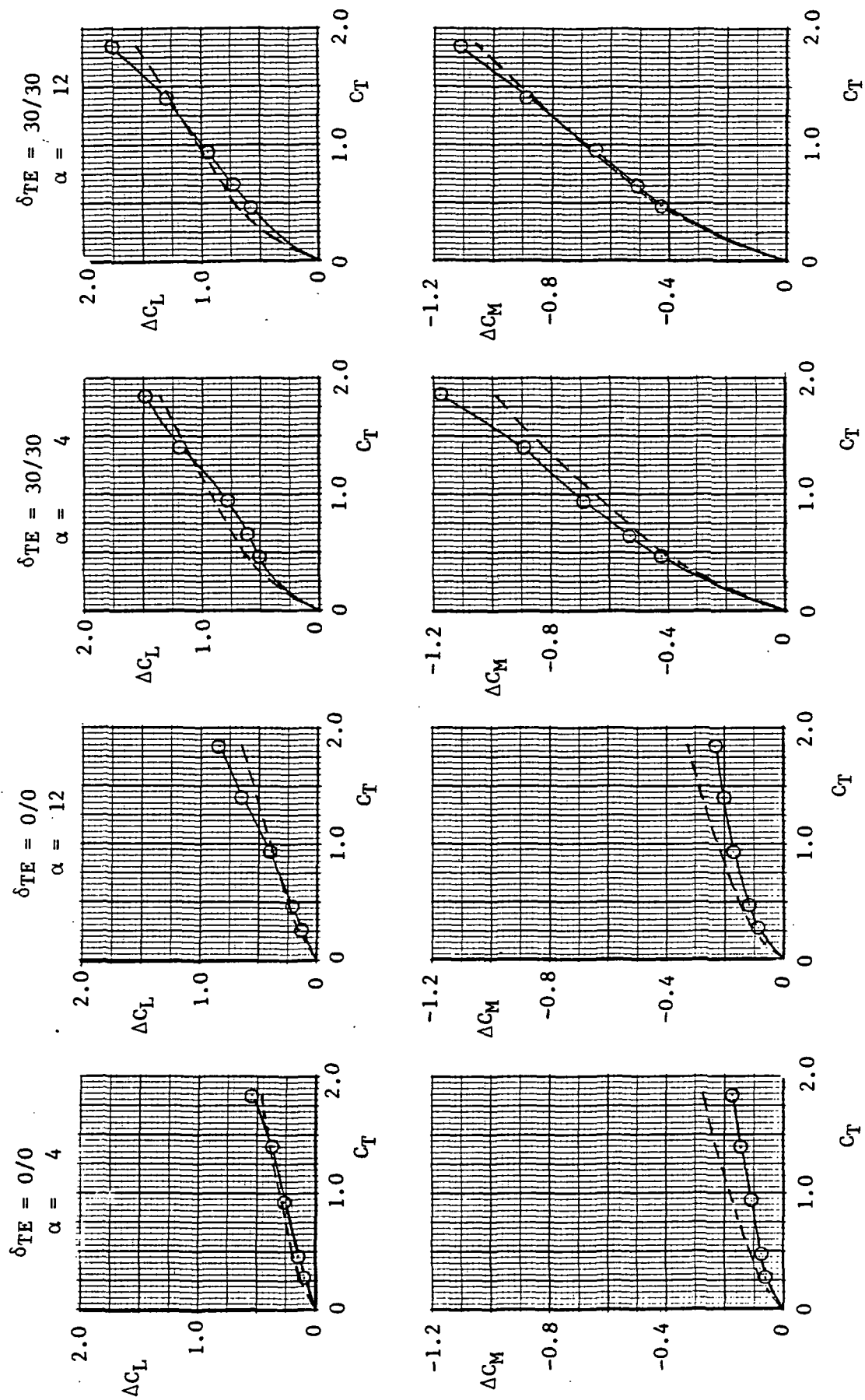


Figure 4-18 Comparison of Data and General Dynamics Prediction Method For Lift and Moment Increments Due to Power

**(This page intentionally left blank.)**



## 5. CONCLUSIONS AND RECOMMENDATIONS

### 5.1 FLOWFIELD

Pressure and thermal data have been used to establish the key flowfield features of the canard, wing, strake, and beaver tail of the STOL Fighter Model, with emphasis on the effects of the integrated propulsion system. An overview of the flowfield is presented in the body of the report, followed by an indepth discussion and presentation of the data.

The most significant feature of the flowfield was a leading-edge vortex that formed naturally on the wing at low alpha and progressively grew stronger and moved inboard as alpha was increased. The vortex outer edge defined a separation line, outboard of which the wing was stalled. Inboard of the separation line, the leading-edge vortex produced a modest increase in local lift. Chordwise blowing significantly enhanced the lift on the wing, both in the stalled and unstalled regions with the lift gains being greatest at high alpha and with wing trailing-edge flaps deflected. Except for the region immediately beneath the vortex, the incremental lift distribution caused by power was fairly evenly distributed over the chord, with only a modest aft shift in the center of pressure. Spanwise blowing effectively enhanced the wing leading-edge vortex, thereby increasing lift and causing a favorable, forward shift in the center of pressure. Traces of the spanwise jet and vortex were identified by a simultaneous analysis of the wing thermal and pressure data. Apparently, the spanwise jet mixed with the wing flowfield within a short distance from the nozzle, as indicated by the maximum temperature measured at the most inboard instrumentation, which was nominally 300 to 350°F. The jet was turned downstream sharply at low alphas as the vortex was being formed along the outboard leading edge, resulting in a large distance between the two streams. At high alphas, the jet unswept as the vortex moved inboard, so that they were much closer, interacting peripherally, but never confluent.

The wing vortex was dominant but not unique; a similar flow pattern also existed on the canard. The canard vortex was positioned above the plane of the wing, and its direct effects on the wing were rarely identifiable. Downwash from the canard, however, was prominent along the inboard section of the wing and it delayed by several degrees in angle of attack the inboard movement of the wing leading-edge vortex. Wing chordwise blowing reduced the canard upper-surface pressures slightly at low alphas, but quite substantially at high alphas. The effects of chordwise blowing were greater on the canard when the wing flaps were neutral than when deflected. The effects on the canard of wing spanwise blowing were similar to those registered by chordwise blowing at the same power setting.

Deflection of the beaver tail created an increase in upper-surface pressures that extended forward on the strake to approximately the wing flap station with corresponding pressure reductions on the lower surface. It was observed that the pressure reduction on the lower surface at most conditions was concentrated mainly along the edge of the beaver tail, and the favorable load did not carry over to the centerline of the surface. Direct influence of the primary nozzle on the beaver tail was identified by a simultaneous analysis of the pressure and thermal data. The only significant heating of the beaver tail occurred (1) near the edge of the surface when the wing flap was neutral or slightly deflected and (2) over the entire upper surface of the beaver tail when the wing flap was deflected upward, thereby causing the exhaust jet to spill inboard onto the area of the strake and beaver tail.

ORIGINAL PAGE IS  
OF POOR QUALITY

C-11

In summary, the primary points realized from the study of the pressure and thermal data are:

- o Leading-edge vortices formed on the upper surfaces of both the canard and wing. The vortices moved from outboard to inboard as  $\alpha$  was increased, leaving separated regions outboard of the vortices.
- o Chordwise blowing decreased the upper surface pressures fairly uniformly over the entire wing. The pressure change was much larger at  $\alpha$ s above wing stall.
- o The chordwise blowing influence, which extended significantly forward, decreased the canard upper surface pressures. The effects were greatest after the canard had stalled.
- o Spanwise blowing caused a decrease in upper-surface pressures directly beneath the jet. It also strengthened the vortex thereby decreasing the pressures over a large portion of the wing, particularly beneath and outboard of the vortex.
- o Chordwise blowing caused a modest aft shift in the wing center of pressure. Spanwise blowing caused a forward shift at  $\alpha$ s greater than about 12 deg.
- o The spanwise jet quickly mixed with freestream air and its temperature was reduced to less than one-half of its original value before it reached the thermal instrumentation.
- o The spanwise jet never became confluent with the leading-edge vortex.
- o The strake pressures were relatively insensitive to most variables.
- o A high-pressure area near the center of the beaver tail lower surface reduced its effectiveness as a pitch control device.

## 5.2 CONFIGURATION DESIGN

Configuration design recommendations are difficult to formulate from pressure data alone without the broader view provided by a study of force data from a test in which design changes were examined. There were, however, several observations made during the analysis of the pressure data that suggest the possibility of improving the flowfield. The simultaneous study of isotherm and isobar patterns indicated that spanwise blowing would be more effective at low  $\alpha$  if the spanwise nozzle were moved forward, nearer the leading edge, the reason being that as the vortex was first being formed on the wing leading edge, the jet was being turned sharply downstream by the wing flowfield and, thus, did not approach the area of the vortex trace. At higher  $\alpha$ , the vortex moved inboard, closer to the jet, and was thereby strengthened. It is felt that a more forward-spanwise-nozzle position would cause the jet to interact more strongly with the vortex in the  $\alpha$  range of 4 to 12 deg.

In the  $\alpha$  range of 20 deg and above, the isobar and isotherm patterns indicated that the vortex aft of the leading-edge was positioned above the wing with the spanwise jet passing beneath it but still interacting with the vortex. It is felt that a nozzle positioned higher above the wing surface would cause the jet to interact more directly with the vortex, thereby making the jet more effective as a vortex enhancer.

Other configuration changes that would strengthen the vortex or cause it to form at a lower  $\alpha$  would also likely improve the lift capability. This could perhaps be accomplished by a sharp leading-edge airfoil on the wing or perhaps a highly-swept strake forward of the wing on the side of the nacelle.

### 5.3 INSTRUMENTATION

The pressure instrumentation on the strake, beaver tail, and nozzle flap was adequate to measure the flow properties in these areas. That provided on the wing and canard, however, was a bare minimum for the determination of the flowfields about those surfaces. Although it was possible to discern the key flowfield features in some detail, this task would have been considerably easier had there been additional chordwise instrumentation along the upper surfaces of the wing and canard. It should be noted that the two chordwise stations that were instrumented were appropriately placed at their respective spanwise locations, and that the high concentration of taps near the upper-surface leading edge proved to be an invaluable aid in the identification of many of the flow features. Although sometimes confusing and often misleading, the spanwise row of instrumentation was ultimately judged to be correctly positioned at mid-chord to measure the effects of spanwise blowing. It should be noted, however, that these taps were generally of little value for spanwise-blowing-off cases except, on occasion, to help determine where the leading-edge vortex crossed over mid-chord. A row positioned further forward on the chord would have been of more value for this purpose.

In the study of the wing data, it was noticed on numerous occasions that the chordwise and spanwise rows of pressure taps did not agree at their intersection. To alleviate this minor problem, it is suggested that future instrumentation be installed so that a pressure measurement can be made from a tap that is common to both the chordwise and spanwise rows as pressures are read along each row. This problem seemed more prevalent when the wing was subjected to a flowfield with high-pressure gradients, such as when it was exposed to spanwise blowing. Consideration should also be given to the use of a slower cycle rate on the scanivalve under these conditions to assure that the pressure at the transducer is stabilized.

As a result of a mixing between the spanwise jet and the local wing flowfield, the temperature in the jet dropped rapidly, having diminished considerably before reaching the most inboard thermal instrumentation. Because of this, the peak thermal impact near the jet was not measured. It is, therefore, recommended that additional thermocouples be placed nearer to the jet in subsequent tests of this type in order to measure the peak thermal impact on the wing surface.

The temperature instrumentation provided on the beaver tail proved to be durable and reliable throughout the tests. Most of the thermocouples on the wing, however, failed shortly after exposure to the spanwise jet. The cause of this problem, which has not been identified, does not seem to be strictly related to temperature alone since the failure rate at the outboard station was almost as high as at the inboard station, even though the temperatures were lower outboard.

The force data were examined in this study only in relationship to their use in the correlation of test data with the analytical predictions. It was discovered, however, that the thrust-removed data contained some discrepancies that cast doubt on the thrust calibration and the engine instrumentation. The single pressure probe, upon which the thrust calibration was made, may have been inadequate for setting the EPR, the reason being primarily that inlet operation may have been somewhat different at static conditions than

in tunnel flow. At static conditions, the periphery of the flow that was sucked into the inlet did not approach from an axial direction, leading to the possibility that the flow may have separated as it negotiated the turn at the inlet lip. This may have led to poor inlet operation and local distortions in the engine-duct flow that affected the total pressure reading, since it was acquired with only one probe. Alternate instrumentation could be provided by mounting several total pressure probes in a uniform matrix within the engine duct, taking care to avoid alignment of the probes with the engine struts. The effects of local distortion would then be minimized by averaging the probe readings to determine the EPR.

## 5.4 TEST PROCEDURES

The test procedures followed in the acquisition of the pressure and thermal data generally provided a good set of data, within the limitations of the instrumentation itself. A minor point might be made, however, concerning the angles of attack that were tested. Pressure data were recorded at intervals of 4 deg in  $\alpha$ , which generally is quite acceptable due to a practical time constraint involved in the acquisition of large amounts of pressure data (not to mention the time for analysis). In these tests, however, quite often abrupt changes in the flowfield occurred between the tested angles of attack, which created difficulty in first formulating the flow model and then tracing the development of some of the flowfield features. As a result of this difficulty, the recommendation is made that pressure data be obtained on a few of the basic configurations at small intervals in angle of attack not to exceed 2 deg. Thereby, the data will be available to establish a more definitive basic flowfield model and an understanding of the basic features before proceeding to an evaluation of the effects of configuration and test variables.

Engine hardware constraints in this test prevented the variation of thrust; therefore, the tunnel  $q$  was varied in order to obtain a  $C_T$  sweep. This test procedure could not have been easily avoided, but the accompanying Reynolds number changes modified the leading-edge stall characteristics and caused some confusion in the interpretation of power effects. It was fortunate that these tests were conducted with a matching  $q$  condition for the  $C_T = 1.4$  and the power-off runs. Test personnel, however, should be alert to the implications of changing tunnel  $q$  and take steps to minimize the impact whenever possible.

A recommended change that would have the most impact on operating procedure is in regard to the manner in which the thrust calibration was obtained. The thrust-removed drag coefficient (a small number 0.05) is defined as the difference between the measured, thrust-included drag and the drag component of the calibrated thrust coefficient (both large numbers 2.0). A high degree of accuracy must be obtained in each of the large numbers if the thrust-removed drag coefficient is to be adequately defined. When the model is moved from the static test stand where the thrust calibration is normally determined to the wind tunnel, there are unavoidable changes in atmospheric conditions and instrumentation. More importantly, there are generally inconsistencies that inherently result when test setups are changed. In order to minimize the error in the thrust-removed drag, it is therefore suggested that final thrust calibrations be performed during the course of the in-tunnel testing. More specifically a static run should be made in the tunnel immediately preceding the wind-on run each time a configuration change is made that could affect the thrust (i.e. nozzle or flap change). It may be argued that this technique adversely affects the thrust calibration since a propulsion-induced flow in the closed circuit of the tunnel develops an aerodynamic load on the model. Loads are indeed produced; however, they are small relative to the propulsive forces, and furthermore, they can be accurately extracted from the load cell forces on the basis of the  $q$  of the induced flow and values of  $C_L$ ,  $C_D$ , and  $C_M$  determined from power-off run at a value of  $q$  approximating that of the propulsion-induced flow.

## 5.5 ANALYTICAL METHODS

Two methods were used to predict the pressures on the fighter model; another was used to estimate the propulsive-induced forces. Then, correlations with the tunnel data were used as the basis for judging the validity of the prediction techniques. The Elementary Vortex Distribution (EVD) method was investigated as an easy-to-use pre-design tool for the estimation of the power-induced pressure changes on the wing. A simple all-wing representation of the model was selected for the paneling scheme. The method was reasonably accurate in the estimation of the isolated trends in wing pressure loads caused by camber and twist, angle of attack, flap deflection, and power. The difficulty in the use of this procedure lies in the fact that the theory is strictly for attached flow, while the model flowfield was often separated. The presence of vortices on the model caused changes in the incremental pressure data that were, of course, not predicted by the EVD method. Therefore, the application of this method must be decided on a case-by-case basis, but the test-to-theory comparisons in Subsection 4.1 should be helpful in making that decision.

The General Dynamics Powered-Lift Prediction Method is a semi-empirical technique that was used to compute thrust-included lift, drag, and pitching moment estimates from the power-off baseline data. An anomaly in the force data prevented a correlation of the minimum drag, but the incremental lift, polar shape, and pitching moment estimates were quite accurate, especially at power setting of  $C_T=1.0$  and below. The procedure is based on correlations that extend only to  $C_T=1.0$ ; extrapolations of the correlation factors are used at higher levels of thrust. Hence, it is not surprising that the method accuracy is somewhat reduced at the higher power settings. The test-to-theory comparisons in Subsection 4.2 should give the user of this method confidence that it can be effectively applied to configurations similar to the STOL Fighter Model at moderate power settings of  $C_T=2.0$  and below.

**(This page intentionally left blank.)**

## REFERENCES

1. Bradley, R. G., Smith, C. W., and Wray, W. O., An Experimental Investigation of Leading-edge Vortex Augmentation by Blowing, NASA CR-132415, April 1974.
2. Bradley, R. G. and Wray, W. O., "A Conceptual Study of Leading Edge Vortex Enhancement by Blowing," Journal of Aircraft, Vol. 11, January 1974, pp. 34-38.
3. Bradley, R. G., Whitten, P. D., and Wray, W. O., "Leading Edge-Vortex Augmentation in Compressible Flow," Journal of Aircraft, Vol. 13, No. 4, April 1976, pp. 238-242.
4. Whitten, P. D., Kennon, I. G., and Stumpfl, S. C., "Experimental Investigation of a Nozzle/Wing Propulsive Lift Concept," AIAA Paper No. 76-625, July 1976.
5. Woodrey, R. W., Whitten, P. D., Smith, C. W., and Bradley, R. G., An Experimental Investigation of a Vectored-Engine-Over-Wing Powered-Lift Concept, Volume I, AFFDL-TR-76-92, September 1976.
6. Whitten, P. D., An Experimental Investigation of a Vectored-Engine-Over-Wing Powered-Lift Concept, Volume II, AFFDL-TR-76-92, March 1978.
7. Whitten, P. D., Kennon, I. G., and Stumpfl, S. C., Experimental Investigation of a Nozzle/Wing Propulsive Lift Concept, AIAA Paper No. 76-625, July 1976.
8. Vectored-Engine-Over Wing Concept Benefits Study, General Dynamics Fort Worth Division Report FZM-6643, 1 February 1977.
9. Heim E. R., Basic Aerodynamic Data for a Vectored-Engine-Over-Wing Configuration, AEDC-TR-78-1, February 1978.
10. Whitten, P. D., and Howell, G. A., Investigations of the VEO-Wing Concept in an Air-to-Ground Role, AFFDL-TR-79-3031, March 1979.
11. Whitten, P. D., Howell, G. A., and Joyce, G. T., Development of STOL VEO-Wing Configurations, General Dynamics Report ERR-FW-2057, 21 December 1979.
12. Harris, Michael J. and Falarski, Michael D., Static Calibration of a Two-Dimensional Wedge Nozzle with Thrust Vectoring and Spanwise Blowing, NASA TM 81161, April 1980.
13. Falarski, M. D., Whitten, P. D., and Harris, M. J., "Aerodynamic Characteristics of a Large-Scale Model of a Highly Maneuverable Supersonic V/STOL Fighter: STOL Configuration," AIAA Paper No. 80-0234, January 1980.
14. White, R. P., Jr., "Wing-Vortex Lift at High Angles of Attack," Paper No. 9-1 in Prediction of Aerodynamics Loading, AGARD CP-204, February 1977.
15. Nicholas, W. U., Jr., A Summary of Aerodynamic Methods for Use in Conceptual Design, General Dynamics Fort Worth Division Report ERR-FW-1576, December 1974.
16. Carlson, W. C. and Mack, R. J., "Studies of Leading-Edge Thrust Phenomena," AIAA Journal of Aircraft, Vol. 17, No. 12, December 1980.

17. Gloss, B. B. and Washburn, K. E., A Study of Canard-Wing interference Using Experimental Pressure Data at Transonic Speeds, NASA Technical Paper 1355, January 1979.
18. Wray, W. O., Jr., Model and Test Information Report, .108-Scale Powered Lift Research Model for NASA Langley Research Center, General Dynamics Report FZT-259, Addendum III, 1 December 1978.
19. Goldhammer, M. I., Lopez, M. L. and Shen, Methods for Predicting the Aerodynamic and Stability and Control Characteristics of STOL Aircraft, Volume I, Basic Theoretical Methods, AFFDL-TR-73-146, December 1973.
20. Goldhammer, M. I. and Wasson, N. F., Methods for Predicting the Aerodynamic and Stability Characteristics of STOL Aircraft, Volume II, STOL Aerodynamic Methods Computer Program, AFFDL-TR-73-146, December 1973.
21. Goldhammer, M. I. and Lopez, M. L., Methods for Predicting the Aerodynamic and Stability Characteristics of STOL Aircraft, Volume III, Engineering Methods, AFFDL-TR-73-146, December 1973.
22. VonBose, D. R. and Whitten, P. D., Evaluation and Modification of the EVD (Elementary Vortex Distribution) Finite-Element Lifting Surface Jet-Flap Computer Procedure, General Dynamics Report, ARM No. 149, 14 May 1975.
23. Whitten, P. D., Semi-Empirical Powered-Lift Methodology Presentation to AFFDL, General Dynamics Report No. ARM 139, April 1974.
24. Spence, D. A., A Treatment of Jet Flap by Thin Airfoil Theory, R.A.E. Report Aero 2568, November 1955.
25. Erickson, J. C., The Pitching-Moment Coefficient of a Jet-Flapped Thin Airfoil, Journal of the Aerospace Sciences, December 1962.
26. Whitten, P. D. and Howell, G. A., Investigations of the VEO-Wing Concept in an Air-to-Ground Role, AFFDL-TR-79-3031, March 1979.



1. Report No. NASA CR-166170		2. Government Accession No.		3. Recipient's Catalog No.	
4. Title and Subtitle EVALUATION OF PRESSURE AND THERMAL DATA FROM A WIND TUNNEL TEST OF A LARGE-SCALE, POWERED, STOL FIGHTER MODEL				5. Report Date June, 1981	
				6. Performing Organization Code	
7. Author(s) G. A. Howell E. L. Crosthwait M. C. Witte				8. Performing Organization Report No.	
9. Performing Organization Name and Address  General Dynamics Fort Worth Division P. O. Box 748, Fort Worth, Texas 76101				10. Work Unit No.	
				11. Contract or Grant No. NAS2-10649	
12. Sponsoring Agency Name and Address Ames Research Center Moffett Field, CA 94035				13. Type of Report and Period Covered Contractor Final Report June 4, 1980-June 4, 1981	
				14. Sponsoring Agency Code	
15. Supplementary Notes  Ames Research Center Technical Monitor: Susan Braden (415) 965-5046					
16. Abstract  A STOL fighter model employing the Vectored-Engine-Over Wing concept was tested at low speeds in the NASA/Ames 40x80-Foot Wind Tunnel. The model, approximately 0.75 scale of an operational fighter, was powered by two General Electric J-97 turbojet engines. Limited pressure and thermal instrumentation were provided to measure power effects (chordwise and spanwise blowing) and control-surface-deflection effects.  An indepth study of the pressure and temperature data revealed many flowfield features - the foremost being wing and canard leading-edge vortices. These vortices delineated regions of attached and separated flow, and their movements were often keys to an understanding of flow-field changes caused by power and control-surface variations.  Chordwise blowing increased wing lift and caused a modest aft shift in the center of pressure. The induced effects of chordwise blowing extended forward to the canard and significantly increased the canard lift when the surface was stalled. Spanwise blowing effectively enhanced the wing leading-edge vortex, thereby increasing lift and causing a forward shift in the center of pressure.  The effects of power on the pressures and forces on the model were estimated with two analytical methods; test-to-theory comparisons are presented for each method.					
17. Key Words (Suggested by Author(s)) Powered-lift Prediction Methods Spanwise Blowing STOL Aerodynamics				18. Distribution Statement	
19. Security Classif. (of this report) Unclassified		20. Security Classif. (of this page) Unclassified		21. No. of Pages 956	
				22. Price*	